3rd Croatian Conference on Earthquake Engineering 3CroCEE

19-22 March 2025, Split, Croatia

Conference Proceedings

Conference Organizers

University of Zagreb
Faculty of Civil
Engineering

UNIVERSITY OF SPLIT,
FACULTY OF CIVIL ENGINEERING,
ARCHITECTURE AND GEODESY

Supporting Organizations

The International
Association for
Earthquake Engineering

The European
Association for
Earthquake Engineering

Croatian
Association for
Earthquake Engineering

Under Auspices of

Government
of the Republic
of Croatia

Copyright © 2025 CroCEE

Title

3rd Croatian Conference on Earthquake Engineering - 3CroCEE

March 19 to 22, 2025· Split

Editors

Josip Atalić

Neno Torić

Marta Šavor Novak

Nikola Grgić

Marina Frančić Smrkić

Boris Trogrlić

Mario Uroš

Nikolina Živaljić

Iva Dasović

Marija Demšić

Ivan Balić

Mirela Galić

ISSN

ISSN 3043-8071

DOI

10.5592/CO/3CroCEE.2025

Published by

University of Zagreb Faculty of Civil Engineering

University of Split Faculty of Civil Engineering, Architecture and Geodesy

Cover page

minimum d.o.o.

Matej Korlaet

Zagreb, March 2025

Copyright © 2025 CroCEE

Proceedings of the 3rd Croatian Conference on Earthquake Engineering

Split, Croatia - March 19 to 22, 2025

Copyright © 2025 CroCEE

3rd Croatian Conference on Earthquake Engineering

CHAIRMEN

Josip Atalić, University of Zagreb
Neno Torić, University of Split

ORGANIZING COMMITTEE

Josip Atalić, University of Zagreb
Mario Bačić, University of Zagreb
Ivan Balić, University of Split
Goran Baloević, University of Split
Maja Baniček, University of Zagreb
Ivan Banović, University of Split
Nina Čeh, University of Rijeka
Domagoj Damjanović, University of Zagreb
Iva Dasović, University of Zagreb
Marija Demšić, University of Zagreb
Marina Frančić Smrkić, University of Zagreb
Mirela Galić, University of Split
Petra Gidak, University of Zagreb
Davor Grandić, University of Rijeka
Nikola Grgić, University of Split
Marin Grubišić, Josip Juraj Strossmayer University of Osijek
Ivica Guljaš, Josip Juraj Strossmayer University of Osijek
Ivo Haladin, University of Zagreb
Alen Harapin, University of Split
Tomislav Kišiček, University of Zagreb
Mladen Kustura, University of Mostar
Senad Medić, University of Sarajevo
Marina Nikolić, University of Split
Marija Smilović Zulim, University of Split
Mislav Stepinac, University of Zagreb
Marta Šavor Novak, University of Zagreb
Petra Šimundić, University of Split
Igor Tomić, École Polytechnique Fédérale de Lausanne
Neno Torić, University of Split
Boris Trogrlić, University of Split
Mario Uroš, University of Zagreb
Damir Varevac, Josip Juraj Strossmayer University of Osijek
Nikolina Živaljić, University of Split

ACADEMIC SCIENTIFIC COMMITTEE

Dražen Aničić, Croatian Academy of Engineering
Josip Atalić, University of Zagreb
Mario Bačić, University of Zagreb
Ivan Balić, University of Split
Goran Baloević, University of Split
Maja Baniček, University of Zagreb
Ivan Banović, University of Split
Ana Baričević, University of Zagreb
Marko Bartolac, University of Zagreb
Paolo Bazzurro, University School for Advanced Studies IUSS Pavia
Vasco Bernardo, University of Minho
Katrin Beyer, École Polytechnique Fédérale de Lausanne
Jelena Bleiziffer, University of Zagreb
Svetlana Brzev, University of British Columbia
Serena Cattari, University of Genoa
Anita Cerić, University of Zagreb
Andrew Charleson, Victoria University of Wellington
Nicola Chieffo, University of Minho
Helen Crowley, EUCENTRE
Nina Čeh, University of Rijeka
Ivan Ćurković, University if Zagreb
Domagoj Damjanović, University of Zagreb
Laurentiu Danciu, ETH Zurich
Iva Dasović, University of Zagreb
Marija Demšić, University of Zagreb
Marco di Ludovico, University of Naples
Matjaž Dolšek, University of Ljubljana
Ivan Duvnjak, University of Zagreb
Amr Elnashai, University of Houston
Peter Fajfar, University of Ljubljana
Radomir Folić, University of Novi Sad
Marina Frančić Smrkić, University of Zagreb
Marco Francesco Funari, University of Surrey
Mirela Galić, University of Split
Petra Gidak, University of Zagreb
Agostino Goretti, Civil Protection Department of Italy

Copyright © 2025 CroCEE

Davor Grandić, University of Rijeka
Nikola Grgić, University of Split
Marin Grubišić, Josip Juraj Strossmayer University of Osijek
Ivica Guljaš, Josip Juraj Strossmayer University of Osijek
Marijana Hadzima-Nyarko, Josip Juraj Strossmayer University of Osijek
Iman Hajirasouliha, University of Sheffield
Sanja Hak, Basler & Hofmann, Zürich
Ivo Haladin, University of Zagreb
Alen Harapin, University of Split
Marijan Herak, University of Zagreb
Sanja Jerković, City of Zagreb
Antonia Jaguljnjak Lazarević, University of Zagreb
Tanja Kalman Šipoš, Josip Juraj Strossmayer University of Osijek
Tomislav Kišiček, University of Zagreb
Meho Saša Kovačević, University of Zagreb
Sergio Lagomarsino, University of Genoa
Damir Lazarević, University of Zagreb
Paulo B. Lourenco, University of Minho
Ivan Lukačević, University of Zagreb
Ana Mandić Ivanković, University of Zagreb
Marko Marinković, University of Belgrade
Senad Medić, University of Sarajevo
Ljubomir Miščević, University of Zagreb
Paolo Morandi, University of Pavia, EUCENTRE
Marija Mustać Brčić, University of Zagreb
Miroslav Nastev, Geoscience for Public Safety Geological Survey of Canada
Marina Nikolić, University of Split
Eva Ocvirk, University of Zagreb
Jelena Pejović, University of Montenegro
Davorin Penava, University of J.J. Strossmayer in Osijek
Ljupko Perić, ETH Zürich
Kyriazis Pitilakis, Aristotle University
Savvas Saloustros, École Polytechnique Fédérale de Lausanne
Marijana Serdar, University of Zagreb
Mahmoud Shaqfa, Massachusetts Institute of Technology
Veronika Shendova, University of SS Cyril and Methodious in Skopje
Neritan Shkodrani, Polytechnic University of Tirana
Zvonko Sigmund, University of Zagreb
Vitor Silva, GEM, EUCENTRE, University of Aveiro
Davor Skejić, University of Zagreb
Ana Skender, University of Zagreb
Marija Smilović Zulim, University of Split
Hrvoje Smoljanović, University of Split
Davor Stanko, University of Zagreb
Mislav Stepinac, University of Zagreb
Marta Šavor Novak, University of Zagreb
Ingrid Tomac, University of California (San Diego)
Igor Tomić, École Polytechnique Fédérale de Lausanne
Neno Torić, University of Split
Thanasis Triantafillou, University of Patras
Boris Trogrlić, University of Split
Mario Uroš, University of Zagreb
Dimitrios Vamvatsikos, National Technical University of Athens
Anđelko Vlašić, University of Zagreb
Mihaela Zamolo, Croatian Society for Earthquake Engineering
Mariano Angelo Zanini, University of Padova
Nikolina Živaljić, University of Split

Copyright © 2025 CroCEE

PREFACE

After the 2020 earthquakes, the initial response was to gather all available resources in Croatia and abroad to address the threat (risk), which is officially designated (in the national strategic documents) as unacceptable. Unity and a thirst for knowledge proved crucial in the aftermath of the earthquakes, and we believe that this remains the guiding principle in our efforts to build a resilient future.

The organization of the First Croatian Conference on Earthquake Engineering (1CroCEE) was symbolic, as it was held on the first anniversary of the 2020 Zagreb earthquake and just a few months after the Petrinja earthquake. This occurred during a period of community recovery, when it was crucial to care for affected citizens, amidst the reconstruction of numerous significant buildings in the nation's capital, and while the country's resources were stretched, and experts were still in the field. Nevertheless, more than 700 researchers, practicing engineers, architects, government representatives (including the Prime Minister), students, and other colleagues from 26 countries participated in the conference. 1CroCEE was a "game-changer" in Croatia, significantly raising the level of knowledge, connecting experts, and maintaining high risk awareness. It highlighted the future reconstruction process as a culmination of post-earthquake activities, where the scientific community demonstrated its value.

The Second Croatian Conference on Earthquake Engineering (2CroCEE), held on the third anniversary of the 2020 Zagreb earthquake, reinforced a continuous and decisive approach to addressing earthquakes in a small and vulnerable country like Croatia. The conference established a new tradition of remembering earthquakes (even if infrequent) and transferring knowledge to new generations. Over 300 participants took advantage of unique technical visits to earthquake-affected areas and reconstruction sites in Zagreb and Petrinja.

The Third Croatian Conference on Earthquake Engineering (3CroCEE), planned for the fifth anniversary of the 2020 Zagreb earthquake, aims to "re(shake)" knowledge sharing and "reunite" efforts to raise awareness of the greatest threat/risk to Croatia. Dalmatian cities, including Split, are prime examples: they are extremely rich in cultural heritage, infinitely beautiful, and attractive for living, yet they contain many traditional buildings with high seismic vulnerability. One of the main goals of the conference is to promote state-of-the-art research and to implement knowledge and experience into prevention activities (minimising the casualties and damage). This is a real test of the lessons learned from the 2020 earthquakes in Zagreb and Petrinja, and a test of the level of seismic risk awareness for preventive measures. Do we have to wait for an earthquake in this part of Croatia or can we try to shake Split with knowledge?

Finally, the organizers of the conference would like to thank all the companies and institutions that supported this conference. Special thanks go to the International Association for Earthquake Engineering, the European Association for Earthquake Engineering and the Croatian Association for Earthquake Engineering, for their assistance and support in organizing this conference. We would like to express our deepest gratitude to the esteemed keynote and invited speakers who, with their expertise and contributions, have elevated this conference to the highest standards of excellence in the field of earthquake engineering. Furthermore, we would like to thank all the authors for their excellent contributions to these proceedings and the members of the Organizing Committee and Academic Scientific Committee, as well as the numerous experts who participated in the review process. The gratitude is also extended to all participants for attending the conference. We believe that these 3CroCEE proceedings will be highly interesting and useful to all experts exhibiting a scientific and professional interest in earthquake engineering.

Copyright © 2025 CroCEE

We conclude with joy and pride that we have once again brought together many leading scientists in earthquake engineering and nearly all experts from Croatia. We firmly believe that the newly acquired knowledge will significantly help to achieve a further step towards an earthquake-resilient future in Croatia. Thank you for joining us at 3CroCEE to (re)shake Croatia (Split) with knowledge and establish a new tradition of reconstructing the past for a resilient future.

Josip Atalić
Neno Torić
Marta Šavor Novak
Nikola Grgić
Marina Frančić Smrkić
Boris Trogrlić
Mario Uroš
Nikolina Živaljić
Iva Dasović
Marija Demšić
Ivan Balić
Mirela Galić

Zagreb, March 2025

Copyright © 2025 CroCEE

CONFERENCE SUPPORT

SUPPORTING ORGANIZATIONS

The European Association for Earthquake Engineering

www.eaee.org

The International Association for Earthquake Engineering

www.iaee.or.jp

The Croatian Association for Earthquake Engineering

Croatian Center for Earthquake Engineering

Branch office of the Faculty of Civil Engineering University of Zagreb

www.hcpi.hr

UNDER AUSPICE OF

GOVERNMENT OF REPUBLIC OF THE REPUBLIC OF CROATIA

The Government of the Republic of Croatia
Trg svetog Marka 2
10000 Zagreb, Croatia
https://vlada.gov.hr/

ACADEMIA SCIENTIARUM ET ARTIUM CROATICA

Croatian Academy of Sciences and Arts
Foundation
Zrinski trg 11
10000 Zagreb, Croatia
www.zaklada-hazu.hr

Copyright © 2025 CroCEE

GENERAL SPONSOR

Croatian Chamber of Civil Engineers

Ulica grada Vukovara 271
10000 Zagreb, Croatia

www.hkig.hr

PLATINUM SPONSORS

Spegra

Ante Petravića 23, 21000 Split, Croatia

www.spegra.hr

GOLDEN SPONSORS

Radnik d.d.

Kralja Tomislava 45, 48260 Križevci, Croata

https://radnik.hr/

FIP MEC S.r.l.

Via Scapacchiò, 41, 35030 Selvazzano Dentro PD, Italy

https://www.fipmec.it

Mapei Croatia d.o.o.

Purgarija 14, Kerestinec, 10431 Sveta Nedelja, Croatia

https://www.mapei.com/hr/

Copyright © 2025 CroCEE

SILVER SPONSORS

Freyssinet Adria Sl, d.o.o.

Žnidarčičeva 37, 5290 Šempeter pri Gorici, Slovenia

www.freyssinet-adria.si

REGUPOL Germany GmbH & Co. KG

Am Hilgenacker 24, 57319 Bad Berleburg, Germany

www.regupol.de

Tromont d.o.o.

Dračevac 11, Split, Croatia

https://www.tromont.hr/

Wienerberger d.o.o.

Donje Pokuplje 2, 47000 Karlovac

www.wienerberger.hr

Ground Zero d.o.o.

Ante Starčevića 49, 21 000 Trogir, Croatia

https://www.gz.hr/

PERI oplate i skele d.o.o.

Banjavčićeva 13, 10 000 Zagreb, Croatia

https://www.peri.com.hr/

Kinemetrics

222 Vista Avenue, Pasadena, CA 91107, U.S.A.

https://kinemetrics.com/

Lavčević d.d.

Bihaćka 2, 21000 Split, Croatia

https://www.lavcevic.hr/

Copyright © 2025 CroCEE

BRONZE SPONSOR

Studio ARHING d.o.o..

Ćire Truhelke 49, 10000 Zagreb, Croatia

https://www.studio-arhing.hr/

U.O.I.G. Tarnik.

Višnjica 29, Zagreb, Croatia

http://www.tarnik-grad.hr/

INSTITUT IGH, d.d..

Janka Rakuše 1, 10000 Zagreb, Croatia

https://www.igh.hr

TODING d.o.o..

Havidićeva 10a, 10000 Zagreb, Croatia

https://toding.hr/

Stabilnost d.o.o..

Kroz Smrdečac 41, 21000 Split, Croatia

https://www.stabilnost.eu/

Copyright © 2025 CroCEE

TABLE OF CONTENTS

KEYNOTE AND INVITED LECTURES: ABSTRACTS

SEISMIC ISOLATION IN LOSS-BASED DESIGN
Gian Michele Calvi.....1

MODELLING AND ANALYSES FOR THE SEISMIC ASSESSMENT OF EXISTING URM BUILDINGS: RESEARCH CHALLENGES AND ENGINEERING-PRACTICE IMPLICATIONS
Serena Cattari.....2

WHY SEISMIC HAZARD MODELLING HAS BECOME A RISKY BUSINESS
Helen Crowley.....3

COMPARISON OF TWO GENERATIONS OF EUROCODES FOR EARTHQUAKE-RESISTANT CONCRETE BUILDINGS THROUGH SYSTEMATIC APPLICATIONS
Michael N. Fardis.....4

MASONRY ENCLOSURES: DAMAGE, APPLICATIONS, LESSONS LEARNED FROM TESTING AND NEW SOLUTIONS
Paulo B. Lourenço.....5

TESTING FOR THE ASSESSMENT OF EARTHQUAKE RESISTANCE OF HERITAGE MASONRY BUILDINGS: NONDESTRUCTIVE VERSUS DESTRUCTIVE, LABORATORY VERSUS IN-SITU TESTING
Miha Tomaževič.....6

EXPLOITING NONLINEAR SOIL-FOUNDATION RESPONSE IN DEFENCE OF THE SUPERSTRUCTURE
Ioannis Anastasopoulos.....7

SEISMIC PERFORMANCE AND FRAGILITY ASSESSMENT OF GLASS CURTAIN WALLS: METHODS AND INFLUENCING PARAMETERS
Chiara Bedon.....8

SEISMIC RISK ASSESSMENT IN URBAN AREAS: INNOVATIVE APPROACHES TO SUPPORT LARGE-SCALE VULNERABILITY EVALUATIONS IN THE DIGITAL AGE
Tiago Miguel Ferreira.....9

EXAMPLES OF APPLICATION OF SEISMIC INTERFEROMETRY IN ENGINEERING SEISMOLOGY
Stefano Parolai.....10

SEISMIC ANALYSIS OF MASONRY STRUCTURES
Hrvoje Smoljanović.....11

SEISMIC DESIGN OF MASONRY STRUCTURES WITH THE SECOND GENERATION OF EUROCODE 8 - BACKGROUND AND APPLICATION
Christoph Butenweg.....12

Copyright © 2025 CroCEE

ENGINEERING SEISMOLOGY

A CAUSAL LENS PERSPECTIVE ON BASIN EFFECTS
Rashid Shams, Chukwuebuka C. Nweke, Chenhao Wu and Henry Burton.....13

COMBINING CONVENTIONAL AND NEXT-GENERATION INTENSITY MEASURES FOR RISK ASSESSMENT OF BRIDGES
Savvinos Aristeidou, Gerard O'Reilly.....15

SEISMIC GROUND MOTION AMPLIFICATION INDUCED BY TOPOGRAPHIC IRREGULARITY IN NORTHERN CROATIA
Davor Stanko, Dragana Dogančić, Sanja Kovač, Jasmin Jug, Stjepan Strelec, Vesna Poslončec Petrić, Marijan Kovačić, Francesco Panzera, Olga-Joan Ktenidou.....27

PATTERNS OF EARTHQUAKE DAMAGE IN STON: A 146-YEAR COMPARISON
Marijan Herak, Davorka Herak.....30

THE ROLE OF SEISMIC GEOPHYSICAL METHODS IN NEAR-SURFACE CHARACTERIZATION
Irena Gjorgjeska, Vlatko Sheshov, Julijana Bojadjieva, Kemal Edip.....32

LOCAL EARTHQUAKES - GROUND MOTION MODELS FOR EPICENTRAL ZONE
Snezana Gjorgji Stamatovska.....40

IMPROVEMENT AND UPDATES OF THE NATIONAL DATABASES FOR SEISMOGENIC SOURCE MODELING IN THE CONTEXT OF REVISING THE NATIONAL HAZARD MODEL FOR NORTH MACEDONIA
Zabedin Neziri, Ljubcho Jovanov, Radmila Salic Makreska, Katerina Drogreshka, Laurentiu Danciu, Jasmina Najdovska, Daniel Tomic.....52

PARAMETRIZATION OF SYNTHETIC NEAR-FAULT SEISMIC WAVEFIELDS FOR THE SOUTHWEST ICELAND TRANSFORM ZONE
Farnaz Bayat, Milad Kowsari, Benedikt Halldórsson.....64

INVESTIGATING TIME-DEPENDENT EARTHQUAKE CLUSTERING IN SHORT-TERM RISK ANALYSIS
Atefe Darzi, Benedikt Halldorsson, Mojtaba Moosapoor.....66

DEVELOPING EARTHQUAKE GROUND MOTION MODELS FOR ICELAND USING BAYESIAN HIERARCHICAL MODELING
Hamed Davari, Milad Kowsari, Benedikt Halldorsson, Birgir Hrafnkelsson, Sahar Rahpeyma, Atefe Darzi.....69

TOWARDS A HYBRID SEISMIC HAZARD MODEL FOR ICELAND
Benedikt Halldorsson, Milad Kowsari, Farnaz Bayat, Atefe Darzi, Hamed Davari.....71

PHYSICS-BASED SITE-SPECIFIC PSHA FOR SEVERAL URBAN CENTERS IN SOUTHWEST ICELAND
Milad Kowsari, Benedikt Halldórsson.....73

Copyright © 2025 CroCEE

GEOTECHNICAL EARTHQUAKE ENGINEERING

LANDSLIDE TRIGGERING AS AN INDIRECT CONSEQUENCE OF AN EARTHQUAKE - CASE STUDY FROM NORTHERN CROATIA
Jasmin Jug, Stjepan Strelec, Kristijan Grabar, Dragana Dogančić, Anja Bek.....75

EFFECTS OF GROUND MOTION INTENSITY IN ASSESSMENT OF SOIL SLOPES IN EARTHFILL DAM
Kemal Edip, Davor Stanko, Julijana Bojadjieva, Radmila Shalic-Makreska, Vlatko Sheshov.....83

THERMO-MECHANICAL BEHAVIOR AND STRUCTURAL DESIGN OF GEOTHERMALLY ACTIVE PILES
Guxim Rrudhani, Josif Josifovski.....91

ANALYSIS OF CANTILEVER RETAINING WALL ACCORDING TO EUROCODES IN DRAINED AND UNDRAINED CONDITIONS
Dejan Ivanovski, Julijana Bojadjieva, Kemal Edip, Vlatko Sheshov, Toni Kitanovski, Jovana Ristova.....103

LABORATORY TESTING OF SMALL-STRAIN MODULI IN NATURAL SANDY DEPOSITS
Toni Kitanovski, Vlatko Sheshov, Julijana Bojadzieva, Kemal Edip, Dejan Ivanovski.....110

ANALYTICAL AND NUMERICAL INVESTIGATION OF THE SITE RESPONSE PERIOD IN THE SAGUENAY REGION, EASTERN CANADA
A S M Fahad Hossain, Ali Saeidi, Mohammad Salsabili, Miroslav Nastev, Juliana Ruiz Suescun.....118

EFFECT OF SEISMIC LOAD ON THE STABILITY OF A DOLOMITE QUARRY IN HUNGARY
Saltanat Yesselbayeva, Máté Urbán, Péter Görög.....128

LIQUEFACTION ASSESSMENT USING A SYNTHETIC CPT DERIVED FROM CORRELATION WITH SHEAR WAVE VELOCITY
Mario Bačić, Lovorka Librić, Meho Saša Kovačević.....135

EXPERIMENTAL TECHNIQUES FOR CHARACTERIZATION OF MATERIALS AND STRUCTURES

TESTING FOR THE ASSESSMENT OF EARTHQUAKE RESISTANCE OF HERITAGE MASONRY BUILDINGS: NONDESTRUCTIVE VERSUS DESTRUCTIVE, LABORATORY VERSUS IN-SITU TESTING
Miha Tomaževič.....146

DYNAMIC EFFECTS IN TALL STEEL STRUCTURES WITH DIFFERENT PURPOSES
Elena Stokuca, Golubka Necevska-Cvetanovska, Milos Stokuca.....163

ADVANCING SEISMIC DESIGN AND ASSESSMENT THROUGH EXPERIMENTAL TESTING: INSIGHTS FROM THE ERIES PROJECT
Gerard J. O'Reilly, Volkan Ozsarac, Davit Shahnazaryan, Igor Lanese, Elisa Rizzo Parisi, Filippo Dacarro, Gian Michele Calvi.....173

Copyright © 2025 CroCEE

INTEGRATION OF THE OMA AND FEMU FOR ESTIMATION MODULUS OF ELASTICITY IN MASONRY STRUCTURES
Suzana Ereiz, Ivan Duvnjak, Janko Košćak, Marko Bartolac, Domagoj Damjanović, Marina Frančić Smrkić.....181

EXPERIMENTAL TESTING OF CIRCULAR RC BRIDGE PIER MODELS SUPPORTING REFINED 3D MICRO-MODELING
Laurent Hakaj, Jelena Ristic, Toni Arangelovski, Danilo Ristic.....189

PROTECTION OF SENSITIVE INFILL IN FRAME BUILDINGS USING SB-UPGRADED ISOLATION SYSTEM: SEISMIC TESTS OF MODEL
Ilir Canaj, Jelena Ristic, Elena Dumova-Jovanoska, Danilo Ristic.....200

TESTING OF THE SEISMIC BEHAVIOUR OF A TRADITIONAL JOINT IN A WOODEN ROOF STRUCTURE
Nives Meštrović, Ivica Guljaš.....212

PUSH-OUT TESTS ON TIMBER-STEEL HYBRID JOINT WITH SCREWS CONNECTIONS. NUMERICAL AND EXPERIMENTAL INVESTIGATIONS
Laura Corti, Giovanni Muciaccia.....221

EXPERIMENTAL IN-SITU TESTING OF AN EXISTING BRIDGE
Antonio Shoklarovski, Aleksandra Bogdanovic, Zoran Rakicevic, Filip Manojlovski, Angela Poposka 229

EXPERIMENTAL ASSESSMENT OF EXISTING BRIDGE STRUCTURE
Angela Poposka Antonio Shoklarovski, Aleksandra Bogdanovic, Zoran Rakicevic, Filip Manojlovski 237

REMOTE TESTING AND ASSESSMENT OF DIFFERENT TYPES OF BRIDGES USING ADVANCED EVALUATION METHODS
Igor Gjorgjiev, Borjan Petreski, Marija Vitanova, Filip Manojlovski, Vlado Micov, Ana Nanevska, Trajche Zafirov.....244

IMPROVING THE BENDING STIFFNESS OF DLT BEAMS: EXPERIMENTAL ANALYSIS AND ANALYTICAL MODEL VERIFICATION
Ana Skender, Marina Frančić Smrkić, Ante Barišić.....256

SAND AND SAND-KAOLINE MIXTURES CYCLIC PROPERTIES UNDER LOW CONFINING STRESS
Vedran Jagodnik, Davor Marušić, Neira Mušić, Ivana Bošnjak 264

HISTORICAL STRUCTURES

A STATE-OF-THE-ART REVIEW: SEISMIC VULNERABILITY ASSESSMENT METHODS FOR MASONRY STRUCTURES
Antonela Moretić, Mislav Stepinac, Karlo Ožić.....274

POST-1979 MONTENEGRO EARTHQUAKE RETROFITTING OF RECTOR'S PALACE IN DUBROVNIK'S OLD CITY: PRESERVING ARCHITECTURAL AND SCULPTURAL HERITAGE
Davorin Penava, Marin Valičnić, Ante Vrban, Lars Abrahamczyk, Vasilis Sarhosis.....282

Copyright © 2025 CroCEE

ASSESSMENT, EVALUATIONS AND RETROFITTING APPLICATIONS METHODS FOR MASONRY OLD STONE STRUCTURE
Naser Kabashi, Enes Krasniqi, Teuta Imeri, Ylli Murati, Alush Shala.....294

SEISMIC ANALYSIS OF DRY STONE MASONRY STRUCTURES WITHIN THE DIOCLETIAN'S PALACE IN SPLIT
Nikolina Živaljić, Ivan Balić, Hrvoje Smoljanović, Boris Trogrlić, Ante Munjiza.....306

PREFABRICATED REINFORCED CONCRETE RESIDENTIAL BUILDINGS: A FOCUS ON THE JUGOMONT SYSTEM
Milica Petrović, Svetlana Nikolić - Brzev.....314

PREDICTION OF MASONRY STRENGTH AND EARTHQUAKE CHARACTERISTICS USING MACHINE-LEARNING ALGORITHMS
Karl Deix, Branko Rusnov.....328

INTEGRATED NON-DESTRUCTIVE APPROACH FOR THE DIAGNOSIS OF HISTORIC MONUMENTS
Jasna Grujoska-Kuneska, Veronika Shendova.....339

ASSESSMENT OF THE PHYSICAL CONDITION OF BYZANTINE CHURCHES IN NORTH MACEDONIA
Jasna Grujoska-Kuneska, Veronika Shendova.....349

SEISMIC EVALUATION OF THE HIGH-RISE RESIDENTIAL BUILDING WITH STRUCTURAL WALLS FROM THE LATE 60'S
Mustafa Hrasnica, Amina Karavelić-Hadžimejlić, Senad Medić, Jelena Medić.....358

ASSESSING MECHANICAL PROPERTIES OF HISTORIC STONE MASONRY: CASE STUDY IN JURDANI (RIJEKA)
Paulo Šćulac, Josipa Mihaljević, Ivana Štimac Grandić, Davor Grandić.....370

TIES IN UNREINFORCED MASONRY STRUCTURES: CASE STUDY IN KRK
Paulo Šćulac, Kristina Galjanić, Davor Grandić, Josipa Mihaljević, Željko Smolčić.....380

SEISMIC ASSESSMENT OF A HISTORIC AUSTRO-HUNGARIAN MASONRY BUILDING IN SARAJEVO'S BAŠČARŠIJA
Ćamil Medanović, Naida Ademović, Marijana Hadzima-Nyarko.....390

PERFORMANCE ANALYSIS OF HISTORICAL CHURCHES AND MOSQUES DURING RECENT EARTHQUAKES – SOME PERSPECTIVES ON APPLICATION OF AI/ ML SYSTEMS
Satwant Rihal, Hisham Assal.....401

SEISMIC VULNERABILITY ASSESSMENT OF COMPLEX HISTORICAL MASONRY AGGREGATES WITH INTERACTIONS BETWEEN STRUCTURAL UNITS
Madalena Ponte, Gabriele Guerrini, Andrea Penna, Rita Bento.....407

ASSESSMENT OF TRAM-INDUCED VIBRATIONS ON EARTHQUAKE-DAMAGED BUILDINGS
Ivo Haladin, Franka Meštrović, Zvonimir Šantek, Katarina Vranešić, Krešimir Burnać.....417

Copyright © 2025 CroCEE

SEISMIC PERFORMANCE OF STRUCTURES

COMPARISON OF RESULTS OBTAINED FROM ANALYTICAL AND EXPERIMENTAL INVESTIGATIONS OF RC BUILDING COLUMNS USING CFRP
Artur Roshi, Golubka Nechevska-Cvetanovska, Jordan Bojadjiev.....425

RAPID VISUAL SCREENING METHOD FOR RC BUILDING STRUCTURES
Burbuqe Shatri, Golubka Nechevska-Cvetanovska.....433

RESEARCH IMPERATIVES FOR ENHANCING THE ANALYSIS AND SEISMIC PERFORMANCE OF JOINTS IN VERTICAL BUILDING EXTENSIONS
Alush Shala, Jelena Bleiziffer.....445

INVESTIGATING THE SEISMIC PERFORMANCE OF THE HONEYCOMB YIELDING DAMPER(HYD)
Zeinolabedin Mortezaali, Peyman Shadman Heidari, Mohammad Ghanooni Bagha.....451

SHAKE TABLE TESTING OF U-SHAPED MASONRY STRUCTURES: OUT-OF-PLANE RESPONSE TO VARYING GROUND MOTION SIGNALS
Babar Ilyas, Dario Vecchio, Nuno Mendes, Paulo B. Lourenco.....467

EFFECTIVE STIFFNESS OF FLANGED REINFORCED CONCRETE STRUCTURAL WALLS: A NUMERICAL APPROACH
Komaravolu Venkata Purneshwar, Nilanjan Samanta, Kaustubh Dasgupta.....480

INFLUENCE OF KINEMATIC SOIL – STRUCTURE INTERACTION ON THE SEISMIC BEHAVIOUR OF REINFORCED – CONCRETE FRAME BUILDINGS
Nikola Petrov, Julijana Bojadjieva, Jordan Bojadjiev.....491

SEISMIC RETROFIT OF "PLINIO IL GIOVANE" SCHOOL BUILDING: MAJOR APPLICATION OF BASE ISOLATION USING HIGH DAMPING RUBBER BEARINGS
Stefano Barone.....503

SEISMIC VULNERABILITY ASSESSMENT OF 1960S REINFORCED CONCRETE FRAME BUILDINGS WITH INFILL MASONRY WALLS
Naser Kabashi, Enes Krasniqi, Florim Grajcevci, Milot Muhaxheri, Ylli Murati, Valon Veseli.....515

PREDICTION OF MODAL FEATURES FOR DIFFERENT DAMAGE STAGES AND RETROFIT METHODS OF A MASONRY BUILDING
Maja Baniček, Mahmoud Shaqfa, Sara Vaing, Josip Atalić.....525

SEISMIC BEHAVIOUR OF PREFABRICATED WALL PANELS: AN OVERVIEW
Anđela Čavčić, Ivan Banović, Nikola Grgić, Alen Harapin.....531

IMPROVED SEISMIC ASSESSMENT OF EXISTING RC FRAME STRUCTURES
Aleksandar Zhurovski, Borjan Petreski, Igor Gjorgjiev.....543

SEISMIC ASSESSMENT OF THE DAMAGE LIMIT STATES OF EXISTING HIGHWAY BRIDGES
Radomir Folić, Miloš Čokić.....554

SEISMIC ASSESSMENT AND COST-BENEFIT ANALYSIS OF RETROFITTING MEASURES FOR POST-WAR MULTI-RESIDENTIAL MASONRY BUILDINGS IN LJUBLJANA
Simon Petrovčič, Petra Prašnikar, Vojko Kilar.....566

Copyright © 2025 CroCEE

THE INFLUENCE OF STRUCTURAL ECCENTRICITY ON THE SEISMIC BEHAVIOR OF TORSIONALLY SENSITIVE STRUCTURES
Riste Volchev, Nikola Postolov, Koce Todorov, Ljupcho Lazarov.....578

PERFORMANCE-BASED SEISMIC ASSESSMENT OF RC FRAME STRUCTURES USING SIMPLIFIED SDOF IDA
Leart Taravari, Koce Todorov.....589

MODELLING THE SEISMIC RESPONSE OF A CONFINED MASONRY BUILDING USING EQUIVALENT STRUT MODELS
Nemanja Krtinić, Matija Gams, Marko Marinković.....601

IN-PLANE BEHAVIOUR OF RC FRAMES WITH TRADITIONAL AND DECOUPLED INFILLS: PARAMETRIC STUDY
Aleksa Milijaš, Marko Marinković, Christoph Butenweg, Sven Klinkel.....613

AUGMENTED MODAL DIMENSIONS FOR SEISMIC EVALUATION OF BUILDINGS
Jui-Liang Lin.....626

BEHAVIOUR OF DUAL STEEL FRAMES WITH INNOVATIVE DOUBLE SKIN COLD-FORMED STEEL CONCRETE COMPOSITE SHEAR WALLS
Ivan Lukačević, Emanuel Krupa-Jurić, Ivan Ćurković, Marko Barišić.....634

NUMERICAL EXPERIMENT FOR SHEAR KEY JOINT BEHAVIOUR SIMULATION IN ARCH DAMS: PART 1 – INVESTIGATING THE INFLUENCE OF THE KEY SHAPE AND ANGLE
Ana Nanevska, Violeta Mircevska.....646

NUMERICAL EXPERIMENT FOR SHEAR KEY JOINT BEHAVIOUR SIMULATION IN ARCH DAMS: PART 2 – INVESTIGATING THE INFLUENCE OF THE ARCH THICKNESS AND APPLIED FORCE
Violeta Mircevska, Ana Nanevska.....658

COMPARATIVE NUMERICAL INVESTIGATION OF TIMBER ADDED FLOORS ON EXISTING RC STRUCTURES
Viktor Hristovski, Trajche Zafirov.....670

NEW PROVISIONS FOR SEISMIC DESIGN OF BRIDGES
Ana Mandić Ivanković, Mladen Srbić, Gordana Hrelja Kovačević.....679

MASONRY WALL-RC SLAB INTERACTION UNDER SEISMIC LOADING
Goran Simonović, Mustafa Hrasnica, Senad Medić.....691

THE EFFECTS OF SOIL-STRUCTURE INTERACTION ON THE SEISMIC DESIGN OF SHALLOW FOUNDATIONS FOR EBFs
Sanda Koboevic, Bardia Ramin Afshar.....698

INFLUENCE OF GROUND MOTION PARAMETERS ON SEISMIC RESPONSE
Tanja Kalman Šipoš, Adriana Brandis.....706

ANALYTICAL INVESTIGATION OF MASONRY INFILL REINFORCED CONCRETE FRAMES UNDER AXIAL AND LATERAL LOADING
Florim Grajçevci, Valon Veseli, Labeat Misini, Zijadin Guri, Ilir Canaj.....717

Copyright © 2025 CroCEE

PUSHOVER ANALYSIS OF TIMBER BUILDINGS WITH LIGHT FRAME TIMBER PANELS FOR ENGINEERING PRACTICE: METHOD DESCRIPTION, DISCUSSION, AND HIGHLIGHTING RESEARCH GAPS
Meta Kržan.....730

ENGINEERING ANALYSIS OF A TYPICAL PRE-CODE URM BUILDING IN ZAGREB
Kenan Omerović, Mario Uroš, Senad Medić.....740

APPLICATION OF THE NEW EUROCODE 8 TO THE SEISMIC ASSESSMENT OF AN EXISTING BUILDING IN ZAGREB
Andrea Brunelli, Silvia Pinasco, Serena Cattari, Sergio Lagomarsino.....752

ANALYSIS OF REINFORCED CONCRETE BEAM-COLUMN JOINT IN ANSYS SOFTWARE
Ivana Drobnjak, Marina Rakočević.....763

IMPACT OF ENVIRONMENT AND CLIMATE CHANGE ON SEISMIC RESISTANCE OF CONCRETE BRIDGES
Marija Kušter Marić, Petra Milić, Anđelko Vlašić, Mladen Srbić, Ana Mandić Ivanković, Dominik Skokandić.....775

SEISMIC ASSESSMENT OF THE PRECODE HIGH RISE BUILDING FRAME USING THE PUSHOVER ANALYSIS
Karlo Grgurić, Mario Uroš.....785

INFLUENCE OF CONNECTING ELEMENTS IN HORIZONTAL LOAD-BEARING SYSTEM OF A MASS TIMBER OFFICE BUILDING
Robert Buzjak, Mario Uroš.....796

REPAIR AND STRENGTHENING OF STRUCTURES

OPTIMAL ESTIMATION OF LINEAR SHEAR-TYPE MODELS FOR BENCHMARK STEEL STRUCTURES IN DYNAMIC ANALYSIS
Maziar Fahimi Farzam, Mohammad Salehi.....810

NUMERICAL VALIDATION OF MASONRY WALL EXPERIMENTS USING THE APPLIED ELEMENT METHOD
Sergey Churilov.....823

BIM APPLICATION IN SEISMIC STRENGTHENING OF REINFORCED CONCRETE BUILDING USING FRP MATERIALS
Goran Chapragoski, Golubka Nechevska-Cvetanovska.....835

TESTS ON SPECIAL ANCHORS FOR MASONRY INFILLS WITH SPECIAL OPPORTUNITY FOR SEISMIC RETROFITTING
Matthias Roik, Caroline Piesker.....844

SEISMIC RETROFIT OF MASONRY WALLS USING REPOINTING WITH TRADITIONAL MORTAR AND POLYPROPYLENE STRIPS - TEST RESULTS
Festim Ademi, Sergey Churilov, Enis Jakupi, Elena Dumova - Jovanoska.....855

BASE ISOLATION OF AN EXISTING REINFORCED CONCRETE BUILDING
Krešimir Todorić, Mario Uroš.....868

Copyright © 2025 CroCEE

DYNAMIC ASSESSMENT OF RC BEAMS FLEXURALY STRENGTHENED WITH CFRP STRIPS
Tomislav Brozović, Tomislav Kišiček.....880

STRUCTURAL RECONSTRUCTION OF THE BELFRY, MONASTERY AND CHURCH OF ST. FRANCIS ON THE KAPTOL IN ZAGREB
Ante Mlinar, Ante Kelava, Ante Borovina, Ante Buzov.....887

POST-EARTHQUAKE RECONSTRUCTION PROCESS

INCREASING STRUCTURAL RESILIENCE: A CASE STUDY OF HOSPITAL RETROFITTING IN ALBANIA
Izet Mehmetaj, Erjon Çobani, Armela Kalliri.....901

POST-EARTHQUAKE RECONSTRUCTION IN THE ZAGREB SETTLEMENTS MARKUŠEVAC AND ČUČERJE
Svirčić Gotovac, Anđelina, Zlatar Gamberožić, Jelena.....911

LESSONS LEARNT FROM EARTHQUAKE DISASTERS

COMPUTED BI-DIRECTIONAL COMBINATION COEFFICIENTS FOR STRUCTURES USING THE FEB. 6TH, 2023 KAHRAMANMARAS EARTHQUAKES' GROUND MOTION DATA
Asma Yahioaui, Oguz Koz, Oguz C. Celik.....923

ANALYSIS OF SGM DATA CHARACTERISTICS FOR BETTER EXPLANATION OF BUILDING DAMAGE DURING THE FEB.6TH, 2023 KAHRAMANMARAS, TURKEY EARTHQUAKES
Oguz Koz, Sinem Guntepe, Oguz C. Celik.....935

RAPID EARTHQUAKE LOSS ASSESSMENT FRAMEWORK: RELAR PROJECT AND ITS APPLICATION ON THE DATA SET FROM THE KRALJEVO (SERBIA) EARTHQUAKE IN 2010
Marko Marinković, Zoran Stojadinović, Miloš Kovačević, Mladen Nikolić, Dejan Marinković, Đorđe Nedeljković, Zoran Babović, Zoran Pucanović, Filip Đorđević, Marija Ivanović, Nevena Simić, Božidar Stojadinović.....947

ENGINEERING EXPERTISE ASPECTS DURING DISASTER RESPONSE – A CASE STUDY OF FLOODS IN FBIH
Ante Pilipović, Karlo Jandrić.....958

SUZI-SAEE EARTHQUAKE IMAGE DATABASE: A FRAMEWORK FOR TAGGING EARTHQUAKE-INDUCED DAMAGE
Filip Đorđević, Marko Radišić, Svetlana Brzev, Marko Marinković.....966

Copyright © 2025 CroCEE

PREPAREDNESS AND EMERGENCY MANAGEMENT

EARTHQUAKE RISK PERCEPTION IN BANJA LUKA: IMPLICATION FOR SEISMIC MANAGEMENT
Vesna Šipka, Mirjana Landika, Ljiljana Popović.....975

DEPLOYING OF SEISMIC ALERT WARNING SYSTEMS IN INDUSTRIAL FACILITY
Igor Gjorgjiev, Marta Stojmanovska.....987

BUILDING RESILIENT COMMUNITIES: ADVANCING STEM EDUCATION AND EARTHQUAKE ENGINEERING RESEARCH
Roberta Apostolska, Vlatko Sheshov, Marija Vitanova, Goran Jekic, Elena Delova, Ana Nanevska, Filip Manojlovski, Dejan Ivanovski.....995

FIELD APPLICATION FOR ASSESSING THE DAMAGE AND USABILITY OF BRIDGES AFTER AN EARTHQUAKE
Anđelko Vlašić, Marta Šavor Novak, Ana Mandić Ivanković, Gordana Hrelja Kovačević, Mladen Srbić, Marija Kušter Marić, Dominik Skokandić, Jelena Bleiziffer.....1005

APPLICATION OF THE BAILEY BRIDGES IN POST-EARTHQUAKE INTERVENTIONS
Marko Šimić, Dražen Brkić, Marija Kušter Marić, Anđela Ivanović.....1017

ENHANCING URBAN DISASTER RISK MANAGEMENT: A TRANSNATIONAL ANALYSIS OF SEISMIC RISK ASSESSMENT FRAMEWORKS IN EUROPE
Jelena Pejovic, Nina Serdar, Maria Polese, René Kastner, Marta Faravelli, Marco Gaetani d'Aragona, Paolo Ricci, Anže Babič, Neja Fazarinc, Serena Cattari, Valerio Poggi, Marco Lazzati, Christina Rechberger, Can Baran Aktaş, Mehmet Fırat Aydın, Özkan Kale, Rıza Secer Orkun Keskin.....1026

A BUILDING CLASSIFICATION SYSTEM FOR SEISMIC RISK ASSESSMENT OF GOSTIVAR, NORTH MACEDONIA
Shpresim Ibraimi, Koce Todorov, Miroslav Nastev, Stanislav Milovanovic.....1038

THE USE OF UAVS IN ASSESSING SEISMIC VULNERABILITY OF EXISTING URM BUILDINGS
Mislav Stepinac, Lucijano Bajić, Milan Domazet.....1050

EMERGE: RAPID MULTI-RISK NEEDS EVALUATION AND PLANNING PLATFORM
Radmila Salic Makreska, Igor Gjorgjiev, Julijana Bojadjieva, Vlatko Sesov, Roberta Apostolska, Goran Chapragoski.....1058

EDUCATION OF EXPERTS FOR DAMAGE ASSESSMENT OF BUILDINGS IMMEDIATELY AFTER AN EARTHQUAKE USING XR – PROJECT PROGRESS
Zvonko Sigmund, Massimo Migliorini, Karlo Jandrić, Elios De Maio, Marina Nadalin.....1066

SEISMIC LOSS AND RISK ANALYSIS

CHALLENGES AND CONSIDERATIONS FOR MODULAR CONSTRUCTION SYSTEMS IN SEISMIC PRONE REGIONS: A STATE-OF-THE-ART REVIEW
Vasco Bernardo, Paulo Candeias, António A. Correia.....1075

Copyright © 2025 CroCEE

SEISMIC PERFORMANCE EVALUATION OF EXISTING REINFORCED CONCRETE BUILDINGS IN SKOPJE
Elena Delova, Aleksandar Zlateski, Marin Grubisic, Veronika Shendova, Zivko Bozinovski, Kemal Edip.....1087

RECENT ADVANCES IN SEISMIC VULNERABILITY ASSESSMENT OF CROATIAN COASTAL URBAN AREA
Željana Nikolić, Elena Benvenuti, Luka Runjić, Nenad Mladineo, Marko Mladineo.....1096

SP-BELA: A STRUCTURAL SEISMIC VULNERABILITY ASSESSMENT METHODOLOGY BASED ON PUSHOVER CURVES
Barbara Borzi, Antonella Di Meo, Marta Faravelli.....1104

ON THE IMPACTS OF STRUCTURE-TO-STRUCTURE DAMAGE CORRELATION FOR REGIONAL SEISMIC RISK ASSESSMENT
Tomas Mejia, Gerard J. O'Reilly.....1116

BRIDGING THE GAP: A SOFTWARE TOOL FOR EFFICIENT GROUND MOTION RECORD SELECTION IN EARTHQUAKE ENGINEERING
Davit Shahnazaryan, Volkan Ozsarac, Gerard J. O'Reilly.....1128

ENHANCING FUNCTIONAL RECOVERY ESTIMATIONS THROUGH STOREY LOSS FUNCTIONS
Davit Shahnazaryan, Gerard J. O'Reilly.....1140

INTEGRATING SEISMIC RISK ASSESSMENT INTO SPATIAL PLANNING: CASE REPUBLIC OF NORTH MACEDONIA
Elena Dumova - Jovanoska, Kristina Milkova, Sergey Churilov, Simona Bogoevska.....1150

A REVIEW OF EXISTING SEISMIC VULNERABILITY FUNCTIONS FOR BUILDINGS IN THE BALKAN REGION
Kristina Milkova, Marta Šavor Novak, Marko Marinkovic, Elena Dumova - Jovanoska.....1157

BUILDING EXPOSURE MODELLING FOR NATIONAL SEISMIC RISK ASSESSMENT IN MONTENEGRO
Nina Serdar, Jelena Pejović.....1169

SCENARIO-BASED SEISMIC RISK ASSESSMENT OF SCHOOL BUILDINGS IN THE SKOPJE AREA, NORTH MACEDONIA
Lisa Jusufi, Roberta Apostolska.....1179

SEISMIC VULNERABILITY ASSESSMENT OF PART OF HISTORIC CENTER OF SKOPJE
Aleksandar Zlateski, Elena Delova, Veronika Shendova.....1191

VULNERABILITY ASSESSMENT AND SEISMIC RISK ANALYSIS OF BUILDINGS IN IRAQ: INSIGHTS FROM BUILDING SURVEYS AND DAMAGE SCENARIOS
Peshawa L. Hasan, Baban A. Bapir, Brwa S. Hama Ali, Lars Abrahamczyk, Serwan Khurshid.....1200

IMPROVEMENT OF THE EXPOSURE MODEL AND PRELIMINARY PHYSICAL RISK ANALYSIS: A PILOT CASE MUNICIPALITY
Daniel Tomic, Radmila Salic Makreska, Marija Vitanova, Zabedin Neziri, Noah Martin.....1212

DEVELOPMENT OF K QUOTIENT METHODOLOGY FOR INTER-CODE LATERAL FORCE COMPARISON
Zoran Milutinovic, Radmila Salic Makreska, Jovan Trajchevski, Daniel Tomic.....1221

Copyright © 2025 CroCEE

APPLICATION OF THE PARAMETRIC PUSHOVER CURVE MODEL FOR SEISMIC LOSS ESTIMATION OF A BUILDING STOCK
Neja Fazarinc, Anže Babič, Matjaž Dolšek.....1233

PHD SPECIAL SESSION

INFLUENCE OF GROUND MOTION RECORD SELECTION ON HIGHER MODE DEMANDS IN RC WALLS: A COMPARISON OF UHS AND CS APPROACHES
Jose Poveda, Gerard J. O´Reilly.....1244

ANALYTICAL APPROACH TO SEISMIC BEHAVIOUR ASSESSMENT OF RC FRAME STRUCTURES WITH RUBBER JOINTED MASONRY INFILL
Liljana B. Mijalkova, Aleksandra Bogdanović, Enrico Tubaldi, Marko Marinković, Bartolomeo Pantò.....1256

EFFECT OF COLUMN BASE ROTATIONAL STIFFNESS ON THE SEISMIC RESPONSE OF STEEL BUILDINGS
Menelaos Papamichelakis, George Papagiannopoulos.....1258

RESPONSE OF THE BUILDING IN AGGREGATES ACCORDING TO THE INTERCONNECTED DIFFERENT PARAMETERS
Maja Mrkonjić, Josip Atalić.....1270

OVERVIEW OF THE DEVELOPMENT, APPLICATION AND CHALLENGES OF NATURAL FIBER REINFORCED CEMENTITIOUS MATRIX (NFRCM)
Mario Žigo, Marina Nikolić, Marija Smilović Zulim, Nikola Grgić 1272

NEAR-DISTANCE SPECTRAL PARAMETER KAPPA CALCULATIONS FOR STATIONS INSTALLED IN N. MACEDONIA
Marina Poposka, Davor Stanko, Radmila Salic Makreska, Dragi Dojcinovski, Marta Stojmanovska.....1285

A COLLABORATIVE FRAMEWORK TO MODEL THE SEISMIC VULNERABILITY OF RC BUILDINGS USING SIMULATED DESIGN
Volkan Ozsarac, Nuno Pereira, Hossameldeen Mohamed, Xavier Romão, Gerard O'Reilly, Helen Crowley.....1295

SEISMIC RISK AND LOSS ASSESSMENT OF REINFORCED CONCRETE FRAME STRUCTURES STRENGTHENED BY THE ADDITION OF MASONRY INFILL WALLS
Marin Grubišić.....1307

EARTHQUAKE RESISTANCE OF POLES ALONG ROADS
Višnja Tkalčević Lakušić, Iva Crnjac.....1319

ADVERTISEMENTS.....1327

Copyright © 2025 CroCEE

Keynote Lecture

SEISMIC ISOLATION IN LOSS-BASED DESIGN

Gian Michele Calvi

Professor and Vice-Rector for Research, IUSS, Scuola Universitaria Superiore, Pavia, Italy, gm.calvi@eucentre.it
Director of Science, EUCENTRE, European Centre for Training and Research in Earthquake Engineering, Pavia, Italy
Executive Vice-President, IAEE, International Association for Earthquake Engineering, Tokyo, Japan
Adjunct Professor, NCSU, North Carolina State University, Raleigh, NCIUSS Pavia, Italy

Abstract

Performance-based design was first envisaged in the early 1990s and has become a mantra in conceptual seismic design. However, practical approaches to be possibly introduced in codes of practice are not readily available, to say the least, though some can be found in the literature. What is essentially missing is some correlation between structural response parameters and expected monetary losses, at a level of simplicity comparable with the force- or displacement-based approaches applied to designing in everyday practice. The basics of a formulation that may evolve into such a practical loss–based approach will be discussed, with a focus on some essential practical questions: is it possible to design for very low expected loss and what will be the associated parametric investment cost?
In this context, seismic isolation, plays a peculiar role, being one of the most accredited candidates to allow a credible design approach for strategic constructions, in which case extremely contained losses should be aimed to for low probability ground motions.
Some example derived from the recent 2023 Turkey earthquake will be introduced and discussed as case studies.

Biography

Gian Michele Calvi is Professor at the IUSS Pavia, Director of Science of the Eucentre Foundation, Italy, and President-elect of the IAEE.
He graduated at the University of Pavia and received a Master of Science from the University of California, Berkeley, a PhD from the Politecnico di Milano and an Honorary Doctorate from the University of Cuyo, Mendoza, Argentina.
He has been the founder of the Eucentre Foundation and of the ROSE School (with M.J.N. Priestley).
In 1996 he created the Journal of Earthquake Engineering (Taylor and Francis), with A.S. Elnashai and N.N. Ambraseys, where he still serves as associate editor.
He is author of hundreds of publications and of a few books, including: Seismic design and retrofit of bridges (with M.J.N. Priestley and F. Seible, 1996), Displacement-Based Seismic Design of Structures (with M.J.N. Priestley and M.J. Kowalsky, 2007), Seismic design and analysis of tanks (with R. Nascimbene, 2023). In the occasion of the WCEE 2024 he has published a “Master Series” monograph, The art of seismic design, by invitation of the IAEE President and Past President.
He has been invited keynote speakers in tens of conferences, including three World and four European Conferences on Earthquake Engineering.
He has been designer, consultant or checker for hundreds of structural projects, including: the Rion-Antirion cable stayed bridge (1999-2004, 2883 m, in Greece); the Anatolian Viaduct (2000-2003, 119 spans, in Turkey); the new housing system after L’Aquila earthquake (2009-2010, with 185 buildings seismically isolated with more than 7,000 devices, completed in about six months); the construction of 103 schools in Costa Rica (2013-2018, for the IAD bank); the assessment and strengthening program in the area of Groningen, in The Netherlands (2013-2024, due to problems of induced seismicity).
He has been always active in conceptual innovation in seismic design, focusing on masonry in his early days, on bridges, displacement–based design and seismic isolation from the nineties.

Copyright © 2025 CroCEE

Keynote Lecture

MODELLING AND ANALYSES FOR THE SEISMIC ASSESSMENT OF EXISTING URM BUILDINGS: RESEARCH CHALLENGES AND ENGINEERING-PRACTICE IMPLICATIONS

Serena Cattari

Professor, University of Genova, Department of Civil, Chemical and Environmental Engineering, Italy, serena.cattari@unige.it

Abstract

The keynote lecture intends highlighting the challenge of, on the one hand, incorporating all available information into numerical models to make them as reliable as possible, and, on the other hand, recognizing the numerous pitfalls that can lead to widely varying and scattered results in the seismic assessment of existing URM buildings.

The lessons learned from the URM Nonlinear Modelling - Benchmark project (funded by the ReLUIS consortium and the Department of Civil Protection) will be shared, offering recommendations with significant implications for engineering practice. This project aimed to compare numerical simulations obtained using different modelling approaches (e.g., finite element models based on various nonlinear constitutive laws and equivalent frame approaches) and software packages, all under consistent modelling assumptions. The primary goal was to identify possible strategies for harmonizing different modelling approaches in the context of seismic assessment according to the format of Codes. Although the project primarily focused on nonlinear static analyses, its insights into modelling choices are also relevant for linear approaches. Key topics which will be discussed include the importance of parameter calibration strategies, the need of a multi-criteria approach to defining ultimate displacement capacity, and the impact of modelling assumptions (such as flange effect).

Biography

Serena Cattari (SC) is Full Professor at the University of Genova, Department of Civil, Chemical and Environmental Engineering. Her core research topics are: numerical modelling and seismic performance-based assessment of existing and historical masonry buildings; seismic risk analysis of the built environment at large scale; structural monitoring. SC is authors of more than 250 contributions (more than 80 peer-reviewed international journal papers) and is the coordinator of the PhD program on Security, Risk and Vulnerability (https://sicurezza.unige.net). SC participated to several projects at national and international scale and is currently Associate Editor of Earthquake Spectra journal. With reference to the expertise in numerical modelling, SC has provided significant contributions to the equivalent frame modelling approach. In particular, she is contributing to the development of the software Tremuri, widely used at national and international scale by both researchers and practitioners. Recently, SC coordinated the "URM nonlinear modelling-Benchmark project" funded by the Italian Department of Civil Protection within ReLUIS research programs. The project was mainly addressed to provide a critical analysis and a systematic comparison of the results obtained by using several modelling approaches and software package tools on selected benchmark examples to outline a useful and qualified reference to the engineering and scientific community. Additionally, she participated to the drafting panel of CNR-DT 212 Document "Guide for the probabilistic assessment of the seismic safety of existing buildings" issued by Italian National Research Council, Rome, Italy.

Copyright © 2025 CroCEE

Keynote Lecture

WHY SEISMIC HAZARD MODELLING HAS BECOME A RISKY BUSINESS

Helen Crowley

Secretary-General, the Global Earthquake Model (GEM) Foundation, helen.crowley@globalquakemodel.org

Abstract

The Joyner Lecture honours the distinguished career of William B. Joyner at the U.S. Geological Survey and his abiding commitment to continuing communication and education at the interface between research findings of earthquake science and the practical realities of earthquake engineering. One such interface that has been the source of much debate in recent years relates to the use of probabilistic seismic hazard assessment (PSHA) models as the basis for seismic design and assessment. Since the publication of the landmark paper by Cornell in 1968, PSHA has become the standard approach for defining the seismic actions in design codes. Before then, following the Messina (Italy) earthquake in 1908, seismic zonation maps based on observed macroseismic intensity from past earthquakes were used to define where, and to what level, buildings should be designed to withstand the lateral forces from earthquakes. These zonation maps were often, and somewhat inevitably, updated after damaging earthquakes. Despite the clear improvements that the use of a PSHA-based approach brought, criticism was frequently placed on the outputs of these models, such as when the ground motions from earthquakes were seen to exceed those underlying the design code, suggesting a widespread misunderstanding of the meaning of the latter. Since the 2000's, there has been a move towards explicitly discussing the levels of risk that are being accepted by the code, together with the consequences expected under the design levels. This has led, in the United States, to the adoption of the so-called risk-targeted approach for defining the seismic actions, which aims at harmonising the probability of collapse of buildings across the region of interest. This methodology has not yet been widely adopted by design regulations in other parts of the world, though in Italy, for instance, a significant effort has been made to evaluate the underlying spatial variation of risk to buildings designed to the latest standards. Whilst a more explicit recognition of the level of risk associated with seismic design codes has been an important step forward in Italy, the latest update to the PSHA model, developed in 2019 by the Italian Geological Survey, has continued to receive criticism and has even been rejected as the basis for an update of seismic actions in the design code. In this lecture, the argument will be made that the onus should now be on structural engineers to demonstrate the impact of these changes in terms of the levels of risk to the building stock, and how resilience has been, and can continue to be, built into the code to accommodate such changes resulting from advances in earthquake science.

Biography

Helen Crowley is the current Secretary-General of the Global Earthquake Model (GEM) Foundation. She holds an M.Eng. in Civil Engineering from Imperial College London and M.Sc. and Ph.D. degrees in Earthquake Engineering from the University of Pavia (ROSE School). She has collaborated closely with both the engineering seismology and earthquake engineering communities in Europe, as a member of the European Plate Observing System (EPOS) Seismology Consortium, and the coordinator of the development of the first, open European Seismic Risk Model (ESRM20), and won the 2009 European Geosciences Union Plinius Medal for her contributions to the field. Her research has touched on many topics related to seismic risk mitigation, from the definition of seismic actions for earthquake loss models and seismic design codes, to the development of regional exposure and vulnerability models for the built environment. She has nearly 200 publications, including more than 70 papers in international peer-reviewed publications, covering many aspects of earthquake engineering with a common thread of earthquake risk estimation. Helen Crowley is currently Editor of Earthquake Spectra, where she previously served as an Associate Editor. She is also the recipient of the 2012 Shah Family Innovation Prize.

Copyright © 2025 CroCEE

Keynote Lecture

COMPARISON OF TWO GENERATIONS OF EUROCODES FOR EARTHQUAKE-RESISTANT CONCRETE BUILDINGS THROUGH SYSTEMATIC APPLICATIONS

Michael N. Fardis

Professor Emeritus, Department of Civil Engineering, University of Patras, Greece, fardis@upatras.gr

Abstract

The rules of both generations of Eurocodes 2 and 8 for earthquake-resistant concrete buildings have been implemented in a computational platform for fully-automated, cloud-based detailed design and assessment of the seismic performance with nonlinear response-history analysis. It includes Ultimate Limit State design for resistance and ductility for seismic and non-seismic actions, Serviceability Limit State design for quasi-permanent or frequent actions and fire rating of elements for the three standard fires in Eurocode 1. The scope covers columns of rectangular, circular, L- or T-section, beams and foundation beams with or without flanges at top and/or bottom, walls of rectangular, L-, or U-section, beam-column connections, rectangular footings and the underlying soil, and storey- or multi-storey-deep perimeter walls of basements. Any layout in plan or elevation is treated. This capability has been applied to three concrete buildings with six storeys above ground and two basements. In one direction the buildings have a wall-, frame-equivalent-dual- or frame-lateral-load-resisting system; in the other, the first two buildings have a wall system and the third a wall-equivalent dual. The design seismic action is in all cases according to the current generation Eurocode 8, scaled to a Peak Ground Acceleration (PGA) on rock of 0.2g or 0.3g. Seismic design is for Ductility Class (DC) Medium of the first generation Eurocode 8, or DC 3 of the second one, which have the same behaviour factors, q, in all structural systems considered; so, in each building seismic action effects from the analysis are the same for the two Eurocode generations. Designs according to the second generation meet the performance goals of Eurocode 8 much better and transparently than with the first generation, and – under certain conditions - at about the same or lower cost. Nonlinear response-history analyses under seven historic bidirectional records scaled to the design PGA of the buildings confirm that the second generation Eurocodes can give more cost-effective designs than the first generation, with overall better performance.

Biography

Michael N. Fardis received his Civil Engineering Diploma from the National Technical University of Athens (1971), MSc Degrees in Civil Engineering (1977) and in Nuclear Engineering (1978) and a PhD in Structural Engineering (1979), all from the Massachusetts Institute of Tehcnology (MIT). He was appointed Assistant Professor of Civil Engineering at MIT in February 1979 and promoted to Associate Professor in 1982. He returned to his home country as Professor of concrete structures at the University of Patras, from which he retired in 2016 as Emeritus Professor. He is Honorary President of the International Federation for Structural Concrete (fib), having served as fib President in 2009 and 2010, Deputy President in 2007 and 2008 and Presidium member from 2002 to 2012. He was Director of the International Association of Earthquake Engineering (IAEE) from 2012 to 2020 and is IAEE Honorary Member. He is Editor of the top journal in earthquake engineering, "Earthquake Engineering and Structural Dynamics" since 2016 and Corresponding Member of the Mexican Academy of Engineering. He led the development of the first generation of the European Standard Eurocode 8 "Design of structures for earthquake resistance" as Chairman of CEN/TC250/SC8 from 1998 to 2005 and has been deeply involved in the development of the second generation of all Eurocodes as Vice Chairman of CEN/TC250 "Structural Eurocodes" from 2013 to 2022 and member of its Management Group till today. He has authored four books on seismic design of concrete structures, published by Springer, CRC Press or Thomas Telford/ICE Publishing (one of them translated to three other languages) and edited four books published by Springer and over 10 other international books. Results of his research, published in over 100 articles in peer-reviewed journals or over 200 papers in conference proceedings, are widely quoted in the international literature and have been extensively adopted in design rules of the first or second generation of Eurocode 8. He has been awarded by ACI the 1993 Wason Medal for the best paper in materials. Last year the President of the Hellenic Republic conferred to him the Prize for Excellence in University Teaching.

Copyright © 2025 CroCEE

Keynote Lecture

MASONRY ENCLOSURES: DAMAGE, APPLICATIONS, LESSONS LEARNED FROM TESTING AND NEW SOLUTIONS

Paulo B. Lourenço

Professor, University of Minho, Department of Civil Engineering, pbl@civil.uminho.pt
ICOMOS ISCARSAH President
ERC Advanced Grant Holder | STAND4Heritage | www.stand4heritage.org

Abstract

Observations of damage in earthquakes across the world related to masonry infills demonstrate that performance is too often inadequate. Images of out-of-plane failures and excessive in-plane damage confirm that lifesaving and economical requirements are not complied with. European regulations make structural designers responsible for the performance of non-structural elements and should lead to changes in the way we build masonry walls in many earthquake-prone countries. It is also known that, even in the absence of earthquakes, the performance of masonry enclosures often needs improvement, particularly with relation to water ingress and cracking. Finally, also the performance of masonry enclosures to exceptional blast loading, e.g. due to war or gas explosion, could be improved.
These aspects call for research on existing and innovative reinforced and unreinforced masonry panel solutions, and also strengthening solutions for existing panels. The lecture will address such topics, including challenges posed to masonry, lessons learned from inadequate performance of enclosures, different testing programmes carried out by University of Minho, numerical simulation tools and design issues.

Biography

Professor and Head of the Structural Group at the Department of Civil Engineering, University of Minho, Guimarães, Portugal. President of ICOMOS ISCARSAH - International Scientific Committee on the Analysis and Restoration of Structures of Architectural Heritage. Experienced in the fields of non-destructive testing, advanced experimental and numerical techniques, innovative repair and strengthening techniques, and earthquake engineering. Specialist in structural conservation and forensic engineering, with work on 100+ monuments including 18 UNESCO World Heritage. Leader of the revision of the European masonry code (EN 1996-1-1). Coordinator of the European Master on Structural Analysis of Monuments and Historical Constructions, with alumni from 70+ countries and European Heritage / Europa Nostra Award (most prestigious in Europe). Editor of the International Journal of Architectural Heritage and advisor of the Conference Series on Structural Analysis of Historical Constructions. Supervised 80 PhD theses and coordinate multiple national and international research projects. Awarded an Advanced European Research Council Grant to develop an integrated seismic assessment approach for heritage buildings. Coordinator of an Innovative Training Network on sustainable building lime applications via circular economy and biomimetic approaches with 15 PhD students across Europe.

Copyright © 2025 CroCEE

Keynote Lecture

TESTING FOR THE ASSESSMENT OF EARTHQUAKE RESISTANCE OF HERITAGE MASONRY BUILDINGS: NONDESTRUCTIVE VERSUS DESTRUCTIVE, LABORATORY VERSUS IN-SITU TESTING

Miha Tomaževič

Professor, Slovenian Building and Civil Engineering Institute, Slovenia, miha.tomazevic@zag.si

Abstract

Traditional masonry is typical composite construction material, mainly consisting masonry units and mortar. Natural raw materials, earth, clay and various types of stone are used for manufacturing the units, whereas the mortar is composed of mud, lime and sand, mixed with water in the prescribed proportions with or without additives, such as cement. Units of various types and shapes are laid in various arrangements, and are expected to act together as a homogeneous structural material when subjected to permanent and temporary actions. Traditionally, masonry was aimed at resisting gravity loads: masonry resists compression, however its capacity to resist tension and shear, caused by seismic forces induced during earthquakes, is rather low. Earthquake ground motion is three-dimensional. During earthquakes, dynamic forces are induced, which, in addition to gravity, act on the structures, cyclically changing directions of action. Besides materials, structural layout is responsible for energy dissipation and displacement capacity of resisting structural systems. To obtain reliable information, needed to assess the resistance of structural systems built of complex structural materials, such as masonry, to complex loads, such as seismic action, testing is indispensable. Various testing methods are available, including non-destrucitve, semi-destructive, and destructive testing, both in-situ and in the laboratory. Experiences show that, since masonry is non-homogeneous, anisotropic and inelastic material, nondestructive tests on the basis of propagation of sonic and seismic waves, as well as radar scanning cannot directly provide values of mechanical properties of masonry. They are good for discovering irregularities, such as voids in the masonry, filling the openings in masonry walls and changes in masonry structure. Semi-destructive tests, like shove-tests in the case of brick masonry or flat jack tests provide information regarding the existing stress state in the structural elements as well as compressive and shear strength. However, careful calibration of test results, which requires destructive testing in each particular case, is needed to obtain reliable values. As a result of non-homogeneity and anisotropy of masonry, material with limited elastic characteristics, it is not possible to reliably assess seismic behavior of masonry structural components and entire structures only on the basis of relatively easily obtained mechanical properties of constituent materials, such as masonry units and mortar. Additional specific testing of structural components and assemblages is needed to assess the values of parameters which determine the seismic behavior, e.g. strength and stiffness degradation and deterioration under repeated lateral load reversals, as well as displacement and energy dissipation capacity. To obtain relevant information, testing methods which simulate actual seismic conditions, should be used. In such a case, in-situ tests are preferred to laboratory testing of laboratory prepared specimens. Ultimately, real earthquakes represent best testing fields. Although expensive in all aspects, information obtained by learning lessons from earthquakes is precious and most valuable, if thoroughly studied and understood. On the basis of such information, supported by testing, methods and procedures can be developed to prevent consequences of future seismic events, if adequately used and timely applied.

Full paper is available in the Proceedings (https://doi.org/10.5592/CO/3CroCEE.2025.1).

Biography

Since 1967, Professor Tomaževič has worked at Slovenian Building and Civil Engineering Institute. He was heading section of earthquake engineering since 1977, and acted as the director of the Institute from 1996 to 2005. He partially retired in 2009 and worked on a half-time basis until 2017. Among other topics, the scope of his work included experimental and analytical research in seismic resistance of masonry buildings. Important part of his research was aimed at reducing seismic vulnerability of existing, including architectural cultural heritage buildings. Professor Tomaževič has been visiting professor to the Universities of Trento, Padua, Brescia, and Trieste in Italy, Universidad de Chile, Technical University of Dresden, Germany, as well as the Indian Institute of Technology in Roorkee. He has given more than 90 lectures and seminars at many universities and research institutes in Europe and the USA, Japan, China, Chile, Mexico, and India. He worked in several national and international technical committees, and served as an expert for Italian and Mexican goverments, UNIDO and the World Bank. He published more than 400 papers and 7 books, collecting almost 4900 citations (Google scholar). Professor Tomaževič is member of Slovenian Academy of Sciences and Arts and Slovenian Academy of Engineers. He is recipient of a number of awards and recognitions in Slovenia and abroad.

Copyright © 2025 CroCEE

Invited Lecture

EXPLOITING NONLINEAR SOIL-FOUNDATION RESPONSE IN DEFENCE OF THE SUPERSTRUCTURE

Ioannis Anastasopoulos

Professor, Head of Department of Civil, Environmental and Geomatic Engineering, ETH Zurich, Switzerland, ioannis.anastasopoulos@igt.baug.ethz.ch

Abstract

The vast majority of existing bridges were built before the 90's, without any or just basic seismic design. Pile group strengthening can be a challenging, costly, and time-consuming operation, calling for optimised solutions. The lecture will look into the behaviour of pile groups under combined Vertical, Horizontal and Moment (*VHM*) loading, combining 3D Finite Element (FE) and centrifuge modelling. Initially, a proof-of-concept study is conducted, inspired by the recent widening of a Swiss bridge. According to conventional design, the existing pile group needs retrofit to accommodate the increased seismic loads due to widening. An unconventional "do-nothing" approach is explored (maintaining the existing foundation), exploiting nonlinear soil response in defence of the superstructure. Such an approach requires improved design methods and better definition of the ultimate capacity of pile groups under combined loading. A fundamental yet representative 2 x 1 bored pile group is tested at the ETH Zurich Geotechnical Centrifuge Centre (GCC). After determining the bearing capacity under vertical loading, pushover loading is employed to measure the moment capacity (M_{ult}) of a lightly- and a heavily-loaded (widening) pile group. In contrast to intuitive expectations, the heavily-loaded system mobilises larger (M_{ult}). Combined loading is performed to derive experimental failure envelopes, confirming their tendency to expand with increasing vertical load. The transition to prototype scale accounts for scale effects, and employs the Concrete Damaged Plasticity (CDP) model for proper simulation of the reinforced concrete (RC) piles. The latter is a key advancement, accounting for the axial load dependency of bending moment capacity.

Biography

Ioannis Anastasopoulos has been Full Professor of Geotechnical Engineering at ETH Zurich since 2016. Since 2023, he is also Head of the Department of Civil, Environmental and Geomatic Engineering. He specializes in geotechnical earthquake engineering and soil–structure interaction, combining numerical with experimental methods. He is the inaugural recipient of the ISSMGE Young Researcher Award in Geotechnical Earthquake Engineering, and winner of the 2012 Shamsher Prakash Research Award. He has been a consultant in major projects in Europe, US and the Middle East. His consulting work ranges from the design of pile-rafts of tall buildings, to bridge foundations, metro stations, tunnels, and quay walls, as well as special design against faulting. He is Editor-in-Chief of Soil Dynamics and Earthquake Engineering, and has been Associate Editor or Editorial Board Member in several Journals, including the JEE and Géotechnique. He is a Director of IAEE, and Chair of ISSMGE TC104 on Physical Modelling.

Copyright © 2025 CroCEE

Invited Lecture

SEISMIC PERFORMANCE AND FRAGILITY ASSESSMENT OF GLASS CURTAIN WALLS: METHODS AND INFLUENCING PARAMETERS

Chiara Bedon

Associate Professor, University of Trieste, Department of Engineering and Architecture, Italy, chiara.bedon@dia.units.it

Abstract

This paper focuses on the development and assessment of a simplified, mechanically optimized finite element (FE) numerical model for the non-linear dynamic analysis of Glass Curtain Walls (GCWs) under seismic loads. It emphasizes the importance of robust design strategies and simulation tools to evaluate the mechanical performance of glass facades, particularly for seismic resistance. The study conducts a fragility analysis using the cloud analysis method to assess the capacity and performance limitations of typical GCWs in accordance with existing construction standards. Two modeling approaches are compared—one refined but expensive (MREF) and one simplified yet computationally efficient (MSIMP)—to analyze both global and local behavior under seismic loads. A parametric sensitivity analysis is performed to evaluate key performance indicators, such as stress and deformation peaks, and to identify influential parameters. The study highlights the need for capturing both global and local failure mechanisms and stresses the necessity for more efficient performance indicators to ensure safe and optimized seismic-resistant GCWs. Additionally, the paper explores the use of fragility curves and the application of Cloud Analysis for the seismic assessment of glass systems, providing a probabilistic approach for evaluating their vulnerability to dynamic loads.

Biography

Associate Professor at University of Trieste, Department of Engineering and Architecture, Italy, where she is the principal instructor for 'Structural Analysis' and 'Steel Structures' lectures. With a PhD degree in 2012, since 2009 she is involved in international research projects and European networks (JRC-ERNCIP, NATO-SPS, COST, etc.). Editorial board member for ISI international journals. Listed "2% Top Scientist" since 2019 (Stanford), "Top Italian Scientist" (engineering) and "Top Italian Women Scientist" (engineering > civil). She collected several research grants and awards, and presently coordinates the international projects HOPgLAz, 3FiRES and CoReng.

Copyright © 2025 CroCEE

Invited Lecture

SEISMIC RISK ASSESSMENT IN URBAN AREAS: INNOVATIVE APPROACHES TO SUPPORT LARGE-SCALE VULNERABILITY EVALUATIONS IN THE DIGITAL AGE

Tiago Miguel Ferreira

Senior Lecturer, Smart and Resilient Cities and Structures at the University of the West of England (UWE Bristol), UK, tiago.ferreira@uwe.ac.uk

Abstract

Urban areas are inherently prone to risk, with many structures and infrastructure systems lacking the capacity to withstand both natural and human-induced hazards. Additionally, increasing urban populations, evolving land use patterns, and climate change further heighten exposure. This talk will explore how seismic vulnerability and risk assessment results can inform risk management and mitigation strategies, as well as how digital technologies—such as GIS-based data collection and risk mapping, virtual reality tools, and machine learning applications—can enhance all stages of the assessment process, from data collection and management to the visualisation of outputs and the reduction of epistemic uncertainty. Furthermore, the interplay between the physical vulnerability of the built environment and the exposure of its users will be discussed, demonstrating how integrated assessments can provide more detailed insights into the actual level of risk and, consequently, support more robust and reliable risk mitigation strategies.

Biography

Dr Tiago Miguel Ferreira is a Senior Lecturer in Smart and Resilient Cities and Structures at the University of the West of England (UWE Bristol), UK, where he also serves as Programme Leader for the MSc Programme in Civil Engineering. Additionally, he is an Invited Associate Professor at the University of Coimbra, Portugal. His research focuses on the structural vulnerability of historical buildings and urban areas to natural and anthropogenic hazards, including earthquakes, fires, floods, and landslides. More recently, his work has expanded to explore the interactions between these hazards and their impacts on physical and social vulnerability, as well as the use of digital technologies to support decision-making and community engagement. Dr Ferreira has been listed among the top 2% of most influential scientists globally by Elsevier BV and Stanford University in 2021, 2022, 2023, and 2024. He has contributed over 200 publications, including more than 90 research articles in leading international journals, and has been actively involved in 13 R&D projects with a total funding of over £10.9 million. In addition, he serves as a reviewer for various international funding bodies, is a member of ICOMOS-UK and ISCARSAH, and is an Editor-in-Chief of the journal GeoHazards. Currently, he coordinates a working group established under Sub-Commission 8 (Eurocode 8) of the Portuguese Technical Commission for Standardization of Structural Eurocodes (CT115), which brings together universities, national and regional research institutes, and industry partners to work on the mechanical characterisation of masonry typologies in Portugal, intended for adoption in the future generation of the Portuguese Annex of Eurocode 8 – Part 3.

Copyright © 2025 CroCEE

Invited Lecture

EXAMPLES OF APPLICATION OF SEISMIC INTERFEROMETRY IN ENGINEERING SEISMOLOGY

Stefano Parolai

Professor, Head of Department of Mathematics, Informatics and Geosciences, University of Trieste, Italy, stefano.parolai@units.it

Abstract

Although the foundations of the methodology behind seismic interferometry, and in particular the use of seismic noise, were laid more than 60 years ago, their use has found increasing development in the past two decades. This methodology has found applications in various branches of seismology and engineering seismology, proving to be an optimal tool for noninvasive surveys and continuous monitoring of the medium.
In this presentation some examples of application of seismic interferometry will be shown and in particular for optimal estimation of seismic input, estimation of attenuation in soft sediments and structures, identification of structure-soil interaction effects, and estimation of 2D/3D site effects and virtual seismograms in sedimentary basins.
Finally, expected results will be presented as part of a new project (MODERN- Advanced Seismic Interferometry Methods and Technologies for Engineering Seismology) in which the application of innovative seismic interferometry-based methodologies and the development of ad hoc instrumentation with private sector components is planned.

Biography

Prof. Stefano Parolai is full Professor in Physics of the Solid Earth and Head of the Department of Mathematics, Informatics and Geosciences of the University of Trieste. Till 2022 he was the Director of the Seismological Research Centre (CRS) of the National Institute of Oceanography and Applied Geophysics- OGS in Italy and Secretary General of the European Seismological Commission (ESC). He has been formerly head of the Centre for Early Warning Systems of the German Research Centre for Geosciences (GFZ) in Potsdam and Apl. Professor at the Technische Universität Berlin, Germany. From 2011 to 2017 he has been Coordinator of Central Asia Global Change Observatory of GFZ and Member of the Scientific Advisory Board of the Central Asian Institute for Applied Geosciences (CAIAG). He was appointed by the Minister of Civil Protection and Sea Policy as a component and substitute contact person in the field of Seismic Risk, of the National Commission for the Forecasting and Prevention of Major Hazards. (Commissione Grandi Rischi) Prof. Stefano Parolai has been involved in several national and international projects, such as SIBYL (SeIsmic monitoring and vulneraBilitY framework for civiL protection), AZEHR (Azerbaijan Earthquake Hazard and Risk), MARsite (New Directions in Seismic Hazard Assessment through Focused Earth Observation in the Marmara Supersit), REAKT (Strategies and Tools for Real Time Earthquake RisK Reduction), MATRIX (New Multi-Hazard and Multi-Risk Assessment Methods for Europe) and CASCADE (Central Asia Cross-Border Natural Disaster), the PNRR Return. He is the PI of the “Advanced SeisMic InterferOmetry MethoDs and TechnologiEs for EngineeRiNg Seismology (MODERN)” project. funded by the "talian Fund for Applied Sciences". Prof. Stefano Parolai is author of 201 publications on international scientific journals. (h-index 43). His main research interests are in the fields of engineering seismology and in particular earthquake early warning, building monitoring, site response analysis and seismic hazard and risk assessment.

Copyright © 2025 CroCEE

Invited Lecture

SEISMIC ANALYSIS OF MASONRY STRUCTURES

Hrvoje Smoljanović

Associate Professor, University of Split, Faculty of Civil Engineering, Architecture and Geodesy, Croatia, hrvojes@gradst.hr

Abstract

Masonry is one of the oldest construction techniques that has been preserved to this day due to its simplicity. Despite the simplicity of building, numerical modelling of masonry structures, for the purpose of assessing their mechanical resistance and stability, is not such a simple task. These difficulties in numerical modelling of masonry structures arise from numerous effects that need to be taken into account, the most significant of which are large displacements, large rotations, material nonlinearity, the appearance and development of cracks, and contact interaction that includes friction between blocks in dry stone masonry structures. To date, a numerous numerical models have been developed for the analysis of masonry structures. Most of these models are based on the Finite Element Method or the Discrete Element Method. Numerical models based on the Finite Element Method are suitable for describing the deformability of a structure, however, they have limitations when modelling discontinuities in the structure that can occur during the appearance and development of cracks, and the inability to model contact interaction between stone blocks in dry stone masonry structures. On the other hand, numerical models based on the Discrete Element Method have the advantage of describing large displacements, large rotations, contact interactions, discontinuities that occur due to cracking of structural parts, but they are limited in describing the deformability of the structure and the nonlinear material behaviour. Recently, numerical models have also appeared that combine the advantages of the Finite and Discrete Element Methods.
This paper will present one such numerical model for the analysis of masonry structures, which is based on the Combined Finite and Discrete Element Method, pioneered by Ante Munjiza. This paper presents a series of examples that demonstrate the advantage of this method in the analysis of masonry structures, with an emphasis on historical masonry structures. Various examples demonstrate the effects that significantly affect the mechanical resistance and stability of the masonry structure during seismic action, but which are often not taken into account in engineering calculations and national standards. The presented numerical analyses can be very useful for structural engineers for: choosing a numerical model for structural analysis, obtaining a better insight into the behaviour of masonry structures due to seismic action, making decisions about the possibly necessary rehabilitation of structures, choosing the method of rehabilitation of the structure.

Biography

Associate Professor at University of Split, Faculty of Civil Engineering, Architecture and Geodesy, Croatia, where he is instructor in courses related to Theory of Structures. With a PhD degree in 2013, since 2010 he is involved in research related to Building Structure, Earthquake Engineering and Virtual Experimentation. Editorial board member for IJIM international journal. Participated in several scientific projects, winner of the University Science Award in 2017.

Copyright © 2025 CroCEE

Invited Lecture

SEISMIC DESIGN OF MASONRY STRUCTURES WITH THE SECOND GENERATION OF EUROCODE 8 - BACKGROUND AND APPLICATION

Christoph Butenweg

Professor, Christoph Butenweg, FH Aachen University of Applied Sciences, christoph.butenweg@fh-aachen.de

Abstract

The seismic design of masonry structures with the second generation of Eurocode 8 offers structural engineers in Europe new possibilities for verification, allowing a much better utilisation of structural load-bearing reserves. The verification at significant damage limit state (SD) can be performed in a problem-oriented manner through three verification levels of increasing complexity: At the first level, verification is achieved through design rules by complying with required shear wall areas to be specified at the national level. At the next level, a force-based verification can be carried out in combination with Eurocode 6, using material- and building-specific behaviour factors. At the third level, a deformation-based verification using pushover analysis is required, by applying normative deformation capacities of individual walls.

The lecture begins with a in-depth explanation of the implementation and development of the three-level verification concept for the second generation of Eurocode 8, based on normative background documents, relevant research and experimental studies. Subsequently, key aspects of practical application are illustrated through examples. The lecture concludes with insights and recommendations for defining nationally determined parameters, based on the experience from European standardisation work. This includes, notably, deriving a table of required minimum shear wall areas that considers the country-specific masonry types, masonry units, architectural styles and constructional practice.

Biography

Prof. Dr.-Ing. Christoph Butenweg obtained his degree in engineering (Dipl.-Ing.) from Ruhr-Universität Bochum in 1994. In 1999, he earned his doctoral degree (Dr.-Ing.) from Universität Essen. In 2016, he became a Professor Dr.-Ing. at FH Aachen University of Applied Sciences. Additionally, he served as a visiting professor at the University of Belgrade in 2021. Between 1994 and 1999, he worked as a research assistant at the Chair of Institute of Structural Mechanics at the University of Essen. From 2000 to 2001, he worked as a structural engineer at the engineering company „Karvanek-Thierauf“ in Essen. He served as Chief Engineer at the Institute of Structural Statics and Dynamics, RWTH Aachen from 2001 to 2015. Since 2006, he has been the manager of SDA-engineering GmbH in Herzogenrath. Since 2016, he has been a professor for Technical Mechanics and Structural Engineering at FH Aachen University of Applied Sciences. Prof. Butenweg gives lectures on various topics such as Linear and Nonlinear Finite Elements, Structural Dynamics, Bionics, Earthquake Engineering, Dynamics, Technical Mechanics, and Structural Engineering. His research areas include Structural Dynamics, Earthquake Engineering, and Computational Structural Mechanics.

He has held several important roles in the field, including Chairman of the national code committee NA 005-51-06 AA "Earthquakes, special tasks" (Sp CEN/TC 250/SC 8) and Chairman of the national code committee NA 005-06-37 AA "Earthquake safety of masonry structures". He also led Project Team 5 for the development of Parts 4 and 6 of Eurocode 8 between 2018 and 2020. Additionally, he is a member of the national code committee 06 – Masonry Structures and a member of Working Group 1 "Masonry structures" of TC250/SC8. He is involved in the Executive Committee of the European Association of Earthquake Engineering (EAEE), and he serves on the executive board of the "Center for Wind and Earthquake Engineering" at RWTH Aachen University. He is also a member of the Research Advisory Board of the German Committee for Masonry Construction e. V. (DAfM) and a qualified structural engineer with the Chamber of Engineers “Bau NRW” in Germany. Since 2006, he has been leading seminars for the Chamber of Engineers Construction NRW in the field of structural dynamics and earthquakes. He served as the President of the German Society of Earthquake Engineering and Structural Dynamics (DGEB) from 2011 to 2015. Additionally, he holds a teaching assignment for the master’s program "Construct" at RWTH Aachen University.

Prof. Butenweg has authored over 250 national and international publications and four specialized books on Structural Dynamics and Earthquake Engineering. A complete list of his publications can be found at https://www.sda-engineering.de/publikationen.

Proceedings of the 3rd Croatian Conference on Earthquake Engineering - 3CroCEE
19–22 March 2025, Split, Croatia
Copyright © 2025 CroCEE
DOI: https://doi.org/10.5592/CO/3CroCEE.2025.3

A CAUSAL LENS PERSPECTIVE ON BASIN EFFECTS

Rashid Shams[a], Chukwuebuka C. Nweke[a], Chenhao Wu[b] and Henry Burton[b]

[a] *Department of Civil and Environmental Engineering, University of Southern California (USC), rashidsh@usc.edu*

[b] *Civil and Environmental Engineering, University of California, Los Angeles (UCLA)*

Keywords: Causal Inference, Basin Effects, Structural Damage, Double Machine Learning

Introduction

Earthquakes pose a significant threat to the safety and well-being of a large portion of the global population. As the rate of urbanization continues to exceed the rate of population growth, the risks associated with seismic hazards intensify, especially in urban areas where vertical expansion through high-rise structures is often the solution to housing demands. These tall structures are particularly susceptible to damage and collapse during earthquake events due to amplification and prolonged ground shaking. These phenomena are exacerbated in sedimentary basins, where two- and three-dimensional seismic wave propagation mechanisms significantly alter ground motion intensity, spectral content, and duration. Despite decades of research, basin effects remain inadequately understood and are often oversimplified in current seismic hazard assessment frameworks.

The effects of sedimentary basins have been observed in several major earthquakes, where damage was concentrated in urban centres built over deep sedimentary deposits. For instance, during the 1985 Michoacán earthquake (M8.1), Mexico City experienced catastrophic damage to tall buildings due to basin-induced amplification (Pilz et al., 2011; Assimaki et al. 2012). A similar pattern of damage was observed in the Seattle basin during the 2001 Nisqually earthquake (M6.8), and in Christchurch, New Zealand, during the Canterbury Earthquake sequence (2010 M7.1 Darfield and 2011 M6.3 Christchurch events.

Methodology

Our research focuses on two key domains: ground motion characterization and structural response/damage assessment. For ground motion characterization, we consider multiple intensity measures (IMs), such as spectral acceleration, peak ground acceleration, Arias intensity, and significant duration, which collectively capture the amplitude, frequency content, and duration of ground shaking. The study employs both empirical data from past earthquakes and simulated ground motions using advanced nonlinear models. This dual approach ensures that our findings are robust and applicable across a range of seismic scenarios.

The structural response and damage assessment component investigates the performance of tall buildings and critical infrastructure within basins under real and simulated ground motion records. Using causal machine learning, we disentangle the effects of basin amplification, ground motion duration, and other confounding factors (e.g., spectral shape, pulse effects) on structural damage metrics. This approach enables us to establish causal relationships rather than mere associations, thereby providing actionable insights for engineering design and policy decisions. The proposed work represents a paradigm shift in how sedimentary basin effects are studied and incorporated into seismic risk assessments. By leveraging causal inference, we move beyond traditional statistical methods to explicitly address the challenges posed by confounding variables. This transition is crucial for developing scientifically rigorous and practically relevant models that can inform effective risk mitigation strategies. We formulate our causal problem as basin/non-basin as treatment, vs30, basin depth, Magnitude, focal depth, geology of site as confounders where PSAs are outcomes. We employ Propensity score methods such as and Double machine learning approach to quantify and explore

Copyright © 2025 CroCEE
DOI: https://doi.org/10.5592/CO/3CroCEE.2025.3

factors contributing to basin effects. The propensity score is calculated using logistic regression or more advanced methods such as machine learning models. This score represents the likelihood of treatment assignment based on observed covariates (Rosenbaum & Rubin, 1983). Individuals in the treatment group are matched with those in the control group based on similar propensity scores, reducing bias due to confounding variables (Austin, 2011). Double machine learning (DML) (Bach et al. 2021) is a statistical method designed to estimate causal effects in high-dimensional settings by leveraging machine learning models. It is particularly useful for constructing unbiased treatment effect estimates from observational data, even when dealing with complex covariates. Preliminary results from our research indicate that causal machine learning methods, such as causal forests and double machine learning, can effectively isolate the effects of individual basin features. The figure 1 below shows a preliminary DAG (Direct Acyclic Graph) to conceptualize both the causal and statistical dependencies between the variables that are considered in seismic intensity and infrastructure damage assessments. The unmeasured influences on Basin Geomorphology (BA), PGA and M are denoted as U_{BA}, U_{PGA} and U_M.

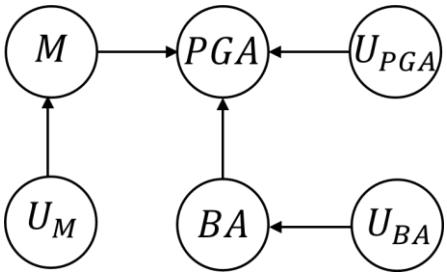


Figure 1. Simple 3-variable DAG where the goal is to isolate the causal effect of BA on PGA

Looking ahead, the insights gained from this research have the potential to significantly improve the accuracy of seismic hazard models and enhance our understanding of infrastructure vulnerability in basins. By explicitly quantifying the causal effects of basin geomorphology, we aim to bridge the gap between seismology and structural engineering, fostering a more holistic approach to seismic risk mitigation.

Conclusion

In conclusion, this study underscores the importance of interdisciplinary research in addressing complex challenges at the intersection of earth sciences and engineering. The integration of causal inference into seismic hazard and risk assessments marks a critical step toward more resilient urban infrastructure in earthquake-prone regions. We believe that the findings from this research will not only advance scientific understanding but also contribute to the development of evidence-based policies and practices that prioritize safety and sustainability.

References

Pilz, M., Parolai, S., Stupazzini, M., Paolucci, R., & Zschau, J. (2011). Modelling basin effects on earthquake ground motion in the Santiago de Chile basin by a spectral element code. Geophysical Journal International, 187(2), 929-945.

Assimaki, D., Ledezma, C., Montalva, G. A., Tassara, A., Mylonakis, G., & Boroschek, R. (2012). Site effects and damage patterns. *Earthquake Spectra*, *28*(1_suppl1), 55-74.

Rosenbaum, P., & Rubin, D. (1983). The central role of the propensity score in observational studies for causal effects. *Biometrika*, 70, 41-55. https://doi.org/10.1093/BIOMET/70.1.41.

Austin, P. (2011). An Introduction to Propensity Score Methods for Reducing the Effects of Confounding in Observational Studies. Multivariate Behavioral Research, 46, 399 - 424. https://doi.org/10.1080/00273171.2011.568786.

Bach, P., Chernozhukov, V., Kurz, M., & Spindler, M. (2021). DoubleML - An Object-Oriented Implementation of Double Machine Learning in R. ArXiv, abs/2103.09603. https://doi.org/10.18637/jss.v108.i03.

Proceedings of the 3rd Croatian Conference on Earthquake Engineering - 3CroCEE
19–22 March 2025, Split, Croatia
Copyright © 2025 CroCEE
DOI: https://doi.org/10.5592/CO/3CroCEE.2025.25

COMBINING CONVENTIONAL AND NEXT-GENERATION INTENSITY MEASURES FOR RISK ASSESSMENT OF BRIDGES

Savvinos Aristeidou [(1)], Gerard O'Reilly [(2)]

[(1)] *Postdoctoral Researcher, Scuola Universitaria Superiore IUSS Pavia, savvinos.aristeidou@iusspavia.it*
[(2)] *Associate Professor, Scuola Universitaria Superiore IUSS Pavia, gerard.oreilly@iusspavia.it*

Abstract

This study investigates seismic risk assessment of bridge structures using a combination of conventional and next-generation intensity measures (IMs). The structures are simplified bridge models, characteristic of European construction, distinguished into regular and irregular bridges depending on the pier height arrangement. The efficacy of multiple IMs is explored, including spectral acceleration, *Sa*, significant duration, *Ds*, average spectral acceleration, Sa_{avg}, and filtered incremental velocity, *FIV*3, in predicting seismic demand. This was done by setting up different ground motion selection schemes, with different conditioning and matching IMs, and performing comparative analyses. Probabilistic seismic hazard analysis (PSHA) is conducted for each conditioning IM to obtain their seismic demand hazard curves and disaggregation. The dispersion IMs given exceedance of a range of engineering demand parameters (EDPs) was quantified, which provided a deeper understanding of the performance of each selection case across various nonlinearity levels. Our findings demonstrate that the cases conditioned on *Sa* exhibit the lowest dispersion in the elastic and early non-linear stages, making them the most reliable for low-intensity seismic events. However, as non-linearity increases, cases with Sa_{avg} as the conditioning IM demonstrate superior performance, showing the least dispersion for low to high non-linear conditions, especially in irregular bridge structures. In cases of high non-linearity and near-collapse scenarios, *FIV*3 outperforms the other IMs by offering the lowest dispersion, especially in regular bridge structures. In addition, the hazard consistency of each selection cases was checked, and a couple of examples are presented here. The case study outcomes provide valuable insights into the benefits of ground motion selection with a combination of next-generation IMs with conventional ones for seismic risk assessments. Additionally, practical guidance is offered on the leverage of recently developed generalised ground motion model (GGMM) and correlation models for achieving more accurate performance-based assessments.

Keywords: Bridges, risk assessment, generalised conditional intensity measure, intensity measures, hazard consistency

1. Introduction

Seismic risk assessment of structures, particularly bridges, has evolved significantly over the years with advancements in ground motion modelling and the development of next-generation intensity measures (IMs). Traditional approaches often relied on simpler IMs, such as *PGA*, which, while convenient, is insufficient in capturing the complex response of multi-modal and multi-component systems like bridges [1,2]. This is because other characteristics of ground motions, such as amplitude, frequency content, duration, and pulses, may significantly influence structural response. Recent research has highlighted the importance of utilising advanced IMs that better reflect the underlying seismic hazard that can be of higher engineering interest (e.g., [3,4]). These advanced (or next generation, as dubbed here) IMs not only improve the accuracy of seismic hazard representation but also enhance the reliability of risk predictions, addressing the limitations of older approaches. Building on this foundation, some IMs of engineering interest were integrated herein with advanced modelling and evaluation techniques to assess the level to which they enhance seismic risk for bridge structures.

A recently developed generalised ground motion model (GGMM) and correlation models [5,6] were leveraged to demonstrate the potential of next-generation IM. These models enabled improved predictive power and more accurate representation of seismic hazard. Also, showcased here is the practical applicability of the aforementioned models in ground motion record selection and risk assessment.

Copyright © 2025 CroCEE
DOI: https://doi.org/10.5592/CO/3CroCEE.2025.25

2. Ground motion selection for performance-based assessment of bridges

The selection and scaling of ground motion input are critical steps in the seismic risk analysis of bridge structures. Ground motions are typically selected and scaled based on seismic scenarios that match the site-specific hazard, coming from either probabilistic seismic hazard analysis (PSHA), or design code requirements. Scaling is usually done to achieve a specific IM value, and subsequent selection to match the spectral shape (or distribution in the probabilistic case). Many studies continue to rely on IM definitions, such as *PGA* or *Sa* at a fixed period [7–9] for regional risk assessments. Although they recognise that IMs like *PGA* are not ideal, they are often used as a baseline standard due to their simplicity and widespread adoption for convenience.

There are several ground motion selection approaches, a few of which listed and briefly described in the following. Advanced methods such as the conditional spectrum (CS) [10] and generalised conditional intensity measure (GCIM) [11] offer a rigorous probabilistic framework, with a more nuanced representation of ground motion variability by conditioning the selection process on a specific intensity measure or multiple IMs. These methods ensure consistency with the PSHA and are particularly suited for performance-based assessments. Scenario-based assessment [12], on the contrary, selects ground motions that represent specific seismic events, such as characteristic earthquakes for a known nearby fault. While this approach provides realistic inputs for scenario-specific studies, it lacks the versatility required for probabilistic risk evaluations.

3. Case study structures

3.1. Description

Seven multi-span bridges, each comprising either 4 or 8 spans of 50 m, were analysed. These bridges, previously studied by Pinho et al. [13] and O'Reilly [14], are representative of typical European bridge designs, featuring reinforced concrete (RC) piers designed according to Eurocode 8 [15]. The piers had a hollow rectangular cross-section, while the deck was continuous, with reinforcement details depicted in Figure 2(left). Pier heights were either 7 m, 14 m, or 21 m, and the bridges were categorised as regular or irregular based on the pier height variations along their length. Table 1 summarises the modal properties of the bridge structures and their classification as either regular or irregular, with additional illustrations shown in Figure 1.

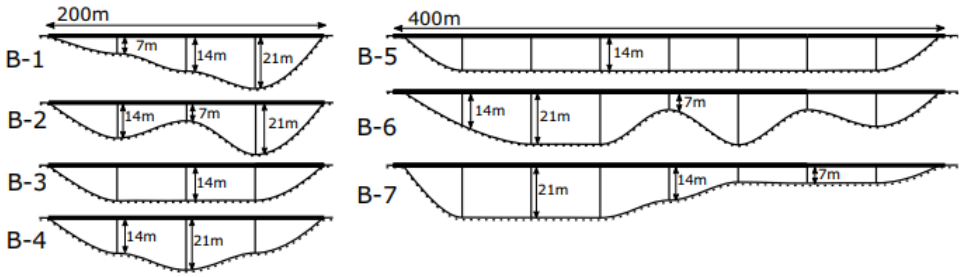


Figure 1. Illustration of the longitudinal profile of the case study bridge structures. Adapted from O'Reilly [14]

Table 1. Modal properties of each case study bridge structure

ID	Type	T_1 [s]	T_2 [s]	T_3 [s]	$\%M_1$	$\%M_2$	$\%M_3$	$\Sigma\%M$
B-1	Irregular	0.555	0.447	0.277	30	8	27	65
B-2	Irregular	0.555	0.474	0.253	30	19	5	53
B-3	Regular	0.483	0.475	0.223	32	0	66	98
B-4	Regular	0.508	0.475	0.307	6	0	77	94
B-5	Regular	0.479	0.479	0.225	16	0	76	92
B-6	Irregular	0.494	0.474	0.36	3	10	29	42
B-7	Irregular	0.556	0.436	0.387	11	7	35	53

Copyright © 2025 CroCEE
DOI: https://doi.org/10.5592/CO/3CroCEE.2025.25

3.2. Numerical modelling

A numerical model for each bridge was adapted to OpenSeesPy [16] from the previous OpenSees model detailed in O'Reilly [14]. The pier elements were represented using lumped plasticity models, with their parameters derived from moment–curvature analysis of the corresponding fibre-based section. This rupture strain was set at 0.10, based on Priestley et al. [17] for reinforcement steel in European bridges. The only difference from the modelling parameters described in O'Reilly and Monteiro [18] and O'Reilly [14] is the use of the *HystereticSM* material for the lumped plasticity hinges. This material was implemented with a pinching factor for deformation during reloading of 0.8, a pinching factor for force during reloading of 0.2, a damage parameter due to ductility of 0.001, and a damage parameter due to energy of 0.0001. Incorporating cyclic and in-cycle stiffness and strength degradation was essential for two main reasons: firstly, to capture the effects of matching (or not) the theoretical GCIM distribution of significant duration, *Ds*, and the implications of filtered incremental velocity, *FIV*3, matching and conditioning; and secondly, to ensure the model exhibits behaviour that more closely approximates real-world structural responses (i.e., it degrades and collapses).

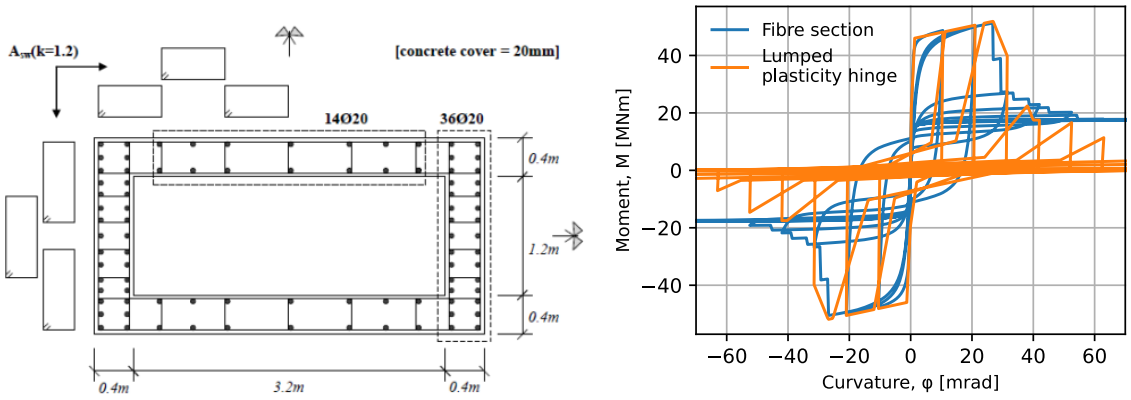


Figure 2. Illustration of structural detailing of the pier cross section [13]. The shorter side of the section is placed in the direction of the bridge deck (left). Moment curvature analysis of bottom section of the Pier with 7 m height. 10 cycles of unloading/reloading are shown here as an example, with equal curvature increments until the target curvature (right).

Modal analysis was performed to determine the dynamic properties of each bridge structure. Table 1 presents the periods, *T*, and modal masses participation factors, *M*, for the first three modes of vibration, as well as their cumulative sum for each structure, focusing exclusively on the transverse direction of response.

In bridge structures, the absence of a dominant mode or a clearly critical element complicates the selection of a suitable engineering demand parameter (EDP). Given the structural configuration of the bridges, the piers were identified as the critical elements susceptible to structural damage and element-specific EDPs were preferred. Specifically, the peak transient section curvature at the base of the piers was monitored during the ground shaking. The maximum curvature among all piers, φ_{max}, was then selected as the EDP. The curvature direction was the transversal, since in the records are applied only in the transversal direction. The collapse limit was assumed to be when the first pier reached 60 mrad of base curvature, since as seen in Figure 2(right) there is almost no moment resisting capacity in the pier at that level of deformation.

4. Hazard Analysis

PSHA was carried out for a site in Erzincan, Turkey using the OpenQuake [19] open-source software for seismic hazard and risk assessment developed by the Global Earthquake Model Foundation. The source model input was the ESHM20 model [20] and the GMM was the one developed by Aristeidou et al. [5]. Erzincan was selected as the case study site as it exhibits one of the highest seismic activities in Europe and Middle East and has been struck by a devastating 7.8 M_w earthquake in 1939, among

Copyright © 2025 CroCEE
DOI: https://doi.org/10.5592/CO/3CroCEE.2025.25

others. This high seismicity makes it easier to characterise the bridges' performance throughout the whole range of non-linear response without needing to reach very high return periods.

The hazard curves of each IM used to analyse bridge 1 are shown in Figure 3. The hazard curves of the IMs at other periods are omitted here for brevity but would be similar and were characterised the same way. Additionally, the hazard disaggregation of *FIV*3(0.555s) is given in Figure 4 as an example. It can be seen that most of the hazard is controlled by source-to-site distances below 30 km and magnitude mostly above 6.5. There are many scenarios contributing to the hazard, especially in low return periods, but for simplicity only the modal rupture scenario was used to select ground motions at each return period as a first-order approximation of the full disaggregation distribution.

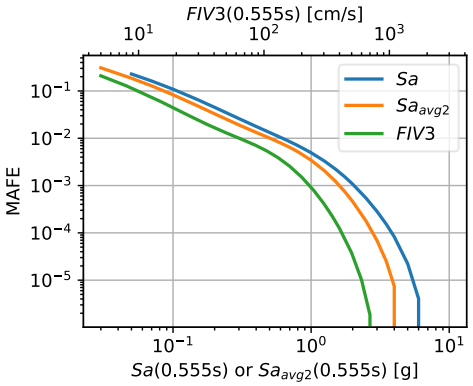


Figure 3. Hazard curves of IM* of bridge 1

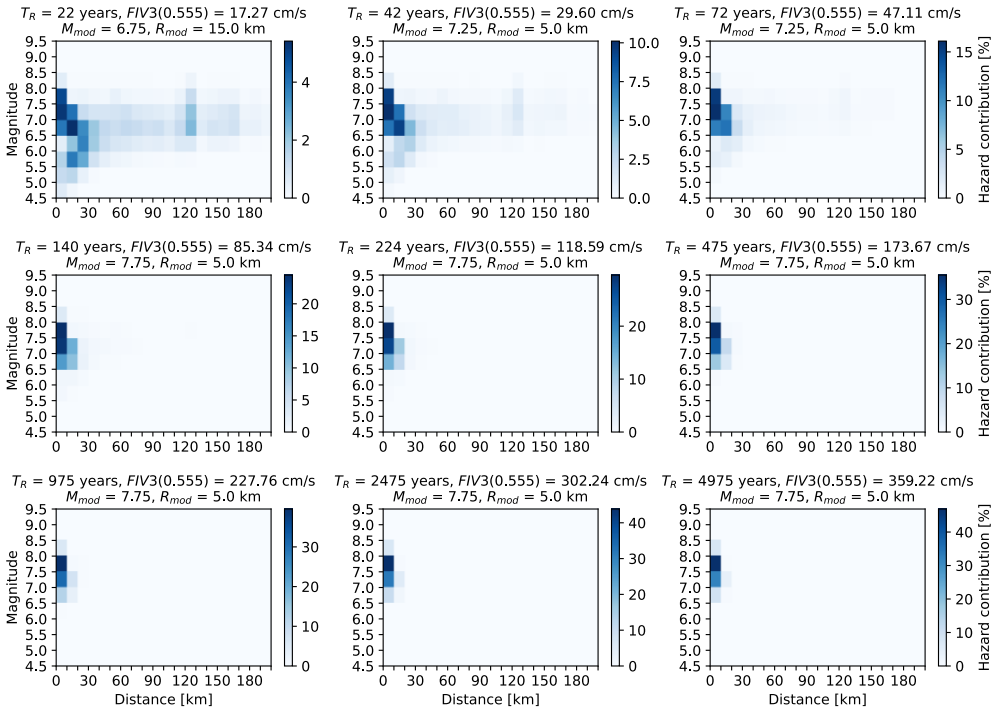


Figure 4. Hazard disaggregation of *FIV*3 at 0.555 s for the nine return periods investigated

5. Ground motion selection cases

The GCIM ground motion selection approach, introduced by Bradley [11], extends the principles of the CS approach [10] by allowing the matching IMs to differ from the conditioning IM. The CS approach is based on the assumption that spectral accelerations follow a multivariate lognormal distribution.

Proceedings of the 3rd Croatian Conference on Earthquake Engineering - 3CroCEE
19–22 March 2025, Split, Croatia
Copyright © 2025 CroCEE
DOI: https://doi.org/10.5592/CO/3CroCEE.2025.25

Building on this, the GCIM approach generalises this concept by proposing that any arbitrary vector of IMs, for a given seismic scenario, follows a multivariate lognormal distribution. Regarding the validity of this assumption, it is widely recognised that most IMs exhibit marginal lognormal distributions, as supported by regression analyses on ln(IM) in empirical GMMs. The conditional mean and standard deviation of the included IMs are therefore expressed in Equations (1) and (2).

$$\mu_{\ln IM_i|\ln IM^*,rup} = \mu_{\ln IM_i|rup} + \sigma_{\ln IM_i|rup} \cdot \rho_{\ln IM_i,\ln IM^*} \cdot \varepsilon_{\ln IM^*} \quad (1)$$

$$\sigma_{\ln IM_i|\ln IM^*,rup} = \sigma_{\ln IM_i|rup} \cdot \sqrt{1 - \rho^2_{\ln IM_i,\ln IM^*}} \quad (2)$$

where, IM_i is the matched IMs, IM* is the conditioning IM, μ is the target mean, σ is the target standard deviation, ρ the cross-correlation coefficient, and ε the normalised residual [21].

In the ground motion selection schemes investigated here, three different conditioning IMs (IM*) were included, namely $Sa(T_1)$, average spectral acceleration, $Sa_{avg2}(T_1)$, and $FIV3(T_1)$. Also, a combination of several IMs, for which the theoretical distribution was also conditionally matched (IM_i), namely $Sa(T)$, Ds_{575}, $Sa_{avg3}(T)$, $FIV3(T)$, and $Sa_{avg2}(T)$, was included. All the different ground motion record selection cases along with their conditioning and matched IMs are listed in Table 2. For the period-dependent IMs, where 'T' is denoted, it means that the whole spectrum at a range of periods was matched, and 'T_1' means that the IM at the first period of each structure was matched. It is noted here that Sa_{avg3} and Sa_{avg2} were calculated from 10 equally spanning periods ranging from $0.2T$ to $3T$, and $0.2T$ to $2T$, respectively.

Table 2. Ground motion input cases

Case No.	IM*	IMi			
0	$Sa(T_1)$	—	—	—	—
1	$Sa(T_1)$	$Sa(T)$	—	—	—
2	$Sa(T_1)$	$Sa(T)$	Ds_{575}	$Sa_{avg3}(T_1)$	$FIV3(T_1)$
3	$Sa(T_1)$	$Sa(T)$	—	$Sa_{avg3}(T_1)$	$FIV3(T_1)$
4	$Sa(T_1)$	$Sa(T)$	Ds_{575}	—	—
5	$Sa_{avg2}(T_1)$	$Sa(T)$	—	—	—
6	$FIV3(T_1)$	$Sa(T)$	—	—	—
7	$Sa_{avg2}(T_1)$	—	—	$Sa_{avg2}(T)$	—
8	$FIV3(T_1)$	—	—	—	$FIV3(T)$
9	$Sa_{avg2}(T_1)$	—	Ds_{575}	$Sa_{avg2}(T)$	—
10	$FIV3(T_1)$	—	Ds_{575}	—	$FIV3(T)$

No rupture parameter limits were applied in the selection of ground motions, but a maximum scale factor of 8 was set. Both horizontal components of the pool of recorded motions were included in the selection pool, in other words the number of possible ground motions to be used for the analysis was double the number of available recordings. This is done because the bridge is excited unidirectionally (transversally). A set of 50 records were selected for each stripe.

The hazard consistency was checked for the ground motion selection cases and two examples are illustrated in Figure 5. The checks are shown for four different periods of Sa, a shorter period than the conditioning one, a period that is close to the conditioning, and two longer periods than the conditioning one. Firstly, it can be observed that the selection Case 0 gives a good match with the seismic hazard curves, except for $T = 0.2$ s, which is an unexpected result since no effort was made in the selection to achieve hazard consistency. It seems to be a circumstantial result, emanating from the interaction between the lower medians and higher dispersions of the selected records of Case 0. This is the case for longer periods than the conditioning one (spectrum not shown here due to space limitations). For shorter periods than the conditioning, it can be seen that the selected records present higher hazard curve than that from PSHA. This is because, while the median of selected records is close in value to the target median, the dispersion of the selected records is higher that the target dispersion.

Proceedings of the 3rd Croatian Conference on Earthquake Engineering - 3CroCEE
19–22 March 2025, Split, Croatia
Copyright © 2025 CroCEE
DOI: https://doi.org/10.5592/CO/3CroCEE.2025.25

Figure 5(right) illustrates the hazard consistency check of ground motion record selection Case 5, which is conditioned on Sa_{avg2}. It can be seen that there is a good match with the hazard curves obtained from PSHA, except for the high annual rate of exceedance part of $T = 2$ s. The source of this mismatch is due to the fact that not all input parameters of the GGMM could be extracted from the hazard disaggregation, only magnitude and distance, therefore some assumptions had to be made for other parameters. Another reason is the choice of the modal scenario of the hazard disaggregation, and not the inclusion of all the scenarios that significantly contribute to hazard.

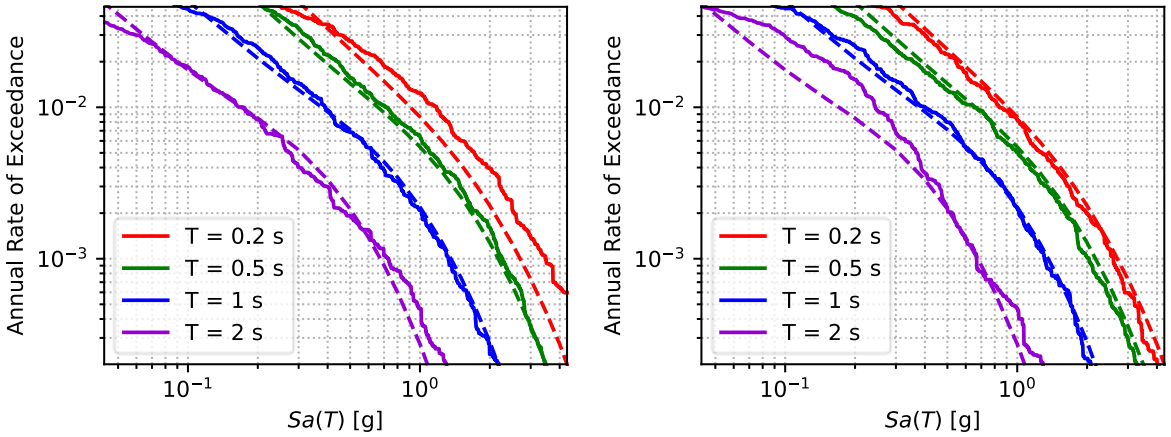


Figure 5. Hazard consistency checks for ground motion input Cases 0 (left) and 5 (right) for bridge B-1. Dashed lines represent the hazard curves and solid lines represent the reconstructed hazard curves obtained from the selected ground motions

6. Results

6.1. Multiple stripe analysis (MSA) results

With the ground motion record sets identified for each selection case, return period, and bridge structure, MSA was carried on the numerical model of each bridge structure. The output of this analysis is an empirical distribution of the bridge response, characterised via an EDP (in this case φ_{max}), versus an IM level corresponding to a specific return period. As an example, the MSA results for the case study bridge B-1 and ground motion selection Case 5 are illustrated in Figure 6. The response ordinates of only the non-collapse cases are shown in the plot, for which the logarithmic mean and ±1 standard deviation are also illustrated. Also shown in the right-hand side of the figure is the probability of collapse in each intensity level.

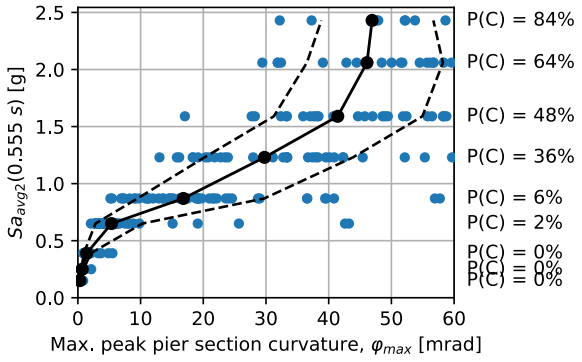


Figure 6. MSA results obtained with the ground motion input 5 on case study bridge B-1. Also depicted is the logarithmic mean and ±1 standard deviation of the non-collapse cases, and the probability of collapse resulting from each intensity level

Copyright © 2025 CroCEE
DOI: https://doi.org/10.5592/CO/3CroCEE.2025.25

6.2. Demand-based evaluation

The probability of an IM causing exceedance of certain damage limit threshold, which is indexed by an EDP value, is often modelled using a lognormal distribution characterised by a median, $\eta_{IM|EDP}$, and dispersion, $\beta_{IM|EDP}$, forming what is known as a seismic fragility function. By integrating this function with the mean hazard curve derived from PSHA, $H(im)$, the mean annual frequency of exceedance (MAFE) of that EDP value is obtained, offering a more comprehensive and consistent measure of seismic risk. The calculation of this MAFE is given in Equation (3), where $\Phi[\cdot]$ represents the standard normal cumulative distribution function.

$$\lambda = \int_0^\infty \Phi\left[\frac{\ln im - \eta_{IM|EDP}}{\beta_{IM|EDP}}\right] |dH(im)| \tag{3}$$

The parameter $\beta_{IM|EDP}$ in Equation (3) is plotted in Figure 7 versus the whole range of EDP response of the structure. The legend indicates each case, with its corresponding short naming scheme. The first IM is the conditioning one, while the IMs after the dash symbol are the ones whose theoretical GCIM distribution is been matched by the record selection. The IMs after the dash that are denoted with "(*T*)" are the ones whose spectrum is matched, whereas for the other period-dependent IMs, without "(*T*)", only at the 1st period of each structure was matched For the regular bridge structures (B-3, B-4, and B-5), Cases 6, 8, and 10 exhibit the lowest dispersion $\beta_{IM|EDP}$ for φ_{max} values exceeding 10 mrad, which spans most of the response range. These cases employ *FIV*3 as the IM*. Among these, Case 10 clearly achieves the lowest dispersion overall by conditioning on *FIV*3 and matching both the *FIV*3 spectrum and Ds_{575}, demonstrating its superior efficiency for these regular bridges, especially for the higher levels of EDP when the structure is responding in its non-linear range since the yield curvature was approximately 1.25 mrad.

In contrast, for the irregular bridge structures, Cases 5, 7, and 9 show the lowest dispersion, particularly in the initial half of the structural response range. These cases condition on $Sa_{avg2}(T_1)$. While the differences among these cases are not pronounced, Case 9 stands out as slightly more efficient. This can be attributed to its matching of the expected duration distribution at the site, which additionally ensures more accurate median response estimates.

For cases using *Sa* as the conditioning IM, dispersion remains low in the initial stages of the response but increases significantly as the structural response becomes more non-linear. Cases 1 and 3 exhibit the highest dispersion, although they differ little from Cases 2 and 4. Interestingly, Case 0—the most basic scenario—exhibits lower dispersion than the other *Sa*-conditioned cases, despite its higher dispersion of the selected records. This unexpected outcome can be explained by the inclusion of records with lower spectral ordinates in longer periods and also lower durations, which artificially raises the efficiency of *Sa* as a conditioning IM. However, this comes at the expense of not adhering to hazard consistent selection rules, as Case 0 fails to represent the site-specific hazard and underestimates risk, particularly at higher EDPs where structural nonlinearity and longer-period motions dominate, as discussed in Section 5.

Finally, it is worth noting that cases incorporating *Ds* as a matched IM consistently achieve lower dispersion compared to corresponding cases where *Ds* is not matched. This highlights the value of including duration-based IMs, like *Ds*, in reducing variability and improving the accuracy of seismic demand predictions.

Copyright © 2025 CroCEE
DOI: https://doi.org/10.5592/CO/3CroCEE.2025.25

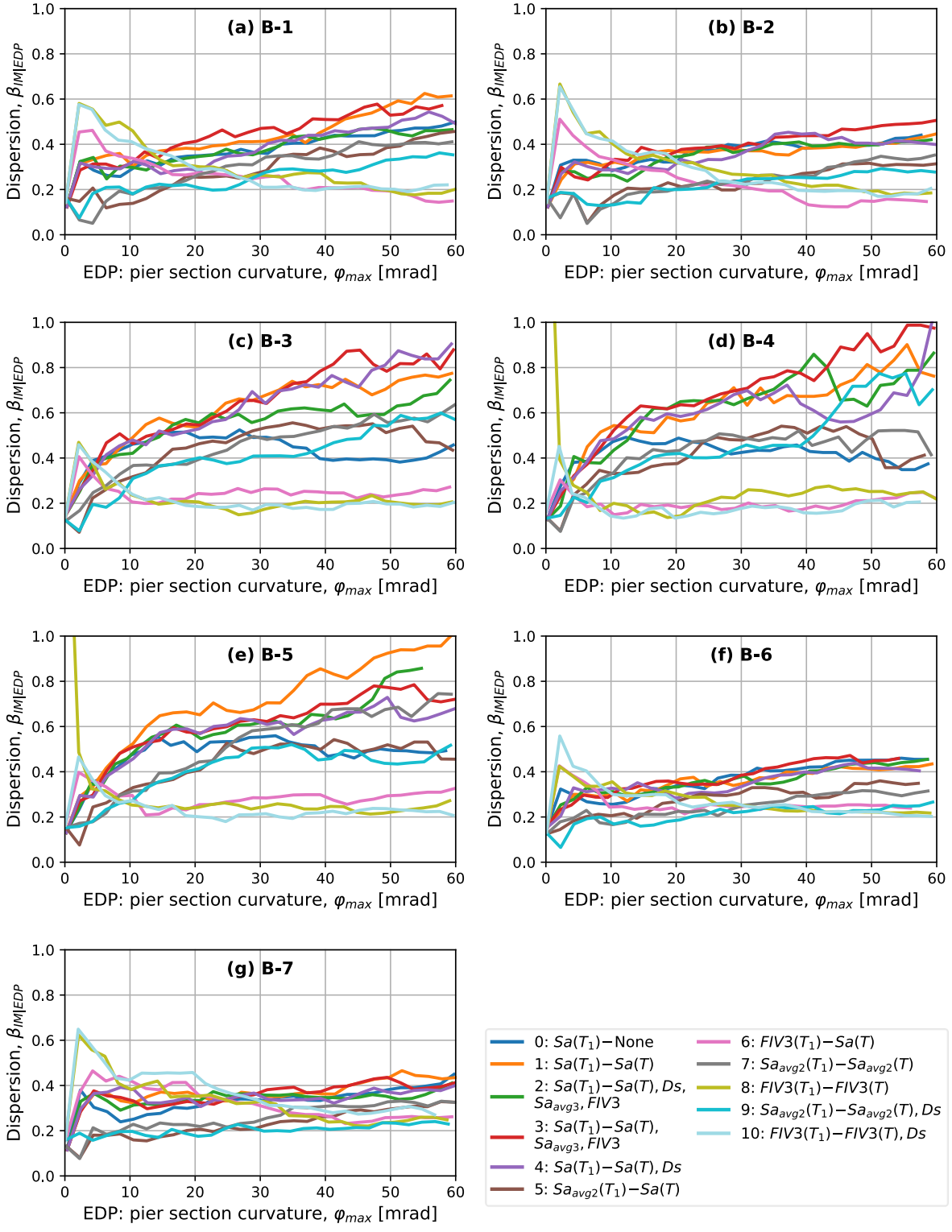


Figure 7. Dispersion of IM given exceedance of EDP

6.3. Risk-based evaluation

It is expected that for the hazard-consistent selection cases the resulting MAFE estimates converge to a similar value for each bridge. These curves can be compared and, in some cases, validated against

Copyright © 2025 CroCEE
DOI: https://doi.org/10.5592/CO/3CroCEE.2025.25

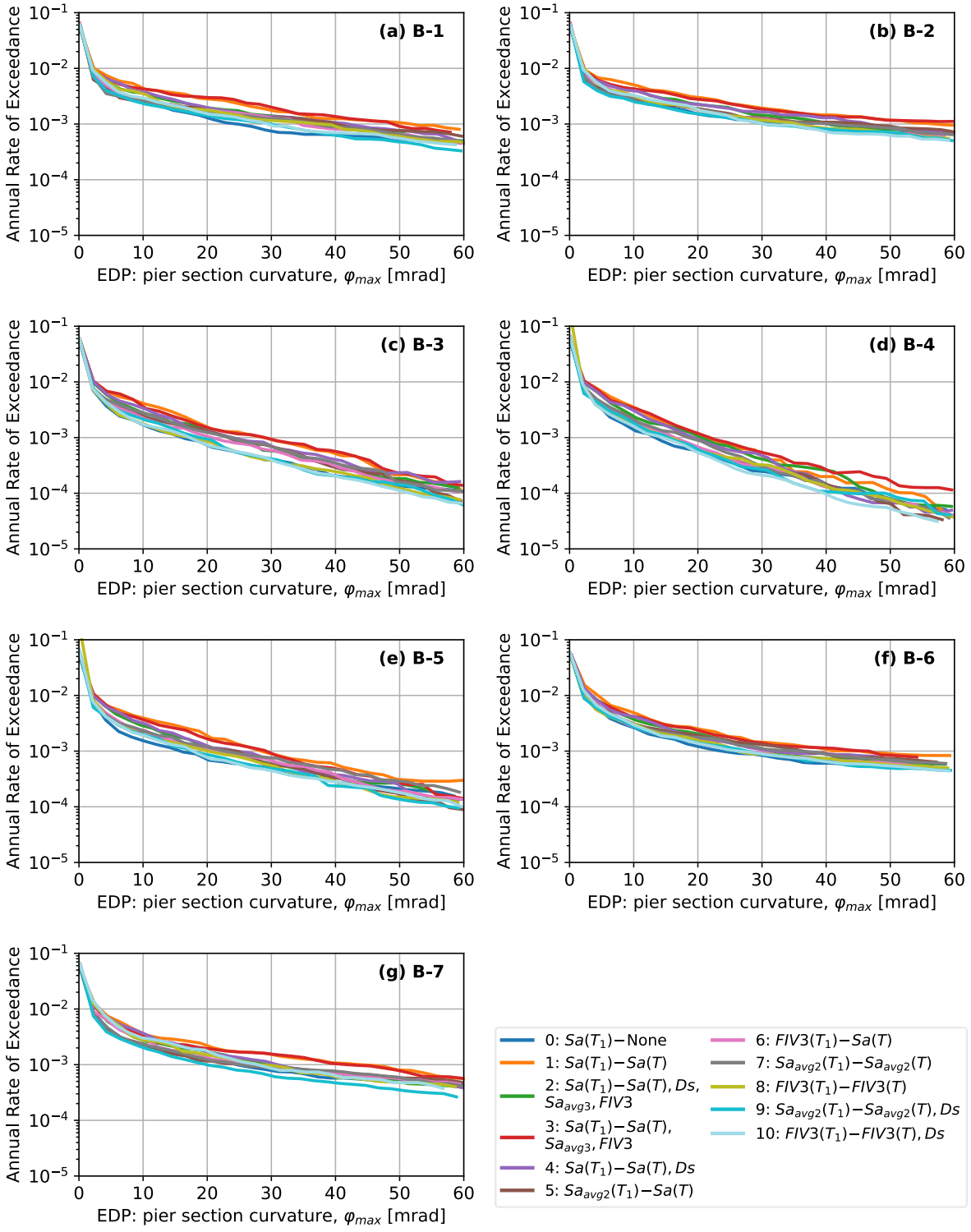


Figure 8. Seismic demand hazard curves of the case study bridges

results from detailed physics-based simulations, as discussed by Bradley et al. [22]. However, such validations would be beyond the scope of this study.

From Figure 8, there are a number of observations that can be made. Regular bridges have lower MAFE, than the irregular bridges, especially in higher EDPs. B-4 has the lowest risk. Cases 1 and 3 consistently gave higher estimates of λ in all the bridge structures. It is interesting to note the Cases 2 and 4 (i.e.,

Copyright © 2025 CroCEE
DOI: https://doi.org/10.5592/CO/3CroCEE.2025.25

conditioning on *Sa* and matching the Ds_{575}) result in MAFE closer to the rest of the cases, which indicates that matching the Ds_{575} GCIM distribution alleviates part of the incompetencies of *Sa* as a conditioning IM. Case 0 gives one of the lowest risk estimates because of its lower-than-expected *Sa* spectrum and Ds_{575} of the records, as already discussed above, hence deeming it the ``worst'' case for what concerns risk estimation.

The difference between Cases 5 and 7 is negligible. The same applies to Cases 6 and 8, which indicates that there is no practical difference in matching the *Sa* or Sa_{avg2} spectrum along with conditioning on Sa_{avg2}, or matching the *Sa* or *FIV*3 spectrum along with conditioning on *FIV*3. This is likely due to the high level of correlation between each of these IMs [6], meaning that these cases are slight variations of each other. It also underlines the importance of hazard-consistent ground motion record selection when compared to Case 0, for example.

Additionally, Cases 9 and 10 give similar MAFE estimates, which are relatively low in value compared to the rest of the cases. All in all, it can be concluded that matching the Ds_{575} distribution makes a notable difference in the risk estimates and is likely what should be focused on for analysts when dealing with non-linear systems with some form of strength degradation.

7. Summary and conclusions

In this conference paper, an analysis was conducted to evaluate the implications of next-generation IMs on the seismic risk assessment of bridge structures. The GGMM and correlation models, developed by Aristeidou et al. [5,6], were employed to facilitate the seismic hazard analyses and selection of ground motions using advanced approaches, such as the GCIM method. The latter approach ensures that key features of ground motions beyond spectral acceleration, such as duration and velocity, are appropriately represented and matched during selection. Ground motion records were selected and scaled according to different strategies, including just scaling to the conditioning IM, CS-based and GCIM-based selection. A suite of multi-span bridge structures with varying pier heights and span configurations was analysed using numerical models built in OpenSeesPy. The MSA method was used to quantify structural demands, and risk estimates were derived for the case study bridges.

Several ground motion selection cases were investigated and the following conclusions regarding the comparisons between them are outlined:

- Cases 0 and 1: Case 0 gave lower IM dispersion for a given EDP exceedance for the majority of EDP range. Additionally, its lower-than-expected *Sa* spectrum was primarily responsible for the lower risk estimates. This highlights the importance of matching target distributions of all pertinent IMs, and not just the conditioning one.
- Cases 1 and 2: The CS approach gave ground motions with higher-than-expected Ds_{575}, which resulted in higher EDP medians, and therefore risk estimates. The dispersions were somewhat lower in Case 2, and therefore presented higher efficiency. Nevertheless, the differences in dispersion were small.
- Cases 1, 2, 3, and 4: Cases 2 and 4 give similar results, while Cases 1 and 3 also exhibit similar results between them. Therefore, we can conclude that the differences between Cases 1 and 2 come solely from matching or not the Ds_{575}.
- Cases 1, 5, and 6: Case 1 resulted in low dispersion only in the initial stages of EDP response, which is the elastic and mildly inelastic stage, and then the dispersion quickly rises. Case 5 was more efficient in the irregular bridges, while Case 6 dominated with regards to efficiency in most of the non-linear response range of the regular bridges.
- Cases 5 and 7: Dispersions and risk estimates are very similar between the two cases. Which suggests that one can select any of the two selection schemes and obtain very similar results.
- Cases 6 and 8: Dispersions and risk estimates are very similar between the two cases, with Case 6 resulting in slightly lower dispersions. This suggests that when conditioning on *FIV*3, matching the *Sa* spectrum will give slightly more accurate results, than matching the *FIV*3 spectrum.

Copyright © 2025 CroCEE
DOI: https://doi.org/10.5592/CO/3CroCEE.2025.25

- Cases 9 and 10, versus all the rest: The CS of Sa_{avg2} and *FIV*3 while matching the Ds_{575} theoretical distribution at the site seem to be best cases. Case 9 was found to be more accurate for the initial and intermediate stages of nonlinearity, while Case 10 was found to be more accurate for the deeper stages of response nonlinearity and near collapse.

By utilising a newly developed GGMM and correlation models, the practical benefits of next-generation IMs, such as *FIV*3 and Sa_{avg2}, in improving both the accuracy and consistency of seismic demand predictions were demonstrated. Specifically, the GCIM-based approach proved highly effective in reducing the dispersion of structural response while maintaining hazard consistency—a critical factor often overlooked in traditional selection methods. The findings further highlighted the sensitivity of IM's performance to structural regularity, with velocity-based IMs like *FIV*3 excelling for regular bridges and Sa_{avg2} exhibiting superior performance for irregular structures.

Overall, this work bridges the gap between state-of-the-art ground motion selection techniques and practical applications for researchers and practitioners who would like to use the IMs utilised here. The tools and methodologies used here can serve as a foundation for future research and implementation in performance-based designs and assessments.

Acknowledgements

This work has been developed within the framework of the projects "Dipartimenti di Eccellenza", funded by the Italian Ministry of Education, University and Research at IUSS Pavia. The authors would also like to acknowledge Davit Shahnazaryan for developing the ground motion selection tool used in this study.

References

1. Luco N, Cornell CA. Structure-specific scalar intensity measures for near-source and ordinary earthquake ground motions. *Earthquake Spectra* 2007; **23**(2): 357–392. DOI: 10.1193/1.2723158.
2. Huang Q, Gardoni P, Hurlebaus S. Probabilistic Seismic Demand Models and Fragility Estimates for Reinforced Concrete Highway Bridges with One Single-Column Bent. *Journal of Engineering Mechanics* 2010; **136**(11): 1340–1353. DOI: 10.1061/(ASCE)EM.1943-7889.0000186.
3. Kohrangi M, Vamvatsikos D, Bazzurro P. Pulse-like versus non-pulse-like ground motion records: Spectral shape comparisons and record selection strategies. *Earthquake Engineering and Structural Dynamics* 2019; **48**(1): 46–64. DOI: 10.1002/eqe.3122.
4. Dávalos H, Miranda E. Evaluation of FIV3 as an Intensity Measure for Collapse Estimation of Moment-Resisting Frame Buildings. *Journal of Structural Engineering* 2020; **146**(10): 1–14. DOI: 10.1061/(asce)st.1943-541x.0002781.
5. Aristeidou S, Shahnazaryan D, O'Reilly GJ. Artificial neural network-based ground motion model for next-generation seismic intensity measures. *Soil Dynamics and Earthquake Engineering* 2024; **184**: 108851. DOI: 10.1016/j.soildyn.2024.108851.
6. Aristeidou S, Shahnazaryan D, O'Reilly GJ. Correlation Models for Next-Generation Amplitude and Cumulative Intensity Measures using Artificial Neural Networks. *Earthquake Spectra* 2024; **0**(0): 1–24. DOI: 10.1177/87552930241270563.
7. HAZUS. *Multi-hazard loss estimation methodology - earthquake model,*. Washington, DC, USA: 2003.
8. Villar-Vega M, Silva V, Crowley H, Yepes C, Tarque N, Acevedo AB, *et al.* Development of a Fragility Model for the Residential Building Stock in South America. *Earthquake Spectra* 2017; **33**(2): 581–604. DOI: 10.1193/010716EQS005M.
9. Del Gaudio C, De Martino G, Di Ludovico M, Manfredi G, Prota A, Ricci P, *et al.* Empirical fragility curves from damage data on RC buildings after the 2009 L'Aquila earthquake. *Bulletin of Earthquake Engineering* 2017; **15**(4): 1425–1450. DOI: 10.1007/s10518-016-0026-1.
10. Baker JW. Conditional Mean Spectrum: Tool for Ground-Motion Selection. *Journal of Structural Engineering* 2011; **137**(3): 322–331. DOI: 10.1061/(asce)st.1943-541x.0000215.

Copyright © 2025 CroCEE
DOI: https://doi.org/10.5592/CO/3CroCEE.2025.25

11. Bradley BA. A generalized conditional intensity measure approach and holistic ground-motion selection. *Earthquake Engineering and Structural Dynamics* 2010; **39**(12): 1321–1342. DOI: 10.1002/eqe.995.

12. Tarbali K, Bradley BA. Ground motion selection for scenario ruptures using the generalised conditional intensity measure (GCIM) method. *Earthquake Engineering & Structural Dynamics* 2015; **44**(10): 1601–1621. DOI: 10.1002/eqe.2546.

13. Pinho R, Monteiro R, Casarotti C, Delgado R. Assessment of continuous span bridges through nonlinear static procedures. *Earthquake Spectra* 2009; **25**(1): 143–159. DOI: 10.1193/1.3050449.

14. O'Reilly GJ. Seismic intensity measures for risk assessment of bridges. *Bulletin of Earthquake Engineering* 2021; **19**(9): 3671–3699. DOI: 10.1007/s10518-021-01114-z.

15. CEN. *Eurocode 8: Design of Structures for Earthquake Resistance - Part 2: Bridges (EN 1998–2:2005)*. Brussels, Belgium: 2005.

16. Zhu M, McKenna F, Scott MH. OpenSeesPy: Python library for the OpenSees finite element framework. *SoftwareX* 2018; **7**: 6–11. DOI: 10.1016/j.softx.2017.10.009.

17. Priestley MJN, Seible F, Calvi GM. *Seismic design and retrofit of bridges*. New York: John Wiley & Sons; 1996. DOI: 10.1002/9780470172858.

18. O'Reilly GJ, Monteiro R. On the efficient risk assessment of bridge structures. *COMPDYN Proceedings*, vol. 1, 2019. DOI: 10.7712/120119.6933.18933.

19. GEM. The OpenQuake-engine User Manual. *Global Earthquake Model (GEM) OpenQuake Manual for Engine Version 3180* 2022. DOI: 10.13117/GEM.OPENQUAKE.MAN.ENGINE.3.18.0.

20. Danciu L, Nandan S, Reyes C, Basili R, Weatherill G, Beauval C, *et al.* The 2020 update of the European Seismic Hazard Model: Model Overview 2021(EFEHR Technical Report 001 v1.0.0): 1–121.

21. Baker JW, Cornell CA. Spectral shape, epsilon and record selection. *Earthquake Engineering & Structural Dynamics* 2006; **35**(9): 1077–1095. DOI: 10.1002/eqe.571.

22. Bradley BA, Burks LS, Baker JW. Ground motion selection for simulation-based seismic hazard and structural reliability assessment. *Earthquake Engineering & Structural Dynamics* 2015; **44**(13): 2321–2340. DOI: 10.1002/eqe.2588.

Proceedings of the 3rd Croatian Conference on Earthquake Engineering - 3CroCEE
19–22 March 2025, Split, Croatia
Copyright © 2025 CroCEE
DOI: https://doi.org/10.5592/CO/3CroCEE.2025.42

SEISMIC GROUND MOTION AMPLIFICATION INDUCED BY TOPOGRAPHIC IRREGULARITY IN NORTHERN CROATIA

Davor Stanko [(1)], Dragana Dogančić [(1)], Sanja Kovač [(1)], Jasmin Jug [(1)], Stjepan Strelec [(1)], Vesna Poslončec Petrić [(2)], Marijan Kovačić [(3)], Francesco Panzera [(4)], Olga-Joan Ktenidou [(4)]

[(1)], *University of Zagreb, Faculty of Geotechnical Engineering, Croatia, davor.stanko@gfv.unizg.hr*
[(2)] *University of Zagreb, Faculty of Geodesy, Croatia, vesna.posloncec-petric@geof.unizg.hr*
[(3)] *University of Zagreb, Faculty of Science, Department of Geology, Zagreb, mkovacic@geol.pmf.hr*
[(4)] *University of Catania, Biological, Geological and Environmental Sciences Department, Italy, francesco.panzera@unict.it*
[(5)] *National Observatory of Athens, Greece, olga.ktenidou@noa.gr*

Keywords: Seismic ground motion, Topographic amplification, Northern Croatia

1. Introduction

After the recent 2020 earthquakes M_L5.5 in Zagreb and M_L6.2 in Petrinja, a considerable part of the reported damages to churches, museums, cultural and older buildings and houses were observed in the areas of pronounced topography of Northern Croatia. It is generally known that these kinds of buildings have been rebuilt/renovated many times throughout history, basically on the foundations of previous ones, especially on the prominent topographical features. It can be assumed that there were several recurring historical earthquake damages at certain locations, where in addition to the condition of the building, the role of topographic irregularity shape, directional effects and geological site properties played important role (Ktenidou et al. 2016). The aim of this study within the Croatian Science Foundation (HRZZ) research project IP-2022-10-1296 SIGMATOPCRO, was to assess and analyse possible topographic and directivity amplification ground motion effects correlated with associated impact on 2020 earthquake damage at these sites.

2. Preliminary results – example of Gornje Jesenje

Investigations include visual damage observations (that still exist) and renovations, spatial position of topographic features in terms of geometry, size, direction, and geological properties with preliminary microtremor measurements to determine the extent of site effects compared to reference rocky outcrops to better understand topographic amplification of seismic ground motion (Del Gaudio et al. 2014). Over 40 topographical sites (features) in Northern Croatia were carefully examined within reports of earthquake damage observations from 2020 events (Figure 1). At the Gornje Jesenje in Krapina-Zagorje County, the Church of St. John (built in 1858.) on the top of a topographic feature (approx. 40 km from the Zagreb and 90 km from the Petrinja earthquake epicentres) sustained damage that was classified as moderate to substantial (grades 2–3) according to the EMS-98 damage classification grade (data provided by the Conservation Department of Krapina). Estimated macroseismic intensity of the Zagreb and Petrinja 2020 earthquakes for that area was V–VI EMS (Seismological Survey of Croatia). This area is also known for landslides. A big road landslide was activated in this area one week after the Petrinja 2020 earthquake (Raspudić et al. 2022). Figure 2 shows a topography map of the studied area (based on LiDAR-inferred topography provided by the State Geodetic Administration of the Republic of Croatia). Slope is relatively high, varying between 24–32 % (14–18 degrees) which by Eurocode 8 (Part 5, Annex A) indicates topographic amplification by a factor of 1.2. Preliminary microtremor measurements were performed (blue triangles). From its eastern and southern sides, numerous primary reference rock outcrops are visible (high frequencies, above 10 Hz, or flat HVSR curves). According to the lithological characteristics and geological map (Figure 3, Avanić et al. 2021), the church (yellow triangle) was built on deposits of Egenburgian age (Lower Miocene) - defined as the Vučji jarek (VuJ) formation known in the older literature as Macelj sandstones. Measured frequencies are around 7 Hz indicating approximately 10-15m of deposits overlying the rock formations. (Stanko & Markušić 2020).

Copyright © 2025 CroCEE
DOI: https://doi.org/10.5592/CO/3CroCEE.2025.42

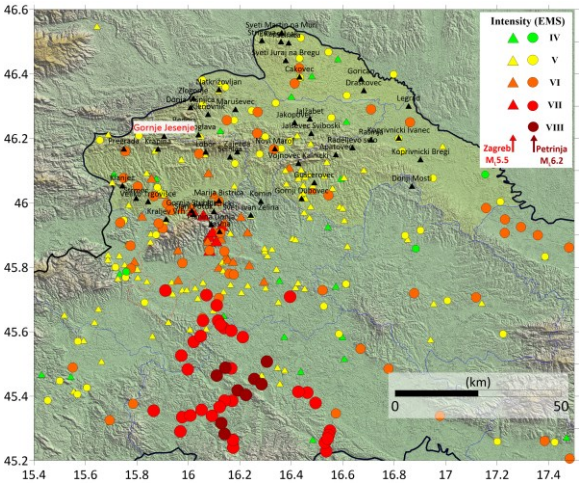


Figure 1. Combined macroseismic intensity map of the 2020 Zagreb (triangles) and Petrinja earthquakes (circles). (Source: Seismological Survey of Croatia)

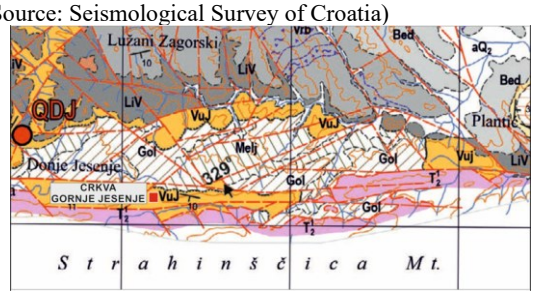


Figure 3. Excerpt of the geological map from Avanić et al. (2021) with the position of the Church in G. Jesenje - Vučji jarek (VuJ) formation - Lower Miocene.

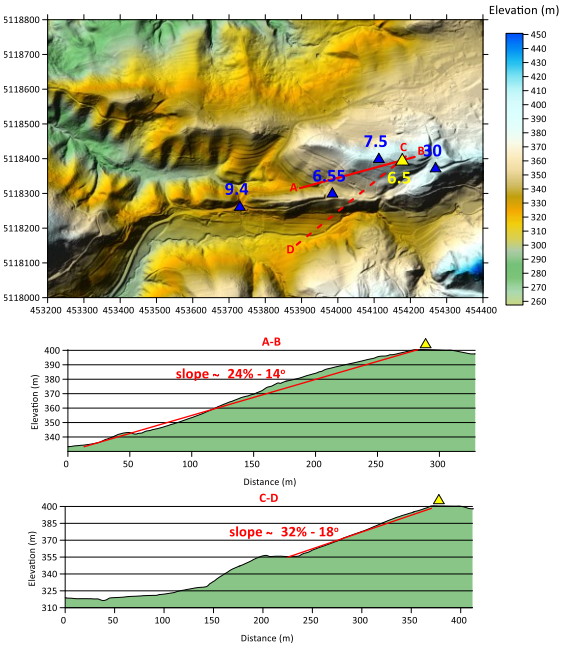


Figure 2. Gornje Jesenje, LiDAR-inferred topography with preliminary microtremor measurements (blue triangles) and estimated frequencies (numbers, in Hz) and topographic 2D profiles (red lines). Yellow triangle indicates location of the Church of St. John.

3. Conclusions and future works

Preliminary results of macroseismic damage observations, 2D topographic irregularity terrain configuration along different directions, geological conditions, and site resonance frequencies of topographic features indicate that topographic amplification effects are very complex compared to stratigraphic amplification. The presence of fractures, water saturations, and human interventions in the topographic environment can be relevant factors in enhancing the susceptibility of slopes to earthquake induced failures and possible occurrences of higher damage effects at certain sites (Del Gaudio et al. 2014). Future multidisciplinary field investigations will be performed to characterize crucial segments along chosen topographical irregularities as an input for 1D and 2D complex numerical seismic response modelling in order to study amplification effects associated with topographical irregularities and possible roles in seismic slope instability. Continuous seismic monitoring will be established at these sites (one instrument at the top and one at the bottom of the hilltop) to compare empirical data with numerical analysis of topographic and stratigraphic amplification effects.

Acknowledgements

This work was supported by the Croatian Science Foundation under the project number [HRZZ-IP-2022-10-1296].

References

Avanić, R., Pavelić, D., Pécskay, Z., Miknić, M., Tibljaš, D., Wacha, L. (2021): Tidal deposits in the Early Miocene Central Paratethys: the Vučji Jarek and Čemernica members of the Macelj formation (NW Croatia). Geologia Croatica, 74, 1, 41-56.

Copyright © 2025 CroCEE
DOI: https://doi.org/10.5592/CO/3CroCEE.2025.42

Del Gaudio, V., Muscillo, S., Wasowski, J., (2014): What we can learn about slope response to earthquakes from ambient noise analysis: An overview. *Engineering Geology* 182, 182–200. https://doi.org/10.1016/j.enggeo.2014.05.010

EN 1998-5 (2004): Eurocode 8: Design of structures for earthquake resistance – Part 5: Foundations, retaining structures and geotechnical aspects [Authority: The European Union Per Regulation 305/2011, Directive 98/34/EC, Directive 2004/18/EC]

Ktenidou O.-J., F.J. Chávez-García, D. Raptakis and K.D. Pitilakis (2016): Directional dependence of site effects observed near a basin edge at Aegion, Greece'. Bull. Earthq. Eng., 14(3), pp. 623-645. https://doi.org/10.1007/s10518-015-9843-x

Stanko, D. & Markušić, S. (2020): An empirical relationship between resonance frequency, bedrock depth and Vs30 for Croatia based on HVSR forward modelling. *Natural Hazards*, 103, 3715-3743 https://doi.org/10.1007/s11069-020-04152-z

Raspudić, S., Žnidarić, L., Martinić, I., (2022): Uzroci pojave klizišta u Općini Jesenje u razdoblju 2012.-2021. Geografski horizont, 2, 43-59.

Proceedings of the 3rd Croatian Conference on Earthquake Engineering - 3CroCEE
19–22 March 2025, Split, Croatia
Copyright © 2025 CroCEE
DOI: https://doi.org/10.5592/CO/3CroCEE.2025.62

PATTERNS OF EARTHQUAKE DAMAGE IN STON: A 146-YEAR COMPARISON

Marijan Herak [(1)], Davorka Herak [(2)]

[(1)] *Prof. emeritus, Department of Geophysics, Faculty of Science, University of Zagreb, mherak@gfz.hr*
[(2)] *Prof. dr. sc., retired, Department of Geophysics, Faculty of Science, University of Zagreb, dherak@gfz.hr*

Keywords: Earthquake damage, variability of earthquake damage, soil amplification, historical seismicity, southern Dalmatia.

1. Introduction

The medieval town of Ston in southern Dalmatia (Croatia) has experienced several significant earthquakes since the mid-19th century, notably the ones o 3 April 1850 and 5 September 1996. While the macroseismic parameters as well as classification of damage to buildings in Ston related to the 1996 event are available from previous studies, the 1850 earthquake has only recently undergone detailed macroseismic analysis [2]. It revealed clear similarities between the two events, including their epicentres (Fig. 1), focal depths (h_{1850} = 9, h_{1996} = 11 km), epicentral intensities ($I_{0,1850}$ = 8.2 MSK, $I_{0,1996}$ = 8.1 MSK) and magnitudes ($M_{mL,1850}$ = 6.0 and $M_{L,1996}$ = 6.0). For more detail see the papers [1, 2].

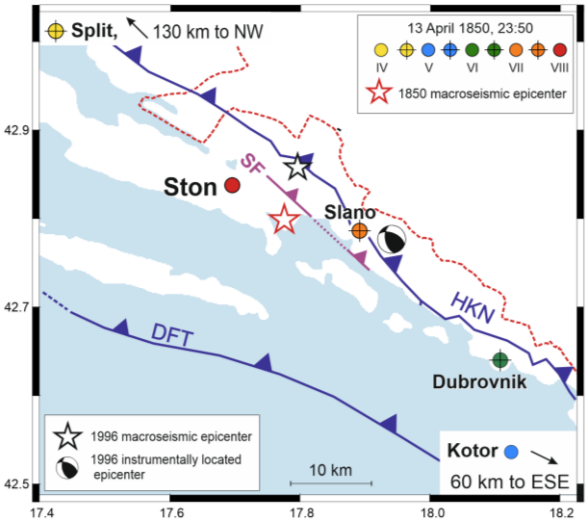


Figure 1. Results of macroseismic inversion. The red-edged star is the final, representative macroseismic epicentre of the 1850 earthquake. The black-edged star is the macroseismic epicentre of the Ston-Slano event of 1996 [1]. DFT, Dalmatian unit frontal thrust; HKN, high karst nappe; SF, Slano fault. Simplified after [2].

To enable comparison of the spatial distribution of damage in Ston from these twin earthquakes, we combined historical damage reports from 1850 with cadastral records from 1837 [3]. This allowed us to geolocate most of the damaged buildings, despite challenges in identifying individual structures due to changes in ownership and building modifications over the intervening years. For full description of archive and cadastral material, data and methods, please see [3].

2. Results

Our study indicates that both earthquakes caused the most significant damage in the plain area below Bartolomija Hill, characterized by a sedimentary cover 10–30 m thick, with expected ground motion amplification by factors between 3 and 5 (Fig. 2).

Copyright © 2025 CroCEE
DOI: https://doi.org/10.5592/CO/3CroCEE.2025.62

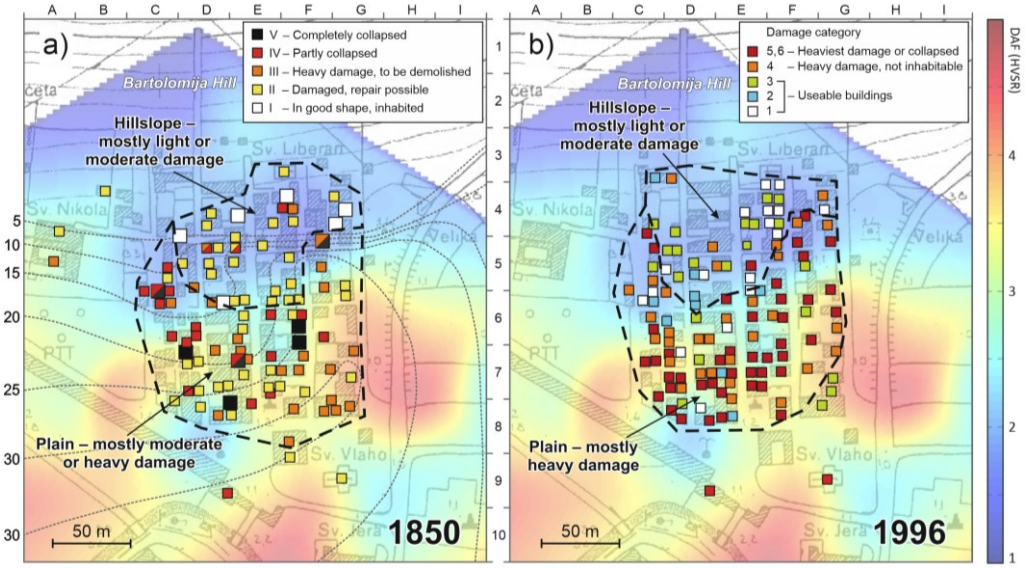


Figure 2. Distribution of damage to houses in Ston after the earthquakes of: a) 13 April 1850 [3], and b) 5 September 1996 [4]. The basemap shows the value of dynamic amplification factor for PGA (DAF, as defined in [5], see the colour-bar on the right) estimated by HVSR measurements. The thickness of Quaternary sediments is also shown in part a) as thin dotted iso-lines with values in meters shown along the left subplot edge. Thick dashed lines show areas of predominantly heavy and light damage. Basemap is the topographic plan of Ston from the second half of the 20th century. Slightly modified after [3].

In contrast, the hillsides of Bartolomija in the northern part of the city, with their shallow or outcropping bedrock, experienced minimal damage from both events. To our knowledge, this observation of the shaking effects for two strong similar earthquakes in a city that has changed little in the 146 years between them is unique in Croatia. It demonstrates consistency of spatial pattern of earthquake ground motion amplification for comparable input earthquake motion.

Acknowledgements

We gratefully acknowledge full support by the Croatian Science Foundation under the grant IP2020-02-3960 (DuFAULT project). We also thank the State Archive in Split, the Dubrovnik State Archive and the Institute for the Restoration of Dubrovnik for cadastral maps from 1837, and documents about damage and restoration of Ston after the earthquakes of 1850 and 1996.

References

[1] Govorčin, M., Herak, M., Matoš, B., Pribičević, B., Vlahović, I. (2020): Constraints on complex faulting during the 1996 Ston–Slano (Croatia) earthquake inferred from the DInSAR, seismological, and geological observations, *Remote Sensing*, **12**, 1157, doi:10.3390/rs12071157.

[2] Herak, D., Herak, M., Vrkić, I. (2024). The Earthquake of 13 April 1850 near Ston, Croatia: Macroseismic Analyses, *Seismological Research Letters*, **95** (2a), 1043–1056, doi: 10.1785/0220230299.

[3] Herak, M., Herak, D. (2024): A Comparative Study of Building Damage in Ston, Croatia, Caused by the Earthquakes of 1850 and 1996, *Seismological Research Letters*, **95** (5), 3070–3081, doi: 10.1785/0220240248.

[4] Herak, M., Allegretti, I., Herak, D., Kuk, K., Kuk, V., Marić, K., Markušić, S., Stipčević, J. (2010). HVSR of ambient noise in Ston (Croatia)—Comparison with theoretical spectra and with the damage distribution after the 1996 Ston-Slano earthquake, *Bulletin of Earthquake Engineering*, **8**, 483–499, doi: 10.1007/s10518-009-9121-x.

[5] Herak, M. (2008): Model HVSR – A Matlab tool to model horizontal-to-vertical spectral ratio of ambient noise, *Computers and Geosciences*, **34** (11), 1514–1526, doi: 10.1016/j.cageo.2007.07.009.

Proceedings of the 3rd Croatian Conference on Earthquake Engineering - 3CroCEE
19–22 March 2025, Split, Croatia
Copyright © 2025 CroCEE
DOI: https://doi.org/10.5592/CO/3CroCEE.2025.123

THE ROLE OF SEISMIC GEOPHYSICAL METHODS IN NEAR-SURFACE CHARACTERIZATION

Irena Gjorgjeska [(1)], Vlatko Sheshov [(2)], Julijana Bojadjieva [(3)]
Kemal Edip [(4)]

(1) PhD, Ss. Cyril and Methodius University in Skopje, IZIIS, R. N. Macedonia, gj_irena@iziis.ukim.edu.mk
(2) Professor, PhD, Ss. Cyril and Methodius University in Skopje, IZIIS, R. N. Macedonia, vlatko@iziis.ukim.edu.mk
(3) Ass. Professor, PhD, Ss. Cyril and Methodius University-Skopje IZIIS, R. N. Macedonia, jule@iziis.ukim.edu.mk
(4) Professor, PhD, Ss. Cyril and Methodius University in Skopje, IZIIS, R. N. Macedonia, kemal@iziis.ukim.edu.mk

Abstract

Near-surface characterization, i.e., determination of the physical-mechanical characteristics of the soil and rock masses that constitute the terrain structure is crucial in avoiding catastrophic consequences during seismic and geotechnical hazards. Geophysical techniques can provide a comprehensive understanding of subsurface conditions, including the presence of weak zones, local anomalies, groundwater levels, slope stability, and tectonic structures, offering valuable information for assessing potential risks and hazards. Surface seismic methods are non-invasive and widely accepted geophysical techniques for near-surface characterization and have been used in IZIIS for an extended period. This paper presents two case studies of geophysical surveys conducted for site characterization purposes. Combined seismic method surveys were performed in Strumica, N. Macedonia, at the site of the Orta Mosque. The primary motivation for this study was the appearance of cracks in the Orta Mosque building, which have progressively expanded over time. A similar procedure was applied at the location for tunnel construction in Aleksinac, Serbia. The main objective in both cases has been definition of the seismo-geological characteristics, potential anomalies, local tectonic deformations, and discontinuities in the terrain structure. The seismic models derived from the seismic refraction survey at the Orta Mosque site indicate layers of unconsolidated deposits, with a maximum recorded depth of over 20 meters. The seismic reflection sections, displayed in 3D to provide a more realistic view of the discontinuities and the slope of the bedrock, indicate deformations and local disturbances in the deeper layers. The variation in the thickness of the surface layers, as recorded in the seismic refraction profiles conducted at the tunnel site in Serbia, indicates anomalies, i.e., unstable zones, which are also identified in the deeper layers through reflection profiles. Interpreted discontinuities and deformations in the terrain structure in both case studies point to underlying dynamic processes.

Keywords: geophysical survey, seismic methods, site characterization, combined approach

1. Introduction

In this paper, the applied methodology and the results of two case studies of geophysical surveys conducted for site characterization purposes are presented.

The first location is situated in Serbia, near the town of Aleksinac, in the southern part of the country [1]. The main goal of the surveys was to perform seismo-geological modeling of the site proposed for tunnel construction. Geophysical surveys were conducted using a combined approach involving two different seismic methods: seismic refraction and seismic reflection [2]. Based on previously conducted geotechnical boreholes, the terrain structure comprises diluvial deposits in the surface layers, which overlay Miocene sediments. The seismic bedrock primarily consists of andesite gneisses and migmatites.

Considering the significant distances between the boreholes, the geophysical surveys conducted at this location were highly important. Combined with data from the drilled boreholes, they enabled advanced seismo-geological modeling and characterization. Seismic refraction surveys allowed the determination of the thickness of the unconsolidated deposits, as well as variations in their physical-mechanical characteristics both laterally and in depth, along with the detection of local anomalies. On the other hand, seismic reflection profiles provided valuable insights into discontinuities and deformations within the terrain structure.

Copyright © 2025 CroCEE
DOI: https://doi.org/10.5592/CO/3CroCEE.2025.123

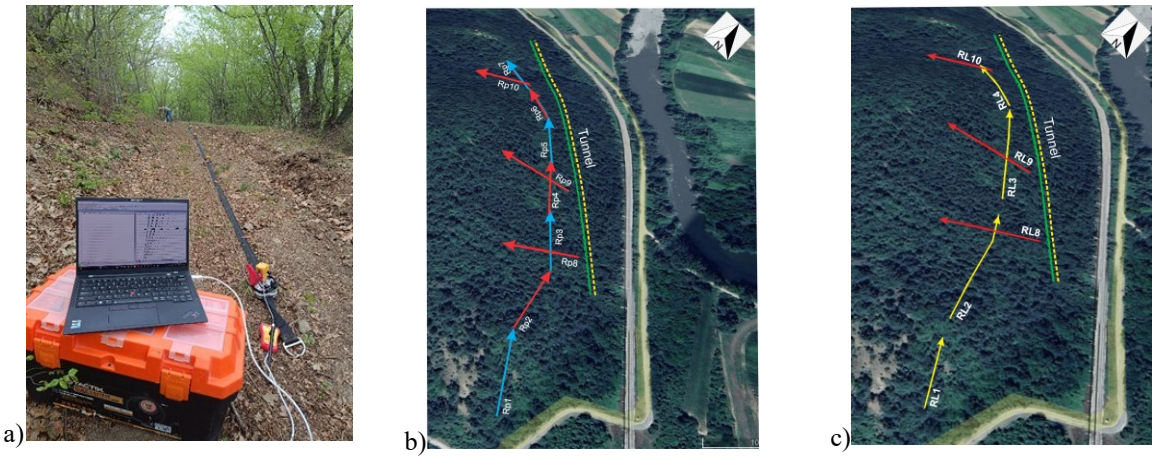


Figure 1. Geophysical surveys in Aleksinac. a) Photo of the survey location; b) Seismic refraction profiles layout; c) Seismic reflection profiles layout.

The second survey location is situated in the city of Strumica, which belongs to the southeastern part of North Macedonia. The motivation for this study stemmed from the appearance of cracks in the Orta Mosque building, which have progressively expanded over time. What is specific about this location is the lack of sufficient geological data, as well as the absence of geomechanical boreholes, which were not conducted due to the inaccessibility of the terrain for drilling machines. As a result, this case study relies only on the results of the geophysical surveys [3].



Figure 2. Geophysical surveys in Strumica – Orta Mosque. a) Seismic profiles layout; b) Photo of the survey location

In both case studies, the geophysical methods of seismic refraction and reflection were applied in a combined approach to achieve more detailed and higher-resolution seismo-geological modeling of the terrain structure [4, 5]. The results are presented primarily as 2D seismic models. A 3D display of the seismic reflection sections from the surveys conducted at the Orta Mosque location provided a more realistic view of the discontinuities and the slope of the bedrock [6].

Proceedings of the 3rd Croatian Conference on Earthquake Engineering - 3CroCEE
19–22 March 2025, Split, Croatia
Copyright © 2025 CroCEE
DOI: https://doi.org/10.5592/CO/3CroCEE.2025.123

2. Research Methodology: Data Acquisition and Processing

In-situ measurements were performed using both seismic refraction and reflection methods with the SoilSpy Rosina multichannel digital seismograph (MoHo - Science & Technology, Italy). Additionally, a seismic landstreamer was employed for seismic reflection measurements, utilizing the roll-along method for data collection. The seismic energy was generated by vertical 10 kg sledgehammer blows on an aluminium plate and was recorded by 4.5 Hz vertical geophones.

The pre-processing of the data was performed using the SoilSpy Rosina software, MoHo - Science & Technology, Italy. The consecutive analyses and interpretation of seismic refraction and reflection data were carried out applying the ReflexW software - Dr. K-J. Sandmeier, Germany.

For the processing of seismic refraction data, the tomographic approach is used. This approach performs better in many situations where traditional refraction techniques fail, such as in modeling subsurface velocity structures with both lateral and vertical velocity gradients. The tomographic concept relies on a gridded initial model for an iterative process, determining the velocity of individual 2-dimensional grids within a profile, rather than modeling the subsurface structure as constant-velocity layers (commonly referred to as 'cake layers'). This method provides higher-resolution modeling of complex subsurface structures. [7, 8].

Processing of the seismic reflection data was performed using the Common Midpoint (CMP) technique, which involves stacking seismic records reflected from the same point at stratigraphic boundaries [9]. Pre-stacking static corrections and 1D and 2D filtering were applied to the raw data, followed by post-stacking depth migration. The complex processing of seismic reflection data enables the precise definition of layer boundaries, seismic bedrock, local deformations, and discontinuities with very high accuracy and resolution.

2.1. Case study: Aleksinac, Serbia – Data aquisition

Geophysical surveys along a total of 4 seismic profiles have been performed on the location planned for tunnel construction in Aleksinac, Serbia (Fig.1). Surveys with application of the seismic refraction method were performed along 1 longitudinal profile which consists of 7 segments (Rp1-Rp7) and 3 transversal profiles (Rp8, Rp9 and Rp10). Seismic reflection surveys were performed along 1 longitudinal profile which consist of 4 segments (RL1, RL2, RL3 and RL4) and 3 transversal profiles (RL8, RL9 and RL10).

Measurements using the seismic refraction method along the seismic profiles were conducted with a geophone spacing of 5.25 meters and a minimal offset (distance between the source and the first receiver) of 5.25 meters. Data acquisition was carried out with a sampling frequency of 512 Hz and a time length of 0.5 seconds.

For the seismic reflection method, the Common Depth Point (CDP) technique was applied with a fixed distribution for seismic profiles RL8, RL9, and RL10, using the same seismic spread as that used for the seismic refraction method. Measurements along seismic profiles RL1, RL2, RL3, and RL4 were performed using the roll-along technique, with a geophone spacing of 3 meters, an excitation step of 6 meters, and a minimum offset of 6 meters.

2.2. Case study: Strumica, N. Macedonia – Data aquisition

In-situ measurements using seismic methods were conducted at the survey locations in a practical and effective manner. The same seismic equipment and, in most cases, the same acquisition parameters were used, ensuring a time- and cost-effective survey for subsurface characterization, using the SoilSpy Rosina multichannel digital seismograph (MoHo - Science & Technology, Italy).

Certain site-specific details on the “in situ” measurements are as follows:

Seismic refraction measurements were conducted along a seismic spread of 17 channels (Rp1, Rp2) with a geophone spacing of 5 meters, a near offset (minimal source-to-receiver distance) of 5 meters,

Copyright © 2025 CroCEE
DOI: https://doi.org/10.5592/CO/3CroCEE.2025.123

an excitation step of 20 meters at 5 points through the seismic spread. Measurements along Rp3 (seismic spread of 13 channels) were performed with a geophone spacing of 2 meters, a near offset of 2 meters.

Seismic reflection measurements were conducted along a fixed seismic spread of 17 channels (RL1, RL2) using the following acquisition parameters: a geophone spacing of 5 meters, an excitation step of 10 meters, a near offset of 6 meters. Measurements along seismic profile RL3 were conducted with a fixed seismic spread of 13 channels, a geophone spacing of 2 meters, an excitation step of 4 meters, a near offset of 3 meters.

In all cases, the seismic record duration was 0.5 seconds, with a sampling frequency of 1024 Hz.

3. Results: Findings and Interpretation

The results from the investigations using the seismic refraction method consist of 2D seismic models that map the lateral variations in Vp and Vs seismic velocities down to a depth of 20-30 meters. Based on these variations, different lithological media have been identified. The results from the seismic reflection survey consist of 2D seismic sections, which help identify local disturbances, deformations, and anomalies in the terrain structure, both in surface media and deeper layers, down to a depth of 150m.

3.1. Results from the Seismic Survey in Aleksinac, Serbia

According to 2D seismic models derived from data analyzed using the seismic refraction method, four lithological media have been identified. These media are characterized by distinct physical-mechanical properties.

The variation in seismic Vp and Vs velocities, combined with existing geological data, indicates the following lithological media:

- Surface layer – deluvial deposits characterized by seismic velocities in the interval of: Vp=240-750 m/s; Vs=120-310 m/s
- Subsurface layer – decomposed sandstones, loose and crushed rock: Vp=750-1150 m/s; Vs=310-430 m/s;
- Intensively fractured rocks -with seismic velocities: Vp=1150-1700m/s; Vs=430 - 630 m/s;
- Intensively to moderately fractured rocks-with seismic velocities: Vp=1700-2000 m/s; Vs=630 - 780 m/s;

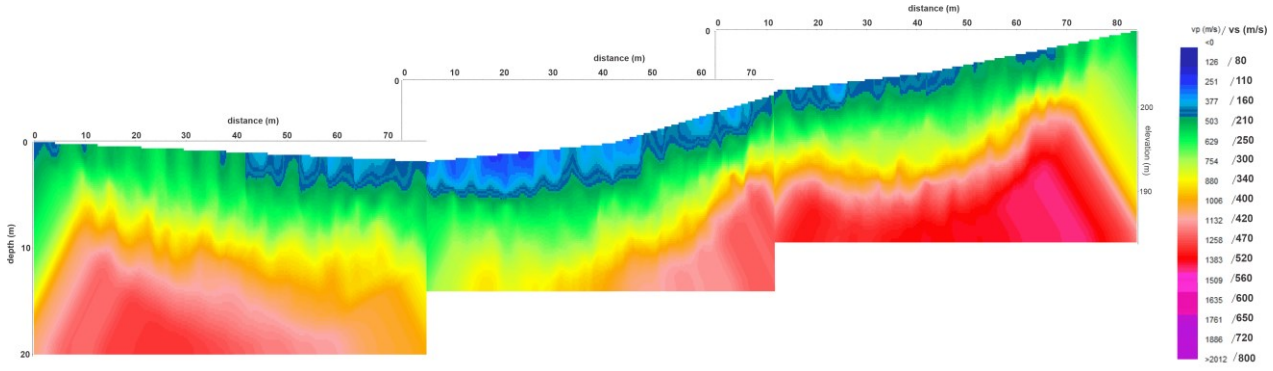


Figure 3. 2D Seismic refraction profiles Rp2, Rp3 and Rp4

Copyright © 2025 CroCEE
DOI: https://doi.org/10.5592/CO/3CroCEE.2025.123

By interpreting the final seismic refraction models, the following conclusions can be drawn:

- Surface layers with relatively weak physical-mechanical characteristics (Vs < 310 m/s) have been identified at depths ranging from a maximum of 3 meters along profile Rp1 to 7 meters along Rp2. At the positions of seismic profiles Rp3 and Rp8, as well as along profiles Rp4 and Rp9, the thickness of this layer varies between 7 and 10 meters. Seismic profiles Rp5, Rp6, and Rp7, indicate shallower deluvial deposits.
- Based on seismic wave propagation velocities (Vs = 310–430 m/s), the subsurface consists of decomposed, loose rocks. Between the end of profile Rp2 and the start of profile Rp3, located near the tunnel's exit, the layer is not detected down to a depth of 20 meters, as shown in Fig. 3, marking the most critical area. This anomaly is also observed along the first half of profile Rp8, which was conducted transversely to Rp3. In the central site, seismic profiles Rp3, Rp4, and Rp9 indicate the layer at depths of 10 to 15 meters. Along profiles Rp5, Rp6, and Rp7, extending from the central part toward the tunnel's entrance, the layer is recorded at a maximum depth of 7 to 10 meters.
- This interpretation is based on 2D seismic refraction profiles conducted along the longitudinal seismic profile, which consists of seven segments in total (Rp1–Rp7), as well as three transverse profiles (Rp8, Rp9, and Rp10) (Fig.1b). This paper presents three segments of the longitudinal profile—Rp2, Rp3, and Rp4—which represent the most critical zone of the survey site in terms of the thickness of the surface loose layers (Fig3).

The variation in the thickness of the surface layers recorded in the seismic refraction profiles indicates discontinuities in the terrain structure of the investigated site, as defined by the 2D reflection sections obtained from these investigations.

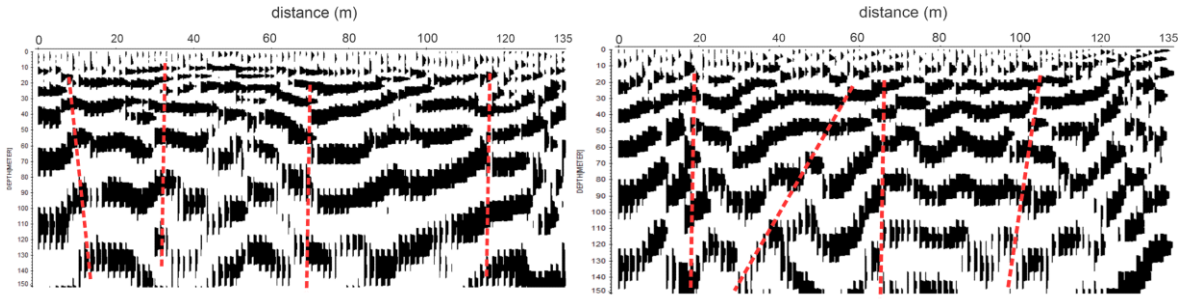


Figure 4. 2D Seismic reflection sections RL2 and RL3

- Very pronounced deformations have been recorded along the seismic reflection profiles conducted at the survey location. The interpreted discontinuities (marked by a red dashed line), observed along seismic reflection profiles RL2 and RL3—which were conducted along the same seismic line as the refraction profiles presented above—indicate anomalies, i.e., unstable zones, even in the deeper layers (depth > 20 m). These deformations, as identified in the seismic reflection profiles, have also been observed at the same positions within the surface layers, as determined from the seismic refraction profiles (Fig.4).

- The interpreted deformations and local disturbances in the terrain structure indicate the presence of internal dynamic processes of tectonic origin.

3.2. Results from the Seismic Survey in Strumica, N. Macedonia

The final results from the geophysical surveys at the Strumica site enabled successful seismo-geological modeling of the terrain structure, including the definition of the surface layer thickness composed of loose, degraded rock, as well as the identification of discontinuities and anomalies in both the surface and deeper layers, which was the main objective of the survey.

According to the final 2D seismic refraction models, the terrain structure at the Orta Mosque site consists of the following lithological media:

Copyright © 2025 CroCEE
DOI: https://doi.org/10.5592/CO/3CroCEE.2025.123

• Surface layer with values of seismic velocities: Vp=200-750 m/s; Vs= 100-280 m/s;

• Subsurface zone consisting of degraded, decomposed, and intensely cracked rocks, with seismic velocity values: Vp=800-1500 m/s; Vs=350-580 m/s;

• Intensively cracked to more compact rocks with seismic velocity values: Vp>1600m/s; Vs>600 m/s

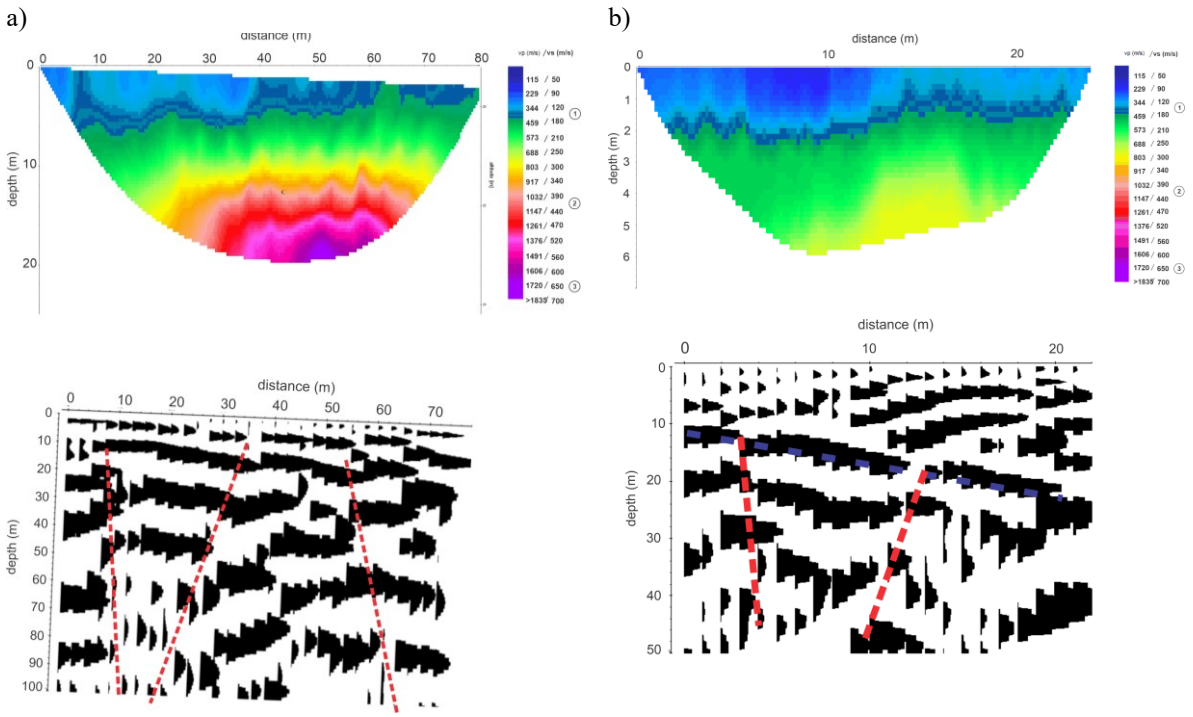


Figure 5. 2D seismic refraction and reflection models a) Rp2 and RL2 with defined discontinuities (red dashed lines). b) Rp3 and RL3 with defined discontinuities (red dashed lines)

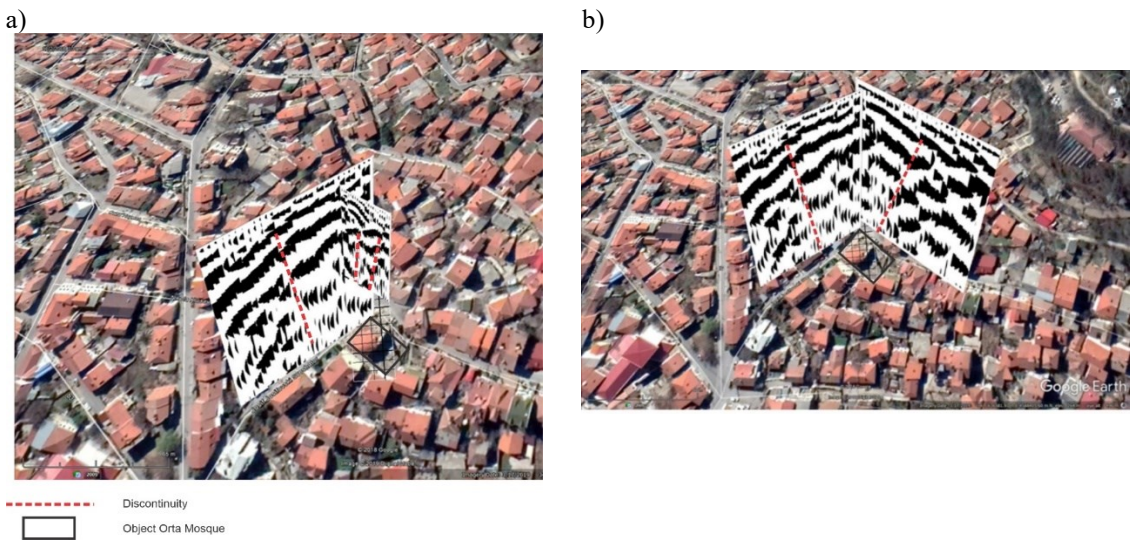


Figure 6. 3D display of the seismic reflection sections. a) RL2 and RL3 with defined discontinuities (red dashed lines). b) RL1 and RL2 with defined discontinuities (red dashed lines)

Based on the interpretation of the final seismic refraction models, the following conclusions can be drawn:

Proceedings of the 3rd Croatian Conference on Earthquake Engineering - 3CroCEE
19–22 March 2025, Split, Croatia
Copyright © 2025 CroCEE
DOI: https://doi.org/10.5592/CO/3CroCEE.2025.123

- Surface layers characterized by quite weak physical-mechanical characteristics (Vs<300m/s) have been recorded at maximum depth of 12 m at each of the performed refraction profiles.
- The subsurface zone, based on the defined seismic velocity values (Vs=350-580m/s), is composed of degraded, decomposed, and intensely cracked rocks, recorded at maximum depths exceeding 20m.

Although the refraction profiles do not indicate significant variations in the surface layers (d < 20 m), the seismic reflection profiles reveal discontinuities in the deeper layers (d > 10 m), suggesting deformations and local disturbances caused by internal dynamic processes. This can especially be concluded from the 2D models shown in Fig. 5, where in both cases, the refraction profiles indicate an improvement in the physical-mechanical characteristics of the rock with the depth, in contrast to the seismic reflection sections, which reveal deeper weak zones and deformations in the terrain structure.

In Fig.6, the seismic reflection sections are presented in 3D to provide a more realistic depiction of the local deformations, discontinuities, and the slope of the bedrock.

4. Conclusions

The results presented above emphasize the importance of applying geophysical methods for seismo-geological modeling of terrain structures and assessing potential risks and hazards.

The primary objective of the surveys conducted at the first location in Aleksinac, Serbia, was to identify critical loose zones that could pose hazards during tunnel construction. While geotechnical surveys offered preliminary insights into the terrain structure, they proved insufficient for detailed forward planning and analysis due to the large gaps between survey points and the lack of data on physical-mechanical characteristics. The application of seismic geophysical methods, using a combined approach, enabled a successful modeling of the terrain structure, determination of surface layer thicknesses, and characterization of seismo-tectonic structures.

In situ measurements using seismic methods at the Orta Mosque site were conducted in a practical and effective manner, using the same seismic equipment and, in most cases, the same acquisition parameters, ensuring a time- and cost-efficient survey for subsurface characterization. Seismic refraction models indicate the presence of unconsolidated deposits extending to a maximum depth of over 20 meters. Seismic reflection sections, presented in a 3D display, provide a more realistic visualization of local deformations, discontinuities, and the slope of the bedrock. These sections point to deformations and disturbances not only in the surface layers but also in the deeper layers. Such anomalies in the terrain structure indicate internal dynamic processes that are considered responsible for the cracks observed in the building.

From the findings presented above, it can be concluded that the most widely used seismic methods—seismic refraction and reflection—have once again demonstrated exceptional effectiveness for near-surface characterization. The methodology is particularly valuable for sites where access to conventional subsurface investigations, including drilling boreholes, is challenging or limited. This carries significant implications for future surveys focused on near-surface characterization, not only in urban environments where traditional invasive methods may be limited or unfeasible due to space constraints, infrastructure disruptions, and high costs, but also in rural or remote settings, such as mountainous regions, where the challenges, though different, are equally significant.

While conventional borehole drilling provides direct measurements of subsurface conditions and is essential for site characterization, surface seismic methods, with their ability to model subsurface structures in detail over larger areas, offer a broad view of subsurface conditions. This makes them invaluable for complementing localized borehole data and enabling more comprehensive assessments. In cases where geotechnical and geological data are insufficient, the combined use of these seismic methods has proven to be the most cost- and time-efficient approach, enabling complex modeling of terrain structures in both case studies presented in this paper.

Copyright © 2025 CroCEE
DOI: https://doi.org/10.5592/CO/3CroCEE.2025.123

References

[1] Sheshov, V., Gjorgjeska, I. (2024): Geophysical Surveys for Characterization of the Tunnel Djunis Site. Results from Field Measurements and Cabinet Processing of Data. *Report IZIIS 2024-25*, Institute of Earthquake Engineering and Engineering seismology, Skopje, N. Macedonia

[2] Gjorgjeska, I., Sesov, V., Stojmanovska, M., Bojadjieva, J., Dojchinovski, D., Edip, K., Poposka, M. (2022): Multi-method approach for seismic site characterization, *3rd European Conference on Earthquake Engineering and Seismology (3ECEES)*, Bucharest, Romania

[3] Gjorgjeska, I., Sheshov, V. (2019): Geophysical surveys for site characterization at the location of a building: Orta Mosque, Strumica, *Report IZIIS 2019-74*, Institute of Earthquake Engineering and Engineering seismology, Skopje, N. Macedonia

[4] Gjorgjeska, I., Sheshov, V., Edip, K. (2019): Advantages of Using Integrated Geophysical Approach to Site Characterization, *8th International Scientific Consultation. Geotechnical Aspects of Construction*, 13-15 November 2019, Vrnjacka Banja, Serbia

[5] Gjorgjeska, I., Sheshov, V., Edip, K. and Dojchinovski, D. (2020): Efficiency Of Integrated Seismic Methods Approach to Near-Surface Characterization, *EGU General Assembly 2020,* Online, 4–8 May 2020, EGU2020-17489, https://doi.org/10.5194/egusphere-egu2020-17489

[6] Gjorgjeska, I., Sheshov, V., Edip, K., Bojadjieva, J., Kitanovski, T., Ivanovski, D. (2022): Combined Seismic Methods and Gpr Application for Shallow Subsurface Investigation - *Fifth symposium of the Macedonian Association for Geotechnics, ISRM specialized conference*, 2022, Macedonian Association for Geotechnics

[7] Tien-When, Lo. And Philips, L. (2002): Fundamentals of Seismic Tomography. *Geophysical Monograph Series; no. 6*, Society of Exploration Geophysicists Tulsa.

[8] White, DJ. (1989): Two-Dimensional Seismic Refraction Tomography, *Geophysical Journal International*, Volume 97, Issue 2, Pages 223–245.

[9] Knapp, W.R & Steeples, W.D. (1986): High-resolution common-depth-point reflection profiling: Field acquisition parameter design. *Geophysics.* 51. 283-294.

Proceedings of the 3rd Croatian Conference on Earthquake Engineering - 3CroCEE
19–22 March 2025, Split, Croatia
Copyright © 2025 CroCEE
DOI: https://doi.org/10.5592/CO/3CroCEE.2025.126

LOCAL EARTHQUAKES - GROUND MOTION MODELS FOR EPICENTRAL ZONE

Snezana Gjorgji Stamatovska[1)]

[(1)] *Full Professor – retired, Ss Cyril and Methodius University, Institute of Earthquake Engineering and Engineering Seismology, Skopje, R.N. Macedonia. snezanagj.stamatovska@gmail.com*

Abstract

Based on records on occurred shallow earthquakes obtained on soil type rock, epicentral distances of $R_e \leq 20km.$, focal depths $h \leq 10\,km.$ and local magnitude $M = 3.9 - 6.1$, ground motion models GMMs for an epicentral zone were developed. Investigated were horizontal acceleration response spectrum *SA* for *5%* of the critical damping and for *221* models of a single-degree-of-freedom system with a natural period ranging from *0.01* to *5.0* seconds.

Two mathematical physical models were selected. In the first one, the horizontal acceleration response spectrum *SA* was dependent on magnitude only, whereas in the second one, it depended on both magnitude and hypocentral distance. For an assumed normal distribution of the natural logarithm of *SA*, a multi-linear regression analysis was carried out. The results were regression coefficients and standard deviations. These are practically applicable for prediction of the expected *SA* in an epicentral zone by deterministic and probabilistic methods.

Keywords: ground motion models, spectral acceleration, epicentral zone, magnitude, epicentral distance

1. Ground motion models – GMMs

GMMs predict the expected level of ground motion depending on magnitude, distance, type of fault structure, local soil layers, azimuth, etc. They are empirical since they are developed by use of data from records of occurred earthquakes and using the regression analysis method. The selected mathematical form will fit in an available or formed databank of records of occurred earthquakes for an assumed normal or log-normal distribution of parameters on which earthquake ground motion depends. The result are regression coefficients and standard deviations. Such GMMs are called conventional /or traditional [1, 7, 8, 12]. Today, GMMs are also developed by use of machine learning approaches ML [6], which cannot be a replacement for the conventional ones. Therefore, the presented conventional GMMs in this paper are important for prediction of the seismic effect in an epicentral zone.

According to summary reviews of a large number of published GMMs [2, 3], it is evident that the number of GMMs for local earthquakes is very small [1, 6, 7, 12].

2. GMMs for Local Earthquakes as a Necessity

As a long year researcher [8, 10, 12] and user of GMMs [9, 11, 13, 14, 15, 16, 17, 18, 19, 20, 21, 22, 23], the author has understood their great importance when probabilistic PSHA [9, 11, 13, 14, 19, 22, 23], and deterministic DSHA [9, 11, 13] methods are used for definition of seismic design parameters. Therefore, the development of GMMs for local earthquake effects is a necessity according to the author. This particularly holds for an epicentral zone and existence of shallow soil layers of weak characteristics that are great amplifiers of local and regional seismic effects upon seismic rock. The dynamic response of their characteristic soil model, upon the ground surface or at the foundation level, known as specific site spectrum SSS, very often surpasses the design spectra recommended and given in the valid standards.

Copyright © 2025 CroCEE
DOI: https://doi.org/10.5592/CO/3CroCEE.2025.126

SSS is particularly important in design of seismically resistant structures of the first class of importance, located in the immediate vicinity of active fault structures with the potential to generate local earthquakes with $M > 6.5$ according to Richter and Eurocode 8 [4, 5], moment magnitudes $M_w > 6.5$, according to UBC 2000 [24], and defined characteristic of local soils. Therefore, the regulations for design of seismically resistant structures [4, 5, 24] also contain defined principles and rules for its determination as well as criteria for its selection as a design spectrum of a site.

2.1. GMMs for Epicentral Zone

GMMs for an epicentral zone were investigated within the frames of the scientific-research project: Ground Motion Models [10]. The created databank of recorded accelerogrammes of occurred earthquakes obtained by SMA- instruments, Kinemetrics, from the strong motion instrument network of former Yugoslavia [8] and the Italian databank ENEA-ENEL (ENEA-ENEL: File ENEAUN TUTTO C VM/HPO 4.2 CMSL–SIAM– 8.4.87) were used. The recorded accelerograms contained in both banks were available as corrected time histories of acceleration.

These were used to create two separate datasets with different distribution of time histories of acceleration per earthquake parameters like magnitude M, epicentral distance R_e, focal depth h and local soil conditions. All this for the purpose of investigating the effect of the distribution of data upon the size of the expected SA in an epicentral zone.

Two sets of data were investigated:

I set *59* data: $h \le 10\,km.,\ R_e \le 20km.\ (M = 3.9\text{-}6.1,\ R_h = 7.-30km.,\ h = 5\text{-}10km.)$

II set *101*data $h \le 20\,km.,\ R_e \le 35km.\ (M = 3.9\text{-}6.5,\ R_h = 7-40km.,\ h = 5\text{-}17km.)$

Computed were the horizontal acceleration response spectra for *5%* of the critical damping $SA(T;\xi = 0.05)$ for *221* models of a single-degree-of-freedom system with periods ranging from *0.01* second to *5.0* seconds for each of the two data sets.

Two mathematical models (equations 1 and 2) were selected and fitted into each of the two created data sets.

ΓMM1: $$lnSA(T;\xi = 0.05) = b_1 + b_2 M + \sigma_{lnSA} P \quad (1)$$

ΓMM2 : $$lnSA(T;\xi = 0.05) = b_1 + b_2 M + b_3 lnR_h + \sigma_{lnSA} P \quad (2)$$

$$R_h = \sqrt{(R_e)^2 + h^2} \quad (3)$$

where: $SA(T;\xi = 0.05)$ is the amplitude of the horizontal acceleration response spectrum for 5% of the critical damping in (cm / s^2), M is local magnitude according to Richter, R_h is hypocentral distnce in *km.*, R_e is epicentral distance in *km.,* h is focal depth in *km.*, b_1, b_2, b_3 are regression coefficients, σ_{lnSA} is standard deviation, and P is random variable, with a value of zero for median and *1* for median plus one standard deviation.

The first GMM1 (Equation 1) is a function of magnitude M, i.e., of the earthquake energy, whereas the second GMM2 is a function of magnitude M and hypocentral distance R_h (Equation 2). In both equations, the term depending on the local soil conditions is omitted since the selected time histories of acceleration are obtained for the same type of soil, i.e., rock.

The size of SA amplutudes is directly proportional to the size of magnitude M and inverseley proportional to the size of distance R_h. Therefore, in the first GMM1, SA depends on M only, whereas in the second GMM2, SA depends on both M and R_h. With the application of both models, the assessment of the seismic effect in the epicentral zone is much more realistic.

A multi linear regression analysis was carried out for an assumed normal distribution for $lnSA$. In it, the dependent parameter was $lnSA$. Independent parameters were M for GMM1, and M and R_h for

Copyright © 2025 CroCEE
DOI: https://doi.org/10.5592/CO/3CroCEE.2025.126

GMM2. For each of both GMMs, *221* regression analyses were performed. Regression coefficients and standard deviations were obtained.

It was for the first time that GMMs obtained with the first set of data (Tables 1 and 2) were published. The results obtained with the second data set (containing also the data from the first set) or a total of *101* horizontal acceleration components, were published in 2008 [12], but are not presented for all *221* models of a single-degree-of-freedom system, but only for selected *43* (Note: equations 1 and 2 of these investigations also hold for the GMMs published in 2008. In these, there is a typing error. Specifically, in the mathematical equations, regression coefficient b_1 without *ln* before it, or the same as in eq. 1 and 2 herein, should be used). GMMs defined with the two sets of data refer to an epicentral zone. The difference is that some of these are for very shallow earthquakes with focal depth of down *to 10 km*, epicentral distances of up to *20 km* and magnitudes between *3.9* and *6.1*, whereas the others are for shallow local earthquakes with focal depths of down to *20 km*, epicentral distances of up to *35 km* and magnitudes between *3.9* and *6.5*.

Using the results shown in Table 1 (GMM1, equation 1), horizontal acceleration response spectra *SA* for an expected earthquake with $M = 6.5$ were computed as median and median + one standard deviation (Figure 1, above). The comparison between these and those computed with GMM2 (Table 2, equation 2) for $M = 6.5$ and $R_h = 7$ *km*, as median and median + *1* standard deviation, is presented type A (Figure 1, above and below). Such a direct comparison between a deterministic spectrum and a probabilistic spectrum, given according to the European standard /or other valid standard, can be made for all cases when such comparison is required by regulations or recommendations. Namely, during definition of maximum possible earthquake on locations of structures of capital importance, particularly when no regulations are elaborated for them, as are large dams [13, 15]. In other cases, it is necessary to compute a probabilistic spectrum by seismic hazard analyses PSHA, for a defined return period, applying GMMs developed for an epicentral zone. If used as alternative in PSHA, they should be given a corresponding weight factor. The results from the PSHA should be compared to the design ones given in Eurocode 8, for corresponding return periods.

In completely the same way as in Figure 1 (above and below), Figure 2 (above and below) shows the horizontal acceleration response spectra *SA* for GMM1 and GMM2, for the same values of magnitude and hypocentral distance ($M = 6.5$, $R_h = 7$*km*), as median and median + *1* standard deviation, for earthquakes with hypocentral depth of down to *20 km* [12].
The effect of *M* and R_h for deeper local earthquakes ($h \leq 20$ *km.*) is given in Figure 3 (above and below). GMMs defined with the two equations and with the second data set, or *101* data [12], were used. The acceleration spectra *SA* for a single value of magnitude, ($M = 6.5$), and varied values of $R_h = 5, 7, 10, 20, 40$ *km* are shown in Figure 3 (above), while for a single value of $R_h = 10$ *km* and varied values of $M = 4.5$ to 6.5, by a step of 0.5, they are given in Figure 3 (below). Figure 3 (above) shows that *SA*, for the range of periods $T > 0.4$ seconds, are decreased with the increase of R_h, whereas for $T < 0.4$ seconds, they are increased (the red line). For the same hypocentral distance, $R_h = 10$ *km*, and increase of magnitude *M*, *SA* are increased for the range of $T > 0.3$ seconds, while they are negligibly reduced for the range $T < 0.3$ seconds (black line).

3. Conclusions

The presented regression coefficients and standard deviations, for two mathematical models of ground motion, for soil type - rock, are practically applicable in defining the seismic design parameters by deterministic and probabilistic methods. While using them, care should be taken for the values of the boundaries of magnitude, epicentral distance and focal depth for which they are used, for the purpose of avoiding the extrapolation effect or making a mathematical error. While using very small hypocentral depths that are smaller than the least included in the data, it is recommended to use a mathematical model in function of magnitude.

The investigations presented herein are a contribution to better inclusion of the effect of local earthquakes in providing seismic resistance of structures.

Proceedings of the 3rd Croatian Conference on Earthquake Engineering - 3CroCEE
19–22 March 2025, Split, Croatia
Copyright © 2025 CroCEE
DOI: https://doi.org/10.5592/CO/3CroCEE.2025.126

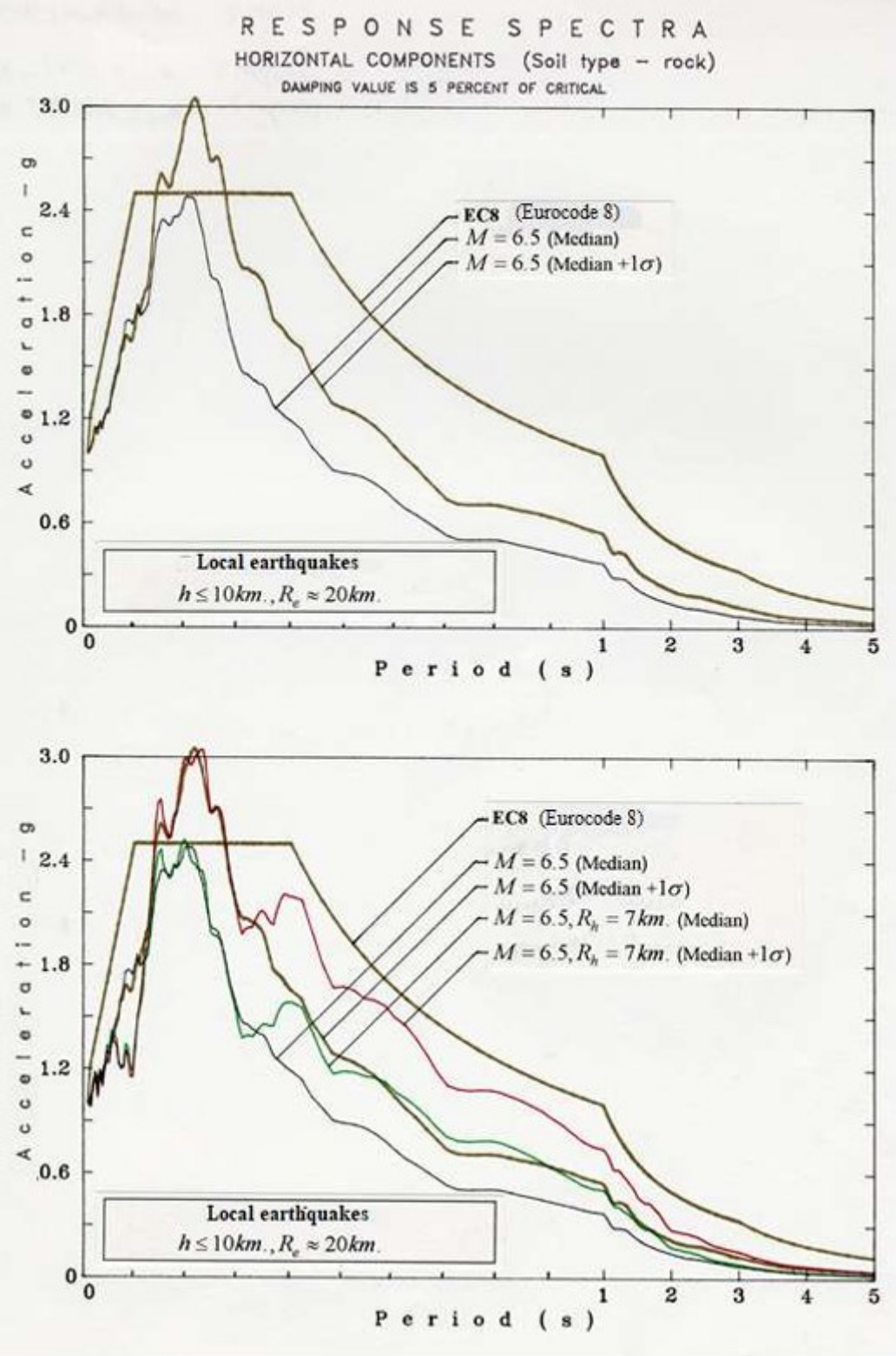


Figure 1. Comparison between expected *SA* (*g*) for an epicentral zone, for GMM1 (the figure above) and GMM2 (the figure below) and Eurocode 8.

Copyright © 2025 CroCEE
DOI: https://doi.org/10.5592/CO/3CroCEE.2025.126

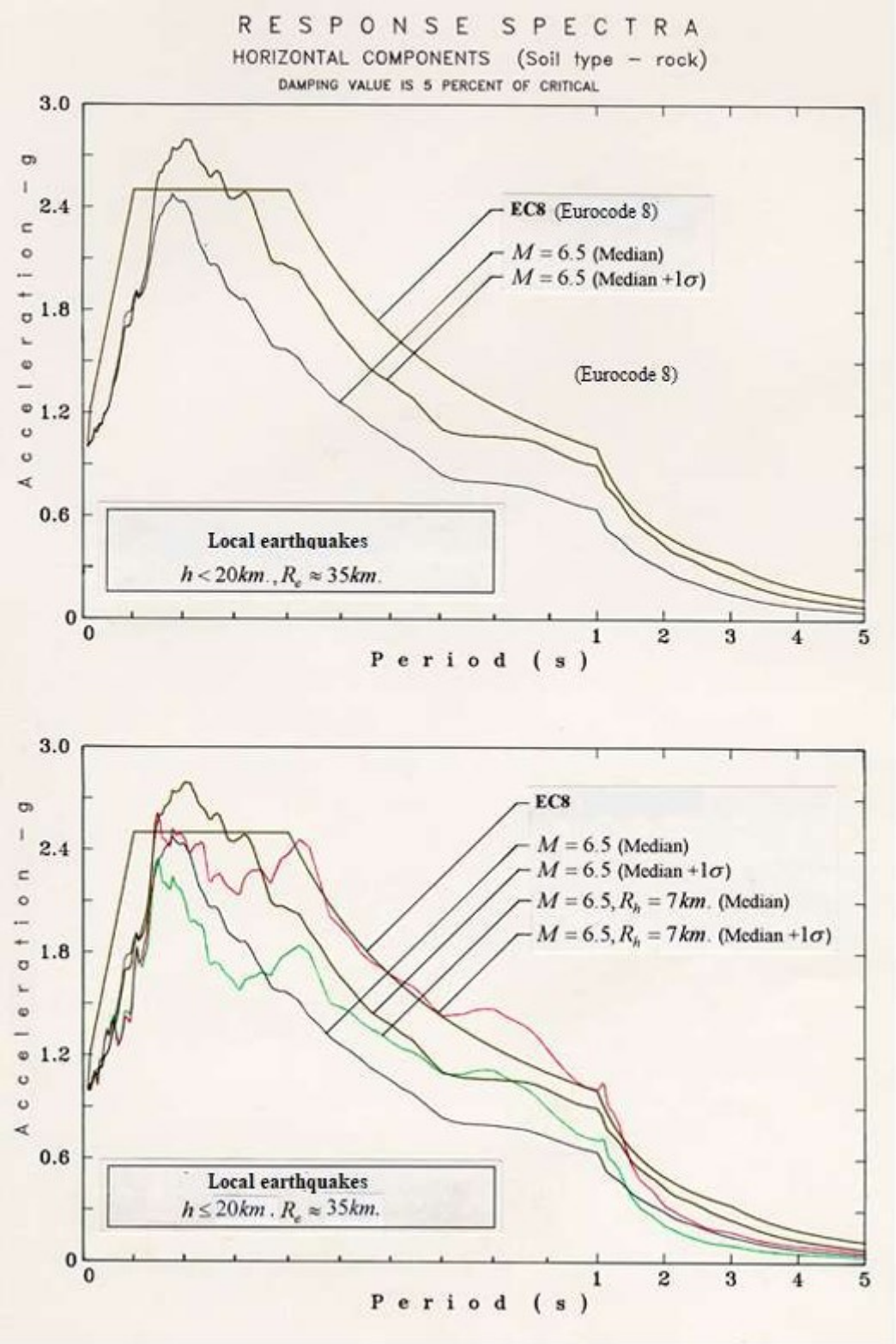


Figure 2. Expected *SA* (*g*) for an epicentral zone, for GMM1 (the figure above) and GMM2 (the figure below) and comparison with Eurocode 8.

Copyright © 2025 CroCEE
DOI: https://doi.org/10.5592/CO/3CroCEE.2025.126

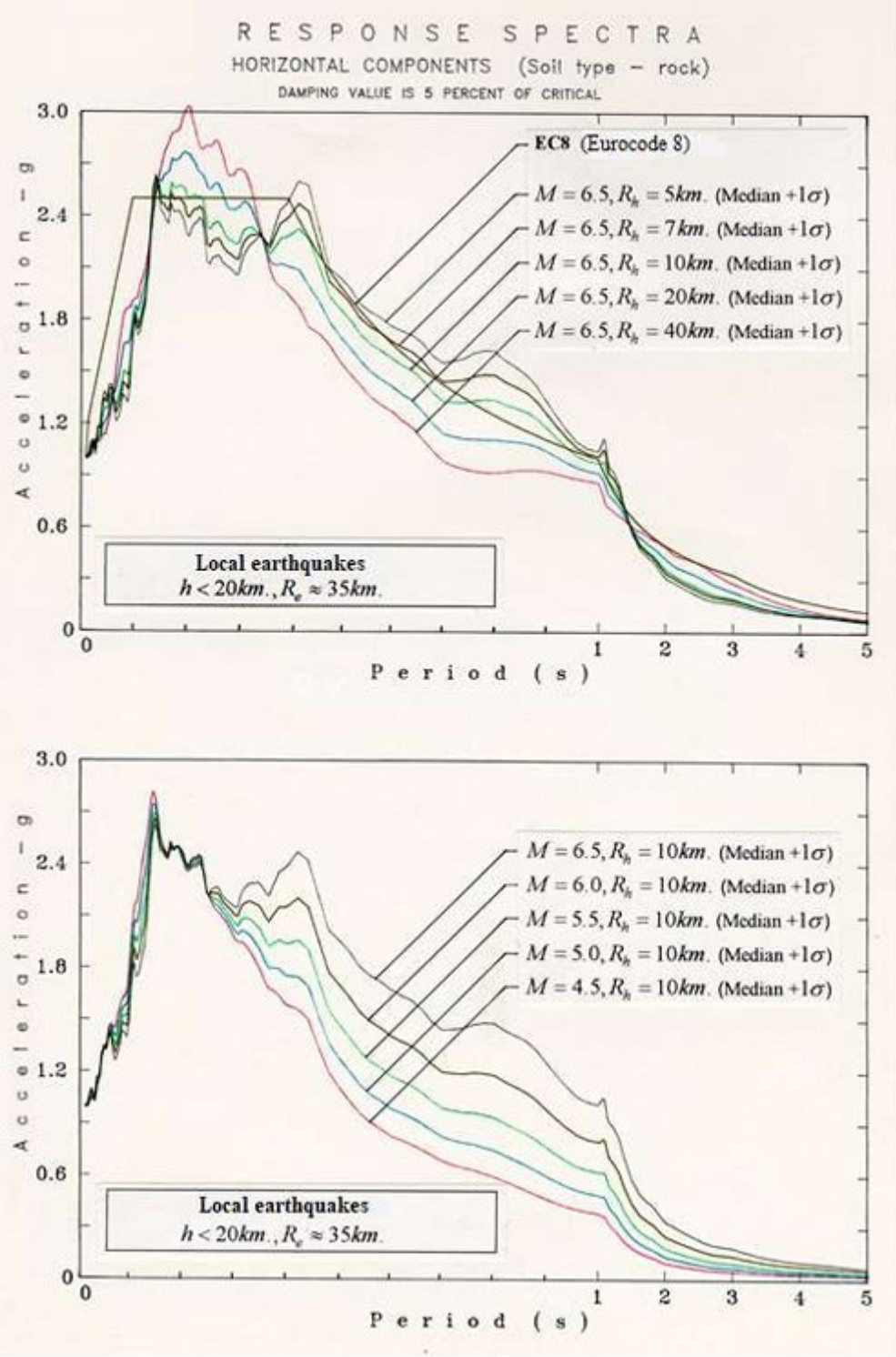


Figure 3. Distribution of expected *SA* (*g*) for an epicentral zone for GMM2 (the figure below) and comparison with Eurocode 8 (the figure above).

Proceedings of the 3rd Croatian Conference on Earthquake Engineering - 3CroCEE
19–22 March 2025, Split, Croatia
Copyright © 2025 CroCEE
DOI: https://doi.org/10.5592/CO/3CroCEE.2025.126

Table 1. Regression coefficients and standard deviation
Mathematical model: $lnSA(T;\xi=0.05)=b_1+b_2M+\sigma_{lnSA}P$

No.	Period T (s)	b_1	b_2	σ_{lnSA}
1	0.0100	2.7280	.2865	.5958
2	0.0145	2.7310	.2908	.5847
3	0.0190	2.6465	.3092	.5920
4	0.0235	2.5599	.3343	.5898
5	0.0280	2.7046	.3101	.5711
6	0.0325	2.6892	.3186	.5766
7	0.0370	2.8587	.2894	.5792
8	0.0415	2.9389	.2839	.5896
9	0.0460	2.9838	.2820	.5797
10	0.0505	3.0690	.2697	.5759
11	0.0550	3.1238	.2725	.5791
12	0.0595	3.2308	.2640	.5633
13	0.0640	3.3098	.2576	.5739
14	0.0685	3.4338	.2414	.5728
15	0.0730	3.4811	.2436	.5830
16	0.0775	3.6054	.2289	.5626
17	0.0820	3.5816	.2419	.5504
18	0.0865	3.6808	.2278	.5407
19	0.0910	3.8249	.2052	.5257
20	0.0955	4.0689	.1656	.5435
21	0.100	4.1839	.1518	.5586
22	0.105	4.1673	.1605	.5794
23	0.110	4.2340	.1446	.6043
24	0.115	4.2185	.1483	.6361
25	0.120	4.2124	.1512	.6525
26	0.125	4.2442	.1486	.6460
27	0.130	4.1652	.1696	.6491
28	0.135	4.0044	.2044	.6777
29	0.140	3.7978	.2454	.6967
30	0.145	3.6550	.2711	.7086
31	0.150	3.5136	.2966	.7051
32	0.155	3.4297	.3099	.6965
33	0.160	3.3998	.3134	.6905
34	0.165	3.4233	.3085	.6858
35	0.170	3.4275	.3086	.6865
36	0.175	3.3737	.3198	.6991
37	0.180	3.3784	.3188	.7184
38	0.185	3.3700	.3207	.7373
39	0.190	3.2925	.3349	.7479
40	0.195	3.1564	.3598	.7583
41	0.200	3.0752	.3731	.7675
42	0.205	3.0150	.3819	.7810
43	0.210	2.9715	.3888	.7953
44	0.215	2.9635	.3887	.8113
45	0.220	2.9640	.3847	.8312
46	0.225	2.9688	.3795	.8427
47	0.230	2.9723	.3754	.8488
48	0.235	3.0277	.3608	.8568
49	0.240	3.0573	.3506	.8661
50	0.245	3.0717	.3424	.8777
51	0.250	3.0281	.3476	.8873
52	0.255	2.9637	.3574	.8959
53	0.260	2.9213	.3626	.9043
54	0.265	2.9259	.3580	.9102
55	0.270	2.9561	.3480	.9141
56	0.275	2.9992	.3359	.9135
57	0.280	3.0841	.3153	.9109
58	0.285	3.1183	.3051	.9095
59	0.290	3.1373	.2971	.9134
60	0.295	3.1592	.2885	.9179
61	0.300	3.1789	.2808	.9278
62	0.305	3.1890	.2755	.9366
63	0.310	3.1782	.2754	.9433
64	0.315	3.1531	.2792	.9452
65	0.320	3.1297	.2816	.9493
66	0.325	3.1090	.2830	.9541
67	0.330	3.0666	.2887	.9579
68	0.335	3.0258	.2935	.9611
69	0.340	2.9773	.3000	.9587
70	0.345	2.9209	.3083	.9516
71	0.350	2.8837	.3122	.9438
72	0.355	2.8660	.3118	.9360
73	0.360	2.8716	.3068	.9301
74	0.365	2.8798	.3012	.9260
75	0.370	2.8609	.3021	.9289
76	0.375	2.8288	.3056	.9299
77	0.380	2.7960	.3090	.9320
78	0.385	2.7676	.3117	.9337
79	0.390	2.7515	.3123	.9314
80	0.395	2.7382	.3129	.9276
81	0.400	2.7329	.3125	.9267
82	0.420	2.6917	.3125	.9386
83	0.440	2.7506	.2894	.9425
84	0.460	2.6613	.2932	.9465
85	0.480	2.5702	.2958	.9498
86	0.500	2.4156	.3173	.9435
87	0.520	2.2638	.3388	.9367
88	0.540	2.0909	.3626	.9277
89	0.560	1.9356	.3808	.9314
90	0.580	1.8709	.3826	.9353
91	0.600	1.8471	.3752	.9441
92	0.620	1.8563	.3628	.9519
93	0.640	1.8525	.3554	.9459
94	0.660	1.8504	.3464	.9364
95	0.680	1.8641	.3335	.9297
96	0.700	1.8539	.3240	.9262
97	0.720	1.8087	.3248	.9324
98	0.740	1.7404	.3340	.9329
99	0.760	1.6249	.3525	.9301
100	0.780	1.5004	.3722	.9273
101	0.800	1.3918	.3878	.9289
102	0.820	1.3242	.3937	.9369
103	0.840	1.2439	.4014	.9474
104	0.860	1.1514	.4123	.9558
105	0.880	1.0699	.4200	.9691
106	0.900	1.0085	.4245	.9770
107	0.920	.9593	.4272	.9816
108	0.940	.9285	.4270	.9815
109	0.960	.9127	.4234	.9826
110	0.980	.8697	.4251	.9817
111	1.000	.8053	.4308	.9806
112	1.020	.7627	.4330	.9815
113	1.040	.7198	.4353	.9857
114	1.060	.6922	.4345	.9891
115	1.080	.7137	.4242	.9922

Proceedings of the 3rd Croatian Conference on Earthquake Engineering - 3CroCEE
19–22 March 2025, Split, Croatia
Copyright © 2025 CroCEE
DOI: https://doi.org/10.5592/CO/3CroCEE.2025.126

Table 1. Regression coefficients and standard deviation (continued)
Mathematical model: $lnSA(T;\xi=0.05)=b_1+b_2M+\sigma_{lnSA}P$

No.	Period T (s)	b_1	b_2	σ_{lnSA}
116	1.100	.7185	.4168	.9936
117	1.120	.6945	.4154	.9950
118	1.140	.6432	.4188	.9977
119	1.160	.5621	.4289	1.0044
120	1.180	.4509	.4457	1.0102
121	1.200	.3473	.4615	1.0132
122	1.220	.2417	.4781	1.0146
123	1.240	.1555	.4908	1.0163
124	1.260	.0765	.5026	1.0172
125	1.280	.0067	.5126	1.0159
126	1.300	-.0708	.5240	1.0119
127	1.320	-.1489	.5354	1.0088
128	1.340	-.2185	.5444	1.0063
129	1.360	-.2647	.5483	1.0036
130	1.380	-.2964	.5489	1.0029
131	1.400	-.3206	.5483	1.0027
132	1.420	-.3414	.5469	1.0014
133	1.440	-.3578	.5454	1.0007
134	1.460	-.3698	.5437	.9982
135	1.480	-.3742	.5400	.9975
136	1.500	-.3852	.5377	.9978
137	1.520	-.3935	.5348	1.0003
138	1.540	-.4067	.5334	1.0022
139	1.560	-.4196	.5323	1.0037
140	1.580	-.4366	.5317	1.0061
141	1.600	-.4587	.5319	1.0091
142	1.620	-.4823	.5324	1.0126
143	1.640	-.5046	.5326	1.0171
144	1.660	-.5295	.5338	1.0212
145	1.680	-.5525	.5344	1.0242
146	1.700	-.5683	.5338	1.0248
147	1.720	-.5975	.5360	1.0254
148	1.740	-.6287	.5383	1.0267
149	1.760	-.6594	.5403	1.0282
150	1.780	-.6846	.5412	1.0297
151	1.800	-.7036	.5408	1.0313
152	1.820	-.7215	.5405	1.0317
153	1.840	-.7630	.5452	1.0305
154	1.860	-.8017	.5489	1.0305
155	1.880	-.8405	.5527	1.0301
156	1.900	-.8718	.5550	1.0290
157	1.920	-.8930	.5554	1.0272
158	1.940	-.9144	.5561	1.0271
159	1.960	-.9402	.5579	1.0271
160	1.980	-.9728	.5609	1.0275
161	2.000	-.9969	.5621	1.0287
162	2.020	-1.0195	.5628	1.0301
163	2.040	-1.0407	.5631	1.0326
164	2.060	-1.0608	.5630	1.0357
165	2.080	-1.0843	.5637	1.0395
166	2.100	-1.1171	.5663	1.0435
167	2.120	-1.1532	.5699	1.0476
168	2.140	-1.1833	.5723	1.0519
169	2.160	-1.2098	.5741	1.0565
170	2.18	-1.2319	.5751	1.0616
171	2.20	-1.2606	.5776	1.0660
172	2.22	-1.2887	.5800	1.0705
173	2.24	-1.3159	.5822	1.0748
174	2.26	-1.3459	.5851	1.0786
175	2.28	-1.3889	.5910	1.0813
176	2.30	-1.4276	.5962	1.0843
177	2.32	-1.4577	.5997	1.0869
178	2.34	-1.4842	.6027	1.0885
179	2.36	-1.5098	.6054	1.0906
180	2.38	-1.5399	.6091	1.0926
181	2.40	-1.5654	.6119	1.0948
182	2.42	-1.5891	.6142	1.0969
183	2.44	-1.6144	.6169	1.0988
184	2.46	-1.6383	.6192	1.1007
185	2.48	-1.6509	.6190	1.1029
186	2.50	-1.6598	.6181	1.1053
187	2.52	-1.6682	.6170	1.1077
188	2.54	-1.6760	.6158	1.1102
189	2.56	-1.6840	.6149	1.1130
190	2.58	-1.6921	.6139	1.1158
191	2.60	-1.6999	.6128	1.1181
192	2.62	-1.7102	.6123	1.1198
193	2.64	-1.7167	.6111	1.1218
194	2.66	-1.7214	.6094	1.1240
195	2.68	-1.7237	.6072	1.1265
196	2.70	-1.7256	.6051	1.1293
197	2.72	-1.7267	.6027	1.1313
198	2.74	-1.7341	.6017	1.1340
199	2.76	-1.7380	.5999	1.1366
200	2.78	-1.7359	.5970	1.1395
201	2.80	-1.7288	.5930	1.1425
202	2.82	-1.7194	.5886	1.1444
203	2.84	-1.7062	.5837	1.1466
204	2.86	-1.6903	.5782	1.1482
205	2.88	-1.6726	.5723	1.1495
206	2.90	-1.6593	.5674	1.1507
207	2.92	-1.6449	.5625	1.1523
208	2.94	-1.6423	.5600	1.1531
209	2.96	-1.6424	.5580	1.1533
210	2.98	-1.6424	.5559	1.1533
211	3.00	-1.6453	.5546	1.1537
212	3.20	-1.6850	.5418	1.1463
213	3.40	-1.6284	.5058	1.1332
214	3.60	-1.5659	.4731	1.1201
215	3.80	-1.4483	.4317	1.1219
216	4.00	-1.4885	.4250	1.1260
217	4.20	-1.4741	.4068	1.1189
218	4.40	-1.5439	.4077	1.1092
219	4.60	-1.5134	.3894	1.1086
220	4.80	-1.4543	.3646	1.1133
221	5.00	-1.3966	.3383	1.1119

Proceedings of the 3rd Croatian Conference on Earthquake Engineering - 3CroCEE
19–22 March 2025, Split, Croatia
Copyright © 2025 CroCEE
DOI: https://doi.org/10.5592/CO/3CroCEE.2025.126

Table 2. Regression coefficients and standard deviation
Mathematical model: $lnSA(T;\xi=0.05)=b_1+b_2M+b_3lnR_h+\sigma_{lnSA}P$

No	Period T (s)	b_1	b_2	b_3	σ_{lnSA}
1	0.0100	3.7204	.4090	-.5851	.5708
2	0.0145	3.6740	.4073	-.5560	.5621
3	0.0190	3.7231	.4421	-.6348	.5612
4	0.0235	3.5984	.4625	-.6123	.5614
5	0.0280	3.5934	.4198	-.5241	.5510
6	0.0325	3.7016	.4436	-.5969	.5491
7	0.0370	3.7999	.4056	-.5549	.5564
8	0.0415	3.9480	.4084	-.5950	.5631
9	0.0460	4.0799	.4173	-.6462	.5467
10	0.0505	4.1313	.4008	-.6263	.5449
11	0.0550	4.1950	.4047	-.6316	.5477
12	0.0595	4.1988	.3835	-.5708	.5378
13	0.0640	4.1840	.3655	-.5154	.5547
14	0.0685	4.1325	.3276	-.4119	.5624
15	0.0730	4.0372	.3123	-.3279	.5787
16	0.0775	4.1435	.2953	-.3173	.5583
17	0.0820	4.1716	.3147	-.3478	.5439
18	0.0865	4.2335	.2960	-.3259	.5353
19	0.0910	4.2510	.2578	-.2512	.5241
20	0.0955	4.4854	.2171	-.2456	.5426
21	0.10	4.7439	.2210	-.3302	.5534
22	0.105	4.8393	.2435	-.3962	.5705
23	0.11	5.0188	.2415	-.4628	.5911
24	0.115	5.0740	.2540	-.5044	.6209
25	0.12	5.2457	.2788	-.6092	.6284
26	0.125	5.2854	.2772	-.6139	.6210
27	0.13	5.2426	.3027	-.6353	.6221
28	0.135	5.0579	.3344	-.6212	.6539
29	0.14	4.8822	.3792	-.6394	.6721
30	0.145	4.7554	.4069	-.6489	.6837
31	0.15	4.5899	.4295	-.6346	.6814
32	0.155	4.4436	.4351	-.5978	.6758
33	0.16	4.4014	.4371	-.5905	.6702
34	0.165	4.4134	.4308	-.5838	.6659
35	0.17	4.4161	.4307	-.5829	.6667
36	0.175	4.3809	.4442	-.5939	.6789
37	0.18	4.3734	.4417	-.5867	.6997
38	0.185	4.4082	.4489	-.6121	.7173
39	0.19	4.3462	.4650	-.6212	.7275
40	0.195	4.1859	.4869	-.6070	.7396
41	0.20	4.0802	.4972	-.5926	.7505
42	0.205	3.9833	.5014	-.5709	.7662
43	0.21	3.9132	.5050	-.5552	.7822
44	0.215	3.9139	.5060	-.5604	.7983
45	0.22	3.9324	.5043	-.5710	.8182
46	0.225	3.9789	.5042	-.5956	.8283
47	0.23	4.0118	.5038	-.6129	.8333
48	0.235	4.0855	.4914	-.6237	.8407
49	0.24	4.0720	.4759	-.5983	.8523
50	0.245	4.0418	.4622	-.5720	.8661
51	0.25	3.9997	.4676	-.5730	.8760
52	0.255	3.9366	.4775	-.5736	.8848
53	0.26	3.8973	.4830	-.5754	.8933
54	0.265	3.9178	.4804	-.5848	.8988
55	0.27	3.9558	.4714	-.5894	.9025
56	0.275	3.9786	.4568	-.5774	.9027
57	0.28	4.0643	.4363	-.5779	.9000
58	0.285	4.0948	.4257	-.5757	.8987
59	0.29	4.1080	.4170	-.5724	.9029
60	0.295	4.1121	.4061	-.5618	.9082
61	0.30	4.1000	.3945	-.5431	.9196
62	0.305	4.0876	.3864	-.5298	.9295
63	0.31	4.1066	.3900	-.5474	.9352
64	0.315	4.0853	.3943	-.5497	.9370
65	0.32	4.0721	.3979	-.5557	.9409
66	0.325	4.0628	.4007	-.5624	.9454
67	0.33	4.0502	.4102	-.5799	.9482
68	0.335	4.0445	.4192	-.6007	.9502
69	0.34	4.0270	.4296	-.6189	.9465
70	0.345	3.9883	.4401	-.6293	.9385
71	0.35	3.9691	.4462	-.6400	.9296
72	0.355	3.9764	.4489	-.6547	.9205
73	0.36	4.0185	.4484	-.6762	.9127
74	0.365	4.0733	.4485	-.7037	.9064
75	0.37	4.1194	.4575	-.7420	.9062
76	0.375	4.1403	.4675	-.7733	.9045
77	0.38	4.1515	.4763	-.7992	.9044
78	0.385	4.1564	.4832	-.8188	.9039
79	0.39	4.1646	.4867	-.8331	.9006
80	0.395	4.1641	.4890	-.8407	.8959
81	0.40	4.1729	.4903	-.8491	.8941
82	0.42	4.1658	.4945	-.8691	.9046
83	0.44	4.2230	.4712	-.8681	.9089
84	0.46	4.0701	.4671	-.8306	.9167
85	0.48	3.9697	.4686	-.8251	.9207
86	0.50	3.8556	.4951	-.8491	.9118
87	0.52	3.7150	.5180	-.8556	.9040
88	0.54	3.5437	.5419	-.8566	.8944
89	0.56	3.4334	.5657	-.8831	.8957
90	0.58	3.4177	.5735	-.9120	.8968
91	0.60	3.4229	.5697	-.9291	.9043
92	0.62	3.4875	.5642	-.9618	.9091
93	0.64	3.4904	.5576	-.9657	.9022
94	0.66	3.4955	.5495	-.9699	.8916
95	0.68	3.5027	.5358	-.9661	.8849
96	0.70	3.5081	.5282	-.9753	.8801
97	0.72	3.4841	.5316	-.9878	.8853
98	0.74	3.4192	.5412	-.9898	.8856
99	0.76	3.3057	.5600	-.9910	.8824
100	0.78	3.1797	.5795	-.9901	.8796
101	0.80	3.0627	.5941	-.9852	.8818
102	0.82	2.9928	.5997	-.9838	.8906
103	0.84	2.9076	.6067	-.9810	.9021
104	0.86	2.7893	.6145	-.9657	.9128
105	0.88	2.6843	.6192	-.9518	.9285
106	0.90	2.5900	.6197	-.9324	.9389
107	0.92	2.5120	.6189	-.9155	.9454
108	0.94	2.4430	.6140	-.8930	.9476
109	0.96	2.3961	.6065	-.8746	.9505
110	0.98	2.3424	.6070	-.8683	.9501
111	1.00	2.2930	.6145	-.8772	.9481
112	1.02	2.2642	.6183	-.8852	.9483
113	1.04	2.2348	.6224	-.8932	.9520
114	1.06	2.2306	.6245	-.9071	.9542
115	1.08	2.2809	.6176	-.9240	.9558

Copyright © 2025 CroCEE
DOI: https://doi.org/10.5592/CO/3CroCEE.2025.126

Table 2. Regression coefficients and standard deviation (continued)
Mathematical model: $lnSA(T;\xi = 0.05) = b_1 + b_2 M + b_3 lnR_h + \sigma_{lnSA} P$

No	Period T (s)	b_1	b_2	b_3	σ_{lnSA}
116	1.10	2.3080	.6130	-.9372	.9559
117	1.12	2.2819	.6114	-.9359	.9576
118	1.14	2.2241	.6140	-.9321	.9608
119	1.16	2.1449	.6243	-.9332	.9677
120	1.18	2.0273	.6403	-.9295	.9743
121	1.20	1.9223	.6560	-.9286	.9775
122	1.22	1.8041	.6710	-.9212	.9797
123	1.24	1.7032	.6819	-.9125	.9824
124	1.26	1.6077	.6916	-.9028	.9843
125	1.28	1.5136	.6986	-.8885	.9842
126	1.30	1.4219	.7083	-.8801	.9808
127	1.32	1.3340	.7184	-.8743	.9781
128	1.34	1.2590	.7268	-.8711	.9758
129	1.36	1.2206	.7317	-.8757	.9725
130	1.38	1.2051	.7343	-.8852	.9708
131	1.40	1.1966	.7356	-.8946	.9697
132	1.42	1.1959	.7367	-.9064	.9673
133	1.44	1.1933	.7369	-.9145	.9657
134	1.46	1.1741	.7343	-.9103	.9635
135	1.48	1.1659	.7302	-.9080	.9630
136	1.50	1.1490	.7271	-.9046	.9636
137	1.52	1.1462	.7249	-.9078	.9660
138	1.54	1.1424	.7246	-.9133	.9675
139	1.56	1.1374	.7245	-.9180	.9686
140	1.58	1.1304	.7252	-.9239	.9705
141	1.60	1.1178	.7265	-.9295	.9731
142	1.62	1.1110	.7291	-.9394	.9758
143	1.64	1.1098	.7320	-.9519	.9793
144	1.66	1.1065	.7357	-.9646	.9823
145	1.68	1.1035	.7389	-.9764	.9843
146	1.70	1.0976	.7395	-.9822	.9844
147	1.72	1.0592	.7405	-.9768	.9856
148	1.74	1.0171	.7415	-.9703	.9877
149	1.76	.9811	.7428	-.9672	.9895
150	1.78	.9537	.7434	-.9659	.9912
151	1.80	.9339	.7429	-.9655	.9930
152	1.82	.9040	.7412	-.9584	.9941
153	1.84	.8288	.7417	-.9385	.9948
154	1.86	.7631	.7421	-.9226	.9961
155	1.88	.6965	.7424	-.9062	.9975
156	1.90	.6310	.7405	-.8860	.9982
157	1.92	.5729	.7364	-.8643	.9983
158	1.94	.5284	.7343	-.8507	.9993
159	1.96	.4790	.7331	-.8368	1.0006
160	1.98	.4279	.7338	-.8258	1.0020
161	2.00	.3951	.7339	-.8207	1.0037
162	2.02	.3772	.7353	-.8235	1.0049
163	2.04	.3699	.7373	-.8317	1.0068
164	2.06	.3677	.7394	-.8423	1.0092
165	2.08	.3620	.7422	-.8527	1.0122
166	2.10	.3404	.7463	-.8594	1.0158
167	2.12	.3072	.7501	-.8610	1.0199
168	2.14	.2787	.7527	-.8620	1.0244
169	2.16	.2585	.7553	-.8657	1.0288
170	2.18	.2453	.7574	-.8710	1.0337
171	2.20	.2215	.7605	-.8738	1.0381
172	2.22	.2003	.7639	-.8779	1.0424
173	2.24	.1810	.7670	-.8825	1.0465
174	2.26	.1527	.7701	-.8836	1.0504
175	2.28	.0926	.7739	-.8735	1.0541
176	2.30	.0425	.7777	-.8668	1.0577
177	2.32	.0046	.7803	-.8622	1.0609
178	2.34	-.0277	.7825	-.8587	1.0628
179	2.36	-.0578	.7847	-.8561	1.0652
180	2.38	-.1021	.7866	-.8477	1.0681
181	2.40	-.1466	.7871	-.8365	1.0712
182	2.42	-.1872	.7873	-.8266	1.0742
183	2.44	-.2291	.7879	-.8168	1.0770
184	2.46	-.2686	.7883	-.8076	1.0797
185	2.48	-.2933	.7866	-.8004	1.0825
186	2.50	-.3146	.7842	-.7932	1.0855
187	2.52	-.3346	.7817	-.7863	1.0885
188	2.54	-.3532	.7791	-.7799	1.0915
189	2.56	-.3723	.7768	-.7734	1.0950
190	2.58	-.3887	.7748	-.7685	1.0982
191	2.60	-.4058	.7725	-.7630	1.1009
192	2.62	-.4261	.7708	-.7571	1.1032
193	2.64	-.4349	.7693	-.7557	1.1053
194	2.66	-.4374	.7680	-.7570	1.1075
195	2.68	-.4353	.7663	-.7596	1.1099
196	2.70	-.4322	.7648	-.7626	1.1126
197	2.72	-.4291	.7629	-.7650	1.1145
198	2.74	-.4403	.7614	-.7628	1.1174
199	2.76	-.4432	.7598	-.7634	1.1201
200	2.78	-.4350	.7576	-.7670	1.1228
201	2.80	-.4182	.7548	-.7728	1.1255
202	2.82	-.3993	.7516	-.7783	1.1271
203	2.84	-.3711	.7486	-.7872	1.1287
204	2.86	-.3426	.7446	-.7946	1.1298
205	2.88	-.3148	.7400	-.8006	1.1307
206	2.90	-.2917	.7362	-.8064	1.1315
207	2.92	-.2599	.7335	-.8166	1.1324
208	2.94	-.2528	.7315	-.8193	1.1331
209	2.96	-.2509	.7298	-.8204	1.1332
210	2.98	-.2503	.7277	-.8208	1.1331
211	3.00	-.2567	.7260	-.8187	1.1337
212	3.20	-.3686	.7043	-.7761	1.1292
213	3.40	-.2705	.6734	-.8006	1.1138
214	3.60	-.2057	.6410	-.8020	1.1002
215	3.80	-.0447	.6049	-.8275	1.1001
216	4.00	-.1111	.5950	-.8121	1.1055
217	4.20	-.0850	.5783	-.8190	1.0977
218	4.40	-.2000	.5736	-.7923	1.0896
219	4.60	-.1900	.5528	-.7802	1.0899
220	4.80	-.1139	.5301	-.7903	1.0940
221	5.00	-.0591	.5034	-.7886	1.0927

Proceedings of the 3rd Croatian Conference on Earthquake Engineering - 3CroCEE
19–22 March 2025, Split, Croatia
Copyright © 2025 CroCEE
DOI: https://doi.org/10.5592/CO/3CroCEE.2025.126

4. References

[1] Akkar S., Cagnan Z. (2010): A Local Ground-Motion Predictive Model for Turkey and Its Comparison with Regional and Global Ground Motion-Models. *BSSA, Vol. 100, No.6. pp. 2978-2995, December 2010. doi: 10.1785/0120090367*

[2] Douglas et al. (2011): Ground Motion Prediction Equations 1964-2010 (and its upgrading up to 2018). *PEER Report 2011/102* Pacific Earthquake Engineering Research Center, Collage of Engineering, Berkeley, California.

[3] Douglas J. (2019): Ground Motion Prediction Equations (1964-2019). Department of Civil and Environmental Engineering, University of Strathclyde, Glasgow, UK.

[4] EUROCODE 8: Design Provisions for Earthquake Resistance of Structures, Seismic Actions and General Requirements for Structures, [2004] EN 1998-1:2004, Stage 51, May 2004.

[5] EUROCODE 8: Design Provisions for Earthquake Resistance of Structures, Part 2-Bridges, [2005] EN 1998-2:2005, December 2005.

[6] Sedaghati, F., M.EERI[1] and Shahram P., M. EERI[2], sagepub.com/journals-permisssions DOI: 10.1177/87552930231191759 journals.sagepub.com/home/eqs (2023). Machine Learning – Based Ground Motion Models for Shallow Crustal Earthquakes in Active Tectonic Regions.

[7] Pacor F., Spallarossa D., Oth A., Luzi A., Puglisa R., Cantore L., Mecuri A., D'Amico M., Bindi D. (2016): Spectral Models for Ground Motion Prediction in the L'Aquila Region. *Geophysical Journal International,* Volume 204, Issue 2, February 2016, Pages 697-718, http://doi.org/10.1093/gji/ggv448

[8] Stamatovska S. (1988): Probability Response of SDFS Exposed to Seismic Loads. Master Thesis (in Macedonian), Institute of Earthquake Engineering and Engineering Seismology, "Ss. Cyril and Methodious" University, Skopje, R. of Macedonia, 1988.

[9] Stamatovska S. (2001): Design Response Spectra–Deterministic and Probabilistic Approach. *Albanian Journal of Natural &Technical Science (AJNTS)*, No.10/2001, pp. 113-123.

[10] Stamatovska S., Paskalov A., Petrovski D., Hadzievski D. (2003). *Ground Motion Models*, Institute of Earthquake Engineering and Engineering Seismology, "Ss. Cyril and Methodius" University, Skopje, Republic of Macedonia, *Report IZIIS-2003-19*, March 2003 (in Macedonian).

[11] Stamatovska S. (2003): Design Response Spectra for a Rock Site in the City of Skopje. *International Conference on Earthquake Engineering to Mark 40 Years from Catastrophic 1963 Skopje Earthquake and Successful City Reconstruction*, Skopje-Ohrid, R. of Macedonia, 26-29 August 2003. Reference: CD: SE-40EEE, 0155.pdf.

[12] Stamatovska S. (2008): Ground Motion Models for Local Earthquakes. Proceedings, Volume 1, *Second International Meeting Civil Engineering - Science and Practice (GNP2008)*, Zabljak, 03-07 March 2008, pp.469-474 (In Serbian)

[13] Stamatovska S. (2008): Evaluation of Seismic Design Parameters of Structures of the HPP Kozjak - ICOLD Method, IZIIS Report 2008 - 67/2, November 2008, Skopje, R. Macedonia (in Macedonian)

[14] Stamatovska S. (2010): Gas Power Plant 'Skopje-East" – Seismic Design Parameters. *3th International Conference - GNP2010*. Zabljak, 15-19 February, 2010. Proceedings, Volume 1, pp.553–558.

[15] Stamatovska S. (2010): Seismic Design Parameters for Large Dams –ICOLD Method. *14th ECEE*, Ohrid, August 30-September 3, 2010, Republic of Macedonia. Paper No.1826.

Copyright © 2025 CroCEE
DOI: https://doi.org/10.5592/CO/3CroCEE.2025.126

[16] Stamatovska S. (2010): Local Soil Response to Seismic Input Compatible to Uniform Hazard Spectra at Bedrock. *Journal of Acta Geodaetica et Geophisica Hungarica*, Volume 45, Number 3, September 2010, pp.273-283. (DOI: 10.1556 /AGeog.45.2010.3.2).

[17] Sesov V., Stamatovska S., Aleksovski D., Zafirova I., Gadza V., Gjorgjeska I. (2010). Evaluation of Seismic Potential of a Site for Preliminary Project on the Ohrid Airport. UKIM-IZIIS, *Report IZIIS 2010-33*, Skopje, May 2010.

[18] Stamatovska S., Sesov V. (2011): "St. Paul the Apostle" Airport in Ohrid - Assessment of Seismic Potential of the Site. *15th International Symposium of MASE (MASE -15)***.** Struga, Macedonia 18-21 September 2013.

[19] Mirakovski G., Stamatovska S., Micajkov S., Aleksovski D., Mircevska V., Zafirova I., Gadza V., Filipovski D., Markovski I. (2011): Geological and Seismogeological Bases for the General Urban Plan of the Wider Urban Area of Skopje City. UKIM-IZIIS, *Report IZIIS 2011-31*, June 2011.

[20] Mirakovski G., Stamatovska S. (2012): Seismic Zoning of the Skopje City Urban Area Using Tomographic Concept. *15thWCEE*, Lisboa, Portugal, 2012. Paper: WCEE2012_1889.pdf

[21] Stamatovska S. (2012): Urban Area Microzonation as Prevention in Managing Earthquake Risk. *Journal of Frontiers in Geotechnical Engineering (FGE),* Volume 1 Issue 1, December 2012. (Online 2012-12), pp. 9-18. www.seipub.org/fge/

[22] Stamatovska S. (2012): Seismic Parameters of Seismic Base of the Location of Antenna Tower on Vodno Mountain. UKIM-IZIIS, *Report IZIIS 2012-44*, October 2012.

[23] Sesov V., Stamatovska S., Gjorgjeska I., Jovanovski Gj. (2012): Definition of Seismic Design Parameters – Structure – State institutions ELEM, Makedonija Str. bb Skopje. UKIM-IZIIS, *Report IZIIS 2012-46*, August 2012.

[24] Uniform Building Code, Volume 2, Division IV, Earthquake Design, 1997. Published regulation of design, A WORLD List -1996, Supplement 2000.

Acknowledgement

The author expresses her gratitude to the Ministry of Education and Science of the Republic of North Macedonia for the financial support to the scientific-research project: **Ground Motion Models.**

Proceedings of the 3rd Croatian Conference on Earthquake Engineering - 3CroCEE
19–22 March 2025, Split, Croatia
Copyright © 2025 CroCEE
DOI: https://doi.org/10.5592/CO/3CroCEE.2025.136

IMPROVEMENT AND UPDATES OF THE NATIONAL DATABASES FOR SEISMOGENIC SOURCE MODELING IN THE CONTEXT OF REVISING THE NATIONAL HAZARD MODEL FOR NORTH MACEDONIA

Zabedin Neziri [(1)], Ljubcho Jovanov [(2)], Radmila Salic Makreska [(3)], Katerina Drogreshka [(4)], Laurentiu Danciu [(5)], Jasmina Najdovska [(6)], Daniel Tomic [(7)]

[(1)] *Assistant, M.Sc., Ss. Cyril and Methodius University in Skopje, Institute of Earthquake Engineering and Engineering Seismology (IZIIS), zabedin@iziis.ukim.edu.mk*
[(2)] *Assistant, M.Sc., Seismological Observatory, Faculty of Natural Sciences and Mathematics (SORM), ljovanov@pmf.ukim.mk*
[(3)] *Prof. Dr., Ss. Cyril and Methodius University in Skopje, Institute of Earthquake Engineering and Engineering Seismology (IZIIS), r_salic@iziis.ukim.edu.mk*
[(4)] *Assoc. Prof. Dr., Seismological Observatory, Faculty of Natural Sciences and Mathematics (SORM), katerinadrogreska@pmf.ukim.mk*
[(5)] *Senior Researcher, ETH Zürich, Swiss Seismological Service (SED), laurentiu.danciu@sed.ethz.ch*
[(6)] *Assoc. Prof. Dr., Seismological Observatory, Faculty of Natural Sciences and Mathematics (SORM), najdovskaj@pmf.ukim.mk*
[(7)] *Assistant, M.Sc., Ss. Cyril and Methodius University in Skopje, Institute of Earthquake Engineering and Engineering Seismology (IZIIS), danielt@iziis.ukim.edu.mk*

Abstract

The official adoption of Eurocode standards in North Macedonia, compared to developed EU countries, was only in recent years, leaving a significant gap that needs to be tackled. The new generation of Eurocode standards is posing demands to seismic hazard assessment's outputs to use the most updated seismic hazard models, which will be crucial for the development of national annexes. To improve and refine the national seismic hazard model, it is essential to update and curate the existing datasets (i.e., earthquake catalogues, tectonics information and active faults), particularly in a country that has shown significant tectonic activity in the past decades with the occurrence of moderate to strong earthquakes. In just the last century, 12 earthquakes with magnitudes greater than 6.0 have occurred within the territory of North Macedonia and the surrounding areas, confirming the constant threat of earthquake to society.

The main task in developing a refined national seismogenic source model is to improve and update the national database by increasing the quality and thoroughness of all available national and regional seismotectonic databases. This activity involves compilation and statistical analyses of the updated national earthquake catalogue that chronologically ranges from 1000 to 2020. In its compiling, priority was given to the national catalogue from the National Seismological Observatory at the Faculty of Natural Sciences and Mathematics (SORM), which was then supplemented by events from the International Seismological Centre (ISC). Additionally, an overview of the latest defined active faults in North Macedonia will be presented, serving as an input for the new national seismic hazard model.

With recently collected and compiled data, along with updated information on seismically active faults in the region, we are now capable of elevating and upgrading the probabilistic seismic hazard assessment of the country, which previously was built primarily upon seismological data, i.e., data from past earthquakes.

Keywords: Seismogenic model, Earthquake catalogue, Active faults, Seismic Hazard, North Macedonia

1. Introduction

The Republic of North Macedonia is located in the Balkan Peninsula, an active seismic region with a complex tectonic structure that causes frequent earthquakes, especially moderate ones. The moderate to high seismicity points out the necessity for comprehensive seismic hazard assessment of the country. This study provides an effort in the enhancement and update of the national databases, more specifically the earthquake catalogue and the fault database, which constitute the backbone of the updated national

Proceedings of the 3rd Croatian Conference on Earthquake Engineering - 3CroCEE
19–22 March 2025, Split, Croatia
Copyright © 2025 CroCEE
DOI: https://doi.org/10.5592/CO/3CroCEE.2025.136

seismogenic source model. The update of the seismogenic source model as an initial part of the new seismic hazard assessment of the country plays a key role in the development of the national annexes for the new generation of Eurocodes.

The compilation and the main features of the updated earthquake catalogue are presented, both for the instrumental period, 1900-2020, and the historical period, pre-1900. The catalogue contains 4993 events, integrating data from the updated national earthquake catalogue of the Seismological Observatory as its core, the International Seismological Centre ISC [1], and other regional sources. For the first time faults are intended to be introduced as a branch tree in the seismogenic model, thus, improvements in the identification and parametrization of active faults have been done. The methodologies and results of such updates are discussed hereinafter, highlighting their importance to improve the probabilistic seismic hazard assessment (PSHA) of the country.

2. Earthquake catalogue

2.1. Catalogue compilation and main characteristics

Understanding the seismicity of a region relies on records of past earthquakes, which are obtained from instrumental data, direct analysis of earthquake-induced damage in recent times, or chronicles from both the recent and distant past [2]. This information is typically compiled into documents known as earthquake catalogues. Earthquake catalogues are the most important seismological product in regions, since earthquake hazard assessments heavily rely on the analysis of historical and instrumental earthquake data [3] [4].

The area of interest is defined by the coordinates 39.8˚N≤φ≤43.3˚N, 19.3˚E≤λ≤24.2˚E which includes the territory of N. Macedonia and the surrounding regions. Thus, assessing the seismic hazard in North Macedonia requires considering contributions from neighbouring regions. In the compilation of the updated and the improved earthquake catalogue that will be used in the refined national seismogenic source model, priority was given to the national earthquake catalogue from the Seismological Observatory at the Faculty of the Natural Sciences and Mathematics (SORM). The latest edition of the national earthquake catalogue [5], still in publishing and updated this year, includes data for earthquakes whose epicentres are located within the territory of the Republic of North Macedonia and its neighbouring regions, extending up to a 100 km buffer from the national borders. This update covers only the instrumental period (1900-2020) while retaining the data for pre-instrumental events from the previous version of the catalogue.

Table 1. Relations between moment magnitude M_w and other earthquake size measures

Eq.	Mag	Catalogue	Relation	Reference
1	**M_{ms}**	national	$M_L = 0.96 * M_{ms} + 0.19$	[6] as referred in [7], eq. 3
2	**M_L**	national	$M_W = 0.9203 * M_L + 0.3989$	[8], as referred in [7], eq. 1
3	**MD**	ISC bulletin	$M_W = 1.472 * M_D - 1.49$	[9], eq. 13
4	**M_S**	ISC bulletin	$M_W = \exp(-0.044 + 0.227 * M_S) + 2.26$	[10], eq. 5
5	**mb**	ISC bulletin	$M_W = \exp(-1.401 + 0.227 * mb) + 2.28$	[10], eq. 6
6	**M_L**	EQs in Albania	$M_W = 1.22 + 0.813 * M_L$	[10], eq. 7
7	**M_L**	EQs in Serbia	$M_W = 0.7 + 0.858 * M_L$	[10], eq. 10
8	**M_L**	EQs in Kosovo	$M_W = 0.56 + 0.913 * M_L$	[10], eq. 11
9	**M_L**	EQs in Montenegro	$M_W = -0.01 + 1.028 * M_L$	[10], eq. 8

Copyright © 2025 CroCEE
DOI: https://doi.org/10.5592/CO/3CroCEE.2025.136

10	**M_L**	EQs in Bulgaria	$M_W = M_L + 0.43$	[11] as referred in [12], Table 2a, Table 2c
11	**M_L**	EQs in Greece	$M_W = M_L + 0.19$, (1969-2007)	[13]
12			$M_W = 0.964 * M_L + 0.147$, (2008-2016)	[14], Figure 7., Area 1

The national earthquake catalogue was then supplemented by events from the European Preinstrumental Earthquake Catalogue – EPICA [15] in the historical period (1000 to 1899) and by events from the reviewed ISC - International Seismological Centre bulletin event catalogue [1] and ISC GEM catalogue in the instrumental period (post 1900) [16] [17] [18] [19]. The renewal was mainly for the surrounding regions, specifically targeting areas of interest not included in SORM's national earthquake catalogue. The earthquake catalogue chronologically ranges from the year 1000 to 2020. The magnitude type for all events in the catalogue is the moment magnitude M_W, as it is the standard magnitude used in PSHA applications. Thus, for the events that were reported not in M_W, but in magnitudes of various types, different published relations were used for conversion to M_W (Table 1).

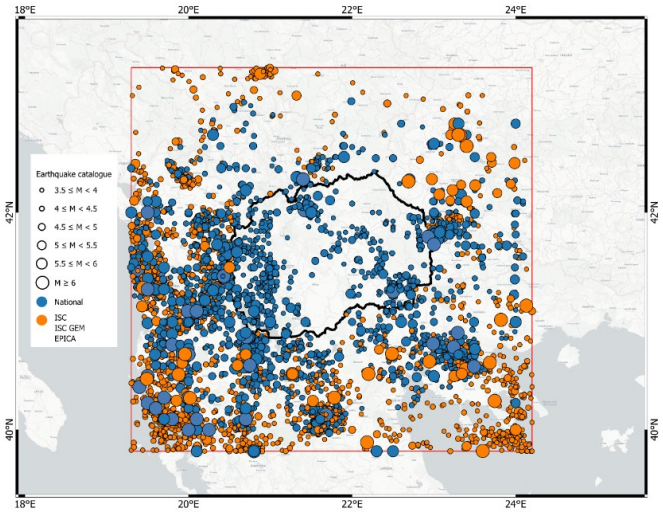


Figure 1. Distribution of historical and instrumental earthquakes observed in North Macedonia and the surrounding regions

The minimum threshold magnitude of the earthquake catalogue was set to 3.5 as a value typically detectable that provides useful data for seismic hazard analysis. While these events aren't usually destructive, they offer important insights into the local seismic activity, helping to improve the accuracy of hazard assessments. Including these smaller but frequent events also contributes to a more comprehensive understanding of long-term seismic risk in the region. The total number of events in the final version of the earthquake catalogue is 4993 (Fig 1).

Most recorded events are small to moderate earthquakes, with magnitudes around 4 being the most frequent (Fig. 2).

The dataset also includes some significant high-magnitude events, which although rare, are crucial and critical for seismic hazard analysis since they often release the most seismic energy and have the greatest potential for damage. The smooth distribution of magnitudes indicates a reliable dataset free from major gaps.

The depth distribution (Fig. 3) shows that most earthquakes occur at shallow depths, with 75% of events occurring at depths of 16 km or less. The average depth of 12.5 km is consistent with typical crustal seismic activity, while the maximum depth of 82.5 km indicates the presence of deeper tectonic activity, potentially fault systems reaching the lower crust. However, the number of events exceeding depths of 40-45 km remains relatively small. The overall shallow-depth concentration of the earthquakes reflects tectonic settings where crustal earthquakes dominate.

The dataset spans from the year 1000 to 2020 (Fig. 4, Fig. 5), with the earliest reported event dating back to 1153. Covering a period of 867 years, it provides a comprehensive historical record of seismic activity, including both instrumentally recorded and historically documented events. In the earlier years, particularly before the 20th century, the records mainly document significant, high-magnitude earthquakes due to the limited capabilities of observation and documentation at the time. During the

Copyright © 2025 CroCEE
DOI: https://doi.org/10.5592/CO/3CroCEE.2025.136

20th century, with advancements in seismic monitoring and record-keeping, the dataset expanded to include smaller and more frequent seismic events.

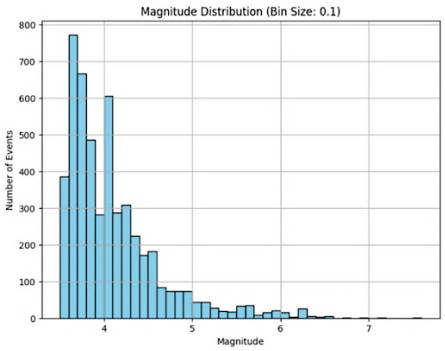


Figure 2. Magnitude distribution of the catalogue

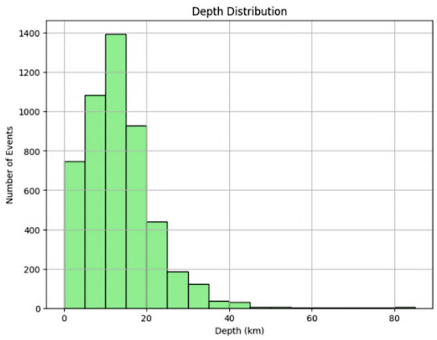


Figure 3. Depth distribution of the catalogue

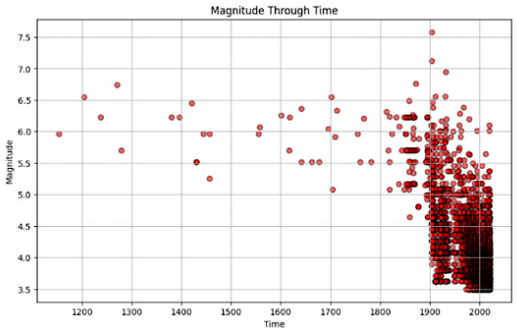


Figure 4. Magnitude-time plot

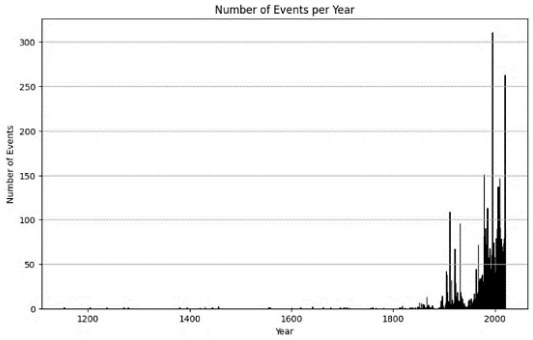


Figure 5. Number of events per year

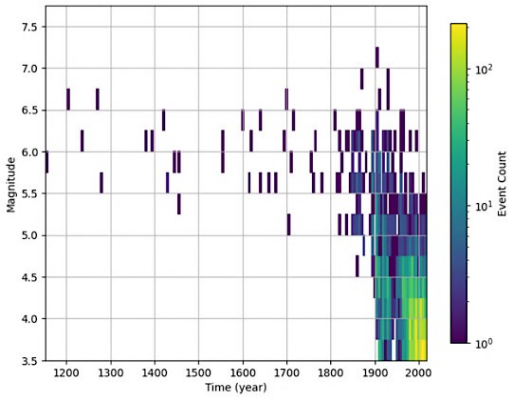


Figure 6. Magnitude - time density plot

This earthquake catalogue offers a comprehensive view of seismic activity over several centuries. The predominance of shallow depths and moderate magnitudes suggests that the data primarily represents crustal earthquakes. Clusters of events over specific time periods point to episodes of increased activity, that could provide insights into tectonic processes. This analysis underscores the importance of maintaining comprehensive and accurate earthquake catalogues for assessing seismic hazard and risk.

2.2. Catalogue completeness

For a catalogue to be considered complete, nearly all events above a certain magnitude threshold must be recorded [20]. One of the most fundamental issues faced in statistical analyses of any catalogue is estimating the intervals of catalogue completeness. It is evident that completeness levels vary over time. For the pre-instrumental era, catalogues only contain data on significant events of higher magnitudes. The shift of completeness levels toward lower magnitudes is driven by the development of

Copyright © 2025 CroCEE
DOI: https://doi.org/10.5592/CO/3CroCEE.2025.136

seismographs, their increased sensitivity, and the substantial and continuous increase in station network density throughout the 20th century [10].

The completeness of catalogues is determined to evaluate their spatial and temporal homogeneity. To obtain more reliable forecast parameters, complete catalogues are an essential requirement.

Identifying completeness thresholds and their temporal and spatial variations is a challenging and often controversial task, with no universal solution. In assessing completeness, the simplified approach proposed by [21] can be used, involving a visual inspection of the cumulative plot of the number of events as a function of time. This method appears to be highly efficient and accurate, even when applied to small datasets. If the most recent change in slope occurs when the data becomes complete for magnitudes above the reference magnitude [22], completeness intervals for different magnitude ranges are shown in Table 3.

The Stepp method [23] is also widely used approach for assessing the completeness of earthquake catalogues. This method is currently implemented in the current version of the Modeller's Toolkit in OpenQuake engine [24].

The Stepp method works by examining the average recurrence rate of earthquakes within predefined magnitude and time intervals. By analysing the standard deviation of the mean rate and its changes over time, the method can determine when the catalogue achieves completeness for specific magnitudes [24].

While the Stepp method is simple and robust, its effectiveness depends on careful selection of magnitude and time intervals, as well as thoughtful interpretation of results [24].

Catalogue completeness analysis was done by using the Stepp method but also the classical visual inspection of the cumulative plot of the number of events as a function of time. In Fig. 7 the completeness of the catalogue is shown in the magnitude-time density plot by the Stepp method.

Cumulative rates of magnitudes are evaluated within each of the magnitude intervals to determine completeness years.

Based on the analysis of the results obtained through both approaches, with priority given to visual inspection, the final decision defines the catalogue's completeness across seven intervals, i.e., the catalogue can be considered complete from the year 1978 for Mw ≥ 3.5, from the year 1963 for Mw ≥ 4.0, from the year 1952 for Mw ≥ 4.5, from the year 1891 for Mw ≥ 5.0, from the year 1846 for Mw ≥ 5.5, from the year 1560 for Mw ≥ 6.0, and from the year 1270 for Mw ≥ 6.5. The cumulative number of events versus year is shown in Fig. 8, while completeness years are given in Table 2. The completed earthquake catalogue contains 4180 events.

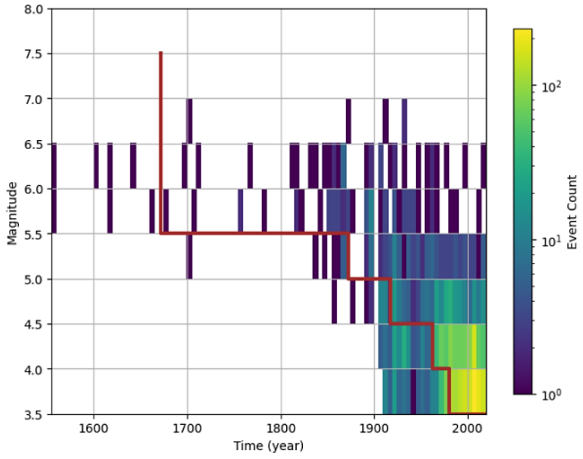


Figure 7. Completeness by Stepp method

Table 2. Completeness years for corresponding magnitude ranges

Magnitude range	Completeness year
$3.5 \leq M_W < 4$	1978
$4 \leq M_W < 4.5$	1963
$4.5 \leq M_W < 5$	1952
$5 \leq M_W < 5.5$	1891
$5.5 \leq M_W < 6$	1846
$5.5 \leq M_W < 6$	1560
$M_W \geq 6.5$	1270

Copyright © 2025 CroCEE
DOI: https://doi.org/10.5592/CO/3CroCEE.2025.136

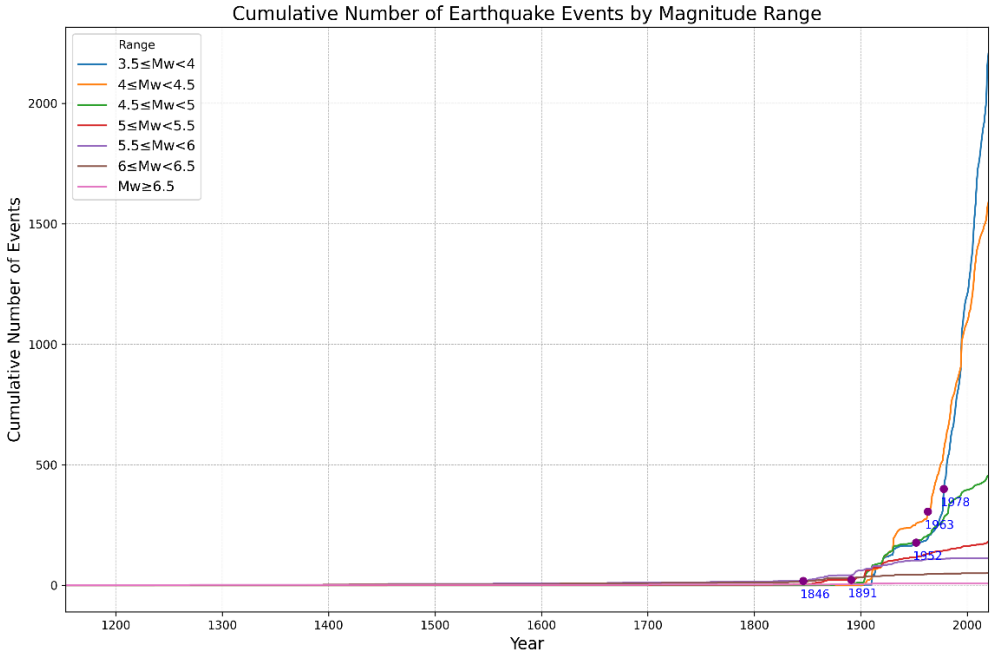


Figure 8. Cumulative number of events for different magnitude ranges – completeness analysis

2.3. Catalogue declustering

The analysis of seismic hazards often treats seismicity as a Poisson process where events are regarded as random, independent, and constant in rate over time [20]. Earthquake sequences, on the other hand, are not independent and typically include dependent events such as aftershocks and foreshocks, which are necessarily associated with a mainshock.

Declustering is the process of removing these dependent events (foreshocks and aftershocks) from seismic catalogues to estimate the long-term average rate of independent seismic events under the assumption of a homogeneous Poisson process [20].

There are numerous algorithms used as declustering techniques, based on different assumptions. One of the most used algorithms are the windowing techniques with space-time windows. These windowing methods function under the premise that all earthquakes in the catalogue from which they were established become aftershocks when certain timing and distance criteria are met in relation to any event [25]. Likewise, foreshocks are identified in this way, except when the largest earthquake happens after the sequence; in such cases, the foreshock is redefined as an aftershock. Hence, the time and space windows are modified according to the size of the maximum earthquake in the sequence [25].

Different adjustments to the time and distance windows have been proposed, as outlined by [26]. The original windows are formulated by Garner and Knopoff [27]. An alternative formulation is proposed by Grünthal (as reported in [26]) and by Uhrammer [28] (as reported in [26]). A sensitivity analysis is done using the three methods regarding the number of events for different magnitude ranges. The frequency-magnitude distribution plot of the main non declustered complete catalogue is shown in Fig.9.

The parameters such as total number of events and number of events for different magnitude ranges are summarized in Table 3. In summary, Uhrhammer's method is the most inclusive, Grünthal's approach is the most selective, and Gardner-Knopoff sits in between.

Copyright © 2025 CroCEE
DOI: https://doi.org/10.5592/CO/3CroCEE.2025.136

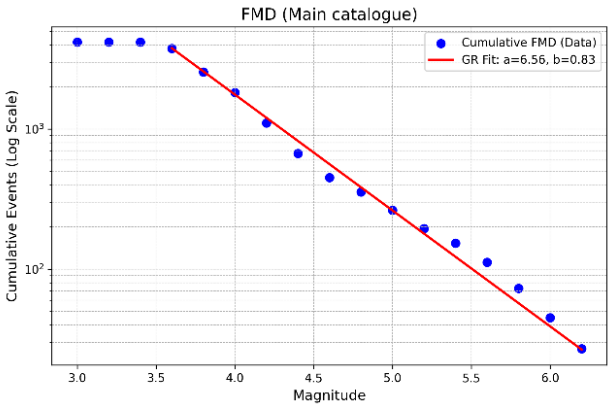


Figure 9. FMD of the non declustered complete catalogue

The Gardner-Knopoff [27] windowing method was chosen for declustering our earthquake catalogue.

It represents a credible windowing technique and the most widely applied windowing method. It classifies aftershocks using predefined time and distance thresholds that scale with the mainshock's magnitude. After applying the Gardner-Knopoff method, 1766 events remained out of 4180

Table 3. Parameters of the main non-declustered catalogue and the declustered catalogue

Parameter	Complete catalogue	Gardner-Knopoff	Grünthal	Uhrhammer
Total number of events	4180	1766	1224	2585
Events with M < 4	2279	839	513	1348
Events with 4 ≤ M < 5	1594	752	556	1040
Events with 5 ≤ M < 6	250	131	113	151
Events with M ≥ 6	57	44	42	46

3. Compilation of the fault database

3.1. Local tectonic setting in North Macedonia

As a result of the complex geotectonic evolution, several tectonic regimes have been altered [29] on the Balkan Peninsula, including the territory of the Republic of North Macedonia. The known cycles of differently oriented geodynamic movements of the South Balkan Extensional System [30], [31], [32], [33] have formed and modified the relief, mostly during the Neogene–Quaternary period.

The present relief on the territory of interest, the Republic of North Macedonia and the neighbouring regions up to 100 km from the state border, is defined as a complex mosaic of uplifting and sinking blocks, divided by edge, boundary faults [34]. Because of the different amplitude of the recent tectonic movement of the blocks, most of the neotectonic and many of the pre-neotectonic faults are active, stipulating less or more intense seismic activity.

Many faults have regional and deep character, longitudinal orientation and spread over the whole terrain, resulting in composite occurrence of earthquakes on both sides of the state border.

Merging all the mentioned, a new neotectonic map of neotectonic and reactivated pre-neotectonic faults located in North Macedonia and neighbouring areas was assembled [35], presenting a complex network of differently oriented and sized rupture structures (Fig. 10), considering the area of frequent and strong seismicity.

The updated neotectonic map consists of 152 faults – 116 on the territory of North Macedonia and 36 from the neighbouring regions added for of the effects of their activity in North Macedonia. Using this map, the tectonic causes of earthquakes can be fully explained.

Proceedings of the 3rd Croatian Conference on Earthquake Engineering - 3CroCEE
19–22 March 2025, Split, Croatia
Copyright © 2025 CroCEE
DOI: https://doi.org/10.5592/CO/3CroCEE.2025.136

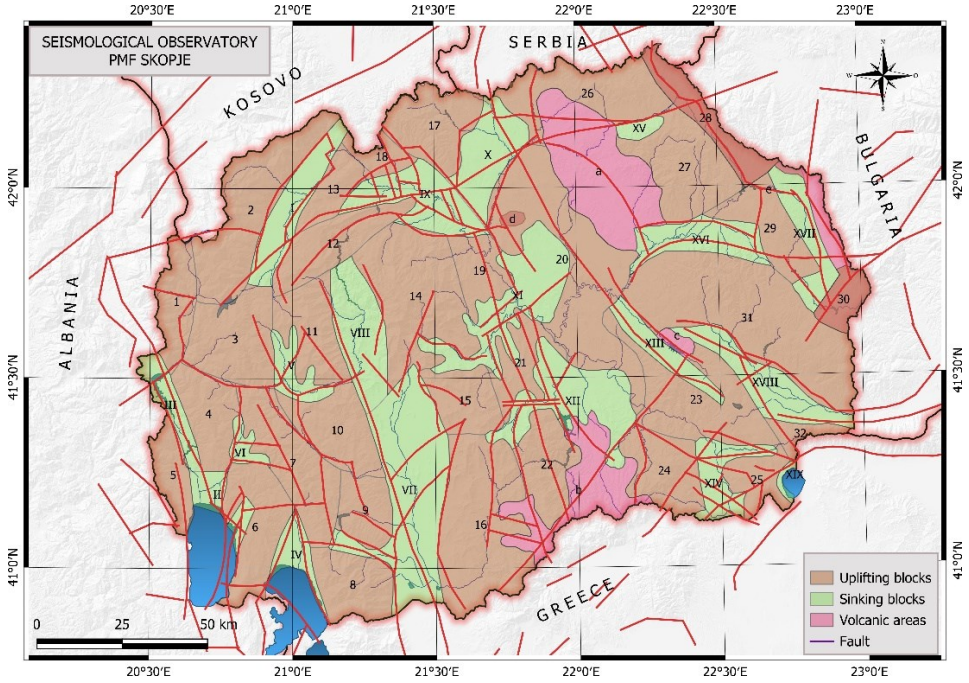


Figure 10. Neotectonic map of North Macedonia and neighbouring regions – block mosaic of the relief and orientation of the faults

3.2. Active faults in North Macedonia

The results of the tectonic characteristics of the territory of North Macedonia, presented in [36], of all defined faults in the tectonic map, distinguish 11 of them as barriers of seismicity in distinct parts of the country, called representative faults.

The representative faults are defined as faults along which the largest number of epicentres of earthquakes are distributed, for which the parameters of the accessible solutions of source mechanisms, determined by the method of the first longitudinal (P) displacements, correspond to spatial and geological characteristics of a given fault [36].

Thus, for the territory of North Macedonia, for the period 1960-2010, as representative faults were defined: Sharplanina, Elbasan-Debar, Galichki, Belchishki, Prespa, Pelister, Skopje-Kustendil, Lakavichki, Valandovo, Kozhuf and Dojransko-Gevgeliski fault, shown in Fig. 11.

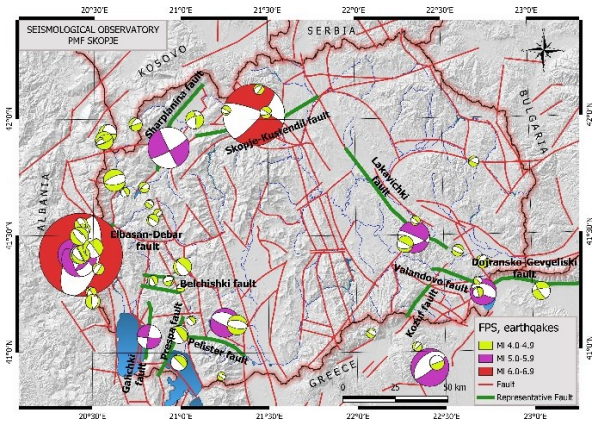


Figure 11. Tectonic map of the representative faults in North Macedonia and the available data for focal mechanisms for the period 1960-2010

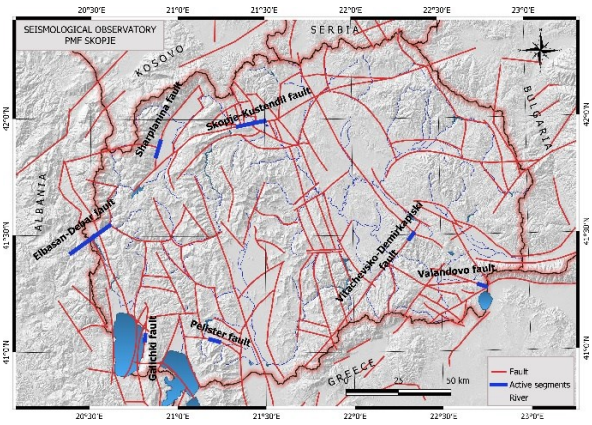


Figure 12. Map of the named active faults and their most active segments (blue lines) in North Macedonia for the period 1960-2010

Proceedings of the 3rd Croatian Conference on Earthquake Engineering - 3CroCEE
19–22 March 2025, Split, Croatia
Copyright © 2025 CroCEE
DOI: https://doi.org/10.5592/CO/3CroCEE.2025.136

For the necessities of seismic hazard assessment and further detailed seismological research, an additional database of active faults is compiled. An active fault is generally defined as a fault that is expected to cause destructive earthquakes (Mw ≥ 5.0). A fault commonly is considered as active if there has been movement observed in the considered period.

Applying these criteria, 6 out of the 11 representative faults can be classified as active. Namely, Sharplanina, Elbasan-Debar, Galichki, Pelister, Skopje-Kustendil and Dojransko-Gevgeliski fault meet the criteria. Additionally, the seismological data that meet the defined criteria permit the Vitachevsko-Demirkapiski fault to be added as an active fault.

Applying the parameters of the focal plane solutions (Fig. 11) and relations for the geometry of the source given in [36], parametrization of the active segments of the faults was obtained.

3.3. Parametrization of the active faults

Combining all the available neotectonic, geodynamic and seismological data, for the first time in the seismological research in North Macedonia, robust parametrization of the defined active faults was made. It is called robust because of the lack of available seismological data for the considered period (1960-2010). However, to determine geometric parameters (strike, dip, slip, length, area, observed M_{max}) of the fault, firstly, the focal mechanism of earthquakes with $M_W \geq 5.0$ were analysed to determine if the source belongs to the same fault. A lower limit of $M_W \geq 5.5$ as worldwide accepted value for active fault definition was defined because of the significance of the soil classification with a high sensitivity at the most vicinities of the active faults. The main criterion of correctness was the acceptable mathematical difference in the values of the segment plane parameters. Confirmation of the results was made with the spatial distribution of the epicentres of the weaker earthquakes. The rest of the parameters of the corresponding segment were determined using the previously defined formulas and relations [36].

Table 4 shows the parameters for the two active faults out of seven, with specific examples The map in Fig. 12 illustrates the spatial distribution of the most active fault segments within the faults.

Table 4. Fault parametrization example (Vitachevo - Demirkapiski fault, Valandovo fault)

Fault Name	**Vitachevo - Demirkapiski**	**Valandovo**
Fault type	Sinistral normal strike-slip	Sinistral normal strike-slip
Max depth	22 km	17 km
Strike [min/max]	24/39	116/133
Dip [min/max]	33/38	69/89
Rake [min/max]	-165/-175	-79/-81
Total fault length [along trace] (km)	77	23.6
Fault width [km]	7.41	11.61
Area (km^2)	68.71	230.14
Slip rate [mm/y]	<1	<1
M_{WMAX}	5.74[37]	6.38[37]
Activity	Active	Active

4. Conclusions

The present study underlines the developments and the updates of the national earthquake and fault databases which are essential in improving and enhancing the seismic hazard model of North Macedonia.

The updated earthquake catalogue includes data from the national Seismological Observatory, the International Seismological Centre (ISC) and regional catalogues. It reports a total number of 4993 events in the time span from 1000-2000 by including historical and instrumental seismicity. Since for use in PSHA applications, all earthquakes are described by moment magnitude M_W, unification of

Copyright © 2025 CroCEE
DOI: https://doi.org/10.5592/CO/3CroCEE.2025.136

moment magnitude was established by different magnitude conversions. Most of the events are small to moderate and occurring at shallow depths.

The completeness analysis demonstrated that the catalogue is reliable with completeness years differing for different magnitude intervals. The complete earthquake catalogue has 4180 events. By doing the completeness we evaluate the spatial and temporal homogeneity of the seismic activity.

For declustering our earthquake catalogue, we selected the Gardner and Knopoff [27] windowing method. This approach is widely recognized and commonly used, as it assumes that any event occurring within a defined time and spatial window of a stronger event is likely dependent on it. The size of these windows is adjusted based on the magnitude of the largest earthquake in the sequence. The method strikes a balance between conservative and non-conservative approaches, making it suitable for standard aftershock removal using well-calibrated time-distance windows. After applying this method, the catalogue was reduced from 4180 events to 1766.

The study also included the update of the fault database with focus on the active faults in North Macedonia and the surrounding regions. A total of 152 faults were mapped. 116 of them on the territory of North Macedonia. Out of 11 representative faults, 6 of them were identified as active based on the focal mechanism analysis and the seismic active criteria. The seismological data satisfying the established criteria allowed also for the inclusion of the Vitachevsko-Demirkapiski fault as an active fault. For the first time, robust parametrization of fault geometries, such as strike, dip, slip rate, and maximum depth, was achieved. Even though as a result of this research parametrization of the active faults for the period 1960-2010 was made, further research is needed. Namely, the detailed seismological observations and analyses brought us valuable information that most faults have block structures and do not have unified fault planes and orientations even if the strike of the fault line has the same orientation. Knowing this, additional research is needed to define the different block parameters of the same faults. However, at this stage, the presented robust results for defining and parameterizing the active faults in North Macedonia provide a good foundation for the seismic hazard assessment.

The work in this study, allow us to refine the seismogenic source model which directly affects the accuracy and the reliability of the national seismic hazard assessment, thereby contributing to the development of national annexes.

References

[1] International Seismological Centre (20XX), On-line Bulletin, https://doi.org/10.31905/D808B830

[2] Michele Caputo, Comparison of five independent catalogues of earthquakes of a seismic region, Geophysical Journal International, Volume 143, Issue 2, November 2000, Pages 417–426, https://doi.org/10.1046/j.1365-246X.2000.01235.x

[3] Lenhardt, W., Svancara, J., Melichar, P., Pazdirkova, J., Havir, J. and Sykorova, Y. (2007). “Seismic activity of the Alpine-Carpathian-Bohemian massif region with regard to geological and potential field data”. Geologica Carpathica, 58, 397-412

[4] Grünthal, G. and GSHAP Region 3 Working Group (1999). “Seismic hazard assessment for central, north and northwest Europe: GSHAP Region 3”. Annali di Geofisicia 42, 999-1011

[5] Catalogue of earthquakes, Seismological Observatory, Faculty of Natural Sciences and Mathematics, Ss. Cyril and Methodius University, Skopje, 2024 (in publishing)

[6] Jordanovski, Lj., Pekevski, L., Chejkovska, V., Chernih, D., Hristovski, B., and N. Vasilevski, 1998, Fundamental Characteristics of the Seismicity of the Territory of the Republic of Macedonia, Skopje, "Ss. Cyril and Methodius" University, Faculty of Natural Sciences and Mathematics, Seismological Observatory. (292 pages with maps and tables; ISBN 9989-631-01-8.) (in Macedonian)

[7] Čejkovska, V., et al. (2016) Report under the project of the Institute for Standardization of the Republic of Macedonia titled 'National Annexes for the Eurocodes'. Skopje: Institute for Standardization of the Republic of Macedonia (in Macedonian)

Copyright © 2025 CroCEE
DOI: https://doi.org/10.5592/CO/3CroCEE.2025.136

[8] Čejkovska, V., 2006-2007: Empirical relations of seismic moment and earthquake moment magnitude to earthquake local magnitude for the Vardar and West Macedonia seismic zones, Contributions, Sec. Math. Tech. Sci., MANU, XXVII-XXVIII, 1-2, pp.93-115 (in Macedonian)

[9] Grünthal, G. and Wahlström, R. (2012) 'The European-Mediterranean Earthquake Catalogue (EMEC) for the last millennium', Journal of Seismology, 16(4), pp. 535–570. doi: 10.1007/s10950-012-9302-y

[10] Markušić, S., Gülerce, Z., Kuka, N., Duni, L., Ivančić, I., Radovanović, S., Glavatović, B., Milutinović, Z., Akkar, S., Kovačević, S., Mihaljević, J., and Šalić, R. (2016) 'An updated and unified earthquake catalogue for the Western Balkan Region', Bulletin of Earthquake Engineering, 14(1), pp. 321–343. doi: 10.1007/s10518-015-9833-z

[11] Baba, A. B., Papadimitiou, E., Papazachos, B. C., Papaioannou, C. A., and Karakostas, B. G.: Unified local magnitude scale for earthquakes of south Balkan area, Pure Appl. Geophys., 157, 765–783, 2000

[12] Bayliss, T. J. and Burton, P. W. (2007) 'A new earthquake catalogue for Bulgaria and the conterminous Balkan high hazard region', Natural Hazards and Earth System Sciences, 7(3), pp. 345–359. doi: 10.5194/nhess-7-345-2007

[13] Roumelioti, Z., Kiratzi, A., and Benetatos, C. (2009) 'The instability of the Mw and ML comparison for earthquakes in Greece for the period 1969 to 2007', Journal of Seismology, 14(2), pp. 309–337. doi: 10.1007/s10950-009-9167-x

[14] Konstantinou, K. I. and Melis, N. S. (2017) 'The relationship between local and moment magnitude in Greece during the period 2008–2016', Pure and Applied Geophysics, 175(4), pp. 851–871. doi: 10.1007/s00024-017-1750-4

[15] Rovida A., Antonucci A., Locati M. (2022). The European Preinstrumental Earthquake Catalogue EPICA, the 1000–1899 catalogue for the European Seismic Hazard Model 2020. Earth System Science Data. https://doi.org/10.5194/essd-14-5213-2022

[16] International Seismological Centre (20XX), ISC-GEM Earthquake Catalogue, https://doi.org/10.31905/d808b825

[17] Storchak, D.A., D. Di Giacomo, I. Bondár, E.R. Engdahl, J. Harris, W.H.K. Lee, A. Villaseñor and P. Bormann (2013). Public Release of the ISC-GEM Global Instrumental Earthquake Catalogue (1900-2009). Seism. Res. Lett., 84, 5, 810-815, doi: 10.1785/0220130034

[18] Storchak, D.A., D. Di Giacomo, E.R. Engdahl, J. Harris, I. Bondár, W.H.K. Lee, P. Bormann and A. Villaseñor (2015). The ISC-GEM Global Instrumental Earthquake Catalogue (1900-2009): Introduction, Phys. Earth Planet. Int., 239, 48-63, doi: 10.1016/j.pepi.2014.06.009

[19] Di Giacomo, D., E.R. Engdahl and D.A. Storchak (2018). The ISC-GEM Earthquake Catalogue (1904–2014): status after the Extension Project, Earth Syst. Sci. Data, 10, 1877-1899, doi: 10.5194/essd-10-1877-2018

[20] Baker, J.W., Bradley, B.A. and Stafford, P.J., 2021. Seismic Hazard and Risk Analysis. Cambridge: Cambridge University Press. DOI: 10.1017/9781108425056

[21] Mulargia F, Gasperini P, Tinti S (1987) Contour mapping of Italian seismicity. Tectonophysics 142:203–216

[22] Gasperini, P. and Ferrari, G. (2000). "Deriving numerical estimates from descriptive information: the computation of earthquake parameters". In Catalogue of Strong Italian Earthquakes from 461 B.C. to 1997, Annali di Geofisica, Vol. 43, N.4, 729-746

[23] Stepp, J. C. (1971). "An investigation of earthquake risk in the Puget Sound area by the use of the type I distribution of largest extreme". PhD thesis. Pennsylvania State University (cited on pages 9, 25–27)

[24] Weatherill, G. A. (2014) OpenQuake Hazard Modeller's Toolkit- User Guide. Global Earthquake Model (GEM). Technical Report

[25] Danciu L., Nandan S., Reyes C., Basili R., Weatherill G., Beauval C., Rovida A., Vilanova S., Sesetyan K., Bard P-Y., Cotton F., Wiemer S., Giardini D. (2021) - The 2020 update of the European Seismic Hazard Model: Model Overview. EFEHR Technical Report 001, v1.0.0, https://doi.org/10.12686/a15

[26] Stiphout, T. van, J. Zhuang, and D. Marsan (2012). Theme V-Models and Techniques for Analysing Seismicity. Technical report. Community Online Resource for Statistical Seismicity Analysis. URL: http://www.corssa.org (cited on page 22)

Copyright © 2025 CroCEE
DOI: https://doi.org/10.5592/CO/3CroCEE.2025.136

[27] Gardner, J. K. and L. Knopoff (1974). "Is the sequence of earthquakes in Southern California, with aftershocks removed, Poissonian?" In: Bulletin of the Seismological Society of America 64.5, pages 1363–1367 (cited on pages 9, 22–24)

[28] Uhrhammer, R. (1986). "Characteristics of Northern and Central California Seismicity". In: Earthquake Notes 57.1, page 21 (cited on pages 22, 23)

[29] Dumurdzanov N., Serafimovski T., Burchfiel B. C., Evolution of the Neogene–Pleistocene Basins of Macedonia, Geological Society of America Digital Map and Chart Series 1 (accompanying notes), 2004

[30] Dumurdzanov N., Serafimovski T., Burchfiel B. C., Cenozoic tectonics of Macedonia and its relation to the South Balkan extensional regime, Geosphere, v.1 n.1, 2005

[31] Matev K., GPS constrains on current tectonics of southwest Bulgaria, northern Greece, and Albania, PhD thesis, Universite de Grenoble, 2006

[32] Burchfiel B. C., Nakov R., Dumurdzanov N., Papanikolaou D., Tzankov T., Serafimovski T., King R. W., Kotzev V., Todosov A., Nurce B., Evolution and dynamics of the Cenozoic tectonics of the Southern Balkan extensional system, Geosphere, v. 4 n. 6, pp. 919–938, 2008

[33] N D'Agostino, A Copley, J Jackson, R Koçi, A Hajrullai, L Duni, N Kuka, Active tectonics and fault evolution in the Western Balkans, *Geophysical Journal International*, Volume 231, Issue 3, December 2022, Pages 2102–2126, https://doi.org/10.1093/gji/ggac316

[34] Arsovski M., Hadzievski D., Correlation between neotectonics and the seismicity of Macedonia, Tectonophysics, vol. 9, pp. 129-142, 1970

[35] Jovanov Lj., Contemporary tectonic and seismic characteristics of the territory of the republic of North Macedonia and neighboring regions, MSc. Thesis, Faculty of Natural Sciences and Mathematics, Ss. Cyril and Methodius University, Skopje, 2024 (in Macedonian)

[36] Drogreshka K., Use of the dislocation theory in defining the epicentral areas and tectonic conditions in the territory of the Republic of Macedonia, Skopje, 2018 (in Macedonian)

[37] Petkovski R., Seismotectonic characteristics of Macedonia, Phd. Thesis, Faculty of Mining and Geology, University of Belgrade, Belgrade, 1992 (in Serbo-Macedonian)

Proceedings of the 3rd Croatian Conference on Earthquake Engineering - 3CroCEE
19–22 March 2025, Split, Croatia
Copyright © 2025 CroCEE
DOI: https://doi.org/10.5592/CO/3CroCEE.2025.158

PARAMETRIZATION OF SYNTHETIC NEAR-FAULT SEISMIC WAVEFIELDS FOR THE SOUTHWEST ICELAND TRANSFORM ZONE

Farnaz Bayat[(1)], Milad Kowsari[(2,1)], Benedikt Halldórsson[(2,1)]

[(1)] *Faculty of Civil and Environmental Engineering, School of Engineering and Natural Sciences, University of Iceland, Reykjavík, Iceland, fab14@hi.is; milad@hi.is; skykkur@hi.is;*

[(2)] *Volcanic activity, earthquakes and deformation dept., Service, and research Division, Icelandic Meteorological Office, Iceland, Reykjavík, Iceland, milad@vedur.is; benedikt@vedur.is;*

Keywords: Directivity effect, CyberShake, kinematic fault rupture modeling, near-fault GMMs

Iceland is one of the northern European countries with the highest seismic activity. The strongest earthquakes take place on two large transform faults, one of which is the densely populated South Iceland Seismic Zone (SISZ), characterized by its unique North-South aligned bookshelf dextral strike-slip faults that are responsible for the long-term release of tectonic strain across the zone. The bookshelf fault system has been shown to be continuous towards West, all along the Reykjanes Peninsula Oblique Rift (RPOR) [1], bringing the Capital region of Reykjavík, in greater proximity to the bookshelf faults. It is well known both from the observations and the physics-based modeling of earthquake rupture and near-fault ground motion simulations, that the most damaging part of near-fault seismic motion is the large-amplitude, long-period velocity pulses found in the forward direction of fault rupture due to the directivity effect. With relatively large North-South striking faults now being mapped directly South of the evermore expanding Capital region, this becomes a cause for great concern. In particular since such effects have not been taken into account in any probabilistic seismic hazard assessment (PSHA) nor incorporated into any modern building standards such as Eurocode 8.

The recorded near-fault data in Iceland, however, is relatively sparse, making it difficult to accurately capture the physical characteristics of near-fault ground motions. Fortunately, the key elements of physics-based ground motion simulation have recently been developed in Southern Iceland, one of which is the 3D finite-fault system model of the bookshelf strike-slip faults in the SISZ-RPOR [2]. The model accounts for the systematic changes in how large the earthquakes can become along the zone by subdividing it into six distinct subzones, with the largest earthquakes (~M_w7) taking place in the Eastern SISZ and the smallest (~M_w5.5) in the Western RPOR, respectively. The fault system allows for both deterministic and random fault locations, and each fault is completely specified in terms of its maximum magnitude, its dimensions, and its long-term slip rate. The new model allows the derivation of the time-independent magnitude-frequency distribution (MFDs) for each subzone and explains the historical earthquake catalogue, thus validating the physics-based fault system model [3]. Kowsari et al [4] extended the 3D model and applied the MFDs in each subzone to generate different sets of physics-based finite-fault synthetic earthquake catalogues. One realization of such catalogue (500-yr long) has been incorporated into CyberShake [5], a high-performance computational platform developed by the Southern California Earthquake Center (SCEC) and the foundation of physics-based seismic hazard models [6]. Variations in the kinematic rupture properties of each fault result in the vast synthetic dataset of low-frequency two-component horizontal velocity time histories that sample the near-fault wavefield variations over a uniform spatial grid of hypothetical stations in Southwest Iceland.

In this study, we parametrize the synthetic waveforms and retrieve information about the source geometries and the kinematic rupture features into a single flat-file. The flat-file includes various intensity measures (e.g., the amplitude of pseudo spectral acceleration, *PSA* at different oscillatory periods) that are retrieved from the processing of velocity time histories in each station. The flat-file thus provides a uniformly processed and high-quality synthetic dataset, enabling the calibration of new scaling laws and predictive models, such as the empirical near-fault term to the ground motion models

Copyright © 2025 CroCEE
DOI: https://doi.org/10.5592/CO/3CroCEE.2025.158

(GMMs). Figure 1 (a) illustrates the spatial distribution of the rotational invariant for two as-recorded horizontal components of the *PSA* at $T = 2$ s for two fault rupture variations, unilateral and bilateral of $M_w 7$. From the figure, it is evident that the unilateral ruptures exhibit positive directivity at the northern end of the fault, along with an increased amplitude of the PSA, similar to the bilateral scenarios at both ends of the strike-slip fault. In summary, this study significantly augments our comprehension of the near-fault seismic wavefield and its correlation with key independent variables of the seismic source model. This advancement facilitates the development of a near-fault GMM, crucial for implementing efficient and physics-based near-fault PSHA in the SISZ-RPOR.

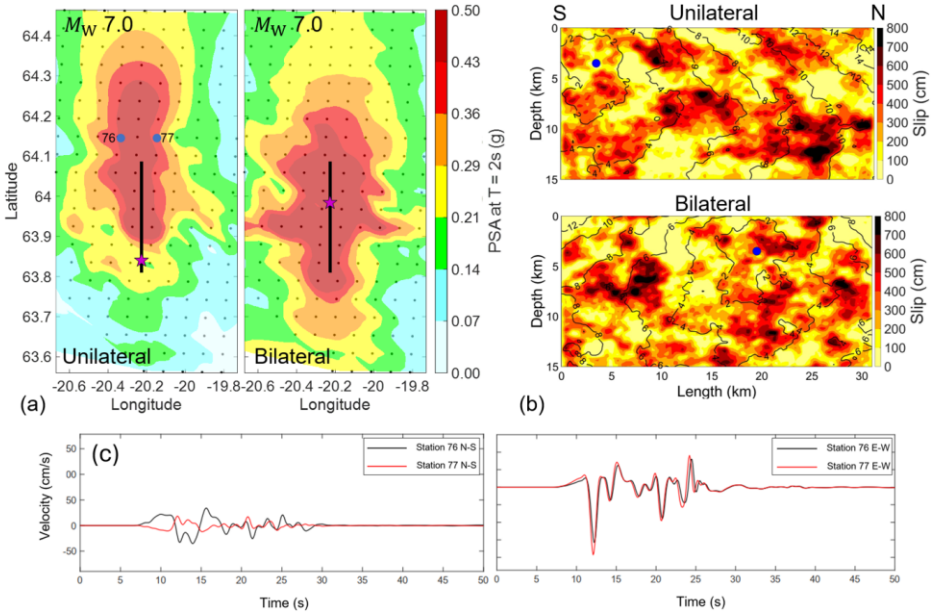


Figure 1. (a) Spatial distribution of rotational invariant *PSA* at $T = 2$ s for a $M_w 7$ earthquake with varying hypocentral locations (b) The slip distribution on the fault plane along with the contours of rupture time. (c) Comparison of two horizontal-component velocity time histories (cm/s) of two stations in blue circles.

Acknowledgements

This study was funded by the "seismic hazard and risk for Reykjanes" project from Icelandic Meteorological Office (No. 3721-0-0019), the Project Grant (No. 196089, SENSHAZ) and the Doctoral Grant (No. 239376) of the Icelandic Research Fund of the Icelandic Centre for Research (RANNIS), the Landsvirkjun Energy Research Fund (No. NÝR-06-2024 and NÝR-28-2024), and the Icelandic Road and Coastal Administration Research Fund (No. 1800-1032).

References

[1] Einarsson P. Mechanisms of Earthquakes in Iceland. In: Beer M, Kougioumtzoglou IA, Patelli E, Au IS-K, editors. Encyclopedia of Earthquake Engineering, Berlin, Heidelberg: Springer Berlin Heidelberg; 2014, p. 1–15. https://doi.org/10.1007/978-3-642-36197-5_298-1.

[2] Bayat F, Kowsari M, Halldorsson B. A new 3-D finite-fault model of the Southwest Iceland bookshelf transform zone. Geophysical Journal International 2022;231:1618–33. https://doi.org/10.1093/gji/ggac272.

[3] Bayat F, Kowsari M, Halldorsson. A simplified seismicity model of the bookshelf fault system of the Southwest Iceland transform zone. Bulletin of Earthquake Engineering 2024.

[4] Kowsari M, Halldorsson B, Bayat F. Preparation of Finite-fault Earthquake Catalogues Enabling Physics-based PSHA in Southwest Iceland. Proceedings of the 3rd European Conference on Earthquake and Engineering Seismology (3ECEES), Bucharest, Romania: 2022, p. 3863-3870 (No. 8441).

[5] Rojas O, Monterrubio-Velasco M, Rodriguez JE, Callaghan S, Abril C, Halldorson B, et al. Earthquake Fault Rupture Modeling and Ground Motion Simulations for the Southwest Iceland Transform Zone using CyberShake. Bulletin of the Seismological Society of America 2024:(in press).

[6] Graves R, Jordan TH, Callaghan S, Deelman E, Field E, Juve G, et al. CyberShake: A physics-based seismic hazard model for southern California. Pure and Applied Geophysics 2011;168:367–81.

Proceedings of the 3rd Croatian Conference on Earthquake Engineering - 3CroCEE
19–22 March 2025, Split, Croatia
Copyright © 2025 CroCEE
DOI: https://doi.org/10.5592/CO/3CroCEE.2025.159

INVESTIGATING TIME-DEPENDENT EARTHQUAKE CLUSTERING IN SHORT-TERM RISK ANALYSIS

Atefe Darzi [1], Benedikt Halldorsson [2, 3], Mojtaba Moosapoor [4]

[1] *Research Specialist, Earthquake Engineering Research Centre, School of Engineering and Natural Sciences, University of Iceland, atefe@hi.is*
[2] *Coordinator of seismic hazard, Service and Research Division, Icelandic Met Office, benedikt@vedur.is*
[3] *Research Professor, School of Engineering and Natural Sciences, University of Iceland, skykkur@hi.is*
[4] *School of Engineering and Natural Sciences, University of Iceland, mom12@hi.is*

Keywords: *time-dependent, ETAS, Aftershock forecast, seismic risk assessment, earthquake clustering, short-term seismic hazard, earthquake sequence,*

1. Abstract

The understanding of earthquake occurrence patterns and their implications for short-term increases in seismic hazard and risk is crucial during ongoing seismic crises. This understanding enables informed decision-making by civil protection and governmental agencies. Aftershocks exacerbate seismic hazards by striking already weakened structures and generating strong ground motions, which sometimes surpass the mainshock effects due to their proximity to exposed assets [1–4]. Recent earthquake sequences, e.g., 2010-2011 Canterbury earthquakes (M_w7.1-6.2) in New Zealand, the 2019 Ridgecrest sequence (M_w6.4-7.1) in the US, and the 2023 Turkey earthquakes (M_w7.8-7.5), highlight the significant role of aftershocks in amplifying losses [5,6]. For example, during the Canterbury sequence, several large aftershocks caused greater ground shaking in urban centers than the mainshock, intensifying losses. Thus, for enhancing post-event planning and emergency responses, shifting from time-invariant to time-variant seismic risk estimates is critical. For this, first and foremost, the forecasting capability of time-dependent short-term seismicity clustering models are assessed via retrospective experiments to ensure the model's reliability in estimating the upcoming aftershock sequences in space and time.

The South Iceland Seismic Zone, a prominent transform zone in southwest Iceland, is prone to strong strike-slip earthquakes followed by intense aftershock sequences. The 2008 Ölfus earthquake (M_w 6.3) was the most recent and costliest event in Iceland, triggering substantial aftershock activity. The Hveragerði town, located near the earthquake's epicenter, experienced significant damage to buildings. Elevated hazard levels persisted for days after the mainshock, posing additional challenges for the affected community [7,8].

Our study develops a framework for time-dependent short-term seismic risk assessment for Hveragerði following the 2008 Ölfus earthquake. The short-term probabilistic hazard framework integrates seismicity forecasts from the Bayesian spatiotemporal epidemic-type aftershock sequence (ETAS) model with Iceland-specific hybrid ground motion models (GMMs) [9]. The ETAS model is well-suited for simulating space-time clustering of earthquakes- quantifying triggering rates, spatial distribution, and temporal decay of aftershocks. To investigate elevated seismicity, stochastic simulations of earthquake catalogs are performed corresponding to a set of sampled posteriors of main ETAS parameters. These spatiotemporal forecasts, which account for uncertainty, are compared with actual recorded events exceeding a specified magnitude threshold during the ongoing active sequence.

Bayesian parameter estimation is applied to quantify the uncertainty in the main ETAS model parameters and incorporate them in the resulting forecasts and consequently in the timed-dependent hazard and risk estimates. To do this, we used informative priors obtained from the last intense sequence of June 2000 sequence, enabling improved model calibration [10–12]. By employing an adaptive prior estimation technique, ETAS parameters are continuously updated throughout the sequence as new data

Copyright © 2025 CroCEE
DOI: https://doi.org/10.5592/CO/3CroCEE.2025.159

become available, enhancing forecast reliability during an active seismic sequence. To estimate short-term time-dependent seismic hazard, we calculate the daily probability of exceeding specified PGA thresholds using two Iceland-specific GMMs: a GMM with simplified site term [13] and a detailed geological site term [14]. The results show a sharp increase in PGA exceedance rates early in the sequence. Rea23 predicted higher PGA values than KSea20, emphasizing the importance of considering local site effects, especially in basaltic lava regions.

A detailed building-by-building seismic risk assessment, using high-resolution exposure data for Hveragerði, is conducted to inform post-earthquake decision-making, particularly in small towns with significant exposure near active fault zones. The assessment incorporates uncertainties in building vulnerability models using empirical Bayesian vulnerability models developed for Iceland [15,16]. Building typologies are identified by material, height, and ductility levels following Icelandic design standards. For each building typology, mean damage ratios are estimated, accounting for uncertainties in ETAS-based seismicity forecasts, ground shaking predictions, and vulnerability model parameters. Our findings indicate that buildings with low ductility levels and masonry structures exhibited the highest risk. Masonry buildings, which have historically shown poor resistance to earthquakes, are no longer used in Icelandic construction practices to improve resilience against damaging ground motions. The study highlights the importance of explicitly modeling aftershock clustering and integrating time-dependent seismic hazard and risk assessments for regions with high exposure and vulnerable infrastructure.

Acknowledgments

This study was funded by the RANNIS Icelandic Research Fund (No. 228782-051, GEOSITEFF2HAZ, No. 218255, OEFICE, and No. 218149, SERICE), and the H2020 TURNkey project (No. 821046).

References

[1] Iervolino, I., Chioccarelli, E., Giorgio, M., et al. (2015). Operational (Short-Term) Earthquake Loss Forecasting in Italy. Bull. Seismol. Soc. Am. 105, 2286–2298. https://doi.org/10.1785/0120140344

[2] Papadopoulos, A.N., Bazzurro, P, Marzocchi, W (2021) Exploring seismic risk assessment accounting for seismicity clustering and damage accumulation: Part I. Hazard analysis. Earthq. Spectra 37, 803–826

[1] Jalayer F, Ebrahimian H. MCMC-based Updating of an Epidemiological Temporal Aftershock Forecasting Model. Vulnerability Uncertain. Risk, Liverpool, UK: American Society of Civil Engineers; 2014, p. 2093–103. https://doi.org/10.1061/9780784413609.210.

[2] Iervolino I, Chioccarelli E, Giorgio M, Marzocchi W, Zuccaro G, Dolce M, et al. Operational (Short-Term) Earthquake Loss Forecasting in Italy. Bull Seismol Soc Am 2015;105:2286–98. https://doi.org/10.1785/0120140344.

[3] Papadopoulos AN, Bazzurro P, Marzocchi W. Exploring probabilistic seismic risk assessment accounting for seismicity clustering and damage accumulation: Part I. Hazard analysis. Earthq Spectra 2021;37:803–26. https://doi.org/10.1177/8755293020957338.

[4] Wang S, Werner MJ, Yu R. How Well Does Poissonian Probabilistic Seismic Hazard Assessment (PSHA) Approximate the Simulated Hazard of Epidemic-Type Earthquake Sequences? 2022;112.

[5] Cattania C, Werner MJ, Marzocchi W, Hainzl S, Rhoades D, Gerstenberger M, et al. The Forecasting Skill of Physics-Based Seismicity Models during the 2010–2012 Canterbury, New Zealand, Earthquake Sequence. Seismol Res Lett 2018;89:1238–50. https://doi.org/10.1785/0220180033.

[6] Bayona JA, Savran WH, Rhoades DA, Werner MJ. Prospective evaluation of multiplicative hybrid earthquake forecasting models in California. Geophys J Int 2022;229:1736–53. https://doi.org/10.1093/gji/ggac018.

[7] Halldorsson B, Gibbons SJ, Sigbjörnsson R. Analysis of the 29 May 2008 Ölfus earthquake and aftershock sequence using three-component array processing on ICEARRAY. Bull Earthq Eng 2012:(manuscript in preparation).

[8] Darzi A, Bessason B, Halldorsson B, Molina S, Kharazian A, Moosapoor M. High spatial-resolution loss estimation using dense array strong-motion near-fault records. Case study for Hveragerði and the M w 6.3 Ölfus earthquake, South Iceland. Int J Disaster Risk Reduct 2022;73:102894. https://doi.org/10.1016/j.ijdrr.2022.102894.

Copyright © 2025 CroCEE
DOI: https://doi.org/10.5592/CO/3CroCEE.2025.159

[9] Darzi A, Halldorsson B, Cotton F, Hrafnkelsson B. Feasibility of short-term seismic hazard forecasting for aftershock sequences in Southwest Iceland. 18th World Conf. Earthq. Eng. 18WCEE, 30 June to 5 July, Milan, Italy: 2024.

[10] Ebrahimian H, Jalayer F. Robust seismicity forecasting based on Bayesian parameter estimation for epidemiological spatio-temporal aftershock clustering models. Sci Rep 2017;7:9803. https://doi.org/10.1038/s41598-017-09962-z.

[11] Darzi A, Halldorsson B, Hrafnkelsson B, Vogfjörð KS. Short-term Bayesian ETAS spatiotemporal forecasting of the Ölfus 2008 earthquake sequence in Iceland. Tectonophysics 2022;839:229522. https://doi.org/10.1016/j.tecto.2022.229522.

[12] Darzi A, Halldorsson B, Hrafnkelsson B, Ebrahimian H, Jalayer F, Vogfjörð KS. Calibration of a Bayesian spatio-temporal ETAS model to the June 2000 South Iceland seismic sequence. Geophys J Int 2023;232:1236–58. https://doi.org/10.1093/gji/ggac387.

[13] Kowsari M, Sonnemann T, Halldorsson B, Hrafnkelsson B, Snæbjörnsson JÞ, Jónsson S. Bayesian Inference of Empirical Ground Motion Models to Pseudo-Spectral Accelerations of South Iceland Seismic Zone Earthquakes based on Informative Priors. Soil Dyn Earthq Eng 2020;132:106075. https://doi.org/10.1016/j.soildyn.2020.106075.

[14] Rahpeyma S, Halldorsson B, Hrafnkelsson B, Darzi A. Frequency-dependent site amplification functions for key geological units in Iceland from a Bayesian hierarchical model for earthquake strong-motions. Soil Dyn Earthq Eng 2023;168:107823. https://doi.org/10.1016/j.soildyn.2023.107823.

[15] Moosapoor M, Bessason B, Hrafnkelsson B, Darzi A, Rupakhety R, Bjarnason JÖ, et al. Seismic vulnerability model development based on Bayesian parameter estimation: Application to the South Iceland loss data. Rev 2023.

[16] Moosapoor M, Bessason B, Hrafnkelsson B, Rupakhety R, Darzi A, Bjarnason JÖ, et al. Bayesian estimation of seismic vulnerability model parameters using south Iceland loss data. 18th World Conf. Earthq. Eng. 18WCEE, Milan, Italy: 2024, p. Paper No.

Proceedings of the 3rd Croatian Conference on Earthquake Engineering - 3CroCEE
19–22 March 2025, Split, Croatia
Copyright © 2025 CroCEE
DOI: https://doi.org/10.5592/CO/3CroCEE.2025.160

DEVELOPING EARTHQUAKE GROUND MOTION MODELS FOR ICELAND USING BAYESIAN HIERARCHICAL MODELING

Hamed Davari[1], Milad Kowsari[2,1], Benedikt Halldorsson[2,1], Birgir Hrafnkelsson[3], Sahar Rahpeyma[4], and Atefe Darzi[1]

[(1)] *Faculty of Civil and Environmental Engineering, School of Engineering and Natural Sciences, University of Iceland, Reykjavik, Iceland. Emails: HD: had6@hi.is; MK: milad@hi.is; AD: atefe@hi.is; BH: skykkur@hi.is*

[(2)] *Department of volcanic activity, earthquakes and deformation, Service and research Division, Icelandic Meteorological Office, Reykjavik, Iceland. Emails: MK: milad@vedur.is; BH: benedikt@vedur.is*

[(3)] *Faculty of Physical Sciences, Department of Mathematics, University of Iceland, Reykjavik, Iceland. Email: birgirhr@hi.is*

[(4)] *Faculty of Geo-Information Science and Earth Observation, Department of Applied Earth Sciences, University of Twente, Twente, Netherland. Email:* s.rahpeyma@utwente.nl

Keywords: Bayesian Hierarchical Modeling, GMMs, Frequency-Dependent Site Effects, Epistemic Uncertainty

Ground motion models (GMMs) are the key element of probabilistic seismic hazard assessment (PSHA). These models predict an earthquake ground motion intensity measure as a function of some independent variables that represent the earthquake source, path and site effects. The latter one can substantially influence the PSHA results since they are critical factors affecting the amplitude, frequency content, and duration of seismic waves. In regions with different geological characteristics, therefore, site effects should be appropriately accounted for in GMMs and thus PSHA. This is the case for southwest Iceland where due to its distinct geological characteristics (e.g., lava layers interbedded with sedimentary deposits), site-specific amplification varies significantly across different geological units, particularly at higher frequencies.

Therefore, in this study we develop a new set of GMMs with frequency-dependent site amplification factors for four site categories (i.e., hard rock, rock, lava, and stiff soil) in Iceland. For this purpose, we use advanced Bayesian hierarchical modeling (BHM). The BHM framework reduces uncertainty and enhances the reliability of predictions. The models also benefit from the inclusion of site-specific parameters, such as frequency-dependent amplification factors, which account for Iceland's unique geological conditions [1]. Moreover, due to the limited strong-motion data in Iceland, particularly for larger magnitudes, developing GMMs with all the essential terms such as magnitude saturation, magnitude-dependent distance scaling and inelastic attenuation terms, is challenging [2]. In this regard, the Bayesian statistical approach can be particularly useful as it allows taking prior information about the model parameters into account and adding it to the information in the likelihood that stems from the observed data. This study utilized 83 strong-motion records from six strike-slip earthquakes (M_w 5.1-6.5), recorded at 34 seismic stations across diverse geological settings.

In GMMs, uncertainty in the median prediction values is epistemic which depends on the GMM's functional form. To consider the epistemic uncertainty therefore, we take different functional forms as those used and proposed in Kowsari et al. [3]. It is worth noting that they proposed a new functional form specifically calibrated to Icelandic strong-motions that incorporates depth-dependent magnitude scaling and frequency-independent site effects to improve the applicability of GMMs in Iceland. Later, this epistemic uncertainty can be taken into account in PSHA using either a backbone or logic tree approach [4,5]. Figure 1 shows the Bayesian hierarchical ground motion models (BH-GMMs) developed in this study. This figure illustrates the attenuation of BH-GMMs for peak ground acceleration (PGA) at four site classes along with the observed Icelandic strong-motions (colored circles) that are color-coded by their corresponding magnitude. The models are evaluated at magnitudes M_w 5.2 (dotted line), M_w 6.4 (solid line), and M_w 7.2 (dashed line).

Copyright © 2025 CroCEE
DOI: https://doi.org/10.5592/CO/3CroCEE.2025.160

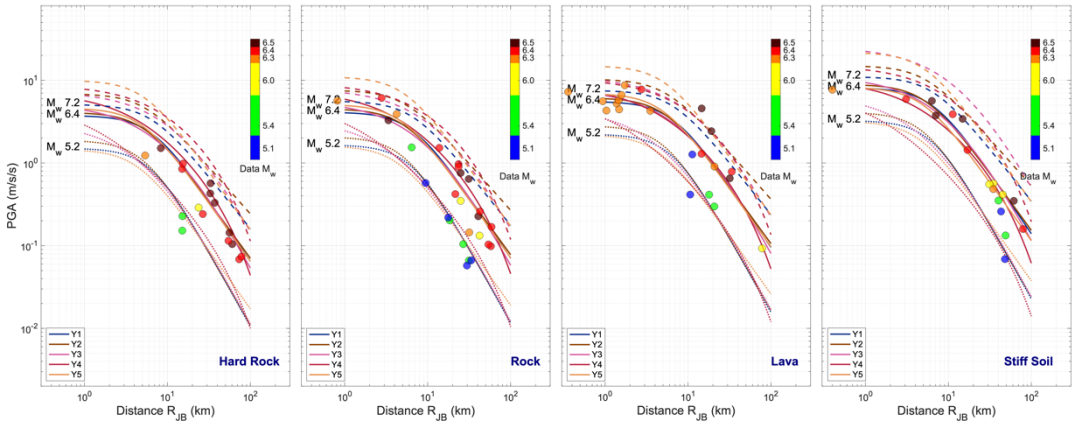


Figure 1. The attenuation of the Bayesian hierarchical ground motion models (BH-GMMs) for peak ground acceleration *PGA* at different site classes. The models are evaluated for magnitudes M_w 5.2 (dotted line), M_w 6.4 (solid line), and M_w 7.2 (dashed line). The circles are observed strong-motions that are color-coded by their corresponding magnitudes.

The results indicated the capability of BH-GMMs to effectively capture the attenuation of *PGA* with distance for varying magnitudes. Moreover, the attenuation trends of observed *PGA*s, align closely with the model predictions for each geological unit, underscoring the importance of incorporating site-specific amplification in PSHA. The distinction in amplification behaviors, particularly at higher frequencies, provides critical insights into the interaction between seismic waves and geological units. This study highlights the critical role of local geological conditions in shaping seismic responses and sets a benchmark for future research in seismic hazard assessment, particularly in regions with complex geological and seismic environments like Southwest Iceland.

Acknowledgments

This study is funded by the “seismic hazard and risk for Reykjanes” project from Icelandic Meteorological Office (No. 3721-0-0019), Icelandic Research Fund (No. 228782-051, GEOSITEFF2HAZ), the national energy company of Iceland, Landsvirkjun (No. NÝR-06-2024 and NÝR-28-2024), and the Icelandic Road Administration, Vegagerðin (No. 1800-1032).

References

[1] Rahpeyma S, Halldorsson B, Hrafnkelsson B, Darzi A. Frequency-dependent site amplification functions for key geological units in Iceland from a Bayesian hierarchical model for earthquake strong-motions. Soil Dyn Earthq Eng 2023;168:107823. https://doi.org/10.1016/j.soildyn.2023.107823.

[2] Kowsari M, Halldorsson B, Hrafnkelsson B, Snæbjörnsson JÞ, Jónsson S. Calibration of ground motion models to Icelandic peak ground acceleration data using Bayesian Markov Chain Monte Carlo simulation. Bull Earthq Eng 2019;17:2841–70. https://doi.org/10.1007/s10518-019-00569-5.

[3] Kowsari M, Sonnemann T, Halldorsson B, Hrafnkelsson B, Snæbjörnsson JÞ, Jónsson S. Bayesian Inference of Empirical Ground Motion Models to Pseudo-Spectral Accelerations of South Iceland Seismic Zone Earthquakes based on Informative Priors. Soil Dyn Earthq Eng 2020;132:106075. https://doi.org/10.1016/j.soildyn.2020.106075.

[4] Kowsari M, Ghasemi S, Farajpour Z, Zare M. Capturing epistemic uncertainty in the Iranian strong-motion data on the basis of backbone ground motion models. J Seismol 2020;24:75–87.

[5] Kowsari M, Ghasemi S, Bayat F, Halldorsson B. A backbone seismic ground motion model for strike-slip earthquakes in Southwest Iceland and its implications for near- and far-field PSHA. Bull Earthq Eng 2023;21:715–38. https://doi.org/10.1007/s10518-022-01556-z.

Proceedings of the 3rd Croatian Conference on Earthquake Engineering - 3CroCEE
19–22 March 2025, Split, Croatia
Copyright © 2025 CroCEE
DOI: https://doi.org/10.5592/CO/3CroCEE.2025.161

TOWARDS A HYBRID SEISMIC HAZARD MODEL FOR ICELAND

Benedikt Halldorsson [1,2], Milad Kowsari[1,2], Farnaz Bayat[1], Atefe Darzi[1], Hamed Davari[1]

[1] *Volcanic activity, earthquakes and deformation dept., Service, and research division, Icelandic Meteorological Office, Iceland, Reykjavík, Iceland, B.H.: Coordinator of Seismic Hazard, benedikt@vedur.is., M.K.: Seismic risk specialist, milad@vedur.is.*

[2] *Faculty of civil and environmental engineering, School of engineering and natural sciences, University of Iceland, Reykjavík, Iceland. B.H.: Research Professor, skykkur@hi.is, M.K.: Research specialist, milad@hi.is, F.B.: Postdoctoral research associate, fab14@hi.is, A.D.: Research specialist, atefe@hi.is, H.D..: Doctoral student, had6@hi.is.*

Keywords: seismic hazard assessment, PSHA, model, physics-based, empirical.

Probabilistic seismic hazard assessment (PSHA) is the international standard practice for seismic risk management worldwide and is used as the foundation for evaluating the basis peak ground motion parameters used by structural building codes for earthquake resistant design (e.g., Eurocode 8). While the existing PSHA map for Iceland, the Icelandic National Annex to Eurocode 8, has effectively not been updated for more than two decades [1], it still is a more realistic map compared to those that recent European efforts have produced, the ESHM13 and ESHM20 [2]. However, the PSHA map for Iceland requires a robust revision that settles the matter of the inconsistencies of the existing map and the European PSHA efforts for Iceland. In recent years, intense efforts have been undertaken in seismic hazard research in Iceland: These are (1) a new harmonized and long-term earthquake catalogue for Iceland [the ICEL-NMAR catalogue, 3]; (2) A new fault system model for the bookshelf transform zone of Southwest Iceland [4] with a new fault system model for the transform zone of North Iceland being in preparation [5]; (3) The corresponding models of seismic activity rates on those transform zones, that effectively explain the historical catalogue [5,6]; The fault system models enable the generation of synthetic finite-fault earthquake catalogues that are consistent both with the model and the historical seismicity [7]; (4) A new suite of hybrid empirical Bayesian ground motion models (GMMs) [8–10] that include uncertainty handling, sensitivity analyses and new methods e.g. the backbone approach [11] and the quantitative selection of GMMs for PSHA [12]; (5) New frequency-dependent seismic wave amplification functions for the four dominant surface geology classes of Iceland [13] and new maps of site amplification in Iceland [14]; (6) The fault system models of transform zones have led to modelling of earthquake rupture scenarios [15–17]; (7) The effects of the new GMMs on PSHA and its uncertainty have been tested [11,18]; (8) Established ETAS models for earthquake aftershock forecasting and short-term seismic hazard assessment [19,20]; (9) Compared the seismic loss estimation results using local vs. European vulnerability models [21]; (10) Proposed a new and provisional seismic source zonation for Iceland [22]. At present therefore, all the fundamental elements for PSHA for Iceland have been updated based on the state-of-the-art methods and data, and are now in place for a timely, robust and much needed revision of the seismic hazard of Iceland using both physics-based and empirical approaches.

References

[1] Standards Council of Iceland / Staðlaráð Íslands (SI), Halldorsson P. Icelandic National Annexes to Eurocodes. Reykjavík, Iceland: Staðlaráð Íslands; 2010.

[2] Woessner J, Laurentiu D, Giardini D, Crowley H, Cotton F, Grünthal G, et al. The 2013 European seismic hazard model: key components and results. Bulletin of Earthquake Engineering 2015;13:3553–96.

[3] Jónasson K, Bessason B, Helgadóttir Á, Einarsson P, Gudmundsson GB, Brandsdóttir B, et al. A Harmonised Instrumental Earthquake Catalogue for Iceland and the Northern Mid-Atlantic Ridge. Natural Hazards and Earth System Sciences 2021;21:2197–214. https://doi.org/10.5194/nhess-21-2197-2021.

[4] Bayat F, Kowsari M, Halldorsson B. A new 3-D finite-fault model of the Southwest Iceland bookshelf transform zone. Geophysical Journal International 2022;231:1618–33. https://doi.org/10.1093/gji/ggac272.

Copyright © 2025 CroCEE
DOI: https://doi.org/10.5592/CO/3CroCEE.2025.161

[5] Halldorsson B, Abril C, Bayat F, Kowsari M. On the Establishment of Physics-based Finite-fault Earthquake Source Models of the Transform Zones of Iceland. Proceedings of the 3rd European Conference on Earthquake and Engineering Seismology (3ECEES), Bucharest, Romania: 2022, p. 3820-3829 (No. 7077).
[6] Bayat F, Kowsari M, Halldorsson B. A simplified seismicity model of the bookshelf fault system of the Southwest Iceland transform zone. Bull Earthquake Eng 2024;22:4959–81. https://doi.org/10.1007/s10518-024-01946-5.
[7] Kowsari M, Halldorsson B, Bayat F. Preparation of Finite-fault Earthquake Catalogues Enabling Physics-based PSHA in Southwest Iceland. Proceedings of the 3rd European Conference on Earthquake and Engineering Seismology (3ECEES), Bucharest, Romania: 2022, p. 3863-3870 (No. 8441).
[8] Kowsari M, Halldorsson B, Hrafnkelsson B, Snæbjörnsson JÞ, Jónsson S. Calibration of ground motion models to Icelandic peak ground acceleration data using Bayesian Markov Chain Monte Carlo simulation. Bull Earthquake Eng 2019;17:2841–70. https://doi.org/10.1007/s10518-019-00569-5.
[9] Kowsari M, Sonnemann T, Halldorsson B, Hrafnkelsson B, Snæbjörnsson JÞ, Jónsson S. Bayesian Inference of Empirical Ground Motion Models to Pseudo-Spectral Accelerations of South Iceland Seismic Zone Earthquakes based on Informative Priors. Soil Dynamics and Earthquake Engineering 2020;132:106075. https://doi.org/10.1016/j.soildyn.2020.106075.
[10] Sonnemann T, Halldorsson B, Hrafnkelsson B, Jónsson S. Bayesian Inference of a Physical Seismological Model to Earthquake Strong-motion in South Iceland. Soil Dynamics and Earthquake Engineering 2020;138:106219. https://doi.org/10.1016/j.soildyn.2020.106219.
[11] Kowsari M, Ghasemi S, Bayat F, Halldorsson B. A backbone seismic ground motion model for strike-slip earthquakes in Southwest Iceland and its implications for near- and far-field PSHA. Bull Earthquake Eng 2023;21:715–38. https://doi.org/10.1007/s10518-022-01556-z.
[12] Kowsari M, Halldorsson B, Hrafnkelsson B, Jonsson S. Selection of earthquake ground motion models using the deviance information criterion. Soil Dynamics and Earthquake Engineering 2019;117:288–99. https://doi.org/10.1016/j.soildyn.2018.11.014.
[13] Rahpeyma S, Halldorsson B, Hrafnkelsson B, Darzi A. Frequency-dependent site amplification functions for key geological units in Iceland from a Bayesian hierarchical model for earthquake strong-motions. Soil Dynamics and Earthquake Engineering 2023;168:107823. https://doi.org/10.1016/j.soildyn.2023.107823.
[14] Darzi A, Halldorsson B, Cotton F, Rahpeyma S. Nationwide frequency-dependent seismic site amplification models for Iceland. Soil Dynamics and Earthquake Engineering 2024;183:108798. https://doi.org/10.1016/j.soildyn.2024.108798.
[15] Rojas O, Monterrubio-Velasco M, Rodriguez JE, Callaghan S, Abril C, Halldorson B, et al. Earthquake Fault Rupture Modeling and Ground Motion Simulations for the Southwest Iceland Transform Zone using CyberShake. Bulletin of the Seismological Society of America 2024:(in press).
[16] Li B, Gabriel A-A, Ulrich T, Abril C, Halldorsson B. Dynamic rupture models, fault interaction and ground motion simulations for the segmented Húsavík-Flatey Fault Zone, Northern Iceland. Journal of Geophysical Research: Solid Earth 2023;128:e2022JB025886. https://doi.org/10.1029/2022JB025886.
[17] Kutschera F, Gabriel A-A, Wirp SA, Li B, Ulrich T, Abril C, et al. Linked and fully coupled 3D earthquake dynamic rupture and tsunami modeling for the Húsavík–Flatey Fault Zone in North Iceland. Solid Earth 2024;15:251–80. https://doi.org/10.5194/se-15-251-2024.
[18] Kowsari M, Halldorsson B, Snæbjörnsson JÞ, Jónsson S. Effects of different empirical ground motion models on seismic hazard maps for North Iceland. Soil Dynamics and Earthquake Engineering 2021;148:106513. https://doi.org/10.1016/j.soildyn.2020.106513.
[19] Darzi A, Halldorsson B, Hrafnkelsson B, Vogfjörð KS. Short-term Bayesian ETAS spatiotemporal forecasting of the Ölfus 2008 earthquake sequence in Iceland. Tectonophysics 2022;839:229522. https://doi.org/10.1016/j.tecto.2022.229522.
[20] Darzi A, Halldorsson B, Hrafnkelsson B, Ebrahimian H, Jalayer F, Vogfjörð KS. Calibration of a Bayesian spatio-temporal ETAS model to the June 2000 South Iceland seismic sequence. Geophysical Journal International 2023;232:1236–58. https://doi.org/10.1093/gji/ggac387.
[21] Darzi A, Bessason B, Halldorsson B, Molina S, Kharazian A, Moosapoor M. High spatial-resolution loss estimation using dense array strong-motion near-fault records. Case study for Hveragerði and the M w 6.3 Ölfus earthquake, South Iceland. International Journal of Disaster Risk Reduction 2022;73:102894. https://doi.org/10.1016/j.ijdrr.2022.102894.
[22] Halldorsson B, Kowsari M, Bayat F, Abril C, Darzi A, Bessason B, et al. A provisional seismic source zonation of Iceland for the ESHM20 based on new physics-based bookshelf fault system models and a revised earthquake catalogue. Proceedings of the 3rd European Conference on Earthquake and Engineering Seismology (3ECEES), 4-9 September, Bucharest, Romania: 2022, p. 3739-3748 (No. 4494).

Proceedings of the 3rd Croatian Conference on Earthquake Engineering - 3CroCEE
19–22 March 2025, Split, Croatia
Copyright © 2025 CroCEE
DOI: https://doi.org/10.5592/CO/3CroCEE.2025.162

PHYSICS-BASED SITE-SPECIFIC PSHA FOR SEVERAL URBAN CENTERS IN SOUTHWEST ICELAND

Milad Kowsari[1,2], Benedikt Halldórsson[1,2]

[1] *Volcanic activity, earthquakes and deformation dept., Service, and research division, Icelandic Meteorological Office, Reykjavík, Iceland, M.K.: Seismic risk specialist, milad@vedur.is; B.H.: Coordinator of Seismic Hazard, benedikt@vedur.is*

[2] *Faculty of civil and environmental engineering, School of engineering and natural sciences, University of Iceland, Reykjavík, Iceland. M.K.: Research Specialist, milad@hi.is; B.H.: Research Professor, skykkur@hi.is*

Keywords: Physics-based, PSHA, FFCAT, Iceland.

Seismic risk assessment is crucial for mitigation of strong earthquakes' effects on communities since it offers a comprehensive framework for minimizing damage, casualties, and economic losses. This can be accomplished through designing earthquake-resistant structures, retrofitting the existing buildings, economic resilience, urban planning, and public education. One of the key elements of seismic risk assessment is to estimate the earthquake hazard in the region of interest. The most acceptable way to evaluate the earthquake hazard in a given region is to perform a probabilistic seismic hazard assessment (PSHA). The seismic hazard and risk are highest in southwest Iceland due to the transform faulting near a relatively populated region with all critical infrastructures and lifelines. The South Iceland Seismic Zone (SISZ) is one of the two major transform zones of Iceland where earthquakes take place on an array of short, near vertical, and north-south trending right-lateral strike slip faults, known as the 'bookshelf fault system'. This bookshelf fault system has been shown to be continuous towards the west along the entire Reykjanes Peninsula Oblique Rift (RPOR) [1]. Based on geological and seismological evidence, seismogenic potential is variable in the SISZ-RPOR, with the increasing seismogenic depth from west to east [2,3]. This results in the maximum magnitudes from∼5.5 in the westernmost part of the RPOR to∼7−7.2 in the easternmost part of the SISZ, which agrees with the seismicity and also historical catalogue in southwest Iceland. Recently, a new physics-based finite-fault system model has been developed for the SISZ-RPOR, calibrated to the steady-state relative plate velocity of transcurrent tectonic motions across the zone [4].

This model, which is constrained by historical and instrumental seismicity, accounts for the variability in inter fault distances guided by fault mapping and relative relocations of seismic swarms. Therefore, the resulting model is completely specified in terms of suites of 3D strike-slip faults along with their corresponding annual slip rates, thus fully capturing the salient characteristics of spatially variable maximum magnitudes and zone-specific magnitude frequency distributions (MFDs). These zone-specific MFDs are entirely compatible with the physical constraints, effectively explain the observed Icelandic catalogues and also avoid the bias introduced by the short duration of earthquake catalogues [5]. This model was further used to simulate a synthetic finite-fault earthquake catalogue (FFCAT) for a long-time interval with random locations across the region [6]. This physics-based approach is in stark contrast to conventional PSHA which relies on simplified seismic source models and simplistic statistics of an earthquake catalogue that for each subzone is effectively incomplete, whereas the finite-fault catalogues fully incorporate the first two key elements of PSHA, the seismic source locations along with their activity rates [7].

In this study, we take advantage of a new physics-based FFCAT and carry out a Monte Carlo PSHA (MC-PSHA) for several major cities and towns in Southwest Iceland. In the MC-PSHA, the ground motion intensity measures of interest are predicted from each finite-fault by several GMMs. However, different ground motions predictions by different GMMs have the largest contributions to the overall epistemic uncertainty. To reduce the epistemic uncertainty, therefore, we use different data-driven GMM-ranking methods to reduce subjectivity in the selection process [8–10]. For inferring the most suitable GMMs, we consider several empirical GMMs developed from local, regional and

Copyright © 2025 CroCEE
DOI: https://doi.org/10.5592/CO/3CroCEE.2025.162

worldwide data. The ranking results favor the Icelandic Bayesian GMMs and thus the logic tree is populated with six Bayesian GMMs with different functional forms for use in PSHA. The PSHA results of this study are shown in terms of hazard curves at different periods. We conclude that this study avoids the use of limited statistics from observed catalogues and is firmly rooted in a physical finite-fault system of Southwest Iceland.

Acknowledgements

This study is funded by the "seismic hazard and risk for Reykjanes" project from Icelandic Meteorological Office (No. 3721-0-0019), the national energy company of Iceland, Landsvirkjun (No. NÝR-06-2024 and NÝR-28-2024), the Icelandic Road Administration, Vegagerðin (No. 1800-1032).

References

[1] Steigerwald L, Einarsson P, Hjartardóttir ÁR. Fault kinematics at the Hengill Triple Junction, SW-Iceland, derived from surface fracture pattern. Journal of Volcanology and Geothermal Research 2020;391:106439. https://doi.org/10.1016/j.jvolgeores.2018.08.017.

[2] Stefánsson R, Halldórsson P. Strain release and strain build-up in the south Iceland seismic zone. Tectonophysics 1988;152:267–76. https://doi.org/10.1016/0040-1951(88)90052-2.

[3] Stefánsson R, Böðvarsson R, Slunga R, Einarsson P, Jakobsdóttir S, Bungum H, et al. Earthquake prediction research in the South Iceland seismic zone and the SIL project. Bulletin of the Seismological Society of America 1993;83:696–716. https://doi.org/10.1785/BSSA0830030696.

[4] Bayat F, Kowsari M, Halldorsson B. A new 3-D finite-fault model of the Southwest Iceland bookshelf transform zone. Geophysical Journal International 2022;231:1618–33. https://doi.org/10.1093/gji/ggac272.

[5] Bayat F, Kowsari M, Halldorsson B. A simplified seismicity model of the bookshelf fault system of the Southwest Iceland transform zone. Bull Earthquake Eng 2024;22:4959–81. https://doi.org/10.1007/s10518-024-01946-5.

[6] Kowsari M, Halldorsson B, Bayat F. Preparation of Finite-fault Earthquake Catalogues Enabling Physics-based PSHA in Southwest Iceland. Proceedings of the 3rd European Conference on Earthquake and Engineering Seismology (3ECEES), Bucharest, Romania: 2022, p. 3863-3870 (No. 8441).

[7] Kowsari M, Ghasemi S, Bayat F, Halldorsson B. A backbone seismic ground motion model for strike-slip earthquakes in Southwest Iceland and its implications for near- and far-field PSHA. Bull Earthquake Eng 2023;21:715–38. https://doi.org/10.1007/s10518-022-01556-z.

[8] Scherbaum F, Delavaud E, Riggelsen C. Model selection in seismic hazard analysis: An information-theoretic perspective. Bulletin of the Seismological Society of America 2009;99:3234–47.

[9] Kale Ö, Akkar S. A new procedure for selecting and ranking ground-motion prediction equations (GMPEs): The Euclidean distance-based ranking (EDR) method. Bulletin of the Seismological Society of America 2013;103:1069–84.

[10] Kowsari M, Halldorsson B, Hrafnkelsson B, Jonsson S. Selection of earthquake ground motion models using the deviance information criterion. Soil Dynamics and Earthquake Engineering 2019;117:288–99. https://doi.org/10.1016/j.soildyn.2018.11.014.

Proceedings of the 3rd Croatian Conference on Earthquake Engineering - 3CroCEE
19–22 March 2025, Split, Croatia
Copyright © 2025 CroCEE
DOI: https://doi.org/10.5592/CO/3CroCEE.2025.16

LANDSLIDE TRIGGERING AS AN INDIRECT CONSEQUENCE OF AN EARTHQUAKE - CASE STUDY FROM NORTHERN CROATIA

Jasmin Jug [(1)], Stjepan Strelec [(2)], Kristijan Grabar [(3)], Dragana Dogančić [(4)], Anja Bek [(5)]

[(1)] *Assistant Professor, University of Zagreb Faculty of Geotechnical Engineering, jasmin.jug@gfv.hr*
[(2)] *Full Professor, University of Zagreb Faculty of Geotechnical Engineering, stjepan.strelec@gfv.hr*
[(3)] *PhD student at Faculty of Geotechnical Engineering, SPP d.o.o., kristijan@spp.hr*
[(4)] *Assistant Professor, University of Zagreb Faculty of Geotechnical Engineering, dragana.dogancic@gfv.hr*
[(1)] *PhD student and Assistant, University of Zagreb Faculty of Geotechnical Engineering, anja.bek@gfv.hr*

Abstract

A landslide is the movement of soil and rocks down a slope as a result of the loss of shear strength in the material that builds the hill. Although various human activities increase the risk of landslides, the most common causes for the loss of shear strength are geological and morphological. Thus, natural triggers for landslides can be the characteristics of the soil and rocks that build the slope, the slope angle, erosion, and water, but this paper will analyse the triggering of landslides as indirect consequences of earthquakes. In 2020, two significant earthquakes hit central Croatia. First, a moderate earthquake was triggered in the area of Zagreb, and towards the end of the year, a strong earthquake hit the regions of Petrinja, Sisak and Glina. In addition to the enormous damage to buildings, the mentioned earthquakes indirectly activated numerous landslides, including in the area of Northern Croatia. The landslide in Slatina Svedruška near Petrovsko was activated immediately after the Zagreb earthquake. This instability potentially threatened the D206 state road corridor. Engineering geological and recent geotechnical-geophysical investigations were applied to define the instability boundaries, the lithological composition of sediments in the subsurface, and the location of the sliding surface. The unfavourable geological structure was determined, as silty sands and clays predominate in the surface layers, and organic clays of low shear strength appear immediately before contact with marl. The mentioned location of the landslide was selected for microtremor measurements that will be carried out as part of the Croatian Science Foundation (HRZZ) project IP-2022-10-1296, SIGMATOPCRO.

Keywords: earthquake, landslide, geotechnical investigations, geological investigations, microtremor.

1. Introduction

Landslides are conditioned by several terrain and geo-environmental factors and can be triggered by different kinds of natural processes (rainfall, earthquakes, etc.) but also by man-made activities [1]. Understanding and mitigating the risks associated with earthquake-induced landslides requires a comprehensive approach tailored to specific geographical regions and local conditions. By recognizing the interactions between seismic events and slope stability, communities can better prepare for and respond to these natural hazards, ultimately reducing loss of life and property damage.

Earthquake-induced ground shaking can trigger landslides by applying horizontal and vertical accelerations to the soil or rock mass along a hillside slope. The critical or yield acceleration, denoted as ac, represents the peak ground acceleration within the sliding mass required to reduce the factor of safety to 1.0. Typically, this acceleration value is determined through pseudo-static slope stability analyses or empirical observations of slope behaviour during past earthquakes and does not depend on the earthquake hazard at the location. Simply, if the earthquake acceleration reached at a certain seismic event is higher than the critical acceleration of the potential sliding mass, landslide induced by earthquake will occur.

Several empirical models have been developed to predict the seismic displacements of sliding masses [2-4]. These models estimate downslope deformations when the induced peak ground acceleration

Copyright © 2025 CroCEE
DOI: https://doi.org/10.5592/CO/3CroCEE.2025.16

within the sliding mass exceeds the critical acceleration. They are grounded on the assumption of a sliding rigid block, providing a measure of dynamic slope performance.

Site amplification related to topography can be also an important factor in coseismic triggering of landslides as an indirect consequence of an earthquake (it can be triggered at some time after mainshock). Furthermore, site response directivity can be relevant in enhancing susceptibility of slopes to earthquake induced failures considering that in most of the observed cases the direction of maximum shaking resulted close to that of the maximum slope [5-7]. Furthermore, site response directivity can be relevant in enhancing susceptibility of slopes to earthquake induced failures considering that in most of the observed cases the direction of maximum shaking resulted close to that of the maximum slope.

Slope response to seismic shaking can be influenced by directional variations of a factor of 2–3 or more prominent, with maxima oriented along local topography features (e.g. maximum slope direction, geotechnical and geological characteristics). This phenomenon appears influenced by slope material properties and has occasionally been detected on landslide-prone slopes, where a down-slope directed amplification could enhance susceptibility to seismically-induced landsliding [6,7].

In 2008 Del Gaudio et al. [5] performed detection of directivity in seismic site response using microtremor (ambient noise) measurements compared with average H/V spectral ratios obtained for low-to-moderate earthquakes recorded by the accelerometric stations. Ambient noise vibrations allow rapid detection and seismic monitoring of dynamic response of topographic slope [8]. It is possible to distinguish unstable areas, slope eigenfrequencies and local amplification levels (due to weak excitation) [9]. Based on the above claims, microtremor measurements were conducted in the case of a landslide in Slatina Svedruška (Fig. 1).

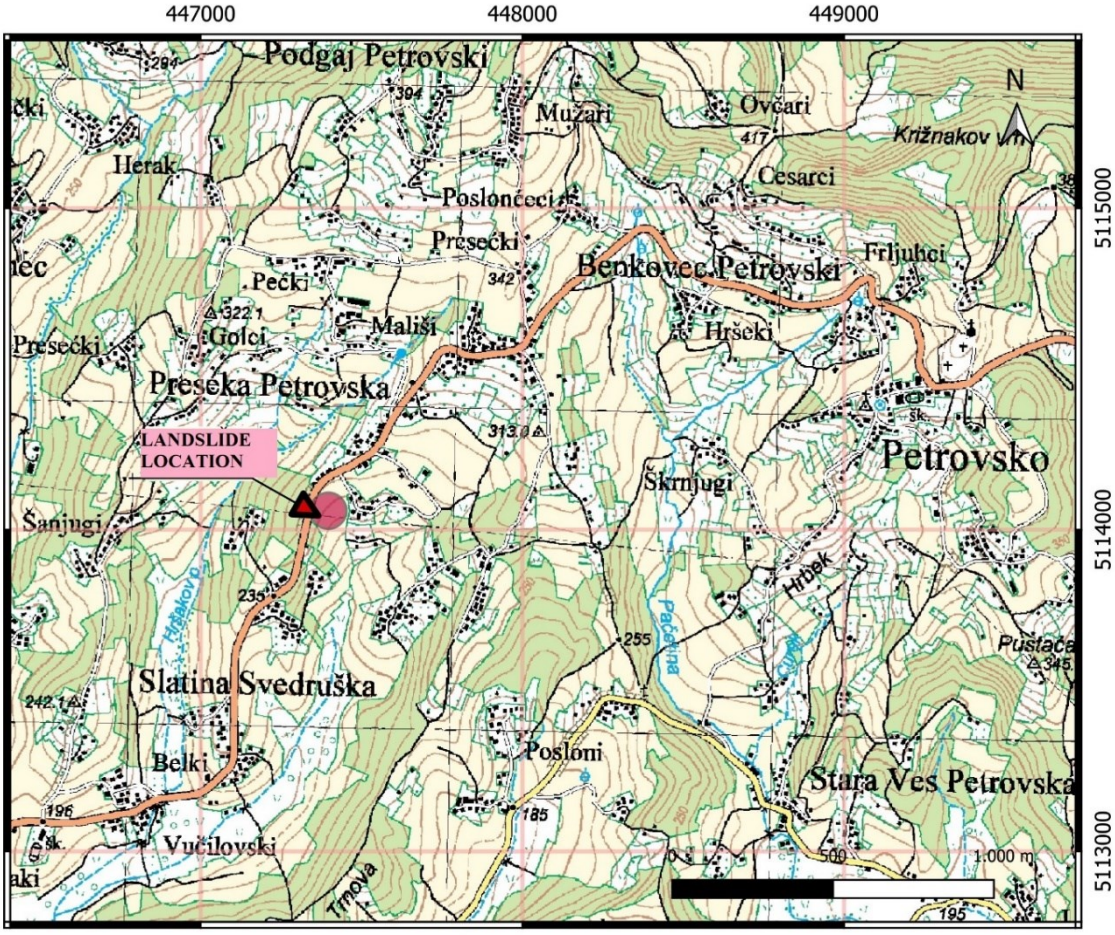


Figure 1. Map of landslide location in Slatina Svedruška near Petrovsko.

Copyright © 2025 CroCEE
DOI: https://doi.org/10.5592/CO/3CroCEE.2025.16

Detailed engineering geological and recent geotechnical-geophysical investigations on the landslide were carried out at the beginning of 2021, and detailed results are available in [10]. In 2024, additional geological and microseismic investigations through microtremor (ambient noise) measurements were carried out as part of the SIGMATOPCRO project.

2. Methods and results of previous investigations from 2021

According to information from residents of the village of Slatina Svedruška near Petrovsko (Fig. 1), a landslide occurred in early 2020, immediately after the earthquake in Zagreb. The D206 state road corridor may have been in danger due to this instability. At the beginning of 2021, detailed engineering geology and geotechnical-geophysical investigations were conducted on a 5000-square-meter landslide. The bounds of instability and the lithological composition of sediments in the subsurface and sliding surface were identified. The sliding surface's depth was assessed using a Dynamic Probe Light (DPL) and a Cone Penetration Test (CPTu). Geophysical investigations were conducted utilizing Electrical Resistivity Tomography (ERT), Seismic Refraction (SRF), and Multichannel Analysis of Surface Waves (MASW).

Sliding elements was evident in the landslide: material pushed into the foot, a forehead with a tensile crack, and a jump of up to h = 2.5 m (Fig. 2). The type of sliding indicates that the landslide is translational-rotational. The entire displacement is roughly 10 meters, and the displaced masses match a volume of about 2000 m^3. Over a distance of 150 meters, the tensile crack is visible. As the landslide is inched, the masses move 30 to 60 meters in courses.



Figure 2. Tensile crack with a jump in the northern part of the landslide.

The investigation's findings provided information on the structure of the soil stratigraphy, which in turn produced the comprehensive geotechnical landslide profile (Fig. 3). The lithological composition of the ground was ascertained by analysing the results of static and dynamic probing and geophysical surveys:

1. The surface soil up to a maximum depth of 6 m is built of siltstone sands and sand-siltstone clays. Klastites are in sedimentary exchange from silty sands (siSaP) to clayey silt, and fine gravel is also present within the sand series. At a depth of 6 m, the CPT probe identified clays with organic impurities, low shear strength. A sliding surface was identified at the same depth. Soil parameters at the 1st interval (0 – 6 m): c_u = 20 - 50 kN/m^2, γ = 14 - 16 kN/m^3, c = 0 - 5 kN/m^2, φ = 25°, V_P = 200 - 500 m/s, V_S = 180 - 300 m/s.
2. Solid marl deeper than 6 m. Soil parameters at the 2nd interval (> 6 m): c_u > 250 kN/m^2, γ = 19 kN/m^3, c = 50 kN/m^2, φ = 25°.

Copyright © 2025 CroCEE
DOI: https://doi.org/10.5592/CO/3CroCEE.2025.16

An unfavourable fact is the geological structure, which is dominated by silty sands and clayey silts, and immediately before contact with marl appear organic clays of low shear strength, which are very sensitive to changes in humidity. The main cause of landslides is the drop in the strength of clay in contact with marl. The exact trigger is not entirely clear, and a possible scenario is a rise in groundwater levels and the effect on pore pressure and the effective pressure of deeper soil layers. Given that nearby Zagreb was hit by a strong earthquake in 2020, the impact of this event is associated with the triggering of a landslide.

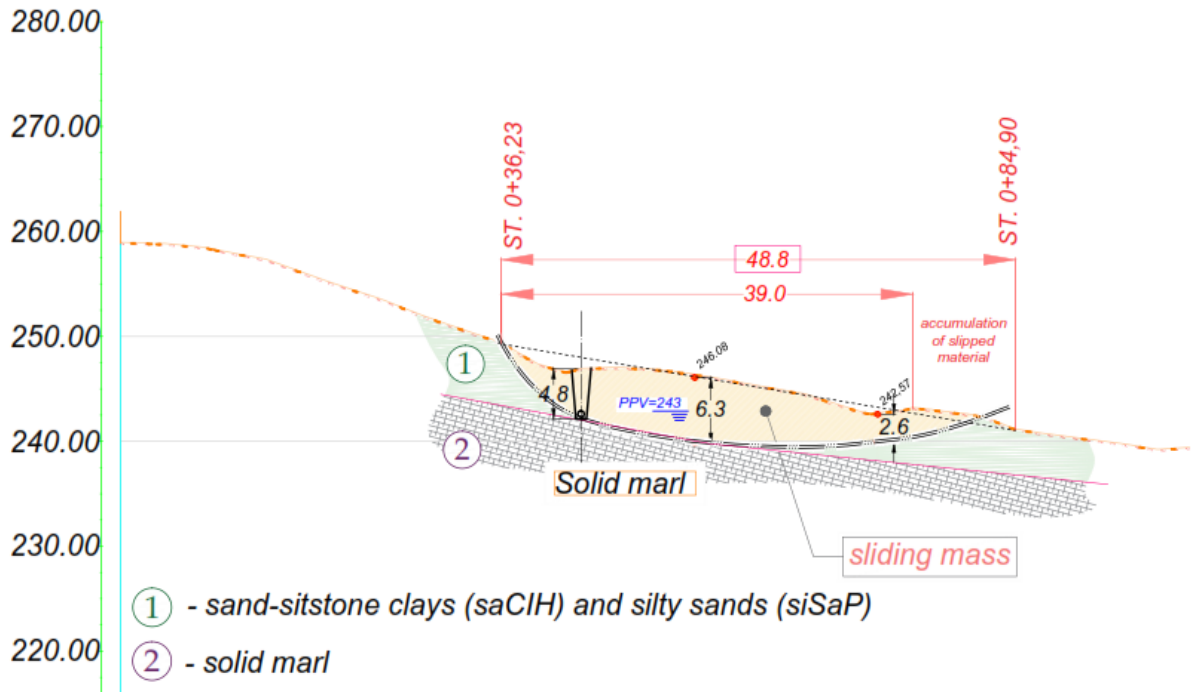


Figure 3. Characteristic geotechnical Slatina Svedruška landslide profile [10].

3. Methods and results of additional investigations from 2024

The landslide in Slatina Svedruška was selected for microseismic investigations through microtremor (ambient noise) measurements that were carried out as part of Croatian Science Foundation (HRZZ) project IP-2022-10-1296, SIGMATOPCRO. However, a detailed geological reconnaissance of the materials that make up the slope was carried out before the microseismic measurements.

3.1. Geological reconnaissance results

On the northern scarp, it is evident that under the humus layer, there is weakly bound to loose sediment (Fig. 4a). It is a poorly sorted clastic sediment whose composition is dominated by particles of pelitic dimensions (silt and clay), but also contains pebbles up to two centimetres in size (Fig. 4b). Sediment can be defined as gravelly clayey silt.

On the southern scarp, massive-looking sand emerges to the surface. The sand is completely loose, well-sorted, fine to medium-grained. Its composition is dominated by quartz, and macroscopically large-foliated micas are clearly visible.

Well-sorted micaceous sands are characteristic of the Upper Miocene deposits in the northern part of the Croatian Zagorje. They were formed as a result of the deposition of sandy detritus of Alpine provenance in the then Pannonian Lake, and their thickness in places exceeds a hundred meters. On the other hand, the poorly sorted gravelly-clayey silt discovered on the northern scarp probably represents a thin surface layer of younger sediments deposited perhaps during the Pliocene or Quaternary [11].

Proceedings of the 3rd Croatian Conference on Earthquake Engineering - 3CroCEE
19–22 March 2025, Split, Croatia
Copyright © 2025 CroCEE
DOI: https://doi.org/10.5592/CO/3CroCEE.2025.16



Figure 4. a) Northern scarp of the landslide in Slatina Svedruška; b) Pebble-clayey silt of massive appearance on the northern scarp.

3.2. Microtremor results

To characterise properties of the topographic irregularity necessary to understand the dynamic behaviour of landslide in Slatina Svedruška, spectral frequency analysis of ambient seismic noise measurements was performed for the detection of possible changes in resonance frequencies at five microlocations (Fig. 5). The Nakamura technique or Horizontal-to-Vertical-Spectral-Ratio (HVSR) [12] is based on short-duration ambient noise measurements, and the spectral ratio is defined as a ratio of the horizontal and the vertical components using small portable seismographs.

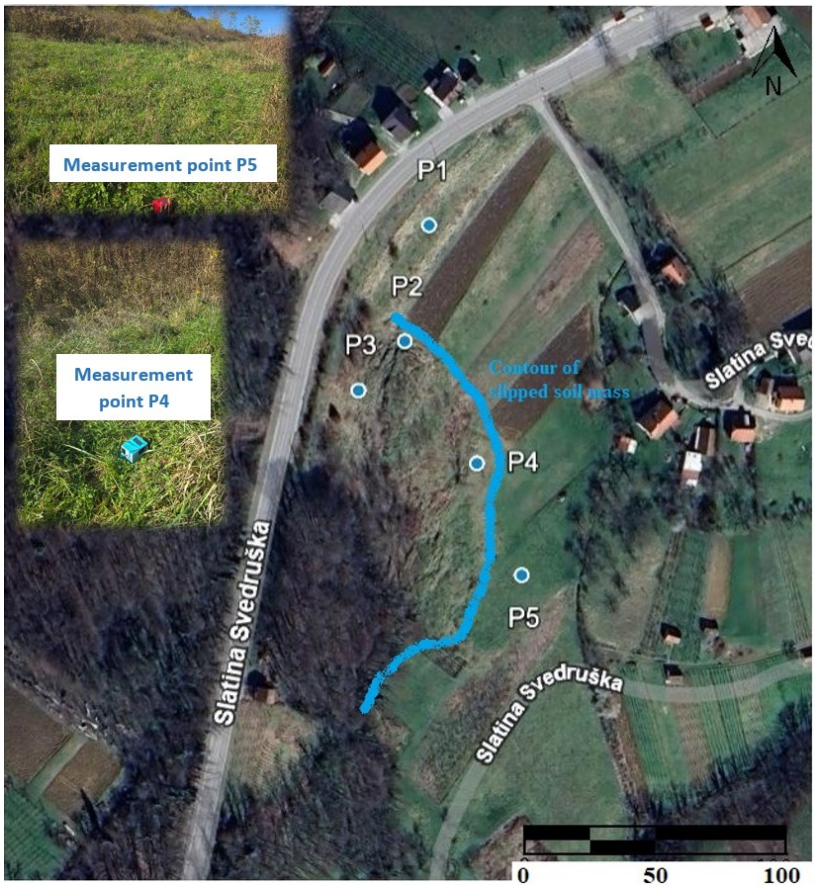


Figure 5. Map of microtremor measurement positions.

Proceedings of the 3rd Croatian Conference on Earthquake Engineering - 3CroCEE
19–22 March 2025, Split, Croatia
Copyright © 2025 CroCEE
DOI: https://doi.org/10.5592/CO/3CroCEE.2025.16

The results of microtremor measurements (Fig. 6) show variable changes of frequencies along the landslide body ranging from 10 to 20 Hz, which is approximately 5 to 12 m of depth to bedrock [13] (solid marl in this case) that is well correlated with investigations results from 2021.

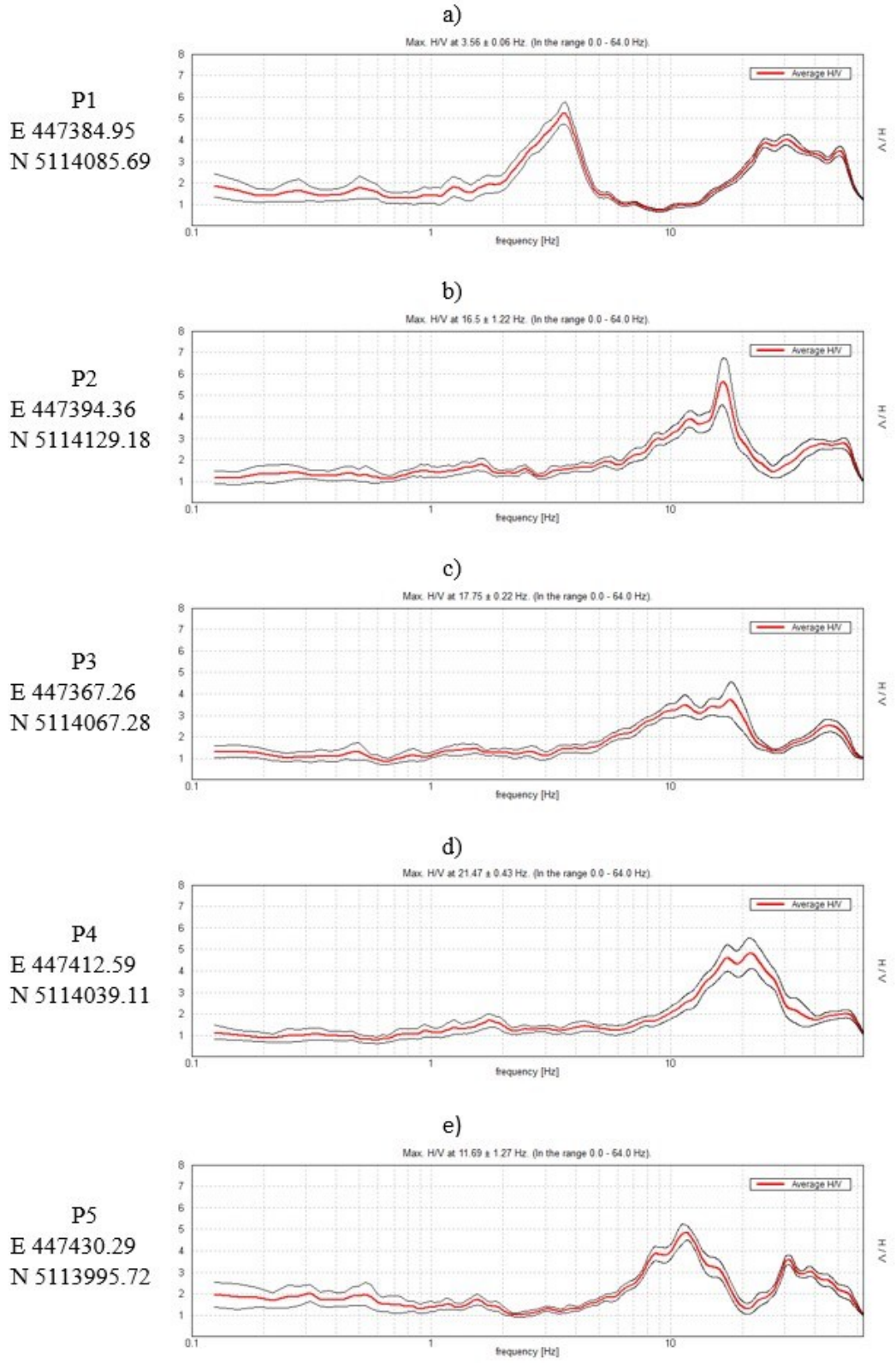


Figure 6. Results of microtremor measurements on the landslide in Slatina Svedruška: a) Measurement point P1; b) Measurement point P2; c) Measurement point P3; d) Measurement point P4; e) Measurement point P5.

Copyright © 2025 CroCEE
DOI: https://doi.org/10.5592/CO/3CroCEE.2025.16

4. Conclusions

Natural causes (e.g., rain or earthquake), as well as anthropogenic ones, can decrease the shear strength of the material in the slope and ultimately cause the soil or rock to move. In Slatina Svedruška, in the municipality of Petrovsko, due to increased amounts of rainfall, there was an increase in the groundwater level and an impact on the pore pressure of deeper soil layers on the slope under the state road corridor D206. In 2020, Zagreb was hit by a strong earthquake, and the impact of that event triggered a landslide on the mentioned slope.

At that location, the majority of research was conducted in 2021, while additional geological and microseismic research was conducted later in 2024. The combination of geological, geophysical and geotechnical research methods provided information on the structure of the soil stratigraphy, which in turn produced the comprehensive geotechnical landslide profile. The lithological composition of the soil begins with the surface layer that has been built of siltstone sands and gravelly clayey silt, up to a maximum depth of 5-7 m. Deeper than that lies solid marl, which represents the bedrock. In this case, the contact zone between those mentioned above was relatively water-permeable surface materials and the marl, which was sensitive to increased humidity and became a sliding surface. In the area of Northern Croatia, there are numerous slopes of the same or similar geological structure, so it can be concluded that they are all potential landslides.

As part of the SIGMATOPCRO project, a spectral frequency analysis of ambient seismic noise measurements was subsequently performed in 2024 to detect possible changes in resonant frequencies. The results of microtremor measurements are well correlated with geotechnical and geophysical investigation results. However, it can be concluded that the use of ambient noise (microtremor) signals is attractive in studies on marginally stable slopes since other approaches require more time and money.

Acknowledgements

This paper was supported by the Croatian Science Foundation under the project number [HRZZ-IP-2022-10-1296].

References

[1] Geertsema, M., Highland, L., Vaugeouis, L. (2009): Environmental Impact of Landslides. In book: Landslides - Disaster risk reduction. Publisher: Springer. Editors: Kyoji Sassa, Paolo Canuti. 1st edition, Germany.

[2] Bray, J. D., Travasarou, T. (2007): Simplified procedure for estimating earthquake-induced deviatoric slope displacements. *Journal of geotechnical and geoenvironmental engineering*, **133** (4), 381-392, doi: http://dx.doi.org/10.1061/(ASCE)1090-0241(2007)133:4(381)

[3] Jibson, R.W. (2007): Regression models for estimating coseismic landslide displacement. *Engineering geology*, **91** (2-4), 209-218, doi: https://doi.org/10.1016/j.enggeo.2007.01.013

[4] Fotopoulou, S.D., Pitilakis, K.D. (2015): Predictive relationships for seismically induced slope displacements using numerical analysis results. *Bulletin of Earthquake Engineering*, **13** (11), 3207-3238, doi: http://dx.doi.org/10.1007/s10518-015-9768-4

[5] Del Gaudio, V., Coccia, S., Wasowski, J., Gallipoli, M. R., Mucciarelli, M. (2008): Detection of directivity in seismic site response from microtremor spectral analysis. *Nat. Hazards Earth Syst. Sci.*, **8** (4), 751–762, doi: https://doi.org/10.5194/nhess-8-751-2008

[6] Del Gaudio, V., Muscillo, S., Wasowski, J. (2014): What we can learn about slope response to earthquakes from ambient noise analysis: An overview. *Engineering Geology*, **182** (4), 182–200, doi: https://doi.org/10.1016/j.enggeo.2014.05.010

[7] Del Gaudio, V., Y. Luo, Y. Wang, J. Wasowski (2018): Using ambient noise to characterise seismic slope response: The case of Qiaozhuang peri-urban hillslopes (Sichuan, China). *Eng. Geol.*, 246 (6), 374–390, doi: https://doi.org/10.1016/j.enggeo.2018.10.008

Proceedings of the 3rd Croatian Conference on Earthquake Engineering - 3CroCEE
19–22 March 2025, Split, Croatia
Copyright © 2025 CroCEE
DOI: https://doi.org/10.5592/CO/3CroCEE.2025.16

[8] Colombero, C., Jongmans, D., Fiolleau, S. et al. (2021): Seismic Noise Parameters as Indicators of Reversible Modifications in Slope Stability: A Review. *Surv Geophys* **42**, 339–375, doi: https://doi.org/10.1007/s10712-021-09632-w

[9] Kleinbrod, U., Burjánek, J., Fäh, D. (2017): On the seismic response of instable rock slopes based on ambient vibration recordings. *Earth Planets Space*, **69** (1), 9 pages, doi: http://dx.doi.org/10.1186/s40623-017-0712-5

[10] Jug, J., Strelec, S., Bek, A., Pažur, I. (2022): Landslide investigation without the application of exploratory drilling. *Fifth symposium of the Macedonian Association for Geotechnics: Engineering problems in soft rocks*, Skopje, Republic of North Macedonia, 8 pages.

[11] Kovačić, M. (2024). Personal correspondence.

[12] Nakamura, Y. (1989): A method for dynamic characteristics estimation of subsurface using microtremor on the ground surface. *QR of RTRI*, **30** (1), 25-33.

[13] Stanko, D., Markušić, S. (2020): An empirical relationship between resonance frequency, bedrock depth and V_{s30} for Croatia based on HVSR forward modelling. *Natural hazards*, **103**, 3715-3743, doi: https://doi.org/10.1007/s11069-020-04152-z

Proceedings of the 3rd Croatian Conference on Earthquake Engineering - 3CroCEE
19–22 March 2025, Split, Croatia
Copyright © 2025 CroCEE
DOI: https://doi.org/10.5592/CO/3CroCEE.2025.27

EFFECTS OF GROUND MOTION INTENSITY IN ASSESSMENT OF SOIL SLOPES IN EARTHFILL DAM

Kemal Edip [(1)], Davor Stanko [(2)], Julijana Bojadjieva [(3)], Radmila Shalic-Makreska [(4)] and Vlatko Sheshov [(5)]

[(1)] *Prof, Ss.Cyril and Methodius University in Skopje, Institute of Earthquake Engineering and Engineering Seismology-IZIIS, kemal@iziis.ukim.edu.mk*
[(2)] *Assist.Prof, University of Zagreb, Faculty of Geotechnical Engineering, Croatia, dstanko@gfv.hr*
[(3)] *Assoc.Prof, Ss.Cyril and Methodius University in Skopje, Institute of Earthquake Engineering and Engineering Seismology-IZIIS, jule@iziis.ukim.edu.mk*
[(4)] *Prof, Ss.Cyril and Methodius University in Skopje, Institute of Earthquake Engineering and Engineering Seismology-IZIIS, r_salic@iziis.ukim.edu.mk*
[(5)] *Prof, Ss.Cyril and Methodius University in Skopje, Institute of Earthquake Engineering and Engineering Seismology-IZIIS, vlatko@iziis.ukim.edu.mk*

Abstract

The cumulative displacement of sloped soil masses in earth-fill dams subjected to seismic loading is fundamentally governed by both the magnitude and frequency characteristics of the seismic excitation. This correlation necessitates comprehensive numerical simulations incorporating diverse acceleration time histories to capture the full spectrum of potential seismic responses.

This manuscript examines the response of an earth dam slope susceptible to seismically-induced instability under various earthquake scenarios with distinct magnitude-frequency characteristics. The accurate modeling of soil media becomes particularly critical in situations where dynamic pore pressure generation occurs within the soil matrix. The coupled numerical approach developed in this study conceptualizes the soil element as a three-phase medium composed of soil grains, pore water and pore air.

The simulation considers a nonlinear behavior with respect to the water retention curves and material model for the solid state and analysis is performed by ANSYS and PLAXIS. The air pressure is assumed to stay atmospheric in the course of the calculation and matric suction is equal to a negative value of the hydrostatic stress in water pressure. The coupled model allows to take into account the deformations of the soil skeleton and simultaneously considers the pore water pressure change during the earthquake excitation. The seismic behavior of the slope gives interesting results considering both deformation and pore water pressure development. The primary objectives of this research are to investigate the seismic response of earth dam slopes under various earthquake scenarios and compare results between ANSYS and PLAXIS software implementations for multiphase soil modeling. The contributions include the development of a comprehensive coupled numerical approach that simultaneously considers soil deformation and pore pressure evolution during seismic loading along with the integration of hypoplastic material model with multiphase flow analysis.

Keywords: Landslide susceptibility, nonlinear modelling, earth-fill dam.

1. Introduction

In the last decades, earthquakes have shown the importance of ground motion intensities in assessment of soil slopes during seismic events. In 1985 a large earthquake with magnitude Mw=8.1 which occurred in Mexican subduction zone proved that the earthquake effects increased in soft soil areas composed mainly of clay layers in the Valley of Mexico [1]. In 2019 during the Durres earthquake with magnitude Mw=6.4 the effects of soil layers played important role in site amplification [2]. The Earthquake in Zagreb, Croatia also showed that the site response amplification should be given importance [3, 4]. In numerical simulation of heterogeneous materials, it is of great interest that the media is simulated as multiphase media [5-7]. In simulation of hydromechanical behavior of dam bodies, the multiphase flow plays an important role in simulation owing to the nonlinear nature of the fluid flow in the pores. The simulation of porous media such as soils, the behavior is governed largely by the interaction of the solid skeleton with water and/or air in the pores. Therefore, coupled problems

Copyright © 2025 CroCEE
DOI: https://doi.org/10.5592/CO/3CroCEE.2025.27

of fluid flow and deformation of solid skeleton are considered in a detailed way. The advances in computational capabilities have enabled more sophisticated modeling approaches that can better capture the complex interactions between seismic forces, pore pressure development and structural deformation.

2. Model analysis-Numerical model

In defining porous media, one of the great difficulties is to mathematically represent the phases involved. In describing these porous soil media, factors like water saturation and pore pressure have a strong impact on the load distribution. In the description of the material, the macroscopic approach has been followed in which the soil behavior is homogenized over a representative volume element. The concept of volume fraction has been used to evaluate the participation of each constituent in formulation of the equilibrium equations for each phase and to take into consideration the interaction among the phases. The spatial discretization is performed by means of interpolation polynomials (shape functions). Usually, for the structural degrees of freedom biquadratic and for the pressure degrees of freedom bilinear approaches are selected. The solution of the differential equation is in compliance with the physical nonlinearity in the time domain. The software Plaxis has this module for simulation of multiphase media in a very smooth manner and is widely used. On the other hand, the software ANSYS which is a general FEM software has option for programming a special multiphase element while its procedure is given in Fig. 1.

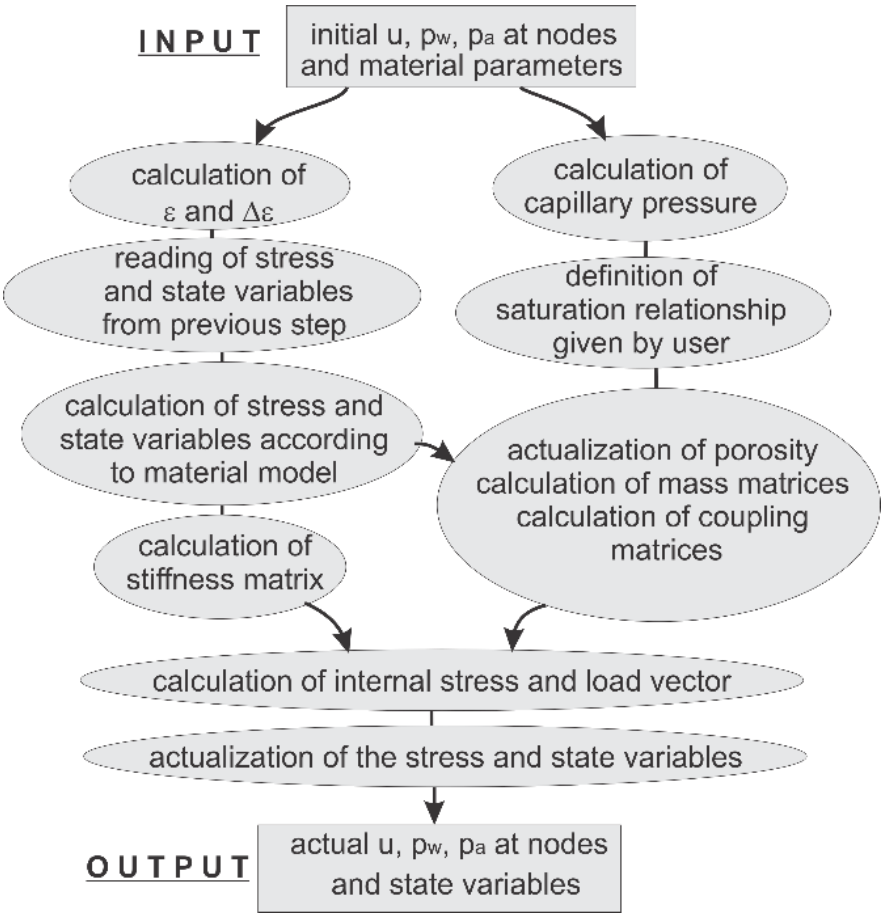


Figure 1. Implementation of the proposed model in ANSYS software [8]

The finite element equations for the numerical model can be summarized as follows:

Copyright © 2025 CroCEE
DOI: https://doi.org/10.5592/CO/3CroCEE.2025.27

$$\begin{pmatrix} \mathbf{M} & \mathbf{0} & \mathbf{0} \\ \mathbf{M_w} & \mathbf{0} & \mathbf{0} \\ \mathbf{M_g} & \mathbf{0} & \mathbf{0} \end{pmatrix} \begin{pmatrix} \ddot{\mathbf{u}} \\ \mathbf{0} \\ \mathbf{0} \end{pmatrix} + \begin{pmatrix} \mathbf{C} & \mathbf{0} & \mathbf{0} \\ \mathbf{C_{sw}}^{\mathbf{T}} & \mathbf{P_{ww}} & \mathbf{C_{wa}} \\ \mathbf{C_{sa}}^{\mathbf{T}} & \mathbf{C_{aw}} & \mathbf{P_{aa}} \end{pmatrix} \begin{pmatrix} \dot{\mathbf{u}} \\ \dot{\bar{\mathbf{p}}}_{\mathbf{w}} \\ \dot{\bar{\mathbf{p}}}_{\mathbf{a}} \end{pmatrix} + \begin{pmatrix} \mathbf{K} & -\mathbf{C_{sw}} & -\mathbf{C_{sa}} \\ \mathbf{0} & \mathbf{H_{ww}} & \mathbf{0} \\ \mathbf{0} & \mathbf{0} & \mathbf{H_{aa}} \end{pmatrix} \begin{pmatrix} \bar{\mathbf{u}} \\ \bar{\mathbf{p}}_{\mathbf{w}} \\ \bar{\mathbf{p}}_{\mathbf{a}} \end{pmatrix} = \begin{pmatrix} \mathbf{f_u} \\ \mathbf{f_w} \\ \mathbf{f_a} \end{pmatrix} \quad (1)$$

The nodal degrees of freedom for displacement, water and air pressure are taken into consideration as u, pw and pa. Their first and second time derivative of solid phase complete the system of equations. The different matrices of the system of equations describe different properties of the numerical model. The indices provide information about the nature and function of the matrix, which can be interpreted as follows. The coupling matrices Csw, Csa describe the interaction of the solid phase with water and air phases. The mutual influence of the fluids with each are represented by Cwa. The compressibility of the various phases and their effects on the entire media is considered by compressibility matrix Pww. The Permeability matrix Hww on the other hand, concerns the flow behaviour.

On the other hand, the PLAXIS [9] software plays important role in simulation of different problems in geotechnical earthquake engineering. The novelty of the proposed method is that both shear stress in soil and pore water pressures are simulated thus describing the effective stress principle in a correct manner in both softwares. The main novelty is the non-linear material model of hypoplasticity which in both softwares has been added as user advancement for the material modelling.

3. Results in simulation of an Earth Dam slope

This particular example shows the implementation of the proposed numerical model in partially saturated soil medium through the numerical simulation of the dam body given in the work of Oettl [10]. The dam body is a compacted earth-fill dam with 52m length and 12 m height. The steady state simulation of the dam is simulated to compare the results of the newly developed coupled model. A typical configuration and finite element mesh for the dam body is generated as shown in Figure 2.

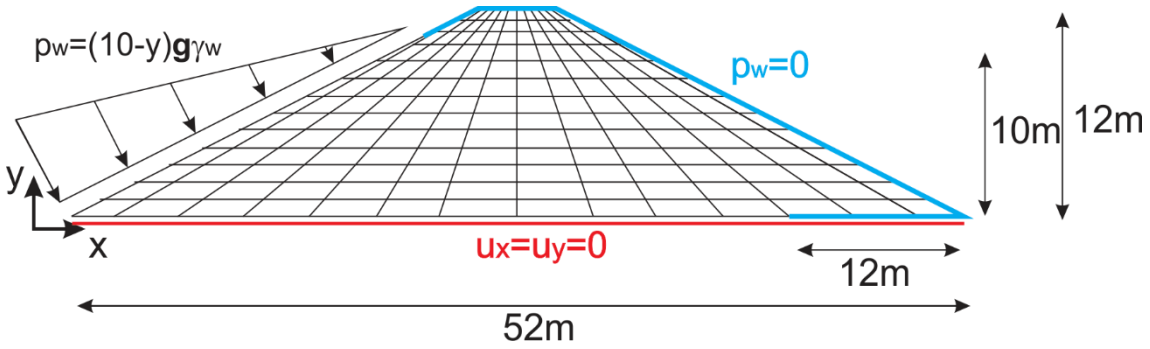


Figure 2. Finite element model of dam

The dam is assumed to be situated above a hard rock formation. Therefore, the base of the dam is assumed to be impermeable and fixed, i.e. the deformability is constrained apart from the drainage which has a length of 12m. The initial effective stress of the dam is obtained after the seepage analysis and static equilibrium has been reached. As can be seen in Figure 4 there is a good correlation between the model simulation of ANSYS and PLAXIS.

Copyright © 2025 CroCEE
DOI: https://doi.org/10.5592/CO/3CroCEE.2025.27

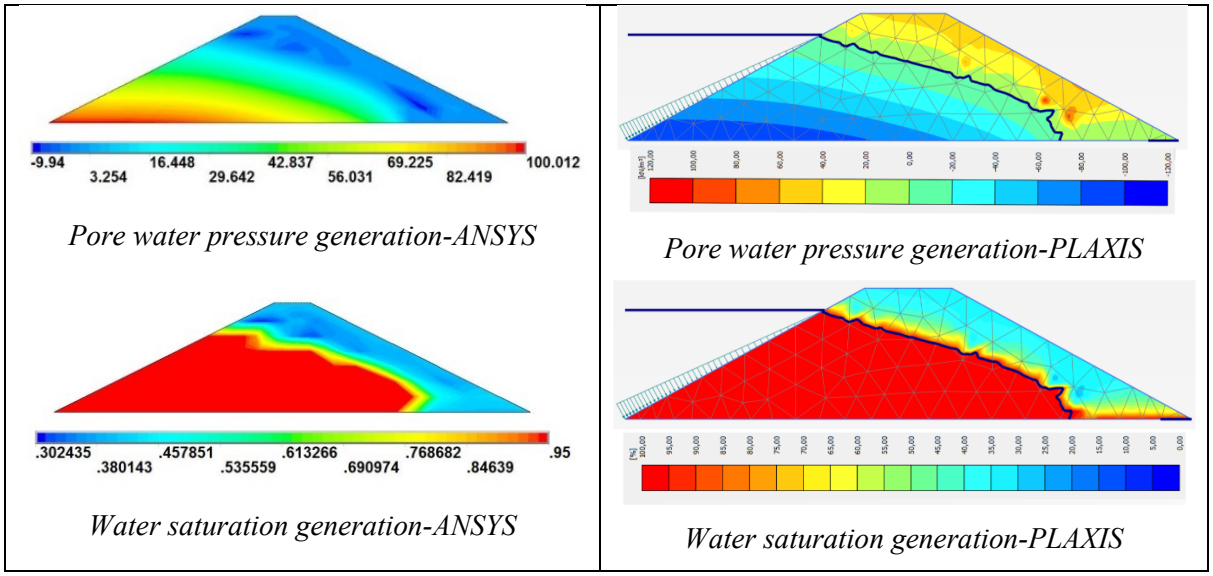


Figure 3. Comparison of pore pressures (left) and water saturation (right) of two softwares ANSYS and PLAXIS

In Figure 3 the water saturations and pressure developments follow a good similarity in which it has to be stated that the fully saturated part is hindered at the right side of the base where the drainage prevents the pore pressure development.

Next, three acceleration histories namely, El Centro N-S, USA, 1940, with magnitude M=6.7; Robic N-S, recorded during the Furlania (Italy) earthquake of 15.09.1976 with magnitude M=6.1., Bitola N-S, recorded on 01.09.1994 with magnitude M=5.2-5.4 have been used in order to analyze the behaviour of the dam body under earthquake excitations. The input earthquake time histories are scaled to 0.25g and are given in the Figure 4:

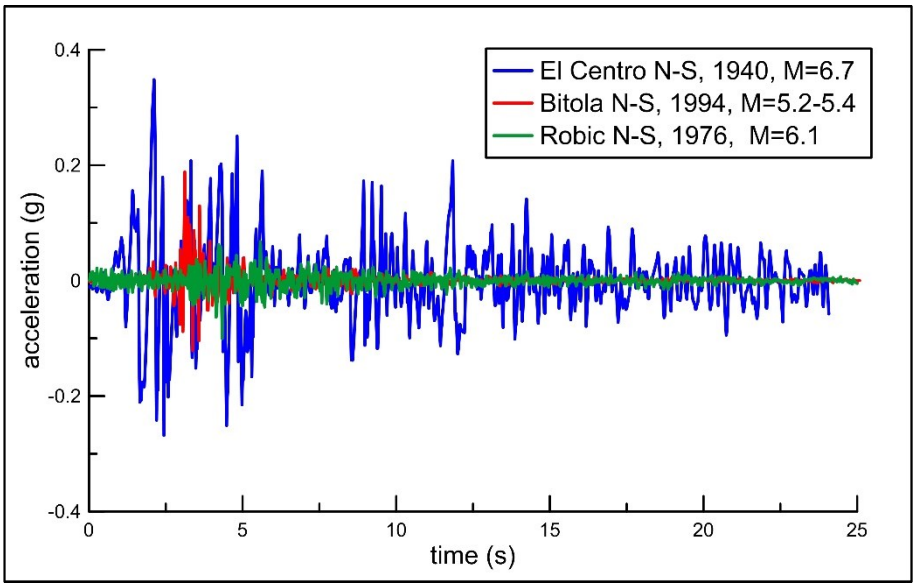


Figure 4. Selected acceleration histories from earthquakes

The earthquake time histories are used as input accelerations at the base of the dam body for analyses in order to estimate the dynamic response of the dam body under strong earthquakes. In the literature, the pore water pressure time histories of dam bodies during earthquakes have been investigated by other authors such as Zienkiewicz [11], [12], etc. In their works, the pore pressure development has caused

Proceedings of the 3rd Croatian Conference on Earthquake Engineering - 3CroCEE
19–22 March 2025, Split, Croatia
Copyright © 2025 CroCEE
DOI: https://doi.org/10.5592/CO/3CroCEE.2025.27

main issues in the stability of the dam bodies. In this paper the numerical results of both pore pressure and of displacement time history are simulated and discussed. The advantage of this model is that the used hypoplastic model takes into account the accumulation of strain in each cycle of the stress – strain relation [13]. In selection of the material model for solid phase the hypoplasticity material model has been used.

Table 1. Material parameters of the dam body

	Parameter	Symbol	Value	Unit
1	Density of solid phase	ρs	2.7	ton/m³
2	Density of water pase	ρw	1.0	ton/m³
3	Permeability	k	1.0×10^{-7}	m/s
4	Compression modulus of solid phase	Ks	10^{9}	kPa
5	Compression modulus of water phase	Kw	2×10^{4}	kPa
6	Dynamic viscosity of water	μw	1.31×10^{6}	kNs/m²
7	Critical internal angle	φc	30	degrees
8	Granulate hardness	hs	1600	MPa
9	Exponent	n	0.39	-
10	Minimum void ratio	ed0	0.62	-
11	Critical void ratio	ec0	0.94	-
12	Maximum void ratio	ei0	1.08	-
13	Numerical parameter	α	0.2	-
14	Numerical parameter	β	1.1	-
15	Numerical parameter	R	0.0001	-
16	Numerical parameter	mr	2.5	-
17	Numerical parameter	mt	9.0	-
18	Numerical parameter	βr	0.25	-
19	Numerical parameter	χ	9.0	-

In simulation of earthquake time histories the duration used for simulation is considered only 25seconds during which the peak of accelerations of all earthquake time histories are found. In Figure 6 the pore pressure development during the El Centro earthquake time history simulation is considered. At the beginning the pore pressure distribution is similar to the steady state pore pressure as given in Figure 4. When the peak acceleration is considered at time=10seconds the development of pore pressure intensifies in the middle of the dam body changing the density and effective stress parameters. As the earthquake effects continue the pore pressure development shifts to the left side of the dam body which influences the overall stability of the dam body.

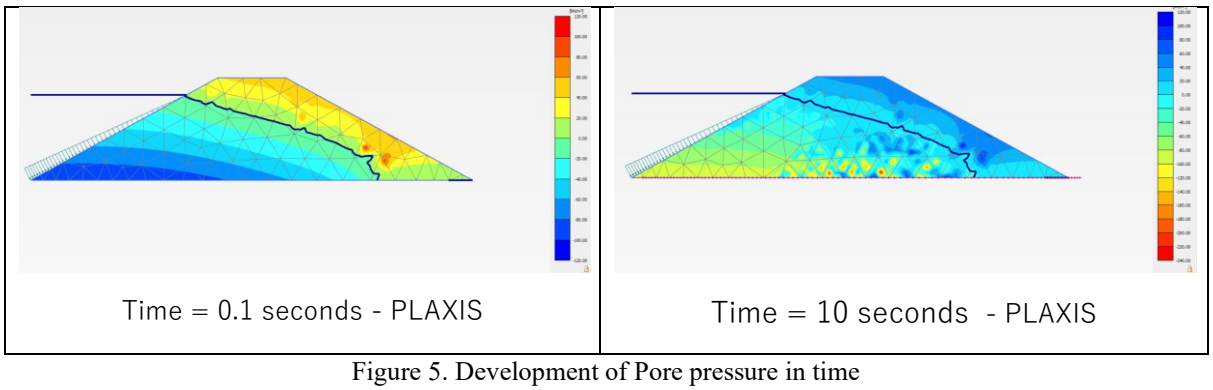


Figure 5. Development of Pore pressure in time

The Figure 6 shows the temporal evolution of pore water pressure distribution in the earth dam. At the beginning of the time the pore pressure is presented as the hydrostatic pressure distribution while at the

Copyright © 2025 CroCEE
DOI: https://doi.org/10.5592/CO/3CroCEE.2025.27

time=10s, there is notable intensification of the pore pressure development in the central region of the dam body. This intensification is significant because it indicates the change in the density and effective stress parameters according to the Hypoplastic material model which has been used for the soil modelling. The detailed presentation for effective stress is given in Figure 6.

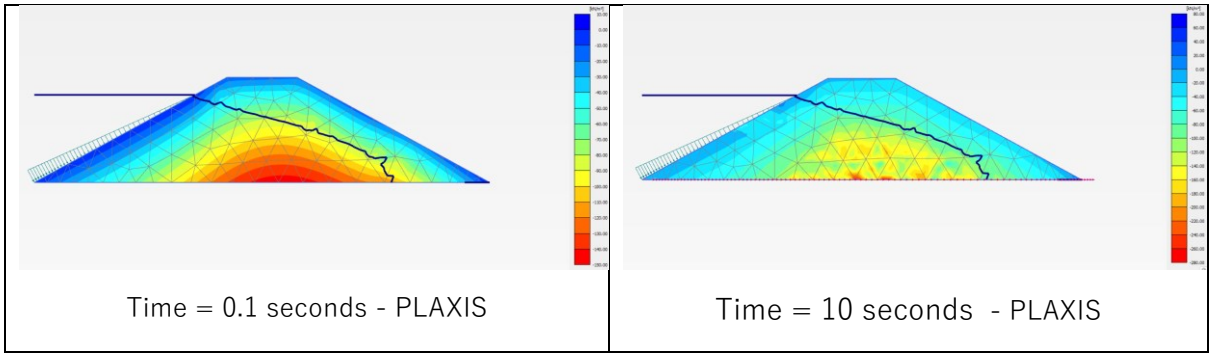


Figure 6. Development of Effective stress in time

As can be seen from Figure 6, the development of effective stress in time during the earthquake simulation follows a gravity induced pattern at the beginning while at the end of time the there is a noteworthy redistribution of effective stresses. This redistribution is directly linked with the pore pressure development as increased pore pressure reduce the effective stress which gives to the multiphase simulation weight in dealing with partially saturated soil media. This reduction in effective stresses is crucial for the stability of the earth dam as it directly affects the shear strength of the soil material.

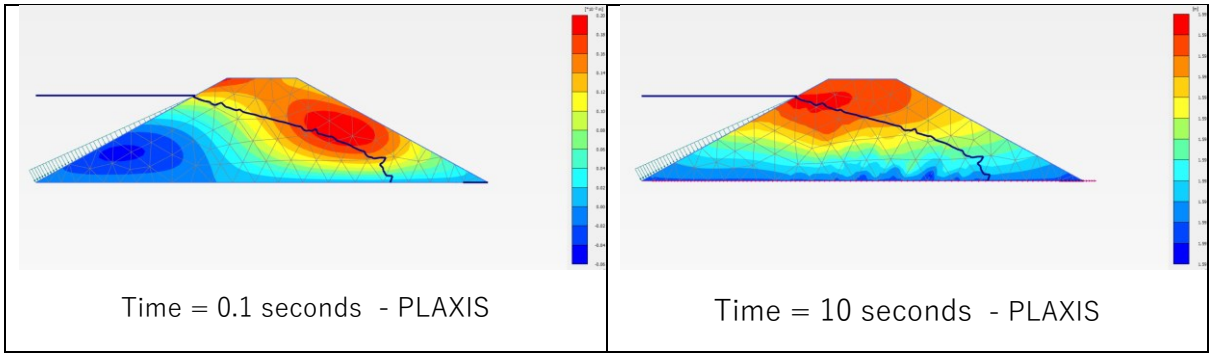


Figure 7. Development of horizontal displacement in time

Figure 7 shows the development of horizontal displacements in the earth-fill dam body in which at the end of the earthquake loading there is a marked increase in horizontal displacement, particularly pronounced in the upper left portion of the dam body. This pattern of displacement in the dam body correlates directly with the previously observed changes in pore pressure (Figure 5) and effective stress (Figure 6).

The earthquakes applied to ANSYS software reveal similar results in simulation of pore pressures at the upstream slope of the body as given in Figure 8.

Copyright © 2025 CroCEE
DOI: https://doi.org/10.5592/CO/3CroCEE.2025.27

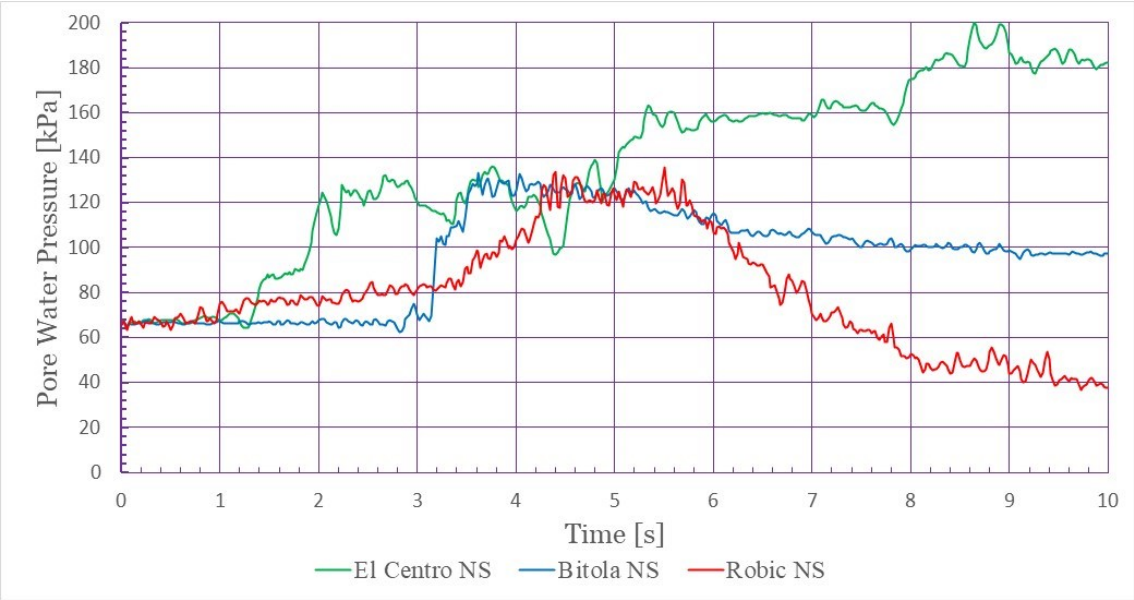


Figure 8. Time history of pore water pressure

As can be seen from Figure 8 the time history of pore pressure developed at the front side of the dam using the software ANSYS has similar forms to those found in PLAXIS above. The observation shows that the increased pore pressure development at the front side (upstream slope) of the dam body correlates with larger displacements which tend to make the dam body unstable. This relationship between pore pressure build-up and horizontal displacement at the upstream slope during seismic loading leads to reduced effective stresses as is also seen in the PLAXIS in Figure6 and should be considered carefully.

4. Conclusions

Based on the analysis of the earth-fill dam's seismic response through simulations using software ANSYS and PLAXIS several significant conclusions can be drawn. The correlation between ANSYS and PLAXIS simulations validates the numerical approaches, demonstrating consistent predictions for both pore pressure distribution and water saturation patterns. It is to be stated that the earthquake loading notably influences both pore pressure development and solid displacements with particularly significant effects observed on the upstream side of the dam body. The displacements have been increased significantly after the peak point of earthquake has ended due to a decrease in pore water pressure which contributed to further increase in overall deformation. The parametric analysis examining different acceleration time histories provides comprehensive understanding of dam response under varying seismic conditions. The coupled approach, simultaneously considering deformations and pore pressures proves essential for accurate prediction of dam behavior. Large horizontal permanent movements observed at the upstream side indicate a critical vulnerability zone with potential for triggering overall dam failure. It is recommended to implement enhanced monitoring systems focusing on pore pressure development at the upstream slope and install additional drainage systems to better control pore pressure development during seismic events.

Acknowledgements

This work was supported in part by the Croatian Science Foundation under the project "Seismic ground motion amplification induced by topographic irregularity in Northern Croatia" [HRZZ-IP-2022-10-1296].

Copyright © 2025 CroCEE
DOI: https://doi.org/10.5592/CO/3CroCEE.2025.27

References

1. Chavez-Garcia, F.J. and P.-Y. Bard, *Site effects in Mexico City eight years after the September 1985 Michoacan earthquakes.* Soil Dynamics and Earthquake Engineering, 1994. **13**(4): p. 229-247.
2. Sheshov, V., et al., *Reconnaissance analysis on buildings damaged during Durres earthquake Mw6. 4, 26 November 2019, Albania: effects to non-structural elements.* Bulletin of Earthquake Engineering, 2021: p. 1-23.
3. Markušić, S., et al., *The Zagreb (Croatia) M5. 5 Earthquake on 22 March 2020.* Geosciences, 2020. **10**(7): p. 252.
4. Atalić, J., et al., *The Mw5. 4 Zagreb (Croatia) earthquake of March 22, 2020: impacts and response.* Bulletin of Earthquake Engineering, 2021. **19**(9): p. 3461-3489.
5. Edip, K., *Development of three phase model with finite and infinite elements for dynamic analysis of soil media*. 2013, Ss. Cyril and Methodius: Institute of Earthquake Engineering and Engineering Seismology.
6. Edip, K., et al., *EFFECTS OF CORE STRUCTURE IN MULTIPHASE SIMULATION OF AN EARTH DAM.* 2023.
7. Edip, K., et al., *Development of coupled numerical model for simulation of multiphase soil.* Computers and Geotechnics, 2018. **96**: p. 118-131.
8. ANSYS. *Fem Software*. 2006.
9. Plaxis, B., *PLAXIS 2D Version 2024-Finite element code for soil and rock analysis.* AA Balkema, Delft, 2024.
10. Oettl, G., R.F. Stark, and G. Hofstetter, *Numerical simulation of geotechnical problems based on a multi-phase finite element approach.* Computers and Geotechnics, 2004. **31**(8): p. 643-664.
11. Zienkiewicz, O.C., et al., *Static and Dynamic Behaviour of Soils: A Rational Approach to Quantitative Solutions. II. Semi-Saturated Problems.* Proceedings of the Royal Society of London. A. Mathematical and Physical Sciences, 1990. **429**(1877): p. 311-321.
12. Khoei, A.R. and T. Mohammadnejad, *Numerical modeling of multiphase fluid flow in deforming porous media: A comparison between two- and three-phase models for seismic analysis of earth and rockfill dams.* Computers and Geotechnics, 2011. **38**(2): p. 142-166.
13. Niemunis, A. and I. Herle, *Hypoplastic model for cohesionless soils with elastic strain range.* Mechanics of Cohesive-frictional Materials, 1997. **2**(4): p. 279-299.

Proceedings of the 3rd Croatian Conference on Earthquake Engineering - 3CroCEE
19–22 March 2025, Split, Croatia
Copyright © 2025 CroCEE
DOI: https://doi.org/10.5592/CO/3CroCEE.2025.63

THERMO-MECHANICAL BEHAVIOR AND STRUCTURAL DESIGN OF GEOTHERMALLY ACTIVE PILES

Guxim Rrudhani [(1)], Josif Josifovski [(2)]

[(1)] *Teaching Assistant, University of Prishtina "Hasan Prishtina", Faculty of Civil Engineering, guxim.rrudhani@uni-pr.edu*
[(2)] *Professor, Ss. Cyril and Methodius University in Skopje, Faculty of Civil Engineering, jjosifovski@gf.ukim.edu.mk*

Abstract

Contemporary living and the need for renewable energy sources demand innovative "green" technologies that offer structural improvement and simultaneously provide more economical and long-term cost-friendly solutions. In geotechnical engineering, shallow thermo-active geo-structures look like one of the most promising concepts. Thermo-active geo-structures may include base slabs, piles, retaining walls, and supporting elements for tunnels, such as linings and anchors, which besides the mechanical (bearing) function have a thermal function working as heat exchanger systems. In most cases, these structures are piles, whose behavior could be predicted using different approaches. Utilizing foundation systems as heat exchangers has received significant public interest worldwide, as these energy geo-structures can constitute a clean, renewable, and economical solution for space heating and cooling. Thermo-active geo-structures are considered innovative alternatives to traditional Ground Source Heat Pump (GSHP) systems for space heating and cooling, having the potential to reduce the upfront cost of the GSHP systems. Hence, the structural element gets an additional thermal function such as piles, retaining walls, tunnel linings pavements, etc. This way they will be loaded by thermal change or difference in temperature which must be considered during the design phase. The most common type of energy geo-structures are energy piles, most likely due to their significant geometrical similarities with the thoroughly studied traditional vertical borehole systems, attempting to adapt the available thermal design methods for the traditional borehole systems for energy pile design, commercial aspects, benefits of using Energy Geotechnical Structures (EGS) compared to standard Borehole heat exchanger systems.

Keywords: Geotechnical engineering, thermos-active structures, geothermal energy, geothermal pile.

1. Introduction

The foundation of a structure represents a connection between the structure and the supporting soil. Through the foundation, mechanical loads are transferred to the soil. In the design of every geostructures, the behavior of soil plays a primary role. For energy geostructures, an energy supply role is added to the conventional role of the foundation as structural support. The so-called Energy piles are generally subjected to monotonic or cyclic temperature changes, depending on the season of operation or daily thermal energy requirements of the building. They are subjected to daily cyclic temperatures from intermittent operations of the ground source heat pump (GSHP) with natural or forced ground thermal recoveries during the non-operating times of the GSHP [1]. The long-term temperature changes that occur along the length of the energy pile, caused by the effects of heating and cooling, can significantly affect the stress state around the pile, and therefore its load-bearing capacity. The cyclic processes of heating and cooling affect the volume changes of the pile, but also the soil surrounding it. The pile elongates when heated, and contracts when cooled, which causes additional axial tensile stress, which further affects the soil-pile interaction. All these additional effects that occur from the activity of the energy piles can affect the load-bearing capacity and stability of the pile. Therefore, it is important to take them into account when designing geothermally active structures. Given that geothermal piles, compared to conventional piles, have additional impacts, there are no precise design methods to verify the geotechnical strength of energy piles [2]. For years, designers have designed buildings with energy piles based on empirical understandings or with a conservative approach, increasing the safety factor (Boönnec, 2009, Knellwolf et al., 2011).

Proceedings of the 3rd Croatian Conference on Earthquake Engineering - 3CroCEE
19–22 March 2025, Split, Croatia
Copyright © 2025 CroCEE
DOI: https://doi.org/10.5592/CO/3CroCEE.2025.63

2. Physical processes involved in exploitation of the energy piles

The exploitation of energy piles involves complex physical processes related to heat transfer and mechanical behavior. Heat transfer in energy piles occurs through conduction within the pile material, convection within the circulating fluid, and conduction or convection in the surrounding soil, depending on moisture content and groundwater flow. These thermal interactions influence the temperature distribution within the pile and the soil, affecting the pile's structural response. Additionally, thermal expansion and contraction of the pile due to temperature variations introduce thermomechanical stresses, which must be considered in design to prevent structural damage or excessive deformation. The efficiency of energy piles depends on factors such as pile material properties, pipe configuration, soil thermal characteristics, and operational conditions. Understanding these physical processes is crucial for optimizing energy pile performance, ensuring both structural stability and effective geothermal energy exchange.

2.1. Principle of the heat transfer in the soil

Soil is a multiphase material with a complex heat transfer mechanism, which includes conduction, convection, radiation, evaporation and condensation, ion exchange and freeze-thaw processes. As shown in Figure 1, the main mechanism of heat transfer in the soil is conduction, followed by convection. The figure illustrates different heat transfer mechanisms in soil based on the D_{10} effective grain size (ranging from clay to gravel) and the degree of saturation. It identifies six key processes: thermal redistribution of moisture, vapor diffusion due to moisture gradients, free convection in water, free convection in air, heat radiation, and heat conduction as the dominant mechanism. The transitions between these processes depend on the soil's particle size and moisture content. Finer soils (clay and silt) are dominated by moisture-driven heat transfer, while coarser soils (sand and gravel) experience convection and radiation effects, particularly at lower saturation levels. Thermal conduction is also possible if there is a phase change of water (latent heat during evaporation and condensation). Radiation is of minimal importance (1%) and is limited to the upper soil layers. Thaw-thaw processes, although they can make heat transfer more effective, are recommended to be neglected for thermo-active foundations for geotechnical reasons. [3]

The total heat transfer q_{tot} can be defined according to the expression (Rees et al. 2000):

$$q_{tot} = q_{cond} + q_{l.conv} + q_{v,conv} + q_{lat}$$

Where q_{tot} represents heat transfer by conduction, $q_{l.conv}$ represents heat transfer by fluid convection, $q_{v,conv}$ represents heat transfer by evaporation, and q_{lat} represents latent heat transfer.

Latent heat transfer occurs as a result of phase changes of pore water (evaporation) and depends on the amount of vapor transfer occurring in the soil pores. It increases with decreasing water content and can be expressed as follows:

$$q_{lat} = L_0 \rho_l \vartheta_v$$

Where L_0 represents the latent heat of vaporization, ρ_l represents the density of water, and ϑ_v represents the rate of evaporation.

Copyright © 2025 CroCEE
DOI: https://doi.org/10.5592/CO/3CroCEE.2025.63

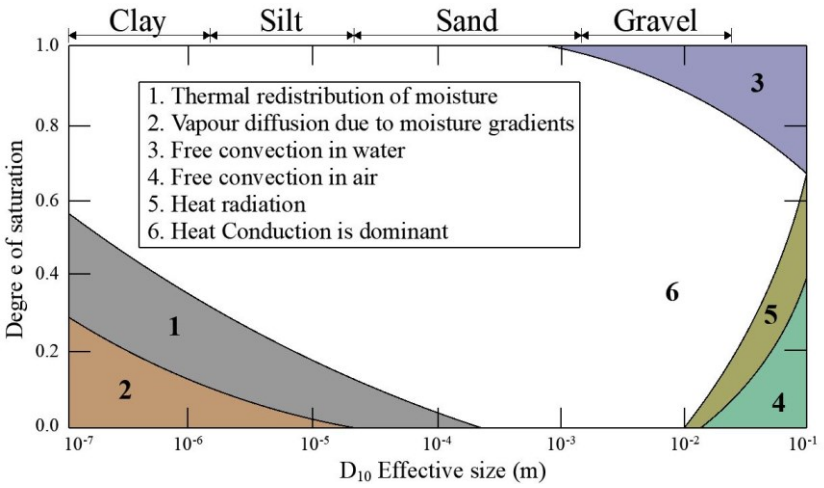


Figure 1. Dominant heat transfer mechanisms in soil in relation to grain size and soil saturation (adapted from Farouki 1986)

Thermal convention occurs between thermodynamic systems that are moving relatively to each other. In soils, the solid phase is static: hence convection can only occur in the water or (pore) gas phase. The heat transfer by fluid convection, $q_{l.conv}$ and the heat transfer for evaporation (pore gas) $q_{v,conv}$, are defined by the following expressions:

$$q_{l,conv} = c_l \rho_l \vartheta_l \Delta T$$

Where c_l is the specific heat capacity of the pore water, ρ_l is the density of the water, ϑ_l is the velocity of the water, and ΔT is the temperature change.

$$q_{v,conv} = c_v \rho_v \vartheta_v \Delta T$$

Where c_v is the specific heat capacity of the soil vapor, ρ_v is, the density of the soil vapor, ϑ_v represents the evaporation rate, and ΔT is the temperature change.

Thermal conduction is a process where heat is transferred from one part of a medium to another, without visible movement in the medium. Thermal energy is transferred from molecule to molecule. According to Fourier's law, the heat flux for a heat volume Q through an arbitrary surface A during a time t is the heat flux per unit area, q_{cond}, generated by conduction is defined by the expression:

$$q_{cond} \frac{Q}{At} = -\lambda \Delta T$$

Where λ represents the thermal conductivity of the medium, Δ is the gradient parameter and T is the temperature.

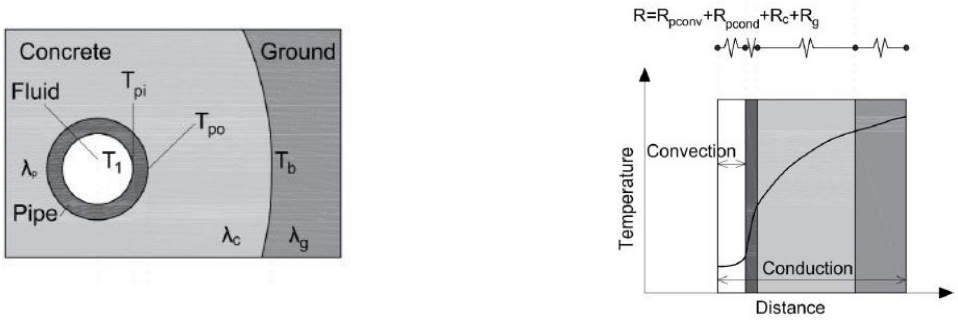
Changes in moisture content of the soil causes changes in the thermal properties of it, especially in unsaturated soils (Farouki 1981). The evaporation of water in the soil induces a temperature gradient and water vapor can move through the pores towards the lower vapor pressure. If the temperature is lower in the new location, condensation occurs, releasing heat and changing the amount of water in the soil. These changes in moisture content affect the thermal properties of the soil by changing the saturation degree but also contribute to the process of heat transfer. This process is important in soil with high porosity and high temperature differences.

2.2. Heat transfer in the Energy Pile

The temperature difference between the ground, the pile, and the fluid that carries the heat through the geothermal installation drives the heat transfer in the geothermal system. The mechanisms involved in this process are shown in Figure 4, namely convective heat flow between the fluid and the pipe, conductive heat flow in the pipe wall, conductive heat flow in the concrete pile, conductive heat flow

Copyright © 2025 CroCEE
DOI: https://doi.org/10.5592/CO/3CroCEE.2025.63

in the soil, and convective heat flow in the soil, if the geothermal water flow rate is greater than 0.5 – 1.0 m/day (Loveridge and Powrie 2012).



a) b)

Figure 2. Heat transfer mechanism in energy piles (a) plan view of the energy pile and surrounding soil (b) lateral view of the energy pile and surrounding soil (Loveridge and Powrie 2012)

According to Lee et al. (2009) the total usable heat extracted through the energy loops can be calculated using the following equation:

$$q_{tot} = Q_{in} - Q_{out} = mc_{fluid}(T_{in} - T_{out})$$

Where m is the mass flux density of the circulating fluid, c_{fluid} is the heat capacity of the circulating fluid, Q is the total heat extracted, T_{in} is the inlet temperature, while T_{out} is the outlet temperature.

In the design of energy piles, the instantaneous steady state is assumed to be the internal heat transfer between the heat fluid and the outer surface of the concrete. The temperature difference between the fluid in the pipes and the edge of the heat exchangers ΔT can be calculated based on the thermal resistance of the heat exchanger:

$$R_{tot} = \frac{T_s - T_f}{q}$$

Where T_s is the temperature of the soil-pile interaction, T_f is the temperature of the fluid carrying the heat and q is the heat flow per meter of the GSHP exchanger. The total thermal resistance can be divided into the thermal resistance of the individual components of the geothermal construction, i.e.:

$$R_{tot} = R_{fluid} + R_{pipe} + R_{concrete} + R_{ground}$$

The thermal resistance of the fluid circulating in the pipes is calculated by the equation:

$$R_{fluid} = \frac{1}{2n\pi r_i h}$$

Where r_i is the inner radius of the pipe, n represents the number of pipes, and h is the coefficient of heat transfer through convection. The value of the thermal resistance depends on the number of pipes, their disposition, the thickness of the concrete layer, as well as the thermal conductivity of the concrete and the thermal characteristics of the fluid that transfers heat.

The thermal resistance of the pipe is represented by the following equation:

$$R_{pipe} = \frac{ln(r_0/r_i)}{2n\pi k_p}$$

Where r_0 is the outer radius of the pipe, while k_p denotes the thermal conductivity of the pipe material.

Regarding the thermal resistance of the concrete cross-section, its steady state can be calculated using the thermal resistance equation of a cylinder, but assuming an effective internal radius of that cylinder r_{eff}. [4]

The thermal resistance of concrete using the equivalent diameter approach is given by:

Copyright © 2025 CroCEE
DOI: https://doi.org/10.5592/CO/3CroCEE.2025.63

$$R_{concrete} = \frac{ln(r_b/r_{eff})}{2\pi k_c}$$

Where r_b is the radius of the circle, k_c is the thermal conductivity of the concrete, and r_{eff} is the effective radius

$$r_{eff} = r_0\sqrt{n}$$

The equivalent cylinder approach does not consider the position of the pipes. The mechanism is graphically shown in the figure below:

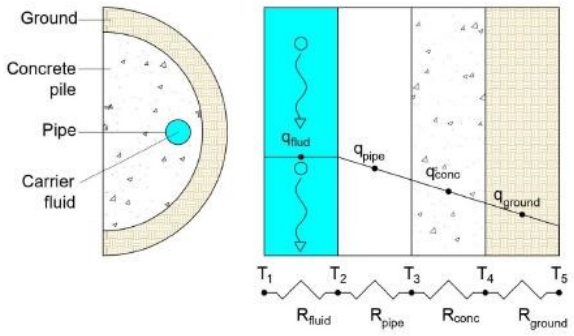


Figure 3. Description of the heat transfer mechanism from the primary circulation of the energy pile to the ground [3]

It should be noted that the concrete layer usually depends on the construction design (the placement of the reinforcement cage) and because it is important to avoid thermal interactions between cold and hot pipes, the value of the shape factor can only be partially optimized. Loveridge et al. (2014) have proposed tables for determining the thermal resistance of piles. According to the tables, it can be concluded that with a larger pile diameter, lower thermal resistance, and thinner concrete layer, thermal contact between the pile and the soil would be better, with an optimal number of pipes according to the diameter of the pile (increasing the number of pipes can cause more thermal interactions between hot and cold pipes and reduce the efficiency of the system). Although these tables can offer a first idea of the characteristic configuration suitable for an energy pile, it is needed to be used more advanced tools for the design of the entire system and for monitoring the long-term behavior of the geothermal system. [4]

3. Thermo-mechanical behavior of energy piles

Thermal and mechanical loads application to energy piles introduces new aspects in the response of these piles compared to conventional piles which are typically subjected to only mechanical loads. This is a result of coupled heat transfer and deformation of materials. Different approaches can be used to investigate the response of energy piles, subjected to mechanical and thermal loads. These include full-scale in situ tests, model-scale laboratory tests, and centrifuge tests. To interpret the response of energy piles these must be considered: idealizations and assumptions, classifications of energy piles, temperature, vertical and radial strains due to thermal loads, vertical displacements, shear stresses and vertical stress due to thermal and mechanically loads, and freedom degrees. [5]

Idealizations and assumptions: Soil layers surrounding the pile are not fully horizontal, also thermal and mechanical loads cause non-uniform variations of the temperature, stress, strain, and displacement within and around the pile. In the calculations of energy piles, soil layers are assumed to be fully horizontal, and it is assumed that temperature, stress, strain, and displacement are uniform and representative of the energy pile response. [6]

Copyright © 2025 CroCEE
DOI: https://doi.org/10.5592/CO/3CroCEE.2025.63

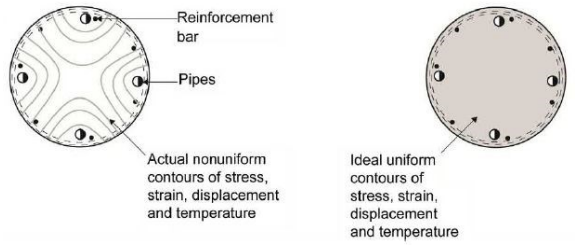


Figure 4. Idealization of stress, strain, displacement and temperature fields within energy piles

In Fig. 4 is shown comparison between the actual and ideal stress, strain, displacement, and temperature distribution in a circular cross-section of a geothermal pile, composed by concrete column with embedded reinforcement bars and pipes. The left side of the figure illustrates the real scenario, where the presence of reinforcement and pipes causes nonuniform contours due to material discontinuities and thermal effects. The right side of the figure represents an idealized condition where these properties are uniformly distributed, assuming a homogenous material without interruptions. This comparison highlights the impact of embedded elements on structural behavior and the challenges in achieving uniform performance

Classification of energy piles: Classification of energy piles can be done according to various criteria. The commonly used classification is related to the technique because of its influence on the response of the energy pile. Another criterion of classification refers to the bearing behavior of the pile [7].

Temperature variations: Due to geothermal operation in energy piles, the temperature can develop notable variations. For known boundary conditions, the rate of temperature variations depends on the thermal power applied to the pile, as well as on the thermohydraulic properties of both surrounding ground and the pile. [8]

Vertical and radial strains due to thermal load: For energy pile under thermal loads, expansive strains are generated during heating and contraction strains during cooling. These strains are usually not uniform with depth. End-restraint provided by the presence of the ground and superstructure determines the evolution of the strains. Besides vertical strains, because of the applied thermal loads also radial strains develop in energy piles. Vertical and radial strains caused by the temperature variations can be observed for the same temperature variation which is applied to the energy pile. But, because of the different dimensions, length, and diameter of energy piles, the vertical and horizontal displacements of the pile, associated with the considered strains are markedly different.[9]

Vertical and shear stress due to thermal and mechanical loads: Thermal loads along energy piles describe at best a linear distribution of the vertical displacement with depth, and at worst scenario a nonlinear distribution of these vertical displacements, which become more prominent with increasing compressibility and slenderness of the pile. These should be taken into consideration during the analysis of both rigid and deformable piles. Shear stress at energy piles are mobilized in opposite directions of the deformations induced by the thermal loads, to ensure equilibrium with the surrounding soil from the so-called null point of the shear stress. Mobilized shear stresses magnitude depends on the restraint conditions.[3]

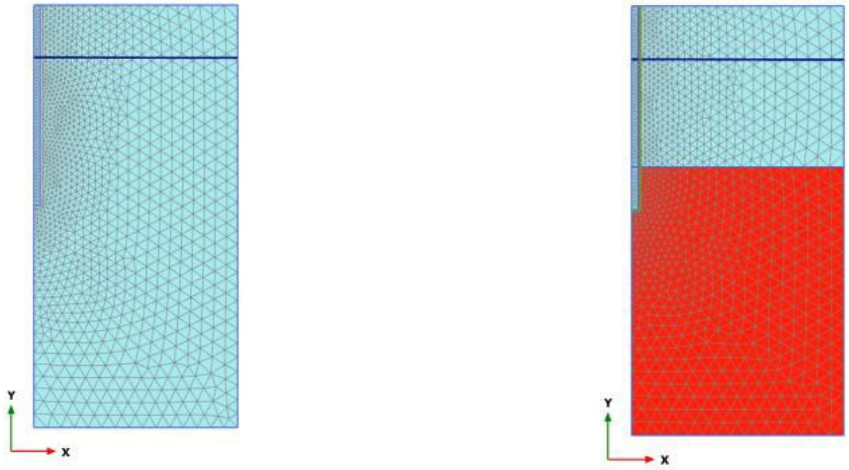
Freedom degrees: Another factor determining the response of the energy pile under mechanical and thermal loads is the end-restraint. In this context, the degree of freedom can effectively characterize the degree of restraint of energy piles.[8]

4. Numerical modelling of the energy piles

Two cases of geothermal piles, free head pile and end bearing pile were analyzed using the software Plaxis 2D. "Plaxis 2D" is a finite element software for geotechnical engineering applications. When working in PLAXIS 2D, the geomaterial is considered in a three-phase (solid/liquid/gas) porous medium, but the gas pressure is taken as constant, which is widely accepted in geotechnical engineering. In both cases, it was used an axisymmetric model, placed in a half-space with dimensions x_{max}=20 m

Copyright © 2025 CroCEE
DOI: https://doi.org/10.5592/CO/3CroCEE.2025.63

and y_{max}=40 m. The piles were modeled with a length of 19.0 m and a diameter of 0.60 m. In the first case for free head pile there is only one layer of clay with the thickness of 40 meters (blue color in the model in Figure 9a), while in the second case for end bearing pile, it consists of two layers, the first layer of clay with 16 meters (blue color in the model, Figure 9b) and the layer of limestone of 24 meters (red color in the model Figure 9b). Material's properties for soil layers and the pile are given in the Table 1. During the analysis, volumetric finite elements were used, with a "fine" finite element mesh.



a) b)

Figure 9. Plaxis models, a) Free head pile in clay layer; b) End bearing pile in clay and limestone layers

The piles were calculated according to the Mohr-Coulomb laws. The load was applied in four phases for both cases. The material parameters for both cases and loading phases are given in the tables below:

Table 1. Material properties of the models

		Case 1 – Free head pile		Case 2 – End-bearing pile		
Parameters	Unit	Concrete	Clay	Concrete	Clay	Limestone
General						
Model*		LE	MC	LE	MC	LE
Unsaturated unit weight	kN/m^3	25.00	21.00	25.00	21.00	25.50
Mechanical						
Young's modulus	kN/m^2	31.5 E6	55.00 E3	31.5 E6	55.00 E3	2.60 E6
Poisson's ratio	-	0.20	0.30	0.20	0.30	0.1517
Cohesion	kPa	-	2.00	-	2.00	
Friction angle	°	-	35.00	-	35.00	
Dilatancy angle	°	-	5.00	-	5.00	
Thermal						
Heat capacity	$J/T/K$	800	890	800	890	784
Thermal conductivity	$W/m/K$	2.100	4.450	2.100	4.450	1.100

Copyright © 2025 CroCEE
DOI: https://doi.org/10.5592/CO/3CroCEE.2025.63

Soil density	t/m^3	2.500	2.735	2.500	2.735	2.250
Thermal expansion	$1/K$	1.0 10E-5	1.0 10E-4	1.0 10E-5	1.0 10E-4	1.0 10E-6

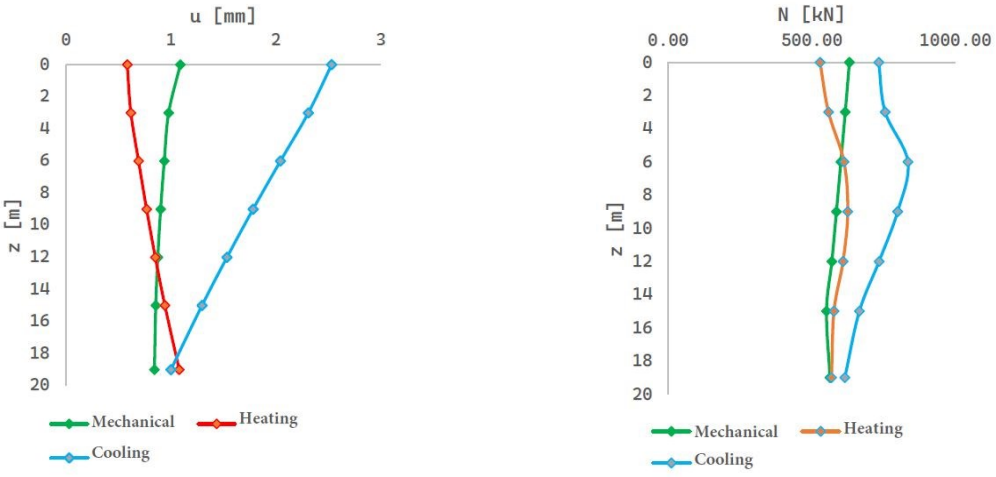
Table 2. Loading phases

Phase	Loading type	Specifics
Phase 1	Starting phase	-
Phase 2	Mechanical load	F=3500 kN
Phase 3	Thermo-mechanical load - heating	Harmonic temperature variation ΔT=8 °C, t=20 days
Phase 4	Thermo-mechanical load - cooling	Harmonic temperature variation ΔT=8 °C, t=20 days

As previously mentioned, a free head pile and end-bearing pile are analyzed in three characteristic phases: (1) mechanical loading, (2) thermomechanical loading – heating and (3) thermomechanical loading – cooling. A linear temperature change of 8 $°K$ is given in the two phases of thermal loading respectively. The aim is to determine the thermomechanical behavior of the pile under the action of mechanical and thermal loads. During the analysis, the most characteristic changes shown are the displacements $[u]$, axial force $[N]$, vertical stresses $[\sigma_{yy}]$ and shear stresses $[\tau]$ along the length of the circle, for mechanical loading, thermomechanical loading-heating and thermomechanical loading-cooling.

4.1. Case 1 – Free head pile

From the obtained results it shows that in the case of a free head pile, under the action of the mechanical load a decrease in the magnitude of the displacements along the length of the pile is shown. This is also due to the increase in the strength of the soil layer along the length of the pile, driven by the activated mobilized friction strength along the length of the pile. In the heating phase of the pile in summer, under the action of the displacement that causes the lifting of the pile head on one side, and on the other hand the mechanical load acts vertically downwards, so finally the total displacements decrease in this phase. This causes additional effects on the state of stress. According to the results, in the cooling phase, an additional increase in the total displacements occurs at the pile head, which follows as a result of a decrease in the axial force (Fig. 10a).



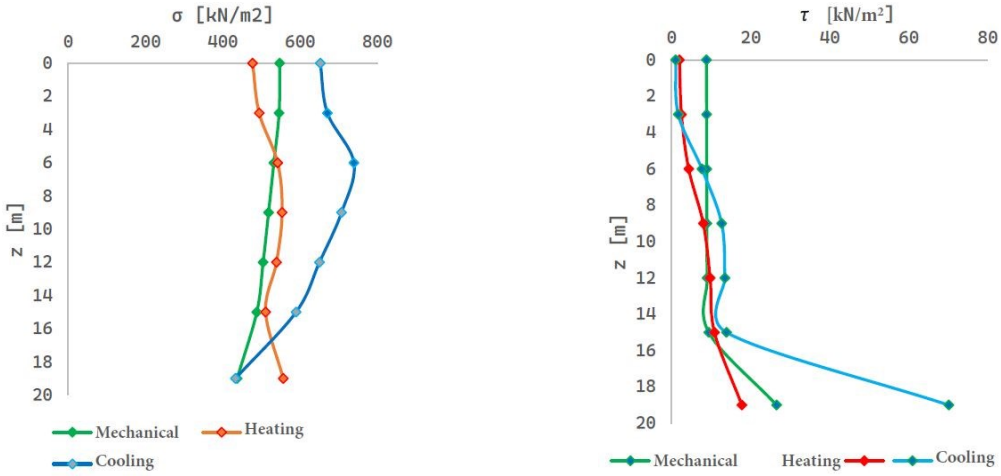
a) b)

Figure 10. a) Change in displacements along the length of the pile from three load cases; b) Change in axial force along the length of the pile from three load cases.

Copyright © 2025 CroCEE
DOI: https://doi.org/10.5592/CO/3CroCEE.2025.63

Considering that during the operation of free head pile, friction is additionally included, and additional mobilized friction stress occurs, the axial force from the mechanical loading phase decreases along the length of the pile. As mentioned earlier, in the thermomechanical loading phase - heating, it is shown a decrease in the total displacements at the pile head, which results in an increase in the axial forces inside the pile. On the other hand, the increase in the displacement of the pile head leads to a reduction in the axial force during the thermomechanical loading phase – cooling (Fig. 10b).

Regarding the normal stresses they decrease with the depth of the pile. From the aspect of the stresses within the pile itself, analogous to the situation with axial forces, in the phase of mechanical loading there is a reduction of the normal stresses along the length of the pile, which is due to the activation of the influence of friction. Regarding the thermomechanical loading - heating, due to the reduced displacements of the pile head, greater normal stresses occur in the pile itself, while due to the increased displacements of the pile head, reduced normal stresses occur (Fig. 11a).



a) b)

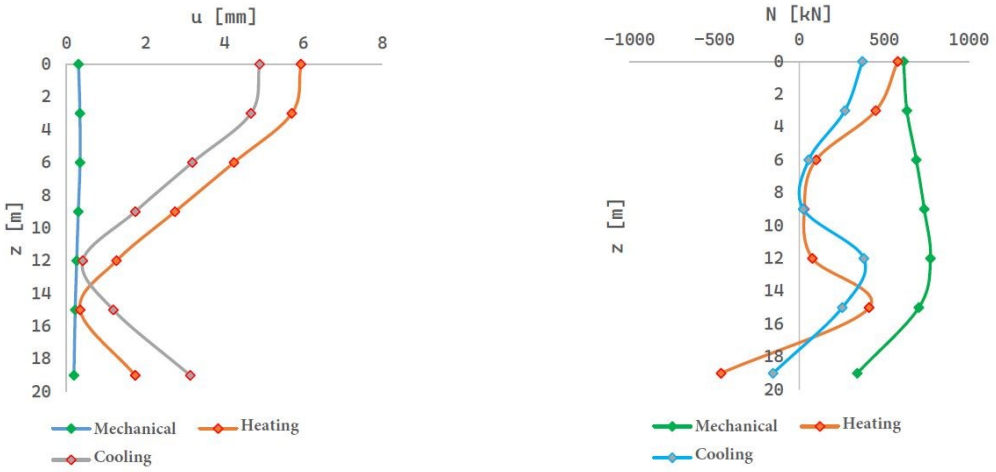
Figure 11. a) Change in normal stresses along the length of the pile from three load cases; b) Change in shear stresses along the length of the pile from three load cases.

Unlike normal stresses, shear stresses are mobilized in the opposite direction of the pile body, to ensure equilibrium with the surrounding soil. According to the analysis, in the case of thermomechanical loading – heating due to the elongation of the pile, the friction strength decreases in the upper part and increases in the lower part of the pile. On the other hand, due to the shrinkage of the pile, the friction strength increases towards the head of the pile, while it decreases towards the base of the pile. By including friction, the bearing capacity of the pile also increases (Fig. 11b).

4.2.Case 2 – End-bearing pile

From the results obtained in the analysis of end-bearing pile, it is shown that under mechanical loading, displacements are approximately equal to zero due to the fixed head of the pile itself. In contrast to this case, in the case of thermomechanical loading – heating of the pile, because the base of the pile is prevented from moving, a larger displacement occurs near the head. On the other hand, in the case of thermomechanical loading – cooling larger displacement near the head of the pile occurs as a result of the shrinkage towards the base of the pile (Fig. 12a).

Copyright © 2025 CroCEE
DOI: https://doi.org/10.5592/CO/3CroCEE.2025.63

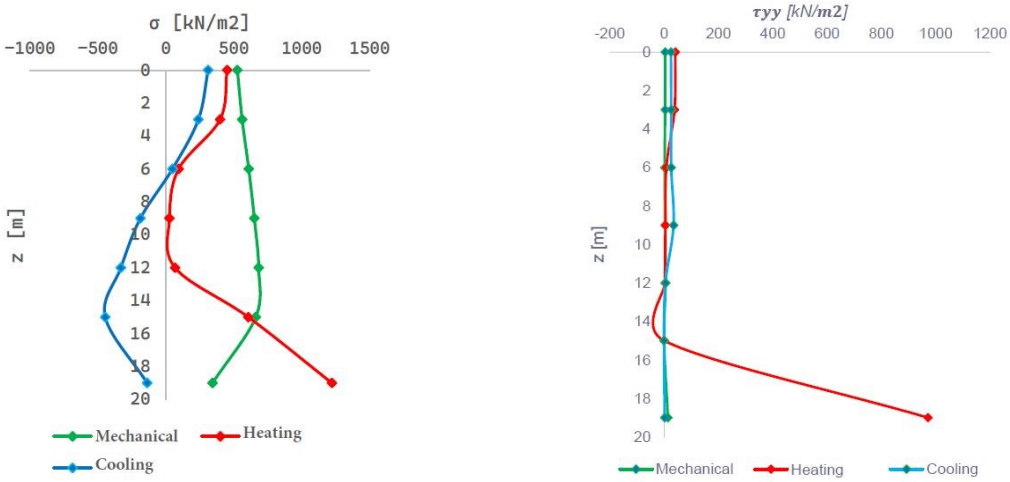


a) b)

Figure 12. a) Change in displacements along the length of the pile from three load cases; b) Change in axial force along the length of the pile from three load cases.

In end-bearing pile, during the thermomechanical loading phase – heating, additional load on the pile head occurs, resulting in an increase in the normal forces and the frictional strength. Additionally, due to the elongation of the pile, the strength of the base of the pile increases. Conversely, during the thermomechanical loading phase – cooling, cooling causes a decrease in the normal forces and the frictional strength. Due to the shrinkage of the pile, the strength of the pile base decreases (Fig. 12b).

From the aspect of normal stresses, it is noticed an increase of them in the case of mechanical loading along the length of the pile. In a heating situation, additional stresses appear at the base of the pile, due to the limitation and inability to move. In the case of cooling, a decrease in normal stress occurs, during which they turn into tension and the pile tends to fracture (Fig. 13a).



a) b)

Figure 13. a) Change in normal stresses along the length of the pile from three load cases; b) Change in shear stresses along the length of the pile from three load cases.

As mentioned earlier, the heating phase causes additional load on the pile head, which in addition to increasing the normal forces, also increases the frictional strength at the pile base and increases the base strength. During the cooling phase, there is a global decrease in the normal forces, and additionally decreases the frictional strength. Due to the shrinkage of the pile, the basic strength also decreases (Fig. 13b).

Copyright © 2025 CroCEE
DOI: https://doi.org/10.5592/CO/3CroCEE.2025.63

5. Conclusions

A numerical analysis was performed using software based on the finite element method, in order to determine the thermomechanical behavior, resulting in important recommendations that could be applied in design in practice. For the design of energy circuits, it is necessary to include all the elements that are crucial for their proper design: (1) determination of thermal actions, (2) displacements of the upper structure, (3) resistance of the pile and (4) resistance of the soil.[12]

Based on the research conducted in this paper, regarding the thermomechanical behavior of energy piles, the following conclusions and recommendations could be drawn:

- Considering that energy piles are loaded with mechanical and thermal actions, their design must consider the effects of temperature changes on the pile and the surrounding soil.
- According to the results obtained, in case of free head pile, under the action of mechanical loading and heating, there is a decrease in the value of the displacements, with the appearance of additional stresses in the pile itself. On the contrary, during the thermomechanical effect of cooling, larger displacements occur, and smaller additional stresses in the pile.
- In the end-bearing pile case, during the heating phase, an additional load occurs on the pile head, which increases the stresses in the cross section, as well as the friction strength. The cooling phase leads to a global decrease in normal forces and frictional strength.
- During the cooling phase, for end-bearing pile the basic strength decreases due to the shrinkage of the circuit. Conversely, during the heating phase, the basic strength increases due to the elongation of the circuit.
- Considering that longer energy piles involve proportionally greater changes in length, it can be concluded that longer energy piles loaded with the same mechanical load are characterized by greater stresses caused by thermal actions.
- In the analysis, the vertical changes in stresses caused by mechanical and thermal actions must be considered along the entire length of the energy piles and the most stressed section along the pile should be checked. Displacements should also be considered, especially at the head of the pile.

References

[1] Laloui, L., Donna, D.A. (2013): *Energy geostructures, Innovation in underground engineering*, USA.

[2] Vasilescu A. R., (2019): Design and execution of energy piles: Validation by in-situ and laboratory experiments, *PhD Dissertation, Institut de Recherche en Genie Civil et Mecanique*.

[3] Raouf, A.M.I., Raouf, M.I.N., Abuel Naga H., Nasser, A.G. (2015): Energy piles: current state of knowledge and design challenges, *Environmental Geotechnics*, V8, pp. 195-210, doi: https://doi.org/10.1680/envgeo.13.00019

[4] Di Girolamo, L., Ausiello, G., Russo, G., Marone, G., (2022): High thermal conductivity concrete for energy piles, Acta Polytechnica CTU Proceedings, p.125 – 132, https://doi.org/10.14311/APP.2022.33.0125

[5] Laloui, L., Loria, R.A.F. (2019): *Analysis and design of energy geostructures, theoretical essential and practical applications*, USA.

[6] Abdelaziz, S., Ozudogru, Y.T. (2016): Non-uniform thermal strain and stresses in energy piles, Environmental Geotechnics, V5, p. 237 – 252, https://doi.org/10.1680/jenge.15.00032

[7] Tomlinson, M., Woodward, J. (2014): *Pile design and construction practice*, 6th edition, USA.

[8] Knellwolf, C., Peron, H., Laloui, L. (2011): Geotechnical analysis of heat exchanger piles, Journal of Geotechnical and Geoenvironmental Engineering, V137, I10, https://doi.org/10.1061/(ASCE)GT.1943-5606.0000513

[9] Dupray, F., Mimouni, T., Laloui, L. (2015): Alternative uses of heat-exchanger geostructures, Acta Geotechnica, V10(4), https://doi.org/10.1002/9781118761809.ch6

Copyright © 2025 CroCEE
DOI: https://doi.org/10.5592/CO/3CroCEE.2025.63

[10] Bourne-Webb, P.J., Amayat, B., Sogat, K., Amis, T., Davidson, C., Payne, P. (2009): Energy pile test at Labeth College, London, Geotechnical and thermodynamic aspects of pile response to heat cycles, Geotechnique, V59(3), p. 237 – 248, https://doi.org/10.1680/geot.2009.59.3.237

[11] Mohamad, Z., Fardoun, F., Meftah, F., (2021): A review on energy piles design, evaluation, and optimization, Journal of Cleaner Production, V292, https://doi.org/10.1016/j.jclepro.2021.126963

[12] Habert, J., Mroueh, H., Szymkiewkz, F., Suyatriyastuti, M.E. (2013): Toward a design approach of bearing capacity of thermo-active piles, *European Geothermal Congress 2013*.

Proceedings of the 3rd Croatian Conference on Earthquake Engineering - 3CroCEE
19–22 March 2025, Split, Croatia
Copyright © 2025 CroCEE
DOI: https://doi.org/10.5592/CO/3CroCEE.2025.78

ANALYSIS OF CANTILEVER RETAINING WALL ACCORDING TO EUROCODES IN DRAINED AND UNDRAINED CONDITIONS

Dejan Ivanovski [(1)], Julijana Bojadjieva [(2)], Kemal Edip [(3)], Vlatko Sheshov [(4)], Toni Kitanovski [(5)], Jovana Ristova [(6)]

[(1)] *Research assistant, PhD Candidate, Ss. Cyril and Methodius University, Institute of earthquake engineering and engineering seismology-IZIIS, Skopje, North Macedonia, ivanovski@iziis.ukim.edu.mk*
[(2)] *Associate professor, Ss. Cyril and Methodius University, Institute of earthquake engineering and engineering seismology-IZIIS, Skopje, North Macedonia, jule@iziis.ukim.edu.mk*
[(3)] *Professor, Ss. Cyril and Methodius University, Institute of earthquake engineering and engineering seismology-IZIIS, Skopje, North Macedonia, kemal@iziis.ukim.edu.mk*
[(4)] *Professor, Ss. Cyril and Methodius University, Institute of earthquake engineering and engineering seismology-IZIIS, Skopje, North Macedonia, vlatko@iziis.ukim.edu.mk*
[(5)] *Research assistant, PhD Candidate, Ss. Cyril and Methodius University, Institute of earthquake engineering and engineering seismology-IZIIS, Skopje, North Macedonia, tonik@iziis.ukim.edu.mk*
[(6)] *M.Sc, Civil Engineering Institute Macedonia, Skopje, North Macedonia, ivanovski@iziis.ukim.edu.mk*

Abstract

Retaining cantilever walls are typically designed under drained conditions, assuming that proper drainage is designed, constructed, and functions throughout the structure's lifespan. Even when appropriate drainage cannot be constructed—such as in walls cutting and retaining a natural slope, where the wall is built adjacent to nearly vertical excavated soil—designers usually use effective soil parameters and effective stresses. This paper analyzes a 6-meter-high cantilever wall, retaining non-cohesive soil (backfill), but founded on different types of soils (non-cohesive and cohesive). Initially, a non-cohesive, granular soil is assumed, with effective soil parameters under drained conditions. The analysis is then repeated under undrained conditions, with a fully saturated backfill and the groundwater table assumed to be at the ground surface behind the wall (for instance, when proper drainage is absent). Both static and seismic conditions are considered. Additionally, a comparison is made between the drained and undrained strength of cohesive material (clay) beneath the wall, using effective and total soil parameters, also under static and seismic conditions. All analyses are conducted according to Eurocode 7 and 8. The differences in the required foundation width of the wall, ensuring stability under static and seismic conditions, are compared by verifying the resistances.

Keywords: cantilever, retaining, wall, drained, undrained, seismic, Eurocode,

1. Introduction

Cantilever retaining walls are important structures widely used in geotechnical engineering to stabilize slopes and prevent soil movement in various civil engineering applications, such as roadways, embankments, and foundations. These walls are typically designed under the assumption that proper drainage is provided, which helps prevent hydrostatic pressures from building up behind the wall. In ideal conditions, effective drainage ensures that the backfill remains dry (in a drained state), allowing for the use of effective soil parameters and stress conditions in the design process. However, there are cases where drainage may not be functional, or may not be included in the structural project, so the retaining wall may experience additional pressure due to the backfill saturation i.e. (undrained state). The analyses are performed using effective soil parameters. The level of groundwater to be considered is specified in Eurocode 7 - Part 1 (EN 1997:1) [1] which states: "Unless the adequacy of the drainage system can be demonstrated and its maintenance ensured, the design ground-water table should be taken as the maximum possible level, which may be the ground surface". According to some authors, the requirements of Eurocode 7 appear more rigorous than what is typically adopted in practice, as it is unusual for the natural water table to rise to the ground surface. Annex E in EC 8-5 (E.5-E.8), addresses

Copyright © 2025 CroCEE
DOI: https://doi.org/10.5592/CO/3CroCEE.2025.78

various water level conditions based on soil permeability and prescribes modifications to the equation for the total design force (static + seismic) acting on the retaining structure.

Additional analyses are conducted with cohesive material (clay) under the foundation, firstly using effective parameters, calculating the drained strength, and then the analysis is repeated with total parameters, calculating the undrained strength. The geomechanical parameters of the soils used are assumed and shown in Table 1. The difference in the required wall's foundation width is assessed as it is the dimension which contributes the most to the stability of a cantilever retaining wall, while all other dimensions shown on Fig. 1 remain the same for all analyses.

The analyses are performed for a 6-meter-high cantilever retaining wall under different conditions (Fig. 1). The procedure prescribed in EC 7-1, design approach 2 – DA-2 is used for the static analyses. Additionally, the analyses are repeated considering the seismic conditions, in accordance with Eurocode 8, part 5 (EN 1998:5) [2], design approach 2 (DA-2) and additionally calculated with design approach 3 (DA-3). According to EC-7, all partial factors for accidental situations, should be taken as 1.0, while partial factors for materials and resistances during accidental (seismic) actions, are not clearly distinguished, neither in EC 7, nor in EC 8. Hence, using DA-2, which applies partial factors to actions and resistances, there is no additional increase in the characteristic value of actions to obtain its design value when performing the seismic analyses. However, DA-3, does not apply partial factors to the actions, but does apply to the materials, so that the seismic analysis is performed with the same partial factors as for the static analysis, resulting in a large increase of the required foundation width. Normally, partial factors for seismic analysis are expected to be lower than those for static analysis.

The pseudo-static approach, according to Mononobe-Okabe theory [4, 5] is used for calculating the seismic forces, applied as horizontal and vertical forces. The ground acceleration is assumed as a_{gR} =0.25g, and the soil type is chosen as type B for the non-cohesive material (corresponding to gravel), and type C for the cohesive material (corresponding to clay), according to Table 3.1 in EN 1998:1 [2]. A reduction coefficient of r=2.0 (EN 1998:5, Table 7.1) [3] is adopted for the performed analyses, so the coefficients k_h and k_v are calculated as:

$$k_h = \alpha * \frac{S}{r} = 0.25 * \frac{1.20}{2} = 0.15 \text{ – non-cohesive material; } k_h = 0.25 * \frac{1.15}{2} = 0.144 \text{ – cohesive material}$$

$$k_v = \pm 0.5\, k_h = \pm 0.075 \text{ – non-cohesive material; } k_v = \pm 0.072 \text{ – cohesive material}$$

The analyses are conducted to satisfy the stability conditions, i.e., the design actions must be less than the resistance to sliding, overturning, and the bearing capacity of the soil i.e.:

$$H_d \leq R_d + R_{pd}; \quad M_{Ed,dst} \leq M_{Ed,st}; \quad V_d \leq R_d$$

The seismic bearing capacity of the ground is given in form of an empirical expression that needs to be satisfied, given in EC 8-5 - annex F.

By comparing the design results under both static and seismic conditions, this study provides a comprehensive understanding of how drainage, soil type, and seismic activity influence the design of cantilever retaining walls according to Eurocodes.

Proceedings of the 3rd Croatian Conference on Earthquake Engineering - 3CroCEE
19–22 March 2025, Split, Croatia
Copyright © 2025 CroCEE
DOI: https://doi.org/10.5592/CO/3CroCEE.2025.78

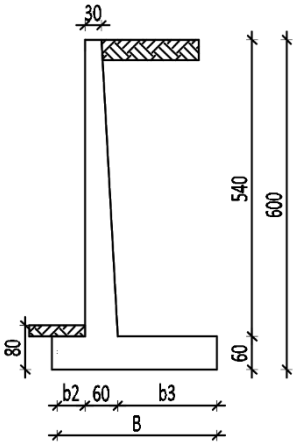


Figure 1: 2D - Scheme of the analyzed wall

Table 1: Assumed geomechanical parameters

Non – cohesive soil (drained analyses)	γ=21 [kN/m3]	φ'=30 [˚]	c'=0 [kPa]
Cohesive soil (effective parameters)	γ=21 [kN/m3]	φ'=19 [˚]	c'=0 [kPa]
Cohesive soil (total parameters)	γ=21 [kN/m3]	/	c_u=50 [kPa]

2. Main differences between drained and undrained conditions in terms of resistance

In the following part, selected main differences in equations for the drained and undrained resistances, important for the aim of this paper are shown:

2.1. Drained conditions

2.1.1. Drained bearing resistance according to EC7-1

The drained bearing resistance of a spread foundation R is given by Eq (1):

$$\frac{R}{A'} = c'N_c b_c s_c i_c + q'N_q b_q s_q i_q + 0.5\gamma' B' N_\gamma b_\gamma s_\gamma i_\gamma \quad (1)$$

where c' is the soil's effective cohesion; q' is the effective overburden pressure at the foundation base; γ' is the effective specific weight of the soil below the foundation; Nc, Nq, and Nγ are bearing capacity factors; b, s and i are factors for base inclination, shape, and inclination, respectively.

2.1.2. Drained sliding resistance according to EC 7-1

The design horizontal resistance Rd for drained conditions (ignoring passive pressure) is given by Eq. (2):

$$\mathrm{R_d} = \frac{(W_{Gd} - U_{Gd})tan\delta_d}{\gamma_{Rh}} \quad (2)$$

where W_{Gd} = the wall's design self-weight, including backfill; U_{Gd} = the design water upthrust beneath the base; δ_d = the design angle of friction between the base and the ground; γ_{Rh} = a partial actor on sliding resistance.

2.2. Undrained conditions

2.2.1. Undrained bearing resistance according to EC 7-1

The undrained bearing resistance of a spread foundation R is given by Eq. (3):

$$\frac{R}{A'} = (\pi + 2)c_u b_c s_c i_c + q \quad (3)$$

Proceedings of the 3rd Croatian Conference on Earthquake Engineering - 3CroCEE
19–22 March 2025, Split, Croatia
Copyright © 2025 CroCEE
DOI: https://doi.org/10.5592/CO/3CroCEE.2025.78

where A' is the footing's effective area, c_u is the soil's undrained shear strength; q the total overburden pressure at the foundation base;

2.2.2. Undrained sliding resistance according to EC 7-1

The characteristic shear resistance τ_{Rk} for undrained conditions (ignoring passive pressure) is given by the expression:

$$R_d = c_{ud} A \tag{4}$$

Where c_{ud} represents the design undrained shear strength of the soil.

3. Results from the performed analyses

3.1. Drained analyses

The 6m wall is analyzed using the software package GEO-5, under different conditions and with different soil types. The minimum required foundation width (100% utilization ratio) is shown for all case-scenarios, allowing for direct comparison. Additionally, the most critical stability verification, which corresponds to the 100% utilization ratio is highlighted. Table 2 presents the results obtained from the drained analysis, using effective parameters. When the wall is analyzed with a dry fill under static conditions, the minimum required foundation width is 2.85m (Fig. 2), with the most critical condition being the bearing resistance. When the backfill is wet, i.e. the ground water table is at the surface behind the wall, the required footing width increases significantly to 7.7m (Fig. 3), to satisfy the sliding resistance which is the most critical stability condition. Of course, sliding resistance can also be increased with introducing a shear key in the foundation, which would reduce the total width required.

Under seismic conditions, the required foundation width is considerably larger than in static conditions. For the dry fill, using design approach 2 (DA-2), the obtained minimum width is 3.8m, while using design approach 3 (DA-3), as mentioned earlier, the required width increases to a minimum of 4.8m. For a wall with a wet fill, achieving the required resistance through foundation width alone is not feasible, even if the width exceeds 10m for both design approaches. However, occurring an earthquake, especially with maximum expected acceleration, during a fully saturated backfill - up to the ground surface, which practically means that there is impermeable soil below the backfill is almost impossible. Therefore, in author's opinion, this case should not be considered a valid load combination for structure design.

In extremely rare cases where designing a retaining structure without drainage is unavoidable, particularly in highly active seismic regions, the groundwater table level behind the wall should be reconsidered. Taking it as the ground surface is overly conservative, even for static conditions. For example, the British practice [6] suggests lowering the water table to approximately H/4 below the surface. Also, other measures could be taken for increasing the sliding resistance, like introducing shear key, pile foundation, etc. The critical resistance (causing utilization ratio of ~100%), is either the bearing or the sliding, while the overturning is not critical in any of the analyzed case-scenarios given the assumed parameters.

Copyright © 2025 CroCEE
DOI: https://doi.org/10.5592/CO/3CroCEE.2025.78

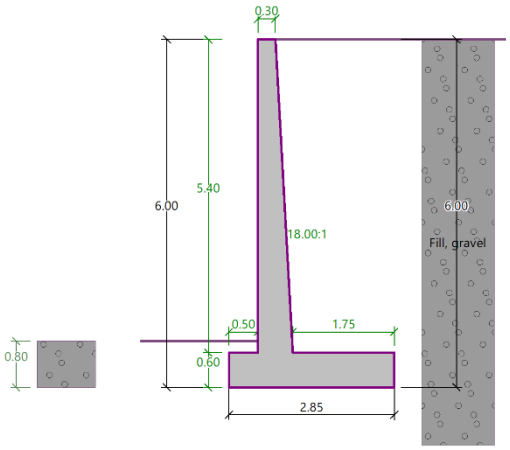


Figure 2. Model geometry - dry fill

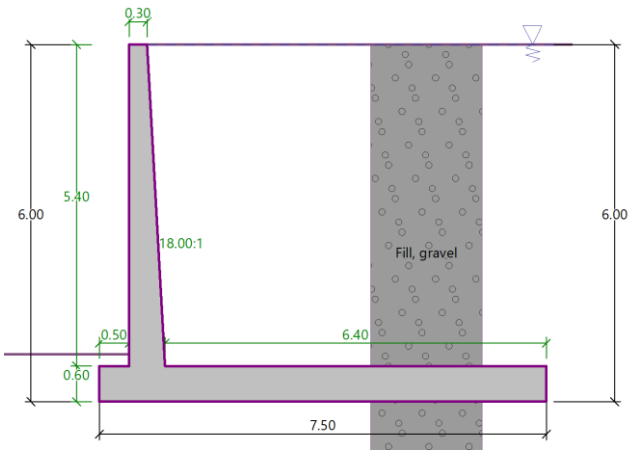


Figure 3. Model geometry - wet fill

Table 2: Results from the drained analysis

Type of analysis	*Foundation width [B]*	*Critical resistance*
Drained - dry fill - static	2.85	Bearing
Drained - wet fill - static	7.7	Sliding
Drained - dry fill - seismic - DA-2	3.8	Bearing
Drained - dry fill - seismic - DA-3	4.8	Sliding
Drained - wet fill - seismic - DA-2	∞	Sliding
Drained - wet fill - seismic - DA-3	∞	Sliding

3.2. Undrained vs. drained strength

Using the same geometry of the wall, several analyses are performed with cohesive soil beneath the wall (Fig. 3) and the same non-cohesive soil as a backfill. The analyses differ only in the input of the geomechanical parameters in the analyses for the cohesive material, shown in Table 1. It is firstly analyzed with total parameters, calculating the undrained strength and then with effective parameters, calculating the drained strength, assuming the parameters are valid for identical soil. Additionally, seismic analyses are carried out, using design approaches 2 and 3 from EC 7, as mentioned earlier.

The results show that there is no significant difference in static conditions, regardless of whether total or effective parameters (undrained or drained strength) are used, although the drained strength is slightly larger than the undrained strength. A larger difference occurs in seismic conditions, so using DA-2, the minimum required foundation width is 5.8m for the undrained strength and 5.0m for the drained strength. Using DA-3, as previously concluded, there is a significantly greater need for foundation width, so the undrained strength requires a width of 10m, while the drained strength requires a narrower width of 7.3m. In other words, the drained strength is larger than the undrained strength for the assumed material. Again, the overturning condition is not critical in any of the performed calculations.

Copyright © 2025 CroCEE
DOI: https://doi.org/10.5592/CO/3CroCEE.2025.78

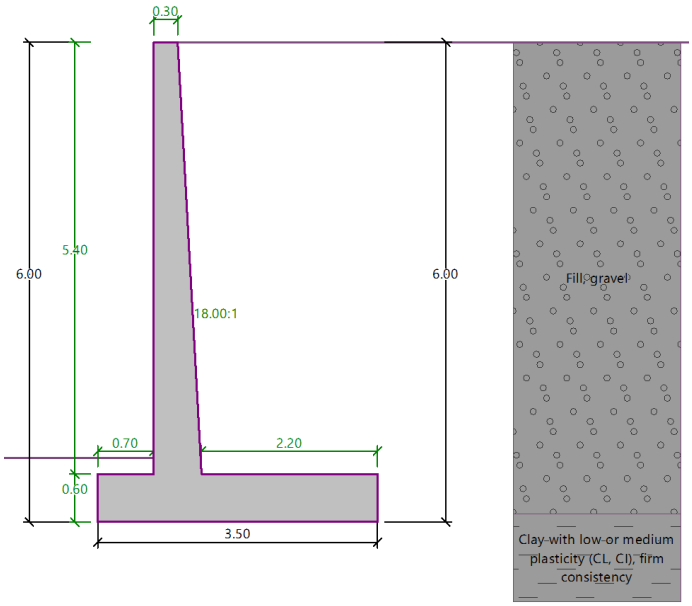


Fig. 3. Model geometry – cohesive soil below foundation

Table 3: Results from the undrained analysis

Type of analysis	*Foundation width [B]*	*Critical resistance*
Undrained strength - static	3.5	Sliding
Drained strength - static	3.4	Bearing
Undrained strength - seismic - DA-2	5.8	Sliding
Undrained strength - seismic - DA-3	10	Sliding
Drained strength - seismic - DA-2	5.0	Sliding
Drained strength - seismic - DA-3	7.3	Sliding

4. Conclusions:

After performing the analyses and making the comparisons, the following conclusions can be drawn:

1. Adding the water table at the surface behind the retaining structure imposes significant additional horizontal pressure, which requires a drastic increase in the foundation width to ensure stability, i.e. resistance of the wall, compared to the width required for a dry fill. This emphasizes the importance of providing appropriate drainage, which should also be regularly maintained
2. The seismic analyses show a significant increase in the required foundation width compared to the static analyses. It is also concluded that design approach 2 (DA-2) results in a smaller required width than design approach 3. However, in author's opinion is that using DA-3 leads to unexpectedly large dimensions of the structure.
3. Seismic analyses with a fully saturated backfill show that it is not possible to meet the required resistance only by increasing the width of the foundation. This scenario is unlikely to happen, and in author's opinion is that it does not have to be considered in the design.
4. Comparing the drained and undrained strength of a cohesive material, it is concluded that generally the drained strength is larger than the undrained one, especially under seismic conditions.

Copyright © 2025 CroCEE
DOI: https://doi.org/10.5592/CO/3CroCEE.2025.78

References:

[1] European Committee for Standardization (2004) Eurocode 7: Geotechnical design - Part 1: General rules. CEN, Brussels, EN 1997-1;

[2] European Committee for Standardization (2004) Eurocode 8: Design of Structures for Earthquake Resistance. Part 1: General rules, seismic actions and rules for buildings. CEN, Brussels, EN 1998-1;

[3] European Committee for Standardization (2004) Eurocode 8: Design of Structures for Earthquake Resistance. Part 5: Foundations, retaining structures and geotechnical aspects. CEN, Brussels, EN 1998-5;

[4] Mononobe, N. and Matsuo, H. (1929) On the Determination of Earth Pressure during Earthquakes. Proceedings of the World Engineering Conference, 9, 176;

[5] Okabe S., 1926 General theory of earth pressure. Journal of the Japanese Society of Civil Engineers, Tokyo, Japan 12 (1);

[6] Bond, A., & Harris, A. (2008). Decoding Eurocode 7. CRC Press;

[7] Fardis, M. et al (2005). Designers' guides to the eurocodes, - Designers' guide to EN 1998-1 and EN 1998-5 Eurocode 8: Design of structures for earthquake resistance general rules, seismic actions, design rules for buildings and retaining structures;

[8] Ivanovski D. et. al. (2024): Evaluation of the coefficient "r" in Eurocode 8-5 and choosing a design approach for seismic analysis of retaining structures, *18th World Conference on Earthquake Engineering, WCEE 2024*, Milan, Italy.

[9] Roje-Bonacci T. (2005). Potporne gradzevine i gradzevne jame, Gradzevinsko-Arhitektonski Fakultet Sveucilista u Splitu (in Croatian);

[10] GEO 5, Fine software, Cantilever wall program, Spread Footing program, Czech Republic;

[11] Mircevski J. (2024). Analysis of structures according to Eurocode in undrained conditions, M.Sc thesis, SS. Cyril and Methodius, Skopje.

[12] Ivanovski D. (2022). Comparative analysis and design of retaining structures according to the current practice and Eurocodes, M.Sc thesis, SS. Cyril and Methodius, Skopje.

Proceedings of the 3rd Croatian Conference on Earthquake Engineering - 3CroCEE
19–22 March 2025, Split, Croatia
Copyright © 2025 CroCEE
DOI: https://doi.org/10.5592/CO/3CroCEE.2025.79

LABORATORY TESTING OF SMALL-STRAIN MODULI IN NATURAL SANDY DEPOSITS

Toni Kitanovski [(1)], Vlatko Sheshov [(2)], Julijana Bojadzieva [(3)], Kemal Edip [(4)], Dejan Ivanovski [(5)]

[(1)] *Research assistant, PhD Candidate, Ss. Cyril and Methodius University, Institute of earthquake engineering and engineering seismology-IZIIS, Skopje, Macedonia, tonik@iziis.ukim.edu.mk*
[(2)] *Professor, Ss. Cyril and Methodius University, Institute of earthquake engineering and engineering seismology-IZIIS, Skopje, Macedonia, vlatko@iziis.ukim.edu.mk*
[(3)] *Associate professor, Ss. Cyril and Methodius University, Institute of earthquake engineering and engineering seismology-IZIIS, Skopje, Macedonia, jule@iziis.ukim.edu.mk*
[(4)] *Professor, Ss. Cyril and Methodius University, Institute of earthquake engineering and engineering seismology-IZIIS, Skopje, Macedonia, kemal@iziis.ukim.edu.mk*
[(5)] *PhD Candidate, Ss. Cyril and Methodius University, Institute of earthquake engineering and engineering seismology-IZIIS, Skopje, Macedonia, ivanovski@iziis.ukim.edu.mk*

Abstract

A vast majority of experimental results have been accumulated to assess the shear modulus of natural sand at very small levels of strains, the so-called small strain modulus or maximum shear modulus, Gmax. This paper presents a part of a long-term study on the dynamic behaviour of alluvial deposits from ancient river terraces in the Skopje valley, Republic of North Macedonia. Extensive laboratory and field measurements have already clarified many aspects of the cyclic stress-strain characteristics of these natural sandy deposits. The main objective in this study is to contribute to improved understanding of the small strain shear modulus using laboratory element testing with advance measuring techniques. Integral static and dynamic triaxial apparatus equipped with bender element was used for testing of soil specimens and measurement of the parameters necessary for calculation of the small strain shear modulus. This reliable and efficient approach is non-destructive, simple to use and suited to perform multiple tests on a single soil specimen Because of the non-destructive nature of the bender elements the same prepared specimens were used to determine the shear methods as in the case of triaxial tests. Additionally, for finer granular soil materials, cyclic simple shear apparatus was also used to perform the cyclic shearing on soil samples for evaluation of the shear modulus in a more explicit way. Soil specimens were first prepared using the wet-tamping method varying the initial relative densities, from Dr=30% to Dr=70%, then confined at four levels of initial effective stress p_0 = 50, 100, 200 and 400kPa before application of loading. Results obtained from element tests show stable relationships between the small strain shear modulus, relative density, effective stress and shear strain amplitude, with strong dependence on the effective stress, which appears to be one of the key parameters.

Keywords: Small shear modulus Gmax, triaxial test, direct simple shear tests, bender elements

1. Introduction

Recent software developments compiled with various numerical techniques represent the most common way of solving geotechnical problems. The maximum shear modulus (Gmax) represents one of the fundamental parameters required for linear and non-linear dynamic analyses, foundation design, prediction of soil settlement prediction, soil improvement, etc. In particular, significant focus is placed on the implementation of Gmax in engineering practices for calculating the settlement and bearing capacity of spread foundations [1]. In earthquake prone regions, a better insight into Gmax of local soils is of vital importance for designing of earthquake-resistant structures. It can be concluded that correctly defined and proper use of shear modulus is of vital importance.

In this study, three types of experimental methods were used to determine the maximum shear modulus (Gmax) under laboratory conditions. The first method used is the cyclic triaxial test which due to overriding popularity in recent decades has become probably the most widely used method for measuring the small strain shear modulus. These tests were conducted herein according to the ASTM D-3999 standard, strain-controlled approach, where 40 cycles of strain were applied with an amplitude of 0.1% axial strain. To improve the output results, all loading cycles were considered in the analysis. The triaxial test first determines the initial elastic modulus Emax, which is then converted to initial shear modulus Gmax. Bender elements (BE), installed along the vertical axis of the triaxial specimen,

Proceedings of the 3rd Croatian Conference on Earthquake Engineering - 3CroCEE
19–22 March 2025, Split, Croatia
Copyright © 2025 CroCEE
DOI: https://doi.org/10.5592/CO/3CroCEE.2025.79

constitute the second method for determining the small strain shear modulus. BE represents an efficient technique due to the non-destructive nature, simple use and ability to perform multiple tests on one specimen. In this way, it is possible to use the same prepared soil specimens from previous method to determine the shear methods as in the case of triaxial tests. ASTM D8295-19 standard prescribes the use of BE in laboratory conditions with the following statement "…*shear wave velocity determination involves very small strains and is non-destructive to a test specimen. As such, bender element shear wave velocity determinations can be made at any time and any number of times during a laboratory test*". Currently, BE can be added to multiple standard laboratory equipment such as triaxial apparatus [2], resonant column [3] or oedometer apparatus [4] and widely used in various scenarios. The third method applied in this study is the direct simple shear test (DSS), which is also commonly used for cyclic shearing of soil samples to evaluate shear modulus in a more explicit way. In this test two cylindrical specimens are simultaneously loaded with shear force while being rigidly restrained in the vertical direction. The soil specimens are placed in a series of Polytetrafluoroethylene PTFE (teflon) coated steel rings and dynamic shear excitation in the form of shear strains is applied in the horizontal direction through the central loading plate placed between the two models. Through the relative horizontal displacement of the rings, the dynamic excitation is uniformly applied along the entire height of the model. Due to simple cyclic shear in the element shear strains will develop and hysteresis relationships are obtained.

2. Testing material and program

The soil material used in this study represents a natural fluvial sand, the so-called "Skopje sand", that has been frequently tested in the laboratory for dynamics of soils and foundation, UKIM-IZIIS [5] and a lot of reports have already been published using the same sand [6,7,8,9]. It consists mainly of silica oxides (about 78%) with particles of subangular shape. With only 2% fines it is highly uniform with mean grain size of d_{50} = 0.26mm and a uniformity coefficient Cu = 1.8. Since it is a natural sand, small differences in each batch can be expected. Initial investigation is therefore necessary to determine the physical properties (Table 1). The void ratios were determined using ASTM D4253-00 standards, where e_{min} = 0.51 and e_{max} = 0.95, at mean pressure p = 0kPa.

Table 1 – Physical properties of Skopje sand

e_{max}	e_{min}	G_s	D_{10} (mm)	D_{50} (mm)	D_{60} (mm)	Cu	Cc	φ (o)	Fines (%)
0.95	0.51	2.615	0.095	0.26	0.19	1.8	0.8	33.5	2

Table 2 – Testing programme

Triaxial apparatus			Bender elements			Direct simple shear apparatus		
No	σ_{eff}	Dr	No	σ_{eff}	Dr	No	σ_{eff}	Dr
1	50	30.73	1	50	32.03	1	50	27.09
2	50	59.26	2	50	56.5	2	50	49.29
3	50	78.2	3	50	73	3	50	71.61
4	100	27.08	4	100	27.14	4	100	29.61
5	100	64.45	5	100	48.15	5	100	49.28
6	100	82.02	6	100	74.65	6	100	69.7
7	200	33.52	7	200	33.38	7	200	33.8
8	200	69.11	8	200	53.53	8	200	50.38
9	200	79.85	9	200	74.19	9	200	69.1
10	400	35.84	10	400	31.14			
11	400	72.89	11	400	47.21			
12	400	86.53	12	400	64			

The testing program consisted of three series of tests according to the testing method/equipment and then grouped by the applied effective stress σ_{eff} and initial relative density Dr (table 2). In total, 33 tests

Copyright © 2025 CroCEE
DOI: https://doi.org/10.5592/CO/3CroCEE.2025.79

were performed. The experiments on triaxial apparatus were confined to four different effective stress levels: 50, 100, 200, 400kPa, while the confining pressure on DSSA was applied only up to a vertical stress of 200 kPa. All soil samples in the triaxial apparatus were reconstituted using the wet-tamping method with an initial water content of 3% [10] height/diameter ratio of around 2, into roughly three groups of initial relative densities.

3. Results from Triaxial tests

The triaxial testing equipment used for the experiments is a feedback-controlled cyclic triaxial system that applies cyclic or dynamic loading to cylindrical soil specimens. This apparatus is a servo pneumatic system, with control on axial stress, confining pressure, and back pressure by incorporated Control and Data Acquisition System (CDAS). During the testing seven transducers were used for measuring the required physical quantities. This includes measurements of the cell, back and pore pressure, using pressure transducers, measurements of the applied axial load with submersible load cell and volume change of water entering or leaving the sample. As well, two axial transducers acquired the deformations directly on the samples. All data acquisition functions, critical control and timing were provided through CDAS (figure 1). The wet-tamping method was used for reconstitution of soil samples, where the sand was placed in identical layers using a three-piece steel cylinder lined with a rubber membrane. To achieve a better saturation, all samples were first saturated using CO_2 and then deaired water was applied to a B-value≥0.95. As mentioned, consolidation of the soil specimens was done at four levels (50, 100, 200 and 400kPa) until stabilization of the volume change. The cyclic loading was applied according to ASTM D-3999 standard, with 40 sinusoidal cycles with an axial strain amplitude of 0.1%.

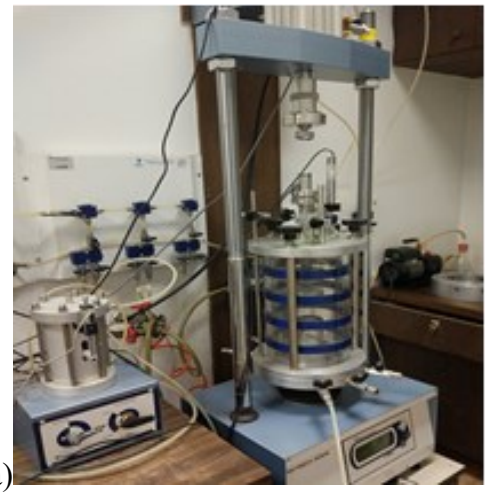
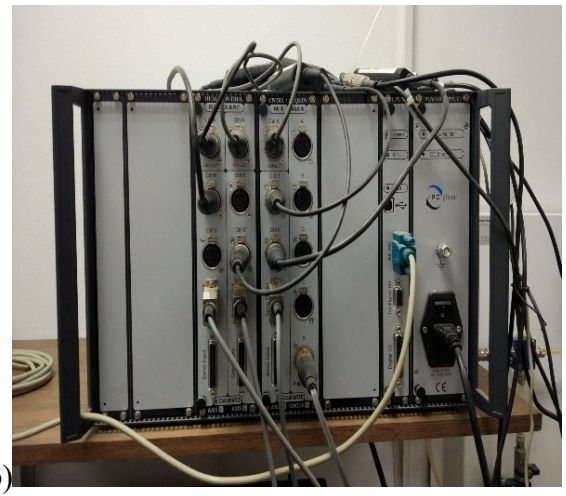
a)  b) 

Figure 1. a) Triaxial and volume change equipment, b) Control and data acquisition system

First notion from the test results is the fact that there is small inconsistency in the amplitude of the axial strain applied on the samples for different experiments, even though in all cases the applied sinusoidal cycles are smooth the amplitudes vary from 0.08% to 0.105%. This limit of accuracy is known in literature and presented as inadequate practice particularly when small strain stiffness of the soil is being investigated [11,12]. Additionally, there is variance in the shear modulus for different cycles during a single experiment. This type of variance is expected and in our case is below the limit of 10% between the highest and lowest value of Gmax (figure 2). Figure 3 represents results from all triaxial experiments presented in terms of shear modulus and initial relative density. From the figure a strong initial pressure-dependence for the shear modulus can be noted, but in terms dependency from relative density no clear conclusion can be made. Inconsistency in applied axial strain significantly affects the scattering in results.

Copyright © 2025 CroCEE
DOI: https://doi.org/10.5592/CO/3CroCEE.2025.79

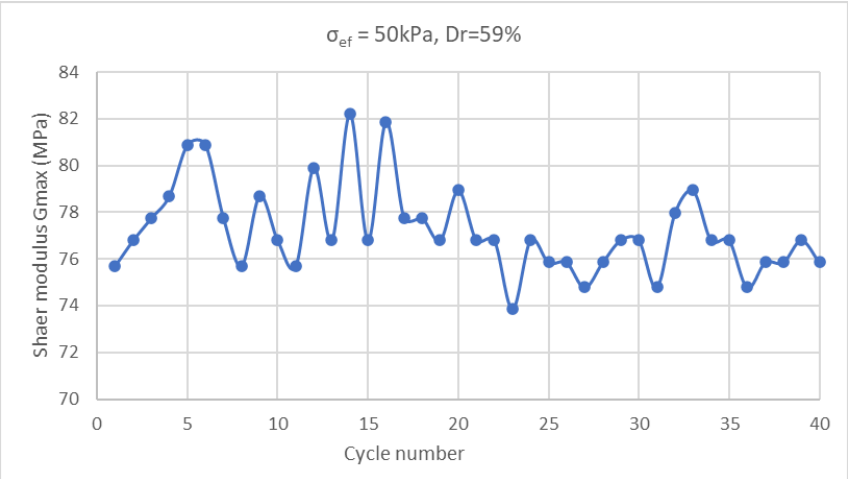


Figure 2. Gmax results for single triaxial experiment

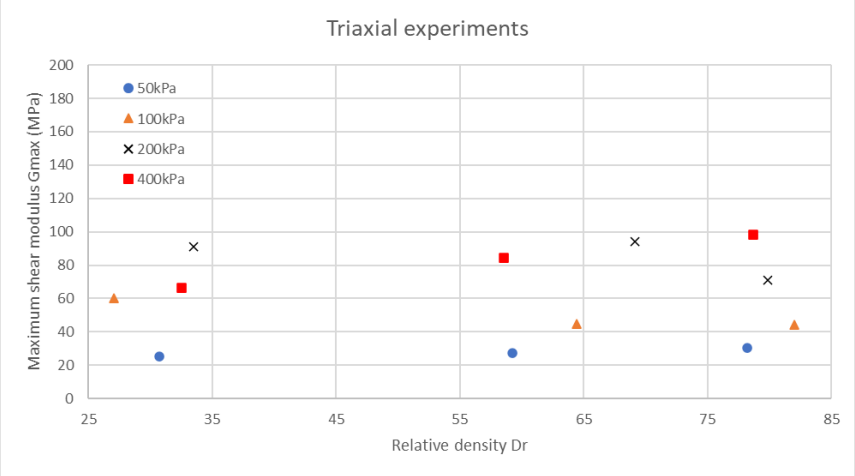


Figure 3. Gmax from triaxial experiments

4. Results from Bender element tests

The practice of using bender elements to determine the shear modulus of a soil sample is becoming widely popular in laboratory testing, especially knowing the previous mentioned limitation the triaxial apparatus. Many researchers have developed bender elements in their laboratories and used them on all types of soils [13,14,15], while for verification of the BE approach resonant column tests, torsional shear tests were used [16,17]. Additionally, because of their non-destructive nature researchers used bender elements multiple times during the experiments to determine the development of shear modulus [18]. The system installed in the laboratory for soil dynamics part of IZIIS represents a Wykeham Farrance bender element system. The bender element system consists of two bender elements (transmitter and receiver) which are connected to a single master signal conditioning control unit (28-WF4200). The unit includes waveform generator, analog-to-PC interface, virtual oscilloscope software and connecting cables. Advanced user-friendly software (figure 4) that automates the analysis is also incorporated. The system allows to measure shear modulus (Gmax) of a soil specimen in the shear strain levels of about 0.0001%. This system is constructed to be used in advanced triaxial systems but also can be used as a standalone product.

Copyright © 2025 CroCEE
DOI: https://doi.org/10.5592/CO/3CroCEE.2025.79

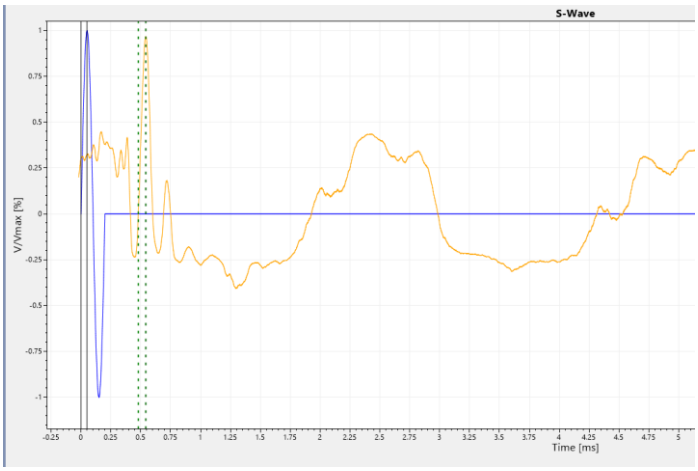


Figure 4. Typical waveforms response curve from bender element

Determination of Vs using bender elements was calculated by three methods: a) start-to-start, b) peak-to-peak and c) cross-correlation, with single sinusoidal input with frequency of 4Hz. This frequency proves to be the most effective and most consistent input parameters for calculating Vs. In the literature it has been recognized that the frequency effect on shear modulus is negligible for clean sands, but there are some authors that have determined that there is frequency dependence of the Vs results especially for high frequencies [17,19]. In this study no dependencies were noticed, bearing in mind that the transition frequency is much greater than the frequency used for standard determination of Vs using BE. The equation for computing Gmax can be written as:

$$\mathbf{G_{max} = V_s^2 \times \rho}$$

where Vs is shear wave velocity at which the wave propagates through the soil specimen, and ρ is the mass density of the soil. The results of the three above-mentioned methods show stable and reliable results for Vs, with max. differences of 2 to 5%. Figure 5 presents the shear modulus for different relative densities and different levels of effective stress. The results show strong pressure-dependence that increases with the increase of relative density.

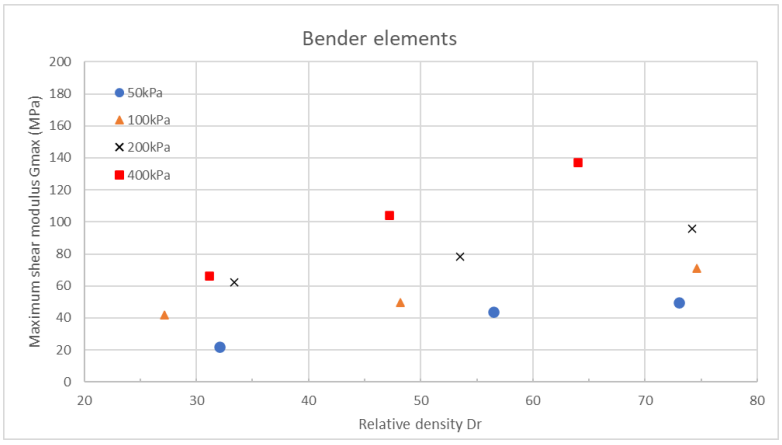


Figure 5. Maximum shear modulus results from bender elements

Copyright © 2025 CroCEE
DOI: https://doi.org/10.5592/CO/3CroCEE.2025.79

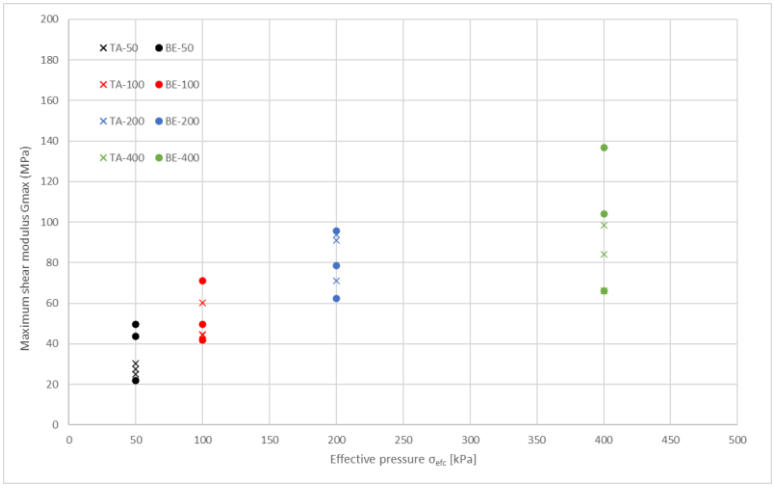


Figure 6. Results for Gmax from triaxial and bender element test

5. Results from Direct simple shear tests

Direct simple shear devices historically have been the most used laboratory apparatus to determine the shear modulus, and it is still present in almost every geotechnical laboratory. The apparatus in the Laboratory for Soil Dynamic DSSA is manufactured by Dames & Moore, London [20], and it is consisted of four main components: testing device, hydraulic pump, data acquisition digital units and response recording PC control console. This apparatus has been in use for more than 35 years [21], improved and digitalized throw out the years. While testing, the device considers simultaneously two dry soil specimens with cylindrical shape of 6.1cm diameter of and height can range from 1.5 to 2cm, restrained in vertical direction, placed between three loading plates. The dynamic excitation in the form of shear strains is applied in horizontal direction through a central loading plate placed between the two models. As shown in Figure 7 shear strain amplitudes that can be applied are raging from $1x10^{-4}$ % up to 5% from which hysteresis curves shear stress-shear strain are obtained successfully. Series of cyclic tests are performed on soil specimens with around 30, 50 and 70% relative densities, while the effective pressure of 50,100 and 200kPa are applied. The dynamic excitation was applied step by step in form of short series of cyclic simple shear loads with frequency of 0.1Hz and constant vertical load by controlling the shear strains.

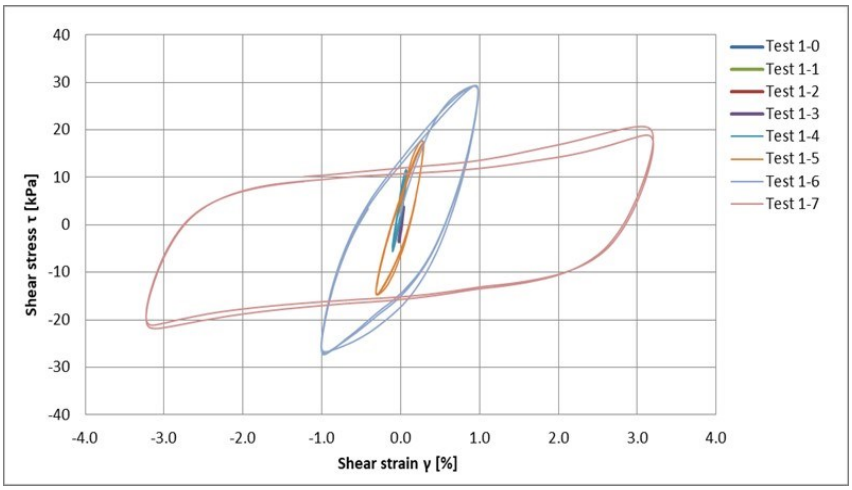


Figure 7. Shear stress–strain relationship from DSS test

Figure 8 presents the summary of the results for DSSA from which some conclusions can be made. Again, strong pressure dependence is noticed that increases with the increase of specimen relative density, contrary to this the

Copyright © 2025 CroCEE
DOI: https://doi.org/10.5592/CO/3CroCEE.2025.79

relative density dependence compared to previous results is lower and only noticeable when specimen are reconstituted with high Dr.

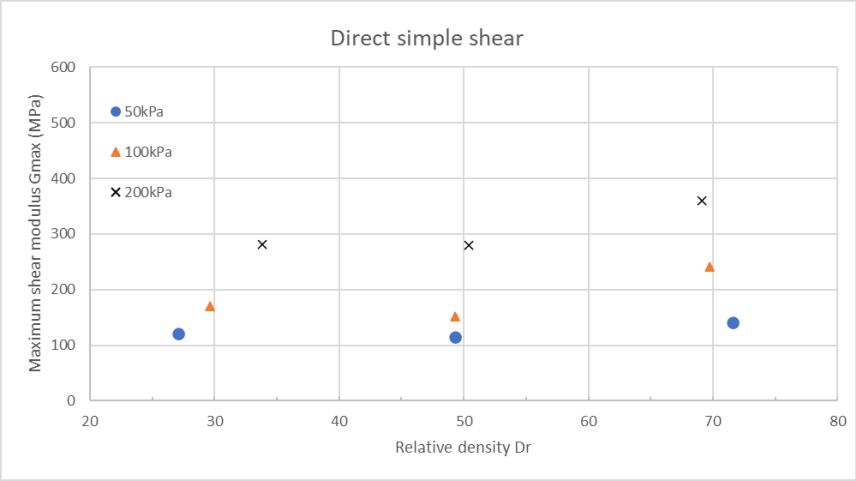


Figure 8. Results from DSSA

6. Conclusions

Extensive laboratory element testing of Skopje sand specimens was performed aiming to better understanding of key parameters which influence the determination of small strain shear modulus Gmax. Triaxial integral system and Direct Simple shear apparatus were used to run the respective triaxial, bender element and direct simple shear tests. Particular attention was paid to investigate the impacts initial stress conditions and relative densities exert on Gmax. Although the above mentioned testing equipment work on different stress states of the soil specimens, the obtained results for Gmax clearly show the significant stress dependency of Gmax (figure 9). The relative density also influenced small strain modules, particularly at high level of initial stresses. These findings are important outputs of the present study and have to be considered during the design and running of element testing for assessment of small strain modulus.

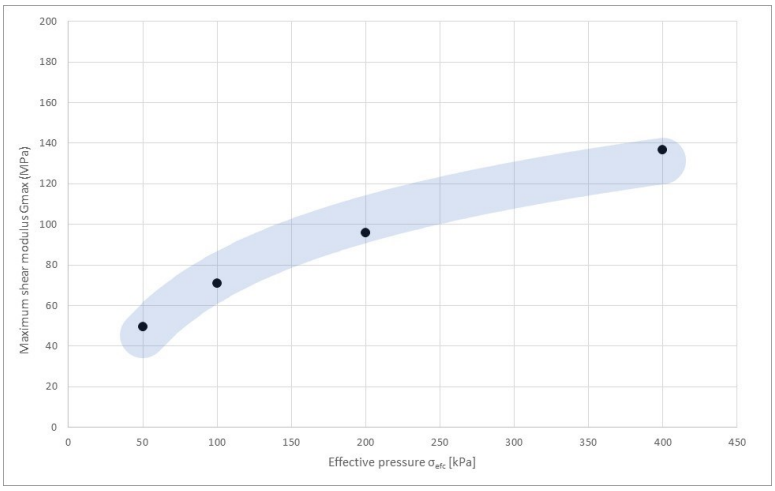


Figure 9. Dependance of the small strain shear modulus to the effective stress – envelope trend

References

[1] Kacar, O., 2014, "*Building a framework for predicting the settlements of shallow foundations on granular soils using dynamically measured soil properties*", From Soil Behavior Fundamentals to Innovations in Geotechnical Engineering, Geo Congress, 629-644

Copyright © 2025 CroCEE
DOI: https://doi.org/10.5592/CO/3CroCEE.2025.79

[2] Lee, J.S., Santamarina, J.C., 2005, "*Bender elements: Performance and signal interpretation*", Journal of Geotechnics and Geo Environmental Engineering, 131(9), 1063-1070

[3] Xiaoqiang; G., Jun Y., Maosong H., 2013, "*Laboratory measurement of small strain properties of dray sands by bender element*", Soils and Foundations 53, 735-745

[4] Lo Presti, D.C.F., Jamiolkowski, M., Lancellota, R., Varcelli, L., 1993, "*Maximum shear modulus measurement using bender elements in oedometer tests*", Rivista Italiana di Geotecnica

[5] Institute of Earthquake Engineering and Engineering Seismology (UKIM-IZIIS) website, https://www.iziis.ukim.edu.mk/en/

[6] J. Bojadjieva, "*Dynamic behavior of saturated cohesionless soils based on element and 1-G experiments*" PhD Thesis University Ss. Cyril and Methodius-Skopje, Macedonia, 2015

[7] Bojadjieva, J., et al. "*Comparison of cyclic simple shear and triaxial tests on natural sand*." XVII European Conference on Soil Mechanics and Geotechnical Engineering. 2019.

[8] T. Kitanovski., et al. "*Laboratory model tests on natural sand from Skopje region*." ce/papers 2.2-3: 689-694, 2018

[9] T. Kitanovski, et al. "*Effect of prior cyclic loading on triaxial monotonic experiments*." Proceedings of the 2nd Croatian Conference on Earthquake Engineering (2CroCEE). 2023.

[10] Tatsuoka F., Ochi K., Fujii S., Okamoto M., (1986) *"Cyclic undrained triaxial and torsional shear strength of sands for different sample preparation methods"* Soils and foundations vol.26, nº3, pp.23-41

[11] Scholey, Graham K., et al. "*A review of instrumentation for measuring small strains during triaxial testing of soil specimens*." Geotechnical Testing Journal 18.2 (1995): 137-156.

[12] Świdziński, W., and J. Mierczyński. "*On the measurement of strains in the triaxial test.*" Archives of Hydro-Engineering and Environmental Mechanics 49.1 (2002): 23-41.

[13] Deniz, Remzi Oguz. "*Bender elements and bending disks for measurement of shear and compressional wave velocities in large sand specimens*". MS thesis. Northeastern University, 2008.

[14] Piriyakul, K., and S. Pochalard. "*Using Shear Wave Velocity to Determine the Cementation Effect of Soft Bangkok Clay Mixed with Cement and Fly Ash*." Multiphysical Testing of Soils and Shales. Berlin, Heidelberg: Springer Berlin Heidelberg, 2012. 311-316.

[15] Suwal, Laxmi Prasad, and Reiko Kuwano. "*Disk shaped piezo-ceramic transducer for P and S wave measurement in a laboratory soil specimen*." Soils and foundations 53.4 (2013): 510-524.

[16] Dyvik, R., and Madshus, C. 1985. "*Lab measurements of Gmax using bender elements. In Advances in the Art of Testing Soils Under Cyclic Conditions*", Proceedings of the ASCE Conference, Detroit, Mich., 24 October 1985. Edited by V. Khosla. American Society of Civil Engineerings (ASCE), New York. pp. 186–196.

[17] Youn, Jun-Ung, Yun-Wook Choo, and Dong-Soo Kim. "*Measurement of small-strain shear modulus G max of dry and saturated sands by bender element, resonant column, and torsional shear tests*." Canadian Geotechnical Journal 45.10 (2008): 1426-1438.

[18] Dutta, T. T., et al. "*Evolution of shear wave velocity during triaxial compression*." Soils and Foundations 60.6 (2020): 1357-1370.

[19] Panuska J., Frankovska J., 2016, "*Effect of A void ratio on the small strain shear modulus Gmax for coarse-grained soils*", Procedia Engineering 161, 1235-1239

[20] Dames & Moore (1981),"*Manual for the Operation of the Cyclic Sample Shear Apparatus*", Dames & Moore, "The Times", 123 Northlake High Street, London

[21] Talaganov, K. (1986), "*Definition of of liquefaction potential of soil- cyclic deformation approach*" Ph.D., Ss. Cyril and Methodius, Skopje

Proceedings of the 3rd Croatian Conference on Earthquake Engineering - 3CroCEE
19–22 March 2025, Split, Croatia
Copyright © 2025 CroCEE
DOI: https://doi.org/10.5592/CO/3CroCEE.2025.94

ANALYTICAL AND NUMERICAL INVESTIGATION OF THE SITE RESPONSE PERIOD IN THE SAGUENAY REGION, EASTERN CANADA

A S M Fahad Hossain[(1)], Ali Saeidi[(2)], Mohammad Salsabili[(3)], Miroslav Nastev[(4)] and Juliana Ruiz Suescun[(5)]

[(1,2)] *Université du Québec à Chicoutimi, 555 Bd de l'Université, Chicoutimi, QC G7H 2B1, Canada*
[(3)] *University of Western Ontario, 1151 Richmond St, London, ON N6A 3K7, Canada*
[(4)] *Geological Survey of Canada, 490 R. de la Couronne, Québec, QC G1K 9A9, Canada*
[(5)] *Hydro Québec, 75 Boul. René-Lévesque O, Montréal, QC H2Z 1A4, Canada*

Abstract

The fundamental vibration period T_0 is often applied with the standard V_{S30} approach to improve the prediction of the seismic site effects. The commonly used equivalent single-layer method ($4H/V_{Savg}$) usually overestimates T_0. The present study applies a multi-layered method to develop empirical correlations for T_0 prediction. Numerical analyses examine the effects of the soil nonlinearity on T_0 shift and reduction of peak amplitude, establishing correlations for different hazard levels. The Saguenay Lac-Saint-Jean region (SLSJ), characterised by moderate seismicity and a strong impedance contrast at the bedrock interface, was selected as the study area. Results indicate that the analytical approach using the multiple soil layer method considerably reduces the T_0 overestimation. Empirical models were developed for site period evaluation using the multiple soil layer method for elastic strain and nonlinear dynamic response.

Keywords: Fundamental site period, Nonlinear site period, nonlinear analysis.

1. Introduction

The local geological and geotechnical properties of soils may lead to rapid variations of the seismic shaking in terms of duration and amplitudes at certain period ranges. In response to cyclic loading during the strong earthquake motion, the shear strains in soil increase, accompanied by a damping increase causing softening of the soil while reducing the amplitude of the ground motion amplification. This phenomenon contributes to a shift of the fundamental site period (T_0) to longer values, referred to as the nonlinear site period. These so-called seismic site effects were well observed during the 1985 Michoacan and 1989 Loma Prieta earthquakes. [1]. In seismic hazard evaluations, site effects are commonly accounted for with simple site conditions proxies, where the time-averaged shear-wave velocity of the top 30 m (V_{S30}), related to soil stiffness, is considered as the primary site parameter [2]. T_0 is also applied as an indicator of the resonance frequency to help improve surface ground motion prediction. It represents a soil column's most extended natural vibration period and can be determined through field measurements, analytical and empirical solutions, and numerical analysis. [3] and [4], demonstrated the benefits of using dominant periods from H/V spectral ratios (HVSR) for consistent site classification across diverse geologies. [5] refined this approach with H/V response spectra, creating new site categories. Studies by [6] and [7] confirmed HVSR's reliability, revealing sediment thickness effects missed by geology-based methods. [8] expanded HVSR analysis with Spanish data, while recent research employs Fourier and response spectra to calculate dominant periods (e.g., [9]; [10]). [11], [12] used nonlinear site response methods to evaluate the role of soil nonlinearity in shifting site periods. These findings underline the importance of considering nonlinear site periods for accurate seismic site classification. [13] analyzed the existing methods to calculate T_0 from shear-wave velocity V_S using various analytical approaches. The simple characteristic site period approximation $T_0=(4H/V_{Savg})$ is mainly applied when the time-averaged shear-wave velocity (V_{Savg}) and the

Copyright © 2025 CroCEE
DOI: https://doi.org/10.5592/CO/3CroCEE.2025.94

thickness of the soil column (H) are known [14]. However, it tends to overestimate T_0 as the nonlinear soil behavior during earthquakes, where stiffness degradation increases the site period, is not accounted for. Also, the equivalent single layer (ESL) assumption with uniform V_S across thick soil deposits, instead of the common increasing velocity depth gradient, shifts the evaluated T_0 to longer periods [11], [12]. To improve accuracy, [15] proposed the multilayer soil Layer (MSL) approach, building on the work of [16] and [17] to account for variations across layers. Therefore, comparing T_0 across different methods is essential, as ESL is frequently used as a secondary proxy in ground motion equations.

The present study is part of the ongoing site categorization in the Saguenay region, eastern Canada. Located near the Charlevoix-Kamouraska seismic zone, the Saguenay region is exposed to strong earthquakes with a predicted magnitude of up to M7.0 and a 2%/50yrs probability of exceedance (PE). The 1988 M5.9 Saguenay earthquake was the strongest recorded earthquake in eastern North America in more than 50 years, highlighting the need to assess the site response during intense seismic events. The study's objective is to investigate the dynamic site response with a focus on the fundamental site period (T_0). Site responses of 52 typical soil profiles in the study area, exposed to synthetic and recorded strong ground motions, are analyzed and compared to existing analytical models. Predictive T_0 models are developed with ESL and MSL approaches using equivalent linear and nonlinear analyses.

2. Materials and Methods

Saguenay, situated 200 km north of Québec City with a population of 147,100, serves as a central hub for commerce and administration. Positioned within the seismically active Saguenay graben, part of the Charlevoix-Kamouraska seismic zone, the city has experienced significant earthquakes, such as those in 1663 and 1988 with magnitudes of 6.0. The region's bedrock is composed of Precambrian rocks from the Grenville Province. At the same time, the lowlands are layered with glacial and postglacial deposits, including till, glaciofluvial gravel, glaciomarine clay, and deltaic sands, creating a geologically diverse landscape. The selection of 52 soil profiles in this area was based on the vertical and geographic distribution of four surface components: sand, gravel, clay, and till, distributed over four cross-sections shown in Figure 1(a), with thickness details for surface soils in Saguenay. 10 to 15 profiles were retrieved for each cross-section, with 52 stratigraphic soil profiles analyzed. The bedrock was modeled as an elastic half-space with specific density and shear-wave velocity parameters. Two earthquake scenarios, with moment magnitudes of M6 and M7 and exceedance probabilities of 1/975 and 1/2475 years, represented Saguenay's seismic hazard (www.seismotoolbox.ca). Four artificial ground movements were selected based on source-to-site distances of 40–60 km, and two accurate earthquake records from eastern Canada were incorporated: the 1988 M5.9 Saguenay earthquake (35 km from the epicenter) and the 2010 M5.1 Val-des-Bois earthquake (22 km from the epicenter). Figure 1(b) illustrates initial acceleration time histories for each ground movement, scaled to target spectra using the SeismoMatch software (www.seismosoft.com/). All site-specific soil properties used in the analysis are shown in Table 1.

The site response analysis was carried out on 52 soil profiles, using six input ground motions, each scaled to five earthquake hazard levels: 2%/50yrs, 3.5%/50yrs, 5%/50yrs, 10%/50yrs and 20%/50yrs PE from NBCC 2020. This analysis employed nonlinear methods in the time domain and equivalent linear methods in the frequency domain. The open-source software DEEPSOIL v7.0 was used and recognized for its reliability in site response analysis. Earlier versions of DEEPSOIL have been extensively validated and shown to replicate observed responses in well-documented soil sites accurately. In DEEPSOIL, the MKZ hyperbolic model, which accounts for pressure dependency, was applied to simulate modulus reduction and shear stress characteristics. The software technical guidelines provide an overview of the methods used for calculating the site response of a soil column discretized into individual layers using a single-

Copyright © 2025 CroCEE
DOI: https://doi.org/10.5592/CO/3CroCEE.2025.94

or multi-degree-of-freedom system and solving the dynamic equilibrium equations. Seismic amplification is the ratio of calculated surface to bedrock response spectral accelerations in time domain solution or Fourier amplitude spectrum ratio from frequency domain solution. The final amplification factor for each model was determined by taking the geometric mean of six responses obtained from different earthquake motions at the surface.

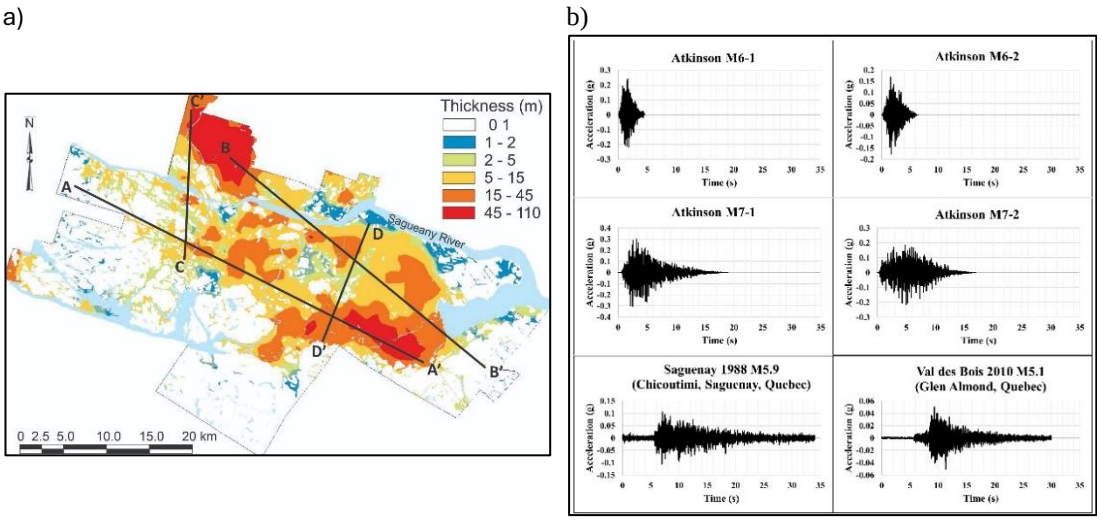


Figure 1. a) Thickness of surficial deposits with four cross-sections for selection of the 52 soil profiles used in the site response analyses (modified from [18] and b) unscaled input time histories.

Table 1. Adopted geotechnical and dynamic properties of soils and rock in the Saguenay region.

	Shear-Wave Velocity vs. Depth (m/s)	Density (kN/m^3)	Shear Modulus Reduction and Damping Ratio curves
Clay	Vs = 114.5 + 9.4 x D$^{0.76}$ [19]	18.7 [20]	[21]
Sand	Vs = 144.9 + 2.55 x D [19]	17.5 [20]	[22]*
Gravel	Vs = 46.861 + 61.55 x D$^{0.5}$ [19]	18.3 [23]*	[24]*
Till	V_{Still} = 582, σ=±174 (Motazedian et al., 2011)	21.0 [26]	Hydro Quebec (internal communication)
Rock	V_{Srock} = 1875, σ=±781 [27]	28.0 [28]	N/A

* Studies conducted in other regions

3. Analytical approach

The fundamental site period of 52 typical vertical profiles was calculated using both the equivalent single layer (ESL; T_0=4H/Vs) and multiple soil layers (MSL) approaches as described in Hadjian (2002). The procedure for calculating the T_0 in MSL profiles is described with equations 1 to 3. The process starts by considering the top two layers with respective fundamental periods T_1 and T_2. The combined fundamental period $T_{i=1}$ of these two layers is determined. In the next step, these two layers are treated as a single layer, and the third layer underneath is incorporated to calculate the combined $T_{i=2}$. This process is repeated iteratively across all the layers until the final T_0 is calculated for each of the 52 soil profiles. The number of iterations equals the number of assumed layers minus 1.

$$\frac{T}{T_1} = \sqrt{\frac{\pi^2}{8}\left[0.75 + \left(\frac{T_2}{T_1}\right)^2\left(1 + 2\frac{H_1}{H_2}\right)\right]} \quad ; \quad \left[\text{For } \frac{T_2}{T_1} > 0.1, H_1 > H_2\right] \tag{1}$$

Copyright © 2025 CroCEE
DOI: https://doi.org/10.5592/CO/3CroCEE.2025.94

$$\frac{T}{T_1} = \left[1 + \beta\left(\frac{T_2}{T_1}\right)^n \left(1 + 2\frac{H_1}{H_2}\right)^n\right]^{\frac{1}{n}} \quad ; \quad \left[\text{For } \frac{T_2}{T_1} > 0.1, H_1 \leq H_2\right] \tag{2}$$

$$\frac{T}{T_1} = \left[1 + \frac{H_1}{H_2}\left(\frac{T_2}{T_1}\right)^2\right] \quad ; \quad \left[\text{For } \frac{T_2}{T_1} \leq 0.1\right] \tag{3}$$

where, $\beta = 1\text{-}0.2\left(\frac{H_1}{H_2}\right)^2$; and $n = 4 - 1.8\frac{H_1}{H_2}$

At the end of the process, an empirical correlation was developed to convert the fundamental site period from TESL to TMSL, as shown in equation 4.

$$T_{MSL} = 0.87 * T_{ESL}^{0.93}; \quad R^2 = 1.00; \quad \sigma = 0.018 \tag{4}$$

The calculated and empirical fundamental site period in multiple soil layered methods is plotted against the calculated site fundamental period in equivalent single-layer methods, as shown in Figure 2. It can be seen in Figure 2 that the fundamental site period calculated using MSL is lower than that using ESL and that the difference increases for soil columns with higher fundamental periods.

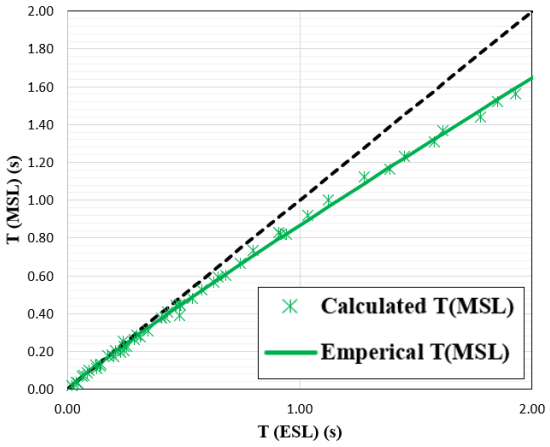


Figure 2. Correlation between the fundamental site periods obtained using the equivalent single layer, T_{ESL}, and the multiple TMSL approaches of soil layering. The black dashed line indicates the 1:1 correlation, where $T_{MSL}=T_{ESL}$.

4. Nonlinear numerical modelling

In response to cyclic loading during the strong earthquake motion, the shear strains in soil increase, accompanied by a damping increase causing softening of the soil and reducing the amplitude of the ground motion amplification. This phenomenon contributes to a shift of the fundamental site period (T_0) to longer values, which becomes more significant for stronger earthquake motions. Nonlinear site response simulations were carried out with the DEEPSOIL software to evaluate the magnitude of the period shift. The results are compared to the standard T_{ESL}. Two sets of 6 ground motions (Figure 1b) were scaled according to the NBCC 2020 hazard for the Saguenay region with a probability of exceedance (PE in the further text) of 2%/50yrs, which corresponds to a return period of 2475yr, and 10%/50yrs PE (475yr; NBCC2020). The nonlinear site period, T_{NL}, was determined from the acceleration response spectra at the ground surface for the period with maximum spectral amplification. The results are shown in Figure 3.

Copyright © 2025 CroCEE
DOI: https://doi.org/10.5592/CO/3CroCEE.2025.94

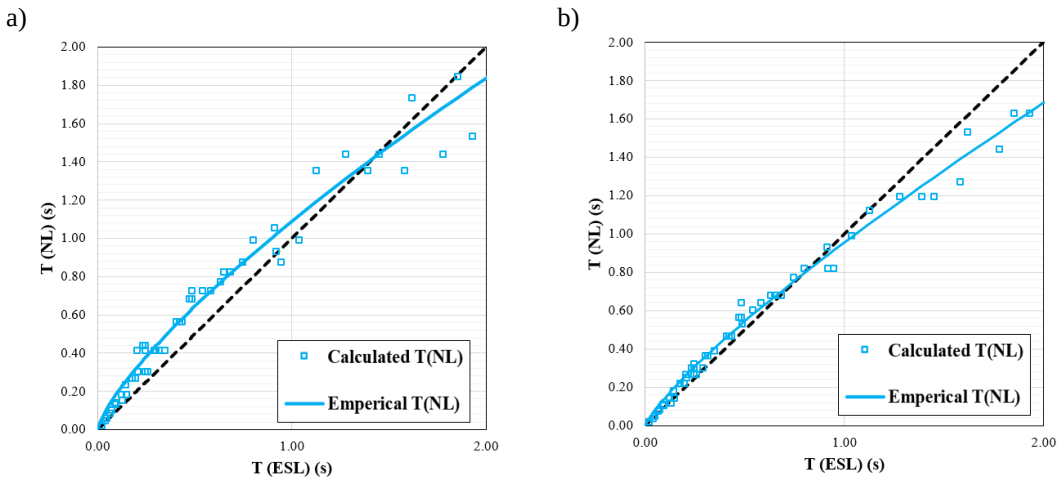


Figure 3. Nonlinear site period of soil for ground motion with a) 2%/50yrs PE and b) 10%/50yrs PE. The black dashed line indicates 1:1 correlation, where T_{NL}=T_{ESL}.

Figure 3 indicates that in the short period range, T_{NL} is higher than T_{ESL} for both hazard levels and shifts toward longer periods. In the longer period ranges, it becomes lower than T_{ESL}. The shift below the 1:1 line first occurs for ground motions scaled to 10%/50yrs PE, at approximately T=0.7s, and then for the ground motions scaled to 2%/50yrs PE, at approximately T=2.0s. Such performance can be explained by the conventional ESL method, which tends to overestimate T_0 values, especially for thicker soil columns. On the other hand, the MSL method provides better T_0 estimates. Also, soil columns with higher V_{Savg} display higher stiffness, resulting in a smaller T_0 shift due to earthquake loading compared to softer soil columns. For both sets of input motions, empirical correlations were developed as described with equations 5 and 6 for 2%/50yrs and 10%/50yrs PE, respectively. Additionally, a relationship between the nonlinear site period T_{NL}, on one hand side, and the peak ground acceleration (PGA) and the fundamental site period (T_0), on the other, was developed considering all five hazard levels with PE of 2%, 3.5%, 5%/, 10% and 20% in 50yrs, equation 7.

$$T_{NL\text{-}2\%/50yrs\ PE} = 1.09 * T_{ESL}^{0.76}; \quad R^2 = 0.97; \quad \sigma = 0.093 \qquad (5)$$

$$T_{NL\text{-}10\%/50yrs\ PE} = 0.96 * T_{ESL}^{0.82}; \quad R^2 = 0.99; \quad \sigma = 0.047 \qquad (6)$$

$$T_{NL} = 1.28 * PGA^{0.14} * T_{ESL}^{0.92}; \quad R^2 = 0.98; \quad \sigma = 0.086 \qquad (7)$$

Figure 4 shows the scatter of nonlinear site period results from all five hazards with the fundamental site periods T(ESL) and T(MSL). In all empirical correlations, the R^2 value is close to 1, indicating low errors in the regression analysis.

In the numerical site response modeling process, it is important to conduct an equivalent linear analysis to compare and validate the results of the nonlinear analysis. To this end, the amplification values were calculated as the ratio between the ground surface acceleration response spectra and Fourier amplitude spectra and their analogs of the input ground motions. In both cases, the site periods were determined to correspond to the maximum amplification. The site period in the frequency domain analysis was defined as the reciprocal value of the frequency. Figures 5 and 6 compare maximum amplification values and the corresponding site periods from the response spectrum using a time-domain nonlinear approach (NL) and

Proceedings of the 3rd Croatian Conference on Earthquake Engineering - 3CroCEE
19–22 March 2025, Split, Croatia
Copyright © 2025 CroCEE
DOI: https://doi.org/10.5592/CO/3CroCEE.2025.94

frequency-domain equivalent linear analysis (EL) corresponding to 2%/50-year and 10%/50-year PE hazard scenarios.

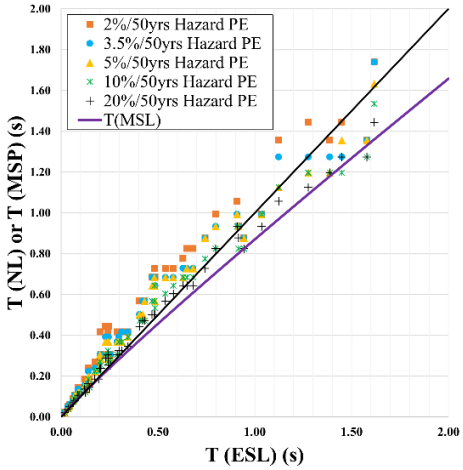


Figure 4. The scatter of nonlinear site periods T(NL) from different soil models for all five hazard levels and T(MSL) against the fundamental site periods T(ESL). The black dashed line indicates a 1:1 correlation, where T_{NL} or T_{MSL}=T_{ESL}.

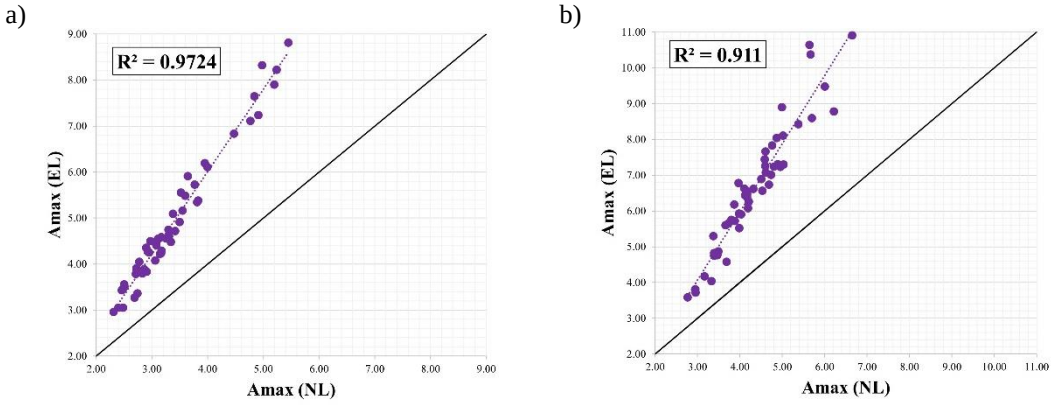


Figure 5. Comparison of the maximum amplifications from nonlinear, Amax (NL), and equivalent linear, Amax (EL), analyses for: a) 2%/50yrs PE and b) 10%/50yrs PE. (Black straight line is the 1:1 line where Amax (EL)=Amax (NL))

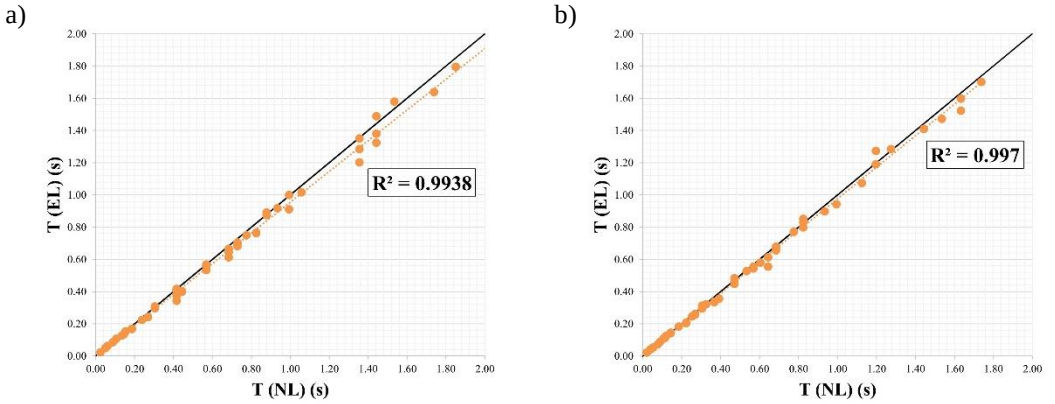


Figure 6. Comparison of the maximum amplification and corresponding site periods from nonlinear, T_{NL}, and equivalent linear, T_{EL}, analyses for a) 2%/50yrs PE and b) 10%/50yrs PE. (Black straight line is the 1:1 line where Amax (EL)=Amax (NL))

Copyright © 2025 CroCEE
DOI: https://doi.org/10.5592/CO/3CroCEE.2025.94

The results in Figures 4 and 5 demonstrate high correlations between the maximum amplifications and fundamental site periods, with R2 values ranging from 0.91 to 0.99 for both hazard levels. Slightly higher deviations among the data points can be observed for higher amplifications and longer periods. These results suggest a stable and predictable relationship between nonlinear and equivalent linear analyses across both hazard scenarios.

5. Resonance Effect

In soil dynamics, the resonance effect occurs when the dominant period range of the incoming seismic waves, where most of the earthquake energy is concentrated, aligns with the fundamental site period or the natural frequency of the soil column. This alignment contributes to amplified seismic shaking at the ground surface. The buildup in the soil vibrations amplitude can potentially lead to permanent soil deformations, such as subsidence, lateral spread, landslide, etc. Site response analyses indicate that maximum amplification occurs when the ratio between the dominant input vibration period and the site response period becomes close or equal to 1 [29]. Here, most of the earthquake energy content is concentrated in the dominant input vibration period. The site response period refers to the maximum period at which the soil vibrates, with T_0 indicating low (elastic) strain conditions and T_{NL} indicating nonlinear soil behavior under earthquake loading. The nonlinear amplification values were plotted with respect to the ratio of the oscillation period and site period, as shown in Figure 7.

The nonlinear analysis correlated against the vibration period to fundamental site period ratio in Figure 7a indicates that a shift in the resonance period occurs due to the considered nonlinearity. However, when nonlinear amplification is compared against the ratio of the oscillation period (T_{osc}) to the nonlinear site period (T_{NL}) derived from the empirical models discussed in section 4, resonance occurs steadily near the ratio of 1 (Figure 7b).

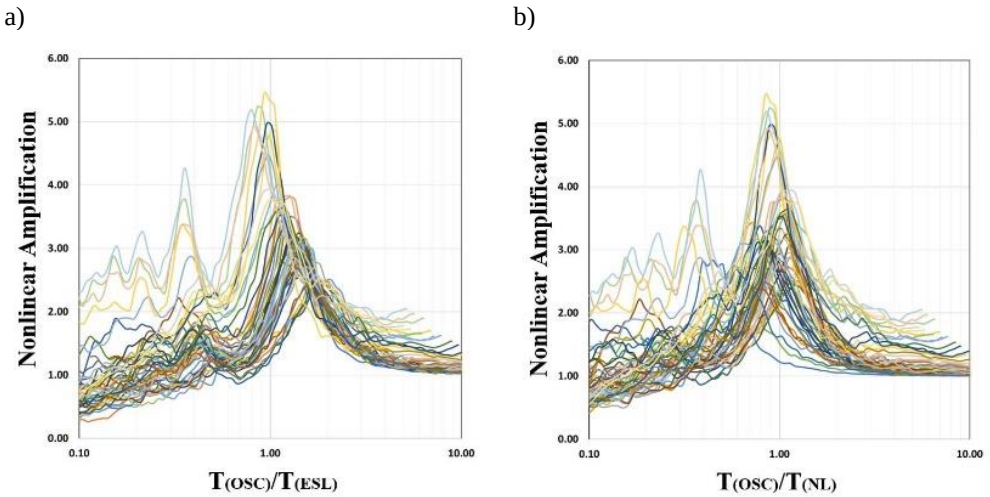


Figure 7. Amplification Values vs. Ratio of Vibration Period to Site Natural Period for 2%/50yrs PE: a) a) Nonlinear amplification vs T_{osc}/T_{ESL} b) Nonlinear amplification vs T_{osc}/T_{NL}.

6. Conclusion

A comprehensive 1D site response analysis was conducted in the Saguenay region on 52 soil profiles with site-specific properties. Both the nonlinear time-domain and the equivalent linear frequency-domain methods were used. This analysis employed hazard levels of 2%, 3.5%, 5%,

Copyright © 2025 CroCEE
DOI: https://doi.org/10.5592/CO/3CroCEE.2025.94

10% and 20% probability of exceedance in 50 years as specified in NBCC2020. Results from both time-domain and frequency-domain methods align well, validating the findings.

Each soil column's fundamental site period was calculated using the widely used equivalent single-layer method and a multiple-soil-layer profile method. The multiple-layer method was observed to be more effective, resulting in less overestimation of the fundamental site period. We developed an empirical correlation for the multiple-layer method, enabling precise calculation of the fundamental site period from the commonly used single-layer method.

Additionally, we calculated the nonlinear site period from the site response analysis by identifying the maximum amplification and developing empirical models for different hazard levels. We highlighted the resonance effect in the Saguenay region, which is critical as it may amplify the amplitudes of the ground motion and cause site-induced damage due to resonance. An amplification model incorporating nonlinear site response and accounts for the resonance effect using the nonlinear site period is essential for accurate assessment in this region.

References

[1] J. H. Steidl, “Site Response in Southern California for Probabilistic Seismic Hazard Analysis,” Bulletin of the Seismological Society of America, vol. 90, no. 6B, pp. S149–S169, Dec. 2000, doi: 10.1785/0120000504.

[2] A. F. Hossain, A. Saeidi, M. Salsabili, M. Nastev, and J. Suescun, “Soil Dynamic Response and Site Amplification Parameters for Saguenay, Eastern Canada,” Japanese Geotechnical Society Special Publication, vol. 10, no. 52, p. v10.OS-41-03, 2024, doi: 10.3208/jgssp.v10.OS-41-03.

[3] J. X. Zhao et al., “An empirical site-classification method for strong-motion stations in Japan using H/V response spectral ratio,” Bulletin of the Seismological Society of America, vol. 96, no. 3, pp. 914–925, Jun. 2006, doi: 10.1785/0120050124.

[4] Y. Fukushima, L. F. Bonilla, O. Scotti, and J. Douglas, “Site Classification Using Horizontal-to-vertical Response Spectral Ratios and its Impact when Deriving Empirical Ground-motion Prediction Equations,” Journal of Earthquake Engineering, vol. 11, no. 5, pp. 712–724, Oct. 2007, doi: 10.1080/13632460701457116.

[5] C. Di Alessandro, L. F. Bonilla, D. M. Boore, A. Rovelli, and O. Scotti, “Predominant-Period Site Classification for Response Spectra Prediction Equations in Italy,” Bulletin of the Seismological Society of America, vol. 102, no. 2, pp. 680–695, Apr. 2012, doi: 10.1785/0120110084.

[6] N. Harinarayan and A. Kumar, “Seismic Site Classification of Recording Stations in Tarai Region of Uttarakhand, from Multiple Approaches,” Geotechnical and Geological Engineering, vol. 36, no. 3, pp. 1431–1446, Jun. 2018, doi: 10.1007/s10706-017-0399-1.

[7] S. Chopra, V. Kumar, P. Choudhury, and R. B. S. Yadav, “Site classification of Indian strong motion network using response spectra ratios,” J Seismol, vol. 22, no. 2, pp. 419–438, Mar. 2018, doi: 10.1007/s10950-017-9714-9.

[8] L. A. Pinzón, L. G. Pujades, A. Macau, E. Carreño, and J. M. Alcalde, “Seismic Site Classification from the Horizontal-to-Vertical Response Spectral Ratios: Use of the Spanish Strong-Motion Database,” Geosciences (Basel), vol. 9, no. 7, p. 294, Jul. 2019, doi: 10.3390/geosciences9070294.

[9] H. Ghofrani, G. M. Atkinson, and K. Goda, “Implications of the 2011 M9.0 Tohoku Japan earthquake for the treatment of site effects in large earthquakes,” Bulletin of Earthquake Engineering, vol. 11, no. 1, pp. 171–203, Feb. 2013, doi: 10.1007/s10518-012-9413-4.

Copyright © 2025 CroCEE
DOI: https://doi.org/10.5592/CO/3CroCEE.2025.94

[10] H. Livaoğlu, E. Şentürk, and F. Sertçelik, "A Comparative Study of Response and Fourier Spectral Ratios on Classifying Sites," Pure Appl Geophys, vol. 178, no. 5, pp. 1745–1759, May 2021, doi: 10.1007/s00024-021-02722-1.

[11] D. Motazedian, K. Khaheshi Banab, J. A. Hunter, S. Sivathayalan, H. Crow, and G. Brooks, "Comparison of Site Periods Derived from Different Evaluation Methods," Bulletin of the Seismological Society of America, vol. 101, no. 6, pp. 2942–2954, Dec. 2011, doi: 10.1785/0120100344.

[12] D. Motazedian, H. Torabi, J. A. Hunter, H. L. Crow, and M. Pyne, "Seismic site period studies for nonlinear soil in the city of Ottawa, Canada," Soil Dynamics and Earthquake Engineering, vol. 136, p. 106205, Sep. 2020, doi: 10.1016/j.soildyn.2020.106205.

[13] S. Wang, Y. Shi, W. Jiang, E. Yao, and Y. Miao, "Estimating Site Fundamental Period from Shear-Wave Velocity Profile," Bulletin of the Seismological Society of America, vol. 108, no. 6, pp. 3431–3445, Dec. 2018, doi: 10.1785/0120180103.

[14] A. F. Hossain, M. Salsabili, A. Saeidi, J. R. Suescun, and M. Nastev, "Effects of Shear Wave Velocity and Thickness of Soil Layers on 1D Dynamic Response in the Saguenay Region, Quebec," in Rocscience International Conference (RIC 2023), Toronto: Atlantis Press, 2023, pp. 165–173. doi: 10.2991/978-94-6463-258-3_17.

[15] A. H. Hadjian, "Fundamental period and mode shape of layered soil profiles," Soil Dynamics and Earthquake Engineering, vol. 22, no. 9–12, pp. 885–891, Oct. 2002, doi: 10.1016/S0267-7261(02)00111-2.

[16] Madera G., "Fundamental period and amplification of peak acceleration in layered systems," 1970.

[17] Dobry, R., Oweis, I., & Urzua, A. (1976). Simplified procedures for estimating the fundamental period of a soil profile. Bulletin of the Seismological Society of America, 66(4), 1293-1321.

[18] M. Salsabili, A. Saeidi, A. Rouleau, and M. Nastev, "Development of empirical CPTu-V correlations for post-glacial sediments in Southern Quebec, Canada, in consideration of soil type and geological setting," Soil Dynamics and Earthquake Engineering, vol. 154, p. 107131, Mar. 2022, doi: 10.1016/j.soildyn.2021.107131.

[19] M. Salsabili, A. Saeidi, A. Rouleau, and M. Nastev, "Probabilistic approach for seismic microzonation integrating 3D geological and geotechnical uncertainty," Earthquake Spectra, vol. 39, no. 1, pp. 310–334, Feb. 2023, doi: 10.1177/87552930221132576.

[20] A.-G. Sanou, A. Saeidi, S. Heidarzadeh, R. V. P. Chavali, H. E. Samti, and A. Rouleau, "Geotechnical Parameters of Landslide-Prone Laflamme Sea Deposits, Canada: Uncertainties and Correlations," Geosciences (Basel), vol. 12, no. 8, p. 297, Jul. 2022, doi: 10.3390/geosciences12080297.

[21] M. Abdellaziz et al., "New model of shear modulus degradation and damping ratio curves for sensitive Canadian clays," Canadian Geotechnical Journal, vol. 60, no. 6, pp. 784–801, Jun. 2023, doi: 10.1139/cgj-2021-0475.

[22] EPRI, "Guidelines for Site Specific Ground Motions," 1993.

[23] K. M. Rollins, M. D. Evans, N. B. Diehl, and W. D. D. III, "Shear Modulus and Damping Relationships for Gravels," Journal of Geotechnical and Geoenvironmental Engineering, vol. 124, no. 5, pp. 396–405, May 1998, doi: 10.1061/(ASCE)1090-0241(1998)124:5(396).

Copyright © 2025 CroCEE
DOI: https://doi.org/10.5592/CO/3CroCEE.2025.94

[24] H. B. Seed, R. T. Wong, I. M. Idriss, and K. Tokimatsu, "Moduli and Damping Factors for Dynamic Analyses of Cohesionless Soils," Journal of Geotechnical Engineering, vol. 112, no. 11, pp. 1016–1032, Nov. 1986, doi: 10.1061/(ASCE)0733-9410(1986)112:11(1016).

[25] D. Motazedian, J. A. Hunter, A. Pugin, and H. Crow, "Development of a Vs 30 (NEHRP) map for the city of Ottawa, Ontario, Canada," Canadian Geotechnical Journal, vol. 48, no. 3, pp. 458–472, Mar. 2011, doi: 10.1139/T10-081.

[26] R. Urgeles, J. Locat, H. J. Lee, and F. Martin, "The Saguenay Fjord, Quebec, Canada: integrating marine geotechnical and geophysical data for spatial seismic slope stability and hazard assessment," Mar Geol, vol. 185, no. 3–4, pp. 319–340, Jun. 2002, doi: 10.1016/S0025-3227(02)00185-8.

[27] S. Ladak, S. Molnar, and S. Palmer, "Multi-method site characterization to verify the hard rock (Site Class A) assumption at 25 seismograph stations across Eastern Canada," Earthquake Spectra, vol. 37, no. 1_suppl, pp. 1487–1515, Jul. 2021, doi: 10.1177/87552930211001076.

[28] A. Saeidi, S. Heidarzadeh, S. Lalancette, and A. Rouleau, "The effects of in situ stress uncertainties on the assessment of open stope stability: Case study at the Niobec Mine, Quebec (Canada)," Geomechanics for Energy and the Environment, vol. 25, p. 100194, Mar. 2021, doi: 10.1016/j.gete.2020.100194.

[29] J. Harmon et al., "Site Amplification Functions for Central and Eastern North America – Part I: Simulation Data Set Development," Earthquake Spectra, vol. 35, no. 2, pp. 787–814, May 2019, doi: 10.1193/091017EQS178M.

Proceedings of the 3rd Croatian Conference on Earthquake Engineering - 3CroCEE
19–22 March 2025, Split, Croatia
Copyright © 2025 CroCEE
DOI: https://doi.org/10.5592/CO/3CroCEE.2025.140

EFFECT OF SEISMIC LOAD ON THE STABILITY OF A DOLOMITE QUARRY IN HUNGARY

Saltanat Yesselbayeva [(1)], Máté Urbán [(2)], Péter Görög [(3)]

[(1)] *PhD student, Budapest University of Technology and Economics, Faculty of Civil Engineering, Department of Engineering Geology and Geotechnics, saltanat.yesselbayeva@edu.bme.hu*
[(2)] *) Geotechnical designer, Mott MacDonald Cz, urban.mate91@gmail.com*
[(3] *Associate professor, Budapest University of Technology and Economics, Faculty of Civil Engineering, Department of Engineering Geology and Geotechnics, gorog.peter@emk.bme.hu*

Abstract

The rock slope stability in seismically active regions is a critical aspect for safe and sustainable quarrying. This study investigates the effect of seismic loading on the stability of a dolomite quarry, integrating traditional analytical methods with advanced two-dimensional finite element models. The site, located near a historically active earthquake zone, provides an ideal environment to explore slope stability under both static and dynamic conditions. Site measurements and rock mass data, supplemented by geological data from comparable formations, inform the development of a comprehensive geotechnical model. The methodology the slope design framework emphasizing kinematic analysis and failure mode evaluation, particularly relevant to the structural integrity of strong, jointed rock masses like dolomite. Regulations, including Eurocode 7 partial factors and criteria for safety and failure probability, frame the analytical approach. Slope stability is first assessed through empirical techniques, such as SMR and Q Slope, then through detailed analytical solutions using RocScience software. Through RocScience RS2 could examine the application of seismic load in finite element models and highlight potential failures under earthquake conditions**.** While optimization of mining slopes is outside the scope, this analysis emphasizes model sensitivity to seismic inputs, joint geometry, and mesh size, demonstrating critical conditions under dynamic loading. Limitations in data availability, particularly historical earthquake data, are addressed with approximate time-history data.

Keywords: rock slope stability, seismic loading, dolomite quarry, geotechnical modelling, jointed rock masses, earthquake effects

1. Introduction

Open-pit mining often involves the excavation of rock masses with complex geological structures, requiring detailed slope stability assessments to ensure operational safety and economic viability. Stable slopes are critical to minimizing the risks of rockfalls or large-scale collapses, which can result in fatalities, equipment damage, and operational disruptions. In regions subject to seismic activity, the risk of slope instability is further exacerbated by dynamic forces, necessitating specialized approaches for slope analysis [1, 2]. This study focuses on addressing these challenges in the context of a dolomite quarry in Vilonya, Hungary, where the interplay of geological conditions and seismicity poses significant engineering concerns.

The Vilonya dolomite quarry is situated in an area of moderate seismic activity, as evidenced by the 1985 Berhida earthquake, which had a moment magnitude of Mw = 5.2 and occurred approximately 5 km from the site. This earthquake highlighted the potential for seismic events to impact local infrastructure and geological stability [3]. Given the quarry's proximity to the epicentre, understanding the seismic response of slopes is essential for designing resilient pit walls. The absence of local acceleration time history data necessitated using comparable seismic records, such as those from the 2004 Parkfield earthquake in California, to model the effects of dynamic loading on slope stability [4].

The primary objective of this study is to assess the stability of a slope in the Vilonya dolomite quarry under both static and seismic conditions. This involves:

Proceedings of the 3rd Croatian Conference on Earthquake Engineering - 3CroCEE
19–22 March 2025, Split, Croatia
Copyright © 2025 CroCEE
DOI: https://doi.org/10.5592/CO/3CroCEE.2025.140

1. Utilizing traditional analytical methods, such as Slope Mass Rating (SMR) and kinematic analysis, to identify potential failure mechanisms.
2. Incorporating advanced numerical modelling techniques using finite element methods (FEM) to simulate the effects of seismic loading.
3. Comparing analytical and numerical results to evaluate the reliability and accuracy of different methods in predicting slope behaviour under varying conditions.
4. Providing recommendations for slope design and monitoring strategies to mitigate the risks associated with seismic activity.

2. Geological and Geotechnical Framework

The Vilonya dolomite quarry is located in western Hungary, within Veszprém County, near the village of Vilonya. The area is predominantly composed of the Budaörs Dolomite Formation, a Triassic-era carbonate rock unit with a thickness of up to 1.5 kilometres. The dolomite is overlain by the Dachstein Limestone Formation and underlain by the Veszprém Marl Formation. These formations provide a stable geological foundation but require detailed characterization to assess their engineering behaviour [5].

The rock mass in the quarry consists predominantly of dolomite, a sedimentary carbonate rock with a fractured and blocky structure. The dolomite is characterized by the following features:

Material Properties: Laboratory testing has determined a uniaxial compressive strength (UCS) of approximately 68.8 MPa and a unit weight of 27.69 kN/m³. The dolomite exhibits a residual UCS of 20-30% of its intact strength under high-stress conditions.

Joint Systems: The rock mass contains significant discontinuities, including a primary joint set with a dip/dip direction of 30°/311°. The joints are rough (mean Joint Roughness Coefficient, JRC = 10) and variably spaced, with a typical interjoint distance of 10 m. These features strongly influence the stability and potential failure mechanisms of the slopes.

Geological Strength Index (GSI): The dolomite is classified within a GSI range of 40–60, reflecting its blocky, interlocked structure with moderate surface weathering. Residual GSI values are lower (20–30), corresponding to degraded conditions after failure [6, 7].

The hydrogeological setting of the quarry has a minimal impact on slope stability. The site is located in the catchment area of the Séd River but lacks significant groundwater sources, springs, or surface water bodies within a 1-kilometer radius. Precipitation and infiltration rates are low due to the region's fractured, karstic nature, which promotes rapid drainage. As a result, the effects of groundwater pressure or hydrodynamic forces on slope stability are considered negligible for this analysis.

3. Seismic Activity and Loading Considerations

The Vilonya dolomite quarry is situated in a region of moderate seismic activity. One of Hungary's largest recorded earthquakes occurred in 1985 near Berhida, just 5 kilometres from the quarry. This earthquake, with a moment magnitude of Mw = 5.2, was caused by strike-slip faulting at a focal depth of approximately 10–12 kilometres [8]. The event generated a peak ground acceleration (PGA) of 0.15g and a peak ground velocity (PGV) of 7 cm/s, which resulted in localized structural damage and heightened awareness of seismic risks in the area. The proximity of the quarry to this epicentre underscores the need for detailed seismic stability assessments on its slopes [9].

A key challenge in the analysis was the absence of detailed acceleration time-history data from the 1985 Berhida earthquake. To address this, comparable seismic events were identified using global earthquake databases. The 2004 Parkfield earthquake in California, which had a moment magnitude of Mw = 6.0, was selected as a reference due to its similar geological setting (strike-slip faulting) and focal depth (7.9 km). The acceleration data from the Turkey Flat #1 Rock South station provided a reliable basis for the analysis, with a peak horizontal ground acceleration of 0.25g, closely matching the design acceleration for the quarry. This selection ensured that the seismic input accurately represented the dynamic forces that might act on the slope during an earthquake.

Copyright © 2025 CroCEE
DOI: https://doi.org/10.5592/CO/3CroCEE.2025.140

Two seismic loading approaches were employed to assess slope stability under earthquake conditions: Pseudo-Static Analysis: A horizontal seismic coefficient (kH) of 0.15g was applied as the design acceleration, representing the region's typical seismic activity. Additionally, a higher kH value of 0.25g, corresponding to the peak acceleration observed in the Parkfield earthquake, was used to simulate extreme conditions. These values were applied in a static framework using analytical methods such as RocPlane and Swedge . Dynamic Analysis: To capture the transient effects of seismic loading, the acceleration time history from the Parkfield earthquake was integrated into the finite element model (FEM) using RocScience RS2 software. This dynamic approach accounted for the progressive buildup and dissipation of seismic forces, providing insights into displacement patterns, joint yielding, and potential failure mechanisms.

4. Methodology

The methodology for assessing the effect of seismic loading on the stability of a dolomite quarry slope near Vilonya, Hungary, integrates field investigations, analytical techniques, and numerical modelling [10] to provide a comprehensive analysis. Field investigations began with data collection on-site, including the measurement of joint properties using geological compasses and Barton comb profilometers to determine key parameters such as the Joint Roughness Coefficient (JRC) and joint stiffness values. The geometry and structure of the slope were recorded, and a photogrammetry-based 3D model of the quarry was developed, incorporating reference points measured on-site to ensure dimensional accuracy Fig. 1. Laboratory tests from a comparable dolomite quarry provided values for the uniaxial compressive strength (UCS), density, and elastic modulus of the rock, which were used alongside field observations to establish Geological Strength Index (GSI) ranges for the generalized Hoek-Brown failure criterion.

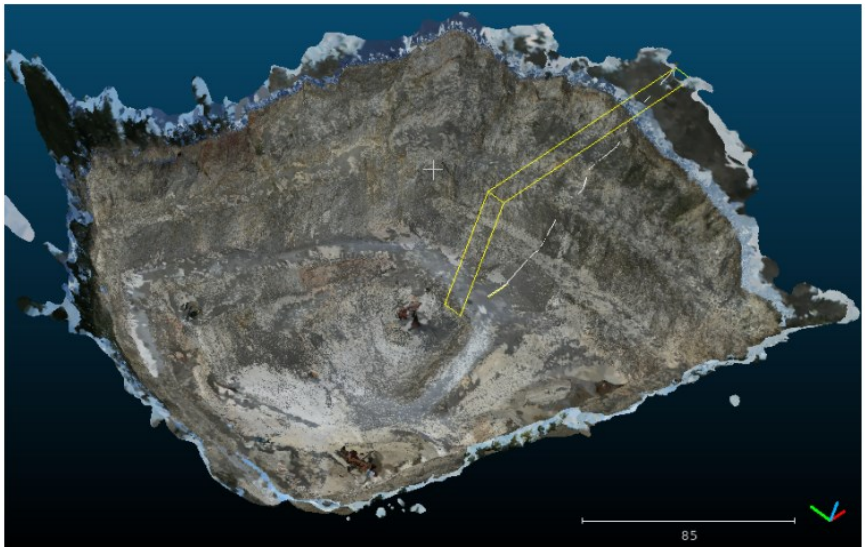


Figure 1. 3D model of the mine generated from photographs. The examined wall can be seen in yellow. (courtesy of Gábor Németh)

Analytical methods included kinematic analysis using stereographic projection to identify potential failure mechanisms such as planar, wedge, and toppling failures Fig. 2. Stability was further assessed using empirical approaches, including the Slope Mass Rating (SMR) and Q-Slope systems. Pseudo-static analysis was conducted with RocScience RocPlane software, calculating the factor of safety (FoS) for seismic coefficients kH=0.15gk and kH=0.25gk. The input parameters for these analyses, including joint orientations and material properties, were derived from field and laboratory data. Numerical modelling was performed using RocScience RS2 software to simulate both static and dynamic conditions [11]. The slope geometry was simplified to reflect typical open-pit mine configurations, and

Copyright © 2025 CroCEE
DOI: https://doi.org/10.5592/CO/3CroCEE.2025.140

finite element models were created with varying mesh densities and boundary conditions to ensure robustness. Dynamic analysis incorporated acceleration time history data from the 2004 Parkfield earthquake, scaled to match the seismic design parameters for the site. Rayleigh damping was applied to simulate realistic energy dissipation during seismic events, and horizontal displacement trends were analysed under different loading conditions [9].

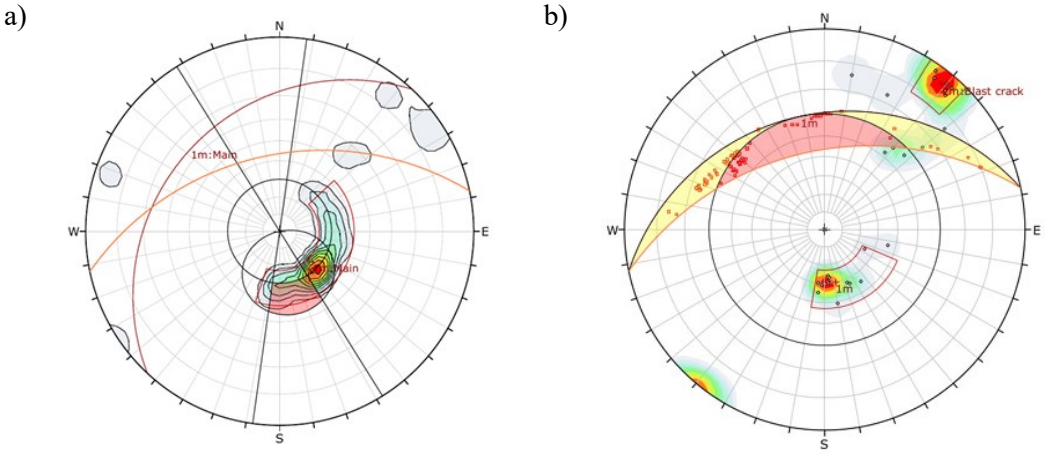
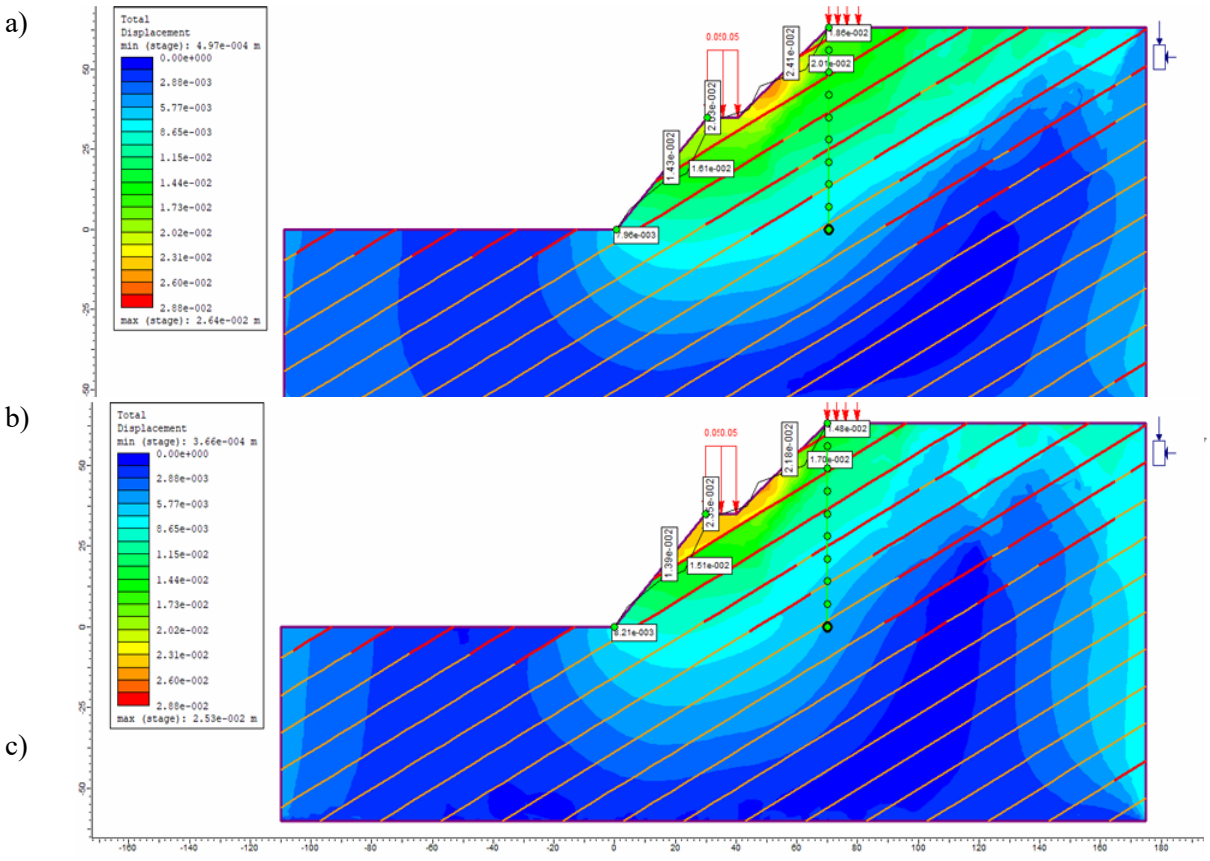


Figure 2. Kinematic analysis of wall 3 a) Possibility of plane failure; b) Possibility of wedge failure

Sensitivity analyses were conducted to examine the effects of mesh density, slope geometry, and joint stiffness on stability outcomes. The robustness of the numerical models was verified through comparative analyses with empirical methods. Figures of total displacements (Fig. 3 and 4) shows critical zones of instability. Horizontal displacements of the dynamic earthquake can be acquired on the base of the ramp geometry and dynamic model with large mesh. These detailed investigations provided a comprehensive understanding of the seismic response of the dolomite slope, forming the basis for recommendations on slope reinforcement and design adjustments.



Copyright © 2025 CroCEE
DOI https://doi.org/10.5592/CO/3CroCEE.2025.140

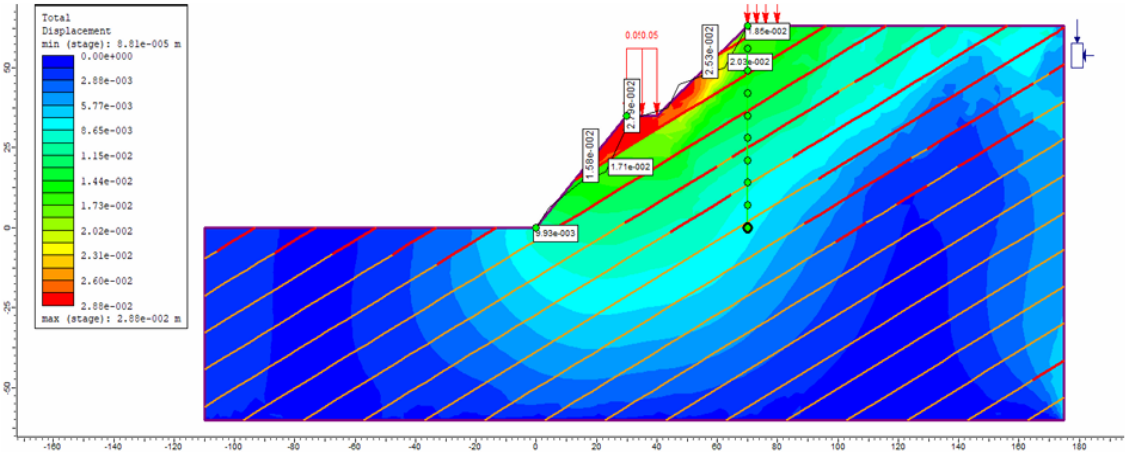
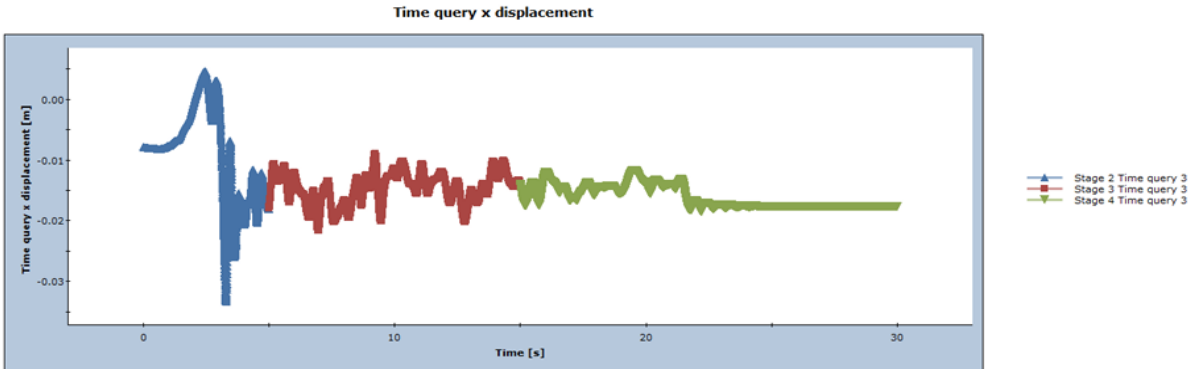
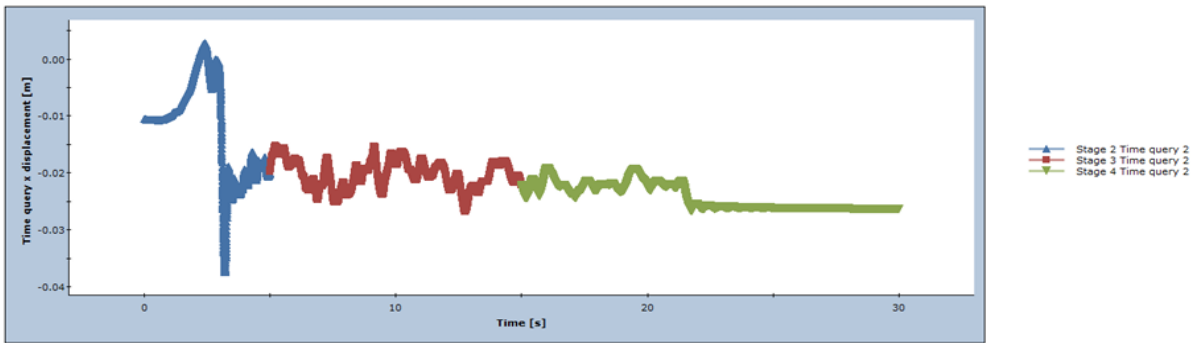


Figure 3. Displacement diagrams of dynamic model showing the yielded joints.
a) Dynamic loading at 5s; b) Dynamic loading at 15s; c) Dynamic loading at 35s

a)



b)



c)

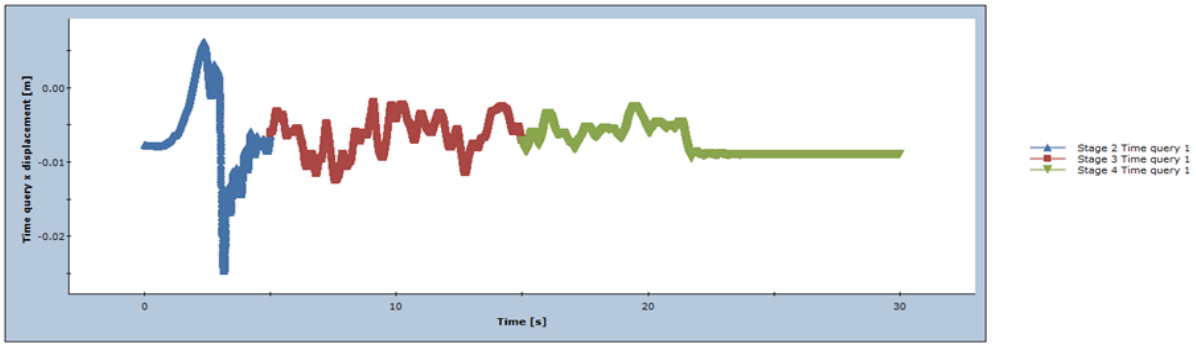


Figure 4. Horizontal displacements during the earthquake shows twofold increase of the static displacements. a) crown; b) ramp; c) base

Proceedings of the 3rd Croatian Conference on Earthquake Engineering - 3CroCEE
19–22 March 2025, Split, Croatia
Copyright © 2025 CroCEE
DOI: https://doi.org/10.5592/CO/3CroCEE.2025.140

5. Results and Discussion

The results of this study highlight critical insights into the stability of dolomite quarry slopes under static and seismic loading conditions. Analytical methods, such as SMR and Q-Slope, classified the slope as stable under static conditions, aligning with conventional expectations for strong, jointed rock masses like dolomite. However, the pseudo-static analysis indicated significant sensitivity to higher seismic accelerations [12, 13], with the factor of safety dropping below the acceptable limit at kH=0.25gk. Dynamic finite element modelling confirmed these findings, showing substantial horizontal displacements and yielded joint zones near the crest and mid-slope regions during peak seismic events. The deformation trends observed in the numerical models underscore the slope's vulnerability to seismic loading beyond the design-level acceleration.

Comparing these findings with existing literature, the observed behaviour aligns with studies on jointed rock masses under seismic loading. For instance, works like those by Sarma (1973) and recent publications on probabilistic seismic slope stability Qing Lu (2019) report similar trends where joint orientation and dynamic acceleration significantly influence failure mechanisms. These studies emphasize the importance of joint geometry and seismic coefficients, consistent with the sensitivity analyses conducted in this research. However, the specific findings for dolomite, particularly the critical role of joint roughness and residual strength, provide a more tailored perspective for regions with similar geological conditions [2].

From a theoretical standpoint, this study demonstrates the necessity of integrating dynamic analyses into slope stability evaluations. While traditional methods provide an initial assessment, they lack the capability to account for time-dependent seismic effects, which finite element models effectively capture. Practical implications include the need for designing slope reinforcements, such as rock bolts and anchors, particularly in areas with a history of significant seismic activity. The findings advocate for a shift towards incorporating seismic loading in quarry planning to ensure operational safety.

However, there are some limitations. The unavailability of site-specific time-history seismic data required the use of approximate data from a comparable event, which may not fully capture the unique seismic characteristics of the region. Additionally, the numerical models were limited to two-dimensional analysis, which does not account for potential three-dimensional effects. Future research opportunities include the development of three-dimensional models to better understand complex failure mechanisms and the integration of probabilistic approaches to account for the variability in seismic and geological parameters.

6. Conclusion

This study investigated the effects of seismic loading on the stability of a dolomite quarry slope, addressing key research questions about the behaviour of jointed rock masses under both static and dynamic conditions. The results directly support the hypothesis that seismic loading significantly influences the stability of slopes in seismically active regions [14]. Analytical methods, including SMR and Q-Slope, demonstrated that the slope is stable under static conditions, but pseudo-static and dynamic analyses revealed reduced stability when subjected to higher seismic accelerations, particularly at kH=0.25gk. The observed yielding of joints and increased horizontal displacements in dynamic finite element models confirm the hypothesis that dynamic seismic effects exacerbate potential failure mechanisms in jointed rock masses.

A clear cause-and-effect relationship was established between seismic loading and slope deformation. The results showed that jointed rock slopes like dolomite are particularly sensitive to dynamic seismic forces, with the magnitude and orientation of joint sets playing a critical role in failure. The study demonstrated that under design-level seismic accelerations, the slope remains stable, but peak accelerations cause significant instability, leading to potential failure. These findings emphasize the importance of considering both joint geometry and seismic inputs in slope design, particularly in regions prone to earthquakes.

The practical significance of these results lies in their application to quarry slope management and safety. The findings suggest that traditional static and pseudo-static methods, while valuable for initial

Copyright © 2025 CroCEE
DOI: https://doi.org/10.5592/CO/3CroCEE.2025.140

assessments, may underestimate risks in seismically active areas. Incorporating dynamic analyses into design practices can help engineers identify critical zones of instability and implement targeted reinforcement measures, such as rock bolts or anchors, to mitigate failure risks. The study also provides a framework for adapting quarry operations to dynamic loading scenarios, ensuring safe and sustainable mining practices.

Theoretically, the study contributes to the understanding of seismic effects on jointed rock masses by integrating empirical methods with advanced finite element modelling. It highlights the necessity of dynamic modelling for capturing time-dependent failure mechanisms that traditional methods overlook. The sensitivity analysis of key parameters, such as joint stiffness and mesh density, offers insights into optimizing numerical models for improved accuracy. Furthermore, the approach demonstrates how approximate seismic time-history data can be effectively used in the absence of site-specific records, broadening the applicability of the findings to similar geological and seismic contexts.

In summary, the results of this study validate the initial hypothesis and provide robust answers to the research questions, linking seismic loading to slope stability in jointed dolomite formations. The cause-and-effect relationships identified and the integration of practical and theoretical insights underline the significance of this work for advancing slope stability analysis and enhancing safety in seismically active quarrying environments.

References

[1] Sarma, S.K. (1973): Stability analysis of embankments and slopes, *Geotechnique*, 23(3), 423–433, doi: https://doi.org/10.1680/geot.1973.23.3.423.

[2] Qing, L., et al. (2019): Probabilistic assessment of seismic stability of rock slopes, *Engineering Geology*, 105210, doi: https://doi.org/10.1016/j.enggeo.2019.105210.

[3] Hoek, E., Bray, J.W. (1981): *Rock slope engineering*, Institution of Mining and Metallurgy, 3rd edition, London, UK.

[4] Barton, N. (1973): Review of a new shear strength criterion for rock joints, *Proceedings of the Symposium on Rock Mechanics*, New York, USA, 10 pages.

[5] Wyllie, D.C., Mah, C.W. (2005): *Rock slope engineering: Civil and mining*, Taylor & Francis, 4th edition, USA.

[6] Rocscience Inc. (2018): RocPlane and RS2 Software Manuals, Rocscience, Canada, https://www.rocscience.com/, (accessed November 26, 2024).

[7] Engineering Strong Motion Data (2018): Turkey Flat earthquake acceleration data from Parkfield, California, https://esm.mi.ingv.it/, (accessed November 26, 2024).

[8] Török, Á. (2007): Properties and applications of dolomites in Hungary, *Hungarian Journal of Geosciences*, 67(1), 89–103.

[9] Görög, P., Bögöly, G. (2018): Structural and geotechnical properties of dolomite quarries in Hungary, *Geotechnical Bulletin*, 47(4), 25–39.

[10] National Highway Institute (1998): Seismic considerations for slopes, *Geotechnical Engineering Guidelines*, 21 pages.

[11] Hoek, E., Carranza-Torres, C., Corkum, B. (2002): Hoek–Brown failure criterion, *Journal of Geotechnical and Geoenvironmental Engineering*, 128(8), 691–695, doi: https://doi.org/10.1061/(ASCE)1090-0241(2002)128:8(691).

[12] ATLAS Observatory (1985): Data from the Berhida earthquake, Hungarian Seismological Database, accessed via https://earthquake.usgs.gov/, (accessed November 26, 2024).

[13] Read, J., Stacey, P. (2009): *Guidelines for open pit slope design*, CSIRO Publishing, Australia.

[14] Pacific Earthquake Engineering Research Center (2017): Dynamic response of geotechnical slopes, *Technical Report PEER 2017/08*, Berkeley, USA.

Proceedings of the 3rd Croatian Conference on Earthquake Engineering - 3CroCEE
19–22 March 2025, Split, Croatia
Copyright © 2025 CroCEE
DOI: https://doi.org/10.5592/CO/3CroCEE.2025.148

LIQUEFACTION ASSESSMENT USING A SYNTHETIC CPT DERIVED FROM CORRELATION WITH SHEAR WAVE VELOCITY

Mario Bačić [(1)], Lovorka Librić [(2)], Meho Saša Kovačević [(3)]

[(1)] *Associate professor, University of Zagreb, Faculty of Civil Engineering, Department of Geotechnics, mbacic@grad.hr*
[(2)] *Associate professor, University of Zagreb, Faculty of Civil Engineering, Department of Geotechnics, llibric@grad.hr*
[(3)] *Professor, University of Zagreb, Faculty of Civil Engineering, Department of Geotechnics, msk@grad.hr*

Abstract

The assessment of liquefaction potential is critical in regions subject to seismic activity due to significant threat it poses to buildings and infrastructure. The reliability of liquefaction potential evaluations is highly dependent on the employed assessment method and the conducted number of representative investigations. This issue is particularly pertinent when assessing linear infrastructure, such as levees, which are often built on sediments prone to liquefaction. This study introduces an innovative approach for evaluating liquefaction potential using synthetic Cone Penetration Test (CPT) parameters, derived from correlations with shear wave velocity (v_s). The proposed methodology involves CPT–v_s correlations based on an extensive dataset, with careful consideration of the effects of averaging thicknesses over which the results are computed. This correlation forms the basis for generation of CPT data from the measured v_s values, which is subsequently utilized to calculate the liquefaction factor of safety and respective probability of liquefaction occurrence. The methodology is validated using data from a test site adjacent to a levee in the Krnjica borough, Croatia, which experienced liquefaction during the 2020 Petrinja earthquake. The findings suggest that the integration of the spatial v_s measurements to generate synthetic CPT parameters provides a relatively reliable tool for estimation of the liquefaction potential. At the end, recommendations are made for improving the applicability and accuracy of the proposed method.

Keywords: soil liquefaction, correlation, shear wave velocity, cone penetration test, Krnjica levee

1. Introduction

Seismic risk assessments are typically focused on the insufficient structural resilience of buildings and infrastructure to earthquake shaking, often overlooking the significant impact of liquefaction. Despite being a relatively rare phenomenon, liquefaction can lead to extensive damage and substantial economic losses [1]. Occurring in saturated, unconsolidated soils during high-magnitude earthquakes, liquefaction results in loss of soil shear strength and stiffness properties, impairing the soil capacity to support foundations of buildings and infrastructure. Recorded cases worldwide indicate that the liquefaction occurrence and intensity can be highly variable at short distances, likely influenced by the numerous factors within the underlying soil profile.

While detailed laboratory tests provide rigorous estimates of the liquefaction potential at specific sites, they are often too tedious and costly to be used for routine liquefaction assessments. As a result, the simplified "cyclic stress approach" is commonly employed for practical assessments. This approach relies on empirical correlations derived from historical data, for which liquefaction charts are developed and periodically updated. The most widely used procedures for assessing liquefaction resistance include in-situ tests such as the Standard Penetration Test (SPT), Cone Penetration Test (CPT), shear wave velocity determination (v_s), and the Becker Penetration Test (BPT). As highlighted by Bačić et al. [2], a significant challenge lies in evaluating the liquefaction potential in soils beneath linear infrastructure, such as levee networks, which can extend over vast areas. This challenge is compounded by the inability to conduct detailed, costly, and time-consuming investigations, especially considering the limited financial resources and time available to infrastructure managers. Additionally, the inherent variability of soil properties makes difficult the prediction of behaviour of individual layers during an earthquake, and as a result, interpreting the data and outcomes of various tests often requires a high level of engineering judgment, introducing subjectivity and variability into the assessment outcomes [3].

Copyright © 2025 CroCEE
DOI: https://doi.org/10.5592/CO/3CroCEE.2025.148

The shear wave velocity (v_s) and Cone Penetration Test (CPT) measurements are widely accepted to assess the liquefaction potential due to their rapidity, cost-effectiveness, and continuous soil profiling. Both methods offer distinct advantages and limitations in the context of liquefaction assessment. For example, although invasive, the CPT method generally does not disturb the soil and offers fast and accurate representation of in-situ conditions. However, some studies suggest that it may overestimate the liquefaction potential in certain soils, likely due to particle crushing and aging effects. Shear wave velocity-based methods, such as the multichannel analysis of surface waves (MASW), present an alternative to penetration methods for assessing liquefaction resistance. These methods provide consistent data on liquefaction resistance, with the advantage of being less influenced by soil disturbance. Despite differing opinions on the applicability of small-strain in-situ methods for estimation of liquefaction resistance, typically associated with large strains, the use of shear wave velocities as an indicator of liquefaction resistance is justified. This is because both shear wave velocity and liquefaction resistance are similarly influenced by factors such as void ratio, stress state, stress history, and geological age. Limitations of the shear wave velocity-based methods include the lack of sensitivity to the stress-strain history of the soil, which plays a significant role in liquefaction resistance. Additionally, the shear wave velocity is closely correlated to the soils void ratio as opposed to the relative density, with latter being a more reliable indicator of the liquefaction potential. This discrepancy complicates the use of shear wave velocity in liquefaction assessments. Also, thinner soil layers with low shear wave velocities, which may be prone to liquefaction, could be missed if the measurement resolution is insufficient. Despite the above-mentioned drawbacks, empirical correlation of the liquefaction potential to CPT data is better established when compared to shear wave velocity measurements, which explains the widespread use of CPT for practical liquefaction assessment. However, CPT assessments are discrete and typically conducted at specific locations, whereas shear wave velocity measurements cover broader soil volumes.

This study combines shear wave velocity (v_s) and Cone Penetration Test (CPT) measurements to assess the liquefaction potential. To leverage the benefits of both approaches, a methodology is proposed based on the correlations between CPT parameters and the shear wave velocity based on an extensive dataset so that v_s can be used in the absence of CPT measurements. This improves the assessment of the liquefaction potential along linear infrastructure by increasing the number of CPTs through the development of synthetic CPTs derived from established correlations with shear wave velocities. A careful consideration was given on the effects of averaging the layer thicknesses over which the results are computed. The methodology is validated using data from a levee in the Krnjica borough, Croatia, that suffered significant liquefaction damage during the 2020 Petrinja earthquake.

2. Methodology Framework

2.1. Study workflow

The workflow of the present study is outlined in Figure 1. The procedure begins with the selection of layer thicknesses over which the in-situ data (CPT and v_s) will be averaged. In this study, the v_s data are derived from interpreted v_s profiles obtained through regression of the measured data, while the CPT data is collected at 2 cm intervals along the investigated depth. For the averaging thickness, this study considers three different values: 1.0 m, 0.5 m, and 0.2 m.

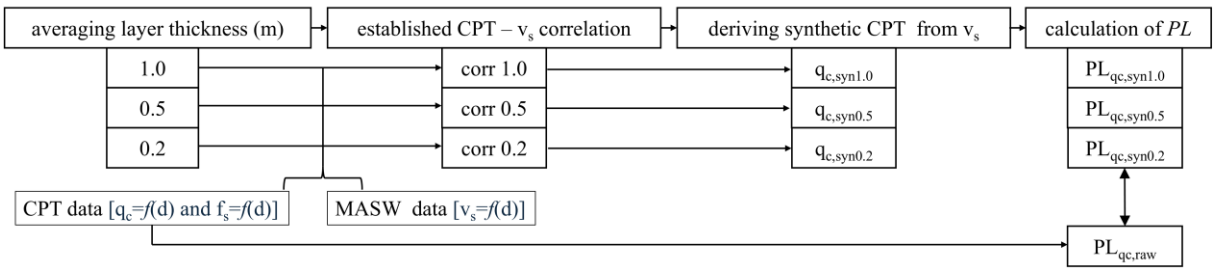


Figure 1. Applied methodology

Proceedings of the 3rd Croatian Conference on Earthquake Engineering - 3CroCEE
19–22 March 2025, Split, Croatia
Copyright © 2025 CroCEE
DOI: https://doi.org/10.5592/CO/3CroCEE.2025.148

The next step includes establishment of the CPT and v_s correlations as described in the section 2.2, depending on the averaging thickness (corr 1.0, corr 0.5 and corr 0.2). These correlations are developed from the larger dataset of measured CPT and v_s values. Once the correlations are established, they enable derivation of synthetic CPT data from known v_s values, again adjusted for the averaging thickness ($q_{c,syn1.0}$, $q_{c,syn0.5}$ and $q_{c,syn0.2}$). This synthetic data serves as the basis for calculating the factor of safety and the probability of liquefaction, as detailed in Section 2.3. In the last step, the synthetic assessments are compared to the liquefaction evaluations derived from the acquired CPT measurements at the specific location ($PL_{qc,raw}$) allowing for the validation of the overall methodology.

2.2. Correlation between the CPT parameters and shear wave velocities

For over 40 years, a number of studies have focused on correlations between shear wave velocities and CPT test results [4]. In addition to measured values of tip resistance (q_c), sleeve friction (f_s), and pore pressure (u), these correlations also accounted for the initial stress state and geological age of soils. Since these correlations are based on data from various locations worldwide, they cannot be directly applied to other regions without proper validation. For example, Robertson [5] used a database of 1,035 CPT - v_s data pairs from the USA to develop a correlation that incorporates the corrected tip resistance (q_t in kPa), soil behavior type index (I_c), vertical total stress in the soil (σ_{vo} in kPa), and atmospheric pressure (p_a in kPa):

$$v_s = \left[10^{0.55 \cdot I_c + 1.68} \cdot \left(\frac{q_t - \sigma_{v0}}{p_a}\right)\right]^{0.5} \tag{1}$$

Another example is McGann et al. [6], who used a database of 513 data pairs from New Zealand to develop a correlation that includes tip resistance (q_c in kPa), sleeve friction (f_s in kPa), and test depth (d in meters):

$$v_s = 18.4 \cdot {q_c}^{0.144} \cdot {f_s}^{0.0832} \cdot d^{0.278} \tag{2}$$

The CPT - v_s correlation form presented in Eq. (2) is also utilized in this study. This choice was based on the fact that the CPT parameters q_c (or q_t), f_s, and d, are directly measured and independent variables, while I_c, σ'_{vo}, and σ_{vo} are derived from the measured parameters. Additional assumptions are also required regarding the unit weight of the soil (γ) and the in-situ pore pressure (u_0). All these assumptions introduce uncertainties in the correlation. Given this, the regression model employed in this study takes the following form:

$$v_s = c_0 \cdot {q_t}^{c_1} \cdot {f_s}^{c_2} \cdot d^{c_3} \tag{3}$$

where, c_0, c_1, c_2 and c_3 are the regression model parameters. By taking the logarithm of both sides of Eq. (3), the established regression model is transformed to:

$$log\ v_s = log\ c_0 + c_1 \cdot log\ q_t + c_2 \cdot log\ f_s + c_3 \cdot log\ d \tag{4}$$

The transformed regression represents a linear regression model, which can be written as:

$$y = a_0 + a_1 \cdot x_1 + a_2 \cdot x_2 + a_3 \cdot x_3 \tag{5}$$

where, $y = \log v_s$, $a_0 = \log c_0$, $a_1 = c_1$, $a_2 = c_2$, $a_3 = c_3$, $x_1 = \log q_t$, $x_2 = \log f_s$ and $x_3 = \log d$.

For (n) measured data, the parameters of the transformed regression model, a_0, a_1, a_2, and a_3, can be determined using the least squares method by minimizing the sum of the squared deviations between the measured and regression values:

$$\min \sum_{i=1}^{n} [y - (a_0 + a_1 \cdot x_1 + a_2 \cdot x_2 + a_3 \cdot x_3)]^2 \tag{6}$$

where, the parameters a_0, a_1, a_2, and a_3 are unknowns. Taking the derivative of Eq. (6) with respect to each of these parameters, results in a system of four equations with four unknowns. By solving these equations, the parameters of the transformed regression model, a_0, a_1, a_2, and a_3, are obtained. Since a_0

Copyright © 2025 CroCEE
DOI: https://doi.org/10.5592/CO/3CroCEE.2025.148

= log c_0, the parameters c_0, c_1, c_2, and c_3 can be determined. If v_s-measured denotes the measured shear wave velocities, and v_s-predicted denotes the shear wave velocity obtained based on the CPT test results using Eq. (3), the representativeness of the regression model can be assessed using the performance metrics: coefficient of determination (R^2), Root Mean Square Error (RMSE), and Mean Absolute Percentage Error (MAPE).

2.3. Calculation of the probability of liquefaction occurrence

The assessment of the liquefaction potential is based on the calculation of the cyclic resistance ratio (CRR), which defines the soil resistance to cyclic loading, and the cyclic stress ratio (CSR). The calculation of CRR is based on the equation provided by Boulanger and Idriss [7], which utilizes CPT data:

$$CRR_{M=7.5,\sigma'_v=1atm} = exp\left(\frac{q_{C1Ncs}}{113} + \left(\frac{q_{C1Ncs}}{1000}\right)^2 - \left(\frac{q_{C1Ncs}}{140}\right)^3 + \left(\frac{q_{C1Ncs}}{137}\right)^4 - 2.80\right) \quad (7)$$

where, q_{C1Ncs} is an equivalent clean-sand penetration resistance, while the calculation of CSR follows the equation proposed by Seed and Idriss [8]:

$$CSR_{M=7.5,\sigma'_v=1atm} = 0.65\frac{\sigma_v}{\sigma'_v}\frac{a_{max}}{g}r_d\frac{1}{MSF}\frac{1}{K_\sigma} \quad (8)$$

where, r_d is a shear stress reduction coefficient, MSF is magnitude scaling factor and K_σ is overburden correction factor.

The procedure then compares CSR and CRR. For CSR> CRR, the analyzed soil is susceptible to liquefaction. In the opposite case when CRR>CSR, the liquefaction will not occur. In terms of the Factor of Safety (FS) this means:

$$FS = \frac{CRR}{CSR} \quad (9)$$

Based on the methodology proposed by Juang et al. [9], the probability of liquefaction (PL) along the depth can be calculated as:

$$PL = \frac{1}{\left[1 + \left({}^{FS}/_{A}\right)^B\right]} \quad (10)$$

where, A = 1.0 and B = 3.3 are selected regression coefficients.

3. Site description

3.1. Location and liquefaction occurrence

To validate the methodology, a levee near the Krnjica borough is selected, Figure 2.



Figure 2. Location of the test site and the levee near the Krnjica borough

Copyright © 2025 CroCEE
DOI: https://doi.org/10.5592/CO/3CroCEE.2025.148

The investigation area is adjacent to the right bank levee of the Kupa River, where the levee reaches a height of up to 4 meters, with a crest width of approximately 3.5 meters and 1:2 slopes. The levee axis is marked in Figure 2a with the dashed blue line, and the investigation area is highlighted on Figure 2b. Following the M6.4 earthquake on December 29, 2020, the levee sustained significant damage, partially losing integrity and functionality, thus compromising its stability during higher water levels. A field inspection of the levee and surrounding area revealed substantial damage, including longitudinal cracks at the base extending over approximately 2 km, as well as transverse cracks along the crest and slopes, Figure 3. The dimensions of the cracks ranged from a few centimeters to several tens of centimeters in width, with depths varying from one meter to several meters. Ejecta of sandy material were also observed, indicating liquefaction had taken place in the foundation soil. It has been reported that once liquefied soils do not necessarily acquire sufficient resistance to liquefaction, i.e. re-liquefaction effect may occur during the subsequent seismic events [10-13]. These studies showed that the soil, which once liquefied, is still very likely susceptible to liquefaction, sometimes even more during the aftershocks than during the first strong shock.



Figure 3. Cracks at the test site developed in the aftermath of the Petrinja 2020 earthquake

3.2. Investigation programme

To evaluate the liquefaction potential of the site in the post-earthquake period, this study employs two in-situ methods: CPT and MASW. The test site is defined as a profile positioned 50 meters from the toe of the levee on the waterside, extending along the levee over length of 500 meters. Along this profile, an MASW investigation was conducted with a 2.0 meter geophone separation, providing a high-resolution shear wave velocity (v_s) profile down to a depth of 30 meters. In addition, a total of eleven (11) CPT investigations were carried out along the profile, reaching a depth of 15 meters, with a consistent separation of 50 meters between each test, as shown in Figure 4. This combined approach allows for a comprehensive assessment of the liquefaction potential across the levee section.

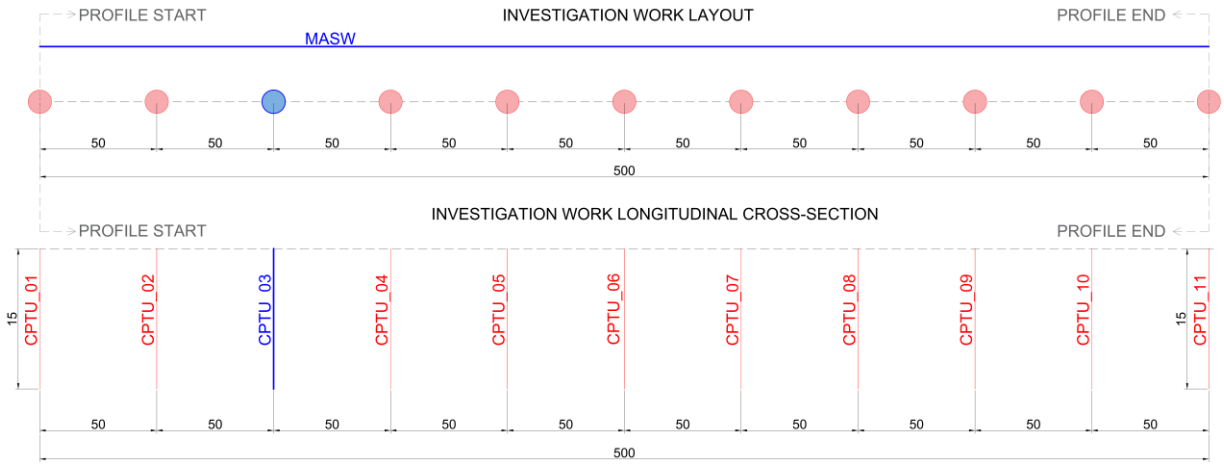


Figure 4. Layout of the investigation programe including MASW and CPT investigations

Proceedings of the 3rd Croatian Conference on Earthquake Engineering - 3CroCEE
19–22 March 2025, Split, Croatia
Copyright © 2025 CroCEE
DOI: https://doi.org/10.5592/CO/3CroCEE.2025.148

4. Results and Discussion

Considering all 11 CPTs obtained at the test site location, as well the v_s values at same locations obtained by means of MASW, a correlation is established for various layer thicknesses (1.0 m, 0.5 m and 0.2 m) over the which averaging is conducted, Figure 5. The correlation was derived for the entire dataset without considering the specific soil layering or the influence of different layers on the established correlations. As a result, the correlation reflects a generalized relationship, which may not fully account for variations in soil composition and behaviour across different depths.

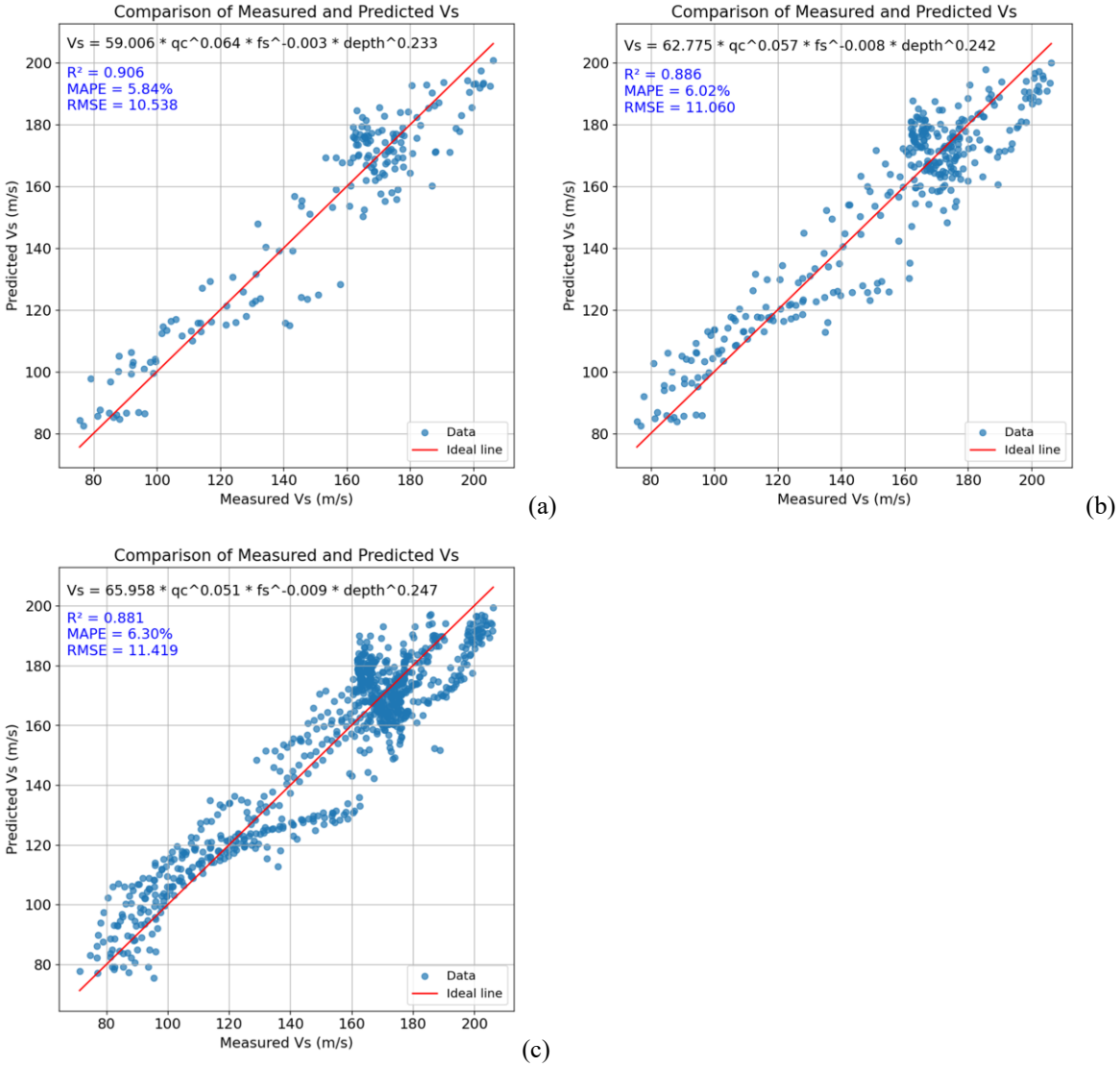


Figure 5. Derived correlations between v_s and CPT parameters for averaging thickness of (a) 1.0 m, (b) 0.5 m and (c) 0.2 m

The obtained correlations are as follows:

$$v_s = 59.006 \cdot {q_c}^{0.064} \cdot {f_s}^{-0.003} \cdot d^{0.233} \quad \text{for 1.0 m averaging thickness} \tag{11}$$

$$v_s = 62.775 \cdot {q_c}^{0.057} \cdot {f_s}^{-0.008} \cdot d^{0.242} \quad \text{for 0.5 m averaging thickness} \tag{12}$$

$$v_s = 65.958 \cdot {q_c}^{0.051} \cdot {f_s}^{-0.009} \cdot d^{0.247} \quad \text{for 0.2 m averaging thickness} \tag{13}$$

Copyright © 2025 CroCEE
DOI: https://doi.org/10.5592/CO/3CroCEE.2025.148

It can be observed that the influence of the CPT shaft friction (f_s) is relatively negligible compared to that of the CPT cone resistance (q_c) and depth (d), and as such, it has been neglected in the further analysis. The coefficient of determination (R^2) increases with the increase in the averaging thickness, although it remains relatively high, ranging from 0.88 to 0.91. MAPE and RMSE, on the other hand, both increase as the averaging thickness decreases, with MAPE ranging from 5.8% to 6.3% and RMSE from 10.5 to 11.4. These results indicate a strong generalized correlation between the CPT and v_s data, regardless of the chosen averaging thickness, suggesting that the established correlation is robust and reliable for further assessment of liquefaction potential across different depths and layer configurations.

The following example is provided to illustrate the potential for using a shear wave velocity (v_s) profile to develop a synthetic CPT for subsequent liquefaction assessment. A synthetic CPT location is selected to overlap with the position of one of the investigated CPTs, allowing for comparison between the synthetic and the actual CPT assessments. For this demonstration, the CPT-03 location (Figure 4) was randomly selected, with the raw data and the interpreted soil profile shown in Figure 6. The raw data reveals an increase in cone resistance (q_c) and sleeve friction (f_s) between depths of 5 to 8 meters, corresponding to soils with SPTn of 6 to 7, which indicate sands to gravelly sands. Several layers of sandy mixtures (with an SPTn of 5) are interspersed with silt mixtures (SPTn of 4) along the profile depth, with the material at the top of the profile classified as very stiff over-consolidated clay (SPTn of 9).

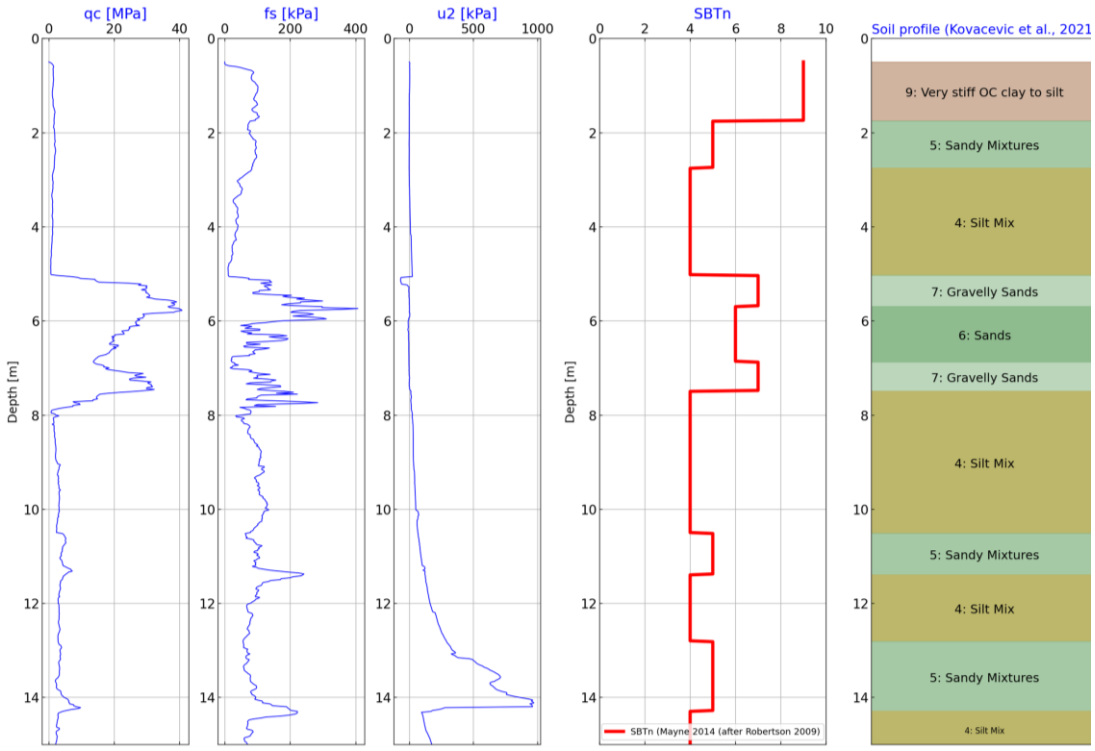
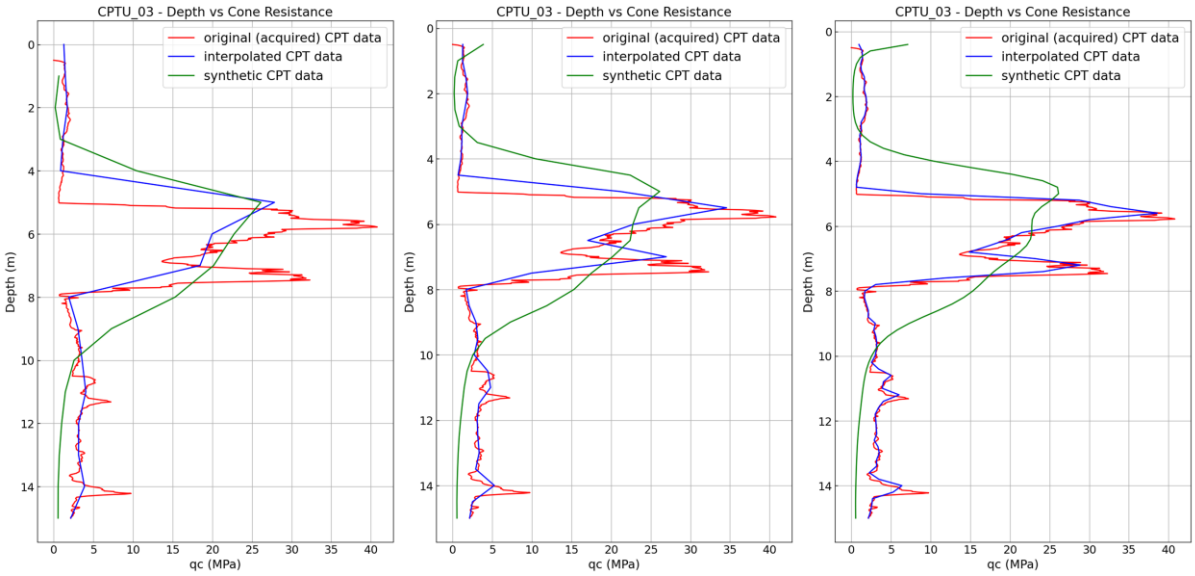


Figure 6. The acquired raw data from CPT-03, along with the interpreted soil profile along the depth

Figure 7 presents a comparison of the q_c – depth curves for various averaging thicknesses. The original data shows the in-situ acquired q_c values from CPT-03 with a sampling thickness of 2 cm. The interpolated data represents the same q_c profile obtained for CPT-03, but with the data averaged over 1.0 m, 0.5 m, and 0.2 m thicknesses. As the averaging thickness decreases, the interpolated profile matches more closely the original data. These profiles are compared with the synthetic CPT data at the same location, where the synthetic q_c values are calculated from the acquired v_s – depth profile using the correlations given with Eq. 11–13. An increase in synthetic q_c is observed at the same depths as in the original data, however, despite the good matching trend, the synthetic data is unable to capture the actual q_c values accurately, leading to their underestimation.

Copyright © 2025 CroCEE
DOI: https://doi.org/10.5592/CO/3CroCEE.2025.148



(a) (b) (c)

Figure 7. Comparison of acquired, interpolated and synthetic CPT data for (a) 1.0 m, (b) 0.5 m and (c) 0.2 m averaging thickness

Once the synthetic CPTU is obtained, it enables the calculation of the factor of safety and the liquefaction occurrence probability using Eq. 9 and 10. For the calculation of the cyclic stress ratio (CSR), a magnitude of 6.5 and a horizontal peak acceleration of 0.25g are considered. These assessments are presented in Figure 8 for an averaging thickness of 1.0 m, in Figure 9 for an averaging thickness of 0.5 m, and in Figure 10 for an averaging thickness of 0.2 m.

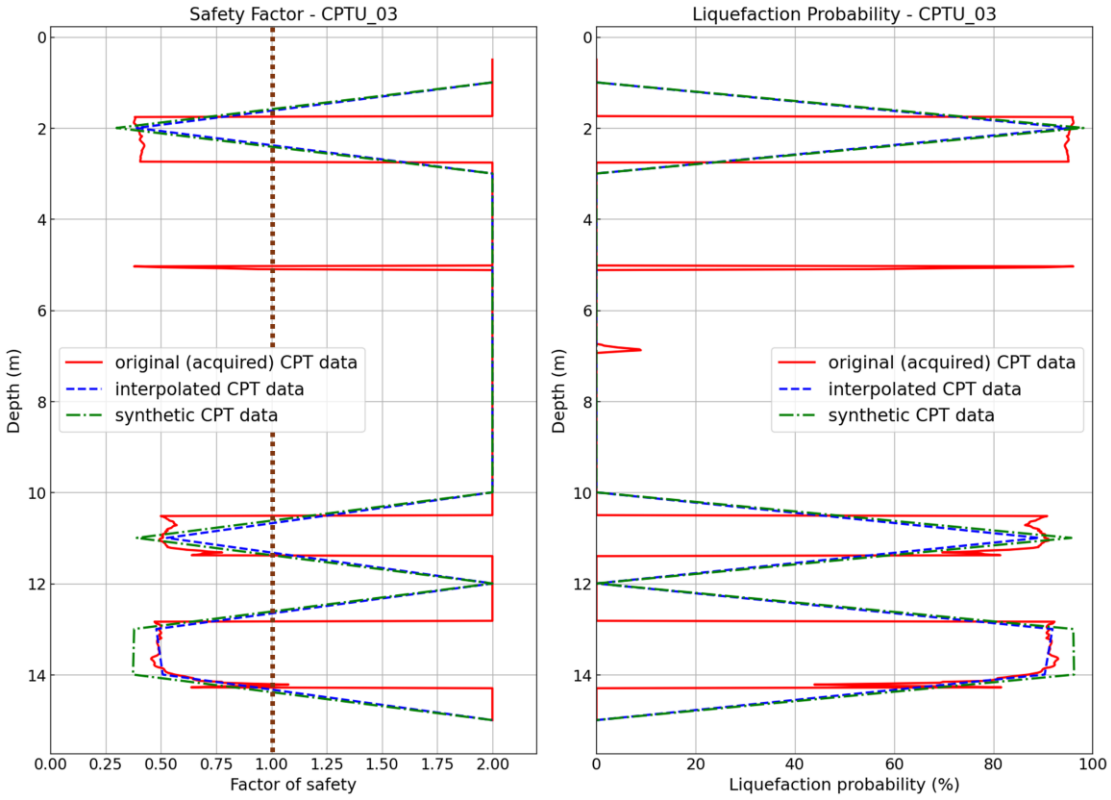


Figure 8. Comparison of factor of safety and probability of liquefaction for averaging thickness of 1.0 m

Copyright © 2025 CroCEE
DOI: https://doi.org/10.5592/CO/3CroCEE.2025.148

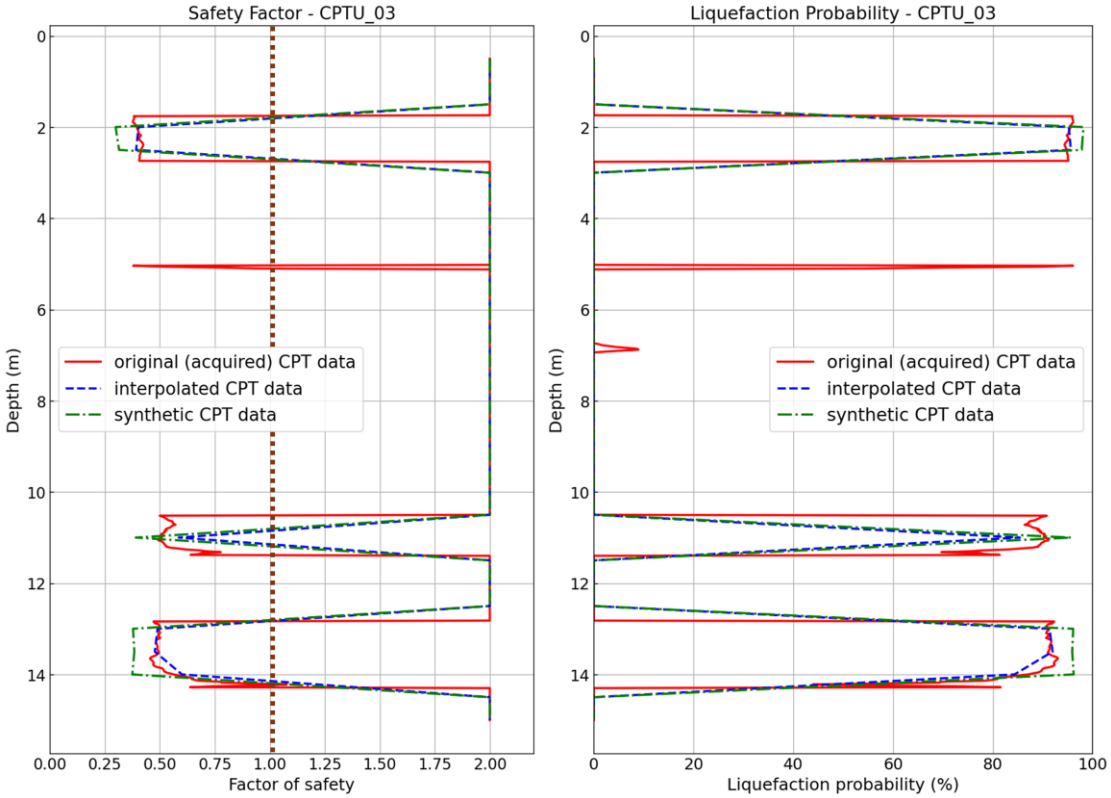


Figure 9. Comparison of factor of safety and probability of liquefaction for averaging thickness of 0.5 m

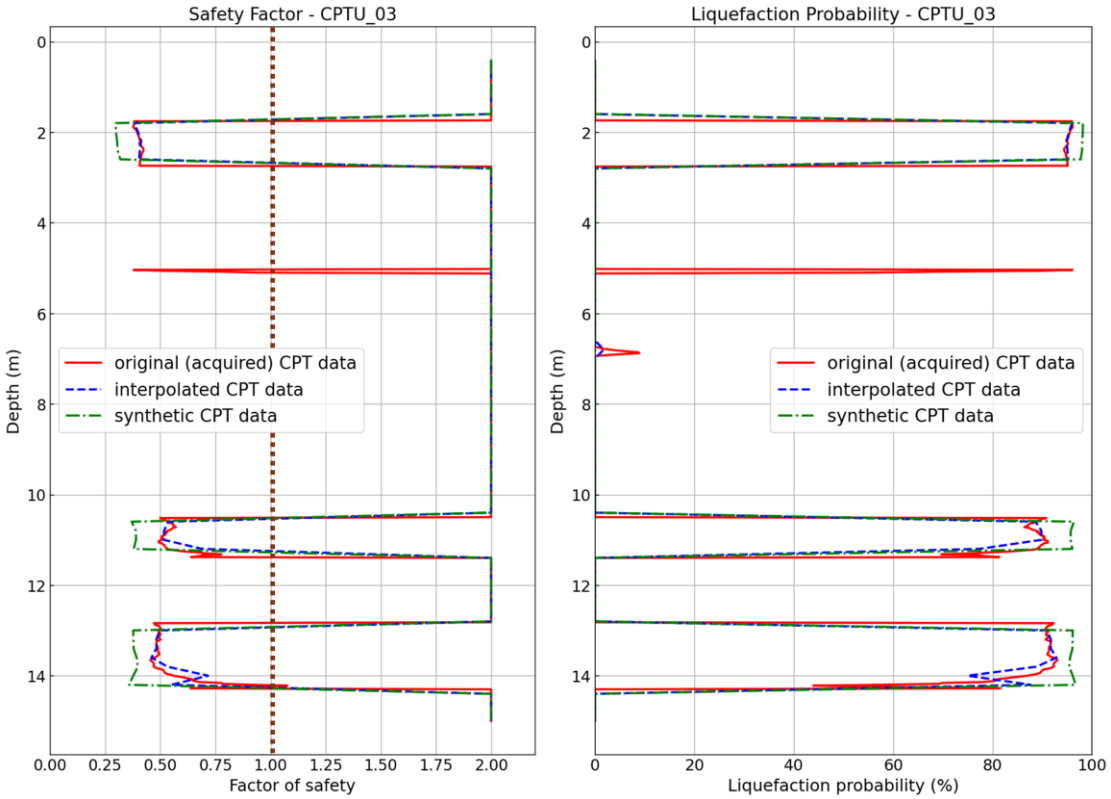


Figure 10. Comparison of factor of safety and probability of liquefaction for averaging thickness of 0.2 m

Proceedings of the 3rd Croatian Conference on Earthquake Engineering - 3CroCEE
19–22 March 2025, Split, Croatia
Copyright © 2025 CroCEE
DOI: https://doi.org/10.5592/CO/3CroCEE.2025.148

Figures 8–10 illustrate that the critical zones in terms of low factor of safety (and high liquefaction probabilities), determined from original (acquired) CPT data, predominantly correspond to soils classified as sandy mixtures, with a thickness of approximately 1 meter. The clean sand layer, which is bounded by thinner layers of gravelly sands, generally does not exhibit significant liquefaction, apart from a single peak observed in the diagrams. This limited likelihood of liquefaction occurrence can largely be attributed to the relatively high q_c values in these zones.

When analysing the factor of safety and liquefaction probability assessments for the 1.0-meter averaging thickness (Figure 8), it becomes clear that the calculated factors of safety <1, along with the associated higher liquefaction probabilities obtained from interpolated CPT and synthetic CPT data, are consistent with those derived from the original CPT measurements. However, assessments based on synthetic CPT data show slightly lower factors of safety and marginally higher liquefaction probabilities when compared to interpolated CPT data. Despite these differences, both interpolated and synthetic CPT results typically exhibit a single peak in the diagrams, in contrast to the relatively broader liquefaction zone identified by the original CPT data.

When the averaging thickness is reduced to 0.5 meters (Figure 9) and further to 0.2 meters (Figure 10), the trends and values of the factor of safety and liquefaction probabilities remain consistent with those observed for the 1.0-meter averaging thickness. The potentially liquefiable layers identified using interpolated and synthetic CPT data now extend over greater thicknesses, aligning more closely with the results obtained from the original CPT data. This suggests that finer resolution in layer thickness provides a more detailed representation of potentially liquefiable zones, highlighting areas that may have been understated in coarser assessments.

Important limitation of using v_s-profile alone for liquefaction assessments is that it does not differentiate between liquefiable and non-liquefiable layers, meaning low-velocity layers may be identified as liquefiable even if they are clayey in nature. To address this issue, the approach in this paper incorporates not only v_s measurements but also CPT data, which helps to identify the known locations of non-liquefiable layers. These identified layers are then excluded from further liquefaction assessments.

5. Conclusions

This paper introduces a methodology for deriving synthetic CPT data based on measured shear wave velocities (v_s), which is subsequently applied to assess liquefaction potential. The approach is demonstrated using data from a test site near the levee in the Krnjica borough, which experienced severe damage due to liquefaction triggered by the 2020 Petrinja earthquake. The study incorporates a total of 11 CPTs investigated over a 500-meter stretch, alongside v_s profiles of the same length, to establish a generalized, non-layering-dependent correlation between CPT parameters and shear wave velocities. This correlation enables the derivation of synthetic CPT data at specific locations using measured v_s values. To evaluate the influence of the averaging thickness on the results, various layer thicknesses were examined. The synthetic CPT data was found to align well with the trends of the acquired CPT measurements, though it typically underestimated q_c values. Despite this, the calculated factor of safety and associated liquefaction potential derived from the synthetic CPT data closely matched those obtained from the original CPT data. Furthermore, using finer averaging thicknesses provided a more detailed representation of potential liquefaction zones, effectively highlighting areas that might have been overlooked with coarser averaging methods.

The presented results provide initial insights into the potential for deriving synthetic CPTs from v_s data, further used for liquefaction assessment. For a more comprehensive spatial assessment of liquefaction potential along the levee or any other linear infrastructure, both vertical and horizontal soil variability, which significantly impacts the assessments, have to be accounted for. Further research will focus on evaluation of the spatial variability of the liquefaction potential. Due to the inherent heterogeneity of soils, this will involve correlation of results from multiple in-situ investigation techniques and development of an algorithm to establish better quantification of uncertainty propagation.

Copyright © 2025 CroCEE
DOI: https://doi.org/10.5592/CO/3CroCEE.2025.148

Acknowledgements

This research was funded by Croatian Science Foundation (HRZZ), GA no° IP–2022–10-7608, project LeveeLiq (Mapping of the spatial variability of liquefaction potential below the levees and modelling of optimal mitigation techniques).

References

[1] Bačić, M.; Ivšić, T.; Kovačević, M. S. (2020): Geotechnics as an unavoidable segment of earthquake engineering, *Građevinar*, 70 (72), 923-936, doi:10.14256/JCE.2968.2020

[2] Bačić, M., Kovačević, M.S., Rossi, N., Librić, L. (2024): Assessing the Soil Liquefaction Susceptibility: A Comparative Study of CPT and MASW Techniques in the Aftermath of Road Failure. *In Proceedings of Road and Rail Infrastructure VIII (CETRA 2024)*. Lakušić, S. (ed.), Zagreb: University of Zagreb Faculty of Civil Engineering, 2024, 783-790, doi: 10.5592/CO/CETRA.2024

[3] Bačić, M., Andačić, K., Gavin, K., Urumović, K. (2024): Soil investigations as a cornerstone for geotechnical design of liquefaction mitigation measures below levees . *Engineering Geology and Geotechnics: Building for the Future* (EUROENGEO 2024). Kovačević, M.S., Librić, L., Bačić, M. (eds.), Zagreb: University of Zagreb Faculty of Civil Engineering, 2024, 218-227, doi: 10.5592/CO/EUROENGEO.2024.257

[4] Žužul, P.; Kovačević, M. S. (2020): Development of correlation for estimating maximum soil stiffness via cone penetration test (CPT). *6th PhD Symposium of Civil Engineering*. Zagreb: University of Zagreb Faculty of Civil Engineering, 2020, 9-20, doi: 10.5592/CO/PhDSym.2020.01

[5] Robertson, P. (2009): Interpretation of cone penetration tests - a unified approach, *Canadian Geotechnical Journal* 46 (11), 1337-1355, doi: doi.org/10.1139/T09-065

[6] McGann, C.R., Bradley, B.A., Taylor, M. L., Wotherspoon, L.M., Cubrinovski, M. (2015): Applicability of existing empirical shear wave velocity correlations to seismic cone penetration test data in Christchurch, New Zealand, *Soil Dynamics and Earthquake Engineering*, 75, 76-86, doi: 10.1016/j.soildyn.2015.03.021

[7] Boulanger, R., Idriss, I. (2014): *CPT and SPT Based Liquefaction Triggering Procedures*, Report No. UCD/CGM-14/01; Center for Geotechnical Modeling, Department of Civil and Environmental Engineering, University of California: Davis, CA, USA

[8] Seed, H. B., Idriss, I. M. (1967): Analysis of liquefaction: Niigata earthquake. *Journal of the Soil Mechanics and Foundations*, 93 (3), 83-108, doi: 10.1061/JSFEAQ.0000981

[9] Juang, C.H., Jiang, T., Andrus, R.D. (2002): Assessing probability-based methods for liquefaction evaluation, *Journal of Geotechnical and Geoenvironmental Engineering*, 128 (7), 580-589, doi: 10.1061/(ASCE)1090-0241(2002)128:7(580)

[10] Ishihara, K., Okada, S. (1978): Effects of stress history on cyclic behavior of sand, *Soils And Foundations*, 18, 31–45, doi: 10.3208/sandf1972.18.4_31

[11] Suzuki, T., Toki S. (1984): Effects of pre-shearing on liquefaction characteristics of saturated sand subjected to cyclic loading, *Soils And Foundations*, 24, 16–28, doi: 10.3208/sandf1972.24.2_16

[12] Olson, S. M., Green, R. A., Obermeier, S. F. (2005): Geotechnical analysis of paleo-seismic shaking using liquefaction features: a major updating, *Engineering Geology*, 76, 235–261, doi: 10.1016/j.enggeo.2004.07.008

[13] Wang, S., Yang, J., Onyejekwe, S. (2013): Effect of Previous Cyclic Shearing on Liquefaction Resistance of Mississippi River Valley Silt, *Journal of Materials in Civil Engineering*, 25 (10), 1415–1423, doi: 10.1061/(ASCE)MT.1943-5533.0000698

Proceedings of the 3rd Croatian Conference on Earthquake Engineering - 3CroCEE
19–22 March 2025, Split, Croatia
Copyright © 2025 CroCEE
DOI: https://doi.org/10.5592/CO/3CroCEE.2025.1

TESTING FOR THE ASSESSMENT OF EARTHQUAKE RESISTANCE OF HERITAGE MASONRY BUILDINGS:

nondestructive versus destructive, laboratory versus in-situ testing

Miha Tomaževič

(1)Scientific Consultant, Retired; Slovenian National Building and Civil Engineering Institute, Ljubljana, Slovenia, miha.tomazevic@zag.si

Abstract

Some considerations, regarding testing methods, aimed at providing information needed to assess earthquake resistance of heritage masonry buildings, are presented. Various testing methods are available, including non-destructive, semi-destructive, and destructive testing, both in-situ and in the laboratory. Because of specific properties of masonry, non-destructive tests on the basis of propagation of sonic and seismic waves, as well as radar scanning cannot directly provide values of mechanical properties of masonry. They are good for discovering irregularities, such as voids in the masonry, filling the openings in masonry walls and changes in masonry structure. Semi-destructive tests, like shove and flat jack tests provide information regarding the existing stress state in the structural elements as well as shear and compressive strength of masonry. Scratch and impact hammer tests provide information regarding the strength of mortar and units. However, careful calibration of test results, which requires destructive testing in each particular case, is needed to obtain reliable values.

Additional specific testing of structural components and assemblages, as well as complete structures, is needed to assess the values of parameters which determine the seismic behavior, such as displacement and energy dissipation capacity, as well as strength and stiffness degradation and deterioration when subjected to cyclic lateral loads. To obtain relevant information, testing methods which simulate actual seismic conditions, should be used. Since it is not easy to reliably reproduce existing masonry in the laboratory, in-situ tests are preferred to laboratory testing of laboratory prepared specimens. Ultimately, real earthquakes represent best testing fields. Although "testing by earthquakes" is expensive by all aspects, from human to material loss, information obtained by learning lessons from earthquakes is precious and most valuable, if thoroughly studied and understood. On the basis of such information, observed phenomena can be simulated by testing, and methods and procedures can be developed to prevent consequences of future seismic events, if timely applied.

Keywords: masonry, assessment of earthquake resistance, testing, non-destructive testing, laboratory testing, in-situ testing

1. Introduction

Traditional masonry is typical composite construction material, mainly consisting of masonry units and mortar. Natural raw materials, earth, clay and various types of stone are used for manufacturing the units, whereas mortar is composed of mud, lime and sand, mixed with water in the prescribed proportions, with or without additives, such as cement. Units of various types and shapes are laid in various arrangements, and are expected to act together as a homogeneous structural material when subjected to permanent and temporary actions. Traditionally, masonry was aimed at resisting gravity loads: masonry resists compression, however its capacity to resist tension and shear, caused by seismic forces induced during earthquakes, is rather low.

Proceedings of the 3rd Croatian Conference on Earthquake Engineering - 3CroCEE
19–22 March 2025, Split, Croatia
Copyright © 2025 CroCEE
DOI: https://doi.org/10.5592/CO/3CroCEE.2025.1

Earthquake ground motion is three-dimensional. During earthquakes, dynamic forces are induced, which, in addition to gravity, act on the structures, cyclically changing direction of action. Besides materials, structural layout is responsible for energy dissipation and displacement capacity of resisting structural systems. Earthquake (seismic) resistance is the capability of the structure to resist the expected seismic loads by load-bearing and energy dissipation capacity (ductility). According to contemporary standards and codes, a new structure should be designed to resist the strongest expected earthquake which may - with a given probability - occur in the region during a given return period so that human lives are protected, damage is limited, and structures important for civil protection remain operational. Depending on the category of use, same requiremens should be taken into consideration in the case of existing, heritage buildings. Residential buildings should be upgraded to the same safety level as required in the case of the new construction. However, reduction of design seismic loads is sometimes permitted because of costs and feasibility of application of strengthening measures. In the case of monumental buildings, each building represents a specific case. Strengthening is a compromise between technical demands and preservation requirements.

In the case of the new construction, structural layout and properties of materials are determined by structural design, subjected to revision. Use of materials with certified quality and inspection on the construction site guarantee the compliance with design requirements. In the case of existing buildings, the structural system and materials exist, however, engineering information needed for earthquake resistance evaluation, is missing. Structural system should be identified, the dimensions of the structure and elements measured and the system checked for possible deterioration and damage. Mechanical properties of materials need yet to be determined.

It is not the aim of this contribution to present state-of-the-art of various methods of testing of masonry materials, structural components and structures. Various details of contemporary testing methods of masonry are discussed elsewhere in the relevant publications, too many to be mentioned at this point. The contribution is based on the author's experience obtained at Slovenian National Building and Civil Engineering Institute, (ZAG) in Ljubljana, Slovenia, where experimental research in seismic behavior of masonry structures, new and existing, including heritage buildings, has been one of the major concerns in the past several decades. Although there have been almost unbelievable improvements made in the last decades regarding testing methods, facilities, measuring and data acquisition systems, the basic principles of testing remained.

2. Assessment of Earthquake Resistance

Assessment of earthquake resistance of an existing building is carried out in order to decide whether the building under consideration should be repaired (if damaged after an earthquake) or strengthened to prevent collapse and/or excessive damage when subjected to expected strong seismic event in the future. In the case where the damage observed in the structure after an earthquake is a consequence of expected energy dissipation processes, the structure will be repaired in order to return the building to its original seismic resistance. In the case where the degree of damage is beyond the expected level and/or the assessed resistance level does not meet the requirements for earthquake resistance, the structural system needs to be strengthened. Assessment of earthquake resistance (structural evaluation) of an existing building is the first step in the process of seismic redesign.

By visual examination of the building, the overall qualitative information about the structural system is obtained and possible errors regarding the structural layout, construction and maintenance are identified. The condition of structural and non-structural elements is verified and possible damage documented and categorized. If needed, the dimensions of the building and individual structural and non-structural elements in plan and elevation are measured so that adequate plans can be prepared for subsequent structural evaluation and redesign.

By digging inspection pits, the category of foundation soil and type and condition of foundations are determined. By removing plaster from the walls at characteristic locations in plan and along the height of the building, basic type of the existing masonry can be determined. In addition,

Copyright © 2025 CroCEE
DOI: https://doi.org/10.5592/CO/3CroCEE.2025.1

parts of the buildings which have been eventually rebuilt, reconstructed, or simply added during the building's life-time, can be identified. By drilling or making holes through the walls, information regarding the type of construction and structure of masonry walls can be obtained, which significantly vary from region to region, from urban to rural areas. By opening the floors, the type, dimensions and condition of floor structure can be determined. By opening the walls and floors, information regarding the existence, position and condition of some other elements, relevant for earthquake resistance (such as wall-ties and similar elements) can be obtained. Sometimes, simple devices, such as Schmidt and pendulum rebound hammer as well scratch testing apparatus, are used during visual inspection of the building to obtain basic information regarding compressive strength of masonry units and mortar. Naturally, the instruments should be calibrated before being used on the site.



Figure 1. Invasive inspection of foundations and walls. a) Foundation of a small church; b) Drilling in a stone masonry wall; c) Removing plaster to inspect wall typology (Photo: Archive ZAG)

In the case where the original design plans are available, the correctness of information regarding the geometry, position and dimensions of structural elements, as well as type and quality of structural materials, should be verified. In the case where no plans exist, the dimensions of the actual structure should be measured and plans of the existing structure prepared.

3. Testing For the Assessment of Earthquake Resistance

Most important information, needed for the assessment of earthquake resistance, however, represent engineering data, i.e. quantitative information regarding the mechanical characteristics of structural materials and systems. In this regard, testing is indispensable. Although tests are sometimes costly and time consuming, the results of tests represent the only reliable basis for the assessment and subsequent decisions on seismic upgrading. On the basis of a thorough structural diagnosis and assessment of earthquake resistance, technical solutions for improving the resistance of the structure can be proposed and costs of structural interventions, which many times represent critical criterion for final decision regarding strengthening, realistically estimated.

In order to determine mechanical properties of existing masonry, samples of stone, brick and mortar are taken from the wall during inspection, brought to the laboratory and tested. However, since masonry is non-elastic, non-homogeneous and anisotropic material, it is as a rule not possible to determine the mechanical properties of masonry only on the basis of tests of constituent materials. This is possible in the case where the material tests serve as an identification of specific type of masonry with mechanical properties already known. Therefore, testing of masonry walls is usually needed, especially in the case where a large number of buildings of the same typology needs to be rehabilitated. Preferably, such tests are carried out in-situ, hence preserving the actual boundary restraints under which the specimens respond to seismic actions.

Copyright © 2025 CroCEE
DOI: https://doi.org/10.5592/CO/3CroCEE.2025.1

3.1.Non-destructive and Minor-destructive Testing

Non-destructive testing (NDT) procedures, which have been originally developed in medical, mechanical, aerospace and geophysical fields for detecting various discontinuities and errors in homogeneous and elastic materials, have first been used in the field of masonry construction 3-4 decades ago. As testing of mechanical characteristics of existing masonry needs destructive interventions, damaging the building (from in-situ testing to taking samples off the building), the mechanical testing is not accepted from preservation and conservation of historic heritage point of view. Therefore, the idea of modifying NDT methods to be used for obtaining information regarding the mechanical properties of masonry, is logical. Several attempts have been already made (for example [1]) to calibrate the results of NDT methods with the results of "classic" testing to determine basic mechanical properties, such as compressive and shear strength, however with no major practical success.

M.Schuller, one of the pioneers of using NDT and minor-destructive testing (MDT) methods for testing masonry in practice [2, 3], recently wrote: "Recent advances in non-destructive testing technology have led to mainstream use of several methods for evaluating masonry construction. Non-destructive approaches such as rebound hardness, stress wave transmission, impact-echo, surface penetrating radar, tomographic imaging, and infrared thermography are useful for qualitative condition surveys as well as identification of internal features such as voids or areas of distress".

By non-destructive testing (NDT), such as ultrasonic and/or seismic waves propagation measurements, or radar testing, qualitative data regarding the general structure of masonry, defining possibly existing non-uniformities of masonry structures, such as irregularities and voids, as well as existing damage, cracks, etc., can be obtained. Non-destructive tests are helpful in order to identify the general, qualitative condition of the building under consideration. NDT methods are also useful in the case of quality control of applications of seismic strengthening solutions, such as grouting and coating of masonry walls. By using minor-destructive testing (MDT) methods, such as flat jack and shove test, information on compressive and shear strength of masonry, respectively, can be obtained.

3.1.1. Radar Method

The radar method is based on the transmission and reflection of short electromagnetic impulses in the band from 50 MHz to 1,5 GHz. The waves are pulsed by a transducer, whereas a receiver reads the signals reflected off changes in materials, inhomogeneities like voids, or burried objects, like metals (Fig. 2a).



a) b) c)

Figure 2. Examples of application of typical NDT methods. a) Radar; b) Impact echo; c) Seismic wave velocity measurements (Photo: Archive ZAG, Onsiteformasonry Project [1])

3.1.2. Impact Echo

With impact echo, the impact hammer strikes a masonry surface, generating an acoustic impulse, which propagates into the material and is recorded with a receiving transducer near a striking point. The input energy from the hammer and the reflected compression wave energy from the receiver are

Copyright © 2025 CroCEE
DOI: https://doi.org/10.5592/CO/3CroCEE.2025.1

processed to evaluate structural integrity and locate irregularities, such as voids and delaminations in the wall (Fig. 2b).

3.1.3. Seismic Wave Velocity Measurements

Similar to impact echo method, the hammer strikes the surface of the wall, however, the seismic surface waves, travelling along the wall, are measured. As almost no energy is passing through the air, voids and delaminations of layers in the wall can be detected.

3.1.4. Flat jack testing

The objective of the flat jack test is to obtain the local state of stress in compression of a masonry element that works under vertical stress. The method, originally developed to determine the stress-state in rock masses [4], is based on stress release. Flat jack is a simple device, made of two thin steel plates, shaped as needed and welded together along the borders, with nozzles fixed to the device to pump oil between the plates. Usually two flat jacks are used during the test, placed one above another at a distance of several courses in the slots, made in the mortar bed joints or cut into the masonry. In the case that the stress state in the masonry is analyzed, the general procedure of this test is based on restoring the vertical displacement, which resulted in the part of the wall after cutting the slots. The distance between three or four points fixed across the slot is measured by gages before and after cutting. After placing the flat jacks in the slots, oil is pumped in the jack until the distance between the gage points is restored to the initial situation. In order to obtain the local state of stress, the restoring pressure has to be corrected taking into account the mechanical characteristic of the flat jack, calibrated in the laboratory, and on the relation between the geometry of the slot and the shape of the flat jack [5]. In case that the value of the compressive strength is looked for, the pressure in the jack is increased until the bricks or parts of masonry between the jacks start cracking. Typical example of flat jack test is shown in Fig. 3a [6].



a) b)

Figure 3. a) Testing compressive strength of a brick masonry wall in Ljubljana [6] and b) Making flat jacks in the laboratory of ANA in Boulder, Co.

Copyright © 2025 CroCEE
DOI: https://doi.org/10.5592/CO/3CroCEE.2025.1

3.1.5. Shove test

Whereas flack jack testing method represents a MDT method to obtain information regarding compressive strength of masonry, shove test is representing an example of MDT method to obtain information regarding the (sliding) shear strength [7].

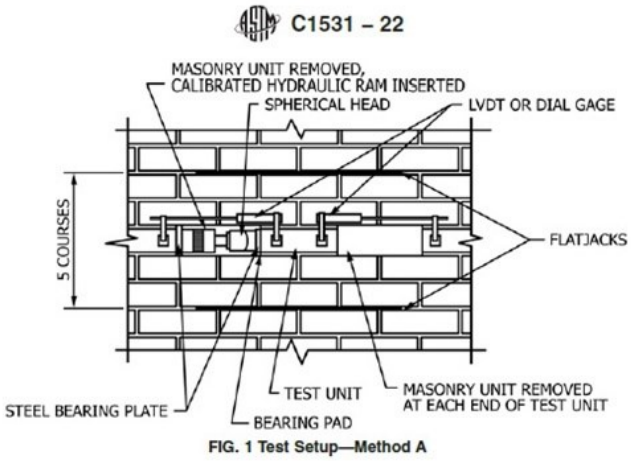


Figure 4. Schematic presentation of a shove test using flat jacks according to [7]

Shove test is applicable to brick masonry, i.e. masonry built of regularly sized units, where sliding shear mechanism (sliding along the bed joints) is one of the possible failure mechanisms. At the selected location, a single masonry unit and a head joint are removed from both opposite ends of the chosen test unit. Using a small hydraulic jack placed in the hole made by removing the unit (or using specially shaped flat jack in the case that only mortar head joint is removed), the test unit is displaced horizontally, relative to the surrounding masonry. The horizontal force required to cause the first movement (sliding) of the test unit provides, as called in the standard, a “measured index of the mortar joint shear strength”. To evaluate the test results, actual compressive stress in the wall at the location of shove tests needs to be evaluated. In the case that the test unit is prestressed by means of flat jacks placed above and below the test brick, compressive stresses acting on the test unit are step-wise increased and pushing of the test brick repeated until movement of the brick occurs under increased compression. Hence, the correlation between the compressive stresses and sliding shear strength can be evaluated, similarly as in the case of the triplet test.

3.2. Laboratory Testing of Masonry Walls

Observed failure mechanisms of masonry walls after earthquakes are simulated by testing specimens either in the laboratory or on site. To determine the parameters of seismic resistance, the specimens of the similar size and geometry should be tested at similar boundary restraints as in the actual structural systems, by subjecting them to similar actions as in the case of an actual earthquake. Knowing the geometry of the walls, boundary restraints and loads acting on the walls during testing, equations based on the observed damage patterns and failure mechanisms can be derived and parameters to be used in these equations evaluated on the basis of test results.

The analysis of earthquake damage indicated that sliding shear, shear (diagonal shear), and flexural (rocking) modes represent typical main failure possible mechanisms. However, in the case of the plain stone and brick masonry buildings, including urban and rural heritage buildings, observations of damage after past earthquakes indicated that shear mechanism predominates (Fig. 5a). Typical loads, acting on a masonry pier in seismic situation, are schematically presented in Fig. 5b. Tensile strength (diagonal shear strength) represents the decisive parameter, controlling the shear failure mode. Typical testing methods, by means of which the values of tensile strength of masonry can be determined are schematically presented in Figure 6. Although testing procedures in the case of racking and diagonal compression (diagonal tension) tests are also standardized [10, 11], cyclic shear

Copyright © 2025 CroCEE
DOI: https://doi.org/10.5592/CO/3CroCEE.2025.1

testing method is recommended, because besides tensile strength, additional important information regarding seismic resistance, can be obtained.

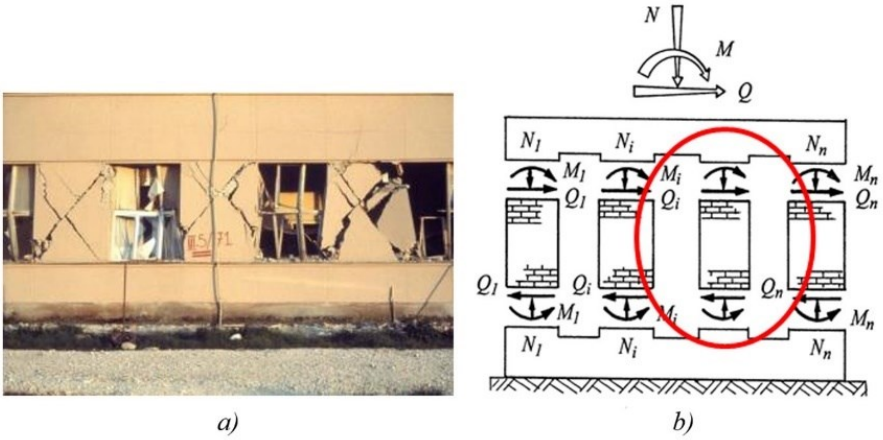


Figure 5. Shear mechanism. a) Failure of brick masonry piers of a school building, Montenegro earthquake, 1979 and b) Forces acting on a masonry pier during earthquake

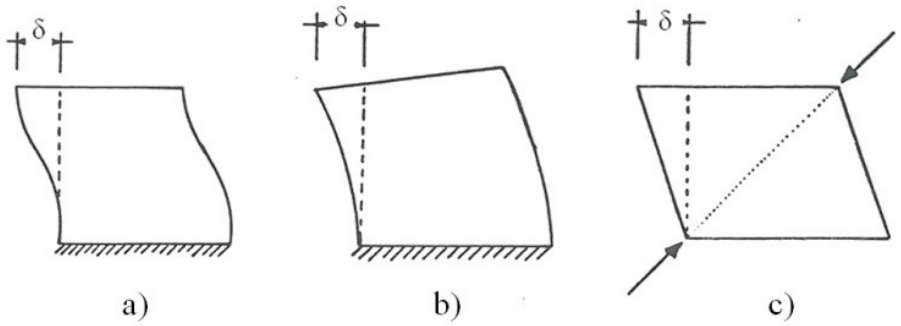


Figure 6. Schematic presentation of different types of tests suitable for evaluation of tensile strength of masonry: a) cyclic test of a fixed-ended wall, b) cyclic or racking test of a cantilever wall, c) diagonal compression test [8]

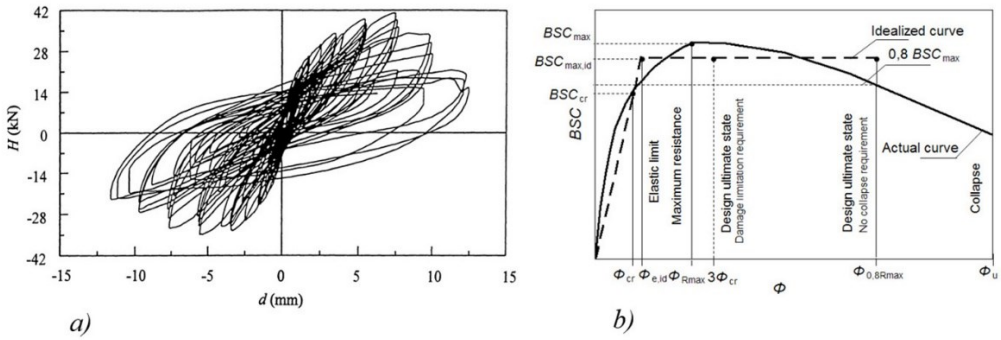


Figure 7. Results of a cyclic shear test. a) Lateral resistance-displacement hysteresis loops b) Idealization of resistance envelope indicating typical limit states

The comparison of test results, carried out on specimens made of the same type of masonry, has indicated that no statistically significant difference in the values of tensile strength, evaluated by using either of the three testing methods, can be expected [11]. Whereas by diagonal compression tests only the values of the tensile strength can be determined, some information regarding deformability properties of masonry, though of limited value for seismic design, can be obtained by racking tests. Cyclic shear tests are preferred for seismic testing, as they yield almost complete information

Copyright © 2025 CroCEE
DOI: https://doi.org/10.5592/CO/3CroCEE.2025.1

regarding the seismic behavior of walls, including stiffness and strength degradation as well as displacement and energy dissipation capacity (Figure 7).

Various testing arrangements and various cyclic lateral load patterns (loading protocols), applied statically or dynamically, are used in testing laboratories.

3.2.1. Boundary restraints

Analyzing typical examples of shear failure of URM walls (see Fig. 5a) it can be assumed that the walls are symmetrically fixed at both ends. This assumption has been followed when designing testing arrangements, which keep the upper and lower boundary of the tested walls parallel during the test. Mechanical devices, usually in the form of parallelograms (pantographs), should prevent the rotation of the specimen directly, when placed on the top of the wall, or indirectly by means of a rigid beam, rigidly connected to the parallelogram in the case when placed laterally. Lateral loads from the actuators are transferred to the wall by means of the horizontally moveable part of the parallelogram, placed on the walls. One of the first devices of the kind, designed at ZAG in the late 1960-ties, is shown in Figure 8a.



a) b)

Figure 8. Cyclic lateral resistance tests of stone masonry walls. a) Specimen tested as symmetrically fixed b) Specimen tested as vertical cantilever

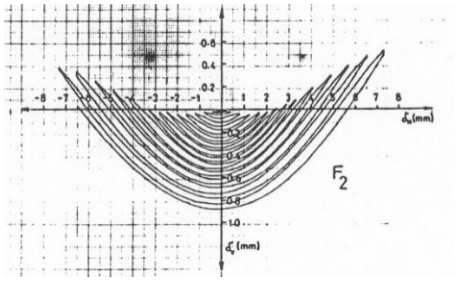


Figure 9. Vertical motion of lower part of the pantograph as a function of lateral displacements, indicating rocking of an URM wall during initial phases of cyclic shear tests [12]

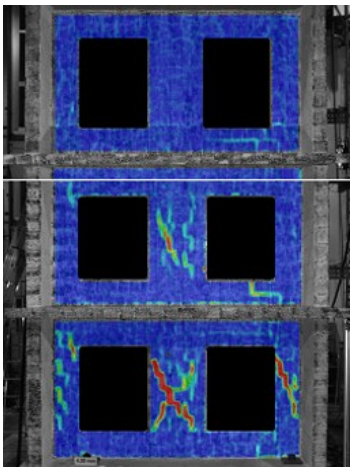


Figure 10. Three story full scale building: digital optical measurements indicate no rocking phenomena of piers [13]

Copyright © 2025 CroCEE
DOI: https://doi.org/10.5592/CO/3CroCEE.2025.1

Control measurements of possible vertical motion of the lower beam of the parallelogram indicated that it moves upwards with increased lateral displacement, imposed to the wall during testing (Fig. 9). This indicates that test specimens rock as rigid bodies when subjects to lateral load until cracks and damage occur, what reduces the rigidity of the specimen and, consequently, rocking.

The walls can be also tested as simple vertical cantilevers. In this case, the foundation block on which the specimen is built, is fixed to the testing floor. Lateral load is imposed by means of a programmable hydraulic actuator, fixed to the upper beam placed on the specimen. Vertical load is applied by means of hydraulic jacks. Roller bearings are placed between the steel beam and steel plates on the top of the specimen to allow for the friction-free lateral motion of the wall during cycling (Fig. 8b). However, the analysis of tests results indicated [14] that the arrangement for application the vertical load prevents free rotation of the upper boundary of the walls. In case where the vertical load is applied by two jacks, the restraint is significant, resulting into changes of position of the moment inflection point in the range of 60-80 % of the wall's height. The analysis indicated, that the walls are not tested as vertical cantilevers, fixed at the bottom, but as partly restrained at both ends.

It can be concluded that the walls, supposed to be tested as fixed-ended, are actually tested as symmetrically restrained. On the other hand, the walls, supposed to be tested as vertical cantilevers, are tested as partly restrained at both ends. These facts do not affect the experimentally obtained information regarding the resistance, but make difficult to correctly evaluate the deformability characteristics, as well as all as the mechanism of behavior in the earlier phases of testing.

In the buildings, restraint conditions may change during the earthquake due to progressive damage and consequent changes in rigidities of the walls and horizontal structural elements. However, only exceptionally observed damage patterns indicated rocking behavior of the walls. This has been also confirmed by in-situ (see Chapter 3.3) and large scale laboratory testing, where the phenomena of rocking of walls have not been observed (Fig. 10).

3.2.2. Application of Lateral Loads

In order to be able to study failure mechanisms and non-linear behavior of masonry buildings when subjected to strong earthquakes, displacements, and not forces, are imposed to test specimens during seismic testing. Because of the cyclic character of seismic loads, various cyclic lateral load patterns, applied statically or dynamically, are used to simulate the seismic loads in different laboratories. The influence of frequency of application of cyclic lateral loads on the strength and ductility of URM walls has been already studied four decades ago [15, 16]. Differences in the observed behavior as a result of different displacement histories and vertical loads have been discussed. Static and dynamic responses of model masonry houses have been also correlated [17].

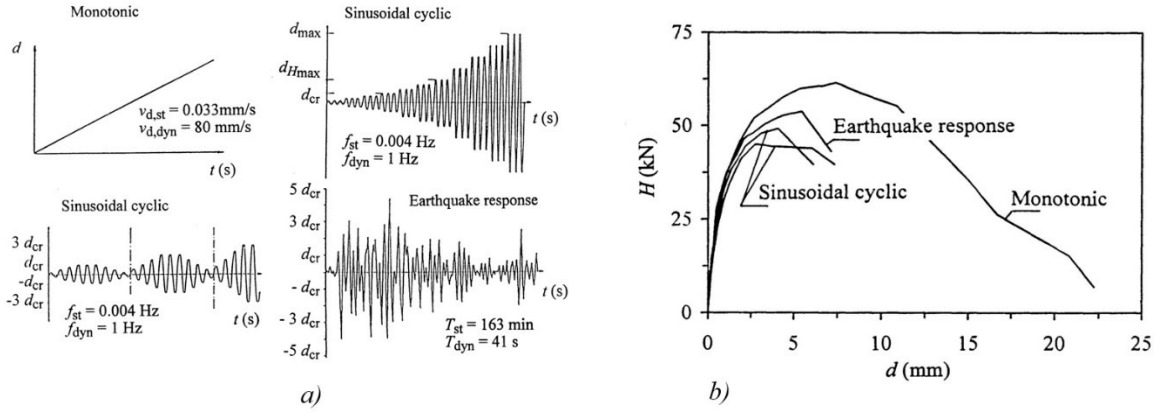


Figure 11. Influence of displacement protocols on test results, a) Test protocols, b) Correlation between resistance envelopes, obtained by application of various displacement protocols [18]

Copyright © 2025 CroCEE
DOI: https://doi.org/10.5592/CO/3CroCEE.2025.1

The analysis of test results obtained by testing 32 equal reinforced-masonry wall specimens at ZAG has further confirmed the influence of shape of the applied displacement time history and velocity of application on test results [18]. The influence of four different lateral load (displacement) patterns, monotonic and cyclic, static and dynamic, on the behavior of the walls has been compared at two levels of vertical load acting on the walls (Fig. 11).

It has been found that higher values of lateral resistance and larger ultimate displacements have been measured in the case of monotonic than in the case of cyclic loading procedures of any type. In the case of cyclic testing, higher values of lateral resistance have been obtained dynamically than statically. However, there was no distinct rule observed regarding the differences in displacement capacity. Similar values of ductility factors resulted from both, static and dynamic type of tests.

The level of vertical load was the decisive parameter in all cases. When subjected to higher level of vertical load, lateral resistance of the wall was improved but deformability and ductility decreased at both, static and dynamic types of loading, at all load patterns. The walls subjected to higher level of vertical load were more rigid than the walls tested at low vertical load, and larger stiffness values were obtained by dynamic than by static tests. However, displacement and energy dissipation capacity were lower. The failure mechanism and propagation of damage was also affected by the level of the imposed vertical load.

These conclusions are in good agreement with previously mentioned investigations as well as with recent proposals [19]. Since different results can be obtained by different methods of testing, the compatibility between the testing methods, used to obtain the values of input parameters for the assessment of seismic resistance, and testing methods, on the basis of which the numerical models for seismic resistance verification have been developed, is of relevant importance.

3.3.In-situ Testing of Masonry Walls

From the point of view of simulating boundary restraints, testing the wall in situ is far more realistic than testing in the laboratory. The wall is tested as part of the structural system, so there is no need to simulate boundary restraints and gravity loads: the same interaction forces between the surrounding horizontal and vertical elements and the tested specimen will develop during lateral resistance test as in the case of the real seismic situation.



a) b)

Figure 11. In situ test of a wall in Gracarjev turn Castle. a) Selection of testing location; b) Diagonal cracks in the wall after the end of test. No horizontal cracks at the ends of the wall are visible

The specimen to be tested is separated from the surrounding masonry by vertical cuts at both sides. Horizontal force is induced at the mid-height of the wall by a system of steel rods and

Copyright © 2025 CroCEE
DOI: https://doi.org/10.5592/CO/3CroCEE.2025.1

supporting beams, with dimensions adjusted to actual situation in the building. Care should be taken to select appropriate location and size of the tested part of the structure. In order to prevent damage to other parts of the building, hydraulic jack should be supported by a strong enough portion of an adjacent wall. In the vertical direction, the surrounding part of the floor structure is supported with wooden posts or otherwise in order to prevent the accidental collapse of the floor in the case of possible sudden collapse of the tested specimen.

Since vernacular masonry is non-homogeneous, it is not easy to reproduce the existing masonry walls in the laboratory, even though existing material is used and very thorough chemical and mechanical analysis of mortar, brick and/or stone may have been carried out. The only reliable method of determining the load-carrying capacity of existing old masonry walls involves the carrying out tests in situ, or cutting out specimens from these walls and test them in the laboratory. However, the method of testing is destructive and will be hardly approved by authorities of conservation and preservations of architectural cultural heritage. If approved, one has to bear in mind that sophisticated laboratory testing equipment cannot be moved to the testing site. Instead of programmable actuators used for cyclic shear tests, simple hydraulic jacks and monotonic cyclic loading test methods (Fig. 12b) are applicable. Therefore, full size specimens are sometimes cut off the building and transported into laboratory. Besides being time consuming, cutting of the specimens, preparation for transport and transport to the laboratory require careful handling.

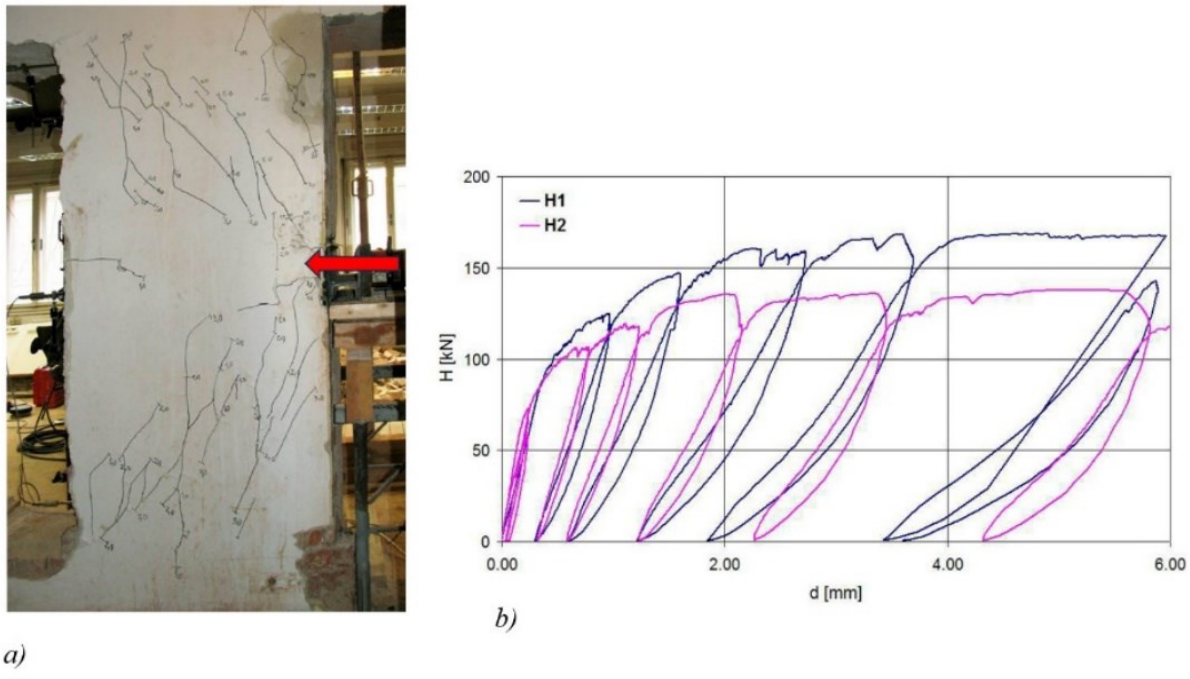


Figure 12. In situ testing of a brick masonry wall. a) Crack pattern after the end of tests. No horizontal cracks at supports can be seen; b) Lateral load-displacement relationships, obtained by monotonic cyclic testing [6]

3.4. Testing of Dynamic Characteristics of Buildings

In the case where information is needed about dynamic characteristics of the building under consideration, such as natural periods of vibration and damping, special tests are carried out. For this purpose, various methods and techniques are available. By means of dynamic exciters, fixed on the floors, vibrations of the building are induced. In this case, the frequency of rotating eccentric masses is electronically controlled and the response of the structure at different points along the height of the building at each frequency of excitation is measured. By evaluating the resonance curves measured during excitation, the coefficient of equivalent viscous damping can be also determined.

Proceedings of the 3rd Croatian Conference on Earthquake Engineering - 3CroCEE
19–22 March 2025, Split, Croatia
Copyright © 2025 CroCEE
DOI: https://doi.org/10.5592/CO/3CroCEE.2025.1

Ambient vibration tests are simpler. In this case, vibrations of the building, induced by seismic microtremors, traffic, wind and other environmental influences are measured with sensitive transducers, placed on the structure at different locations along the height of the structure. The vibrations are measured for sufficiently long time and analyzed. Again, on the basis of the calculated Fourier response spectra, information is obtained about the structure's natural vibration periods and structural damping.

One has to bear in mind, that such information is obtained at small energies of excitation, where the tested structural system behaves more or less elastically. They represent dynamic characteristics of buildings in the initial phases of seismic excitation and cannot be considered as "effective" when assessing the seismic resistance.

4. Testing of Small-scale Models on Simple Earthquake Simulators

To understand seismic behavior of structures, testing of individual components is not enough. Since the basic principles of earthquake resistant design assume that energy is dissipated by means of non-linear response, i.e. damage occurring to the structures when subjected to design level earthquakes, not only linear elastic, but also inelastic response of the system in the non-linear range should be known. The understanding of mechanism of behavior in the non-linear range is needed not only to develop and validate sophisticated numerical models, but also to assess reliable values of many code-required coefficients used in the process of earthquake resistant design. To obtain such information, the observed earthquake damage to buildings should be reproduced by testing the entire structural systems, not only individual structural components, under simulated earthquake loading conditions.

Nowadays, development of high technologies made possible the installation of large, multi-degree of freedom shaking-tables which are capable of driving large masses of prototype-sized structures with a high degree of accuracy of simulation of the spatial, recorded or artificial seismic ground motion. Of course, the response of the tested structure to spatial ground motion, taking into consideration in-plane, out-of-plane and vertical components of seismic action on structural system and components, is close to the actual seismic response. There is no better way to simulate seismic behavior of a structure in the laboratory. Unfortunately, costs of installation, maintenance as well as experiments by using such devices are high. Therefore, structures at reduced scale, i.e. physical models of structures, are still tested on simple earthquake simulators in many laboratories.

There are advantages and disadvantages of model testing. Such tests are cheaper than full scale tests. Testing facilities are simpler and in many cases, hydraulic actuators, used to drive the platform when used as a shaking table, can be dismantled and used for other kinds of testing. The construction of models is cheaper, although many times not simpler than the construction of prototype. Adequate model materials, whose characteristics depend on the modelling scale, should be used (developed), depending on the modelling scale. To develop such materials and verify how the mechanical characteristics of model and prototype materials comply with the similitude laws, takes time. In the case where the prototype is tested, no such problems need to be resolved. Modelling techniques can be adjusted to possibilities which, however, this requires caution when interpreting the test results.

Generally, only the overall behavior of structural system and its global failure mechanism can be determined by testing small-scale masonry building models, and not the behavior of structural elements and details. When reducing the physical dimensions of the model, the effects of many parameters, such as stress and strain gradients, bond between reinforcement and mortar (or grout), adhesion between mortar and masonry units, etc., on the overall behavior of the structure, change. In most cases, the possibility of modelling the influence of these parameters on the structural behavior to an acceptable degree of accuracy limits the reduction of the size of the masonry building models.

The excitation is usually one-directional, which provides better control of the observed mechanisms of structural behavior. However, one has to bear in mind that sometimes seismic actions in other directions (out-of-plane, vertical) influence the observed mechanism.

Proceedings of the 3rd Croatian Conference on Earthquake Engineering - 3CroCEE
19–22 March 2025, Split, Croatia
Copyright © 2025 CroCEE
DOI: https://doi.org/10.5592/CO/3CroCEE.2025.1

Accuracy of simulation of seismic motion represents a technological problem of test control. As the experience shows, it is important that the induced shaking's spectral characteristics are similar to actual characteristics of earthquakes. In case that the actual shaking table motion is accurately recorded, matching the input and output motions is not of relevant importance. Earthquakes with the same dynamic characteristics, duration and acceleration time histories, never occur twice: when analyzing the response of the model, the recorded motion of the shaking table represents the earthquake to be considered as the dynamic input, and not the scaled actual earthquake.

By testing models of buildings on shaking tables, phenomena observed on the buildings during earthquakes are simulated, and physical quantities, which determine the seismic response, are measured in order to analyze the behavior. Obviously, it is the similitude of behavior and failure mechanisms of a real building, subjected to an actual earthquake, and its reduced size replica (model), subjected to simulated earthquake, which is the measure of success and accuracy of the testing procedure. Damage patterns and failure mechanisms obtained during model tests should be similar to those observed on the prototype buildings during earthquakes. If the failure mechanisms of structural elements and the entire building are accurately simulated and the boundary conditions and loads which acted on the elements during the experiment are known, the measured data can be used for reliable prediction of seismic response of the prototype.

4.1. Model materials, models and similitude

The modelling techniques and similitude conditions are discussed elsewhere [20, 21]. Basic relationships between physical quantities measured on the prototype and model are determined on the basis of dimensional analysis [22] and depend on the mechanical properties of materials used for the construction of the model and modelling scale. In the case where elastic behavior if the structure under static loads is studied, the relationships between the prototype and model structures are straightforward. However, if the dynamic behavior in the nonlinear range and failure mechanisms are investigated, model materials and testing techniques should be carefully selected in order to reliable reproduce the behavior of the prototypes.

Although the theoretical requirements for model similitude are sometimes difficult to fulfill, two basic conditions should be fulfilled in order to obtain reliable information:

- the distribution of masses and stiffnesses along the height of the model and prototype should be similar (similitude in dynamic behavior);
- the working stress in masonry walls/compressive strength of masonry ratio in the case of the model and prototype walls should be similar (similitude in failure mechanisms).

If both conditions are fulfilled, the seismic response and failure mechanisms of the model and prototype will be similar. This will make possible the conversion of values of physical quantities, measured on the model, to the prototype in accordance with similitude laws. Whereas the similitude in dynamic behavior is not always of decisive importance, care should be taken to fulfil the similitude in failure mechanism.

Usually, model materials are manufactured on the basis of experience by using trial-and-error procedures. Although the mechanical properties of constituent materials, model masonry units and mortar, are modelled to a required degree of accuracy, the final correlation between the model and prototype masonry is assessed by comparing the results of tests of model and prototype walls at both, compression and cyclic shear loads. Prior to shaking-table model tests, scaled masonry wallets are tested. Since the seismic behavior is concerned, besides mechanical properties of masonry, failure mechanism and damage propagation, as well as displacement and energy dissipation capacity, are also correlated.

4.2. Earthquake simulator and modelling of seismic ground motion

The idea of using simple, single-directional shaking table, driven by multi-purpose hydraulic actuator, to study the seismic behavior of building structures, is based on the following considerations.

Copyright © 2025 CroCEE
DOI: https://doi.org/10.5592/CO/3CroCEE.2025.1

Although actual earthquake ground motion is three-dimensional, vertical components of the ground motion do not significantly affect the seismic behavior of regular structures, such as masonry buildings. Also, many important data regarding the seismic behavior of the structure can be obtained by subjecting the tested model to simulated seismic excitation, acting in one of the two principal directions of the building, or askew to one of them. The earthquake ground motion is a stochastic phenomenon, the characteristics of which depend on the source mechanism and on local soil conditions. However, as the deterministic, dynamic phenomenon, the earthquake will never again occur in the same form. Therefore, the decision regarding the type of the shaking table motion is usually taken by considering the similarity between the response spectra of the acceleration time history, used to drive the shaking table, and the design response spectra, required by the codes (Fig. 14a). In this regard, synthetic accelerograms, calculated on the basis of the design spectra, can be also used. Once the decision is made, accurate simulation of the chosen seismic input does not represent serious problems. Usually, earthquake simulator motion is calibrated by considering the capacity of the actuator, payload (mass of the model and its foundation slab, including mass of the moveable platform), and modelling scale.

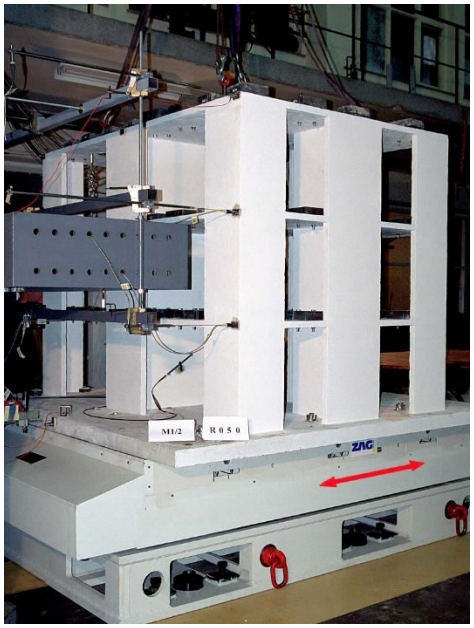


Figure 13: Earthquake simulator at ZAG

For example, earthquake simulator at ZAG (Fig. 13) consists of a rigid foundation steel box, fixed to the r.c. laboratory testing floor, and a moveable, 2.0/3.2 m box-type steel platform, onto which the foundation slab with the model is bolted and which is moved by means of a programmable hydraulic actuator. Depending on the actuator coupled to platform, the simulator is able to accurately drive the payload of up to 5000 kg mass with motion of typical earthquake spectral characteristics, needed when testing models at up to 1:5 scale. Displacement time history, used to drive the actuator, is obtained by double integration of the chosen earthquake accelerogram. Nevertheless, accelerations measured on the shaking table during the tests, match the input acceleration record surprisingly well (Fig. 14b). The calibration measurements have shown that the moveable platform is rigid enough for carrying the bending loads, developed as a result of interaction between the model and platform during the shaking tests.

Copyright © 2025 CroCEE
DOI: https://doi.org/10.5592/CO/3CroCEE.2025.1

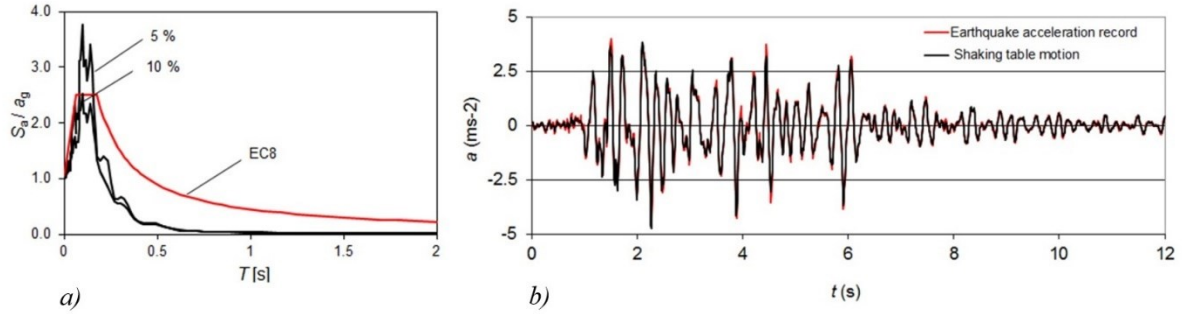


Figure 14. a) Response spectrum of the model earthquake in correlation with EC8 spectrum
b) Typical correlation between the input and output accelerogram, measured on the simulator

4.3. Example: testing the influence of steel ties on the seismic behaviour of stone masonry houses

As an example of usefulness of model testing on simple simulators, the study of effectiveness and mechanism of action of wall ties, which connect the walls at floor levels, prevent disintegration and ensure integrity of structural system when subjected to strong earthquakes, will be briefly presented [23]. A series of models of simple stone masonry houses with wooden floors, with and without wall ties placed at floor levels, as well as with r.c. floors or brick vaults replacing wooden floors, have been tested on the shaking table by subjecting them to a series of simulated ground motions with increased intensity of motion in each subsequent test run. Acceleration time history, recorded during an actual strong earthquake, scaled according to modelling scale, has been used to drive the earthquake simulator. The intensity of motion has been gradually increased up until the collapse of the models. Typical situation of the models with wooden floors, with and without ties at the end of tests is shown in Fig. 15.



Figure 15. Failure mechanisms obtained by shaking table tests of stone masonry models
a) Model without ties; b) Model with wall ties

As can be seen, the upper storey of the model without wall ties disintegrated and collapsed, whereas in the case of the model with wall ties, separation and disintegration of the walls was prevented. The model collapsed because of the shear failure of the load-bearing walls in the first

Copyright © 2025 CroCEE
DOI: https://doi.org/10.5592/CO/3CroCEE.2025.1

storey. Both models resisted the approximately same base shear, however, the model with wall ties resisted repeated seismic action with intensity 50 % stronger than the earthquake which caused the collapse of the model without ties. Information of this kind could have been obtained only by shaking table test.

By measuring strains in the walls ties, mechanism of tie action has been defined and a model for designing the dimensions of ties proposed.

5. Conclusions

Assessment of earthquake resistance of heritage/existing masonry buildings is a complex procedure. By visual inspection, investigations and measurements, the type, geometry and conditions of the building and structural elements are determined. However, destructive, or at least minor destructive tests are indispensable to obtain engineering data. In this regard, existing information obtained on similar buildings of similar typology may reduce the amount of testing provided that similarity in typology and construction materials has been proved by identification testing. Destructive tests are also the only means to validate the efficiency of proposed strengthening methods.

Initial dynamic characteristics of the building's structural system may be defined by forced vibration or ambient vibration techniques. Sometimes, the structure is monitored and short and long-term observations and measurements are performed to collect the relevant information for structural evaluation. On the basis of the obtained data, standard or sophisticated computational models are developed, seismic resistance is verified and, consequently, decision can be made as regards the necessary structural interventions.

NDT methods are helpful in identifying the overall situation of the structure. They represent the best means for quality control of interventions for structural strengthening.

Acknowledgements

The paper is based on the author's long-time experience obtained by conducting experimental research at Slovenian National Building and Civil Engineering Institute. Additional details can be found in referenced publications and elsewhere.

References

[1] European Commission, Directorate-General For Research And Innovation (2006): *Onsiteformasonry project: on-site investigation techniques for the structural evaluation of historic masonry buildings*, Köpp, C.(editor), Maierhofer, C.(editor), Binda, L.(editor), Publications Office, Brussels

[2] Suprenant, B.A., Schuller, M. (1995): *Non destructive evaluation & testing of masonry structures*, The Aberdeen Group, Addison, USA

[3] Schuller, M. (2003): Non-destructive testing and damage assessment of masonry structures. *Progress In Structural Engineering and Materials,* 5 (4), 239–251, doi.org/10.1002/pse.160

[4] Rossi, P. (1985): Flat jack test for the analysis of the mechanical behaviour of brick masonry structures; *Proceedings 7th International Brick Masonry Conference*, Melbourne, Australia, 136-148

[5] ASTM (1999): *Standard test method for in situ compressive stress within solid unit masonry estimated using the flat-jack method*. ASTM C 1196-95, ASTM.

[6] Lutman, M., Bohinc, U., Gams, M., Tomaževič, M. (2012): In situ tests for the assessment of seismic strengthening historic brick masonry walls with carbon fiber fabric. *Proceedings 15th World Conference on Earthquake Engineering*, Lisbon, Portugal, 10 pages

[7] ASTM (2022): *Standard test methods for in situ measurement of masonry mortar joint shear strength index*. ASTM C 1531-22, ASTM

[8] CIB (1987): *Publication 94: International recommendations for design and erection of unreinforced and reinforced masonry structures*. Rotterdam, International Council for Building.

Copyright © 2025 CroCEE
DOI: https://doi.org/10.5592/CO/3CroCEE.2025.1

[9] ASTM (2015). *Standard test methods of conducting strength tests of panels for building construction*. ASTM E 72-15, ASTM

[10] ASTM (2022). *Standard test method for diagonal tension (shear) in masonry assemblage.* ASTM E 519/E 519M-22, ASTM

[11] Bernardini, A., Modena, C., Turnšek, V., Vescovi, U. (1980): A comparison of three laboratory test methods used to determine the shear resistance of masonry walls, *Proceedings 7th world conference on earthquake engineering*, Istanbul, Vol.7, 181-184

[12] Tomaževič, M., Žarnić, R. (1984). Shaking table study of a four storeyed masonry building model. *Proceedings 8th world conference on earthquake engineering,* San Francisco, Vol. 6, 847-854.

[13] Triller, P., Tomaževič, M., Gams, M. (2018). Seismic behaviour of masonry buildings built of low compressive strength units. *Bulletin of earthquake engineering.* **16** (12), 6191-6219, doi: 10.1007/s10518-018-0418-5.

[14] Tomaževič, M., Gams, M. (2009). Shear resistance of unreinforced masonry walls. *Ingegneria sismica*, **26** (3), 5-18

[15] Williams, D., Scrivener, J.C. (1974). Response of reinforced masonry shear walls to static and dynamic cyclic loading. *Proceedings 5th world conference on earthquake engineering*, Rome, 1491-1494

[16] Terčelj, S., Sheppard, P., Turnšek, V. (1977). The influence of frequency on the shear strength and ductility of masonry walls in dynamic loading tests. *Proceedings 6th world conference on Earthquake Engineering*, New Delhi, Vol. 3, 2992-2999

[17] Paulson, T.J., Abrams, D.P. (1990). Correlation between static and dynamic response of model masonry structures. *Earthquake spectra,* **6** (3), 573-591

[18] Tomaževič, M., Lutman, M., Petković, L. (1996). Seismic behavior of masonry walls: experimental simulation. *Journal of Structural Engineering*, ASCE, **122** (9), 1040-1047

[19] Mergos, P.E., Beyer, K. (2014). Loading protocols for European regions of low to moderate seismicity. *Bulletin of earthquake engineering* **12**, 2507-2530

[20] Carvalho E.C. [1998]. Seismic testing of structures. *Proceedings 11th European conference on earthquake engineering*, Paris, France, 53-64. Rotterdam: Balkema.

[21] Harris, G.H., Sabnis, G.M. [1999]. *Structural modeling and experimental techniques*. CRC Press, Boca Raton, Florida.

[22] Langhaar, H.L. (1951). *Dimensional analysis and theory of models*. New York: John Wiley & Sons.

[23] Tomaževič, M., Lutman, M., Velechovsky, T. (1993). Aseismic strengthening of old stone-masonry buildings: is the replacement of wooden floors with R. C. slabs always necessary? *European earthquake engineering.* **7** (2), 34-46

Proceedings of the 3rd Croatian Conference on Earthquake Engineering - 3CroCEE
19–22 March 2025, Split, Croatia
Copyright © 2025 CroCEE
DOI: https://doi.org/10.5592/CO/3CroCEE.2025.21

DYNAMIC EFFECTS IN TALL STEEL STRUCTURES WITH DIFERENT PURPOSES

Elena Stokuca [(1)], D-r. Golubka Necevska-Cvetanovska [(2)], D-r. Milos Stokuca [(3)]

[(1)] CEO in STO-SEH doo Skopje, N. Macedonia, Doctoral candidate in the Institute of Earthquake Engineering and Engineering Seismology, Ss. Cyril and Methodius University in Skopje, elena.stokuca@stokuca.com.mk
[(2)] Prof. Emeritus at Institute of Earthquake Engineering and Engineering Seismology, Ss. Cyril and Methodius University in Skopje, golubkapero@yahoo.com
[(3)] CEO in STOKUCA dooel Skopje, N. Macedonia, milos.stokuca@stokuca.com.mk

Abstract

In the initial stages of structure design, precisely defining the loads that a structure must support is of utmost importance. While structures are generally designed to handle live loads effectively, they must also be capable of accommodating other types of loads. The dominant types of loads that a structure must withstand can differ based on the materials used and the type of structure.

For instance, steel structures, which have a lower self-weight, are particularly susceptible to horizontal wind loads. On the other hand, reinforced concrete (RC) structures, due to their higher self-weight, are more affected by horizontal seismic forces. Despite these differences, wind loads are a significant factor for high-rise buildings regardless of whether they are made of steel or reinforced concrete.

This paper explores the impact of wind loads on tall structures, with a particular focus on the role of shape coefficients. It provides a comparison between values obtained through experimental measurements and those specified in regulatory standards. Additionally, the paper includes a practical analysis of various types of structures to illustrate how wind loads affect different designs.

By examining these aspects, the paper aims to shed light on the effectiveness of current regulations and practices related to wind load calculations. It will discuss any discrepancies between experimental data and theoretical predictions, and offer insights into the implications for engineering practice. This analysis is intended to enhance the understanding of wind load effects on high-rise buildings and inform future design approaches.

Keywords: wind, structure, shape coefficients, dampening, steel structures.

1. History

Designing the proper wind speeds for the design of structures is a first and critical step towards the calculation of the wind loads. Moreover, it is also the most inaccurate and uncertain step of the design process for the design of wind loads, and requires a static analysis of written wind speeds over a period of time.

In the 1930es, the dominant school of thought suggested using a symmetrical bell shaped distribution (a Gaussian distribution) to display the extreme wind speeds in order to have a base for the design of the long-term wind speeds which will be used for design. However, this manner for the calculation of the wind load does not take into account earlier theoretical research which take into account the borderline shapes of distribution of the biggest (or smallest) value in a fixed sample. The identification of the three types of distribution of extreme values plays a great role in the development of the probabilistic approach in engineering in general.

The analysis of wind gusts lags behind when using extreme values for wind design speeds. As a result of this circumstance and a number of studies conducted in the 1950s and 1960s, some nations adopted the wind gust principle in accordance with the extreme value analysis as a method of wind speed prediction. Research in the 1960s led to the rapid adoption of probability and statistics by many engineers, which form the foundation of the current method for calculating wind loads.

Copyright © 2025 CroCEE
DOI: https://doi.org/10.5592/CO/3CroCEE.2025.21

Even though, the structure failures of the 1970s and 1980s (the Tracy cyclone in Australia and the strong winds exceeding 60 km/h in Europe) demonstrated that the actual wind loads were significantly higher than those that were planned.

Therefore, additional research was conducted in the following areas:

- errors in gathering data on written value samples (mostly from less than 50 years ago)
- categorizing information from various storm types.

In general, the design's integration of probabilistic methods developed concurrently with their application in wind engineering. This research and development theory, also referred to as the theory of load bearing capability, has been used in design since the 1970s.

2. Introduction

The wind load on structure is very unpredictable and infrequent because of the turbulent nature of the wind speeds. Consequently, a dynamic resonant response of the structures, or segments of them, with a natural frequency below 1Hz could appear. Different wind intensity levels at different times are highlighted by the structure's resonant response. As a result, the resonant response of the structures is dependent on both the wind gust that is occurring at the moment and the wind gusts that have preceded the monitored moment.

The primary focus of the work in this section is upon that the analysis of the dynamic response of the structures to wind, as well as some basis of aero-elasticity and fatigue effects on the structures and the method of equivalent or effective distribution of the static load.

3. Principles of dynamic response

As previously mentioned, the ability of wind loads to vary in terms of force, pressure, and speed can result in a considerable resonant vibration of the structures or their elements if the damping and natural frequencies are low enough.

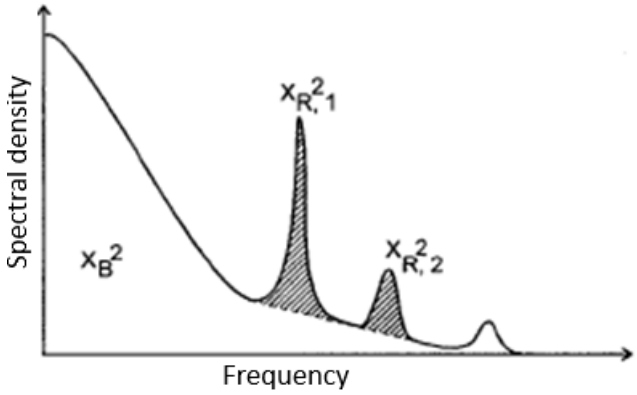


Figure 1. Density of the spectral response under wind loading

There should be a difference between the resonant dynamic response and the background fluctuations that the structure experiences. The density of the spectral response under wind loading is plotted in the figure 1. In reality, the mean square of the fluctuating response is represented by the surface of the entire curve.

The graph's hatched area represents the first two modes' resonant response. Low frequencies (generally under the lowest natural frequency) make up the majority of the background response. In fact, it has the largest percentage of wind loading in the wind direction and produces the highest yield in the graph above. With this in mind, the resonant response will become increasingly important after a certain amount of wind loading, to eventually become the dominant effect. This effect happens when the structures are high and slender compared to their cross section, and their mode becomes smaller.

Copyright © 2025 CroCEE
DOI: https://doi.org/10.5592/CO/3CroCEE.2025.21

Figure 2 (a) shows the characteristics of the data at a specific time period of the forces that act in the wind load direction. The figure 2 (b) shows the response of a structure with a high frequency of natural oscillations, while figure 2 (c) shows the response of a structure with a low frequency. It is evident from the graphs that the resonance, as well as vibration component, appears to have a negligible impact on the structure response. The resonance's close proximity to the time variation of the forces acting on the structure explicitly states. The resonant response of the first mode is crucially significant in the second scenario, while the response of the higher modes can be simply ignored.

In actuality, the large percentage of the structures we come across during the design process would figure under 2 (b) and would not respond at all, or only minimally, to a resonant dynamic response. Furthermore, it is common practice to avoid designing buildings with a natural mode lower than 1Hz. In addition, the damping, the aerodynamic characteristics, and the structure itself all affect the amount of the dynamic response.

For illustration, a dynamic response should be used to influence high voltage power lines, which typically have a natural mode well below 1Hz. But because of their extremely high aero dynamical damping value (roughly 25% of the critical), the resonant response is significantly reduced. Because of their low mass, the lattice and truss structures in this impact have a bigger coefficient of aero dynamical damping. Furthermore, the sorts of connections used for such structures enable the emergence of an absorption mechanism in the connections, whereby the forces from the wind loads are dissipated through friction, thereby reducing the resonant response.

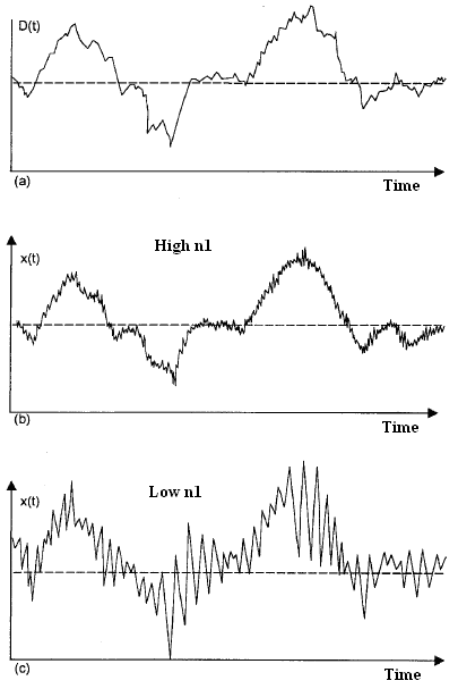


Figure 2. Time response (a) wind load, (b) high period structure response (c) low period structure response

When a resonant response occurs, it may temporarily result in intricate interactions that, when paired with the structure's deflections, may give rise to extra aero-elastic forces. In severe situations, such as the Tacoma Narrows Bridge, this scenario may lead to a structure failure. These are rare scenarios that should, of course, be avoided. However, the dynamic coefficient is superposed over the dominant mean and the background fluctuating response in most cases where the structure has a significant resonant dynamic response.

The primary and most evident cause of the fluctuating wind load is the wind's turbulent flow, which results from the hear effects that occur when the wind passes over non-flat areas of the terrain. The

Copyright © 2025 CroCEE
DOI: https://doi.org/10.5592/CO/3CroCEE.2025.21

formation of vortexes behind structures with cross sections that produce higher aerodynamic resistance (such as square or circular cross sections) is another main reason of the fluctuating load.

To balance the wind forces, the opposing forces inside the structure will first come into play if it can be altered in a way that produces a dynamic reaction.

The primary offenders are:

- The internal forces are proportionate to the structure's mass.
- The damping or energy-absorbing forces are proportional to speed in their purest form, although this is not always the case.
- Rigid or elastic forces that are proportionate to the structure's deflection

Regarding mostly horizontal loads, it is crucial to note the primary differences between the dynamic responses of structures to earthquakes and wind. The following are the primary differences between these forces:

- Earthquakes are regarded as incident loads since they have a substantially shorter duration of impact than wind loads.
- An earthquake's dominant frequency is typically 10–50 times higher than that of a full-fledged storm. This explains why some structures up to a certain height can react significantly to wind loads while remaining totally inert to seismic loads.
- There will be a direct correlation between the height of the structure and the movement of the earthquake load along it. However, the wind load will be partially correlated because of the vortices that form along the height of the structure.

The figure 3 also illustrates the range of frequencies that cause structures to be excited by earthquake and wind loads.

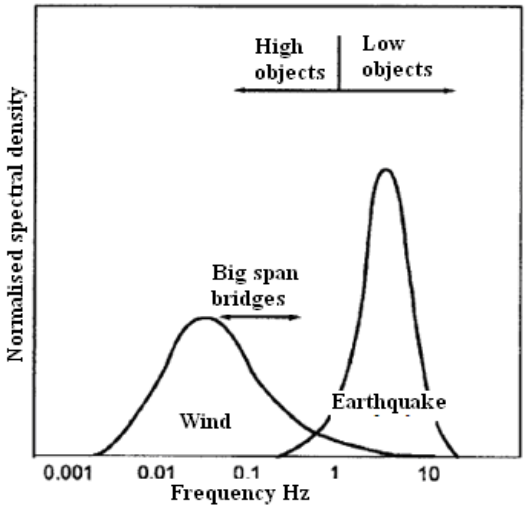


Figure 3. Dynamic response of structures to wind and earthquake loads

4. Calculation

A comparative analysis of multiple structures made of different materials (steel and RC) and for various uses (a 50m mast, a 200m industrial chimney, a 30m radar, and 30m silos) was conducted for the purposes of this work. Under the influence of wind loads, the elements were analyzed both as linear and shell elements, taking into account the shapes of the structure as well as the used method to determine wind intensity. Of course, in order to obtain data about the main loads in the structures dimensioning, the structures were loaded with additional loads that are typical for their respective purposes.

Proceedings of the 3rd Croatian Conference on Earthquake Engineering - 3CroCEE
19–22 March 2025, Split, Croatia
Copyright © 2025 CroCEE
DOI: https://doi.org/10.5592/CO/3CroCEE.2025.21

For all the structures at hand, the analysis has been done with the aid of the program SAP2000 according to EUROCODE2.

4.1. Analysis of mast elements

The 3D model used for determining of the influence of the loads on the use of the structure, was made of shell elements, of which the dimensions are shown in Table 1. In the calculation done in tower, frame elements were used.

From the results obtained, shown on figure 4, one can conclude that the horizontal wind loads W have a dominant role in the use of the mantles from the chimney, which entails 80%. On the other hand, the seismic loads Sx and Sy have an insignificant influence of 5% and 10%. The effect of the vertical loads is inversely proportional to the mantle thickness, where the mantle thickness of 5mm takes only 30% in the participation of the elements use.

Table 1. Mast's mantle thickness

dp=9mm – Mantle thickness 9mm (segment 0m-10m)
dp=8mm – Mantle thickness 8mm (segment 10m-20m)
dp=7mm – Mantle thickness 7mm (segment 20m-40m)
dp=5mm – Mantle thickness 5mm (segment 40m-50m)

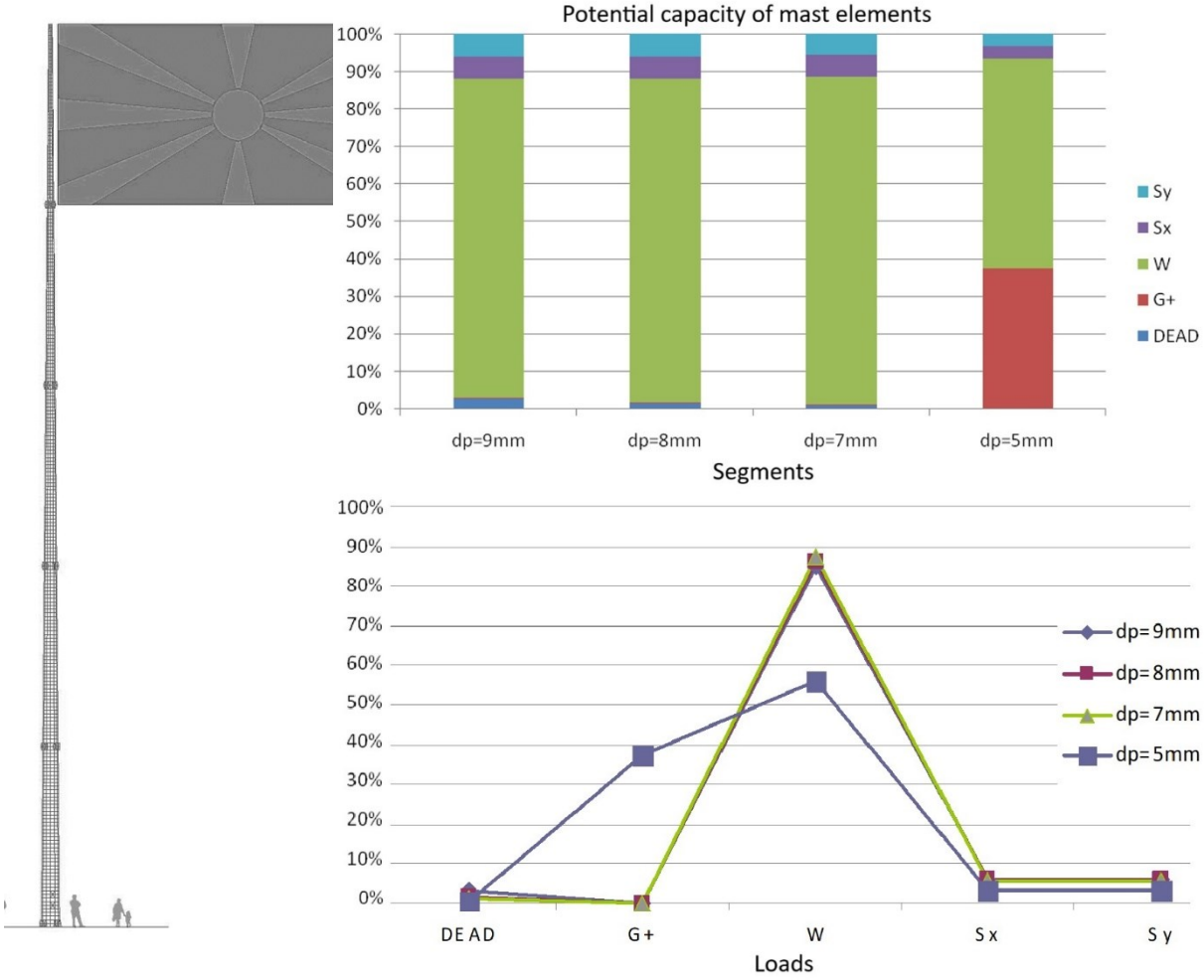


Figure 4. Percentage of load participation in the stress of the elements of a MAST

Copyright © 2025 CroCEE
DOI: https://doi.org/10.5592/CO/3CroCEE.2025.21

4.2. Analysis of radar tower elements

In the static analysis for radar tower, the elements are modeled as frame elements. In this static calculation own weight of the elements has been applied directly through the program and the other loads were applied manually – the other permanent loads (the radar itself); operational and survival wind loads; temperature and ice coating. In table 2 the naming of the constructive elements is shown.

On figure 5, the results of the analysis, i.e. the usage of the elements in percentages is shown, for every constructive elements for every different load case. From this analysis it can be concluded that the biggest percentage of the use of the constructive elements entiles to the horizontal wind loads W_{maxX} и W_{maxY}. On the other hand, the bigger use from vertical load cases is displayed only in the columns(C 24-30).

Table 2. Radar tower elements

C 0-12 – Column 0-12	HD – Horizontal beam Down
C 12-24 – Column 12-24	HU – Horizontal beam Up
C 24-30 – Column 24-30	BD – Bracing Down
	BU – Bracing Up

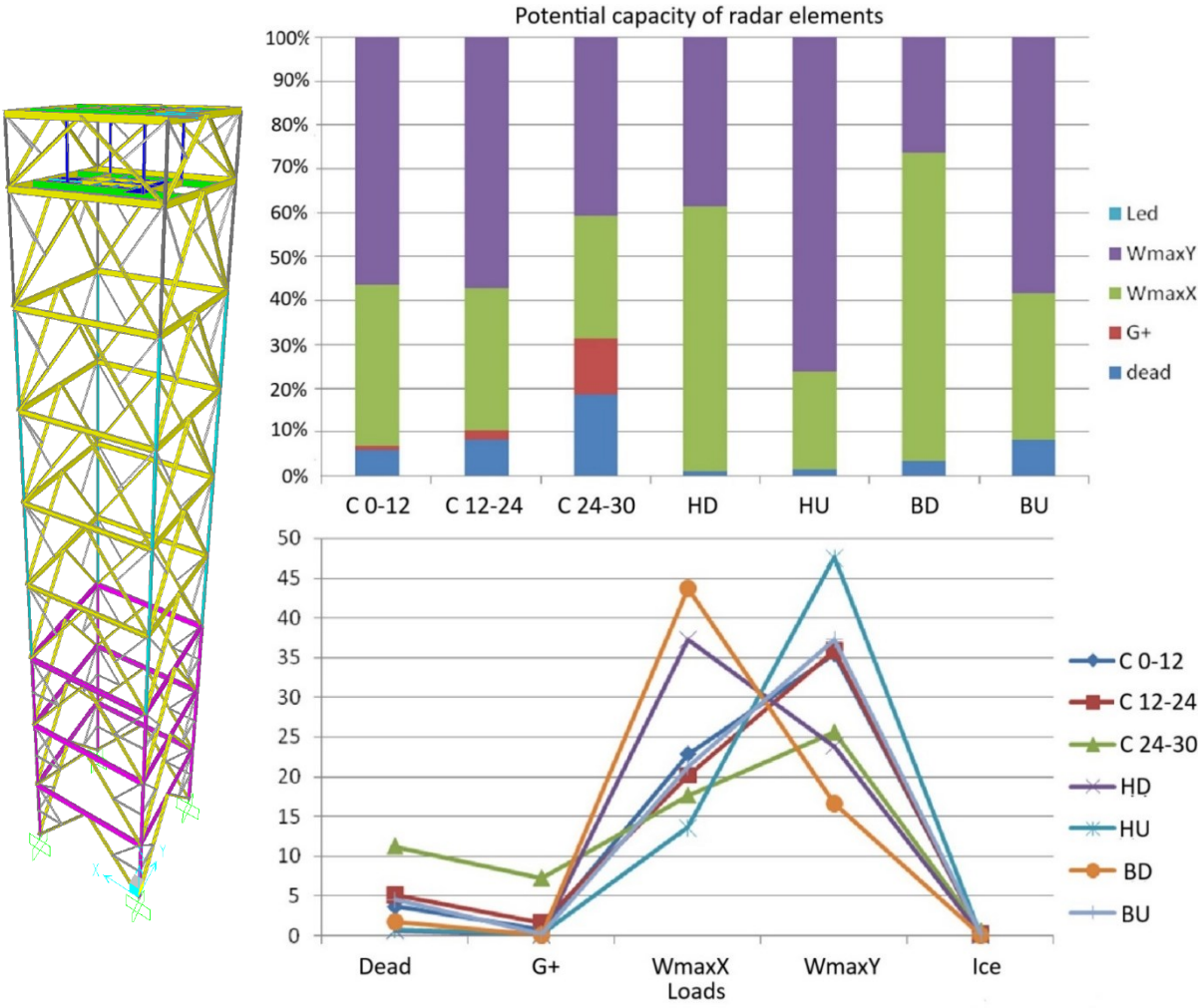


Figure 5. Percentage of load participation in the stress of the elements of a RADAR TOWER

Copyright © 2025 CroCEE
DOI: https://doi.org/10.5592/CO/3CroCEE.2025.21

4.3. Analysis of silo elements

The mathematical analysis model is designed as a spatial system made of frame elements (table 3), with joint connections with the foundations, while the silos are modeled as shell elements (table 4). In this analysis case, different constructive elements have different behavior on outside influences. On figure 6 the percentage use of the steel elements of the structure are displayed for different load cases.

On the mantle of the silo (figure 7), the horizontal dynamic pressure has a dominant influence on the use of up to 80%, and as such (albeit reduced) again as dominant is transferred to the load bearing structure.

Table 3. Silo elements

ECD – End Column Down	MCU – Middle Column Up
ECU – End Column Up	BD – Beam Down
MCD – Middle Column Down	BU – Beam Up
Mantle thickness 8mm and 6mm	B – Bracing

Table 4. Silo's mantle thickness

dp=9mm – Mantle thickness 9mm (segment 0m-10m)
dp=8mm – Mantle thickness 8mm (segment 10m-30m)
dp=7mm – Mantle thickness 7mm (segment 30m-40m)
dp=5mm – Mantle thickness 5mm (segment 40m-50m)

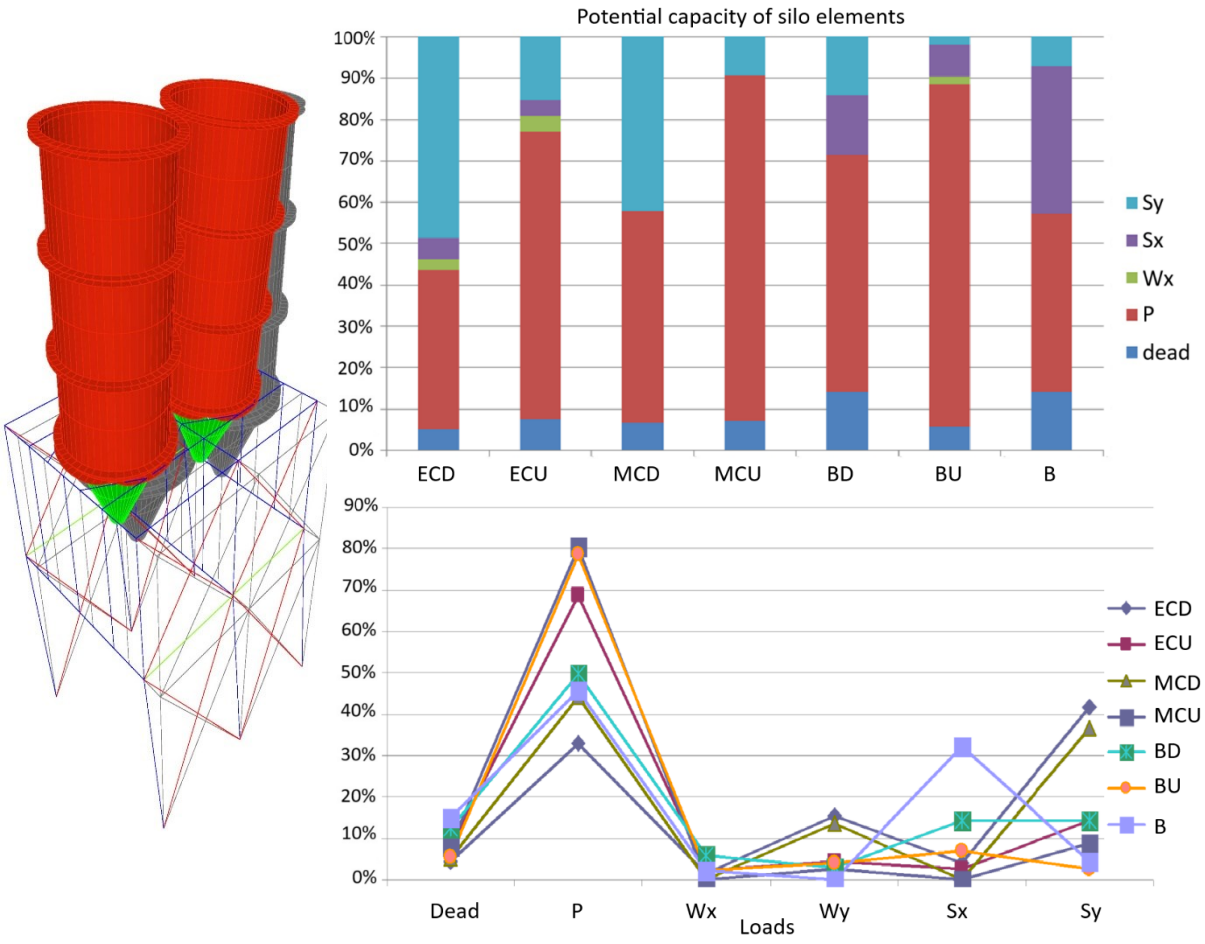


Figure 6. Percentage of load participation in the stress of the elements of a SILO

Copyright © 2025 CroCEE
DOI: https://doi.org/10.5592/CO/3CroCEE.2025.21

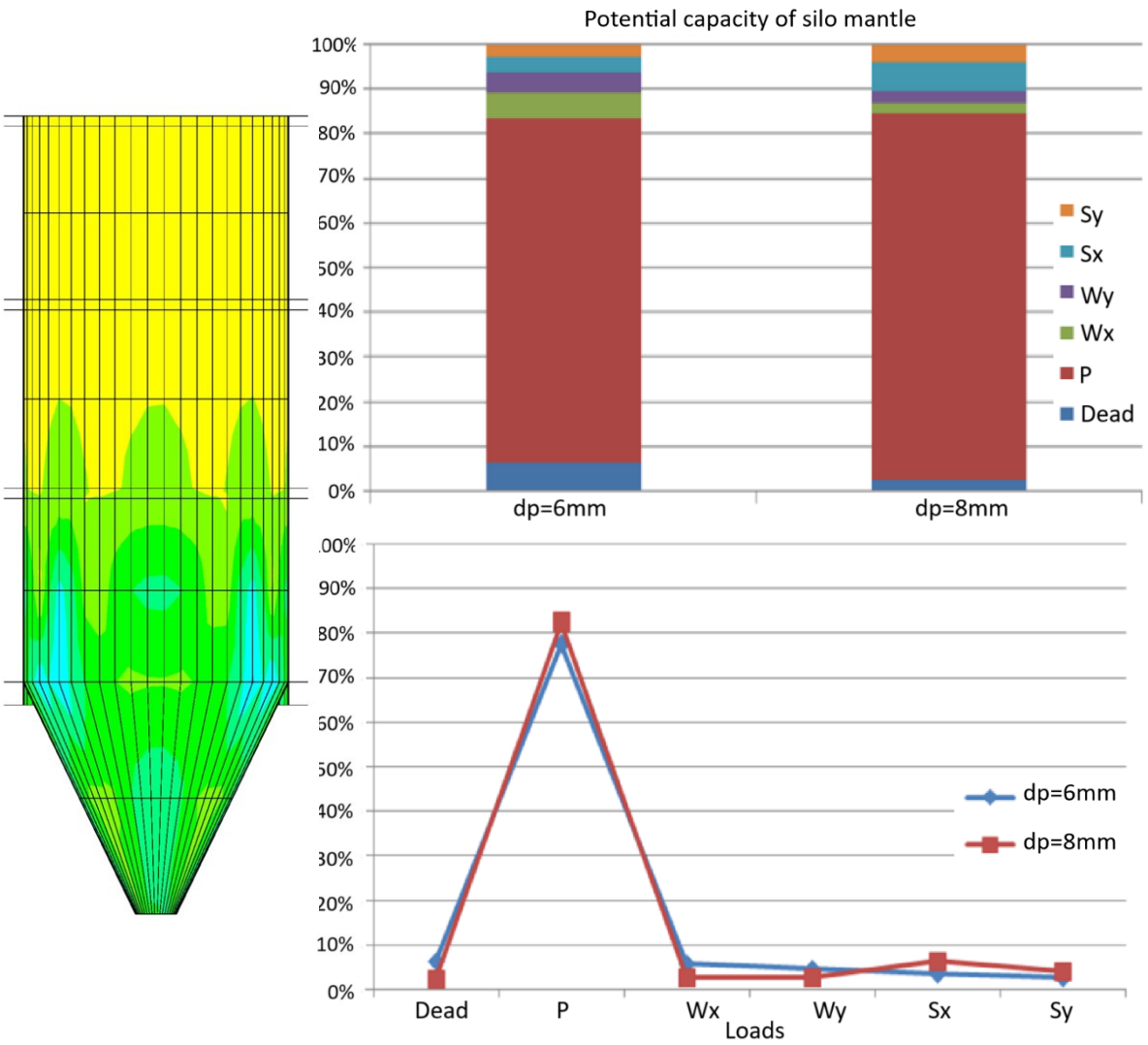


Figure 7. Percentage of load participation in the stress of the elements of a SILO MANTLE

4.4. Analysis of chimney elements

All chimney elements are with 30cm thickness, but in order to achieve finer transparency, the chimney is divided in segments in regard with the different wind loads along the height of the chimney. From the analysis one can conclude that as the height of the chimney increases, the influence of the dynamic horizontal loads is more dominant, with the seismic load of up to 50% in the overall use of the load capacity of the elements, and on second place is the dynamic wind load with 30% (figure 8). With the decrease of the height of the chimney and the increase of the thickness of the mantle, the influence of the vertical loads in the overall use of the elements increase, but only up to 15%.

Copyright © 2025 CroCEE
DOI: https://doi.org/10.5592/CO/3CroCEE.2025.21

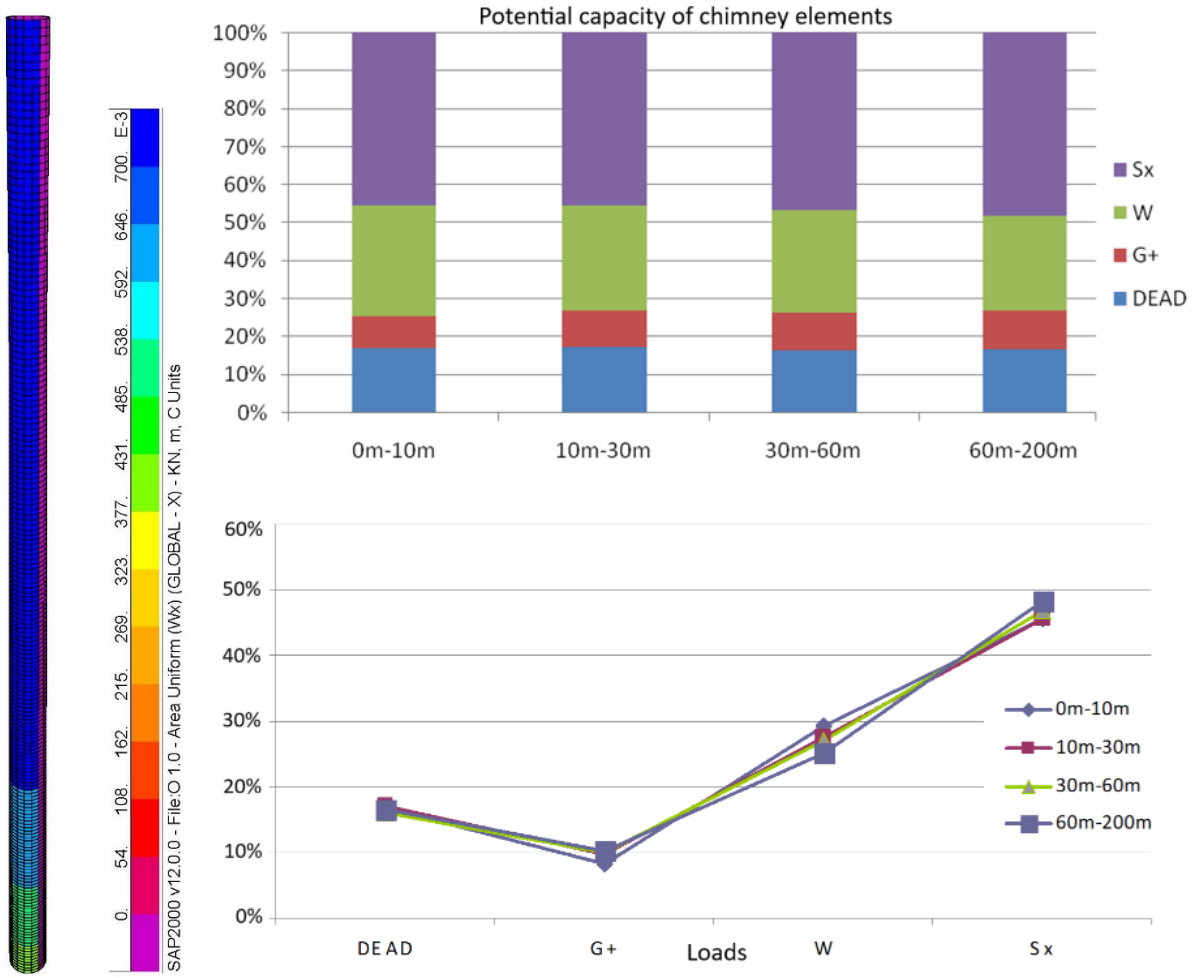


Figure 8. Percentage of load participation in the stress of the elements of a CHIMNEY

5. Conclusion

The following conclusions can be drawn from the experimental and the theoretical research:

- An overall analysis of the entire structure with all of its elements and loads should be preferred over generalizing the wind load on the overall design of the elements for individual objects (such as columns, beams, girders, etc.). Specifically, the mantle will experience significant deformations if only empty silos with wind load are examined. On the other hand, the loads cancel each other out if the mantle is examined with wind and live load.
- Compared to reinforced concrete, the wind load has a far greater impact on the design of steel structural elements. Specifically, steel structures are far more vulnerable to wind loads than concrete ones (which are more vulnerable to seismic loads) because of their small mass. However, the wind load effect can be minimized to be less than the seismic load effects when choosing the constructive solution for a steel structure.
- Additionally, the structures can be significantly stabilized with minor interventions. The silo mantle, in particular, shows a rapid increase in stiffness after adding horizontal rings as stiffeners (just 2% more material), which decreased the material's deformation and stress.
- The stress of the constructive elements also depend by the type of structure, whether it is open or closed. The material experiences less stress in closed objects than in directly exposed elements of open structures because of the interaction between the cladding and the constructive elements.

Proceedings of the 3rd Croatian Conference on Earthquake Engineering - 3CroCEE
19–22 March 2025, Split, Croatia
Copyright © 2025 CroCEE
DOI: https://doi.org/10.5592/CO/3CroCEE.2025.21

- The height and width of a structure determine how the wind affects it. In other words, wind increases the stress on tall building's materials than it does on low, wide structures. According to the previously mentioned calculations, the mast had the highest material stress while the silos had the lowest. However, compared to open structures (like radar towers or power lines), closed structures, where the surface for wind load application is precisely defined, can be designed with much more precision and certainty. The effect that ice and snow deposits have on the increase of the surface for wind loads is one topic that was not covered in this work and that provides room for additional study. Specifically, as was the case with numerous power lines during the winter of 2012–2013, these deposits have the potential to drastically increase the surface area for wind loads and even completely change the structure from an open to a closed type, which can lead to failure. The stress would have been lowest in a typical warehouse, according to the analysis.

References

[1] *Eurocode 0*. European Committee for Standardization. Brussels: CEN, 2002

[2] Pakvor, A. (1997): *Eurocode 1, Osnove Proračuna i dejstva na konstrukcije*. Građevinski fakultet Univerziteta Srbije, Beograd, Serbia

[3] Kappos, A. (2002): *Dynamic Loading and Design of Structure.* Spon Press, New York, USA.

[4] Ragheb, M. (2008): *Dynamics and structural loading in wind turbines*. New York University Press, New York, USA.

[5] Stephanopoulos, T.; Baniotopoulos, C. (2007): *Wind Effects on Buildings and Design of Wind-Sensitive Structures.* Springer, New York, USA.

[6] Ole Hansen, S. (1997): *Wind Loads on Structures.* John Wiley & Sons, New York, USA.

[7] Holmes, J. (2001): *Wind Loading on Structures.* Taylor & Francis, London, Great Britain.

Proceedings of the 3rd Croatian Conference on Earthquake Engineering - 3CroCEE
19–22 March 2025, Split, Croatia
Copyright © 2025 CroCEE
DOI: https://doi.org/10.5592/CO/3CroCEE.2025.33

ADVANCING SEISMIC DESIGN AND ASSESSMENT THROUGH EXPERIMENTAL TESTING: INSIGHTS FROM THE ERIES PROJECT

Gerard J. O'Reilly [(1)], Volkan Ozsarac [(2)], Davit Shahnazaryan [(3)], Igor Lanese [(4)], Elisa Rizzo Parisi [(5)], Filippo Dacarro [(6)], Gian Michele Calvi [(8)]

[(1)] *Associate Professor, Scuola Universitaria Superiore IUSS Pavia, Italy, gerard.oreilly@iusspavia.it*
[(2)] *Postdoctoral Researcher, Scuola Universitaria Superiore IUSS Pavia, Italy, volkan.ozsarac@iusspavia.it*
[(3)] *Postdoctoral Researcher, Scuola Universitaria Superiore IUSS Pavia, Italy, davit.shahnazaryan@iusspavia.it*
[(4)] *Researcher, EUCENTRE Foundation, Pavia, Italy, igor.lanese@eucentre.it*
[(5)] *Researcher, EUCENTRE Foundation, Pavia, Italy, elisa.rizzoparisi@eucentre.it*
[(6)] *Laboratory Director, EUCENTRE Foundation, Pavia, Italy, filippo.dacarro@eucentre.it*
[(8)] *Professor, Scuola Universitaria Superiore IUSS Pavia, Italy, gm.calvi@iusspavia.it*

Abstract

Seismic design and assessment of structures hinge on accurately quantifying the non-linear behaviour of various structural and non-structural elements within the built environment. Experimental testing has become a cornerstone of earthquake engineering, providing invaluable insights into key structural behaviours that can be either designed for or mitigated against. This paper presents ongoing experimental activities at the Eucentre Foundation, under the auspices of the ERIES project, funded by the European Union. The project facilitates collaboration between research groups across Europe and leading research infrastructures as part of the transnational access and joint research initiative. The experimental facilities such as 9DLAB and MOBILAB at the Eucentre Foundation play a central role in these efforts, offering unparalleled flexibility, mobility, and adaptability in test setups—capabilities that are unique on a global scale. This study highlights several experimental research efforts, including the characterisation of the energy dissipation capacity of masonry infill walls and the exploration of sustainable retrofitting solutions for enhancing the capacity of rubble stone walls. Additionally, the paper discusses innovative in-situ testing of base-isolated buildings using a mobile shaking table. These advanced and adaptable experimental testing facilities not only deepen our understanding of the seismic behaviour of structures but also pave the way for new research directions in earthquake engineering. By harnessing these capabilities, researchers can better address the challenges of seismic resilience, leading to safer and more sustainable designs.

Keywords: experimental testing; structural performance; built environment; seismic performance.

1. Introduction

Natural disasters continue to inflict significant harm globally, impacting buildings and infrastructure, as well as causing profound economic and societal disruptions. Recent seismic events, such as those in L'Aquila (2009), Central Italy (2016-2017), Samos Island in the Aegean Sea (2020), Albania (2019), and Croatia (2020), have had considerable societal effects. For instance, the 2020 Aegean Sea earthquake resulted in an estimated €400 million in economic losses and left around 15,000 people homeless. In Albania, the November 2019 earthquake claimed 52 lives, injured 3,000 individuals, displaced 14,000 people, and destroyed more than 14,000 buildings. The Petrinja earthquake in Croatia also caused extensive damage, with additional challenges in reconstruction due to geotechnical issues, soil liquefaction, and the formation of sinkholes.

The ongoing impacts of these disasters underline the need for further research and technological innovations. Addressing this need, the ERIES project (European Research Infrastructures for European Synergies, www.eries.eu) responds to the European Commission's Horizon Europe call INFRA-2021-SERV-01-07. ERIES aims to provide transnational access (TA) to advanced research infrastructures in structural, seismic, wind, and geotechnical engineering, enabling ground-breaking research. This project offers access to leading experimental facilities, facilitating research that addresses hazard-related losses, risk management, and the development of innovative solutions for a greener, more sustainable society.

Proceedings of the 3rd Croatian Conference on Earthquake Engineering - 3CroCEE
19–22 March 2025, Split, Croatia
Copyright © 2025 CroCEE
DOI: https://doi.org/10.5592/CO/3CroCEE.2025.33

This paper offers an overview of the experimental work at the Eucentre Foundation in Pavia, Italy, as part of ERIES. Researchers from Portugal, Turkey, the UK, and the Netherlands contribute to these activities, all aligned with ERIES' broader research goals. Each TA project is introduced, along with a summary of current achievements.

2. Developments at EUCENTRE Foundation testing facilities

To date, four Transnational Access (TA) projects (Table 1) have been completed at the EUCENTRE Foundation, utilising the advanced facilities of 9DLAB and MOBILAB. The following details summarise each project, including information on the user group leader, the institution, and the country of origin of each transnational access team. The subsections below offer an overview of each project, highlighting the experimental activities conducted at EUCENTRE Foundation to date.

Table 1. List of transnational access projects currently hosted at the Eucentre Foundation

Project Acronym	**Title**	**User Group Leader**	**Institution**
ERIES-RESTORING	REtrofitting of STOne masonRy using INnovative Grid-based composites	Rita Bento	Instituto Superior Técnico, University of Lisbon
ERIES-ENFRAG	ENhancing state-dependent FRAGility through experimentally validated Energy-Based Approaches	Roberto Gentile	University College London, United Kingdom
ERIES-SUPREME	Seismic oUt-of-Plane REsponse of Masonry gablEs	Francesco Messali	Technische Universiteit Delft, The Netherlands
ERIES-PASFIT	Long-Term Performance Assessment of Base Isolated Buildings through Field Testing	Haluk Sucuoglu	Middle East Technical University, Turkiye

2.1. ERIES-RESTORING

2.1.1. Overview of project

The seismic assessment/retrofit of existing masonry buildings has become in the past years a matter of high priority in seismically prone countries with a significant presence of built cultural heritage, such as several European and Mediterranean countries, accentuated by recent and mandatory legal sources. Moreover, the change of focus from building replacement to rehabilitation of the existing stock is a step towards greater sustainability, a topic for which more and more awareness is being raised.

The proposed project aims at spanning the information gap about factors affecting the seismic effectiveness of Composite Reinforced Mortars (CRM) applied to existing rubble stone masonry buildings by experimental research. The in-plane cyclic behaviour of innovative strengthening solutions compatible with historic masonry materials will be tested on full-size rubble stone masonry piers and will be compared with the non-retrofitted pier response. CRM, consisting of a glass-FRP mesh embedded in natural hydraulic mortar, will be applied to one or both sides of the specimen. Imposing double-fixed boundary conditions, two different aspect ratios will also be investigated. Moreover, the influence of the horizontal load rate will be studied by performing in-plane cyclic shear-compression tests with quasi-static and high-rate protocols.

The outcomes will provide useful data for the future development of design guidelines and building code requirements, currently missing, about the design of CRM as a strengthening solution for existing masonry structures. This will contribute to the reduction of their vulnerability and of the associated losses after earthquake events.

2.1.2. Experimental activities to date

The ERIES-RESTORING project has successfully completed its main phases. Key achievements include the design and construction of test specimens (see Figure 1) and setups, detailing the geometry and materials (masonry, mortar, CRM components, connectors), and adapting existing facility

Copyright © 2025 CroCEE
DOI: https://doi.org/10.5592/CO/3CroCEE.2025.33

components. Essential structures, such as RC elements and test wallets for material characterisation, have been built. Comprehensive material tests have been conducted, covering CRM components, mortar, and masonry wallets under vertical and diagonal compression. Seven full-scale cyclic test piers were constructed and tested to evaluate their performance. Currently, the user group is analysing the data, interpreting results, and engaging in joint dissemination activities.

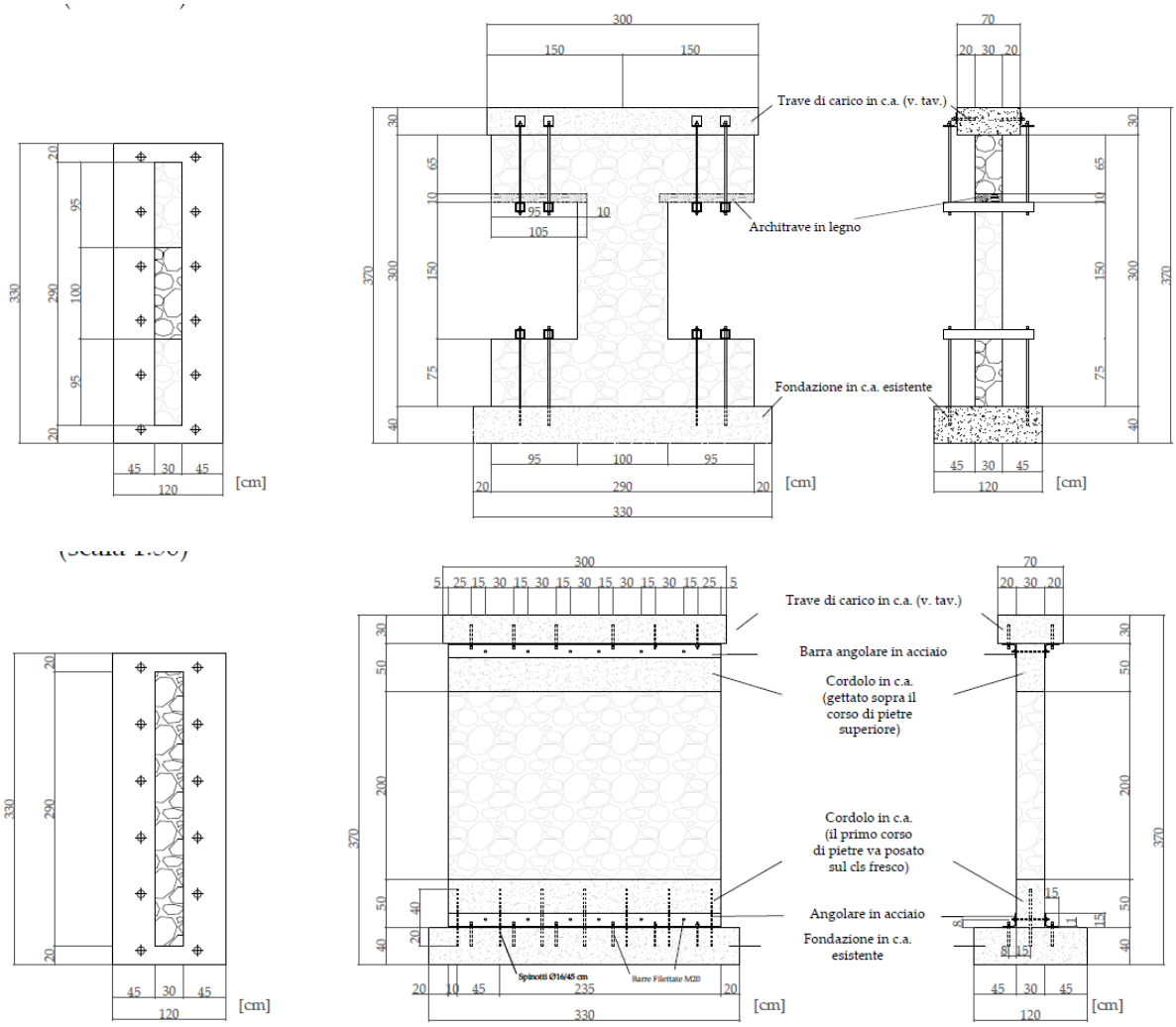


Figure 1. Specimen typologies and geometry for the ERIES-RESTORING project

2.2. ERIES-ENFRAG

2.2.1. Overview of project

ERIES-ENFRAG advances state-dependent earthquake fragility assessment methodologies. The project focuses on masonry infill walls experiencing cumulative states of damage due to combinations of in-plane (IP) and out-of-plane (OOP) actions, commonly quantified through two different peak-based engineering demand parameters (EDPs). ERIES-ENFRAG explores the experimental validation of hysteretic energy-based fragility assessment approaches, which are: 1) currently based only on analytical and/or numerical validations; 2) only considering one type of action/damage mechanism. ERIES-ENFRAG will pave the way for similar cumulative-damage tests for different structures/structural components while providing experimental data on the IP and OOP response of masonry infills. ERIES-ENFRAG aims at a robust consideration of damage-accumulation, particularly

Copyright © 2025 CroCEE
DOI: https://doi.org/10.5592/CO/3CroCEE.2025.33

relevant in mainshock-aftershock conditions, and will also shed further light on the appropriateness of IP and OOP loading protocols used in experimental testing.

2.2.2. Experimental activities to date

The ERIES-ENFRAG project has completed all main phases, focusing on integrating numerical simulations with experimental efforts. Numerical models were improved and calibrated using EUCENTRE's existing test database on similar specimens. Construction included three main infill specimens, wallettes, and material samples for characterization tests, minimising uncertainties from environmental factors and labour variations. Comprehensive testing was performed (see Figure 2), covering IP and OOP mixed protocols, as well as wallettes and material samples. Data processing by EUCENTRE staff has delivered clean datasets for analysis. Currently, user groups are engaged in data analysis, interpretation of results, and collaborative dissemination activities.



Figure 2. Test setup for the ERIES-ENFRAG project

2.3. ERIES-SUPREME

2.3.1. Overview of project

Typical low-rise existing masonry buildings in Europe commonly feature unreinforced masonry (URM) walls, complemented by diverse pitched roof configurations supported or finished by masonry gables. Such buildings also constitute a large part of the building stock for several seismic-prone countries, including both areas subject to natural hazard and induced seismicity. In such buildings, the masonry gables are often associated with the highest seismic vulnerability. The evidence of this seismic vulnerability has been widely documented in the aftermath of past earthquakes. This vulnerability can be attributed to multiple factors, including their high slenderness, poor connections to the roof structure, and their positioning at the uppermost part of the building, exposing them to amplified seismic excitation with respect to the ground motion while being subjected to low values of overburden load. Additionally, the interaction of the gables with flexible roof diaphragms can also contribute to the seismic vulnerability of the coupled system, due to the possible further amplification of the seismic motion through the timber elements. However, the amount of experimental data regarding the performance of URM gables is extremely limited, and it can be mostly inferred from tests that simulate a complete building and are not specifically focused on these structural elements.

The project here proposed aims therefore at improving the understanding of the seismic out-of-plane response of masonry gables within existing masonry buildings, a subject of fundamental interest to enhance the safety and seismic performance of existing masonry structures.

Copyright © 2025 CroCEE
DOI: https://doi.org/10.5592/CO/3CroCEE.2025.33

The project will produce novel experimental data on the dynamic behaviour of URM gables, which is currently missing from published literature. The experiments will adopt idealised and easily numerically replicable boundary conditions, which can be simulated conveniently via numerical simulations. The tests will therefore be used as benchmarks to allow refinement and calibration of existing numerical modelling approaches, as well as the development of new tools based on single-degree of freedom systems. A blind-prediction contest open to international research groups will be set up to foster the calibration process. The generated experimental data and the calibrated numerical models will serve as basis for the improvement of available guidelines for the OOP seismic assessment of URM gables in existing masonry buildings. The results of the test results and of the prediction contest, as well as the recommendations to improve assessment guidelines will be published on a special issue of a peer-reviewed journal.

2.3.2. Experimental activities to date

The ERIES-SUPREME project has successfully completed all primary phases. Key milestones include the design and construction of the dynamic test setup (see Figure 3), incorporating steel elements and RC foundations, and the incremental dynamic testing of URM gables. Complementary material characterisation tests were performed at the University of Pavia to ensure representativeness. Numerical modelling was conducted to define dynamic seismic inputs, simulating interactions between gables and flexible or semi-rigid retrofitted roof diaphragms. Dynamic tests of three gable walls were performed using the EUCENTRE 9D System. Data processing, analysis, and interpretation of results are complete, while dissemination activities and the final test report are currently underway.

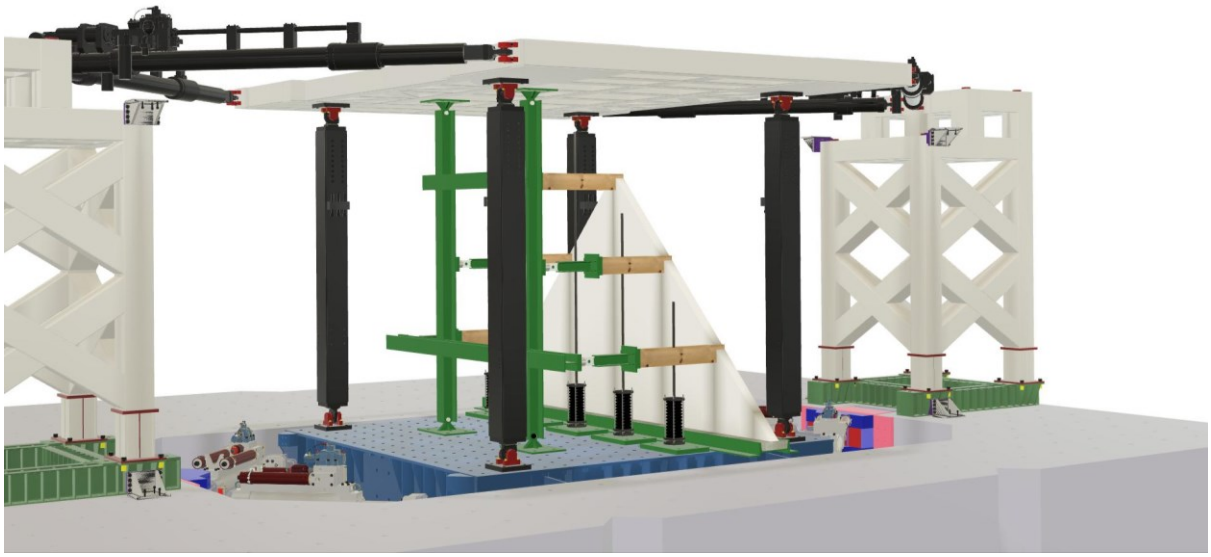


Figure 3. Test setup for the ERIES-SUPREME project

2.4. ERIES-PASFIT

2.4.1. Overview of project

Base isolation has emerged as one of the most effective and elegant strategies for protecting infrastructure and their contents under seismic loading, both in the context of new construction and in the retrofit of existing systems. The benefits of base isolation are twofold: first, by increasing the fundamental period of vibration and adding damping, the structural response is shifted into a more favourable regime and overall forces are lowered, and second, by changing the mode shape of the structure, displacement is concentrated into the isolation layer, greatly minimising storey drifts.

However, understanding of the performance of isolated buildings is primarily based on component level testing of new isolation bearings. Less well understood is the performance of large groups of isolators,

Copyright © 2025 CroCEE
DOI: https://doi.org/10.5592/CO/3CroCEE.2025.33

each of which may have a slight variation in properties within the allowable design limits. Furthermore, interaction with the sub- and superstructure have the potential to change the demands on the bearing. On top of this, it is understood that the long-term behaviour of a base isolation system may differ significantly from its original as-designed behaviour. While this has been explored on rare occasions for individual aged bearings, generating sparse data points, there are no previous studies testing system-level aged isolated buildings.

ERIES-PASFIT will conduct full-scale in-situ testing of buildings, base isolated via laminated rubber bearings and friction pendulum (FP) systems that have been in service for approximately 15 years. The results of these field tests will be the first of their kind, and will be used to fill important research gaps pertaining to the characterization of the response and performance of base isolated buildings, including aspects of system-level response in conjunction with aging, deterioration and, more generally, variability of the mechanical properties of the isolation devices. Thus, this will have important implications on base isolation design, assessment and modelling strategies.

2.4.2. Experimental activities to date

The ERIES-PASFIT project has successfully completed its primary phases, focusing on the evaluation and performance assessment of base-isolated structures. The project began with identifying and characterizing case-study buildings in collaboration with local authorities and the EUCENTRE team, collecting essential data such as base isolator properties, structural layouts, and material details. Non-linear numerical analyses were conducted to assess the nominal as-designed response and theoretical aged response of these buildings (see Figure 4), using empirical aging factors from the literature. Subsequently, an in-situ testing setup was designed and implemented based on numerical simulation results. Preliminary activities, including system configuration programming and interface component production, ensured the readiness of the testing setup. In-situ testing of the case-study building was conducted, employing quasi-static reversed cyclic and dynamic loading protocols. Currently, the project is processing experimental results to assess the impact of bearing aging on structural and non-structural performance, validating findings through comparisons between numerical and experimental outcomes, and evaluating the applicability of existing design and modelling recommendations.



Figure 4. Rendering of building typology in L'Aquila, Italy considered for ERIES-PASFIT

3. Overall impacts within ERIES Research Goals

The collective efforts of these individual projects under the ERIES initiative have made substantial contributions towards its overarching research goals, particularly in advancing knowledge, testing, and developing guidelines for seismic resilience and mitigation in structural engineering. The research goals for earthquake hazards in the ERIES project focus on three primary objectives:

- First, the project aims to advance loss-driven design and mitigation approaches by addressing gaps in current seismic design and retrofit methods, emphasizing loss-based assessments and performance optimization. This includes experimental testing and database development using

Proceedings of the 3rd Croatian Conference on Earthquake Engineering - 3CroCEE
19–22 March 2025, Split, Croatia
Copyright © 2025 CroCEE
DOI: https://doi.org/10.5592/CO/3CroCEE.2025.33

cutting-edge facilities, such as shake tables and wind tunnels, to reduce risk in buildings, critical infrastructure, and industrial facilities.

- Second, ERIES emphasizes risk quantification and prioritization to improve societal resilience and robustness. This involves probabilistic seismic and wind risk analysis, addressing soil-structure interaction effects, and developing systemic approaches for interconnected infrastructure networks, enabling better preparedness and prioritization of interventions.
- Third, the project integrates green and sustainable development across its activities by promoting innovative materials and designs that reduce environmental impact and improve energy efficiency. Examples include recycled materials for seismic isolation and testing renewable energy solutions like wind turbines and photovoltaic systems, contributing to a resilient, low-carbon built environment.

The ERIES-RESTORING project has significantly advanced understanding in the seismic assessment and retrofitting of rubble stone masonry buildings, which are particularly vulnerable to earthquakes due to their lack of specific seismic provisions. Through a comprehensive experimental campaign involving cyclic tests under various retrofit and loading conditions, the project contributes toward developing guidelines for CRM retrofit solutions. These outcomes directly support Research Goal 1 (Loss-driven Design and Mitigation Approaches) by providing critical insights into effective retrofit strategies that could reduce seismic risk for a wide range of structures, from residential buildings to historical landmarks.

ERIES-ENFRAG addresses both Research Goal 1 and Research Goal 2 (Risk Quantification and Prioritization) by experimentally examining masonry infills, a common feature in European buildings, especially in the Mediterranean region. The project's experimental tests, which include developing fragility functions for these infills, are essential for assessing in-plane (IP) and out-of-plane (OOP) behaviour under seismic loading. This work aids in understanding seismic vulnerabilities and advancing models that quantify and prioritize risks for better mitigation strategies.

The ERIES-SUPREME project focuses on the seismic vulnerability of gable walls in URM low-rise buildings, structures highly susceptible to out-of-plane motion. The experimental campaign and blind-prediction contest contribute to Research Goal 1 by enhancing understanding of gable wall capacity and interactions with roof structures, which are critical to seismic resilience. The project also aligns with Research Goal 3 (Green and Sustainable Development) by evaluating a timber-based retrofitting technique, encouraging the use of environmentally sustainable materials over conventional concrete solutions in seismic strengthening.

ERIES-PASFIT uniquely contributes to Research Goal 1 by conducting pioneering tests on the in-situ behaviour of aged, seismically isolated buildings. The project also addresses Research Area 2 (Critical Infrastructures) as it examines base isolation technology used in critical facilities. By characterizing long-term performance and advancing design and assessment strategies, PASFIT provides valuable insights into how seismic isolation systems perform over time, ensuring that buildings meet or exceed design standards in real-world conditions.

Collectively, these projects reinforce ERIES' mission by driving forward the scientific understanding, risk management, and sustainable practices required to mitigate the impact of natural disasters on the built environment. The experimental results generated through these projects not only enhance current seismic assessment methodologies but also lay the groundwork for more resilient, sustainable construction practices across Europe.

4. Summary

This paper presents the ongoing experimental activities and findings of the ERIES project to advance seismic design, assessment, and resilience through cutting-edge experimental testing and international collaboration. Utilizing world-class facilities like 9DLAB and MOBILAB at the EUCENTRE Foundation, the initiative addresses critical gaps in seismic performance knowledge and sustainable retrofitting techniques. Key projects include the seismic retrofitting of masonry buildings (ERIES-

Copyright © 2025 CroCEE
DOI: https://doi.org/10.5592/CO/3CroCEE.2025.33

RESTORING), cumulative damage assessment of masonry infills (ERIES-ENFRAG), dynamic testing of vulnerable masonry gables (ERIES-SUPREME), and the long-term performance evaluation of base-isolated buildings (ERIES-PASFIT). These efforts contribute to loss-driven design, risk quantification, and sustainable development, fostering more resilient and environmentally friendly infrastructure while enhancing seismic risk mitigation across Europe.

Acknowledgements

This work provides an overview of several transnational access projects whose contributions to the summary presented here were fundamental to their successes. It is also part of the Engineering Research Infrastructures for European Synergies (ERIES) project (www.eries.eu), which received funding from the European Union's Horizon Europe Framework Programme under Grant Agreement No. 101058684. This is ERIES publication number C37.

Proceedings of the 3rd Croatian Conference on Earthquake Engineering - 3CroCEE
19–22 March 2025, Split, Croatia
Copyright © 2025 CroCEE
DOI: https://doi.org/10.5592/CO/3CroCEE.2025.44

INTEGRATION OF THE OMA AND FEMU FOR ESTIMATION MODULUS OF ELASTICITY IN MASONRY STRUCTURES

Suzana Ereiz [(1)], Ivan Duvnjak [(2)], Janko Košćak [(3)], Marko Bartolac [(4)], Domagoj Damjanović [(5)], Marina Frančić Smrkić [(6)]

[(1)] *Postdoctoral fellow, Politecnico di Milano, University of Zagreb Faculty of Civil Engineering, suzana.ereiz@polimi.it, suzana.ereiz@grad.unizg.hr*
[(2)] *Associate professor, University of Zagreb Faculty of Civil Engineering, ivan.duvnjak@grad.unizg.hr*
[(3)] *Senior research assistant, University of Zagreb Faculty of Civil Engineering, janko.koscak@grad.unizg.hr*
[(4)] *Associate Professor, University of Zagreb Faculty of Civil Engineering, marko.bartolac@grad.unizg.hr*
[(5)] *Full-time professor, University of Zagreb Faculty of Civil Engineering, domagoj.damjanovic@grad.unizg.hr*
[(6)] *Assistant professor, University of Zagreb Faculty of Civil Engineering, marina.francic.smrkic@grad.unizg.hr*

Abstract

The recent seismic activity in Croatia has inflicted significant damage on numerous buildings, with masonry structures being especially vulnerable. For the effective rehabilitation and restoration of these structures, it is critical to assess key mechanical properties such as the modulus of elasticity, compressive strength, tensile strength, and shear strength. Conventional methods for determining these properties often involve labour-intensive field tests and laboratory analysis of masonry samples. This paper introduces an innovative methodology that integrates Operational Modal Analysis (OMA) with Finite Element Model Updating (FEMU) to estimate the modulus of elasticity in masonry structures. By leveraging dynamic parameters, including natural frequencies and mode shapes derived from OMA, the methodology allows for the updating of a numerical sub-model of the masonry. This integrated approach was applied to a real structure, with results compared to those obtained using traditional testing methods. The findings indicate that the proposed method is not only more efficient but also yields highly accurate estimations of mechanical properties, particularly the modulus of elasticity, with minimal disruption to the structure. The reduced need for invasive testing, coupled with its precision, positions this approach as a compelling alternative to traditional methods for assessing the structural integrity of masonry structures following seismic events.

Keywords: Operational modal analysis (OMA), Finite element model updating (FEMU), Modulus of elasticity, masonry structures, seismic activity

1. Introduction

Recent seismic events in Croatia, particularly those affecting Zagreb and Petrinja, have resulted in extensive damage to numerous buildings, with masonry structures being especially susceptible. The necessity of rehabilitating and reconstructing these buildings to ensure their load-bearing capacity and functional integrity has underscored the importance of comprehensive structural assessments. Consequently, experimental investigations and structural condition evaluations have become indispensable components of the rehabilitation process. The restoration and retrofitting of earthquake-damaged structures is a complex and time-consuming endeavour, requiring thorough preliminary investigations and in-depth material testing to ensure compliance with current regulatory standards. Traditionally, these investigations involve a range of testing methods to determine key mechanical properties. These are modulus of elasticity, compressive strength, tensile strength, and shear strength of masonry materials [1]. Investigation methods can be categorized into destructive, semi-destructive, and non-destructive approaches [2]. Destructive testing methods, such as core extraction [3] and flat-jack testing [4]–[6], are commonly used in laboratory analyses. However, these approaches are often limited by the availability of representative masonry samples and the challenges associated with establishing reliable correlations between material hardness and strength. Semi-destructive methods, including rebound hammer testing [7]–[9] and endoscopy [10], are frequently employed to provide information

Copyright © 2025 CroCEE
DOI: https://doi.org/10.5592/CO/3CroCEE.2025.44

about the hardness of brick and mortar as well as the internal condition of walls. Despite their utility, these techniques are constrained by localized application and potential subjective interpretation by investigators. Non-destructive testing methods, such as ground-penetrating radar [10]–[12] ultrasonic testing [13], and infrared thermography [14], offer the advantage of damage detection without significantly compromising the integrity of the structure. While these methods yield valuable insights into the condition of masonry elements, they require considerable expertise for accurate result interpretation. Additionally, acoustic emission [15] techniques are employed to monitor crack propagation over extended periods, but their primary limitation lies in the time-intensive nature of the monitoring process.

Beyond field testing, numerical modelling plays a critical role in the rehabilitation process [16][17]. Numerical analysis aims to predict the actual behavior of structures by considering their geometry, mechanical properties, and boundary conditions. The development of robust numerical models, commonly referred to as "digital twins" is crucial for assessing load-bearing capacity and formulating effective restoration strategies that align with current building codes.

This paper presents an integrated approach for estimating the mechanical properties of materials of masonry structures that combines experimental investigations with numerical modelling. Specifically, it leverages the integration of Operational Modal Analysis (OMA) [18] and Finite Element Model Updating (FEMU)[19]. The methodology begins with dynamic testing to perform modal identification, from which natural frequencies and mode shapes are extracted. A finite element model of a representative masonry wall segment is then developed and calibrated using the OMA results to estimate the modulus of elasticity accurately. The proposed methodology was applied to the case study of the earthquake-damaged School of Medicine, University of Zagreb. Dynamic testing and modal identification were conducted on a representative masonry wall sample, and a corresponding local model of the wall was calibrated using FEMU. Additionally, traditional testing methods were performed on the same wall to determine mechanical properties, and the results from both approaches were compared. The findings demonstrate that the integrated approach, which minimizes structural disruption, is more efficient and yields accurate estimations of mechanical properties compared to conventional methods.

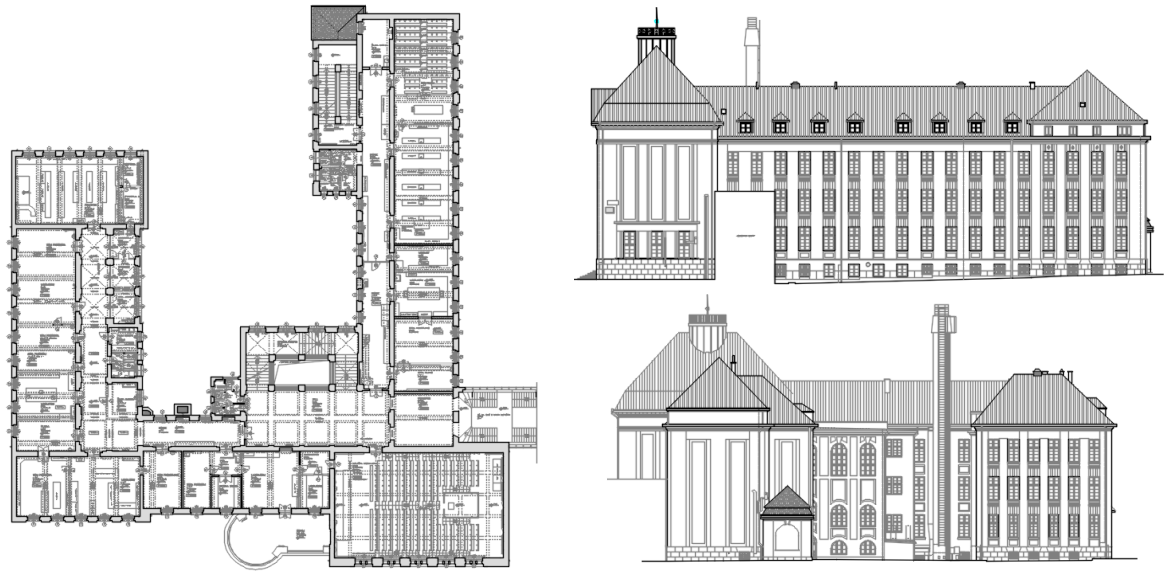
The paper is organized as follows: Section 2 describes the experimental campaign and its results. Section 3 outlines the finite element model updating process for the representative wall segment. Section 4 discusses the iterative FEMU results, while Section 5 provides concluding remarks on the methodology's efficiency and accuracy.

2. Experimental campaign

2.1. Description of the structure

The Building at Šalata 3 is a key facility of the School of Medicine, University of Zagreb supported by auxiliary structures. The building has an irregular footprint, with a basement, ground floor, two upper floors, and an attic. Its footprint dimensions are approximately 58.92 x 68.49 meters, with a cornice height of 17.78 meters and an overall height of 28.45 meters. The gross floor area is 8,452 square meters. Load-bearing walls are constructed of solid brick, from 45 to 94 cm thick, with inter-floor slabs made of 10 cm reinforced concrete supported by a T-beam grid system. A T-beam system also supports the floors and ceilings in the large auditorium and central corridor. In the ground-floor foyer and part of the left wing’s first floor, a three-flight staircase features masonry vaults, with a 10 cm reinforced concrete slab above them. Vertical access is provided by two double- and triple-flight staircases, likely of precast reinforced concrete on steel supports. The building lacks vertical and horizontal ties, and the wooden roof is gabled and tiled.

Proceedings of the 3rd Croatian Conference on Earthquake Engineering - 3CroCEE
19–22 March 2025, Split, Croatia
Copyright © 2025 CroCEE
DOI: https://doi.org/10.5592/CO/3CroCEE.2025.44



(a) (b)

Figure 1. Documentation of the current condition of the School of Medicine, University of Zagreb building: (a) ground floor plan, (b) west and north façades of the building

2.2. On site - determination of mechanical properties

On the building previously described, a series of investigation works were carried out to assess the structural condition and determine the quality of the materials used (Figure 2.). These includes the flat jack and shear test.



(a) (b) (c)

Figure 2. Determination of the mechanical properties (a) vertical stress (b) modulus of elasticity (c) shear strength of masonry wall on the first floor of the School of Medicine, University of Zagreb

Based on the performed test using flat jack and a small hydraulic press the values of different important mechanical properties are obtained (Table 1). The obtained results are used to compare the one obtained using the proposed method.

Table 1. Determined values of mechanical properties of materials of wall at the School of Medicine, University of Zagreb

Mechanical property	Experimentally determined value
Vertical Stress, σ_0, MPa	0.35
Modulus of elasticity, E, MPa	1393
Shear strength, f_{v0}, MPa	0.15
Coefficient of friction, μ	0.30

Copyright © 2025 CroCEE
DOI: https://doi.org/10.5592/CO/3CroCEE.2025.44

2.3. Operational modal analysis of the representative wall

Within the experimental analysis of the School of Medicine, University of Zagreb building by classical operational modal analysis the dynamic properties (natural frequencies and mode shapes) of the representative wall were determined. The location of the cut was strategically selected close to the door opening in the load-bearing wall, ensuring that the structural behavior around the opening could be effectively evaluated while minimizing the influence of boundary conditions on the sides; the cut itself was made with a width of 5 mm (red line, Figure 3 a)). The OMA was conducted by roving four accelerometers (Figure 3 b)) in several points on the wall on which the connection between the wall and accelerometer was made using the round metal plate (Figure 3 b)). One accelerometer was used as a referent (orange point, Figure 3.c)). Frequency domain decomposition (FDD) was used to estimate the values on natural frequency and mode shapes (Figure 4.).

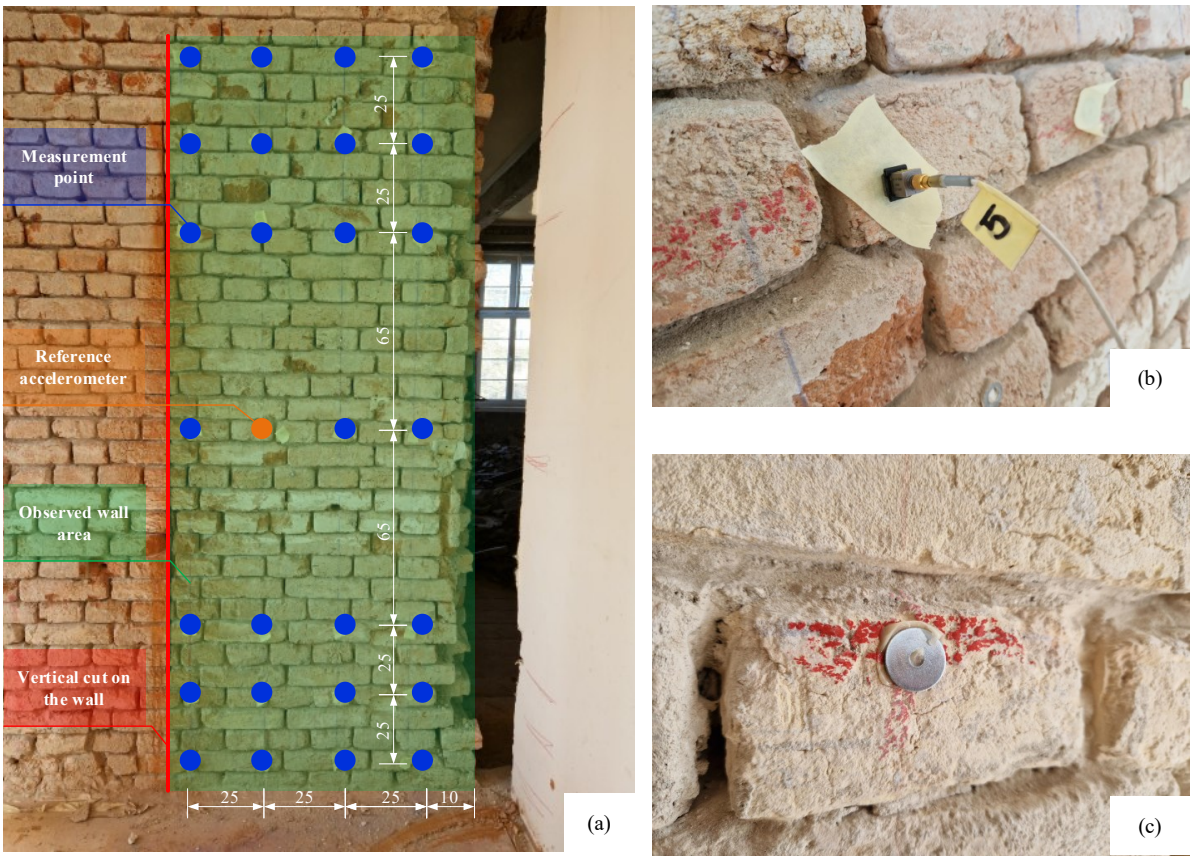
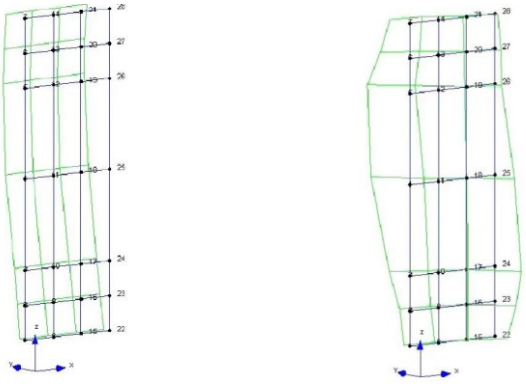


Figure 3. Operational modal analysis set up (a) arrangement of the measurement points (b) accelerometer Brüel & Kjær Type 4508 (c) round metal plate on used during the measurement to place the accelerometers on the wall



29.2 Hz 92.4 Hz

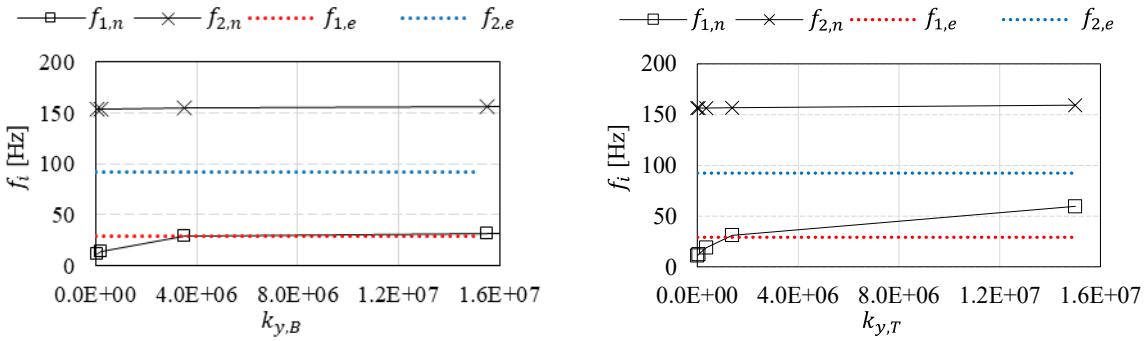
Copyright © 2025 CroCEE
DOI: https://doi.org/10.5592/CO/3CroCEE.2025.44

Figure 4. Results of the modal identification of the representative wall on the first floor of the School of Medicine, University of Zagreb

3. Finite element modelling and updating

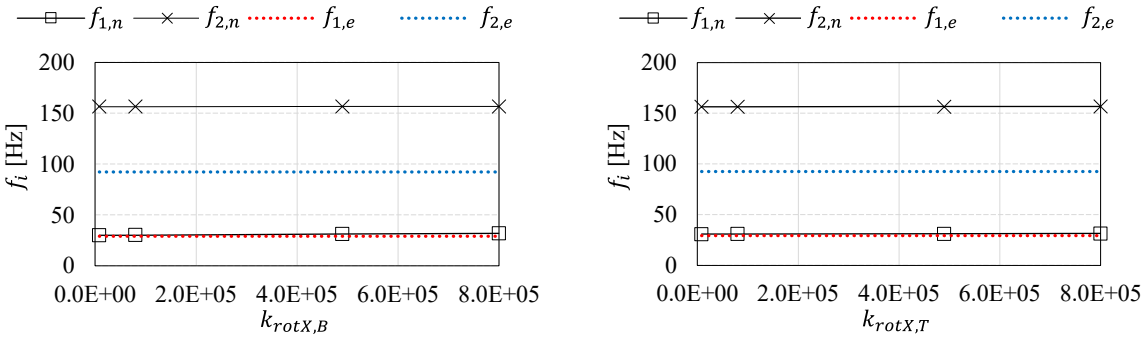
3.1. Initial numerical model and manual calibration

The experimentally obtained results were used to update the local numerical model of the wall. Numerical modelling of the wall was performed using commercial FE package Ansys and personal computer with the processor 3.59 Hz and 16 GB RAM memory. FE model was developed using (i) four node shell elements with six degrees of freedom, SHELL 181, and (ii) COMBIN14 for modelling support with lateral and rotational spring elements. It is assumed that the vertical displacement was constrained. The developed model was meshed using 108 elements. The initial values of the mechanical properties of numerical model were assumed as follows. The modulus of elasticity was proposed as: E_x = 1393 MPa and E_y = 1393 MPa, the material density, ρ = 1700 kg/m3, shear modulus G_{xy} = 557.2 MPa and G_{xz} = 557.2 MPa, Poisson ratio= 0.25. The boundary conditions were determined based on the iteration of the spring stiffness until matching between mode shapes are not reached (Figure 5. and Figure 6.).



(a) (b)

Figure 5. Dependence of the change in numerically obtained first $(f_{1,n})$ and second $(f_{2,n})$ natural frequency on the change in stiffness of the translational spring in the y direction at (a) the bottom of the wall $(k_{y,B})$ (b) the top of the wall $(k_{y,T})$ with the highlighted values of the experimentally determined first $(f_{1,e})$ and second $(f_{2,e})$ natural frequency



(a) (b)

Figure 6. Dependence of the change in numerically obtained first $(f_{1,n})$ and second $(f_{2,n})$ natural frequency on the change in stiffness of the rotation spring around the x axis at (a) the bottom of the wall $(k_{rotX,B})$ (b) the top of the wall $(k_{rotX,T})$ with the highlighted values of the experimentally determined first $(f_{1,e})$ and second $(f_{2,e})$ natural frequency

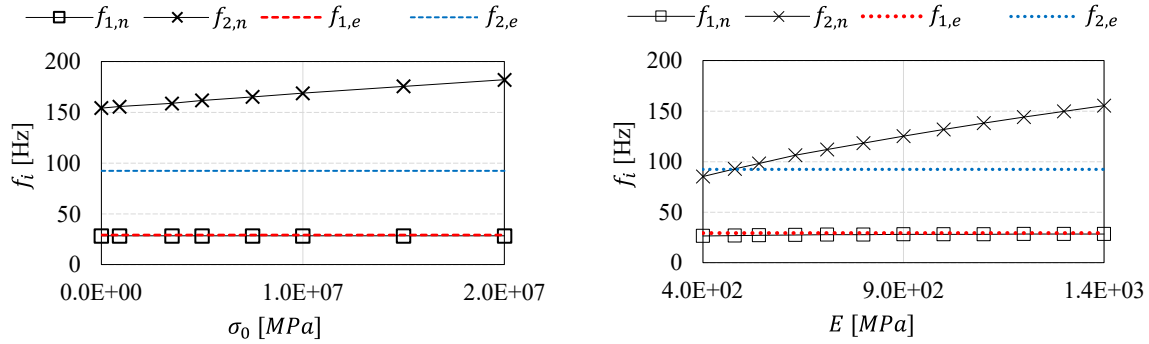
The obtained stiffness of the spring elements was determined based on the values that results in the highest values of MAC factors (0.959 for the first and 0.791 for the second mode). These values are: $k_{y,B} = 1.55 \cdot 10^7 N/m$; $k_{rotX,B} = 4.90 \cdot 10^5 Nm/rad$ for the bottom of the wall and $k_{y,T} = 1.38 \cdot$

Copyright © 2025 CroCEE
DOI: https://doi.org/10.5592/CO/3CroCEE.2025.44

$10^6\ N/m$; $k_{rotX,T} = 4.90 \cdot 10^5\ Nm/rad$ for the top of the wall. For the determined values of the spring stiffness, the calculated values of first two natural frequencies were $f_{1,num}$= 31.13 Hz for the first and $f_{2,num}$= 156.63 Hz for the second mode. Despite the good correlation of the manually optimized numerical model with springs of different stiffness values, the residual of the natural frequency for the second mode remains high (48.32%). To reduce the residual, automated FEMU is applied using Harmony search optimization algorithm [20] in the following.

3.2. Harmony search based finite element model updating

The automated process of the finite element model updating start with the manually calibrated initial finite element model from the previous section. In the first step, numerical model is automated calibrated by updating the spring stiffness values. Based on the manually performed FEMU the obtained values of spring stiffness were: $k_{y,B} = 4.42 \cdot 10^6$; $k_{rotX,B} = 1.78 \cdot 10^5$ for the bottom of the wall and $k_{y,T} = 1.06 \cdot 10^6$; $k_{rotX,T} = 5.32 \cdot 10^4$ for the top. The calculated values of the spring stiffness result in the MAC factor 0.982 for the first and 0.784 for the second mode shape and they correspond to the 28.39 Hz for the first and 154.86 Hz for the second mode. To decrease the changes in natural frequencies updated numerical model is updated in the second step by changing the values of the mechanical properties of materials. This was done by iterating the modulus of the elasticity of masonry between the interval $[40 - 1400]$ MPa while it has been concluded that vertical stress does not affect much the natural frequency value (Figure 7 a)).



(a) (b)

Figure 7. Changing in first $(f_{1,n})$ and second $(f_{2,n})$ numerically obtained natural frequency depending on the change in (a) vertical stress (σ_0) (b) modulus of the elasticity of the masonry (E) with the highlighted values of the experimentally determined first $(f_{1,e})$ and second $(f_{2,e})$ natural frequency

4. Discussion

In the following figure (Figure 8.), the trend of changes in natural frequency values across iterations is presented. The initial models, based on different traditional boundary conditions, did not demonstrate satisfactory agreement between experimentally and numerically obtained frequency and mode shape values. Thus, updating FEM of masonry wall was performed using an automated Harmony Search optimization algorithm.

The first iteration focused on updating the stiffness of translational springs in the y-direction at the top and bottom of the wall, as well as the rotational springs around x axis at the same points, to more accurately simulate the actual boundary conditions. From the graphical representations of natural frequency variations relative to spring stiffness, it can be concluded that the translational springs in the y-direction have the greatest influence on frequency changes. The differences between experimentally and numerically obtained frequencies were 0.27% for the first mode shape and 3.70% for the second, indicating satisfactory results that justified the use of the developed model in the next iteration step. The second iteration examined the effect of varying the vertical stress on the masonry wall natural frequencies. Results showed that the natural frequency was not significantly affected by changes in vertical stress. Consequently, the vertical stress level was set to the values for which was shown that it minimize the residual between the second experimental and numerical natural frequencies. The third

Copyright © 2025 CroCEE
DOI: https://doi.org/10.5592/CO/3CroCEE.2025.44

iteration involved the final assessment of the masonry elasticity modulus, utilizing experimentally obtained modal characteristics. The differences between the experimental and numerical natural frequencies were 1.39% for the first and 0.83% for the second mode, with an elasticity modulus value of 1310 MPa. The difference between the adopted elasticity modulus, determined by calibrating the numerical model based on experimental results, and the modulus obtained through flat-jack testing was 6.33%.

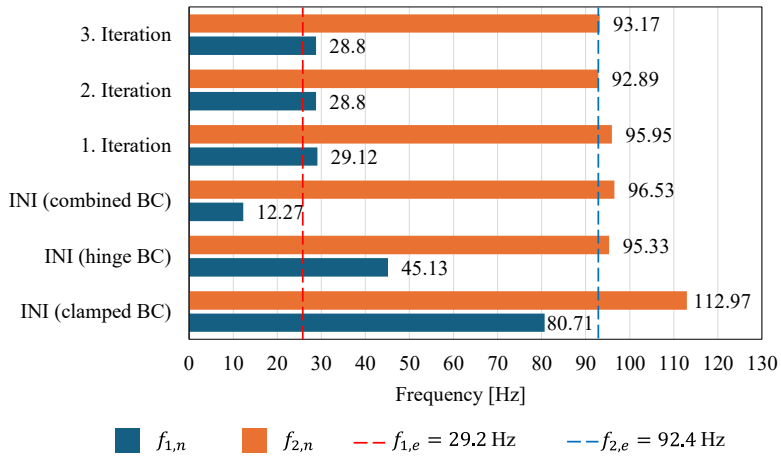


Figure 8. Changing in first $(f_{1,n})$ and second $(f_{2,n})$ numerically obtained natural frequency trough the performed iterations steps with the highlighted values of the experimentally determined first $(f_{1,e})$ and second $(f_{2,e})$ natural frequency

5. Conclusion

This paper presented an innovative approach for estimating the modulus of elasticity in masonry structures by integrating Operational Modal Analysis (OMA) with Finite Element Model Updating (FEMU). The methodology leverages dynamic parameters, such as natural frequencies and mode shapes obtained from OMA, to accurately update a numerical model of the masonry wall. The application of this approach to a real structure demonstrated that it is not only more efficient but also highly accurate, significantly reducing the need for invasive testing that could potentially damage the structure. Results from the optimization process, conducted using the Harmony Search algorithm, revealed that changes in the stiffness of translational springs in the y-direction had the most substantial impact on frequency variations. Although variations in vertical stress had a lesser effect on natural frequencies, the iterative calibration process effectively refined the mechanical property estimates. The modulus of elasticity obtained using the proposed approach differs only slightly from the value determined through the flat-jack method, demonstrating that this approach enables highly accurate estimation of the modulus of elasticity. The method offers a significant advantage in terms of precision and minimal structural impact, establishing itself as a robust alternative to conventional techniques for assessing the mechanical properties of earthquake-damaged masonry buildings.

Acknowledgements

This project has received funding from the European Union's Horizon 2020 research and innovation programme under the Marie Skłodowska-Curie grant agreement No [101151734].

References

[1] Lulić , L., Ožić , K., Kišiček , T., Hafner , I., Stepinac , M. (2021): Post-earthquake damage assessment-case study of the educational building after the zagreb earthquake. *Sustain.*, **13**,,

[2] Furtado , A., Rodrigues , H., Arêde , A., Varum , H. (2020): Mechanical properties characterization of different types of masonry infill walls. *Front. Struct. Civ. Eng.*, **14**, 411–434,

Copyright © 2025 CroCEE
DOI: https://doi.org/10.5592/CO/3CroCEE.2025.44

[3] Arêde , A., Almeida , C., Costa , C., Costa , A. (2019): In-situ and lab tests for mechanical characterization of stone masonry historical structures. *Constr. Build. Mater.*, **220**, 503–515,

[4] Vicente , R., Ferreira , TM., Mendes da Silva , JAR., Varum , H. (2015): In Situ Flat-Jack Testing of Traditional Masonry Walls: Case Study of the Old City Center of Coimbra, Portugal. *Int. J. Archit. Herit.*, **9**, 794–810,

[5] Carpinteri , A., Invernizzi , S., Lacidogna , G. (2009): Historical brick-masonry subjected to double flat-jack test: Acoustic emissions and scale effects on cracking density. *Constr. Build. Mater.*, **23**, 2813–2820,

[6] Stepinac , M., Kisicek , T., Renić , T., Hafner , I., Bedon , C. (2020): Methods for the assessment of critical properties in existing masonry structures under seismic loads-the ARES project. *Appl. Sci.*, **10**,,

[7] Debailleux , L. (2019): Schmidt hammer rebound hardness tests for the characterization of ancient fired clay bricks. *Int. J. Archit. Herit.*, **13**, 288–297,

[8] Matysek , P., Łątka , D. (2012): Comments on the application of the sclerometric method in the diagnostics of brick masonry..

[9] Marastoni , D., Benedetti , A., Pelà , L., Pignagnoli , G. (2017): Torque Penetrometric Test for the in-situ characterisation of historical mortars: fracture mechanics interpretation and experimental validation. *Constr. Build. Mater.*, **157**, 509–520,

[10] Palieraki , V., Vintzileou , E., Miltiadou-Fezans , A., Delinikolas , N. (2008): The use of radar techniques and boroscopy in investigating old masonry: The case of dafni monastery. *Int. J. Archit. Herit.*, **2**, 155–186,

[11] Arêde , A. … Gonçalves , R. (2017): Experimental characterization of the mechanical behaviour of components and materials of stone masonry railway bridges. *Constr. Build. Mater.*, **153**, 663–681,

[12] Martini , R., Carvalho , J., Barraca , N., Arêde , A., Varum , H. (2017): Advances on the use of non-destructive techniques for mechanical characterization of stone masonry: GPR and sonic tests. *Procedia Struct. Integr.*, **5**, 1108–1115,

[13] Strength estimation of concrete masonry units using stress-wave methods..

[14] Meola , C. (2007): Infrared thermography of masonry structures. *Infrared Phys. Technol.*, **49**, 228–233,

[15] Invernizzi , S., Lacidogna , G., Lozano-Ramírez , NE., Carpinteri , A. (2019): Structural monitoring and assessment of an ancient masonry tower. *Eng. Fract. Mech.*, **210**, 429–443,

[16] Ereiz , S., Duvnjak , I., Damjanović , D., Bartolac , M. (2021): Analysis of seismic action on the tie rod system in historic buildings using finite element model updating. *Buildings*, **11**,,

[17] Duvnjak , I., Ereiz , S., Smrkić , MF., Damjanović , D. (2023): Post-Earthquake Dynamic Performance of Intact Masonry Building Based on Finite Element Model Updating. *Appl. Sci.*, **13**, 9042,

[18] Zahid , F BIN., Ong , ZC., Khoo , SY. (2020): A review of operational modal analysis techniques for in-service modal identification. *J. Brazilian Soc. Mech. Sci. Eng.*, **42**, 398,

[19] Mottershead , J., Friswell , M. (2013): Finite Element Model Updating in Structural Dynamics. *Springer Sci. Bus. Media.*, **38**,.

[20] Ereiz , S., Duvnjak , I., Fernando Jiménez-Alonso , J. (2022): Review of finite element model updating methods for structural applications. *Structures*, **41**, 684–723,

Proceedings of the 3rd Croatian Conference on Earthquake Engineering - 3CroCEE
19–22 March 2025, Split, Croatia
Copyright © 2025 CroCEE
DOI: https://doi.org/10.5592/CO/3CroCEE.2025.48

EXPERIMENTAL TESTING OF CIRCULAR RC BRIDGE PIER MODELS SUPPORTING REFINED 3D MICRO-MODELING

Laurent Hakaj [(1)], Jelena Ristic [(2)], Toni Arangelovski [(3)], Danilo Ristic[(4)]

[(1)] *PhD student, Faculty of Civil Engineering, Ss. Cyril and Methodius University, Skopje, Republic of North Macedonia, e-mail: laurent.hakaj123@gmail.com*
[(2)] *Assoc. Prof. Dr. Sc., Faculty of Engineering, Department of Civil Engineering, International Balkan University (IBU), Skopje, Republic of North Macedonia, e-mail: risticjelenaibu@gmail.com*
[(3)] *Prof. Dr. Sc., Faculty of Civil Engineering, Ss. Cyril and Methodius University, Skopje, Republic of North Macedonia, e-mail: arangelovskitoni@gf.ukim.edu.mk*
[(4)] *Prof. Dr. Sc., Institute of Earthquake Engineering and Engineering Seismology (IZIIS), Ss. Cyril and Methodius University, Skopje, Republic of North Macedonia, e-mail: danilo.ristic@gmail.com*

Abstract

This paper shows the original results obtained from the realized laboratory tests of nonlinear response of the constructed typical large-scale prototype models of circular RC bridge piers under simulated interactive effects of earthquake-like cyclic horizontal loads and different levels of axial loads. Considering the obtained test results, the most important observations regarding refined analytical modeling and accurate earthquake response analysis of RC bridges can be briefly summarized: (1) The inelastic behaviour of reinforced concrete bridge piers is characterized by a variety of complex influencing phenomena directly resulting from the successive degradation of mechanical properties of the used steel and concrete material. The complex inelastic material response mainly results from the induced complex interactive effects of vertical and horizontal loading. To achieve a realistic analytical simulation of such a complex nonlinear process, the effects of the most important influencing factors should be analytically modeled. This can be achieved through the development of an experimentally proved advanced nonlinear (micro) analytical model based on the results obtained from the conducted representative experimental tests. (2) The presented experimental results indicate that the inelastic behaviour of the tested RC bridge pier models is directly affected by their actual geometry and by the applied level of axial load. The earthquake-induced large time-variation of axial forces in critical bridge piers can introduce complex effects on the overall inelastic structural response. To predict the inelastic earthquake response of specific bridges involving large spans and very tall RC bridge towers, the analytical model should be capable of accounting for the induced instantaneous interactive effects of bending and time-varying axial forces. The development of an advanced nonlinear analytical 3D micro-model to realistically simulate the above-stated complex phenomena represents the specific study objective of the next research phase.

Keywords: bridge, concrete, column, nonlinear response, bending forces, axial forces

1. Introduction

Based on damage observations following strong earthquakes that occurred in the past, it was confirmed that the existing RC bridge piers were commonly exposed to the critical interactive effects of induced cyclic bending and varying axial loads [1-6]. The interactive effects of bending and varying axial loads are particularly relevant and can be critical in the case of modern large-span cable-stayed or cable-suspended bridges having very high RC bridge piers (towers), often constructed with a specific A-shaped geometry [7-10]. Due to this specific axial loading phenomenon, severe damages were also observed to the most frequent regular multi-span RC girder bridges during past earthquakes. These types of bridges are commonly supported by piers with different but harmonized stiffness characteristics, representing a combination of long or flexural failure bridge piers and short or shear failure bridge piers. Heavy damages to bridge structures were recorded almost in all seismic regions worldwide. Different types of damages are evident as shown in many published reports about each

Proceedings of the 3rd Croatian Conference on Earthquake Engineering - 3CroCEE
19–22 March 2025, Split, Croatia
Copyright © 2025 CroCEE
DOI: https://doi.org/10.5592/CO/3CroCEE.2025.48

specific event, for example, the earthquake in Japan [1], the earthquake in Chile [2], the earthquakes in the USA and in China [3], etc.

Renowned research centers worldwide have been performing continuous research toward reducing catastrophic earthquake consequences through the improvement of regulations for the design and construction of structures in seismically active regions [11-17]. Recently, extensive research involving shaking table tests on large-scale models has been conducted by the second and the fourth author and their collaborators, mainly targeted to seismic upgrading of isolated structures with specific energy dissipation devices, [18-24]. Shaking table tests of scaled bridge models have intensively been carried out by many researchers, [25-26], exploring the established, practically applicable model similarity conditions [27].

The presented experimental testing of circular RC bridge pier models was conducted to generate original background experimental data supporting the development of a refined analytical 3D micro-model. The study results will contribute to the improvement of the seismic design and seismic safety of RC columns of common bridges and also of very tall RC towers (often taller than 100 m) supporting large-span cable-stayed or suspended bridges. The presented extensive and original experimental tests of the constructed large-scale circular RC bridge prototype models were performed at the RESIN Laboratory, Skopje, established as a regional research centre by Prof. D. Ristic, (PPD project director), in the framework of the innovative NATO Science for Peace and Security Project: Seismic Upgrading of Bridges in South-East Europe by Innovative Technologies (SFP: 983828).

2. Study Objectives

Bending rarely occurs in reinforced concrete members without axial load being present. In the case of columns, dominant axial loads exist even initially, while very large bending moments can be additionally imposed during structural earthquake response, producing stress-strain state beyond material elastic limit. Reinforced concrete members decrease their stiffness with the development of cracks in concrete and plastic strains in steel. However, many structures could have avoided severe damages or total collapse during past strong earthquakes, with induced loads that were even larger than the design ones, because of the favorable nonlinear characteristics of their reinforced concrete members. To introduce effective and rational earthquake-resistant design of reinforced concrete structures, an understanding of the real inelastic response characteristics of the structural members appears to be essential. The most convenient method to achieve this goal is experimental testing of various reinforced-concrete members under expected loading conditions. The nonlinear behaviour testing is especially useful because the obtained experimental results may be widely applied:

- to evaluate the seismic performances of newly designed reinforced-concrete structural members under realistically simulated expected loading patterns;
- to provide necessary evidence for calibration and improvement of existing seismic design regulations, and
- to generate a sufficient volume of representative experimental data needed for the development and verification of analytical predictive models, etc.

Although numerous experimental investigations were conducted in the past, the urgent need for further experimental studies and advanced analytical modeling of the inelastic behaviour of reinforced-concrete members under various loading conditions has been pointed out by many researchers. To solve complex design problems of modern structures, an advanced analytical model applicable for the realistic simulation of complex inelastic response of reinforced concrete columns is needed. The conducted extensive experimental research was mainly directed to such specific study objectives.

3 Testing of Circular RC Flexural Failure Bridge Pier Models

3.1 Circular RC Flexural Failure Prototype Models

Copyright © 2025 CroCEE
DOI: https://doi.org/10.5592/CO/3CroCEE.2025.48

The presented experimental program involving laboratory testing of reinforced concrete flexural failure (FF) bridge pier models was elaborated based on consideration of various representative design and testing aspects, including: (1) selection of circular cross-section of the piers because it is frequently applied in real bridge structures as a very convenient shape from structural, aesthetic and hydraulic point of view; (2) consideration of long, or flexural failure bridge prototype models (Ml-A and M1-B) because their application is common in bridges located in seismic areas and it is important to experimentally test their inelastic response and failure modes under interactive loads; (3) selection of cantilever type bridge piers for testing, simulating fixation in the footings and hinges at the top, because this type of connection represents the main differences between bridge piers and building columns. In practice, hinge conditions at the top of the piers are usually provided by the installation of bridge bearings, supporting the superstructure mass; (4) consideration of piers' aspect ratio of H/D = 6.22 to investigate the characteristics of the dominant flexural failure during their inelastic response. The symbols D and H represent the pier diameter and distance between the pier fixation level and the level of applied lateral load, respectively; (5) assuming the same design conditions for both tested flexural failure models, M1-A and M1-B including, geometry, concrete class, reinforcement arrangement, laboratory test set-up, etc., to study the effect of different levels of applied axial loads on the hysteretic response of the piers, and (6) design of adequate and identical pin-type mechanisms for application of axial and cyclic lateral loads, and identical fixation system of the footings to provide realistic simulation of loading of the piers in laboratory conditions.

The geometrical properties of the model, the reinforcing steel layout and the designed elements for application of reversed cyclic lateral and compressive vertical load are presented in Fig. 1.

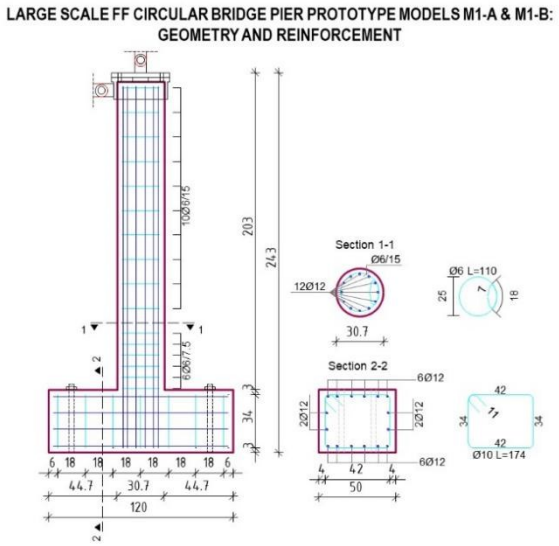


Figure 1. Geometry and reinforcement of the tested flexural failure circular RC bridge pier prototype models M1-A and M1-B.

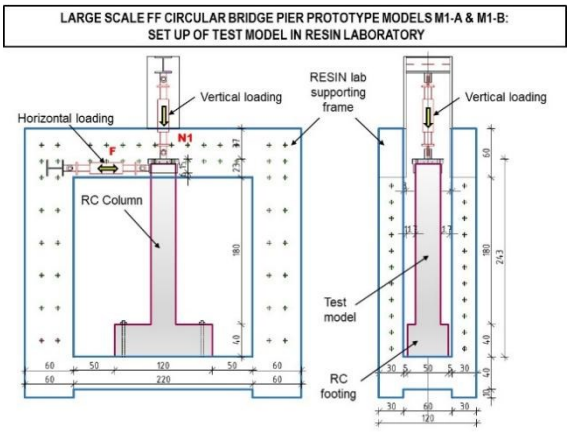


Figure 2. Set-up of flexural failure circular RC bridge pier models M1-A and M1-B in the RESIN laboratory testing frame.

The pier body was designed to be 200 cm in height and 30.7 cm in diameter and be fixed in the reinforced-concrete footing with dimensions 120 x 50 x 40 cm. Four circular holes were provided at both sides of the footing and used to fix it to the laboratory stiff testing frame. A square steel plate, 400 x 400 x 30 mm, was anchored at the top of the pier. In the steel plate, a central hole of 120 mm in diameter was provided for casting of the RC concrete column in a vertical position. Additional four holes ϕ30 mm at the steel plate corners were used for connecting the pin-joint device to the hydraulic actuator for the application of the axial load. A similar pin-joint device was installed between the iron ring placed at the upper end of the pier and the hydraulic actuator for application of reversed lateral force. There was a longitudinal reinforcement of 12 ϕ 12 mm steel bars, grade 240/360, providing a

Copyright © 2025 CroCEE
DOI: https://doi.org/10.5592/CO/3CroCEE.2025.48

percentage of reinforcement of 1.83 in total. Transverse reinforcement was provided by single stirrups (hoops) 6 mm in diameter, placed at a distance of 7.5 cm near the fixed end, the expected plastic hinge region, and at a distance of 15 cm in the remaining part of the pier. The reinforcement of the footings consisted of 16 ϕ 12 mm steel bars, confined by stirrups placed at a distance of 18 cm. The volumetric ratio of the pier transverse reinforcement at the fixed end region was p_s = 0.00395, and half of this was in the remaining part. After arrangement of the reinforcing steel, it was placed in the previously prepared steel forms, equipped with mechanisms for easy assembling and disassembling. Casting of the concrete was carried out in a vertical position and an internal vibrator was used for its compaction. River gravel with a maximum grain size of D = 16 mm was applied, while its remaining characteristics (strength, grain size distribution, etc.) were designed based on the existing design requirements. Portland cement with attested quality was applied for concrete preparation. Concrete compressive strength was determined as an average value of the tested sample cubes proportioned 20 x 20 x 20 cm, taken during the casting of the specimens. The average concrete compressive strength amounted to 45.6 MPa. The typical set-up of the flexural failure circular RC bridge pier models M1-A and M1-B in the RESIN laboratory stiff testing frame is shown in Figure 2.

3.2 Testing Program and Results from Cyclic Tests of FF Prototype Models

For experimental testing of the prototype model M1-A, the laboratory testing frame was used, Fig. 2. The experimental test was carried out under the simulated effect of constant vertical and cyclic horizontal load. As shown in Fig. 1, a vertical compressive load was applied upon the RC column with intensity N1 = 149.0 kN by using the respective hydraulic actuator. A horizontal reversed cyclic load was applied by using the horizontal hydraulic actuator located at the top of the circular RC column model. The loading process upon experimental model M1-A was realized in two loading phases. In the first phase, a vertical load was slowly applied with an incremental increase of loading of the RC column at each successive discrete step. Following the achievement of the assigned constant value of vertical load N1 = 149.0 kN, loading in the second phase was continued by the application of cyclic horizontal loading. The cyclic loading of the model was efficiently provided through the successively applied positive and negative displacement increments, according to the prescribed full history of cyclic displacements. To provide insight into the development of cracks in concrete, very small but well-adjusted displacement increments were applied.

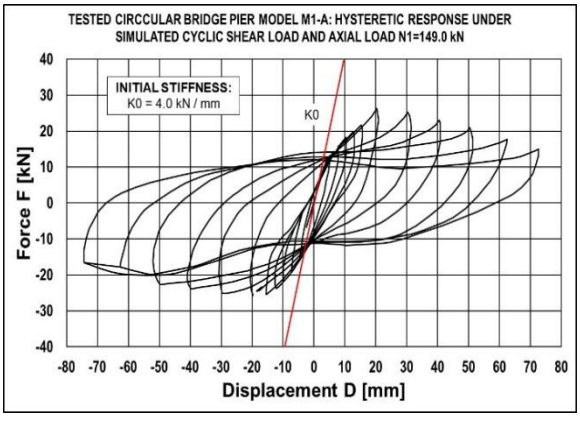


Figure 3. Hysteretic response of RC model M1-A tested under interactive effects of cyclic horizontal and vertical load N1 = 149.0 kN.

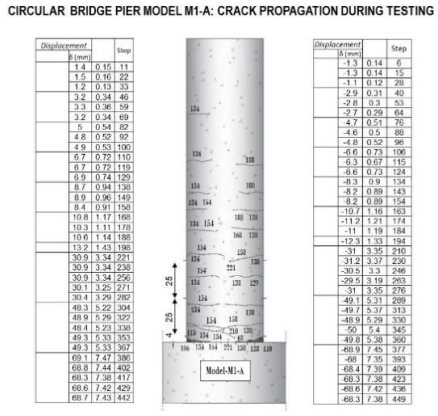


Figure 4. Typical propagation of cracks in concrete during experimental testing of flexural failure RC prototype model M1-A.

During the tests, the applied electronic instrumentation system provided acquisition of a large set of numerical values of measured quantities, including the measured values of displacements Di (mm) and corresponding restoring force Fi (kN) at each loading step. Using the recorded numerical values of force and displacement, the hysteretic nonlinear response of the tested experimental model M1-A was obtained for a quite large range of cyclic deformations, Fig. 3. The obtained hysteretic relationship very successfully represents the real nonlinear response of the tested model considering that almost

Copyright © 2025 CroCEE
DOI: https://doi.org/10.5592/CO/3CroCEE.2025.48

symmetrical hysteretic relationship was obtained in the domain of positive and negative deformations. The resulting hysteretic relationship was used to obtain the representative envelope curve and to successfully define the major envelope segments for the positive and the negative sides with defined characteristic points Y, U and L that were also almost symmetrical, Fig. 7. Point Y represents the yielding point, point U indicates the recorded maximum value of the restoring force F, whereas point L defines the maximum deformation D. Generally, the obtained hysteretic relationship points to a very stable nonlinear response and expected good ductility of the experimentally tested prototype model M1-A. Fig. 4 graphically shows the pattern of the recorded propagation of initial and enlarged cracks in concrete during the experimental testing of flexural failure RC prototype model M1-A.

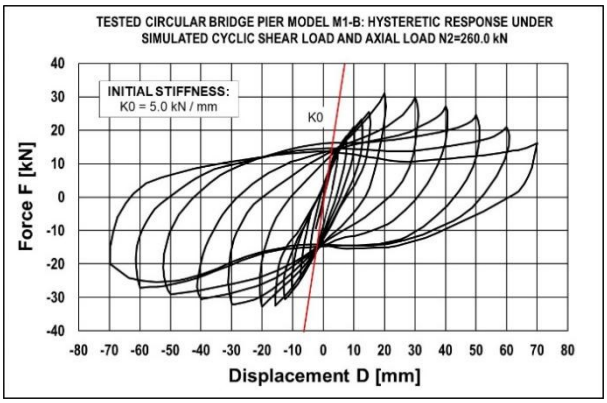


Figure 5. Hysteretic response of RC model M1-B tested under interactive effects of cyclic horizontal and vertical load N2 = 260.0 kN.

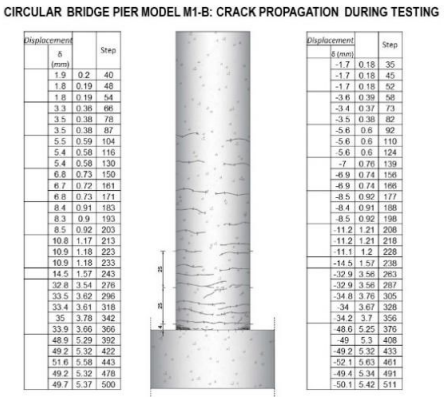


Figure 6. Typical propagation of cracks in concrete during experimental testing of flexural failure RC prototype model M1-B.

Similarly, the loading process upon experimental model M1-B was realized also in two loading phases. After achieving the prescribed larger value of vertical load N2 = 260.0 kN, loading in the second phase was continued with the application of cyclic horizontal loading. Using the recorded time histories of force and displacement, the hysteretic response of the tested experimental model M1-B was obtained and presented in Fig. 5. From the resulting hysteretic relationship, the representative envelope curve was obtained for the positive and the negative displacements with defined characteristic points Y, U and L that were also almost symmetrical, Fig. 7. Fig. 6 graphically shows the crack propagation pattern in concrete during the experimental testing of the flexural failure RC prototype model M1-B.

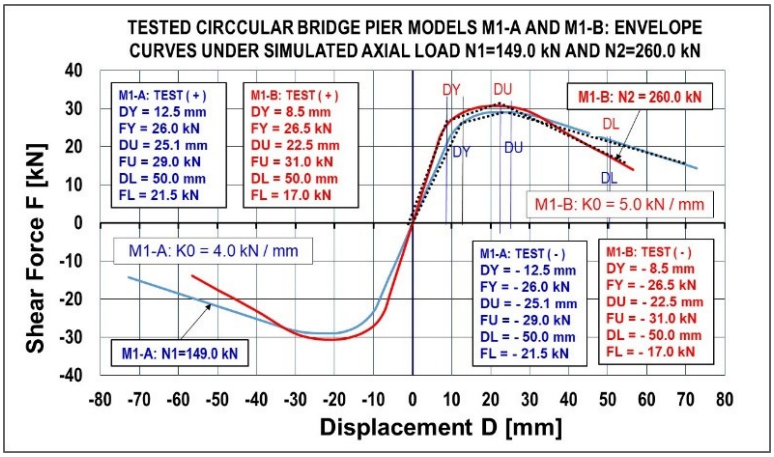


Figure 7. Comparative envelope curves recorded from the tests on models M1-A and M1-B under simulated interactive effects of cyclic horizontal load and vertical loads N1 = 149.0 kN and N2 = 260.0 kN.

Copyright © 2025 CroCEE
DOI: https://doi.org/10.5592/CO/3CroCEE.2025.48

• ***Observation from experimental testing of FF models:*** Based on the original results obtained from the conducted experimental tests on circular RC flexural failure bridge pier prototype models, important observations can be derived. Considering the comparatively presented envelope curves in Fig. 7 for the tested FF models M1-A and M1-B under simulated interactive effects of cyclic horizontal and vertical loads at two levels, N1 = 149.0 kN and N2 = 260.0 kN, significant differences are evident.

(a) The plotted load-displacement hysteretic relationships for both flexural failure (FF) specimens indicate a recorded greater initial stiffness and larger lateral load-carrying capacity of the model tested under higher axial load.

(b) However, in the range characterized by imposed larger displacement, typical for structural response due to strong ground motion, a higher applied axial load produced more intensive degradation of the model ductility and ultimate lateral load carrying capacity.

(c) The observation mentioned under (b) points out the high importance of taking into account the actual level of the imposed axial loads in the analysis of the inelastic earthquake response of reinforced concrete structures. This is especially important for structures exposed to severe earthquakes when during large inelastic deformations, there is a high variation of axial forces.

(d) The experimental results show that the inelastic behaviour of the critical cross-sections can be greatly affected by the level of applied axial load. The resulting moment-curvature relationship for the critical cross-sections will show a similar tendency as the previously presented one for the load - displacement response. Then, in practice, it is equally important to calculate the hysteretic response of the RC sections considering the interactive effects of bending and varying axial loads.

(e) The change in axial load mainly influences the inelastic responses of the RC columns due to the following two effects: (1) the effect of the initially induced different stress-strain state in concrete and reinforcing steel, and (2) the effect of the induced additional moment along the member due to the imposed lateral displacement, commonly referred to as the P-delta effect.

(f) During nonlinear cyclic tests of circular RC flexural failure bridge pier models, the orientation of the cracks in concrete in a horizontal direction was generally recorded. The recorded generally horizontal cracks mainly resulted from the dominant effect of bending loads.

4 Testing of Circular RC Shear Failure Bridge Pier Models

4.1 Circular RC Shear Failure Prototype Models

The second experimental program involving laboratory testing of reinforced concrete shear failure (SF) bridge pier models was elaborated based on consideration of identical all basic design parameters.

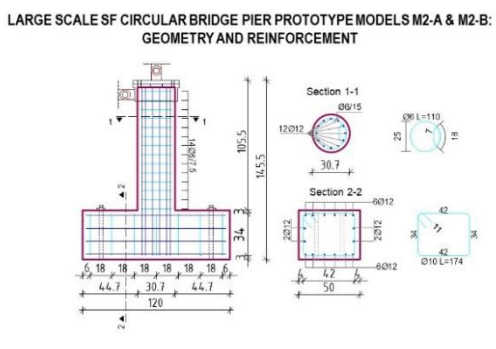


Figure 8. Geometry and reinforcement of the tested shear failure circular RC bridge pier prototype. Models M2-A and M2-B.

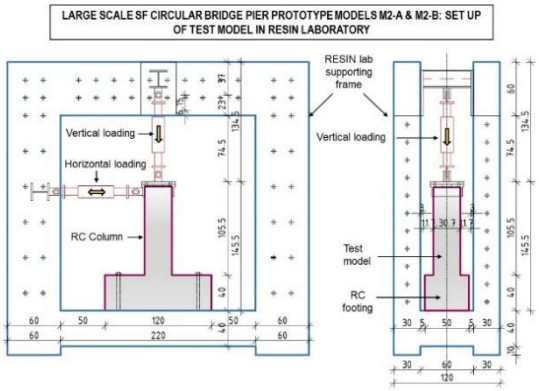


Figure 9. Set-up of the shear failure circular RC bridge pier models M2-A and M2-B in the RESIN laboratory testing frame.

Copyright © 2025 CroCEE
DOI: https://doi.org/10.5592/CO/3CroCEE.2025.48

Actually, the pier geometry, concrete class, reinforcement arrangement and laboratory test set-up were considered identical to provide conditions to evaluate the effect of the defined identical set of different levels of applied axial loads on hysteretic response. However, for comparative purposes, in the design of short or shear failure bridge prototype models (M2-A and M2-B), only their different height was considered, Fig. 8. The typical set-up of shear failure circular RC bridge pier models M2-A and M2-B is shown in Fig. 9. The term shear failure models refers to short piers where, besides flexural deformations, shear deformations produce a very significant effect on their hysteretic response.

4.2 Testing Program and Results from Cyclic Tests of SF Prototype Models

To perform experimental testing of prototype models M2-A and M2-B, the respective connections and the laboratory testing frame were properly adjusted and used, Fig. 9. The first experimental test of prototype models M2-A, representing shear failure specimens, was carried out under the simulated effect of constant vertical and cyclic horizontal load. The vertical compressive load upon the RC column model M2-A was applied with lower intensity N1 = 149.0 kN using the respective hydraulic actuator. Using the recorded time histories of force and displacement, the hysteretic nonlinear response of the tested experimental model M2-A was obtained and it is presented in Fig. 10.

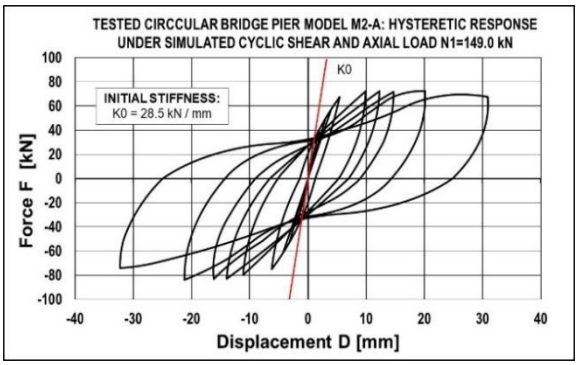


Figure 10. Hysteretic response of RC model M2-A tested under interactive effects of cyclic horizontal and vertical load N1 = 149.0 kN.

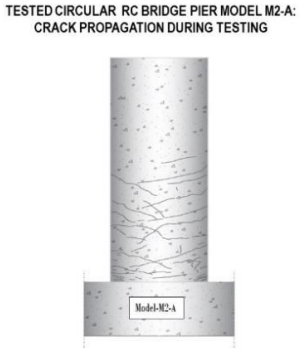


Figure 11. Typical propagation of cracks in concrete during experimental testing of shear failure RC prototype model M2-A.

The resulting, nearly symmetrical hysteretic relationship was used to define the representative envelope curve with the respective characteristic points Y, U and L that were also almost symmetrical, Fig. 14. Fig. 11 graphically shows the pattern of the recorded cracks in concrete during the experimental testing of the shear failure RC prototype model M2-A.

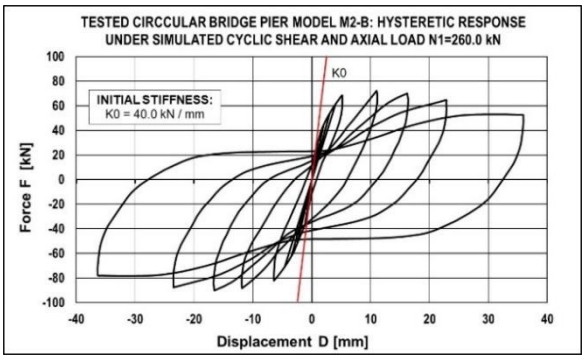


Figure 12. Hysteretic response of RC model M2-A tested under interactive effects of cyclic horizontal and vertical load N1 = 149.0 kN.

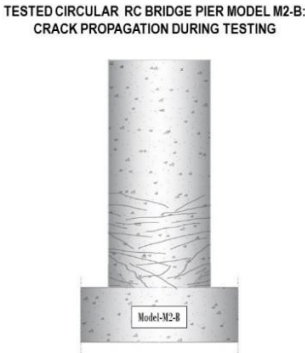


Figure 13. Typical propagation of cracks in concrete during experimental testing of shear failure RC prototype model M2-A.

Copyright © 2025 CroCEE
DOI: https://doi.org/10.5592/CO/3CroCEE.2025.48

The recorded pattern of cracks in this case is very complex due to the complex mixed effect of bending and shear deformations. Analogously, the loading process upon experimental model M2-B was realized also in two loading phases. After the prescribed larger value of vertical load N2 = 260.0 kN was applied, loading in the second phase was continued with the application of cyclic horizontal loading. Using the recorded time histories of force and displacement, the hysteretic response of the tested experimental model M2-B was obtained and it is presented in Fig. 12. From the resulting hysteretic relationship, the representative envelope curve was obtained for the positive and the negative displacements with defined characteristic points Y, U and L that were also almost symmetrical, Fig. 14. Fig. 13 graphically shows the crack pattern recorded during testing of the RC shear failure prototype model M2-B.

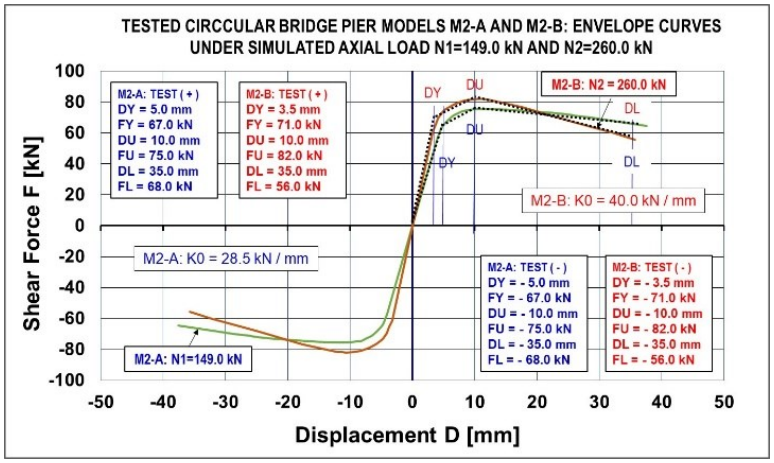


Figure 14. Comparative envelope curves recorded from the tests on models M2-A and M2-B under simulated interactive effects of cyclic horizontal load and vertical loads N1 = 149.0 kN and N2 = 260.0 kN.

• ***Observation from experimental testing of SF models:*** Considering the results obtained from the experimental testing of circular RC shear failure bridge piers prototype models, respective conclusions were drawn. From the comparatively presented envelope curves in Fig, 14, for models M2-A and M2-B tested under simulated cyclic horizontal and vertical loads at two levels, N1 = 149.0 kN and N2 = 260.0 kN, significant differences were also recorded.

(a) The presented load - displacement relationships for both tested shear failure models in Fig. 14, clearly indicate a greater initial stiffness and a larger lateral load carrying capacity in the case of the specimen tested under higher axial load.

(b) However, in the domain characterized with larger displacements, the higher applied axial load produced more intensive degradation of the lateral load capacity. This is specifically important in the cases where the induced inelastic deformations are large and the variation of axial forces is high.

(c) The experimental results show that the effect of shear deformations in this case is very significant, since a very complex pattern of cracks was recorded. Therefore, the commonly computed moment-curvature relationship for the critical cross-sections will be incorrect.

(d) The change in axial load and height of the specimens mainly influences the inelastic responses of the SF models due to the following effects: (1) the effect of the initially induced different stress-strain state in concrete and reinforcing steel, and (2) the effect of the induced large shear deformations due to the effective shear force.

(d) During nonlinear cyclic tests of circular RC shear failure bridge pier models, a complex orientation of cracks was recorded. Suh complex pattern of cracks mainly resulted from the dominant integrative effect of shear and bending deformations.

Copyright © 2025 CroCEE
DOI: https://doi.org/10.5592/CO/3CroCEE.2025.48

• ***Observation from experimental testing of FF and SF models:*** Considering the integral results obtained from the conducted experimental testing of RC flexural failure and shear failure bridge pier prototype models, very important observations were made. From the comparatively presented envelope curves in Fig, 15, for the FF models M1-A and M1-B and for the SF model M2-A and M2-B tested under simulated cyclic horizontal and different vertical loads N1 = 149.0 kN and N2 = 260.0 kN, very significant differences were recorded.

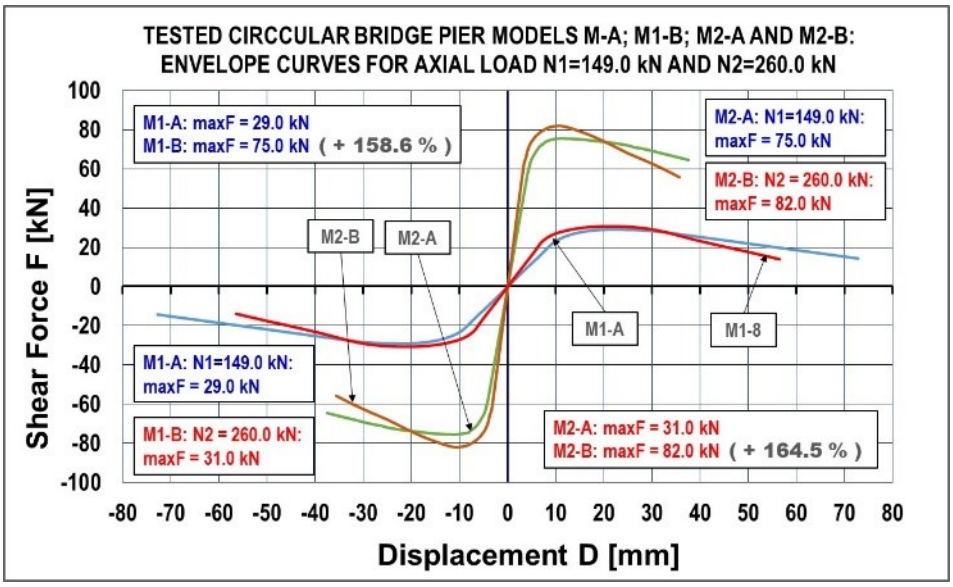


Figure 15. Comparative overview of the recorded nonlinear envelope curves from the experimentally tested flexural failure and shear failure RC bridge pier prototype models under simulated effects of cyclic horizontal and different levels of vertical loads N1 = 149.0 kN and N2 = 260.0 kN

The presented original experimental results obtained from the conducted extensive laboratory tests on large-scale RC flexural and shear failure bridge pier models are directly expressing the high importance of the presented extensive experimental research. Derived from the conducted experimental study was an essential experimental database needed for advancing modern practical applications and for the development of advanced nonlinear analytical micro-models.

5 Conclusions

Analyzing the comparatively obtained original experimental results from the performed experimental testing of circular RC flexural failure and shear failure bridge pier models, several very important conclusions are drawn: (1) The recorded hysteretic responses of the FF bridge pier models show a very good symmetry, stable hysteretic cyclic curves and very good ductility. The hysteretic relationships of the model tested under higher axial load indicate a greater initial stiffness and a larger lateral load capacity. However, in the range of larger displacement, the higher axial load produced more intensive degradation of the model ductility and ultimate lateral load carrying capacity; (2) The hysteretic responses of the SF bridge pier models show a similar behaviour tendency. The envelope curve of the model tested under a higher axial load also indicates a greater initial stiffness and a larger lateral load capacity, but in the range of the larger displacement, the higher axial load produced more intensive degradation of the ductility and lateral load-bearing capacity. However, compared to the FF models, the tested SF bridge pier models showed a much higher lateral load-bearing capacity ranging up to 164.5 %. (3) The recorded initial stiffness of the FF and SF bridge pier models was continuously reduced with the increase of deformations and became increasingly smaller during larger deformations, reaching the zero value at point “U”. The repeated cyclic curves evidently show the regularity of the stiffness deterioration regarding the repeated segments of loading and unloading; (4) The first initiation and

Copyright © 2025 CroCEE
DOI: https://doi.org/10.5592/CO/3CroCEE.2025.48

propagation of cracks in the tested FF bridge pier models occur in the critical tension zones located in the segments close to the fixations of the columns into the RC foundation. During the experimental tests of the prototype models M1-A and M1-B, nearly identical wider zones of occurrence of cracks in concrete were recorded. The orientation of the cracks in this case was dominantly horizontal; (5) In the case of the tested SF bridge pier models, the propagation of cracks occurred with different patterns but also in critical zones located close to the fixations of the columns into the RC foundation. During the experimental tests of the prototype models M2-A and M2-B, similar wider zones of occurrence of cracks in concrete were recorded. The orientation of cracks, in this case, was very complex due to the dominant effect of shear deformations; (6) The obtained original experimental results regarding the nonlinear behaviour characteristics of the tested RC circular FF and SF bridge pier prototype models represent a unique and harmonized database of great importance for experimental validation of the formulated advanced nonlinear analytical micro-models.

Acknowledgements

The experimental tests of the constructed large-scale circular RC bridge prototype models were performed in the RESIN Laboratory, Skopje, established as a regional research centre by Prof. Danilo Ristic, PPD, in the framework of the innovative NATO Science for Peace and Security Project: *Seismic Upgrading of Bridges in South-East Europe by Innovative Technologies (SFP: 983828).* The authors express sincere thanks for the extended cooperation in the testing research.

REFERENCES

[1] Kazuhiko Kawashima, Kenji Kosa, Yoshikazu Takahashi, Mitsuyoshi Akiyama, Tsutomu Nishioka, Gakuho Watanabe, Hirohisa Koga, and Hiroshi Matsuzaki (2011) Damage of Bridges During 2011 Great East Japan Earthquake.

[2] Denis Mitchell, Sharlie Huffman, Robert Tremblay, Murat Saatcioglu, Dan Palermo, René Tinawi, and David Lau. (2010) Damage to Bridges due to the 27 February 2010 Chile Earthquake1, Accepted 5 April 2012: www.nrcresearchpress.com/cjce on June 2012

[3] Wang, Z.; Lee, G.C. A Comparative Study of Bridge Damage Due to the Wenchuan, Northridge, Loma Prieta and San Fernando Earthquakes. Earthq. Eng. Eng. Vib. 2009, 8, 251–261. [CrossRef]

[4] Hashimoto, S.; Abe, M.; Fujino, Y. Damage Analysis of Hanshin Expressway Viaducts during 1995 Kobe Earthquake. III: Three-Span Continuous Girder Bridges. J. Bridge Eng. 2005, 10, 61–68. [CrossRef]

[5] Han, Q.; Du, X.; Liu, J.; Li, Z.; Li, L.; Zhao, J. Seismic Damage of Highway Bridges during the 2008 Wenchuan Earthquake. Earthq. Eng. Eng. Vib. 2009, 8, 263–273. [CrossRef]

[6] Wotherspoon, L.; Bradshaw, A.; Green, R.; Wood, C.; Palermo, A.; Cubrinovski, M.; Bradley, B. Performance of Bridges during the 2010 Darfield and 2011 Christchurch Earthquakes. Seismol. Res. Lett. 2011, 82, 950–964. [CrossRef]

[7] Zhu, J.; Zhang, W.; Zheng, K.F.; Li, H.G. Seismic Design of a Long-Span Cable-Stayed Bridge with Fluid Viscous Dampers. Pract. Period. Struct. Des. Constr. 2016, 21, 04015006. [CrossRef]

[8] Li, X.; Li, J.; Zhang, X.; Gao, J.; Zhang, C. Simplified Analysis of Cable-Stayed Bridges with Longitudinal Viscous Dampers. ECAM 2020, 27, 1993–2022. [CrossRef]

[9] Xu, Y.; Tong, C.; Li, J. Simplified Calculation Method for Supplemental Viscous Dampers of Cable-Stayed Bridges under Near-Fault Ground Motions. J. Earthq. Eng. 2021, 25, 65–81. [CrossRef]

[10] Abdel Raheem, S.E.; Hayashikawa, T.; Dorka, U. Ground Motion Spatial Variability Effects on Seismic Response Control of Cable-Stayed Bridges. Earthq. Eng. Eng. Vib. 2011, 10, 37–49. [CrossRef]

[11] Nigel Hewson and Gerard Parke, (2008) ICE Manual of Bridge Engineering, Second Edition, Published by Thomas Telford Ltd, 1 Heron Quay, London E14 4JD, UK. www.thomastelford.com.

[12] American Association of State Highway and Transportation Officials. AASHTO Guide Specifications for LRFD Seismic Bridge Design, 2nd ed.; American Association of State Highway and Transportation Officials: Washington, DC, USA, 2011; ISBN978-1-56051-521-0.

Copyright © 2025 CroCEE
DOI: https://doi.org/10.5592/CO/3CroCEE.2025.48

[13] Chen, W. F. and Duan, L. [2000] Bridge Engineering, Handbook (CRC Press).

[14] EC8 [1994] Eurocode 8 Design Provisions for Earthquake Resistence of Structures — Part 1-1: Seismic Actions and General Requirements of Structures, ENV 1998-1-1; Part 2: Bridges, ENV 1998-2, Comite Europeen de Normalisation, Brussels.

[15] Wilson, E.L. Three-Dimensional Static and Dynamic Analysis of Structures; Computers and Structures: Walnut Creek, CA, USA, 2001.

[16] Xiang, N.; Goto, Y.; Obata, M.; Alam, M.S. Passive Seismic Unseating Prevention Strategies Implemented in Highway Bridges: A State-of-the-Art Review. Eng. Struct. 2019, 194, 77–93. [CrossRef]

[17] Kowalsky, M. J. and Priestley, M. J. N. [2000] "Improved Analytical Model for Shear Strength of Circular Reinforced Concrete Columns in Seismic Regions," ACI Structural Journal 97(3), 388–396

[18] Ristic, J., Misini, M., Ristic, D., Guri, Z., Pllana, N. (2017): Seismic Upgrading of Isolated Bridges with SF-ED Devices: Shaking Table Tests of Large-Scale Model, *Gradjevinar*, 2147-2017. [DOI]

[19] Ristic, J., Brujic, Z., Ristic, D., Folic, R., Boskovic, M. (2021): Upgrading of Isolated Bridges with Space-Bar Energy-Dissipation Devices: Shaking Table Test, Advances in Structural Engineering, June 23, 2021; pp. 2948–2965.

[20] Ristic, J. (2016): Modern Technology for Seismic Protection of Bridge Structures Applying Advanced System for Modification of Earthquake Response, PhD Thesis, Institute of Earthquake Engineering and Engineering Seismology (IZIIS), "SS Cyril and Methodius" University, Skopje, Macedonia.

[21] Ristic, D. (1988): Nonlinear Behavior and Stress-Strain Based Modeling of Reinforced Concrete Structures under Earthquake Induced Bending and Varying Axial Loads, Doctoral Dissertation, School of Civil Engineering, Kyoto University, Japan.

[22] Ristic, D., Ristic J. (2012): Advanced Integrated 2G3 Response Modification Method for Seismic Upgrading of New and Existing Bridges, 15th World Conf. on Earthquake Engineering, (WCEE), Lisbon.

[23] Ristic, J., Ristic D., Behrami, R., Hristovski, V., (2024): Adaptive Seismic Upgrading of Isolated Bridges with C-Gapped Devices: Model Testing, Civil Engineering Journal, Vol. 10, No. 09, September, 2024.

[24] Ristic, J., Veseli V., Misini, L., Ristic, D., (2023): Seismic Potection of Masonry and Infilled Frame Buildings Using Upgraded Sliding Isolation System with SF Devices, Proceedings of the 2nd Croatian Conference on Earthquake Engineering - 2CroCEE, Zagreb, Croatia - March 22 to 24, 2023.

[25] Guo, W.; Li, J.; Guan, Z. Shake Table Test on a Long-Span Cable-Stayed Bridge with Viscous Dampers Considering Wave Passage Effects. J. Bridge Eng. 2021, 26, 04020118. [CrossRef]

[26] H. Sun, B. Li, K. Bi, N. Chouw, J. W. Butterworth and H. Hao, (2011) Shake Table Test of a Three-Span Bridge Model, Proceedings of the Ninth Pacific Conference on Earthquake Engineering, Auckland, New Zealand.

[27] Candeias, P., Costa, A. C., Coelho, E. (2004): Shaking Table Tests of 1:3 Reduced Scale Models of Four-Story Unreinforced Masonry Buildings, 13th World Conference on Earthquake Engineering, Vancouver, Paper: 2199.

Proceedings of the 3rd Croatian Conference on Earthquake Engineering - 3CroCEE
19–22 March 2025, Split, Croatia
Copyright © 2025 CroCEE
DOI: https://doi.org/10.5592/CO/3CroCEE.2025.52

PROTECTION OF SENSITIVE INFILL IN FRAME BUILDINGS USING SB-UPGRADED ISOLATION SYSTEM: SEISMIC TESTS OF MODEL

Ilir Canaj[(1)], Jelena Ristic [(2)], Elena Dumova-Jovanoska [(3)], Danilo Ristic[(4)]

[(1)] *PhD student, Faculty of Civil Engineering, Ss. Cyril and Methodius University, Skopje, Republic of North Macedonia, e-mail: ilirshcanaj@gmail.com*
[(2)] *Assoc. Prof. Dr. Sc., Faculty of Engineering, Department of Civil Engineering, International Balkan University (IBU), Skopje, Republic of North Macedonia, e-mail: risticjelenaibu@gmail.com*
[(3)] *Prof. Dr. Sc., Faculty of Civil Engineering, Ss. Cyril and Methodius University, Skopje, Republic of North Macedonia, e-mail: dumova@gf.ukim.edu.m*
[(4)] *Prof. Dr. Sc., Institute of Earthquake Engineering and Engineering Seismology (IZIIS), Ss. Cyril and Methodius University, Skopje, Republic of North Macedonia, e-mail: danilo.ristic@gmail.com*

Abstract

This article presents an innovative construction system that provides efficient earthquake protection for sensitive infill panels in RC frame buildings. With qualitative upgrading of buldog sliding base (SB) isolation system by incorporated novel uniform C-gaped energy dissipation devices, created was the new advanced sliding base C-gaped (SBC) system for seismic protection of buildings. Capability of the new seismic protection system of masonry infilled frame buildings was demonstrated with the conduccted extensive seismic shaking table tests of large-scale model constructed with application of sliding base isolation system and created uniform C-gaped energy dissipation devices. The specific research segment devoted to development of the present SBC upgraded building system was originally initiated by the second and the fourth author and represent a part of the integral research project realized in the Institute of Earthquake Engineering and Engineering Seismology (IZIIS), Ss. Cyril and Methodius University in Skopje, during three and a half years research in the frames of the innovative NATO Science for Peace and Security Project "Seismic Upgrading of Bridges in South-East Europe by Innovative Technologies (SFP: 983828)", involving five European countries. The composed upgraded isolated sliding system with uniform C-gaped energy dissipation (ED) devices represent suitably integrated passive mechanical building system providing harmonized response of integral buildings subjeted to strong earthquakes. The adopted system is based on global optimization of seismic energy balance, ahieved through utilization of newly designed energy dissipation devices as a supplementary damping to building isolation. The new SBC seismic protection system is based on incorporation of the following three integrated complementary systems: (1) Sliding base isolation system, (2) Created C-gaped energy dissipation (ED) system and (3) Displacement limiting (DL) system. The created SBC building system represents a qualitatively new construction strategy providing qualitativelly upgraded seismic strutural safety and efficient seismic protection of sensitive infill in rapidly constructed RC frame buildings located in seismically active regions.

Keywords: frame building, masonry, framed masonry, seismic isolation, energy dissipation

1. Introduction

The urgent need for seismic protection of frame buildings with sensitive infill is becoming clear from the recorded heavy damages of these structures during many earthquakes that have occurred worldwide (Japan, Turkey, South Europe, China, the USA, Italy, Taiwan, Chile, New Zealand, etc.). The initial studies in the field are documented in the published review of seismic base isolation research [1]. The renowned research centers worldwide have been performing continuous research toward reducing catastrophic earthquake consequences through improvement of regulations for design and construction of structures in seismically active regions, [2-6]. To increase the energy dissipation of the isolated system, specific U-shaped steel dampers have been studied and recommended for application, [7-9]. Earthquake damaging phenomena have been experimentally studied to define possible solution options, [10-12]. Many research projects have been initiated based on post-earthquake investigations of

Proceedings of the 3rd Croatian Conference on Earthquake Engineering - 3CroCEE
19–22 March 2025, Split, Croatia
Copyright © 2025 CroCEE
DOI: https://doi.org/10.5592/CO/3CroCEE.2025.52

earthquake consequences related to existing types of structures, [13-15]. Recently, extensive research involving shaking table tests on large-scale models have been conducted by the second and forth author and their collaborators, mainly targeted to seismic upgrading of isolated structures with specific energy dissipation devices, [16-18]. The basic design concept of reduced scale models for to be used for shaking table tests under simulated earthquakes, was adopted considering the data available from a completed similar research, [19]. The developed response modification method for seismic upgrading of new and existing building structures offers a very wide potential for practical application, particularly if refined nonlinear models and specific expert analysis procedures are consistently used, [20-23]. Presented in this paper is the developed innovative, multi-directional and uniform system applicable for advanced seismic protection of masonry and infilled frame masonry buildings. The new SBC building system was created based on adopted advanced upgrading of the initial sliding isolation system with the created new, efficient and experimentally proved C-gaped energy dissipation devices.

2. SBC Building System

Extensive experimental and analytical study was performed in the Institute of Earthquake Engineering and Engineering Seismology (IZIIS), Ss. Cyril and Methodius University (Skopje), as part of the NATO Science for Peace and Security Project "Seismic Upgrading of Bridges in South-East Europe by Innovative Technologies" (SFP: 983828), led by the fourth author. The developed SBC system represents a specific product of the extended part of the integrated research.

The new uniform building SBC-system has been developed based on the created compact passive C-gaped energy dissipation device providing uniform multi-directional response and qualitatively improved safety upgrading of buildings exposed to very strong earthquakes. The system has been formulated based on adopted concept of global optimization of the seismic energy balance. The designed C-gaped energy dissipation devices used as supplementary damping represent a qualitative system improvement in respect to the used building isolation only. The SBC system is based on incorporation of three complementary systems: (1) Basic seismic isolation system (SI system) providing low stiffness in horizontal direction; (2) The new C-gaped energy dissipation system to provide sufficient damping through dissipation of seismic energy, and, (3) Building displacement limiting (DL) devices to reduce or eliminate excessive displacements under strong impact effects. The intention was to create innovative SBC System with extended capability providing seismic protection of buildings exposed to strong near field and specific far field earthquakes, Figure 1.

3 C-gaped Devices

The new seismic energy dissipation system installed in the tested SBC building prototype model was composed of the developed advanced horizontal C multi-gap (HC-MG or C-gaped) energy dissipation (ED) devices. The original C-gaped energy dissipation devices of the proposed type, Fig.2, have been developed for bridges by the second author, [18]. The basic types of the created C-gaped ED components are presented in Table 1.

Table 1. Types of prototype models of C-Gaped (HC-MG) components

No.	Type	L1(mm)	do(mm)	d1(mm)	n
1	HC-1.1	L1 = 180 mm	do = 18.0 mm	d1 = 25.0 mm	25
2	HC-1.2	L1 = 180 mm	do = 12.0 mm	d1 = 18.5 mm	25
3	HC-1.3	L1 = 180 mm	do = 12.0 mm	d1 = 15.0 mm	25
4	HC-2.1	L2 = 150 mm	do = 18.0 mm	d1 = 25.0 mm	25
5	HC-2.2	L2 = 150 mm	do = 12.0 mm	d1 = 18.5 mm	25
6	HC-2.3	L2 = 150 mm	do = 12.0 mm	d1 = 15.0 mm	25

With conducted experimental testing under cyclic loading, Fig. 3, and with refined 3D nonlinear analytical modelling, the hysteretic responses of the created C-gapped energy dissipation components were defined. With the computed original results, it was confirmed that the adopted representative

Copyright © 2025 CroCEE
DOI: https://doi.org/10.5592/CO/3CroCEE.2025.52

gaped-bilinear analytical model could be implemented to realistically model the hysteretic behavior of the individual device components.

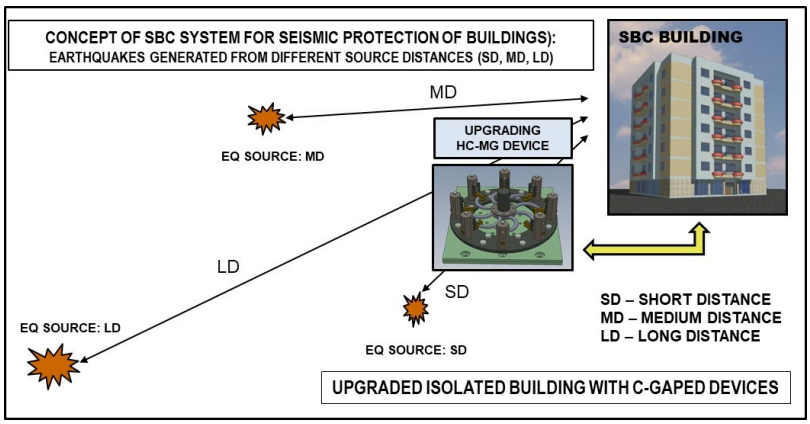


Figure 1. Concept of innovative SBC System for seismic protection of buildings

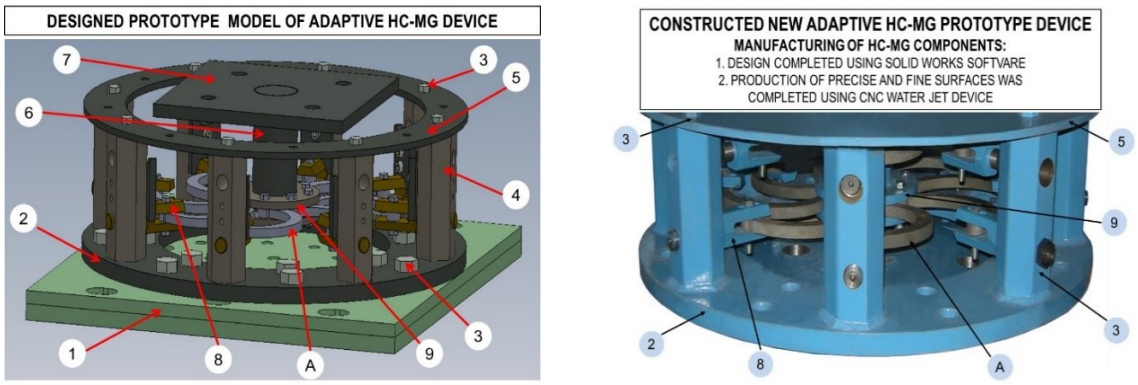


Figure 2. Designed and constructed prototype model of C-Gaped (HC-MG) device consisting of: 1. Bottom fixing plate; 2. Base ring plate; 3. Connecting bolts; 4. Vertical side supports; 5. Upper ring plate; 6. Central support; 7. Upper fixing plate; 8. Gap hinge device; 9. Central hinge device; A. HC-MG components at level L1. Figure right shows the prototype device with assembled HC-MG components of type HC-1.2 (at level L1 with gap G1 and at level L2 with gap G2), *Originally developed for bridges [18].*

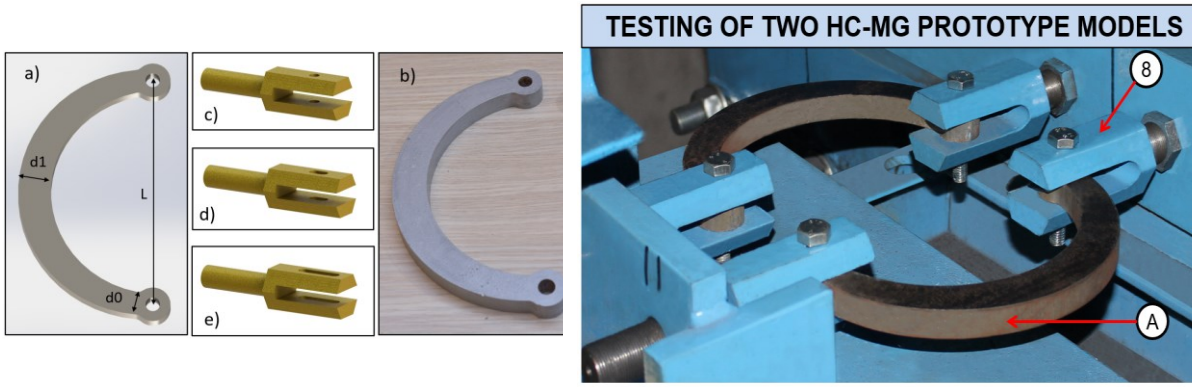


Figure 3. Constructed and tested gapped HC-MG energy dissipation components: prototypes of HC-MG components and supporting devices (left) and test setup for testing of two HC-MG prototype models (right)

Copyright © 2025 CroCEE
DOI: https://doi.org/10.5592/CO/3CroCEE.2025.52

4 Models of Isolation and Displacement Limiting Devices

4.1 Models of DSSSB isolation devices

The present isolation system used for the experimental SBC building model was assembled by use of the developed scaled models of double spherical sliding seismic bearing (DSSSB) devices with two large-radii of spherical surfaces, Fig. 4. The DSSSB devices were originally designed, constructed and used in a previous investigation carried out by Ristic, J., et al., 2023, [23]. The targets that were set prior to the design and construction of the device were fulfilled: (1) very small horizontal reaction and friction forces (reaching maximum 4.3% of the vertical load), and (2) stable hysteretic behavior along the entire range of large displacements. It was confirmed that the hysteretic behavior of the implemented DSSSB devices could be successfully simulated with the experimentally defined representative bilinear analytical model.

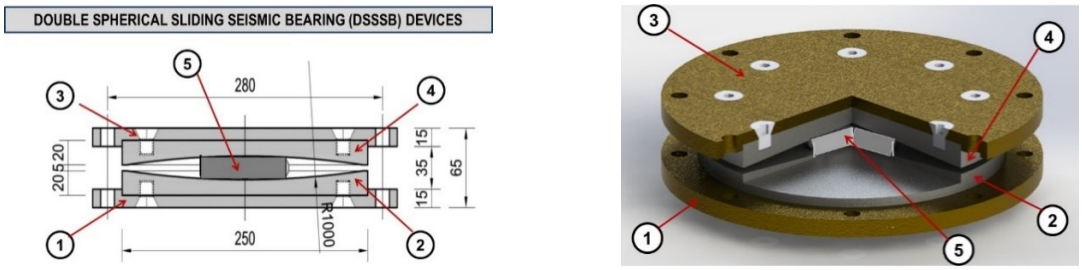


Figure 4. Components of the constructed and used prototypes of DSSSB devices: (1) lower end metal plate; (2) lower spherical plate; (3) upper end metal plate; (4) upper spherical plate; (5) metallic slider.

Actually, the model was controlled by four parameters, DY=1.0 mm, FY=0.32 kN, DU=50.0 mm, FU=0.92 kN, defined experimentally under simulated vertical load and cyclic displacements with increasing amplitudes.

4.2 Models of displacement limiting devices

The constructed and implemented DL system in the tested SBC model consisted of built-in four limiting devices marked by (6) in Fig. 7. The implemented DL devices were installed with a predefined gap. In practice, the new, specially designed and experimentally tested rubber buffers [18] can be an advanced solution.

5 Seismic Tests of SBC Building Model

5.1 Construction of SBC building model

The constructed model of the innovative SBC building prototype is shown in Fig. 5 and Fig. 6. The concept of the created model was specifically targeted on assuring conditions for realistic experimental simulation of pre-defined important testing objectives. The basic geometrical characteristics of the SBC building model, the available size of the seismic shaking table and the implemented instrumentation system of the SBC building model, were considered and harmonized accordingly. Regarding the shaking table dimensions, its loading capacity and related characteristics, a geometric scale factor, l_r, of 1:4 was adopted. In order to preserve the model similarity, all the other characteristics related to the dynamic tests needed to be properly scaled. Considering the important factors addressed, the combined true replica-artificial mass simulation model was adopted as the most adequate. The scale factors for different physical quantities were defined as a function of the geometrical scale factor, according to the similitude law, [18] and [19]. The building prototype model, Fig. 5, Fig. 6 and Fig. 7, was constructed with dimensions of a=314.0 cm and b=174.0 cm at plan, while the considered total model height was h=231.0 cm. The frame system of the model consisted of RC columns (8) with section dimensions 12.0 cm x 12.0 cm, horizontal RC beams, in both directions, with section dimensions 12.0 cm x 12.0 cm and

Copyright © 2025 CroCEE
DOI: https://doi.org/10.5592/CO/3CroCEE.2025.52

two integrating monolithic RC slabs with thickness of 8.0 cm, spaced between the RC beams. The masonry walls (9) having characteristic door and window openings (10), were constructed using plain brick with a width of 9.0 cm. The model-base isolated monolithic RC slab (7) was constructed with thickness of 15.0 cm. The upper part of the building model (the superstructure part) rested on four DSSSB devices (4) placed on constructed four special steel spacers (3). At both ends, between the DSSSB isolators, the two new C-gaped devices (5) for energy dissipation were installed, Fig. 7.

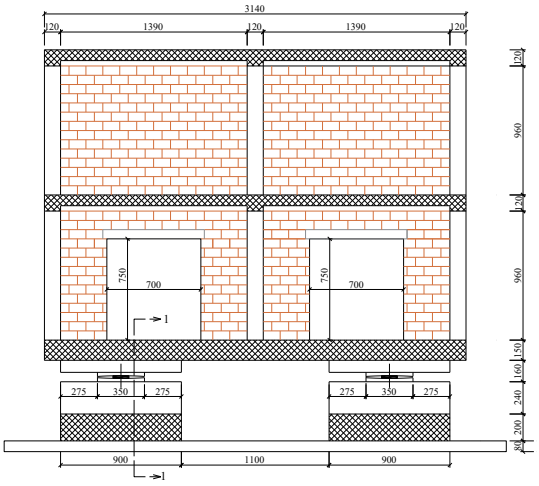


Figure 5. Side view of seismically tested SBC large-building scale prototype model.

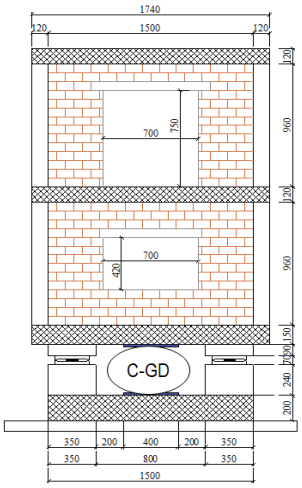


Figure 6. Front of seismically tested SBC large-scale building prototype model.

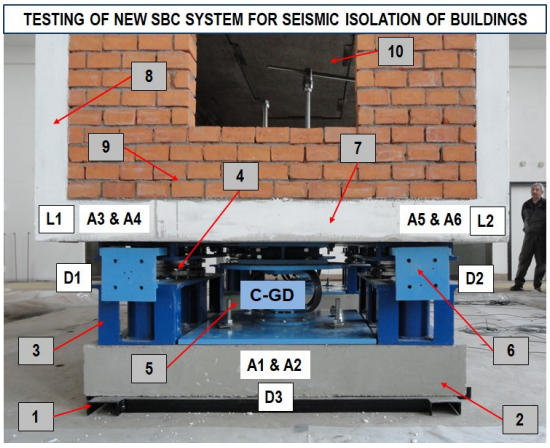


Figure 7. Isolation system of the SBC model: Installed four DSSSB devices (4), Installed two novel C-gaped energy dissipation devices (5) and the implemented four DL devices (6).

Similarly, at each model end, there were provided two DL devices in a cylindrical form that were tested before as special rubber buffers, (6). The integral SBC system was supported by two RC slabs (2), proportioned 90 x 150x 20 cm, connected to the integrating base-metal frame (1), fixed to the seismic shaking table. Eight metal elements with bulk density of 400 kg each were installed on the three RC model slabs to appropriately increase the total mass of the model. Their distribution per story was 2+2+4. The DL devices were installed at 50mm gaps to prevent the destructive effects of possible excessive displacements. All steel parts were manufactured to a reduced scale by use of S355 steel material, while concrete C25/30 was used for construction of all RC parts of the constructed model. The existing laboratory seismic shaking-table was square-shaped (5.0 by 5.0 m). Seismic input could be applied in one horizontal and in vertical direction. To adapt the large-scale SBC model for seismic testing, its longitudinal axis was positioned to coincide with the direction of motion of the shaking table,

Copyright © 2025 CroCEE
DOI: https://doi.org/10.5592/CO/3CroCEE.2025.52

Fig. 8. In that way, generation of seismic forces was enabled in longitudinal direction of the SBC model. The SBC test model was integrally assembled on the shaking table and equipped with the defined instrumentation system. For seismic testing of the SBC prototype model, the model superstructure (isolated building) rested on four DSSSB isolators spaced at the two model ends (using pairs of devices at each end), Fig. 7 and Fig. 8. The two C-gaped energy dissipation devices at both model ends were installed between the installed DSSSB seismic isolators, Fig. 7.

5.2. SBC building model instrumentation

To ensure acquisition of all the required data during the conducted dynamic tests, a well-designed instrumentation system was installed. The SBC large-scale prototype model assembled on the seismic shaking table was experimentally tested under compressed real strong earthquakes, according to the model scaling and similarity conditions. The selected strong earthquakes were simulated in the considered representative longitudinal direction of the constructed model. Actually, the designed instrumentation system of the model consisted of three different types of sensors, Fig. 7 and Fig. 8:
(a) Transducers of the type of LVDT, representing displacement sensors: Three displacement sensors were installed to measure relative displacements in longitudinal direction. The first two transducers of the type of LVDT, marked as D1 and D2, were used for recording time histories of relative displacements between the base-support of the isolation system and the bottom RC model slab located just above the seismic isolation devices. In addition, the third transducer of the type of LVDT, marked as D3, was used to measure possible relative displacements between the shaking table and the lowest fixed steel segment supporting the entire model structure;
(b) Transducers of the type of LP, representing linear potentiometers: Six sensors of the type of LP were used to measure the total displacements of the isolated building model in longitudinal direction. The first two transducers marked as L1 and L2 were located on the left and the right side of the bottom RC model slab, the next two transducers, L3 and L4, were installed on the left and the right side of the middle RC slab, and the last two transducers, L5 and L6, were spaced at respective locations on the top RC model slab. To assure conditions for such measurement, the second ends of the linear potentiometers were connected to the provided appropriate connection points. The required connection points were located in the constructed additional steel frame directly fixed to the existing, no excited, laboratory floor, spaced with a respective gap around the moving shaking table.

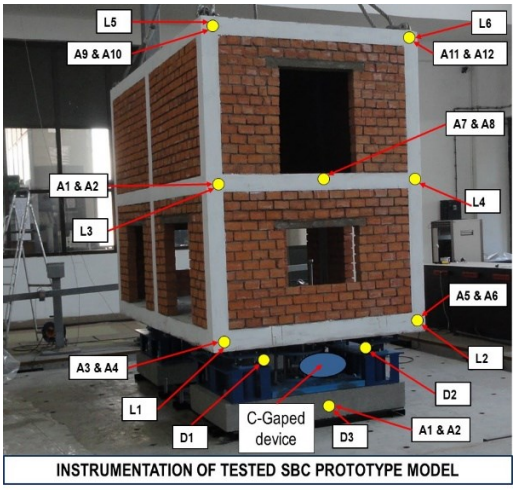


Figure 8. Used acquisition points and sensors for recording channels of SBC building model tested on seismic shaking table under simulated strong earthquakes.

(c) Transducers of the type of ACC, representing acceleration sensors: A total of twelve sensors of the type of ACC were installed, providing thus a pair of sensors at each of the selected six characteristic locations. The first and the second ACC sensor at each considered location were properly directed to measure acceleration time-histories in longitudinal (L) and transversal (T) direction, respectively. In the

Proceedings of the 3rd Croatian Conference on Earthquake Engineering - 3CroCEE
19–22 March 2025, Split, Croatia
Copyright © 2025 CroCEE
DOI: https://doi.org/10.5592/CO/3CroCEE.2025.52

first (the lowest) ACC location, there were provided two measuring channels (A1 & A2), recording accelerations in longitudinal (L) and transversal (T) direction, respectively. Following the same instrumentation concept, at each of the next five ACC locations, two measuring channels were similarly provided. The first and the second channel (Ai & Aj) at each location were similarly used for recording accelerations in longitudinal (L) and transversal (T) direction, respectively.

5.3 Seismic tests of SBC building model

(a) SBC Model assembling: The new SBC building prototype model, Fig. 8, was assembled, incorporating four DSSSB isolation devices, two C-gaped energy dissipation devices and four displacement limiting (DL) devices, Fig. 7. The created C-gaped energy dissipation devices were composed by installation of pre-defined four prototypes of energy dissipation components, Table. 1.

(b) Tests with sine-sweep: The dynamic tests carried out by simulated sine-sweep dynamic inputs, 0.02g and 0.04g, covering a range of frequencies from 1 to 35Hz and the use of the provided data sources, enabled definition of: (1) the initial fundamental period amounting to T_o=0.461s, corresponding to the case of the building model with installed DSSSB devices only. The new C-gaped devices were not connected and not activated; and (2) Damping between 3.0 and 3.4%.

(c) Comparative testing: To assess the contribution of the C-gaped devices to energy dissipation, the model was first tested with installed DSSSB isolators only, under simulated Petrovac earthquake scaled to PGA = 0.47 g. The comparative relative displacements recorded under equal test conditions for the system composed with and without C-gaped devices are presented in Fig. 10. It was shown that the building model with installed C-gaped devices represented a highly favorable upgrading option. For the system with seismic isolation only, an unacceptable relative displacement amounting to De = 42.6 mm was obtained. This excessive response actually represented the critical state, because the displacement limit of the used seismic isolators was 40.0 mm. However, regarding the SBC system with the new C-gaped devices, the relative displacement was reduced to a fully controlled value of Dc = 24.69 mm, representing an important reduction of -38.2%.

(d) Summary of testing conditions and selected results, including:

d1) Seismic input: Seismic testing of the new SBC building model was carried out using four selected real earthquake records. Actually, to obtain representative experimental data, representative earthquake intensities were considered in all testing cases. The seismic input intensities were generated considering controlled high (possible) values of peak ground accelerations amounting to PGA=0.42g for the El Centro (1940) record, PGA=0.48g for the Petrovac (Montenegro, 1979) record, PGA=0.51g for the Landers record and PGA=0.29g for the Northridge record, respectively. Following the similitude law. the original earthquake records were time compressed for a time factor of 1/2, as a square root of lr.

Table 2. Maximum positive and negative relative displacements recorded by the installed LVDT sensors, during the conducted four original seismic tests of SBC prototype model

No.	O-T1: C-El-Centro, PGA=0.42G			O-T2: C-Petrovac, PGA=0.48G		
	Channel	MaxD (-) (mm)	MaxD (+) (mm)	Channel	MaxD (-) (mm)	MaxD (+) (mm)
1	LVDT-01	-30.27	24.60	LVDT-01	-21.90	21.62
2	LVDT-02	-36.34	24.38	LVDT-02	-24.69	21.69
3	LVDT-03	-8.79	6.49	LVDT-03	-6.37	6.61

No.	O-T1: C-Landers, PGA=0.51G			O-T2: C-Nortrige, PGA=0.29G		
	Channel	MaxD (-) (mm)	MaxD (+) (mm)	Channel	MaxD (-) (mm)	MaxD (+) (mm)
1	LVDT-01	-22.95	27.72	LVDT-01	-31.40	20.92
2	LVDT-02	-26.11	29.50	LVDT-02	-36.36	20.98
3	LVDT-03	-8.52	6.62	LVDT-03	-9.06	0.00

Copyright © 2025 CroCEE
DOI: https://doi.org/10.5592/CO/3CroCEE.2025.52

d2) Data acquisition: Extensive experimental data files were recorded from each acquisition channel. The integral data recording system included the full set of 21 channels instrumented with sensors according to the model instrumentation plan and additional extra sensors were used for full control of the shaking table. Having such an extensive instrumentation system and refined data sampling rate from each seismic test, about 5 million numerical values were recorded. The testing process consisting of nine seismic tests, was completed very successfully and all sensors provided correct and complete experimental records continuously. The representative results showing the actual system response were selected, presented and discussed.

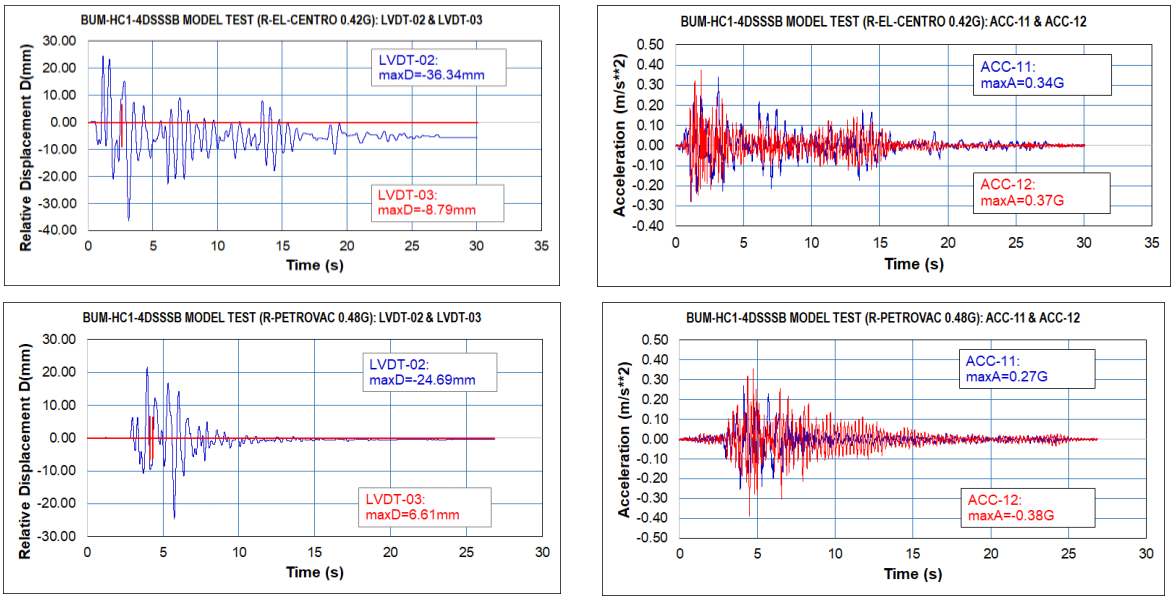


Figure 9. Relative displacements of the SBC model-base (left) and recorded acceleration responses by ACC-11 & ACC-12 (right) during the tests carried out under simulated El-Centro and Petrovac earthquake.

Table 3. Maximum positive and negative displacements recorded by the installed LP sensors during the conducted four original seismic tests of the new SBC prototype model

No.	O-T1: C-El-Centro, PGA=0.42G			O-T2: C-Petrovac, PGA=0.48G		
	Channel	MaxD (-) (mm)	MaxD (+) (mm)	Channel	MaxD (-) (mm)	MaxD (+) (mm)
1	LP-01	-47.49	-47.49	LP-01	-20.96	16.89
2	LP-02	-51.89	-51.89	LP-02	-22.22	15.96
3	LP-03	-48.80	-48.80	LP-03	-22.08	17.71
4	LP-04	-52.95	-52.95	LP-04	-23.19	16.59
5	LP-05	-49.64	-49.64	LP-05	-22.90	18.13
6	LP-06	-54.08	-54.08	LP-06	-23.93	16.90

No.	O-T1: C-Landers, PGA=0.51G			O-T2: C- Nortrige, PGA=0.29G		
	Channel	MaxD (-) (mm)	MaxD (+) (mm)	Channel	MaxD (-) (mm)	MaxD (+) (mm)
1	LP-01	-12.40	21.51	LP-01	-52.59	41.58
2	LP-02	-14.03	21.26	LP-02	-55.23	41.14
3	LP-03	-13.72	22.60	LP-03	-54.14	42.45
4	LP-04	-15.05	22.29	LP-04	-56.09	42.23
5	LP-05	-14.53	23.28	LP-05	-54.91	43.45
6	LP-06	-15.75	22.96	LP-06	-57.30	42.18

Proceedings of the 3rd Croatian Conference on Earthquake Engineering - 3CroCEE
19–22 March 2025, Split, Croatia
Copyright © 2025 CroCEE
DOI: https://doi.org/10.5592/CO/3CroCEE.2025.52

Table 4. Maximum positive and negative accelerations recorded by the installed ACC sensors during the conducted four original seismic tests of the new SBC prototype model

No.	O-T1: C-El-Centro, PGA=0.42G					O-T2: C-Petrovac, PGA=0.48G				
	Channel	MaxAG (-)	DAF	MaxAG (+)	DAF	Channel	MaxAG (-)	DAF	MaxAG (+)	DAF
1	ACC-01	-0.40	0.95	0.43	1.02	ACC-01	-0.51	1.06	0.40	0.82
2	ACC-02	-0.09	0.21	0.10	0.23	ACC-02	-0.07	0.14	0.07	0.14
3	ACC-03	-0.30	0.71	0.31	0.73	ACC-03	-0.29	0.60	0.21	0.43
4	ACC-04	-0.22	0.52	0.24	0.57	ACC-04	-0.21	0.43	0.32	0.66
5	ACC-05	-0.23	0.54	0.31	0.73	ACC-05	-0.22	0.45	0.21	0.43
6	ACC-06	-0.22	0.52	0.24	0.57	ACC-06	-0.20	0.41	0.32	0.66
7	ACC-07	-0.21	0.50	0.24	0.57	ACC-07	-0.20	0.41	0.19	0.39
8	ACC-08	-0.23	0.54	0.19	0.45	ACC-08	-0.25	0.52	0.31	0.64
9	ACC-09	-0.32	0.76	0.34	0.80	ACC-09	-0.28	0.58	0.35	0.72
10	ACC-10	-0.29	0.69	0.38	0.90	ACC-10	-0.39	0.81	0.36	0.75
11	ACC-11	-0.27	0.64	0.34	0.80	ACC-11	-0.25	0.52	0.27	0.56
12	ACC-12	-0.28	0.66	0.37	0.88	ACC-12	-0.38	0.79	0.35	0.72

No.	O-T1: C-Landers, PGA=0.51G					O-T2: C- Nortrige, PGA=0.29G				
	Channel	MaxAG (-)	DAF	MaxAG (+)	DAF	Channel	MaxAG (-)	DAF	MaxAG (+)	DAF
1	ACC-01	-0.54	1.05	0.44	0.86	ACC-01	-0.20	0.68	0.31	1.06
2	ACC-02	-0.07	0.13	0.09	0.17	ACC-02	-0.05	0.17	0.05	0.17
3	ACC-03	-0.37	0.72	0.29	0.56	ACC-03	-0.22	0.75	0.28	0.96
4	ACC-04	-0.33	0.64	0.31	0.60	ACC-04	-0.16	0.55	0.19	0.65
5	ACC-05	-0.32	0.62	0.30	0.58	ACC-05	-0.23	0.79	0.29	1.00
6	ACC-06	-0.32	0.62	0.31	0.60	ACC-06	-0.16	0.55	0.19	0.65
7	ACC-07	-0.21	0.41	0.22	0.43	ACC-07	-0.20	0.68	0.25	0.86
8	ACC-08	-0.28	0.54	0.33	0.64	ACC-08	-0.15	0.51	0.14	0.48
9	ACC-09	-0.34	0.66	0.36	0.70	ACC-09	-0.23	0.79	0.30	1.03
10	ACC-10	-0.39	0.76	0.37	0.72	ACC-10	-0.11	0.37	0.23	0.79
11	ACC-11	-0.34	0.66	0.31	0.60	ACC-11	-0.22	0.75	0.29	1.00
12	ACC-12	-0.38	0.74	0.36	0.70	ACC-12	-0.11	0.37	0.23	0.79

(d3) Relative displacements: The relative peak displacements, including positive and negative pulses, recorded during the seismic tests of the SBC system under the simulated El-Centro, Petrovac, Landers and Northridge earthquake are presented in Table 2. Comparatively, Fig. 9 (left) shows the recorded time-histories of relative displacement responses in longitudinal (L) direction during the tests carried out by simulation of the El-Centro and Petrovac earthquake, respectively. Regarding the presented experimental results, the following important observations were made: (1) The recorded relative displacements in L direction (direction of earthquake excitation) were dominant; (2) It was confirmed that the test model was successfully fixed to the shaking table since the relative displacements in L direction recorded by LVDT-03 were very small in all test cases; (3) The absolute maximum recorded relative displacement amounting to Dmax = 36.36 mm was below the critical (allowable) relative displacement of the seismic isolators amounting to Da = 40.0 mm, and (4) Seismic response of the assembled SBC system that was tested repeatedly twice appeared to be very similar. The results from the conducted original series of tests-1 are presented (O-Ti) in Tables 2 to 4. Consequently, the series of repeated seismic tests-2 (not presented) were realized using the same four earthquakes. Only small, negligible differences of maximum displacements were observed.

(d4) Accelerations: The representative time-histories of accelerations recorded by sensors ACC-11 and ACC-12, respectively in L and T-direction, during the seismic tests on the SBC model conducted under the simulated El-Centro and Petrovac earthquakes are comparatively shown in Fig. 9 (right).

Copyright © 2025 CroCEE
DOI: https://doi.org/10.5592/CO/3CroCEE.2025.52

However, Table 4 shows the representative peak accelerations recorded by all sensors, namely, ACC-01 to ACC-12. At each measuring point, accelerations were recorded in L and in T-direction during the seismic tests on the SBC model conducted under the simulated all four representative earthquakes. Considering the presented results, it was confirmed that: (1) The recorded accelerations at the superstructure, respectively in L and T-direction, were quite small (without amplification); and (2) Due to the present regular fluctuation, the recorded accelerations at the superstructure in L and T-direction were with similar peak values and in the expected range; (3) The new SBC system showed sustainability since the response parameters recorded during the original (O) tests-1 and the repeated tests-2 were quite similar, and (4) Generally, the DAF (dynamic amplification factor) values presented in the same Table 4 were quite small (smaller than 1.0), demonstrating favorable and consistent response. It was confirmed that the obtained relations between the maximum response and the maximum input acceleration (DAF = Ar/PGA) were within the expected ranges in all cases.

(d5) Absolute displacements: The absolute displacement responses (in L -direction) recorded by the six LP sensors, Table 3, installed on the SBC model, proved existence of small inter-story drifts and successful control of the shaking table in all realized testing cases.

(d6) System advances: Generally, the new SBC system exhibited safe and very favorable behavior under strong earthquake excitations. Considering the processing of more than 50.000.000 recorded original numerical values obtained from the realized fifteen shaking table tests, the main qualitative advances of the innovative SBC system upgraded with C-gaped energy dissipation devices, are summarized in Fig. 10. Stable, reliable and safe seismic response was observed in all test cases due to the provided significant reduction of maximum relative displacements amounting to 9.1%, 38.2%, 26.2% and 9.1%, respectively, in the case of the simulated El Centro, Petrovac, Landers and Northridge earthquakes. All recorded peak values were lower than the defined allowable design displacement of Da=40.0mm for the seismic isolators. The importance of upgrading the isolated masonry and infilled frame buildings with the new C-gaped devices was experimentally validated and confirmed with the conducted initial quantification test of the model with the installed seismic isolation only. Under the simulated strong Petrovac earthquake, the tested system without C-gaped devices showed an unsafe response to the recorded excessive relative displacement amounting to maxD=42.6 mm, Fig. 10.

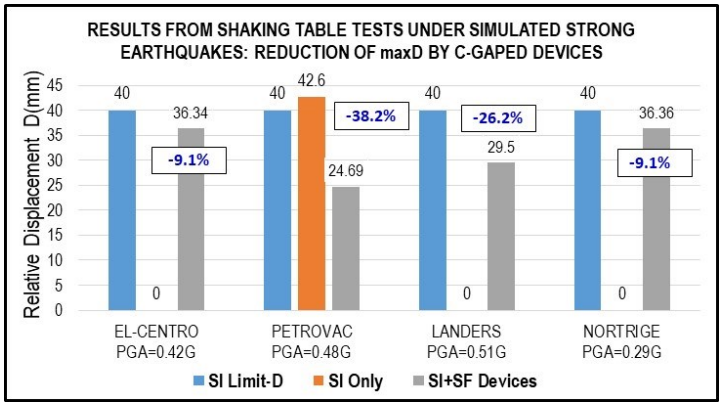


Figure 10. Advances of the SBC system: Reduction of maximum relative displacements defined from the conducted seismic tests under simulated strong earthquakes.

6 Conclusions

Considering the results obtained from the conducted experimental study, the following conclusions are derived: (1) The new SBC building system represents efficient and experimentally proved option for seismic protection of framed masonry buildings and their sensitive infill. The system provided significant modification of seismic response of the integral structure, resulting in efficient protection of buildings subjected to strong near field earthquakes; (2) The originally designed, constructed and implemented double spherical sliding bearing (DSSSB) devices [18], were confirmed as favorable types

Copyright © 2025 CroCEE
DOI: https://doi.org/10.5592/CO/3CroCEE.2025.52

of isolation bearings for the new SBC isolation system; (3) The created uniform C-gaped energy dissipation devices exhibited very good energy dissipation capacity. Their capability to exhibit stable hysteretic response under arbitrary earthquake excitation was clearly confirmed. In addition, the new C-gaped energy dissipation devices preserve their dissipation capability even in the cases of repeated strong earthquake loading; (4) The displacement limiting (DL) devices of the building should be considered as an obligatory constituent element of the created SBC system serving as the last defense line against excessive displacements of the integral building. Their appropriate design is an important step toward providing their activation only in the critical cases of very strong and abrupt earthquakes; (5) The three-dimensional, hysteretic, uniform and multi-directional response of the new C-gaped energy dissipation devices can be successfully predicted by application of the refined nonlinear micro-modeling with the adopted bilinear kinematic hardening steel material model; (6) The present study resulted in development of an experimentally proved design concept. The developed design concept can assure practical application of the new SBC system for seismic protection of framed masonry buildings located in seismic regions.

Acknowledgements

The present study represents a supplemental part of the long-term innovative NATO Science for Peace and Security Project: Seismic Upgrading of Bridges in South-East Europe by Innovative Technologies (SFP: 983828). The extended NATO support to the realization of the extensive innovative research is highly appreciated.

References

[1] Kelly, J. M. (1986): Aseismic Base Isolation: A Review and Bibliography, *Soil Dynamics and Earthquake Engineering* 5, 202-216. [DOI]

[2] Robinson, W. H. (1982): Lead-Rubber Hysteretic Bearings Suitable for Protecting Structures During Earthquakes, *Earthquake Engineering and Structural Dynamics* 10, 593-604. [DOI]

[3] Iemura, H., Taghikhany, T., Jain, S. K. (2007): Optimum Design of Resilient Sliding Isolation System for Seismic Protection of Equipment, *Bulletin of Earthquake Engineering* 5, 85–103. [DOI]

[4] Zayas, V. A., Low, S. S., Mahin, S. A. (1990): A Simple Pendulum Technique for Achieving Seismic Isolation, *Earthquake Spectra* 6, 317-334. [DOI]

[5] Mokha, A., Constantinou, M. C., Reinhorn, A. M. (1990): Teflon Bearings in Seismic Base Isolation I: Testing, *Journal of Structural Engineering* 116, 438-454. [DOI]

[6] Skinner, R. I., Kelly, J. M., Heine, A. J. (1975): Hysteretic Dampers for Earthquake Resistant Structures, *Earthquake Engineering and Structural Dynamics* 3, 287-296. [DOI]

[7] Ene, D., Yamada, S., Jiao, Y., Kishiki, S., Konishi. Y. (2017): Reliability of U-shaped Steel Dampers Used in Base-Isolated Structures Subjected to Biaxial Excitation, *Earthquake Engineering & Structural Dynamics* 46, 621–639. [DOI]

[8] Oh, S., Song, S., Lee, S., Kim, H. (2013): Experimental Study of Seismic Performance of Base-Isolated Frames with U-shaped Hysteretic Energy-Dissipating Devices, *Engineering Structures* 56, 2014-2027. [DOI]

[9] Jiao, Y., Kishiki, S., Yamada, S., Ene, D., Konishi, Y., Hoashi, Y., Terashima, M. (2014): Low Cyclic Fatigue and Hysteretic Behavior of U-shaped Steel Dampers for Seismically Isolated Buildings under Dynamic Cyclic Loadings, *Earthquake Engineering Structural Dynamics* 44(10): 1523–1538. [DOI]

[10] Jankowski, R., Seleemah, A., El-Khoribi, S., Elwardany, H. (2015): Experimental Study on Pounding between Structures During Damaging Earthquakes, *Key Engineering Materials* Vol. 627, 249-252. [DOI]

[11] Serino, G., Occhiuzzi, A. (2003): A Semi-Active Oleodynamic Damper for Earthquake Control: Part 1: Design, Manufacturing and Experimental Analysis of the Device. *Bulletin of Earthquake Engineering* 1: 269–301. [DOI]

Copyright © 2025 CroCEE
DOI: https://doi.org/10.5592/CO/3CroCEE.2025.52

[12] Tian, L., Fu, Z., Pan, H., Ma, R., Liu, Y. (2019): Experimental and Numerical Study on the Collapse Failure of Long-Span Transmission Tower-Line Systems Subjected to Extremely Severe Earthquakes, *Earthquakes and Structures* 16 No. 5. [DOI]

[13] UNCRD (1995): Comprehensive Study of the Great Hanshin Earthquake, UNCRD Research Report Series No. 12, United Nations Centre for Regional Development (UNCRD), Nagoya, Japan.

[14] Ghasemi, H., Cooper, J. D., Imbsen, R., Piskin, H., Inal, F., Tiras, A. (2000): The November 1999 Duzce Earthquake: Post- earthquake Investigation of the Structures on the TEM, Publication No. FHWA-RD-00-146, Federal Highway Administration Report.

[15] Erdik, M. (2001): Report on 1999 Kocaeli and Duzce (Turkey) Earthquakes, *Structural Control for Civil and Infrastructure Engineering*, pp. 149-186 (2001). [DOI]

[16] Ristic, J., Misini, M., Ristic, D., Guri, Z., Pllana, N. (2017): Seismic Upgrading of Isolated Bridges with SF-ED Devices: Shaking Table Tests of Large-Scale Model, *Gradjevinar*, 2147-2017. [DOI]

[17] Ristic, J., Brujic, Z., Ristic, D., Folic, R., Boskovic, M. (2021): Upgrading of Isolated Bridges with Space-Bar Energy-Dissipation Devices: Shaking Table Test, Advances in Structural Engineering, June 23, 2021; pp. 2948–2965.

[18] Ristic, J. (2016): Modern Technology for Seismic Protection of Bridge Structures Applying Advanced System for Modification of Earthquake Response, PhD Thesis, Institute of Earthquake Engineering and Engineering Seismology (IZIIS), "SS Cyril and Methodius" University, Skopje, Macedonia.

[19] Candeias, P., Costa, A. C., Coelho, E. (2004): Shaking Table Tests of 1:3 Reduced Scale Models of Four-Story Unreinforced Masonry Buildings, 13th World Conference on Earthquake Engineering, Vancouver, Paper: 2199.

[20] Ristic, D. (1988): Nonlinear Behavior and Stress-Strain Based Modeling of Reinforced Concrete Structures Under Earthquake Induced Bending and Varying Axial Loads, Doctoral Dissertation, School of Civil Engineering, Kyoto University, Japan.

[21] Ristic, D., Ristic J. (2012): Advanced Integrated 2G3 Response Modification Method for Seismic Upgrading of New and Existing Bridges, 15th World Conf. on Earthquake Engineering, (WCEE), Lisbon.

[22] Ristic, J., Ristic D., Behrami, R., Hristovski, V., (2024): Adaptive Seismic Upgrading of Isolated Bridges with C-Gapped Devices: Model Testing, Civil Engineering Journal, Vol. 10, No. 09, September, 2024.

[23] Ristic, J., Veseli V., Misini, L., Ristic, D., (2023): Seismic protection of masonry and infilled frame buildings using upgraded sliding isolation system with SF devices, Proceedings of the 2nd Croatian Conference on Earthquake Engineering - 2CroCEE, Zagreb, Croatia - March 22 to 24, 2023.

Proceedings of the 3rd Croatian Conference on Earthquake Engineering - 3CroCEE
19–22 March 2025, Split, Croatia
Copyright © 2025 CroCEE
DOI: https://doi.org/10.5592/CO/3CroCEE.2025.56

TESTING OF THE SEISMIC BEHAVIOUR OF A TRADITIONAL JOINT IN A WOODEN ROOF STRUCTURE

Nives Meštrović[(1)], Ivica Guljaš[(2)]

[1] *MSc student, University of Josip Juraj Strossmayer in Osijek, Faculty of Civil Engineering and Architecture Osijek mestrovic@gfos.hr*
[2] *Professor, University of Josip Juraj Strossmayer in Osijek, Faculty of Civil Engineering and Architecture Osijek, iguljas@gfos.hr*

Abstract

The roof timber constructions are and have been used extensively to support floors and roofs, nowadays as well as traditionally. They consist of plain timber elements and carpentry joints that work together mainly by contact pressure and friction. The structural response of roof frameworks (especially those in historical buildings) is highly dependent on the behaviour of their joints, particularly, their capacity for rotation and energy dissipation. Nevertheless, the seismic response in newly designed timber structures relies on the mechanical behaviour of connections. In historical timber structures, carpentry joints transmit forces between timber elements by direct contact and friction, whereas metal connectors, when present, only safeguard the connection against exceptional actions that could relieve contact and separate parts. Carpentry joints are built based on traditional practice based on empirical rules, or at most designed with extremely simplified models that are not supported by sufficient experimental and analytical evidence and consequently they may not comply with the safety levels that are now imposed, particularly for seismic action.

With that in mind, a small research program has been carried out by the authors for characterizing the mechanical behaviour of carpentry joints. The so called bird-mouth joint typology most frequently used in simple timber structures, with special attention to roof trusses, have been considered in the study. In the paper, some results are presented, with special attention to the rotational behaviour of these joints and to the effects of possible seismic strengthening operations in the elastic and post-elastic field.

Keywords: wooden roofs, carpentry joints, mechanical seismic behaviour, experimental testing.

1. Introduction

Traditional carpentry joints, which make up the majority of joints in historic timber structures, transmit forces primarily through direct contact and friction. Traditional timber connections are most often constructed with notches, wedges, bearing surfaces, grooves. These joints are often supplemented with metal parts, some of which were added during construction to enable the joints to withstand tensile forces, or to increase their strength or stiffness, while some are added later, to repair or reinforce joints that have deteriorated. Metal elements are extremely important in rehabilitation, i.e. subsequent reinforcement of the joint. The need for reinforcement arises for several reasons, e.g. deterioration due to poor maintenance, change of purpose of the building and the need for greater strength due to cracks, etc. Metal elements in the joint, when present, prevent the joint from separating in exceptional situations and can thus reduce pressure or act outside the plane of the joint. Given the brittleness of wood, it is important to ensure that the wooden elements remain elastic. Under critical conditions, the post-elastic behavior of joints, which involves the interaction between metal and wood, is crucial for meeting modern safety standards, [1].

The vast majority of regions around the world are located in seismically active areas, and earthquake damage can be catastrophic. Therefore, it is important to understand how different building structures, including roofs, respond to seismic forces.

Copyright © 2025 CroCEE
DOI: https://doi.org/10.5592/CO/3CroCEE.2025.56

Seismic damage in old wooden roof structures can mainly be attributed to inadequate joint performance until significant damage to the wooden elements occurs. Damage also occurs due to poor connection of the main load-bearing structure and secondary elements. Often, in seismic strengthening of existing buildings, wooden structures were removed and replaced with new elements of industrial origin, which would often lead to poor outcomes because the interaction of new structures, with high stiffness and mass, with the surrounding walls, often of modest quality, would result in poor seismic performance, or even greater damage or even collapse.

The key issues when it comes to traditional wooden roofs are the weight of the material and weak connections. Since traditional roofs often use materials such as tiles and wood, they increase the load on the structure. During an earthquake, this load can cause greater forces to act on the walls and foundations. Traditional roofs have less effective connections, which can lead to the roof separating or collapsing during an earthquake. Another important factor is stiffness, as reduced stiffness can cause the building to not adapt to the vibrations caused by the earthquake, which can increase the risk of damage.

In their research paper, Parisi et al. [2] consider the quality of the wood-to-wall connection, the type and quality of the wood-to-wood connection, and the general state of preservation for seismic loading. They developed a procedure for assessing the seismic vulnerability of wooden roof structures. They divided it into two steps. In the first part, data on the structure is collected based on a visual inspection, and in the second step, specific vulnerability indicators are determined by analysis.

Kasal and colleagues [3] conducted research that focused on investigating the behavior of glulam frames under dynamic loading simulating an earthquake. They tested two types of frames, one without reinforcement and one of a new design with glass fiber reinforcements to improve the durability of the joints. The results showed that the wooden structures, thanks to their low density and high ductility, can withstand heavy loads well while maintaining the load capacity and energy absorption capacity, which makes them very resistant to earthquakes.

Many factors, such as urbanization, excessive tourism, climate changes, people's neglect and loss of traditional knowledge, affects this tangible heritage. Additionally, the vulnerability of historic buildings is greater in seismic prone regions as earthquakes pose a big treat to the stability of the buildings and may cause irreversible damage.

2. Typical carpentry joints

The most frequent layout of roof structures is given by a series of parallel trusses, usually connected by simple purlins or, seldom, by more elaborated transversal elements. Depending on the surface to be covered, trusses may reach considerable size and complexity. The rafter-to-tie beam connection has always been considered the most important node of a truss, as may be seen, for instance, consulting traditional design manuals. Figure 1 presents the forms of this joint that are most frequently found.

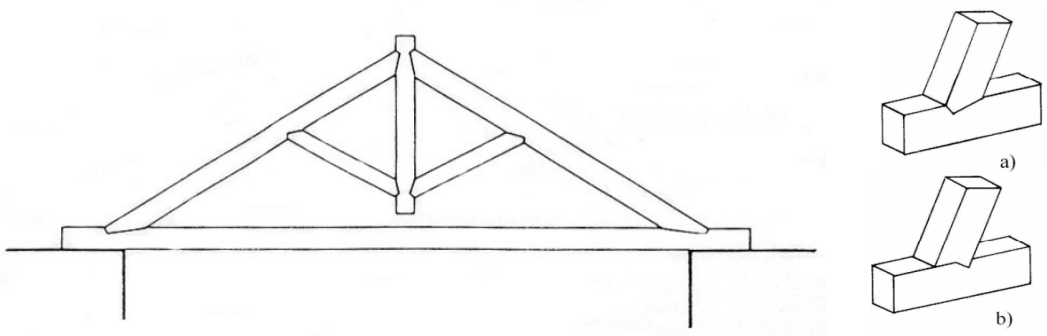


Figure 1. Typical roof truss (left), (a) birdsmouth joint; (b) its reversed form.

The most common joint in existing timber roof structures is the "birdsmouth joint with a single tooth", (a) in Figure 1, usually presenting a skew angle of about 30° between the tie beam and the rafter,

Copyright © 2025 CroCEE
DOI: https://doi.org/10.5592/CO/3CroCEE.2025.56

although geometry varies with joint location in the truss, and the joint bearing capacity is function of skew angle, notch depth and length of the toe. The load transmission relies on direct contact and friction between facing surfaces. Metal ties or fasteners are not mean to transmit forces directly; they are mainly used for positioning and maintaining the functionality of the joint in adverse or unpredictable conditions.

Common timber roof structures are usually modelled with perfect hinges at the extremities of each element. However, these joints offer a significant moment resistance and may be better classified as semi-rigid. The lack of practical though realistic models for the joints in old traditional timber structures generally leads to very conservative retrofits and upgrades to satisfy new safety and serviceability requirements. Moreover, the misunderstanding of the global behavior of traditional roof trusses can result in unacceptable stresses in the members as a consequence of inappropriate joint strengthening (in terms of stiffening). Joint strengthening can be done in a number of possible ways: from simple replacement or addition of fasteners, to the use of metal plates, glued composites or even full injection with fluid adhesives. Each solution presents unique consequences in terms of the joint final strength, stiffness and ductility.

3. Testing and numerical analysis

The behaviour of carpentry joints in historical timber structures plays an important role in their overall structural response to applied loads, especially during seismic events. This has been the subject of several research projects, mostly in countries with high seismic activity. In these countries, roof framework joints employ a typical birdsmouth connection for joined timber elements, as shown in Figure 1.

The birdsmouth joint has been studied most extensively, because of its preminence among possible connection solutions. Its rotational behavior has been characterized by numerical analysis and experimentally in monotonic conditions, in the elastic and post-elastic field up to failure. Monotonic tests were performed on unreinforced joints and on strengthened ones. During the tests a constant pressure is applied to the rafter, while a lateral force is applied to generate moment and rotation at the node. The experimental setting permits load reversal.

3.1 Test specimens

An experimental research was carried out at the Laboratory of Faculty of Civil Engineering and Architecture Osijek, including monotonic tests of full-scale traditional timber connections. A series of monotonic tests on unstrengthened specimens was performed in order to study the primary behaviour characteristics of the connection, as well as its sensitivity to a few parameters. Subsequently, connections strengthened with basic metal devices were tested under monotonic loading. The purpose of these tests was to uncover any advantages and deficiencies in the behaviour of the connection and the device itself, as well as to determine a need for different types of strengthening. Tests on assembled connections were preceded by accurate material characterization, determining the mechanical properties of the timber elements used for all full-scale models

A total of 6 tests were performed. Three (3) models were made with varying angles between the rafter and the beam (30°, 45°, 60°). First, an unreinforced joint (carpenter's joint) was tested, which was held in place by a single screw, then a reinforced joint with a metal plate and screws was tested. Monotonic tests were applied in 4 steps, being 2 in each loading direction (positive and negative) under a compression level in the rafter of 5.0 MPa corresponding to the Service Limit State conditions.

Copyright © 2025 CroCEE
DOI: https://doi.org/10.5592/CO/3CroCEE.2025.56

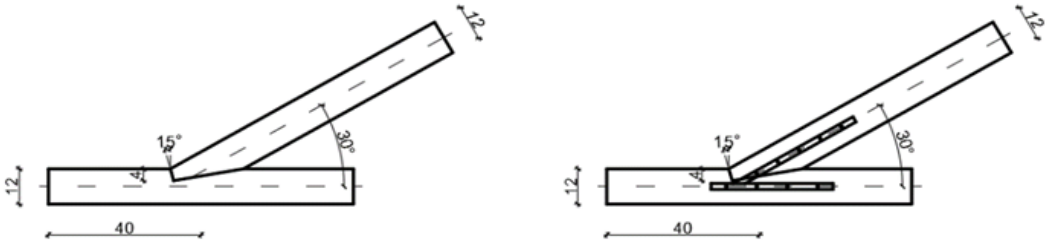


Figure 2. Geometrical scheme of the joint at an angle of 30°: basic unreinforced (left) and strengthened (right).

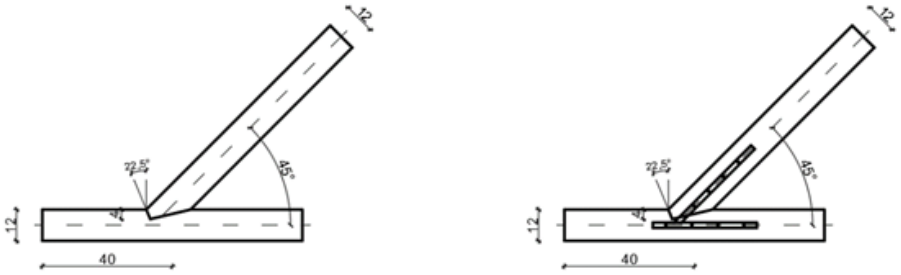


Figure 3. Geometrical scheme of the joint at an angle of 45°: basic unreinforced (left) and strengthened (right).

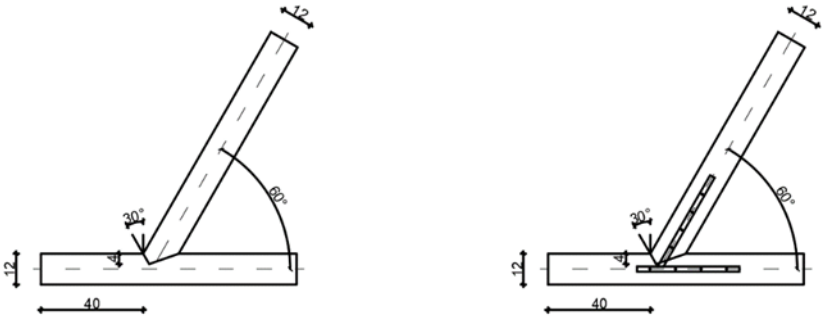


Figure 4. Geometrical scheme of the joint at an angle of 60°: basic unreinforced (left) and strengthened (right).

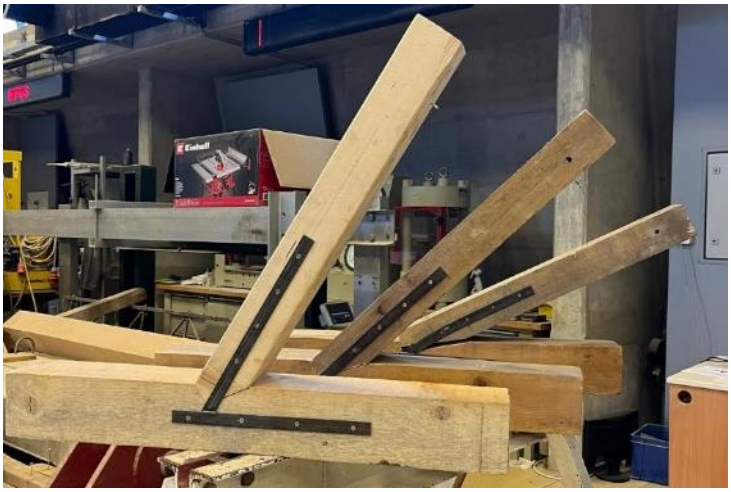


Figure 5. Test specimens of the joint at an angle of 60°, 45° and 30°.

Copyright © 2025 CroCEE
DOI: https://doi.org/10.5592/CO/3CroCEE.2025.56

The notch lengths t_v and the length l_v (length of timber outside the notch - heel) are given as functions of the angle of inclination and the cross-sectional dimensions. The general design procedure assumes a hinged connection and involves defining the load paths between the members, resolving the pressure from the rafters into components perpendicular to the notch surfaces (a) and defining the corresponding shear surfaces to accommodate these stresses (b) [4].

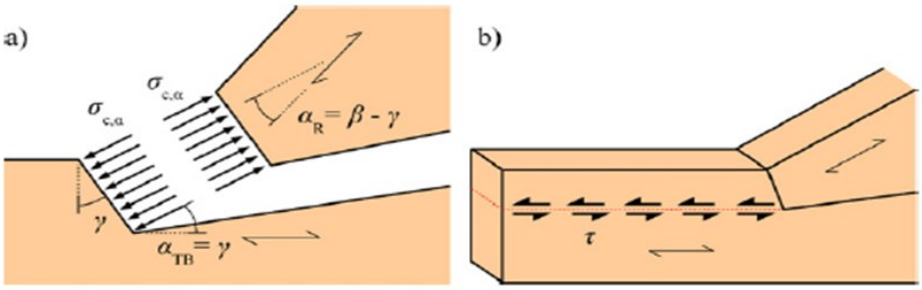


Figure 6. (a) Compressive stresses in the notch, (b) Shear stresses in the heel [4].

Regarding the rotational behavior of the horn-beam joint, Parisi and Piazza [2] presented two simplified physical models (for rotations in both directions) to predict the moments of simple butt-joints without metal parts. These models are based on equilibrium considerations and are shown in the figure below.

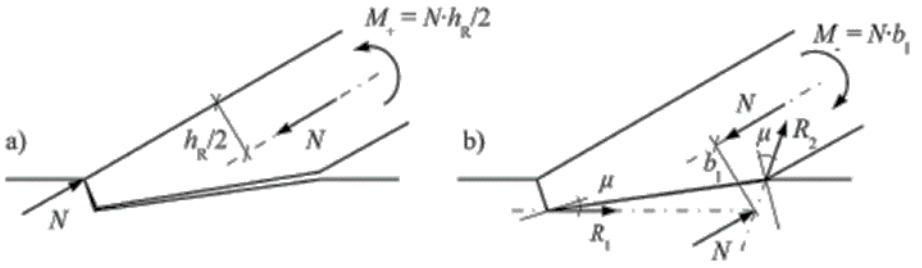


Figure 7. Prediction of moments of simple front mortise joints without metal parts [2].

When opening the tilt angle (a), the maximum moment M_{max} is given by the equation:

$$M_{max+} = N\frac{h_R}{2}$$

where N is the compressive force in the horn, and h_R is the horn height (max moment does not depend on the depth of the notch, but on the level of compressive load in the horn).

When closing the bank angle (b), the maximum moment M_{max} is given by the equation:

$$M_{max-} = N \cdot b_l$$

where N is again the compressive force in the horn, and b_l is the lever arm between N and the intersection of the lines of action of the corresponding notch reactions. The lever arm b_l depends on the geometric parameters of the joint (depth, length and angle of the notch) and on the coefficient of friction.

A groove is a cutout in a wooden beam that allows a tongue to be inserted into another component. This form of connection provides a larger contact surface between the two elements, which increases the strength of the connection. The groove can be of various dimensions and shapes, depending on the needs of the structure and the size of the wooden elements. It is usually made in such a way that the tongue fits tightly into the groove, minimizing movement and oscillation.

The tongue-and-groove joint provides greater stability and resistance to horizontal forces, which is especially important in areas prone to earthquakes or winds. This type of joint is relatively simple to

Copyright © 2025 CroCEE
DOI: https://doi.org/10.5592/CO/3CroCEE.2025.56

make, which makes the carpenter's work easier and reduces construction time. This joint must be properly protected to prevent moisture from penetrating, which can cause the wood to rot or warp over time. The tongue-and-groove joint can allow for some flexibility in the structure, which is important for resistance to earthquake forces. This flexibility helps to reduce the transfer of forces to other parts of the structure.

For the purpose of testing, a carpenter's joint, or the connection of a rafter and a beam, known as a groove joint, was performed. More precisely, the rafter rests on a groove in the beam, which is additionally (in this case) fastened with a single screw. This connection relies exclusively on compressive forces and friction forces that are generated and transmitted on the contact surfaces. The main force transmitted through the rafter is compressive force. As the rafter supports the weight of the roof and loads (e.g. snow, wind), these loads create a compressive force along the axis of the rafter. This compressive force is transmitted through the groove to the beam, thus ensuring the stability of the connection. For the purpose of testing, this compressive force was introduced into the rafter as a prestressing force of 5 kN.

Tensile forces occur because the beam, as a horizontal element, must maintain the tendency of the rafter to move apart or separate from the structure due to the horizontal component of the load on the rafter. Shear forces occur on the contact surfaces between the rafter and the beam. These forces act parallel to the surfaces of the connection and are caused by the weight that the rafter transfers to the beam. Bending forces also occur due to the load that the rafter transfers to the beam.

3.2 Test arrangement and procedure

The arrangement allows independent control of two forces (Figure 8). First, aligned with the rafter, induced constant compression throughout the test by prestressing. The other, a double-acting jack, positioned above the center of the connection, applied a transversal force, with a programmed load cycle, and generated a moment at the connection. Force (F) versus displacement (d) curves were measured. Tests were performed under displacement control for the typical birdsmouth connection skew angle of 30º , 45 º and 60º. For all the specimens, the cross sections of the elements were 10x120 cm^2, the notch depth was 40 mm and the notch length varied according to the skew angle.

The first step of the loading procedures was the application of an axial compression force on the rafter, which was kept constant during the test. In the subsequent loading steps, a transversal force (F) was employed, acting perpendicular to the rafter axis. When the skew angle increased, it was defined as the positive direction and when the skew angle decreased, it was defined as the negative direction. Monotonic tests were performed to determine the elastic behavior, in particular, the apparent elastic limit displacement d_{e+} and d_{e-}. Under displacement control, a maximum displacement value of 50 mm was imposed.

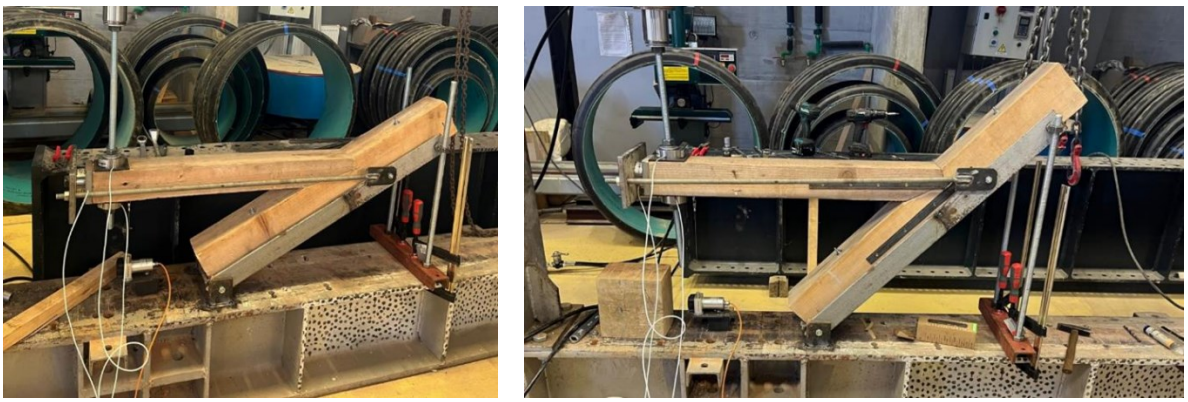


Figure 8. Test setup of joints without (left) and with metallic strengthening parts (right).

Proceedings of the 3rd Croatian Conference on Earthquake Engineering - 3CroCEE
19–22 March 2025, Split, Croatia
Copyright © 2025 CroCEE
DOI: https://doi.org/10.5592/CO/3CroCEE.2025.56

3.3 Some test results

In the seismic response of timber structures, joints are the key elements because they may either contribute to fragility, or develop, to some extent, a dissipating behavior. In the perspective of seismic strengthening of timber structures, general criteria for strengthening the connections to resist the effect of seismic action are needed, considering that traditional intervention methods in timber construction are generally conceived in view of a static behavior under vertical loads. The results of an experimental and numerical research program on the behavior of carpentry joints have been outlined here focusing on the semi-rigid behavior of carpentry joints. The measurement is carried out in four (4) steps and was based on the pushover analysis principle, i.e. the method of gradual pushing until a certain level of deformation is reached.

Table 1. Test results, steps #1 and #2

Test sample		Step #1			Step #2	
		Force [N]	Displacement [m]	Joint stiffness [kN/m]	Force [N]	Displacement [m]
30°	basic	1000	0,0293	34,095	1601	0,0298
	strengthened	1000	0,0163	61,538	1938	0,0161
45°	basic	1000	0,0314	31,888	1409	0,0255
	strengthened	1000	0,0255	39,154	1210	0,0261
60°	basic	1000	0,0347	28,794	1851	0,0301
	strengthened	1000	0,0263	38,037	2301	0,0263

Table 2. Test results, steps #3 and #4

Test sample		Step #3		Step #4	
		Force [N]	Displacement [m]	Force [N]	Displacement [m]
30°	basic	1931	0,0502	1688	0,0501
	strengthened	2051	0,0502	2956	0,0502
45°	basic	1872	0,0530	2986	0,0502
	strengthened	1852	0,0525	3566	0,0501
60°	basic	2000	0,0510	2122	0,0502
	strengthened	2182	0,0516	2991	0,0501

The results of the pushover analysis are shown graphically below. They are shown graphically in relation to force/displacement (curve F/d) and in relation to moment/turning angle [curve M/φ]. The curves in the first quadrant (d>0 and F>0) correspond to the tested joints opening the curvature angle. The curves in the fourth quadrant (d<0 and F<0) represent the tested connections where the curvature angle closes. The M/φ curve will only be shown for the first test step since it is crucial to obtain the stiffness input to the model.

Before the actual analysis and processing of the data, it is important to note that the reinforcements were placed on previously tested non-strengthened models and that they had already acquired certain defects there.

Copyright © 2025 CroCEE
DOI: https://doi.org/10.5592/CO/3CroCEE.2025.56

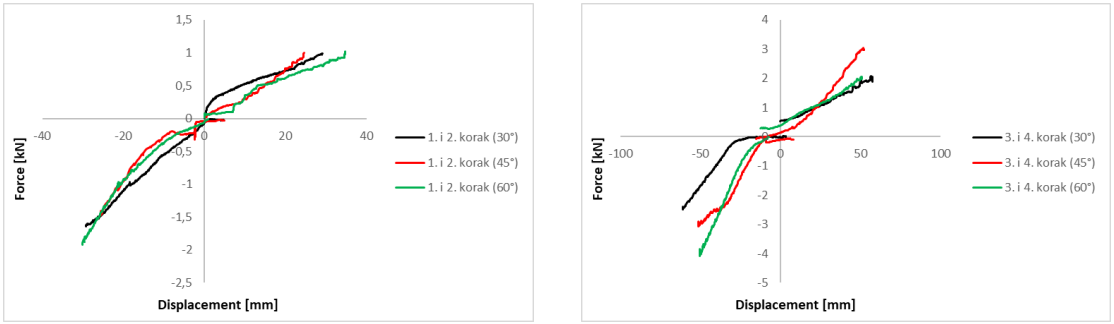


Figure 9. Force – displacement curves obtained for non-strengthened joints and various skew angles.

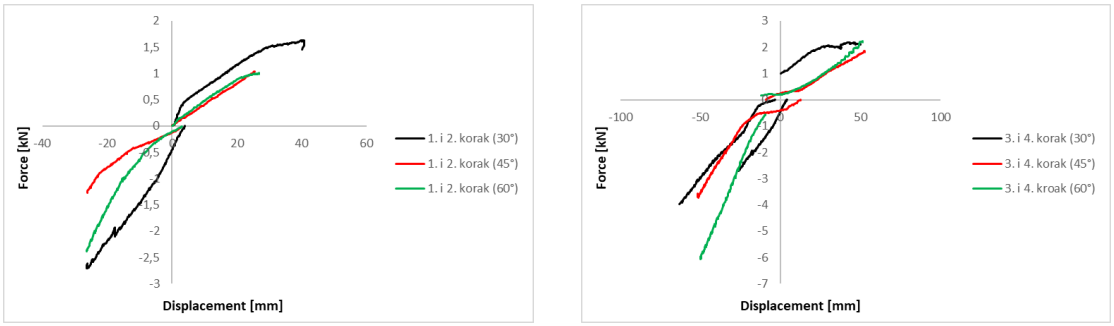


Figure 10. Force – displacement curves obtained for strengthened joints and various skew angles.

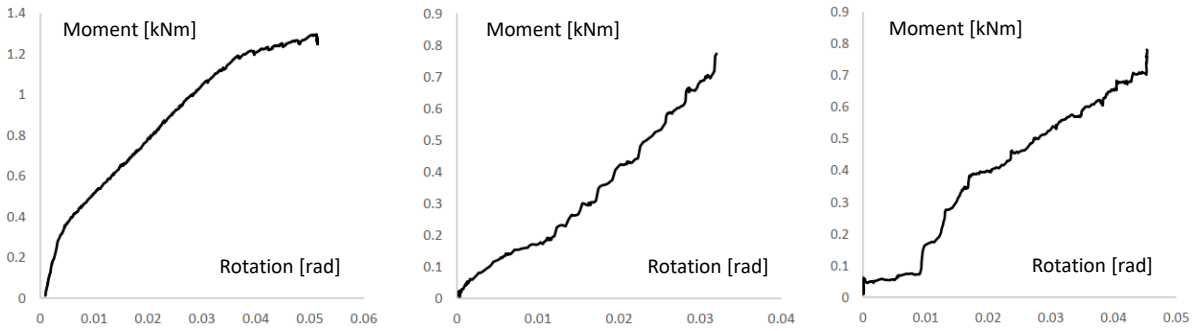


Figure 11. M – φ diagrams for non-strenghtened rafter to tie beam joints with skew angle of 30°, 45° and 60°.



Figure 12. Final deformed shapes of non-strengthened / strengthened joints for 30° skew angle.

Proceedings of the 3rd Croatian Conference on Earthquake Engineering - 3CroCEE
19–22 March 2025, Split, Croatia
Copyright © 2025 CroCEE
DOI: https://doi.org/10.5592/CO/3CroCEE.2025.56

4. Conclusion

With this work, we paid attention to traditional wooden roofs, which are mostly represented in our area and are made of ordinary wooden elements, and the joints are usually carpentry with or without reinforcement.

A total of six tests were conducted where the joints were exposed to monotonic loading, observing their behavior, the influence of the reinforcement itself and the angles between the rafter and the tie beam.

By analyzing the data, it was determined that the reinforcement itself in this case of loading, where the behavior of the joint under seismic load was analyzed, did not prove to be effective. The reason for this is that the connection to the groove itself works on the principle that the horn is wedged when the force acts downwards, while in the case when the force acts upward, the horn comes out of the connection and this reinforcement that we used does not sufficiently prevent it. For such a load case, it would be necessary to put a thicker metal plate or even better to make a screw connection through both elements in order to connect the elements in that direction as well.

Also, from the tests, we come to the conclusion that roofs with a greater slope are more suitable for this type of load, since they have a better distribution of forces and reduce horizontal loads during an earthquake. That was noticed during this test champagne since the model with an angle of 30° responded in the same way during the test in the case with/without reinforcement, that is, the rafter rose out of the tie beam and when the downward force was applied, it did not form a wedge again, which was not the case with the other two models proving their better performance.

In any case, it is necessary to additionally examine the behavior of classic wooden joints, since their stiffness plays an important role in the calculation of the global structure. This is important in order to know how to carry out the reconstruction or assessment of safety and remaining service life in the correct way.

Traditional timber connections, even without any strengthening device, usually have a significant moment-resisting capacity. Therefore, they should not be represented by common constraint models, like perfect hinges, but should be considered semi-rigid and friction based. The test results performed by the authors show that this capacity is function of the compression stress applied to the rafter and of the skew angle, the height of the rafter cross section and the friction angle The experimental analysis has been of fundamental importance in order to understand the real behavior, by pointing out some important aspects like force transmission mechanisms, failure modes and guidance for appropriate strengthening solutions.

5. References

[1] Parisi M.A, Piazza M. Seismic Strengthening of Traditional Carpentry Joints. The 14t^{h} World Conference on Earthquake Engineering. Beijing; China, 2008.

[2] Parisi, M.A., Piazza, M. Mechanics of plain and retrofitted traditional timber connections, Journal of Structural Engineering, ASCE, 126 (12), 1395-1403. 2000.

[3] Kasal, B.; Pospíšil, S.; Jirovský, I.; Heiduschke, A.; Drdácký, M.; Haller, P. Seismic performance of laminated timber frames with fiber-reinforced joints. J. Earthq. Eng. Struct. Dyn. 2004, 33, 633–646.

[4] Palma P, Garcia H, Ferreira J, Appleton J, Cruz H. Behaviour and repair of carpentry connections – Rotational behaviour of the rafter and tie beam connection in timber roof structures. Journal of Cultural Heritage. 2012 Sep;13(3): S 64–73.

[5] Poletti E, Vasconcelos G, Branco JM, Koukouviki AM. Performance evaluation of traditional timber joints under cyclic loading and their influence on the seismic response of timber frame structures. Construction and Building Materials. 2016 Nov;127:321–34.

[6] Branco, J.M.; Piazza, M.; Cruz, P.J.S. Experimental evaluation of different strengthening techniques of traditional timber connections. Eng. Struct. 2011, 33, 2259–2270.

Proceedings of the 3rd Croatian Conference on Earthquake Engineering - 3CroCEE
19–22 March 2025, Split, Croatia
Copyright © 2025 CroCEE
DOI: https://doi.org/10.5592/CO/3CroCEE.2025.77

PUSH-OUT TESTS ON TIMBER-STEEL HYBRID JOINT WITH SCREWS CONNECTIONS. NUMERICAL AND EXPERIMENTAL INVESTIGATIONS

Laura Corti[1], Giovanni Muciaccia[2]

(1) *PhD candidate, Politecnico di Milano, laura.corti@polimi.it*
(2) *Professor, Politecnico di Milano, giovanni.muciaccia@polimi.it*

Abstract

The increasing spread of timber as structural material strongly seeks for deeper investigations concerning its behaviour, in static and, even more, in cyclic conditions. It is well known that timber is characterised by several favourable properties, as lightness (significantly lower than e.g., concrete and steel), high strength-to-weight ratio, proneness to reusability and recyclability (under certain conditions taken into account since the early design phases), but some other properties are detrimental and should be handled. One of the main unfavourable characteristics that is source of several issues in timber structures is the material low ductility, especially in tension and shear where brittle behaviour is acknowledged. In order to provide adequate ductility, avoiding significant unexpected strength loss, proper design of connections is the key to guarantee ductile structural behaviour; moreover, it is very common to combine timber with steel, giving rise to timber-steel composite (STC) assemblies, where desirable properties of both materials are highlighted. This solution allows for significant environmental advantages with comparable structural performance in terms of static loading with reference to traditional solutions, according to available literature findings; on the other hand, very few experimental campaigns with cyclic loading conditions were encountered and this issue was the reason behind the motivation of this research: timber structures are now spreading in areas, as southern Europe, where seismicity is generally significantly higher than e.g., northern Europe where timber is very common but seismicity is low. This paper presents the outcomes of both static and cyclic push-out tests, carried out according to European Standard EN 12512. The results are compared with the predictions of numerical investigations, carried out in advance such to select optimal conditions for experimental activities. Screw shear connectors with two diameters (8 mm and 12 mm) are considered. On the basis of results, equivalent viscous damping is calculated, acknowledging effects of screw diameter.

Keywords: ***Timber-steel hybrid joint, screw connections, numerical modelling, cyclic tests, ductility, viscous damping, sustainability.***

1. Introduction

Timber is experiencing an outstanding popularity as an environmentally sustainable material, due to its carbon sequestration capacity [1]. When an engineered timber product (ETP) like Cross-Laminated Timber (CLT) or Glued-Laminated Timber (Glulam) is manufactured, carbon naturally contained in wood is preserved from emission in the atmosphere and it is stored at least up to building End-of-Life (EOL). From this point on, different scenarios may be practicable; in case the timber member is reused or recycled the carbon is maintained stored, while if it incinerated (with or without energy recovery) or landfilled carbon is released in the atmosphere with different timing and modalities [2].

However, timber EOL scenario cannot be merely chosen according to environmental considerations, but awareness on structural conditions is needed [3]; in case a total reuse of the structural member is foreseen, no damage should be present, and no extraordinary load or excessive deflections should have been experienced. Clear understanding of structural behaviour is the key to allow for a sustainable choice in the EOL phase. In particular, it is worth considering nowadays trends for timber buildings, as they broadly are hybrid; it is common to observe timber-concrete and timber-steel hybrid buildings [4, 5], in order to take advantage of every possible favourable properties of each material. Moreover, some unfavourable characteristics of each material are minimized, e.g., timber brittleness

Copyright © 2025 CroCEE
DOI: https://doi.org/10.5592/CO/3CroCEE.2025.77

and low ductility, concrete high environmental impact and high specific weight, steel high initial cost. The hybridization concept is quite a novelty in the building sector, such that existing heritage is limited with respect to pure timber one and even more compared to traditional reinforced concrete (RC) or steel buildings.

It is also worth considering that timber buildings are traditionally widespread – in the European context – in regions characterised by low seismicity levels, such that lateral stability is dominated by wind action, while seismic one is generally not addressed [6]. However, timber buildings are becoming more common solutions even in previously unpopular areas, and a proper seismic design is required [7]; this necessity, coupled with limited real case studies, highlights the importance to shed a light on this topic. In particular, some literature on timber-steel hybrid joints tested under static loading conditions is available [8, 9, 10], while a few investigations present tests with cyclic loading conditions [11]. This lack of experience unveils some urgent issues to be faced, such as strength and stiffness degradation, change in the failure mode, energy dissipation, etc.

The systematic literature research developed for this study lead to identification of a representative configuration for a timber-steel hybrid joint [9]; two connectors – screws and bolts – were examined with numerical modelling in previous studies [12, 13], and modelling technique is hereby refined. Thereafter the configuration with screw connectors is tested during an experimental campaign, with two different diameters (12 mm and 16 mm), both in static and cyclic loading conditions. European standards are adopted to define test methods and loading procedures in the planning phase, and relevant parameters calculations during the analysis phase. Considering tests carried out under static and cyclic loads, European standards are adopted [14, 15]. Moreover, new generation of Eurocode 8 [16] includes direct mention to EN 12512:2001 [15], such that harmonization process is encouraged. Finally, observation of specimens after testing enabled considerations in a life cycle thinking perspective; damage extent after load was applied is directly correlated with reuse potential.

The paper is organised as follows: the methodology is explained in Section 2, results are presented in Section 3, and discussion and conclusions are respectively outlined in Section 4 and Section 5.

2. Method

In order to identify a representative configuration for numerical and experimental modelling, a literature review was carried out and one of the investigation examined was selected as reference [9]; however, being such research focused on static loading conditions, some modifications to the setup were introduced to the scope of testing also in cyclic loading conditions, like the position of screws, which are, in the modified test setup, at equal distance from steel beam end to CLT top end (Figure 1). Numerical modelling methodology is mostly described in previous authors' studies [12, 13], but in this case two refinements are developed:

- Specimens tested with numerical analysis are adapted, and they precisely represent those ones designed for experimental tests;
- Cyclic loading procedure is assessed after laboratory statics tests, so that it is accurately established.

Test plan is presented in Table 1. Static and cyclic loading procedures are designed according to European standards, respectively EN 26891:1991 [14], and EN 12512:2001 [15]. According to results obtained from static tests, yield slip is defined (V_y), such that in 1st and 2nd cycles the specimen is loaded until $0.25V_y$ and $0.5V_y$ both in compression and in tension; 3rd cycle (up to $0.75V_y$ slip) is repeated three times, and the same procedure is repeated for the following ones (V_y, $2V_y$, $4V_y$, etc.). The test is finished when either failure or 30 mm slip is reached, according to the standard.

Copyright © 2025 CroCEE
DOI: https://doi.org/10.5592/CO/3CroCEE.2025.77

Table 1. Test plan

Test #	Screw diameter (mm)	Load type
1	12	Static
2	12	Cyclic
3	12	Cyclic
4	12	Cyclic
5	16	Static
6	16	Cyclic
7	16	Cyclic
8	16	Cyclic

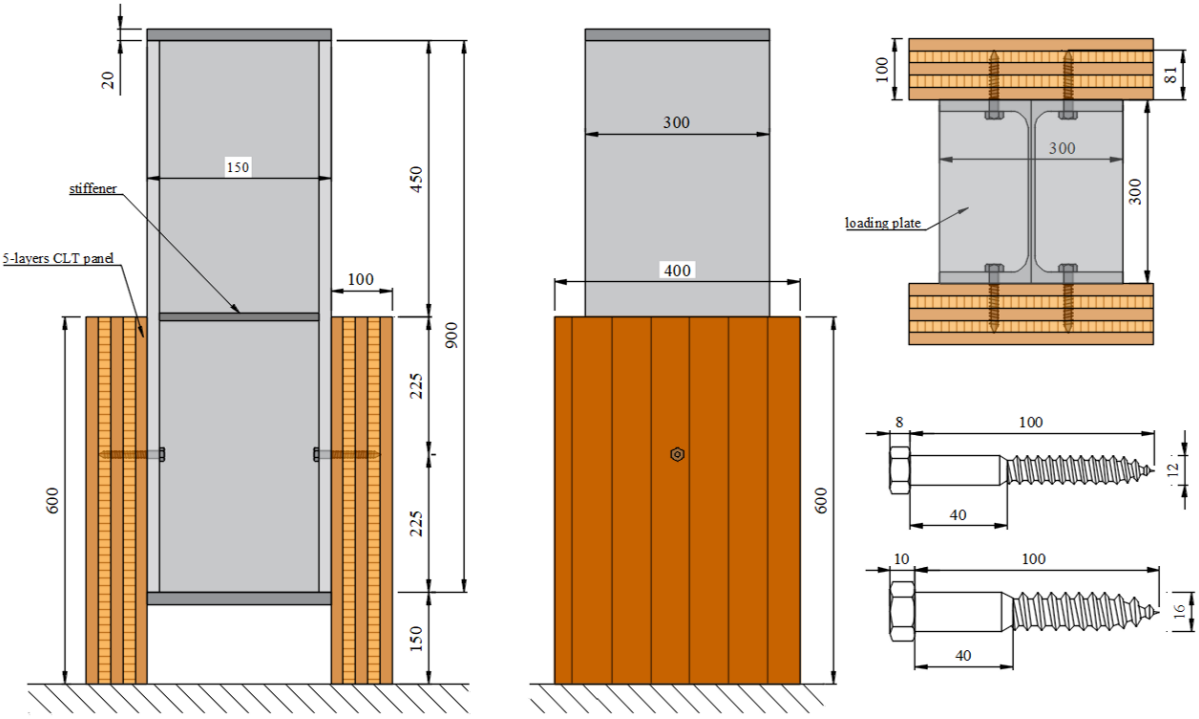


Figure 1. Configuration of specimen for experimental campaign. Screws used as timber-to-steel connections are represented. Picture adapted from a previous study [13].

Numerical analysis is used to estimate specimens' behaviour, especially in cyclic loading conditions, and to easily identify the most damaged regions to monitor during experimental campaign. Considering both EN 12512:2001 [15] and draft of the new Eurocode 8 [16], two parameters are selected to determine joints properties: impairment of strength (IS), equivalent viscous damping at 1st cycle (EVD1), and equivalent viscous damping at 3rd cycle (EVD3). Impairment of strength is referred to the reduction of load capacity of a joint that is undergoing cyclic loading; it is evaluated calculating the ratio between measured capacities of the first and third cycles, each time at the maximum reached amplitude. Equivalent viscous damping measures the hysteresis properties of a joint subjected to cyclic loading, according to Eq. (1).

$$\mathrm{EVD} = \frac{E_d}{2\pi \cdot E_p} \tag{1}$$

Where:

- E_d is the energy dissipated in one half-cycle
- E_p is the available potential energy

Available potential energy is calculated with a MATLAB code designed on purpose; considering that data do not present relevant noise, an easy numerical integration technique is selected, in particular

Copyright © 2025 CroCEE
DOI: https://doi.org/10.5592/CO/3CroCEE.2025.77

the trapezoidal rule is applied. It is worth mentioning that in the considered standard [15], there is not specific instruction on which cycle has to be used to compute EVD, so that it is calculated at first (EVD1) and third (EVD3) cycles. In this way, EVD1 is a measure of early-stage dissipation properties and EVD3 provides a more stable representation of the dissipation characteristics, since transient effects may affect 1st cycle.

The last step is visual analysis of tested specimens, with identification of the following features:

- Screw failure modes
- CLT panel damage extension
- Possibility to disassemble the specimen without increasing timber damage

3. Results and discussion

Results from both numerical analysis and experimental tests are hereby presented. Load-displacement curves from static tests and backbone curves from cyclic tests are shown in Figure 2.

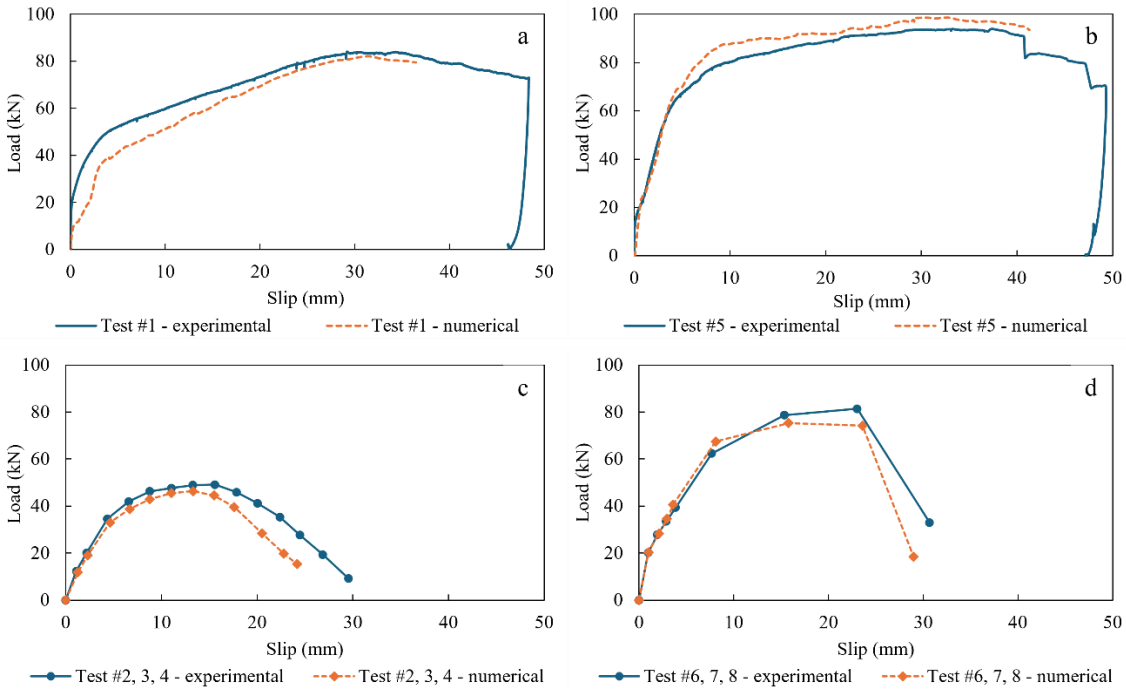


Figure 2. Load-slip results from analytical modelling and experimental tests. Static tests (a, b) and backbone curves from cyclic tests (c, d).

Effects of different screws diameters is evident from comparing Figure 2a and Figure 2b, where maximum capacities in static loading conditions are identified, as they are respectively 82 kN and 93 kN on the other hand ductility of test #1 and test #5 are very similar, given that the peak load is recorded at very similar slips, respectively 30 mm and 35 mm (Table 2). It is worth noticing that numerical modelling correctly represents the specimens load-slip curves detected in the experimental campaign; initial stiffness is correctly caught for test #5, while slightly underestimated for test #1, probably also due to some slackening in the setup.

Focusing on Figure 2c and Figure 2d, effects of cyclic loading conditions can be observed and, moreover, parameters listed in Table 2 provide a clear picture of the situation; impairment of strength (IS) is much more evident in tests #2, 3, 4 for 15 mm slip, while at 30 mm slip strong strength reductions are noticed for every joint, which almost lost almost of their capacities, with very high results variability. Focusing on equivalent viscous damping, significant energy dissipation is calculated for EVD1 at 15 mm for tests #6, 7, 8, while moderate energy dissipation capacity is recorded for tests #2, 3, 4. Considering EVD calculated for 3rd cycle, deterioration of the specimen dissipation capacity is

Copyright © 2025 CroCEE
DOI: https://doi.org/10.5592/CO/3CroCEE.2025.77

acknowledged for tests #6, 7, 8; on the other hand, results obtained for tests #2, 3, 4 are very similar for EVD1 and EVD3, so that deterioration is recorded from low slip values.

Results presented in Table 2 are focused on two specific slip values: 15 mm and 30 mm. The first slip value is useful to compare static and cyclic behaviours, since this is the limit slip suggested by EN 26891:1991 [15]; on the other hand, the second slip value is prescribed in the new Eurocode 8 [16]. However, both these two slip values may also be considered from an environmental perspective:

- Slip=15 mm corresponds to a "sustainability serviceability limit state", given that deterioration resulting from this deformation are still controlled and demountability is not totally compromised;
- Slip=30 mm corresponds to a "sustainability ultimate limit state", since deterioration is extended in the surroundings of the screw holes and easy demountability is not possible.

Table 2. Experimental tests results analysis: peak load, slip at peak load, load at 15 mm, impairment of strength at 15 mm, impairment of strength at 15 mm, impairment of strength at 30 mm, equivalent viscous damping at 1st cycle at 15 mm, equivalent viscous damping at 1st cycle at 30 mm, equivalent viscous damping at 3rd cycle at 15 mm, equivalent viscous damping at 3rd cycle at 30 mm.

Test #	Peak load (kN)	Slip at peak load (mm)	Load at 15 mm (kN)	IS at 15 mm	IS at 30 mm	EVD1 at 15 mm	EVD1 at 30 mm	EVD3 at 15 mm	EVD3 at 30 mm
1	82	30	67	-	-	-	-	-	-
2	49	16	48	85%	59%	10%	8%	8%	7%
3	46	13	43	75%	x	8%	x	8%	x
4	52	13	50	79%	48%	9%	7%	7%	7%
5	93	35	85	-	-	-	-	-	-
6	85	15	85	89%	x	14%	x	8%	x
7	84	23	81	87%	64%	15%	11%	6%	7%
8	82	23	79	89%	35%	15%	9%	7%	x

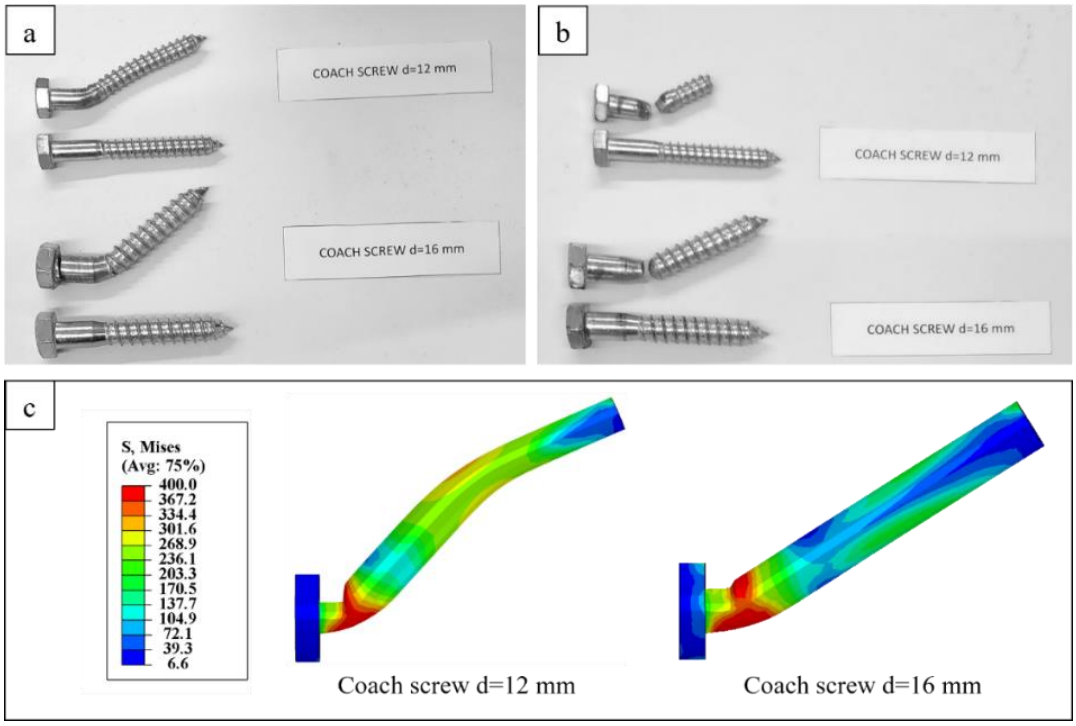


Figure 3. Screws failure modes in static (a) and in cyclic (b) loading conditions. Experimental findings match with results from numerical modelling in static loading conditions (c), refined from a previous study [12].

Copyright © 2025 CroCEE
DOI: https://doi.org/10.5592/CO/3CroCEE.2025.77

In order to properly understand differences arisen from considering screws with 12 mm and 16 mm diameters, failure modes are shown in Figure 3: greater bending deformation as a result of higher slenderness ratio of 12 mm-screws is highlighted; initiation of 2nd plastic hinge is detected in Figure 3a (test #1), while 2 clear plastic hinges are noticed for the same screws used in the specimens tested in cyclic loading conditions (Figure 3b, tests #2, 3, 4), as described in Table 3. On the other hand, greater strength of 16 mm-screws results in a less ductile failure mode, due to higher stress concentration, with 1 plastic hinge.

Moreover, numerical modelling carried out before experimental testing phase correctly predicted screws failure modes (Figure 3), with greater high stress concentration region for 16 mm-screw.

Table 3. Failure modes description

Test #	Failure mode
1	Screws with 1 evident plastic hinge and initiation of 2nd plastic hinge. CLT damage extended for 20 cm along holes direction
2, 3, 4	Screws with 2 plastic hinges and ruptures in their correspondences
5	Screws with 1 plastic hinge. CLT damage extended for 30 cm along holes direction
6, 7, 8	Screws with 1 plastic hinge and rupture in their correspondence

Finally, it is worth focusing on the surroundings of connections locations, in order to explore whether CLT damages (crushing, splitting, delamination, etc.) are correlated with screws failure modes. First of all, focusing on Figure 4a and Figure 4c, it is evident that timber is strongly damaged and splitting failure is detected; damage extent is greater in Figure 4c, as it also reached the CLT end, as an acknowledgement of the fact that a less ductile screw failure mode results into larger panel deterioration. On the other hand, greater screw ductility (12 mm diameter screw) takes advantage of timber embedment strength, resulting in more ductile specimen. Considering Figure 4b and Figure 4d, timber deterioration is noticed to be less extended, confirming the concept previously mentioned of "sustainability ultimate limit state", even though screws failures occur abruptly during testing; post-testing observed failure modes are the same with respect to static ones, except for fully development of both plastic hinges in tests #2, 3, 4.

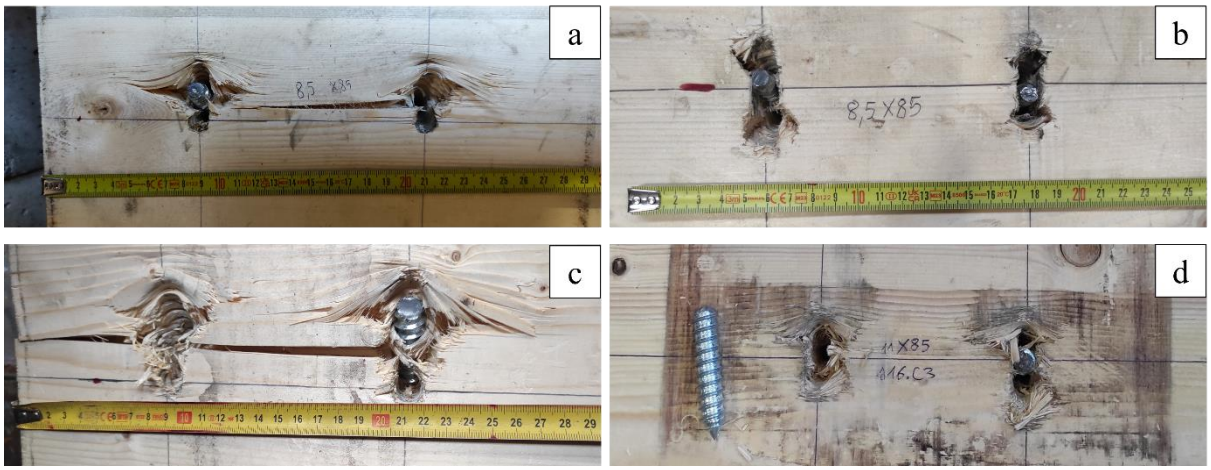


Figure 4. CLT panels in the surroundings of screw holes after testing. Specimen with 12 mm screw tested in static loading conditions (a); specimen with 12 mm screw tested in cyclic loading conditions (b); specimen with 16 mm screw tested in static loading conditions (c); specimen with 16 mm screw tested in cyclic loading conditions (d).

4. Conclusions

This research aims at providing a benchmark for future studies on timber-steel hybrid joints, which are expected to become increasingly widespread. The main focus is understanding of joints behaviour in

Copyright © 2025 CroCEE
DOI: https://doi.org/10.5592/CO/3CroCEE.2025.77

cyclic loading conditions, but remarks and observations towards environmental sustainability are constantly proposed.

Existing literature provides a quite defined frame for timber-steel hybrid joints subjected to static loading conditions, however a few investigations focus on cyclic tests, so that possible issues that may cause sudden strength or stiffness loss can be overlooked with unexpected consequences. This gap should be filled in the next years since timber-hybrid solutions are now becoming of prominent interest, and their popularity now crossed the traditional boundaries. This investigation moves in this direction, since comparison between static and cyclic tests are carried out, with calculation of parameters related to cyclic loading conditions, as impairment of strength and equivalent viscous damping.

The choice of investigating two different diameters for screws was relevant because some differences is noticed between tests #1, 2, 3, 4 (with 12 mm-screw diameter) and tests #5, 6, 7, 8 (with 16 mm-screw diameter); this last set of tests highlighted minor strength loss under repeated loading, but failure mode is less ductile with respect to the other set of tests. It is fundamental to ensure ductile failure modes for connections, since in case the whole ductility is demanded to the timber panel, brittle failures as e.g., splitting, row and/or block shear develop; on the other hand, in case two plastic hinge evolve, overcome of timber embedment strength is facilitated and abrupt cracking is limited. In this context, the abovementioned concept of "sustainability limit states" is the key to read the whole research: this concept involves both structural (serviceability and ultimate limit states) and environmental perspectives, considering that reuse End-of-Life scenario can be foreseen just in case the slip – and consequently joint deterioration – is limited (e.g., for slips lower than 15 mm). Focusing on this serviceability limit state, it is worth mentioning the concept of demountability easiness, which can be applied just in case connectors deformations are small. On the other hand, experience has shown that multiple EOL scenarios are necessary to smooth some of the uncertainties linked to this stage, so that e.g., lower reuse percentages may be planned in case a strong seismic event hit the building and large drifts are experienced.

Future developments include testing on different connections systems – e.g., bolts – to better understand the link between structural performances and environmental sustainability. Moreover, additional tests on similar specimens within "sustainability serviceability limit states" are foreseen, in order to define a limit below that connectors demountability is possible without extending damage in the CLT panel. Considering the possibility of a seismic event, it is also essential to evaluate demountability easiness in the perspective of ready connections substitution, such that not just environmental sustainability is guaranteed, but also social and economic one, given that inconveniences caused to inhabitants are reduced and extended and expensive post-seismic repair are avoided.

Acknowledgements

Authors want to express their gratitude to ROTHOBLAAS SRL for providing steel screws to carry out experimental laboratory tests presented in this study.

References

[1] Zeng, N., King, A. W., Zaitchik, B., Wullschleger, S. D., Gregg, J., Wang, S., & Kirk-Davidoff, D. (2013): Carbon sequestration via wood harvest and storage: an assessment of its harvest potential. *Climatic Change*, **118**, 245-247, doi: https://doi.org/10.1007/s10584-012-0624-0

[2] Cordier, S., Blanchet, P., Robichaud, F., & Amor, B. (2022): Dynamic LCA of the increased use of wood in buildings and its consequences: Integration of CO2 sequestration and material substitutions. *Building and Environment*, **226**, 109695, doi: https://doi.org/10.1016/j.buildenv.2022.109695

[3] Corti, L., & Muciaccia, G. (2023): Impact of end-of-life stage in cradle-to-cradle LCA analysis of timber and timber-hybrid buildings. *IALCCE 2023 - The Eighth International Symposium on Life-Cycle Civil Engineering*, Milan, Italy, doi: https://doi.org/10.1201/9781003323020

Copyright © 2025 CroCEE
DOI: https://doi.org/10.5592/CO/3CroCEE.2025.77

[4] Pastori, S., Mazzucchelli, E. S., & Wallhagen, M. (2022): Hybrid timber-based structures: A state of the art review. *Construction and Building Materials*, **359**, 129505, doi: https://doi.org/10.1016/j.conbuildmat.2022.129505

[5] Yeoh, D., Fragiacomo, M., De Franceschi, M., & Heng Boon, K. (2011): State of the art on timber-concrete composite structures: Literature review. *Journal of Structural Engineering*, *137*(10), 1085-1095, doi: https://doi.org/10.1061/(ASCE)ST.1943-541X.0000353

[6] Follesa, M., Fragiacomo, M., Casagrande, D., Tomasi, R., Piazza, M., Vassallo, D., Canetti, D., Rossi, S. (2018): The new provisions for the seismic design of timber buildings in Europe. *Engineering Structures*, **168**, 736-747, doi: https://doi.org/10.1016/j.engstruct.2018.04.090

[7] Stepinac, M., Šušteršič, I., Gavrić, I., & Rajčić, V. (2020): Seismic design of timber buildings: Highlighted challenges and future trends. *Applied sciences*, **10**(4), 1380, doi: https://doi.org/10.3390/app10041380

[8] Loss, C., Piazza, M., & Zandonini, R. (2016): Connections for steel–timber hybrid prefabricated buildings. Part I: Experimental tests. *Construction and Building Materials*, **122**, 781-795, doi: https://doi.org/10.1016/j.conbuildmat.2015.12.002

[9] Hassanieh, A., Valipour, H. R., & Bradford, M. (2016): Load-slip behaviour of steel-cross laminated timber (CLT) composite connections. *Journal of Constructional Steel Research*, **122**, 110-121, doi: doi.org/10.1016/j.jcsr.2016.03.008

[10] Imakawa, K., Ochiai, Y. A., Hori, N., Takemura, A., & Yamaguchi, T. (2022): Mechanical properties of hybrid joints in timber structures. *Journal of Wood Science*, **68**(1), doi: http://dx.doi.org/10.1186/s10086-022-02043-4

[11] Gavric, I., Fragiacomo, M., & Ceccotti, A. (2015): Cyclic behaviour of typical metal connectors for cross-laminated (CLT) structures. *Materials and Structures*, **48**, 1841–1857, doi: https://doi.org/10.1617/s11527-014-0278-7

[12] Corti, L., & Muciaccia, G. (2024): Numerical modelling of timber-steel hybrid structures: challenges and innovative strategies. *Proceedings in civil engineering*, **7**(1-2), 92-101, doi: https://doi.org/10.1002/cepa.3026

[13] Corti, L., & Muciaccia, G. (2024): A numerical investigation of mechanical connectors in steel-timber joints under cyclic loading. *18th World Conference on Earthquake Engineering (WCEE2024)*, Milan, Italy.

[14] European Committee for Standardization (1991): *EN 26891:1991 Timber structures - Joints made with mechanical fasteners - General principles for the determination of strength and deformation characteristics*.

[15] European Committee for Standardization (2001): *EN 12512:2001 Timber structures - Test methods - Cyclic testing of joints made with mechanical fasteners*.

[16] European Committee for Standardization (2024): *EN1998-1-1:2024 Eurocode 8 – Design of structures or earthquake resistance - Part 1-1: General rules and seismic action* (draft).

Proceedings of the 3rd Croatian Conference on Earthquake Engineering - 3CroCEE
19–22 March 2025, Split, Croatia
Copyright © 2025 CroCEE
DOI: https://doi.org/10.5592/CO/3CroCEE.2025.91

EXPERIMENTAL IN-SITU TESTING OF AN EXISTING BRIDGE

Antonio Shoklarovski [(1)], Aleksandra Bogdanovic [(2)], Zoran Rakicevic [(2)], Filip Manojlovski [(1)], Angela Poposka [(3)]

[(1)] *Res. Assist.,MSc, Institute of Earthquake Engineering and Engineering Seismology, University "Ss. Cyril and Methodius", Skopje, North Macedonia, antonio@iziis.ukim.edu.mk, filipmanojlovski@iziis.ukim.edu.mk*
[(2)] *Prof. PhD, Institute of Earthquake Engineering and Engineering Seismology, University "Ss. Cyril and Methodius", Skopje, North Macedonia, saska@iziis.ukim.edu.mk, zoran_r@iziis.ukim.edu.mk*
[(3)] *Res. Assist.,PhD, Institute of Earthquake Engineering and Engineering Seismology, University "Ss. Cyril and Methodius", Skopje, North Macedonia, angela@iziis.ukim.edu.mk*

Abstract

The assessment of the condition of existing bridges is of great importance, particularly for bridge structures that have been in operation for a long time and for which no adequate technical documentation exists. The behavior and condition of these bridges change over time, making it necessary to perform specific experimental tests and additional analyses to determine their actual load-bearing capacity and usability.

This paper presents the results of experimental in-situ tests conducted on a steel bridge. The experimental activities were divided into two phases. The first phase involved determining the dynamic characteristics of the bridge using the ambient vibration method, while the second phase focused on evaluating the bridge's behavior under static and dynamic loading. The equipment used for determining the dynamic characteristics included accelerometers, a data acquisition system, and a computer. For the static and dynamic loading tests, strain gauges, accelerometers, and linear potentiometers were used.

The results of these tests form the basis for further numerical analyses of the bridge's load-bearing capacity and stability.

In conclusion, following detailed analyses and investigations, conclusions regarding the condition of the bridge structure were drawn.

Keywords: bridge, ambient vibration, static and dynamic loading

1. Introduction

The behavior and condition of existing bridges changes over time. Therefore, to obtain an accurate assessment of their load-bearing capacity and usability, it is necessary to perform specific experimental tests and additional analyses. This paper presents the results of experimental investigations conducted on a steel bridge located in the municipality of Negotino, near the village of Krivolak, Republic of N. Macedonia [1][2][3]. The experimental activities for this structure were divided into two phases. The first phase included tests to determine the dynamic characteristics of the bridge using the ambient vibration method, while the second phase involved tests to evaluate the bridge's behavior under static and dynamic loading. Selected results from these investigations are presented in this paper.

2. Description of the structure

The bridge is a steel structure built in the 1940s, using construction techniques typical of that time (Fig. 1). The structure is straight, with two traffic lanes and steel railings on both sides. It provides a reliable crossing over the Vardar River, connecting the local road from the Krivolak military area to surrounding areas, ensuring the safe passage of motor vehicles.

Copyright © 2025 CroCEE
DOI: https://doi.org/10.5592/CO/3CroCEE.2025.91



Figure 1. View of the bridge

The bridge consists of five spans, each representing a static simply supported beam system. Each span measures 34.0 meters in length. The main load-bearing elements are two longitudinal steel trusses, divided into seven sections, each 4.85 meters long. These trusses are interconnected by transverse girders and braces on the upper side, as well as transverse and longitudinal girders and braces on the lower side.

On the lower longitudinal and transverse girders, a steel sheet is placed, over which a reinforced concrete slab is cast. The total height of the truss is 5.0 meters, and the distance between the two main trusses is also 5.0 meters. All components, including the main trusses, longitudinal and transverse girders on both the upper and lower sides, are made of steel "L," "U," "I," and plate elements. These are connected to form complex cross-sections. The elements of the bridge are interconnected using rivets, providing rigid connections.

The main girders are supported on bearings that are fixed on one side and movable on the other. The usable width of the bridge is 4.0 meters, with an open bridge deck. The deck structure consists of a composite reinforced concrete slab over trapezoidal steel sheeting and a finishing layer of cast asphalt. The thickness of the reinforced concrete slab is 40 cm.

The abutments and central piers are constructed of stone, while the exact foundation type remains unknown.

3. Methodology of testing

The bridge under investigation is a steel structure for which no construction design documentation is available. Consequently, the design loads, characteristics of the structural elements, type of bearings, and calculated deflections and deformations from the design are unknown. Due to these limitations, the testing procedure could not fully comply with the MKS 1019:2018 standard for bridge testing [4]. Instead, the testing was adapted to the on-site conditions and the resources available.

Another significant challenge was the lack of information regarding the bridge's foundation. The condition of the foundation plays a vital role in the overall stability of the structure, particularly under future operational loads.

The tests conducted on the bridge were categorized as control tests, as specified in Section 4.1 of MKS 1019:2018, and performed during its operational phase. Since no documentation was available, an initial visual inspection was carried out. Based on this inspection, a testing program was developed, which included the following tasks described in Section 5.2 of MKS 1019:2018:

- Definition of the size and distribution of loads for each phase;
- Identifying measurement points where maximum deflections and deformations were expected;
- Development of an organizational plan for the application of the loads.

Both static and dynamic load tests were performed in accordance with Section 4.3 of MKS 1019:2018.

Copyright © 2025 CroCEE
DOI: https://doi.org/10.5592/CO/3CroCEE.2025.91

The static load tests provided the following results (as per Section 5.4 of MKS 1019:2018):

- Measurements of vertical deflections at the midspan of the bridge;
- Occurrence of cracks in the structural elements;
- Measurements of deformations at places of expected extreme effects;
- Measurements of residual deflections and deformations after the removal of the loads.

Unfortunately, due to limited access, it was not possible to measure displacements at the bridge bearings.

The dynamic load tests provided the following results:

- Measurements of vertical deflections at the midspan during the passage of a moving load;
- Measurements of the speed at which the load traveled across the bridge.

Additional measurements during the dynamic tests included:

- Deformations at critical locations under extreme effects;
- Transverse and longitudinal displacements at the midspan of selected spans;
- Remaining dynamic characteristics of the bridge structure.

The experimental setup included PCB Piezotronics 393B12 accelerometers, Kyowa KC-70-A1-11 strain gauges, and Micro-Epsilon WDS-1000-P60-SR-U linear potentiometers to measure accelerations, strains, and displacements, respectively. Data acquisition was performed using National Instruments cDAQ 9188 and National Instruments cDAQ 9178 systems, connected to a portable laptop for real-time monitoring and recording.

Some of the results are presented in this paper.

4. Determination of the bridge's dynamic characteristics using the ambient vibration method

4.1. Testing procedure and Instrument layout

The testing procedure consisted of recording real-time accelerations and processing the data in both the time and frequency domains. Accelerometers were placed at predefined points on the bridge structure. The arrangement of these measurement points was designed to maximize the number of necessary records to accurately determine the required dynamic characteristics [5][6][7].

At each point, three accelerometers were installed to measure accelerations in the transverse, longitudinal, and vertical directions. One point (Point 13, Fig. 2) was selected as a reference point, where the accelerometers remained in a fixed position throughout all measurements. The other 12 accelerometers were moved across the remaining predefined points. In total, 42 measurement points were defined for the bridge. Fig. 2 illustrates the placement of the accelerometers at these measurement points.

To record the acceleration time histories at all predefined points, 11 measurements were conducted. Each dataset consisted of acceleration time histories with a duration of 300 seconds and a sampling frequency of 2048 Hz (2048 samples per second). During the field measurements, the bridge and surrounding structures were in a state of rest. A bandpass filter ranging from 0.5 Hz to 35 Hz was applied to remove low-frequency drift and high-frequency noise, ensuring accurate measurement of the structural response.

This methodology ensured that the collected data could be used to accurately determine the dynamic characteristics of the bridge.

Copyright © 2025 CroCEE
DOI: https://doi.org/10.5592/CO/3CroCEE.2025.91

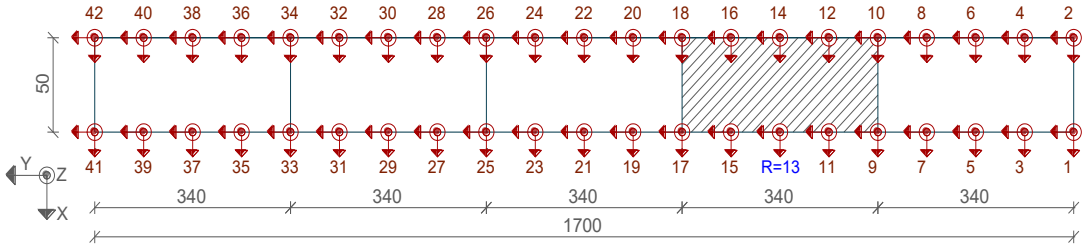


Figure 2. Position of accelerometers at measuring points

4.2. Results and Discussion

The recorded ambient vibration data were analyzed and processed using the ARTeMIS Modal software (version 7.1), developed by Structural Vibration Solutions A/S [8]. The dynamic characteristics of the bridge—natural frequencies, mode shapes in different directions, and damping coefficients—were determined using the Peak Picking (PP) technique, an identification method applied in the frequency domain to the recorded data. Table 1 presents the identified dominant frequencies of the bridge and their corresponding mode shapes.

Table 1. Dominant frequencies of the structure – model of the integral bridge

Frequency [Hz]	Mode
5.4	First mode – vertical direction
6.9	First mode – transverse direction
9.1	First mode - torsion
11.0	Second mode – vertical direction

By analyzing the determined dynamic characteristics of the bridge, it can be concluded that the fundamental natural frequencies are relatively clearly defined, and the mode shapes exhibit a continuous deformation pattern. This suggests a uniform distribution of stiffness across the structure. The modes of vibrations are given in Fig. 3, Fig. 4, and Fig. 5.

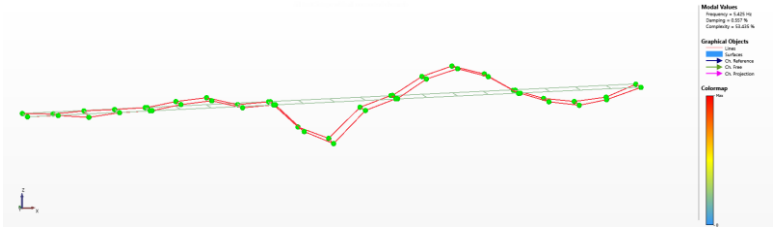


Figure 3. First mode – vertical direction [5.4Hz]

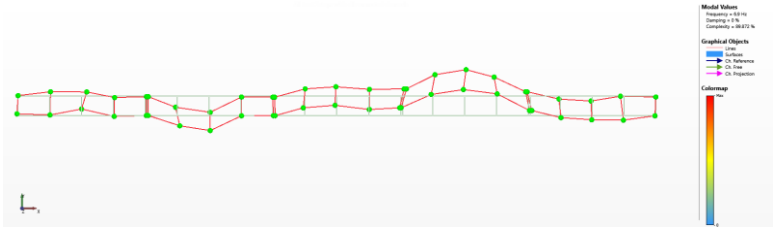


Figure 4. First mode – transverse direction [6.9Hz]

Copyright © 2025 CroCEE
DOI: https://doi.org/10.5592/CO/3CroCEE.2025.91

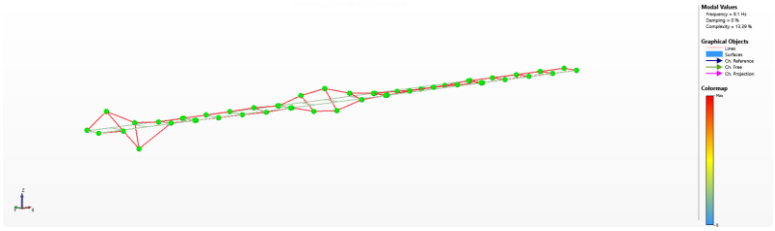


Figure 5. First mode - torsion [9.1Hz]

5. Static and Dynamic loading

To determine the control parameters during serviceability of the bridge, appropriate instrumentation was installed, as shown in Fig. 6. A total of 29 instruments were placed, including 10 strain gauges (SG) positioned at key locations to measure strains, 15 accelerometers (ACC) placed at five points to measure acceleration in the three directions (x, y, and z), and 4 linear potentiometers (LP) for measuring deflections (vertical deformations).

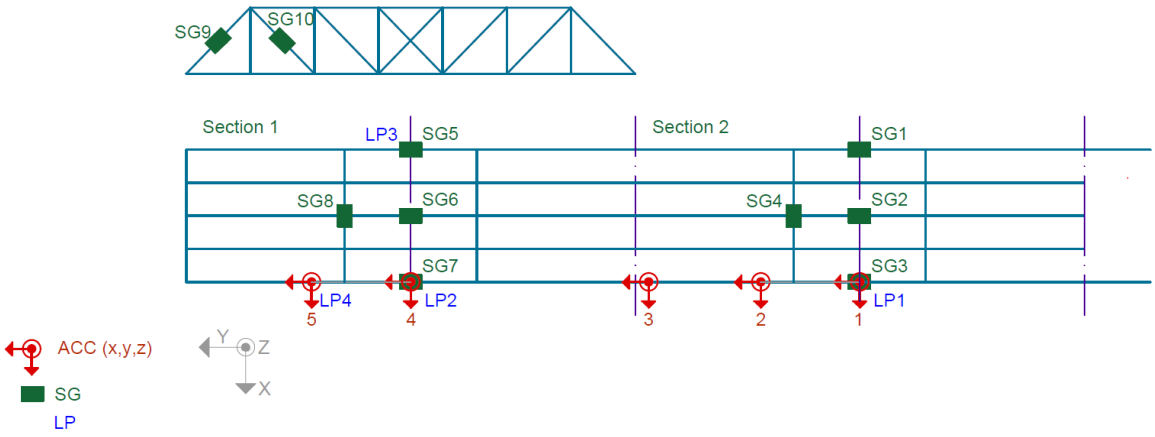


Figure 6. Scheme of instruments on the steel bridge

For the static and dynamic loading tests, two types of trucks were used, with a total of four trucks. The characteristics of the trucks used, Truck A and Truck B, are provided in Fig. 7 and Table 2, along with a more detailed presentation of the distribution of forces on the wheels during the static loading test.



Figure 7. Axial distance of wheels of trucks A and B

Table 2. Axial distribution of forces in the wheels of trucks A and B

Truck A ≈ 24.8t		**Truck B ≈ 24.5t**	
Point	Force [kN]	Point	Force [kN]
1	46.5	3	46
2	31.5	4	31.9

Copyright © 2025 CroCEE
DOI: https://doi.org/10.5592/CO/3CroCEE.2025.91

Initially, the section marked as 2 was loaded, starting with one truck positioned at the center, as shown in Fig. 8, with a load of 24.0 tons, for a duration of three minutes. Consequently, the load was increased by adding two, and then four trucks, resulting in a total load of 48.0 tons and 96.0 tons, respectively (Fig. 8). Between all the tests, unloading was performed, and a baseline (empty) measurement was taken without any load, lasting three minutes.

It is important to note that due to a lack of space to place the four trucks as a concentrated load in the midspan of section, they were arranged in a line along the entire length of the field. Fig. 9 shows a photo of the sixth static loading test of section 2.

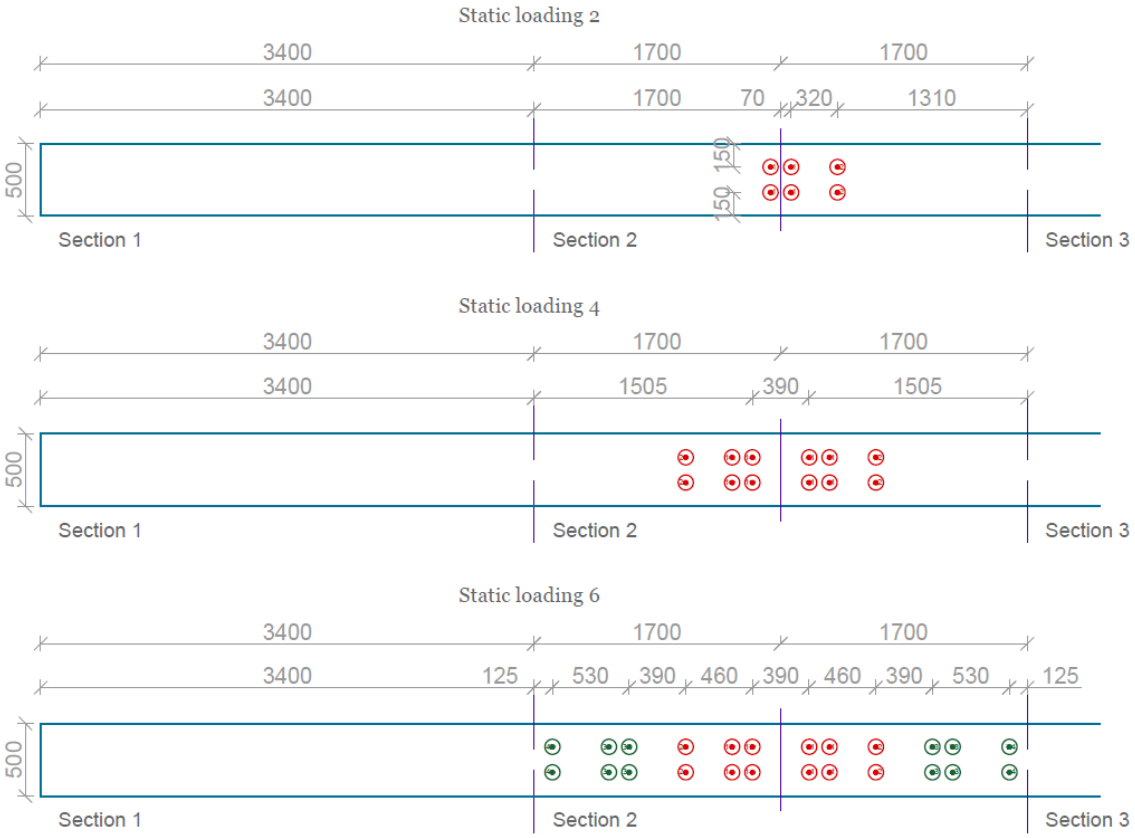


Figure 8. Position of trucks during static tests in section 2



Figure 9. Photo of static loading of section 2

Proceedings of the 3rd Croatian Conference on Earthquake Engineering - 3CroCEE
19–22 March 2025, Split, Croatia
Copyright © 2025 CroCEE
DOI: https://doi.org/10.5592/CO/3CroCEE.2025.91

Table 3 presents the maximum values of strains and deflections under characteristic loadings for section 2. From the results of the vertical displacements, it can be concluded that the measured vertical deformations are smaller than the allowable limit of L/750. Fig. 10 shows the strains measured by the strain gauges.

Table 3. Maximum values from instruments under static trial loading of section 2

	SG1 [mstr]	SG2 [mstr]	SG3 [mstr]	SG4 [mstr]	LP1 [mm]
Static loading 2	44.72	134.99	45.32	81.50	2.5
Static loading 4	65.31	34.82	70.04	93.97	3.62
Static loading 6	73.08	38.43	89.54	93.11	4.12

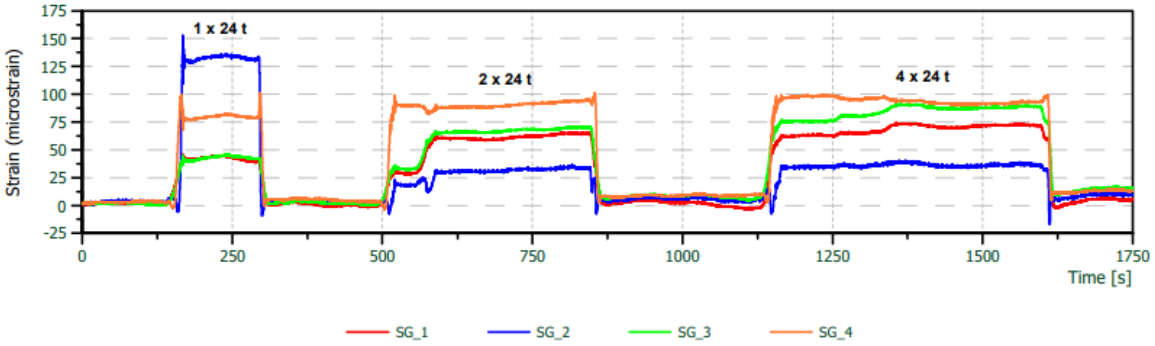


Figure 10. Time histories from strains measured by strain gauges during static loading of section 2

Residual deformations were analyzed to assess their significance. The results indicate that the maximum residual deformation does not exceed 10%, corresponding to approximately 10-15 microstrains. This is a small value and within acceptable limits, meaning it does not pose any structural concerns. The minor residual strain is likely due to measurement sensitivity or localized material behavior, and it does not affect the overall stability of the bridge.

The dynamic loading was carried out through three different tests, simultaneously on section 1 and section 2. The trucks passed over the bridge at various characteristic speeds (5 km/h – 20 km/h). A metal plate obstacle was placed at the third points of the bridge, in section 1 and 2, to simulate an impulsive dynamic excitation. Table 4 presents the maximum deflections (vertical deformations).

Table 4. Tabular presentation of deflections during the dynamic tests

Instrument	Vertical deformation due to static load [mm]	Vertical deformation due to dynamic load – 5km/h [mm]	Vertical deformation due to dynamic load – 10km/h [mm]	Vertical deformation due to dynamic load – 20km/h [mm]
LP1	4.12	1.27	2.11	2.73
LP2	4.73	1.8	2.32	285
LP1	4.12	1.27	2.11	2.73

6. Conclusions

Based on the conducted experimental investigations, the following conclusions can be drawn:

– Dynamic characteristics: The dynamic properties of the bridge, such as natural frequencies and mode shapes, were clearly defined. The bridge shows a consistent deformation pattern, indicating a uniform distribution of stiffness across its structure.

Copyright © 2025 CroCEE
DOI: https://doi.org/10.5592/CO/3CroCEE.2025.91

- Deflections and deformations: Both static and dynamic deflections and deformations were within acceptable limits set by the standards. The vertical deflections after unloading were well below the allowed limits for steel and composite bridges.
- Impact on functionality: The deflections and vibrations do not affect the bridge's use, safety, or appearance. Vibrations did not cause discomfort for users, showing that the bridge works well under the applied loads.
- Conformance to standards: Although the tests could not fully follow the MKS 1019:2018 standard due to missing design data, the methods were adjusted to fit the available conditions on-site, ensuring reliable results.
- Further investigations: More studies are needed to check the condition of the foundation, as the lack of detailed information about it could affect the bridge's overall stability and long-term performance.

Based on all the results obtained, it was determined that the bridge is in good condition and performs well under the loads applied during the tests.

References

[1] Testing of Allowed Loads and Other Important Characteristics of the Steel Bridge Near the Village of Krivolak, IZIIS Report 2022-42 (in Macedonian).

[2] Load Test of Bridges – MKC 1019:2018, Macedonian Standard.

[3] A. Bogdanovic, M. Vitanova, J. Bojadjieva, Z. Rakicevic, V. Sesov, K. Edip, N. Naumovski, F. Manojlovski, A. Poposka, A. Shoklarovski, T. Kitanovski, D. Ivanovski, I. Markovski, and D. Filipovski, "Structural Parameter Diagnosis of Old Steel Truss Bridge Using Numerical and Experimental Techniques," *Earthquake Engineering & Dynamics for a Sustainable Future - SECED*, September 14-15, 2023, Cambridge, UK.

[4] A. Shoklarovski, A. Bogdanovic, Z. Rakicevic, A. Poposka, and F. Manojlovski, "Experimental Tests of Bridge Structures," *Proceedings of the 20th International Symposium of MASE*, September 28-29, 2023, DoubleTree by Hilton, Skopje, ISBN: 978-608-66946-2-3.

[5] M. Venglár, M. Sokol, R. Ároch, and J. Jur, "Ambient Vibration Measurements of Steel Truss Bridges," *Journal of Measurements in Engineering*, vol. 6, no. 4, December 2018.

[6] T. Yin and H.-P. Zhu, "Probabilistic Damage Detection of a Steel Truss Bridge Model by Optimally Designed Bayesian Neural Network," *Sensors*, 2018.

[7] L. Marcheggiani, F. Clementi, and A. Formisano, "Static and Dynamic Testing of Highway Bridges: A Best Practice Example," *Journal of Civil Structural Health Monitoring*, 2019.

[8] *Structural Vibration Solutions: User Manual SVS*.

Proceedings of the 3rd Croatian Conference on Earthquake Engineering - 3CroCEE
19–22 March 2025, Split, Croatia
Copyright © 2025 CroCEE
DOI: https://doi.org/10.5592/CO/3CroCEE.2025.93

EXPERIMENTAL ASSESSMENT OF EXISTING BRIDGE STRUCTURE

Angela Poposka [(1)] Antonio Shoklarovski [(2)], Aleksandra Bogdanovic [(3)], Zoran Rakicevic [(3)], Filip Manojlovski [(2)]

[(1)] *Res. Assist.,PhD, Institute of Earthquake Engineering and Engineering Seismology, University "Ss. Cyril and Methodius", Skopje, North Macedonia, angela@iziis.ukim.edu.mk*
[(2)] *Res. Assist.,MSc, Institute of Earthquake Engineering and Engineering Seismology, University "Ss. Cyril and Methodius", Skopje, North Macedonia, antonio@iziis.ukim.edu.mk, filipmanojlovski@iziis.ukim.edu.mk*
[(3)] *Prof. PhD, Institute of Earthquake Engineering and Engineering Seismology, University "Ss. Cyril and Methodius", Skopje, North Macedonia, saska@iziis.ukim.edu.mk, zoran_r@iziis.ukim.edu.mk*

Abstract

Assessing existing bridges is an important task in the sustainable management of infrastructure, particularly for those structures that have been in service for extended periods and lack comprehensive technical documentation. In fact, due to the old age of a large part of the infrastructure assets and the deteriorating conditions affecting the structural elements, their safety with respect to the ultimate limit states may be compromised, making it essential to conduct experimental assessments and additional analyses to accurately determine their current load-bearing capacity and functional viability.

Experimental tests performed on an existing concrete bridge built in the 90s are presented in this paper. The bridge is a single-bay structure with a simply supported beam structural system and a 12.8-meter span. The testing process was divided into two phases. In the first phase, the dynamic characteristics of the bridges were evaluated using the ambient vibration method, while the second phase focused on assessing the bridges' behavior under static and dynamic loads. More in detail, the second phase was carried out through static and dynamic load testing. To measure dynamic characteristics, accelerometers, data acquisition systems, and a PC were employed, whereas strain gauges, accelerometers, and linear potentiometers were used for static and dynamic loading tests.

The results from these experimental tests can be utilized to calibrate and enhance the accuracy of the numerical analyses for the bridge, so more complex analyses and seismic assessment could be performed. Following comprehensive analyses and investigations, conclusions were reached regarding the condition of the bridge structure.

Keywords: bridge, ambient vibration, static and dynamic loading

1. Introduction

The condition and performance of existing bridges built in the past evolve over time. Consequently, obtaining an accurate evaluation of their load-bearing capacity and functionality requires specific experimental testing and additional analyses. This paper discusses the findings from experimental studies conducted on an existing concrete bridge [1] [7] situated in the municipality of Negotino, R. N. Macedonia. The experimental process for this structure involved assessing the dynamic characteristics of the bridge using the ambient vibration method and evaluating its response to static and dynamic loading. Key results from these investigations are presented in this paper.

2. Description of the structure

The bridge is a concrete structure built in the 90s, using construction techniques typical of that time. The bridge is a single-bay structure with a simply supported beam structural system and a 12.8-meter span. The structure consists of eight longitudinal reinforced concrete girders placed side by side, supporting a cast-in-place reinforced concrete slab. The girders have a variable cross-section along their length. At the middle of the span, they have a "T" cross-section with a height of 80 cm, a web width of 20 cm, and a flange thickness of 15 cm. Toward the ends, the cross-section of the girders gradually

Copyright © 2025 CroCEE
DOI: https://doi.org/10.5592/CO/3CroCEE.2025.93

transitions into a rectangular shape with dimensions of 50/80 cm. The reinforced concrete slab consists of the flanges of the girders, which are tightly positioned to each other, and a leveling layer of concrete of 5 cm, over which a layer of asphalt is applied. The primary longitudinal girders are interconnected by transverse girders, positioned at each quarter of the span of the main girders. The main girders are positioned directly on the end columns, which has resulted in localized detachment of surface concrete layers, (Fig. 1).



Figure 1. Location and appearance of the concrete bridge.

3. Methodology of testing

The bridge under investigation is an existing concrete structure for which no construction design documentation is available. Consequently, the design loads, characteristics of the structural elements, type of bearings, and calculated deflections and deformations from the design are unknown. Due to these limitations, the testing procedure could not fully comply with the MKS 1019:2018 standard for bridge testing [2]. Instead, the testing was adapted to the on-site conditions and the resources available [8]. Another major challenge was the absence of detailed information about the bridge's foundation, which condition is crucial to ensuring the structure's overall stability, especially when subjected to future operational loads.

The tests conducted on the bridge were classified as control tests, in accordance with Section 4.1 of MKS 1019:2018 [2], and were carried out during the bridge's operational phase. Due to the lack of documentation, an initial visual inspection was performed. Following this inspection, a testing program was developed, incorporating the tasks outlined in Section 5.2 of MKS 1019:2018:

- Definition of the size and distribution of loads for each phase;
- Identifying measurement points where maximum deflections and deformations are expected;
- Development of an organizational plan for the application of the loads.

Both static and dynamic load tests were performed in accordance with Section 4.3 of MKS 1019:2018.

The static load tests provided the following results (as per Section 5.4 of MKS 1019:2018):

- Measurements of vertical deflections at the midspan of the bridge;
- Occurrence of cracks in the structural elements;
- Measurements of deformations at places of expected extreme effects;
- Measurements of residual deflections and deformations after the removal of the loads.

Unfortunately, due to limited access, it was not possible to measure displacements at the bridge bearings.

The dynamic load tests provided the following results:

- Measurements of vertical deflections at the midspan during the passage of a moving load;
- Measurements of the speed at which the load traveled across the bridge.

Copyright © 2025 CroCEE
DOI: https://doi.org/10.5592/CO/3CroCEE.2025.93

Additional measurements during the dynamic tests included:

- Deformations at critical locations under extreme effects;
- Transverse and longitudinal displacements at the midspan of selected spans;
- Remaining dynamic characteristics of the bridge structure.

Some of the results are presented in this paper.

4. Determination of the bridge's dynamic characteristics using the ambient vibration method

4.1. Testing procedure and Instrument layout

The ambient vibration method was used for determination of the current dynamic characteristics of the bridge. The testing procedure involved capturing real-time accelerations and analyzing the data in both the time and frequency domains. Accelerometers were strategically placed at predefined locations on the bridge structure. The placement of these measurement points was carefully planned to ensure the collection of sufficient data for accurately determining the required dynamic characteristics [3][4][5].

Ten measurement points were defined for the bridge. At each point, three accelerometers were installed to measure accelerations in the transverse, longitudinal, and vertical directions, total 30 accelerometers. One point (Point 2, Fig. 2) was selected as a reference point, where the accelerometers remained in a fixed position throughout all measurements. The other 27 accelerometers were moved across the remaining predefined points. Fig. 2 illustrates the placement of the accelerometers at these measurement points. To record the acceleration time histories at all predefined points, 3 measurements were conducted. Each dataset consisted of acceleration time histories with a duration of 300 seconds and a sampling frequency of 2048 Hz (2048 samples per second). During the field measurements, the bridge and surrounding structures were in a state of rest.

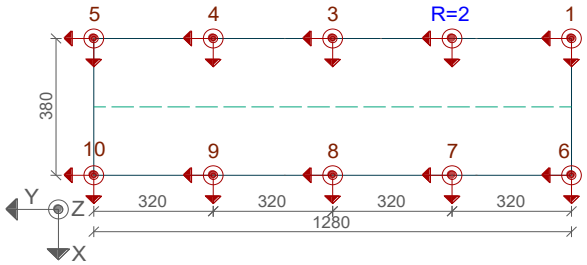


Figure 2. Position of accelerometers at measuring points

4.2. Results and Discussion

The recorded ambient vibration data were analyzed and processed using the ARTeMIS Modal software (version 7.1), developed by Structural Vibration Solutions A/S [6]. The dynamic characteristics of the bridge—natural frequencies, mode shapes in different directions, and damping coefficients—were determined using the Peak Picking (PP) technique, an identification method applied in the frequency domain to the recorded data. Table 1 presents the identified dominant frequencies of the bridge and their corresponding mode shapes.

Table 1. Dominant frequencies of the structure – model of the integral bridge

Frequency [Hz]	Mode
11.0	First mode – vertical direction
14.0	First mode - torsion
17.8	Second mode – vertical direction

Copyright © 2025 CroCEE
DOI: https://doi.org/10.5592/CO/3CroCEE.2025.93

By analyzing the determined dynamic characteristics of the bridge, it can be concluded that the fundamental natural frequencies are in general clearly defined, and the mode shapes exhibit a continuous deformation pattern. This suggests a uniform distribution of stiffness across the structure. The modes of vibrations are given in Fig. 3, Fig. 4, and Fig. 5.

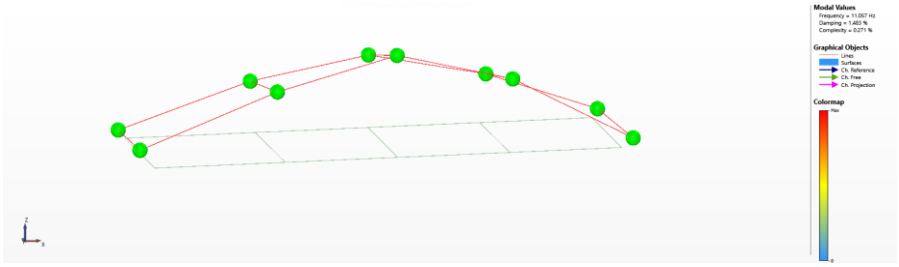


Figure 3. First mode – vertical direction [11.0 Hz]

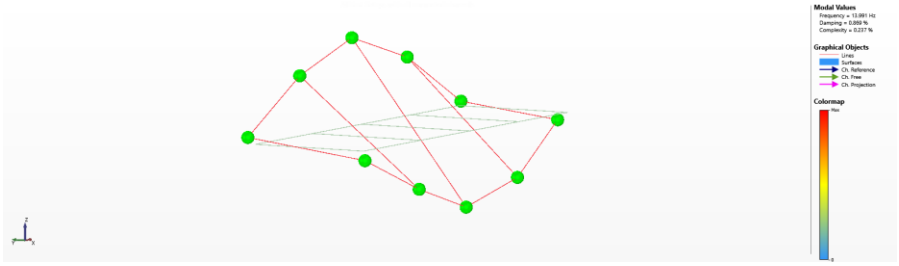


Figure 4. First mode – torsion [14.0 Hz]

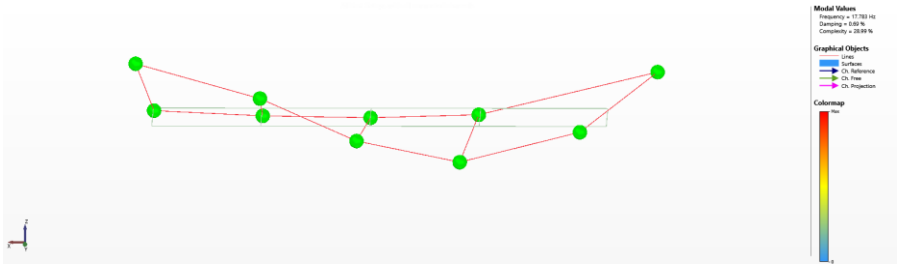


Figure 5. Second mode – vertical direction [17.8 Hz]

5. Static and Dynamic loading

To determine the control parameters during serviceability of the bridge, appropriate instrumentation was installed, as shown in Fig. 6. A total of 21 instruments were placed, including 4 strain gauges (SG) positioned at key locations to measure strains, 15 accelerometers (ACC) placed at five points to measure acceleration in the three directions (x, y, and z), and 2 linear potentiometers (LP) for measuring deflections (vertical deformations).

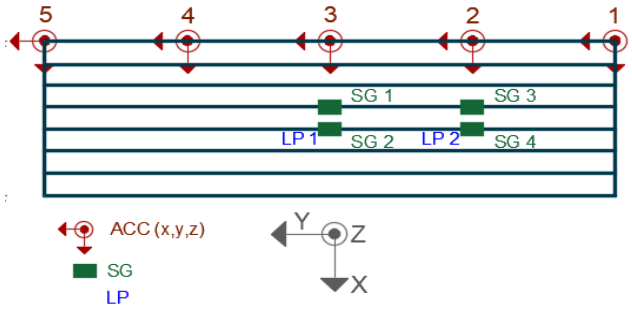


Figure 6. Scheme of instruments on the bridge

Copyright © 2025 CroCEE
DOI: https://doi.org/10.5592/CO/3CroCEE.2025.93

For the static and dynamic loading tests, two types of trucks were used, with a total of four trucks. The characteristics of the trucks used, Truck A and B, along with a the distribution of forces on the wheels during the static loading test are provided in Fig. 7.



Truck A ≈ 24.8t	
Point	Force [kN]
1	46.5
2	31.5
Truck B ≈ 24.5t	
Point	Force [kN]
3	46
4	31.9

Figure 7. Axial distance of wheels of trucks A and B

According to the size of the bridge and the trucks, the test loading was conducted using a maximum of two trucks. Initially, the bridge was loaded with a single truck, weighing approximately 24.8 tons, of which around 18.6 tons were on the rear wheels. Subsequently, the load was increased by adding another truck of the same type, resulting in an additional load of 24.8 tons. Between the static load tests, unloading (empty measurements without load) were performed. All tests lasted three minutes, Table 2.

Table 2. List of static loadings

No of loading	Duration	Mass [t]
1	3 min	0
2	3 min	24
3	3 min	0
4	3 min	48
5	3 min	0

It is important to note that due to insufficient space to position both trucks as a concentrated load in the middle of the span, they were aligned lengthwise along the entire span. Consequently, the maximum concentrated load at the center of the span was approximately 37 tons, while the maximum applied mass of nearly 49 tons acted as a uniformly distributed load across the entire span. The technical positioning of the trucks, for static loading, is illustrated in Fig. 8, whereas Fig. 9 presents photograph of the static loading number 4.

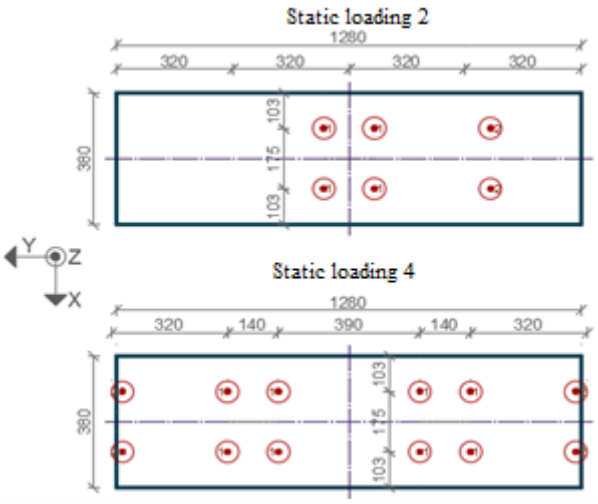


Figure 8. Position of trucks during static loading 2 and 4, respectively

Copyright © 2025 CroCEE
DOI: https://doi.org/10.5592/CO/3CroCEE.2025.93



Figure 9. Photo of static loading 4

Table 3 presents the maximum values of strains and deflections under characteristic static loadings. From the results of the vertical displacements, it can be concluded that the measured vertical deformations are smaller than the allowable limit of L/750. Furthermore, Fig. 10 shows the strains measured by the strain gauges during static loadings.

Table 3. Maximum values from instruments under static trial loadings

	SG1 [mstr]	SG2 [mstr]	SG3 [mstr]	SG4 [mstr]	LP1 [mm]	LP2 [mm]
Static loading 2	77.28	86.84	34.32	33.24	1.62	1.35
Static loading 4	167.94	161.02	171.76	142.18	1.84	1.26

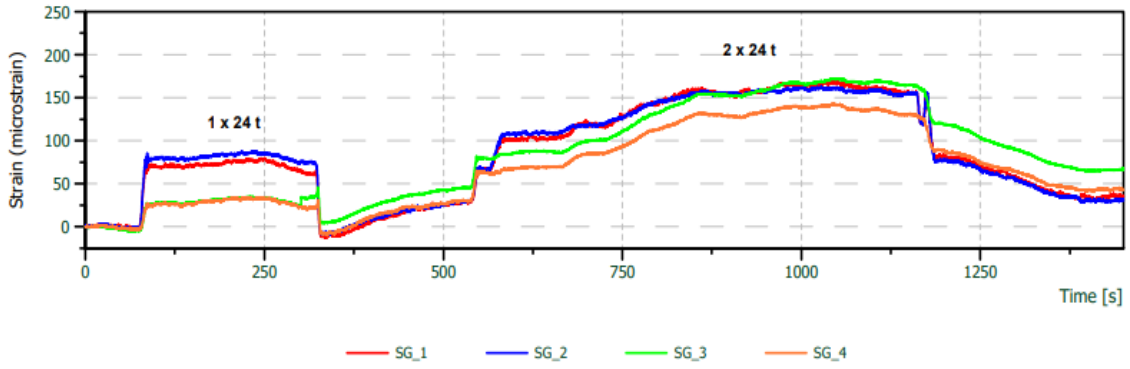


Figure 10. Time histories from strains measured by strain gauges during static loading

The dynamic loading was conducted through two different tests. Specifically, the trucks crossed the bridge at various characteristic speeds (5 km/h – 10 km/h). A metal plate obstacle was placed at the first third point of the bridge, to simulate an impulsive dynamic excitation. Table 4 presents the maximum deflections (vertical deformations) during the dynamic tests.

Table 4. Tabular presentation of deflections during the dynamic tests

Instrument	Vertical deformation due to static load [mm]	Vertical deformation due to dynamic load – 5km/h [mm]	Vertical deformation due to dynamic load – 10km/h [mm]
LP1	2.64	2.04	2.25
LP2	2.05	1.41	1.56

Copyright © 2025 CroCEE
DOI: https://doi.org/10.5592/CO/3CroCEE.2025.93

6. Conclusion

Based on the experimental investigations conducted, the following conclusions can be drawn:

- Dynamic characteristics: The dynamic properties of the bridge, such as natural frequencies and mode shapes, were clearly defined. The bridge shows a consistent deformation pattern, indicating a uniform distribution of stiffness across its structure.
- Deflections and deformations: Both static and dynamic deflections and deformations were within acceptable limits set by the standards. The vertical deflections after unloading were below the allowed limits for reinforced concrete bridges.
- Impact on functionality: The deflections and vibrations do not affect the bridge's use, safety, or appearance. Vibrations did not cause discomfort for users, showing that the bridge works well under the applied loads.
- Conformance to standards: Although the tests could not fully follow the MKS 1019:2018 standard due to missing design data, the methods were adjusted to fit the available conditions on-site, ensuring reliable results.
- Further investigations: More studies are needed to check the condition of the foundation, as the lack of detailed information about it could affect the bridge's overall stability and long-term performance.

Based on all the results obtained, it was determined that the bridge is in good condition and performs well under the loads applied during the tests. Furthermore, the findings from these experimental tests can be used to calibrate and improve the numerical model for the bridge, enabling more advanced evaluations and a more precise seismic assessment according to the current codes.

References

[1] Testing of Allowed Loads and Other Important Characteristics of the Concrete Bridge Near the Village of Krivolak, IZIIS Report 2022-43 (in Macedonian).

[2] Load test of bridges – MKC 1019:2018, Macedonian standard

[3] Michal Venglár, Milan Sokol, Rudolf Ároch, Jur. Ambient Vibration Measurements of Steel Truss Bridges, Journal of Measurements in Engineering, December 2018, Volume 6, Issue 4.

[4] Tao Yin, Hong-ping Zhu. Probabilistic Damage Detection of a Steel Truss Bridge Model by Optimally Designed Bayesian Neural Network, Sensors 2018.

[5] Marcheggiani Laura, Clementi Francesco, Formisano Antonio. Static and Dynamic Testing of Highway Bridges: A Best Practice Example, Journal of Civil Structural Health Monitoring, 2019.

[6] Structural Vibration Solutions. User Manual SVS.

[7] A. Shoklarovski, A. Bogdanovic, Z. Rakicevic, A.Poposka, F. Manojlovski, Experimental tests of bridge structures, 19th International Symposium of MASE, 28-29 September 2023, Skopje, North Macedonia, ISBN: 978-608-66946-3-0

[8] A. Bogdanovic, M. Vitanova, J. Bojadjieva, Z. Rakicevic, V. Sesov, K. Edip, N. Naumovski, F. Manojlovski, A. Poposka, A. Shoklarovski, T. Kitanovski, D. Ivanovski, I. Markovski, D. Filipovski Structural parameter diagnosis of old steel truss bridge using numerical and experimental technics, Earthquake Engineering & Dynamics for a Sustainable Future - SECED 14-15 September 2023, Cambridge UK

Proceedings of the 3rd Croatian Conference on Earthquake Engineering - 3CroCEE
19–22 March 2025, Split, Croatia
Copyright © 2025 CroCEE
DOI: https://doi.org/10.5592/CO/3CroCEE.2025.99

REMOTE TESTING AND ASSESSMENT OF DIFFERENT TYPES OF BRIDGES USING ADVANCED EVALUATION METHODS

Igor Gjorgjiev [(1)], Borjan Petreski [(2)], Marija Vitanova [(3)], Filip Manojlovski [(4)], Vlado Micov [(5)], Ana Nanevska [(6)], Trajche Zafirov [(7)]

[(1)] *Prof. Dr., Ss. Cyril and Methodius University in Skopje, Institute of Earthquake Engineering and Engineering Seismology, Skopje, Republic of North Macedonia, igorg@iziis.ukim.edu.mk*
[(2)] *Ass. Prof. Dr., Ss. Cyril and Methodius University in Skopje, Institute of Earthquake Engineering and Engineering Seismology, Skopje, Republic of North Macedonia, borjan@iziis.ukim.edu.mk*
[(3)] *Assoc. Prof. Dr., Ss. Cyril and Methodius University in Skopje, Institute of Earthquake Engineering and Engineering Seismology, Skopje, Republic of North Macedonia, marijaj@iziis.ukim.edu.mk*
[(4)] *Ass., Ss. Cyril and Methodius University in Skopje, Institute of Earthquake Engineering and Engineering Seismology, Skopje, Republic of North Macedonia, filipmanojlovski@iziis.ukim.edu.mk*
[(5)] *Prof. Dr., Ss. Cyril and Methodius University in Skopje, Institute of Earthquake Engineering and Engineering Seismology, Skopje, Republic of North Macedonia, micov@iziis.ukim.edu.mk*
[(6)] *Ass., Ss. Cyril and Methodius University in Skopje, Institute of Earthquake Engineering and Engineering Seismology, Skopje, Republic of North Macedonia, nanevska@iziis.ukim.edu.mk*
[(7)] *Ass., Ss. Cyril and Methodius University in Skopje, Institute of Earthquake Engineering and Engineering Seismology, Skopje, Republic of North Macedonia, trajce@iziis.ukim.edu.mk*

Abstract

This paper presents the procedure for remote testing of various categories of bridges, incorporating both static and dynamic assessment methodologies. The investigated structures include different types of bridges categorized by the structural system and materials, as well as different categories of bridges according to their usage. Therefore, the study incorporates a cable-stayed steel pedestrian bridge, a simply supported steel girder railway bridge and a prestressed reinforced concrete road bridge. The objective of the testing was to evaluate the structural performance, safety, and long-term serviceability of these diverse bridge types under varying load conditions. For the testing phase, an advanced radar technique called microwave interferometry is employed. Using a high-precision interferometric radar system to remotely monitor deflection patterns, any subtle displacements with millimetre-level accuracy were detected. Additionally, accelerometer devices were employed to record the resulting accelerations and vibration patterns, enabling a detailed analysis of the structural behaviour under dynamic loads and confirming the accuracy of the interferometric remote testing procedure. The combination of static and dynamic testing allowed for a thorough evaluation of the bridges' stiffness, damping characteristics, and overall structural integrity. The findings highlight key insights into the current condition and performance of the various types of bridges. Overall, the study emphasizes the necessity of integrating static and dynamic testing methodologies for accurate structural assessment, especially in complex traffic networks. The findings provide a strong basis for informed decision-making regarding maintenance strategies, ensuring the continued safety and serviceability of these critical infrastructures. Regular monitoring and timely intervention based on these insights are essential to extending the lifespan and reliability of the bridges.

Keywords: bridges, testing, remote, assessment, interferometry, static, dynamic.

1. Introduction

Bridges are critical components of modern infrastructure, providing essential connections for transportation and commerce. As these structures age and become subjected to increasing loads and environmental challenges, their safety and performance must be regularly evaluated. The importance of effective assessment methodologies cannot be overstated, particularly given the possible consequences of structural failures, which can lead to significant economic loss and pose threats to public safety.

Beginning with the design, continuing onto the construction phase and concluding with the exploitation of the bridge structures, obtaining the correct and up-to-date data is crucial for assessment of their

Proceedings of the 3rd Croatian Conference on Earthquake Engineering - 3CroCEE
19–22 March 2025, Split, Croatia
Copyright © 2025 CroCEE
DOI: https://doi.org/10.5592/CO/3CroCEE.2025.99

behaviour. From a simple routine maintenance to check the serviceability of the bridge, through visual inspection to assess the condition of the bridge, the thorough inspections require detailed engineering investigation using various testing methods and theoretical structural analysis. The technology has advanced greatly, thus the use of unmanned aerial systems (UAS) has already been widely accepted and implemented as a method for obtaining key information on structural condition of bridges [1-7]. Moreover, machine learning (ML), as part of the rapidly advancing artificial intelligence (AI) application in engineering, through its deep learning models provides state of the art results to problems that are initially considered to be intuitively solved by humans [8]. Using the benefits of highly developed computer vision solutions, new frameworks for monitoring of bridges can be implemented as well [9].

In recent years, advancements in testing technologies have opened new avenues for the remote evaluation of bridges, allowing engineers to gather detailed information about structural performance without the need for intrusive measures. Therefore, techniques such as digital image correlation (DIC), interferometer radar, LiDAR systems, total stations etc. have been successfully incorporated into the monitoring plans for bridges. Garnica et al. [10] have reviewed the various sensors and measuring techniques that are applicable to load testing of concrete bridges and found that deflections can be accurately measured with an interferometric radar and that non-contact techniques are the better choice for bridges that are difficult to access. Employing microwave interferometry, an advanced radar technique, deflection patterns can be monitored to achieve millimetre-level accuracy in detecting subtle displacements. The interferometric radar's most significant advantage over other remote sensing techniques is its high precision evaluated in laboratory environments [11, 12]. It can be used as a single radar measuring the vertical displacements of the bridge structure with high frequency and accuracy, or different configurations using two or more radars can be implemented in order to tackle the monitoring problems associated with more complicated geometries or bridge types [13, 14].

This paper presents a comprehensive procedure for remote testing of various categories of bridges, incorporating both static and dynamic assessment methodologies and using interferometric radar in all case studies. The study investigates a range of bridge types, specifically focusing on a cable-stayed steel pedestrian bridge, a simply supported steel girder railway bridge, and a prestressed reinforced concrete road bridge. This diversity in structural systems and materials underscores the complexity of bridge assessment and the necessity for tailored evaluation techniques. By emphasizing the necessity of comprehensive testing methodologies, it is aimed at supporting the development of effective maintenance strategies that safeguard public safety and enhance the serviceability of bridges.

2. Bridge inspection overview

2.1. Methodology for bridge monitoring and assessment

This section outlines the systematic approaches used to monitor and assess the health of bridges. The methodology typically involves four key components: monitoring techniques, data acquisition, structural assessment and evaluation methods.

Bridge monitoring involves the use of a wide range of tools and techniques to investigate structural performance. These can involve visual inspection, structural health monitoring (SHM) systems, non-destructive tests (NDT), remote monitoring systems and smart materials and sensors. The visual inspection is usually performed by experienced engineers and it can result in detection of cracks, spalling of concrete or corrosion of the steel and reinforcement. SHM systems are more advanced tools for monitoring of bridge structures and they incorporate automated systems with sensors, data acquisition units and analytical software solutions. They can be differentiated via the character of the monitoring as static or dynamic and they can also provide monitoring data in long-term and in real-time. NDTs are one of the most frequently used techniques for assessing the material properties of the bridge structures as they provide very useful data without causing damage to the structural elements. Finally, the remote monitoring systems and smart materials and sensors are the state-of-the-art

Proceedings of the 3rd Croatian Conference on Earthquake Engineering - 3CroCEE
19–22 March 2025, Split, Croatia
Copyright © 2025 CroCEE
DOI: https://doi.org/10.5592/CO/3CroCEE.2025.99

technologies for structural monitoring that are used for data obtaining without the need of physical proximity of the investigated structure.

After the suitable inspection and monitoring method is selected, accurate data acquisition and efficient data management are crucial for effective bridge monitoring. The data acquisition procedure consists of proper sensor placement and calibration, the possibility of real-time data acquisition, robust data storage and management systems and big data and analytics techniques to process large volumes of monitoring data as well as identify patterns, anomalies and predict failures.

After monitoring data is collected, structural assessment and modelling help interpret the data. To provide an accurate interpretation of the physical engineering parameters from the monitoring phase, a robust finite element modelling (FEM) for simulation of the bridge behaviour under various load conditions is required. Numerical modelling can also be employed to perform model updating using the monitoring data to improve accuracy. The dynamics principles can therefore be applied for identifying changes in modal properties, while the mechanics principles and suitable material behaviour properties can be utilized for detecting excessive deformation and cracking. The most advanced ML and AI techniques such as the deep learning are more frequently used for supervised and unsupervised learning for anomaly detection and damage classification and prediction.

The final step involves evaluating the health of the bridge and assessing associated risks. Thus, development of a quantifiable index to represent the overall condition of the bridge which combines data from various monitoring sources is required. Probabilistic methods are applied to evaluate the likelihood of failure under specific conditions with focus on load-carrying capacity, fatigue, and environmental factors. These measures result in integration of monitoring and assessment data into a overall management system which facilitates prioritization of maintenance, repair, or replacement activities.

Bridge inspection frameworks in developed countries emphasize routine inspections, advanced technologies, and centralized data systems for managing bridge infrastructure. They mandate regular inspections to assess structural integrity and safety. Generally, the regular inspections are conducted more frequently to visually assess all accessible parts of the structure [15-19]. Additionally, thorough inspections are performed, involving detailed visual checks and load-bearing capacity evaluations [20]. Also, many of the bridge inspection standards include post-event inspections following extreme weather or seismic events that involve more comprehensive assessment of the structure. While commonalities exist, variations in environmental conditions, traffic demands, and regulatory standards have shaped unique approaches in each region, Table 1. Continuous innovation, including the adoption of AI, digital twins, and IoT, will further enhance these frameworks, enabling proactive maintenance and improved safety.

Table 1. Comparison of bridge inspection frameworks in developed countries

Country	Inspection frequency		Technologies used	Unique feature
	Routine	Other		
Australia	2-5 yrs	Risk-based	IoT sensors, NDT	Multi-level inspection hierarchy
Canada	Not defined	Post-event	GPR, LiDAR, SHM	Focus on extreme weather resilience
UK	2 yrs	6 yrs (risk-based)	Drones, condition indices	Risk-based inspection prioritization
USA	2 yrs	Risk-based	NDT, drones, SHM, ML	Centralized NBI for data management
Japan	5 yrs	Post-disaster	SHM	Advanced SHM adoption for seismic resilience
Germany	1 yr	6 yrs	Drones, SHM	Sustainable bridge management

Copyright © 2025 CroCEE
DOI: https://doi.org/10.5592/CO/3CroCEE.2025.99

Regarding the advanced technologies that enhance the bridge inspection procedures, several authors have proposed suitable adjustments of the existing frameworks [21-23]. Others have detected the need for evaluating the remote sensing technologies for the next generation bridge inspection methodologies. They noted that monitoring the condition of a bridge using remote sensors can eliminate the need for traffic disruption or total lane closure because remote sensors do not come in direct contact with the structure [24].

2.2. Instrumentation

Laser sensors are a possible non-contact technique for monitoring large structures such as bridges. Consequently, a remote microwave sensor able to provide displacement measurements with sub-millimeter accuracy and a sampling rate high enough to track the transient movements of an architectural structure was developed [25]. The microwave interferometric radar measures the static deflections of several points on a large structure, as well as vibrations to identify resonant frequencies and mode shapes. The IBIS-FS interferometric radar is a ground-based remote sensing system widely used for monitoring the stability and deformation of structures such as bridges, dams, and buildings. It employs radar interferometry to measure sub-millimetre displacements over large areas in real time, offering a non-contact, high-precision solution for structural health monitoring (SHM). The system uses electromagnetic waves to detect changes in the structure's surface, providing continuous data without requiring physical sensors or extensive setup, Fig. 1. Its portability and ability to operate under diverse environmental conditions make it particularly valuable for both short-term assessments and long-term monitoring applications. It is therefore the main instrument used for this investigation, applied on all of the varying case study structures.

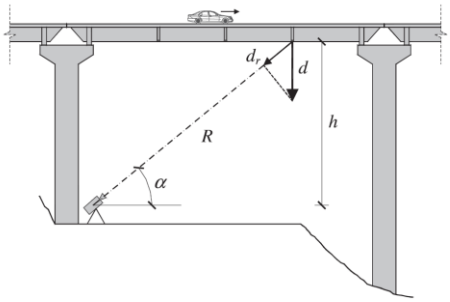


Figure 1. Typical setup of interferometric radar IBIS-FS for bridge static and dynamic measurement [26].

Simultaneously, accelerometers were used to record the resulting accelerations and vibration patterns, facilitating a thorough analysis of structural behaviour under dynamic loading conditions. This dual approach enables a comprehensive assessment of important parameters such as stiffness, damping characteristics, and overall integrity of the bridges.

During one of the case studies, UAS inspection was also conducted. For that purpose, a sophisticated drone technology was used. The DJI Phantom 4 Pro V2.0 is an advanced unmanned aerial vehicle (UAV) designed for professional applications such as structural inspections of structures and bridges [27]. Its 1-inch 20-megapixel CMOS camera ensures high-resolution imagery and 4K video recording at 60 fps, while the mechanical shutter eliminates rolling shutter distortion, crucial for accurately capturing structural details during fast movements. The drone's intelligent battery supports a flight time of up to 30 minutes, reducing the need for frequent landings and enabling efficient coverage of large structures. User-friendly controls and automated flight modes, make the Phantom 4 Pro V2.0 accessible to both novice and experienced operators. The included controller connects with mobile phone or tablet, ensuring clear visibility even in direct sunlight, which is critical during field inspections. The OcuSync 2.0 HD transmission system provides a stable and reliable video feed up to 8 km, enhancing the ability to monitor inspections in real time. Additionally, the drone's five-direction obstacle sensing, enabled by infrared and stereo vision sensors, enhances safety during operations in confined or complex environments.

Proceedings of the 3rd Croatian Conference on Earthquake Engineering - 3CroCEE
19–22 March 2025, Split, Croatia
Copyright © 2025 CroCEE
DOI: https://doi.org/10.5592/CO/3CroCEE.2025.99

3. Case studies

In order to assess the suitability of state-of-the-art technologies for remote bridge inspection, a pilot project involving three case studies was conducted. The case studies involved different types of bridges according to their function, structural type and structural material. Also, each case study incorporated different remote inspection techniques varying by the detail level of the inspection and the condition of the bridge structure. One thing in common for all the case studies was the implementation of the interferometric radar instrumentation in order to demonstrate the advantages of using this technique for different types of bridge inspection and their location in seismic prone area.

3.1. Simply supported steel girder railway underpass

Firstly, the investigation considered an older bridge structure located in urban area with little or no maintenance over the course of existence. The first case study structure is a simply supported steel girder railway underpass with 4 spans constructed roughly 50 years ago. The length of the longest middle spans is 14m. This bridge is frequently used as it is positioned on the main railway line in N. Macedonia (Fig. 2 – left) that reaches the main station in the capital Skopje. It is in constant exploitation with passenger and freight trains and undergoes cyclic loading and deformation a few times a day. Due to the lack of maintenance strategy and non-existence of bridge inspection procedures, the exposed steel superstructure of the bridge is heavily corroded (Fig. 2 - right). Additionally, there is spalling of concrete visible at the column faces resulting in removal of the concrete cover and reinforcement being exposed to external influences. The bearings and the rivetted connections are also heavily corroded.



Figure 2. View above (left) and below (right) the simply supported steel girder underpass.

The investigation of this bridge structure was performed using visual routine inspection and the interferometric radar IBIS-FS. Since the bridge is in full operation throughout the year, the passing of a freight train was chosen as the suitable loading for obtaining the information required.

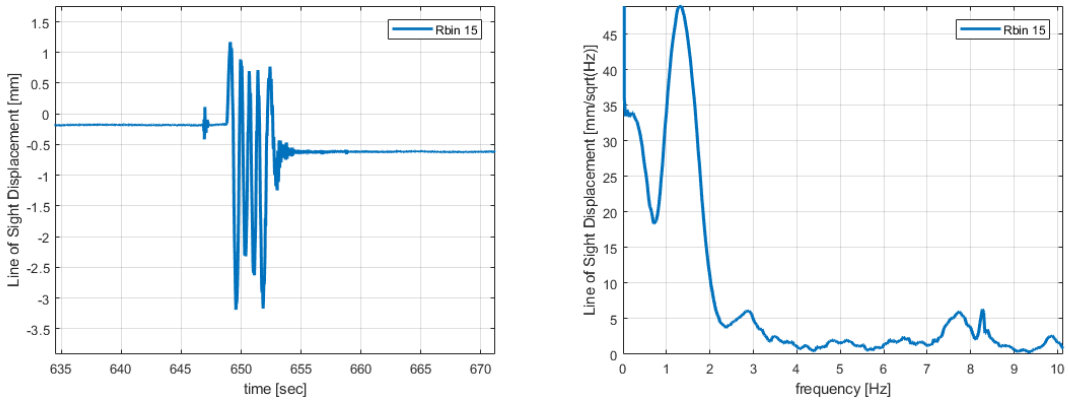


Figure 3. Time history of the bridge deformation (left) and frequency analysis of its superstructure (right).

Copyright © 2025 CroCEE
DOI: https://doi.org/10.5592/CO/3CroCEE.2025.99

Without disruption of the traffic above and below the bridge structure, several key structural parameters were obtained. A line of sight (LOS) absolute displacement of 4.1mm was measured (Fig. 3 – left) which results in 13.3mm total vertical displacement from the freight train dynamic loading. The measured displacement represents 1/1050 of the length of the structure which is a parameter that can be compared with the prescribed values for maximum allowed deformations under live loading in bridge structures. It is interesting to note that a small permanent deformation was observed which can be accounted to the static system of the bridge and the small movement in the bearings during the cyclic loading from the trains. After the dynamic loading of the bridge, frequency analysis was performed on the free oscillations from the deformation time-history. The first frequency of the superstructure was evaluated at 1.3Hz (Fig. 3 – right) and that parameter gives valuable information about the condition and the behaviour of the structure, especially when considering the response of the structure during seismic events that occur frequently in this area. It was therefore concluded that the remote sensing technology can easily be implemented for fast assessment of the deformability and behaviour of the bridge structures in urban areas without disrupting the rail and road traffic during regular inspections and after seismic events.

3.2. Cable-stayed pedestrian bridge

The next case study structure is a cable-stayed pedestrian bridge over the river Vardar in Skopje. The main span is 55m long and as is the case with the steel girder railway underpass, the bridge is with little or no maintenance over the course of existence. It was constructed around 25 years ago. Figure 4 – top shows the view from the side of the bridge while Figure 4 – bottom depicts the entire bridge structure taken from the top using the UAV described in Section 2.



Figure 5. Side view (top) and view from aerial perspective (bottom) of the cable-stayed pedestrian steel bridge.

Copyright © 2025 CroCEE
DOI: https://doi.org/10.5592/CO/3CroCEE.2025.99

From the visual inspection of the structural elements of the bridge, heavily corroded bridge deck and girders were observed. Additionally, the lower side connections of the stays with the girders and the substructure of the bridge were also corroded (Fig. 6). Since the upper side of the bridge stays was far from the accessible range for visual inspection, UAV was employed. Using the UAV inspection, the condition of the upper side of the stay connections with the pylons was inspected. As expected, corrosion was detected at the connection and in other parts of the upper bridge structure (Fig. 6).



Figure 6. Corrosion detection following visual and UAV inspection.

Copyright © 2025 CroCEE
DOI: https://doi.org/10.5592/CO/3CroCEE.2025.99

Then, the behaviour of the case study bridge was investigated using instrumentation for evaluation of its dynamic characteristics. As previously mentioned, the interferometric radar was employed in all case study structures. Additionally, seismic sensors such as accelerometers were installed on the bridge deck to assess the accuracy of the radar measurements. The bridge was dynamically excited by applying a vertical periodic load at the midspan of the bridge in the form of pedestrians jumping on the bridge midspan. The measurements of the transversal and vertical displacement time history were obtained after the removal of the periodic load to avoid the interference from the periodic loading. The tests and measurements were performed several times for repeatability. Finally, the results of the transversal and vertical frequency analyses using the accelerometers and interferometric radar are presented in Fig. 7.

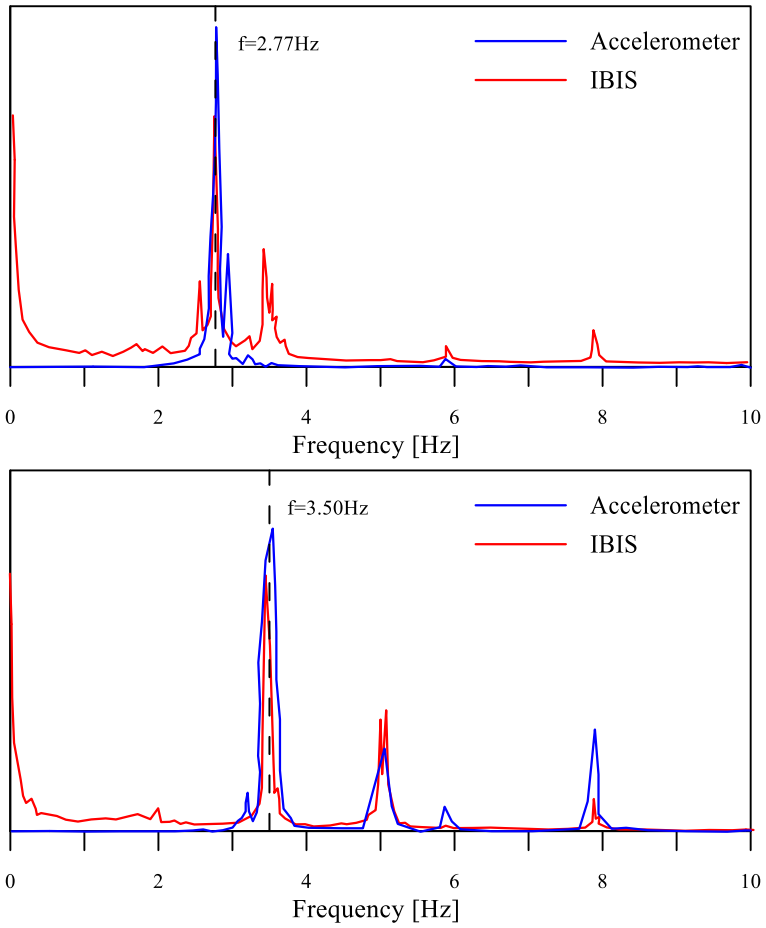


Figure 7. Frequency analysis of the pedestrian bridge deck structure for transversal (top) and vertical (bottom) direction using accelerometers and interferometric radar.

It is observed that the frequencies from the frequency analyses using the accelerometers and the interferometric radar for transversal and vertical direction are matching. Since the main characteristic of the interferometric radar is evaluation of displacements in its line of sight (LOS), the setup of the instrument with regard of the structure main axis is very important. It should be noted that for obtaining the transversal direction frequency the interferometric radar was installed on the side of the bridge. Hence, the highest amplitude peak from Fig. 7 – top displays the transversal frequency of the structure while also depicting the vertical frequencies obtained with the radar with lower amplitudes due to the three dimensionality of the displacement vector. In contrast, the accelerometer obtained only one peak in the transverse direction depicting the first transverse frequency of the structure. The same values for the vertical frequencies can be observed on Fig. 7 – bottom, which was obtained from a measurement of the bridge deck using the interferometric radar placed directly beneath the bridge structure. As a result, it was demonstrated that the interferometric radar technology for remote testing of bridge structures can accurately be employed for assessing the behaviour of cable-stayed pedestrian bridge

Proceedings of the 3rd Croatian Conference on Earthquake Engineering - 3CroCEE
19–22 March 2025, Split, Croatia
Copyright © 2025 CroCEE
DOI: https://doi.org/10.5592/CO/3CroCEE.2025.99

without the need of additional arrangements for loading or access to the bridge deck. Combined with the thorough visual inspection using UAV, it can give detailed information on the condition of the bridge structure under consideration and can be employed without any obstacles during regular inspections and after significant seismic events.

3.3. Prestressed reinforced concrete road overpass

Finally, the last case study involves the implementation of the remote sensing technology for bridge inspection on a newly constructed bridge structure. In this situation, the interferometric radar instrument is employed to identify the modal properties of a newly built road overpass and measure the deformations under live loading. The newly constructed overpass is 21.5m long and finished with construction in 2024, Fig. 8. It consists of 6 prestressed T-section girders resting on 120cm thick end columns. Reinforced concrete slab with 15cm thickness is cast over the bridge girders.



Figure 8. View of the prestressed reinforced concrete overpass with the installed radar for measurement.

The investigation of this bridge structure involved both static and dynamic testing procedures. Namely, the static test involved placement of the live load at midspan and leaving it for 1 minute before removing it from the bridge and measuring the residual deformations (Fig. 9 – left). The dynamic test was performed using the same live load (loaded truck) and letting it move with 30km/h over the bridge (Fig. 9 – right). Displacements in the range of 1/12000-13500 of the length of the structure were observed during both measurements. However, in this case study, the weight of the live load was not measured and the efficiency of the load testing was not evaluated.

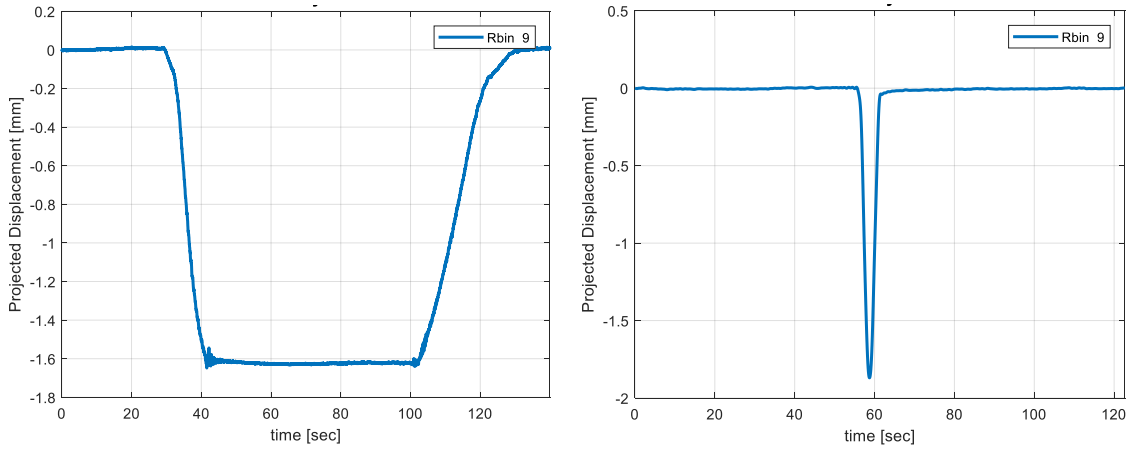


Figure 9. Deformation time-history during bridge testing: static (left) and dynamic (right).

Additionally, to produce significant excitation for modal properties estimation, an obstacle was placed at midspan and the corresponding frequency analysis was performed on the free oscillating segment of

Copyright © 2025 CroCEE
DOI: https://doi.org/10.5592/CO/3CroCEE.2025.99

the dynamic time history recording. This is the common procedure for load testing of newly constructed or repaired and retrofitted bridges. The modal properties of the case study bridge were estimated using the interferometric radar and additional seismic sensor. The accelerometer was installed on the bridge deck to assess the accuracy of the radar measurements regarding this particular type of bridges. The measurements of the vertical displacement time history were obtained from the free oscillations after the live load excitation. The results of the vertical frequency analyses using a state-of-the-art accelerometer and interferometric radar are presented in Fig. 10.

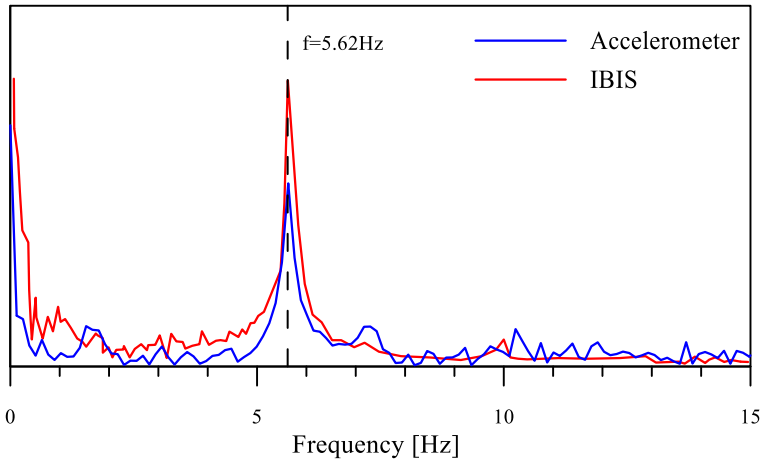


Figure 10. Frequency analysis of the prestressed road bridge deck structure for vertical direction using accelerometer (top) and interferometric radar (bottom).

It was again observed that the frequencies from the frequency analyses using the accelerometer and the interferometric radar are matching, obtaining values of 5.62Hz in both cases. Hence, it was demonstrated that the interferometric radar technology for remote testing of bridge structures can accurately be employed for assessing the behaviour of newly built prestressed reinforced concrete road bridge without the need of access to the bridge deck. The remote sensing technology using the microwave interferometric radar is evaluated to provide accurate results for both static and dynamic testing of bridges. The results from the static and dynamic load testing can be used for estimation of the real dynamic coefficient of the bridge structures and monitoring the condition of newly built bridges in a comprehensive asset management system. Additionally, the results obtained from these analyses can provide strong basis for evaluation of the structural behaviour during regular inspection and after significant seismic events in order to ensure safety of the critical infrastructure assets.

4. Conclusion

This study has provided critical insights into the current condition and performance of various bridge types, highlighting the effectiveness of integrating different testing methodologies. These methods form a robust framework for structural assessment, which is crucial for making informed decisions regarding maintenance and rehabilitation strategies. The findings emphasize the importance of regular monitoring and timely interventions to extend the lifespan and ensure the reliability of essential infrastructures during regular exploitation and after significant seismic events.

A key outcome of this research is the validation of remote sensing technology as a practical solution for the rapid assessment of deformability and behaviour of bridge structures in urban environments. The significant advantage of this approach is its ability to operate without disrupting rail and road traffic, making it particularly valuable for densely populated areas.

The study has demonstrated that interferometric radar technology can be effectively employed for the remote testing of bridge structures. Specifically, it has proven to be an accurate tool for assessing the behaviour of cable-stayed pedestrian bridges without the need for additional loading arrangements or access to the bridge deck. When combined with thorough visual inspections using unmanned aerial

Copyright © 2025 CroCEE
DOI: https://doi.org/10.5592/CO/3CroCEE.2025.99

vehicles (UAVs), this approach provides a comprehensive and detailed evaluation of the condition of the bridge structure.

Furthermore, the application of interferometric radar technology has been shown to be equally effective for newly built prestressed reinforced concrete road bridges. The capability of microwave interferometric radar to deliver precise results for both static and dynamic testing underscores its value in modern bridge assessment practices. These results can be utilized to estimate the actual dynamic coefficient of bridge structures and to monitor the condition of newly constructed bridges within a comprehensive asset management system.

In conclusion, this study affirms the transformative potential of remote sensing technologies in the field of structural engineering. By enabling accurate, non-intrusive, and efficient assessments, these technologies represent a significant step forward in ensuring the safety, reliability, and longevity and a crucial tool for post-earthquake assessment of critical infrastructure assets.

References

[1] Morgenthal, G., Hallermann, N., Kersten, J., Taraben, J., Debus, P., Helmrich, M., Rodehorst, V. (2019): Framework for Automated UAS-Based Structural Condition Assessment of Bridges. *Automation in Construction*, 97, 77-95, doi: https://doi.org/10.1016/j.autcon.2018.10.006

[2] Chen, S., Laefer, D. F., Mangina, E., Zolanvari, S. I., Byrne, J. (2019): UAV Bridge Inspection Through Evaluated 3D Reconstructions. *Journal of Bridge Engineering*, 24(4), 05019001, doi: https://doi.org/10.1061/(ASCE)BE.1943-5592.0001343

[3] Dorafshan, S., Maguire, M. (2018): Bridge Inspection: Human Performance, Unmanned Aerial Systems and Automation. *J Civil Struct Health Monit* 8, 443–476, doi: https://doi.org/10.1007/s13349-018-0285-4

[4] Duque, L., Seo, J., Wacker, J. (2018): Bridge Deterioration Quantification Protocol Using UAV. *Journal of Bridge Engineering*, 23(10), 04018080, doi: https://doi.org/10.1061/(ASCE)BE.1943-5592.0001289

[5] Kim, I.-H., Jeon, H., Baek, S.-C., Hong, W.-H., Jung, H.-J. (2018): Application of Crack Identification Techniques for an Aging Concrete Bridge Inspection Using an Unmanned Aerial Vehicle. *Sensors*, 18(6), 1881, doi: https://doi.org/10.3390/s18061881

[6] Lei, B., Wang, N., Xu, P., Song, G. (2018): New Crack Detection Method for Bridge Inspection Using UAV Incorporating Image Processing. *Journal of Aerospace Engineering*, 31(5), 04018058, doi: https://doi.org/10.1061/(ASCE)AS.1943-5525.0000879

[7] Tomiczek, A. P., Whitley, T. J., Bridge, J. A., Ifju, P. G. (2019): Bridge Inspections with Small Unmanned Aircraft Systems: Case Studies. *Journal of Bridge Engineering*, 24(4), 05019003, doi: https://doi.org/10.1061/(ASCE)BE.1943-5592.0001376

[8] Bai, Y., Zha, B., Sezen, H., Yilmaz, A. (2023): Engineering Deep Learning Methods on Automatic Detection of Damage in Infrastructure Due to Extreme Events. *Structural Health Monitoring*, 22(1), 338-352, doi: https://doi.org/10.1177/14759217221083649

[9] Bai, Y., Sezen, H., Yilmaz, A., Qin, R. (2023): Bridge Vibration Measurements Using Different Camera Placements And Techniques Of Computer Vision And Deep Learning. *Advances in bridge engineering*, 4(1), 25, doi: https://doi.org/10.1186/s43251-023-00105-1

[10] Garnica G., Lantsoght E., Yang Y. (2022): Monitoring Structural Responses During Load Testing of Reinforced Concrete Bridges: A Review. *Structure and Infrastructure Engineering*, 18 (10-11), 1558-1580, doi: https://doi.org/10.1080/15732479.2022.2063906

[11] Michel, C., Keller, S. (2021): Advancing Ground-Based Radar Processing for Bridge Infrastructure Monitoring. *Sensors*, 21, 2172. doi: https://doi.org/10.3390/s21062172

[12] Schill, F., Michel, C., Firus, A. (2022): Contactless Deformation Monitoring of Bridges with Spatio-Temporal Resolution: Profile Scanning and Microwave Interferometry. *Sensors*, 22, 9562, doi: https://doi.org/10.3390/s22239562

[13] Olaszek, P., ´Swiercz, A, Boscagli, F. (2021): The Integration of Two Interferometric Radars for Measuring Dynamic Displacement of Bridges. *Remote Sensing*, 13, 3668, doi: https://doi.org/10.3390/rs13183668

Copyright © 2025 CroCEE
DOI: https://doi.org/10.5592/CO/3CroCEE.2025.99

[14] Talich, M., Havrlant, J., Soukup, L., Plachý, T., Polák, M., Antoš, F., Ryjáˇcek, P., Stanˇcík, V. (2023): Accuracy Analysis and Appropriate Strategy for Determining Dynamic and Quasi-Static Bridge Structural Response Using Simultaneous Measurements with Two Real Aperture Ground-Based Radars. *Remote Sensing,* 15, 837, https://doi.org/10.3390/rs15030837

[15] Australian Standard (2004): Bridge Design Part 7: Rating of existing bridges (AS5100.7). *Standards Australia International Ltd*, Sydney, Australia.

[16] Canadian Standards Association (2006): CAN/CSA-S6-06. Canadian highway bridge design code. *Canadian Standards Association*, Toronto, Canada.

[17] Atkins, W.S. (2005): Management of highway structures – a code of practice. *The Stationery Office*, London, UK.

[18] FHWA (Federal Highway Administration) (2004): National bridge inspection standards. *Federal Register*, 69(239), 74419-39.

[19] Ministry of Land, Infrastructure, Transportation, and Tourism (2014): Manual for Bridge Periodic Inspection, *Ministry of Land, Infrastructure, Transportation, and Tourism*, Tokyo, Japan.

[20] Deutsches Institut fur Normung e.V. DIN (1999): Bauwerksprufung nach DIN 1076 - Bedeutung, Organisation, Kosten, Dokumentation, *Beuth Verlag*, Berlin, Germany.

[21] Nettis, A., Saponaro, M., Nanna, M. (2020): RPAS-Based Framework for Simplified Seismic Risk Assessment of Italian RC-Bridges. *Buildings*, 10(9), 150, doi: https://doi.org/10.3390/buildings10090150

[22] Sacks, R., Kedar, A., Borrmann, A., Ma, L., Brilakis, I., Hüthwohl, P., Muhic, S. (2018): Seebridge as Next Generation Bridge Inspection: Overview, Information Delivery Manual and Model View Definition. *Automation in Construction*, 90, 134-145, doi: https://doi.org/10.1016/j.autcon.2018.02.033

[23] Seo, J., Duque, L., Wacker, J. (2018): Drone-Enabled Bridge Inspection Methodology and Application. *Automation in construction*, 94, 112-126, doi: https://doi.org/10.1016/j.autcon.2018.06.006

[24] Vaghefi, K., Oats, R. C., Harris, D. K., Ahlborn, T. T. M., Brooks, C. N., Endsley, K. A., Dobson, R. (2012) Evaluation of Commercially Available Remote Sensors for Highway Bridge Condition Assessment. *Journal of Bridge Engineering*, 17(6), 886-895, doi: https://doi.org/10.1061/(ASCE)BE.1943-5592.0000303

[25] Pieraccini, M., Parrini, F., Fratini, M., Atzeni, C., Spinelli, P., Micheloni, M. (2007): Static and Dynamic Testing of Bridges Through Microwave Interferometry. *Ndt & E International*, 40(3), 208-214, doi: https://doi.org/10.1016/j.ndteint.2006.10.007

[26] Gentile, C., Bernardini, G. (2008): Output-Only Modal Identification of a Reinforced Concrete Bridge from Radar-Based Measurements. *Ndt & E International*, 41(7), 544-553, doi: https://doi.org/10.1016/j.ndteint.2008.04.005

[27] DJI, DJI Phantom 4, https://www.dji.com/global/support/product/phantom-4, (accessed January 20, 2025).

Proceedings of the 3rd Croatian Conference on Earthquake Engineering - 3CroCEE
19–22 March 2025, Split, Croatia
Copyright © 2025 CroCEE
DOI: https://doi.org/10.5592/CO/3CroCEE.2025.134

IMPROVING THE BENDING STIFFNESS OF DLT BEAMS: EXPERIMENTAL ANALYSIS AND ANALYTICAL MODEL VERIFICATION

Ana Skender [(1)], Marina Frančić Smrkić [(1)], Ante Barišić

[(1)] *Department of Engineering Mechanics, Faculty of Civil Engineering, University of Zagreb, Croatia*

Abstract

The search for environmentally friendly building materials has led to the development of dowel laminated timber (DLT), a product in which sawn timber boards are laminated using hardwood dowels. The dowels in DLT reduce the need for metal fasteners and synthetic adhesives. However, the application of DLT beams is challenged by the relatively low bending stiffness resulting from the low composite action. In this research, we evaluated the effectiveness of the dowel composite connection depending on different dowel angle positions to improve the bending stiffness and further enhance the environmental benefits of DLT beams. Double shear tests were performed on three-layer connections assembled with beech wood dowels. Three-layer beams were then fabricated and tested under four-point bending load. The efficiency of the composite action and the resulting flexural behaviour were evaluated. The results show that the angular position of the dowels can improve the bending stiffness by up to 50 %. The simplified design method, also known as the γ-method, was used to estimate the efficiency of composite beams. A comparison of the experimental and theoretical results helps to verify the feasibility of the EC5 model for composite beams for use with DLT beams.

Keywords: dowel laminated timber, bending stiffness, experimental analysis, analytical model

1. Introduction

Timber constructions have proven to be a viable construction option in recent decades. To meet the increasing demand for timber constructions, there is a growing interest in laminated timber elements with larger dimensions or higher load-bearing capacity. Glulam and cross-laminated timber (CLT), both glue-laminated products, are widely used due to their strength, stiffness and reliability. However, non-glue-laminated timber is also gaining increasing attention in both the academic and industrial sectors. This type of timber, which does not require adhesives, has a lower environmental impact and produces fewer pollutants [1]. Its easy disassembly and the possibility of reuse increase its ecological efficiency, especially in terms of carbon sequestration and energy savings. While there is limited experience in producing non-glued wood, the manufacturing process requires only basic techniques and equipment, making it accessible to small manufacturers. Despite its potential in circular economy, there is little data on the structural behaviour of unglued wood. In particular, the structural properties of beams made from unglued wood have not yet been sufficiently researched and their bending properties need further investigation. Various factors can influence the effectiveness of dowel composite connection: different dowel angle positions and number of dowels [2], different lamination techniques or different materials [3].

Despite the increasing importance of DLT in modern construction, Eurocode 5 lacks specific provisions for its unique properties. EC5 primarily addresses more established engineered wood products such as glulam and CLT, which are widely used in modern timber construction. As DLT is relatively new compared to these products, its specific design properties and performance in various structural applications have not been included in the Eurocode standards. The only given solution is the design approach of the "γ-method", which can be used to assess the load-bearing capacity of composite beams. The accuracy of this analytical model for assessing the composite behaviour of DLT beams needs to be validated by comparing experimental data with theoretical predictions. To address these concerns, full-scale bending tests were conducted in this study and the results were compared with analytical assessments.

Proceedings of the 3rd Croatian Conference on Earthquake Engineering - 3CroCEE
19–22 March 2025, Split, Croatia
Copyright © 2025 CroCEE
DOI: https://doi.org/10.5592/CO/3CroCEE.2025.134

Two types of connections were analysed: Dowels inserted at an angle of 45° to the plane of the layers and at an angle of 90°. The slip modulus was determined on five specimens of each connection type by a double shear test according to EN 26891 [5]. The modulus of elasticity was determined by four-point bending test according to EN 408 [6] on five simply supported specimens. Two series of three-layer beams measuring 80 x 57 x 1000 mm were then tested in the four-point bending test, with load and deflection being monitored. The experimentally determined stiffness values were compared with the analytical values.

2. Analytical calculation

Using the "γ - method" from Eurocode 5 [4], the effective bending stiffness of a simply supported composite beam consisting of three layers can be approximated as follows:

$$(EI)_{eff} = \sum_{i=1}^{3} (E_i \cdot I_i + \gamma_i \cdot E_i \cdot A_i \cdot e_i^2) \tag{1}$$

$$\gamma_i = \frac{1}{1 + \frac{\pi^2 \cdot E_i \cdot A_i \cdot s_i}{k_s \cdot L^2}} \tag{2}$$

$$k_s = (\rho^{1.5} \cdot \frac{d}{23}) \tag{3}$$

where I_i, A_i and E_i represent the second moment of inertia, the area and the elasticity modulus of the wood layers, s_i is the spacing between the dowels, L is the span of the beam, k_s is the slip modulus and e_i is the distance between the center of each layer and the neutral axis of the beam, Figure 1. In eq. (3), ρ is the wood density and d is the diameter of a dowel.

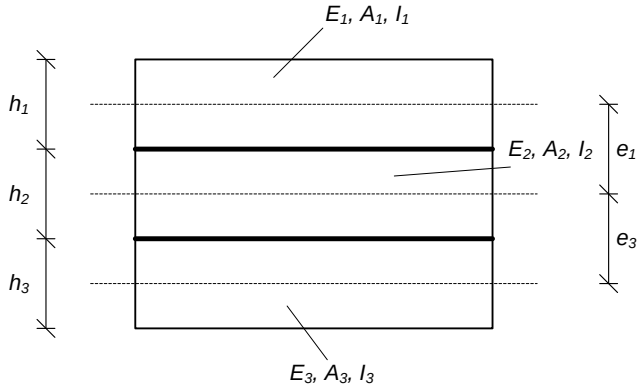


Figure 1. Cross-section of a three-layer beam with dowel connection

In previous equations, $\gamma = 1$ represents a fully bonded system (composite connection), while $\gamma = 0$ represents no shear transition between the layers.

The normal stress in the composite cross-section of the individual wood layers at mid-span can be calculated as follows:

$$\sigma_i = \frac{0{,}5 \cdot E_i \cdot h_i + \gamma_i \cdot E_i \cdot e_i}{(EI)_{eff}} \cdot M_d, \tag{4}$$

and deflection can be calculated as:

$$w_{max} = \frac{F \cdot a}{48(EI)_{eff}} (3 \cdot L^2 - 4 \cdot a^2), \tag{5}$$

Copyright © 2025 CroCEE
DOI: https://doi.org/10.5592/CO/3CroCEE.2025.134

where F is the applied force in the four-point bending test, w_{max} is the deflection at mid-span, M_d is the maximum bending moment, L is the span and a is the distance between the load grip and a support.

3. Experimental study

Fir wood with a moisture content of 12 % and a density of 452 kg/m^3 was used for the construction of the multi-layered element. Each layer was 19 mm thick. Commercially available fluted beech dowels with a diameter of 10 mm and a length of 100 mm were used for the assembly. The dowels were inserted at 90° and 45° angles to determine whether transferring the applied stress from shear only to a combination of shear and tension could result in higher shear strength.

The slip modulus was determined on five specimens according to EN 26891 [5], Figure 2. During all experiments, the load was applied by a servo-hydraulic actuator with a capacity of 50 kN. For each series, a preliminary test was first conducted to determine the estimated load. The load was then applied up to 40 % of the estimated force and held for 30 s. The load was then reduced to 10 % of the estimated force and held for an additional 30 s. Thereafter, the load was increased to the ultimate load or a slip of 15 mm. The slip modulus is calculated as follows:

$$k_s = \frac{0{,}4F_{est}}{v_{i,mod}}, \tag{6}$$

$$v_{i,mod} = \frac{4}{3}(v_{04} - v_{01}), \tag{7}$$

where F_{est} is the estimated maximum load, $v_{i,mod}$ is the modified initial slip, v_{01} and v_{04} are the slip values at $0.1F_{est}$ and $0.4F_{est}$ respectively.

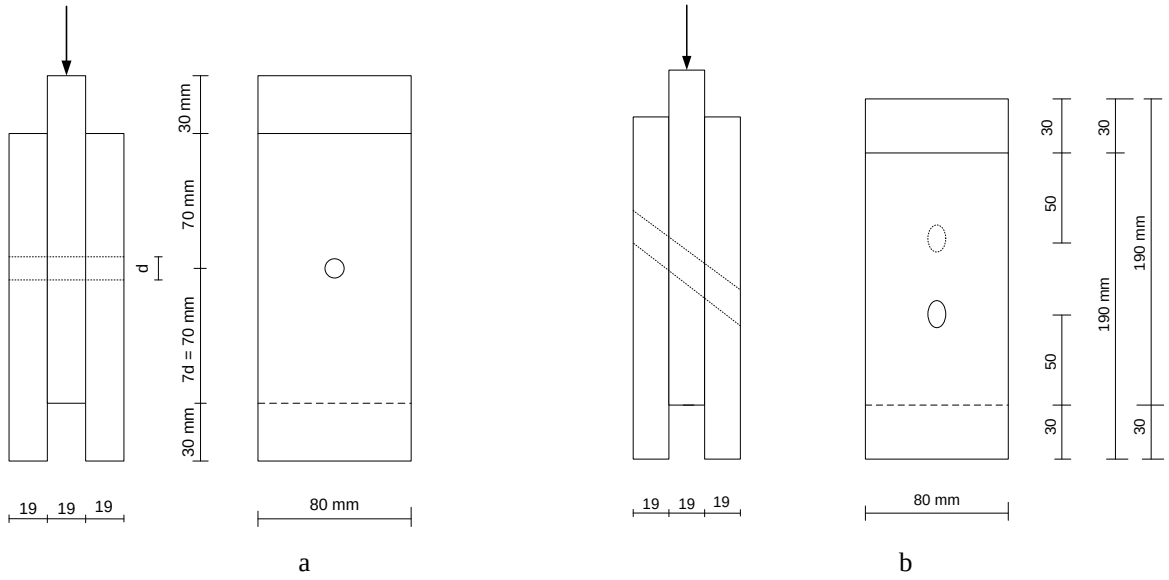


Figure 2. Specimens for slip modulus testing: a) dowel connection at 90°, b) dowel connection at 45°

The elasticity modulus was determined by four-point bending according to EN 408 [6] on five simply supported monolithic specimens with dimensions 80 x 57 x 1000 mm (labelled M), Figure 3. The load was applied at a displacement-controlled rate of 8 mm/min. Two linear variable differential transformers (LVDT) HBM WA 50 mm were used to measure the vertical displacements. They were positioned at mid-span on the neutral axis of the specimen, one on each side of the specimen, Figure 4. The test was performed until failure of the specimen to determine the flexural strength.

Copyright © 2025 CroCEE
DOI: https://doi.org/10.5592/CO/3CroCEE.2025.134

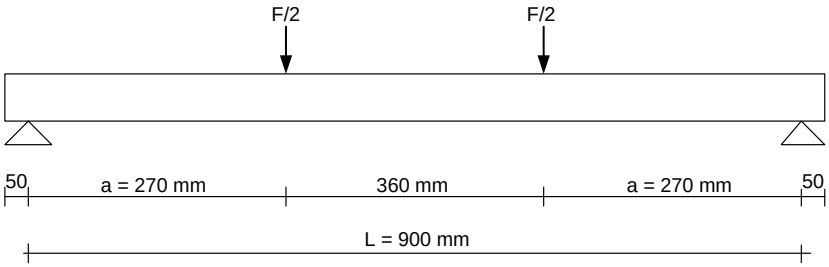


Figure 3. Test set-up for elasticity modulus testing

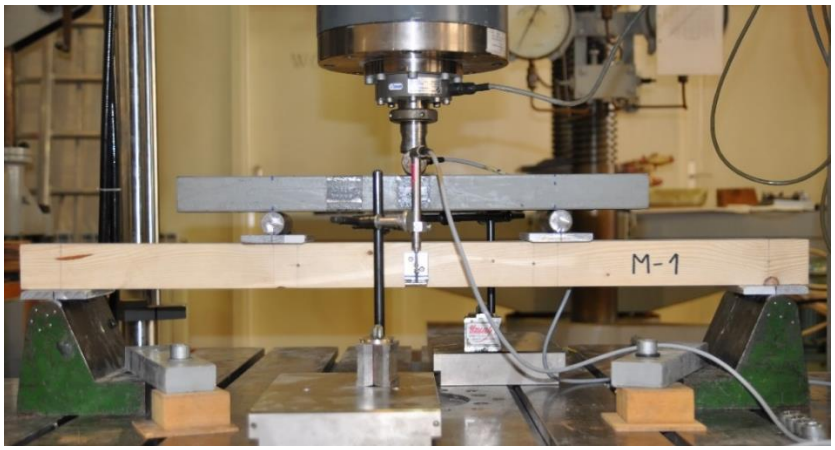


Figure 4. Modulus of elasticity test set-up

The global elasticity modulus was calculated as follows:

$$E_{m,g} = \frac{3aL^2 - 4a^3}{2bh\left(2\frac{w_2 - w_1}{F_2 - F_1} - \frac{6a}{5Gbh}\right)}, \tag{8}$$

where $F_2 - F_1$ is a load increments in newtons on the regression line with a correlation coefficient of 0.99 or better, $w_2 - w_1$ is the deformation increment corresponding to $F_2 - F_1$ in millimeters, and G is the shear modulus, which can be assumed to be infinite.

Two series of three-layer beams were assembled: with dowels inserted at an angle of 45° to the plane of the layers, labelled DLT-45 (Figure 5) and at an angle of 90°, labelled DLT-90. Each series consisted of six specimens, with each layer measuring 80 x 19 x 1000 mm. The final dimensions of the three-layer beam were b x h x L = 80 x 57 x 1000 mm. The holes were drilled at a distance of 50 mm. Due to the geometry, the 90° beams were assembled with 20 dowels and the 45° beams with 18 dowels. The dowels were soaked in sunflower oil for 10 minutes before insertion to ensure a better connection. The dowels were hammered in while the lamellas were under the clamp. The test setup was the same as for the elasticity modulus test, Figure 3 and Figure 4.



Figure 5. Laminated beam with dowels inserted at 45° (DLT-45)

Copyright © 2025 CroCEE
DOI: https://doi.org/10.5592/CO/3CroCEE.2025.134

4. Results and discussion

The slip modulus was determined on five specimens of each connection type by a double shear test according to EN 26891 [5]. The load-slip curves of the test specimens are shown in Figure 6 and

Figure 7. The shear capacity and shear stiffness results are listed in Table 1. The plastic behaviour results from the embedding of the wooden dowels in the lamellas during loading. The failure mechanism of the dowel connection was associated with the compression and fracture of the dowels at the two shear surfaces. The shear capacity F_s was defined as the maximum load observed during the test. In general, the shear strength of a 45° series is 8 % lower than that of a 90° series. The slip modulus of a 45° series was 48 % lower than that of a 90° series. For comparison, the slip modulus calculated according to eq. (3) is $k_s = 4178\ \mathrm{N/mm}$, which significantly overestimates the experimentally determined values.

Table 1. Slip test results

Specimen	F_s (kN)	k_s (N/mm)
45-1	3.6	1024
45-2	3.5	825
45-3	3.6	930
45-4	3.1	737
45-5	3.2	994
Average 45	**3.4**	**902±120**
90-1	4.4	1705
90-2	4.0	1497
90-3	3.5	1993
90-4	2.8	1429
90-5	3.8	2093
Average 90	**3.7**	**1741±291**

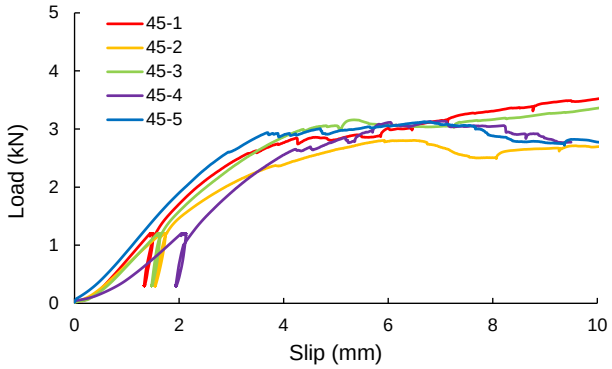
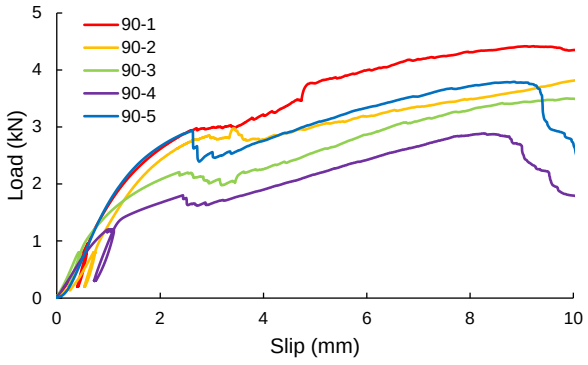


Figure 6. Load-slip curves of 45° series



Copyright © 2025 CroCEE
DOI: https://doi.org/10.5592/CO/3CroCEE.2025.134

Figure 7. Load-slip curves of 90° series

The elasticity modulus and bending strength are calculated on monolithic specimens based on EN 408 [6]. The results are summarized in Table 2. The variations in the results are relatively small.

Table 2. Physical and mechanical properties of the timber

Specimen	Elasticity modulus (MPa)	Flexural strength (MPa)	Density (kg/m^3)	Moisture content (%)
M-1	11064	52.4	437.2	12.0
M-2	12768	63.9	455.2	12.5
M-3	12130	49.2	466.6	12.6
M-4	12152	54.6	451.3	12.0
M-5	12667	60.8	444.9	11.5
Average	**12156±605**	**56.2±5.4**	**452.2±9.9**	**12.1±0.4**

Two series of three-layer beams were tested in the four-point bending test, with load and deflection being monitored. Five specimens were tested for each connection type. The typical failure mode was bending (Figure 8), meaning that the dowels resisted well to shear loading in the mid-plane of the composite beam. Figure 9 and Figure 10 show the experimentally determined load-displacement curves for each specimen. A certain non-linearity can be seen just before the peak load. Table 3 summarises the results of the maximum load, flexural strength and initial stiffness for all tested specimens. It is noticeable that the 45° series shows better flexural behaviour than the 90° series, which is consistent with the results of previous studies [7]. When comparing the two test series, it is noticeable that the 45° series has 35% higher values for load-bearing capacity and 49% higher values for stiffness than the 90° series.

Figure 9 and Figure 10 also show the result of an analytical calculation. The accuracy of the calculation depends on the experimentally determined values of the slip modulus, the modulus of elasticity and the flexural strength. It can be seen that the analytical model for the 45° series predicts the behaviour of the composite beam quite well, while the analytical model for the 90° series overestimates the load-bearing capacity by 46 % and the stiffness by 40 %. This could be due to the fact that the load bearing capacity is most strongly influenced by the value of the slip modulus. In the 90° series, the dowel is subjected to pure shear during the shear test, whereas in the 45° series the dowel is subjected to shear and tension simultaneously. The stress state specified for the 45° specimen corresponds better to the dowel conditions that occur in the four-point bending test. This difference between the experimental and analytical results would be even more pronounced if the calculated value of the slip modulus according to the eq. (3) given by EC5 was used instead of the experimental results of the slip modulus.

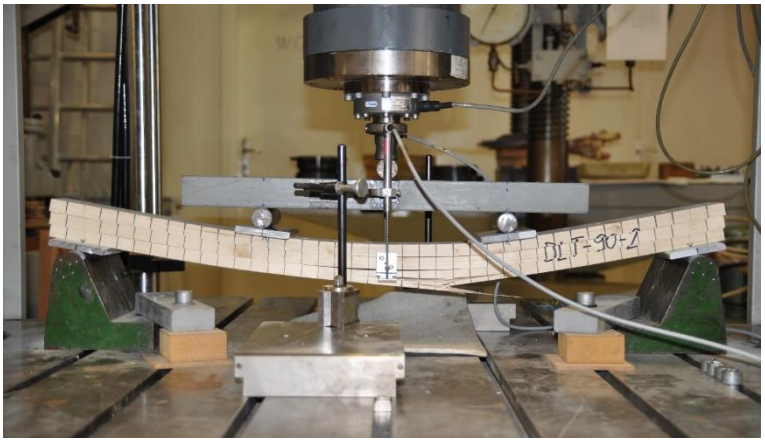


Figure 8. Failure mode

Copyright © 2025 CroCEE
DOI: https://doi.org/10.5592/CO/3CroCEE.2025.134

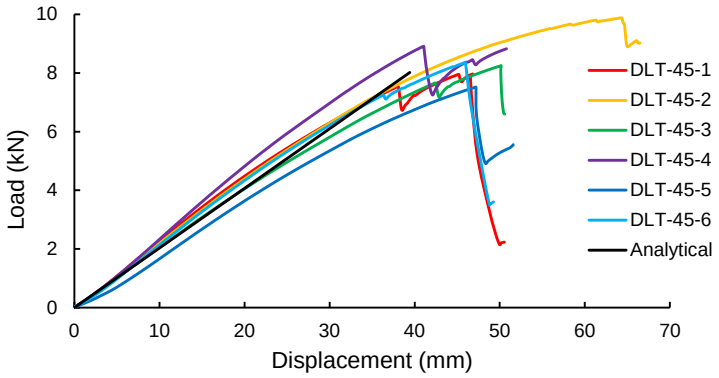


Figure 9. Load – displacement curve of 45° connection DLT beam

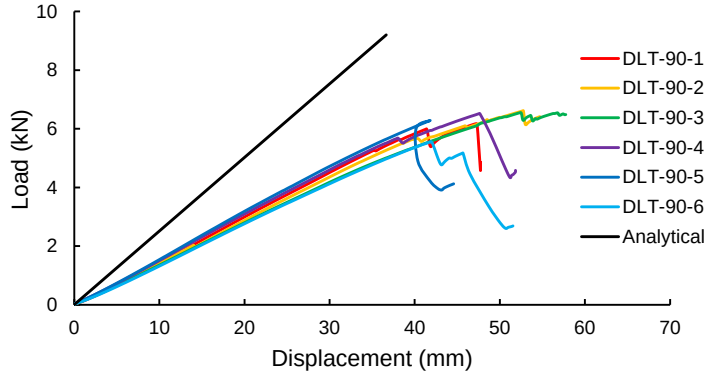


Figure 10. Load-displacement curve of 90° connection DLT beam

Table 3. Maximum load, flexural strength and initial stiffness for all tested specimens

Specimen	**Maximum load (kN)**	**Flexural strength (MPa)**	**Stiffness (N/mm)**	
			Experimental	Analytical
DLT-45-1	7.97	8.28	235.1	
DLT-45-2	9.88	10.26	228.2	
DLT-45-3	8.25	8.57	205.1	
DLT-45-4	8.90	9.25	255.4	**203.3**
DLT-45-5	7.52	7.81	197.7	
DLT-45-6	8.36	8.69	228.7	
Average 45	**8.48 ± 0.75**	**8.81 ± 0.78**	**225.0 ± 19.1**	
DLT-90-1	6.17	6.41	154.9	
DLT-90-2	6.62	6.87	144.3	
DLT-90-3	6.55	6.81	143.4	
DLT-90-4	6.53	6.78	159.0	**251.0**
DLT-90-5	6.28	6.53	163.6	
DLT-90-6	5.56	5.78	142.6	
Average 90	**6.29 ± 0.36**	**6.53 ± 0.37**	**151.3 ± 8.27**	

Copyright © 2025 CroCEE
DOI: https://doi.org/10.5592/CO/3CroCEE.2025.134

5. Conclusion

In this study, the effectiveness of the dowel composite connection is evaluated depending on different dowel angle positions to improve bending stiffness. The dowels were inserted at 90° and 45° angles to determine whether transferring the applied stress from pure shear to a combination of shear and tension could result in higher shear strength. The results obtained on five specimen series of 1 m long beams show that the 45° angle position of the dowels can improve the bending stiffness by up to 50 % and the load bearing capacity by 35 %.

The lack of specific regulations for DLT design in Eurocode 5 reflects the general challenge of standardizing emerging construction technologies. Whilst EC5 is comprehensive for more established products such as CLT and glulam, it has yet to catch up with the unique design considerations of DLT. Currently, the only given solution for DLT is the design approach of the "γ-method", which can be used to assess the load-bearing capacity of composite beams. A key factor in this calculation is the slip modulus, which is determined here on five specimens per series in accordance with EN 26891. The results show that the analytical model greatly overestimates the load-bearing capacity and stiffness of the beams in case of the 90° series. This difference between experimental and analytical results would be even more pronounced if the calculated value of the slip modulus according to EC5 was used instead of the experimental value. Future experimental tests need to be conducted to update EC5, overcome the provisions gap and provide clearer guidance for DLT design.

References

[1] A. Sotayo, D. Bradley, M. Bather, P. Sareh, M. Oudjene, I. El-Houjeyri, A. M. Harte, S. Mehra, C. O'Ceallaigh, P. Haller, S. Namari, A. Makradi, S. Belouettar, L. Bouhala, F. Deneufbourg, Z. Guan; Review of state of the art of dowel laminated timber members and densified wood materials as sustainable engineered wood products for construction and building applications; Developments in the Built Environment 2020; 1; doi.org/10.1016/j.dibe.2019.100004.

[2] C. O'Loinsigh, M. Oudjene, H. Ait-Aider, P. Fanning, A. Pizzi, E. Shotton, E.-M. Meghlat; Experimental study of timber-to-timber composite beam using welded-through wood dowels; Construction and Building Materials; 2012; 36; 245-250, doi.org/10.1016/j.conbuildmat.2012.04.118.

[3] Derikvand M, Hosseinzadeh S, Fink G. Mechanical properties of dowel laminated timber beams with connectors made of salvaged wooden materials. J Archit Eng 2021;27. doi.org/10.1061/(ASCE)AE.1943-5568.0000513

[4] EN 1995-1-1:2004 - Eurocode 5: Design of timber structures - Part 1-1: General - Common rules and rules for buildings. Eurocode 5 2004;1:1–123.

[5] EN 26891:1991 - Timber Structures. Joints Made With Mechanical Fasteners. General Principles For The Determination Of Strength And Deformation Characteristics (ISO 6891:1983). 1991.

[6] EN 408:2003 - Timber structures - Structural timber and glued laminated timber - Determination of some physical and mechanical properties Structures. 2010.

[7] N. Dourado, F.A.M. Pereira, J.L. Lousada, M.F.S.F. de Moura, Experimental and numerical analyses of wood boards joining using wood-pin connectors, Construction and Building Materials, 2019.; 222; 556-565; doi.org/10.1016/j.conbuildmat.2019.06.179.

Proceedings of the 3rd Croatian Conference on Earthquake Engineering - 3CroCEE
19–22 March 2025, Split, Croatia
Copyright © 2025 CroCEE
DOI: https://doi.org/10.5592/CO/3CroCEE.2025.137

SAND AND SAND-KAOLINE MIXTURES CYCLIC PROPERTIES UNDER LOW CONFINING STRESS

Vedran Jagodnik [1,4], Davor Marušić [2], Neira Mušić [3], Ivana Bošnjak [3]

[1] *Associated professor, University of Rijeka, Faculty of Civil Engineering, Radmile Matejčić 3, 51000 Rijeka, vedran.jagodnik@gradri.uniri.hr*
[2] *PhD student, University of Rijeka, Faculty of Civil Engineering, Radmile Matejčić 3, 51000 Rijeka, davor.marusic@gradri.uniri.hr*
[3] *Graduate student, University of Rijeka, Faculty of Civil Engineering, Radmile Matejčić 3, 51000 Rijeka*
[4] *Center for Artificial Intelligence and Cybersecurity, University of Rijeka, Radmile Matejčić 2, 51000 Rijeka*

Abstract

The dynamic behaviour of sand and sand mixtures containing low-plasticity fines at low confining stresses is of crucial importance for geotechnical engineering, especially in regions prone to seismic activity. Such materials can be found as natural or man-made deposits or produced in the laboratory. For these mixtures, the accurate assessment and representation of the initial void ratio, defined by the phase relationship or intergranular void ratio, is essential for understanding their cyclic behaviour. The initial void ratio has a direct influence on the response of sand-fines aggregate mixtures under cyclic loading, especially when fines aggregate fills the voids between the sand grains.

Although the cyclic shear threshold for pore water pressure tends to increase with higher plasticity indices, the behaviour of sand mixtures with low plasticity fines remains highly susceptible to liquefaction at low confining stresses. These mixtures exhibit a rapid build-up of pore water pressure and undergo faster cyclic degradation under seismic loads. The problem becomes particularly apparent when the void ratio is calculated using standard phase relationships, which may not fully capture the complex interactions between sand and fines.

This paper presents preliminary findings on the role of fines in filling the voids between sand grains and investigates the behaviour of sand-kaolinite mixtures under dynamic conditions. A series of cyclic triaxial tests were conducted under undrained conditions using both strain and stress-controlled approaches as well as resonant column tests. The results highlight the critical role of intergranular void ratio and effective confining stress in determining the susceptibility to liquefaction and overall cyclic behaviour of sand and sand-kaolinite mixtures under low confining stresses. These results provide important insights into the factors influencing soil stability in seismic environments and emphasise the need for further research on the interaction of sand and low-plasticity fines.

Keywords: stiffness degradation, pore water pressure build-up, sand-kaolinite mixtures, cyclic triaxial test, resonant column test, low confining stress

1. Introduction

The cyclic behaviour of sand mixtures with fines, particularly those containing silt and clay, has attracted significant attention in geotechnical engineering. This interest arises from the need to predict their performance under dynamic conditions such as earthquakes and other vibration induced loading. Research conducted by Thevanayagam [1], Lade et al. [2] and Seed [3], established the influence of fines content and confining stress on the monotonic and cyclic soil behaviour. Recent works, including Othman et al. [4], Akhila et al. [5–7] and Swamy et al. [7], have made some advancement in the understanding of such behaviour, focusing on sand-kaolinite mixtures.

Initial studies on sand-fines mixtures emphasised understanding of their monotonic behaviour, exploring how fines content affects strength and compressibility properties. Later research extended this work to investigate the materials' cyclic loading response, revealing the significant role of fines and how they are influencing liquefaction resistance and cyclic strength degradation. For example, the

Copyright © 2025 CroCEE
DOI: https://doi.org/10.5592/CO/3CroCEE.2025.137

research by Othman et al. [4] highlighted the complex interaction between kaolinite clay and sand particles, and how this interaction can profoundly influence the overall mechanical properties of the mixed material.

Clay minerals introduce complexities in interparticle contacts. Benessalah et al. [8] demonstrated how low-plasticity fines significantly impact instability stress while Nougar et al. [9] and Dafalla et al. [10] found that increasing fines content reduces dilatancy and strength. Wu et al. [11] emphasized the role of fines to creep and secondary compression in sand-clay mixtures.

Fines content and confining stress strongly influence cyclic properties. Studies reveal a non-linear relationship where cyclic strength decreases until fines reach approximately 20%, beyond which it increases [12]. Hyodo et al. [13] noted that strength increases at approximately 30% fines, while Fei & Xu [14] observed fading effects of coarse particles under high cyclic loads. Karim & Alam [15], found that pore pressure generation stabilizes at higher fines content (approximately 35%).

Low confining stresses intensify cyclic strength degradation, particularly in soils with high fines content. Noorzad & Shakeri [16] reported a decrease in post-cyclic monotonic strength at higher fines levels, while Shan et al. [17] described transitional failure behaviours in sand-clay mixtures. For sands with 15–30% fines, cyclic loading significantly alters ultimate strength, with negligible effects in cleaner sands.

Void ratio is critical for predicting soil behaviour, whether the soil is under undrained or drained conditions and whether the soil is loaded monotonically or cyclically. Research has shown that the silty sands' void ratios differ from the void ratios determined for sands using standardized testing procedures and conventional phase relations [1,2,18]. Existing analytical models provided by Chang et al. [19] have been used to redefine the tested silty sands' minimum and maximum void ratios for specimen reconstitution at a targeted relative density. The paper presents the preliminary finding on the role of fines in sand-kaolinite mixtures below fines threshold at low confining stress. Series of cyclic tests were performed on three different material types under the same relative density, based on the redefined void ratios. Focus of the presented results are on the degradation of stiffness and pore water pressure rise.

2. Methodology of performed research

2.1. Materials used

Uniform sand (SK0) and sand-kaolinite mixtures with 10% (SK10) and 15% (SK15) kaolinite content were prepared to examine their cyclic behaviour under low confining stress. Tests were conducted at confining stresses of 25 kPa and 50 kPa, representative of conditions in many geotechnical applications. The sand used was a clean, uniform material with a specific gravity of 2.7. The kaolinite, a commercially available product with a specific gravity of 2.6, was mixed in dried condition with the sand to ensure homogeneity prior to preparing specimens for dynamic properties testing.

Key properties, such as particle size distribution and Atterberg limits, were determined following standardized procedures. Sieve analysis was conducted following European standard [20]. As mentioned, void ratios e_{min} and e_{max} were obtained with existing analytical methods for binary soil mixtures provided by Chang et al. [19]. Liquid and plastic limits were easily obtained for kaolinite, following the procedure according to European standards [21]. For the samples made of sand-kaolinite mixture, the fall cone procedure [22] was used due to the difficulties on the consistency limit determination. The complexity behind the determination of consistency limits for such mixtures are presented in the work done by Marušić and Jagodnik [23]. Physical properties of the material used in laboratory testing are summarized in Table 1.

Proceedings of the 3rd Croatian Conference on Earthquake Engineering - 3CroCEE
19–22 March 2025, Split, Croatia
Copyright © 2025 CroCEE
DOI: https://doi.org/10.5592/CO/3CroCEE.2025.137

Table 1. Physical properties of materials used in research, [24–26]

Physical property	SK0	SK10	SK15	SK100
Specific gravity, G_s (-)	2.7	2.69	2.67	2.6
Eff. Particle size, D_{10} (mm)	0.183	0.054	0.0045	0.00258
Minimum void ratio, e_{min} (-)	0.641	0.473	0.390	0.850
Maximum void ratio, e_{max} (-)	0.911	0.716	0.619	1.640
Plastic limit, w_{PL} (%)	N/A	5.8	9.6	21.6
Liquid limit, w_{LL} (%)	N/A	17.9	17.9	48.3

N/A- non applicable

2.2.Testing equipment

Dynamic properties of artificially sand-kaolinite mixtures were determined using two types of advanced testing systems: (i) Resonant Column device and (ii) Cyclic triaxial device. The two types of system were used due to their possibility to control confining stress and to ensure the full saturation of samples. This ensured the accurate measurement of pore water pressure.

2.2.1. Resonant column device

Resonant column testing is a widely used laboratory method to determine the dynamic properties of soil samples, specifically the shear modulus and damping ratio [27,28]. It involves vibrating a cylindrical soil specimen at different frequencies until resonance is achieved. By measuring the resonant frequency and the rate of decay of vibrations, the shear modulus and damping ratio can be calculated [29,30]. These parameters are crucial for understanding how soil behaves under dynamic loading, such as earthquakes or machine vibrations [31,32].

Recently, the use of the chirp method in resonant column testing has been reported in the literature, e.g. [33–36]. In this approach, the specimen is excited with a frequency sweep rather than a single frequency. This allows for a more comprehensive assessment of the sample's non-linear dynamic response across a broad range of strain amplitudes, providing valuable insights into the soil's behaviour under large deformation conditions.

2.2.2. Cyclic triaxial device

Cyclic triaxial testing was carried out in accordance with ASTM standard [37,38]. Cylindrical specimens, prepared at the same relative densities as the resonant column tests, were subjected to sinusoidal axial loading under constant confining stresses of 25 kPa and 50 kPa. Pore pressure measurements allowed for the evaluation of excess pore pressure ratios r_u during cycling. The cyclic triaxial system's capabilities and calibration details are described in work done by Jagodnik et al. [24,39–41]. Membrane corrections were applied following established methods Duncan & Seed [42] and Lade [43].

2.3.Sample preparation

Samples were prepared using the moist compaction method [44], to ensure uniform density and an even distribution of the soil constituents, thereby preventing fines segregation. The specimens were compacted in ten uniform layers within a latex membrane at the undercompaction of 5%. The initial parameters, including water content, relative density, and void ratio, are detailed in Table 2.

Table 2. Initial parameters of tested materials

Initial parameters	SK0	SK10	SK15
Initial water content, w_i (%)	2	5.8	9.6
Saturated water content, w_{max} (%)	20.5	16.2	14
Relative density, D_r (%)	80	80	80
Initial void ratio, e_0 (-)	0.692	0.681	0.738

Proceedings of the 3rd Croatian Conference on Earthquake Engineering - 3CroCEE
19–22 March 2025, Split, Croatia
Copyright © 2025 CroCEE
DOI: https://doi.org/10.5592/CO/3CroCEE.2025.137

2.4. Test procedures

Specimen prepared using undercompaction method mentioned above were subjected to resonant column tests to characterize the dynamic properties. The testing protocol involved exciting the soil specimen with a frequency sweep and measuring the amplitude, phase response, and torsional shear. Samples were saturated and consolidated to confining stresses of 25 and 50 kPa. After consolidation the samples were loaded with torsional strain amplitude, defined with Table 3. The shear modulus and damping ratio were then calculated from the resonant frequency and rate of decay of the vibrations. Tests were performed in undrained conditions.

Table 3. Initial parameters of tested materials

Test system type	Loading type	Loading values
Resonant column	Torsional shear amplitude [Vol]	0.001, 0.002, 0.005, 0.01, 0.02, 0.05, 0.075, 0.1
Dynamic triaxial test	Cyclic axial strain [%]	0.005, 0.0067, 0.013, 0.033, 0.05, 0.067, 0.13

For cyclic triaxial testing, soil specimens were prepared in the same manner as the resonant column tests. The cylindrical samples were then mounted in the triaxial cell and subjected to sinusoidal axial cyclic strain under constant confining pressures of 25 kPa and 50 kPa, after saturation and consolidation.

3. Results and discussion

This paper presents experimental results of resonant column and cyclic triaxial tests performed to investigate the cyclic shear behavior of soils under low confining stresses. The study focuses on the variation of stiffness degradation, shear modulus and viscous damping as functions of cyclic shear strain, with comparisons to reference trends for soils with different plasticity indices. The results illustrate the dynamic response of soils with low plasticity under different strain amplitudes and confining pressures and provide insights into their stiffness degradation and damping properties.

The Figure 1 illustrates the variation of stiffness degradation via normalized shear modulus $G_s/G_{s,max}$ and equivalent viscous damping ratio λ as functions of cyclic shear strain γ, derived from experimental results of Resonant Column (RC) and Torsional Shear (TS). Tests were conducted at effective confining stresses of 25 kPa and 50 kPa. The experimental data are compared against reference trends for soils with plasticity indices of 0 and 15. For $G_s/G_{s,max}$ the experimental results predominantly follow the trend of the reference curve, especially in the low-to-moderate strain range ($0.001\% \leq \gamma \leq 0.01\%$). At these strain levels, the degradation of shear modulus is minimal, with normalized values remaining above 0.6. This alignment with PI=0 suggests that the tested soil exhibits behavior consistent with non-plastic or low-plasticity materials under cyclic loading.

At higher strains ($\gamma > 0.01\%$), slight deviations from the PI=0 curve are observed, with some data points exhibiting faster degradation of $G_s/G_{s,max}$ These deviations could be attributed to differences in soil fabric, sample preparation methods, or the specific test conditions (e.g., confining pressure and loading history). Nonetheless, the overall trends remain reasonably consistent with the PI=0 reference, indicating that the plasticity of the tested soil is negligible.

For the equivalent viscous damping ratio λ, the experimental results also follow the expected upward trend observed in the PI=0 reference curve. At low strains ($\gamma < 0.01\%$), damping remains relatively low, consistent with typical behavior of low-plasticity soils. As strain increases, the damping ratio exhibits a progressive increase, aligning closely with the reference curve for PI=0.

Copyright © 2025 CroCEE
DOI: https://doi.org/10.5592/CO/3CroCEE.2025.137

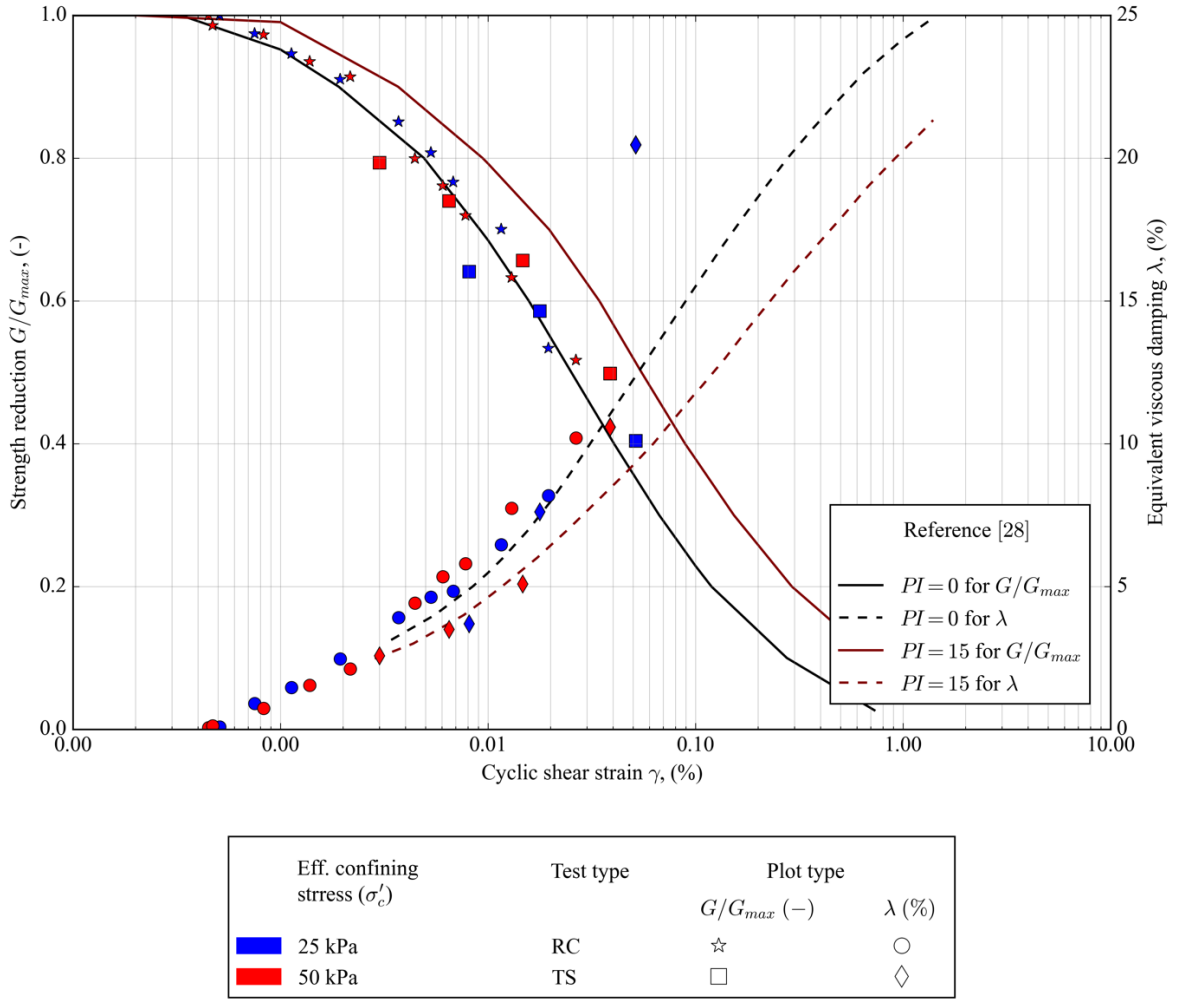


Figure 1. Strength reduction of SK15 mixtures along with equivalent viscous damping

The agreement between experimental data and the PI=0 curve supports the classification of the tested soil as a low-plasticity material. This is consistent with the known characteristics of soils with low or negligible fines content, where plasticity plays a minimal role in dynamic response.

The Figure 2 shows the relationship between normalized pore water pressure (r_u) and stiffness degradation (δ) for cyclic shear strain amplitudes of 0.01%, 0.05%, and 0.1% under effective confining stresses of 25 kPa and 50 kPa. Each subplot corresponds to a specific shear strain amplitude and highlights the progression of stiffness degradation as r_u increases. At low r_u values, stiffness degradation remains minimal, with δ close to 1.0, indicating negligible loss in stiffness, Figure 2a. As r_u approaches 0.65, marked by a dashed vertical line, the stiffness degradation becomes more pronounced, Figure 2b, with greater reductions observed at higher cyclic shear strain amplitudes, Figure 2c. The data also reveal consistent trends across different effective confining stresses, with degradation intensifying at larger strain levels and nonlinear behaviour of material at low cyclic shear strain (Figure 2b and c).

Proceedings of the 3rd Croatian Conference on Earthquake Engineering - 3CroCEE
19–22 March 2025, Split, Croatia
Copyright © 2025 CroCEE
DOI: https://doi.org/10.5592/CO/3CroCEE.2025.137

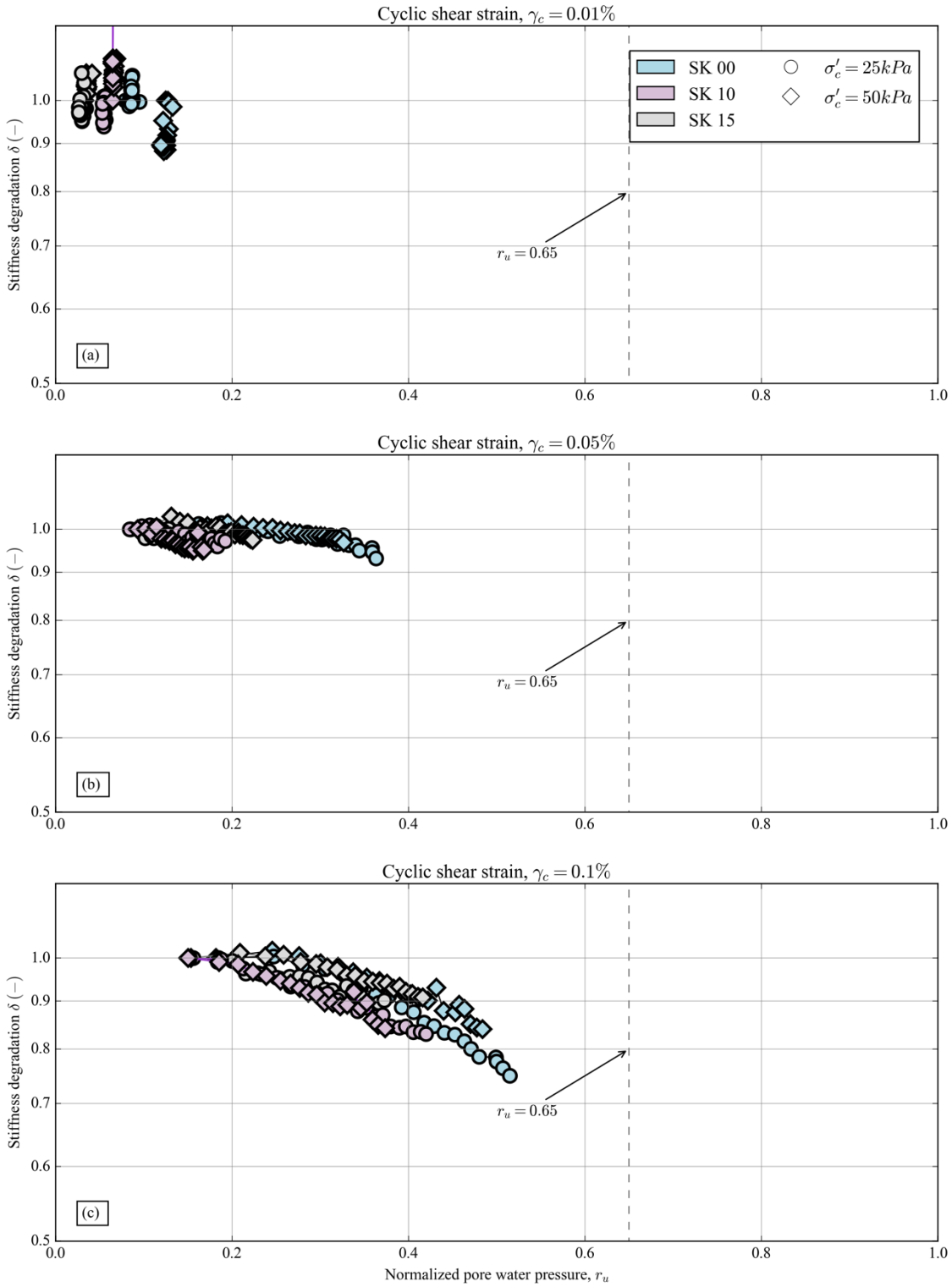


Figure 2. Relation of stiffness degradation and normalized pore water pressure: (a) Cyclic shear strain $\gamma_c = 0.01$ %, (b) Cyclic shear strain $\gamma_c = 0.05$ % and (c) Cyclic shear strain $\gamma_c = 0.1$ %,

Proceedings of the 3rd Croatian Conference on Earthquake Engineering - 3CroCEE
19–22 March 2025, Split, Croatia
Copyright © 2025 CroCEE
DOI: https://doi.org/10.5592/CO/3CroCEE.2025.137

4. Conclusions

This study investigates the dynamic properties of sand-kaolinite mixtures using a comprehensive laboratory test programme that includes resonant column and cyclic triaxial tests. Several important results can be derived:

- Increasing the fines content leads to a reduction in shear modulus at small strains, probably due to the softer nature of the clay fraction.
- Higher fines contents lead to a greater accumulation of excess pore pressure during cyclic loading, indicating an increased susceptibility to liquefaction, especially at lower confining pressures.
- With increasing fineness, the sand-kaolin mixtures experience a greater reduction in stiffness during cyclic loading, as can be seen from the normalised curves for shear modulus degradation.
- Higher limiting stresses lead to higher shear modulus values, lower pore pressure accumulation and less pronounced stiffness degradation.

In summary, it can be said that the dynamic behavior of sand-kaolinite mixtures is significantly influenced by the fines content and the confining stress. A higher fines content reduces the shear modulus at small strains, increases the susceptibility to pore pressure accumulation and accelerates the stiffness degradation under cyclic loading. Conversely, higher limiting stresses improve the shear modulus, reduce the build-up of pore pressure and reduce the reduction in stiffness

Acknowledgements

The tests were conducted in the Geotechnical Laboratory at the Faculty of Civil Engineering, University of Rijeka, within the Project Research Infrastructure for Campus-based Laboratories at the University of Rijeka, (RC.2.2.06-0001) funded by Ministry of Science, Education and Sports of the Republic of Croatia. This project has been co-funded by the European Fund for Regional Development (ERDF); this support is gratefully acknowledged.

The research was funded by the University of Rijeka, Croatia through the project “Physical and laboratory tests of interparticle behavior of sand and clay mixtures at low overburden stresses" (uniri-iskusni-tehnic-23- 183 212).

The help of a former graduate students from the Faculty of Civil Engineering, University of Rijeka, Croatia, Martina Turković and Duje Katalinić in conducting several cyclic tests is sincerely appreciated.

References

[1] Thevanayagam, S., (1998), Effect of Fines and Confining Stress on Undrained Shear Strength of Silty Sands, Journal of Geotechnical and Geoenvironmental Engineering, **124**(6), 479–491, https://doi.org/10.1061/(ASCE)1090-0241(1998)124:6(479).

[2] Lade, P. V, Liggio, C. D., and Yamamuro, J. A., (1998), Effects of Non-Plastic Fines on Minimum and Maximum Void Ratios of Sand, Geotechnical Testing Journal, **21**(4), 336–347, https://doi.org/10.1520/gtj11373j.

[3] Seed, R. B., (2010), *Soil Liquefaction During Earthquakes*, [Online]. Available: https://vulcanhammernet.files.wordpress.com/2017/01/liquefactionreview.pdf.

[4] Othman, B. A., Marto, A., Uzuoka, R., Ueda, K., and Satar, M. H. M., (2022), Liquefaction Resistance of Sand-Kaolin Mixtures: Effect of Sand Sizes, IOP Conference Series: Earth and Environmental Science, **1103**(1), 12026, https://doi.org/10.1088/1755-1315/1103/1/012026.

[5] Akhila, M., Rangaswamy, K., and Sankar, N., (2019), Liquefaction Susceptibility of Silty Sands and Low Plastic Clay Soils, International Journal of Geotechnical Earthquake Engineering, **10**(2), 1–17, https://doi.org/10.4018/IJGEE.2019070101.

Copyright © 2025 CroCEE
DOI: https://doi.org/10.5592/CO/3CroCEE.2025.137

[6] Akhila, M., Rangaswamy, K., and Sankar, N., (2019), Undrained Response and Liquefaction Resistance of Sand–Silt Mixtures, Geotechnical and Geological Engineering, **37**(4), 2729–2745, https://doi.org/10.1007/s10706-018-00790-0.

[7] Ranga Swamy, K., Akhila, M., and Sankar, N., (2021), Effects of Fines Content and Plasticity on Liquefaction Resistance of Sands, Proceedings of the Institution of Civil Engineers - Geotechnical Engineering, **174**(6), 697–706, https://doi.org/10.1680/jgeen.19.00270.

[8] Benessalah, I., Arab, A., and Meziane, E.-H., (2021), Intergranular Void Ratio and Undrained Monotonic Behavior of Chlef Sand Containing Low Plastic Fines, Acta Mechanica, **232**(4), 1621–1640, https://doi.org/10.1007/s00707-020-02923-0.

[9] Nougar, B., Brahimi, A., Bouri, D. E., Arab, A., and Benessalah, I., (2021), Laboratory Investigation into the Effect of Fines Plasticity on the Mechanical Behavior of Sand/Fines Mixtures, Transportation Infrastructure Geotechnology, **8**(3), 438–451, https://doi.org/10.1007/s40515-020-00144-5.

[10] Dafalla, M., Shaker, A., Elkady, T., Almajed, A., and Al-Shamrani, M., (2020), Shear Strength Characteristics of a Sand Clay Liner, Scientific Reports, **10**(1), 18226, https://doi.org/10.1038/s41598-020-75188-1.

[11] Wu, Z., Deng, Y., Cui, Y., Chen, Y., Wang, Q., and Feng, Q., (2019), Investigations on Secondary Compression Behaviours of Artificial Soft Sand-Clay Mixtures, Soils and Foundations, **59**(2), 326–336, https://doi.org/10.1016/j.sandf.2018.11.008.

[12] Balreddy, M. S., Dinesh, S. V, and Sitharam, T. G., (2021), Liquefaction Behavior of Low to Medium Plasticity Sand-Fines Mixtures, 181–191, https://doi.org/10.1007/978-981-33-4001-5_17.

[13] Hyodo, M., Yamamoto, Y., and Sugiyama, M., (1994), Undrained Cyclic Shear Behaviour of Normally Consolidated Clay Subjected to Initial Static Shear Stress, Soils and Foundations, **34**(4), 1–11, https://doi.org/10.3208/sandf1972.34.4_1.

[14] Fei, K., and Xu, J., (2017), Dynamic Behavior of Clay-Aggregate Mixtures, Advances in Materials Science and Engineering, **2017**, 1–10, https://doi.org/10.1155/2017/2479507.

[15] Karim, M. E., and Alam, Md. J., (2014), Effect of Non-Plastic Silt Content on the Liquefaction Behavior of Sand–Silt Mixture, Soil Dynamics and Earthquake Engineering, **65**, 142–150, https://doi.org/10.1016/j.soildyn.2014.06.010.

[16] Noorzad, R., and Shakeri, M., (2017), Effect of Silt on Post-Cyclic Shear Strength of Sand, Soil Dynamics and Earthquake Engineering, **97**, 133–142, https://doi.org/10.1016/j.soildyn.2017.03.013.

[17] Shan, Y., Cui, J., Wen, H., Yu, S., and Li, Y., (2022), Analysis of Dynamic Properties and Transitional Failure of Clay–Sand Mixture in Fine-Grained Soil Based on Mineral Composition, Engineering Geology, **296**, 106464, https://doi.org/10.1016/j.enggeo.2021.106464.

[18] Thevanayagam, S., Fiorillo, M., and Liang, J., (2000), Effect of Non-Plastic Fines on Undrained Cyclic Strength of Silty Sands, *Soil Dynamics and Liquefaction 2000*, American Society of Civil Engineers, Reston, VA, 77–91, https://doi.org/10.1061/40520(295)6.

[19] Chang, C. S., Wang, J.-Y., and Ge, L., (2015), Modeling of Minimum Void Ratio for Sand–Silt Mixtures, Engineering Geology, **196**, 293–304, https://doi.org/10.1016/j.enggeo.2015.07.015.

[20] HRS CEN ISO/TS 17892-4:2016, (2016), *Geotehničko Istraživanje i Ispitivanje – Laboratorijsko Ispitivanje Tla – 4. Dio: Određivanje Granulometrijskog Sastava*.

[21] HRS CEN ISO/TS 17892-12:2008, (2008), *Geotehničko Istraživanje i Ispitivanje - Laboratorijsko Ispitivanje Tla -- 12. Dio: Određivanje Atterbergovih Granica*.

Copyright © 2025 CroCEE
DOI: https://doi.org/10.5592/CO/3CroCEE.2025.137

[22] HRS CEN ISO/TS 17892-6:2008, (2008), *Geotehničko Istraživanje i Ispitivanje - Laboratorijsko Ispitivanje Tla -- 6. Dio: Pokus s Padajućim Šiljkom*.

[23] Marušić, D., and Jagodnik, V., (2023), Determination of the Atterberg Limits Using a Fall Cone Device On Low Plasticity Silty Sands, Rudarsko-geološko-naftni zbornik, **38**(3), 133–145, https://doi.org/10.17794/rgn.2023.3.11.

[24] Jagodnik, V., and Arbanas, Ž., (2022), Cyclic Behaviour of Uniform Sand in Drained and Undrained Conditions at Low Confining Stress in Small-Scale Landslide Model, Sustainability, **14**(19), 12797, https://doi.org/10.3390/su141912797.

[25] Marušić, D., and Jagodnik, V., (2023), DETERMINATION OF THE ATTERBERG LIMITS USING A FALL CONE DEVICE ON LOW PLASTICITY SILTY SANDS, Rudarsko-geološko-naftni zbornik, **38**(3), 133–145, https://doi.org/10.17794/rgn.2023.3.11.

[26] Pajalić, S., Peranić, J., Maksimović, S., Čeh, N., Jagodnik, V., and Arbanas, Ž., (2021), Monitoring and Data Analysis in Small-Scale Landslide Physical Model, Applied Sciences (Switzerland), **11**(11), https://doi.org/10.3390/app11115040.

[27] Hardin, B. O., and Drnevich, V. P., (1972), Shear Modulus and Damping in Soils: Design Equations and Curves, Journal of Soil Mechanics & Foundations Div, **98**(sm7).

[28] Vucetic, M., and Dobry, R., (1991), Effect of Soil Plasticity on Cyclic Response, Journal of Geotechnical Engineering, **117**(1), 89–107, https://doi.org/10.1061/(ASCE)0733-9410(1991)117:1(89).

[29] Iwasaki, T., Tatsuoka, F., and Takagi, Y., (1978), Shear Moduli of Sands under Cyclic Torsional Shear Loading, Soils and Foundations, **18**(1), 39–56.

[30] Drnevich, V. P., (1978), Resonant-Column Testing—Problems and Solutions, *Dynamic Geotechnical Testing*, ASTM International, 100 Barr Harbor Drive, PO Box C700, West Conshohocken, PA 19428-2959, 384–384–15, https://doi.org/10.1520/STP35687S.

[31] Seed, H. B., and Idriss, I. M., (1970), *Soil Moduli and Damping Factors for Dynamic Response Analyses*.

[32] Vucetic, M., (1994), Cyclic Threshold Shear Strains in Soils, Journal of Geotechnical Engineering, **120**(12), 2208–2228, https://doi.org/10.1061/(ASCE)0733-9410(1994)120:12(2208).

[33] Jagodnik, V., Đomlija, P., Oštrić, K., and Arbanas, Ž., (2019), Strength Reduction Curve of Soils from Eluvial Deposits in Vinodol Valley, Croatia, *Proceedings of the 4th Regional Symposium on Landslides in the Adriatic - Balkan Region*, Društvo za geotehniku u Bosni i Hercegovini, 109–114, https://doi.org/10.35123/ReSyLAB_2019_18.

[34] Cavallari, A., (2016), Resonant Column Testing Challenges, *1st IMEKO TC4 International Workshop on Metrology for Geotechnics, MetroGeotechnics 2016*, 149–156.

[35] Moin, S., and Qasim, S., (2024), Effect on Dynamic Parameters of Waste Reinforced Soil under Vibrations Generated through Traffic Loading: Experimental Evaluation, Journal of Engineering Research (Kuwait), https://doi.org/10.1016/j.jer.2023.12.011.

[36] Khan, Z. H., Cascante, G., El Naggar, M. H., and Lai, C. G., (2008), Measurement of Frequency-Dependent Dynamic Properties of Soils Using the Resonant-Column Device, Journal of Geotechnical and Geoenvironmental Engineering, **134**(9), 1319–1326, https://doi.org/10.1061/(asce)1090-0241(2008)134:9(1319).

[37] ASTM, (1996), ASTM D5311-92(1996) Standard Test Method for Load Controlled Cyclic Triaxial Strength of Soil, https://doi.org/10.1520/D5311-92R96.

Copyright © 2025 CroCEE
DOI: https://doi.org/10.5592/CO/3CroCEE.2025.137

[38] ASTM, (2011), ASTM D3999/D3999M-11e1 Standard Test Methods for the Determination of the Modulus and Damping Properties of Soils Using the Cyclic Triaxial Apparatus (Withdrawn 2020), https://doi.org/10.1520/D3999_D3999M-11E01.

[39] Jagodnik, V., and Sulovsky, T., (2025), *Degradation of Fully Saturated Uniform Sand at Small Strain Undrained Cyclic Shearing (in Review)*.

[40] Jagodnik, V., Turković, M., and Arbanas, Ž., Preliminary Results on the Undrained Cyclic Behavior of Uniform Sand at Low Confining Stress.

[41] Jagodnik, V., Marušić, D., Peranić, J., Vivoda Prodan, M., Arbanas, Ž., and Katalinić, D., (2024), Cyclic Properties of Sand-Clay Mixtures at Low Confining Stresses, *Geotechnical Engineering Challenges to Meet Current and Emerging Needs of Society*, CRC Press, London, 554–559, https://doi.org/10.1201/9781003431749-82.

[42] Duncan, J. M., and Seed, H. B., (1967), Corrections for Strength Test Data, Journal of the Soil Mechanics and Foundations Division, **93**(5), 121–137.

[43] Lade, P. V, (2016), *Triaxial Testing of Soils*, Wiley, [Online]. Available: https://books.google.hr/books?id=bytECwAAQBAJ.

[44] Ladd, R. S., (1978), Preparing Test Specimens Using under Compaction, Geotechnical Testing Journal, **1**(1), 16–23, https://doi.org/10.1520/GTJ10364J.

Proceedings of the 3rd Croatian Conference on Earthquake Engineering - 3CroCEE
19–22 March 2025, Split, Croatia
Copyright © 2025 CroCEE
DOI: https://doi.org/10.5592/CO/3CroCEE.2025.4

A STATE-OF-THE-ART REVIEW: SEISMIC VULNERABILITY ASSESSMENT METHODS FOR MASONRY STRUCTURES

Antonela Moretić [(1)], Mislav Stepinac [(2)], Karlo Ožić [(3)]

[(1)] *Research assistant, Faculty of Civil Engineering, University of Zagreb, antonela.moretic@grad.unizg.hr*
[(2)] *Associate Professor, Faculty of Civil Engineering, University of Zagreb, mislav.stepinac@grad.unizg.hr*
[(3)] *Research assistant, Faculty of Civil Engineering, University of Zagreb, karlo.ozic@grad.unizg.hr*

Abstract

Seismic vulnerability assessment is a comprehensive process that involves evaluating the susceptibility of structures to potential damage or failure during seismic events. This assessment is crucial for understanding and mitigating the impact of earthquakes on structures. Still, it is necessary to emphasize that vulnerability assessment is not a singular procedure: it varies based on the scale of analysis and the specific goals of the assessment. Conducting such assessments requires significant technical expertise as well as human and financial resources, which are often limited. These challenges are particularly evident in historic urban areas due to the unique characteristics of historical buildings, including complex materials, construction techniques, and the difficulty of quantifying their cultural value and significance.

Methods for assessing structural vulnerability can be categorized into empirical, analytical, expert-based, or hybrid approaches.

The paper discusses the existing vulnerability assessment methods presented by various authors, emphasizing the advantages and disadvantages of each and examining their practical applications.

Keywords: vulnerability, review, empirical methods, analytical methods, expert-based methods, hybrid methods

1. Introduction

Earthquakes, though relatively rare, can exert some of the most significant horizontal forces on structures, causing not only physical destruction but also loss of life and other far-reaching consequences. Seismic risk is assessed using three key factors: seismic hazard, exposure, and vulnerability. Seismic hazard refers to the probability of earthquakes causing destructive effects in a specific area, often expressed as the likelihood of exceeding certain ground motion parameters (PGA) within a defined period and depicted on seismic hazard maps. Exposure represents the concentration of human activity and assets, such as buildings and infrastructure, in the observed area. Vulnerability reflects the susceptibility of structures to the damage caused by seismic forces, enabling the estimation of the probability of specific damage levels during an earthquake. Understanding these three factors allows for better evaluation and mitigation of seismic risk, contributing to safer design and disaster preparedness [1]. The seismic hazard is given by natural geological processes; therefore, it is beyond the human control. Exposure theoretically can be altered, by measures such as relocating the population or organizing new settlements through urban planning. Nevertheless, such an approach is difficult to implement in practice. On the other hand, the vulnerability of the building stock is the easiest factor to influence. Still, in order to decrease it, in case of existing structures, firstly, it needs to be assessed. There are several distinct approaches to assessing seismic vulnerability, commonly grouped into empirical, analytical, expert-based, and hybrid methods.

The authors are conducting a large-scale vulnerability assessment of Lower Town, historical centre of Zagreb. The preliminary assessment based on existing methods has been performed and the scatter between expected and observed damage was noted [2]. The modified method applicable for Croatia is being developed, hence the state-of-the-art review is essential to navigate the numerous existing approaches.

Proceedings of the 3rd Croatian Conference on Earthquake Engineering - 3CroCEE
19–22 March 2025, Split, Croatia
Copyright © 2025 CroCEE
DOI: https://doi.org/10.5592/CO/3CroCEE.2025.4

2. Empirical methods

Empirical methods are often associated with the statistical analysis of post-earthquake inspection data, usually represented in the form of damage probability matrices (DPM). A damage probability matrix, introduced by Whitman et al. in 1973 [3], systematically represents the likelihood of a structure reaching a specific damage level (damage state) under varying seismic intensities. These methods can be further divided into two categories: Rapid Visual Screening (RVS) assessment methods and vulnerability index methods [4]. RVS methods are the simplest vulnerability assessment techniques, based on visual surveys that don't involve detailed calculations or investigations. These methods rely solely on external building observations, ignoring interior factors. RVS is particularly useful for quick, preliminary vulnerability assessments in cases of urgency or limited data access, helping prioritize actions. It is also suitable for large building stocks since it can be completed in under 30 minutes. The RVS method defines 17 building types and assigns each a "Basic Structural Hazard" (BSH) score, which reflects the probability of structural collapse. The BSH score is then adjusted by score modifiers (SM) based on factors such as the number of stories, building height, plan and vertical irregularities, soil type, and construction age. RVS methods have been developed and implemented in countries such as United States, Canada, Japan, New Zealand, Turkey and Greece.

The Vulnerability Index Method (VIM) is widely used for seismic vulnerability assessment due to its straightforward approach, involving seismic hazard analysis, vulnerability analysis, and damage evaluation via the damage probability matrix. In recent decades, the GNDT (National Group of Defense from Earthquakes) approach in Italy has been vocal in developing vulnerability index methods. These methods are classified into two levels: "GNDT level I" and "GNDT level II." "GNDT level I" classifies buildings into typological classes and defines vulnerability classes A, B, and C, while "GNDT level II" integrates the work of Benedetti et al [5]. The method, based on extensive damage data and building stock information, defines parameters that influence seismic response and applies a weighting process, considering the importance of each parameter through expert judgment (Table 1).

Table 1 Vulnerability index method [5]

Parameter	Class				Weight factor
	A	B	C	D	
1. Connection of walls	0	5	20	45	1,00
2. Type of walls	0	5	25	45	0,25
3. Soil condition	0	5	25	45	0,75
4. Total shear resistance of walls	0	5	25	45	1,50
5. Plan regularity	0	5	25	45	0,50
6. Elevation regularity	0	5	25	45	(*)
7. Horizontal diaphragms	0	5	15	45	(*)
8. Roof	0	15	25	45	(*)
9. Details	0	0	25	45	0,25
10. General maintenance conditions	0	5	25	45	1,00

A modified version of the VIM developed by Benedetti and Petrini [5], was proposed by Formisano et al [6]. This method introduces five additional parameters with corresponding weight factors to capture the aggregate effect more accurately (Table 2). These parameters were selected based on a thorough review of previous studies and expert judgment. To justify the weight factors, several pushover analyses were conducted for each new parameter. Diverse boundary conditions among adjacent structural units were simulated, and the pushover analyses were performed using the 3MURI software, which employs the Frame by Macro-Elements (FME) method. The structural response was evaluated using the mechanical vulnerability index (IM) in both isolated and aggregate conditions, calculated as the ratio of demand to capacity in terms of displacement. This modified VIM is commonly used in both research and practice to assess the collective impact of various factors on structural vulnerability.

Proceedings of the 3rd Croatian Conference on Earthquake Engineering - 3CroCEE
19–22 March 2025, Split, Croatia
Copyright © 2025 CroCEE
DOI: https://doi.org/10.5592/CO/3CroCEE.2025.4

Table 2 Parameters that capture the aggregate effect [6]

Parameter	Class				Weight factor
	A	B	C	D	
1. Presence of adjacent buildings with different height	-20	0	15	45	1,00
2. Position of the building in the aggregate	-45	-25	-15	0	1,50
3. Presence and number of staggered floors	0	15	25	45	0,50
4. Effect of either structural or typological heterogeneity among adjacent structural unit	-15	-10	0	45	1,20
5. Percentage difference of opening areas among adjacent facade	-20	0	25	45	1,00

The applicability of empirical methods is often constrained to specific regions. For instance, the VIM method was applied to the case study from Croatian building stock [7], [8] revealing significant discrepancies between the expected [2] and actual damage outcomes [9], [10].



Figure 1 Preliminary assessemnt in Zagreb; case studies [2]

A similar approach for considering the aggregate effect was proposed by Ferreira et al. [11]. The authors identified key factors in generating the aggregate effect, including height irregularities, misalignments of floors and/or openings, the quality of masonry, location, soil conditions, and the plan geometry.

In 1999, the European Union supported the RISK-UE project, aiming to develop a comprehensive seismic risk assessment methodology for European countries [4]. This initiative arose from the lack of a unified system across Europe. As part of the Risk-UE project, two models were proposed: a macroseismic model, intended to be used with macroseismic intensity hazard maps, and a mechanical-based model, designed for when the hazard is represented by peak ground accelerations and spectral values [12]. The macroseismic model introduced the VIM as an effective tool for vulnerability assessment, which was implemented in seven European cities. The VIM classifies buildings (including masonry, reinforced concrete, steel, and wooden structures) into six vulnerability classes (A to F). Each class is assigned a vulnerability index, which is then adjusted by a Behaviour Modifier Factor / Response Modification Factor, based on expert judgment, and a Regional Vulnerability Factor, derived from both historical data and expert judgment. Additionally, the approach categorizes damage into five grades, from slight damage to complete collapse, using the EMS-98 scale (D1 to D5).

However, it is important to note that producing an overall seismic risk assessment may not always be feasible due to the unique characteristics of different building stocks. For example, in one study [13], the authors compared the seismic vulnerability models for masonry and reinforced concrete structures

Proceedings of the 3rd Croatian Conference on Earthquake Engineering - 3CroCEE
19–22 March 2025, Split, Croatia
Copyright © 2025 CroCEE
DOI: https://doi.org/10.5592/CO/3CroCEE.2025.4

from the Risk-UE project with experimental dynamic properties of buildings in France. They observed significant discrepancies between the proposed vulnerability curves and the experimental data. The authors recommended deriving curves for typological classes based on the number of stories, as they concluded that the elastic period (or frequency) is a function of building height and/or number of stories [13].

3. Analytical methods

Unlike empirical methods, which rely on observations, analytical methods depend on numerical models and simulations to assess the physical vulnerability of structures to seismic forces. Recently, advancements in structural modelling tools have broadened the scope of analytical approaches, allowing for the creation of vulnerability and fragility curves without relying on data from previous seismic events. Analytical methods can generally be categorized into detailed and simplified approaches. Detailed methods involve complex numerical simulations, including static or dynamic nonlinear analyses. However, due to the significant effort involved, simplified analytical methods have emerged as a more practical alternative. These simplified methods can be further divided into three subgroups: collapse mechanism-based (CMB) methods, capacity spectrum-based (CSB) methods, and fully displacement-based (FDB) methods.

CMB methods focus on predefined collapse mechanisms, such as in-plane and out-of-plane failures, and calculate corresponding collapse multipliers. The critical collapse mechanism is determined by identifying the lowest collapse multiplier, derived from the strength ratio of the structural walls' shear or flexural properties. This is calculated using the principle of virtual work, aligned with the static theorem of limit analysis. An example of this approach is discussed by the authors in [14], who suggested an automated procedure to evaluate local collapse mechanisms in masonry aggregates. In contrast, CSB methods derive the capacity curve through nonlinear analysis, which is then compared to the seismic demand. FDB methods, similar to CSB, also compare displacement capacities to seismic demands, but with the added complexity of accounting for changes in stiffness as a result of structural deformation and variations in period values [14].

Numerical modelling and seismic response simulations are crucial for analytical methods. Numerical modelling strategies fall into four categories: block-based models, continuum models, microelement models and geometry-based models. Each has unique features suited to specific applications:

1. **Block-Based Models**: These represent masonry as individual elements (blocks) bonded by mortar, reflecting its heterogeneity. Blocks can be modelled as rigid or deformable, with interactions defined by methods such as interface elements, contact-based, textured continuum, limit analysis, or extended finite element (FE) approaches. While highly detailed, they are computationally intensive and time-consuming.
2. **Continuum Models**: These treat masonry as a homogeneous, continuous material, omitting individual block and mortar distinctions. They are faster to compute since mesh size doesn't depend on masonry details but require complex constitutive laws to accurately represent the material.
3. **Macroelements Models**: These divide the structure into large-scale components, like piers and spandrels, based on geometry. They focus on in-plane behaviour and typically ignore out-of-plane failure mechanisms.
4. **Geometry-Based Models**: These represent structures as rigid bodies, emphasizing equilibrium and collapse mechanisms using static or kinematic theorems.

The research [15] by Tomić et al. confirms the impact of numerical modelling to the results. The study included conducting a shake table test with a case study consisting out of two masonry structural units. Afterwards, the input data had been provided to other researchers and engineers from practice in order to perform seismic analysis. A significant scatter was recorded among the output data and shake table test results.

Proceedings of the 3rd Croatian Conference on Earthquake Engineering - 3CroCEE
19–22 March 2025, Split, Croatia
Copyright © 2025 CroCEE
DOI: https://doi.org/10.5592/CO/3CroCEE.2025.4

The process of deriving fragility and vulnerability curves through analytical methods is computationally intensive and time-consuming. These methods also face challenges due to the many uncertainties involved throughout the modelling process. Despite these difficulties, analytically derived curves have proven useful, especially when empirical data from past seismic events is unavailable. One such analytical method, META-FORMA [16], is an automated procedure for seismic performance assessment of masonry aggregates. It utilizes mechanical and geometrical parameters of structural units in a masonry aggregate as inputs to a vulnerability algorithm. Using MATLAB, the procedure interacts directly with structural analysis software (POR2000) to generate and analyse numerous numerical models, producing bilinear capacity curves and capacity/demand ratios. This method was successfully applied in a pilot study in the historical centre of Foggia, Italy. Its key advantage lies in its ability to quickly and simply estimate the seismic behaviour of masonry aggregates with minimal input data. A similar study conducted in the Azores on traditional stone masonry aggregates [16] focused on the overall seismic response of buildings, considering the interactions with adjacent buildings of varying heights. The global response was determined using nonlinear static analyses, emphasizing the importance of modelling the structure and adjacent buildings accurately to assess expected damage.

FaMIVE (Failure Mechanism Identification and Vulnerability Evaluation) method [17] is an analytical comprehensive method designed specifically for unreinforced masonry (URM) buildings. The method identifies failure mechanisms within masonry structures, focusing on in-plane, out-of-plane, and combined failure mechanisms (13 in total), and calculates collapse load factors for each façade, considering masonry properties and connections between structural elements. This analysis generates capacity curves and identifies the most probable failure mechanism. FaMIVE's versatility allows it to be used to generate vulnerability functions for various masonry structures globally.

4. Expert-based and hybrid methods

Expert-based methods involve conducting vulnerability assessments grounded in the knowledge and experience of specialists. Hybrid methods, on the other hand, represent a combination of these expert-based approaches with other methodologies. A notable example of such a hybrid approach is demonstrated in the work of Kappos et al., where damage probability matrices were developed to enhance risk assessment [18].

One comprehensive hybrid methodology is the HAZUS framework, which addresses natural hazards such as earthquakes, floods, and hurricanes [18]. This method integrates empirical data, analytical techniques, and expert knowledge. The HAZUS framework is organized into six interdependent modules, designed to support detailed and flexible loss estimation studies. Depending on the user's needs and the intended application, this modular structure allows for adjustments in the level of detail and precision [18]. A key feature of the HAZUS methodology is its classification system for buildings. Structures are categorized based on their use or occupancy to estimate economic losses and by their structural characteristics to predict damage. The method distinguishes 28 occupancy categories and 36 building typologies, classifying structures by factors such as structural type, material, height, and period.

5. Discussion and conclusion

The paper provides a brief state-of-the-art review and highlights aspects that require special attention when conducting vulnerability assessment. Seismic vulnerability assessment methods vary in approach and complexity, catering to different objectives and data availability. Empirical methods rely on observed damage patterns and statistical relationships to estimate vulnerability. The methods analyse historical earthquake data and are efficient for large-scale assessments but lack accuracy for individual buildings. Analytical methods, on the other hand, use structural modelling to simulate how buildings respond to seismic forces. While these methods provide more accurate results, they require extensive data and computational

Proceedings of the 3rd Croatian Conference on Earthquake Engineering - 3CroCEE
19–22 March 2025, Split, Croatia
Copyright © 2025 CroCEE
DOI: https://doi.org/10.5592/CO/3CroCEE.2025.4

resources. Expert-based methods leverage specialists' judgment to assess vulnerability qualitatively, making them valuable for limited data scenarios or complex structures. These methods are particularly useful when data is limited or when dealing with complex structures that don't fit standard models. Hybrid methods combine empirical, analytical, and/or expert-based approaches, merging the strengths of each to offer a more comprehensive assessment. By using empirical data to validate analytical models and integrating expert insights, hybrid methods improve both the accuracy and practical applicability of seismic vulnerability evaluations. These methods can also be categorized as direct or indirect, depending on the steps involved in estimating earthquake damage. Direct methods establish a direct relationship between damage levels and earthquake intensity, while indirect methods include an additional step, typically involving the definition of a vulnerability index. Tools like the Analytic Hierarchy Process (AHP) and Geographic Information Systems (GIS) further support modern assessments.

Table 3 Comparison between vulnerability assessment methods

Methods	**Empirical**	**Analytical**	**Expert - based**	**Hybrid**
Strengths	Provides practical insights from past experiences	Systematic, repeatable, and data-driven	Useful when data is scarce, incorporates experience	Balances real-world data with theoretical analysis
Limitations	Limited to a certain area (also geological properties)	Requires time and computational efforts	Subjective and prone to biases	High data and resource requirements
Required data	Historical damage records, case studies	Physical properties, probability models	Expert knowledge and qualitative data	Combination of past data and theoretical models
Application scale	Local, urban, regional, national	Individual buildings, local	Local, urban	Local, urban, regional
Accuracy	Depends on data availability and relevance	High in controlled environments, but may not fully capture real-world complexity	Varies based on expert experience and knowledge	Generally more accurate than individual methods

Finally, seismic vulnerability assessments vary in methodology based on their specific aims and scale. The scale of assessment influences data collection, precision, and mitigation strategies At the individual building level, detailed surveys and numerical modelling provide precise assessments. At local and urban scales, methods focus on collective vulnerabilities, integrating empirical data, geospatial tools, and probabilistic models for broader insights. Regional and national assessments rely on simplified models and statistical analyses to identify large-scale trends. Given resource constraints, simpler methods are often used for large-scale evaluations while balancing accuracy and variability in building types. To conclude, method selection depends on the assessment's goals, with validation through post-earthquake data remaining essential.

Acknowledgements

This research is funded by the Croatian Science Foundation, grant number UIP-2019-04-3749 (ARES project—assessment and rehabilitation of existing structures—development of contemporary methods for masonry and timber structures), project leader: Mislav Stepinac.

Proceedings of the 3rd Croatian Conference on Earthquake Engineering - 3CroCEE
19–22 March 2025, Split, Croatia
Copyright © 2025 CroCEE
DOI: https://doi.org/10.5592/CO/3CroCEE.2025.4

References

[1] Atalić, J., Novak, M. Š., and Uroš, M., Seismic risk for Croatia: Overview of research activities and present assessments with guidelines for the future, *Gradjevinar*, vol. 71, no. 10, pp. 923–947, 2019, doi: 10.14256/JCE.2732.2019.

[2] Moretić, A., Chieffo, N., Stepinac, M., and Lourenço, P. B., Vulnerability assessment of historical building aggregates in Zagreb: implementation of a macroseismic approach, *Bull. Earthq. Eng.*, no. 0123456789, 2022, doi: 10.1007/s10518-022-01596-5.

[3] Whitman, R. V., Damage Probability Matrices for Prototype Buildings. Seismic Design Decision Analysis, *Natl. Sci. Found.*, no. 380, p. 162, 1973.

[4] Kassem, M. M., Mohamed Nazri, F., and Noroozinejad Farsangi, E., The seismic vulnerability assessment methodologies: A state-of-the-art review, *Ain Shams Eng. J.*, vol. 11, no. 4, pp. 849–864, 2020, doi: 10.1016/j.asej.2020.04.001.

[5] Benedetti, D., Benzoni, G., and Parisi, M. A., Seismic vulnerability and risk evaluation for old urban nuclei, *Earthq. Eng. Struct. Dyn.*, vol. 16, pp. 183–201, 1988.

[6] Formisano, A., Mazzolani, L. F., Landolfo, R., and Florio, G., A quick methodology for seismic vulnerability assessment of historical masonry aggregates, 2010.

[7] Ožić, K., Markić, I., Moretić, A., and Lulić, L., The Assessment and Retrofitting of Cultural Heritage—A Case Study of a Residential Building in Glina, *Buildings*, vol. 13, no. 7, 2023, doi: 10.3390/buildings13071798.

[8] Moretić, A., Stepinac, M., and Lourenço, P. B., Seismic upgrading of cultural heritage – A case study using an educational building in Croatia from the historicism style, *Case Stud. Constr. Mater.*, vol. 17, no. May, p. e01183, 2022, doi: 10.1016/j.cscm.2022.e01183.

[9] Novak, M. Š. *et al.*, Zagreb earthquake of 22 March 2020 – Preliminary report on seismologic aspects and damage to buildings, *Građevinar*, vol. 72, no. 10, pp. 843–867, 2020, doi: 10.14256/JCE.2966.2020.

[10] Stepinac, M., Lourenço, P. B., Atalić, J., Kišiček, T., Uroš, M., Baniček, M., and Šavor Novak, M., Damage classification of residential buildings in historical downtown after the ML5.5 earthquake in Zagreb, Croatia in 2020, *Int. J. Disaster Risk Reduct.*, vol. 56, Apr. 2021, doi: 10.1016/j.ijdrr.2021.102140.

[11] Ferreira, T. M. and Vicente, R., Vulnerability assessment of building aggregates: A macroseimic approach Wall Cladings and Structural Masonry View project SafEarth-Seismic protection of earthen construction heritage View project, no. January, 2012, [Online]. Available: https://www.researchgate.net/publication/236117520

[12] Lagomarsino, S. and Giovinazzi, S., Macroseismic and mechanical models for the vulnerability and damage assessment of current buildings, *Bull. Earthq. Eng.*, vol. 4, no. 4, pp. 415–443, Nov. 2006, doi: 10.1007/s10518-006-9024-z.

[13] Michel, C., Guéguen, P., Lestuzzi, P., and Bard, P. Y., Comparison between seismic vulnerability models and experimental dynamic properties of existing buildings in France, *Bull. Earthq. Eng.*, vol. 8, no. 6, pp. 1295–1307, 2010, doi: 10.1007/s10518-010-9185-7.

[14] Grillanda, N., Valente, M., Milani, G., Chiozzi, A., and Tralli, A., Advanced numerical strategies for seismic assessment of historical masonry aggregates, *Eng. Struct.*, vol. 212, no. November 2019, p. 110441, 2020, doi: 10.1016/j.engstruct.2020.110441.

[15] Tomić, I. *et al.*, Seismic Testing of Adjacent Interacting Masonry Structures – Analysis of a Blind Prediction, *RILEM Bookseries*, vol. 47, pp. 1053–1064, 2024, doi: 10.1007/978-3-031-

Copyright © 2025 CroCEE
DOI: https://doi.org/10.5592/CO/3CroCEE.2025.4

39603-8_84.

[16] Leggieri, V., Ruggieri, S., Zagari, G., and Uva, G., Appraising seismic vulnerability of masonry aggregates through an automated mechanical-typological approach, *Autom. Constr.*, vol. 132, no. December, p. 103972, Dec. 2021, doi: 10.1016/j.autcon.2021.103972.

[17] D'Ayala;, D. and Speranza, E., An Integrated Procedure for the Assessment, *12th Eur. Conf. Earthq. Eng.*, no. January 2002, 2002.

[18] Kappos, A., Pitilakis, K., Stylianidis, K., Morfidis, K., and Asimakopoulos, N., Cost - benefit analysis for the seismic rehabilitation of buildigns in Thessaloniki, based on a hybrid method of vulnerability assessment.

Proceedings of the 3rd Croatian Conference on Earthquake Engineering - 3CroCEE
19–22 March 2025, Split, Croatia
Copyright © 2025 CroCEE
DOI: https://doi.org/10.5592/CO/3CroCEE.2025.5

POST-1979 MONTENEGRO EARTHQUAKE RETROFITTING OF RECTOR'S PALACE IN DUBROVNIK'S OLD CITY: PRESERVING ARCHITECTURAL AND SCULPTURAL HERITAGE

Davorin Penava [(1)], Marin Valičnić [(2)], Ante Vrban[(3)], Lars Abrahamczyk[(4)], Vasilis Sarhosis[(5)]

[(1)] *Full Professor, Head of Department, Josip Juraj Strossmayer University of Osijek, Faculty of Civil Engineering and Architecture Osijek, Osijek, Croatia, davorin.penava@gfos.hr*
[(2)] *MEng, Josip Juraj Strossmayer University of Osijek, Faculty of Civil Engineering and Architecture Osijek, Osijek, Croatia, marin.valincic@gfos.hr*
[(3)] *MArch, Josip Juraj Strossmayer University of Osijek, Faculty of Civil Engineering and Architecture Osijek, Osijek, Croatia, ante.vrban@gfos.hr*
[(4)] *Assistant Professor, Head of Department, Bauhaus-Universität Weimar, Faculty of Civil Engineering and Environmental Engineering, Weimar, Germany, lars.abrahamczyk@uni-weimar.de*
[(4)] *Full Professor, University of Leeds, Faculty of Engineering and Physical Sciences, Leeds, UK, V.Sarhosis@leeds.ac.uk*

Abstract

Building codes on earthquake-resistant design, construction, and retrofitting are being improved based on observations of building performance during strong earthquakes, with the aim of mitigating earthquake risk in proportion to the corresponding hazard. In the Republic of Croatia, prior to introduction of Eurocodes in 2005 and 2011, an example is the earthquakes M_L6.9 in North Macedonia in 1963 and M_L7.2 in Montenegro in 1979, which resulted in construction regulations in 1964 and 1981, respectively. The urban built environment was therefore constructed in compliance with building codes from different time periods, which do not provide the same level of earthquake protection as the most recent codes. Special attention is required for built heritage of outstanding significance, such as the Old City of Dubrovnik, which was included in the UNESCO World Heritage list after the M_L7.2 earthquake in Montenegro in 1979 ($I_{MCS,MAX}$ = IX–X, and of very strong intensity, i.e., I_{MCS} = VI-VII in Dubrovnik). One of the most representative buildings in the Old City is the Rector's Palace, which dates back to the 13th century but has been reconstructed several times throughout history. Due to structural damage sustained in the aforementioned earthquake, the building was comprehensively retrofitted on two occasions: 1982-1984 and 2015-2017. The objective of this study was to review the effectiveness of the retrofitted built heritage construction against contemporary design-level earthquake shaking, focusing particularly on the atrium and arcades, which are the most vulnerable structural parts of the Rector's Palace and possess significant architectural and sculptural value. The discussion will also address the structure's performance levels and provide recommendations for achieving reasonable earthquake protection within affordable means while avoiding irretrievable damage to heritage construction.

Keywords: 1979 Montenegro Earthquake, Retrofitting, Rector's Palace in Dubrovnik, Built Heritage Construction

1. Introduction

Building codes on earthquake-resistant design, construction, and retrofitting are being improved based on observations of building performance during strong earthquakes, with the aim of mitigating earthquake risk in proportion to the corresponding hazard. In the Republic of Croatia, prior to introduction of Eurocodes in 2005 and 2011, an example is the earthquakes M_L6.9 in North Macedonia in 1963 and M_L7.2 in Montenegro in 1979, which resulted in regulations in 1964 [1] and 1981 [2], respectively. The urban built environment was therefore constructed in compliance with building codes from different time periods, which do not provide the same level of earthquake protection as the most recent codes, without subsequent retrofitting. Special attention is required for historical and cultural heritage buildings of outstanding significance, such as the Old City of Dubrovnik, which was included

Copyright © 2025 CroCEE
DOI: https://doi.org/10.5592/CO/3CroCEE.2025.5

in the UNESCO World Heritage list after the M_L7.2 earthquake in Montenegro in 1979 ($I_{MCS,MAX}$ = IX–X, and of very strong intensity, i.e., I_{MCS} = VI-VII in Dubrovnik). This led to the establishment of the Institute for the Restoration of Dubrovnik, which has been overseeing the retrofitting efforts.

The Old City of Dubrovnik is located in the southernmost part of Croatia, in the historical region of Dalmatia, on the eastern coast of the Adriatic (Fig. 1), at an elevation of 3 meters above sea level, at the foot of Mount Srđ. It is located in a seismically very active area, as evidenced by the Croatian Earthquake Catalogue (CEC), which records the epicentres of earthquakes throughout history, including those of the highest intensities (up to I_{MCS}=X) and the greatest values of horizontal peak ground accelerations of ground type A (a_{gR}).

a) b)



Figure 1. Old City of Dubrovnik with the location of Rector's Palace: a) view from the southeast; b) view from the northwest (source: [3])

One of the most representative buildings in the Old City is the Rector's Palace (Fig. 2), which dates back to the 13th century but has been reconstructed several times throughout history. The Rector's Palace, located on the eastern edge of the Old City of Dubrovnik, next to the city walls and the harbour. Due to severe structural damage sustained in the aforementioned earthquake, the building was comprehensively retrofitted on two occasions: 1982-1984 and 2015-2017 [3]. The objective of this study was to review the effectiveness of the retrofitted built heritage construction against contemporary design-level earthquake shaking (e.g., 475-year hazard level), focusing particularly on the atrium and arcades, which are the most vulnerable structural parts of the Rector's Palace and possess significant architectural and sculptural value. The discussion will also address the structure's performance levels and provide recommendations for achieving reasonable earthquake protection within affordable means while avoiding irretrievable damage to heritage construction.

2. Soil and Structure Characteristics

The ground beneath the structure consists of compacted sands and clays of medium to high plasticity, extending from 13 to 27 meters to the bedrock. The groundwater level is approximately 1.5 meters below the surface and about 0.75 meters above sea level. The walls of the building are founded on strip foundations made of roughly hewn stone bonded with preserved lime-clay mortar, while the columns of the atrium are founded on stacked irregular stone fragments bound with a binder of minimal or no strength. Geotechnical boreholes in the stone foundations of the atrium columns of the Rector's Palace revealed remnants of wooden piles on which the atrium columns were supported.

In compliance with the building codes applicable during the reconstruction period (1982-1984) and according to the current building codes, the building is irregular in plan and height. The structural system of the Rector's Palace consists of three layers of masonry, predominantly with a thickness of 0.45-1.2 m. The outer layers are made of finely cut stone and lime mortar, while the central layer is composed of a larger quantity of stone rubble and fill with added lime mortar. The ceiling structures consisted originally of stone vaults and wooden joists. The vaults are made of light, porous limestone and are cross, cross-ribbed, barrel, mirrored, and combined, with a thickness of approximately 25-27 cm at the apex, with material fill up to 50 cm.

Copyright © 2025 CroCEE
DOI: https://doi.org/10.5592/CO/3CroCEE.2025.5



a) b) c)

Figure 2. The Rector's Palace in Dubrovnik's Old City: a) the palace portico; b) view of the building from the southwest; c) the atrium (source: 2nd author)

The portico is located on the western facade of the building, and its construction consists of circular stone columns with Corinthian capitals on top, supporting cross-ribbed vaults. The portico, together with the entire western facade, represents the most valuable element of the Rector's Palace from a cultural-historical standpoint. The atrium extends from the ground floor to the roof height. The intermediate floor structures consist of travertine cross vaults, filled with material to floor level. The inner facade of the entire atrium is made up of columns, onto which semi-circular arches rest, except for the northern facade of the ground floor, where there are no columns, but a stone wall instead.

The roof structure of the atrium is flat, while the rest of the building contains gable and multi-gable roofs with various static systems. The roof of the western wing is gabled with a double-chair static system, the southern wing has a gabled roof with a triple-chair static system and an added column on the inner eaves, the eastern wing has a gabled corneal roof with a ridge, the southeast tower has a four-pitched roof with a presumed single-chair static system, and the roof of the northwest tower is presumed to be single-pitched.

3. History of Structural Interventions

The design of the Rector's Palace has changed throughout history, from the 13th century to the present, due to accidental actions that caused significant damage or the collapse of parts of the structure. In 1435, part of the structure was destroyed due to a gunpowder explosion and fire. The rehabilitation was completed in 1443 under the supervision of the Neapolitan builder Onofrio della Cava. The explosion in the armoury in 1463 caused the collapse of the western facade and the destruction of the second floor.

Copyright © 2025 CroCEE
DOI: https://doi.org/10.5592/CO/3CroCEE.2025.5

The building was restored by the Florentine architect Salvi di Michiele. The earthquakes of 1520 and 1639 (I_{MCS} = VIII), damaged parts of the building, while the 1667 earthquake (I_{MCS} = IX–X), caused severe structural damage, but not collapse. The walls of the western facade began to tilt out of their plane, and part of the atrium collapsed. The restoration involved connecting the walls with steel ties and rebuilding the atrium. The first documented retrofitting including repairs and addition of steel ties, was completed in 1704. In 1843, steel ties were installed to support the western facade, along with several rough construction interventions that disrupted the building's structural system. Due to the poor condition of the building, improvement efforts were made in 1952, including relieving the terrace around the atrium, restoring the roof structure, and structure strengthening. The 1962 M_L=5.9 earthquake near Makarska (Croatia) and the 1968 M_L=5.5 earthquake on the Montenegrin coast highlighted that the safety of the Rector's Palace was once again at risk. As a result, in 1968, investigative work was initiated by the Dubrovnik Institute for the Protection of Cultural Monuments, aiming to assess the building's condition. The 1979 Montenegro earthquake, caused structural damage to the Palace. The walls separated from the ceiling structures, cracks appeared in the vaults, and additional tilting of the walls of the western facade occurred, with the wall tilting 23 cm from the vertical. The Palace was given priority in the restoration, and in 1981, the main restoration project was developed, with the works commencing in 1982.

3.1. Structural Interventions 1982-1984

The restoration began in 1982 and was completed in 1984 (Fig. 3) [4], in compliance with the building code [2], and conservation requirements. The masonry strip foundations were strengthened by adding reinforced concrete beams measuring 30/80 cm alongside them, connected by steel anchors (d=20 mm). In the atrium, reinforced concrete beams were installed on both sides of the existing foundations of the stone columns. Stone walls were reconstructed in locations where they had been removed in 1843, while several partition walls were demolished. Two structural walls were reinstated on the ground floor, mezzanine, and first floor. Steel anchors along the full height of the wall-ceiling connection lines were added. The walls were interconnected with reinforced concrete slabs and/or diagonal steel ties at three levels: at the foundation level, at the mezzanine ceiling level, and at the first-floor ceiling level. The atrium was reinforced at the mezzanine ceiling level with a system of perpendicular steel ties. At the first-floor ceiling level, reinforced concrete slabs were installed in the towers, similar to the mezzanine ceiling level. Between the towers on the western façade at the first-floor level, there is a space without structural walls perpendicular to the façade. To prevent further tilting of the façade out of its plane, a very rigid diaphragm was constructed. The strengthening at the first-floor level created a closed ring of reinforced concrete ties, connecting all four wings of the building with the atrium. An expansion joint was constructed between the Rector's Palace and the City Hall, except in the south-eastern section, which was omitted due to heritage sensitivity, and the eastern wing, where structural ties to the city walls made it unfeasible.

a) b)

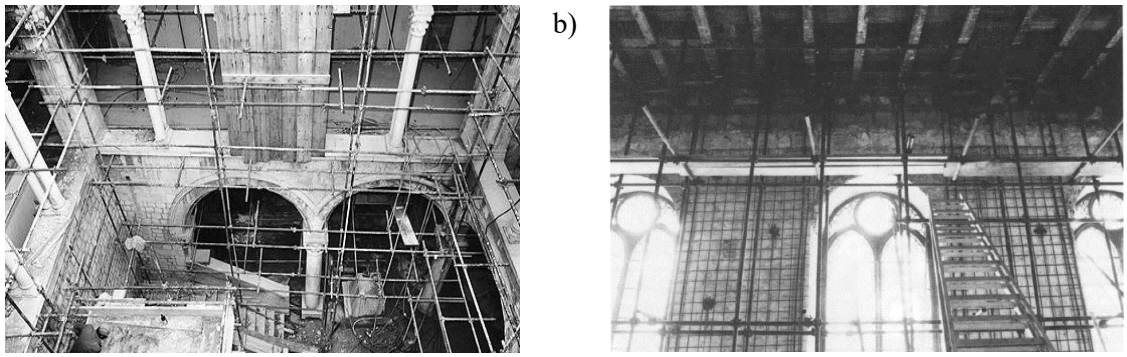


Figure 3. Rehabilitation of the Rector's Palace Following the 1979 M_L=7.2 Montenegro Earthquake a) atrium; b) inner spaces (source: [3])

Copyright © 2025 CroCEE
DOI: https://doi.org/10.5592/CO/3CroCEE.2025.5

3.2.Structural Interventions 2015-2017

Due to the appearance of numerous cracks in the atrium, construction work began at the end of 2015 and was carried out in three phases [3]:

1) the structural rehabilitation of the foundations and the sub-foundation zone of the atrium. Additionally, the first phase included the structural rehabilitation of the foundations and the sub-foundation zone of the atrium, preceded by investigative works using probes and boreholes. The results of these investigations did not align with the design assumptions, as the load-bearing rock was found to be at a greater depth than anticipated. The foundations were strengthened using load-bearing micropiles, secondary piles, and the grouting of the space enclosed by micropiles beneath the isolated footings, resulting in a compact foundation body supporting the ground-floor columns of the atrium. Full-scale 1:1 model testing of the ground-floor and upper-floor columns under actual loading conditions was also conducted.
2) the structural rehabilitation of the stone columns on the ground floor and the paired columns of the north façade on the upper floor, the installation of ties at the springing points of the vaults, and the completion of work on the roof terrace.
3) the rehabilitation of the stone paired columns of the east, west, and south façades on the upper floor, the installation of ties at the springing points of the upper-floor vaults in the atrium, the paving of the atrium ground floor, and the remaining conservation and restoration works.

The retrofitting performed in the atrium are of a local nature, meaning they improve the seismic performance of the atrium but not the building as a whole.

4. Characteristics of construction materials

The construction materials of the built heritage in the Old City of Dubrovnik, and generally along the eastern Adriatic coast, consist primarily of high-quality processed limestone blocks obtained from nearby quarries, bonded with lime mortar (see Fig. 4).

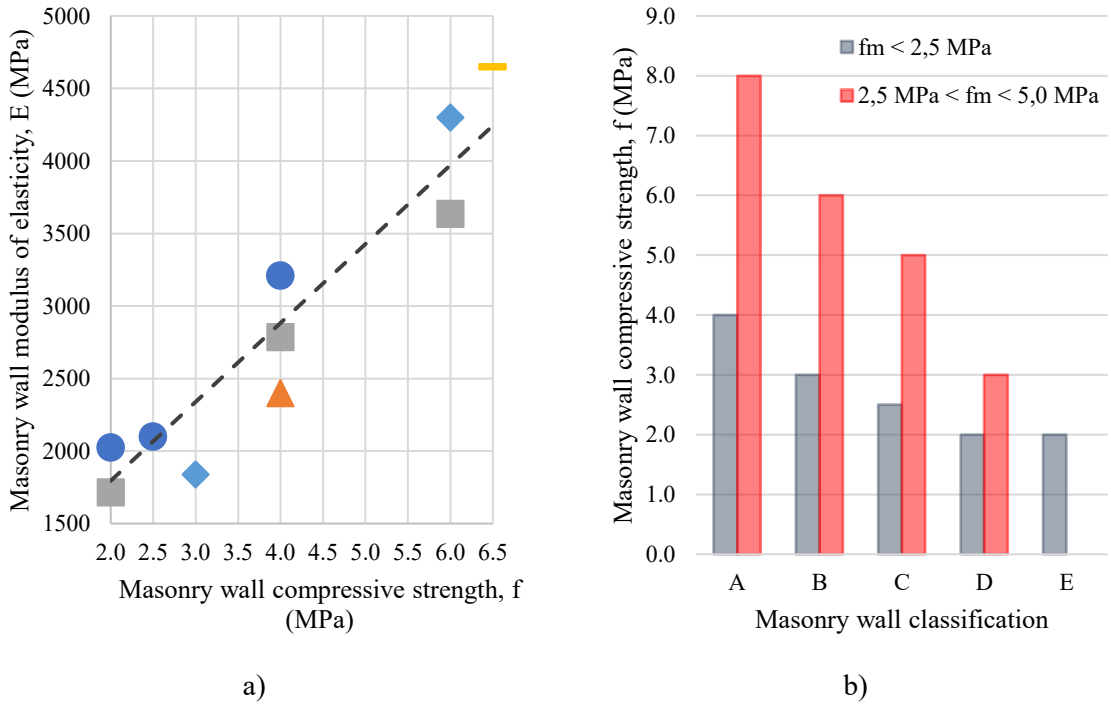


Figure 4. Material characteristics of stone masonry units and walls belonging to eastern Adriatic coast: a) unit and wall compressive strength relation; b) wall classification and compressive strength relation [5]

Copyright © 2025 CroCEE
DOI: https://doi.org/10.5592/CO/3CroCEE.2025.5

The wall classification (A-E) in Figure 2b. as proposed by [5] where letter symbols refer to: A designates walls made of finely dressed and properly arranged stone blocks, without intermediate layers; B walls made of large regularly dressed stone blocks with a relatively narrow central layer filled with fill material and stone chippings; C walls made of large irregularly dressed stone blocks with a relatively narrow central layer filled with fill materials and stone chippings; D walls made of roughly dressed irregular stone blocks with a large quantity of stone chippings and fill material in the central layer, and with irregular joints; E walls made of undressed stone with a large quantity of fill. Other materials used are wood and steel (ties), and a concrete class of C25/30 was assumed (retrofitting).

5. Vibrational characteristics of the building

Measurement of ambient vibrations at the Rector's Palace was conducted in 1981 (on the damaged building) and in 2023. The 1981 measurements recorded values of 0.36 s for the north-south direction and 0.37 s for the east-west direction for the first mode of vibration. In the 2023 measurements, repeated at the same locations as in 1981 with additional measurements around the atrium, values of 0.30 s were observed for both the north-south and east-west directions. Period values of 0.34 s were determined near the atrium. More details on the measurement process and the obtained data are available in [6–8] and are omitted from this report for brevity.

6. Spatial FEM Model of Rector’s Palace

6.1. Development of the Structural Model

The spatial structural FEM model for simulating the seismic behaviour of the Rector's Palace was created using the SCIA Engineer 22.1 [9] software, based on architectural and 3D scans of the Rector's Palace (see Figs. 5 to 9). The walls were modelled as 2D "Wall" elements, columns as 1D "1D Member" elements, and vaults as 2D "Shell" elements. The roof was not modelled, and the load was applied to the walls of the upper floor. The connection between the walls and the foundation soil was simulated using linear pinned supports, while point supports were used for the columns. Displacements were constrained at the locations where the Palace connects with the Old City walls and adjacent buildings.

In the second model, applied were the strengthening measures of the 1982-1984 restoration (see Sec. 3.1). A dilation joint was also added to the northern part of the Palace. The reinforced concrete slabs were modelled as 2D "Plate" elements, steel ties and horizontal ring beams as 1D "1D Member" elements, with only the transverse ring beams modelled, while the longitudinal ones were applied as loads on the model.

The third model refers to the state of the building after the reconstruction carried out between 2015 and 2017. At the locations of missing ties in the atrium on the ground and upper floors, steel ties were added to the spring points of the vaults, modelled as 1D "1D Member" elements.

a) b)

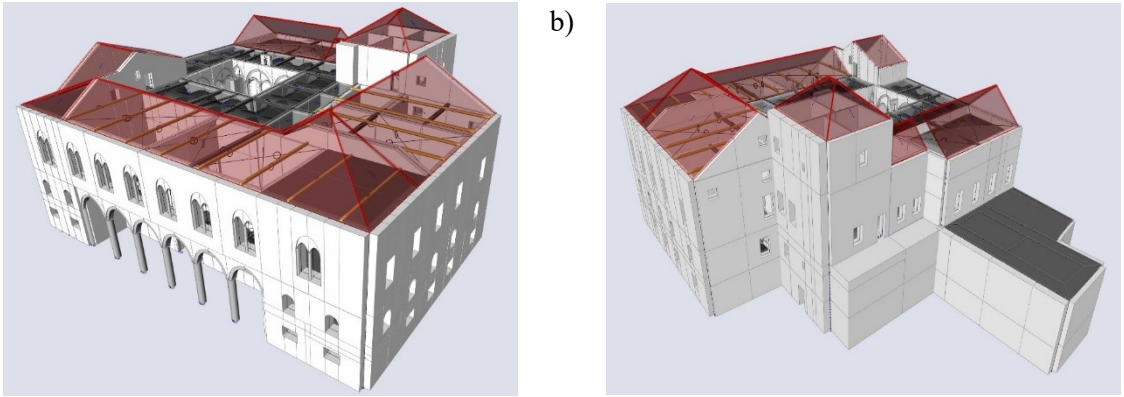


Figure 5. Finite Element Method (FEM) spatial model of Rector’s Palace: a) view from the southwest; b) view from the southeast [8]

Copyright © 2025 CroCEE
DOI: https://doi.org/10.5592/CO/3CroCEE.2025.5

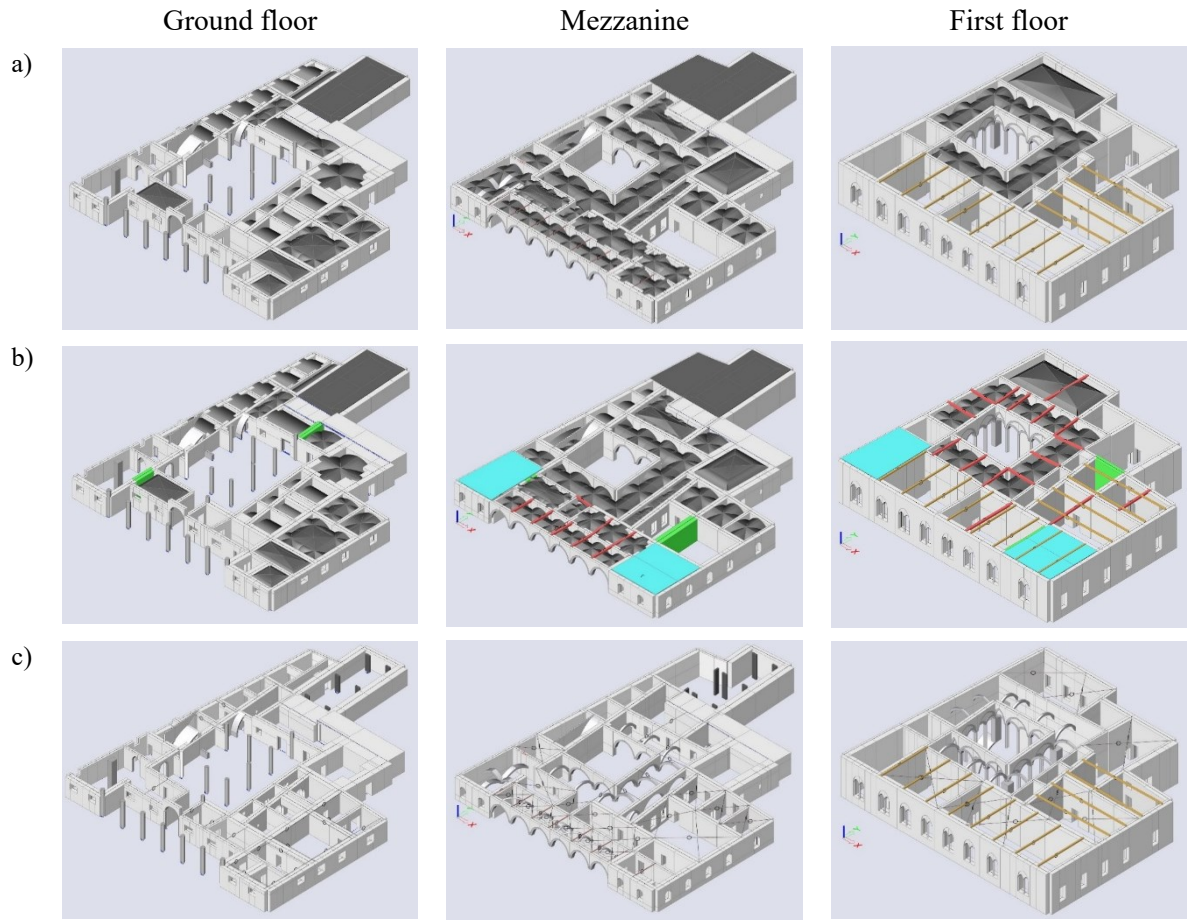


Figure 6. Retrofitting of Rector's Palace – pre-1979 earthquake and post-1982-1984 interventions: a) condition prior to the 1979 earthquake; b) condition after the 1982–1984 restoration, including: stone walls (green), reinforced concrete slabs (cyan), and horizontal tie beams (red); c) connection of stone walls with steel ties during the same period (shown separately for clarity) [8]

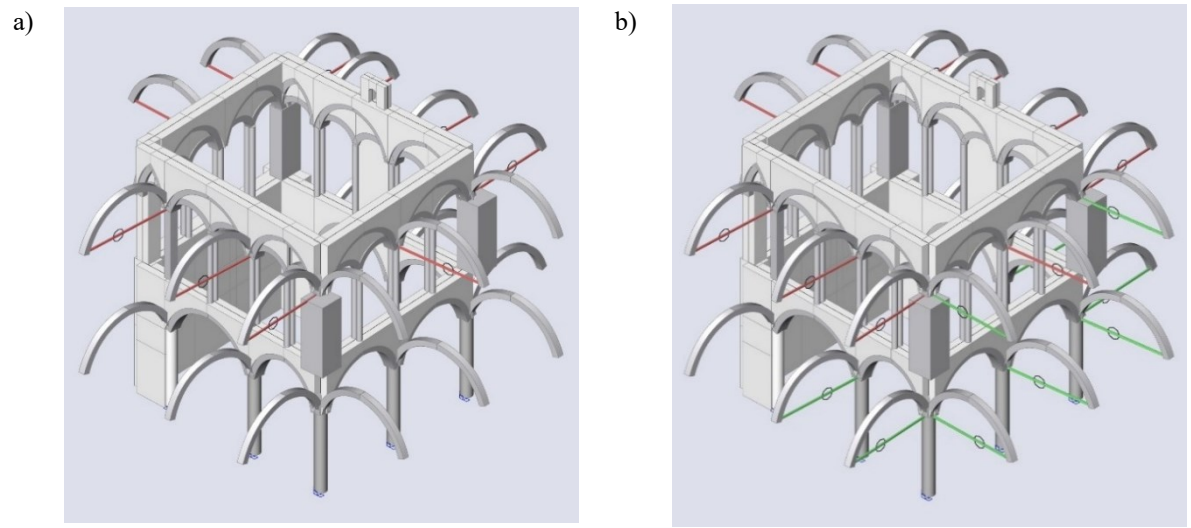


Figure 7. Retrofitting of Rector's Palace Atrium Completed in 2015–2017: a) condition before and after the 1982–1984 restoration with the existing steel ties at the atrium floor level (red); b) condition after the 2015–2017 restoration with the newly installed steel ties at the springing points of the atrium cross vaults (green) [8]

Copyright © 2025 CroCEE
DOI: https://doi.org/10.5592/CO/3CroCEE.2025.5

a) b)

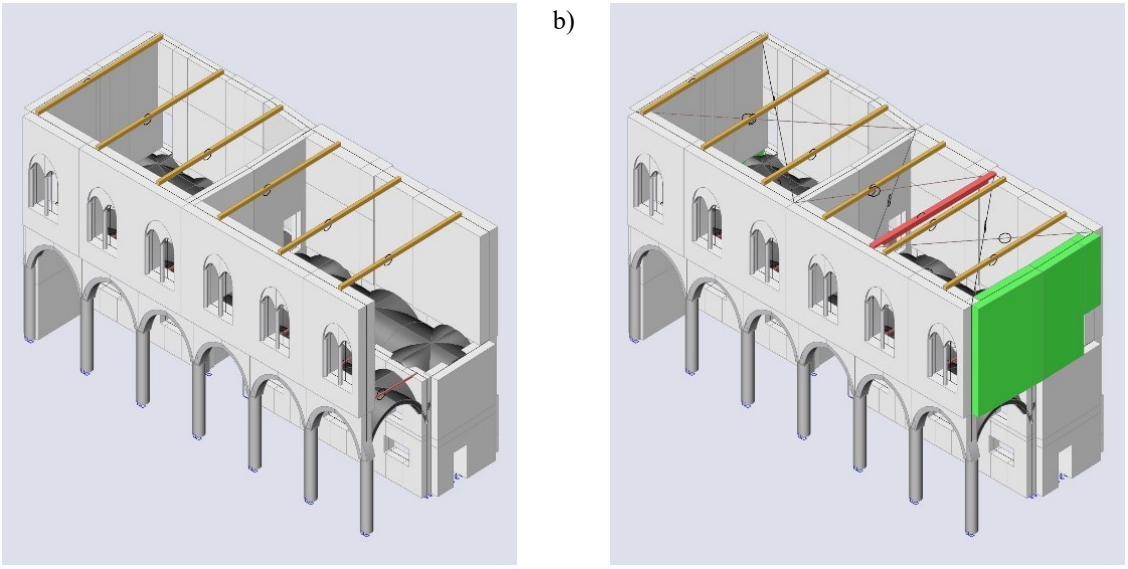
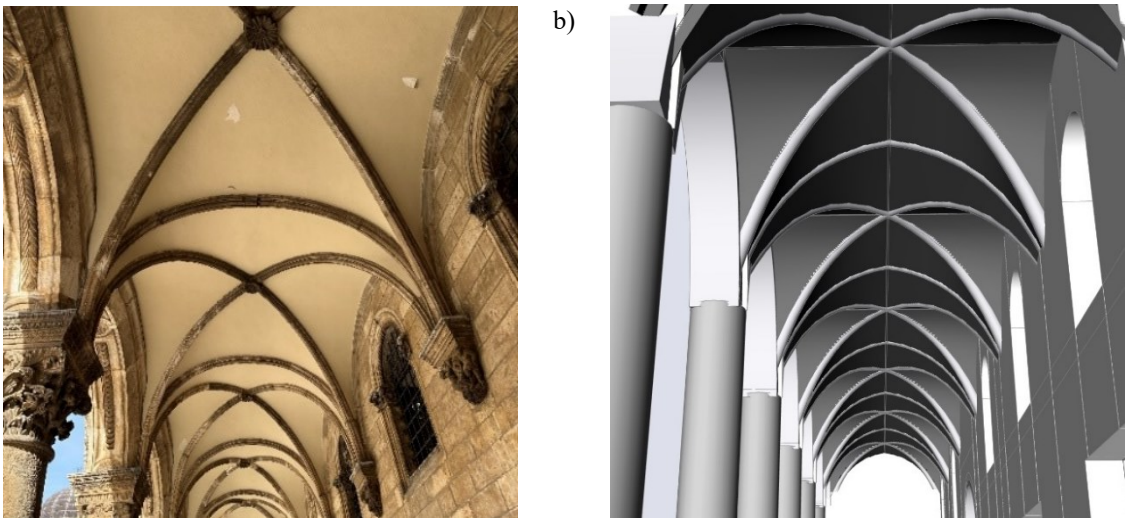


Figure 8. Portrayal of the west facade portico in the structural model: a) before and; b) after the 1982-1984 restoration [8]

a) b)



c) d)

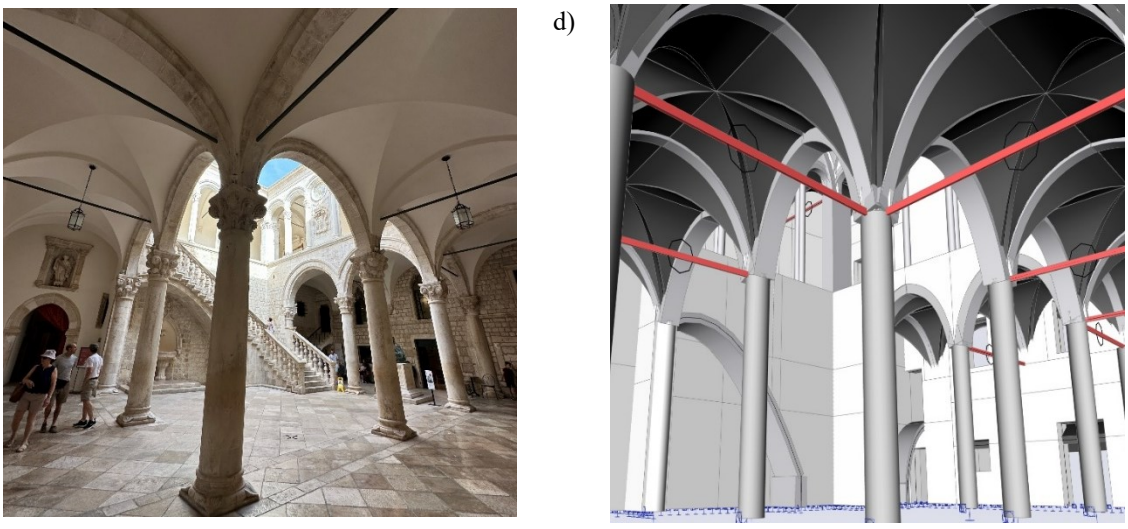


Figure 9. Representation of the structure in reality and in the computational model: a) ribbed cross vaults of the arcade; b) cross vaults of the atrium [3,8]

Copyright © 2025 CroCEE
DOI: https://doi.org/10.5592/CO/3CroCEE.2025.5

6.2. Actions on the structure

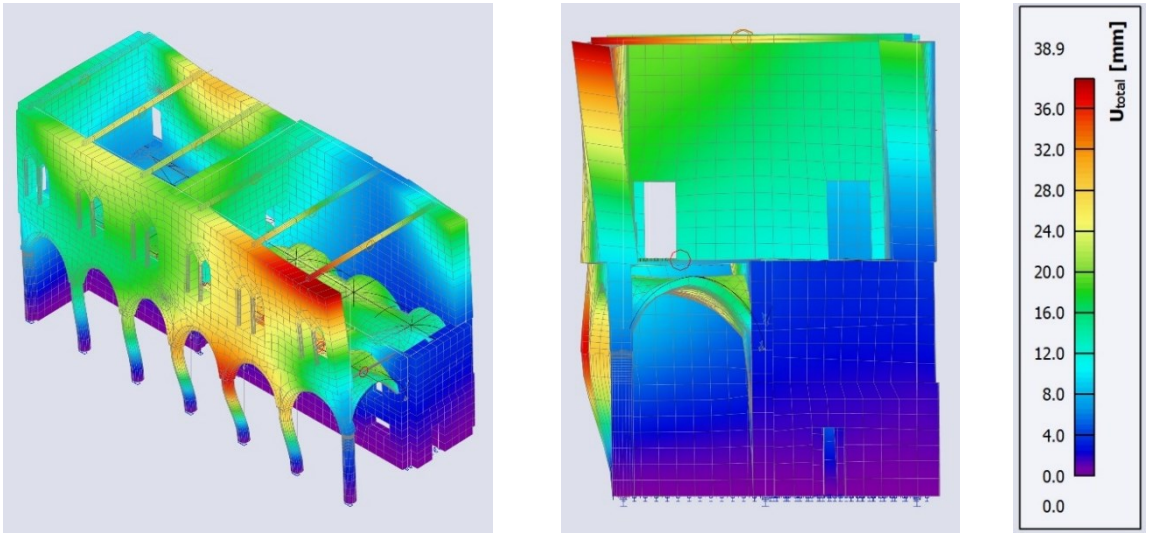
The following actions on the structure were considered: permanent (G), variable (Q), and accidental action (A) [10–14]. The self-weight of the stone walls at 25 kN/m³, the embankments above the vaults (fill material and floor layers) at 14 kN/m³, wooden beams (wooden structure and floor layers) at 8 kN/m³, and the roof structure (wooden structure and tiles) at 5.8 kN/m³ were adopted. The Rector's Palace falls under the C3 usage category, so the floor load for intermediate floor structures is taken as 5 kN/m³, and for the roof over the atrium (slope < 20°), based on the H usage category, the floor load is 0.75 kN/m³. Snow load is neglected due to the very small values of the load on the building's roof structure, as well as wind load, which has no impact on massive masonry structures. Seismic action was considered using the design response spectrum for a return period of 475 years (10% exceedance probability in 50 years), as well as the response spectrum for the actual 1979 Mne earthquake recorded at Herceg Novi station. A Type 1 response spectrum with a damping ratio of 0.05 was used. According to [15], soil type B was assumed for the location of the Rector's Palace. The peak ground acceleration for soil type A at a return period of 475 years for the city of Dubrovnik is 0.30g, the importance factor for the selected building was 1.2, and the behaviour factor 1.5. Non-seismic and seismic combinations of actions were considered as shown in Table 1. Due to the brevity and purpose of the study, only the seismic combinations of actions and their results are presented.

Table 1. Seismic combination of actions considered (the x-axis is parallel to the western façade, extending in the north-south direction; the y-axis is extending in the east-west direction)

No.	Seismic combination of actions	Rspns. spectr.
1	$G + E_{Ed,x} + 0{,}30 \cdot E_{Ed,y} + \sum \Psi_2 \cdot Q$	EN1998-1
2	$G + 0{,}30 \cdot E_{Ed,x} + E_{Ed,y} + \sum \Psi_2 \cdot Q$	
3	$G + E_{Ed,x} + 0{,}30 \cdot E_{Ed,y} + \sum \Psi_2 \cdot Q$	1979 Mne eq.
4	$G + 0{,}30 \cdot E_{Ed,x} + E_{Ed,y} + \sum \Psi_2 \cdot Q$	

7. Outcomes of the analysis

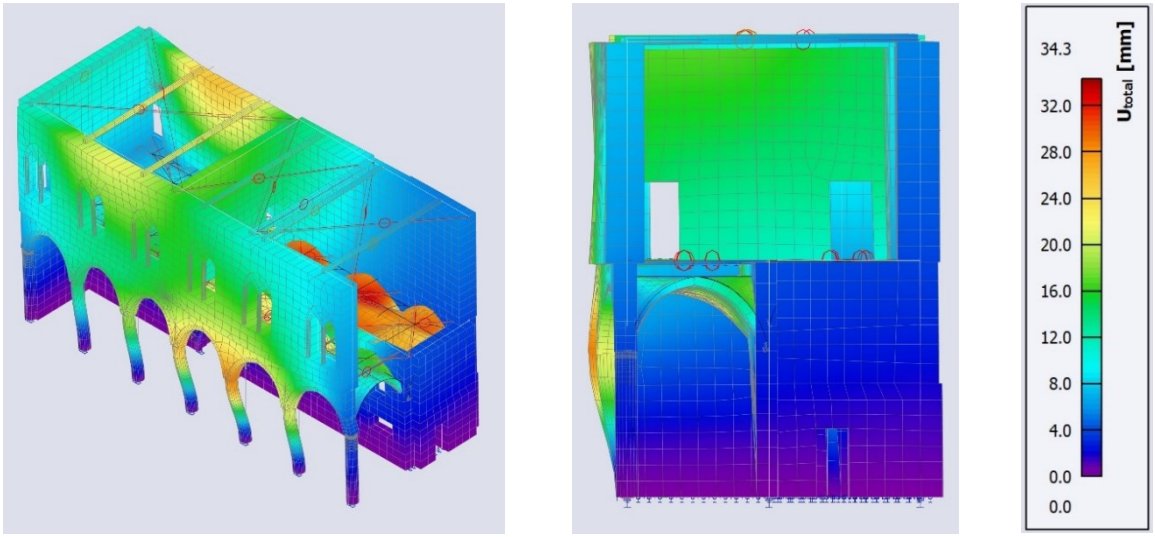
Outcomes of the analysis are shown in form of spatial displacements in Figs. 10 & 11.



a)

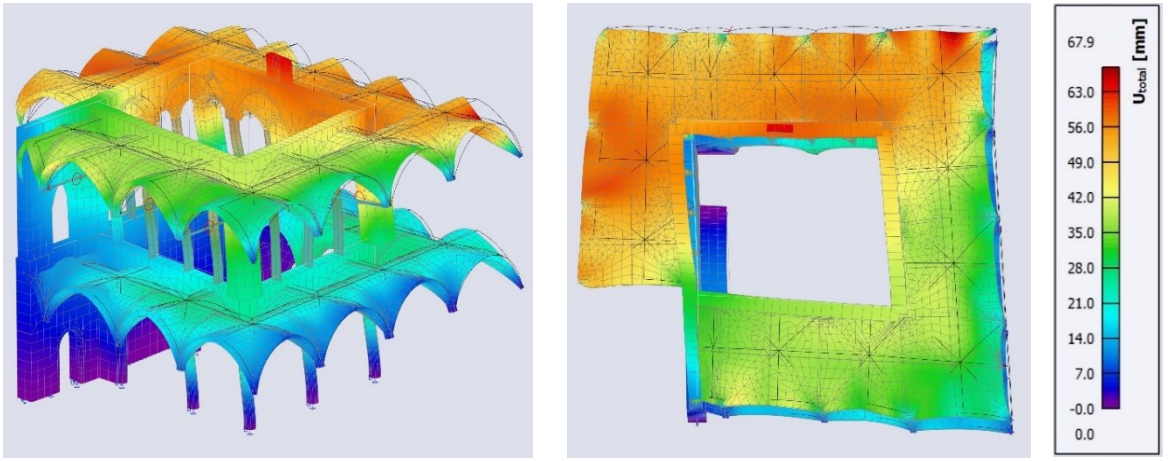
Figure 10. Portrayal of the west facade portico in the structural model: a) before and; b) after the 1982-1984 restoration

Copyright © 2025 CroCEE
DOI: https://doi.org/10.5592/CO/3CroCEE.2025.5

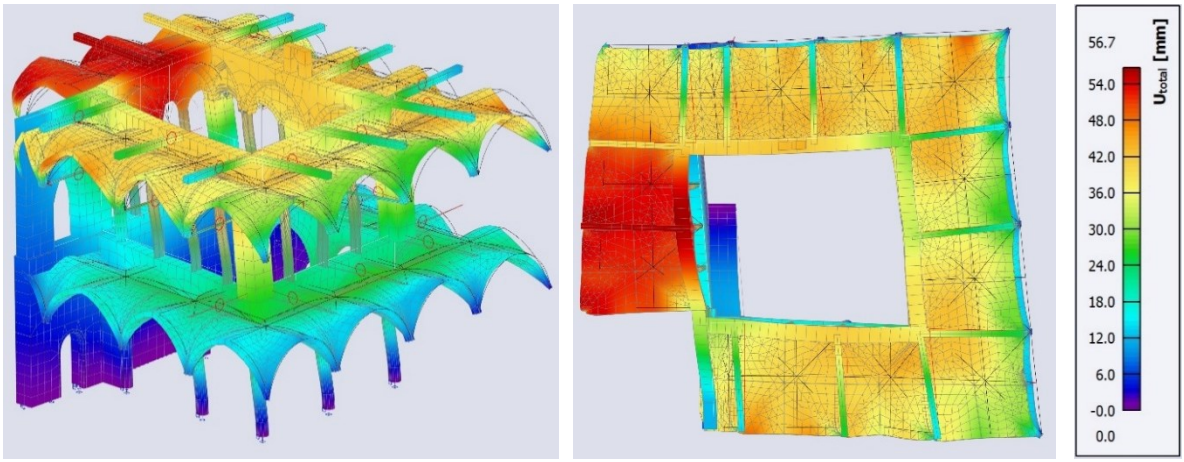


b)

Figure 11. *continuation …*



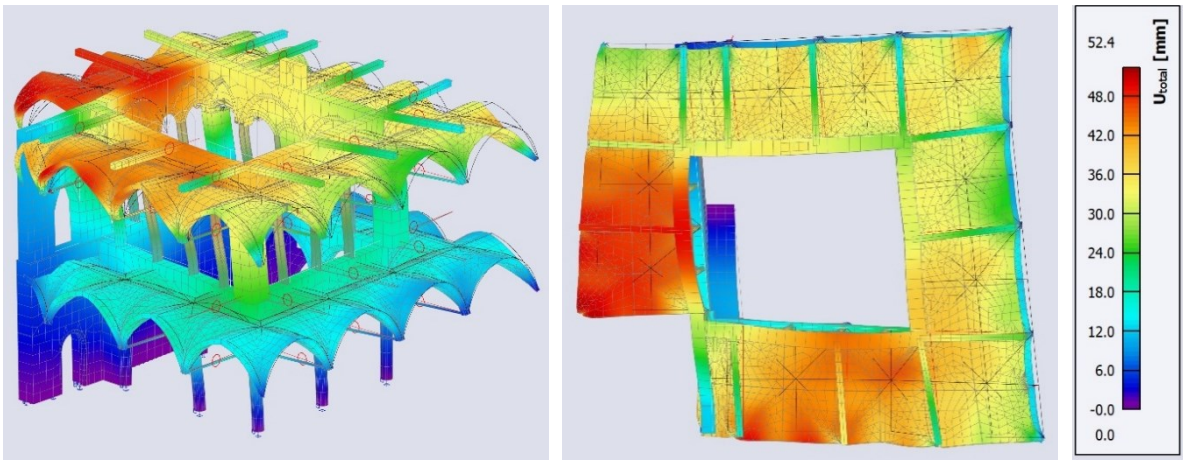
a)



b)

Figure 11. Spatial displacements of the atrium for seismic combination of actions no. 3: a) before 1982-1984 restoration; b) after the 1982-1984 restoration; c) after 2015-2017 restoration

Copyright © 2025 CroCEE
DOI: https://doi.org/10.5592/CO/3CroCEE.2025.5



c)

Figure 12. *continuation …*

By conducting a sensitivity study of the finite element mesh, a mesh density of 0.5 m was adopted. Comp. model was calibrated against first natural period from 1981 measurements (see Sec. 5). A modal analysis, i.e., the analysis of natural vibrations of the Rector's Palace, was conducted for the first six vibration modes across three computational models. For the measured vibration period of 0.37 s, a mean elasticity modulus of 1750 MPa for the B-grade walls was adopted for the entire building. Figs. 1 & 2 illustrate the spatial displacements for the most unfavourable seismic combination, i.e., combination no. 3, as outlined in Table 1.

8. Conclusions

The monumental heritage of the Old City of Dubrovnik, constructed with stone, generally does not meet the design criteria and construction standards for earthquake-resistant buildings in compliance with EN 1998-1:2004 and EN 1996-1-1:2005 codes. The assessment of Rector's Palace was conducted by means of a computational model on both global and local levels (atrium and arcades) for non-seismic and seismic combinations of actions, supported and calibrated with field measurements and laboratory tests. Seismic combinations with the response spectrum of the 1979 M_L=7.2 Montenegro earthquake, resulted in higher spatial displacements, as compared to those with the EN1998-1 design spectrum for a return period of 475 years.

In the global analysis, seismic combinations with dominant earthquake action in the x direction cause the largest spatial displacements in the atrium area, while for the dominant y direction, the greatest values occur at the wall above the arcade on the western façade, where the wall is missing. With the addition of reinforcement, the building deforms the most in the atrium area for both seismic directions. Displacements in the atrium vaults are reduced due to the transverse horizontal tie beams in the post-1982-1984 restoration model and the tie rods at the vault spring points in the post-2015-2017 restoration model, as well as on the western façade due to the high effectiveness of the reinforced concrete slab reinforcement and the horizontal tie beams and rods system.

In the local analysis, retrofitting lead to a reduction in displacements, which coincide with the tilt points of the western façade wall following previous earthquakes. The atrium deforms the most in the eastern wing during the seismic combination with dominant action in the x direction, while in the y direction, larger displacements occur in all four wings. With the addition of strengthening, the western and eastern parts of the atrium on the upper floor experience the greatest deformations due to the lower degree of lateral support of the walls compared to the eastern and southern wings, where there are no transverse structural walls to stiffen the supporting walls of the vaults.

A detailed study of the seismic performance of the arcades is recommended due to the proposed implementation of additional strengthening.

Copyright © 2025 CroCEE
DOI: https://doi.org/10.5592/CO/3CroCEE.2025.5

Acknowledgements

We would like to express our sincere gratitude to the City of Dubrovnik authorities, the Institution for the Restoration of Dubrovnik, the Association of Friends of Dubrovnik Antiquities, and the Dubrovnik Museums for their invaluable support throughout the course of this research. This research was conducted within the framework of the Croatian Science Foundation Research Project IP-2020-02-3531, entitled Seismic RIsk Assessment of Cultural Heritage Buildings in CROatia (acr. SeisRICHerCRO), and their support is gratefully acknowledged.

References

[1] Official Journal SFRY No. 39/64 (in Croatian: Službeni List SFRJ 39/64). O*rdinance on Temporary Technical Regulations for Construction in Seismic Areas* (in Croatian: *Pravilnik o privremenim tehničkim propisima za gradenje u seizmičkim područjima*). Belgrade, SR Serbia, Federal Republic of Yugoslavia (FRY): 1964.

[2] Official Journal SFRY No. 31/81, 49/82, 29/83 (in Croatian: Službeni List SFRJ 31/81, 49/82, 29/83). *Ordinance on Technical Standards for the Construction of High-Rise Buildings in Seismic Areas* (in Croatian: *Pravilnik o tehničkim normativima za izgradnj*u. Belgrade, SR Serbia, SFR Yugoslavia: Official Journal No. 31/81, 49/82, 29/83, 20/88, 52/90 (in Croatian:Službeni list SFRJ 31/81, 49/82, 29/83, 20/88, 52/90); 1981.

[3] Zavod za obnovu Dubrovnika. *Institute for the Restoration of Dubrovnik* (in Croatian: Zavod za obnovu Dubrovnika) 2021. https://zod.hr/ (accessed December 13, 2024).

[4] Aničić D, Steinman V. *Seismic Strengthening of Rector's Palace in Dubrovnik*. In: Mijušković S, editor. Sci. Gatherings. Vol. 10. Balk. Cult. Herit. Seism. Probl. Proceedings., Titograd (Today's Podgorica), SR Montenegro, SFR Yugoslavia: Montenegrin Academy of Sciences and Arts (in Croatian: Crnogorska akademija nauka i umjetnosti); 1983, p. 209–24.

[5] Morić D. Seismic Resistance of Stone Masonry Buildings Regarding Permissible Retrofitting Measures on Floor Structures. Ph.D. Thesis. University of Zagreb, 1998.

[6] Petrovski J, Jurukovski D, Bojadžiev M. *Defining Basic Frequencies at the Rector's Palace Building by Measuring Ambient Vibrations. Report IZIIS 81-34* (in original: *Definisanje osnovnih frekvencija na objektu Knežev dvor mjerenjem ambijent vribracija. Izveštaj IZIIS 81-34*). Skopje, SR Macedonia, SFR Yugoslavia: 1981.

[7] Penava D, Valinčić M, Vrban A, Abrahamczyk L, Guljaš I, Kraus I. *The Effects of Strong Earthquakes on Built Heritage: A Preliminary Case Study of Rector's Palace in Dubrovnik's Old City*. Sustainability 2023;15:14926. doi:10.3390/SU152014926.

[8] Valinčić M. *Earthquake assessment of Rector's Palace in Dubrovnik*. Graduate Thesis. Josip Juraj Strossmayer University of Osijek, 2024.

[9] ALLPLAN. *SCIA Engineer v.22.1* 2023.

[10] CEN. *Eurocode: Basis of structural design (EN 1990:2002+A1:2005+A1:2005/AC:2010)*. Brussels: Comité Européen de Normalisation; 2010.

[11] CEN. *Eurocode 8: Design of Structures for Earthquake Resistance - Part 1: General Rules, Seismic Actions and Rules for Buildings (EN 1998-1:2004)*. Brussels: European Committee for Standardization; 2004.

[12] CEN. *Eurocode 6: Design of masonry structures - Part 1-1: General rules for reinforced and unreinforced masonry structures (EN 1996-1-1:2005)*. Brussels: European Committee for Standardization; 2005.

[13] CEN. *Eurocode 8: Design of structures for earthquake resistance -- Part 3: Assessment and retrofitting of buildings (EN 1998-3:2005+AC:2010)*. Brussels: European Committee for Standardization; 2010.

[14] CEN. *Eurocode: Basis of structural design - National Annex (HRN EN 1990:2011/NA:2011)*. Brussels: European Committee for Standardization; 2011.

[15] Stanko D, Korbar T, Markušić S. *Evaluation of the Local Site Effects and Their Implication to the Seismic Risk of the UNESCO World Heritage Site Old City of Dubrovnik (Croatia)*. J Earthq Eng 2023:1–29. doi:10.1080/13632469.2023.2220029.

Proceedings of the 3rd Croatian Conference on Earthquake Engineering - 3CroCEE
19–22 March 2025, Split, Croatia
Copyright © 2025 CroCEE
DOI: https://doi.org/10.5592/CO/3CroCEE.2025.55

ASSESSMENT, EVUALATIONS AND RETROFITING APPLICATIONS METHODS FOR MASONARY OLD STONE STRUCTURE

Naser Kabashi [(1)], Enes Krasniqi [(2)], Teuta Imeri[(3)],Ylli Murati[(4)], Alush Shala[(5)]

[(1)] *Prof.dr, University of Prishtina, naser.kabashi@uni-pr.edu*
[(2)] *Teaching Assistent, University of Prishtina, enes.krasniqi@uni-pr.edu*
[(4)]*Teaching Assistent, University of Prishtina, ylli.murati@uni-pr.edu*
[(3)]*Alb-Architect Company, Prishtina, teutaimeri@albarchitect.com*
[(5)]*Alb-Architect Company, Prishtina, alushshala@albarchitect.com*

Abstract

The deterioration of old masonry structures, particularly from the Middle Ages, poses significant challenges due to material degradation and structural deficiencies. This study focuses on assessing and strengthening a traditional stone masonry "Kulla," addressing the need to preserve its historical character while improving its structural performance to meet modern building codes. The research objectives are to identify material and structural deficiencies, evaluate the impact on load-bearing capacity, and develop effective retrofitting techniques. A combination of non-destructive and destructive testing methods was used to analyze material properties and structural elements such as stone foundations, walls, roofs, and floors. The results revealed substantial material deterioration, particularly in the stone masonry, leading to the design of a tailored retrofitting strategy focused on strengthening key elements. This retrofitting approach significantly improves the building's seismic and structural resilience, with comparisons showing a marked improvement between the building's current and retrofitted conditions. The study highlights the importance of integrating material analysis and retrofitting techniques to preserve the structural integrity and historical value of ancient masonry structures in seismic regions.

Keywords: Masonry structures, Retrofitting, Material testing, Seismic resilience, Historical preservation

1. Introduction

Historical buildings are an important part of the cultural heritage, because of their architectural value, materials and techniques of building in different years or eras. Their conservation over the centuries is a responsibility of our society, in order to pass on to future generations. The diagnosis of the present conditions of the building can be made by a complete interdisciplinary knowledge based on historical notes, technological survey, non-destructive testing, destructive testing, procedures and the interpretation of crack and decay patterns. Slow and inevitable aging processes might affect the current structural stability due to different possible origins. In this concept more effected factors are the materials deterioration in scope of time and environmental effects.[1].

In different buildings one or more of threes parameters will lead to the damages in buildings in slowly time effect, which are under the Institutions for evaluations the Cultural Heritage Buildings:

- behavior the buildings under natural hazards (floods, earthquake, fire,etc). The seismic assessment of existing buildings is a complex task, basically for two different reasons:
- the difficulty of interpreting and modelling the seismic response; and
- the difficulty of acquiring as-built information on material parameters and structural details, due to their spatial variability in the buildings and the need of avoiding invasive testing.

A detailed assessment through proper procedures and models allows to avoid collapse and useless interventions. The analyses need to involve more different knowledge in different specific fields.

Proceedings of the 3rd Croatian Conference on Earthquake Engineering - 3CroCEE
19–22 March 2025, Split, Croatia
Copyright © 2025 CroCEE
DOI: https://doi.org/10.5592/CO/3CroCEE.2025.55

2. Architectural and structural assessment of existing Cultural Heritage Buildings

Architectural and structural assessment of Cultural Heritage Buildings is a crucial process that preserves, restore and maintenance the structures, more focused in specific important buildings which represent the autochthony of country and populations. The assessment involves several stages, for better understanding the building's current conditions, historical importance and the measurements to ensure its durability of structures.[1].

2.1. The origin and establishment of the survey concept

During the analyzing the survey concept and eventually intervention on the Cultural Heritage Buildings, it is essentially to analyses the documents for current conditions of the structural components stability and state of the materials actually in buildings. The documents should explain the specific reasons for selections the materials and methods in preservation efforts. The rational approach for the survey stage must keep guided by the following general principles:

- Each traditional building has different and singular aspects that make them unique, leading to slightly different survey needs, from case to case.
- The selection of the means of inspection, appraisal and recording must be adaptable to the nature of the building, physical and in situ limitation of survey actions and available resources;
- The survey actions should be based on the general scope and most important and critical aims of the project. Any repair, maintenance, refurbishment action or intervention strategy should reflect the technical and financial effort made in the survey phase;
- The survey is a multidisciplinary task, including the surveyor teams (engineers, architects, historians, archaeologists, etc.) with expertise opinion is very valuable.
- The use of other sources of information, such as the documentary information is
- Also, very valuable and should be considered.

The establishment of survey concept in case Study: Kulla e Ymer Poges, is result of:

- Geometric measurements (using a laser scanner and direct measurements)
- Site visits and direct observation of the monument's condition
- Interviews with local residents (who provided insights into the monument's functional history)
- Photographs and videos

2.2. Functionality of Cultural Heritage Buildings –Case Study Kulla-Ymer Poga

The analyzing building is type of traditional residence of tower type, characterized with plane dimensions 6.35 x 6.35 m and three stories high. The primary function of the building was residential, with the ground floor serving as a stable, the first floor designated for the residents of the house, while the second floor housed the guest room. For a period, the tower is said to have served as a mosque. This is evidenced by the dome found in the guest room, making the tower unique in construction style in Kosovo and beyond.[2]. The entrance to the tower was made through two doors: one located on the ground floor used by family members, and the other, now walled up, located again on the northeast side on the second floor of the tower, used for guest entry. This door is thought to have been accessed via movable external stairs. Detail of the ground floor, first floor and second floor are presented in figure 1.

Proceedings of the 3rd Croatian Conference on Earthquake Engineering - 3CroCEE
19–22 March 2025, Split, Croatia
Copyright © 2025 CroCEE
DOI: https://doi.org/10.5592/CO/3CroCEE.2025.55

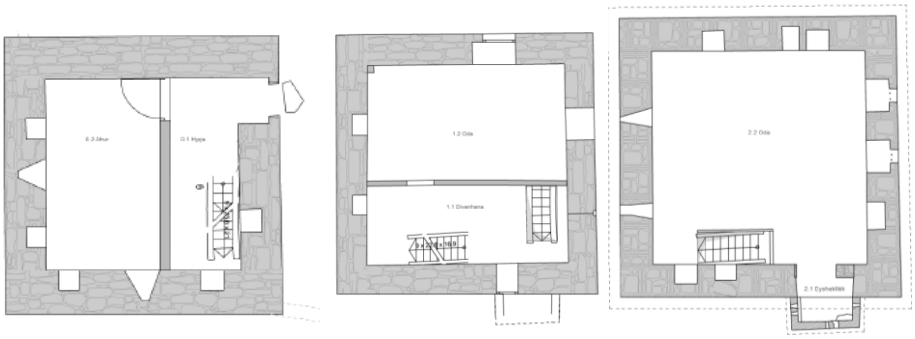


Figure 1. Three floors space of Kulla- Ymer Poga

2.3. Interventions over the Years on the building

Comparing surveys over the years, we can determine the changes that the structure and its surrounding context have undergone. The changes from the original state, identified through the survey between 1990-2001, are marked in blue. Notably, the rosette on the southeast wall was walled up, as well as the door leading to the guest room on the northeast side. Changes following the 2013 survey are marked in red and yellow, where yellow indicates demolition interventions, and red marks new elements. Demolition interventions primarily involve clearing the surfaces of the building from plaster and demolishing a one-story structure built adjacent to the northeast side of the tower. A new element is the roof, which was restored in 2013 by adding a waterproofing membrane and a wooden floor under the flag stone elements, presented in fig 2.

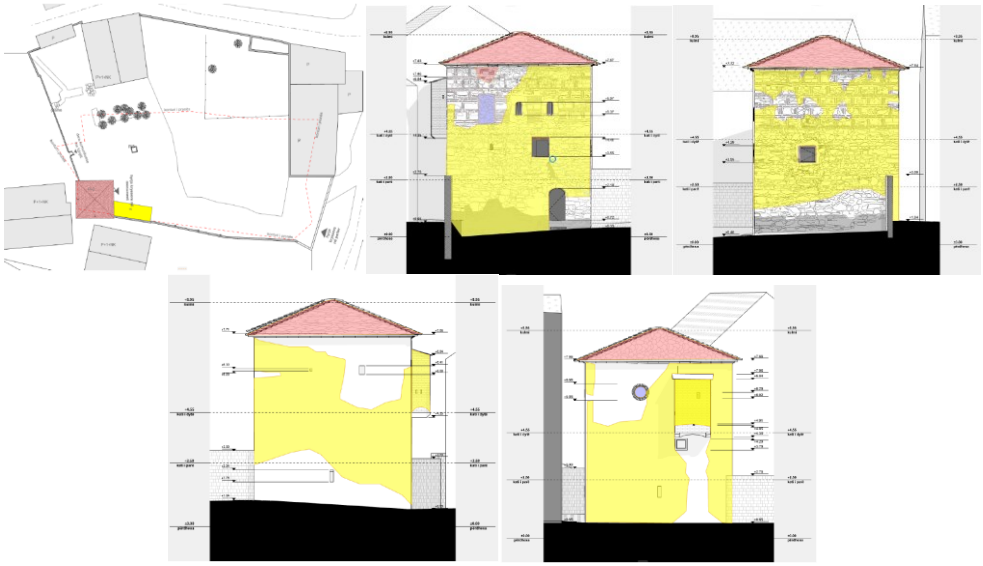


Figure 2. Interventions over the years in building-Kulla Ymer Poga

2.3.1. Conservation and Restoration Interventions

The building represents historical value, as one of the oldest examples of tower-type Kulla- buildings in Kosovo. Additionally, it stands out for its characteristic facade treatment and the semi-spherical dome covered by a four-sided roof.
Based on Point 5 of the Conservation Principles of the Charter on Built Vernacular Heritage (1999), ratified by the 12th General Assembly of ICOMOS, in Mexico, October 1999: "Vernacular includes not only the physical form and shell of buildings, structures, and spaces, but also how they are used and

Copyright © 2025 CroCEE
DOI: https://doi.org/10.5592/CO/3CroCEE.2025.55

understood, as well as the intangible traditions and relationships attached to them.", the base steps are listed as follows:

- Consolidation interventions (walls, the dome, and floors)
- Supplementary interventions (elements that have partial or total deficiencies)
- Liberating interventions (walls added with inappropriate materials or in positions that compromise the unity and values of the monument)
- Restorative interventions (plastering, windows, internal stairs, ground floor

The approach to the project is closely related to the exceptionally unique historical and architectural values that this monument represents, as one of the oldest towers in Kosovo (if not the oldest that is still intact). Based on this fact, the project aims to preserve the authentic features of the monument as much as possible, making minimal interventions, which consist of consolidating the building and avoiding other adaptive interventions [3].

2.3.2. Proposal Interventions in Restoration process

The interventions are oriented in each damaged positions, carefully taking into account the typical characteristics of the monument. These interventions encompass all key structural and architectural components, including the walls, floors, ceilings, stairs, and roof, ensuring the restoration maintains the tower's original, integrity and cultural authenticity.

2.3.2.1. External stone walls

In scope of the interventions steps for the wall positions are apply:
-Clean the surface of the stone walls
-Replacement the damages horizontal wood beams
-Replacement the lime mortar and eventually reinforced the structures with injection filling method
-Replacement the stone elements in perimeter of windows
-Replacement the stone elements in perimeter of wall foundation in needed positions
Based on the actually state of buildings are presented through the photos in fig.3.



Figure 3. Proposed interventions in stone walls

The stone walls represent the stability of the structure and this is reason for starting the interventions in these positions using the different methods and materials.

2.3.2.2. Restorations and demolition process of ground floor

Recommended parameters for interventions are based on the previous state and remove all the interventions in over the years realized without any concept for Cultural Heritage Buildings.
The monument maintains its planar layout on the 1st and 2nd floors, while on the ground floor the plan is restored to its original state. The first scenario on remove the interior wall , realized in over the years is presented in fig.4.

Proceedings of the 3rd Croatian Conference on Earthquake Engineering - 3CroCEE
19–22 March 2025, Split, Croatia
Copyright © 2025 CroCEE
DOI: https://doi.org/10.5592/CO/3CroCEE.2025.55

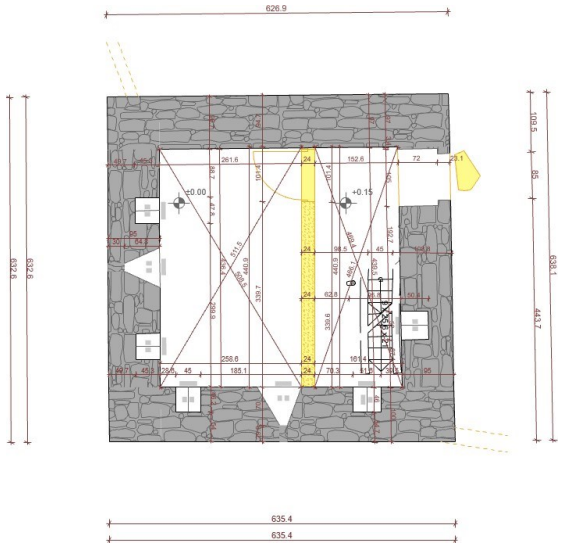


Figure 4. Demolition and remove the interior wall

2.3.2.3. Restorations the floors

Interventions in ground floor are oriented in stone floor with flag stone elements, based on the entrance door model to create the stiff ground floor system using the heavyweight of the stone elements, presented in fig.5.

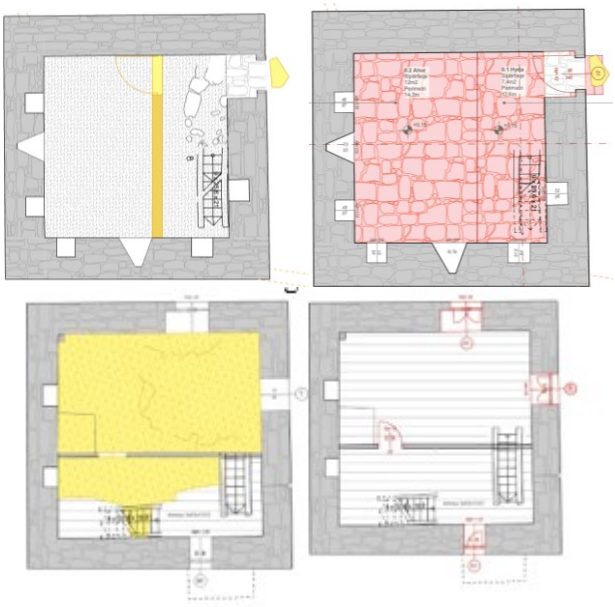
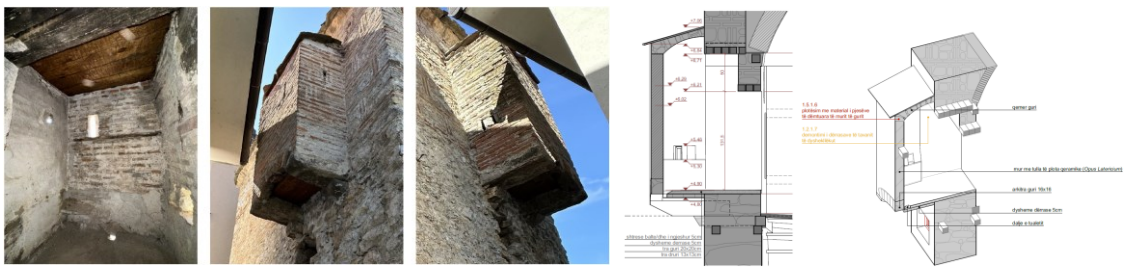


Figure 5. Restorations the ground floor with stone elements and floor restoration (right photos)

The demolishing and restorations of the first and second floor based on the actual system and materials: wood boards in combinations with clay will replace with new wood board, following all the parameters for Cultural Heritage Buildings, in scope of the typically view, presented in figure 5.



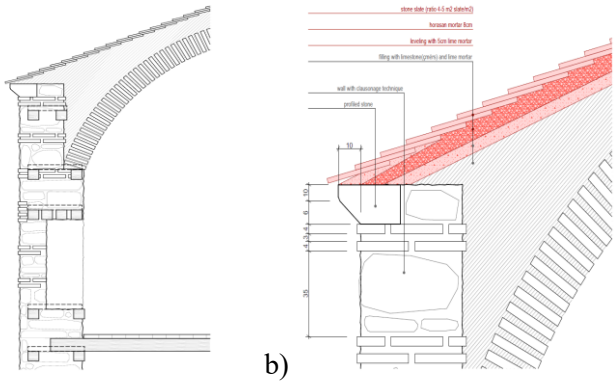
Copyright © 2025 CroCEE
DOI: https://doi.org/10.5592/CO/3CroCEE.2025.55

Figure 6. Analyze and proposal for restorations the protruding gallery

One of the main features of the monument's plan is the perimeter outside space(protruding gallery-dyshekllak) located at the 2nd floor level, which was an element not commonly used in these tower-kulla typologies, presented in figure 6.

2.3.2.4. Restorations the roof-dome

Specifically the roof restorations is one of the important Cultural Heritage element, because it's dome surface , characteristics in this typology of building , including the elements and materials, presented in Fig 7.a &b

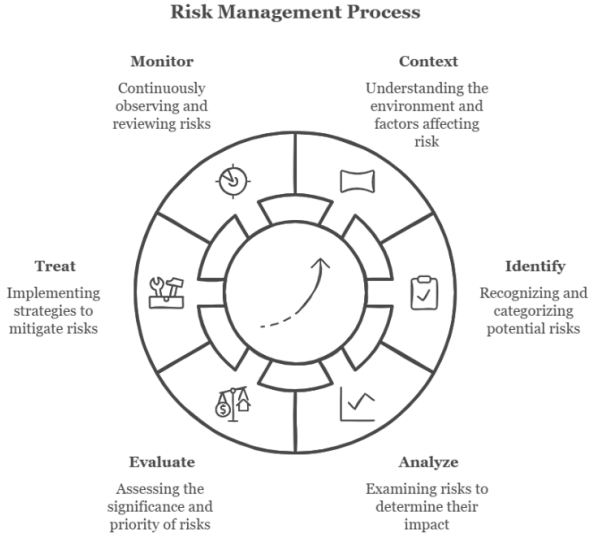


a) b)

Figure 7. Roof – dome existing section(a) and Roof – dome proposed layers(b)

2. Risk management of Cultural Heritage Buildings

To the heritage sites, risk management is the process that involves managing losses of value an impacts in order to minimize them and to reach a balance between opportunities gained and lost. Climate change impacts on cultural heritage are illustrated by several incidents such as flash floods, earthquake in different years results with damages on the existing buildings. However, one of the international standards of the risk tool is ISO 31000:2009[4]. Management Principles and Guidelines. Fig. 8 shows the main six steps in the historical and heritage risk management cycle (context, identify, analyze, evaluate, treat, then monitoring). This risk management principle was considered in this study.[5]. Risks to heritage sites are dependent on the nature, specific characteristics, inherent vulnerability and geographical environment of the site. From another perspective they are dependent on the nature of the external threats affecting the heritage itself.[12]



Copyright © 2025 CroCEE
DOI: https://doi.org/10.5592/CO/3CroCEE.2025.55

Figure 8. Risks and agents of deterioration potentially affecting the integrity of heritage sites © UNESCO

2.1. Risk in Practice-Cultural Heritage Buildings

From developmental perspective, the most critical risks to heritage properties would be to people, property and livelihoods. But from conservation perspective, risk assessment of these properties would mean consideration for three important heritage elements, which may be at risk in themselves and for their interrelationships: local communities, ecology and standing as traditional structures. The Cultural Heritage at risk would imply risk to one or all of these elements of structures.[6]. Risk analysis is the scientific and technical study of risks, leading to a full description and model of the processes causing the risks to cultural heritage properties. Based on the information sets collected from various sources, hazards and vulnerability factors can be analyzed as follows: Analyzing the external sources and agents of risk hazards; Analyzing the external sources and agents of risks-hazards; Analyzing vulnerability factors that expose various elements of the property to risk from hazards.[12]. The building risk scenarios can be of various types and the typical concept is presented in figure 9.



Figure 9.The risk analysis framework with the elements risk assessment, risk management and risk communication [8]

3. Structural analyses of building-Case Study: Kulla Ymer Poga

The analyzing building is typical Albanian tower-Kulla, built more than 3 centuries ago. In scope of the analyzing the element of structures, it characterized with thick walls made from stone , such building material at that time. The floors are from the wood materials, including the wooden beams and wooden elements in combinations with clay. The roof is typical design, constructed in dome shape with clay bricks and lime mortar, support in four points. From visual inspections in scope of the structures it result with high damages from different factors, specifically the environmental factors. The detail analyses of taken samples for testing in laboratory are done in Laboratory IBMS-Prishtine, and based on the outputs of testing, using the software ETABS , is simulated current and possibility retrofitting conditions of the structure. The numerical analyses and create the model provide e realistic view of reactions the building and level of absorptive the capacity under applied loads. In table 1- are presented the properties of testing materials.[9].

Table1. Properties of testing materials

Materials	**f_b (MPa)**	**f_m (MPa)**	**f_k (MPa)**	**E (MPa)**	**G (MPa)**	**E_m (MPa)**	**G_m (MPa)**
Non damage wood-Humidity 12%	7.10			96 000	38 400		
Damage wood	0			0	0		
No damage stone	203.51			35 000	14 000		
Damages stone for basements	22.52			22 520	9 008		

Copyright © 2025 CroCEE
DOI: https://doi.org/10.5592/CO/3CroCEE.2025.55

Mortar		7		7 000	2 800		
Clay Bricks	5.47			5 470	2 188		
Stone wall			74.04			33 318	13 327.2
Damage stone wall			15.86			7 137.4	2 854.96
Dome with clay bricks			5.89			2 650.5	1 060.2

The calculation of the characteristic value of the masonry using the characteristic values for brick and mortar is taken from EC6, the characteristic compressive strength of masonry should be determined from equation 1.

$$f_k = K f_b^{\alpha} f_m^{\beta} \quad (1)$$

f_k – characteristic compression strength of masonry
K – is constant from tab.3.3 page 37, EC 6-1-1 2006

α, β – are constants
f_b – normalised mean compressive strength of units
f_m – is the compressive strength of mortar.

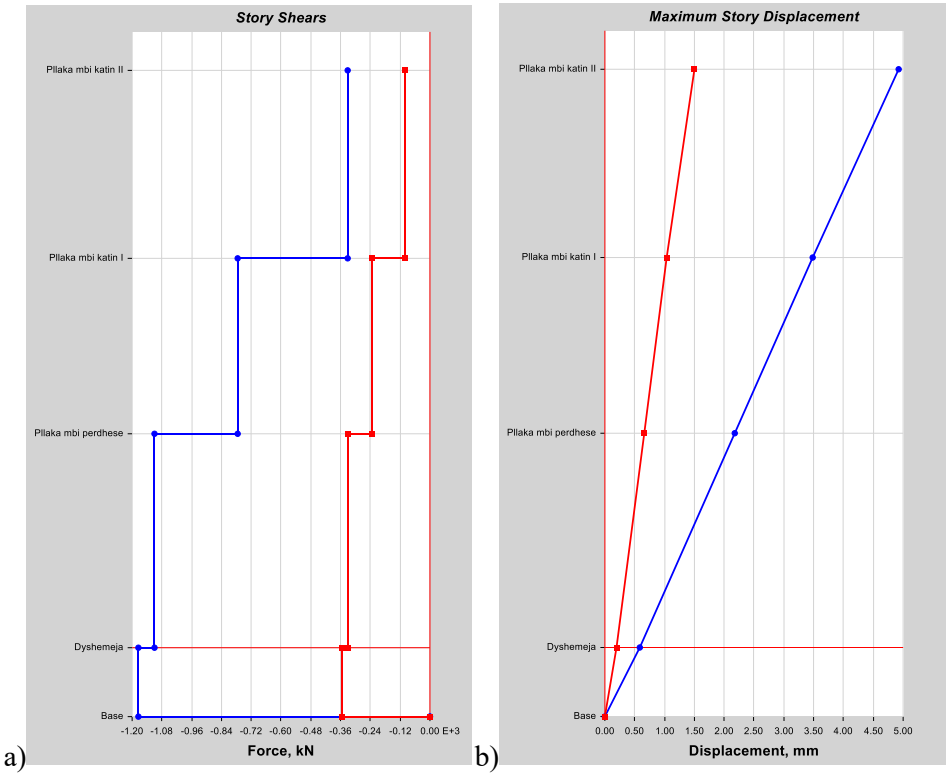
Based on the calculations the continues process is Modulus of Elasticity and Modulus of Shear

$$E_m = 1000\ f_k;\ G_m = 0.4\ E_m \quad (2)$$

Under the given earthquake of peak ground acceleration (PGA) of 0.24 ag/g, the response of the masonry structure was analyzed to assess its performance. Since the structure is composed of stones and lacks structural elements that can absorb the energy and it does not possess designated zones for plastic deformation, leading to the adoption of a behavior factor q=1.5. From the analysis, it was determined that the structure can withstand base shear forces up to 1200 kN. The maximum deflections observed were 4 mm, and the presence of cracks was confined to the zones experiencing tension stresses, indicating the points of vulnerability under seismic loading. The following figure represents the building response before retrofitting.

Figure 10.a) illustrates the distribution of shear forces across the stories of the structure under seismic loading. Higher forces are typically observed at the lower stories due to the cumulative effect of inertia from the upper levels, while the forces decrease progressively towards the top of the structure. The second figure, 10.b), represents the displacement profile of the structure, showcasing the lateral movement experienced by each story due to the earthquake. The maximum displacement observed is 4.6mm.

Copyright © 2025 CroCEE
DOI: https://doi.org/10.5592/CO/3CroCEE.2025.55



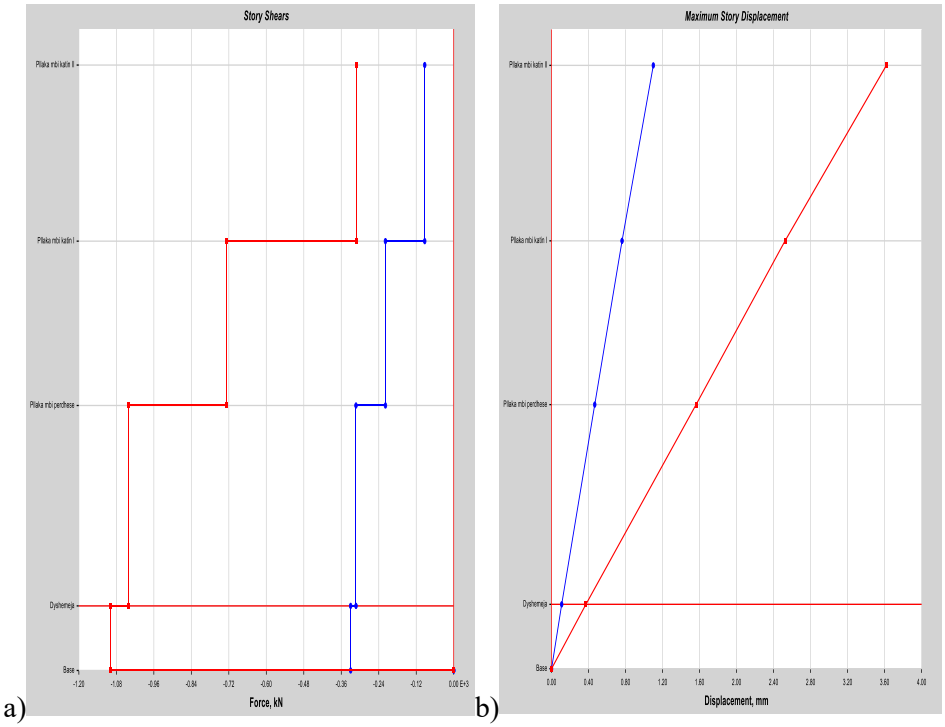
a) b)

Figure 10. Story shears and maximum story displacements, before retrofitting.

Retrofitting measures were implemented, primarily aimed at increasing the stiffness of the walls, which resulted in a noticeable reduction in the structure's fundamental period. This reduction in period correlates with a shift to a lower pseudo-acceleration range, thereby decreasing the seismic forces acting on the walls as per the analysis. Consequently, while cracks remain a factor under tension zones, the retrofitted structure demonstrates a more favorable response under the seismic conditions analyzed, showcasing the benefits of the strengthening measures applied. The retrofitting measures implemented not only enhanced the stiffness of the structure but also provided critical confinement to the masonry units. This confinement significantly improved the durability of the individual stone elements, ensuring they did not shatter or break apart like Lego pieces during the seismic event. The increased cohesion among the masonry units allowed the structure to maintain its integrity beyond the initial impact of the earthquake, providing resistance and stability throughout the seismic motion.

The following figure 11 presents the elastic response of the system after incorporating the effects of retrofitting into the model. This response reflects the improved performance of the structure, showcasing how the retrofitting measures enhanced its ability to withstand seismic forces. By increasing the stiffness of the masonry walls and providing confinement to the structural elements, the retrofitted model demonstrates a more favorable elastic behavior, effectively reducing deformations and mitigating potential damage under seismic loading conditions.

Copyright © 2025 CroCEE
DOI: https://doi.org/10.5592/CO/3CroCEE.2025.55



a) b)

Figure 11. Story shears and maximum story displacements, after retrofitting.

Figure 11.a) illustrates the distribution of shear forces across the stories of the structure under seismic loading. The second figure, 11.b), represents the displacement profile of the structure. The maximum displacement observed is 3.6mm.

Figure 12 illustrates the distribution of stresses, measured in MPa, within the wall under a seismic load combination. This stress map provides critical insights into how the seismic forces are distributed across the structure, identifying areas of high stress concentration that may be prone to cracking or failure.

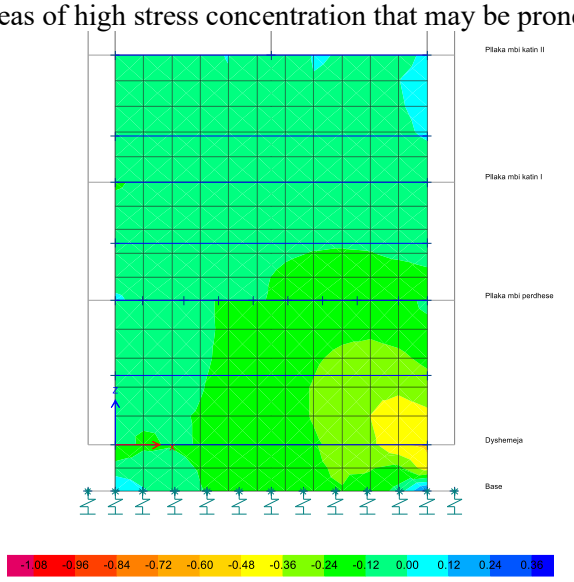


Figure 12. Normal stresses on the wall.

Table 2. Comparing retrofitted structure and non retrofitted structure behavior.

Materials	Shear at base	Displacement	Tension on the wall	Period
Non retrofitted structure	1150kN	4.8 mm	0.06MPa	0.186s
Retrofitted structure	1100 kN	3.6 mm	0.05MPa	0.184s

Copyright © 2025 CroCEE
DOI: https://doi.org/10.5592/CO/3CroCEE.2025.55

After the statically analyses and proposal for restoration is presented in figure 13.

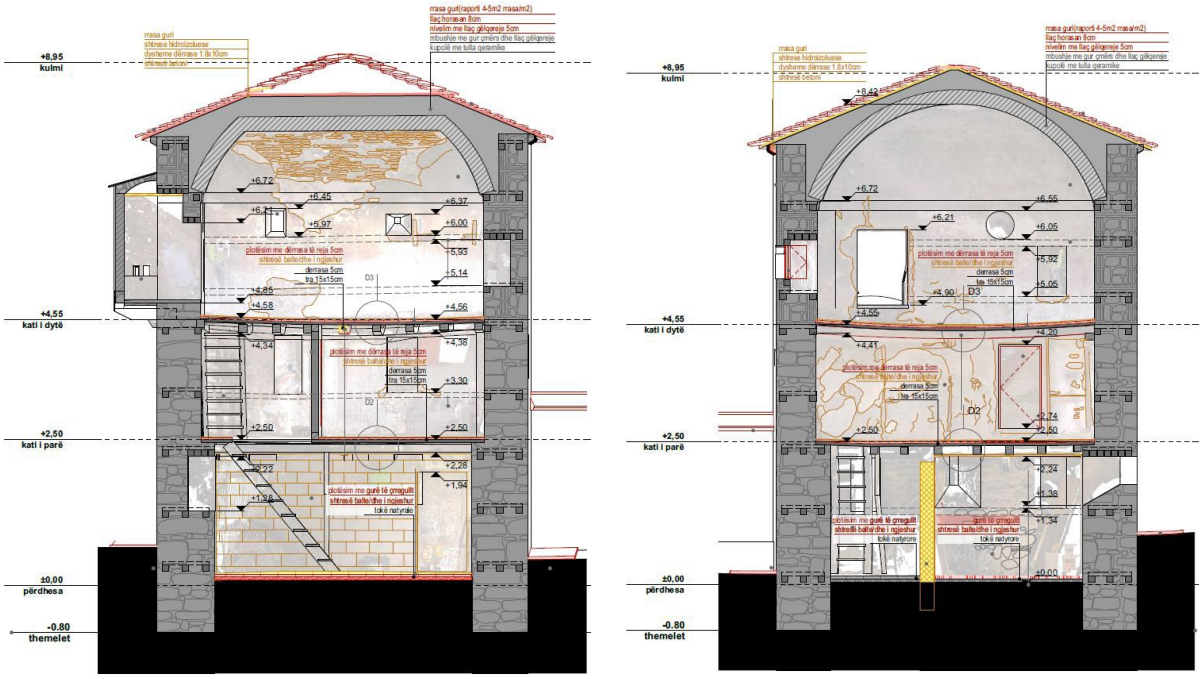


Figure 13. Proposal for Restoration the Kulla Ymer Poga

4. Conclusions and recommendations

The analysis conducted in this project aims to validate a protocol for Cultural Heritage Buildings and risk management, demonstrating its effectiveness as a tool for maintenance, conservation, and restoration efforts. Based on our case study and findings, we present insights that may interest engineers and architects engaged in theoretical research, material analysis, and restoration proposals:

- Involve technical specialists (architects, engineers, chemists, physicists, historians, archaeologists, and economists) from various disciplines in an integrated approach to managing Cultural Heritage Buildings.
- Develop a comprehensive quantitative and qualitative assessment of the environmental, economic, and social impacts of the entire restoration process.
- Define criteria and methods to identify, prioritize, and engage all stakeholders at every stage of the restoration, conservation, and valorization process.
- Design a complete framework of impact indicators to ensure the sustainable restoration of Cultural Heritage.
- Regarding the Kulla-Tower, the analysis of supporting conditions and the mechanical properties of its materials confirms that the numerical model satisfactorily reproduces the structure's dynamic response.

Recommendations Based on the Case Study:

- Design a detailed activity plan for the demolition process and verify stability after each step.
- Adjust the process steps as needed, incorporating preventive measures to address potential changes in structural stability.
- Pay particular attention to wall constructions, as these elements are critical for the structure's load-bearing capacity.
- Recognize that roof systems vary from building to building, and wood deterioration differs, necessitating detailed material testing for accurate assessment.

Copyright © 2025 CroCEE
DOI: https://doi.org/10.5592/CO/3CroCEE.2025.55

Acknowledgements

All authors contributed to study conception and supported from **Ministry of Educations Science and Technology**, through bilateral project: **Repairing the structure using the methods and applications the FRP**

References

[1] Romeu Vicente,Sergio Lagomarsino,TiagoMiguel Ferreira. : Cultural Heritage Monuments and Historical Buildings:Conservation Works and Structural Retrofiting: Chapter, Springer Nature,2017(pp 25-57).

[2] https://gjakovaportal.com/al/trashegimia/kulla-e-ymer-pog235s

[3] Fatemeh Hedieh Arfa,Hielkje Zijlstra,Barbara Lubelli,Wido Quist, Adaptive Reuse of Heritage Buildings: From a Literature Review to a Model of Practice, DOI:10.1080/17567505.2022.2058551,2022

[4] Sesana Elena,Gagnon Alexandre S,Ciantelli Chiara,Casser Joann,Hughes John J. Climate change impacts on cultural heritage: A literature review, DOI 10.1002/wcc.710,July 2021

[5] Jose Luiz Pedersoli Jr, A Guide to Risk Management of Cultural Heritage,2016

[6] Rohit Jigyasu , Risk Assessment of Cultural Heritage : Tools & Methodology,2019

[7]. Maarten Nauta, Rikke Andersen, Kirsten Pilegaard, Morten Poulsen, Meeting the challenges in the development of risk-benefit assessment of foods, DOI: 10.1016/j.tifs.2018.04.004,2018

[8]. Tiago M. Ferreira, Xavier Romão, Paulo B. Lourenço, Esmeralda Paupério &Nuno Martins. Risk and Resilience in Practice: Cultural Heritage Buildings, DOI: 10.1080/15583058.2020.1759007,2021

[9] Liubov Lisienkova 1*, Tatyana Shindina 2, Tatiana Lisienkova 3, Development of a Methodology for Assessing the Technical Level of Cultural Heritage Objects in Construction, 2021

[10] Anna Paolini,Azadeh Vafadari,Giorgia Cesaro. Mario Santana Quintero,Koen Van Balen,Ona Vileikis. Risk management at heritage sites:A case study of the petra world heritage site,2012

[11] Florina Jerliu,Kaltrine Thaci,Building typology of Albanian Kulla stone houses in the Balkans,2024

[12] Fatma ELaradi,Saber Kh.Elmabrouk, Risk Assessment at Heritage Sites: A Case Study of Tripoli Old City, Libya,2018

Proceedings of the 3rd Croatian Conference on Earthquake Engineering - 3CroCEE
19–22 March 2025, Split, Croatia
Copyright © 2025 CroCEE
DOI: https://doi.org/10.5592/CO/3CroCEE.2025.57

SEISMIC ANALYSIS OF DRY STONE MASONRY STRUCTURES WITHIN THE DIOCLETIAN'S PALACE IN SPLIT

Nikolina Živaljić [(1)], Ivan Balić [(1)], Hrvoje Smoljanović [(1)], Boris Trogrlić [(1)], Ante Munjiza [(1)]

[(1)] *Associate Professor, University of Split, Faculty of Civil Engineering, Architecture and Geodesy, nzivaljic@gradst.hr*
[(2)] *Associate Professor, University of Split, Faculty of Civil Engineering, Architecture and Geodesy, ibalic@gradst.hr*
[(3)] *Associate Professor, University of Split, Faculty of Civil Engineering, Architecture and Geodesy, hsmoljanovic@gradst.hr*
[(4)] *Full Professor (tenure), University of Split, Faculty of Civil Engineering, Architecture and Geodesy, btrogrlic@gradst.hr*
[(5)] *Full professor (tenure), University of Split, Faculty of Civil Engineering, Architecture and Geodesy, amunjiza@gradst.hr*

Abstract

A large number of cultural heritage buildings, especially in the Mediterranean area, belong to dry masonry stone structures. In order to be able to make decisions about possibly necessary rehabilitation techniques and to preserve them for future generations, it is necessary to have insight into their behaviour due to expected actions, the most destructive of which is an earthquake. As part of this work, an assessment of the seismic resistance of four dry stone masonry structures in the old centre of Split in Croatia was carried out: the bell tower of the Cathedral of Saint Domnius, the colonnade in front of the Cathedral, the Prothyron and the southeast tower in Diocletian's Palace. Numerical analyses were performed on plane models by the computer program Y-2D, which is based on the finite-discrete element method. In the conducted analyses, each stone block was modelled as one discrete element that can be found in mechanical interaction with other stone blocks. The mechanical interaction between discrete elements in the performed analyses was modelled through potential contact forces including frictional forces between blocks as the most important mechanism of seismic energy dissipation in these types of structures. Numerical analyses were performed for three different earthquakes whose acceleration amplitudes were incrementally increased until the complete collapse of the structure. The advantage of using such a numerical model is that, along with the assessment of the seismic resistance of the structure, it gives the expected mode of failure mechanism. This is very important information for taking measures in case of possibly necessary repairs of this type of construction.

Keywords: cultural heritage, dry stone masonry structures, finite-discrete element method, seismic resistance of the structure.

1. Introduction

The history of Split is inextricably linked to the Roman Emperor Diocletian and his stunning palace, which was built for his retirement in 305 AD. Diocletian's Palace is certainly at the top of any list of Split attractions. It is one of the best-preserved and most impressive monuments of the Roman era in Europe, and has been on the UNESCO World Heritage List since 1979.

The palace was built for several purposes, including an imperial residence, a military fortress and a fortified city. It is believed that the construction of the palace took about 10 years. It was built from stone brought from the island of Brač, marble from Italy and Greece, and columns and 12 sphinxes from Egypt. The palace actually contained an entire city with streets, squares and buildings that served different purposes. The southern facade of the palace was located right on the coast. The other three facades were located on the mainland and, together with the southern facade, closed the rectangular shape of the palace. The palace was conceived as a rectangle in its ground plan, but adaptation to the terrain, during construction, imposed minor deviations. The front walls of the palace are massive and simple in their lower parts without openings, and in the upper parts they are openable with large arched windows that are simple towards the mainland, i.e. on the western, northern and eastern facades, and divided by cornices, consoles and half-columns on the southern facade towards the sea. The outer walls of the palace, except for the western one, are mostly well preserved to this day.

Copyright © 2025 CroCEE
DOI: https://doi.org/10.5592/CO/3CroCEE.2025.57

Sixteen towers on the front walls towards the mainland give the palace the character of a fortress. The four towers at the corners have a square ground plan. Two of the six towers with an octagonal ground plan each framed three land entrances, while the six towers with a rectangular ground plan were located between the corner and octagonal ones. To this day, three corner towers (except the southwestern one) have been partially preserved, as well as only the remains of the octagonal and rectangular ones.

The Split Peristyle is a square in front of the Cathedral of St. Domnius in the Old Town of Split. On the sides, it is bordered by two rows of Corinthian-style columns connected by arches. The Prothyron, which was located on the south side, also contributed to the importance of the Peristyle, because from it the Emperor Diocletian addressed the inhabitants of the other part of the palace. It also connected, in fact separated, the northern part of the palace for servants, the army, etc. from the southern part where the emperor resided.



Figure 1. a) Peristyle in Diocletian's Palace, b) Diocletian's Palace [1].

In this paper an assessment of the seismic resistance of four dry stone masonry structures in the old centre of Split in Croatia was carried out: the bell tower of the Cathedral of Saint Domnius, the colonnade in front of the Cathedral, the Prothyron and the southeast tower in Diocletian's Palace. Numerical analyses were performed on plane models by the computer program Y-2D, which is based on the finite-discrete element method. The advantage of using such a numerical model is that, along with the assessment of the seismic resistance of the structure, it gives the expected mode of failure mechanism. This is very important information for taking measures in case of possibly necessary repairs of this type of construction.

2. The combined finite-discrete element method

The combined finite-discrete element method [2] comprises a large number of particles. These particles are represented by a single discrete element that interacts with its neighbouring discrete elements. Each discrete element has its own finite element mesh that is used to analyse the particle deformability. The material non-linearity including elastic hysteresis, fracture and fragmentation of the discrete elements is considered through contact elements implemented within the finite element mesh.

Discretization of a dry-stone masonry structure in the framework of FEM/DEM method is shown in Fig. 2. Each stone block is modelled as a discrete element that is discretized by constant strain triangular finite elements.

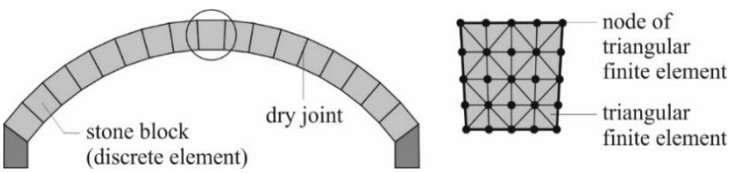


Figure 2. Discretization of a dry-stone masonry structure.

Copyright © 2025 CroCEE
DOI: https://doi.org/10.5592/CO/3CroCEE.2025.57

The material behaviour of the finite element is linear-elastic. The mechanical interaction between discrete elements in the performed analyses was modelled through potential contact forces including frictional forces between blocks as the most important mechanism of seismic energy dissipation in these types of structures.

Since the strength of stone is much greater than the effective stress level that occurs in stone structures, and therefore the failure of the structure occurs due to the loss of stability caused by the relative displacements between the blocks under the influence of horizontal force, the collapse of stone structures occurs mainly due to the loss of stability. In the performed numerical analyses, the cracking of stone blocks has not been considered as a possibility [3].

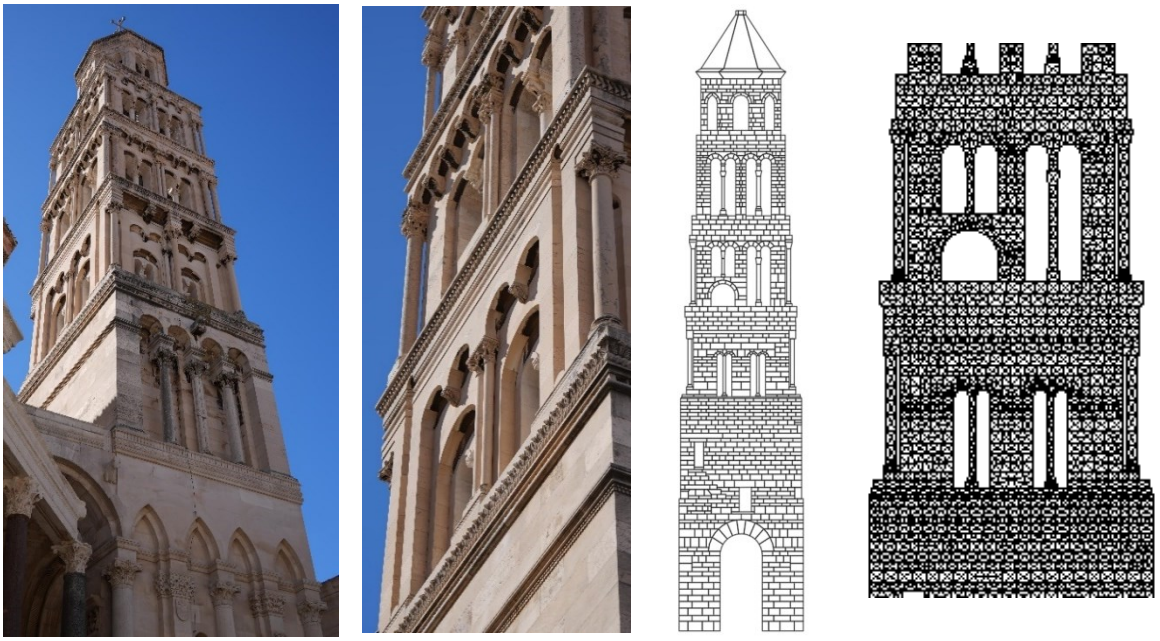
In the presented numerical analyses, the bell tower of the Cathedral of Saint Domnius, the colonnade in front of the Cathedral, the Prothyron and the southeast tower in Diocletian's Palace are exposed to horizontal and vertical ground acceleration from the recorded accelerograms of three real earthquakes recorded on the rock soil. The horizontal and associated vertical amplitudes were gradually increased until the collapse of the structure.

The earthquake accelerograms are adopted from the European Strong-Motion Database [4]. The selected earthquakes Petrovac 1979 (Montenegro), Campano Lucano 1980 (Italy), and South Iceland 2000 (Iceland). Material characteristics used in the numerical analyses are shown in Table 1.

Table 1. Material characteristics of stone

Density ρ (kg/m^3)	Modulus of elasticity E (MPa)	Friction coefficient μ	Damping coefficient $\overline{\mu}$
2190	48400	0.6	$4.5 \cdot 10^6$

Fig. 3 presented the analysed bell tower of the Cathedral of Saint Domnius. The geometry of the eastern facade shown in the Fig. 3c was adopted for the numerical analysis. The model was discretized with 9693 finite elements.



a) b) c) d)

Figure 3. Cathedral of Saint Domnius tower: a) View of the eastern part of the bell tower; b) Detail of the eastern facade, c) Geometry; d) Discretization.

Copyright © 2025 CroCEE
DOI: https://doi.org/10.5592/CO/3CroCEE.2025.57

Since Split is located in an area where the horizontal peak ground acceleration for a return period of 475 years is 0.22g, all numerical analyses were first performed for this acceleration value for all three earthquakes. After that, the acceleration increased incrementally until the structure collapsed.

For an acceleration of 0.22g, no damage occurred to the structure, while for an acceleration of 0.4g, the structure completely collapsed due to the Petrovac earthquake. From the analysis of the cathedral tower, it can be seen that the Petrovac earthquake was the relevant one. Namely, for an acceleration of 0.22g, the maximum displacement for the Petrovac earthquake is 0.39 cm, for the Campano Lucano it is 0.12 cm, while for the South Iceland it is 0.13 cm.

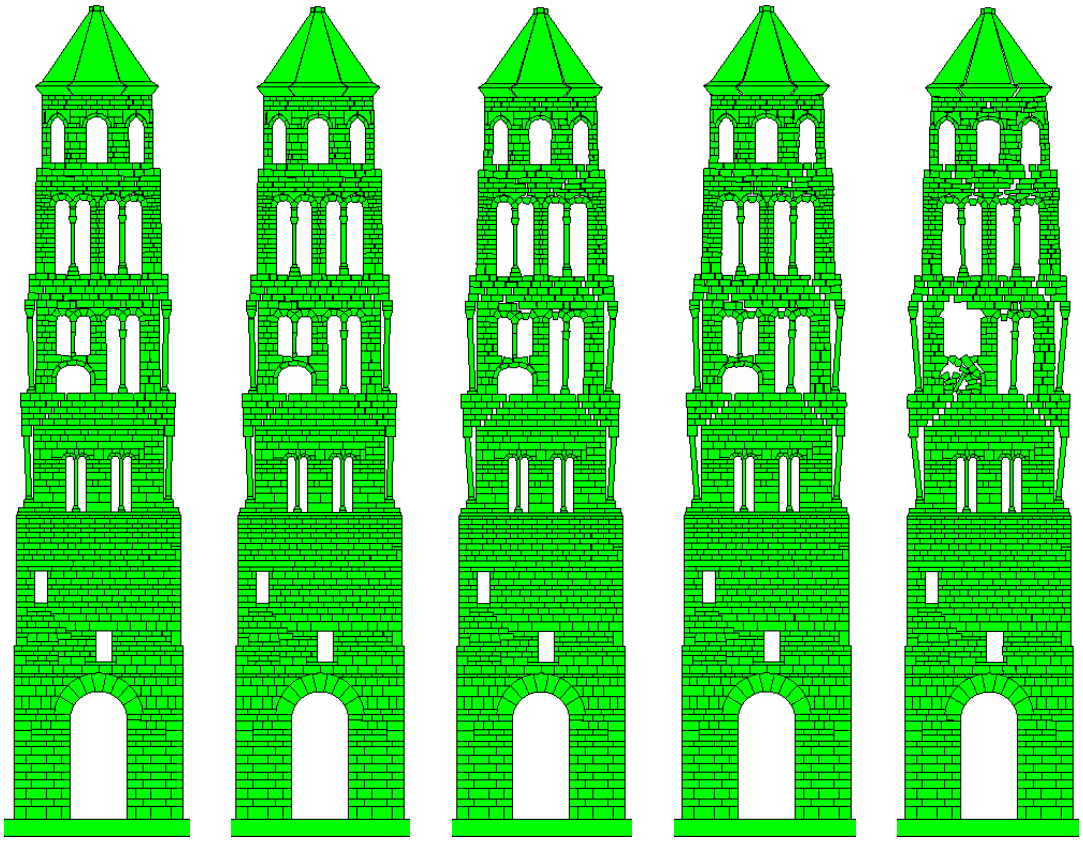


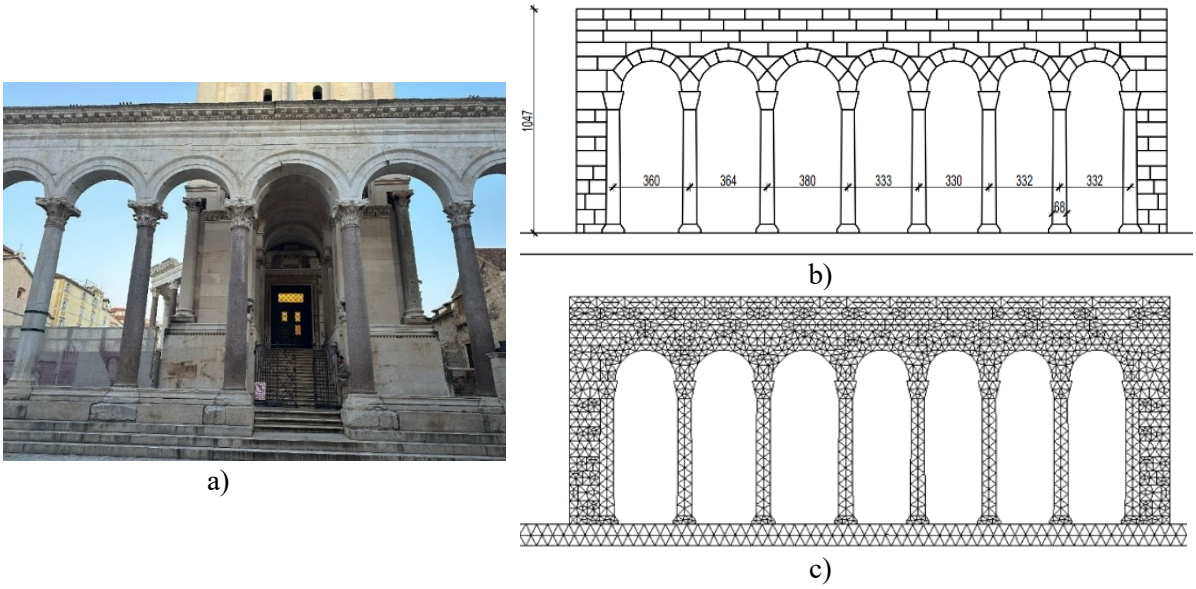
Figure 4. Behaviour of the bell tower of the Cathedral of Saint Domnius exposed to failure peak ground acceleration (a_g=0.40g) of earthquake Petrovac in time.

The complete collapse of the structure occurred for an acceleration of 0.40g and the effects of the Petrovac earthquake, as shown in the Fig. 4. For accelerations of 0.50g due to the Campano Lucano earthquake, a displacement of 11.5 cm was achieved, while for South Iceland a displacement of 0.26 cm was achieved. For both earthquakes, there was no significant damage to the structure.

Fig. 5 present the eastern colonnade on the Peristyle. The geometry of the colonnade includes seven arches supported by capitals on columns. The building's plan dimensions are 27.73 x 1.00 meters, while the height of the colonnade is 10.47 meters. The geometry and finite element mesh of the colonnade is shown in Fig. 5. The structure is discretized with 3031 triangular finite elements.

Numerical analyses of eastern colonnade on the Peristyle were first performed for 0.22g acceleration value for all three earthquakes. After that, the acceleration increased incrementally until the structure collapsed. For an acceleration of 0.22g, no damage occurred to the structure. The results of numerical analyses showed that the observed structure suffers the greatest damage and first loses stability for the Petrovac earthquake, which is why we consider it relevant for the analysis of the observed structure.

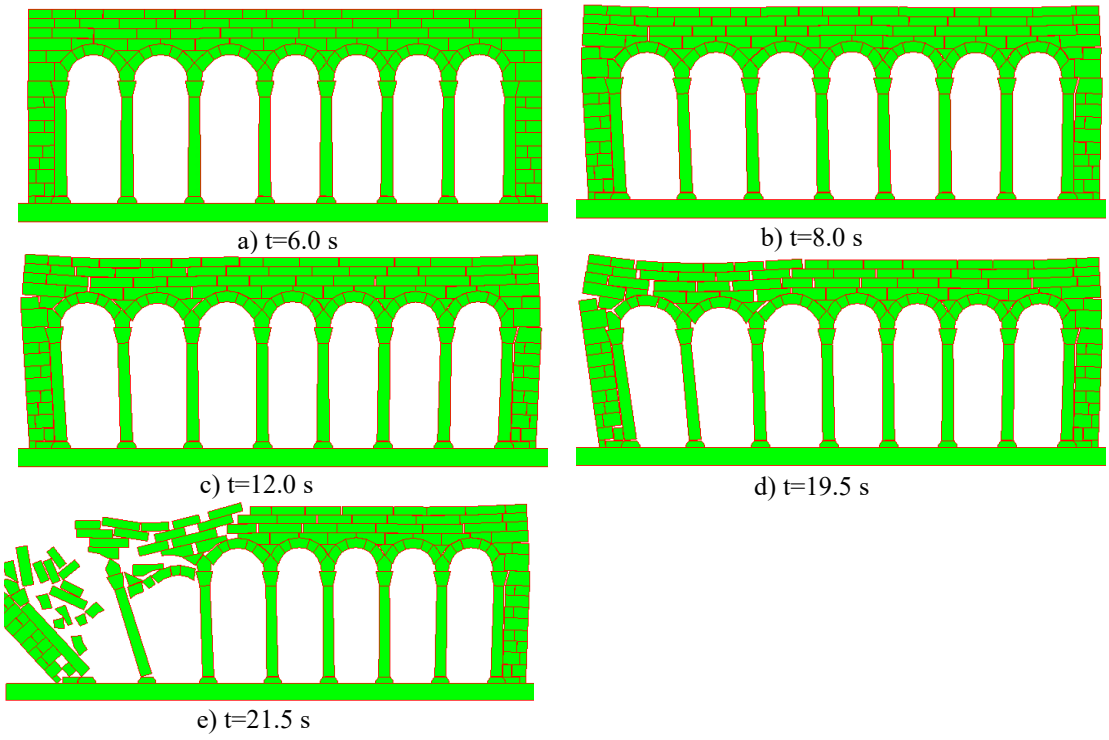
Copyright © 2025 CroCEE
DOI: https://doi.org/10.5592/CO/3CroCEE.2025.57



a) b) c)

Figure 5. a) Eastern colonnade on the Peristyle; b) Geometry; c) Discretization.

For peak ground acceleration of 0.80g, the structure completely collapsed due to the Petrovac earthquake. Namely, for an acceleration of 0.22g, the maximum displacement for the Petrovac earthquake is 6.50 cm, for the Campano Lucano it is 0.19 cm, while for the South Iceland it is 0.62 cm.



a) t=6.0 s b) t=8.0 s c) t=12.0 s d) t=19.5 s e) t=21.5 s

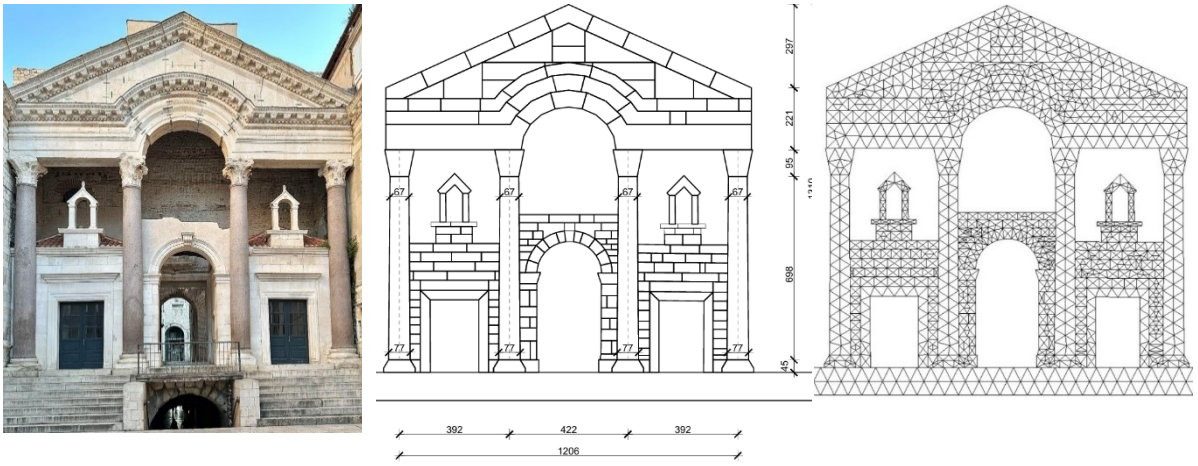
Figure 6. Behaviour of the Eastern colonnade on the Peristyle exposed to failure peak ground acceleration (a_g=0.90g) of earthquake Petrovac in time.

The complete collapse of the structure occurred for an acceleration of 0.80g and the effects of the Petrovac earthquake. A displacement of 20.30 cm was achieved. For accelerations of 0.80g due to the Campano Lucano earthquake, a displacement of 1.11 cm was achieved, while for South Iceland a displacement of 4.71 cm was achieved. For both earthquakes, there was no significant damage to the

Copyright © 2025 CroCEE
DOI: https://doi.org/10.5592/CO/3CroCEE.2025.57

structure. Behaviour of the Eastern colonnade on the Peristyle exposed to failure peak ground acceleration 0.90g of earthquake Petrovac in time is shown in the Fig.6.

The Prothyron on the Peristyle, its geometry and the discretization of the structure are shown in Fig. 7. The model of Prothyron was discretized with 2539 finite elements.



a) b) c)

Figure 7. a) Prothyron; b) Geometry; c) Discretization.

For an acceleration of 0.22g, no damage occurred to the structure and the maximum displacements for Petrovac, Campano Lucano and South Iceland earthquakes are 4.47 cm, 0.10 cm and 0.37 cm respectively.



a) t = 6.95 s b) t = 8.50 s c) t = 8.90 s

d) t = 11.50 s e) t = 12.75 s f) t = 14.25 s

Figure 8. Behaviour of the Prothyron on the Peristyle exposed to failure peak ground acceleration (a_g=0.75g) of earthquake Petrovac in time.

Copyright © 2025 CroCEE
DOI: https://doi.org/10.5592/CO/3CroCEE.2025.57

For peak ground acceleration of 0.70g, the structure completely collapsed due to the earthquake Petrovac. From the analysis of the Prothyron on the Peristyle, it can be seen that the Petrovac earthquake was the relevant one. For peak ground acceleration of 0.70g due to the Petrovac, Campano Lucano and South Iceland earthquakes, displacements of 23.83 cm, 11.50 cm and 0.26 cm was achieved respectively. For Campano Lucano and South Iceland earthquakes, there was no significant damage to the structure.

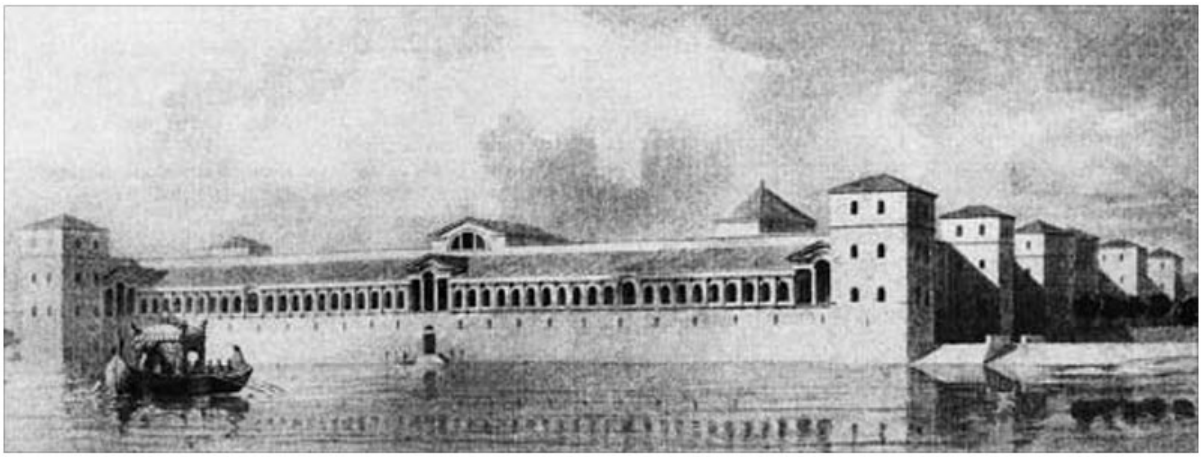
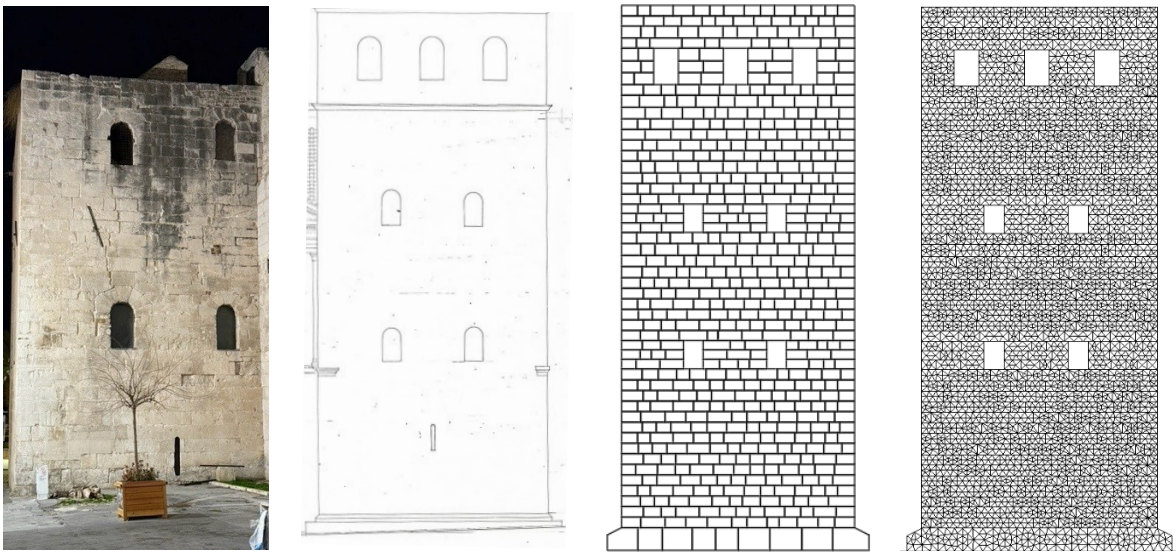


Figure 9. G. Niemann: South façade of Diocletian's apartments, original appearance [1]

The southeast tower of Diocletian's Palace in its original state had a ground floor and three floors, and today it is preserved in the form of a ground floor and two floors [1]. In the numerical analyses presented in this paper, the original geometry of the tower shown in Fig.10b was adopted. The tower is discretized with 8143 finite elements. The geometry and discretization of the structure are shown in Fig. 10.



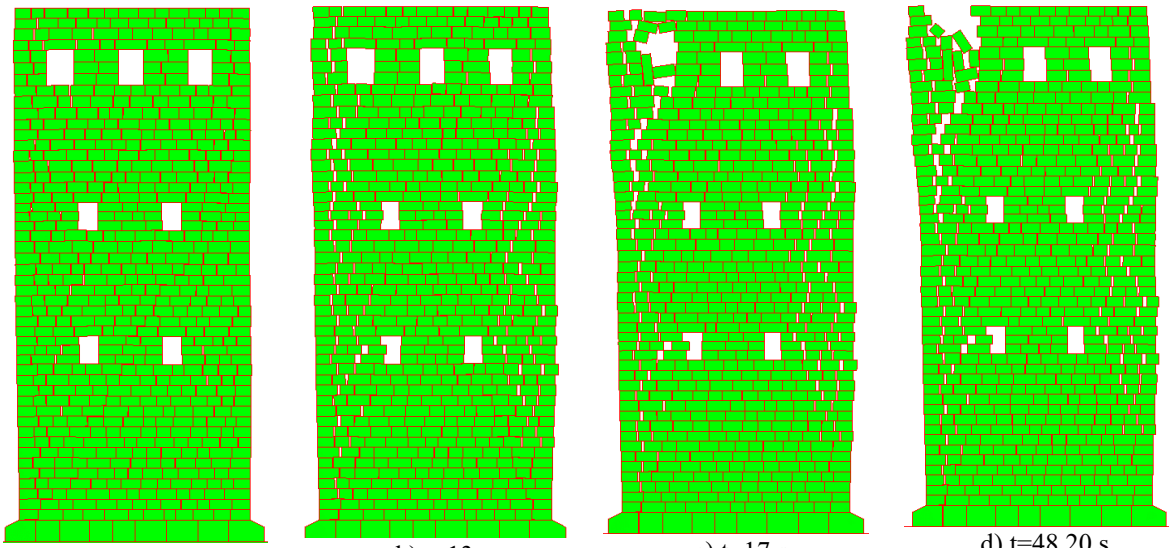
a) b) c)

Figure 10. a) Southeast tower of Diocletian's Palace; b) Geometry [5]; c) Discretization.

The results of numerical analyses showed that the observed structure suffers the greatest damage and first loses stability for the Petrovac earthquake, which is why we consider it relevant for the analysis of the observed structure. The other two earthquakes did not cause the structure to collapse, although significantly higher ground acceleration values were used. For an acceleration of 0.22g, no damage occurred to the structure and the maximum displacements for Petrovac, Campano Lucano and South

Copyright © 2025 CroCEE
DOI: https://doi.org/10.5592/CO/3CroCEE.2025.57

Iceland earthquakes are 0.29 cm, 0.12 cm and 0.22 cm respectively. For peak ground acceleration of 1.50g, the structure completely collapsed due to the earthquake Petrovac as it is shown in Fig.11.



a) t=7.25 s b) t=13 s c) t=17 s d) t=48.20 s

Figure 11. Behaviour of the Southeast tower of Diocletian's Palace exposed to failure peak ground acceleration (a_g=1.50g) of earthquake Petrovac in time.

For peak ground acceleration of 1.50g due to the Petrovac, Campano Lucano and South Iceland earthquakes, displacements of 27.0 cm, 1.6 cm and 8.2 cm was achieved respectively. For Campano Lucano and South Iceland earthquakes, there was no significant damage to the structure.

From the analyses of all four buildings located in Diocletian's Palace, it can be seen that for the peak ground acceleration value of a_g = 0.22 g, which is relevant for the city of Split, the structure did not sustain any damage, which leads us to the conclusion that the building in question has good seismic resistance for the area in which it is located. The advantage of using such a numerical model is that, along with the assessment of the seismic resistance of the structure, it gives the expected mode of failure mechanism. This is very important information for taking measures in case of possibly necessary repairs of this type of construction.

Acknowledgements

This research was partially supported through project KK.01.1.1.02.0027, a project co-financed by the Croatian Government and the European Union through the European Regional Development Fund - the Competitiveness and Cohesion Operational Programme.

References

[1] Marasović, T., Alujević, T. (2007): Dioklecijanov stan u splitskoj palači / The Apartments of Diocletian's Palace in Split. PROSTOR, **15** (2), 155-179.

[2] Munjiza, A. (2004): *The combined finite-discrete element method*. John Wiley & Sons, London. U.K.

[3] Balić, I., Živaljić, N., Smoljanović, H., Trogrlić, B. (2016): Seismic resistance of dry stone arches under in-plane seismic loading. *Structural Engineering and Mechanics*, **58** (2), 243-257, doi: https://doi.org/10.12989/sem.2016.58.2.243

[4] European Strong-Motion Database, available at: https://esm-db.eu/#/event

[5] Marasović, J., Marasović, T. (1978): Istraživanje i obnova jugoistočne kule Dioklecijanove palače, https://hrcak.srce.hr/file/240093

Proceedings of the 3rd Croatian Conference on Earthquake Engineering - 3CroCEE
19–22 March 2025, Split, Croatia
Copyright © 2025 CroCEE
DOI: https://doi.org/10.5592/CO/3CroCEE.2025.59

PREFABRICATED REINFORCED CONCRETE RESIDENTIAL BUILDINGS: A FOCUS ON THE JUGOMONT SYSTEM

Milica Petrović [(1)], Svetlana Nikolić - Brzev [(2)]

[(1)] *Assistant Project Engineer, Zoling d.o.o., Serbia, milica.petrovic.ml@gmail.com*
[(2)] *Adjunct Professor, Department of Civil Engineering, University of British Columbia, Canada, sbrzev@mail.ubc.ca*

Abstract

The second half of the 20th century was marked by the rise of prefabricated concrete systems used as the best solution for fast construction after the vast devastation of the building stock after WWII. In Yugoslavia, several innovative structural systems were used for mass construction of multi-family housing blocks. Two large groups of prefabricated systems were: 1) large panel and 2) dual frame-wall systems. Some of these systems were adapted from other European countries by local construction companies, such as Rad-Balency, but over time engineers developed new ones, the most famous being the IMS building system developed by Professor Branko Žeželj at the Institute IMS in Belgrade. A construction boom from 1964-1980 brought new urban projects and developments, such as Novi Beograd (New Belgrade) in Serbia, Novi Zagreb (New Zagreb) and Split 3 in Croatia, Nova Gorica in Slovenia, and the reconstruction of Skopje, North Macedonia after the 1963 earthquake. This paper presents a case study on Blok 28 building complex in New Belgrade, the largest urban development in Serbia and former Yugoslavia and a polygon for experiments in architecture and construction technologies. Architectural and structural features of the Jugomont prefabricated reinforced concrete system are outlined in the paper, with a focus on the features that influence the seismic performance of buildings constructed using this system and the failure mechanisms of prefabricated wall structures composed of panels and their connections under seismic actions. The paper is expected to contribute towards the understanding of the architectural and structural design concepts related to prefabricated reinforced concrete buildings which are a part of the existing building stock in urban areas of the countries within the territory of former Yugoslavia.

Keywords: prefabricated reinforced concrete panels, seismic behaviour, failure mechanisms, mid-20th century heritage, New Belgrade, Jugomont

1. Introduction

The objective of this paper is to analyse the mid-20th-century building stock in the Western Balkans and to discuss the architectural and structural aspects of prefabricated multi-family housing built during this period. Most of these structures were built between the 1960s and 1980s with the idea of increasing the building stock in major cities in former Yugoslavian republics. They stand as vital examples of the region's heritage and were recognised internationally, and presented in 2018 at the Museum of Modern Art in New York as part of the exhibition *Toward a Concrete Utopia: Architecture in Yugoslavia, 1948 -1980* [1]. These buildings are examples of modernist architectural and engineering achievements and need to be preserved and rehabilitated.

The increasing need for housing in the post-war Yugoslavia, led architects and engineers to develop prefabricated systems due to ease of production of elements off the construction site and fast assembly. These structures reflect the relationship between modernist design principles and the socio-political context of the time. This paper focuses on residential multi-family buildings built using reinforced concrete (RC) panel elements in the Jugomont system.

This paper presents an overview of housing construction practices in the second half of the 20th century in Yugoslavia, focusing on prefabricated multi-family housing, its characteristics, external influences and the seismic characteristics of the structures. A typical residential community in New Belgrade, Serbia, Block 28, was selected for this study since it features the buildings constructed in the Jugomont system, which was developed in Croatia. The paper showcases the diversity of architectural and engineering solutions for that period and the seismic vulnerability of these buildings.

Proceedings of the 3rd Croatian Conference on Earthquake Engineering - 3CroCEE
19–22 March 2025, Split, Croatia
Copyright © 2025 CroCEE
DOI: https://doi.org/10.5592/CO/3CroCEE.2025.59

Recent earthquakes in the Western Balkans and the neighbouring region, that is, the November 26, 2019 Durres, Albania earthquake (M 6.4) and the March 22, 2020 Zagreb, Croatia earthquake (Mw 5.4), highlighted the seismic vulnerability of urban building stock. Lessons from these earthquakes provided valuable insight into the seismic performance of the affected building typologies. Prefabricated RC buildings in urban centres of Albania were exposed to the earthquake but exhibited relatively minor damage compared to cast in-situ RC frame buildings and unreinforced masonry buildings, demonstrating the resilience of these systems under moderate seismic actions [2, 3]. The buildings affected by the 2020 Zagreb earthquake were mostly older unreinforced masonry structures, which are not the subject of this paper (note that prefabricated RC buildings were not affected by the earthquake).

The aim of this paper is to provide an overview of architectural and structural design concepts of post-WWII urban construction in former Yugoslavia, with a focus on prefabricated RC construction practices. Specifically, the focus is on the Jugomont system, which was developed in Zagreb, Croatia, and was applied throughout the region. Key structural elements and their connections were described in the context of identifying possible seismic failure mechanisms of buildings constructed using the system and the consequences on the seismic performance of these buildings.

2. Building Context in Post-War Yugoslavia

The post-World War II period in Europe was marked by the (re)construction of damaged cities and the design of new city centres. Urban planning relied on modernist principles outlined in the Athens Charter during the 1933 CIAM meeting. Based on architect Le Corbusier's concept of the Radiant City—"a city of sunlight, space, and greenery" [4]—new urban plans required vast areas to implement large-scale interventions with varied functions aligned with emerging state ideologies. A product of the CIAM meeting, which involved participation from over half of Europe's nations, was the concept of the *functional city*. The meeting showcased plans for 33 cities, including Zagreb.

The functional city concept was founded around four essential activities—housing, work, recreation, and transportation—and their comprehensive integration into new urban plans [5]. In former Yugoslavia, encompassing six current Balkan countries, the development of Belgrade as the country's capital exemplified the planning and construction of a new urban area guided by these principles. The planning of New Belgrade, located on the left bank of the Sava River, drew from modernist legacies but was adapted to political ideologies. Early plans for New Belgrade were abandoned when Yugoslavia distanced itself from other Eastern European socialist countries and pivoted towards Western Europe. Between 1950 and 1960, the focus shifted from governance-related urban design to addressing housing issues. The ideas of broad roads and buildings surrounded by ample green spaces were retained, and the construction of several public facilities such as the Central Committee building, Federal Executive Council palace and hotel "Yugoslavia" began. Numerous architectural competitions based on the initial plan for New Belgrade attracted architects from across Yugoslavia, resulting in "the creation of a new architectural discourse and architectural-urban planning practice of the new Yugoslavia" [6]. New Belgrade bears witness to the collaboration between architects and engineers in constructing numerous residential buildings that reflect a cohesive post-war architectural language in Yugoslavia.

After WWII, Belgrade saw an influx of new residents who needed housing. Urban planning aimed to make Belgrade a city of millions, though the ideal of "free housing for all" proved unfeasible. Construction technology struggled to keep pace with rapid population growth. The drive for rapid and cost-effective construction led to the development of more than 20 prefabrication systems, which gradually dominated residential construction across Yugoslavia. Housing quality was defined not only by its commodification but also by its functional value [7]. Notable prefabricated systems include the IMS system developed in 1957 and various forms of panel systems, such as Jugomont, Rad-Balency, etc. Prefabricated elements were often combined with cast in-situ RC components such as walls and foundations.

Due to a unified housing policy, residential buildings across Yugoslavia utilised similar or identical prefabricated systems and construction technologies in general. The first five-year construction plan prioritised urbanisation in Belgrade, Ljubljana, and Titograd (now Podgorica) [8]. Major modernisation

Copyright © 2025 CroCEE
DOI: https://doi.org/10.5592/CO/3CroCEE.2025.59

efforts between 1950 and 1960 focused on New Belgrade (Serbia), New Zagreb (Croatia), and Nova Gorica (Slovenia), alongside new industrial centres nationwide. The 1970s saw Split's expansion and the development of Skopje's reconstruction after the earthquake in 1963. "The modernism inherited from the pre-WWII period was a solid foundation, but implementing large-scale mass urbanisation required new knowledge, such as urban development management, construction process organisation, and prefabricated mass production. This knowledge was less about aesthetics and more about broader modernisation, while socialist urbanisation aimed to reduce societal disparities across the region" [9]. The aim was to construct buildings economically, using prefabrication that was simple to produce and could be completed at a faster pace compared to traditional cast in-situ construction practices.

To maximise the number of apartments within a short time, the building designs included mostly two-bedroom apartments. The architects provided design solutions with expanded dining rooms that could accommodate a bed if needed. This approach enabled economical social housing construction for a larger population [10]. Limited construction technology and a shortage of skilled labour necessitated innovative structural solutions tailored to the context. In New Belgrade, the challenges of building on marshland, including the high cost of pile foundations, led to structural innovations aimed at reducing construction weight while ensuring simplicity and cost-effectiveness [11]. The prestressed concrete prefabricated spatial frame system, developed at the IMS institute by engineer Branko Žeželj, was tested during the construction of Blocks 1 and 2 in New Belgrade. Remarkably, Žeželj consulted architects to determine optimal spans for residential design, leading to the adoption of a 4.2x4.2m module which was compatible with available site equipment. Cranes of the time could lift slabs up to 17 square meters, earning the nickname "crane architecture" for post-war construction [11].

The synthesis of architectural and engineering expertise—architects trained at leading European modernist schools and civil engineers implementing contemporary construction systems—placed Yugoslav projects on the 20th-century architectural map alongside major European countries. However, the unique context of Yugoslavia's housing policy and construction produced distinctive architecture and unparalleled mass housing. Prefabricated systems accommodated architectural designs by modifying elements on-site, resulting in a unique architectural style [12]. Despite architects striving to align designs to accommodate the use of prefabricated systems, the government prevented monopolies by ensuring that multiple companies participated in the construction, leading to a predominance of hybrid systems. While this hindered the economic efficiency of mass production, it contributed to unique architectural outcomes. "A region as a space of authentic architectural imagination, which is still to be inscribed on the international map of modernity" [9].

The cultural, social, and political context, combined with technological advancements, shaped the architectural expression of structures where their structural form became prominent. Studies translated and published in numerous journals of the period, including *Tehnika*, *Arhitektura Urbanizam Beograda*, *Arhitektura Urbanizam*, and internal publications by the Urban Planning Institute and Construction Centre provided architects and engineers with a broad knowledge base for designing structures aligned with state policies promoting progress. Ideas for large-scale urban plans, individual buildings, and innovative construction techniques showcased fairs and competitions that raised public awareness of construction and state development. Although urbanisation was not fully realised, the constructed legacy of that period represents a significant 20th-century architectural heritage that remains present in contemporary architectural contexts.

3. New Belgrade Central Zone – Block 28

The central zone of New Belgrade comprises nine blocks, with a central axis of three blocks with public buildings oriented towards the Federal Executive Council building on the north side and a proposed Central railway station on the south side. Designed as an urbanistic entity, this zone draws inspiration from Le Corbusier's city plans. The corner blocks, numbered 21, 23, 28, and 30, feature high towers at their corners, enclosing the central zone. The axis towards the Federal Executive Council building houses compact business districts and public areas, surrounded by 12 high towers. The buildings in the neighbouring blocks around the central axis provide shelter in the interior of the block for its inhabitants

Copyright © 2025 CroCEE
DOI: https://doi.org/10.5592/CO/3CroCEE.2025.59

(Fig. 1). Each block in the central zone is a harmonious blend of typologies, including high-rise buildings, mid-rise residential buildings called lamellae, and public buildings like schools, kindergartens and local community buildings.

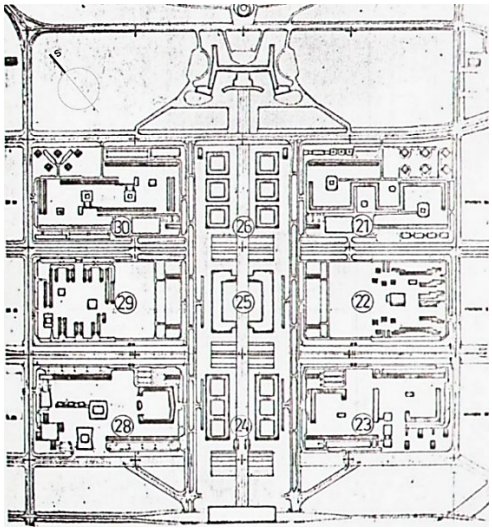


Figure 1. New Belgrade Central Zone (Blocks 21 to 30) with Federal Executive Council building in the northeast [11]

The central zone blocks on the axis (24, 25 and 26) were never fully realised as designed. The idea was to build a new centre equivalent to the historical city centre of Belgrade, but the project primarily focused on constructing apartment buildings and supporting public facilities. Nevertheless, the blocks located along the perimeter of the central zone stand as a witness to this project.

Each block in the central zone of New Belgrade was developed following an architectural competition, which resulted in a diverse array of individual designs for both the block and its buildings. Since the monopoly of companies was prohibited, multiple prefabricated systems, both in terms of construction methods and architectural elements, were implemented. This resulted in unique designs that distinguished each block and left a lasting impact on the modernist architectural heritage.

In this paper, Block 28 will be discussed in detail, specifically in terms of structural design and the application of the Jugomont prefabricated panels. The detailed urban design of Block 28 was proposed based on the design conception for the New Belgrade central zone. The design envisioned nine buildings in total (labelled 1 to 9, see Fig.2), aligning with the planned dynamics for other blocks. Public buildings, including a community council, kindergarten, and school, were strategically positioned in the central area to ensure equal accessibility for all residents (Fig. 3) [14, 15, 16]. Along the perimeter of the block, two long 10-storey buildings (lamellae, numbered 1 and 6) were positioned parallel to the main boulevards. In the western corner, the design envisioned four 16-storey high-rise buildings enclosing the central zone blocks (number 4). Notably, the design proposed a truly unique 4-storey building in the area (number 7), located along the central zone axis, called “Potkovica” (en. horseshoe) for its horseshoe-like shape in plan. The concept behind this shape was to create a barrier towards the public blocks and provide a more private space for the inhabitants of Block 28.

The Block 28 established itself as Yugoslav. The urban concept was set in Belgrade; a team from Ljubljana won the design competition for the block, the prefabricated systems were the IMS system from Belgrade and the Jugomont system from Zagreb, and the contractor was “Hidrogradnja” from Čačak. The success of the project depended on all participants. The constant presence of the investor "Jingrap" played a crucial role in coordinating the construction of the buildings in the block. Communication between the urban planners and the designers of individual buildings, who served as a link with the contractor, resulted in turning all the ideas into reality [14]. This block presents a true

Copyright © 2025 CroCEE
DOI: https://doi.org/10.5592/CO/3CroCEE.2025.59

collaboration of all participants in the project and reflects the idea of the collaboration between architectural design and prefabricated construction technologies [16].

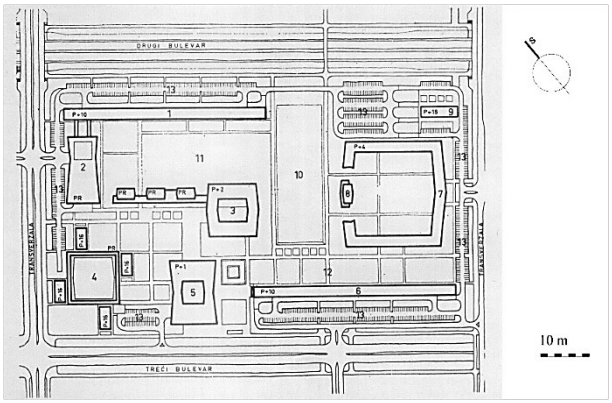


Figure 2. Plan of Block 28, New Belgrade [15]



Figure 3. A 3D view of Block 28 [17]

The architectural and structural design of the "Potkovica" building in Block 28 makes it an important one to date. The unique shape of the building and its construction from the prefabricated system Jugomont demand special attention in architectural heritage. Built in the period from 1969 to 1971 and designed by the architect Ilija Arnautović, the building consists of 24 modules, creating a zig-zag contour on its facade. The design resembled a block of terraced houses and created a more human-scale building. The building has four floors, with four apartment types, the largest one being a two-bedroom apartment with an area of 81.87 m^2. A typical floor for one module of the building had two of these apartments in mirror with a vertical communication in between [15]. The Jugomont prefabricated system was chosen for this building because of the 3,60 m span, which was convenient for this type of apartment. The typical floor plan of the apartment (Fig. 4), clearly shows that each bedroom has a 3.60 m span, as well as the living room and the kitchen/dining room/bathroom area. Another advantage of the Jugomont system was the adaptability to the building shape. [18] The building façade was also designed using the Jugomont prefabricated panel elements, leaving the connections visible and a natural treatment of the surface – flat or washed concrete. The façade elements changed between closed elements and the ones with openings for windows or balcony doors. The terraces were made as separate elements, seemingly only leaning onto the main structure (Fig. 5).

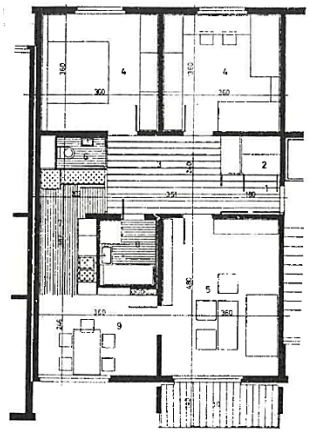


Figure 4. Apartment floor plan.

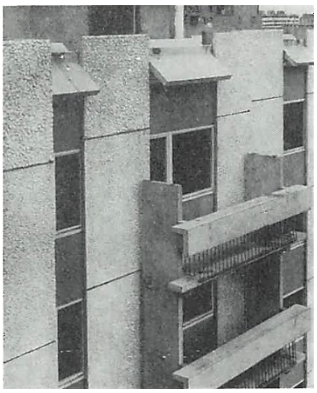


Figure 5. An exterior view of the façade.

According to the architect Ilija Arnautović, the architecture of Block 28 was enriched by using prefabrication systems (contrary to popular opinion). This project could only be completed through constant collaboration of all participants. The "Potkovica" building is a prime example of how, at the

Proceedings of the 3rd Croatian Conference on Earthquake Engineering - 3CroCEE
19–22 March 2025, Split, Croatia
Copyright © 2025 CroCEE
DOI: https://doi.org/10.5592/CO/3CroCEE.2025.59

same time, prefabricated systems can be flexible and adaptable to the urban and architectural design of buildings [18].

4. Jugomont system: a structural and seismic engineering perspective

4.1. Introduction

Use the decimal system for headings with no more than three levels. Jugomont semi-prefabricated large panel system was originally developed in 1959 (JU-59 system), and it further evolved through its variants developed in 1960 (JU-60), 1961 (JU-61), and 1971 (JU-71). The system was named after a Zagreb-based engineering firm, which was established in 1955. The main structural components of the system were prefabricated RC wall and floor panels, which were interconnected along the horizontal and vertical joints. The buildings had cast-in-situ strip foundations. Information related to the Jugomont system and its applications is available in local technical literature dating back to 1960s and 1970s [19].

The Jugomont system was used for construction of mid-rise residential buildings throughout former Yugoslavia. Most buildings were 5-storey high (P+4), which was a common building height for residential buildings at the time when these buildings were constructed (the 1960s and 1970s); however, building height was also limited by structural features of the system, especially for the JU-59 and JU-60 variants. Taller buildings were constructed in the JU-61 system - for example, 6-storey buildings were constructed in Maribor, Slovenia, in 1964 [20], and the system was suitable for the construction of buildings of up to 8-storey height [15].

Plan dimensions of these buildings varied depending on the project and variant of the system. Plan shape was usually regular (rectangular), with a fixed width (approximately 10 m), while the length ranged from approximately 40 m (JU-60) to 77 m (JU-61) [21]. In the case of buildings where architectural design envisaged an irregular shape, buildings were separated into regular blocks by means of construction joints (seismic gaps), e.g., “Potkovica” building, Blok 28, New Belgrade, Serbia [15].

The layout of structural walls in a building, which is very important from the perspective of its response to seismic actions, also evolved over time and varied depending on the variant of the system. The JU-59 variant had only transverse structural walls, while the JU-60 variant comprised of transverse walls plus a single interior longitudinal wall [15]. Finally, the JU-61 variant comprised of transverse walls plus two interior longitudinal walls.

4.2. Key building components and their connections

Sizes of panel elements varied over time, but the objective was to arrange the panels to match the basic cell (room) size (4 m x 4 m plan dimensions). Wall panels in the JU-59, JU-60, and JU-61 systems were 14 cm thick, 1.2 m wide, and 2.6 m high (equal to the floor height) (Fig. 6). Floor panels were 12 cm thick, while their length and width were variable. The main difference between the JU-60 and JU-61 variants was in the material strengths (e.g. concrete grade was increased from MB-160 to MB-220), and improving panel connections.

Both floor and wall panels were reinforced with two layers of steel mesh. The size of horizontal and vertical reinforcing bars was rather small (ranging from 5-8 mm in diameter). Wall panels in the Jugomont system are considered as lightly reinforced according to the modern RC design standards, especially for buildings subjected to seismic actions.

Further evolution of the system led to new variants characterized by larger panel elements (JU-71). The original variants of the system were developed using smaller panel sizes due to limited construction equipment and low labour costs, however construction considerations changed over time - the new goal was to achieve faster building construction (faster assembly of panels at the construction site). As a result, wall panel length increased to 614 cm (compared to the previous 120 cm length), and the thickness was increased to 16 cm (compared to 14 cm thickness), while the height remained the same (258 cm - equal to the floor height). The thickness of floor panels remained unchanged (12 cm), while typical plan dimensions were 360 cm x 310 cm and 240 cm x 310 cm.

Copyright © 2025 CroCEE
DOI: https://doi.org/10.5592/CO/3CroCEE.2025.59

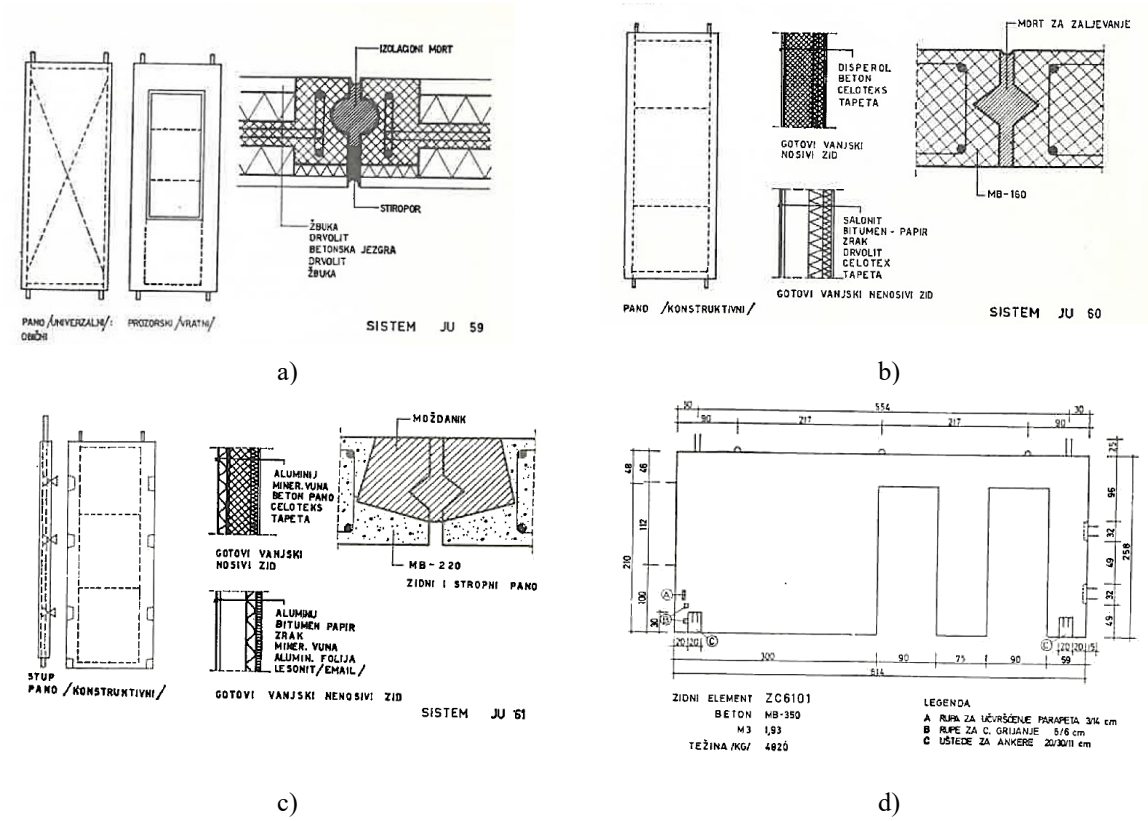


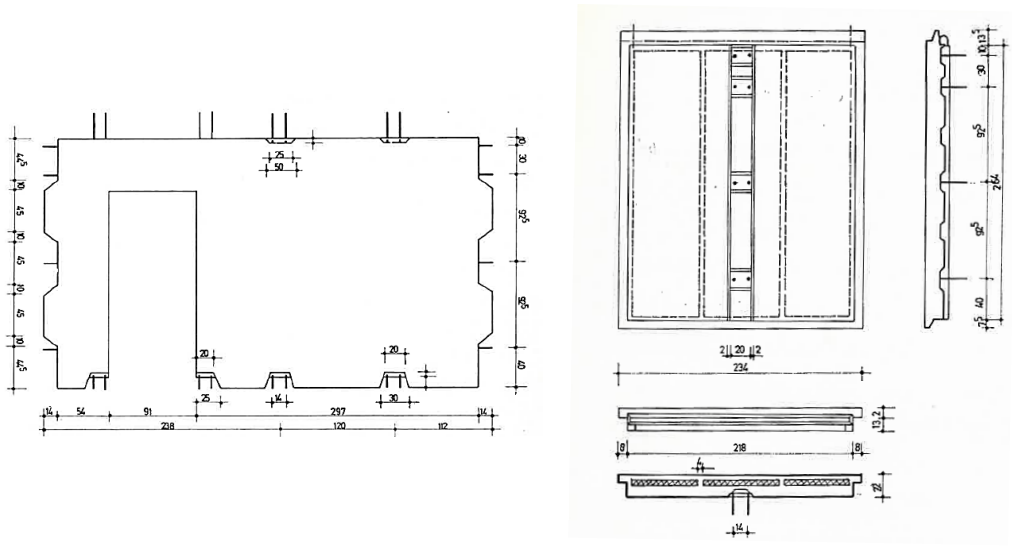
Figure 6. Variants of the Jugomont system – key structural elements: a) JU-59; b) JU-60; c) JU-61 and d) JU-71 [19]

Another variant of the Jugomont system, known as HG-68, was custom-developed for the construction of the "Potkovica" building in Blok 28, New Belgrade. The key structural components were based on the Jugomont system, however some improvements were introduced by the design team, which comprised of local engineers and a few engineering experts from the Soviet Union retained by the United Nations [22]. A typical wall panel in the HG-68 system was similar to the one characteristic for the JU-71 variant, except for more robust connections along horizontal and vertical joints (Fig. 7). For example, a larger number of extended vertical bars were provided along the horizontal joints, the configuration of shear keys along the vertical joints was changed, and extended horizontal bars were provided along the vertical joints [23].

Buildings constructed using the "Jugomont" system were known as "Limenke" (*cans* in English) due to the appearance of their façade elements, some of which were constructed using corrugated aluminium sheet cladding. Exterior walls were constructed either as structural or non-structural panels with 22 cm thickness. Structural exterior wall panels had 11 cm thick interior RC core, exterior thermal insulation and cladding (e.g. corrugated aluminium sheet), and interior finishing (e.g. wallpaper). Some of the façade panels were constructed with extended horizontal bars, which were intended for achieving connections between exterior and interior wall panels.

Wall panels at adjacent floors were connected by welding the vertical steel bars extended at the ends of the wall panels. Connections between the adjacent panels at the same floor were achieved through shear keys distributed along vertical joints. Voids between the panels were filled with cementitious grout (referred to as "mortar" in the technical literature related to this system) (Fig. 8a). Since no reinforcement was provided in the joints along the wall panel height, horizontal reinforcement in RC tie-beams at floor levels significantly contributed to the overall shear resistance of vertical joints (Fig. 9). It should be noted that the vertical connections were further improved in the JU-61 variant by inserting discrete RC (or steel) shear key elements between the adjacent wall or floor panels, see Fig. 8b [21, 25].

Copyright © 2025 CroCEE
DOI: https://doi.org/10.5592/CO/3CroCEE.2025.59



a) b)

Figure 7. Prefabricated wall panels, "Potkovica" building in New Belgrade (HG-68 variant): a) interior wall panel and b) exterior wall panel [23]

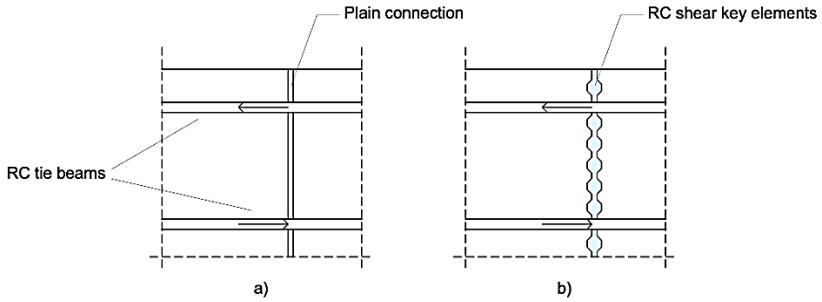


Figure 8. Vertical joints between adjacent wall panels: a) unreinforced shear keys and RC tie-beams at floor levels, JU-59 and JU-60 variants [24] and b) reinforced concrete shear keys, JU-61 and later variants [21]

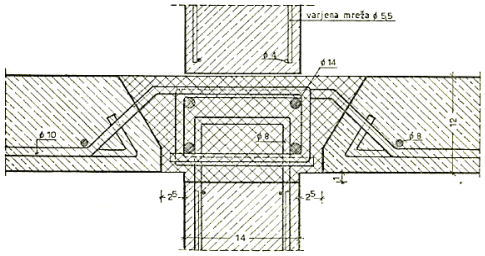


Figure 9. Horizontal joints – vertical section through a wall-to-floor panel joint, showing cast in-situ RC tie-beam, JU-61 [20]

4.3.Structural/seismic design philosophy

Reported case studies on the Jugomont applications for building construction in the 1960s and 1970s are invaluable for understanding the seismic design methodology for these buildings [20, 23]. Seismic design loads were determined according to the 1964 Yugoslav seismic design code [26], which was enforced at the time of original construction, but did not contain specific seismic design provisions for prefabricated concrete structures. Internal seismic forces in a building were determined according to the equivalent static analysis procedure. Distribution of shear forces to individual walls was performed in proportion to their relative stiffnesses, considering both flexural and shear effects [23]. The effect of spandrel beams was ignored (a cantilever model was used for the analysis).

Copyright © 2025 CroCEE
DOI: https://doi.org/10.5592/CO/3CroCEE.2025.59

For the seismic design of the "Potkovica" building in New Belgrade, Serbia (constructed using a variant of the JU-61 system), seismic actions in longitudinal direction were solely resisted by the interior longitudinal walls, hence the contribution of exterior longitudinal walls in resisting seismic actions was ignored [23]. Since the exterior walls in that building had many openings and did not have spandrel beams, it was considered that they were rather flexible and would not be able to resist significant shear forces. Seismic shear forces in transverse direction were applied to all walls in proportion to their relative stiffnesses. It should be noted that earlier variants of the system (e.g. JU-59) did not have any longitudinal walls, which is considered a seismic deficiency since there is no lateral load resisting system for resisting seismic effects in that direction. Design of wall and floor panels was performed according to the Yugoslav design code for RC structures which was applicable at the time of construction and was based on the Allowable Stress Design approach.

Seismic design of panel connections is of particular interest since their integrity has a significant influence on the seismic behaviour and failure mechanisms for these buildings. The evidence related to the connection design and experimental proof testing is limited. It was reported that connections for the "Potkovica" building were designed according to the approach followed in the Soviet design practice, but the actual material properties were used in design calculations. It was also stated that the connections were tested experimentally and that the results confirmed a good agreement between the calculated design values and the experimental results [23].

4.4. Seismic behaviour and failure mechanisms of joints in wall panels

A lateral force-resisting system in an RC prefabricated panel building consists of vertical elements (walls), horizontal elements (diaphragms), and their connections. When these buildings are subjected to seismic loads, wall panels act as shear walls, and floor/roof slabs act as diaphragms. These diaphragms need to have sufficient strength and stiffness to permit rotation and deformation of the entire floor, hence connections between the slab panels need to be sufficiently strong. The diaphragms transfer lateral forces to wall panels through the connections at the interface between the diaphragms and wall panels.

Shear walls in these buildings need to resist seismic shear forces which are transferred from the diaphragms at each floor level, and transmit these forces and bending moments to the foundations. These shear walls are composed of prefabricated wall panels connected by means of horizontal joints at each floor level and vertical joints along the building height. Seismic behaviour and failure mechanisms for these buildings are significantly influenced by the integrity of panel connections. Seismic performance of prefabricated large panel buildings in the November 26, 2019 Durres, Albania earthquake is well documented [27].

A prefabricated RC shear wall is expected to perform like a cast-in-situ RC shear wall, provided that horizontal and vertical wall panel joints are sufficiently strong (Fig. 10a). However, when prefabricated RC shear walls have weak vertical joints between adjacent wall panels, a relative vertical slip may take place along the interface of adjacent wall panels, which may be subjected to rocking caused by overturning moments ("weak vertical joints") (Fig. 10b). Alternatively, when horizontal joints between the adjacent panels are weak, a horizontal (shear) slip may occur along the joints ("weak horizontal joints") (Fig. 10c).

Connections between adjacent wall panels in the Jugomont system are critical for transferring vertical shear forces along the joints (Fig. 11). As discussed earlier in this section, vertical panel joints were grooved along the panel height, and the voids were filled with grout/mortar (JU-59 and JU-60 variants) - this is similar to a plain surface connection (Fig. 8a). In subsequent variants of the system (e.g. JU-61), discrete shear keys were created along the vertical joints, and in some cases RC or steel elements were provided in these shear keys (Fig. 8b).

Copyright © 2025 CroCEE
DOI: https://doi.org/10.5592/CO/3CroCEE.2025.59

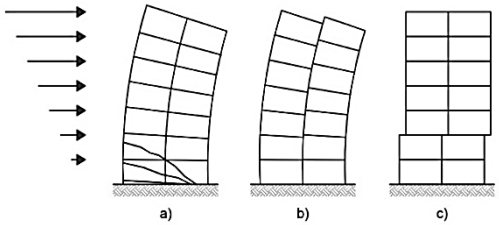


Figure 10. Seismic behaviour of RC structural walls composed of prefabricated wall panels: a) monolithic behaviour; b) weak vertical joints, and c) weak horizontal joints (based on [28])

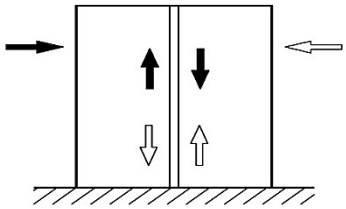


Figure 11. Lateral seismic forces and the corresponding internal vertical shear forces along a vertical joint between adjacent panels [29]

Structural behaviour of vertical connections in wall panels subjected to vertical shear forces depends on the connection type. A conceptual vertical shear force vs displacement (slip) relationship [29] shows differences in the capacity and displacements (slip) for a monolithic RC connection (cast in-situ wall), a plain connection of prefabricated panels (similar to the JU-59 and JU-60 variants), and a shear key connection (similar to JU-61 system) (Fig. 12). It is clear that a monolithic connection is characterized by the largest capacity and smallest displacements, while plain and shear key connections are expected to experience significantly larger displacements. It is also expected that the capacity of a shear key connection is going to be significantly larger than a plain connection.

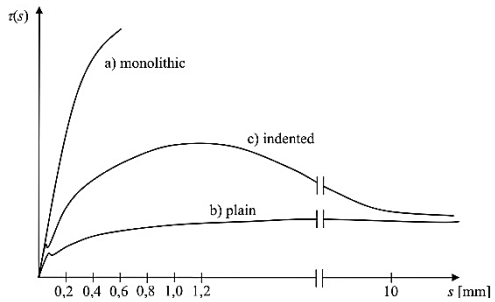


Figure 12. Vertical shear force versus displacement (slip) relationship for different RC panel connections [29]

Structural behaviour of RC wall panel connections with shear keys subjected to monotonic shear loading has been studied for more than 50 years. An early study on the structural behaviour and shear capacity of a shear key connection was performed by Cholewicki [30], who considered a shear key connection along the panel height and horizontal (longitudinal) reinforcement in RC tie-beams at floor levels. There are two distinct phases of progressive failure of the connection (Phase I and Phase II) (Figure 13). Initially, a shear key connection is very stiff, and adhesion between the panel surface and grout effectively transfers shear stresses between the panels (Phase I). With an increase in the applied shear force, cracking takes place at the interface between the panel and the grout, resulting in relative slippage (this is referred to as splitting). Once the slippage commences along the vertical cracks (Phase IIa), the shear is transferred by means of shear friction through horizontal reinforcement in RC tie beams. Finally, diagonal cracks occur across the shear keys and are aligned in the direction of principal stresses within a shear key (Phase IIb). At that stage, the connection is expected to attain the ultimate resistance.

Copyright © 2025 CroCEE
DOI: https://doi.org/10.5592/CO/3CroCEE.2025.59

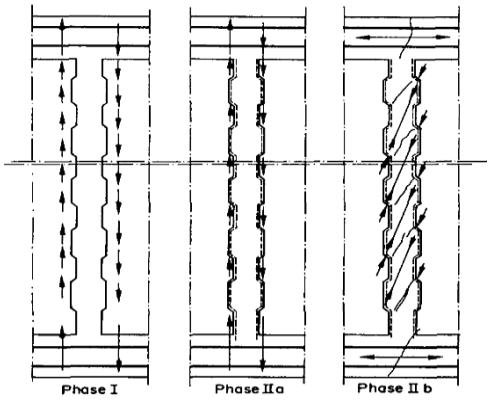


Figure 13. Progressive failure of a shear key connection between adjacent prefabricated RC wall panels [30]

Experimental studies on RC panel specimens with different configurations of shear key connections and a plain surface connection were performed by Rizkalla et al. [31] and Foerster, Rizkalla, and Heuvel [32]. Based on the experimental results, the authors proposed a shear force versus displacement (slip) relationship for a shear key connection (Fig. 14). The authors also proposed equations for estimating the capacities of the connection at critical stages (cracking, maximum, and ultimate).

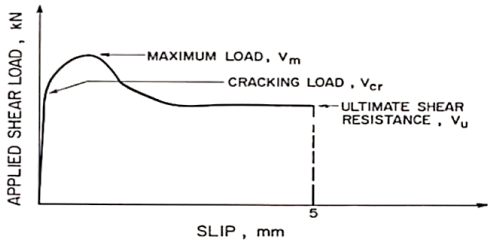


Figure 14. Vertical shear force versus displacement relationship for a shear key connection in a wall panel [31]

The experimental results showed a significant effect of the type of connection on the capacity of panel connections based on the testing of 7 large-scale specimens [31] (Fig. 14). A shear key arrangement (large versus small shear keys) did not have a significant effect on the connection performance: specimen 1LK2 (with large shear keys) demonstrated a similar performance like specimen 2SK2 (with small shear keys). The effect of compression stress perpendicular to the connection was significant: specimen 1LK2 (subjected to 2 MPa compression) attained a significantly lower maximum capacity than specimen 2LK4 (subjected to 4 MPa compression).

Horizontal connections between wall panels are critical for maintaining their integrity under lateral seismic loads. The following three types of failure mechanisms are possible for RC panels subjected to combined effects of lateral seismic forces and gravity loads (Fig. 15): a) shear sliding failure along a horizontal panel joint, b) flexural tensile failure, characterized by tensile deformations, and possibly a failure of vertical reinforcement within tensile zone of the connection, and c) flexural compression failure, characterized by high compression stresses and crushing of concrete within the compressed wall end zone.

These failure mechanisms may be possible in the context of buildings constructed using the Jugomont system. A sliding failure mechanism along horizontal panel joints may develop when shear friction resistance, contributed by vertical reinforcing bars and frictional resistance along the mortar interface, is not adequate to resist the applied seismic loads. Shear friction resistance along interfaces in RC structures is well established, and can be estimated according to design codes for RC structures, e.g. Eurocode 2 [33].

Copyright © 2025 CroCEE
DOI: https://doi.org/10.5592/CO/3CroCEE.2025.59

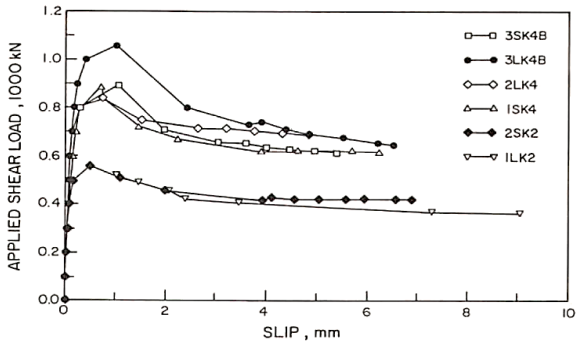


Figure 14. Experimental results for vertical shear force versus slip response for six wall panel connections with different shear key arrangements [31]

A flexural tension failure of the wall panels in the Jugomont system is governed by tensile resistance provided by extended vertical reinforcing bars, which were welded at the construction site (at the assembly stage). Given the small size and number of extended bars at wall panel ends, it is expected that their tensile capacity is relatively small. On the other hand, quality of field welding may be deficient in some cases (and is difficult to determine after the construction has been completed). When a prefabricated RC shear wall is subjected to significant overturning moments induced by seismic actions, either a reinforcing bar fracture or weld failure may take place.

Finally, a flexural compression failure could take place in prefabricated RC shear walls due to large seismic overturning moments, which may induce crushing of compressed concrete at the wall base (toe). This mechanism may be possible in prefabricated RC shear walls in buildings constructed using the Jugomont system, especially given a relatively small concrete compressive strength and a small wall thickness (14 -16 cm).

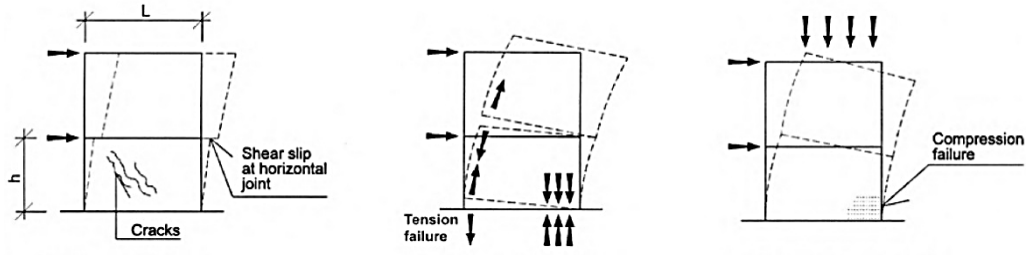


Figure 15. Failure mechanisms for horizontal panel connections: a) shear slip along a horizontal joint; b) flexural tension failure, and c) flexural compression failure (based on [24]).

5. Conclusions

Prefabricated RC buildings constitute a significant fraction of the existing building stock in urban areas of Eastern European and Central Asian countries. Majority of these buildings were constructed using prefabricated RC panel systems during the post-WWII period. Jugomont system was one of the most popular prefabricated RC panel systems in former Yugoslavia, hence there are many existing buildings constructed using that system in the region.

Some of the buildings constructed using “Jugomont” system are located in areas characterized by moderate to high seismic hazard, especially in urban areas of Croatia and Slovenia. In order to assess seismic risk associated with these buildings it is necessary to understand the original architectural and structural/seismic design concepts. Possible failure mechanisms of these structures due to seismic actions are generally well established. It is possible to quantify characteristic force versus displacement response for panels and their connections, and the corresponding acceptance criteria needed for seismic assessment of these buildings. Challenges associated with numerical modelling of these structures are associated with input parameters such as mechanical characteristics of panel materials and their

Copyright © 2025 CroCEE
DOI: https://doi.org/10.5592/CO/3CroCEE.2025.59

connections. Particular challenge is associated with the behaviour of connections under seismic actions, given that available experimental studies related to structural response of panel connections subjected to monotonic and especially reversed cyclic loading are extremely scarce. Comprehensive analytical studies, considering numerical models or prefabricated RC walls with variable mechanical properties of construction materials and connection types, are needed in the context of seismic risk assessment for urban building portfolios.

References

[1] Towards A Concrete Utopia: Architecture in Yugoslavia, 1948-1980, MoMA Museum of Modern Art, New York USA, Version: https://www.moma.org/calendar/exhibitions/3931 (accessed December 27, 2024)

[2] Nikolić-Brzev, S., Marinković, M., Milićević, I. & Blagojević, N. (2020). Posledice zemljotresa u Albaniji od 26.11.2019. na objekte i infrastrukturu (Consequences of the November 26, 2019 Albania earthquake on the buildings and infrastructure), *Serbian Association for Earthquake Engineering* (SUZI-SAEE), Belgrade, Serbia (in Serbian), 80 p. (ISBN 978-86-7466-843-6)

[3] Andonov, A., Baballëku, M., Baltzopoulos, G., Blagojević, N., Bothara, J., Brûlé, S., Brzev, S., ... & Veliu, E. (2022): EERI earthquake reconnaissance team report: M6.4 Albania Earthquake on November 26,2019,Version: http://learningfromearthquakes.org/images/earthquakes/2019_Albania_Earthquake/EERI_Earthquake_Reconnaissance_Report_-_M6.4_Albania_Earthquake_on_November_26_2019.pdf

[4] Frampton, K. (2020): *Modern Architecture: A Critical History*. Thames & Hudson 5th Edition, New York, USA.

[5] Le Corbusier (1973): *The Athens Charter*. Grossman Publishers. New York, USA.

[6] Blagojević, Lj. (2007): *Novi Beograd: Osporeni modernizam*. Zavod za udžbenike, Arhitektonski fakultet Univerziteta, Zavod za zaštitu spomenika, Beograd, Srbija.

[7] Blagojević, Lj. (2005): Back to the future of New Belgrade: Functional past of the modern city, *AESOP 2005 Annual Congress The Dream of a Greater Europe*, Vienna, Austria, 8 pages.

[8] Jovanović, J., Grbić, J., Petrović, D. (2012): Prefabricated Construction in Former Yugoslavia. Visual and Aesthetic Features and Technology of Prefabrication, Version: https://www.academia.edu/1985956/Prefabricated_Construction_in_Former_Yugoslavia_Visual_and_Aesthetic_Features_and_Technology_of_Prefabrication (accessed December 07, 2024)

[9] Mrduljaš, M. (2012): Architecture and urban planning in the former Yugoslavia and the successor states, In *Unfinished Modernisations – Between Utopia and Pragmatism*, ed. Maroje Mrduljaš and Vladimir Kulić, Zagreb, Croatia.

[10] Damljanović Conley, T., Jovanović, J. (2012): Belgrade residential architecture 1950-1970, A privileged dwelling for a privilege-free society, In *Unfinished Modernisations – Between Utopia and Pragmatism*, ed. Maroje Mrduljaš and Vladimir Kulić, Zagreb, Croatia.

[11] Jovanovi, J. (2017): Mass Heritage of New Belgrade: Housing Laboratory and So Much More. *Periodica Polytechnica Architecture*, **48** (2), doi: https://doi.org/10.3311/PPar.11621

[12] Jovanović, J., Grbić, J., Petrović, D. (2012): Prefabricated construction in socialist Yugoslavia from 'system' to 'technology', In *Unfinished Modernisations – Between Utopia and Pragmatism*, ed. Maroje Mrduljaš and Vladimir Kulić, Zagreb, Croatia.

[13] Fototeka stanova Centralna zona Novog Beograda II (1979), Centa za stanovanje IMS, Version https://drive.google.com/file/d/1YxT0TdPv-3guHI4aOUbY20WBLAT1OyJY/view (accessed December 15, 2024)

[14] Glavički, M. (1971): Urbanistička koncepcija bloka 28. *Izgradnja*, **5**, 12-16.

[15] Mecanov, D. (2015): Sustav prefabricirane gradnje Jugomont iz Zagreba: Zgrada 'Potkovica' u bloku 28 u Novom Beogradu. *Prostor* **1** (49), UDK 721.013:69.002.2 (497.5, 497.11, Beograd)

Copyright © 2025 CroCEE
DOI: https://doi.org/10.5592/CO/3CroCEE.2025.59

[16] Docomomo Srbija (2003): Stambena zgrada u obliku potkovice, blok 28, šifra RES-RS-011-b-0005, Novi Beograd, Version: http://www.docomomo-serbia.org/code/uploads/2018/03/13-RES-RS-011-b-0005-Blok-28-NBG-Potkovica-SR.pdf (accessed December, 15, 2024)

[17] Google Maps (n.d.): Block 28, New Belgrade, Serbia. Retrieved: January 27, 2025.

[18] Arnautović, I. (1971): Objekti u bloku 28 građeni po montažnom sistemu. *Izgradnja*, **5**, 17-29.

[19] Knežević, G. and Kordiš, I. (1972): *Stambene i javne zgrade*. Tehnička Knjiga, Zagreb, Croatia.

[20] Majaron, B. (1966): Prvi montažni stanovanjski blok v Mariboru (The first block of flats built of precast units in Maribor). *Gradbeni vestnik*, **15** (6-7), 137-142.

[21] Šavor Novak, M., Uroš, M., Demšić, M., Jevtić Rundek, R., Pilipović, A., and Atalić, J. (2024): Detailed Structural Typology of Existing Substandard Masonry and Reinforced Concrete Buildings in the City of Zagreb, Croatia. *Buildings*, **14** (11), 3644, doi: https://doi.org/10.3390/buildings14113644

[22] Vlak, N. (1971): Projektovanje i gradnja stambenog bloka 28. *Izgradnja*, **5**, 4-11.

[23] Gendelman, L. B. (1971): Konstruktivna rešenja stambenih zgrada Bloka 28. *Izgradnja*, **5**, 47-54.

[24] BCA (2001): *Structural Precast Concrete Handbook*, Building and Construction Authority, Singapore.

[25] Jevtić-Rundek, R. et al. (2024): Failure Mechanism and Load Bearing Capacity of a Typical Pre-Code Wall Panel System. *Proceedings of the 18th World Conference on Earthquake Engineering*, Milan, Italy.

[26] PTP-12 (1964): PTP-12 Privremeni tehnički propisi za građenje u seizmičkim područjima (Provisional Technical Regulations for Construction in Seismic Regions). Yugoslav Institute for Standardization, *Official Gazette of SFRY No. 39/64*. Belgrade, Yugoslavia.

[27] Guri, M., Brzev, S., Lluka, D. (2021): Performance of Prefabricated Large Panel Reinforced Concrete Buildings in the November 2019 Albania Earthquake. *Journal of Earthquake Engineering*, **26** (11), 5799-5825, doi: https://doi.org/10.1080/13632469.2021.1887010

[28] UNIDO (1983): Design and construction of prefabricated reinforced concrete frame and shear-wall buildings. Building Construction Under Seismic Conditions in the Balkan Region. Volume 2. *UNDP/UNIDO Project RER/79/015*, Vienna.

[29] FIB (2008): Structural connections for precast concrete buildings. *Bulletin 43*, International Federation for Structural Concrete (fib), Lausanne, Switzerland.

[30] Cholewicki, A. (1971): Loadbearing Capacity and Deformability of Vertical Joints in Structural Walls of Large Panel Buildings, *Building Science*, 6 (4), 163-184, doi: https://doi.org/10.1016/0007-3628(71)90009-0

[31] Rizkalla, S.H., Serrette, R.L., Heuvel, J.S. and Attiogbe, E.K. (1989): Multiple Shear Key Connections for Precast Shear Wall Panels. *PCI Journal*, **34** (2), 104-120, doi: https://doi.org/10.15554/pcij.03011989.104.120

[32] Foerster, H.R., Rizkalla, S.H., Heuvel, J.S. (1989): Behavior and Design of Shear Connections for Loadbearing Wall Panels. *PCI Journal*, **34** (1), 102-119, doi: https://doi.org/10.15554/pcij.01011989.102.119

[33] EN 1992-1-1 (2004): Eurocode 2: Design of concrete structures - Part 1-1: General rules and rules for buildings. European Committee for Standardization, Brussels, Belgium.

Proceedings of the 3rd Croatian Conference on Earthquake Engineering - 3CroCEE
19–22 March 2025, Split, Croatia
Copyright © 2025 CroCEE
DOI: https://doi.org/10.5592/CO/3CroCEE.2025.64

PREDICTION OF MASONRY STRENGTH AND EARTHQUAKE CHARACTERISTICS USING MACHINE-LEARNING ALGORITHMS

Karl Deix [(1)], Branko Rusnov [(2)]

[(1)] *Ass. -Prof., Techn. Universität Wien, karl.deix@tuwien.ac.at*
[(2)] *Ingenieurkonsulent für Bauwesen, branko.rusnov@rusnov.at*

Abstract

„Gründerzeit houses“ in Vienna/Austria, which were built between 1848 and 1918, are an essential part of the Viennese building infrastructure with a number of approx. 30,000. Since 1992, the masonry properties of over 200 buildings with over 2,000 test positions have been determined and evaluated by the authors. These were determined in the context of the engineering expertise in order to carry out the load-bearing capacity and earthquake verifications for the refurbishment.

Based on the results of the investigations, a comprehensive data set was created containing the coordinates of the buildings, district, construction period, use, building type, number of storeys, type of test, moisture, compressive strength of the brick and mortar, compressive strength of the masonry, etc. This data set contains approx. 40,000 independent numerical and categorical values.

This data set is analysed for clusters and correlations using machine learning algorithms. Among others, the unsupervised learning algorithms “Hierarchical Clustering”, “k-means” and the dimension-reducing algorithm “t-SNE” are used. The correlations found are statistically evaluated and visualized. The most important results will be presented.

In the second part, various prediction models based on machine learning algorithms are used to predict the masonry strengths of existing objects as well as the earthquake resistance according to Eurocode 8. The algorithms used include “neural networks”, “random forest”, “k-nearest neighbours”, etc. With regard to the earthquake resistance, shear-tables are used, with which the compliance factor can be quickly specified using a few building parameters, such as the number of storeys, the floor plan shapes and the ground parameters. These values are calibrated with “push-over” calculations for different building geometries and are thus incorporated into the prediction models. The aim is to find and compare data-based models in order to enable an evaluation of all Viennese “Gründerzeit” buildings with regard to the expected strengths and earthquake values.

Keywords: ***earthquake, machine learning, Vienna, prediction, Gründerzeit houses***

1. Introduction

The period from 1848 to 1918 is referred to as the Viennese Gründerzeit. The buildings were erected using specific construction principles in solid brickwork with thicknesses of 30 to 115 cm as main walls and slabs as wood constructions where the partition walls (18 - 22 cm with plaster) go through without contact with slabs.

The publicly accessible building information of the City of Vienna [1] can be used to determine the number and exact location as well as other characteristics of all buildings in Vienna. The large number of around 30,000, which accounts for 46.5 % of all Viennese buildings, shows the intense building activity at the time. Fig.1 show the location of the buildings depending on the construction period in Vienna.

Copyright © 2025 CroCEE
DOI: https://doi.org/10.5592/CO/3CroCEE.2025.64

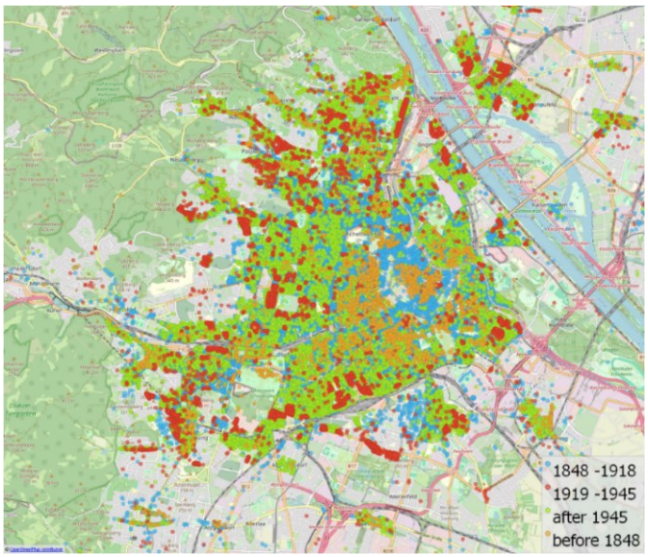


Figure 1. Location of buildings by construction period using Openstreetmap and [1].

2. Materials and Methods

2.1. Masonry examination

Until 2016, component testing based on mortar and brick samples was common practice. Pieces of bed joint mortar about the size of the hand, which were leveled with plaster on both sides, were tested in a compression test using a round stamp d = 25 mm or a square stamp 40 x 40 mm. The conversion to the standardized mortar strength was carried out according to [2]. The bricks were also tested in a compression test in accordance with ÖNORM EN 772-1 [3] after the appropriate grinding or adjustment with cement mortar. For the standardized brick compressive strength, a shape factor that takes into account the brick width and height was used.

The disadvantage of component testing is that relatively large holes in the masonry have to be created, which may reduce the stability of the building. Since 2013, the long-established penetration method [4] has therefore also been used for mortar testing in accordance with ÖNORM B 1996-3 [5]. On a 40 cm × 40 cm wall surface, a wedge-shaped cutting edge is struck into the joint mortar using a test hammer and the penetration depth between the first and tenth strike is measured (Fig. 2). The test hammer type L is used, which has a lower impact energy of 0.735 Nm. The measured value in mm is multiplied by 8 as a reciprocal value, resulting in the penetration strength f_E of the mortar, which is converted to the mortar compressive strength f_m in the second step in accordance with [4]. The compressive strength of the brick is determined - analogous to the concrete test - with the rebound hammer type N on the already exposed brick surfaces and converted to the standardized compressive strength of the brick f_b. The two tests are carried out ten times per sample location and the mean value and the standard deviation are determined.

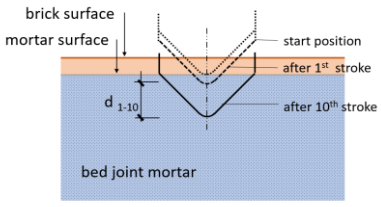


Figure 2. Penetration method with the hammer type L.

Proceedings of the 3rd Croatian Conference on Earthquake Engineering - 3CroCEE
19–22 March 2025, Split, Croatia
Copyright © 2025 CroCEE
DOI: https://doi.org/10.5592/CO/3CroCEE.2025.64

The characteristic compressive strength of the masonry f_k is calculated according to ÖNORM B 4008-1 [6] using the formula Eq. (1) based on the compressive strength of the brick and mortar.

$$f_k = 0.80 \cdot 0.60 \cdot f_b^{0.65} \cdot f_m^{0.25} \quad (1)$$

f_k … characteristic compressive strength of the masonry in MPa.

f_b … standardized compressive strength of bricks in MPa

f_m … compressive strength of the masonry mortar in MPa

2.2. Earthquake values

The seismic safety of existing buildings from the Gründerzeit is verified according to the currently applied standards ÖNORM EN 1998-3:2013 [7] and ÖNORM B 1998-3:2018 [8]. In accordance with ÖNORM B 1998-1:2017 [9], the expected seismic risk is specified according to the zone map with the reference ground acceleration of a_{gR} = 0.80 m/s^2. Furthermore, the ground classes are essential for the seismic design according to ÖNORM EN 1998-1:2013, whereby in Vienna those with B and C are available. This results in the corresponding response spectrum for the ground.

The 'limit state of significant damage (SD)' according to ÖNORM B 1998-3:2018 is decisive for the design in Austria, whereby the relevant damage mechanisms for existing, unreinforced masonry structures are 'components subjected to bending and longitudinal force' and 'components subjected to shear stress' under consideration of the respective applicable limit state. ÖNORM B 1998-3:2018 [8] introduces the compliance factor 'α' in Annex A as the quotient of design resistance and design earthquake action, where $\alpha = R_d/E_d$. R_d is the design resistance, expressed in terms of force, acceleration or displacement, and E_d is the design earthquake action. The compliance factor α is of central importance and must be greater than or equal to 1.0 for new buildings. As this value cannot be achieved for many older buildings, especially those without shear-resistant ceiling systems, it is at least 0.25 for Gründerzeit buildings. Furthermore, the partition walls extend through the ceilings up to the last storey, whereby these are connected to the centre wall and the outer wall in every third or fourth brick, so that the failure of these shear walls is 80 % decisive.

The "pushover" method, which is based on the N2 method with the inelastic response spectra approach, is mainly used to perform the stability check. The pushover calculation is carried out under constant weight loads and monotonically increasing horizontal forces.

In [10] shear-tables are described that specify α_{min} for different numbers of storeys (building heights), the effective wall lengths as a function of the ground classes. This is based on investigations into the masonry parameters, number of storeys, wall lengths, influenced areas and ground classes, which were analysed in parameter studies.

The single wall systems are considered to be simple, vibration-capable systems due to the predominantly shear-soft floor systems in the form of tram and dippler beam floors. In the overall system, each shear wall is stressed in the respective building direction (transverse and longitudinal direction of the building) based on its spatial geometric area of influence in the design case earthquake, whereby a failure of the weakest shear wall implies a failure of the entire building. Due to the shear-soft floor systems, the earthquake-induced action is not assigned to the stiffening shear walls in proportion to their stiffness, but rather in proportion to their area.

Copyright © 2025 CroCEE
DOI: https://doi.org/10.5592/CO/3CroCEE.2025.64

The α-values do not change by varying the material parameters ($f_{b,k}$ and $f_{m,k}$) for partition walls, but only for load-bearing outer and centre walls and solid fire walls. Furthermore, the mean values of the component strengths have an influence on the masonry strength, the initial bond shear strength and the stiffness properties in the uncracked and cracked state. This shear-table shows the following value ranges for the number of storeys 3, 4 and 5 for different ground vailues and depending on the wall length:

3 storeys: B: 0.36-0.38, C: 0.31-0.33

4 storeys: B: 0.47, C: 0.40-0.41

5 storeys: B: 0.59-0.61, C: 0.48-0.51

The layout of the Viennese Gründerzeit houses is also essential for the assessment. These can be reduced to four main types according to [11]. These are: W3.1: single line house, W3.2: side wing house, W3.4: doubled sided house with court and W3.7: corner house. A total of six pushover-calculations were carried out using 3muri [12] and the compliance factor α was calculated and the failure mode specified. Fig. 3 shows the buildings, the calculated compliance factor α and the reason for the failure for the 4 different types.

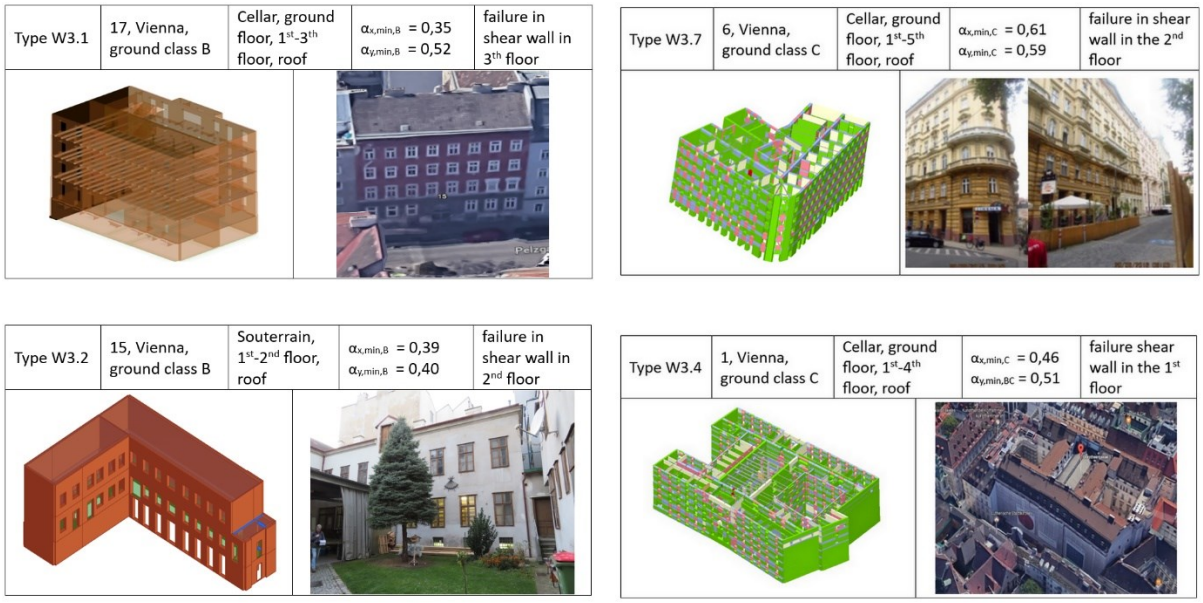


Figure 3. Results of pushover-calculations for 4 different types.

There are different ground categories (B and C), the failure occurred due to the yielding of the shear-stressed partition wall in different storeys, in one case (not in Fig. 3) in the external walls due to bending. The results were included in the calculations according to chapter 5.

2.3. Creation of the data set

Examination reports are available for 207 buildings with 2,054 examination points that were examined using the two methods described. These were used to create the data set described in Table 1. The classification into “type” and “role” required for machine learning and the range of values are also listed.

Proceedings of the 3rd Croatian Conference on Earthquake Engineering - 3CroCEE
19–22 March 2025, Split, Croatia
Copyright © 2025 CroCEE
DOI: https://doi.org/10.5592/CO/3CroCEE.2025.64

Table 1. Description of the dataset

No.	Name	Source	Type	Role	Values
1	Object		text	meta	
2	District	BIV *1)	categorical	feature	1-23
3	Location - Longitude	BIV *1)	numeric	feature	16.2642 - 16.4555
4	Location - Latitude	BIV *1)	numeric	feature	48.1351 - 48.2770
5	Building type Use	BIV *)1 BIV *1)	categorical	feature	W3.1, W3.2, W3.4, W3.7
6	Number of storeys above basement	BIV *1)	categorical	feature	2-6
7	Date of examination	measurement	date	feature	2013 - 2022 1992 - 2017
8	Examination storey	measurement	categorical	feature	Cellar, ground floor, 1st to 5th floor,
9	Position of the wall	measurement	categorical	feature	Exterior wall on the courtyard side (awh), street side (aws), middle wall (mw), firewall (fm), supports (st)
10	Used examination method	measurement	categorical	feature	Plaster window and component testing
11	Standardized brick strength f_b - Medium	measurement	numeric	feature	7.55 - 45.2
11	Standardized brick strength f_b - Standard deviation		numeric	feature	0 - 12.0
12	Standardized mortar strength f_m - Medium	measurement	numeric	feature	0.44 - 5.11
13	Standardized mortar strength f_m – Standard deviation	measurement	numeric	feature	0.03 - 1.26
14	Masonry strength f_k	calculated	numeric	feature, target	1.70 - 8.08
15	Medium standard brick strength $f_{b\text{-}m}$	calculated	numeric	feature, target	10.3 - 30.0
	Medium mortar strength $f_{m\text{-}m}$	calculated	numeric	feature, target	0.79 - 3.3
13	$\alpha_{y,min,B}$	Shear-tables	numeric	target	0.28 - 0.69
14	$\alpha_{x,min,B}$	Shear-tables	numeric	target	0.35 - 1.34
15	$\alpha_{y,min,C}$	Shear-tables	numeric	target	0.20 - 0.59
16	$\alpha_{x,min,C}$	Shear-tables	numeric	target	0.21 - 1.18

*1) Building information Vienna according to [1]

3. Exploratory Data Analysis (EDA)

The data is analysed with Python scripts using the Python-based open-source software environment SciPy [14] and "Orange" [15]. Orange is a toolkit for data visualization, machine learning and data mining. In the first step, a "Hierarchical Clustering Analysis" was carried out to identify and exclude rare attributes that are not representative, such as very high brick and mortar compressive strengths (originating from clinker bricks and cement mortar).

In the next step, the t-disseminated stochastic neighbourhood implantation (t-SNE) was used for data analysis. This is a dimension-reducing, probabilistic method. Similar data are displayed together as a cluster.

Copyright © 2025 CroCEE
DOI: https://doi.org/10.5592/CO/3CroCEE.2025.64

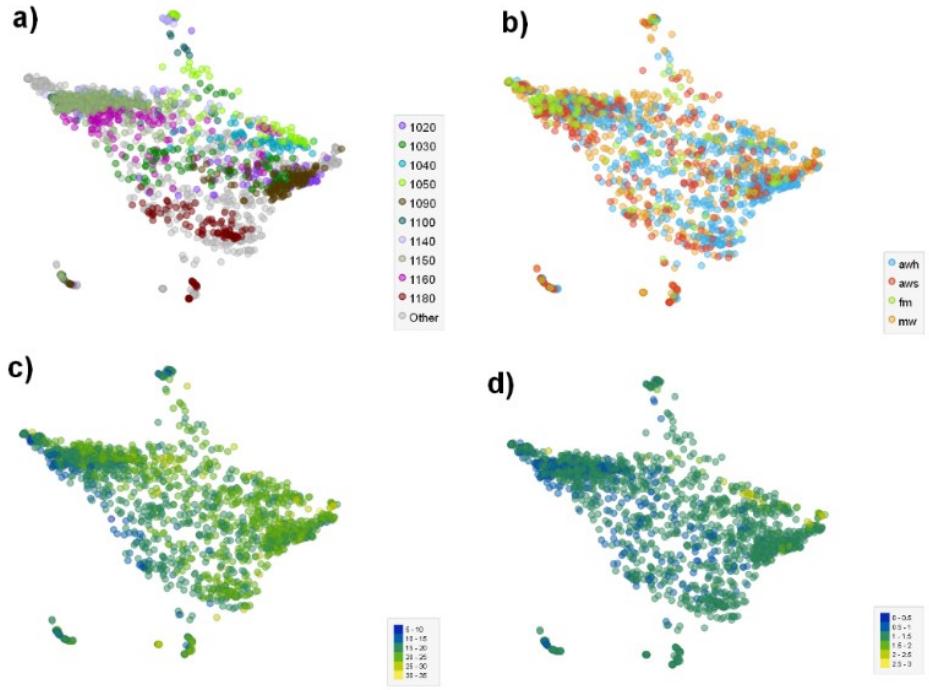


Figure 4. t-SNE analyse: a) district; b) position of the wall; c) strength of the bricks; d) strength of the mortar.

Fig. 4 show some examples of the results. In summery the calculations showed that the strength of the wall components barely depends on the floor under investigation and the location of the wall in the house. Furthermore, the geographical location, the district and the number of storeys had little influence. However, the construction period, the building type and in particular the test method used are significant.

4. Statistic Results of bricks and mortar

The correlations found in chapter 3 using machine learning algorithms are analyzed below. An important statement for the seismic and structural analysis is the strength of the components depending on the position of the wall. Fig. 5 shows the determined brick and mortar compressive strengths grouped by storey, whereby the “violin plot” is used for graphical representation.

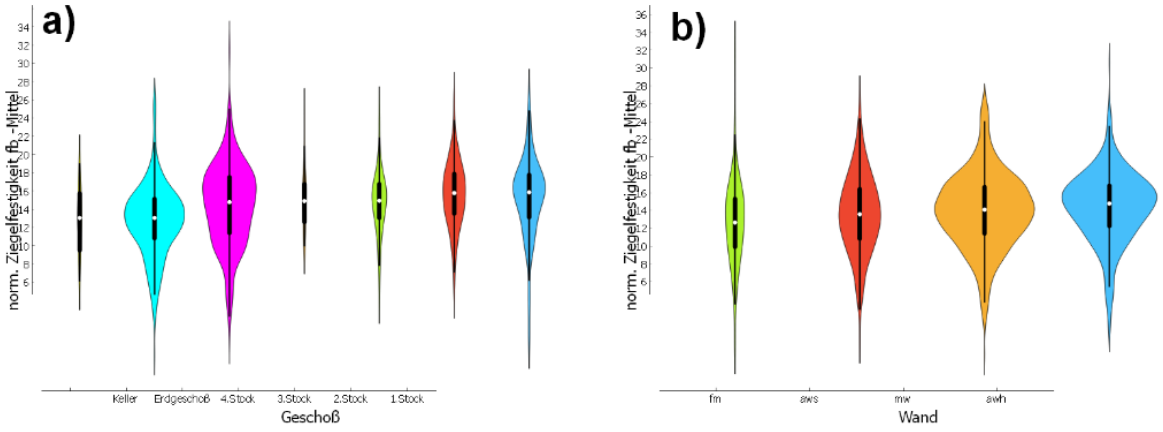


Figure 5. Brick strength according to a) storey and b) wall position.

Proceedings of the 3rd Croatian Conference on Earthquake Engineering - 3CroCEE
19–22 March 2025, Split, Croatia
Copyright © 2025 CroCEE
DOI: https://doi.org/10.5592/CO/3CroCEE.2025.64

The overall mean value for the standardised brick strength is 19.8 N/mm². At 18.9 N/mm², slightly lower compressive strengths were measured in the cellar and roof storey than in the other storeys at 20 to 21 N/mm², although there were no significant deviations between them. This is consistent with the experience that lower brick qualities were often used in the basement. In the attic, on the other hand, there is a very low ballast, which has an effect on the impact test.

The lower brick compressive strengths of the firewall are attributed to the comparatively low wall thickness and often poor quality of the workmanship, which is reflected in the empirical data. With a mean value of 1.18 N/mm², the mortar strengths show no significant deviations between the storeys, although it is to be expected that the basement has lower mortar compressive strengths due to moisture.

5. Results

5.1. General

The machine learning algorithms are divided into ‘unsupervised’, where no labels are available (see chapter 3), and ‘supervised’, where labels are available. The former are used for clustering and dimension reduction, the second for regression and classification. For the prediction of the masonry strength f_k, the average brick and mortar strength and the alpha-values, the following algorithms are used and tested.

Random forest builds a set of decision trees. Each tree is developed from a bootstrap sample from the training data. When developing individual trees, an arbitrary subset of attributes is drawn (hence the term "random"), from which the best attribute for the split is selected. The final model is based on the majority vote from individually developed trees in the forest [15].

Support vector machine (SVM) is a machine learning technique that separates the attribute space with a hyperplane, thus maximizing the margin between the instances of different classes or class values [15].

k-nearest neighbourhood (kNN) searches for k closest training examples in feature space and uses their average as prediction [15].

A neural network (NN) consists of layers of nodes: an input layer, one or more hidden layers, and an output layer. Each node connects to others, and has its own associated weight and threshold. If the output of any individual node is above the specified threshold value, that node is activated, sending data to the next layer of the network.

These algorithms allow variation of their hyperparameters, such as for neural networks the number of layers and neurons and the activation function, for kNN the number of neighbours, etc. These were varied accordingly to obtain the best results for the predictions with values such as mean square error (MSE), root means square errors (RMSE), mean absolute error (MAE) and coefficient of determination (R^2 - proportion of the variance in the dependent variable that is predictable from the independent variable), which were determined using cross validation, were evaluated. Furthermore, a visual evaluation is made based on the distribution in the Vienna map as well as the mean value and variance.

5.2. Masonry strength

K-Means [16] forms clusters from similar data points by optimizing the quadratic deviations between data points to a mean value (centroid). It was used with the feature “masonry strength”, which is calculated from the brick and mortar strength, and the coordinates to find zones with higher and lower

Copyright © 2025 CroCEE
DOI: https://doi.org/10.5592/CO/3CroCEE.2025.64

strength. Fig. 6 shows the clusters found with a selected number of 6. The colour assignment of the data points to the clusters is shown on the left and the centroids with the boundaries are shown on the right.

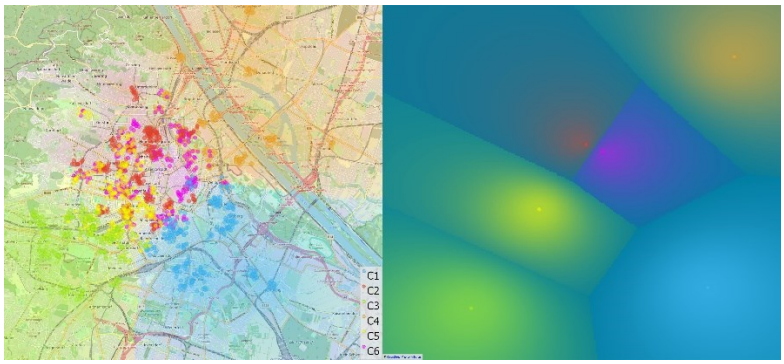


Figure 6. K-means: cluster and centroide.

The calculations show that certain areas with similar masonry compressive strength do exist, but are not very clear and the clusters also overlap. As an example, the 1st district should be mentioned: Here, there are high masonry qualities on representative, public buildings, whereas other buildings in the district "only" have medium masonry compressive strengths.

Based on the Vienna data, a second data set was created containing the following attributes of the approx. 25,000 Viennese Gründerzeit houses: Object with geographical location (longitude and latitude), district, number of storeys and building type. In the first step, the masonry strength was selected as the target criterion and the following models were used: neural network, kNN, SVM and random forest. Fig. 7 shows the results of the different methods in comparison.

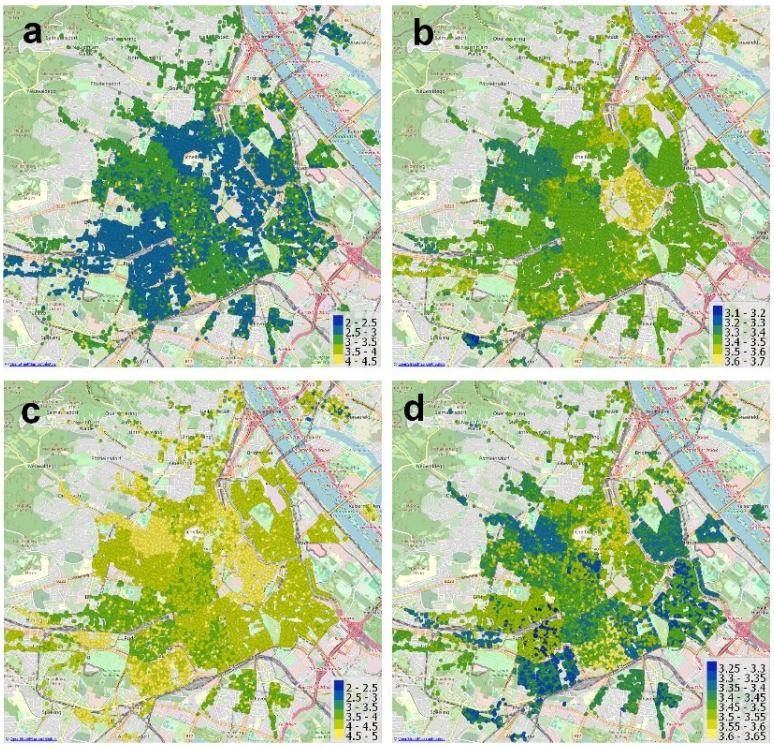


Figure 7. Prediction of f_k: a) neural network; (b) random forest; c) SVM; d) kNN.

Copyright © 2025 CroCEE
DOI: https://doi.org/10.5592/CO/3CroCEE.2025.64

Table 2. Results of the cross validation

No.	Model	MSE	RMSE	MAE	R^2
1	Neural network	0.015	0.123	0.089	0.916
2	Random Forest	0.061	0.248	0.172	0.661
3	Support vector machine	0.577	0.760	0.526	-
4	K nearest neighbourhood	0.019	0.137	0.103	0.896
5	Stack	0.018	0.133	0.096	0.902

Table 2 shows the cross validation of the different models, as described above. The best value is shown here by the neural network (MSE = 0.015), consisting of 4 hidden layers with 200 neurons each, the "tanh" -activation and the solver "Adam". kNN also shows good values (MSE = 0.019), slightly larger random forest (MSE = 0.061). A stack in the form of a combination of these three algorithms results in an MSE of 0.018. The SVM shows significantly larger values here and is therefore unusable. An examination of the distributions shows that these models enable a prediction of the masonry strength for all "Gründerzeit" houses with good probability. This is also due to the relatively large number (approx. 200) of test objects which accounts for approx. 0.8 % of all "Gründerzeit" houses and test points (> 2,000).

5.3. Prediction of masonry strength and the earthquake compliance factor α

The failure of a shear wall is assumed to be a failure of the entire building. The α values are available for 60 objects, which are used for predictions. The following four cases are presented as examples of the many results with the different algorithms and features:

For the case $\alpha_{x,min,B}$, Fig. 8a shows the predicted values using the neural network. Here, however, there are also smaller and larger values than specified, namely from 0.47 - 1.34 according to Table 1. Random forest, on the other hand, shows a smaller distribution that corresponds approximately to the target range. In the first case, however, $R^2 = 0.95$, and larger in the second case is only $R^2 = 0.85$.

For $\alpha_{y,min,C}$, which are the decisive values as they apply to the longitudinal direction of the buildings and are smaller, a range of 0.20-0.59 is given in Table 1. Random forest shows the distribution shown in Fig. 8c with all features and in Fig. 8d without the "district" feature ($R^2 = 0.96$). It can be seen that the district boundaries are less pronounced here. There is a better fit with random forest than with the neronal network ($R^2 = 0.78$).

Copyright © 2025 CroCEE
DOI: https://doi.org/10.5592/CO/3CroCEE.2025.64

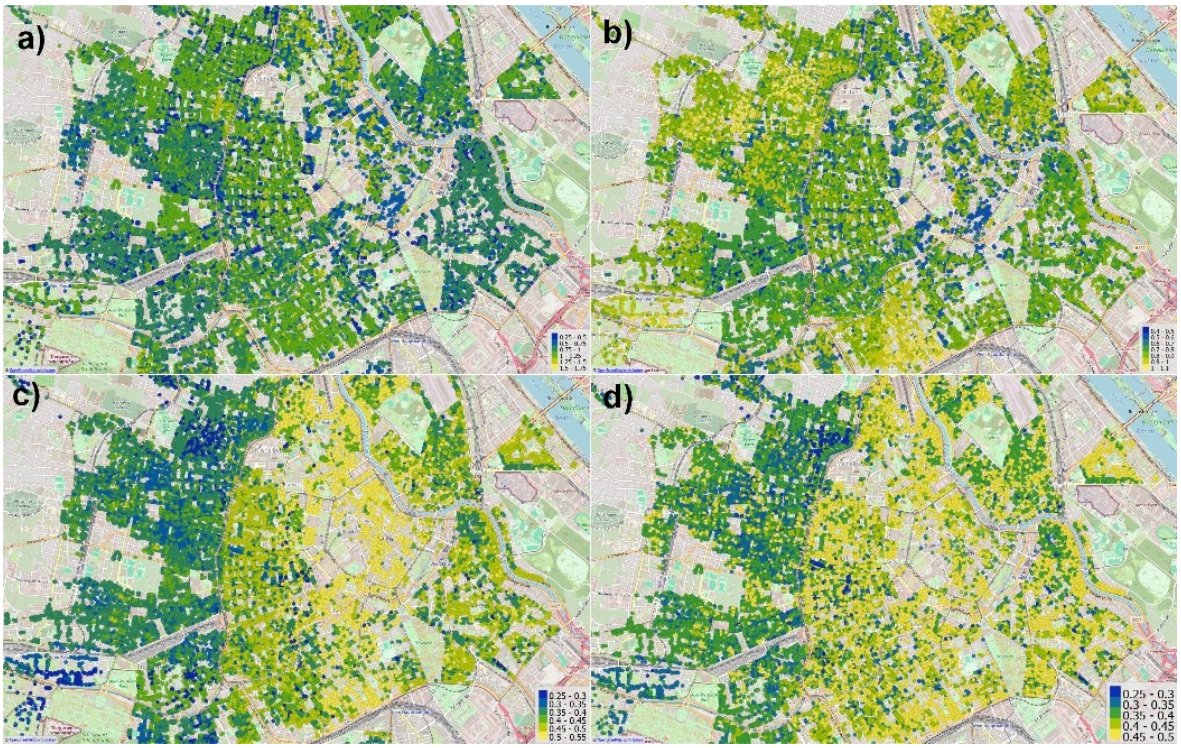


Figure 8. Prediction of α: a) $\alpha_{x,min,B}$ with neural network, b) with random forest; c) $\alpha_{y,min,C}$ with random forest with all features und d) without the features "district".

In summary, due to the smaller number of values determined using the pushover-methdo and shear-tables (60), the prediction shows greater variations and these vary depending on the features taken into account.

6. Summary

The calculations show that the dimension-reducing algorithms (t-SNE) can recognise the significant features very well by means of machine learning and can therefore be statistically evaluated.

Using cluster analyses (K-means), important results, such as the masonry strength, can already be assigned to geographical zones in the first step. Based on the prediction models used (kNN, NN, SVM, random forest), it is also possible to provide specific values for all 25,000 Gründerzeit houses. It is favourable that data from a large number of test objects (207) and test points (> 2,000) is available here. These results, together with other building data, can be used to evaluate the existing building structure and the expected renovation or reconstruction costs.

The compliance factor of 60 buildings was calculated using pushover calculations and shear-tables. However, as this depends on the number of storeys and the ground class, this only represents a small amount of data. This means that a good prediction with the uses algorithms is subject to greater uncertainties.

Copyright © 2025 CroCEE
DOI: https://doi.org/10.5592/CO/3CroCEE.2025.64

References

[1] Gebäudeinformation Wien, Datenquelle: Stadt Wien, https://data.wien.gv.at [accessed October 18, 2021].

[2] Undesch H. (1990): *Versuche zur Ermittlung der Druckfestigkeit von Mauermörtel nach unterschiedlichen Verfahren.* Diplomarbeit, Technische Universität Wien.

[3] ÖNORM EN 772-1: 2015 (2015): Prüfverfahren für Mauersteine – Teil 1: Bestimmung der Druckfestigkeit. Austrian Standards, Wien.

[4] Schmiedmayer, R., Pech, A. (1995): *Bestimmung der Festigkeit von Mauermörtel mittels Schlagversuchen: Grundlagenversuche zur Entwicklung eines In-Situ Prüfverfahrens*. Forschungsvorhaben H34/93, Technische Universität Wien.

[5] ÖNORM B 1996-3:2009 (2009): Eurocode 6: Bemessung und Konstruktion von Mauerwerksbauten - Teil 3: Vereinfachte Berechnungsmethoden für unbewehrte Mauerwerksbauten - Nationale Festlegungen und Ergänzungen zur ÖNORM EN 1996-3, Austrian Standards, Vienna.

[6] ÖNORM B 4008-1:2018 (2018): Bewertung der Tragfähigkeit bestehender Tragwerke Teil 1: Hochbau. Austrian Standards, Vienna.

[7] ÖNORM EN 1998-3:2013 (2013): Eurocode 8: Auslegung von Bauwerken gegen Erdbeben - Teil 3: Beurteilung und Ertüchtigung von Gebäuden, Austrian Standards, Vienna.

[8] ÖNORM B 1998-3:2013 (2013): Eurocode 8 - Auslegung von Bauwerken gegen Erdbeben - Teil 3: Beurteilung und Ertüchtigung von Gebäuden - Nationale Festlegungen zu ÖNORM EN 1998-3 und nationale Erläuterungen, Austrian Standards, Vienna.

[9] ÖNORM B 1998-1:2017 (2017): Eurocode 8: Auslegung von Bauwerken gegen Erdbeben - Teil 1: Grundlagen, Erdbebeneinwirkungen und Regeln für Hochbauten - Nationale Festlegungen zu ÖNORM EN 1998-1 und nationale Erläuterungen, Austrian Standards, Vienna.

[10] Karic, A., Sonnek, R., Deix, K., & Kolbitsch, A. (2023): *Nachbemessungsstrategie für gemauerte, gründerzeitliche Schubwände*. Bauingenieur, 98(1–2), 18–27. https://doi.org/10.37544/0005-6650-2023-01-02-46

[11] Rusnov, B. (2006): *Analyse von erdbebengefährdeten Bauwerken mit dem Schwerpunkt auf alten und historischen Gebäuden, Dissertation*. Technische Universität Wien.

[12] 3muri. Erdbebennachweis von Mauerwerk, www.ingware.com/de/produkte/3muri, (accessed November 10, 2024).

[13] Deix, K., Rusnov, B., Dzudzevic, E., & Huber, C. (2023): *Analyse von Mauerwerksuntersuchungen von Gründerzeithäusern in Wien*. Bautechnik,. https://doi.org/10.1002/bate.202300018

[14] *Scientific Python Scipy*, https://scipy.org, (accessed April 15, 2021).

[15] *Orange,* https://orangedatamining.com, (accessed April 15, 2021).

[16] MacKay D. (2003): *Information Theory, Inference and Learning Algorithms*. Cambridge University Press, ISBN 0-521-64298-1, Chapter 20. An Example Inference Task: Clustering, S. 284–292.

Proceedings of the 3rd Croatian Conference on Earthquake Engineering - 3CroCEE
19–22 March 2025, Split, Croatia
Copyright © 2025 CroCEE
DOI: https://doi.org/10.5592/CO/3CroCEE.2025.70

INTEGRATED NON-DESTRUCTIVE APPROACH FOR THE DIAGNOSIS OF HISTORIC MONUMENTS

Jasna Grujoska-Kuneska[(1)], Veronika Shendova[(2)]

[1] *PhD student, Institute of Earthquake Engineering and Engineering Seismology-Skopje, jasnagrujoska@yahoo.com*
[2] *Professor, Institute of Earthquake Engineering and Engineering Seismology-Skopje, veronika@iziis.ukim.edu.mk*

Abstract

As part of the tangible cultural heritage, historic buildings hold great importance for today's societies. These are buildings that have persisted for hundreds or thousands of years as visible witnesses of the past generations and their traditions, and as such deserve special attention and treatment.

A particular challenge is the protection of historical buildings located in seismic regions, where in addition to the climatic and human factors, these buildings are exposed to the effects of earthquakes, and so despite their visually good condition they exist today with many hidden weaknesses. Historic buildings respond to earthquakes, among other things, depend on the correct treatment and conservation practice. In order to achieve all that, a solid diagnostic study that will ensure an accurate assessment of its current condition is an essential prerequisite.

This paper presents the non-invasive methodology carried out to one Byzantine monument – the church of St. Nikita near Skopje, North Macedonia, using the available Non-Destructive Techniques (NDTs): visual inspections, microscopy, infrared thermography, 3D laser scanning and ambient vibration tests. The use of the above mentioned NDTs enabled to evaluate the current condition of the monument in a relatively short time without affecting its authenticity, which is especially significant for this type of buildings. Additionally, the use of the 3D laser scanner generated digital documentation of the monument, accessible at any time.

Keywords: tangible heritage, byzantine churches, conservation, diagnostic study, non-destructive techniques, digital documentation

1. Introduction

Cultural heritage, both tangible and intangible, holds great importance in today's societies, acting like a bridge that connects us to the past. It promotes our identity and can contribute to economic development, poverty reduction and sustainable development, [1].

Significant part of the cultural heritage in North Macedonia consists of historic buildings from different periods, which symbolize diverse cultures and people who lived before. Byzantine churches are among the most preserved and numerous monuments characterized by exceptional architectural and artistic values. These medieval monuments range from monumental basilica-type churches, conch and domed square-in-plane concepts, to small single nave churches, [2][3].

Many factors, such as urbanization, excessive tourism, climate changes, people's neglect and loss of traditional knowledge, affects this tangible heritage. Additionally, the vulnerability of historic buildings is greater in seismic prone regions as earthquakes pose a big treat to the stability of the buildings and may cause irreversible damage, [4].

The earthquake that struck Skopje in 1963 is one of the biggest natural disasters in the recent history of North Macedonia. With magnitude of 6.1 degrees (Richter scale) the earthquake caused minor to major damage to all cultural-historical buildings in Skopje and nearby. The buildings located in the old bazaar, dating from different periods (churches, mosques, baths, shops) were significantly damaged. Many Ottoman buildings (15th-16th centuries) were affected and few were almost entirely destroyed. The Byzantine churches (9th-14th centuries) also suffered some damages, [5].

Proceedings of the 3rd Croatian Conference on Earthquake Engineering - 3CroCEE
19–22 March 2025, Split, Croatia
Copyright © 2025 CroCEE
DOI: https://doi.org/10.5592/CO/3CroCEE.2025.70

Even with the technological advancements we cannot predict earthquakes, neither to reduce their intensity, [4] but what we can do is to take preventive measures to reduce the vulnerability and potential damages to the heritage buildings. The seismic performance of these buildings depends on many aspects, including the correct and professional treatment and conservation practice. In that perception, the diagnostic study that provides an accurate assessment on the building's condition and consequently suitable conservation measures is imposed as vital step in the long-term process of heritage protection, [6].

2. Representative Byzantine monument: St. Nikita church

The church of St. Nikita is a typical late Byzantine monument from 14th century with exceptional architectural, artistic and historic values. It is located outside the city of Skopje, on the slopes of Skopska Crna Gora in the village of Banjani. Typologically, the church belongs to group cross-in-square plans with a single-dome, which is one of the most common typology in the country. The church contains two main clearly defined units: the central naos and an altar area, without narthex. Structural system consists of massive facade walls and columns (in the interior) that support the vaulted roof elements and the central dome. Different types of stones (mainly limestone and sandstone), bricks and lime mortar were used in the construction of the building. Special attention is paid to the construction of the facades, using three dimensional polychrome, shallow niches and pilasters, (fig. 2.1). The pentagonal apse, on the east side, is visually enriched with double niches with brick arches. The interior surfaces of the church are plastered and painted with frescoes, preserved on a larger scale, (fig. 2.2). The original frescoes, from 14th century, symbolize the rich artistic Byzantine life which adds up to the artistic values of the monument, [2][7].

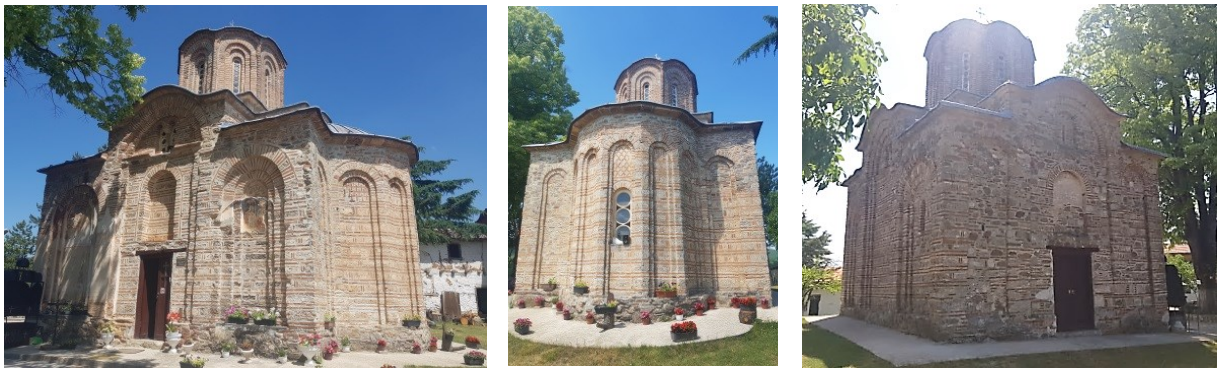


Figure 2.1 Facades of St. Nikita church

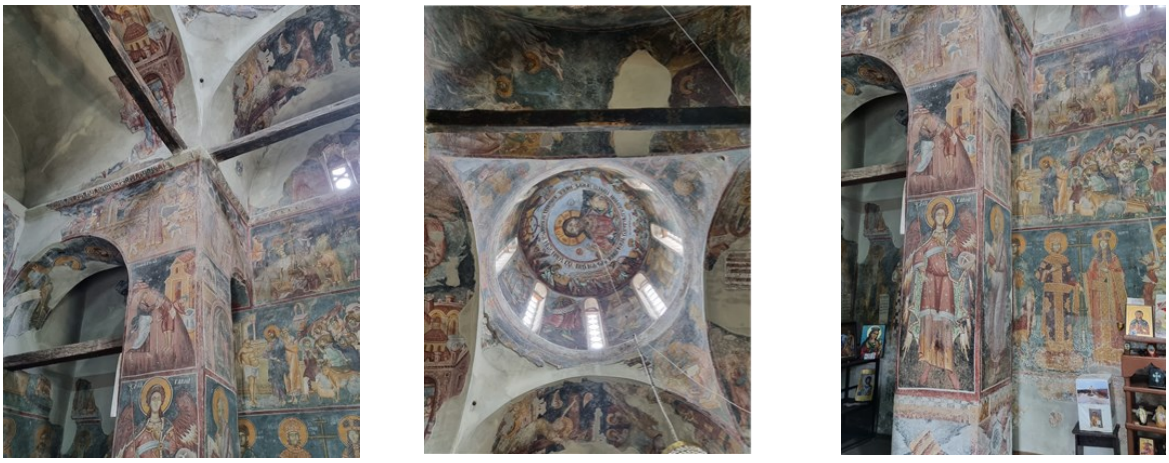


Figure 2.2 Interior of St. Nikita church

Copyright © 2025 CroCEE
DOI: https://doi.org/10.5592/CO/3CroCEE.2025.70

3. Diagnostic study on St. Nikita church

For the selected monument an integrated diagnostic study was carried out to assess its existing state. This study included different phases – archival research, documents review, field surveys and recording. The archival research and the review of the existing documentation enabled insight into the different historical stages of the building and previous interventions, (table 3.1).

Table 3.1 Review of historical changes on St. Nikita church, [7][8][9]

1307	The church was built on the base of an older building from XI or XII century
Ottoman period	Addition of small single nave structure on the south side of the church (demolished in 1928)
XIX century	Reconstruction activities on the dome of the church addition of a closed porch on the south and west side (demolished in 1928)
1963 (Skopje earthquake)	Damages in the interior of the church in form of cracks and detachments of the frescoes
1967	Conservation activities on the frescoes in the interior
1968	Conservation activities on the architecture
1978-80	Extensive intervention on the roof parts: restoration of the roof and replacement of the roof tiles with a lead sheet

During the field survey the monument's condition was assessed using the available non-destructive techniques: visual inspections assisted by drone, digital microscopy, infrared thermography, 3D laser scanning and ambient vibration tests.

3.1 Visual inspections assisted by drone

The visual inspections were conducted on the facades of the church and on the inside, and provided information regarding the visible surface irregularities and damage. Inspections on the facades pointed to certain irregularities, such as evident porosity of the limestone and carbonization of the lime mortar; presence of capillary moisture in the lower zones of the northern and western walls; presence of lichens in the lower and middle zones on each facade, (fig. 3.1). However, the general condition of the facades was assesses as relatively good and preserved, without the presence of major damages that could pose a further threat to the monument.



Figure 3.1 Surface irregularities on the facades of St. Nikita church: porosity on limestone (left), presence of moisture (middle), presence of lichens (right)

Copyright © 2025 CroCEE
DOI: https://doi.org/10.5592/CO/3CroCEE.2025.70

The interior of the church is completely plastered and covered with frescoes, preserved on a larger scale; therefore the condition of the structure materials cannot be investigated. Fine cracks were observed in several spots of the upper zones in the walls and vaults. It was also noticed that one of the wooden ties was disrupted, (fig. 3.2).



Figure 3.2 Damage in the upper zones of the church

Use of the drone enabled to investigate some challenging areas that were difficult to access during visual inspections. The high-quality photographs from an aerial perspective presented the wider context of the church within the surrounding and also provided an opportunity to investigate the roof's covering. The lead sheet (cover material) is well preserved, apart from the segment of the dome (fig. 3.3 right) where some cracks were noticed, probably due to unprofessional fixing of the joints.



Figure 3.3 Aerial perspectives of the church

3.2 Digital microscopy

The images from the microscope (magnification 40x) allowed more detailed view of the different types of lichen that are present on the facades of the church, (fig. 3.4). The presence of the lichens can be correlated to some minor micro cracks on the facades, but had not significantly affected the condition of the materials. Additionally, most of the lichens form kind of crust that firmly attach to the substrate; therefore their mechanical removal on large areas is particularly difficult and could damage the original materials. So, at this point, removing the lichens would cause more damage than benefits.

Copyright © 2025 CroCEE
DOI: https://doi.org/10.5592/CO/3CroCEE.2025.70



Figure 3.4 Different types of lichens present on the facades of the church (magnification 40x)

3.3 Infrared thermography

Infrared thermography is an evaluation technique that uses a thermal imaging camera to records the infrared radiation emitted by materials as a result of natural heating or cooling process and to correlate these variations to material's condition and properties, [10][11]. The thermal imaging surveys on the church of St. Nikita enabled to investigate large areas of the facades and the interior of the church.

On the facades, the technique was used to detect the distribution of moisture within the walls. Thermal image (fig. 3.5) shows irregular shapes of thermal anomalies, characteristic for the presence of moisture. The lower zones, which are actually the moisture zones, show lower temperatures (presented with blue and yellow colors) compared to the rest of facade surface. The moisture is mainly present at the contact zone between the wall and the sidewalk and rises up to 60-80cm of the wall's height.

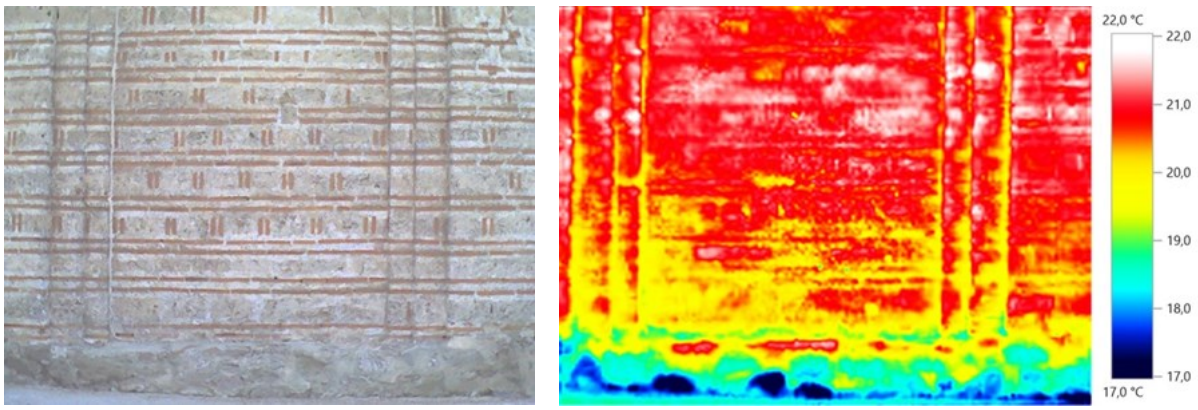


Figure 3.5 Segment of the north facade wall of St. Nikita church and corresponding thermal image

In the interior, the technique enabled to investigate the frescoes in a non-destructive way, which is important because due to their value there is no possibility for sampling. Most of the frescoes in the interior of the church are original, date back from 14th century. In the later periods (15th and 19th century) some of the damaged frescoes have been partially restored and others have been painted on a new layer of plaster. Since the restorer masters have followed the original work, it's difficult to separate the new of the old frescoes, but they vary in their composition and characteristics, and consequently, have different emissive values that can be observed with the thermal camera. Figure 3.6 shows a composition on the southern wall, where no surface changes are visually noticeable. However, the thermal image of this part shows temperature variations, i.e. a zone with a lower temperature (marked with a black circle) which may indicate to different material properties and different period of origin.

Copyright © 2025 CroCEE
DOI: https://doi.org/10.5592/CO/3CroCEE.2025.70

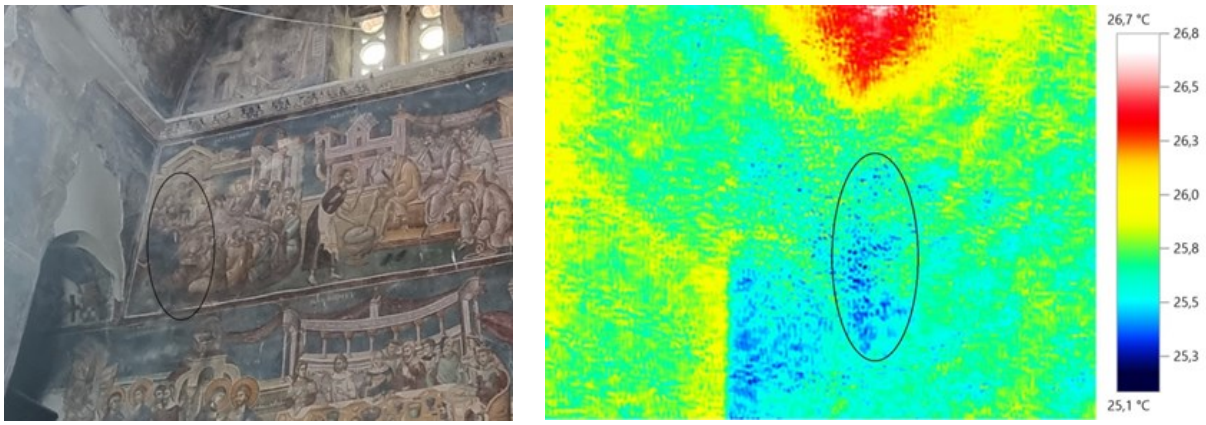


Figure 3.6 Composition on the south wall and corresponding thermal image

3.4 3D Laser Scanning

This is a fast non-invasive acquisition technique that uses laser lights for measuring 3D coordinates of points on surfaces, providing dense point cloud. The point cloud is a collection of millions of points into a common Cartesian (x,y,z) coordinate system that defines the structure's geometry in great detail. The color of the surface at each point can be added to the coordinate and intensity information by the imagery from the embedded camera. Specialized software are used to process the point cloud and create a digital representation of the building, [12].

In the case of St. Nikita church the Leica ScanStation P40 scanner was used, which is one of the latest models of scanners with exceptional precision. The use of the laser scanner enabled to record the entire building and to create a precise 3D model, i.e. a digital replica of the monument, (fig. 3.8). To ensure complete coverage of the building, multiple scans from different angles in the exterior and interior of the church were taken, (fig. 3.7). Combined with the data from the drone recording it gives a complete and precise definition on the building's geometry and structural details.

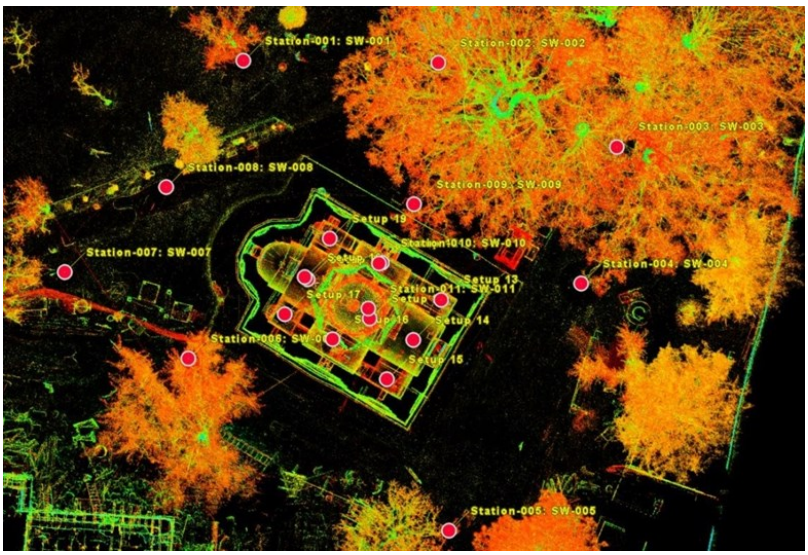


Figure 3.7 Position of the measuring points in the exterior and interior of the church

Copyright © 2025 CroCEE
DOI: https://doi.org/10.5592/CO/3CroCEE.2025.70

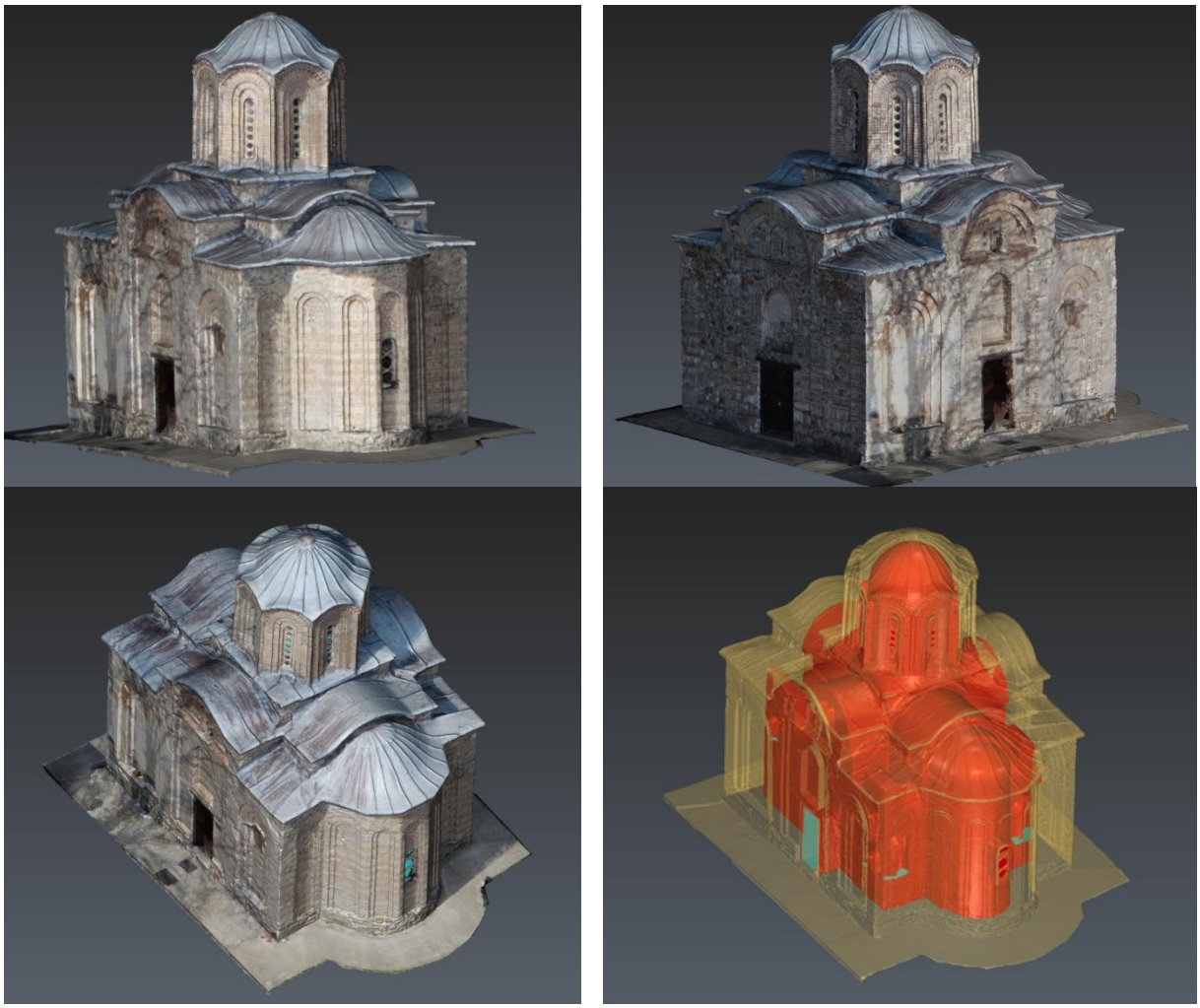


Figure 3.8 Virtual 3D model of the church generated from laser scanning

This 3D model serves as valuable resource for analysis and documentation. It gives opportunity to architects, engineers, conservators and other specialists to visualize and manage building from different angles, regardless the real physical limitations. The precision of the model could be used to measure any dimension of the elements (fig. 3.9) and identify even the smallest details, which facilitated the creation of the mathematical model for further structural analyzes. Additionally, the model was imported into AutoCad program which provided detailed 2D drawings (floor plans) of the building, (fig. 3.10). At this point, all required 2D drawings (section, elevations, floor plans) can be attained and with some additional work they can become valuable digital documentation of the monument, available at any time, without the need for repeated inspection.

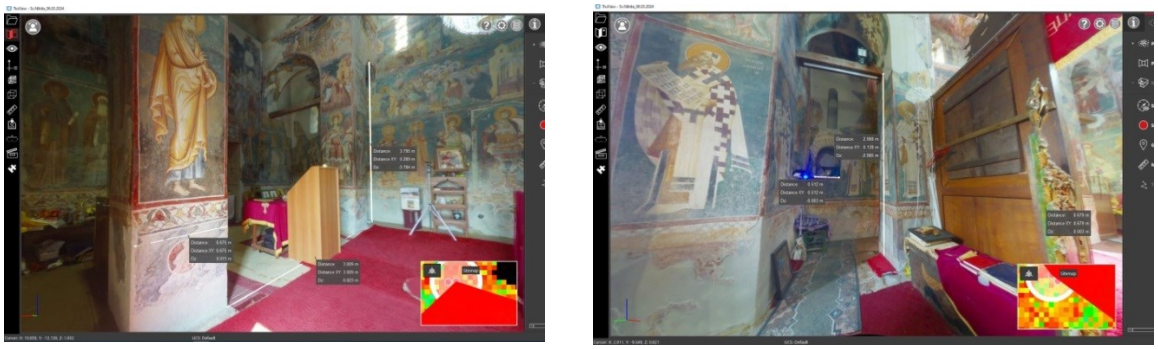


Figure 3.9 Representation of the interior of the church with measurements

Copyright © 2025 CroCEE
DOI: https://doi.org/10.5592/CO/3CroCEE.2025.70

This type of information is the basis for monitoring the building's condition and aids the future conservation or restoration processes. Also, it preserves all the physical, historical and cultural aspects of the monument for the future generations.

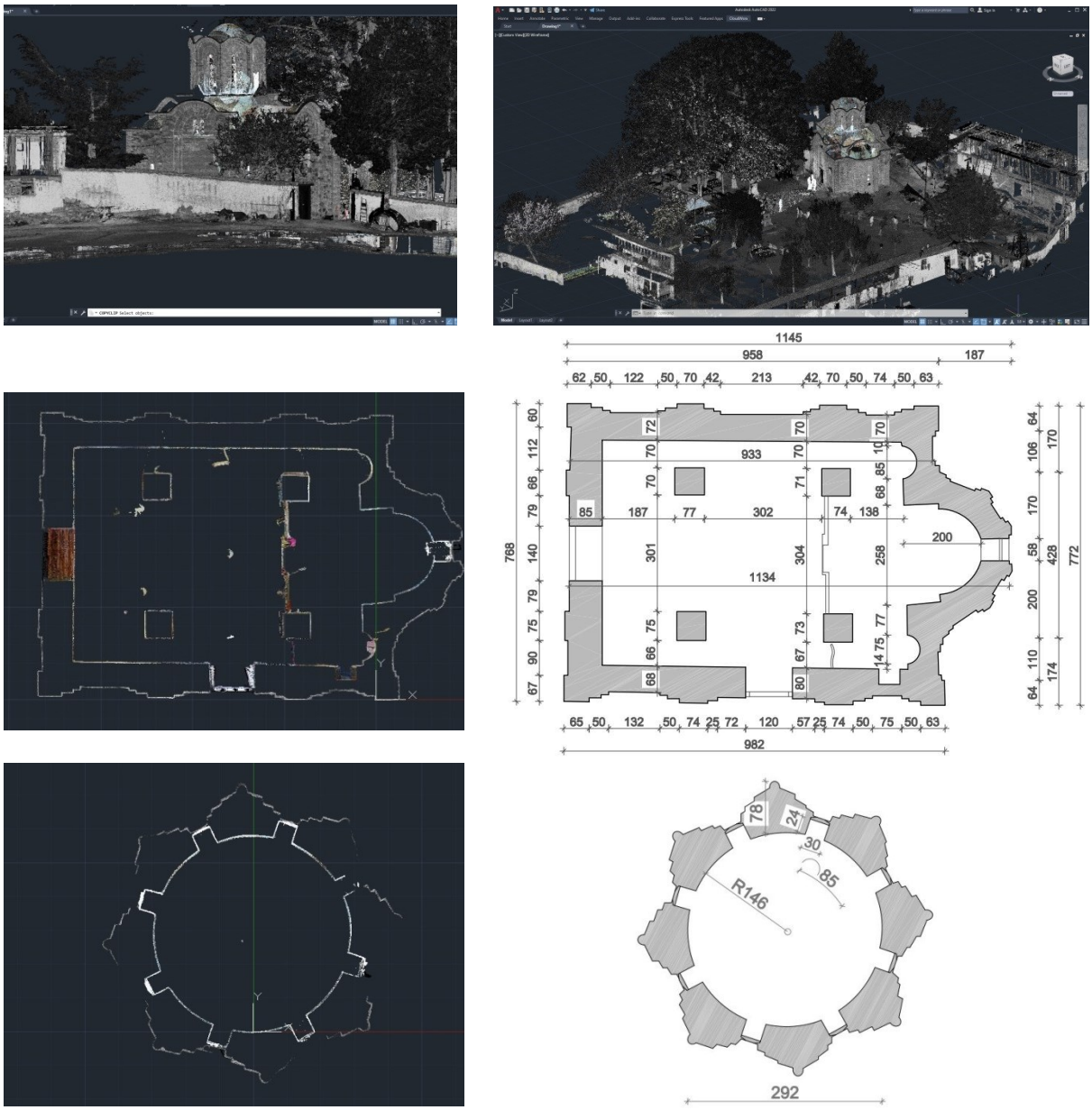


Figure 3.10 3D Model in Cad setting, 2D drawings generated from the model

3.5 Ambient vibration method

This technique has proved to be practical and cost-effective way for the determination of the dynamic properties of the structures, especially suitable in the field of built cultural heritage. The method involves real-time measurements of the small structural vibrations caused by ambient forces like the wind and processing the recorded data, [13].

The dynamic parameters of the structure are related to its physical and mechanical properties like mass, stiffness and energy dissipation, so any major structural change in the system will also be reflected on the dynamic parameters, hence the importance of monitoring. In the case of St. Nikita church, the ambient vibration method was used to determine the dynamic parameters - periods of

Copyright © 2025 CroCEE
DOI: https://doi.org/10.5592/CO/3CroCEE.2025.70

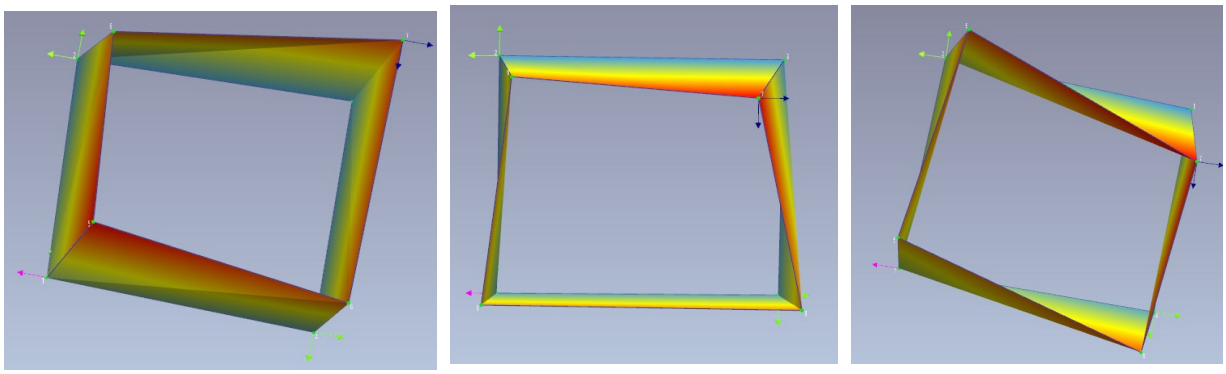
vibration and mode shapes, [14]. Eight sensitive accelerometers were used with different arrangement and measurement locations at levels 0.00 and +5.40, (fig. 3.11).



Figure 3.11 Positions of the accelerometers

The tests enabled to obtain the natural frequencies in both orthogonal directions: $f_{E\text{-}W}$=5.98Hz and $f_{N\text{-}S}$= 4.70Hz, and sequently the characteristic periods $T_{E\text{-}W}$= 0.167sec $T_{N\text{-}S}$= 0.212sec.

The mode shapes (fig. 3.12) indicate synchronized behavior of the facade walls which contribute to the overall stiffness and stability of the building as one global entity. The displacements in both, longitudinal and transversal directions are generally translational with insignificant presence of rotation more pronounced in the longitudinal direction. Such forms are expected considering the lack of symmetry due to the presence of the semi-circular apse at the altar area.



f=5.98 Hz
(longitudinal direction E-W)

f=4.70 Hz
(transverse direction N-S)

f=8.05 Hz
(torsion)

Fig. 3.12 Frequencies and mode shapes

The results of this research compared to data from similar tests conducted in 1990s -calculated mode shapes were $f_{E\text{-}W}$=6Hz, $f_{N\text{-}S}$=4.8Hz (project "Conservation, rehabilitation and strengthening of Byzantine churches in Macedonia", [2]), indicate that there were no changes in the dynamic parameters of the building's structure in the past 30 years, i.e. the past earthquakes, especially the earthquake of 2016 in Skopje did not cause additional damages to the church's structure.

4. Conclusion

Historic buildings are an integral part of our shared heritage. They serve as a connecting bridges to the past, representing the cultural development of the civilizations. Over the years, these buildings are exposed to many impacts (human, natural, climatic, etc.) so despite the visually good condition they may hold many hidden weaknesses. The buildings located in seismic-prone regions are particularly vulnerable, so the precaution to mitigate potential devastation must exist. The diagnostic study that will provide accurate condition assessment and consequently lead to appropriate conservation activities is an essential part of the long-term process of heritage building protection.

Copyright © 2025 CroCEE
DOI: https://doi.org/10.5592/CO/3CroCEE.2025.70

This paper describes an integrated diagnostic study conducted on a medieval monument in North Macedonia – church of St. Nikita near city of Skopje. The study involved archival research, documents review and in-situ surveys using non-destructive techniques: visual inspections aided by drone, microscopy, infrared thermography, 3D laser scanning and ambient vibration tests. The combination of these techniques provided valuable information regarding visible (surface) and hidden irregularities. The use of drone provided additional information for the less accessible areas of the building (aerial perspective). Furthermore, 3D laser scanning technology proved to be valuable resource for the purpose of heritage digital documentation.

5. References

[1] Stanton-Geddes Z, Soz SA. Promoting Disaster Resilient Cultural Heritage. Washington: Word Bank; 2017.

[2] Gavrilović P, Ginell SW, Shendova V, Šumanov L. Conservation and Seismic Strengthening of Byzantine Churches in Macedonia. Los Angeles: Getty Publications; 2004.

[3] Shendova V. Doctoral dissertation: Seismic strenghtening and repair of Byzantine churches (Сеизмичко зајакнување и санација на Византиски цркви). Institute of Earthquake Engineering and Engineering Seismology, IZIIS, Ss. Cyril and Methodius University in Skopje, 1997.

[4] Feilden B. Conservation of Historic Buildings. 3rd Edition. Oxford; Burlington, MA: Architectural Press; 2003.

[5] RZZSK, Kosicki I. Republic Institute for the Protection of Cultural Monuments Skopje, 1963-1983; 1983.

[6] Grujoska-Kuneska J. Doctoral dissertation: Modern approach in existing state diagnosis of cultural-historical monuments - architectural perspective (Современ пристап во дијагностика на состојбата на културно историски споменици-архитектонска перспектива). Institute of Earthquake Engineering and Engineering Seismology, IZIIS, Skopje, 2024.

[7] Markovic M. St. Nikita near Skopje (Свети Никита код Скопља). Belgrade: Sluzben Glasnik; 2015.

[8] NI Conservation Center - Skopje. Written documentation for the church of St. Nikita. 1978.

[9] NI Conservation Center - Skopje. Record documents. Skopje: 1980.

[10] Moropoulou A, Labropoulos KC, Delegou ET, Karoglou M, Bakolas A. Non-destructive techniques as a tool for the protection of built cultural heritage. Constr Build Mater 2013;48:1222–39. https://doi.org/10.1016/j.conbuildmat.2013.03.044.

[11] Kilic G. Using advanced NDT for historic buildings: Towards an integrated multidisciplinary health assessment strategy. J Cult Herit 2015;16:526–35. https://doi.org/10.1016/j.culher.2014.09.010.

[12] Historic England. 3D Laser Scanning for Heritage. 2018.

[13] Birtharia A, Jain SK. Application of ambient vibration testing: an overview. Int Res J Eng Technol 2015;02.

[14] Grujoska-Kuneska J, Jekic G, Shendova V. Comparative Analysis of Dynamic Characteristics of the St. Nikita Church. 19 Symp. MASE, Ohrid: 2022.

Proceedings of the 3rd Croatian Conference on Earthquake Engineering - 3CroCEE
19–22 March 2025, Split, Croatia
Copyright © 2025 CroCEE
DOI: https://doi.org/10.5592/CO/3CroCEE.2025.71

ASSESSMENT OF THE PHYSICAL CONDITION OF BYZANTINE CHURCHES IN NORTH MACEDONIA

Jasna Grujoska-Kuneska(1), Veronika Shendova(2)

1 PhD student, Institute of Earthquake Engineering and Engineering Seismology- Skopje, jasnagrujoska@yahoo.com
2 Professor, Institute of Earthquake Engineering and Engineering Seismology-Skopje, veronika@iziis.ukim.edu.mk

Abstract

Byzantine civilization is one of the longest-lived cultures, well known for the large number of constructed religious buildings, which today represent part of the world cultural heritage. Byzantine churches are a significant part of North Macedonia's tangible heritage; one of the most valuable and numerous medieval monuments, with exceptional architectural and artistic values. These churches appear in several characteristic concepts: basilica, conch, cross-in-square and smaller single-nave buildings. During their long-term existence they have been exposed to diverse impacts including earthquakes, so despite the visually good physical condition, they may hide many weaknesses.

This paper presents the investigation campaign carried out on 50 Byzantine churches in North Macedonia that included archival searches, review of church documentation and field inspections. The main objective was to assess the current state of the buildings, based on previously defined methodology and criteria for physical condition assessment. This research resulted in a data-base for Byzantine churches and their classification to several criteria: construction period, typology, previous intervention, current condition and authenticity. The collected data enabled to propose the future measures for their protection, graded as: monitoring, regular maintenance, repair or emergency protection.

Keywords: Byzantine churches, uniform methodology, assessment, physical condition, data base, classification

1. Introduction

The Byzantine Empire, lasting from the 4th to the 15th century, stands as one of the longest-lasting civilizations, enduring for over eleven centuries before being conquered by the Ottoman Empire in the 15th century. As a continuation of the Roman Empire, centered in Constantinople, it represented a link between the antiquity and the modern world, [1]. During the centuries, the Empire possessed territories of Asia Minor, Balkans, Greece, Italy and North Africa. The Byzantines developed their own culture, mainly presented by the architecture and art, [2].

The Byzantine architectural style developed as a combination of Roman traditions and innovative engineering techniques. While Byzantine buildings still incorporated Classical orders, they became more eclectic and irregular, with a greater emphasis on functionality over strict adherence to form. Byzantines continued to build baths, amphitheaters, villas and other arched structures, but also added new structures like churches, monasteries and fortifications. To support the spread of Christianity, a large number of churches were erected. Following the Roman design, the early churches (4^{th} - 5^{th} century) were basilica type – designed as long halls with timber roofs. In the 6^{th} century the timber roof was replaced with a dome-vault roof system. By the 9^{th} century these monumental structures were replaced with smaller churches and the domed cross-in-square plans became the most common typology. Over time, the high of the central dome was raised using polygonal drum, [3]. In the later period (13^{th} - 14^{th} century) there was a variability in the churches plans, which in a way reflected the political condition of the Empire, [1]. One of the most famous Byzantine buildings is Hagia Sophia in Istanbul, built in the 6^{th} century. The dome of the church has a span of 31.8m and rests on the system of arches and pendentives which is a significant architectural achievement of that period. The interior of the church was originally decorated with wall paintings and mosaics, [3].

Copyright © 2025 CroCEE
DOI: https://doi.org/10.5592/CO/3CroCEE.2025.71

During the existence of the Byzantine Empire, the territory of today's North Macedonia was influenced by various cultures, including the Byzantine one. The development of the cultural values in this region began in the second half of the 9th century. At the same time significant architectural achievements were made, particularly in the realm of sacred architecture. Most churches from this period are characterized by a structural concept influenced from the Near East and presence of byzantine ornamental features, [2]. There are still many fine examples of Byzantine churches (9th – 14th century) preserved on the territory of North Macedonia and today they represent significant part of the tangible heritage in the country.

2. Byzantine churches in North Macedonia - general information

Byzantine churches are one of the most preserved and numerous medieval monuments in the territory of North Macedonia. So far, 54 Byzantine churches have been registered, built between from 9th - 14th century. These churches appear in several different concepts–basilica, conch, cross-in-square and small single-nave structures, (fig. 2.1). Although there are some variations, generally, the structural system of these buildings consists of peripheral walls, inner columns and vaults. The vaulted (roof) structure generally rests on a system of arches, pendentives and columns, except for the single-nave churches where the vaulted structure rests directly on the walls. In most churches there is also an additional wooden system of horizontal belts placed into the walls and visible timber ties in the interior upper zones. This wooden system improves the stability of the structure, especially during seismic actions, [4][5].

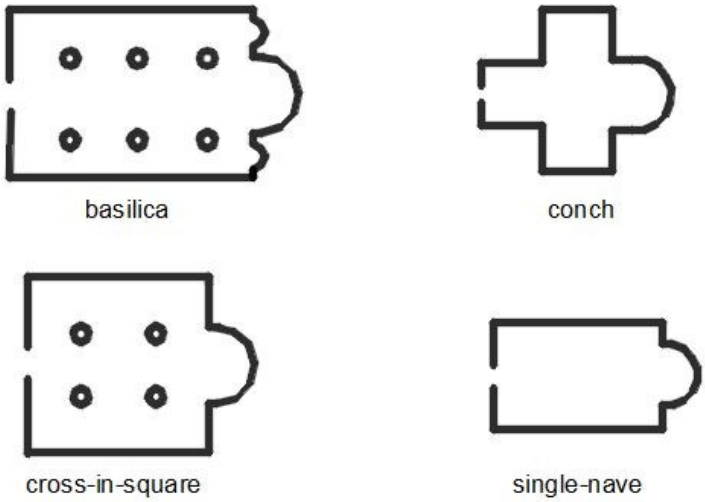


Figure 2.1 Main concepts of the Byzantine churches

The building materials are local stones, bricks and lime mortar. The walls usually consist of two outer layers of horizontal stone and brick masonry, separated by the core of rubble masonry and lime mortar. The columns are often constructed as monolithic elements of granite or marble blocks, or in some cases, from the same materials as the walls. Vaults are mainly built of limestone, and for the construction of drum and dome, bricks and lime-mortar are most often used, [4].

The domes are the most symbolic structural elements in Byzantine churches, which historically suffered most damage and sometimes were completely destroyed. The drum is a particularly significant element in the overall dome appearance. The octagonal drum is the most common shape, which corresponds to the span of the domes in most buildings, which ranges between 3.0 - 3.5m. Twelve-sided drum rarely exists in the medieval architecture; one example is the church of St. Demetrius in Prilep from 13th century. The apses are another specific element in the facade design of the churches. They appear in several forms - polygonal, semi-circular and often as three-sided, [6].

Copyright © 2025 CroCEE
DOI: https://doi.org/10.5592/CO/3CroCEE.2025.71

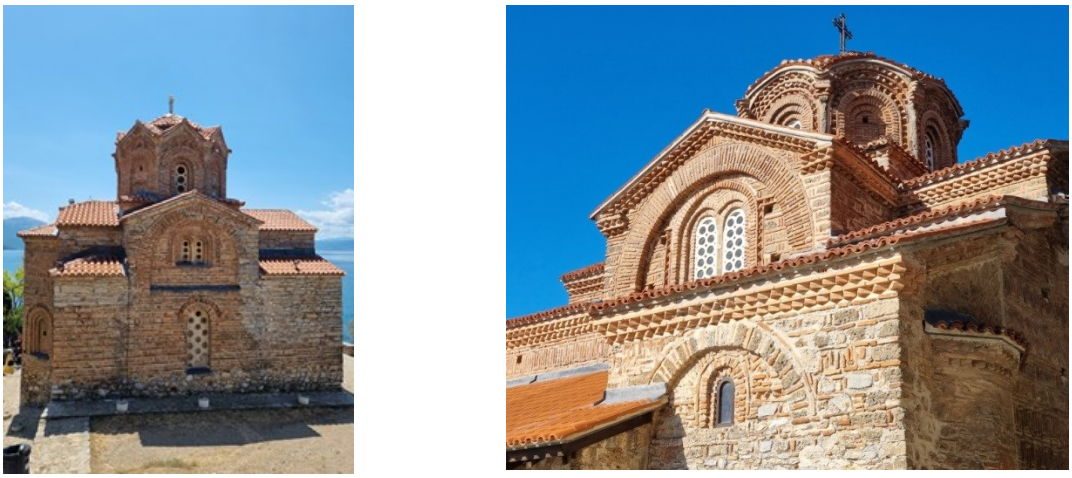


Figure 2.2 Dynamic facades of the Byzantine churches in the Ohrid region

The facades of the churches (fig. 2.2) are characterized by vibrant and dynamic appearance, combining pilasters, arches, niches and cornices with three-dimensional effects. In some Byzantine churches the facade surfaces are formed in a so called "cloisonné" technique, where alternating rows of stone and brick are combined with two vertically placed bricks in the joints to create a distinct pattern. In the church of St. Jonh the Theologian in Ohrid this technique is most consistently implemented. The rich ornamentation of the facades (fig. 2.3) is mainly achieved using bricks placed in different patterns - horizontally, vertically, inclined, which creates different forms of fishbone, zigzag stripes, rhombs, letter shapes etc. Combination of bricks and limestone is used for shaping the decorative arches and inscriptions. The polychromatic effect is gained using stones in diverse colors and mortar ranging from white to light rose, [4][6].



Figure 2.3 Ornamental facades of Byzantine churches: St. Nicholas in Varosh (left), St. John the Theologian in Ohrid (middle), St. Archangel Michael in Shtip (right)

The interior surfaces of the Byzantine churches have perforations for windows or blind niches. These surfaces were originally covered with frescoes (fig. 2.4) depicting various scenes from the Bible, in accordance with certain canons. Some of the most preserved examples of these frescoes can be found in the church of St. George in Kurbinovo (12th century), St. Nicholas in Varosh (late 13th century), St. Nikita in Banjani (14th century) etc. Floors of the churches are moderately finished with stones and sometimes bricks in a mosaic pattern (original floors of the churches St. Sophia in Ohrid and St. Holy Mother Eleusa in Veljusa), [4].

Copyright © 2025 CroCEE
DOI: https://doi.org/10.5592/CO/3CroCEE.2025.71



Figure 2.4 Interior of the church of George, Kurbinovo (left) and of St. Nicholas in Varosh, Prilep (right)

3. Classification of the investigated churches

The investigation included a total of 50 Byzantine churches within its scope. They are located in several regions across the country, but mostly in Ohrid, Skopje, Prilep and Shtip region, (fig. 3.1).



Figure 3.1 Location of Byzantine churches in the territory of North Macedonia

The investigation began with archival research and a systematic review of historical documents and records related to the churches. This process yielded valuable information regarding the historical context, construction phases, and changes over time. Additionally, field surveys were conducted to assess the physical condition of both the exterior and interior of the churches, highlighting any past

Copyright © 2025 CroCEE
DOI: https://doi.org/10.5592/CO/3CroCEE.2025.71

interventions. The field activities took place between 2021 and 2023, with some being part of the "Monitoring of the Orthodox Cultural Heritage" project organized by ICOMOS Macedonia., [7].

For the purpose of this research, a uniform recording form was designed (fig. 3.2) and completed for each church during the field surveys, thus representing an ID sheet for the monument that includes both general and specific information.

General information			photo
Name			
Date of built			
Corresponding institution			
Location and surrounding			
Address			
Coordinates			
Altitude			
Surrounding			
Seismicity zone			
Architecture			
Typology			
Functional units			
Horizontal plan			
Arch. / structural elements			
Exterior	Surfaces		
	Ornament		
	Specific features		
	Damages		
	Condition		
Interior	Surfaces		
	Damages		
	Condition		
Previous interventions			
Level of authenticity			
Future measures			

Figure 3.2 Designed recording form

The data collected in this manner allowed for the classification of the churches based on several criteria: construction period, typology, condition, interventions, and authenticity. The condition of the churches, referring to an evaluation of their tangible state and considering the extent to which they have deteriorated or been altered over time due to natural elements, human activity, insufficient or incorrect maintenance, was assessed using predefined criteria and rated as good, satisfactory, poor, or very poor. Past interventions were categorized into structural and non-structural, closely linked to their level of authenticity, which was rated as high, medium, or low. The data led to the final conclusion in the recording form (fig. 3.2) which refers to proposed future measures for the churches, graded as monitoring, regular maintenance, repair or emergency measures.

The churches were built between 9th and 14th century (fig. 3.3). Among the oldest are the first phase of the church of St. Leontius in the village of Vodocha (7th -9th century), St. George in the village of Goren Kozjak (9th century), St. Sophia in Ohrid (11th century), St. Holy Mother Eleusa in Veljusa (11th century) and St. George in Staro Nagorichane (11th century). Few churches were built during 12th and 13th century and most of the churches (over 60%) were built in the 14th century.

Copyright © 2025 CroCEE
DOI: https://doi.org/10.5592/CO/3CroCEE.2025.71

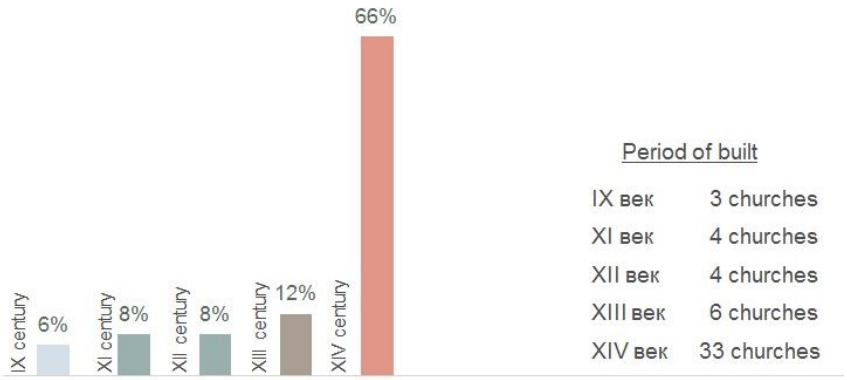


Figure 3.3 Classification of the churches - period of built

In relation to their typology, the most numerous are the domed cross-in-square and the small single nave buildings, (fig. 3.4). In the Skopje region most of the churches belong to the typology cross-in-square (fig. 3.5) – St. Nikita in Banjani, St. Panteleimon in Nerezi, St. Nicholas in Ljuboten, St. Holy Mother in Matka etc. Many examples of the small single-nave churches could be found in Ohrid region (fig. 3.6) - St. Cosmas & Damian, St. Demetrius, St. Holy Mother Bolnichka, St. Nicholas Bolnichki, Small St. Clement etc. Basilicas are rarely present. The church of St. Sophia in Ohrid and St. Nicholas in Mariovo belong to this typology. The conch churches appear as three-conch (St. Andrea in Matka and St. Holy Mother in Leshok) and four-conch (St. Holy Mother Eleusa in Veljusa). The only example of a two-nave concept is the church of St. Holy Mother Chelnichka in Ohrid. Some of the churches are combination of two typologies - inscribed cross and basilica, like the churches St. George in Staro Nagorichane, St. Holy Mother in Drenovo and St. Leontius in Vodocha.

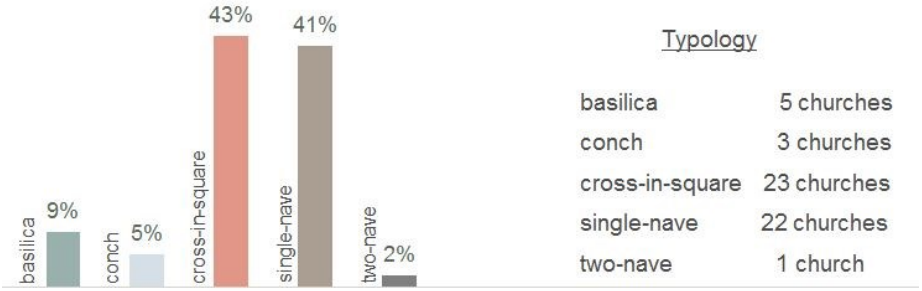


Figure 3.4 Classification of the churches – typology



Figure 3.5 Cross-in-square churches in the Skopje region

Copyright © 2025 CroCEE
DOI: https://doi.org/10.5592/CO/3CroCEE.2025.71



Figure 3.6 Single-nave churches in the Ohrid region

Field inspections enabled to visually assess the condition of the churches and to identify some visible damage/irregularities on the exterior and interior surfaces. Although these churches existed for centuries it was noted that most churches (around 85%) are in a "good" or "satisfactory" physical condition, fig. 3.7. More severe damages, such as: structural cracks, material degradation or poor structural connections were observed at six churches - St. John the Baptist in Shtip, St. Stefan in Konche, St. George in Staro Nagorichane, St. Holy Mother in Drenovo, St. Holy Mother in Treskavec Monastery and St. Nicholas in Shishevo. The condition of these buildings was assessed as "bad". The one church in a "very bad" condition is located in the Prilep region – church St. Atanasius in Varosh, (fig. 3.8). This building is completely abandoned and overgrown with vegetation. The roof structure and the upper parts of the walls are completely destroyed and the wooden elements in the walls are burnt and rotted due to previous fire. Since the building is in high risk, emergency measures are proposed.

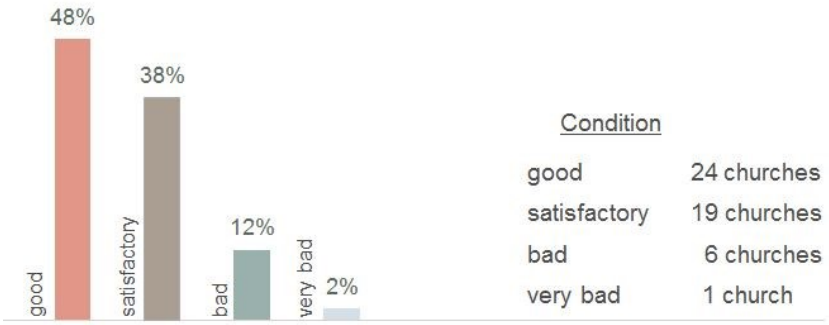


Figure 3.7 Classification of the churches - condition



Fig. 3.8 Exterior and interior of the St. Atanasius church in Varosh, Prilep

Copyright © 2025 CroCEE
DOI: https://doi.org/10.5592/CO/3CroCEE.2025.71

The documentation review and the visual inspections indicated that all churches have undergone some past interventions on a smaller or larger scale. Additions in form of porch or narthex were often built in the later periods, fig. 3.9. Facade, structural and interior interventions were also performed. These interventions range from minor protective works (replacement of the roof or floor material, rearrangement of the cornices, injection of cracks, forming drainage channels), up to extensive works (structural strengthening with reinforce concrete, reconstruction of damaged parts, partial or complete replacement of the roof structure etc.). Such extensive works were noted in a few churches – St. Panteleimon in Nerezi, St. Holy Mother Perivlepta in Ohrid, St. Sophia in Ohrid, St. Holy Mother in Drenovo, St. Archangel Michael in Varosh, St. Nicholas in Mariovo and St. Holy Mother in Trescavec Monastery. The church of St. Athanasius in Varosh is the only church with no records for past conservation activities or other interventions.



Figure 3.9 Additions from later periods in form of narthex and porch

The authenticity of these churches (fig. 3.10) is directly related to the scope and type of the past interventions. Part of the churches (30%) are preserved true to their origins in terms of materials, forms and structure, so these churches have high level of authenticity (St. Archangel Michael in Shtip, St. John the Theologian in Ohrid, St. Nicholas in Varosh, St. Nikita in Banjani, etc). Most of the churches (over 60%) have medium level of authenticity, due to later additions or conservation efforts that somehow impacted the original appearance of the monuments. The only church with low level of authenticity is the church of St. Panteleimon in Ohrid since it was completely rebuilt in 2002 on the remains of the original walls and modern materials were used.

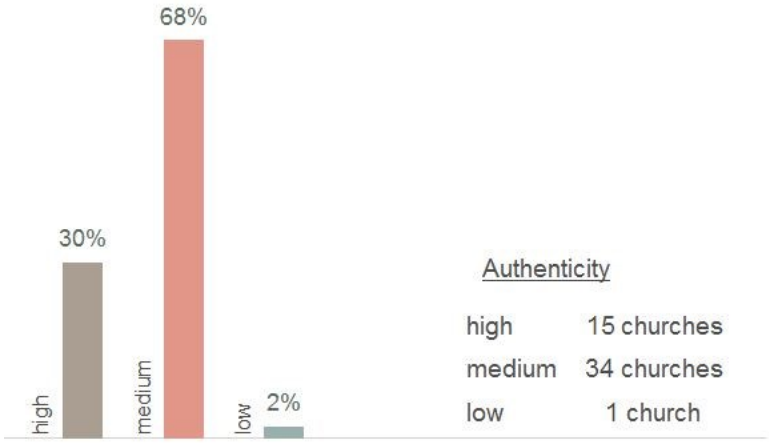


Figure 3.10 Classification of the churches - authenticity

4. Conclusion

Byzantine churches (9th-14th century) are a significant part of the tangible heritage in North Macedonia. These medieval monuments hold exceptional architectural and artistic value, and today, they serve as a bridge that connects us to the culture and people who created them.

Copyright © 2025 CroCEE
DOI: https://doi.org/10.5592/CO/3CroCEE.2025.71

The presented investigation provides information on the current state of the Byzantine churches in North Macedonia (a total of 50 churches), using a uniform methodology with clearly defined criteria for condition assessment. The methodology included archival research, a review of available documentation, and field surveys for each church. Based on the collected data, the churches were categorized according to several criteria: construction period, typology, condition, degree of interventions, and authenticity.

Within the presented research, a database for the Byzantine churches in North Macedonia was created, offering new and updated information on their condition, all in one place. This database can can help update and synchronize official national registers, support future conservation efforts, and provide a deeper understanding of the country's Byzantine heritage. Additionally, some of the relevant information could serve as an exposure model for national risk assessment activities related to potential natural hazards and climate change.

5. References

[1] Gregory TE. A History of Byzantium: 306-1453 (Blackwell History of the Ancient World). 1 st Editi. John Wiley & Sons; 2005.

[2] Boshkovic Dj. Medieval architecture (Архитектура средњег века). 4th issue.Belgrade: Naucna kniga; 1976.

[3] Byzantine Architecture. World Hist Encycl 2018. https://www.worldhistory.org/Byzantine_Architecture/ (accessed November 24, 2024).

[4] Gavrilović P, Ginell SW, Shendova V, Šumanov L. Conservation and Seismic Strengthening of Byzantine Churches in Macedonia. Los Angeles: Getty Publications; 2004.

[5] Shendova V. Doctoral dissertation: Seismic strenghtening and repair of Byzantine churches (Сеизмичко зајакнување и санација на Византиски цркви). Institute of Earthquake Engineering and Engineering Seismology, IZIIS, Ss. Cyril and Methodius University in Skopje, 1997.

[6] Korunovski S. Church architecture in Macedonia in 13th century (Црковната архитектура во Македонија во XIII век). Ss. Cyril and Methodius, Skopje, 2000.

[7] ICOMOS Macedonia. Monitoring of Orthodox Cultural Heritage 2022. https://monitoring.icomos.org.mk/home (accessed April 14, 2024).

Proceedings of the 3rd Croatian Conference on Earthquake Engineering - 3CroCEE
19–22 March 2025, Split, Croatia
Copyright © 2025 CroCEE
DOI: https://doi.org/10.5592/CO/3CroCEE.2025.107

SEISMIC EVALUATION OF THE HIGH-RISE RESIDENTIAL BUILDING WITH STRUCTURAL WALLS FROM THE LATE 60'S

Mustafa Hrasnica [(1)], Amina Karavelić-Hadžimejlić [(2)], Senad Medić [(3)], Jelena Medić [(4)]

[(1)] *Professor, University of Sarajevo – Faculty of Civil Engineering, hrasnica@bih.net.ba*
[(2)] *Assistant, University of Sarajevo – Faculty of Civil Engineering, amina.karavelic148@gmail.com*
[(3)] *Professor, University of Sarajevo – Faculty of Civil Engineering, senad_medic@yahoo.com*
[(4)] *Senior Lecturer, University of Sarajevo – Faculty of Civil Engineering, jecacuric@yahoo.com*

Abstract

Extensive construction of buildings with structural system made of reinforced concrete walls had been started in the early 60s of the last century, as a continuation of the rebuild of Europe after the World War II. This was especially true in the Western Balkan region. In some way these buildings replaced multi-storey masonry buildings, enabled significantly higher number of floors and a larger number of apartments. A specific construction technology with the so-called tunnel formwork was applied, which enabled rapid construction progress in terms of the height of the building. Seismic resistant structure of the buildings consisted mainly of reinforced concrete slabs and walls, whereby the reinforcement detailing was performed according to the old technical codes and the ancient state of the art of the building's construction. Regarding the structural system, the way of the construction and structural detailing of these buildings, they can be classified as a recent historical heritage. A high-rise building in Sarajevo, with 20 residential floors, about 55 years old, with a load-bearing system made of reinforced concrete walls and slabs, almost without any beams, was analysed. According to the modern state of the praxis, the building does not meet the requirements of contemporary seismic codes, and this especially applies to the reinforcement design and detailing. Taking into account seismic vulnerability classification of the European Macroseismic Scale the building could suffer substantial damages when exposed to the stronger earthquake motions. We tried to capture the specific design of the existing reinforced concrete walls applying more sophisticated structural models, including confined and unconfined concrete. The mechanical properties of the built-in building materials in existing slabs and walls were obtained experimentally. The results of the nonlinear analysis show a relatively satisfactory global response of the structure, but with possible damages due to the rather poor reinforcement quantity in the walls. Just to mention that some of the main structural walls possess only few longitudinal reinforcement bars in the corners. An improvement of the structural system, in order to achieve a ductile response with the dissipation of the energy introduced by the earthquake, as proposed by the latest seismic codes and recommendations, has been discussed as well.

Keywords: seismic analysis, existing buildings, R.C. walls, multi-storey buildings.

1. Introduction

Reinforced concrete structures prevailed in construction of multi-storey residential and public building in great reconstruction of the devastated European towns after the World War II. Implementations of specialized construction techniques enabled faster progress of construction along the height of the building in comparison with "classical" reinforced concrete frame structures. This is especially true for the Balkan region, where the construction of residential buildings with structural R.C. walls started in late 60's, continued in 70's and 80's. High-rise residential buildings with 15-20 floors were very popular and they were built all over former Yugoslavia. Such type of housing was very cost-effective. It could accommodate a lot of flats, which was one of the main goals in former political system, while fast growing cities urgently needed new apartments. Construction companies, some of them with few thousand employees, developed so-called tunnel formwork, especially designed for the structural system, made of reinforced concrete walls and slabs. In well organised construction procedure, they achieved progress form one floor to another in just few days. The tunnel formwork could be pulled out and reassembled again very quickly. Similar type of the residential buildings was built in other part of the Europe as well. Just to mention "Plattenbauten" in Germany.

Copyright © 2025 CroCEE
DOI: https://doi.org/10.5592/CO/3CroCEE.2025.107

Seismic resistance and good seismic performance are important issues in every day structural designs in seismic active regions. High-rise residential buildings with reinforced concrete walls, built in 60's to 80's, usually possess regular structural system with uniform structure from the bottom to the top of the building, including mostly symmetrical distribution of walls, viewed in the plan [1]. And this is one of the important structural properties in order to achieve good seismic performance. However, they are not built according to the modern structural codes and recommendations. It concerns, especially, design and detailing of the reinforcement, which will be presented in the example building further in this paper. The main vertical structure, made of concrete walls could be simply evaluated as poor reinforced, according to the contemporary state of the praxis. But it should be recalled, that the structural codes for concrete structures and seismic analysis, existing in the time of the construction, didn't provide enough rules and instruction for the design of the reinforced concrete walls.

2. Seismic vulnerability of the existing R.C. wall buildings

Within European Macroseismic Scale [EMS] structural systems of buildings are classified according to vulnerability classes depending on building materials, structural system and seismic design. Vulnerability classes are A – F, where class A stands for the weakest seismic structures and class F for those that are expected to have very good seismic performance [2], see Table 1.

Table 1. Vulnerability classes according to EMS

Type of Structure		Vulnerability Class A B C D E F
REINFORCED CONCRETE (RC)	frame without earthquake-resistant design (ERD)	
	frame with moderate level of ERD	
	frame with high level of ERD	
	walls without ERD	
	walls with moderate level of ERD	
	walls with high level of ERD	

The classification of vulnerability, presented in Table 1, is extract from the EMS classification and concerns only reinforced concrete buildings. It can be easily observed that the existing buildings with walls, built without or with moderate earthquake resistant design could be ordered in the vulnerability classes C or D. However, they are slightly more favourable compared to ordinary masonry buildings.

On the other hand, damages are classified in degrees/grades from 1 to 5, which ranges from irrelevant damages or only damages of non-structural elements that correspond to damage grade1, to destruction or even building collapse that corresponds to damage grade 5.

Short description of damages to reinforced concrete buildings with walls, according to [2] are listed here for convenient:

- Grade 1: Negligible to slight damage (no structural damage). Fine cracks in walls at the base.

- Grade 2: Moderate damage (slight structural damage). Cracks in structural walls.

- Grade 3: Substantial to heavy damage (moderate structural damage). Cracks at the base and at joints of coupled walls. Spalling of concrete cover, buckling of reinforced rods.

- Grade 4: Very heavy damage (heavy structural damage). Large cracks in the walls with compression failure of concrete and fracture of rebars.

- Grade 5: Destruction (very heavy structural damage). Collapse of ground floor or parts of building

Copyright © 2025 CroCEE
DOI: https://doi.org/10.5592/CO/3CroCEE.2025.107

Within the European Macroseismic Scale [2] there are short descriptions of effects that could be expected for the specific degree of seismic intensity, provided in 12-degree European Macroseismic Scale (very similar to the former MSK-scales). So, the vulnerability classes, damage grades and seismic intensities cold be mutually correlated. As the result, at existing multi-storey buildings with poor earthquake design of the structural walls, classified in seismic vulnerability classes C and D, for the seismic zones in Bosnia and Herzegovina (Western Balkan), damage grades 2 or 3 are to be expected [3]. This corresponds generally to moderate or heavy damages or slight to moderate structural damages.

Previous classifications refer to some average design and constructed buildings or to relatively regular structures. That means: the layout of the structural walls in a plan is approximately symmetrical and the stiffness is almost uniform or proportional along the height of the building. Each irregularity increases seismic vulnerability of the structure, which was confirmed during past earthquakes in the Balkan region [3]. Just to recall irregular distribution of walls in a plan of the building resulting in relatively large eccentricity between mass and stiffness centre, or non-uniform stiffness distribution along the height of the building which has a consequence in the formation of soft-story mechanism [1].

3. Seismic response of the buildings with structural walls

When considered multi-storey building with structural walls, we should make distinction between recently constructed buildings, designed and built according to the modern seismic provisions [4] and older reinforced concrete buildings, built in the past without implementation of the seismic codes. They were no existing, or they were in very early stage of the development, with very few considerations about structural detailing.

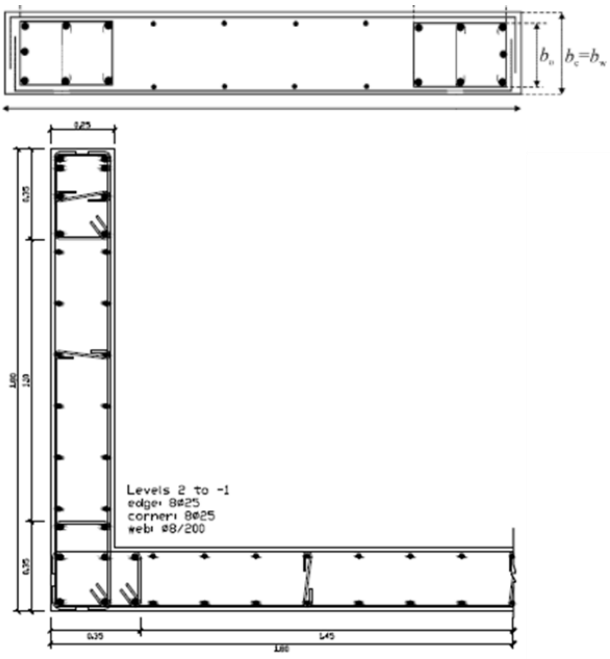


Figure 1. Contemporary details of the wall reinforcement.

Generally, structural walls provide significant resistance to lateral loads caused by earthquakes. Compared to the R.C. frames they reduce the lateral displacement and inter-storey drift, which could be critical for the overall stability of high-rise buildings. Increased stiffness and strength reduce structural damages significantly [5].

Modern buildings with high level of earthquake-resistant design should have only light and predictable damages in the case of stronger earthquakes. They are design according to modern seismic codes and fulfil the rules of capacity design procedures [1, 4]. The reinforced concrete walls are designed and detailed in the way to develop ductile behaviour and dissipation of the energy introduced in the structure

Copyright © 2025 CroCEE
DOI: https://doi.org/10.5592/CO/3CroCEE.2025.107

by the earthquake. Some layout of the structural walls corresponding to the modern recommendation are shown on the Fig. 1.

Buildings with poor or moderate earthquake resistant design can hardly develop ductile response. Typical older multi-storey building with R.C. walls is shown in the following chapter No. 4.

Another important goal of the good seismic design is to avoid brittle failure. Appropriate amount of transverse reinforcement, stirrups and ties, longitudinal reinforcement ratio and minimum wall thickness are to be considered. A typical damage at the bottom of the vertical reinforced concrete element is presented on the Fig. 2.



Figure 2. Damage at the bottom of the vertical reinforced concrete element.

Overall seismic response of the multi-storey wall building depends significantly on the regularity of the structural system. Even buildings with well-designed structural elements could suffer heavy damages in the case of larger non-symmetry or existence of the soft-story.

4. Example building (case study)

As an example of the older existing building with reinforced concrete walls a high-rise residential building, built in 1969 in Sarajevo, Bosnia and Herzegovina has been chosen. Different photos of the building are shown on the Fig.3 and Fig. 4. Five, almost same buildings had been built at the same time in the new part of the city (60 years ago) close to the iconic football stadium "Grbavica". With some adjacent, significantly lower building, they surround the Square of Heroes in the city quarter Hrasno. During the aggression on the town of Sarajevo the buildings were exposed to bombing and suffered structural and non-structural damages. There were fires due to bombing with special ammunition, which usually included several floors in few cases almost third or half of the building.

Several years after the war the buildings were reconstructed. Damages due to shelling were repaired, holes caused by shell hits have been closed, buildings physics generally improved. The rehabilitation process is presented on the Fig. 4.

The example building has 23 floors, 20 of them are residential. In that time, they were the tallest building in the city and they were given the name “skyscrapers”. The height of the building is almost 66 m, dimensions in a plan of the building are 21 × 21 m. Thus, overall slender ratio of the building H/L is about 3. Story height is 2.7 m, only the ground floor itself is 5.4 m high. Eight small flats were accommodated on each floor.

Copyright © 2025 CroCEE
DOI: https://doi.org/10.5592/CO/3CroCEE.2025.107



Figure 3. The high-rise buildings in Sarajevo (case study).



Figure 4. View of the building before, during and after repair.

The main structural system comprises reinforced concrete walls and slabs. The structure is regular along the height of the building and the floor plan is constant for all residential floors (see Fig. 5). The thickness of all walls is 20 cm and the slabs are just 16 cm thick. The structure was adjusted for the construction technique using so called tunnel formwork, as mentioned earlier. The maximum span of the slab (in shorter direction) is about 6 m. The foundation slab is only 60 cm thick and it is stiffened with 40 cm thick walls.

According to the construction time, structural design in general and especially reinforcement quantity, are governed by the principle to build in as less building material as possible. This presented real challenge for the structural engineers, while the overall structural reliability had to be guaranteed, as well. Reinforcement steel of the wall was built in a way that lower parts of the wall were reinforced completely in the length of the wall, and above certain floor level (depending on the wall, 3rd, 4th or 5th floor) only edge reinforcement was retained up to the top of the building. This can be observed on the Fig. 6. That means that at least 2/3 of the height of the concrete walls were unreinforced, apart 6 longitudinal bars, diameter 16 mm, closed by very few stirrups at the wall edges. The stirrups and ties

Copyright © 2025 CroCEE
DOI: https://doi.org/10.5592/CO/3CroCEE.2025.107

of the longitudinal bars at the edges of the walls were built in very economically, usually stirrups diameter of 6 mm at distance of 25 cm along the height of the wall. Generally, there are no meshes, only the reinforcing bars were built in.

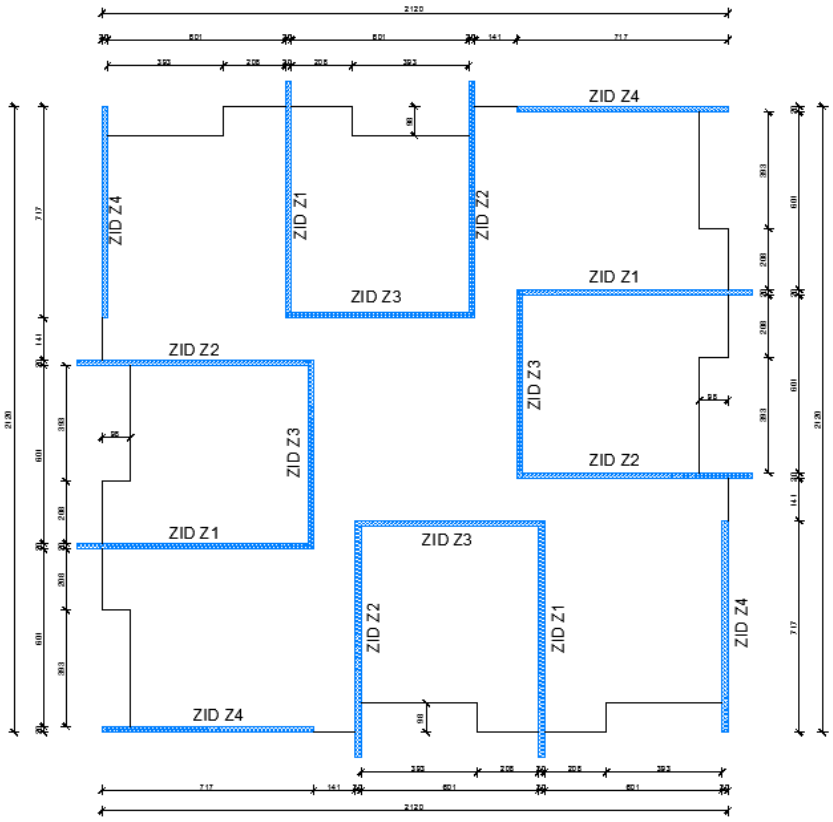


Figure 5. Floor plan, distribution of R.C. walls.

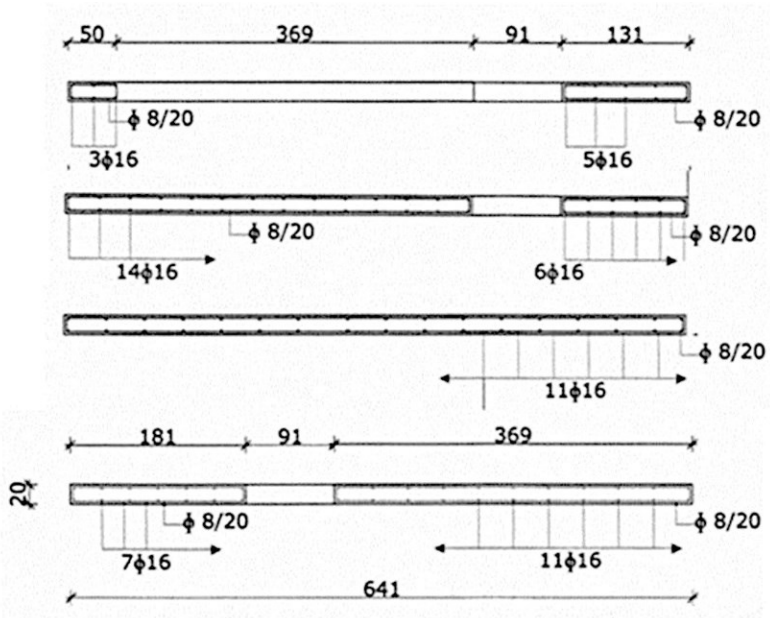


Figure 6. Reinforcement of the walls.

Copyright © 2025 CroCEE
DOI: https://doi.org/10.5592/CO/3CroCEE.2025.107

During rehabilitation works in order to repair war damages on the building, testing of the mechanical properties of concrete and reinforcement steel were performed. The tests showed a quality class of concrete MB 20 according ancient concrete code, corresponding to C16/20 as per Eurocode 2 [6], and reinforcement steel, only plain bars, corresponds to GA 240/360, old label as well, having yield strength of 240 N/mm^2. It should be recall that the applied reinforcement has generally good ductile behaviour.

Former design of the building does not meet the requirements of contemporary technical codes. The mechanical properties of the existing concrete are at the lowest tolerated limit for reinforced concrete structures. But it is current state of the existing structures. These buildings, and there are a lot of them all over Europe, could be in some way also marked as a type of "newer" historical buildings, especially in the sense of their seismic resistance and performance.

5. Seismic analysis of the example building

Seismic response of the previously described high-rise building is without doubt of the interest. First step is to form appropriate numerical/mechanical model for the seismic analysis. In the case of stronger earthquake motions nonlinear response of the building structure could be expected. In addition, three-dimensional dynamic analysis of the whole building would be preferred choice [7, 8]. Adequate numerical model, covering both issues should be chosen.

Seismic analysis was performed using SAP2000 [9] software. Earthquake loading for time history analysis is described by recorded accelerograms. "Classical" accelerogram El Centro of the Imperial Valley earthquake and recently recorded accelerogram of the Zagreb earthquake (2020) were applied. In order to capture nonlinear behaviour of the reinforced concrete walls, caused by stronger earthquake, nonlinear shell layer element was chosen (see Fig. 7).

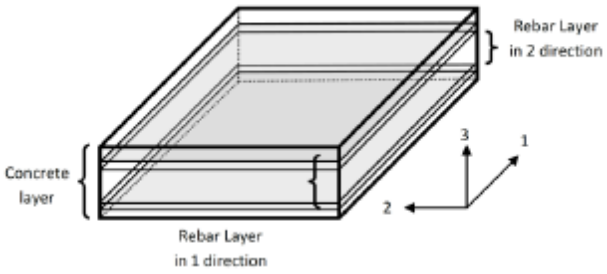


Figure 7. Shell layer element (SAP2000).

The main parts of the elements are layers of the different building materials of the R.C. wall, concrete and reinforcing steel. Further, it is possible to make a difference between confined and unconfined concrete. Well known Mander model [10] for confined/unconfined concrete, already implemented in software, is shown on the Figure 8.

Strength and ductility of the confined concrete, could be together labelled as capacity as well, is strongly dependent on the stirrups or hooks quantity, their diameter and distance [11]. It should be mentioned here, that the existing reinforced concrete walls have in 2/3 or even 3/4 of the wall's height very few stirrups at the edges of the walls and mostly unreinforced concrete. Tension capacity of the concrete was neglected. Stress-strain model of the reinforcing steel is shown on the Fig. 9. Assuming same form in the tension and compression.

Copyright © 2025 CroCEE
DOI: https://doi.org/10.5592/CO/3CroCEE.2025.107

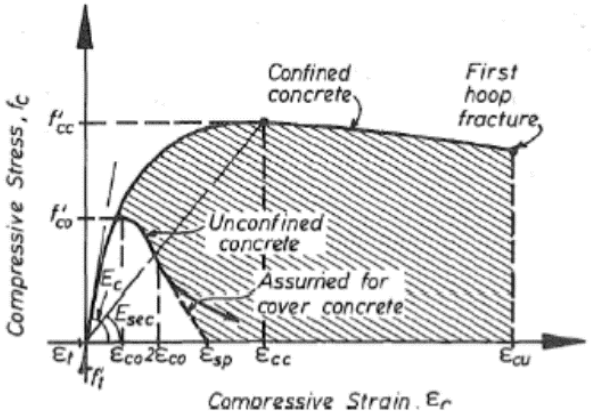


Figure 8. Mander model of confined concrete.

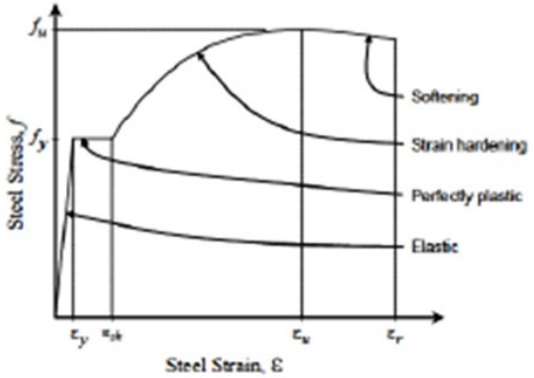


Figure 9. Stress-Strain model for the reinforcement.

In order to gain better insight in deformation or crack development another model and seismic analysis of the same building was done in DIANA [12] software as well.

The eigenforms and periods of oscillation were calculated using both software. The first few periods of oscillation are shown in the Table 2.

Table 2. Periods of oscillation

Period	SAP2000	DIANA FEA
T1 [s]	1,41	1,45
T2 [s]	1,00	1,07
T3 [s]	0,99	1,07

Good agreements of the results obtained using two different software could be observed. First eigenform is dominantly in torsion, second and third eigenform, numerically fast identical, are predominantly translational forms in both mutually perpendicular direction viewed in the plan of the building. The eigenforms are shown on the Fig. 10.

The high-rise building is symmetrical in relation to the main diagonal. One could conclude that the building does not possess enough torsional stiffness. There are some practical formulas [13] (details in Schneider) which can be used to estimate, roughly, if one multi-storey building has satisfactory level of stiffness, in torsional or translational sense. Brief control using simple formulas yield that the torsional stiffness demand is not slightly fulfilled, while translational stiffness demand is slightly

Copyright © 2025 CroCEE
DOI: https://doi.org/10.5592/CO/3CroCEE.2025.107

fulfilled. One must take into account that those formulas give just rough estimation and that they are based on elastic property of the structure concerned.

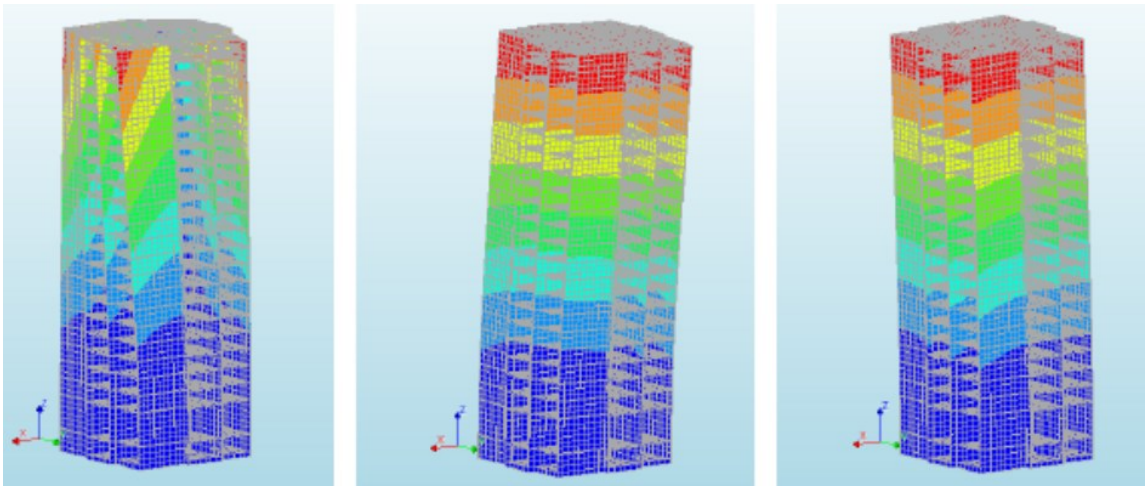


Figure 10. Eigenforms corresponding to periods T_1, T_2 and T_3.

6. A few interesting results of the seismic analysis

On the Fig. 12. And Fig. 13 two accelerograms used for nonlinear time history analysis of the building structure are shown.

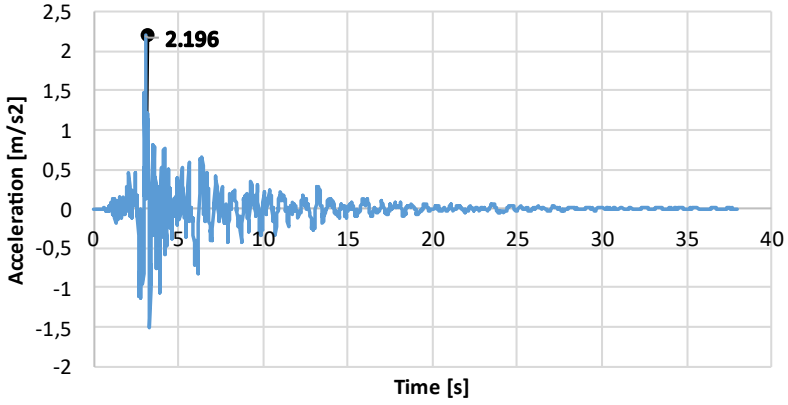


Figure 12. Accelerogram Zagreb 2020.

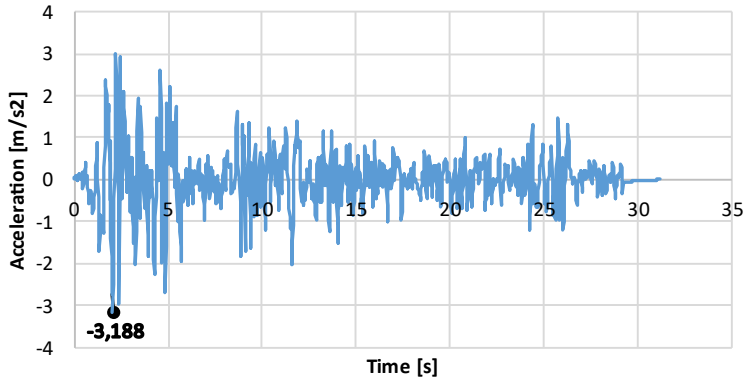


Figure 13. Accelerogram El Centro (Imperial Valley) 1940.

Copyright © 2025 CroCEE
DOI: https://doi.org/10.5592/CO/3CroCEE.2025.107

Assumed nonlinear material behaviour was discussed in previous chapter. Horizontal displacements at the top of the high-rise building are without doubt one of the most interesting parameters to describe seismic response of the existing building. For the earthquake record in Zagreb, they are shown on the Fig. 14. with the highest value of 5.1 cm.

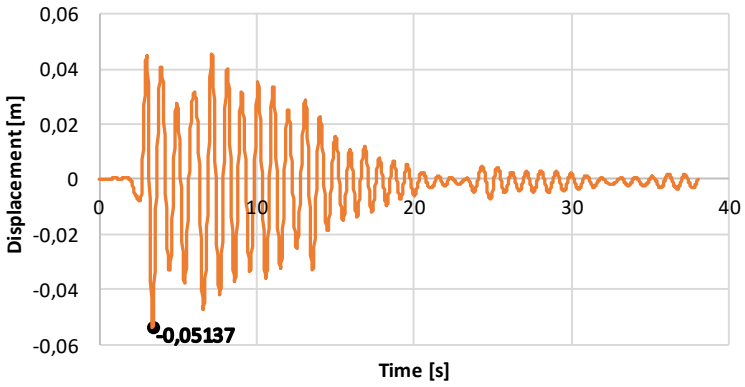


Figure 14. Maximal horizontal displacement at the top of the building, acc. Zagreb.

It should be emphasized here, that either yielding of vertical reinforcement bars or exceeding of compressive strength in concrete were not recorded. According to available data, similar buildings in Zagreb did not suffer significant damages, some minor cracks were reported.

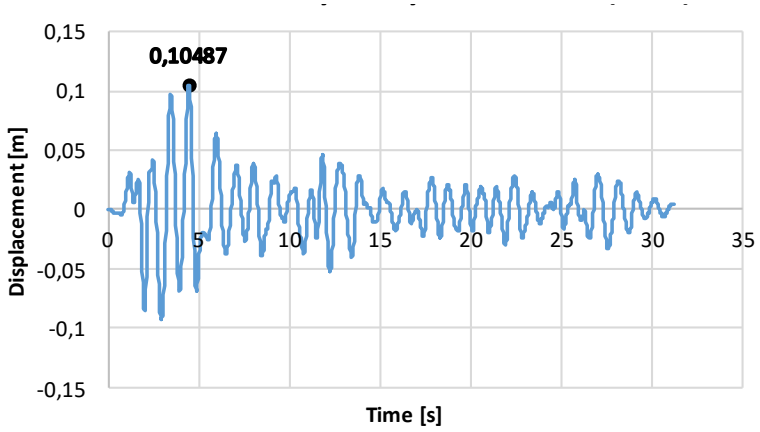


Figure 15. Horizontal displacements at the top of the building, acc. El Centro.

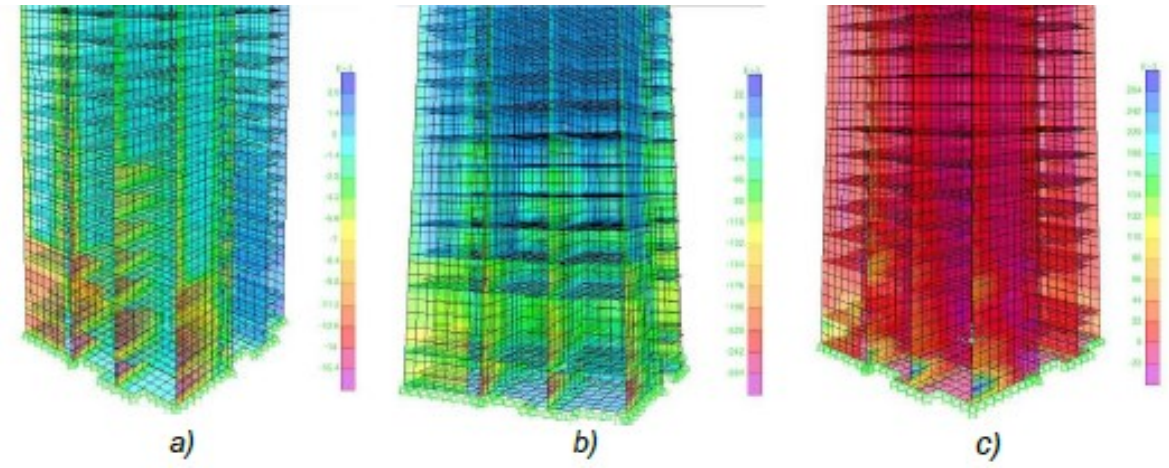


Figure 16. (a) Exceeding of concrete compressive strength, (b) Yielding of reinforcement in compression, (c) Yielding of reinforcement in tension.

Proceedings of the 3rd Croatian Conference on Earthquake Engineering - 3CroCEE
19–22 March 2025, Split, Croatia
Copyright © 2025 CroCEE
DOI: https://doi.org/10.5592/CO/3CroCEE.2025.107

The top displacements due to El Centro earthquake record are presented on the Fig. 15. with maximal horizontal displacement of 10.5 cm.

In the lower part of the building nonlinear behaviour was observed, yielding of reinforcement and exceeding of compressive strength in the concrete, see Fig. 16. Quick remark, due to low ratio of horizontal reinforcement, effect of confinement for the compressive strength of concrete could be fast neglected.

Another time history analysis was performed for the accelerogram Zagreb, simply scaled by factor of 2. The results showed maximal horizontal displacement of 9.5 cm at the top of the building (see Fig. 17.).

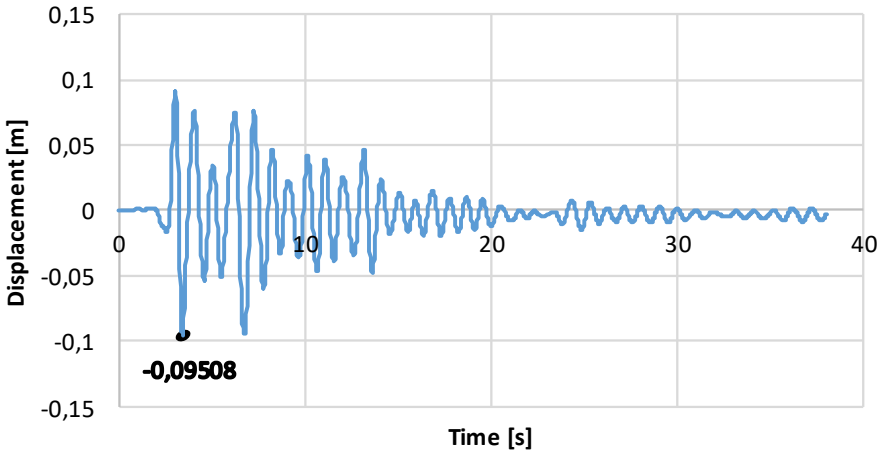


Figure 17. Horizontal displacements at the top of the building, acc. Zagreb, SF=2.

In order to capture some cracks development, building structure was analysed implementing DIANA software as well. Due to limitation in the size and number of finite elements, nonlinear behaviour was assumed only in lower part of the reinforced concrete walls. For the Zagreb accelerogram the cracks up to the width of 8 mm were observed at the bottom of some walls. The developing of the cracks during nonlinear dynamic analysis (time history analysis) is presented on the Fig. 18. It should be taken in the account that the cracks appear already by exceeding of tension strength in the concrete.

The magnitudes of horizontal displacements are not generally very large. The inter-storey drifts are all under the Eurocode 8 limit of 1%.

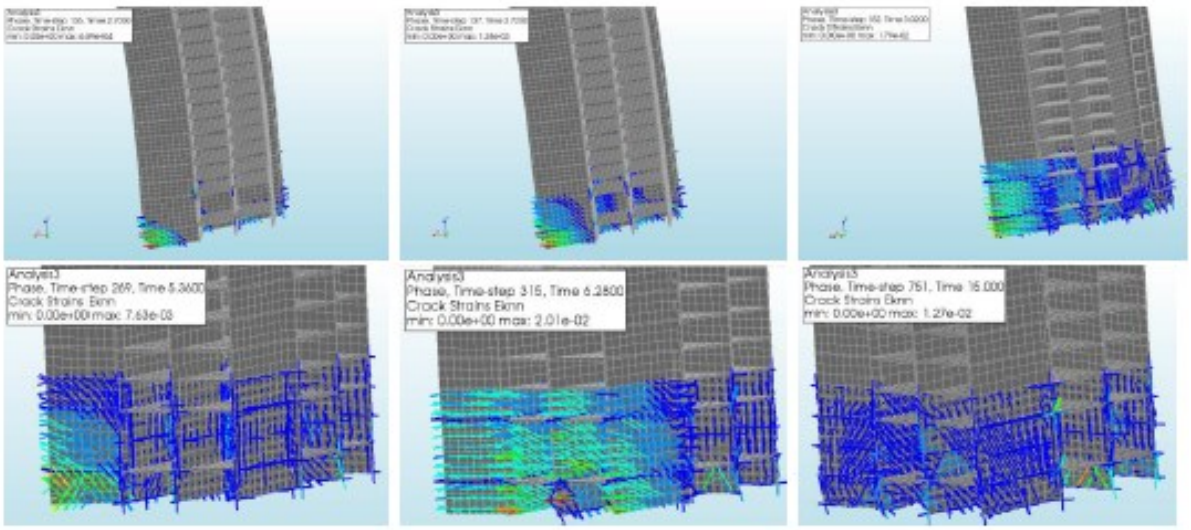


Figure 18. Cracks development.

Proceedings of the 3rd Croatian Conference on Earthquake Engineering - 3CroCEE
19–22 March 2025, Split, Croatia
Copyright © 2025 CroCEE
DOI: https://doi.org/10.5592/CO/3CroCEE.2025.107

7. Conclusions

The aim of the paper was to report about seismic analysis of the existing high-rise residential building, which was designed and built before introduction of the modern seismic code. Additional features of interest are structural system made entirely of reinforced concrete walls and slabs and extremely reduced amount of reinforcement at the upper three quarter of the walls height. The building is 66 m high with 23 floors and its structure is regular along the height. Time history analysis using two different software packages were performed.

Seismic analysis showed relatively good seismic performance. Time history analysis of the building, when exposed to the stronger earthquake motion yield nonlinear behaviour of the walls at the lower part of the building, which was expected. When exposed to moderate earthquake, like accelerogram of the Zagreb earthquake in 2020, the considered building structure remains mostly in the elastic range of the behaviour. This corresponds to the seismic performance of similar buildings, which were situated at the city of Zagreb, relatively close to the epicentre of the earthquake mentioned previously. Maximal horizontal displacement at the top of the building, exposed later to the stronger earthquakes was about 11 cm. Further on, for the Zagreb accelerogram scaled 200%, which means twice larger soil accelerations, nonlinearity, respectively plastic behaviour was developed at the bottom of the structure. The cracks up to 8 mm were developed in the bottom part of the walls.

However, it should be noted that the nonlinear dynamic analysis of an entire high-rise building depends significantly on computational model, variety of material behaviour modelling and earthquake loading input.

References

[1] Hrasnica, M. (2012): *Aseizmičko građenje (Aseismic buildings)*. Faculty of Civil Engineering, University of Sarajevo, Bosnia and Herzegovina *(*in Bosnian).

[2] EMS-98 (1998): *European Macroseismic Scale*, Editor G. Grüntal, European Seismological Commission, Luxembourg.

[3] Hrasnica M (2009): Damage Assessment for Masonry and Historic Buildings in Bosnia and Herzegovina. In: Ibrahimbegovic A, Zlatar M (eds) *Damage Assessment and Reconstruction after War or Natural Disaster*. NATO Science for Peace and Security Series C: Environmental Security, Springer Netherlands, pp. 333-356.

[4] *Eurocode 8* (EC8) European Standard EN 1998-1 2004. Design of structures for earthquake resistance, Part 1: General rules, seismic actions and rules for buildings, CEN European Committee for Standardization, Brussels, EU.

[5] Hrasnica, M. (2018): Seizmička otpornost nosivih sistema sa zidovima (Seismic resistance of the structural systems with walls), *Lecture notes, Research project YODA*, Faculty of Civil Engineering, University of Zagreb, Croatia (in Croatian).

[6] *Eurocode 2* (EC2) European Standard EN 1992-1 2004. Design of concrete structures Part 1-1: General rules and rules for buildings, CEN European Committee for Standardization, Brussels, EU.

[7] Chopra, A.K. (1995): *Dynamics of Structures,* Prentice Hall, USA.

[8] Wilson, E. L. (2002): *Three dimensional static and dynamic analysis of structures: a physical approach with emphasis on earthquake engineering.* Computers and Structures, Inc., California, USA.

[9] SAP2000. (2018). *User´s Manual*. Computers and Structures Inc., California, USA.

[10] Mander, J. B. (1988): Theoretical stress-strain model for confined concrete. *Journal of structural engineering*, 114(8), 1804-1826.

[11] Karavelić-Hadžimejlić, A. (2024): Efekat utezanja armiranobetonskih zidova (Effects of confinement by R.C. walls), *Report for doctoral studies*, University of Sarajevo-Faculty of Civil Engineering, Bosnia and Herzegovina (in Bosnian).

[12] DIANA FEA (2020): *DIANA - User´s Manual*, Material library. Delft, The Netherlands.

[13] Schneider, K-J. (2024*): Bautabellen für Ingenieure*. Werner Verlag, Germany

Proceedings of the 3rd Croatian Conference on Earthquake Engineering - 3CroCEE
19–22 March 2025, Split, Croatia
Copyright © 2025 CroCEE
DOI: https://doi.org/10.5592/CO/3CroCEE.2025.113

ASSESSING MECHANICAL PROPERTIES OF HISTORIC STONE MASONRY: CASE STUDY IN JURDANI (RIJEKA)

Paulo Šćulac [(1)], Josipa Mihaljević [(2)], Ivana Štimac Grandić [(3)], Davor Grandić [(4)]

[(1)] *Assistant Professor, University of Rijeka, Faculty of Civil Engineering, Croatia, paulo.sculac@uniri.hr*
[(2)] *Assistant, University of Rijeka, Faculty of Civil Engineering, Croatia, josipa.mihaljevic@gradri.uniri.hr*
[(3)] *Professor, University of Rijeka, Faculty of Civil Engineering, Croatia, istimac@gradri.uniri.hr*
[(4)] *Professor, University of Rijeka, Faculty of Civil Engineering, Croatia, dgrandic@gradri.uniri.hr*

Abstract

Assessment of mechanical properties of unreinforced stone masonry depends on the material used and the construction techniques applied. In this paper we explore the mechanical properties of stone masonry components on a case study - a more than 200-year-old historical building near Rijeka, which is currently being renovated and repurposed, as part of the ongoing research project on stone masonry in the Kvarner Littoral in Croatia. The stone masonry walls of the case study building were visually inspected, while stone and mortar specimens from the walls were used to determine their mechanical and chemical properties. This case study aims to contribute to a better understanding of the variability of the mechanical properties of stone masonry, especially in traditional buildings in the Kvarner Littoral.

Keywords: Kvarner Littoral, historic buildings, stone masonry, case study, mechanical properties, laboratory tests, earth mortars

1. Introduction

Assessment of the mechanical properties of stone masonry, especially in historic buildings, presents a particular challenge due to the variability of materials and construction techniques. In addition, the construction methods employed by masons vary, which further complicates the assessment of mechanical properties. The primary material – stone, is characterized by considerable regional variation, what can greatly affect their mechanical properties. The second component of stone masonry is mortar and its properties play a crucial role in the overall performance of the masonry (lime mortar is commonly used in historic stone masonry).

The mechanical properties of stone masonry can vary considerably, even within the same country, due to the shape and size of the blocks, the type of stone and the way the blocks are stacked in the wall (typology) which is in fact controlled by the local possibilities of stone supply and the availability of high-quality masons. The properties of mortar, such as the mortar strength, the thickness of the bed joints and possible degradation have a primarily influence on the performance of the stone masonry in an earthquake, rather than the stone blocks of incomparably greater strength [1].

After the 1979 Montenegro Earthquake extensive research on stone masonry, including the testing of masonry walls, was carried out in Croatia [2]. However, the results provided only approximate estimates of the material strengths [3].

In case of listed buildings, destructive testing methods are prohibited, and even non-destructive or semi-destructive techniques are often subject to strict restrictions. On the other hand, for private buildings not subject to listed building control, the investigation process is less restricted, as no cooperation with the heritage authorities is required.

As part of the ongoing research project to determine the material properties of stone masonry in the Kvarner Littoral (Croatia), field and laboratory tests were carried out on masonry components (stone and mortar) of a historic family house in Jurdani near Rijeka. The compressive strength of stone was determined by laboratory tests on 4 test specimens taken from the stone blocks of a partially collapsed

Copyright © 2025 CroCEE
DOI: https://doi.org/10.5592/CO/3CroCEE.2025.113

wall. The mortar was tested using non-destructive and destructive methods. The non-destructive methods, which were carried out in-situ, did not provide any results due to the wear and low strength of the mortar. Using destructive laboratory tests, the flexural strength was determined on 6 specimens from the mortar scraped from the wall, while the compressive strength of the mortar was determined on 12 specimens that remained after the flexural tensile test. The mortar was also subjected to chemical analysis using FTIR spectroscopy.

2. Case study

The building is located in Jurdani, in the vicinity of Rijeka. The year of construction is not known, but the house is displayed on the Second Habsburg cadastral survey from the 1819 [4]. The land lot contains a main building (the case study building) with a former livestock facility situated behind it. The case study building features a rectangular floor plan measuring 11,0 × 6,0 m and comprises of a partially buried ground floor and an upper floor (Fig. 1). The load-bearing walls measure 80 cm at the ground floor and 65 cm on the first floor (including the plaster layer). No iron ties have been detected within the building. The layout of the openings on the front façade is asymmetrical, and their dimensions differ between the ground and first floors, with the ground-floor openings being slightly larger. The building has a gable roof with a ridge height of 6,5 m. However, the roof structure, and consequently also the timber floor structure, have collapsed, so the interior of the building is exposed to weather conditions.

The masonry consists of irregular rubble stone blocks (limestone) of varying dimensions (Fig. 2a)), primarily composed of stone blocks with dimensions of s/h/l = 25/35/40 cm, where s represents the width, h the height, and l the length of the stone block. The largest stone blocks, exceeding 60 cm in length, are concentrated at the corners of the building (Fig. 1b)).

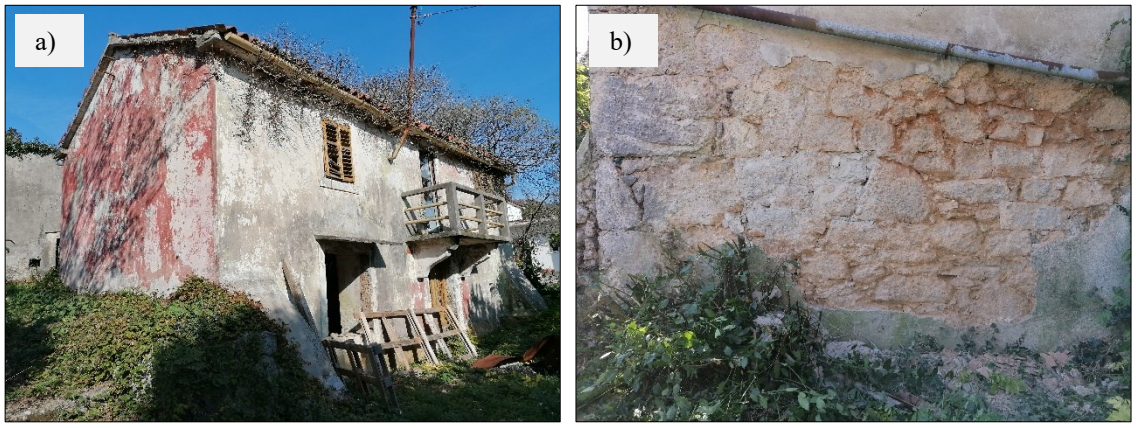


Figure 1. Case study building: a) front façade; b) side view.

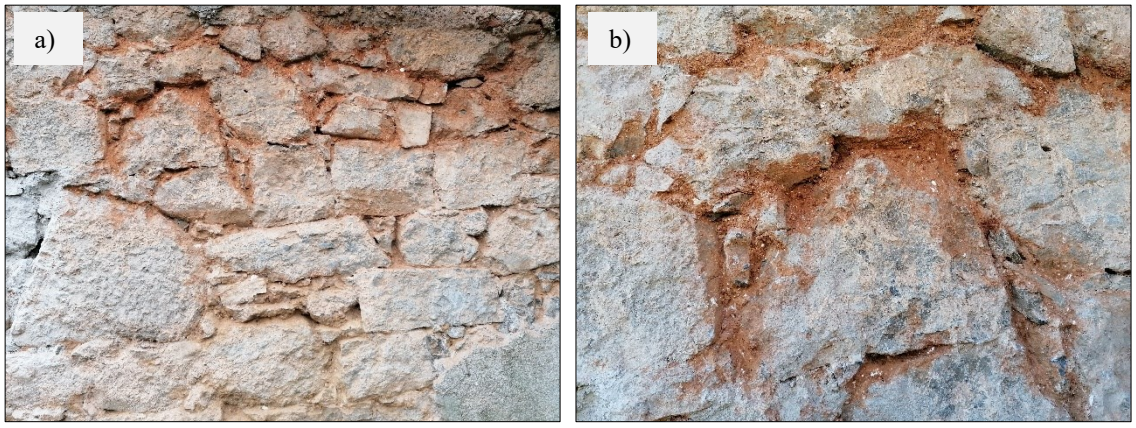


Figure 2. a) Masonry typology; b) detail of earth mortar with lime.

Copyright © 2025 CroCEE
DOI: https://doi.org/10.5592/CO/3CroCEE.2025.113

Non-degraded rubble stone blocks are bonded with a weak mortar. In this case study, instead of lime mortar, an earth mortar with a small addition of lime was observed, as indicated by the presence of white lumps visible in Fig. 2b). The surface layer of the mortar is crumbling. The vertical joints are mostly aligned, while the horizontal joints are discontinuous. Due to large dimensions of the stone blocks, the masonry contains a sufficient number of wedges to ensure the monolithicity of the wall.

3. Material properties of historic stone masonry components

In this section we present results of laboratory tests on stone and mortar specimens performed at the Faculty of Civil Engineering in Rijeka, together with mortar characterization by optical microscope and FTIR analysis, performed by an external laboratory [5].

The original plan was to assess the mechanical properties of the mortar using non-destructive methods, such as the mortar penetrometer or the mortar rebound hammer, but we encountered a mortar that was not lime-based and which was severely degraded in the bed joints near wall surface due to exposure to moisture (Fig. 2).

The mortar penetrometer (Fig. 3a)) measures the response of mortar to needle penetration and correlates it to the mechanical performance of the material, providing information regarding the quality and homogeneity of the mortar [6]. However, the needle penetration depth was so high (Fig. 3b)) that no correlation was possible (i.e. the mortar strength was so small that it was outside the calibration curve).

The mortar rebound hammer (Fig. 3c)) works on the same principle as the concrete rebound hammers: by measuring of the rebound of a spring-controlled mass that strikes a plunger that is in contact with the investigated material [7], except it has a different spring stiffness – the hammer we used may be applied for mortars with strength higher than 1,5 MPa [8]. However, due to low mortar strength the impact plunger just pressed into the mortar (Fig. 3d)), so correlation was not possible.



Figure 3. Application of NDT methods on mortar: a) and b) penetrometer; c) and d) rebound hammer.

Copyright © 2025 CroCEE
DOI: https://doi.org/10.5592/CO/3CroCEE.2025.113

3.1. Mechanical properties of stone

Four stone blocks have been extracted from the neighbouring livestock facility, which is nowadays connected to the case study building (assumed to have been built at the same time since as it is also listed on the cadastral survey [4]). From each block one cylindrical specimen was prepared (Fig. 4), in such a way that the diameter and height match the dimensions prescribed by the Standard [9] equal to 50 ± 5 mm.

The specimens were loaded continuously at a constant stress rate of 1 MPa/s until failure (Fig. 5) according to [9]; the results of uniaxial compressive strength are given in Table 1. Result determined for specimen No. 4 was rejected from statistical analysis due to the large difference in compressive strength (58,6 MPa) and its failure mode during the testing which both indicates probability of the defect in the specimen. The compressive strength values determined in the range of 131,4 MPa to 145,0 MPa (for specimens 1 to 3) correspond to the limestone expected to be built with at the building location.



Figure 4. Preparation of stone specimens: a) stone blocks; b) drilling of cylinders; c) extracted stone cylinders; d) specimens ready for testing.

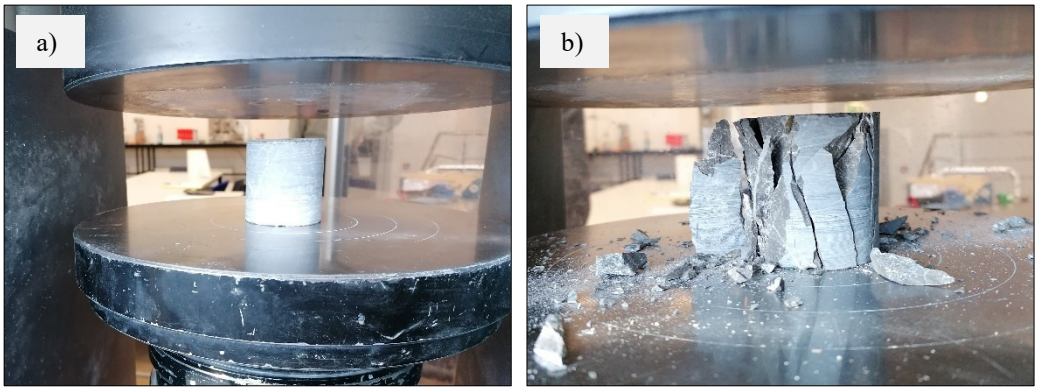


Figure 5. Uniaxial testing of stone cylinders: a) specimen No. 3 before; b) after test.

Copyright © 2025 CroCEE
DOI: https://doi.org/10.5592/CO/3CroCEE.2025.113

Table 1. Compressive strength of stone specimens

Specimen	Height, h (mm)	Diameter, D (mm)	Weight (g)	Density, γ (kg/m^3)	Max load, F (kN)	Strength, f_s * (MPa)
1	53,2	54,2	325	2648	305,1	132,3
2	54,8	54,1	337	2675	333,4	145,0
3	57,7	54,2	355	2667	303,1	131,4
4	62,4	54,1	384	2677	134,6	58,6
Mean value +				2663 +		136,2 +
St. dev. +				14,0 +		7,6 +

* $f_s = 4 \cdot F/(D^2 \cdot \pi)$
+ for specimens 1-3

3.2. Mechanical and chemical properties of mortar

Although the authors did not expected this, based on their previous knowledge on masonry buildings in the Croatian coastal region, after removing the plaster from the ground floor walls of the house in this case study, it was detected that earth mortar had been used (Fig. 2 a)). The similar earth mortar has been observed in another building not fare away from the case study building. There is a high probability that there are many more applications of earthen mortars in our country, but this has not yet been sufficiently researched.

Earth-based mortars (also referred as mud mortar or clay mortar) have been used as filling materials and plasters in adobe, fired brick and stone masonry worldwide [7]. They can be found not only in rural areas but also in European historic centres [10, 11]. Recent restauration works in Scotland have shown that clay mortars are much more common than previously realised [12].

Recent earthquakes revealed that buildings with earth-based mortars behaved poorly, but this shouldn't be attributed only to the mortar but also to the construction techniques. Kumar Bothara et al. [1] report of a large number of destroyed stone masonry buildings with mud mortar located in remote rural areas of India in 2015 Gorkha earthquake. The recent earthquakes in Turkey revealed that earth mortar binders were commonly used in traditional unreinforced masonry buildings in rural areas till 1960s [13, 14]. Kuruscu et al. [13] note that the harsh environmental conditions (freeze-thaw cycles during winter) caused the disintegration of the earth mortars, what significantly decreased the shear capacity of the masonry walls.

Sorrentino et al. [11] and D'Ayala et al. [10] report of performance of historical buildings with mud mortar during the Central Italy earthquakes. As stated in [11], at least until 60-70 years ago,mortar was produced from a soil pit where the excavated ground was mixed with enough water until adequate plasticity was achieved. Cantù et al. [15] report of mortars mixtures consisting of soil and small amount of quicklime (less than 5% of weight) in Cremona. A detailed analysis of earthen mortars in Central and Northern Italy including the petrographic, textural, mineralogical and chemical analysis may be found in [15, 16].

Earth based mortars are regaining its place as building materials for plastering, rendering and repair of earthen walls [17]. In recent studies, the effect of adding fibres or mineral binders as stabilisers was investigated [17], and new methodologies for mortar mix design when adding sand are proposed [18].

Clay mortars are considered to be inferior materials, due to their negligible tensile strength and vulnerability to external conditions (exposure to water). However, the primary function of the mortar is to support the blocks in a masonry wall and to enable a uniform distribution of the compressive stresses and earth based mortars commonly have sufficient compressive strength to conduct this function [12].

Fig. 6 b) presents an image of mortar specimen, which was extracted undisturbed from the bed joints of the case study building, obtained using light microscope with a 10x magnification: it consists of the brown matrix - earth (soil) with a small proportion of lime in the form of white lumps. The admixtures of organic origin (i.e. plant remains) are also visible as black areas in the figure [5].

Proceedings of the 3rd Croatian Conference on Earthquake Engineering - 3CroCEE
19–22 March 2025, Split, Croatia
Copyright © 2025 CroCEE
DOI: https://doi.org/10.5592/CO/3CroCEE.2025.113

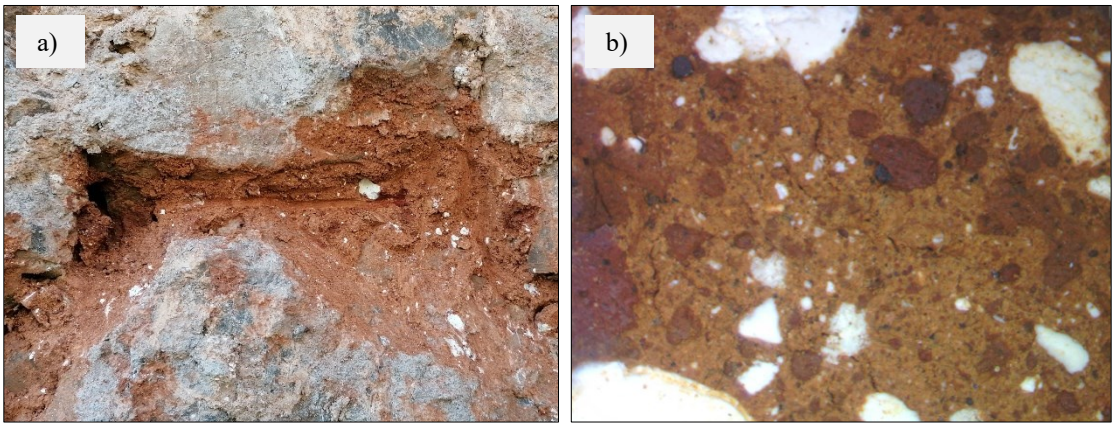


Figure 6. a) Detail of the earth mortar with white lime lumps; b) microscope image of a mortar specimen (10x magnification) [5].

FTIR Spectroscopy was used to identify the composition of the mortar [5]. Two milligrams of both the white lumps as well as the brown matrix were mixed with potassium bromide (KBr) and pressed into pellets. The obtained spectra are the result of the mean value of 20 recorded spectra per sample, with a recording resolution of 4 cm^{-1} in the spectral range from 4000 to 400 cm^{-1}.

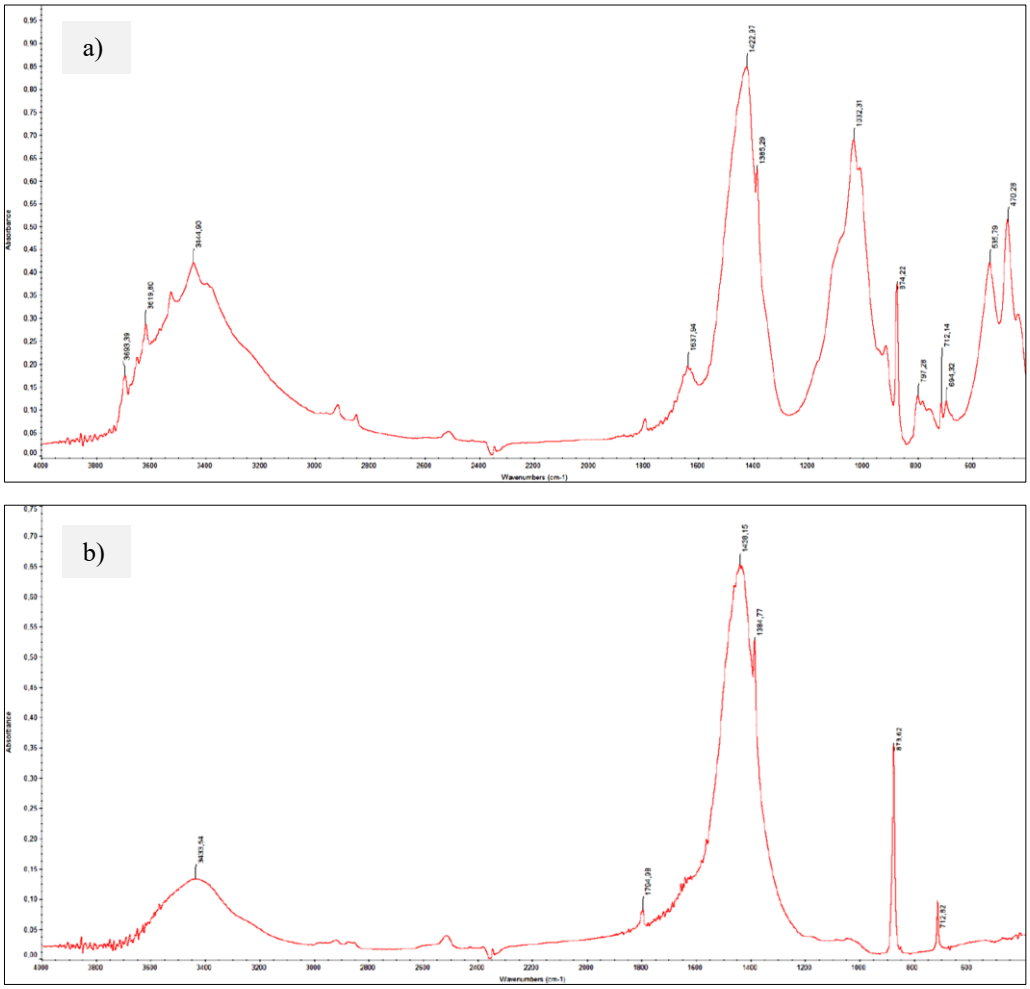


Figure 7. FTIR analysis of mortar: a) brown matrix (soil); b) white lumps (lime) [5].

Copyright © 2025 CroCEE
DOI: https://doi.org/10.5592/CO/3CroCEE.2025.113

The FTIR analysis (Fig. 7) showed that the brown-colored binding matrix consists of minerals typically found in soil (silicates and iron-aluminosilicates such as Illite, Montmorillonite…) and white lime lumps. Additionally, a band at 1385 cm^{-1} is visible in both spectra, indicating the presence of nitrates in the sample. Salts containing nitrates are typically found in buildings in rural areas or tombstones, i.e. in structures that are in direct contact with the soil. Considering that this sample contains a high proportion of the soil, it is possible that nitrates were present from the beginning as components of the soil from which the mortar was made [5].

Since the mortar has degraded, it was possible to extract it from the bed joints in a powder form by simple scratching. The extracted powder was then used to prepare mortar prisms 160 x 40 x 40 mm for flexural and compressive strength testing – enough water was added to ensure good workability (although certain amounts of air pockets were noticed after drying). The metal moulds were filled with mortar in two approximately equal layers, each layer being compacted by 25 strokes of the tamper. The specimens were then stored in polyethylene bags for 7 days and afterwards for another 21 days in laboratory conditions. A total of 6 specimens were prepared (Fig. 8).

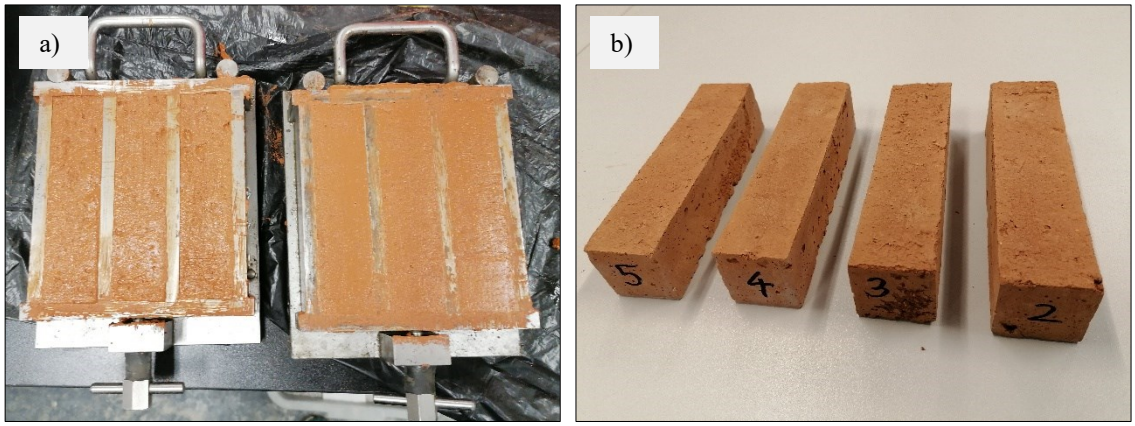


Figure 8. Mortar specimens: a) preparation in metal moulds; b) prisms before testing.

The specimens were tested at an age of 28 days after casting. The flexural strength of mortar was determined by three point loading to failure (Fig. 9) according to [19], and the results are presented in Table 2. The values of flexural strength between 0,18 and 0,3 MPa, with the mean value of 0,26 MPa, are rather low, as expected.



Figure 9. Flexural strength test – three point loading scheme.

Copyright © 2025 CroCEE
DOI: https://doi.org/10.5592/CO/3CroCEE.2025.113

Table 2. Flexural strength of mortar specimens

Specimen	Width, b (mm)	Depth, d (mm)	Max load, F (N)	Strength, f_b * (MPa)
1	39	38,5	100	0,26
2	39	38,3	100	0,26
3	38,6	38,6	70	0,18
4	38,5	38	112,5	0,30
5	38,7	38,2	113	0,30
6	38,6	38,3	103	0,27
Mean value				0,26
St. dev				0,04

* $f_b = 1{,}5 \cdot (F \cdot l)/(b \cdot d^2)$, l =100 mm (distance between the support rollers)

The compressive strength of the mortar given in Table 3 is determined according to [19] on the two parts of the specimens resulting from the flexural strength test (Fig. 10). The average compressive strength of the mortar cubes is 2,36 MPa (standard deviation 0,12). The results are comparable with results reported in [1]: average compressive strength of the mortar cubes 50,8 x 50,8 mm according to ASTM C-109 was 1.73 MPa (CoV 29,2%).

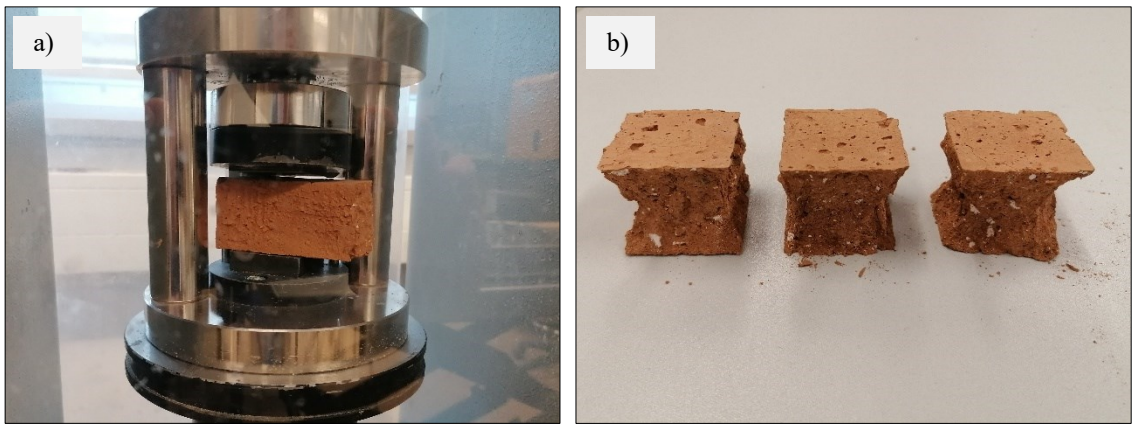


Figure 10. a) Compression test setup; b) hour-glass mortar specimens after testing with visible lime lumps.

Table 3. Compressive strength of mortar specimens

Specimen	Width, b (mm)	Max load, F (N)	Strength, f_c * (MPa)
1	39	3470	2,22
2	39	3630	2,33
3	39	3710	2,38
4	39	3460	2,22
5	38,6	3670	2,38
6	38,6	3730	2,42
7	38,5	4080	2,65
8	38,5	3620	2,35
9	38,7	3770	2,44
10	38,7	3590	2,32
11	38,6	3630	2,35
12	38,6	3420	2,22
Mean value			2,36
St. dev.			0,12

* $f_c = F/(b \cdot a)$, a =40 mm (bearing plate length)

Proceedings of the 3rd Croatian Conference on Earthquake Engineering - 3CroCEE
19–22 March 2025, Split, Croatia
Copyright © 2025 CroCEE
DOI: https://doi.org/10.5592/CO/3CroCEE.2025.113

4. Conclusions

This paper presents results of an on-site inspection of masonry and laboratory tests on stone and earth mortar from a more than 200-year-old stone masonry building in Jurdani near Rijeka. The selected case study building is a typical rural house in the Kvarner Littoral in Croatia. It is a two-storey building, with ground floor partially buried into the ground.

The on-site examination of the stone masonry walls of the case study building and the laboratory tests led to the following conclusions:

- The walls consist of rubble stone masonry with wedges between the blocks and corner stones of larger size.
- The stone used in the case study building is characterized by the high compressive strength typical for limestone.
- Instead of lime mortar, earth mortar with a small amount of lime added is used (it does not contain sand or gravel).
- The results of the FTIR spectroscopy of the earth mortar indicate that the mortar was made from local soil deposits.
- The earth mortar in the bed joints near the wall surface was degraded due to exposure to moisture, so that the non-destructive testing methods on-site test failed.
- The flexural strength of the earth mortar specimens is low, while the compressive strength is comparable to the compressive strength of lime mortar.
- Earth-based mortars are probably more widespread than may be expected in buildings which are part of the built heritage in the Kvarner Littoral.

The most valuable discovery of the case study presented is the usage of earth mortar in stone masonry, which had not been expected. Although there are numerous researches worldwide related to various aspects of earth-based mortars, this type of mortar has not been sufficiently researched in Croatia. Also, the earth mortar of the case study building is of particular interest because it does not contain sand or gravel, which distinguishes it from the commonly used historic earth mortars in which clay minerals serve as a binder for sand and silt particles.

Since mortar properties have a significant influence on the behaviour of stone masonry during earthquakes, further research is therefore required to determine the mechanical properties of rubble stone masonry in which this type of earth mortar is used.

Acknowledgements

This research was financially supported by the University of Rijeka through grant No. *uniri-iskusni-tehnic-23-198: Adjustment of the methodology for assessing the seismic resistance of existing masonry buildings in the Kvarner Littoral.*

References

[1] Kumar Bothara, J., Ahmad, N., Ingham, J.M., Dizhur, D. (2023): Mechanical properties of stone masonry set in mud mortar and contained by steel wire mesh, *Construction and Building Materials*, **405**, 133348, 1-20, doi: https://doi.org/10.1016/j.conbuildmat.2023.133348

[2] Aničić, D., Fajfar, P., Petrović, B., Szavitz-Nossan, A., Tomaževič, M. (1990): *Zemljotresno inženjerstvo – visokogradnja*, Građevinska knjiga, Beograd.

[3] Sorić, Z. (2016): *Zidane konstrukcije*, Zagreb, In Croatian.

[4] https://a4view.archiviodistatotrieste.it/patrimonio/d59786d9-0a27-41b9-8627-209af8655d94/204-b-02-mappa-catastale-del-comune-di-giordani-foglio-ii-sezione-ii-1819-sec-xix-primo-quarto, (accessed November 20, 2024).

Copyright © 2025 CroCEE
DOI: https://doi.org/10.5592/CO/3CroCEE.2025.113

[5] Test Report 26/2024 (2024): Mortar characterization by optical microscope and FT-IR analysis. MarLab d.o.o., Pula, Croatia.

[6] Penetrometer striker RSM, User Manual, Diagnostic Research Company (DRC Srl), Italy, 2015.

[7] Gambilongo, L., Barontini, A., Silva, R.A., Lourenco, P.B. (2023): Evaluation of non-destructive techniques for mechanical characterisation of earth-based mortars in masonry joints, *Construction and Building Materials*, **392**, 131960, 1-14, doi: https://doi.org/10.1016/j.conbuildmat.2023.131960

[8] Sclerometro tipo M, User manual, PASI, Italy, 2009.

[9] HRN EN 1926:2008, Natural stone test methods - Determination of uniaxial compressive strength (EN 1926:2006), HZN.

[10] D'Ayala, D.F., Paganoni, S. (2011): Assessment and analysis of damage in L'Aquila historic city centre after 6th April 2009, *Bulletin of Earthquake engineering*, **9**, 81-104, https://doi.org/10.1007/s10518-010-9224-4

[11] Sorrentino, L., Cattari, S., Da Porto, F., Magenes, G., Penna, A. (2019): Seismic behaviour of ordinary masonry buildings during the 2016 central Italy earthquakes, *Bulletin of Earthquake Engineering*, **17**, 5583-5607, doi: https://doi.org/10.1007/s10518-018-0370-4

[12] Curtis, R. (2015): Clay mortars for masonry buildings. INFORM-Information for historic building owners, Historic Scotland, Edinburgh, UK.

[13] Kuruscu, A.O., Güney, D., Görün, A. (2014): Seismic behaviour of vernacular masonry buildings during 2010 and 2011 earthquakes in Turkey, 9th International Masonry Conference, Guimarães, Portugal, 10 pages.

[14] Günaydin, M., Atmaca, B., Demir, S., Altunişik, A.C., Hüsem M., Adanur, S., Ateş, S., Angin, Z. (2021): Seismic damage assessment of masonry buildings in Elazığ and Malatya following the 2020 Elazığ-Sivrice earthquake, Turkey, *Bulletin of Earthquake Engineering*, **19**, 2421-2456, doi: https://doi.org/10.1007/s10518-021-01073-5

[15] Cantù, M., Giacometti, F., Landi, A.G., Riccardi, M.P., Tarantino, S.C., Grimoldi, A. (2016): Earthen mortars from Cremona (Northern Italy): The evolution through centuries of a manufacturing tradition, Construction and Building Materials, **125**, 520-532, doi: http://dx.doi.org/10.1016/j.conbuildmat.2016.07.139

[16] Artioli, G., Secco, M., Mazzoli, C., Coletti, C., Valuzzi, M.R., da Porto, F. (2010): Characterisation of stone masonry panels consolidated by injection of grouts in buildings damaged by the 2009 Abruzzo earthquake, 2nd Historic Mortar Conference HMC2010 and RILEM TC 203-RHM Final Workshop, Prague, Czech Republic.

[17] Gomes, M.I., Faria, P., Gonçalves, T.D. (2018): Earth-based mortars for repair and protection of rammed earth walls. Stabilization with mineral binders and fibers, *Journal of Cleaner Production*, **172**, 2401-2414, doi: https://doi.org/ 10.1016/j.jclepro.2017.11.170

[18] Duriez, M., Vieux-Champagne, F., Trad, R., Maillard, P., Aubert, J.E. (2020): A methodology for the mix design of earth bedding mortar. *Materials and Structures*, **53** (1), 16, doi: https://doi.org/10.1617/s11527-020-1443-9

[19] HRN EN 1015-11:2019, Methods of test for mortar for masonry - Part 11: Determination of flexural and compressive strength of hardened mortar (EN 1015-11:2019), HZN.

Proceedings of the 3rd Croatian Conference on Earthquake Engineering - 3CroCEE
19–22 March 2025, Split, Croatia
Copyright © 2025 CroCEE
DOI: https://doi.org/10.5592/CO/3CroCEE.2025.114

TIES IN UNREINFORCED MASONRY STRUCTURES: CASE STUDY IN KRK

Paulo Šćulac [(1)], Kristina Galjanić [(2)], Davor Grandić [(3)], Josipa Mihaljević [(4)], Željko Smolčić [(5)]

[(1)] *Assistant Professor, University of Rijeka, Faculty of Civil Engineering, Croatia, paulo.sculac@uniri.hr*
[(2)] *GP KRK d.d., Stjepana Radića 31, 51500 Krk, Croatia, kristina.galjanic@gp-krk.hr*
[(3)] *Professor, University of Rijeka, Faculty of Civil Engineering, Croatia, dgrandic@gradri.uniri.hr*
[(4)] *Assistant, University of Rijeka, Faculty of Civil Engineering, Croatia, josipa.mihaljevic@gradri.uniri.hr*
[(5)] *Associate Professor, University of Rijeka, Faculty of Civil Engineering, Croatia, zeljko.smolcic@uniri.hr*

Abstract

This paper examines the use of ties in a 19th century stone masonry building in Krk, Croatia. To prevent the out-of-plane failure mechanisms buildings should have adequate structural integrity. The beneficial details in this case study include: i) timber ring beams inserted into the walls acting as horizontal ties; ii) connections between the timber floor beams and the masonry walls via anchoring iron ties; and iii) connections of the attic walls and the floor beams using diagonal iron ties. The mechanical properties of wrought iron ties have also been investigated.

Keywords: heritage buildings, unreinforced masonry, structural integrity, wrought iron ties, timber ring beams

1. Introduction

The recent earthquakes in Croatia in 2020 have reminded us again that heritage masonry buildings are highly vulnerable to seismic actions. In this paper we will focus on the prevention of out-of-plane failure mechanisms in masonry structures, which result from scarce wall-to-wall and wall-to-floor connections. Masonry buildings should have adequate structural integrity, i.e. they should behave like a box, in order to switch from the undesirable out-of-plane failure mechanisms to in-plane failure mechanisms. This includes: quoins - larger stone blocks at the corners of the building, appropriate bond pattern between the intersection walls, metal ties between the floor structure and the walls, etc. [1].

Detecting the elements that ensure the integrity of an existing building is very rarely possible since the skeleton of the building is covered by plaster, claddings and façade. The in-depth inspection of the skeleton of the building is only possible: (i) during a renovation or (ii) less favourable, in the event of a major earthquake, during a damage inspection. Although it is not desirable, a post-earthquake damage inspection can provide valuable information about the effectiveness of certain elements in historic buildings [1-4]. This is how construction details that ensured good performance in a previous earthquake was handed down to builders over generations [3].

The ties and quoins aim to enhance the box-like behaviour. Ties should be regularly spaced over the façade and appropriately connected to the walls and to the floor structure, in order to make the constraints effective [1]. The recent earthquakes in Central Italy proved that metal ties, when combined with a reasonably quality masonry, contributed to preventing collapse of the buildings [2]. When the quality of the masonry at the corners is enhanced by the presence of quoins, the vertical overturning of the façade will be prevented. However, the effectiveness of the quoins is limited when coupled with masonry with poor bond pattern or unconnected multi-leaf walls, as wall leafs tend to separate [1].

Lagomarsino [3] performed damage assessment on churches, being the most vulnerable among historical buildings, after the L'Aquila earthquake. He reports of horizontal wooden logs embedded into the masonry walls during construction and connected to the external walls by means of metal flats and anchor metal bars (Italian "capochiave con paletto") acting as ties. The anchor bars are often very small in size (about 60 cm long), since the anchoring is not limited only to the external wall but is diffused due to friction that develops over the entire length of the wooden log. However, the weak point was always found at the connection of the two nails between the metal anchor and the wooden log or in the

Copyright © 2025 CroCEE
DOI: https://doi.org/10.5592/CO/3CroCEE.2025.114

insufficient overlapping. Günaydin et al. [4] showed that masonry buildings with horizontal timber bond beams in rural areas in Turkey behaved more stable than those in which timber bond beams were not used or partially used during the 2020 earthquake. They also report of poor splicing details of the beams, which contributed to their failure.

In this paper we will present a case study building explored as part of an ongoing research project on traditional stone masonry structures in the Kvarner Littoral. The building was recently reconstructed and adapted for a new purpose, and due to the replacement of the floor and roof structures an in-depth inspection of the building skeleton was possible. Structural connections between the walls, floors and the roof will be explained in detail. Also, the material and mechanical properties of several wrought iron ties extracted from the building were investigated.

2. Case study

The building is located in Krk, Croatia, incorporated into the old part of the city, which is listed as a cultural-historical urban complex in the Register of Cultural Properties. Over the years, the building has undergone various reconstructions. It consists of a central L-shaped part (consisting of two rectangular parts that were formerly two different buildings) and two smaller rectangular parts, added afterwards, making an E-shaped ground plan (Fig. 1b). The year of construction is not known, but the central L-shaped part of the building is displayed on the Second Habsburg cadastral survey from the 1819 [5].

It consists of a ground floor, two storeys and an attic, with approximate floor plan dimensions 20 x 12,5 m. The height of the roof cornice is around 10 m. It has an almost symmetrical arrangement of the openings on the front façade (Fig. 1a); the windows are rather large and extend over almost the entire floor (except on the attic).

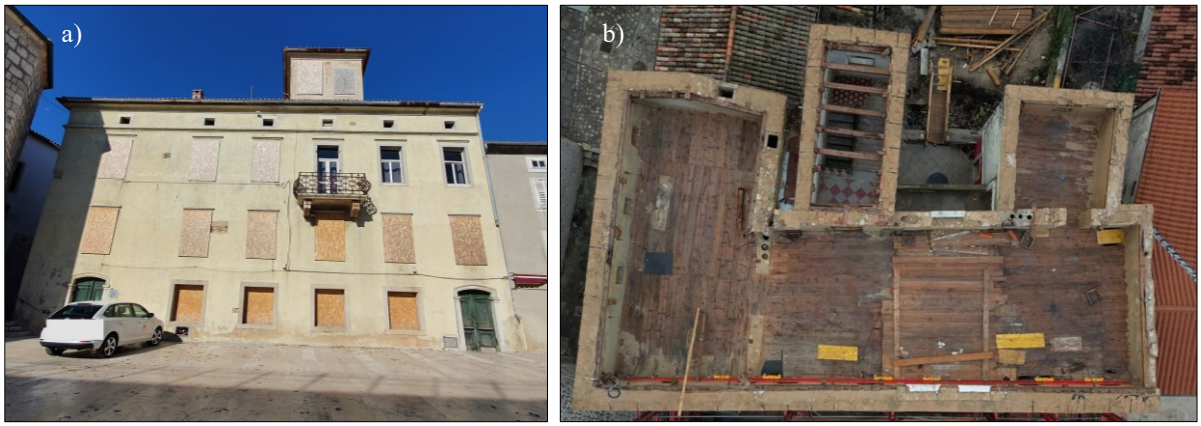


Figure 1. a) Front façade; b) Building plan at the roof level [6].



Figure 2. Masonry typology.

Proceedings of the 3rd Croatian Conference on Earthquake Engineering - 3CroCEE
19–22 March 2025, Split, Croatia
Copyright © 2025 CroCEE
DOI: https://doi.org/10.5592/CO/3CroCEE.2025.114

The floor structures are made of timber beams and boards, as common in this region, while the roof structure is a king-post, covered with tiles. The walls may be categorized into rubble stone masonry (wall thickness 65 cm), though some later added walls are built of brick. The stone blocks are mostly of the same size, with considerably larger dimensions at the corners or at the openings (Fig. 2)

3. Ties

Since the floor is flexible in-plane additional elements have been provided to connect the walls and to ensure the global box-like behaviour. This includes horizontal timber ring beams embedded into the walls just below the floor level and floor-to-wall connections via both the horizontal and diagonal wrought iron ties.

3.1. Timber ring beams

The use of timber ring beams as ties is quite common in adobe masonry [7-9]. A traditional method to reinforce the adobe masonry includes the installation of beams at the corners or at the perimeter of the building, spaced at every 60 to100 cm over the wall height. The ring tie beams are usually made of timber, concrete, steel or straw bars and enable the building to behave as a box, increasing its resistance against the wind or the seismic loads [7].

Although the use of timber ring beams as ties is quite common in adobe masonry, it is not so common in stone masonry. D'Ayala and Paganoni [1] report of timber ties in residential buildings, inserted just below the floor level or above the openings, while Lagomarsino [3] reports of timber logs in churches, both in Aquila. Sorrentino et al. [2] indicate on the application of timber ties in Central Italy. Al Qablan et al. [10] report on timber string-courses embedded in ashlar buildings in Jordan, as an anti-seismic device.

Timber beams have been also used as ties in domes (it is well known that Brunelleschi used timber ring beams to absorb the horizontal thrusts in the dome of Florence [11]) and in arched structures (for example in churches in Albania [12].

Authors of this paper have not so far detected timber ring beams embedded into masonry in the Kvarner Littoral, so the discovery of the timber beams in Krk was the motive for presenting this unique case study. These beams have minimum dimensions 13 x 19 cm, and are made continuous like a ring around the perimeter walls (Fig. 3): at the joint of two beam ends wrought iron ties have been used. At the positions of the opening for chimney in the cross-section of the wall, timber beams have been omitted (since there isn't enough width, but also due to heating) and instead replaced with iron ties (denoted with a red arrow in Fig. 4). The ring beams have also been provided in the inner walls.

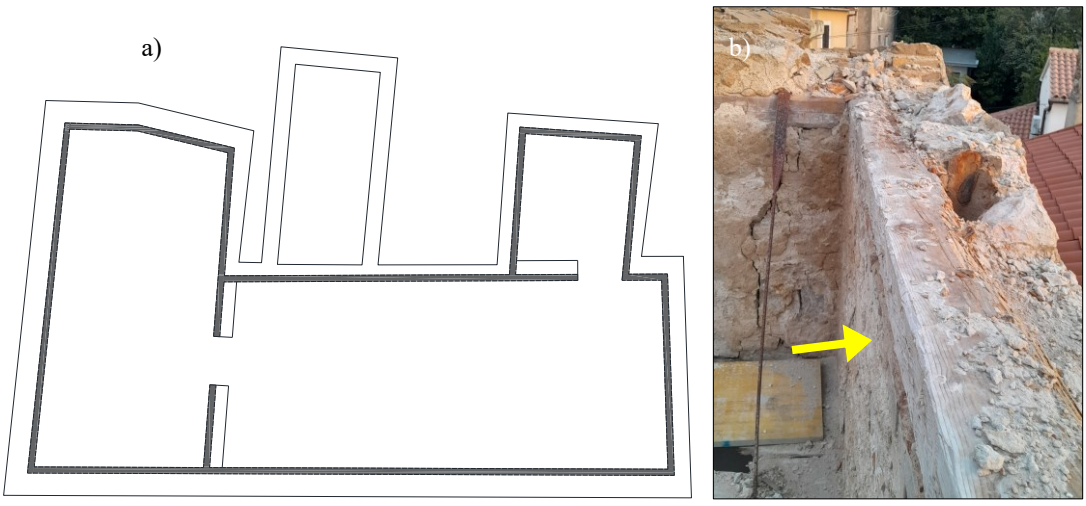


Figure 3. Timber ring beams at the roof level: a) Ground plan; b) Detail.

Copyright © 2025 CroCEE
DOI: https://doi.org/10.5592/CO/3CroCEE.2025.114



Figure 4. Timber ring beams at the roof level.

The timber ring beams are provided at the floor levels and at the roof level (at the top of the attic walls). Note the connection of two beam ends using an iron tie (in order to ensure continuity), indicated with a red arrow in Fig. 5. No ring beams have been detected above the ground floor. This can be explained by the possibility that the ground floor had been probably built in an earlier period.

The ring beams at one corner of the attic walls have been additionally connected by a cross iron tie at the top to prevent their separation (Fig. 6).



Figure 5. Timber ring beams at the floor levels.

Copyright © 2025 CroCEE
DOI: https://doi.org/10.5592/CO/3CroCEE.2025.114

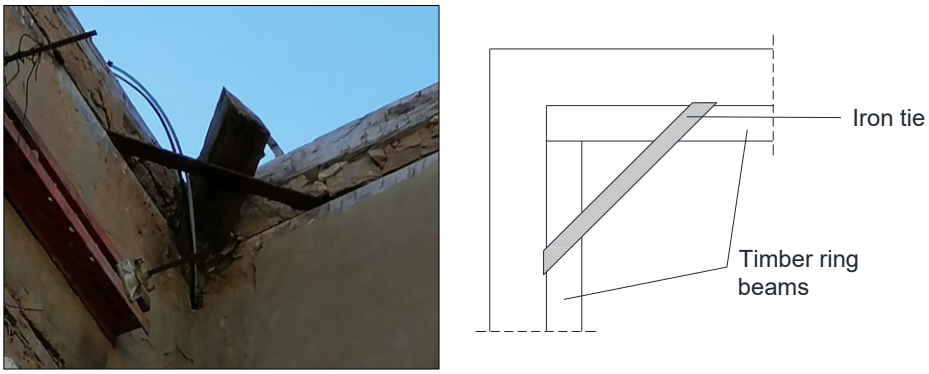


Figure 6. Connection of timber ring beams at a corner via iron ties.

3.2. Horizontal wall-to-floor connections

Wall-to-floor connections play a crucial role in the global stability of masonry buildings under seismic actions [13]. In this case study, connections between the timber floor beams and the masonry walls are placed at every fourth beam in the floor (Fig. 7). Wrought iron ties are anchored to the external walls by means of anchor iron bars (red arrow on Fig. 7). Three nails are used to connect the iron flat and the timber beam.

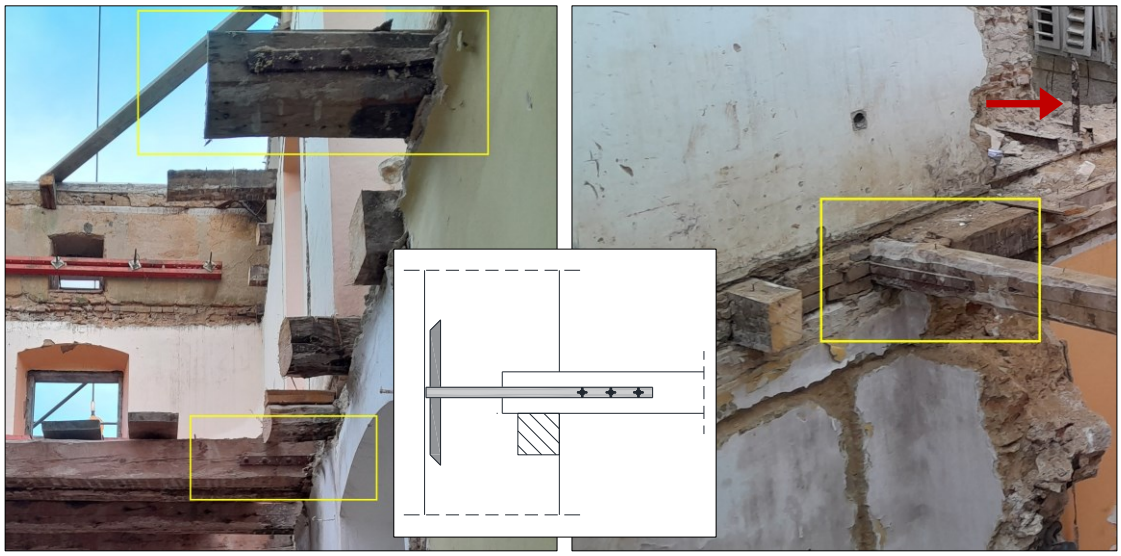


Figure 7. Horizontal wall-to-floor ties.

3.3.Diagonal wall-to-floor ties

Diagonal iron ties are used to connect the attic walls and the floor beams, placed at every fourth or fifth floor beam (Fig. 4, Fig. 8). These ties have a “hockey stick” shape so that they can be attached to the floor beam by two nails, while the upper part of the tie is twisted by 90° and then bent into an L shape, so that it encompasses the timber ring beam (Fig. 8). The ties have a uniform rectangular cross-section measuring 45 mm in width, while the thickness varied from 8,5 to 12,5 mm, depending on the element.

4. Material properties of wrought iron ties

Material and mechanical properties of iron ties were inspected on seven diagonal wall-to-floor ties extracted from the attic. From each diagonal tie one testing specimen was prepared. One sample was used to obtain chemical composition (Fig. 9) - the GDS analysis provided an insight into the concentrations of the secondary elements [14].

Copyright © 2025 CroCEE
DOI: https://doi.org/10.5592/CO/3CroCEE.2025.114



Figure 8. a) Diagonal wall-to-floor iron ties.

4.1. Chemical properties of wrought iron ties

Table 1 shows the mean values of the measured weight percentage *w* of individual elements and their standard deviation *SD* obtained using glow-discharge spectrometer (GDS)[14]. The cross-section was prepared by polishing. According to the very low carbon content, a soft but very ductile material can be expected, what will be confirmed by tensile testing.



Figure 9. a) Cross section of a diagonal tie; b) Detail of forged connection confirming it is wrought iron.

Table 1. Chemical composition obtained via glow-discharge spectrometer [14]

Element	C	Mn	Si	P	S	Mo	Ni	Cr	Cu	Al	Sn	As
w (%)	0,0199	0,32	0,0553	0,0589	0,0186	0,0016	0,0197	0,0038	0,0801	0,0065	0,0312	0,0021
SD (%)	18,42	3,65	-	33,66	36,37	48,8	-	37,33	-	-	38,3	-

4.2. Mechanical properties of wrought iron ties

Testing specimens were prepared by waterjet cutting, using a high-pressure jet of a mixture of water and an abrasive substance (Fig. 10). This cutting method was selected because it does not heat the metal,

Copyright © 2025 CroCEE
DOI: https://doi.org/10.5592/CO/3CroCEE.2025.114

which is preferable since exposure to high temperatures can change its characteristics. According to [15] it is possible to test specimens as-manufactured (without the cross-section reduction), but there is a possibility that the fracture may then occur outside the extensometer length. The surface of the specimens was additionally sanded with an 80 grit flap disc to remove the rust and old paint.

The dimensions of the specimens have been selected to match the so-called proportional specimens [15], in which the gauge length L_o is in direct relationship with the cross-sectional area by the equation $L_o = 5{,}65 \cdot (a_o \cdot b_o)^{1/2}$. However, since the thickness of the specimens after sanding a_o varied from 8,1 to 12,1 mm (i.e. the gauge length would be different for each specimen), due to the ease of testing it was decided to adopt the extensometer gauge length L_e equal to 100 mm (corresponding to the specimen with the largest thickness) for all specimens. A transition radius R of 25 mm was selected between the gripped ends and the parallel (reduced) length (Fig. 11). The following symbols are used: L_t – specimen length (L_t = 500 mm), L_c – length of the parallel reduced section (L_c = 130 mm), b – specimen width, b_o and a_o – width and thickness of the parallel length (reduced section) respectively.

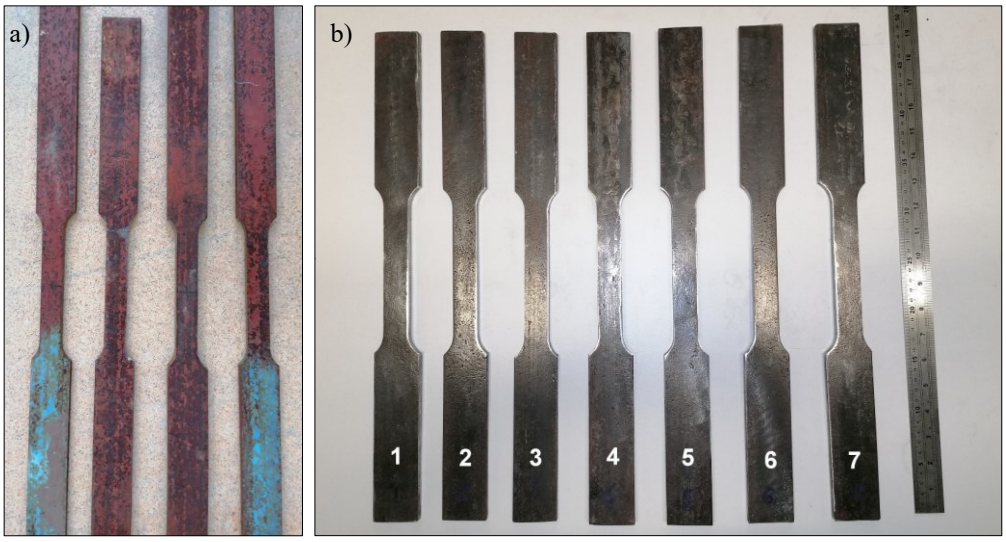


Figure 10. Preparation of specimens: a) after waterjet cutting; b) after sanding.

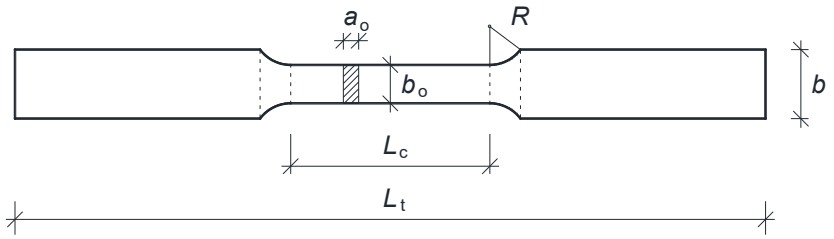


Figure 11. Specimen details.

Specimens were tested on Zwick Röll Z600E (Fig. 12) according to method A1 [15] with strain rate control, based on the feedback obtained from the extensometer in the range up to yielding (recommended strain rate 0,00025 s^{-1} was applied). In the yielding range, the strain rate control over the parallel length (L_c =130 mm) achieved by controlling the crosshead separation rate was used (strain rate equal to 0,00025 s^{-1} was applied), while after the yielding phase the strain rate was increased to 0,0067 s^{-1} (crosshead separation rate). Grip to grip length was 334 mm.

The results of the tensile tests are presented in Table 2, while the stress-strain relationships are given in Fig. 13. The following symbols are used: R_{eH} – upper yield strength, R_m – tensile strength (stress corresponding to maximum load), A_{gt} – deformation at maximum load, A_t – deformation at

Copyright © 2025 CroCEE
DOI: https://doi.org/10.5592/CO/3CroCEE.2025.114

fracture and m_E – slope of the elastic part of the graph corresponding to the tangent of the angle of inclination of the line of linear regression in the stress-strain diagram between 10% and 40% of R_{eH}.

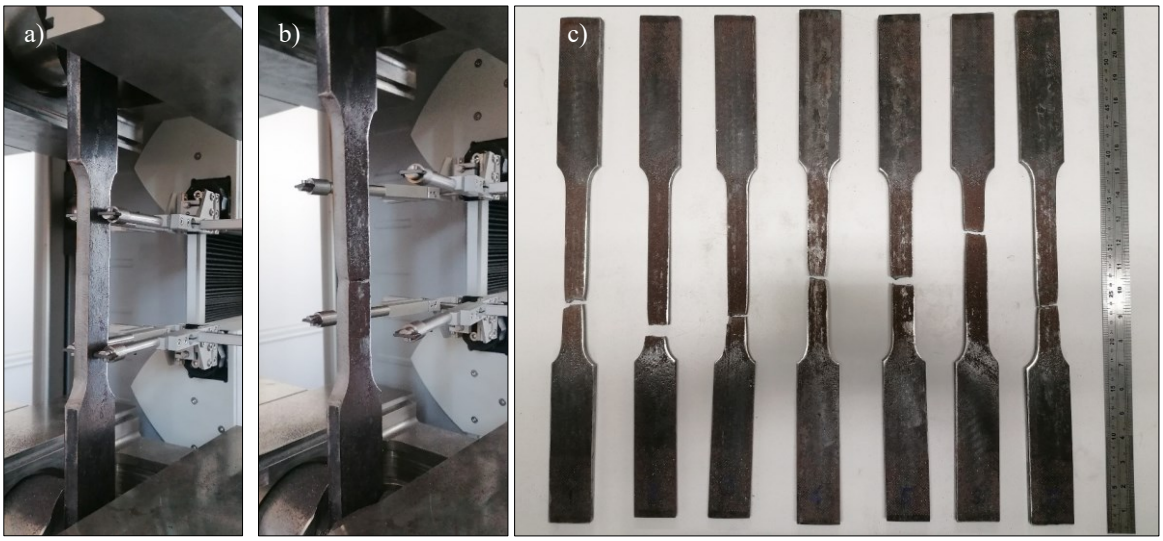


Figure 12. a) Testing setup; b) Specimen 7 just after fracture; c) Specimens after testing.

Table 2. Tensile testing of ties

Specimen	b (mm)	b_o * (mm)	a_o * (mm)	R_{eH} (MPa)	R_m (MPa)	A_{gt} (%)	A_t (%)	m_E (GPa)
1	45,8	24,78	9,70	278,7	359,2	18,6	27,5	198,8
2	44,8	24,63	8,07	239,1	318,9	16,4	16,9	187,1
3	44,8	24,75	8,10	243,3	325,5	18,5	26,7	160,1
4	45,8	24,83	12,00	230,6	339,4	20,4	35,4	194,6
5	45,6	24,87	12,13	233,8	346,7	17,1	20,2	174,2
6	45,2	24,55	8,03	241,8	327,8	18,2	26,7	182,9
7	45,3	24,65	8,13	239,1	330,3	20,0	34,4	154,8
mean				243,8	335,4	18,5	26,8	178,9
SD				16,0	13,9	1,4	6,7	16,7

* average value of 3 measurements within the parallel length

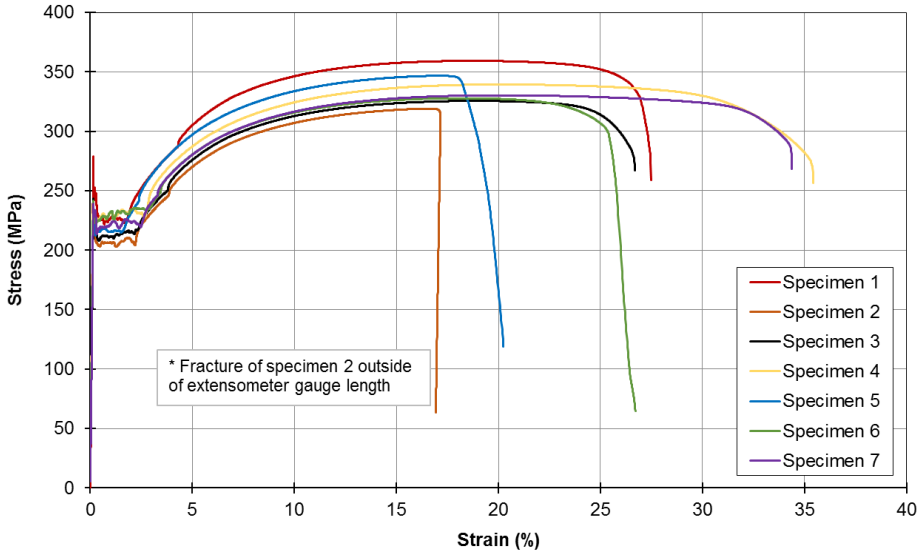


Figure 13. Stress-strain diagram of iron ties.

Copyright © 2025 CroCEE
DOI: https://doi.org/10.5592/CO/3CroCEE.2025.114

The following values were obtained: mean yield strength 244 MPa, mean tensile strength 335 MPa and mean elongation at fracture 26,8 %. When compared with the results of tensile test of ties from Czech Republic [16] or Italy [17], differences may be noticed, what can be attributed to the different composition of wrought iron and different periods of production, so special care should be taken when assuming mechanical properties from different periods and different countries.

Fig. 14 presents the fracture surfaces of two specimens, where the foliar fractures may be noted. Specimen 2 had a smaller tensile strength and significantly smaller deformation A_t, what can be attributed to the defect in the cross section visible as a white spot in Fig. 14a.

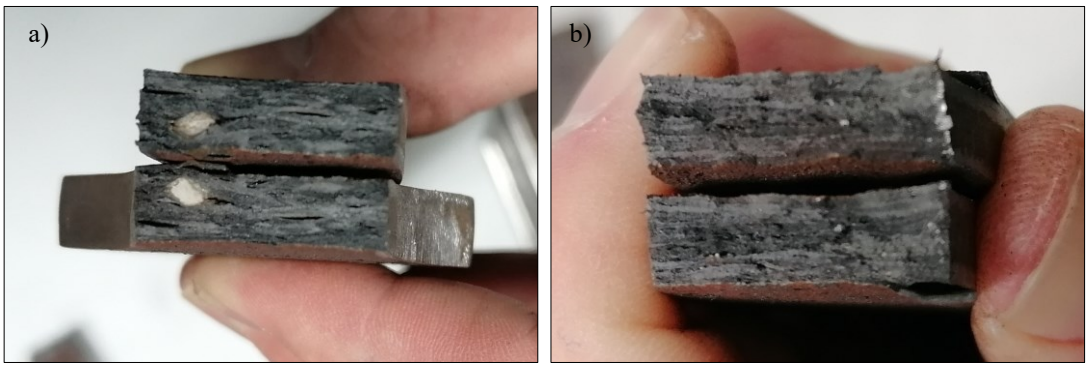


Figure 14. Fracture surfaces: a) Specimen 2; b) Specimen 3.

5. Conclusions

In this paper we presented the application of ties in a stone masonry building located in Krk, Croatia, placed in order to insure an adequate structural integrity, a property that masonry structures often lack. Detecting the elements that ensure the integrity of the building is very rarely possible; this kind of inspection of the skeleton of the building is possible during a renovation or unfortunately in the event of a major earthquake, during a damage inspection.

The in-depth inspection of the case study building and related tensile testing showed the following:

- Horizontal timber ring beams have been embedded into the masonry at the floor and at the roof level. The timber beams were connected by metal flats at their ends to ensure their continuity. Authors of this paper have not so far detected timber ring beams embedded into masonry in the Kvarner Littoral. There may be more such cases in our country, but they still have not been documented.
- Horizontal wall-to-floor connections were obtained by wrought iron flats anchored into the external walls.
- Diagonal wall-to-floor connections via iron ties were used at the roof level. Exceptional level of craftsmanship was noted.
- Tensile testing of diagonal iron ties gave the following results: mean yield strength 244 MPa, mean tensile strength 335 MPa, mean elongation at fracture 26,8 %.

Acknowledgements

This research was financially supported by the University of Rijeka through grant No. uniri-iskusni-tehnic-23-198: *Adjustment of the methodology for assessing the seismic resistance of existing masonry buildings in the Kvarner Littoral*. We also express our gratitude to *GP KRK d.d.* for their cordiality and assistance during the in-depth inspection of the case study building.

Copyright © 2025 CroCEE
DOI: https://doi.org/10.5592/CO/3CroCEE.2025.114

References

[1] D'Ayala, D.F., Paganoni, S. (2011): Assessment and analysis of damage in L'Aquila historic city centre after 6th April 2009, *Bulletin of Earthquake engineering*, **9**, 81-104, doi: https://doi.org/10.1007/s10518-010-9224-4

[2] Sorrentino, L., Cattari, S., Da Porto, F., Magenes, G., Penna, A. (2019): Seismic behaviour of ordinary masonry buildings during the 2016 central Italy earthquakes, *Bulletin of Earthquake Engineering*, **17**, 5583-5607, doi: https://doi.org/10.1007/s10518-018-0370-4

[3] Lagomarsino, S. (2012): Damage assessment of churches after L'Aquila earthquake (2009), *Bulletin of Earthquake Engineering*, **10,** 73-92, doi: https://doi.org/10.1007/s10518-011-9307-x

[4] Günaydin, M., Atmaca, B., Demir, S., Altunişik, A.C., Hüsem M., Adanur, S., Ateş, S., Angin, Z. (2021): Seismic damage assessment of masonry buildings in Elazığ and Malatya following the 2020 Elazığ-Sivrice earthquake, Turkey, *Bulletin of Earthquake Engineering*, **19**, 2421-2456, doi: https://doi.org/10.1007/s10518-021-01073-5

[5] https://www.youtube.com/watch?v=FL2rFZRrsvc, (accessed October 17, 2024).

[6] https://a4view.archiviodistatotrieste.it/patrimonio/c604d646-86b6-42a1-a810-e72d874ae61c/646-a-all01-mappa-catastale-del-comune-di-veglia-foglio-xix-allegato-1-mappa-in-doppia-scala-della-citta-di-veglia-1821-post-1873 (accessed October 17, 2024).

[7] Xekalakis, G., Christou, P., Pitilakis, D., Kyriakides, N. (2023): Quantitative contribution of timber ring beams in the dynamic response of adobe masonry structures, *CivilEng*, **4**, 1182–1197, doi: https://doi.org/10.3390/civileng4040065

[8] Yardimli, S., Mıhlayanlar, E. (2016): The use of beams in traditional masonry structures of Anatolia and Thrace, International Conference on Innovations in Civil and Structural Engineering (ICICSE'16), Phuket, Thailand, 27-32.

[9] Michiels, T.L.G. (2015): Seismic retrofitting techniques for historic adobe buildings, *International Journal of Architectural Heritage*, **9**, 1059-1068, doi: http://doi.org/10.1080/15583058.2014.924604

[10] Al Qablan, H., Rababeh, S., Katkhuda, H., Al-Qablan, T. (2019): On the use of wooden beams as an anti-seismic device in stone masonry in Qasr el-Bint, Petra, Jordan, *Journal of Building Engineering*, **21**, 82-96, doi: https://doi.org/10.1016/j.jobe.2018.10.002

[11] Ottoni, F., Blasi, C. (2016): Hooping as an ancient remedy for conservation of large masonry domes, *International Journal of Architectural Heritage*, **10**:2-3, 164-181, doi: http://doi.org/10.1080/15583058.2015.1113335

[12] Sajeva, S. (2014): Pitture murali, I degrade di origine meccanica, Manuale per restauratori ed ingegneri, DEI Tipografia del genio civile, Roma.

[13] Solarino, F., Oliveira, D.V., Giresini, L. (2019): Wall-to-horizontal diaphragm connections in historical buildings: A state-of-the-art review, *Engineering Structures*, **199**, 109559, doi: https://doi.org/10.1016/j.engstruct.2019.109559

[14] Test Report 10/2024 (2024): Determination of the elemental composition of metals and alloys using optical emission spectrometer - GDS. MarLab d.o.o., Pula, Croatia.

[15] HRN EN ISO 6892-1:2019, Metallic materials - Tensile testing - Part 1: Method of test at room temperature (ISO 6892-1:2019; EN ISO 6892-1:2019), HZN.

[16] Králíková, M., Cikrle, P., Daněk, P., Bilíková, I., Misák, P. (2016): The properties of historical wrought iron tie rods, *Key Engineering Materials*, **714**, 207-212, doi: https://doi.org/10.4028/www.scientific.net/KEM.714.207

[17] Matteis, P., Scavino, G. (2019): Mechanical performance of historical wrought iron rods, *Archaeometry*, **61**(5), 1053-1065, doi: https://doi.org/10.1111/arcm.12470

Proceedings of the 3rd Croatian Conference on Earthquake Engineering - 3CroCEE
19–22 March 2025, Split, Croatia
Copyright © 2025 CroCEE
DOI: https://doi.org/10.5592/CO/3CroCEE.2025.121

SEISMIC ASSESSMENT OF A HISTORIC AUSTRO-HUNGARIAN MASONRY BUILDING IN SARAJEVO'S BAŠČARŠIJA

Ćamil Medanović [(1)], Naida Ademović [(2)], and Marijana Hadzima-Nyarko[(3)]

[(1)] *Mag.Ing.Aedif., RAD BH d.o.o., camilsagf@gmail.com*
[(2)] *Full Professor, University of Sarajevo-Faculty of Civil Engineering, Patriotske lige 30, 71000 Sarajevo, Bosnia and Herzegovina, naidadem@yahoo.com*
[(3)] *Faculty of Civil Engineering Engineering and Architecture Osijek, Josip Juraj Strossmayer University of Osijek, Vladimira Preloga 3, 31000 Osijek, Croatia, mhadzima@gfos.hr*

Abstract

The main purpose of this paper is to assess the seismic resistance of a masonry building from the Austro-Hungarian period in Sarajevo. The building is situated in Sarajevo's old Baščaršija, which is well-known for its marketplace of tiny adobe and wooden buildings from the Ottoman era. It is characterized by specific Austro-Hungarian architecture from the rebuilt Latin district next to the Miljacka River. European construction rules were created following a fire in 1879. The structure is notable for its size and design, which combines Ottoman surroundings with Austro-Hungarian influences. The original structure had two floors A business area occupied the ground floor, while residential apartments occupied the top floor of the original building, which was recorded by the Governmental Building Department in 1903. It was a typical residential rental building at the time. Later, a second level was constructed while keeping the same layout and structural elements. Typical Austro-Hungarian solid bricks from that era were used to construct the load-bearing walls, with lime mortar for the joints. Sand infill serves as fire-resistant insulation between the wooden beams and boards that form the floor structure. The original pitched roof was made of wood.

Numerical modeling and nonlinear static (*pushover*) analysis were conducted using the 3Muri software package. The 3Muri software package, specialized in analyzing masonry structures, employs the innovative Frame by Macro Element (FME) method, enabling detailed seismic behavior analysis of walls. This paper presents detailed pushover analysis results, covering the distribution of lateral forces (uniform and static) for horizontal acceleration in the X and Y directions, considering the significant damage state for a 475-year return period. The main parameter monitored during the analysis was the vulnerability indexes.

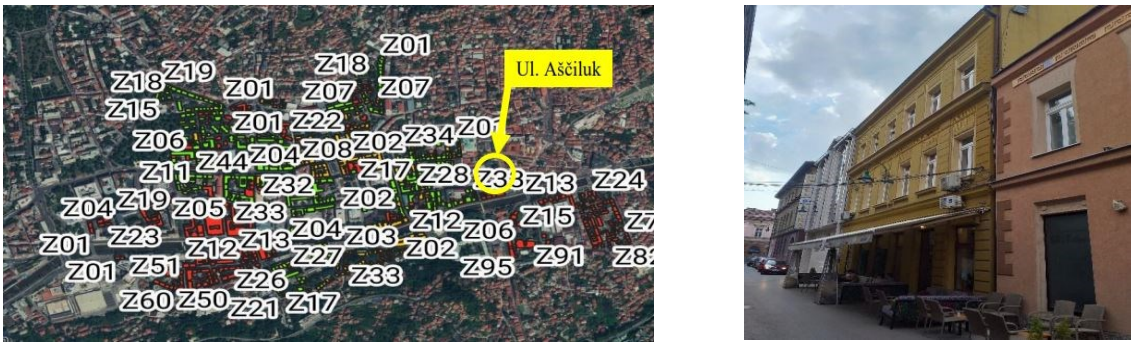
Results are presented for all walls, and wall damage was analyzed relative to the direction of seismic action, identifying walls most affected by bending or shear forces.

Keywords: masonry; pushover analysis; Austro-Hungarian buildings, timber floor, 3Muri software, historical structures

1. Introduction

Recently, frequent and intense ground shaking has occurred in the Balkan region. In Bosnia and Herzegovina (BiH), significant tremors were felt following the earthquake in Croatia in 2020. The epicenter of this earthquake was located in Petrinja, with a magnitude of 6.7 on the Richter scale. In November 2019, Albania was struck by an earthquake with a recorded magnitude of 6.4. More recently, in April 2022, BiH experienced an earthquake with a magnitude of 5.7 on the Richter scale, with its epicenter near Stolac. According to the Federal Hydrometeorological Institute, this earthquake was considered stronger than the one that occurred in 1969 in Banja Luka [1].
The initial phase of this research involved field investigations of 700 buildings (Fig. 1a) which provided the necessary parameters to establish a database for calculating the seismic vulnerability of buildings under earthquakes of varying intensities [2]. Seismic analysis was conducted for a residential building located at Aščiluk Street (Fig.1b), as it was included in the field study and was identified by Ademović et al. [2] as the most vulnerable among the buildings in its neighborhood. This building was constructed in 1903 during the Austro-Hungarian period, in accordance with the regulations enforced at that time.

Proceedings of the 3rd Croatian Conference on Earthquake Engineering - 3CroCEE
19–22 March 2025, Split, Croatia
Copyright © 2025 CroCEE
DOI: https://doi.org/10.5592/CO/3CroCEE.2025.121



a) b)

Figure 1. a) Location of the analyzed building; b) Building in the Aščiluk Street [2].

2. Building Description

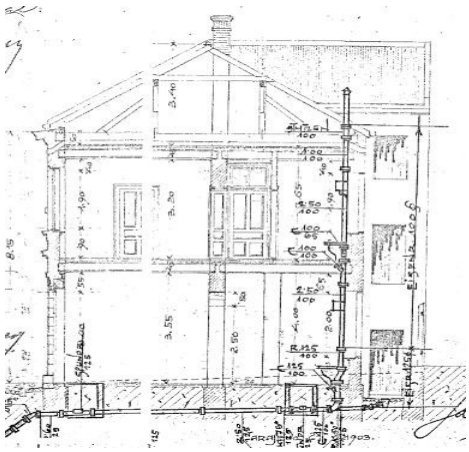
2.1. Structural Geometry and Material Specifications of Load-bearing walls

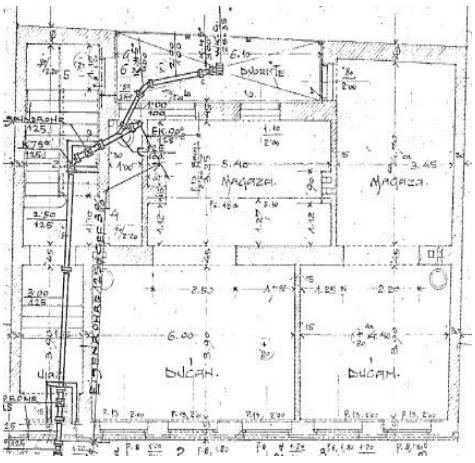
The building represents a typical unreinforced masonry structure (URM) with wooden floor structures, characteristic of the time it was constructed. The building consists of a ground floor, one upper floor, and an attic. The original blueprints were obtained from the Institute for Protection of Cultural-Historical and Natural Heritage of Canton Sarajevo and are presented in Fig. 2. As per the original site plan, the building was designed as an infill structure between two adjacent buildings. Its longer side, measuring 13.30 meters, is aligned in a north-south orientation, with the façade facing the street situated to the south, the shorter side is 10.40 m and has a total height of 10.15 m.

Two external load-bearing walls, positioned longitudinally and transversely, make up the building's structural system. The longitudinal load-bearing walls govern the layout of both floors. Chimneys are part of a central longitudinal load-bearing wall that is 4.35 meters from the façade that faces the street. A transverse load-bearing wall on the ground floor is situated 2.15 meters away from the outside transverse wall on the west side. The first 0.95 meters of this 4.80-meter-long wall are 45 cm thick, whereas the following portion is only 30 cm thick.

The first and second levels have partition walls built above this wall. At a distance of 2.50 meters from the center wall, another transverse wall varies in thickness from 30 cm over 3.70 meters to 45 cm over 1.85 meters. The transverse wall and the staircases run through the two higher stories and are situated in the northwest corner. The arrangement of the 15 cm thick partition walls is depicted in Fig. 2.

Sand infill serves as fire-resistant insulation between the wooden beams and boards that make up the floor structure. For fire safety considerations, the structural floor was separated from the lower level, and the original pitched roof was constructed of wood.





Copyright © 2025 CroCEE
DOI: https://doi.org/10.5592/CO/3CroCEE.2025.121

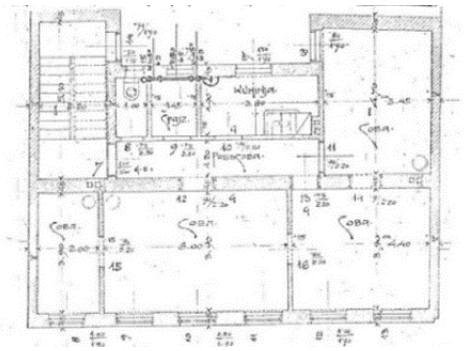


Figure 2. The building's original designs, including the cross-section, ground floor, and first-floor layout (Source: The Cantonal Institute for the Protection of Cultural, Historical and Natural Heritage, Sarajevo)

The structural system from the Austro-Hungarian period is based on longitudinal/medium load-bearing walls, the thickness of which depends on the regulations of the *Construction Code*. The walls of the lower floors, primarily made of brick and unreinforced, can be up to one meter thick [3]. Fig. 3 shows the walls around the elevator in the basement, while those on the upper floors are reduced by 15 cm. According to the *Construction Cod*e, the thickness of the load-bearing walls on the top floor must be at least 45 cm, increasing by 15 cm on each lower floor. The examined building has two floors, with the middle and outer load-bearing walls remaining 45 cm thick. The arrangement of load-bearing walls in only one direction may lead to structural failure due to an earthquake, as illustrated by the example of the 1963 Skopje earthquake [4].

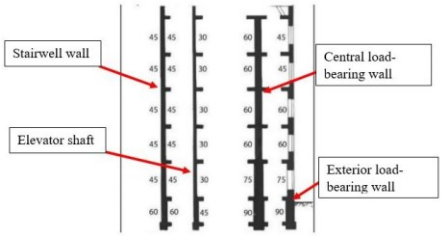


Figure 3. Thickness of the walls according to the Construction Code [5].

2.2.Structural Geometry and Material Specifications of the Timber Slab

The floor-ceiling assemblies characteristic of the Austro-Hungarian period are constructed of flexible wooden systems, with spans ranging between 4 m and 6 m and thicknesses varying from 45 cm to 55 cm. The floor structure layout of the building is depicted in Figure 4 and has been modeled using the 3Muri software for advanced seismic analysis. Fig. 4 shows the orientation of the timber joists (20x26cm) located between the boards. These transversely oriented joists are supported by the central longitudinal wall and the façade walls.

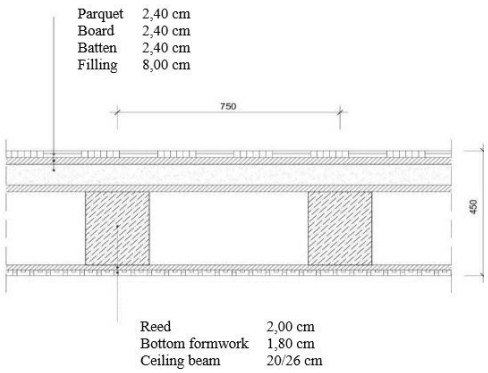


Figure 4. Cross-section of the timber floors [6].

Copyright © 2025 CroCEE
DOI: https://doi.org/10.5592/CO/3CroCEE.2025.121

Wooden ceilings are the oldest and most widespread type of ceiling until the introduction of reinforced concrete in the 21st century. Flexible ceilings, typically made as beams supported by walls, distribute lateral seismic forces to vertical load-bearing elements based on the corresponding surface area. Unlike rigid ceilings, flexible ones are not capable of redistributing forces caused by torsional deformations of the structure.

The consideration of the stiffness or flexibility of ceilings aims to determine the way seismic forces are distributed to load-bearing elements (walls), and whether the forces are distributed based on the stiffness of the walls or the surface area. In the case of rigid ceilings, the load is transferred proportionally to the stiffness of the vertical elements, while in flexible ceilings, the load is transferred according to the surface area. The distribution of seismic forces depends on the stiffness of the ceilings and the vertical load-bearing elements. According to El Sherbeny [7], most ceilings have characteristics that are between rigid and flexible.

Flexible ceilings can cause torsional effects due to the varying stiffness of the vertical load-bearing elements, but they are not stiff enough to transfer forces to walls perpendicular to the seismic movement direction, which can lead to structural failure. On the other hand, rigid ceilings distribute torsional forces to vertical elements in proportion to their stiffness. Torsional effects can cause damage at different levels, making it essential to pay attention to the type of ceiling, especially in irregularly shaped structures. As shown in Fig. 5, with rigid ceilings, each wall takes on a portion of the force proportional to its stiffness relative to the total stiffness of the structure, while with flexible ceilings, the force distribution follows the surface area, so the middle wall takes on twice the force share (V/2) compared to the outer walls (V/4).

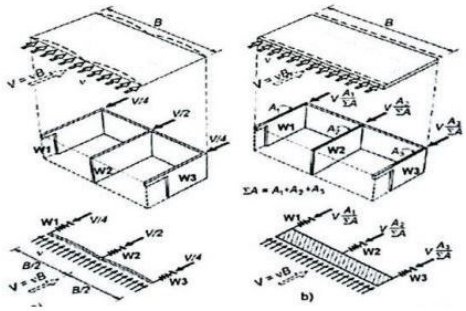


Figure 5. Distribution of seismic forces to vertical load-bearing elements (walls) [7].

Based on observed damage from strong earthquakes, insufficient structural integrity, and weak connections between vertical walls, and between the walls and ceiling structures can cause the separation of load-bearing walls at corners and joints, leading to the collapse of gable or vertical walls in the direction of seismic ground movement [4]. Experimental studies [8, 9] show that ceiling structures with beams supported only by walls cannot prevent wall separation, which may lead to a partial collapse of upper floors (Fig. 6a). However, connecting the walls with steel ties ensures structural integrity and fully utilizes the resistance of the walls (Fig. 6b).

Copyright © 2025 CroCEE
DOI: https://doi.org/10.5592/CO/3CroCEE.2025.121

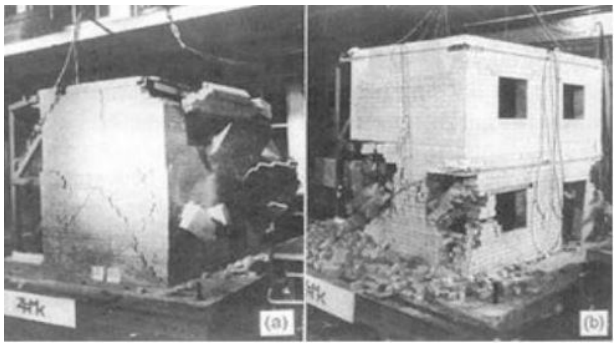


Figure 6. Failure mechanism of the masonry building models made of brick: a) Without wall ties; b) With wall ties [4].

Table 1. Material parameters for masonry [6]

Characteristics-masonry	Symbol	Value
Compressive strength	f_c	3.9 N/mm^2
Tensile strength	f_t	0.02 N/mm^2
Youngs modulus	E	2730 N/mm^2
Shear modulus	G	910 N/mm^2
Mass density	ρ	13.44 kN/mm^3

Table 2. Material parameters for timber [6]

Characteristics-timber	Symbol	Value
Youngs modulus	E	7000 N/mm^2
Shear modulus	G	440 N/mm^2

3. Numerical model

3.1. Pushover analysis

Pushover analysis is conducted under a constant gravitational load combined with an incrementally increasing horizontal load that simulates seismic effects. Horizontal forces are applied at floor levels, where masses are concentrated, following two primary distributions: a uniform distribution along the building height or a modal distribution corresponding to the deformation shape of specific natural vibration modes. This method tracks the structural response to a monotonically increasing static horizontal load until structural instability is reached. It is particularly suited for assessing existing buildings and incorporates nonlinear material behavior.

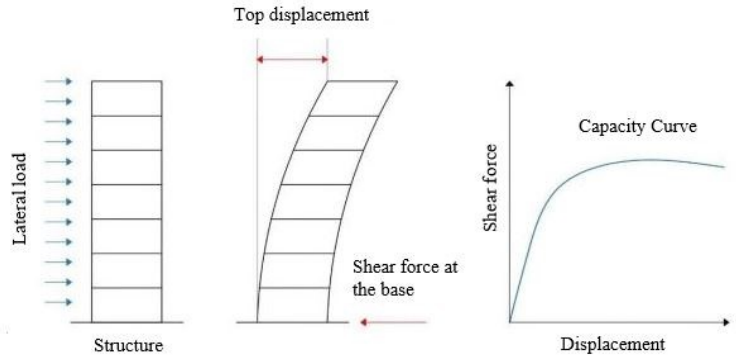


Figure 7. Capacity Curve [6].

Copyright © 2025 CroCEE
DOI: https://doi.org/10.5592/CO/3CroCEE.2025.121

The process involves applying incrementally increasing forces while monitoring the structural response. Given the nonlinear nature of the analysis, appropriate nonlinear material behavior is assumed. The seismic response considers parts of the structure transitioning into nonlinear behavior, which is crucial for evaluating load-bearing systems. The analysis tracks the displacement of the top floor relative to the applied horizontal force, serving as a reference. The result is an F-Δ diagram, or capacity curve, which illustrates the relationship between the total lateral force and the building's top displacement (Fig.7).

3.2.Numerical modeling using 3Muri software

Seismic analysis was conducted using the 3Muri software package, which specializes in the analysis of masonry structures. 3Muri employs the Frame by Macro Element (FME) method, specifically designed for masonry structure analysis. After modeling the walls and floor diaphragms, the software automatically generates a mesh. The innovative FME method schematically represents the structure as an equivalent frame composed of macro elements. This approach facilitates a deeper understanding of seismic behavior and provides the designer with essential information for a detailed review of the results.

The equivalent frames offer a comprehensive mechanism for analyzing in-plane damage, including shear and combined axial loading, while out-of-plane wall collapse is not considered. Due to their simplicity and satisfactory accuracy, equivalent frames are considered the most suitable tool for relatively quick assessments of the seismic resistance of masonry structures.

According to the equivalent frame method, the numerical model consists of vertical load-bearing elements ("piers") and horizontal elements ("spandrels"), which are connected by rigid nodes ("rigid portions") as illustrated in Fig .8 ([10], [11]).

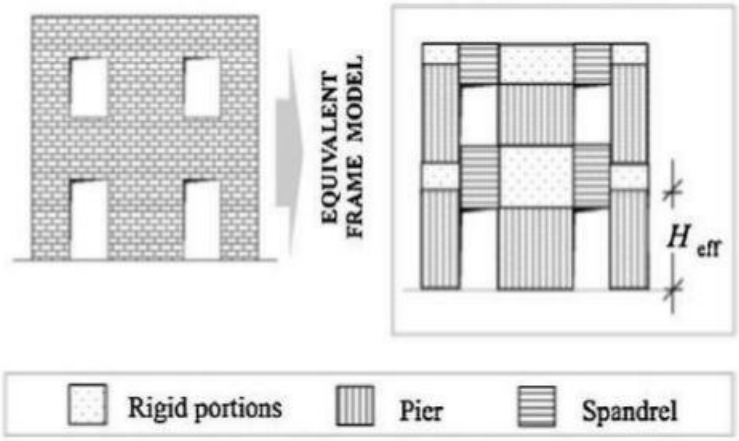


Figure 8. Idealization of a wall using the Equivalent Frame Method [11].

The 3D model of the analyzed structure is presented in Fig 9. The 3Muri software package operates on the principle of simplified numerical models for the analysis of masonry structures, where equivalent frames are formed before the actual calculation. In this method, the numerical model consists of vertical load-bearing elements and spanning elements connected by nodes, as shown in Fig. 9.

Proceedings of the 3rd Croatian Conference on Earthquake Engineering - 3CroCEE
19–22 March 2025, Split, Croatia
Copyright © 2025 CroCEE
DOI: https://doi.org/10.5592/CO/3CroCEE.2025.121

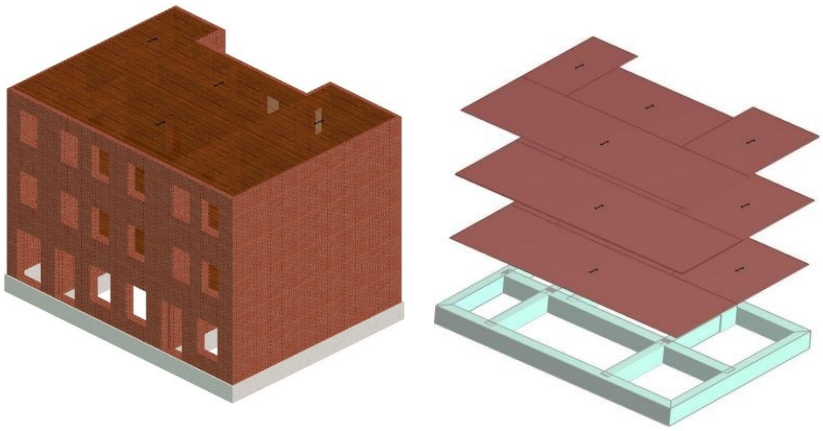
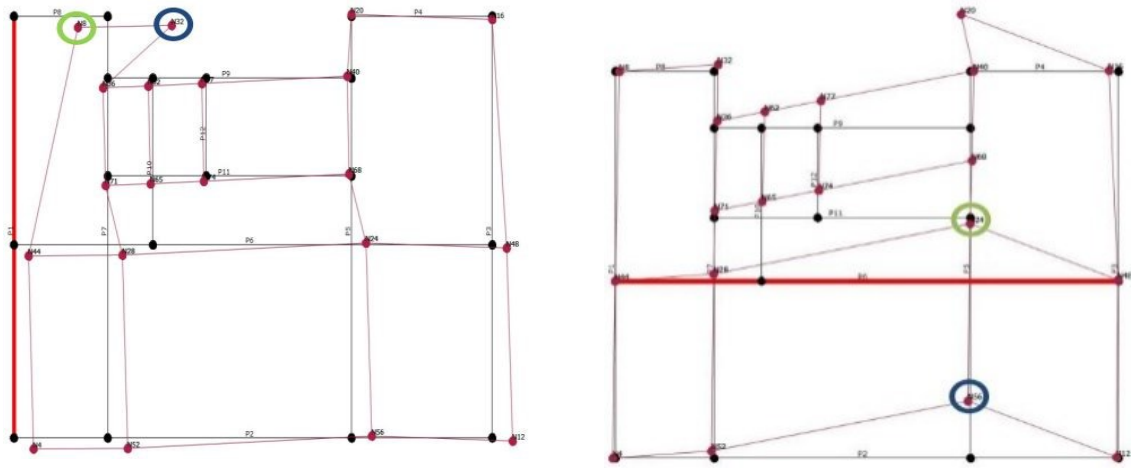


Figure 9. 3D model of the structure [6].

A static analysis was performed to verify the structure's capacity to withstand vertical loads, and the results were satisfactory.

Before conducting the pushover analysis, a modal analysis is performed to determine the fundamental dynamic characteristics of the structure, such as its natural frequencies and mode shapes. Based on the mode shapes, i.e., the deformation patterns of the structure, control points are selected for both directions (X and Y) on the highest floor of the building, as shown in Figs. 10a and 10b.



a) b)

Figure 10. Modal analysis: a) Control displacement in X direction; b) Control displacement in Y direction.

Table 3 displays the results from the modal analysis, including the natural periods and mass participation coefficients for the relevant directions. The first mode (shown in green) occurs in the Y direction and activates 35.82% of the mass, while the second mode (shown in red) occurs in the X direction, activating 43.78% of the mass.

Copyright © 2025 CroCEE
DOI: https://doi.org/10.5592/CO/3CroCEE.2025.121

Table 3. Modal analysis results.

Active in pushover X dir.	Active in pushover Y dir.	Mode	T [s]	mx [kg]	Mx [%]	my [kg]	My [%]	mz [kg]	Mz [%]
☐	☐	1	0,28842	39.230,51	11,09	0,64	0,00	0,13	0,00
☐	☐	2	0,19648	194,46	0,05	126.730,54	35,82	2,19	0,00
☐	☐	3	0,17448	2.135,09	0,60	54.384,92	15,37	7,10	0,00
☐	☐	4	0,14122	26.957,38	7,62	5.264,41	1,49	2,11	0,00
☐	☐	5	0,13819	154.894,53	43,78	10.152,23	2,87	35,97	0,01
☐	☐	6	0,12775	46.396,23	13,11	3.043,70	0,86	3,31	0,00
☐	☐	7	0,11889	6.252,65	1,77	24.377,84	6,89	20,54	0,01
☐	☐	8	0,10682	41.553,43	11,74	3.058,91	0,86	2,47	0,00
☐	☐	9	0,09198	8.909,66	2,52	29.796,31	8,42	5,16	0,00
☐	☐	10	0,08451	310,50	0,09	32.419,18	9,16	31,12	0,01
☐	☐	11	0,07745	595,95	0,17	3.454,62	0,98	31,25	0,01
☐	☐	12	0,07323	394,41	0,11	18.182,98	5,14	4,60	0,00

The pushover analysis was conducted for Node 8 in the X direction, as it exhibited the greatest displacement response. Additionally, considering the significance of the middle longitudinal bearing wall in Austro-Hungarian construction, especially for buildings of this period [3], Node 24, located on the longitudinal bearing wall (P6), was also selected for analysis. The pushover analysis was performed for Node 24 in both horizontal directions, resulting in a total of 24 distinct calculations. The analysis was carried out across four lateral force application directions (+X, -X, +Y, -Y), with two distinct lateral force distributions (uniform and static), and with or without seismic force eccentricity, which could be either positive or negative.

4. Results of numerical analysis

The distribution of transverse forces was analyzed under both uniform and static force distributions, with calculations performed for horizontal accelerations in the X and Y directions. The analysis was carried out for two limit states: limited damage and significant damage, corresponding to return periods of 95 and 475 years, respectively. The results are presented for various structural elements, including the middle longitudinal bearing wall (45 cm thickness), the street-facing wall (45 cm thickness), external and internal walls (30 cm thickness), and partition walls (15 cm thickness).

To evaluate the limit state of significant damage, as per Eurocode 6 [12], the condition (1) is applied:

$$d_t^{SD} \leq d_m^{Sd} \tag{1}$$

In the pushover analysis, the key parameter is the damage index, denoted as α (seismic vulnerability), which is calculated for three limit states: Near Collapse (NC), Significant Damage (SD), and Damage Limitation (DL). For the Significant Damage (SD) state, the displacement is taken from the capacity curve at the point where the horizontal force drops below 80% of the maximum force. For the Damage Limitation (DL) state, the displacement corresponds to the point where the first plastic hinges form and the structure transitions into the plastic regime.

The damage index α is calculated for each limit state as indicated in equation (2)

$$\alpha_{SD} = \frac{PGA_{CSD}}{PGA_{DSD}} \tag{2}$$

where PGA_{CSD} represents the peak ground acceleration at significant damage, and PGA_{DSD} refers to the spectral peak ground acceleration at significant damage. The damage index α represents the ratio of the ultimate displacement $d_m$to the target displacement d_t for each limit state. If this ratio exceeds 1.0, the limit state is considered to be satisfied.

For this analysis, the significant damage limit state (SD) is considered the governing factor, while the limited damage (DL) state is not relevant. As a result, for all 24 combinations tested, the conditions defined by Eurocode 8 are not met, and the cells representing the DL state are marked in red.

Copyright © 2025 CroCEE
DOI: https://doi.org/10.5592/CO/3CroCEE.2025.121

4.1. Comparison of Static and Uniform Force Distribution for the X-Direction

When evaluating load-bearing capacity, ultimate displacement at the Significant Damage (SD) limit state, the shape of the capacity curve, and structural ductility during the analyses with static and uniform force distributions, no significant differences are observed, as indicated by the capacity curves shown in Fig. 11. However, disparities emerge in the damage sustained by specific walls, particularly the external 30 cm thick wall in the Y direction, as presented in Fig. 12. In the static force distribution analysis, this wall remains undamaged, whereas, in the uniform force distribution analysis, it experiences initial bending damage at the ultimate displacement. Conversely, the street-facing and central longitudinal load-bearing walls exhibit nearly identical behavior in both analyses, as noted in Fig. 12.

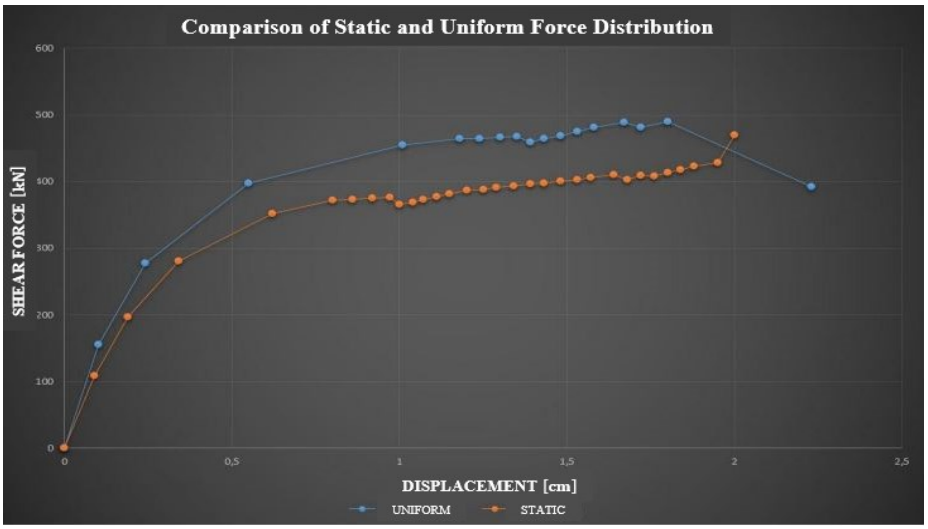


Figure 11. Comparison of Static and Uniform Force Distribution for the X Direction.

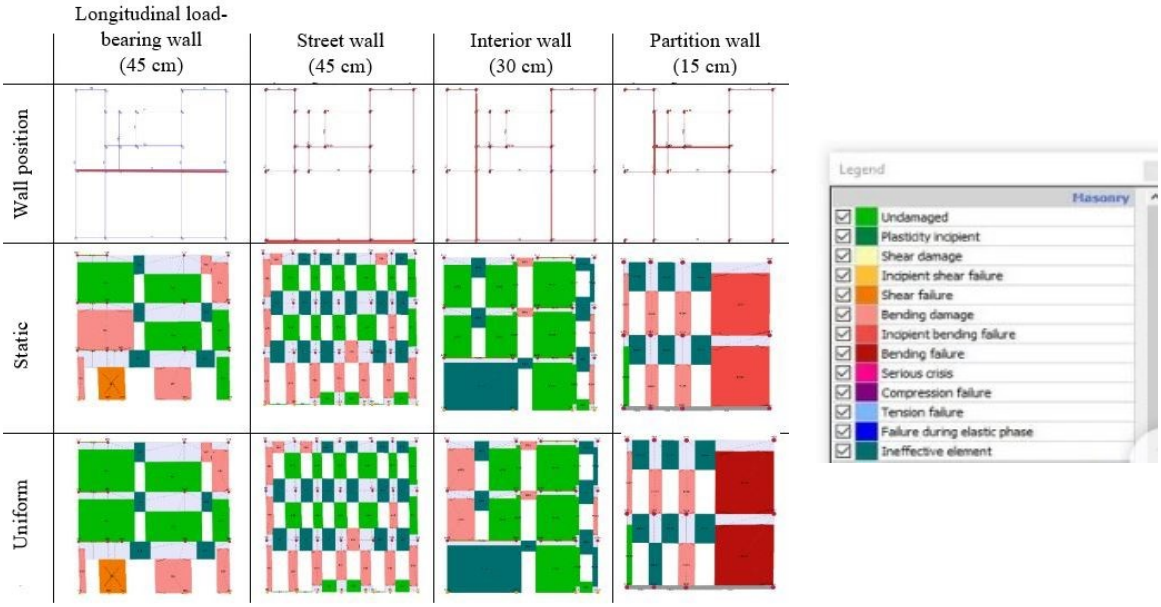


Figure 12. Damage to Walls Depending on Force Distribution – X Direction.

4.2. Representation of Wall Damage in the Analyzed Structure Relative to the Direction of Action

Fig. 13 presents the observed damage to the structural walls under horizontal loading in both the X and Y directions. The analysis indicates that under horizontal action in the X direction, the central longitudinal load-bearing wall experiences bending failure, while in the Y direction, this wall remains

Copyright © 2025 CroCEE
DOI: https://doi.org/10.5592/CO/3CroCEE.2025.121

relatively undamaged. The street-facing wall exhibits initial bending cracks under horizontal loading in both directions, with similar damage patterns observed in each case. The external walls (30 cm thick) remain undamaged under horizontal loading in both directions.

Internal walls show no damage under horizontal action in the X direction; however, under horizontal loading in the Y direction, bending cracks and failures are evident, along with shear failures in certain elements. The backyard load-bearing wall sustains bending failures on the first and second floors under horizontal loading in the Y direction but remains undamaged under the X direction. Partition walls incur bending failures under horizontal loading in both directions.

Based on these observed damage patterns, the subsequent section will discuss potential approaches for repair and strengthening of the affected structural elements.

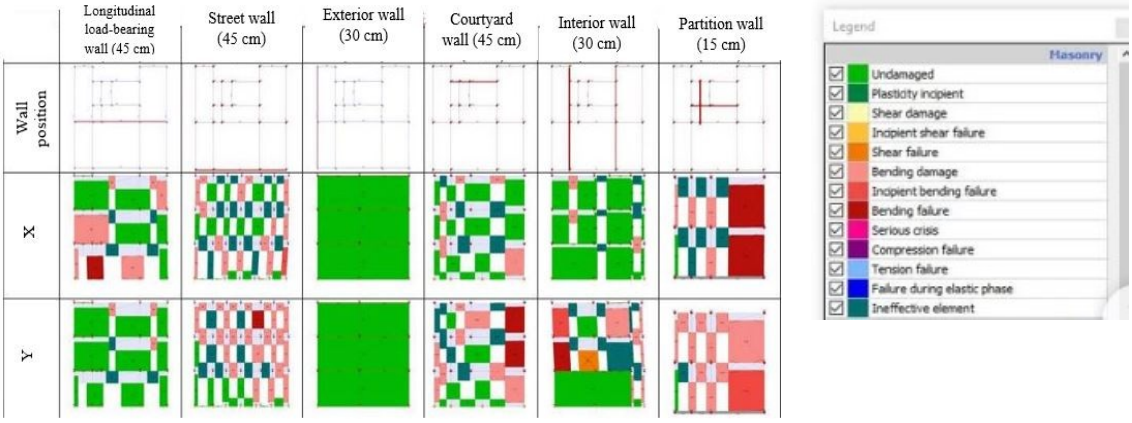


Figure 13. Representation of Wall damage relative to the direction of action.

5. Conclusions

The pushover analysis revealed that the primary damage to the building occurs due to bending and shear, irrespective of the direction of horizontal loading. A key parameter monitored during this analysis was the damage index (α), which represents the ratio of the ultimate displacement (dm) to the target displacement (dt) for each limit state. The comparison between uniform and static load distribution analyses indicated that the static load distribution provides greater structural capacity. Specifically, in the X direction, the capacity is approximately 500 kN with $\alpha = 0.743$, while in the Y direction, the capacity is about 400 kN with $\alpha = 0.733$.

Under applied loads in the X direction, the central longitudinal load-bearing wall (45 cm thick) exhibited bending damage, with failure occurring in one element. In contrast, no significant damage was observed in the Y direction. The pushover curves further indicated that the structure behaves more ductile under horizontal action in the Y direction.

A characteristic feature of Austro-Hungarian buildings is the presence of numerous openings in the walls, which often lead to significant damage. This was evident in the observed damage to this structure. Predictably, partition walls (15 cm thick) suffered bending failures across all floors, with some damage occurring at the early stages of horizontal load application. This confirms that partition walls bear part of the seismic load and should not be overlooked in seismic analysis.

Considering that the building was constructed in 1903, without explicit seismic design considerations, it is not surprising that some analyses did not meet the criteria for significant and limited damage limit states. Many Austro-Hungarian buildings in Sarajevo hold cultural, historical, architectural, and aesthetic value. Strengthening these structures must be approached cautiously to preserve their authenticity and significance. Following the 2020 Zagreb and Petrinja earthquakes, which caused significant damage to similar buildings, it is crucial to implement appropriate repair and strengthening measures to enhance seismic resistance.

Copyright © 2025 CroCEE
DOI: https://doi.org/10.5592/CO/3CroCEE.2025.121

Acknowledgements

The research presented in this article is part of the project titled "Development of Methodology for Earthquake Risk Reduction with the Aim of Preventing and Mitigating the Spread of Infectious Diseases Caused by the COVID-19 Pandemic within the Urban Area of Sarajevo Canton (RIZEMK)." This project is funded by the Ministry of Science, Higher Education, and Youth of Sarajevo Canton. It was selected through a public call for co-financing research and development projects, programs, and scientific and artistic studies from the Sarajevo Canton budget for 2021. The support provided by the Ministry is greatly appreciated.

References

[1] Federal Hydrometeorological Institute, https://www.fhmzbih.gov.ba/latinica/SEIZMO/Skarakteristike.php

[2] Ademović, M., Hadzima-Nyarko, M., Zagora, N., Stojnović, V. (2024): Various numerical modeling procedures of XIX-century masonry building. *Engineering Structures* **301** Vol. 117361, https://doi.org/10.1016/j.engstruct.2023.117361

[3] Spasojević, B. (1999): *Arhitektura stambenih palata austrougarskog perioda u Sarajevu*. Svjetlost, 2nd edition, Bosnia and Herzegovina

[4] Tomaževič, M. (1999): *Earthquake-Resistant Design of Masonry Buildings*, World Scientific Publishing Co. Re. Ltd., Imperial College Press, 1st Edition, United Kingdom

[5] Kolbitsch, A. (1989): *Altbaukonstruktionen – Charakteristika, Rechenwerte, Sanierungsansatze*. Springer-Verlag Wien, 1st Edition, Vienna, Austria, https://doi.org/10.1007/978-3-7091-9033-3

[6] Medanović, Ć. (2024): *Seismic Analysis of an Existing Austro-Hungarian Period Building in Sarajevo*. Master Thesis, University of Sarajevo-Faculty of Civil Engineering (in Bosnian language)

[7] El Sherbeny, H. A. (1999): *Behavior of reinforced concrete flexible floor diaphragms under seismic loads*. Faculty of Engineering, Cairo University Giza, Egypt (Available at (PDF) BEHAVIOR OF REINFORCED CONCRETE FLEXIBLE FLOOR DIAPHRAGMS UNDER SEISMIC LOADS)

[8] Tomaževič, M., Lutman, M., Velechovsky, T. (1993): *Aseismic strengthening of old stonemasonry buildings: is the replacement of wooden floors always necessary?* European Earthquake Engineering 2, pp. 34–46, Pàtron Editore, Bologna, Italy.

[9] Tomaževič, M., Lutman, M., Weiss, P. (1996): *Seismic upgrading of old brick-masonry urban houses: tying of walls with steel ties.* Earthquake Spectra **12** (3), 599–622, Earthquake Engineering Research Institute, Oakland, https://doi.org/10.1193/1.1585898

[10] 3Muri S.T.A. DATA, http://www.3muri.com/en/, Accessed 15.08.2020.

[11] Lagomarisino, S., Penna, A., Galasco, A., Cattari, S. (2013): TREMURI program: An equivalent frame model for the nonlinear seismic analysis of masonry buildings, Engineering Structures **56**, 1787–1799, https://doi.org/10.1016/j.engstruct.2013.08.0

[12] CEN (2004): *Eurocode 8: Design of Structures for Earthquake Resistance. Part 1: General Rules, Seismic Actions, and Rules for Buildings*. European Standard EN 1998-1:2004, Comité Européen de Normalisation, Brussels.

Proceedings of the 3rd Croatian Conference on Earthquake Engineering - 3CroCEE
19–22 March 2025, Split, Croatia
Copyright © 2025 CroCEE
DOI: https://doi.org/10.5592/CO/3CroCEE.2025.141

PERFORMANCE ANALYSIS OF HISTORICAL CHURCHES AND MOSQUES DURING RECENT EARTHQUAKES – SOME PERSPECTIVES ON APPLICATION OF AI/ ML SYSTEMS

Satwant Rihal [(1)], Hisham Assal [(2)]

[(1)] *Professor Emeritus, School of Architecture and Environmental Design, Cal Poly State University, San Luis Obispo, California, U.S.A., srihal@calpoly.edu*
[(2)] *Lecturer, Noyce School of Applied Computing, Cal Poly State University, San Luis Obispo, California U.S.A., hhassal@calpoly.edu*

Abstract

The world has witnessed widespread damages and losses suffered by precious cultural heritage structures during recent earthquakes e.g. Emilia-Romagna, Italy 2012; Central Italy 2016; Turkey /Syria 2023; Morocco 2023; Tohoku, Japan 2011; Puebla, Mexico 2017; Nepal 2015; Christchurch, New Zealand 2011; Iran 2017, among others. Based on traditional surveys and reconnaissance using 3D documentation technologies e.g photogrammetry, TLS etc. following the destructive earthquakes, extensive amounts of observed damage data about the damages of historical churches and mosques etc. has been accumulated over the years.

This paper presents the results of attempts to systematically analyze the damage data for historical churches and mosques to identify the lessons we can learn therefrom, determine their patterns of damage, and evaluate the possible causes of damage. The paper first documents the deep experience and knowledge base of performance of Churches in Italy during the past major earthquakes. The results of an analysis of the observed damage data from the historical colonial churches that suffered extensive damages and losses during the 2017 Puebla, Mexico earthquake, are presented next. The paper then analyzes the available data on the performance and damages suffered by historical mosques during the catastrophic Turkey earthquake of 2023; and the Al Houz, Morocco earthquake of 2023, to classify the types of damage, identify the patterns of damage, and possible causes of damage. The results of this study will help in the structural assessment of damaged historical churches and mosques and the development of the plans for their repair and restoration.

This paper further plans to explore the potential application of Artificial Intelligence and Machine Learning (AI/ML) systems for the systematic analysis of observed damage image data for historical Churches and Mosques, including classification of features, types of damage, and determining the patterns of damage of historical churches and mosques during catastrophic earthquakes.

Many data types and sources describe historical buildings, including 3D scans, photogrammetry, survey images and videos. This wealth of data requires the support of deep learning systems to identify types of damage due to natural disasters. The analysis of this large volume of data also offers the opportunity to compare before-and-after images to determine requirements of restoration projects.

Keywords: Heritage Churches, Historical Mosques, Earthquakes, 3D Documentation, Damage Data, Patterns of Damage, AI/ML Applications

1. Background

This paper is an attempt to learn from the extensive damages and huge losses suffered by religious heritage structures during the catastrophic earthquakes around the world during the past decades e.g.

Emilia-Romagna, Italy 2012; Central Italy 2016; Turkey / Syria 2023; Morocco 2023; Tohoku, Japan 2011; Puebla, Mexico 2017; Nepal 2015; Christchurch, New Zealand 2011; Iran 2017, among others. It has been observed that the heritage churches and mosques that were subjected to the fury and aftermath of these catastrophic earthquakes, not only served as places of worship but also as an emergency shelter, and an emotional support system for the affected communities in the aftermath of the devastation brought on by these catastrophic earthquakes.

Copyright © 2025 CroCEE
DOI: https://doi.org/10.5592/CO/3CroCEE.2025.141

2. Objective

The objective of the paper is to explore potential applications of AI/ML methods to systematically analyze the available damage data acquired from reconnaissance surveys for historical churches and mosques following previous catastrophic earthquakes to identify the patterns of damage, possible causes of the observed damage, and the lessons we can learn therefrom as follows:

Documentation of the deep experience and knowledge base of performance of heritage churches in Italy during previous catastrophic earthquakes.

Analysis of the observed damage data from historical colonial churches that were seriously damaged during the Puebla, Mexico earthquakes of September 2017

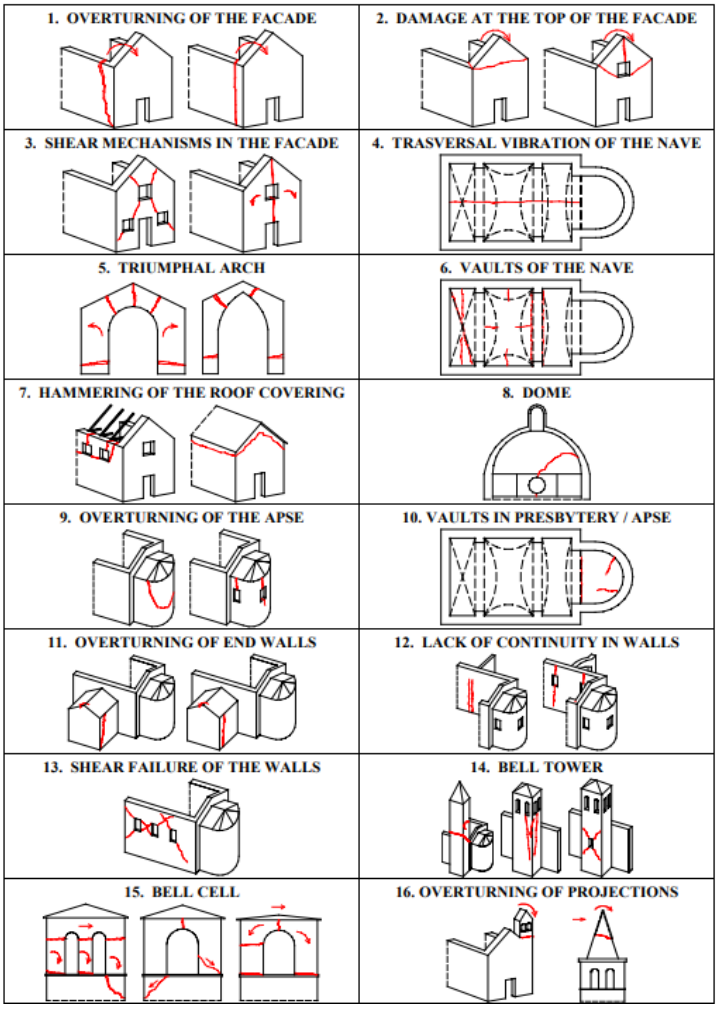
Analysis of the available data on the performance and damages suffered by the historical mosques during the catastrophic Turkey earthquake of 2023, and the Al Houz, Morocco earthquake of 2023

3. Lessons from Churches and Mosques

3.1. Historical Churches in Italy

The records of observed damage data on the beautiful historical churches damaged by catastrophic earthquakes in Italy over the past fifty years and beyond, provide a very important knowledge base for extracting lessons from this massive amount of damage data.

Table 1. Abacus of the damage mechanisms in the macroelements of the church. Source: Lagomarsino [1]



Copyright © 2025 CroCEE
DOI: https://doi.org/10.5592/CO/3CroCEE.2025.141

Lessons from the damages and losses suffered by historical churches during the catastrophic earthquakes in Italy over the past fifty years can best be described in the form of macroelements and damage mechanisms as first proposed by Lagomarsino [1], as presented in Table 1.

An analysis of the observed damage to thirty-six masonry churches during the 2016 Central Italy earthquake has been presented by Ferracuti et. al. [2]. The analysis highlighted the most frequent damage mechanisms and the most vulnerable macro-elements, including development of a damage index based on the observed damage and the macro-elements present in the surveyed churches.

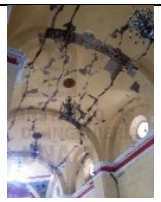
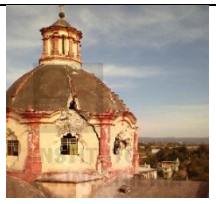
Damage data sets containing images and 3D Point Cloud data have been collected for many of the damaged churches by the Universita di Firenze, and Politecnico di Milano, among others, and archived for later processing and analysis. Point Cloud data presents unique opportunities to perform wellness analysis for undamaged structures as well as documentation of damage after an earthquake.

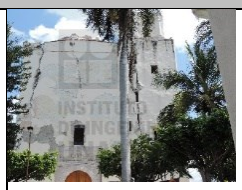
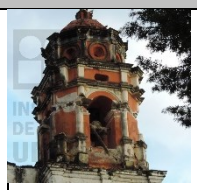
3.2 Colonial Churches in Mexico

The widespread damages suffered by colonial churches during the September 2017 Puebla earthquakes, were systematically surveyed and recorded by survey teams from UNAM, and compiled in the form of a database as reported by Peña in [3].

Classification and patterns of damages and losses suffered by historical colonial churches in Mexico during the Puebla, earthquakes of September 2017 have been presented by Peña as shown in Table 2.

Figure 2. Patterns of Damage of Colonial Churches in Mexico.

Observed Damage by UNAM				
Features	Vaults/Arches	Domes	Domes and Drums	Facades
Structural Damage Pattern	Cracks in vaulted ceilings/roofs	Severe damage in domes	Severe damages	Diagonal Cracks
Description	Tensile cracks in vaults/ arches	Radial and meridian cracks	Shear cracks	

Observed Damage by UNAM				
Features	Bell Towers	Facades / Bell Towers	Facades	Bell Towers
Structural Damage Pattern	Most damaged elements	Separation between Façade and side walls	Out-of-plane behavior	Most damaged elements
Description	Diagonal shear damage in belfries	Vertical cracks in joints	Horizontal or vertical cracks in the joint between elements	Tension Cracks in structural framing system elements

Copyright © 2025 CroCEE
DOI: https://doi.org/10.5592/CO/3CroCEE.2025.141

3.2. Mosques in Turkiye and Syria

The results of surveys to systematically document the performance and behavior of historical mosques heavily damaged during the February 2023 Kahramanmaras, Turkey earthquake has been presented by Ertugrul et. al. [4].

Severe damage and collapse of the Habib-i-Necca mosque in Anatolia is presented in Figure 2.



Figure 3. Habib-i-Necca Mosque one of the first mosques in Anatolia destroyed. Source: ArkeoNews (https://arkeonews.net/)

Some examples of the types and patterns of damage suffered by historical mosques during previous earthquakes in Turkey has been presented by Kocaman, et. al. [5]

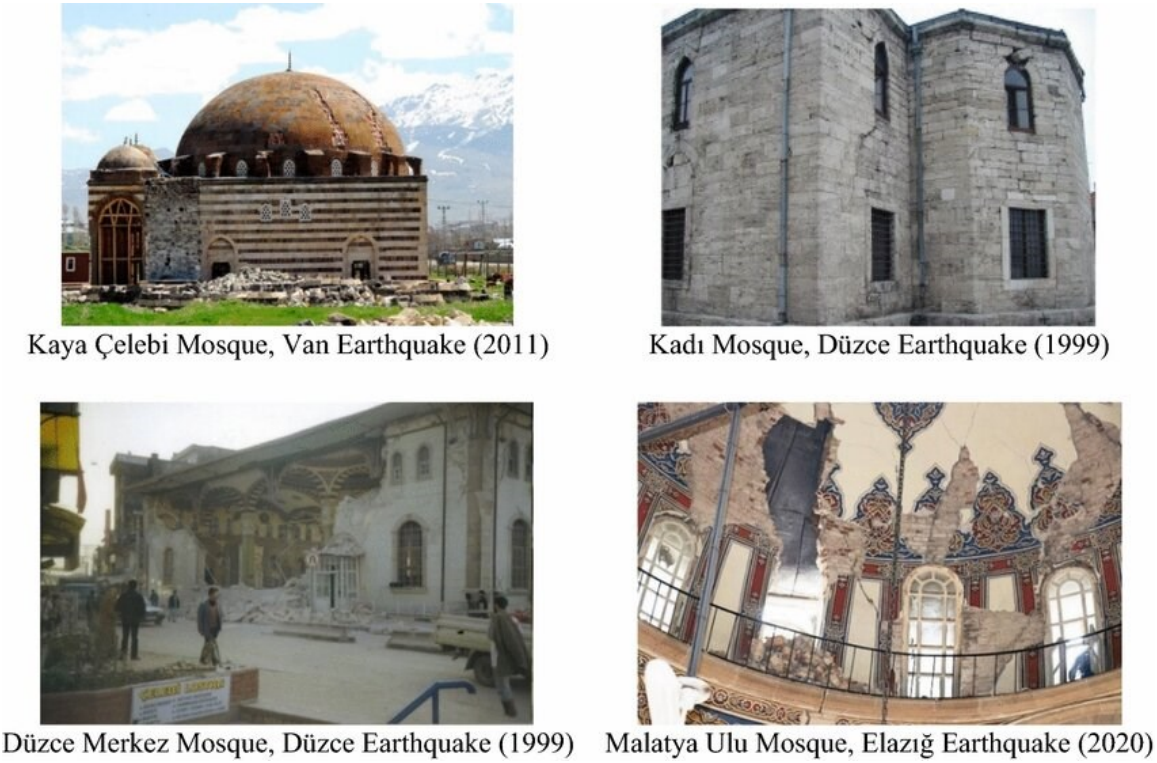


Figure 4. Examples of earthquake damage in historical mosques in Turkiye
Source: DOI: 10.1007/s10518-023-01613-1

Copyright © 2025 CroCEE
DOI: https://doi.org/10.5592/CO/3CroCEE.2025.141

3.3. Historical Mosques in Morocco

The historical Tinmel mosque, considered as a notable example of Almohad architecture, and dating back to the 12th Century, was severely damaged by the 2023 Al Houz, Morocco earthquake, while it was under restoration, as shown in Figure 4.



Figure 5. The Tinmel Mosque – Left: before earthquake, Right: after the earthquake

4. AI/ML Applications

Recent advances in the field of Artificial Intelligence and Machine Learning (AI/ML) offer great opportunities in processing large volumes of data and extract common patterns and lessons to be learned from damage data that is collected after earthquakes, Rihal et. al. [6]. This data includes images, videos, 3D scans and other formats. The benefits of using AI/ML include:

1. *Damage Assessment*: a) Image and Video Analysis: Drones and robots equipped with cameras can capture high-resolution images and videos of damaged heritage sites. AI-powered computer vision algorithms can analyze these images to identify and quantify damage, such as cracks, collapses, or deformations. b) 3D Modeling and Reconstruction: AI/ML can process LiDAR (Light Detection and Ranging) data or photogrammetry to create detailed 3D models of heritage structures before and after an earthquake. Comparing these models helps in assessing the extent of damage. c) Automated Damage Classification: ML models can classify damage into categories (e.g., minor, moderate, severe) based on predefined criteria, enabling rapid prioritization of restoration efforts.
2. *Cultural Value Preservation:* a) Digital Twins: AI can create digital twins of heritage structures, which are virtual replicas that simulate real-world conditions. These twins can be used to test restoration strategies and predict outcomes without risking further damage to the actual structure. b) Material Analysis: AI can analyze the materials used in heritage structures to determine their composition, age, and degradation patterns. This information is crucial for selecting appropriate restoration materials and techniques. c) Cultural Data Integration: AI can integrate historical, architectural, and cultural data to ensure that restoration efforts preserve the original design, aesthetics, and cultural significance of the structure.
3. *Decision Support Systems:* a) Resource Allocation: AI/ML can optimize the allocation of resources (e.g., manpower, materials, funding) for the restoration of multiple heritage sites based on the severity of damage and cultural importance. b) Scenario Simulation: AI can simulate various earthquake scenarios and their potential impact on heritage structures, helping policymakers and conservationists develop effective disaster preparedness and response plans.

Copyright © 2025 CroCEE
DOI: https://doi.org/10.5592/CO/3CroCEE.2025.141

5. Conclusion

Surveys and reconnaissance after a devastating earthquake provide large volumes of data in many formats and require intelligent tools to process and extract useful knowledge to support decision making for recovery and restoration.

AI/ML offers powerful tools for assessing and mitigating earthquake damage to heritage structures, enabling faster, more accurate, and culturally sensitive responses. By leveraging these technologies, we can better preserve our cultural heritage for future generations while enhancing resilience against natural disasters.

6. References

[1] Lagomarsino, S. 1998. Seismic damage survey of the churches in Umbria. Proceedings of the Works on Seismic Performance of Monuments, Lisbon, Portugal, 167–76.

[2] Ferracuti, Barbara; Imperatore, Stefania; Zucconi, Maria & Colonna, Silvia, "Damage to Churches after the 2016 Central Italy Seismic Sequence", Geosciences 12, 122 (2022)

[3] Satwant Rihal, Hisham Assal, Fernando Peña (2023). Deep Learning Modelling of Earthquake Damage Data for Identification of Patterns of Damage in Heritage Structures. In: Endo, Y., Hanazato, T. (eds) Structural Analysis of Historical Constructions. SAHC 2023. RILEM Bookseries, vol 46. Springer, Cham. https://doi.org/10.1007/978-3-031-39450-8_103

[4] Ertuğrul A., Özdemir T.Z., Al Ragabi H. (2023). Report on The Damage Caused by the February 2023 Kahramanmaraş Earthquake on Islamic Cultural Heritage in Türkiye. Research Centre for Islamic History, Art and Culture, İstanbul, Türkiye.

[5] Kocaman, I. et.al., "Global drift ratio limits for historical masonry mosques", Bulletin of earthquake engineering, January 2023, 21 (5)

[6] Satwant Rihal, Hisham Assal. (2024). "Deep Learning Ontology for Documentation and Assessment of Earthquake Damage to Heritage Structures". 18th World Conference on Earthquake Engineering. June 30th-July 5th 2024, Milan, Italy.

Proceedings of the 3rd Croatian Conference on Earthquake Engineering - 3CroCEE
19–22 March 2025, Split, Croatia
Copyright © 2025 CroCEE
DOI: https://doi.org/10.5592/CO/3CroCEE.2025.146

SEISMIC VULNERABILITY ASSESSMENT OF COMPLEX HISTORICAL MASONRY AGGREGATES WITH INTERACTIONS BETWEEN STRUCTURAL UNITS

Ponte, Madalena [(1)*], Guerrini, Gabriele [(2)], Penna, Andrea [(3)], Bento, Rita [(4)]

[(1)] *Pos-doc researcher, Department of Civil Engineering and Architecture (DICAR), University of Pavia, Italy. Email: madalena.ponte@unipv.it, gabriele.guerrini@unipv.it, andrea.penna@unipv.it*
[(2)] *Assistant Professor, Department of Civil Engineering and Architecture (DICAR), University of Pavia, Italy. Email: gabriele.guerrini@unipv.it, andrea.penna@unipv.it*
[(2)] *Full Professor, Department of Civil Engineering and Architecture (DICAR), University of Pavia, Italy. Email: andrea.penna@unipv.it*
[(3)] *Full Professor, Civil Engineering Research and Innovation for Sustainability (CERIS), Instituto Superior Técnico, Universidade de Lisboa, Portugal. email: rita.bento@tecnico.ulisboa.pt*

Abstract

Large scale complex historical buildings, such as palaces or historical city centres, are usually composed of aggregates that were built or connected in different phases. Consequently, under seismic action, there will be an interaction between the buildings that needs to be taken into account when performing their seismic vulnerability assessment. As seen by past seismic events, historical masonry aggregates present a high vulnerability to seismic action.

In this paper, different types of connections will be modeled between adjacent bodies and their effects on the global seismic response will be studied. The National Palace of Sintra, Portugal, an excellent example of large-scale irregular complex rubble stone masonry historic buildings, will be considered as a case study. The Palace is composed of several units built during different time epochs, starting from the XIII Century until the XVII. A collection of the different cases of connections between the units presented in the Palace will be organized and delivered here, according to the presence of different heights and/or floor levels, walls that are connected in same direction or perpendicular to each other, and other irregular cases that were found.

Using some units of the Palace as an example, the modeling approach considered for each type of interaction between the units by means of EFM will be described. The results of the global seismic assessment carried out with nonlinear static analyses will be presented and discussed. A comparison regarding the models with and without considering the connections of the adjacent buildings will also be delivered. The results presented here will be useful for the seismic rehabilitation of the historical buildings composed of aggregates. Engineers in common design practice will be able to model the interactions between units following this approach that uses the EFM, a low time consuming and computational effort numerical method, in the design of strengthening interventions of complex masonry aggregates.

Keywords: Historical aggregates, interactions between buildings, equivalent frame modeling, nonlinear static analyses.

1. General Considerations

The evaluation of seismic vulnerability in existing masonry buildings is a key step in devising effective mitigation strategies and enhancing the resilience of urban infrastructure. This importance is underscored by the significant damage observed during past seismic events ([1], [2], [3], and [4]). Unreinforced masonry (URM) structures, which are widespread in both historical and urban settings, present a variety of materials, construction methods, and irregular geometries that complicate their seismic performance. This complexity is further heightened by their frequent inclusion in building aggregates, where structural connections can vary in type and effectiveness. Factors such as differing construction techniques from various time periods, inconsistent materials, irregular roof and floor

Copyright © 2025 CroCEE
DOI: https://doi.org/10.5592/CO/3CroCEE.2025.146

heights, and suboptimal renovations often weaken the overall structural behavior [5], thereby increasing the seismic vulnerability of these aggregates [6], as shown in Fig. 1.



Figure 1. Local mechanism and in-plane damage in existing aggregates in Amatrice, Italy, after the 2016 Central Italy earthquake (Photo: A. Penna/G. Guerrini).

Understanding how the units within an aggregate interact presents a significant challenge, particularly when historical documentation is limited and on-site surveys are constrained. Identifying individual units within an aggregate can be difficult. Given these aggregate effects, it is essential to assess the seismic vulnerability of the entire aggregate rather than evaluating isolated units. These complexities highlight the need for a robust methodological framework for evaluating seismic vulnerability in masonry aggregates. Recent studies, such as those by [7], [8], and [9], have begun developing models and methods to better understand and calibrate interactions within historical aggregates.

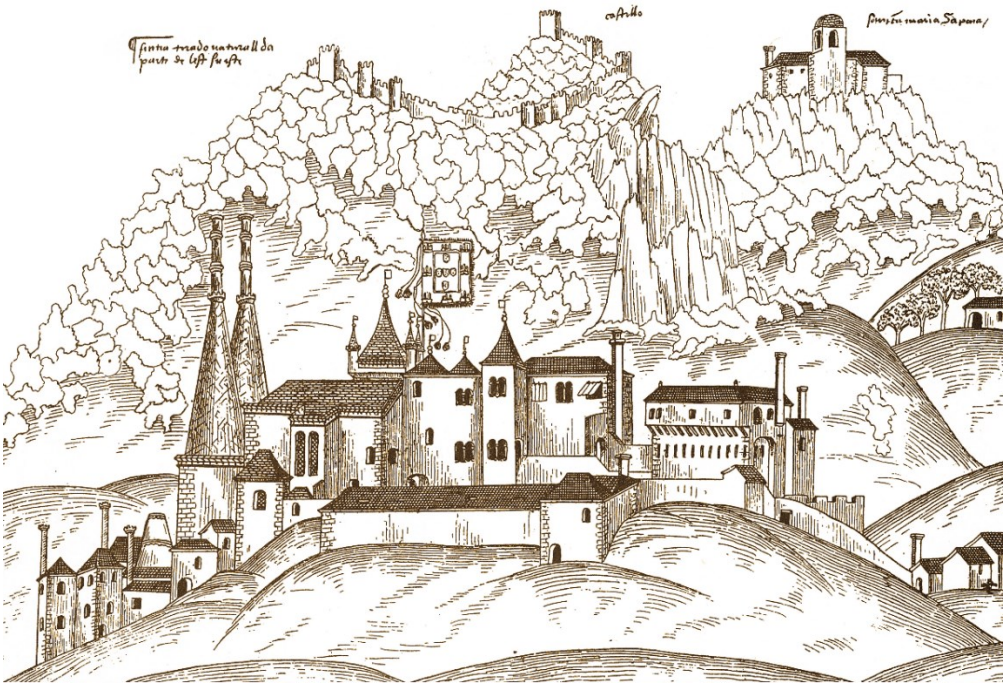
This study examines the interactions between units in irregular aggregates, focusing on the role of connections between adjacent units and their impact on seismic behavior. The research uses the National Palace of Sintra as a case study, a complex aggregate structure built over multiple periods, representative of many historical palaces and ancient urban centers. Numerical models are developed for both standalone units and those integrated within the aggregate. A previously developed aggregate model featuring monolithic connections ([10]) has been further refined and adapted for this study. The findings provide detailed insights into the in-plane seismic response of irregular URM walls and the interactions between neighboring units, analyzed through pushover curves.

2. Case Study

The National Palace of Sintra (NPS), situated in the village of Sintra on the outskirts of Lisbon, Portugal, comprises a series of royal residences that form a complex of buildings developed through successive construction phases, additions, and adaptations over several centuries. The exact foundation date of the oldest section of the Palace remains unknown. It is believed that the initial structures were built around the 10th or 11th century during the Moorish rule of Sintra, corresponding to the foundations of the northern part of the Palace. However, the primary construction and renovation phases occurred during the reign of King João I (1357–1433), with significant additions made later during the reign of King Manuel I (1469–1521). It was during the period of this last mentioned king, that by his order the first official drawings of the Palace were made. Fig. 2 presents the North façade of the Palace in 1507 and a current image of said façade. It is possible to observe that the three main central units remain similar in time with minor differences, comprising (from left to right) the kitchen with two large chimneys, the

Copyright © 2025 CroCEE
DOI: https://doi.org/10.5592/CO/3CroCEE.2025.146

cross-shaped chapel (from here on identified as Unit 2), and, on the right, adjacent to the chapel, a large building with four rooftops and a protrusion in its center (from here on identified as Unit 1). The National Palace of Sintra exemplifies the aggregate building process, illustrating how such constructions evolve naturally through the growth of isolated units, with additional structural elements incorporated over time.



a)



b)

Figure 2. North Façade of the National Palace of Sintra: a) 1507 drawing by Duarte D'Armas, and b) current photo captured by the drone of IST.

Copyright © 2025 CroCEE
DOI: https://doi.org/10.5592/CO/3CroCEE.2025.146

Identifying the main construction periods of the Palace required an initial extensive investigation into the Palace's history, supported by the historian team from Parques de Sintra - Monte da Lua (PSML). This research was complemented by a comprehensive experimental campaign, with sample removal and analysis, flat-jack tests, ambient vibration tests and ground-penetrating radar tests, and a detailed geometric survey using laser scanning and drone technology [10]. However, detecting the connections between sections built in different periods presents significant challenges due to the limited historical records on the construction phases and subsequent structural modifications. Consequently, some uncertainty remains regarding the precise nature of these connections. The identified connections between these sections were categorized into in-plane and in-height connections. The in-plane connections were further subdivided into (i) connections formed by the thickening of existing walls or (ii) connections created by the intersection of walls. The in-height connections, on the other hand, were classified based on the misaligned floor levels between adjacent buildings, where the storey height difference was either (i) smaller or (ii) greater than the thickness of the dividing wall. To analyze the interactions within the aggregates, four units of the oldest part of the NPS complex were selected (as identified in Fig. 3), corresponding to a former residential area, previously identified as Unit 1, and its adjacent buildings.

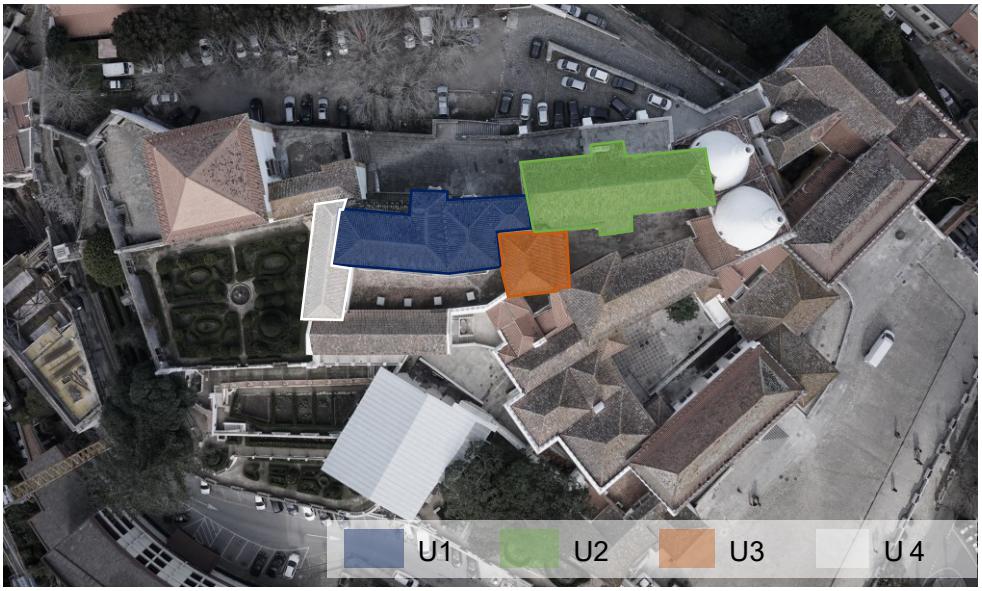


Figure 3. Case study units (Photo: IST drone)

Acquiring accurate geometry using traditional methods is highly challenging for buildings as complex, expansive, and irregular as the National Palace of Sintra. Consequently, the geometrical data were collected using laser scanning and drone surveys, as described in [11]. Unit 1 comprises three to four levels, including an intermediate floor in the central area, with floor heights varying between 2.4 m and 5.8 m. Unit 2, which serves as the chapel, on the other hand, stands at a height of 11 m and features an internal balcony positioned near its connection with Units 1 and 3. Unit 3 serves as a passage between Unit 1 and Unit 2, presenting three floors. Unit 4, also a residential area, was built more recently and presents three floors. The external walls of these buildings range in thickness from 0.65 to 0.88 m. Unit 1 is built atop an uneven and elevated bedrock, resulting in ground floor levels that differ significantly across the unit. Most of the ground floor walls are constructed directly against the bedrock. Moreover, Units 2, 3, and 4 are built at a lower ground floor level than Unit 1.

Ground Penetration Radar (GPR) revealed that Unit 2's walls are constructed with two stone leaves, with the outer leaf measuring 0.30 m thick and containing stones approximately 30–40 cm in size. At the top floor of Unit 1, the GPR identified two types of masonry: one more structured and the other less organized, with significant voids that may explain the visible cracks in the walls. All floors are flexible

Copyright © 2025 CroCEE
DOI: https://doi.org/10.5592/CO/3CroCEE.2025.146

timber constructions, typically supported by main beams connected to the façades. In some areas, the timber boards are overlaid with tiles.

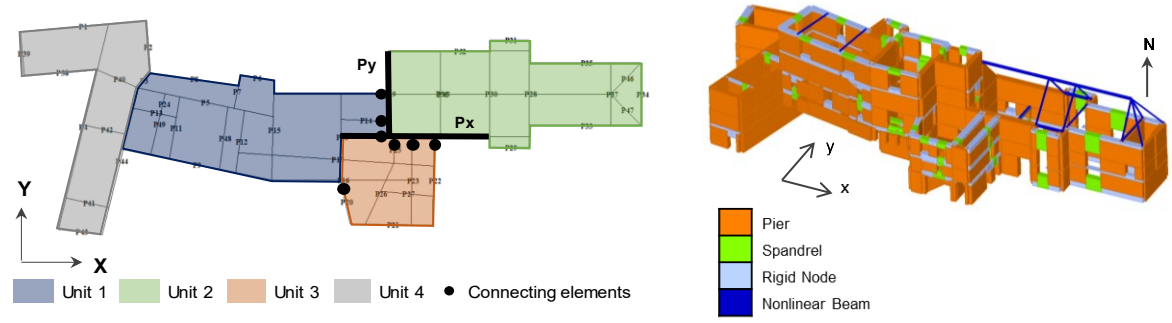
Additionally, previous interventions introduced tie-rods into Unit 1 and Unit 2. In Unit 1, two tie-rods are located on the upper floor of the main room, to prevent out-of-plane displacements of the two primary façades. Similarly, Unit 2 contains two rows of tie-rods linking its main façades, preventing out-of-plane movements. One alignment of tie-rods overlaps with the masonry arch that separates the choir from the chancel on the eastern side of the transept, while another alignment overlaps with the arch separating the chancel from the altar—a later addition to the structure. Each alignment includes two tie-rods placed at different heights: one integrated into a roof truss and another at the ceiling level, visible from the building's interior.

The case study, particularly Units 1 and 2, has been previously examined by [12] and [13]. However, in these studies, their analyses have always considered the connections to adjacent units as monolithic.

3. Numerical Study of the Interactions

3.1. Equivalent Frame Modeling

The Equivalent Frame Method (EFM) was used to model the aggregates under the assumption of monolithic connections. The 3Muri software [14] was employed for constructing the models, while modifications of the geometry and refinements of the mesh were carried out in Tremuri ([15], [16]). This approach was particularly suitable for modeling complex aggregates like the National Palace of Sintra, as it significantly reduces time and computational demands. Fig. 4 illustrates the plan and 3D view of the numerical model of the four structural units in the aggregate, as obtained from the 3Muri software prior to mesh refinements.



a) b)

Figure 4. a) Plan view of the numerical model with the identification of the connecting elements; b) 3D view of automatically generated EF mesh.

Three different levels of interaction between the structural units were considered: negligible interaction, in which structural units were modeled as isolated, partial, and perfect connections. For the latter, the adjacent units were directly linked by sharing nodes at their intersections, eliminating the need for additional elements. On the other side, the integration of the individual units into an aggregate with partial connections was modeled using spandrel elements. The spandrels are designed to resist only compression and shear forces, with no capacity to withstand tensile stresses. Each spandrel was assigned a length equal to half the thickness of the shared transverse wall, simulating the embedded portion of the walls within the existing structure. For the case-study units, only connections between walls oriented perpendicularly were modeled. Floor misalignments were considered when modeling full or partial connections by dividing the pier at the height of each floor. Given the numerous irregularities in the case-study aggregate, the analysis concentrated on the response of Unit 1 to different types of interactions with the adjacent units, considering only partial connections on one side of Unit 1 (located in Fig. 4), specifically with Units 2 and 3. The connections with Unit 4 on the opposite side were simplified and modeled as perfect.

Proceedings of the 3rd Croatian Conference on Earthquake Engineering - 3CroCEE
19–22 March 2025, Split, Croatia
Copyright © 2025 CroCEE
DOI: https://doi.org/10.5592/CO/3CroCEE.2025.146

The materials were characterized through the extensive experimental campaign outlined in [10]. A numerical model, assuming perfect connections between four Units, was employed to calibrate the mechanical properties of the masonry. For small vibrations, such as those recorded during ambient vibration tests, the connections between the units were assumed to behave monolithically. The masonry properties used in the numerical model are listed in Table 1.

Young's modulus (E) and shear modulus (G) were calibrated using the dynamic characterization results obtained from ambient vibration tests conducted in Units 1 and 2. Observations of the masonry in exposed inspection areas revealed disorganized, irregular rubble stone in Unit 1 and roughly dressed rubble masonry in Unit 2. Based on the calibrated values of E and G, other material properties, such as tensile strength (f_t), compressive strength (f_p), and weight (w), were proportionally derived from reference values in the Italian Standard [17] for the identified masonry types. The double flat-jack test results were found to be inconsistent and unreliable for determining compressive strength and Young's modulus, so only the stress levels from single flat-jack tests were used to calibrate the masses in the numerical model.

Additionally, the top floor of Unit 1 was determined to be in poor condition, exhibiting significant cracks. Consequently, the masonry properties for this level were reduced by half. For the unit located adjacent to the west side of Unit 1 (not included in this study), the same calibration methodology was applied to a separate model. No experimental tests were performed on Unit 3, and its material properties were assumed to match those of Unit 2, given its good state of preservation and similar construction period. The material properties for Unit 4 were calibrated using ambient vibration tests conducted on another unit adjacent to Unit 4, built during the same era.

Table 1. Masonry properties (adapted from [10])

	***Young's modulus, E* (GPa)**	***Shear modulus, G* (GPa)**	***Tensile strength, f_t* (MPa)**	***Compressive strength, f_c* (MPa)**	***Weight, w* (kN/m³)**
Disorganized irregular stone masonry					
MIT (2019) [17]	0.69 – 1.05	0.23 – 0.35	0.03 – 0.048	1.0 – 2.0	19
Unit 1	0.80	0.26	0.036	1.24	18
Unit 4	1.20	0.40	0.063	2.43	18
Roughly dressed rubble masonry with varying leaf thickness					
MIT (2019) [17]	1.02 – 1.44	0.34 – 0.48	0.0525 – 0.0765	2.0	20
Unit 2 / Unit 3	1.44	0.48	0.08	3.00	19

3.2. Numerical Results

3.2.1. Nonlinear Static Analysis

Nonlinear static analyses were carried out in the X direction (longitudinal) and Y direction (transverse) for a uniform loading, proportional to the mass. Fig. 5 presents the pushover curves for the three types of connections in terms of the base shear coefficient of Unit 1 versus the average top-floor horizontal

Copyright © 2025 CroCEE
DOI: https://doi.org/10.5592/CO/3CroCEE.2025.146

displacement of the same structural unit. The base shear coefficient was determined by calculating the ratio of the total horizontal force to the total vertical force at the base of the first floor without a supporting wall built against the bedrock. Each curve is displayed up to the ultimate displacement of Unit 1, defined as the point at which either a lateral strength reduction of at least 20% or the formation of a collapse mechanism is observed.

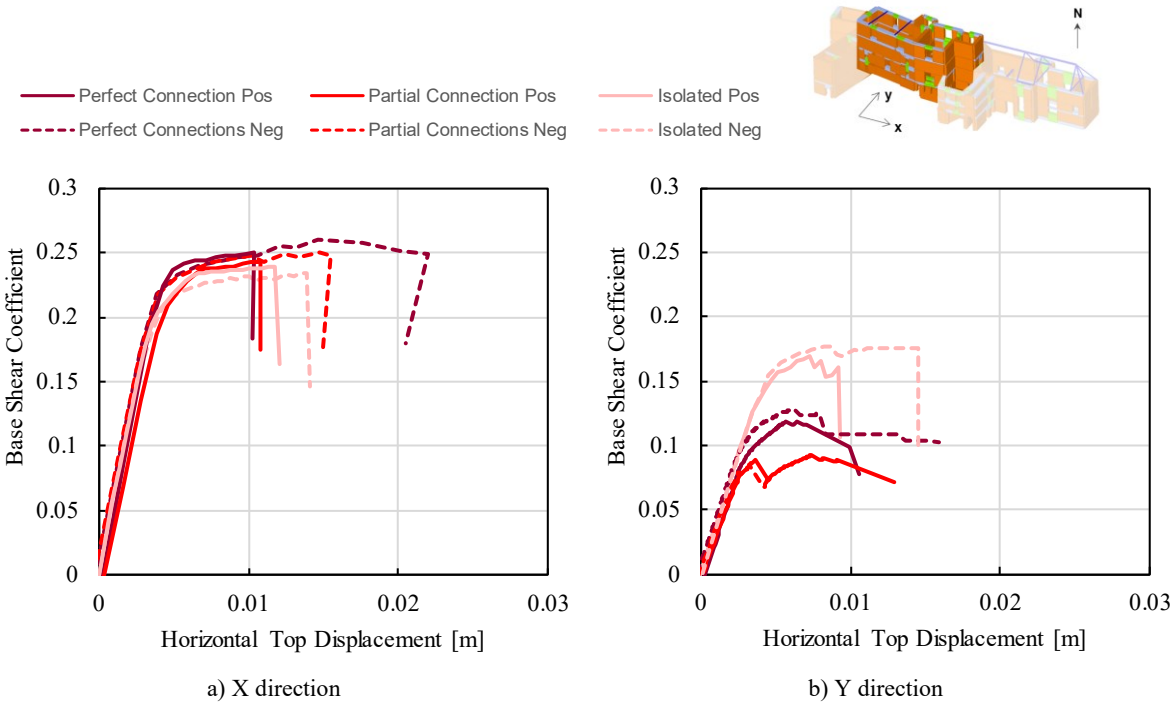


Figure 5. Pushover curves of Unit 1: a) X direction, b) Y direction, considering a uniform loading.

The pushover curves indicate that the aggregate effect does not significantly influence the behavior of Unit 1 in the longitudinal direction of the aggregate (X direction). Units 1 and 2 exhibit similar stiffness, while Units 3 and 4 have a minimal impact on the overall stiffness of Unit 1. Consequently, when subjected to loading in the X direction, the aggregate moves cohesively. In fact, regardless of the connection type, Unit 1's collapse is always governed by a soft-story mechanism in the same façade wall. This mechanism is characterized by a concentration of damage on a single floor preceding failure, resulting in a sudden loss of lateral strength. However, although the same collapse mechanism occurred for the three connection types and the global behavior is not influenced in this direction by the type of connection, not all walls presented the same behavior. For example, Fig. 6 shows the damage pattern that changes with the type of connection in a wall in the X direction shared between Unit 1 and Unit 2, named Px as identified in Fig. 4. The isolated model presents higher concentrated damage at the lower levels, while for the model with perfect connections, the damage is shared between the two buildings on the upper floors. In addition, for partial connections, the connecting elements present tensile stresses, allowing the opening of a gap between the two structural units.

Copyright © 2025 CroCEE
DOI: https://doi.org/10.5592/CO/3CroCEE.2025.146

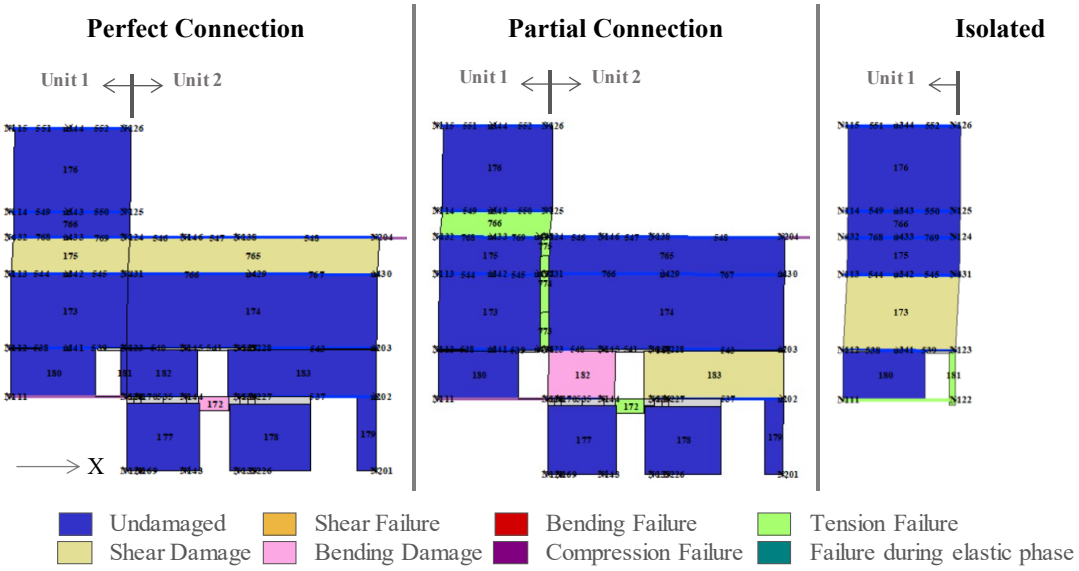


Figure 6. Damage pattern of a wall Px for a top-of-wall horizontal displacement of 0.01 m.

Unlike the X direction, the Y direction reveals a significant aggregate effect on Unit 1's behavior. This influence is not manifested in stiffness changes, largely dictated by the position, geometry, and height of adjacent units in the aggregate. Instead, it affects the behavior of the walls, leading to variations in collapse mechanisms and lateral strengths. Among the three models, the isolated configuration demonstrates the highest strength, followed by the models with perfect and partial connections. Unit 4 restrained Unit 1 within the aggregate, introducing slight torsion. In fact, in the aggregate, the wall shared between those two units presented low force values and remained in the elastic phase when the model started losing resistance. In addition, the different connections introduced different mechanisms of collapse, as presented in Fig. 7. For perfect connections, the damage on wall Py (identified in Fig. 4) is localized in two floors, and the collapse starts to occur on the upper floor with damage (as shown in Figure 7a); while, with partial connections, the wall presented lower strength due to the soft-story collapse localized on an upper floor (Figure 7b). On the other side, for the isolated model, the damage is distributed in height between three floors (Figure 7c).

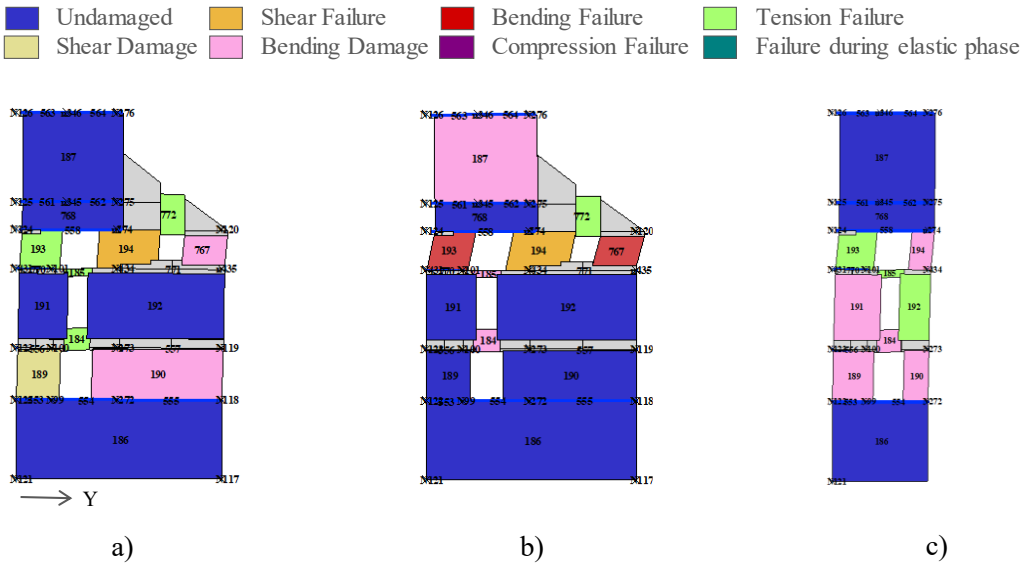


Figure 7. Damage pattern of wall in Y direction shared between Unit 1 and Unit 2, for a top wall horizontal displacement of 0.02 m.

Copyright © 2025 CroCEE
DOI: https://doi.org/10.5592/CO/3CroCEE.2025.146

In terms of displacement capacity, the results varied depending on the direction and connection type. In the positive X direction, displacement capacity remained similar regardless of the connection type, whereas in the negative X direction, it increased with the level of connection. In the Y direction, the model with perfect connections exhibited a slightly higher displacement capacity compared to the isolated model. The partial connection model demonstrated the highest displacement capacity in the positive Y direction, while in the negative Y direction, the collapse of Unit 1 was not reached due to the premature failure of wall Py.

4. Conclusions

The study explores the modeling of complex building aggregates using the Equivalent Frame Method (EFM), using the National Palace of Sintra in Portugal as a case study. This historic structure, originating in the 10th century, has undergone extensive modifications and expansions over the centuries, both horizontally and vertically. The investigation focuses on a specific section of the aggregate, comprising four structural units, which were analyzed both as isolated and as part of the aggregate. Particular attention was given to the type of connections between three of these units, considering two configurations: a monolithic connection representing perfect continuity, with shared nodes between the adjacent units, and a partial connection characterized by spandrel elements made of rubble stone masonry without tensile strength. The impact of varying story heights on the behavior of adjacent piers was also assessed by segmenting the pier next to the connection.

Nonlinear static analyses were performed to evaluate the in-plane response of these connections. The pushover curves reveal notable differences in the behavior of the unit only in the Y (transverse) direction when modeled as isolated or part of the aggregate. Modeling the connections as perfect, as would be done when designing a retrofit solution, allows for taking advantage of the lateral strength of Unit 1, resulting in a strength increase compared to models with partial connections. However, the lateral strength of the aggregate models remains lower than that of the isolated model, which offers a conservative approach, while the deformation capacity is slightly greater. These varying levels of connection influence the collapse mechanisms of the aggregate, thereby affecting its lateral strength and ultimate displacement. In the X (longitudinal) direction, the global pushover curves remain largely unaffected by the type of connection; however, differences were observed in the damage patterns of individual walls. Despite minimal global influence in this direction, this highlights the localized impact of connection variations within the aggregate.

While the results of such a complex case study did not allow for generalized conclusions about whether the aggregate effect was beneficial or detrimental, it was evident that incorporating spandrels resulted in a more realistic representation of damage patterns. Further research is suggested to test alternative connection modeling techniques and to expand the analysis to other units within the aggregate. Additional insights would require conducting nonlinear dynamic analyses to generalize the aggregate effect.

Acknowledgments

The authors would like to thank Dr. Cláudio Marques for all his help as an expert in the history of the National Palace of Sintra. The authors would like to acknowledge the financial support by DPC-ReLUIS project (2024-2026) through WP5 “Integrated and sustainable interventions for existing buildings” and WP10 “Masonry constructions” funded by the Italian Department of Civil Protection, and by the Portuguese Foundation for Science and Technology (Ministry of Science and Technology of the Republic of Portugal) through a PhD scholarship [grant number SFRH/BD/145571/2019] and CERIS project UIDB/04625/2020.

Copyright © 2025 CroCEE
DOI: https://doi.org/10.5592/CO/3CroCEE.2025.146

References

[1] Guerreiro, L., Azevedo, J., Proença, J., Bento, R., Lopes, M. (2000): Damage in ancient churches during the 9th of July 1998 Azores earthquake, *XII World Conference on Earthquake Engineering*, Auckland, New Zealand.

[2] D'Ayala, D.F., Paganoni, S. (2011): Assessment and analysis of damage in L'Aquila historic city centre after 6th April 2009, *Bulletin of Earthquake Engineering,* 9(1),81–104, doi: 10.1007/s10518-010-9224-4

[3] Penna, A., Morandi, P., Rota, M., Manzini, C.F., da Porto, F., Magenes, G. (2014): Performance of masonry buildings during the Emilia 2012 earthquake, *Bulletin of Earthquake Engineering*, 12, 2255–2273, doi: 10.1007/s10518-013-9496-6

[4] Sorrentino, L., Cattari, S., Da Porto, F., Magenes, G., Penna, A. (2019): Seismic behaviour of ordinary masonry buildings during the 2016 central Italy earthquakes, *Bulletin of Earthquake Engineering*, 17(10), 5583-5607, doi: 10.1007/s10518-018-0370-4

[5] Carocci, C. F. (2012): Small centres damaged by 2009 L'Aquila earthquake: on site analyses of historical masonry aggegates, *Bulletin of Earthquake Engineering*, 10, 45-71, doi: 10.1007/s10518-011-9284-0

[6] Cardinali, V., Cristofaro, M.T., Ferrini, M., Nudo, R., Paoletti, B., Tanganelli, M. (2021): A Multiscale Approach for the Seismic Vulnerability Assessment of Historical Centres in Masonry Building Aggregates: Cognitive Approach and Interdisciplinary Perspectives, *International Journal of Architectural Heritage*, 16(6), 839–64, doi: 10.1080/15583058.2021.1992536

[7] Angiolilli, M., Pinasco, S., Cattari, S., Lagomarsino, S. (2023): On the vulnerability features of historical masonry buildings in aggregate, *Procedia Structural Integrity*, 44, 2074–2081, doi: 10.1016/j.prostr.2023.01.265

[8] Gagliardo, R., Godio, M., Portioli, F.P.A., Landolfo, R. (2023): Seismic analysis of failure mechanisms in adjacent interacting stone masonry buildings via rigid block modeling, *Bulletin of Earthquake Engineering*, 22(12), 6195-6224, doi: 10.1007/s10518-023-01659-1

[9] Tomić, I., Beyer, K. (2023): Shake-table test on a historical masonry aggregate: prediction and postdiction using an equivalent-frame model, *Bulletin of Earthquake Engineering*, 22, 6225-6258, doi: 10.1007/s10518-023-01765-0

[10] Ponte, M., Bento, R., Vaz Silva, D. (2019): A multi-disciplinary approach to the seismic assessment of the National Palace of Sintra, *International Journal of Architectural Heritage*, 757-778, doi: 10.1080/15583058.2019.1648587

[11] Godinho, M., Machete, R., Ponte, M., Falcão, A.P., Gonçalves, A.B., Bento, R. (2019): BIM as a resource in heritage management: An application for the National Palace of Sintra, Portugal, *Journal of Cultural Heritage,* 43, 153-162, doi: 10.1016/j.culher.2019.11.010

[12] Malcata, M., Ponte, M., Tiberti, S., Bento, R., Milani, G. (2020): Failure analysis of a Portuguese cultural heritage masterpiece: Bonet building in Sintra, *Engineering Failure Analysis*, 115, 104636, doi: 10.1016/j.engfailanal.2020.104636

[13] Ponte, M., Bento, R., Costa, A., Quelhas, B., Guedes, J.M., Ilharco, T., Lopes, V. (2021): Reduction of earthquake risk of the National Palace of Sintra in Portugal: The palatine chapel, *International Journal of Disaster Risk Reduction*, 60, 102172, doi: 10.1016/j.ijdrr.2021.102172

[14] S.T.A. DATA.: *3Muri* [Computer Program]. Italy, Version: 11.5, 2018, Available at https://www.servizi.stadata.com/download/?lang=en&sw=3muri+project

[15] Lagomarsino, S., Penna, A., Galasco, A., Cattari, S. (2013): TREMURI program: an equivalent frame model for the nonlinear seismic analysis of masonry buildings, *Eng. Struct.,* 56, 1787–1799, doi: 10.1016/j.engstruct.2013.08.002

[16] Penna, A., Lagomarsino, S., Galasco, A. (2014): A nonlinear macro-element model for the seismic analysis of masonry buildings, *Earthquake Engineering & Structural Dynamics*, 43(2), 159-179, doi: 10.1002/eqe.2335

[17] MIT. (2018): DM 17/01/2018. Norme Tecniche per le Costruzioni. In *Gazzetta Ufficiale della Repubblica Italiana*. Rome, Italy.

Proceedings of the 3rd Croatian Conference on Earthquake Engineering - 3CroCEE
19–22 March 2025, Split, Croatia
Copyright © 2025 CroCEE
DOI: https://doi.org/10.5592/CO/3CroCEE.2025.149

ASSESSMENT OF TRAM-INDUCED VIBRATIONS ON EARTHQUAKE-DAMAGED BUILDINGS

Ivo Haladin[(1)], Franka Meštrović[(2)], Zvonimir Šantek[(3)], Katarina Vranešić[(2)], Krešimir Burnać[(2)]

[(1)] Associate professor, University of Zagreb Faculty of Civil Engineering, ivo.haladin@grad.unizg.hr
[(2)] Assistant, University of Zagreb Faculty of Civil Engineering, franka.mestrovic@grad.unizg.hr
[(3)] Associate of Supervising Construction Work Engineer, VIZ-EX d.o.o., z.santek76@gmail.com

Abstract

Operation of rail vehicle induces dynamic forces that can be transmitted to and have a harmful effect on people and structures in vicinity of rail infrastructure. When considering historical masonry structures and earthquake-damaged buildings, vibrations induced by closely positioned rail infrastructure can pose a significant challenge for structural engineers and urban planners, particularly in densely populated, heritage-rich city centres. This paper examines the impact of vibrations induced by tram traffic on the structure of earthquake-damaged buildings, through a case study of a historical masonry structure damaged in 2020 Zagreb earthquake. The main goal was to develop an analytical model for assessing the transmission of tram-induced vibrations to the foundation of an earthquake-damaged building. By utilizing transfer functions derived from measured vibration data on both the building and tram vehicle, the study aimed to evaluate the impact of track irregularities and different tram operating conditions on the vibrations affecting the building. This approach enables the assessment of potential risks associated with elevated vibration levels in the vicinity of seismically damaged buildings and provides insights for mitigating their effects on buildings structure. Results indicate that certain operational scenarios, such as track irregularities and higher tram speeds notably increase vibration amplitudes, potentially leading to progressive building damage over time. This analysis highlighted the cumulative effects of low-amplitude but repetitive vibrations on earthquake-damaged masonry, including the propagation of micro-cracks and loss of material ductility. The study emphasizes the importance of mitigating tramway-induced vibrations by incorporating these insights into structural maintenance and infrastructure planning, to protect damaged structures and enhance sustainable urban resilience in regions affected by earthquakes. Recommendations include implementation of advanced monitoring systems to promptly address and mitigate these risks, enabling targeted maintenance of tram tracks, particularly repairs of irregularities and optimization of tramway operations.

Keywords: vibrations; tram traffic; earthquake; vibro-acoustic analysis; urban resilience

1. Overview

The earthquake that struck Zagreb in 2020, with a magnitude of 5.5 (ML), highlighted decades of insufficient maintenance and inadequate construction practices, primarily within the historic city centre. The affected area spans approximately 22.2 million square meters, with residential zones accounting for 82% of this territory. Within the protected historic urban area, damage was reported to a total of 6,651 structures, of which 2,163 were classified as either unusable or temporarily unusable. Masonry buildings have been shown to exhibit significant vulnerability to seismic activity, a conclusion corroborated by historical earthquake events in Croatia. A key characteristic of Zagreb's pre-1960s building stock is its construction typology, comprising of masonry walls with timber floors and roofs, making such buildings especially susceptible to damage even under moderate seismic loads [1].

Zagreb's extensive tramway network constitutes a critical component of the city's public transport infrastructure. The tramway infrastructure, traverses the historic city centre and is characterized by its integration into narrow streets and close proximity to adjacent buildings. Fig. 1 illustrates the tramway network layout relative to earthquake-damaged buildings within Zagreb's historic city centre. The alignment of tram routes through the urban core highlights the proximity of tram-induced vibrations to the damaged masonry structures. This paper focuses on the post-earthquake evaluation of the impact of

Copyright © 2025 CroCEE
DOI: https://doi.org/10.5592/CO/3CroCEE.2025.149

tram-induced vibrations on the historic masonry buildings that sustained extensive structural damage and are located in the immediate vicinity of tram infrastructure.

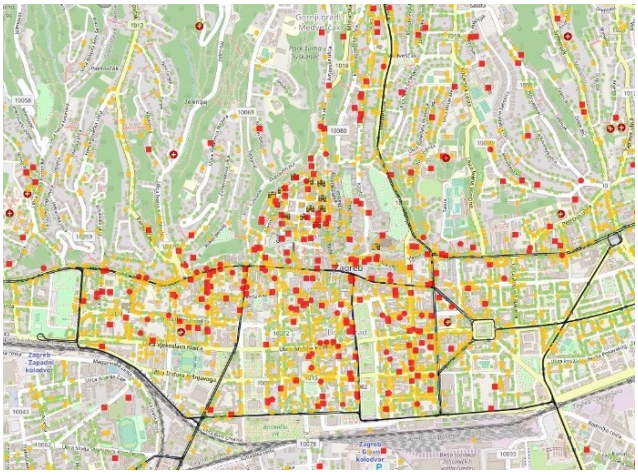


Figure 1. Tram network (black line) and buildings damaged by the earthquake categorized by initial inspections (yellow squares - temporarily unusable; red squares - permanently unusable) [2]

Buildings which are already in an unstable state are significantly more vulnerable to possible damage from vibrations or other disturbances [3]. Traffic-induced vibrations, under extreme conditions, can be detrimental to historic masonry structures. Due to their inability to resist tensile stresses, vibrations can negatively impact the structure of masonry buildings, especially under repeated loading cycles. The lack of tensile strength in masonry materials often leads to mortar deterioration and the detachment of masonry elements, ultimately reducing the overall strength of the structure. Structures with foundation settlement issues or those previously damaged in earthquakes are particularly at risk from vibrations [4]. Noticeable alterations in wall properties often emerge after exposure to tens or thousands of vibration cycles, highlighting the significance of vibration amplitude and duration as critical parameters. Traffic-induced vibrations can lead to the formation of microcracks in plaster and the gradual disintegration of walls, reducing ductility and consequently diminishing the seismic resistance of buildings [5].

The loss of vibration energy occurs during the transmission of vibrations from the source, through the surrounding soil, to the final recipient (typically the building foundations). During transmission through the soil, the attenuation is notably slower, resulting in vibration levels at the recipient being reduced by 2 to 15 dB [6]. The severity of vibration-induced damage to buildings decreases as the distance from tramway tracks increases, due to reduced transmission of vibration energy over greater distances. A minimum distance of 10 meters is recommended to effectively mitigate such vibrations [7]. Measurements of vibrations induced by rail vehicles at varying distances from the track were conducted in [8]. Once vibrations reach the building foundations, they are transmitted throughout the structure, inducing vibrations in floors, ceilings, and walls. As demonstrated in [9], horizontal particle velocities increase with height within the structure, whereas vertical velocities and accelerations remain constant. It can thus be concluded that vibration intensities are consistently greater on the upper floors of buildings. Measurements reported in [4] indicate that vertical velocity levels for foundation slabs exceed horizontal levels. Consequently, vertical vibrations are a key factor in the design strategies aimed at mitigating vibration transmission to upper floors [4].

Establishing universal and accurate thresholds for ground motions to predict structural damage is complex, as such predictions require advanced calculations. Building responses are influenced by dynamic characteristics, structural systems, material properties, and the cumulative effects of vibrations over time [10]. In evaluating the effects of vibrations on building components, peak particle velocity (PPV) has been identified as the most reliable single parameter for correlating with case history data on vibration-induced damage [3]. Unlike peak displacement and peak acceleration, PPV is relatively

Proceedings of the 3rd Croatian Conference on Earthquake Engineering - 3CroCEE
19–22 March 2025, Split, Croatia
Copyright © 2025 CroCEE
DOI: https://doi.org/10.5592/CO/3CroCEE.2025.149

frequency-independent, making it a robust descriptor [4]. Various standards and guidelines propose different PPV limits, which are summarized in Table 1.

Table 1. Examples of acceptable vibration threshold values for buildings and occupants

PPV [mm/s]	Effect on Humans or Buildings	Reference
0.3	Perceptible for humans	[11]
1.0	Cause of complaint in residential environments	[12]
1.0	Structural damage on buildings	[13]
1.5	Structures and buildings which are especially vibration-sensitive and require protection	[14]
2.5	Strongly perceptible for humans	[11]
2.5	Limit for buildings particularly sensitive to vibrations	[15]

A peak particle velocity (PPV) of 1 mm/s is recommended as the most conservative threshold to prevent damage to buildings of cultural and historical significance, as proposed in [17]. According to HRN DIN 4150-3 [15], the maximum allowable vibration levels depend on the type of structure. For historic or sensitive buildings exposed to long-term vibrations, the standard specifies a limit of 2.5 mm/s. The European standard HRN ISO 4866:2018 [16], which addresses the measurement and assessment of vibrations' impact on structures, provides the following expected ranges for traffic-induced vibrations: frequency from 1 to 100 Hz, amplitude from 1 to 200 µm, vibration velocity between 0.2 and 50 mm/s, and acceleration ranging from 0.02 to 1.0 m/s².

2. Objectives and Methodology

The primary objective of this research was to develop a functional analytical model for the transmission of vibrations, measured at the bogie of the tram, to the foundation of the subject building. This model is based on transfer functions and utilizes recorded vibration data from both the building and tram vehicles. The study aimed to investigate the effects of specific track irregularities and varying tram operating conditions on the vibrations acting upon the building. Furthermore, by establishing transfer functions that adapt source excitation to the excitation at the building foundation, it becomes possible to assess the influence of elevated vibration levels on the earthquake-damaged buildings. The research ultimately seeks to quantify the dynamic response of the building under different tram-induced vibration scenarios, thereby providing a framework for evaluating the potential risks associated with tram traffic near earthquake-damaged buildings.

When analysing the causes of elevated vibration levels induced by tram traffic, several factors have been identified as key contributors:

- **Damaged rails** can lead to structural issues, with factors such as rail head cracks, substandard welds, and surface corrugation requiring proper maintenance to prevent further deterioration;
- **Irregularities in switch geometry** caused by poor design or inadequate maintenance can disrupt the wheel's rolling path and introduce irregularities at crossings;
- **Misaligned or deteriorated crossing profiles** at intersections require thorough maintenance, as irregular transitions in the rail surface can contribute to vibration peaks;
- **Condition of track fastenings** plays a significant role in maintaining track stability, issues such as bearing failures or displacement of concrete slabs can compromise track integrity;
- **Increased tram speeds** exacerbate dynamic forces acting on the track and surrounding infrastructure, contributing to higher vibration and noise levels.

Additionally, the evaluation sought to identify the most effective methods for small-scale, long-term vibration monitoring across multiple buildings. The initial evaluation of a typical earthquake-damaged masonry building exposed to significant tram vibrations focused on two primary locations: bogie of the tram vehicle and the masonry building itself. By instrumenting a reference tram vehicle and the affected building with accelerometers, vibration levels were measured at both the source (wheel–rail interface)

Copyright © 2025 CroCEE
DOI: https://doi.org/10.5592/CO/3CroCEE.2025.149

and various locations within the structure. The collected data was then analysed using vibro-acoustical methods to determine the transfer function, allowing for the assessment of track conditions, vibration propagation, and their potential impact on the structure of the earthquake-damaged building (Fig. 2).

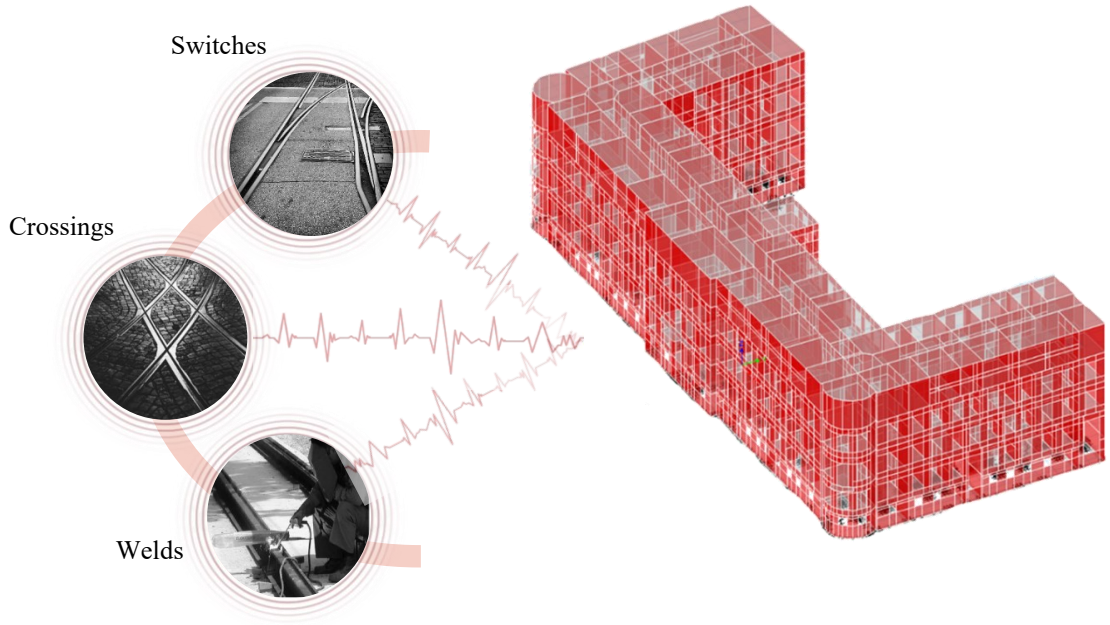


Figure 2. Conditions on rail running surface that can induce significant vibrations that can propagate to nearby masonry structures

3. Measurements and Analysis

The evaluation of tram-induced vibrations on buildings focused on assessing their transmission from tram vehicles to the track structure and, ultimately, to the masonry building, including attenuation of vibrations as they propagate through the surrounding soil. The initial phase involved measuring vibrations at the source and within the observed building during the passage of the reference tram. This was followed by a vibro-acoustical analysis to define the transfer functions. These functions were subsequently used to calculate vibration levels at various measurement points within the building, by applying the vibration levels measured at various track events on the tram network, in order to assess the impact in case they (or levels of vibrations) were to occur in the vicinity of the observed building.

3.1. Instrumentation and Measurement of Vibrations

While measuring vibrations directly at the building was essential, the tram traffic itself served as the main source of excitation. To comprehensively analyse the influence of tram vibrations, a representative tram vehicle was instrumented to measure vibration levels at the bogie level. This allowed for the assessment of track conditions and vibration amplitudes at the source (wheel–rail interface) during tram passages in front of the observed building. For the initial tests, measurements were conducted using tram TMK 2224, a 70-meter-long low-floor tram with five modular compartments, operating on three bogies in a Bo'Bo'Bo' configuration, further referred to as the reference tram. The central bogie of the tram was instrumented with accelerometers placed on the left and right sides in both the vertical and transverse directions (Z and Y respectivelly), as shown in Fig. 2. Acceleration data was collected using 10 mV/g accelerometers synchronized in time, with data recorded at a sampling rate of 4096 Hz.

Copyright © 2025 CroCEE
DOI: https://doi.org/10.5592/CO/3CroCEE.2025.149

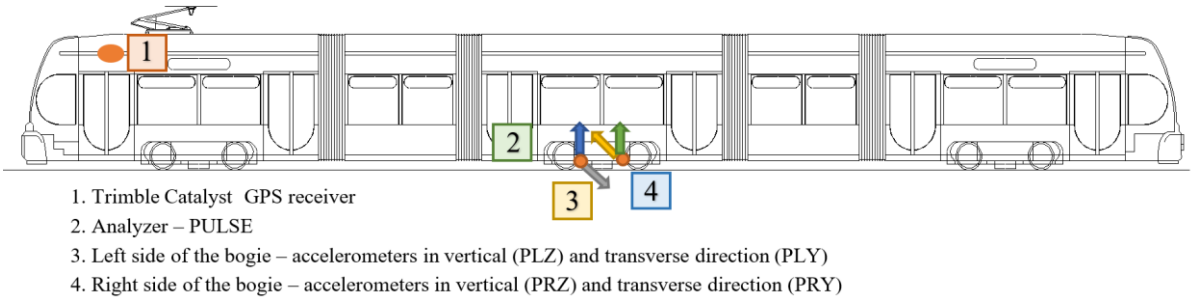


Figure 2. Position of accelerometers and GPS on reference tram TMK 2224

The testing was conducted at a masonry structure built in 1903 that exemplifies Zagreb's historic downtown architecture. The building is located in close proximity to the tram tracks, with the centerline of the nearest track only 5 meters from the building's façade. Observed building comprises of three wings (east, south, and west) and five levels, including the basement, ground floor, first, second, and third floor. Given that the south wing, which is closest to the track, was fully evacuated after the earthquake, it provided an ideal location for conducting an initial investigation into the effects of tram-induced vibrations on an earthquake-damaged structures. Following an initial inspection of the building layout and the damage caused by the earthquake, five measurement points for triaxial accelerometers were identified, as depicted in Fig. 3. The accelerometer positions were strategically selected to capture vibrations at equivalent locations across all floors. The accelerometer placements adhered to the recommendations of HRN DIN 4150-3 [15]. Data was recorded using 500 mV/g accelerometers synchronized in time, with a sampling rate of 1024 Hz.

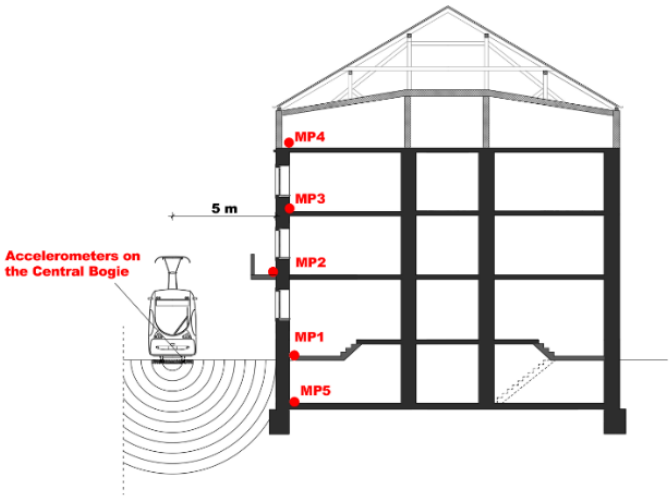


Figure 3. Positions of accelerometers and track distance from the observed building

3.2. Vibro-Acoustical Analysis

Following the measurements of vibration levels on the reference tram (Fig. 2) and measurement points within the building (Fig. 3), vibro-acoustical analysis was conducted using the DIAdem software. The primary objective was to determine the transfer function, which can subsequently be applied to calculate the impact of specific track conditions and driving scenarios on the induced vibration levels, as well as their effect on the building and the vibration levels within the structure. The transfer function is a dimensionless parameter used to calculate vibrations from various locations in the tram network under different deteriorated conditions. The data processing procedure is shown in Fig. 4.

Copyright © 2025 CroCEE
DOI: https://doi.org/10.5592/CO/3CroCEE.2025.149

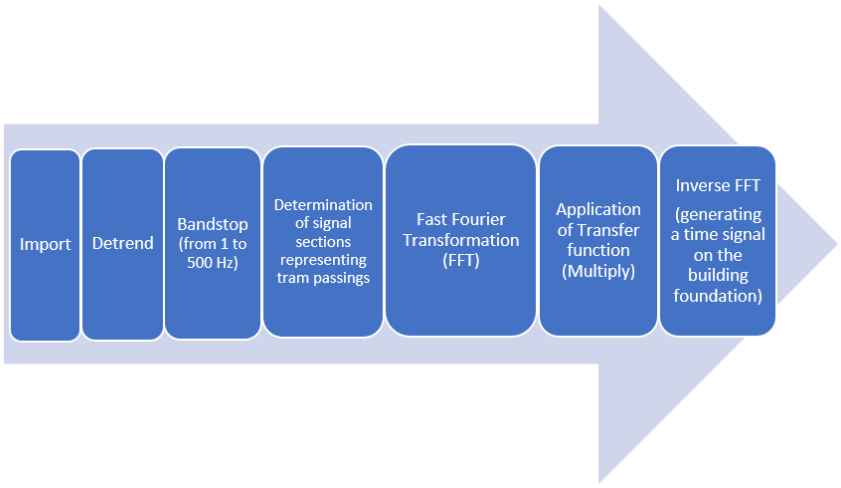


Figure 4. Diagram showing steps of data processing in DIAdem software

Tram network locations where track events generate vibration levels exceeding 150 dB were identified, which according to the study [17], are considered to potentially induce harmful vibrations (PPV>2.5 mm/s) in nearby buildings. Table 2 presents vibration levels recorded on 5 track cases of the tram network, which could cause considerable levels of PPV in the observed building at MP4, if they were to occur on the section of tram tracks in question. Most of the 5 chosen track events could cause PPV values which exceed the conservative threshold value of 1 mm/s [13], while PPV value caused by the track event on location L3 exceeds the maximum allowable level of 2.5 mm/s defined for culturally and historically important buildings [15]. Calculated levels of peak particle velocities were determined using transfer functions defined in DIAdem software.

Increased levels of vibrations at selected track events occur due to:

- L1 and L2 → degradation of the rail profile at crossings and the discontinuity of the rail profile,
- L3, L4 and L5 → degradation of the rail profile at crossings.

Measurements conducted for these track events exhibit pronounced Z-direction vibrations, primarily attributed to rail profile degradation at crossings, especially degradation of the rail head. This suggests that such vibrations are predominantly caused by rail surface discontinuities and rail wear in these track events. Given that vibrations have been analysed at the foundation level (MP5), and considering [9], it can be concluded that calculated horizontal particle velocities would be even more pronounced on higher floors of the building, as shown in the Table 2.

Table 2. Comparison of PPV values measured on the reference tram with values on MP5 and MP4 values calculated with transfer functions

Track events	**PPV [mm/s]**					
	MP5 (Z)	**ΔZ**	**MP5 (Y)**	**ΔY**	**Calculated (MP4) - Z**	**Calculated (MP4) - Y**
REF	0.14	-	0.09	-	-	-
L1	0.83	0.69	0.50	0.41	**1.96**	**1.18**
L2	0.66	0.51	0.48	0.39	**1.56**	**1.13**
L3	1.20	1.06	0.55	0.45	**2.83**	**1.30**
L4	0.55	0.41	0.40	0.30	**1.30**	**0.94**
L5	1.01	0.87	0.39	0.30	**2.38**	**0.92**

Proceedings of the 3rd Croatian Conference on Earthquake Engineering - 3CroCEE
19–22 March 2025, Split, Croatia
Copyright © 2025 CroCEE
DOI: https://doi.org/10.5592/CO/3CroCEE.2025.149

4. Conclusions

This research provides valuable insights into the impact of tram-induced vibrations on earthquake-damaged buildings and highlights the importance of maintaining track infrastructure to mitigate vibration transmission. Tram vibrations, despite their small amplitude compared to those caused by earthquakes, can considerably affect historically sensitive masonry structures due to the high number of cyclic loadings. The analysis focused on vibration levels at the foundation level, identifying critical elements that amplify vibration levels recorded on the reference tram, such as degradation of rail profile geometry at crossings and turnouts, discontinued rail surface, substandard welds, and higher speeds.

Through vibro-acoustic analysis, transfer functions were derived from vibration signals recorded on the reference tram and the observed building using DIAdem software. These functions provide insight into how tram-induced vibrations propagate through the surrounding soil and impact nearby buildings. By modeling the vibration responses of 5 track events, from locations on the tram network in Zagreb, the study demonstrated the potential of utilizing transfer functions for assessing vibration levels at various measurement points within the building. This is particularly important if similar track events were to occur in front of the observed structure, or if significant vibration levels were to occur in the vicinity of a similar masonry building.

The research also revealed that tram vibration impacts are specially pronounced in areas where rail surfaces are degraded, such as at intersections or turnouts, leading to amplified vertical and horizontal vibrations. Given these findings, it is clear that continuous monitoring and regular maintenance of tramway infrastructure is crucial for minimizing excessive vibration levels and their transmission to buildings, especially those damaged by earthquakes. Future research should focus on the numerical modeling of building responses to tram vibrations and the development of strategies for further reducing vibration levels to safeguard the structure of sensitive buildings as well as railway infrastructure.

References

[1] M. Stepinac, T. Kisicek, T. Renić, I. Hafner, and C. Bedon, "Methods for the assessment of critical properties in existing masonry structures under seismic loads-the ARES project," Mar. 01, 2020, *MDPI AG*. doi: 10.3390/app10051576.

[2] I. Haladin, M. Bogut, and S. Lakušić, "Analysis of tram traffic-induced vibration influence on earthquake damaged buildings," *Buildings*, vol. 11, no. 12, Dec. 2021, doi: 10.3390/buildings11120590.

[3] R. Thornely-Taylor *et al.*, *Measurement & Assesment of Groundborne Noise & Vibration*, 3rd ed. Suffolk: Association of Noise Consultants, 2020.

[4] A. Erkal, "Transmission of Traffic-induced Vibrations on and around the Minaret of Little Hagia Sophia," *International Journal of Architectural Heritage*, vol. 11, no. 3, pp. 349–362, Apr. 2017, doi: 10.1080/15583058.2016.1230657.

[5] M. Tomaževič, A. Žnidarič, I. Klemenc, and I. Lavrič, "The influence of traffic induced vibrations on seismic resistance of historic stone masonry buildings," in *Proceedings of the 12th European Conference on Earthquake Engineering*, London, UK: Wales, Sep. 2002, p. 631.

[6] F. Ribes-Llario, S. Marzal, C. Zamorano, and J. Real, "Numerical Modelling of Building Vibrations due to Railway Traffic: Analysis of the Mitigation Capacity of a Wave Barrier," *Shock and Vibration*, vol. 2017, 2017, doi: 10.1155/2017/4813274.

[7] Y. E. Ibrahim and M. Nabil, "Finite element analysis of multistory structures subjected to train-induced vibrations considering soil-structure interaction," *Case Studies in Construction Materials*, vol. 15, Dec. 2021, doi: 10.1016/j.cscm.2021.e00592.

[8] G. Kouroussis, H. P. Mouzakis, and K. E. Vogiatzis, "Structural impact response for assessing railway vibration induced on buildings," *Mechanics and Industry*, vol. 18, no. 8, 2017, doi: 10.1051/meca/2017043.

Copyright © 2025 CroCEE
DOI: https://doi.org/10.5592/CO/3CroCEE.2025.149

[9] M. Stepinac *et al.*, "Damage classification of residential buildings in historical downtown after the ML5.5 earthquake in Zagreb, Croatia in 2020," *International Journal of Disaster Risk Reduction*, vol. 56, p. 102140, Apr. 2021, doi: 10.1016/J.IJDRR.2021.102140.

[10] S. Casolo, "A numerical study on the cumulative out-of-plane damage to church masonry façades due to a sequence of strong ground motions," *Earthq Eng Struct Dyn*, vol. 46, no. 15, pp. 2717–2737, Dec. 2017, doi: 10.1002/eqe.2927.

[11] J. F. Wiss, "Construction Vibrations: State-of-the-Art," *Journal of the Geotechnical Engineering Division*, vol. 107, no. 2, pp. 167–181, Feb. 1981, doi: 10.1061/AJGEB6.0001095.

[12] *Code of practice for noise and vibration control on construction and open sites-Part 2: Vibration*. 2014.

[13] M. Crispino and M. D'Apuzzo, "Measurement And Prediction Of Traffic-Induced Vibrations In A Heritage Building," *J Sound Vib*, vol. 246, no. 2, pp. 319–335, Sep. 2001, doi: 10.1006/JSVI.2001.3648.

[14] "SN-640312a: Les ´Ebranlements—Effet des ´Ebranlements sur les Constructions; Swiss Standard on vibration effects on buildings; Schweizerische Normen-Vereinigung: Winterthur, Switzerland, 1992."

[15] "HRN DIN 4150-3:2016 Vibrations in Buildings—Part 3: Effects on structures; Deutsches Institut für Normung: Berlin, Germany, 2020."

[16] "HRN ISO 4866:2018. Mechanical Vibration and Shock—Vibration of Fixed Structures—Guidelines for the Measurement of Vibrations and Evaluation of their Effects on Structures; HRN ISO: Zagreb, Croatia, 2018."

[17] I. Haladin, K. Vranešić, and K. Burnać, "Monitoring stanja tračničke infrastrukture na temelju podataka prikupljenih konvencionalnim tračničkim vozilima," Dani HKIG, Opatija, 2023.

Proceedings of the 3rd Croatian Conference on Earthquake Engineering - 3CroCEE
19–22 March 2025, Split, Croatia
Copyright © 2025 CroCEE
DOI: https://doi.org/10.5592/CO/3CroCEE.2025.8

COMPARISON OF RESULTS OBTAINED FROM ANALYTICAL AND EXPERIMENTAL INVESTIGATIONS OF RC BUILDING COLUMNS USING CFRP

Artur Roshi [(1)], Golubka Nechevska – Cvetanovka [(2)], Jordan Bojadjiev [(3)]

[(1)] *Ph.D., Metropolitan University, Tirana, Albania, artur.roshi@yahoo.com*
[(2)] *Emerutis Professor, Ph.D., UKIM-IZIIS Ss. Cyril and Methodius University-Skopje, R.N.Macedonia, golubkapero@yahoo.com*
[(3)] *Ass. Professor, International Balkan University, Skopje, R.N.Macedonia, bojadziev@gmail.com*

Abstract

The focus of the research in this paper is Quasi-static tests on RC building columns strengthened with CFRP (Carbon Fiber Reinforced Polymers). To present the possibilities and the benefits of use of these materials, laboratory research for definition of the characteristics and experimental investigations of RC columns strengthened by CFRP by variation of concrete class, reinforcement percentage and different technologies of strengthening, are carried out at the Institute of Earthquake Engineering and Engineering Seismology – IZIIS, Skopje. Some recommendations and outcomes regarding the approach and technology of practical application of these materials, will be given.

Selected results from laboratory testing of built-in materials, part of analytical results and part of quasi-static experimental investigations of models designed and constructed by use of CFRP-materials are presented. Based on the analysis of values obtained from nonlinear static and nonlinear time history analyses, it can be concluded that the ductility capacity for displacement of models strengthened with CFRP is greater than 60%, while its strength capacity is greater than 7.7% when compared to the values obtained for the models without CFRP.

It can generally be concluded that CFRP systems are a very practical tool for strengthening and retrofitting RC building structures, as they can extensively improve flexural strengthening, shear strengthening, column confinement and ductility, thus, contributing towards better seismic resilience of the structures.

Keywords: RC columns; quasi-static tests; innovative materials; CFRP; strength; ductility.

1. INTRODUCTION

The field of research in the frames of this paper is application of innovative materials for repair and strengthening of RC buildings in seismic active regions. In order to make a contribution towards development and application of new innovative materials in engineering practice, experimental, quasi-static tests were carried out in the Dynamic Testing Laboratory at UKIM-IZIIS – Skopje, R.N. Macedonia. Laboratory tests on materials were done at the Institute for Material Testing – ZIM, AD Skopje,R.N. Macedonia. To define the real bearing and deformability capacity of the built column models, the values on quality of built-in concrete and reinforcement obtained for both vertical and transverse reinforcement, as well as the type of used CFRP were tested.

To contribute to definition of the joint behaviour of concrete, reinforcement and CFRP materials in the nonlinear range and develop a methodology and criteria for application of these materials in seismically active regions, for the needs of this study, an original research program involving experimental investigations on a series of two elements-models (columns) was defined. The main objective of the research programme was to define the strength and deformability of the elements constructed of innovative materials, as a function of a number of selected parameters that were varied in the course of the experiments. Within the frames of the experimental programme realized at UKIM-IZIIS, the percentage of longitudinal and transverse reinforcement was varied. The concrete class and the CFRP type were the same for both models. The behaviour of the models exposed to cyclic loads (quasi-static

Copyright © 2025 CroCEE
DOI: https://doi.org/10.5592/CO/3CroCEE.2025.8

tests) up to failure was investigated by visual monitoring of occurrence of cracks and development of failure mechanism.

In this paper, selected results from laboratory testing of built-in materials, part of analytical results and part of quasi-static experimental investigations of models designed and constructed by use of CFRP-materials are presented.

2. EXPERIMENTAL PROGRAM

For the needs of own experimental investigations, two column elements were designed. The column models were designed as fixed cantilever girders with a constant length of both models of 200 cm (the column was treated only up to the inflection point, i.e., half of the total height) and cross-section of 30/30 cm.In both models, the varying parameters were, the percentage of longitudinal and transverse reinforcement and the axial forces. The concrete class, i.e., the compressive strength of concrete and the type of the FRP was same for both models. The elements were designed to the geometrical scale of 1:1.

Presented further are photos taken during construction of the models (Model M1 and Model M2), Fig. 1 and Fig. 2 , and presented further are photos and results taken in the process of quasi-static tests on Model M1 and Model M2 with photos of characteristic damage (Fig. 3, Fig.4 and Fig.5) [1].

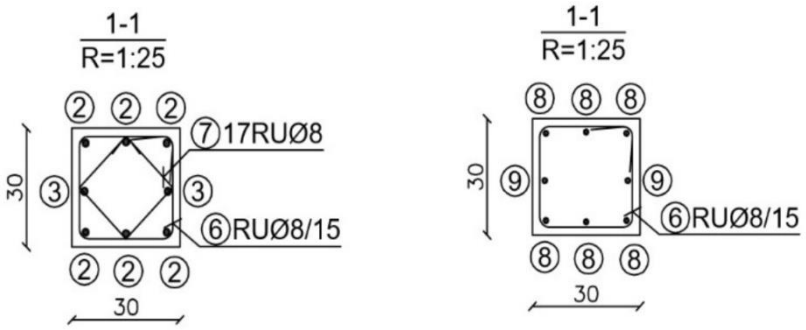


Fig. 1. Construction of the column models (Model M1 and Model M2) for experimental tests.



Fig. 2. Construction of the column models for experimental tests and photos taken during application of CFRP on the models.

Copyright © 2025 CroCEE
DOI: https://doi.org/10.5592/CO/3CroCEE.2025.8

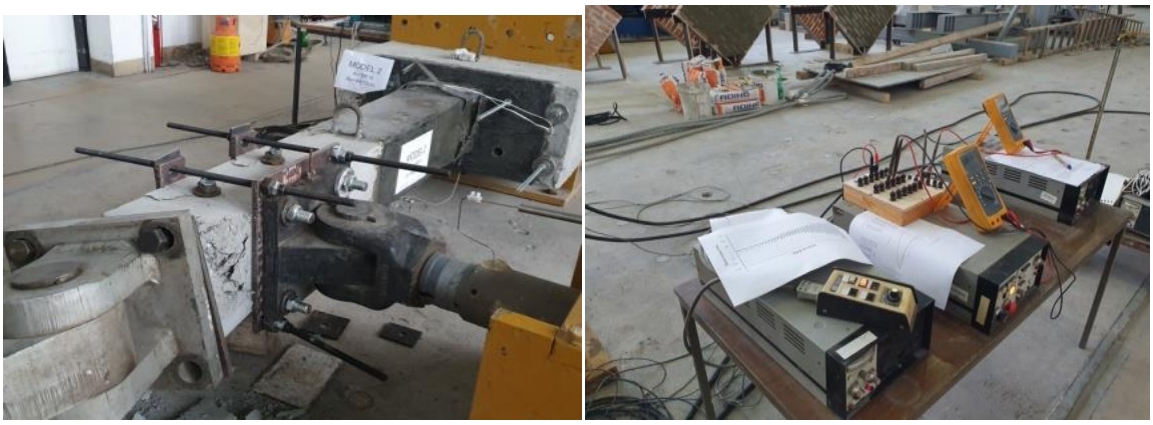


Fig. 3. Photos during the quasi static testing of the column models – Model M1and M2

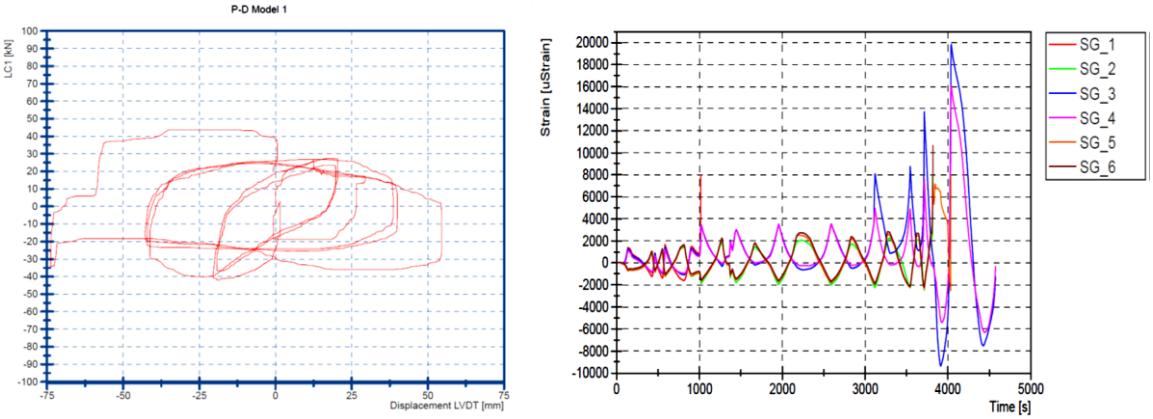


Fig. 4. Force – displacement relationship and time histories of strains for model M1[10]



Fig. 5. Observed damages during the quasi static testing of Model M1 and Model M2.

3. LABORATORY TESTS ON MATERIALS BUILT-IN MODELS FOR EXPERIMENTAL RESEARCH

During concreting of the models for experimental quasi-static tests, two models and three trial specimens- concrete cubes proportioned 15/15/15 were taken from the supports - beams and three trial cubes proportioned 15/15/15 were taken from the columns, in addition to the nine (9) cylinders

Copyright © 2025 CroCEE
DOI: https://doi.org/10.5592/CO/3CroCEE.2025.8

proportioned 15/30 cm (Fig. 6). To define compressive strength and concrete class, laboratory tests were performed at stock holding company-GIM-Skopje (for the cubes) and ZIM –Skopje (for the cylinders), while the tests for definition of the modulus of elasticity of the built-in concrete were done at ZIM – Skopje.

Using the trial concrete specimens – cylinders, three series of tests of compressive strength and tests for definition of the modulus of elasticity of the built-in concrete were carried out as follows:

- Series 0- concrete cylinders without CFRP- plain concrete
- Series 1- concrete cylinders wrapped with 1 (one) CFRP layer
- Series 2- concrete cylinders wrapped with 2 (two) CFRP layers

Presented further are photos and results taken during laboratory tests for definition of compressive strength and Modulus of elasticity of concrete and for the three series. It must be pointed out that the collapse of the models from the first and the second series was explosive, with big crushing of concrete wrapped with CFRP. This was particularly pronounced in Series 2 where concrete was wrapped with two CFRP layers.

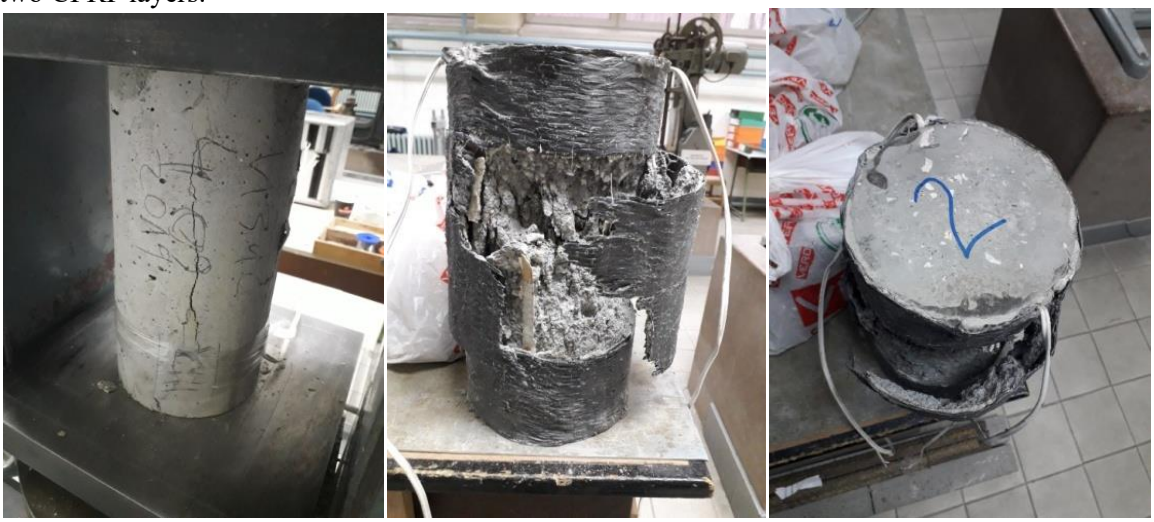


Fig. 6. Testing of the Compressive strength and modulus of elasticity of all three series.

From the results obtained, it can be concluded that the force inducing failure of concrete cylinders without CFRP amounts to 296.0 kN. For the cylinder with one CFRP layer, it amounts to 670.0 kN., while for the cylinder with two CFRP layers, it amounts to 955.0 kN. The compressive strength amounts to 16.8 Mpa, 37.0 Mpa and 54.1 Mpa, for all three series, and static modulus of elasticity are 28200.Mpa, 33000.Mpa And 43500.Mpa respectively.
The results obtained are presented graphically in Fig. 7.

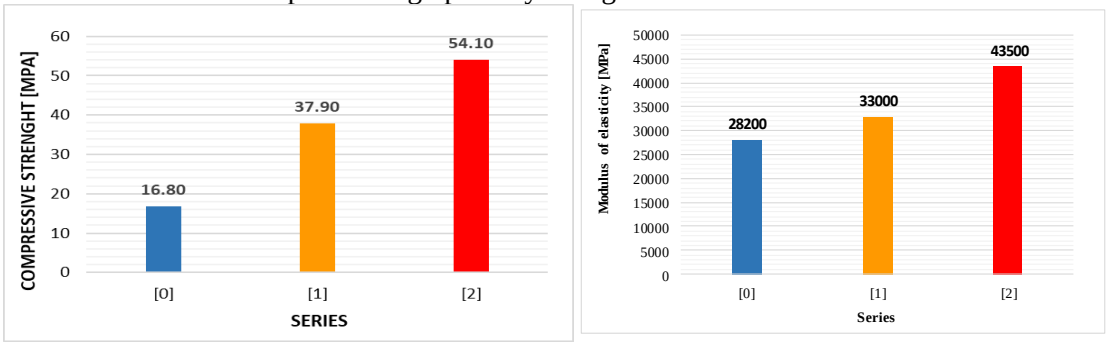


Fig. 7. Diagram of compressive strength and static modulus of elasticity for each series.

In general, it can be concluded that the compressive strength and modulus of elasticity becomes higher with the increase of the number of CFRP layers.

Copyright © 2025 CroCEE
DOI: https://doi.org/10.5592/CO/3CroCEE.2025.8

3.1 Definition of Real Strength and Deformability Capacity of Column Models

To define the real bearing and deformability capacity of the built column models, the values on quality of built-in concrete and reinforcement obtained for both vertical and transverse reinforcement, as well as the type of used CFRP were used. In the first phase, the real M-Φ (moment – curvature) relationships of the column cross-sections were computed by applying axial force, the real M-N diagrams, and then, based on the obtained M-Φ diagrams, the strength and deformability capacity of each model was defined [1].
The strength and deformability characteristics (M-N) and (M-Φ) at cross-section level, and Nonlinear Static Pushover Analysis and Nonlinear Time-History Analysis were analytically defined by use of the SAP2000 computer software. The following analyses were carried out:

(1) For Model M1, definition of the M-Φ diagram for Nv = 500 kN and M-N diagram (Fig. 8) for the following values for 0.1, 0.2, 0.3 series:
• For the designed concrete class (DC) (EC-25/30) with quality and quantity of reinforcement.
• For the built-in concrete class (CC) (EC-16/20) with quantity and quality of reinforcement.
• For the built-in concrete class with one layer of CFRP (CC-FRP) (38/46) with quantity and quality of reinforcement.

(2) For Model M2, definition of the M-Φ diagram for Nv = 300 kN and M-N diagram (Fig. 9) for the following values for 0.1, 0.2, 0.3 series:
• For the designed concrete class (DC) (EC-25/30) with quality and quantity of reinforcement.
• For the built-in concrete class (CC) (EC-16/20) with quantity and quality of reinforcement.
• For the built-in concrete class with one layer of CFRP (CC-FRP) (38/46) with quantity and quality of reinforcement.

Presented further are the results obtained from these analyses for Model M1 and Model M2.

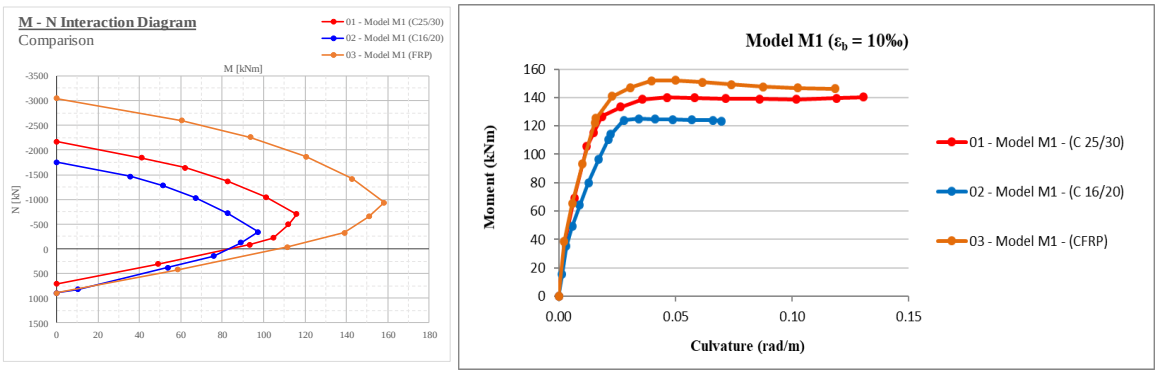


Fig. 8. M-N and M-Φ Diagrams for Model M1 - Comparison

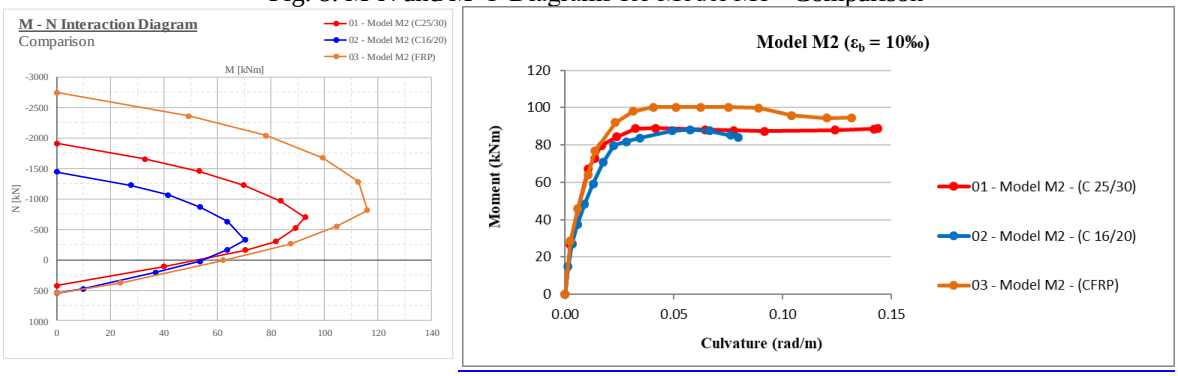


Fig. 9. M-N and M-Φ Diagrams for Model M2 – Comparison

Copyright © 2025 CroCEE
DOI: https://doi.org/10.5592/CO/3CroCEE.2025.8

Based on this analyses (Fig. 8 and Fig.9) and the results from Table 1, it can be concluded that the ductility to rotation for Model M1 is 2.049 greater for the model with CFRP, while the ductility to displacementt is greater in respect to the ductility of Model M1 without CFRP for 76.7%.
In the case of Model M2, the ductility to rotation is higher in the case of the Model with CFRP for 64 %, while the ductility to displacements is higher compared to the ductility of the Model M2 without CFRP for 46.1%.

Table 1. Rotation and displacement capacity for Model M1 and Model M2

Specimen	Rotation		Ductility	Displacement		Ductility
	Φy [rad/m]	Φu [rad/m]	DΦ	dy [cm]	du [cm]	Dd
Model M1-02	0.0127	0.0696	5.48	1.056	2.626	2.487
Model M1-03	0.0154	0.1730	11.23	1.281	5.631	4.306
Model M2-02	0.0128	0.0663	5.18	1.065	2.542	2.387
Model M2-03	0.0231	0.1963	8.50	1.922	6.702	3.487

From the Nonlinear Static Pushover Analysis and Nonlinear Time-History Analysis analysis of the values obtained, it can be concluded that the ductility capacity of Model M1 strengthened with CFRP is greater for 64.6% and for Model M2 is greater for 60% , while the strength capacity for Model M1 is greater for 21.1% and for Model M2 is greater for 7.7% compared to the model without CFRP (Fig.10 and Fig.11 and Table 2 and Table 3).

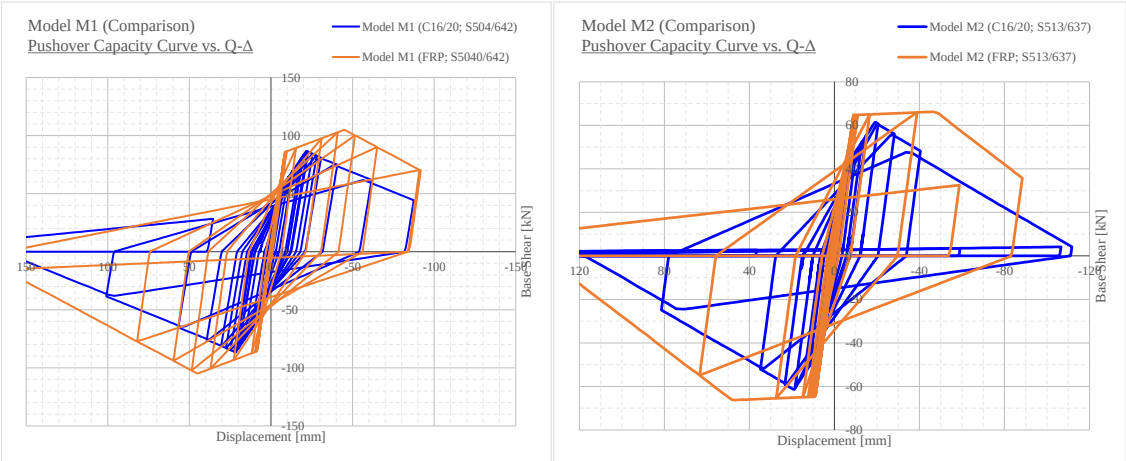


Fig. 10. Q – d diagram for Model M1 and Model M2 – comparison for series 02 and 03.

Copyright © 2025 CroCEE
DOI: https://doi.org/10.5592/CO/3CroCEE.2025.8

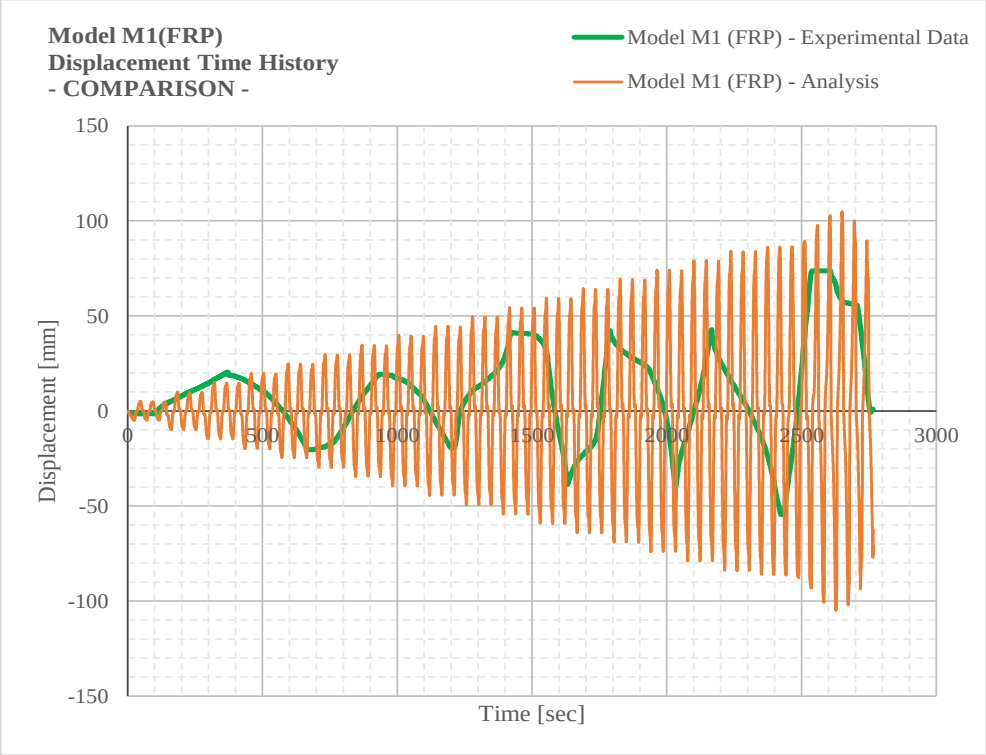


Fig. 11. Time history of displacements for Model M1- comparison between experimental and analytical results.

Table 2. Forces and displacements capacities, obtained from Pushover analysis for Model M1

Specimen	Displacement		Ductility	Shear force	
	dy [cm]	du [cm]	D_d	Qy [kN]	Qu [kN]
Model M1-01	0.864	3.564	4.125	81.41	99.01
Model M1-02	0.676	2.164	3.20	56.54	87.07
Model M1-03	0.855	4.506	5.27	86.15	105.39

Table 3. Forces and displacements capacities, obtained from Pushover analysis for Model M2

Specimen	Displacement		Ductility	Shear force	
	dy [cm]	du [cm]	D_d	Qy [kN]	Qu [kN]
Model M2-01	0.637	3.633	5.70	51.65	62.77
Model M2-02	0.578	1.916	3.31	41.96	61.88
Model M2-03	0.904	4.803	5.31	65.10	66.70

4. CONCLUSION

As a result of the comprehensive laboratory tests on concrete cylinders for: Series 0 - concrete cylinders without CFRP- plain concrete; Series 1- concrete cylinders wrapped with 1 (one) CFRP layer; Series 2- concrete cylinders wrapped with 2 (two) CFRP layers; It can be concluded that the compressive strength and Modulus of Elasticity becomes higher with the increase of the number of FRP layers.

Copyright © 2025 CroCEE
DOI: https://doi.org/10.5592/CO/3CroCEE.2025.8

Sample analytical analyses were carried out to define the strength and deformability capacity (M-N) and (M-Φ) at cross-section level were analytically defined by use of the SAP2000 computer programme. Based on the obtained M-Φ diagrams, the strength and ductility capacity of each model was defined.
The following analyses were carried out:
The moment capacity obtained for cross-section of Model M1 with CFRP is greater for 21.07 % than that of cross-section without CFRP and the ductility to rotation is higher in the case of the model with CFRP for 98 %. The moment capacity obtained for cross-section of Model M2 with CFRP is greater for 7.7 % than that of cross-section without CFRP and the ductility to rotation is higher in the case of the model with CFRP for 64 %.
Generally, it can be concluded that FRP systems represent a very practical tool for strengthening and retrofitting of concrete structures and are appropriate for flexural strengthening, shear strengthening and column confinement and ductility improvement.

REFERENCES

[1] Roshi, A., (2020). Application of innovative buildings materials for repair and strengthening of RC columns in seismically active regions, Doctoral dissertations, Ukim Iziis Skopje, Macedonia
[2] Nechevska-Cvetanovska, G., & Roshi, A. (2019). Rehabilitation of RC buildings in seismically active regions using traditional and innovative materials. Građevinski materijali i konstrukcije, 62(3), 19-30.
[3] Nechevska-Cvetanovska, G., Roshi, A., & Bojadjieva, J. (2019). Seismic strengthening of existing rc buildings structures using concrete jacketing and frp materials. E-GFOS, 10(19), 68-80.
[4] Roshi, A., Nechevska- Cvetanovska, G. (2019). Repair and Strengthening of RC Buildings using Traditional and Innovative Materials, 18th International Symposium organized by Macedonian Association of Structural Engineers (MASE), October 4-7, 2019, Ohrid, Macedonia
[5] Necevska-Cvetanovska, G., Apostolska, R. (2012). Methodology for Seismic Assessment and Retrofitting of RC Building Structures, Proc. of 15 World Conference on Earthquake Engineering (Paper ID 2149), 24-28 September 2012, Lisboa, Portugal.
[6] Necevska – Cvetanovska, G., Roshi, A. "Rehabilitation of RC Buildings in Seismically Active Regions Using Traditional and Innovative Materials", Journal Building Materials and Structures, Novi Sad, Serbia, 62 (2019) 3 (19-30).
[7] G. Necevska-Cvetanovska and R. Petrushevska (2000). " Methodology for Seismic Design of R/C Building Structures ". 12WCEE, New Zeland
[8] M. DI ludovico, A. Prora, G.Manfredi and E.Gosenza, "Seismic Strengthening of an Under-design RC Structure with FRP", Department of Structural Engineering, University of Naples Federico II, Naples, Italy, Published online 24 August 2007 in Wiley InterScience;
[9] CNR-DT 200/2004. Guide for the Design and Construction of Externally Bonded FRP Systems for Strengthening, 2004 (Downloaded free from: http://www.cnr.it/sitocnr/IlCNR/Attivita/NormazioneeCertificazione/NormazioneeCertificazione file/IstruzioniCNR DT200 2004 eng.pdf).
[10] Krstevska, L., Nechevska- Cvetanovska, G. (2019), Quasi-static testing of column models strengthened by FRP, UKIM-IZIIS, IZIIS Report 2019-75.

Proceedings of the 3rd Croatian Conference on Earthquake Engineering - 3CroCEE
19–22 March 2025, Split, Croatia
Copyright © 2025 CroCEE
DOI: https://doi.org/10.5592/CO/3CroCEE.2025.12

RAPID VISUAL SCREENING METHOD FOR RC BUILDING STRUCTURES

Burbuqe Shatri [(1)], Golubka Nechevska-Cvetanovska [(2)]

[(1)] *Teaching Assistant, University of Pristina, Faculty of Civil Engineering, Prishtina, Republic of Kosova, PhD Student at Institute of Earthquake Engineering and Engineering Seismology (IZIIS), "Ss. Cyril and Methodius" University, Skopje, Republic of North Macedonia, e-mail: burbuqe.shatri@uni-pr.edu*
[(2)] *Prof. Emeritus Dr., Institute of Earthquake Engineering and Engineering Seismology (IZIIS), "Ss. Cyril and Methodius" University, Skopje, Republic of North Macedonia, e-mail: golubkapero@yahoo.com*

Abstract

The destruction caused by recent earthquakes worldwide highlights the urgent need to assess buildings, especially those in medium-high-seismic-prone areas. Over the past few decades, advances in earthquake engineering have led to new methods to evaluate the hazard levels in buildings. Several seismic evaluation methods have been developed across the world. One such method, which is both rapid and cost-effective, is Rapid Visual Screening (RVS). In this paper, a detailed investigation has been done on the developed RVS methodologies in the field. Seismic evaluation guidelines from, the USA, Canada, Japan, and New Zealand, are reviewed from the perspective of their applicability. Each method is briefly outlined, highlighting its key features, applications, and contributions to seismic vulnerability assessment of RC building structures. According to most of the guidelines used worldwide, the work of various researchers was also presented.

Keywords: rapid visual screening (RVS), RC structues, assessment, methodolgies, scale, rapid, preliminary, detailed

1. Introduction

It is well known that as a consequence of earthquakes there is ground motion experienced on the surface resulting from the transmission of energy waves released from source and then undergoing certain modifications while travelling through soil layers as the energy reaches the earth surface. Many of these are of small intensity and do not cause significant damage to structures. However, there are cases when earthquakes of larger intensity in the urban areas cause considerable damage to the buildings and sometimes even a loss of life. During the last few decades, the urban areas have experienced very rapid population growth due to economic factors, such as the decrease in economic opportunities in rural areas, resulting in migration to urban areas. As a result of this migration, rapid construction in urban areas often leads to the spread of poorly designed and constructed buildings. Additionally, the older buildings were built to the relevant standards at the time of their construction and may not comply with the requirements of the latest building codes and standards. These buildings are at greater risk of considerable damage during a future earthquake, which can pose significant risks to human life and result in substantial economic losses in densely populated areas. Meanwhile, reinforced concrete (RC) buildings are among the most populated construction types in many developing countries. Most developing countries have emphasized the need to assess the seismic vulnerability of buildings in urban areas as an essential component of a comprehensive earthquake risk management policy. There are many methods available for seismic assessment of structures, which need a lot of time, cost, effort, a complex technical background, and procedure. Alternative methods have been developed to filter and prioritize buildings for a comprehensive, time- and resource-saving evaluation. These range from the most complex procedures to simpler ones. Amongst the simplified ones, Rapid Visual Screening (RVS) methodologies have been recently developed and proposed and their application is particularly useful in regions characterized by high seismicity or where a significant part of buildings are not designed according to seismic provisions. Rapid visual screening (RVS) is the basic key to measuring the seismic capacity of buildings. RVS helps to quickly categorize buildings into risk levels based on factors such

Copyright © 2025 CroCEE
DOI: https://doi.org/10.5592/CO/3CroCEE.2025.12

as building height, structural system, age, condition, and irregularities, and it provides a framework for identifying those at higher risk of significant damage during an earthquake. By identifying vulnerable buildings early, RVS enables authorities to focus their efforts on structures that need urgent attention, ensuring that the most at-risk buildings are prioritized for retrofitting or detailed evaluation.

2. Approaches to seismic vulnerability assessment

Over the past few decades, RVS has become an essential approach for quickly identifying vulnerable buildings, particularly in areas with a large number of older structures or those that do not meet modern seismic standards. The Rapid Visual Screening, (RVS) methodology has undergone several adaptaions and improvements, over the years to increase its accuracy and applicability. Fig. 1 illustrates the chronological evolution of widely used RVS methods for assessing seismic vulnerability which can be broadly divided into two categories:

a) Instrumental and quantitative data-based techniques

These methods rely on sophisticated instruments (e.g., accelerometers) to gather detailed quantitative data on the building's seismic performance.

b) Methods combining quantitative and qualitative data

This category includes the RVS method which uses a combination of visual inspection (qualitative data) and basic measurements (quantitative data) to assess a building's seismic vulnerability.

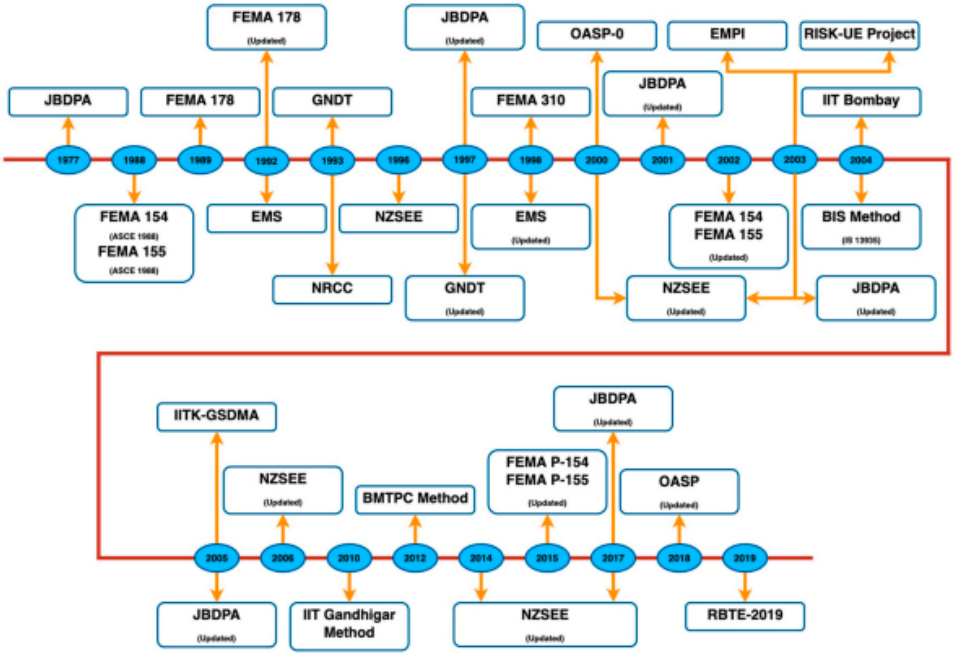


Figure 1. Timeline graphic of the development of the RVS methods

JBDPA: Japan Building Disaster Prevention Association
ASCE: American Society of Civil Engineering
GNDT: Gruppo Nazional per la Difesa dai Terremoti (National Earthquake Protection)
NZSEE: New Zealand Society for Earthquake Engineering
EMPI: Earthquake Master Plan of Istanbul

BMTPC: Building Materials and Technology Promotion Council

FEMA: Federal Emergency Management Agency

EMS: European Macro-seismic Scale
NRCC: National Research Council of Canada

OASP: Earthquake Planning and Protection Organization
IITK-GSDMA: Indian Institute of Technology Kanpur – Gujarat State Disaster Mitigation Authority

Copyright © 2025 CroCEE
DOI: https://doi.org/10.5592/CO/3CroCEE.2025.12

2.1 Application scales of seismic vulnerability assessment methodologies

The choice of methodology primarily depends on the number of buildings under assessment and the level of detail required. Based on the scale of applications the assessment procedures can be classified into three groups, as is illustrated in Fig. 2: a) single building scale, b) building stock scale, and c) large scale.



Figure 2. Different scales of the seismic vulnerability assessment procedures: (a), (b) & (c)

At the single building scale, the assessment focuses on evaluating the seismic vulnerability of individual structures. This method provides the most detailed analysis of a building's structural integrity and its ability to withstand seismic forces. It typically requires in-depth inspection, detailed design reviews, and sometimes the development of complex numerical models, including finite element analysis. This level of assessment is often used for high-value or high-risk buildings, where the cost of failure would be catastrophic.

At the building stock scale, the assessment aims to evaluate the seismic vulnerability of a group of buildings within a specific urban zone or district.

The approach begins by identifying sample buildings that represent the main building typologies within the area. These buildings act as representative models for the broader building stock, considering various factors such as the construction material, structural system, and the age of the buildings.

The second step in this process involves applying the vulnerability values from the sample buildings to the other structures in the zone by referring to their characteristics. This method allows for a more generalized but still relatively accurate assessment of a larger number of buildings, and it is useful for understanding the overall seismic risk in a particular area.

In large-scale applications, the methodology is employed to assess seismic vulnerability across an entire city or region. This involves the assessment of a large number of buildings over a wide area, often using simplified methods, such as Rapid Visual Screening (RVS), to evaluate large building stocks quickly. Large-scale assessments are generally used for city-wide seismic risk mapping and urban planning, where the goal is to prioritize interventions and resources for retrofitting or improving building codes across a broad geographic area [1].

3. Review of RVS documents

Rapid Visual Screening (RVS) methodology was first developed by "Applied Technology Council" in the late 1980's and published in FEMA 154 in 1988 by the United States as a standard guideline methodology for rapid vulnerability assessment. Several national seismic codes were further developed by various other countries worldwide, each of them being specific to local factors of construction methods and design philosophies.

The common RVS methodologies adopted by various countries across the globe include: RVS by the USA (FEMA), Rapid Evaluation method by the New Zealand Society of Earthquake Engineering (NZSEE), RVS by Canada developed by the National Research Council (NRC), Japanese method developed by the Japanese Building Disaster Prevention Association (JBDPA), Greek method by Earthquake Planning and Protection Organization (OASP), Indian approach based on FEMA 154

Proceedings of the 3rd Croatian Conference on Earthquake Engineering - 3CroCEE
19–22 March 2025, Split, Croatia
Copyright © 2025 CroCEE
DOI: https://doi.org/10.5592/CO/3CroCEE.2025.12

developed by IIT Kanpur, Turkish method developed by the Structural Engineering Research Unit (TERU), and the Italian method by the National Earthquake Defense Group (GNDT) all of which serve as approximate seismic vulnerability assessment techniques. These methodologies typically involve a three-level procedure: rapid, preliminary, and detailed assessments.

Rapid Visual Screening (RVS) is the initial stage of the assessment process, aimed at quickly evaluating a large number of buildings to determine their level of seismic risk. This stage involves visual inspections of buildings to identify key structural and non-structural vulnerabilities that may affect their performance during an earthquake. Following RVS, buildings identified as having significant seismic vulnerabilities undergo a more detailed preliminary assessment. PVA involves more comprehensive evaluations, including structural analysis and assessment of specific vulnerabilities identified during the RVS stage. Buildings requiring further consideration based on RVS and PVA results are subject to a detailed vulnerability assessment. DVA involves in-depth structural analysis, often utilizing advanced engineering techniques and computer modeling, to assess the building's behavior under seismic loading.

Throughout the years, numerous studies have been conducted to develop a more accurate and efficient Rapid Visual Screening (RVS) approach, primarily in seismically active regions.

One such study by Moustafa Moufid Kassem et al. (2020) [2], presents a comprehensive review of seismic vulnerability assessment methodologies. This review provides a detailed examination of the most common empirical and analytical techniques, summarizing findings from various research works. It also discusses the history and basic concepts of vulnerability assessment, screening procedures, the development of screening techniques, and the advancements in technology.

In another study, Mohd Danish et al. (2014) review the Rapid Visual Screening (RVS) method, highlighting its speed and cost-effectiveness. The study explains how the RVS score is calculated and assessed for various purposes related to seismic risk mitigation. It emphasizes the importance of RVS as a tool for identifying buildings that require further simplified vulnerability assessments and for identifying critical structures that need more detailed evaluations. This approach helps prioritize buildings for retrofitting or additional analysis, ultimately reducing seismic risks [3].

3.1. The method of the U.S.A. by the Federal Emergency Management Agency

The RVS methods that were developed for the seismic assessment of buildings in the United States consist of FEMA 154 and FEMA 155 which was first published in 1988 and revised in 2002. In January 2015, FEMA issued a third edition of procedures for FEMA P-154 and FEMA P-155.

The FEMA P-154 Rapid Visual Screening (RVS) method incorporates two levels of screening forms, Level 1 and Level 2, tailored for each seismicity region, which can be classified as moderate, moderately high, high, and very high.

- Level 1 screening form in the first section of the data collection form includes public information about the building, such as address, location, usage, and construction date, along with scores for various parameters based on the building type.

- Level 2 screening form is more detailed, including additional screening measures (SMs) for evaluating the final score (FS), and it requires a more qualified screener. While it is optional, it provides a more comprehensive assessment. At the end of the Level 2 screening, some nonstructural screening properties are also considered.

This two-tiered approach allows flexibility in the level of detail and expertise required, making it easier to comprehensive seismic risk assessments depending on needs and available resources.

The FEMA P-154 method provides forms for different seismicity regions, with the appropriate form selected based on seismic classification as shown in Fig. 3.

Copyright © 2025 CroCEE
DOI: https://doi.org/10.5592/CO/3CroCEE.2025.12

Rapid Visual Screening of Buildings for Potential Seismic Hazards — **Level 1**
FEMA P-154 Data Collection Form — **HIGH Seismicity**

PHOTOGRAPH

SKETCH

Address: _____ Zip: _____
Other Identifiers: _____
Building Name: _____
Use: _____
Latitude: _____ Longitude: _____
S_S: _____ S_1: _____
Screener(s): _____ Date/Time: _____

No. Stories: Above Grade: ____ Below Grade: ____ Year Built: ☐ EST
Total Floor Area (sq. ft.): _____ Code Year: _____
Additions: ☐ None ☐ Yes, Year(s) Built: _____

Occupancy: Assembly, Commercial, Emer. Services, ☐ Historic, ☐ Shelter; Industrial, Office, School, ☐ Government; Utility, Warehouse, Residential, # Units: _____

Soil Type: ☐A Hard Rock ☐B Avg Rock ☐C Dense Soil ☐D Stiff Soil ☐E Soft Soil ☐F Poor Soil DNK *If DNK, assume Type D.*

Geologic Hazards: Liquefaction: Yes/No/DNK Landslide: Yes/No/DNK Surf. Rupt.: Yes/No/DNK

Adjacency: ☐ Pounding ☐ Falling Hazards from Taller Adjacent Building

Irregularities: ☐ Vertical (type/severity) _____ ☐ Plan (type) _____

Exterior Falling Hazards: ☐ Unbraced Chimneys ☐ Heavy Cladding or Heavy Veneer ☐ Parapets ☐ Appendages ☐ Other: _____

COMMENTS:

☐ Additional sketches or comments on separate page

BASIC SCORE, MODIFIERS, AND FINAL LEVEL 1 SCORE, S_{L1}

FEMA BUILDING TYPE — Do Not Know	W1	W1A	W2	S1 (MRF)	S2 (BR)	S3 (LM)	S4 (RC SW)	S5 (URM INF)	C1 (MRF)	C2 (SW)	C3 (URM INF)	PC1 (TU)	PC2	RM1 (FD)	RM2 (RD)	URM	MH
Basic Score	**3.6**	**3.2**	**2.9**	**2.1**	**2.0**	**2.6**	**2.0**	**1.7**	**1.5**	**2.0**	**1.2**	**1.6**	**1.4**	**1.7**	**1.7**	**1.0**	**1.5**
Severe Vertical Irregularity, V_{L1}	-1.2	-1.2	-1.2	-1.0	-1.0	-1.1	-1.0	-0.8	-0.9	-1.0	-0.7	-1.0	-0.9	-0.9	-0.9	-0.7	NA
Moderate Vertical Irregularity, V_{L1}	-0.7	-0.7	-0.7	-0.6	-0.6	-0.7	-0.6	-0.5	-0.5	-0.6	-0.4	-0.6	-0.5	-0.5	-0.5	-0.4	NA
Plan Irregularity, P_{L1}	-1.1	-1.0	-1.0	-0.8	-0.7	-0.9	-0.7	-0.6	-0.6	-0.8	-0.5	-0.7	-0.6	-0.6	-0.7	-0.4	NA
Pre-Code	-1.1	-1.0	-0.9	-0.6	-0.6	-0.8	-0.6	-0.2	-0.4	-0.7	-0.1	-0.5	-0.3	-0.5	-0.5	0.0	-0.1
Post-Benchmark	1.6	1.9	2.2	1.4	1.4	1.1	1.9	NA	1.9	2.1	NA	2.0	2.4	2.1	2.1	NA	1.2
Soil Type A or B	0.1	0.3	0.5	0.4	0.6	0.1	0.6	0.5	0.4	0.5	0.3	0.6	0.4	0.5	0.5	0.3	0.3
Soil Type E (1-3 stories)	0.2	0.2	0.1	-0.2	-0.4	0.2	-0.1	-0.4	0.0	0.0	-0.2	-0.3	-0.1	-0.1	-0.1	-0.2	-0.4
Soil Type E (> 3 stories)	-0.3	-0.6	-0.9	-0.6	-0.6	NA	-0.6	-0.4	-0.5	-0.7	-0.3	NA	-0.4	-0.5	-0.6	-0.2	NA
Minimum Score, S_{MIN}	*1.1*	*0.9*	*0.7*	*0.5*	*0.5*	*0.6*	*0.5*	*0.5*	*0.3*	*0.3*	*0.3*	*0.2*	*0.2*	*0.3*	*0.3*	*0.2*	*1.0*

FINAL LEVEL 1 SCORE, $S_{L1} \geq S_{MIN}$:

EXTENT OF REVIEW
Exterior: ☐ Partial ☐ All Sides ☐ Aerial
Interior: ☐ None ☐ Visible ☐ Entered
Drawings Reviewed: ☐ Yes ☐ No
Soil Type Source: _____
Geologic Hazards Source: _____
Contact Person: _____

LEVEL 2 SCREENING PERFORMED?
☐ Yes, Final Level 2 Score, S_{L2} _____ ☐ No
Nonstructural hazards? ☐ Yes ☐ No

OTHER HAZARDS
Are There Hazards That Trigger A Detailed Structural Evaluation?
☐ Pounding potential (unless S_{L2} > cut-off, if known)
☐ Falling hazards from taller adjacent building
☐ Geologic hazards or Soil Type F
☐ Significant damage/deterioration to the structural system

ACTION REQUIRED
Detailed Structural Evaluation Required?
☐ Yes, unknown FEMA building type or other building
☐ Yes, score less than cut-off
☐ Yes, other hazards present
☐ No
Detailed Nonstructural Evaluation Recommended? *(check one)*
☐ Yes, nonstructural hazards identified that should be evaluated
☐ No, nonstructural hazards exist that may require mitigation, but a detailed evaluation is not necessary
☐ No, no nonstructural hazards identified ☐ DNK

Where information cannot be verified, screener shall note the following: EST = Estimated or unreliable data OR DNK = Do Not Know

Legend: MRF = Moment-resisting frame; BR = Braced frame; RC = Reinforced concrete; SW = Shear wall; URM INF = Unreinforced masonry infill; TU = Tilt up; MH = Manufactured Housing; LM = Light metal; FD = Flexible diaphragm; RD = Rigid diaphragm

Figure 3. Data collection form for high seismicity region (FEMA, 2015)

The classification of levels of seismicity is based on the spectral response acceleration values, as shown in Table 1, where S_S the spectral response acceleration parameter for a 5%-damped maximum

Proceedings of the 3rd Croatian Conference on Earthquake Engineering - 3CroCEE
19–22 March 2025, Split, Croatia
Copyright © 2025 CroCEE
DOI: https://doi.org/10.5592/CO/3CroCEE.2025.12

considered earthquake (MCER) at a period of 0.2 seconds, and S_1 is the spectral response acceleration parameter for a 5%-damped MCER at a period of 1 second, assuming Soil Type B.

Table 1. Range and median *MCER* spectral response acceleration values in each seismic region

Seismicity Region	Range of Response Values for Each Region	Median Response Values for Each Region	Range of Response Values for Each Region	Median Response Values for Each Region
	$S_{S(g)}$	$S_{1(g)}$	$S_{S,\ avg\ (g)}$	$S_{1,\ avg\ (g)}$
Low(L)	S_S<.0.25g	S_1<0.1g	0.2	0.08
Moderate (M)	0.25g≤S_S <.0.5g	0.1g≤S_1<.0.2g	0.4	0.16
Moderately High (M)	0.5g≤S_S <.1g	0.2g≤S_1<.0.4g	0.8	0.32
High (H)	1g≤S_S<.1.5g	0.4g≤S_1<.0.6g	1.2	0.48

The assessment begins by selecting a suitable Basic Score for each building, which is derived from the building's general characteristics, such as its construction type and age. This Basic Score represents the initial evaluation of the building's seismic performance before accounting for specific vulnerabilities or mitigation measures. A lower Basic Score indicates higher vulnerability.

The classification of damage is then based on the Final Score, which incorporates additional screening measures and detailed evaluation. The Final Score, as outlined in Table 2, helps determine the extent of potential damage and the necessary steps for improving the building's seismic resilience.

Table 2. Structural scores with damage potential

Rapid Visual Screening Score	Damage Potential
S<0.3S	High probability of Grade 5 damage; Very high probability of Grade 4 damage
0.3<S<0.7	High probability of Grade 4 damage; Very high probability of Grade 3 damage
0.7<S<2	High probability of Grade 3 damage; Very high probability of Grade 2 damage
2.0<S<2.5	High probability of Grade 2 damage; Very high probability of Grade 1 damage
S>2.5S>2.5	Probability of Grade 1 damage

The Final Score (FS) is a crucial metric in assessing a building's seismic performance, determined by summing the Basic Score and adjustments from all applicable Score Modifiers. The Final Score ranges from 0 to 7, where: 0 indicates a potential for collapse and 7 signifies better expected seismic performance. The building categorization can be divided into the following ranges based on the final score (FS):

- **Acceptable Seismic Performance (2 < FS ≤ 7):** Buildings within this range are considered to have a level of seismic safety that is considered acceptable.

- **Seismically Hazardous (0 ≤ FS ≤ 2):** Buildings in this range are considered to be at risk and require further detailed assessment to understand the potential risks in case of seismic events. These buildings may not meet current seismic safety standards and could pose a significant risk in the event of an earthquake.

By evaluating and adjusting scores through this method, the Rapid Visual Screening (RVS) process offers a comprehensive assessment of a building's seismic vulnerability. This approach helps prioritize buildings for more detailed evaluations and necessary seismic upgrades, enhancing the overall safety and resilience of the built environment [4].

Copyright © 2025 CroCEE
DOI: https://doi.org/10.5592/CO/3CroCEE.2025.12

The FEMA P-155 supports the RVS process, which is a preliminary assessment method used to quickly evaluate the seismic performance of buildings and identify those that require more detailed evaluation. For buildings identified as needing further evaluation, FEMA P-155 provides guidelines for conducting more comprehensive assessments and designing appropriate retrofits. The goal of FEMA P-155 is to help reduce the risk of earthquake damage and enhance the resilience of buildings, contributing to overall community safety and preparedness [5]. The steps of RVS survey for seismic vulnerability assessment (FEMA, 2015) are illustrated as in Fig. 4.

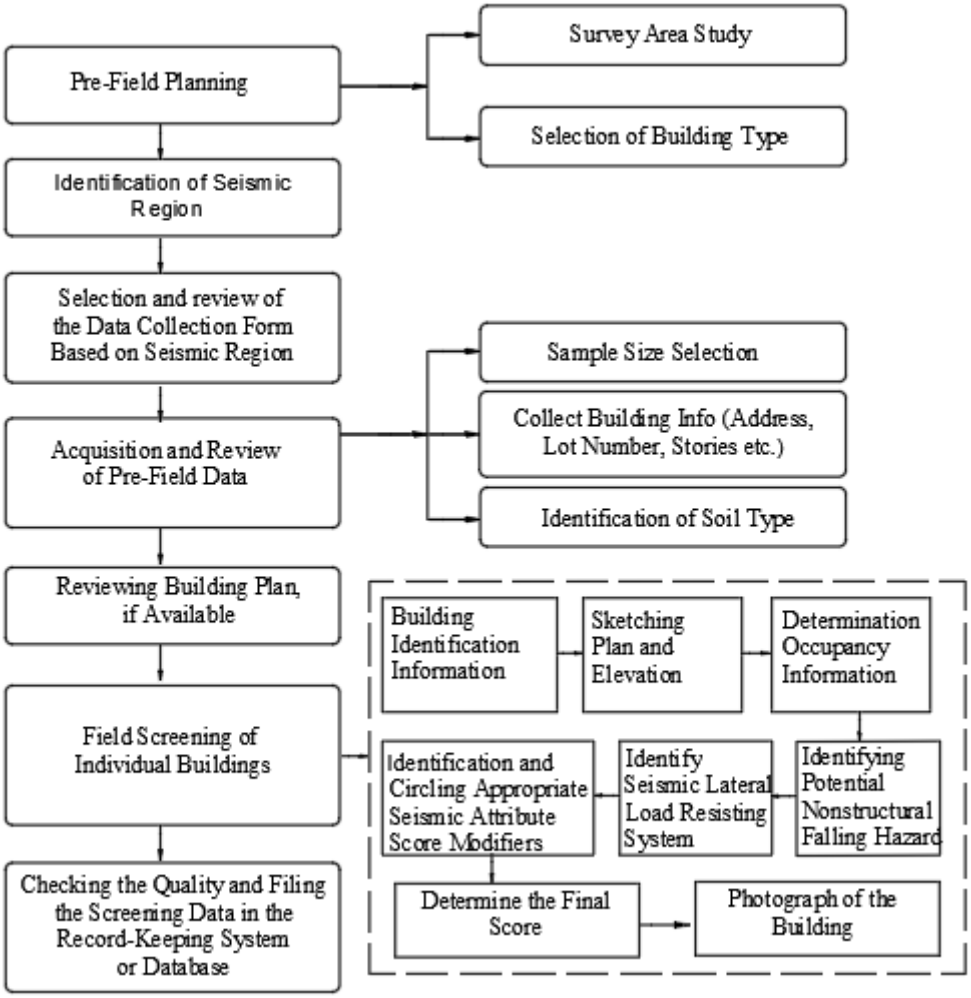


Figure 4. Steps of RVS survey for seismic vulnerability assessment (FEMA, 2015)

The RVS methods that were developed for the seismic assessment of buildings in the United States, have been widely used for seismic assessments by various researchers, as illustrated in studies such as those by Apostolska Roberta et al. (2017) [6,7], who conducted a comprehensive two-level, multi-group approach to assess the seismic performance of existing buildings in Karposh, a significant municipality in Skopje, Macedonia. The study began with rapid visual screening (level 1) on 161 buildings. For two case studies, various steps from the level 2 activities were implemented. The results indicated that the multidisciplinary approach led to a realistic assessment of the structural integrity of the buildings in relation to potential earthquakes.

Additionally, Nechevska-Cvetanovska Golubka et al. (2014) [8,9], introduced a methodology for geo-referenced inventory and monitoring of existing structures, with a focus on seismic stability and safety in the municipality of Karposh, Skopje. The methodology was applied to 161 buildings, using FEMA 154 level 1 rapid visual inspection steps. Three selected buildings were then analyzed further using FEMA 154 level 2 methods to assess seismic safety and stability.

Copyright © 2025 CroCEE
DOI: https://doi.org/10.5592/CO/3CroCEE.2025.12

The review of RVS methods, including FEMA P-154 Level 1, FEMA P-154 Level 2, and the Indian and Bangladesh methods, was used to assess the seismic safety of 26 low-rise RC buildings in Mandalay, Myanmar, in a study by Moe Myat Myat Aung et al. (2021) [10]. Based on the results, the FEMA P-154 methods gave the highest risk estimates, which were found to be overestimated and are therefore not recommended. The Indian method was recommended for low-rise buildings, while the Bangladesh method was found to be more suitable for assessing high-rise buildings.

Furthermore, Sameh A. El-Betar et al. (2016) [11] applied a seismic evaluation to two case studies: one representing GLD buildings and the other representing buildings designed according to Egyptian codes. The study used Level 1 FEMA P-154 score modifiers and conducted pushover analysis to investigate the buildings' vulnerability. Simplified parameters were used to determine the safety index, and both structural and non-structural factors were considered in the evaluation.

3.2. Japanese Seismic Index Method by the Japanese Board of Disaster Prevention Association

The Japanese Board of Disaster Prevention Association (JBDPA) developed three-stage screening procedures for assessing the seismic vulnerability of buildings in Japan. This procedure was developed in 1977 and underwent revisions in 1990 and 2001. In the first screening stage, the seismic assessment is conducted with a simplified approach. The ultimate strengths of the vertical resisting members are used to quantify the structure's response behavior during lateral seismic loading. The second screening stage, a more comprehensive evaluation of seismic building capacity is conducted. This level considers not only the strength but also the ductility of the resisting members. While the third screening stage, represents the most detailed and comprehensive assessment. It considers not only the strength and ductility of columns and walls but also the strength and ductility of beams for evaluating the structural performance during the earthquake movements.

In the Japanese standard, the seismic performance of a building is expressed by the seismic index of the structure (IS-index), where for each story and in each principal horizontal direction of the structure the calculation is done based on the product represented by Eq. (1):

$$IS = EO * SD * T \tag{1}$$

Where, (EO), is basic seismic index, (SD), is irregularity index and (T), is time index.

The basic seismic index of structure (EO) for different screening levels, calculated differently, however, is generally approximated by multiplying the shear modification factor, strength index and ductility index of each story. The irregularity index (SD) is introduced to adjust the basic seismic index by measuring the effects of horizontal and vertical shapes, and the mass and stiffness irregular distribution of the structure following engineering judgment. The time index (T) considers the effects of cracks, deflection, and aging of building. Once the Seismic Index of Structure (IS) is determined, it is compared with the Seismic Demand Index (ISO) using Eq. (2):

$$ISO = ES * Z * G * U \tag{2}$$

Where, (ES) for the first level of assessment is taken as 0.8 and 0.6 for the second and third levels; (Z) represents the seismicity of the region corresponding to the building's location; (G) symbolizes the ground index and (U) the usage index. There are two possibilities in comparing IS and IS0, in the first one, if: IS > IS0, this means it has low vulnerability condition, and for the second one, if IS < IS0 it will correspond to high vulnerability condition [12].

The Japanese seismic assessment procedures, based on the seismic index, are widely used by researchers, such as those outlined by Ercan IŞIK et al. (2015) [13]. In their study, the Japan Seismic Index Method was applied alongside the Canadian Seismic Screening Method and the Turkish First Stage Evaluation Method to assess a building damaged during the 2003 Bingöl earthquake. The building, a three-story structure constructed in the 1990s, sustained significant damage during the May 2003 Bingöl earthquake. Each method was used separately to calculate the building's performance score, and the results were found to be identical.

Proceedings of the 3rd Croatian Conference on Earthquake Engineering - 3CroCEE
19–22 March 2025, Split, Croatia
Copyright © 2025 CroCEE
DOI: https://doi.org/10.5592/CO/3CroCEE.2025.12

3.3. Canada Seismic Screening Method by the National Research Council

The methodology widely used in Canada for screening buildings for seismic investigation is outlined in the "Manual for Screening of Buildings for Seismic Investigation," published in 1993 by the National Research Council (NRC).

The methodology utilizes a scoring system similar to FEMA 154 but focuses on different factors. By considering these additional factors, the NRC approach enables a more comprehensive analysis of the consequences of building failure. Its purpose is to establish a Seismic Priority Index (SPI), which serves as a ranking system for buildings based on their seismic vulnerability.

The Seismic Priority Index is calculated by combining two indices: the Structural Index and the Non-Structural Index. The structural index (SI) considers a range of parameters related to seismicity, soil conditions (ground motions), structure type, structural irregularities, and building importance.

In contrast, the non-structural index (NSI) focuses on life safety against falling hazards in post-disaster scenarios, building importance, and soil conditions. SI is the structural index developed based on the product of five parameters.

These parameters along with their corresponding letters are: (A) seismicity index; (B) soil conditions; (C) type of structure; (D) building irregularities; and (E) importance of the building; (F) Max (F_1, F_2): (F_1) Failing Hazards to life; (F_2) Hazards to vital operations. Each of the parameters is calculated using the coefficient that is given in the Seismic Examination Method of Canada.

In first step, the structural index (SI) is calculated based on the product represented by Eq. (3):

$$SI = A * B * C * D * E * F \tag{3}$$

The non-structural index (NSI) which is the product of three parameters (B), (E), and (F) is calculated based on Eq. (4):

$$NSI = B * E * F \tag{4}$$

Where, F is the maximum value between F_1 for falling hazards to life and F_2 for hazard to vital operations. The formula for calculating the Seismic Priority Index (SPI), which is the sum of the Structural Index (SI) and the Non-Structural Index (NSI) is calculated based on Eq. (5):

$$SPI = SI + NSI \tag{5}$$

The score obtained by using the survey classifies the seismic vulnerability classes of the buildings as “low”, “medium”, and “high” seismic assessment stages. Then, the obtained results are the primary criteria that contributed to this screening score with the limit values given in Table 3:

Table 3. Priority levels for buildings in Canada Seismic Screening Method (Çelik, 2007)

Score type	Limit values	Priority Level
SPI	<10	Low priority buildings
SPI	10-20	Middle priority buildings
SPI	>20	High priority buildings
SPI	>30	Very hazardous buildings
SI/NSI	1.0-2.0	Sufficient seismic safety

If the SPI value of the evaluated building is less than 10, it is classified as “low”; if it is in the range from 10 to 20, it is classified as “medium”; and if the value is more than 20, then it is classified as being of the “high” seismic vulnerability class in terms of the priority of a further detailed assessment. A building constructed in compliance with the National Building Code of Canada (NBCC) is intended to have an SPI index score of 2.0. By considering these factors and calculating the SPI, this methodology

Proceedings of the 3rd Croatian Conference on Earthquake Engineering - 3CroCEE
19–22 March 2025, Split, Croatia
Copyright © 2025 CroCEE
DOI: https://doi.org/10.5592/CO/3CroCEE.2025.12

provides a systematic approach to prioritize buildings for further investigation or retrofitting efforts aimed at improving their seismic stability [14].

In the study by Ibrahim Baran Karasin et al. (2016) [15], the Canadian Seismic Screening Method was applied to assess the seismic risk of 37 RC buildings in Ahlat, located in the Lake Van Basin, an area known for its high seismic activity in Turkey. According to the Canadian seismic regulations, the evaluation categorized the buildings as follows: 14% as low priority, 41% as medium priority, 35% as high priority, and 10% as very risky. This evaluation represents the first stage, aiming to determine the risk priority of the buildings and guide further detailed analysis.

3.4. Rapid evaluation method by the New Zealand Society for Earthquake Engineering

The seismic assessment procedures in New Zealand (2017) are based on guidelines provided by the New Zealand Society for Earthquake Engineering (NZSEE) which incorporates elements from the FEMA methodology.

The NZSEE recommends a two-stage seismic risk assessment procedure, consisting of an initial assessment phase (IAP), which is the rapid evaluation stage and a detailed seismic assessment phase (DSA), which consists of two parts: one for potential earthquake-prone buildings (EPBs) and one for non-EPBs only. The IAP procedure presents an initial evaluation phase of the existing buildings based on the new building design standards (NBS).

The New Building Standard (NBS) is derived based on the characteristic features, such as the design year, the previous retrofitting interventions, the building importance, the fault distance, the site soil properties, and the vertical and plan irregularities integrated into the building area.

The % NBS value is calculated using this information given in Table 4, providing an initial indication of the building's seismic performance.

Table 4. Priority levels for buildings in Canada Seismic Screening Method (Çelik, 2007)

% NBS	Building Status	Seismic Risk Assessment
%NBS < 33	Vulnerable	Requires detailed seismic assessment and possible retrofitting
33 ≤ %NBS ≤ 67	Moderate Risk	Requires a more sophisticated assessment than RVS to determine seismic performance
%NBS > 67	Acceptable Seismic Performance	Considered capable of withstanding future earthquakes: no immediate action needed

If the % NBS is less than 33, the building is considered vulnerable, requiring a more detailed assessment. If it's greater than 67, the building is deemed capable of withstanding future earthquakes. For % NBS values between 33 and 67, the structural system should be examined in a method that is more sophisticated than RVS.

The earthquake rating evaluation is given in Eq. (5):

$$NBS = (Ultimate\ Capacity\ Seismic)/ULS\ \ (Seismic\ Demand) * 100 \quad (5)$$

The DSA can be used to verify the accuracy of the results obtained from the Initial Assessment Procedure (IPA). If the IPA indicates a need for further evaluation, the DSA provides a more detailed and comprehensive analysis to confirm the initial findings [16].

The seismic assessment procedures in New Zealand (2017) are based on guidelines widely used in countries with high seismic risk, as discussed by Kapetana, P. et al. (2007) [17]. Their study provides an overview of various rapid visual screening methods developed in seismic-prone regions such as the

Copyright © 2025 CroCEE
DOI: https://doi.org/10.5592/CO/3CroCEE.2025.12

USA, Greece, New Zealand, India, and Canada. These methods were applied to a sample of 456 reinforced concrete buildings in Athens, Greece, for which structural characteristics and damage levels from the 1999 Athens earthquake were already known. The earthquake caused 93 building collapses, 201 buildings sustained severe damage, 69 experienced moderate damage, and 93 had light damage. Each building was assessed using the scoring systems of the applied methods, resulting in eight different scores for each building. The study aimed to evaluate the reliability of these methods in identifying potentially seismically hazardous buildings.

4. Conclusion

Many structures in the current building stock, including reinforced concrete (RC) buildings, were constructed without considering seismic design standards, or with lower seismic design criteria, making them vulnerable to potential earthquakes. This paper highlights key factors that should be considered when selecting an appropriate seismic vulnerability assessment method for buildings. The Rapid Visual Screening (RVS) method is an effective tool for quickly assessing the seismic vulnerability of existing buildings. It provides a cost-effective and efficient way to identify RC structures and other structures that may need further detailed evaluation or retrofitting to reduce their seismic risk. By utilizing a set of predefined criteria, the RVS method helps prioritize buildings for more in-depth seismic analysis, ensuring that limited resources are directed toward the most critical structures at risk. This paper also provides a review of some of the most significant contributions to the field of vulnerability assessment.

References

[1] Shabani A., Kioumarsi M., Zucconi M. (2021): State of the art of simplified analytical methods for seismic vulnerability assessment of unreinforced masonry buildings,https://doi.org/10.1016/j.engstruct.2021.112280

[2] Moustafa M.K., Fadzli M.N., Ehsan N.F. (2020): The seismic vulnerability assessment methodologies -A state-of-the-art review, *Ain Shams Engineering Journal,* Volume 11, Issue 4, Pages 849-864, https://doi.org/10.1016/j.asej.2020.04.001

[3] Danish, M., Mohammad, Z., Gupta, H., Shariq, M., Masood, A. (2014): Importance of Rapid Visual Screening (RVS): An Overview, *3rd International Conference on Emerging Trends in Engineering & Technology*, College of Engineering, Teerthanker Mahaveer University, Meerut, India.

[4] Federal Emergency Management Agency (FEMA), FEMA P-154 (2015): Rapid Visual Screening of Buildings for Potential Seismic Hazards, *A Handbook*; Applied Technological Council (ATC), Washington, DC, USA.

[5] Federal Emergency Management Agency (FEMA), FEMA P-155 (2015): Rapid Visual Screening of Buildings for Potential Seismic Hazards. *Supporting Documentation,* Applied Technological Council (ATC), Washington, DC, USA.

[6] Apostolska, R., Nechevska-Cvetanovska, G., Shendova, V., Bojadjieva, J. (2017): Seismic performance assessment of hybrid&quot structures using two-level multy group GIS oriented approach-case studies, *Bulletin of Earthquake Engineering*, *BEEE-D-17-00063R2,* Institute of Earthquake Engineering and Engineering Seismology (IZIIS), Skopje, Macedonia.

[7] Nechevska-Cvetanovska, G., Apostolska, R. (2012): Methodology for seismic assessment and retrofitting of RC building structures, Proceedings *of 15th World Conference on Earthquake Engineering* (WCEE), Lisbon, Portugal.

[8] Necevska-Cvetanovska, G., Apostolska, R., Shendova, V., Vitanova, M., Bojaddjieva, J. (2014): Geo-referenced Inventory toward Seismic Safety of Existing Building – Case Study Karposh Municipality Skopje, *Proceeding on the Second European Conference on Earthquake Engineering and Seismology*, Istanbul, Turkey.

[9] Nechevska-Cvetanovska, G. (2013): Upgrading of Information System with New Attributes for Inventorying and Monitoring of Seismic Stability and Safety of Existing Structures in Karposh Municipality – GIS

Copyright © 2025 CroCEE
DOI: https://doi.org/10.5592/CO/3CroCEE.2025.12

Environment, Volume 1, Visual Inspection and Opinion about Existing State of Structures in Karposh Municipality and Inventorying in the Defined Form, *IZIIS Report No.* 2013-47, Institute of Earthquake Engineering and Engineering Seismology (IZIIS), Skopje, Macedonia.

[10] Aung, M.M., Aye, M.N. (2012): Seismic Safety Assessment of Existing Low-Rise RC Buildings with Rapid Visual Screenings and Preliminary Evaluation Methods, *ASEAN Journal on Science & Technology for Development* Vol 38, No 1, 29–36, DOI:10.29037/ajstd.649

[11] El-Betar, S.A. (2016): Seismic vulnerability evaluation of existing R.C. buildings, *HBRC Journal*. Housing and Building National Research Center, Egypt, https://doi.org/10.1016/j.hbrcj.2016.09.002

[12] Japan Building Disaster Prevention Association (JBDPA). (2017): Standard for Evaluation of Seismic Capacity of Existing Reinforced Concrete Buildings, *Japan Building Disaster Prevention Association (JBDPA)*, Tokyo, Japan.

[13] Işık, E. (2015): Investigation of an Existing RC Building with Different Rapid Assessment Methods, Bitlis Eren Univ J Sci & Technol 5 (2), 71-74. E - ISSN 2146-7706.

[14] National Research Council of Canada (NRCC). (1993): Manual for Screening of Buildings for Seismic Investigation, *Canadian Standard,* Ottowa, Canada.

[15] Karasin, B.I., Işık, E., I., Antep, B. (2016): A Case Study of Canadian Seismic Screening Method in Lake Van Basin, *IOSR Journal of Mechanical and Civil Engineering (IOSR-JMCE)* e-ISSN: 2278-1684, p-ISSN: 2320-334X, Volume 13, Issue 1 Ver. III, PP 91-95.

[16] New Zealand Society for Earthquake Engineering (NZSEE). (2017): The Seismic Assessment of Existing Buildings*, Technical Guidelines for Engineering Assessments-Initial Seismic Assessment-Part B,* New Zealand Society for Earthquake Engineering (NZSEE), Wellington, New Zealand.

[17] Kapetana, P., Dritsos, S. (2007): Seismic assessment of buildings by rapid visual screening procedures, *WIT Transactions on The Built Environment*, Vol 93, ISSN 1743-3509, https://doi:10.2495/ERES070391

Proceedings of the 3rd Croatian Conference on Earthquake Engineering - 3CroCEE
19–22 March 2025, Split, Croatia
Copyright © 2025 CroCEE
DOI: https://doi.org/10.5592/CO/3CroCEE.2025.23

RESEARCH IMPERATIVES FOR ENHANCING THE ANALYSIS AND SEISMIC PERFORMANCE OF JOINTS IN VERTICAL BUILDING EXTENSIONS

Alush Shala [(1)], Jelena Bleiziffer [(2)]

[(1)] *Senior Project Manager, Alb-Architect L.L.C., 10000 Prishtina, Kosovo, alushala@gmail.com*
[(2)] *Assistant professor, Faculty of Civil Engineering Zagreb, jelena.bleiziffer@grad.unizg.hr*

Abstract

There are many cases around the world where vertical extensions of existing buildings are favored as alternatives to the erection of new buildings, which would entail demolishing the old structure as well. Such solutions with vertical extensions have certain benefits, but the design characteristics of the base structures and their condition after years of service urge careful consideration of the joint between the new and old structural members and how it affects the global performance of the entire system. The risk to human lives, as well as environmental, economic, and social implications – including pollution and carbon emissions contributing to the greenhouse effect – serve as a strong motivation for researching these connections. This issue becomes especially critical in regions prone to frequent tectonic activity, where errors in the design and execution of additional floors on existing buildings are often observed. The errors observed on-site during the execution and design of additional floors on existing buildings are notable. This paper will discuss the research needs for improving the seismic behavior of the structural detailing and subsequent modeling for structural analysis of this connection between the vertically added floors and the base structure, focusing on the reinforced concrete frame structure solutions. The connection between the new floor and the old structure might not be rigid as is often treated in the design phase, and the behavior of the joint in response to dynamic forces might differ from what is projected thus the joint might not be adequately addressed from a seismic behavior perspective. The treatment of this issue will be discussed taking into consideration the conditions in the on-site execution and the provisions of Eurocodes standards, namely the EC2 part 4.

Keywords: vertical extension, joint connection, seismic behavior, on-site execution

1. Introduction: background and research motivation

The observation of recent construction trends in the Republic of Kosovo, where it is a relatively frequent occurrence to erect additional floors on top of old buildings, raises concerns about their safety. Vertical extensions on old buildings pose higher risk than constructing the entire (higher) structure anew, especially so if executed beyond building permits, which may also happen in Kosovo, as there is a "widespread phenomenon of illegal buildings" [1]. These constructions violate current laws and regulations, making them illegal under existing legislation. Inspired by these developments and the need to address the impact of new construction on agricultural land, there was a motivation to explore innovative approaches to adding stories to existing buildings.

2. Preliminary review of the relevant research and numerical study

Although the research motivation stems from the experience and practices observed in Kosovo, the relevant research was reviewed to examine state-of-the-art around the world. An extensive discussion of the literature review is available from the previous publication [2]. A widespread interest was observed in various aspects of adding extra floors to buildings of various types, from more global and multicriteria and multidisciplinary perspectives, including:

- methods for adding floors to buildings considering the need for more space, associated costs, financial implications, and societal impacts [3],

Proceedings of the 3rd Croatian Conference on Earthquake Engineering - 3CroCEE
19–22 March 2025, Split, Croatia
Copyright © 2025 CroCEE
DOI: https://doi.org/10.5592/CO/3CroCEE.2025.23

- global issue of increasing urban populations, emphasizing the risk to green spaces and productive land due to new construction, thus proposing adding new floors to old buildings [4],
- the reasons for adding extra floors to existing buildings, considering financial, social, and environmental factors, legal constraints, and permitting issues [5],
- the need to expand the capacities of existing structures due to significant population growth [5],

to the very specific ones, focusing on structural issues, for instance:

- analyses of the behavior, load-bearing capacity, and materials of old buildings, along with geometric aspects and foundation conditions for adding floors [7],
- examination of how to extend buildings constructed according to old building codes, utilizing elastic analysis and the capacity reserve in old structures [8],
- analyses of the joint connecting beams and columns, emphasizing its importance in a building's survival during seismic events [9],
- assessment of strengthening scheme of existing buildings extended by adding additional floors [10].

Overall, it was noted that the population growth worldwide drives the need for additional housing, and adding new stories to old buildings offers economic, environmental, and social benefits by eliminating the need to relocate residents temporarily. Environmental concerns also motivate exploring alternatives to demolishing existing structures, reducing financial costs and environmental impacts.

From the structural behavior and safety point of view, as the risks associated with adding floors and their response to the base building continue to rise, investigating the column-beam connection becomes crucial. The literature review [2] thus also encompassed the examples of treatment of similar structural details:

- the *fib* Task Group 6.2's guide Structural Connections for Precast Concrete Buildings explores connections between precast concrete elements, covering various connection types [11],
- Eurocode 2, Part 1-1 provides general rules and guidelines for reinforced concrete structures but does not address connections between columns and beams in superimposed elements [12],
- Eurocode 8, Part 1 focuses on design for earthquake resistance, including requirements for beam-column connections, including also the discussion on precast elements and their connections, specifying conditions for connection [13],
- ACI 550.2R-13 provides a design guide for connections in precast jointed systems, detailing conditions and behavior based on the type of joint and seismic zone [14]
- ACI 318-11 addresses connections in structural concrete [15],
- ACI 550.1R-01 covers various connections and seismic aspects in precast concrete structures [16]
- Eurocode 2, Part 4 focuses on the design of supplementary elements to be installed as structural or non-structural components, including anchoring with ribbed reinforcement in accordance with European technical regulations. It encompasses rules regarding the spacing of anchors and their distances from the edges of concrete members, as well as technical requirements for the load-bearing capacity of anchors and their modes of failure [17].

Following the preliminary review of the relevant research, it was decided to narrow the investigation to the connections between newly added floors of vertical extension and the old, existing building constructed as reinforced concrete (RC) frame structure. The earthquake risk further underscores the importance of researching this structural detail. Thus, a preliminary numerical study was conducted [2]. The assumption that these connections are monolithic, or rigid might not be held up in practice, as various factors affect their behavior, especially in seismic regions. The study demonstrated that under dynamic loads, new floors do not respond as if constructed simultaneously due to differences in materials and dowels anchoring. The design principle of strong columns and weak beams aims to ensure building stability. However, inadequately rigid connections between columns and old joints may lead to plastic hinge formation, jeopardizing the stability of added floors. The type of connection between the column and the old joint significantly influences the building's fundamental modes of oscillation. A

Proceedings of the 3rd Croatian Conference on Earthquake Engineering - 3CroCEE
19–22 March 2025, Split, Croatia
Copyright © 2025 CroCEE
DOI: https://doi.org/10.5592/CO/3CroCEE.2025.23

significant motivation for addressing this phenomenon is the lack of clear guidance in codes regarding the effects of dynamic loads. No consensus exists on joint modelling techniques, despite extensive research, leaving room for improvement [18]. Similar concerns apply to joints on additional floors connected to old or base buildings. Retrofitting is a viable solution for most existing buildings that exhibit deficiencies and are vulnerable to future earthquakes. By using research findings and conclusions from various studies, the aim is to make a valuable contribution to addressing these structures, benefiting both society and the environment. This strong motivation drives to further develop this study on the connection between the new column and the old top column-beam node (corner frame joint), ensuring safety in existing multi-story buildings with added stories, as well as those to be constructed in the future.

3. Research objectives and hypotheses

The research objective is to investigate and address the challenges associated with adding new stories to existing buildings, particularly focusing on the connection between the new column and the old joint (corner frame joint in a RC frame structure). The aim is to understand the behavior of these connections, their impact on structural stability, and the response to dynamic loads, ultimately contributing to the safety and resilience of multi-story buildings. Specifically, the objectives are consequently formulated as follows:

1. analysis and assessment of joints in vertically extended RC buildings,
2. comparison of joint rigidity levels in joints connecting additional floors to an existing building under seismic influences,
3. determination of the joint rigidity coefficient in joints connecting additional floors to a base building for design purposes,
4. determination of the type of joint formation: fully rigid, semi-rigid or hinged,
5. determination of the load-bearing capacity of joints connecting additional floors to a base building,
6. evaluation of the advantages of constructing additional floors in existing and new buildings from economic, environmental, and social perspectives.

With research focusing on the new column and the old joint of the base building constructed as a RC frame structure, the hypotheses relate to the fact that the level of rigidity in this connection significantly impacts the structural stability and response to dynamic loads, thus rendering properly addressing this connection crucial for ensuring the safety of both existing and newly constructed multi-story buildings. The level of rigidity of the subject connection for RC frame buildings with added floors is not the same as for the new structures of the same number of floors, and therefore a coefficient that can be used to simulate the actual rigidity of the connection for calculation purposes when vertical extension of the structure is designed needs to be determined. The hypotheses were formulated as follows:

1. often-used assumption of full rigidity of a joint connecting vertical extension to an existing RC frame building is not accurate for construction practices in Kosovo and the region,
2. incorporating appropriate rigidity coefficients in the structural analysis of a vertically extended RC frame will provide a more realistic prediction of behavior under dynamic (seismic) loads.

4. Research plan and methodology

The following, six step research plan and program was put forward consisting of an experimental campaign to test scaled RC frame models and complementary numerical simulations, in line with the research objectives and hypotheses.

1. Firstly, the experiment's groundwork is laid, involving the preparation of experimental samples and models, thorough testing to assess the quality of the materials used, and the careful selection and calibration of testing equipment for reliable results.
2. Then the second step focuses on ensuring the validity of the experiment's outcomes. This involves not only the verification of results obtained from individual experiments through

Proceedings of the 3rd Croatian Conference on Earthquake Engineering - 3CroCEE
19–22 March 2025, Split, Croatia
Copyright © 2025 CroCEE
DOI: https://doi.org/10.5592/CO/3CroCEE.2025.23

additional experiments but also a detailed analysis of results from similar experiments with analogies to the ongoing experiment. The establishment of experimental boundaries is crucial to guarantee validity and accuracy by thoroughly verifying the methodology used in obtaining results.

3. Moving on to the third step, numerical simulations and project methodology take center stage. Advanced computer methods will be employed for numerical simulations to analyze the behavior of connections at nodes and verify the design methodology. Additionally, the calibration of hysteretic shape parameters will be performed to establish a reliable relationship with experimental results.
4. The fourth step revolves around the exploration of various connection types. A diverse range, including those with anchoring and prefabricated elements with similarities, will be thoroughly examined. The implementation of connections is a critical aspect of this phase, serving to validate the design methodology of experimental connection. Furthermore, a specific connection will be proposed as an experimental solution, ensuring complete testing adequacy.
5. As progress to the fifth step is made, design guidelines will be proposed based on the technical rules and codes in force for design. These guidelines will be informed by the experimental findings, considering the intricacies of each technology used. Practical recommendations for the execution of connections during the experiment will be included to ensure structural stability. Valuable input from researchers and practitioners regarding both existing and new connections will be incorporated into the experiment's framework.
6. The final step, seismic evaluation, delves into the investigation of seismic effects on connections used during new additions to old structures. The analysis of previously used and proposed connections will provide insights into the seismic response of the frame. Sophisticated micro and macro nonlinear models will be employed, considering calibrated characteristics and hysteretic parameters, to accurately simulate connection behavior. This phase aims to gain essential knowledge about modifications in ductility and energy dissipation capacity within the structural system resulting from the application of proposed connection types. The seismic sustainability capacities of connections will be assessed, drawing appropriate conclusions for both used and proposed connections.

5. Research progress

The current activities are focusing on the last stages of the experimental campaign. The experimental frames were developed to represent the characteristics of a commercial building made of reinforced concrete, with a single span in the global X direction, and several spans in the global Y direction. First, a single span two-story RC frame was cast-in-site to represent an “old” (base) building with monolithic column-beam connections, and then, after several days, an additional frame of one story was added. The connection between the two-story base frame and its vertical extension with an additional single-story frame was made with anchoring executed by first opening the holes in the base structure and then placing the reinforcement bars as anchors and securing them using cement-based adhesive material. Both the two-story model representing the old i.e. base building, and the three-story model representing the vertically extended building are tested. The experimental model was designed as a frame with strong columns and weak beams to meet the ductility conditions of the structure as best as possible.

The quasi-static testing method is used for testing under seismic load action. The experiment needs to provide the results for the tested models for ductility, displacements, capacity, and stiffness of separate elements but also as a whole of the experimental model. Previously, testing of samples to obtain different characteristics of materials used in the experimental model was carried out. Figs. 1 a) and b) illustrate various specimens used to experimentally determine different materials’ characteristics, while c) and d) show scaled frame models and quasi-static testing one of the frames in the laboratory.

Copyright © 2025 CroCEE
DOI: https://doi.org/10.5592/CO/3CroCEE.2025.23



Figure 1. a) Samples for testing different characteristics of the materials; b) pull out of anchors under tensile testing; c) Scaled two- and three-story RC frame models; d) Quasi-stating testing one of the frame models.

6. Conclusion

As vertical extensions of buildings are becoming more attractive solutions with some clear advantages in urban spaces, research was launched into investigating the dynamic (seismic) behavior of such buildings as this might be an important, even decisive design and execution criterion in seismically active regions. The research was narrowed to the building typology that is very common in the region in which both the base (old) structure and the vertical extension (added floor) are RC frame structures. The research is aimed at determining the stiffness coefficient of the joint that connects the added floor to the existing base structure. This would lead to refinement of advanced numerical modelling techniques for more precise simulation of column-beam connection joints in such structures, which in turn might serve as a valuable model for future practical applications. The research is also expected to further knowledge of internal forces in the column-beam corner frame joint, thus providing input to

Proceedings of the 3rd Croatian Conference on Earthquake Engineering - 3CroCEE
19–22 March 2025, Split, Croatia
Copyright © 2025 CroCEE
DOI: https://doi.org/10.5592/CO/3CroCEE.2025.23

develop improvements in joint design, detailing and execution as well as global design of vertically extended buildings. The testing of scaled non-extended and extended RC frames is currently underway and the completion of the research is expected in 2025 with subsequent publication of its results.

References

[1] Spahiu, F., Jashari, R. (2015): The legalization process challenges on Illegal constructions in Kosovo, *UBT Int. Conf.* 61, 58-63.

[2] Shala, A., Bleiziffer, J. (2024): Seismic Performance of Reinforced Concrete Frames with Added Floors: Emphasizing the Influence of Structural Joints in the Context of Sustainable Vertical Extensions, *Buildings* **14**, no. 2, 370, 19 pages.

[3] Johansson, B., Thyman, M. (2013): Strengthening of buildings for storey extension, *Master of Science Thesis in the Master's Programme Structural Engineering and Building Technology, Department of Civil and Environmental Engineering Division of Structural Engineering, Chalmers University of Technology,* Göteborg, Sweden, Master's Thesis 2013:113.

[4] Soikkeli, A. (2016): Additional floors in old apartment blocks, *SBE16 Tallinn and Helsinki Conference, Build Green and Renovate Deep*, Tallinn and Helsinki, Energy Procedia 96, 1-4, Elsevier Ltd., 815-823.

[5] Sundling, R. (2019): A development process for extending buildings vertically – based on a case study of four extended buildings", *Construction Innovation*, Vol. **19** No. 3, 367-385.

[6] Bahrami, A., Deniz, S., Moalin, H. (2022): Vertical Extension of a Multi-Storey Reinforced Concrete Building, *Int. J. of Applied Mechanics and Engineering*, vol. **27**, No.1, 1-20.

[7] Zhulidova, M. (2019): Reconstruction of an existing building with one additional storey, Saimaa University of Applied Sciences Technology, Lappeenranta, Double Degree Programme in Civil and Construction Engineering, Bachelor's Thesis 2019.

[8] Kyakula, M., Kapasa, S., Opus, A.E. (2006): Considerations in Vertical Extension of Reinforced Concrete Structures, *Int. Conf. on Advances in Engineering and Technology 2006*, Entebbe, Uganda, 109-116.

[9] Shihoara H. (2004): Quadruple Flexural Resistance in R/C Beam-Column Joints; *13th World Conference on Earthquake Engineering*, Vancouver, B.C., Canada, paper no. 491., 15 pages.

[10] Al-Nu'man, B.S. (2016): Assessment of Strengthening Scheme of Existing Buildings Extended by Adding Additional Floors, *Eurasian Journal of Science & Engineering* Vol. **2** No. 1, 28-40.

[11] Engström, B. et al. (2008): Structural connections for precast concrete buildings, Guide to good practice prepared by Task Group 6.2, International Federation for Structural Concrete (*fib*).

[12] CEN (2004): EN 1992-1-1 Eurocode 2: Design of concrete structures - Part 1-1: General rules and rules for buildings, Brussels.

[13] CEN (2004): EN 1998-1 Eurocode 8: Design of structures for earthquake resistance – Part 1: General rules, seismic actions and rules for buildings, Brussels.

[14] American Concrete Institute (2013): ACI 550.2R-13 Design Guide for Connections in Precast Jointed Systems, Reported by Joint ACI-ASCE Committee 550.

[15] American Concrete Institute (2011): Building Code Requirements for Structural Concrete (ACI 318-11) An ACI Standard and Commentary; Reported by ACI Committee 318.

[16] American Concrete Institute (2001): ACI 550.1R-01: Emulating Cast in Place Detailing in Precast Concrete Structures; Reported by Joint ACI-ASCE Committee 550.

[17] CEN (2018): EN 1992-4 Eurocode 2: Design of concrete structures - Part 4: Design of fastenings for use in concrete, Brussels.

[18] Masi, A., Santarsiero, G., Verderame, G.M., Russo, G., Martinelli, E., Pauletta, M., Cortesia, A. (2009): Capacity Models of Beam-Column Joints: Provisions of European and Italian Seismic Codes and Possible Improvements; *Eurocode 8 Perspectives from the Italian Standpoint Workshop,* Doppiavoce, Napoli, Italy, 145-158.

Proceedings of the 3rd Croatian Conference on Earthquake Engineering - 3CroCEE
19–22 March 2025, Split, Croatia
Copyright © 2025 CroCEE
DOI: https://doi.org/10.5592/CO/3CroCEE.2025.26

INVESTIGATING THE SEISMIC PERFORMANCE OF THE HONEYCOMB YIELDING DAMPER(HYD)

Zeinolabedin Mortezaali [(1)], Peyman Shadman Heidari [(2)*], Mohammad Ghanooni Bagha [(3)]

(1) Department of Civil Engineering, East Tehran Branch, Islamic Azad University, Tehran, Iran, zizomortezaali@yahoo.com
(2) Department of Civil Engineering, East Tehran Branch, Islamic Azad University, Tehran, Iran, peyman.shademan@iau.ac.ir
(3) Department of Civil Engineering, East Tehran Branch, Islamic Azad University, Tehran, Iran,mohammad_ghanooni@yahoo.com

Abstract

Today, the use of energy-dissipating system such as yielding metal damper in structures can improve the seismic performance of structures. One of the characteristics of metal yielding dampers is the ability to dissipate high energy and increase the ductility of the structural system, which can improve the ductility and energy absorption characteristics of the metal frame equipped with braces and prevent the brace from buckling during an earthquake. The purpose of this research is introduce a new form of yielding dampers called honeycomb yielding damper (HYD) in 28 numerical models with different dimensions and thickness along with evaluating and comparing the force-displacement diagrams and investigating the seismic parameters of this type of yielding damper. All modeling and validation of numerical samples were done by Ansys software. Non-linear analysis method is used in this research. The hysteresis curves are obtained under in-plane cyclic loads. The mechanical parameters such as ductility ratio, initial hardness, effective hardness and damping coefficient can be determin. The results of this research showed that, the effective stiffness increases with the increase in the length of the sample and the Ductility ratio and damping of the equivalent viscous damping. Also, as the thickness of the sample increases, the effective stiffness, the Ductility ratio and the equivalent viscous damping also increases. As the height of the sample increases, the effective stiffness decreases, and the Ductility ratio, the equivalent viscous damping have increased.

Keywords: Yielding honeycomb damper, Ductility ratio, Initial stiffness, Effective stiffness, Equivalent viscous damping.

1. Introduction

Earthquakes are the natural disasters that have occurred in recent years around the world, causing human and financial losses. damping systems are the most popular energy dissipation tools and are used in most projects. These instruments can a large amount of incoming earthquake energy with a predictable performance. In general, seismic control systems are divided into two categories, active control and passive control. Therefore, the use of passive control seismic design methods, such as yielding metal dampers that have the ability to dissipate the incoming energy of earthquake to structures, can improve the seismic performance of structures. The performance of metal dampers based on their non-linear behavior is one of the most effective mechanisms of damping and absorption of energy input to the structure during an earthquake. Kelly et al [1] used the idea of metallic dampers to absorb earthquakes energy in the structure. They introduced several hysteretic energy absorption mechanisms in structures. Skinner et al [2, 3] proposed several yielding metal dampers, including torsion beam dampers, bending beam dampers, and U-shaped dampers. Kasai and Popov [4] presented yielding damper using steel plate and stiffener. They tested it and introduced the hysteresis curve. Bergman and Goel [5] proposed flexural yielding metallic dampers. They tested added damping and stiffness (ADAS) and Triangular-ADAS (TADAS) systems. In ADAS and TADAS dampers are used parallel X and V shaped steel plates, respectively. Whittaker et al [6] tested X-shaped metallic dampers as ADAS under cyclic load. Tsai et al [7], in order to fix the defects of the XADAS dampers, studied TADAS triangular steel plate dampers. Also, they developed a simple mathematical model for force-displacement, which was reasonably accurate compared to laboratory

Copyright © 2025 CroCEE
DOI: https://doi.org/10.5592/CO/3CroCEE.2025.26

work. Dargush and Soong [8] conducted a more detailed study of the phenomenon of fatigue in low cycles based on the behavioral theories of TADAS dampers and developed their analytical models. Gang Li and Hongnan Li [9] presented a new idea for designing metallic damper. They tested dual functions metallic damper (DFMD) with quasi-static loading. Soni and Sanghvi [10] described a technique to find out combined stiffness of model equipped with ADAS damper. They proposed a mathematical model. Teruna et al [11] investigated four steel damper specimens with specific geometry. They obtained energy absorption capabilities, hysteresis loop and stiffness in specimens. Sahoo et al [12] investigated passive energy dissipation of steel plates in both flexure and shear yielding under cyclic loading. Their specimens consist of two flexure (end) plates of X-shape and a shear (web) plate of rectangular shape. Garivani et al [13] introduced a new type of flexural yielding metallic damper and they called comb-teeth damper (CTD). Their damper included number of teeth steel plates that absorb energy through in-plane flexural yielding. Ghaedi et al [14] introduced a new hysteretic metallic bar damper that they named bar damper (BD). BD included three simple steel plates and a number of solid bars which dissipate input energy due to vibration loads through flexural yielding. Kiani [15] designed a model of yielding damper with the hip, chevron, gate, diagonal and knee braces, whose performance reduced the base shear of the system. Moghadisi and Namazi [16] regarding the design of three earthquake-resistant systems, including a structure with a damper, a structure without a damper, and a structure with a chevron brace, which showed that the base shear in a structure with a yield damper is reduced compared to other structures. They also showed that the performance of the structure with yielding damper is better during earthquakes. Yang et al [17] investigated the experimental results of the new HSF honeycomb structure, which shows that the use of the proposed HSF honeycomb structure can provide stable energy dissipation capability as an efficient metal damper for earthquake parameters. Yang et al [18] in a detailed experimental study on the new metal WWFF damper in order to investigate the effect of design parameters such as aspect ratio and slenderness on structural response such as yield strength and stiffness showed that this damper has a stable energy dissipation capacity and can It can be used as an efficient and strong metal damper. Peyman Shadman Heidari [19] presented a new type of metal shear yielding damper in which a perforated shear plate is used and by changing the location and diameter of the holes in DPMD dampers, he investigated the mechanical characteristics of different samples of DPMD dampers.

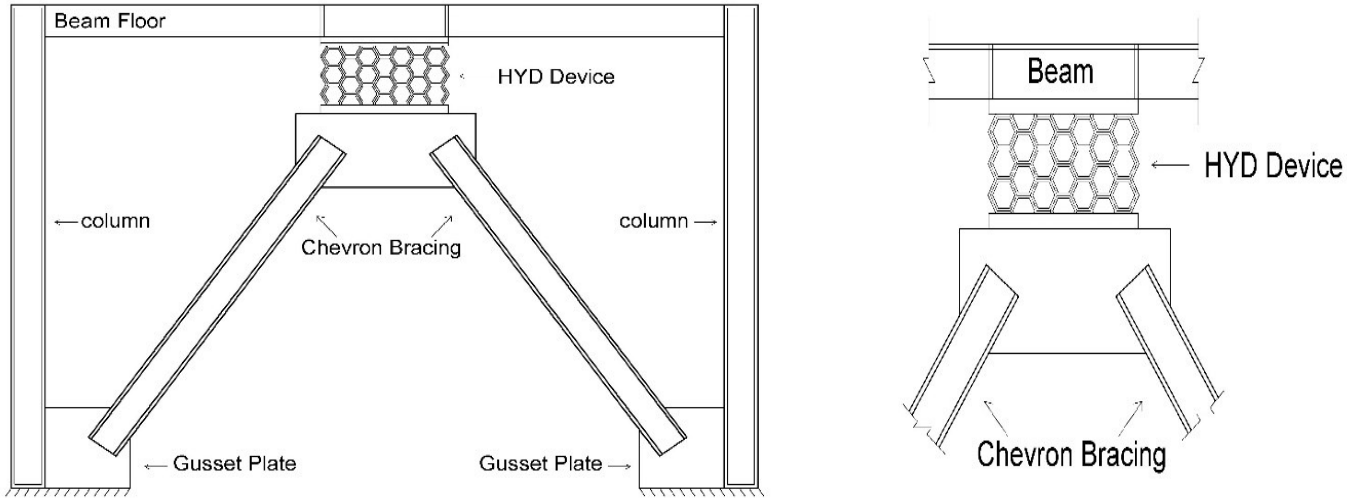
The purpose of this research is introduce the new form of yielding dampers with different geometry under the name of honeycomb yielding dampers (HYD) with different dimensions and thicknesses. In this reaserch determines their mechanical and seismic characteristics of samples were investigated with the hysteresis curves of the honeycomb yielding damper samples under in-plane cyclic load can determined mechanical parameters such as ductility ratio, initial stiffness, effective stiffness, total dissipated energy, dissipated energy in the last cycle, elastic strain energy, equivalent viscous damping (EVD) and equivalent plastic strain (EPS).

2. Honeycomb yielding damper (HYD)

2.1. Geometry of Honeycomb damper

ADAS dampers are usually used in steel bracing frames, as shown in Figure 1. The HYD dampers can create by drilling a hexagonal shape on a metal sheet and use in metal frame with a chevron brace as shown in Figure 1.

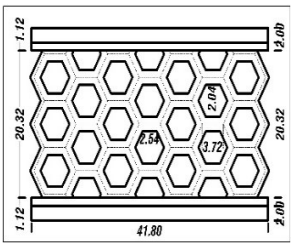
Proceedings of the 3rd Croatian Conference on Earthquake Engineering - 3CroCEE
19–22 March 2025, Split, Croatia
Copyright © 2025 CroCEE
DOI: https://doi.org/10.5592/CO/3CroCEE.2025.26



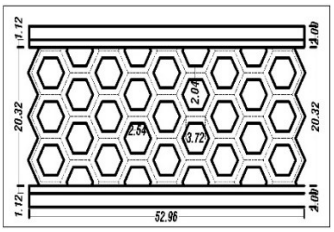
(a) (b)

Figure 1. a) Frame system and HYD position, b) Connection of HYD to beam and bracing

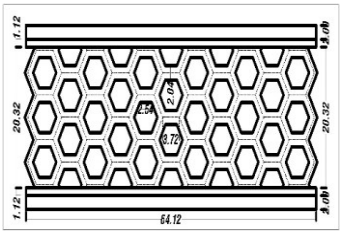
In this research, 28 numerical models are proposed based on different thickness, length and height. The thickness of all samples was considered as 0.48, 0.72, 0.96 and 1.44 cm, respectively. The length of all samples are 41.80, 52.96, 64.12 and 75.28 cm, respectively. Also, samples were considered with different heights of 20.32, 26.76, 33.20 and 39.65 cm. The length of each side of the hexagon is 2.5423 cm and the angle between the sides is 120 degrees. Figure 2 shows the modeling of the honeycomb damper with different lengths, heights and thicknesses. Table 1 shows the specifications and dimensions of the HYD dampers. The Table 1 shows specifications and different dimensions of HYD dampers.



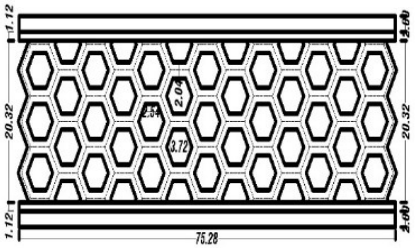
HYD-1-1-1-2



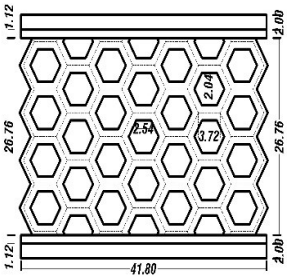
HYD-1-2-1-2



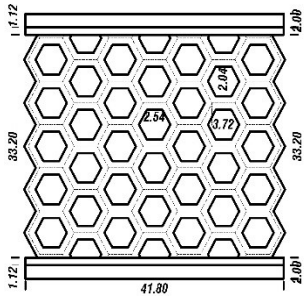
HYD-1-3-1-2



HYD-1-4-1-2

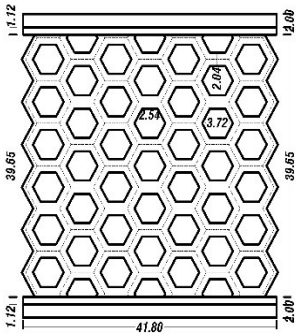


HYD-1-1-2-2

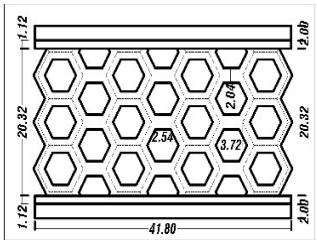


HYD-1-1-3-2

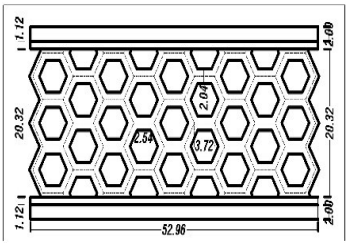
Proceedings of the 3rd Croatian Conference on Earthquake Engineering - 3CroCEE
19–22 March 2025, Split, Croatia
Copyright © 2025 CroCEE
DOI: https://doi.org/10.5592/CO/3CroCEE.2025.26



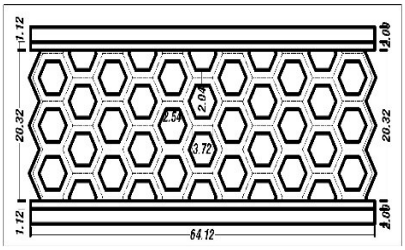
HYD-1-1-4-2



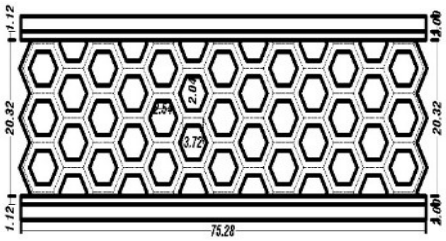
HYD-2-1-1-2



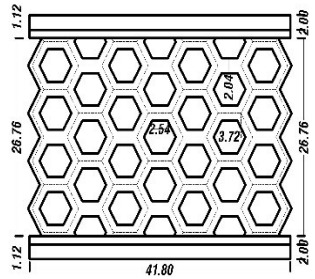
HYD-2-2-1-2



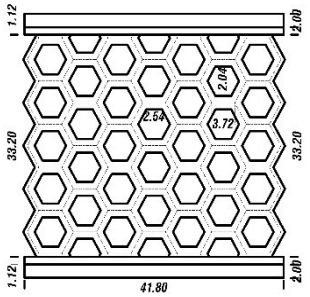
HYD-2-3-1-2



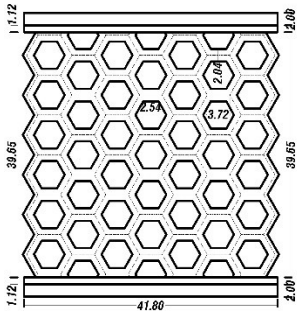
HYD-2-4-1-2



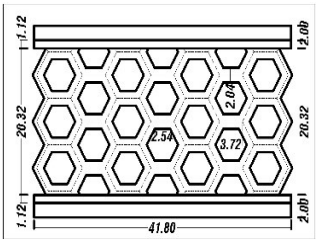
HYD-2-1-2-2



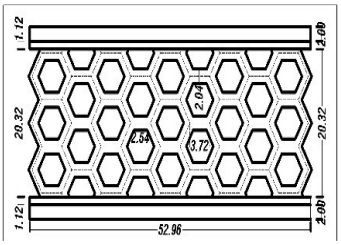
HYD-2-1-3-2



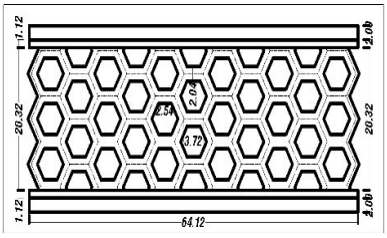
HYD-2-1-4-2



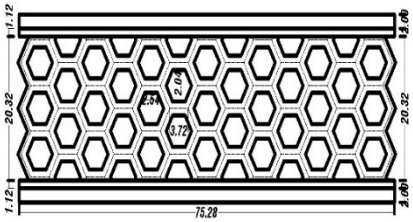
HYD-3-1-1-2



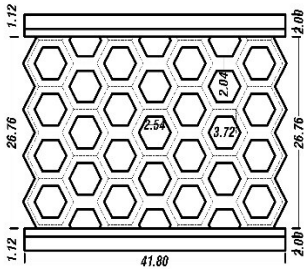
HYD-3-2-1-2



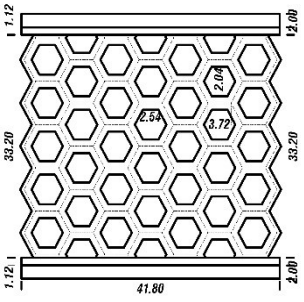
HYD-3-3-1-2



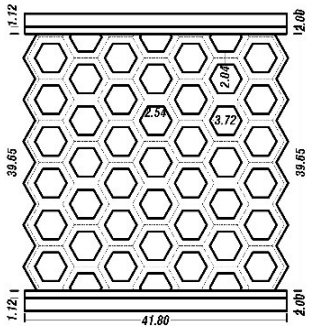
HYD-3-4-1-2



HYD-3-1-2-2



HYD-3-1-3-2



HYD-3-1-4-2

Copyright © 2025 CroCEE
DOI: https://doi.org/10.5592/CO/3CroCEE.2025.26

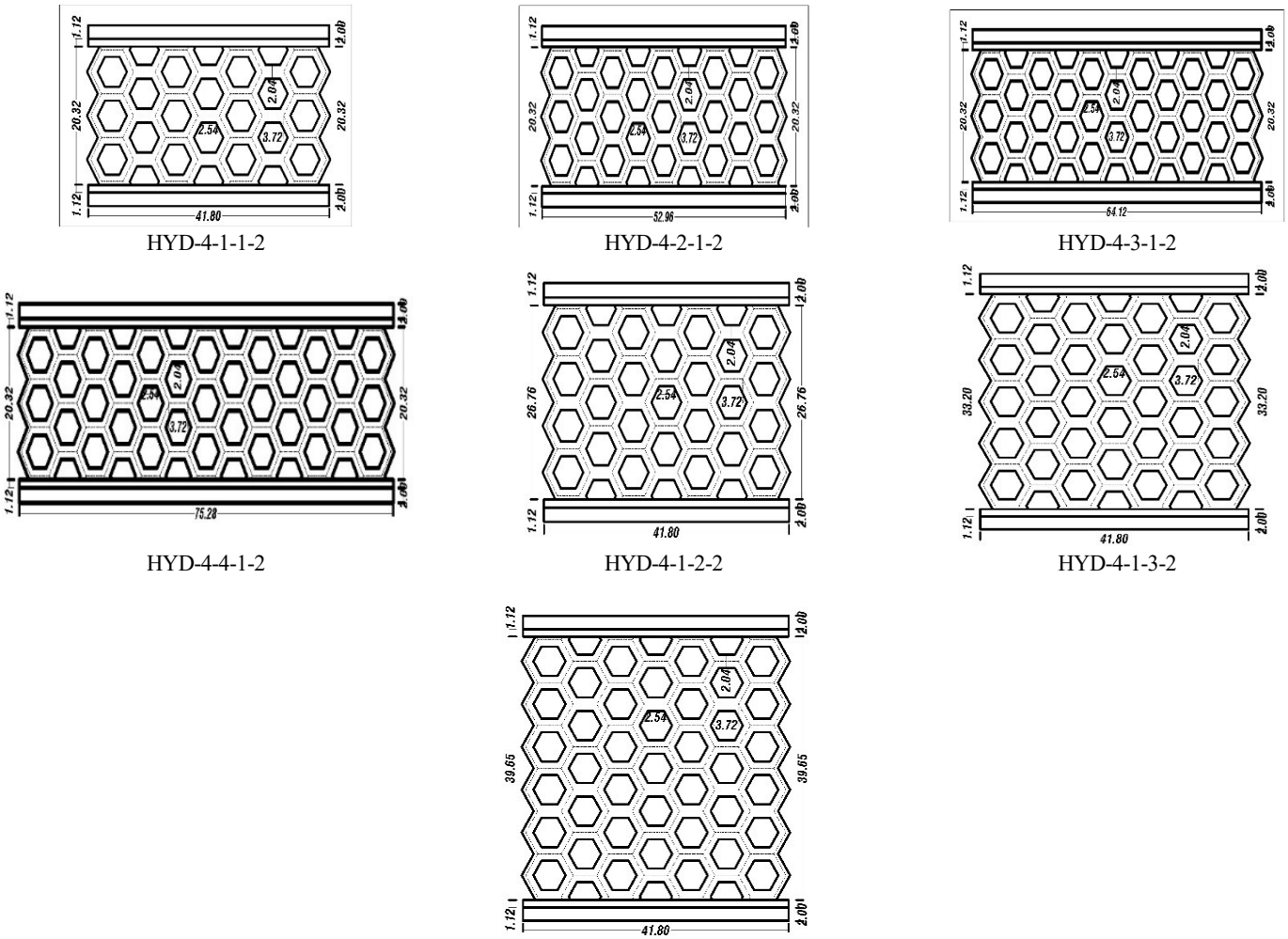


Figure.2. HYD damper modeling with different lengths, heights and thicknesses.

Table 1. Specifications and different dimensions of HYD dampers

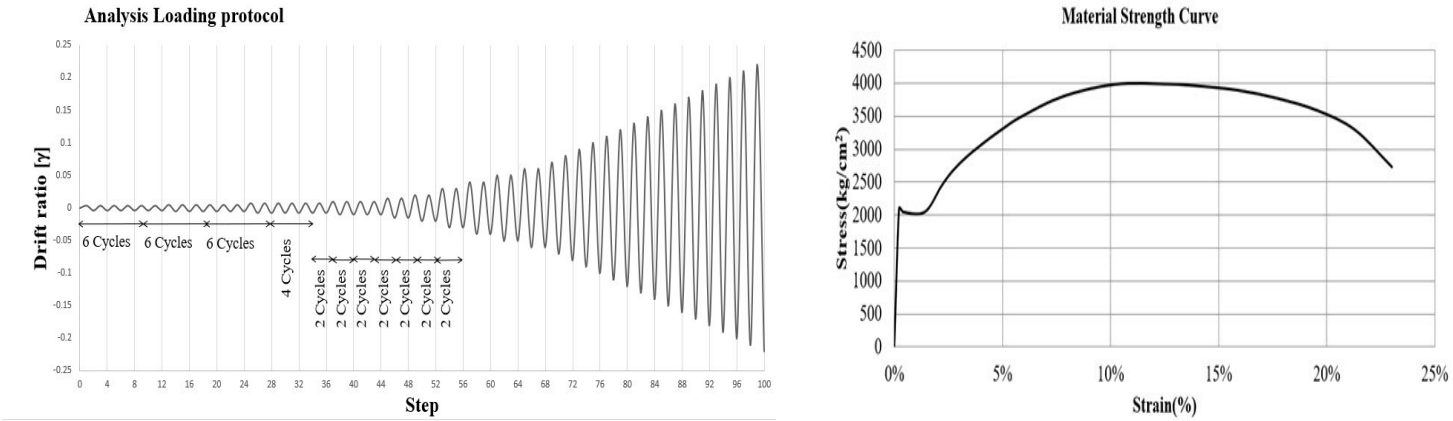
Number	Sample	thickness t_p (cm)	Length L(cm)	Hight H(cm)	Length of the hexagon h(cm)
1	HYD-1-1-1-2	0.48	41.80	20.32	2.5423
2	HYD-1-2-1-2	0.48	52.96	20.32	2.5423
3	HYD-1-3-1-2	0.48	64.12	20.32	2.5423
4	HYD-1-4-1-2	0.48	75.28	20.32	2.5423
5	HYD-1-1-2-2	0.48	41.80	26.76	2.5423
6	HYD-1-1-3-2	0.48	41.80	33.20	2.5423
7	HYD-1-1-4-2	0.48	41.80	39.65	2.5423
8	HYD-2-1-1-2	0.72	41.80	20.32	2.5423
9	HYD-2-2-1-2	0.72	52.96	20.32	2.5423
10	HYD-2-3-1-2	0.72	64.12	20.32	2.5423
11	HYD-2-4-1-2	0.72	75.28	20.32	2.5423
12	HYD-2-1-2-2	0.72	41.80	26.76	2.5423
13	HYD-2-1-3-2	0.72	41.80	33.20	2.5423
14	HYD-2-1-4-2	0.72	41.80	39.65	2.5423
15	HYD-3-1-1-2	0.96	41.80	20.32	2.5423
16	HYD-3-2-1-2	0.96	52.96	20.32	2.5423
17	HYD-3-3-1-2	0.96	64.12	20.32	2.5423

Copyright © 2025 CroCEE
DOI: https://doi.org/10.5592/CO/3CroCEE.2025.26

18	HYD-3-4-1-2	0.96	75.28	20.32	2.5423
19	HYD-3-1-2-2	0.96	41.80	26.76	2.5423
20	HYD-3-1-3-2	0.96	41.80	33.20	2.5423
21	HYD-3-1-4-2	0.96	41.80	39.65	2.5423
22	HYD-4-1-1-2	1.44	41.80	20.32	2.5423
23	HYD-4-2-1-2	1.44	52.96	20.32	2.5423
24	HYD-4-3-1-2	1.44	64.12	20.32	2.5423
25	HYD-4-4-1-2	1.44	75.28	20.32	2.5423
26	HYD-4-1-2-2	1.44	41.80	26.76	2.5423
27	HYD-4-1-3-2	1.44	41.80	33.20	2.5423
28	HYD-4-1-4-2	1.44	41.80	39.65	2.5423

2.2. Loading pattern and material properties

In order to evaluate the performance of honeycomb yielding dampers was used AISC 341-16[20] cyclic loading pattern. The relative deformation between the upper and lower plates of the damper is equal to 0.00375 radians for steps 1 to 12 in 6 cycles. for steps 13 to 24 for 6 cycles, the relative deformation between the upper and lower plates of the damper is equal to 0.005 radians for steps 25 to 36 in 6 cycles, the relative deformation is equal to 0.0075 radians for steps 37 to 44 in 4 cycles, the relative deformation is equal to 0.01 radians for steps 45 to 48 in 2 cycles, the relative deformation between the upper and lower plates of the damper is equal to 0.015 radians for steps 49 to 52 in 2 cycles, the relative deformation is equal to 0.02 radians for steps 53 to 56 in 2 cycles, the relative deformation between the upper and lower plates of the damper is equal to 0.03 radians for steps 57 to 60 in 2 cycles, the relative deformation between the upper and lower plates of the damper is equal to 0.04 radians and for steps 61 to 100 in 2 cycles, the relative deformation between the upper and lower plates of the damper is equal to 0.01 radians according to Figure 3-a. In this research, materials with the characteristics of the stress-strain curve used according to Figure 3-b.



(a) (b)

Figure 3. a) AISC 341-16[20] cyclic loading pattern, b) Stress-strain curve

3. Finite Element Modeling procedure

3.1. FEMs of HYD

To study the mechanical parameters of the honeycomb metallic damper used nonlinear finite element (FEM) analyses with ANSYS R16 FEM [21] software. The 28 finite element models were modeled with different thickness, length and height. Steel plate elements were modeled using a 3D solid element. SOLID 185 (brick 8 node 185) element was used for modeling of proposed samples. Multilinear kinematic hardening plastic model [21] was used to model the plasticity and cyclic inelastic behavior of steel material, respectively. The transitional degree of freedom in the Z and Y

Copyright © 2025 CroCEE
DOI: https://doi.org/10.5592/CO/3CroCEE.2025.26

directions are closed in order to prevent out of plane buckling of the end plate. Mesh sensitivity analysis was performed to find proper element sizes in the FEMs. Figure 4 shows the FEMs of the HYD-1-1-1-2, HYD-1-2-1-2, HYD-1-3-1-2, HYD-1-4-1-2, HYD-1-1-2-2, HYD-1-1-3-2 and HYD-1-1-4-2.

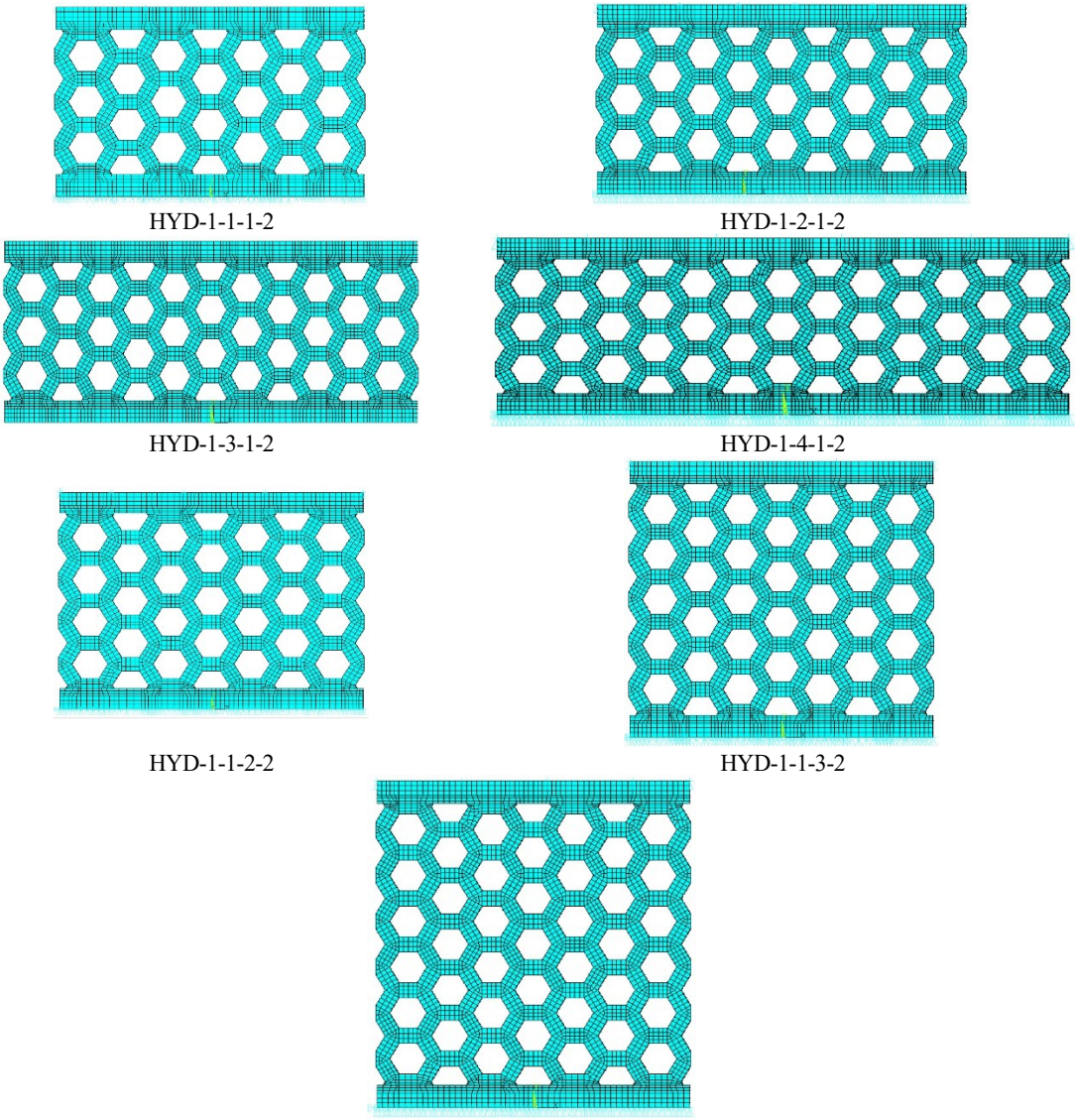
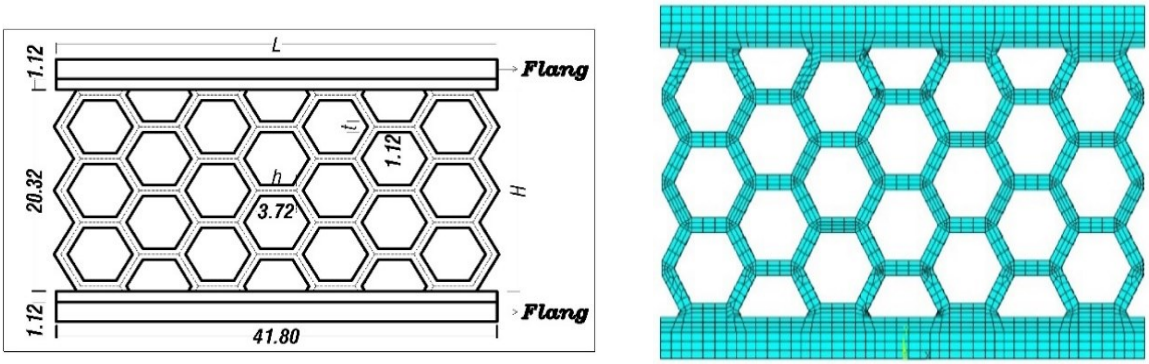


Figure 4. Finite element models of HYD sample

3.2. FEM of HSF experimental specimen

The experimental specimen (HSF [17]) was modeled in ANSYS R16 FEM [21] software in order to validate the FEMs. The displacement ratio applied in the upper sample is γ=10%. The details of the experimental specimen and finite element modeling with ANSYS R16 FEM software [21] show in the Figure 5 respectively.

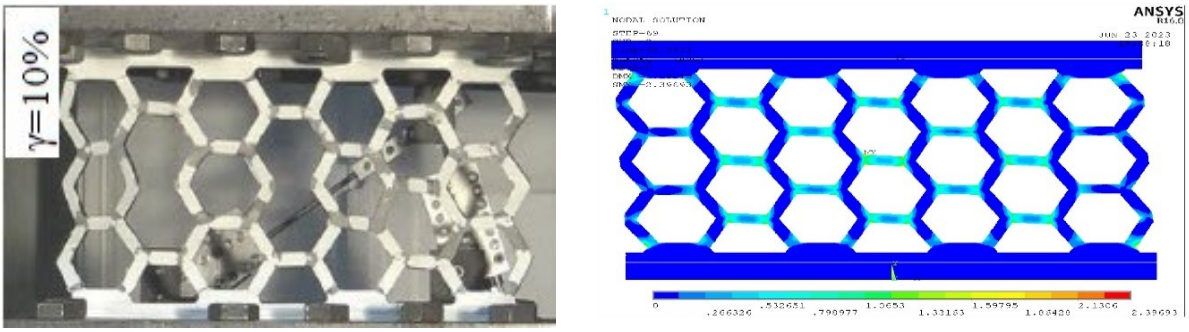
Copyright © 2025 CroCEE
DOI: https://doi.org/10.5592/CO/3CroCEE.2025.26



(a) (b)

Figure 5. a) Details of HSF experimental specimen [17], b) Finite element modeling of HSF experimental sample [17]

The results of analytical analysis were compared experimental results. there is an acceptable agreement between the results of analytical and experimental studies according to Figure 6.



(a) (b)

Figure 6. a) Deformation after loading in HSF experimental specimen [17], b) Deformation after applying loading in the FEM sample with ANSYS R16 FEM[21]

Figure 7 shows the comparison between the hysteresis curves of the HSF experimental specimen [17] and the FEM hysteresis curves.

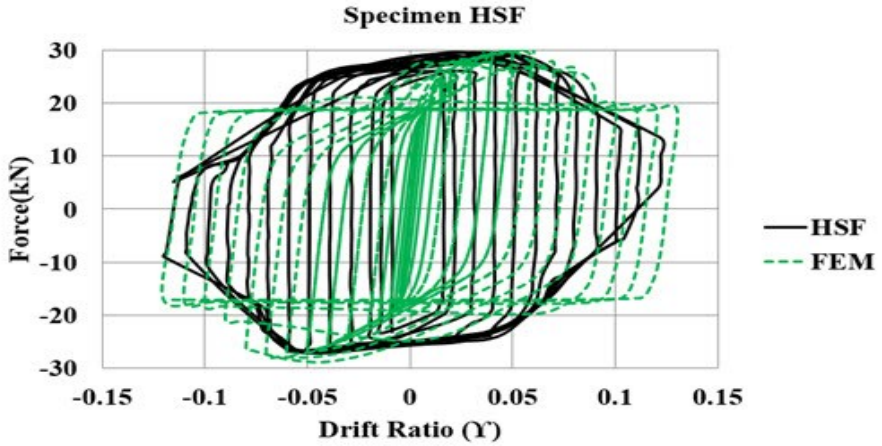
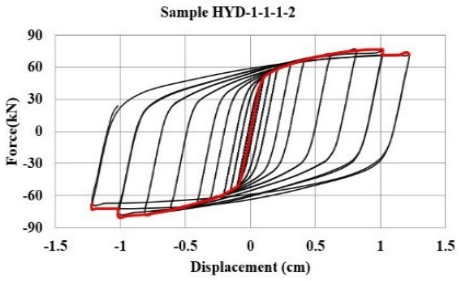


Figure 7. Comparison between the hysteresis curve of the HSF experimental specimen [17] and the FEM sample with ANSYS R16 FEM software [21]

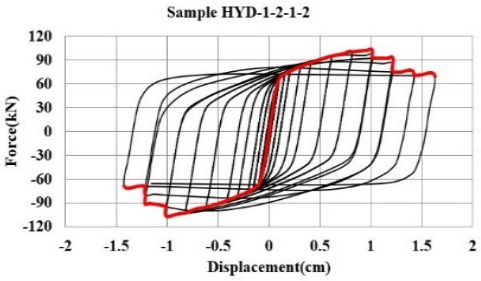
Proceedings of the 3rd Croatian Conference on Earthquake Engineering - 3CroCEE
19–22 March 2025, Split, Croatia
Copyright © 2025 CroCEE
DOI: https://doi.org/10.5592/CO/3CroCEE.2025.26

3.3. Hysteresis behavior of HYDs

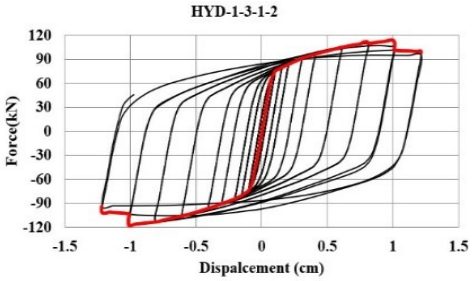
Hysteresis curves used to determine the mechanical parameters of the HYD proposed damper. In the force-displacement hysteresis curve can be obtained parameters such as yield force, yield displacement, ultimate force, and ultimate displacement. For this purpose, force-displacement hysteresis curves of analytical samples were determined. Figure 8 shows the force-displacement hysteresis curves of the HYD dampers.



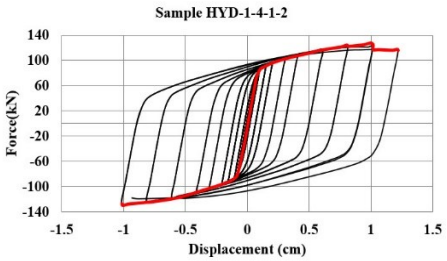
HYD-1-1-1-2



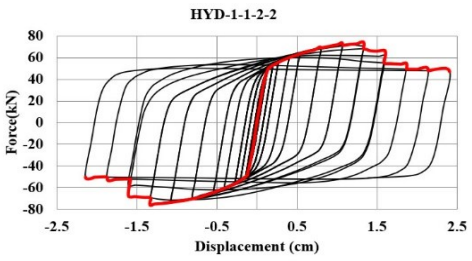
HYD-1-2-1-2



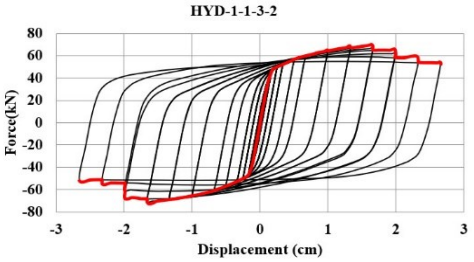
HYD-1-3-1-2



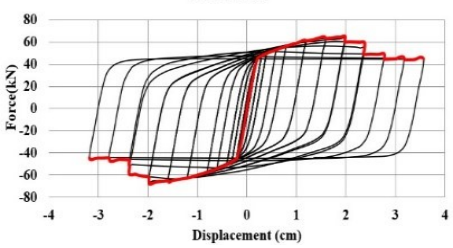
HYD-1-4-1-2



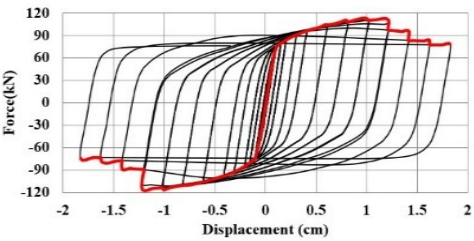
HYD-1-1-2-2



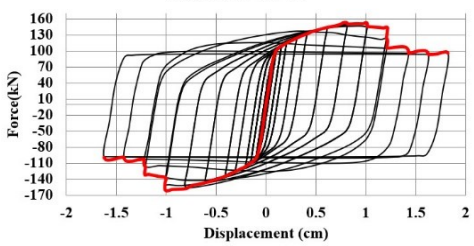
HYD-1-1-3-2



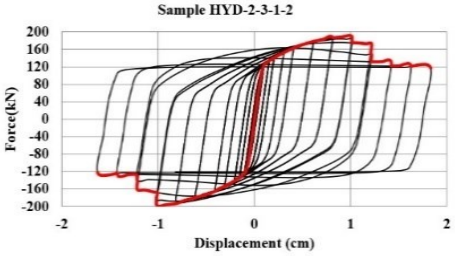
HYD-1-1-4-2



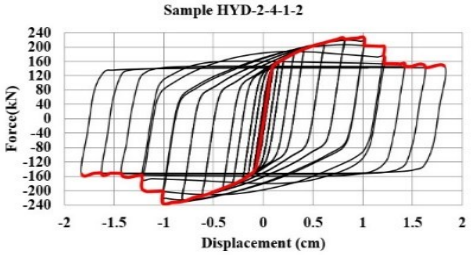
HYD-2-1-1-2



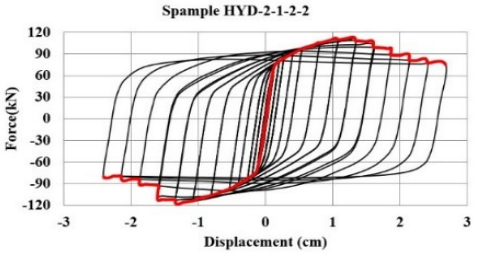
HYD-2-2-1-2



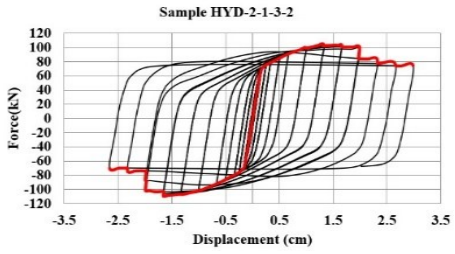
HYD-2-3-1-2



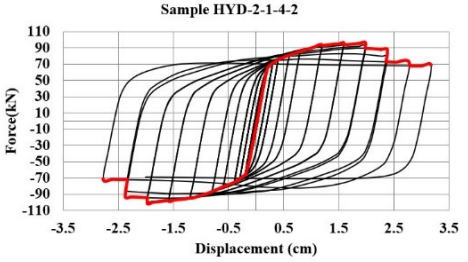
HYD-2-4-1-2



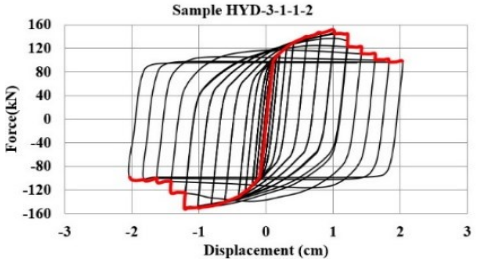
HYD-2-1-2-2



HYD-2-1-3-2



HYD-2-1-4-2



HYD-3-1-1-2

Proceedings of the 3rd Croatian Conference on Earthquake Engineering - 3CroCEE
19–22 March 2025, Split, Croatia
Copyright © 2025 CroCEE
DOI: https://doi.org/10.5592/CO/3CroCEE.2025.26

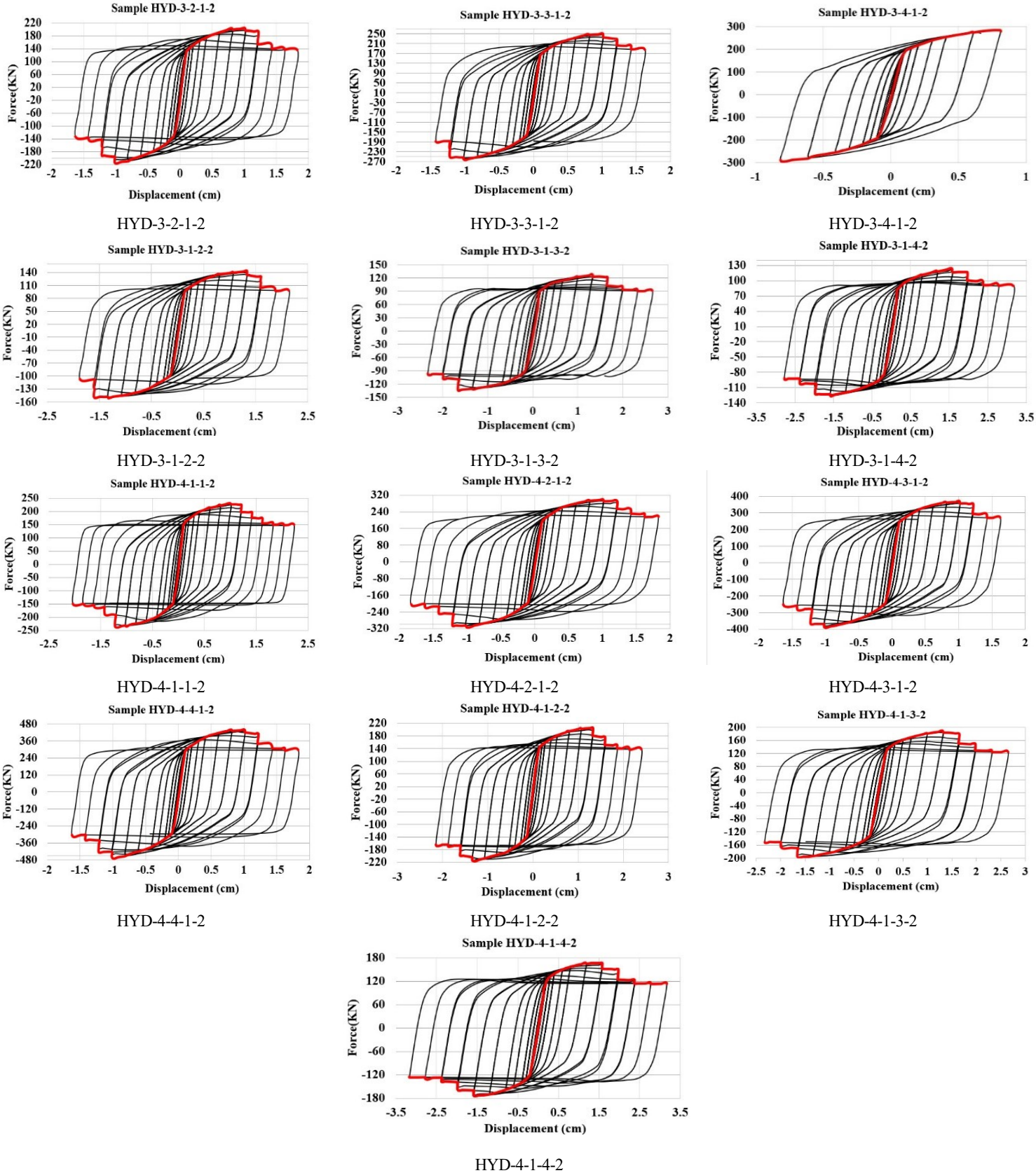


Figure. 8 Force-displacement hysteresis loops of the HYD and backbone curves

Copyright © 2025 CroCEE
DOI: https://doi.org/10.5592/CO/3CroCEE.2025.26

4. Mechanical parameters of HYD dampers

4.1. Ductility ratio, effective and initial stiffness

Ductility ratio can be defined as the ratio of maximum deformation capacity to the deformation level corresponding to a yield deformation. The value of ductility ratio is given by:

$$\mu = \frac{\Delta_{max}}{\Delta_y} \tag{1}$$

Where Δ_{max} and Δ_y are ultimate displacement and yield displacement, respectively. In each loop of the force-deformation hysteresis curve the secant or effective stiffness can be defined. The effective stiffness for maximum displacement was obtained as the average from minimum and maximum force over the average from minimum and maximum displacement, respectively. According to Figure 9, effective stiffness equation is obtained as follows:

$$K_{eff} = \frac{\frac{|P_{max}|+|P_{min}|}{2}}{\frac{|\Delta_{max}|+|\Delta_{min}|}{2}} = \frac{P_{ave}}{\Delta_{ave}} \tag{2}$$

Where Δ_{max} , Δ_{min} , Δ_{ave} , P_{max} , P_{min} and P_{ave} are ultimate displacement, minimum displacement, average displacement, ultimate force, minimum force, average force in each loop, respectively. In this research, effective stiffness was calculated for maximum displacement and last loop of the force displacement hysteresis curves of the HYD samples. Also, initial stiffness is calculated as follows:

$$K_{initial} = \frac{P_y}{\Delta_y} \tag{3}$$

Where Δ_y and P_y are yield displacement and yield force, respectively. In this paper, initial stiffness was calculated for first loop of the force-displacement hysteresis curves of the HYD samples. Effective stiffness represents the damping force in response to the desired displacement. The ultimate displacement and yield displacement values were obtained from the force-displacement hysteresis curve. Table 2 illustrates the ductility ratio, effective stiffness and initial stiffness for the HYD samples. Figure 9 shows the effective stiffness, dissipated energy, and elastic strain energy in the last loop of the hysteresis curve[19]. Figure 10 show the Ductility ratio (μ) and effective stiffness (K_{eff}) of HYD samples.

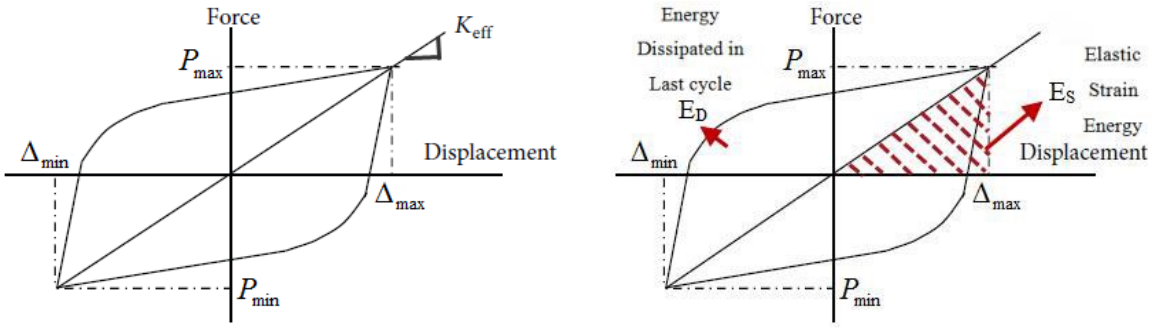


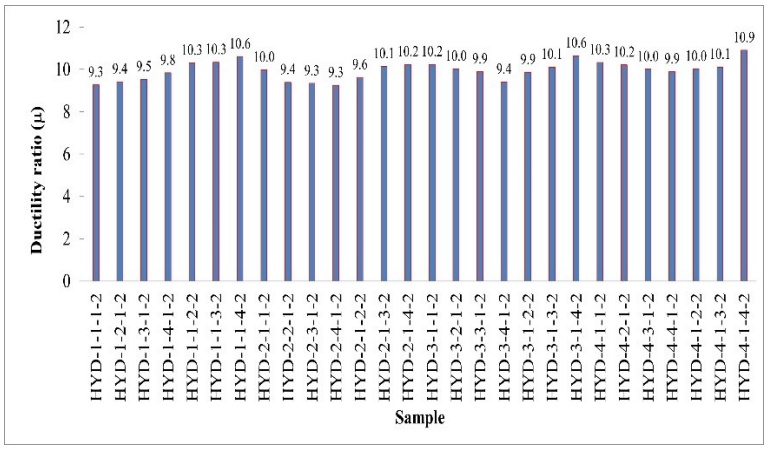
Figure. 9 Effective stiffness, dissipated energy and elastic strain energy in the last loop of the hysteresis curve [19]

Proceedings of the 3rd Croatian Conference on Earthquake Engineering - 3CroCEE
19–22 March 2025, Split, Croatia
Copyright © 2025 CroCEE
DOI: https://doi.org/10.5592/CO/3CroCEE.2025.26

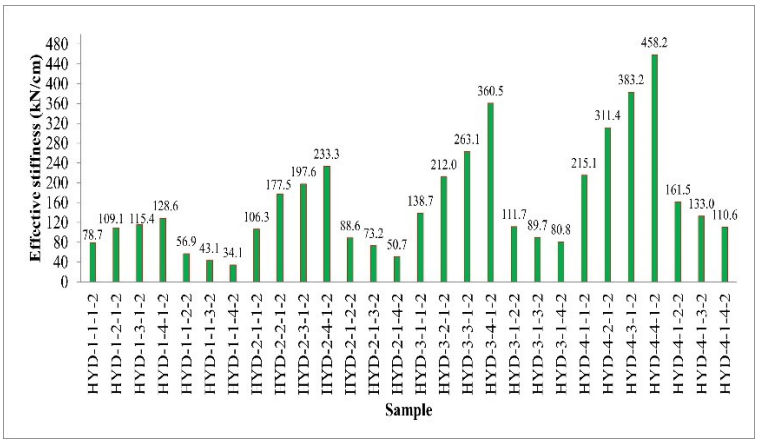
Table 2. Ductility ratio, effective stiffness and initial stiffness of HYD samples

Number	Sample	Δ_y (cm)	Δ_{max} (cm)	Δ_{min} (cm)	Δ_{ave} (cm)	P_y (KN)	P_{min} (KN)	P_{max} (KN)	P_{ave} (KN)	μ	k_{inital} (KN/ cm)	k_{eff} (KN/cm)
1	HYD-1-1-1-2	0.109	1.0096	-0.992	1.00	50.53	-80.53	76.96	79	9.26	463.6	78.66
2	HYD-1-2-1-2	0.1066	1.0038	-0.902	0.95	67.80	-104.2	103.7	104	9.41	635.7	109.1
3	HYD-1-3-1-2	0.1049	0.9992	-1.009	1.00	75.49	-117.7	114.1	116	9.52	719.5	115.4
4	HYD-1-4-1-2	0.1013	0.9961	-1.004	1.00	86.09	-129.7	127.7	129	9.83	749.5	128.5
5	HYD-1-1-2-2	0.1289	1.3286	-1.314	1.32	47.57	-76.03	74.37	75	10.30	368.9	56.90
6	HYD-1-1-3-2	0.1595	1.6483	-1.637	1.64	44.48	-72.43	69.14	71	10.33	278.9	43.09
7	HYD-1-1-4-2	0.1848	1.9596	-1.959	1.96	40.87	-68.17	65.51	67	10.60	221.1	34.11
8	HYD-2-1-1-2	0.0979	0.9767	-1.193	1.09	69.52	-117.6	113.2	115	9.97	709.8	106.3
9	HYD-2-2-1-2	0.8545	0.8017	-0.970	0.89	94.69	-160.9	153.7	157	9.38	1108.3	177.4
10	HYD-2-3-1-2	0.1055	0.9852	-0.990	0.99	125.3	-199.1	191.3	195	9.33	1187.8	197.5
11	HYD-2-4-1-2	0.1083	1.0023	-0.985	0.99	149.1	-237.0	226.6	232	9.25	1376.0	233.2
12	HYD-2-1-2-2	0.1352	1.3012	-1.312	1.31	72.76	-118.6	112.8	116	9.62	537.80	88.55
13	HYD-2-1-3-2	0.1292	1.3097	-1.626	1.47	60.12	-109.9	105.1	108	10.14	465.30	73.23
14	HYD-2-1-4-2	0.1923	1.9677	-1.954	1.96	62.53	-102.0	96.99	100	10.23	325.0	50.74
15	HYD-3-1-1-2	0.0964	0.9867	-1.205	1.10	93.11	-152.6	151.3	152	10.24	965.80	138.6
16	HYD-3-2-1-2	0.0999	1.0015	-0.977	0.99	129.9	-215.6	204.0	210	10.02	1300.3	212.0
17	HYD-3-3-1-2	0.0983	0.9726	-0.979	0.98	158.7	-263.7	249.8	257	9.89	1614.4	263.1
18	HYD-3-4-1-2	0.0858	0.806	-0.798	0.80	172.7	-295.4	283.2	289	9.40	2012.8	360.5
19	HYD-3-1-2-2	0.1341	1.3223	-1.327	1.33	94.62	-151.0	144.8	148	9.86	705.4	111.6
20	HYD-3-1-3-2	0.1298	1.3121	-1.63	1.47	81.93	-134.8	129.0	132	10.11	631.2	89.68
21	HYD-3-1-4-2	0.1455	1.5487	-1.571	1.56	80.52	-127.6	124.5	126	10.64	553.5	80.81
22	HYD-4-1-1-2	0.0961	0.9923	-1.191	1.09	138.4	-239.7	230.0	235	10.32	1440.2	215.1
23	HYD-4-2-1-2	0.0979	0.9999	-0.975	0.99	182.9	-314.4	300.7	308	10.21	1867	311.3
24	HYD-4-3-1-2	0.1003	1.0032	-0.988	1.00	231.2	-391.3	371.6	381	10.00	2304.6	383.1
25	HYD-4-4-1-2	0.1004	0.9934	-0.993	0.99	283.6	-469.6	440.7	455	9.89	2823.6	458.2
26	HYD-4-1-2-2	0.1325	1.3273	-1.298	1.31	134.3	-216.6	207.2	212	10.01	1013.5	161.4
27	HYD-4-1-3-2	0.1290	1.3048	-1.617	1.46	110.2	-198.3	190.3	194	10.11	853.7	133.0
28	HYD-4-1-4-2	0.1421	1.5486	-1.552	1.55	101.7	-175.3	167.6	171	10.90	715.7	110.5

Proceedings of the 3rd Croatian Conference on Earthquake Engineering - 3CroCEE
19–22 March 2025, Split, Croatia
Copyright © 2025 CroCEE
DOI: https://doi.org/10.5592/CO/3CroCEE.2025.26



(a)



(b)

Figure 10. a) Ductility ratio (μ) of HYD samples, Figure 10. b) Effective stiffness (K_{eff}) of HYD samples.

According to Figure 10-a by increasing the sample length from 41.80 cm to 75.28 cm, the Ductility ratio in HYD samples decreases and by increasing the height from 20.32 cm to 33.20 cm, this ratio increases and by increasing the thickness this ratio increases. In sample HYD-2-1-1-2 with a length of 41.80 cm and a Ductility ratio of 9.97, with an increase in length of 52.96 cm in sample HYD-2-2 1-2- The Ductility ratio decreased to 9.38 and by increasing the length again to 75.28 cm in sample HYD-2-4-1-2, the Ductility ratio was 9.25 it has decreased by 7.49% compared to HYD-2-1-1-2 sample. In the HYD-1-1-1-2 sample with a height of 20.32 cm and a thickness of 0.48 cm and a Ductility ratio of 9.26, with a height increase of 39.65 cm in the HYD-1-1-4-2 sample, the Ductility ratio has increased to 10.60, and the Ductility ratio has increased by 13.49% compared to HYD-1-1-1-2 sample. In sample HYD-1-1-1-2 with a thickness of 0.48 cm, with the increase the thickness in sample HYD-2-1-1-2 by 0.72, the Ductility ratio increased to 9.97 and by increasing the thickness of the sample to 0.96 cm in the HYD-3-1-1-2 sample, the Ductility ratio has increased to 10.24 which increases by 7.38% and 10.05% compared to HYD-1-1-1-2 sample and as a result, due to the increase in the thickness of the samples, it can be expected that the Ductility ratio in the samples will increase.

According to the values obtained from Figure 10-b, HYD-1-1-1-2 sample with a length of 41.80 cm has an effective stiffness of 78.66 KN/cm, which increases to 52.96, 64.12 and 75.28 cm in HYD -1-2-1-2, HYD-1-3-1-2 and HYD-1-4-1-2, samples respectively, amounting to 109.10, 115.44 and 128.57 KN/cm have increased, and the effective stiffness has increased by 32.42%, 37.89%, and 48.16%, respectively, compared to HYD-1-1-1-2 sample. In sample HYD-1-1-1-2 with a height of 20.32 cm, which by increasing the height to 26.76, 33.20 and 39.65 cm in samples HYD-1-1-2-2, HYD-1-1-3-2 and HYD-1-1-4-2 The effective stiffness decreased to 56.90, 43.09 and 34.11 KN/cm, respectively, which compared to HYD-1-1-1-2 sample, respectively, by It has decreased by 32.10%, 58.43% and 79.01%. Regarding the increase in thickness, the effective stiffness of the HYD-1-1-1-2 sample is 78.66 KN/cm, which by increasing the thickness to 1.44 cm in the HYD-4-1-1-2 sample is 215.14 KN/cm increases, which has increased by 92.90%.

4.2. Hysteresis damping coefficient

The equivalent viscous damping (EVD) or effective damping is effective index in evaluating the seismic performance of passive energy dissipation systems. The EVD has defined the combined effects of elastic and hysteretic damping. The EVD concept was first proposed by Jacobsen [17, 18]. The value of EVD based on Jacobsen's approach can be calculated with equation 4. The ξhyst represents the dissipation energy due to the hysteretic behavior.

$$\zeta_{hyst} = \frac{E_D}{4\pi E_S} = \frac{E_D}{2\pi K_{eff} {\delta_{ave}}^2} \quad (4)$$

Proceedings of the 3rd Croatian Conference on Earthquake Engineering - 3CroCEE
19–22 March 2025, Split, Croatia
Copyright © 2025 CroCEE
DOI: https://doi.org/10.5592/CO/3CroCEE.2025.26

Table 3 shows the value of ζhyst for 28 HYD samples for the ultimate displacement.

Table 3. Total dissipated energy (ET), dissipated energy in the last cycle (ED)elastic strain energy (ES) and EVD of HYD samples and proposed formula

Number	Sample	E_T (KN.cm)	E_D (KN.cm)	E_S (KN.cm)	$\frac{E_D}{E_T}$	$\frac{E_S}{E_T}$	ζhyst (%)
1	HYD-1-1-1-2	1760.40	257.60	39.40	14.60%	2.20%	52.00
2	HYD-1-2-1-2	3062.30	402.20	49.60	13.10%	1.60%	64.20
3	HYD-1-3-1-2	2579.80	356.90	58.20	13.80%	2.30%	48.80
4	HYD-1-4-1-2	2511.20	385.00	64.30	15.30%	2.60%	47.60
5	HYD-1-1-2-2	3214.90	429.30	49.70	13.40%	1.50%	68.70
6	HYD-1-1-3-2	3553.90	496.10	58.10	14.00%	1.60%	67.90
7	HYD-1-1-4-2	4241.40	566.80	65.50	13.40%	1.50%	68.90
8	HYD-2-1-1-2	4058.70	524.20	62.60	12.90%	1.50%	66.60
9	HYD-2-2-1-2	5294.60	633.70	69.70	12.00%	1.30%	72.30
10	HYD-2-3-1-2	6441.50	792.00	96.50	12.30%	1.50%	65.30
11	HYD-2-4-1-2	8244.90	1018.40	115.20	12.40%	1.40%	70.30
12	HYD-2-1-2-2	6032.80	757.20	75.60	12.60%	1.30%	79.70
13	HYD-2-1-3-2	5705.00	770.50	79.00	13.50%	1.40%	77.70
14	HYD-2-1-4-2	5843.90	795.60	97.60	13.60%	1.70%	64.90
15	HYD-3-1-1-2	6330.10	755.20	83.30	11.90%	1.30%	72.20
16	HYD-3-2-1-2	6907.50	893.10	103.80	12.90%	1.50%	68.50
17	HYD-3-3-1-2	7439.80	1067.60	125.30	14.30%	1.70%	67.80
18	HYD-3-4-1-2	2913.90	582.40	116.10	20.00%	4.00%	39.90
19	HYD-3-1-2-2	5644.80	756.80	98.00	13.40%	1.70%	61.40
20	HYD-3-1-3-2	6299.10	885.50	97.00	14.10%	1.50%	72.60
21	HYD-3-1-4-2	7410.60	1027.20	98.40	13.90%	1.30%	83.10
22	HYD-4-1-1-2	10238.80	1202.00	128.20	11.70%	1.30%	74.60
23	HYD-4-2-1-2	10722.50	1436.30	151.90	13.40%	1.40%	75.20
24	HYD-4-3-1-2	11871.20	1618.20	189.90	13.60%	1.60%	67.80
25	HYD-4-4-1-2	15267.10	1969.60	226.10	12.90%	1.50%	69.30
26	HYD-4-1-2-2	9544.10	1277.40	139.10	13.40%	1.50%	73.10
27	HYD-4-1-3-2	9658.90	1309.80	142.00	13.60%	1.50%	73.40
28	HYD-4-1-4-2	11192.40	1467.60	132.90	13.10%	1.20%	87.90

According to table 3, the hysteresis damping of the sample HYD-1-1-1-2 with a thickness of 0.48 cm is 52.00%. Compared to the sample HYD-4-1-1-2 with a thickness of 1.44 cm, this amount has decreased by 74.60%. Therefore, with the increase in the thickness of the sample, the hysteresis damping decreases. Also, by increasing the height of the HYD-1-1-4-2 sample by 39.65 cm, the hysteresis damping increases by 68.90% compared to the HYD-1-1-1-2 sample.

Copyright © 2025 CroCEE
DOI: https://doi.org/10.5592/CO/3CroCEE.2025.26

5. Conclusions

In this research, a new type of yielding metal dampers called honeycomb dampers was introduced. According to the analysis, it was found that the effective stiffness increases with the increase in the length of the sample and the Ductility ratio and damping of the equivalent viscous damping. Also, as the thickness of the sample increases, the effective stiffness, the Ductility ratio and the equivalent viscous damping also increases. As the height of the sample increases, the effective stiffness decreases, and the Ductility ratio, the equivalent viscous damping have increased. The highest effective stiffness value related to the HYD-4-4-1-2 sample, which has the longest length and the largest thickness, and its effective stiffness is equal to 121.57 KN/cm. The highest effective stiffness value is related to the HYD-4-4-1-1 sample, which has the longest length and the largest thickness, and its effective stiffness is equal to 458.20 KN/cm which has increased by 141.39% compared to HYD-1-1-1-2 sample. The highest Ductility ratio value is related to the HYD-4-1-4-2 sample, and it has a Ductility ratio to 10.90. In the end, it is suggested that the performance of the honeycomb yielding damper is improved by increasing the length and thickness.

References

[1] Kelly J.M, Skinner R.1, Heine A.J. Mechanisms of Energy Absorption in Special Devices for Use in Earthquake Resistant Structures. Bulletin of N. Z. Society of Earthquake Engineering, Vol. 5 No. 3, 1972.

[2] Skinner R.1, Kelly J.M, Heine A.J. Hysteretic Dampers for Earthquake Resistant Structures. Earthquake Engineering and Structural Dynamics, 287- 296, 1975.

[3] Skinner R.1, Tyler R.G, Heine A.J, Robinson W.H. Hysteretic Dampers for the Protection of Structures from Earthquakes. Bulletin of N. Z. Society of Earthquake Engineering, Vol 13. No 1, 1980.

[4] Kasai K, Popov E.P. General behavior of WF steel shear link beams. J. Struc. Eng, 112(2): 362-382, 1986.

[5] Bergman D. M, Goel S.C. Evaluation of cyclic testing of steel plate device for added damping and stiffness. Report No. UMCE 87-10, the University of Michigan, Ann Arbor, MI, 1987.

[6] Whittaker A.S, Bertero V.V, Thompson C. L, Alonso L.J. Seismic Testing of Steel Plate Energy Dissipation Devices. Earthquake Spectr; 7(4): 563-604, 1991.

[7] Tsai K.C, Chen H.W, Hong C.P, Su Y.F. Design of steel triangular plate energy absorbers for seismic-resistance construction. Earthquake Spectra; 9(3): 505-528, 1993.

[8] Dargush G.F, Soong T.T. Behavior of Metallic Plate Dampers in Seismic Passive Energy Dissipation Systems. Earthquake Spectra; 11(4): 545-568, 1995.

[9] Gang Li, Hongnan Li. Earthquake resistant design of RC frame with dual functions metallic damper. The 14th World Conference on Earthquake Engineering. Beijing, China, 2008.

[10] Soni A.H, Sanghvi C.S. Mathematical modeling of ADAS damper element and nonlinear time history analysis of SDOF steel structure using ETABS. Journal of Engineering Research and Studies, 2012.

[11] Teruna D.R, Majid T.A, Budiono B. Experimental Study of Hysteretic Steel Damper for Energy Dissipation Capacity. Advances in Civil Engineering, Article ID 631726, 12 pages, 2015.

[12] Sahoo D.R, Singhal T, Taraithia S.S, Saini A. Cyclic behavior of shear-and-flexural yielding metallic dampers. Journal of Constructional Steel Research; (114): 247–257, 2015.

[13] Garivani S, Aghakouchak A.A, Shahbeyk S. Numerical and Experimental Study of Comb-Teeth Metallic Yielding Dampers. International Journal of Steel Structures; 16(1): 177-196, 2016.

[14] Ghaedi K, Ibrahim Z, javanmardi A. A new metallic bar damper device for seismic energy dissipation of civil structures. 14th International Conference on Concrete Engineering and Technology, 2018.

[15] Kiai, M. Evaluation of the performance of metal yielding dampers in steel structures, Faculty of Civil Engineering, Noshirvan University of Technology, Babol, 2018.

[16] Moghadasi M, Namazi A. Assessment of pearformance of TADAS dampers for the Seismic rehabilitation of buildings. International Journal of Applied Engineering Research; 11(21): 10516-10523, 2016.

Copyright © 2025 CroCEE
DOI: https://doi.org/10.5592/CO/3CroCEE.2025.26

[17] Yang T.Y, Tianyi Li, Tobber L, Pan X. Experimental Test of Novel Honeycomb Structural Fuse. The 14th Nordic Steel Construction Conference, Copenhagen, Denmark, 451-456, 2019.

[18] Yang T.Y, Banjuradja W, Tobber L. Experimental Test of Welded Wide Flange Fuses. key Engineering Materials; (763): 414-422, 2018.

[19] Shadman Heidari P. numerical study on mechanical parameters of novel drilled plate metallic damper (DPMD). Proceedings of the 2nd Croatian Conference on Earthquake Engineering, 505-516, 2023.

[20] ANSI/AISC 341-16. Seismic provisions for structural steel buldings. An american national standard, 9.1-148, 2016.

[21] ANSYS Meshing User's Guide, (2016), Release 16.0. ANSYS, Inc.

[22] Jacobsen L.S. Steady forced vibration as influenced by damping. Transactions of ASME, 52, 169-181, 1930.

[23] Jacobsen L.S. Damping in composite structures, Proceedings of the Second World Conference on Earthquake Engineering, Vol 2, 1029-1044, (1960).

Proceedings of the 3rd Croatian Conference on Earthquake Engineering - 3CroCEE
19–22 March 2025, Split, Croatia
Copyright © 2025 CroCEE
DOI: https://doi.org/10.5592/CO/3CroCEE.2025.28

SHAKE TABLE TESTING OF U-SHAPED MASONRY STRUCTURES: OUT-OF-PLANE RESPONSE TO VARYING GROUND MOTION SIGNALS

Babar Ilyas [(1)], Dario Vecchio [(2)], Nuno Mendes [(3)], Paulo B. Lourenco [(4)]

[(1)] *PhD Student, University of Minho, ISISE, Department of Civil Engineering, babarilyas7@gmail.com*
[(2)] *PhD Student, University of Minho, ISISE, Department of Civil Engineering, dariovecchio4@yahoo.it*
[(3)] *Auxiliar Researcher, University of Minho, ISISE, Department of Civil Engineering, nunomendes@civil.uminho.pt*
[(4)] *Full Professor, University of Minho, ISISE, Department of Civil Engineering, pbl@civil.uminho.pt*

Abstract

Historical structures consisting of unreinforced masonry are highly vulnerable to seismic forces, with out-of-plane failure mechanisms being a primary concern. This vulnerability has often resulted in the collapses of the masonry structures during seismic events. Masonry walls tend to rock and overturn in the out-of-plane direction due to the dynamic loading, leading to either one-way or two-way bending. These mechanisms mainly depend on the boundary conditions and the degree of connectivity between the structural elements. Previously the one-way and the two-way bending mechanisms of masonry structures have been explored to some extent. However, research is still needed to develop reliable analytical and numerical models for predicting the mechanism under seismic action. This paper presents an extensive experimental campaign carried out on the shake table at the University of Minho (PT) to assess the sensitivity of the out-of-plane behavior of U-shape structures to varying ground motions. Two signals were chosen from the database to enable a comprehensive analysis of how different types of seismic events influence the structural response. To replicate the behavior of historical unreinforced masonry structures, the specimen was constructed using dry-stack granite blocks in U-shaped configuration, consisting of a façade and two orthogonal walls. Dry joints allow the walls to be rebuilt after each test, ensuring the repeatability at large displacements. The structural response was evaluated under varying intensities of two distinct ground motion inputs. The outcomes of the experimental campaign are expected to contribute to the development of better predictive models for seismic risk assessment and conservation strategies for historical URM structures.

Keywords: Shake-table Testing, Out-of-Plane, Historical Structures, Unreinforced Masonry, Collapse Mechanism.

1. Introduction

Unreinforced masonry (URM) structures make up a substantial portion of the architectural heritage in many earthquake-prone regions, such as Italy, Portugal, and Greece, where they also reflect profound cultural and historical significance [1]. These structures are typically built with thick vertical load-bearing walls without consideration for lateral seismic actions, making them highly vulnerable to earthquake-induced damage. This observation is supported by many post-earthquake in-situ observations. For example, the February 6, 2023, Kahramanmaras Earthquake occurred in Turkiye, demonstrating the destructive effects of seismic activity on masonry structures, further emphasizing the importance of addressing their vulnerability [2]. In New Zealand, for instance, URM built heritage is a vital element of the architectural landscape, yet, it represents a severe vulnerability under seismic activity [3]. Similarly, in India, the wide prevalence of URM buildings in densely populated urban areas under high seismic vulnerability highlights the potential for catastrophic outcomes during earthquakes [4]. Therefore, it is apparent the urgent need to protect such structures, to avoid human casualties and economic losses. Research has consistently shown that URM structures frequently sustain damage and experience collapses when subjected to seismic forces because of their limited tensile strength, brittle nature, and lack of lateral resistance [5]. This vulnerability to cracking, severe damage, and collapse

Copyright © 2025 CroCEE
DOI: https://doi.org/10.5592/CO/3CroCEE.2025.28

under seismic loads is often increased by non-ductile construction techniques such as the absence of reinforcement and the rigid connections between structural components [6]. However, a complete understanding of all the possible mechanisms of energy dissipation, the occurrence of large displacements and the probability of collapses is still not completely understood, especially when dealing with dynamic forces.

Depending on their direction, URM walls can experience both in-plane (IP) and out-of-plane (OOP) collapse mechanisms during an earthquake event. Largely and yet not clearly understood are the OOP mechanisms that have proven to be highly destructive due to the tendency of masonry walls to rock and overturn, leading to sudden collapses and substantial damage [7]. They are triggered in situations of poor connection between the façade and diaphragm/roof systems, when the seismic forces act perpendicular to the walls. They can result in pronounced rocking, bending, and eventually overturning, as illustrated in **Figure 1.** The OOP vulnerability has been observed in numerous earthquake events, where URM have exhibited distinctive one-way and two-way bending mechanisms influenced by various factors such as boundary conditions, degree of connectivity between structural elements, and slenderness ratios.



Figure 1. OOP failure mechanisms observed in URM structures [8].

One-way bending mechanisms are due to either poor lateral connection between two elements or the presence of an opening. Upon the existence of such a configuration, a wall/panel may undergo a sustained rocking motion over the base, after the creation of a three-hinge system. Two hinges are formed at the top and the bottom boundary conditions, while the latter forms along the height of the wall/panel [9]. This failure was also observed in isolated walls which have insufficient later support along the vertical edges. As a result, they exhibit significant rotational displacement, which leads to the complete overturning of the wall, especially when the slenderness ratio is high [10]. In contrast, two-way bending mechanisms involve both horizontal and vertical bending, creating more complex displacement patterns and rotational behavior. The two-way mechanism has been observed in wider facades, supported by structural elements or boundary conditions that prevent free OOP displacements, but allow rotations on both vertical and horizontal edges [7].

Copyright © 2025 CroCEE
DOI: https://doi.org/10.5592/CO/3CroCEE.2025.28

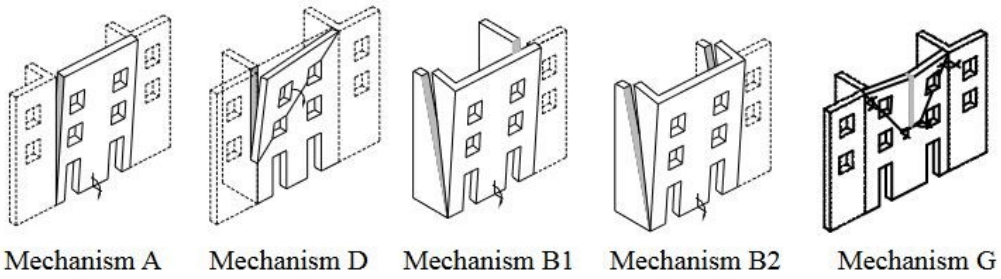


Figure 2: Example OOP mechanisms reported in various studies [11].

As shown in **Figure 2,** many OOP mechanisms in URM structures have been previously investigated with the use of analytical and numerical models. However, most of these studies focused on a priori selection of a specific mechanism and the application of quasi-static loading patterns. Despite the highly non-linear problem, force and displacement-based static tools lack the accuracy needed to predict the seismic response/capacity of URM under dynamic loading. In addition, due to the complex interaction between the characteristics of a ground motion, these models often lead to overly conservative strengthening and retrofitting solutions [12].

As mentioned, several factors, such as walls' geometry, boundary conditions, degree of connectivity between structural elements, and type of seismic excitation, may contribute to the complex nature of OOP collapse mechanism. This highlights the necessity of developing reliable analytical and numerical models to predict the capacity of OOP mechanisms, based on the dynamic response of URM structures. Such analytical and numerical models are crucial for assessing structural safety and guiding retrofitting efforts, particularly in historical contexts where structural interventions must be minimized to conserve heritage value. However, the accuracy of these models depends on the calibration and validation against extensive experimental data. Indeed, the existing studies have primarily focused on more straightforward configurations or limited testing scenarios, leaving a gap in comprehensive OOP assessment for more varying scenarios in terms of seismic excitations.

Shake table testing is one of the most advanced techniques used for experimental dynamic testing, because it can replicate real ground excitations in a controlled laboratory environment. Numerous studies have used shake table testing to assess the behavior of both reinforced and URM under varying seismic intensities and geometric configurations [7], [13], [14], [15], [16]. However, previous studies have largely concentrated on simpler wall configurations, often overlooking the distinctive structural behavior of 3D masonry systems under seismic forces. Additionally, the effect of varying ground motion signals on OOP responses remains insufficiently investigated. This paper addresses this gap by conducting an extensive experimental campaign within the framework of the Stand4Heritage project. The Stand4Heritage project aims to develop new standards and methodologies for seismic assessment and preservation of built cultural heritage. Dry-stacked granite blocks configured in a U-shape assembly, consisting of a façade and two orthogonal walls, are tested on the shake table at the Structural Laboratory of the University of Minho (PT). Through the application of two different ground motion signals on the same specimen, this study provides a broader understanding of how URM structures behave in the OOP direction under excitations of different characteristics. In the following sections the experimental campaign is presented including the test setup, ground motion signals selection and the outcomes of the campaign.

2. Experimental Setup

2.1. Description of Specimen

The experimental study used a U-shape URM specimen, constructed with dry-joint masonry blocks to replicate the seismic vulnerability of historical masonry structures. The specimen's configuration consisted of a 1.5-meter-long façade wall oriented perpendicular to the direction of the shake table's

Copyright © 2025 CroCEE
DOI: https://doi.org/10.5592/CO/3CroCEE.2025.28

motion to allow the occurrence of OOP failure mechanisms. Each return wall measured 1.65 m in length, connected to the facade forming a U-shape configuration.

The specimen has a total height of 1.5 m, constant across all the walls. Two types of blocks were used, and they are as follows: (a) Type 1, with dimensions of 30 cm x 30 cm x 15 cm, (b) Type 2 with dimensions of 15 cm x 15 cm x 15 cm. The masonry was built with granite blocks, disposed of in a typical stretcher bond pattern. The use of dry-stacked granite blocks, typical of historical masonry practices (especially in the country of Portugal), allowed for easy disassembly and reassembly, enhancing the repeatability in successive tests under varied seismic inputs. **Figure 3(a)** shows a view of the specimen constructed on the top of the shake table.

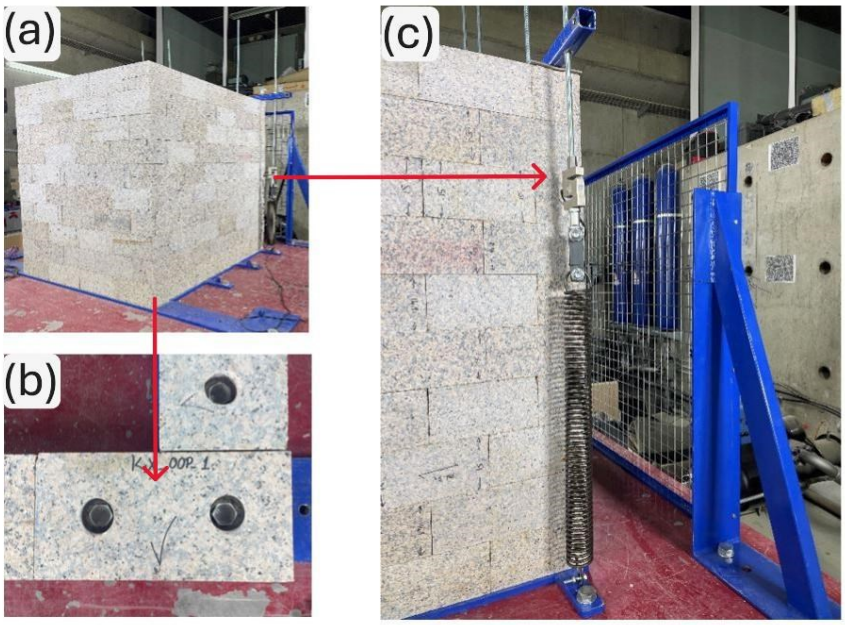


Figure 3: Test setup: (a) U-shape specimen, (b) anchoring system of the base course, and (c) spring-load cell connection in the precompression system.

2.2.Shake Table Specifications

The shake table facility available at the Structural Laboratory at the University of Minho, (PT) was used for this extensive experimental campaign. The shake table has a platform of 2.9 m x 2.9 m, with one degree of freedom (DOF), i.e., unidirectional. The shake table is operated by a hydrodynamic actuator, working up to a pressure of 300 kN, thus allowing the construction of specimens up to 3 tons. Note that the shake table weighs 3 tons. The shake table can work within a frequency range of 0-50 Hz, which covers the typical relevant frequency range for civil engineering structures. The main features of the shake table are given in **Table 1**. The shake table is equipped with a control station comprising two chassis. The primary chassis manages system operations, including the actuator's hydraulic system, while the secondary chassis offers expansion capabilities for additional instrumentation as needed. The surface of the shake table is provided with a grid of M27 holes, enabling bolted connections to anchor specimens directly to the platform, which is critical for simulating realistic seismic conditions without slippage or unintended movement. **Figure 4** shows a view of both the shake table and actuator.

Table 1: Shake table features.

Dimensions [m]	Frequency [Hz]	PTA[a] [g]	PTV[b] [cm/s]	PTD[c] [cm]	M_{ST}[d] [kg]	M_{ST}[e] [kg]
2.9 x 2.9	0-50	5	85	±12.5	3000	3000

a) Peak table acceleration, b) Peak table velocity, c) Peak table displacement, d) Mass of shake table, e) Maximum payload

Copyright © 2025 CroCEE
DOI: https://doi.org/10.5592/CO/3CroCEE.2025.28



Figure 4: The 1DOF shaking table installed at the University of Minho (PT).

2.3. Test setup and Instrumentation

The specimen was designed with a height of 1.5 m, with a total of 10 horizontal courses. To replicate realistic boundary conditions, the base of the specimen was anchored to the shake table platform. Each masonry block in the first course was connected to steel plates using two M18 threaded bolts embedded within the blocks. Next, the plates were fixed to the shake table's platform with M27 bolts, thereby simulating a rigid foundation and preventing any unintended sliding during seismic excitation, as shown in **Figure 3(b)**.

At the ends of the east and west return walls, a precompression force of 2 kN was applied on each wall via spring mechanisms to further establish a fixed boundary condition, as shown in **Figure 3(c)**. No additional restraints were applied to the top of the façade, allowing for a free upper boundary. This configuration reflects the case of a façade poorly connected to either a diaphragm or a roof system, which has the potential of triggering a complete overturning (see **Figure 2**).

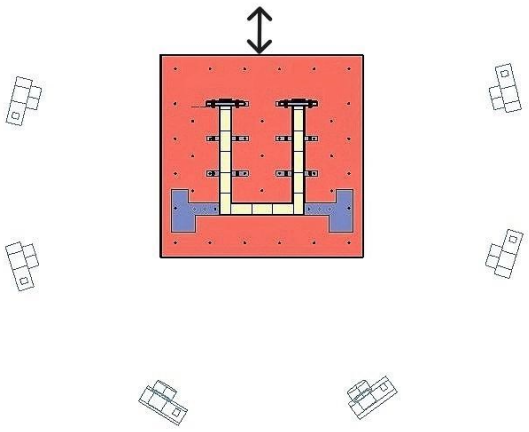


Figure 5: Schematic diagram of DIC cameras setup (top view).

To accurately capture the dynamic response of the masonry structure during testing, a Digital Image Correlation (DIC) system was employed as the data recording tool. The DIC system provides a contactless method of measurement, capable of recording displacement and strain data across the specimen surfaces. The system includes six high-speed cameras, each operating at a frequency of 145 Hz, ensuring that displacements are captured with high accuracy. The cameras were properly positioned surrounding the structure, with two cameras assigned to monitor each wall. **Figure 5** shows a top view of the camera location around the shake table (in red). This arrangement allowed for comprehensive, multi-angle coverage of the façade and both return walls, facilitating accurate data recording across the entire structure. Before testing, the cameras were calibrated and adjusted to account for lighting

Proceedings of the 3rd Croatian Conference on Earthquake Engineering - 3CroCEE
19–22 March 2025, Split, Croatia
Copyright © 2025 CroCEE
DOI: https://doi.org/10.5592/CO/3CroCEE.2025.28

conditions. Also, the cameras were paired to create stereo vision, enhancing the system's ability to capture displacement and deformation accurately across the three-dimensional geometry of the specimen. Additionally, the table is featured by a high precision accelerometer (±5g), enabling the real-time monitoring of the peak table acceleration (PTA).

2.4. Testing Protocols

Considering the operational limits of the shake table, both selected ground motion signals required scaling to achieve the desired test intensities. The HOR signal, which exhibited moderately impulsive characteristics, was scaled up to twice its original amplitude, with increments of 25% applied for each test stage. Due to its less impulsive nature, the ARG2 signal was scaled to 3.5 times its original amplitude, maintaining the same 25% incremental increases. Before testing, according to well-known protocols, each scaled signal was calibrated to ensure response spectra matching by using equivalent rigid masses bolted on the shake table.

A low-amplitude pink noise signal having a frequency range of 0-50 Hz was used to conduct dynamic identification tests on the specimen. Dynamic identification tests aimed to determine the natural frequencies and their corresponding mode shapes to understand the dynamic characteristics of test the specimen.

The testing followed an incremental dynamic loading approach, divided into two phases: **General Run** and **Collapse Area**. In the General Run, the specimen was subjected to incremental increases, starting from a 0.25 scale factor up to 2.0 times the original PGA of HOR and up to 3.5 times for ARG2, with each increment of 25%. This phase provided a broad view of the structural response across a varying excitation level, with a major focus on the measured maximum displacement. In the second phase, tests were concentrated around specific PGAs, where collapses were observed. This stage aimed to deepen the understanding of the randomness of collapse occurrence, allowing the reconstruction of fragility curves.

3. Ground Motion Signal

Testing URM structures under a variety of ground motion signals is critical due to the unique responses caused by different seismic characteristics. Also, OOP mechanisms may be extremely sensitive to velocity rather than acceleration content. As a result, several numerical analyses have already focused on the URM response under pulse-like ground motions, which usually release most of the energy in small-period velocity pulses. By experimentally applying both impulsive and non-impulsive signals, researchers can replicate a broader spectrum of real-world seismic events, allowing a more comprehensive understanding of OOP failure mechanisms. This approach helps ensure that the structural responses observed during the tests closely reflect real-world conditions. Such a consideration is fundamental for URM structures, which are highly sensitive to changes in frequency, due to their non-linear behavior.

3.1. Selection and Characteristics of Ground Motion Signals

The selection of appropriate ground motion signals to investigate the OOP responses of URM structures was a critical aspect of this experimental campaign. Given the demanding nature of shake table testing, the selection of the signal was guided by two criteria: (1) each signal should be capable to initiate the targeted failure mechanisms, and (2) each signal had to comply with the operational limitations of the shake table, including capacity constraints in acceleration, velocity and displacement. The compliance with these criteria ensured that the selected signals would generate the desired seismic responses without exceeding the mechanical limits of the experimental setup.

The European Strong-Motion (ESM) database was used to search for potential candidate signals. Preliminary Non-Linear-Time-History-Analyses (NLTHA) based on a discontinuous model and the use of an explicit algorithm to facilitate the computational efforts, were conducted on 20+ ground motion records. According to the occurrence of collapses encountered in the NLTHAs, seven ground motion

Copyright © 2025 CroCEE
DOI: https://doi.org/10.5592/CO/3CroCEE.2025.28

signals, as shown in **Table 2**, were shortlisted based on their capacity to induce significant rocking, overturning, and bending behavior.

Table 2: Ground motion suite selected for the dynamic campaign: main characteristics.

Event name	Year	M_w	PGA [g]	PGV [cm/s]	PGD [cm]	LDV*	IPR**	IP***
GMN	1976	6.4	0.33	37.26	4.12	337.56	1.0	9.06
NRC	2016	6.0	0.72	56.78	5.67	752.64	1.0	13.26
HOR	1998	6.2	0.37	35.16	3.82	532.93	1.0	15.16
NRC	2016	6.0	0.36	30.33	5.43	680.1	0.86	22.42
MZ28	2016	6.6	0.76	29.49	7.0	886.28	0.36	30.05
4629	2023	7.7	0.34	28.32	9.17	1090.9	0.04	38.52
ARG2	2014	6.2	0.35	21.65	3.49	861.56	0.02	39.8

* Development length of velocity time series, ** Impulsivity index by regression, *** Impulsivity index

3.2. Rationale for Categorizing Ground Motion Signals

Given the goal of investigating the pulse-like behavior on the U-Shape specimen, the seven ground motions were analyzed in terms of their impulsivity content. Such an analysis is based on the observation of the velocity time series to classify the pulse-like (impulsive) and non-impulsive signals [17]. The classification procedure involved the following steps:

1. **Development Length of Velocity (Ldv)**: The Ldv parameter was calculated for each ground motion signal by summing the incremental variation in velocity over time. The "length" of the velocity time history provides a quantitative measure of the impulsive nature of the signal, with shorter lengths typically associated with stronger impulsive characteristics. LDv was calculated using Eq. (1).

$$\mathrm{LDv} = \sum_{i+1}^{n} \left(\sqrt{(\Delta t)^2 + (\Delta V)^2}\right) \tag{1}$$

2. **Peak Ground Velocity (PGV)**: PGV was measured for each signal, representing the peak recorded value of velocity within its time history. This value, in combination with Ldv, helps to identify signals that exhibit sharp, high-velocity pulses indicative of impulsive signals.

3. **Impulsivity Index by Regression (IP_R):** A logistic regression model was used to predict the nature of a ground motion signal. This regression used PGV and Ldv values as predictors, assigning each signal to an impulsive category (e.g., impulsive or non-impulsive) based on historical earthquake records with known impulsive characteristics. This additional step minimizes subjectivity in impulsivity classification and provides a statistically backed approach to selecting signals. The IP_R was calculated using Eq. (2).

$$\mathrm{IP_R} = \frac{1}{1 + e^{(5 - 0.45(\mathrm{PGV}) + 0.01(\mathrm{LDv})}} \tag{2}$$

4. **Impulsivity Index (IP)**: IP is the ratio of development length of velocity time series to peak ground velocity. Lower IP values correspond to higher impulsivity, which is typical of pulse-like ground motions.

5.

6. **Table** *3* shows the thresholds to classify signals into different levels of impulsivity, allowing for the differentiation of highly impulsive signals from those with more distributed or vibratory characteristics [17]. The IP was calculated using Eq. (3):

$$\mathrm{IP} = \frac{\mathrm{LDv}}{\mathrm{PGV}} \tag{3}$$

Copyright © 2025 CroCEE
DOI: https://doi.org/10.5592/CO/3CroCEE.2025.28

Table 3: Classification of Impulsivity Levels.

IP	Impulsivity
IP ≤ 12	Highly Impulsive
12 < IP ≤ 20	Moderate Impulsive
20 < IP ≤ 35	Low Impulsive

Using this classification, two signals were selected to provide the targeted OOP responses: one moderately impulsive signal and one less impulsive or vibratory signal. The first signal, recorded during the Azores Earthquake in 1998 (HOR), exhibited characteristics of a moderately impulsive event, making it suitable for testing immediate and forceful OOP responses. The second signal, from the 2014 Western Greece (ARG2) earthquake, represented a non-impulsive event. **Figure 6** shows the acceleration, the velocity, and the displacement time histories for each signal. By combining the results of the NLTHAs and regression-based impulsivity classification, this selection of two contrasting signals, one moderately impulsive and one non-impulsive, which supports the assessment of URM structures under variable seismic conditions.

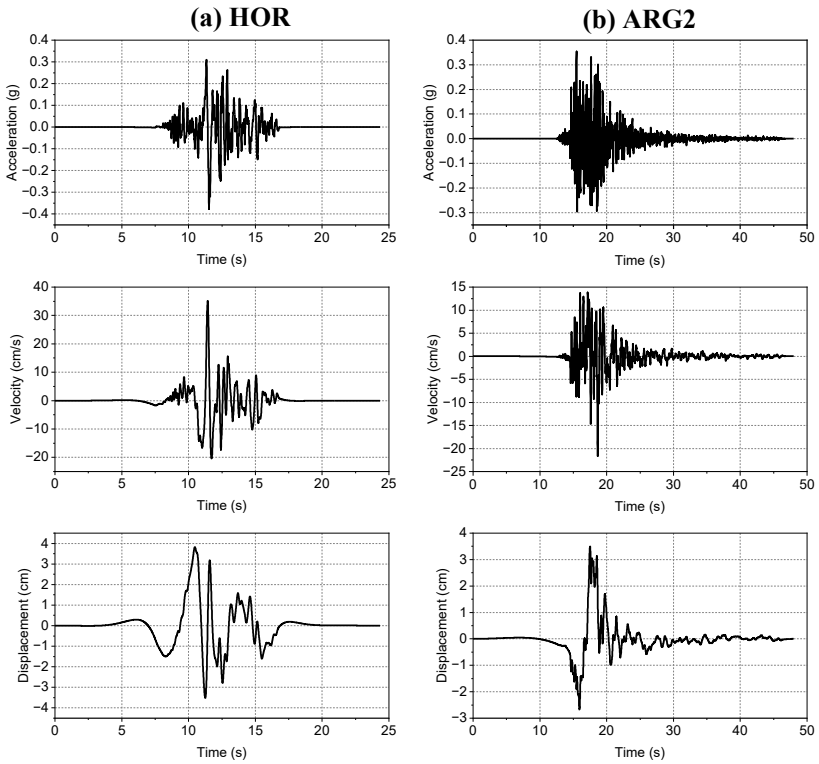


Figure 6: Time histories of the signals: (a) HOR, (b) ARG2.

4. Observed Structural Response

The U-shape specimen was subjected to incremental dynamic testing using the two ground motion signals, namely HOR and ARG2, selected using the criteria mentioned above. For each test, the specimen was returned to its original undamaged state, allowing for the assessment of distinct failure mechanisms at varying intensity levels.

Copyright © 2025 CroCEE
DOI: https://doi.org/10.5592/CO/3CroCEE.2025.28

4.1.Impulsive Signal

The response of the specimen under the moderate impulsive ground motion was a complex occurrence of two distinct mechanisms, the horizontal bending of the façade, due to the return walls' opening, and the overturning of the façade, due to shear-diagonal cracking in the orthogonal walls. Note that in the case of dry-stacked masonry structures, cracking is associated with detachment of the blocks at the common interface. At low PGA levels, up to 0.2g, the structure remained stable with no notable damage. Minor bending of the façade was first observed around 0.25g, though without any substantial cracking or structural damage. This response suggested that the specimen could initially withstand low-to-moderate seismic forces without substantial impact. As the PGA increased beyond 0.3g, more visible deformation was observed in the top courses of the façade, however, the overall response was still dictated by the bending of the façade. Around 0.4g, the response started showing a combination of bending and (minor) rocking, suggesting the initiation of a complex dynamic OOP response, where the shift from one to the other mechanism was dictated by the increasing energy of the velocity pulse. Around 0.5g, the structure exhibited higher interaction between bending forces and rocking, particularly in the façade and at the connections with the return walls, where diagonal cracks were highly visible.

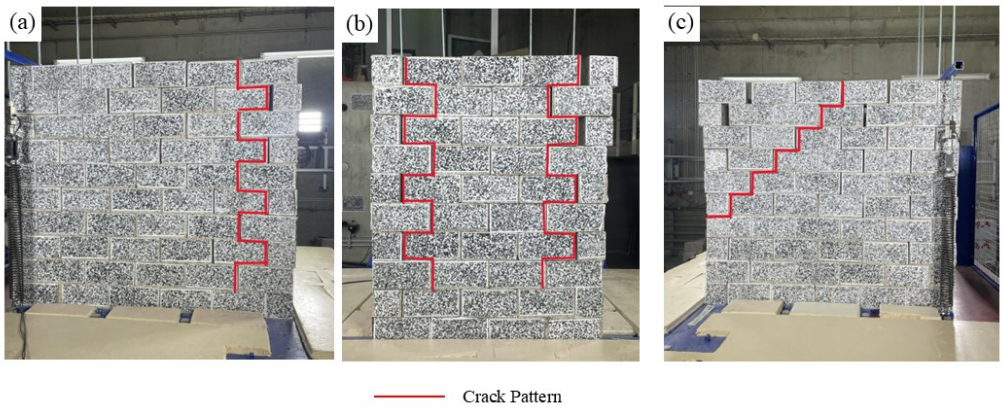


Figure 7: Observed damage before the collapse at 0.524 g: (a) interface separation of the facade from west return wall, (b) return walls opening seen in the facade, and(c) diagonal crack in the east return wall.

In the higher intensity range, specifically between 0.5g and 0.6g, the deformation pattern became significantly more pronounced. Large residual displacements were evident in the façade, and the cracks at the junctions between the façade and return walls widened. At 0.56g, substantial deformation was observed in the façade, accompanied by noticeable separation at the interface with the return walls. This stage marked a critical threshold for structural stability, as further increases in PTA pushed it towards collapse. **Figure 7** illustrates the residual deformation in the façade and the cracking patterns in the return walls. At a PTA of around 0.6g, the façade underwent a partial collapse due to overturning, with recorded peak table velocity (PTV) and peak table displacement (PTD) values of 54.41 cm/s and 5.61 cm, respectively.

Copyright © 2025 CroCEE
DOI: https://doi.org/10.5592/CO/3CroCEE.2025.28

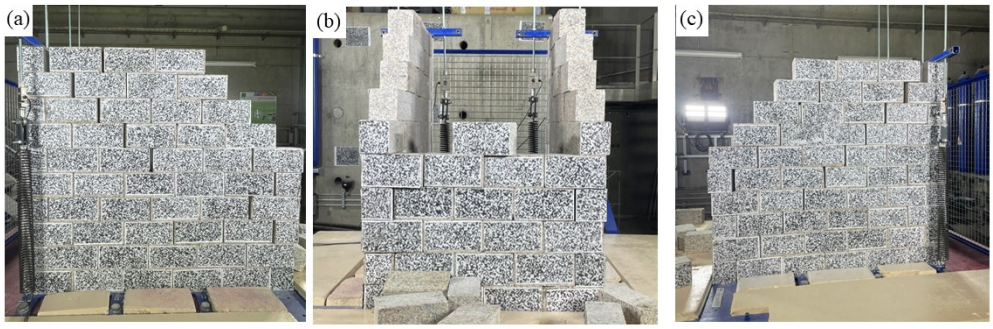


Figure 8: Observed collapse at 0.766 g: (a) top corner of the west return wall involved in the collapse, (b) overturning of the façade, and (c) widened diagonal cracks in the east return wall.

The collapse was characterized by concentrated damage in the OOP façade, where blocks in the upper courses began to separate and dislodge. Concurrently, significant diagonal cracking extended from the base to the top corners of the return walls, reflecting intense lateral stresses acting on these elements. Although the overall testing showed the development of symmetric deformation patterns, notable variations were noted between the left and right sides of the structure. This clearly suggested the existence of asymmetric in the structure, despite the application of a 1 DOF signal input.

At PGAs exceeding 0.7g, the façade experienced all collapse, with widespread block separation and substantial dislodgement along the upper courses. The return walls, although exhibiting extensive diagonal cracking, resisted full overturning due to their in-plane stiffness, which provided some degree of lateral stability despite severe damage. **Figure 8** captures the post-collapse condition of the façade, along with the diagonal cracks that formed in the return walls.

4.2.Non-Impulsive Signal

The structural response of the U-shape URM specimen to the non-impulsive ARG2 ground motion signal differed notably from the behavior experienced under the impulsive HOR signal. At lower PTAs (up to approximately 0.5g), the specimen displayed mild rocking and bending, characterized by incremental lateral displacements in both the façade and return walls. These early displacements were not accompanied by significant structural damage, suggesting that the initial phases of this non-impulsive signal allowed the structure to accommodate seismic forces with minimal deformations. As the PTA increased beyond 0.5g, bending became visible in the upper courses of the façade, along with the formation of diagonal cracks in the return walls. These cracks gradually widened with increased loading but did not immediately compromise structural stability, indicating a tolerance for progressive deformation under non-impulsive forces. At higher PTAs, nearing 1.0g, the specimen continued to display OOP bending and rocking without the sudden collapse observed. Prominent OOP bending mechanism was observed in the façade which extended down to the lower courses, as illustrated in **Figure 9**. Residual displacement in the return walls was higher because of the very high intensity of this vibratory signal. The collapse was first observed at a PTA of 1.31g, where the recorded PTV and PTD were 63.4 cm/s and 11.93 cm, respectively.

Copyright © 2025 CroCEE
DOI: https://doi.org/10.5592/CO/3CroCEE.2025.28

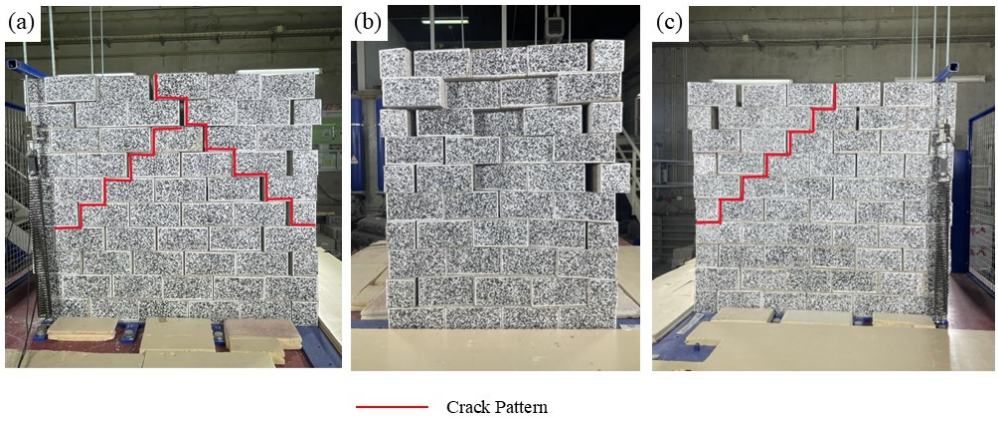


Figure 9: Observed damage before collapse at 1.14 g: (a) crack opening due to in-plane rocking of two macro-blocks in west return wall, (b) displaced blocks in OOP façade shows bending and opening of return walls, and (c) large displacements in east return wall along with crack showing formation of macro-blocks.

The failure mechanism, in this case, was markedly different from that under impulsive loading; the collapse occurred gradually, initiated by progressive rocking and severe bending in the façade along with the outward opening of the return walls. In-plane rocking was also observed in both return walls, forming two macro-blocks in the return walls. This behavior led to a gradual dislodgement of blocks, particularly in the upper courses of the façade, rather than a sudden collapse. **Figure 10** captures the state of the structure following the initial collapse, showing both the gradual dislodgement of the facade, and the damage progression in the return walls.



Figure 10: Observed collapse at 1.31 g: (a) top corner involved in collapse along with a wide diagonal crack in the west return wall, (b) Disintegration of the blocks in the facade, and (c) separation of interfaces with wide cracks in the east return wall.

5. Conclusion

This paper describes a shake table campaign conducted on a U-Shape dry-stacked masonry specimen to enhance the understanding of the out-of-plane collapse mechanism of unreinforced masonry structures under varying seismic ground motion characteristics. By applying both impulsive and non-impulsive ground motion signals, the experiments revealed distinct structural responses to each type. The impulsive signal triggered rapid damage progression and sudden collapse due to overturning in the façade, with significant diagonal cracking in the return walls. In contrast, the non-impulsive signal allowed for a gradual rocking and bending response, delaying collapse initiation even at higher peak ground accelerations. Thus, the final collapse was dictated by the higher frequency content in the acceleration time history, rather than by a significant pulse in the velocity time history. It was possible to state that the collapse happened due to the disintegration of the masonry.

Copyright © 2025 CroCEE
DOI: https://doi.org/10.5592/CO/3CroCEE.2025.28

Notably, the impulsive HOR signal led to collapse at lower PTA, PTV, and PTD levels than the non-impulsive ARG2 signal, underscoring the significant influence of ground motion impulsivity on URM structural failure mechanisms. These findings highlight the importance of incorporating ground motion characteristics into seismic assessments, especially for historical masonry structures.

Finally, this research underscores the need for predictive models that account for ground motion impulsivity when evaluating URM seismic vulnerability. The results emphasize the value of using varied seismic signals in experimental testing to capture realistic structural responses, contributing to the creation of valuable data for the conservation of heritage masonry structures in earthquake-prone areas.

Acknowledgements

This investigation has been partly funded by the STAND4HERITAGE project that has received funding from the European Research Council (ERC) under the European Union's Horizon 2020 research and innovation program (Grant agreement No. 833123), as an Advanced Grant. This work was also partly financed by FCT/MCTES through national funds (PIDDAC) under the R&D Unit Institute for Sustainability and Innovation in Structural Engineering (ISISE), under reference UIDB/04029/2020, and under the Associate Laboratory Advanced Production and Intelligent Systems ARISE under reference LA/P/0112/2020.

References

[1] C. Modena, F. Da Porto, and M. Valluzzi, Eds., Brick and Block Masonry: Proceedings of the 16th International Brick and Block Masonry Conference, Padova, Italy, 26-30 June 2016. CRC Press, 2016. doi: 10.1201/b21889.

[2] V. Kahya et al., "Evaluation of earthquake-related damages on masonry structures due to the 6 February 2023 Kahramanmaraş-Türkiye earthquakes: A case study for Hatay Governorship Building," Eng. Fail. Anal., vol. 156, p. 107855, Feb. 2024, doi: 10.1016/j.engfailanal.2023.107855.

[3] A. Marotta, L. Sorrentino, D. Liberatore, and J. M. Ingham, "Seismic Risk Assessment of New Zealand Unreinforced Masonry Churches using Statistical Procedures," Int. J. Archit. Herit., vol. 12, no. 3, pp. 448–464, Apr. 2018, doi: 10.1080/15583058.2017.1323242.

[4] R. Maheshwari, B. K. Singh, and R. Marques, "Seismic vulnerability assessment and strengthening of an existing typical Indian unreinforced masonry building in a high-risk seismic zone-a comprehensive application," Innov. Infrastruct. Solut., vol. 9, no. 11, p. 424, Nov. 2024, doi: 10.1007/s41062-024-01728-7.

[5] D. D'Ayala and E. Speranza, "Definition of Collapse Mechanisms and Seismic Vulnerability of Historic Masonry Buildings," Earthq. Spectra, vol. 19, no. 3, pp. 479–509, Aug. 2003, doi: 10.1193/1.1599896.

[6] S. Cattari, M. Angiolilli, S. Alfano, A. Brunelli, and F. De Silva, "Investigating the combined role of the structural vulnerability and site effects on the seismic response of a URM school hit by the Central Italy 2016 earthquake," Structures, vol. 40, pp. 386–402, Jun. 2022, doi: 10.1016/j.istruc.2022.04.026.

[7] F. Graziotti, U. Tomassetti, S. Sharma, L. Grottoli, and G. Magenes, "Experimental response of URM single leaf and cavity walls in out-of-plane two-way bending generated by seismic excitation," Constr. Build. Mater., vol. 195, pp. 650–670, Jan. 2019, doi: 10.1016/j.conbuildmat.2018.10.076.

[8] E. Işık et al., "Structural damages in masonry buildings in Adıyaman during the Kahramanmaraş (Turkiye) earthquakes (Mw 7.7 and Mw 7.6) on 06 February 2023," Eng. Fail. Anal., vol. 151, p. 107405, Sep. 2023, doi: 10.1016/j.engfailanal.2023.107405.

[9] L. Sorrentino, R. Masiani, and M. C. Griffith, "The vertical spanning strip wall as a coupled rocking rigid body assembly," Struct. Eng. Mech., vol. 29, no. 4, pp. 433–453, Jul. 2008, doi: 10.12989/SEM.2008.29.4.433.

Copyright © 2025 CroCEE
DOI: https://doi.org/10.5592/CO/3CroCEE.2025.28

[10] L. F. Restrepo Vélez, G. Magenes, and M. C. Griffith, "Dry Stone Masonry Walls in Bending—Part I: Static Tests," Int. J. Archit. Herit., vol. 8, no. 1, pp. 1–28, Jan. 2014, doi: 10.1080/15583058.2012.663059.
[11] D. D'Ayala and Y. Shi, "Modeling Masonry Historic Buildings by Multi-Body Dynamics," Int. J. Archit. Herit., vol. 5, no. 4–5, pp. 483–512, Jul. 2011, doi: 10.1080/15583058.2011.557138.
[12] S. Lagomarsino, "Seismic assessment of rocking masonry structures," Bull. Earthq. Eng., vol. 13, no. 1, pp. 97–128, Jan. 2015, doi: 10.1007/s10518-014-9609-x.
[13] U. Tomassetti, A. A. Correia, P. X. Candeias, F. Graziotti, and A. Campos Costa, "Two-way bending out-of-plane collapse of a full-scale URM building tested on a shake table," Bull. Earthq. Eng., vol. 17, no. 4, pp. 2165–2198, Apr. 2019, doi: 10.1007/s10518-018-0507-5.
[14] M. Mongelli, A. Giocoli, I. Roselli, G. D. Canio, G. D. Felice, and S. D. Santis, "SHAKING TABLE TESTS ON C-SHAPED MASONRY WALLS: DISPLACEMENT FIELD DATA DETECTED BY 3D MOTION CAPTURE SYSTEM AT ENEA CASACCIA RESEARCH CENTER".
[15] F. Graziotti, U. Tomassetti, S. Kallioras, A. Penna, and G. Magenes, "Shaking table test on a full scale URM cavity wall building," Bull. Earthq. Eng., vol. 15, no. 12, pp. 5329–5364, Dec. 2017, doi: 10.1007/s10518-017-0185-8.
[16] S. Kallioras, A. A. Correia, P. X. Candeias, A. Campos Costa, and F. Graziotti, "Dataset from the dynamic shake-table experiments on a full-scale unreinforced clay-brick masonry building with chimneys," Data Brief, vol. 52, p. 109813, Feb. 2024, doi: 10.1016/j.dib.2023.109813.
[17] D. S. Panella, M. E. Tornello, and C. D. Frau, "A simple and intuitive procedure to identify pulse-like ground motions," Soil Dyn. Earthq. Eng., vol. 94, pp. 234–243, Mar. 2017, doi: 10.1016/j.soildyn.2017.01.020.

Proceedings of the 3rd Croatian Conference on Earthquake Engineering - 3CroCEE
19–22 March 2025, Split, Croatia
Copyright © 2025 CroCEE
DOI: https://doi.org/10.5592/CO/3CroCEE.2025.36

EFFECTIVE STIFFNESS OF FLANGED REINFORCED CONCRETE STRUCTURAL WALLS: A NUMERICAL APPROACH

Komaravolu Venkata Purneshwar [(1)], Nilanjan Samanta [(2)], Kaustubh Dasgupta [(3)]

[(1)] *MTech student, Department of Civil Engineering, Indian Institute of Technology, Guwahati, India, p.komaravolu@alumni.iitg.ac.in*
[(2)] *PhD student, Department of Civil Engineering, Indian Institute of Technology, Guwahati, India, nsamanta@iitg.ac.in*
[(3)] *Associate Professor, Department of Civil Engineering, Adjunct Faculty, Centre for Disaster Management and Research, Indian Institute of Technology, Guwahati, India, kd@iitg.ac.in*

Abstract

For high rise buildings, Reinforced Concrete (RC) shear walls have emerged as a preferred structural element due to their significant contributions to global lateral strength, stiffness, and ductility. The lateral stiffness RC structural walls provide to the building system effectively mitigates structural and non-structural damage by limiting excessive deformation. Therefore, accurately estimating the effective stiffness of structural components under design basis earthquake is crucial for determining the design forces on various structural elements and for assessing the global drift of the building system. Under design basis earthquake the concrete cracks over a significant portion of the shear walls and the reinforcement yields in concentrated locations, and thereby there is a reduction of the initial uncracked stiffness. Various international standards and design codes have prescribed effective stiffness of the RC structural wall as a constant reduction factor to the gross moment of inertia of the wall section. Two major limitations of the constant reduction factor prescribed by current design codes are the lack of identification of the key parameters that influence effective stiffness and the inability to consider the geometrical shape of RC structural walls. The present study has tried to address these two major gap areas. In the current study, a flanged RC structural wall from a previous experimental study is selected, and a finite element (FE) modeling is employed to develop the numerical model. Displacement-controlled nonlinear static analyses are conducted. From past studies on rectangular and non-rectangular RC structural walls, the major influencing parameters related to the effective stiffness of the RC structural wall are identified. Based on the determined parameters, a parametric study is conducted, and finally, an empirical equation of the effective stiffness of the L-shaped wall is presented. The accuracy of the empirical equation is assessed by estimating the coefficient of variation (COV) between the predicted effective stiffness and the FE model-derived effective stiffness.

Keywords: effective stiffness, flanged shear wall, L-shaped structural wall, nonlinear static analysis.

1. Introduction

Over the past few decades, seismic design standards have had a transition from the force-based approach to the displacement-based approach. This shift necessitates the quantification of the deformation behavior of structures. In the case of reinforced concrete (RC) wall structures, their stiffness characteristics play a pivotal role in determining the fundamental period, deformation, and distribution of internal force responses among walls. The reduction in the gross stiffness of the RC structural wall depends on the level of earthquake hazard (design basis earthquake or maximum considered earthquake) considered in the design of the RC structures. Typically, under the design basis earthquake (DBE) the yielding of the RC structural wall is expected; hence the effective stiffness of an RC structural wall up to the point of yielding is determined using its cross-sectional moment of inertia (MOI), adjusted by a reduction factor to account for the effects of flexural and shear cracking [1]. In general, the stiffness modifier is prescribed in various design codes to take into account for (a) concrete cracking, (b) the effect of axial load, (c) bond-slip of reinforcement, and (d) anchorage extension. In various design standards, the reduction factors vary between 0.35–0.70 [1]. Previous studies [2,3] have examined the reduction factor and proposed various methods to increase the accuracy of stiffness predictions. For RC structural walls, research has primarily concentrated on developing approaches that incorporate additional design parameters and account for shear deformation in the effective stiffness. However,

Copyright © 2025 CroCEE
DOI: https://doi.org/10.5592/CO/3CroCEE.2025.36

investigations on non-rectangular RC structural walls [1,4] suggest that the findings applicable to rectangular RC structural walls may not be directly transferable to non-rectangular configurations. A past study [1] proposed effective stiffness values for T-shaped and U-shaped RC structural walls under different loading directions. However, no research has been identified that specifically addresses the effective stiffness of L-shaped RC structural walls, which are commonly used at the corners of building layouts. Therefore, the present study focuses on the nonlinear behavior of L-shaped RC structural walls and ultimately proposes a simplified expression for their effective stiffness.

2. Significance of Present Study

RC structural elements crack immediately after the application of the lateral load which makes the RC structure more flexible than the uncracked condition. Therefore, the uncracked stiffness is modified under the action of the lateral load to get a reasonable structural response (base shear, deformation, etc.). In general, many design codes specify the constant stiffness modifier which has a lack of identification of the salient parameters that contribute to the effective stiffness. Moreover, previous proposals of effective stiffness for rectangular RC structural walls are not applicable to flanged RC structural walls. In the present study empirical expressions of the effective stiffness of the L-shaped RC structural wall are developed which has taken into account both the significant influencing parameters to the effective stiffness as well as the geometrical shape of the RC structural wall.

3. Definition of Effective Stiffness

For RC structural members, effective stiffness can be defined in different ways, though two methods are predominantly used [1]. The first approach estimates the effective stiffness as the secant slope of the lateral force versus lateral displacement curve, evaluated at the point where the applied force reaches 75% of the nominal flexural strength. The second approach defines the effective stiffness as the stiffness of the wall at the onset of yielding, which occurs when either the first longitudinal reinforcing bar yields or the maximum compressive strain in the concrete at the critical section reaches 0.002.

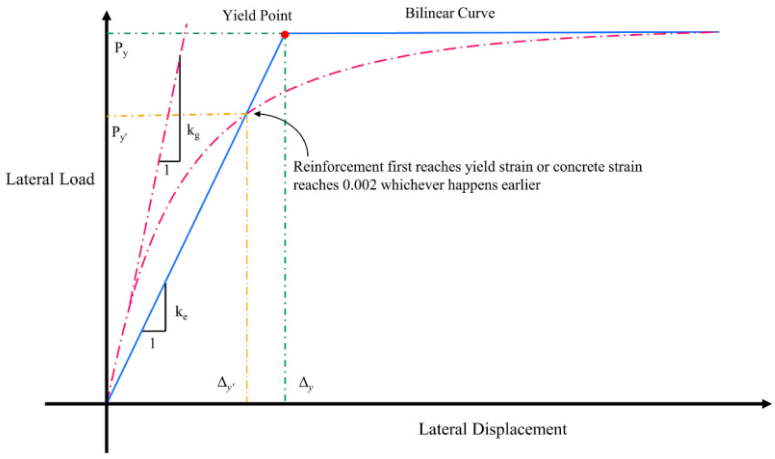


Figure 1. Definition of effective stiffness.

4. Salient Past Studies on Effective Stiffness of Rectangular RC Structural Wall

Based on the parametric study, Fenwick and Bull [2] proposed a relationship between the effective moment of inertia (I_e) and the moment of inertia of an uncracked concrete section (I_g) for cantilever walls which is expressed in Eq. (1) such as:

$$\frac{I_e}{I_g} = 0.267\left(1 + 4.4\frac{N}{A_g f_c'}\right)\left(0.62 + \frac{190}{f_y}\right)(0.76 + 0.005 f_c') \quad (1)$$

Proceedings of the 3rd Croatian Conference on Earthquake Engineering - 3CroCEE
19–22 March 2025, Split, Croatia
Copyright © 2025 CroCEE
DOI: https://doi.org/10.5592/CO/3CroCEE.2025.36

Paulay and Priestley [3] proposed Eq. (2) to relate the effective moment of inertia of the wall cross-section at first yield in the extreme fiber (I_e) to the moment of inertia of the uncracked gross concrete section (I_g). The expression was proposed considering the effect of yield strength of longitudinal reinforcement (f_y) and axial load ratio ($P_u/(f_c' A_g)$).

$$I_e = \left(\frac{100}{f_y} + \frac{P_u}{f_c' A_g}\right) I_g \tag{2}$$

Unlike previous researchers, Paulay and Priestley [3] accounted for shear deformation contributions also to the wall stiffness and proposed the following Eq. (3) to evaluate the effective stiffness for structural walls with aspect ratios less than 4.0.

$$I_w = \frac{I_e}{1.2+F} \quad , where \quad F = \frac{30 I_e}{H^2 t_w l_w} \tag{3}$$

In the above equation, the shear deformation contribution to effective wall stiffness is reflected by wall height(H), wall thickness(t_w), and wall length (l_w).

5. Salient Past Studies on Effective Stiffness of Flanged RC Structural Wall

Numerous studies have been carried out to examine the seismic performance of non-rectangular RC walls. It is worth mentioning here that compared to rectangular RC walls, experimental or numerical investigations regarding flanged or non-rectangular RC walls are limited. A few experimental investigations conducted by Beyer et al. [5], Thomsen and Wallace [4], and Brueggen [6] have helped us to understand the behavior of flanged shear walls. Thomsen and Wallace [4] found that the stiffness of the T-shaped walls is much higher compared to that of the rectangular RC walls of similar height they tested. Brueggen [6] reported that the effective stiffness of the T-shaped wall for web parallel flange-in-tension direction loading was around 30% larger than that of the effective stiffness for flange-in-compression direction loading. Zhang and Li [1] performed a numerical study to find out the effective moment of inertia of flanged RC shear walls and proposed empirical equations for T-shaped RC structural walls for both web parallel flange-in-tension and flange-in-compression. The proposed empirical equations are:

For T-shaped RC structural wall for web parallel flange-in-tension

$$\frac{I_e}{I_g} = 2.35 \frac{P_u}{f_c' A_g} + \frac{185}{f_y} \tag{4}$$

For T-shaped wall for web parallel flange-in-compression

$$\frac{I_e}{I_g} = 1.75 \frac{P_u}{f_c' A_g} + \frac{125}{f_y} \tag{5}$$

6. Formulation of Stiffness Modifier

The in-plane behaviour of RC structural walls is widely considered as single curvature bending. Furthermore, most of the design standards assume cantilever action under the action of lateral load for RC structural wall; therefore, the effective stiffness commonly expressed in the form of stiffness modifier (κ) such as:

$$\kappa = \frac{K_e}{K_g} = \frac{I_e}{I_g} \tag{6}$$

Where K_e is the effective stiffness of the structural member and the K_g is the gross stiffness of the structural member. The effective MOI is related to effective stiffness such as:

$$K_e = \frac{3 E_c I_e}{H^3} \tag{7}$$

Where E_c is the concrete modulus elasticity and H is the wall height. Shear deformation in slender RC structural walls has been observed to contribute a significant portion of the total deformation [3]. To

Copyright © 2025 CroCEE
DOI: https://doi.org/10.5592/CO/3CroCEE.2025.36

determine the shear deformations of the RC shear wall, the diagonal deformation is measured at the bottom storey of the wall according to Massone and Wallace [7]. The schematic diagram of the shear deformations at the wall base is presented in Fig. 2. Finally, based on Eq. (8) the original shear deformation is estimated.

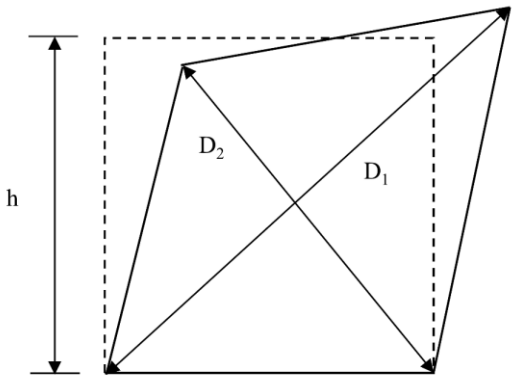


Figure 2. Estimation of shear deformation at the wall base.

$$\Delta_{S_original} = \frac{\sqrt{D_1^2-h^2}-\sqrt{D_2^2-h^2}}{2} \tag{8}$$

However, Massone and Wallace [7] have indicated that this method is erroneous if the center of rotation of the bottom story does not coincide with the geometric center of the storey height; hence the shear deformation is coupled with flexural deformation. In the present study, according to the suggestion of Massone and Wallace [7], the following correction is made in the measurement of shear deformation:

$$\Delta_{S_Corrected} = \Delta_{S_Original} + (0.5 - \alpha\theta h) \tag{9}$$

Where θ is storey level rotation, h is the storey height and α is the relative distance from the top of the first story to the centroid of the curvature distribution. In the current study, α is taken as 0.67 considering the triangular distribution of curvature [7]. Finally, to get the effective flexural stiffness (K_w), the effective stiffness of the wall (K_e) is reduced by taking into account the influence of the shear deformation such as:

$$K_w = \frac{K_e\Delta_f}{\Delta_f+\Delta_s} = P_f K_e \tag{10}$$

Considering the pure cantilever action, the following expression can be written:

$$I_w = P_f I_e \tag{11}$$

Where Δ_f and Δ_s are the flexural and shear deformation of the wall at first yield, respectively. P_f is the portion of flexure deformation in total deformation for the wall at first yield.

7. Numerical Modelling and Validation

In the current study, the numerical model i.e., a three-dimensional (3D) finite element (FE) model is developed for the parametric analysis in the general-purpose software suite ABAQUS 6.14 which is capable of solving both linear and nonlinear problems. Ni and Lu [8] investigated the seismic behavior of three T-shaped RC walls built with high-strength reinforcement using quasi-static reverse cyclic load. One of the T-shaped wall specimens designated as T-0.1 F in the study of Ni and Lu [8] has been considered in the current study for the verification of the accuracy of the FE model. The details of the crack pattern of the test specimen are also available in previous literature [8]. The aspect ratio (H/l_w) of the test specimen was 2 which qualifies the wall to be slender and exhibit flexural-dominant behavior.

Copyright © 2025 CroCEE
DOI: https://doi.org/10.5592/CO/3CroCEE.2025.36

The axial load ratio of the test specimen was 0.1 and the specimen was built with high-strength steel (HRB 600) except for boundary element stirrups (HRB 400). The average characteristic compressive strength of the concrete for the test specimen T-0.1 F was found to be 35 MPa.

The constitutive model of concrete is defined according to the isotropic concrete damage plasticity (CDP) model. The CDP parameters considered in the adopted FE model of the current study are specified in Table 1. According to past studies [9,10], the uniaxial compressive and tensile response of concrete is determined whereas the response of the rebar is taken according to the experimental results. The constitutive model of concrete and steel rebar is presented in Fig. 3.

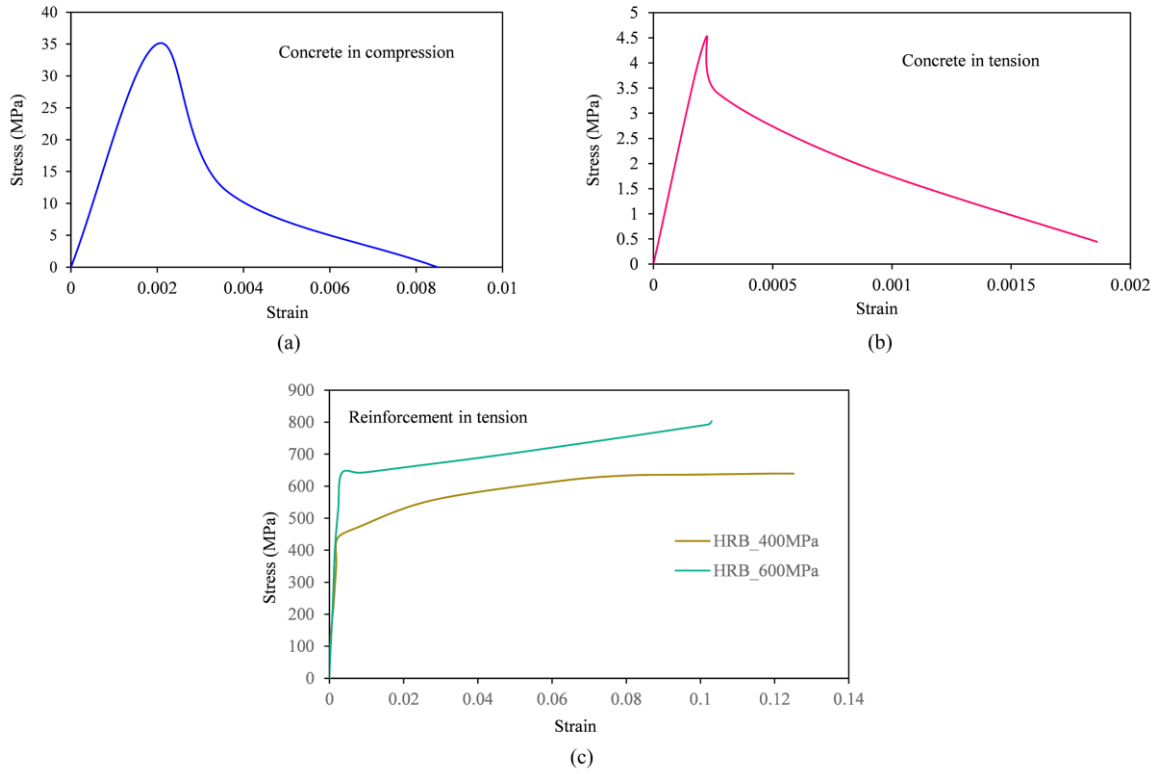


Figure 3. Stress-strain relationship for a) Concrete in uniaxial compression; b) Concrete in uniaxial tension; c) Steel reinforcement.

Concrete elements are modeled as eight-node solid linear brick elements having reduced integration with hourglass control (C3D8R) from ABAQUS/Standard element library. Reinforcement bars are modeled as wire features integrated with the two-node 3D linear truss element (T3D2). Reinforcement bars are considered to be embedded into concrete by using the embedded element constraints which ensures strain compatibility of reinforcement with adjacent concrete. Tie constraints are used in the interface of the loading beam and T-shaped RC wall which ensures no relative motion between them. Similarly, Tie constraints are also used in the interface of the T-shaped RC wall and the pedestal base. All degrees of freedom (DOFs) at the bottom of the pedestal base are considered to be restrained. In the current study, the rotational degrees of freedom (DOF) about the X-axis, the rotational DOF about the Y-axis, and the translational DOF about the Z-axis are made restrained which facilitates the avoidance of the web parallel out-of-plane bending of T-shaped RC wall and rotational movement of T-shaped RC shear walls about the vertical axis of the wall which mimics the actual experimental boundary condition. Fig. 4 shows the typical FE model of the T-shaped RC wall.

Table 1. CDP parameters considered for the material definition of concrete

ψ	e	σ_{b0}/σ_{c0}	K_c	μ
55°	0.1	1.16	0.667	0.01

Proceedings of the 3rd Croatian Conference on Earthquake Engineering - 3CroCEE
19–22 March 2025, Split, Croatia
Copyright © 2025 CroCEE
DOI: https://doi.org/10.5592/CO/3CroCEE.2025.36

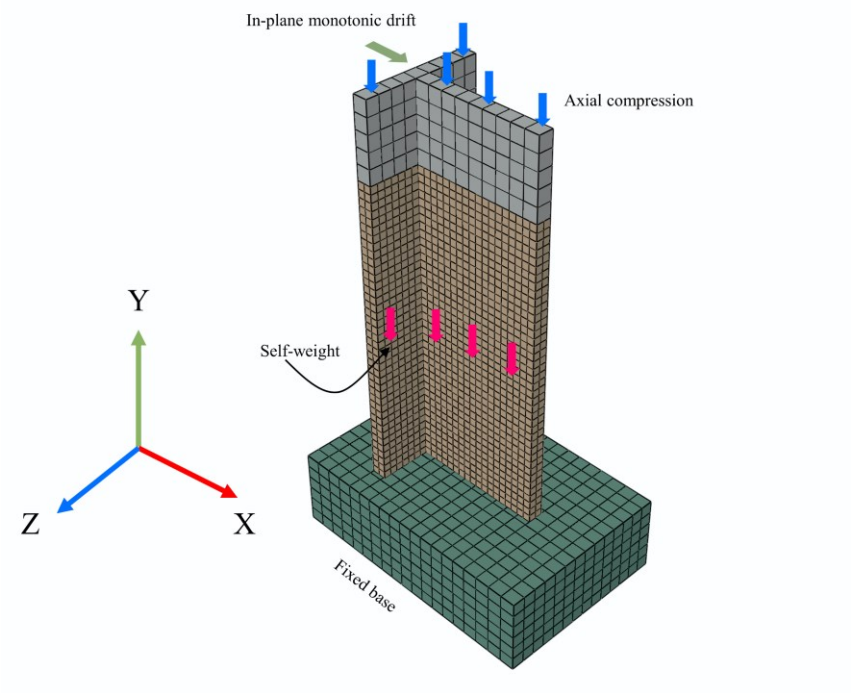


Figure 4. FE model of the T-shaped RC structural wall.

In the current study, the loading is applied in two phases. In the first phase, the self-weight and external axial load is applied and in the second phase, the monotonic load is given in a displacement-controlled manner at the reference point which kinematically couples all nodes of the loading beam. Although analysis involving reverse slow cyclic displacement is the best method to predict the response of the wall, nonetheless the current study adopts monotonic displacement due to time constraints. The monotonic load-drift relationship is compared with the backbone curve of the experimental load-drift relationship of T-0.1 F which is shown in Fig. 5a. Mesh-sensitivity analysis is also accomplished which is shown in Fig. 5b and based on the convergence, the optimum mesh size is decided as 50 mm.

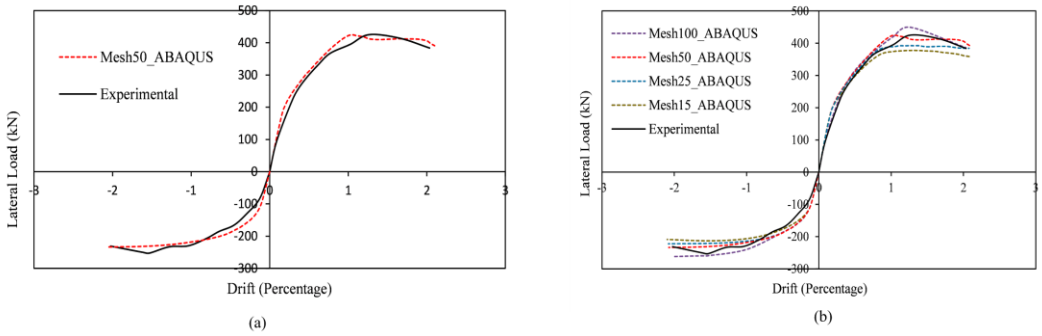


Figure 5. Lateral load-drift relationship for T-0.1 F: a) Numerical result vs. experimental result; b) Mesh sensitivity study

8. Parametric Study for Effective Stiffness

Based on the previous studies [1,3], the following parameters are found to be sensitive for estimating the effective stiffness such as axial load ratio (ALR), aspect ratio (H/l_w) of the wall, yield strength of longitudinal steel rebar (f_y), flange length (b_w). The range of these considered parameters are presented

Copyright © 2025 CroCEE
DOI: https://doi.org/10.5592/CO/3CroCEE.2025.36

in Table 2. It is worth mentioning here that unless otherwise specified, the parametric study with zero axial load ratio invariably means that only the self-weight of the structural wall is considered. In this study, the aspect ratio of the numerical L-shaped RC structural wall is taken as 2 which ensures flexure dominant failure mode. All the walls are considered to have characteristic cube compressive strength of 30 MPa. The percentage of longitudinal reinforcement in the web and flange is kept at 0.5% and the spacing between both longitudinal and transverse web rebar is kept at 150mm.

Table 2. Summary of the parameters considered

Aspect ratio	*Flange length (b_w) in meter*	*ALR*	*Yield strength (MPa)*
2,3,4	0.5,1,1.2,1.5,1.7,2.4,3.4,3.6,5.1	0,0.05,0.1,0.2	415,550

9. Results and Discussion

To determine the effective stiffness of L-shaped RC structural walls, the initial load-deformation responses of all the models are recorded. Using these responses, the effective stiffness of each numerical model is calculated based on the previously explained second method. Finally, the effective stiffness is adjusted by applying a reduction factor to account for the influence of shear deformation, as discussed in earlier sections.

9.1. Influence of Axial Load Ratio (ALR)

The influence of axial load ratio on the effective flexural stiffness ratio (K_w/K_g) of L-shaped RC structural walls is presented in Fig. 6a and Fig. 6b for web parallel flange-in-tension and flange-in-compression direction respectively.

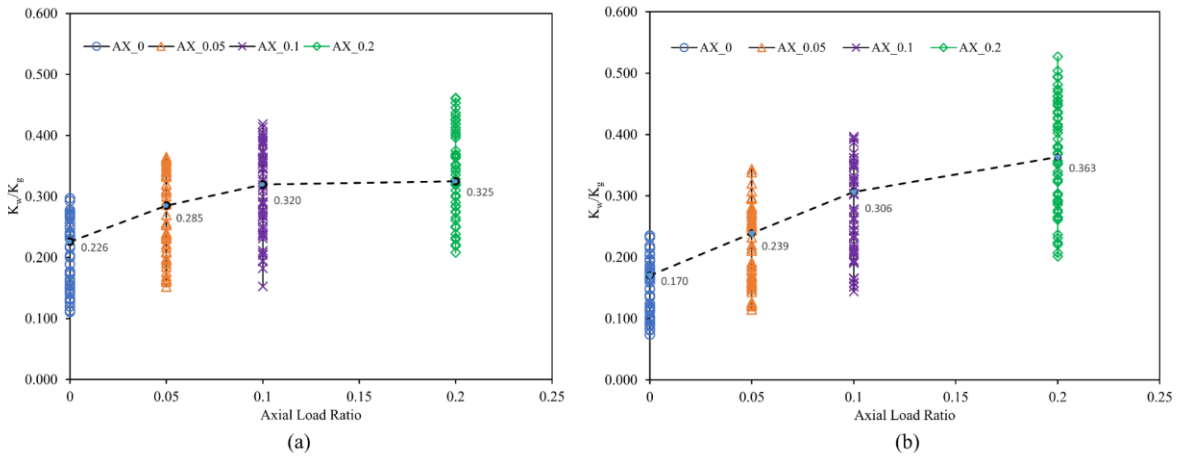


Figure 6. Influence of axial load ratio (ALR) on effective flexural stiffness ratio (K_w/K_g) for (a) Web parallel flange-in-tension; (b) Web parallel flange-in-compression

The results show that as the axial load ratio increases, the effective flexural stiffness ratio also rises. To provide better clarity, the average values corresponding to different axial loads are plotted. For web parallel flange-in-tension loading, an increase in the axial load ratio from 0.0 to 0.2 leads to a 43% rise in the effective flexural stiffness ratio. Although the yield drift increases with higher axial loads, the substantial gain in lateral strength of the RC structural walls ultimately results in an overall increase in the effective flexural stiffness ratio. Despite significant differences in the load-carrying capacity of the wall under web parallel flange-in-tension loading versus flange-in-compression loading, the effective stiffness ratio exhibits less variation. This is attributed to the earlier onset of yielding in the flange-in-compression direction, which leads to a lower yield drift compared to the web-parallel flange-in-tension direction.

Copyright © 2025 CroCEE
DOI: https://doi.org/10.5592/CO/3CroCEE.2025.36

9.2. Influence of Aspect Ratio (H/l_w)

The influence of aspect ratio on the effective flexural stiffness ratio (K_w/K_g) of L-shaped RC structural walls is illustrated in Fig. 7a and Fig. 7b for web parallel flange-in-tension and flange-in-compression direction respectively.

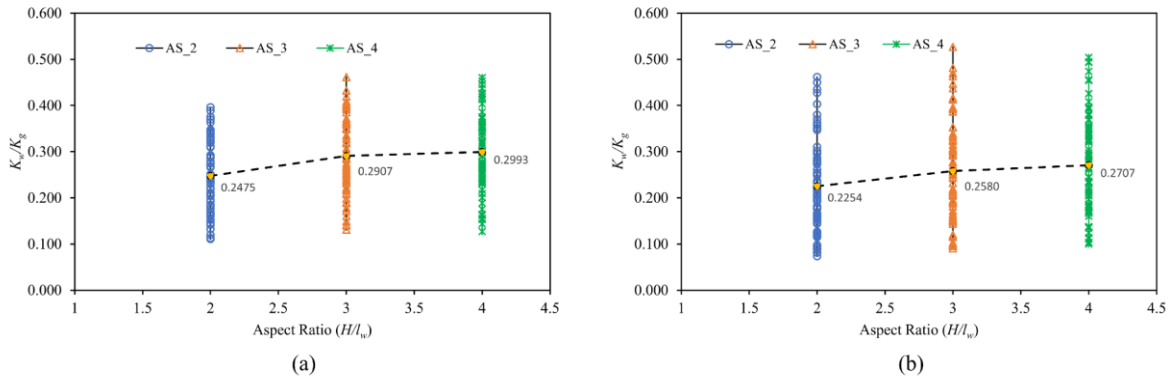


Figure 7. Influence of aspect ratio on effective flexural stiffness ratio (K_w/K_g) for (a) Web parallel flange-in-tension; (b) Web parallel flange-in-compression

From the results, it is quite clear that with an increase in aspect ratio, the effective flexural stiffness ratio (K_w/K_g) increases by 21% for web parallel flange-in-tension direction and by 20% for web parallel flange-in-compression direction. Generally, as the aspect ratio increases, the load-carrying capacity decreases, and the yield drift increases, reducing the effective stiffness ratio K_e/K_g. However, the overall K_w/K_g increases as shear deformation is significant for walls with lower aspect ratios, whereas shear deformation is negligible for walls with higher aspect ratios.

9.3. Influence of Yield Strength (f_y) of Longitudinal Rebar

The influence of the yield strength (FE 415 and FE 550) of vertical rebar on the effective flexural stiffness ratio (K_w/K_g) of L-shaped RC structural walls is shown in Fig. 8a and Fig. 8b for web parallel flange-in-tension and flange-in-compression direction respectively. From the results, it is observed that with an increase in yield strength of vertical rebar, the effective flexural stiffness ratio (K_w/K_g) decreases by about 34% for web parallel flange-in-tension and by about 37% for web parallel flange-in-compression direction. This is expected because with the increase in yield strength of vertical rebar, that load carrying capacity increases marginally but the yield drift increases significantly which finally results large reduction of the effective flexural stiffness ratio.

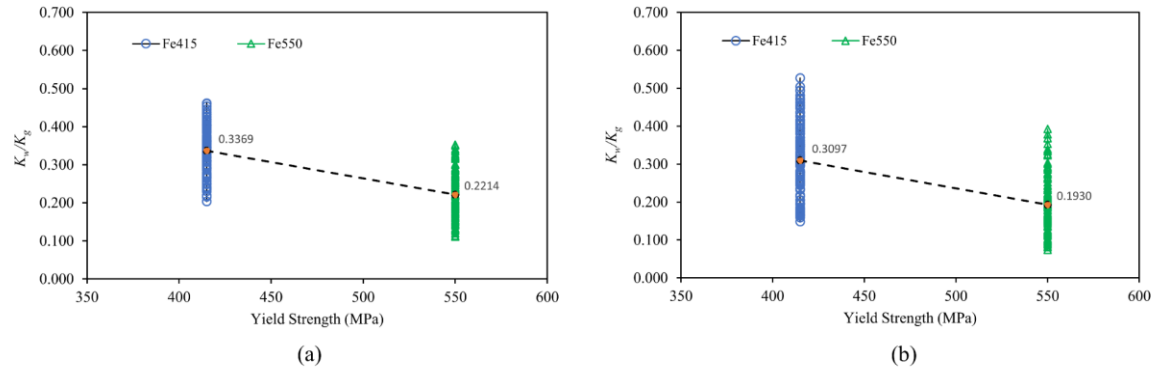


Figure 8. Influence of yield strength (f_y) of longitudinal rebar on effective flexural stiffness ratio (K_w/K_g) for (a) Web parallel flange-in-tension; (b) Web parallel flange-in-compression

Copyright © 2025 CroCEE
DOI: https://doi.org/10.5592/CO/3CroCEE.2025.36

9.4. Influence of Flange length (b_w)

In this study, for all numerical models, there are three types of flange lengths such as (a) flange length equals one-third of wall length, (b) flange length equals two-thirds of wall length, and (c) flange length equals wall length. The influence of flange length on the effective flexural stiffness ratio is presented in Fig. 9a and Fig. 9b for web parallel flange-in-tension and flange-in-compression direction respectively.

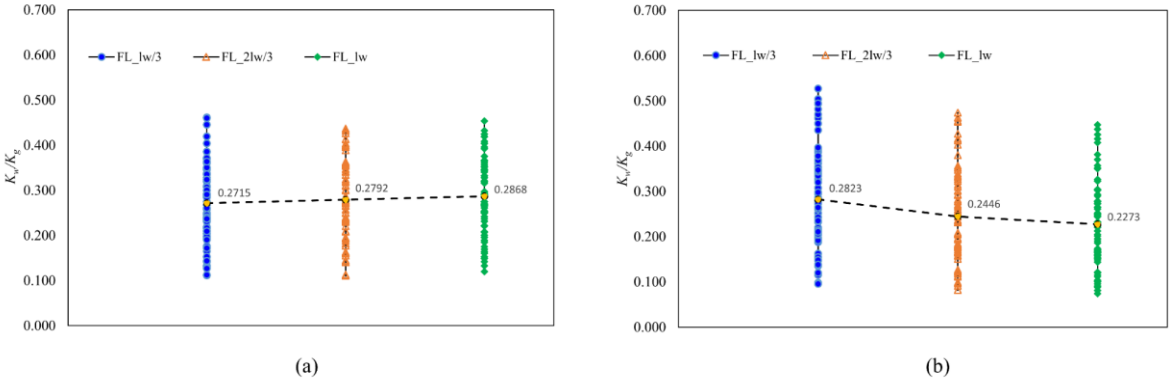


Figure 9. Influence of flange length on effective flexural stiffness ratio (K_w/K_g) for (a) Web parallel flange-in-tension; (b) Web parallel flange-in-compression

For the L-shaped walls web parallel flange-in-tension direction, increasing the flange length from $l_w/3$ (33.3% of the wall length) to l_w (100% of the wall length) does not have a distinct effect on the K_w/K_g ratios. The average value slightly changed from 0.2715 to 0.2868 which indicates a marginal increase in K_w/K_g ratios for any value of flange length in the case of flange-in-tension direction loading. For the web parallel flange-in-compression direction, the average K_w/K_g ratios exhibit a significant decline, dropping from 0.282 to 0.227, corresponding to an approximate 19% reduction. The increase of the flange length increases the gross stiffness (K_g) of the wall section. On the other hand, the K_w of the wall section does not increase proportionally, and the K_w/K_g ratios of the investigated models generally reduce with an increase in the flange length which is evident for the web parallel flange-in-compression direction loading. In the case of web parallel flange-in-tension direction loading, there is a marginal increase of K_w/K_g is observed because the longer flange can be less effective due to the shear lag effect.

9.5. Proposed Empirical Equation of Effective Flexural Stiffness Ratio

Based on the parametric study, the empirical equations for evaluation of the effective stiffness of L-shaped RC structural walls are proposed for different directions of loading with the aid of multiple linear regression following a similar form of equation proposed by Paulay and Priestley [3].

For L-shaped RC structural walls web parallel flange-in-tension direction

$$\frac{K_e}{K_g} = 0.8\frac{P_u}{f_c' A_g} + \frac{123}{f_y} \tag{12}$$

For L-shaped RC structural walls web parallel flange-in-compression direction

$$\frac{K_e}{K_g} = 1.21\frac{P_u}{f_c' A_g} + \frac{98}{f_y} \tag{13}$$

Finally, for considering the shear deformation in L-shaped RC structural walls Eq. (13), and Eq. (14) are prescribed. The reduction factors are derived from the empirical relationships of the portions of the flexure deformations with the wall height and the wall length from the FE results.

For L-shaped RC structural walls for web parallel flange-in-tension direction

Copyright © 2025 CroCEE
DOI: https://doi.org/10.5592/CO/3CroCEE.2025.36

$$P_f = \frac{1}{1.2+\frac{22I_e}{H^2 b_w l_w}} \tag{14}$$

For L-shaped RC structural walls for web parallel flange-in-compression direction

$$P_f = \frac{1}{1.2+\frac{15I_e}{H^2 b_w l_w}} \tag{15}$$

Finally, the effective flexural stiffness ratio of L-shaped RC structural walls is determined as:

$$\frac{K_w}{K_g} = P_f \frac{K_e}{K_g} \tag{16}$$

Finally, the FE model-derived K_w/K_g is compared with the results obtained from the proposed formulae which are shown in Fig. 10. As the figure illustrates, the proposed empirical expression can predict the effective flexural stiffness ratio of these models quite accurately. The mean value and coefficient of variation (COV) for the predicted K_w/K_g ratio over the FE-derived K_w/K_g ratio are 1.12 and 0.199 respectively. The results suggest that the predictions are reasonably consistent and fairly reliable with some scatter.

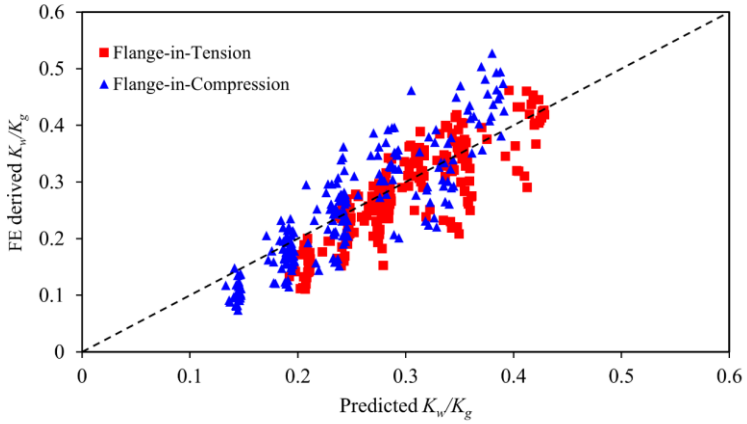


Figure 10. Comparison between Predicted K_w/K_g and FE-derived K_w/K_g

10. Conclusion

The effective flexural stiffness of flanged RC structural walls, as examined in this study, has received limited attention. To address this gap, empirical expressions have been proposed for estimating the effective flexural stiffness of L-shaped RC structural walls frequently used at building layout corners. The major conclusions of the current study can be summarised as:

- The flange in L-shaped RC walls significantly increases the effective stiffness of the wall. The K_w/K_g ratios of L-shaped RC walls are in general higher than those of the rectangular RC walls for the same parameters.
- For the investigated models of L-shaped walls, the average K_w/K_g ratio for the web parallel flange-in-tension direction is higher than that of the flange-in-compression direction.
- An increase in the axial load ratio leads to a rise in the K_w/K_g ratio, while a higher aspect ratio also results in a marginal increase in the K_w/K_g ratio.
- The length of the flange of the L-shaped RC walls reduces the K_w/K_g ratio for web parallel flange-in-compression direction whereas for web parallel flange-in-tension direction the variation of K_w/K_g ratio is insignificant.
- An increase in reinforcement grade of longitudinal reinforcement significantly reduces the K_w/K_g ratio.

Copyright © 2025 CroCEE
DOI: https://doi.org/10.5592/CO/3CroCEE.2025.36

- Empirical equations of effective flexural stiffness ratio are proposed by taking into account the shear deformation which will help practical designers to quickly estimate the effective flexural stiffness of L-shaped RC structural walls.

Acknowledgments

The support and resources provided by the Department of Civil Engineering; Indian Institute of Technology, Guwahati are gratefully acknowledged by the authors.

References

[1] Zhang, Z., Li, B. (2018): Effective Stiffness of Non-Rectangular Reinforced Concrete Structural Walls. *Journal of Earthquake Engineering*, **22**(3), 382-403, doi: https://doi.org/10.1080/13632469.2016.1224744

[2] Fenwick, R. and Bull, D. (2000): What is the stiffness of reinforced concrete walls, *SESOC Journal* **13**(2), 23–32.

[3] Paulay, T. and Priestley, M. J. N. (1992): *Seismic Design of Concrete and Masonry Structures*, John Wiley and Sons, New York.

[4] Thomsen, J., Wallace, W (1995): Displacement based design of reinforced concrete structural walls: An experimental investigation of walls with rectangular and T-shaped cross-sections, *Report No.CU/CEE-95-06*, Civil and environmental engineering, Clarkson university

[5] Beyer, K., Dazio, A., Priestley, M. J. N. (2008): Quasi-static cyclic tests of two U-shaped reinforced concrete walls. Journal of earthquake engineering, 12(7), 1023-1053, doi: https://doi.org/10.1080/13632460802003272

[6] Brueggen (2009): Performance of T-shaped Reinforced Concrete Structural Walls under Multi-Directional Loading, *Dissertation*, University of Minnesota

[7] Massone, M., Wallace, W (2004): Load-Deformation Responses of Slender Reinforced Concrete Walls, *ACI Structural Journal*,101-S12, doi: doi:10.1016/j.engstruct.2017.02.050

[8] Ni, X., Lu, N. (2022): Cyclic tests on T-shaped concrete walls built with high-strength reinforcement. *Journal of Earthquake Engineering*, **26**(11), 5721-5746, doi: https://doi.org/10.1080/13632469.2021.1884626

[9] Karthik, M. M., Mander, J. B. (2011): Stress-block parameters for unconfined and confined concrete based on a unified stress-strain model. *Journal of Structural Engineering*, **137**(2), 270-273, doi: https://doi.org/10.1061/(ASCE)ST.1943-541X.0000294

[10] Wahalathantri, B., Thambiratnam, D., Chan, T., Fawzia, S. (2011): A material model for flexural crack simulation in reinforced concrete elements using ABAQUS, *In Proceedings of the first international conference on engineering, designing and developing the built environment for sustainable wellbeing* (pp. 260-264), Queensland University of Technology.

Proceedings of the 3rd Croatian Conference on Earthquake Engineering - 3CroCEE
19–22 March 2025, Split, Croatia
Copyright © 2025 CroCEE
DOI: https://doi.org/10.5592/CO/3CroCEE.2025.39

INFLUENCE OF KINEMATIC SOIL – STRUCTURE INTERACTION ON THE SEISMIC BEHAVIOUR OF REINFORCED – CONCRETE FRAME BUILDINGS

Nikola Petrov [(1)], Julijana Bojadjieva [(2)], Jordan Bojadjiev [(3)]

[(1)] *PhD Candidate, Institute of Earthquake Engineering and Engineering Seismology, N. Macedonia, petrovnikola93@gmail.com*
[(2)] *Assoc. Prof. Dr., Institute of Earthquake Engineering and Engineering Seismology, N. Macedonia, jule@iziis.ukim.edu.mk*
[(3)] *Assis. Prof. Dr., International Balkan University, N. Macedonia, bojadziev@gmail.com*

Abstract

In earthquake-prone areas, soil–structure interaction (SSI) may play a key role in ensuring structural safety. This study investigates the effects of SSI on the seismic response of a six-storey reinforced concrete (RC) frame building, using guidelines from American codes and Eurocode 8 for soil types B and C. The analysis compares the building's behavior under various soil conditions and foundation embedment configurations. To accurately assess these effects, four models were analyzed: a fixed base model, a flexible base model, a model incorporating soil conditions beneath the foundation and on the basement walls to simulate the effects of embedment, and a model with reduced spectral acceleration due to the kinematic SSI effects. A linear-elastic analysis was conducted for all models to evaluate the structural response in terms of base shear forces, storey moments, storey displacements, and inter-storey drifts. The results show that SSI lengthens the period of the structure, which affects the values of the base shear forces. SSI generally reduces the base shear forces, but in case of very stiff structures it may increase its values. In any case, the inclusion of SSI leads to an increase in storey displacements and inter-storey drifts, particularly in models with flexible foundations and embedded basements, due to the release of rotations on the foundation level. The model with reduced spectral acceleration due to kinematic SSI effects demonstrated how the kinematic soil – structure interaction effects influence the overall seismic response of the structure. These findings highlight the importance of accounting for SSI in the structural design of buildings located in seismic regions, as neglecting these interaction can lead to an underestimation of critical design parameters such as shear forces, moments, and displacements. Incorporating SSI effects ensures more accurate seismic performance predictions and enhances the resilience of structures in earthquake-prone areas.

Keywords: soil-structure interaction, kinematic interaction, period lengthening, linear analysis, embedding

1. Introduction

With the development of earthquake engineering, the need for design of structures that can safely withstand even the strongest earthquakes by suffering damages, but avoiding complete collapse, has been increased. Each building exposed to earthquake forces responds appropriately based on its structural characteristics. Recent researches and experts in structural and geotechnical engineering [1] indicate that the response of structures to seismic events depends not only on the structural system, but also on the interaction among three interconnected systems, namely:

- Structure;
- Foundation; and,
- Surrounding soil.

This relationship is known as 'soil-structure interaction' in literature and deals with the overall response of the complex system to an earthquake [2]. In Eurocode 8 - Part 5, in Chapter 6 and Appendix D [3], essential information is provided regarding the role of the 'soil-structure interaction' phenomenon in structures. It outlines which types of structures and soils are significantly influenced by this interaction, as well as the impact it has on their inherent periods and mode shapes. However, particular attention is

Proceedings of the 3rd Croatian Conference on Earthquake Engineering - 3CroCEE
19–22 March 2025, Split, Croatia
Copyright © 2025 CroCEE
DOI: https://doi.org/10.5592/CO/3CroCEE.2025.39

not paid to the influence of the foundation type and embedment depth of the structure. The same applies to most of the codes, as many researches [4] in this field have stated it.

Unlike Eurocode 8, American researches and pre-code guidelines delve deeper into this issue. The NIST guidelines titled 'Soil-Structure Interaction for Building Structures' [5], as well as FEMA P-2019 – 'Practical Guide for Soil-Structure Interaction' [6], provide comprehensive guidelines for incorporating soil conditions into analyses and understanding their impact on the structural response. Among other things, Eurocode 8 - Part 5 emphasizes that noticeable soil-structure interaction occurs when structures are founded in exceptionally poor soils with shear wave velocities $v_s \leq 100$ m/s. As to the American researches and regulations, the fundamental preliminary condition for assessing the magnitude of soil-structure interaction effects is expressed as:

$$\frac{h'}{v_s \cdot T} \tag{1}$$

Where, h' - effective height of the structure; v_s - shear wave velocity; T - natural period of oscillation.

Values greater than 0.1 [6] indicate the potential for significant influence of the soil-structure interaction on the response of a structure.

Hence, it can be concluded that the contribution of the soil-structure interaction to the structural response depends not only on the soil type, but also on the height of the structure and its natural period of vibration.

This study explores seismic structural responses of a RC frame structures set on Type B and C soils per Eurocode 8, focusing on soil-structure interaction effects. The analysis examines the influence of embedment depth and foundation type on structural behavior. Linear analysis and modal response spectrum methods were used to calculate seismic forces, assessing story displacements, inter-story drifts, moments, and shear forces. The results emphasize the importance of considering soil conditions and kinematic interactions to enhance design accuracy and prevent potential issues in structural performance.

2. Analysis methods

According to the literature [6], two fundamental methods are commonly employed for modelling the interconnection of a structure, foundation, and soil:

- the substructure approach, and
- the direct approach.

In the substructure method, the soil is represented by springs [6], with their stiffness properties calculated to simulate the behaviour of the soil under the foundation. Springs are typically placed at the foundation base (oriented normally) to prevent horizontal translation. For embedded structures, horizontal springs (oriented normally to basement walls) illustrate the horizontal translation of the foundation relative to the soil.

Conversely, the direct analysis method employs finite elements [7] to model both the structure and the soil, extending the soil medium around and beneath the structure to replicate real conditions with greater precision. While the substructure method is widely used in practice, the direct approach is reserved for critical structures like nuclear power plants and major infrastructure [8].

In this paper, two analyses were performed. A modal analysis with 12 mode shapes provided natural periods and mode shapes, followed by a linear-elastic spectral analysis to calculate seismic forces, moments, and deformations. The substructure approach was adopted to account for SSI effects.

3. Soil – Structure interaction effects

The effective ground displacement applied at the ends of the springs, which simulate soil conditions, differs from the actual displacement adjacent to the foundation. This discrepancy arises due to the

Proceedings of the 3rd Croatian Conference on Earthquake Engineering - 3CroCEE
19–22 March 2025, Split, Croatia
Copyright © 2025 CroCEE
DOI: https://doi.org/10.5592/CO/3CroCEE.2025.39

influence of the structure and deformations occurring in the springs (representing the soil medium) [9]. As these deformations increase, a portion of the energy dissipates, which is attributed to soil-structure interaction (SSI) effects, specifically kinematic and inertial interactions.

Kinematic interaction primarily involves:

- Base slab averaging effects, and;
- Embedment effects.

Base slab averaging effects occur because of the incoherent propagation of seismic waves across the foundation's surface. Embedment effects, observed in embedded structures, reduce excitation at the foundation level due to the decreasing ground motion with depth below the surface.

Inertial interaction, on the other hand, is a dynamic interaction involving the structure, foundation, and soil. Its effects include:

- Period lengthening, caused by increased foundation flexibility;
- Foundation damping, which consists of:
    - Radial damping, from seismic wave propagation, and;
    - Soil damping, similar to viscous damping in structures [5].

SSI effects are especially significant for structures with large foundation systems, embedded structures, or those with high stiffness relative to the soil. These effects influence seismic force magnitudes and structural behavior during earthquakes.

3.1. Kinematic soil-structure interaction effects

3.1.1. Base slab averaging

Base slab averaging is the first kinematic interaction effect between the soil and the structure. This phenomenon depends exclusively on the structure and the geometry of the foundation. The reduction in spectral acceleration occurs due to the incoherence of ground motions beneath the foundation. This incoherence can result from differences in the time intervals at which seismic waves reach various points of the foundation, as well as variations in wave characteristics due to non-uniform soil conditions. As a result, one side of the structure may move in one direction while the opposite side moves in another, resisting deformation and leading to overall smaller deformations.

American guidelines provide equations to calculate the reduction coefficient for spectral acceleration under this effect. The coefficient depends on the foundation's surface area A_{base} and the average seismic wave propagation velocity v_s in the effective soil profile. The effective side length of the foundation is determined as $b_e = \sqrt{A_{base}}$ [10], with a maximum limit of 80 m [6], based on studies of real structures with effective dimensions up to 80 m.

The next step is to calculate the coefficient b_0:

$$b_0 = 0.0023\left(\frac{b_e}{T}\right) \tag{2}$$

The minimum value for T (natural period of oscilation) is prescribed to be not less than 0.2 [6].

Following b_0, the next for calculation is the coefficient B_{bsa}:

$$B_{bsa} = 1 + b_0^2 + b_0^4 + \frac{b_0^6}{2} + \frac{b_0^8}{4} + \frac{b_0^{10}}{12} \text{ for } b_0 \leq 1 \tag{3.1}$$

$$B_{bsa} = \exp\left(2 \cdot b_0^2\right)\left[\frac{1}{\sqrt{\pi \cdot b_0}}\left(1 - \frac{1}{16 \cdot b_0^2}\right)\right] \text{ for } \; b_0 > 1 \tag{3.2}$$

The values of the reduction coefficient for this kinematic effect of SSI are then calculated for each period value of the spectrum according to the following expression:

Copyright © 2025 CroCEE
DOI: https://doi.org/10.5592/CO/3CroCEE.2025.39

$$RRS_{bsa} = 0.25 + 0.75\left\{\frac{1}{b_0^2}\left[1 - \left(exp\left(-2 \cdot b_0^2\right)\right) \cdot B_{bsa}\right]\right\} \quad (4)$$

The value of this coefficient is limited to 0.7 in order to ensure safety [6].

3.1.2. Embedment effects

Embedment effects reduce spectral acceleration, similar to base slab averaging. Deeper embedding results in greater reduction due to kinematic interaction, as seismic wave amplitudes decrease with foundation depth [11]. This diminishes ground motion intensity at the foundation, reducing seismic forces on the structure. The spectrum reduction coefficient is calculated using foundation depth „*e*“ and the average shear wave velocity v_s in the effective soil profile.

$$RRS_e = 0.25 + 0.75 \cdot \cos\left(\frac{2\pi e}{T v_s}\right) \quad (5)$$

where,

- e is the foundation depth, and its value is limited to 6 meters. A condition is set that a minimum of 75% of the foundation structure should be at the level considered for embedding. For structures on a sloping terrain, a less shallow depth is taken as a foundation depth.

- v_s is the average effective shear wave velocity in a given soil medium, in the layers where embedding is performed, and its value should not be less than 200 m/s.

- T is the period of natural vibration of the spectrum being analyzed, and its minimum value is constrained to 0.2 s.

As for the first kinematic effect of soil – structure interaction, the value of this coefficient is also limited to 0.7 in order to ensure safety [6].

3.2.Inertial soil – structure interaction effects

3.2.1. Period lengthening

When a structure has significantly greater stiffness compared to the soil, rotations and translations of the foundation are "released," resulting in additional displacements. This process simultaneously increases the natural period of the system [12]. The increase in the natural period has a direct impact on the spectral acceleration used to calculate the design seismic force. Depending on the location of the fixed-base model's natural period within the response spectrum, incorporating soil conditions and lengthening the period can either increase or decrease the spectral acceleration [5], as illustrated in Figure 1. However, regardless of whether the spectral acceleration increases or decreases, period lengthening due to soil conditions consistently leads to higher spectral displacements.

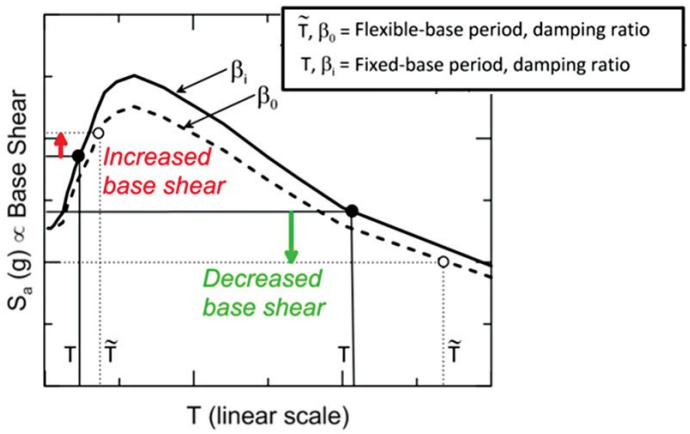


Figure 1. Example of acceleration and displacement spectra.

Copyright © 2025 CroCEE
DOI: https://doi.org/10.5592/CO/3CroCEE.2025.39

4. Calculation of springs' stiffness

Vertical spring elements contribute to the vertical stiffness of the foundations, affecting the rotation of the system around its base. The rotation of the system around its base causes greater deformations when the system is subjected to horizontal (seismic) loads. There are three methods for calculating the stiffness characteristics of these spring elements [5], depending on the purpose and the type of analysis to be performed, and these are:

- Method 1 - Rigid foundation and flexible soil;
- Method 2 - Flexible foundation and nonlinear flexible soil; and,
- Method 3 – Flexible foundation and linear flexible soil.

For the purposes of this project, the stiffness characteristics of the spring elements were calculated using Method 1, and their values were then modified because, in the mathematical model, they were introduced as uniformly distributed spring elements under the entire foundation slab. Figure 2 illustrates the various methods used to calculate the stiffness characteristics of vertical spring elements.

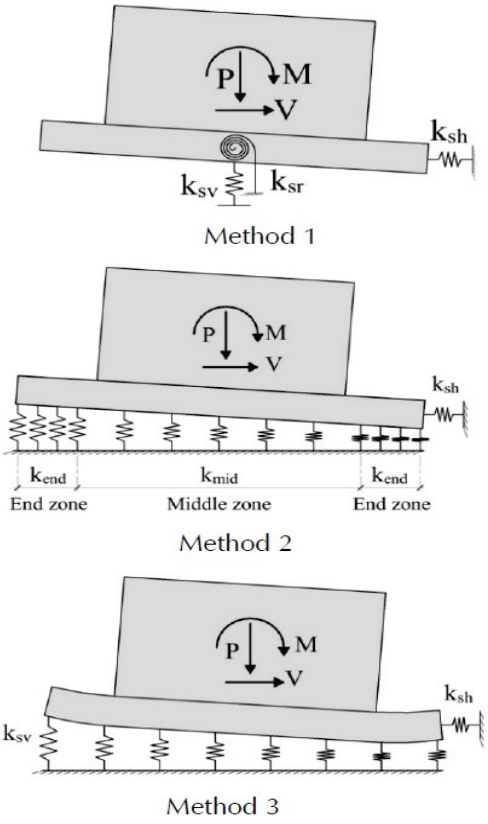


Figure 2. Three methods for foundation modeling approaches with vertical and rotational springs presented in ASCE/SEI 41 from FEMA (2018).

In ASCE/SEI 41-17 [9], equations are provided for calculating the stiffness characteristics of vertical spring elements for six degrees-of-freedom. The stiffness characteristics of the spring elements applied in the model studied in this paper were calculated according to the following expressions (Pais and Kussel, 1998) [5][13].

$$K_{z,sur} = \frac{G \cdot B}{1-v}\left[3.1\left(\frac{L}{B}\right)^{0.75} + 1.6\right] \quad (6.1)$$

$$K_{y,sur} = \frac{G \cdot B}{2-v}\left[6.8\left(\frac{L}{B}\right)^{0.65} + 0.8\left(\frac{L}{B}\right) + 1.6\right] \quad (6.2)$$

$$K_{x,sur} = \frac{G \cdot B}{2-v}\left[6.8\left(\frac{L}{B}\right)^{0.65} + 2.4\right] \quad (6.3)$$

$$K_{zz,sur} = G \cdot B^3\left[4.25\left(\frac{L}{B}\right)^{2.45} + 4.06\right] \quad (6.4)$$

$$K_{xx,sur} = \frac{G \cdot B^3}{1-v}\left[3.2\left(\frac{L}{B}\right) + 0.8\right] \quad (6.5)$$

$$K_{yy,sur} = \frac{G \cdot B^3}{1-v}\left[3.73\left(\frac{L}{B}\right)^{2.4} + 0.27\right] \quad (6.6)$$

Where $K_{z,sur}$, $K_{y,sur}$ and $K_{x,sur}$ represent the translational stiffness of the spring elements, and $K_{zz,sur}$, $K_{yy,sur}$ and $K_{xx,sur}$ represent the rotational stiffness about the respective axes. B and L in the expressions refer to half the values of the width and length of the foundation. The same authors (Pais and Kussel, 1998) [5][13] have provided expressions for calculating correction coefficients, which serve to increase

Copyright © 2025 CroCEE
DOI: https://doi.org/10.5592/CO/3CroCEE.2025.39

the stiffness of the spring elements due to the embedding of the structures [14]. They are calculated using the following expressions [5][13]:

$$\acute{\eta}_z = \left[1.0 + \left(0.25 + \frac{0.25}{\frac{L}{B}}\right)\left(\frac{D}{B}\right)^{0.8}\right] \quad (7.1)$$

$$\acute{\eta}_y \approx \acute{\eta}_x = \left[1.0 + \left(0.33 + \frac{1.34}{1 + \frac{L}{B}}\right)\left(\frac{D}{B}\right)^{0.8}\right] \quad (7.2)$$

$$\acute{\eta}_{zz} = \left[1.0 + \left(1.3 + \frac{1.32}{\frac{L}{B}}\right)\left(\frac{D}{B}\right)^{0.9}\right] \quad (7.3)$$

$$\acute{\eta}_{yy} = \left[1.0 + \frac{D}{B} + \left(\frac{1.6}{0.35 + \frac{L}{B}^4}\right)\left(\frac{D}{B}\right)^2\right] \quad (7.4)$$

$$\acute{\eta}_{xx} = \left[1.0 + \frac{D}{B} + \left(\frac{1.6}{0.35 + \frac{L}{B}}\right)\left(\frac{D}{B}\right)^2\right] \quad (7.5)$$

where $\acute{\eta}_z$, $\acute{\eta}_y$ and $\acute{\eta}_x$ are correction coefficients for translational stiffness calculated according to the aforementioned expressions, while $\acute{\eta}_{zz}$, $\acute{\eta}_{yy}$ and $\acute{\eta}_{xx}$ are correction coefficients for rotational stiffness.

5. Case study

The structure analyzed in this project, shown in Figure 3 (left), is a reinforced - concrete frame building with a basement, ground floor, and four upper floors (B+GF+4). This structural system was selected for analysis as it represents the most commonly used building type in the area of interest. The building dimensions are 27.00 m x 26.00 m at the basement and ground floor levels and 17.00 m x 16.00 m at the upper floors. Each floor has a height of 3 m, and the layout is symmetric with respect to the X and Y axes. Spans in the X direction are 5m–6m–5m–6m–5m, while in the Y direction, spans are 5m–6m–4m–6m–5m.

Columns are sized at 50 x 50 cm, except in the central part of the structure where they are 60 x 60 cm. Beams are dimensioned 35 x 50 cm, and slabs are 16 cm thick. The basement, fully embedded in the ground, includes perimeter reinforced concrete walls 20 cm thick. The foundation consists of a reinforced concrete slab 80 cm thick. Dimensions were calculated following PBAB '87 [15] and PIOVS '81 [16], which have been the primary regulations for decades. These norms were used to define the cross-sections of the structural elements, as all buildings designed in our country in the past decades adhere to these regulations. In recent years, there has been a transition towards the use of the Eurocodes. During this, parallel use of PBAB '87 and PIOVS '81 and the Eurocodes is permitted.

Linear analysis was performed using CSI ETABS 20. Seismic force calculations were based on spectral analysis in accordance with Eurocode 8 [17], employing Spectrum Type 1 for soil types B and C, with A_g=0.24g and a behaviour factor q=3.9. The chosen A_g value represents the seismic hazard of the area of interest.

For the purposes of the study, different variants (Figure 3 (right)) of the described model were considered:

- Model 1: Fixed base;
- Model 2: Foundation with vertical springs;
- Model 3: Foundation with vertical and horizontal springs; and,
- Model 4: Model 3 with a reduced spectrum accounting for kinematic interaction effects.

Further on, to each model, /B or /C label was added, referring to which soil type the model was analysed for. In this way two sub-models were generated for each model, resulting in models 1/B through 4/C.

Copyright © 2025 CroCEE
DOI: https://doi.org/10.5592/CO/3CroCEE.2025.39

Model 1/B, Model 2/B, Model 3/B and Model 4/B analysed for Soil type B, and Model 1/C Model 2/C, Model 3/C and Model 4/C analysed for Soil type C.

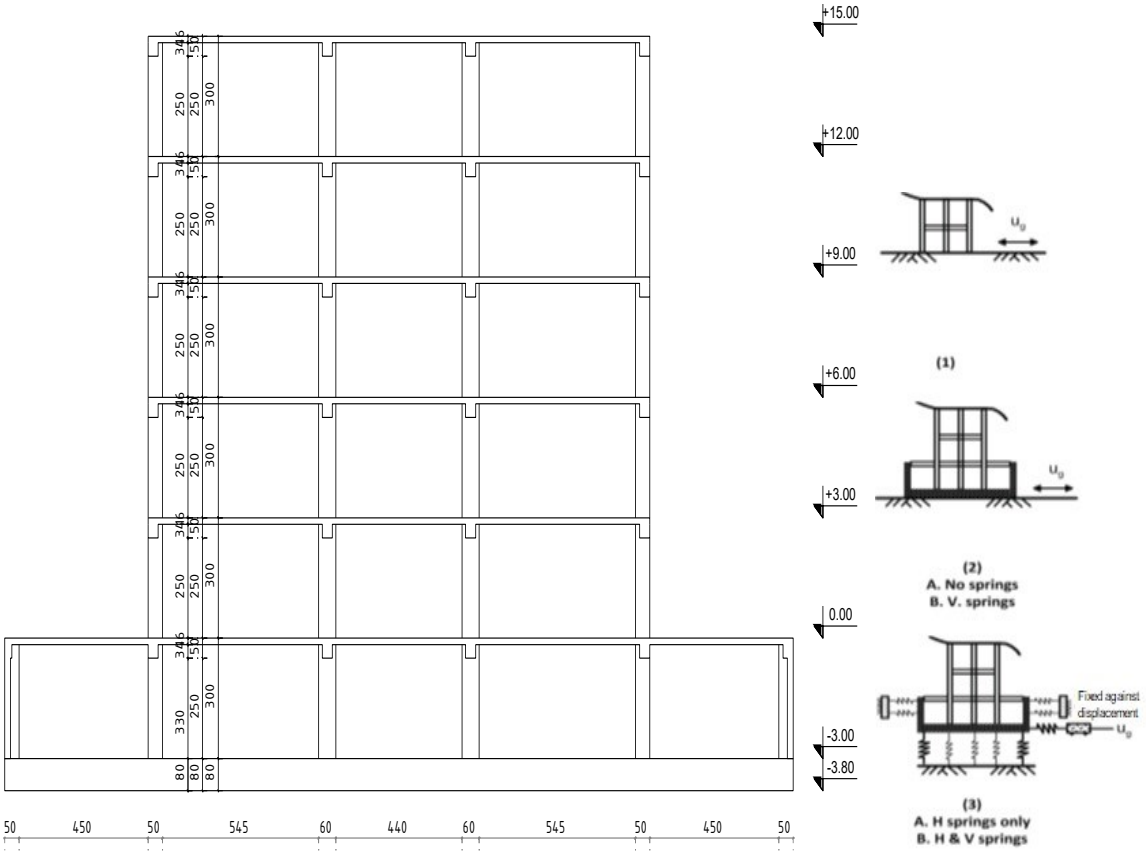


Figure 3. Elevation view of the case study structure (left) and model variants: Model 1 (1), Model 2 (2), Model 3 and Model 4 (3) (right).

6. Calculation of the springs' stiffness characteristics

According to the provided equations for calculating the stiffness characteristics of the spring elements for all three translations and rotations, as well as the equations for calculating the coefficients due to embedding of structures, calculations were performed for soil types B and C [17][18][19] according to Eurocode 8.

6.1. Soil type B

For soil type B, soil with the following characteristics was theoretically considered:

$V_s = 400\ m/s$ and $G = 70000\ kN/m^2$. The embedding depth was e=3.00m.

Based on the specified input parameters, calculation of the spring characteristics as well as the correction factor for the effects of embedment was performed. The values are presented in Table 1.

6.2.Soil type C

The same calculations were carried out for soil type C with the following characteristics:

$V_s = 250\ m/s$ and $G = 14000\ kN/m^2$. The embedding depth was e=3.00m.

Based on the specified input parameters, calculation of the spring characteristics as well as the correction factor for the effects of embedment was performed. The values are presented in Table 1.

Copyright © 2025 CroCEE
DOI: https://doi.org/10.5592/CO/3CroCEE.2025.39

Table 1. Springs' stiffness and correction coefficients – Soil type B and Soil type C

Pais and Kussel (1988)	Soil type B		Soil type C	
	Spring stiffness	Correction coefficient due to embedding	Spring stiffness	Correction coefficient due to embedding
Degree of freedom	$\frac{kN}{m}$ / $\frac{kN/m}{rad}$		$\frac{kN}{m}$ / $\frac{kN/m}{rad}$	
Translation in z direction	6225700	1.32	1245140	1.32
Translation in y direction	5031574	1.53	1006315	1.53
Translation in x direction	5015104	1.53	1003021	1.53
Rotation around z axis	1341312106	2.64	268262421	2.64
Rotation around y axis	956491364	1.29	191298273	1.29
Rotation around x axis	905840000	1.29	181168000	1.29

7. Coefficients for spectral reduction

7.1. Base slab averaging

Using the expressions provided in 3.1.1, all the parameters necessary to determine the values of the spectrum reduction coefficient due to the first kinematic effect, base slab averaging, were calculated. The values were computed for each period (T) of the corresponding spectrum, adhering to the condition that the minimum value of the period should be taken as 0.20s. The calculated values are graphically shown in Figure 4, where it can be observed that the contribution to the spectrum reduction by the base slab averaging effect slightly occurs in structures with low periods of natural vibration. However, it should be noted that these coefficient values are related to the foundation with dimensions and geometry according to the analyzed case study.

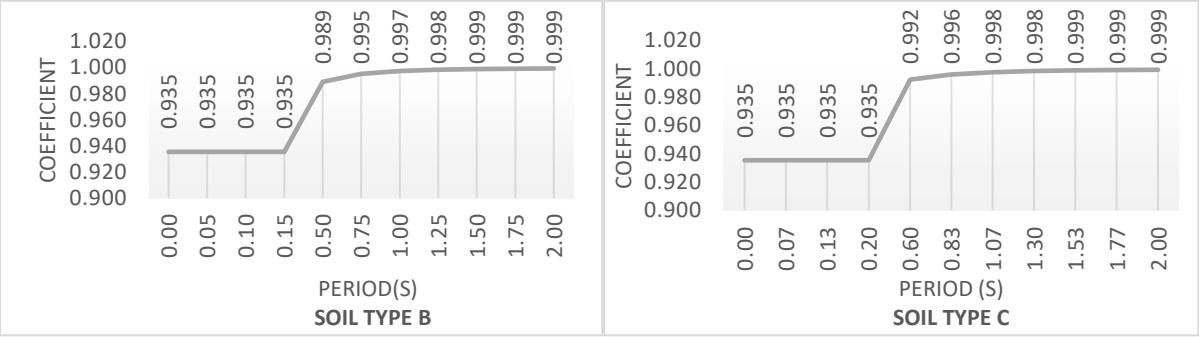


Figure 4. Spectrum reduction coefficient – Base slab averaging – Soil type B (left) and Soil type C (right)

7.2. Embedment effect

In a similar manner, based on the expressions provided in 3.1.2, calculations were performed, and the values of the coefficients for reduction of the spectral acceleration under the influence of the second kinematic effect, embedment effects, were determined.

According to the conditions of the analyzed structure, the foundation depth was established to be 3m. In accordance with this, the values of the reduction coefficient for the spectral acceleration were computed. The results for soil type B and C are graphically presented in Figure 5.

Copyright © 2025 CroCEE
DOI: https://doi.org/10.5592/CO/3CroCEE.2025.39

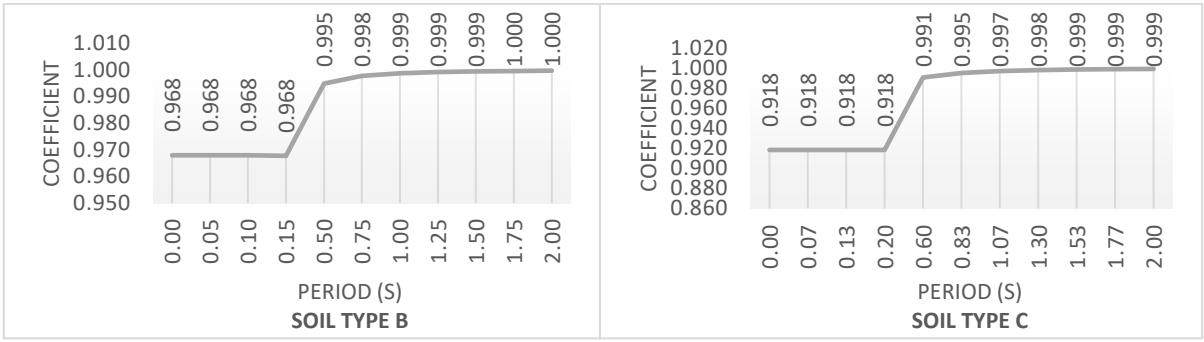


Figure 5. Spectrum reduction coefficient – Embedment effects – Soil type B (left) and Soil type C (right)

7.3.Reduced spectra

The product of the calculated values of the reduction coefficients for Spectrum Type 1, for the sorresponding soil type, from both kinematic interaction effects (RRS_{bsa} and RRS_e) and the acceleration value for the corresponding period from the design spectrum, represents a reduced value of the design spectral acceleration ($A_{g,red.}$):

$$A_{g,red.} = RRS_{bsa} \cdot RRS_e \cdot A_{g,ori.} \tag{8}$$

The values of the spectral acceleration for Spectrum Type 1, soil type B and soil type C, as well as their reduced values, are shown on a comparative graph in Figure 6.

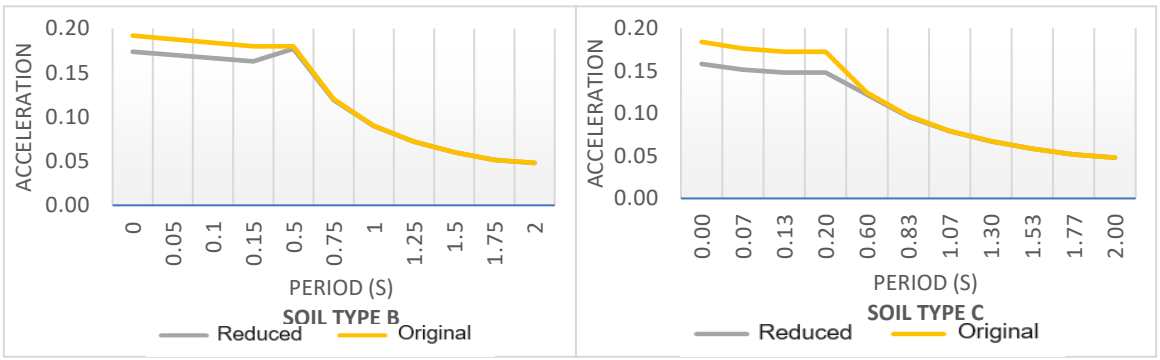


Figure 6. Original and reduced spectra – Soil type B (left) and Soil type C (right)

Hence, it can be concluded that a greater reduction in spectral acceleration is achieved for unfavorable soil conditions, as in the case of soil type C. Therefore, in the seismic analysis of the models, lower values for the seismic force were obtained for the model analyzed with springs and calculated for soil type C.

8. Linear analysis with SSI

A linear analysis of the structural model [18][19] was performed to determine static quantities (moments, forces), dynamic characteristics, seismic forces (via spectral analysis), displacements, and inter-story drifts. The analysis was conducted using ETABS for four models with soil types B and C.

Modal analysis was carried out to calculate 12 natural vibration periods and mode shapes, meeting Eurocode 8 [17] requirements (4.3.3.3.1 (2)P and (3)). Using these periods, seismic analysis was performed per Eurocode 8 [17]. Base and top displacements, as well as base moments, were then calculated.

Models with fixed bases exhibited identical dynamic characteristics, with differences arising in seismic responses due to the use of Spectrum Type 1 for soil types B (Model 1/B) and C (Model 1/C). Models

Copyright © 2025 CroCEE
DOI: https://doi.org/10.5592/CO/3CroCEE.2025.39

incorporating soil conditions showed longer natural periods due to inertial interaction [18][19]. Increased flexibility led to higher deformations, proportional to period lengthening [12]. Figure 7 graphically illustrates the first-mode periods for all analyzed models.

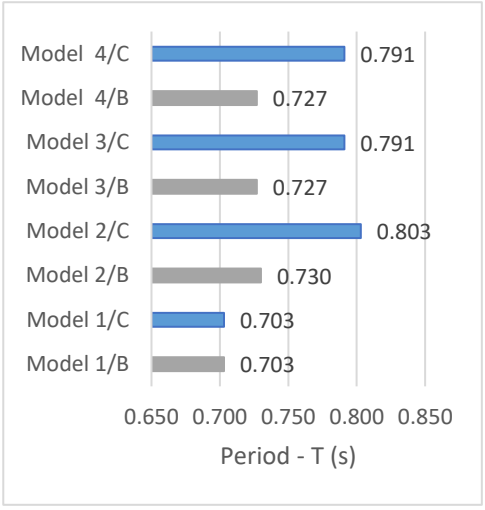


Figure 7. Natural periods of the first mode shapes

The period lengthening was more significant for the structural system on soil type C, with a 14% increase due to greater translation and rotation release. For the model on soil type B, the increase was only 4%, reflecting its stiffer foundation. Consequently, greater differences in seismic force, moments, story drifts, and inter-story drifts are obtained for models on soil type C. Linear analysis results focus on shear force, moments, story displacements, and inter-story drifts (Figures 8–11), presented in different colors for clarity. Due to the system's symmetry, results are shown only for the X direction. These results highlight the differences in the response of structural models caused by local soil conditions and the kinematic interaction effects between soil and structure [18][19].

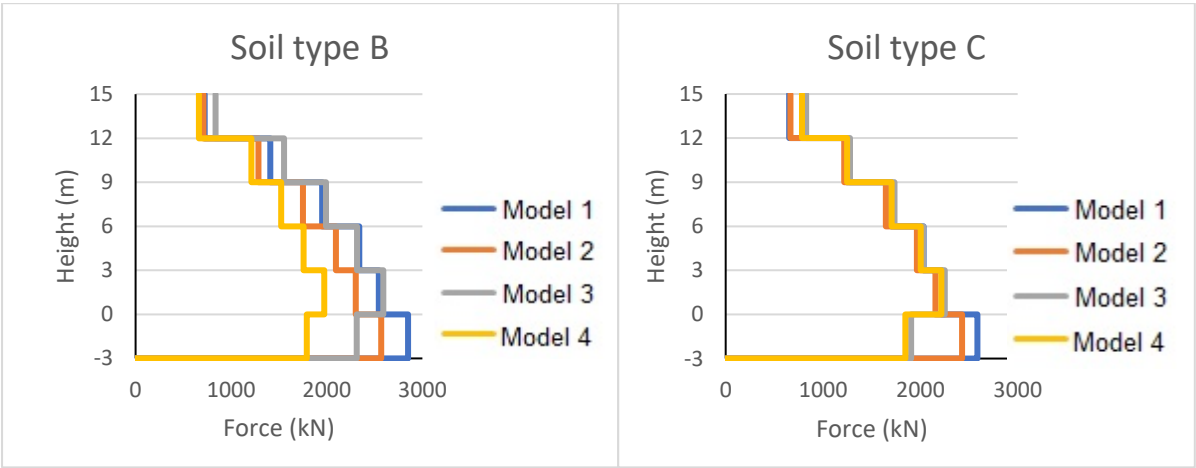


Figure 8. Story shear forces

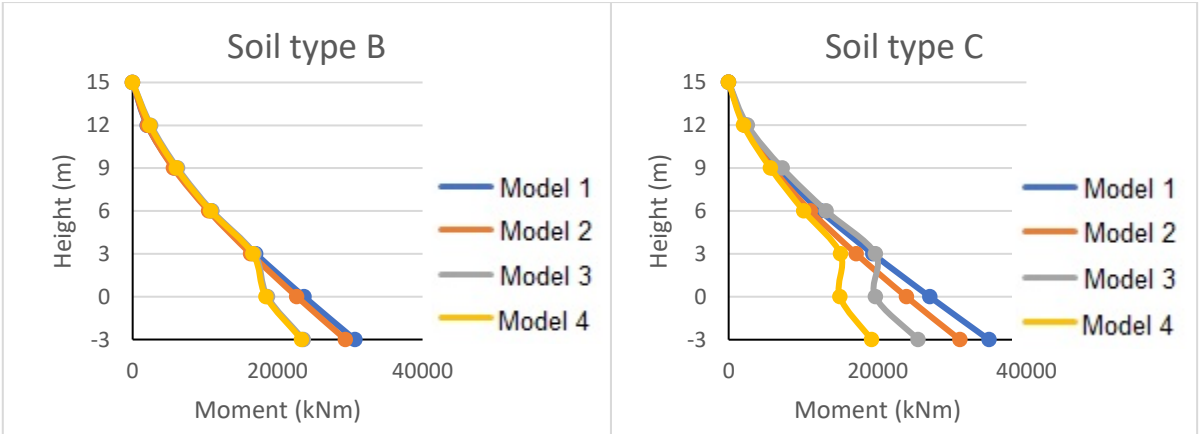


Figure 9. Story moments

Copyright © 2025 CroCEE
DOI: https://doi.org/10.5592/CO/3CroCEE.2025.39

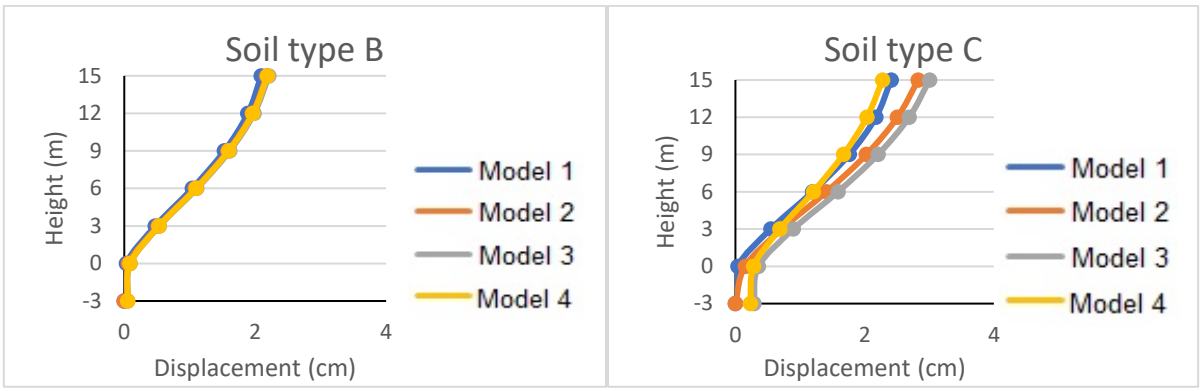


Figure 10. Story displacements

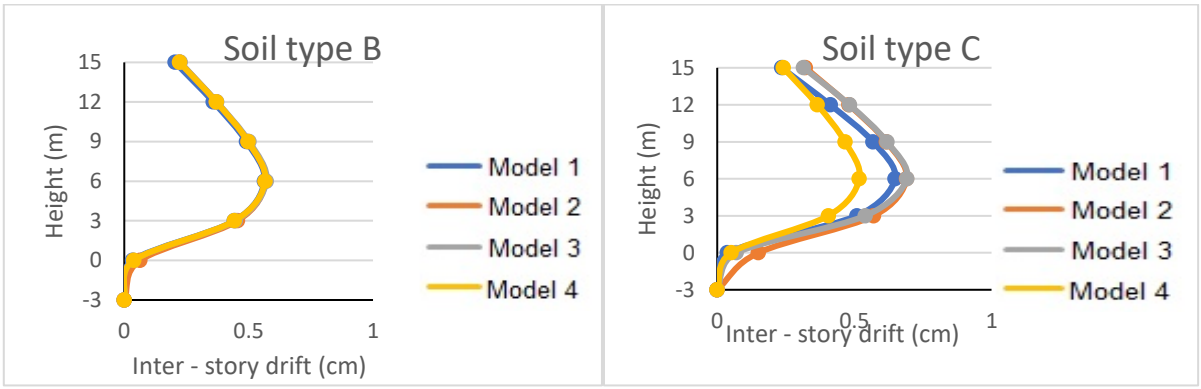


Figure 11. Inter-Story drifts

9. Conclusion

To examine the effects of soil-structure interaction (SSI) and kinematic interaction in line with American guidelines for modeling soil conditions, mathematical models of a six-story reinforced-concrete frame structure were developed. The structure was regular in plan and elevation, and modal and linear-elastic analyses were performed using ETABS. Stiffness characteristics of the springs, simulating soil conditions for soil types B and C (per Eurocode 8), were calculated based on American guidelines. From the modal, spectral and linear analysis results, the following conclusions were drawn:

- Soil conditions affect the natural vibration period, with embedment springs along basement walls slightly reducing the period compared to models with only vertical springs;
- For soil type B, the higher shear modulus (G = 70000 kN/m²) adds restraint at the embedded floor, significantly reducing seismic forces;
- For soil type C, the lower shear modulus (G = 14000 kN/m²) increases flexibility, amplifies seismic waves, and slightly increases seismic forces while reducing rotational restraint at the foundation;
- Soil type C's flexibility reduces foundation-level moments, but leaves upper-story moments largely unchanged as the moments are released on the foundation level;
- Storey displacements and drifts increase compared to fixed base models, with type B showing a 3.27% increase and type C a 21.46% increase;
- Despite spectral acceleration differences, local soil effects cause higher actual displacements than fixed base models.

This research highlights the need for a comprehensive approach to SSI and its kinematic effects during earthquakes. Structures on even favorable soils exhibit different behavior than those analyzed with fixed

Copyright © 2025 CroCEE
DOI: https://doi.org/10.5592/CO/3CroCEE.2025.39

bases, underscoring the importance of including soil conditions. Unlike regulations that focus on weak soils, modeling local soil conditions is crucial for understanding changes in seismic force intensity and structural deformations. These deformations, influenced by modified seismic forces and embedment, cannot be accurately captured with fixed-base models, emphasizing the importance of incorporating soil effects for structural safety. However, this research is limited to the selected structural type, seismic hazard, and soil parameters, expressed by the shear modulus (G) and shear wave velocity (V_s). Hence, it does not provide a general consideration of soil types B and C.

References

[1] Bačić, M., Ivšić, T., Kovačević, M. S. (2020): Geotechnics as an Unavoidable Segment of Earthquake Engineering, *GRAĐEVINAR*, **72** (10), 923-936

[2] Zogh, P., Motamed, R., Ryan, K. (2021): Empirical Evaluation of Kinematic Soil-Structure Interaction Effects in Structures with Large Footprints and Embedment Depths, *Soil Dynamics and Earthquake Engineering*, **149** (106893).

[3] European Committee for Standardization (2004): *Eurocode 8: Design of Structures for Earthquake Resistance - Part 5: Foundations, Retaining Structures and Geotechnical Aspects*, CEN, Brussels.

[4] Vishwajit, A. (2018): Soil-Structure Interaction: A State-of-the-Art Review, *Structures*, **16**, 317-326.

[5] NEHRP Consultants Joint Venture (2012): *Soil-Structure Interaction for Building Structures*, First edition, U.S. Department of Commerce - National Institute of Standards and Technology, Gaithersburg, MD.

[6] Applied technology council (2020): *A Practical Guide to Soil-Structure Interaction*, First edition, Federal Emergency Management Agency (FEMA), Washington, DC.

[7] Edip, K., Garevski, M., Sheshov, V., Bojadjieva, J. (2017): Boundary Effects in Simulation of Soil-Structure Interaction Problems, *Soil Mechanics and Foundation Engineering*, **54** (4), 239-243

[8] Lou, M., Wang, H., Chen, X., Zhai, Y. (2011): Structure–Soil–Structure Interaction: Literature Review, *Soil Dynamics and Earthquake Engineering*, **31** (12), 1724-1731.

[9] ASCE/SEI 41-17 (2017): *Seismic Evaluation and Retrofit of Existing Buildings*, Second edition, American Society of Civil Engineers, Reston, Virginia.

[10] ASCE/SEI 7-16 (2017): *Minimum Design Loads and Associated Criteria for Buildings and Other Structures*, American Society of Civil Engineers, Reston, Virginia.

[11] Thusoo, S., Modi, K., Kumar, A., Kumar, R. (2016): Dynamic Soil Structure Interaction in Buildings, *International Journal of Civil and Environmental Engineering*, **10** (5), 617-622.

[12] Khalil, L.; Sadek, M.; Shahrour, I. (2007): Influence of the Soil–Structure Interaction on the Fundamental Period of Buildings, *Earthquake Engineering Structural Dynamics*, **36** (15), 2445–2453.

[13] Pais, A.; Kausel, E. (1988): Approximate Formulas for Dynamic Stiffnesses of Rigid Foundations. *Soil Dynamics and Earthquake Engineering*, **7** (14), 213–227.

[14] Brandis, A., Kraus, I., Petrovčič, S. (2021): Simplified Numerical Analysis of Soil–Structure Systems Subjected to Monotonically Increasing Lateral Load, *Applied Sciences*, **11** (9).

[15] Sojuzen zavod za standardizacija (1987): *Pravilnik za tehnicki normative za beton I armiran beton*, Sluzben list na SFRJ, **11**, 309-352.

[16] Sojuzen zavod za standardizacija (1981): *Pravilnik za tehnicki normativi za izgradba na objekti na visokogradba vo seizmicki podracja*, Sluzben list na SFRJ, **31**, 844-854.

[17] European Committee for Standardization (2004): *Eurocode 8: Design of Structures for Earthquake Resistance - Part 1: General Rules, Seismic Actions and Rules for Buildings*, CEN, Brussels.

[18] Petrov, N. (2023): *Kinematic Soil – Structure Interaction Effects on Seismic Performance of RC Frames*, Institute of Earthquake Engineering and Engineering Seismology, Skopje.

[19] Petrov, N. Bojadjieva, J. and Bojadjiev, J. (2024): Kinematic SSI effects on seismic performance of RC structures, *GRAĐEVINAR*, **76** (7), 647-658. https://doi.org/10.14256/JCE.3913.2023

Proceedings of the 3rd Croatian Conference on Earthquake Engineering - 3CroCEE
19–22 March 2025, Split, Croatia
Copyright © 2025 CroCEE
DOI: https://doi.org/10.5592/CO/3CroCEE.2025.41

SEISMIC RETROFIT OF "PLINIO IL GIOVANE" SCHOOL BUILDING: MAJOR APPLICATION OF BASE ISOLATION USING HIGH DAMPING RUBBER BEARINGS

Stefano Barone [1]

[1] *Area Sales Manager - Bearings and seismic devices, FREYSSINET, stefano.barone@freyssinet.com*

Abstract

Seismic retrofitting of critical structures, such as schools, military facilities, and essential infrastructure, is crucial in earthquake engineering. These buildings need to meet higher performance standards than typical structures, aiming to withstand design-level seismic events (Life Safety Limit State, LSLS) and ensure functionality immediately after an earthquake. This involves not only protecting the structural components but also minimizing damage to internal equipment. For strategic buildings, maintaining operational capability post-event is essential.

In seismic zones, traditional retrofit methods like roof and floor anchoring, wall bracing, and diaphragm strengthening often fall short and are invasive, altering the building's architecture and functionality. Seismic base isolation presents a non-invasive, highly effective alternative by reducing seismic demands with anti-seismic devices that offer high horizontal flexibility.

The "Plinio Il Giovane" school in Città di Castello, Italy, constructed in the 1970s, serves as a case study. The building has a non-symmetrical L-shaped floor plan with three above-ground floors for educational use and is built with brick-cement floors and a reinforced concrete and brick roof. Città di Castello is in a high seismic hazard area with peak ground accelerations of 0.30g for a 712-year return period (LSLS) and 0.36g for a 1462-year return period (Collapse Limit State, CLS).

For this project, Freyssinet provided 94 ISOSISM® HDRB-S 500x108 High Damping Rubber Bearings (HDRBs) and 42 elastomeric sliders (Type CE 300x69 and CE 400x75). These devices enable the building to withstand 100% of the design seismic action, effectively eliminating its seismic vulnerability.

The paper details the dynamic behaviour of these isolators through experimental tests and outlines the construction phases and technical details of the isolation process.

Keywords: base isolation, high damping rubber bearings, masonry buildings, seismic retrofit.

1. Introduction

Seismic retrofitting of structures is a highly relevant topic in earthquake engineering. Strategic buildings, such as schools, military facilities, bridges, and infrastructure, must not only withstand earthquakes but also ensure immediate occupancy and full functionality following a seismic event. For masonry buildings located in regions of medium to high seismic risk and originally designed to bear static loads, traditional retrofit methods (e.g., anchoring walls to roofs and floors, out-of-plane bracing, and diaphragm reinforcement) are insufficient to protect the structure from the design-level seismic action. While these methods allow for damage without collapse, they fail to guarantee immediate post-earthquake occupancy. Additionally, such techniques often compromise the architectural and functional integrity of the building. In this context, seismic isolation frequently emerges as the most effective strategy for safeguarding structures against earthquakes.

Seismic isolation, a well-established method for earthquake protection, has become increasingly common in existing buildings due to its minimal impact on occupants and functionality during implementation. The approach involves decoupling the building's motion from ground movement by incorporating anti-seismic devices with low horizontal stiffness. This adjustment elongates the building's natural period, reducing lateral acceleration demands while increasing lateral displacement

Copyright © 2025 CroCEE
DOI: https://doi.org/10.5592/CO/3CroCEE.2025.41

at the isolation level. The dynamic performance of an isolated building is largely determined by the properties of the isolators, which must both recentre the structure after seismic activity and dissipate seismic energy. Various seismic devices, including elastomeric isolators, curved surface sliders, and dampers, can be employed and combined, as extensively studied in general literature [1, 2] and in specific applications to historic buildings [3, 4, 5, 6, 7, 8].

This paper focuses on the application of seismic isolation to protect the "Plinio Il Giovane" school institute, a masonry building located in Città di Castello, Umbria, Italy, built in the 1970s. The implemented isolation system includes 94 High Damping Rubber Bearings ISOSISM® HDRB-H 500x108 and 42 elastomeric flat sliders Type CE 400x75 and 300 x 69, provided by Freyssinet, a global leader in specialized civil engineering solutions.

This paper details the isolators' performance characteristics, focusing on their testing behavior, and offers an in-depth look at the construction phases and technical measures necessary to apply seismic isolation to a masonry structure.

2. The case study

2.1. Seismic vulnerability of "Plinio Il Giovane" school institute

The selected case study focuses on the "Plinio Il Giovane" masonry school building, situated in Città di Castello, a historic medieval city in the Province of Perugia, Italy.



Figure 1. Location of the building

The building, constructed in the 1970s, is characterized by a non-symmetrical L-shaped floor plan with three above-ground floors used for education. It is made by brick-cement floors and a reinforced concrete and brick roof, which replaced the original wooden roof in 1978. The main vulnerabilities of the building are identified below:

• irregular vertical configuration of the structure, with an L-shape in plan and section of varying heights

• presence of staggered floors in elevation

• absence of transverse stiffening walls in certain parts of the building

Città di Castello is in an area prone to medium-to-strong seismic activity, with a peak ground acceleration (PGA) on rock soil estimated at 0.261g for a return period of 712 years (equivalent to a 10% probability of exceedance in 50 years). The building exhibits high stiffness, with a fundamental vibration period of approximately 0.27 seconds, corresponding to a design horizontal acceleration of 0.720g. Fig. 2 illustrates the elastic acceleration response spectrum for the specified return period (associated with the Life Safety Limit State), including the reduction due to the additional damping provided by the isolation system (ξ_{eq} = 12.5%).

Copyright © 2025 CroCEE
DOI: https://doi.org/10.5592/CO/3CroCEE.2025.41

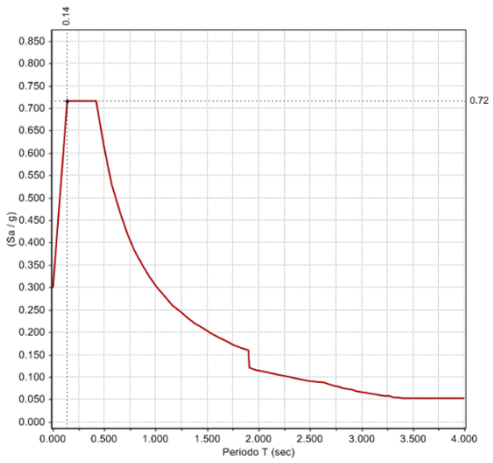


Figure 2. Elastic acceleration response spectrum for 712 years return period

The building exhibits significant structural deficiencies and high seismic vulnerability, with risk indicators nearing zero for out-of-plane actions (refer to Table 1).

The retrofit strategy must enhance seismic safety, at least for the design seismic action, while minimizing invasive interventions on the building. Conventional methods, such as adding new structural walls, installing metal hoops, or strengthening with fiber-reinforced polymers, can reduce seismic vulnerability but often conflict with the architectural preservation and conservation goals. Moreover, traditional approaches do not ensure damage prevention - both structural and non-structural - nor do they guarantee the functionality of the structure following a seismic event.

2.2. Seismic protection through base isolation

As outlined in the introductory chapter, seismic isolation is a widely adopted design strategy globally, both for new constructions and the retrofitting of existing structures. By decoupling the motion of the superstructure from ground movements through the installation of anti-seismic devices with low horizontal stiffness, the fundamental period of the structure is significantly extended. This results in a substantial reduction in seismic accelerations affecting the superstructure. Consequently, damage to superstructure elements can be effectively eliminated due to the drastic decrease in interstory drifts and floor shear forces. Fig.3 illustrates the comparison between the response of the original fixed-base structure and the structure with base seismic isolation.

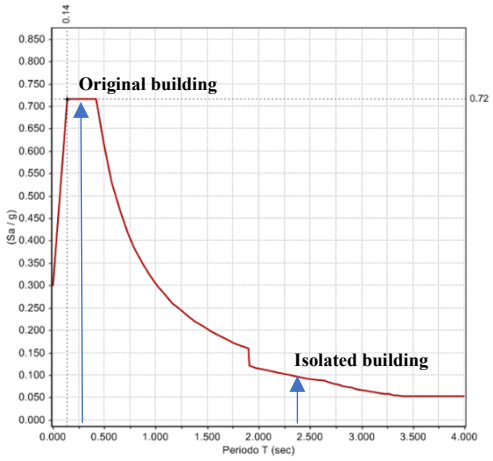


Figure 3. Performance point of original building and base isolated building

Analysing Fig. 3, the primary benefits of seismic isolation can be qualified as follows:

Copyright © 2025 CroCEE
DOI: https://doi.org/10.5592/CO/3CroCEE.2025.41

• significant reduction in seismic accelerations transmitted to the superstructure, by a factor of more than 7

• increased system damping up to 12.5%, which further reduces accelerations transmitted to the building and limits displacements at the isolation level

• high decoupling of the superstructure motion from the ground motion, with an isolation ratio of $T_{iso}/T_{fixed} = 7.4$

For the building's isolation system, Freyssinet supplied 94 High Damping Rubber Bearings ISOSISM® HDRB-H 500x108 and 42 elastomeric flat sliders of two types: CE 400x75 (5 units) and 300x69 (37 units). Fig. 4 provides a rendering of the implemented isolation system at the base of the structure.

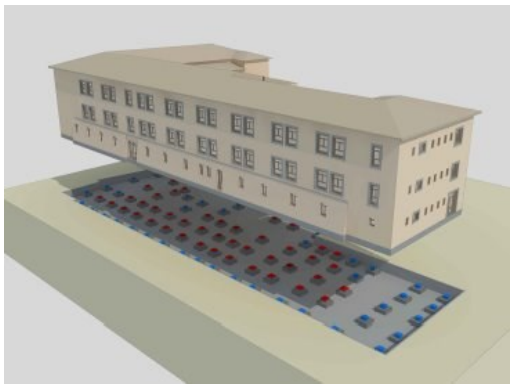


Figure 4. Identification of the base isolation level

The isolators and sliders are strategically positioned to ensure optimal alignment between the centre of mass and the centre of stiffness, effectively minimizing torsional effects during a seismic event. The layout of the devices is illustrated in Fig. 5.

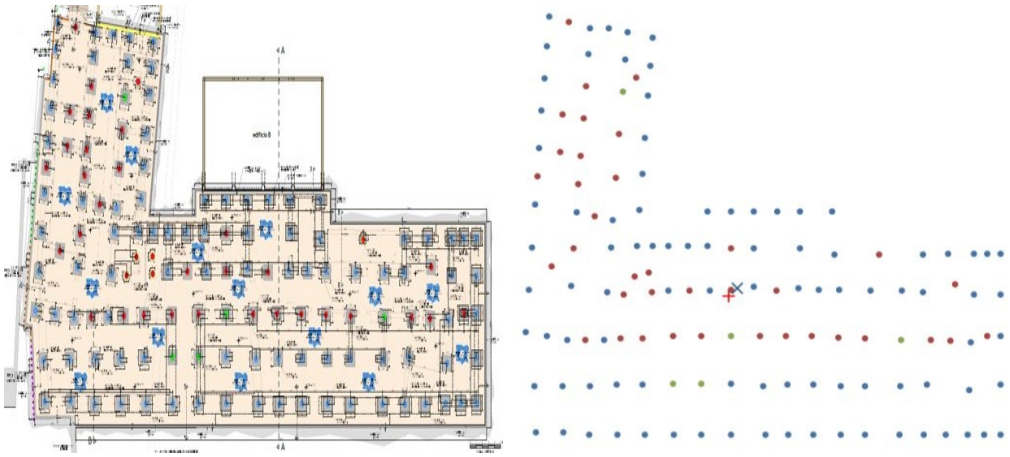


Figure 5. Plan view of the isolation system (left), identification of stiffness center "x" and mass center "+" (right). Isolators in blue, sliders in red.

Finally, Fig. 6 provides an overview of the finite element model of the building, while Fig. 7 illustrates the first three vibration modes. With just the first three modes, more than 90% of the building's mass is engaged.

Copyright © 2025 CroCEE
DOI: https://doi.org/10.5592/CO/3CroCEE.2025.41

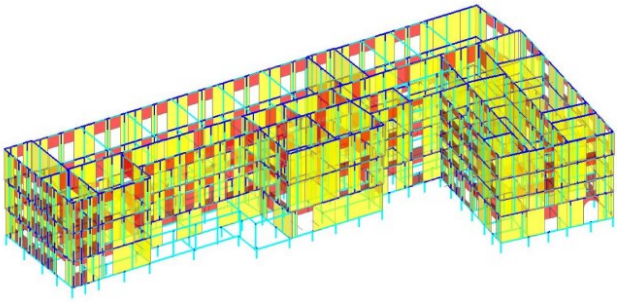


Figure 6. Finite Element Model of the building

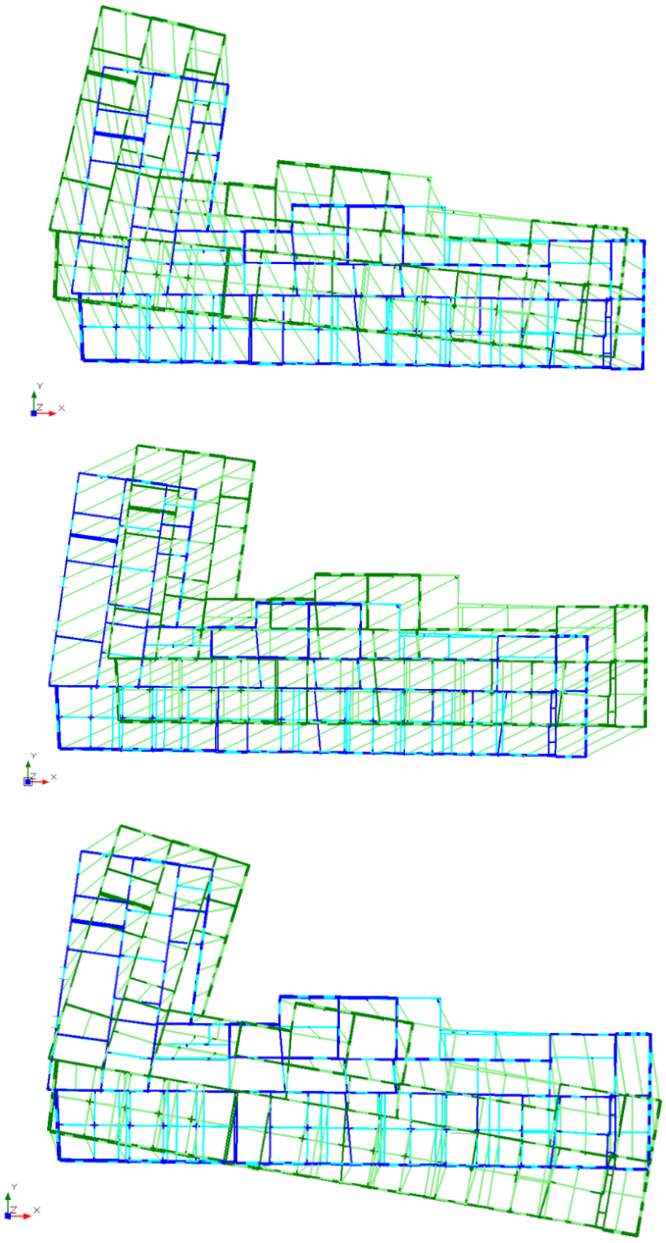


Figure 7. T_1 = 2.38 sec (top), T_2 = 2.35 sec (middle) and T_3 = 2.19 sec (bottom)

Thanks to the isolation system, the building is now able to withstand the design seismic action. Table 1 presents the changes in the risk index before and after the implementation of the isolation system.

Copyright © 2025 CroCEE
DOI: https://doi.org/10.5592/CO/3CroCEE.2025.41

Table 1. Risk index for the Life Safety Limit State

Parameter	Unit	Value
Fundamental period of vibration of original building, T_{fixed}	sec	0.270
Fundamental period of vibration of isolated building, T_{iso}	sec	2.380
Isolation ratio, T_{iso}/T_{fixed}	-	7.438
Pseudo spectral acceleration at T_{fixed}, $S_a(T_{fixed})$	g	0.720
Pseudo spectral acceleration at T_{iso}, $S_a(T_{iso})$	g	0.100
Pseudo spectral acceleration ratio, $S_a(T_{iso})/S_a(T_{fixed})$	-	0.139
PGA demand, PGA_D	g	0.300
Return period demand, TR_D	years	712
RISK INDEX – ORIGINAL BUILDING		
PGA capacity, PGA_C	g	0.000
PGA ratio, PGA_C/PGA_D	-	0.000
Return period capacity, TR_C	years	0.000
Return period ratio, TR_C/TR_D	-	0.000
RISK INDEX – ISOLATED BUILDING		
PGA capacity, PGA_C	g	0.300
PGA ratio, PGA_C/PGA_D	-	1.000
Return period capacity, TR_C	years	712
Return period ratio, TR_C/TR_D	-	1.000

3. Freyssinet seismic devices

3.1. ISOSISM® HDRB and Type CE: performance overview

The ISOSISM® HDRB elastomeric isolators are reinforced rubber bearings composed of alternating layers of hot-vulcanized rubber and steel laminates. These isolators are characterized by high vertical stiffness, low horizontal stiffness, and a suitable damping capacity. These properties enable them to effectively resist vertical loads without significant deformation, extend the fundamental vibration period of the structure, and limit the horizontal displacements of the isolation system.

For the seismic isolation of the school building, 94 ISOSISM® HDRB-H 500x108 isolators were supplied, featuring an elastomeric compound with high stiffness and damping capacity. Fig. 8 illustrates the 3D exploded view of the isolator, while Table 2 outlines the key design parameters.

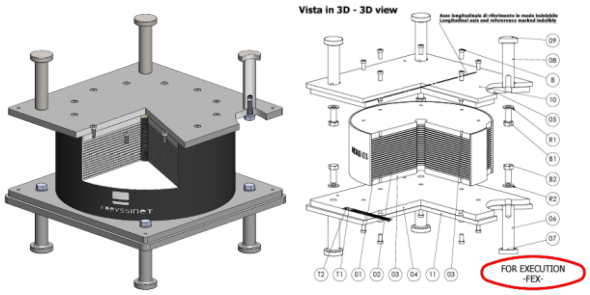


Figure 8. Rendering of ISOSISM® HDRB-H 500x108 (left) and its exploded view (right)

Copyright © 2025 CroCEE
DOI: https://doi.org/10.5592/CO/3CroCEE.2025.41

Table 2. Design parameters of ISOSISM® HDRB-H 500x108

Parameter	Unit	Value
Rubber diameter, D_r	mm	500
Rubber height, T_r	mm	108
Total height, H	mm	226
Side length of outer steel plates, B	mm	550
Weight, W	kg	331
Maximum static vertical load, $N_{ULS,max}$	kN	6000
Maximum seismic vertical load, $N_{Ed,max}$	kN	2800
Design displacement, d_{bd}	mm	±180
Displacement capacity, d_c	mm	±250
Effective horizontal stiffness, $K_{eff}(d_{bd})$	kN/mm	0.88
Vertical stiffness, K_v	kN/mm	≥ 704
Equivalent viscous damping, $\xi_{eq}(d_{bd})$	-	12.5%

The isolators are combined with elastomeric flat sliders of Type CE 400x75 and 300x69 to reduce the eccentricity between the center of mass and the stiffness. Fig. 9 provides the 3D exploded view of the slider, while Table 3 presents the design parameters.

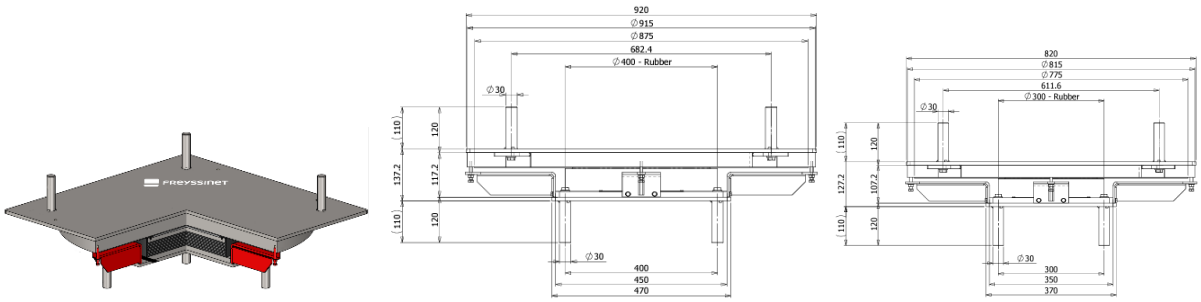


Figure 9. Rendering of Type CE slider (left), front view of Type CE 400x75 (middle) and 300x69 (right)

Table 3. Design parameters of Type CE 400x75 and 300x69

		Type CE 400x75	Type CE 300x69
Parameter	Unit	Value	Value
Rubber diameter, D_r	mm	400	300
Rubber height, T_r	mm	75	69
Total height, H	mm	137	127
Side plate diameter, D_S	mm	915	815
Weight, W	kg	361	256
Maximum vertical load, $N_{ULS,max}$	kN	4000	2500
Horizontal force, F_H	kN	-	-
Displacement capacity, d_c	mm	±250	±250

All the devices are fitted with upper and lower masonry plates, facilitating easy installation and potential future replacement if necessary.

3.2. Testing of ISOSISM® HDRB

The isolators underwent full-scale testing to evaluate their performance. In accordance with European Standard EN 15129:2009 and the Italian Standard "Norme Tecniche per le Costruzioni 2018", 20% of the production (a total of 20 units) were subjected to vertical compression and horizontal dynamic tests to thoroughly characterize the response of the devices and compare it to the theoretical behavior. The tests were conducted by Politecnico di Milano (responsible for execution and certification) at the ISOLAB laboratory (Montebello della Battaglia, Italy), the testing facility of Freyssinet. Table 4

Copyright © 2025 CroCEE
DOI: https://doi.org/10.5592/CO/3CroCEE.2025.41

outlines the test protocol for the devices, while Fig. 10 depicts one device during testing and its response.

Table 4. Factory Production Control Test protocol

test name	main dof [-]	max displ [mm]	max vel [kN/min]	load shape [-]	vertical load [kN]	cycles [-]
Compression stiffness	vert	-	165	ramp	1650	1
Horizontal characteristics under cyclic deformation	hor	±162 mm	509	sine	1178	3

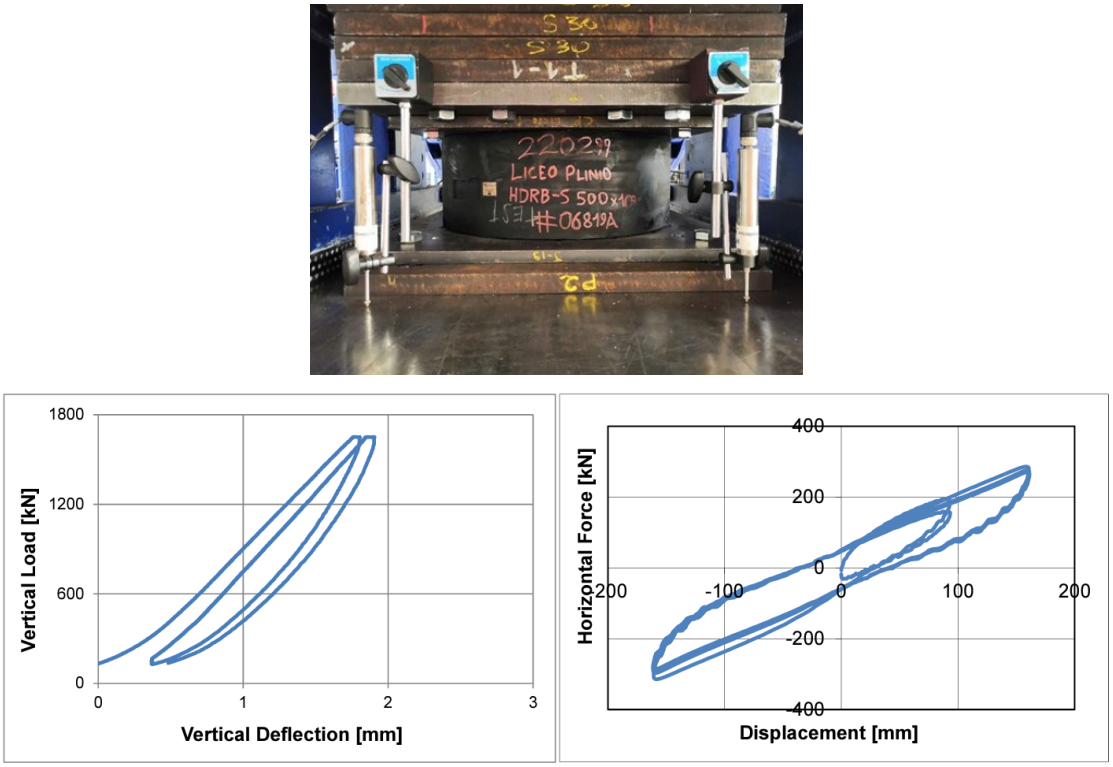


Figure 10. ISOSISM® HDRB-H 500x108 during testing (top), vertical (left) and horizontal response (right)

Fig. 11 displays the response of all the isolators in terms of effective stiffness and damping at the third cycle, along with the maximum tolerance (±20%) permitted by the standard.

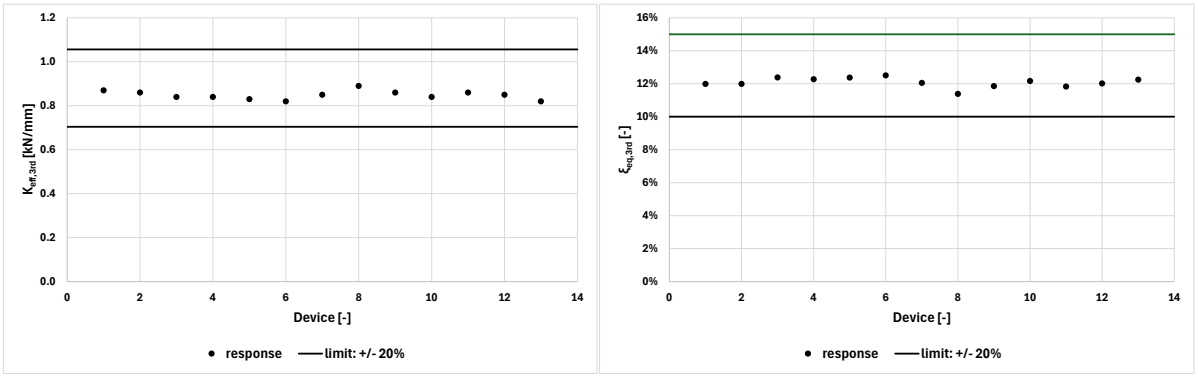


Figure 11. Hysteretic results: $K_{eff,3rd}$ (left) and $\xi_{eq,3rd}$ (right)

After testing, all the devices were shipped for on-site installation.

Copyright © 2025 CroCEE
DOI: https://doi.org/10.5592/CO/3CroCEE.2025.41

4. Implementation of the isolation level

To implement a seismic isolation system for a masonry building, a series of complex site activities are required. This includes reinforcing weaker masonry walls through localized reconstruction, excavating and removing soil from the building's rooms to a depth of approximately two meters below the basement level, and excavating sections of the foundations and soil beneath the walls. Two new reinforced concrete foundations are then built: the first is a foundation slab resting on the ground, while the second consists of curb beams placed at the base of the masonry walls. Seismic isolation devices are inserted between these two foundations, effectively isolating the building from seismic forces. Concrete caps are added to the foundation slab at the locations of the devices for support. Flat jacks, filled with injected epoxy resin, redirect part of the upper structure's load to the devices and the new foundation, helping to prevent differential settlements during construction. Fig. 12 visually illustrates these new elements at the base of the isolated building.

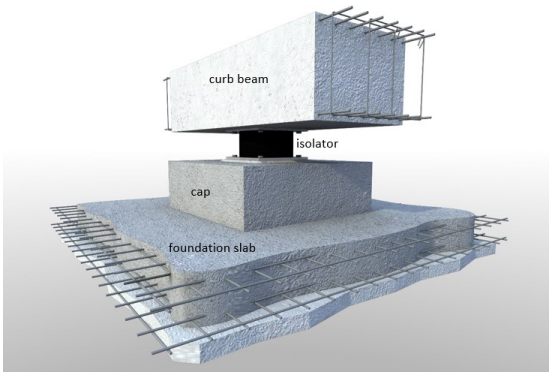


Figure 12. New foundation slab, cap, device and curb beam

Seismic isolation at the base enables the building to move independently of the ground during seismic events. A concealed perimeter cavity, covered by a sidewalk, accommodates this movement. Fig. 13 shows typical construction details at the isolation level.

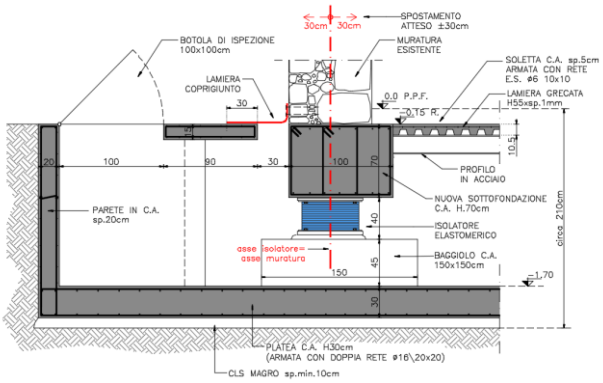
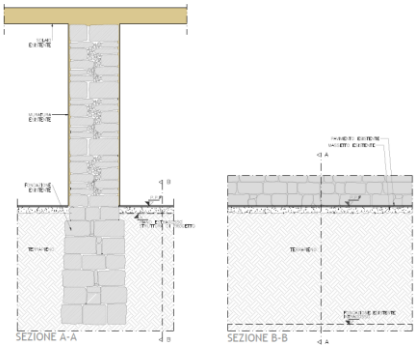


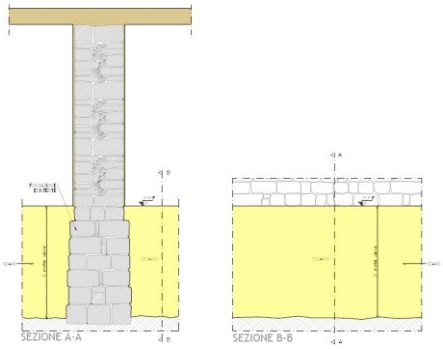
Figure 13. Details of the isolation system along the perimeter of the building

Fig. 14 illustrates the sequence of the various phases described earlier.

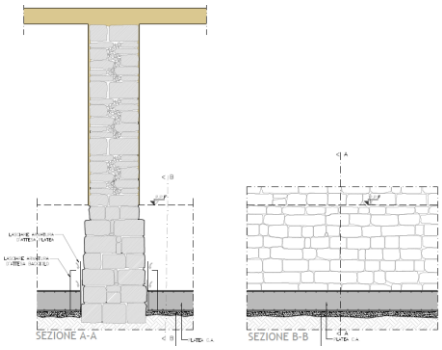
Proceedings of the 3rd Croatian Conference on Earthquake Engineering - 3CroCEE
19–22 March 2025, Split, Croatia
Copyright © 2025 CroCEE
DOI: https://doi.org/10.5592/CO/3CroCEE.2025.41



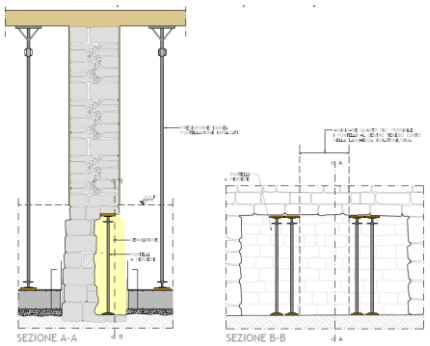
Phase 0: Existing masonry wall



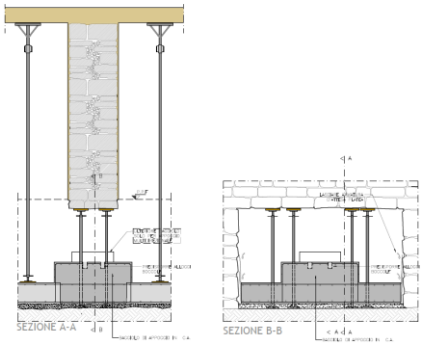
Phase 1: Excavation and removal of soil



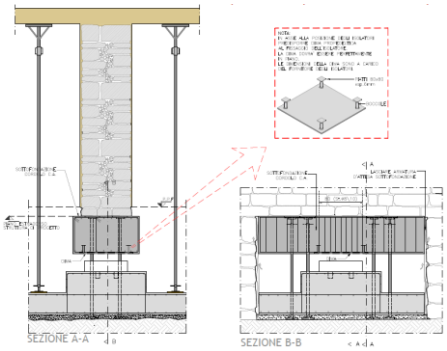
Phase 2: Construction of RC foundation slab



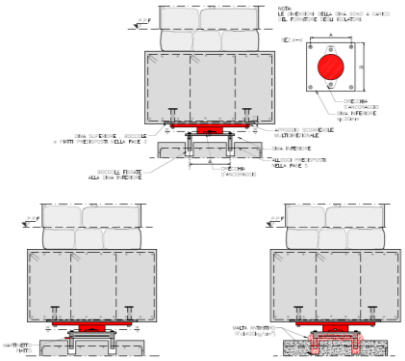
Phase 3: Shoring of slab and demolition of masonry portion



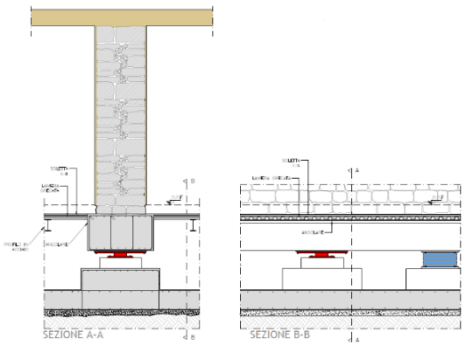
Phase 4: Construction of RC cap



Phase 5: Construction of RC beam at the base of masonry wall



Phase 6: device installation, flat jack loading, lowering anchors casting



Phase 7: Removal of floor supports, cutting of formworks supports, construction of ground floor

Figure 14. Construction phases of the isolation system

Copyright © 2025 CroCEE
DOI: https://doi.org/10.5592/CO/3CroCEE.2025.41

The final step involves constructing the new base floor, which includes a technical compartment for device maintenance and inspection. This construction approach ensures that the building remains fully operational, albeit with a slightly reduced usable area. Work is carried out in temporarily unoccupied sections, which are later reoccupied after the installation of the devices. The only exception is the ground floor immediately above the isolation level, which remains unusable throughout the construction process.

It is important to emphasize that this approach allows the school to remain operational, despite the reduction in usable surface area. The construction framework permits work in macro areas of the building that are temporarily unused, which are then reoccupied once the devices are installed. Only the ground floor directly above the isolation level remains unavailable for the entire duration of the construction.

5. Conclusions

This paper presents the application of seismic isolation at the base of an existing masonry building. The "Giacomo Matteotti" school was originally designed for vertical loads only, as seismic design was not required by law at the time of its construction. The building is highly vulnerable to seismic activity due to its static structural design and the high seismic hazard of the site. Moreover, the building holds significant historical value. For these reasons, seismic isolation retrofitting was chosen as an alternative to conventional methods. This technique not only protects the building from earthquakes but also allows it to remain fully operational with minimal impact on the architectural integrity of the structure.

Seismic isolation significantly reduces the accelerations transmitted to the superstructure (by a factor of more than 7), increases system damping (up to 12.5%), and effectively decouples the superstructure's motion from the ground motion ($T_{iso}/T_{fixed} = 7.4$). The isolation system comprises 94 ISOSISM® HDRB-H 500x108 anti-seismic rubber devices and 42 elastomeric flat sliders (Type CE 400x75, total 5; Type CE 300x69, total 37) supplied by Freyssinet, a global leader in specialized civil engineering. 20% of the isolators were tested according to EN 15129:2009 and NTC 2018 standards, meeting the required acceptance criteria.

The installation of the isolation system at the base of the masonry building involved a range of complex construction activities, including the demolition of the existing foundation and the construction of two new concrete foundations: a base slab resting on the ground and curb beams placed beneath the masonry walls. The devices were then installed between these two newly constructed elements.

The retrofit process was implemented progressively in macro areas of the building, allowing the school to remain operational throughout the entire construction period.

References

[1] Braga, F., Faggella, M., Gigliotti, R., Laterza, M. (2005): Nonlinear dynamic response of HDRB and hybrid HDRB-friction sliders base isolation systems, *Bullettin Earthquake Eng*, **3**, 333–353, doi: 10.1007/s10518-005-1242-2.

[2] Martelli, A., Forni, M. (1998): Seismic isolation of civili buildings in Europe, *Progress Struct. Eng. Mater.*, **1**, 286-294, doi: 10.1002/pse.2260010310.

[3] De Luca, A., De Mele, E., Molina, J., Verzeletti, G., Pinto, A.V. (2001): Base isolation for retrofitting historic building: evaluation of seismic performance through experimental investigation, *Earthquake Eng. Struct. Dynam*, **30**, 1125-1145, doi: 10.1002/eqe.54.

[4] Tomazevic, M., Klemenc, I., Weiss, P. (2009): Seismic upgrading of old masonry buildings by seismic isolation and CFRP laminates: a shaking-table study, *Bulletin Earthquake Eng.*, **7**, 293–321, doi: 10.1007/s10518-008-9086-1.

[5] Petrovčič, S., Kilar, V. (2017): Seismic retrofitting of historic masonry structures with the use of base isolation – modeling and analysis aspects, *Int. J. Archit. Heritage*, **11**, 229-246, doi: 10.1080/15583058.2016.1190881.

Copyright © 2025 CroCEE
DOI: https://doi.org/10.5592/CO/3CroCEE.2025.41

[6] Kawamura, S., Sugisaki, R., Ogura, K., Maezawa, S., Tanaka, S. (2000): Seismic isolation retrofit in Japan, *12th World Conference on Earthquake Engineering*, Auckland.

[7] Barone, S., Vetturini, R., Cecchini, W., Trombettoni, L. (2024): Retrofit of existing masonry buildings through seismic isolation: recent applications in Italy, *18th World Conference on Earthquake Engineering*, Milan.

[8] Barone, S., Vetturini, R. (2023): Seismic retrofit of strategic masonry structures with base isolation technique: the case study og "Giacomo Matteotti" school building in Gubbio, Italy, *2nd Croatian Conference on Earthquake Engineering*, Zagreb.

[9] Barone, S. (2023): Seismic isolation of existing masonry buildings: three case studies in Italy, *XXIV Congreso Nacional De Ingenierìa Sismica*, Guadalajara.

Proceedings of the 3rd Croatian Conference on Earthquake Engineering - 3CroCEE
19–22 March 2025, Split, Croatia
Copyright © 2025 CroCEE
DOI: https://doi.org/10.5592/CO/3CroCEE.2025.43

SEISMIC VULNERABILITY ASSESSMENT OF 1960S REINFORCED CONCRETE FRAME BUILDINGS WITH INFILL MASONRY WALLS

Naser Kabashi [(1)], Enes Krasniqi [(2)], Florim Grajcevci[(3)], Milot Muhaxheri[(4)],Ylli Murati[(5)], Valon Veseli[(6)]

[(1)] *Prof.dr, University of Prishtina, naser.kabashi@uni-pr.edu*
[(2)] *Teaching Assistant, PhD Cand, University of Prishtina, enes.krasniqi@uni-pr.edu*
[(3)] *Prof.asst.dr, University of Prishtina, florim.grajcevci@uni-pr.edu*
[(4)] *Prof.asst.,University of Prishtina, milot.muhaxheri@uni-pr.edu*
[(5)] *Teaching Assistant, PhD Cand, University of Prishtina, yllimurati@uni-pr.edu*
[(6)] *Teaching Assistant, PhD Cand, University of Prishtina, valon.veseli@uni-pr.edu*

Abstract

This study investigates the seismic performance of low-rise and mid-rise reinforced concrete (RC) structures with and without masonry infills through nonlinear static and dynamic analyses. The research emphasizes the role of confined masonry in enhancing structural stiffness and strength, as well as its contribution to the overall seismic resilience of buildings. Field testing, including ambient vibration measurements, and historical records were integrated to calibrate the numerical models and refine capacity curves. Results indicate that masonry infills significantly improve base shear capacity and limit state performance, particularly in terms of Damage Limitation (DL) and Significant Damage (SD). In the absence of infills, structures exhibited increased vulnerability to seismic forces, leading to potential collapse. The influence of material properties, such as masonry strength and concrete grade, was evaluated through parametric studies. The findings highlight the necessity of accurate material characterization and proper assessment methodologies, aligning with the guidelines of Eurocode 8 and recent advances in seismic engineering. Additionally, the importance of ambient vibration testing for model calibration is underscored, offering a non-invasive approach to assess the dynamic properties of existing buildings. This research contributes to the ongoing efforts to improve the seismic assessment and retrofitting of vulnerable structures in earthquake-prone regions.

Keywords: Reinforced concrete frame, Seismic performance, Material testing, Model calibration, Retrofitting.

1. Introduction

Kosova lies in a moderate seismic vulnerable zone. The records from different sources shows that there are a number of magnitude VI or VII that occurred in Kosovo in the last 500 years. In this paper, for the stock of buildings selected, the building codes at the time of their construction did not prioritize seismic activity as much as they do today. The selected buildings were constructed during the period from 1960 to 1970. These structures were built using in situ concrete and prefabricated slab decks, consisting of a concrete frame structure combined with masonry walls, with materials categorized according to the standards of that time. Currently, the design of buildings complies with Euro norms, and earthquake intensity is measured in terms of PGA. In Kosovo, the peak ground acceleration ranges from 0.05 to 0.20 ag/g. Concrete frame structures, often with infilled masonry, were first constructed in Kosovo during the 1950s and 1960s. These buildings were typically not high-rise structures but rather 4- to 6-story buildings. In such cases, although earthquakes affect the structure, their impact may not be as significant as it would be on 10- to 14-story buildings [1]. Nevertheless, a proper risk assessment requires foreseeing any possible risk that may arise during the lifetime of the building, and one of them is also seismic activity [2][3].

A building's inadequate seismic response is mainly caused by poor execution of key structural elements, connections, and assembly, as well as the use of materials such as smooth rebar, low-quality concrete, and outdated design principles. Consequently, in European seismic-prone countries, the

Copyright © 2025 CroCEE
DOI: https://doi.org/10.5592/CO/3CroCEE.2025.43

assessment of existing structures is a priority since most residential buildings were designed using old versions of seismic codes or without applying the codes. In many of these buildings, there are significant uncertainties regarding their nonlinear behavior [4]. The seismic vulnerability of existing reinforced concrete (RC) structures infilled with masonry walls is evident from the observed damages to failed structures across Europe after earthquakes. The infills in a building can enhance its performance; however, in some cases, they may also have a negative impact. Infills can induce different failure mechanisms. For instance, infill from the first floor upward could affect the global structure and, under seismic loading, create a soft-story mechanism. They may also cause short-column mechanisms or result in localized failure mechanisms [5]. Several studies have highlighted the impact of masonry infills on building performance, as masonry walls can exhibit shear strength [6][7].

A full-scale test on a three-story building strengthened with infill brick walls showed that the addition of these walls prevented slab collapse and increased both the strength and stiffness of the original frame structure [8]. Similarly, Dolsek and Fajfar observed that infill walls enhance the stiffness and strength of a structure, provided the seismic demand does not exceed the deformation capacity of the infill walls [9]. To mitigate the devastating effects of seismic events, it is crucial to evaluate the vulnerability of buildings to plan effective mitigation policies and structural strengthening interventions. Assessing the performance of a building involves a combination of in situ tests, laboratory tests, and numerical analysis. These methods allow for an analysis of the structure's behavior under permanent, transient, and seismic loads. Numerical analysis alone is insufficient, as the influence of infill walls on building performance cannot be neglected for this type of structure. Additionally, not all walls may affect the structure's behavior under seismic loads. To address this, material testing and ambient vibration tests were conducted to evaluate the material properties and the dynamic characteristics of the buildings [10].

Ambient vibration testing records real-time vibrations of the structure, typically caused by environmental factors such as wind, occupants, or other micro-vibrations [11]. Based on the in situ data, a validated structural model was developed to simulate and calibrate the building's behavior. In this study, an existing concrete frame structure with masonry infill was analyzed. The 3D numerical model was created using software such as CSI and Seismosoft package [12][13]. This model was calibrated with results obtained from ambient vibration tests. A parametric study was conducted to evaluate the influence of the infills on the structure and to determine how the mechanical properties of materials affect global behavior. Non-linear static analysis was performed to assess the seismic vulnerability of the building [14].

2. Description of structure

2.1. General Description

A large neighborhood, known for its replicated buildings, has been selected for this study. The buildings in this neighborhood share the same year of construction, materials, construction technology, and structural system. The selected building is a 6-story reinforced concrete structure with infilled walls, located in Prishtina, the capital city of Kosovo. A view of the location is presented in Fig. 1.

Proceedings of the 3rd Croatian Conference on Earthquake Engineering - 3CroCEE
19–22 March 2025, Split, Croatia
Copyright © 2025 CroCEE
DOI: https://doi.org/10.5592/CO/3CroCEE.2025.43



Figure 1. Series of replicated buildings

The buildings are aligned with joints between the individual group of apartments with the same geometry and other parameters. The selected building has 2 bays in “Y” direction and 5 bays in “X” direction. The maximum span between columns is 3.85 m in “X” direction and 5.60 m in “Y” direction , with rectangular section and designed with characteristic resistance f_{ck}=22.0 N/mm^2 in basement and other floors , except third and fourth floor with lower value. All columns are reinforced with 4Ø16 mm main bars in the basement, ground, first and second floor and 4Ø14 mm bars on the third and fourth floor. The stirrups are Ø6/25 cm are in general for all columns. In scope of the construction methodology during the built are used the horizontal RC beams, reinforced with Ø8/10 cm and characteristics of concrete f_{ck}=20.0 N/mm^2. The typical floor plan is presented in fig.2 and section in fig.3.

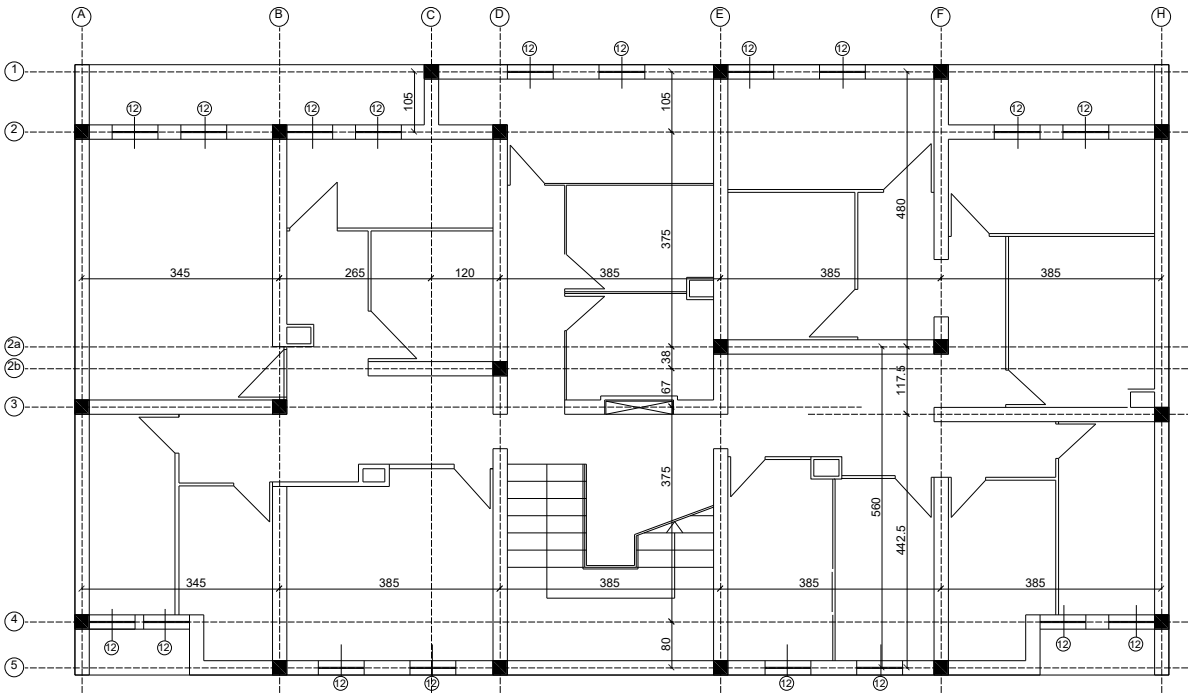


Figure 2. Geometry of typical floor plan

Copyright © 2025 CroCEE
DOI: https://doi.org/10.5592/CO/3CroCEE.2025.43

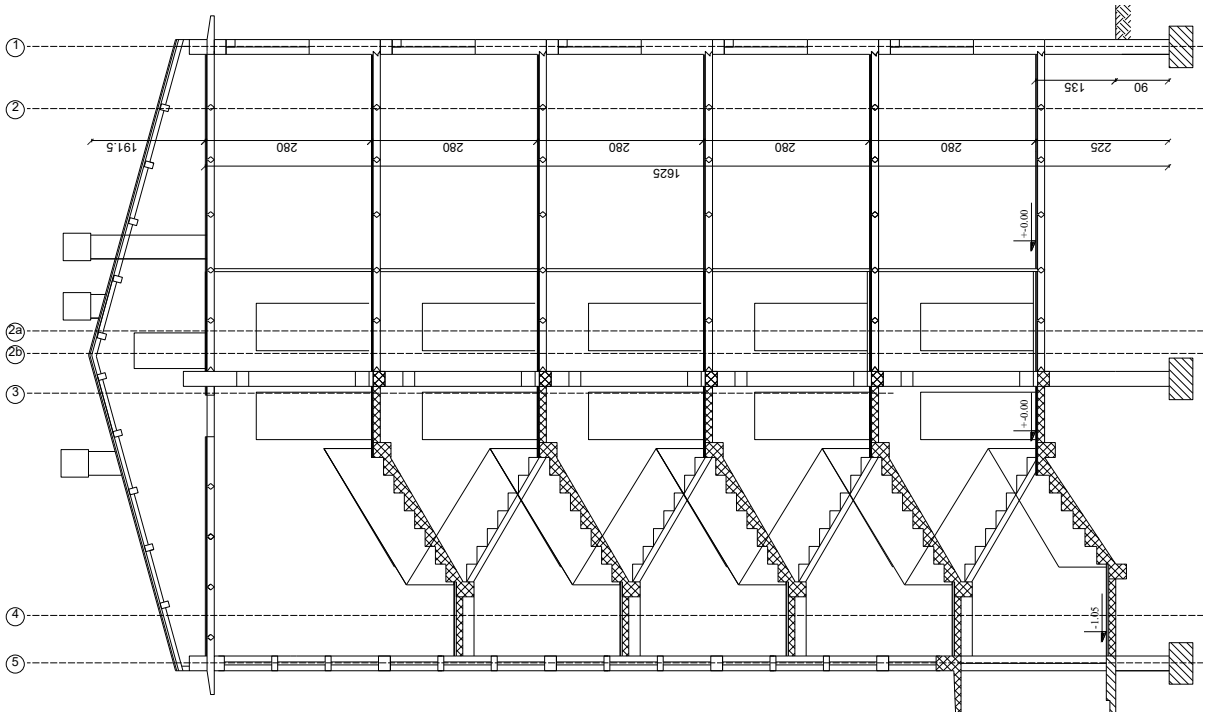


Figure 3. Vertical cross section

2.2. Testing of structural elements

2.2.1. Description the proposed Methodology

The proposed methodology for assessing the seismic vulnerability of existing reinforced concrete (RC) structures with masonry infills is structured into the following systematic steps:

1. **Collection of Technical Information**: Comprehensive data collection is undertaken to enhance the structural knowledge of the building. This includes archival research, construction drawings, and field investigations to identify critical design parameters and material properties.
2. **Estimation of Structural Capacity**: The structural system's capacity is evaluated with respect to the Life Safety (LS) performance limit state. This step involves analyzing the structural integrity under seismic loads to ensure compliance with LS criteria.
3. **Demand Evaluation (PGAc)**: The seismic demand is assessed by determining the Peak Ground Acceleration (PGA) corresponding to the building's location and seismic zone. This evaluation considers regional seismic hazard data and site-specific factors.
4. **Identification of Vulnerability Class**: Based on the assessed capacity and demand, the vulnerability class of the structure is identified. This classification aids in prioritizing retrofitting measures and informs risk mitigation strategies.

2.2.1.1. In situ testing - Characteristic value of concrete quality – Schmidt hammer test

As part of the evaluation, the quality of concrete in the structural elements was assessed using the non-destructive Schmidt Hammer Test. The testing procedure adhered to the requirements of Standards EN 12504-2, ensuring consistency and reliability in the results. Table 1 summarizes the findings obtained from different structural positions.

Proceedings of the 3rd Croatian Conference on Earthquake Engineering - 3CroCEE
19–22 March 2025, Split, Croatia
Copyright © 2025 CroCEE
DOI: https://doi.org/10.5592/CO/3CroCEE.2025.43

Table 1. Non-destructive testing results for different positions

Position	Age (days)	Mean reading	Calibrated Strength	fck (N/mm²)
Column	>28	42	37.87	30
Foundation	>28	36	24.5.6	20
Horizontal Beams	>28	44	38.8	30

A comparative analysis of these results against the original design specifications and in situ tests revealed that the concrete has not experienced significant chemical degradation over time. Consequently, the material properties have remained stable, ensuring structural reliability.

2.2.2. Laboratory tests - Testing the masonry unit-clay bricks

Samples of masonry units were carefully extracted from the building for detailed compression strength testing in the laboratory of the Faculty of Civil Engineering. A total of six clay bricks, each with standardized dimensions of 250 × 120 × 62 mm, were selected and grouped into three representative testing samples. The structural behavior of wall elements is intrinsically linked to the mechanical properties of the masonry units, which play a pivotal role in the overall seismic and load-bearing performance of the infill walls.

In this context, the infill walls of the studied building were partially constructed using clay bricks. Compression strength tests were carried out in strict compliance with Standards EN 772, ensuring the reliability and accuracy of the obtained results. These tests provided valuable insights into the mechanical characteristics of the masonry units, including their ability to withstand compressive forces under operational conditions. The findings are summarized in Table 2, which presents a detailed overview of the compression properties of the sampled materials.

Table 2. Testing results of clay bricks

Sample	Load (kN)	Mean value (N/mm²)	Shape factor	f_b (N/mm²)	
S"1"	770	24.3			
S"2"	706	23.5	0.75	16	
S"3"	460	16.0			

2.3. In situ testing - Ambient Vibration Test

Ambient vibration testing is a non-destructive technique utilized to evaluate the dynamic properties of structures by examining their responses to natural environmental excitations, such as wind, traffic-induced vibrations, or human activity. This approach is widely applied to determine critical parameters including natural frequencies, mode shapes, and damping ratios of the structural system [15].
Measurement points were strategically located according to the prescribed measurement protocol, ensuring that the selected positions were free from steady-state vibrations caused by eccentric machinery or other rotary influences. In instances where transient frequencies were identified, they were carefully filtered out during the signal processing phase to ensure the accuracy of the results [16].
The testing process employed standard equipment for structural analysis, which included accelerometers, advanced data acquisition systems, signal processing software, and controlled excitation sources. Key considerations during the procedure involved minimizing environmental interference, optimizing sensor placement, and maintaining high data quality. This method offers several advantages, including its non-invasive nature, speed, and simplicity, allowing it to be performed

Copyright © 2025 CroCEE
DOI: https://doi.org/10.5592/CO/3CroCEE.2025.43

on active structures without disrupting their normal operations. Since the vibration amplitudes in such tests are small, ambient vibration testing effectively captures the linear behavior of structures. Previous studies have demonstrated that results obtained from ambient vibration tests are consistent with those from forced vibration experiments conducted within the linear excitation range [17].
Data acquisition involved the conversion of analog signals from the sensing devices into digital formats, followed by permanent storage for subsequent analysis. Rigorous checks were performed to address potential errors arising from quantization, aliasing, filtering, and signal leakage. These steps were essential to ensure the integrity of the data and to derive accurate parameter estimates [18]. The detailed layout of the measurement points and the testing plan for each floor are illustrated in Fig. 4.

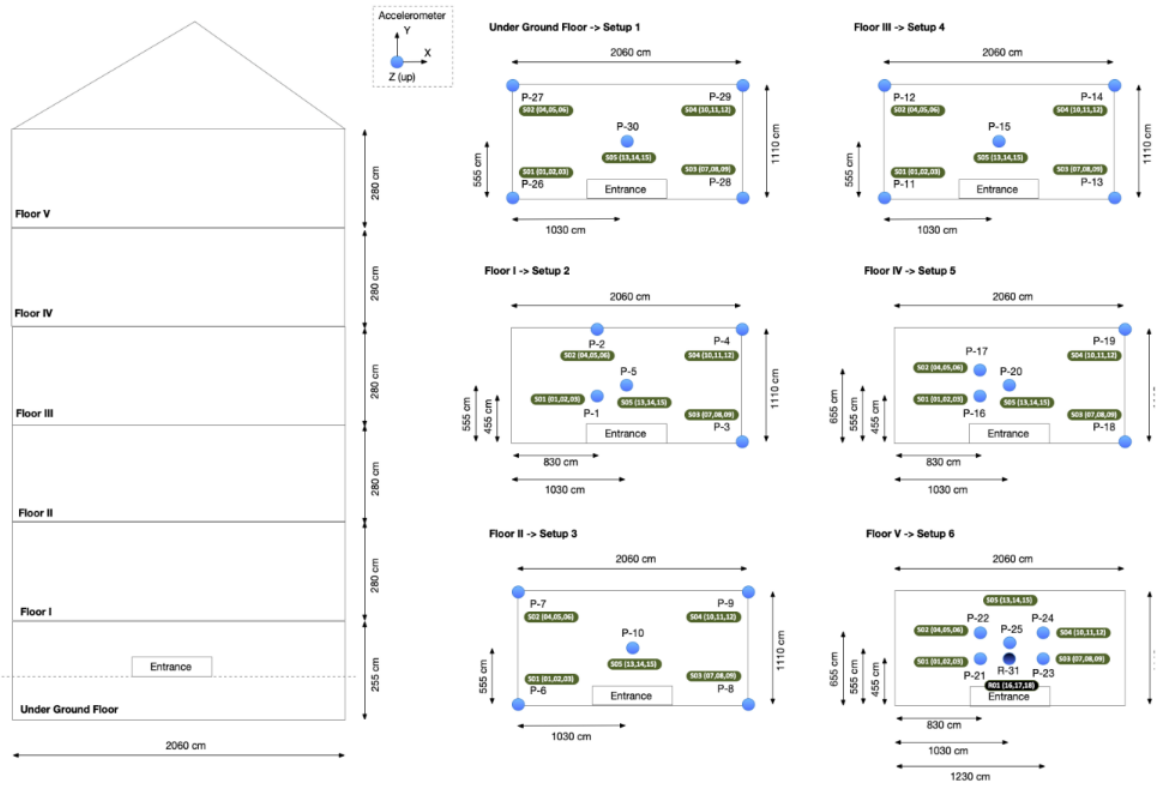


Figure 4. Layout of locations the accelerometers

2.3.1. Testing results

The measurements were conducted on April 20, 2024, starting from 9:30 a.m. and concluding at 1:00 p.m. Each measurement lasted a total of 300 seconds, equivalent to 5 minutes. Given the analysis of multiple measurement series, the calculated singular values were averaged to display the curves effectively. Additionally, the identified mode shapes, along with their corresponding direction, frequency (f), and period (T), are summarized in Table 3. Fig. 5 present singular values of spectral densities.[15].

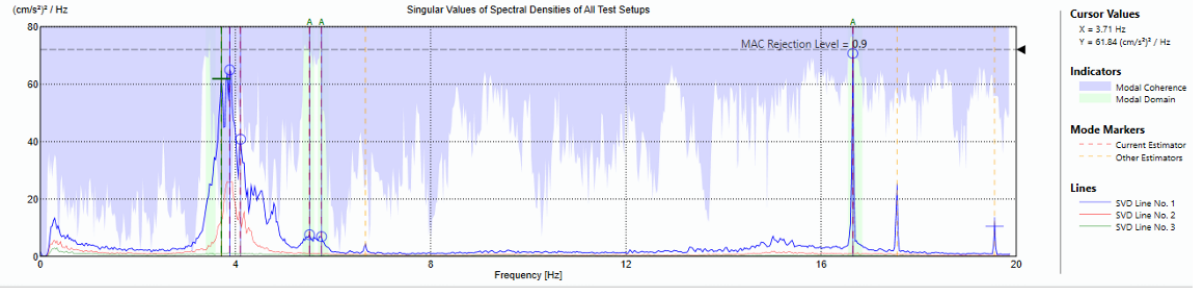
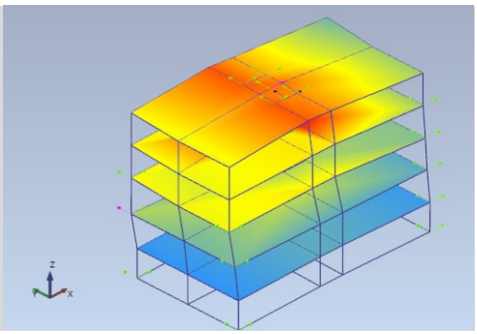


Figure 5. EFDD singular values of spectral density for all setups[14]

Proceedings of the 3rd Croatian Conference on Earthquake Engineering - 3CroCEE
19–22 March 2025, Split, Croatia
Copyright © 2025 CroCEE
DOI: https://doi.org/10.5592/CO/3CroCEE.2025.43

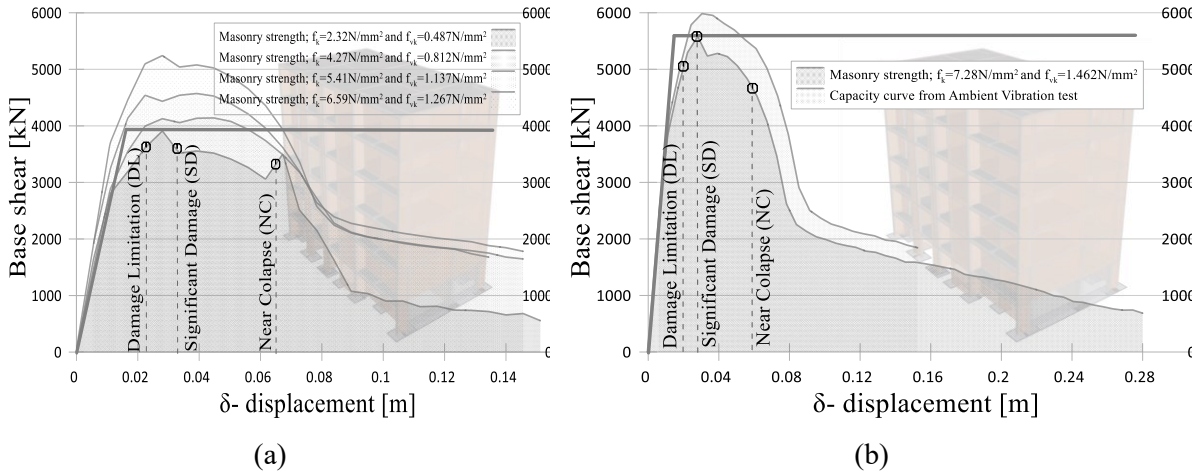
The analysis identified a total of 8 mode shapes, among which 4 can be considered global mode shapes with frequencies f1=3.711 Hz, f2=4.102 Hz, f3=5.518 Hz and f4=5.762 Hz. The remaining mode shapes are local, signifying independent oscillations of individual or adjacent. structural elements [15].

Table 3. Identified dynamic properties of study case

Mode shape	Description	f(Hz)	T(sec)	
1	Translations in Y direction slight rotation	3.711	0.269	
2	Translations in X direction slight rotation	4.102	0.244	
3	Torsion	5.5.18	0.181	

3. Parametric study

Infill walls significantly influence the global and local behavior of structures. Globally, they enhance stiffness and strength, improving seismic performance and dynamic characteristics. Locally, they affect load distribution and may induce failure mechanisms like soft-story or short-column effects. To study these impacts, a nonlinear static analysis was conducted, calibrated with in situ test data. This method, essential for assessing buildings in seismic regions, involves pushover analyses under constant gravity loads (1.00G + 0.30Q) and incremental lateral forces to simulate seismic inertia. Self-weight and additional slab loads are included in the 3D model, with two vertical load patterns: uniform (simulating soft-story mechanisms) and modal (aligned with the fundamental mode shape). Analyses consider both positive and negative lateral directions, with accidental eccentricities to address mass and seismic motion uncertainties. Each pushover analysis produces a capacity curve (base shear vs. horizontal displacement at a control node). Comparing capacity with demand from a 5% damped Linear Response Spectrum determines Limit States (Near Collapse, Significant Damage, or Damage Limitation). Structural demands, verified against Eurocode 8 - Part 3, account for brittle and ductile behaviors, material nonlinearity, and section interaction effects.



(a) (b)

Figure 6. Calibration of capacity curves: (a) Influence of masonry properties on structural dynamic behavior; (b) Field-test-based comparison

The initial model assumes masonry with moderate mechanical performance, simulating a scenario where lower-cost, lower-performance masonry products are used. This assumption leads to discrepancies in modal periods and frequencies compared to the calibrated model. Despite this moderate

Copyright © 2025 CroCEE
DOI: https://doi.org/10.5592/CO/3CroCEE.2025.43

characterization, the overall influence of the masonry on the structure's behavior is relatively high, with a notable 25% difference observed in the DL state between the initial and calibrated model (fig. 6(a)).

Experimental tests on the masonry units demonstrated performance exceeding the characteristic strength determined in laboratory conditions. However, while the structure includes confined masonry, the initial modeling treated all masonry as unconfined, introducing inconsistencies in the calibration of the final model, which incorporates test-based properties as represented in fig. 6(b). As the project documentation does not explicitly identify the confined masonry elements, further field investigations are needed to refine the capacity curves and address these uncertainties.

To account for the influence of confined masonry, assumptions were made based on the construction techniques likely employed during the building's execution. Masonry along the perimeter and near the main corridor was presumed to be confined. As illustrated in Fig. 7(b), incorporating these assumptions reduces the discrepancy in base shear, bringing the differences in DL and SD states to below 10%. However, additional destructive and non-destructive testing is essential to verify the locations and properties of the confined masonry.

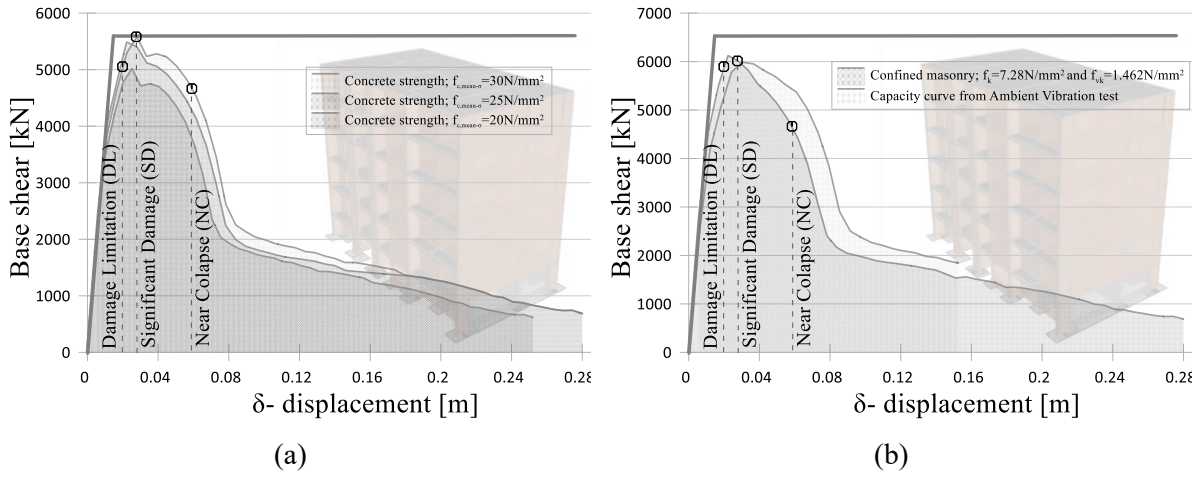


Figure 7. Calibration process of capacity curves; (a)impact of concrete strength, (b)calibration considering confined masonry

Field testing of concrete mechanical properties revealed that the in-situ performance of the concrete exceeds the specifications outlined in the project documentation. The observed mechanical properties suggest a higher concrete strength class than initially assumed in the design phase. This discrepancy highlights the potential for underestimation of the concrete's structural contribution in the original project specifications.

To evaluate the impact of concrete strength on structural behavior, a series of parametric study cases was conducted, each representing different levels of concrete strength. These cases examine variations in stiffness, load-bearing capacity, and overall structural performance under seismic and gravitational loads. The results, as illustrated in Fig. 7(a), provide a comparative analysis of how variations in concrete strength influence the capacity curve, particularly in terms of base shear and displacement thresholds. This analysis demonstrates the critical role of accurate characterization of material properties in structural modeling and the potential benefits of higher-than-expected concrete performance for improving the building's seismic resilience.

4. Results

The analysis presented in this study further highlights the critical role of historical records in understanding and improving the structural knowledge of the analyzed building. Data collected from the city archive was instrumental in defining the structural layout and characteristics, enabling accurate

Copyright © 2025 CroCEE
DOI: https://doi.org/10.5592/CO/3CroCEE.2025.43

modeling and assessment. Detailed structural analysis revealed that the building's capacity is sufficient to withstand the Peak Ground Acceleration (PGA) for the designated seismic zone, primarily due to the stabilizing effect of the infill walls. However, the absence of these infills significantly compromises the structural integrity, making it prone to severe damage and potential unusability. Additionally, the displacement associated with the limit states is reduced as masonry strength increases, indicating better overall structural integrity under seismic loads. For higher masonry strength, the range between DL and SD states narrows, suggesting a stiffer response and a reduced likelihood of intermediate damage during seismic events. These findings emphasize the critical role of masonry strength and infill walls in determining the structure's seismic performance. Accurate material characterization, combined with historical data, proves essential for reliable predictions and improved structural resilience, underlining the importance of integrating both engineering analysis and historical research in the assessment of heritage structures.

The results in Fig. 6(a) demonstrate a significant influence of masonry strength on the structural response. Variations in masonry strength impact both the base shear capacity and the displacement thresholds corresponding to the DL, SD, and NC states. Specifically, masonry with higher strength (f_m=6.59 N/mm^2) exhibits a notable increase in peak base shear capacity, approximately 35–40% higher than that of the lowest strength masonry (f_m=2.32 N/mm^2). This improvement reflects the enhanced stiffness and strength provided by higher-performance masonry materials, which contribute to greater resistance against lateral forces.

Variations in concrete strength as depicted in fig. 7(a) directly affect the base shear capacity and displacement thresholds corresponding to the DL, SD, and NC states. Structures with higher concrete strength exhibit an approximately 10–15% increase in peak base shear capacity compared to those with lower strength, reflecting their enhanced resistance to lateral forces. Additionally, higher-strength concrete reduces displacements at all limit states, indicating improved structural stiffness and overall seismic resilience.

As illustrated in fig. 7(b) The results underscore the critical role of confined masonry in enhancing structural performance under seismic loading. The incorporation of confined masonry with properties of significantly improves the capacity curve, as evidenced by increased base shear capacity and better alignment with the capacity curve derived from Ambient Vibration tests. Confined masonry contributes to higher stiffness and strength, which delays the transition between the Damage Limitation (DL), Significant Damage (SD), and Near Collapse (NC) states.

The enhanced confinement effects narrow the gap between numerical predictions and field-test results, reducing discrepancies in both displacement and base shear. These findings highlight the necessity of accurate field validation and appropriate modeling of confined masonry to capture its stabilizing effects. Confined masonry, particularly near the building perimeter and structural corridors, plays a pivotal role in ensuring seismic resilience and must be prioritized in assessment and retrofitting strategies.

Acknowledgements

All authors contributed to the study conception and were supported by the Ministry of Education Science and Technology through a bilateral project: “Assessment and repairing of buildings in Ulpiana-Prishtina”.

References

[1] Meena, D., Bansal, A., Bharathi, M. (2024): Seismic analysis of low-rise and high-rise buildings and their foundation design. *Asian Journal of Civil Engineering,* 25, 5215–5226, doi: 10.1007/s42107-024-01108-7.

Copyright © 2025 CroCEE
DOI: https://doi.org/10.5592/CO/3CroCEE.2025.43

[2] Pereira, E., Andrade, R., Leitão, F., Carobeno, C., Siqueira, G. (2024): Seismic risk evaluation of non-ductile low-rise RC buildings in Brazil: Time-based and intensity-based assessments considering different performance metrics. *Journal of Building Engineering,* 88, 109147, doi: 10.1016/j.jobe.2024.109147.

[3] Akkar, S., Bommer, J.J. (2010): Empirical Equations for the Prediction of PGA, PGV, and Spectral Accelerations in Europe, the Mediterranean Region, and the Middle East. *Seismological Research Letters,* 81 (2), 195–206, doi: 10.1785/gssrl.81.2.195.

[4] Mpampatsikos, V., Nascimbene, R., Petrini, L. (2008): A Critical Review of the R.C. Frame Existing Building Assessment Procedure According to Eurocode 8 and Italian Seismic Code. *Journal of Earthquake Engineering,* 12, 52–82, doi: 10.1080/13632460801925020.

[5] Varum, H., Furtado, A., Rodrigues, H., Oliveira, J., Vila-Pouca, N., Arêde, A. (2016): Seismic performance of the infill masonry walls and ambient vibration tests after the Ghorka 2015, Nepal earthquake. *Bulletin of Earthquake Engineering,* doi: 10.1007/s10518-016-9999-z.

[6] Meli, R. (1973): Behavior of Masonry Walls under Lateral Loads. *Fifth World Conference on Earthquake Engineering,* Tokyo-Kyoto, Japan, VI.

[7] Alcocer, S., Meli, R. (1995): Test Program on the Seismic Behaviour of Confined Masonry Walls. *The Masonry Society Journal,* Boulder, USA.

[8] Pujol, S., Climent, A.B., Rodriguez, M.E., Smith-Pardo, J.P. (2008): Masonry Infill Walls: An Effective Alternative for Seismic Strengthening of Low-Rise Reinforced Concrete Building Structures. *The 14th World Conference on Earthquake Engineering,* Beijing, China.

[9] Dolsek, M., Fajfar, P. (2008): The effect of masonry infills on the seismic response of a four-storey reinforced concrete frame – A deterministic assessment. *Engineering Structures,* 30, 1991–2001, doi: 10.1016/j.engstruct.2008.01.001.

[10] Birtharia, A., Jain, S.K. (2015): Applications of Ambient Vibration Testing: An Overview. *International Research Journal of Engineering and Technology (IRJET),* 2 (5), August 2015.

[11] Trifunac, M.D. (1970): Ambient Vibration Test of Thirty-Nine Storey Steel Frame Building. *Report No. EERL 70-02,* National Science Foundation, California Institute of Technology, Pasadena, California.

[12] SeismoSoft (2006): *SeismoStruct—A Computer Program for Static and Dynamic Nonlinear Analysis of Framed Structures* [Online]. Available at: http://www.seismosoft.com.

[13] ETABS: *A Computer Program for Static and Dynamic, Linear and Nonlinear Analysis of Structures.* Available at: https://www.csiamerica.com/etabs.

[14] Abdelaziz, M., Gomaa, M., El-Ghazaly, H. (2019): Seismic evaluation of reinforced concrete structures infilled with masonry infill walls. *Asian Journal of Civil Engineering,* 20, doi: 10.1007/s42107-019-00158-6.

[15] Churilov, S., Micevski, S., Dumova-Jovanoska, E. (2018): Ambient vibration testing of public unreinforced masonry buildings from the beginning of the 20th century.

[16] Noroozinejad Farsangi, E., Bogdanovic, A., Rakicevic, Z., Poposka, A., Stojmanovska, M. (2021): Structural response of unreinforced masonry buildings under ambient vibration tests. *Earthquake Engineering Research Reports,* Belgrade, Serbia.

[17] Trifunac, M.D. (1970): Ambient Vibration Test of Thirty-Nine Storey Steel Frame Building. *Report No. EERL 70-02,* National Science Foundation, California Institute of Technology, Pasadena, California.

[18] Omenzetter, P., Beskhyroun, S., Shabbir, F., Chen, G.W., Chen, X., Wang, S., Zha, W. (2013): Forced and Ambient Vibration Testing of Full-Scale Bridges. *Report to Earthquake Commission Research Foundation,* Project No. UNI/578.

Proceedings of the 3rd Croatian Conference on Earthquake Engineering - 3CroCEE
19–22 March 2025, Split, Croatia
Copyright © 2025 CroCEE
DOI: https://doi.org/10.5592/CO/3CroCEE.2025.45

PREDICTION OF MODAL FEATURES FOR DIFFERENT DAMAGE STAGES AND RETROFIT METHODS OF A MASONRY BUILDING

Maja Baniček [(1)], Mahmoud Shaqfa [(2)], Sara Vaing [(3)], Josip Atalić [(4)]

[(1)] *Postdoctoral Researcher, Croatian Centre for Earthquake Engineering, University of Zagreb, mbanicek@grad.hr*
[(2)] *Senior Scientist, Croatian Centre for Earthquake Engineering, University of Zagreb, mshaqfa@grad.hr*
[(3)] *PhD Student, Croatian Centre for Earthquake Engineering, University of Zagreb, svaing@grad.hr*
[(4)] *Professor, Department of Engineering Mechanics, Faculty of Civil Engineering, University of Zagreb, atalic@grad.hr*

Abstract

Under seismic and gravity loads, existing unreinforced masonry (URM) cultural heritage buildings are vulnerable and prone to damage. With careful calibration and thorough validation, credible results can be obtained from numerical tools, but this process requires reliable experimental data. Therefore, various blind prediction contests have been held recently. This paper discusses the results of a blind prediction contest of a two-story URM building that consists of a masonry vault above the ground floor and timber floor above the first floor. This contest was launched in 2023 under the DETECT-AGING project to test the damage detection capabilities of the (Structural Health Monitoring) SHM system and the reliability of numerical tools.

After generating the macro-model of the URM building, we used the implicit finite element (FEM) scheme to test the model using Abaqus software. Parametric analyses were held to calibrate key parameters of the numerical model, such as the activation and deactivation of installed steel anchors and horizontal ties, stiffness of the orthotropic timber material and the material parameters of the Concrete Damage Plasticity (CDP) model for masonry. This calibration was held following the experimental data provided included in the published competition documentation. The results of the numerical model represent the submitted prediction sheet. In general, the numerical results showed differences in modal shapes and frequencies compared to a reference state with a significant change in the damaged states.

Keywords: masonry, numerical modelling, modal parameters, non-invasive retrofitting methods

1. Introduction

Unreinforced masonry (URM) buildings and cultural heritage are vulnerable to seismic and vertical loads. While significant attention has been given to the seismic vulnerability of URM structures, less focus is on damage from aging, degradation, and soil settlement [1]. Retrofitting for seismic and vertical resilience includes invasive and non-invasive techniques. Invasive methods are time and cost-intensive, whereas non-invasive options are more economical, preventive, and often allow residents to stay in place [2]. Non-invasive methods use fiber-reinforced polymers (FRP), fabric-reinforced cementitious (FRCM) systems, and steel ties or anchors to enhance structural performance with minimal changes in the structure itself.

Engineers have tailored numerical tools and multiple methodologies to assess the performance of damaged structures and the impact of non-invasive retrofitting approaches on existing URM buildings. (maybe add examples with REFs). With careful calibration, credible results can be obtained from numerical tools, however, this process requires reliable experimental data for validation. During the last two decades, various blind prediction contests and experiments have been held to obtain reliable experimental data to test different approaches for numerical modelling of URM structures. One of the recent examples of shake table tests of a full-scale stone masonry structure was performed at the EUCENTRE laboratory [3], where the strengthening methods were applied to the structure in the mean of steel ties, steel ring beam and extra layer of planks to study the influence of the retrofit on the structure response during the seismic loading. More recently, another blind prediction contest of shake table test of a stone masonry aggregate buildings [4] were conducted. The latter contest focused on

Copyright © 2025 CroCEE
DOI: https://doi.org/10.5592/CO/3CroCEE.2025.45

assessing the strengthening strategies applied upon significantly damaged building unit via anchoring the timber beams to the walls to prevent out-of-plane failure.

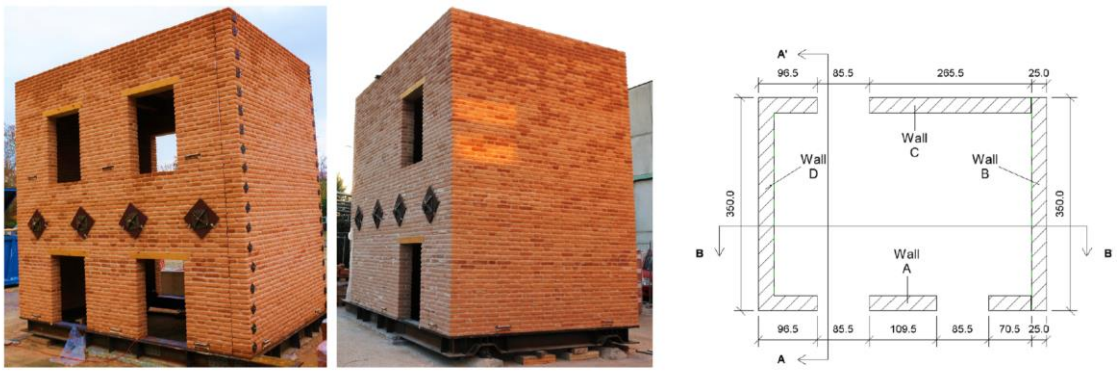
To test different approaches for numerical modelling of a URM structure in a different stages of non-invasive retrofit and damage, four Italian universities (Bologna, Genoa, Napoli Federico II, and Perugia) have launched a blind prediction contest in 2023 as part of the DETECT-AGING (Degradation Effects on sTructural safEty of Cultural heriTAGe constructions through simulation and health monitoring) project to test the damage detection capabilities of the SHM system and the reliability of different types of numerical models [5]. For the blind prediction test, a two-story masonry building was built, consisting of a single room with a masonry barrel vault above the ground floor and a wooden floor above the first floor. Measurements were carried out using the hybrid SHM system based on vibration measurements (with accelerometers) and strain measurements (with a smart brick system).

In our research, for building the model of the structure we used macro-modelling approach, where masonry is modelled as continuum with 3D solid elements. A series of sensitivity analyses were performed to calibrate key parameters of the numerical model, such as the wall-to-wall connection by tensioning steel anchors, activation and deactivation of the horizontal steel ties, stiffness parameters of the timber floor and parameters of CDP (Concrete Damage Plasticity) material model for masonry walls and vaults, by comparing experimental data included in the published competition documentation.

2. Geometry of the structure and structural elements

As a sample of the blind prediction, a two-story full-scale masonry building was built, with main dimensions of the building footprint measured 4.72 m by 3.50 m, and its total height was 4.67 m. The structure incorporates a single chamber with a masonry barrel vault of thickness 12 cm above the ground level and a wooden floor at the first level (Fig 1). The timber floor on the first floor is made of wooden planks of thickness 50 mm nailed to wooden beams of dimensions of 200 mm × 280 mm × 3250 mm supported by masonry walls A and C. Above each door or window opening, wooden lintel beams were installed with cross sectional dimensions 250 × 100 mm.

While walls A, B, and C collectively form a structural connected part of the structure, wall B is initially structurally separated from walls A, B and C and is subsequently joined to the other walls using 18 tensioned anchors on each vertical side of the wall B to ensure structural integrity. Additionally, above the ground floor, four steel ties were installed during the construction of the building connecting walls A and C.



a. b.

Figure 1. a) The real constructed a full-scale URM structure; b) footprint of the model

3. Numerical model

To construct the geometry of a detailed numerical model incorporating all structural components, we utilized the Computer-Aided Design (CAD) tool Rhino [6] alongside a visual script developed in Grasshopper [7]. For numerical modeling and analysis, we employed the Computer-Aided Engineering (CAE) software ABAQUS [8]. A flowchart illustrating the process of generating a numerical model of

Copyright © 2025 CroCEE
DOI: https://doi.org/10.5592/CO/3CroCEE.2025.45

the structure is illustrated in Fig 2. The numerical model was developed in phases, corresponding to the six experimental cases, as outlined below:

Case A: Initial Configuration. The referent model represents a masonry building consisting of three structurally connected walls (A-D-C) and one structurally separated wall (B). In this configuration, wall B is strongly connected to walls A and C via anchors applying 14 kN of force per connection. All steel ties are pre-installed during the construction phase and activated in case A. The structure includes a barrel-vaulted masonry ceiling above the ground floor and a wooden floor system composed of beams and a single layer of wooden planks at the upper level. Additionally, gravel and concrete blocks are assigned as additional mass loads on the vault and timber floor in all simulated cases.

Case B: Weak connection simulation. In this case, the anchor connections between walls B and A-C are released, reducing the force in each anchor to 0 kN to simulate weak connections.

Case C: Stiffened wooden floor. The upper-level wooden floor is reinforced by adding a second layer of wooden planks placed perpendicular to the original layer, enhancing its stiffness.

Case D: Reduced floor stiffness and tie release. This case reverts Case C floor stiffening by removing the second plank layer and releasing two middle steel ties.

Case E: Mortar removal simulation. 2.5 cm of mortar is removed from both the inner and outer surfaces of masonry walls A and C, up to a height of one meter from the base, simulating degradation or intentional material reduction.

Case F: Foundation settlement simulation. A 10 mm foundation settlement is introduced beneath wall D to assess structural response to differential settlement.

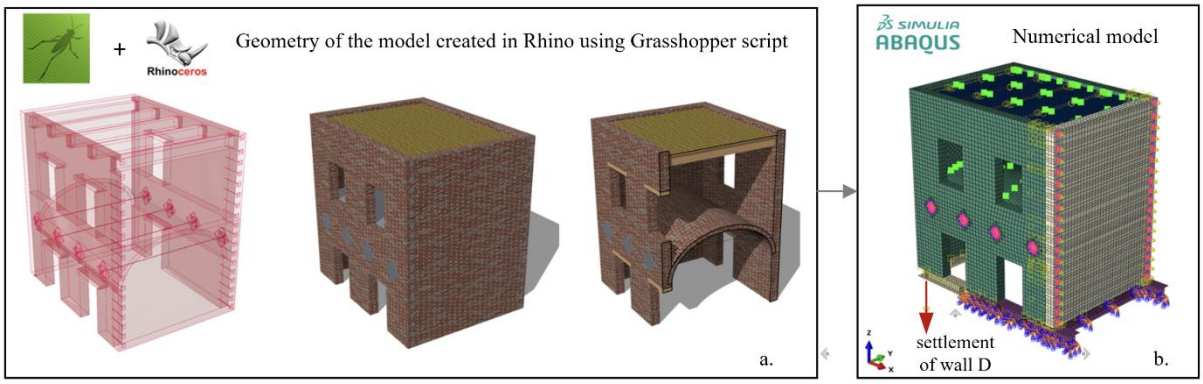


Figure 2. a) 3D view of Grasshopper and Rhino model with a cross section; b) numerical model

3.1.Loads

The model accounted for self-weight, incorporated as mass density, and additional gravel and concrete block loads applied to the vault and wooden floor. Tensile forces of 14 kN per anchor ensured structural integrity of wall B with walls A and C. Furthermore, tension bolt forces were applied to activate all four steel ties connecting walls A and C. In Case F, the foundation settlement beneath wall D was introduced by imposing a 10 mm displacement on the steel foundation beams, simulating ground movement effects.

3.2. Material properties

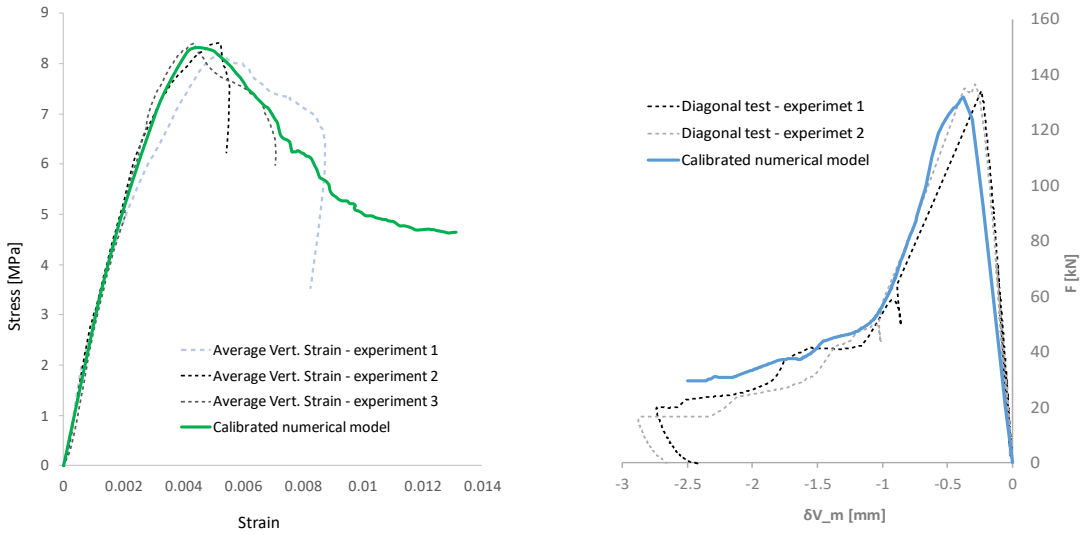
The numerical model incorporates steel for anchors, ties, and foundation beams, while timber is used for lintels and wooden beams, assuming isotropic mechanical properties. The timber planks above the first floor are modeled as an orthotropic shell, accounting for different stiffness values in the two principal orthogonal directions. In Case C, the thickness and mechanical properties of the wooden floor are modified during later analysis steps to simulate the installation of an additional plank layer oriented orthogonally to the first layer.

Copyright © 2025 CroCEE
DOI: https://doi.org/10.5592/CO/3CroCEE.2025.45

For modelling of masonry material for walls and vault in ABAQUS, we utilized the Concrete Damage Plasticity (CDP) model [9]. The material properties were calibrated through parametric analysis, using experimental data to fine-tune the CDP parameters. To streamline this process, we developed a visual script in Grasshopper, allowing for interactive modification of the material properties within the ABAQUS numerical model. This approach significantly enhanced the efficiency of the calibration process. The mechanical properties of the masonry material were determined through vertical and diagonal compression tests [5], resulting in average values listed in Table 1. The material model was first calibrated using compression test data, followed by diagonal test data validation. The results of the final calibrated model for both test simulations are presented in Fig. 3a and Fig. 3b.

Table 1. Elastic properties of masonry material

Parameters	***fc* [MPa]**	**E [MPa]**	**ν (-)**	***ft* [MPa]**
Values	8.33	2976	0.34	0.21



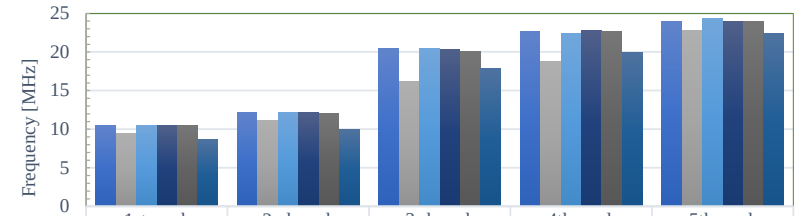
a. b.

Figure 3. Numerical simulations of experiments: a) compression test (stress-strain), b) diagonal compression test (force- relative vertical displacement of speciment)

4. Analysis and results

Figure 4 presents a comparative analysis of the frequencies corresponding to the first five significant modes across all six cases. As observed, the most significant frequency shifts occur in Cases B and F, which is expected, as both scenarios simulate structural damage. Case B represents a weak vertical wall-to-wall connection between wall B and the rest of the structure, significantly reducing the global stiffness of the structure and leading to notable frequency changes. Case F simulates foundation settlement beneath wall D, inducing structural deformations and further altering the modal characteristics. In contrast, Cases C, D, and E, which involve non-invasive strengthening methods, exhibit no significant frequency variations in the first four modes. However, a slight increase in frequency is observed in the fifth mode, indicating a minor influence of these modifications on the higher-order dynamic response of the structure.

Copyright © 2025 CroCEE
DOI: https://doi.org/10.5592/CO/3CroCEE.2025.45



	1st mode	2nd mode	3rd mode	4th mode	5th mode
Case A	10.511	12.163	20.388	22.63	24.02
Case B	9.434	11.182	16.12	18.811	22.804
Case C	10.542	12.205	20.416	22.462	24.375
Case D	10.511	12.147	20.324	22.794	24.011
Case E	10.464	12.009	20.137	22.606	23.884
Case F	8.727	10.011	17.812	19.888	22.415

Figure 4. Values of frequencies that correspond for each mode and case

To better understand the changes in modal shapes between a case with a good (Case A) and a poor (Case B) wall-to-wall connection, we compared the modal displacements of the first three modes, as shown in Figure 5. The differences between these modal shapes are further visualized in Figure 6.

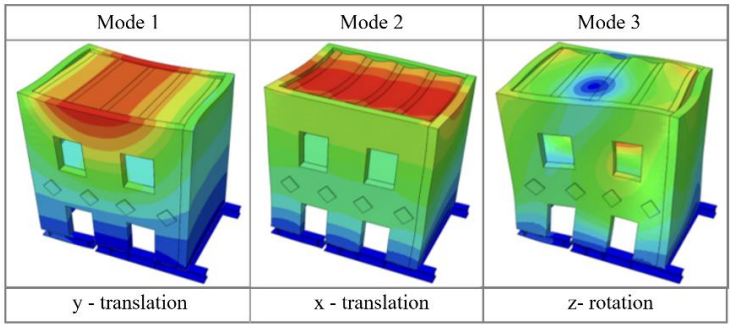


Figure 5. First three modal shapes for the difference in displacements between case "A" and "B"

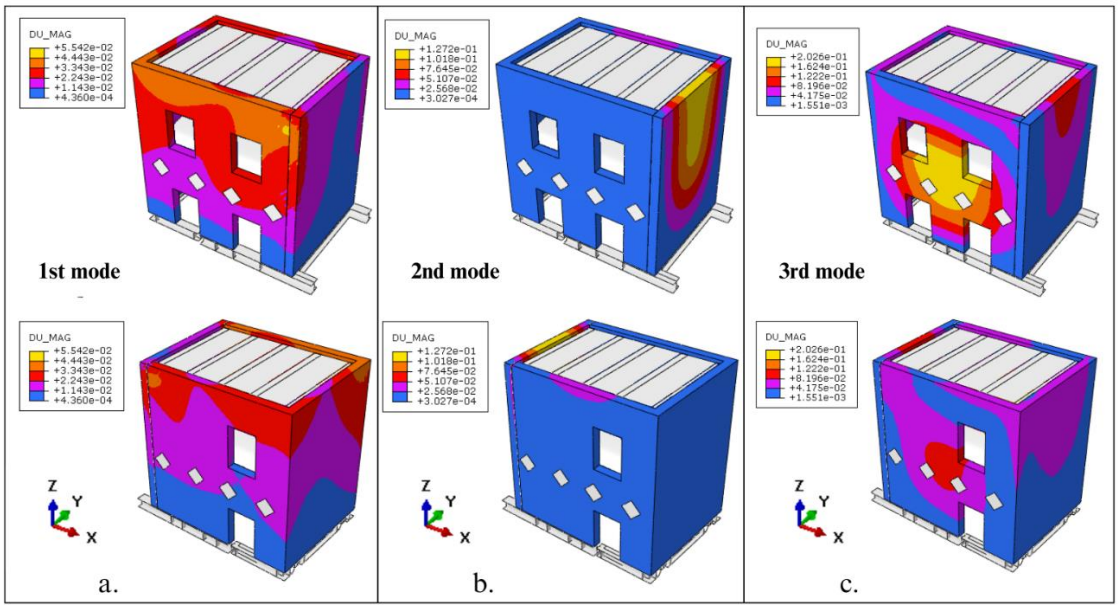


Figure 6. 3D visualization of differences in displacement of the first three modal shapes: between case "A" and "B": a) in y – displacement, b) x – displacement and c) z - rotation

Copyright © 2025 CroCEE
DOI: https://doi.org/10.5592/CO/3CroCEE.2025.45

5. Conclusion and future work

The results obtained with the numerical model showed differences in modal shapes and frequencies compared to a referent case "A" with a significant change in the damaged states "B" and "F". The cases with applied non-invasive retrofit methods did not show significant change in the frequencies, but these methods are crucial for out-of-plane.

This study is of a significant value for the Croatian engineering community as nearly all the constructed buildings in the historical center of Zagreb Downtown are URM structures Such structures are known for their high vulnerability to seismic activity, a fact highlighted by the recent 2020 earthquakes in central Croatia. These buildings, predominantly constructed in the late 19th and early 20th centuries, exhibit weak structural integrity between walls and floors. While the objective of the blind prediction competition was to assess damage accumulation from ageing, degradation, and soil settlement, the findings could also substantially contribute to numerical models for cost-effective, preventive and non-invasive retrofitting strategies for existing URM buildings against earthquake impacts in Zagreb Downtown.

For the future, we envisage working on first cross validating the current findings with other beam element models. Next, we will compare our results with the experimental findings and work on a post-diction paper. In that paper, we will use evolutionary algorithms (ES) to auto-calibrate our material properties and see how close we can get to the experimental results and the current numerical ones. The latter will also shed light on the reliability and trust of current engineering practices using commercial numerical software.

Acknowledgements

This research was funded by the Croatian Centre for Earthquake Engineering and Croatian Ministry of Science, Education and Youth, grant number A679117 – HPC – Research project in the field of Earthquake Engineering.

References

[1] Ertürk Atmaca, E., Genç, A. F., Altunişik, A. C., Günaydin, M., & Sevim, B. (2023). Numerical Simulation of Severe Damage to a Historical Masonry Building by Soil Settlement. *Buildings*, *13*(8), 1973. https://doi.org/10.3390/buildings13081973

[2] Dizhur, D., Ismail, N., Knox, C., Lumantarna, R., & Ingham, J. M. (2010). Performance of unreinforced and retrofitted masonry buildings during the 2010 Darfield earthquake. *Bulletin of the New Zealand Society for Earthquake Engineering*, *43*(4), 321–339. https://doi.org/10.5459/bnzsee.43.4.321-339

[3] Guerrini, G., Senaldi, I., Graziotti, F., Magenes, G., Beyer, K., & Penna, A. (2019). Shake-Table Test of a Strengthened Stone Masonry Building Aggregate with Flexible Diaphragms. *International Journal of Architectural Heritage*, *13*(7), 1078–1097. https://doi.org/10.1080/15583058.2019.1635661

[4] Tomić, I., Penna, A., DeJong, M. *et al.* (2024). Shake table testing of a half-scale stone masonry building aggregate. *Bull Earthquake Eng* **22**, 5963–5991. https://doi.org/10.1007/s10518-023-01810-y

[5] N. Buratti, S. Cattari, G. Lignola, A. Meoni, F. Parisi, F. Ubertini & G. Virgulto (2023). DETECT-AGING blind prediction contest: a benchmark for structural health monitoring of masonry buildings, *Procedia Structural Integrity*, 44, 2128-2135, doi: https://doi.org/10.1016/j.prostr.2023.01.272.

[6] R. McNeel and Associates: *Rhinoceros 3D*, www.rhino3d.com, 15.1.2024

[7] R. McNeel and Associates: *Grasshopper 3D*, www.grasshopper3d.com, 15.1.2024

[8] Dassault Systèmes: SIMULIA, User Assistance 2020, 2020.

[9] Lubliner, J., Oliver, J., Oller, S., & Oñate, E. (1989). A plastic-damage model for concrete. *International Journal of Solids and Structures*, 25(3), 299-326.

Proceedings of the 3rd Croatian Conference on Earthquake Engineering - 3CroCEE
19–22 March 2025, Split, Croatia
Copyright © 2025 CroCEE
DOI: https://doi.org/10.5592/CO/3CroCEE.2025.51

SEISMIC BEHAVIOUR OF PREFABRICATED WALL PANELS: AN OVERVIEW

Anđela Čavčić [(1)], Ivan Banović [(2)], Nikola Grgić [(3)], Alen Harapin [(4)]

[(1)] *Research and teaching assistant, PhD student, University of Split, Faculty of Civil Engineering, Architecture and Geodesy, acavcic@gradst.hr*
[(2)] *Assistant Professor, University of Split, Faculty of Civil Engineering, Architecture and Geodesy, ibanovic@gradst.hr*
[(3)] *Associate Professor, University of Split, Faculty of Civil Engineering, Architecture and Geodesy, ngrgic@gradst.hr*
[(4)] *Full Professor (tenure), University of Split, Faculty of Civil Engineering, Architecture and Geodesy, harapin@gradst.hr*

Abstract

Recent global events such as earthquakes, the COVID-19 pandemic, wars, floods, and similar crises, which have also affected Croatia, have highlighted the urgent need for rapidly deployable emergency shelters, hospitals, and both temporary and permanent housing solutions. Simultaneously, cities worldwide are grappling with accelerated population growth, creating a huge need for residential areas.

Prefabricated construction is an efficient solution to these challenges. It enables the faster construction of a greater number of industrial and residential units, helping to reduce demand while lowering the cost per square meter of housing or commercial space. In addition, prefabricated construction is considered sustainable as it minimizes the amount of waste and optimizes the use of materials [1]- a key advantage in today's construction industry.

Prefabricated wall panels, a fundamental component of such structures, are increasingly being used worldwide. However, these panels must meet stringent mechanical resistance and stability requirements to withstand all foreseeable impacts. It could be said that prefabricated wall panel systems are particularly susceptible to seismic (dynamic) actions. Numerous scientific studies have addressed this issue and undoubtedly established that the seismic resistance of these systems, and therefore of the entire prefabricated construction, is largely dependent on the quality of the joints between the panels.

The increasing number of prefabricated buildings, coupled with the growing frequency of earthquakes worldwide, has amplified the need for in-depth research on the seismic resistance of prefabricated reinforced concrete structures, where the greatest emphasis is placed precisely on prefabricated wall panels, i.e. on their mutual connections. For this reason, this paper aims to compile and analyze the conclusions and observations of previous research conducted by scientists worldwide on the topic of prefabricated reinforced concrete wall panels and their connections under the influence of earthquakes.

Keywords: seismic behaviour, prefabricated wall panels, prefabrication, connections, earthquake, etc.

1. Introduction

Conventional monolithic construction implies on-site building, which demands extensive space, labor, and machinery. Additionally, it is limited by weather conditions and other site-specific factors. This method reduces the potential for reusing and recycling materials, resulting in higher energy and time consumption and, consequently, increased CO_2 emissions. Higher CO_2 emissions contribute to climate change and atmospheric warming, leading to extreme weather events such as floods and droughts. This is a pressing global issue, underscored by the commitment made in the Kyoto Protocol, where EU member states and several other countries committed to cutting greenhouse gas emissions by 20% by 2020. The EU has since raised its target, committing to a 55% reduction by 2030 [1]. On the other hand, prefabricated construction is faster, more sustainable, and uses less time and energy, as components are

Proceedings of the 3rd Croatian Conference on Earthquake Engineering - 3CroCEE
19–22 March 2025, Split, Croatia
Copyright © 2025 CroCEE
DOI: https://doi.org/10.5592/CO/3CroCEE.2025.51

manufactured in factories, delivered to the site, and assembled on the location. This approach minimizes the dependency on weather and site conditions while allowing for greater quality control in production. Prefabricated elements can be easily reused, disassembled, and reassembled at different locations, making recycling much more feasible. Consequently, this reduces waste, and the energy required for production and recycling, ultimately lowering pollution levels. In addition, prefabricated components can be constructed with advanced insulating materials that improve their energy efficiency and the overall performance of the building, particularly in terms of thermal and acoustic insulation. Precast walls can also be designed with pre-installed ducts for utilities which significantly speeds up the installation of electrical, plumbing, and other systems. This reduces the need for additional construction work, saving both time and effort during the building process. Controlled factory environments make it easier to maintain consistent quality, and the use of advanced machinery, resulting in highly consistent outcomes and fewer structural issues. This is in contrast to traditional monolithic construction, where quality can vary significantly due to unstable weather conditions, human error, and various complications on site. Achieving consistent quality across all areas of a project is more challenging in conventional construction, as environmental and logistical factors are harder to manage.

Furthermore, rapid population growth demands quick solutions to meet housing needs. There is an increasing demand for residential units in the shortest possible time, and prefabricated construction provides a practical solution to this challenge. Unfortunately, the use of prefabricated construction is limited due to the lower load-bearing capacity of prefabricated structures under dynamic loads. For example, the 2012 Emilia earthquake led to the collapse of structures that were not properly connected. There have been several other instances where such structures sustained damage, primarily due to an insufficient understanding of the behaviour of joints and structural systems under stress [2]. Table 1 summarizes the key differences between prefabricated and monolithic construction based on specific criteria.

Although prefabricated construction offers numerous advantages, one notable drawback lies in the limited understanding of the behaviour of such structures, particularly under dynamic loads, such as earthquakes. Consequently, research into the behaviour of prefabricated structures has increased recently, with significant progress made over the past decade. In 1989, Foerster et al. [3] studied the behaviour of shear connections in prefabricated wall panels. Similar research continued through the 1990s, further exploring and refining the performance of these connections [4], [5], [6], [7]. In 2011, Pavese and Bournas [8] conducted an experimental study on the behaviour of prefabricated sandwich wall panels, both with and without openings, varying the dimensions of the openings, under seismic loading. They simulated the behaviour of fixed-end walls and cantilever walls. The tests revealed a strong interaction between shear and flexure due to the squat geometry of the panels. In their 2016 study, Palermo and Trombetti [9] proposed a new structural system that is consisted of lightly reinforced concrete sandwich panels characterized by a small proportion of reinforcement and a thin concrete layers. The system was tested under cyclic loading, and a non-linear model was developed, showing a strong correlation between experimental results and model predictions. It was concluded that the seismic performance of this structural system, in terms of ductility, strength, and stiffness, is comparable to that of monolithic RC (reinforced concrete) walls. However, greater attention needs to be given to the connections between such panels and the foundations. Research in this field continues, with Xu et al. in 2017 [10] investigating the seismic behaviour of wall panels with sleeve connections. Their study compared the performance of these panels to that of cast-in-place specimens and proposed several types of wall panel connections. Vaghei et al. [11] introduced an innovative method for connecting vicinal wall panels using two U-shaped channels joined through a male-female mechanism, secured with bolts and nuts. To enhance performance, a rubber element was integrated into the connection to effectively dissipate vibrations. Guo et al. [12] developed a new dry connection using high-strength bolts and plates, which was tested under shear loading and tension.

As prefabricated construction gained popularity, the number of published studies on this topic also increased, along with the variety of proposed and investigated types of wall panels, their

Copyright © 2025 CroCEE
DOI: https://doi.org/10.5592/CO/3CroCEE.2025.51

interconnections, and their connections to foundations and floor systems. According to the graph presented by Martins et al. [1] in Figure 2, the number of publications related to prefabricated wall panels (or their connections) rose after 2019, indicating a growing interest in prefabricated construction overall. This surge can likely be attributed to the COVID-19 pandemic, which created a pressing need for rapid construction of hospitals capable of accommodating large numbers of patients. A prime example of the capabilities of prefabricated construction is the Huoshenshan Hospital in China, built in just 10 days using prefabrication.

As mentioned earlier, 2019 saw an increase in interest in prefabricated construction, alongside a growing focus on sustainable building practices and climate change. Sebaibi et al. [13] focused on exploring methods to enhance energy efficiency in the prefabricated construction industry by minimizing the environmental impact of concrete through the incorporation of ground granulated blast furnace slag (GGBS) and ultrafine Portland cement (UC) and by removing thermal treatment. Conversely, a growing emphasis on innovative solutions is evident, both in the development of connection systems and the design of prefabricated wall types. Zhou et al. [14] introduced a novel dry connection method, referred to as sleeve and box connections, demonstrating its potential in prefabricated construction. Similarly, Han et al. [15] conducted a detailed investigation into the behaviour of double composite walls, with a particular focus on the influence of bolts within shear-loaded wall connections, providing valuable insights into their structural performance.

The analyzed data provide valuable insights into the benefits of prefabricated construction. However, there is still room for improvement and the development of advanced prefabricated wall panels and connection systems with enhanced seismic performance. These opportunities for progress extend beyond structural optimization, encompassing economic efficiency and sustainability considerations, thereby highlighting the necessity for further innovation in the field of prefabricated construction. The main purpose of this research is to provide a comprehensive review of the existing literature on this topic. The aim is to offer insights into innovations related to types of wall panels and their connections, as well as to provide an overview of the seismic testing methods that have been conducted so far. Additionally, the paper seeks to trace the progress of research over time and summarize the key findings of researchers worldwide. It also aims to highlight the existing gaps in the field, identify areas that require further investigation, suggest potential improvements, and provide recommendations for future research directions.

Table 1. Summary table

Criteria	Prefabrication	Monolithic construction
Construction time	Faster, simultaneous with site preparation	Slower, sequential
Quality control	High, standardized in factories	Variable, dependent on site conditions
Waste	Minimal, factory reuse possible	Higher due to reuse on-site
Energy consumption	Lower due to efficient production	Higher due to extended on-site work
Environmental impact	Minimal on-site, lower pollution	Higher site disruption, noise, and dust
Design flexibility	Moderate, modular focused	High, adaptable to custom designs
Cost	Potentially lower, with less labor	Often higher, with more labor required
Safety	Safer, controlled environment	More hazardous, dynamic on-site risks
Sustainability	Higher, easier to recycle	Lower, difficult to deconstruct

2. Types of precast walls

Progress in the study of wall panels and their response to seismic loads have driven the development of innovative ideas and increasingly effective design solutions. This progression has led to the emergence of various panel types, distinguished by differences in core materials and cross-sectional configurations. According to the literature, wall panels can be systematically categorized based on their assembly techniques and cross-sectional characteristics. These classifications primarily include three types:

Copyright © 2025 CroCEE
DOI: https://doi.org/10.5592/CO/3CroCEE.2025.51

sandwich wall panels, plain wall panels, and double wall panels. The following presents recent research by scientists regarding the previously mentioned types of walls.

2.1.Sandwich wall panels

In a study conducted in 2011 [8], the seismic performance of prefabricated sandwich wall panels was investigated through experimental testing. The panels were composed of two layers of sprayed concrete reinforced with wire mesh and a core of Expanded Polystyrene foam. Experimental tests were performed on specimens with and without openings, simulating the structural behaviour of cantilever and fixed-end walls. The results indicated that the proposed panel system shows potential for use in regions characterized by moderate and, potentially, high seismic activity. In his recent study, Hou, Hetao [16] proposed a novel type of wall sandwich panel consisting of an EPS (expanded polystyrene) core serving as insulation, flanked by two external panels reinforced with wire mesh. The external panels are interconnected by diagonal steel bars welded to the wire mesh reinforcement. The reinforced panels' inner surface can be either ribbed or flat. The study concluded that the diagonal bars are sufficient to transfer shear forces between the external panels, enabling the system to achieve full composite action for bending moment resistance. Additionally, it was noted that while the ribbed surface of the reinforced panels reduces the overall mass of the system, it may, on the other hand, lead to decreased flexural resistance in the sandwich wall panel. Figure 1. shows these types of sandwich wall panels. Ricci et al. [17] experimentally investigated the seismic performance of a novel type of sandwich squat wall panel. The structural system comprises a central layer of expanded polystyrene with a thickness ranging from 60 to 160 mm, enclosed by two outer layers of sprayed reinforced concrete. Seismic tests were conducted on the walls and their connections, leading to the conclusion that these panels exhibit behaviour closely resembling that of reinforced concrete wall panels. It is also important to highlight that this system is particularly well suited for low-rise residential buildings, where walls are longer than they are wide.



Figure 1. A novel type of sandwich wall panel investigated by Hou, Hetao [16]

2.2.Plain wall panels

Todut's 2014 study [18] presents findings from an experimental program examining the seismic performance of precast reinforced concrete wall panels with and without openings. All tested panels exhibited shear-type failure, significantly influenced by the type and size of openings, with critical areas and insufficient reinforcement observed in specific regions. Experimental observations revealed extensive cracking across all panel regions, reinforcement yielding, concrete crushing, and diagonal cracks in the piers. Panels with large openings showed notable reductions in stiffness and lateral resistance, along with reduced energy dissipation compared to panels with smaller openings. However, panels with larger openings demonstrated a greater deformation capacity. Overall, panels with small

Copyright © 2025 CroCEE
DOI: https://doi.org/10.5592/CO/3CroCEE.2025.51

openings were more effective in dissipating seismic energy, while large-opening panels exhibited increased deformability at the cost of reduced structural stiffness and energy dissipation. Figure 2. shows the manufacturing process of prefabricated reinforced concrete wall panels.



Figure 2. Manufacturing process for plain wall panel [18]

Bruno Dal Lago [19] explored the structural performance of a novel lightweight precast concrete wall system, developing two distinct solutions. The first solution involves a fully lightened wall, where selected hollow cavities are filled with in-situ concrete after the placement of reinforcing steel cages. The second solution features a partially lightened wall, where solid sections are cast during production, and the connections are formed using pre-installed mechanical devices, like rebar couplers. In his 2017 study, Guoshan Xu [10] investigated the seismic performance of a precast RC shear wall with a single-row grout-filled sleeve connection, designed for six-story precast box-modular structures with RC shear walls. The paper introduces a force-displacement mixed control method to manage the seismic response. Experimental results demonstrated that this method effectively controlled rotations, lateral deformations, and axial forces in specimens subjected to quasi-static cyclic loading. Additionally, a comparison between the prefabricated sandwich wall panels and a cast-in-situ specimen showed similar behaviour in terms of inter-story drift angle, failure mode, stiffness degradation, ultimate force, energy dissipation capacity, and ductility under combined axial-flexural-shear loading.

2.3. Double wall panels

Mackechnie, James R. in his 2013 study [20], explored the thermal performance of a 250 mm thick double wall composed of multiple layers shown in Figure 3. Toward the exterior, a 125 mm lightweight layer was placed, serving as thermal insulation, followed by a transition layer, and finally, a 75 mm thick heavyweight layer. The heavyweight layer was reinforced and provided thermal mass. The research progressed with the work of Han S. [15], who investigated the behaviour of double walls composed of two reinforced wall panels with ribbed cross-sections, connected using bolts. The space between the panels was then filled with cast-in-place (CIP) concrete. The specimens varied in design, including differences in the filling material, which was tested in reinforced and non-reinforced configurations. In a further advancement, Kim, Seungho [21] proposed an innovative double precast wall panel type consisting of two thin panels interconnected by lattice bars. The study aimed to improve the efficiency of retaining wall construction and to address existing challenges in reinforced concrete systems, offering a more effective solution for modern construction applications.

Copyright © 2025 CroCEE
DOI: https://doi.org/10.5592/CO/3CroCEE.2025.51

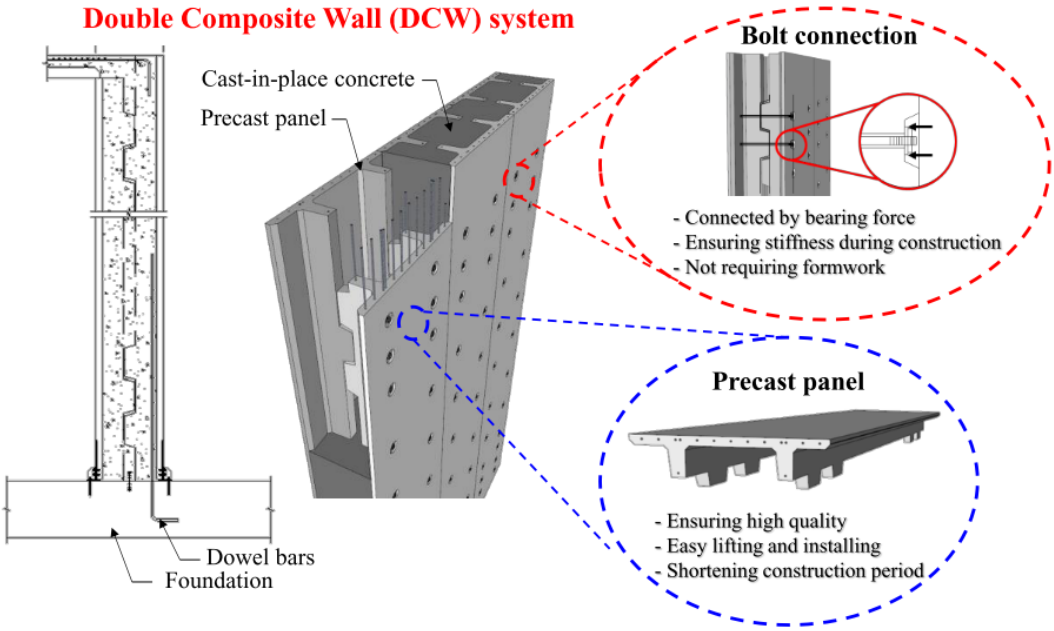


Figure 3. DCW system explored by Mackechnie, James R [20]

3. Precast wall connections

Load-bearing walls, including precast reinforced concrete walls, are required to effectively transmit vertical and horizontal loads without exceeding the ultimate or serviceability limit states. The connections between precast wall panels represent critical components in structural systems, as they must accommodate stresses induced by structural displacements caused by external loading or inherent concrete deformations, such as shrinkage, swelling, and thermal effects. Moreover, these connections play a key role in maintaining the overall stability of structural systems under seismic loading. It is well established that the seismic performance of precast wall systems is significantly affected by the design and implementation of panel connections.

To achieve satisfactory load-bearing capacity of the structural system, particularly under seismic actions, wall panels must be properly connected to the foundations, floor systems, and adjacent panels through both vertical and horizontal joints. These joints can be classified based on the type of structural elements they link or the technology employed in their construction. Depending on the construction methodology and materials utilized, joints are broadly categorized into wet and dry connections. Table 2. presents a chronological summary of scientific research and proposed joint typologies, predominantly assessed under shear stress conditions. These investigations aim to develop joint configurations that exhibit superior performance when subjected to seismic loads.

Table 2. Literature review on types of connections

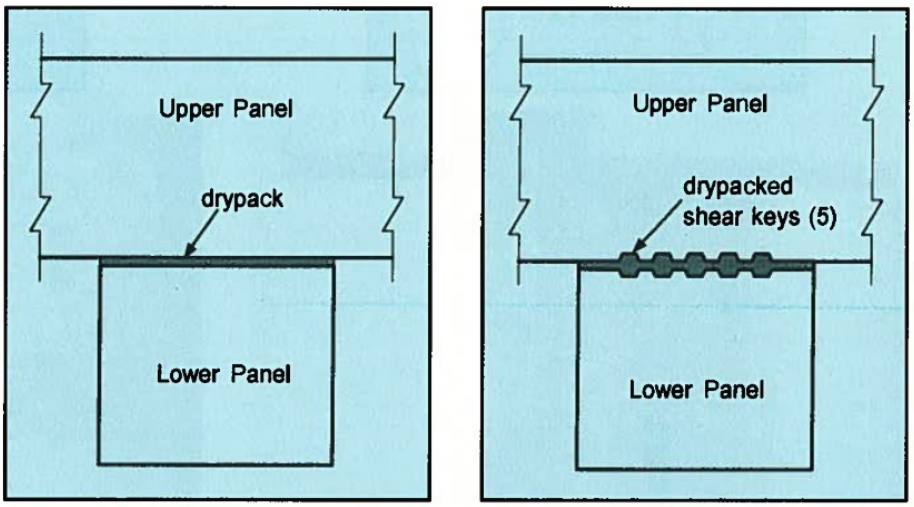
Type of connection	Authors	Year	Proposed/investigated types of connections
Wet connections	Soudki, Khaled A et al. [6]	1996	(a) The dry pack plain surface connection features a flat surface area filled with dry pack; (b) Multiple shear keys - The shear keys and the space between the panels are entirely filled with dry pack grout. There is no vertical reinforcement included at the connection interface to examine the effect of the shear keys only; (c) Rebars welded to the steel angle- The connection comprises a flat surface area featuring two mild steel bars. The straight bars extending from the top panel are welded to a steel angle located in an open pocket in the lower panel. After the welding process, the space between the panels is embedded with dry pack grout.

Proceedings of the 3rd Croatian Conference on Earthquake Engineering - 3CroCEE
19–22 March 2025, Split, Croatia
Copyright © 2025 CroCEE
DOI: https://doi.org/10.5592/CO/3CroCEE.2025.51

	Xu, Guoshan et al. [10]	2017	(a) a horizontal connection between walls where longitudinal reinforcement is indirectly spliced using grout-filled sleeves arranged in a single row; (b) a vertical connection between walls, featuring a stirrup that is bolted to vertical reinforcement; and (c) a non-composite floor slab joint
	Li, Jianbao et al. [22]	2017	Vertical seam connection that is divided into two groups (I and II) based on the placement of the columns' longitudinal reinforcement. Group I specimens, the longitudinal reinforcement is partially embedded in the prefabricated section, with the rest placed in the cast-in-place section. In contrast, all longitudinal reinforcement in Group II specimens is arranged entirely within the cast-in-place section.
	Biswal, Aparup et al. [23]	2019	Plane joint with U-bars at 250 mm spacing, plane joint with loop boxes at 250 mm spacing, plane joints with U-bars at 125 mm spacing, castellated joint with U-bars at 300 mm spacing, castellated joint with loop boxes at 300 mm spacing, and castellated joint with edge lips and loop boxes at 300 mm spacing
	Seifi, Pouya et al. [24]	2019	Connections with grouted metal ducts where bars are extending from the foundation, embedded within metal ducts later filled with non-shrinkage grout, while another end of the reinforcement was anchored into the foundation with a standard 90-degree hook. Variations were made in the shape and amount of reinforcement within the connection, as well as in the wall thickness.
	Kothandapani, Karthikeyan et al. [25]	2019	In the first set of specimens, rebars were used as dowels, with varying diameters, quantities, and spacing, as well as their position. Diameters of 10 mm and 12 mm were used at a spacing of 300 mm, 250 mm, and 150 mm. In the second set of specimens, gusset plates, steel angles, and bolts were used at the joint to connect the top and the bottom section either vertically, diagonally, or combined.
Dry connections	Foerster, Harry R et al. [3]	1989	(a) 20 mm wide dry pack grouted connection, (b) 25M continuity bars with dry pack grout, (c) 25M continuity bars with dry pack grout and type A shear connectors, (d) 25M continuity bars with dry pack grout and type B shear connectors, (e) dry pack grouted shear keys.
	Rizkalla, Sami H et al. [26]	1989	Three types of connections were tested: (a) a plain surface connection, 20 mm thick, and two types of shear key connections: (b) Small key consisting of four 50 mm high and 70 mm wide slots and (c) Large key consisting of two slots 100 mm high and 90 mm wide. The space in between was filled with a dry pack composed of sand, Portland cement, and water in a ratio of 2:1:0.2.
	Soudki, Khaled A et al. [6]	1996	(a) Dry pack Plain Surface specimen had a plain surface region that was filled with dry pack. This specimen was used as a controlled specimen to determine the impact of the dry pack on the connection behaviour. (b) Multiple dry packed shear keys without any reinforcement to focus on the shear keys' influence only. (c) A specimen with two mild rebars welded to a steel angle in the lower panel projecting into the upper panel. Following the welding, the gap between the panels is filled with a dry pack grout. (d) Post-tensioned strand connection is provided using two seven-wire strands positioned within galvanized steel ducts embedded in the panels. After the post-tensioning process, the ducts were infused with expansive grout. (e) Post-tensioned bars type of connection was the same as the previous one with the difference in the diameter and grade of the bars. Here, two 15.8 mm diameter prestressing bars with 1080 grade were used.
	Crisafulli, F. J. et al. [27]	2003	A welded steel consisting of a rectangular steel plate with a centrally located circular hole, measuring five hole diameters in length and 1.6 hole diameters in high welded with a weld thickness of *t*.
	Brunesi, E. et al. [28]	2017	The connection is achieved by leaving a hole of specified dimensions, which is subsequently grouted with mortar. Inside the hole, there is a hook connected to the longitudinal reinforcement using bolts and a steel plate.
	Wang, Wei et al. [29]	2018	The connection is established by welding the longitudinal reinforcement of the lower and upper panels to the connecting steel plates. A layer of high-strength mortar is cast on top of the lower panel beforehand. The steel plates

Copyright © 2025 CroCEE
DOI: https://doi.org/10.5592/CO/3CroCEE.2025.51

		from the lower panel are inserted into pre-formed channels in the upper panel. The positions of the upper and lower plates are adjusted to align the pre-defined holes on the plates, through which a bolt is inserted and tightened, securing the connection.
Psycharis, Loannis N. et al. [30]	2018	(a) Rebar connections are achieved using reinforcement bars that protrude from the panels and fit into prepared ducts within the beams while the space between the reinforcement bars and ducts is filled with non-shrinking, high-strength grout or epoxy resin. (b) Wall shoe connections are constructed using an anchor bolt set into the beam and a steel "wall shoe" built into the panel. (c) Steel plate connections use steel nests embedded in both the beam and the panel, which are secured to one another via a connecting plate.
Vaghei, Ramin et al. [11]	2019	Connection is achieved by utilizing two steel U-shaped channels attached to the sides of the walls. These channels are fastened together as male and female joints using bolts and nuts to ensure a secure connection. Additionally, a U-shaped rubber element is placed between the two channels to help dissipate vibrations within the structure.
Cai, Gaochuang et al. [31]	2019	Demountable vertical bolted joints were created using three reinforced concrete blocks, detachable steel bolts, and steel plates. The steel bolts and plates were arranged and the concrete blocks were joined together with secured bolts to form specimens.
Sun, Jian et al. [32]	2019	The horizontal connection between two wall panels is achieved using an H-connector and high-strength bolts. First, the top and bottom steel units, which have pre-drilled holes for the bolts, are cast onto the wall panels. Then, the H-connector and high-strength bolts are used to complete the connection.
Guo, Wei et al. [12]	2019	A new dry connection proposed here consists of high-strength bolts and anchored steel plate. The steel plate is made of Q345 steel, and is anchored using welded HRB400 rebars. To secure the walls, 10.9-grade high-strength bolts are used.
Zhou, Yun et al. [14]	2021	The sleeve connector and box connector are embedded within concrete wall panels or footing slabs. At the connection point, a 16 mm diameter screw bolt extending from the sleeve connector is inserted into a corresponding 16 mm hole in the box connector, securing the connection between the sleeve and box connectors. Finally, the gap between the connectors is filled with high-strength grout.



Copyright © 2025 CroCEE
DOI: https://doi.org/10.5592/CO/3CroCEE.2025.51

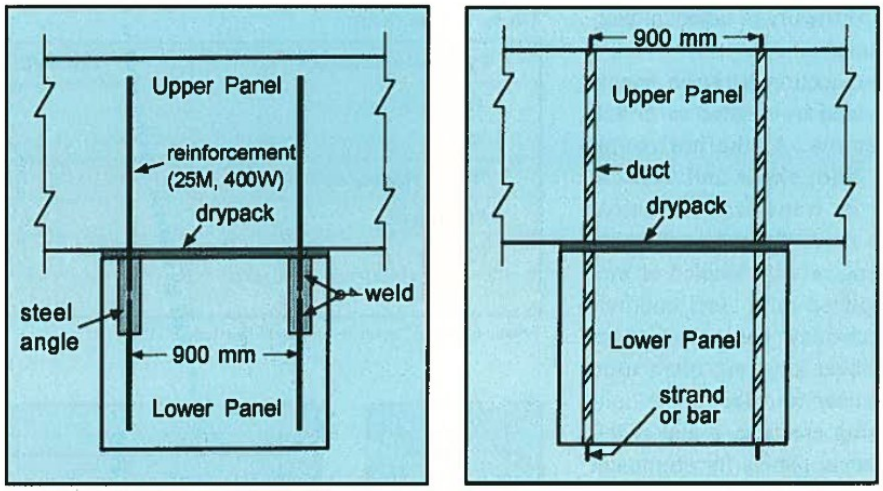


Figure 4. Respectively: dry pack grout-only connection; shear keys connection; reinforcing bars with welded connection; post-tensioned connection using strands or bars [6]

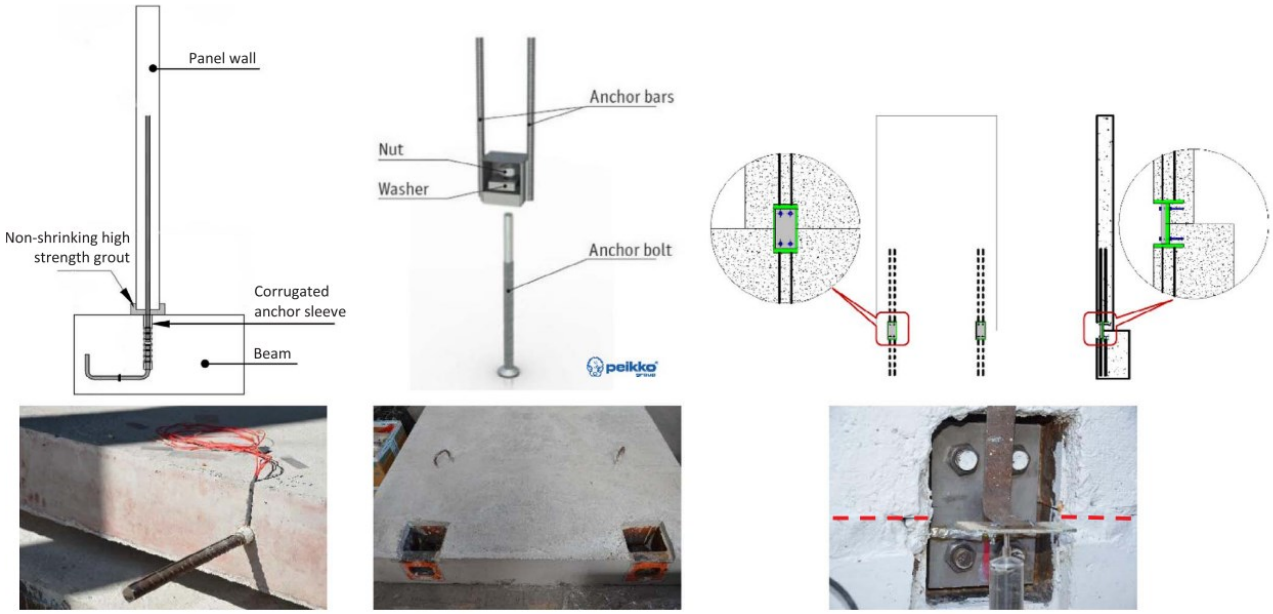


Figure 5. Types of connections considered in the research by Psycharis, Ioannis N. (2018) [30] respectively: "'Rebar' connections','Wall shoe' connections and 'Steel plate' connections"

4. Conclusion

The review of scientific studies, presented in this paper, offers a comprehensive analysis of prefabricated wall panels and their seismic performance, focusing on panel types and connection methods. The investigation encompassed three main types of wall panels - double panels, sandwich panels, and plain panels - highlighting their structural behaviour under earthquake-induced loads. Experimental studies reviewed in the literature emphasize the advantages and limitations of each panel type, particularly in terms of strength, stiffness, energy dissipation and deformation. Double panels, while providing simple solutions, may exhibit increased material usage, whereas sandwich panels show superior thermal performance and moderate seismic resistance. Plain panels, being simpler in design, may be less effective under significant seismic loads but offer cost efficiency.

Additionally, two principal connection systems, wet and dry joints, were evaluated, with detailed descriptions of variations tested in the reviewed works. Wet joints, often involving concrete infill or

Copyright © 2025 CroCEE
DOI: https://doi.org/10.5592/CO/3CroCEE.2025.51

grouted connections, demonstrated enhanced stiffness and continuity but could be labor-intensive and sensitive to construction quality. Dry joints, typically utilizing mechanical fasteners or interlocking elements, provided greater flexibility and ease of assembly but there can be a challenge in achieving optimal energy dissipation. The findings collectively underscore the critical influence of panel and joint selection on the seismic resilience of prefabricated structures.

In conclusion, the reviewed studies suggest that an optimized combination of panel type and joint configuration is essential to balance structural performance, construction efficiency, and cost. Future research should focus on optimizing these systems to enhance seismic resistance, sustainability, cost efficiency, and adaptability to diverse construction demands. The findings contribute important insights to the field of prefabricated construction, supporting informed decision-making in the design and implementation of modern building systems.

References

[1] R. Martins, R. do Carmo, H. Costa, and E. Júlio, "A review on precast structural concrete walls and connections," Adv. Struct. Eng., vol. 26, no. 14, pp. 2600–2620, 2023, doi: 10.1177/13694332231191073.

[2] S. Singhal, A. Chourasia, S. Chellappa, and J. Parashar, "Precast reinforced concrete shear walls: State of the art review," Struct. Concr., vol. 20, no. 3, pp. 886–898, 2019, doi: 10.1002/suco.201800129.

[3] H. R. Foerster, S. H. Rizkalla, and J. S. Heuvel, "Behavior and Design of Shear Connections for Loadbearing Wall Panels," PCI J., vol. 34, no. 1, pp. 102–119, 1989, doi: 10.15554/pcij.01011989.102.119.

[4] R. L. Hutchinson, S. H. Rizkalla, M. Lau, and S. Heuvel, "Horizontal post-tensioned connections for precast concrete loadbearing shear wall panels," PCI J., vol. 36, no. 6, pp. 64–75, 1991, doi: 10.15554/pcij.11011991.64.76.

[5] P. S. Walls, "Seismic Response of Friction Jointed Precast l [Tlii I · t 1- I I I I," 1988.

[6] K. A. Soudki, J. S. West, S. H. Rizkalla, and B. Blackett, "Horizontal connections for precast concrete shear wall panels under cyclic shear loading," PCI J., vol. 41, no. 3, pp. 64–80, 1996, doi: 10.15554/pcij.05011996.64.80.

[7] C. R. Newkirk, "Make Ideal Housing Components".

[8] A. Pavese and D. A. Bournas, "Experimental assessment of the seismic performance of a prefabricated concrete structural wall system," Eng. Struct., vol. 33, no. 6, pp. 2049–2062, 2011, doi: 10.1016/j.engstruct.2011.02.043.

[9] M. Palermo and T. Trombetti, "Experimentally-validated modelling of thin RC sandwich walls subjected to seismic loads," Eng. Struct., vol. 119, pp. 95–109, 2016, doi: 10.1016/j.engstruct.2016.03.070.

[10] G. Xu et al., "Seismic performance of precast shear wall with sleeves connection based on experimental and numerical studies," Eng. Struct., vol. 150, pp. 346–358, 2017, doi: 10.1016/j.engstruct.2017.06.026.

[11] R. Vaghei, F. Hejazi, A. A. Firoozi, and M. S. Jaafar, "Performance of Loop Connection in Precast Concrete Walls Subjected to Lateral Loads," Int. J. Civ. Eng., vol. 17, no. 3, pp. 397–426, 2019, doi: 10.1007/s40999-018-0366-0.

[12] W. Guo, Z. Zhai, Z. Yu, F. Chen, Y. Gong, and T. Tan, "Experimental and Numerical Analysis of the Bolt Connections in a Low-Rise Precast Wall Panel Structure System," Adv. Civ. Eng., vol. 2019, 2019, doi: 10.1155/2019/7594132.

[13] N. Sebaibi and M. Boutouil, "Reducing energy consumption of prefabricated building elements and lowering the environmental impact of concrete," Eng. Struct., vol. 213, no. September 2019, p. 110594, 2020, doi: 10.1016/j.engstruct.2020.110594.

[14] Y. Zhou et al., "Tensile and shear behavior of box connector for precast concrete shear walls," Eng. Struct., vol. 245, no. July, p. 112983, 2021, doi: 10.1016/j.engstruct.2021.112983.

Copyright © 2025 CroCEE
DOI: https://doi.org/10.5592/CO/3CroCEE.2025.51

[15] S. J. Han, I. Heo, J. H. Kim, K. S. Kim, and Y. H. Oh, "Experimental and numerical studies on the structural performance of a double composite wall," Appl. Sci., vol. 11, no. 2, pp. 1–19, 2021, doi: 10.3390/app11020506.

[16] H. Hou, K. Ji, W. Wang, B. Qu, M. Fang, and C. Qiu, "Flexural behavior of precast insulated sandwich wall panels: Full-scale tests and design implications," Eng. Struct., vol. 180, no. November 2018, pp. 750–761, 2019, doi: 10.1016/j.engstruct.2018.11.068.

[17] I. Ricci, M. Palermo, G. Gasparini, S. Silvestri, and T. Trombetti, "Results of pseudo-static tests with cyclic horizontal load on cast in situ sandwich squat concrete walls," Eng. Struct., vol. 54, pp. 131–149, 2013, doi: 10.1016/j.engstruct.2013.03.046.

[18] C. Todut, D. Dan, and V. Stoian, "Theoretical and experimental study on precast reinforced concrete wall panels subjected to shear force," Eng. Struct., vol. 80, pp. 323–338, 2014, doi: 10.1016/j.engstruct.2014.09.019.

[19] B. Dal Lago, M. Muhaxheri, and L. Ferrara, "Numerical and experimental analysis of an innovative lightweight precast concrete wall," Eng. Struct., vol. 137, pp. 204–222, 2017, doi: 10.1016/j.engstruct.2017.01.073.

[20] J. R. Mackechnie and L. A. Bellamy, "Thermal performance of variable density wall panels made using Portland cement or inorganic polymer concrete," Mater. Struct. Constr., vol. 48, no. 3, pp. 643–651, 2013, doi: 10.1617/s11527-013-0206-2.

[21] S. Kim, D. E. Lee, Y. Kim, and S. Kim, "Development and application of precast concrete double wall system to improve productivity of retaining wall construction," Sustain., vol. 12, no. 8, 2020, doi: 10.3390/SU12083454.

[22] J. Li, Y. Wang, Z. Lu, and J. Li, "Experimental study and numerical simulation of a laminated reinforced concrete shear wall with a vertical seam," Appl. Sci., vol. 7, no. 6, 2017, doi: 10.3390/app7060629.

[23] A. Biswal, A. M. Prasad, and A. K. Sengupta, "Study of shear behavior of grouted vertical joints between precast concrete wall panels under direct shear loading," Struct. Concr., vol. 20, no. 2, pp. 564–582, 2019, doi: 10.1002/suco.201800064.

[24] P. Seifi, R. S. Henry, and J. M. Ingham, "In-plane cyclic testing of precast concrete wall panels with grouted metal duct base connections," Eng. Struct., vol. 184, no. December 2018, pp. 85–98, 2019, doi: 10.1016/j.engstruct.2019.01.079.

[25] K. Karthikeyan and M. Helen Santhi, "Experimental investigation on precast wall connections," J. Adv. Res. Dyn. Control Syst., vol. 11, no. 6 Special Issue, pp. 1672–1678, 2019.

[26] S. H. Rizkalla, R. L. Serrette, J. S. Heuvel, and E. K. Attiogbe, "Multiple Shear Key Connections for Precast Shear Wall Panels," PCI J., vol. 34, no. 2, pp. 104–120, 1989, doi: 10.15554/pcij.03011989.104.120.

[27] F. J. Crisafulli and J. I. Restrepo, "Ductile steel connections for seismic resistant precast buildings," J. Earthq. Eng., vol. 7, no. 4, pp. 541–553, 2003, doi: 10.1080/13632460309350463.

[28] E. Brunesi and R. Nascimbene, "Experimental and numerical investigation of the seismic response of precast wall connections," Bull. Earthq. Eng., vol. 15, no. 12, pp. 5511–5550, 2017, doi: 10.1007/s10518-017-0166-y.

[29] W. Wang, A. Li, and X. Wang, "Seismic performance of precast concrete shear wall structure with improved assembly horizontal wall connections," Bull. Earthq. Eng., vol. 16, no. 9, pp. 4133–4158, 2018, doi: 10.1007/s10518-018-0348-2.

[30] I. N. Psycharis, I. M. Kalyviotis, and H. P. Mouzakis, "Experimental investigation of the response of precast concrete cladding panels with integrated connections under monotonic and cyclic loading," Eng. Struct., vol. 159, no. November 2017, pp. 75–88, 2018, doi: 10.1016/j.engstruct.2017.12.036.

[31] G. Cai, F. Xiong, Y. Xu, A. S. Larbi, Y. Lu, and M. Yoshizawa, "A Demountable connection for low-rise precast concrete structures with DfD for construction sustainability-A preliminary test under cyclic loads," Sustain., vol. 11, no. 13, 2019, doi: 10.3390/su11133696.

[32] J. Sun, H. Qiu, and H. Jiang, "Experimental study and associated mechanism analysis of horizontal bolted connections involved in a precast concrete shear wall system," Struct. Concr., vol. 20, no. 1, pp. 282–295, 2019, doi: 10.1002/suco.201800113.

Proceedings of the 3rd Croatian Conference on Earthquake Engineering - 3CroCEE
19–22 March 2025, Split, Croatia
Copyright © 2025 CroCEE
DOI: https://doi.org/10.5592/CO/3CroCEE.2025.51

Proceedings of the 3rd Croatian Conference on Earthquake Engineering - 3CroCEE
19–22 March 2025, Split, Croatia
Copyright © 2025 CroCEE
DOI: https://doi.org/10.5592/CO/3CroCEE.2025.58

IMPROVED SEISMIC ASSESSMENT OF EXISTING RC FRAME STRUCTURES

Aleksandar Zhurovski [(1)], Borjan Petreski [(2)], Igor Gjorgjiev [(3)]

[(1)] *Asst. Prof., Ss. Cyril and Methodius University in Skopje, Institute of Earthquake Engineering and Engineering Seismology (IZIS), Skopje, N. Macedonia, zurovski@iziis.ukim.edu.mk*
[(2)] *Asst. Prof, Ss. Cyril and Methodius University in Skopje, Institute of Earthquake Engineering and Engineering Seismology (IZIIS), Skopje, N. Macedonia, borjan@iziis.ukim.edu.mk*
[(3)] *Prof, Ss. Cyril and Methodius University in Skopje, Institute of Earthquake Engineering and Engineering Seismology (IZIIS), Skopje, N. Macedonia, igorg@iziis.ukim.edu.mk*

Abstract

The seismic performance of building structures is governed by the lateral stiffness which is provided by the geometrical and material characteristics of their structural elements and their arrangement in plan and elevation. In general, the procedure for designing the structures to withstand the code-prescribed lateral loads is quite straightforward. However, the performance of the building subjected to realistic seismic loading is also important beyond the deterministically defined safety points that ensure life-safety at fixed return periods. Building structures in North Macedonia are designed according to an outdated code that does not consider the modern developments in the field of performance-based earthquake engineering such as ductility of the cross-section. Thus, the ratio of the column dimensions is not a matter of consideration when designing a structure and the weak beam – strong column concept is ignored in the designer's check list. Therefore, because of the need for open architectural spaces and aligned interior walls and columns, the designers often rotate the shorter cross-section dimension along the longer beam span. With the aim of investigating the effect of the orientation of the columns in plan on the seismic performance of reinforced concrete frame structures, an existing residential building is analyzed. The existing structure is compared with alternatively designed structural models with different column cross-sections or different orientation of the existing column cross-section in plan. The comparison is performed using nonlinear analysis of the existing structures and the proposed models. Then, a simplified probabilistic assessment of the structural configurations is performed, and the results are presented. Finally, the results are used to stress the need for assessment of the existing structures with the modern approaches employed in the more up-to-date design codes and performance-based earthquake engineering principles.

Keywords Seismic Assesment; RC frame structures; PERFORM 3D; probabilistic estimation:

Copyright © 2025 CroCEE
DOI: https://doi.org/10.5592/CO/3CroCEE.2025.58

1. Introduction

North Macedonia is located in the central part of the Balkan Peninsula, a region often in the history exposed by the devastating nature of strong earthquakes [1]. Therefore, the whole territory of the country is seismically active and intensity VII-IX earthquakes according to European intensity scale frequently occur. In the recent past, there have been several earthquakes that resulted in significant economic damage and social disruption. The most significant of them happened in 1963, when a 6.1 magnitude earthquake killed over 1000 people. After that earthquake, great effort was made in order to develop the building practice and improve the building stock in the country and in Europe in general. The building stock of North Macedonia is generally characterized by 2 types of buildings. The first type incorporates the buildings that were built prior to 1969 when the first seismic building code was implemented. These buildings do not meet the current seismic design standards and only a few of them are designed to resist lateral loads such as wind. The second type contains the structures designed to resist seismic forces, following the code from 1969 and the revised and more refined code from 1981. The newly built structures are also part of this type since the last revision of the seismic code is dating back to 1981.

Given that the structural response under earthquake loading is essential for structure's seismic resilience, especially beyond safety point defined by the code, it is crucial to design each structural element properly. Unfortunately, North Macedonia is one of the last European countries that uses outdated codes for seismic design of structures. Even though the 1981 code provides considerably good guidelines for design of earthquake resistant structures, it is based on general interpretation of the good seismic design practices and does not give details of the design details. Since the code has not been modified for a long time, it does not contain the state-of-the-art advancements in the earthquake engineering field such as the ductile capacity design. For example, in the current seismic code there are no strict guidelines for following the "strong column / weak beam" principle such as the capacity design guidelines in Eurocode 8 (EC8), CEN (2005) [2], apart from a recommendation that the formation of plastic hinges in the columns and joints should be avoided.

The architectural demand for open space very often implies the design of rectangular columns with small dimensions fully incorporated within the width of the infill wall (usually 25cm). Additionally, in some plan arrangements, the smaller side of the rectangular cross-section is oriented along a longer span. This results in a very small column capacity in the smaller side direction whereas the beam possesses greater dimensions and capacity to satisfy the span to depth ratio. Consequently, the smaller column capacity affects the global structural response under earthquake excitation.

To investigate the influence of the ratio of section sides of rectangular columns on the seismic performance of structures, an existing reinforced concrete (RC) frame structure designed according to Macedonian codes of practice was selected for analysis. The analyzed structure is a three-story residential building regular in plan and elevation. Nonlinear static pushover (SPO) analysis was performed on the existing structural configuration and its performance was evaluated through a SPO curve. The characteristic values regarding the current seismic code limits were plotted on the performance curve and the structural design was assessed. Then, additional three structural configurations were examined to demonstrate the performance differences between the structure designed with the current seismic code and the alternative configurations. Initially, the SPO response of the four models was investigated and compared. Due to the need to compare the response of the models for higher levels of nonlinearity, up to collapse of the structure, an improved procedure involving effective tool for estimating structure-specific seismic fragility curves was employed. Finally, the models were investigated for several performance levels and the performance differences were discussed.

Copyright © 2025 CroCEE
DOI: https://doi.org/10.5592/CO/3CroCEE.2025.58

2. Nonlinear Static Analysis Approach

2.1. Structural description of the building

The residential building being investigated is a three-story RC frame structure with story height of 2.9m. To achieve greater open space and flat interior walls, the columns were made rectangular. The building's plan shape is rectangular and can be classified as regular, as shown in Figure 1. The spans in x-direction measure 6.4m and 5.65m, while the spans in y-direction measure 3.4m and 4.5m. The beams are rectangular with dimensions of 25/40cm and 25/45cm, while all columns have dimensions of 25/45cm.

The structural design of the building is performed using the current Macedonian seismic code dating back to 1981. The loads are applied using the current codes of practice as well and their values are 1.50kN/m^2 dead load and 1.50kN/m^2 live load for residential areas. The snow load is applied on the third floor and it is taken as 0.75kN/m^2. According to the seismic code, the masses for calculation of the modal parameters and seismic forces are taken with coefficient 1.0 for dead load and snow load, while the coefficient for the live load is 0.5. Therefore, the floors' masses are 136t, 115t and 83t for the first, second and third floor accordingly. After the definition of masses, modal analysis is performed and translational modes in both principal directions are obtained. The first period in x-direction is 0.37s, while the first period in y-direction is 0.33s. The structure is located in zone IX of the seismicity zonation according to the European intensity scale and the seismicity coefficient for the calculation of base shear force is 0.1. Consequently, the total base shear force for the structure in x and y-directions is 335kN.

The effect of column cross-section orientation on the seismic response of the structure was investigated using four structural analytical models. In Model 1, the shorter section side of all columns is oriented along y-direction (C1 - 45/25 cm), while in Model 2, the shorter section side of all columns is oriented along x-direction (C2 - 25/45 cm). In the third analytical model, columns C1 and C2 are arranged in a mixed arrangement as it was originally designed. The need for the layout of the structure in Figure 1 is a result of architectural demands. Thus, there are columns that are oriented with shorter section sides along the longer span. The last model, Model 4, is a structure that has a square cross-section of all columns (C4 - 35x35cm), which the authors consider the most suitable column cross-section for such a building providing equal resistance in both directions.

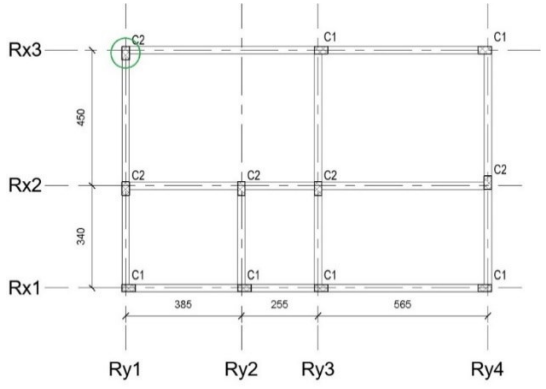


Figure 1. Characteristic floor plan of the example building (Model 3).

2.2. Numerical modelling

The SPO analysis was performed using the Perform3D software for nonlinear analysis and design [3]. Depending on the modelling requirements, there are several different types of elements available for use. Each element consists of numerous basic components that are used to simulate the nonlinear behaviour of all types of structural elements. For this case study, the basic components used for the modelling are as follows:

Copyright © 2025 CroCEE
DOI: https://doi.org/10.5592/CO/3CroCEE.2025.58

- Inelastic non-buckling steel material was defined for the reinforcement according to the provisions given in the national standard. The stress-strain relationship of the reinforcement was modelled as trilinear, with strength loss (at point L), without cyclic stiffness degradation. The model curve is shown in Figure 2 (left).
- A macro model with Mander stress-strain relationship is most frequently used to describe the working condition of confined concrete in uniaxial compression [4], which is related to section shape and the configuration condition of the stirrup. By the program, the model is transferred in the standard force-deformation (F-D) relationship. Hence, for the design quality of concrete, a concrete model curve was computed according to the Mander model, mean value of concrete's strength and elastic modulus (Figure 2 - right).

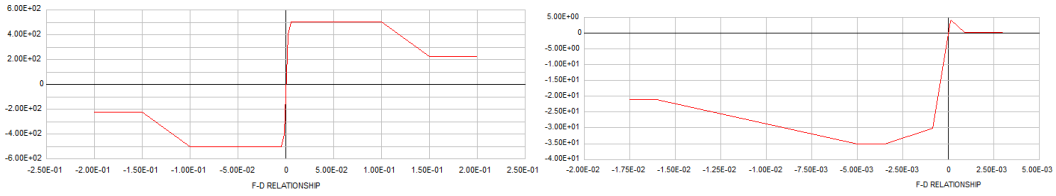


Figure 2. Material models for reinforcement (left) and confined concrete (right) from Perform3D, Computers and Structures, Inc. (2018).

The properties of steel material are defined by a yield strength of fy=400MPa, a yield strain of εy=2‰, an ultimate strength of fu=500MPa and an ultimate strain of εu =25‰. The Mander stress-strain model for confined concrete is used to determine the properties of the concrete material. Hence, the typical values are fco'=30MPa, fcc'=35MPa, εco=2‰, εco=3.5‰ and εcu=17.5‰ (the ultimate compressive strain εcu is obtained at first hoop fracture).

Inelastic fiber sections were used for modelling of the columns. They were assigned at the corresponding lengths of the elements to simulate the plastic hinge region, with the rest of the element remaining elastic. The beams were modelled following the lumped plasticity approach using inelastic rotational moment hinges. The joints were considered as fully rigid and they were modelled using rigid elements.

2.3. Analysis procedure

The use of nonlinear static analyses has been increasing recently, in contrast to ductility-modified spectra analyses. Nonlinear static analysis, also known as pushover analysis, accurately defines the deformation curve of a structure and demonstrates its capacity through a pushover curve. This method is considered a step forward from the use of linear analysis and ductility-modified response spectra because it is based on a more accurate estimate of the distributed yielding within a structure, rather than an assumed, uniform ductility [5]. Nonlinear response analysis is performed for many reasons, including the design of new buildings and assessing the performance of existing and new buildings, as per the NEHRP classification [6]. Furthermore, a number of codes and guidelines have designated it as the preferred assessment procedure [7].

The performance of the investigated structural configurations was evaluated through static pushover analyses. A predefined set of lateral forces was applied to the structures stepwise, based on their masses and first mode shape vectors. The stiffness matrices were updated at each step of the analyses to account for the yielding of beams or columns. The pushover analyses were executed until the structures collapsed.

Because of the outdated Macedonian seismic design code, the performance levels for the assessment of structures were obtained from more advanced contemporary codes of practice. As an example, the Italian National Code defines 4 limit states: Operational, Damage Control, Life Safety and Collapse Prevention [8]. Based on FEMA 273 recommendations [9], [10], [11], for concrete frames, drift limit indicators are provided following the structure's response to different performance levels. FEMA 273 categorizes the drift limitations in three classes: 1) immediate occupancy, represented with 1% transient

Copyright © 2025 CroCEE
DOI: https://doi.org/10.5592/CO/3CroCEE.2025.58

and negligible residual drift, 2) life-safety, exhibiting maximum of 2% transient and 1% residual drifts, and 3) collapse prevention, limited with 4% of transient and residual drifts. Therefore, in this study, a combination of the codes of practice can be observed as the FEMA 273 performance assessment limits are used for concrete frames designed following the Macedonian code of practice.

The deformation capacities for the components or the so-called performance acceptance criteria corresponding to different building performance levels were defined in terms of plastic rotation capacities. In the present study, plastic rotation capacities for Immediate Occupancy (IO), Life Safety (LS) and Collapse Prevention (CP) levels were used for the column and beam elements (Table 1). In the analysis, only one criterium was used for performance-based evaluation. Namely, the performance of the structure was evaluated based on the flexural behavior of the columns only. It was assumed that the flexural behavior of the columns governs the structure's behavior, and the columns define the structure's failure mechanism. For the analysis, the rotation capacities in columns were used as referent. The damaged state of the structure corresponded to reaching the specified level of rotation in columns.

Table 1. Rotation capacities and colour designation for the structural elements used in the analysis.

Performance Level	Column Rotation Capacities (rad)	Beam Rotation Capacities (rad)	Colour
IO	0.005	0.005	
LS	0.025	0.025	
CP	0.035	0.050	

2.4.Column cross-section ductility calculation

The moment-curvature relationships of a column section are very important to assess the ductility of the element, the amount of the possible redistribution of stresses and its resistance against dynamic loading. Calculation of the moment-curvature relationship of the three implemented column cross-sections was performed using the tool developed by Bentz and Collins [12]. Moment-curvature relationships of the column cross-sections were calculated along the local x-axis for columns C1(45x25cm), C2(25x45cm) and C3(35x35cm) for predefined axial force from the gravity loads (Figure 3). The reinforcement area in the column cross-sections is taken as 1% of the concrete section area, proportionally distributed along the section sides.

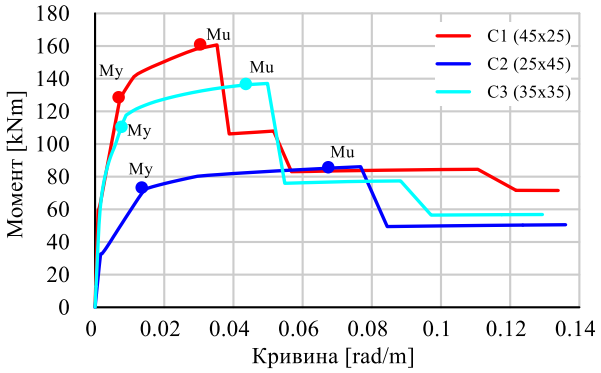


Figure 3. Moment-curvature relationships of the column cross-sections for gravity loads axial force.

Column C1 has the largest moment capacity, while column C2 has the lowest moment capacity, as observed in Figure 3. The yielding moment My for column C1 is 134kNm for C2 is 76kNm and for C3 is 112kNm. Column C1 has an ultimate moment Mu of 167kNm, column C2 has an ultimate moment Mu of 92kNm, and column C3 has an ultimate moment Mu of 141kNm.

Table 2 presents the calculated curvatures at yield and ultimate moments of the columns for three different levels of axial force. The curvature ductility of all concrete columns is calculated accordingly. It is defined as the ratio of ultimate curvature to yield curvature and it presents a metric for warning of

Proceedings of the 3rd Croatian Conference on Earthquake Engineering - 3CroCEE
19–22 March 2025, Split, Croatia
Copyright © 2025 CroCEE
DOI: https://doi.org/10.5592/CO/3CroCEE.2025.58

failure. C1 has a ductility of 5.05 for design gravity axial load, while C2 and C3 have a ductility of 6.73. The square column C3 exhibits a balanced behaviour in terms of ductility and moment capacity along both axes compared to the rectangular columns investigated. Two additional axial load levels are included in Table 2 to display the variations in axial load in the column due to the pushover analysis.

Table 2. Characteristic curvature and curvature ductility values for the investigated column cross-sections.

Column	N = 380kN			N = 300kN			N = 550kN		
	φ_y [rad/m]	φ_u [rad/m]	μ_φ	φ_y [rad/m]	φ_u [rad/m]	μ_φ	φ_y [rad/m]	φ_u [rad/m]	μ_φ
C1	0.00767	0.03878	5.05	0.00767	0.03525	4.59	0.00844	0.03878	4.59
C2	0.01141	0.07678	6.73	0.01141	0.07678	6.73	0.01256	0.07678	6.12
C3	0.00741	0.04986	6.73	0.00741	0.04986	6.73	0.00815	0.04986	6.12

2.5. Evaluation of the seismic performance

The results obtained from the nonlinear static analysis in terms of Pushover curves (Base shear vs. Top Drift) for the four models in both x and y orthogonal directions are shown in Figure 4. The diagrams display various top drift levels arranged in regions (cyan, orange, red). The lines that lie in these regions were set by following the response of the structure under the increasing displacement in the analysis and the nonlinear response of the columns, as they are governing the stability of the building structure. Table 1 rotation capacities are the basis for the acceptance criteria. Roof drifts when the structures reach IO, LS, and CP damage states (acceptance criteria) are designated in the figure.

Figure 4 shows that the base shear capacity is highly influenced by the column cross-section orientation in plan. Model 1 has the greatest base shear capacity in the x-direction (the direction of the longer column cross-section side), while Model 2 has the greatest base shear capacity in the y-direction. It is noted that the base shear capacity of Models 3 and 4 is similar and demonstrates uniformity in both directions. This is a demonstration of how a balanced choice of column cross-section orientation for Model 3 and a good choice of rectangular column cross-sections for Model 4 can be achieved. On the other hand, Models' 1 and 2 base shear capacity in both orthogonal directions shows differences of more than 30%.

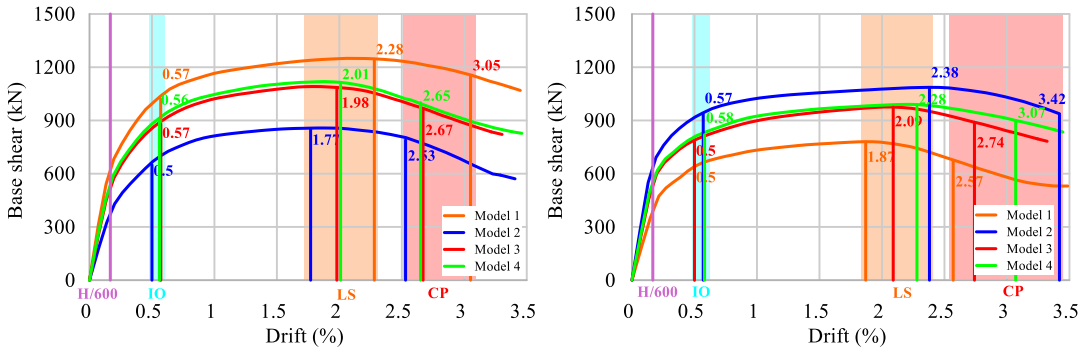


Figure 4. Pushover curves for Models 1, 2, 3 and 4 in x-direction (left) and y-direction (right).

Regarding the Macedonian code of practice and its total horizontal deflection limitations (H/600, where H is the total height of the structure), it is observed that the IO performance criteria are reached at greater drift level for every model. This demonstrates the stringency of the Macedonian seismic code of practice since the total drift limitation is at 1/3 of the earliest plastic rotation capacity of a column as per the IO performance criterium.

The design base shear is another parameter that has been investigated in accordance with the Macedonian seismic code. The structures are designed with a total base shear load of 335kN, for which the previously mentioned total drift limitation is assessed. This study demonstrates that the drift of the

Copyright © 2025 CroCEE
DOI: https://doi.org/10.5592/CO/3CroCEE.2025.58

lowest capacity models in each direction is closest to the H/600 limitation, while Models 3 and 4 exhibit lower drifts for the same base shear load.

The models' responses to the performance criteria levels vary as well. The IO performance level region is quite narrow, and the results for each model are similar, with the highest difference being 16%. On the other hand, the behaviour of the models in the LS and CP regions is more varied. The drift regions are wider and are associated with the plastic rotation capacities of the columns for LS and CP performance levels. Variation in global structural ductility of the models investigated is indicated by the difference in the width of the LS and CP regions and the narrowness of the IO performance level region. In the next chapter, the seismic response of the structural configurations is evaluated probabilistically for all performance levels, and this variance is investigated.

Figure 5 contains the damage state of the structure and the performance of the columns when the IO damage state is reached. It should be noted that the color when a column reaches a certain rotation capacity limit is given in table 1 and it corresponds to the colors given in the diagrams and figures.

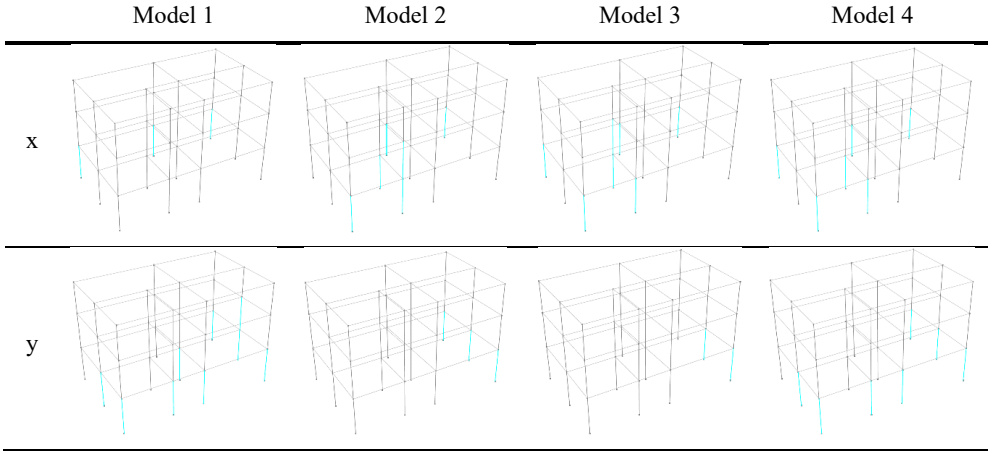


Figure 5. IO damage states in x and y-direction for Models 1, 2, 3 and 4.

The models investigated have some similarities, as shown in Figure 5. It was previously established that the response of the four models for IO performance level is similar. Thus, figure 5 additionally shows that IO is reached only for the ground floor columns for every model. However, the pattern for each model is different and governed by the column cross-section orientation and span length. The three-dimensional analysis additionally allows for different redistribution of loads for each model and affects the varying plastic rotation demand pattern.

3. Probabilistic Estimation of Seismic Response

When considering design of new structures or assessment of existing ones, the codes of practice usually provide limit values for deterministic assessment of structural performance. That is the only method available for design and assessment of structures subjected to earthquake loading, especially in more outdated seismic codes. The more up-to-date codes of practice provide the designers with some possibilities to choose probabilistic techniques for more realistic evaluation of the seismic response of the structural system. Since nothing is perfect and one needs to look at the problems probabilistically, especially in highly nonlinear behaviour where many uncertainties are involved, the probabilistic evaluation supplies seismic response evaluation in form of fragility functions.

Performance-based earthquake engineering (PBEE) is a structural engineering paradigm that fully embraces the intrinsic uncertainty associated with strong ground motion and employs probabilistic tools to evaluate structural performance in seismic areas [13]. The fragility functions are represented via a lognormal distribution that represents the probability of some ‘failure’, defined by a median η and dispersion β. They are usually derived from Incremental Dynamic Analysis (IDA) given in Vamvatsikos

Copyright © 2025 CroCEE
DOI: https://doi.org/10.5592/CO/3CroCEE.2025.58

and Cornell [14] or Multiple Stripe Analysis (MSA) which matches the building code intensity-based approach.

For the purpose of probabilistic evaluation of the seismic response of the structural configurations investigated, a simplified SPO-based procedure for estimating structure-specific seismic fragility curves of buildings is employed. The utilized SPO2FRAG tool simplifies the computationally demanding IDA by taking advantage of the SPO2IDA algorithm [15]. Basically, it accepts as input static pushover results obtained from the structural analysis software package of the user's choice and allows the user to control the IDA simulation and fragility estimation procedure at its various steps and intervene where one deems necessary [16]. The fragility function parameters are estimated as in Equation 1, where the terms $Sa_{f,x\%}^{LS}$ represent the x% fractile of the structural intensity causing exceedance of each limit state LS.

$$\begin{cases} \eta = \ln(Sa_{f,50\%}^{LS}) \\ \beta = \ln(Sa_{f,50\%}^{LS} / Sa_{f,16\%}^{LS}) \end{cases} \quad (1)$$

It is straightforwardly inferred from the above that such a simplified methodology for substituting a complex analytic procedure such as IDA involves many approximations and assumptions. Some of the basic assumptions for performing the simplified fragility curve calculation procedure include:

- As a consequence from IDA's intensity measure based (IM-based) fragility function development, the EDP random variable conditioned on the IM is independent of other ground motion features needed to evaluate the seismic hazard for the site, such as magnitude and source-to-site distance.
- Transformation from multi degree of freedom (MDoF) to single degree of freedom (SDoF) system with equivalent period of vibration T*.
- A quadrilinear fit of the SDoF backbone curve according to De Luca et al. [17].
- Use of approximate equations for the lateral post-yield deformation profile suggested in FEMA P-58-1 (FEMA 2012) to convert the IDAs into interstorey drift ratio (IDR).

The simplified methodology for fragility curve estimation offers implementation of other sources of variability. Hence, the user is allowed to account for variability at nominal yield due to higher-mode effects and modelling uncertainty. According to Baltzopoulos et al. [16] there is a good agreement between the SPO2FRAG and analytically derived estimate of the fragility curves even without considering estimation uncertainty. Therefore, it is decided that for the sake of simplicity, there is no need for addition of variabilities for the investigated simple RC moment frame structures.

In order to be consistent with previous research and the examples provided by the developers of SPO2FRAG tool, the three-dimensional structure of this study is substituted with selected frames in both directions and turned into a two-dimensional problem. For the probabilistic estimation of seismic response, frames Rx3 and Ry1 of the structure are analyzed and SPO curves obtained. Figure 6 presents the SPO curves of the selected frames.

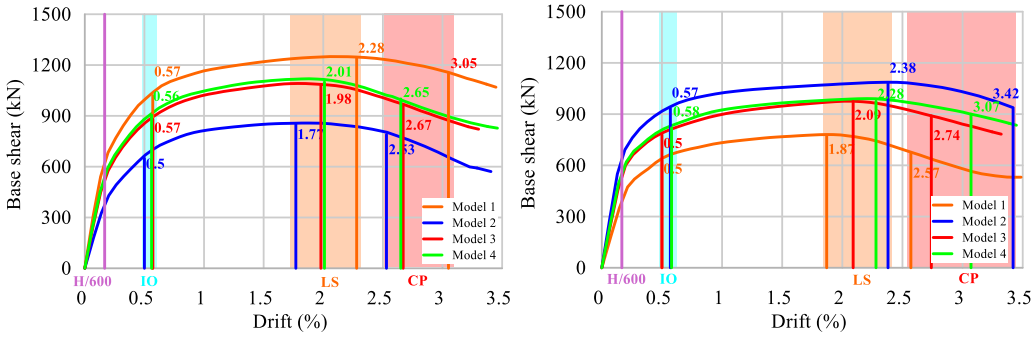


Figure 6. Pushover curves for selected frames from Models 1, 2, 3 and 4: frame Rx3 (left) and Ry1 (right).

Copyright © 2025 CroCEE
DOI: https://doi.org/10.5592/CO/3CroCEE.2025.58

Five performance levels for the development of structure-specific seismic fragility curves are defined by the user. The software tool incorporates the following limit states: fully operational (FO), immediate occupancy (IO), life safety (LS), collapse prevention (CP) and side-sway collapse (C). The FO limit state is set to 0.5% IDR while the C limit state is added by SPO2FRAG automatically when the quadrilinear fit of the backbone curve exhibits strength degradation in the form of a negative-stiffness branch. The other three performance levels (IO, LS and CP) are defined using the SPO curves and previous research studies. Results from the fragility curves development using the SPO2FRAG tool are given in Tables 3 and 4.

Table 3. Lognormal fragility function parameter estimates from SPO2FRAG – frame Rx3.

Limit state	**Rx3**							
	M1		**M2**		**M3**		**M4**	
	η (g)	***β***	***η (g)***	***β***	***η (g)***	***β***	***η (g)***	***β***
FO	0.283	0	0.161	0	0.259	0	0.246	0
IO	0.453	0	0.258	0	0.414	0	0.394	0
LS	1.128	0.157	0.670	0.156	1.038	0.173	0.992	0.155
CP	2.054	0.316	1.285	0.301	1.891	0.326	1.821	0.312
C	2.969	0.421	1.690	0.370	2.594	0.416	2.539	0.404

Table 4. Lognormal fragility function parameter estimates from SPO2FRAG – frame Ry1.

Limit state	**Ry1**							
	M1		**M2**		**M3**		**M4**	
	η (g)	***β***	***η (g)***	***β***	***η (g)***	***β***	***η (g)***	***β***
FO	0.418	0	0.625	0	0.584	0	0.553	0
IO	0.659	0.097	0.961	0.092	0.902	0.097	0.860	0.089
LS	1.428	0.311	1.978	0.303	1.875	0.308	1.800	0.301
CP	2.344	0.463	3.173	0.463	3.030	0.467	2.906	0.460
C	2.851	0.516	4.110	0.553	3.793	0.537	3.603	0.525

The results from the fragility estimation of the investigated models show consistent trends in several aspects regarding both frames, Figure 7. For the frame Rx3, the FO and IO results show similar values for the median value of the IM Sa(T*). The only difference is observed in Model 2 which shows significantly smaller values of exceedance for those performance levels. This is due to the orientation of the cross-section of the rectangular columns. When considering the ranges with considerable inelastic behaviour of the structures, the differences between the structural response of the model increases. However, Models 3 and 4 tend to present matching results even in these performance regions. Similar results have been observed for Ry1 as well. In this case study, Model 1 exhibits the exceedance of the structural demands at lower IM values. From this example it is clearly observed that the differences between the models are increasing as the nonlinearity of the problem increases. Regarding the comparison in the behaviour between both frames it is obvious that Ry1 shows better performance for all limit states and the reason for that is the lower tributary mass for that frame according to the structural configuration shown in Figure 1 and the smaller beam spans.

Copyright © 2025 CroCEE
DOI: https://doi.org/10.5592/CO/3CroCEE.2025.58

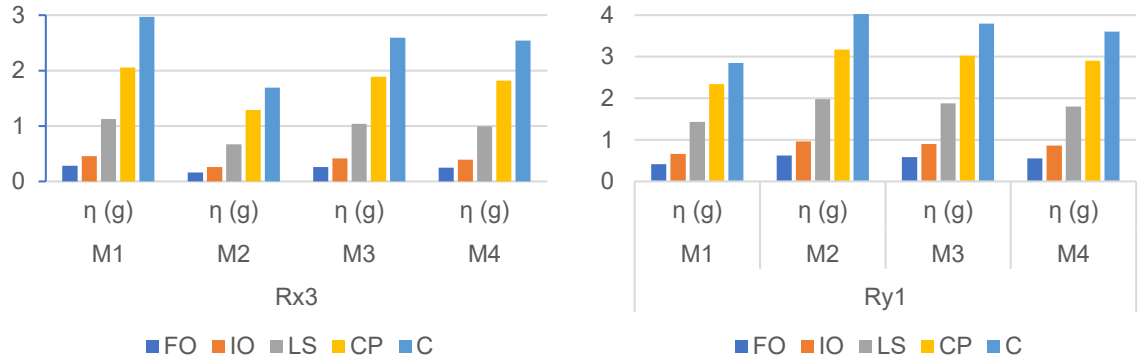


Figure 7. Median Sa(T*) intensities for each performance level for Rx3 (left) and Ry1 (right)

Another important point is the distribution of the dispersion values among the different limit states, which is an indicator of the IM efficiency. This distribution is shown in Figure 8. From Figure 8, one can observe the similarity of dispersion values for the LS limit state across all models. This suggests that Sa(T*) is a solid indicator of structural response for structures responding in their linear elastic range. Additionally, one can also observe the absence of dispersion values for FO and IO performance levels for Rx3 and only FO for Ry1. This shows the uniformness of the responses in the linear region of the structures. However, when considering highly nonlinear response of the frames, the dispersion increases. Comparing these dispersion values to some existing values in the literature, the values appear reasonable and of the same order of magnitude, with FEMA P695, FEMA (2009), proposing values of β between 0.10 and 0.50 depending on how well the model represents the actual structural behaviour and how robust that numerical model is O'Reilly and Sullivan (2018).

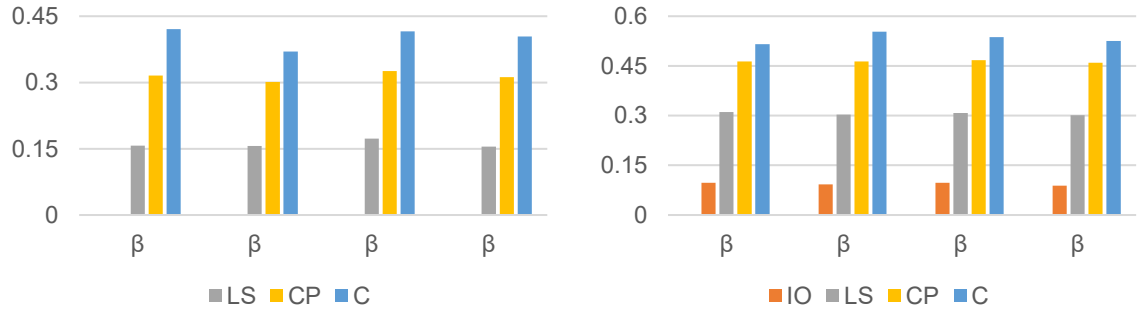


Figure 8. Dispersion values for each performance level for Rx3 (left) and Ry1 (right)

4. Conclusion

This study depicted a comparison arising from an ongoing problem in the structural engineering field. A number of cases were examined using a more sophisticated nonlinear analysis to evaluate the structural response of low-rise reinforced concrete residential buildings designed according to outdated seismic code. The results from the performed analyses emphasize the need for selecting suitable reinforced concrete column cross-sections and arranging them properly in plan. When selecting rectangular cross-sections with one relatively small section side, greater attention should be given to the arrangement of the columns in plan in order to provide satisfactory capacity and deformability of the structure in both directions. Even though, the global behaviour of the structure can be optimized by applying these measures, it is doubtful whether this type of columns assures resilience of the structure. Additionally, the capacity of the columns is strictly limited in the up-to-date seismic codes when one needs to follow the “strong column / weak beam” principle. In any case, it is established that the square column sections demonstrated balanced behaviour in both orthogonal directions. The response of the

Copyright © 2025 CroCEE
DOI: https://doi.org/10.5592/CO/3CroCEE.2025.58

structure designed with rectangular columns only is somewhat similar in x and y-directions which represents the desired behaviour in seismic design.

The use of more sophisticated, even though simplified, analysis procedure demonstrates the need for application of these techniques when considering highly nonlinear behaviour of the structures. The SPO analysis itself is providing solid information about the performance of the investigated structures. However, the fragility analysis of the same structures contributes by supplying more detailed data about the performance beyond the safety points defined by the codes.

References

[1] INFRANAT (2019). Increased Resilience of Critical Infrastructure under Natural and Human-induced Hazards (INFRA-NAT), *Deliverable D1.1*, INFRANAT Project, Italy.

[2] CEN (2005). EN 1998-3:2005. Eurocode 8: Design of structures for earthquake resistance - Part 3: Assessment and retrofitting of buildings, Comité Européen de Normalisation, Brussels.

[3] Computers and Structures Inc. (2018). CSI PEFRORM-3D- Components and Elements. Version 7.

[4] Mander J.B., Priestley M.J.N., Park R. (1988). Theoretical stress-strain model for confined concrete, *ASCE Journal of Structural Engineering*, **114** (8): 1804-1826.

[5] Elghazouli, A. (Ed). (2009). Seismic Design of Buildings to Eurocode 8, 1st Ed., *CRC Press*.

[6] Haselton C., Whittaker A., Hortacsu A., Baker J., Bray J. & Grant D. (2012). Selecting and scaling earthquake ground motions for performing response-history analyses, *Proceedings of the 15th World Conference on Earthquake Engineering*, Lisbon, Portugal.

[7] Sullivan, T.J., Saborio-Romano, D., O'Reilly, G.J., Welch D.P., Landi L. (2018). Simplified Pushover Analysis of Moment Resisting Frame Structures, *Journal of Earthquake Engineering*, **25** (4): 621-648.

[8] O'Reilly G.J., Sullivan T.J. (2018). Quantification of modelling uncertainty in existing Italian RC frames, *Earthquake Engineering & Structural Dynamics*, **47**: 1054-1074.

[9] FEMA (1997). NEHRP Guidelines for the Seismic Rehabilitation of Buildings. Report No. 273, *Federal Emergency Management Agency*, Washington DC.

[10] FEMA (2009). FEMA P695: Quantification of Building Seismic Performance Factors. Washington, DC, USA.

[11] FEMA (2012). FEMA-58-1: seismic performance assessment of buildings volume 1—methodology. *Prepared by ATC for FEMA*, Washington, DC.

[12] Bentz, E.C., Collins, M.P. (2000). Response 2000. Software program for load-deformation response of reinforced concrete section.

[13] Cornell C. A., Krawinkler H. (2000). Progress and challenges in seismic performance assessment. *PEER Center News* 3(2): 1–3.

[14] Vamvatsikos D., Cornell C. A. (2002). Incremental dynamic analysis. *Earthquake Engineering & Structural Dynamics*, **31** (3): 491–514.

[15] Vamvatsikos D., Cornell C. A. (2006). Direct estimation of the seismic demand and capacity of oscillators with multi-linear static pushovers through IDA. *Earthquake Engineering & Structural Dynamics*, **35**:1097–1117.

[16] Baltzopoulos, G., Baraschino, R., Iervolino, I. & Vamvatsikos, D. (2017). SPO2FRAG: software for seismic fragility assessment based on static pushover. *Bull Earthquake Eng*, **15**: 4399–4425.

[17] De Luca F., Vamvatsikos D., Iervolino I. (2013). Near-optimal piecewise linear fits of static pushover capacity curves for equivalent SDOF analysis. *Earthquake Engineering & Structural Dynamics* **42** (4):523–543.

Proceedings of the 3rd Croatian Conference on Earthquake Engineering - 3CroCEE
19–22 March 2025, Split, Croatia
Copyright © 2025 CroCEE
DOI: https://doi.org/10.5592/CO/3CroCEE.2025.65

SEISMIC ASSESSMENT OF THE DAMAGE LIMIT STATES OF EXISTING HIGHWAY BRIDGES

Radomir Folić [(1)], Miloš Čokić [(2)]

[(1)] *Professor Emeritus, University of Novi Sad, Faculty of Technical Sciences, Novi Sad, Republic of Serbia, r.folic@gmail.com or folic@uns.ac.rs*
[(2)] *Structural engineer, Termoenergo inženjering, Belgrade, Republic of Serbia, cokicmilos@gmail.com*

Abstract

The majority of existing bridges originate from various periods of design and construction. Due to their age, they have been exposed to environmental influences, often exacerbated by increased traffic loads and different hazards. For bridges located in areas prone to seismic activity, including our region, it is particularly important whether the structure was designed and built according to codes that do not meet modern seismic performance requirements. Environmental effects contribute to gradual deterioration, but de-icing salts and the aggressiveness of the environment lead to corrosion, which can often result in faster deterioration. Therefore, assessing the load-bearing capacity and seismic performance of beam bridges, which are the most common type of bridge, is crucial. For this purpose, it is necessary to apply appropriate assessment methods, especially for structures that were not built according to modern code requirements and for older bridges with a higher degree of deterioration and thus reduced load-bearing capacity.

This paper presents a review of relevant literature, codes, and recommendations related to the pre-earthquake evaluation of bridges from countries frequently affected by strong earthquakes, including the USA, Japan, India, New Zealand, Turkey, and others. Based on this and the analysis of fragility curves (for substructures), this paper lists some recommendations for bridge evaluation as a case study, serving as a basis for making decisions on the type of structural intervention on the bridge or its demolition and removal.

Considering that for bridges, unlike reinforced concrete buildings, the condition is set that the deck structure does not exhibit yielding, which dissipates the energy of an earthquake, it is recommended that yielding occurs first in the elements of the lower structure (columns, abutments, and even foundations). Therefore, numerical analyses are focused on the sub-structure.

A comparative numerical analysis of six bridge mid-column models, featuring identical superstructures but differing substructures was performed in the paper. The prestressed concrete bridges, spanning 88 meters with configurations of 24.0+40.0+24.0m, were designed according to both old JUS design standard (three models) and new EN standards (three models). The substructures consist of RC columns with foundations and a prestressed beam of variable height (1.40m to 2.60m). Models type 1 has massive rectangular mid-columns, while types 2 and 3 consist of two columns with a crossbeam—type 2 features rectangular columns, and type 3 has circular columns. Using nonlinear analysis, the study evaluates how these design choices impact seismic damage limit states and column responses for different damage limit states. The results show significant differences in structural resilience and vulnerability, emphasizing the importance of design factors in enhancing seismic performance and ensuring safety.

Keywords: Concrete road bridges, pre-earthquake evaluation, deterioration, damage state, performance, seismic fragility

1. Introduction

Seismic assessment analysis of an existing bridge is to determine the level of risk associated with loss of serviceability, severe damage, or collapse. It depends on the age of the bridge, soil conditions, structural type, and site seismicity. Seismicity includes site-specific information on the expected ground motion. Ideally, it should consist of a basic response spectrum shape, or shapes, with peak ground acceleration related to annual probability of exceedance, and should be appropriate to the soil conditions of the site. Vulnerability represents the susceptibility to damage or collapse and is related primarily to

Proceedings of the 3rd Croatian Conference on Earthquake Engineering - 3CroCEE
19–22 March 2025, Split, Croatia
Copyright © 2025 CroCEE
DOI: https://doi.org/10.5592/CO/3CroCEE.2025.65

structural aspects. The vulnerability will depend on the structural form and topography. Importance relates to the consequences of damage or failure and typically includes consideration of traffic volume, type of crossing, length of detour resulting from bridge closure, and the significance of the bridge to lifeline operations such as the passage of emergency services vehicles to hospitals [1].

In the book [1], chapter 7 is devoted to the seismic assessment of existing buildings. A detailed methodology for the evaluation of bridges and their elements is presented in [2]. For the assessment and design of bridges in Europe, EN 1998 [3] is used. Additionally, the methodology for the design of concrete bridges is discussed in [1], [4], and [5], and retrofitting of bridges is analyzed in detail in [1]. In assessing the condition of bridges, evaluating their damage is crucial, as covered in works [6], [7]. Post-earthquake rapid assessment of bridges (Case study Glina County) is discussed in [8].

In most studies, it is shown that inspections of structures form the basis for assessing the performance of existing bridges. Inspection methods according to different codes are analyzed in [9], generally, and in [10] for the assessment and retrofitting using state-of-the-art approaches. For assessing the condition and durability of deteriorated bridges, the work [10] can be used, and for bridges exposed to chloride corrosion [11]. Corrosion of steel reinforcements is a major factor causing seismic performance deterioration of reinforced concrete (RC) bridges. This phenomenon is considered regarding the seismic performance assessment of aging RC bridges [12].

Corrosion of reinforcing steel is one of the primary sources of durability problems in reinforced concrete (RC) bridges. Authors of the paper [13] quoted that most structures designed and constructed after 1990 have performed well. However, there are a significant number of older major infrastructure artifacts that are located in an aggressive environment and are suffering from material aging and deterioration. This will increase the probability of failure of deteriorated structures in big earthquakes. It can also result in significant permanent damage in smaller earthquakes.

All bridges become more vulnerable to seismicity due to corrosion deterioration. Therefore, neglecting the effects of corrosion deterioration may lead to unconservative estimates of seismic damage risk [14].

Most existing bridges were designed according to outdated codes that did not address current requirements, including seismic resistance. In this regard, it is necessary to emphasize that bridges perform a strategic function in civil protection plans for emergency management and must remain functional in the aftermath of an extreme event. Therefore, the assessment of their potential performance in the case of ground motions is of great importance in earthquake-prone countries [15].

For more accurate assessments, various numerical and analytical procedures of different complexity and accuracy are used. Assistance in choosing analysis methods can be obtained using methods for fragility analysis. Fragility functions for assessing seismic risk of typical concrete bridges by means of nonlinear static analysis (NSA) and nonlinear dynamic analysis (NDA) are described in [16]. In the study [15], linear and nonlinear performance analyses of multi-span bridges are compared. Seismic resilience assessment of bridges considering both maximum and residual displacements is the subject of [16], and displacement-based seismic performance of RC bridge piers is discussed in [17].

Examples from the application of fragility curve development for seismic evaluation of RC bridges in Algeria are presented in [18]. Seismic fragility analysis of continuous girder bridges with varying pier heights is the subject of [2], and a bridge exposed to corrosion is discussed in [19]. A special case of seismic fragility and resilience improvement of conventional bridges supported by double-column piers is analyzed in [20], and seismic performance assessment of deteriorated two-span reinforced concrete bridges in [21]. Seismic vulnerability assessment of deteriorated bridges is analyzed in [22].

This paper presents a comparative numerical analysis of three bridge models which have identical super-structures but different sub-structures, specifically the supporting mid-columns. The analyzed prestressed concrete bridges span 88 meters and they are located on the same site. The design solutions for the frame structural system were selected based on terrain characteristics and project requirements, adhering to European standards EN1990 [23], EN1991 [24], EN1992 [25], and EN1998-2 [3]. Each bridge has two lanes (3.50 m width) and two pedestrian paths (1.5 m width) (Fig. 1), with spans of

Copyright © 2025 CroCEE
DOI: https://doi.org/10.5592/CO/3CroCEE.2025.65

24.0+40.0+24.0m (Fig. 2). The substructure includes RC columns with foundations and a prestressed beam with a variable-height box cross-section (1.40m to 2.60m), cast in situ.

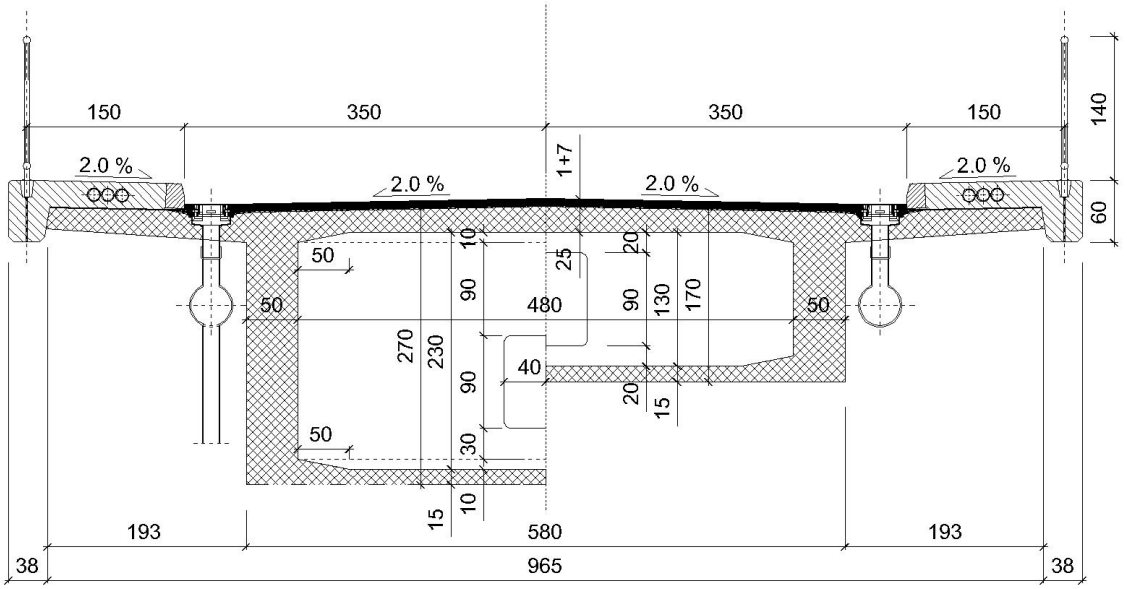


Figure 1. Upper deck cross-section of bridge models (M1, M2 and M3)

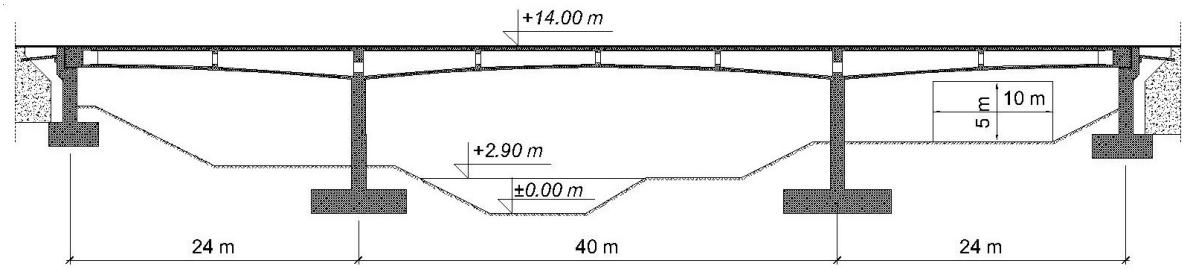


Figure 2. Bridge model 1 (M1) – longitudinal view

The paper analyzes how these design choices according to different (EN [3], [23-25] and JUS [26-28]) standards impact seismic fragility and bridge column responses using nonlinear analysis methods. Structural damage can lead to significant material loss, compromising the bridge's functions and posing risks to nearby areas. Therefore, damage limit states were calculated using NSA, which was conducted and compared to NDA results in the paper [29] and it gave a valid match of the calculated values.

Fragility curves were calculated using NDA results and earthquake time-history (TH) data. The structural responses of bridge columns were compared across different damage states, contributing to the assessment of seismic damage and resilience. The findings enhance understanding of differences between (EN [3], [23-25] and JUS [26-28]) standards and various design factors affect the seismic response and fragility of the bridge structural system.

2. Methodology of the analysis

2.1. Geometric and material properties of the structures

The analyzed concrete bridges, have an 88 meters span, with configurations of 24.0+40.0+24.0m (Fig. 1). In Model 1 (M1) in Fig. 3, the mid-columns are massive and designed as DCL and in models 2 (Fig. 4) and 3 (Fig. 5) (M2 and M3), the mid-columns are designed as DCM elements. For M2 and M3, the mid-columns construction comprises three elements. These consist of two piers and a crossbeam, which

Copyright © 2025 CroCEE
DOI: https://doi.org/10.5592/CO/3CroCEE.2025.65

are rigidly connected to the main deck. In M2, the mid-columns have a rectangular cross-section, while in M3, the mid-columns have a circular cross-section. The crossbeams have a rectangular cross-section.

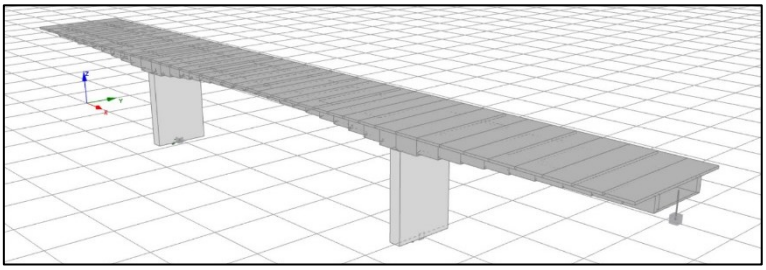


Figure 3. Bridge model 1 (M1), [32]

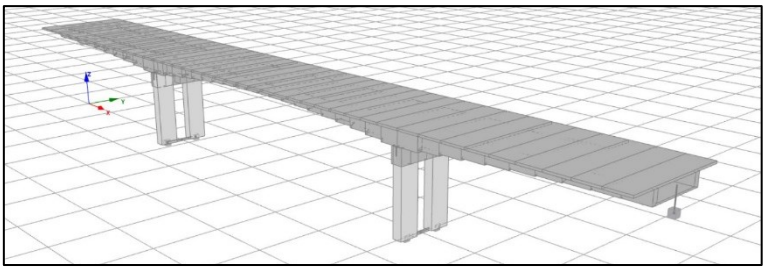


Figure 4. Bridge model 2 (M2), [32]

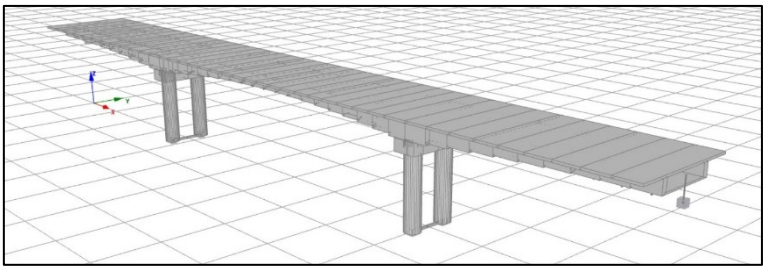


Figure 5. Bridge model 3 (M3), [32]

The bridge structures are of the rigid frame type, restrained perpendicular to the bridge alignment at the abutments. The mid-columns are fixed at the bottom and they all have a height of H_C = 8.45 m. Concrete of grade C30/37 and steel B500 for reinforcement were used in calculation according to EN standards [3], [23-25]. Concrete of grade MB40 (which has similar properties to C30/37) and steel RA400/500 for reinforcement were used in calculation according to JUS standards [26-28]. The bridge mid-columns in M1, M2, and M3 were designed in accordance with the both standards (EN [3], [23-25] and JUS [26-28]).

The calculations were carried out using the software packages *Radimpex Tower* [30] (linear analysis), *CSi SAP2000* [31] (damage limit state thresholds calculation), and and *Seismosoft Seismostruct* [32] (nonlinear analysis). For the calculation of seismic forces, 20% of traffic load was included in the seismic combination and modal analysis of the structures. The structures were designed to design spectrum type 1, soil type E, and horizontal design acceleration of 0.1g according to [3] and for soil of category III and seismic zone VIII, according to [26].

The assessment of damage limit states in the mid-columns was conducted on three different models to compare and analyze the values at which these damage limit states (LS) occur. The current modeling approach of analyzed structures (Table 1) provides a balanced framework for the assessment of bridge performance, with nonlinear analysis of critical components (mid-columns) and simplified modeling of other structural elements. Table 2 provides a detailed comparison of the geometric and material properties of the mid-columns in each model.

Proceedings of the 3rd Croatian Conference on Earthquake Engineering - 3CroCEE
19–22 March 2025, Split, Croatia
Copyright © 2025 CroCEE
DOI: https://doi.org/10.5592/CO/3CroCEE.2025.65

Table 1. Structural element type used in the models

Element	Structural element type in the models
Mid-column	Nonlinear element with hinges
Mid-column foundation	Restraints
Cross-beam	Linear element
Bridge deck	Linear element
Abutments	Restraints

Table 2. Geometric and material properties of the mid-columns in each model

Cross-section properties	M1	M2	M3
	EN | JUS		
Ductility class:	DCL (q = 1.5) (EN)	DCM (q = 3.0) (EN)	DCM (q = 3.0) (EN)
Crossbeam:	/	d/b/l = 1.2/1.6/6.2m	d/b/l = 1.2/2.4/6.2m
Cross-section height: d [m]	6.0	2.0	Diameter D = 1.6m
Cross-section width: b [m]	1.2	1.0	
Longitudinal rebars in columns (EN | JUS):	132 Ø25 | 120 Ø22 As = 648.1 cm^2 | 456.0 cm^2	44 Ø25 | 44 Ø22 As = 216.0 cm^2 | 167.2 cm^2	36 Ø28 | 36 Ø22 As = 221.4 cm^2 | 136.8 cm^2
Stirrups in column:	Ø12/15 | Ø10/20, Confinement bars: 4 x 7 | 2 x 7	Ø12/15 | Ø10/20 Confinement bars: 5 x 8 | 1 x 5	Ø12/15 | Ø10/20 Confinement bars: 1 hoop

2.2. Damage limit state threshold values

Table 3 defines different levels of damage and their threshold values for the mid-columns of the bridge models and how these thresholds are used to evaluate the structural performance. To determine the damage limit LS values, NSA was performed. By analysing the response of the structures, the damage states for various conditions were assessed. Similar approach to the definition of damage or limit state values is used in paper [33], [29].

Table 3. Description of the damage state threshold values

Nr.	Limit state (LS)	Description	M1	M2	M3
	EN | JUS				
1	**Small damage (SD)**	Depends on steel and concrete values. SD occurs either in the first step, when reaching the reinforcement yield limit ($\varepsilon_s \geq \varepsilon_{sy}$) or the stress limit of concrete with maximum strength in the protective layer of concrete ($\varepsilon_c \geq \varepsilon_{c1}$).	$\varepsilon_s \geq \varepsilon_{sy} = 0.0025$ *or* $\varepsilon_c \geq \varepsilon_{c1} \approx 0.002$		
2	**Moderate damage (MD)**	This level of damage is assumed to occur when reaching the stress limit in the protective layer of concrete ($\varepsilon_c \geq \varepsilon_{cu,1}$) or the maximum stress of the confined concrete core ($\varepsilon_{c,c} \geq \varepsilon_{cc,1}$)	$\varepsilon_c \geq \varepsilon_{cu,1} = 0.0035$ *or* $\varepsilon_{c,c} \geq \varepsilon_{cc,1} = 0.0030 \mid 0.0023$	$\varepsilon_c \geq \varepsilon_{cu,1} = 0.0035$ *or* $\varepsilon_{c,c} \geq \varepsilon_{cc,1} = 0.0037 \mid 0.0022$	$\varepsilon_c \geq \varepsilon_{cu,1} = 0.0035$ *or* $\varepsilon_{c,c} \geq \varepsilon_{cc,1} = 0.0024 \mid 0.0024$
3	**Extensive damage (ED)**	Occurs in the first step, when the ultimate stress is reached in the confined concrete core ($\varepsilon_{c,c} \geq \varepsilon_{cc,u}$).	$\varepsilon_{c,c} \geq \varepsilon_{cc,u} = 0.0069 \mid 0.0049$	$\varepsilon_{c,c} \geq \varepsilon_{cc,u} = 0.0142 \mid 0.0106$	$\varepsilon_{c,c} \geq \varepsilon_{cc,u} = 0.0077 \mid 0.0065$
4	**Complete damage (CD)**	This state results in the case of tensile fracture of longitudinal reinforcement bars ($\varepsilon_s \geq \varepsilon_{s,u}$), the mid-column drift reaches ($\theta \geq \theta_u$) and the loss of system balance.	$\varepsilon_s \geq \varepsilon_{s,u} = 0.05$ *or* $\theta \geq \theta u$	$\varepsilon_s \geq \varepsilon_{s,u} = 0.05$ *or* $\theta \geq \theta u$	$\varepsilon_s \geq \varepsilon_{s,u} = 0.05$ *or* $\theta \geq \theta u$

Copyright © 2025 CroCEE
DOI: https://doi.org/10.5592/CO/3CroCEE.2025.65

2.3. Incremental NDA

Nonlinear time-history analysis (THA) is conducted by using ten particular accelerograms [34-35] (Fig. 6 and Table 4) in only one direction, perpendicular to the bridge deck alignment, because of its simplicity and the wide application of this method of analysis.

The main criterion for selecting earthquake records was that the mean of the selected and scaled records should match the elastic response spectrum EN1998-1 [3] used in the analysis.

THA data were scaled with a common scale factor $F_S = 0.8$, which was obtained using the least-squares method. Scaled accelerograms are used for NDA, with the increment of $\Delta PGA = 0.1g$, in a total scaling factor range of $0.1–1.0g$.

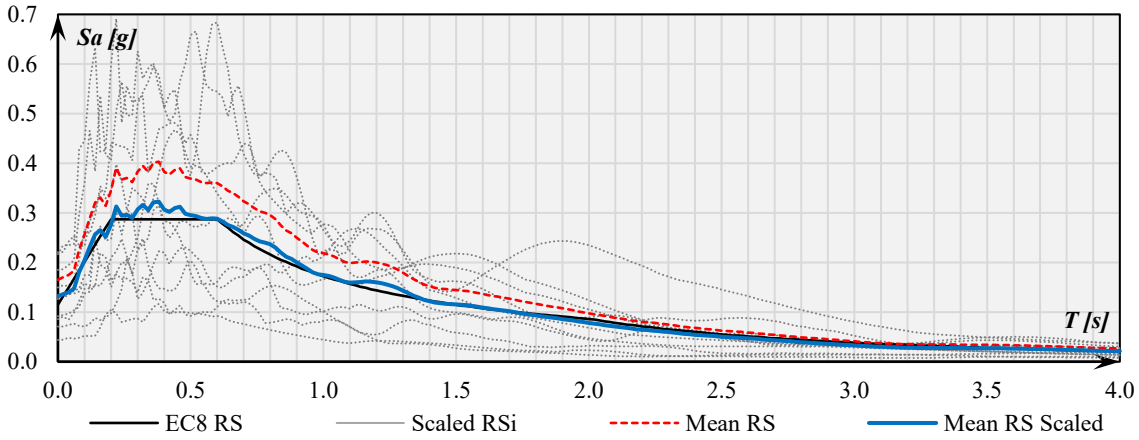


Figure 6. Response spectra used in the analysis (scaled RS_i, mean RS and mean scaled RS)

Table 4. Main properties of the earthquakes that were used in NDA

ID	Earthquake Location	Earthquake ID (Component/Orientation)	Station ID/Code	Date/Time	M_W	Original PHA [cm/s²]
EQ01	*Spitak, Armenia*	213 (Y)	173	07.12.1988. 07:41:24	6.7	179.580
EQ02	*Manjil, Western Iran*	230 (Y)	189	20.6.1990. 21:00:08	7.4	87.045
EQ03	*Umbria Marche, Central Italy*	286 (Y)	221	26.9.1997. 09:40:30	6.0	218.340
EQ04	*Umbria Marche, Central Italy*	286 (Y)	224	26.9.1997. 09:40:30	6.0	106.660
EQ05	*Alkion, Greece*	559 (X)	214	15.6.1995. 00:15:51	6.5	55.501
EQ06	*Düzce, Turkey*	497 (Y)	3139	12.11.1999. 16:57:20	7.2	112.320
EQ07	*Umbria, Central Italy*	EMSC-20161030_0000029 (N-S)	CNE	30.10.2016. 06:40:18	6.5	288.280
EQ08	*Emilia-Romagna, Italy*	IT-2012-0011 (N-S)	MOG0	29.5.2012. 07:00:02	6.0	167.075
EQ09	*Adana, Turkey*	TK-1998-0063 (E-W)	0105	27.6.1998. 13:55:53	6.2	271.955
EQ10	*Emilia-Romagna, Italy*	IT-2012-0011 (N-S)	MIR08	29.5.2012. 07:00:02	6.0	242.970

Copyright © 2025 CroCEE
DOI: https://doi.org/10.5592/CO/3CroCEE.2025.65

3. Discussion of the results

3.1. Damage state values

The NSA results are shown in Fig. 7. Mid-column drift values for the analysed models for different damage limit states (LS) provide the insights into the seismic performance of the bridge structures designed according to EN [3], [23-25] and JUS [26-28].

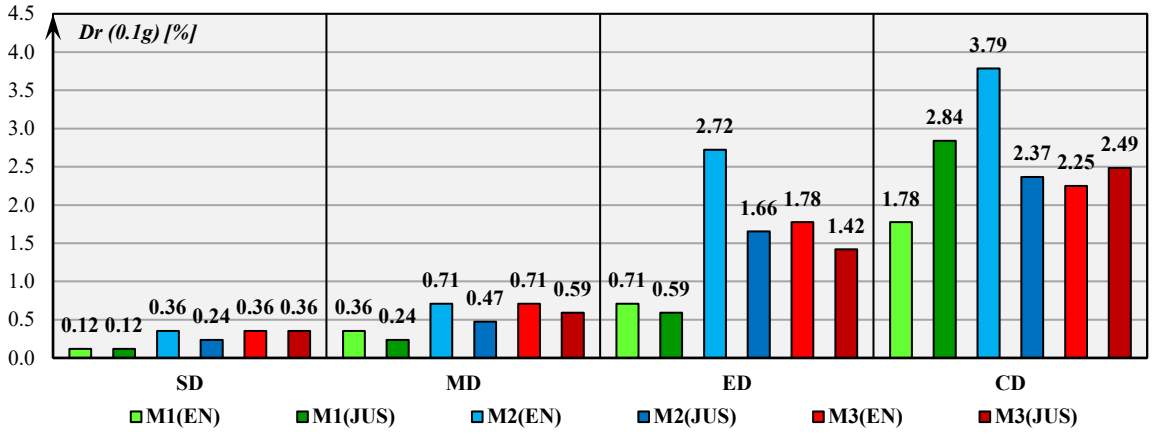


Figure 7. Comparison of drift values of mid-column for M1, M2 and M3, derived from NSA

At the Small Damage (SD) state, both M1 (EN) and M1 (JUS) have the same drift value of 0.118%, indicating similar behaviour in the massive rectangular columns. For M2, the drift values are higher, with 0.355% for M2 (EN) and 0.237% for M2 (JUS), while M3 has an equal drift value of 0.355% for both standards, suggesting that circular columns are more flexible.

In the Moderate Damage (MD) state, M1 (EN) allows a higher drift (0.355%) compared to M1 (JUS) at 0.237%. M2 (EN) also shows a higher drift (0.710%) than M2 (JUS) (0.473%), while M3 (EN) at 0.710% is greater than M3 (JUS) at 0.592%, indicating that the columns designed according to EN standard will achieve higher deformation value before moderate damage state is reached.

In the Extensive Damage (ED) state, the difference between the two standards becomes more pronounced. M1 (EN) has a drift of 0.710%, while M1 (JUS) is at 0.592%. M2 (EN) shows a much larger difference at 2.722% compared to 1.657% for M2 (JUS). M3 (EN) is at 1.775%, while M3 (JUS) is at 1.420%, that the columns designed according to EN standard will achieve higher deformation before reaching extensive damage state.

At the Complete Damage (CD) state, M1 (JUS) has a drift of 2.840%, compared to 1.775% for M1 (EN). M2 shows an even larger gap, with 3.787% for M2 (EN) and 2.367% for M2 (JUS). M3 shows slightly different values for each standard, with 2.249% for M3 (EN) and 2.485% for M3 (JUS).

Overall, the EN standards [3], [23-25] allow higher drift values across all models, indicating that these structures are more ductile before reaching the damage states. This suggests a greater deformation capacity when the structure is designed according to EN, while JUS standards [26-28] impose more conservative drift values, meaning that damage occurs at lower drift levels.

3.2. Fragility analysis

Fragility curves are calculated as the empirical fragility curves. An empirical fragility function is one that is created by fitting a function to approximate observational data. The observational data in this case represents number of assets exposed to some level of excitation, and the number of those that failed when subjected to the environmental excitation (i.e., reaching or exceeding the specified limit state). Fragility curves give insights into the probability of exceeding certain damage limit states (SD, MD, ED, CD) under varying ground motion peak ground acceleration (PGA).

Copyright © 2025 CroCEE
DOI: https://doi.org/10.5592/CO/3CroCEE.2025.65

In the case of the calculation of fragility curves, an engineering demand parameter (EDP) is used as a referent value in order to calculate the probability of the occurrence of a defined damage state (DS) at a particular intensity measure (IM) value $\left(P_{DS_i|IM_j}\right)$, using the expression:

$$P_{DS_i|IM_j}\left(\mu_{LN,IM_j}^{EDP_i}, \sigma_{LN|IM_j}^{EDP_i}\right) = 1 - \Phi\left(\frac{\ln EDP - \mu_{LN,IM_j}^{EDP_i}}{\sigma_{LN|IM_j}^{EDP_i}}\right) \quad (1)$$

where $\mu_{LN,IM_j}^{EDP_i}$ and $\sigma_{LN|IM_j}^{EDP_i}$ are the mean and standard deviation in log-log space of the probability density function (PDF) of the variable $\ln EDP$ for a particular $\ln IM_j$ value. $\ln EDP_i$ is the lognormal value of a DS threshold. These fragility curves are calculated using methods of statistical analysis and probability described in [36], [37]. The results of the analysis are shown in Fig. 8 – 12.

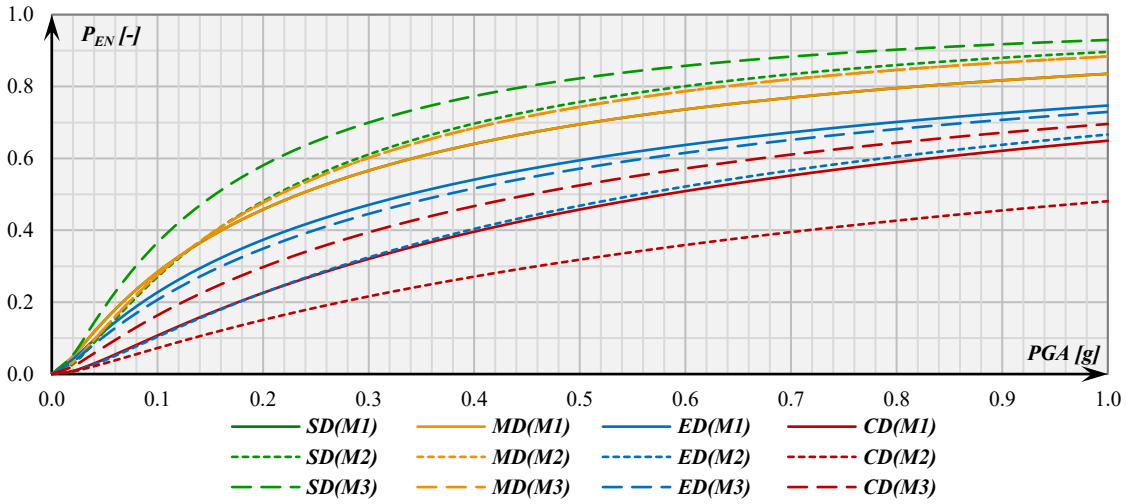


Figure 8. Fragility curves for M1, M2 and M3, according to EN

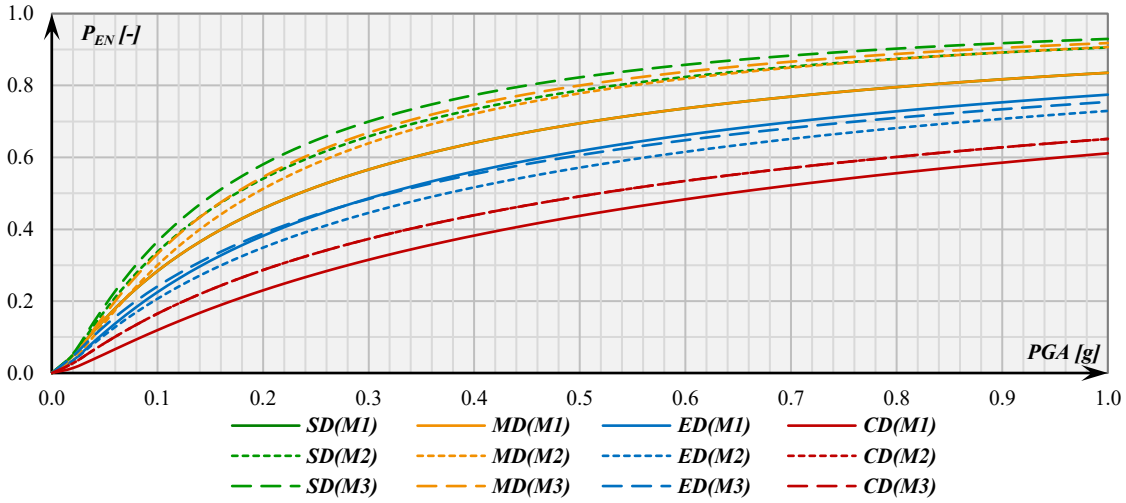


Figure 9. Fragility curves for M1, M2 and M3, according to JUS

Copyright © 2025 CroCEE
DOI: https://doi.org/10.5592/CO/3CroCEE.2025.65

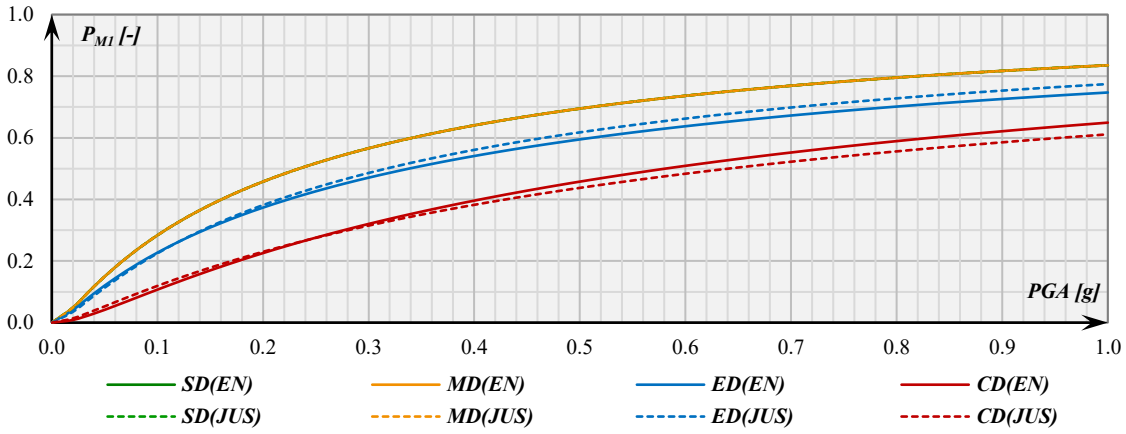


Figure 10. Fragility curves for M1(EN) and M1(JUS), for damage LS: SD, MD, ED, CD

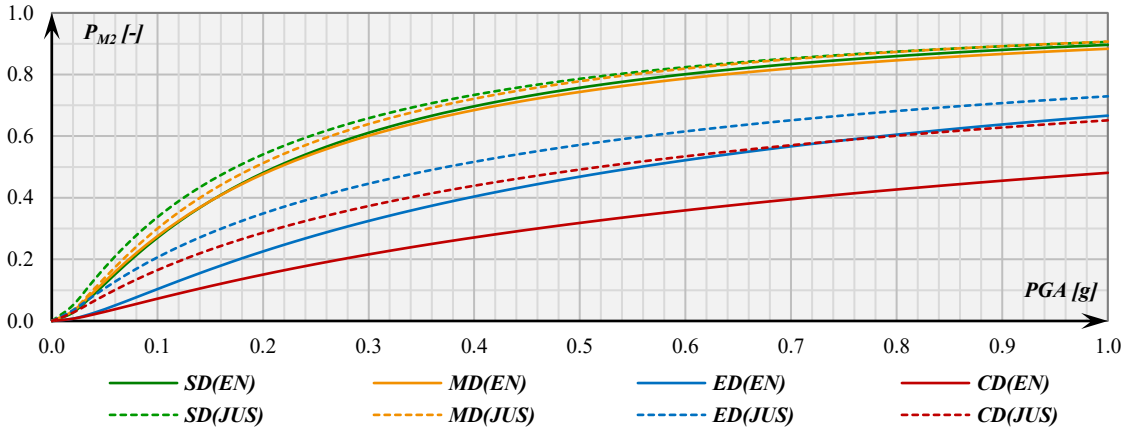


Figure 11. Fragility curves for M2(EN) and M2(JUS), for damage LS: SD, MD, ED, CD

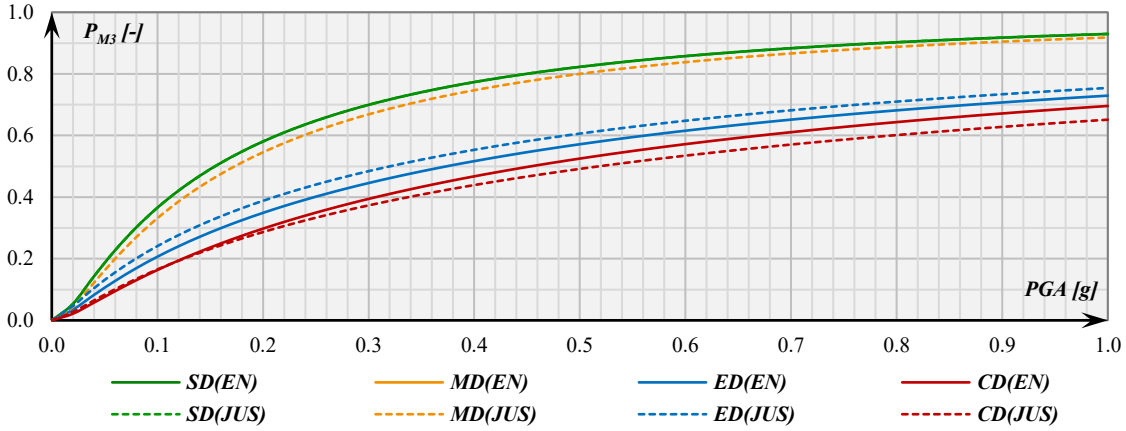


Figure 12. Fragility curves for M3(EN) and M3(JUS), for damage LS: SD, MD, ED, CD

The results provided represent fragility curves for three models (M1, M2, and M3) under two different design codes (EN and JUS). The fragility analysis typically evaluates the probability of a system or structure reaching different damage states (SD - Slight Damage, MD - Moderate Damage, ED - Extensive Damage, CD - Complete Damage) at various ground accelerations (PGA, in g).

Proceedings of the 3rd Croatian Conference on Earthquake Engineering - 3CroCEE
19–22 March 2025, Split, Croatia
Copyright © 2025 CroCEE
DOI: https://doi.org/10.5592/CO/3CroCEE.2025.65

These results allow for a comparison of how each model behaves under varying intensities of seismic loading, as well as how the two design codes (EN and JUS) influence the fragility curves.

3.3. Comparison between M1, M2, and M3

M1 shows a higher level of resistance to damage at lower PGA values, with a gradual increase in the probability of reaching MD and ED as PGA increases. At higher PGAs, the probability of reaching ED and CD rises significantly. M2 and M3 follow a similar pattern but with lower resistance at lower PGAs compared to M1.

M2 shows a higher probability of MD and ED damage, while M3 exhibits a slightly higher probability of damage in the Moderate to Complete Damage states compared to M2, particularly at higher PGAs. The progression toward severe damage states is more pronounced in M2 and M3, with the probability of reaching CD being higher for both models compared to M1. However, the transition from MD to ED to CD in M3 occurs more gradually than in M2, suggesting greater vulnerability in the higher PGA range for M3.

M1 shows a gradual increase in probability of damage as PGA increases, but it maintains a higher overall level of resilience across all damage states. This suggests that M1 is more robust against seismic actions. M2 and M3 show similar trends, with a higher sensitivity to seismic excitation. This is reflected in a faster rapid progression from SD to MD and ED as PGA increases.

3.4. Comparison between EN and JUS

EN appears to define a more resilient structural design, particularly at lower PGAs, as seen in the lower probabilities of damage across all models. This could indicate that the EN code may impose stricter or more robust safety requirements for building design and performance under seismic events.

On the other hand, JUS appears to be more sensitive to higher seismic accelerations, as the damage states progress more quickly with increasing PGA, indicating either a less strict design for moderate shaking or a faster progression to failure in structures designed under JUS.

The fragility results suggest that structures designed according to EN may have a greater margin of safety in terms of resilience to seismic events, especially for lower-magnitude earthquakes. However, structures designed under JUS may face more significant damage at higher PGA values, necessitating more robust reinforcement for earthquake-resilient designs. EN design standards seem to offer better performance in terms of damage mitigation at both low and high seismic intensities.

The analysis reveals that the models exhibit different behaviours under seismic loading, with M1 being more resilient than M2 and M3. Additionally, structures designed according to EN standards demonstrate better resistance to damage at both low and high PGAs compared to those designed according to JUS. The results indicate a more conservative approach in EN, particularly in mitigating damage under low to moderate seismic loads, while JUS standards predict higher damage probabilities at higher PGAs, especially for the more sensitive models.

4. Conclusions

This study shows the importance of the assessment of the seismic performance and lateral load-bearing capacity of existing bridges, especially those not designed to modern seismic standards. The research focused on comparison of the bridge models with different substructures (massive rectangular mid-columns, and two-column frame mid-column) designed under old (JUS [26-28]) and modern (EN [3], [23-25]) standards. The results from nonlinear static and dynamic analyses show that bridges designed according to the EN standard exhibited greater seismic resilience, allowing higher deformation before reaching critical damage states compared to those designed using JUS standards.

Fragility analysis results show the significance of design choices in order to enhance the seismic performance of beam bridges, particularly in earthquake-prone regions. The results show that bridges with circular columns and dual-column frame mid-columns (M2 and M3) are more flexible and

Copyright © 2025 CroCEE
DOI: https://doi.org/10.5592/CO/3CroCEE.2025.65

experience larger drift values before reaching damage limit states, than massive rectangular mid-columns (M1) which can influence seismic resilience. Additionally, the columns designed according to the EN standard consistently show the greater deformation capacity before critical damage states, suggesting a more ductile behaviour under seismic actions.

In general, the results suggest that bridges designed with modern seismic codes exhibit improved resilience, which is crucial for maintaining functionality and safety during seismic events. Moreover, this study underscores the need for comprehensive evaluations and retrofitting of older bridges to meet current seismic performance standards, ensuring their long-term safety and serviceability.

References

[1] Priestley M.J.N, Seible F, Calvi G.M, (1996): Seismic design and retrofit of bridges, John Wiley & Sons Inc, NY.

[2] Cao, Y., Liang, Y., Huai, C. Yang J., Mao, R.: Seismic Fragility Analysis of Multispan Continuous Girder Bridges with Varying Pier Heights considering Their Bond-Slip Behavior, Advances in Civil Engineering, (2020), Article ID 8869921

[3] EN 1998-Part 2: Bridges, 2005; Part 3; Designers' guide to EN 1992-2 (Ed. C. R. Hendy and D. A. Smith) TT, 2007.

[4] Lee, G.C., Tong, M., Yen. W. P.: Design Higway Bridges against extreme hazard Events; Issues, Principles and Approaches. MCEER, University at Buffalo, June 30, 2008, MCEER-08-SP06

[5] Zhang, Qi, Alam, M.S.: Performance-based seismic design of bridges: a glabal perspective and critical review of passt, pezent and future direction, Structure and Inrfa. Eng. 2018, P 1558269.

[6] Folić, R. Čokić, M. Folić, B.: Some damage of RC bridges after strong Earthquakes, Conf. VSU 2023, Proc. Ed. I. Stoynova, pp. 438 - 450.

[7] Folić, R., Radonjanin, V., Prokić, A., Malešev, M.: Earthquake damage to RC bridges and review of recommendation for its repair and strengthening, Str. Fault and Repair, Edinburgh, Ed. M. Forde, 2016

[8] Vlašic, A. Srbic, M. et al. Post-Earthquake Rapid Damage Assessment of Road Bridges in Glina County, Buildings 2022, 12, 42. https://doi.org/10.3390/buildings12010042

[9] Folić, R., Čokić, M., Folić, B.: Post-earthquake evaluation of concrete bridges, XXIV Intern. Scientific Conf. VSU2024, PL 2Č: 18p.

[10] Skokandić,D., Vlašić, A., Kušter Marić, M., Srbić, M., Mandić Ivanković, A.: Seismic assessment and retrofitting of existing road breidges: State of the art review, Materials 2022, 15, 2523

[11] Liu, X., Zhang,W., Sun, P., Liu, M (2022).: Time-dependent seismic fragility of tipical concrete girder bridges under chloride-induced corrosion, Materials, 15, 5020

[12] Kibboua,A., Kehila, F., Bechtoula, H., Mehani, Y. Remki, M.: Development of fragility Curves for Seismic Evaluation of a RC Bridges, 2nd ECEES, Istanbul, Aug. 25-29, 2014

[13] Lee, G.C., Tong, M., Yen. W. P.: Design Higway Bridges against extreme hazard Events; Issues, Principles and Approaches. MCEER, University at Buffalo, June 30, 2008, MCEER-08-SP06

[14] Randi, R., Okumus, P., Wang,H.: Seismic vulnerability assessment of deteriorated bridges, Rep. CAIT-UTC-REG29, University at Buffalo, 2021. 60p.

[15] Pettorruso, C., Quaglini, V.: Comparison of Linear and Nonlinear Procedures for the Analysis of thw Seismic Performance of Stright Multi-Span RC Bridges, Buildings (2024), 14, 464

[16] Wei, B. Jia, J. Bai, Y. Du, X. Guo, B. Guo, H.: Seismic resilience assessment of bridges considering both maximum and residual displacements, Engineering Structures 291, 2023; 116420

[17] Taipe, J.F., Fernandez-Davila, V.I.: Displacement-based seismic performance of RC bridge pier, Advances in Bridge Engineering, (2023) 4:17

[18] Kibboua,A., Kehila, F., Bechtoula, H., Mehani, Y. Remki, M.: Development of fragility Curves for Seismic Evaluation of a RC Bridges, 2nd ECEES, Istanbul, Aug. 25-29, 2014

Copyright © 2025 CroCEE
DOI: https://doi.org/10.5592/CO/3CroCEE.2025.65

[19] Choe, D-E., Gardony, P., Rosowsky, D., Haukas,T.: Seismic fragility estimates for RC bridges subjected to corrosion, Structural safety, 31, 2009, 275-283.

[20] Hong, Y., Ye, L., Xie, W.: Seismic Fragility and Resilience improvement of convential Bridges supported by double-column piers utilizing shear links, Structures 57 (2023) 105309

[21] Kim, T-H.: Seismic performance assessment of deteriorated two-span reinforced concrete bridges, Int J Concr Struct Mater, 2022,16:4; https//doi.org/10.1186/s40069-022-00498-9

[22] Randi, R., Okumus, P., Wang,H.: Seismic vulnerability assessment of deteriorated bridges, Rep. CAIT-UTC-REG29, University at Buffalo, 2021. 60p.

[23] EN 1990: European Committee for Standardization. (2002). Eurocode - Basis of structural design. EN 1990:2002.

[24] EN 1991: European Committee for Standardization. (2002). Eurocode 1: Actions on structures. Part 1-1: General actions - Densities, self-weight, imposed loads for buildings. EN 1991-1-1:2002.

[25] EN 1992-2: European Committee for Standardization. (2005). Eurocode 2: Design of concrete structures. Part 2: Concrete bridges - Design and detailing rules. EN 1992-2:2005.

[26] Collection of Yugoslav Regulations and Standards for Building Structures, Book 1 (*in serbo-croatian: Zbirka jugoslovenskih pravilnika i standarda za građevinske konstrukcije, Knjiga 1*), Association of Civil Engineers and Technicians of Yugoslavia, Belgrade, 1995

[27] Regulations on Technical Standards for the Design and Construction of Concrete and Reinforced Concrete Structures, PBAB/87 – Part 1: General Provisions, Calculation, and Design, Federal Institute for Standardization, Belgrade, 1987

[28] Regulations on Technical Standards for the Design and Construction of Concrete and Reinforced Concrete Structures, PBAB/87 – Part 2: Execution and Control, Federal Institute for Standardization, Belgrade, 1987

[29] Čokić, M., Folić, R., Drča, J., Folić, B., Nonlinear Fragility Analysis of Three Different Concrete Bridge Mid-Column Structural Types, Proceedings of the 11th International Conference on Bridges in Danube Basin, November 2024, pp. 409-418, doi:10.14459/icbdb24.37

[30] Radimpex Tower, Software for Structural Analysis and Design

[31] Computers and Structures, Inc., SAP2000: Structural Analysis and Design Software

[32] Seismosoft SeismoStruct: Structural Analysis Software for Seismic Design

[33] Parisi, F., Scalvenzi, M., Brunesi, E.: Performance limit states for progressive collapse analysis of reinforced concrete framed buildings, Structural Concrete, 20 (2019) 1; pp. 68–84 https://doi.org/10.1002/suco.201800039

[34] Ambraseys, N., Smit, P., Sigbjornsson, R., Suhadolc, P., Margaris, B.: Internet-site for European Strong-motion Data, European Commission, Research-directorate General, Environment and Climate Programme, http://www.isesd.hi.is, 1.1.2021.

[35] ORFEUS: Engineering Strong Motion Database, https://esm-db.eu/, 11.1.2021.

[36] Porter, K.A.: Beginner's Guide to Fragility, Vulnerability and Risk, University of Colorado Boulder, Boulder, CO, USA, 2015., DOI:10.1007/978-3-642-35344-4_256.

Proceedings of the 3rd Croatian Conference on Earthquake Engineering - 3CroCEE
19–22 March 2025, Split, Croatia
Copyright © 2025 CroCEE
DOI: https://doi.org/10.5592/CO/3CroCEE.2025.85

SEISMIC ASSESSMENT AND COST-BENEFIT ANALYSIS OF RETROFITTING MEASURES FOR POST-WAR MULTI-RESIDENTIAL MASONRY BUILDINGS IN LJUBLJANA

Simon Petrovčič [(1)], Petra Prašnikar [(2)] and Vojko Kilar [(3)]

[(1)] *Assistant Professor, University of Ljubljana, Faculty of Architecture, Slovenia, simon.petrovcic@fa.uni-lj.si*
[(2)] *Researcher, University of Ljubljana, Faculty of Architecture, Slovenia, petra.prasnikar@fa.uni-lj.si*
[(3)] *Full Professor, University of Ljubljana, Faculty of Architecture, Slovenia, vojko.kilar@fa.uni-lj.si*

Abstract

This study presents an integrated approach to seismic assessment and retrofitting of multi-residential masonry buildings constructed between 1945 and 1963 in Ljubljana, Slovenia. These buildings, characterized by unreinforced masonry walls and prefabricated floor slabs, represent a significant portion of the urban housing stock and are highly vulnerable to seismic loading.

The paper develops a standardized typology classification based on building shape, number of stories, and number of cores, identifying over 400 buildings across Ljubljana. Four representative building types were selected for detailed seismic performance assessment using the equivalent frame approach in 3Muri software. Two retrofitting scenarios using Fibre Reinforced Cementitious Matrix (FRCM) systems were evaluated: selective strengthening of critical elements and comprehensive strengthening of all load-bearing walls.

Results show that while FRCM retrofitting improves seismic performance, most retrofitted configurations fail to fully meet Eurocode 8 requirements. Cost-benefit analysis reveals that selective retrofitting requires 5-8% of property value investment, while comprehensive strengthening demands 17-23%, suggesting that additional strengthening measures may be necessary despite economic considerations.

The research provides critical insights for developing economically viable seismic risk mitigation strategies that balance structural safety requirements with financial constraints. This approach offers valuable guidance for addressing similar challenges in seismic-prone regions with comparable post-war building stocks.

Keywords: Seismic vulnerability assessment, Unreinforced masonry buildings, Post-war residential architecture, Building typology classification, Nonlinear static analysis, Seismic retrofitting, FRCM strengthening, Cost-benefit analysis.

1. Introduction

Multi-residential masonry buildings constructed between 1945 and 1963 in urban centres across former Yugoslavia represent a significant portion of the housing stock and are highly vulnerable to seismic loading [1], [2], [3], which became very clear after the 1963 Skopje earthquake [4]. These buildings, characterized by unreinforced masonry walls and prefabricated floor slabs, require a comprehensive approach to seismic vulnerability assessment and retrofitting measure planning.

Existing research indicates that these buildings often fail to meet modern seismic safety requirements. This is particularly concerning in cities with high seismic hazard, such as Ljubljana, where these buildings constitute a substantial portion of the multi-residential housing stock. Although many buildings have undergone energy efficiency renovations, most have not received structural reinforcement to improve their seismic resistance.

This study develops a standardized typology classification and conducts detailed seismic performance assessments using the equivalent frame approach. The research focuses on four representative building types from Ljubljana, which are analysed using 3Muri software – a commercial version of TREMURI, originally developed by Lagomarsino and co-authors [5]. Special attention is given to evaluating the

Copyright © 2025 CroCEE
DOI: https://doi.org/10.5592/CO/3CroCEE.2025.85

effectiveness of various retrofitting strategies, particularly Fibre Reinforced Cementitious Matrix (FRCM) systems, both in terms of structural improvement and economic feasibility.

The study also incorporates cost estimations for retrofitting measures based on current market prices and compares these to potential property value increases and avoided seismic losses. This cost-benefit analysis considers both structural safety and architectural preservation, as these buildings often represent an important part of cities' cultural identity.

The results of this research will provide valuable insights for policymakers and stakeholders involved in urban renewal and seismic risk mitigation across the former Yugoslavia region. The research contributes to developing sustainable strategies for enhancing urban resilience against seismic hazards, balancing safety, economic considerations, and architectural preservation. This approach offers valuable guidance for addressing similar challenges in seismic-prone regions with comparable post-war building stocks.

2. Building Identification and Typological Classification

2.1. Post-war Residential Neighbourhoods

In the first two decades following World War II, Slovenia experienced significant socio-economic changes and accelerated industrialization, leading to increased migration from rural areas to cities [6]. Additionally, there was substantial immigration from other Yugoslav republics to major Slovenian cities. This created an intense housing shortage, prompting large-scale construction of multi-residential buildings to address the urgent need for housing.

The first large multi-residential neighbourhoods began to appear in Ljubljana and other major Slovenian cities, following modernist architectural patterns. These neighbourhoods were characterized by their functional design, standardized construction methods, and community-oriented planning. Two pioneer neighbourhoods in Ljubljana, "Litostrojsko naselje" [7] and "Savsko naselje" [9], stand out as early examples of post-war modernist development.



Figure 1: Aerial photograph of "Litostrojsko naselje".

These buildings were typically constructed using traditional techniques in the earlier period, later incorporating prefabricated elements. The buildings are predominantly low- to medium-rise with flat or gently sloped roofs, adhering to modernist principles of simplicity and practicality. Their facades are

Proceedings of the 3rd Croatian Conference on Earthquake Engineering - 3CroCEE
19–22 March 2025, Split, Croatia
Copyright © 2025 CroCEE
DOI: https://doi.org/10.5592/CO/3CroCEE.2025.85

characterized by rhythmic window arrangements, often complemented by balconies or loggias, contributing to the cohesive and utilitarian aesthetic of Ljubljana's post-war urban landscape.

The vertical load-bearing structure typically consisted of unreinforced masonry walls, with varying materials and mortar types used at different levels. The ground and intermediate floors often utilized solid clay brick masonry with lime-cement mortar for added strength, while hollow clay bricks were occasionally employed. Floor structures were commonly constructed using semi-prefabricated systems, consisting of reinforced concrete joists alternated with hollow clay elements, topped by a thin reinforced concrete compressive slab.

It is worth noting that the construction quality in these post-war residential developments varied significantly. The rapid pace of construction and the large-scale nature of these developments, coupled with material shortages and the need for quick housing solutions, often led to compromises. The construction process frequently involved local residents, which, while fostering a sense of community ownership, meant that not all workers had professional construction experience, potentially affecting the overall quality and consistency of the buildings.

Today, these neighbourhoods represent a significant portion of Ljubljana's housing stock, with many buildings requiring both energy efficiency improvements and seismic retrofitting. Understanding their architectural and structural characteristics is crucial for developing appropriate intervention strategies that respect both their historical significance and the need for modern safety standards.

2.2. Criteria and Parameters for Typological Classification

To identify suitable buildings for our study, we utilized publicly accessible spatial information system databases within the City Municipality of Ljubljana (MOL). The collected data was processed using a commercial GIS software package, focusing on MOL due to the extensive available data. The selection criteria given in Table 1 were considered.

Table 1. Selection criteria for identification of buildings.

Selection Criteria	Parameter Range
Construction period	1945-1963
Number of stories	3-7 above-ground floors
Number of apartments	≥ 9 units

This selection process identified over 400 structures that met these criteria, distributed across various clusters in Ljubljana. The identified buildings were then categorized into distinct typologies based on their geometric and structural characteristics. For each identified typological class, we gathered data on architectural features, load-bearing structure design, materials used, and construction details from original project documentation in various archive records [9]. Complete data was obtained for 62 buildings, including original architectural plans and technical reports. This detailed information allowed for accurate characterization of each building type's structural system and potential seismic vulnerabilities.

A naming convention is used, where the first segment (S, R, CS, or CR) describes the building's shape, the second segment indicates the number of above-ground floors, and the last segment indicates the number of entrances that indicate individual building cores. The shape of the building is further divided into three groups:

- **S**: Square or nearly square buildings with a length-to-width ratio between 1.0 and 1.2.
- **R**: Rectangular buildings with a length-to-width ratio greater than 1.2 or less than 1.0.
- **CS/CR**: Compound shape formed by combining two identical S-shape buildings (CS) or compound shape formed by combining one S-shape and one R-shape building (CR).

Copyright © 2025 CroCEE
DOI: https://doi.org/10.5592/CO/3CroCEE.2025.85

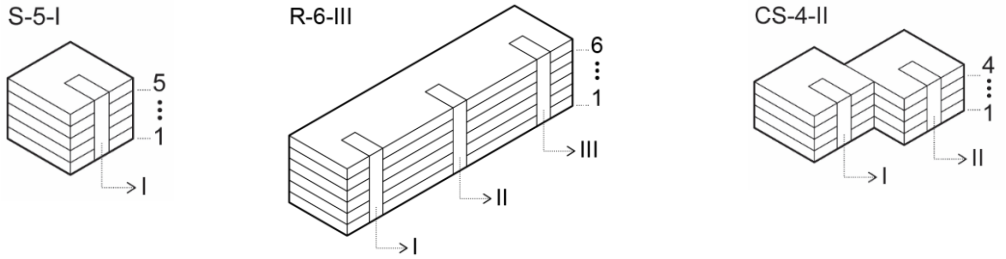


Figure 2: Schematic typology representation.

The classification coding system combines these parameters. For example, "R-4-II" represents a rectangular-shaped building with 4 stories and 2 communication cores. This standardized approach enables systematic analysis of similar building types.

The classification methodology proved particularly valuable for seismic vulnerability assessment as it groups buildings with similar structural characteristics and expected seismic behaviour. This approach allows for estimating the seismic vulnerability of a large number of buildings without performing detailed individual evaluations, which would be costly and time-consuming. Furthermore, it helps identify the most common and critical building types in the region, facilitating the prioritization of seismic retrofitting interventions.

Significant variations were observed across the typological classes in terms of:

- floor plan dimensions and configurations,
- wall-to-floor area ratios,
- structural system arrangements,
- construction materials and techniques,
- building height and slenderness ratios.

This classification system provides a framework for developing targeted seismic assessment and retrofitting strategies appropriate for each building type, considering their specific structural characteristics and vulnerabilities.

3. Seismic Performance Assessment and Retrofitting Strategies

3.1. Numerical Modelling and Performance Assessment

To evaluate the seismic performance of typical post-war masonry buildings in Ljubljana, four representative building prototypes were selected based on their prevalence and geometric characteristics. As shown in Figure 3, Building S (S-5-I) represents a compact, nearly square five-story structure measuring 16.6 x 14.8 meters, with a centralized communication core and symmetrically distributed apartments. It exhibits notably different wall ratios in its principal directions, with 6.5% in the longitudinal direction versus 2.9% in the transversal direction. Building R (R-6-III) presents a contrasting configuration as a six-story rectangular building spanning 62.8 meters in length, featuring three communication cores. Its elongated form results in reversed wall ratios compared to Building S, with 2.8% longitudinal and 6.5% transversal, reflecting its distinct structural arrangement.

The compound-shaped buildings, CS (CS-4-II) and CR (CR-6-III), represent more complex geometric configurations. Building CS combines two four-story square structures arranged in an L-shape, with dimensions of 15.6 x 13.5 meters and two communication cores. It maintains relatively balanced wall ratios of 6.1% longitudinal and 4.1% transversal, reflected in its similar fundamental periods of vibration (0.40s and 0.48s respectively). Building CR, a six-story structure combining rectangular and square forms over a 32.6-meter length, features three communication cores and demonstrates more balanced structural characteristics with wall ratios of 5.5% longitudinal and 6.4% transversal. As depicted in the floor plans and 3D representations in Figure 3, these four prototypes encompass key

Copyright © 2025 CroCEE
DOI: https://doi.org/10.5592/CO/3CroCEE.2025.85

variations in shape, height, and structural configuration found across Ljubljana's post-war residential buildings, providing a comprehensive basis for seismic assessment while representing distinct approaches to multi-residential construction of that era.

The seismic performance of these four representative building typologies was evaluated using nonlinear static (pushover) analyses in the 3Muri software. For this analysis it was crucial to define the longitudinal and transverse direction since there is quite a difference between the percentage of the walls, between the two directions, in some building prototypes, which greatly impacts the results. As seen in Figure 3 we defined the longitudinal direction as the axis aligned with the longer side of the building or the main entrance. The 3Muri software employs an equivalent frame modelling approach, where masonry walls are represented as piers, spandrels, and rigid nodes, allowing for an efficient assessment of buildings' capacity to resist seismic actions considering material nonlinearity. Similar modelling approaches using the 3Muri software have been successfully applied in previous studies to analyse historical unreinforced masonry buildings, such as those damaged during the 2020 Zagreb earthquake [11]. The analysis generated capacity curves which were compared with inelastic response spectra using the N2 method. Each building's response was analysed in both longitudinal and transversal direction to assess their vulnerabilities and identify potential retrofitting needs.

3.2.Numerical Modelling and Performance Assessment

Each prototype was analysed in three structural states to capture the impact of retrofitting measures. Beside the first state, which represents the original unreinforced masonry (URM), characterized by the vulnerabilities inherent in historic masonry structures, two additional retrofitting scenarios were developed to evaluate the effectiveness of different strengthening strategies, the position of the application of FRCM for these scenarios, can be seen on Figure 4. The first scenario, Selective Retrofitting (RET), focused on reinforcing critical structural elements. These included the building cores (BC), which are the central stairwells essential for overall stability, the outer piers (OP), which are vertical elements on the external walls that experience significant vertical force variation, and the outer walls (OW) in the Y-direction, which provide additional lateral stability.

The second scenario, All Walls Retrofitting (RET-AW), involved a more comprehensive application of FRCM to all load-bearing walls throughout the structure. This approach encompassed not only the elements included in the RET scenario—building cores, outer piers, and outer walls—but also internal vertical elements in the X-direction, referred to as inner piers (IP), and internal walls in the Y-direction, known as inner walls (IW). This strategy aimed to achieve uniform strengthening across the entire structure. These retrofitting configurations were tailored to each building's structural characteristics. For example, Building R's elongated shape and numerous openings necessitated a larger increase in retrofitted wall area under the RET-AW scenario compared to RET. Conversely, Building S saw significant increases in both directions with RET-AW, effectively doubling the strengthened area longitudinally.

The study followed guidelines from CNR-DT 215/2018 [12], using alkali-resistant (AR) glass fibres for FRCM reinforcement. AR glass fibres were selected for their durability in alkaline environments and strong mechanical properties. The FRCM was applied symmetrically on both sides of masonry elements, covering piers, walls, and spandrels in a bi-directional configuration. This approach not only increased in-plane capacity but also enhanced crack control and system integrity, particularly after cracking onset. Preliminary analysis showed that both longitudinal (X-direction) and transverse (Y-direction) strengthening were necessary for the studied buildings [9], [13]. Both retrofitting approaches were complemented by the installation of horizontal steel ties around the building perimeter at each floor level. These ties enhanced the structure's box-like behaviour, reducing the risk of out-of-plane

Copyright © 2025 CroCEE
DOI: https://doi.org/10.5592/CO/3CroCEE.2025.85

wall failure during seismic events. By improving load distribution, the ties bolstered the overall effectiveness of FRCM strengthening in both scenarios.

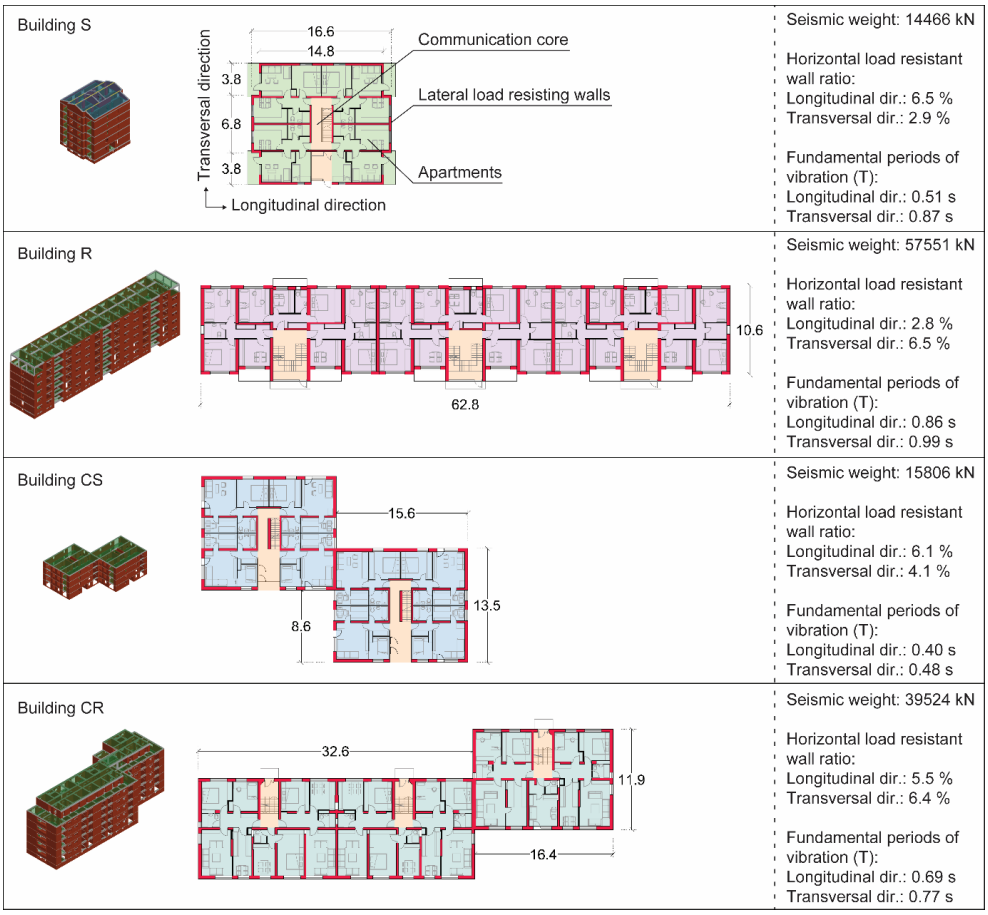


Figure 3: Four representative building prototypes and their key characteristics.

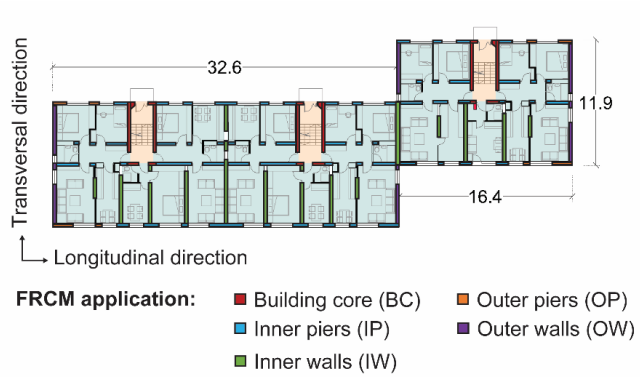


Figure 4: Schematic representation of FRCM retrofit positions for building CR. Similar strengthening configurations were applied to other selected building types.

Material properties of URM were derived from prior studies of similar unreinforced masonry (URM) buildings [14], [15], [16], [17], [18], [19]. These reference values, along with the properties of the FRCM system used in the numerical analysis, are presented in Table 2 and formed the basis for our analyses.

The assessment followed Eurocode 8 – Part 3 guidelines, focusing on two limit states: Damage Limitation (DL) and Significant Damage (SD), corresponding to different levels of structural damage

Proceedings of the 3rd Croatian Conference on Earthquake Engineering - 3CroCEE
19–22 March 2025, Split, Croatia
Copyright © 2025 CroCEE
DOI: https://doi.org/10.5592/CO/3CroCEE.2025.85

and seismic return periods. Lateral load-resistant wall ratios (ρ_w), a key parameter for seismic resistance [20], were calculated for each building typology.

Table 2: Reference mechanical properties of URM and properties of FRCM used in numerical analysis.

URM Properties	
Property	**Reference value**
Compressive strength (f_c)	4.00 MPa
Tensile strength (f_t)	0.14 MPa
Young's modulus (E)	1800 MPa
Shear modulus (G)	360 MPa

Properties of FRCM	
Parameter	**Reference value**
Equivalent thickness of reinforcing mesh (t_f)	0.028 mm
Young's modulus of elasticity of dry fibre (E_f)	280 GPa
Ultimate tensile strain of dry fibres (ε_f)	0.67%
Environmental conversion factor (η_a)	0.8

Building S exhibited higher wall ratios in the longitudinal direction (6.5%) compared to the transversal direction (2.9%) due to its compact and symmetrical configuration. Conversely, Building R showed the reverse trend, with a longitudinal wall ratio of 2.8% versus 6.5% in the transversal direction, attributed to its elongated rectangular shape with numerous openings in the longitudinal facades. These asymmetries suggest potential vulnerabilities requiring targeted strengthening. Building CS displayed a moderate asymmetry in wall ratios (6.1% longitudinal and 4.1% transversal), reflecting its compound square shape with a low slenderness ratio. Despite this, its seismic behaviour appeared balanced, with similar fundamental periods of vibration in both directions. Building CR exhibited near-symmetrical wall ratios (5.5% longitudinal and 6.4% transversal), likely due to its compound rectangular configuration, combining the characteristics of square and rectangular layouts. This balance may contribute to more uniform seismic behaviour, though its geometric complexity could introduce other performance challenges. Overall, the analysis underscored the significance of geometry and wall distribution in seismic vulnerability. Asymmetries in Buildings S and R highlight potential weaknesses, whereas the more balanced configurations in Buildings CS and CR suggest relatively stable performance. However, their intricate geometric layouts could also pose unique challenges that may affect their seismic behaviour in unexpected ways. These insights inform the need for tailored seismic retrofitting strategies to address the unique challenges posed by each typology.

Table 3: Horizontal load resistant retrofitted wall ratio ($\rho_{w,R}$).

	Longitudinal direction		**Transversal direction**	
Building	**RET**	**RET AW**	**RET**	**RET AW**
S	2.6%	6.5%	1.6%	2.9%
R	1.2%	2.8%	2.7%	6.5%
CS	2.1%	6.9%	1.9%	4.0%
CR	1.2%	5.5%	3.4%	5.9%

The horizontal load-resistant retrofitted wall ratio ($\rho_{w,R}$) was calculated for each building and scenario and is presented in Table 3. The RET-AW scenario consistently resulted in higher $\rho_{w,R}$ values, providing more comprehensive strengthening. However, the RET scenario achieved targeted improvements with reduced intervention, making it a more economical choice in some cases. For instance, Building CR benefited from strategically applied reinforcement in the RET scenario, which effectively addressed vulnerabilities in the longitudinal direction without the extensive disruption associated with RET-AW.

To assess the effectiveness of FRCM retrofitting measures across building typologies and directions, we utilized the seismic performance indicator α, defined as the ratio between d_C and d_D. This ratio provides a clear metric for assessing seismic performance improvement and compliance with EC8-3 requirements for both DL and SD limit states, where $\alpha \geq 1.0$ indicates that the structure meets the code-based compliance criteria. For URM buildings, the α values predominantly fall between 0.30 and 0.60,

Copyright © 2025 CroCEE
DOI: https://doi.org/10.5592/CO/3CroCEE.2025.85

significantly below the required threshold of 1.00, indicating inadequate seismic performance across all examined cases. The effectiveness of the FRCM strengthening system across different building typologies and directions is presented in Table 4. To more accurately assess the impact of the selected retrofitting measures, a new metric (η) was defined as: $\eta = \alpha / \rho_w$ for the case of URM and $\eta = \alpha / \rho_{w,R}$ for the two retrofitted scenarios RET and RET AW. The η ratio normalizes the seismic performance indicator (α) by the total available shear wall ratio (ρ_w) for URM structures, or by the ratio of strengthened walls ($\rho_{w,R}$) for retrofitted scenarios. This normalization allows for a more precise comparison of retrofitting efficiency by considering only the walls that have been strengthened. A higher η value indicates greater effectiveness of the FRCM system relative to the wall area utilized, whether this reflects better inherent seismic performance in URM cases or more substantial performance improvements in retrofitted scenarios.

Table 4: Performance indicator α and retrofitting efficiency metric η.

Principal Direction	Building	Limit State	α [-]			η [-]		
			URM	RET	RET AW	URM	RET	RET AW
Transversal	CR	DL	0.62	0.77	0.81	9.6	22.4	12.6
		SD	0.42	0.47	0.43	6.5	13.5	6.7
	CS	DL	0.31	0.42	0.56	7.7	13.5	13.9
		SD	0.35	0.65	0.72	8.5	21.2	17.8
	R	DL	0.73	0.80	0.85	11.3	29.3	13.2
		SD	0.53	0.81	0.82	8.1	30.0	12.6
	S	DL	0.50	0.56	0.67	17.1	34.0	22.8
		SD	0.75	0.88	0.93	25.6	53.7	31.9
Longitudinal	CR	DL	0.61	0.91	0.96	11.1	76.1	17.6
		SD	0.40	0.51	0.61	7.4	42.1	11.2
	CS	DL	0.40	0.55	0.64	6.6	23.4	10.5
		SD	0.71	0.90	0.97	11.6	38.4	16.0
	R	DL	0.48	0.49	0.64	17.0	40.6	23.0
		SD	0.47	0.58	0.73	16.9	48.0	26.2
	S	DL	0.91	1.10	1.15	14.0	41.7	17.7
		SD	0.55	0.56	0.59	8.5	21.5	9.1

4. Cost-benefit analysis

4.1. Methodological Framework

This study employs a comprehensive methodology for evaluating the economic feasibility of seismic retrofitting measures. The analysis follows a systematic approach that enables detailed building-specific assessments [21].

The cost-benefit analysis process begins with a detailed examination of selected retrofit interventions, particularly focusing on selected FRCM systems with alkali-resistant glass fibre. For each intervention type, we developed a comprehensive list of cost items and their associated unit prices, as presented in Table 6. These baseline costs include material expenses, labour requirements, and auxiliary work such as surface preparation and finishing. The cost estimation first involved detailed quantity surveying for individual prototype buildings, providing precise cost estimates for specific structural configurations.

Copyright © 2025 CroCEE
DOI: https://doi.org/10.5592/CO/3CroCEE.2025.85

4.2. Building Characteristics and Market Values

To establish accurate market values for the analyzed building types, we utilized data from the Real Estate Market Register (ETN) maintained by the Surveying and Mapping Authority of the Republic of Slovenia [22]. The ETN database provides a comprehensive and reliable foundation for market value assessment, capturing at least 95% of all real estate transactions in Slovenia. The property values presented in Table 5 represent median prices derived from actual transactions, offering a balanced view where half of the transactions fall above and half below these reference points.

Our analysis reveals significant variations in both apartment sizes and market values across the four building typologies. Building R contains the largest apartments with a mean floor area of 56.6 m², while Building CS features notably smaller units averaging 40.2 m². Buildings S and CR fall between these extremes, with mean apartment sizes of 49.9 m² and 53.0 m² respectively. These size variations reflect the different architectural approaches and social priorities of post-war residential development.

Market prices per square meter demonstrate equally noteworthy differences among the building types. Building CS commands the highest value at 3833.9 €/m², suggesting strong market appreciation for its architectural characteristics and location. In contrast, Building R exhibits the lowest market value at 2832.4 €/m², while Buildings S and CR maintain intermediate positions at 3253.1 €/m² and 3169.5 €/m² respectively. These price variations likely reflect a combination of factors including location, building condition, and local market dynamics.

The reliability of these market value assessments is strengthened by the ETN's comprehensive coverage of the real estate market and its standardized methodology for recording and analyzing transaction data. These baseline values prove essential for our subsequent analysis of retrofitting costs and their economic implications, allowing us to evaluate the financial feasibility of different intervention strategies in relation to current property values. This market context becomes particularly relevant when considering the substantial investments required for seismic retrofitting and their potential impact on property values.

Table 5: Apartment size and mean market price.

Building	Total floor area of apartments [m²]	Mean floor area of single apartment [m²]	Mean market value per square meter [€/m²]
S	998.0	49.9	3253.1
R	1286.4	40.2	2832.4
CS	3058.8	56.6	3833.9
CR	2542.8	53.0	3169.5

4.3. Building-Specific Cost Analysis and Economic Performance Indicators

The detailed cost analysis was conducted for both retrofitting scenarios (RET and RET-AW) across all four prototype buildings, considering their specific geometric characteristics and apartment configurations. The analysis incorporated both the base retrofit costs and an optional thermal insulation component (TI), though our primary focus remains on the seismic strengthening aspects.

Using the unit costs from Table 6, which includes basic operations like plaster removal (16 €/m²), FRCM system installation (120 €/m²), and finishing works, we calculated the total intervention costs per square meter of net apartment area. As shown in Figure 5, the results demonstrate significant variations across building types and retrofitting scenarios. For the RET scenario without thermal insulation, Building S exhibits costs of 276.3 €/m² of net apartment area, while Buildings CS, R, and CR show costs of 299.6 €/m², 191.3 €/m², and 186.7 €/m² respectively. The addition of thermal insulation (TI) increases these costs by approximately 30%.

The more comprehensive RET-AW scenario naturally results in higher costs across all building types, as illustrated by the orange bars in Figure 5. Without thermal insulation, Building S requires 599.6 €/m²,

Copyright © 2025 CroCEE
DOI: https://doi.org/10.5592/CO/3CroCEE.2025.85

Building CS needs 584.3 €/m², Building R demands 642.0 €/m², and Building CR requires 585.0 €/m². Again, the inclusion of thermal insulation further increases these costs.

Table 6: Retrofitting measures - cost items and unit prices.

Cost item	Cost €/m²
FRCM system	120.00
Removal of existing plaster	16.00
Plaster finishing (internal / external)	12.00
Wall painting (internal / external)	2.50
Thermal insulation (optional cost)	52.00

Figure 5 also presents the relationship between retrofit costs and the efficiency metric η for the Significant Damage (SD) limit state. The solid lines show efficiency in the longitudinal direction, while the dashed lines represent the transverse direction. Interestingly, the RET scenario often achieves higher η values despite lower absolute costs, particularly in the longitudinal direction, suggesting better cost-effectiveness of targeted interventions.

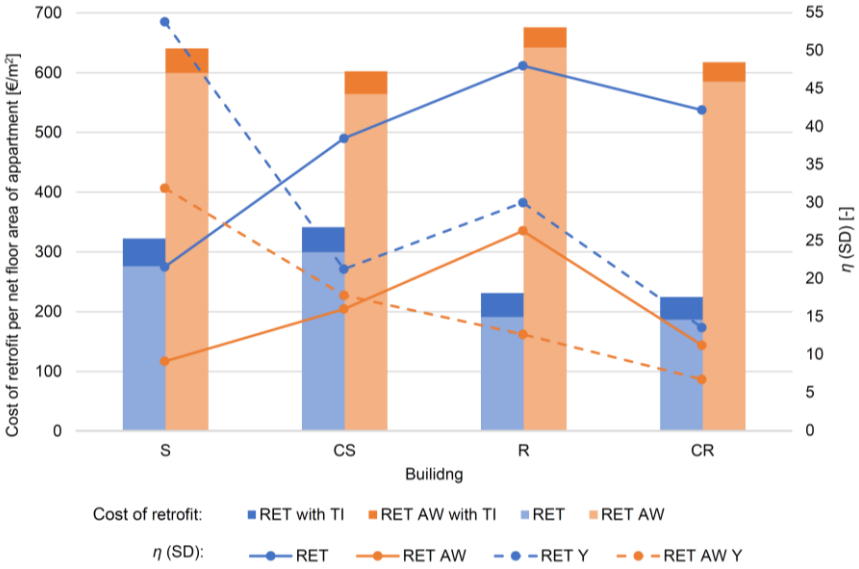


Figure 5: Correlation between retrofit cost and η.

When comparing these costs to current market values, Figure 6 reveals the retrofitting investments as percentages of property value. For the basic RET scenario, the investment ranges from about 5% to 8% of current market value. Adding thermal insulation increases this to 6-10%. The more extensive RET-AW scenario requires significantly higher investments, ranging from 17% to 23% without thermal insulation, and reaching up to 24% with thermal insulation included. This substantial difference in investment requirements highlights the importance of careful consideration when selecting retrofitting strategies.

The analysis reveals that buildings with higher initial market values (like Building CS at 3833.9 €/m²) tend to justify more comprehensive retrofitting strategies, as the relative cost impact remains manageable while providing enhanced structural safety. Conversely, buildings with lower market values may benefit more from targeted interventions that optimize the cost-benefit ratio. This finding suggests that strategic placement of strengthening measures may offer a more economically viable approach to seismic risk mitigation, particularly for buildings with limited financial resources for renovation.

Copyright © 2025 CroCEE
DOI: https://doi.org/10.5592/CO/3CroCEE.2025.85

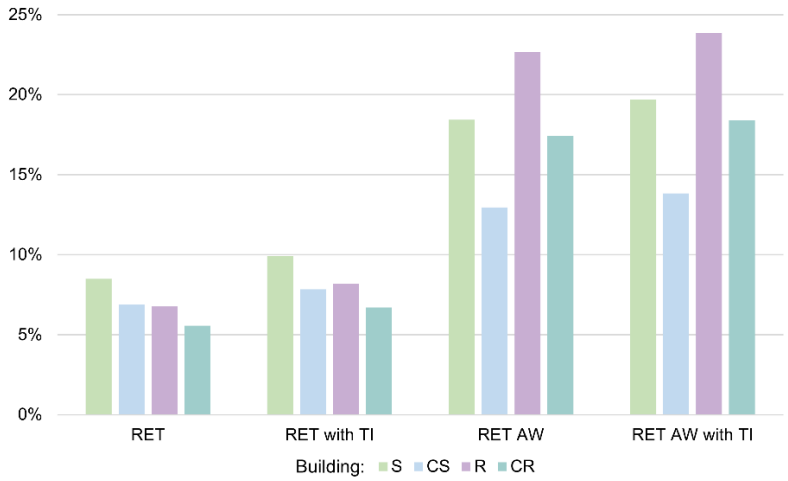


Figure 6: Retrofit cost as percentage of apartment market value.

5. Conclusions

This study provides valuable insights into the economic feasibility and structural effectiveness of FRCM retrofitting for post-war masonry buildings in Ljubljana. The cost analysis reveals that selective retrofitting (RET) requires investments ranging from 5-8% of current property values, while comprehensive strengthening (RET-AW) demands 17-23%. When considering the efficiency metric η, the RET scenario demonstrates higher values despite lower absolute costs, suggesting better cost-effectiveness of targeted interventions versus full-building strengthening.

However, the seismic performance analysis indicates that FRCM strengthening alone may be insufficient to achieve full EC8-3 compliance. While several retrofitted configurations achieve α values between 0.6 and 0.8 for both damage limitation (DL) and significant damage (SD) limit states, only one case reaches $\alpha \geq 1.0$ (Building S, longitudinal direction, DL state). This suggests that additional rigorous strengthening measures, such as the addition of new structural walls or cores, may be necessary to meet current seismic code requirements. Future research should explore combining FRCM with other retrofit techniques to achieve both economic feasibility and adequate seismic performance.

Acknowledgements

The research presented in this paper was conducted in the scope of the research program “Sustainable planning for the quality living space” and is funded by the Slovenian Research and Innovation Agency (ARIS) under grant no. P5-0068. This support is gratefully acknowledged.

References

[1] Brzev, S., Blagojević, P., & Cvetković, R. (2023): Seismic retrofitting of post-WWII mid-rise unreinforced masonry residential buildings in the Balkans, *2nd Croatian Conference on Earthquake Engineering - 2CroCEE*, Zagreb, Croatia. doi: https://doi.org/10.5592/CO/2CroCEE.2023.90

[2] Atalić, J., Šavor Novak, M., & Uroš, M. (2019): Seismic risk for Croatia: Overview of research activities and present assessments with guidelines for the future. Građevinar, 71, 923-947. doi: https://doi.org/10.14256/JCE.2732.2019

[3] Kilar, V., & Kušar, D. (2009): Assessment of the earthquake vulnerability of multi-residential buildings in Slovenia. *Acta Geographica Slovenica*, 49(1). doi: https://doi.org/10.3986/ags49103

[4] Petrovski, J.T. (2004). Damaging effects of July 26, 1963 Skopje earthquake. Middle East Seismological Forum, Cyber Journal of Geoscience, Volume Two.

[5] Lagomarsino, S., Penna, A., Galasco, A., & Cattari, S. (2013): TREMURI program: an equivalent frame model for the nonlinear seismic analysis of masonry buildings, *Engineering Structures*, 56, 1787-1799. doi: https://doi.org/10.1016/j.engstruct.2013.08.002

Copyright © 2025 CroCEE
DOI: https://doi.org/10.5592/CO/3CroCEE.2025.85

[6] Petelin, D. (2017): Stanovanjske razmere v Ljubljani v letih 1945–1965. *Kronika*, 65(1), 1-18. [In Slovenian].

[7] Nikšič, M., Goršič, N., Mihelič, B., Mujkić, S., & Tominc, B. (2013): Smernice za vzdrževanje in prenovo karakterističnih območij mesta Ljubljane, Litostrojsko naselje. Mestna občina Ljubljana. [In Slovenian].

[8] Nikšič, M., Goršič, N., Mihelič, B., Mujkić, S., & Tominc, B. (2013): Smernice za vzdrževanje in prenovo karakterističnih območij mesta Ljubljane, Savsko naselje. Mestna občina Ljubljana. [In Slovenian].

[9] Prašnikar, P., Kilar, V., Petrovčič, S. (2024): Typology and seismic assessment of multi-residential post-war masonry buildings in Ljubljana, *18th World Conference on Earthquake Engineering*, Milan, Italy.

[10] Petrovčič, S., Kilar, V., Prašnikar, P., Azinović, B., Bradeško, T., Gjura Godec, M., Grulja, S.N., Krznarič, E., Anil, A., Rogelj, J.: Project results "Aggregation of data on post-war architectural structures in Slovenia for the assessment of their seismic resistance", University of Ljubljana Repository, https://repozitorij.uni-lj.si/IzpisGradiva.php?lang=slv&id=164800, Version: 01.12.2023, (accessed December 15, 2024).

[11] Uroš, M., Demšić, M., Šavor Novak, M., Atalić, J., Baniček, M., Jevtić Rundek, R., & Prevolnik, S. (2024): Damage Evaluation and Seismic Assessment of a Typical Historical Unreinforced Masonry Building in the Zagreb 2020 Earthquake: A Case Study—Part I. *Buildings*, 14(2), 474. doi: https://doi.org/10.3390/buildings14020474

[12] CNR (2018): Guide for the Design and Construction of Externally Bonded Fibre Reinforced Inorganic Matrix Systems for Strengthening Existing Structures. Advisory Committee on Technical Recommendations for Construction, Rome, Italy.

[13] Petrovčič, S., Prašnikar, P., & Kilar, V. (2023): Seismic Performance and Retrofit of a Mid-Rise Post-second World War Residential Building Made of Unreinforced Masonry, *13th International Conference on Structural Analysis of Historical Constructions*, Kyoto, Japan. pp. 929-943. doi: https://doi.org/10.1007/978-3-031-39603-8_75

[14] Bosiljkov, V., Antolinc, D., Čepon, F., Jursinovič, B., Siebenreich., N. (2016): Poročilo o analizi nosilnosti in potresne odpornosti objekta UL ALUO na Erjavčevi 23 v Ljubljani. *Report No. P 001/3/16*, University of Ljubljana, Faculty of Civil and Geodetic Engineering [In Slovenian], Ljubljana, Slovenia.

[15] Lutman, M. (2018): Ocena potresne ogroženosti stavbe Praprotnikova ulica 15 v Ljubljani. *Report No. P 331/18-610-1*, Slovenian National Building and Civil Engineering Institute [In Slovenian], Ljubljana, Slovenia.

[16] Bilgin, H., & Huta, E. (2018): Earthquake performance assessment of low and mid-rise buildings: Emphasis on URM buildings in Albania. *Earthquakes and Structures*, 14(6), 599–614. doi: https://doi.org/10.12989/EAS.2018.14.6.599

[17] Mendes, N., & Lourenço, P.B. (2014): Sensitivity analysis of the seismic performance of existing masonry buildings. *Engineering Structures*, 80, 137-146. doi: https://doi.org/10.1016/j.engstruct.2014.09.0055

[18] Bompa, D.V., & Elghazouli, A.Y. (2020): Compressive behaviour of fired-clay brick and lime mortar masonry components in dry and wet conditions. *Materials and Structures*, 53(3), 60. doi: https://doi.org/10.1617/s11527-020-01493-w

[19] Soleymani, A., Najafgholipour, M.A., & Johari, A. (2022): An experimental study on the mechanical properties of solid clay brick masonry with traditional mortars. *Journal of Building Engineering*, 58, 105057. doi: https://doi.org/10.1016/j.jobe.2022.1050577

[20] Blagojević, P., Brzev, S., & Cvetković, R. (2021): Simplified seismic assessment of unreinforced masonry residential buildings in the Balkans: The case of Serbia. *Buildings*, 11(9), 392. doi: https://doi.org/10.3390/buildings11090392

[21] Follador, V., Donà, M., Carpanese, P., Saler, E., D'Alpaos, C., & da Porto, F. (2024): Seismic retrofit cost model for Italian masonry residential buildings to support territorial-scale risk analysis, *International Journal of Disaster Risk Reduction*, 105, 104373. doi: https://doi.org/10.1016/j.ijdrr.2024.104373

[22] Geodetska uprava Republike Slovenije. Trg nepremičnin. Dostopno na: https://www.e-prostor.gov.si/podrocja/trg-in-vrednosti-nepremicnin/trg-nepremicnin/?acitem=1967-2418 (accessed June 6, 2024).

Proceedings of the 3rd Croatian Conference on Earthquake Engineering - 3CroCEE
19–22 March 2025, Split, Croatia
Copyright © 2025 CroCEE
DOI: https://doi.org/10.5592/CO/3CroCEE.2025.87

THE INFLUENCE OF STRUCTURAL ECCENTRICITY ON THE SEISMIC BEHAVIOR OF TORSIONALLY SENSITIVE STRUCTURES

Riste Volchev [(1)], Nikola Postolov [(2)], Koce Todorov [(3)], Ljupcho Lazarov [(4)]

[(1)] *Teaching Assistant, MSc, Faculty of Civil Engineering - Skopje, R. Macedonia, volcev@gf.ukim.edu.mk*
[(2)] *Teaching Assistant, MSc, Faculty of Civil Engineering - Skopje, R. Macedonia, postolov@gf.ukim.edu.mk*
[(3)] *Professor, PhD, Faculty of Civil Engineering - Skopje, R. Macedonia, todorov@gf.ukim.edu.mk*
[(4)] *Professor, PhD, Faculty of Civil Engineering - Skopje, R. Macedonia, lazarov@gf.ukim.edu.mk*

Abstract

The focus of this research is to determine the impact of structural eccentricity on the seismic behaviour of torsionally sensitive structures. To achieve this, two groups of single-storey structural models with different levels of irregularity were analysed. The dimensions of the structures at the base are 6 m x 5 m, with a storey height of 3 m. The total external load on each structure is 300 KN. In the first group of structures, the center of mass was shifted by redistributing the load over a smaller area. In the second group, the center of stiffness was altered by increasing the cross-sectional dimensions of the columns on one side of the structure. Analyses were conducted for structural eccentricity ranging from 5% to 30%. In accordance with the criteria provided in Eurocode 8 and ASCE 7-22, the torsional regularity of the analysed structures was assessed. For the same value of eccentricity, a comparison of the levels of irregularity between the two groups was made. Through the results obtained from the nonlinear static analysis, a relationship between the level of irregularity and the level of damage was established. Additionally, an evaluation of the torsional irregularity criteria in both regulations was conducted, highlighting the advantages and disadvantages of each approach.

Keywords: eccentricity, torsion, irregularity, Eurocode 8, ASCE 7-22.

1. Introduction

Torsion, as a phenomenon contributing to significant structural damage during earthquakes, has been recognized since the 1950s. Despite significant attention over the past few decades, the issue remains unresolved. This is evidenced by differences in the provisions for torsional irregularity in modern building codes, as well as the conflicting perspectives within the scientific community. Torsional response of structures arises from several factors: eccentricity between the center of mass and center of stiffness of vertical lateral force resisting elements, accidental torsion due to the rotational component of ground motion about a vertical axis, the discrepancy between assumed and actual stiffness and mass, uncertainties in the distribution of live and dead loads, etc. The position of centre of stiffness can vary depending on the assumptions in the mathematical model, this comparison is made by Postolov et al. [1]. With the advancement of powerful computational tools in recent years, the seismic behaviour of irregular structures has increasingly been analysed using multi storey building models. Nevertheless, single-storey models continue to attract researchers as they represent the most extreme idealization of plan irregular buildings and remain adequate for obtaining general insights into the torsional behavior of asymmetric buildings, particularly from a qualitative perspective.

Extensive early researches on this issue were carried out by Kan and Chopra, Dempsey and Irvine, Kung and Pecknold, Chandler and Hutchinson and others, [2,3,4,5]. These studies, primarily analysed the elastic torsional response of single-storey models. One of the first attempts to study the torsional response in the nonlinear region was conducted by Stathopoulos and Anagnostopoulos [6]. The same researchers, in 2014, provided a detailed and critical review of the state of the art in the field of irregular structures [7]. In the development of nonlinear static analysis, which is one of the most commonly used procedures for obtaining the nonlinear response of torsionally irregular structures, significant contributions were made by Chopra, De Stefano, Fajfar, among others, [8, 9, 10].

Proceedings of the 3rd Croatian Conference on Earthquake Engineering - 3CroCEE
19–22 March 2025, Split, Croatia
Copyright © 2025 CroCEE
DOI: https://doi.org/10.5592/CO/3CroCEE.2025.87

2. Torsional irregularity criteria in modern codes

Structural irregularities were introduced in codes in the 1980s and have continuously evolved since. These provisions were implemented to differentiate between various analysis methods and, in some cases, to prevent inclusion of irregularities in structures. Modern seismic provisions have introduced criteria for determining whether a structure is torsionally sensitive, along with corresponding design guidelines. Generally, these criteria are based on either the dynamic characteristics of the structure or storey drifts. However, they differ in two key aspects: the definition of the required parameters and their numerical limits. These differences in approach can lead to the same structure being classified differently depending on the code applied. Numerous studies have compared the criteria for regularity across different codes, including those by Rutenberg, Shahini, De Stefano, Athanatopoulou, and others, [11, 12, 13, 14]. This highlights the need for further research to establish generally accepted criteria for defining torsional irregularity.

2.1. Torsional irregularity in Eurocode 8

According to Eurocode 8 [15], specific criteria must be met for structure to be considered regular. Some of these conditions are qualitative, and can be checked during preliminary design stage, but others are quantitative, regarding additional calculations based on parameters such as the eccentricity between the center of mass and center of stiffness or torsional radius. In order to achieve satisfactory seismic behaviour, conventionally designed structures must exhibit approximately symmetrical lateral stiffness and mass distribution in plan with respect to two orthogonal axes. The following are the quantitative structural regularity conditions:

The slenderness ratio, $\lambda=L_{max}/L_{min}$, of the structure should not exceed 4, where L_{max} and L_{min} are the largest and smallest plan dimensions of the structure, measured along two orthogonal directions.

At each level and for each direction of analysis, the structural eccentricity $e_{0x/y}$, defined as the distance between the floor center of mass and the floor center of stiffness, should not exceed 30% of the corresponding storey torsional radius $r_{x/y}$, as shown in Eq. (1).

$$e_{0x/y} \leq 0.30 r_{x/y} \tag{1}$$

The torsional radius of the storey in each of the two orthogonal horizontal directions should not be less than the radius of gyration of the floor mass l_s, as shown in Eq. (2).

$$r_{x/y} \geq l_s \tag{2}$$

If the criteria are not met, meaning the structure is torsionally irregular, this implies limited structural nonlinear behaviour. Therefore, Eurocode 8 prescribes the use of a reduced behaviour factor, a 3D mathematical model for analysis, and at least a modal analysis to obtain the seismic response of the structure.

2.2. Torsional irregularity in ASCE 7-22

According to US code ASCE 7-22 [16], two levels of torsional irregularity are defined, based on the ratio between the maximal and average storey drift, shown in Fig. 1. The drifts are obtained using the equivalent lateral force procedure with the application of 5% accidental torsion.

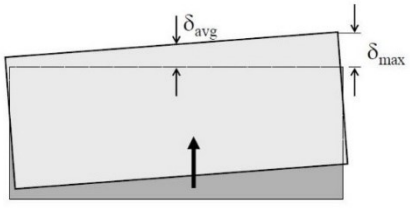


Figure 1. Maximal and average storey drift.

Copyright © 2025 CroCEE
DOI: https://doi.org/10.5592/CO/3CroCEE.2025.87

$$\delta_{max} \geq 1.2 \cdot \delta_{avg} \tag{3}$$

$$\delta_{max} \geq 1.4 \cdot \delta_{avg} \tag{4}$$

The structure is considered torsionally irregular if the maximal displacement is 1.2 times greater than the average, Eq. (3). If this ratio exceeds 1.4, the structure is considered extremely torsionally irregular, Eq. (4). The average displacement is calculated as follows $\delta_{avg} = (\delta_L + \delta_R) / 2$. For torsionally irregular structures, accidental torsion should be magnified using the amplification factor, A_x:

$$A_x = \left(\frac{\delta_{max}}{1.2 \cdot \delta_{avg}}\right)^2, \text{where } 1 < A_x < 3 \tag{5}$$

Structures with extreme irregularity are prohibited in areas with high seismic activity, as well as for buildings of public interest (such as public institutions, industrial structures, etc.).

3. Description of analysed structures

To investigate the impact of structural eccentricity on the seismic behaviour of torsionally sensitive structures, an ideally symmetrical single-storey structure (S0) was analysed, along with two groups of six single-storey structures (CM1-6 and CS1-6) with different degree of torsional irregularity. All analysed structures are rectangular in plan and consist of two frames in x and y direction. The distance between the frames is 6 m and 5 m, respectively, while the storey height is 3 m. All beams are with rectangular cross-section 35/45 cm. The slab thickness is 15 cm. All columns at the first model (S0), have a 35 cm square cross-section. This structure is loaded with a uniformly distributed load of 10 KN/m^2, i.e. a total equivalent load of 300 KN.

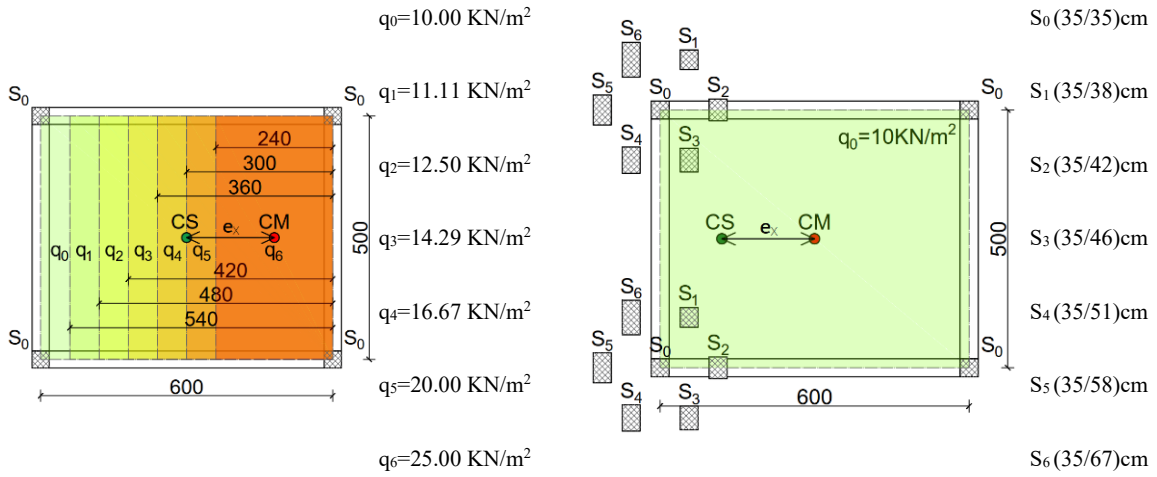


Figure 2. Layout of structures: a) Models S0, CM1-6; b) Models S0, CS1-6.

In the first group of six structures (CM1-6), the center of mass was shifted by redistributing the load over a smaller area, whereby the total equivalent load remains the same. In this group, the position of the center of stiffness remains constant. The structural eccentricity ranges from 5% to 30% from the structure's length, increasing in increments of 5% for each next structure from CM1 to CM6. The uniformly distributed load ranges from 10 KN/m^2 to 25 KN/m^2, respectively, as shown in Fig. 2.a).

In the second group of six structures (CS1-6), the square cross-section columns on the left side were replaced with rectangular cross-section columns, thereby shifting the center of stiffness by the same structural eccentricity values as in the previous group. In this group, the position of the center of mass remains constant. The dimensions of the columns range from 35/38 cm to 35/67 cm, respectively, as shown in Fig. 2.b). All structures from this group are loaded with uniformly distributed load of 10 KN/ m^2.

Proceedings of the 3rd Croatian Conference on Earthquake Engineering - 3CroCEE
19–22 March 2025, Split, Croatia
Copyright © 2025 CroCEE
DOI: https://doi.org/10.5592/CO/3CroCEE.2025.87

4. Criteria for plan regularity

All analysed structures are regular with respect to the x-axis, as they are symmetrical in terms of mass distribution, loads, stiffness and load-bearing capacity. The check for torsional irregularity criteria is performed with respect to the y-axis. Table 1. presents the values for the torsional radius and the radius of gyration of the floor mass for all analysed structures. According to Eurocode 8 (EN 1998-1), the characteristics of single-storey buildings are uniquely defined and can be determined using the moments of inertia of the cross-section of vertical elements. The torsional radius is defined relative to the centre of lateral stiffness. To verify the regularity in accordance with ASCE 7-22, an equivalent static analysis was performed, considering a 5% accidental eccentricity. The calculated intensity of the lateral seismic force is 225 KN. The obtained results are shown in Table 2.

Table 1. Regularity check according to Eurocode 8.

Structural eccentricity	Structure	e_x [m]	r_x [m]	l_s [m]	$e_x \leq 0.3 \cdot r_x$				$r_x \geq l_s$			
$e_x = 0\%$	S0	0.00	3.90	2.26	0.00	<	1.17	✓	3.90	>	2.26	✓
$e_x = 5\%$	CM1	0.30	3.90	2.13	0.30	<	1.17	✓	3.90	>	2.13	✓
	CS1	0.30	3.83	2.26	0.30	<	1.15	✓	3.83	>	2.26	✓
$e_x = 10\%$	CM2	0.60	3.90	2.01	0.60	<	1.17	✓	3.90	>	2.01	✓
	CS2	0.60	3.74	2.26	0.60	<	1.12	✓	3.74	>	2.26	✓
$e_x = 15\%$	CM3	0.90	3.90	1.89	0.90	<	1.17	✓	3.90	>	1.89	✓
	CS3	0.90	3.61	2.26	0.90	<	1.08	✓	3.61	>	2.26	✓
$e_x = 20\%$	CM4	1.20	3.90	1.79	1.20	>	1.17	✗	3.90	>	1.79	✓
	CS4	1.20	3.45	2.26	1.20	>	1.04	✗	3.45	>	2.26	✓
$e_x = 25\%$	CM5	1.50	3.90	1.69	1.50	>	1.17	✗	3.90	>	1.69	✓
	CS5	1.50	3.26	2.26	1.50	>	0.98	✗	3.26	>	2.26	✓
$e_x = 30\%$	CM6	1.80	3.90	1.61	1.80	>	1.17	✗	3.90	>	1.61	✓
	CS6	1.80	3.00	2.26	1.80	>	0.90	✗	3.00	>	2.26	✓

Table 2. Regularity check according to ASCE 7-22.

Structural eccentricity	Structure	δ_L [mm]	δ_R [mm]	δ_{avg} [mm]	$\delta_{max} \leq 1.2 \cdot \delta_{avg}$				$\delta_{max} \leq 1.4 \cdot \delta_{avg}$			
$e_x = 0\%$	S0	7.57	8.51	8.04	8.51	<	9.65	✓	8.51	<	11.26	✓
$e_x = 5\%$	CM1	7.11	9.03	8.07	9.03	<	9.68	✓	9.03	<	11.30	✓
	CS1	6.45	8.21	7.33	8.21	<	8.80	✓	8.21	<	10.26	✓
$e_x = 10\%$	CM2	6.61	9.46	8.04	9.46	<	9.64	✓	9.46	<	11.25	✓
	CS2	5.45	7.92	6.69	7.92	<	8.02	✓	7.92	<	9.36	✓
$e_x = 15\%$	CM3	6.14	9.94	8.04	9.94	>	9.65	✗	9.94	<	11.26	✓
	CS3	4.55	7.63	6.09	7.63	>	7.31	✗	7.63	<	8.53	✓
$e_x = 20\%$	CM4	5.66	10.41	8.04	10.41	>	9.64	✗	10.41	<	11.25	✓
	CS4	3.73	7.35	5.54	7.35	>	6.65	✗	7.35	<	7.76	✓
$e_x = 25\%$	CM5	5.19	10.89	8.04	10.89	>	9.65	✗	10.89	<	11.26	✓
	CS5	3.00	7.07	5.04	7.07	>	6.04	✗	7.07	>	7.05	✗
$e_x = 30\%$	CM6	4.56	11.06	7.81	11.06	>	9.37	✗	11.06	>	10.93	✗
	CS6	2.32	6.84	4.58	6.84	>	5.50	✗	6.84	>	6.41	✗

Copyright © 2025 CroCEE
DOI: https://doi.org/10.5592/CO/3CroCEE.2025.87

According to Eurocode 8, models with a structural eccentricity of up to 15% are considered regular. Models with a structural eccentricity of 20% or more are classified as torsionally irregular, as they do not satisfy the criterion that the structural eccentricity should be less than 30% of the torsional radius. These regulations do not provide a gradation of irregularity, resulting in a sharp boundary between regular and irregular structures. In contrast to Eurocode, ASCE 7-22 relates both criteria to the ratio between the maximum and average displacement, with different values assigned based on the prescribed level of irregularity. According to this provision, the analysed models with a structural eccentricity up to 10% are considered regular. Models with a structural eccentricity of 15% or more are torsionally irregular because they do not satisfy the first criterion, $\delta_{max}<1.2\cdot\delta_{avg}$. The models CS5, CM6, and CS6 do not satisfy neither the second criterion $\delta_{max}<1.4\cdot\delta_{avg}$, and are therefore classified as extremely torsionally irregular structures.

From this, the initial inconsistency between the two provisions becomes apparent. The CM3 and CS3 structures are considered regular according to Eurocode 8, whereas ASCE 7-22 classifies them as irregular. Structures deemed extremely torsionally irregular under ASCE 7-22, are also classified as irregular under Eurocode 8, as along with all other structures with a lower level of irregularity but fail to meet certain criteria. As mentioned in Section 2, this classification has significant implications and limitations in the design process. Fig. 3.a) and Fig. 3.b) present diagrams showing the regularity check of the structures through normalized values of each criterion, indicating how many a certain criterion is satisfied or not.

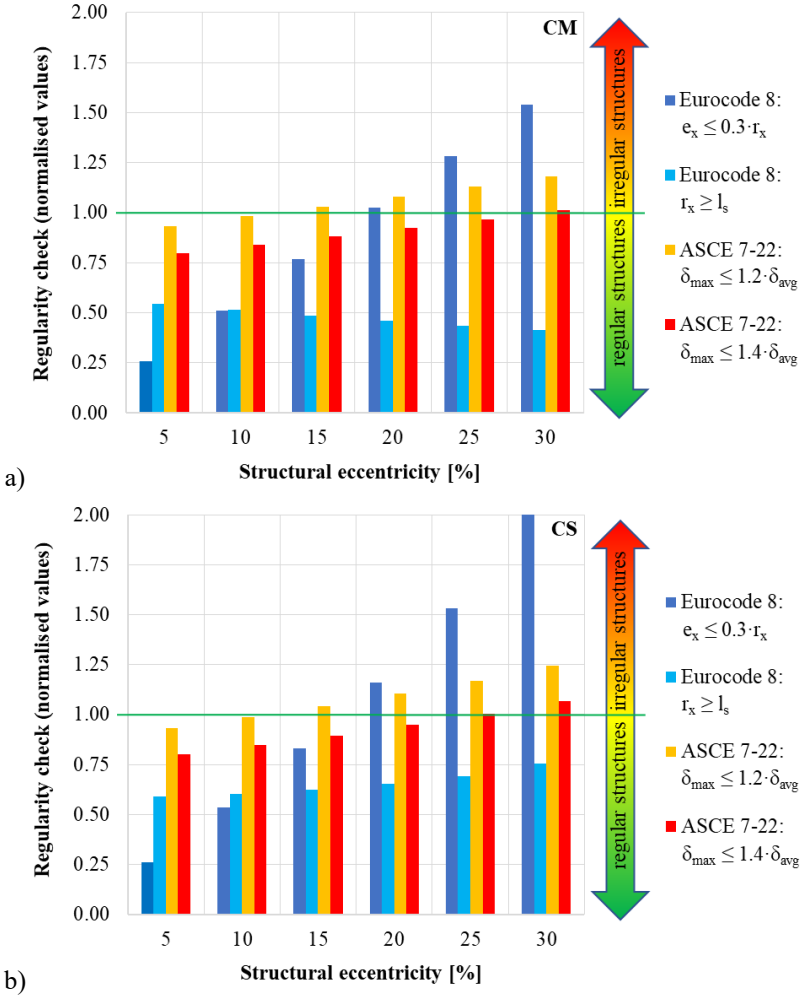


Figure 3. Regularity check (normalized values) a) Models S0, CM1-6; b) Models S0, CS1-6.

Copyright © 2025 CroCEE
DOI: https://doi.org/10.5592/CO/3CroCEE.2025.87

A value less than 1 signifies that the criterion is met and the structure is considered regular, whereas a value greater than 1 indicates that the criterion is not met, requiring the structure to be analysed as irregular. According to both provisions, the level of irregularity is directly proportional to the increase in structural eccentricity and is more pronounced in structures with a shifted center of stiffness. Under ASCE 7-22, the regularity criterion is exceeded by no more than 25%, whereas according to Eurocode 8, it is exceeded by as much as 100%. In addition to the gradation of irregularity, another advantage of the US provision is that the amplification factor for accidental eccentricity A_x, Eq. (5), also depends on the maximum and average displacement. The value of this factor ranges from 1 to 3. In contrast, under European provisions, irregular structures are assigned a lower basic value for the behaviour factor q_0, meaning they are analysed with higher design forces. This value is not directly dependent on the level of irregularity of the structure, unless it has been determined through a nonlinear static analysis.

5. Nonlinear seismic assessment of analysed structures

To determine the required reinforcement in the RC beams and columns of the analysed structures, a multimodal analysis was performed. The following input parameters were used: reference peak ground acceleration $a_g = 0.30g$, soil category C, spectrum type 1, importance class II ($\gamma = 1$), and ductility class DCM. The analysed structures are subjected to seismic forces in the y direction only. For designing, concrete class C25/30 and reinforcement class B500C were used. The required reinforcement in the beams was determined from the analysis of the S0 structure, where an accidental eccentricity of 5% was also considered. For the columns, a minimum reinforcement of 1% was adopted, which exceeds the required reinforcement area obtained from the analyses. The adopted reinforcement in all cross-sections is shown in Fig. 4. The nonlinear static analysis was performed using the SeismoStruct software package, which is based on the distributed plasticity method. The nonlinear behaviour of the structural elements is defined using the inelastic frame element (infrmFBPH), where the nonlinearity is concentrated over a precisely defined length of the element, as proposed by Scott and Fenves [17]. The length of the plastic hinges is 16.67% of the element length. The beam elements are modelled as "Γ" cross-sections, with an effective width of 75 cm and 83 cm for the beams in the x and y directions, respectively. The cross-section of the beam elements is divided into 82 fibres, while the cross-section of the columns is divided into 62 fibres. The previously applied area load is distributed onto the beam elements as a linear load, proportional to their respective surface area. To obtain the capacity curves, a reference point was selected at the top of the rightmost column of the structure.

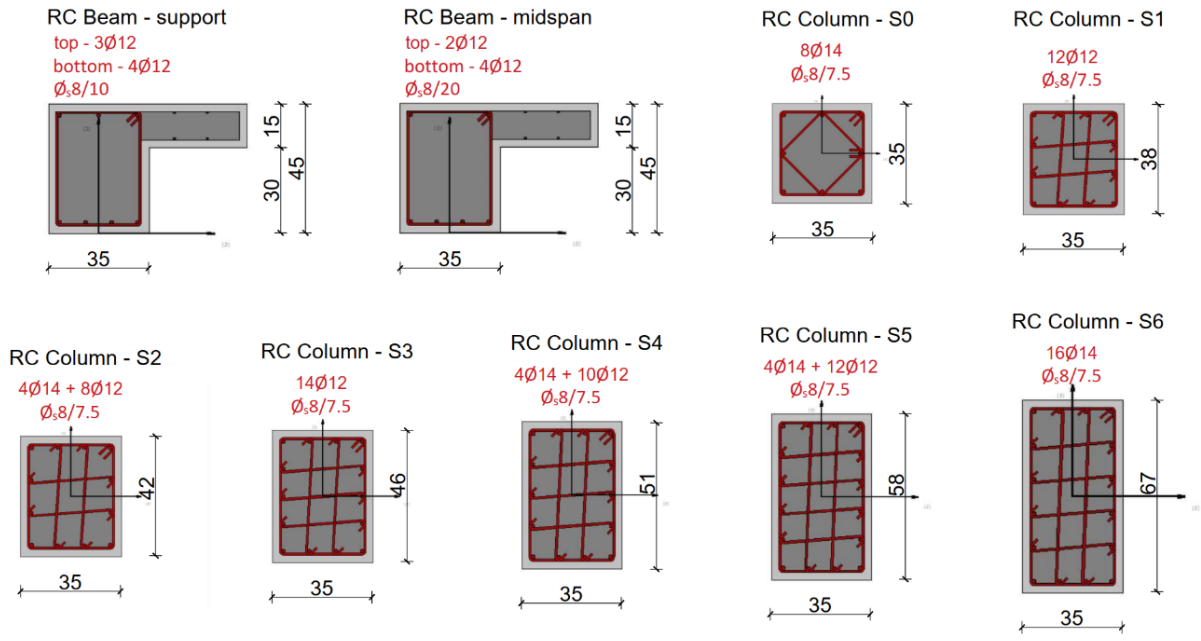


Figure 4. Reinforcement details.

Copyright © 2025 CroCEE
DOI: https://doi.org/10.5592/CO/3CroCEE.2025.87

6. Comparison of results

After conducting the analyses and obtaining the results, the nonlinear response was compared among the symmetric structure S0, the group of structures with a shifted center of mass CM, and the group with a shifted center of stiffness. Fig. 5 shows the capacity curves of the analysed structures. As structural eccentricity increases and the level of irregularity rises, the load bearing capacity decreases in the group of structures with a shifted center of mass, as shown in Fig. 5.a). The load bearing capacity of the CM6 structure is up to 20% lower than that of the S0 structure. In contrast, the increased load bearing capacity of the structures with a shifted center of stiffness is attributed to the enlargement of the column dimensions on the left side of the structure, as shown in Fig. 5.b).

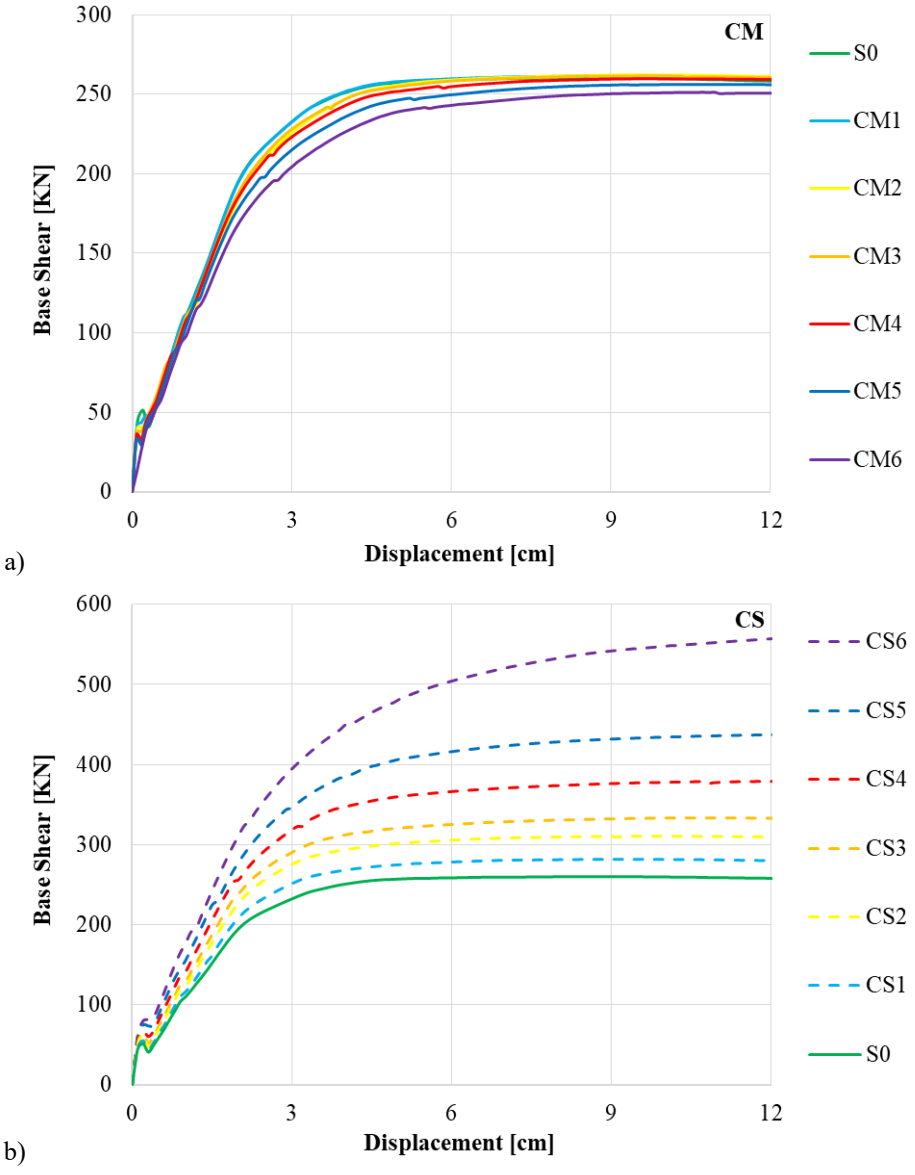


Figure 5. Pushover curves a) structures SO, CM(1-6); b) structures SO, CS(1-6).

In all structures, despite the differences in capacity curves, an increasing level of irregularity leads to a greater tendency for unevenly damage at both ends of the structure, resulting in gradual shift of the center of stiffness over time. This raises concerns about the reliability of structural responses obtained from the linear analysis, which assumes a fixed position for the center of stiffness. Table 3. presents the maximum displacement of the observed node in the y direction and the base shear force for four characteristic states in the structure: (1) the development of the first plastic hinge on the right side,

Copyright © 2025 CroCEE
DOI: https://doi.org/10.5592/CO/3CroCEE.2025.87

(2) the development of a plastic hinge on the left side, (3) the formation of a mechanism on the right side, and (4) the formation of a mechanism on the left side. The first plastic hinges on both sides of the structure develop at maximum displacements ranging from 1.6 cm to 2.4 cm, which represents a relative difference of about 0.25% of the story height of the analysed structures. The ratio between the maximum displacement at the formation of a mechanism on the right and left side of the structure ranges from 1.1 to 2.3 for the group of structures with a shifted center of mass, and from 1.0 to 1.6 for the group of structures with a shifted center of stiffness.

Table 3. Maximum displacement and base share force for characteristic states in the structure.

Structural eccentricity	Structure	1st Plastic Hinge - R		1st Plastic Hinge - L		Plastic Hinge Mechanism - R		Plastic Hinge Mechanism - L	
		d_y [cm]	F_b [KN]	d_y [cm]	F_b [KN]	d_y [cm]	F_b [KN]	d_y [cm]	F_b [KN]
$e_x = 0\%$	S0	1.8	180	1.8	180	2.7	224	2.7	224
$e_x = 5\%$	CM1	1.8	180	1.8	180	2.7	224	2.9	230
	CS1	1.7	183	1.7	183	2.7	241	2.7	241
$e_x = 10\%$	CM2	1.7	161	2.0	185	2.7	217	3.5	238
	CS2	1.7	200	1.7	200	2.7	265	2.8	269
$e_x = 15\%$	CM3	1.7	165	2.1	196	2.6	216	3.9	246
	CS3	1.7	211	1.6	199	2.7	280	2.9	287
$e_x = 20\%$	CM4	1.7	165	2.2	197	2.5	208	4.4	248
	CS4	1.6	218	1.6	218	2.8	308	3.0	318
$e_x = 25\%$	CM5	1.7	159	2.3	193	2.3	193	4.6	243
	CS5	1.6	230	1.8	256	2.8	338	3.6	373
$e_x = 30\%$	CM6	1.6	146	2.4	187	2.1	175	4.8	237
	CS6	1.6	257	1.9	299	2.8	380	4.5	464

The diagrams in Fig. 6. illustrate the amplification of rotations for the structures in each of the two groups. For the previously defined four states, the ratio of rotations between each structure and those of the CM1 and CS1 structures is presented, respectively. As structural eccentricity increases in each state, a greater amplification of rotations is observed, with the most significant amplification occurring in the group of structures with a shifted center od stiffness.

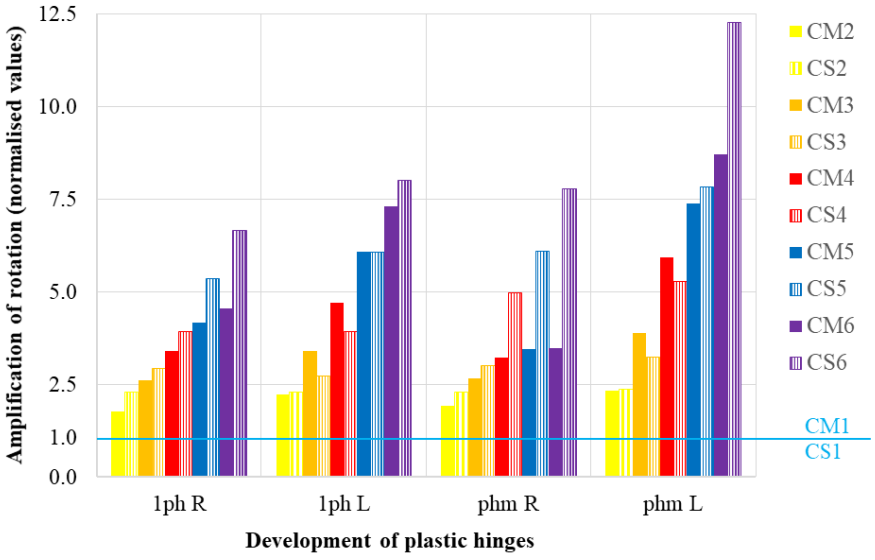


Figure 6. Amplification of rotation for characteristic states in the structure.

Copyright © 2025 CroCEE
DOI: https://doi.org/10.5592/CO/3CroCEE.2025.87

When a mechanism forms on the left side of the structure, the rotation amplification for the CS6 structure reaches nearly 12.5 times. In the same state, the rotation amplification for the CM5 structure is approximately 8.5 times.

The diagrams in Fig. 7. illustrate the relationship between the ratio $\delta_{max}/\delta_{avg}$, and the maximum displacement at the observed point. The trend and shape of the curves are similar for all the analysed structures. A peak appears in the diagrams at a maximum displacement of approximately 0.1% of the storey height. According to ASCE 7-22, at this displacement level, some structures would be classified one level higher in terms of irregularity. The structures CM1 and CM2, previously considered regular, would be reclassified as torsionally irregular, while CM5, previously classified as torsionally irregular, would be categorized as extremely torsionally irregular. Although these displacements are generally very small, attention should be given to this phenomenon in the case of impulsive seismic action, due to dynamic effects such as torsional motion. Beyond this stage, the curve values for almost all structures fall below the initially unsatisfied criterion, indicating that the linear analysis remains on the safe side. The only exceptions are structures CM5 and CS6, whose curve values exceed the criterion up to a maximum displacement of approximately 2% of the floor height. However, this effect has been accounted for in the linear analysis.

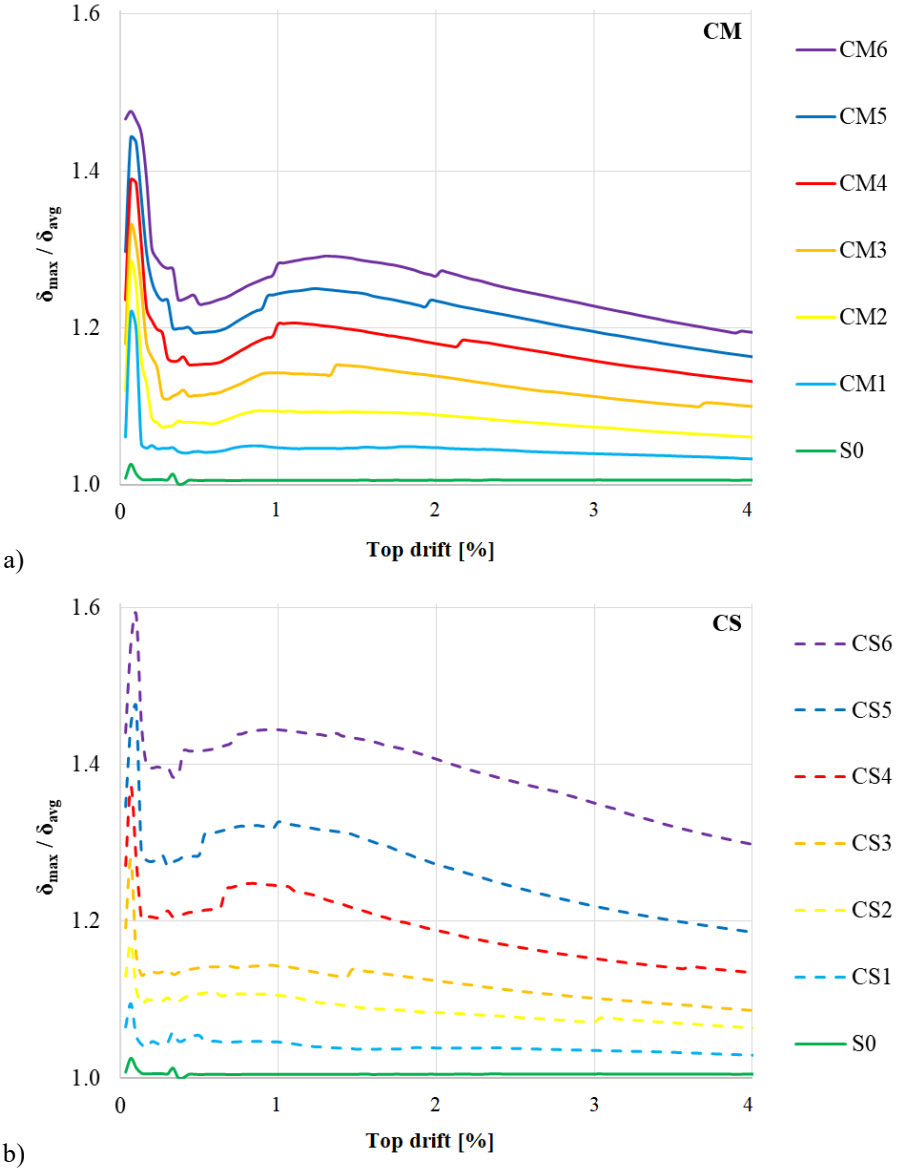


Figure 7. $\delta_{max}/\delta_{avg}$ - top drift diagrams a) structures SO, CM(1-6); b) structures SO, CS(1-6).

Copyright © 2025 CroCEE
DOI: https://doi.org/10.5592/CO/3CroCEE.2025.87

Since all curves exhibit a similar trend, only the diagram for structure CS6 is shown in Fig. 8. Characteristic points are marked, and the order of plastic hinges development is indicated for the four characteristic states. The peak of the curves occurs due to the uneven formation of cracks on both sides of the structure. Up to point C on the diagram, cracks develop only in the columns on the right side of the structure. The maximum is reached when cracks also begin to form in the columns on the left side of the structure, after which the curve declines. Another local maximum occurs at a maximum displacement of approximately 1% of the storey height, corresponding to the formation of a mechanism on the right side of the structure, (point phm R). If the influence of cracks is neglected, i.e. if the tensile strength of concrete is taken as f_{ctm}=0, the curve would follow the path of the light-coloured line. In this case, no peak would appear in the initial phase, and after the formation of a mechanism on the left side of the structure, (point phm L), the curves would completely overlap.

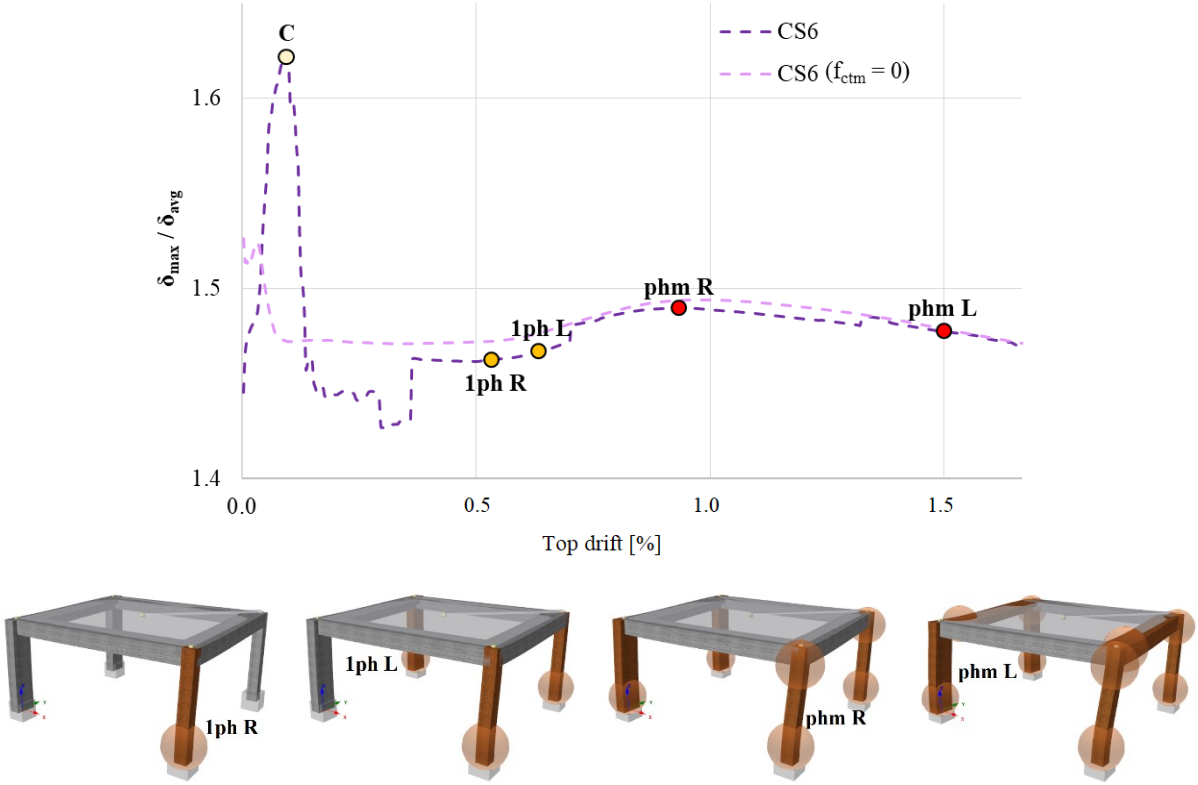


Figure 8. Order of plastic hinges development for characteristic states in the structure.

7. Final remarks

Several conclusions can be drawn from this research. A larger structural eccentricity, whether caused by a shifted center of mass or stiffness, generally has an unfavorable impact on the structural behavior. The criteria for torsional regularity in the utilized codes are based on two fundamentally different approaches. Eurocode 8 relies on the dynamic characteristics of the structure, whereas ASCE 7-22 classifies the level of irregularity based on displacements obtained from seismic analysis. An inconsistency may arise because one structure can be classified as torsionally regular by the one code and torrsionaly irregular by the other. Additionally, the two codes differ in how they penalize irregularity. Eurocode 8 mandates an increase in the design seismic forces, while ASCE 7-22 applies an amplification of the accidental eccentricity. These differences create an opportunity for further research aimed to establishing generally accepted criteria for torsional regularity in modern codes.

Copyright © 2025 CroCEE
DOI: https://doi.org/10.5592/CO/3CroCEE.2025.87

References

[1] Postolov, N., Volcev, R., Todorov, K., Lazarov, Lj. (2020): Effects of Modelling Assumptions on the Plan Irregularity Criteria for Single Storey Buildings, *Seismic Behaviour and Design of Irregular and Complex Civil Structures III. Geotechnical, Geological and Earthquake Engineering*, vol 48. Springer, Cham. https://doi.org/10.1007/978-3-030-33532-8_19.

[2] Kan, C. L., Chopra, A. K. (1977): Elastic earthquake analysis of torsionally-coupled multi-storey buildings, *Earthquake Engineering & Structural Dynamics*, Vol. 5, 395-412.

[3] Dempsey, K.M., Irvine, H.M. (1978): A Note on the Numerical Evaluation of Duhamel's Integral, *Earthquake Engineering & Structural Dynamics*, Vol. 6, 511-515.

[4] Kung, S. Y., Pecknold, D. A. (1984): Seismic response of torsionally coupled single-storey structures, *Proceedings of the 8th World Conference of Earthquake Engineering*, Vol. 4, California, 235-242.

[5] Chandler, A. M., Hutchinson, G. L. (1986): Torsional coupling effects in the earthquake response of asymmetric buildings, *Engineering Structures*, Vol. 8, Issue 4, 222-236.

[6] Stathopoulos, K.G., Anagnostopoulos, S. A. (2005): Inelastic torsion of multistory buildings under earthquake excitations, *Earthquake Engineering & Structural Dynamics*, 34 (12): 1449-1465.

[7] Anagnostopoulos, S. A., Kyrkos, M.T., Stathopoulos, K.G. (2013): Earthquake Induced Torsion in Buildings: Critical Review And State Of The Art, *ASEM 13*, Jeju, Korea.

[8] Chopra, A. K., Goel, R. K. (2004): A Modal Pushover Analysis Procedure to Estimate Seismic Demands for Unsymmetric - Plan Buildings, *Earthquake Engineering & Structural Dynamics*, 33 (8): 903-927.

[9] De Stefano, M., Mariani, V. (2014): Pushover Analysis for Plan Irregular Building Structures, *Perspectives on European Earthquake Engineering and Seismology. Geotechnical, Geological and Earthquake Engineering*, vol 34. Springer, Cham. https://doi.org/10.1007/978-3-319-07118-3_13.

[10] Fajfar, P. (2021): *The Story of the N2 Method*. International Association for Earthquake Engineering, Vol. 2.

[11] Chandler, A. M., Duan, X. N., Rutenberg, A. (1996): *Seismic torsional response: assumptions, controversies and research progress*, European Earthquake Engineering, (1), 37-51.

[12] Shahini, M., Mirghaderi, S. R., Keyhani, A. (2010): How Different Seismic Codes Define Torsionally Unbalanced Structure?, *9th US National and 10th Canadian Conference on Earthquake Engineering*.

[13] Alecci, V., De Stefano, M., Galassi, S., Lapi, M., Orlando, M. (2020): An Assessment of American Criterion for Detecting Plan Irregularity, *Seismic Behaviour and Design of Irregular and Complex Civil Structures III. Geotechnical, Geological and Earthquake Engineering*, vol 48. Springer, Cham. https://doi.org/10.1007/978-3-030-33532-8_18.

[14] Athanatopoulou, A. M., Manoukas, G. E. (2021): Torsional sensitivity criteria in seismic codes, *Earthquakes and Structures*, vol 21, Number 1, pages 1-10, DOI: https://doi.org/10.12989/eas.2021.21.1.001.

[15] CEN (2004a): European Standard EN 1998-1: 2004 Eurocode 8: Design of structures for earthquake resistance, Part 1: General rules, seismic actions and rules for buildings, Comite Europeen de Normalisation, Brusells.

[16] ASCE (2022): Minimum Design Loads and Associated Criteria for Buildings and Other Structures, American Society of Civil Engineers, Reston, Virginia, United States of America.

[17] Scott, M. H., Fenves, G. L. (2006): Plastic hinge integration methods for force-based beam–column elements, *ASCE Journal of Structural Engineering*, Vol. 132, No. 2, pp. 244-252.

Proceedings of the 3rd Croatian Conference on Earthquake Engineering - 3CroCEE
19–22 March 2025, Split, Croatia
Copyright © 2025 CroCEE
DOI: https://doi.org/10.5592/CO/3CroCEE.2025.92

PERFORMANCE-BASED SEISMIC ASSESSMENT OF RC FRAME STRUCTURES USING SIMPLIFIED SDOF IDA

Leart Taravari[(1)], Koce Todorov[(2)]

[(1)] PhD Candidate, Faculty of Civil Engineering, University "Ss. Cyril and Methodius", leart1taravari@gmail.com
[(2)] Professor, Faculty of Civil Engineering, University "Ss. Cyril and Methodius", todorov@gf.ukim.edu.mk

Abstract

The following paper focuses on the conducted performance-based analyses of 8 representative reinforced concrete frame structures. These structures encompass a range of stories, including 2, 3, 5, and 7, and feature varying bay numbers of 3 and 4. The frames are designed to represent the central frame of a reinforced concrete spatial frame structure. The RC frame structures are designed following Eurocode 0 and Eurocode 2 recommendations. The seismic analyses and design of the RC frame structures are conducted using equivalent lateral force method, in line with Eurocode 8 capacity design recommendations. The analysed frame structures are classified as ductile moment resisting frame structures and it is assumed that they are located in Skopje, N. Macedonia.

Based on the final design of the frame structures, several incremental dynamic analyses on the RC frames have been conducted. The incremental dynamic analyses are performed for four intensity measures: PGA, PGV, the ξ=5% damped spectral acceleration at the respective structure's fundamental period (S_a (T_1, 5%)) and the average spectral acceleration (avg S_a); plotted against the same engineering demand parameter – the maximum interstorey drift of the frame (Θ_{max}). The incremental dynamic analyses of the RC frame are performed for 20 ground motion records. The selected ground motions are obtained from the EU-funded INNOSEIS project. To reduce the computational effort required by the demanding IDAs of multi-degree-of-freedom (MDOF) systems, this paper proposes a simplified and approximate method which is based on the response parameters obtained via a pushover analysis of the respective MDOF system and on the nonlinear dynamic analysis of the equivalent single-degree-of-freedom (SDOF) system. This paper also presents the obtained IM-based fragility functions of the RC frames, from the performed incremental dynamic analyses on the MDOF systems and on the equivalent SDOF systems. Respective conclusions on the obtained differences of the IM-based fragility functions, have been drawn.

Keywords: PBEE, incremental dynamic analyses, multi-degree-of-freedom (MDOF) systems, equivalent single-degree-of-freedom (SDOF) systems, IM-based fragility functions

1. Introduction

It is known that fragility functions express the conditional probability of reaching or exceeding a specific damage state, hence a specific threshold of the selected EDP given an intensity measure which is used to describe an earthquake-induced ground motion [1]. The most reliable approach for obtaining analytic fragility functions is by conducting a series of nonlinear dynamic analyses on the respective mathematical model of the multi-degree-of-freedom (MDOF) system.

In recent years, simplified and approximate methods have been developed to reduce the computational effort required by the demanding IDAs of multi-degree-of-freedom (MDOF) systems. These methods rely on response parameters via pushover analyses of the respective MDOF systems and on the nonlinear dynamic analysis of the equivalent single-degree-of-freedom (SDOF) systems. In this paper we present the obtained results of performed IDAs on various MDOF systems and on their equivalent SDOF counterparts.

2. Incremental dynamic analyses of multi-bay and multi-storey RC frames

The following paper presents the conducted incremental dynamic analyses on eight RC planar frame structures and on their respective equivalent SDOF systems. The frame structures are designed in accordance Eurocode 8, using equivalent lateral force method and detailing recommendations.

Proceedings of the 3rd Croatian Conference on Earthquake Engineering - 3CroCEE
19–22 March 2025, Split, Croatia
Copyright © 2025 CroCEE
DOI: https://doi.org/10.5592/CO/3CroCEE.2025.92

Classified as ductile moment resisting frame structures, these structures are regular in plan and elevation. The analysed planar frame structures represent central frames of their respective spatial RC frame structures. The analysed frame structures are designated as R1 through R8 and consist of 2, 3, 5 and 7 stories. Each pair of consecutive frames shares the same number of stories, however odd-numbered RC frames (R1, R3, R5 and R7) have three bays, while the even-numbered (R2, R4, R6 and R8) have four bays. The first-storey height of all the analysed RC frames is 4 m, while the heights of the upper stories remain uniform at 3 m. The bays of the RC frames each have a uniform length of 5 m. It is assumed that the RC frames are constructed from C25/30 concrete and B500B reinforcement. Fig. 1 illustrates the dimensions of the cross-sections and the longitudinal reinforcement details for the beams and columns of frames R1 through R8. On the ground level (±0.00 m), the columns are fixed to the foundations, meaning that in those particular joints, restraints are applied to all 6 DOFs.



Copyright © 2025 CroCEE
DOI: https://doi.org/10.5592/CO/3CroCEE.2025.92

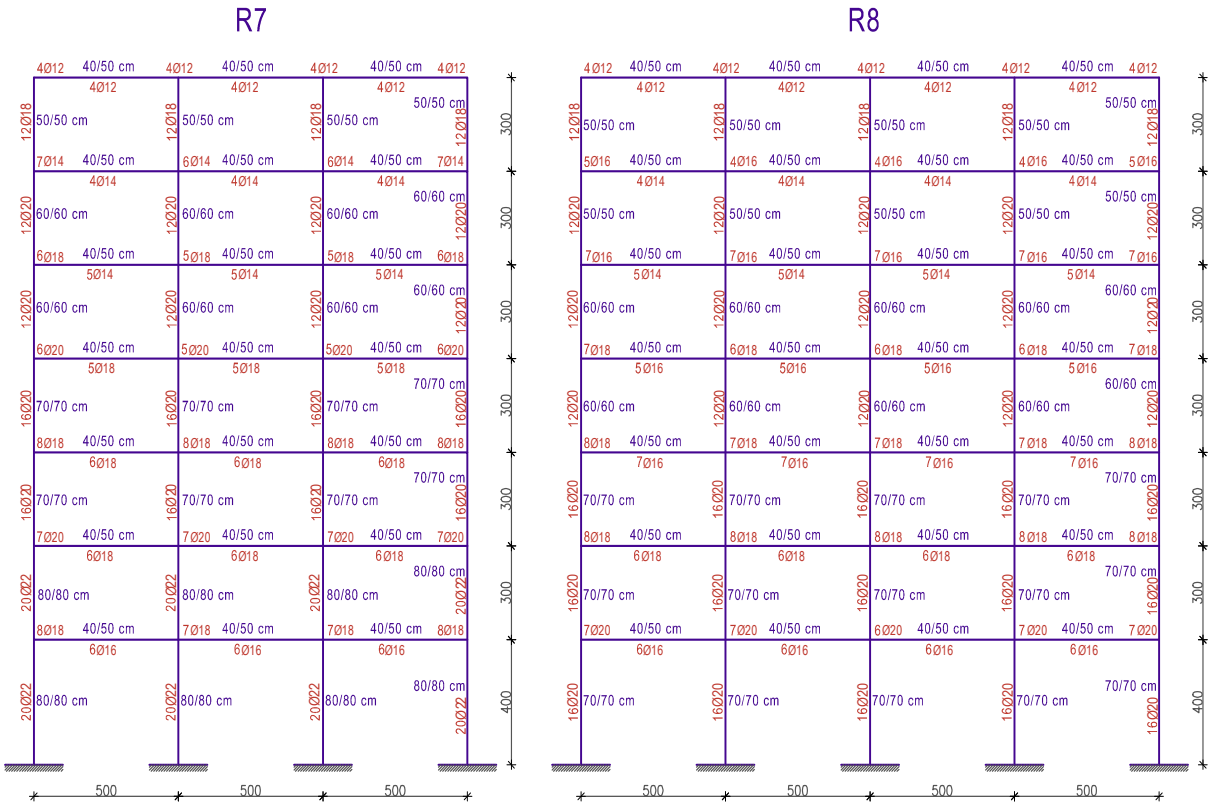


Figure 1. Cross-sectional dimensions and longitudinal reinforcement details for RC frames R1-R8.

The structural models of the RC frames are built in *SeismoStruct*. Nonlinear mathematical modelling of the RC frames was achieved through the use of the distributed plasticity approach. The inelastic behaviour of the beam-column elements of the RC frames was captured through the use of the inelastic displacement-based frame element types [4][7]. This nonlinear modelling approach provides satisfactory accuracy for short, inelastic elements. For this reason, to achieve an accurate assessment of the nonlinear behaviour of structural systems, it is necessary to discretize the constituent beam-column elements (typically into four or five sub-elements). In our case, each beam-column element is discretized into four sub-elements, with the end two sub-elements (where plastic deformations are expected to develop) having a length of 15%, while the middle two sub-elements have a length equal to 35% of the total length of the beam-column element (Fig. 2).

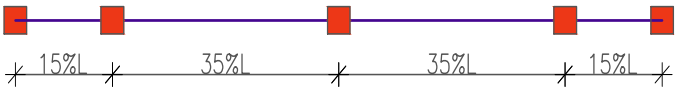


Figure 2. The utilised discretization of the beam-column elements into 4 sub-elements.

Fibre models, through numerical integration, distribute plasticity along the height of the cross-section and the length of the element. In fibre models, the cross-section of the element is divided into a finite number of layers or fibres. Constitutive relationships at section level, e.g. bending moment-curvature, are obtained through the integration of the nonlinear uniaxial stress-strain response of the individual fibres in which the section has been subdivided. Adequate material modelling or in other words, adequate definition of the stress-strain relationships of constituent materials, is thus a key element of the fibre-based discretization. In our study, we have adopted the Menegotto and Pinto uniaxial steel model, supplemented by Monti and Nuti's model to describe the post-elastic buckling behaviour of reinforcing bars under compression, alongside the Mander model for unconfined and confined concrete.

Copyright © 2025 CroCEE
DOI: https://doi.org/10.5592/CO/3CroCEE.2025.92

For numerical integration, the cross-sections at the Gauss integration points are discretized using a triangular mesh of fibres, with a mesh density of approximately 200 fibres per cross-section. For our case, this configuration represents an optimal number of fibres per cross-section. The number of fibres is dependent on the type of section, the target of the analysis and the degree of accuracy sought. Refined subdivisions with a large number of fibres or monitoring points increase exponentially the computations required in the analysis [3]. To determine an optimal number of fibres per cross-section, balancing computational efficiency with analysis accuracy, we conducted a series of sensitivity analyses.

Beam-column joints were assumed to be rigid, and no shear mechanisms were modelled since the design of the RC frame structures followed capacity design criteria, in line with Eurocode 8. In our study, we assume that the elements of the RC frame structures are reinforced with ribbed bars and that the required lapping lengths for the longitudinal reinforcement are satisfied. Therefore, we assume that the bond loss between the concrete and the longitudinal reinforcement is negligible. Consequently, when conducting nonlinear analyses, bar slippage effects were not taken into account. Hysteretic damping, which typically accounts for the majority of energy dissipation caused by earthquake actions, is implicitly included within the nonlinear fibre model formulation of the inelastic frame elements. In this paper, additional sources of non-hysteretic damping are neglected.

To fully capture the behaviour of the RC frame structures in future earthquake events, from elasticity to yielding and finally global dynamic instability, the analyses are performed for 20 different ground motions, with at least 15 intensity increments per ground motion. In the general case, the intensity increments are not equal to each other. This means that for each case, we have performed at least 300 nonlinear dynamic analyses of the nonlinear mathematical model of the respective RC frame. The selected ground motions are obtained from the EU-funded INNOSEIS Project [5]. The selected ground motions for the IDA consider sites with high and medium seismicity. The 5%-damped elastic acceleration response spectra of the unscaled ground motion records are depicted in Fig. 3.

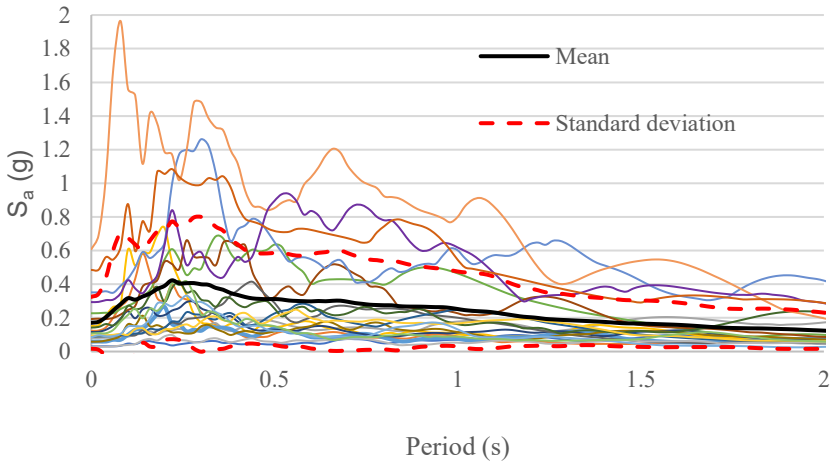


Figure 3. The 5%-damped linear elastic acceleration response spectra of the utilised 20 ground motions.

Fig. 3 provides a graphical summary of the mean and standard deviation of the linear elastic acceleration response spectra for the 20 ground motion records used in the incremental dynamic analyses. The standard deviation quantifies the variability of the response spectra relative to the mean.

The incremental dynamic analyses are performed for four different IMs: PGA, PGV, the ξ=5% damped spectral acceleration at the structure's fundamental period ($S_a(T_1, 5\%)$ and the average spectral acceleration (avg S_a). It is known that the latter two are based on the peak response of linear elastic SDOF systems.

The average spectral acceleration is defined as the geometric mean of the elastic spectral values ($S_a(T_i)$) over a predefined period range [T_{lower}, T_{upper}]. According to Kohrangi et al. [6], for ductile RC frames without masonry infills, this period range is defined as [$0.2 \cdot T_1$, $1.5 \cdot T_1$], where T_1 is the first

Proceedings of the 3rd Croatian Conference on Earthquake Engineering - 3CroCEE
19–22 March 2025, Split, Croatia
Copyright © 2025 CroCEE
DOI: https://doi.org/10.5592/CO/3CroCEE.2025.92

mode elastic period of vibration of the structure. In our analyses, we have adopted this definition of the period range, with 10 equally spaced elastic spectral ordinates between the lower and upper limit of the period range. While the geometric mean and arithmetic mean values are generally very similar, the former has some advantages for computing the average spectral acceleration as it is less sensitive to extreme spectral ordinates, which may significantly influence the arithmetic mean value, Eads et al. [2].

Interstorey drift represents a direct indicator of the structural integrity of a building during earthquake lateral loadings. Due to this, the maximum (along the height) peak (in time) storey drift (Θ_{max}) is chosen as the EDP of interest for all of the aforementioned IMs. The global dynamic instability limit-state (collapse) of the respective analysed structure is defined at 5% of the selected EDP. The maximum peak storey drift (Δ_i) between two adjacent stories of the RC frame i and i-1, is defined as (Eq. (1)):

$$\Delta_i = \frac{\Delta u_i(t)}{h} = \frac{u_i(t) - u_{i-1}(t)}{h} \tag{1}$$

where h is the storey height, while $u_i(t)$ and $u_{i-1}(t)$ are the lateral displacements of two adjacent stories of the analysed RC frame i and i-1, in a particular moment in time t.

The maximum peak storey drift (*MPSD*) of the frame is defined as (Eq. (2)):

$$MPSD = \Delta_{i,max} = \max(\Delta_1, \dots, \Delta_i) \; where \; i = n \tag{2}$$

In Eq. (2), the parameter n represents the total number of stories of the analysed RC frame.

Plotted below (Fig. 4) are the obtained 16%, 50% and 84% fractile curves from the performed incremental dynamic analyses of the considered MDOF systems for four different IMs. The 16% and 84% fractile curves represent the dispersion of the IDA curves around the mean IDA curve (50% fractile curve). In other words, these curves correspond to one standard deviation below and above the mean, assuming a Gaussian distribution. The 16% and 84% fractile curves are represented by dashed lines while the respective 50% fractile curve is represented by a solid line.

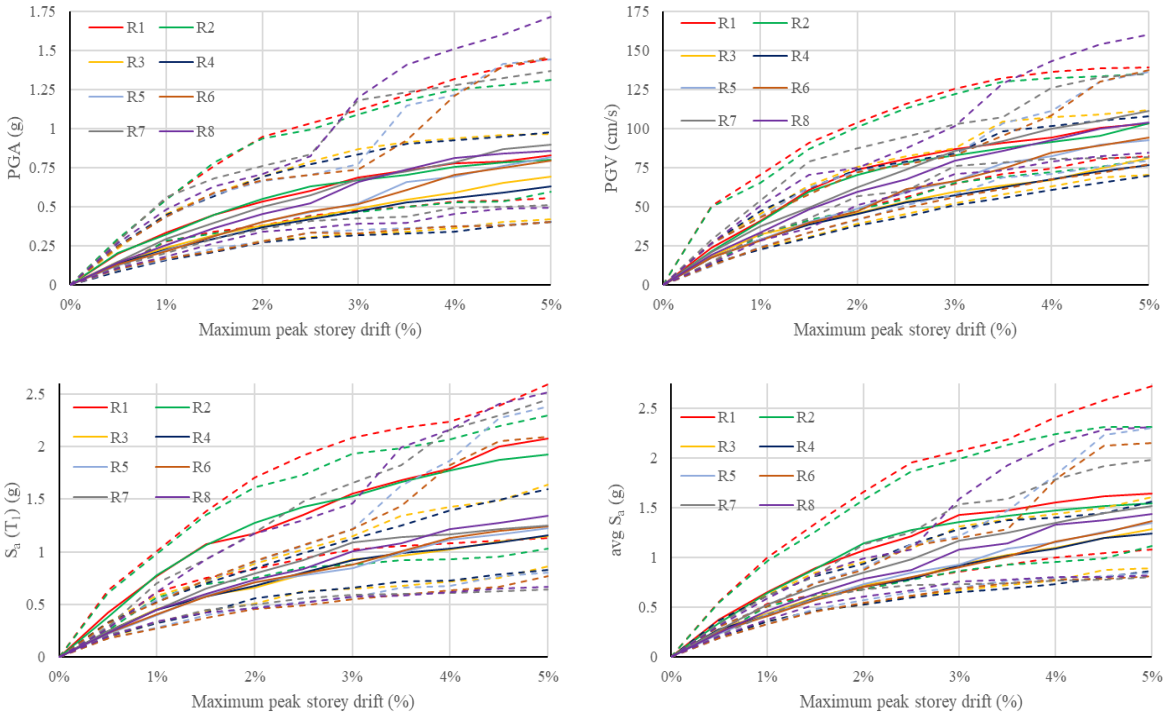


Figure 4. 16%, 50% and 84% fractile curves for PGA, for PGV, for $S_a(T_1)$ and for avg S_a, derived from IDA for 20 ground motion records (top to bottom).

Copyright © 2025 CroCEE
DOI: https://doi.org/10.5592/CO/3CroCEE.2025.92

3. Incremental dynamic analyses of equivalent SDOF systems

If a MDOF system's seismic response is first-mode dominated, which is common for simple, not overly flexible systems, then assessing the seismic performance of the MDOF system can be simplified by analysing the corresponding equivalent SDOF system. This part of the paper deals with the performed IDAs of the equivalent SDOF systems of the aforementioned RC frames. The IDAs were performed by using the same ground motion records that were used for conducting IDAs on the MDOF systems. When conducting IDAs on equivalent SDOF systems, each system is subjected to each ground motion record individually. In the general case, the corresponding intensity was scaled using the same increments that were applied during the IDAs of the MDOF systems. The IDAs of the equivalent SDOF systems were performed for the same intensity measures that were used for the MDOF systems: PGA, PGV, $S_a(T_0, 5\%)$ and avg S_a. Analogously, for the IDAs of equivalent SDOF systems, the lower limit of the period range is defined as $0.2 \cdot T_0$, while the upper limit is defined as $1.5 \cdot T_0$, where T_0 is the elastic natural period of vibration of the corresponding equivalent SDOF system. Within this period range, 10 spectral ordinates, equally spaced from one another, are considered.

While retransforming the maximum displacements of the equivalent SDOF system ($\Delta_{SDOF,max}$) to the MDOF level using $\delta_{max}=\Gamma \cdot \Delta_{SDOF,max}$, a constant lateral displacement profile along the height of the corresponding frame structure is assumed. This assumption is made to determine the maximum peak storey drifts of the retransformed MDOF systems. In this paper, the constant lateral displacement profiles along the heights of the RC frames are based on the first-mode shapes of the eight analysed frames, R1 through R8.

One of the main steps of defining the properties of the equivalent SDOF system is the multi-linearisation and transformation of the SPO curve which is used to describe the lateral response of the MDOF system in terms of nominal base shear and roof displacement. In order to obtain the static pushover curves of the MDOF systems, we have performed a series of displacement-controlled pushover analyses. It is worth mentioning that the lateral load vectors necessary for the static nonlinear analyses, are derived from the eigen mode (Φ_i) corresponding to the fundamental period (T_1) of the respective model of the RC frame. In other words, a modal pattern corresponding to the fundamental eigen mode of the respective mathematical model of the RC frame is used as a vertical distribution of the lateral loads. In our paper, we have adopted a multi-linearisation of the respective SPO curve, that utilises six segments. The multi-linear idealisation is conducted based on a simple technique of curve matching through two control parameters: matching of the obtained SPO curve and matching of the secant lateral stiffness degradation. Each characteristic point that defines the start and/or the end of the segment, viewed on a global level, is closely associated to reaching a specific limit state in the structural elements, which is reflected in changes to the properties of the corresponding SPO curve. Fig. 5 illustrates the application of this technique for RC frame R5.

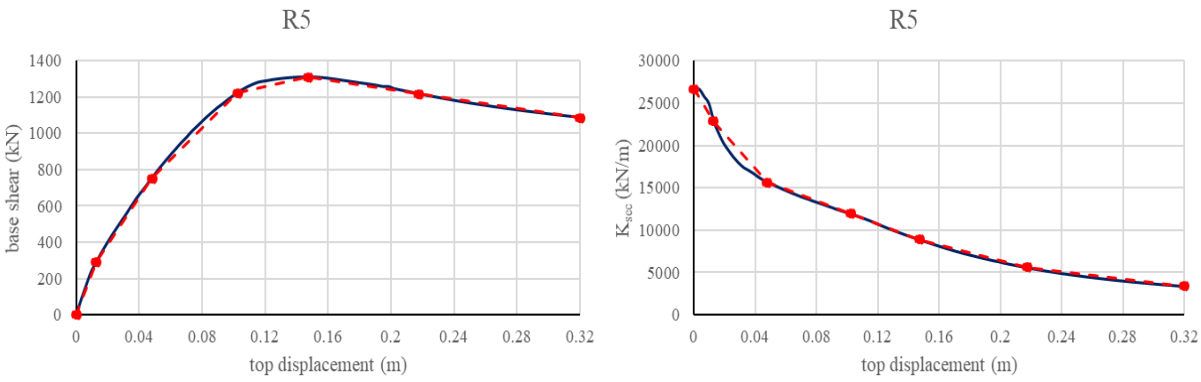


Figure 5. Multi-linear idealisation technique of the SPO curve for RC frame R5.

Proceedings of the 3rd Croatian Conference on Earthquake Engineering - 3CroCEE
19–22 March 2025, Split, Croatia
Copyright © 2025 CroCEE
DOI: https://doi.org/10.5592/CO/3CroCEE.2025.92

The transformation of the continuous SPO curve of the MDOF system, which defines the properties of the equivalent SDOF system, expressed in terms of equivalent base shear $V_{b,SDOF}$ and displacement Δ_{SDOF}, is performed as follows (Eq. (3), (4) and (5)):

$$\Delta_{SDOF} = \frac{\Delta_{roof}}{\Gamma} \tag{3}$$

$$V_{b,SDOF} = \frac{V_{base}}{\Gamma} \tag{4}$$

$$\Gamma = \frac{\sum_1^n m_i \varphi_{1,i}}{\sum_1^n m_i \varphi_{1,i}^2} = \frac{m^*}{\sum_1^n m_i \varphi_{1,i}^2} \tag{5}$$

where Γ is the first-mode transformation factor computed via Eq. (5) assuming a first-mode based non-torsional behaviour of the RC frame structure, m^* is the effective mass of the equivalent SDOF system, m_i is the mass at floor i while $\varphi_{1,i}$ is the displacement amplitude at floor i of the fundamental mode shape, normalised to have a unit maximum amplitude.

In addition to determining the envelope capacity curve of the equivalent SDOF system, defining an appropriate hysteresis rule is essential for conducting nonlinear dynamic analyses of the equivalent SDOF system. Hysteretic models are used to represent the cyclic behaviour of structural elements within a specific system under cyclic loading. In other words, hysteretic models represent the variation of the force–displacement relationship of structural elements under a given cyclic loading. The global hysteretic behaviour of MDOF systems, represented in the format: nominal base shear versus roof displacement, is the result of the influence of the local hysteretic behaviours of individual structural elements, as well as the influence of the higher mode response of the MDOF system [9]. In order to perform the IDAs on the equivalent SDOF systems, we have adopted the Takeda hysteretic model [8], which is a suitable model for representing the cyclic behaviour of RC elements.

4. IM-based fragility functions from IDA

From the obtained IDA curve sets of the MDOF systems and their equivalent SDOF systems, for 20 ground motion records, we have plotted the IM-based fragility functions. The IM-based fragility functions represent the distributions of intensities needed to exceed a certain limit of a defined EDP. The IM-based fragility functions are generated using the maximum likelihood estimation. The IM-based fragility functions are plotted for three threshold levels of EDP (Maximum peak storey drift, θ_{max}): 0.5%, 2.0% and 5.0% (collapse).

It is known that the median values of fragility functions correspond to a 50% probability of exceeding a specified threshold level of EDP. The median values for the IM-based fragility functions, derived from performed IDAs on the MDOF systems and on their equivalent SDOF systems, are given in Table 1.

Proceedings of the 3rd Croatian Conference on Earthquake Engineering - 3CroCEE
19–22 March 2025, Split, Croatia
Copyright © 2025 CroCEE
DOI: https://doi.org/10.5592/CO/3CroCEE.2025.92

Table 1. The median values (η) of the IM-based fragility functions, computed from IDA for 20 ground motion records.

RC frame	MPSD (%)	PGA (g)		PGV (cm/s)		S_a (T_0, T_1) (g)		avg S_a (g)	
		MDOF	e. SDOF	MDOF	e. SDOF	MDOF	e. SDOF	MDOF	e. SDOF
R1	$\eta_{0.5\%}$	0.197	0.329	24.901	41.579	0.414	0.668	0.377	0.619
	$\eta_{2.0\%}$	0.56	0.779	70.801	98.434	1.163	1.58	1.06	1.465
	$\eta_{5.0\%}$	0.859	1.126	108.536	142.256	1.78	2.284	1.622	2.118
R2	$\eta_{0.5\%}$	0.193	0.317	24.417	40.098	0.392	0.644	0.364	0.597
	$\eta_{2.0\%}$	0.552	0.751	69.792	94.882	1.121	1.523	1.039	1.413
	$\eta_{5.0\%}$	0.827	1.099	104.46	138.863	1.677	2.23	1.555	2.067
R3	$\eta_{0.5\%}$	0.149	0.218	18.811	27.491	0.25	0.378	0.266	0.397
	$\eta_{2.0\%}$	0.4	0.586	50.527	74.083	0.668	1.02	0.716	1.07
	$\eta_{5.0\%}$	0.68	0.903	85.861	114.03	1.136	1.569	1.216	1.647
R4	$\eta_{0.5\%}$	0.145	0.216	18.332	27.28	0.249	0.375	0.264	0.394
	$\eta_{2.0\%}$	0.39	0.581	49.304	73.383	0.669	0.976	0.71	1.06
	$\eta_{5.0\%}$	0.653	0.889	82.55	112.302	1.12	1.493	1.189	1.622
R5	$\eta_{0.5\%}$	0.14	0.182	17.647	22.965	0.219	0.288	0.237	0.309
	$\eta_{2.0\%}$	0.428	0.535	54.017	67.552	0.672	0.848	0.725	0.91
	$\eta_{5.0\%}$	0.793	0.854	100.151	107.873	1.246	1.354	1.344	1.453
R6	$\eta_{0.5\%}$	0.144	0.182	18.221	22.99	0.225	0.289	0.242	0.31
	$\eta_{2.0\%}$	0.421	0.533	53.151	67.338	0.656	0.845	0.707	0.907
	$\eta_{5.0\%}$	0.79	0.848	99.8	107.176	1.233	1.346	1.327	1.444
R7	$\eta_{0.5\%}$	0.169	0.192	21.485	24.302	0.247	0.29	0.274	0.315
	$\eta_{2.0\%}$	0.528	0.622	66.945	78.618	0.768	0.937	0.853	1.021
	$\eta_{5.0\%}$	0.869	1.07	110.223	135.158	1.265	1.611	1.404	1.755
R8	$\eta_{0.5\%}$	0.155	0.183	19.641	23.131	0.233	0.272	0.248	0.292
	$\eta_{2.0\%}$	0.48	0.598	60.613	75.58	0.719	0.887	0.765	0.954
	$\eta_{5.0\%}$	0.863	1.021	109.018	128.946	1.294	1.514	1.377	1.628

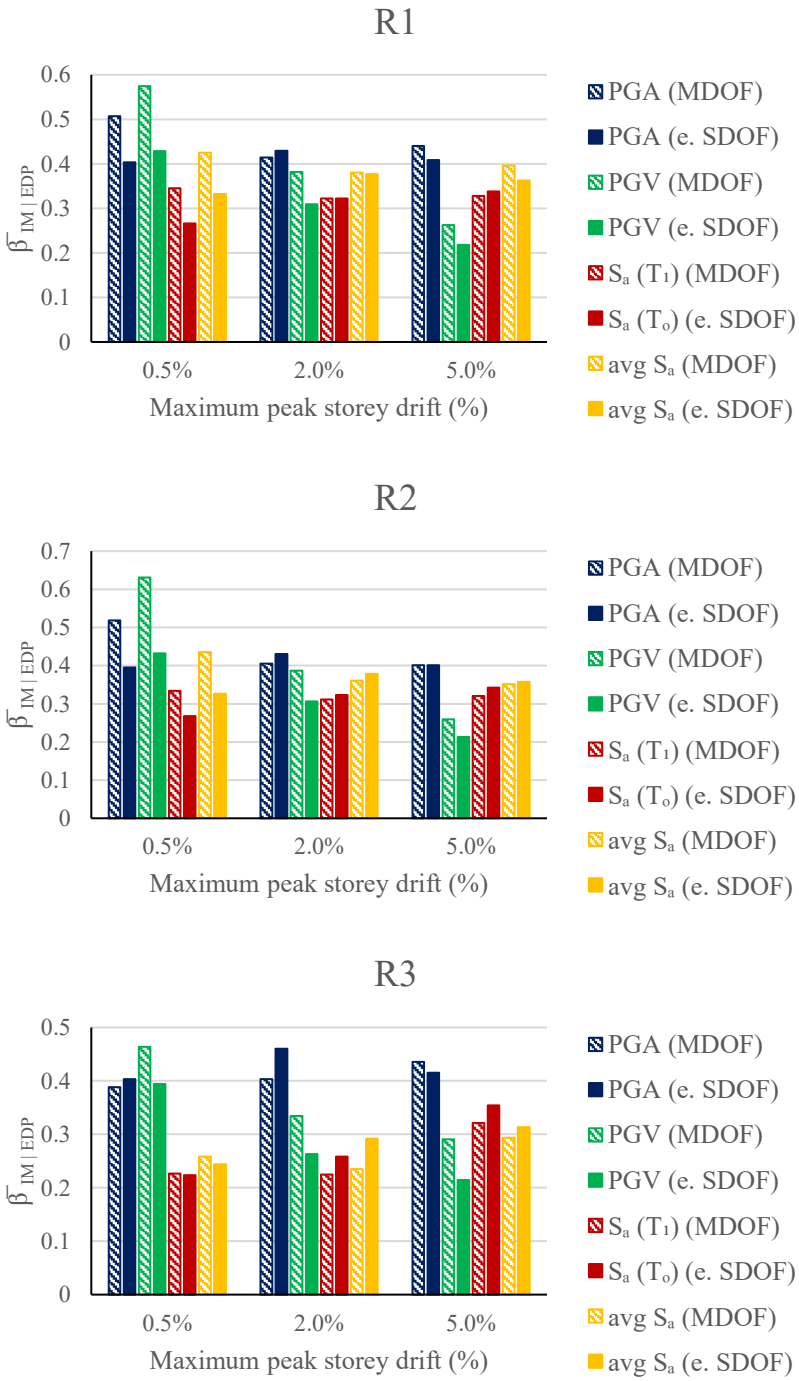
It is known that dispersion values are indicators of the efficiency of a selected IM [11]. The dispersion values influence the slope of the fragility function and reflect the level of uncertainty in the analysis results. The overall level of uncertainty encompasses two main sources of uncertainty. The aleatory or record-to-record uncertainty (β_{RTR}) reflects the variability in the response of the structures due to the stochastic nature of ground motions. The epistemic or modelling uncertainty ($\beta_{modelling}$) is mainly due to lack of knowledge about the real properties of the structural elements. The combination of these two sources of uncertainty is performed according to Tzimas et al. [10] (Eq. (6)):

Copyright © 2025 CroCEE
DOI: https://doi.org/10.5592/CO/3CroCEE.2025.92

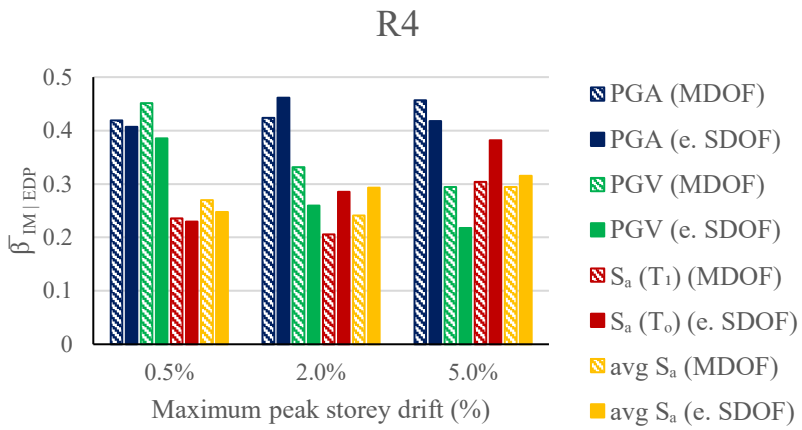
$$\beta_{Total} = \sqrt{\beta_{RTR}^2 + \beta_{modelling}^2} \tag{6}$$

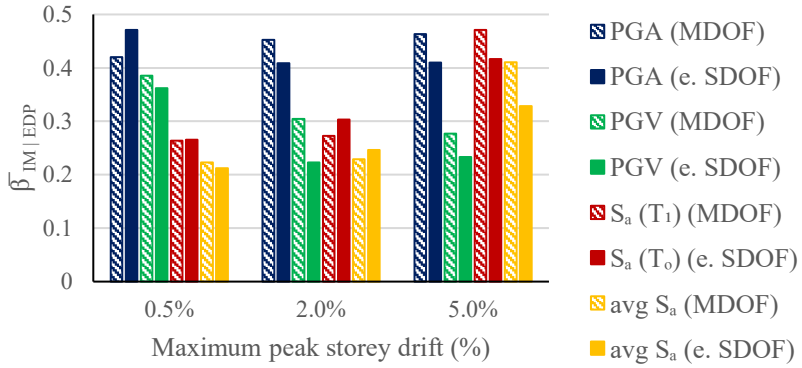
In our study, we have assumed that $\beta_{modelling}=0$, hence we have assumed that the total dispersion value arises solely from the stochastic nature of ground motions. In other words, $\beta_{Total} = \beta_{RTR} = \beta_{IM\,|\,EDP}$.

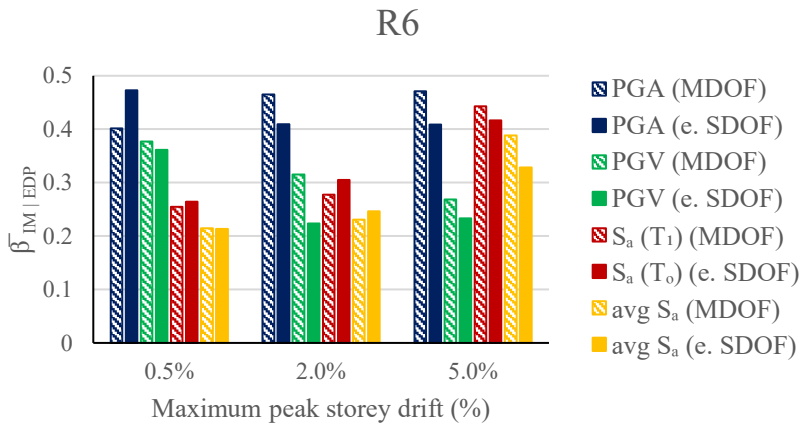
Plotted below (Fig. 6) are the variations of the normalised dispersion values ($\bar{\beta}_{IM\,|\,EDP}$) of the IM-based fragility functions, derived from performed IDAs on the MDOF systems and on their equivalent SDOF systems. The normalised dispersion values of the IM-based fragility functions are obtained as the ratio of the standard deviation of the respective intensity measure values, corresponding to a given maximum peak storey drift, and their arithmetic mean.



Copyright © 2025 CroCEE
DOI: https://doi.org/10.5592/CO/3CroCEE.2025.92







Copyright © 2025 CroCEE
DOI: https://doi.org/10.5592/CO/3CroCEE.2025.92

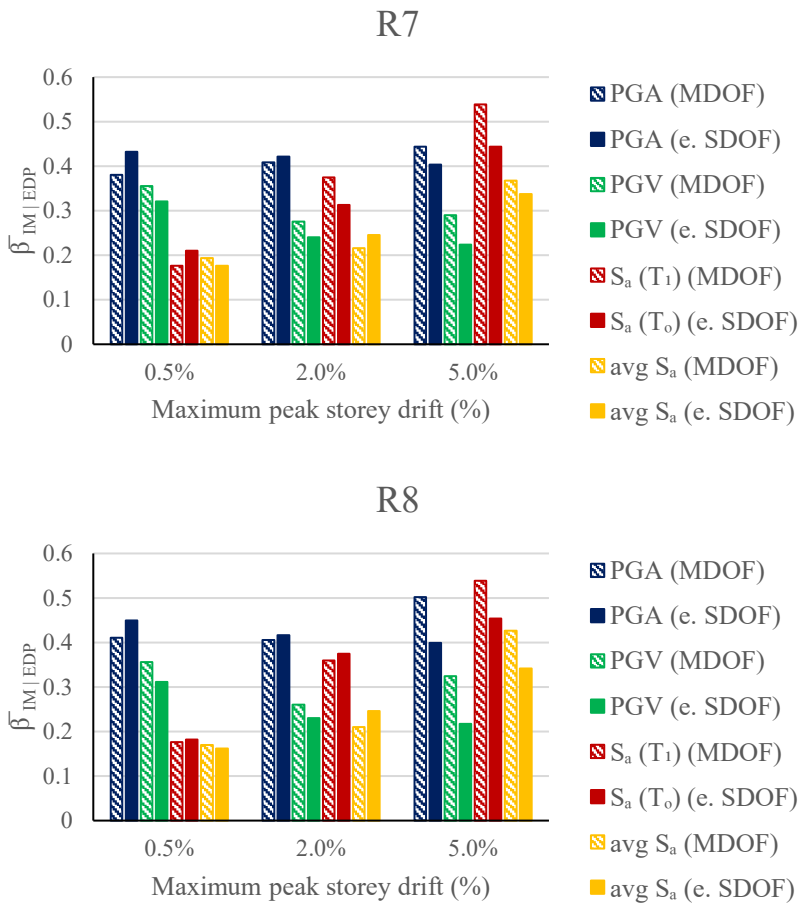


Figure 6. The normalised dispersion values ($\bar{\beta}_{IM|EDP}$) of the IM-based fragility functions, computed from IDA for 20 ground motion records.

The IM-based fragility functions for frame R5 and for the avg S_a case, computed from IDAs of the MDOF system (dashed lines) and of the equivalent SDOF system (solid lines), are plotted in Fig. 7.

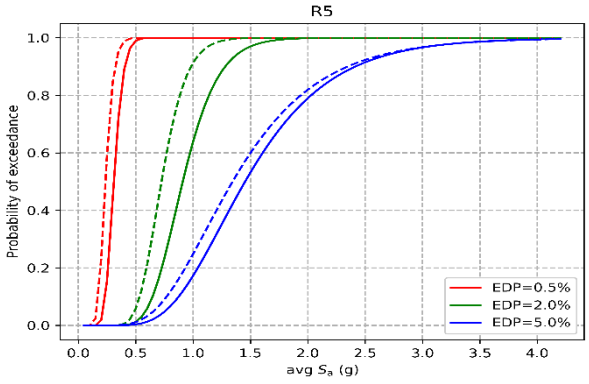


Figure 7. IM-based fragility functions for RC frame R5, computed from IDA curves, for avg S_a.

5. Conclusions

From the generated IM-based fragility functions of the MDOF systems and of their equivalent SDOF systems, obtained from IDA for 20 ground motions, for three threshold levels of EDP, it is obtained that the lower frames R1-R4 exhibit larger deviations in the median values of the IM-based fragility functions for all considered IMs, compared to the respective values obtained from IDA of the equivalent

Copyright © 2025 CroCEE
DOI: https://doi.org/10.5592/CO/3CroCEE.2025.92

SDOF systems. It is also observed that for a given RC frame, at a specified threshold level of EDP, the deviations in the median values of the IM-based fragility functions are of similar magnitude for all four considered IMs. For RC frames R1-R5, increasing the threshold level of EDP results in a reduction in most of the deviations in the median values of the IM-based fragility functions.

From the conducted analyses, it is obtained that in all cases, the PGA as an IM displays relatively large dispersion values. Additionally, from the conducted incremental dynamic analyses of the equivalent SDOF systems, it has been observed that for the case of PGV, in the lower frames R1-R4 and in frames R7-R8, as the EDP increases, the dispersion value decreases. It is worth mentioning that in these frames, there is a more rapid reduction of the dispersion values when increasing the EDP from 0.5% to 2.0%, compared to the increase from 2.0% to 5.0%. Nonetheless, in all analysed RC frames, at an EDP of 0.5%, PGV as an intensity measure exhibits high dispersion values.

From the IDAs of equivalent SDOF systems, for RC frames R1-R4 and for low values of EDP, $S_a(T_0, 5\%)$ exhibits the lowest normalised dispersion values. The normalised dispersion values obtained from these analyses are slightly lower than the analogous values obtained from IDAs performed on MDOF systems. Even at the collapse states of these RC frames, hence at a 5.0% maximum peak storey drift, the dispersion values remain relatively low. It can be concluded that from the conducted IDAs on the MDOF systems of R1-R4 and on their equivalent SDOFs, $S_a(T_0, T_1, 5\%)$ represents an efficient IM.

From the performed IDAs, it is obtained that for the taller frames R5-R8, the average spectral acceleration as an IM exhibits relatively low dispersion values across all considered levels of EDP. From the IDAs of equivalent SDOF systems it is observed that for these taller frames (R5-R8), at an EDP of 0.5%, the average spectral acceleration demonstrates the lowest dispersion values.

References

[1] Di Sarno, Luigi, Elnashai, S., Amr, (2021): *Seismic Fragility Relationships for Structures*, part of: Akkar, S., Ilki, A., Goksu, C., Erdik, M., *Advances in Assessment and Modeling of Earthquake Loss*, Springer Tracts in Civil Engineering, Springer, Cham.

[2] Eads, L., Miranda, E., Lignos, G.D. (2015): Average spectral acceleration as an intensity measure for collapse risk assessment, *Earthquake Engineering and Structural Dynamics*, 44: 2057-2073.

[3] Elnashai, S., Amr, di Sarno, Luigi, (2008): *Fundamentals of Earthquake Engineering*, John Wiley & Sons, Inc, UK and USA.

[4] Hellesland, Jostein, Scordelis, C., Alex, (1981): Analysis of R.C. Bridge Columns under Imposed Deformations, *IABSE Colloquium on Advanced Mechanics of Reinforced Concrete*, Delft, Holland.

[5] INNOSEIS (2016). GM Records. Available from: http://innoseis.ntua.gr.

[6] Kohrangi, M., Bazzurro, P., Vamvatsikos, D., Spillatura, A. (2017): Conditional spectrum-based ground motion record selection using average spectral acceleration, *Earthquake Engineering and Structural Dynamics*, 46: 1667-1685.

[7] Mari, A., Scordelis, C., Alex, (1984): Nonlinear geometric, material and time dependent analysis of three dimensional reinforced concrete and prestressed frame, *UC SESM Report no. 84/12*, EERC, Berkeley, California, USA.

[8] Takeda, T., Sozen, A., Mete, Nielsen, N.N., (1970): Reinforced Concrete Response to Simulated Earthquakes, *Journal of Structural Engineering Div.*, ASCE, 96:12, 2557-2573.

[9] Todorov, K. (2014): *Сеизмички перформанси на исполнети армиранобетонски рамки со отворен прв кат* – PhD Thesis (in Macedonian). Faculty of Civil Engineering – University of Ss. Cyril and Methodius, Skopje, R. of Macedonia.

[10] Tzimas, A.S., Kamaris, G.S., Karavasilis, T.L., Galasso, C., (2016): Collapse risk and residual drift performance of steel buildings using post-tensioned MRFs and viscous dampers in near-fault regions, *Bulletin of Earthquake Engineering*, 14(6), pp. 1643-1662.

[11] Vamvatsikos, Dimitrios, Cornell, C., Allin, (2004), Applied Incremental Dynamic Analysis, *Earthquake Spectra*, Volume 20, No.2, pp. 523-553.

Proceedings of the 3rd Croatian Conference on Earthquake Engineering - 3CroCEE
19–22 March 2025, Split, Croatia
Copyright © 2025 CroCEE
DOI: https://doi.org/10.5592/CO/3CroCEE.2025.95

MODELLING THE SEISMIC RESPONSE OF A CONFINED MASONRY BUILDING USING EQUIVALENT STRUT MODELS

Nemanja Krtinić [(1)], Matija Gams [(2)], Marko Marinković [(3)]

[(1)] *PhD student, Faculty of Civil and Geodetic Engineering, University of Ljubljana, nkrtinic@fgg.uni-lj.si*
[(2)] *Assistant professor, Faculty of Civil and Geodetic Engineering, University of Ljubljana, mgams@fgg.uni-lj.si*
[(3)] *Assistant professor, Faculty of Civil Engineering, University of Belgrade, mmarinkovic@grf.bg.ac.rs*

Abstract

Confined masonry (CM) technology is extensively employed in many parts of the world for the construction of residential buildings due to its improved seismic performance compared to the unreinforced masonry (URM). This study focuses on the numerical simulation of seismic response of CM walls and a three-storey model of a CM building using Equivalent Strut Models (ESM) in OpenSees framework. Different strut and constitutive models available in the literature were used. The primary objective is to identify the most suitable model for simulating the global response of CM walls and structures. Firstly, different numerical models of the CM wall were compared against two full-scale shear compression tests, which enabled us to identify the most suitable and accurate model. The most suitable model was then used to develop a numerical model of the three-storey CM building, and the results of the simulations were compared with the experiment.

Keywords: confined masonry, equivalent strut model, numerical modelling, pushover analysis, OpenSees.

1. Introduction

The European masonry industry is developing new products and construction technologies that offer improved thermal properties, thereby reducing energy consumption for heating and cooling, while also enhancing the comfort of occupants. One such technology involves the use of polyurethane (PU) adhesive instead of thin-bed mortar, which reduces joint thickness to almost zero, preventing heat transfer through the joints. Additionally, this technology enables faster construction and building at lower temperatures. Typically, the PU glue is applied only in bed-joints, while head joints remain unfilled. Masonry blocks are also evolving, with new types featuring larger cavities filled with insulation material, which further reduces thermal conductivity of walls. This construction technology is often employed in the seismic-prone regions, such as Southeastern Europe, where masonry structures are built using confined masonry (CM) technology with reinforced concrete (RC) vertical and horizontal tie-elements, also known as tie-columns and tie-beams, respectively.

The seismic response of CM built with the new type of masonry, incorporating new masonry products and construction with PU glue, was recently experimentally tested through shear-compression tests on two full-scale CM wall test specimens under constant compressive loading [1], as well as by investigating a three-storey full-scale CM building [2]. Numerical modelling of this type of masonry is relatively poorly researched. However, modelling is a promising alternative to expensive and challenging full-scale experiments, offering a valuable complement to and extension of experimental research. Numerical approaches for seismic analysis of CM structures vary, ranging from detailed micro models to simplified micro models and macro models, with the choice depending on the objectives of the analysis and the required level of detail. The Equivalent Strut Model (ESM) is a widely used macro-modelling approach that balances accuracy and computational efficiency, making it suitable for routine design.

The main objective of this study is to numerically model the seismic response of CM walls using equivalent diagonal strut models. To identify the most suitable mathematical model, three different

Copyright © 2025 CroCEE
DOI: https://doi.org/10.5592/CO/3CroCEE.2025.95

constitutive laws were applied to the single ESM models. These numerical 2D models were developed using the open-source software OpenSees [3].

First, numerical simulations of CM walls were conducted, and by comparing the results with experimental results, the most suitable model was identified. The selected model was then used to numerically simulate the seismic response of the three-storey CM building. The aim of the study is to evaluate whether equivalent strut models, which are simple enough for practical use, can accurately and reliably represent the global response of walls and buildings constructed with the previously described new type of CM.

2. Brief overview of the previous experimental campaigns

2.1. Walls

Two confined masonry (CM) walls, labelled W7 and W8, were tested in a laboratory, as detailed in [1]. Both walls were built with identical dimensions: 175 cm in length, 195 cm in height, and 38 cm in thickness (Fig. 1a). The tie-columns measured 25 x 25 cm (Fig. 1b), and were reinforced with 4 Ø 14 mm bars, providing a longitudinal reinforcement ratio of 1 %. The transverse reinforcement consisted of Ø 8 mm stirrups spaced approximately 20 cm apart. The dimensions of the vertical tie-columns exceeded the requirements outlined in Eurocode 8/1 [4], while the reinforcement complied with the Eurocode 8/1 requirements, which mandate at least 1 % longitudinal reinforcement and transverse reinforcement of at least Ø5/15 cm.

A notable feature of these CM walls is that the tie-columns do not cover the full thickness of the wall. Specifically, they are positioned flush with one surface of the masonry, while on the opposite side, they are depressed by 13 cm, as shown in Fig. 1a.

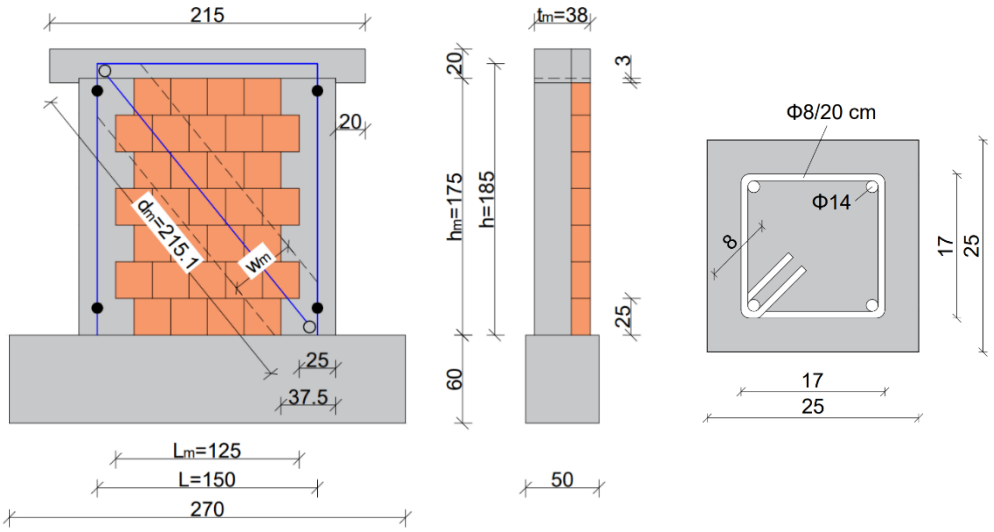


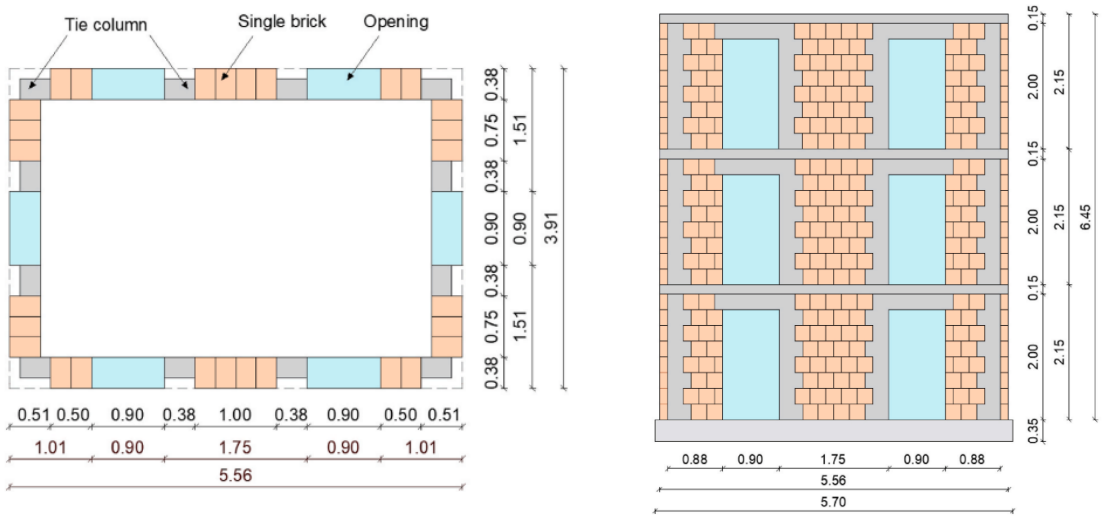
Figure 1: a) CM wall test specimen (dimensions in cm); b) Tie-column reinforcement [1].

2.2. Three-storey masonry building

The three-storey CM building model, tested at nearly full scale in a laboratory, is detailed in a separate study by Gams et al. [2]. The floor plan dimensions of the building were 5.6 x 3.9 m (Fig. 2a), and due to the spatial limitations of the laboratory, the storey height was reduced to 2.15 m, with a clear storey height of 2.0 m. The thickness of the RC floor slabs was 15 cm. The model was doubly symmetric, with two shear walls loaded in their plane and two cross walls providing stability. Cross walls are fully confined with tie-columns at both ends of piers. The shear walls consisted of three piers and two openings, each measuring 0.9 x 1.75 m (Fig. 2b). The central pier, which was longer than the side piers,

Copyright © 2025 CroCEE
DOI: https://doi.org/10.5592/CO/3CroCEE.2025.95

had a length of 1.75 m. Note that the central pier and tie-columns were identical to those used in walls W7 and W8 (placed on both sides). The shorter piers had tie-columns only on one end due to their length of about 1m. Above the openings, lintels with dimensions of 25 x 25 cm were placed, with longitudinal reinforcement consisting of four Ø14 bars and stirrup reinforcement of Ø8/20 cm.



a) b)

Figure 2: Plan of the three-storey building: a) floor plan, b) side view [2]. All dimensions are in meters.

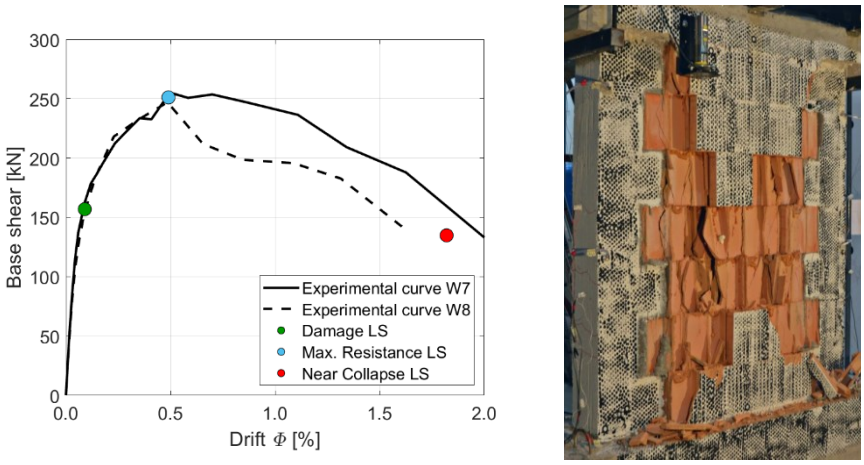
2.3. Brief overview of the test results

The walls W7 and W8 were tested under in-plane shear compression conditions, with a constant vertical stress of 0.63 MPa. Fixed-fixed boundary conditions were applied (no rotation at the top, with constant vertical force), while horizontal displacements were cyclically applied at the bond beam level. Each displacement amplitude was repeated three times in both directions to simulate seismic loading in a standard manner [5]. The displacement amplitude was progressively increased until near-collapse. The amplitude was gradually increased until nearing collapse. A Digital Image Correlation (DIC) system was used to measure displacement and strain fields across the surface of the wall. Further details regarding the experimental setup, instrumentation, loading protocol, and comprehensive test results are provided in [1].

Fig. 3a shows the hysteretic response envelopes for both walls, obtained as the average response in both the push and pull directions. The envelopes also highlight different limit states (LSs): the green circle represents the damage LS, the blue circle indicates the maximum resistance LS, and the red circle marks the near-collapse LS.

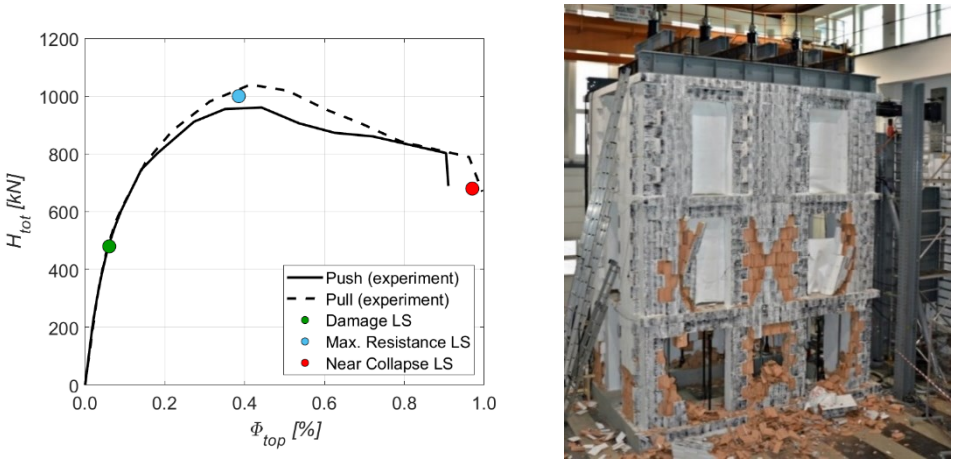
The seismic response of the tested CM walls was as expected, with dominant shear behaviour. However, the observed damage was unexpected. An interesting phenomenon occurred at the interface between the masonry and tie-columns, where initial cracking initiated by tie-columns and damage spread towards the centre of the wall. This damage was primarily caused by the geometry of the blocks, which featured larger individual holes (6 % of the total volume), and a total hole volume of 59 %. These values exceed the Eurocode 6 [5] limits for load-bearing walls (2 % and 55 %, respectively). The protruding part of masonry, which was not fully confined by tie-columns, was significantly damaged already at the maximum resistance LS (at about 0.5 % drift) and completely sheared off at a drift of 1.3 % (Fig. 3b).

Copyright © 2025 CroCEE
DOI: https://doi.org/10.5592/CO/3CroCEE.2025.95



a) b)

Figure 3: a) Experimentally obtained envelope curves of the two tested CM walls W7 and W8, with marked limit states; b) Cracking in the plane of the wall due to tie-columns at 1.3 % drift.



a) b)

Figure 4: a) Experimentally obtained envelope curve (base shear against top drift) of a three-storey masonry building with highlighted limit states; b) Masonry building close to the Near Collapse LS.

The three-storey building model was tested in the same manner as CM walls. First, a vertical load was applied to the model, inducing a compressive stress state of approximately 0.63 MPa in the walls, corresponding to about 20 % of the characteristic compressive strength of the masonry (f_k). This vertical stress was caused by a total force of 2395 kN. Part of this force was contributed by the self-weight of the walls and floor slabs, while the remaining portion was applied using four hydraulic actuators positioned at the top of the building. After the vertical load was applied, the building was subjected to a cyclic lateral load with an inverted triangular distribution, applied three times for each load level. The test was displacement-controlled at the first storey, and the measured force in the first storey was scaled accordingly for the upper two stories. The hysteretic response envelope, shown separately for pushing and pulling direction, is presented in Fig. 4a, with limit states indicated by the same symbols used for the walls. The damage LS was reached at a drift of 0.07–0.08 %, while the significant damage LS was observed at a drift of 0.55 %. The near-collapse LS, indicating the building was close to the failure, was reached at a drift of 1 % for the entire structure, and at 1.75 % drift for the bottom storey (see Fig. 4b).

Copyright © 2025 CroCEE
DOI: https://doi.org/10.5592/CO/3CroCEE.2025.95

3. Numerical macro-modelling

In this Section, the classical model with an equivalent diagonal strut [7] is used to simulate the global seismic response of walls and buildings built using CM technology. Although the ESM model was originally developed for reinforced concrete (RC) frame structures with infills, it can be adapted for CM structures (see e.g., [5], [8]). Since the model is relatively simple, it is also suitable for practical applications. The main drawback is that the model is unable to capture local phenomena, which are often not of interest in design.

The model of the RC members and the strut for CM walls used in this work is essentially the same as that for RC frame structures with infills, except that plastic hinges are assumed not to develop in the bond beam. This is because the masonry and the top beam are strongly connected (the concrete is poured directly onto the masonry), and because no such damage was observed during the tests. In this paper, three commonly used simple ESMs with one single strut are applied, namely the models of Panagiotakos and Fardis model [9], the Decanini et al. model [10], and the Liberatore et al. model [11]. Since a detailed description of each model exceeds the scope of this paper, only brief descriptions and the calculated characteristic points of the strut models are provided, in the form of graphs of strut force–strut displacement.

The ESM model of the considered CM walls is shown in Fig. 1a, where L is the length of the wall measured between the central axes of the tie-columns, L_m is the length of the masonry panel, h is the specimen height, h_m is the height of the masonry panel, w_m is the width of the equivalent strut, d_m is the length of the equivalent strut, t_m is the masonry wall thickness, and θ is the inclination angle of the strut.

3.1. Equivalent strut models

3.1.1. Model by Panagiotakos and Fardis [9]

The classical ESM describes the behaviour of strut with four linear segments, as shown in Fig. 5. The initial state is followed by the cracked state up to the point of maximum resistance. After that, there is a segment of strength degradation, eventually leading to residual strength. The graph shows only the response of the wall panel without the contribution of the RC ties. The characteristic points of the strut, calculated for walls W7 and W8, are summarized in Table 1.

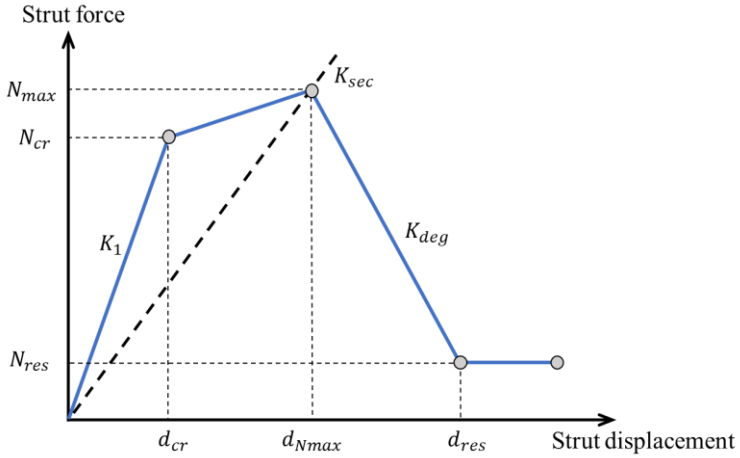


Figure 5: Constitutive model of the strut [9].

Proceedings of the 3rd Croatian Conference on Earthquake Engineering - 3CroCEE
19–22 March 2025, Split, Croatia
Copyright © 2025 CroCEE
DOI: https://doi.org/10.5592/CO/3CroCEE.2025.95

Table 1: Characteristic points of the ESM model according to the model of Panagiotakos and Fardis [9]

Limit state	**Strut displacement *d* [mm]**	**Wall drift *Φ* [%]**	**Strut force *N* [kN]**
Crack	0.34	0.03	237.0
Max. resistance	3.41	0.32	308.1
Residual	11.25	1.05	30.8
Ultimate	34.87	3.24	30.8

3.1.2. Model by Decanini et al. [10]

The constitutive law of the equivalent strut proposed by Decanini et al. [10] is also composed of four linear segments (see Section 3.1.1, Fig. 5). The key difference lies in how the characteristic points are calculated. The most notable difference is in the calculation of the maximum resistance $N_{\max}$, which, in the case of the Decanini et al. [10] model, requires evaluating four different failure mechanisms and selecting the most critical one.

The critical stresses for all four mechanisms are shown in Table 2.

Table 2: Estimation of the failure stress in the masonry panel [10]

Equation	**Stress [MPa]**	**Failure mode**
$\sigma_{m,a} = \dfrac{1.16 f_{md} \tan\theta}{K_1 + K_2 \lambda_h} t_w d$	8.31	Diagonal compression failure
$\sigma_{m,b} = \dfrac{1.12 f_{md} \sin\theta \cos\theta}{K_1 (\lambda_h)^{-0.12} + K_2 (\lambda_h)^{-0.88}}$	3.13	Corner crushing
$\sigma_{m,c} = \dfrac{(1.2\sin\theta + 0.45\cos\theta) f_{v0} + 0.3\sigma_V}{w_m / d_m}$	1.57	Sliding of bed joints
$\sigma_{m,d} = \dfrac{0.6 f_{md} + 0.3\sigma_V}{w_m / d_m}$	1.63	Diagonal tensile failure

* σ_V is the vertical compressive stress in the masonry panel (equal to 0.63 MPa). The tensile strength of the masonry was evaluated from tests conducted for this purpose and $f_{md} = f_{mt}$ is equal to 0.29 MPa [1].

$$N_{\max} = t_m \cdot b_m \cdot \min\left(\sigma_{m,a}, \sigma_{m,b}, \sigma_{m,c}, \sigma_{m,d}\right) \tag{1}$$

The values in the middle column of Table 2 indicate that the critical failure mechanism is sliding along the bed joints. However, the actual tests revealed that the CM walls failed due to diagonal tensile cracking. Since the difference in prediction for both failure modes is only 0.06 MPa, the discrepancy is not crucial for the model of Decanini et al. [10]. The maximum resistance of the strut based on Eq. (1) is 286 kN. The remaining characteristic values of the strut model are shown in Table 3.

Table 3: Characteristic points of the ESM model according to the model of Decanini et al. [10]

Limit state	**Strut displacement *d* [mm]**	**Wall drift *Φ* [%]**	**Strut force *N* [kN]**
Crack	0.23	0.02	228.8
Max. resistance	1.54	0.14	286.0
Residual	26.56	2.47	100.1
Ultimate	29.06	2.70	100.1

Proceedings of the 3rd Croatian Conference on Earthquake Engineering - 3CroCEE
19–22 March 2025, Split, Croatia
Copyright © 2025 CroCEE
DOI: https://doi.org/10.5592/CO/3CroCEE.2025.95

3.1.3. Model by Liberatore et al. [11]

The ESM model proposed by Liberatore et al. [11] is based on the statistical analysis of 162 experimental results and consists of four linear segments with four characteristic points, as shown in Fig. 6. Unlike earlier ESM models, it provides explicit values for the displacements corresponding to these points, rather than deriving them through equations describing mechanical behaviour. This allows the model to scale these points according to the material properties of the masonry.

The strut properties are calculated by determining the reference strength $N_{max,ref}$ following the procedure outlined in Section 3.1.2. For the analysed walls, this value is 286.0 kN. The remaining characteristic points of the constitutive law are calculated using regression coefficients provided in [11]. As an example, it is shown only the calculation of the maximum resistance, which requires only a modification for vertical holes and it is modified with the parameter 0.98 [11]:

$$N_{max} = 0.98 \cdot N_{max,ref} \tag{2}$$

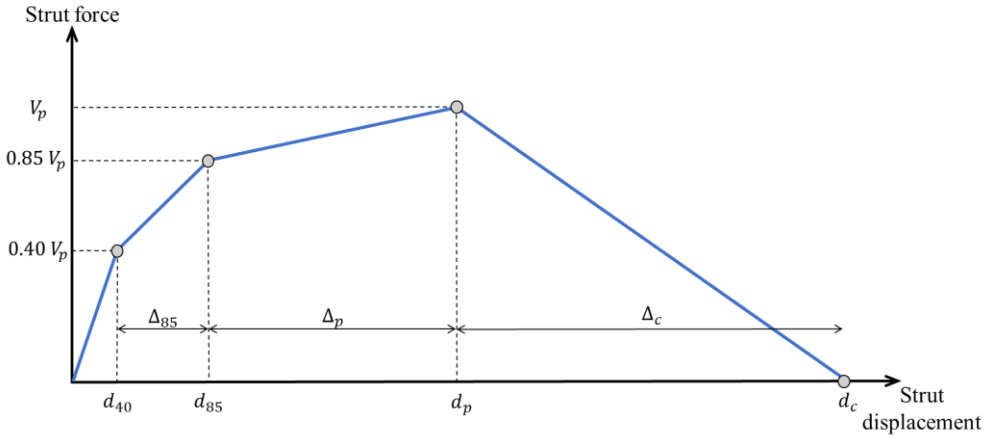


Figure 6: Constitutive model of the strut [11].

The characteristic points of the strut model by Liberatore et al. [11] for CM walls are given in Table 4.

Table 4: Characteristic points of the ESM model according to the model of Liberatore et al. [11]

Limit state	**Strut displacement *d* [mm]**	**Wall drift *Φ* [%]**	**Strut force *N* [kN]**
Crack	0.25	0.02	112.1
Max. resistance	2.31	0.21	238.2
Residual	5.45	0.51	280.3
Ultimate	35.97	3.34	0

3.1.4. Comparison of the ESM models

The constitutive material models of the ESMs are shown in Fig. 7. While good agreement is shown in terms of maximum resistance, significant differences are observed in other aspects. The largest differences appear in the degradation part of the curves (the slope after reaching the maximum load capacity), where the model by Panagiotakos and Fardis stands out significantly. The models by Liberatore et al. and Decanini et al. show the most significant differences within the range between the initial cracking and the maximum load capacity state.

Copyright © 2025 CroCEE
DOI: https://doi.org/10.5592/CO/3CroCEE.2025.95

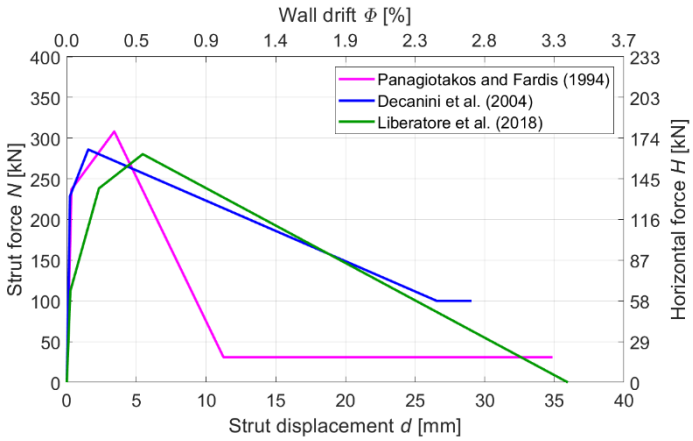


Figure 7: Comparison of the strut force–strut displacement (horizontal force–wall drift) curves for ESMs proposed by various authors.

3.1.5. Numerical model and validation

The numerical model of the CM wall was built in the OpenSees software package [3]. In the ESM model, the RC ties (tie-columns and bond beam) are represented as RC frame elements, while the masonry wall is modelled using pin-joined diagonal strut element (Fig. 8a). The strut element in the model shown in Fig. 8a has a nonlinear relationship between wall resistance (axial force) and (axial) displacement. The vertical load on the vertical RC tie-elements was determined based on the stiffness ratio between the masonry panel and the vertical ties (in the model, vertical force acts only on the ties) and was set to 150 kN per tie-column. After applying the vertical force, the wall was loaded with a monotonically prescribed horizontal displacement in the upper left corner (Fig. 8a) up to the same drift as in the experiment. The P-Delta effects were included in the static nonlinear analysis.

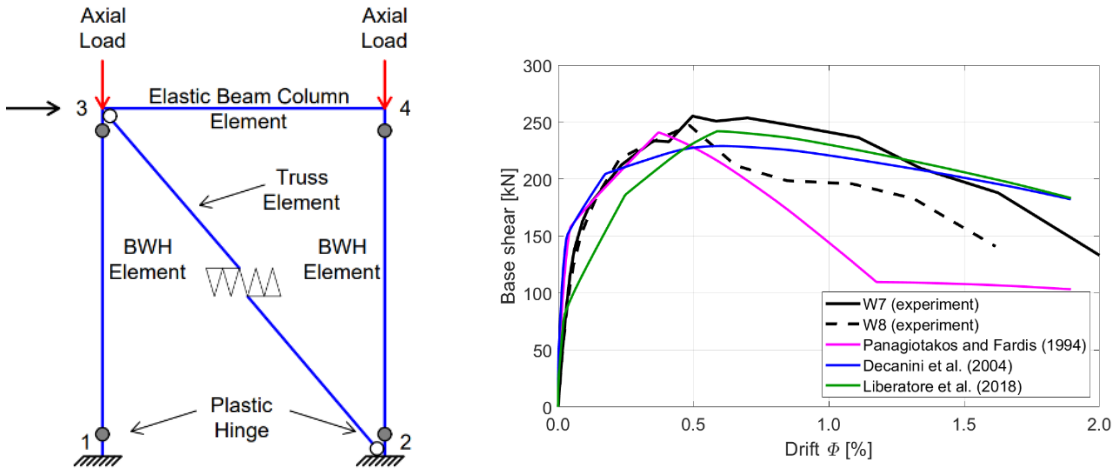
The tie-columns were fixed at the base, and modelled using the "*Beam With Hinges*" (BWH) *element*, which assumes that plastic hinges can only form at the ends of the elements. The length of the plastic zone (plastic hinge length) was calculated according to the recommendations in Eurocode 8-3 [12]:

$$L_{pl} = \frac{L_v}{30} + 0.2h + 0.11\frac{d_{bL} f_y}{\sqrt{f_c}} = 23.6 \text{ cm} \tag{3}$$

where L_v is the shear span (assuming a contra-flexure point at the mid-height of tie-column), h is the depth of the cross-section, f_c is the concrete compressive strength, and f_y and d_{bL} are the yield strength and the diameter of longitudinal bars, respectively.

Since no damage was observed in the bond beam and because the displacement of the bond beam was prevented by the masonry at the bottom and by the steel support at the top, the bond beam was modelled as an elastic element (*Elastic Beam Column Element* in [3]).

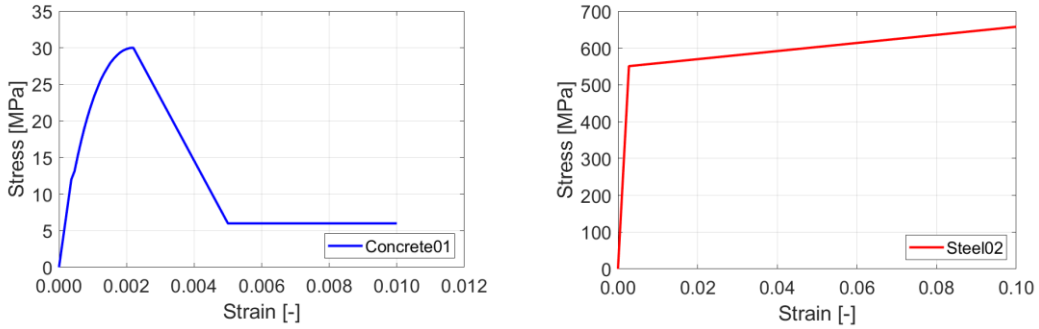
Copyright © 2025 CroCEE
DOI: https://doi.org/10.5592/CO/3CroCEE.2025.95



a) b)

Figure 8: a) Schematic representation of the 2D ESM for considered CM wall; b) Comparison of numerical simulations with experimental results.

The cross-section of the tie-columns was modelled using a fibre section with special fibres for the longitudinal bars. Given that the stirrups were Ø8 spaced at approximately 20 cm, the effect of confinement was negligible, and the entire section was treated as unconfined. For concrete, the material model Concrete01 [3] without tensile strength was used, as presented in Fig. 9a. The steel bars were modelled using the Steel02 model with a hardening ratio of 0.55 % (Fig. 9b). The nonlinear behaviour of the equivalent single strut in the form of strut force-strut displacement was modelled using the *Pinching4* model, which allows the definition of the multi-linear curve with four points.



a) b)

Figure 9: Uniaxial material response: a) concrete and b) steel.

The comparison between numerical simulations and the experimental envelope curves is shown in Fig. 8b. The numerical (magenta) curve represents the model of Panagiotakos and Fardis model [9], which slightly overestimates the initial stiffness compared to the experiment (solid and dashed black lines) but accurately predicts the maximum load capacity of the CM wall. However, it underestimates the drift at peak load capacity by 25 % and predicts faster degradation than observed experimentally.

The blue curve, based on Decanini et al. model [10], slightly overestimates the stiffness and underestimates the maximum load capacity by 10 %, as seen in Fig. 8b. It should be noted that the numerical curve aligns well with the experimental response in terms of stiffness degradation.

The prediction of the Liberatore et al. model [11] is shown in Fig. 8b with the green curve. While the model accurately predicts the maximum load and load degradation, the model poorly captures the

Copyright © 2025 CroCEE
DOI: https://doi.org/10.5592/CO/3CroCEE.2025.95

behaviour from the initial crack to the peak load stage. The model predicts the maximum load capacity at 0.58 % drift, while in the experiment it was achieved at 0.5 %.

Overall, the Decanini et al. model [10] provides the closest match and was selected as the most suitable for numerically modelling the seismic response of a three-storey masonry building.

3.3. Numerical model of a three-storey masonry building and results

Since the building's response was primarily translational, the numerical model of a three-storey masonry building was simplified by modelling only one shear wall and half of the cross walls (see Fig. 2a). The tie-columns from the cross walls incorporated into the RC ties at the extreme left and right edges of the considered shear wall. As only half of the building was modelled, the calculated load capacity was doubled to account for the entire structure.

The 2D numerical model of the building, shown in Fig. 10, was developed similarly to the CM wall model (see Fig. 8a). The masonry wall was represented using equivalent struts with a nonlinear response. It was observed during the experiment that the failure of the edge piers (confined on only one side) occurred at a drift of 0.5 %, and this was also incorporated into the numerical model. The vertical RC tie-elements were modelled as line elements with plastic hinges. Since minor cracks were observed during the test in the horizontal RC ties above the openings, the tie-beams were modelled using elements with plastic hinges in these regions. The parts of the horizontal RC ties above the piers were modelled using “rigid” elements (see Fig. 10).

The vertical load was applied to the numerical model first, followed by the application of the horizontal load, in accordance with the experimental setup. The load was distributed in a triangular pattern along the building height, and, as in the experiment, the displacement was applied at the first-floor level.

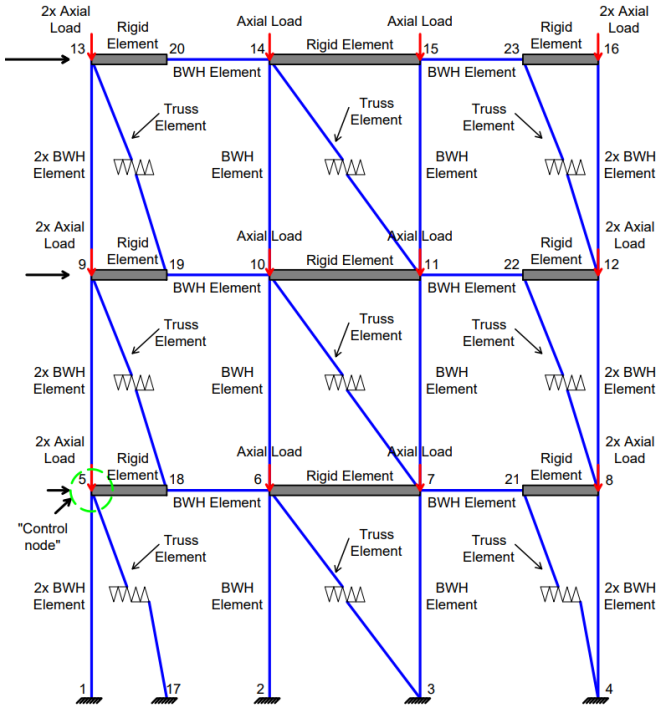


Figure 10: Numerical model of the three-storey CM building.

Fig. 11 presents a comparison between the numerical simulation and the experimentally obtained envelope curves for both directions in terms of a pushover curve. The simulation slightly overestimates the initial stiffness and reaches the maximum load at a drift of 0.37 %, whereas the drift reached during the experiment was 0.44 % (pushing) and 0.41 % (pulling). The peak capacity predicted by the model

Copyright © 2025 CroCEE
DOI: https://doi.org/10.5592/CO/3CroCEE.2025.95

was nearly aligned with the experimental load capacity, with a minor underestimation of 3 % in the pushing direction and 10 % in the pulling direction.

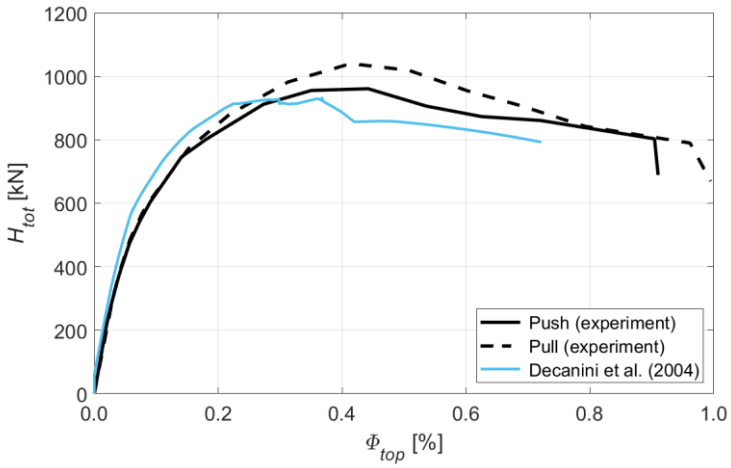
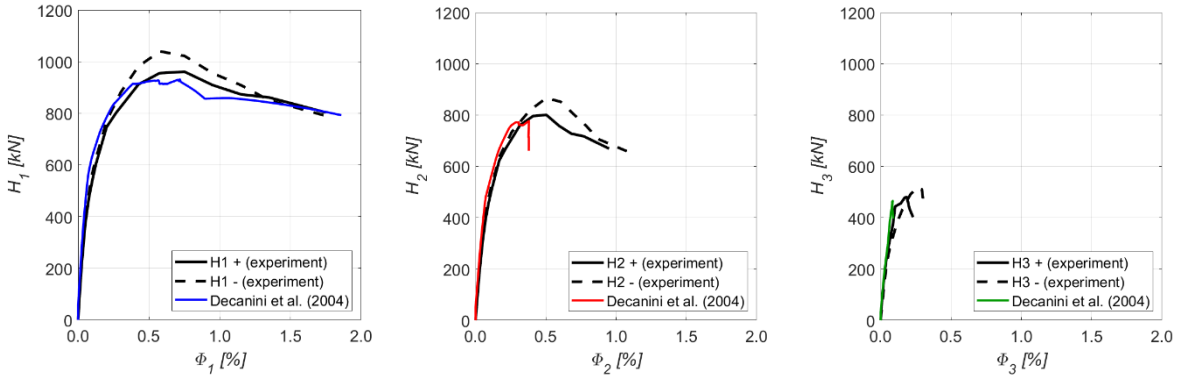


Figure 11: Comparison of the numerical simulation and the experimental response of the three-storey building.

The comparison of the building responses for each individual floor is shown in Fig. 12. The response of the ground floor in Fig. 12a shows a very good match between the simulation and the experiment, indicating that damage concentration and eventual failure occur in the ground floor. However, the response in the upper floors (Fig. 12b and Fig. 12c) shows a significant deviation from the experimental results. The issue with the model is that the upper floors are relieved when damage occurs in the ground floor.



a) b) c)

Figure 12: Comparison of the numerical simulation and experimental envelope curves along the floors.

4. Conclusions

The equivalent diagonal strut models, using different constitutive laws for the struts, were analysed to determine the most suitable approach for modelling CM built from the new type of masonry and PU glue. The experimental envelope curves for both walls (average response) obtained from shear-compression tests were compared with the numerical results from the ESM models using constitutive laws (for strut) proposed by Panagiotakos and Fardis [9], Decanini et al. [10], and Liberatore et al. [11]. The results showed that the Decanini et al. model provided the best match with the experimental response, with an error in initial stiffness of 10 %, the peak load capacity underestimated by 8.8 %, and the drift at peak load capacity by only 0.1 %. Therefore, this model was used in the next phase to

Copyright © 2025 CroCEE
DOI: https://doi.org/10.5592/CO/3CroCEE.2025.95

simulate the seismic response of the three-storey CM building, for which the actual experimental response was also known.

The response of the three-storey building model was generally well-aligned with the experiment. The pushover curve for the entire building and the ground floor was excellently captured, with the peak load capacity being underestimated for the entire building by only 3 % for pushing and 10 % for pulling. However, the seismic response of the first and second floors was somewhat less accurate. Future work will focus on refining the numerical model to better capture the damage distribution across the floors.

Acknowledgements

The research was sponsored by the Slovenian Research and Innovation Agency (programme P2-0185).

References

[1] Gams, M., Triller, P., Jäger, A. (2023): In-plane seismic behaviour of URM and confined masonry built from vertically perforated blocks and polyurethane glue, *Structures*, **58**, 105528, doi: 10.1016/j.istruc.2023.105528

[2] Gams, M., Triller, P., Tomaževič, M., Jäger, A. (2024): Test of three-storey confined masonry structure built from clay blocks and PU glue, *Journal of Building Engineering*, **91**, 109696, doi: 10.1016/j.jobe.2024.109696

[3] McKenna, F., Fenves, G. L., Scott, M. H., & Jeremic, B. (2000): Open system for earthquake engineering simulation (OpenSees). Pacific Earthquake Engineering Research Center, University of California, Berkeley, CA, USA.

[4] EN 1998-1 (2004): Eurocode 8: Design of structures for earthquake resistance – Part 1: General rules, seismic actions and rules for buildings, European Committee for Standardization.

[5] Tomaževič, M. (1999): *Earthquake-Resistant Design of Masonry Buildings*, Imperial College Press, 1st edition, London, U.K.

[6] EN 1996-1-1 (2005): Eurocode 6: Design of masonry structures – Part 1-1: General rules for reinforced and unreinforced masonry structures, European Committee for Standardization.

[7] Tarque, N., Candido, L., Camata, G., Spacone, E. (2015): Masonry infilled frame structures: State-of-the-art review of numerical modelling, *Earthquakes and Structures*, **8** (1), 225–251, doi: 10.12989/eas.2015.8.3.733

[8] Lang, A.F., Crisafulli, F.J., Torrisi, G.S. (2014): Overview and assessment of analysis techniques for confined masonry buildings, *10th National Conference in Earthquake Engineering*, Anchorage, Alaska, USA.

[9] Panagiotakos, T.B., Fardis, M.N. (1994): Proposed Nonlinear Strut Models for Infill Panels, 1st year Progress Report of HCM-PREC8 Project, University of Patras.

[10] Decanini, L., Mollaioli, F., Mura, A., Saragoni, R. (2004): Seismic performance of masonry infilled R/C frames, *13th World Conference on Earthquake Engineering 13WCEE*, Vancouver, B.C., Canada.

[11] Liberatore, L., Noto, F., Mollaioli, F., Franchin, P. (2018): In-plane response of masonry infill walls: Comprehensive experimentally-based equivalent strut model for deterministic and probabilistic analysis. *Engineering Structures*, **167**, 533-548, doi: https://doi.org/10.1016/j.engstruct.2018.04.057

[12] EN 1998-3 (2005): Eurocode 8: Design of structures for earthquake resistance – Part 3: Assessment and retrofitting of buildings, European Committee for Standardization.

Proceedings of the 3rd Croatian Conference on Earthquake Engineering - 3CroCEE
19–22 March 2025, Split, Croatia
Copyright © 2025 CroCEE
DOI: https://doi.org/10.5592/CO/3CroCEE.2025.96

IN-PLANE BEHAVIOUR OF RC FRAMES WITH TRADITIONAL AND DECOUPLED INFILLS: PARAMETRIC STUDY

Aleksa Milijaš [(1)], Marko Marinković [(2)], Christoph Butenweg [(3)], Sven Klinkel [(4)]

[(1)] *PhD Student, Chair of Structural Analysis and Dynamics, RWTH Aachen University, Aachen, Germany, e-mail address: milijas@lbb.rwth-aachen.de*
[(2)] *Assistant Professor, Chair of Engineering Mechanics and Theory of Structures, Faculty of Civil Engineering, University of Belgrade, Belgrade, Serbia, e-mail address: mmarinkovic@grf.bg.ac.rs*
[(3)] *Professor, Center of Wind and Earthquake Engineering, RWTH Aachen University, Aachen, Germany, e-mail address: butenweg@lbb.rwth-aachen.de*
[(4)] *Professor, Chair of Structural Analysis and Dynamics, RWTH Aachen University, Aachen, Germany, e-mail address: klinkel@lbb.rwth-aachen.de*

Abstract

Masonry infills are used as outer and inner partitions in reinforced concrete (RC) frame buildings. Although regarded as non-structural elements, masonry infills are activated under seismic actions. Because of this activation, masonry infills experience life-threatening damage. Moreover, they affect the seismic response of the whole RC frame structure, as they modify the dynamic characteristics of the structure. An innovative decoupling solution is developed to improve the seismic response of the infilled RC frames. In this paper, the in-plane behaviour of the RC frames with traditional and innovative decoupled infills is investigated by means of the simplified micro-model developed in Abaqus. Firstly, the numerical model is validated against the in-plane experimental tests on the RC frames, fully infilled with traditional and decoupled infill. Afterwards, a parametric study is carried out, focusing on the effect of the brick thickness and infill height-to-length ratio on the in-plane behaviour of the infilled RC frames. The level of the frame-infill interaction is evaluated through a comparison of the numerical results on the referent bare RC frame and RC frames with traditional and decoupled infills. The damage on masonry infills and surrounding RC frames, infill contribution forces and initial in-plane stiffness of the RC frames are observed. Additionally, a distribution of internal forces on the RC frames is evaluated in the post-processing of the results, which represents an important novelty of the study. Numerical results show that the decoupling system significantly reduces the activation of the decoupled infills, for all investigated infill geometries. Furthermore, the overall in-plane response of the RC frames with decoupled infills is very similar to the in-plane response of the bare RC frame up to 2.0 % of in-plane drift, which is certainly not the case for the traditionally infilled RC frames.

Keywords: Traditional infill, Decoupled infill, INODIS, brick thickness, height-to-length ratio

1. Introduction

Buildings composed of load-bearing reinforced concrete (RC) frames are widespread all over the world. In these buildings, after the erection of the RC frame elements, masonry walls are usually built as inner and outer partitions, with a stiff mortar connection to the surrounding RC frame. These walls are called masonry infills, and in seismic design, they are commonly regarded as non-structural elements. Therefore, while carrying out the design of the RC frame structures, the effect of masonry infills is taken only as an additional vertical line load on the RC load-bearing element. However, masonry infills interact with the surrounding RC frames under seismic loads. This plays an important role, as masonry infills can significantly affect the in-plane response of the RC frame structure considered in the design. This raises questions about the accuracy of the whole design of the RC frame structure and its safety. The severe damage to masonry infills and RC frames in recent earthquakes in Albania (2019) [1], Croatia (2020) [2], and Turkey (2023) [3], for instance, confirms that neglecting masonry infills in the design is far from conservative and can therefore have serious consequences for the economy of the affected regions and the safety of the inhabitants.

RC frames with masonry infills have been intensively investigated for decades. Most of the research work is focused on the in-plane behaviour of infilled RC frames. Some relevant experimental studies have been carried out by Dawe and Seah (1989) [4], Mehrabi et al. (1994) [5], Flanagan and Bennett

Proceedings of the 3rd Croatian Conference on Earthquake Engineering - 3CroCEE
19–22 March 2025, Split, Croatia
Copyright © 2025 CroCEE
DOI: https://doi.org/10.5592/CO/3CroCEE.2025.96

(1999a) [6], Stylianidis (2012) [7], Morandi et al. (2017a) [8], and Di Trapani et al. [9]. In these studies, it has been recognised that numerous parameters (frame-infill interface conditions, brick thickness, height-to-length ratio, openings) influence the in-plane response of the infilled RC frames. With the development of computers, the number of research studies that use numerical models to investigate the behaviour of infilled RC frames has largely increased. For instance, some authors [10,11] have developed complex micro-models that can genuinely replicate the behaviour of experimental specimens, while others [12,13] have developed less complicated but faster macro-models that can be applied for the studies of the infilled frames on the building level. Despite the significant amount of both experimental and numerical research, simple and efficient approaches to considering masonry infills in engineering codes are still absent.

Recently, a lot of the work by research teams has been dedicated to developing solutions that can improve the seismic performance of infilled RC frames. For instance, groups of authors propose strengthening masonry infills and thus increasing their load-bearing capacity, e.g., [14,15]. However, a major disadvantage of strengthening measures is that masonry infills become part of the load-bearing system, and they need to be carefully designed, along with the frames around them, which is already a problem. The second direction is to increase the ductility of masonry infills, for instance, by installing horizontal [16] or vertical sliding joints [17]. These solutions can efficiently improve the in-plane response of infilled RC frames. However, the shear demand on the columns can increase due to the sliding along the horizontal joints [18]. In addition to this, a significant disadvantage is the absence of vertical arching to carry the out-of-plane loads, which results in more complicated and rather expensive solutions for addressing out-of-plane loads. The third direction is to decouple masonry infills from the RC frame. This can be achieved by inserting soft material between the infill and the frame, as done in [19,20], for example. The idea of decoupling appears to be the most promising one, and it is already recommended in some codes [21,22]. However, providing out-of-plane stability to the infill can be challenging for decoupled infills.

In the present work, RC frames with traditional infills and decoupled infills are investigated. RC frames with decoupled infills are made with the innovative decoupling system INODIS. The efficiency of the system has already been proved in an extensive experimental campaign [23]. In this study, the in-plane behaviour of RC frames with decoupled infills and traditional infills is investigated numerically. A three-dimensional model developed by Marinković and Butenweg (2022) [24] is employed, calibrated, and validated against the results of the experimental tests [23,25]. Afterwards, the numerical model is used for the parametric study. The investigated parameters are brick thickness and height-to-length infill (frame) ratio. The in-plane behaviour of different RC frames with traditional and decoupled infills is compared with the in-plane behaviour of the referent bare RC frame. Based on the numerical results, conclusions regarding the level of frame-infill interaction of RC frames with traditional and decoupled infills are derived.

2. Experimental specimens

The basis for the numerical simulations carried out in this work is a large experimental campaign. The first part of the experimental campaign addresses the behaviour of RC frames with traditional infills [25] and the second part of the experimental campaign addresses the behaviour of RC frames with decoupled infills [23]. Detailed information on the construction of the experimental specimens, materials used and experimental results can be found in [23,25]. In this study, in-plane parts of the experimental tests on the RC frames fully infilled with traditional (test T2) and decoupled infill (test D2) are used for the calibration and validation of numerical model.

For the construction of both traditional and decoupled infills modern hollow clay bricks are used, with a thickness 30 cm. Bed joints are filled with the thin layer mortar, while head joints are made as dry joint connections, following the usual practice. Traditional infill is connected to the surrounding RC frame with the mortar. On the other side, between RC frame and decoupled infill, the decoupling system called INODIS is installed. It consists of three strips made of recyclable elastomeric material. The middle strip is glued to the RC frame elements, and the outer strips to the masonry infill. This

Copyright © 2025 CroCEE
DOI: https://doi.org/10.5592/CO/3CroCEE.2025.96

distribution of elastomeric strips is important for providing stable boundary conditions at the infill parameter against out-of-plane loads. The strips between columns and infill are softer and thicker, in order to absorb the frame deformation under in-plane drifts, while strips at the infill top and bottom are stiffer because of the out-of-plane load safety requirements. In addition to this, bottom surface of the middle elastomer at the top beam is covered with a sliding surface, as well as the top surfaces of the outer elastomers at the infill top. This significantly reduces the friction between frame and infill. More details about the decoupling system can be found in [23].

3. Numerical modelling

The three-dimensional numerical model developed in [24] is used for conducting numerical simulations. The numerical model consists of concrete elements (columns and beam), brick units, and elastomer strips (in case of the decoupled infill), which are modelled with three dimensional 8-node hexahedral continuum finite elements, with reduced integration (C3D8R), and reinforcement, which is modelled with truss elements (T3D2) elements that are embedded in the solid concrete elements. The stiff and strong bottom beam of the experimental frame is replaced by three discrete rigid plates in order to reduce the number of elements and calculation time. Two rigid plates are tied with the columns of the RC frame, and the middle one is tied with the masonry infill. In this way reaction forces of RC columns and masonry infill are separately measured, which presents a small difference to the original model described in [24].

Brick units are modelled as parts, while mortar in bed joints is not modelled with separate elements, but its effect is accounted for by defining a specific interaction that can simulate its response. This technique is called “simplified micro-modelling”. More information on the definition of interactions can be found in [24].

The concrete damage plasticity (CDP) model available in Abaqus [26] is used as a constitutive model for concrete and masonry. In this model, different stress-strain and stress-displacement relationships can be used to define the response of the material under compression and tension, respectively. In addition, the CDP model can define different damage characteristics in compression and tension. Material curves of the concrete and masonry with detailed explanations can be found in [24]. To define the stress-strain curve of reinforcement bars experimental data are used.

In decoupled infills, the hyperfoam material model available in Abaqus [26] is used to simulate the hyperelastic material of elastomers. This model allows using the stress-strain curves obtained from experimental tests on the softer and stiffer elastomer mixtures. The experimental curves used in the model can be found in [23]. Furthermore, to model the sliding surface a new interaction is defined, with a friction coefficient of 0.1.

It should be pointed out that brick units and mortar used in this study have different material characteristics than in [24]. Therefore, a number of parameters that are necessary to calibrate the material models and interaction properties had to be calibrated again. The validation of the numerical model against the experimental tests on RC frame with traditional (T2) and decoupled infill (D2) are presented in Section 4.

In addition to this, a novelty of this numerical study is a detailed post-processing of the results, which enables the extraction of internal forces (bending moments and shear forces) along columns of the RC frame. This is an important step in the analysis of the results, as there are fewer studies in the literature that investigate the internal forces on the RC frame with a simplified micro-model.

Copyright © 2025 CroCEE
DOI: https://doi.org/10.5592/CO/3CroCEE.2025.96

4. Numerical simulations of experimental tests

4.1. Validation of numerical model

Numerical simulations of experimental tests consist of three loading steps that simulate the loading conditions in the in-plane loading phases of experimental tests: gravity load, vertical loads on columns (200 kN per column) and in-plane displacements. In-plane displacements in the experimental tests have a form of the quasi-static cyclic loads, while in numerical simulations they are applied only in one direction (from left to the right) and increase monotonically up to the target value. Due to this, numerical force-drift curves are compared with the envelopes of the experimental force-drift curves. More detailed information on the loading conditions in the experimental tests can be found in [23,25], and in the numerical model in [24].

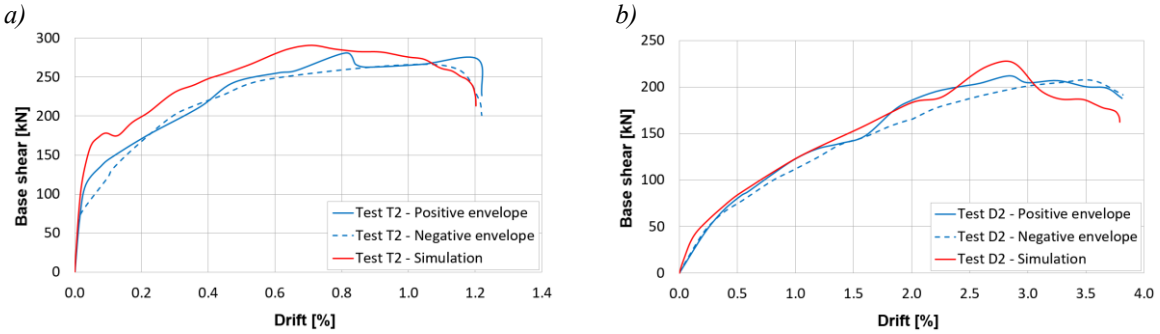


Figure 1. Comparison of numerical and experimental in-plane force-drift curves: a) Test T2 and b) Test D2

Firstly, the in-plane loading phase of a test on the traditionally fully infilled RC frame is simulated (Test T2). Figure 1a shows that the calibrated numerical model can quite accurately reproduce the in-plane response of an experimental specimen. Additionally, Figure 2a shows the major strain propagation on the experimentally tested traditional infill, whereas Figure 2b shows the tensile damage propagation in numerical simulation, at 1.2 % of in-plane drift. It can be seen that the cracking pattern in the numerical simulation corresponds to the one observed in the experimental test.

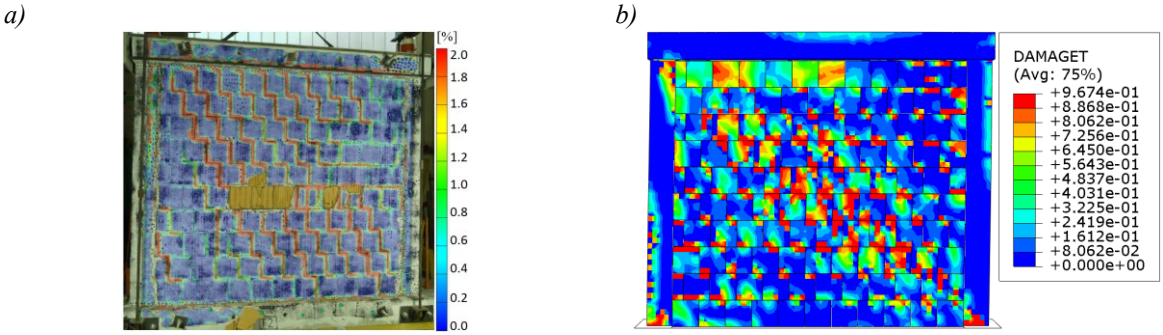


Figure 2. a) Major strain propagation on masonry infill in test T2 at 1.2 % of in-plane drift [25]; b) Tensile damage propagation in numerical simulation of test T2 at 1.2 % of in-plane drift

In-plane loading phases of the experimental test on the RC frame with a decoupled infill (Test D2) are simulated too. A good match between experimental and numerical force-drift curves can be seen in Figure 1b. Furthermore, Figures 3a and 3b show that the numerical model can quite well predict the crack propagation on decoupled masonry infill too. It can be observed that at 2.0 % of in-plane drift only stepwise cracks are visible on decoupled masonry infill, both in test D2 and its numerical simulation.

Copyright © 2025 CroCEE
DOI: https://doi.org/10.5592/CO/3CroCEE.2025.96

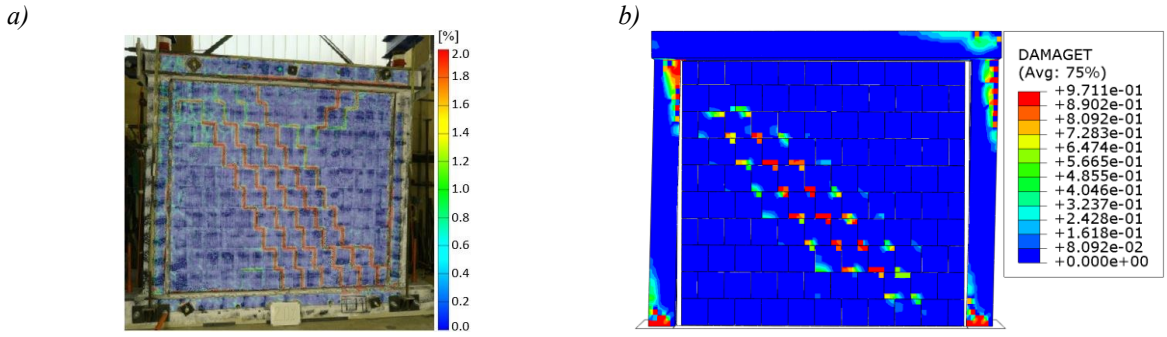


Figure 3. a) Major strain propagation on masonry infill in test T2 at 2.0 % of in-plane drift [23]; b) Tensile damage propagation in numerical simulation of test T2 at 2.0 % of in-plane drift

4.2. Comparison of in-plane behaviour of RC frame with solid traditional and decoupled infill

In this section, frame-infill interaction effects are further investigated by comparing numerical force-drift curves of infilled RC frames and a bare frame and numerical force-drift curves of masonry infill contribution of traditional and decoupled infill (Fig. 4). Because of the decoupling system, the initial stiffness of the RC frame infilled with the decoupled infill (D-TOTAL) remains unchanged in comparison to the initial stiffness of the bare RC frame (BF-TOTAL). On the other side, the initial stiffness of the traditionally infilled RC frame (T-TOTAL) is significantly higher because of the infill activation at in-plane drifts lower than 0.1 %. The activated traditional infill contributes significantly to the stiffness and total horizontal force up to around 0.8 % of in-plane drift. At this point, the maximum in-plane force is reached by traditional infill, and its contribution starts to decline. Because of the delayed activation of the decoupled infill, a more significant discrepancy between the force-drift curve of the RC frame infilled with decoupled infill and bare RC frame can be noticed only after 2.0 % of in-plane drift when the first cracks appear on masonry infill. The contribution of decoupled masonry infill to the total stiffness and force up to this point is rather small. Furthermore, Figure 5a shows that the traditional infill suffers significant damage already at around 0.7 % of in-plane drift. The decoupled infill gets activated at around 2.0 % of in-plane drift and experiences significant damage at around 3.0 % of in-plane drift (Fig. 5b).

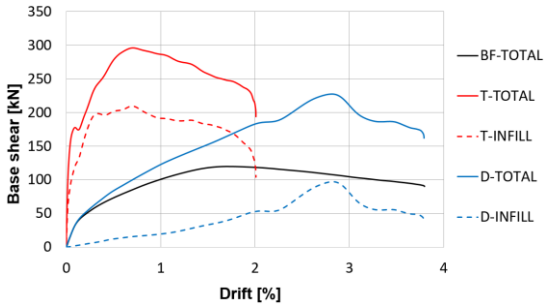


Figure 4. Force-drift curves of bare RC frame, infilled RC frames and masonry infills

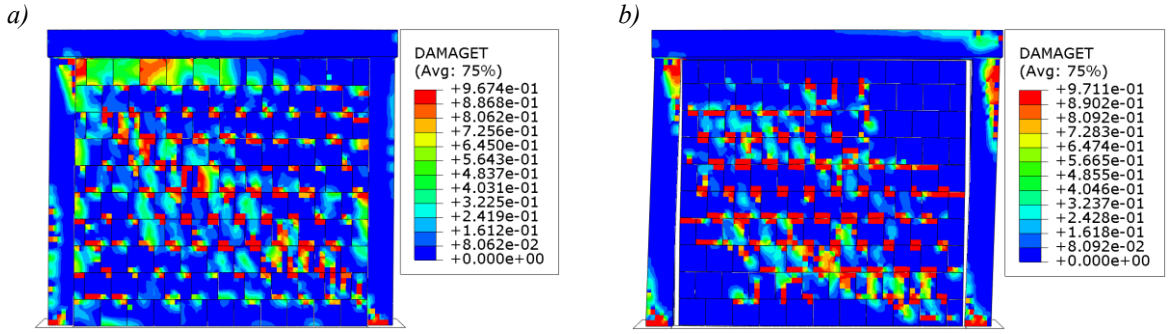


Figure 5. Significant damage on a) traditional infill (Δ = 0.7 %) and b) decoupled infill (Δ = 3.0 %)

Copyright © 2025 CroCEE
DOI: https://doi.org/10.5592/CO/3CroCEE.2025.96

In the post-processing of numerical results internal forces on the bare RC frame (BF), RC frame with traditional infill (T) and RC frame with decoupled infill (D) are determined. For instance, distribution of bending moments on the left column is compared between bare RC frame and traditionally infilled RC frame in Figure 6a and between bare RC frame and RC frame with decoupled infill in Figure 6b. Interaction between RC frame and traditional infill significantly affects the bending moment propagation on the left column, starting already at 0.1 % of in-plane drift. Opposite to this, there is almost no difference in bending moments of the bare RC frame and RC frame with decoupled infill. The effect of infill activation can only be seen at 2.0 % of in-plane drift. The result of the strong frame-infill activation in the case of traditional infill can be observed in Figure 5a too. Because of the increased bending moments, left column experiences cracking up to half of its height. On the other side, damage propagation on the RC frame with decoupled infill corresponds to the common damage propagation of bare RC frames, concentrated in the column corners (Fig. 5b).

The numerical results are compared in the similar way for the distribution of shear forces in Figure 7a. An early activation of traditional masonry infill imposes high shear forces on the top left corner of the RC frame. For instance, at 0.1 % of in-plane drift, shear force in the top left corner of the traditionally infilled RC frame is around 2.76 times larger than the shear force in the bare RC frame. At 0.5 % and 1.0 % of in-plane drift, this ratio is equal to 2.39. At 1.5 % and 2.0 % of in-plane drift it drops to 2.17 and 1.84, respectively, due to the damage to the infill. On the other side, the decoupling system reduces the local effects in the top left corner of the RC frame, in comparison to the traditionally infilled RC frame. More significant increase of the shear forces in the top left corner can be noticed at around 1.5 % and 2.0 % of in-plane drift. For instance, at 1.5 % and 2.0 % of in-plane drift shear force on the RC frame with decoupled infill is around 1.45 and 1.76 larger than the shear force on the bare RC frame, respectively (Fig. 7b).

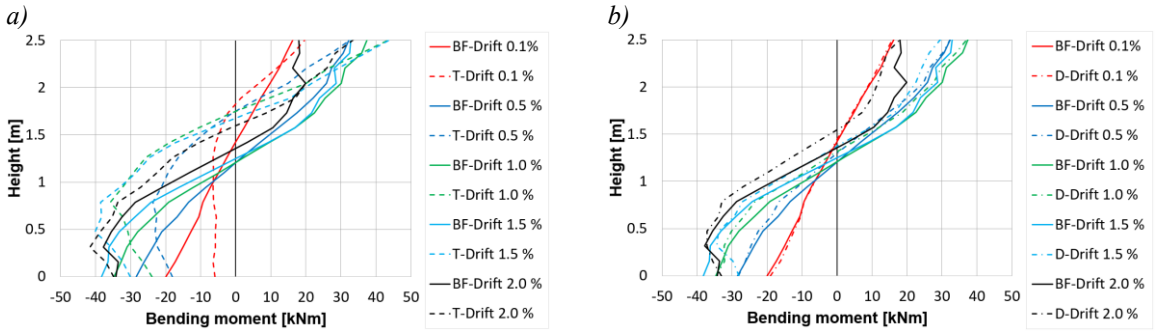


Figure 6. a) Bending moments on the left column of the bare frame and RC frame with traditional infill and (b) bare frame and RC frame with decoupled infill

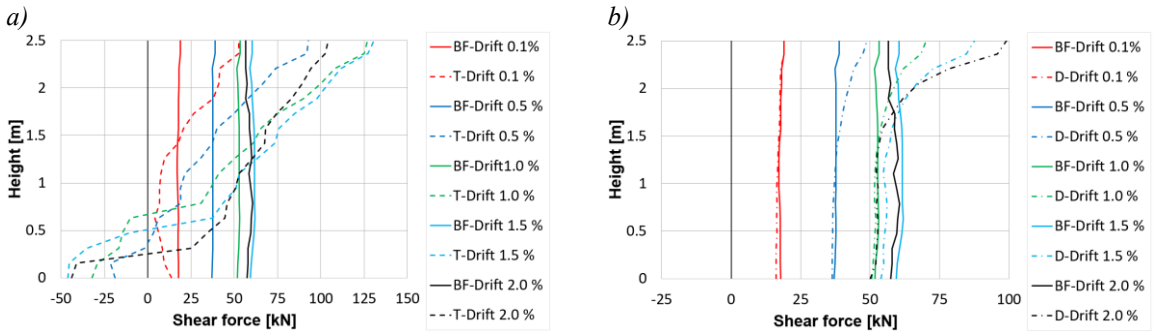


Figure 7. a) Bending moments on the left column of the bare frame and RC frame with traditional infill and (b) bare frame and RC frame with decoupled infill

Proceedings of the 3rd Croatian Conference on Earthquake Engineering - 3CroCEE
19–22 March 2025, Split, Croatia
Copyright © 2025 CroCEE
DOI: https://doi.org/10.5592/CO/3CroCEE.2025.96

5. Parametric study

In the parametric study, parameters that represent infill geometry are varied, such as brick thickness and infill (frame) height-to-length ratio. The level of frame-infill interaction is evaluated through the comparison of force-drift curves of infilled frames and masonry infills, initial in-plane stiffness, ratio of the horizontal force of the infilled frame to the horizontal force of the bare RC frame (H_{IF}/H_{BF}), ratio of the horizontal force of decoupled masonry infill to the horizontal force of the bare RC frame (H_{INF}/H_{BF}), and ratio of the shear force in the top left corner of the infilled frame to the bare RC frame ($V_{TL,IF}/V_{TL,BF}$).

5.1. Brick thickness

The effect of brick thickness of 10 cm, 20 cm, 30 cm and 36.5 cm is investigated. The results of the RC frame with 30 cm thick masonry infill are presented in Section 4 in detail. In Figure 8 and Table 1 it can be seen that all traditional infills (T) significantly affect the in-plane response of the RC frame. The force-drift curves of traditionally infilled RC frames have high initial stiffness, and the maximum horizontal forces are reached at around 0.6 – 0.9 % of in-plane drift, depending on the brick thickness (Fig. 8a). Due to the damage to traditional infills, the horizontal forces of infilled RC frames start to drop. Force-drift curves of traditional infills also point that traditional infills strongly contribute to the total horizontal force up to around 0.8 % of in-plane drift. Expectedly, larger brick thickness leads to a higher infill contribution (Fig. 8b). The force-drift curves of RC frames with decoupled infills (D) are very similar to the force-drift curves of the bare RC frame. For instance, up to 1.0 % of in-plane drift, almost no difference can be seen between the curves of the RC frames with decoupled infills and bare RC frame. For in-plane drifts between 1.0 % and 2.0 % horizontal forces of the RC frames with decoupled infills slowly start to increase (Fig. 8a). However, the first stepwise cracks in all investigated decoupled infills appear at around 2.0 % of in-plane drift. This is followed by a more noticeable increase of the horizontal force, which is more pronounced for the infills with a brick thickness of 30 cm (T30-D) and 36.5 cm (T36.5-D) and less for infills with a thickness of 20 cm (T20-D) and 10 cm (T10-D) (Fig. 8b).

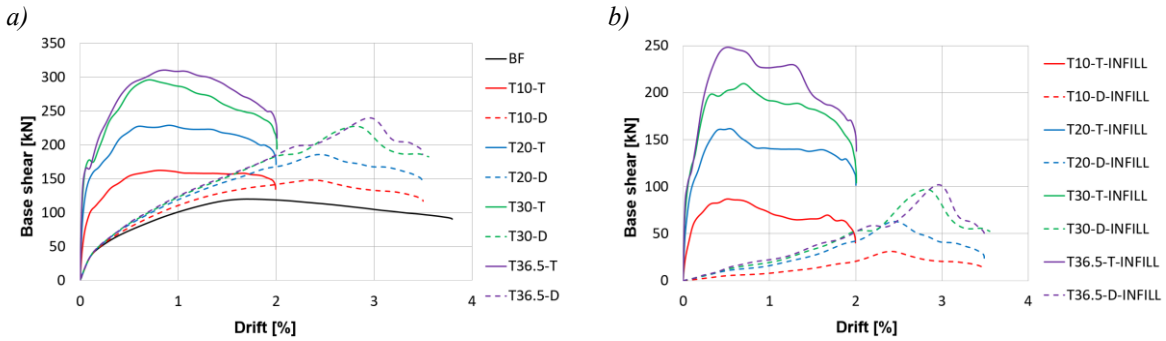


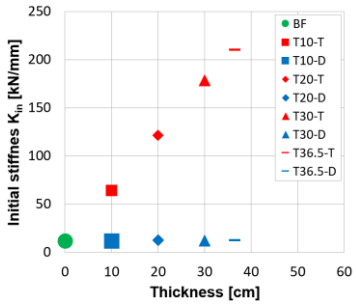
Figure 8. a) Force-drift curves of infilled RC frames; b) Force-drift curves of masonry infills with different brick thicknesses

For a direct comparison, the results of numerical simulations are summarised in Table 1. It can be seen that there is no difference between the initial stiffness of the bare RC frame and RC frame with decoupled infills, for all investigated thicknesses. On the other side, the initial stiffnesses of the traditionally infilled RC frames are around 5, 10, 15 and 17 times higher than the initial stiffness of the bare RC frame for the infill thicknesses of 10 cm, 20 cm, 30 cm and 36.5 cm, respectively. Furthermore, it can be seen that the H_{IF}/H_{BF} ratio for traditional infills takes the highest values at already 0.1 % of in-plane drift. For instance, at 0.1 % of in-plane drift horizontal force of the traditionally infilled RC frame (H_{IF}) is around 2.9, 4.4, 5.1 and 4.8 times larger than the horizontal force of the bare RC frame (H_{BF}), for infill thickness of 10 cm, 20 cm, 30 cm and 36.5 cm respectively. With an increase of in-plane drift, this ratio decreases because of the propagating damage to the masonry infill and surrounding RC frame. On the other side, at 0.1 % of in-plane drift, the H_{IF}/H_{BF} ratio is equal to 1.0 for decoupled infills with

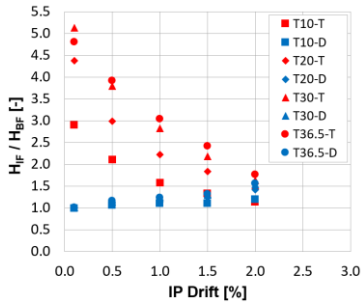
Copyright © 2025 CroCEE
DOI: https://doi.org/10.5592/CO/3CroCEE.2025.96

all thicknesses. Because of the decoupling system, the H_{IF}/H_{BF} slowly increases with an increase of the in-plane drift. For instance, for the infills with thicknesses of 30 cm and 36.5 cm, it is around 1.6 and 1.7 at 2.0 % of in-plane drift, whereas for thinner infills, it is even smaller (1.1 and 1.4 for 10 cm and 20 cm thick decoupled infill, respectively). In Table 1 the H_{INF}/H_{BF} is presented only for decoupled infills. At 0.1 % of in-plane drift, the horizontal forces of decoupled infill are less than 2 % of the horizontal force taken by the horizontal force of the bare RC frame. The diagram shows that the H_{INF}/H_{BF} ratio increases for higher in-plane drifts, but at 1.5 % of in-plane drift it is still less than 0.3 for all configurations. At 2.0 % of in-plane drift, the H_{INF}/H_{BF} ratio is equal to 0.44 for decoupled infills with thicknesses of 30 cm and 36.5 cm. For decoupled infills with thicknesses of 20 cm and 10 cm it is around 0.35 and 0.17, respectively. The negative effects of the traditional infills on the frame behaviour can also be seen in Table 1. The $V_{TL,IF}/V_{TL,BF}$ ratio is around 3 for the 36.5 cm thick traditional infill, up to 1.0 % of in-plane drift, and at 1.5 % and 2.0 % of in-plane drift, it takes the values of around 2. The 30 cm and 20 cm thick traditional infills also impose shear forces on the top left corner of the left column of the RC frame that are around 2-3 times larger than the shear forces of the bare RC frame, up to 2.0 % of in-plane drift. Even the $V_{TL,IF}/V_{TL,BF}$ ratio for infill with a 10 cm thickness is larger than 2.0 for in-plane drifts of 0.5 % and 1.0 %, and between 1.5 and 2.0, for in-plane drifts between 1.0 % and 2.0 %. These results indicate that traditional infills impose shear forces that are much higher than the shear forces that act on the RC frame without traditional infills, which can lead to additional damage to the RC frame column. If the decoupling system is installed, the $V_{TL,IF}/V_{TL,BF}$ ratio is equal to 1.0 for all infill thicknesses at 0.1 % of in-plane drift, and it remains smaller than 1.5 for all infill thicknesses up to 1.5 % of in-plane drift, with a rather small differences in the $V_{TL,IF}/V_{TL,BF}$ ratios for different thicknesses. Only at 2.0 % of in-plane drift, the $V_{TL,IF}/V_{TL,BF}$ ratio is around 1.75 for 30 cm and 36.5 cm thick decoupled infills, 1.6 for the 20 cm thick decoupled infill, and 1.3 for 10 cm thick decoupled infill.

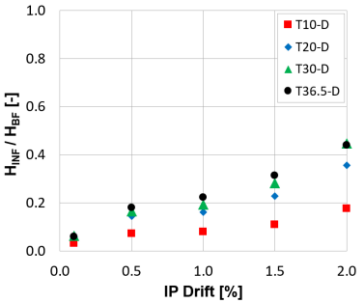
Table 1. Summary of results on RC frames with traditional and decoupled infills with different brick thicknesses



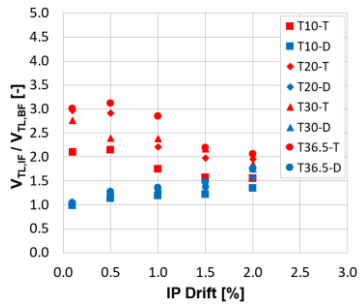
Initial stiffnesses



H_{IF}/H_{BF} ratio in function of in-plane drift



H_{INF}/H_{BF} ratio in function of in-plane drift



$V_{TL,IF}/V_{TL,BF}$ ratio in function of in-plane drift

Copyright © 2025 CroCEE
DOI: https://doi.org/10.5592/CO/3CroCEE.2025.96

5.2. Height-to-length ratio

In addition, the influence of the height-to-length ratio is investigated by varying the infill length. Other parameters are kept the same, and the considered brick thickness is 30cm. Three infill lengths are considered: 1.5 m (short infill-S), 2.77 m (infill that is also investigated experimentally) and 4.5 m (long infill-L). The results of the RC frame with 2.77 m long masonry infill are presented in Section 4 in detail. Bare RC frames with different opening lengths are also investigated: BF-S ("short" bare frame), BF (experimentally tested bare frame with 2.77 m long opening) and BF-L ("long" bare frame). Force-drift curves in Figure 9a show that all investigated bare RC frames (BF) have an almost identical in-plane response. The in-plane response of all traditionally infilled RC frames (T) is recognisable by the high initial stiffness. However, it can be seen that the RC frame with the short traditional infill (T_Short) reaches a significantly smaller maximum horizontal force than the other two traditionally infilled RC frames. Furthermore, RC frames with a 2.77 m long traditional masonry infill and a 4.5 m long traditional masonry infill reach the maximum horizontal forces at around 0.7 % and 1.1 % of in-plane drift, respectively, and the RC frame with a 1.5 m long traditional masonry infill at around 1.5 % of in-plane drift. However, the horizontal force of the RC frame with a 1.5 m long traditional masonry infill is almost constant at in-plane drifts larger than 1.0 %. Force-drift curves of traditional infills show that the longer the infill, the higher its contribution to the total horizontal force (Fig. 9b). Additionally, the traditional infill force-drift curves also indicate that the short infill can experience a more drastic loss of the force capacity because of the high compressive stresses developed in the infill that lead to the severe damage. Force-drift curves of RC frames with decoupled infills indicate that the in-plane response of the RC frames with decoupled infills with different lengths (D) is similar to the in-plane response of corresponding bare RC frames (Fig. 9a). Up to 1.0 % of in-plane drift, there is no significant discrepancy between the curves of the RC frames with decoupled infills and corresponding bare RC frames. Between 1.0 % and 2.0 % of in-plane drift, a rather slow increase in the horizontal force can be seen for RC frames with two longer infills, while the horizontal force of the RC frame with a short decoupled infill is dominantly constant after around 1.3 % of in-plane drift. This is because the short decoupled infill is activated sooner, at around 1.3 % of in-plane drift, which can be observed by the jump of the horizontal force of decoupled infill in Fig. 9b. The first stepwise cracks appear later on other two decoupled infills, at around 2.0 % of in-plane drift, when the more pronounced increase in the horizontal force on both decoupled infill and infilled RC frame can be observed (Fig. 9a,b).

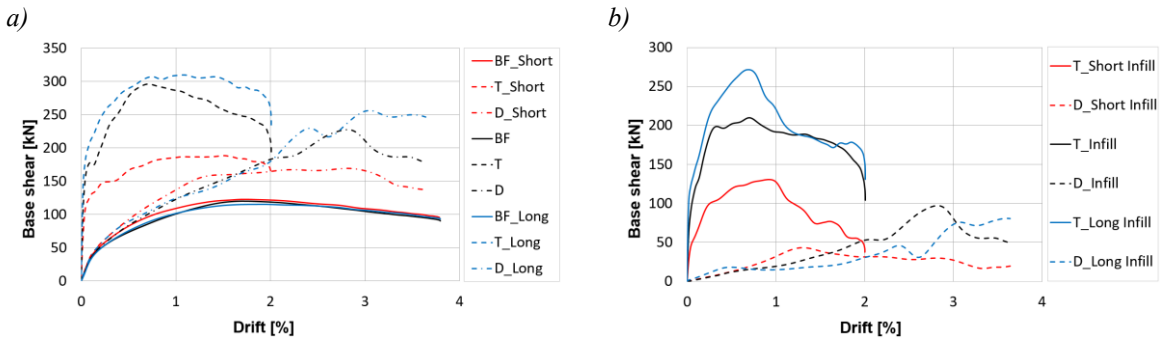


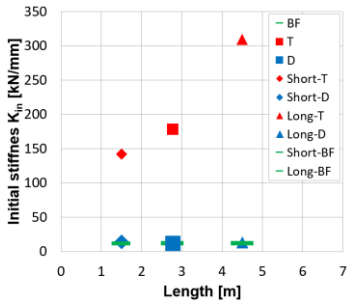
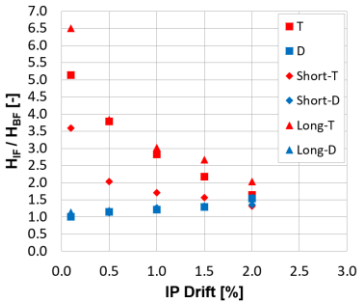
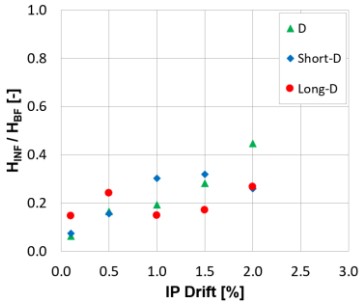
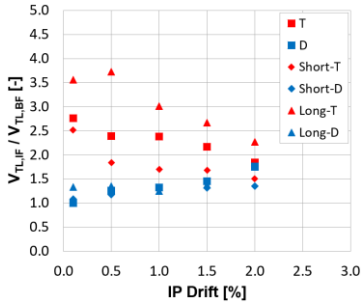
Figure 9. a) Force-drift curves of infilled RC frames; b) Force-drift curves of masonry infills with different height-to-length ratios

Table 1 summarises the results of the numerical simulations on bare RC frames infilled RC frames with different height-to-length ratios (H/L). Firstly, it can be seen that the change of the infill (and frame) length has no influence on the initial stiffness of bare RC frames, as well as on the initial stiffness of the RC frames with decoupled infills. In the case of traditional infills, the initial stiffness of the short-infilled RC frame is around 12, and of the long-infilled RC frame, 26 times larger than the initial stiffness of corresponding bare RC frames. Furthermore, the H_{IF}/H_{BF} ratio for RC frames with traditional and decoupled infills with different infill lengths is presented. At 0.1 % of in-plane H_{IF}/H_{BF} is around 6.5, 5.1 and 3.6 for long infill, almost square infill, and short infill, respectively. At 0.5 % of in-plane drift, this ratio drops to around 2 for the short infill and to around 3.8 for the other two cases. With

Copyright © 2025 CroCEE
DOI: https://doi.org/10.5592/CO/3CroCEE.2025.96

further damage to traditional infills, the H_{IF}/H_{BF} ratio further reduces. The opposite can be seen in the case of the RC frames infilled with decoupled infills. At 0.1 % of in-plane drift, there is no difference in the horizontal forces of the infilled and bare RC frames. At larger in-plane drifts, the H_{IF}/H_{BF} ratio increases slowly, taking similar values for different infill lengths. At 2.0 % of in-plane drift, the H_{IF}/H_{BF} values are 1.4 for the short and around 1.6 for the almost square and long infill. Table 1 also presents the H_{INF}/H_{BF} ratio for decoupled infills. It can be seen that the horizontal forces of decoupled infills are rather low in comparison with the horizontal force of the corresponding bare RC frame. For instance, horizontal forces of all decoupled infills are less than 30 % of the horizontal force of the bare RC frame. Only at 2.0 % of in-plane drift, the H_{INF}/H_{BF} ratio is 0.44 for the almost square decoupled infill. A high $V_{TL,IF}/V_{BF}$ ratio can be seen for all traditional infills. For instance, up to 1.0 % of in-plane drift, long traditional infill imposes shear forces in the top of the left column that are more than 3 times larger than the shear forces of the corresponding bare RC frame, and for in-plane drifts of 1.5 % and 2.0 % the $V_{TL,IF}/V_{BF}$ ratio is around 2.5. For the RC frame with the almost square traditional infill, the $V_{TL,IF}/V_{BF}$ ratio is around 2-3 times larger than for the corresponding bare RC frame, with the largest shear forces imposed at the lower in-plane drifts. At 0.1 % of in-plane drift, the short traditional infill imposes shear forces 2.5 times larger than the shear forces on the corresponding bare RC frame. For higher in-plane drifts, this ratio is between 1.5 and 2.0 because of the propagating damage to the short traditional infill. On the other side, the decoupling system reduces the local effects. For instance, at 0.1 % of in-plane drift, the $V_{TL,IF}/V_{TL,BF}$ ratio is around 1.3 for the long infill, and around 1.0 for other two configurations. Up to 1.5 % of in-plane drift, the ratio slowly increases, but it is lower than 1.5 for all configurations. Only at 2.0 % of in.plane drift, $V_{TL,IF}/V_{BF}$ is around 1.75 for the long and almost square infill, but still around 1.4 for the short decoupled infill.

Table 2. Summary of results on RC frames with traditional and decoupled infills with different H/L ratios

	
Initial stiffnesses	H_{IF}/H_{BF} ratio in function of in-plane drift
	
H_{INF}/H_{BF} ratio in function of in-plane drift	$V_{TL,IF}/V_{TL,BF}$ ratio in function of in-plane drift

6. Conclusions

In this paper, the in-plane behaviour of RC frames with traditional and decoupled infills is investigated by means of numerical simulations. Traditional infills represent common masonry infills connected to the RC frame by the mortar, while decoupled infills refer to masonry infills decoupled from the RC frame by the innovative decoupling system INODIS. After validation of the numerical model against the available experimental results, a parametric study is carried out. The parameters varied are brick thickness and infill height-to-length ratio. The results of numerical simulations clearly show the benefits

Copyright © 2025 CroCEE
DOI: https://doi.org/10.5592/CO/3CroCEE.2025.96

of the decoupling system for all investigated infill configurations. All traditional infills activate at low in-plane drifts. Due to this, the initial in-plane stiffnesses of the traditionally infilled RC frames are between 5 and 26 times larger than the initial stiffness of the corresponding bare RC frame. Furthermore, for all investigated configurations, the horizontal forces of the traditionally infilled RC frames are at least 2-3 times larger than the horizontal forces of the corresponding bare RC frames, already at in-plane drifts up to 0.5 %. Because of the significant damage to traditional infills, the H_{INF}/H_{BF} ratio has a descending trend. Moreover, the strong infill action imposes shear forces at the top of the left column that are at least around 2 times larger than the shear forces of the bare RC frame, already at in-plane drifts of 0.1 % and 0.5 %. It can be concluded that neglecting traditional masonry infills in the seismic design is incorrect and dangerous, as they change the response of the bare RC frame, and suffer significant damage at low in-plane drifts. However, the level of their activation strongly depends on the brick thickness and height-to-length ratio, which complicates the development of a design concept for their verification. On the contrary, the frame-infill interaction is significantly reduced between decoupled infills and RC frames. Firstly, the initial in-plane stiffnesses of the RC frames with decoupled infills obtain the same values as the initial in-plane stiffnesses of the corresponding bare RC frames. In addition to this, the H_{IF}/H_{BF} ratio has an increasing trend because of the slow infill activation, and it takes the values between 1.0 and 1.5 up to the in-plane drift of 1.5 %. At 2.0 % of in-plane drift, the H_{IF}/H_{BF} ratio is slightly over 1.5 just for three investigated configurations. The horizontal forces of decoupled infills also remain low, and up to 1.5 % of in-plane drift, they are less than 30 % of the bare frame horizontal force, whereas at 2.0 % of in-plane drift only three configurations obtain infill horizontal forces that are between 35 % and 45 % of the bare frame horizontal force. Additionally, the decoupling system reduces the local effects. The shear forces at the top of the left column slowly increase with the increase of the in-plane drift, but even at 2.0 % of in-plane drift, the $V_{TL,IF}/V_{TL,BF}$ ratio is lower than 1.5 for most of the infill configurations, and it is around 1.75 for only three considered configurations. Finally, the in-plane behaviour of all considered RC frames with decoupled infills is similar, as no big differences in the in-plane response can be observed, up to 2.0 % of in-plane drift. After 2.0 % of in-plane drift, most of the decoupled infills get more activated and some differences in their behaviour can be noticed. However, the in-plane response for in-plane drifts larger than 2.0 % is not important for the practice, as 2.0 % of in-plane drift usually represents the design limit value. Therefore, based on the observed in-plane response of RC frames with decoupled infills, the development of a simple design concept seems promising. In future work, authors plan to study the effect of other important parameters, such as openings in the infills, and derive recommendations regarding the seismic design of RC frames with decoupled infills, applicable in the engineering practice.

References

[1] Marinković, M., Baballëku, M., Isufi, B., Blagojević, N., Milićević, I., Brzev, S. (2022): Performance of RC cast-in-place buildings during the November 26, 2019 Albania earthquake. *Bulletin of Earthquake Engineering,* 20:5427-5480. https://doi.org/10.1007/s10518-022-01414-y

[2] Marinković, M., Brzev, S., Baballëku, M., Isufi, B., Blagojević, N., Milićević, I., Žugić, Ž., Bursać, P. (2021): Out-of-plane behaviour of loadbearing and non-structural masonry walls during recent earthquakes. In Conference proceedings from 1st Croatian Conference on Earthquake Engineering-1CroCEE, 22nd to 24th March 2021, Zagreb, 2021 (Vol. 64, pp. 213-207). University of Zagreb, Faculty of Civil Engineering.

[3] Dilsiz A. et al. (2023): "StEER: 2023 Mw 7.8 Kahramanmaras, Türkiye Earthquake Sequence Preliminary Virtual Reconnaissance Report (PVRR)", in StEER- February 6, 2023, Kahramanmaras, Türkiye, Mw 7.8 Earthquake. DesignSafe-CI. https://doi.org/10.17603/ds2-7ry2-gv66

[4] Dawe, J.L., Seah, C.K. (1989): Behaviour of masonry infilled steel frames. *Canadian Journal of Civil Engineering*, *16*(6), 865-876.

[5] Mehrabi, A.B., Shing, P.B., Schuller, M.P., Noland, J.L. (1994): Performance of Masonry-Infilled R/C Frames under in-Plane Lateral Loads; Report No. CU/SR-94-6; Department of Civil, Environmental, and Architectural Engineering, University of Colorado: Denver, CO, USA

Copyright © 2025 CroCEE
DOI: https://doi.org/10.5592/CO/3CroCEE.2025.96

[6] Flanagan, R.D., Bennett, R.M. (1999a): In-plane behavior of structural clay tile infilled frames. *Journal of Structural Engineering,* 125(6): 590-599. https://doi.org/10.1061/(ASCE)0733-9445(1999)125:6(590)

[7] Stylianidis, K.C. (2012): Experimental investigation of masonry infilled RC frames. The Open Construction *& Building Technology Journal,* 6 (1):194-212. https://doi.org/10. 2174/1874836801206010194

[8] Morandi, P., Hak, S., Magenes, G. (2017a): Experimental and numerical seismic performance of strong clay masonry infills. In Appendix: guideline proposal for seismic design of masonry infills. Research Report 2017a/02. EUCENTRE Foundation

[9] Di Trapani, F., Khan, N. A., Zhou, L., Demartino, C., Monti, G. (2024): Cyclic response of infilled RC frames with window and door openings: Experimental results and damage interpretation. *Earthquake Engineering & Structural Dynamics*, *53*(1), 43-67. https://doi.org/10.1002/eqe.4005

[10] Stavrdis, A., Shing, P.B. (2010): Finite-element modelling of nonlinear behaviour of masonry-infilled RC frames. *Journal of Structural Engineering*, 136(3), 285-296.

[11] Nasiri, E., Liu, Y. (2017): Development of a detailed 3D FE model for analysis of the in-plane behaviour of masonry infilled concrete frames. *Engineering Structures*, 143, 603-616.

[12] Di Trapani, F., Shing, P.B., Cavaleri, L. (2018): Macroelement Model for in-plane and out-of-plane responses of masonry infills in frame structures. *Journal of Structural Engineering,* 144(2):04017198. https:// doi. org/ 10. 1061/(ASCE) ST. 1943- 541X. 00019 26

[13] Kubalski, T. (2023): Modellierung von seismisch beanspruchten Mauerwerksausfachungen in Stahlbetonrahmentragwerken (Doctoral dissertation, RWTH Aachen Univresity, 2022)

[14] Koutas, L., Bousias, S.N., Triantafillou, T.C. (2015): Seismic strengthening of masonry-infilled RC frames with TRM: Experimental study. *Journal of Composites for Construction,* 19(2):04014048. https://doi.org/10.1061/(ASCE)CC.1943-5614.0000507

[15] da Porto, F., Donà, M., Verlato, N., Guidi, G. (2020): Experimental testing and numerical modeling of robust unreinforced and reinforced clay masonry infill walls, with and without openings. *Frontiers in Built Environment,* 6:591985. https://doi.org/10.3389/fbuil.2020.591985

[16] Morandi, P., Milanesi, R.R., Magenes, G. (2018a): Innovative solution for seismic-resistant masonry infills with sliding joints: in-plane experimental performance. *Engineering Structures,* 176:719-733. https://doi.org/10.1016/j.engstruct.2018.09.018

[17] Preti, M., Bolis, V. (2017): Masonry infill construction and retrofit technique for the infill-frame interaction mitigation: test results. *Engineering Structures,* 132:597-608. https://doi.org/10.1016/j.engstruct.2016.11.053

[18] Bolis, V., Stavridis, A., Preti, M. (2017): Numerical investigation of the in-plane performance of masonry-infilled RC frames with sliding subpanels. *Journal of Structural Engineering*, 143(2), 04016168. https://doi.org/10.1061/(ASCE)ST.1943-541X.0001651

[19] Tsantilis, A.V., Triantafillou, T.C. (2018a): Innovative seismic isolation of masonry infills using cellular materials at the interface with the surrounding RC frames. *Engineering Structure,s* 155:279-297. https://doi.org/10.1016/j.engstruct.2017.11.025

[20] Jin, W., Zhai, C., Zhang, M., Liu, W., Wei, Y., Xie, L. (2023): Experimental investigation on the in-plane and out-of-plane interaction of isolated infills in RC frames. *Engineering Structures*, *293*, 116569. https://doi.org/10.1016/j.engstruct.2023.116569

[21] GB 50011-2010 (2010) Code for Seismic Design of Buildings, Architecture & Building Press, Beijing, China (In Chinese)

[22] Standards New Zealand (2004) NZS 4230:2004, Design of Reinforced Concrete Masonry Structures, Standards New Zealand, Wellington, New Zealand.

[23] Milijaš, A., Marinković, M., Butenweg, C., Klinkel, S. (2024): Experimental investigation on the seismic performance of reinforced concrete frames with decoupled masonry infills: Considering in-plane and out-of-plane load interaction effects. *Bulletin of Earthquake Engineering*, 22, 7489-7546, https://doi.org/10.1007/s10518-024-02012-w

Copyright © 2025 CroCEE
DOI: https://doi.org/10.5592/CO/3CroCEE.2025.96

[24] Marinković, M., Butenweg, C. (2022): Numerical analysis of the in-plane behaviour of decoupled masonry infilled RC frames. *Engineering Structures*, *272*, 114959. https://doi.org/10.1016/j.engstruct.2022.114959

[25] Milijaš, A., Marinković, M., Butenweg, C., Klinkel, S. (2023): Experimental results of reinforced concrete frames with masonry infills with and without openings under combined quasi-static in-plane and out-of-plane seismic loading, *Bulletin of Earthquake Engineering*, 21:3537-3579. https://doi.org/10.1007/s10518-023-01664-4

[26] Simulia, Abaqus, User Manual. Version 6.13. Providence, RI, USA: DS SIMULIA Corp., 2013. URL https://www.3ds.com/products-services/simulia/products/abaqus/

Proceedings of the 3rd Croatian Conference on Earthquake Engineering - 3CroCEE
19–22 March 2025, Split, Croatia
Copyright © 2025 CroCEE
DOI: https://doi.org/10.5592/CO/3CroCEE.2025.103

AUGMENTED MODAL DIMENSIONS FOR SEISMIC EVALUATION OF BUILDINGS

Jui-Liang Lin [1]

[1] Research Fellow, National Center for Research on Earthquake Engineering, Taiwan, R.O.C., jllin@narlabs.org.tw

Abstract

An N-degree-of-freedom structure can be represented by using N single-degree-of-freedom modal sticks/oscillators, which form an N-dimensional modal space. Because each modal stick represents a modal equation of motion, we always take it for granted that a modal stick is one-dimensional. This paper shows that a modal equation of motion could be multi-dimensional. Accordingly, the corresponding modal stick/oscillator is also multi-dimensional. In other words, we can augment the dimensions of a modal space. It is worth recalling that with the imaginary unit, the one-dimensional real number axis was augmented into the two-dimensional complex plane, which is influential in mathematics and science. Likewise, augmented modal dimensions are influential in seismic evaluation of structures. For instance, a three-degree-of-freedom modal stick can simultaneously reflects the three force-displacement relationships of a two-way asymmetrical building subjected to its modal inertia force. Moreover, a multi-degree-of-freedom modal stick allows the modal responses in the three directions to be different from each other. This feature is appealing for modal analysis of non-proportionally damped buildings, such as buildings with supplemental damping, or buildings with soil-structure interaction. On the other hand, it is common to use multiple tuned mass dampers to control a translation-rotation coupled vibration mode. Nevertheless, based on the concept of augmented modal dimensions, a translation-rotation coupled tuned mass damper was developed to control a translation-rotation coupled vibration mode. That novel tuned mass damper is a straightforward and simple solution to the modal control of asymmetrical buildings. Moreover, through conducting modal fusion, a self-mass damper, designated as top-story mass damper, was developed for the seismic control of the first triplet of vibration modes of two-way asymmetrical buildings. In short, augmented dimensions of modal space push the boundaries of seismic evaluation of structures.

Keywords: modal dimension, modal space, modal analysis, structural dynamics, seismic analysis and design, asymmetric-plan building, non-proportionally damped building, tuned mass damper.

1. Introduction

In physical space, the degree of freedom of a numerical model of a building can be very large or small. The smallest dimension is of course equal to one. An N-degree-of-freedom structure can be represented by using N single degree-of-freedom (SDOF) modal sticks, which form an N-dimensional modal space. Because each SDOF modal stick reflects a modal equation of motion, it always takes for granted that a modal stick is a one-dimensional oscillator. The SDOF modal oscillator is a cornerstone of structural dynamics and earthquake engineering. Nevertheless, Lin and Tsai [1, 2] demonstrated that a modal equation of motion can be expressed in a format of multiple degrees of freedom. Accordingly, the corresponding modal stick is no longer a one-dimensional oscillator. In other words, the dimension of the original N-dimensional modal space is augmented. The augmented modal dimension is useful for many aspects of earthquake engineering. It is worth recalling that augmenting the one-dimensional real axis into a two-dimensional complex plane through complex numbers significantly advanced mathematics, physics, and engineering.

Asymmetrical buildings are vulnerable to earthquakes because of their translation-rotation coupled response. It is also challenging to do seismic evaluation and design of such buildings. For a two-way asymmetrical building, every vibration mode simultaneously has two translational and one rotational deformation, i.e., a three-dimensional deformation. Therefore, using one-dimensional modal systems for asymmetrical buildings is inconsistent with the visual reality. Moreover, translational and

Copyright © 2025 CroCEE
DOI: https://doi.org/10.5592/CO/3CroCEE.2025.103

rotational modal properties are mixed up (i.e., unclear) in terms of SDOF modal systems. Finally, SDOF modal systems can not reflect the fact that the modal deformations in the three directions are possibly non-proportional to each other, e.g., buildings with supplemental damping. In contrast, a three-degree-of-freedom (3DOF) modal equation of motion explicitly reveals those properties of a vibration mode of a two-way asymmetrical building [1, 2]. It is like to discover the ratios between protons, neutrons, and electrons in composition of an atom mass. Accordingly, some trends in torsional effects in asymmetrical buildings were further understood [3]. Moreover, for non-proportionally damped two-way asymmetrical buildings, the 3DOF modal equation of motion maintains the characteristic of non-proportional damping at a modal level. That characteristic benefits the modal response history analysis of asymmetrical buildings with supplemental damping [4, 5, 6]. Because the 3DOF modal system can reflect the non-proportionality between modal translations and modal rotation while asymmetrical buildings go into inelastic excursions, the augmented modal dimensions also benefit the seismic analysis of inelastic asymmetrical buildings [1, 2]. Based on the encouraging results, Lin et al. [7] further applied the augmented modal dimensions to the seismic analysis of buildings with specific vertical irregularities.

Moreover, Lin et al. [8, 9] applied the augmented modal dimensions to develop novel tuned mass dampers (TMDs). In contrast with the typical approach of employing multiple SDOF TMDs for the seismic control of asymmetrical buildings, the proposed approach used a single translation-rotation coupled TMD straightforwardly controlling a translation-rotation coupled vibration mode. Through modal fusion of the first triplet of vibration modes, which are the fundamental vibration modes in each of the three directions, Lin [10, 11] further developed a novel self-mass damper that simultaneously controls the three fundamental vibration modes.

The present paper shows the derivation of the 3DOF modal equation of motion as well as numerical examples. The present paper aims at briefing the theory and application of the augmented modal dimensions for seismic evaluation of buildings.

2. Theoretical background

2.1. 3DOF modal equation of motion

In order to be consistent with the coordinate system used in previous study [1, 2], the X- and Z-axes are used as the two plan axes. The positive direction of the Y-axis is opposite to the direction of gravity. The center of rigidity (CR) of a two-way asymmetric-plan buildings is not aligned with the center of mass (CM) in both plan axes. The two horizontal components of seismic ground motions are simultaneously applied along the x- and the z-directions. The equation of motion for an elastic N-story two-way asymmetric-plan building with each floor simulated as a rigid diaphragm is:

$$\begin{aligned}
&\mathbf{M}\ddot{\mathbf{u}}+\mathbf{C}\dot{\mathbf{u}}+\mathbf{K}\mathbf{u}=-\mathbf{M}\boldsymbol{\iota}_x\ddot{u}_{gx}(t)-\mathbf{M}\boldsymbol{\iota}_z\ddot{u}_{gz}(t)\\
&=-\sum_{n=1}^{3N}\mathbf{s}_{xn}\ddot{u}_{gx}(t)-\sum_{n=1}^{3N}\mathbf{s}_{zn}\ddot{u}_{gz}(t)=-\sum_{n=1}^{3N}\Gamma_{xn}\mathbf{M}\boldsymbol{\varphi}_n\ddot{u}_{gx}(t)-\sum_{n=1}^{3N}\Gamma_{zn}\mathbf{M}\boldsymbol{\varphi}_n\ddot{u}_{gz}(t)\\
&=-\sum_{n=1}^{3N}\left(\Gamma_{xn}\ddot{u}_{gx}+\Gamma_{zn}\ddot{u}_{gz}\right)\mathbf{M}\boldsymbol{\varphi}_n
\end{aligned} \tag{1}$$

where the displacement vector, $\mathbf{u}$, mode shape, $\boldsymbol{\varphi}_n$, mass matrix, $\mathbf{M}$, stiffness matrix, $\mathbf{K}$, influence vectors, $\boldsymbol{\iota}_x$, $\boldsymbol{\iota}_z$, modal inertia force vectors, $\mathbf{s}_{xn}$, $\mathbf{s}_{zn}$, and modal participation factors, Γ_{xn}, Γ_{zn}, are defined as:

Copyright © 2025 CroCEE
DOI: https://doi.org/10.5592/CO/3CroCEE.2025.103

$$\mathbf{u}=\begin{bmatrix}\mathbf{u}_x\\ \mathbf{u}_z\\ \mathbf{u}_\theta\end{bmatrix}_{3N\times 1},\quad \boldsymbol{\varphi}_n=\begin{bmatrix}\boldsymbol{\varphi}_{xn}\\ \boldsymbol{\varphi}_{zn}\\ \boldsymbol{\varphi}_{\theta n}\end{bmatrix}_{3N\times 1},\quad \mathbf{M}=\begin{bmatrix}\mathbf{m}_x & \mathbf{0} & \mathbf{0}\\ \mathbf{0} & \mathbf{m}_z & \mathbf{0}\\ \mathbf{0} & \mathbf{0} & \mathbf{I}_0\end{bmatrix}_{3N\times 3N},\quad \mathbf{K}=\begin{bmatrix}\mathbf{k}_{xx} & \mathbf{k}_{xz} & \mathbf{k}_{x\theta}\\ \mathbf{k}_{zx} & \mathbf{k}_{zz} & \mathbf{k}_{z\theta}\\ \mathbf{k}_{\theta x} & \mathbf{k}_{\theta z} & \mathbf{k}_{\theta\theta}\end{bmatrix}_{3N\times 3N}$$

$$\boldsymbol{\iota}_x=\begin{bmatrix}\mathbf{1}\\ \mathbf{0}\\ \mathbf{0}\end{bmatrix},\quad \boldsymbol{\iota}_z=\begin{bmatrix}\mathbf{0}\\ \mathbf{1}\\ \mathbf{0}\end{bmatrix},\quad \mathbf{s}_{xn}=\Gamma_{xn}\mathbf{M}\boldsymbol{\varphi}_n,\quad \mathbf{s}_{zn}=\Gamma_{zn}\mathbf{M}\boldsymbol{\varphi}_n,\quad \Gamma_{xn}=\frac{\boldsymbol{\varphi}_n^T\mathbf{M}\boldsymbol{\iota}_x}{\boldsymbol{\varphi}_n^T\mathbf{M}\boldsymbol{\varphi}_n},\quad \Gamma_{zn}=\frac{\boldsymbol{\varphi}_n^T\mathbf{M}\boldsymbol{\iota}_z}{\boldsymbol{\varphi}_n^T\mathbf{M}\boldsymbol{\varphi}_n} \tag{2}$$

When the force $-\left(\Gamma_{xn}\ddot{u}_{gx}+\Gamma_{zn}\ddot{u}_{gz}\right)\mathbf{M}\boldsymbol{\varphi}_n$ is applied to the building only, the equation of motion (Eq. 1) becomes:

$$\mathbf{M}\ddot{\mathbf{u}}_n+\mathbf{C}\dot{\mathbf{u}}_n+\mathbf{K}\mathbf{u}_n=-\left(\Gamma_{xn}\ddot{u}_{gx}+\Gamma_{zn}\ddot{u}_{gz}\right)\mathbf{M}\boldsymbol{\varphi}_n=-\left(\Gamma_{xn}\ddot{u}_{gx}+\Gamma_{zn}\ddot{u}_{gz}\right)\mathbf{s}_n,\quad n=1\sim 3N \tag{3}$$

where $\mathbf{s}_n=\mathbf{M}\boldsymbol{\varphi}_n$ is the modal inertia force of the *n*th vibration mode; $\mathbf{u}_n$ is the *n*th modal displacement response and $\mathbf{u}=\sum_{n=1}^{3N}\mathbf{u}_n=\sum_{n=1}^{3N}\boldsymbol{\varphi}_n D_n$. D_n is the generalized modal coordinate, which is a scalar. Notably, $\mathbf{s}_n$ and $-\left(\Gamma_{xn}\ddot{u}_{gx}+\Gamma_{zn}\ddot{u}_{gz}\right)$ respectively reflect the distribution of seismic force in the space and the variation of the seismic force along with time. By replacing $\mathbf{u}_n$ of Eq. 3 with $\boldsymbol{\Phi}_n\mathbf{D}_n$, where

$$\boldsymbol{\Phi}_n=\begin{bmatrix}\boldsymbol{\varphi}_{xn} & \mathbf{0} & \mathbf{0}\\ \mathbf{0} & \boldsymbol{\varphi}_{zn} & \mathbf{0}\\ \mathbf{0} & \mathbf{0} & \boldsymbol{\varphi}_{\theta n}\end{bmatrix}_{3N\times 3},\quad \mathbf{D}_n=\begin{bmatrix}D_{xn}\\ D_{zn}\\ D_{\theta n}\end{bmatrix}_{3\times 1} \tag{4}$$

, and then multiplying both sides of Eq. 3 with $\boldsymbol{\Phi}_n^T$, the 3DOF modal equation of motion for the *n*th vibration mode is obtained as:

$$\mathbf{M}_n\ddot{\mathbf{D}}_n+\mathbf{C}_n\dot{\mathbf{D}}_n+\mathbf{K}_n\mathbf{D}_n=-\left(\Gamma_{xn}\ddot{u}_{gx}+\Gamma_{zn}\ddot{u}_{gz}\right)\mathbf{M}_n\mathbf{1},\quad n=1\sim 3N \tag{5}$$

where:

$$\mathbf{M}_n=\begin{bmatrix}\boldsymbol{\varphi}_{xn}^T\mathbf{m}_x\boldsymbol{\varphi}_{xn} & 0 & 0\\ 0 & \boldsymbol{\varphi}_{zn}^T\mathbf{m}_z\boldsymbol{\varphi}_{zn} & 0\\ 0 & 0 & \boldsymbol{\varphi}_{\theta n}^T\mathbf{I}_0\boldsymbol{\varphi}_{\theta n}\end{bmatrix}_{3\times 3},\quad \mathbf{1}=\begin{bmatrix}1\\ 1\\ 1\end{bmatrix}_{3\times 1}$$

$$\mathbf{C}_n=\begin{bmatrix}\boldsymbol{\varphi}_{xn}^T\mathbf{c}_{xx}\boldsymbol{\varphi}_{xn} & \boldsymbol{\varphi}_{xn}^T\mathbf{c}_{xz}\boldsymbol{\varphi}_{zn} & \boldsymbol{\varphi}_{xn}^T\mathbf{c}_{x\theta}\boldsymbol{\varphi}_{\theta n}\\ \boldsymbol{\varphi}_{zn}^T\mathbf{c}_{zx}\boldsymbol{\varphi}_{xn} & \boldsymbol{\varphi}_{zn}^T\mathbf{c}_{zz}\boldsymbol{\varphi}_{zn} & \boldsymbol{\varphi}_{zn}^T\mathbf{c}_{z\theta}\boldsymbol{\varphi}_{\theta n}\\ \boldsymbol{\varphi}_{\theta n}^T\mathbf{c}_{\theta x}\boldsymbol{\varphi}_{xn} & \boldsymbol{\varphi}_{\theta n}^T\mathbf{c}_{\theta z}\boldsymbol{\varphi}_{zn} & \boldsymbol{\varphi}_{\theta n}^T\mathbf{c}_{\theta\theta}\boldsymbol{\varphi}_{\theta n}\end{bmatrix}_{3\times 3},\quad \mathbf{K}_n=\begin{bmatrix}\boldsymbol{\varphi}_{xn}^T\mathbf{k}_{xx}\boldsymbol{\varphi}_{xn} & \boldsymbol{\varphi}_{xn}^T\mathbf{k}_{xz}\boldsymbol{\varphi}_{zn} & \boldsymbol{\varphi}_{xn}^T\mathbf{k}_{x\theta}\boldsymbol{\varphi}_{\theta n}\\ \boldsymbol{\varphi}_{zn}^T\mathbf{k}_{zx}\boldsymbol{\varphi}_{xn} & \boldsymbol{\varphi}_{zn}^T\mathbf{k}_{zz}\boldsymbol{\varphi}_{zn} & \boldsymbol{\varphi}_{zn}^T\mathbf{k}_{z\theta}\boldsymbol{\varphi}_{\theta n}\\ \boldsymbol{\varphi}_{\theta n}^T\mathbf{k}_{\theta x}\boldsymbol{\varphi}_{xn} & \boldsymbol{\varphi}_{\theta n}^T\mathbf{k}_{\theta z}\boldsymbol{\varphi}_{zn} & \boldsymbol{\varphi}_{\theta n}^T\mathbf{k}_{\theta\theta}\boldsymbol{\varphi}_{\theta n}\end{bmatrix}_{3\times 3} \tag{6}$$

D_{xn}, D_{zn}, and $D_{\theta n}$, are referred to as the x- and z-directional modal translations and modal rotation, respectively. $\mathbf{D}_n$ is a vector augmented from the generalized modal coordinate D_n. $\mathbf{D}_n$ reserves the possibility that D_{xn}, D_{zn}, and $D_{\theta n}$ are not equal to each other. Moreover, $\mathbf{M}_n$, $\mathbf{C}_n$, and $\mathbf{K}_n$ reveal the coupled and uncoupled modal properties in the three directions. It is worth noting that the summation of the nine elements of each of the matrices $\mathbf{M}_n$, $\mathbf{C}_n$, and $\mathbf{K}_n$ is equal to the mass, damping, and stiffness

Copyright © 2025 CroCEE
DOI: https://doi.org/10.5592/CO/3CroCEE.2025.103

of the *n*th SDOF modal equation of motion, respectively. In other words, the mass, damping, and stiffness of the *n*th SDOF modal equation of motion are expanded into $\mathbf{M}_n$, $\mathbf{C}_n$, and $\mathbf{K}_n$, respectively.

A 3DOF modal stick (Fig. 1a) is constructed in order to represent the 3DOF modal equation of motion (Eq. 5). The degrees of freedom of the 3DOF modal stick (denoted as $\tilde{D}_{xn}$, $\tilde{D}_{zn}$, $\tilde{D}_{\theta n}$) are defined at the lumped mass, which has the x and z-translational masses (denoted as m_{xn}, m_{zn}), and mass moment of inertia (denoted as I_n). The lumped mass is at the end of a rigid beam, whose projected lengths on the X-Y and Z-Y planes are e_{xn} and e_{zn}, respectively. The beam is connected to a rigid column through a rotational spring with stiffness $k_{\theta n}$. The column, which has a unit length, is connected to the ground with two rotational springs with stiffness k_{xn} and k_{zn}. There is an angle β_n between the two rotational springs with stiffness k_{xn} and k_{zn}. For such a simple structure shown as Fig. 1a, its displacement vector, mass matrix, and stiffness matrix are expresses as

$$\tilde{\mathbf{D}}=\begin{bmatrix}\tilde{D}_{xn}\\ \tilde{D}_{zn}\\ \tilde{D}_{\theta n}\end{bmatrix}_{3\times1},\quad \tilde{\mathbf{M}}=\begin{bmatrix}m_{xn}&0&0\\0&m_{zn}&0\\0&0&I_n\end{bmatrix}_{3\times3},\quad C=\cos\beta_n,\quad S=\sin\beta_n$$

$$\tilde{\mathbf{K}}=\begin{bmatrix}k_{xn}C^2 & & \textit{symm.}\\ k_{xn}SC & k_{zn}+k_{xn}S^2 & \\ -e_{zn}k_{xn}C^2+e_{xn}k_{xn}SC & -e_{zn}k_{xn}SC+e_{xn}\left(k_{zn}+k_{xn}S^2\right) & k_{\theta n}+e_{xn}^2k_{zn}+\left(e_{xn}S-e_{zn}C\right)^2k_{xn}\end{bmatrix}_{3\times3} \tag{7}$$

By letting $\tilde{\mathbf{D}}=\mathbf{D}_n$, $\tilde{\mathbf{M}}=\mathbf{M}_n$, $\tilde{\mathbf{K}}=\mathbf{K}_n$, the elastic properties of the *n*th 3DOF modal stick are determined as follows (Eq. 8):

$$\beta_n=\tan^{-1}\left(\frac{\boldsymbol{\varphi}_{zn}^T\mathbf{k}_{zx}\boldsymbol{\varphi}_{xn}}{\boldsymbol{\varphi}_{xn}^T\mathbf{k}_{xx}\boldsymbol{\varphi}_{xn}}\right),\quad k_{xn}=\frac{\boldsymbol{\varphi}_{xn}^T\mathbf{k}_{xx}\boldsymbol{\varphi}_{xn}}{C^2},\quad k_{zn}=\boldsymbol{\varphi}_{zn}^T\mathbf{k}_{zz}\boldsymbol{\varphi}_{zn}-k_{xn}S^2$$

$$\begin{bmatrix}e_{xn}\\ e_{zn}\end{bmatrix}=\begin{bmatrix}k_{xn}SC & -k_{xn}C^2\\ k_{zn}+k_{xn}S^2 & -k_{xn}SC\end{bmatrix}^{-1}\begin{bmatrix}\boldsymbol{\varphi}_{xn}^T\mathbf{k}_{x\theta}\boldsymbol{\varphi}_{\theta n}\\ \boldsymbol{\varphi}_{zn}^T\mathbf{k}_{z\theta}\boldsymbol{\varphi}_{\theta n}\end{bmatrix},\quad k_{\theta n}=\boldsymbol{\varphi}_{\theta n}^T\mathbf{k}_{\theta\theta}\boldsymbol{\varphi}_{\theta n}-e_{xn}^2k_{zn}-\left(e_{xn}S-e_{zn}C\right)^2k_{xn}$$

$$m_{xn}=\boldsymbol{\varphi}_{xn}^T\mathbf{m}_x\boldsymbol{\varphi}_{xn},\quad m_{zn}=\boldsymbol{\varphi}_{zn}^T\mathbf{m}_z\boldsymbol{\varphi}_{zn},\quad I_n=\boldsymbol{\varphi}_{\theta n}^T\mathbf{I}_0\boldsymbol{\varphi}_{\theta n} \tag{8}$$

β_n is approximately equal to zero (i.e. $\mathbf{k}_{zx}$ is neglected) for buildings with all lateral force resisting elements placed along either the X- or Z-axes.

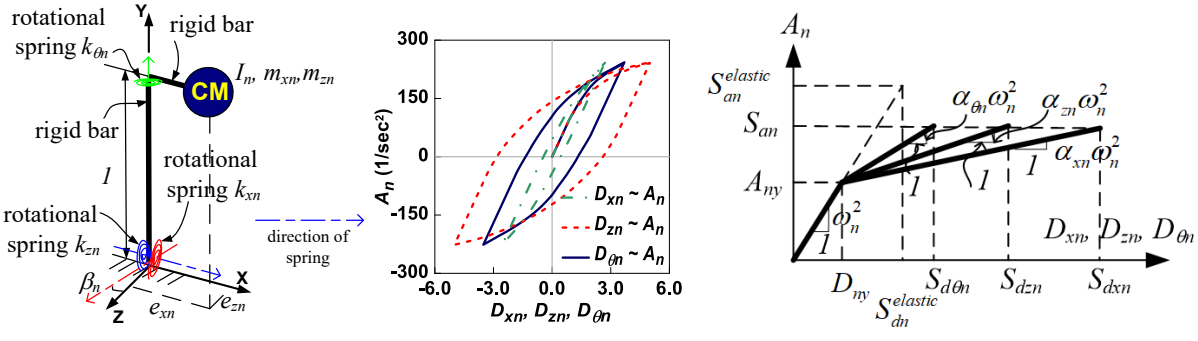


Figure 1. (a) A 3DOF modal stick, (b) three force-displacement curves, (c) three bilinear force-displacement curves.

Proceedings of the 3rd Croatian Conference on Earthquake Engineering - 3CroCEE
19–22 March 2025, Split, Croatia
Copyright © 2025 CroCEE
DOI: https://doi.org/10.5592/CO/3CroCEE.2025.103

While applying a modal inertia force vector to a symmetrical building, there is only one force-displacement curve, which represents the roof displacement versus base shear relationship. However, while applying a modal inertia force vector to an asymmetrical building, there are three force-displacement curves, which represents two roof displacement-base shear relationships and one roof rotation-base torque relationship (Fig. 1b). The SDOF modal system is capable of describing the one force-displacement relationship. However, the SDOF modal system is obviously insufficient to describe the three force-displacement relationships simultaneously. By converting the three force-displacement curves into the acceleration-displacement-response-spectra (ADRS) format, the three curves overlap when the building is elastic. In addition, the three force-displacement curves bifurcate when the building becomes inelastic (Fig. 1b). This bifurcation indicates that the modal responses in the three directions are different from each other (i.e., non-proportional) when asymmetrical buildings are in an inelastic state. By bi-linearizing the three force-displacement curves, the post-yielding stiffness ratios α_{xn}, α_{znn}, $\alpha_{\theta n}$, as well as the yielding accelerations A_{yxn}, A_{yzn}, $A_{y\theta n}$ are obtained (Fig. 1c). Using these parameter values, the inelastic properties of the 3DOF modal system, including the yielding moments (denoted as M_{yxn}, M_{yzn}, $M_{y\theta n}$) and inelastic stiffness of the three rotational springs (denoted as k'_{xn}, k'_{zn}, $k'_{\theta n}$) are determined and shown as Eq. 9.

$$M_{yxn} = A_{xny} m_{xn}, \quad M_{yzn} = A_{zny} m_{zn} \tag{9a}$$

$$M_{y\theta n} = A_{\theta ny} I_n + A_{xny} m_{xn} e_{zn} - A_{zny} m_{zn} e_{xn} \tag{9b}$$

$$k'_{xn} = \frac{m_{xn}}{\dfrac{m_{xn}}{k_{xn}} + \dfrac{\left(I_n + m_{xn} e_{zn} - m_{zn} e_{xn}\right) e_{zn}}{k_{\theta n}} - \dfrac{\left(I_n + m_{xn} e_{zn} - m_{zn} e_{xn}\right) e_{zn}}{k'_{\theta n}}} \tag{9c}$$

$$k'_{zn} = \frac{m_{zn}}{\dfrac{m_{zn}}{k_{zn}} - \dfrac{\left(I_n + m_{xn} e_{zn} - m_{zn} e_{xn}\right) e_{xn}}{k_{\theta n}} + \dfrac{\left(I_n + m_{xn} e_{zn} - m_{zn} e_{xn}\right) e_{xn}}{k'_{\theta n}}} \tag{9d}$$

$$k'_{\theta n} = k_{\theta n} \cdot \alpha_{\theta n} \tag{9e}$$

Up to here, all the elastic and inelastic properties of a 3DOF modal stick are determined (Eqs. 8 and 9). By solving (using the step-by-step integration as an example) the 3DOF modal equation of motion (Eq. 5), the nth modal response history $\mathbf{D}_n$ can be obtained. The total displacement response $\mathbf{u}$ of the original building is then calculated as:

$$\mathbf{u} = \sum_{n=1}^{3N} \mathbf{u}_n = \sum_{n=1}^{3N} \mathbf{\Phi}_n \mathbf{D}_n = \sum_{n=1}^{3N} \begin{bmatrix} \boldsymbol{\varphi}_{xn} & \mathbf{0} & \mathbf{0} \\ \mathbf{0} & \boldsymbol{\varphi}_{zn} & \mathbf{0} \\ \mathbf{0} & \mathbf{0} & \boldsymbol{\varphi}_{\theta n} \end{bmatrix}_{3N \times 3} \begin{bmatrix} D_{xn} \\ D_{zn} \\ D_{\theta n} \end{bmatrix}_{3 \times 1} \tag{10}$$

Certainly, there are three vibration modes for each 3DOF modal system. In order to avoid confusion with the vibration modes of the original asymmetrical building, these three modes of a 3DOF modal system are called ‘sub-modes’. It has been mathematically demonstrated that one of the sub-modes is active with modal participation factor equal to one. The other two sub-modes are spurious as modal participation factors are equal to zero, i.e. the spurious sub-modes do not contribute to the vibration of an elastic 3DOF modal system. Moreover, the vibration period of the active sub-mode is equal to the nth vibration period of the original asymmetrical building. The mode shape of the active

Copyright © 2025 CroCEE
DOI: https://doi.org/10.5592/CO/3CroCEE.2025.103

sub-mode is equal to $[1\ 1\ 1]^T$, i.e. $D_{xn} = D_{zn} = D_{\theta n}$ for elastic 3DOF modal systems. Therefore, the 3DOF modal system is identical to the conventional SDOF modal system in an elastic state. In other words, the 3DOF modal system, a result of the augmented modal dimensions, completely complies with the basic principle of structural dynamics. Nevertheless, the non-proportionality between modal translations (D_{xn} and D_{zn}) and modal rotation ($D_{\theta n}$) of an inelastic asymmetrical building can be captured by using the proposed 3DOF modal systems.

2.2. Non-proportional damping reflected at a modal level

When an N-story asymmetrical building is proportionally damped (i.e., $\mathbf{C} = \alpha\mathbf{M} + \beta\mathbf{K}$), its corresponding 3DOF modal stick is also proportionally damped, i.e.,

$$\mathbf{C}_n = \begin{bmatrix} \boldsymbol{\varphi}_{xn} & \mathbf{0} & \mathbf{0} \\ \mathbf{0} & \boldsymbol{\varphi}_{zn} & \mathbf{0} \\ \mathbf{0} & \mathbf{0} & \boldsymbol{\varphi}_{\theta n} \end{bmatrix}^T \mathbf{C} \begin{bmatrix} \boldsymbol{\varphi}_{xn} & \mathbf{0} & \mathbf{0} \\ \mathbf{0} & \boldsymbol{\varphi}_{zn} & \mathbf{0} \\ \mathbf{0} & \mathbf{0} & \boldsymbol{\varphi}_{\theta n} \end{bmatrix} = \begin{bmatrix} \boldsymbol{\varphi}_{xn} & \mathbf{0} & \mathbf{0} \\ \mathbf{0} & \boldsymbol{\varphi}_{zn} & \mathbf{0} \\ \mathbf{0} & \mathbf{0} & \boldsymbol{\varphi}_{\theta n} \end{bmatrix}^T (\alpha\mathbf{M} + \beta\mathbf{K}) \begin{bmatrix} \boldsymbol{\varphi}_{xn} & \mathbf{0} & \mathbf{0} \\ \mathbf{0} & \boldsymbol{\varphi}_{zn} & \mathbf{0} \\ \mathbf{0} & \mathbf{0} & \boldsymbol{\varphi}_{\theta n} \end{bmatrix}$$
$$= \alpha\mathbf{M}_n + \beta\mathbf{K}_n \tag{11}$$

Therefore, when an N-story asymmetrical building is non-proportionally damped (i.e., $\mathbf{C} \neq \alpha\mathbf{M} + \beta\mathbf{K}$), its corresponding 3DOF modal stick is also non-proportionally damped, i.e., $\mathbf{C}_n \neq \alpha\mathbf{M}_n + \beta\mathbf{K}_n$. That is to say, the damping characteristic of an N-story building is retained at a modal level. Hence, the augmented modal dimensions allow the modal responses in the three directions to be different from each other when asymmetrical buildings are non-proportionally damped. This feature benefits the modal response history analyses of asymmetrical buildings with supplemental damping or with soil-structure interaction [6].

Lin and Tsai [5] investigated a three-story building with linear viscous dampers placed in both the x and z-directions. The damping coefficients were assigned so that the damping ratio in each direction is 30%. Figure 2a-c shows the three-directional modal responses (i.e., $\tilde{D}_{xn}$, $\tilde{D}_{zn}$, $\tilde{D}_{\theta n}$) of the 1st, 2nd, and 3rd vibration modes of the building, respectively, subjected to a scaled bi-directional El Centro earthquake. It indicates that the three-directional modal responses of each vibration mode are obviously different from each other because of the supplemental damping effect. Figure 2d-f shows the response histories of the 3rd, 2nd, and 1st stories of the building, respectively. In Fig. 2d-f, the abbreviation 3MA stands for the seismic responses obtained from using the 3DOF modal response history analysis. Additionally, the abbreviation SMA stands for the seismic responses obtained from the response history analysis of the complete finite element model of the building. Figure 2d-f indicates that the modal response history analysis with 3DOF modal systems effectively estimated the floor displacement histories of the non-proportionally damped building. The excellent feature of augmented modal dimensions for seismic evaluation of non-proportionally damped buildings is verified.

3. Conclusions

The augmented modal dimensions explicitly reveal the translational and rotational modal properties of each vibration mode of asymmetrical buildings. In addition, the augmented modal dimensions is capable of reflecting the non-proportional modal responses in the three directions when asymmetrical buildings are inelastic or non-proportionally damped. The augmented modal dimensions can be applied not only to asymmetrical buildings but also to vertically irregular buildings. Furthermore, the concept of augmented modal dimensions benefits the development of novel tuned mass dampers. It is worth putting more effort on the study of augmented modal dimensions in the future.

Copyright © 2025 CroCEE
DOI: https://doi.org/10.5592/CO/3CroCEE.2025.103

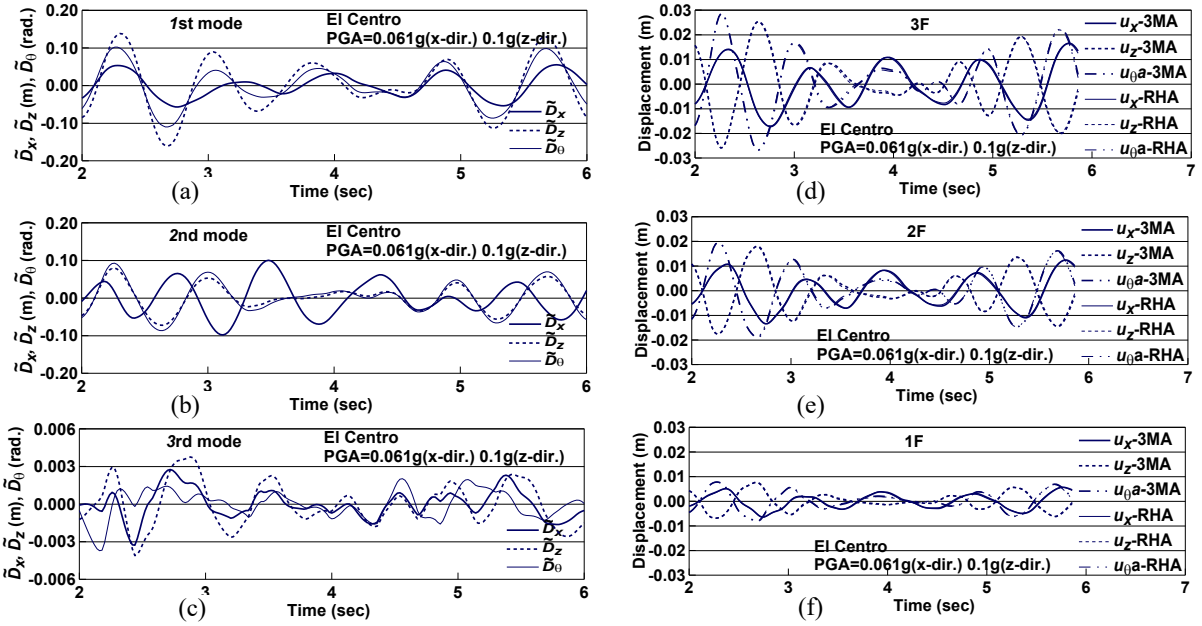


Figure 2. The three-directional modal responses of the (a) 1st, (b) 2nd, and (c) 3rd vibration modes of a non-proportionally damped three-story building. The response histories of the (d) 3rd, (e) 2nd, and (f) 1st floors of the three-story building.

References

[1] Lin, J.L., Tsai, K.C. (2007a): Simplified seismic analysis of asymmetric building systems. *Earthquake Engineering and Structural Dynamics*, **36** (4), 459-479, doi: https://doi.org/10.1002/eqe.635

[2] Lin, J.L., Tsai, K.C. (2008a): Seismic analysis of two-way asymmetric building systems under bi-directional seismic ground motions. *Earthquake Engineering and Structural Dynamics*, **37** (2), 305-328, doi: https://doi.org/10.1002/eqe.759

[3] Lin, J.L., Tsai, K.C., Chuang, M.C. (2012): Understanding the trends in torsional effects in asymmetric-plan buildings. *Bulletin of Earthquake Engineering*, **10**, 955-965, doi: https://doi.org/10.1007/s10518-012-9339-x

[4] Lin, J.L., Tsai, K.C. (2007b): Simplified seismic analysis of one-way asymmetric elastic systems with supplemental damping. *Earthquake Engineering and Structural Dynamics*, **36** (6), 783-800, doi: https://doi.org/10.1002/eqe.653

[5] Lin, J.L., Tsai, K.C. (2008b): Seismic analysis of non-proportionally damped two-way asymmetric elastic buildings under bi-directional seismic ground motions. *Journal of Earthquake Engineering*, **12** (07), 1139-1156, doi: https://doi.org/10.1080/13632460802003371

[6] Lin, J.L., Tsai, K.C., Miranda, E. (2009): Seismic history analysis of asymmetric buildings with soil-structure interaction. *ASCE, Journal of Structural Engineering*, **135** (2), 101-112, doi: https://doi.org/10.1061/(ASCE)0733-9445(2009)135:2(101)

[7] Lin, J.L., Tsaur, C.C., Tsai, K.C. (2019): Two-degree-of-freedom modal response history analysis of buildings with specific vertical irregularities. *Engineering Structures*, **184**, 505-523, doi: https://doi.org/10.1016/j.engstruct.2019.01.106

[8] Lin, J.L., Tsai, K.C., Yu, Y.J. (2010): Coupled tuned mass dampers for the seismic control of asymmetric-plan buildings. *Earthquake Spectra*, **26** (3), 749-778, doi: https://doi.org/10.1193/1.3435347

[9] Lin, J.L., Tsai, K.C., Yu, Y.J. (2011): Bi-directional coupled tuned mass dampers for the seismic response control of two-way asymmetric-plan buildings. *Earthquake Engineering and Structural Dynamics*, **40** (6), 675-690, doi: https://doi.org/10.1002/eqe.1054

Copyright © 2025 CroCEE
DOI: https://doi.org/10.5592/CO/3CroCEE.2025.103

[10] Lin, J.L. (2017): Top-story mass dampers for seismic control of the first triplet of vibration modes of two-way asymmetric-plan buildings. *Journal of Vibration and Control*, **23** (18), 2962-2976, doi: https://doi.org/10.1177/1077546315624997

[11] Lin, J.L. (2018): Seismic effectiveness of top-story mass dampers for inelastic two-way asymmetric-plan buildings. *Engineering Structures*, **161**, 118-133, doi: https://doi.org/10.1016/j.engstruct.2018.02.005

Proceedings of the 3rd Croatian Conference on Earthquake Engineering - 3CroCEE
19–22 March 2025, Split, Croatia
Copyright © 2025 CroCEE
DOI: https://doi.org/10.5592/CO/3CroCEE.2025.105

BEHAVIOUR OF DUAL STEEL FRAMES WITH INNOVATIVE DOUBLE SKIN COLD-FORMED STEEL CONCRETE COMPOSITE SHEAR WALLS

Ivan Lukačević[(1)], Emanuel Krupa-Jurić [(2)], Ivan Ćurković [(3)], Marko Barišić [(4)]

[(1)] *Associate Professor, University of Zagreb, Faculty of Civil Engineering, ivan.lukacevic@grad.unizg.hr*
[(2)] *Research Assistant, University of Zagreb, Faculty of Civil Engineering, emanuel.krupa.juric@grad.unizg.hr*
[(3)] *Assistant Professor, University of Zagreb, Faculty of Civil Engineering, ivan.curkovic@grad.unizg.hr*
[(4)] *PhD Student, University of Zagreb, Faculty of Civil Engineering, marko.barisic@student.grad.unizg.hr*

Abstract

Dual systems that combine moment-resisting frames with innovative replaceable bracing systems offer significant advantages over conventional solutions. The key benefits of these systems include energy dissipation at specific locations and a re-centring capability, which substantially reduces repair costs. However, the design of such systems must meet specific requirements, such as using higher steel grades to ensure the part of the system remains elastic and structural solutions for the double skin cold formed shear wall filled with concrete, which ensures the system's ductile behaviour. This paper presents an assessment of a dual system using finite element analysis that integrates a moment-resisting multi-story frame with an innovative double-skin cold-formed steel concrete composite shear wall. The steel frame consists of three bays, with a central bay being a braced frame and two adjacent bays being moment-resisting frames. The shear wall, acting as a bracing system, consists of corrugated cold-formed steel sheets filled with concrete, which are connected with intermediate shear connectors and form a sandwich steel-concrete-steel panel. In the first step, non-linear analyses of individual shear wall panels are conducted considering influences of steel sheet thickness, concrete strength and type of shear connection. Afterwards, pushover analyses are performed using the resulting load-displacement behaviour of the analysed shear walls. The performance of the analysed systems is discussed in terms of collapse mechanisms, capacity curves, overstrength ratios, behaviour factors, and potential improvements for the shear wall's performance. The analysed systems demonstrated their dual behaviour and re-centring capabilities, but further research on different shear wall typologies will provide deeper insights into their practical applications.

Keywords: dual systems, re-centring capability, cold-formed steel double skin concrete shear walls, non-linear static pushover method, capacity curve, overstrength ratio, collapse mechanism

1. Introduction

Modern codes require ductile behaviour during earthquakes and seismic energy dissipation through inelastic deformation. The capacitive design ensures seismic energy dissipation through the yielding of structural components at specific locations within the structure. Even though inelastic deformations are localised, damage is irreversible, and repair is complex, sometimes even impossible. In addition, the repair costs could be very high. A possible solution can be found to improve the stated issues when applying dual systems. The idea of dual systems, formed by combining moment-resisting frames (MRF) and replaceable bracing systems, is that seismic energy is dissipated through the yielding of the bracing system while MRFs remain elastic and enable re-centering of the structure. MRF design may require higher-grade steel to ensure elastic behaviour, while the bracing system must be sufficiently rigid and ductile [1]. In [2] the authors summarised the experimental and numerical behaviour of re-centring dual eccentrically braced frames (EBFs) with removable links. Experimental tests on full-scale dual eccentrically braced structures were conducted to test the re-centring capability and feasibility of the link removal. Results showed excellent behaviour at serviceability limit state (SLS) and ultimate limit state (ULS) earthquakes. Small permanent deformations were observed but within the erection tolerance. Two case study buildings were evaluated using pushover analysis. The analysis showed that MRFs remained elastic before reaching ULS deformations in the removable links of the EBF, which confirmed the dual behaviour of the structures. In paper [3] the authors investigate replaceable shear

Copyright © 2025 CroCEE
DOI: https://doi.org/10.5592/CO/3CroCEE.2025.105

panels as lateral load-resisting and dissipative systems as alternatives to traditional systems. The results showed that shear panels are efficient bracing systems with stable cyclic behaviour and good ductility. The analysis showed that yielding occurs in replaceable shear panels while MRFs remain elastic. Also, re-centering analysis showed that residual drift is not present after unloading. However, slender shear panels may buckle during the early stages of lateral loading.

Also, a possible solution for lateral stabilisation can be the usage of different composite steel-concrete systems. Combining concrete and steel can achieve both rigidity and ductility of the bracing system [4]. Composite systems, where steel sheets are connected with screws, bolts, or diaphragms and filled with concrete first saw used in the nuclear industry and steel frames of highrise buildings. Such systems showed excellent behaviour regarding lateral resistance and ductility. One of the ways of optimal use of materials is the application of cold-formed steel profiles and elements. In papers [5,6], the application of corrugated steel sheets was investigated, and it was shown that corrugated sheets provide greater resistance and stiffness than conventional steel sheets. However, in highly seismic areas for the stabilisation of medium-rise and highrise buildings, the disadvantage of such systems is insufficient shear resistance, which can be increased by introducing concrete. In paper [7], the authors conducted a numerical analysis which showed potentially favourable characteristics of a shear wall composed of corrugated steel sheets and concrete.

This paper presents an assessment of dual systems, based on finite element analysis, that integrates multi-story MRFs with innovative double-skin cold-formed steel concrete composite shear walls. In the first step, non-linear analyses of individual shear wall panels are conducted considering influences of steel sheet thickness, concrete strength, and shear connection type. Afterwards, pushover analyses are performed using the resulting load-displacement behaviour of the analysed shear walls.

2. Analysed system

The structure consists, in the x direction, of two three-bay moment resisting frames with the shear walls in the central bay and in the y direction of four one-bay moment resisting frames, of which two with the bracing system. The shear wall, acting as a bracing system, consists of corrugated cold-formed steel sheets filled with concrete, which are connected with intermediate shear connectors and form a sandwich steel-concrete-steel panel.

The structure has eight floors with a floor height of 4,2 m, and the span of the bay is 8 m. The structure is regular in plan and height, as shown in Figs. 1. and 2. In addition, Fig. 2. shows the schematic view of the structure's re-centering capability.

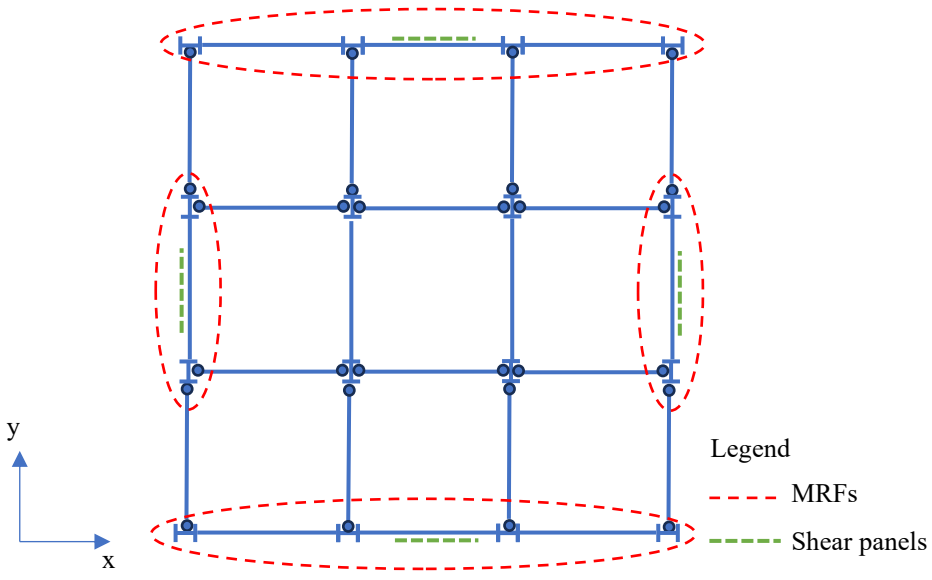


Figure 1. Building plan

Copyright © 2025 CroCEE
DOI: https://doi.org/10.5592/CO/3CroCEE.2025.105

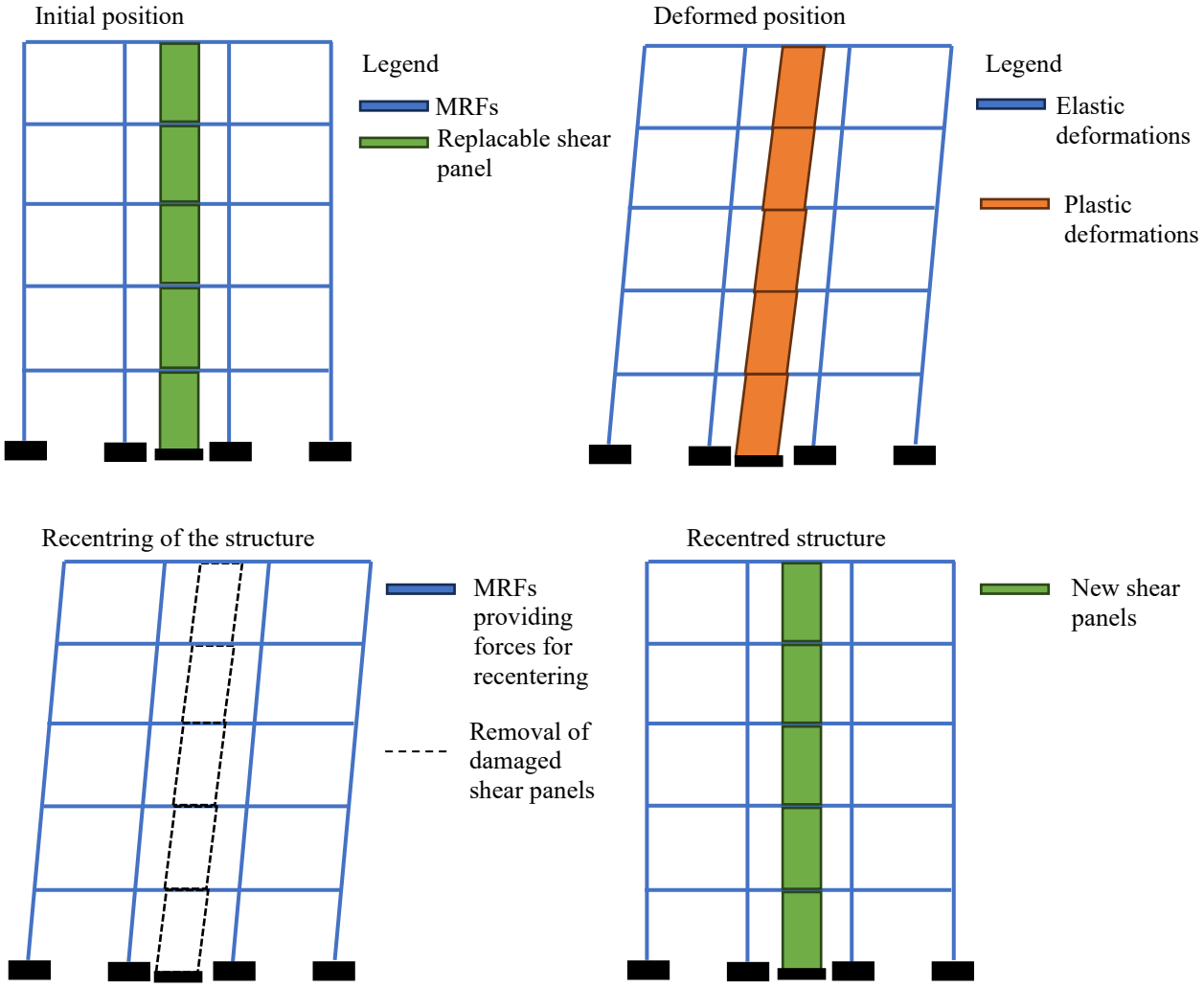


Figure 2. Building elevation and schematic view of the structure's re-centering capability

3. Numerical analysis of the shear wall

Numerical analysis of composite shear walls was performed with Abaqus software [8] by using Explicit Solver.

3.1. Geometry and Components

The shear wall consists of double skin cold formed corrugated steel sheets filled with concrete, which are connected with intermediate shear connectors forming a sandwich steel-concrete-steel panel, as shown in Fig. 4. The shear wall is 2.2 m wide and 4.2 m tall with an average thickness of 120 mm. Details regarding geometry are provided in [9]. Cold-formed corrugated steel sheets were modelled using homogenous shell elements, type S4R and the concrete slab was modelled using homogenous solid elements, type C3D8R. Intermediate shear connectors were modelled using beam elements B31.

3.2. Material

All materials were assigned elastic and plastic behaviour. Material properties of steel used for corrugated sheets were obtained by experimental tests [10]. The elastic behaviour of steel was modelled as isotropic with Young's modulus equal to E = 210 000 MPa and Poisson's ratio of ν = 0.3. Plastic material properties were modelled using a true stress-strain relationship.

Copyright © 2025 CroCEE
DOI: https://doi.org/10.5592/CO/3CroCEE.2025.105

The elastic behaviour of the concrete was modelled as isotropic with Young's modulus equal to $E = 31\,476$ MPa and $E = 32\,836$ MPa for classes of concrete C25/30 and C30/37, respectively and Poisson's ratio of $v = 0.2$. The plastic behaviour of the concrete was simulated with the Concrete Damage Plasticity (CDP) model according to research provided in paper [11].

3.3. Boundary conditions and interactions

At the bottom of the shear wall, displacements and rotations in all three directions are prevented at all points of the corrugated steel sheet. At the top of the shear wall, out-of-plane displacement is prevented. Also, all points of the corrugated steel sheet edge are connected using the coupling constraints with a reference point through which the horizontal load was applied using the displacement control method.

The shear connection between concrete and corrugated steel sheets is realised with bolts embedded in the concrete and a "tie constraint" corresponding to a full shear connection. "MPC constraint"-Multi-point constraints were used to attach bolts to corrugated steel sheets.

Contact between bolts and concrete was modelled with tangential behaviour with a friction coefficient equal to 0.3 and normal behaviour as "hard" contact.

3.4. Mesh convergence analysis

A mesh sensitivity test was conducted to determine the influence of mesh size on the results. Varied mesh sizes are 5, 10, 15, and 25 mm for the corrugated steel sheets and 10, 15, 20, 25, and 50 mm for the concrete filling. The results are presented with a force-displacement curve shown in Fig. 3. Table 1 shows the ultimate force P_u and displacement u_u for models with different mesh sizes

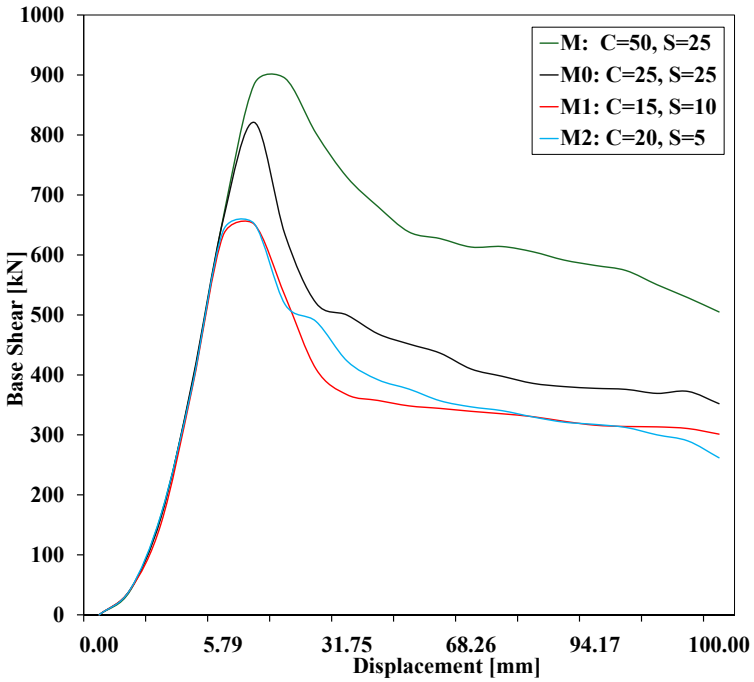


Figure 3. Comparison of the force-displacement curves for different mesh sizes

Table 1. Models with different mesh sizes and corresponding ultimate force and displacement

MODEL	MESH	P_u [kN]	u_u [mm]
CCFSSW_03_03_16_M	CCFS-25, C-50	894,47	16,32
CCFSSW_03_03_16_M0	CCFS-25, C-25	821,00	10,36
CCFSSW_03_03_16_M1	CCFS-10, C-15	651,60	10,34
CCFSSW_03_03_16_M2	CCFS-5, C-20	652,46	10,35

Proceedings of the 3rd Croatian Conference on Earthquake Engineering - 3CroCEE
19–22 March 2025, Split, Croatia
Copyright © 2025 CroCEE
DOI: https://doi.org/10.5592/CO/3CroCEE.2025.105

The optimal mesh size is determined by considering the convergence of the results. Models with a mesh configuration denoted CCFSSW_03_03_16_M and CCFSSW_03_03_16_M0 have significant deviations in the results. Convergence of results is observed for models with a mesh configuration denoted CCFSSW_03_03_16_M1 and CCFSSW_03_03_16_M2. Therefore, the adopted mesh configuration is CCFSSW_03_03_16_M1.

3.5. Parametric analysis

In order to determine the optimal structural design of the shear wall, parametric analysis was performed. The assumption is that the following parameters mostly influence the behaviour of the shear wall: the thickness of the corrugated steel sheets, concrete strength, the diameter of the bolts and the arrangement of the bolts. Therefore, these parameters were varied. Also, the influence of mesh sensitivity on the results was tested. The behaviour of each analysed shear wall is represented with a numerical load-displacement curve. Table 2 lists all varied parameters and Fig. 4. shows different cases of bolt arrangement.

Table 2. Parameters varied within the parametric study

Steel sheet thickness	Concrete strength	Diameter of bolts	Shear connection type
1 mm, 3 mm	C25/30, C30/37	M12, M16	SW1, SW2, SW3

The influence of the parameter change is best seen by comparing numerical force-displacement curves. In a comparison of the results for different shear connection types and bolt arrangements, shown in Fig. 5. a), it can be concluded that the shear wall with bolt configuration SW2 has the greatest capacity, followed by a shear wall with full shear connection. In contrast, the shear wall with bolt arrangement SW3 has the lowest capacity. A larger bolt diameter leads to a slight increase in the shear wall's capacity, as represented in Fig. 5. b).

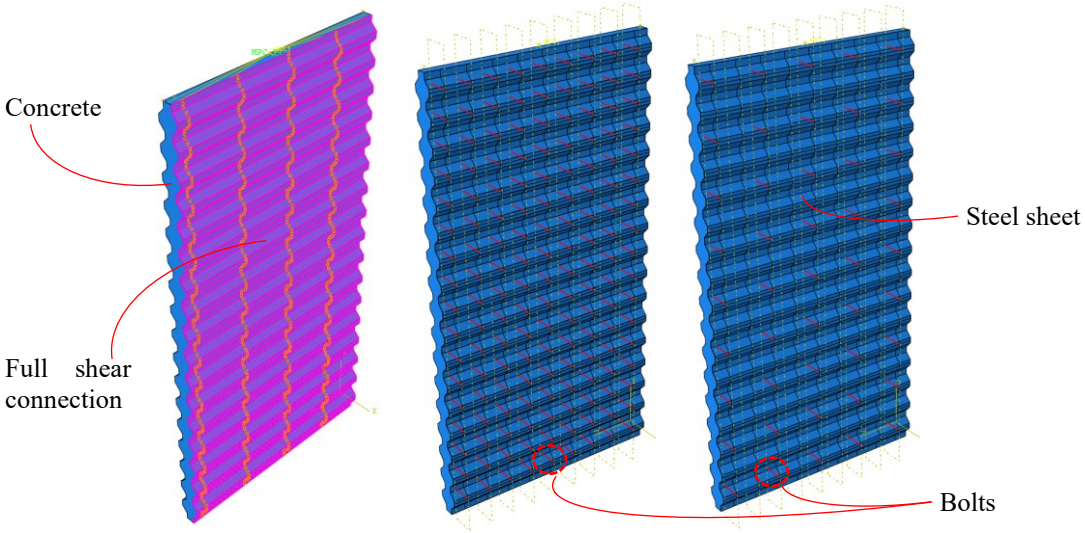


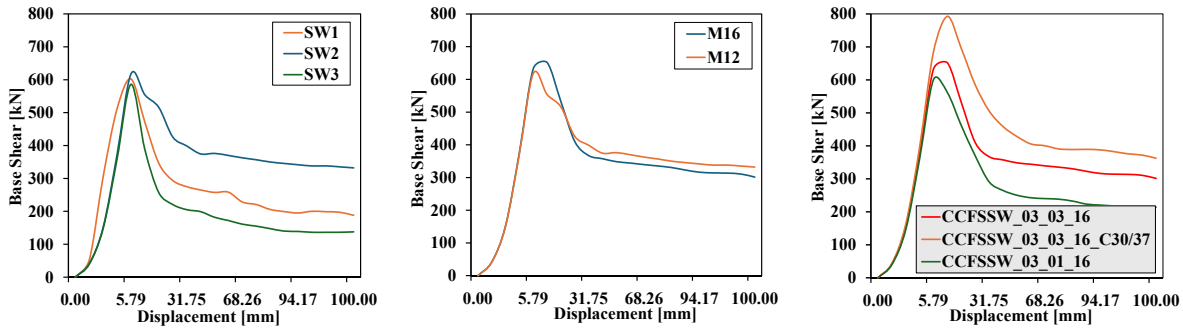
Figure 4. Type of the shear connection and bolt arrangement SW1, SW2 and SW3 in the given order

By comparing numerical force-displacement curves of the shear walls with the same bolt arrangement and diameter, shown in Fig. 5. c), it can be seen that the highest capacity has the shear wall with concrete strength C30/37 and steel sheet thickness of 3 mm, followed by the shear wall with concrete strength C25/30 and steel sheet thickness of 3 mm. The lowest capacity shear wall is composed of concrete strength C25/30 and a steel sheet thickness of 1 mm.

Based on the parametric study, the increase in the strength of the concrete and the type of the shear connection makes the most significant contribution to the capacity of the shear wall. In contrast, the

Copyright © 2025 CroCEE
DOI: https://doi.org/10.5592/CO/3CroCEE.2025.105

increase in the thickness of the steel sheets and bolt diameter results with a minor contribution to the wall strength.



a) b) c)

Figure 5. a) Influence of the shear connection type, b) Influence of the bolt diameter on the capacity of the shear wall, c) Influence of the concrete strength and steel sheet thickness on the capacity of the shear wall

4. Seismic analysis

4.1. Selection of the analysis method

For performance-based design and damage control, the most suitable are non-linear methods. Therefore, the non-linear static (pushover) method will be used. Furthermore, pushover analysis gives better insight into the structure's behaviour than the conventional approach using elastic response spectrum reduced with behaviour factor q for several reasons. First, values of behaviour factors are approximate and may not be suitable for specific structures. Analysis based on the q factor does not consider redistribution of internal forces and deformation when inelastic deformations occur [12]. Moreover, the collapse mechanism cannot be predicted using the elastic distribution of forces and deformations. The assessment of the structure behaviour has been done using the non-linear static (pushover) method - N2 method. The analysis results ar provided as a characteristic force-displacement relationship that gives key information about structure: strength, stiffness and ductility.

4.2. Overview of the N2 method

The steps of the N2 method, according to [13], are:

1. Data

The analysis begins by defining the 2D structural model, the force-deformation relationship for structural elements, and seismic demand, which is determined in the form of an elastic pseudo-acceleration spectrum where spectral acceleration is a function of the period of the structure.

2. Seismic demand in Acceleration-displacement format

The acceleration response spectrum is transformed into AD format using the following relation:

$$S_{de} = \frac{T^2}{4\pi^2} S_{ae} \tag{1}$$

where S_{de} and S_{ae} are values of displacement and acceleration, respectively, corresponding to the response spectrum in AD format for a fundamental period and fixed viscous damping ratio.

For an inelastic Single degree of freedom (SDOF) system with a bilinear force-deformation relationship, the acceleration spectrum and the displacement spectrum can be determined using the following relations:

$$S_a = \frac{f_y}{m} = \frac{S_{ae}}{R_\mu} \tag{2}$$

Proceedings of the 3rd Croatian Conference on Earthquake Engineering - 3CroCEE
19–22 March 2025, Split, Croatia
Copyright © 2025 CroCEE
DOI: https://doi.org/10.5592/CO/3CroCEE.2025.105

$$S_d = \frac{\mu}{R_\mu} S_{de} = \frac{\mu}{R_\mu} \frac{T^2}{4\pi^2} S_{ae} = \mu \frac{T^2}{4\pi^2} S_a \tag{3}$$

where μ is the ductility factor and R_μ is the reduction factor due to ductility.

For determining R_μ, factor concerning the period T, N2 method, as implemented in EC8, uses bilinear relation between R_μ and T:

$$R_\mu = (\mu - 1)\frac{T}{T_c} + 1; T < T_c \tag{4}$$

$$R_\mu = \mu; T \geq T_c \tag{5}$$

where T_c is the transition period of the short-period range and the medium-period range.

In the medium-period and long-period range, the equal displacement rule applies as stated in equation (5). Now, the demand spectra in AD format can be obtained.

3. Pushover analysis

The structure is subjected to a monotonically increasing pattern of lateral forces and constant gravitational load. Lateral forces represent inertial forces due to earthquakes. There is no exact solution for the distribution of lateral forces. A reasonable solution is to use two different displacement shapes and to envelop the results. Commonly used load patterns are uniform and modal distribution. The main assumption of the method is that the structure vibrates in a single time-invariant mode. Therefore, the modal distribution of lateral forces would equal the effective (inertial) forces acting upon the structure during an earthquake. It is important to emphasise that this method is not applicable to structures that vibrate in higher modes. The vector of lateral loads is:

$$P = p\boldsymbol{\Psi} = p\boldsymbol{M}\boldsymbol{\Phi} \tag{6}$$

where p controls magnitude. Distribution of lateral forces $\boldsymbol{\Psi}$ related to diagonal mass matrix $\boldsymbol{M}$ and assumed displacement shape $\boldsymbol{\Phi}$.

Loading of a structure is displacement-controlled, i.e., the load is applied until predefined displacement is achieved. By incrementally increasing the load, elements progressively yield, leading to overall stiffness loss. The analysis results in a characteristic non-linear force-displacement curve, most commonly related to base shear and rooftop displacement.

4. Equivalent SDOF system

In the N2 method, seismic demand is determined by using response spectra given for SDOF systems, and the Multi degree of freedom (MDOF) system has to be transformed into an equivalent SDOF system.

The equation of motion of the MDOF system is:

$$\boldsymbol{M}\ddot{\boldsymbol{U}} + \boldsymbol{R} = \boldsymbol{M}\boldsymbol{1}a \tag{7}$$

where $\boldsymbol{M}$ is a diagonal mass matrix, and $\boldsymbol{U}$ and $\boldsymbol{R}$ are displacement and internal forces vectors, respectively. 1 is the unit vector and a is the ground acceleration. Dumping is included in the design spectrum. When assuming a constant displacement shape, the displacement vector $\boldsymbol{U}$ is defined as:

$$\boldsymbol{U} = \boldsymbol{\Phi} D_t \tag{8}$$

where D_t is time-dependent top displacement. $\boldsymbol{\Phi}$ is normalised such that the top component is equal to 1.

Equilibrium of forces:

Proceedings of the 3rd Croatian Conference on Earthquake Engineering - 3CroCEE
19–22 March 2025, Split, Croatia
Copyright © 2025 CroCEE
DOI: https://doi.org/10.5592/CO/3CroCEE.2025.105

$$\boldsymbol{P} = \boldsymbol{R} \tag{9}$$

where R represents internal forces and P statically applied external forces.

Expanding equation (9) and multiplying from the left-hand side with Φ^T the following equation is obtained:

$$\boldsymbol{\Phi^T M \Phi \ddot{D}_t} + \boldsymbol{\Phi^T M \Phi} p = -\boldsymbol{\Phi^T M 1} a \tag{10}$$

Dividing the left-hand side with $\boldsymbol{\Phi^T M 1}$, equation of motion of equivalent SDOF system is:

$$m^* \ddot{D}^* + F^* = -m^* a \tag{11}$$

Where m^* is the mass of the equivalent SDOF system:

$$\sum_i^n m_i^* \cdot \Phi_i \tag{12}$$

and D^* and F^* are the displacement and force of the equivalent SDOF system:

$$D^* = \frac{d_t}{\Gamma} \tag{13}$$

$$F^* = \frac{V}{\Gamma} \tag{14}$$

Base shear of the MDOF system:

$$V = \{\Phi\}^T [M]\{1\} p = p m^* \tag{15}$$

The constant Γ of transformation of the MDOF system to the SDOF system and vice versa is defined as:

$$\Gamma = \frac{\{\Phi\}^T [M]\{1\}}{\{\Phi\}^T [M]\{\Phi\}} = \frac{\sum m_i \Phi_i}{\sum m_i \Phi_i^2} \tag{16}$$

Constant Γ is applied for the transformation of both displacements and forces, as shown in equations (13) and (14), force-displacement curve of the equivalent SDOF system has the same shape and initial stiffness as one for the MDOF system. The obtained force-displacement curve of equivalent SDOF is then simplified to a bilinear elastoplastic curve. To determine the initial stiffness of the idealised system, EC8 suggests using the principle of equal energy of the real and idealised curve. The period of the idealised system can be determined as follows:

$$T^* = 2\pi \sqrt{\frac{m^* d_y^*}{F_y^*}} \tag{17}$$

where d_y^* and F_y^* are yield displacement and yield force, respectively. Finally, the capacity diagram in AD format is obtained using the following equation:

$$S_a = \frac{F^*}{m^*} \tag{18}$$

5. Seismic demand

Seismic demand can be determined using a graphical procedure by plotting demand spectra, inelastic spectra in AD format, obtained from elastic demand spectra using ductility factor, and capacity diagram

Copyright © 2025 CroCEE
DOI: https://doi.org/10.5592/CO/3CroCEE.2025.105

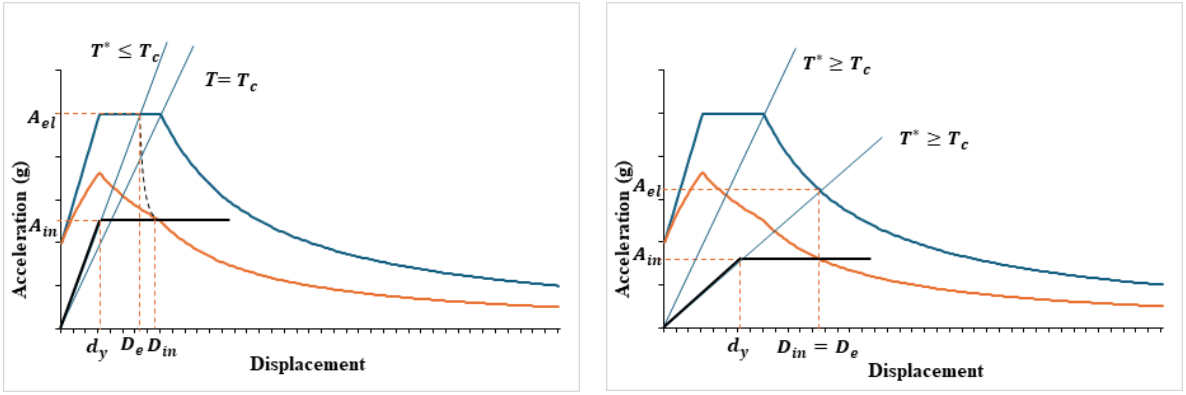
in the same graph, presented in Figs. 6. a) and 6. b). Elastic demand is determined by the intersection of the radial line corresponding to the elastic period of the idealised bilinear system, T^*, with elastic demand spectra. Inelastic displacement demand depends on the period of the system.

For periods shorter than T_c, inelastic displacement demand can be determined using the following relation:

$$S_d = \mu D_y^* = \frac{S_{de}}{R_\mu}\left(1 + (R_\mu - 1)\frac{T_C}{T^*}\right) \tag{19}$$

For periods larger than T_c, the equal displacement rule applies, i.e.:

$$S_d = S_{de}(T^*) \tag{20}$$



a) b)

Figure 6. a) Seismic demand for equivalent SDOF system with a period in short range b) Seismic demand for equivalent SDOF system with a period in medium/long-period range

Then, the MDOF system's displacement demand is determined using equations (13) and (14).

Pushover analysis is then performed until target displacement is reached, after which resistant capacity and floor drifts are verified.

4.3. Pushover analysis modelling and results

The pushover analysis was conducted in SAP2000 [14]. The structure is regular in plan and elevation and vibrates predominantly in the first mode, therefore, pushover analysis is applicable. A single three-bay moment resisting frame with the shear walls is analysed. P-Δ effects were not included in the analysis as the structure is not sensitive to its effects [9]. Half of the overall structural mass was taken into account.

Non-linear plastic hinges were assigned at the ends of the MRF's beams and columns. The shear walls were modelled with link elements. The behaviour of the link element is determined by the capacity curve obtained from the non-linear analysis of the individual shear wall in Abaqus software, as shown in Fig. 5. c).

The load pattern is defined using equation (6) by determining the diagonal mass matrix and the first mode of the structure, which is determined by conducting the modal analysis. The load is applied using the displacement control method. The structure is loaded until the roof displacement of 0.3 m is reached. The first model used a shear wall with concrete C25/30 and 1 mm thick steel sheets. In the second model, a shear wall with concrete C25/30 and 3 mm thick steel sheets was used, and in the third model, a shear wall with concrete C30/37 and a 3 mm thick steel sheet was used.

During the analysis, in all three models, yielding was not observed in the MRFs, while the shear walls yielded. Therefore, all three systems satisfy the requirements of dual systems.

Copyright © 2025 CroCEE
DOI: https://doi.org/10.5592/CO/3CroCEE.2025.105

The analysis results are represented with so-called capacity curves, showing the relationship between base shear and rooftop displacement. Seismic demand is given for the SDOF system. Therefore, the capacity curve of the MDOF system has to be transformed into the capacity curve of the equivalent SDOF system by using the transformation factor Γ. Using the equal energy principle, the obtained curve is idealised into the bilinear curve. The calculation of yield displacement, elastic periods of the idealised SDOF systems, and target displacements for the equivalent SDOF systems and corresponding MDOF systems are presented in Table 3. Fig. 8. shows the capacity curves of the equivalent SDOF system with corresponding bilinear curves.

Table 3. Calculation of the target displacement [15]

	CCFSSW_03_01_16	CCFSSW_03_03_16	CCFSSW_03_03_16_C30/37
m^*		763.88	
Γ		1.262	
E_m^*	191.37	209.66	232.256
d_m^*	0.23772	0.23772	0.23772
F_y^*	854.6	948.5	1051
$d_y^* = 2(d_m^* - E_m^*/F_y^*)$	0.028	0.033	0.033
$T^* = 2\pi\sqrt{(m^* d_y^*/F_y^*)}$	0.99	1.03	0.98
$S_e(T)$	2.97	2.85	3
$d_{et}^*{}_{SDOF} = S_e(T^*)(T^*/2\pi)$	0.073	0.077	0.073
$d_{et}^*{}_{MDOF} = \Gamma d_{et}^*{}_{SDOF}$	0.092	0.097	0.092

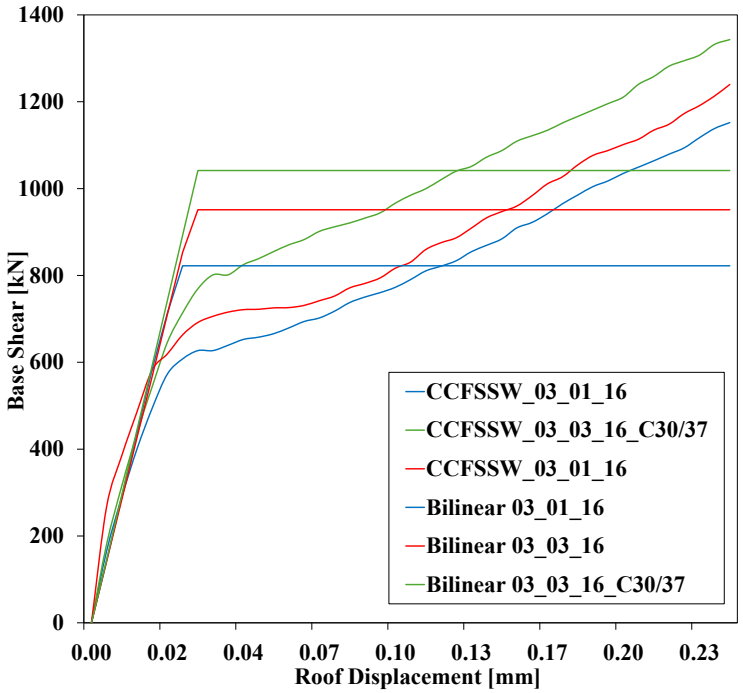


Figure 7. The capacity curves for equivalent SDOF systems and corresponding bilinear idealisations

The overstrength factor can be determined by comparing the base shear at the formation of the plastic mechanism and the base shear at the beginning of the yielding. After obtaining the overstrength factor, the behaviour factor can be calculated as presented in Table 4.

Table 4. Calculated behaviour factors [15]

	CCFSSW_03_01_16	CCFSSW_03_03_16	CCFSSW_03_03_16_C30/37
α_u/α_1	1.35	1.31	1.28
q_0		$4.5 \cdot \alpha_u/\alpha_1$	
$q = q_0 \cdot k_w$, $k_w = 1.00$	6.1	5.9	5.8

Copyright © 2025 CroCEE
DOI: https://doi.org/10.5592/CO/3CroCEE.2025.105

Pushover analysis proved that all three models satisfy the requirements of the dual systems. The shear walls yielded while MRFs remained elastic, thus enabling re-centering. The most notable difference is in the capacity. Comparing the capacity curves of the global models, presented in Fig. 8., with the capacity curves of the individual shear walls, presented in Fig. 5. c), it is evident that the two correlate. The difference in the overstrength ratio and the behaviour factor is not significant. Obtained values of the behaviour factors suggest that the structures can be designed using much smaller forces.

5. Conclusions

Dual structural systems have shown increased attention in recent years because of their re-centring capabilities. The paper analyses dual systems based on finite element analysis that integrate multi-story MRFs with innovative double-skin cold-formed steel concrete composite shear walls. The steel frame consists of three bays, a central braced frame, and two adjacent moment-resisting frames. The shear wall, acting as a bracing system, consists of corrugated cold-formed steel sheets filled with concrete, which are connected with intermediate shear connectors and form a sandwich steel-concrete-steel panel. In this system, the double skin composite shear wall has the function of energy dissipation during an earthquake, while the MRFs remain elastic to provide re-centring forces once the shear walls are removed from each floor. Pushover analysis confirmed the system's dual behaviour. All three shear walls proved to be an effective form of lateral stabilisation. The behaviour factors and overstrength ratios are similar for all three models. The only significant difference is in the capacity of the system, which correlates with the capacity of the individual shear wall. The increase in capacity of the individual shear wall and the global system is achieved primarily by increasing concrete strength, while steel sheet thickness and bolt diameter contribute less. Such structures have the potential of high sustainability after a significant earthquake since replacing the dissipative elements restores the structure to its original position. This paper highlights the benefits of systems with re-centring capabilities, emphasising their potential to reduce repair costs and enhance sustainability. However, further research is needed to optimise these systems and explore different shear wall typologies, which could provide deeper insights into their practical applications.

References

[1] Lukačević I, Maleta T, Dujmovic D. Behaviour of dual eccentrically braced steel frames with short and long seismic links, 2019, p. 1673–80. https://doi.org/10.2749/newyork.2019.1673.

[2] Chesoan A, Stratan A, Dubina D. Design implementation of re-centring dual eccentrically braced frames with removable links. Soil Dynamics and Earthquake Engineering 2018;112:174–84. https://doi.org/10.1016/j.soildyn.2018.05.015.

[3] Dubina D, Dinu F. Experimental evaluation of dual frame structures with thin-walled steel panels. Thin-Walled Structures 2014;78:57–69. https://doi.org/10.1016/j.tws.2014.01.001.

[4] Androić B, Dujmović D, Lukačević I. Projektiranje spregnutih konstrukcija prema Eurocode 4. Zagreb: IA Projektiranje; 2012.

[5] Zhang W, Mahdavian M, Li Y, Yu C. Experiments and Simulations of Cold-Formed Steel Wall Assemblies Using Corrugated Steel Sheathing Subjected to Shear and Gravity Loads. Journal of Structural Engineering 2017;143. https://doi.org/10.1061/(ASCE)ST.1943-541X.0001681.

[6] Zhang W, Mahdavian M, Lan X, Yu C. Cold-Formed Steel Framed Shear Walls with In-Frame Corrugated Steel Sheathing. Journal of Structural Engineering 2021;147. https://doi.org/10.1061/(ASCE)ST.1943-541X.0003182.

[7] Vlaho Žuvelek, Ivan Ćurković, Ivan Lukačević, Andrea Rajić. Numerical Investigation of Double-Skin Cold-Formed Steel Shear Wall Filled with Concrete. In: Ungureanu V, Bragança L, Baniotopoulos C, Abdalla KM, editors. International Conference" Coordinating Engineering for Sustainability and Resilience", Springer Nature Switzerland; 2024, p. 105–15.

[8] ABAQUS User Manual 2014.

Copyright © 2025 CroCEE
DOI: https://doi.org/10.5592/CO/3CroCEE.2025.105

[9] Emanuel Krupa-Jurić. Non-linear analysis of multy-storey steel building with innovative shear wall bracing system. University of Zagreb, Faculty of Civil Engineering, 2024.

[10] Ivan Lukačević, Marko Bartolac, Ivan Ćurković, Andrea Rajić, Vlaho Žuvelek. Laboratory Tests of Lightweight Composite Floor System LWT-FLOOR. Zagreb: n.d.

[11] Lukačević I, Ćurković I, Rajić A, Bartolac M. Lightweight Composite Floor System-Cold-Formed Steel and Concrete-LWT-FLOOR Project. Buildings 2022;12:209. https://doi.org/10.3390/buildings12020209.

[12] Mitrović S, Čaušević M. Non-linear static seismic analysis of structures. Građevinar 2009:521–31.

[13] Fajfar P. Structural analysis in earthquake engineering – a breakthrough of simplified non-linear methods. 12th European Conference on Earthquake Engineering, Elsevier Science Ltd.; 2002.

[14] SAP2000 Integrated Software for Structural Analysis and Design, ” Computers and Structures Inc., Berkeley, California. n.d.

[15] Eurocode 8: Design of structures for earthquake resistance - Part 1: General rules, seismic actions and rules for buildings n.d.

Proceedings of the 3rd Croatian Conference on Earthquake Engineering - 3CroCEE
19–22 March 2025, Split, Croatia
Copyright © 2025 CroCEE
DOI: https://doi.org/10.5592/CO/3CroCEE.2025.111

NUMERICAL EXPERIMENT FOR SHEAR KEY JOINT BEHAVIOUR SIMULATION IN ARCH DAMS: PART 1 – INVESTIGATING THE INFLUENCE OF THE KEY SHAPE AND ANGLE

Ana Nanevska [(1)], Violeta Mircevska [(2)]

[(1)] *Research Assistant, Institute of Earthquake Engineering and Engineering Seismology, University of Ss. Cyril and Methodious, Skopje, R. N. Macedonia., nanevska@iziis.ukim.edu.mk*
[(2)] *Professor, Institute of Earthquake Engineering and Engineering Seismology, University of Ss. Cyril and Methodious, Skopje, R. N. Macedonia., mircevska@iziis.ukim.edu.mk*

Abstract

Nonlinear behaviour of contraction joints in arch dams, such as joint opening and sliding caused by hydrostatic pressure and temperature variations can affect the dam's serviceability. Furthermore, strong seismic events can additionally alter the response in dynamic conditions, impacting the natural period and stress redistribution in the arches and cantilevers. In order to enhance structural integrity with additional shear strength, shear key elements are usually installed along these joints. However, traditional modeling with the actual shear key geometry results in complex analyses. This paper presents a novel approach for simulating shear key behaviour by modifying the flat joint concept in ADAD-IZIIS software. The method introduces additional tangential stiffness to the flat joint's stiffness matrix to simulate shear resistance derived from the key geometry. The model uses a uniaxial constitutive law for nonlinear behaviour in normal and Coulomb's friction law in the tangential direction. This paper presents the first part of a comprehensive study examining the influence of the key shape and angle through numerical experiments using refined FE models of flat, bevelled, and unbevelled shear key joints. The additional shear resistance $F_{\tau,add}$ is calculated by increasing the initial modulus of elasticity $E_{n,\tau}$ in the local shear direction as $E_{n\tau,add}=k_{ad}*E_{n,\tau}$, applying the additional tangential stiffness coefficient k_{ad}, derived from the experimental analyses. Results indicate that the shape and angle of the key greatly influence the element's shear resistance. Unbevelled shear key joint increases tangential stiffness by approximately 60%, while the bevelled joint by 23% compared to the flat joint. Although tangential stiffness minimally affects the extreme joint openings at the top edge, the unbevelled joint significantly reduces openings along the joint length. The research confirms the efficiency of the proposed approach in simulation of the complex nonlinear behavior of an arch dam constructed with shear key joints.

Keywords: contraction joint, nonlinear behaviour, shear key, numerical experiment.

1. Introduction

Arch dams are highly efficient structures that transfer large compressive stresses to the supports through their curved arch geometry [1]. In order to control tensile stresses development caused by expansion and contraction during concreting, temperature variations, as well as seismic activity, arch dams are constructed in monolithic blocks separated by vertical joints [2]. These joints, however, are potential weak points due to imperfections in the grouting process, making them susceptible to initial damage from temperature variations and strong earthquakes [3]. During strong earthquakes, the monoliths undergo relative displacements, resulting in joint opening and shear sliding, causing significant redistribution of internal forces both during the seismic action and afterward due to residual joint openness. Several studies [4][5][6][7][8] have demonstrated that the nonlinear behaviour of these joints in arch dams, including their opening and shear sliding increases the natural period of the dam and leads to a significant redistribution of stresses in the arches and cantilevers. Therefore, accurate numerical simulation of these behaviours is critical for evaluating the static and seismic stability of arch dams.

To improve the compactness, shear strength and enhance the overall integrity of arch dams, shear key elements are often incorporated along the joints in the radial and/or longitudinal directions. These elements are designed to provide additional shear resistance when joints experience normal

Proceedings of the 3rd Croatian Conference on Earthquake Engineering - 3CroCEE
19–22 March 2025, Split, Croatia
Copyright © 2025 CroCEE
DOI: https://doi.org/10.5592/CO/3CroCEE.2025.111

displacements, i.e. opening in the normal direction [9]. While shear keys offer significant advantages, including improved monolithic integrity particularly in thinner arch dams, their analytical modeling remains challenging. Despite advancements over the last four decades, comprehensive analysis of arch dams with shear key joints remains limited. Namely, over the past four decades, number of different constitutive models have been applied for joint behaviour simulation, progressing from models that include only the normal displacement of joints, to models that include the relationship between the opening and shear sliding in the contact.

Early modeling efforts include contact elements derived from rock mechanics, such as finite elements for soft material contacts that do not work in tension [10][11][12]. Beer, 1985 [13] developed a contact element using special quasi-continuum finite elements with a small thickness and a prescribed reduced stiffness. However, further studies are needed to extend the applicability of this method for simulation of dynamic behaviour. Further developments introduced nonlinear spring models [14], which also failed to incorporate the most important mechanical properties of the shear key elements, including initial tensile stresses from grouting and shear strength loss due to dilation. Later studies incorporating 3D contact elements were limited to simulating the behaviour of the joint in the normal direction only, neglecting the interaction effects between normal and tangential displacements [4]. The first FE models with a discrete crack in the joint were developed for tensile failure for a prescribed lower limit only for static load [15] or not considering all physical properties of the joint [16].

A gap element introduced into the ADINA software assumed identical movement of contact element points in the vertical and radial directions, an assumption that does not align with the observed behaviour of shear key joints [17]. Similarly, a nonlinear contact element incorporated in the ADAP-88 software considered both normal and tangential displacements but didn't consider the geometric characteristics of the shear key elements [18]. Another approach employed a zero-thickness contact element to model structural joints, considering opening, closing, and shear effects, as well as limiting relative tangential displacements based on a predefined slip limit specified according to the joint's geometry [5]. While this method achieves satisfactory accuracy for prevented slip in the contact, under conditions of partial slip with partial joint openness its efficiency needs to be improved.

The discrete crack contact model proposed by Ahmadi et al., 2001 [3] was used to capture the nonlinear interaction between shear and tension behavior, making it an important advancement in understanding the key mechanical properties of joints. This model incorporates partial tangential sliding that depends on normal displacements, assuming elastic behavior for closed joints and fully plastic behavior when the shear strength is exceeded. Additional efforts to model contact elements include elements with zero thickness [19] as well as linear springs [20], both of which ignore the most important shear key effects. More precise joint configurations have been adopted in numerical simulations to achieve realistic representations of shear key joint behaviour [21]. However, analyses' results show significant stress concentrations at sharp contact angles, that highlights the need for further model refinements. Additional developments, such as the introduction of additional tangential nonlinear spring elements with enhanced stiffness to simulate shear key effects address some of these challenges [22]. Still, further improvements remain necessary, as current models lack comprehensive consideration of different shear key geometries.

Simulating the nonlinear behavior of joints presents a significant challenge, particularly in accounting for all influencing factors and addressing computational limitations. A major difficulty is accurately modeling of the complex shear key geometry, as the dense finite element mesh required for precise representation often leads to computational impracticalities. To address this, it is necessary to develop a constitutive law that will integrate the effect of material nonlinearity of the grouting mass with the restrictive shear effect of the shear key geometry. In this study, a nonlinear constitutive model for simulating the behavior of shear key joints is developed. The model integrates existing research insights and introduces modifications based on numerical experiments to accurately replicate shear key behavior. The model is based on a 3D flat joint contact element previously integrated into the ADAD-IZIIS software [23]. This paper presents the first part of a comprehensive study, focusing on results of

Copyright © 2025 CroCEE
DOI: https://doi.org/10.5592/CO/3CroCEE.2025.111

numerical experiments that investigate the influence of the key shape and angle on the behaviour of shear key joints in arch dams.

2. 3D flat contact element implemented in the ADAD-IZIIS software

The flat joint behaviour in the software [23] is simulated using a 3D contact element positioned between two adjacent finite elements (representing concrete monoliths) with different mechanical properties. The finite elements can be modelled with 6, 8, 15 or 20 points, while the contact elements with 6, 8, 12 or 16 points. Each pair of nodes has identical global coordinates, with one node on the lower contact surface (Π1) and the corresponding node on the upper contact surface (Π2). Fig. 1 illustrates these contact surfaces, representing the faces of two different finite elements in the contact, each defined by eight points.

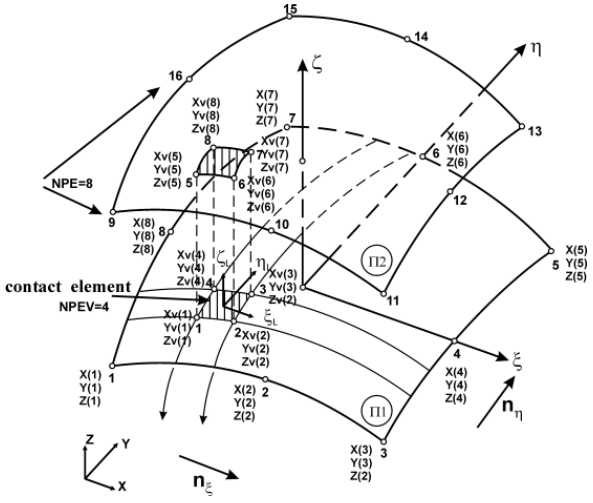


Figure 1. Schematic representation of the 8-point contact element

The contact element follows a uniaxial constitutive law for the nonlinear behaviour in the normal direction (Fig. 2a) and Coulomb's law of friction for the two tangential directions (Fig. 2b), capturing a coupled effect of the stresses in all three directions of the contact. The mechanical properties of the grouting mass are adopted with slightly lower values than the concrete in the monoliths, namely: modulus of elasticity in the normal and tangential directions $E=25.5*10^7$ kPa, tensile strength $\sigma_{t,doz}=1000$ kPa, compressive strength $\sigma_{c,doz}=25500$ kPa, compressive dilation $\varepsilon_c=0.2*10^{-3}$ m, compressive dilation $\varepsilon_{fail}=0.3*10^{-3}$ m when the compressive strength drops to $\sigma_{c,fail}=20\ 000$ kPa and shear strength $\tau=2000$ kPa. The monoliths assume linear behaviour of concrete corresponding to C25/30, with the following characteristics: modulus of elasticity $E_n=31.5*10^7$ kPa, Poisson's ratio $\nu=0.2$ and bulk density $\gamma_{con}=24.0$ kN/m^3.

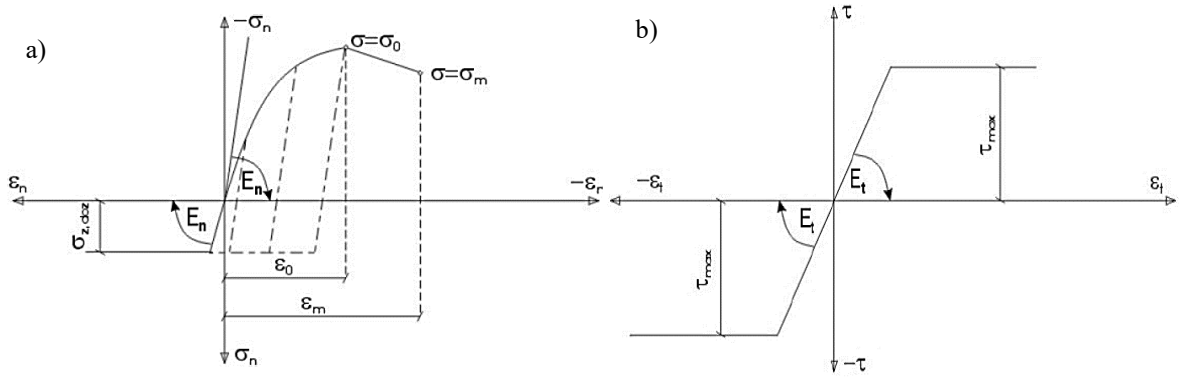


Figure 2. Constitutive relations for the behaviour of the grouting mass in construction joints in the a) normal direction and b) two tangential directions

Copyright © 2025 CroCEE
DOI: https://doi.org/10.5592/CO/3CroCEE.2025.111

3. Numerical experiment for shear key joint behaviour simulation in arch dams

The simulation of shear key joint behaviour in the study incorporates modifications to the flat element concept in the tangential direction, introducing additional shear resistance that is induced by the geometric shear resistance of the shear key element. Further key assumptions are:

1. The tangential shear resistance combines the Coulomb's friction force, and an additional shear resistance attributed to the shear key geometry when the element is activated:

$$F\tau = F\tau_f + Fc + F\tau_{ad} = (\mu\sigma_n + c) + F\tau_{ad} \quad (1)$$

2. When the joint opens, the shear resistance depends solely on the joint's geometry until shear failure occurs within the key.
3. The behaviour of shear key joints results from the interaction between relative normal and tangential stresses.
4. The additional tangential force is obtained by increasing the initial modulus of elasticity in the direction of the shear key element. The increased modulus of elasticity $E_{1\,\tau,add}$ is expressed as:

$$E_{1\,\tau,add} = k_{ad} * E_{1,\tau} \quad (2)$$

where k_{ad} is the additional tangential stiffness coefficient, and $E_{1,\tau}$ is the initial tangential modulus of elasticity. The coefficient k_{ad} is determined through numerical experiments using three very refined finite element models, one with a flat joint configuration (Model 1, Fig. 3 a), and two models with different geometry of the shear key joint, a bevelled shear key joint with a 30° angle (Model 2, Fig.3 b) and an unbevelled shear key joint (Model 3, Fig. 3 c). These models enable the quantification of the additional stiffness effects influenced by the shear key geometry, its shape and key angle.

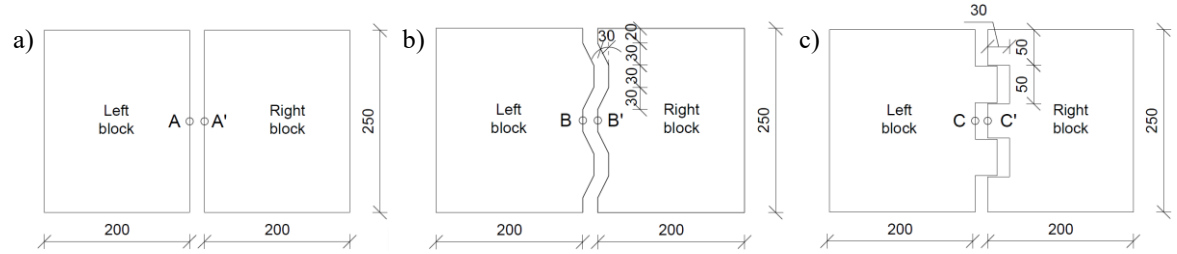


Figure 3. Geometric characteristics: a) Model 1, b) Model 2, and c) Model 3

Fig. 4 shows the finite element mesh and boundary conditions applied to the analysed models. In each configuration, the left side is fixed, while a horizontal static force is applied incrementally in 20 steps on the right side. The force is incremented according to the linear relation $F_{fmi} = F_s * f_{mi}$, where the multiplier f_{mi} ranges from 1 to 50, while the horizontal static force applied at the first loading step has a magnitude of 25000 kN. The experiment is conducted until the uniaxial compressive strength in the contact's normal direction is reached. For Models 2 and 3, a constant tangential modulus of elasticity is adopted, while for Model 1 different coefficients of additional tangential stiffness k_{ad} are applied until the contact slip values between the flat joint and shear key joints coincide. This approach easily determines the values of k_{ad} that effectively replicate the shear resistance effects induced by the shear key geometry, allowing these effects to be easily incorporated into the flat joint model.

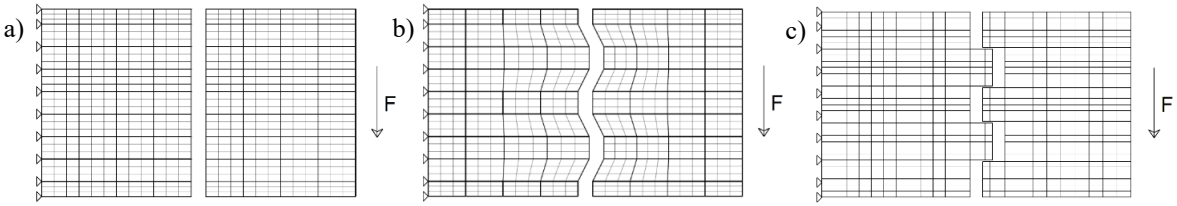


Figure 4. Finite element mesh and boundary conditions for: a) Model 1, b) Model 2 and c) Model 3

Copyright © 2025 CroCEE
DOI: https://doi.org/10.5592/CO/3CroCEE.2025.111

4. Results from numerical experiments

The conducted numerical experiments in the first part of this study offer a comprehensive evaluation of the behaviour of different types of shear key joints compared to flat joints under incremental loading conditions. The shear key joints are analysed separately and compared with the flat joint, using various coefficients of additional tangential stiffness k_{ad}. For the bevelled shear key (Model 2) comparisons were made with the flat joint (Model 1) using coefficients k_{ad}=1.0 (equal tangential stiffness for both models), k_{ad}=1.08, k_{ad}=1.18 and k_{ad}=1.23. For the unbevelled shear key joint (Model 3), coefficients with values of k_{ad}=1.0, k_{ad}=1.23, k_{ad}=1.49 and k_{ad}=1.60 were adopted for the flat joint (Model 1).

Fig. 5 shows the horizontal displacements in the monolithic blocks in both global directions for incremental load factor f_{mi}=50: a) Model 1 with k_{ad}=1.0, b) Model 2 and c) Model 3. Fig. 6 illustrates the zones of open contact elements in the joints for the same load factor (f_{mi}=50) for Model 1 with k_{ad}=1.0, Model 2 and Model 3. For all joint types, the concentration of open elements occurs predominantly in the upper half of the contact zone, which aligns with the action of a bending force. The stress-strain relationships for all models are shown in Fig. 7, focusing on the contact elements where extreme responses occur. The figure shows the stress-strain relationships for: Model 1 with k_{ad}=1.0 in the contact elements in which the maximum: a) opening in the direction of the normal (CE 586) and b) sliding in the direction of the shear key element (CE 275) occur; Model 2 in the contact elements in which the same extremes occur, shown in the corresponding elements: c) CE 586 and d) CE 132 and Model 3 in the contact elements where the extremes occur: e) CE 370 and f) CE 617. Each figure also highlights the position of these elements.

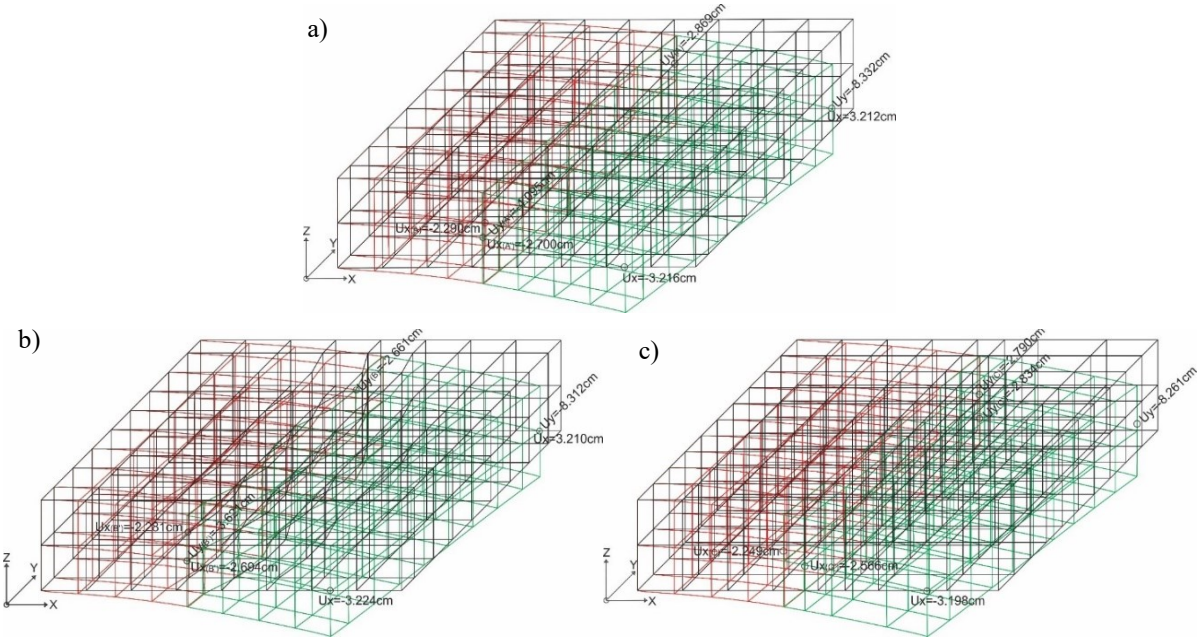


Figure 5. Horizontal displacements in the monoliths in both global directions (f_{mi}=50): a) Model 1 with k_{ad}=1.0, b) Model 2 and c) Model 3

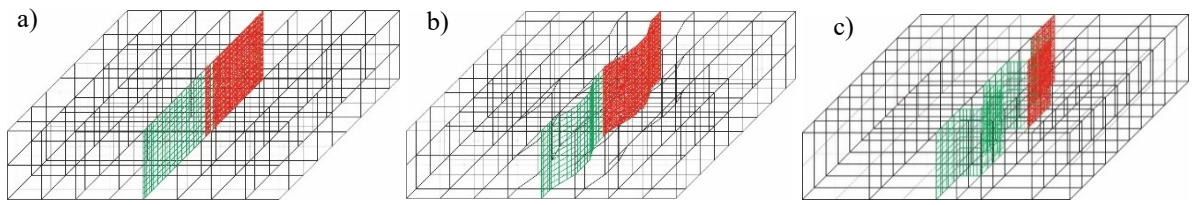


Figure 6. Open contact elements (f_{mi}=50): a) Model 1 with k_{ad}=1.0 (46% open elements), b) Model 2 (45% open elements) and c) Model 3 (35% open elements)

Copyright © 2025 CroCEE
DOI: https://doi.org/10.5592/CO/3CroCEE.2025.111

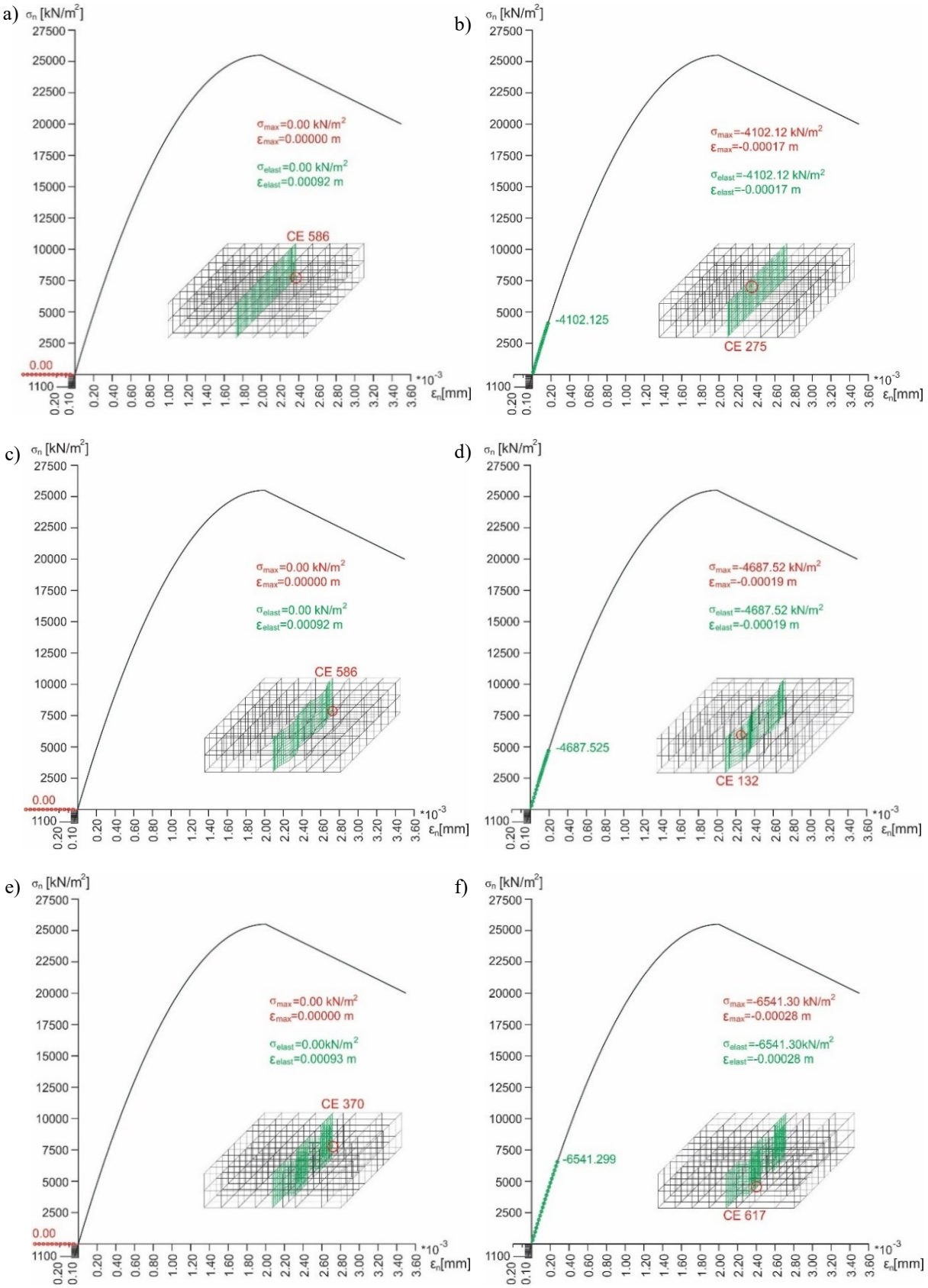


Figure 7. Normal stress–strain relationship (f_{mi}=50) in Model 1 (k_{ad} =1.0) for elements with maximum: a) opening in the direction of the normal (CE 586), b) sliding in the direction of the element (CE 275); Model 2: c) opening (CE 586), d) sliding (CE 132); and Model 3: e) opening (CE 370) and f) sliding (CE 617)

Proceedings of the 3rd Croatian Conference on Earthquake Engineering - 3CroCEE
19–22 March 2025, Split, Croatia
Copyright © 2025 CroCEE
DOI: https://doi.org/10.5592/CO/3CroCEE.2025.111

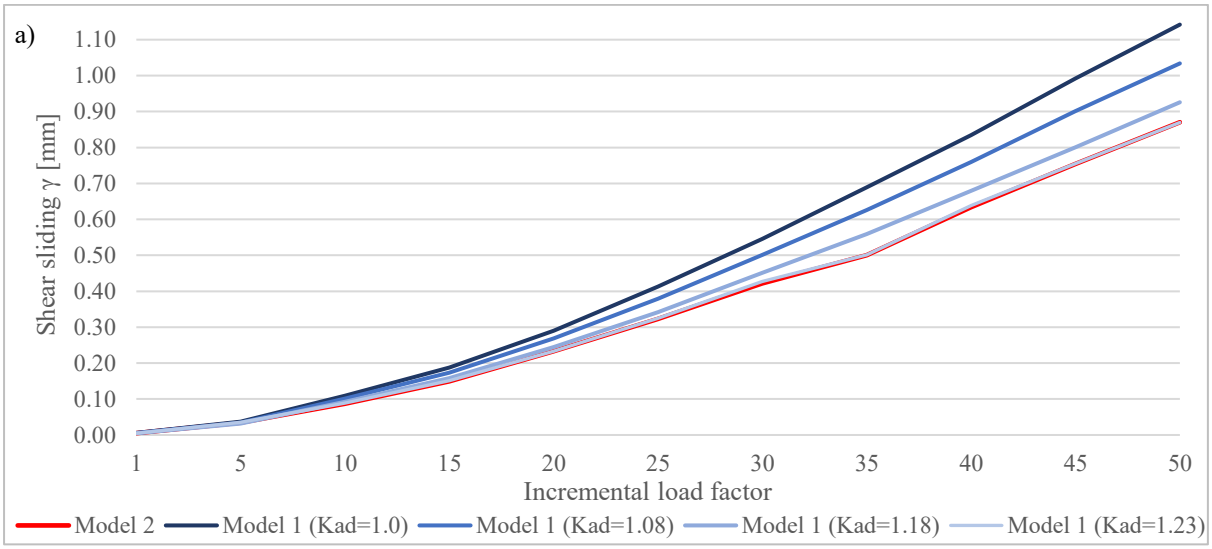
The histories of maximum values of characteristic parameters, including shear sliding deformations, contact openings and horizontal displacements in the left and right monolithic blocks in the global y-direction are shown in Fig. 8 to Fig. 11. These parameters are calculated as functions of the incremental loading factor for Models 2 and 3 (shear key joints) and Model 1 (flat joint) with all coefficients of additional tangential stiffness k_{ad}. The results highlight significant differences in behaviour between the models.

The largest differences between the two models that are compared are in the contact shear sliding deformations. According to Fig. 8, the largest differences occur between Model 1 with k_{ad}=1.0 and Models 2 and 3, i.e. when all models have equal modulus of elasticity in the tangential direction. The maximum sliding deformation in the bevelled shear key joint (Model 2) is γ_{max}=0.87 mm, 24% smaller than the maximum deformation observed in the flat joint (γ_{max}=1.14 mm), Fig. 8a. For the unbevelled shear key joint (Model 3), the maximum sliding deformation is γ_{max}=0.54 mm, more than 50% smaller than the slip in the flat joint, Fig 8b. As the coefficient k_{ad} increases, the maximum sliding values in the flat joint converge towards those in the shear key joints. A good agreement in the values between the flat and bevelled shear key joints is achieved for k_{ad}=1.23, and between the flat and unbevelled shear key joints for k_{ad}=1.60. These shear sliding extremes for all types of joints occur near the middle of the contact zone (Figure 7b, d, f), immediately after maximum opening zones (Figure 6), consistent with the applied boundary conditions and forces.

Insignificant differences in values of maximum opening are observed across all models, with δ_{max}=0.923 mm for Model 2, δ_{max}=0.926 mm for Model 3, and δ_{max}=0.924 mm for Model 1 with k_{ad}=1.0 (Figure 9). This indicates that under pure bending loads, the additional tangential stiffness has a minimal impact on the maximum joint opening. Shear key joints (Models 2 and 3) exhibit increased tangential stiffness, resulting in dominant opening behaviour over sliding. For Model 1, as the loading factor f_{mi} exceeds 30, sliding deformations become more pronounced due to plastic yielding after exceeding the allowable shear stress. The maximum openings occur at the upper edge of the contact zone (Figure 7a, c, d), where the bending curvature is uniform across all analysed models, explaining their similar behaviour. That's why it's also useful to discuss openings in other characteristic elements along the contact. Additional analyses of openings in three characteristic contact elements along the joint, at the first key, the mid-point of the contact, and the second key (not shown in the paper) reveal that the unbevelled shear key joint (Model 3) more significantly reduces contact openings compared to the bevelled joint (Model 2). The shear sliding deformation ratios between Model 2 and Model 1 are 9% for the first contact element, 0% for the second (mid-part element), and 3% for the third contact element. For Model 3, these slip ratios are 51%, 70% and 51% for the three points, respectively. The same can be concluded by analysing the open elements zones, 35% open elements in Model 3, compared to 45% in Model 2 and 46% in Model 1 with k_{ad}=1.0.

Horizontal displacements in both monolithic blocks show the largest differences when comparing models with equal tangential stiffness, with differences decreasing as k_{ad} increases. While values for the flat joint approach those of the shear key joints when k_{ad} increases, they do not fully converge. For all joint types, the left monolithic block shows smaller maximum displacements compared to the right block, as dictated by the boundary conditions. In Model 3, the maximum displacement in y-direction in the left block (u_y=27.90 mm) is slightly higher than in Model 2 (u_y=26.61 mm), though both are smaller than the displacements in the flat contact, Model 1 with k_{ad}=1.0 (u_y=28.69 mm), Fig. 10. In the right block, maximum displacements in y-direction are u_y=36.21 mm for Model 2 and u_y=28.34 mm for Model 3, both smaller than the flat joint (u_y=40.95 mm), Fig. 11. The relative horizontal displacements between the blocks are significantly smaller in Model 3 (Δu_y=0.45 mm) compared to Model 2 (Δu_y=9.61 mm), with both being smaller than Model 1 (Δu_y=12.26 mm). The bevelled shear key joint reduces relative displacement by 20%, while the unbevelled shear key joint achieves over a 90% reduction. These results align with the reduced shear sliding deformation and increased tangential stiffness of the unbevelled shear key joint.

Copyright © 2025 CroCEE
DOI: https://doi.org/10.5592/CO/3CroCEE.2025.111



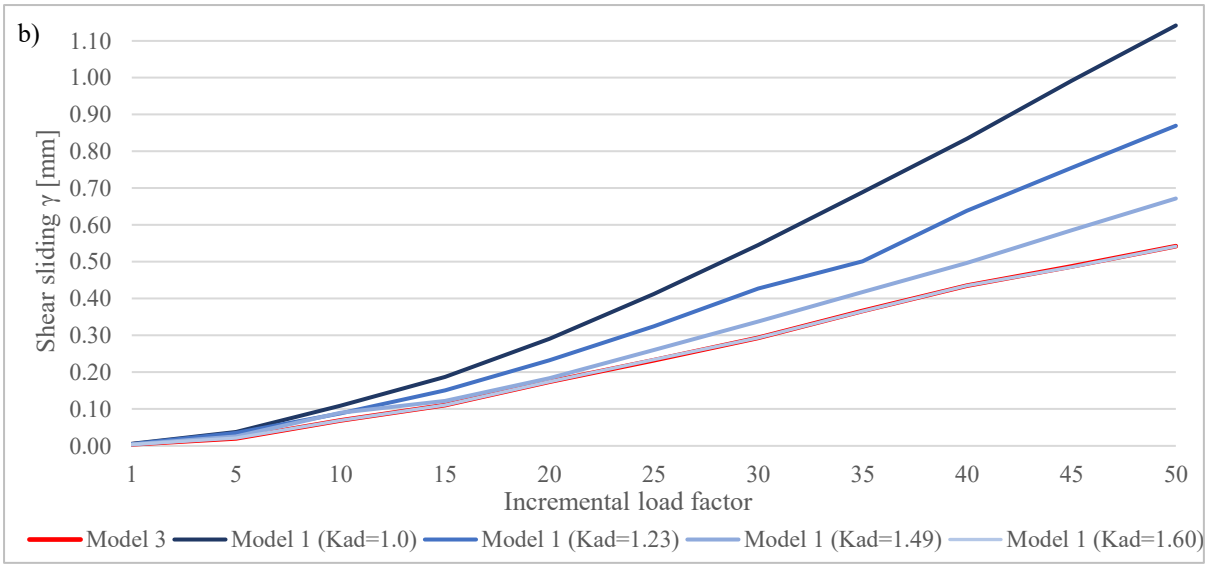
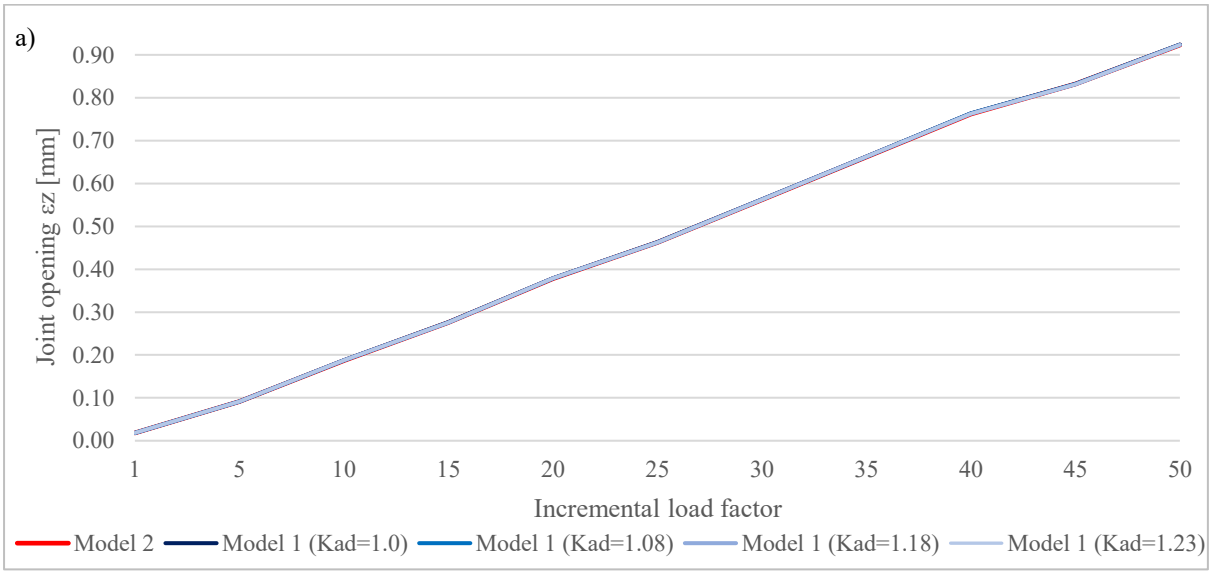


Figure 8. History of maximum shear sliding in the contact as a function of the incremental load factor for: (a) Model 1 and Model 2, (b) Model 1 and Model 3



Copyright © 2025 CroCEE
DOI: https://doi.org/10.5592/CO/3CroCEE.2025.111

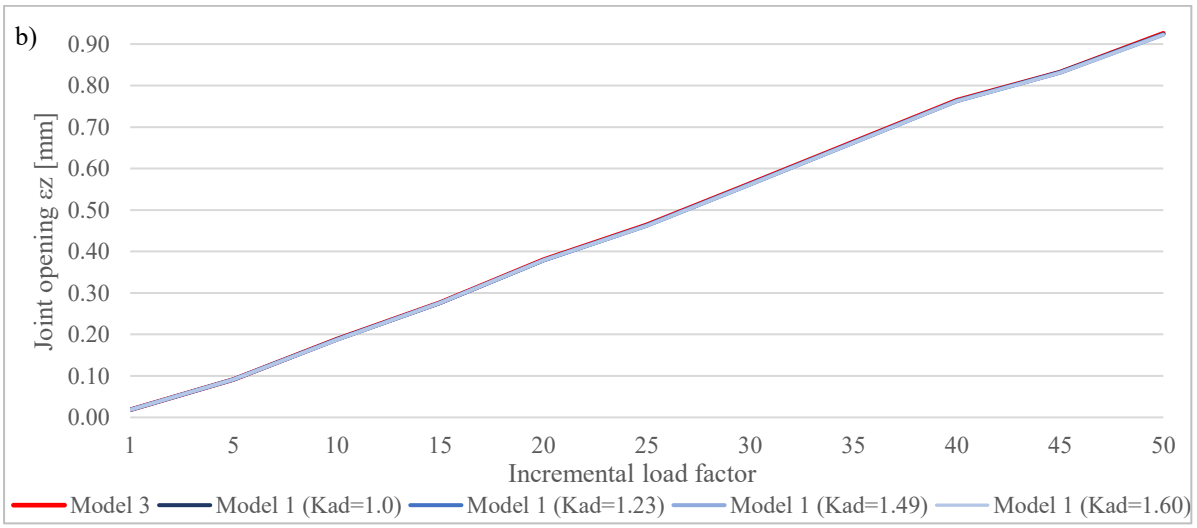
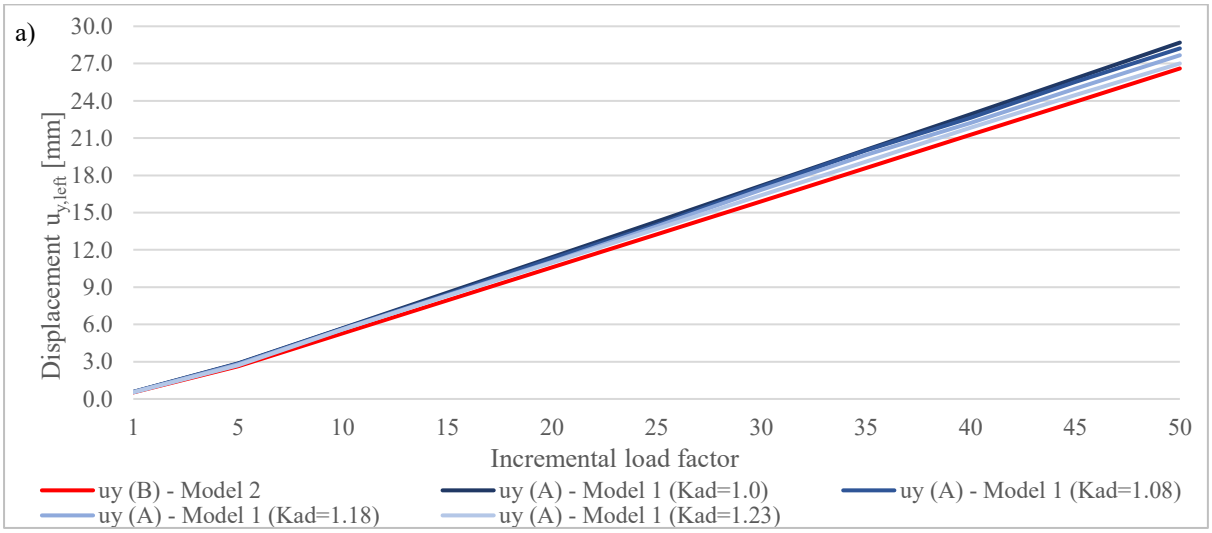


Figure 9. History of maximum opening in the contact as a function of the incremental load factor for: (a) Model 1 and Model 2 and (b) Model 1 and Model 3



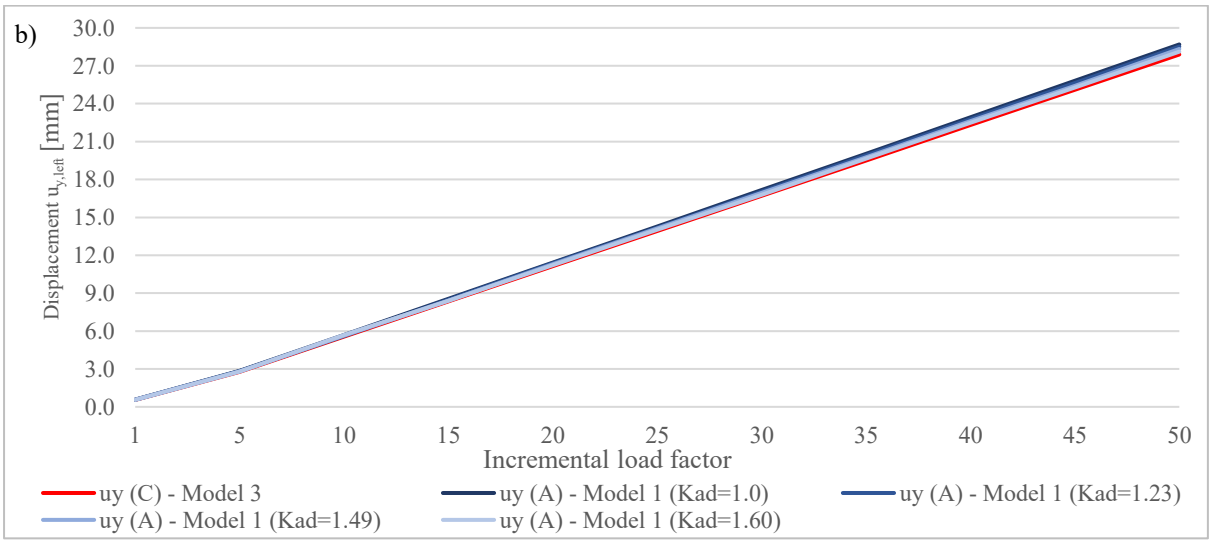


Figure 10. History of maximum horizontal displacements in the global y-direction in the left monolithic block as a function of the incremental load factor for: (a) Model 1 and Model 2 and (b) Model 1 and Model 3

Copyright © 2025 CroCEE
DOI: https://doi.org/10.5592/CO/3CroCEE.2025.111

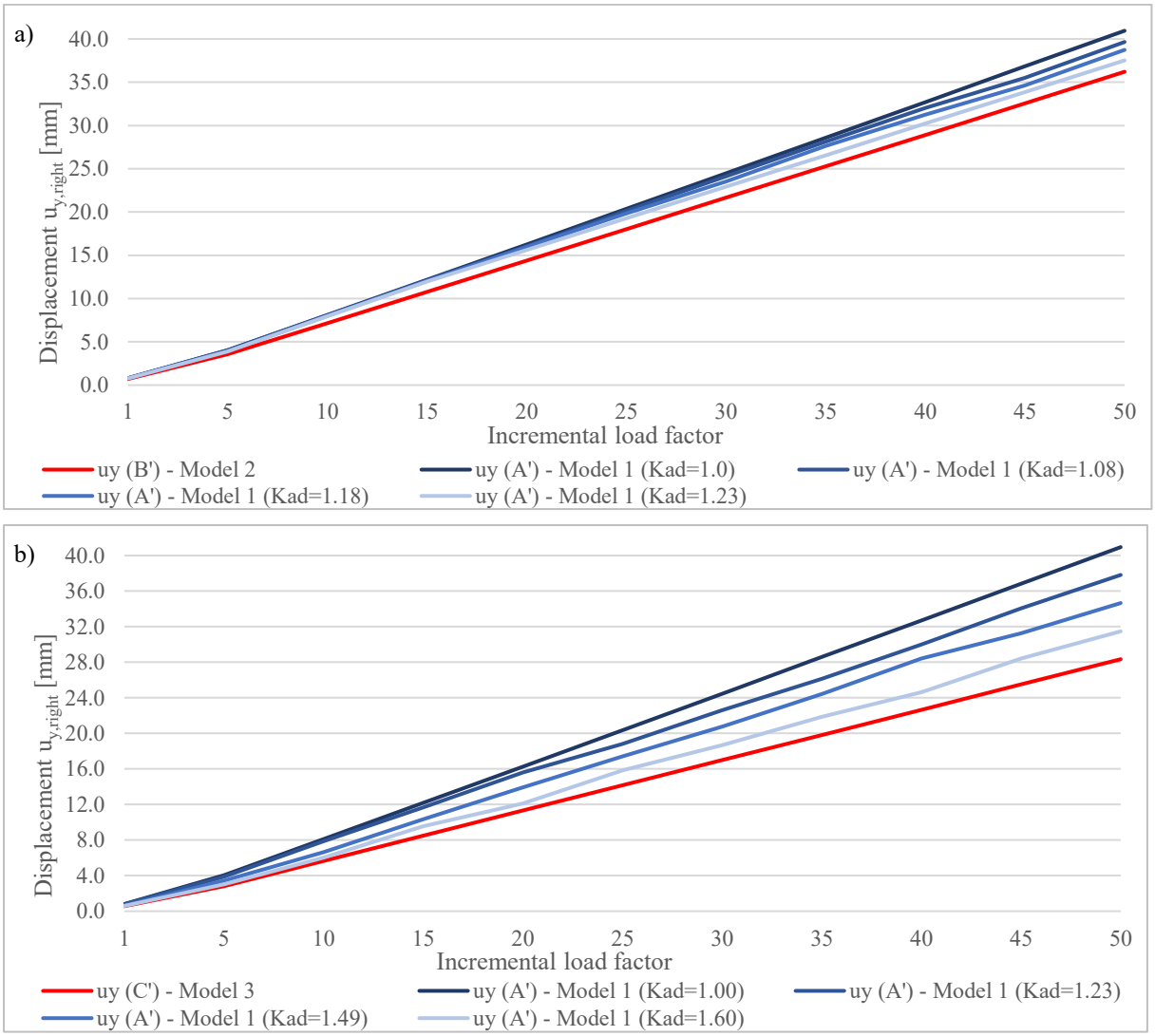


Figure 11. History of maximum horizontal displacements in the global y-direction in the right monolithic block as a function of the incremental load factor for: (a) Model 1 and Model 2 and (b) Model 1 and Model 3

5. Discussion of the results and conclusions

The aim of this research is to quantify the additional tangential stiffness representing the shear resistance of shear key joint elements with various geometries. The main focus is to derive these tangential stiffness values that can be applied to flat joints, thereby eliminating the need for detailed geometric modeling to capture the complexity of shear key joint geometry and behavior. These computed values, expressed as additional tangential stiffness coefficient are integrated into the flat joint contact elements' stiffness matrix, modifying the constitutive law to accurately simulate nonlinear behavior of the joint in the direction of the shear key elements, which may be implemented in one or two directions. The first part of the study focuses on the influence of shear key joint's geometry, with particular emphasis on key shape and angle.

The most pronounced differences among the analysed parameters are observed in the shear sliding deformations at the contact. The tangential stiffness coefficient k_{ad} is determined by equating the sliding deformations of the flat joint with various values of k_{ad}, to those observed in the shear key joints. The results indicate that replicating the shear resistance of the bevelled shear key joint requires a 23% increase in the tangential stiffness, while for the unbevelled shear key joint, an increase of 60% is

Copyright © 2025 CroCEE
DOI: https://doi.org/10.5592/CO/3CroCEE.2025.111

needed. These findings underscore the significant impact of shear key geometry on the overall stiffness of the model, with each joint configuration contributing differently to the tangential resistance.

Despite different sliding behavior, all models exhibit nearly identical joint opening values, with the maximum occurring at the upper edge of the contact where the bending curve remains consistent across all models. This uniformity suggests that tangential stiffness has a negligible influence on the maximum joint opening. However, analyses of openings across different contact elements along the contact, reveal that the unbevelled shear key joint not only enhances tangential stiffness and shear sliding resistance, but also significantly reduces openings along the contact. Maximum horizontal displacements in the global y-direction within the contact zone, as well as relative displacements between the monolithic blocks, correspond closely to the observed shear sliding behavior. Furthermore, the response curves for all joint types demonstrate consistent trends across the analysed parameters.

The study findings confirm that the favourable shear key joint geometry (of both analysed types) significantly increases the tangential stiffness compared to flat joints. The geometry of the joints, particularly the shape and angle of the shear key element are key factors influencing the shear resistance. It should be noted that the segment analysed in this first part of the study corresponds to the lower part of the arch dam, where the greater thickness minimizes slippage and joint openings. The second part of the study, titled "*Numerical experiment for shear key joint behaviour simulation in arch dams: Part 2 – Investigating the influence of the arch thickness and applied force*", will examine an upper dam segment, highlighting the need of incorporating arch thickness as a critical parameter in future analyses. It is particularly important to evaluate the role of arch thickness in influencing tangential stiffness for identical shear key configurations. Additionally, the second part of the study will also explore the effects of varying applied forces.

The research confirms the efficiency of the proposed approach in simulation of the complex nonlinear behavior of an arch dam constructed with shear key joints, eliminating the need for explicit geometric modeling. The model will be applied to simulate contraction joints in an arch dam, evaluating the impact of the different joint types on stress redistribution and the overall structural response under static and dynamic loading conditions.

References

[1] Talatahari, S., Salami M., Parsiavash, R. (2016): Optimum design of double curvature arc dams using a quick hybrid charged system search algorithm. *Iran University of Science & Technology*, **6**, 227-243, Corpus ID: 53392743.

[2] Du, C. B., Jiang, S. Y. (2010): Effects of contraction joints and key slots on the seismic responses of arch dam (in Chinese). *Journal of Hydroelectric Engineering*, **29** (5), 1–5.

[3] Ahmadi, M. T., Izadinia, M., Bachmann, H. (2001): A discrete crack joint model for nonlinear dynamic analysis of concrete arch dam. *Computers and Structures,* **79** (4), 403-420, https://doi.org/10.1016/S0045-7949(00)00148-6.

[4] Fenves, G. L., Mojtahedi, S., Reimer, R. B. (1992): Effect of contraction joints on earthquake response of an arch dam. *Journal of Structural Engineering*, **118** (4), 1039—1055, https://doi.org/10.1061/(ASCE)0733-9445(1992)118:4(1039).

[5] Lau, D. T., Noruziaan, B., Razaqpur, A. G. (1998): Modelling of contraction joint and shear sliding effects on earthquake response of arch dams. *Earthquake Engineering and Structural Dynamics*, **27**, 1013-1029, https://doi.org/10.1002/(SICI)1096-9845(199810)27:10<1013::AID-EQE765>3.0.CO;2-0.

[6] Tzenkov, A. D., Lau, D. T. (2002): Seismic analysis of concrete arch dams with contraction joints and non-linear material models, *7th U.S. National Conference on Earthquake Engineering*, Boston, Massachusetts.

[7] Toyoda, Y., Ueda M., Shiojiri, H. (2002): Study of joint opening effects on the dynamic response of an existing arch dam, *15th ASCE Engineering Mechanics Conference*, Columbia University, New York.

[8] Noble, C. R., Solberg J. (2004): Nonlinear seismic analysis of Morrow Point dam. *A Study for the United States Bureau of Reclamation*, UCRL-TR-202545.

Copyright © 2025 CroCEE
DOI: https://doi.org/10.5592/CO/3CroCEE.2025.111

[9] Guerra, A. (2007): Shear key research project – Literature review and finite element analysis. Dam Safety Technology Development Program, U.S. Department of the Interior, Bureau of Reclamation, *Report DSO-07-05*.

[10] Ricketts, R. E. Zienkiewicz, O. C. (1975): *Preformed 'cracks' and their influence on behaviour of concrete dams*. Criteria and assumptions for numerical analysis of dams, UK.

[11] Row, D., Schricker, V. (1984): Seismic analysis of structures with localized nonlinearities, *8th World Conference on Earthquake Engineering*, San Francisco, California.

[12] O' Connor, J. P. F. (1985): The modeling of cracks, potential crack surfaces and construction joints in arch dams by curved surface interface elements, *15th International Conference on Large Dams*, Lausanne, Switzerland.

[13] Beer, G. (1985) An isoperimetric joint/interface element for finite element analysis. *International Journal for Numerical Methods in Engineering*, **21**, 585-600, https://doi.org/10.1002/nme.1620210402.

[14] Dowling, M. J., Hall, J. F. (1989): Nonlinear seismic analysis of arch dams. *Journal of Engineering Mechanics, ASCE*, **115** (4), 768-89, https://doi.org/10.1061/(ASCE)0733-9399(1989)115:4(768).

[15] Ahmadi, M. T., Razavi, S. (1992): A three-dimensional joint opening analysis of an arch dam. *Computers and Structures*, **44** (1-2), 187–192, https://doi.org/10.1016/0045-7949(92)90237-T.

[16] Lotfi, V. (1996): Comparison of discrete crack and elasto-plastic models in nonlinear dynamic analysis of arch dams. *Dam Engineering*, **7** (1).

[17] Mays, J. R., Roehm, L. H. (1993): Effect of vertical contraction joints in concrete arch dams. *Computers & Structures*, **47** (4-5), 615-627, https://doi.org/10.1016/0045-7949(93)90346-F.

[18] Azmi, M., Paultre P. (2002): Three-dimensional analysis of concrete dams including contraction joint non-linearity. *Engineering Structures*, **24**, 757–771, https://doi.org/10.1016/S0141-0296(02)00005-6.

[19] Arabshahi, H. R., Lotfi, V. (2009): Nonlinear dynamic analysis of arch dams with joint sliding mechanism. *Engineering Computation*, **26** (5), 464–482, https://doi.org/10.1108/02644400910 970158.

[20] Wang, J. T., Jin, F., Zhang, C. H. (2011): Seismic safety of arch dams with aging effects. *Science China Technological Sciences*, **54** (3), 522–530.

[21] Du, C. B., Jiang, S. Y. (2010): Effects of contraction joints and key slots on the seismic responses of arch dam (in Chinese). *Journal of Hydroelectric Engineering*, **29** (5), 1–5.

[22] Jiang S. Y., Du C. B., Yuan, J. W. (2011): Effects of shear keys on nonlinear seismic responses of an arch – gravity dam. *Technological Sciences*, Science China Press and Springer, Verlag Berlin 2011.

[23] ADAD-IZIIS – Software for analysis and design of arch dams. *Institute of Earthquake Engineering and Engineering Seismology*, University of Ss. Cyril and Methodious, Skopje, R. N. Macedonia.

Proceedings of the 3rd Croatian Conference on Earthquake Engineering - 3CroCEE
19–22 March 2025, Split, Croatia
Copyright © 2025 CroCEE
DOI: https://doi.org/10.5592/CO/3CroCEE.2025.112

NUMERICAL EXPERIMENT FOR SHEAR KEY JOINT BEHAVIOUR SIMULATION IN ARCH DAMS: PART 2 – INVESTIGATING THE INFLUENCE OF THE ARCH THICKNESS AND APPLIED FORCE

Violeta Mircevska [(1)], Ana Nanevska [(2)]

[(1)] *Professor, Institute of Earthquake Engineering and Engineering Seismology, University of Ss. Cyril and Methodious, Skopje, R. N. Macedonia., mircevska@iziis.ukim.edu.mk*
[(2)] *Research Assistant, Institute of Earthquake Engineering and Engineering Seismology, University of Ss. Cyril and Methodious, Skopje, R. N. Macedonia., nanevska@iziis.ukim.edu.mk*

Abstract

Nonlinear behavior of contraction joints in arch dams, such as joint opening and sliding caused by hydrostatic pressure and temperature variations, can affect the dam's serviceability. Furthermore, strong seismic events can additionally alter the response in dynamic conditions, impacting the natural period and stress redistribution in the arches and cantilevers. In order to enhance structural integrity with additional shear strength, shear key elements are usually installed along these joints. However, traditional modeling with the actual shear key geometry results in complex analyses. This paper presents a novel approach for simulating shear key behavior by modifying the flat joint concept in ADAD-IZIIS software. The method introduces additional tangential stiffness to the flat joint's stiffness matrix to simulate shear resistance derived from the key geometry. The model uses a uniaxial constitutive law for nonlinear behavior in normal and Coulomb's friction law in the tangential direction. This paper presents the second part of a comprehensive study examining the influence of the arch thickness and applied force through numerical experiments using refined FE models of flat and bevelled shear key joints. The additional shear resistance $F_{\tau,add}$ is calculated by increasing the initial modulus of elasticity $E_{n,\tau}$ in the local shear direction as $E_{n\tau,add}=k_{ad}*E_{n,\tau}$, applying the additional tangential stiffness coefficient k_{ad}, derived from the experimental analyses. Results show that shear resistance is primarily influenced by arch thickness, while the applied force has a lesser effect. In the lower segment, the bevelled shear key increases tangential stiffness by 23% to 27% compared to the flat joint, depending on the applied force. In an upper segment, the same shear key joint exhibits 46% increase, meaning this factor has to be considered in further analysis. The research confirms the efficiency of the proposed approach in simulation of the complex nonlinear behavior of an arch dam constructed with shear key joints.

Keywords: contraction joint, nonlinear behaviour, shear key, numerical experiment

1. Introduction

Arch dams are highly efficient structures that transfer large compressive stresses to the supports through their curved arch geometry, ensuring strength and stability [1]. In order to control tensile stresses development caused by expansion and contraction during concreting, temperature variations, as well as seismic activity, arch dams are constructed in monolithic blocks separated by vertical contraction joints [2]. While these joints enhance construction feasibility, they introduce potential weak points due to imperfections in the grouting process, making them vulnerable to initial damage from temperature variations and strong earthquakes [3]. During a seismic event, relative displacements between monoliths cause joint opening and shear sliding, significantly redistributing internal forces both during and after the seismic event due to residual joint openness. Previous research [4][5][6][7][8] has shown that the nonlinear behavior of these joints, including their opening and shear sliding, increases the natural period of the dam and leads to a significant redistribution of stresses in the arches and cantilevers. This emphasizes the importance of accurate numerical simulation of contraction joint behaviour for evaluating the static and seismic stability of arch dams.

To improve the compactness, shear strength and enhance the overall integrity of arch dams, shear key elements are often incorporated along the joints in the radial and/or longitudinal directions. These elements improve monolithic integrity and provide additional shear resistance especially in thinner

Copyright © 2025 CroCEE
DOI: https://doi.org/10.5592/CO/3CroCEE.2025.112

dams, by resisting normal displacements caused by joint opening [9]. However, their analytical modeling remains complex due to challenges in representing their specific geometry, as well as proper modeling of the interaction effects between opening and sliding in the joints.

The first part of this study titled "*Numerical experiment for shear key joint behaviour simulation in arch dams: Part 1 – Investigating the influence of the key shape and angle*", focused on the numerical simulation of shear key joint behavior, specifically investigating the influence of shear key shape and angle. Part 1 also provided a comprehensive review of the existing literature on the subject, discussing the development and application of various numerical models for simulating the nonlinear behavior of construction joints in arch dams. To avoid redundancy, this literature review will not be reiterated here; however, readers are encouraged to refer to Part 1 for a review of the state-of-the-art research and background on the topic.

This second part of the study builds on the findings, established methodology and nonlinear constitutive model for simulating shear key joint behavior developed in Part 1. This part of the study further expands the investigation to explore the effects of additional critical parameters, such as arch thickness and applied force on the shear key joint behavior. Additional numerical experiments are conducted using the same constitutive model and the 3D flat joint contact element previously implemented in the ADAD-IZIIS software [10]. By analysing additional parameters, the study offers a deeper exploration of the mechanical behavior of shear key joints and provides valuable insights into their performance under varying loading and geometric conditions. Together, these two parts establish a robust and comprehensive framework for assessing the static and seismic stability of arch dams with shear key joints, contributing valuable insights to both research and practical engineering applications.

2. 3D flat contact element implemented in the ADAD-IZIIS software

The modeling approach is based on the 3D flat contact element previously integrated into the ADAD-IZIIS software [10], as described in Part 1. A schematic representation of this contact element is provided in Fig. 1, illustrating the contact surfaces that represent the two faces of two different finite elements in the contact, defined by eight points each.

This contact element simulates the nonlinear behavior of flat joints by capturing coupled effects in all three directions of the contact. The nonlinear behaviour in the normal direction is governed by follows a uniaxial constitutive law (Fig. 2a),while the tangential behavior adheres to the Coulomb's law of friction in both tangential directions (Fig. 2b). The mechanical properties of the grouting joint material are slightly lower than those of the concrete in the monoliths, with nonlinear behaviour modelled in the joints and linear behaviour in the monoliths. Readers are referred to Part 1 for a detailed description of the material properties.

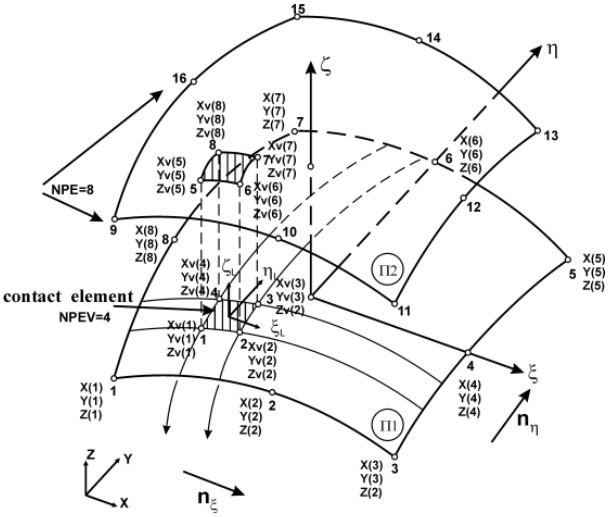


Figure 1. Schematic representation of the 8-point contact element

Copyright © 2025 CroCEE
DOI: https://doi.org/10.5592/CO/3CroCEE.2025.112

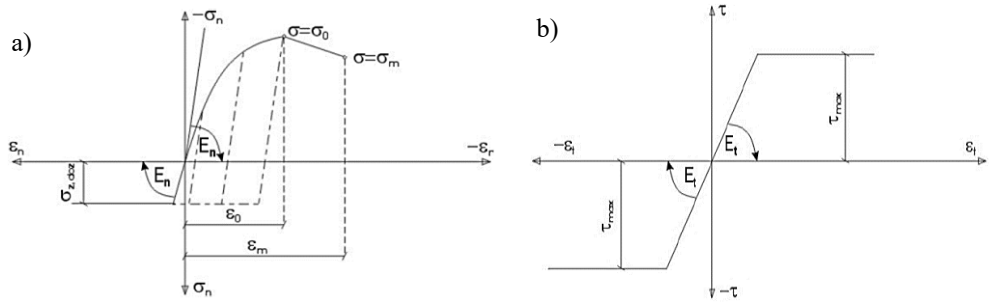


Figure 2. Constitutive relations for the behaviour of the grouting mass in construction joints in the a) normal direction and b) two tangential directions

3. Numerical experiment for shear key joint behaviour simulation in arch dams

The numerical experiment builds upon the same foundational approach and assumptions established in Part 1 of the study, with modifications to the flat element concept in the tangential direction by introducing an additional tangential stiffness induced by the geometric shear resistance of the shear key element. The tangential shear resistance is modelled as:

$$F\tau = F\tau_f + Fc + F\tau_{ad} = (\mu\sigma_n + c) + F\tau_{ad} \quad (1)$$

where $F\tau_{ad}$ represents the additional shear resistance obtained by increasing the initial modulus of elasticity ($E_{1,\tau}$) in the direction of the shear key element, as described by:

$$E_{1\,\tau,add} = k_{ad} * E_{1,\tau} \quad (2)$$

Here, k_{ad} is the coefficient of additional tangential stiffness, determined through numerical experiments. In this part of the study, different numerical experiments are conducted to investigate the impact of arch thickness. The finite element models are adopted with smaller thickness (140 cm) to represent a segment in the higher part of the dam. One model has the flat joint configuration (Model 4, Fig. 3a) while the other two have are with the bevelled shear key joint (Model 5, Fig. 3b) and unbevelled shear key joint (Model 6, Fig. 3c).

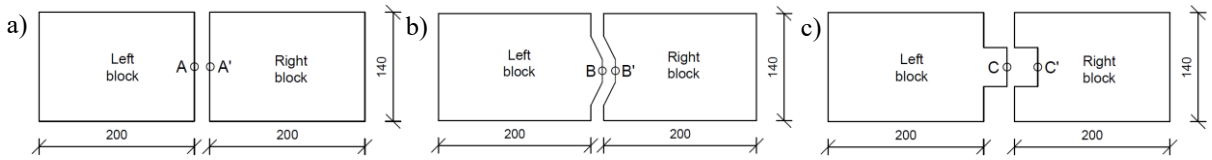


Figure 3. Geometric characteristics: a) Model 4, b) Model 5, and c) Model 6

The finite element meshes and boundary conditions for these models are presented in Fig. 4 and follow the same setup as in Part 1, ensuring consistency in the numerical experiments. For all models, the left side is fixed, and a horizontal static force is applied at the end (not shown in the figures) and along the contact, simulating both bending and shearing force, respectively. The static force is incremented according to $F_{fmi} = F_s * f_{mi}$, where the multiplier f_{mi} ranges from 1 to 50 and the experiment continues until the uniaxial compressive strength in the contact's normal direction is reached. Models 5 and 6 use a constant tangential modulus of elasticity, while for Model 4 various coefficients k_{ad} are employed until the contact shear sliding values between the flat joint and shear key joints coincide.

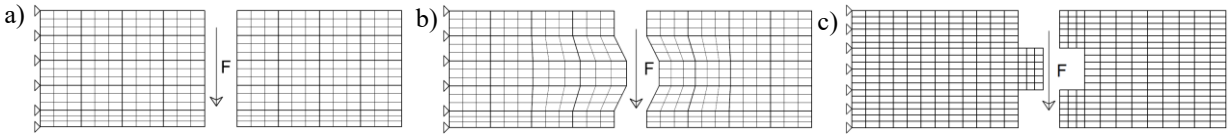


Figure 4. Finite element mesh and boundary conditions for: a) Model 4, b) Model 5 and c) Model 6

Proceedings of the 3rd Croatian Conference on Earthquake Engineering - 3CroCEE
19–22 March 2025, Split, Croatia
Copyright © 2025 CroCEE
DOI: https://doi.org/10.5592/CO/3CroCEE.2025.112

4. Results from numerical experiments

The numerical experiments conducted in the second part of the study provide an in-depth evaluation of the behaviour of shear key joints with a particular emphasis on the influence of arch thickness and applied forces. Separate analyses are performed for both bevelled and unbevelled shear key joints, with comparisons made against the flat joint with various adopted coefficients k_{ad}. For the bevelled shear key joint (Model 5), comparisons with the flat joint model (Model 4) were made for k_{ad} values of k_{ad}=1.0 (equal tangential stiffness for both models), k_{ad}=1.15, k_{ad}=1.30 and k_{ad}=1.46. For the unbevelled shear key joint (Model 6), k_{ad} values of k_{ad}=1.0, k_{ad}=1.30, k_{ad}=1.46 and k_{ad}=1.86 were employed in Model 4 for comparative analysis. The results presented are derived from the analysis conducted under a pure shear force acting along the length of the contact.

The horizontal displacements of the monolithic block in both directions for an incremental load factor of f_{mi}=50 are presented in Fig. 5 for: a) Model 4 with k_{ad}=1.0, b) Model 5 and c) Model 6. Fig. 6 highlights the zones of open contact elements across all joints for the same load factor. The spatial distribution of open contact elements is along the contact, which is consistent with the acting shearing force. The percentage differences underscore reduced openings in the unbevelled shear key joint compared to the similar values in the bevelled and flat joint models.

Fig. 7 presents the stress-strain relationships in critical contact elements in which extreme responses, such as maximum opening and shear sliding are observed. The figures shows the stress-strain relationships for: Model 4 with k_{ad}=1.0 in the contact elements in which the maximum: a) opening in the direction of the normal (CE 25) and b) sliding in the direction of the shear key element (CE 154) occur; Model 5 in the contact elements in which the same extremes occur in the corresponding elements: c) CE 25 and d) CE 154 and Model 6 in the contact elements where the extremes occur: e) CE 25 and f) CE 77. The position of these contact is illustrated in each subfigure and highlights the localized responses unique for each joint configuration.

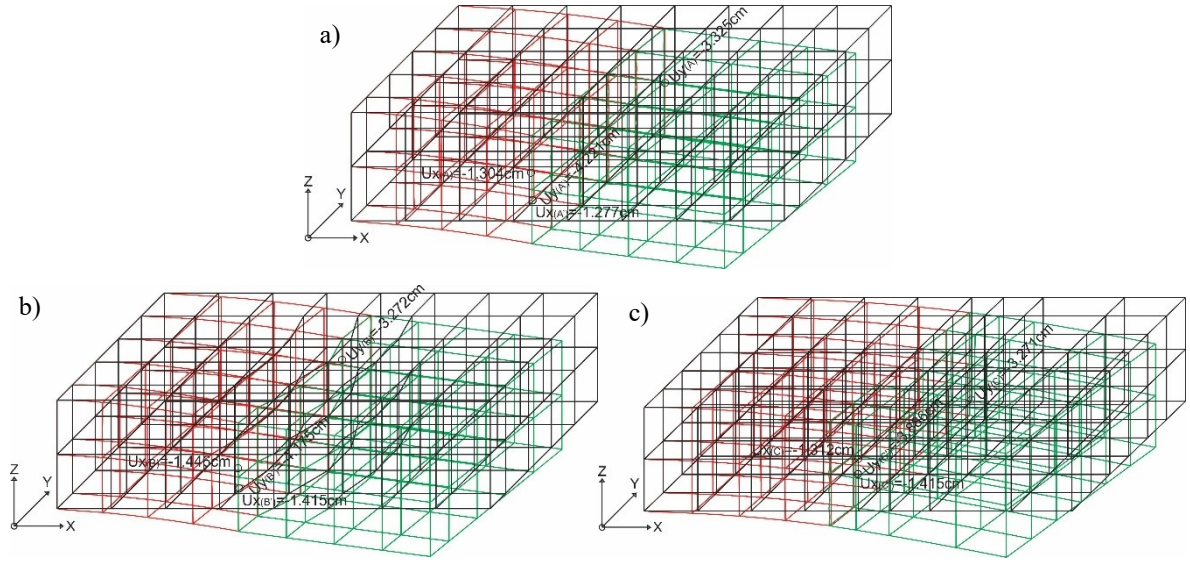


Figure 5. Horizontal displacements in the monoliths in both global directions (f_{mi}=50): a) Model 4 with k_{ad}=1.0, b) Model 5 and c) Model 6

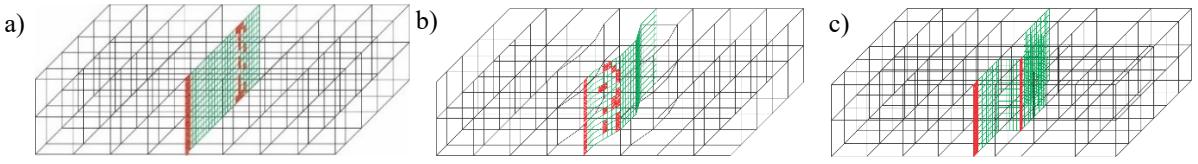


Figure 6. Open contact elements (f_{mi}=50): a) Model 4 with k_{ad}=1.0 (18% open elements), b) Model 5 (18% open elements) and c) Model 6 (17% open elements)

Copyright © 2025 CroCEE
DOI: https://doi.org/10.5592/CO/3CroCEE.2025.112

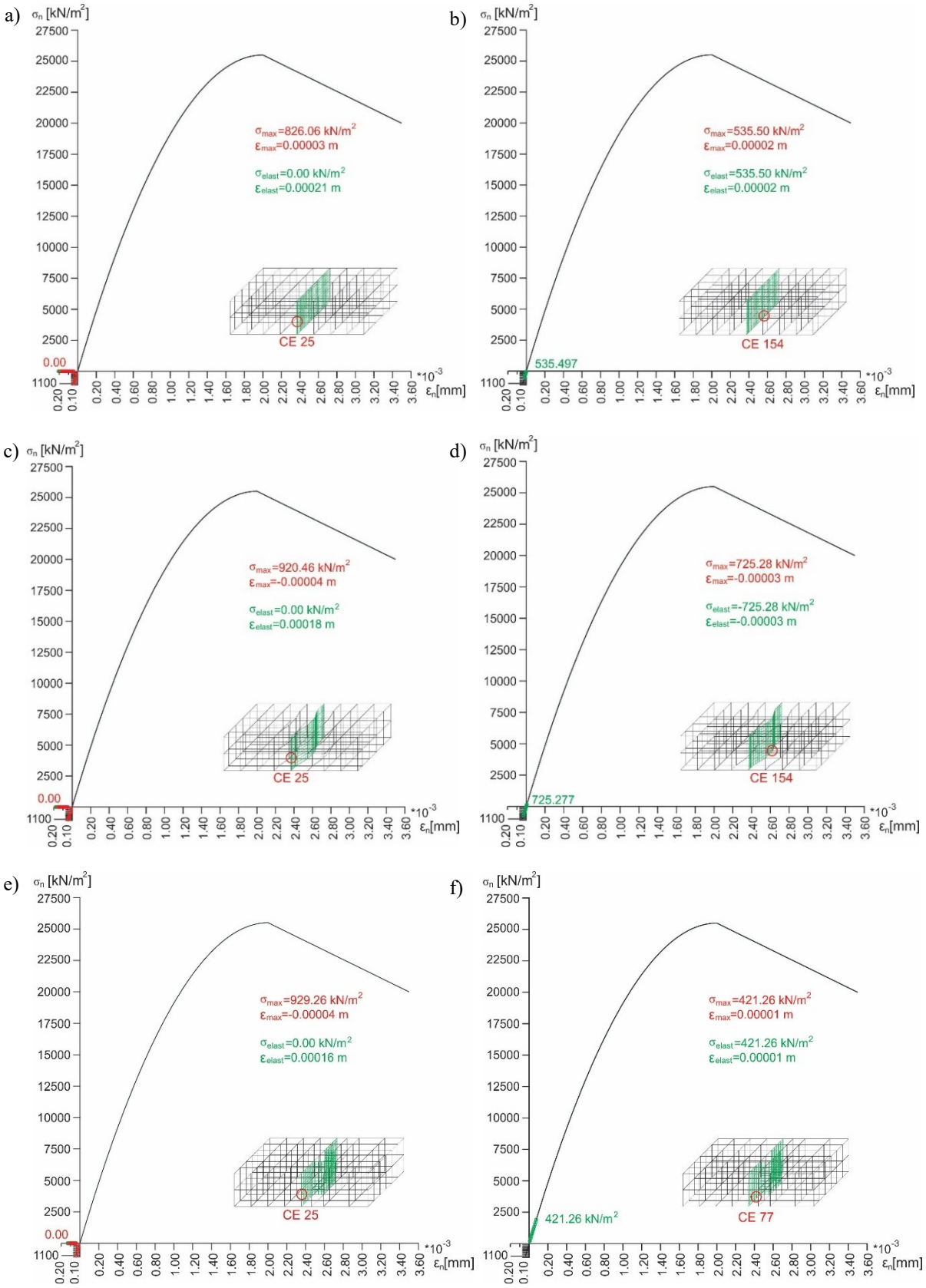


Figure 7. Normal stress–strain relationship (f_{mi}=50): Model 4 (k_{ad} =1.0) for elements with maximum: a) opening in the direction of the normal (CE 25), b) sliding in the direction of the element (CE 154); Model 5: c) opening (CE 25), d) sliding (CE 154); and Model 6: e) opening (CE 25) and f) sliding (CE 77)

Proceedings of the 3rd Croatian Conference on Earthquake Engineering - 3CroCEE
19–22 March 2025, Split, Croatia
Copyright © 2025 CroCEE
DOI: https://doi.org/10.5592/CO/3CroCEE.2025.112

For these analysed upper dam segments, Fig. 8 to Fig. 11 illustrate the histories of extremes of key parameters, including shear sliding deformations, contact openings, and horizontal displacements in the y-direction for both the left and right blocks. These parameters are calculated as a function of the incremental load factor across Models 5 and 6, and Model 4 with all of the calculated coefficients of additional tangential stiffness k_{ad}.

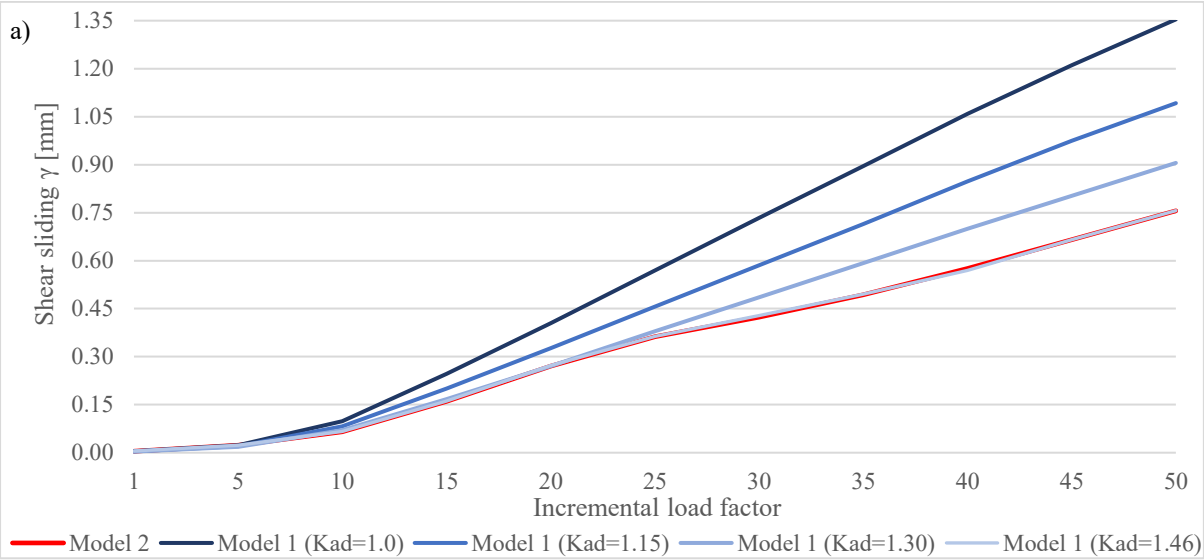
The most pronounced differences between the two models that are compared are observed in sliding deformations when all models have the same modulus of elasticity (k_{ad}=1.0), as shown in Fig. 8. Under a loading factor of f_{mi}=50, the flat joint (Model 4 with kad=1.0) exhibits a maximum shear sliding of γ_{max}=1.35 mm, whereas the bevelled shear key joint (Model 5) reduces the deformation by 44% with a maximum value of γ_{max}=0.76 mm. The unbevelled shear key joint model (Model 6) demonstrates even greater resistance, with a 68% reduction of shear sliding compared to the flat joint, with maximum value of γ_{max}=0.43 mm. As the coefficient k_{ad} increases, the sliding deformation in the flat joint approaches that of shear key joints. Good agreement is achieved for k_{ad}=1.46 between the sliding values of flat and bevelled shear key joint, while for the unbevelled and flat joint the sliding values are equal for k_{ad}=1.85. These values represent the resistance effects of the different shear key types in the upper dam segments. The shear sliding extremes are concentrated near the middle to lower part of the contact zone for all models (Figure 7b, d, f).

Consistent with the applied shear force, sliding dominates over the contact openings across all analysed models. Maximum openings occur at the lower edge of the contact zone (Figure 7a, c, d) in contact element CE 25 for all of the models. For all loading factors, the bevelled shear key joint (Model 5) shows smaller maximum contact openings, δ_{max}=0.179 mm, compared to the flat joint (Model 4), δ_{max}=0.213 mm, even with increased tangential stiffness (Fig. 9 a). Similarly, the unbevelled shear key joint (Model 6), exhibits maximum openings δ_{max}=0.165 mm, much smaller than those in flat joint (Model 4), even for various values of k_{ad} and increased tangential stiffness, Fig 9b.

Horizontal displacements in the monolithic blocks exhibit larger differences when models have equal tangential stiffness, with differences decreasing as k_{ad} increases. While the displacements of the flat joint approach those of the shear key joints, they do not fully converge. The left monolithic block, constrained by boundary conditions shows smaller maximum displacements than the right block (Fig. 11 and 12). In the bevelled shear key joint (Model 5), maximum displacements are u_y=41.75 mm in the right (Fig. 12a) and u_y=32.72 mm in the left block (Fig 11.a). These displacements are both larger than the corresponding values in the flat joint (Model 4 with k_{ad}=1.0), with values u_y=44.36 mm in the right and u_y=35.80 mm in the left block. For the unbevelled shear key joint (Model 6), the maximum displacement are u_y=44.36 mm in the right (Fig. 12b) and u_y=36.68 mm in the left block (Fig. 11b). All of these displacements are notably higher than those observed in the joints of the lower dam segment (Part 1 of the study). The reduction in relative displacements is greater in the unbevelled shear key joint compared to the bevelled shear key joint, which is consistent with its superior sliding resistance behavior shown in earlier results.

Based on the results of the numerical experiments and their comparison with lower dam segment results, a linear interpolation was performed to determine the k_{ad} values needed for increasing the tangential modulus of elasticity $E_{1,t}$ for both shear key types as a function of arch cantilever thickness (Fig. 12). This approach allows straightforward calculation of the additional tangential stiffness for joints of each shear key type across varying dam cantilever thicknesses that will be applied to different segments along the dam height. The calculated stiffness values are integrated into the contact element stiffness matrix, ensuring necessary adjustments in the numerical model.

Copyright © 2025 CroCEE
DOI: https://doi.org/10.5592/CO/3CroCEE.2025.112



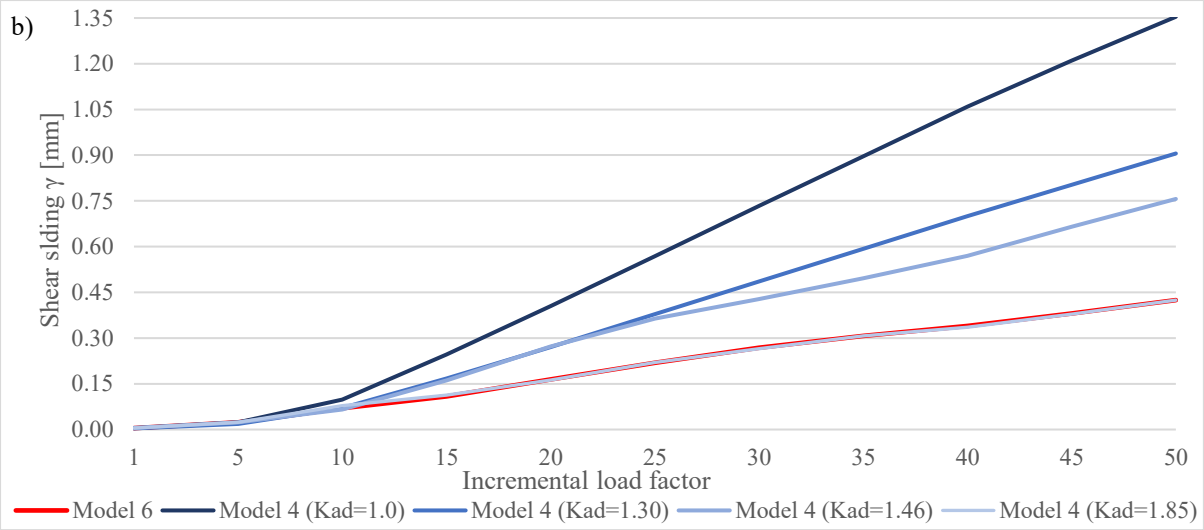
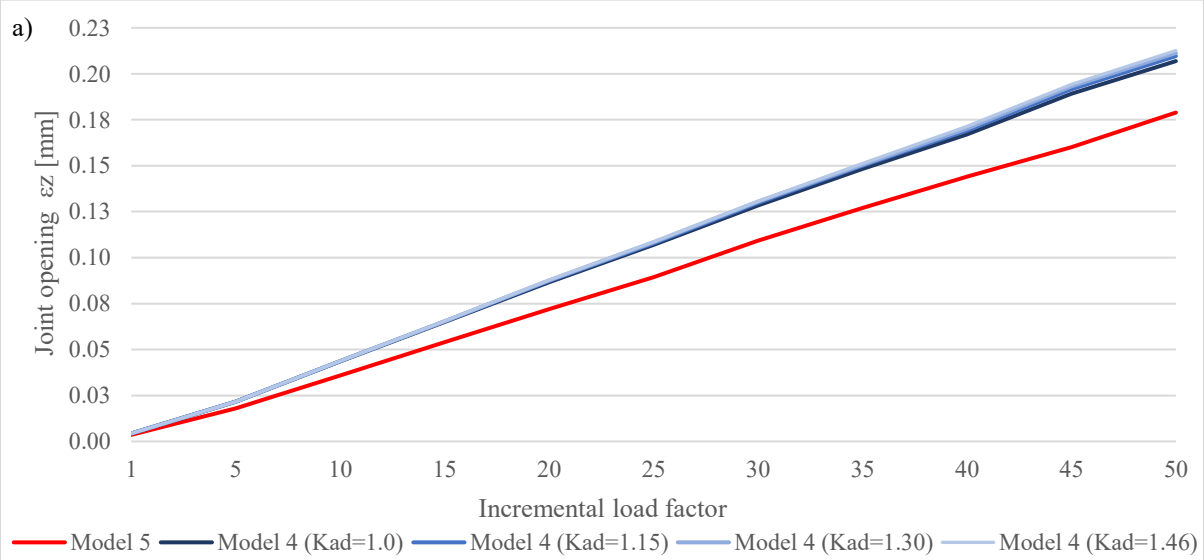


Figure 8. History of maximum shear sliding in the contact as a function of the incremental load factor for: (a) Model 1 and Model 2, (b) Model 1 and Model 3



Proceedings of the 3rd Croatian Conference on Earthquake Engineering - 3CroCEE
19–22 March 2025, Split, Croatia
Copyright © 2025 CroCEE
DOI: https://doi.org/10.5592/CO/3CroCEE.2025.112

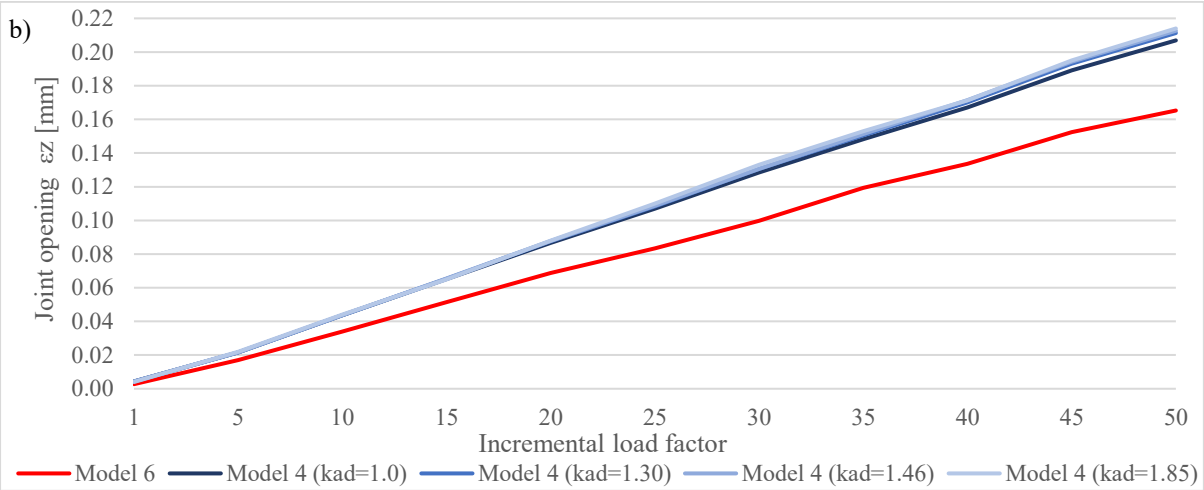
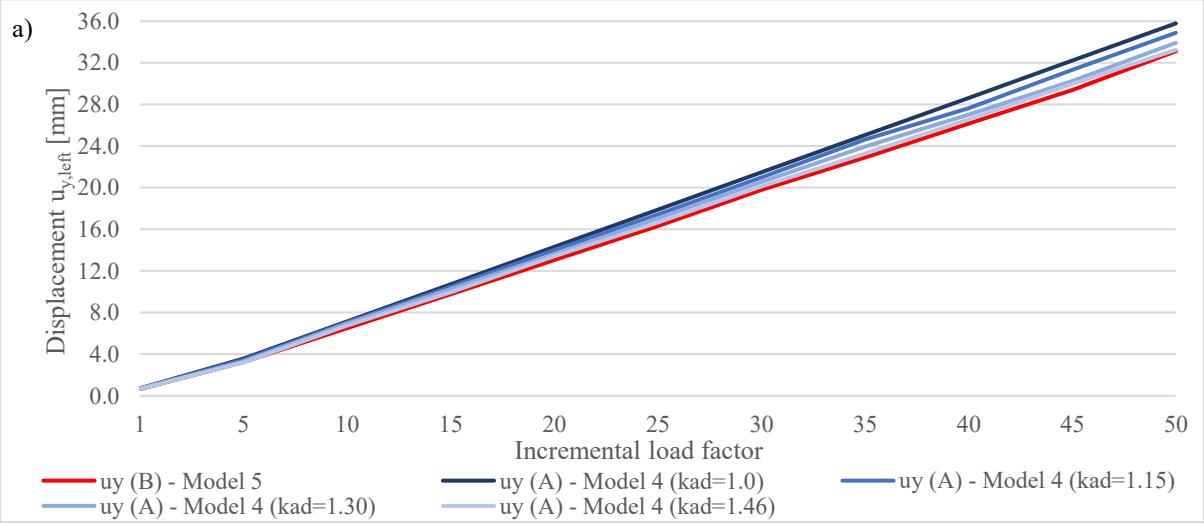


Figure 9. History of maximum opening in the contact as a function of the incremental load factor for: (a) Model 1 and Model 2 and (b) Model 1 and Model 3



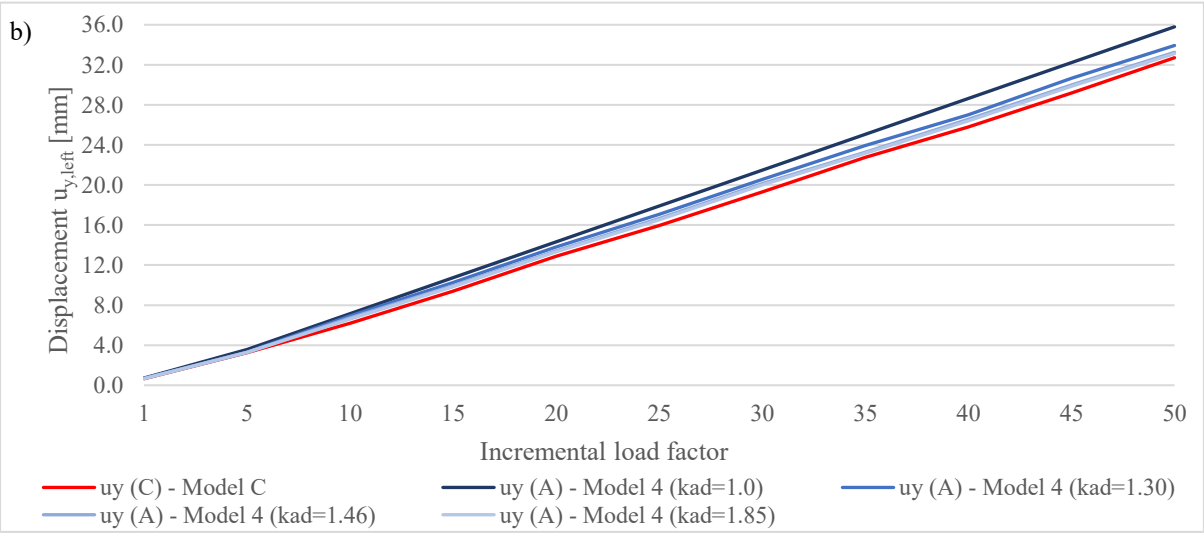


Figure 10. History of maximum horizontal displacements in the global y-direction in the left monolithic block as a function of the incremental load factor for: (a) Model 1 and Model 2 and (b) Model 1 and Model 3

Copyright © 2025 CroCEE
DOI: https://doi.org/10.5592/CO/3CroCEE.2025.112

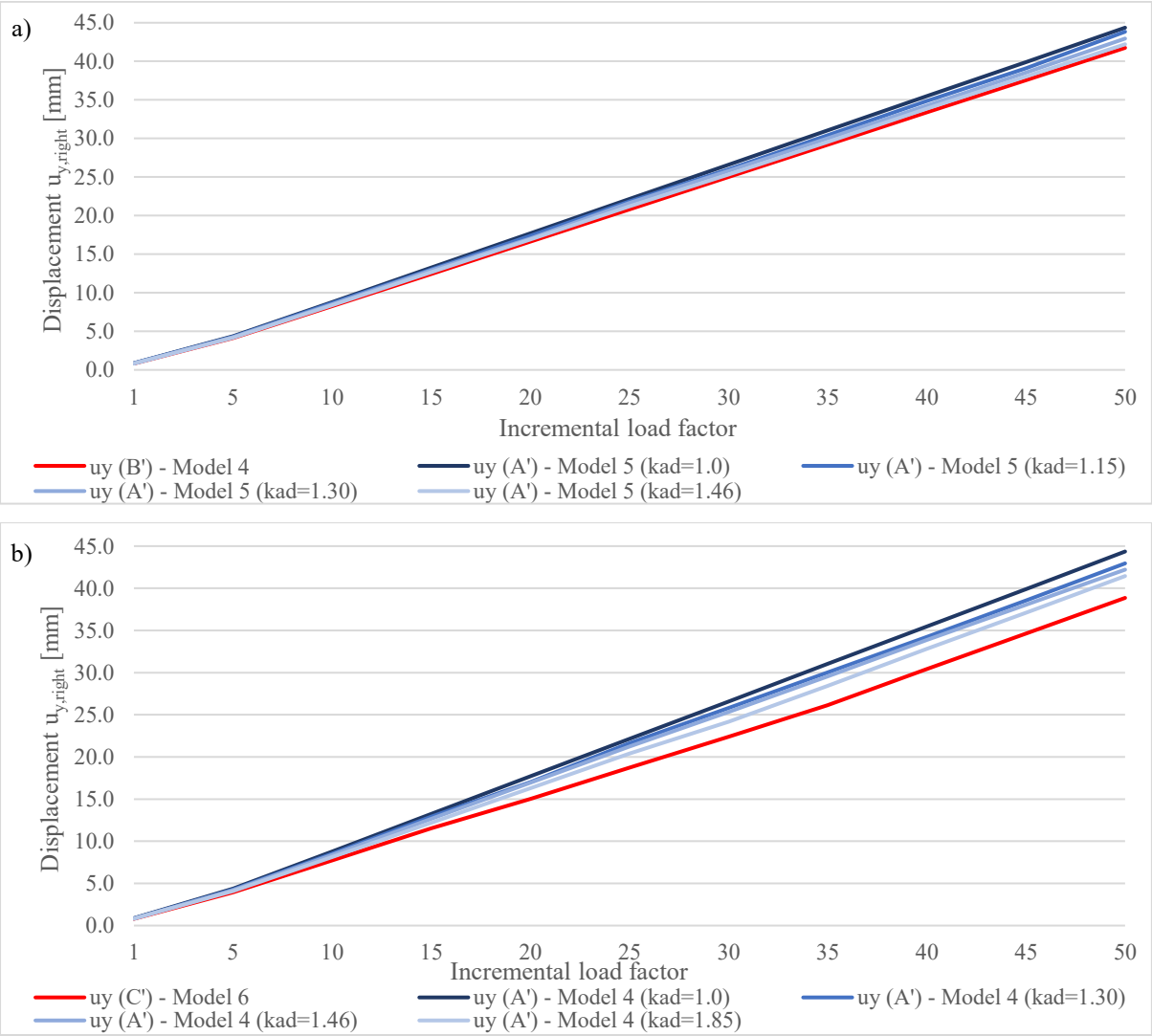


Figure 11. History of maximum horizontal displacements in the global y-direction in the right monolithic block as a function of the incremental load factor for: (a) Model 1 and Model 2 and (b) Model 1 and Model 3

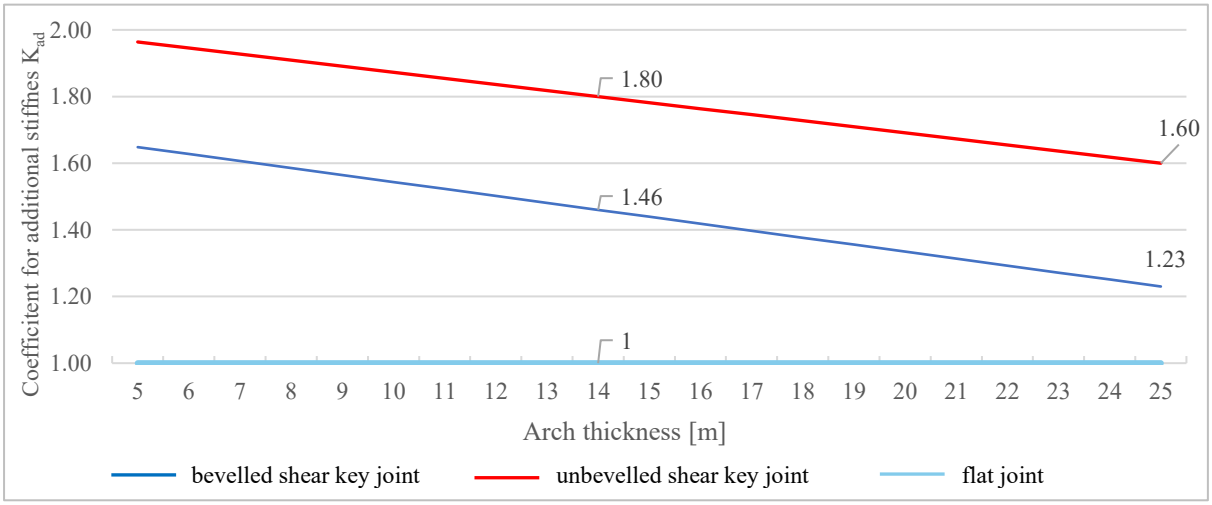


Figure 12. Calculation of the coefficient for additional tangential stiffness k_{ad} needed for increase of the tangential modulus of elasticity $E_{1,t}$ as a function of the arch thickness

Proceedings of the 3rd Croatian Conference on Earthquake Engineering - 3CroCEE
19–22 March 2025, Split, Croatia
Copyright © 2025 CroCEE
DOI: https://doi.org/10.5592/CO/3CroCEE.2025.112

The same models in the lower dam segment from Part 1 of the study (Models 1, 2, and 3) are analysed again, this time to examine the effects of a shearing force. Fig. 13 presents the histories of maximum sliding deformations for Models 2 and 3, compared to Model 1 under varying adopted values for k_{ad}. For the unbevelled shear key joint (Model 3), sliding deformations in the lower dam segment under a sliding force are reduced by 50%, with γ_{max}=0.68 mm, compared to the flat joint (Model 1 with k_{ad}=1.0), where γ_{max}=1.40 mm (Fig. 13b). This reduction is consistent regardless of whether the applied force is bending or shear force. For the bevelled shear key joint (Model 2), the reduction under a shearing force is smaller compared to Model 3, showing a 30% decrease in sliding deformation, γ_{max}=0.96 mm compared to the flat joint, γ_{max}=1.40 mm (Model 1 with k_{ad}=1.0), as shown in Fig. 13a. Under bending force, as examined in Part 1 of the study, the shear sliding reduction in the bevelled shear key joint is approximately 25%. Comparing these findings with the bending force results from Part 1 confirms that the type of applied force has minimal to no impact on the additional tangential stiffness needed to model shear key joints effectively.

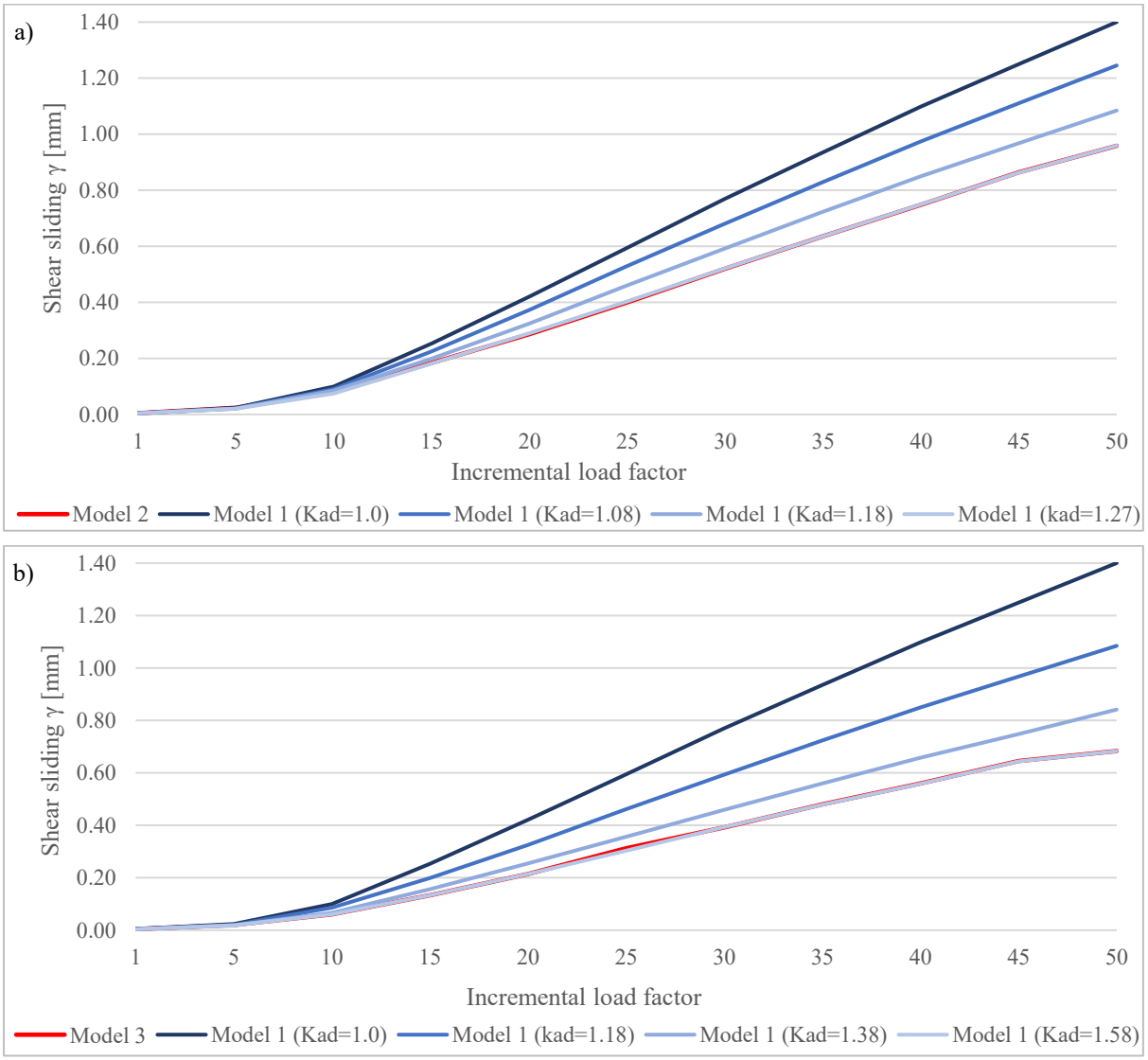


Figure 13. History of maximum shear sliding in the contact as a function of the incremental load factor for shearing force acting along the contact: (a) Model 1 and Model 2, (b) Model 1 and Model 3

Proceedings of the 3rd Croatian Conference on Earthquake Engineering - 3CroCEE
19–22 March 2025, Split, Croatia
Copyright © 2025 CroCEE
DOI: https://doi.org/10.5592/CO/3CroCEE.2025.112

5. Discussion of the results and conclusions

The aim of this research is to quantify the additional tangential stiffness representing the shear resistance of shear key joint elements with various geometries. The main focus is to derive these tangential stiffness values that can be applied to flat joints, thereby eliminating the need for detailed geometric modeling to capture the complexity of shear key joint geometry and behavior. These computed values, expressed as additional tangential stiffness coefficient are integrated into the flat joint contact elements' stiffness matrix, modifying the constitutive law to accurately simulate nonlinear behavior of the joint in the direction of the shear key elements, which may be implemented in one or two directions. The second part of the study focuses on investigating the influence of arch thickness and applied force.

The most pronounced differences among the analysed parameters are observed in the sliding shear deformations at the contact. The tangential stiffness coefficient k_{ad} is determined by equating the sliding deformations of the flat joint to those of the shear key joints. In the upper dam segments, the bevelled shear key shows a 46% increase in tangential stiffness, compared to 27% in the lower parts. The unbevelled shear key exhibits a 70% increase, emphasizing the impact of arch thickness. These results affirm that the segment thickness directly influences tangential stiffness, with each joint configuration contributing differently to the resistance in tangential direction. In both parts of the study, it is confirmed that the tangential stiffness increase varies depending on the type of shear key, with unbevelled joints consistently showing greater stiffness increase than bevelled joints. Furthermore, Part 2 confirms that arch thickness significantly affects shear key behavior, even for the same joint configuration.

In the upper segments under shear force, both shear key joint types of exhibits reduced joint openings compared to the flat joint, with differences that do not diminish with the increase of tangential stiffness. However, these differences remain relatively small, around 0.034 mm for the bevelled and 0.049 mm for the unbevelled shear key joint. It can be concluded that despite variations in sliding deformations, joint openings are exhibit similar values across all modes. Regarding open element zones, the unbevelled shear key joint shows fewer open elements, concentrated on the key element within a small area near the contact's end. In contrast, the bevelled shear key joint displays open elements in both upper and lower key regions, with more pronounced openings in the lower section, aligning with the maximum observed openings in that area. Maximum horizontal displacements in the global y-direction, as well as relative displacements between the monolithic blocks, closely correspond to the observed shear sliding behavior. Arch thickness significantly influences these displacements, with larger values observed in the thinner upper sections compared to the thicker lower section of the dam, which is expected. Additionally, the response curves for all joint types demonstrate strong consistency across the analysed parameters for all types of joints.

The study findings confirm that the favourable shear key joint geometry (of both analysed types) significantly increases the tangential stiffness compared to flat joints. The key factors influencing shear resistance include not only the geometry of the joints (shape and angle of the key element), but also the arch segment's thickness, and, to a lesser extent, the type of applied force. Notably, the segment's thickness plays a critical role even for joints with identical shear key configurations, highlighting the need to account for this parameter in further analyses.

The research confirms the efficiency of the proposed approach in simulation of the complex nonlinear behavior of an arch dam constructed with shear key joints, eliminating the need for explicit geometric modeling. The model will be applied to simulate contraction joints in an arch dam, evaluating the impact of the different joint types on stress redistribution and the overall structural response under static and dynamic loading conditions.

Copyright © 2025 CroCEE
DOI: https://doi.org/10.5592/CO/3CroCEE.2025.112

References

[1] Talatahari, S., Salami M., Parsiavash, R. (2016): Optimum design of double curvature arc dams using a quick hybrid charged system search algorithm. *Iran University of Science & Technology*, **6**, 227-243, Corpus ID: 53392743.

[2] Du, C. B., Jiang, S. Y. (2010): Effects of contraction joints and key slots on the seismic responses of arch dam (in Chinese). *Journal of Hydroelectric Engineering*, **29** (5), 1–5.

[3] Ahmadi, M. T., Izadinia, M., Bachmann, H. (2001): A discrete crack joint model for nonlinear dynamic analysis of concrete arch dam. *Computers and Structures,* **79** (4), 403-420, https://doi.org/10.1016/S0045-7949(00)00148-6.

[4] Fenves, G. L., Mojtahedi, S., Reimer, R. B. (1992): Effect of contraction joints on earthquake response of an arch dam. *Journal of Structural Engineering*, **118** (4), 1039—1055, https://doi.org/10.1061/(ASCE)0733-9445(1992)118:4(1039).

[5] Lau, D. T., Noruziaan, B., Razaqpur, A. G. (1998): Modelling of contraction joint and shear sliding effects on earthquake response of arch dams. *Earthquake Engineering and Structural Dynamics*, **27**, 1013-1029, https://doi.org/10.1002/(SICI)1096-9845(199810)27:10<1013::AID-EQE765>3.0.CO;2-0.

[6] Tzenkov, A. D., Lau, D. T. (2002): Seismic analysis of concrete arch dams with contraction joints and non-linear material models, *7th U.S. National Conference on Earthquake Engineering*, Boston, Massachusetts.

[7] Toyoda, Y., Ueda M., Shiojiri, H. (2002): Study of joint opening effects on the dynamic response of an existing arch dam, *15th ASCE Engineering Mechanics Conference*, Columbia University, New York.

[8] Noble, C. R., Solberg J. (2004): Nonlinear seismic analysis of Morrow Point dam. *A Study for the United States Bureau of Reclamation*, UCRL-TR-202545.

[9] Guerra, A. (2007): Shear key research project – Literature review and finite element analysis. Dam Safety Technology Development Program, U.S. Department of the Interior, Bureau of Reclamation, *Report DSO-07-05*.

[10] ADAD-IZIIS – Software for analysis and design of arch dams. *Institute of Earthquake Engineering and Engineering Seismology*, University of Ss. Cyril and Methodious, Skopje, R. N. Macedonia.

Proceedings of the 3rd Croatian Conference on Earthquake Engineering - 3CroCEE
19–22 March 2025, Split, Croatia
Copyright © 2025 CroCEE
DOI: https://doi.org/10.5592/CO/3CroCEE.2025.119

COMPARATIVE NUMERICAL INVESTIGATION OF TIMBER ADDED FLOORS ON EXISTING RC STRUCTURES

Viktor Hristovski [(1)], Trajche Zafirov [(2)]

[(1)] *Professor, Institute of Earthquake Engineering and Engineering Seismology (IZIIS), viktor@iziis.ukim.edu.mk*
[(2)] *Assistant, , Institute of Earthquake Engineering and Engineering Seismology (IZIIS), trajce@iziis.ukim.edu.mk*

Abstract

As urban areas become increasingly dense, the vertical extension of existing structures has gained importance, especially in seismically active regions. The challenge is more pronounced for older buildings designed with minimal or no seismic provisions. Light frame timber systems are often preferred for vertical extensions due to their low mass, which minimizes additional seismic forces on the existing structure. At the Institute of Earthquake Engineering and Engineering Seismology (IZIIS) in Skopje, experimental shaking-table tests were performed on two-story reinforced concrete (RC) structures with timber-added floors to assess their structural performance. The goal of these tests was to examine the impact of vertical extension on the structural behavior under seismic loads. To validate the experimental findings, numerical analyses using OpenSees software were conducted. Initially, modal (eigen) analyses were performed to determine the natural frequencies and vibration mode shapes of the structure. This was followed by pushover analyses using a nonlinear static procedure in both the transverse and longitudinal directions. Modal force patterns based on the first mode of vibration were applied to simulate the loading conditions. Lastly, dynamic analyses under seismic ground motion were performed to further assess the behavior of the structure with timber-added floors. The comparative study highlights the effectiveness of using timber for vertical extensions, providing insight into its impact on the seismic performance of existing RC structures.

Keywords: Adding floors, vertical extension, Light frame timber, XLAM,

1. Introduction

A significant number of studies have been conducted on the dynamic behavior of lightweight structures made of wood and steel [1],[2],[3],[4],[5],[6],[7]. However, their behavior when used as materials for vertical extensions on existing structures has not been sufficiently investigated.

To address this, experimental tests were carried out at the Institute of Earthquake Engineering and Engineering Seismology (IZIIS) in Skopje on a shaking table. The tests focused on different extension systems applied to existing two-story RC structures. The aim of this research is to fill the existing knowledge gap by clarifying how the extension interacts with the existing structure and how it alters the dynamic characteristics and behavior of the integral system. Furthermore, the purpose of these tests is to comparatively investigate the impact of each type of extension system on the overall structural behavior.

Numerous dynamic tests were performed on the shaking table at the IZIIS laboratory. The investigation involved harmonic, synthetic, and real earthquake records as input in a single horizontal direction. To verify the test results, numerical analyses were subsequently carried out using the OpenSees software. Initially, modal (eigenvalue) analyses were performed to obtain natural frequencies and mode shapes. Then, a nonlinear static pushover analysis was conducted in two directions using modal forces corresponding to the first mode shape. Finally, dynamic analyses were performed using time histories of real and synthetic earthquakes. It should be noted that these analyses are preliminary, as much of the nonlinear behavior of materials and connections has not been considered.

Copyright © 2025 CroCEE
DOI: https://doi.org/10.5592/CO/3CroCEE.2025.119

This study focuses on RC two-story models without infill walls (RCF1), RC two-story models with infill walls (RCF2), and extension systems made of steel (STL) and lightweight timber (LFT). The paper first presents the geometry of the models and material characteristics. Then, the methods for measuring the models are explained. Afterward, test results and experimental outcomes are presented. Finally, numerical investigations of the basic and extension systems using steel and lightweight timber applied to existing RC structures are discussed.

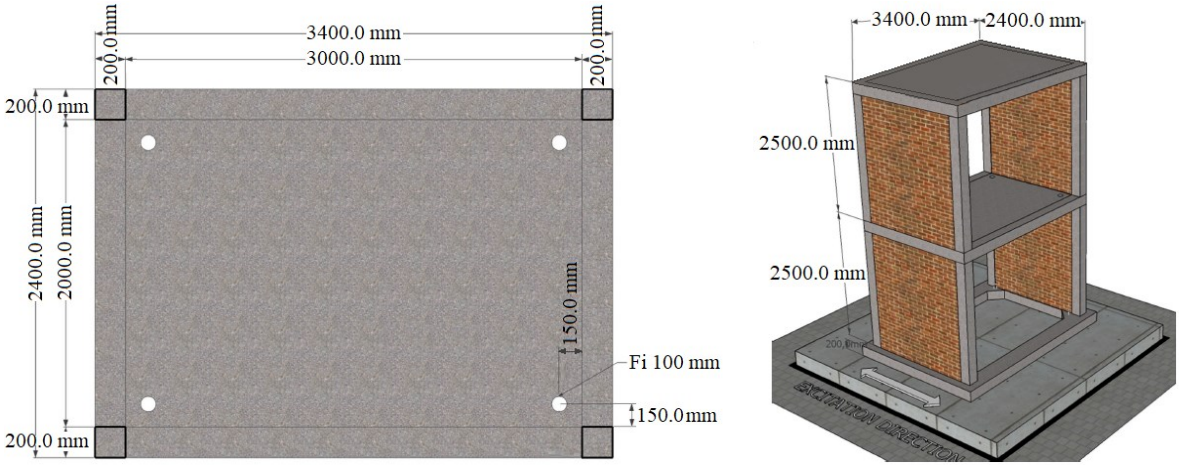
2. Experimental Investigation

2.1. Description of the Models

The basic 3D RC model (referred to in the text as model RCF1) represents a simple two-story structure with a single span and base dimensions of 340cm x 240cm (Fig. 1 and 2 a)). It consists of RC columns (20x20cm), RC beams (20x20cm), and RC slabs with a thickness of 7cm. The columns are reinforced with 4 longitudinal reinforcement bars of Φ16mm and stirrups of Φ8mm/10(20)cm. The beams are symmetrically reinforced in both the top and bottom zones, with a total of 4 longitudinal bars of Φ14mm and stirrups of Φ8mm/10(20)cm.

The RC foundation beams are designed with a height of 20cm and are fixed to the vibration platform using special anchors. Symmetrical longitudinal reinforcement consisting of 4 bars of Φ14mm is placed in the foundation beams, with stirrups of Φ8mm/8(20)cm.

The story height of the model is h = 2.5m (see Fig. 2). A two-story RC frame is rotated by 90 degrees (referred to as model RCF2), and masonry infill (modular hollow blocks, 19x19x29cm) is installed along the shorter direction.



a) b)

Figure 1. a) Building plan view, b) Building 3D view (RCF2)

The XLAM upgrade structure, depicted in Fig. 2 (b), was entirely constructed from 3-layer cross-laminated panels with a thickness of 10 cm. The wall elements were designed so that the outer two layers of the panel, each with a thickness of 3 cm, were oriented vertically, while the middle layer, with a thickness of 4 cm, was oriented horizontally. The XLam roof panel was oriented perpendicular to the direction of the extension. A CLT roof panel was secured to the CLT wall elements with 8 mm self-tapping screws.

Along the shorter side, two wall segments measuring 240 cm each were installed. On the longer side, three segments, each 80 cm in length, were placed—two on one side and one on the opposite. The CLT walls were fixed to the RC slab using 100 mm reinforced angle brackets supplied by Rothoblaas (Jancar et al., 2013).

The light timber frame upgrade (LTF), see Fig. 2 (c), consists of timber frame walls and a CLT roof panel. Two external timber frame wall elements (2.4 × 2.4 m) are placed along the shorter direction,

Copyright © 2025 CroCEE
DOI: https://doi.org/10.5592/CO/3CroCEE.2025.119

while in the longer direction one wall segment measuring 1.2 × 2.4 m is placed on each side. In order to observe differences in dynamic behavior due to changes in stiffness, no mechanical connection was made between adjacent perpendicular wall elements in the LTF 1 and LTF 3 specimens. Where connections were made, self-tapping screws with a diameter of 8 mm were used at a spacing of 100 mm center to center.

The light timber frame wall consists of a timber frame (10/8 cm, C24), with studs placed at 62.5 cm spacing. Each wall is sheathed with three 12 mm thick OSB panels, which are attached to the timber frame using metal staples. The wall elements are anchored to the reinforced concrete slab using 100 mm reinforced angle brackets (Jancar et al., 2013).

To simulate the live load, the first- and second-floor slabs were each loaded with eight lead ingots of 400 kg each (see Fig. 2 a)). In addition, two 400 kg ingots were placed on top of the upgrade systems.



a) b) c)

Figure 2. a) RCF1 model, b) RCF1+XLAM, c) RCF1+LFT1

2.2. Dynamic Excitations

To gain insight into the elastic behavior of the models, tests were conducted using synthetic earthquake records with low amplitude (a modified Landers earthquake) and real earthquake records (El Centro and Petrovac) up to 0.1 g. The acceleration spectra of the aforementioned records are shown in Fig. 3.

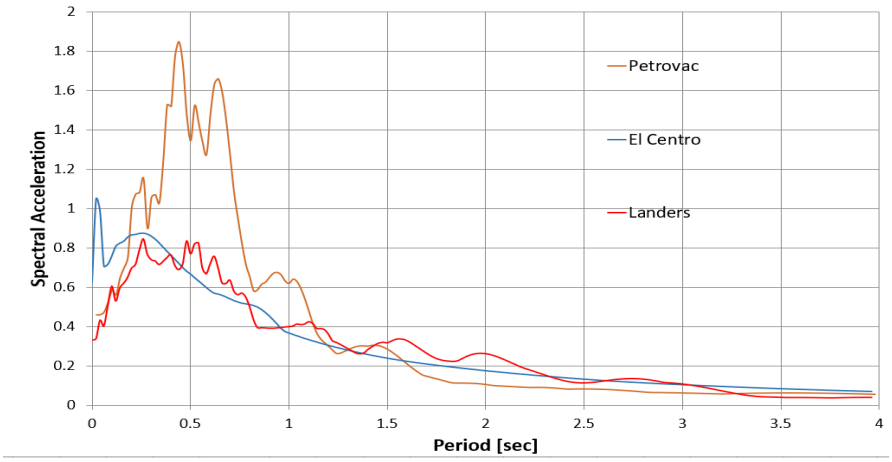
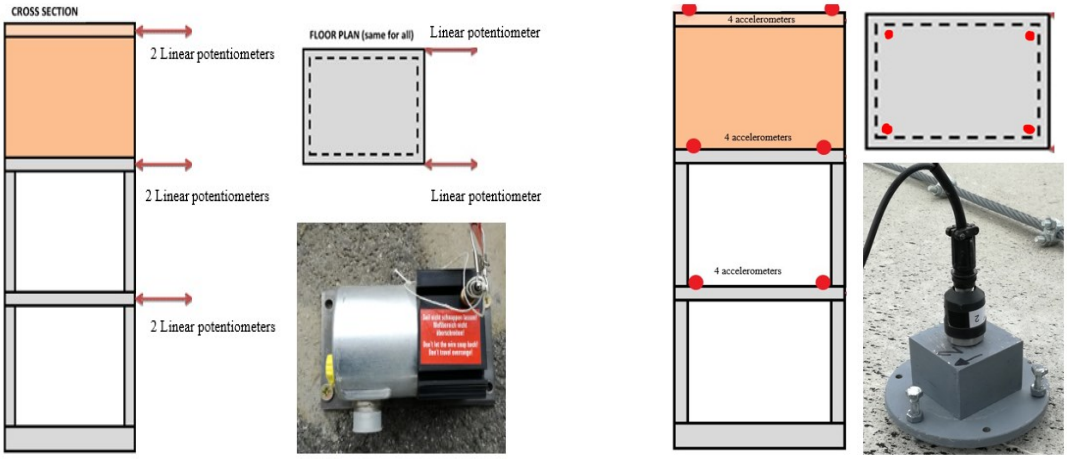


Figure 3. Acceleration spectrum for PGA 0.1g from the modified records used in the tests.

Copyright © 2025 CroCEE
DOI: https://doi.org/10.5592/CO/3CroCEE.2025.119

2.3. Instrumentation

The instrumentation concept for the model is shown in Fig. 4 a) and b). Two linear potentiometers were installed on each floor to measure absolute displacements (a total of 6). Additionally, two accelerometers in the transverse direction and two accelerometers in the longitudinal direction were placed on each floor to measure absolute accelerations (a total of 12).



a) b)

Figure 4. a) Two linear potentiometers on each floor, b) Four accelerometers on each floor

2.4. Experimental structure response

Some of the comparative results from the shaking table tests are shown in Fig.. 5-7. Fig. 5 presents the response of the basic two-story model RCF1, while Fig. 11 shows the response of the three-story model RCF1 + LFT1. It can be observed that the displacement amplitudes of the third story in the upgraded model RCF1 + LFT1 are smaller than those of the second story. This leads to the conclusion that higher mode shapes become more significant in the dynamic response when using materials like steel for upgrading RC structures. This phenomenon was also visually observed during the tests.

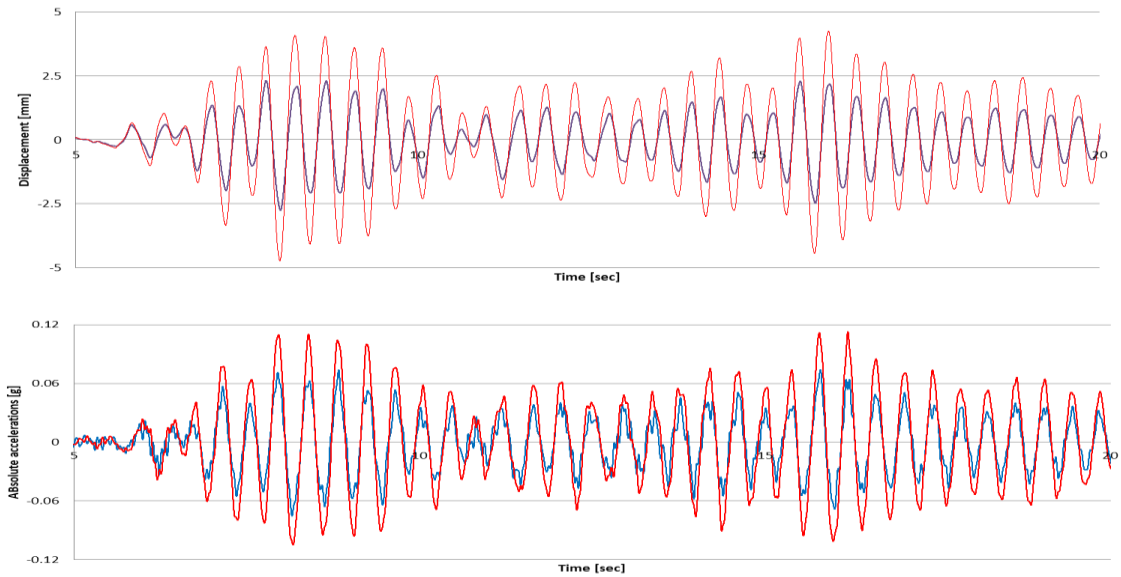


Figure 5. Experimentally obtained relative displacements and acceleration time histories for the RCF1 model: blue line – first floor, red line – second floor (Test 03).

Copyright © 2025 CroCEE
DOI: https://doi.org/10.5592/CO/3CroCEE.2025.119

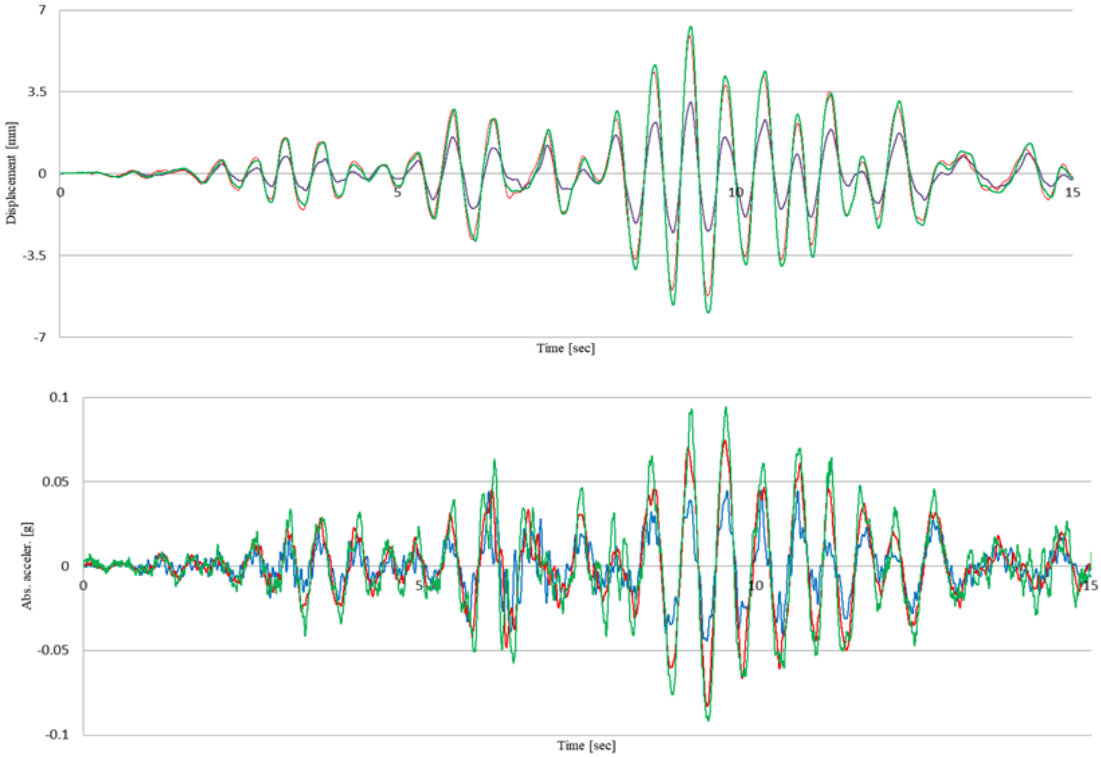


Figure 6. Experimentally obtained relative displacement and acceleration time histories for specimen RCF1+XLAM2: blue line – 1st story, red line – 2nd story, green line – 3rd story (Test 17)

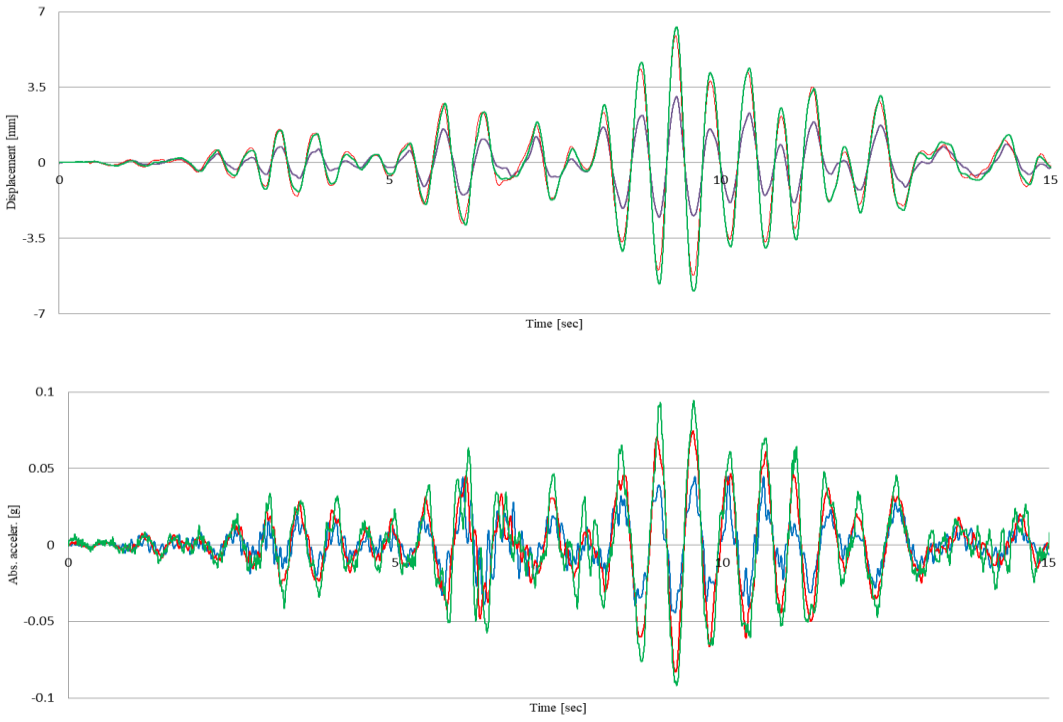


Figure 7. Experimentally obtained relative displacements and acceleration time histories for the RCF1+LFT model: blue line – first floor, red line – second floor, green line – third floor (Test 26).

Copyright © 2025 CroCEE
DOI: https://doi.org/10.5592/CO/3CroCEE.2025.119

3. Numerical Investigation

3.1. Computer Model of the Specimen

Nonlinear analyses were conducted in OpenSees. The columns and beams were modeled as single-plasticity elements, consisting of an elastic element with two "fiber" sections at each end of the elastic element. For modeling in OpenSees, "Beam with Hinges" elements were used. The nonlinear behavior of the masonry was modeled by replacing the wall with an equivalent diagonal strut. The nonlinear behavior of the diagonals was defined by a force-displacement relationship, following the procedure proposed by Fardis et al. [9].

In OpenSees, truss elements were used to model the masonry, with the behavior of the masonry represented by a hysteretic uniaxial material. Rigid diaphragms were assigned at each floor level. The total mass and moment of inertia of the structure were applied to specific nodes located at the center of mass. The mass nodes from the total weight were horizontally connected with a rigid beam element to the center of the structure. Vertical loading was applied as concentrated loads at the columns.

The second-order effect (P-Delta theory) was also considered. The columns were fully fixed at the base. Since the columns and beams are well-reinforced with adequate transverse reinforcement (stirrups), it is assumed that their shear behavior remains elastic. The effective width of the slab in the inverted T-section of the beams was calculated using the method proposed by Eurocode 2 (SIST EN 1992-1-1, 2004) [10]. The plastic hinge length for the RC elements was determined according to Eurocode 8 (SIST EN 1998-3, 2005). The three-dimensional layout of the mathematical model is shown in Fig. 8.

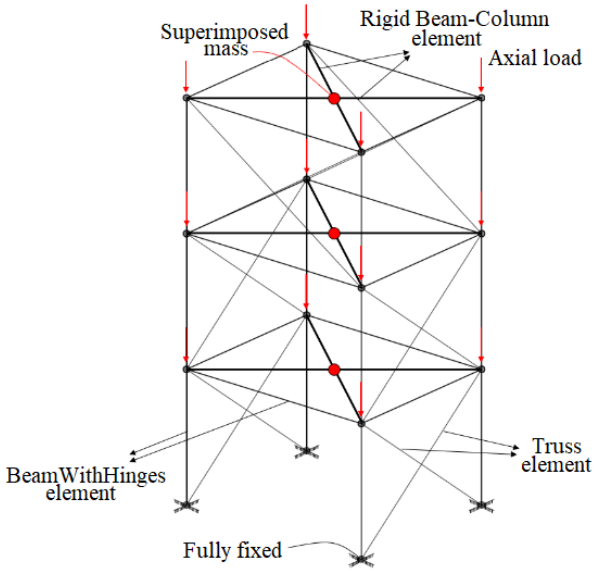


Figure 8. Three-dimensional representation of the mathematical model.

Proceedings of the 3rd Croatian Conference on Earthquake Engineering - 3CroCEE
19–22 March 2025, Split, Croatia
Copyright © 2025 CroCEE
DOI: https://doi.org/10.5592/CO/3CroCEE.2025.119

3.2. Modal analysis

First, modal (eigenvalue) analyses were performed, and the results for the obtained periods and mode shapes of vibration were compared with the experimental results obtained from the shaking table tests. The correlation between the test results and the analysis results is presented comparatively in Table 2 (values in parentheses correspond to the simply supported model).

Table 1. Dynamic properties of models

Model		RCF1	RCF2	RCF1+STL	RCF1+XLAM	RCF1+LFT1
Values from experiment						
Mode	1	0.390	/	0.510	0.55	0.542
	2	0.320	/	0.460	0.27	0.478
	3	0.190	/	0.250	0.14	0.21
	4	0.120	/	0.210	0.12	0.125
Analytically obtained values						
Mode	1	0.399	0.398	0.467 (0.617)	0.490	0.683
	2	0.357	0.118	0.403 (0.454)	0.468	0.676
	3	0.177	0.077	0.249 (0.372)	0.340	0.41
	4	0.118	0.052	0.204 (0.302)	0.117	0.36

3.3. Dynamic analysis

- **General**

Dynamic analyses were performed using a stepwise increase in vibration amplitude (10%, 25%, 50%, and 100% of the Kobe earthquake amplitude). The dynamic analyses were conducted separately in both directions. The results presented for the RCF1 model correspond to excitation in the longitudinal direction, while those for the RCF2 model correspond to excitation in the transverse direction. In the dynamic analysis, 5% proportional mass damping was considered.

- **Response of the RCF1 Model**

The floor displacements and acceleration response history corresponding to the Kobe 100% record are shown in Fig. 9. The maximum displacement of approximately 80 mm was observed at the top of the structure during the final excitation. This corresponds to a 1.6% drift at the top. The peak acceleration at the top of the building, under excitation with the same intensity, reached approximately 1g. The maximum base shear force was approximately 100 kN.

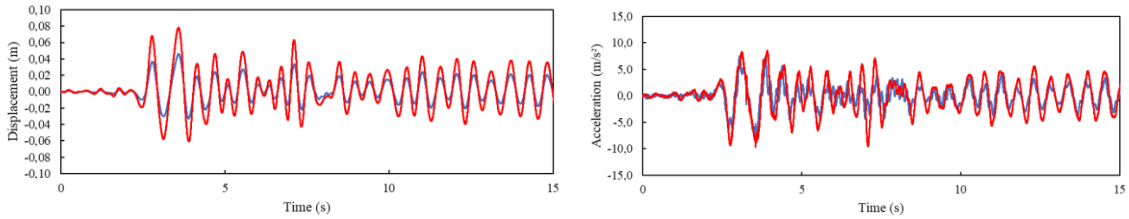


Figure 9. Analytically obtained relative displacements and acceleration time histories for the RCF1 model: blue line – first floor, red line – second floor (Kobe Test 100%).

- **Response of the RCF1+XLAM Model**

The floor displacements and acceleration response history corresponding to the Kobe 100% record are shown in Fig. 10. The maximum displacement of approximately 163 mm was observed at the top of the structure during the final excitation. This corresponds to a 3% drift at the top. The gradually reduced stiffness of the structure can be observed from the presented results. A nonlinear response of the building was obtained during the final excitation. The maximum base shear force was approximately 120 kN.

Copyright © 2025 CroCEE
DOI: https://doi.org/10.5592/CO/3CroCEE.2025.119

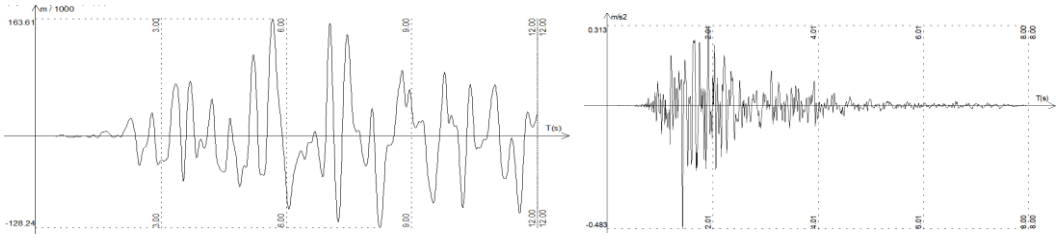


Figure 10. Analytically obtained relative displacements and acceleration time histories for the RCF1+XLAM

- **Response of the RCF1+LFT Model**

The floor displacements and acceleration response history corresponding to the Kobe 100% record are shown in Fig. 11. The maximum displacement of approximately 179 mm was observed at the top of the structure during the final excitation. This corresponds to a 3.5% drift at the top. The gradually reduced stiffness of the structure can be observed from the presented results. A nonlinear response of the building was obtained during the final excitation. The maximum base shear force was approximately 120 kN.

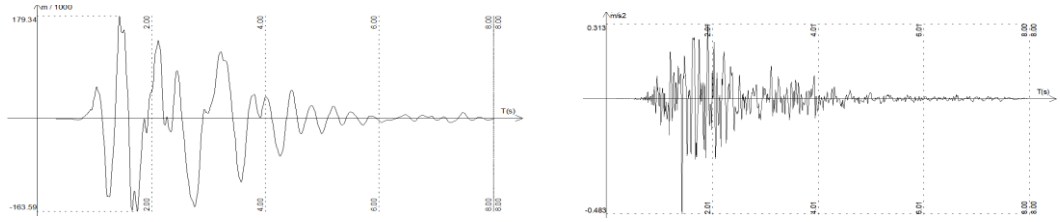


Figure 11. Analytically obtained relative displacements and acceleration time histories for the RCF1+LFT model: third floor (Kobe Test 100%).

4. Conclusion

From this research, as observed from the tested specimens, it can be concluded that all upgrades contribute differently to the overall dynamic response of the integral system. In this case, higher mode shapes were shown to be more significant. The lightweight timber structure(LFT) exhibited improved behavior compared to the steel structure. The connections with the concrete slab certainly had an impact on the response mechanism of the extension. the most favorable behavior due to compactness and properly distributed stiffness along the height has been observed in the case of the X-Lam panel upgrade (XLAM). The masonry also contributed to the different responses of the base and upgraded models. From the numerical analysis conducted, it was concluded that the model closely resembled the real structure in terms of modal analysis. The results from the earthquake records (Kobe) indicated similar characteristics to the real model. The displacement time history showed larger amplitudes in models without masonry. The model with masonry and a steel extension exhibited significantly higher amplitudes in the acceleration time history. In the future, a more detailed analysis will be conducted, including all earthquake records, as well as upgrades made from cross-laminated timber (CLT) and composite structures of wood and glass, to determine the behavior factor for this type of structures.

Copyright © 2025 CroCEE
DOI: https://doi.org/10.5592/CO/3CroCEE.2025.119

References

[1] Ceccotti A (2008). New Technologies for Construction of Medium-Rise Buildings in Seismic Regions: The Xlam Case, *Structural Engineering International*, 2008(2), pp. 156-165 doi: 10.2749/101686608784218680

[2] Chen S, Chengmou F, Jinglong P (2010). Experimental Study on Full-Scale Light Frame Wood House under Lateral Load, *ASCE Journal of Structural Engineering*, Vol. 136, No. 7, pp. 805-812

[3] Filiatrault A, Christovasilis I, Wanitkorkul A, John W. van de Lindt (2010). Experimental Seismic Response of a Full-Scale Light-Frame Wood Building. *ASCE Journal of Structural Engineering*, Vol. 136, No. 3, pp. 246-254.

[4] Hristovski V, Dujic B, Stojmanovska M, Mircevska V (2013). Full-Scale Shaking-Table Tests of XLam Panel Systems and Numerical Verification: Specimen 1, *ASCE Journal of Structural Engineering*, Vol. 139, No. 11, pp. 2010-2018

[5] Hristovski V, Jančar J, Dujic B, Garevski M (2014). Comparative Shaking-Table Tests of Various Upgrade Systems Applied on Existing Two-Storey RC Structures with and without Masonry Infill – Preliminary Results, *Proceedings of the 2nd European Conference on Earthquake Engineering and Seismology*, 24-29 August, Istanbul, Turkey.

[6] John W. van de Lindt, Shiling Pei, Pryor S. E., Shimizu H, Isoda H (2010). Experimental Seismic Response of a Full-Scale Six-Story Light-Frame Wood Building, *ASCE Journal of Structural Engineering*, Vol. 136, No. 10, pp. 1262-1272.

[7] Popovski M, Schneider J, Schweinsteiger M (2010). Lateral Load Resistance of Cross-Laminated Wood Panels. Proc. 11th World Conference on Timber Engineering WCTE , Trentino, Italy, June 20-24, 2010, ID Paper 171.

[8] CEN. European standard EN 1992-1-1: 2004. *Eurocode 2: Design of concrete structures – Part 1-1: General rules and rules for buildings*. European Committee for Standardization, Brussels, December, 2004.

[9] Fardis, M.N., (ed.). 1996. *Experimental and numerical investigations on the seismic response of RC infilled frames and recommendations for code provisions*. ECOEST/PREC8 Report No. 6, Lisbon, LNEC – Laboratotio Nacional de Engenharia.

[10] CEN. European standard EN 1998-3: 2005. *Eurocode 8: Design of structures for earthquake resistance. Part3: Assessment and retrofitting of buildings*. European Committee for Standardization, Brussels, June, 2005.

Proceedings of the 3rd Croatian Conference on Earthquake Engineering - 3CroCEE
19–22 March 2025, Split, Croatia
Copyright © 2025 CroCEE
DOI: https://doi.org/10.5592/CO/3CroCEE.2025.120

NEW PROVISIONS FOR SEISMIC DESIGN OF BRIDGES

Ana Mandić Ivanković [1], Mladen Srbić [2], Gordana Hrelja Kovačević [3]

[1] Prof. PhD, Faculty of Civil Engineering, Department of Structural Engineering, ana.mandic.ivankovic@grad.unizg.hr
[2] Assis. Prof. PhD, Faculty of Civil Engineering, Department of Structural Engineering, mladen.srbic@grad.unizg.hr
[3] Faculty of Civil Engineering, Department of Structural Engineering, gordana.hrelja.kovacevic@grad.unizg.hr

Abstract

The paper presents an overview of the new provisions of the second generation of the EN 1998 standards dedicated to design of bridges for earthquake resistance based on available phase of development of standards. Main document Eurocode 8 – Design of structures for earthquake resistance – Part 2: Bridges (FprEN 1998-2:2024) is analysed in relation to the introductory Part 1-1: General rules and seismic action (FprEN 1998-1-1:2024) and basic document on Basis of structural and geotechnical design (FprEN 1990:2022) together with Part 1 on New structures (prEN 1990-1:2024). Authors aim to reveal the changes in the determination of seismic actions and in the approach to design of bridges for earthquake resistance and to emphasise the most important novelties.

Keywords: Eurocode 8, bridges, seismic action, consequence classes, limit states, ductility classes, modelling, analysis, detailing

1. Introduction

The first-generation of Eurocode 8 deals with seismic design and assessment of bridges through Part 1: General rules, seismic actions and rules for buildings (EN1998-1 or in Croatia HRN EN 1998-1:2008) [1], Part 2: Bridges (EN 1998-2 or in Croatia HRN EN 1998-2:2008) [2] and Part 3: Assessment and retrofitting of buildings (EN1998-3 or in Croatia HRN EN 1998-3:2008) [3]. Part 1 presents a traditional approach to seismic design, based on linear analysis and force-reduction, through the "behaviour factor" q, accounting for ductility, redundancy, and overstrength. Capacity design is enforced to ensure that the structure possesses the necessary global ductility [1, 4]. Part 2 follows this approach and provides provisions for seismic action, analysis, strength verification and detailing of bridges. It also includes a special section on seismic isolation with provisions covering the application of this method of seismic protection to bridges [2]. In addition, it offers 11 Annexes among which is the informative one on static non-linear (pushover) analysis. Part 3, at the time of release, among its main novelties, included nonlinear static analysis and displacement-based assessment. One further novelty of Part 3 was a framework to deal with the specific uncertainty of existing structures [3, 4]. Although the European standard EN 1998-3 [3] covers the assessment and retrofitting of buildings, and its Part 2 [2] focuses primarily on the seismic design of new bridges, a combination of these normative prescriptions may be used in the assessment of the existing bridges, but with additional improvement of certain aspects, such has been shown on the example of seismic assessment of existing reinforced-concrete arch bridges [5].

The second generation of Eurocode 8 is more clearly reconstructed in three levels covering: (i) seismic action & general rules in EN 1998-1-1, (ii) design of new structures, buildings in EN 1998-1-2 and bridges in EN 1998-2 and (iii) assessment of existing structures, both buildings and bridges, in EN 1998-3 [6]. Main document for bridge design *Eurocode 8 – Design of structures for earthquake resistance – Part 2: Bridges* (FprEN 1998-2:2024) [7] on one hand introduces new parts such are specific rules for cable stayed and extradosed bridges and integral abutment bridges and some additional information on timber bridges but on the other hand is very much reduced in size as seismic action is mainly covered in FprEN 1998-1-1 [8] and majority of previous annexes are removed to either FprEN 1998-1-1 [8] or FprEN 1990 [9] or to standards dedicated to seismic isolators [10].

In this paper the main provisions for earthquake resistant bridges based on current phase of development of standards will be overviewed aiming to reveal the changes in the determination of seismic actions

Proceedings of the 3rd Croatian Conference on Earthquake Engineering - 3CroCEE
19–22 March 2025, Split, Croatia
Copyright © 2025 CroCEE
DOI: https://doi.org/10.5592/CO/3CroCEE.2025.120

and in the approach to design of new bridges and to emphasise the most important novelties. Specific rules mentioned above, and annexes will not be discussed here as they are still to be further analysed and are beyond the scope of the basic approaches elaborated in this paper.

2. Basic requirements

2.1. Bridges in different Consequence Classes

Importance classes (I less than average, II average and III bridges of critical importance for maintaining communications) that were used to reliability differentiation in the first-generation of Eurocode 8 are being replaced by Consequence Classes (CC) which are given in Annex A2 of FprEN 1990 [6,9] on bridges, table A.2.1 as a Nationally Defined Parameters (NDP) so each country may adapt these definitions to its own need. Most bridges will fall within CC2 which covers normal consequence or CC3a which is the lower class of the high consequence class which covers railway bridges on main railway lines, bridges over main railway lines and bridges over and under major roads. Major roads are not just those roads considered as major in terms of volume of traffic or velocity such are highways or motorways. Those are also roads that have a major role for civil protection like i.e. the only road that connects an industrial plant or a small town to the main road network [10].

Table 1. Bridges in different consequence classes as in [9] and values of coefficient δ provided as NDP in [7]

Consequence class	Description of consequence	Bridge examples	Coefficient δ
CC4	Highest	-	-
CC3b	High (upper class)	Where an increased level of reliability is required, when specified by the relevant authority or, where not specified, agreed for a specific project by the relevant parties	1,60
CC3a	High (lower class)	Railway bridges on main railway lines, bridges over main railway lines, bridges over and under major roads	1,25
CC2	Normal	Bridges not in other consequence classes	1,00
CC1	Low	Short span bridges on local roads with little traffic (provided they do not span over main railway lines or major roads)	0,60
CC0	Lowest	Elements other than structural	-

Consequence class will influence the choice of coefficient δ which is one of the parameters necessary to define the seismic action index $S_\delta = \delta\, F_\alpha\, F_T\, S_{\alpha,475}$. In this formula δ is a coefficient that depends on the consequence class of the considered structure, F_α is the site amplification factor, F_T is the topography amplification factor and $S_{\alpha,475}$ is the reference maximum spectral acceleration for the return period of 475 years. The values of δ applicable to bridges (Table 1) are provided in FprEN 1998-2 [7] as Nationally Defined Parameters (NDP) so each country may adapt these definitions to its own need. Depending on the range of S_δ values, seismic action classes are defined in FprEN 1998-1-1 [8] as *very low* seismic action class with a range of seismic action index $S_\delta < 1{,}30$ m/s^2, *low* with a range $1{,}30$ m/s^2 $\leq S_\delta < 3{,}25$ m/s^2, *moderate* with a range $3{,}25$ m/s^2 $\leq S_\delta < 6{,}50$ m/s^2 and *high* with a range $S_\delta \geq 6{,}50$ m/s^2.

2.2. Limit states

In the first generation of Eurocodes limit states (No Collapse and Damage Limitation) defined in the parts 1 [1] and 2 [2] for new structures were not consistent with those defined in part 3 [3] for existing structures (Near Collapse, Significant Damage, Damage Limitation). Therefore, second generation of Eurocode 8 provides a homogenisation of limit states definition through all its parts with better consistency with definition of Ultimate Limit States and Serviceability Limit States in Eurocode 0, introducing, in addition, a new Fully Operational limit state [6,7,8,9]. At least one Ultimate Limit State verification is mandatory to reach the safety of the structure and the choice of Serviceability Limit States

Proceedings of the 3rd Croatian Conference on Earthquake Engineering - 3CroCEE
19–22 March 2025, Split, Croatia
Copyright © 2025 CroCEE
DOI: https://doi.org/10.5592/CO/3CroCEE.2025.120

to be verified is up to National Annex or the contract [6]. To satisfy the seismic performance requirements for new structures the non-exceedance of the SD limit state shall be verified and the choice of other limit states to be verified could be defined in National Annex.

Table 2. Details of ultimate and serviceability limit states for seismic design situations

Limit states		**Quantitative definition [8]**
Ultimate Limit States ULS	Near Collapse NC	LS of Near Collapse (NC) shall be defined as one in which the structure is heavily damaged, with large permanent drifts, but retains its vertical load bearing capacity; most ancillary components, where present, have collapsed.
	Significant Damage SD	LS of Significant Damage (SD) shall be defined as one in which the structure is significantly damaged, possibly with moderate permanent drifts, but retains its vertical load bearing capacity; ancillary components, where present, are moderately damaged. The structure is expected to be repairable but, in some cases, it may be uneconomic to repair.
Serviceability Limit States SLS	Damage Limitation DL	LS of Damage Limitation (DL) shall be defined as one in which the structure is only slightly damaged and economic to repair, with negligible permanent drifts, undiminished ability to withstand future earthquakes and structural members retaining their full strength with a limited decrease in stiffness; ancillary components exhibit only minor damage that can be economically repaired.
	Operability OP	Fully Operational LS (OP) shall be defined as one in which the structure is only slightly damaged and economic to repair, allowing continuous operation of systems hosted by the structure.

3. Seismic action

Seismic action is defined in FprEN 1998-1-1 [8] and design seismic action is specified either in terms of return period $T_{LS,CC}$ or in terms of the performance factor $\gamma_{LS,CC}$ both given in FprEN 1998-2 [7], tables 4.2 (NDP) and 4.3 (NDP) respectively, as a function of the limit state and the consequence class. Return periods and performance factors for bridges are the same as for buildings for the same limit state and consequence class. Return periods $T_{LS,CC}$ and performance factors $\gamma_{LS,CC}$ depend on the target reliability indices $\beta_{t,LS,CC}$ which is suggested in Annex F.3 of FprEN 1998-1-1 [8] and are both Nationally Defined Parameters. Target reliability indices $\beta_{t,LS,CC}$ is related to the probability of failure of the bridge or of exceedance of the limit state. In the first generation of Eurocode 8 importance factors were used so, for comparison, for the significant damage for a less than normal important bridge (CC1) this factor previously was 0,85 now it is 0,80 (* Table 4) and for more important bridges (CC3) it was 1,30 now it is 1,1 or 1,25 (** Table 4) [10].

Table 3. Return period $T_{LS,CC}$ for bridges provided as NDP values in [7] (in years)

Limit state	**Consequence class**			
	CC1	**CC2**	**CC3a**	**CC3b**
NC	600	1600	2500	5000
SD	275	475	600	900
DL	100	115	125	140

Table 4. Performance factor $\gamma_{LS,CC}$ for bridges provided as NDP values in [7]

Limit state	**Consequence class**			
	CC1	**CC2**	**CC3a**	**CC3b**
NC	1,10	1,50	1,75	2,20
SD	0,80*	1,00	1,10**	1,25**
DL	0,60	0,60	0,65	0,65

Copyright © 2025 CroCEE
DOI: https://doi.org/10.5592/CO/3CroCEE.2025.120

An important aspect of seismic action for bridges is how to deal with the topographic amplification because these are not single point facilities but extended structure. Guidance for the evaluation of the topographic amplification factor F_T for bridges is given in FprEN 1998-2 [7]. Since the bridge has different points of contact of the structure at the supports with the ground it would be necessary to come up with a set of values of topographic amplification factor F_T, one per each support. Unless spatial variability is considered in the analysis, an average value of the topographic amplification factor will have to be used to amplify the uniform excitation applied to the bridge. This is applicable when the bridge model does not include the soil domain with its geometry which is in majority of all cases when regular fixed based model or a simple model with soil structure interaction is used [10].

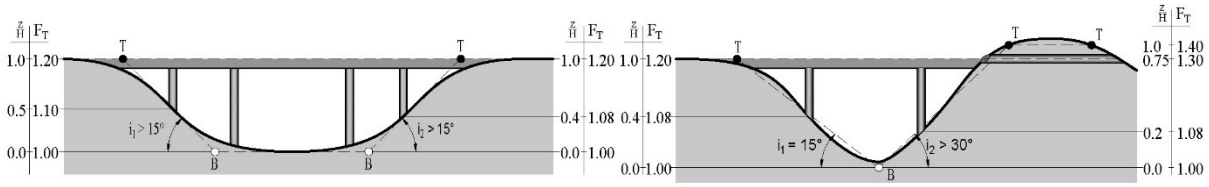


Figure 1. Calculation of topographic amplification factors F_T at supports in the case of wide valleys (left) and narrow valleys (right) where H is a slope height, z is height of support with respect to slope base point B and i is inclination angle of slope, reproduced based on [7]

3.1. Site consideration

When designing the bridge that will be built in close vicinity to active and shallow faults, permanent displacements arising from ground failure or fault rupture can result in imposed deformations with severe consequences for bridges. In this case the code FprEN 1998-2 [7] gives a recommendation that ground permanent displacements should be evaluated through specific studies as this problem is not manageable with a simplified treatment [10]. Some information on the seismic part of the differential displacement at the fault crossing can be found in prEN 1998-4:2023 [11], Annex E as pipelines share the same vulnerability with bridges due to their extended nature [10]. For other considerations regarding the site, as stability of slopes or liquefaction susceptibility, reference is made to prEN 1998-5:2024 [12].

4. Characteristics of earthquake resistant bridges

Strategies recommended for satisfying the performance requirements of non-exceedance of the limit states for the given seismic action can be achieved with either energy dissipation in members or anti-seismic devices or both as combining both strategies is common situation in bridges. Bridge foundations should not intentionally be used as a source of energy dissipation mainly due to limited asses for repairs [7,10].

Further important issue, which was already introduced in the first generation of Eurocode 8, is that the global torsional resistance of a bridge around the vertical axis should not rely on the torsional rigidity of a single pier. For example, a highway overpass with a middle pier, transversally fixed at abutments is fine in this sense, but if it has sliding bearings at the abutments or if the bridge is a single span one, this phenomenon has to be considered [7,10].

4.1. Primary and secondary members

Distinction between primary and secondary members is introduced in the general part FprEN 1998-1-1 [8] for buildings and other structures and the part for bridges FprEN 1998-2 [7] reads that supporting members (piers and abutments) resisting the seismic force in the given direction (longitudinal or transverse) should be designated as primary emphasising that the number of primary members may be less than a total number of supporting members.

Example is a continuous bridge over four spans with two abutments, one short and two taller piers (Figure 2). Unidirectional longitudinally sliding bearings on the abutments and short pier will result those supporting members to be considered as secondary members in longitudinal direction. Taller piers which are connected to the deck, because the deck is used to restrain the top displacement of relatively

Copyright © 2025 CroCEE
DOI: https://doi.org/10.5592/CO/3CroCEE.2025.120

slender piers, are considered as primary members in the longitudinal direction. In addition, if, in moderate and high seismic action class, deck is connected to one abutment through dampers or anti seismic devices or rigid connection, engaging its vibration to reduce displacement, this abutment will also be considered as primary seismic member in the longitudinal direction. In the above-described case, as sliding bearings are unidirectional longitudinally, all supports are considered as primary in the transverse direction [7,10]. In addition, FprEN 1998-2 [7] defines a sacrificial element, typically abutment's back walls, which can be designed to fail in the event of an impact with a deck as long as they are easily repairable and are protecting the remaining parts, i.e. deck joint [10]. Guidelines for design of the abutment's back walls should be provided so that damage is minimal and controlled.

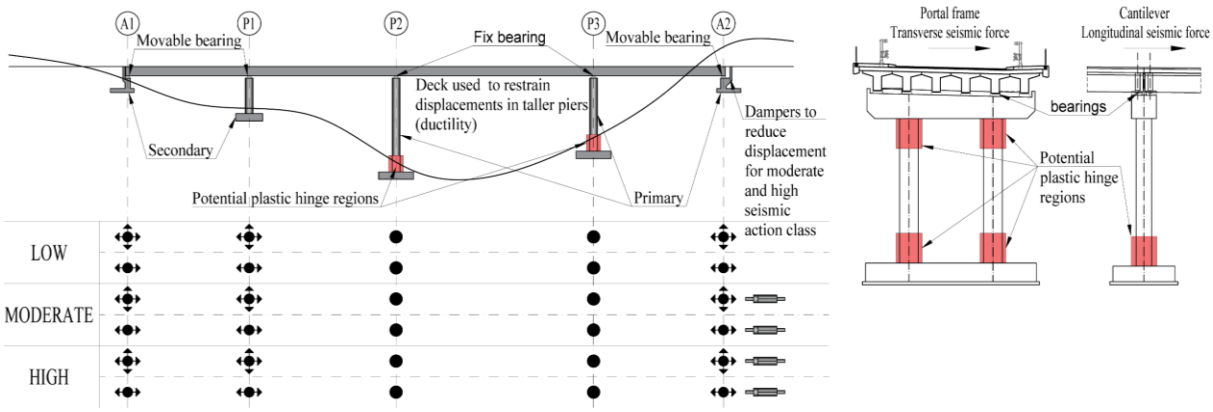


Figure 2. Primary and secondary members of the bridge example and the location of potential plastic hinges, reproduced based on [10]

4.2. Choice of Ductility Class

For bridges that are exploiting ductility to satisfy performance requirements (and not those who rely on seismic isolation) the following provisions are given. The primary structure should be assigned a ductility class according to FprEN 1998-1-1 [8]. Ductility classes are described based on the structure deformation capacity and cumulative energy dissipation capacity in the table 5.

Table 5. Provisions for choosing ductility class depending on the seismic action class and consequence class of the bridge

Ductility		**Seismic action class**		
Ductility class categories	Description of the structure deformation capacity and cumulative energy dissipation capacity	**Low**	**Moderate**	**High**
DC1	The overstrength capacity is taken into account, while the inelastic deformation capacity and energy dissipation capacity are disregarded.	+ (all CC)	-	-
DC2	The local overstrength capacity, the local deformation capacity and the local energy dissipation capacity are taken into account. Global plastic mechanisms are controlled by limited verifications.	+ (all CC)	+ (all CC)	+ (CC1)
DC3	The ability of the structure to form a global plastic mechanism at SD limit state is verified and its local overstrength capacity, local deformation capacity and local energy dissipation capacity are taken into account.	+ (all CC)	+ (all CC)	+ (CC2, CC3)

This ductility class should be unique for the bridge - the same for all members and in all directions. Assigning the unique ductility does not mean the same as that the behaviour factor q will be unique, unique ductility means that approach to detailing will be the same for all primary structures as ductility class determines detailing and not just the value of behaviour factor *q* [10]. Not all ductility classes can

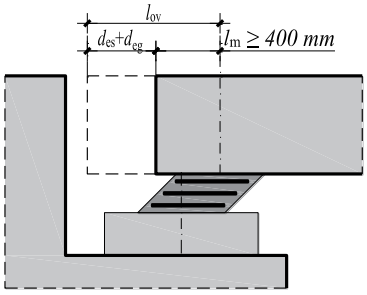
Copyright © 2025 CroCEE
DOI: https://doi.org/10.5592/CO/3CroCEE.2025.120

be used irrespective of seismic action class or seismic intensity. In high seismic action class, bridges of CC2 and higher should be designed for DC3 but bridge of CC1 could be designed for DC2. In addition, seismic design for DC1, which exploit overstrength capacity only, should not be adopted in moderate and high seismic action classes which altogether leads to the provisions for choosing ductility class for bridges as presented in the table 5 [7,10].

The locations of critical zones should be chosen to ensure accessibility for inspection and repair. Such locations should be clearly indicated in the appropriate design documents. For DC2 and DC3 structures, a dependably stable partial or full mechanism should develop in the structure through the formation of flexural plastic hinges [7]. Potential plastic hinges may not be foreseen wherever, they are usually in the piers and not necessary in all piers, i.e. in the longitudinal direction they will form in the primary members only as indicated in Figure 2 [10]. The bridge deck should remain within the elastic range except in the case of adjacent simply supported spans made of precast concrete girders beams connected with continuity slabs [7]. Plastic hinges are allowed in the continuity slabs, but they cannot be relied upon for energy dissipation [10].

4.3. Unseating and pounding

Important principle when designing connections between supporting and supported members is to avoid unseating which is provided with appropriate overlap lengths (Figure 3). In addition, pounding between adjacent parts which can oscillate and get in contact should be avoided. An exception is the sacrificial back wall, but it cannot be provided in all cases as the deck should be tolerant to this pounding as well. For example, large shock forces on sensitive components such as prestressing anchorages at the prestressed concrete girder head should be prevented by ductile/resilient members or special buffers [7].



$\boldsymbol{l_{ov}} = l_m + d_{eg} + d_{es}$	**overlap length**
$\boldsymbol{l_m}$	**minimum support length** (>400mm)
$\boldsymbol{d_{eg}} = (2d_g / l_g) l_{eff} \leq 2d_g$	**relative displacement** (spatial variation)
d_g	expected ground displacement
l_g	distance parameter
l_{eff}	effective length of the deck
$\mathbf{d_{es}}$ (= d_{Ed} or $d_{Ed}+s$)	**effective seismic displacement** (s, the link slack)

Figure 3. Minimum overlap length at connections, reproduced based on [13,14 & 7]

In order to size the gaps to avoid unseating and pounding the evaluation of displacements is necessary [10] which is done through the formula which is the same as in the first generation of Eurocode 8: $d_{Ed} = d_G$ "+" d_E "+" $\psi_2 d_T$; where d_G is the governing value between the short-term (opening) and long-term (end of design service life) values of the relative displacement due to the permanent and quasi-permanent actions (e.g. post-tensioning, shrinkage and creep for concrete decks), d_E is the design relative displacement due to seismic action (displacement of adjacent portions), d_T is the design relative displacement due to thermal movements and ψ_2 is the combination factor for the quasi-permanent value of thermal action, given in FprEN 1990, Table A.2.7(NDP) [9]. For timber bridges the above equation should also include d_ω which is the displacement due to average moisture content variation Δ_ω [10]. It should be noted that even when the bearings are dimensioned for sufficient displacement, dimensioning the expansion joint devices for smaller displacements may result in the superstructure pounding the abutment wall, therefore its appropriate design is necessary as mentioned above.

5. Modelling & Analysis

5.1. Mass, stiffness and damping

In terms of modelling the first issue is to add non-structural masses to structural ones. These are the masses due to traffic and masses due to water. The proportion of the mass corresponding to traffic needs

Copyright © 2025 CroCEE
DOI: https://doi.org/10.5592/CO/3CroCEE.2025.120

to be added only for road and railway bridge with severe traffic conditions and this is by employing coefficient $\psi_{E,I}$ with the value 0,2 for road and 0,3 for traffic bridges. It has to be noted that load models for traffic are different and only uniformly distributed load of the corresponding load model (LM1 for loads and LM71 for railways) should be considered for the evaluation of additional masses [10]. Calculation of the added mass of entrained water for immersed piers is the same as it was in the first generation of Eurocode 8 and covered with the only Annex left (Annex B) from this previous Eurocode version [10].

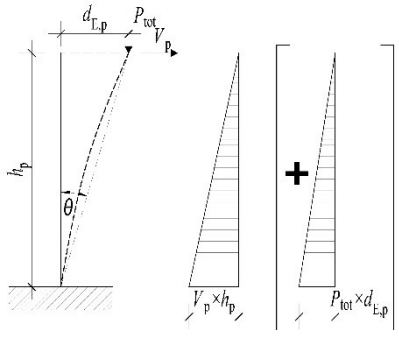
When designing bridges for ductility classes DC2 and DC3, in critical regions of primary seismic members, where energy dissipation is considered as a part of the seismic design strategy, the elastic stiffness of each member should correspond to its secant effective stiffness at the elastic limit. For reinforced concrete piers this is estimated as secant stiffness of the cracked section at the initiation of the yield of the reinforcement which is approximated as 50% of the corresponding stiffness of the uncracked members for the force-based approach. In the bridge deck where no inelastic action happens, the gross stiffness of 100 % should be considered with the reduction to 25% for the continuity slabs where plastic hinges are allowed but they cannot be relied upon for energy dissipation [7,10].

When cracking occurs, torsional stiffness of the deck decreases in a much more relevant manner which is the reason why for open sections or slabs torsional stiffness is taken with 0% of the uncracked torsional stiffness which means it is neglected, and for box sections it is proportional to 50% or 30 % depending on whether the box is made of prestressed or reinforced concrete respectively. Particular care should be dedicated to curved bridges where torsion contributes to the static equilibrium. Curved bridge is the bridge with an angle between the initial and final tangents to the curved longitudinal axis larger than 25° [7,10].

When elastic response spectrum analysis is used weighting factors for damping are 0,02 for welded steel, 0,04 for bolted steel, 0,05 for reinforced concrete and 0,02 for prestressed concrete based on the material of the members where larger part of the deformation energy is dissipated during the seismic response, which is the same as in the first generation of Eurocode with an added value 0,03 for timber. For response history analysis individual damping should be assigned to each component and when the q-factor approach is used, there is no correction of damping in the reduced spectrum [7,10].

5.2. Second order effects

Second order effects (P-Δ effects) may be neglected when pier top displacement sensitivity coefficient θ is less than 0,1. This sensitivity coefficient presenting the ratio of second order moments over first order moments (or $P_{tot}d_{E,p}$ over $V_p h_p$, where P_{tot} is vertical force; $d_{E,p}$ pier top displacement, V_p shear force and h_p pier hight) is computed differently depending on whether linear force-based approach (L-FBA) or non-linear displacement-based approach (NL-DBA) is used [7,8,10].



L-FBA:
$\theta = (P_{tot}d_{E,p}) / (q_R q_S V_p h_p)$
$d_{E,p} = q_{disp} d_r$

NL-DBA:
$\theta = (P_{tot}d_{E,p}) / (V_p h_p)$
$d_{E,p} = d_t^*$

d_r displacement calculated under the reduced spectrum associated to the design seismic action

q_{disp} $= q;$ if $T_1 \geq T_B$,
$= [1+(q-1)\ T_B/T_1]; \leq 3q;$ if $T_1 < T_B$

d_t^* target displacement of the equivalent single degree of freedom oscillator

Figure 4. P-Δ effects and corresponding terms

5.3. Vertical component of seismic action

Vertical component of the seismic force should be considered when verifying: (i) structural members of prestressed concrete decks because prestressed members are sensitive to vertical loads, (ii) structural

Copyright © 2025 CroCEE
DOI: https://doi.org/10.5592/CO/3CroCEE.2025.120

members in cable stayed bridges which have inclined forces and axial forces in pylon, (iii) anti-seismic devices which may be very sensitive to axial forces or (iv) inclined piers where both vertical and horizontal component of seismic force lead to axial force variations in the members. On the other hand, effects of vertical component may be omitted for piers in low or moderate seismic intensities [7,10].

5.4. Behaviour factors for the force-based approach (linear analysis)

In the force-based approach, the seismic action should take the form of a reduced spectrum, derived from the elastic response spectrum by introducing the behaviour factor q, which accounts for overstrength, deformation capacity and energy dissipation capacity [8].

The values of behaviour factors for the force-based approach have basically not changed with respect to those in the first generation of Eurocode 8 but they have been split so their contribution is clearly separated into contribution of overstrength (which is taken with q_s=1.5, which means that for DC1 the final q = 1,5) and in the contribution coming from redundancy q_R and ductility q_D which are specified in the table 6 depending on the type of ductile member and for ductility classes DC2 and DC3 for which all three components are to be added to the final value q [7,10].

Table 6. Example of maximum values of behaviour factors for reinforced concrete piers and abutments, extracted from [7]

Type of Ductile Members	q_R	q_D		$q = q_S\, q_R\, q_D$	
		DC2	**DC3**	**DC2**	**DC3**
Multiple double-bending vertical RC piers (i.e. more than one monolithically connected pier in longitudinal direction or multicolumn piers in transverse direction)	1,2	1,3λ(a_s)	2,0λ(a_s)	2,3λ(a_s)	3,6λ(a_s)
Multiple single-bending vertical RC piers (i.e. more than one pin-connected pier in longitudinal direction or single-column piers in transverse direction)	1,0	1,3λ(a_s)	2,0λ(a_s)	2,0λ(a_s)	3,0λ(a_s)
Inclined RC struts in bending	1,1	1,0λ(a_s)	1,3λ(a_s)	1,6λ(a_s)	2,1λ(a_s)
Abutments rigidly connected to the deck	1,1	1,0	1,1	1,6	1,8
Abutments of integral abutment bridges	1,0	1,0	1,0	1,5	1,5
$\lambda(a_s) = \sqrt{1/3}$ if a_s<1; $\lambda(a_s) = \sqrt{a_s/3}$ if 3 > $a_s \geq 1$; $\lambda(a_s)$ =1 if $a_s \geq 3$; where $a_s = Lv/h$ is the shear span ratio, ratio between the distance from the plastic hinge to the point of zero moment and the cross-section height in the plane of deformation					

Nevertheless, second generation of Eurocode 8 introduces accounting for the foundation flexibility when selecting the behaviour factor [7]. If soil-structure interaction is considered in the bridge model, the ductility should be reduced because the deformation of the soil-foundation system absorbs a portion of overall deformation. Ductility will need to be reduced also for (i) high axial force, (ii) non-accessibility of critical zones for inspection and repair and for (iii) irregular inelastic demand. The latter applies as for the application of the force-based approach, bridges should be considered to have regular seismic behaviour. If bridges have irregular seismic behaviour, they should be designed either by using a reduced q value or by employing the displacement-based approach [10].

It needs to be emphasised, while the ductility class for the bridge is unique as explained in the previous chapter 4.2, different values of the behaviour factor q may be used in each of the two horizontal directions. When the bridge is curved or skew and different ductility is available in different directions for each supporting pier, the lower q of the primary members govern the ductility class. When the bridge is neither curved nor skew, the higher value of q may be used in the direction of higher available ductility, while using lower value of q in the orthogonal, less ductile direction [7]. This is a typical case

Copyright © 2025 CroCEE
DOI: https://doi.org/10.5592/CO/3CroCEE.2025.120

of a straight bridge with wall type piers where ductility is very different in the longitudinal and transversal direction.

5.5. Displacement-based approach (nonlinear analysis)

Methods used to implement the displacement-based approach are: (i) non-linear static analysis and (ii) response history analysis. Single mode non-linear static (pushover) method is an invariant of N2 version of the method. N2 was first proposed and applied to buildings in 1987, and in 1997 it was applied to the example of a bridge with appropriate adaptations. The N2 method includes two types of calculation and two structural models: 1) non-linear static calculation on the real structural model - model with multiple degrees of freedom and 2) non-linear dynamic calculation on a simplified model - model with one degree of freedom. The static calculation determines the properties of the structure (e.g. stiffness) that are required for the dynamic calculation. Compared to the non-linear calculation of the dynamic time response, the calculation according to the N2 method is significantly simplified, as it is performed on a simplified model. Moreover, in the N2 method, the seismic load is usually defined by nonlinear response spectra determined on the basis of standard elastic spectra, which avoids difficulties and doubts in the selection of accelerograms required for the nonlinear calculation of the time response. Due to the simplification of the method, it also has certain limitations. It is suitable for the calculation of structures where there is no major influence of higher vibration modes and where the dominant vibrations do not change significantly with different intensities of seismic loading [15, 16].

Single mode pushover method is applicable only to straight bridges (less than 25°) with two modes having modal mass larger than 60% in the two plan directions [10]. Assuming the influence of the pier masses to be minor, the above condition is always met in the longitudinal direction of approximately straight bridges. The condition is also met in the transverse direction when the distribution of the stiffness of piers along the bridge provides an approximately uniform lateral support to a relatively stiff deck. This is the most common case for bridges where the height of the piers decreases towards the abutments or does not present intense variations. When, however, the bridge has one stiffer and unyielding pier, located between groups of regular piers, the system cannot be approximated in the transverse direction by a single degree of freedom and pushover analysis can lead to unrealistic results. A similar exception holds for long bridges, when very stiff piers are located between groups of regular ones, or in bridges in which the mass of some piers has a significant effect on the dynamic behaviour, in either of the two directions. When possible and expedient, such irregular arrangements can be avoided, e.g. by providing sliding connection between the deck and the pier(s) that cause the irregularity [7]. Single pushover method, N2 method is a simple and it should stay simple as indicated with the note that verification are carried out independently in the longitudinal and in the transversal direction [7].

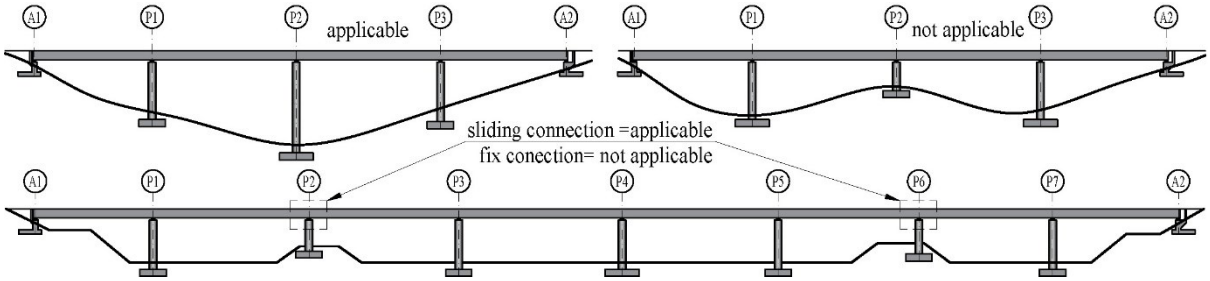


Figure 5. Applicability of single mode pushover method

When single pushover method (N2) method is not possible, Eurocode [7,8] allows to use alternative methods. Non-linear static analysis methods accounting for the response of higher modes such are modal pushover methods are permitted with the standard, but they are not further explained, and their limitations are noted, emphasising they are not of general applicability. This means that when N2 method is not possible, modal pushover method may be applied but better way is to use non-linear response analyses [10]. The choice of number and type of input motions, as well as calculation of seismic action effects, should in this case comply with FprEN 1998-1-1 [8].

Proceedings of the 3rd Croatian Conference on Earthquake Engineering - 3CroCEE
19–22 March 2025, Split, Croatia
Copyright © 2025 CroCEE
DOI: https://doi.org/10.5592/CO/3CroCEE.2025.120

5.6. Combination of the seismic action with other actions

The design value E_d of the effects of actions in the seismic design situation should be determined in accordance with FprEN 1990:2022 [9] with following provisions of FprEN 1998-2:2024 [7]. Action effects due to imposed deformations may be neglected except in the case of bridges in which the seismic action is resisted by elastomeric laminated bearings. In this case, the action effects due to imposed deformations (caused by temperature, shrinkage, settlements of supports, residual ground movements due to seismic faulting) should be accounted for. Displacement due to creep does not normally induce additional stresses to the system and can therefore be neglected. Creep also reduces the effective stresses induced in the structure by long-term imposed deformations (e.g. by shrinkage) [7].

6. Verification of structural members to limit states

Clause 6 of FprEN 1998-2:2024 [7] should be applied to the earthquake resisting system of bridges designed for DC1, DC2 or DC3. This clause provides provisions for the design of structural members and for the detailing of the critical regions of each member type. Outside the critical regions, the detailing of structural members should satisfy relevant provisions in standards dedicated to concrete, steel or composite structures.

Verification of Significant Damage (SD) limit state according to the force-based approach should be carried out in terms of local resistances while demand on non-ductile members should be obtained as capacity design effects. Brittle and other undesired failure mechanisms should be avoided by deriving design action effects from capacity design if not exceeding those obtained with q=1. Formula for overstrength moment of a flexural plastic hinge M_o, associated variables, graphical representation of capacity design bending moment within the length of a member developing plastic hinges are provided in relevant subclauses of FprEN 1998-2:2024 [7]. It has to be noted that values of the overstrength partial factor γ_{Rd} (recommended as 1,1 when M_o is used to calculate seismic action effects on the shear mechanism, and 1,0 otherwise) may be adapted as a Nationally Defined Parameters (NDP) [13]. Flexural resistance of sections in critical regions of concrete members should be satisfied with $M_{Ed} \leq M_{Rd}$ where M_{Rd} is the design flexural resistance of the section in accordance with standard for concrete structures. For structures of DC1 M_{Ed} is derived from analysis for the seismic design situation, including second-order effects if needed; and for shear resistance verification, seismic action effect A_{Ed} should be multiplied by the behaviour factor q. For structures of DC2 and DC3 M_{Ed} is the design moment accounting for capacity design effects and for shear resistance verification, design action effect should account for capacity design effect. In addition, for structures of DC2 and DC3 any joint between a vertical ductile pier and the deck or a foundation member adjacent to a plastic hinge in the pier should be designed in shear to resist the capacity design effects of the plastic hinge in the relevant direction. Definition of variables, stress condition and formulas are provided in relevant subclauses of FprEN 1998-2:2024 [7]. It needs to be mentioned that no significant yielding should occur in the deck and elastic response of foundation members is preferred for bridges [13].

In case the Near Collapse (NC) limit state is used, verifications should be carried out with the displacement-based approach, via non-linear static or response-history analysis since the seismic action for this limit state can drive the structure into the non-linear range to an extent where results of a linear analysis are less reliable than they are at the SD limit state [7]. In case the DL or OP limit state is required, verification may be carried out with the force-based or the displacement-based approach [7].

7. Detailing for ductility

Detailing for ductility should be applied to primary seismic members (piers and abutments) of bridges designed for DC2 and DC3 through plastic hinging and aims to ensure a minimum level of curvature/rotation ductility at the plastic hinges. General requirement is that in concrete piers longitudinal reinforcement ratio ρ_L should be higher than 0,5% (in the previous version it was 1,0%) and the diameter of the bar d_{bL} should be equal or higher than 16 mm. Further on several requirements for critical regions in concrete piers will be elaborated.

Copyright © 2025 CroCEE
DOI: https://doi.org/10.5592/CO/3CroCEE.2025.120

Length of critical regions l_{cr} is estimated as the largest of the: (i) the depth of the pier section within the plane of bending perpendicular to the axis of rotation; (ii) distance between M_{max} and 0,8 M_{max} locations but not larger than 1,5xdepth of the pier section from (i). This is for the cases when ratio $\eta_k = N_{Ed}/A_c f_{ck} \leq 0{,}3$, while for $0{,}3 < \eta_k \leq 0{,}6$ critical length should be increased by 50%. It has to be noted that this length of critical regions is only used for detailing of the reinforcement and not for estimating the plastic hinge rotation [7, 13]. The longitudinal reinforcement should remain constant and fully effective over the length of the critical region l_{cr} without splicing by lapping or welding.

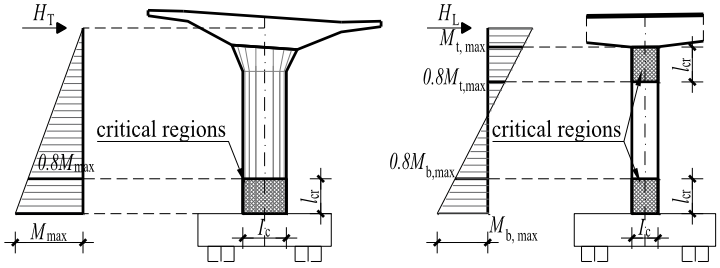


Figure 6. Location of critical regions in concrete piers: for the transversal (left), for longitudinal direction (right), reproduced based on [13]

Confinement should be ensured within the critical regions of the primary seismic members, through rectangular or circular hoops and/or cross ties and spirals, with dimeter $d_{bT} \geq 10$ mm. The quantity of confining reinforcement should be defined through the mechanical reinforcement ratio $\omega_{wd} = \rho_w (f_{yd}/f_{cd})$ where ρ_w is transverse reinforcement volumetric ratio, presented in the table 7 together with the minimum amount of confining reinforcement $\omega_{wd,min}$. This minimum amount is to be provided over the entire length of the critical region, it may be reduced gradually outside the critical region but not less than 50% over an additional adjacent length l_{cr}. In addition, outward buckling of longitudinal reinforcement shall be avoided along potential hinge areas by restraining it by transverse reinforcement (hoops or cross-ties) perpendicular to the longitudinal bars at a spacing $s_L \leq 5d_{bL}$ and $s_T \leq 200$mm.

Table 7. Provisions for confining reinforcement extracted from [7]

Section type	**Type of reinforcement**	**ρ_w**	**$\omega_{wd,min}$**		**s_L and/or s_T**
			DC2	**DC3**	
Rectangular	Hoops or ties	$\rho_w = A_{sw}/(s_L b)$	0,08	0,12	$s_L \leq 6d_{bL}$; $s_L \leq 1/5 b_{min}$ $s_T \leq 1/3 b_{min}$ or 200mm for $b_{min} \leq$1,0m or 300mm for b_{min}>1,5m
Circular	Spiral or hoop bars	$\rho_w = 4A_{sp}/(D_{sp} s_L)$	0,12	0,18	$s_L \leq 6d_{bL}$; $s_L \leq 1/5 b_{min}$
A_{sw} is the total area of a layer of hoops or ties in the direction of confinement under consideration; s_L is the spacing of confining reinforcement in the longitudinal direction; b is the dimension of the concrete core perpendicular to the direction of the confinement under consideration, measured to the outside of the perimeter hoop; s_T is the transverse distance between hoop legs; b_{min} smallest dimension of confined concrete core; d_{bL} longitudinal bar diameter; A_{sp} is the area of the spiral or hoop bar; D_{sp} is the diameter of the spiral or hoop bar					

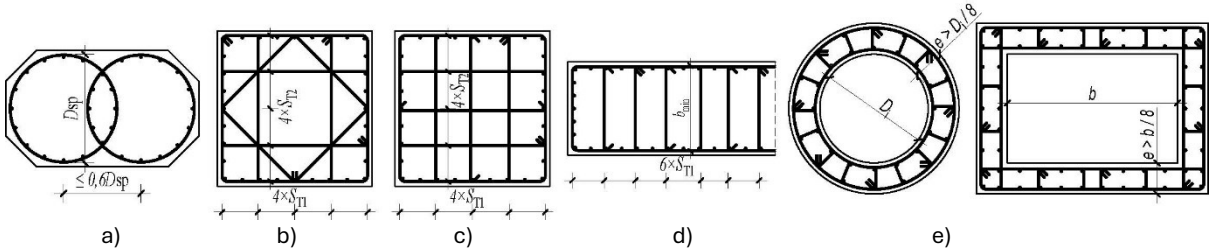


Figure 7. Confinement details in concrete piers using (a) interlocking spirals/hoops in polygonal cross section; (b) 4 closed overlapping hoops; (c) 3 closed overlapping hoops plus cross-ties; (d) closed overlapping hoops plus cross ties in wall type rectangular cross section; (e) closed overlapping hoops plus cross ties in hollow piers, reproduced based on [7]

Proceedings of the 3rd Croatian Conference on Earthquake Engineering - 3CroCEE
19–22 March 2025, Split, Croatia
Copyright © 2025 CroCEE
DOI: https://doi.org/10.5592/CO/3CroCEE.2025.120

8. Conclusions

In this paper authors overviewed the main provisions for earthquake resistant bridges introduced with the 2nd generation of Eurocodes. The most important novelties are (i) the determination of seismic action as a function of the clearly defined limit state and the consequence classes defined for bridges, (ii) choosing ductility class of the bridge depending on the seismic action class and consequence class of the bridge and further on (iii) clear separation of behaviour factor into contribution of overstrength, redundancy and ductility. The work on Croatian National Annex of EN 1998-2, contemplating allowable national choice through the value of Nationally Determined Parameters, is under progress and will be the subject of a further publication. It should be emphasized that a complete insight into the benefits of the 2nd generation of Eurocode will only be possible by reviewing and developing of all standards and national annexes related to bridges, and only the experience with actual bridge projects will reveal whether one of the main goal, simpler application in practice, is reached.

References

[1] EN 1998-1:2004. Eurocode 8: Design of structures for earthquake resistance Part 1: General rules, seismic actions and rules for buildings, CEN- European Committee for Standardization, Bruxelles, 2004.

[2] EN 1998-2:2005. Eurocode 8: Design of structures for earthquake resistance, Part 2: Bridges, CEN- European Committee for Standardization, Bruxelles, 2005.

[3] EN 1998-3:2005. Eurocode 8: Design of structures for earthquake resistance, Part 3: Assessment and retrofitting of buildings, CEN- European Committee for Standardization, Bruxelles, 2005.

[4] Franchin, P., Noto, F.(2023): Reliability-based partial factors for seismic design and assessment consistent with second-generation Eurocode 8, *Earthquake Engineering & Structural Dynamics*: Volume 52, Issue 13, https://doi.org/10.1002/eqe.3840

[5] Franetović, M., Mandić Ivanković, A., Radić, J. (2014): Seismic assessment of existing reinforced-concrete arch bridges, *Građevinar* 66, 8, 691-703

[6] Bisch, P. (2022): EC8 Webinars Second Generation of Eurocode, Webinar 1-1.1 *Organisation and concepts of EN 1998*, 30th March 2022, https://ec8webinars.org/, (accessed September 21, 2024).

[7] FprEN 1998-2:2024. Eurocode 8: Design of structures for earthquake resistance Part 2: Bridges, CEN-European Committee for Standardization, Bruxelles, 2024.

[8] FprEN 1998-1-1:2024. Eurocode 8: Design of structures for earthquake resistance Part 1-1: General rules and seismic action, CEN- European Committee for Standardization, Bruxelles, 2023.

[9] FprEN 1990:2022. Eurocode - Basis of structural and geotechnical design & prEN 1990-1:2024 Part 1: New structures, CEN- European Committee for Standardization, Bruxelles, 2023.

[10] Franchin, P. (2024): EC8 Webinars Second Generation of Eurocode, Webinar 2.1 *Bridge classification and structural analysis*, 5th April 2024, https://ec8webinars.org/, (accessed September 21, 2024).

[11] prEN 1998-4:2023. Eurocode 8: Design of structures for earthquake resistance Part 4: Silos, tanks, pipelines, towers masts and chimneys, CEN- European Committee for Standardization, Bruxelles, 2023.

[12] FprEN 1998-5:2024. Eurocode 8: Design of structures for earthquake resistance Part 5: Geotechnical aspects, foundations, retaining and underground structures, CEN, Bruxelles, 2023.

[13] Davi, D. (2024): EC8 Webinars Second Generation of Eurocode, Webinar 2.3: Verifications of structural members and detailing for ductility, 5th April 2024, https://ec8webinars.org/, (accessed September 21, 2024).

[14] Panagiotakos, T. (2024): EC8 Webinars Second Generation of Eurocode, Webinar 2.4: Bridges equipped with antiseismic devices, 5th April 2024, https://ec8webinars.org/, (accessed September 21, 2024).

[15] Mandić Ivanković A., Srbić M., Skokandić D., Friedl P. (2024): Application of Pushover Analysis in Seismic Assessment of 50 years old Bridge. Report of the IABSE Congress San Jose 2024: Beyond Structural Engineering in Changing World. ISBN: 978-3-85748-205-2. Pg 201-208

[16] Isaković T., Fischinger M. (2009): Simplified nonlinear method for the analysis of concrete bridges, *Građevinar,* 61 (7)

Proceedings of the 3rd Croatian Conference on Earthquake Engineering - 3CroCEE
19–22 March 2025, Split, Croatia
Copyright © 2025 CroCEE
DOI: https://doi.org/10.5592/CO/3CroCEE.2025.122

MASONRY WALL-RC SLAB INTERACTION UNDER SEISMIC LOADING

Goran Simonović [(1)], Hrasnica Mustafa [(2)], Senad Medić [(3)]

[(1)] *Associate professor, University of Sarajevo-Faculty of Civil Engineering, goransimonovic@yahoo.com*
[(2)] *Full professor, University of Sarajevo-Faculty of Civil Engineering, hrasnica@bih.net.ba*
[(3)] *Associate professor, University of Sarajevo-Faculty of Civil Engineering, senad.medic@gf.unsa.ba*

Abstract

In conventional engineering practice, masonry walls are typically analyzed independently from the rest of the structure. The gravity load is determined, and a horizontal load is applied under the assumption that RC slabs behave as rigid diaphragms, distributing horizontal forces according to the relative stiffness of the walls. The wall load-bearing capacity is then assessed in a separate model, considering the effects of bending moments, and normal and shear forces. However, spatial models that incorporate structural elements connected with masonry walls are rarely developed. This study focuses on slender masonry walls, where the height exceeds the length, a characteristic feature in traditional engineering structures. In such structures, reinforced concrete ring beams are commonly placed atop these walls, often transitioning into lintels or beams supporting the RC slab. The objective of this research is to investigate whether these elements, along with the RC slab as a whole, influence the seismic behavior of walls. Experimental studies and post-earthquake damage reports indicate that wall behavior varies significantly depending on the level of normal stress. Key influencing factors include the wall's position within the structure, load intensity, connection details, and material and geometric properties. Less-loaded walls, typically found on upper slabs, are prone to rocking failure, with or without edge crushing. Sliding failure is common under low normal forces combined with high shear stresses, whereas diagonal cracking occurs under specific stress conditions. This study develops a numerical model to explore the interaction between slender walls and RC slabs, particularly in relation to rocking and toe crushing. It aims to answer whether walls should be considered isolated or part of spatial frame systems.

Keywords: masonry walls, frame, rocking, sliding, uplifting, ring beams, stress redistribution.

1. Introduction

Although masonry structures have been used since the beginnings of civilization, a generally acceptable engineering model has not yet been developed to analyze them in practice, especially under seismic loads. There are many reasons, and they should primarily be sought in the difference in the construction traditions of different regions and the material used for masonry structures. The material characteristics of masonry walls are one of the primary unknowns. The physical properties of walls depend on the choice of binders and masonry blocks, type of loading, masonry method, quality control, geometry and many other factors. In engineering design, empirical forms are usually employed to determine the material characteristics of walls and rarely experimentally obtained data. Modulus of elasticity, compressive and shear strength of the wall, which can be determined empirically or experimentally for the proposed analysis method, are of interest for this work.

Originally, the slabs of masonry structures were made of wood as beams laid freely on the walls, followed by the use of numerous typical prefabricated beams that were subsequently monolithically connected with the structure. Today, reinforced in-situ concrete dominates in the construction of slabs. There are relatively thick plates without horizontal tie-beams in northern Europe, or thinner plates with horizontal tie-beams in the southern parts of Europe. Tie-columns are also commonly used in seismically active areas, which is not the case, for example, for German masonry tradition. For buildings where the slab is made with prefabricated single-beam elements, which are later monolithic in some way or not, the slab can usually be considered rigid in its plane. In the vertical plane, such a slab is a system of simply supported beams that transmit the gravity load to the corresponding walls. To sustain

Copyright © 2025 CroCEE
DOI: https://doi.org/10.5592/CO/3CroCEE.2025.122

the seismic load, the walls can be considered as a system of cantilevers hinged at the top [1]. Distribution of the seismic force depends on material and geometric properties of individual walls and an example is shown in Fig. 1a. The presented 2D model is calculated using finite elements, and it is obtained that approximately 92% of the seismic force is resisted by the central wall (Fig. 1b). An almost identical value would be obtained if the distribution of the seismic force was basically calculated as a percentage of the individual moment of inertia of the wall in the sum of the moments of inertia of all the walls in the model.

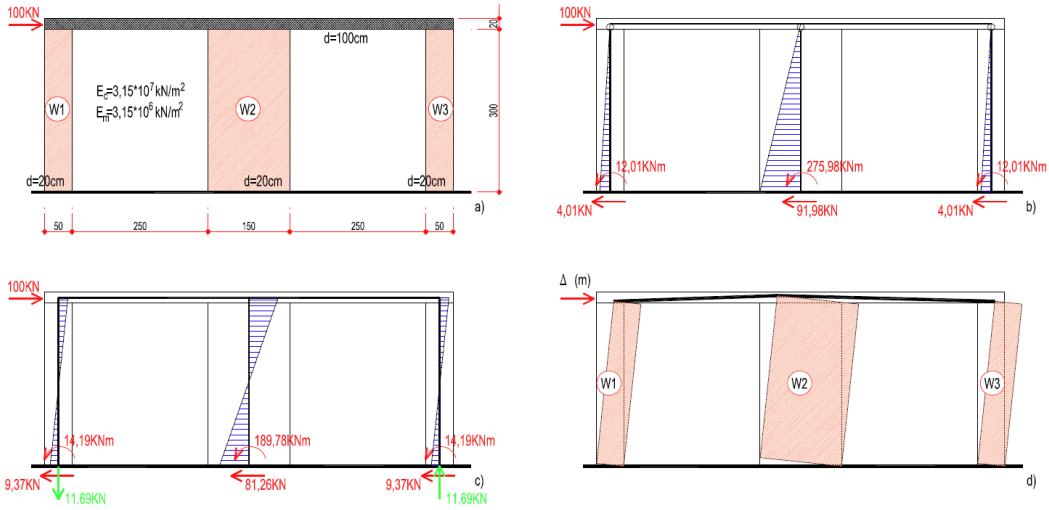


Figure 1. Structural models: a) 2D view, b) system of cantilever walls, c) frame structure, d) assumed behavior.

In the case of monolithic RC slabs, a 2D model in which the slab is modeled as a 100/20cm beam element, a different distribution of cross-sectional forces is obtained (Fig. 1.c). Such a distribution is typical for frame structures. The presented values will vary depending on the specific case, and in this case, a reduction of the transverse force in the middle wall by approx. 10% and a different distribution of bending moments in the wall plane is noticeable. For rigid RC slabs, which also have tie-beams, these framing effects come to the fore even more significantly. It is interesting to emphasize that a coupling of forces is formed in the edge walls of the frame, and that this moment partly takes over the moment from the horizontal force on the slab. This combination of forces in the left wall reduces the normal force from the gravity load, and in the right increases, which will be discussed in detail later in the text. For the example shown, this coupling takes up approx. 27% of the moment, which is not negligible.

Previous analyzes were performed for linear behavior. The assumption is that in the case of non-linear behavior of the walls, the situation will change more significantly, because after reaching the tensile strength of the coupling, the walls start to rotate more noticeably. The rotation of the wall, especially the central one from the previous example (Fig1d), acts on the slab above, attempting to lift it up, which is explored in this paper. How the wall will affect the slab depends on many factors, most of all on the type of wall failure. Below is a brief overview of wall failures types under seismic loads.

2. Masonry wall failure types

For buildings with openings (Fig. 2.b), which are the subject of research, less loaded walls located on the top slabs, will fail mainly due to the rotation of the complete wall as a rigid body (rocking). This rotation can also cause lifting of the slabs on top of the building. A similar failure occurs on the slabs below, where the compressed edge of the joint is crushed without pronounced rotation of the wall. Wall sliding occurs at relatively low intensities of normal forces and significant transverse stresses, while the characteristic diagonal failure occurs at a certain intensity of transverse and normal stresses.

The failure types of solid walls shown in Fig. 2a are also of interest for the work. In the analyzed example of the building, these walls are perpendicular to the earthquake action and in them, in addition

Proceedings of the 3rd Croatian Conference on Earthquake Engineering - 3CroCEE
19–22 March 2025, Split, Croatia
Copyright © 2025 CroCEE
DOI: https://doi.org/10.5592/CO/3CroCEE.2025.122

to failure perpendicular to the wall plane, local tensile failure that may occur due to the interaction of walls and slab, which was already hinted at in the introduction, are also numerically registered.

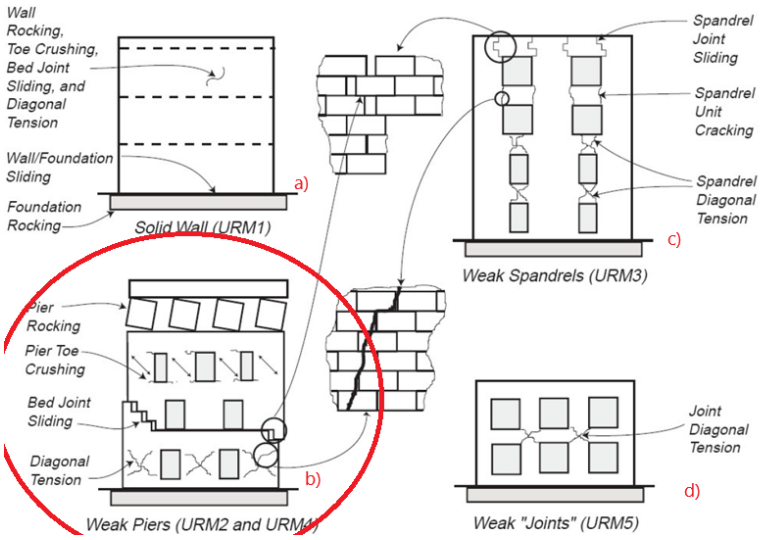
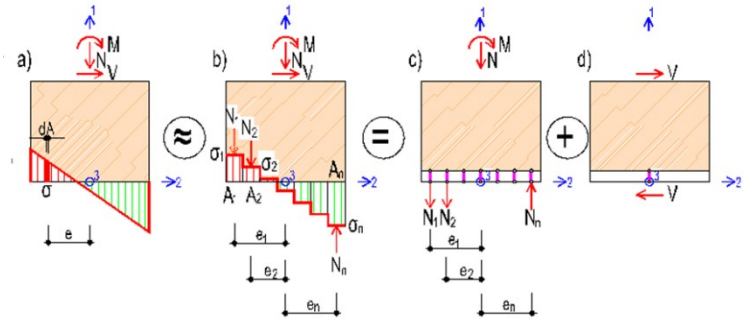


Figure 2. Types of masonry wall failures - FEMA [2].

For newer buildings, the walls with openings shown in Fig. 2c are mostly executed as parapets that are built later and are therefore not of interest to the work. For the case of buildings shown in Fig.2d, beams executed as horizontal tie-beams can yield, which is discussed below.

3. Proposed model

The normal force in the wall by definition represents the integral of the normal stresses on the surface of the cross-section of the wall, while the bending moment in the plane of the wall is equal to the integral of the product of the normal stresses and the distance from the center of gravity of the section. If we divide the wall into a sufficient number of segments, it is possible to repslace the integral dependence with the discrete one and present the normal force as the sum of normal stresses in individual segments. In that case, the in-plane moments of the wall are equal to the product of the normal stresses in the segments and the distance between the centers of gravity of the segment and the wall.



$$N = \int_A \sigma \cdot dA \approx \sum_{i=1}^{n} \sigma_i \cdot A_i = \sum_{i=1}^{n} N_i$$

$$M = \int_A \sigma \cdot e \cdot dA \approx \sum_{i=1}^{n} \sigma_i \cdot A_i \cdot e_i = \sum_{i=1}^{n} N_i \cdot e_i$$

$$M_{Rd} \geq M = \sum_{i=1}^{n} N_i \cdot e_i$$

$$N_{i,Rd} = f_d \cdot A_i \geq N_i$$

$$V_{Rd} \geq V$$

Figure 3.Stress distribution a) normal stress, b) normal forces in wall segment, c) axial force in nlink elements, d) sliding.

The idea is to use universal software packages such as SAP2000nl [3] and the elements readily available in the program. The width of the segment for which we are looking for the force N_i is actually determined by the FE discretization of the wall. In the part of the wall that is connected to the rest of the structure, i.e. at the top and bottom of the wall, we introduce an artificially formed joint where parts of the wall are replaced by non-linear connecting elements in SAP2000 known as nlink elements. Direction 1 defines the axial direction of the nlink element, and direction 2 the plane of the wall. N-Δ

Copyright © 2025 CroCEE
DOI: https://doi.org/10.5592/CO/3CroCEE.2025.122

dependence can be assigned to axial bonds. The load-bearing capacity of an individual connection is defined by the surface to be connected and the compressive strength of the wall while in this case, tension is neglected. The sum of all forces in the nlink elements of the joint gives the normal force in the wall, and the sum of the products of the normal forces and the eccentricity gives the bending moment in the wall where the joint is introduced. Regarding the transverse force load bearing capacity, there is only one nlink in direction 2 [4, 5]. Before the introduction of links in which nonlinearity is introduced, it is desirable to create a linear elastic model without additional connecting elements for comparison of response to gravity load.

In the first steps of the analysis, a FEM model made of finite and nlink elements is created, a gravity load is applied, and in the next steps of the analysis, the model is gradually pushed to the required tip displacement or, in the case of time history analysis, the supports of the model are excited with accelerograms. The behavior of one such simple cantilever wall model is shown in Fig.4.

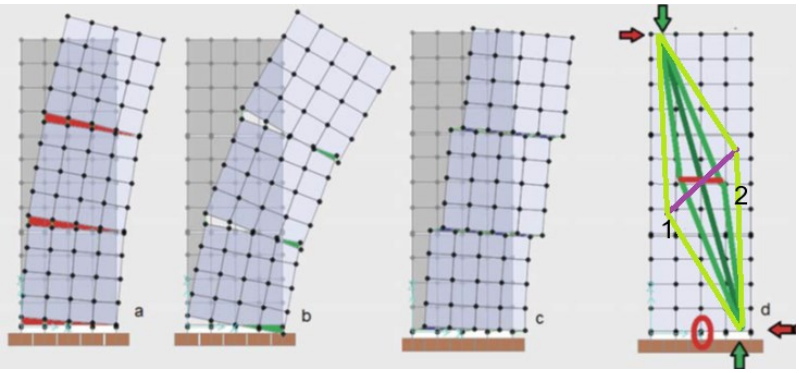


Figure 4. Wall failure: a) rocking; b) toe chrushing; c) sliding or diagonal tension; d) V_{Rd}.

Bending failure without crushing of the compressed edge is shown in Fig.4.a. The force in the far-right link does not reach the assigned compression bearing capacity. The stressed block is relatively narrow and its length is less than half the length of the associated finite element. All tensioned connections are open because no tension capacity has been assigned. The block of finite elements behaves like a rigid body and rotates around the support point. In the case of a higher normal force, the stress block is longer, which results that the last nlink element yields in compression, while the others follow the length of the stress block, so depending on the degree of stress, they can be in the linear or non-linear range. For this failure, depending on the normal force in the wall, in addition to crushing the right edge of the joint, it is possible for the left edge of the joint to open for tension. Wall sliding is shown in Fig4c. Depending on whether the relevant slip failure is V_{Rd2} or a diagonal failure V_{Rd1}, the calculated resistance is assigned to the transverse nlink element and this failure is simulated as sliding.

4. Wall -RC slab interaction

If the walls of a masonry structures are modeled as columns of a frame system, node A will move to node A' according to the pushover analysis, where it will have a horizontal, vertical and rotational component of movement (Fig.5a). If, on the other hand, the wall is modeled in the suggested way, due to the strong rotation of the wall as a rigid body, open joints are observed, left down and right up for the shown direction of pushing (Fig.5b). By opening the connection, a hinge is formed. Two opposite compressed hinges clearly indicate that a compression diagonal was formed in the model (Fig.5c). The diagonal in the wall is controlled by the width and strength of the compression block, i.e. the force N_{Rd}, and also by the shear bearing capacity of the wall V_{Rd}. By rotating the wall, the wall acts on the slab, tending to lift it up (Fig.5d), which is clearly visible from the display of model displacements. On the other hand, the slab, which is supported by other structural elements, resists this effect, which results in an increase in the normal force in the rotating wall. By increasing the normal force, its resistance to the action of the transverse force also increases. The gravity load of a structure is constant, so an increase

Copyright © 2025 CroCEE
DOI: https://doi.org/10.5592/CO/3CroCEE.2025.122

in the normal force in a rotating wall leads to a decrease in the normal forces in other walls of that structure. The key element in this redistribution is the rigidity and load-bearing capacity of the slab.

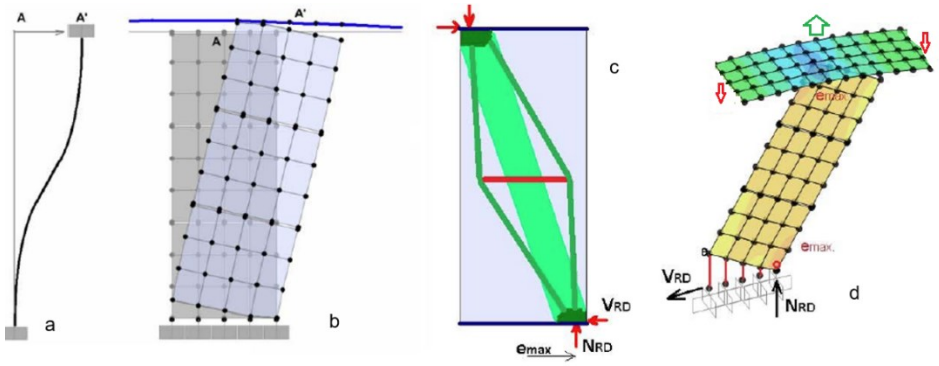


Figure 5. Columns/wall model, compressed diagonal, uplifting/increasing wall force

Refined models show more complex behavior. Fig. 6a shows the characteristic node of the model, i.e. the connection of the wall and the slab with stress components. Overturning of the wall above node shown in Fig.6c occurs when the normal force in that wall reaches the extreme eccentricity $N_{Ed,w}$. On the slab, the gravity load from that slab is entered automatically through the software and numerical model $N_{Ed,s}$. The total normal force on the wall below is the sum of those two forces, and its position is determined by the length of the stress block, which is formed using nlink elements automatically in the software. At any point in the pushover analysis, sliding may occur if the transverse force in the wall reaches the bearing capacity of the transverse connection (Fig.6d). If all the walls reach the assigned bearing capacity for the transverse force, that step is considered a collapse.

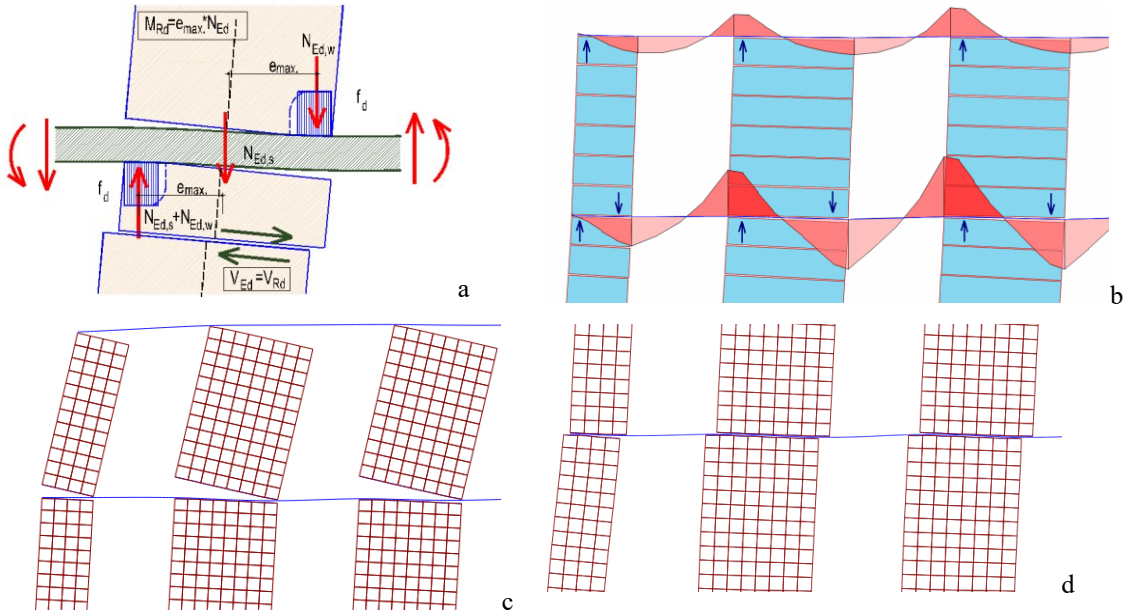


Figure 6. a) model, b) bending moment, c) rocking/crushing, d) sliding.

Figure 6b shows the diagram of the moments in the beams of the top slabs of a three-story building during the last steps of the pushover analysis. The beams of the last slab are raised, resting on the left ends of the walls when pushed from left to right, and can be imagined as a continuous beam supported on the compressed parts of the walls of the last slab. The length of the support is actually the length of the formed tension block, and the resulting force represents the gravity load from the top slab. In this case, the combination of all elements in the structure comes to full expression. This scenario is possible if and only if the beams of this slab have the capacity to act as continuous beam. Namely, in everyday

Copyright © 2025 CroCEE
DOI: https://doi.org/10.5592/CO/3CroCEE.2025.122

structural planning, it is common to design these beams as simply supported beams on the clear length of the opening. By rotating the wall, the system length of the opening changes and increases to the length of the span, because the beam loses most of its support when the wall is rotated. Depending on the disposition of the slab and the associated gravity load, and the beam reinforcement layout, it is possible that minimum reinforcement in the beam enables such a scenario. It is even possible for the slabs to physically separate from the walls in a second direction locally, i.e. that tension appears in those walls.

The situation is much more complex on the slab below. At the left ends of the walls under the last slab, the supports of the imaginary continuous beam are formed, and the slab above acts as a concentrated load in the opposite corner of the wall above, as indicated. The walls under the last slab in the analyzed building models show a tendency to fail due to crushing of the compressed edge. Due to crushing, the rotation is not expressed because the wall adapts to the deformed shape of the beam. If the beams above the opening are reinforced for the gravity load only (which is usual), they are not able to resist the imposed distribution, so the behavior of the model approaches the scenario shown in Fig.2d. If, on the other hand, the building is analyzed as a frame system, these beams are usually designed as fixed. The diagram shown in Fig.6b corresponds to certain moments if we ignore the hatched part of the wall where the moment sign change occurs.

For frame structures where nonlinearity is analyzed, it is common for plastic hinges to appear at the ends of the beams. An analysis of this kind shows that due to the opening in tension and crushing hinges, the appearance of hinges in beams can also be expected in parts of the beam that continuously pass through the wall, and that the position of the plastic hinge in the beam is not known in advance and depends in many respects on the behavior of the wall. On the other hand, the slabs, which can take over the shown redistributions, in many ways affect the walls through a change in the intensity of the normal force in the wall, and indirectly thereby also on the bearing capacity of the wall to transverse forces, because this bearing capacity depends on the intensity of the normal force in the wall.

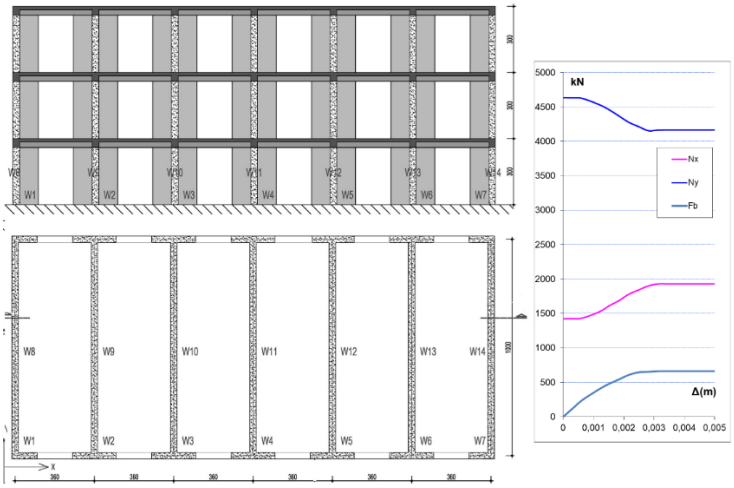


Figure 7. Building, normal forces in walls, capacity curve.

It is clear, for the building shown in the previous figure, that the main bearing walls are in the y direction. The walls in the x direction take about 23% of the total gravity load. The Nx-Δ curve shows the total normal force in all x-direction walls, and the Ny-Δ curve shows the total normal force in all y-direction walls. By following the steps of the pushover analysis, an interesting change of the normal forces in the structure is observed, which occurs due to the cooperation of all the elements of the structure. By rotating the walls in the x direction, they act on the slab tending to lift it up. The slab mainly rests on the walls of the y direction, so lifting the slab reduces the normal force in the walls of the y direction. As the total gravity load is constant for the entire pushover analysis, there is an increase in the normal force in the x direction, which in the last steps of the pushover analysis takes over by redistributing almost 32% of the gravity load. Previously, in Figure 1c, the coupling of forces that occurs during linear

Copyright © 2025 CroCEE
DOI: https://doi.org/10.5592/CO/3CroCEE.2025.122

analysis of frame structures was mentioned, so in the left wall a decrease in the normal force was registered, and in the right an increase. At the beginning of the non-linear analysis, this trend exists only in the first steps for the edge walls W1 and W7, so that after the joints are opened and the wall is attached to the slab during rotation in all walls in the x direction, the normal force will increase.

The Fb-Δ curve in Figure 7 shows the building capacity curve. Independent calculations in 3MURI [6] and MINEA [7] software yielded consistent results. By using specialized software for masonry structures, these effects remain unnoticed by the user.

5. Conclusion

Masonry structures are not even a system of interconnected walls, and especially not frame systems. Their behavior is somewhere between these two models. The common design approach of analyzing buildings as a system of walls separated from the structure and connected to each other by axially rigid RC slabs gives unrealistic wall stresses because a certain frame effect certainly exists. This effect is partly investigated in the paper. To what extent it will be realized depends on many factors, the most important of which is the rigidity and load-bearing capacity of the slab.

In addition to this effect, by modeling step by step as briefly described in the paper, many other interesting features can be observed that remain hidden by using specialized software for masonry structures. The disadvantage of the approach is that it takes considerable time to analyze the specific building, so the approach can be applied mainly for research purposes. Finally, we must say that from the point of view of usability, these scenarios are questionable, and that in the case of the errection of new buildings, much more attention should be paid to proper general design than the numerical proof of load-bearing capacity.

References

[1] Meskouris, K., Butenweg C., Geller,t C., Erdbebensicheres Bauen – Kalksandstein, Verlag Bau+Technik GmbH, Düsseldorf, Germany, 2008

[2] FEMA 306: „Evaluation of earthquake damaged concrete and masonry wall buildings – Basic Procedures Manual“, Applied Technology Council (ATC), Publication No. 306, Federal Emergency Management Agency, Washington D.C., 1998

[3] CSI Computers & Structures Inc. (2002), SAP2000 - Analysis reference manual, Berkley

[4] Simonović, G., Proračunski modeli za trodimenzionalnu analizu seizmičke otpornosti zidanih zgrada, disertacija, Građevinski fakultet Univerziteta u Sarajevu, 2014.

[5] Simonović, G., Hrasnica, M., Medić. S. Engineering model for analysis of masonry structures, Proceedings of the 2nd Croatian Conference on Earthquake Engineering - 2CroCEE, Zagreb, Croatia 2023.

[6] S.T.A. DATA (2009), 3muri - manuale d'uso, S.T.A. DATA srl - C.so Raffaello, Torino

[7] SDA-engineering GmbH MINEA, Programm für den Nachweis von Mauerwerksbauten nach DIN4149

Proceedings of the 3rd Croatian Conference on Earthquake Engineering - 3CroCEE
19–22 March 2025, Split, Croatia
Copyright © 2025 CroCEE
DOI: https://doi.org/10.5592/CO/3CroCEE.2025.125

THE EFFECTS OF SOIL-STRUCTURE INTERACTION ON THE SEISMIC DESIGN OF SHALLOW FOUNDATIONS FOR EBFs

Sanda Koboevic [(1)], Bardia Ramin Afshar [(2)]

[(1)] *Associate professor, Department of Civil Engineering, Polytechnique Montreal, Montreal, QC, Canada, email: sanda.koboevic@polymtl.ca*
[(2)] *Former M.Sc. student, Department of Civil Engineering, Polytechnique Montreal, Montreal, QC, Canada, email: ushanthan.murugananthan@gmail.com*

Abstract

Past research has demonstrated that foundation rocking can reduce demands on the superstructure by dissipating a portion of earthquake energy through soil-structure interaction (SSI). Canadian seismic provisions allow two approaches for foundation design: capacity-protected (CP) and not-capacity-protected (NCP). CP foundations are designed to fully develop the resistance of the seismic force-resisting system (SFRS), thereby concentrating inelastic activity within the superstructure. In contrast, NCP foundations are designed to develop only a partial capacity of the SFRS, leading to foundation uplift and rotation, which limit the forces transmitted to the superstructure. In practice, Canadian design often results in large foundations for steel frame buildings, significantly increasing construction costs and potentially favouring alternative structural materials. Previous studies on concentrically braced frames have shown that, on competent soils, such large foundations may not be necessary, and satisfactory performance can be achieved even without considering frame overstrength in design.

To further validate the applicability of Canadian seismic provisions for foundation design of steel frames, this study investigates 3- and 8-storey steel buildings with eccentrically braced frames located in Vancouver, Canada. Two site classes (C and E) were considered. Foundation designs followed Canadian seismic design provisions (NBCC 2020 and CSA A23.3-19), with an additional comparison to a design approach without capacity considerations, similar to US practice. Non-linear time history analyses were conducted using the STKO/OpenSees platform, incorporating both inelastic frame behavior and nonlinear soil response. The results indicate that for foundations on competent soil (site class C), even without applying capacity design principles, the inter-storey drift and soil capacity limits were satisfied. This design approach resulted in smaller foundations and reduced ductility demands on the superstructure.

Keywords: Eccentrically braced frames, Seismic foundation design, Soil-structure interaction, Nonlinear time-history analysis.

1. Introduction

The foundation of a structure plays a key role in seismic performance, acting as the interface between the superstructure and the ground to transfer earthquake forces. Traditional foundation design aims to keep the foundation elastic and undamaged, directing energy dissipation into the superstructure. The required foundation strength varies depending on the seismic force resisting system (SFRS) and design philosophy. In Canada, foundations with unrestrained rotations can be designed as capacity-protected (CP) or not-capacity-protected (NCP). CP foundations must resist an overturning moment corresponding to the full capacity of the SFRS, ensuring energy dissipation occurs only in the superstructure. The SFRS capacity depends on the ductility level of the system. In contrast, NCP foundations do not need to fully develop the SFRS capacity. Instead, they allow uplift and rocking, and can limit force demands on the structure but introduce more prominent foundation rotations and increased inter-storey drifts, requiring careful structural design.

Eccentrically braced frames (EBFs) provide an effective balance of stiffness, strength, and ductility by dissipating seismic energy through inelastic deformations in a beam segment called the link. All links are expected to yield simultaneously, creating a shear yielding mechanism that influences force demands on all protected elements, including foundations. Previous studies on concentrically braced

Copyright © 2025 CroCEE
DOI: https://doi.org/10.5592/CO/3CroCEE.2025.125

frames (CBFs) [1,2] suggest that current Canadian foundation design provisions, originally developed for reinforced concrete shear walls, may not fully account for distributed yielding, sometimes resulting in overly conservative foundation designs. Given that EBFs exhibit the same yielding mechanism, albeit differently achieved, it is crucial to assess whether existing foundation design requirements remain appropriate or require modification.

This study evaluates the applicability of Canadian seismic foundation design provisions, provided in National Building Code of Canada [3], and reinforced concrete design standard CSA A23.3-19 [4], for EBFs through nonlinear time history analyses of 3- and 8-storey shear-link EBF buildings designed for Vancouver, Canada. Two soil categories were considered. For comparison, an alternative foundation design omitting capacity requirements, similar ti U.S. practice, was examined. The soil-foundation-structure response was analysed using STKO/OpenSees, incorporating inelastic frame behaviour and nonlinear soil response. A fixed-base scenario was also analysed for comparison. The effects of soil-structure interaction (SSI) on the frame-foundation-soil system were evaluated by examining overturning moments, foundation uplift, permanent soil settlements, maximum spring forces, foundation rotations, shear forces in yielding links, and inter-story drifts.

2. Frame and foundation design

2.1. Design of the superstructure

Chevron-type EBFs with shear-critical links were designed for 3- and 8-storey buildings in Vancouver, BC (VCR3 and VCR8), considering Class C (very dense soil or soft rock; 360 m/s ≤ v_s ≤ 760 m/s) and Class E (soft soil; v_s ≤ 180 m/s) site conditions. In the studied N-S direction, seismic resistance is provided by four EBFs, with a system ductility factor R_d = 4 and a system overstrength factor R_o = 1.5. In the E-W direction the buildings are braced by perimeter moment-resisting frames.

Fig. 1 illustrates the typical floor plan of the buildings and the design gravity loads. The braced bay width is 8 m, with typical storey heights of 4 m and a first-storey height of 4.5 m, resulting in total building heights of 12.5 m for the 3-storey frames and 32.5 m for the 8-storey frames. A link length of 600 mm was selected. Brace-to-beam connections were designed as moment-resistant, while all other connections were considered pinned.

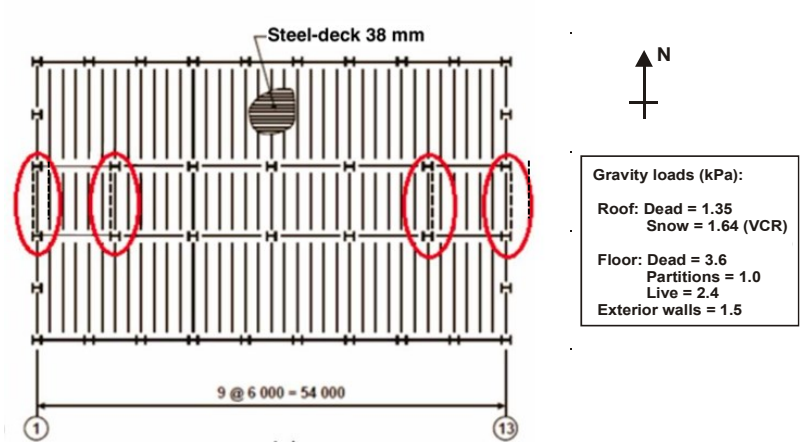


Figure 1. Plan view of the studied buildings and design gravity loads

The frames were designed in accordance with NBCC 2020 [3] and Canadian strandard for Steel structures CSA S16-19 [5]. The seismic design base shear was determined using response spectrum analysis under fixed-base conditions, as NBCC 2020 does not require consideration of soil-structure interaction in design. Dynamic base shear was calibrated against $0.8V_d$, as permitted for regular structures. The seismic base shear V_d was determined using the NBCC 2020 equivalent static procedure: $V_d = S(T_a)M_vI_EW / (R_dR_o)$, where $S(T_a)$ is the design spectral acceleration at the fixed-base fundamental

Proceedings of the 3rd Croatian Conference on Earthquake Engineering - 3CroCEE
19–22 March 2025, Split, Croatia
Copyright © 2025 CroCEE
DOI: https://doi.org/10.5592/CO/3CroCEE.2025.125

period T_a, M_v accounts for higher mode effects, I_E is the importance factor, and W is the seismic weight. The fundamental periods from modal analysis (VCR3-C: 0.54 s, VCR3-E: 0.45 s, VCR8-C: 1.33 s, VCR8-E: 0.98 s) were used to calculate V_d, as they exceeded the NBCC 2020 empirical values (VCR3: 0.31 s, VCR8: 0.81 s) but remained within the allowable limit of twice the empirical period. The resulting seismic design base shears were 761 kN, 1057 kN, 1148 kN, and 2455 kN for VCR3-C, VCR3-E, VCR8-C, and VCR8-E, respectively.

Frame members were sized to meet ductility requirements and then checked for all relevent load combination including wind and seismic loading. Links were selected from W-shapes having sufficient inelastic shear resistance for factored seismic loads, including P-Delta effects. Braces and outer beams were designed as beam-columns, resisting forces from $1.3R_y$ times the nominal link shear resistance, V_p. Beams were selected from W-shapes and braces from an HSS section database, with beams assumed fully laterally supported out-of-plane by floor slabs. Bending moments combined with axial tension governed outer beam design, while brace design was controlled by compressive axial loads and bending moments. At link ends, bending moments were initially distributed between the brace and outer beam based on their elastic flexural stiffness. When the moment assigned to the outer beam exceeded its resistance, the remaining moment was transferred to the brace, allowing yielding of the outer beam segment. Columns were considered continuous over the building height. Axial forces from gravity loads were combined with forces from yielding links ($1.3R_yV_p$ for top tiers, $1.17R_yV_p$ for lower tiers). Bending moments due to column continuity and storey drifts were also considered per CSA S16-19.

2.2. Design of foundation

The overturning capacity of CP foundations is determined based on the ductility of the SFRS. If the ratio R_dR_o/γ_w exceeds 2.5, the foundation must resist the lateral load corresponding to the probable overturning capacity of the SFRS, in addition to the applied factored gravity load. In this expression, γ_w represents the system overstrength. Conversely, NCP foundations are not required to develop the full capacity of the SFRS. Instead, their overturning resistance must be sufficient to withstand factored gravity loads and the greater of: (i) 75% of the nominal overturning capacity of the SFRS, or (ii) the overturning moment resulting from the design load combinations that include earthquake effects, calculated using $R_dR_o = 2$.

Table 1. Summary of soil properties and foundation dimensions for studies frames

	Footing dimensions (m)	VCR-C	VCR-E	Soil properties*	Site C	Site E
3-storey EBF		Capacity-protected foundations (CP)				
	Length (L)	11.2	16.8	q_{ult} (kPa)	3000	400
	Width (B)	4.5	6	q_f (kPa)	1500	200
	Depth (d)	1.3	1.7	G (MPa)	100	20
		No capacity design (NCD)				
	Length (L)	11.2	16.8			
	Width (B)	2	5			
	Depth (d)	1.3	1.7			
8-storey EBF		Capacity-protected foundations (CP)				
	Length (L)	16	24			
	Width (B)	6	12			
	Depth (d)	1.5	2			
		No capacity design (NCD)				
	Length (L)	16	24			
	Width (B)	3.5	9			
	Depth (d)	1.5	2			

* q_{ult}: ultimate bearing soil resistance
q_f: factored bearing soil resistance
G: shear modulus

For all EBFs studied, the probable overturning moment ($M_{probable}$) was found to be lower than the overturning moment calculated using $R_dR_o = 2$, so all foundations were designed as CP foundations. The impracticality of NCP foundations can be attributed to the high ductility of the EBF systems. The

Proceedings of the 3rd Croatian Conference on Earthquake Engineering - 3CroCEE
19–22 March 2025, Split, Croatia
Copyright © 2025 CroCEE
DOI: https://doi.org/10.5592/CO/3CroCEE.2025.125

design overturning capacities of the frames were determined based on full probable link resistances, considering direct summation. For comparison, an alternative design (NCD) was conducted similarly to the US design approach, in which capacity considerations were not included to determine foundation design forces.

Table 1 presents a summary of the soil properties used for design, along with the final footing dimensions for the studied cases. The factored bearing resistances (q_f) for site classes C and E were derived from field data, while the ultimate bearing resistance (q_{ult}) and shear modulus (G) were determined using the Canadian Foundation Engineering Manual [6]. Although q_{ult} varies with foundation dimensions, an analysis of the soil friction angles considered in this study indicated that its impact on foundation sizing was negligible. As a result, as shown in Table 1, the same factored bearing resistance values were applied to all foundations within the same site class.

3. Modelling and ground motion selection for non-linear time history analysis

Nonlinear time history analysis (NLTHA) of the soil-foundation-structure system was done using OpenSeeS [7]. Scientific Toolkit for OpenSees (STKO) [8], an advanced GUI, was used to facilitate the preparation of the OpenSees models and the visualisation of the analysis results.

The links were modelled using force-based fiber elements, with a section aggregator included to account for nonlinear shear behaviour. The shear response was represented using the Steel02 material model, where the yield strength was defined as the probable link shear resistance ($V_{pr}=R_yV_p$, where $R_y = 1.1$), and the initial shear stiffness was given by GA_v, with G being the shear modulus and A_v the shear area of the link. The strain hardening ratio was set to 0.003. The isotropic hardening parameters (a1, a2, a3, a4) were assigned values of 0.033, 1, 0.033, and 1.0, respectively, while the elastic-plastic transition parameters (R0, cR1, cR2) were set to 18.5, 0.925, and 0.15 following the recommendations by Yang et al. [9] who verified the model's accuracy by comparison with experimental data from tests conducted by Dusicka and Lewis [10].

The outer beam segments and diagonals were modelled using eight nonlinear beam-column elements with fiber discretization of the cross-section. This approach allowed for the representation of cross-sectional yielding and flexural buckling. Each element contained four integration points, and the cross-section was modeled using 16 fibers, as recommended by Agüero et al. [11]. To account for the end restraint conditions induced by the gusset plates, rotational spring elements were incorporated into the model. In contrast, the columns were modelled using elastic beam-column elements.

A flexible boundary substructure approach was employed to model the soil–foundation system, capturing rocking and permanent settlement. The nonlinear soil–foundation interaction was represented using the Beam-on-Nonlinear-Winkler-Foundation (BNWF) model. The foundation was idealized as an elastic beam supported by a finite number of vertical nonlinear springs of the q-z type. To account for the increased reactions that develop in the end zones under vertical loads, the springs were assigned variable stiffness. Following the recommendations in [12], the footing end-length ratio (L_{end}/L) was set at 20%, and a spring spacing ratio (Ie/L) of 4% was chosen, ensuring a minimum of 25 springs along the footing length. Further details on the frame and soil–foundation modelling can be found in [13].

Ground motion records were selected based on the magnitude-distance scenarios that have the most significant contribution to the seismic hazard for the studied design cases [14]. To ensure a representative selection, two distinct ground motion sets were established, corresponding to site class categories selected for this study. Each set consisted of 15 historical ground motion records, categorized into three subsets of five records, representing the dominant tectonic sources for Vancouver: crustal, in-slab, and interface earthquakes. The selected ground motions were then scaled and calibrated to match the NBCC 2020 design spectra, following the methodology outlined in [15]. This approach ensured consistency in spectral characteristics while preserving the natural variability of the recorded motions.

Proceedings of the 3rd Croatian Conference on Earthquake Engineering - 3CroCEE
19–22 March 2025, Split, Croatia
Copyright © 2025 CroCEE
DOI: https://doi.org/10.5592/CO/3CroCEE.2025.125

4. Results and discussion

The response of the superstructure–foundation–soil system was evaluated based on link shear force demand, inter-story drifts, foundation overturning moments, foundation uplift, soil settlement, and maximum forces in the nonlinear soil springs. For comparison, results were also obtained for the fixed-base (FB) system. The values presented in this section correspond to the mean of the five largest peak response values from individual ground motion records, as recommended in [14].

Table 2– Summary of the results for the overturning moments on foundations

Building	Foundation type	$M_{f\ SSI}$ (kNm)	$M_{f\ FB}$ (kNm)	M_d (kNm)	$M_{f\ SSI}/Mf_{FB}$	M_d/M_{FB}
VCR3-C	CP	18338	18472	16719	0.99	0.91
VCR3-E		27685	28201	23448	0.98	0.83
VCR8-C		69549	71318	66735	1.04	0.94
VCR8-E		145148	151432	126472	0.96	0.84
VCR3-C	NCD	16055	18472	7672	0.87	0.42
VCR3-E		29110	28201	11189	1.03	0.40
VCR8-C		65634	71318	30108	0.92	0.42
VCR8-E		136023	151432	67273	0.90	0.44

To evaluate the impact of including soil-structure interaction (SSI) in the analysis, Table 2 compares the overturning moment demand on the foundation obtained from the analysis of superstructure-foundation-soil system ($M_{f\,SSI}$) with the foundation overturning moment obtained from nonlinear time-history analysis (NLTHA) for fixed-base conditions ($M_{f\,FB}$). The ratio of design moment M_d to $M_{f\ FB}$ is also provided to validate design predictions. For capacity-protected (CP) foundations, the design overturning moment M_d corresponds to the probable overturning resistance of the frame (M_p), considering that all shear links have reached their probable shear resistance ($1.3R_yV_p$). In contrast, for foundations designed without capacity considerations (NCD), the design overturning moment is determined at the base of the frames using response spectrum analysis.

As shown in Table 2, the ratio of design moment to the fixed-based overturning moment demand (M_d/ $M_{f\ FB}$) varies between 0.83 and 0.94, suggesting that the design estimates are somewhat unconservative. This underestimation is likely due to greater strain hardening in yielding links than anticipated in the design. Indeed, the maximum link shear forces reveal that strain-hardening factors recorded in fixed-base analyses exceed the 1.3 assumed in design by approximately 10% for 3-storey frames (1.41) and 20% for 8-storey frames (1.6). The ratio $M_{f\,SSI}/M_{f\ FB}$ remains close to one for CP foundations on Class C site, indicating that the foundation provides sufficient resistance to ensure energy dissipation primarily through inelastic frame response. However, for the 8-storey frame on a Class E site, a lower $M_{f\,SSI}/M_{f\ FB}$ ratio suggests increased energy dissipation through the foundation-soil system. As the foundation size decreases (NCD foundation), $M_{f\ SSI}/M_{f\ FB}$ also decreases, indicating a greater contribution of the soil-foundation system to seismic energy dissipation. This trend is further supported by the analysis of maximum link shear forces, which reveals that smaller foundations result in reduced inelastic demand on the links and smaller strain-hardening factors (1.33 and 1.47 for 3- and 8-storey frames, respectivelly). These reductions confirm that energy dissipation is distributed between the superstructure and the foundation-soil system, rather than being primarily concentrated in the frame.

The results for foundation uplift in 3-storey frames with CP foundations (VCR3-C: 1.5 mm, VCR3-E: 1.8 mm) and permanent soil settlements (VCR3-C: 2.2 mm, VCR3-E: 17 mm) suggest that some inelastic response of the foundation-soil system occurred. On the Class C site, such response was minimal and primarily involved limited rocking. In contrast, on the Class E site, the response was more pronounced, combining inelastic soil deformation with some rocking.

Copyright © 2025 CroCEE
DOI: https://doi.org/10.5592/CO/3CroCEE.2025.125

As the size of the NCD foundation decreased, the impact of soil-structure interaction became more evident. On the Class C site, the foundation experienced increased uplift (21 mm), while on the Class E site, greater permanent settlement was observed (29 mm), slightly exceeding the acceptable limit of 25 mm. For the Class C site, the maximum forces in the soil springs remained within acceptable limits, reaching $0.13q_{ult}$ for the CP foundation and $0.33q_{ult}$ for the NCD foundation. On the Class E site, the recorded values were higher ($0.6q_{ult}$ for CP and $0.65q_{ult}$ for NCD) but still considered acceptable, particularly since these peaks occurred at extreme foundation springs and only for very short durations.

For 8-storey frames, regardless of site class or foundation type, the maximum recorded spring forces were similar to those observed in 3-storey frames. As expected, uplift and permanent soil settlements were greater than those recorded for the 3-storey frames, particularly for the NCD foundation. However, for frames on the Class C site, these values remained well within acceptable limits, with maximum uplift reaching 24 mm and maximum permanent settlement reaching 8 mm for the system with an NCD foundation. For Class E site, on the other hand, for which inelastic soil deformations dominated the response, high values of permanent soil settlement were observed (61mm and 101 mm for CP and NCD foundations, respectively), exceeding the acceptable values by a large margin.

One of the unique aspects of seismic foundation design in Canada is the requirement to account for the increase in inter-story drifts caused by the rotations of unanchored foundations in the superstructure design. Previous studies on concentrically braced frames (CBFs) [1,2] have shown that this increased drift can become a governing factor in frame design, potentially leading to larger foundation sizes to mitigate the effects of foundation rotations.

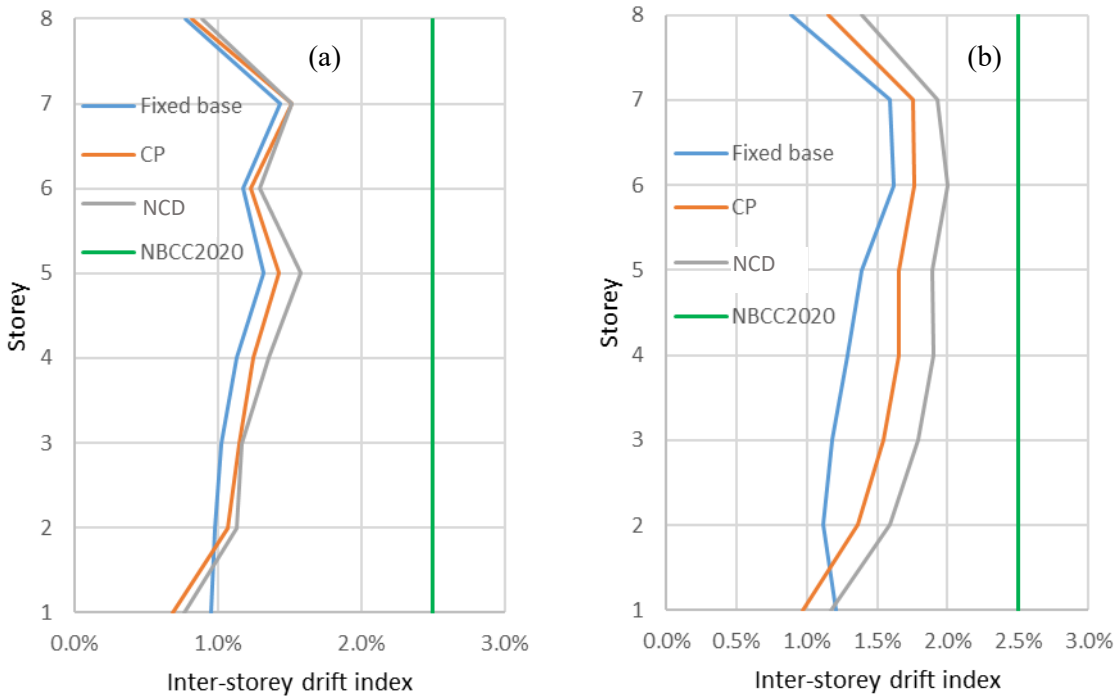


Figure 2. Inter-storey drift index for Vancouver 8-storey frame on (a) Class C and (b) Class E sites

In Fig. 2 inter-story drift ratios for 8-storey frames with CP and NCD foundations, obtained from nonlinear time-history analysis (NLTHA) and normalized by the story height, are compared to the 2.5% limit specified in the National Building Code of Canada (NBCC). For reference, results for the fixed-base scenario are also included. As the foundation size decreases, inter-story drift increases. For the 8-storey building on a Class C site, the highest inter-story drift occurs at the 5th level, reaching

Proceedings of the 3rd Croatian Conference on Earthquake Engineering - 3CroCEE
19–22 March 2025, Split, Croatia
Copyright © 2025 CroCEE
DOI: https://doi.org/10.5592/CO/3CroCEE.2025.125

approximately 1.6%. On the Class E site, the maximum drift index of 2% is recorded at the 6th level. Despite these variations, all drift values remain within the NBCC limit. For the 3-storey frames, in all cases studied, drift values remain well below the design limit, with a maximum of approximately 1%.

5. Conclusions

In this study, Canadian seismic foundation design requirements are applied to 3-storey and 8-storey steel buildings with eccentrically braced frames to assess their applicability to steel structures. The frames are designed for Vancouver, considering both Class C (competent soil) and Class E (soft soil) site conditions. Only capacity-protected (CP) foundations, sized to develop the full capacity of the frame, could be designed under Canadian provisions. For comparison, foundations were also designed without capacity considerations (NCD), following an approach similar to U.S. practice. The seismic response of the building-foundation-soil system was investigated through nonlinear time-history analysis using the OpenSees software platform. The numerical model incorporated inelastic frame behaviour and nonlinear soil response. A fixed-base scenario was also analysed for comparison. The effects of soil-structure interaction (SSI) on the frame-foundation-soil system were evaluated by examining overturning moments, foundation uplift, permanent soil settlements, maximum spring forces, foundation rotations, shear forces in yielding links, and inter-story drifts.

The following conclusions can be drawn from this study:

- Contrary to previous observations for concentrically braced frames (CBFs), non-capacity-protected (NCP) foundations were not a viable design option for the eccentrically braced frames (EBFs) studied. This limitation stems from the higher ductility coefficients assigned to EBFs compared to CBFs, which lead to lower design moments for fully developing the seismic force-resisting system's capacity. As a result, these moments fall below the minimum required for NCP foundation design, making the approach impractical.
- For both CP and NCD foundations, energy dissipation occurred through a combination of superstructure response and foundation-soil interaction. In CP foundations, the overturning moment demand closely matched fixed-base predictions, particularly on Class C sites, indicating that the foundation provided sufficient resistance to concentrate energy dissipation primarily within the inelastic response of the frame. In contrast, for NCD foundations, the reduction in overturning moment demand led to a greater share of seismic energy being dissipated through foundation rocking and inelastic soil deformation. While inelastic demand on the frame also decreased, the reduction was less significant than previously observed for CBFs on Class C sites when foundation dimensions were reduced.
- Inter-story drift values remained below the NBCC limit in all cases, though drift increased with greater foundation flexibility. For 8-storey frames, the highest drift occurred at mid-height levels, with Class E sites exhibiting slightly larger values than Class C. However, even with NCD foundations, drift remained within the 2.5% NBCC limit. This suggests that strict CP foundation design may not always be necessary for drift control and raises questions about the accuracy of current methods for estimating the impact of foundation rotations on inter-story drifts.
- The results suggest that for steel frames on competent soils, applying CP foundation principles may lead to over-conservative foundation sizing, increasing construction costs without significant performance benefits. Allowing some level of foundation flexibility through NCD design could lead to cost-effective solutions while maintaining adequate seismic performance. However, on softer soils, careful consideration is needed, as excessive soil deformations could compromise overall structural performance.

While these findings provide valuable insights into the seismic response of eccentrically braced frames with different foundation designs, certain limitations should be acknowledged. This study focuses on two specific site classes (Class C and Class E), which may not fully represent the wide range of soil conditions encountered in practice. The findings are based on ground motions calibrated for Vancouver,

Copyright © 2025 CroCEE
DOI: https://doi.org/10.5592/CO/3CroCEE.2025.125

meaning the results may not be directly applicable to other seismic regions with different soil characteristics and tectonic settings. Ongoing research aims to extend these analyses to a broader range of soil conditions and seismic environments to further generalize the conclusions.

Acknowledgements

The financial support of the Natural Sciences and Engineering Research Council of Canada (NSERC) is gratefully acknowledged. The authors also thank Profs. Lydell Wiebe and Peijun Guo from McMaster University for valuable advice as well as engineers M. Andy Metten and M. Trevor Withney (Bush, Bohlman & Partners LLP, Vancouver, BC) for sharing their experience related to seismic design of steel braced frames and their foundations.

References

[1] Murugananthan, U. (2018): *Influence of soil-structure interaction on the design of shallow foundations for concentrically braced steel frames.* Master's Thesis. Polytechnique Montréal. (*in French*)

[2] Reyes-Fernandez, A. (2023): *Impact of soil-structure interaction on seismic design of steel frames foundations*. Master's Thesis. Polytechnique Montréal.

[3] CSA. (2020): *National Building Code of Canada 2020*. NRCC, Ottawa, ON, Canada.

[4] CSA. (2019): *CSA-A23.3-19: Design of Concrete Structures*. CSA, Mississauga, ON, Canada.

[5] CSA. (2019): *CAN/CSA-S16-19: Design of Steel Structures*. CSA, Toronto, ON, Canada

[6] Canadian Geotechnical Society. (2023): *Canadian foundation engineering manual. 5th ed*. Richmond, BC, Canada.

[7] McKenna, F., Fenves, G.L. (2004): *Open System for Earthquake Engineering Simulation (OpenSees)*. Pacific Earthquake Engineering Research Center, Berkeley, CA, USA.

[8] ASDEA. (2020): *The scientific toolkit for OpenSees (STKO)*. https://asdeasoft.net/?home.

[9] Yang, T.Y., Neitsch, J., Al-Janabi, M., Tung, D.P. (2020): Seismic performance of eccentrically braced frames designed by the conventional and equivalent energy procedures. *Soil Dynamics and Earthquake Engineering*, 139, 106322, doi: https://doi.org/10.1016/j.soildyn.2020.106322

[10] Dusicka, P., Lewis, N. (1995): Behaviour of bolted link-column joints in eccentrically braced frames. *Canadian Journal of Civil Engineering*, 22(4), 745–758, doi: https://doi.org/10.1139/l95-085

[11] Aguero, A., Izvernari, C., Tremblay, R. (2006) : Modelling of the seismic response of concentrically braced steel frames using the OpenSees analysis environment. *International Journal of Advanced Steel Construction, 2*(3), 242-274, doi: https://doi.org/10.18057/IJASC.2006.2.3.5

[12] Gajan, S., Raychowdhury, P., Hutchinson, T. C., Kutter, B. L. and Stewart, J. P. (2010). Application and validation of practical tools for nonlinear soil-foundation interaction analysis. *Earthquake Spectra, 26*(1), 111-129, doi: https://doi.org/10.1193/1.3263242

[13] Ramin Afshar, B. (2024): *The effect of soil-structure interaction on seismic design of eccentrically braced frames foundations.* Master's Thesis. Polytechnique Montréal.

[14] Atkinson, G. M. (2009). "Earthquake time histories compatible with the 2005 National building code of Canada uniform hazard spectrum". *Canadian Journal of Civil Engineering, 36*(6), 991-1000, doi: https://doi.org/10.1139/L09-044

[15] Tremblay, R., Atkinson, G., Bouaanani, N., Daneshvar, P., Léger, P., Koboevic, S. (2015): *Selection and scaling of ground motion time histories for seismic analysis using NBCC 2015.* 11th Canadian Conference on Earthquake Engineering, Victoria, BC, Canada.

Proceedings of the 3rd Croatian Conference on Earthquake Engineering - 3CroCEE
19–22 March 2025, Split, Croatia
Copyright © 2025 CroCEE
DOI: https://doi.org/10.5592/CO/3CroCEE.2025.128

INFLUENCE OF GROUND MOTION PARAMETERES ON SEISMIC RESPONSE

Tanja Kalman Šipoš [(1)], Adriana Brandis [(2)]

[(1)] *Associate Professor, Faculy of Civil Engineering and Architecture Osijek, tkalman@gfos.hr*
[(2)] *Senior Teaching and Research Assistant, Faculy of Civil Engineering and Architecture Osijek, acerovecki@gfos.hr*

Abstract

In order to establish a connection with structural vulnerability, ground motions generate intricate datasets that are distinguished by a variety of properties. The objective of the investigation is to evaluate the impact of specific seismic record characteristics on the nonlinear structural response of buildings, with the ultimate goal of determining the characteristics that have the most significant impact on structural vulnerability. An experimental model, the ICONS, was employed to calibrate a numerical nonlinear model for the study. This model depicts existing buildings that were constructed without regard for seismic regulations. These buildings are prevalent in cities such as Zagreb and Dubrovnik, which are located in highly seismically precarious regions of Croatia. The analysis comprised 30 seismic records that were selected based on parameters such as peak ground acceleration (PGA), magnitude (M), and distance from the epicentre (R), following the disaggregation and uniform hazard spectrum results for city of Zagreb. Storey displacement data was generated from the records through dynamic time-history analysis, which allowed for the calculation of maximum interstorey drift ratios (IDR) as a metric for structural damage. A substantial correlation between structural damage and seismic record characteristics was discovered during the analysis. Peak ground velocity (PGV), specific energy density (SED), and Housner intensity (HI) were identified as the most significant factors influencing structural vulnerability. Consequently, they should be prioritised when selecting seismic records for structural damage assessments.

Keywords: ground motion parameters, time history analysis, maximum inter-story drifts, peak ground velocity.

1. Introduction

Prediction of the response of structures to seismic forces is, therefore, the cornerstone of earthquake engineering; earthquakes have resulted in devastation and loss of life very many times. Numerical modeling and the availability of more detailed seismic data have greatly enhanced our ability to assess structural vulnerabilities due to seismic loading [1][2]. This development is particularly helpful for those regions where seismic activities are higher, and any reasonable accurate assessment will reduce risks of disasters.Nonlinear dynamic analysis is the primary tool for simulating complex inelastic behavior of structures during seismic events [3]. Different from the linear model, these methods consider geometric nonlinearities and material properties, hence providing a realistic representation of the structural behavior under extreme loads [4]. Nonlinear modeling is uniquely suited to capture major seismic events inducing cracking, plastic deformation, and collapse phenomena [3][5]. This capability is of particular importance for older structures built before the implementation of modern seismic codes [6].The complexity of seismic response modeling depends on structural type, soil-structure interaction, and characteristics of ground motion inputs. Selection of representative ground motion records is the most critical task for dynamic analysis. Many research studies emphasize developing region-specific seismic data based on local tectonic features and ground motion characteristics [5][7]. Traditional intensity measures include PGA, PGV, and SA that are in common use but very often result in poor correlation for nonlinear responses with structural damage [8].
In this direction, research for improving seismic analysis has put greater emphasis on energy-based and velocity-sensitive measures such as cumulative absolute velocity, spectral shape parameters, which present stronger correlation with structural damage in systems with moderate to low seismic resistance

Copyright © 2025 CroCEE
DOI: https://doi.org/10.5592/CO/3CroCEE.2025.128

[9]. These metrics are especially relevant for the assessment of the performance of older structures, since their performance tends to deviate from that of modern code-compliant designs [6].
The interplay between ground motion characteristics and architectural properties is another key area of investigation. For reinforced concrete (RC) buildings, seismic performance depends on material properties, construction practices, and geometric configurations [3]. Advanced numerical simulations, validated through experimental data, improve our ability to predict the seismic performance of such structures [10]. Calibration against empirical observations enhances predictive accuracy, facilitating more reliable assessments of seismic vulnerability [4][10].
Despite these advances, some important gaps remain. Most studies focus on traditional parameters such as PGA and do not consider the increasing energy-based and frequency-dependent metrics that are really essential to understand damage potential [8]. Very few studies have investigated pre-code structures-buildings designed before modern seismic code provisions-even though their vulnerabilities and damage often differ substantially [6].
This research will complement these studies through the analysis of nonlinear seismic behaviour of older reinforced-concrete buildings focusing on energy-based ground motion parameters by using calibrated numerical models, which represent experimental data. It basically determines which seismic parameters give the most insight into structural damage.

2. Ground motion parameters

Earthquake records are highly complex data sets that require numerous parameters to describe them adequately. The definition of earthquake records outlines the intensity of seismic excitation and connects seismic hazard with the structural data needed to address engineering problems. The most significant characteristics of earthquake records from the perspective of earthquake engineering are amplitude, frequency content, and record duration. Some intensity measures are associated with one or more of these three characteristics.

Intensity measures that relate to more than one characteristic of earthquake records are more reliable for describing ground motion and reflecting the potential damage ground motion can cause to structural systems [11]. The characteristics of earthquake records explored in this study include: peak ground acceleration (PGA), peak ground velocity (PGV), peak ground displacement (PGD), specific energy density (SED), Housner intensity (HI), magnitude (M), and distance from epicenter (R).

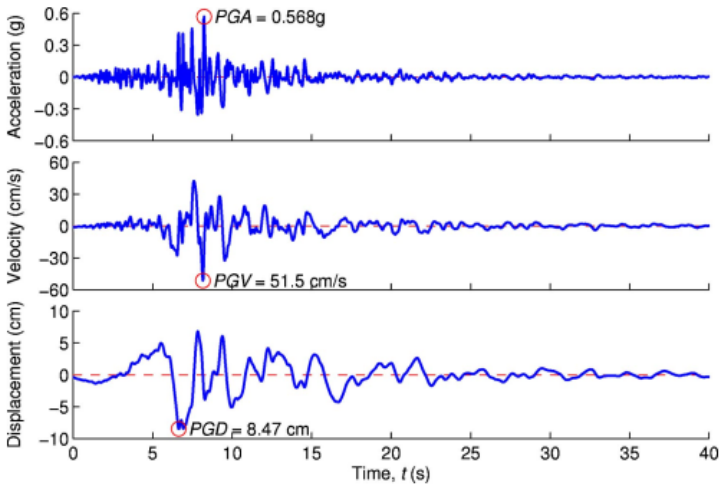


Figure 1. Overview of Peak Ground Acceleration, Velocity, and Displacement for the Horizontal Component of the 1994 Northridge Earthquake [12]

Peak ground acceleration (PGA) is a critical parameter in earthquake engineering, representing the maximum ground acceleration recorded during an earthquake. It serves as a measure of the amplitude of ground shaking intensity at a specific location. PGA is determined from the accelerogram, a time-history record of ground acceleration during seismic events. Unlike measures such as the Richter scale,

Proceedings of the 3rd Croatian Conference on Earthquake Engineering - 3CroCEE
19–22 March 2025, Split, Croatia
Copyright © 2025 CroCEE
DOI: https://doi.org/10.5592/CO/3CroCEE.2025.128

which describe the total magnitude of an earthquake, PGA focuses solely on the local intensity of ground motion.

The horizontal peak ground acceleration (PHA) is widely utilized in construction and is expressed in terms of gravitational acceleration (g = 9.81 m/s²). This parameter is instrumental in the development of seismic hazard maps and is a key input in structural design codes aimed at improving the resilience of buildings and infrastructure to seismic forces.

Peak ground velocity (PGV) is another important measure of seismic amplitude, indicating the maximum velocity of ground motion during an earthquake. Like PGA, PGV is derived from the accelerogram but provides additional insight into the dynamic characteristics of seismic waves (Figure 1).

Peak ground displacement (PGD) represents the maximum displacement of the ground during an earthquake. It is also derived from the accelerogram and provides a measure of the total movement experienced at a specific location.

Specific Energy Density (SED) is defined as the integral of the square of velocity (Equation 1) [13]. It represents a measure of the total energy of an earthquake record. A higher SED value indicates greater earthquake energy and consequently greater expected damage potential.

$$SED = \int_0^{t_{ror}} [v(t)]^2 dt \tag{1}$$

Housner intensity (HI) is a measure of ground motion intensity during an earthquake [14], defined as:

$$HI(\xi) = \int_{0.1}^{2.5} Sv(\xi, T) dt \tag{2}$$

Magnitude (M) is a measure of the size or energy released by an earthquake. It is typically quantified using the Richter scale or moment magnitude scale (Mw). The magnitude reflects the amplitude of seismic waves recorded by seismographs, with higher magnitudes indicating more powerful earthquakes. A higher magnitude generally corresponds to more significant damage and a greater potential for ground shaking.

Epicenter distance (R) refers to the horizontal distance between the location where the earthquake is being observed and the epicenter, which is the point on the Earth's surface directly above the earthquake's focus (the point of origin). The closer the epicenter distance is to the observation point, the stronger the shaking is typically experienced, as seismic waves weaken with distance from the epicenter.

3. Earthquake record selection

The primary goal of design processes is to achieve predictable and reliable levels of safety across various seismic activity scenarios. Despite advancements in structural analysis, the reliability of these analyses and subsequent evaluations depends heavily on input data related to ground motion during earthquakes.

To address this need, numerous computational methods have been developed to select seismic records from databases of historically recorded earthquakes or to artificially generate and modify ground motion records to match desired earthquake characteristics.

The process of selecting earthquake records for this study involved the use of the Uniform Hazard Spectrum (UHS) and site-specific disaggregation based on magnitude (M) and epicentral distance (R) for city of Zagreb, as shown in Figure 2. These values guide the selection of earthquake records from [16].

Copyright © 2025 CroCEE
DOI: https://doi.org/10.5592/CO/3CroCEE.2025.128

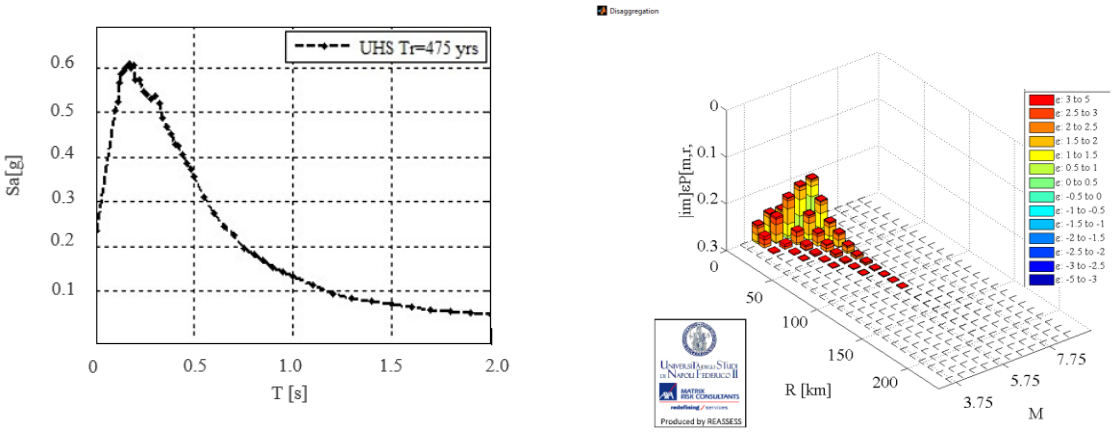


Figure 2. Uniform Hazard Spectrum (UHS) and site-specific disaggregation for city of Zagreb [15]

Based on the defined ranges of magnitude (M) and distance from the epicenter (R) for the Zagreb region, 30 earthquake records were selected to simulate potential seismic hazards for the area. The magnitude and epicentral distance values serve as boundaries. The selected earthquakes are characterized by their magnitude and distance values, illustrated in Figure 3.a). The figure shows that most epicentral distances (R) are within 25 km, while the majority of earthquake magnitudes fall between 4.5 and 6.0, with two outlier values.

Figure 3.a) presents the average ground acceleration for the 30 selected records, which is 2.60 m/s². This value corresponds to the observed peak ground acceleration (PGA) of 0.26g, and confirms the consistency between the initial and final selected parameters used to define the seismic scenario for Zagreb.

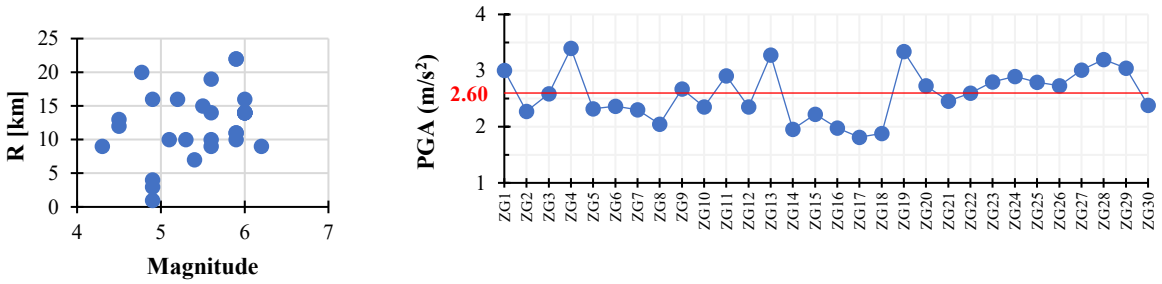


Figure 3. a) Relationship between magnitudes and epicentral distances for 30 selected earthquakes for Zagreb; b) Peak ground accelerations (PGA) for all earthquake records in scenario for Zagreb

Table 1. Ranges of characteristic values of selected earthquake records for the city of Zagreb

	PGA (m/s²)	PGV (cm/s)	PGD (cm)	SED (cm²/s)	HI (cm)	M	R (km)
Minimum value	1,81	30,70	5,28	285,59	41,59	4,3	1
Maximum value	3,40	315,94	90,16	63314,56	1132,44	6,2	22
Mean value	2,6	139,99	27,40	11387,50	361,93	5,48	12,43
Standard deviation	0,44	74,40	24,21	15487,99	272,29	0,54	4,93
Coefficient of variation (%)	17,16	53,15	88,36	136,01	75,23	9,88	39,66

For further analysis, seven earthquake record characteristics influencing the nonlinear structural response, along with their ranges, average values, and variability, are detailed in Table 1.

Copyright © 2025 CroCEE
DOI: https://doi.org/10.5592/CO/3CroCEE.2025.128

4. Validation of nonlinear numerical model for dynamic analysis

Since the earthquake scenarios were developed for the city of Zagreb, where there is a large number of buildings that were not constructed according to the seismic standards that required mandatory implementation of seismic regulations for defining the behavior of structures under earthquake loading, a structure was selected that corresponds to the group of existing buildings.

The ICONS model, shown in Figure 4, presented in detail in [17] is a four-story reinforced concrete frame representing a structure designed without seismic regulations, intended only for vertical loads, which was common practice in construction about 40 years ago in much of Europe. The ICONS model was dimensioned by LNEC (National Laboratory for Civil Engineering) in Lisbon, Portugal, then constructed at full scale and tested in a moderate-strength earthquake at the ELSA laboratory (European Laboratory for Structural Assessment) in Ispra, Italy, for the purpose of assessing the seismic vulnerability of the frame. The model was subjected to earthquake loading with peak ground acceleration of 0.22g and a return period of 475 years. Numerical model for analysis is made in Seismostruct [18].



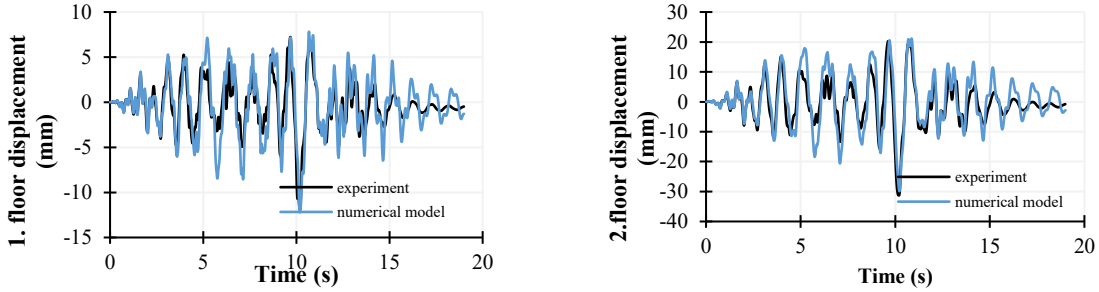
Figure 4. a) ICONS experimental model [17], numerical model of ICONS frame [18]

By comparing the fundamental dynamic characteristics of the experiment and the numerical model after the modal analysis, the first match between the models was confirmed (Table 2).

Table 2. Comparison of natural periods for numerical model evaluation

Mode	experiment	numerical model	error (%)
1	0,68	0,672	1,2
2	0,231	0,226	2,2
3	0,142	0,135	5

The results obtained from the numerical analysis correlate excellently with the experimental results. By comparing the floor displacements, it can be concluded that the numerical model fully replicates the behavior of the model during the experiment (Figures 5.14 and 5.15), which reflects the stiffness and load-bearing capacity of the structure.



Copyright © 2025 CroCEE
DOI: https://doi.org/10.5592/CO/3CroCEE.2025.128

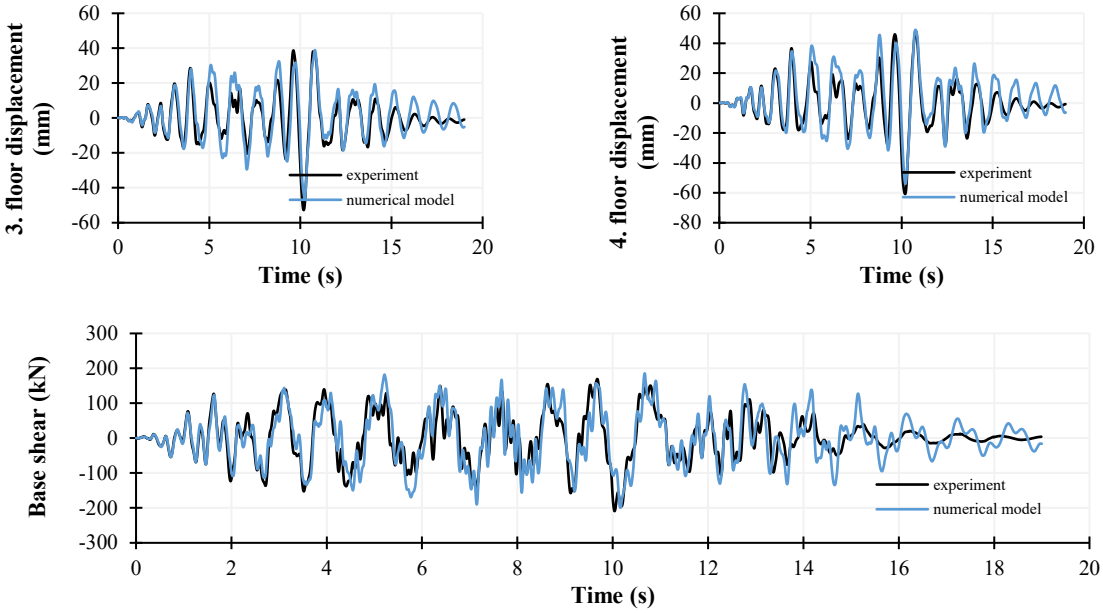


Figure 5. Comparison of displacements at all floors and base shear between the experiment and numerical model.

It is evident that the nonlinear model achieves excellent results with minimal deviations from the experimental test results. The maximum average relative error and deviation from full correlation are 12% for displacements. Based on this, it can be concluded that the model can reliably predict the system's behavior, and it can directly be applied to analyze the impact of earthquake record characteristics on the system's response.

5. Analysis of the impact of earthquake record parameters on seismic response

The previously calibrated numerical model ICONS was used to analyze the structure under time-history earthquake records. The analysis involves applying the selected earthquake records to the model and calculating the structural response by defining maximum interstory drift ratios.

According to [19] it is possible to define structural performance levels for different structural systems, which describe the state of the structure after an earthquake, as shown in Table 3. In Table 4, the maximum values of interstory displacements are marked, and based on Table 3, the behavior areas are defined to draw conclusions about the performance of such types of buildings in the observed seismic area.

It is evident that the model's condition is most critical under the action of earthquakes ZG9 and ZG11, with the maximum interstory displacements occurring on the 2nd and 3rd floors of the structure.

This indicates that the building experiences significant displacement on the higher floors under seismic loading, which may imply potential structural concerns. These results can guide further analysis, focusing on improving the building's ability to withstand seismic forces, particularly in the most affected areas of the structure (the 2nd and 3rd floors).

Table 3. Comparison of IDR (%) according to performance levels and structural type [19]

Structural performance level	Infilled frames	RC walls	RC frames
Slight damage	<0,10	<0,20	<0,20
Moderate damage	<0,40	<0, 80	<1,0
Extensive damage	>0,40	>0,80	>1,0
Near collapse	>0,80	>2,5	>3

Copyright © 2025 CroCEE
DOI: https://doi.org/10.5592/CO/3CroCEE.2025.128

Table 4. Values of interstory drifts for 30 earthquake records

floor	ZG1	ZG2	ZG3	ZG4	ZG5	ZG6	ZG7	ZG8	ZG9	ZG10	ZG11	ZG12	ZG13	ZG14	ZG15
4	0,36	0,23	0,13	0,26	0,20	**0,29**	0,16	**0,09**	0,62	0,49	0,75	0,53	0,69	0,18	0,17
3	**0,52**	**0,38**	**0,17**	**0,46**	0,40	**0,29**	0,26	0,08	**1,32**	0,83	**1,96**	**0,74**	**1,19**	**0,27**	**0,19**
2	0,38	0,23	0,14	0,33	**0,43**	0,20	**0,28**	0,07	1,02	**0,92**	1,60	0,65	0,78	0,19	0,14
1	0,20	0,14	0,09	0,19	0,29	0,15	0,20	0,07	0,58	0,71	1,27	0,48	0,43	0,14	0,08

floor	ZG16	ZG17	ZG18	ZG19	ZG20	ZG21	ZG22	ZG23	ZG24	ZG25	ZG26	ZG27	ZG28	ZG29	ZG30
4	0,17	0,04	0,18	0,16	0,18	0,14	0,57	0,16	0,12	0,12	0,11	0,20	0,41	0,45	0,34
3	**0,18**	**0,05**	0,37	**0,26**	**0,27**	**0,16**	0,86	**0,20**	**0,11**	0,09	**0,12**	0,37	**0,57**	**0,47**	**0,44**
2	0,13	**0,05**	**0,39**	0,25	0,24	0,13	**0,89**	0,17	**0,11**	**0,12**	0,11	**0,39**	0,46	0,30	0,40
1	0,07	0,03	0,24	0,15	0,16	0,09	0,68	0,10	0,08	0,08	0,09	0,26	0,31	0,22	0,23

Slight damage	IDR<0,20%
Moderate damage	0,20% ≤ IDR<1,0%
Extensive damage	1,0% ≤ IDR<3,0%
Near collapse	IDR ≥ 3,0%

Figures 6-7 illustrate the relationships between various characteristics of the earthquake records and the maximum interstory displacements. The aim is to identify the characteristics of earthquake records that have the most significant impact on the values of interstory displacements.
In analyzing the graphs comparing the curves of earthquake record characteristics and maximum interstory drifts, the objective is to find a curve trajectory that is as similar as possible. More specifically, the goal is for the trajectory of the earthquake record characteristic curve to closely follow the trajectory of the maximum interstory drift curve. Additionally, the jumps and dips in both curves should occur at the same points, indicating a strong correlation between certain characteristics of the earthquake records and the resulting structural response.

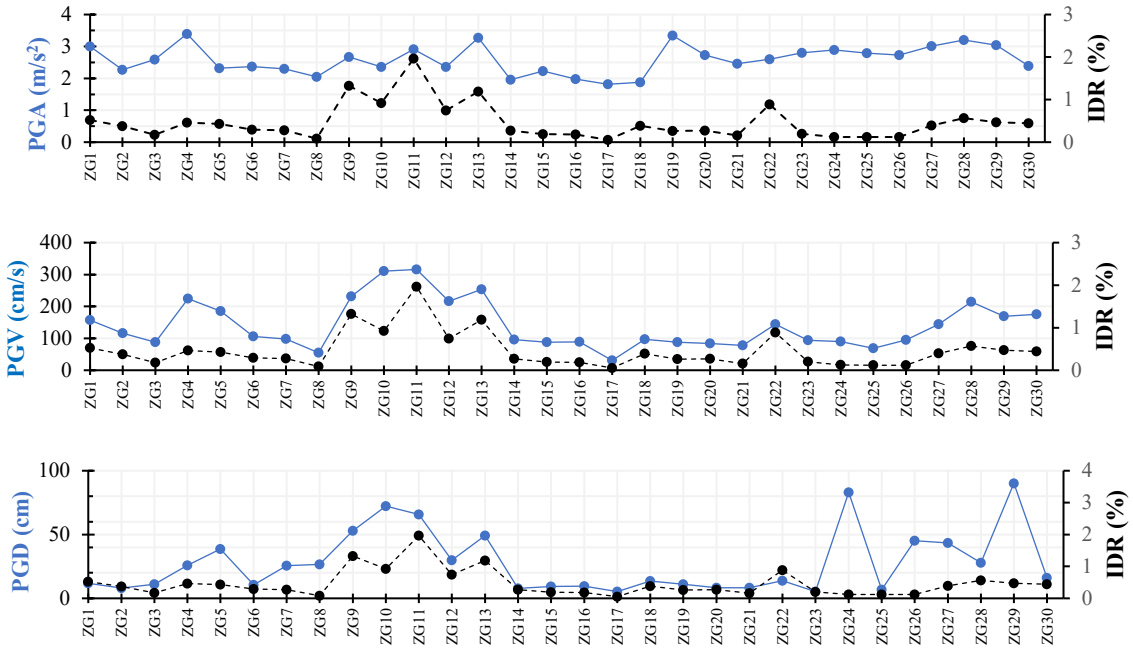


Figure 6. Comparison of peak ground acceleration, velocity and displacement curves and maximum inter-story drifts for all earthquakes for the city of Zagreb

Copyright © 2025 CroCEE
DOI: https://doi.org/10.5592/CO/3CroCEE.2025.128

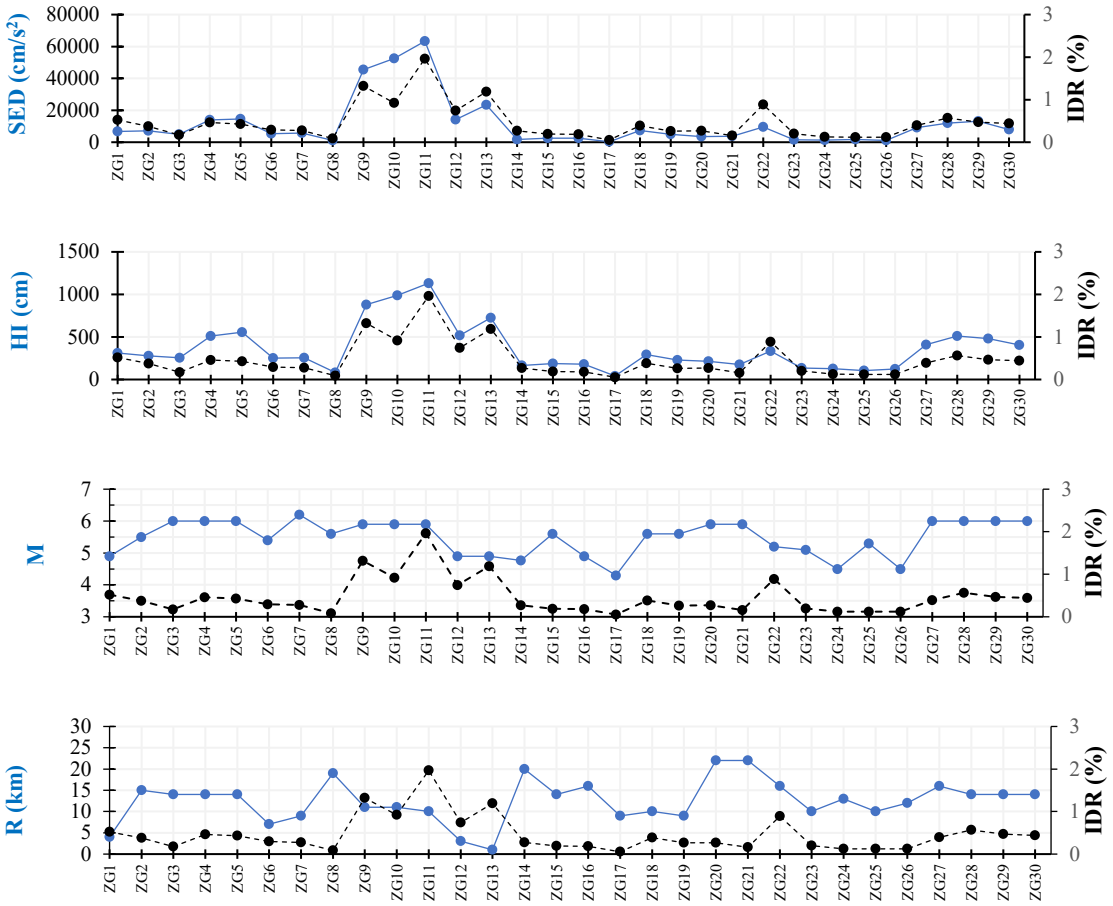


Figure 7. Comparison of specific energy density (SED), Housner intensity (HI), magnitude and epicenter distance and maximum inter-story drifts for all earthquakes for the city of Zagreb

6. Results of the analysis and selection of the most important earthquake record parameters

Based on the results of the comparisons, it can be concluded that there is a significant correlation between certain characteristics of earthquake records and the maximum inter-story drift as a measure of damage. This is because the trends of the PGV, SED, and HI characteristic curves align closely with the trend of the maximum inter-story drift curve. However, to ensure the comparison is measurable, given the differing units of measurement, all earthquake record characteristics and inter-story drift values were normalized to a range of 0–1. Correlation analysis was then used to determine the strength of influence and the degree of alignment corresponding to the changes in the observed parameters.
The correlation results for both observed earthquake areas are presented in Table 5, demonstrating that the characteristics PGV, SED, and HI have the greatest impact on the nonlinear response of the structure. This is evidenced by the fact that the correlations of the normalized values of these three characteristics reach approximately 90%, distinguishing them from other earthquake record characteristics.

Table 5. Comparison of corellation for normalized values

	PGA	PGV	PGD	SED	HI	M	R
	(g)	(cm/s)	(cm)	(cm²/s)	(cm)		(km)
Zagreb	0,30	**0,86**	0,47	**0,90**	**0,91**	0,21	0,34

Copyright © 2025 CroCEE
DOI: https://doi.org/10.5592/CO/3CroCEE.2025.128

The analysis of 30 earthquake records revealed that peak ground velocity (PGV), as a characteristic of amplitude-based intensity measures, has a significant impact on the nonlinear response of structures and their vulnerability. As PGV values increase, the maximum inter-story drift values also rise. These two variables show a high percentage of correlation, as illustrated in Figure 7. According to the analysis specific energy density (SED), which captures the instantaneous values of kinetic energy generated during the earthquake, exhibits an exceptional correlation with maximum inter-story drift values and, consequently, with structural vulnerability. Specifically, higher energy levels correspond to greater structural vulnerability.

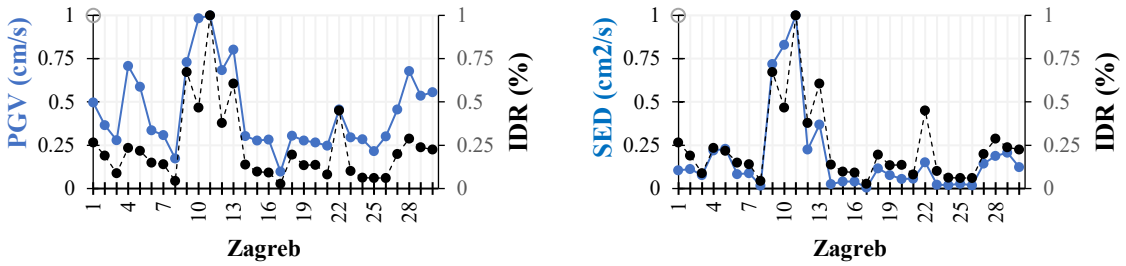


Figure 7. Comparison of normalized values of opeak ground acceleration and specific energy density (SED)and maximum inter-story drifts for all earthquakes for the city of Zagreb

As shown in Figure 8, the analysis of 30 earthquake records confirmed the statement that Housner intensity is the most effective parameter for correlating the severity of seismic events with structural vulnerability. Housner intensity exhibits an exceptional correlation with maximum inter-story drift values as a measure of structural vulnerability. This means that changes in HI values correspond to changes in maximum inter-story drift values (IDR) as a measure of vulnerability.

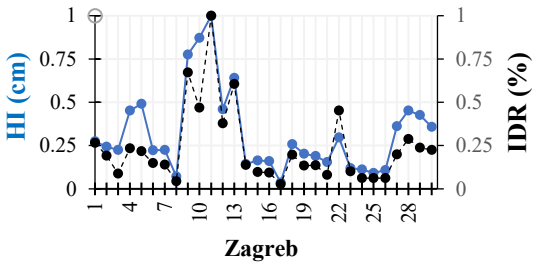


Figure 8. Comparison of normalized values of Housner intensity (HI) and maximum inter-story drifts for all earthquakes for the city of Zagreb

7. Conclusion

Seismic activity is an unexpected and sudden event and is considered one of the greatest global disasters, as it leads to a significant number of casualties and substantial property losses. During an earthquake, there is a sudden release of energy, causing the ground to shake, which is recorded by various devices. This creates complex datasets described by numerous characteristics, with the aim of linking them to the damage to structures. With the increasing frequency of earthquakes due to numerous climate changes, the number of seismic analyses has also risen, driven by the desire to reduce their consequences.

The objective of this analysis was to investigate the impact of specific seismic record characteristics on the nonlinear response of buildings and to define the characteristics with the most significant influence on structural damage. The analysis was carried out using a previously calibrated nonlinear model based on the experimental ICONS model, representing "existing buildings" designed without earthquake regulations approximately 40 years ago.

Copyright © 2025 CroCEE
DOI: https://doi.org/10.5592/CO/3CroCEE.2025.128

The analysis involved the process of selecting seismic records based on magnitude (M) and epicentral distance (R), which are the results of the disaggregation, as well as peak ground acceleration (PGA). For each of the observed areas, 30 seismic records were chosen.
For each seismic record, an analysis of 7 seismic characteristics was performed. By analyzing seismic records in time on a nonlinear numerical model of a four-story building, the displacements of the floors were obtained, from which curves comparing the maximum interstory displacements were calculated as measures of structural damage.
The comparison of the maximum interstory displacements of the building and individual seismic characteristics led to the conclusion that there is a significant correlation with certain characteristics of the seismic records. Peak ground velocity (PGV), specific energy density (SED), and Housner intensity (HI) were the seismic characteristics that proved to be the most influential on the damage to the structures and, therefore, these characteristics are the most reliable for assessing structural damage.
Similarly, the characteristics used in the selection of seismic records (PGA, M, and R) were not sufficiently reliable for detailed seismic calculations of earthquake-induced damage, as they did not show a good correlation in the analysis. When selecting critical seismic records, it is essential to assess the peak ground velocity (PGV) based on the primary characteristics, as this would yield more realistic results for the observed areas.

References

[1] Krawinkler, H. (1996): Cyclic Loading Histories for Seismic Experimentation on Structural Components. *Earthquake Spectra*, **12**(1), 1-12. doi: https://doi.org/10.1193/1.1585

[2] Moehle, J. P. (2015): *Seismic Design of Reinforced Concrete Buildings*. McGraw-Hill Education, USA.

[3] Chopra, A. K. (2017). Dynamics of Structures: Theory and Applications to Earthquake Engineering. Prentice Hall, USA

[4] Luco, N., Ellingwood, B. R., Hamburger, R. O., Hooper, J. D., Kimball, J. K., & Kircher, C. A. (2007): Risk-Targeted versus Current Seismic Design Maps for the Conterminous United States. Structural Engineering International, 17(2), 157-161.

[5] Atkinson, G. M., & Boore, D. M. (2006). Earthquake ground-motion prediction equations for eastern North America. *Bulletin of the seismological society of America*, **96** (6), 2181-2205. doi: https://doi.org/10.1785/0120050245

[6] Bommer, J. J., & Acevedo, A. B. (2004). The Use of Real Earthquake Accelerograms as Input to Dynamic Analysis. *Journal of Earthquake Engineering*, **8**, 43-91. doi: https://doi.org/10.1080/13632460409350521

[7] Kalkan, E., & Kunnath, S. K. (2006). Effects of Fling Step and Forward Directivity on Seismic Response of Buildings. *Earthquake Spectra*, **22**(4), 803-825. doi: https://doi.org/10.1193/1.2192560

[8] Pampanin, S. (2012). Reality-Check and Renewed Challenges in Earthquake Engineering: Implementing Low-Damage Structural Systems – From Theory to Practice. *Bulletin of the New Zealand Society for Earthquake Engineering*, **45**(4), 137-160. doi: https://doi.org/10.5459/bnzsee.45.4.137-160

[9] Bento R, Simões A. (2021): Seismic Performance Assessment of Buildings. *Buildings*. **11**(10):440. doi: https://doi.org/10.3390/buildings11100440

[10] Iervolino, I., Galasso, C. & Cosenza, E. (2010) REXEL: Computer aided record selection for code-based seismic structural analysis. *Bull Earthquake Eng* **8**, 339–362 doi:https://doi.org/10.1007/s10518-009-9146-1

[11] Grubišić, M.(2016) Models for Strengthening Assessment of Reinforced Concrete Frames by Adding the Infills for Earthquake Action. Ph.D. Thesis, Faculty of Civil Engineering Osijek, University of Osijek, Osijek, Croatia.

[12] Malhotra p.K. (2003). Strong-Motion Records for Site-Specific Analysis*, Earthquake Spectra,* **19**, 3. 557–578. doi: https://doi.org/10.1193/1.1598439

[13] Kramer, S. L. (1996). Geotechnical Earthquake Engineering. Prentice Hall, USA.

[14] Housner, G.W., 1959. Behavior of Structures during earthquakes, Journal of the Engineering Mechanics Division, ASCE, Vol. 85., N° EM14, 109-129.

Copyright © 2025 CroCEE
DOI: https://doi.org/10.5592/CO/3CroCEE.2025.128

[15] Chioccarelli, E., Cito, P., Iervolino, I. et al. (2019) REASSESS V2.0: software for single- and multi-site probabilistic seismic hazard analysis. *Bull Earthquake Eng 17*, 1769–1793. doi: https://doi.org/10.1007/s10518-018-00531-x

[16] Luzi L., Lanzano G., Felicetta C., D'Amico M. C., Russo E., Sgobba S., Pacor, F., & ORFEUS Working Group 5 (2020). Engineering Strong Motion Database (ESM) (Version 2.0). Istituto Nazionale di Geofisica e Vulcanologia (INGV).doi: https://doi.org/10.13127/ESM.2

[17] Pinto A, Verzeletti G, Molina J, Varum H, Pinho R, Coelho E. (2002)Pseudo-Dynamic Tests on Non-Seismic Resisting RC Frames (Bare and Selective Retrofit). EUR 20244 EN. 2002 JRC23144

[18] SeismoStruct—A Computer Program for Static and Dynamic Nonlinear Analysis of Framed Structures. Available online: www.seismosoft.com

[19] Ghobarah A (2004). On Drift Limits Associated with Different Damage Levels, International Workshop on Performance-Based Seismic Design, Department of Civil Engineering, McMaster University, Ontario,Canada,June 28 - July 1.

Proceedings of the 3rd Croatian Conference on Earthquake Engineering - 3CroCEE
19–22 March 2025, Split, Croatia
Copyright © 2025 CroCEE
DOI: https://doi.org/10.5592/CO/3CroCEE.2025.132

ANALYTICAL INVESTIGATION OF MASONRY INFILL REINFORCED CONCRETE FRAMES UNDER AXIAL AND LATERAL LOADING

Florim Grajçevci [1], Valon Veseli [2], Labeat Misini [3], Zijadin Guri [4], Ilir Canaj [5]

[1] Professor, University of Prishtina , Faculty of Civil Engineering, florim.grajcevci@uni-pr.edu
[2] Teaching Assistant, University of Prishtina, Faculty of Civil Engineering, valon.veseli@uni-pr.edu
[3] Teaching Assistant, University of Prishtina, Faculty of Civil Engineering, labeat.misini@uni-pr.edu
[4] Professor, University of Prishtina, Faculty of Civil Engineering, zijadin.guri@uni-pr.edu
[5] Teaching Assistant, University of Prishtina , Faculty of Civil Engineering, ilir.canaj@uni-pr.edu

Abstract

The structural behavior of framed reinforced concrete (RC) structures with and without infill is investigated in this work under axial and horizontal loading scenarios. Using sophisticated software and micro modelling approaches, the structural performance of RC frames of various geometrical performances lengths both bare and infilled is assessed, with a focus on rigidity, ductility, and load-bearing capacity. The RC frames were designed according to Euro code (EC) standards to ensure compliance with current design regulations, providing a reliable basis for analysis. The analysis thoroughly examines the structural behavior of these frames and how they react to combined loading situations. The findings imply that the frame slot space and the masonry infill have a major impact on the structures' lateral stiffness and load-bearing capability. The masonry infill within the RC exhibits enhanced resistance frames to horizontal forces, demonstrates with reduced significant horizontal displacement, were on the other hand, bare RC frames without infill show less stiffness and load-bearing ability, were highlights the importance of the slot space, RC frame length, and the infill in enhancing the overall structural performance. The investigation further emphasizes how important these elements are to improving the seismic resilience of RC frames. Across all frame lengths, infilled frames provide better stability and resistance to lateral stresses than plain frames. In order to ensure better performance, structural stability, and safety under both axial and lateral loading circumstances, this research advances optimum design methodologies for RC frames in seismic regions. The findings give engineers and designers important new information by showing how the thoughtful application of masonry infill and frame slot space variations can significantly improve the structural behavior of RC frames. These observations offer useful advice for enhancing stability and resilience in real-world engineering applications, and they can be applied to both new construction and retrofit projects.

Keywords: Reinforced concrete frames, infill walls, axial and lateral loading, structural performance, seismic performance, analytical investigations.

1. Introduction

Reinforced concrete (RC) frames represent a fundamental structural system widely employed in contemporary construction, particularly in seismic-prone areas. Their versatility, strength, and ability to withstand various types of loading make them an essential choice for high-performance buildings. However, optimizing their behavior under different loading scenarios requires a nuanced understanding of their interaction with non-structural components, such as infill walls. Infill walls, typically composed of masonry or bricks, are often integrated within RC frames to partition spaces and enhance lateral stiffness [1]. Despite being considered non-structural elements, these walls significantly influence the overall behavior of the frame, especially under lateral loading conditions [1, 2]. The presence of infill can increase stiffness, reduce displacements, and improve energy dissipation during seismic events. However, these benefits depend on factors such as material properties, wall placement, and the

Proceedings of the 3rd Croatian Conference on Earthquake Engineering - 3CroCEE
19–22 March 2025, Split, Croatia
Copyright © 2025 CroCEE
DOI: https://doi.org/10.5592/CO/3CroCEE.2025.132

dimensions of the frame. The structural performance of RC frames also varies with their geometry and dimensions. Longer or taller frames may exhibit reduced stiffness and greater susceptibility to lateral displacements, whereas shorter frames tend to provide higher stability. Understanding how frame dimensions interact with infill characteristics is crucial for designing resilient structures capable of withstanding axial and lateral forces effectively. This study explores the complex interplay between RC frame dimensions, infill integration, and loading scenarios. Specifically, two frame configurations with dimensions of 2.5 m height by 4 m and 2.5 m height by 6 m width were analyzed. Comparing these configurations provides insights into the effect of varying frame lengths on performance metrics such as lateral stiffness, ductility, and load-bearing capacity. By employing advanced analytical tools and adhering to Eurocode standards, this work contributes to the development of safer and more efficient building systems for seismic regions. In this study, the analysis focuses on a single-story reinforced concrete frame with fixed supports at the base. Since the structure consists of just one story, the concept of interstory drift is not presented for evaluating its performance. Instead, the force-displacement diagrams are used to capture the structural response under lateral loads, which is sufficient for assessing the behavior of the frame in this context. This approach ensures a clear understanding of the frame's lateral stiffness and load-bearing capacity without the need for interstory drift considerations. Additionally, the findings hold relevance for both new construction projects and the retrofitting of existing buildings, ensuring compliance with modern engineering practices and safety requirements [3, 4, 5].

2. Methodology

The analysis was conducted using advanced finite element modelling techniques, leveraging state-of-the-art software to achieve accurate simulations. Micro-modelling was employed to capture the nuanced interaction between reinforced concrete (RC) frames and infill walls, ensuring a detailed representation of the structural behavior. The study considered various parameters, including frame lengths, to evaluate the impact of geometry on structural performance, and infill configurations, analyzing frames both with and without infill walls to assess their contribution to stiffness and load-bearing capacity. Realistic loading scenarios were applied, incorporating axial and lateral loads to simulate conditions such as seismic events. Structural performance metrics such as lateral stiffness, ductility, and load-bearing capacity were carefully evaluated to provide comprehensive insights into the behavior of the frames under different conditions [2, 7, 8].

2.1. Micro-Modelling in DIANA FEA

Micro-modelling in DIANA FEA is an advanced simulation approach used to capture detailed interactions within reinforced concrete frames and masonry infill walls. This methodology enables a precise representation of material behavior, geometric configurations, and boundary conditions. Micro modelling of infilled frames involves detailed representation of the reinforced concrete (RC) frame, the bricks infill material, and the interfaces between these components. This approach is essential for accurately capturing the nonlinear behavior of the frame and infill, including cracking, crushing, and interactions at the frame-infill interface. Brick infill exhibits distinct mechanical properties, such as its lightweight nature, low tensile strength, and relatively brittle behavior compared to traditional masonry. These characteristics pose challenges in finite element modelling, particularly under axial and lateral loading conditions. The strategy for finite element analysis of Brick-infilled RC frames is outlined in this chapter. To simulate real-world conditions and ensure a high level of precision in the analysis, fixed supports were implemented at the base of the RC frames to replicate realistic structural constraints, while interface elements were carefully employed to model the complex interaction between the RC frames and infill walls, accounting for parameters such as friction and cohesion to reflect the behavior of the interface under loading. Axial loads were applied vertically to represent the self-weight of the structure as well as additional gravity loads, while incremental lateral loads were introduced to simulate seismic forces and to assess the lateral stiffness, ductility, and overall structural response under extreme conditions. A fine meshing strategy was adopted for both the RC frames and the infill walls, with a particular focus on critical regions such as interfaces, corners, and stress concentration zones, enabling

Copyright © 2025 CroCEE
DOI: https://doi.org/10.5592/CO/3CroCEE.2025.132

the accurate capture of localized stress distributions and potential failure mechanisms in nonlinear analyses, thereby providing reliable insights into areas prone to cracking or structural instability under combined loading scenarios [16, 17, 18, 19].

2.2. Geometry Definition

The geometry of structure illustrates a reinforced concrete frame with masonry infill, designed for both 4.0 m (Model M1.1) and 6.0 m (Model M2.1) lengths, with the only variation being the frame width. The frame consists of two vertical columns with cross-sectional dimensions of 50x30 cm, connected by a horizontal beam with a T-shaped cross-section, having a flange width of 40 cm and a depth of 20 cm. The overall height of the frame is 260 cm, while the foundation beneath the columns has a rectangular cross-section of 110x60 cm to provide stability and support for load distribution. The masonry infill spans the space between the columns and beam, with a height of 240 cm. For the 4.0 m frame, the masonry infill has a width of 350 cm, while in the 6.0 m frame, it spans 550 cm. The infill is composed of bricks with dimensions of 20x10x5 cm, arranged in a uniform bonded pattern to ensure structural integrity and efficient load transfer. Both models share the same reinforcement and structural design, maintaining a uniform reinforcement ratio of 1.2%. This approach ensures comparable performance in terms of stiffness, load-bearing capacity, and interaction between the frame and infill, while accommodating the differing frame lengths to study their behavior under various loading scenarios.

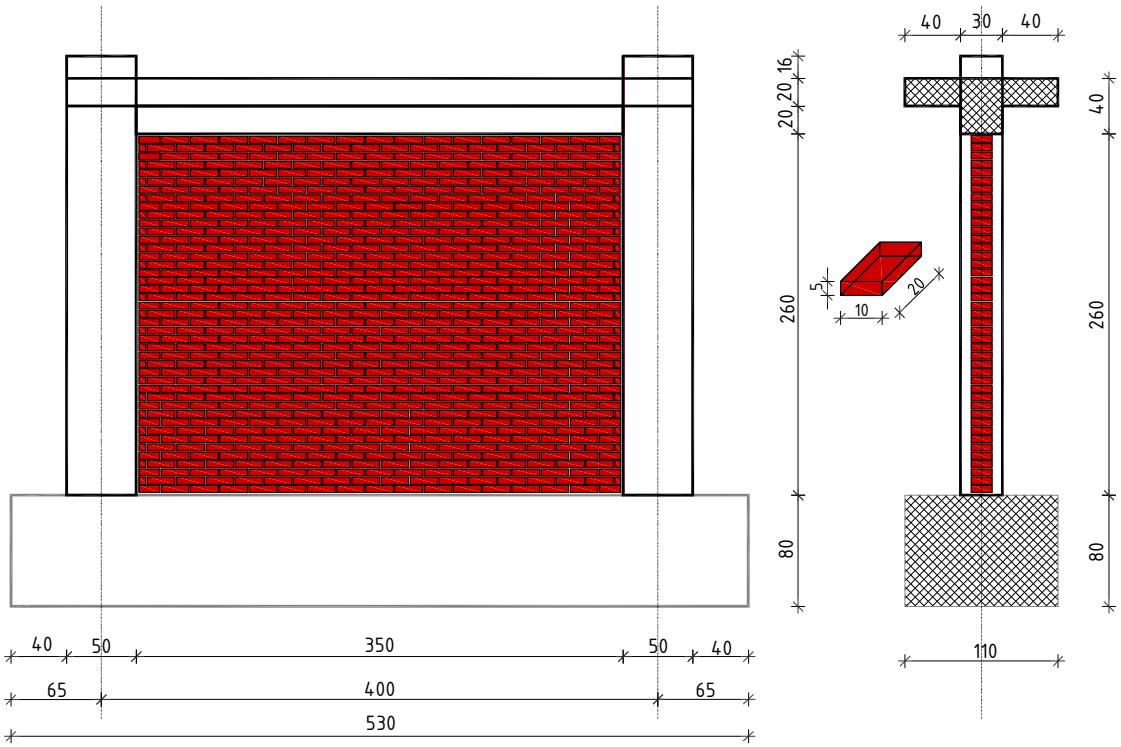


Figure 1. Geometry of Infilled RC frame (4m' length)

The reinforcement for the RC frame (Fig. 2) is designed with a consistent reinforcement ratio of 1.2%, utilizing specific bar diameters to ensure structural integrity across all elements. Columns are reinforced with Ø18 mm and Ø16 mm longitudinal bars, supported by Ø12 mm stirrups for shear resistance and confinement. Beams incorporate Ø20 mm longitudinal bars for both the top and bottom reinforcement, complemented by Ø10 mm stirrups to provide adequate shear capacity. Foundations are reinforced with Ø20 mm longitudinal bars, along with Ø12 mm stirrups or ties for shear stability, ensuring axial and bending resistance. Beam-to-column connections are strengthened with Ø16 mm bars to enhance joint ductility and structural performance. Both Model M1 and Model M2 utilize the same reinforcement

Copyright © 2025 CroCEE
DOI: https://doi.org/10.5592/CO/3CroCEE.2025.132

design, with the only difference being their lengths. This consistent approach ensures reliability and compliance with design standards while addressing the unique demands of different frame lengths.

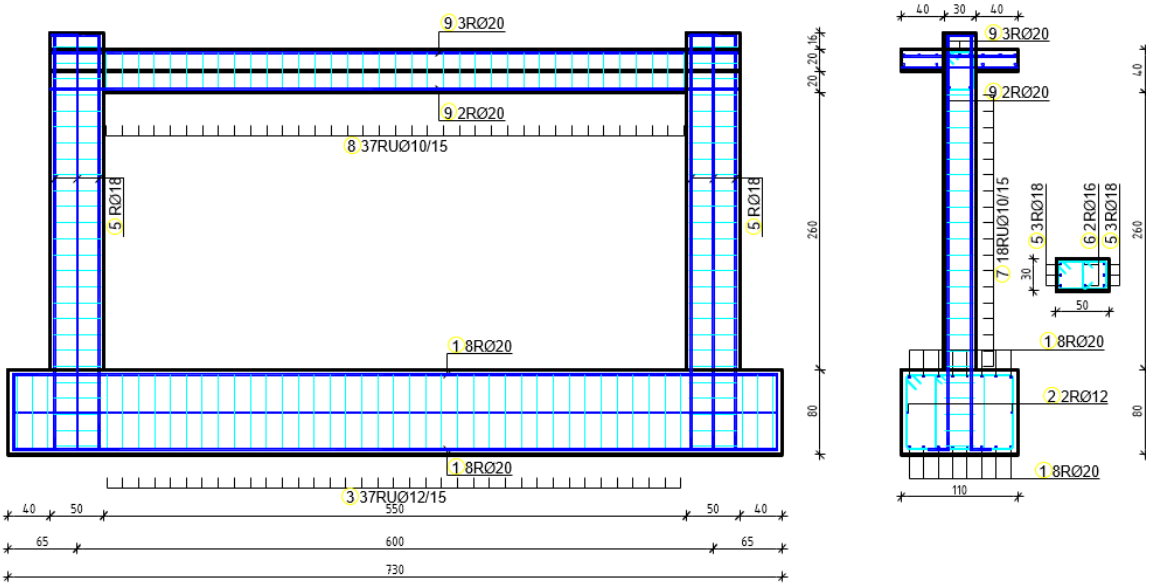


Figure 2. Reinforcement of RC frame (6m' length)

2.3. Material Properties

The material properties used in the analysis were obtained from established literature, ensuring they are well-founded and appropriate for accurately modelling the structural behavior under the specified loading conditions [2, 7, 16].

Table 1. Material used for analysis

Material	Property	Value
Concrete (RC Frame)	Compressive Strength (fc)	30 MPa
	Young's Modulus (E)	25,000 MPa
	Poisson's Ratio (ν)	0.2
Masonry (Infill)	Compressive Strength (fc)	10 MPa
	Tensile Strength (ft)	0.5 MPa
	Young's Modulus (E)	5,000 MPa
	Poisson's Ratio (ν)	0.15
Reinforcement Steel	Yield Strength (fy)	500 MPa
	Young's Modulus (E)	200,000 MPa
	Density (ρ)	7,850 kg/m³

Table 2. Material properties used for analysis in software

Material	Property	Value
Brick (Linear Elastic)	Young's Modulus	1.74E+10 N/m²
	Poisson's Ratio	0.15
	Mass Density	1700 kg/m³
Total strain module	Young's Modulus (X)	4E+9 N/m²
	Young's Modulus (Y)	6E+9 N/m²

Copyright © 2025 CroCEE
DOI: https://doi.org/10.5592/CO/3CroCEE.2025.132

	Shear Modulus	2E+9 N/m²
	Mass Density	1700 kg/m³
	Tensile Strength (Bed Joint)	250,000 N/m²
	Compressive Strength	8.5E+6 N/m²
	Fracture Energy in Compression	15,000 N/m
Brick (Nonlinear)	Young's Modulus	1.74E+10 N/m²
	Poisson's Ratio	0.15
	Mass Density	1700 kg/m³
	Tensile Strength	250,000 N/m²
	Compressive Strength	8.5E+6 N/m²
	Fracture Energy in Compression	15,000 N/m
Concrete	Young's Modulus	3E+10 N/m²
	Poisson's Ratio	0.15
	Mass Density	2200 kg/m³
Linear Interface	Normal Stiffness	1.0E+12 N/m³
	Shear Stiffness	1.0E+12 N/m³
Interface (Plastic Model)	Normal Stiffness	8.3E+10 N/m³
	Shear Stiffness	3.6E+10 N/m³
	Tensile Strength	250,000 N/m²
	Fracture Energy	18 N/m
	Compressive Strength	8.5E+6 N/m²
Interface (Friction)	Normal Stiffness	8.3E+10 N/m³
	Shear Stiffness	3.6E+10 N/m³
	Friction Angle	0.643501 rad
Interface (No Tension)	Normal Stiffness	8.3E+10 N/m³
	Critical Normal Interface Opening	3E-6 m
	Normal Stiffness Reduction Factor	1E-5

3. Results and Discussion

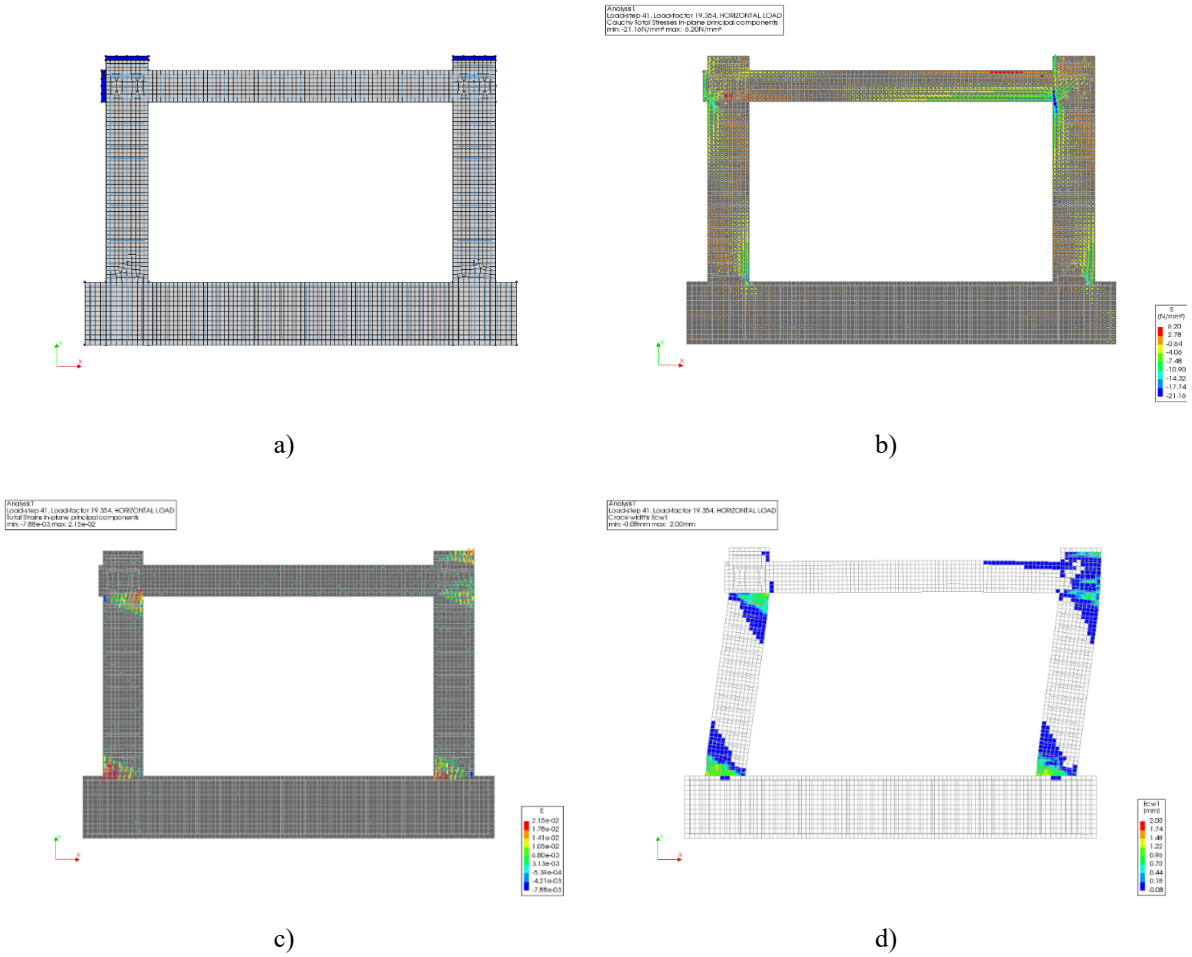
In reinforced concrete (RC) frame systems, masonry infills significantly contribute to enhancing the load-bearing capacity of the structure. However, it is important to clarify that the infill should not be considered a structural element or a rigid surface. While masonry infills are brittle, weak, and have a reduced load-bearing capacity compared to the RC frame, they play a crucial role in improving the overall performance of the frame by enhancing its lateral stiffness. The RC frame, being made of reinforced concrete, has significantly higher shear strength and load-bearing capacity than the masonry wall. As such, the design of the system must ensure that lateral displacements remain within limits, preventing excessive forces from being transmitted to the infill that could lead to failure. This is especially crucial, as masonry walls have a limited ability to resist shear forces and large displacements. There is a substantial body of research demonstrating the beneficial contribution of masonry infills to RC frame systems. However, it is important to note that this contribution varies depending on factors such as the type of masonry units used, the construction methods, mortar layers, and the dimensions of the infill walls. This interaction is evident when comparing the displacement values of frames with and without masonry infills, considering variations in wall height and length.

For the current study, a series of models should be constructed to experimentally validate the theoretical analysis, with a focus on assessing the contribution of masonry infills in improving lateral stiffness and

Copyright © 2025 CroCEE
DOI: https://doi.org/10.5592/CO/3CroCEE.2025.132

load-bearing capacity under axial and lateral loads. It should be noted that, for single-story frames, the effects of interstory drift are not as prominent. However, this analysis is particularly relevant in the context of multi-story buildings. Lastly, it is important to emphasize that the RC frame in this analysis is considered in-plane, not out-of-plane, as out-of-plane behavior of masonry infills is outside the scope of this study.

Fig. 3a (Model 1) illustrates the meshed structural model used for finite element analysis. The mesh is carefully constructed to ensure that the structural response to various loading conditions can be accurately simulated, providing a foundation for the assessment of stresses, strains, and deformations. Fig. 3b presents the stress distribution across the structure, offering a visual representation of how internal forces are distributed as the structure reacts to applied loads. This allows for an understanding of the load-bearing capacity and the regions where stresses are concentrated. Fig. 3c depicts the strain distribution, demonstrating the extent of deformation experienced by the structure under the specified loading conditions. This visualization is crucial for identifying potential zones of significant deformation or instability. Lastly, fig. 3d shows the crack patterns that develop in the structure as a result of the applied forces. The depiction of crack propagation provides insights into the structural integrity, durability, and the areas most affected by the loading, aiding in evaluating the overall performance of the structure [7, 8, 16, 17, 18].



a) b)

c) d)

Figure 3. a) The meshed structural model used for finite element analysis; b) Stress distribution across the structure; c) The strain distribution; d) The crack patterns

The graph in Fig. 4 illustrates the force-displacement response of Model M1 (L=4.0m) under one-way loading. Initially, the steep rise in the curve represents the elastic behavior, where the frame resists load with minimal deformation. The peak force of approximately 260 kN marks the maximum load-bearing

Copyright © 2025 CroCEE
DOI: https://doi.org/10.5592/CO/3CroCEE.2025.132

capacity, followed by a gradual decline indicating nonlinear behavior due to cracking or plastic deformations. The plateau region reflects the post-yield behavior, showcasing the frame's ability to sustain resistance under increased displacements. This diagram highlights the frame's stiffness, strength, and ductility under one-way loading [7, 16, 17].

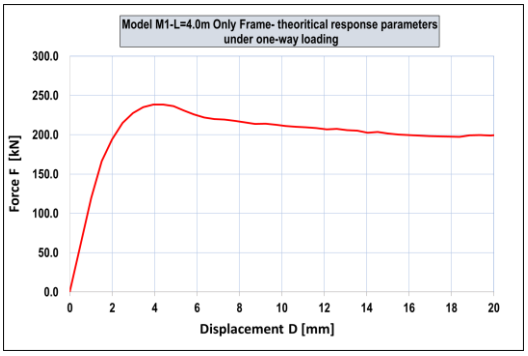
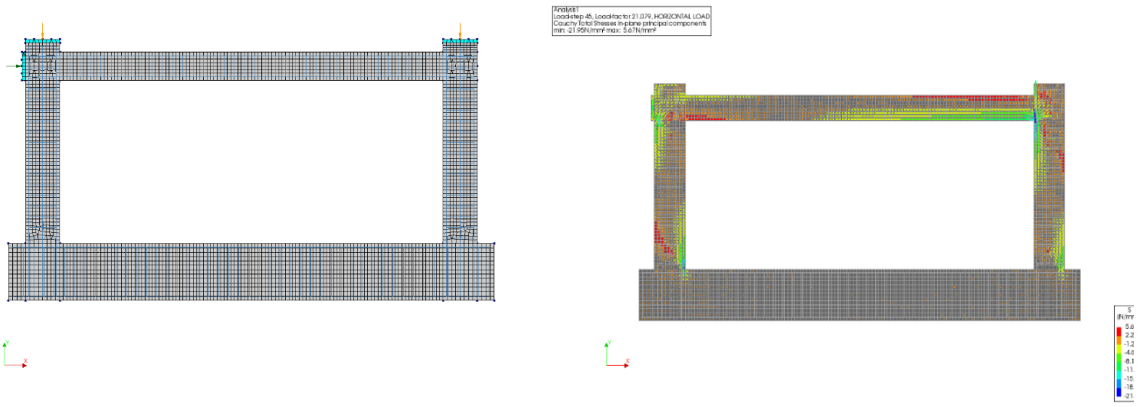


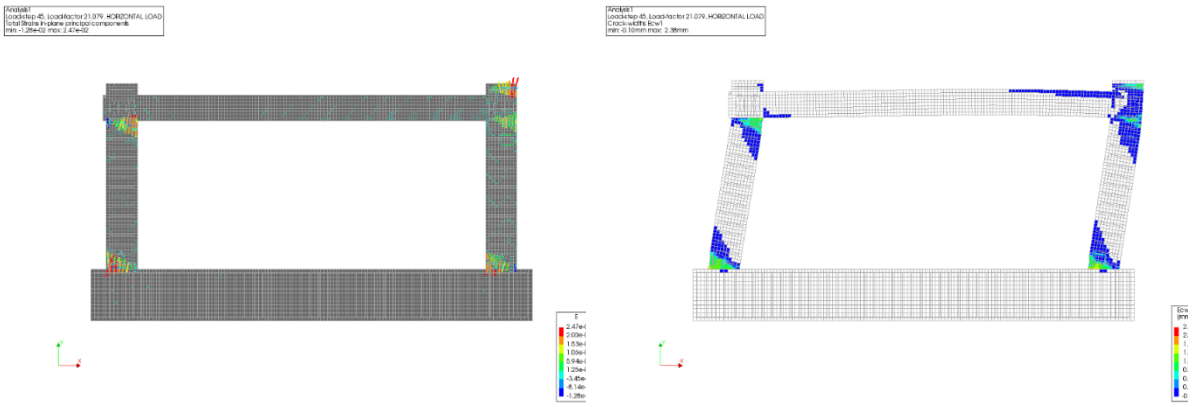
Fig 4. Force-Displacement Diagram for Model M1 (L=4.0m) Under One-Way Loading

The results presented in Fig. 5 (Model 2) provide a comprehensive understanding of the structural behavior of the RC frame with a 6 m length under applied loading conditions. The meshing ensures detailed analysis and accurate representation of the frame's response. The stress distribution illustrates how forces are transferred within the structure, highlighting areas of internal resistance. The strain distribution reflects the deformation experienced by the frame, offering insights into its structural flexibility and potential weaknesses. The crack pattern visualization identifies the development and propagation of cracks, which are critical for assessing the structural integrity and overall performance of the frame under applied forces. Together, these results demonstrate the frame's capacity to handle loading conditions while revealing potential vulnerabilities and areas for improvement.



a) b)

Proceedings of the 3rd Croatian Conference on Earthquake Engineering - 3CroCEE
19–22 March 2025, Split, Croatia
Copyright © 2025 CroCEE
DOI: https://doi.org/10.5592/CO/3CroCEE.2025.132



c) d)

Figure 5. a) The meshed structural model used for finite element analysis (L=6m'); b) Stress distribution across the structure; c) The strain distribution; d) The crack patterns

The graph shown in Fig. 6 represents the force-displacement diagram for Model M2 (L=6.0m) under one-way loading, capturing the structural response of the frame during the application of lateral forces. The curve shows an initial steep increase, indicating the elastic behavior of the structure, where the frame resists applied forces with minimal deformation. The peak force, around 250 kN, represents the maximum load-bearing capacity of the frame. Beyond this point, a slight drop in force is observed, marking the transition to nonlinear behavior caused by material cracking, localized failures, or yielding in critical sections. Following this, the curve transitions into a nearly horizontal plateau, indicating post-yield behavior, where the frame maintains a consistent resistance to increasing displacements.

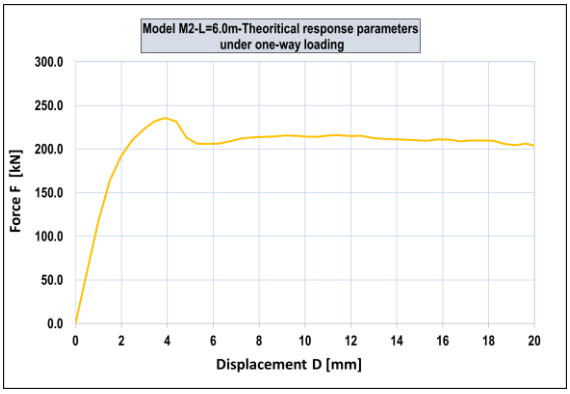
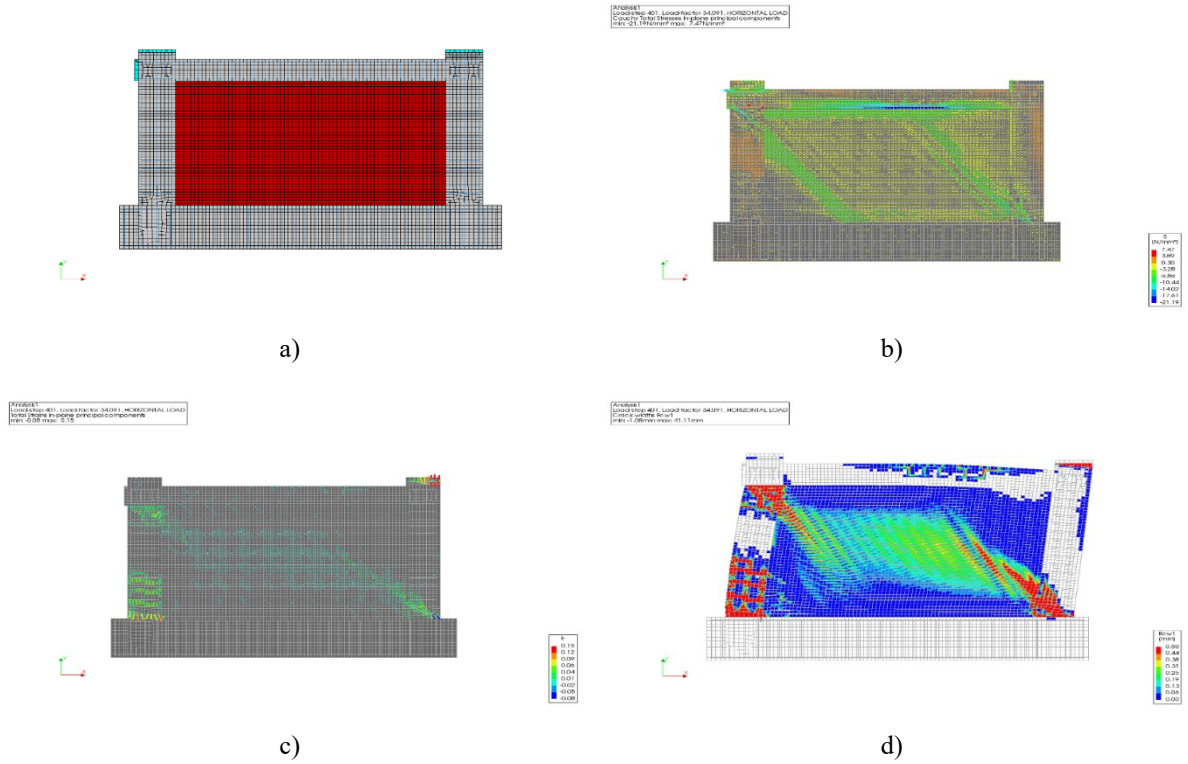


Figure 6. Force-Displacement Diagram for Model M2 (L=6.0m) Under One-Way Loading

Fig. 7 illustrates the analysis results for the RC frame with a length of 4 meters, infilled with masonry (Model 1.1). These results provide a comprehensive understanding of the structural behavior under applied horizontal loading. The meshed model represents the finite element discretization, ensuring accurate simulation of the interaction between the frame and the infill. The distribution of stresses offers valuable insights into how forces are transferred throughout the structure, highlighting the interplay between the frame and the infill under external loading conditions. Similarly, the strain distribution reflects the deformation characteristics of the structure, demonstrating the material's response to the applied forces and identifying areas of potential weakness or instability. The crack pattern visualization further complements this understanding by showcasing the extent and progression of cracking within the frame and infill. Together, these results allow for a detailed assessment of the structural integrity, durability, and overall performance of the system, providing critical information for evaluating the structural behavior and its capacity to withstand horizontal loads [16, 17, 18].

Copyright © 2025 CroCEE
DOI: https://doi.org/10.5592/CO/3CroCEE.2025.132



a) b)

c) d)

Figure 7. a) The meshed structural model used for finite element analysis RC Frame with infill (L=4m'); b) Stress distribution across the structure; c) The strain distribution; d) The crack patterns

Fig. 8 represents the force-displacement diagram for Model M1.1 (L=4.0m) with an infill under one-way loading. The curve exhibits an initial steep rise, indicating the elastic behavior of the frame with infill as it resists applied forces. The peak force of approximately 550 kN demonstrates the enhanced load-bearing capacity due to the presence of the infill, significantly higher compared to the bare frame. Beyond the peak, the curve transitions into a near-horizontal plateau, showcasing the post-yield behavior where the structure maintains consistent resistance despite increasing displacements. This diagram highlights the significant role of the infill in improving the stiffness, strength, and overall performance of the frame under lateral forces, reflecting its ability to enhance structural resilience and maintain stability during loading. The results for the RC frame with an infill and a length of 6 meters provide a detailed understanding of the structural behavior under horizontal loading (fig 9). The meshed model ensures a precise representation of the geometry, allowing for accurate simulation of interactions between the frame and the infill [3, 7]. The stress distribution highlights how forces are transferred and concentrated within the structure, reflecting the response of the materials under the applied loads. The strain visualization demonstrates the deformation characteristics, showing the extent of material elongation and compression. Finally, the crack pattern and width distribution reveal critical insights into the structural integrity, illustrating areas of crack initiation, propagation, and potential failure. These results collectively offer a comprehensive view of the structural performance, emphasizing the frame's load-bearing capacity, flexibility, and durability under horizontal forces.

Copyright © 2025 CroCEE
DOI: https://doi.org/10.5592/CO/3CroCEE.2025.132

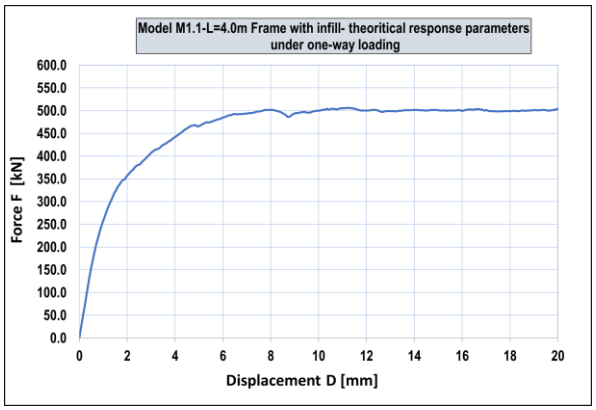
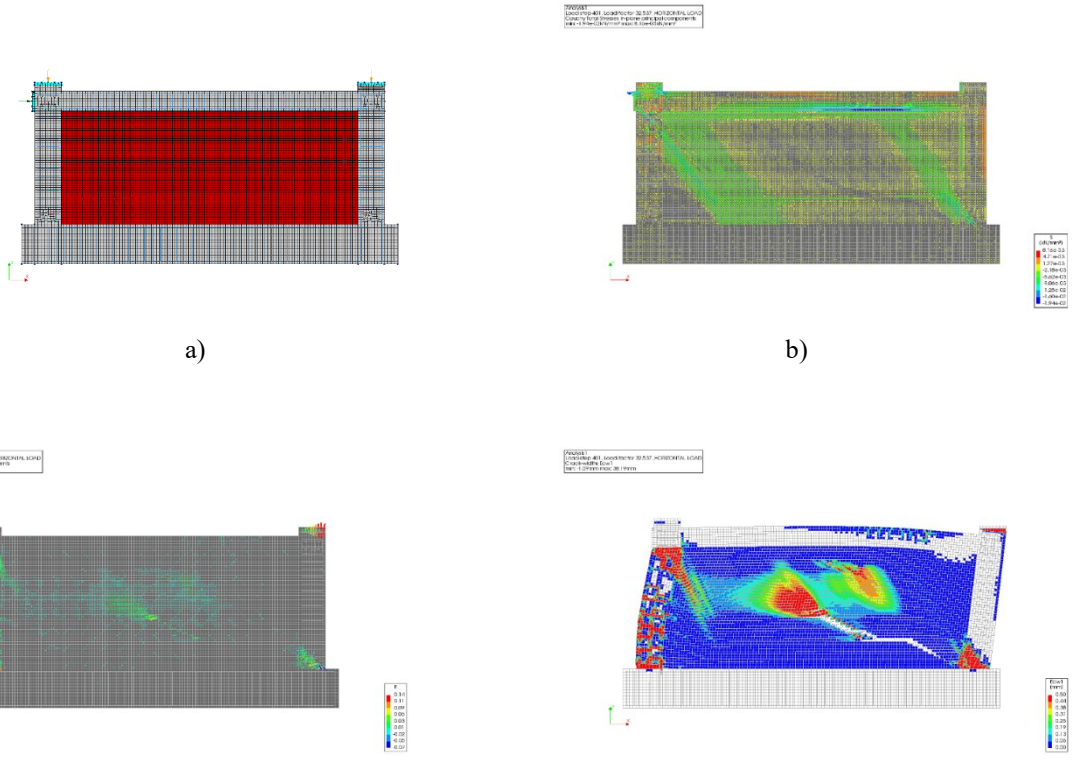


Figure 8. Force-Displacement Diagram for Model M1.1 (L=4.0m) Under One-Way Loading



a) b)

c) d)

Figure 9. a) The meshed structural model used for finite element analysis RC Frame with Infill (L=6m'); b) Stress distribution across the structure; c) The strain distribution; d) The crack patterns

Force-displacement response for Model M2.1 (L=6.0m) with an infill under one-way loading conditions is prescribed in Fig 10. The curve begins with a sharp rise, indicating the elastic behavior of the structure as it resists increasing loads with minimal deformation. The peak force, around 550 kN, demonstrates the frame's enhanced capacity due to the infill's contribution, which significantly improves its strength. Following the peak, the curve flattens into a plateau, representing the post-yield phase, where the structure continues to bear load despite increased displacements. This response reflects the combined action of the frame and infill, which contributes to the stability, ductility, and sustained load-bearing performance of the structure, even under extensive deformation. The diagram emphasizes the importance of infill in maintaining structural integrity and overall resilience in longer frames under lateral loads.

Copyright © 2025 CroCEE
DOI: https://doi.org/10.5592/CO/3CroCEE.2025.132

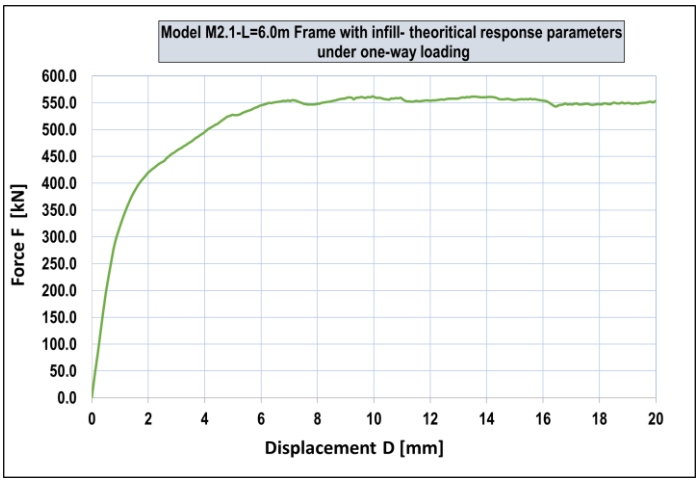


Figure 10. Force-Displacement Diagram for Model M2.1 (L=6.0m) Under One-Way Loading

3.1. Results discussion

The comparative analysis of Model M1, Model M1.1, Model M2, and Model M2.1 highlights the significant impact of masonry infill and frame length on the structural performance of reinforced concrete frames under one-way loading conditions. Model M1 (4.0 m frame without infill) shown in Fig. 11a, and Model M1.1 (4.0 m frame with infill) demonstrate the critical role of infill in enhancing structural stiffness and load-bearing capacity, as evidenced by the steeper initial slope and higher peak force in the force-displacement curve for Model M1.1. The inclusion of infill not only improves stiffness but also provides greater residual strength and ductility, enabling the frame to better resist lateral forces. Similarly, the comparison between Model M2 (6.0 m frame without infill) and Model M2.1 (6.0 m frame with infill) reveals that masonry infill significantly enhances stiffness, peak force, and residual strength (Fig 11b). The infill in Model M2.1 contributes to a more uniform stress distribution, lower strain concentrations, and reduced crack development, whereas Model M2 exhibits localized stress and strain concentrations, along with larger and more severe cracks near beam-column joints and column bases. When comparing Model M1.1 and Model M2.1, which both include infill but differ in frame length, the results demonstrate that the longer frame (Model M2.1) achieves a higher peak force and improved post-peak performance. This can be attributed to the larger dimensions of the masonry infill, which enhance load transfer and lateral stiffness, as well as the longer span allowing for a more distributed stress pattern. Model M1.1, with a shorter length, reaches its residual strength more quickly, indicating higher stress concentrations and reduced load distribution (Fig 11c). Overall, the comparative analysis underscores the critical influence of masonry infill and geometric dimensions on the structural performance of reinforced concrete frames. Numerous studies demonstrate the contribution of masonry infills to RC frames, but there is variability based on factors like the type of masonry units used, the construction methods, mortar layers, and the dimensions of the walls. Additionally, studies from earthquakes, such as those in Durrës in 2019, show how large displacements of the frame could cause significant damage to infill walls, especially when the walls are constructed with certain masonry units or improperly oriented.

Furthermore, the interaction between the RC frame and infill is critical. This can be observed when comparing displacement values for frames with and without masonry infills, considering the length and height of the walls.

These findings highlight the importance of optimizing both material properties and geometric configurations to achieve superior structural performance in reinforced concrete frames [9, 10]. The comparison fig 11.c illustrates the slight variation in stiffness and ductility between the two models (M1 and M2), useful for evaluating structural resilience. Both models exhibit a steep elastic phase followed by a peak load (around 260 kN), with Model M1 showing a slightly higher stiffness. Post-peak behavior

Copyright © 2025 CroCEE
DOI: https://doi.org/10.5592/CO/3CroCEE.2025.132

indicates a gradual decline, highlighting material cracking or plastic deformations, with both models maintaining a comparable plateau phase [2, 3, 4].

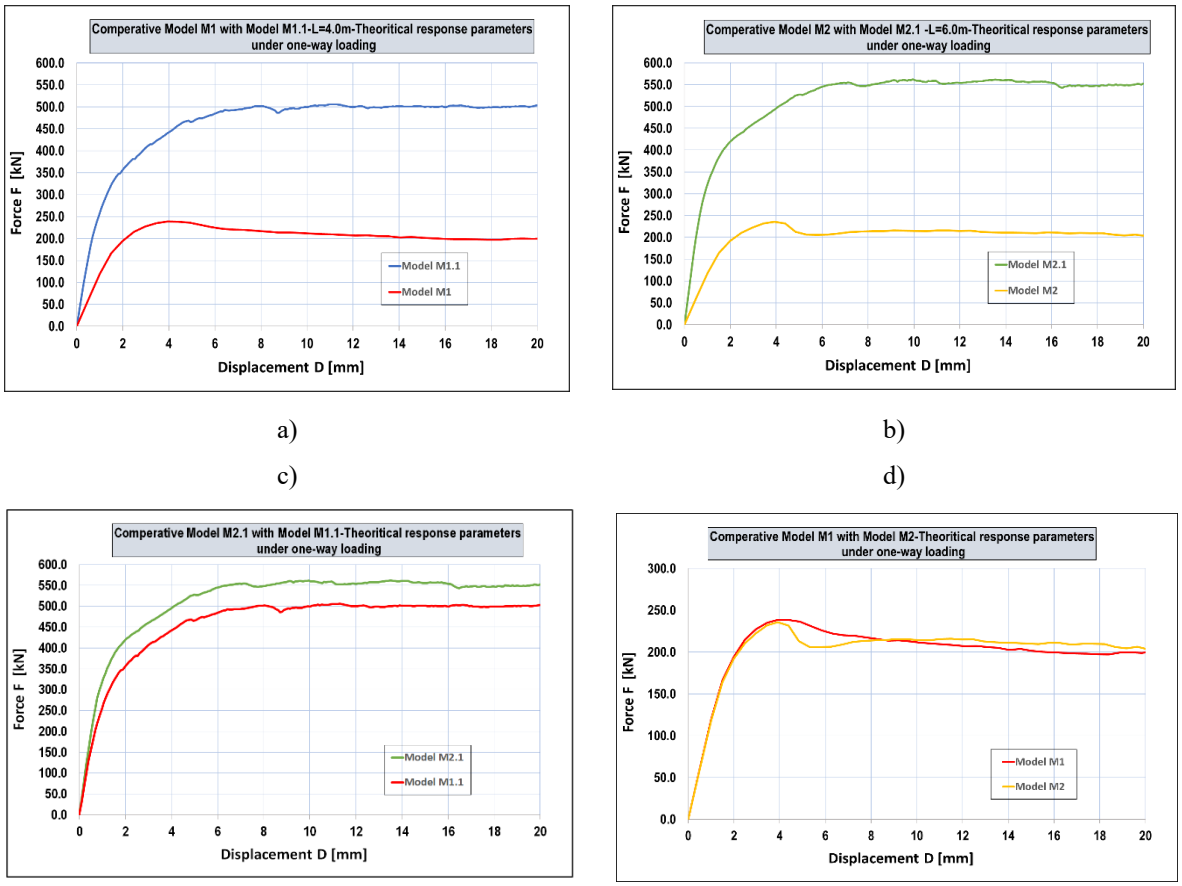


Figure 11. a) Force-Displacement Diagram for Model M1 and Model M1.1; b) Force-Displacement Diagram for Model M2 and Model M2.1; c) Force-Displacement Diagram for Model M2.1 and Model M1.

4. Conclusions

- In reinforced concrete (RC) frame systems, masonry infills provide significant contributions to increasing the load-bearing capacity of the structure. However, it's important to recognize that masonry infills should not be treated as structural elements or rigid surfaces. While the infill is brittle and has reduced load-bearing capacity compared to the RC frame, it still plays a crucial role in enhancing the lateral stiffness of the system. The frame itself, made from reinforced concrete, possesses much higher shear strength and capacity compared to the masonry wall. The engineer must design the system in such a way that lateral displacements are kept within limits so that the infill does not experience excessive forces that could cause failure. This is especially important because masonry walls have a limited capacity to withstand large shear forces.
- Infill walls significantly influence the seismic behavior of reinforced concrete (RC) frames, often with contradictory findings in the literature. While infills may enhance the lateral stiffness and load-bearing capacity of frames, numerous studies and experimental campaigns highlight their potential to cause adverse effects during earthquakes. A critical aspect is the infill/frame interaction, which can induce additional shear forces on RC columns. This phenomenon is particularly detrimental in cases of short columns, where the increased shear demand can lead to brittle failure.

Proceedings of the 3rd Croatian Conference on Earthquake Engineering - 3CroCEE
19–22 March 2025, Split, Croatia
Copyright © 2025 CroCEE
DOI: https://doi.org/10.5592/CO/3CroCEE.2025.132

- Longer frames, such as Model M2.1 (6.0 m), exhibit greater load capacity and more distributed stress patterns compared to shorter frames like Model M1.1 (4.0 m), demonstrating the critical role of geometric dimensions in structural performance.
- Longer frames with infill experience more evenly distributed and less severe cracking, while shorter frames show higher stress concentrations and localized crack formations near beam-column joints and column bases.
- Advanced finite element modelling and micro-modelling techniques provided detailed insights into the structural response under varying lengths, infill configurations, and loading scenarios, accurately capturing critical performance metrics like stiffness, ductility, and energy dissipation

References

[1] MagPage, A. W. (1978). "Finite element model for masonry." *Journal of Structural Division, ASCE*, 104(8), 1267–1285.

[2] Florim Grajcevci, Flamur Grajcevci, Fatos Tahiri, Hamdi Kurteshi, "Preliminary Seismic Vulnerability Assessment of Existing Historic Masonry Building in Pristina, Kosovo", World Academy of Science, Engineering and Technology, International Journal of Geological and Environmental Engineering,

[3] J Ristic, V Veseli, L Misini, D Ristic; "Seismic protection of masonry and infilled frame buildings using upgraded sliding isolation system with sf devices", 2CROCEE, Zagreb , Croatia, 2023.

[4] B Nela, F Grajçevci - Proceedings of the Congresso de Mīetodos Numīericos , "Numerical approach: fem testing of masonry specimens with different bond configurations of units" …, 2019

[5] Lourenço, P. B. (1996). "Computational strategies for masonry structures." *Ph.D. Dissertation*, Delft University of Technology, Netherlands.

[6] Tomaževič, M. (1999). *Earthquake-Resistant Design of Masonry Buildings*. Imperial College Press, London. ISBN: 978-1860940660.

[7] Roca, P., Molins, C., & Marí, A. R. (2005). "Strength capacity of masonry wall structures by the equivalent frame method." Journal of Structural Engineering, 131(10), 1601–1610.

[8] Grajcevci, Florim, Dumova-Jovanoska, Elena, "Vulnerability of existing masonry buildings in function of their heights" Scientific Journal of Civil Engineering, 2019

[9] Kaushik, H. B., Rai, D. C., & Jain, S. K. (2007). "Stress-strain characteristics of clay brick masonry under uniaxial compression." *Journal of Materials in Civil Engineering*, 19(9), 728-739.

[10] Paulay, T., & Priestley, M. J. N. (1992). Seismic Design of Reinforced Concrete and Masonry Buildings. Wiley.

[11] Lourenço, P. B., & Rots, J. G. (1997). "Multisurface Interface Model for Analysis of Masonry Structures." Journal of Engineering Mechanics, 123(7), 660–668.

[12] EN 1996-1-1: Eurocode 6: Design of Masonry Structures – Part 1-1: General Rules for Reinforced and Unreinforced Masonry Structures.

[13] Dolšek, M., & Fajfar, P. (2008). "The effect of masonry infills on the seismic response of a four-story reinforced concrete frame—a probabilistic assessment." Engineering Structures, 30(11), 3186-3192.

[14] Kose, M. M. (2009). "Parameters affecting the fundamental period of RC buildings with infill walls." Engineering Structures, 31(1), 93-102.

[15] Fardis, M. N. (2009). Seismic Design, Assessment, and Retrofitting of Concrete Buildings: Based on EN-Eurocode 8. Springer.

[16] DIANA FEA BV. (2023). DIANA User's Manual.

[17] DIANA FEA BV. (2023). Engineering Masonry Module – User Guide.

[18] DIANA FEA BV. (2023). Tutorials for Nonlinear Analysis.

[19] DIANA FEA BV. (2023). Material Models for Masonry and Concrete.

Proceedings of the 3rd Croatian Conference on Earthquake Engineering - 3CroCEE
19–22 March 2025, Split, Croatia
Copyright © 2025 CroCEE
DOI: https://doi.org/10.5592/CO/3CroCEE.2025.133

PUSHOVER ANALYSIS OF TIMBER BUILDINGS WITH LIGHT FRAME TIMBER PANELS FOR ENGINEERING PRACTICE: METHOD DESCRIPTION, DISCUSSION, AND HIGHLIGHTING RESEARCH GAPS

Meta Kržan [(1)]

[(1)] *Senior researcher, Slovenian National Building and Civil Engineering Institute (ZAG), meta.krzan@zag.si*

Abstract

Timber construction is increasingly recognized as a sustainable building solution due to its low carbon footprint, renewability, and prefabrication efficiency. Its lightweight nature, combined with steel connectors, makes it especially suitable for seismic regions where reducing mass and enabling energy dissipation are vital for resilience. Prefabricated timber systems also offer economic and practical advantages, enhancing their appeal in earthquake-prone areas.

This study presents a simplified pushover analysis method developed for timber buildings with light frame panels, and designed for practical use by structural engineers. Previous research at the Slovenian National Building and Civil Engineering Institute (ZAG), in collaboration with an industrial partner, involved extensive experimental testing of light frame timber panels. These panels, made of cement-particle boards stapled to timber frames, were subjected to full-scale cyclic shear tests. Results showed that panels with cement-particle boards exhibited more ductile behavior compared to those with gypsum-fibre boards.

The study aimed to determine the behavior factor (q-factor) for a timber building under seismic loading, providing performance validation for the manufacturer's systems and design assumptions. It also addresses a gap in current research and standards, as behavior factors for timber frames with stapled sheathing are not clearly defined in design codes, complicating engineering practice. Findings contribute valuable data for improving seismic design codes, particularly Eurocode 8 (EC8).

A pushover analysis, based on the SREMB method, was conducted on an existing building, assuming a critical-story failure mechanism. The methodology and its assumptions regarding the nonlinear behavior of timber panels are discussed, highlighting implications for seismic performance. The study underscores the need for further research and experimental validation to support the broader adoption of non-linear shar wall behaviour assumptions in engineering practice.

Keywords: Light-frame timber wall panels, Timber buildings, Simplified non-linear static (pushover) analysis, Critical storey mechanism, Shear wall nonlinear behaviour, EC5, Behaviour factor.

1. Introduction

The seismic design of timber buildings is typically carried out using linear elastic response spectrum analysis, where behavior factors (q-factors) prescribed by Eurocode 8 (EC8, i.e. EN 1998-1:2005: Eurocode 8: Design of structures for earthquake resistance - Part 1: General rules, seismic actions and rules for buildings [1]) are applied to account for the ductile capacity of the structure, depending on the type of structural system used. These q-factors reduce the elastic seismic demand to a design level by considering the expected energy dissipation capacity and ductility of the structure. However, for the tested type of wall panels used in construction - cement-bonded particle boards fastened to timber frames with metal staples [2] - the conservative q-factors recommended by EC8 may not accurately reflect their true seismic performance compared to other panel types. While experimental tests provide valuable insights into the resistance and ductility of individual panels, they do not directly allow for the evaluation of the overall behavior factor at the building level. The seismic response of a timber structure depends not only on the mechanical properties of individual panels but also on the

Copyright © 2025 CroCEE
DOI: https://doi.org/10.5592/CO/3CroCEE.2025.133

overall building configuration, including the interaction of structural elements and load distribution mechanisms.

Modern timber buildings, particularly residential and commercial structures, often feature irregular architectural layouts in both plan and elevation. Design trends such as large open spaces, extensive glazing on southern facades, and open-plan ground floors introduce significant structural irregularities. These irregularities can lead to uneven load distribution and complex seismic behavior, which linear elastic analysis may not fully capture. As a result, an accurate assessment of the global lateral deformation capacity of such structures is crucial to ensure reliable seismic performance. Nonlinear seismic analysis provides a more realistic evaluation by considering the behavior of structural systems beyond the elastic limit, capturing effects such as yielding, stiffness degradation, and energy dissipation. However, practical challenges exist in applying nonlinear analysis methods. Engineers often lack access to detailed structural properties, and the setup of sophisticated numerical models requires significant time and computational resources. Consequently, simplified yet reliable methods are needed to facilitate the assessment of timber structures in engineering practice, balancing accuracy with practical feasibility.

This paper presents a simplified pushover analysis method that is well-suited for engineering practice. The method is validated through a parametric study involving different nonlinear behavior assumptions for timber wall panels, derived from both experimental investigations and analytical models available in the current timber design standard, Eurocode 5 (EC5, i.e. EN 1995-1-1:2004: Eurocode 5: Design of timber structures - Part 1-1: General - Common rules and rules for buildings, [3]). The study, conducted on a real timber building, highlights the significant influence of panel behavior assumptions on the calculated seismic response and underlines the need for practical guidelines for nonlinear seismic analysis of light-frame timber buildings. Additionally, based on the obtained results, the study provides an assessment of the actual seismic performance of the building under lateral loading, contributing valuable insights to support future standardization efforts.

2. Simplified pushover analysis incorporating nonlinear shear behavior of Light Frame Timber Wall Panels (LFTWPs)

2.1. Short overview of the critical storey pushover analysis method (POR/SREMB Method)

The method upgraded and used for the presented analysis of timber building with LFTP is a simple pushover analysis initially developed for the nonlinear static analysis of masonry buildings in the 1970s', i.e. POR Method [4], in engineering practice also commonly referred to as SREMB (Seismic Resistance Masonry Buildings). With certain adjustments in assumptions, it can also be applied also to other types of structure if the failure mechanism is such that the model is appropriate. The program is based on a simplified nonlinear static analysis, where vertical-loadbearing elements alone of the assumed critical story are modelled and, in the analysis, subsequently loaded with a shear force in the direction of seismic forces through controlled incremental displacements of the mass centre of the floor. At each step, the shear load and displacement of all individual load-bearing elements in the critical story are calculated and checked considering their capacity. As the walls gradually enter the plastic range, the overall stiffness of the structure decreases until the maximum shear capacity of the story is reached. Afterwards, with increasing displacement, the shear capacity of the story decreases. The limit deformation is reached either when the force drops to 80% of the maximum capacity, when a certain portion of structural elements fails, or when a specified story drift is exceeded.

The key results of the nonlinear static analysis are the information on the damage mechanism of load-bearing elements and finally the shear capacity curve or the hysteresis envelope of the critical story. This curve shows the sum of all horizontal forces in the critical story, i.e. total base shear force F_b, in dependence of the horizontal displacement of the mass centre at the top of the story d_{et} in the loading direction of the loading force F_b. The analysis is conducted separately for both orthogonal directions of the building.

Proceedings of the 3rd Croatian Conference on Earthquake Engineering - 3CroCEE
19–22 March 2025, Split, Croatia
Copyright © 2025 CroCEE
DOI: https://doi.org/10.5592/CO/3CroCEE.2025.133

The seismic resistance assessment is based on identifying the critical capacity curve that provides the lowest results in terms of evaluated intensity measure, which commonly are either the PGA (peak ground acceleration) or the SRC (seismic resistance coefficient, calculated as ratio of building shear resistance capacity to building weight).

2.2.Main assumptions of the method and input data

This method is particularly effective for assessing buildings with distinct structural characteristics and failure mechanism. The main assumptions on which the method is based are the following:

- The walls are adequately connected with horizontal ties and floor structures that are rigid within their plane, ensuring a uniform distribution of horizontal loads and imposed displacements across the walls based on their stiffness.
- The damage and failure occur in vertical load-bearing structural elements of critical storey - only vertical load-bearing elements (wall segments) between openings are considered, modelled as linear elements with a bilinear elasto-plastic response.
- Wall elements are fixed to the floor structures at their top and bottom edges.
- The seismic resistance of the story is determined by the stiffness, load-bearing capacity, and deformation capacity of the walls. Additionally, wall deformations are influenced by their position within the story due to torsional effects.
- The contribution of walls oriented both parallel and perpendicular to the earthquake direction is considered, even though the latter affects seismic resistance and stiffness to a lesser extent than walls aligned with the seismic load direction.
- Walls carry their share of the horizontal load until their deformations exceed limit deformations (failure).

The input data for the analysis therefore include:

- Wall geometry, which defines the shear response of the walls and how seismic forces are distributed to individual wall elements.
- Wall layout in the floor plan, crucial for identifying the storey mass and stiffness centre. Asymmetric distribution can lead to increased torsional effects and larger displacements of elements under the same forces.
- Individual walls' predicted shear response in terms of the shear force–horizontal displacement diagram of wall tops. This is a critical assumption that serves to predict wall behaviour under seismic loading by identifying where plastic deformations in the walls will occur and how individual wall elements will carry seismic loads.
- Vertical load on individual structural elements, used to define the seismic loads (determined by the weight of the structure) and analyse the potential overloading of wall elements, also commonly impacting the individual's walls shear capacity.

In our analyses, the shear load-bearing capacity and deformation capacity were evaluated using distinct approaches. For each individual wall, the input parameters included wall dimensions, vertical load, and the precalculated characteristic points of the assumed bilinear shear force–horizontal displacement diagrams, as described below. The assumed nonlinear behaviour of the wall panels forms the foundation of the presented method and analysis.

2.3.Variations of the nonlinear shear response models for LFTWPs

In the analyses conducted, three variations of assumptions were adopted for the nonlinear shear force–horizontal displacement response of the panels: one based on experimental tests and two models derived from analytical calculations of the wall's shear load-bearing capacity $F_{i,v,Rd}$ according to Eurocode 5 (EC5). Yield deformation and wall effective stiffness k_w for the analytical models were derived from a model in the literature. For all models, the ultimate deformation capacity ($u_{i,frame,u}$) was evaluated based on the calculated yielding point ($u_{i,frame}$, $F_{i,v,Rd}$) and the minimum ductility factor μ of 4, obtained from experimental tests for the assumed wall panel type.

Copyright © 2025 CroCEE
DOI: https://doi.org/10.5592/CO/3CroCEE.2025.133

For comparison, the average values of the experimentally obtained and analytically calculated shear capacities, F_v, displacements at the elastic limit, u_{frame}, and shear stiffnesses, k_w, for the 250 cm wide panels used in construction are presented in Table 1.

Table 1. Various assumed bi-linear responses for B12-12 LFTWP of 250 cm length

Bi-linear wall response model	**Sheathing-to-timber frame connection lateral load capacity**	**F_v [kN]**	**u_{frame} [mm]**	**k_w [kN/mm]**	**μ_w [/]**
Method A, Källsner et al	$F_{f,m,EC5}$	22.7	2.8	8.19	4
	$F_{f,m,EXP}$	38.0	4.6	8.19	4
Method B, Källsner et al	$F_{f,m,EC5}$	45.8	5.6	16.4	4
	$F_{f,m,EXP}$	76.7	9.4	16.4	4
Experimental	/	76.0	15.0	5.07	4

Note: A staple spacing of 0.75 mm was used in the presented experimentally tested panels and in the calculations. In Method B, the shear capacity of the panel is calculated taking into account a uniform vertical panel load of 25 kN/m, i.e. the load that the panels were also subjected to in the experimental tests.

Experimental Model: This model utilizes the shear capacity F_v and effective shear stiffness k_w of wall panels determined from experimental cyclic shear tests, presented in Figure 1 [2]. The B12-12 panels tested and used in the building construction and therefore considered in the analysis are briefly described in the following chapter. For wall panels of different lengths, both F_v and k_w are assumed proportional to the 250 cm wall length, as presented in Table 1.

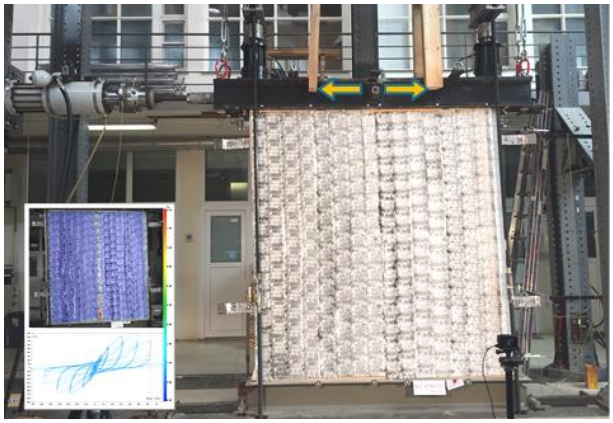


Figure 1: Test setup of experimental tests with some results for LFTWP, used for construction of the analysed timber building [2].

Analytical Models: For the other two variations, the shear capacity of individual wall panels F_v is calculated using either Method A (Eq. (1)) or Method B (Eq. (2)) from EC5. The effective shear stiffness k_w is derived from a displacement model for panels (u_{frame}) proposed by [5] according to Eq. (8), (9).

In Eq. (1)-(9), $F_{f,m}$ represents the lateral capacity of the timber-to-sheathing board connection with mechanical fasteners. The width and height of the sheathing panel are denoted by b and h, respectively. The parameter s refers to the distance between fasteners, while c is a factor that accounts for the panel's length-to-height ratio. The base distance between fasteners, s_0, is defined in Eq. (3) and depends on the fastener diameter (d) and the characteristic density of the timber frame (ρ_k).

Adjustment factors k_d, k_q, k_s, and k_n are used to account for various influences on panel behaviour: k_d is determined by panel dimensions (Eq. (4)), k_q by uniformly distributed vertical load (Eq. (5)), k_s by the arrangement of fasteners (Eq. (6)), and k_n by the contribution of sheathing boards on both sides of the panel (Eq. (7)). The terms $F_{v,Rd,max}$ and $F_{v,Rd,min}$ denote the design shear capacities of the stronger and weaker sides of the panel, respectively.

Proceedings of the 3rd Croatian Conference on Earthquake Engineering - 3CroCEE
19–22 March 2025, Split, Croatia
Copyright © 2025 CroCEE
DOI: https://doi.org/10.5592/CO/3CroCEE.2025.133

$$F_v = \frac{F_{f,m}\, b\, c}{s} \tag{1}$$

$$F_v = \frac{F_{f,m}\, b}{s_0} k_d k_q k_s k_n \tag{2}$$

$$s_0 = \frac{9700\, d}{\rho_k} \tag{3}$$

$$k_d = \frac{b}{h} \text{ for } \frac{b}{h} \leq 1.0 \tag{4}$$

$$k_q = 1+(0.083q - 0.0008q^2)\left(\frac{2.4}{b}\right)^{0.4} \tag{5}$$

$$k_s = \frac{1}{0.86\frac{s}{s_0} + 0.57} \tag{6}$$

$$k_n = \frac{F_{v,max}+0.5\, F_{v,min}}{F_{v,max}}, \text{ for panels with sheathing panels on both sides} \tag{7}$$

$$u_{frame} = \frac{4.52\, h\, s_r}{k_{ser} b} \tag{8}$$

$$k_w = \frac{F_v}{u_{frame}} \tag{9}$$

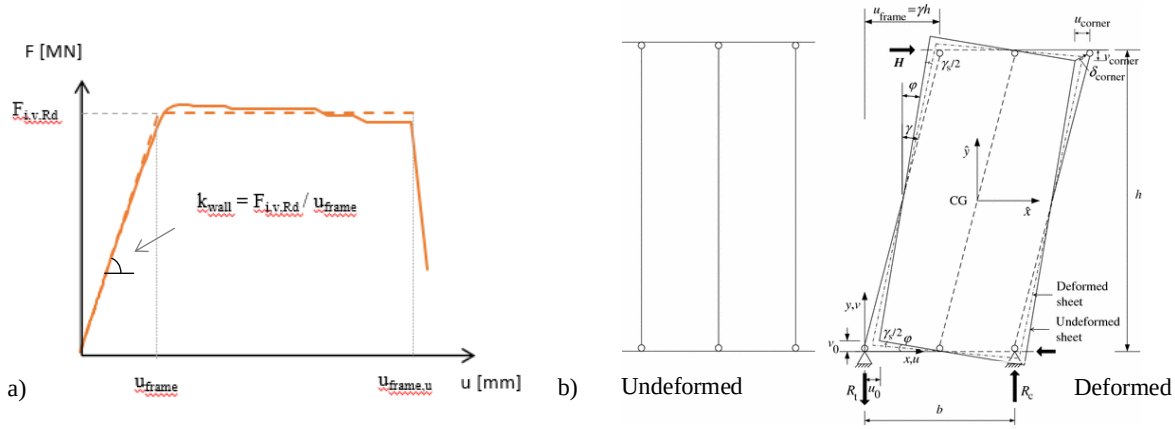


Figure 2: a) Bi-linear shear wall response model; b) model of wall panel deformation according to [5].

For both Method A and Method B, the panels analytical shear capacity F_v is linearly dependent on the lateral load-bearing capacity of the dowel-type connectors $F_{f,m}$ (staples in this case). The parametric building pushover analyses incorporated both the EC5-estimated mean shear capacity of the stapled connection ($F_{f,m,EC5}$ = 0.681 kN, evaluated as 125% of the characteristic value) and the experimentally determined shear capacity ($F_{f,m,EXP}$ = 1.14 kN). Due to the significant difference in the lateral capacities of the sheathing-to-timber connections, the analytically estimated wall shear resistances also differ notably. However, the slip modulus of the connection is consistent between the EC5 calculation and experimental tests. A slip modulus (K_{ser}) of 1.11 kN/mm was assumed for all wall properties in subsequent analytical calculations.

3. Comments and Discussion on the Assumptions of the Nonlinear Static Analysis Methods and the Bi-linear Shear Response of Wall Panels

In buildings with a regular distribution of vertical load-bearing elements across the height, damage does not occur solely at the critical floor. Therefore, the adopted method is most suitable for single-storey buildings and can provide informative conservative results for buildings with one or two floors regarding shear resistance.

Proceedings of the 3rd Croatian Conference on Earthquake Engineering - 3CroCEE
19–22 March 2025, Split, Croatia
Copyright © 2025 CroCEE
DOI: https://doi.org/10.5592/CO/3CroCEE.2025.133

The assumption of a rigid diaphragm and proportional distribution of shear load according to shear stiffness may be questionable in buildings with flexible timber floors or poor wall-to-wall and wall-to-timber connections. However, in modern timber buildings, floor construction should ensure adequate load transfer.

A critical factor in the global seismic response of buildings is the assumed wall shear stiffness, which in our model directly influences the ultimate deformation capacity, as it is defined through ductility in relation to yield displacement. Assuming shear stiffness proportional to wall length in the experimental model results in a numerically stiffer response for panels with a lower length-to-height ratio, potentially underestimating displacements due to rocking (under equal vertical stress and anchoring).

In the analytical calculations, wall stiffness is also assumed to be proportional to panel length. The model considers wall yield deformation dependent on panel height, sheathing-to-timber connection slip modulus, and fastener spacing—all consistent across similarly constructed panels—leaving panel length as the primary variable. This assumption leads to a stiffer response than in actual behaviour, as it neglects displacements from uplift, anchor system shear deformation, and panel shear deformation.

Although future EC models will address panel deformation estimation issues by incorporating geometry, angle bracket characteristics, and vertical load, they currently lack consideration of wall-to-perpendicular wall connections, which could significantly enhance the actual shear stiffness of the building.

Lastly, the assumed ductility in evaluating deformation capacity may limit the accuracy of predicting real panel behaviour under seismic loads, potentially underestimating deformation demands and overestimating safety. While high ductility was experimentally confirmed for the specific panels used, such behaviour is not guaranteed for panels in general and must be verified experimentally before use in analysis. These considerations are essential when interpreting results and comparing them with design standards.

4. Case study building

4.1. Building

To apply the method and investigate the buildings non-linear shear behavior and the influence of panel behaviour assumptions, a real residential building with a regular architectural design in Styria, Austria, was selected as the case study. The building measuring 11.4 m in length and 11.1 m in width, consists of three floors with a floor height of 2.67 m. It features a gable roof with a 22° slope. The first floor differs structurally from the upper floors due to integrated garage spaces. A staircase, measuring 4.4 m in length and 2.4 m in width, is positioned on the left side of the building across all three floors. The total floor area, including the staircase, is 136 m². The ground floor plan, highlighting the arrangement of the light frame timber wall panels, can be seen in Figure 1.

The building's load-bearing system is composed of light frame timber wall panels, timber floors, and a timber roof structure. For the presented building seismic analyses, already mentioned B12-12 panel type was considered for the construction and analysis. This panels consist of a solid timber frame sheathed on both sides with 12 mm thick cement-particle boards, attached to the timber frame using 1.53 x 11.25 x 45 mm metal staples with a characteristic tensile strength of 800 MPa, designed for effective load transfer between the sheathing and the frame. The panels exhibit ductile failure with plastic deformations of the staple under panel shear loading.

4.2. Seismic load

The building's mass for seismic performance assessment is determined by applying a vertical load that according to Eurocode combines various effects as defined in Eq. (10), where G_{kj} represents the characteristic value of the permanent load j, Q_{ki} denotes the characteristic value of the variable load i, and Ψ_{Ei} is the combination factor for the variable load i. In the non-linear static analysis, the vertical

Proceedings of the 3rd Croatian Conference on Earthquake Engineering - 3CroCEE
19–22 March 2025, Split, Croatia
Copyright © 2025 CroCEE
DOI: https://doi.org/10.5592/CO/3CroCEE.2025.133

load on each floor is uniformly distributed across the walls in both horizontal directions. The calculation of vertical loads includes the self-weight of the wall panels, assumed to be 3.0 kN/m³. For the seismic load combination, the total vertical load is considered as 2.7 kN/m² for the floors above the ground and first floors, and 1.7 kN/m² for the roof. The total weight calculated for the building analysis is 1.12 kN.

$$\sum G_{kj} \text{ "+" } \sum \psi_{Ei} Q_{ki} \qquad (10)$$

5. Results of the pushover analysis and comparison of the results

The analysis offers insight in the building deformation and damage mechanisms. In Figure 3, the wall panels lateral displacements in longitudinal (x) seismic loading direction are presented for two characteristic limit states, i.e. at first panel damage $d_{1.cr}$ and maximum shear resistance F_{max}, respectively. Furthermore, Figure 4 present the utilisation of the ultimate deformation capacity of individual walls, i.e. ration of achieved lateral displacements to ultimate available displacement capacity, for limit states at maximum shear resistance F_{max} and ultimate buildings deformation capacity d_u.both again for the critical longitudinal loading direction. All results are presented for analysis case with considered shear wall nonlinear behaviour according to experimental tests.

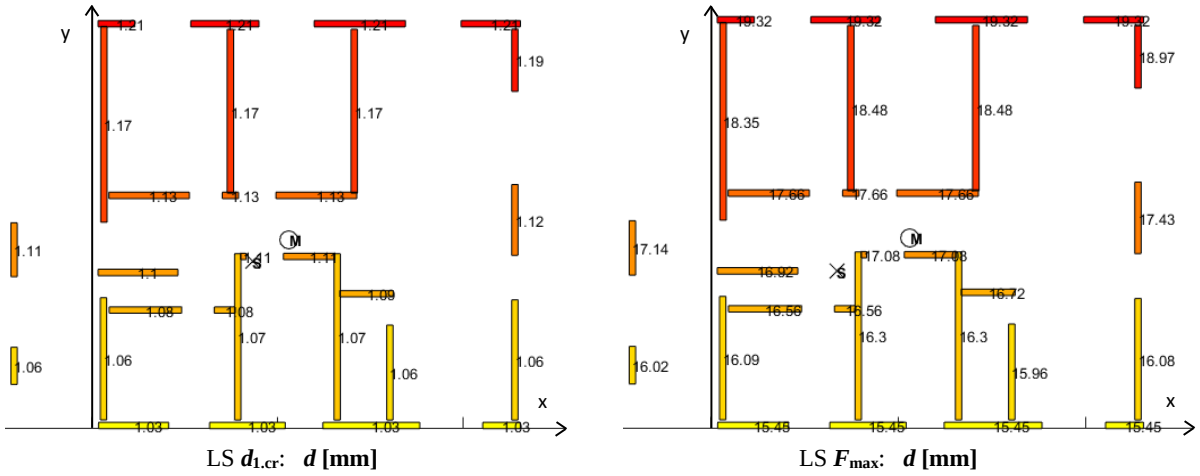


Figure 3: Walls displacements in characteristic limit states of obtained capacity curves in critical loading direction (x) at damage of the 1st panel pa $d_{1.cr}$ and maximum shear load-bearing resistance F_{max}.

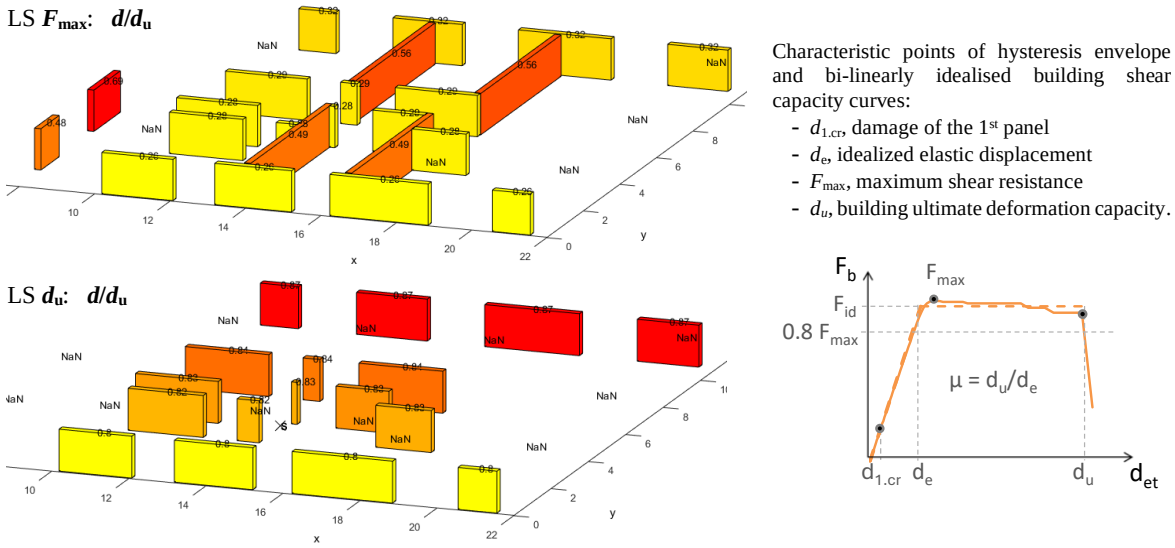


Figure 4: Walls' displacements to ultimate displacements ratio d/d_u in critical loading direction (x) for characteristic limit states at F_{max} and d_u of the building hysteresis envelope capacity curve.

Copyright © 2025 CroCEE
DOI: https://doi.org/10.5592/CO/3CroCEE.2025.133

Building global capacity curves, i.e. base shear force in dependence of lateral displacement of the mass centre, obtained for different panels' nonlinear shear behaviour model assumptions, are for the two directions of loading presented in Figure 5. The results clearly confirm the significant influence of the different assumptions and show, that the seismic loading in longitudinal (x) direction results in lower base shear capacity as well as in lower ultimate lateral displacements than the transversal (y) direction.

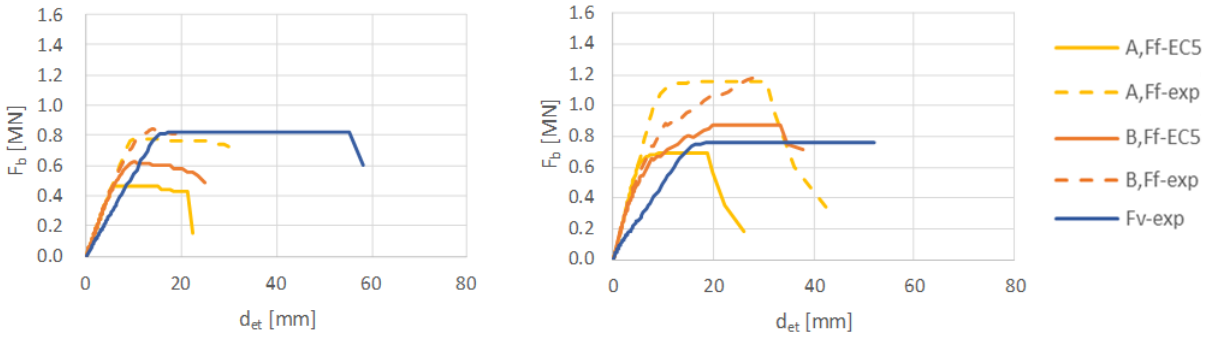


Figure 5: Pushover capacity curves obtained for x (left) and y (right) loading directions in analysis with different panel nonlinear shear behaviour assumptions.

To determine the more critical results in terms of chosen intensity measure, the results are idealised considering equal energy criteria of hysteresis envelope and bi-linearly idealised capacity curves. For all the conducted analyses the results are in terms of characteristic points of bi-linearly idealised curves (presented in Figure 4, right) summarised in Table 2. Furthermore, from the total shear capacity and ductility of the bi-linear capacity curves, the behaviour factors, denoted as $q_{,\mathrm{dej}}$, and the limit ground accelerations $a_{\mathrm{g,u}}$, that the structure can sustain in ultimate limit states, were calculated using the N2 method [6]. Since the assumed shape of the seismic loading is uniform, the participation factor for conversion of a multi-degree-of-freedom system to a single-degree-of-freedom system is equal to 1, and the ratio of the ductility μ to the behaviour factor $q_{,\mathrm{dej}}$ calculated according to Eq. (11), where T^* is the equivalent modal time period calculated from the seismic curves and the value of T_c adopted as specified in the EC8 standard. The values of the q_{dej} factors are given in Table 2, as well as $a_{\mathrm{g,u}}$ for the individual results of the response curves corresponding to the significant damage limit state ("SD"), which should according to the standards achieve the project ground acceleration for 475 year return period earthquake. It is according to EC8 evaluated as 3/4 of ultimate ("NC") displacement d_{u}.

$$q = (\mu - 1)\frac{\mathrm{T}^*}{T_C} + 1, T < T_C \qquad (11)$$

Table 2. Results of analyses - characteristic values of idealised seismic capacity curves

Assumed wall nonlinear shear response	F_{id} **[MN]**	d_{e} **[cm]**	T^* **[s]**	d_{u} **[cm]**	μ	$q_{\mathrm{dej,SD}}$	$a_{\mathrm{g,u}}$ **[g]**	F_{id} **[MN]**	d_{e} **[cm]**	T^* **[s]**	d_{u} **[cm]**	μ	$q_{\mathrm{dej,SD}}$	$a_{\mathrm{g,u}}$ **[g]**
	X direction							Y direction						
Meth. A, $F_{\mathrm{f,m,EC5}}$	0.45	5.09	0.227	21.5	4.23	1.82	0.29	0.68	5.49	0.192	19.9	3.63	1.55	0.38
Meth. A, $F_{\mathrm{f,m,EXP}}$	0.76	8.59	0.227	31.9	3.71	1.67	0.45	1.13	9.17	0.192	32.5	3.54	1.53	0.62
Meth. B, $F_{\mathrm{f,m,EC5}}$	0.58	6.56	0.227	24.4	3.72	1.68	0.34	0.79	6.41	0.192	37.9	5.91	2.10	0.60
Meth. B, $F_{\mathrm{f,m,EXP}}$	0.78	8.79	0.227	32.1	3.65	1.66	0.46	1.06	8.58	0.192	50.7	5.91	2.10	0.80
Experimental	0.81	14.8	0.289	57.4	3.88	1.92	0.55	0.71	9.30	0.244	52.0	5.59	2.30	0.58

Comment: the values of μ refer to d_{u} (Figure 4) and the "NC" limit state, respectively, and $q_{\mathrm{dej,SD}}$ and $a_{\mathrm{g,u}}$ are calculated for the "SD" limit state according to the N2 method.

Copyright © 2025 CroCEE
DOI: https://doi.org/10.5592/CO/3CroCEE.2025.133

For the analyzed building, assuming analytical models for panel behavior, the longitudinal (x) direction is found to be critical in terms of shear resistance capacity across all analyses. In contrast, when experimentally obtained panel behavior is considered, the transverse (y) direction becomes critical, although the difference in capacity between the two directions is relatively minor.

Regarding the limiting accelerations the structure can withstand $a_{g,u}$, the x-direction remains the critical direction for all assumed panel behavior models. However, the difference in performance between the two directions is very small under experimental assumptions. This is primarily due to the greater ductility observed in the y-direction compared to the x-direction in the experimental model, as well as the smaller stiffness difference between the two directions compared to analytical assumptions based on Methods A and B or literature-based stiffness models.

Furthermore, the y-direction exhibits notably higher ductility in the experimental model and when using the Method B panel behavior model, whereas this trend is not necessarily observed in the Method A model.

These findings highlight the influence of panel behavior assumptions on the building's seismic response showing how different combinations of stiffness, base shear resistance capacity and deformation capacity yield various behaviour factors and peak ground accelerations that the building can sustain. Furthermore, the calculated behaviour factors are in fact lower than the ones assumed according to the EC8 for the type of panel, since they are for critical direction in all cases lower than 2.0. This presents a challenge for the EC8 guidelines regarding certain other panel types, as the analysis presented here assumes a relatively high ductility value of 4 for the panels.

6. Conclusions

This study presents a simplified and conservative nonlinear static analysis using a modified POR method, applied to a real timber building constructed with light frame timber wall panels type tested in the preceding experimental campaign. The goal was to assess how different assumptions about panel shear behaviour affect the building's nonlinear seismic response. Three modelling approaches were used: one based on experimental shear tests and two analytical models following Eurocode 5 (EC5). These models accounted also for different stapled connections load-bearing capacity assumptions, directly impacting panels' shear capacity.

The results revealed significant differences in the building's seismic resistance depending on the assumed panel behaviour, highlighting the sensitivity of the analysis to shear capacity and stiffness assumptions. This underscores the need for clear and standardized guidelines for assessing the seismic performance of light frame timber buildings, as current standards like Eurocode 8 (EC8) lack more detail information on which assumptions to adopt for such systems in the analysis.

Key research gaps include the method's limited suitability for multi-storey buildings, simplifications in modelling wall shear stiffness, and the assumption of rigid diaphragms, which may not reflect real structural behaviour. Additionally, the assumed ductility may overestimate safety without broader experimental validation. Addressing these gaps through experimental tests, refined modelling and improved design standards is essential for the reliable seismic design of timber structures.

Acknowledgements

The development of the method and numerical research was financially supported by the Slovenian Research and Innovation Agency (ARIS) through Research Core Funding No. P2-0273. The preceding experimental tests and their analyses were funded under Project No. C3330-19-952045 "Raziskovalci-2.1-ZAG-952045" and "Operational Programme TIGR4smart", both co-financed by the Republic of Slovenia, Ministry of Education, Science and Sport, and the European Regional Development Fund through the EU Cohesion Policy 2014-2020. The valuable contribution of Lucija Balant in conducting parametric numerical analyses is sincerely acknowledged and greatly appreciated.

Copyright © 2025 CroCEE
DOI: https://doi.org/10.5592/CO/3CroCEE.2025.133

Special thanks are also extended to Jelovica Hiše for motivation and support in the development of this study, generously providing the building design plans.

References

[1] "EN 1998-1:2005: Eurocode 8: Design of structures for earthquake resistance - Part 1: General rules, seismic actions and rules for buildings," 2005.

[2] M. Kržan, T. Pazlar, and B. Ber, "Improved seismic response of light-frame-timber panels with cement-particle-board sheathing of various thicknesses and different configurations of fasteners," *Eng. Struct.*, vol. 253, p. 113757, 2022, doi: https://doi.org/10.1016/j.engstruct.2021.113757.

[3] "EN 1995-1-1:2004: Eurocode 5: Design of timber structures - Part 1-1: General - Common rules and rules for buildings," 2004, *CEN*.

[4] M. Tomazevic, "The computer program POR: institute for testing and research in materials and structures-ZRMK," *Ljubl. Slov.*, 1978.

[5] B. Källsner and U. A. Girhammar, "Plastic models for analysis of fully anchored light-frame timber shear walls," *Eng. Struct.*, vol. 31, no. 9, pp. 2171–2181, 2009, doi: https://doi.org/10.1016/j.engstruct.2009.03.023.

[6] P. Fajfar, "A Nonlinear Analysis Method for Performance-Based Seismic Design," *Earthq. Spectra*, vol. 16, no. 3, pp. 573–592, 2000, doi: 10.1193/1.1586128.

Proceedings of the 3rd Croatian Conference on Earthquake Engineering - 3CroCEE
19–22 March 2025, Split, Croatia
Copyright © 2025 CroCEE
DOI: https://doi.org/10.5592/CO/3CroCEE.2025.135

ENGINEERING ANALYSIS OF A TYPICAL PRE-CODE URM BUILDING IN ZAGREB

Kenan Omerović [(1)], Mario Uroš [(2)], Senad Medić [(3)]

[(1)] *Mag.ing.aedif., INFRA Ltd, kenan.omerovic@infra.ba*
[(2)] *Associate professor, University of Zagreb – Faculty of Civil Engineering, mario.uros@grad.unizg.hr*
[(3)] *Associate professor, University of Sarajevo – Faculty of Civil Engineering, senad.medic@gf.unsa.ba*

Abstract

This paper evaluates the seismic resistance and vulnerability of an existing unreinforced masonry (URM) building in Zagreb's Folnegovićevo neighborhood. The building with potentially low seismic resistance was erected in the 60s, a period characterized by the introduction of the first seismic code in practice. It has a rectangular plan 36.9 m x 10.7 m and consists of a basement, a ground floor and four floors totaling 17 m in height. The solid brick walls with variable thickness are evenly distributed in both directions and they run continuously from the foundation to the top. The reinforced concrete slabs are 14 cm thick rigid diaphragms made of MB 20 concrete class with smooth rebars GA 240/360.Two structural variants were analyzed: one with reinforced tie-beams and one without. Equivalent Static Analysis was conducted manually and, a Time-History Linear Dynamic Analysis was performed with the Tower Radimpex software for preliminary assessment. This method provided a basic assessment of the building's seismic resistance, while also comparing manual and numerical results. Two advanced methods, Nonlinear Time-History Analysis (NLTH) and Pushover Analysis, were conducted with Diana FEA software employing Engineering masonry constitutive law to describe the highly nonlinear behaviour of masonry walls which can crush, crack, or fail in shear. NLTH simulated the building's response to the 2020 earthquake, identifying critical structural components and potential damage. The Pushover Analysis evaluated how the building responded to increasing lateral loads, focusing on seismic resilience and collapse mechanisms. This research provides an in-depth comparison of different analytical approaches, contributing to the methodology for assessing and strengthening existing buildings. Conclusions drawn from these analyses emphasize recommendations for modifications to improve structural performance and safety.

Keywords: pre-code URM building, macro-modeling, equivalent static analysis, NLTH

1. Introduction

The city of Zagreb, Croatia, experienced a strong earthquake on March 22, 2020, with an initial magnitude of 5.5 on the Richter scale. Within a little over 24 hours after the initial earthquake, the region of Zagreb recorded a total of 57 additional seismic events. These ground tremors resulted in extensive and significant damage to existing masonry structures in Zagreb. In order to assess earthquake response, static and dynamic analyses are conducted for an existing residential building located in the Folnegovićevo neighborhood in Zagreb, selected as a structure with potentially low seismic resistance. The analysis of the current state of the residential building was based on a review of documentation from the State Archive in Zagreb. This review revealed that, according to the development program for the Folnegovićevo, Trnsko, and Selska Street neighborhoods, standard designs for four-story blocks with low and high ground floors were created in 1960. Three standard units were designed—types A, B, and C—which allowed for the combination of multiple units.

As a consequence of the catastrophic earthquake in Skopje in 1963, the 1964 Provisional Technical Regulations for Construction in Seismic Areas were introduced. These regulations brought the first national seismic map with seismic zones ranging from VI to IX based on the Mercalli-Cancani-Sieberg scale, derived from the 1950 version. According to this map, the residential building is located in the IX seismic zone [1].

Proceedings of the 3rd Croatian Conference on Earthquake Engineering - 3CroCEE
19–22 March 2025, Split, Croatia
Copyright © 2025 CroCEE
DOI: https://doi.org/10.5592/CO/3CroCEE.2025.135

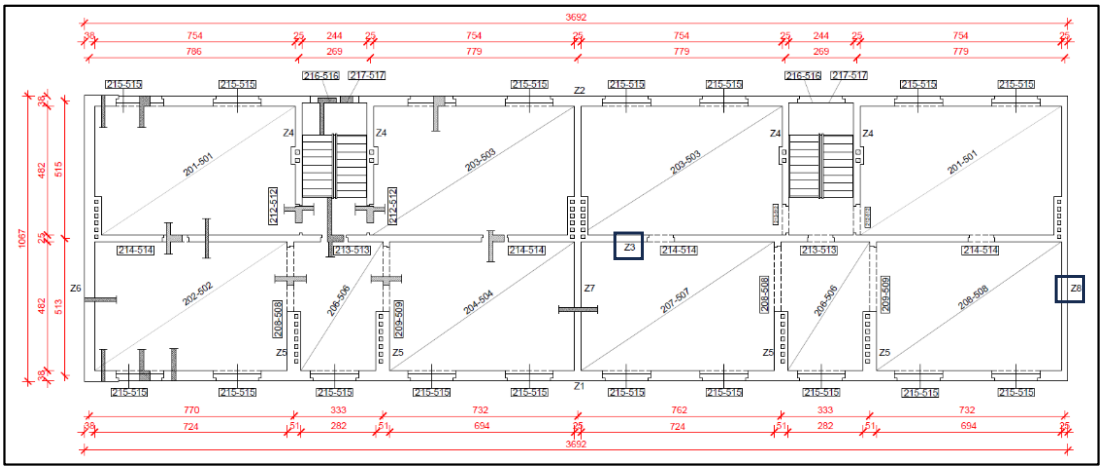
Residential buildings of the Bartolić type were designed in 1960 and were not planned in accordance with the Regulation on Provisional Technical Standards for Construction in Seismic Areas. A review of documentation from the State Archives in Zagreb revealed that most of these buildings were under construction at the time the new regulations were adopted. In 1964, a commission for the technical inspection of buildings was established. A series of structural measures aimed at strengthening residential buildings against earthquake forces were introduced, focusing on the construction of vertical reinforced concrete ties (columns and ring beams) and the connection of load-bearing walls with horizontal reinforced concrete ring beams.

Based on the documentation from the State Archives in Zagreb, it was determined that, as a result of these structural measures, some buildings were constructed with ring beams, while others were not. For this reason, this study will analyze a building in which, in one case, the vertical load-bearing system for resisting seismic forces consists of masonry without ring beams, and in the other case, masonry bounded by ring beams.

1.1. Building description

The building was designed in 1960 and consists of a basement, ground floor, and four upper floors. The residential building has a rectangular floor plan with maximum dimensions of 36.9 m x 10.7 m, and the total floor area of one story is 394.8 m². The height of the basement is 2.56 m, while the height of the other floors is 2.66 m each. The total height of the building is 17 m. The roof is flat and designed as an inaccessible terrace with rolled gravel, thermal insulation, and water proofing.

a)



b)

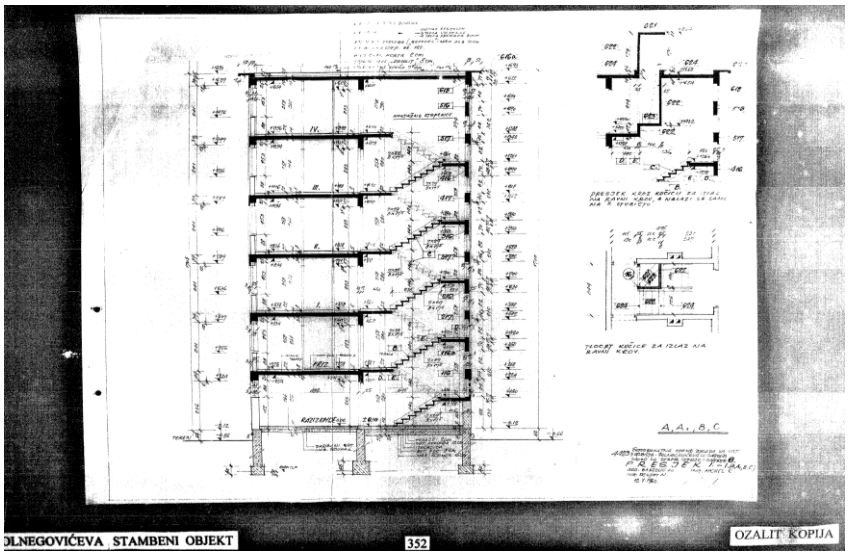


Figure 1. a) Building plan; b) Cross – section (State Archive in Zagreb).

Copyright © 2025 CroCEE
DOI: https://doi.org/10.5592/CO/3CroCEE.2025.135

The structure consists of interconnected solid brick walls evenly distributed in both directions. The exterior load-bearing walls in the basement are 38 cm thick and made of brick, while the central wall is 25 cm thick and made of concrete (MB-110). Load-bearing walls in the ground floor and upper floors are made of brick, with brick grades and mortars specified for each floor according to the structural calculations. One external load-bearing wall is 25 cm thick (in the shorter direction), while the other external load-bearing walls are 38 cm thick. The thickness of the internal load-bearing walls is 25 cm. Based on the test data for solid bricks conducted by the IGH Institute Zagreb, it was determined that the bricks correspond to grade M15. The project specifies that the mortar should have a volumetric ratio of 1:2:6 = cement:lime:sand, which approximately corresponds to mortar grade M5. If no experimental data are available, the characteristic compressive strength of masonry constructed with general-purpose mortar can be determined using empirical formulas.

All load-bearing walls run continuously from the foundation to the top of the building, ensuring that the structure meets vertical regularity criteria. The share of the surface area of lateral load-bearing walls in the total gross floor area of the building's floor plan for the X direction is 5.58 % (4.96 % in Y).

Partition walls are made of hollow Troskanit blocks with a thickness of 15 cm. The staircase wall is 25 cm thick. Window lintels in the basement and upper floors are monolithic, while door lintels are prefabricated. The stairs are prefabricated, supported by beams in the stair landing, which is the same height as the landing.

The floor structure is constructed as a 14 cm thick reinforced concrete slab, which can be considered an axially rigid diaphragm, meaning deformations at the ceiling level can be neglected. The structure is made of concrete (MB 20) and reinforcement steel (smooth bars GA 240/300). The floor structure is directly supported on the brick walls but is not adequately connected to the walls to allow for proper distribution of seismic forces across individual walls or to prevent separation during seismic events.

2. Modeling strategies for masonry

Masonry is a composite material that consists of units and mortar. While experimental investigations are crucial for understanding the structural behavior of masonry, numerical modeling serves as a valuable complement, offering additional insights. Masonry structures are typically analyzed using finite element methods (FEM), and computational strategies are traditionally classified into three categories based on the level of detail: micro-, meso-, and macro-modeling techniques. Another group of modeling approaches includes the discrete element method (DEM) and hybrid methods combining finite and discrete elements (FEM/DEM). The equivalent frame (macro-element) approach is specifically designed for analyzing masonry panels and piers. No single modeling strategy can be universally preferred, as each is suited to different applications.

2.1. Micro-modeling

Micro-modeling, a detailed approach to analyzing masonry, aims to represent all the constitutive elements of a masonry structure, including units, mortar, and the unit/mortar interface. In this method, mortar and brick units are discretized using continuum elements with corresponding failure criteria, while interface elements between the mortar and units introduce discontinuities in the displacement field to account for potential cracking. However, due to its complexity, micro-modeling is rarely employed.

This method is most suitable for analyzing small structural elements, particularly when there is a need to investigate strongly heterogeneous stress and strain states to gain deeper insight into local behavior [2]. The primary goal of micro-modeling is to accurately represent masonry by incorporating the properties of each constituent and their interactions. The required experimental data must be derived from laboratory tests conducted on the individual components and small masonry samples.

Proceedings of the 3rd Croatian Conference on Earthquake Engineering - 3CroCEE
19–22 March 2025, Split, Croatia
Copyright © 2025 CroCEE
DOI: https://doi.org/10.5592/CO/3CroCEE.2025.135

2.2. Meso-modeling

In meso-modeling, wall geometry is slightly simplified by homogenizing the mortar joints and mortar-brick contact into a single discontinuous interface element, while the brick units are expanded to maintain the overall geometry. Masonry is treated as an assembly of bricks connected by potential fracture or slip lines at the joints. Additionally, an interface can be added at the midpoint of each brick to account for potential cracking.

This approach omits the Poisson effect of mortar, which generates biaxial tension in the brick units, limiting the model's ability to capture all possible failure modes [3].

2.3. Macro-modeling

Macro-modeling is suitable for structures composed of solid walls with sufficiently large dimensions, where stresses and strains can be averaged over a macro-length. In large-scale, practice-oriented analyses, the interaction between units and mortar is typically negligible for the overall structural behavior. These models approximate a heterogeneous masonry wall as a single, uniform material, with discretization independent of the brick layout—units, mortar, and the unit-mortar interface are effectively smeared into a continuum. This phenomenological approach requires material properties to be derived from tests on masonry samples of sufficient size under homogeneous stress conditions. A comprehensive macro-model must account for orthotropic behavior, incorporating different compressive and tensile strengths along material axes and distinct inelastic behaviors for each axis. However, the complexity of introducing orthotropic properties means that only a few macro-models have been developed.

Macro-modeling is practice-oriented, offering reduced computational time and memory requirements and simplified mesh generation [4,5, 6, 7]. It is particularly valuable when a balance between accuracy and efficiency is necessary. Nevertheless, capturing the complex failure mechanisms of masonry walls remains challenging, as various failure modes can occur independently or in combination. Numerical issues may arise in cases of strong localization with prominent macro-cracks. In macro-models, cracking is smeared across a characteristic length, which does not accurately reflect real conditions.

In this paper Engineering Masonry model is used for nonlinear modeling of masonry behavior in DIANA [8, 9]. The model has been proposed by DIANA FEA and the Technical University of Delft to evaluate the building masonry stock after a series of earthquakes caused by gas extraction in the Groningen area [10]. Engineering Masonry model is an orthotropic total-strain continuum model with smeared cracking and it can be used with membrane or shell elements. The model is capable of simulating compression, tensile and shear failure modes and it can crack in the X-horizontal bed joint, the Y-vertical head-joint as well as diagonally in the form of staircase. In comparison with the Total Strain Crack model [8], the Engineering Masonry model defines unloading behavior in compression more realistically by assuming combined damage-plasticity model. Coulomb friction failure criterion is included to model typical shear failure. The tensile behavior is defined by linear loading and softening curves.

2.4. Discrete modeling

When significant geometric and material nonlinearity arises in masonry structures, such as fracturing or crushing, finite element methods (FEM) can struggle to accurately account for material damage and discontinuity. To address these challenges, the discrete element method (DEM) offers an alternative approach, modeling fragmentation by representing the medium as an assembly of discrete elements [11]. The DEM model requires relatively few material properties, as the complexity of its response stems from the collective behavior of simple individual elements. While the elements themselves are generally linear elastic, their overall behavior can exhibit nonlinearity, dilation related to mean stress, transitions from brittle to ductile behavior, hysteresis, and more. Additionally, DEM inherently captures phenomena such as localization (e.g., fractures in brittle solids or shear bands in granular materials), which can pose challenges for mesh-based models. However, a key limitation of the discrete approach

Copyright © 2025 CroCEE
DOI: https://doi.org/10.5592/CO/3CroCEE.2025.135

lies in determining the required material properties, such as normal and shear stiffness, damping coefficients, and interparticle bonds. These parameters can only be established through macroscopic experiments, where input values are calibrated against experimental results.

A method which combines finite element and discrete element method is called FEM/DEM [12, 13, 14]. The method uses advantages of both approaches. Namely, the fragmentation process (strong discontinuity between elements) is modeled employing DEM, and the deformation in the element inside is modeled using FEM.

3. Analysis

The structure does not meet the criteria for regularity in the floor plan, as it has unevenly distributed openings and the mass is not symmetrically distributed relative to the horizontal axis. Additionally, not all gable walls are symmetrically positioned with respect to the vertical axis. The result of these asymmetries is eccentricity, which represents the distance between the center of mass and the center of rigidity (Fig. 2).

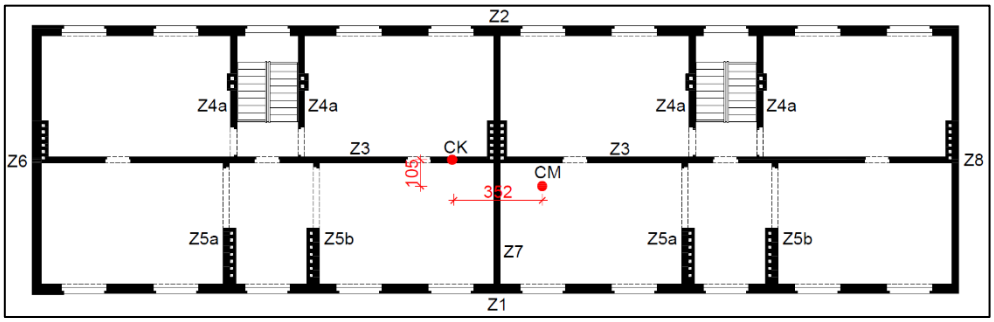


Figure 2. Center of mass (CM) and center of rigidity (CK).

Based on the seismic hazard map of the Republic of Croatia, the value of the reference peak ground acceleration (PGA) for a return period of 475 years was determined. For the residential building located in the Folnegovićevo neighborhood, the reference value is a_{gR} = 0.243g. The identification of the soil for the residential building cannot be determined with certainty, but soil category C has been selected, with a description and parameter values typical for this area.

The behavior factor *q* is an approximation of the ratio between the seismic forces that would act on the structure if its response were fully elastic with 5% relative viscous damping and the forces that can be used in the analysis with a conventional linear elastic model while still ensuring a satisfactory structural response. The ductility of the structure, which enables the dissipation of energy introduced by the earthquake, is accounted for using the behavior factor q = 1.5.

The methods for analysis of structures exposed to seismic action include:

- Linear methods (calculation using the equivalent static method and the response spectrum method)
- Nonlinear static analysis using the pushover method
- Linear and nonlinear dynamic analysis using earthquake accelerograms

Although linear analysis methods are permitted for the assessment of existing masonry buildings, preference is given to nonlinear analysis. Such analysis can be conducted using one of the previously mentioned approaches to structural modeling. The pushover method can also be applied to a detailed model. The choice depends on the capabilities of the numerical model and the assumptions made during its creation. Additionally, simple methods that provide a qualitative understanding of structural behavior are desirable, along with verification of the prescribed methods. One such method is checking the total surface area of load-bearing walls. However, this cannot be used to assess the building's overall load-bearing capacity. Verification is carried out based on limit state criteria for each component as well as

Proceedings of the 3rd Croatian Conference on Earthquake Engineering - 3CroCEE
19–22 March 2025, Split, Croatia
Copyright © 2025 CroCEE
DOI: https://doi.org/10.5592/CO/3CroCEE.2025.135

at the global level. This means that a specific limit state is not satisfied if even one component fails to meet the criteria. Furthermore, an engineering assessment is required to ensure that a less significant element does not limit the load-bearing capacity of the entire building [15].

Linear elastic analysis for existing masonry buildings should be used with great caution. This is not only due to the difficulty in reliably estimating the behavior factor q but also because of the material properties and the distribution of sectional forces within the structure. Masonry elements have very low tensile strength, and the limit stress exceedance occurs even under small loads. Additionally, stress concentrations and singularities arise that are not realistic, meaning the stress values obtained through linear analysis are highly dependent on the density of the finite element mesh. Since linear analysis does not account for stress and force redistribution, an unrealistic force flow within the structure may be obtained, along with inaccurate sectional forces. For these reasons, linear elastic analysis is used primarily for preliminary assessments and should generally be avoided for detailed analysis of existing masonry structures.

When nonlinear methods are used for structural analysis, the force distribution varies in comparison to linear analysis [16]. This difference arises from the varying load-bearing capacities of walls, influenced by axial forces and bending moments. In nonlinear analysis, forces are distributed based on capacity as a function of displacement, while in linear analysis, force distribution is based on stiffness, independent of displacement magnitude.

In verifying the structure using linear elastic methods, if one load-bearing element exceeds its capacity, the limit state is not satisfied. An engineering assessment of the element's impact on the overall structural behavior and the building's global performance is necessary. Additionally, attention should be paid to the robustness of the structural system, ensuring that any potential load redistribution can relieve the overstressed element.

3.1. Equivalent static method

The equivalent static method (ESM) is the oldest and simplest procedure for calculating the seismic response of structures suitable also for "hand calculations". It assumes that the building predominantly responds in its fundamental mode, and the effect of ground motion is represented by horizontal static forces applied at the floor levels, i.e., at points where the largest masses are concentrated. The entire structure can be represented as an equivalent cantilever beam. It can be conditionally stated that the cross-section of this equivalent cantilever beam corresponds to the building's floor plan. For buildings up to 40 m the fundamental period T_1 can be approximated by Eq. 1 which yields $T_1 = 0.41$ s (plateau of the response spectrum):

$$T_1 = C_t \cdot H^{3/4} \tag{1}$$

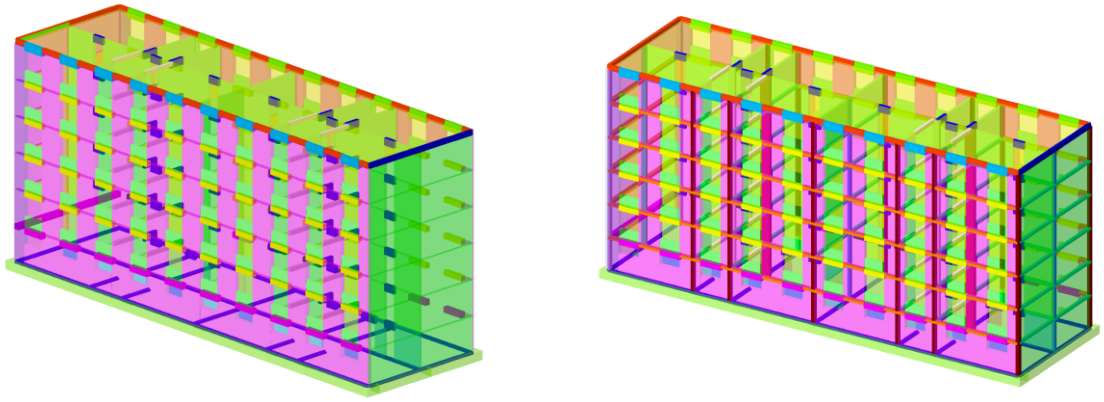
After distributing seismic forces on walls, the largest shear force acts on Z3d in X direction ($V_x = 913$ kN) and Z8 in Y direction ($V_y = 2738$ kN). Both walls fail to comply with load-bearing requirements for shear and bending implying damage in case of stronger ground motions.

The same ESM was applied in commercial software Tower 8 [17] assuming that the build has or has not tie beams (tie columns) (Fig. 3). Although regulations currently do not prohibit the use of this method, it cannot fully provide a high-quality analysis for seismic retrofitting. Masonry is a highly nonlinear material, and its stiffness under cyclic loading is not easily defined. In linear analysis, there is no redistribution of stresses and forces, resulting in an unrealistic flow of forces in the structure and, consequently, inaccurate internal forces. For these reasons, linear analysis should be used with caution. Modes of vibration are shown in Fig. 4. The first eigen-mode is translation in shorter transverse direction (Y) with $f_1 = 3.1$ Hz ($f_{1c} = 3.5$ Hz for the confined model), the second mode is translation in longitudinal direction (X) with $f_2 = 3.8$ Hz ($f_{2c} = 3.9$ Hz) and the third mode pertains to torsion with $f_3 = 4.2$ Hz ($f_{3c} = 4.6$ Hz) (Fig. 4).

The relevant sectional forces in the analyzed walls for the unconfined model amount to $V_x = 889$ kN (Z3d in X) and $V_y = 2469$ kN (Z8 in Y) which is almost equal to the "hand calculation". The confined

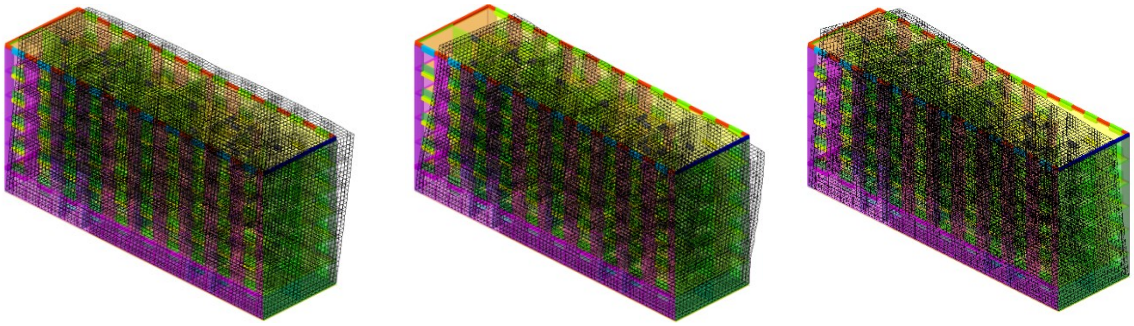
Copyright © 2025 CroCEE
DOI: https://doi.org/10.5592/CO/3CroCEE.2025.135

model yields reduced values V_x = 514 kN and V_y = 1482 kN which is attributed to the larger behaviour factor q = 2.5.



a) b)

Figure 3. 3D model of the building: a) w/o tie beams (columns), b) with confinement.



a) b) c)

Figure 4. Eigen-modes of the building: a) translation in Y, b) translation in X, c) torsion.

3.2. Linear time history analysis

The linear time history analysis was performed using the earthquake record from the Zagreb event on March 20, 2020 (Fig. 5). Accelerations were applied simultaneously in the X and Y directions, with a maximum acceleration of 2.196 m/s² in the N-S direction and 1.769 m/s² in the E-W direction, over a duration of 8 seconds with an integration time step of 0.01 seconds.

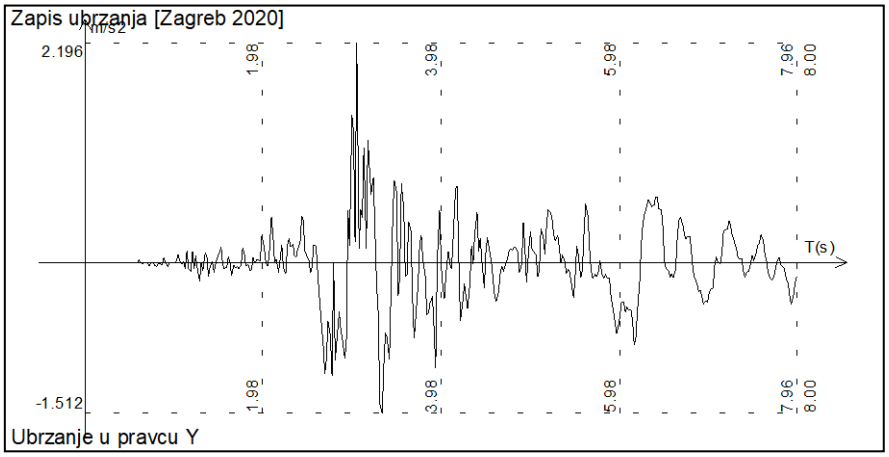


Figure 5. Acceleration record (N-S component) of Zagreb event.

Copyright © 2025 CroCEE
DOI: https://doi.org/10.5592/CO/3CroCEE.2025.135

The displacement history of the center of mass (CM) at the top of the building is shown in Fig. 6. For the building without tie-beams/columns, the maximum displacement of CM in Y direction is $u_{max,y}$ = 6.58 mm (approximately H/2500, where the building height above the basement is H = 16.7 m) at $\ddot{u}_g$ = 2.196 m/s^2. For the confined building, the corresponding displacement is $u_{max,y}$ = 5.4 mm. The maximum shear forces for the unconfined building are V_x = 342 kN and V_y = 600 kN which are three to four times smaller than those obtained from ESM.

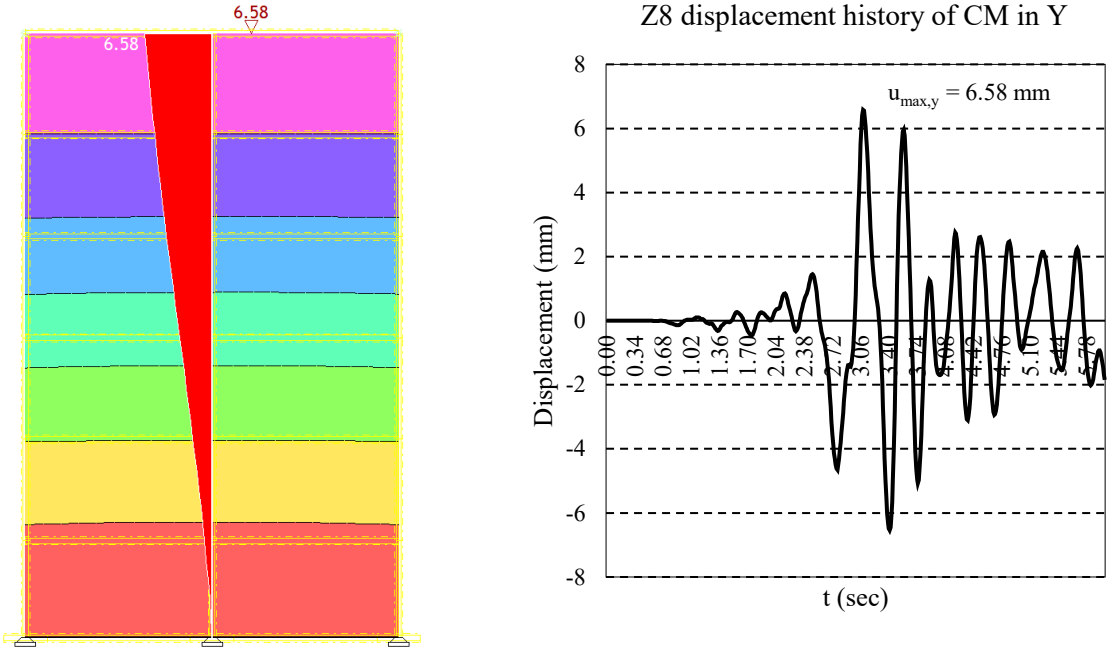


Figure 6. Displacements in Y direction: a) maximum displacement of the CM for $\ddot{u}_g$ = 2.196 m/s^2, b) history of displacements of CM at the top of the building.

3.3.Nonlinear time history analysis

Nonlinear analysis was performed using DIANA. Engineering masonry constitutive model was employed was description of walls and the material parameters are listed in Tabel 1. Results of modal analysis are in excellent agreement with the previously shown model. Displacement history of the center of mass at the top of the building is shown in Fig. 7. The maximum displacement for the unconfined model equals to 13.2 mm (11.5 mm for the confined model) which is almost double the displacement obtained from the linear elastic THA. Interstory drifts are provided in Fig. 8 where it can be noticed that structural performance is far better than required by EC 8 or FEMA 356 for the Life-Safety Level. Number of cracks in integration point and crack widths are shown in Fig. 9. Crack widths of 3 mm and higher occur only locally, while the rest of the walls generally sustains the crack widths of 0.5 mm.

Table 1 – Parameters of the engineering masonry model for the analyzed building

Parameter	Value	Parameter	Value	Parameter	Value
E_x	3000 MPa	G_{ft}	10 N/m	G_{fs}	20 N/m
E_y	3000 MPa	HEADTP	NO	f_c	4,9 MPa
G_{xy}	1200 MPa	h	Rots	n	4
ρ	1600 kg/m^3	c	0,2 MPa	G_c	17000 N/m
f_{tx}	0,15 MPa	ϕ	32 °	λ	1

Copyright © 2025 CroCEE
DOI: https://doi.org/10.5592/CO/3CroCEE.2025.135

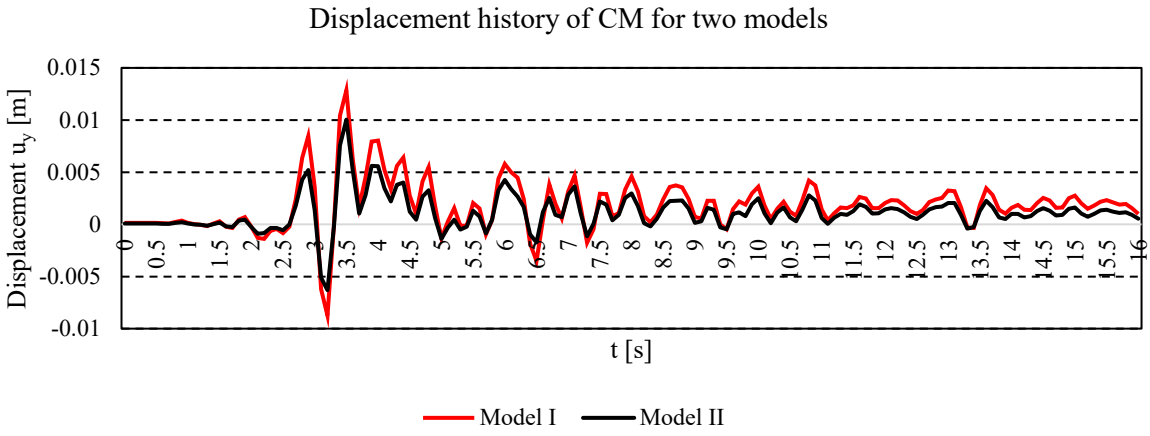


Figure 7. History of displacements of CM at the top of the building.

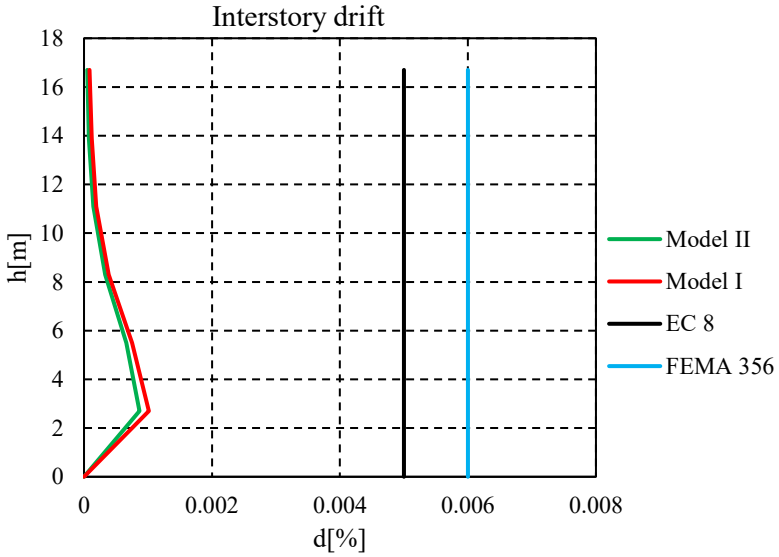
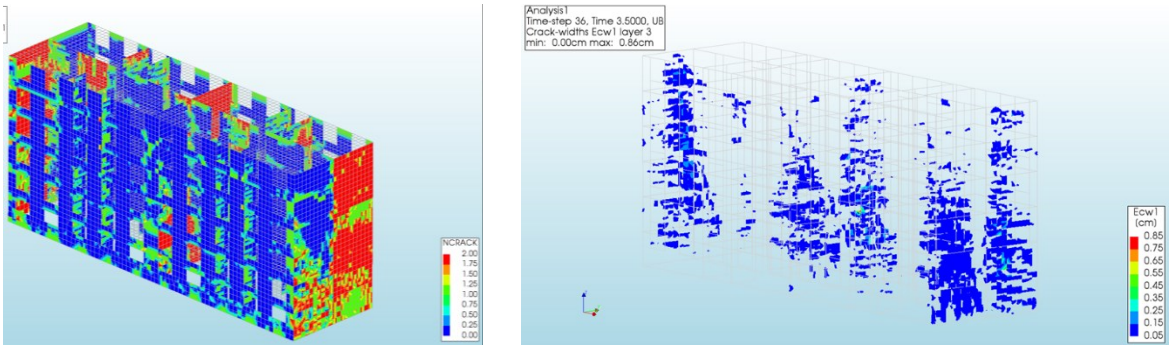


Figure 8. Interstory drifts for the analyzed building.



a) b)

Figure 9. Cracking parameters: a) NCRACK – number of cracks in integration point, b) crack width

3.4. Pushover analysis

The pushover analysis is a nonlinear static procedure where the lateral load on a structure increases monotonically until failure, while the load distribution remains constant. The load is applied in a

Copyright © 2025 CroCEE
DOI: https://doi.org/10.5592/CO/3CroCEE.2025.135

predefined pattern, typically following the fundamental mode from elastic analysis. The relationship between the control node displacement (usually at the building's roof center of mass) and the base shear is plotted as a capacity curve (pushover curve). Fig. 10 presents pushover curves for two different models, showing base shear versus center-of-mass displacement. As expected, Model I, without confinement, exhibits lower stiffness and load-bearing capacity. Pushover analysis (PO) is a static method, whereas nonlinear time history (NLTH) analysis is dynamic and better represents seismic loading. Therefore, NLTH should be considered the reference, with the structural state from PO evaluated at the maximum displacement obtained from NLTH. While their overall behavior is expected to be similar, comparing PO and NLTH should focus on global response rather than direct results. This approach helps identify critical failure locations, determine failure causes, and provide insight into the structural response. Crack strains pertaining to opening (left) and crushing (right) of the gable wall Z8 are shown in Fig. 11.

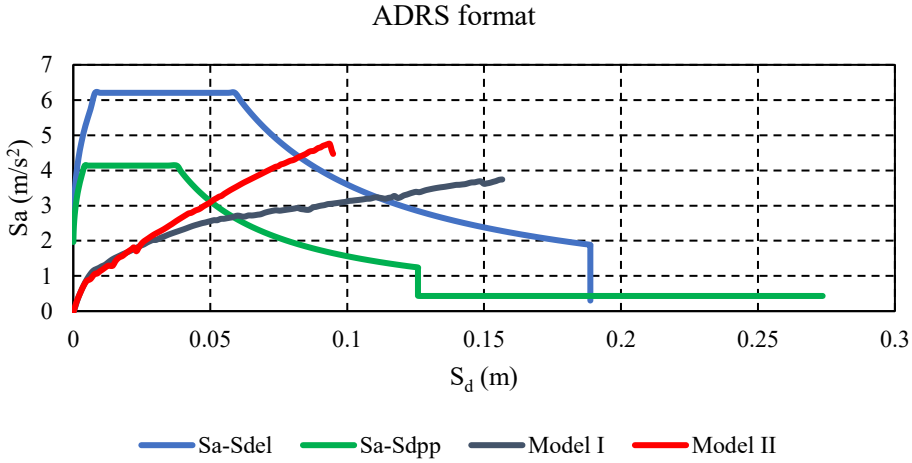


Figure 10. Pushover curves in ADRS format.

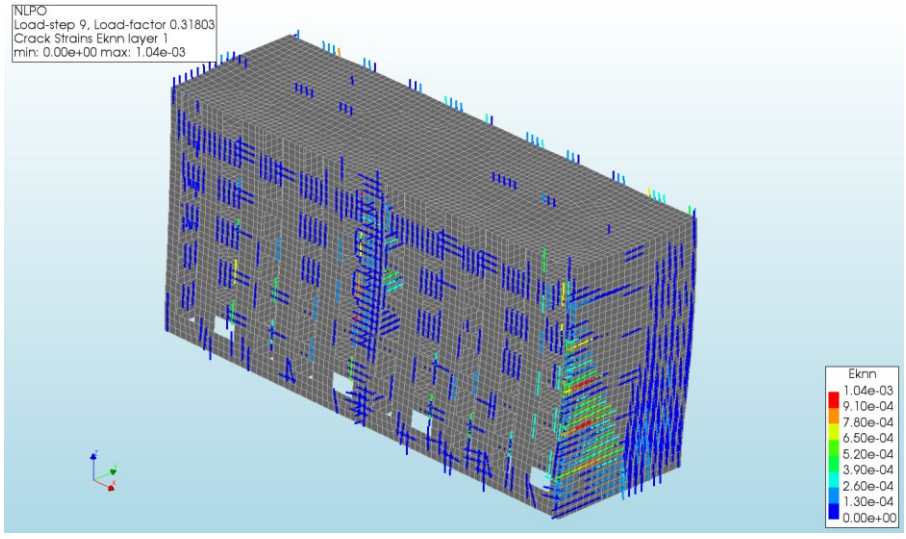


Figure 11. Crack strains in pushover analysis.

4. Damage categorization

To assess structural damage, engineers determine the damage severity (DS) level and evaluate its extent separately for each load-bearing direction. Based on this, the building's overall usability is assessed. Engineers rely on professional judgment, supported by guidelines, criteria, and reference photographs. The initial post-earthquake inspection template was based on Italian experiences. After the Zagreb

Proceedings of the 3rd Croatian Conference on Earthquake Engineering - 3CroCEE
19–22 March 2025, Split, Croatia
Copyright © 2025 CroCEE
DOI: https://doi.org/10.5592/CO/3CroCEE.2025.135

earthquake, engineers struggled to classify buildings with damage levels II and III, similar to challenges in Italy. To improve assessments, additional criteria from Greek methodologies were introduced, providing clearer guidance on crack characteristics and their impact on usability, especially for masonry and reinforced concrete buildings. When categorizing damage, it is crucial to assess whether the building, despite reduced resistance, can withstand another earthquake of similar intensity.

The most widely referenced classification for damage assessment and building usability evaluations is based on the EMS-98 (European Macroseismic Scale), commonly used to determine earthquake intensity [18]. Masonry buildings exhibit significant structural diversity due to variations in materials, construction methods, and structural elements. Key factors to consider include wall condition, floor structure, arches, vaults, roof properties, and hazardous non-structural elements [15].

Considering crack types and maximum widths, Model I (8.5 mm in Y, 4.53 mm in X) aligns with damage level III, while Model II (6.7 mm in Y, 2.61 mm in X) corresponds to damage level II under EMS-98.

5. Conclusion

The conclusions of this study highlight key insights into the seismic performance of a typical pre-code unreinforced masonry (URM) building in Zagreb and offer recommendations for future assessments and retrofitting. Linear elastic analysis, while useful for preliminary assessments, tends to be overly conservative. It often predicts failure at force levels far below the actual capacity of the structure due to the inability to account for stress redistribution and plastic deformations. Because masonry has low tensile strength, this method frequently results in unrealistic stress concentrations, making it unreliable for detailed seismic evaluations.

Nonlinear analysis methods, such as Nonlinear Time-History Analysis (NLTH) and Pushover Analysis, provide a much more accurate representation of structural behavior under seismic loads. These approaches allow for stress redistribution, capturing the effects of material degradation, plasticity, and progressive damage, thereby offering a more realistic assessment of seismic performance. The study compared two structural configurations: an unconfined masonry model without tie beams and a confined model with tie beams. The unconfined model exhibited higher displacement and concentrated damage in specific areas, making it more vulnerable to shear and bending failures during strong ground motions. On the other hand, the confined model demonstrated better seismic performance by reducing displacement, improving force distribution, and increasing ductility, making it more compliant with modern seismic safety standards.

To classify the extent of damage, the study referenced the European Macroseismic Scale (EMS-98). The unconfined model aligned with Damage Level III, indicating moderate to substantial structural damage, while the confined model was categorized as Damage Level II, suggesting moderate damage but still being structurally usable with appropriate repairs. The study also incorporated damage classification methodologies from Greece and Italy to enhance accuracy in post-earthquake assessments.

Based on the findings, several retrofitting strategies are recommended to improve seismic resilience. The addition of horizontal and vertical tie beams can significantly enhance the building's ductility, reducing the risk of sudden failure. Strengthening connections between floor slabs and walls would improve overall force distribution, while reinforcing critical load-bearing walls would help mitigate failure risks. Moreover, conducting site-specific soil investigations is essential to refine seismic hazard assessments and improve future structural evaluations.

This research contributes to the methodology for assessing and strengthening URM buildings, providing a framework that can be applied to similar structures in seismic-prone regions. It underscores the importance of employing advanced nonlinear analysis techniques over traditional linear methods to achieve more reliable seismic evaluations. Additionally, the findings could support updates to policies

Copyright © 2025 CroCEE
DOI: https://doi.org/10.5592/CO/3CroCEE.2025.135

and regulations governing the retrofitting of pre-code masonry buildings in Croatia and other regions facing similar challenges.

Acknowledgements

The authors wish to acknowledge the support of this research effort by the Croatian Science Foundation (grant number UIP-2020-02-1128).

References

[1] Kahle, D. (2021): Građevni i urbanistički propisi u Hrvatskoj od 1956. do 1971. godine. *Časopis za suvremenu povijest*, **53** (3), doi: https://doi.org/10.22586/csp.v53i3.17912

[2] Radnić, J., Harapin, A., Matešan, D., Trogrlić, B., Smilović, M., Grgić, N., Baloević, G. (2011): Numerički model za statički i dinamički proračun zidanih konstrukcija. Građevinar, 63(06.), 529-546.

[3] Lourenço, P. B. (1997): Computational strategies for masonry structures. Delft University Press, The Netherlands.

[4] Osmanović, N., Medić, S., Hrasnica, M. (2019): Seismic Assessment of Existing Masonry Building: *Advanced Technologies, Systems, and Applications III: Proceedings of the International Symposium on Innovative and Interdisciplinary Applications of Advanced Technologies (IAT),* Volume 2, Springer International Publishing, 10 pages, doi: https://doi.org/10.1007/978-3-030-02577-9_7

[5] Hrasnica, M., Medić, S. (2021): Seismic response of unreinforced masonry buildings from 1950's: *Proceedings of the 1st Croatian Conference on Earthquake Engineering - 1CroCEE,,* Zagreb, Croatia, 11 pages, https://doi.org/10.5592/CO/1CroCEE.2021.137

[6] Kadić, A., Medić, S., Penava, D. (2021). Macromodel of RC frame with masonry infill for detailed assessment of structural performance: *Proceedings of the 1st Croatian Conference on Earthquake Engineering - 1CroCEE,* Zagreb, Croatia. https://doi.org/10.5592/CO/1CroCEE.2021.105

[7] Jusufbašić. V., Medić, S., Uroš, M. (2023): Nonlinear static and dynamic analysis of a typical masonry building in Palmotićeva Street in Zagreb*: Proceedings of the 2nd Croatian Conference on Earthquake Engineering – 2CROCEE*, Zagreb, Croatia, 10 pages, doi: https://doi.org/10.5592/CO/2CroCEE.2023.99

[8] TNO Diana BV: DIANA—User's Manual. Material library, Delft, The Netherlands

[9] Schreppers, G.J., Garofano, A., Messali, F., Rots, J.G. (2016): DIANA Validation Report for Masonry Modelling. DIANA FEA BV and TU Delft, Delft.

[10] Noortman, F. (2019): Applicability of the pushover method for the seismic assessment of URM structures in Groningen , Master thesis, Delft University of Technology, The Netherlands.

[11] Cundall, P. A. (1971): A computer model for simulating progressive, large-scale movement in blocky rock system, Proceedings *of the international symposium on rock mechanics*, Nancy, France, 8 pages.

[12] Munjiza, A. (2004): *The combined finite-discrete element method*. John Wiley & Sons.

[13] Smoljanović, H., Živaljić, N., Nikolić, Ž. (2013). A combined finite-discrete element analysis of dry stone masonry structures. *Engineering structures*, *52*, 89-100, doi: https://doi.org/10.1016/j.engstruct.2013.02.010

[14] Smoljanović, H., Nikolić, Ž., Živaljić, N. (2015): A combined finite–discrete numerical model for analysis of masonry structures. *Engineering fracture mechanics*, *136*, 1-14, doi: https://doi.org/10.1016/j.engfracmech.2015.02.006

[15] Uroš, M., Todorić, M., Crnogorac, M., Atalić, J., Šavor Novak, M., Lakušić, S. (2021): Potresno inženjerstvo—Obnova zidanih zgrada. *University of Zagreb, Faculty of Civil Engineering: Zagreb, Croatia*.

[16] Magenes, G., Menon, A. (2009): A review of the current status of seismic design and assessment of masonry buildings in Europe. *Journal of Structural Engineering*, *5*(6), 443-452.

[17] RADIMPEX Software for Civil Engineers: https://www.radimpex.rs/en/tower

[18] EMS-98 (1998): *European Macroseismic Scale*, Editor G. Grüntal, European Seismological Commission, Luxembourg.

Proceedings of the 3rd Croatian Conference on Earthquake Engineering - 3CroCEE
19–22 March 2025, Split, Croatia
Copyright © 2025 CroCEE
DOI: https://doi.org/10.5592/CO/3CroCEE.2025.144

APPLICATION OF THE NEW EUROCODE 8 TO THE SEISMIC ASSESSMENT OF AN EXISTING BUILDING IN ZAGREB

Andrea Brunelli [(1)], Silvia Pinasco [(1)], Serena Cattari [(1)], Sergio Lagomarsino [(1)]

(1) Department of Civil, Chemical and Environmental Engineering, University of Genoa, Italy

andrea.brunelli@edu.unige.it, silvia.pinasco@edu.unige.it, serena.cattari@unige.it, sergio.lagomarsino@unige.it

Abstract

The second-generation of Eurocode 8 (EC8) has reached an advanced stage of development and some validations have already been made. With reference to the seismic assessment of existing masonry buildings, the nonlinear static analysis is the main pathway to proceed, but linear analysis may also be used, both in terms of strength (q-factor approach) and deformation. Even if some of these methods are already in use within some existing codes, including the Italian one, the EC8 draft incorporates new assumptions and refined criteria. These updates specifically address the verification and modelling criteria for masonry elements (piers and spandrels); in particular, spandrels may be explicitly modelled or considered indirectly. In the context of nonlinear static analysis, new criteria are outlined for defining the equivalent single-degree-of-freedom system and the limit states conditions. The implications of these newly proposed methods are investigated, with reference to an existing building in downtown Zagreb, constructed in the early twentieth century and representing a significant piece of the built heritage in the town. Buildings of this type suffered extensive damage after the earthquakes in 2020, especially within Zagreb's historic centre. The selected URM building has a rectangular floor plan and five-stores in elevation, providing a suitable case study to examine the effectiveness and adaptability of the EC8 methodologies in addressing the vulnerabilities of heritage masonry buildings under seismic actions.

Keywords: seismic assessment, linear and nonlinear static analyses, seismic verifications

1. Introduction

The activities in Croatia following the two earthquakes in 2020 (the first in Zagreb on March 22, with a magnitude of 5.3 M_w, and the second in Petrinja on December 29, with a magnitude of 6.4 M_w) have highlighted that the seismic vulnerability of the exposed building stock is a relevant issue. These earthquakes caused widespread damage to buildings in Zagreb, and particularly in Petrinja, as well as in the nearby towns of Glina and Sisak (see [1,2,3]).

The historic centre of Zagreb features a very old building stock, consisting mainly of unreinforced masonry (URM) buildings ranging from three to five stories, predominantly constructed after the 1880 Zagreb earthquake (see [4]) within 'row' aggregates. Issues contributing to the inadequate seismic design of these buildings include flexible timber floors that lack the "box-like" behaviour, poor material quality (especially mortar), poorly constructed spandrels affecting wall connections, inadequate connections between load-bearing walls and the horizontal diaphragms, and uneven stiffness distribution in the vertical elements [5].

This paper examines the in-plane seismic response of a five-story URM building in Zagreb. Specifically, the study focuses on the verification of this building according to the provisions of the draft Eurocode 8-3 [6]. Three primary verification approaches from the EC8-3 draft are compared: (1) linear static analysis (LSA) with the design spectrum, reduced by the behaviour factor q, for the force-based approach, (2) LSA with the displacement-based approach, and (3) non-linear static analysis (NLSA). A numerical model was developed for both the linear and non-linear static analyses. The model was created using the equivalent-frame modelling approach, implemented in the 3Muri software [7].

Proceedings of the 3rd Croatian Conference on Earthquake Engineering - 3CroCEE
19–22 March 2025, Split, Croatia
Copyright © 2025 CroCEE
DOI: https://doi.org/10.5592/CO/3CroCEE.2025.144

2. Case study

The case study focuses on a representative residential building located in Zagreb's Lower Town, a historic area characterized by a distinctive urban fabric composed of row buildings in aggregate. The urban development of Zagreb's Lower Town was largely shaped by the reconstruction efforts following the earthquake of 1880. The area features a dense grid layout, adapted to pre-existing obstacles, resulting in irregularly shaped blocks that are predominantly rectangular or trapezoidal. Row aggregates, which are a defining characteristic of this area, typically consist of five or more adjacent buildings on each side, with spanning lengths between 50 and 150 meters.

These row buildings, constructed from the late 19th century until the early 20th century, do not share common walls but are built in close proximity, with no gaps or seismic expansion joints between them. Structural configurations within these aggregates vary depending on the building's position, whether located within a row or at the corner of an aggregate. Buildings situated within the row are the most common typology, and their structural system relies heavily on longitudinal load-bearing walls, while the transverse direction often lacks sufficient structural elements, except for staircase walls and the two peripheral transverse walls [8].

The specific building analyzed herein, constructed in 1908, is part of a row building aggregate, which is typical in Zagreb's Lower Town. It has a rectangular plan measuring 19,20 x 12,35 meters, a basement, a ground floor, three upper floors, and an attic (Figure *1*). The total height of the building is 22,70 meters, with floor heights of 3 meters for the basement, 3,85 meters for the ground and upper floors, and 4,20 meters for the attic. Load-bearing walls are constructed of solid bricks, with wall thickness ranging from 75 cm at the base to 30 cm at higher levels, reflecting a gradual reduction in thickness with height [9]. Notably, the building does not include reinforced concrete ring beams to connect walls at the level of horizontal diaphragms. The basement's horizontal structure consists of shallow brick barrel vaults supported by steel beams, while the upper floors utilize wooden beam systems filled with rubble material. The beams are oriented transversely, resting on the facade and the central longitudinal wall. This configuration results in greater stiffness in the longitudinal direction, while the transverse direction is structurally weaker due to the lack of adequate connections between floors and walls [8].

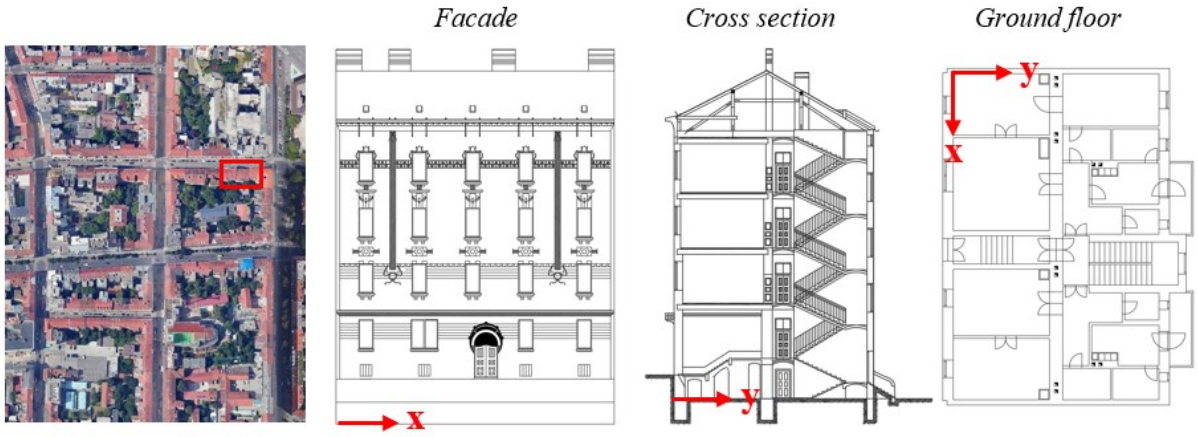


Figure 1. Aggregate to which the analyzed building belongs and a graphical representation of the main façade, the transversal vertical section, and the ground floor plan [8].

The building was modelled according to the equivalent frame approach, by using the program Tremuri [7]. The model is the same used in [8], where the aggregate effect was investigated. In this paper, for the sake of simplicity, the building is assumed as isolated (or the interaction with adjacent buildings, which are structurally independent, is neglected). The geometric model and 3D equivalent frame model are shown in Fig. 2.

The mechanical characteristics assumed are in accordance with the mean values of Table C.1 in Annex C of [6] for *solid clay brick masonry and lime mortar*. The mechanical elastic properties are reported in Table 1: E and G are the Young and shear modulus, w is the specific weight, f_m is the

Copyright © 2025 CroCEE
DOI: https://doi.org/10.5592/CO/3CroCEE.2025.144

compressive strength, f_t is the diagonal tensile strength, f_{v0} is the shear strength in the absence of vertical load and f_b is the normalized compressive strength of the units (as defined in [10]).

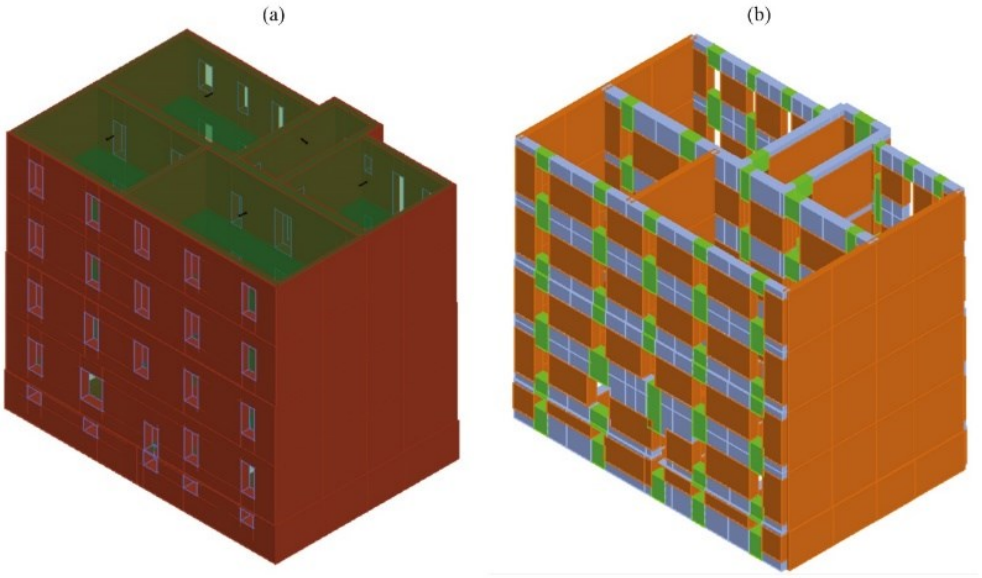


Figure 2. (a) Geometrical model and (b) 3D equivalent frame model of case study,

Table 1 – Mechanical properties

E [MPa]	G [MPa]	w [kN/m^3]	f_m [MPa]	f_t [MPa]	f_{v0} [MPa]	f_b [MPa]
1500	500	18	3.4	0.114	0.160	10

The flexural modulus is defined in accordance with [10]: for piers (in orange in the Fig. 2b) the Young modulus is reduced by multiplying the elastic value by 0.5, G by 0.35. For spandrels (in green in Fig. 2b) both moduli are reduced by multiplying the elastic values by 0.25, as proposed in EC8-1.2 [11]. The Knowledge Level (KL) is defined in function of three categories: Geometry (KLG), construction Details (KLD) and Material properties (KLM). The first two parameters are used to reduce drift in terms of drift capacity, and the third to reduce resistance. For all the three categories KL2 has been assumed, consistently with the guidance in chapter 5.4 of EC8-3.
The reference spectral acceleration is defined as S_α=2.45 m/s^2 consistent with Annex A of EC8-1.1 [12]. As defined in [8], the soil is classifiable as type C, in according with EC8-1.1, being $V_{S,30}$ equal to 275 m/s. Therefore, the site amplifications proposed in EC8-1.1 were considered, while a flat soil was assumed.

3. Seismic assessment in accordance with second-generation of EC8 part 3

In this section, a brief description of the new features of EC8-3 and the subsequent results obtained for the case study under consideration are given. The seismic action is defined using the criterions defined in the next generation of Eurocode 8 (see [12,13]), associated with the site's hypotheses described in previous section at 475 years return period for Significant Damage (SD) verification, and also 975 years for Near Collapse (NC) verification, in the case of Static Non-Linear analyses.

3.1. Linear static analysis with the reduced spectrum for the Force-based approach

This analysis reduces the elastic spectrum of a q-factor equal to 1.5 for masonry buildings.
The estimation of the fundamental period (T_1) of the building, for each direction, may be calculated with Eq. (1).

Proceedings of the 3rd Croatian Conference on Earthquake Engineering - 3CroCEE
19–22 March 2025, Split, Croatia
Copyright © 2025 CroCEE
DOI: https://doi.org/10.5592/CO/3CroCEE.2025.144

$$T_1 = 2\sqrt{\frac{\Sigma m_i s_i^2}{\Sigma m_i s_i}} \tag{1}$$

where s_i is the horizontal displacement at node i obtained by applying horizontal acceleration equal to the gravity and m_i is the mass at node i. Therefore, the execution of a preliminary linear analysis to estimate the fundamental period is required. A new aspect respect to previous Eurocode [11] or other present codes (for example the Italian code [14]) is the distribution of forces to be applied to the structure; the recommended distribution is hence defined in Eq. (2).

$$F_i = F_b \frac{s_i m_i}{\Sigma s_j m_j} \tag{2}$$

where s_i and m_i are the same displacements and masses used for the calculation of fundamental periods and F_b is the total seismic equivalent force (see [12]), evaluated by the acceleration response spectrum at the estimated fundamental period T_1 in the direction of analysis. The point of application of the forces F_i considers a minimum eccentricity requirement, whose recommended value is equal to 5% of the corresponding length of the building including the natural eccentricity between centre of mass and centre of stiffness varies among the stories, if the natural eccentricity is lower than the minimum eccentricity.
The safety check to be performed on the masonry elements is defined by Eq. (3).

$$\gamma_{Sd}\, V \leq \frac{V_R}{\gamma_{Rd}} \tag{3}$$

where γ_{Sd} is the partial factor depending on the present state of the building, which should be assumed equal to 1 in the case of undamaged structures, γ_{Rd} is the partial factor in the resistance, V is the shear force from the analysis at the SD limit state, V_R is the strength defined as minimum among the possible failure modes:

- Failure in flexure

$$V_{R,f} = \frac{DN}{2H_0}\left(1 - \frac{N}{Dtf_m\eta_f}\right) \tag{4}$$

where D is the length in the case of piers and depth for spandrels, t is the thickness of the masonry element, H_0 is the distance between the section where the flexural resistance is attained and the contraflexure point, N is the compression value obtained from the analysis, f_m is the mean compressive strength of masonry and η_f is assumed equal to 0.85. In this case γ_{Rd}=1.85 for KLM equal to 2.

- Failure by shear sliding

$$V_{R,s}=\min\begin{cases} D't\left(f_{v0} + \dfrac{\mu N}{D't}\right) \\ 0.065\, f_b D't \end{cases} \tag{5}$$

where D' is the depth of compressed area at the end section of the pier, t is the pier thickness, μ is the masonry friction coefficient, which is assumed equal to 0.5, f_{v0} is the shear strength in the absence of vertical load, f_b is the normalized compressive strength of the units in agreement with [10]. In this case γ_{Rd}=1.50 for KLM equal to 2.

- Failure by diagonal cracking

Proceedings of the 3rd Croatian Conference on Earthquake Engineering - 3CroCEE
19–22 March 2025, Split, Croatia
Copyright © 2025 CroCEE
DOI: https://doi.org/10.5592/CO/3CroCEE.2025.144

$$V_{R,d}=\min\begin{cases}\frac{Dt}{\mathrm{b}}\left(\frac{f_{v0}}{1+\mu_i\Phi}+\frac{\mu_i N}{(1+\mu_i\Phi)Dt}\right)\\ \frac{Dt}{\mathrm{b}}\frac{0.1f_b}{2.3}\sqrt{1+\frac{N}{0.1Dtf_b}}\end{cases} \tag{6}$$

where D and t are the dimensions of pier or spandrel, f_{v0} is the shear strength in the absence of vertical load, f_b the normalized compressive strength of the units in agreement with [10], $b = {}^{H}/_{D}$ (but not greater than 1.5 and not lower than 1), μ_i is the local friction coefficient which is assumed equal to 0.6, Φ is the interlocking coefficient assumed equal to 0.5. In this case γ_{Rd}=1.55 for KLM equal to 2.

The results of the four linear static analyses (X or Y directions, positive or vertical) are shown in Table 2 and Table 3. The most punishing verification is that associated to shear sliding, especially in the top section of piers at the last level. This depends on the very low level of compression (axial force), which in a few cases from the equivalent frame model becomes a tensile axial force. Also, the verification of the spandrels is problematic (see Table 4).

Table 2 – Capacity/demand ratios for top and bottom section of piers and percentage of elements verified in case of flexural or shear sliding failure

	Top section of piers				**Bottom section of piers**			
	+100%F_x -30%F_y	**-100%F_x +30%F_y**	**+100%F_y -30%F_x**	**-100%F_y +30%F_x**	**100%F_x -30%F_y**	**-100%F_x +30%F_y**	**100%F_y -30%F_x**	**-100%F_y +30%F_x**
Verified cases	100%	99%	99%	98%	100%	100%	100%	100%
$min\left(\frac{V_{R,f}}{\gamma_{Rd}V}\right)$	1	1	1	1	2.91	56.5	106	104
Verified cases	82%	88%	79%	78%	89%	91%	84%	85%
$min\left(\frac{V_{R,s}}{\gamma_{Rd}V}\right)$	0.01	0.01	0.04	0.03	0	0.04	0.07	0.08

Table 3 – Capacity/demand ratios for top and bottom section of piers and percentage of elements verified for diagonal cracking

	+100%Fx -30%Fy	**-100%Fx +30%Fy**	**+100%Fy -30%Fx**	**-100%Fy +30%Fx**
Verified cases	96%	98%	99%	99%
$min\left(\frac{V_{R,d}}{\gamma_{Rd}V}\right)$	0.76	0.91	0.9	0.71

Table 4 – Capacity/demand ratios for spandrels and percentage of elements verified

	+100%Fx -30%Fy	**-100%Fx +30%Fy**	**+100%Fy -30%Fx**	**-100%Fy +30%Fx**
Verified cases	26%	31%	70%	66%
$min\left(\frac{V_{R,d}}{\gamma_{Rd}V}\right)$	0.18	0.16	0.21	0.24

Therefore, the building is not verified by this procedure with the equivalent frame model. This result is similar to that already observed for the design of new masonry buildings with EC8-1.2 [15]. To

Proceedings of the 3rd Croatian Conference on Earthquake Engineering - 3CroCEE
19–22 March 2025, Split, Croatia
Copyright © 2025 CroCEE
DOI: https://doi.org/10.5592/CO/3CroCEE.2025.144

overcome the critical issues of force-based verification by linear analysis, that are in masonry piers with very low strength but also low seismic demand, an attempt was made by modifying the numerical model by not explicitly modeling the last level spandrels, thus neglecting the contribution of the spandrels at the upper level (option 2). To this aim, the constraint at the top of the piers at the last level in the upper section has been assumed as a hinge, thus having a zero-bending moment and so the top section of the last level piers (the critical section in previous analyses) is entirely compressed (D'=D).

In Table 5 and Table 6 the results for the three typology of failure are reported; for the sake of brevity, the verification of the spandrels is not reported, because the results are similar to those shown in Table 4. The most punishing verification is always the shear sliding, although it improves over the previous configuration, the flexural verification is satisfied in almost all sections of the piers.

Anyway, even if the modified structural model reduces the number of critical piers, this model is found to be unverified at the site under consideration using LSA with the Reduced spectrum for the Force-based approach.

Table 5 – Capacity/demand ratios for top and bottom section of piers and percentage of elements verified in case of flexural or shear sliding failure (option 2 –spandrels neglected at the upper level)

	Top section of piers				**Bottom section of piers**			
	+100%Fx -30%Fy	**-100%Fx +30%Fy**	**+100%Fy -30%Fx**	**-100%Fy +30%Fx**	**100%Fx-30%Fy**	**-100%Fx +30%Fy**	**100%Fy-30%Fx**	**-100%Fy +30%Fx**
Verified cases	100%	100%	100%	100%	100%	100%	99%	100%
$min\left(\frac{V_{R,f}}{\gamma_{Rd}V}\right)$	1	1	1	1	1	1	0.86	1
Verified cases	91%	92%	87%	86%	88%	87%	85%	84%
$min\left(\frac{V_{R,s}}{\gamma_{Rd}V}\right)$	0.01	0.11	0.04	0.07	0.03	0	0.01	0.03

Table 6 – Capacity/demand ratios for top and bottom section of piers and percentage of elements verified for diagonal cracking (option 2 –spandrels neglected at the upper level)

	+100%Fx -30%Fy	**-100%Fx +30%Fy**	**+100%Fy -30%Fx**	**-100%Fy +30%Fx**
Verified cases	97%	99%	99%	99%
$min\left(\frac{V_{R,d}}{\gamma_{Rd}V}\right)$	0.76	0.92	0.81	0.72

3.2. Linear static analysis with the Displacement-based approach

This verification is allowed in [6] for existing masonry buildings, while it cannot be performed for new masonry buildings, according to EC8-1.2 [11]. The verification consists of performing a linear static analysis, as described in the previous chapter, with the elastic response spectrum not reduced by the q-factor. The purpose of this verification is to check that the deformation demand is lower than the deformation capacity in elements not verified in strength. Specifically, the same verification in terms of strength as described in the previous chapter is performed, and for the unverified elements a verification in deformation is performed using Eq. (7).

$$\gamma_{Sd}\, f_{SD}\theta \leq \frac{\theta_{SD}}{\gamma_{Rd}} \tag{7}$$

Proceedings of the 3rd Croatian Conference on Earthquake Engineering - 3CroCEE
19–22 March 2025, Split, Croatia
Copyright © 2025 CroCEE
DOI: https://doi.org/10.5592/CO/3CroCEE.2025.144

where θ is the deformation demand drift ratio from the analysis at the SD limit state, γ_{Sd} is equal to 1 in a undamaged structure, γ_{Rd} is the partial factor in the resistance, in terms of drift capacity, for the several damage mechanisms defined in the previous section, and f_{SD} is defined in Eq. (8).

$$f_{SD} = u_{LS}\left[1 + \left(\frac{1-u_{LS}}{u_{LS}}\right)\frac{T_C}{T_1}\right] \geq 1 \tag{8}$$

where u_{LS} is equal to 0.33 being a SD verification (otherwise it would have been 0.25 for NC), T_1 the fundamental period of the building and T_C the characteristic period of the response spectrum.
This verification procedure may be used if the ratio $\rho_{max}/\rho_{min} \leq 2.5$, where $\rho = \frac{V_{Ed}}{V_{Rd}}$ in all critical zones of unverified piers. The θ_{SD} and γ_{Rd} (for KLM=2) are defined in EC8-3 in function of the typology of damage as shown in Table 7.

Table 7 – Displacement capacity and partial factor γ_{Rd} for each typology of damage

Flexure		**Shear sliding**		**Diagonal cracking**	
θSD [%]	γ_{Rd}	**θSD [%]**	γ_{Rd}	**θSD [%]**	γ_{Rd}
(1-ν)	1.85	0.5	1.50	0.6	1.55

with $\nu=\sigma_0/f_m$

This linear static analysis has been made by using the model that neglects the contribution of the last level spandrels (option 2), to limit the number of critical elements. Then, the value of ρ_{max}/ρ_{min} was calculated for all elements not verified with the equation of section 3.1 to assess whether this verification is applicable.
Table 8 shows the calculated ρ_{max}/ρ_{min} values for the four analyses. As shown in section 3.1, the shear sliding failure is the most punitive; in fact, it is observed that considering this verification in the calculation of ρ_{max}/ρ_{min}, this ratio is much higher than the limit imposed by [6]. Consequently, linear static analysis with Displacement-based approach would not be applicable. It should be pointed out that practically ρ_{max}/ρ_{min} coincides with ρ_{max}, as ρ_{min} is usually slightly larger than 1.

Table 8 – ρ_{max}/ρ_{min} for the four analyses in two cases: with and without the shear sliding failure

	+100%Fx -30%Fy	**-100%Fx +30%Fy**	**+100%Fy -30%Fx**	**-100%Fy +30%Fx**
With shear sliding failure	76.72	33.68	97.19	118.90
Without shear sliding failure	1.83	1.53	2.24	2.46

Analyzing in detail the results for the critical piers under shear sliding verification, it is observed that these are located not only at the top floor being lightly loaded, but also where a significant flange effect is activated by the equivalent frame model. Fig. 3 shows some cases of piers (in black square) where the ρ_{max}/ρ_{min} value is very large, and this occurs because, in the equivalent frame model, piers of two intersecting walls are perfectly connected, forming a T section in which the flange or the web result unloaded. In particular, in Figure 3 the perimetral transversal wall and half of the back façade are shown (see Figure 2); the pushover analysis is along the transversal direction, and elements 195, 200 and 210 resulted unloaded because connected to elements 4, 8 and 16 of the orthogonal wall, respectively (please note that they are connected to nodes 8, 9 and 11; analogously, element 13 in the transversal wall is unloaded because strictly connected through node 5 to the main façade.
To overcome this issue, the equivalent frame model could be modified, by vertically disconnecting the orthogonal piers, to verify each pier as independent and limit the redistribution of axial forces.
Anyway, with the aim of understanding the potential of linear static analysis with displacement-based verification, the verification of deformation capacity (see Eq. (7)) was considered even if ρ_{max}/ρ_{min}

Copyright © 2025 CroCEE
DOI: https://doi.org/10.5592/CO/3CroCEE.2025.144

is larger than 2.5. Table 9 shows the capacity-demand ratios in terms of deformation and all elements are found to be verified, even where the verification is largely unsatisfied in terms of strength.
Therefore, while ASL with q-factor is very punitive and the method is practically unusable, the verification in terms of deformation is not very demanding even where the resistance is very low.

Table 9 – Capacity/demand ratios in deformation in each four analyses

	+100%Fx -30%Fy	-100%Fx +30%Fy	+100%Fy -30%Fx	-100%Fy +30%Fx
θ_{Rd}/θ_{Ed} min	1.374	1.438	1.002	1.039

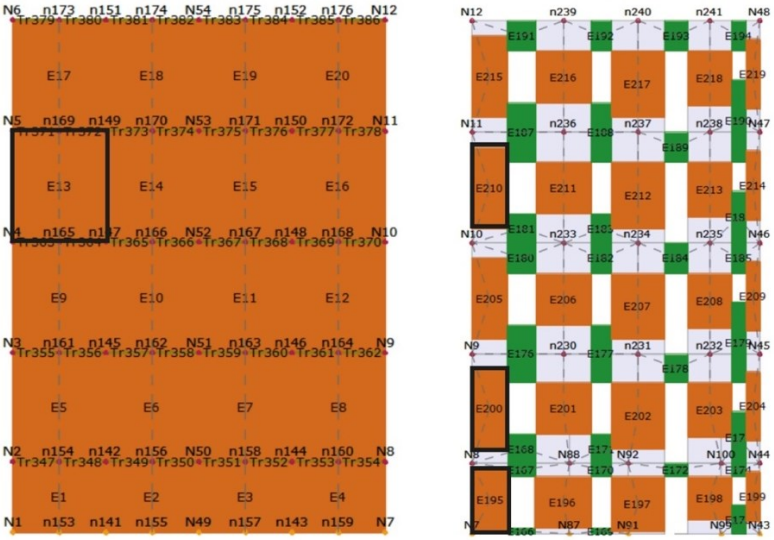


Figure 3. Example of piers in black square that fail in terms of strength due to a relevant flange effect.

3.3. Non-Linear static analysis

The verification with NLSA for building with stiff diaphragms is done using a triangular pattern based on lateral forces that are proportional to masses, considering an inverted profile in elevation (as other actual code e.g. [14]). This load pattern is preferred to the one obtained by modal analysis, which in the absence of a rigid diaphragm usually presents a limited mass participation in each mode, to avoid that only few masonry walls are loaded.
The ultimate drifts are $\theta_u=4/3\theta_{SD}$. For regular masonry piers, the force reduction corresponding to θ_u, for flexure, is assumed to be 10% of shear resistance, for spandrels the reduction is 20%. For shear sliding the reduction is in function of the compression level. Finally for diagonal cracking the reduction is for piers 50%, for spandrels 90%. The values of θ_{SD} are reported in Table 7.
The definition of the bilinear curve of the equivalent single degree of freedom (SDoF) system is done with the procedure described in [12] that recommends the adoption of a stiffness of the SDoF system equal to the secant stiffness, whereas the allowed yield strength is obtained through the equivalence of areas up to the ultimate point.
The definition of displacement capacity (d_u) of the SDoF system at the NC limit state depends on the first of three criteria:

a) the total lateral resistance (base shear) has dropped below 80% of the peak resistance of the building.
b) the damage level associated with the drift θ_{NC} is reached in all piers at any level of any masonry walls.
c) one member has researched a drift ratio corresponding to 1.5 times that corresponding to the NC damage.

Copyright © 2025 CroCEE
DOI: https://doi.org/10.5592/CO/3CroCEE.2025.144

The d_u, defined as minimum of the three conditions, is reduced with a factor equal to 1.8 being the KL equal to 2. The characteristic displacement is the average displacement among those of different walls, weighed by the corresponding seismic masses, because the diaphragms are stiff but not rigid. Instead, the displacement capacity at the SD limit state is defined as the mean value between $d_{u,NC}$ (d_u of the SDoF system at the NC limit state as described in previous section) and d_y. Also in this case, the SD limit state is reduced with factor equal to 1.8 being the level knowledge equal to 2.

Table 10 shows the values of the capacity/demand ratio (in terms of displacements) obtained for the four nonlinear static analyses, in the case of the SD and NC limit state. At NC limit state, the verification is largely satisfied for X direction, while are barely verified in the Y direction. On the contrary, at SD limit state is not verified (0.913) in the Y direction. As an example, Fig. 4 shows the capacity curves (pushover in black and equivalent bilinear in red) for the analysis in the +X and +Y direction with the SD and NC thresholds (in the first case the displacement capacity after the application of γ_{Rd} factors is also shown with a light blue dot, the second with blue dot). The spectra are in dashed line for ND (T_R=795 years), in light blue, and for SD state limit (T_R=475 years), in blue.

In Fig. 4a and b it can be seen how the ultimate NC displacement is associated with condition (a), equally is the case in the other two analyses not shown, at a slightly larger displacement condition (c) is triggered, while condition (b) is never triggered and is not, at least for this case study, significant. Fig. 4a shows how the target (the cross) at both SD and NC is less than d_u, while in the +Y analysis (Fig. 4b) it is verified only at the NC limit state. The verification at SD is more punitive than at NC in the case where the bilinear plateau length (distance between d_y and $d_{u,NC}$) is big since it is possible to take advantage of the increase in drift at NC compared with that at SD value.

Table 10 – Values of capacity/demand ratio (in terms of displacements) for each analysis

	+X	-X	+Y	-Y
NC limit state	1.782	1.602	1.001	1.097
SD limit state	1.420	1.296	0.926	0.913

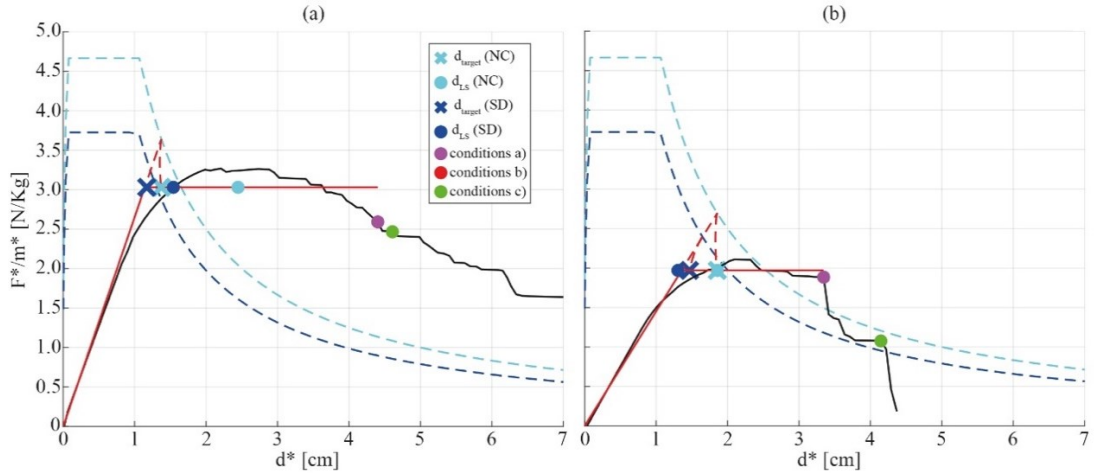


Figure 4. (a) Capacity curve and elastic response spectrum (return period 475 and 975 years) for analysis +X and (b) for +Y.

4. Conclusions

By considering a five-story URM building in Zagreb's Lower Town, built in the early 20th century, three verification procedures for the seismic assessment of existing masonry buildings have been investigated, according to the rules proposed in the current draft of the new Eurocode 8-3 [6]. In particular, it emerges that results can differ even considerably by passing from linear to non linear methods, and from force-based to displacement-based approaches.

It is confirmed how the LSA with the q-factor (force-based approach) is particularly punitive for

Copyright © 2025 CroCEE
DOI: https://doi.org/10.5592/CO/3CroCEE.2025.144

masonry buildings in that even in medium hazard sites such as the one analyzed. This is due to the assumption that verification is in local terms, that is it fails even if the critical condition is attained only in one masonry element. Within the different failure mechanisms for masonry piers, particularly punitive is the shear sliding verification, which is requested only for regular masonry piers.
On the contrary, LSA with unreduced response spectrum and verification in deformation (displacement-based approach) appears to be an effective procedure to assess the seismic behaviour at SD limit state. However, in the present formulation the condition that allows the applicability of the method only when the overcoming in terms of strength is below 2.5 limits the large applicability of this method. Particularly problematic in this case is the verification of elements with low axial force, especially with reference to shear sliding failure. Therefore, for LSAs, it is recommended to make models in which spandrels are not explicitly modeled, especially on the top level. In addition, a critical issue is related to the use of linear analysis in building modelled by the equivalent frame approach because the significant redistribution of generalized forces between masonry elements due to the so-called flange effect. A possible approach to consider the flange effect in equivalent frame model was proposed by [16].
Finally, NLSA turns out to be an effective approach to assess existing masonry buildings, in particular when the verification is made in global terms, by checking the ultimate displacement capacity, instead to check the attainment of drift capacity in any single masonry element. In the specific case study, NC limit state is verified, while SD limit state is slightly overcome.

5. References

[1] Atalić, J., Demšić, M., Baniček, M., Uroš, M., Dasović, I., Prevolnik, S., Kadić, A., Šavor Novak, M., Nastev, M. (2023): The December 2020 magnitude (Mw) 6.4 Petrinja earthquake, Croatia: seismological aspects, emergency response and impacts. *Bulletin of Earthquake Engineering* **21**, 5767–5808, https://doi.org/10.1007/s10518-023-01758-z.

[2] Pinasco, S., Cattari, S., Lagomarsino, S., Demšić, M., Novak, M.S., Uroš, M. (2023): Numerical investigation on the seismic response of an unreinforced masonry residential building hit by Zagreb earthquake in 2020. *2nd Croatian Conference on Earthquake Engineering*, Zagreb, Croatia.

[3] Moretić, A., Chieffo, N., Stepinac, M., Lourenço, P.B. (2022): Vulnerabilit assessment of historical building aggregates in Zagreb: implementation of a macroseismic approach, *Bulletin of Earthquake Engineering*, ***0123456789***, https://doi:10.1007/s10518-022-01596-5.

[4] Šavor Novak, M., Uroš, M., Atalić, J., Herak, M., Demšić, M., Baniček, M., Lazarević, D., Bijelić, N., Crnogorac, M., Todorić, M. (2020): Zagreb earthquake of 22 March 2020-preliminary report on seismologic aspects and damage to buildings. *J Croatian Assoc Civil Eng*, **72** (10),843–867, https://doi.org/10.14256/JCE.2966.2020.

[5] Atalić, J., Uroš, M., Šavor Novak, M., Demšić, M., Nastev, M. (2021): The Mw5.4 Zagre (Croatia) earthquake o March 22, 2020 impacts and response. *Bulletin of Earthquake Engineering*, **19** (9), 3461-3489, https://doi.org/10.1007/s10518-021-011:17-w.

[6] CEN (2023): prEN 1998-1-2. Eurocode 8 - Design of structures for earthquake resistance - Part 1-2: Buildings, April 2023, Comité Européen de Normalisation, Brussels.

[7] Lagomarsino, S., Penna, A., Galasco, A., Cattari, S. (2013): TREMURI program: an equivalent frame model for the nonlinear seismic analysis of masonry buildings. *Engineering Structures*, **56**, 1787-1799, https://doi.org/10.1016/j.engstruct.2013.08.002.

[8] Pinasco, S., Demšić, M., Pilipović, A., Novak, M.S., Uroš, M., Lagomarsino, S., Cattari, S. (2025): Seismic fragility assessment of existing masonry buildings in aggregate located in Zagreb. *Bulletin of Earthquake Engineering (*submitted).

[9] Demšić, M., Pinasco, S., Pilipović, A., Cattari, S., Lagomarsino, S., Šavor Novak, M.S., Uroš, M. (2024): Development of fragility curves of masonry buildings build in a regular row aggregate. *18th World Conference on Earthquake Engineering*, 30 June - 5 July 2024, Milan, Italy.

Copyright © 2025 CroCEE
DOI: https://doi.org/10.5592/CO/3CroCEE.2025.144

[10] CEN (2021): prEN 1996-1-1. Eurocode 6 - Design of masonry structures - Part 1-1: General rules for reinforced and unreinforced masonry structures, October 2021, Comité Européen de Normalisation, Brussels.

[11] CEN (2023): prEN 1998-1-2. Eurocode 8 - Design of structures for earthquake resistance - Part 1-2: Buildings, April 2023, Comité Européen de Normalisation, Brussels.

[12] CEN (2023): prEN 1998-1-1. Eurocode 8 - Design of structures for earthquake resistance - Part 1-1: General rules and seismic action, June 2023, Comité Européen de Normalisation, Brussels.

[13] Labbé, P., Paolucci, R. (2022): Developments relating to seismic action in the Eurocode 8 of next generation. In: Vacareanu, R., Ionescu, C. (eds) "*Progresses in European Earthquake Engineering and Seismology*", ECEES 2022. Springer Proceedings in Earth and Environmental Sciences. Springer. https://doi.org/10.1007/978-3-031-15104-0_29.

[14] NTC (2018) Aggiornamento delle Norme tecniche per le costruzioni. Italian Ministry of Infrastructure and Transportation, G.U. n. 42, 20 February 2018, Rome, Italy (in Italian).

[15] Lagomarsino, S., Penna, A., Cattari, S., Rota, M., Brunelli, A., Bracchi, S. (2024): Unresolved issues in the design of URM buildings: a critical review of linear and nonlinear methods. *18th World Conference on Earhquake Engineering,* 30 June – 5 July 2024, Milan, Italy.

[16] Cattari, S., Alfano, S., Lagomarsino, S. (2023): A Practice-Oriented Proposal to Consider the Flange Effect in Equivalent Frame Modeling of Masonry Buildings. *Buildings*, **13**(2), 462, https://doi.org/10.3390/buildings13020462.

Proceedings of the 3rd Croatian Conference on Earthquake Engineering - 3CroCEE
19–22 March 2025, Split, Croatia
Copyright © 2025 CroCEE
DOI: https://doi.org/10.5592/CO/3CroCEE.2025.145

ANALYSIS OF REINFORCED CONCRETE BEAM-COLUMN JOINT IN ANSYS SOFTWARE

Ivana Drobnjak [(1)], Marina Rakočević [(2)]

[(1)] *Teaching Assistant, University of Montenegro, Faculty of Civil Engineering, ivanadrobnjak25@gmail.com*
[(2)] *Full professor, University of Montenegro, Faculty of Civil Engineering, marinara@ucg.ac.me*

Abstract

In many countries, such as Montenegro, numerous existing reinforced concrete (RC) buildings were designed and built before the adoption of modern seismic codes. These buildings make up a significant portion of Montenegro's RC building stock, making their assessment, retrofitting, and strengthening an urgent research topic. This shortcoming because of insufficient transverse reinforcement, poor energy dissipation, and plastic hinges in critical areas, making shear failures in RC beam-column joints one of the most common structural failure types. Examining and modelling these RC joints and comparing results with experimental data is essential for advancing seismic resilience. The primary goal of this paper was to improve understanding of RC joints, focusing on their vulnerability and critical role in structural integrity. Although these joints represent a local failure point, their breakdown can lead to the collapse of the entire structure. Another aim is to create a foundation for further research, focusing on numerical and experimental analyses of strengthened/retrofitted RC joints. A nonlinear static analysis of an RC joint was conducted using ANSYS software (version 24.2) with selected material models (CPT215 and REINF264) representing the nonlinear behaviour of concrete and reinforcement, respectively. The load was applied as displacement at the beam end in two steps, with a constant axial force in the column. Vertical force-displacement diagrams were compared with experimental results and those in the ANSYS guide (version 19.1) to verify the convergence and accuracy of results. Mesh density was varied, using finite elements (FE) of different sizes and shapes, including hexahedral and prismatic forms. Results showed that element size significantly affects numerical accuracy. Additionally, prismatic elements with triangular base achieving faster convergence. The runtime analysis using different mesh densities and finite element types underscored how mesh and element selection impact the balance between modeling accuracy and computational efficiency.

Keywords: Reinforced Concrete joints, Numerical and experimental analysis, Nonlinear static analysis, ANSYS software

Proceedings of the 3rd Croatian Conference on Earthquake Engineering - 3CroCEE
19–22 March 2025, Split, Croatia
Copyright © 2025 CroCEE
DOI: https://doi.org/10.5592/CO/3CroCEE.2025.145

1. Introduction

Many countries did not design reinforced concrete (RC) structures to effectively withstand seismic forces before the 1970s. These structures often exhibit insufficient reinforcement details and inadequate transverse reinforcement, which compromise their lateral strength, energy dissipation capacity, and resistance to plastic hinge formation during earthquakes [1]. In Montenegro, seismic design regulations were first implemented in 1964 after the Skopje earthquake, and today, Eurocodes serve as the sole applicable standards. Common failure mechanisms include shear failure at beam-column joints, column shear failure, and weak-story collapse. RC joints are particularly susceptible to damage, potentially leading to the collapse of the entire structure, as illustrated in Figures 1–3.



Figure 1. Northridge Earthquake, California, 1994, [2]



Figure 2. Izmir Earthquake, Turkey, 1999, [2]



Figure 3. Kocaeli Earthquake, Turkey, 1999, [1]

The "weak column-strong beam" mechanism contradicts the principles of performance-based design, which prioritise ductile joints and follow a "strong column-weak beam" strategy. Allowing beams to lose strength is preferable to column failure, as plastic hinges forming at beam-column connections can compromise the overall stability of the structure, rendering this mechanism inappropriate for design purposes.

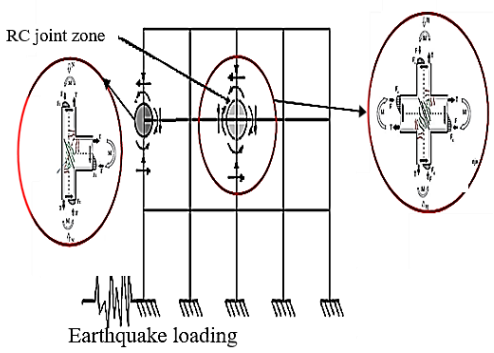


Figure 4. Forces that arise in the beam-column joint zone during an earthquake, [3-4]

In a two-dimensional RC frame exposed to an earthquake, both columns and beams are subjected to shear and bending forces, as shown in Figure 4. Beams primarily endure shear forces and bending moments, while columns must withstand not only these forces but also gravitational loads. Compressive and tensile forces in columns and beams are transmitted through corresponding stresses within the joint.

A widely adopted mechanism for shear transfer in joints is the diagonal strut-and-tie model [5], as illustrated in Figure 5. According to Paulay, Park, and Priestley [5], the strength of the diagonal strut governs the RC joint's capacity before failure. As the shear force at the beam-column connection rises, diagonal cracks develop in the joint core, ultimately causing joint failure due to concrete crushing within the core.

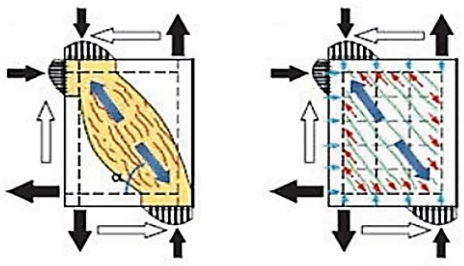


Figure 5. Forces that arise in the beam-column joint zone during an earthquake, [4]

2. Literature review

Since the 1960s, extensive research has been conducted on the behaviour of joints under seismic forces [6]. Hanson and Connor [7] performed some of the earliest experiments, with subsequent advancements reported in [8–11]. Ehsani and Wight [12] investigated the influence of transverse beams, while Pessiki et al. [13] studied joints lacking transverse reinforcement, revealing significant shear cracking upon failure [6]. Tsonos et al. [14] emphasised the effectiveness of inclined overlapping reinforcement in enhancing seismic resistance. An experiment detailed in [15] analysed corner beam-column joints in existing RC structures subjected to low axial pressure to assess their seismic performance.

Copyright © 2025 CroCEE
DOI: https://doi.org/10.5592/CO/3CroCEE.2025.145

The analytical model for RC joints, developed by Park and Paulay [16] and later refined by Paulay et al. [5], identified two primary shear resistance mechanisms under seismic loading. Shear is transferred through a diagonal concrete strut, assuming a perfect bond between concrete and reinforcement. Bond slip occurs when longitudinal reinforcement displaces relative to the concrete due to a loss of bond strength.

The interaction between concrete and reinforcement in joints was examined by Viwathanatepa et al. (1979) [18] and Eligehausen et al. (1983) [19]. While most models assume rigid joints, [20] proposed an alternative approach where the joint core remains elastic during seismic events, even if the surrounding beams and columns sustain damage.

Bracci et al. [21] proposed reducing beam and column stiffness by applying experimentally derived or calculated coefficients. Models that incorporate the behaviour of reinforcement, concrete, and bonding are discussed in [22], while the effects of shear and bond slip are examined in [23, 24]. Shear strength predictions for non-seismically designed joints are provided in [25], and the impact of shear reinforcement is analysed in [26].

Since the 1960s, joint behaviour modelling has advanced significantly, with approaches categorised into plastic hinge models [17, 27–28], component-based models [29–31], and finite element methods (FEM) [3], each offering distinct strengths and limitations.

In software like ETABS and SAP2000, RC structures are modelled with the assumption of rigid beam-column connections. However, this assumption is valid only when failures occur in weaker structural elements rather than in the RC joints themselves [32]. The use of high-strength concrete has reduced column dimensions, increasing the likelihood of joint failures during earthquakes, as observed in Turkey and Taiwan in 1999. Consequently, joints cannot be assumed rigid and are identified as vulnerable structural components, as emphasised in Section 1.

For detailed joint analysis, FEM tools like ANSYS [33] and ABAQUS [34] are widely employed. ABAQUS, extensively used in both engineering practice and academia [35–39], simulates concrete behaviour using damage parameters for compression and tension and models reinforcement with an elastoplastic response to capture steel yielding and failure. The accuracy of such simulations relies heavily on the proper calibration of input parameters against experimental data.

Numerous numerical simulations of RC joints under monotonic loading have been performed [40]. An experimental and numerical study focused on enhancing seismic performance through additional transverse reinforcement in RC joints is presented in [41]. Similarly, [42] provides a numerical analysis in ANSYS of RC joint specimens under cyclic loading to replicate earthquake effects.

3. ANSYS software

3.1. General

In this study, ANSYS software [33] was utilised to simulate the behaviour of RC joints, accurately modelling the properties of both concrete and reinforcement. ANSYS, a leading FEM-based tool, facilitates both static and dynamic analyses for materials that are linear or nonlinear, allowing for the simulation of elastic, inelastic, or viscous behaviours [43]. It enables incremental analysis of stress and strain in RC elements, with capabilities to model large deformations, torsional stress, and contact interaction.

Copyright © 2025 CroCEE
DOI: https://doi.org/10.5592/CO/3CroCEE.2025.145

Model validation was conducted by comparing the results from ANSYS with experimental data to ensure accuracy. The study employed the user-friendly Workbench interface, which is ideal for beginners, while also utilising the APDL scripting language for advanced automation and customization. ANSYS Workbench, Figure 6, supports a wide range of simulations, including structural, thermal, and fluid dynamics analyses. Key features of ANSYS Workbench include an integrated environment (a unified platform for various simulations using ANSYS tools), pre-processing (advanced CAD import and geometry simplification for time efficiency), solution technology (precise simulation of complex phenomena with detailed insights), post-processing (tools for visualising and analysing results through 2D/3D plots, animations, and reports), and model optimisation (optimisation algorithms to enhance performance and reduce costs).



Figure 6. ANSYS Workbench

3.2. Modelling in ANSYS

The general process for conducting any analysis in ANSYS, as shown in Figure 7, whether for simple or complex problems, includes the following steps:

- Pre-processor: Define the geometry, material properties, loads, boundary conditions, and finite element (FE) mesh.
- Analysis: Solve the numerical model defined in the preprocessing phase.
- Post-processor: Analyse and visualise the results.

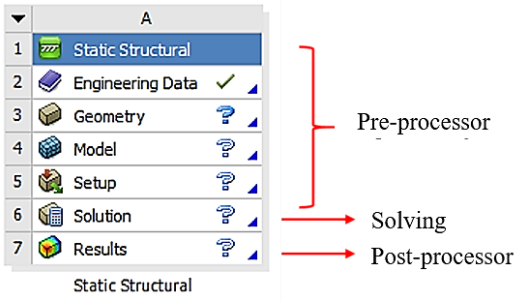


Figure 7. General steps for modelling in ANSYS

Selecting appropriate materials is crucial for modelling and analysing structures, as it significantly impacts the behavior, properties, and durability of the modeled structure or component. ANSYS provides an extensive material library that users can select from and modify as needed. Users can also define and add custom materials with specific properties. The software supports various material types, including linear elastic, isotropic, orthotropic, hyperelastic, viscoelastic, and many other combinations.

In ANSYS, essential material properties include the modulus of elasticity, volumetric density, thermal expansion coefficient, and thermal conductivity. When temperature effects are disregarded, material properties can be treated as linear, requiring only a single iteration. However, properties like the stress-strain relationship are nonlinear and necessitate iterative solutions. Material properties are specified at the element's centre or integration points, depending on the element type [44]. Accurately defining concrete and reinforcement properties in the model module is a critical step for simulating their behaviour and interaction.

In this paper, concrete was modelled using the Coupled Damage-Plasticity (CDP) microplane model, which is well-suited for materials with diverse characteristics. This model accounts for stiffness degradation and material softening, challenges that were previously difficult to simulate, Figure 8.

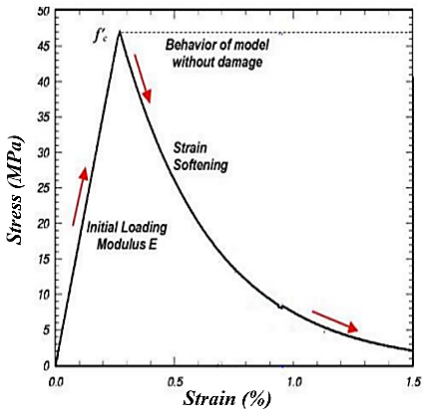


Figure 8. Strain softening effect due to gradual damage of the material

This variant, developed by Zreid in collaboration with ANSYS [45], was designed to incorporate nonlocal interactions, ensuring mesh-independent results. The model represents plasticity using effective stress (in the undamaged space) and employs plastic deformations to capture the resulting damage [45]. Concrete's response under varying stress triaxiality is simulated using the Drucker-Prager function,

Copyright © 2025 CroCEE
DOI: https://doi.org/10.5592/CO/3CroCEE.2025.145

Figure 9. This involves defining the Drucker-Prager yield surface, which considers compressive, tensile, and linear regions.

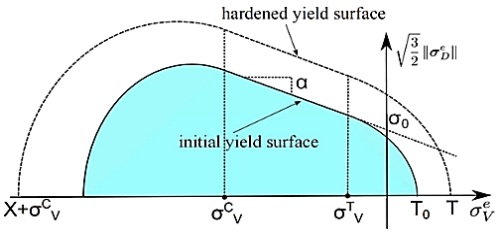


Figure 9. Drucker-Prager function for Microplane model

The initial yield surface defines the boundary of a material's elastic behavior. When the applied stress surpasses this boundary, the hardening process initiates. During this phase, plastic deformations occur, and the elastic region gradually expands until it reaches the hardened yield surface. This new boundary represents the material's updated stress capacity, which will not be exceeded even with further increases in stress. At this stage, material strength decreases, initiating the softening phase, [45]. Defining the CDP microplane model requires specifying 13 parameters, which influence the stress-strain curve, Figure 9.

The concrete material model in ANSYS is implemented using three-dimensional elements (CPT214, CPT215, and CPT216) and two-dimensional elements (CPT211, CPT212, and CPT213). In this study, the CPT215 element was selected, with further details provided in later sections. Reinforcement was modelled using the REINF264 element, with its nonlinear behaviour defined by a bilinear stress-strain isotropic hardening model, which will be explained in more detail subsequently.

To ensure the numerical model accurately represents the physical structure, defining loads and boundary conditions is essential. Loads can include forces applied to faces, edges, or vertices; remote forces or moments applied at distant points; pressures such as fluid, wind, or internal loads; temperature variations; and displacements, commonly used in boundary conditions. Support configurations range from fixed and displacement-defined supports to more advanced options like cylindrical or spherical supports. Proper application of loads and supports is critical to achieving accurate results. Furthermore, generating the finite element mesh is a key step in the simulation process, with ANSYS Workbench offering powerful tools to streamline this task.

Creating the finite element (FE) mesh is a crucial modelling step. ANSYS Workbench provides automated tools with user control over mesh methods, scaling, and edge divisions. This study uses a mesh of hexahedral and prismatic elements with triangular bases to discretize the RC joint, as detailed later.

After preprocessing, ANSYS generates stiffness and mass matrices and load vectors for each element. These are assembled into equations that govern system behavior, solved using methods such as:

- Direct solver: For small to medium models
- Iterative solver: For complex models
- Time integration: For dynamic analyses
- Nonlinear solver: For nonlinear materials or large deformations

If solutions fail to converge, the software adjusts settings or iterations, providing error guidance if needed. Upon successful analysis, users can view results such as displacements, stresses, and deformations through contour plots, animations, graphs, or exported data.

4. Numerical example

This section presents the nonlinear static analysis of an RC exterior joint in ANSYS (version 24.2), validated using experimental data from reference [47] and results from the ANSYS modeling guide (version 19.1), [48]. The paper also investigates how mesh density and element type (hexahedral versus prismatic) influence the speed of solution convergence and the sensitivity of results in nonlinear analysis. Figures 10 - 11 illustrate the geometry of the analysed RC exterior joint [47] and the corresponding geometry model in ANSYS, respectively.

The reinforcement used has the following properties:

Copyright © 2025 CroCEE
DOI: https://doi.org/10.5592/CO/3CroCEE.2025.145

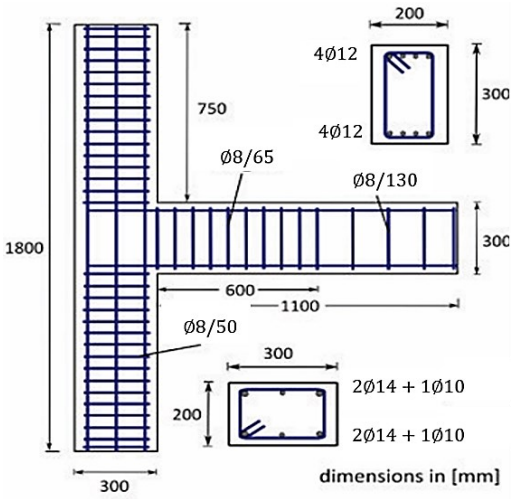


Figure 10. Geometry of the analysed RC joint and reinforcement detailing of the cross sections

$\sigma_y = 470\ MPa$ – yield strength of steel,

The elastic properties of the concrete are:

$f_{uc} = 31.6\ MPa$– compressive strength of concrete,

$\nu = 0.3$ – Poisson's ratio,

$E = 20\ 000\ MPa$ – modulus of elasticity,

$f_{bc} = 36.34\ MPa$ – biaxial strength of concrete

$f_{tc} = 3MPa$ – tensile strength of concrete.

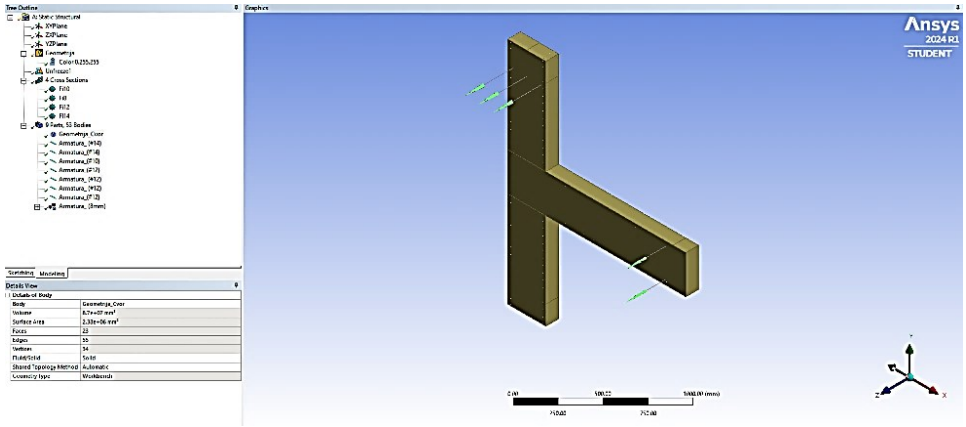


Figure 11. Geometry in ANSYS

Figure 12 shows the APDL commands for defining the CPT215 element and the parameters for the Drucker-Prager model in ANSYS. The REINF264 element from the ANSYS library was used for modelling reinforcement. This element is particularly useful for simulating reinforcement with arbitrary orientations. The nonlinear behavior of reinforcement in the RC joint was defined based on the Bilinear Isotropic Hardening model, as shown in Table 2.

```
!   Commands inserted into this file will be executed just prior to the ANSYS SOLVE command.
!   These commands may supersede command settings set by Workbench.

!   Active UNIT system in Workbench when this object was created:  Metric (mm, kg, N, s, mV, mA)
!   NOTE:  Any data that requires units (such as mass) is assumed to be in the consistent solver unit system.
!                See Solving Units in the help system for more information.


/PREP7
et,matid,CPT215 !define matid to CPT215
KEYOPT,matid,18,2
MP,EX,matid,20000 ! Define Elasticity Modulus (enter a value for E)
MP,NUXY,matid,0.2 ! Define Poisson's ratio
TB,MPLA,matid,,,DPC !Define Drucker-Prager
TBDATA,1,31.6,36.34,3,1,40000,-35 !fuc,fbc,fut,Rt,D,sigVc
TBDATA,7,2,0,2e-5,3000,2000 !R,gamt0,gamc0,betat,betac
TB,MPLA,matid,,,NLOCAL
TBDATA,1,1600,2.5 !nonlocal interaction range c, over nonlocal parameter m

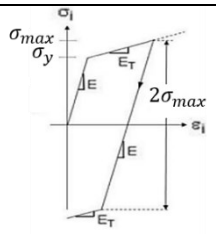
! Replace SOLID185 with CPT215
allsel
esel,s,ename,,SOLID185
emodif,all,type,matid
allsel
! Print out the result:
etlist,all
/SOLU
OUTRES,ALL,ALL
```

Figure 12. APDL commands for defining the CPT215 element and Drucker-Prager parameters

Copyright © 2025 CroCEE
DOI: https://doi.org/10.5592/CO/3CroCEE.2025.145

Table 2. The bilinear isotropic model for steel

The material model for steel - *Bilinear Isotropic Hardening*	
Modulus of elasticity E_s	190 000 MPa
Poisson's ratio, ν_s	0.3
Yield strength, σ_y	470 MPa
Tangent modulus, E_T	1000 MPa



Defining proper boundary conditions is key to accurately modelling the RC joint and replicating rotational supports from the experiment, Figure 13. Load is applied as a constant axial force of 94.80 kN on the column, and an 80 mm displacement at the beam end, Figure 14.

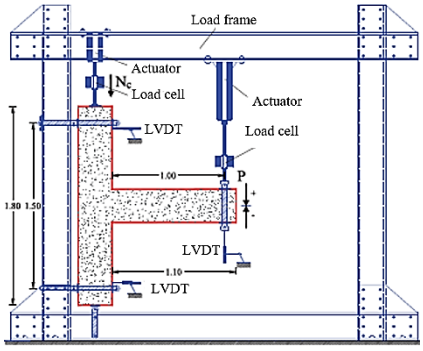


Figure 13. Experiment – analysed specimen with boundary conditions, [48]

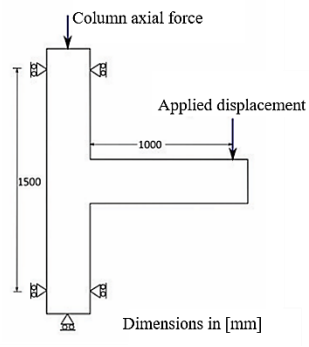


Figure 14. Shematic representation of the model – boundary conditions and loading

Two time steps are considered: $t_1 \in [0,1]$, $t_2 \in [1,2]$, t in seconds. The axial force on the column is applied in time step t_1, and it remains constant at time step t_2. 80 mm displacement is defined in time step t_2.at the beam end.

A finite element (FE) mesh was used to evaluate the accurancy and convergence of numerical solutions. The mesh consisted of hexahedral elements with a size of 25mm, as illustrated in Figure 15.

4.1. Convergence and accurancy of the numerical solutions

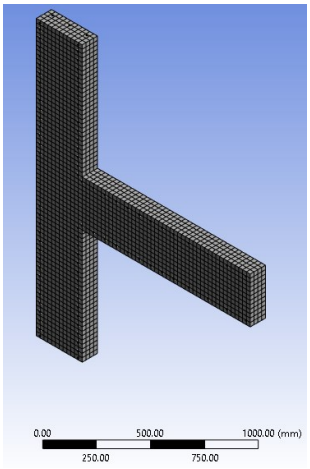


Figure 15. Model discretised with hexahedral finite elements

To verify the convergence and accuracy of the numerical solutions for the RC joint in ANSYS, vertical force–displacement (at the end of the beam) curves were compared with those from the ANSYS guide (version 19.1) and experimental data (Figure 16, Table 3).

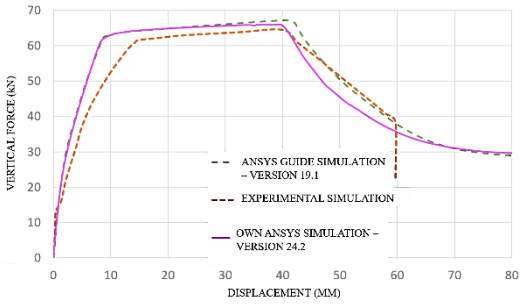


Figure 16. Comparison of vertical force-displacement curves at the end of the beam

The results of the developed model align closely with those from the ANSYS guide, particularly in the curve segment representing elastic behaviour and material hardening. However, material softening in the developed model begins at a displacement of 35 mm, whereas it

Proceedings of the 3rd Croatian Conference on Earthquake Engineering - 3CroCEE
19–22 March 2025, Split, Croatia
Copyright © 2025 CroCEE
DOI: https://doi.org/10.5592/CO/3CroCEE.2025.145

starts at 42 mm in the ANSYS guide model. Beyond this point, as displacement increases, the results converge, with a final discrepancy of 3.51% observed at an 80 mm displacement.

The results in Table 3 are displayed as whole numbers, reflecting the original data format. To maintain consistency, the developed model's results have also been presented in this manner.

Table 3.

a) Comparison of results obtained from the ANSYS guide with results from the own model

ANSYS GUIDE SIMULATION – VERSION 19.1		OWN ANSYS SIMULATION – VERSION 24.2		DIFFERENCE (%)
DISPLACEMENT (MM)	FORCE (kN)	DISPLACEMENT (MM)	FORCE (kN)	
0	0	0	0	0
1	10	1	11	10.18
1	20	1	18	12.11
2	30	2	29	4.50
4	40	4	40	0.15
6	50	6	47	6.59
8	60	8	61	2.36
8	62	8	61	1.02
9	63	9	62	1.35
12	64	12	64	0.07
20	65	20	65	0.13
35	67	35	66	1.16
40	67	40	66	1.84
42	67	42	62	8.19
42	66	42	62	6.84
43	64	43	60	6.46
45	60	45	53	13.70
46	57	46	51	11.88
49	51	49	47	9.56
52	47	52	43	10.70
57	42	57	38	9.43
60	38	60	35	7.62
63	35	63	34	2.33
67	32	67	32	1.15
71	30	71	31	1.11
76	29	76	30	2.26
80	29	80	30	3.51

b) Comparison of results obtained from the own model with results from experiment

EXPERIMENT		OWN ANSYS SIMULATION – VERSION 24.2		DIFFERENCE (%)
DISPLACEMENT (MM)	FORCE (kN)	DISPLACEMENT (MM)	FORCE (kN)	
0	0	0	0	0.00
0	0	0	0	0.00
0	13	0	11	18.92
1	16	1	18	10.32
2	21	2	29	25.98
3	27	3	36	24.23
4	32	4	40	19.63
5	36	5	45	19.45
6	42	6	47	10.88
8	46	8	61	24.01
10	53	10	63	16.50
13	59	13	64	7.59
14	61	14	64	5.41
15	62	15	64	3.67
17	62	17	65	4.51
23	63	23	65	2.92
32	64	32	66	3.22
40	65	40	66	2.16
43	61	43	60	1.36
46	57	46	51	10.79
49	53	49	47	12.52
53	48	53	42	14.31
56	44	56	39	11.69
58	41	58	37	10.20
60	38	60	35	9.74
60	22	60	35	35.98

An investigation into discrepancies between ANSYS versions 19.1 and 24.2 revealed that variations may arise from differences in operating systems, processor cores, and software configurations. Additional factors include the lack of specific details regarding the ANSYS guide model's load distribution and incremental application. Furthermore, the tolerance value used in the Newton-Raphson method significantly affects numerical accuracy—lower tolerances require more iterations, while higher tolerances increase the risk of errors if convergence is not achieved.

The force-displacement curve from the developed ANSYS model closely matches the experimentally obtained curve in terms of shape. However, the most significant deviations occur during the material softening phase. Additionally, it is important to note that experimental results may be influenced by both instrumental and random errors.

4.2. Variation in Finite Element mesh density and type

The finite element (FE) mesh density was initially formed using hexahedral elements, followed by prismatic elements, and the resulting data was analysed and compared. Meshes with element sizes of 35 mm, 50 mm, and 100 mm were generated, as shown in Figure 17, and evaluated against a 25 mm mesh, which served as the benchmark for accuracy and convergence. This methodology was employed to assess the sensitivity of nonlinear numerical analysis results to changes in FE mesh density and to determine the impact of mesh refinement on the accuracy of the results.

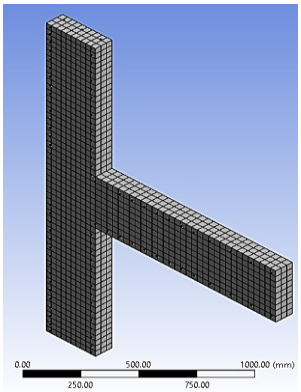


Figure 17. a) Discretisation of the RC joint using finite elements of size 35 mm

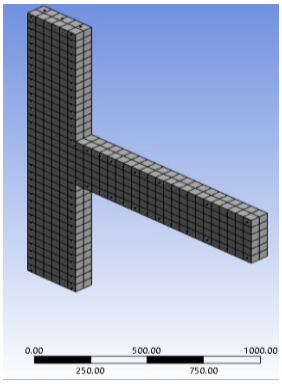


Figure 17. b) Discretisation of the RC joint using finite elements of size 50 mm

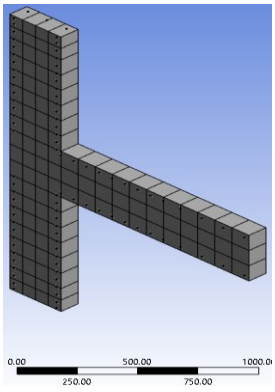


Figure 17. c) Discretisation of the RC joint using finite elements of size 100 mm

Copyright © 2025 CroCEE
DOI: https://doi.org/10.5592/CO/3CroCEE.2025.145

The next section presents the force-displacement curves for models created using different finite element (FE) sizes in the mesh generation process, as illustrated in Figure 18. The size of the finite elements has a significant influence on mesh generation and the accuracy of results, particularly in nonlinear analyses. While variations in FE mesh density have little effect during the elastic phase, discrepancies become more pronounced in later stages. As shown in Figure 18, meshes with element sizes of 100 mm and 50 mm fail to deliver satisfactory results, whereas the 35 mm mesh closely approaches the accuracy of the 25 mm mesh. Smaller elements enhance precision but require longer simulation times and better computational resources.

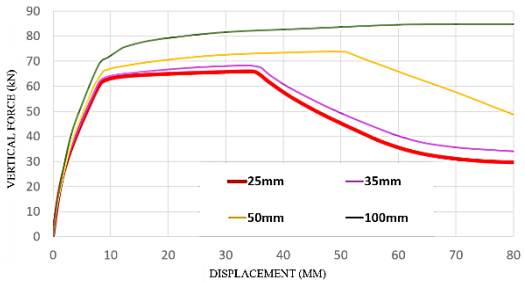


Figure 18. Curve vertical force-displacement at the end of the beam relative to the variation in finite element size

In addition to the element size comparison, the study also evaluated results obtained using hexahedral element meshes alongside models generated with prismatic elements with triangular bases. The prismatic element meshes were created with the same element sizes—35mm, 50mm, and 100mm—as in the previous analysis, Figure 19.

Figure 20 presents a comparison of the vertical force-displacement curves for both types of finite elements used to discretize the analysed RC joint.

It is evident that models with meshes generated using prismatic elements with triangular bases demonstrate faster convergence compared to those with hexahedral elements, particularly for cases involving 35mm element sizes.

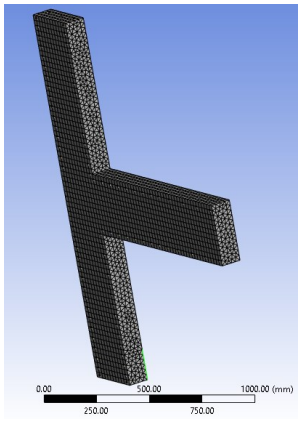


Figure 19. a) Discretisation of the RC joint using prismatic finite elements of size 35 mm

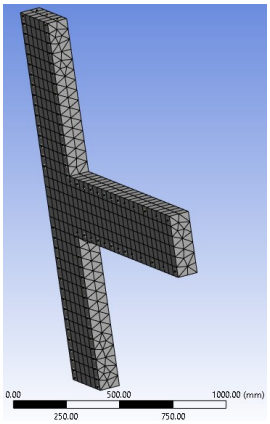


Figure 19. b) Discretisation of the RC joint using prismatic finite elements of size 50 mm

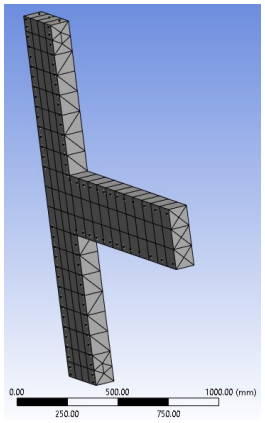


Figure 19. c) Discretisation of the RC joint using prismatic finite elements of size 100 mm

Copyright © 2025 CroCEE
DOI: https://doi.org/10.5592/CO/3CroCEE.2025.145

5. Conclusion

This study conducted a nonlinear static analysis of a reinforced concrete (RC) joint using ANSYS software (version 24.2) to better understand RC joint behaviour and evaluate the feasibility of such connections. It also aimed to provide a foundation for future research involving numerical and experimental analysis of strengthened RC joints. Nonlinear behaviour was modelled using ANSYS material models (CPT215 and REINF264), with loads applied in two steps: displacement at the beam's end and a constant axial force on the column.

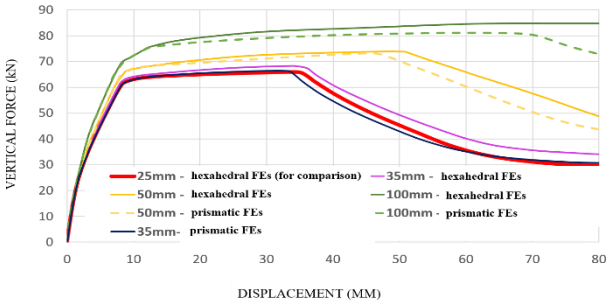


Figure 20 Curve vertical force-displacement at the end of the beam relative to the variation in finite element type

Force-displacement curves from the numerical model were compared with experimental data and results from the ANSYS guide (version 19.1) to validate convergence and accuracy. The force-displacement curve generated by own ANSYS model closely aligns in shape with the experimentally obtained curve. However, the most notable discrepancies are observed during the material softening phase. It is also essential to consider that experimental results may be affected by both random and instrumental errors.

Analysis of finite element (FE) mesh density, element size, and type (hexahedral versus prismatic elements with triangular bases) revealed that even for simple geometries, element size has a significant impact on numerical accuracy. Additionally, prismatic elements with triangular bases achieved faster convergence compared to hexahedral elements.

Future research could focus on analysing RC joints under various loading conditions, exploring alternative material models or input parameters, and modelling strengthening techniques for these connections. This would enhance understanding of the factors influencing joint behaviour and performance, contributing to improved design and strengthening of RC structures.

References

[1] Sharbatdar, K., Fakharifar, M. (2009): The Finite Element analysis of RC joints strengthened with external FRP composites, *3rd International Conference on Concrete & Development,* Iran

[2] Hassan, W.M., Park, S., Lopez, R. R., Mosalam, K.M., Moehle, J. P. (2010): Seismic response of older-type reinforced concrete corner, *Proceedings of the 9th U.S. National and 10th Canadian Conference on Earthquake Engineering, Toronto,* Canada

[3] Pan, Z. (2016): Modeling of interior beam-column joints for nonlinear analysis of reinforced concrete frames, *Master thesis, University of Toronto, Department of Civil Engineering*

[4] Coşgun, C. (2013): Retrofit of 3D Reinforced Concrete Beam-Column Joint with FRP, *PhD thesis, Istanbul Technical University, Institute of Science and Technology*

[5] Paulay, T., Park,, R., Priestley, M.J.N. (1978): Reinforced Concrete Beam-Column Joints under Seismic Actions, *ACI Structural Journal 75*

[6] Coşgun, T. et al (2019).: Ispitivanja rubnih spojeva greda-stup postojećih AB konstrukcija na djelovanje potresa, *Časopis Građevinar*, broj 71

[7] Hanson, N.W., Connor, H.W. (1967): Seismic Resistance of Reinforced Concrete Beam- Column Joints, *Journal of the Structural Division - ASCE, 93*

[8] Zhang, L., Jirsa, J.O. (1982): A study of shear behavior of reinforced concrete beam– column joints, *PMFSEL Report 82–1, University of Texas*, Austin, USA

[9] Sarsam ,K.F., Phipps, M.E. (1985): The shear design of in situ reinforced concrete beam– column joints subjected to monotonic loading, *Magazine of Concrete Research, no. 37*

Copyright © 2025 CroCEE
DOI: https://doi.org/10.5592/CO/3CroCEE.2025.145

[10] Pantazopoulou, S., Bonacci, J. (1992): Consideration of questions about beam–column joints, *Aci Structural Journal, 89*

[11] Hwang, J., Lee, H.J. (1999): Analytical model for predicting shear strengths of exterior reinforced concrete beam–column joints for seismic resistance, *Aci Structural Journal 96*

[12] Ehsani, M.R., Wight, J.K. (1986): Effect of beams and slab on behavior of reinforced concrete beam-to-column connections, *Aci Structural Journal, 82*

[13] Pessiki, S.P., Conley, C.H., Gergely,, P., White, R.N. (1990): Seismic behavior of lightly reinforced- concrete column and beam-column joint details, *Technical Report NCEER- 90-0014, National Centre for Earthquake Engineering Research*

[14] Tsonos,, A.G., Tegos, I.A., Penelis, G. (1992): Seismic resistance of type 2 exterior beamcolumn joints reinforced with inclined bars, *Aci Structural Journal, 89*

[15] Higazy, E.M.M., Elnashai,, A.S., Agbabin, M.S. (1996): Behavior of beam column connections under axial column tension, *Journal of Structural Engineering*

[16] Park, R., Paulay, T. (1975): *Reinforced concrete structures*. John Wiley & Sons, Inc., Newyork

[17] Altoontash, A. (2004): Simulation and Damage Models for Performance Assessment of Reinforced Concrete BeamColumn Joints." P*hD Thesis, Department of Civil and Environmental Engineering, Stanford University, California,* United States

[18] Viwathanatepa, S., Popov, E.P., and Bertero, V.V. (1979): Effects of Generalized Loadings on Bond of Reinforcing Bars Embedded in Confined Concrete Blocks, *Rep. No. UCB/ERRC-79/22 ERRC, Univ. of California, Berkeley, CA*

[19] Eligehausen, R., Popov, E.P. and Bertero, V.V. (1983): Local bond Stress-Slip Relationship of Deformed Bars under Generalized Excitations, *EERC Report 83/23, University of California*

[20] Pessiki, S.P., Conley, C.H., Gergely, P., White, R.N. (1990): Seismic behavior of lightly reinforced - concrete column and beam-column joint details, *Technical Report NCEER- 90-0014, National Centre for Earthquake Engineering Research*

[21] Bracci, J.M., Reinhom, A.M., Mander, J.B. (1992): Seismic resistance of R/C frame structures designed only for gravity loads, Part III experimental performance and analytical study of structural model, *Technical Report NCEER-92-0029, National Centre for Earthquake Engineering Research*

[22] Fleury, F., Reynouard, J-M., Merabet, O. (2000): Multicomponent model of reinforced concrete joints for cyclic loading, *Journal of mechanical Engineering 10*

[23] Pantazopoulou, S.J., Bonacci, J.F. (1994): On earthquake-resistant reinforced concrete frame connections, *Canadian Journal of Civil Engineering 21*

[24] Elmorsi, M.S.E. (1998): Analytical modeling of reinforced concrete beam column connections for seismic loading, *PhD thesis, McMaster University, Ontario*, Canada

[25] Hegger, J., Sherif A., Roeser W. (2003): Nonseismic design of beam column joints, *ACI Structural Journal 100*

[26] Hwang, S.J., Lee, H.J., Liao, T.F., Wang, K.C., Tsai, H.H. (2005): Role of hoops on shear strength of reinforced concrete beam-column joints, *ACI Structural Journal 102*

[27] Alath, S., Kunnath, S.K. (1995): Modeling Inelastic Shear Deformation in RC Beam-Column Joints, *Proceedings of the 10th Conference, University of Colorado at Boulder*

[28] Shin, M., LaFave, J.M. (2004): Modeling of Cyclic Joint Shear Deformation Contributions in RC Beam-Column Connections to Overall Frame Behavior, *Structural Engineering and Mechanics, 18(5)*

[29] Ghobarah, A., Youssef, M. (2001): Modeling of RC Beam-Column Joints and Structural Walls, *Journal of Earthquake Engineering, 5(1), 91-111*

[30] Lowes, L.N., Alttontash, A.: (2003): Modeling Reinforced Concrete Beam-Column Joints Subjected to Cyclic Loading, *Journal of Structural Engineering 129(12)*

Copyright © 2025 CroCEE
DOI: https://doi.org/10.5592/CO/3CroCEE.2025.145

[31] Mitra, N., Lowes, L.N. (2007): Evaluation, calibration, and verification of a Reinforced Concrete Beam-Column Joint Model., *Journal of Structural Engineering* 133(1)

[32] Aoyama, H., Otani S., Kitayama K. (1988): Design critiria for reinforced concrete interior beam-column connections, *Proceedings of 9th World Conference on Earthquake Engineering,* Tokyo-Kyoto, Japan

[33] ANSYS Workbench Product Release Notes (2005), USA

[34] ABAQUS 6.12 (2012) – Analysis User's Manual, USA

[35] Ellobody, E., Baile C.G. (2008): Behaviour of unbonded posttensioned one-way concrete slabs*", Advance Structural Engineering, Vol. 11, No.* 1

[36] Zhang, H.M., Lu, X.L., Duan, Y.F., Li J.B. (2011): Experimental study and numerical simulation of partially prefabricated laminated composite RC walls", *Advances in Structural Engineering, Vol. 14, No. 5,* 2011

[37] Alemdar, Z.F., Matamoros, A.B., Browning, J. (2013): High resolution modeling of reinforced concrete bridge columns under seismic loading, *ACI Structural Journal, Vol. 110, No. 5*

[38] Henriques, J., Silva, L.S, Valente I.B. (2013): Numerical modeling of composite beam to reinforced concrete wall joints Part I: Calibration of joint component, *Engineering Structures, Vol. 52*

[39] Abbas, A.A., Mohsin, S.M.S. and Cotsovos, D.M. (2014): Seismic response of steel fibre reinforced concrete beam-column joints", *Engineering Structures, Vol. 59*

[40] Patil, S.S., Manekari, S.S. (2013): Analysis of reinforced beam-column joint subjected to monotonic loading", *IJEIT*

[41] Bindhu, K.R., Jaya, K.P. (2012): Strength and Behavior of Exterior Beam Column Joints with Diagonal cross Bracing Bars. *Asian Journal of Civil Engineering (Building and Housing), 11*

[42] Sohailuddin, S. i Shaikh, M.G. (2013): Finite element modelling of reinforced concrete beam – column joint using ANSYS, *IJSCER*

[43] Lazzari, B.M. (2015): Análise por elementos finitos de peças de concreto armado e protendido sob estados planos de tensão, *Dissertação (Mestrado em Engenharia) – Programa de Pós-Graduação em Engenharia Civil, Universidade Federal do Rio Grande do Sul, Porto Alegre*

[44] *ANSYS Mechanical APDL Element Reference* (2010), USA

[45] Zreid, I., Kaliske, M. (2018): A gradient enhanced plasticity–damage microplane model for concrete, *Computational Mechanics*

[46] Pirket, M. (2020): Non-linear seismic analysis of a concrete gravity dam using a microplane material model, *Master's Thesis, Graz University of Technology, Hydraulics and Geotechnical Engineering*

[47] Chalioris, C.E., Favvata, M. J., Karayannis, C.G. (2008): Reinforced concrete beam–column joints with crossed inclined bars under cyclic deformations, *Earthquake Engineering and Structural Dynamics*

[48] ANSYS Documentation, Release 19.1 (2019), *Demonstration guide – reinforced concrete*

[49] https://www.ansys.com/blog/what-is-apdl, Accessed 21st November 2024

[50] Dr. Daylo APDL Commands - https://cutt.ly/IjsHW8c, Accessed 21st November 2024

Proceedings of the 3rd Croatian Conference on Earthquake Engineering - 3CroCEE
19–22 March 2025, Split, Croatia
Copyright © 2025 CroCEE
DOI: https://doi.org/10.5592/CO/3CroCEE.2025.150

IMPACT OF ENVIRONMENT AND CLIMATE CHANGE ON SEISMIC RESISTANCE OF CONCRETE BRIDGES

Marija Kušter Marić [(1)], Petra Milić [(2)], Anđelko Vlašić [(3)], Mladen Srbić [(4)], Ana Mandić Ivanković[(5)], Dominik Skokandić [(6)]

[(1)] *Associate professor, Faculty of Civil Engineering, University of Zagreb, marija.kuster.maric@grad.unizg.hr*
[(2)] *PhD student, Faculty of Civil Engineering, University of Zagreb, petramilic7@gmail.com*
[(3)] *Full professor, Faculty of Civil Engineering, University of Zagreb, andjelko.vlasic@grad.unizg.hr*
[(4)] *Assistant professor, Faculty of Civil Engineering, University of Zagreb, mladen.srbic@grad.unizg.hr*
[(5)] *Full professor, Faculty of Civil Engineering, University of Zagreb, ana.mandic.ivankovic@grad.unizg.hr*
[(6)] *Assistant professor, Faculty of Civil Engineering, University of Zagreb, dominik.skokandic@grad.unizg.hr*

Abstract

In seismic design and assessment, it is often assumed that the seismic resistance of the structure remains constant over time, although it is subjected to deterioration processes. However, structure exposure to its environment and local climate lead to several degradation mechanisms, which impact structure durability and load-bearing capacity. By neglecting the influence of the environment and changing climate during the service life, the structure resistance can be significantly overestimated, especially in extreme events such as an earthquake. The focus of this article is on concrete bridges exposed to aggressive environmental and climate conditions (de-icing salts, sea, carbon dioxide concentration in air, high winds, floods, etc.). Concrete bridges and similar structures without surface protection such as facades, coatings, etc. are susceptible to many degradation processes caused by their environment and the local climate. Since corrosion of reinforcement in concrete is the most common degradation process of concrete structures, its effects on seismic resilience are analysed in more detail. In the first part of the article, an overview of numerical and experimental investigations is given to explain and quantify how much the corrosion process can reduce the seismic capacity of the structure. The second part of the article discusses the effects of climate change on the durability and seismic resistance of concrete bridges in the future. In the third part, several bridges in Croatia are presented as case studies where a combination of deterioration processes and seismic action led to damage of the structure. Finaly, recommendation for optimal assessment and management of concrete bridges exposed to multi-hazard environment (earthquake, climate change, aggressive environment) will be given in conclusion.

Keywords: durability, concrete structures, climate change, environment, seismic resistance.

1. Introduction

Currently, seismic design does not assume that the seismic resistance of a structure will change over time. It is considered constant throughout the service life of the structure [1,2]. Thus, the effects of their environment and local climate on the structures, material deterioration, the influence of previous earthquakes and other damage were not considered [3]. This means that the seismic capacity of a structure at the beginning of its service life, which is not corroded or undamaged, is equated with a structure that is at the end of its service life and is exposed to the long-term influence of climate, environmental conditions, damage and other degradation mechanisms. This assumption is not only incorrect, but also not on the side of safety. This fact becomes even more important considering that a significant number of earthquake-prone structures are designed before modern seismic standards and as such pose a hazard due to the additional degradation mechanisms over time [4].

The focus of this article is on concrete bridges exposed to aggressive environmental and climate conditions (de-icing salts, sea, carbon dioxide concentration in air, high winds, floods, etc.). Concrete bridges and similar structures without surface protection such as facades, coatings, etc. are susceptible to many degradation processes caused by their environment and the local climate, e.g. carbonation, freezing-thawing cycles, penetration of chloride in concrete, thermal stresses, etc. Among all possible

Proceedings of the 3rd Croatian Conference on Earthquake Engineering - 3CroCEE
19–22 March 2025, Split, Croatia
Copyright © 2025 CroCEE
DOI: https://doi.org/10.5592/CO/3CroCEE.2025.150

degradation mechanism, corrosion of reinforcement in concrete is the most common and causes the highest repair costs. Moreover, reinforcement corrosion in advanced stage decreases load bearing capacity and seismic resilience of the structure. In the first part of the article, an overview of numerical and experimental investigations is given to explain and quantify how much the corrosion process can reduce the seismic capacity of the structure.

Reinforcement corrosion in concrete as well as other degradation processes of concrete structures may be accelerated by climate change. Moreover, climate change can have multiple negative impact on concrete bridges and other structures [5]. Hence, the effects of climate change on the durability and seismic resistance of concrete bridges are discussed in the second chapter.

To illustrate the impact of various degradation mechanisms on seismic resistance of structures, several bridges in Croatia are presented as case studies where a combination of deterioration processes and seismic action led to damage of the structure. Finally, recommendation for optimal assessment and management of concrete bridges exposed to multi-hazard environment (earthquake, climate change, aggressive environment) will be given.

2. Impact of reinforcement corrosion in concrete on seismic resistance of structures

Most of the infrastructure in Croatia is made of concrete, and the situation is similar worldwide. The main mechanism for the degradation of concrete structures is reinforcement corrosion, which can be triggered by the presence of carbon dioxide, causing carbonation, or by chloride ions from de-icing salts or seawater. Reinforcement corrosion in concrete is not just an aesthetic problem and a maintenance issue. Advanced corrosion reduces the load-bearing capacity and structure resistance to action. If maintenance and repair of structure are not carried out in time, the structure may collapse, especially in extreme events such as an earthquake.

From a seismic design perspective, the consequences of corrosion are the reduction of bearing capacity and deformability, as well as the reduction of energy dissipation capacity, changes in the dynamic properties of the structure, ductility and collapse mechanisms [6-9]. Effects of corrosion on mechanical behaviour of reinforced concrete structures is shown in Fig. 1. Although pitting corrosion induced by chloride is more vulnerable than uniform corrosion caused by carbonation, both types include an electrochemical process of iron dissolution and rust forming. Direct consequences of this process are: (i) reduction of the reinforcement bar area and ductility and (ii) volume expansion of corrosion products [10-13]. A reduced area of the reinforcement leads to reduction of the load-bearing capacity for bending, shear and fatigue. Furthermore, not only the ductility of the reinforcing bars is reduced, but also the stiffness of the structure, the redistribution of internal forces and the load-bearing capacity of a statically indeterminate system [14,15].

Pitting corrosion can significantly reduce the cross-section of the reinforcement, affect the load-bearing capacity and fatigue strength and can lead to brittle fracture of high-strength steel cables for concrete prestressing [16]. The danger of localised corrosion is also reflected in the fact that the degree (depth) of damage can progress considerably before the signs become visible on the surface of the concrete [17]. Furthermore, volume growth of the corrosion products, which is two to six times greater than the original volume of the reinforcement steel, causes additional stresses in the concrete, leading to cracking and possible spalling of the concrete cover. This leads to a reduction of the concrete cross section area.

If the spalling of the concrete cover occurs on the compression side of the cross-section, the arm of the internal forces and thus the bending moment is reduced. Cracks and spalling of the concrete in the area of the reinforcing bars lead to a reduction of the bond strength between concrete and reinforcement and to a reduction of the shear strength. Cracks in the concrete in the tensile zone mean that the tensile strength of the concrete has been reached, and any additional tensile stress leads to further opening of the existing cracks or the formation of new cracks in the concrete [15].

Copyright © 2025 CroCEE
DOI: https://doi.org/10.5592/CO/3CroCEE.2025.150

Cracked concrete reduces the protection of the reinforcement and allows easier and more direct penetration of aggressive substances in concrete to the reinforcement level, reducing the load-bearing capacity of the structure in the long term. Depending on the direction of the cracks, they can also affect the stiffness and the re-distribution of internal forces in the structure [15,16,18].

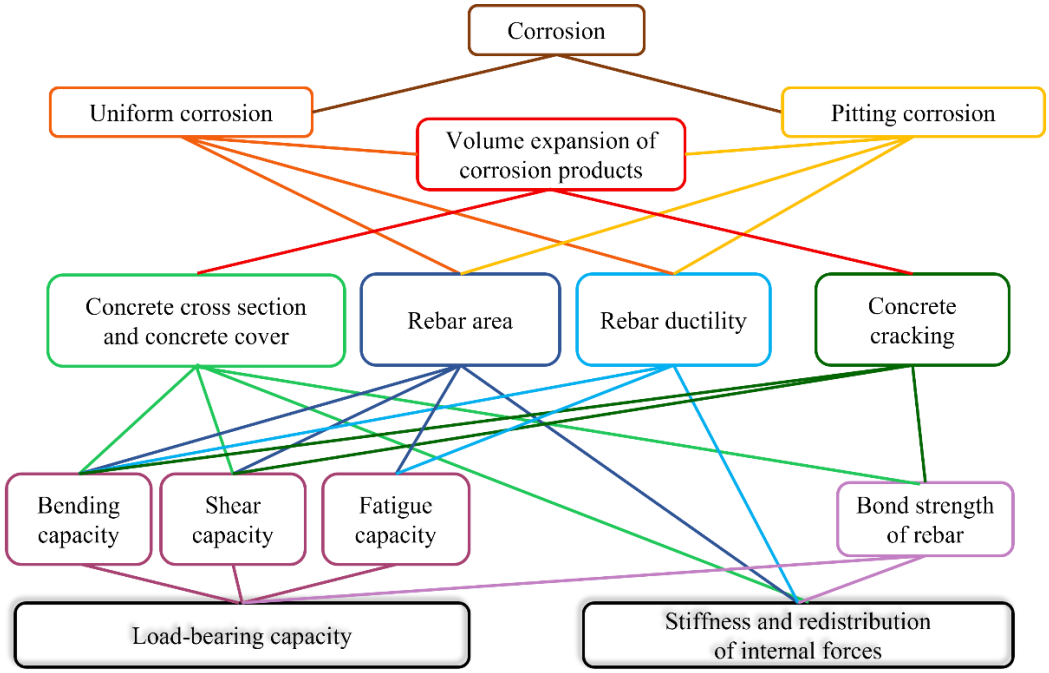


Figure 1. Effects of reinforcement corrosion in concrete on seismic resistance and mechanical behaviour of structure in general

Seismic assessment of existing structures is essential since older structures are designed according to older codes and regulations requiring lower or none seismic resistance in comparison with newer structures. On the other hand, older structures are long-term exposed to degradation processes due to environment and climate action. Damage on older structure additionally reduces their load-bearing capacity, hence their probability of failure may be multiplied.

Many researches on impact of reinforcement corrosion in concrete on seismic capacity have been conducted in recent years [1-4;6-26]. An overview of the results of numerical, laboratory and on-site tests is presented in following chapters. Although each research has some assumption and restriction, since it is difficult to define and predict environment effect on the long-term structural performance, presented findings are valuable for management of all concrete bridges and other infrastructure located in area of high seismicity.

Bridge locations characterized by aggressive maritime environment and high seismicity can be found in Croatian Adriatic regions but also worldwide. To quantify impact of seismic hazard and reinforcement corrosion on seismic resistance during the service life of structure, a probabilistic model is developed and illustrated on Japanese case study [21]. Three bridges in Japan with different seismic vulnerability and distance to coastline are analysed: selected bridge closest to coastline (d=0.1 km, blue line) with the highest corrosion vulnerability has the lowest seismic action, while the bridge farthest from the sea (d=1.0 km, red line) has the highest seismic vulnerability. Corrosion hazard is presented by amount of airborne chloride, while seismic vulnerability in term of annual probability of exceedance of maximum velocity of ground motion (Fig. 2).

For seismic assessment and reinforcement corrosion simulation RC bridge piers are analysed and modelled with single degree of freedom. The plastic hinge with longitudinal rebars buckling of the pier

Copyright © 2025 CroCEE
DOI: https://doi.org/10.5592/CO/3CroCEE.2025.150

was considered as the sole limit state when estimating seismic failure probability. Reinforcement corrosion analysis include estimation of time to rebar corrosion initiation and the time to cover cracking, and estimation of rebar weight loss.

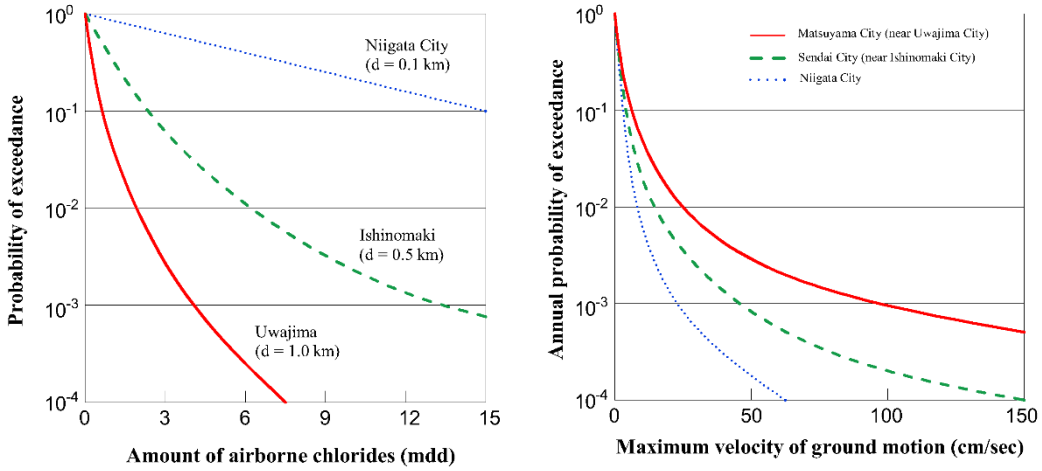


Figure 2. Corrosion vulnerability presented by amount of airborne chloride (left) and seismic hazard presented as velocity of ground motion (right) (adapted from [21])

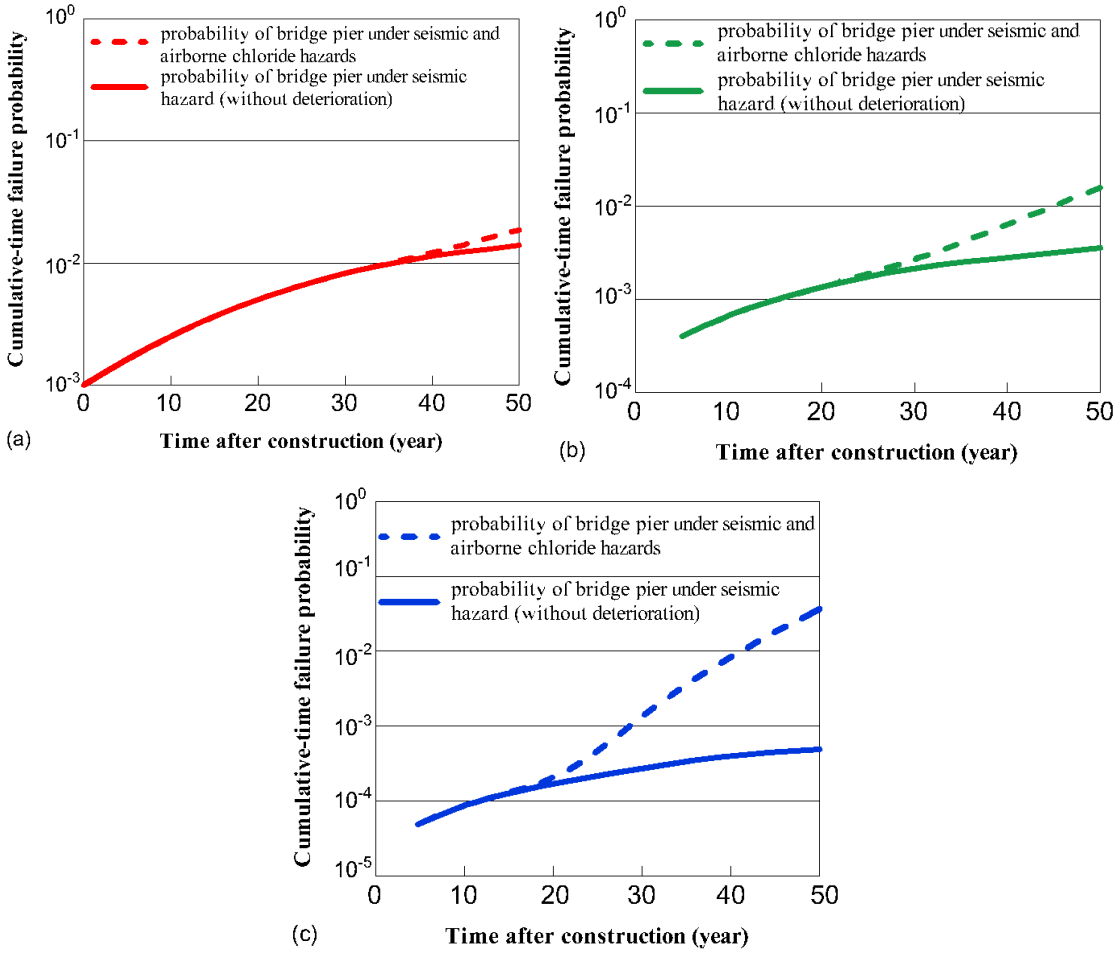


Figure 3. Relationship between time and cumulative-time failure probability: (a) Uwajima City; (b) Ishinomaki City; and (c) Niigata City (adapted from [21])

Proceedings of the 3rd Croatian Conference on Earthquake Engineering - 3CroCEE
19–22 March 2025, Split, Croatia
Copyright © 2025 CroCEE
DOI: https://doi.org/10.5592/CO/3CroCEE.2025.150

Fig. 3 shows the comparison of cumulative time failure probability over the years between piers with considered deterioration due to chloride ingress and without deterioration, for each city. At the start of service life the failure probability only depends on the seismic hazard which is the highest for the bridge in the city of Uwajima (red line). However, greater hazard associated with airborne chloride in the Niigata City results in increased cumulative-time failure probability of RC bridge pier during its service life (blue line). Moreover, even though Niigata city has the lowest seismicity of the three cities, at 50 years of service life the cumulative-time failure probability of RC bridge pier in Niigata City is the highest.

The findings show that the life-cycle reliability of RC bridge piers depends on both the seismic and airborne chloride hazards, and that the cumulative-time failure probabilities of RC bridge piers located in seismic zones can be dramatically affected by the effect of airborne chlorides.

Another research [26] proposed time-dependent corrosion damage model for more successful seismic performance assessment of RC bridges. After comprehensive analysis [26], it is concluded that for smaller peak accelerations (ag < 0.1 g) the influence of corrosion can be neglected. For higher peak accelerations, the reduction in capacity is not too great for both corroded and non-corroded bridges up to a service life of about 25 years. For example, for moderate seismic vulnerability, probability of failure is 14.1% for uncorroded structure. For moderate corrosion damage, values of probability of failure increase with structure age and amount: 24.5%, 47.8%, 74.6% and 98.0% for 25, 50, 75 and 90 years of service life, respectively [26].

Results of numerous research show that corrosion changes the failure mechanism from ductile (yielding of the reinforcement) to brittle failure (concrete crushing), which is always less desirable [4,16,18]. On the other hand, reinforcement corrosion in concrete has a greater effect on structure ductility than on flexural capacity.

3. Impact of climate change on seismic resistance of structures

Analysis of the climate change projection for Croatia for the periods up to 2040 and 2070 with possible impacts on infrastructure [5] leads to conclusion that the effects of climate change on infrastructure have been felt in all areas of civil engineering, from hydraulic engineering, geotechnics and load-bearing structures to building materials, construction organization and management, as well as in all regions in Croatia. Similar analyses are provided for various countries and regions worldwide and unfortunately proofs are already seen in everyday news.

Climate change has multiple and complex effects on infrastructure. However, those effects of climate change on infrastructure can be systemized into two groups (Fig. 4): extreme events and progressive changes. Extreme weather conditions such as flooding and heavy rainfall lead to bridge scour, soil liquefaction and foundation collapse, insufficient capacity of drainage systems, landslides, road and railway damage, accelerated material degradation and reduced slope stability. Strong storms and gusts of wind lead to the failure of structural elements (light roofs, façades) and the collapse of light and/or temporary structures. Heat waves and sudden temperature fluctuations lead to major thermal stresses, deformations, unserviceability of structures and infrastructure due to buckling of rails, as well as problems and delays on the construction site due to poor working conditions. Droughts and forest fires can lead to traffic disruptions, problems with supplies and the functionality (destruction) of infrastructure. Fires can sometimes destroy entire infrastructures, as in August 2023 on Hawaii, when an entire tourist resort was destroyed or in January 2025 in California where at least 12,000 structures are destroyed.

Progressive changes include rising sea levels, the concentration of greenhouse gases, relative humidity and air temperature. Sea level rise can lead to flooding in coastal areas and other associated problems similar to intense rainfall, e.g. foundation problems, damage to buildings and facilities, etc. In addition, seawater contains salt, which is very aggressive to materials and causes corrosion of steel in metal and reinforced concrete structures. All progressive changes (rise in sea level, relative humidity, temperature and greenhouse gases concentration) lead to accelerated material degradation.

Copyright © 2025 CroCEE
DOI: https://doi.org/10.5592/CO/3CroCEE.2025.150

Impact of progressive climate changes on material deterioration will be illustrated on reinforcement corrosion in concrete. Climate change can accelerate carbonation, chloride penetration in concrete and active corrosion of reinforcement in several ways. The most influencing parameters are increase of relative humidity and temperature which effect the concrete diffusivity, transportation processes, but also electrochemical processes of active corrosion: corrosion rate and production of rust. On the other hand, sea level and salinity rise increase chloride concentration on concrete surface, while increase of greenhouse gases concentration increase risk of carbonatization [5].

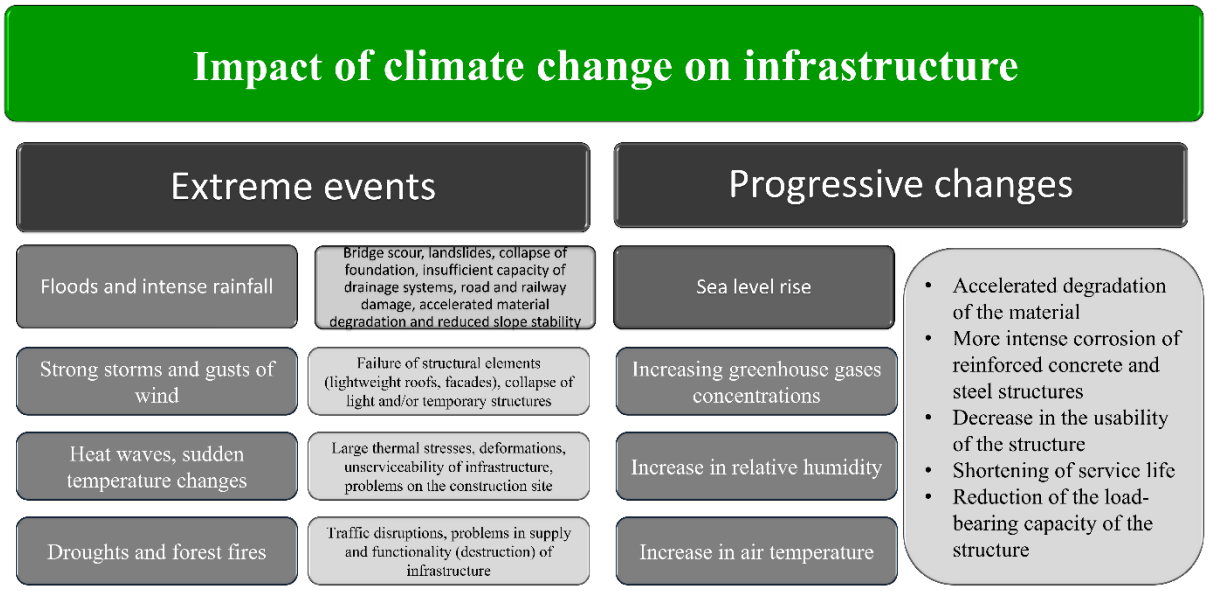


Figure 4. Impact of climate change on infrastructure

While climate change generally brings warmer weather and less snow, in mountain regions it also means more frequent changes in the freeze-thaw cycles, which may not reduce salt consumption. It is the freeze-thaw cycle that leads to degenerative changes in concrete structures, usually in the form of cracks, while the huge amount of used de-icing salts increases the risk of reinforcement corrosion in concrete [5].

In addition to the fact that climate change reduces the resistance of the structure due to accelerated degradation, it also has the effect of increasing the action on the structures. Climate change therefore has a double unfavourable effect on buildings. The only positive effect on buildings may be a reduction in the snow load. On the other hand, many other actions will increase due to climate change, such as wind load, thermal stresses, ground settlement, load on foundation, etc.

It is well known that climate change will increase intensity, frequency and area affected of the extreme events, therefore, the probability of two or more extreme events occurring simultaneously will increase. Therefore, the probability of an earthquake and an extreme event related to climate change occurring simultaneously increases, which can negatively affect the load-bearing capacity of the structure, but also, more importantly, the evacuation and rescue of people. An example of the negative impact of weather on post-earthquake evacuation was during the earthquake in Zagreb on March 22, 2020, when earthquake happened at the same time as a sudden cold snap and snowfall in the spring during the lock-dawn caused by covid-19 pandemic crisis, which further complicated the evacuation of people, especially vulnerable groups such as patients in hospitals.

4. Case studies

As case studies, seven concrete bridges are presented to demonstrate interaction between pre-earthquake deterioration and damage caused by earthquake that happened in December 2020, in Northwestern Croatia with a magnitude of ML = 6.3 (Table 1). Bridges are located 10–15 km from the

Proceedings of the 3rd Croatian Conference on Earthquake Engineering - 3CroCEE
19–22 March 2025, Split, Croatia
Copyright © 2025 CroCEE
DOI: https://doi.org/10.5592/CO/3CroCEE.2025.150

epicentre, the town of Petrinja. Most of these bridges were built in the previous century and are now 50 or more years old. There are only noted two exception bridges (numbered 6 and 7 in Fig. 4) that were built in the last 30 years. All bridges were found to have simply supported or continuous girders and have spans between 7 and 20 m. The superstructures were found to be either concrete slabs (bridges 2, 3 and 7) or composite steel-concrete ribbed cross-section (bridges 1, 3, 4 and 5) [27].

Table 1. Case studies with presented pre-earthquake damage and results of post-earthquake assessment

No	Figure	Water leakage	Corrosion of reinforcement			Other damage types		Soil and river		Equipment			Post-Earthquake Rapid Assessment	
		Concrete efflorescence	Brown spots	Cracks	Delamination of concrete cover	Cracks in concrete	Delamination of concrete cover	Erosion of soil/slope	Scour	Bearing degradation	Deterioration of expansion joins	Cracking of asphalt	Grade	Main issue
1		■	■	■	■			■	■	○	○	■	! (×)	Translation and rotation of abutment due to ground movements and soil erosion
2		■	■	■	□	□	□	□		○	○	■	✓	Bridge footways and cornices heavily degraded due to lack of waterproofing and reinforcement corrosion
3		■	□	□				□		○	○	□	✓	Noticeable water leakage due to failed waterproofing and drainage
4		■	□	□	□					○	○	■	✓	Heavy water leakage due to non-existent drainage and waterproofing, corrosion
5		■	■	■	■	■		□					✓	Poor drainage and asphalt, reinforcement corrosion and possible scour on column
6		□	□							○	■	□	✓	Expansion joints are deteriorated
7		■	■	■	■	■				○	○		✓	Maintenance related problems, limited displacement capacity, earthquake-related damage

PRE-EARTHQUAKE DAMAGE: = damage not present, □ = damage present, ■ = damage highly present, ○ = element not present
ASSESSMENT GRADE: ✓ = bridge can be used, × = bridge should be closed, ! = prescribed immediate action
SOURCE OF MAIN ISSUE: ■ = earthquake, ■ = lack of maintenance

Copyright © 2025 CroCEE
DOI: https://doi.org/10.5592/CO/3CroCEE.2025.150



(a) (b)

Figure 5. (a) Risk of abutment collapse on bridge 1 due to earthquake, slope erosion and possible scour; (b) longitudinal and transverse movements of the bridge 7 due to earthquake visible on cracked asphalt layer and heavy damaged abutment side walls

The main problem of all bridges, which became evident during the post-earthquake rapid assessment, was the lack of maintenance, which, in combination with poor waterproofing, led to progressive material deterioration and subsequent damage to the structural and non-structural parts of the bridges. The most common types of this damage were concrete spalling, the corrosion of reinforcement, the corrosion of steel girders, the corrosion of railings, bearing degradation, the clogging of expansion joints, the cracking of asphalt, and the erosion of abutment slopes [27]. Although most of the inspected bridges were found to be deteriorated due to old age and lack of maintenance, most of the bridges performed well in the earthquake. Only two of them showed significant damage from the earthquake: bridge 1 with major damage and bridge 7 with minor damage [27].

After post-earthquake rapid assessment, bridge 1 needed closure and immediate strengthening measures. Namely, west abutment of the bridge showed signs of slippage and rotation, hence its stability and integrity were compromised (Fig. 5a). The immediate danger of collapse was even more emphasized due to heavy rains that followed in the days after the earthquake, which caused the water level to rise and further erode the west riverbank that had already shown scour signs under the abutment foundation. Additionally, multiple aftershocks threatened the unstable balance of the abutment wall. Hence, immediate strengthening measures and usage restrictions are required for the bridge 1. The immediate strengthening measures included stabilization of the abutment using large stone block material and filling the slope of the riverbank up to the top of the abutment [27].

Bridge 7 is the longest of all the bridges, with relatively large spans and tallest columns, so the seismic action was certainly the highest here. On the other hand, the bridge is built in 1987 and seismic resistance was considered during design according to valuable codes at that time. The bridge has no drainage system, no bearings, and no expansion joints, all of which resulted in durability problems and limited displacement capacity. The bridge showed signs of heavy water leakage from the superstructure on abutment walls, causing concrete degradation and spalling, and reinforcement corrosion on both the superstructure and substructure. Earthquake-related damage was recorded on several elements of the bridge. It was evident that the bridge superstructure moved both longitudinally and transversely at a notable rate (Fig. 5b). Longitudinal movements induced by the earthquake are visible on the cracked, waved and delaminated asphalt layer at the ends of the bridge superstructure. This movement also caused the fracture of bridge cornice. Transverse movements caused heavy damage to abutment side walls, thus cracking and completely fracturing parts of them [27]. Lack of maintenance and advanced

Copyright © 2025 CroCEE
DOI: https://doi.org/10.5592/CO/3CroCEE.2025.150

reinforcement corrosion on structural elements additionally contributed to the increase in the level of damage.

5. Conclusion

Older structures are vulnerable to seismic hazards, not only because they are not appropriately designed for seismic loads, but also due to the fact that they deteriorate over time and degradation processes decrease significantly their initial load-bearing capacity.

Infrastructures, such as bridges, have a service life of 100 years or more. Existing and new structures are exposed to the current and future effects of changing climate and aggressive environment. Climate change has multiple impacts on reducing the stability, load-bearing capacity, serviceability and functionality of structures and infrastructure. By neglecting the influence of the environment and changing climate during the service life, the structure resistance can be significantly overestimated – especially in extreme events such as an earthquake. Besides impact on mechanical behaviour of structures, climate change can additionally complicate the post-earthquake interventions such as evacuation and rescue of people.

Climate change has a double unfavourable effect on structures – it reduces the resistance of the structure due to accelerated degradation and increase the action on the structures. Hence, codes and requirements for structures must be adapted to new environmental conditions and climate changes in order to make new buildings more resilient to extreme weather conditions and natural disasters.

Presented case studies of concrete bridges showed that significant damage due to the earthquake happened on bridges already damaged before the earthquake due to climate and environment impact: erosion and scour on bridge 1 and reinforcement corrosion on bridge 7. Moreover, damage caused by environment and climate, as well as damage caused by earthquake could have been avoided if proper design rules had been followed and timely maintenance had been performed to prevent further deterioration due to water leakage and corrosion of the reinforcement.

References

[1] Titi, A. and Biondini, F., Probabilistic seismic assessment of multistory precast concrete frames exposed to corrosion, Bulletin of Earthquake Engineering, 12 (2014) 6, pp.2665–2681, doi:10.1007/s10518-014-9620-2

[2] Skokandić D., Vlašić, A., Kušter Marić, M., Srbić, M., Mandić Ivanković, A. (2022) Seismic Assessment and retrofitting of Existing Road Bridges; State of the Art Review, Materials, 15 (2022) 7, 2523,23 doi:10.3390/ma15072523

[3] Karapetrou, S., Manakou, M., Bindi, D., Petrovic B. and Pitilakis, K., „Time-building specific“ seismic vulnerability assessment of a hospital RC building using field monitoring data, Engineering Structures, 112 (2016), pp. 114-132, doi: 10.1016/j.engstruct.2016.01.009

[4] Afsar Dizaj, E., Madandoust, R., Kashani, M.M., Modelling the effect of corrosion on failure modes of RC columns subject to lateral seismic loading, Proceedings of the 16th European Conference on Earthquake Engineering, 2018.

[5] Milić, P., Kušter Marić, M.: Climate change effect on durability of bridges and other infrastructure, GRAĐEVINAR, 75 (2023) 9, pp. 893-906, doi: https://doi.org/10.14256/JCE.3756.2023

[6] Franciškoviċ, J.: Corrosion protection in reinforced-concrete structures, GRAĐEVINAR, 56 (2004) 12

[7] Böhni, H., Corrosion in reinforced concrete structures, Woodhead Publishing Limited, Cambridge, 2005.

[8] Yoon, I., Copurouglu, O., Park, K, Effect of global climatic change on carbonation progress of concrete, Atmospheric environment, 41 (2007) 34, pp. 7274–7285, doi: 10.1016/j.atmosenv.2007.05.028

[9] Sousa M.L., Dimova S., Athanasopoulou A et al., Expected implications of climate change on the corrosion of structures, EUR 30303 EN, Publications Office of the European Union, Luxembourg, 2020, ISBN 978-92-76-20782-5, doi:10.2760/05229, JRC121312

Copyright © 2025 CroCEE
DOI: https://doi.org/10.5592/CO/3CroCEE.2025.150

[10] fib Task Group Bond Models, Bond of Reinforcement in Concrete – State-of-art report, fib Bulletin 10 (2000), Lausanne, International Federation for Structural Concrete, doi:10.35789/fib.BULL.0010

[11] Cairns, J., Plizzari, G. A., Du, Y. et al., Mechanical properties of corrosion-damaged reinforcement, ACI Materials Journal, 102 (2005) 4, pp. 256-264.

[12] Du, Y. G., Clark, L. A., Chan, A. H. C., Effect of corrosion on ductility of reinforcing bars, Magazine of Concrete Research, 57 (2005) 7, pp. 407-419.

[13] Du, Y. G.; Clark, L. A. & Chan, A. H. C. Residual capacity of corroded reinforcing bars, Magazine of Concrete Research, 57 (2005) 3. pp. 135-147.

[14] Rodriguez, J., Ortega, L. M., Casal, J., Load carrying capacity of concrete structures with corroded reinforcement, Construction and Building Materials, 11 (1997) 4, pp. 239-248.

[15] Zandi Hanjari, K., Structural Behaviour of Deteriorated Concrete Structures. PhD thesis.Gothenburg, Sweden: Chalmers University of Technology – Department of Civil and Environmental Engineering – Division of Structural Engineering, Concrete Structures, 2010

[16] Kušter Marić, M., Service life prediction of reinforced concrete bridges exposed to chlorides. PhD thesis, University of Zagreb, Croatia, 2013.

[17] RILEM 2022, Benchmarking Chloride Ingress Models on Real-life Case Studies—Marine Submerged and Road Sprayed Concrete Structures, Koenders E., Imamoto K., Soive A., Springer Cham. 2022, https://doi.org/10.1007/978-3-030-96422-1

[18] Kušter Marić, M., Radić, J., Ožbolt, J. et al., Analysis on durability of reinforced concrete bridges in maritime environment, Annual 2015 of the Croatian Academy of Engineering, 22 (2016), pp. 57-78.

[19] Kušter Marić, M., Ivanković, A. M. ., Vlašić, A., Bleiziffer, J., Srbić, M., Skokandić, D. (2019). Assessment of reinforcement corrosion and concrete damage on bridges using non-destructive testing, GRAĐEVINAR, 71 (10), 843-862, doi: https://doi.org/10.14256/JCE.2724.2019

[20] Karapetrou S.T., Fotopoulou S.D., Pitilakis K.D., Seismic Vulnerability of RC Buildings under the Effect of Aging, Procedia Environmental Sciences, 38 (2017), pp. 461–468, doi: 10.1016/j.proenv.2017.03.137

[21] Akiyama M., Frangopol D.M., Matsuzaki H., Life-cycle reliability of RC bridge piers under seismic and airborne chloride hazards, Earthquake Engng Struct. Dyn. 2011; 40:1671–1687. DOI: 10.1002/eqe.1108

[22] Biondini F., Camnasio E., Palermo A., Lifetime seismic performance of concrete bridges exposed to corrosion, Structure and Infrastructure Engineering: Maintenance, Management, Life-Cycle Design and Performance, 10 (2014) 7, pp. 880-900, doi:10.1080/15732479.2012.761248

[23] Afsar Dizaj, E., Kashani, M.M. Numerical investigation of the influence of cross-sectional shape and corrosion damage on failure mechanisms of RC bridge piers under earthquake loading. Bull Earthquake Eng ,18 (2020), pp. 4939–4961, doi:10.1007/s10518-020-00883-3

[24] Cheng, H., Li, HN., Yang, Y.B. et al., Seismic fragility analysis of deteriorating RC bridge columns with time-variant capacity index. Bull Earthquake Eng 17 (2019), pp. 4247–4267, doi:10.1007/s10518-019-00628-x

[25] Zanini, M.A., Pellegrino, C., Morbin, R. et al. Seismic vulnerability of bridges in transport networks subjected to environmental deterioration, Bull Earthquake Eng, 11 (2013), pp- 561–579, doi:10.1007/s10518-012-9400-9

[26] Deng P., Zhang C., Shiling P., Jin Z., Modeling the Impact of Corrosion on Seismic Performance of Multi-Span Simply-Supported Bridges, Construction and Building Materials, 185 (2018), pp. 193-205. doi:10.1016/j.conbuildmat.2018.07.015

[27] Vlašić A, Srbić M, Skokandić D, Mandić Ivanković A. Post-Earthquake Rapid Damage Assessment of Road Bridges in Glina County. Buildings 2022;12,42. https://doi.org/10.3390/buildings12010042.

[28] Hajdin, R.; Kušar, M.; Mašović, S.; Linneberg, P.; Amado, J.; Tanasić, N. COST Action TU1406: Quality Specifications for Roadway Bridges, Standardization at a European Level; WG3 Technical Report: Establishment of a Quality Control Plan; COST: Brussels, Belgium, 2018.

Proceedings of the 3rd Croatian Conference on Earthquake Engineering - 3CroCEE
19–22 March 2025, Split, Croatia
Copyright © 2025 CroCEE
DOI: https://doi.org/10.5592/CO/3CroCEE.2025.152

SEISMIC ASSESSMENT OF THE PRECODE HIGH RISE BUILDING FRAME USING THE PUSHOVER ANALYSIS

Karlo Grgurić [(1)], Mario Uroš [(2)]

[(1)] *Structural Engineer, XXL STEEL d.o.o., Zagreb, Croatia, karlo.grguric12@gmail.com*
[(2)] *Associate professor, University of Zagreb, Faculty of Civil Engineering, Zagreb, Croatia, .mario.uros@grad.unizg.hr*

Abstract

A large part of the housing stock of the Republic of Croatia consists of buildings that were built in the first half of the 20th century, when seismic regulations were poorly developed. Such buildings do not have quality details and have a high seismic risk. In this work a pushover analysis of a reinforced concrete historic high rise building in Zagreb was carried out in order to assess its seismic resistance. Given that the building is symmetrical in plan and has a frame structural system, one planar multi-story frame in week direction was chosen for analyses. The quality of materials, dimensions of the cross-sections, and position of reinforcement in the elements were obtained from the building's archival documentation, along with non-destructive tests that were carried out on the building. A numerical model was established, and plastic hinges were defined for the columns and beams of the observed frame, with corresponding load-bearing capacity curves based on Eurocode 8-3. The analyses were carried out using the nonlinear static pushover analysis method (N2) in the ETABS software. The capacity curves of the structure and the significant structural damage index (SDI) were obtained for the observed direction of the building. At the end, a critical review of the analysis method and the original conception of the historical high rise building construction was made, and a proposal for strengthening the building was provided.

Keywords: seismic assessment, pushover analysis, high rise building

1. Introduction

Most of the buildings in the Lower Town of Zagreb were constructed at the end of the 19th and the beginning of the 20th century. Following a series of earthquakes in 2020 that struck the Zagreb (5,5 on the Richter scale [1]) and Petrinja (5,0 and 6,2 on the Richter scale [2]) areas, significant damage occurred to both non-structural and structural elements. The reason for this is that structural engineers of that period were not aware of designing structures to withstand seismic actions. This work will provide an assessment of the seismic resistance of a historic high-rise building in Zagreb dating back to the 1950s. The structural system of the mentioned high-rise building consists of a reinforced concrete frame in both dominant directions, with a lightly reinforced concrete stairwell core in the center [3]. The main deficiency of building is the insufficient amount of transverse reinforcement in the columns to resist lateral forces, with the dominant brittle shear failure. To obtain a reliable picture of the structure's behavior under seismic action, the nonlinear methods were used. In this work, the nonlinear pushover method will be applied. In addition to the nonlinear static method, a spectral analysis will also be performed. Given that the structure is symmetrical in plan, for simplicity of analysis, a one planar multi-story frame in the weaker direction of the structure will be extracted from the entire structure. The numerical analyses will be performed in software Etabs [4] on one planar multi-story frame using concentrated plastic approach with moment and shear plastic hinges in the columns and beams. The characteristics of materials, dimensions of the cross-sections, and position of reinforcement in the elements were obtained from the building's archival documentation [3], along with non-destructive tests that were carried out on the building.

Copyright © 2025 CroCEE
DOI: https://doi.org/10.5592/CO/3CroCEE.2025.152

The data on the quantity and distribution of reinforcement in the columns and beams is crucial for the application of the pushover method, as the reinforcement in the structural elements dictates the ductility of the elements and their seismic resistance. As an assessment of seismic resistance, the Significant Damage Index (SDI) will be obtained. The SDI index represents the ratio of the ground acceleration at which the structure reaches the limit state of Significant Damage (SD) and the ground acceleration according to regulations, considering a return period of 475 years [5].

2. Methodology of the analysis and structural modelling

2.1 Geometric and material properties of the structure

A one planar multi–story reinforced concrete frame (Ground floor + 10 floors) is analyzed, which is part of an existing reinforced concrete frame structure built in the 1950s in Zagreb [3]. The concrete material is C25/30 and reinforcement GA240, where the mean material values were applied ($f_{cm} = f_{ck} + 8$ [N/mm²] and $f_{ym} = 1{,}15 * f_{yk}$). The modulus of elasticity of is 31 GPa for concrete, and 210 GPa for steel [3]. The geometry of the selected frame along with the corresponding reinforcement in the columns and beams is shown below [3]:

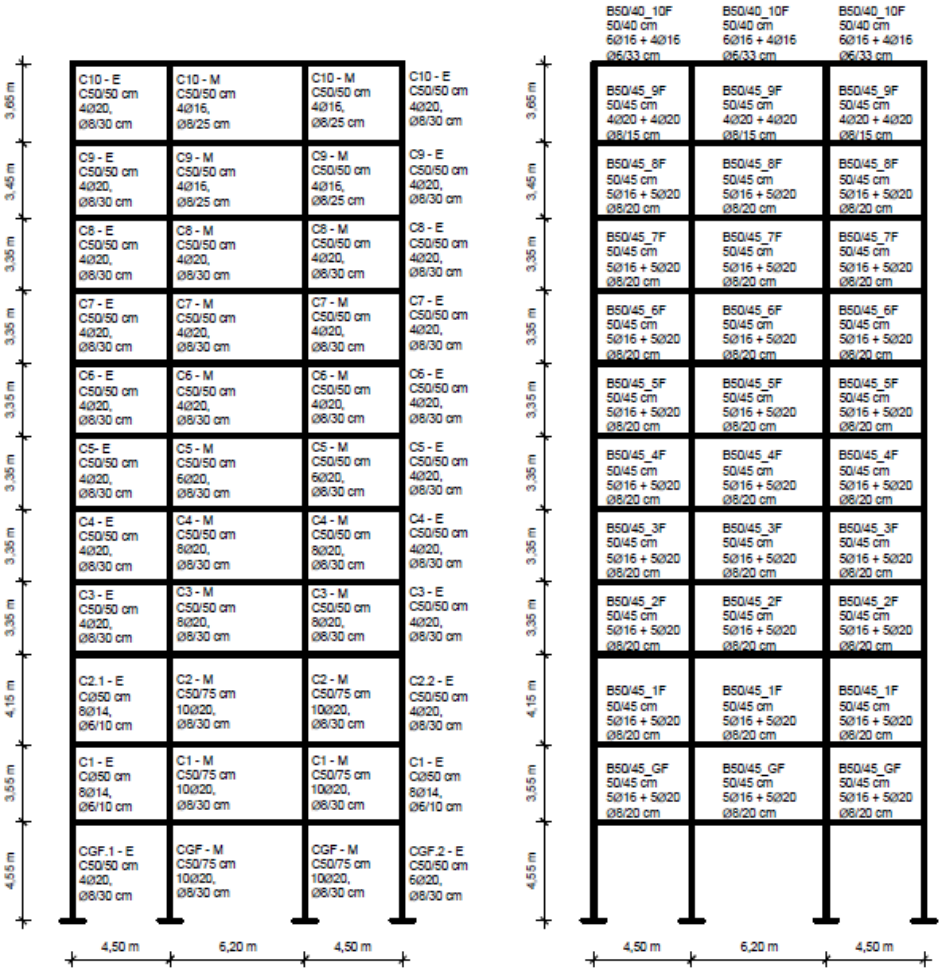


Figure 1. Geometric characteristics of elements and reinforcement of columns (left) and beams (right)

Regarding the labels of the elements, the first row indicates the position of the column or beam. The second row refers to the cross-sectional dimensions, the third row provides information about longitudinal reinforcement, and the fourth row specifies the transverse reinforcement of the columns and beams.

Copyright © 2025 CroCEE
DOI: https://doi.org/10.5592/CO/3CroCEE.2025.152

The first and third spans are length 4,5 m, while the middle span is 6,2 m. The floor heights vary and they are shown in Figure 1, with the total height of the structure being 39,45 m. The interaction with the ground has been simplified for the model using fixed hinge supports, as individual foundations are present. All load-bearing elements of the columns and beams are modeled as frame elements. The numerical model does not include the basement level, and it will not be considered in this study.

Below is the representation of the reinforcement in the characteristic column and beam [3]:

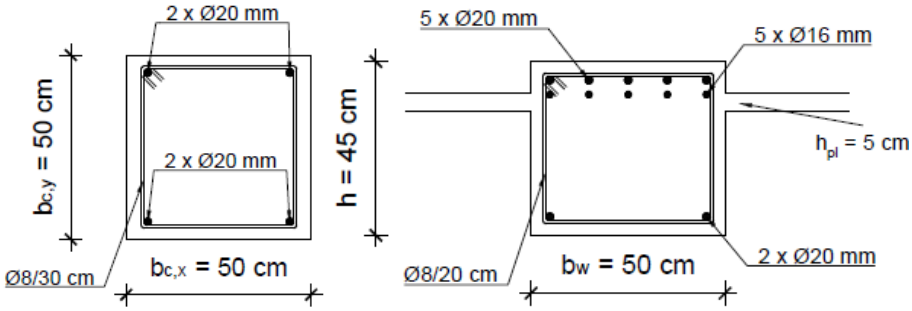


Figure 2. Reinforcement of the characteristic column (left) and beam (right)

2.2 Loads and actions

The loads acting on the structure include self-weight, additional permanent, live and seismic loads. To determine the exact load acting on the observed frame, it is necessary to convert loads such as additional permanent and live loads from surface (kN/m²) to linear (kN/m), where the spacing of the main frames is 4,22 m [3]. The additional permanent load 4,0 kN/m² [3] includes the weight of all layers and partition walls, resulting in a linear load of 28,4 kN/m. The live load varies depending on the floor level. The 1st and 2nd floors are office spaces, and according to [6], the live load is 3,0 kN/m², corresponding to a linear load of 12,66 kN/m, while the higher floors are residential, with a live load of 2,0 kN/m², corresponding to a linear load of 8,44 kN/m. As for the seismic load, the peak ground acceleration at the site of the building is 0,254 g [7] for a return period of 475 years, with a confidence factor of ,1,0 [8] and a behavior factor of 1,5, which is used in the design response spectrum analysis. The low value of the behavior factor is taken because a low level of ductility in the cross-sections is assumed.

2.3 Modal analysis

The modal analysis was performed to determine the dynamic parameters of the structure (structural periods and modes of vibration). The total weight of the frame for the MASS combination, which accounts for self-weight, additional permanent, and 0,3 of the live load, is 7203 kN. Since this is a planar frame, the first mode of vibration is dominated by translation with a period of 2,97 s, where over 90% of the frame's mass is activated. Below is the deformation shape for the first two modes of vibration of the frame:

Copyright © 2025 CroCEE
DOI: https://doi.org/10.5592/CO/3CroCEE.2025.152

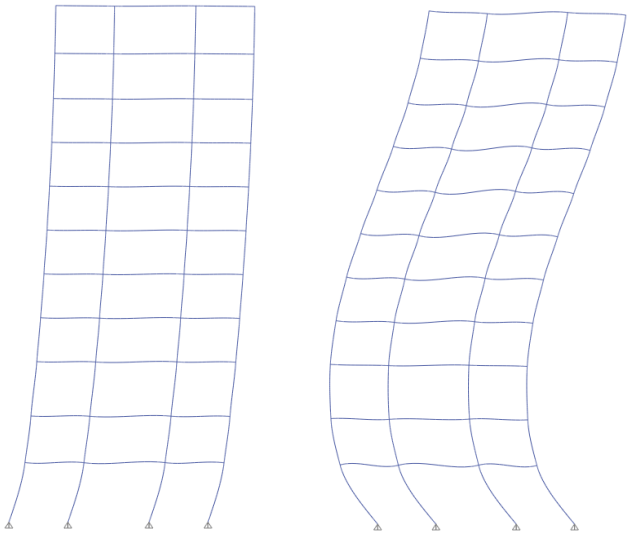


Figure 3. The first mode of vibration on the left (T_1 = 2,97 s) and the second mode of vibration on the right (T_2 = 0,91 s)

3. Methodology and structural modelling

3.1 Geometric and material properties of the structure

For the analysis of the one planar multi-story structure, the [4] was used with certain assumptions and simplifications. The reduction of stiffness of elements according to [9] takes into account the occurrence of cracks in the elements. The shear and elastic bending stiffness of the beams, columns and RC plates were reduced to 50 %. [9]. Regarding the compressive strength of concrete cross-sections and the yield strength of reinforcement, their mean values were used.

3.2 Properties of plastic hinges

Before assigning plastic hinges to the elements, it is necessary to properly define their parameters. To define the moment plastic hinges, it is first necessary to perform a cross-section analysis with the corresponding cross-sectional geometry, longitudinal and transverse reinforcement, as described in [10], in order to obtain the capacity curve of the cross-section from which the values of the section curvature at yielding and failure, as well as the plastic moment, are taken. According to [8], there are three limit states, which are Damage Limitation (DL), Significant Damage (SD) and Near Collapse (NR).

Furthermore, the curvatures at the limit states are determined according to [8]:

$$L_{pl} = 0{,}1 \cdot L_V + 0{,}17 \cdot h + 0{,}24 \cdot \frac{d_{bL} \cdot f_y(MPa)}{\sqrt{f_c}\,(MPa)} \tag{1}$$

$$\theta_y = \Phi_y \cdot \frac{L_V + a_V z}{3} + 0{,}0014 \cdot \left(1 + 1{,}5 \cdot \frac{h}{L_V}\right) + \Phi_y \cdot \frac{d_{bL} \cdot f_y}{8 \cdot \sqrt{f_c}} \tag{2}$$

Proceedings of the 3rd Croatian Conference on Earthquake Engineering - 3CroCEE
19–22 March 2025, Split, Croatia
Copyright © 2025 CroCEE
DOI: https://doi.org/10.5592/CO/3CroCEE.2025.152

$$\theta_m = \frac{1}{\gamma_{el}} \cdot \left(\theta_y + (\Phi_u - \Phi_y) \cdot L_{pl} \cdot \left(1 - \frac{0{,}5 \cdot L_{pl}}{L_V}\right)\right) \quad (3)$$

$$\theta_{SD} = \frac{3}{4} \cdot \theta_m \quad (4)$$

Where the coefficients are:

L_{pl} – Length of the plastic zone
L_V – (M/V) ratio at the end of the element
h – Height
d_{bL} – Diameter of tension reinforcement
f_y – Yield strength of reinforcement
f_c – Concrete compressive strength
θ_y – Curvature at the limit state of Damage Limitation
Φ_y – Curvature at yielding
a_vz – Displacement of the axial force diagram
θ_m – Curvature at the limit state of Near Collapse
$\gamma_{el} = 1{,}8$
Φ_u – Curvature at failure
θ_{SD} – Curvature at the limit state of Significant Damage

These values of the cross-sectional curvature at the limit states and the plastic moment are input data for defining plastic hinges in [4]. Moment plastic hinges are assigned to beams and columns at a distance of 0,5 m from the edges. To define shear plastic hinges, it is necessary to determine the design value of the cross-sectional resistance to shear force. This quantity is obtained according to [8]:

$$V_R = \frac{1}{\gamma_{el}} \left[\frac{h-x}{2L_V} \cdot min(N; 0{,}55 \cdot A_C \cdot f_C) + \left(1 - 0{,}05 \cdot min\left(5; \mu_\Delta^{pl}\right)\right)\right] \cdot$$

$$\cdot \left[0{,}16 \cdot max(0{,}5; 100 \cdot \varphi_{tot}) \cdot \left(1 - 0{,}16 \cdot \left(5; \frac{L_V}{h}\right)\right) \cdot \sqrt{f_C} \cdot A_C + V_W\right] \; [MN \; and \; m] \quad (5)$$

Where the coefficients are:

$\gamma_{el} = 1{,}15$
h – Height
x – Compression zone depth
N – Axial force
A_c – Concrete cross–section area
f_c – Concrete compressive strength
$\gamma_M = 1{,}5$
L_V – (M/V) ratio at the end of the element
φ_{tot} – Total longitudinal reinforcement ratio
μ_Δ^{pl} – Ductility factor of transverse deflection due to shear stress or fiber rotation θ normalized to fiber rotation at the moment of yielding θ_y; $\mu_\Delta^{pl} = (\theta_u / \theta_y)$
V_W – Contribution of transverse reinforcement to shear resistance

$$V_w = \varphi_w \cdot b_w \cdot z \cdot f_{yw} \quad (6)$$

Coefficients are:

φ_w – Ratio of transverse reinforcement
bw – Width of the beam web
z – Length of section internal lever arm
f_{yw} – Yield strength of transverse reinforcement

Copyright © 2025 CroCEE
DOI: https://doi.org/10.5592/CO/3CroCEE.2025.152

Regarding the curvature at the previously mentioned limit states, since a brittle shear failure is assumed, a small value of curvature is assigned. This value must not be too small to avoid numerical issues during the nonlinear static analysis using plastic hinges. For the moment hinges of the columns, we have a symmetrical M_{pl}-φ curve because the reinforcement in the columns is symmetrical. In the case of the beam, the situation is different due to the asymmetric reinforcement, so an asymmetric M_{pl}-φ curve must be defined. The reason for this is that the moment from the MASS combination and the moment from the seismic combination may not act on the same side, so this approach covers both cases. The asymmetric M_{pl}-φ curve is obtained by rotating the cross-section with the corresponding reinforcement by 180º during its definition, and the rest of the plastic hinge definition is the same as for the symmetrical M_{pl}-φ curve. Below are graphical and tabular representations of the M_{pl}-φ curves for the moment hinges of the columns and beams:

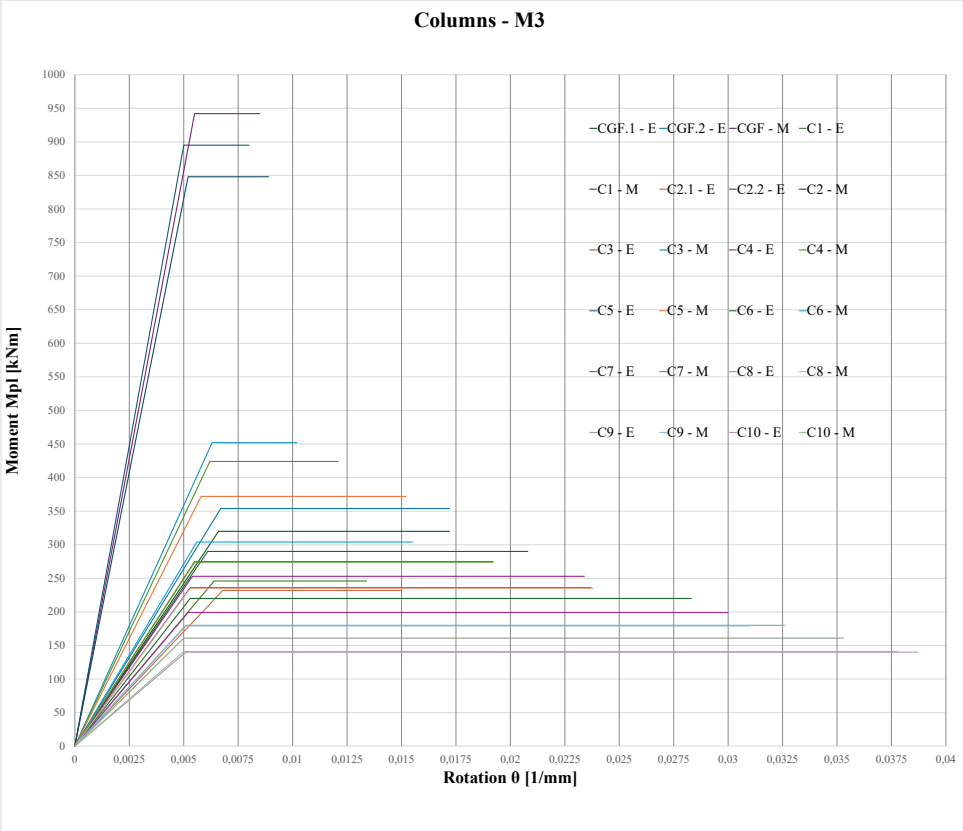


Figure 4. M_{pl} – φ curves for columns

In Figure 4, it can be observed that the values of the middle columns of the ground floor and the first two floors deviate from the rest of the columns, showing a significantly higher value of the plastic moment and a lower capacity for cross-sectional rotation.

Copyright © 2025 CroCEE
DOI: https://doi.org/10.5592/CO/3CroCEE.2025.152

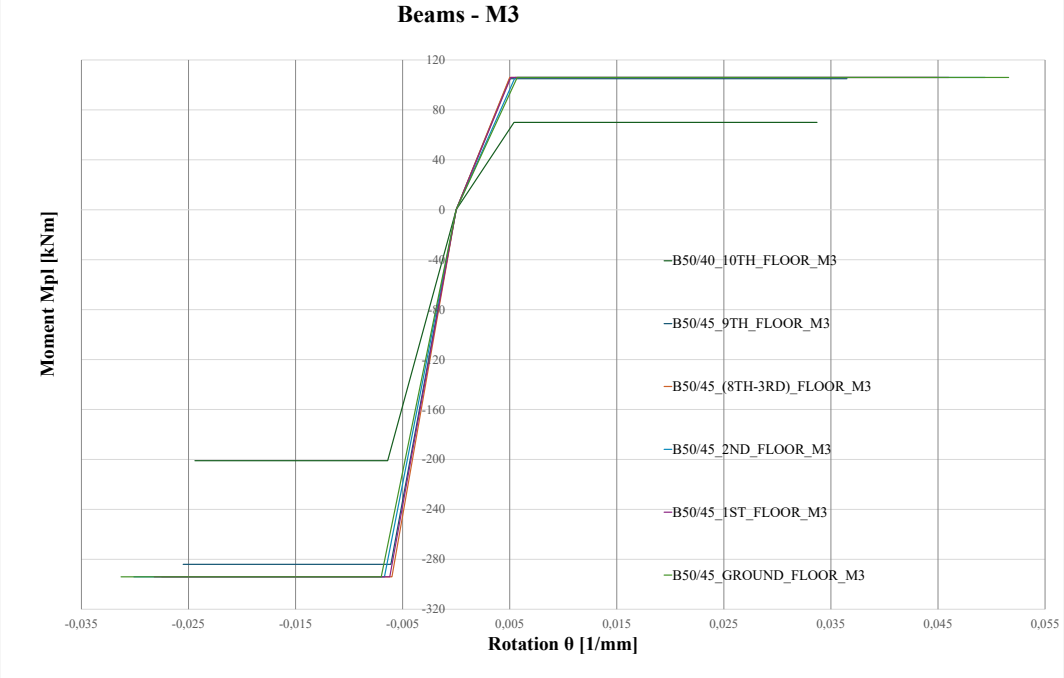


Figure 5. M_{pl} – φ curves for beams

From Figure 5, it can be observed that the curves are identical for all beams with the same cross-sectional height, regardless of the floor they are located on. The only exception is the beam on the 10th floor, which has a cross-sectional height of 40 cm, and it stands out slightly.

Table 1 Tabular representation of column parameters

MARK	H (m)	Lpl (m)	θ_y (1/mm)	θ_{SD} (1/mm)	θ_U (1/mm)	Mpl (kNm)	P (kN)	Vrd (kN)
CGF.1-E	4,55	0,54	0,0066	0,0129	0,0172	320	1153	45
CGF.2-E	4,55	0,54	0,0067	0,0129	0,0172	354	1166	55
CGF-M	4,55	0,59	0,0055	0,0064	0,0085	942	2442	90
C1-E	3,55	0,42	0,0064	0,0101	0,0134	246	1053	55
C1-M	3,55	0,54	0,0050	0,0060	0,0080	895	2189	85
C2.1-E	4,15	0,45	0,0068	0,0112	0,0150	232	950	55
C2.2-E	4,15	0,52	0,0061	0,0156	0,0208	290	961	45
C2-M	4,15	0,57	0,0052	0,0067	0,0089	848	1948	85
C3-E	3,35	0,48	0,0055	0,0144	0,0192	275	853	45
C3-M	3,35	0,48	0,0063	0,0077	0,0102	452	1710	70
C4-E	3,35	0,48	0,0054	0,0176	0,0234	253	751	45
C4-M	3,35	0,48	0,0062	0,0091	0,0121	424	1492	70
C5-E	3,35	0,48	0,0053	0,0178	0,0237	236	646	45
C5-M	3,35	0,48	0,0058	0,0114	0,0152	372	1276	62
C6-E	3,35	0,48	0,0053	0,0212	0,0283	220	540	45
C6-M	3,35	0,48	0,0056	0,0116	0,0155	304	1062	50
C7-E	3,35	0,48	0,0052	0,0225	0,0300	199	432	45
C7-M	3,35	0,48	0,0055	0,0144	0,0192	274	849	50
C8-E	3,35	0,48	0,0051	0,0245	0,0326	180	324	45
C8-M	3,35	0,48	0,0053	0,0178	0,0238	235	638	50
C9-E	3,45	0,49	0,0050	0,0265	0,0353	161	214	45
C9-M	3,45	0,44	0,0051	0,0233	0,0310	179	427	50
C10-E	3,65	0,50	0,0051	0,0290	0,0387	140	103	45
C10-M	3,65	0,45	0,0050	0,0284	0,0378	141	217	50

Proceedings of the 3rd Croatian Conference on Earthquake Engineering - 3CroCEE
19–22 March 2025, Split, Croatia
Copyright © 2025 CroCEE
DOI: https://doi.org/10.5592/CO/3CroCEE.2025.152

In Table 1, the parameters of the columns used in defining the plastic hinges are shown. It can be observed here that the governing failure mechanism will be due to shear force.

Table 2. Tabular representation of column parameters

MARK	H (m)	Lpl (m)	θ_y (1/mm)	θ_{SD} (1/mm)	θ_U (1/mm)	Mpl (kNm)	Vrd (kN)
B50/40_10TH_ FLOOR	3,65	0,43	0,0054	0,0252	0,0337	70	150
	3,65	0,43	-0,0064	-0,0183	-0,0244	-201	150
B50/45_9TH_ FLOOR	3,45	0,48	0,0050	0,0274	0,00365	105	150
	3,45	0,48	-0,0061	-0,0192	-0,0255	-284	150
B50/45_(8-3)TH_FLOOR	3,35	0,47	0,0050	0,0336	0,0449	106	150
	3,35	0,47	-0,0060	-0,0206	-0,0275	-294	150
B50/45_2ND_ FLOOR	4,15	0,51	0,0055	0,0370	0,0494	106	150
	4,15	0,51	-0,0067	-0,0226	-0,0301	-294	150
B50/45_1ST_ FLOOR	3,55	0,48	0,0051	0,0345	0,0460	106	150
	3,55	0,48	-0,0062	-0,0211	-0,0282	-294	150
B50/45_GR_ FLOOR	4,55	0,53	0,0057	0,0387	0,0516	106	150
	4,55	0,53	-0,0070	-0,0235	-0,0313	-294	150

In Table 2, the parameters of the mentioned asymmetric M_{pl}-φ curve can be observed. The shear capacity is also shown, and it is the same for all beams, regardless of the size of the cross-section or the position of the floor.

4. Results

A linear spectral analysis was performed, and the value of the maximum shear force 528 kN at the ground floor was obtained from the design spectrum for a return period of 475 years. The ratio of the maximum shear force to the structure's weight for the MASS combination is 7,33%.

The nonlinear pushover analysis was carried out with three loading cases. The first load case has the form caused by constant ground acceleration "Push_Acceleration_X," [5]. The second load case has a distribution corresponding to the quasi-static seismic force "Push_Earthquake_X," and the third load case is in the direction of the first modal shape and is named "Push_Mode_X" [5]. However, it is first necessary to balance the structure for vertical loads, which include its own weight, additional permanent load, and 0,3 of the live load, before proceeding with the pushover method [5]. Below is the capacity curve for reaching the limit state of significant damage, show for the numerical model with moment and shear plastic hinges, as these values are relevant for evaluating the seismic resistance of the structure. Along with the given structural parameters at the limit states, the deformation shape of the frame with the corresponding plastic hinges is shown. Plastic hinges for the Significant Damage State (SD) are marked in blue.

Copyright © 2025 CroCEE
DOI: https://doi.org/10.5592/CO/3CroCEE.2025.152

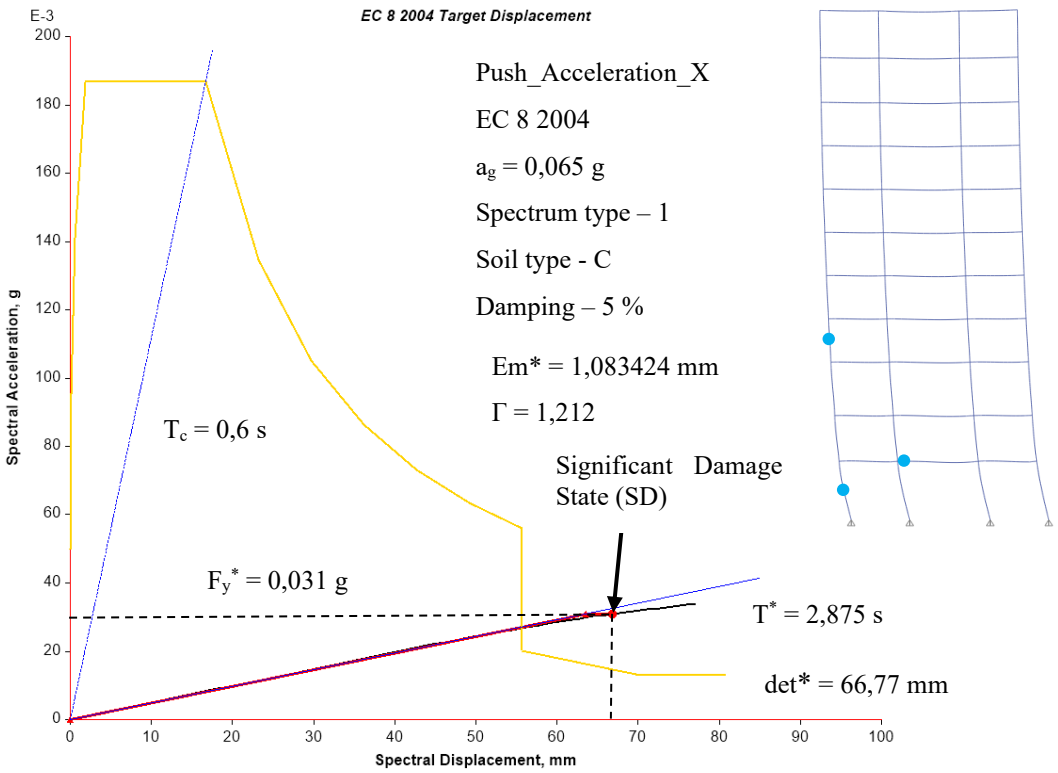


Figure 6 Capacity curve and deformation of the frame for the load case "Push_Acceleration_X"

For the load case "Push_Acceleration_X", the Significant Damage limit state is reached at a peak ground acceleration (PGA) of 0,065 g, and the Significant Damage Index (SDI) is 0,256. The force at this limit state is 204 kN, with a displacement of 80 mm.

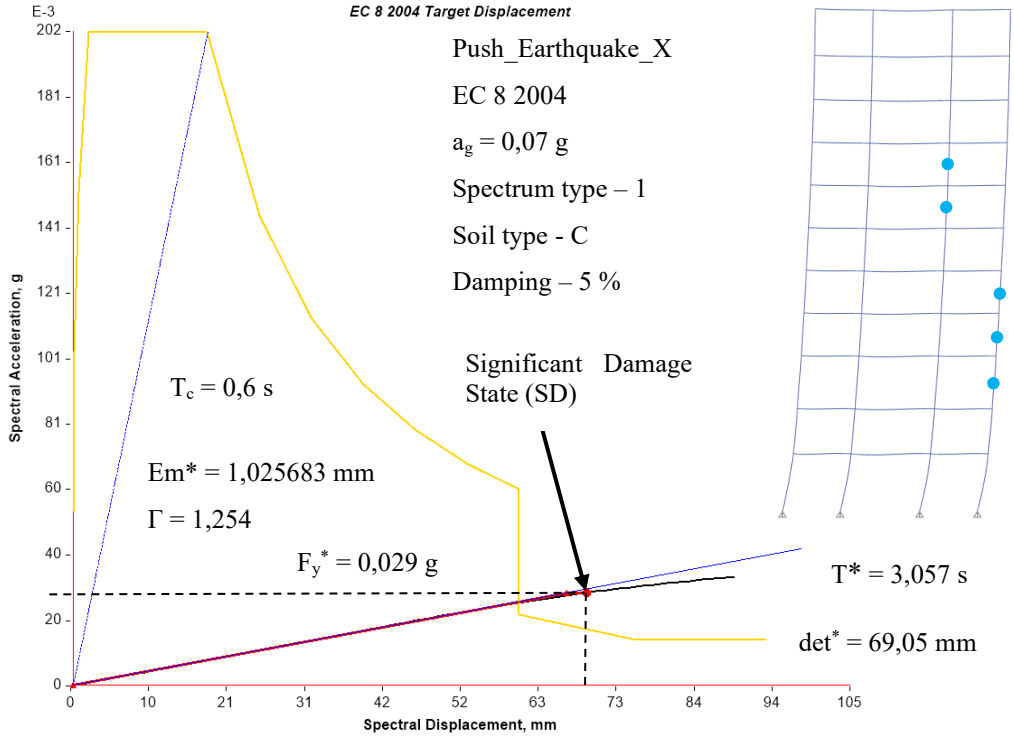


Figure 7 Capacity curve and deformation of the frame for the load case "Push_Earthquake_X"

Copyright © 2025 CroCEE
DOI: https://doi.org/10.5592/CO/3CroCEE.2025.152

For the load case "Push_Earthquake_X", the Significant Damage limit state occurs at a peak ground acceleration (PGA) of 0,07 g, and the Significant Damage Index (SDI) is 0,276. The force at this state is 185 kN, with a displacement of 86 mm.

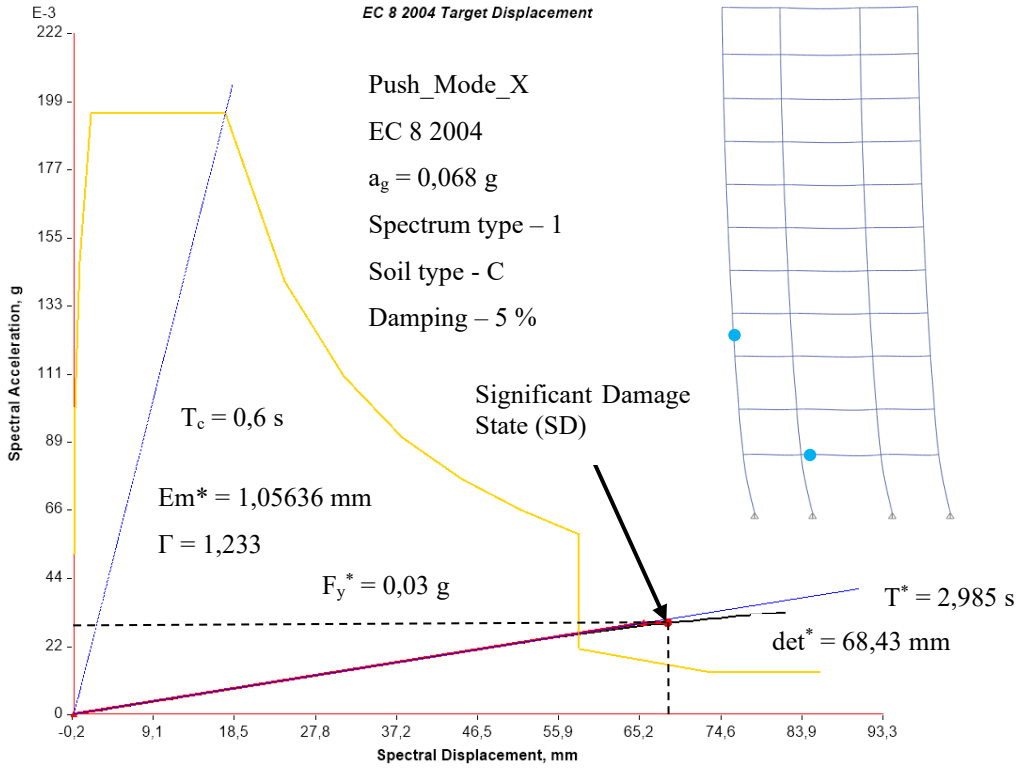


Figure 8 Capacity curve and deformation of the frame for the load case "Push_Mode_X"

For the load case "Push_Mode_X", the Significant Damage limit state of significant damage occurs at a peak ground acceleration (PGA) of 0,068 g, and the significant damage index (SDI) is 0,268. The force at this state is 194 kN, with a displacement of 84 mm.

5. Conclusions

The analysis of the one planar multi-story frame, based on the displacements of the frame, has shown that the observed frame lacks sufficient ductility. The limiting factor is that the building does not have adequate transverse reinforcement and reinforcement detailing to withstand seismic forces without significant damage to elements. The structural system of the mentioned high-rise building consists of a reinforced concrete frame in both dominant directions, with a lightly reinforced concrete stairwell core in the center. The observed reinforced concrete one planar multi-story frame has a relatively high first vibration period of 2,97 s, with dominant translation and mass activation over 90%. The load-bearing capacity of the building is exhausted by shear failure of the concrete due to transverse forces, and this mechanism is brittle and very dangerous as it leads to sudden and unexpected failure of structural elements. The nonlinear static method showed a peak ground acceleration of 0,065 g at which a Significant Damage (SD) limit state occurs. The result is far from satisfactory considering today's seismic regulations. The SDI factor obtained at the Significant Damage (SD) limit state is 0,256. If shear brittle failure is prevented in the structure and a bending failure mechanism is allowed at the joints, the seismic resistance of the structure is significantly increased, as a much more ductile failure mechanism of the elements is achieved. To achieve this, it is necessary to wrap the frame joints with FRP strips or fabrics. This method increases the ductility and shear resistance of the structure, thereby reducing the risk of brittle failure and improving the seismic resistance of the building.

Copyright © 2025 CroCEE
DOI: https://doi.org/10.5592/CO/3CroCEE.2025.152

Acknowledgements

This work was created as part of the Master's thesis titled "ASSESSMENT OF THE LOAD BEARING CAPACITY OF THE EXISTING HIGH RISE BUILDING USING THE PUSHOVER ANALYSIS" in collaboration with my mentor, Associate Professor Mario Uroš.

References

[1] Two years since the Zagreb earthquake. University of Zagreb, Faculty of Science – Department of Geophysics. Available online: https://www.pmf.unizg.hr/geof/seizmoloska_sluzba/o_zagrebackom_potresu_2020 (accessed on 12th February 2025)

[2] Analysis of accelerograms for the earthquakes near Petrinja. University of Zagreb, Faculty of Science – Department of Geophysics. Available online: https://www.pmf.unizg.hr/geof/seizmoloska_sluzba/potresi_kod_petrinje_2020# (accessed on 12th February 2025)

[3] Croatian Museum of Architecture, Croatian Academy of Sciences and Arts: OAF Drago Ibler, (accessed on 25th September 2023)

[4] ETABS, version 20, Computers and Structures, Inc., Berkeley, California, USA, 2022.

[5] Uroš M., Todorić M., Crnogorac M., Atalić J., Šavor Novak M., Lakušić S. (eds.), Earthquake Engineering: Restoration of Masonry Buildings, Zagreb: University of Zagreb, Faculty of Civil Engineering, 2021.

[6] EN1991, Eurocode 1: Actions on Structures—Part 1-1: General Actions—Densities, Self-weight, Imposed Loads for Buildings; European Committee for Standardization (CEN): Brussels, 2002.

[7] Seismic zoning maps of the Republic of Croatia, (accessed on 12th February 2025)

[8] EN1998—Part 3, Eurocode 8: Design of Structures for Earthquake Resistance—Part 3: Assessment and retrofitting of buildings; European Committee for Standardization (CEN): Brussels, Belgium, 2005.

[9] EN1998—Part 1, Eurocode 8: Design of Structures for Earthquake Resistance—Part 1: General Rules, Seismic Actions and Rules for Buildings; European Committee for Standardization (CEN): Brussels, Belgium, 2004.

[10] SAP2000, version 18, Computers and Structures, Inc., Berkeley, California, USA, 2016.

Proceedings of the 3rd Croatian Conference on Earthquake Engineering - 3CroCEE
19–22 March 2025, Split, Croatia
Copyright © 2025 CroCEE
DOI: https://doi.org/10.5592/CO/3CroCEE.2025.166

INFLUENCE OF CONNECTING ELEMENTS IN HORIZONTAL LOAD-BEARING SYSTEM OF A MASS TIMBER OFFICE BUILDING

Robert Buzjak [(1)], Mario Uroš [(2)]

[(1)] *Structural Engineer, Zagreb, Croatia, robert@studio-arhing.com*
[(2)] *Associate professor, University of Zagreb, Faculty of civil engineering, Fra Andrije Kačića-Miošića 26, Zagreb, Croatia, mario.uros@grad.unizg.hr*

Abstract

This paper presents an analysis of the behaviour of a wooden building and its dynamic parameters, considering different methods of modelling the connections between elements, with a focus on the structural elements that are part of the horizontal load-bearing system. The building's structural elements are made of GLT, CLT, and LVL components, with a unique horizontal load-bearing structure consisting of diagonals and a core made of CLT panels. Special attention is given to the connections of the core and the modelling of their impact on the response of the structure. A parametric analysis was conducted on four models, each employing different methods of modelling the connections between the CLT panels of the core. Based on these models, a comparison of the primary dynamic parameters, internal forces in the elements, and internal forces in the connections was made. Finally, the conclusion is drawn regarding the impact of different modelling methods on the dynamic parameters and internal forces.

Keywords: CLT building, dynamic parameters, connection stiffness, CLT core, seismic analysis

1. Introduction

New construction in seismically active regions, particularly in Croatia, typically involves reinforced concrete structures or masonry. The use of materials such as steel and wood is mainly reserved for industrial buildings or those with specific aesthetic requirements, or when construction speed dictates the choice of material. While wood was traditionally used for house construction in the interior of Croatia, building with wood requires expertise and skills that have gradually faded over time. The widespread use of reinforced concrete and masonry was also driven by greater economic efficiency. The emergence of wood-based products has expanded the potential for using wood as a construction material, simplifying construction processes, and the growing global emphasis on environmental preservation, renewable energy, and reducing energy consumption during construction has played a significant role [1].

With the development of wood-based composite materials such as Cross-Laminated Timber (CLT), Glue-Laminated Timber (GLT), and Laminated Veneer Lumber (LVL), the potential for incorporating wood into structures has greatly increased, meeting the demands of modern construction [2]. Elements made from these materials can meet nearly all structural requirements and can effectively compete with conventional materials in high-rise buildings. The load-bearing structure for vertical loads consists of traditional elements like GLT beams and columns, as well as CLT floor slabs and walls [3]. Horizontal stability is typically achieved through diagonal braces that form stabilizing ties or braced frames. The development of CLT also allows for the use of walls to ensure horizontal stability. Some manufacturers conduct tests focusing on seismic actions and highlight the importance of connection components, providing engineers with the opportunity to design entire structures using wood.

In structural engineering practice, connections between elements are generally modelled using idealized assumptions, rather than incorporating their actual stiffness, as these models are considered sufficient for satisfactory results. The specific geometry of the building in question raised the issue of how the stiffness of connections affects the structure’s response and the distribution of internal forces

Copyright © 2025 CroCEE
DOI: https://doi.org/10.5592/CO/3CroCEE.2025.166

within the load-bearing system under horizontal forces. This study focuses on the diagonals forming stabilizing ties in the façade planes, as well as the core composed of CLT walls.

2. Structural system and methodology of the analysis and structural modelling

The subject of the analysis is an office building (Fig. 1) with 3 levels (ground floor + 2 stories). The structure has a rectangular floor plan with dimensions of 30 x 10 meters. The height of the first story is 4,48 m, the height of the second story is 3,2 m and height of the third story is 4 m. Total height of the building 11.8 m.

The load-bearing structure for vertical loads is made up of slabs, beams, columns, and walls. The slabs are freely supported on beams and walls, and they bear loads only in the transverse direction of the building. Thickness of slabs is d = 18 cm. They rest on beams that extend longitudinally through the building along three axes, spaced at 5-meter intervals. The column grid is defined with a 5.0 x 5.0 meter spacing. The longitudinal beams are made of glued laminated timber (glulam) of class GL28h, b/h = 24/50 cm while two massive transverse beams, replacing columns in axes C and E, are made of laminated veneer lumber (LVL), of class GL75 b/h = 30/60 cm.

Horizontal load-bearing system consists of diagonals that form bracing in the facade planes, as well as a core made of CLT panels. The core of the structure is made of CLT (Cross-Laminated Timber) and consists of three walls positioned next to one facade plane of the building as shown in Fig. 1. Two walls are placed in the shorter direction of the building, each with a length of 3.7 meters, and they do not have openings. A wall extends along the longitudinal direction, with a length of 5 meters, and has openings for doors. Thickness of walls at ground level is d = 22 cm, and d = 14 cm on the first and second floor. The longitudinal wall should cover width of 5 meters, but since the panels are made of CLT, they are limited by one shorter side, which most manufacturers produce up to 3.5 meters Therefore, it was decided that the wall in the longitudinal direction would be made of two panels, which are connected by connectors that ensure that panels act as a one part. The braces (diagonals) are made of glued laminated timber (glulam) of class GL28h, with cross-section dimensions of b/h = 24/24 cm.

First, a model with rigid connections (Model 1) was created and presented, and then flexible connections will be modelled using links in the critical parts of the structure (Model 2). A model was also created that uses links to connect elements, but the links are rigid (Model 3). A comparison was made between models with rigid connections and those with flexible connections. This paper presents but also expands authors' master thesis and contributes to it. New improvements were made in terms of modelling flexibility of bracing connections to columns and beams.

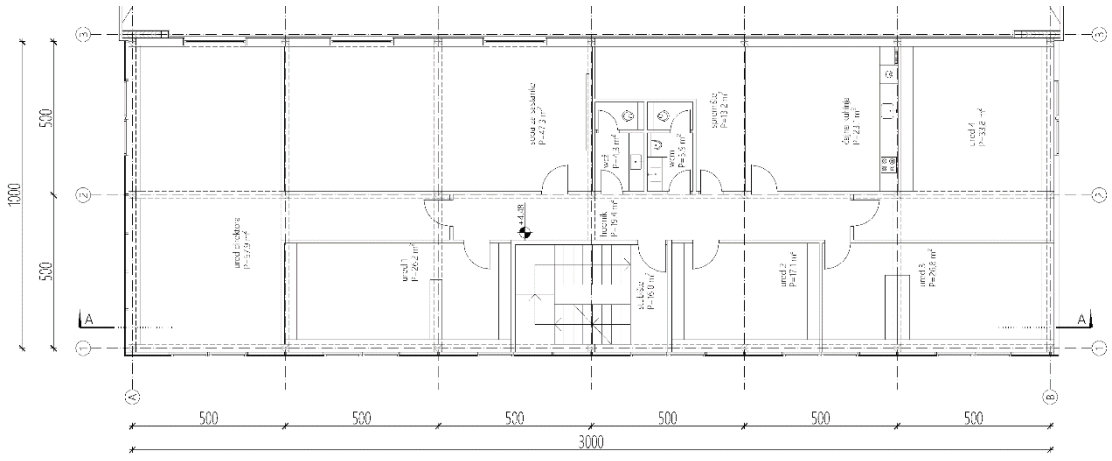


Figure 1. Characteristic floor plan of the building

Copyright © 2025 CroCEE
DOI: https://doi.org/10.5592/CO/3CroCEE.2025.166

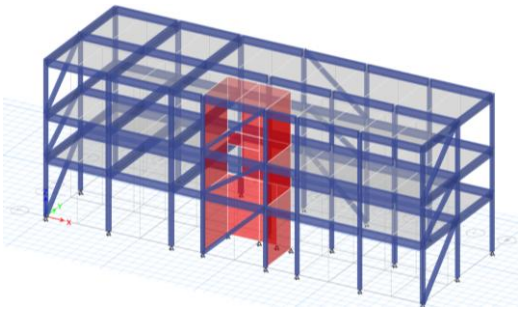
2.1 Numerical model with rigid joints (Model 1)

In this chapter modelling of an idealised numerical model with rigid joints will be presented. This model (Model 1) was used for design of structural elements and its results will be compared to and verified with a more complex model that includes flexibility of joints. End releases for bending moment were used to model correct behaviour of the core and slabs. Moment release was also applied on ends of bracing elements.

2.1.1 Geometric and material properties of model with rigid joints

The plan view of the characteristic floor and 3D model of the structure are shown in Fig. 2 In the next models this won't be shown, because general layout of the model is the same. Emphasis will be put on modelling of connections.

a)



b)

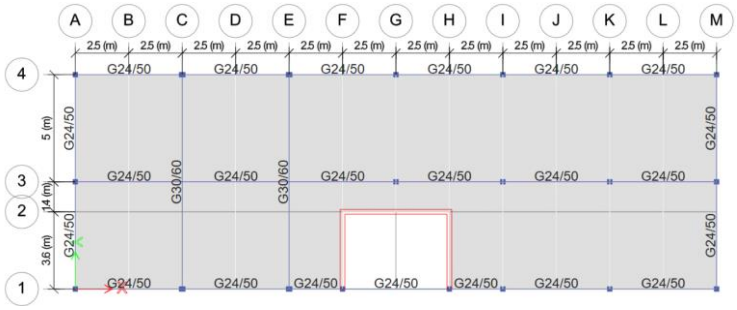


Figure 2. a) Numerical model; b) Ground floor plan with cross sections

CLT panels have properties that are defined by the arrangement of the laminations, depending on the layers. Since CLT is a composite (laminate), the mechanical properties were calculated using composite theory [10]. The modulus of elasticity differs in two orthogonal directions in the plane of the panel. The panel is made of wood of quality grade C24, and the manufacturer offers CLT panels with three, five, or seven layers [6]. For the walls on the upper floor and slabs, CLT elements with five layers were chosen, while for the ground floor walls, elements with seven layers were selected. Characteristics of materials and cross sections are given in Tables 1, 2 and 3.

Table 1. – Characteristics of materials [4] [5] [6]

Material	**E1** [Mpa]	**E2** [Mpa]	**E3** [Mpa]	**G12** [Mpa]	**G13** [Mpa]	**G23** [Mpa]	**ν**	**γ** [kN/m^3]
GL28H	10200	420	420	780	780	780	0,2	4,1
GL75	15300	470	470	850	850	850	0,2	8,9
CLT, d = 14 cm	7972	3411	311	690	690	690	0,2	5
CLT, d = 18 cm	7465	3367	3367	690	690	690	0,2	5
CLT, d = 22 cm	8160	3367	3367	690	690	690	0,2	5

Copyright © 2025 CroCEE
DOI: https://doi.org/10.5592/CO/3CroCEE.2025.166

Table 2. – Characteristics of beam and column cross sections

Cross section	Material	Height [mm]	Width [mm]	I22	I33
G24/50	GL28H	500	240	0.5	0.5
G30/60	GL75	600	300	0.5	0.5
S24/24	GL28H	240	240	0.5	0.5
S24/30	GL75	300	240	0.5	0.5

Table 3. – Characteristics of CLT panel cross sections

Cross section	Modelling	Material	Thickness [mm]	m11	m22	m12
d = 18 cm	Shell thin	CLT, d = 18 cm	180	0.5	0.000001	0.5
d = 14 cm	Shell thin	CLT, d = 14 cm	140	0.5	0.5	0.5
d = 22 cm	Shell thin	CLT, d = 22 cm	220	0.5	0.5	0.5

Bending stiffness of all cross sections were reduced in according to Eurocode 8 [7]. The design of structural elements and connections was carried out according to Eurocode 5 [8] and CLT Engineer Manual [9].

2.1.2 Load Analysis

In this chapter analysis for vertical and horizontal loads is given with summary of load cases and load combinations. Only load cases and combinations that are needed for dynamic and seismic analysis of the structure will be considered because design of structural elements was carried out in master's thesis [10]. Wind load is not considered because dominant horizontal load is seismic load. This load analysis applies to all models that will later be presented.

2.1.2.1 Vertical loads

Permanent loads are taken as follows according to norms: HRN EN 1991-1-1:2012 [11] and national annex HRN EN 1991-1-1:2012/NA:2012 [12] :

- Dead load of all structural elements is taken into account automatically in ETABS (*Dead*)
- Additional dead load is taken into account (*DS*) ; shown in Table 4

Service loads are taken for each floor according to norms: HRN EN 1991-1-1:2012 [11] and national annex HRN EN 1991-1-1:2012/NA:2012 [12]. Their intensities are shown in Table 4.

Snow load is taken for the roof according to norms: HRN EN 1991-1-3:2012 [13]; national annex HRN EN 1991-1-3:2012/NA:2012 [14]. Intensity are shown in Table 4.

Table 4. – Load intensity for vertical loads

Level	Δg (kN/m^2)	q (kN/m^2)	s (kN/m^2)
Roof	0,80	0,60	1,00
2nd floor	2,00	3,00	/
1st floor	2,50	2,00	/

Copyright © 2025 CroCEE
DOI: https://doi.org/10.5592/CO/3CroCEE.2025.166

2.1.2.2 Horizontal load

Horizontal loads acting on this structure are wind and seismic load. Wind load will not be considered in this paper because seismic load is governing horizontal load as it is proven in the thesis [10] [15] [16].

Data needed for spectral analysis:

- Ground type: C
- Behaviour factor: q = 2,5
- Peak ground acceleration for T_p = 95 years: a_g = 0,133 g [17]
- Peak ground acceleration for T_p = 475 years: a_g = 0,266 g [17]

2.1.3. Load cases and combinations

Load cases for vertical and horizontal loads were made:

- Vertical loads: Dead, Additional dead, Live and Snow
- Horizontal loads – load cases for 95-year and 475-year return period were made, also for both return periods response spectrum 1 and response spectrum 2 were considered

Load combinations that are of importance in this paper are seismic load combinations because we are observing behaviour of the structure under horizontal loading. Seismic load combination according to Eurocode 8[7] is: 1,0 x Dead + 1,0 x Additional dead + 0,3 x Live + 1,0 x Seismic load case

2.2 Numerical model with flexible joints (Model 2)

After selection of connections between structural elements, Model 2 was made. Flexibility of the joints was added in elements that make horizontal load bearing system, which includes bracing and CLT core. In this chapter nature of modelled connections and modelling of flexible joints is explained, with calculations of their stiffness and the way it was considered in structural analysis.

2.2.1 Slip modulus and stiffness of connections

For connecting CLT core panels Rothoblaas connectors were used [18]. There are three basic connectors that are analysed in this paper and are shown in Fig. 3 and Fig. 4:

1. Tension angle brackets (THT) → WHTPT 720 and WHT 740
2. Shear angle brackets (TITAN S) → TCS 240 and TTS 240 (Fig.4)
3. Connectors for structural panels → SLOT (Fig.4)

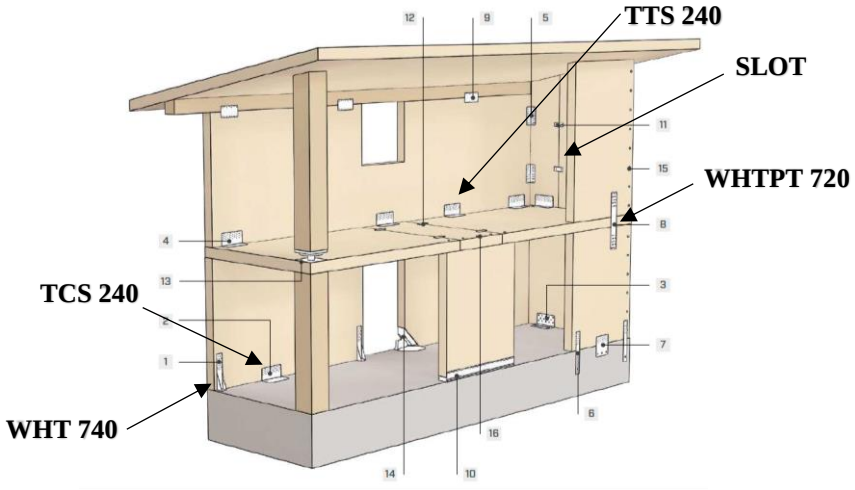


Figure 3. Illustrative representation of CLT wall connectors in a building [18]

Copyright © 2025 CroCEE
DOI: https://doi.org/10.5592/CO/3CroCEE.2025.166

a) b)

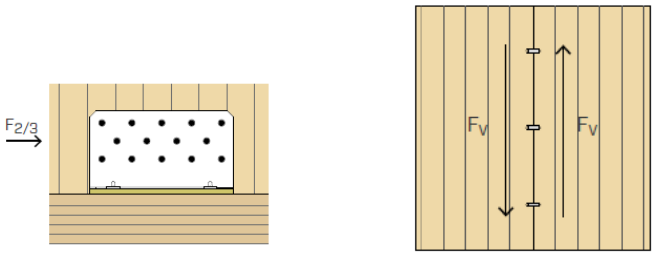


Figure 4. a) Scheme of TTS 240/TCS 240 [11]; b) Scheme of SLOT connector [18]

For calculation of joint stiffness Eurocode 5 is used. According to Eurocode slip modulus K_{ser} is a numerical value that defines stiffness of a connection. It can be used to define the translational stiffness of each joint. [7]

$$K_{ser} = n \cdot \frac{{\rho_m}^{1,5} d^{0,8}}{30} \left[\frac{N}{mm}\right]$$

Rotational stiffness is something that shouldn't be neglected, especially when discussing the connections between the wall and the foundation, as they are directly connected to the fixed restraint. Rotational stiffness for connections used in this model wasn't given, but will instead be taken from the scientific paper (work) [20].

Axial stiffness of a connection between bracing and columns/beams is also considered as bracing is important part of horizontal load bearing system. It is crucial that all elements that take part in transfer of horizontal loads are modelled with flexible joints. Rigid joint in axial direction of the bracing would make it too stiff, and realistic distribution of internal forces wouldn't be achieved. Translational stiffness of all connections is given in Rothoblass catalogue [11] but will not be used in this paper, it's given only for informative purposes. With their use Stiffness of all joints in Model 2 is calculated according to Eurocode 5 [7] and Eq. (1). In Table 5 stiffness of used connections is given.

Table 5. - Slip modulus and rotational stiffness of observed connections

Connection type	**K_{ser} (EC5)**	**K_{ser} (Rothoblaas)**	**Rotational stiffness**
	kN/m	kN/m	kNm/rad
TCS 240 – wall to foundation (shear)	37072	8200	390
TTS 240 – floor to wall (shear)	37072	5600	390
WHTPT 720 – wall to wall (tension)	74144	-	-
WHT 740 – wall to foundation (tension)	130462	-	-
SLOT – wall to wall (in plane shear)	25000	-	-
Bracing – column/beam connection	49718	-	-

2.2.2 Flexible joints in structural model and analysis

Flexible joints in Model 2 were modelled as link elements. Link element is an element that joins two nodes. Each link element can be modelled with six degrees of freedom that are represented with six flexible springs [21]. Stiffness of each spring can be defined as linear or non-linear. In this model all springs were given linear properties. Parameter that is used to define linear properties of links is effective stiffness. Effective stiffness that is attributed to specific links is slip modulus of a connection that is presented in Table 5.

Stiffness modelled with slip modulus is taken account in specific direction for each link. In Table 6 propertied of each link element are given.

Copyright © 2025 CroCEE
DOI: https://doi.org/10.5592/CO/3CroCEE.2025.166

Table 6. - Effective stiffness of joints in CLT core

Link element	U1 [kN/m]	U2 [kN/m]	U3 [kN/m]	R3 [kNm/rad]
Link 1	100000000	-	100000000	-
Link 2 (TTS 240)	100000000	37072	100000000	390
Link 3	100000000	-	100000000	-
Link 4 (TCS 240)	100000000	74144	100000000	780
Link 5 (SLOT)	-	25000	fixed	-
Link 5.2 (SLOT)	-	50000	fixed	-
Link 6 (TTS 240)	37072	37072	37072	390

Axial stiffness of bracing end joints that is presented in Table 5 is modelled as flexible end release. In Fig.5 isometric view of modelled links and mesh is shown. Link elements are modelled with length of 10 cm, and mesh is created so that it represents realistic spacing between connectors.

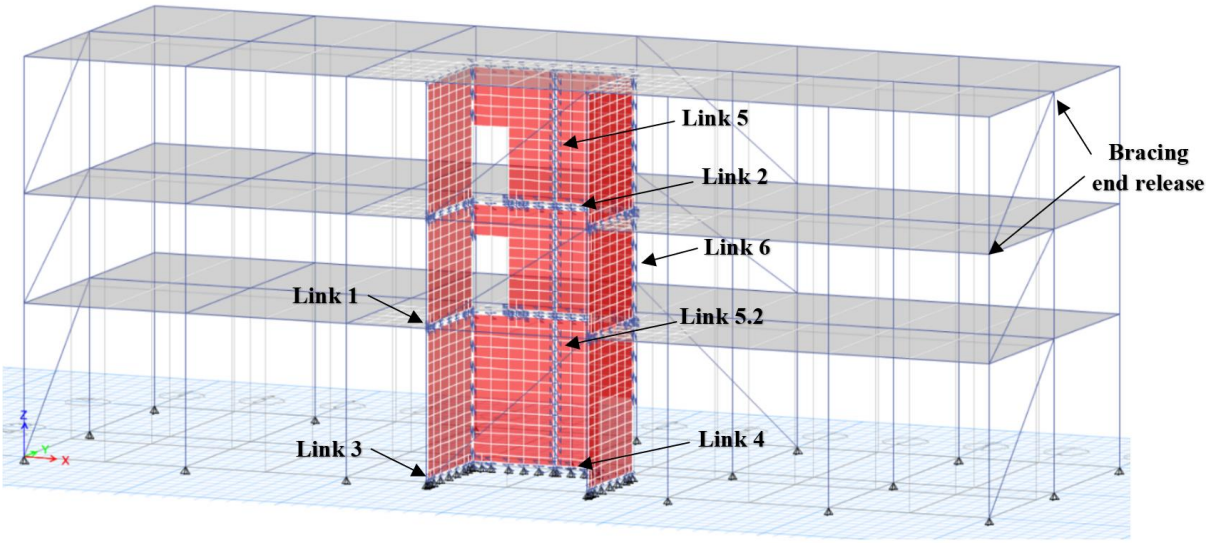


Figure 5. Isometric view of Model 2 with emphasis on CLT core and link elements

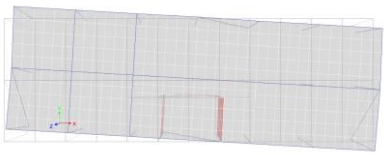
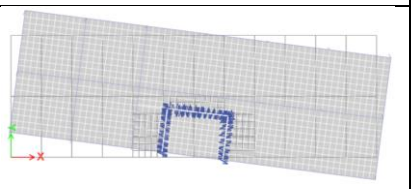
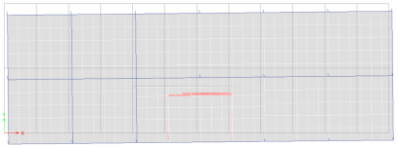
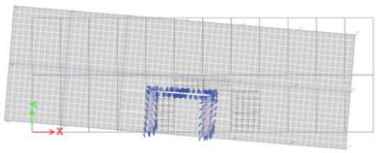
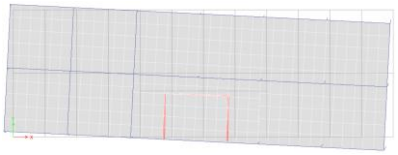
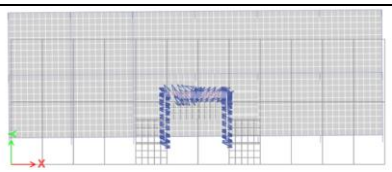
Dynamic and seismic analysis results and comparison

3.1 Comparison of dynamic parameters

In this chapter results of modal analysis are given trough comparison of Model 1 and Model 2. Table 7 shows comparison of mode shapes with corresponding vibration periods and Fig.6 and Fig.7 comparison of mass activation by mode shapes in different directions. It is expected that the structural model with flexible joints will be softer than the one with rigid joints. That should show trough higher numerical values of vibration periods. Mode shapes and mass activation are expected to stay similar.

Proceedings of the 3rd Croatian Conference on Earthquake Engineering - 3CroCEE
19–22 March 2025, Split, Croatia
Copyright © 2025 CroCEE
DOI: https://doi.org/10.5592/CO/3CroCEE.2025.166

Table 7. - Graphical display of mode shapes and corresponding vibration periods

Mode shape	Model 1		Model 2	
	Period [s]	3D view	Period [s]	3D view
1	0,371		0,623	
2	0,342		0,545	
3	0,327		0,495	

a) b)

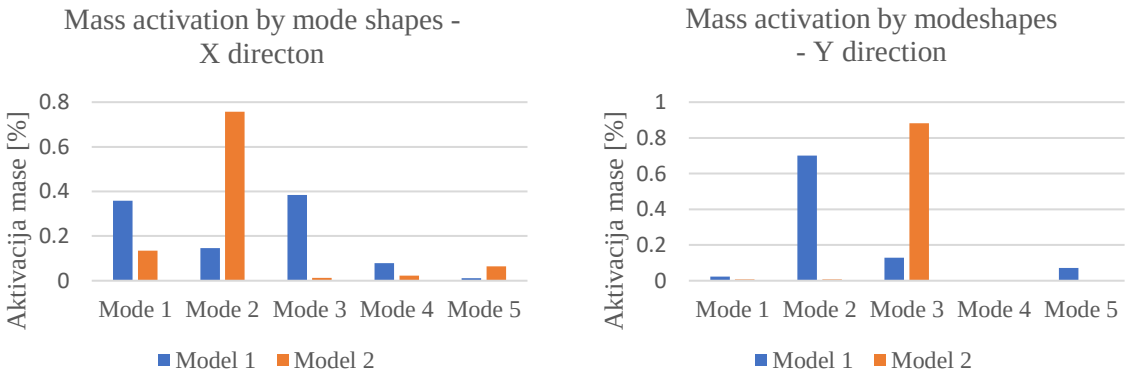


Figure 6. a) Translation in X direction by modes; b) Translation in Y direction by modes

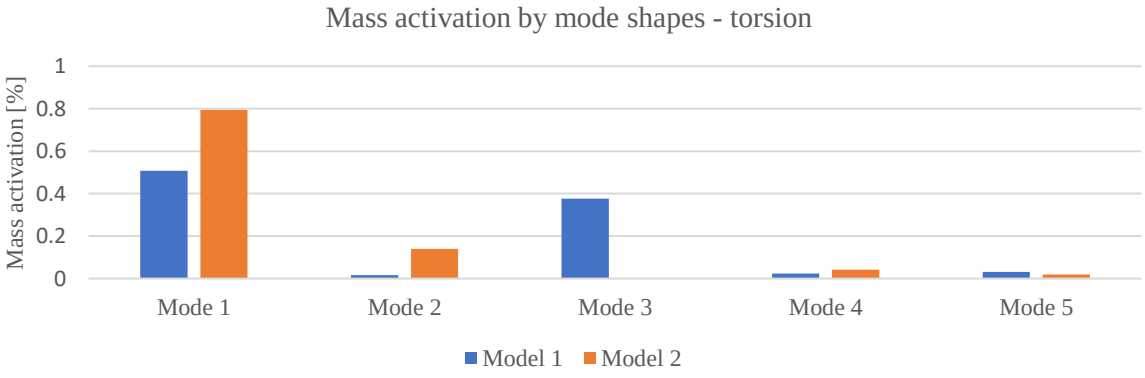


Figure 7. Graphic display of mass activation by modal shapes - torsion

Proceedings of the 3rd Croatian Conference on Earthquake Engineering - 3CroCEE
19–22 March 2025, Split, Croatia
Copyright © 2025 CroCEE
DOI: https://doi.org/10.5592/CO/3CroCEE.2025.166

It is visible from the results that first mode stayed in torsion but with significantly higher vibration period and mass activation. Second mode shape changed, in Model 1 building translates in Y direction and in Model 2 structure translates in X direction. Accordingly, the third mode change too, Model 1 translates in X direction and Model 2 in Y direction. Overall, it is visible that the vibration periods are higher.

3.2 Displacements and deformation

In Fig.8 and Fig.9 maximum story displacement and in story drift are shown for both models. Fig.10 and Fig.11 display shear force distribution in all stories for both response spectrums. In Fig.12 maximum displacement of chosen elements that are representative is shown, one corner column and CLT core wall in axis 2.

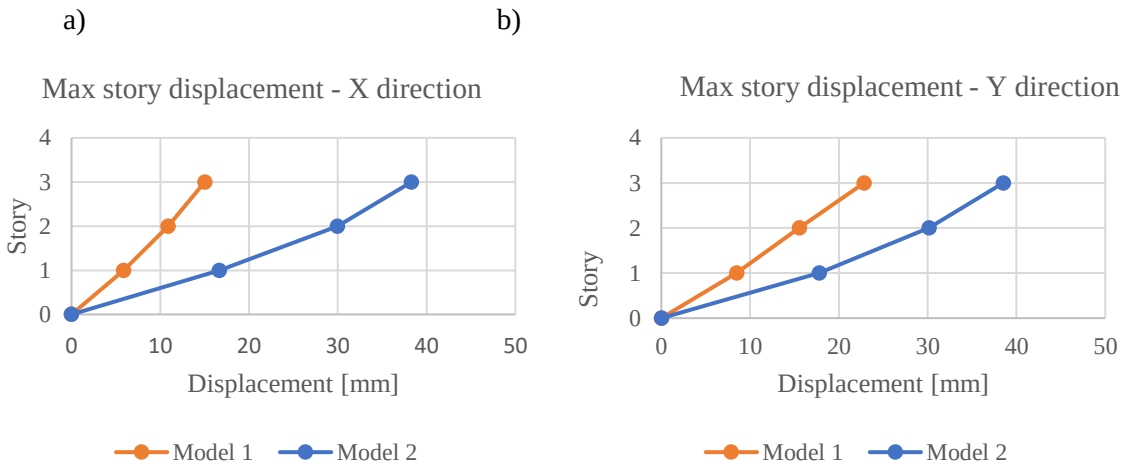


Figure 8. a) Graphic display of maximal story displacement in X direction; b) Graphic display of maximal story displacement in y direction

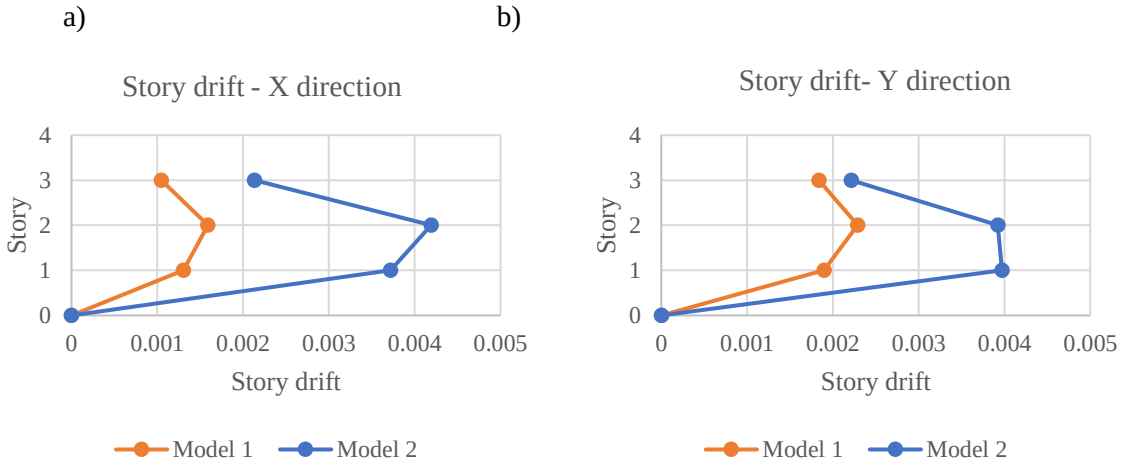


Figure 9. a) Graphic display of story drift in X direction; b) Graphic display of story drift in Y direction

As expected, both maximum story displacement and story drift are higher in Model 2. Less stiffness leads to bigger displacements and deformation. One information is interesting and that's shift in maximum story drift from story 2 to story 1 in Y direction when we compare Model 2 to Model 1.

Proceedings of the 3rd Croatian Conference on Earthquake Engineering - 3CroCEE
19–22 March 2025, Split, Croatia
Copyright © 2025 CroCEE
DOI: https://doi.org/10.5592/CO/3CroCEE.2025.166

a) b)

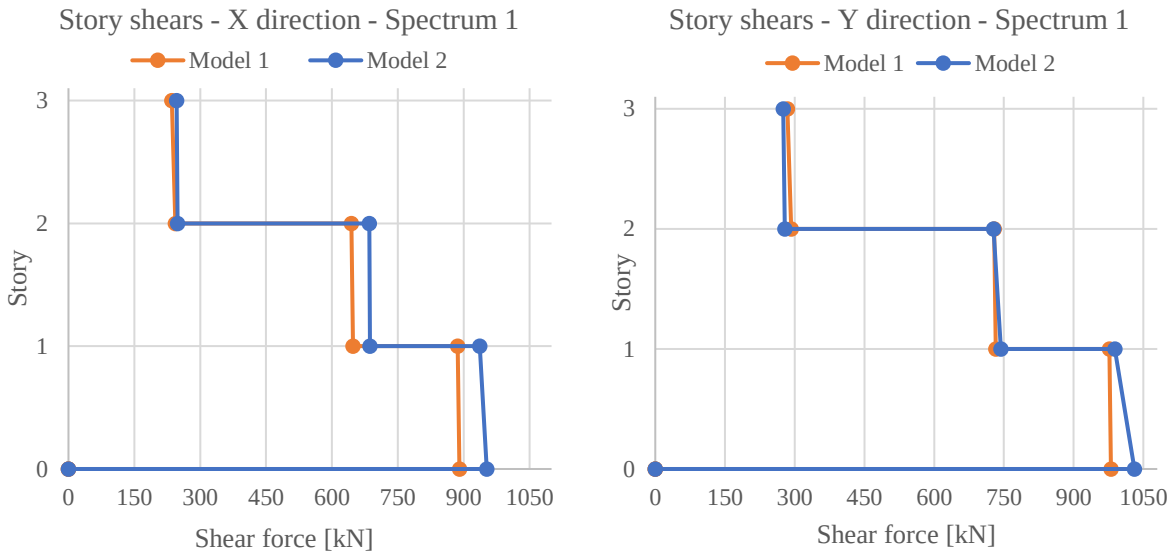


Figure 10. a) Graphic display of story shears in X direction for spectrum 1; b) Graphic display of story shears in Y direction for spectrum 1

a) b)

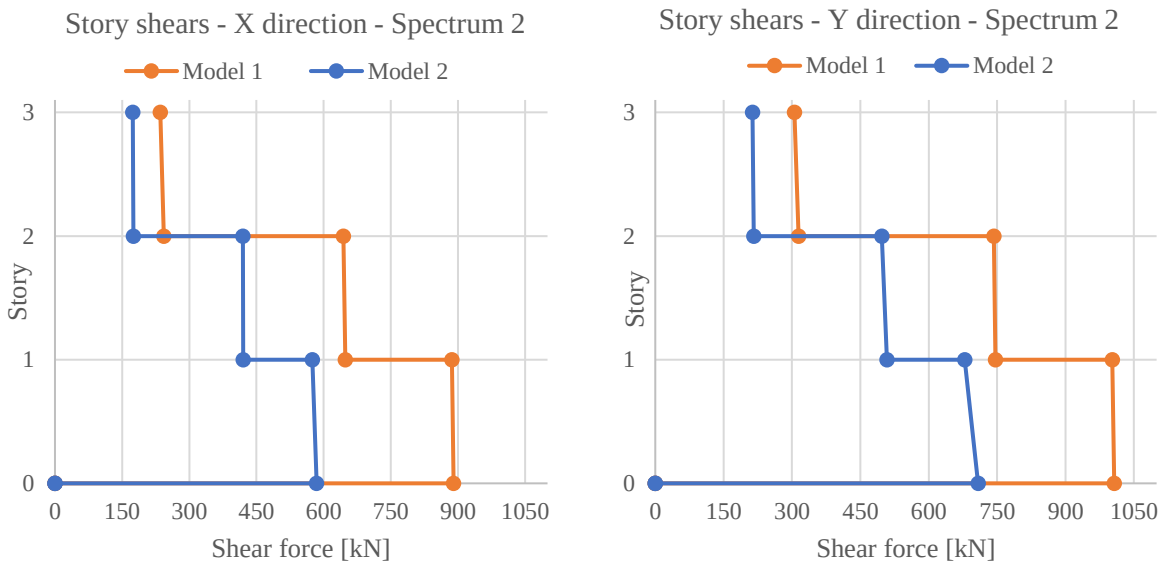


Figure 11. a) Graphic display of story shears in X direction for response spectrum 1; b) Graphic display of story shears in Y direction for response spectrum 2

It is visible that governing response spectrum for Model 2 is spectrum 1. In comparison with response of Model 1, Model 2 has more visible difference between base shear values considering both response spectrums. This is due to higher period of vibration. Base shear in Model 1 isn't very much different when comparing two response spectrums.

Proceedings of the 3rd Croatian Conference on Earthquake Engineering - 3CroCEE
19–22 March 2025, Split, Croatia
Copyright © 2025 CroCEE
DOI: https://doi.org/10.5592/CO/3CroCEE.2025.166

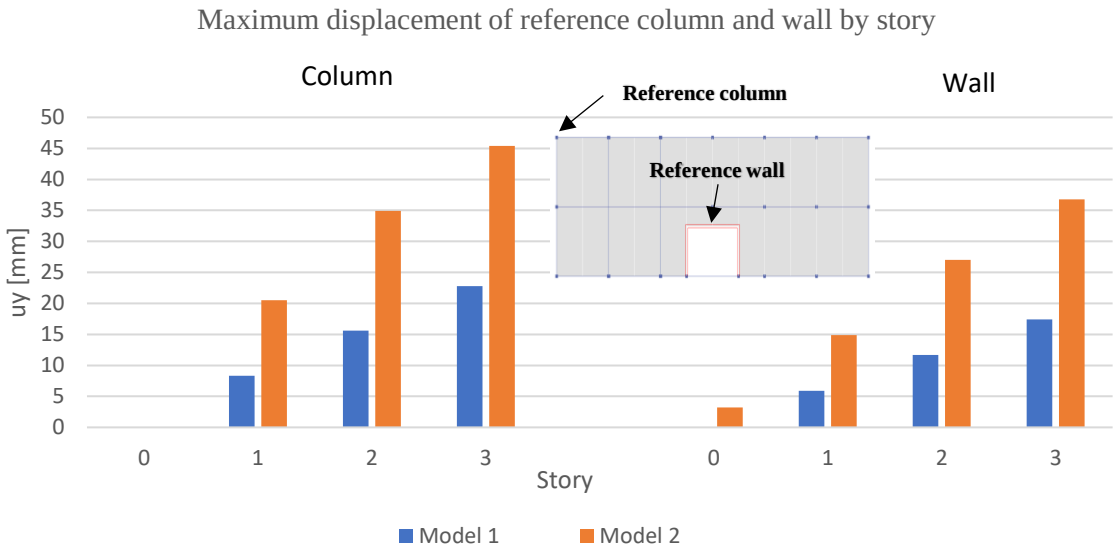


Figure 12. Graphic display of maximum displacement of reference column and wall by story

Fig. 12 shows that horizontal displacement of chosen column and beam are much higher in Model 2. Column was chosen so that it's far enough from the core walls, but as it is visible change in displacement is the same and values are similar.

Results shown in Fig. 8 – 11 are expected, they confirm that horizontal stiffness of Model 2 is lesser than that of Model 1, since Model 2 has flexible joint connections in all its structural elements that partake in horizontal load bearing system. As a result, displacement and relative displacement is greater in Model 2 and governing response spectrum for seismic analysis is response spectrum 1.

3.3 Internal forces in the elements of the structure

In this chapter graphic displays of internal forces are given for structural elements that make horizontal load bearing system. In Fig.13 values of moment and shear force on the bottom of the ground floor wall and on Fig.14 of the first floor wall are shown. Fig.15 shows axial force in reference bracing element. Since Model 2 is softer horizontally than Model 1, different distribution of internal forces is expected.

a) b)

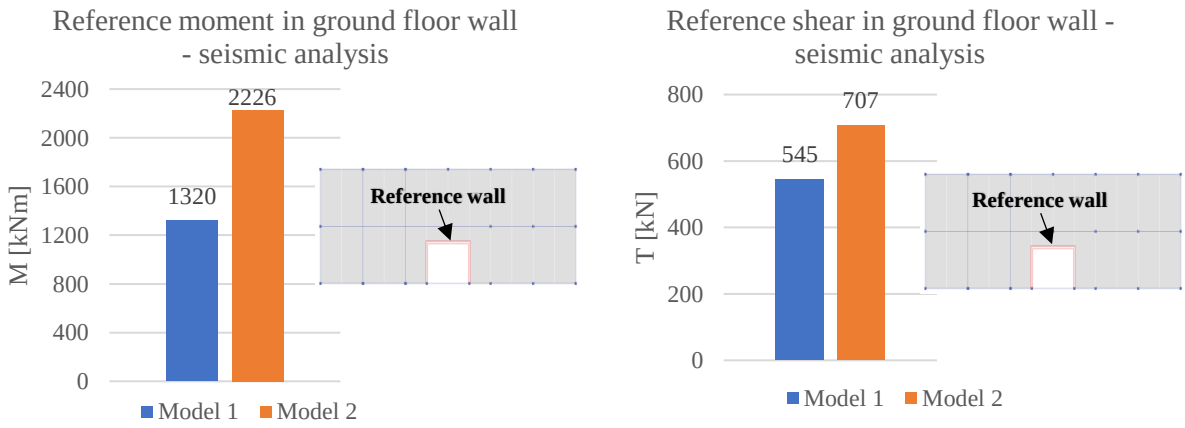


Figure 13. a) Bending moment comparison in reference wall – ground floor; b) Shear force comparison in reference wall – ground floor

Copyright © 2025 CroCEE
DOI: https://doi.org/10.5592/CO/3CroCEE.2025.166

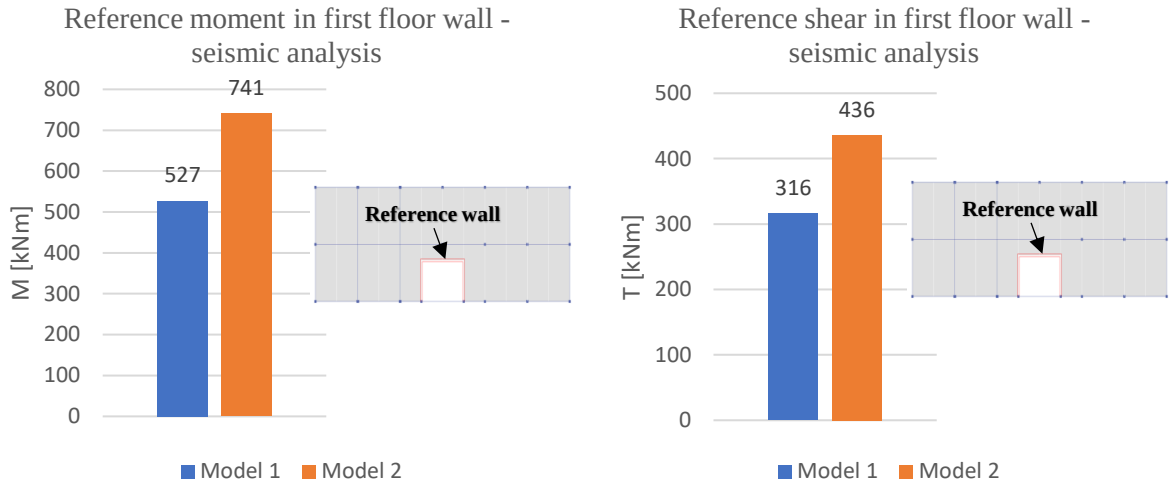


Figure 14. a) Bending moment comparison in reference wall – first floor; b) Shear force comparison in reference wall – first floor

In Fig.13 and Fig.14 bending moment and shear force on the bottom of reference walls are shown. Raise of both values of bending moment and shear force are observed. Which is interesting, since stiffness of core is lower than in Model 1.

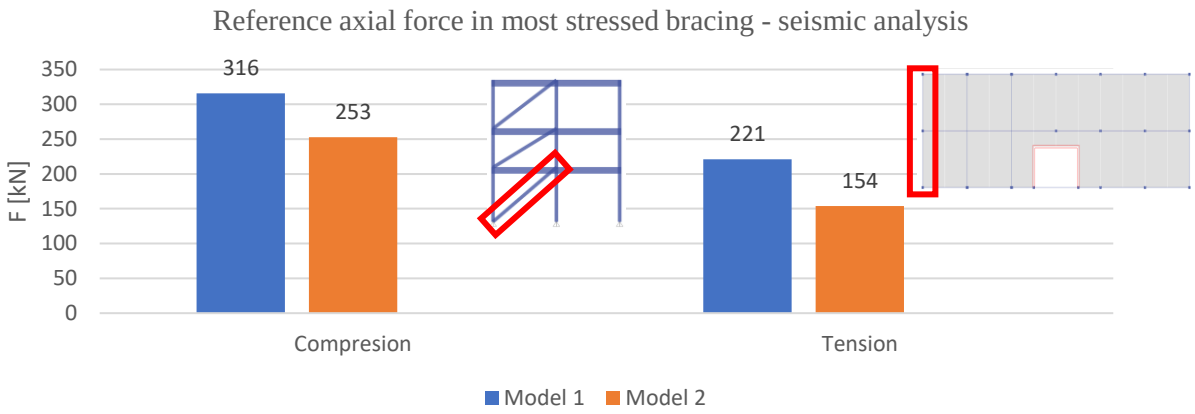


Figure 15. Graphic display of axial force in most stressed bracing element for seismic combination

In Fig.15 it's visible that there's a decrease in axial force in bracing elements in Model 2 and is expected since flexibility of bracing connections was introduced in Model 2.

Results clearly show that CLT core took more shear force from seismic load and that axial force in bracing has decreased. Since we introduced axial flexibility for bracing elements this internal force distribution is not unusual, it shows that CLT core is stiffer than bracing when joint connection flexibility is introduced in these elements. Drops are not gigantic, but they are significant and show how the structure behaves. It can be assumed that if needed we can increase stiffness of bracing connections with columns and beams to alleviate the CLT core and its connectors.

Copyright © 2025 CroCEE
DOI: https://doi.org/10.5592/CO/3CroCEE.2025.166

3.4 Model 3 and forces in link elements

For last comparison and result showcase, a new model is introduced. From now on it will be called Model 3. Model 3 is similar to Model 2 because it also has link elements connecting joints, but all link elements in this model are rigid. In this way we can obtain forces from links and compare them to forces in flexible links from Model 2. Results of forces in link elements are shown in Fig.16.

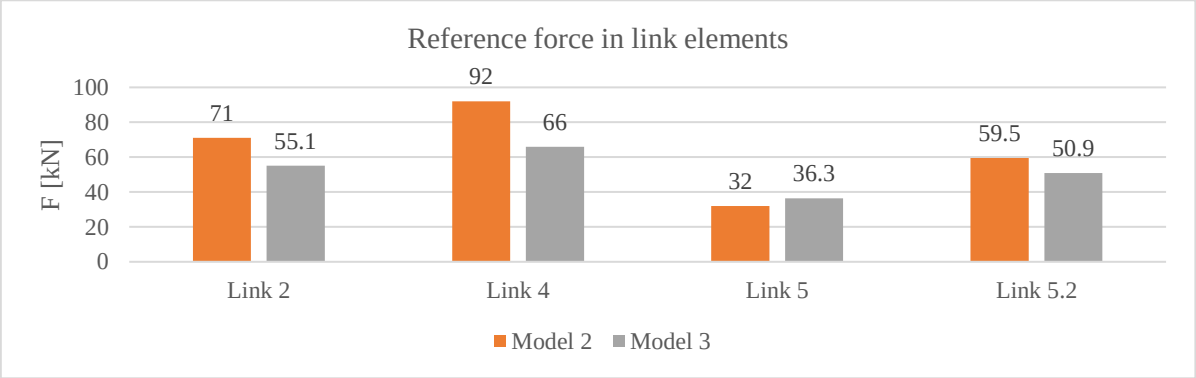


Figure 16. Graphic display of shear force in link elements

Viewing results of forces in link elements clearly shows us that forces in shear connectors (Links 2 and Link 4) are higher in Model 2, which corresponds with previous chapter and greater shear force in core walls. It can also be seen that forces in link elements 5 and 5.2 are similar.

4. Conclusion

In this paper influence of modelling connection stiffness in horizontal load-bearing system of a mass timber building was observed. Two structural models were made with real dimensions of structural elements, one with rigid joint connections and the other with flexible links that connect the joints. Horizontal load -bearing system consists of diagonal bracing and a core made of CLT wall panels. Connections between CLT wall panels and diagonal bracing end connections were taken into account with calculation of slip modulus that represented effective stiffness of link elements that connected the joints. Dynamic parameters, displacements, deformations and internal forces of the structure were observed and compared.

Comparison of models with rigid joint connections (Model 1 and Model 3) and the one with flexible joint connections (Model 2) lead to following conclusions:

- Flexible joint connections in the diagonal bracing and CLT core result in changes to the dynamic parameters, an increase in the vibration period, and a shift in the vibration modes
- Maximum displacement and story drift increase with introduction of flexible joint connections.
- Change in vibration periods leads to change of reference response spectrum.
- Distribution of internal forces in horizontal load bearing elements changes with introducing flexibility of its connections.
- Modelling joint connections with link elements gives a more accurate way of determining internal forces that are used for the design of connections. With correct mesh and distribution of links we can be close to real layout of connectors and forces that they transfer.
- Connections are critical elements of a structure with its design we can impact dynamic parameters, distribution of internal forces and displacements of a structure.

Acknowledgements

This paper presents and calls upon the master's thesis of the co-author that was mentored by Associate professor Mario Uroš as a culmination of two-year master's program attended at the Faculty of Civil engineering, University of Zagreb.

Copyright © 2025 CroCEE
DOI: https://doi.org/10.5592/CO/3CroCEE.2025.166

References

[1] Kuzman, K. M. 'Drvo kao građevni materijal budućnosti', Građevinar, vol.62 4, pp. 313 – 318; 2010. Available: http://casopis-gradjevinar.hr/assets/Uploads/JCE-62-2010-04-04.pdf

[2] Bogdan, A. 'Drvo u modernom graditeljstvu', Građevinar, vol.72, pp. 70–76; 2020. Available: http://casopis-gradjevinar.hr/assets/Uploads/JCE-72-2020-8-Zelenaa.pdf

[3] Jeleč, M., Varevac, D., Rajčić, V. 'Cross-laminated timber (CLT) - a state of the art report', *Građevinar, vol. 70* 2, pp. 75-95, Available: https://doi.org/10.14256/JCE.2071.2017

[4] Bjelanović A, Rajčić V. Drvene konstrukcije prema europskim normama. Second issue. Zagreb: Faculty of civil engineering, University of Zagreb, Hrvatska sveučilišna naklada, Zagora-Zagorje d.o.o.; 2007

[5] Pollmeier, 'Baubache GL75 - Declaration of performance' , str. 3, 2022. Available: https://www.pollmeier.com/product/beam-baubuche-gl75/#gref

[6] 'CLT by Stora Enso – Technical brochure' [Interent]. Available: https://www.storaenso.com/-/media/documents/download-center/documents/product-brochures/wood-products/clt-by-stora-enso-technical-brochure-en.pdf

[7] Eurocode 8: Design of structures for earthquake resistance -- Part 1-1: General rules, seismic actions and rules for buildings, HRN EN 1998-1:2011. Zagreb: Croatian Standards Institute, 2011

[8] Eurocode 5: Design of timber structures - Part 1-1: General - Common rules and rules for buildings, HRN EN 1995-1-1:2013. Zagreb: Croatian Standards Institute, 2013.

[9] 'CLT Engineer Manual' [Internet]. Available: https://calculatis.storaenso.com/Dokumentation/CLT-Engineer_Manual.pdf

[10] Buzjak R, Influence of connecting elements on the dynamic parameters of a wooden building [master's thesis]. Faculty of civil engineering: University of Zagreb

[11] Eurocode 1: Actions on structures - Part 1-1: General actions - Densities, self-weight, imposed loads for buildings, HRN EN 1991-1-1:2012. Zagreb: Hrvatski zavod za norme, 2012.

[12] Eurocode 1: Actions on structures - Part 1-1: General actions - Densities, self-weight, imposed loads for buildings – National annex, HRN EN 1991-1-1:2012/NA:2012. Zagreb: Hrvatski zavod za norme, 2012.

[13] Eurocode 1 - Actions on structures - Part 1-3: General actions - Snow loads, HRN EN 1991-1-3:2012. Zagreb: Hrvatski zavod za norme, 2012.

[14] Eurocode 1 - Actions on structures - Part 1-3: General actions - Snow loads – National annex, HRN EN 1991-1-3:2012/NA:2012. Zagreb: Hrvatski zavod za norme, 2012.

[15] Eurocode 1: Actions on structures - Part 1-4: General actions - Wind actions, HRN EN 1991-1-4:2012. Zagreb: Hrvatski zavod za norme, 2012.

[16] Eurocode 1: Actions on structures - Part 1-4: General actions - Wind actions – National annex, HRN EN 1991-1-4:2012/NA:2012. Zagreb: Hrvatski zavod za norme, 2012.

[17] "Karte potresnih područja Republike Hrvatske." Available: http://seizkarta.gfz.hr/hazmap/karta.php (Accessed 18.1.2025).

[18] 'Plates and connectors for timber' [Internet]. Available: https://www.rothoblaas.com/catalogues-rothoblaas

[19] 'European Technical Assessment ETA-19/0167', 2019. Available: https://www.rothoblaas.com/products/fastening/brackets-and-plates/angle-brackets-and-plates-for-buildings/slot#documents

[20] Vojnovic, L., Toumpanaki E. , and Norman J.A.P. 'Experimental study of a typical external wall-floor-wall connection in a CLT platform type construction.' *The 13th World Conference on Timber Engineering*. 2023. Available : https://www.proceedings.com/content/069/069179-0187open.pdf

[21] Computers & Structures, Inc. [CSI] (2019.) CSI Analysis Reference Manual For SAP 200, ETABS, SAFE and CSiBridge.

Proceedings of the 3rd Croatian Conference on Earthquake Engineering - 3CroCEE
19–22 March 2025, Split, Croatia
Copyright © 2025 CroCEE
DOI: https://doi.org/10.5592/CO/3CroCEE.2025.15

OPTIMAL ESTIMATION OF LINEAR SHEAR-TYPE MODELS FOR BENCHMARK STEEL STRUCTURES IN DYNAMIC ANALYSIS

Maziar Fahimi Farzam [(1)], Mohammad Salehi [(2)]

[(1)] *Department of Civil Engineering, Faculty of Engineering, University of Maragheh, m.farzam@maragheh.ac.ir*
[(2)] *Graduated Student from the University of Maragheh, mohammadsalehicivil70@gmail.com*

Abstract

Reducing the degree of freedoms of building models significantly decreases the computational costs in time consuming structural engineering problems like dynamic analysis of structures, nonlinear analysis or any optimal design of structural systems. In this study, the finite element models of 3- and 9-story benchmark steel buildings with numerous degrees of freedoms are simplified to 3- and 9-degree-of-freedom linear shear-type buildings and reduced to just 3- and 9-degree of freedom buildings, respectively. First, initial linear shear-type models were derived by estimating the stiffness of the stories, ensuring that their fundamental frequency matches the corresponding frequencies of the finite element models. Then, an optimization problem is defined and solved using a Genetic Algorithm (GA) to achieve more significant accuracy in the higher frequencies of the initial linear shear-type models. Two objective functions were established and assessed for the optimization problem: one is the difference in frequencies between the finite element models and the initial linear shear-type models with equal weighting, and the other is the first objective function improved with the modal participation percent weighting. The stiffness of the stories in the shear models are selected as the design variables in both optimization problems. Finally, the models are subjected to four benchmark earthquake excitations and different structural responses are compared with those of finite element models to evaluate the accuracy of optimal linear shear-type models based on the time responses of buildings under natural ground motions. The Root Mean Square (RMS) and peak of the displacement, velocity, and absolute acceleration of the building's roofs have been selected and compared as the performance criteria of the proposed objective functions. The results show that the model derived from the weighted objective function outperformed the objective function with equal weighting. Moreover, by comparing the proposed optimal 3- and 9-story models with those of available in the literature, it can be shown that the proposed optimal linear shear-type models are significantly more accurate both in frequency and time-history analysis.

Keywords: Dynamic Analysis, Finite Element Models, Degrees of Freedom, Shear-Type Models, Genetic Algorithm, Benchmark Steel Structures, Benchmark Earthquake Excitations.

1. Introduction

Engineering structures are increasingly being constructed on a larger scale, leading to greater structural sophistication and more detailed design requirements. Various methods have been employed for analysis and design. This analysis involves calculating displacements, deformations and stresses within a structure over a specified period under defined dynamic loads. Therefore, reliable dynamic analysis tools are essential throughout the design process [1]. Dynamic analysis can be conducted analytically for simple structures under specific loading conditions. However, advanced computational methods are necessary for more complicated structures and intricate loading conditions. The introduction of the Finite Element (FE) [2] method marked a pivotal milestone in the history of computational dynamic analysis. FE techniques are essential in structure analysis, design, and control. The more precise these methods are, and the more accurate the results they can provide, the more complex and computationally intensive the modeling and computational effort required becomes [3].

Unfortunately, FE models often possess hundreds of thousands of degrees of freedom (DoF), making dynamic response computations extraordinarily time-consuming and costly. When multiple designs and loading conditions require evaluation, completing a dynamic assessment of the system within a reasonable time duration becomes unfeasible [4]. Engineers must balance two conflicting objectives to achieve accurate and precise modeling while minimizing time, cost, and computational effort. Model

Copyright © 2025 CroCEE
DOI: https://doi.org/10.5592/CO/3CroCEE.2025.15

Order Reduction (MOR) techniques present a valuable and practical approach for approximating the original model with a significantly more subordinate order. In other words, these techniques create a Reduced-Order Model (ROM) that simulates the behavior of large-scale dynamic systems. So this allows for reduced computation time, cost, and effort while maintaining the accuracy of the analysis results [5]. Today, FE analysis is widely used to analyze and design structural systems, making the need for MOR techniques essential in this context.

Reducing DoF in engineering structures serves various purposes, such as seismic performance assessment, seismic demand analysis, health monitoring, damage detection, damage evaluation, and control system design. Engineering structures, such as buildings, often possess many DoF and are simplified and reduced to lower-order models, including single-degree-of-freedom (SDoF) and shear-type models.

Guyan introduced the concept of reducing DoF in 1965 by reducing mass and stiffness matrices [6]. After Guyan, other researchers have also employed reducing DoF and using ROMs in their studies. Qu et al. reduced the order of the mass and stiffness matrices of a 40-story shear-type building, where ROM is updated iteratively until the desired ROM is achieved [7]. Liu et al. proposed a simplified method for the preliminary design of structural dampers, which simplified 3, 9, and 20-story benchmark steel strutures to a shear-type models [8]. Bagchi proposed an iterative method for reducing the DoF in 6 and 12-story concrete buildings, where these were reduced to SDoF models [9]. Cimellaro et al. simplified a 9-story benchmark steel structure by deriving an equivalent linear shear-type model. This purpose is achieved by minimizing the natural frequencies and mode shapes discrepancies between the FE model and ROM [10]. Larki and Hosseini introduced a method to reduce the DoF in high-rise shear-type models, precisely 40 and 60-story models, by condensing them into 10 and 15-story models [11].

Alonso-Rodríguez and Miranda introduced a method for simplifying large-scale buildings, which was applied to a 20-story building [12]. Niti et al. proposed a fundamental analytical formulation for evaluating high-rise buildings' natural frequencies and mode shapes in the early design stages for dynamic response assessment. This method reduces the structural systems' DoF to 3 per floor [13]. Ghara et al. proposed a matrix-based analytical approach for assessing the behavior of friction-damped structures. In this approach, the DoF are divided into primary and subsidiary groups, with frictional connections modeled using 4 DoF, ultimately condensing the primary structure's matrices [14]. Ahmadi Amiri et al. presented a practical method for seismic risk analysis, which reduces both the DoF in the FE model and the number of iterative nonlinear time history analyses (NLTHA) required [15]. Fiore et al. developed a heuristic algorithm for obtaining a structures' mass and stiffness matrices and determining natural frequencies, requiring minimal input data and accelerating the process compared to traditional FE methods [16].

In this paper, an optimal linear shear-type model of 3 and 9-story benchmark structures is estimated based on the study by Ohotori et al., achieving a very high level of accuracy [17]. Initially, a preliminary shear-type model is created by estimating the story stiffness values, although it shows a considerable discrepancy with the FE model. By adjusting the coefficient in the stiffness equation for each structure, the initial frequencies of the preliminary models are matched to those of the FE models.

An optimization problem is defined to enhance the accuracy of these preliminary models, which is solved using a weighted sum approach. Two objective functions are defined based on the frequency discrepancies between the preliminary shear-type and the FE models, with one function weighted equally and the other weighted by modal participation percent weighting. The design variables in the optimization problem are the story stiffness values, and the search space is set within the range [2/3k, 4/3k], where k represents the stiffness of each story in the preliminary shear-type model. Upon solving the optimization problem for both objective functions, the solutions in which the story stiffness values are identified and corresponding shear-type models are modeled and compared to FE models in terms of frequency and time-history analysis accuracy.

The floor masses in both structures are identical to those in the Ohotori et al. study, and the damping matrix is derived using Rayleigh damping with a 2% damping ratio for the first and second modes. For

Copyright © 2025 CroCEE
DOI: https://doi.org/10.5592/CO/3CroCEE.2025.15

time-history analysis comparison, the optimized and FE models are subjected to identical inputs from four benchmark ground motions: two far-field earthquakes (Elcentro and Hachinohe) and two near-field earthquakes (Kobe and Northridge). The differences in their time-history responses, including peak and RMS values for the roof floor's displacement, velocity, and absolute acceleration, are compared.

2. Structures

2.1. Description of Case Studies

This study employs the 3 and 9-story benchmark buildings designed for the SAC Phase II Steel Project. Although these structures have not been constructed, they conform to seismic design codes and represent typical low, mid and high-rise buildings in Los Angeles, California. These buildings were selected as benchmark structures for SAC studies, providing a broader basis for comparative analysis of the results [17]. Details of these structures are supplied in [18]. The benchmark structures, as studied by Ohtori et al., have been modeled by Farzam and Kalajahi [19] using FE software, achieving significantly higher accuracy compared to Ohtori's models. These models serve as the foundation for the FE models utilized in this article. Figures (1,2) show the schematic diagram, plan, and connection details of the 3 and 9-story structures, along with the specifications of the beams and columns, respectively.

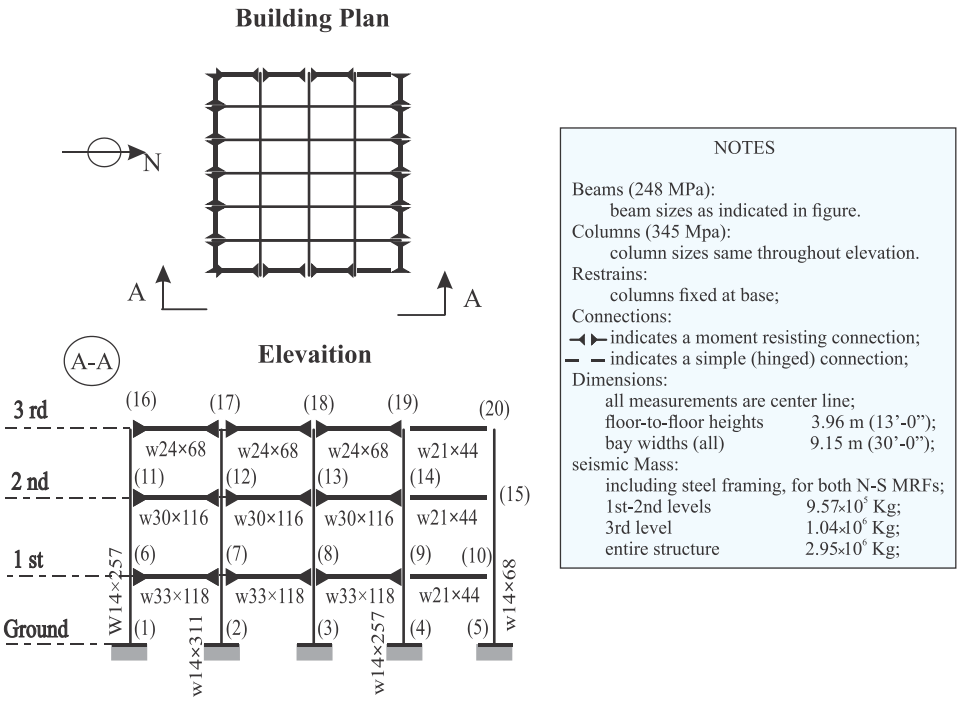


Figure 1. 3-story benchmark building north–south moment-resisting frame

2.2. Preliminary Shear-Type Models

A ROM is essential to simplify and reduce the DoF in the benchmark structures. For this purpose, a linear shear-type model is estimated, and the 3 and 9-story FE models, with 33 and 185 DoF, respectively, are reduced to 3 and 9 DoF shear-type models. In this approach, each floor acts as a rigid diaphragm, and the horizontal displacement of each floor's DoF is linked to the motion of the rigid floor, with the masses concentrated at each floor level. Consequently, the mass matrix of the structure is diagonal. The floor stiffness is calculated for each story, encompassing all cross-sections, and because the structures are modeled linearly, the principle of superposition applies; thus, the stiffness of each

Copyright © 2025 CroCEE
DOI: https://doi.org/10.5592/CO/3CroCEE.2025.15

floor is obtained by summing the stiffnesses of the beams and columns on that floor. With the mass and stiffness matrices established, the damping matrix of the structure is also determined. Figure (3) illustrates an N-story shear-type model subjected to earthquake excitation.

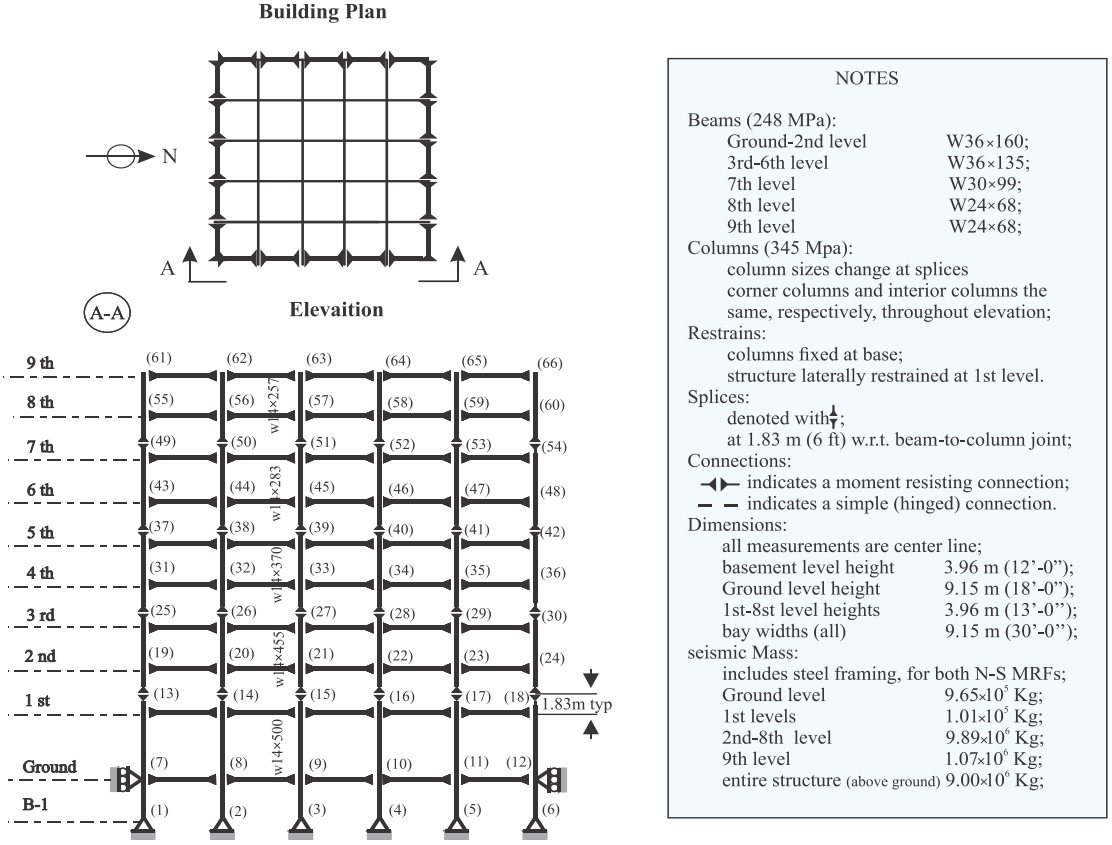


Figure 2. 9-story benchmark building north–south moment-resisting frame

To estimate the story stiffness in moment-resisting frames, a simplified method based on engineering judgment is provided by [8] to develop linear shear-type models for benchmark structures. The lateral stiffness in moment frames can be approximated from the lateral force and the resulting displacement. For frames with strong columns and weak beams, the total displacement under lateral force combines column and beam displacements, with approximately 0.4 and 0.6 contributions to the total displacement. Therefore, the lateral stiffness is estimated as follows:

$$K=\sum_{columns}\frac{4.8\times EI_c}{h^3} \tag{1}$$

E represents the modulus of elasticity of the columns, I_c denotes the moment of inertia of the column section, and h refers to the story height. The benchmark 3 and 9-story structures feature a moment-resisting frame system with a strong column and weak beam design approach. Therefore, the lateral stiffness K for each story in all structures is calculated using Equation (1). In Equation (1), a coefficient of 4.8 is utilized; however, comparing the first frequencies of the linear shear-type and the FE models reveals a significant discrepancy. Therefore, the lateral stiffness K for each story in all structures is calculated using Equation (1). In Equation (1), a coefficient of 4.8 is utilized; however, comparing the first frequencies of the linear shear-type and the FE models reveals a significant discrepancy. Since aligning the initial frequencies, mainly the first frequency, is essential for establishing an accurate preliminary shear-type model, the coefficient of 4.8 was adjusted for both the 3 and 9-story structures.

Copyright © 2025 CroCEE
DOI: https://doi.org/10.5592/CO/3CroCEE.2025.15

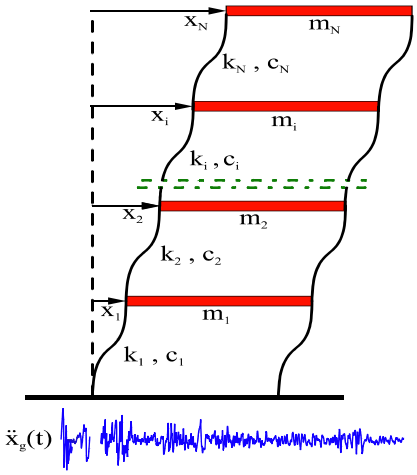


Figure 3. Sketch of an N-story shear-type model under earthquake excitation

The adjusted coefficients are 4.655 for the 3-story structure and 3.891 for the 9-story structure, which ensures that the first frequencies of the preliminary shear-type models match those of the FE models. Table 1. compares the first to third frequencies of the preliminary shear-type and the FE models. The closer the initial shear-type model represents the finite element model in terms of initial frequencies, mainly the first frequency, the less effort the Genetic Algorithm requires to solve the optimization problem. Based on the modification coefficients, as the number of stories and the structure height increase, the stiffness equation coefficient value decreases further. The preliminary model of the 9-story structure exhibits more accurate frequencies than the preliminary model of the 3-story structure.

Table 1. Comparison of natural frequencies of preliminary shear-type and FE models

	Frequency (Hz)			
Structure	**Error (%)**	**Preliminary**	**FE**	**No.Mode**
3-Story	0	0.979	0.979	1
	9.302	2.769	3.053	2
	27.523	4.042	5.577	3
9-Story	0	0.442	0.442	1
	1.180	1.200	1.186	2
	0.148	2.035	2.032	3

3. Genetic Optimization Algorithm

Genetic algorithms (GA) are exploratory search approaches that can be applied to various optimization problems. This flexibility makes them particularly appealing for various practical optimization challenges. Since the early 1980s, extensive research has been conducted on applying and developing GA across different fields. Using GA to optimize various engineering problems has proven successful in structural engineering. GAs are based on the principle of evolution, a concept first introduced by Charles Darwin [20]. Holland initially proposed GA in 1975, and researchers such as Goldberg [21] have further developed and refined them.

Proceedings of the 3rd Croatian Conference on Earthquake Engineering - 3CroCEE
19–22 March 2025, Split, Croatia
Copyright © 2025 CroCEE
DOI: https://doi.org/10.5592/CO/3CroCEE.2025.15

4. Mathematical Formulation

4.1. Governing Equation of Motion

To determine the response of a structure under seismic earthquake excitation, it is necessary to establish the mathematical relationships governing the dynamic displacements of the structure. Subsequently, by solving these relationships, the time-history responses of the structure can be obtained, where the most fundamental response in a dynamic analysis is its displacement. The equation of motion for a system with n DoF subjected to an earthquake is expressed as follows [22]:

$$M\ddot{x} + C\dot{x} + Kx = -M\Gamma\ddot{x}g \tag{2}$$

M, C, and K are the structure's n×n mass, damping, and stiffness matrices, respectively. Additionally, x is the n-dimensional displacement vector, and $\ddot{x}g$ represents the ground acceleration. The matrix Γ is of size n×1 and indicates the ground acceleration. Solving the above equation determines the structural response values.

Equation (2) can be expressed in state space form as follows:

$$\dot{Z} = AZ + E\ddot{x}g \tag{3}$$

In the above relation, Z is a 2n-dimensional state vector defined as follows:

$$Z = \begin{bmatrix} x \\ \dot{x} \end{bmatrix} \tag{4}$$

Additionally, A is the state matrix of the system with dimensions 2n×2n, and E is the earthquake position matrix, which has dimensions 2n×1. These matrices are defined as follows:

$$A = \begin{bmatrix} O(n,n) & I(n,n) \\ -M^{-1}K & -M^{-1}C \end{bmatrix} \quad E = \begin{bmatrix} O(n,1) \\ -\Gamma \end{bmatrix} \tag{5}$$

4.2. Definition Optimization Problem

An optimization problem is formulated to identify a linear shear-type model of benchmark structures that closely approximates FE models. This problem minimizes the frequency discrepancies between preliminary shear-type and FE models. A GA and weighted sum method are used to solve it. In this approach, the objective functions in the problem are combined through weighted coefficients to create a final objective function. The weight of each objective function depends on its significance, with more critical objectives assigned larger weights [23]. The objective function for this problem is defined as follows:

$$f(X) = \sum_{i=1}^{k} w_i f_i(x) \tag{6}$$

In the defined optimization problem, the design variables are the story stiffnesses, which are identified by finding the optimal stiffness of each story according to the specified objective function in the search space. The optimization problem is unconstrained, and the objective function aims to minimize the frequency discrepancies between the preliminary shear-type and FE models. Since matching the initial frequencies of FE models with shear-type models is highly important, the weighting coefficients for the objective functions associated with initial frequency discrepancies are assigned larger values. Appropriate weights are determined based on the dynamic characteristics of the FE models, assigning higher weights to more critical objective functions. Modal participation percent and period-based weightings from FE models can be used as possible weightings. Here, modal participation percent is employed as a weight in this optimization problem. Two objective functions are defined to account for

Proceedings of the 3rd Croatian Conference on Earthquake Engineering - 3CroCEE
19–22 March 2025, Split, Croatia
Copyright © 2025 CroCEE
DOI: https://doi.org/10.5592/CO/3CroCEE.2025.15

frequency differences between the preliminary shear-type and the FE models: one with equal weights and the other with weights proportional to the modal participation percent. The model obtained from the equally weighted objective function is designated Model 1, while the model derived from the objective function weighted by modal participation percent is designated Model 2. The search space for stiffness is defined within the range [2/3k, 4/3k], where k is the stiffness of each story in the preliminary shear-type model. The optimal story stiffnesses are determined by solving the optimization problem for both objective functions, and corresponding shear-type structures are modeled. These optimized shear-type models are then compared with the FE models in terms of frequency and time-history responses to identify the most optimal model. The story masses for both structures are set equal to those in Ohotori et al.'s article, and the damping matrix is derived using Rayleigh damping with a 2% damping ratio for the first two modes.

5. Results Analysis and Comparison

5.1. Frequency Analysis

In the 3 and 9-story structures for Model 1, where the objective function applies equal weighting, the discrepancies of all frequencies relative to their counterparts in the FE model are reduced uniformly. In contrast, for Model 2, where modal participation percent weights are applied to the objective function, the primary frequencies have more minor discrepancies compared to the FE model frequencies. Tables (2,3) present the first three frequencies of the 3 and 9-story models, comparing them with their respective values in the FE model.

Table 2. Comparison of frequencies between optimized the 3-story and FE models

Frequency (Hz)				
3-Story	**Error (%)**	**Optimum**	**FE**	**No.Mode**
Model 1	6.843	1.046	0.979	1
	0	3.053	3.053	2
	17.464	4.603	5.577	3
Model 2	0	0.979	0.979	1
	2.915	2.964	3.053	2
	18.002	4.573	5.577	3

Table 3. Comparison of frequencies between optimized the 9-story and FE models

Frequency (Hz)				
9-Story	**Error (%)**	**Optimum**	**FE**	**No.Mode**
Model 1	4.29	0.423	0.442	1
	1.096	1.173	1.186	2
	1.033	2.011	2.032	3
Model 2	0	0.442	0.442	1
	0	1.186	1.186	2
	0.147	2.035	2.032	3

Copyright © 2025 CroCEE
DOI: https://doi.org/10.5592/CO/3CroCEE.2025.15

In each structure, Model 2 is undoubtedly the more optimal choice. For both the 3 and 9-story structures, model 2 is compared in terms of frequency with the FE and the preliminary model, as shown in Figures (4,5). In the 3-story structure, the optimized model 2 achieves a 0% discrepancy for the first frequency, 2.915% for the second, and 18.002% for the third, demonstrating greater accuracy than the preliminary model and the optimized model 1. Similarly, in the 9-story structure, model 2 shows a 0% discrepancy for the first and second frequencies and 0.147% for the third, surpassing the preliminary model and optimized model 1 in accuracy. At higher frequencies, only the fifth frequency of the preliminary model shows a smaller discrepancy than that of the optimized Model 2.

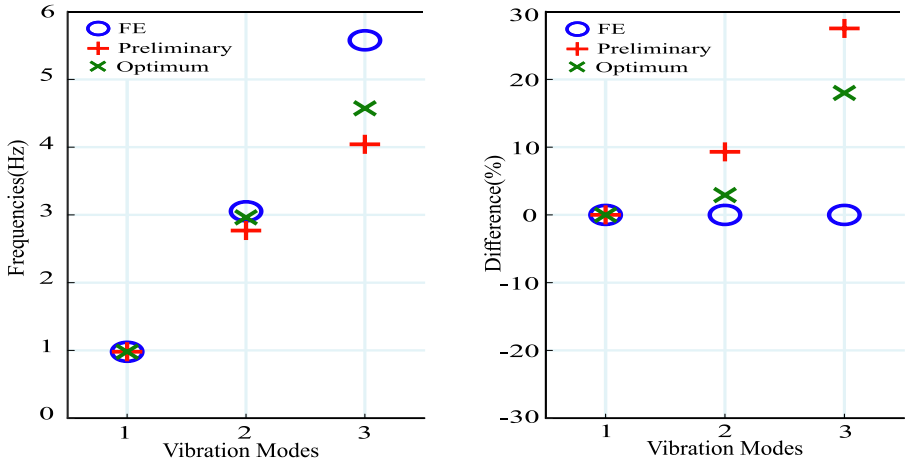


Figure 4. Comparison of Frequencies between Optimized Model 2 of the 3-Story Structure, the FE model, and the Preliminary Shear-type Model

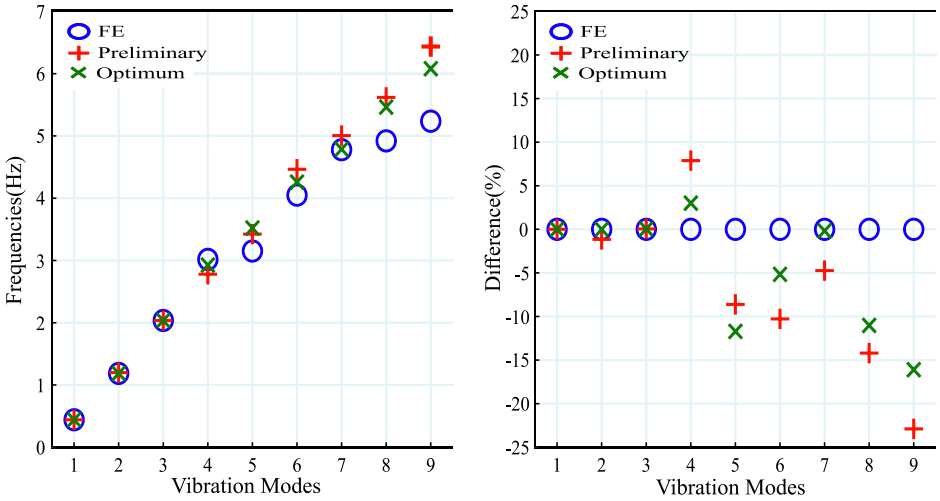


Figure 5. Comparison of Frequencies between Optimized Model 2 of the 9-Story Structure, the FE model, and the Preliminary Shear-type Model

Figures (6,7) illustrate the average absolute discrepancy across all modes during the optimization process and the convergence of preliminary shear-type model frequencies to the FE model frequencies for optimized Model 2 of the 3 and 9-story structures. In the upper figures, the vertical axis represents the percentage, while the horizontal axis denotes the number of analyses. The green curve indicates a reduction in the average absolute discrepancy across all modes throughout the optimization process, with a more pronounced decrease observed in the 9-story structure. The lower figures show the comparison of frequencies between the FE model and optimized Model 2 throughout the optimization process. Across various analyses, the frequencies of the preliminary shear-type model rapidly converge to the FE model frequencies, indicating both a highly accurate initial model and an improvement in its accuracy as the optimization progresses.

Copyright © 2025 CroCEE
DOI: https://doi.org/10.5592/CO/3CroCEE.2025.15

5.2. Time-History Analysis

This section analyzes the time-history responses of optimized Models 1 and 2 for the 3 and 9-story structures. The FE and optimized models are subjected to four benchmark earthquake excitations, and their time-history response discrepancies are evaluated and compared. For this purpose, a time-history response has been obtained by subtracting the time-history response of the finite element model from that of the optimized model. Subsequently, the resulting time-history response Peak and RMS were compared. The model with lower values is considered more optimal and accurate.

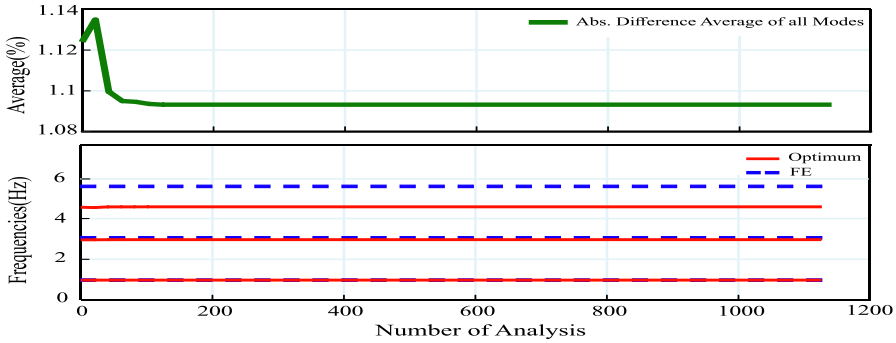


Figure 6. Iteration history of the optimization process in optimized Model 2 of the 3-story structure

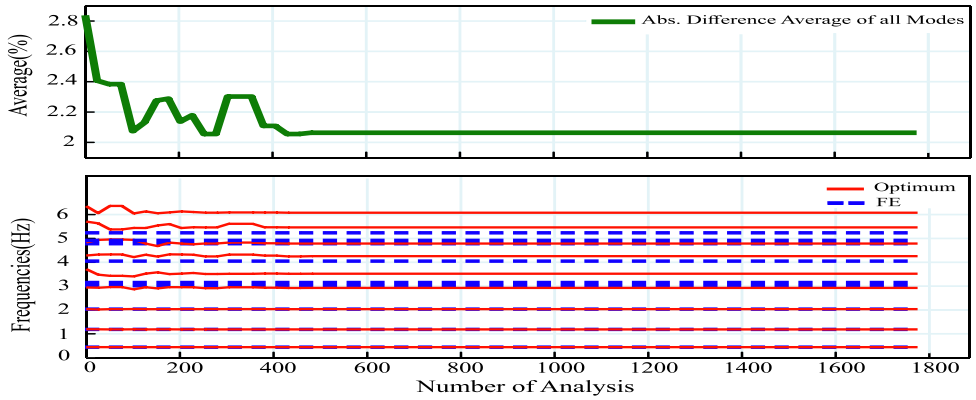


Figure 7. Iteration history of the optimization process in optimized Model 2 of the 9-story structure

This comparison approach is applied to roof responses, including displacement, velocity, and absolute acceleration, which are analyzed, with the results shown in Tables (4,5). Optimized Model 2 demonstrates significantly higher accuracy for both buildings, showing more minor discrepancies than optimized Model 1. The results reveal that the most minor discrepancies in both Peak and RMS occur for displacement. In contrast, the most significant discrepancies are observed in absolute acceleration, particularly under the Kobe and Northridge earthquakes. The large discrepancy in Peak response is due to the rapid and intense oscillation in the absolute acceleration response curve, with slight misalignment in time between the FE and optimized models. The Peak responses in the FE and optimized models do not coincide, resulting in a slight delay and contributing to more significant Peak discrepancies in absolute acceleration at the roof story. For example, in the Model 2 of 3-story structure under the Northridge earthquake, the Peak absolute acceleration in the FE model is 17.85 m/s². In contrast, in optimized Model 2, it is 16.20 m/s² with a difference of 1.65 m/s², and the Peak discrepancy in response to the proposed comparison approach is 10.03 m/s².

If the comparison had been limited to evaluating the differences in Peak and RMS values without utilizing the proposed comparison approach, achieving accurate results from the time-history analysis regarding the precision of the optimized models would not have been possible. Figure (8) presents the roof displacement time-history response of optimized Model 2 for the 3-story structure under the

Proceedings of the 3rd Croatian Conference on Earthquake Engineering - 3CroCEE
19–22 March 2025, Split, Croatia
Copyright © 2025 CroCEE
DOI: https://doi.org/10.5592/CO/3CroCEE.2025.15

Elcentro earthquake. It shows excellent alignment with the FE model time-history response and demonstrates the high accuracy of optimized Model 2.

Table 4. Statistical comparison of response discrepancies between optimized models of the 3-story structures to the FE model

3-Story		**Model 1**		**Model 2**	
Earthquake	**Response Type**	**Statistical**		**Statistical**	
		Peak	**RMS**	**Peak**	**RMS**
Elcentro	Displacement(m)	0.174	0.047	0.014	0.002
	Velocity(m/s)	1.100	0.302	0.172	0.025
	Abs. Acceleration(m/s^2)	7.528	1.993	3.969	0.636
Hachinohe	Displacement(m)	0.171	0.071	0.013	0.004
	Velocity(m/s)	1.089	0.455	0.123	0.036
	Abs. Acceleration(m/s^2)	6.822	2.947	2.896	0.711
Kobe	Displacement(m)	0.568	0.148	0.047	0.010
	Velocity(m/s)	3.563	0.935	0.431	0.082
	Abs. Acceleration(m/s^2)	25.720	6.041	9.724	1.694
Northridge	Displacement(m)	0.246	0.054	0.033	0.004
	Velocity(m/s)	1.620	0.341	0.389	0.069
	Abs. Acceleration(m/s^2)	10.180	2.301	10.03	1.531

Table 5. Statistical comparison of response discrepancies between optimized models of the 9-story building to the FE model

9-Story		**Model 1**		**Model 2**	
Earthquake	**Response Type**	**Statistical**		**Statistical**	
		Peak	**RMS**	**Peak**	**RMS**
Elcentro	Displacement(m)	0.235	0.102	0.028	0.006
	Velocity(m/s)	0.714	0.284	0.154	0.040
	Abs. Acceleration(m/s^2)	3.110	0.950	2.338	0.384
Hachinohe	Displacement(m)	0.249	0.100	0.020	0.005
	Velocity(m/s)	0.733	0.268	0.115	0.028
	Abs. Acceleration(m/s^2)	2.416	0.827	1.572	0.292
Kobe	Displacement(m)	0.310	0.128	0.068	0.012
	Velocity(m/s)	1.101	0.386	0.519	0.092
	Abs. Acceleration(m/s^2)	7.954	1.805	6.072	0.918
Northridge	Displacement(m)	1.026	0.435	0.060	0.015
	Velocity(m/s)	2.830	1.182	0.434	0.064
	Abs. Acceleration(m/s^2)	7.901	3.322	5.043	0.708

Copyright © 2025 CroCEE
DOI: https://doi.org/10.5592/CO/3CroCEE.2025.15

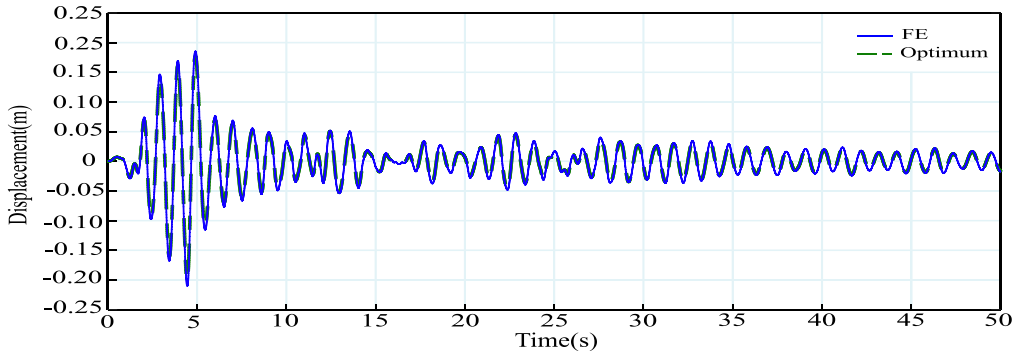


Figure 8. Comparison of roof displacement response history between the FE model and optimized Model 2 of the 3-story structure under the Elcentro earthquake

5.3. Comparison to Other Articles

This section compares the optimized shear-type Model 2 in the 9-story building with the model from Cimellaro et al. [10]. The authors did not find a linear shear-type model for the 3-story structure. The comparison focuses on dynamic parameters and time-history responses. Figure (9) displays the frequencies and mode shapes of the first to the third modes of the FE model, optimized Model 2, and the model from [10]. Optimized Model 2 demonstrates higher accuracy across most frequencies, particularly at lower frequencies, while exhibiting nearly identical accuracy in mode shapes compared to Model [10]. The first three frequencies of the optimized Model 2 show no deviation in the first and second frequencies and only a slight difference of 0.147% in the third frequency compared to the FE model. In contrast, Model [10] exhibits more significant deviations of 3.393%, 8.094%, and 1.820% in the first, second, and third frequencies compared to the FE model. Furthermore, comparing the mode shapes for the first three modes of the optimized Model 2 and Model [10] comparative to the FE model suggests that both models achieve nearly identical overall accuracy.

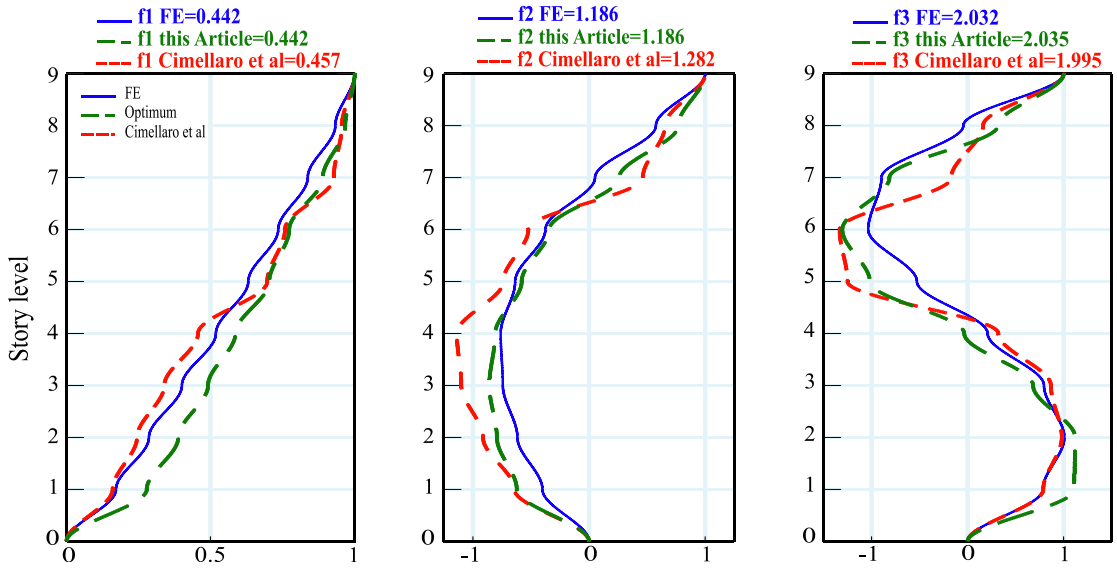


Figure 9. Comparison of frequencies and mode shapes of the optimized Model 2 and the Cimellaro et al. model with the FE model of the 9-story structure

Additionally, Figure (10) presents the roof displacement time-history response under the Elcentro earthquake for the three models: the FE model, the optimized Model 2, and the model from [10]. The analysis results indicate that optimized Model 2 achieves a much higher accuracy in this study.

Copyright © 2025 CroCEE
DOI: https://doi.org/10.5592/CO/3CroCEE.2025.15

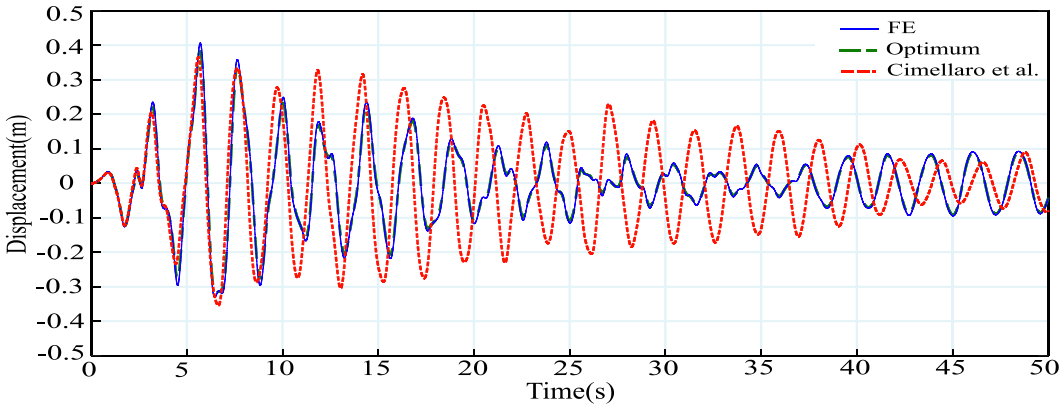


Figure 10. Comparison of roof displacement response time-history between the FE, optimized Model 2 and Cimellaro et al. model of the 9-story structure under the Elcentro earthquake

6. Conclusion

This article addresses the reduction of degrees of freedom in 3 and 9-story benchmark structures to reduce computational time, cost and effort. An optimized shear-type model was developed for these structures using a genetic algorithm, exhibiting high accuracy compared to finite element models. Initially, a preliminary shear-type model was created for each structure by adjusting the coefficient in the stiffness equation for each structure, ensuring that the fundamental frequency matched that of the finite element models.

An optimization problem is defined to enhance the accuracy of these preliminary models, which is solved using a weighted sum approach. The design variables were the story stiffnesses of the preliminary shear-type model. Two objective functions were defined: one minimizes the difference between the frequencies of the FE model and the preliminary shear-type model with equal weighting, and the other uses modal participation percent weighting. By solving the optimization problem, the optimal stiffness for each story was determined according to the defined objective functions within the search space. Frequency comparison between the finite element and the optimized shear-type models showed that the optimal model obtained using the weighted objective function showed significantly higher accuracy, demonstrating that the optimization process improved the accuracy of the preliminary shear-type model.

For time history analysis, the finite element and optimized shear-type models were subjected to four benchmark earthquake excitations, and the displacement, velocity, and absolute acceleration responses at the roof story were compared. Peak and RMS differences in these responses by the proposed comparison approach were evaluated, showing that the optimized Model 2 had much more minor discrepancies than optimized Model 1 in both structures. Furthermore, the optimized Model 2 of the 9-story structure was compared to another model from a different study in terms of dynamic parameters and time-history responses, and it was discovered to have significantly higher accuracy. The optimized Models 2 of the 3 and 9-story benchmark buildings presented in this article highly represent finite element models. They can be used for dynamic analysis and other structural and earthquake engineering purposes.

References

[1] Koutsovasilis, P.(2009): Model order reduction in structural mechanics: coupling the rigid and elastic multi body dynamics. Technische Universität München.

[2] Clough, R.W.(1960): The finite element in plane stress analysis. *Proc. 2^< nd> ASCE Confer. On Electric Computation, 1960*.

[3] Yoo, E.J.(2010): Parametric model order reduction for structural analysis and control. Technische Universität München.

Copyright © 2025 CroCEE
DOI: https://doi.org/10.5592/CO/3CroCEE.2025.15

[4] Besselink, B.,Tabak, U.,Lutowska, A.,Van de Wouw, N.,Nijmeijer, H.,Rixen, D.J.,Hochstenbach, M.and Schilders, W.(2013): A comparison of model reduction techniques from structural dynamics, numerical mathematics and systems and control. *Journal of Sound and Vibration*, 332(19), 4403-4422. DOI: 10.1016/j.jsv.2013.03.025.

[5] Wu, L.(2018): Model order reduction and substructuring methods for nonlinear structural dynamics. DOI: https://doi.org/10.4233/uuid:f9736e8b-d00f-4e25-b456-48bd65b43788.

[6] Guyan, R.J.(1965): Reduction of stiffness and mass matrices. *AIAA journal*, 3(2), 380-380. DOI: https://doi.org/10.2514/3.2874.

[7] Qu, Z.Q.,Shi, Y.and Hua, H.(2001): A reduced‐order modeling technique for tall buildings with active tuned mass damper. *Earthquake engineering & structural Dynamics*, 30(3), 349-362. DOI: https://doi.org/10.1002/eqe.10.

[8] Liu, W.,Tong, M.and Lee, G.C. (Year): Simple procedure for preliminary design of structural damper. in *Proc. 13th World Conference on Earthquake Engineering*. 2004. pages.

[9] Bagchi, A.(2004): A simplified methd of evaluating the seismic performance of buildings. *Earthquake Engineering and Engineering Vibration*, 3(223-236.

[10] Cimellaro, G.,Soong, T.and Reinhorn, A.(2009): Integrated design of controlled linear structural systems. *Journal of Structural Engineering*, 135(7), 853-862. DOI: https://doi.org/10.1061/(ASCE)ST.1943-541X.0000032.

[11] Larki, M.H.A.A. (2011): Physically simplified model of multi-story buildings for their quick dynamic analysis. in *3rd International Conference on Computational Methods in Structural Dynamics and Earthquake Engineering*. 2011 of Conference. Corfu, Greec. 12 pages.

[12] Alonso-Rodríguez, A.and Miranda, E.(2018): Assessment of effects of reductions of lateral stiffness along height on buildings modeled as elastic cantilever shear beams. *Journal of Earthquake Engineering*, 22(4), 553-568. DOI: 10.1080/13632469.2016.1244132.

[13] Nitti, G.,Lacidogna, G.and Carpinteri, A.(2021): An analytical formulation to evaluate natural frequencies and mode shapes of high-rise buildings. *Curved and Layered Structures*, 8(1), 307-318. DOI: https://doi.org/10.1515/cls-2021-0025.

[14] Gharra, K.,Khanlari, K.and Marnani, J.A.(2022): A Simplified Matrix Analysis Approach to Multi-story Buildings Involving a Friction Damper. *Periodica Polytechnica Civil Engineering*, 66(1), 75-85. DOI: 10.3311/PPci.18558.

[15] Ahmadie Amiri, H.,Hosseini, M.and E. Estekanchi, H.(2022): Efficient seismic risk assessment of irregular steel‐framed buildings through endurance time analysis of consistent fish‐bone model. *The Structural Design of Tall and Special Buildings*, 31(2), e1901. DOI: https://doi.org/10.1002/tal.1901.

[16] Fiore, I.,Greco, A.and Pluchino, A.(2022): On Damage Identification in Planar Frames of Arbitrary Size. *Shock and Vibration*, 2022(1), 4736992. DOI: https://doi.org/10.1155/2022/4736992.

[17] Ohtori, Y.,Christenson, R.,Spencer Jr, B.and Dyke, S.(2004): Benchmark control problems for seismically excited nonlinear buildings. *Journal of engineering mechanics*, 130(4), 366-385. DOI: https://doi.org/10.1061/(ASCE)0733-9399(2004)130:4(366).

[18] Gupta, A.(1999): Seismic Demands for Performance Evaluation of Steel Moment Resisting Frame Structures. *The John A.*

[19] Farzam, M.F.and Kalajahi, T.D. (2023): STATISTICAL SEISMIC PERFORMANCE ASSESSMENT OF VISCOUS DAMPER IN BENCHMARK BUILDINGS UNDER FAR-FAULT AND NEAR-FAULT EARTHQUAKES. in *2nd Croatian Conference on Earthquake Engineerin, Conference*. 2023 of Conference. 11 pages.

[20] Darwin, C.(2007): On the origin of species (1859). *Evolution and creationism*, 43-50.

[21] Golberg, D.E.(1989): *Genetic algorithms in search, optimization, and machine learning*. 1st ed. Addion wesley. Vol. 1989. 372, Addison-Wesley Professional.

[22] Chopra, A.K.(1998): *Dynamics of structures*. fourth ed., earson Education India. .

[23] Marler, R.T.and Arora, J.S.(2010): The weighted sum method for multi-objective optimization: new insights. *Structural and multidisciplinary optimization*, 41(853-862. DOI: 10.1007/s00158-009-0460-7.

Proceedings of the 3rd Croatian Conference on Earthquake Engineering - 3CroCEE
19–22 March 2025, Split, Croatia
Copyright © 2025 CroCEE
DOI: https://doi.org/10.5592/CO/3CroCEE.2025.24

NUMERICAL VALIDATION OF MASONRY WALL EXPERIMENTS USING THE APPLIED ELEMENT METHOD

Sergey Churilov [(1)]

[(1)] *Professor, Ss. Cyril and Methodius University in Skopje, Faculty of Civil Engineering Skopje, curilov@gf.ukim.edu.mk*

Abstract

This paper presents an investigation of unreinforced masonry (URM) walls under cyclic in-plane loading using the Applied Element Method (AEM). Due to their historical nature, masonry structures are highly relevant in modern construction; however, they normally pose certain challenges with regards to structural analysis because of their composite nature and nonlinear behaviour. While experimental investigations provide critical information about masonry behaviour, numerical modelling offers an efficient way to extend the understanding of structural performance under various loading conditions. The study combines experimental validation with numerical modelling to evaluate the seismic performance of masonry structures. Two full-scale URM walls with varying vertical pre-compression levels tested experimentally were selected for the validation. The walls exhibited shear-dominated failure mechanisms with diagonal cracking patterns. A simplified micro-modelling approach was implemented in AEM, incorporating nonlinear material behaviour and contact mechanisms. The numerical models accurately captured the experimental force-displacement relationships, with deviations in lateral strength predictions ranging from 2% to 10%. The simulations successfully reproduced the observed failure mechanisms, including crack initiation and propagation patterns. Initial stiffness was slightly overestimated, while displacement at peak lateral strength showed reasonable agreement with experimental results. The study demonstrates AEM's capability to model complex masonry behaviour, while the findings validate AEM as a reliable tool for seismic assessment of masonry structures, with important implications for both historic building conservation and modern masonry design.

Keywords: unreinforced masonry, applied element method (AEM), in-plane cyclic behaviour, seismic performance, numerical modelling, experimental validation.

1. Introduction

Masonry structures represent one of humanity's oldest construction forms, yet their structural analysis remains challenging due to their composite nature and material heterogeneity [1]. The complex dynamic behaviour of unreinforced masonry (URM) structures, characterized by heterogeneous composition and directionally dependent properties, presents significant challenges for seismic assessment [2]. Traditional analytical methods often fail to capture the intricate failure mechanisms and load-distribution patterns observed in real structures [3].

Recent advances in computational mechanics have enabled more sophisticated approaches to masonry analysis. While finite element methods (FEM) have emerged as powerful tools [4], the reliability of numerical models heavily depends on proper validation against experimental data. As noted by Theodossopoulos and Sinha [5], validation processes serve to verify computational results and refine understanding of masonry behaviour under various loading conditions.

The Applied Element Method (AEM), initially developed by Meguro and Tagel-Din [6], represents a significant advancement in structural analysis techniques. Unlike traditional FEM, AEM discretizes structures into small rigid elements connected by normal and shear springs [7, 8], allowing simulation from initial loading through complete collapse [9]. In AEM, masonry structures are modelled using brick springs (connecting elements within bricks) and brick-mortar interface springs (connecting elements between different bricks), effectively capturing the composite nature of masonry [8–10]. AEM offers several advantages for masonry analysis. As demonstrated by Eraky et al. [11], it can analyse

Proceedings of the 3rd Croatian Conference on Earthquake Engineering - 3CroCEE
19–22 March 2025, Split, Croatia
Copyright © 2025 CroCEE
DOI: https://doi.org/10.5592/CO/3CroCEE.2025.24

structural behaviour without requiring prior assumptions about crack locations or propagation directions. The method excels in representing complex mechanical behaviours, particularly rigid body motion and element collision scenarios, while typically requiring less modelling time compared to FEM approaches [11]. One key advantage over FEM is that no transition elements are needed, as elements are connected at faces, allowing partial connectivity [12]. The reliability of AEM has been validated through several studies comparing numerical predictions with experimental observations. These comparisons have shown remarkable concordance, particularly in the prediction of failure patterns and load-displacement relationships. Recent studies have validated AEM's effectiveness for masonry analysis both in-plane and out-of-plane and progressive collapse scenarios, with predictions achieving accuracy within 20% of experimental results [13–16]. While highly effective, the method requires careful material parameter calibration and faces computational intensity challenges with complex models [13, 14, 17, 18].

Despite these advances, several critical research gaps remain in the application of AEM to masonry structures, particularly regarding historic construction and dynamic behaviour. The interaction between in-plane and out-of-plane forces remains underexplored, especially in the context of complex wall assemblies typical in historic buildings [13]. While static and quasi-static analyses are well-documented, there is limited research on dynamic response simulation [7], creating a significant knowledge gap in understanding seismic behaviour. Current methods often prove too complex and computationally intensive for practical implementation in heritage conservation projects [8]. Although AEM has been successfully applied to simple URM structures, studies on complex geometries and irregular layouts characteristic of historic construction are scarce [14]. Current AEM models often use simplified material properties for masonry, neglecting variability due to aging and environmental factors [13]. Perhaps most significantly, while some studies have validated AEM results against experimental data, there is a notable scarcity of comparisons with full-scale URM building tests under dynamic loading up to collapse [13, 14]. This gap is particularly relevant for heritage structures where understanding complete collapse mechanisms is essential for seismic risk assessment.

While significant progress has been made in understanding the in-plane behaviour of masonry, the integration of experimental and numerical methods must continue to address the complexities of real-world applications, particularly in seismic-prone areas. This paper presents a comprehensive study of URM walls using AEM, incorporating experimental validation through comparison with shear behaviour tests. The research aims to establish reliable modelling strategies for predicting the seismic response of masonry structures while addressing current challenges in numerical simulation methods.

2. Experimental Program

The experimental investigation focused on evaluating the in-plane cyclic behaviour of unreinforced masonry walls under seismic loading conditions [19, 20]. Four unreinforced masonry wall (URM) specimens were constructed using solid clay bricks and lime mortar to represent typical historical masonry construction, out of which two were selected in this study. Both URM walls were constructed using solid clay bricks (250×120×65 mm^3) and traditional lime mortar mix (1:3 lime:sand ratio). Material properties were experimentally determined through standardized testing procedures as shown in Table 1.

Masonry compressive strength tests on three wall specimens (520×320×125 mm^3) yielded a characteristic mean strength of $f_k = 3.0$ N/mm^2 and elastic modulus of $E = 2874.8$ N/mm^2 Shear strength characterization using nine masonry triplets under varying pre-compression stress levels (0.2, 0.6 and 1.0 N/mm^2) revealed a friction coefficient $\mu = 0.66$ (friction angle $\theta = 33.4°$). These material properties provided essential input parameters for subsequent numerical modelling and analysis of the masonry wall behaviour under various loading conditions. The relatively low strength values obtained are typical for historical masonry construction using lime mortar [21–23].

The test matrix comprised identical wall geometries (squat walls) under two vertical pre-compression levels of 0.5 N/mm^2 and 1.0 N/mm^2 (URM1, URM3), see Table 2.

Copyright © 2025 CroCEE
DOI: https://doi.org/10.5592/CO/3CroCEE.2025.24

Table 1. Experimental material properties for bricks and mortar [19, 20]

Property	Brick	Mortar
Density, γ [kg/m^3]	1922.6	1384.7
Compressive strength, f_k [N/mm^2]	10.8	0.6
Tensile flexural strength, $f_{t,fl}$ [N/mm^2]	2.7	0.1

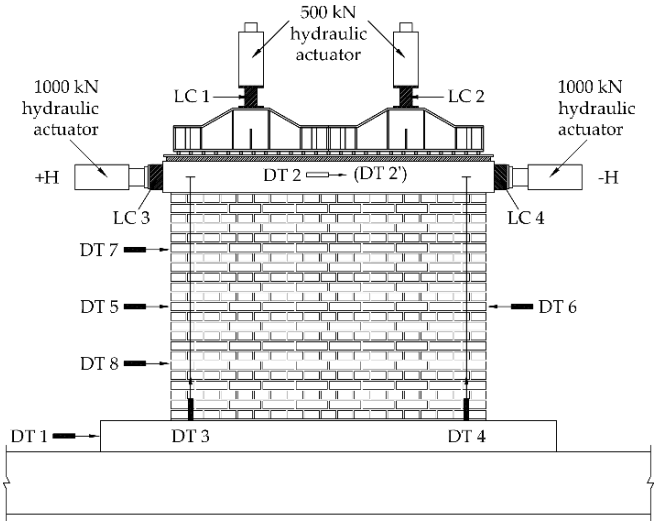
Table 2. Test specimen configuration and vertical compression stresses [20]

Walls	Length, L [mm]	Height, H [mm]	Slenderness ratio (H/L)	Vertical stress, σ_0 [N/mm^2]	σ_0/f_k ratio
URM1	2520	1820	0.72	1.0	0.33
URM3	2520	1820	0.72	0.5	0.17

The specimens were constructed on 250x400 mm^2 pre-casted RC foundation beams anchored to the rigid laboratory floor, with a pre-casted 250x250 mm^2 RC top beams incorporating steel roller bearings and elastomeric bearings to enable horizontal movement while maintaining vertical load distribution. Concrete with compressive strength of $f_c = 30$ N/mm^2, reinforced with 3Ø12 mm longitudinal rebars ($f_y = 400$ N/mm^2) and rectangular stirrups Ø8/100/200 mm were used [19].

The experimental investigation was conducted using a purpose-built steel testing frame equipped with both vertical and horizontal hydraulic actuators. Vertical actuators maintained constant axial loads throughout testing, while horizontal actuators imposed cyclic lateral displacements. The test setup incorporated a monitoring system consisting of strategically placed load cells (LC1-LC4) and displacement transducers (DT1-DT8), Figure 1a. Load cells monitored both vertical and horizontal forces, while displacement transducers tracked in-plane and out-of-plane deformations at critical locations along the wall height, Figure 1b.

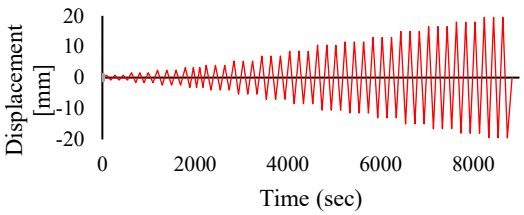
The testing protocol followed a systematic approach, beginning with the application of vertical precompression loads. These loads were gradually applied and maintained constant throughout the test duration. Subsequently, quasi-static cyclic lateral loading was introduced following a predetermined displacement history as illustrated in Figure 1c.



a) Schematics of the key components of the test setup and measuring points locations



b) DT2 sensor on the top RC beam



c) Horizontal displacement protocol

Figure 1. Experimental test setup [19, 20]

Copyright © 2025 CroCEE
DOI: https://doi.org/10.5592/CO/3CroCEE.2025.24

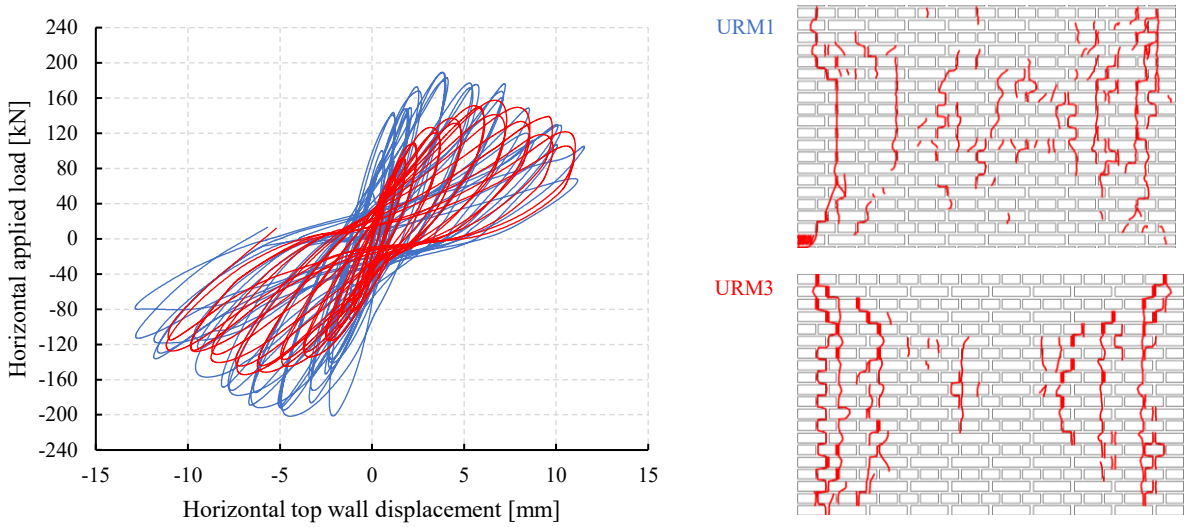


Figure 2. Experimental force-displacement hysteresis diagrams and failure of URM walls

Each displacement amplitude was repeated for three complete cycles to assess strength and stiffness degradation. Loading rates were carefully controlled between 0.2 and 0.5 kN/s to minimize dynamic effects while ensuring test efficiency. Throughout testing, the vertical actuators were manually controlled to prevent in-plane rotation of the top RC beam, maintaining the desired "double-fixed" boundary conditions. The experimental investigation revealed consistent behaviour patterns across all specimens, characterized predominantly by shear-dominated failure mechanisms.

Both URM walls (URM1 and URM3) primarily developed vertically oriented cracks passing through bricks or along head joints, Figure 2. The force-displacement relationships demonstrated almost symmetrical behaviour in both positive and negative loading directions. Initial response remained elastic until the formation of first cracks, occurring at drift ratios between 0.03% and 0.04%. The influence of precompression levels emerged as a significant factor affecting overall performance. URM1 subjected to higher vertical stress (1.0 N/mm^2) demonstrated increased lateral load capacity compared to its counterpart under lower precompression (0.5 N/mm^2).This behaviour aligns with previous research [24–28] and can be attributed to the higher principal tensile stresses required for wall failure. This enhancement in lateral strength was accompanied by improved energy dissipation capabilities, particularly evident in the post-peak response region. The force-displacement relationships exhibited peak lateral forces typically occurring at drift ratios of 0.29% and 0.46%, and drift ratios of 0.67% and 0.72% at the ultimate resistance levels for walls URM1 and URM3, respectively [19]. The precompression level had minimal influence on ultimate displacements, with URM3 actually achieving higher ultimate displacement than URM1. Stiffness degradation followed a consistent pattern across both walls, characterized by a power function relationship between normalized stiffness and displacement ductility. The equivalent viscous damping coefficient, calculated from hysteretic energy dissipation, averaged 12.6% at ultimate displacement levels for both walls, indicating significant energy dissipation capacity despite the brittle nature of the masonry material [20].

3. Numerical Modelling

3.1. Modelling strategy and assumptions

The Applied Element Method (AEM) offers a novel approach to structural analysis, especially for modelling collapse scenarios. The method differs fundamentally from traditional FE methods by representing structures through small, discrete elements interconnected by distributed normal and shear springs along their faces [6]. These spring sets effectively capture the complete mechanical behaviour: stresses, strains, and deformations of the corresponding material volume, as illustrated in Figures Figure 3-Figure 5.

Copyright © 2025 CroCEE
DOI: https://doi.org/10.5592/CO/3CroCEE.2025.24

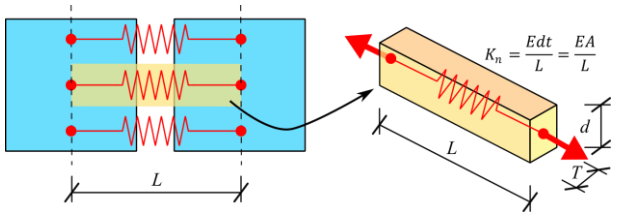


Figure 3. Stiffness of normal springs [29]

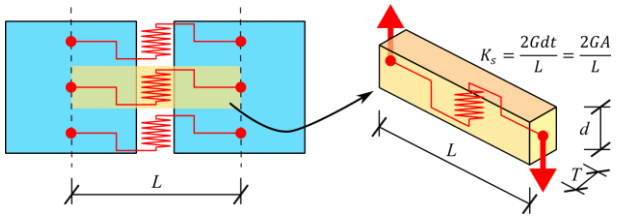


Figure 4. Stiffness of shear springs [29]

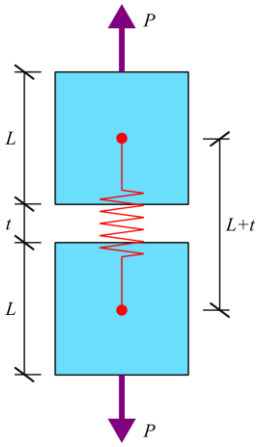


Figure 5. Modelling mortar thickness by averaging the properties for brick and mortar [29]

AEM's distinctive capability lies in its comprehensive simulation of structural response across all loading phases, from initial elastic behaviour through progressive damage and ultimate collapse [29]. Unlike traditional FEM approaches, AEM effectively handles discontinuous behaviour through automatic element separation and collision detection when spring elements exceed their ultimate strain limits. The stiffnesses of normal K_n and shear K_s springs are calculated as shown in (1).

$$K_n = \frac{EdT}{L} = \frac{EA}{L}; \qquad K_s = \frac{2GdT}{L} = \frac{2GA}{L} \tag{1}$$

where, E is tangent stiffness of the normal stress-normal strain curve, G is tangent stiffness of the shear stress-shear strain curve, d is distance between springs, T is thickness of the element, $A = dT$ is cross sectional area of the volume represented by the spring and L is distance between the centers of gravity of the connected elements [29].

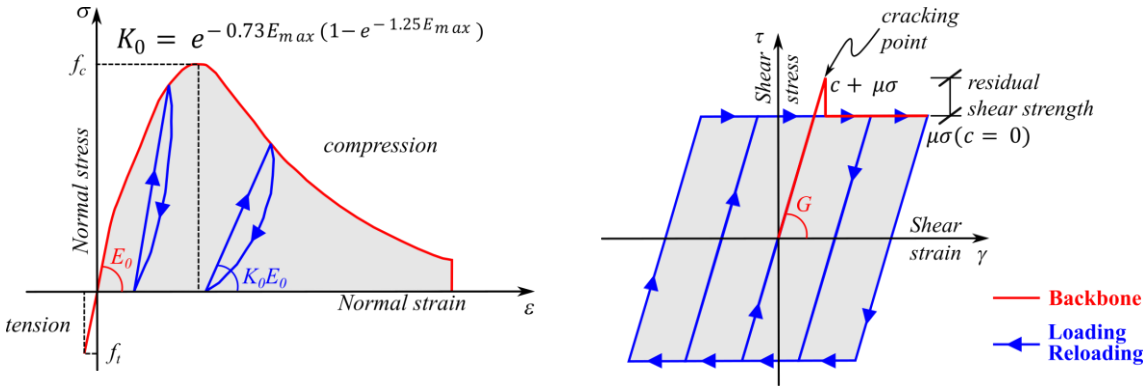
The general formulation of AEM applied to masonry structures is discussed in detail in e.g. [6, 8, 29]. AEM offers three approaches for modelling masonry structures: detailed micro-modelling (units and mortar as rigid elements with spring interfaces), simplified micro-modelling (expanded units as rigid elements with lumped mortar behaviour in springs), and macro-modelling (homogeneous continuum approach) [30]. A simplified micro-modelling strategy approach was implemented in this study, building on established methodologies from multiple studies [7, 8, 13, 16, 17, 31, 32].

The simplified micro-modelling approach, implemented through the Extreme Loading for Structures (ELS) software, provides an optimal balance between computational efficiency and accuracy. In this approach, bricks are modelled in staggered configuration with zero-thickness springs representing mortar joints. In AEM the mass is concentrated in the rigid elements. Each brick can be further subdivided into smaller elements to allow for crack development within the brick itself. The composite brick-mortar behaviour is handled through equivalent springs with modified properties, considering brick and mortar as springs in series. As shown in Figure 5, the AEM accounts for the actual geometry of brick (length L) and mortar joint (thickness t) by using equivalent springs with modified (averaged) properties. The effective stiffness of these springs is derived by considering the brick and mortar as springs in series, leading to the formulation shown in (2):

$$K = \frac{E^* A}{L + t}; \qquad E^* = \frac{E_b E_m}{E_b t + E_m L} \times (L + t) \tag{2}$$

where, K is effective stiffness of the springs, E^* is the equivalent Young's modulus of elasticity for the spring, E_b and E_m are Young's modulus of elasticity for bricks and mortar, L is brick element size and t is mortar thickness.

Copyright © 2025 CroCEE
DOI: https://doi.org/10.5592/CO/3CroCEE.2025.24



a) Normal springs b) Shear springs

Figure 6 Constitutive models for concrete and masonry [29]

The model's primary source of energy dissipation comes from hysteretic damping, which occurs during crack opening/closure and progressive damage evolution. This simplified damping approach has proven effective across numerous AEM applications, successfully analysing collapse mechanisms in both continuous and discrete blocky systems [15, 33].

The masonry nonlinear behaviour was modelled using the Concrete Maekawa model [34, 35], featuring a pseudo-parabolic compression envelope with tension cut-off and an elastic-plastic fracture model for cyclic loading, developed by El-Kashif and Maekawa [36] and shown in Figure 6. The model incorporates an elastic-plastic fracture response for compression, accounting for cyclic damage accumulation, while tensile behaviour follows a simplified linear failure envelope (brittle constitutive law without normal stiffness degradation) with a defined tensile strength limit (f_t) at zero shear stress.

The compression model incorporates three key parameters: initial Young's modulus (E_0), compressive plastic strain (ε_p) and a fracture parameter (K_0) governing stiffness and strength degradation. The fracture parameter is dynamically calculated using an exponential function of the maximum equivalent strain (E_{max}), as shown in Figure 6a and detailed in [33, 35]. In the shear response, the cohesion (c) reduces to zero once the maximum shear strength is reached (Figure 6b). The model incorporates Mohr-Coulomb yield criteria for shear behaviour without including shear stiffness degradation (Figure 6b). While the model effectively captures material capacity, hysteretic response, and deformation characteristics, it conservatively neglects residual shear strength under tensile conditions. The model's dynamic behaviour was handled through a sophisticated contact mechanism. Matrix springs are eliminated upon exceeding the separation strain threshold (default resultant of 0.1), while new contact springs form during re-contact, effectively simulating the interaction between distinct rigid bodies [29].

3.2. AEM model development for simulation of the in-plane cyclic tests

A simplified micro-modelling approach of a 3-D computational models of URM walls was applied using the AEM analysis implemented through ELS software [29], Figure 7. The masonry walls were modelled using their actual geometry, with clay bricks 255×125×70 mm^3 adjusted to accommodate mortar joint thicknesses of 10 mm arranged in an English-bond pattern. Individual bricks were represented as 3-D solid elements (rigid bodies) with eight nodes (3x8 DOF). Mortar joints were simulated through a grid of 25 nonlinear springs (5×5 pattern) at contact surfaces between bricks, following previously validated approaches [6–8], simulating the mechanical properties of bed and head joints. Mesh convergence analysis comparing full-sized and half-sized brick elements was performed to validate the block size selection. Joint behaviour incorporated Mohr-Coulomb failure criteria with complete post-failure cohesion degradation to zero for shear strength (Figure 6b), while tension followed a linear relationship with no post-peak response (Figure 6a). Material characterization integrated both experimental data [19, 20] and literature-derived parameters [7, 8, 10, 13, 30]. The calibration process involved iterative refinement of "preliminary" models, initially parameterized using experimental properties, to achieve optimal correlation with observed behaviour, as shown in Table 3.

Copyright © 2025 CroCEE
DOI: https://doi.org/10.5592/CO/3CroCEE.2025.24

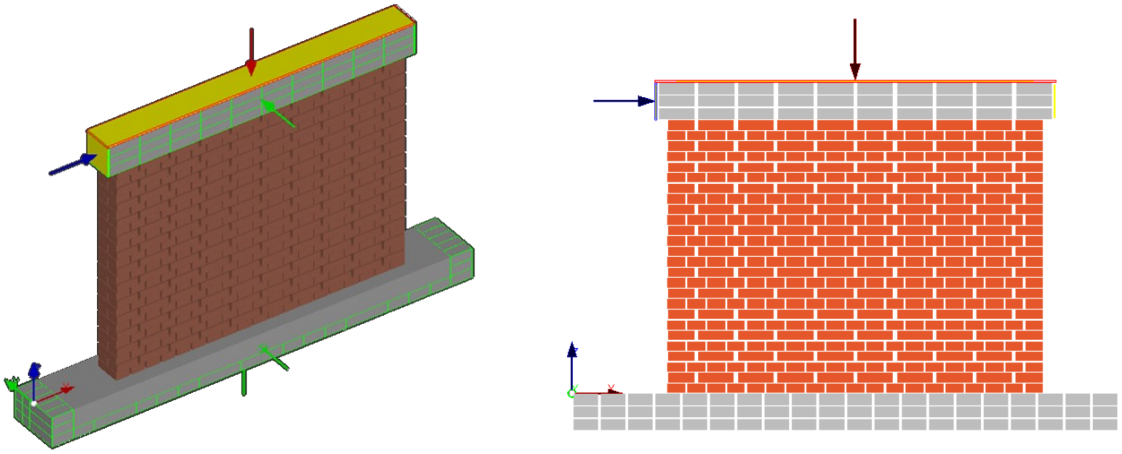


Figure 7 Developed AEM model (bricks and RC beams are shown as shrank)

Models were systematically calibrated against experimental data, resulting in so called "calibrated" models. In cases of limited experimental data, the Young's modulus (E) for the bricks can be estimated as $(200-1000)f_c$, where f_c is compressive strength, while the Poisson's ratio (ν) typically ranges 0.15-0.25 for masonry materials [30]. Direct tensile characterization remains challenging due to testing complexities.

The tensile strength (f_t) typically ranges $(0.03-0.1)f_c$, or can be determined by $f_t = 2.12\ln(1+0.075f_c)$ [30]. For the preliminary model, the Young's modulus of the bricks was estimated as $1{,}000f_c$, and the shear modulus (G) was calculated utilizing the equation $G = E/(2(1+\nu))$, with an assumed Poisson's ratio (ν) of 0.25. In situations where detailed experimental data is unavailable, the coefficient of friction (μ) can be approximated as 0.75 and in this study, it was varied in a range of 0.6-0.8. Furthermore, as established by Lourenço [37], the cohesion (c) can be estimated through its relationship with the tensile bond strength (f_t), expressed as $c = 1.4f_t$. The nonlinear material response was described through fracture energies. The recommended fracture energy in compression (G_c) was calculated with $G_c = 32/(10+f_c)$ and the fracture energy in tension with $G_f = 0.07\ln(1+0.17f_c)$ as shown in [30]. The Young's modulus of the lime mortar in the preliminary model for a compressive strength of 0.6 N/mm^2 linear interpolation yielded $E = 1{,}160$ N/mm^2 with the typical range of 1000-5000 N/mm^2 for $f_c = 0.5-3$ N/mm^2 [22].

The calibrated model parameters, optimized against experimental force-displacement curves, showed significant variations from preliminary values. Brick elements exhibited reduced Young's and shear moduli (-26%), decreased compressive strength (-9.2%), and increased tensile strength (+13.1%).

Table 3. Material properties applied to AEM models

Property	**Experimental (B/M)**	**AEM initial (B/M)**	**AEM calibrated (B/M)**
Density, γ [kg/m^3]	1,923/1,385	1,923/1,385	1,923/1,385
Young's modulus, E [N/mm^2]	-/-	10,800/1,160	7,992/1,765
Compressive strength, f_k [N/mm^2]	10.8/0.6	10.8/0.6	9.81/1.28
Tensile strength, f_t, [N/mm^2]	2.7/0.1*	1.26/0.09	1.42/0.07
Cohesion, c [N/mm^2]	0**	1.76/0.12	0.98/0.10
Friction coefficient, μ [-]	0.66**	0.8/0.6	0.6/0.6
Compressive fracture energy (N/mm)	-/-	16.61/1.81	19.61/2.94
Tensile fracture energy (N/mm)	-/-	0.07/0.007	0.073/2.94
Residual shear strength factor	-/-	0/0	1/0

B/M=Brick/Mortar, * Tensile flexural strength, ** Masonry

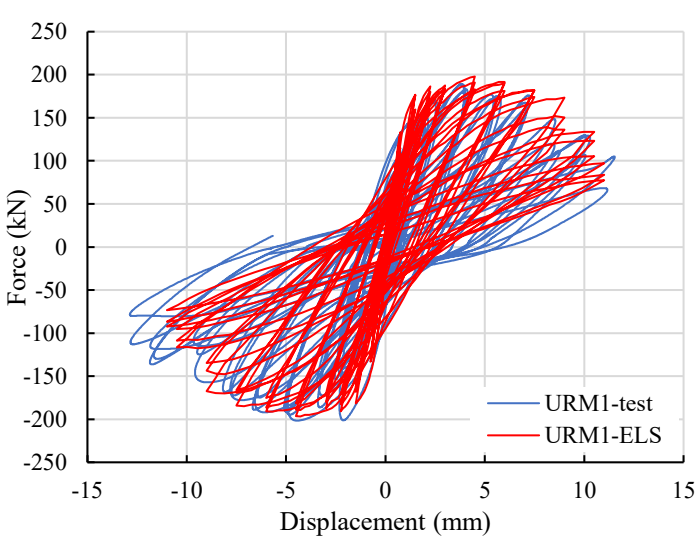
Copyright © 2025 CroCEE
DOI: https://doi.org/10.5592/CO/3CroCEE.2025.24

Joint springs representing mortar demonstrated more substantial modifications: increased Young's and shear moduli (+52.2%), doubled compressive strength (0.6 to 1.275 N/mm²), and reduced cohesion (-25.1%). Fracture energies for brick varied slightly (compression: +18.0%, tension: -0.5%), while mortar showed substantial increases (compression: +62.5%, tension: 0.0068 to 2.942 N/mm). RC beams and steel loading plates maintained elastic properties. It should be noted that the calibrated material properties in ELS for the mortar actually represent the stiffnesses of the joint normal and shear springs.

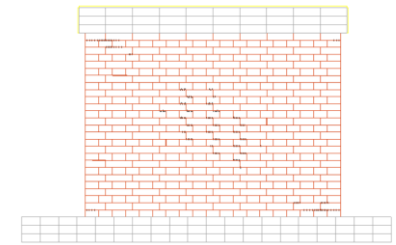
The mechanical response of URM walls exhibits marked sensitivity to boundary conditions. To ensure fidelity with experimental conditions, the analytical model explicitly incorporated the reinforced concrete (RC) beam elements that served dual purposes: the application of vertical pre-compression forces (red arrow in Figure 7) and fully fixed boundary conditions at the wall's base (green arrow in Figure 7). Out-of-plane behaviour was prevented through top RC beam restraint. Loading protocol followed three sequential stages: self-weight (two equal increments), vertical pre-compression (ten equal increments), and cyclic in-plane loading matching experimental patterns, as shown in Figure 1c. Dynamic solution employed 50 time-step intervals between calculations and 20 subdivisions per time step.

4. Results and Discussion

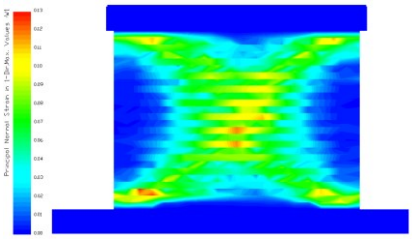
A comparative analysis was conducted between numerical simulations and experimental results for walls URM1 and URM3, examining force-displacement hysteresis and damage progression patterns. Displacement measurements were taken at the load application point on the top beam, with numerical damage characterized through strain patterns and spring corresponding to an ‘open crack’ state in the AEM framework. In AEM and ELS modelling [29], cracks form when spring normal strains exceed zero under specified criteria, allowing simulation of cyclic crack behaviour. Both specimens exhibited shear failure with diagonal and vertical mortar joint cracking and distinctive crack patterns: URM1 initiated damage at diagonal corners at approximately 88 kN during the first loading cycle, before propagation to the centre of the wall, while URM3 showed initiation in the centre at about 84.5 kN with bidirectional expansion. Both walls demonstrated symmetric hysteretic responses, achieving lateral strengths of 197.5 kN and 174.6 kN at displacements of 4.05 mm and 4.4 mm for URM1 and URM3 respectively. At the end of the simulations, comprehensive crack patterns were revealed throughout the wall surfaces, indicating cyclic opening and closing behaviour. The numerical simulation results for URM1, illustrated in Figure 8, demonstrated strong correlation with experimental observations.



a) Force-displacement hysteresis



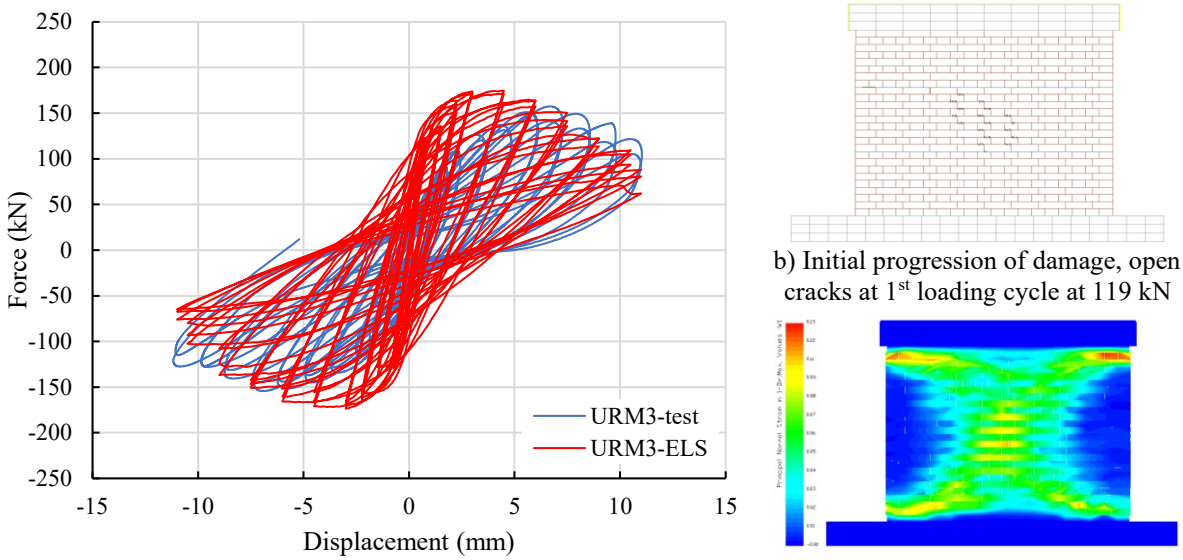
b) Initial progression of damage, open cracks at 1st loading cycle at 119 kN



c) Final principal normal strains

Figure 8. Comparison between numerical and experimental response for URM1

Copyright © 2025 CroCEE
DOI: https://doi.org/10.5592/CO/3CroCEE.2025.24



a) Force-displacement hysteresis

b) Initial progression of damage, open cracks at 1st loading cycle at 119 kN

c) Final principal normal strains

Figure 9. Comparison between numerical and experimental response for URM3

The numerical model accurately captured initial and progressive cracking patterns, with lateral strength predictions deviating only 2% from experimental values for URM1 and 10% for URM3. While both models overestimated initial stiffness, they showed good agreement in predicting peak lateral strength displacements (URM1: 4.44 mm experimental vs. 4.05 mm numerical; URM3: 6.67 mm experimental vs. 4.41 mm numerical). URM3's model successfully reproduced the central crack initiation, bidirectional propagation, and diagonal shear failure, though with a slightly different sequence than observed experimentally, as shown in Figure 9.

The overestimated initial stiffness was due to various interrelated factors, including modelling assumptions and experimental testing procedures. The simplified micro-modelling approach is a computationally efficient approach that idealizes certain aspects of masonry behaviour, particularly in the elastic range. Despite carefully calibrating material properties, the model may not fully capture the complex interactions at brick-mortar interfaces, especially during the initial loading phases. Real masonry structures typically contain pre-existing micro-cracks and construction imperfections that influence their initial response, making numerical modelling of such structures quite challenging. Modelling boundary and loading conditions present another significant challenge. The ELS models explicitly incorporated RC beams and attempted to replicate experimental conditions, but certain idealizations were unavoidable. They assumed perfect connection between the masonry wall and RC beams and introduce idealized restraints at the base. However, physical experiments frequently demonstrate unintended flexibility or minor slips at these connections, resulting to a more complex response. The loading apparatus was simplified in the numerical models and assumes perfect vertical and horizontal load applications. During the experiments, the loading control is critical challenge and often some deviations from the idealized conditions are present. From a theoretical perspective, the modelling approach itself introduces certain limitations. The representation of mortar joints through zero-thickness springs, while effective for overall behaviour, may not perfectly capture initial deformation mechanisms. The Concrete Maekawa constitutive model, selected for its robust representation of nonlinear behaviour, might exhibit excessive stiffness in the elastic range. Furthermore, the discrete nature of the AEM could potentially overlook some continuous deformation behaviours characteristic of early loading stages.

Generally, the ELS models successfully captured key physical characteristics of the masonry walls, including maximum forces, displacement limits, and hysteretic behaviour. The simulations accurately represented essential masonry response features such as stiffness degradation and pinching effects near zero force, reflecting progressive damage and cyclic crack behaviour. This strong correlation validates the model's ability to represent complex masonry wall behaviour under seismic loading.

Proceedings of the 3rd Croatian Conference on Earthquake Engineering - 3CroCEE
19–22 March 2025, Split, Croatia
Copyright © 2025 CroCEE
DOI: https://doi.org/10.5592/CO/3CroCEE.2025.24

5. Conclusions and Recommendations

The present study validated the effectiveness of the Applied Element Method modelling unreinforced masonry walls under cyclic in-plane loading. The numerical models demonstrated high accuracy, with lateral strength predictions deviating only 2-10% from experimental values. The simulations successfully captured key behavioural aspects including crack initiation, propagation patterns, stiffness degradation, and pinching effects which are essential features for understanding seismic performance.

While the models effectively predicted overall behaviour, they overestimated initial stiffness. Additionally, computational demands increased significantly with model complexity when replicating the steel loading elements above the top RC beams, potentially limiting applications to large-scale analyses. Nevertheless, the validated approach provides engineers with a reliable tool for seismic assessment, offering calibrated material parameters as references for similar masonry types.

The practical implications of this research are significant for both research and engineering practice, providing engineers with a reliable tool for seismic assessment of masonry structures. The methodology demonstrates particular promise for implementation in performance-based design and assessment frameworks. However, several practical challenges must be addressed for widespread adoption in engineering practice. These include the need for straightforward procedures for material parameter calibration and integration with existing structural analysis software platforms. Additionally, guidelines for verification of AEM models in practice need to be established.

The findings can be cautiously extended to other masonry typologies beyond the lime mortar and clay brick combinations. The fundamental mechanics captured by the AEM approach, including interface behaviour and discrete crack propagation, are applicable to various masonry systems. Yet, the specific material parameters would need recalibration for different combinations such as cement-based mortars, natural stone units, or historical materials. The methodology's ability to capture brittle failure mechanisms suggests particular applicability to heritage structures built with traditional materials.

Future research should address combined in-plane and out-of-plane loading effects, development of more computationally efficient methods. Additional validation through full-scale dynamic testing, different strengthening techniques applied to existing masonry assemblages and incorporation of aging effects would further enhance the method's applicability to historical structures. The study's findings contribute significantly to masonry modelling knowledge while highlighting areas requiring continued development to expand AEM's practical applications in structural engineering.

Acknowledgements

In this paper, I would like to thank Professor Elena Dumova-Jovanoska, Ss. Cyril and Methodius University in Skopje, Faculty of Civil Engineering Skopje, for the encouragement she gave me during my work as a doctoral student, more than twelve years ago that continues to be relevant even in this research work.

The author gratefully acknowledges Mr. Ayman Elfouly, P.E., Senior Consulting Engineer at Applied Science International, LLC (ASI) for his invaluable support and technical expertise in the ELS software analysis, which significantly enhanced the quality of this research.

References

[1] Roca, P., Cervera, M., Gariup, G., Pela, L. (2010): Structural analysis of masonry historical constructions. Classical and advanced approaches, *Archives of Computational Methods in Engineering*, **17** (3), 299–325, https://doi.org/10.1007/s11831-010-9046-1.

[2] Magenes, G., Calvi, G.M. (1997): In-plane seismic response of brick masonry walls, *Earthquake Engineering & Structural Dynamics*, **26** (11), 1091–1112, https://doi.org/10.1002/(SICI)1096-9845(199711)26:11.

[3] Asteris, P.G., Sarhosis, V., Mohebkhah, A., Plevris, V. (2015): (2015), Numerical modeling of historic masonry structures, in *Handbook of Research on Seismic Assessment and Rehabilitation of Historic Structures, IGI Global*, 213–256. https://doi.org/10.4018/978-1-4666-8286-3.

Copyright © 2025 CroCEE
DOI: https://doi.org/10.5592/CO/3CroCEE.2025.24

[4] Giordano, A., Mele, E., Luca, A. (2002): Modelling of historical masonry structures: comparison of different approaches through a case study, *Engineering Structures*, **24** (8), 1057–1069, https://doi.org/10.1016/S0141-0296(02)00033-0.

[5] Theodossopoulos, D., Sinha, B. (2013): A review of analytical methods in the current design processes and assessment of performance of masonry structures, *Construction and Building Materials*, **41**, 990–1001, https://doi.org/10.1016/j.conbuildmat.2012.07.095.

[6] Meguro, K., Tagel-Din, H. (2000): Applied Element Method for structural analysis: Theory and application for linear materials, *Structural Engineering/Earthquake Engineering*, **17** (1), 31–45.

[7] Malomo, D., Pinho, R., Penna, A. (2018): Using the Applied Element Method to simulate the dynamic response of full-scale URM houses tested to collapse or near-collapse conditions, in *Proceedings of 16th European Conference on Earthquake Engineering*, Thessaloniki, Greece.

[8] Malomo, D., Pinho, R., Penna, A. (2018): Using the applied element method for modelling calcium silicate brick masonry subjected to in-plane cyclic loading, *Earthquake Engineering & Structural Dynamics*, **47** (7), 1610–1630, https://doi.org/10.1002/eqe.3032.

[9] Mayorca, P., Meguro, K. (2003): Modeling Masonry Structures using the Applied Element Method, *Seisan-Kenkyu*, **55** (6), 123–126.

[10] Christy, D.L., Pillai, T.M.M., Nagarajan, P. (2018): Analysis of Brick Masonry Wall using Applied Element Method, *IOP Conference Series: Materials Science and Engineering*, **330**, 012128, https://doi.org/10.1088/1757-899X/330/1/012128.

[11] Eraky, A., Mustafa, S.A., Badawy, M. (2021): Structural Analysis using Applied Element Method: A Review, *The Egyptian International Journal of Engineering Sciences and Technology*, **34** (1), 16–27, https://doi.org/10.21608/eijest.2021.56786.1043.

[12] Gohel, V., Patel, P.V., Joshi, D. (2013): Analysis of Frame using Applied Element Method (AEM), *Procedia Engineering*, **51**, 176–183, https://doi.org/10.1016/j.proeng.2013.01.026.

[13] Khattak, N., Derakhshan, H., Thambiratnam, D.P., Malomo, D., Perera, N.J. (2023): Modelling the in-plane out-of-plane interaction of brick and stone masonry structures using Applied Element Method, *Journal of Building Engineering*, **76**, 107175, https://doi.org/10.1016/j.jobe.2023.107175.

[14] Adhikari, R.K., Parammal Vatteri, A., D'Ayala, D. (2023): Seismic Performance Assessment of Low-Rise Unreinforcedand Confined Brick Masonry School Buildings Using the Applied Element Method, *Buildings*, **13**, 159, https://doi.org/10.3390/buildings13010159.

[15] Karbassi, A., Nollet, M.-J. (2013): Performance-Based Seismic Vulnerability Evaluation of Masonry Buildings Using Applied Element Method in a Nonlinear Dynamic-Based Analytical Procedure, *Earthquake Spectra*, **29** (2), 399–426, https://doi.org/10.1193/1.4000148.

[16] Pandey, B., Meguro, K. (2004): Simulation Of Brick Masonry Wall Behavior Under Inplane Lateral Loading Using Applied Element Method, in *13th World Conference on Earthquake Engineering*, Vancouver, B.C., Canada, August.

[17] Sharma, S., Marasca, A., Ponte, M., Bento, R. (2022): Modelling the in-plane cyclic behaviour of typical Portuguese rubble stone masonry using the applied element method, *Structures*, **46**, 1224–1242, https://doi.org/10.1016/j.istruc.2022.10.107.

[18] Canditone, C., Parisi, F. (2024): Numerical simulation of soft stone masonry under simple compression using the Applied Element Method, in *18th World Conference on Earthquake Engineering*, Milan, Italy.

[19] Churilov, S. (2012): *Experimental and analytical research of strengthened masonry*. PhD dissertation, Ss. Cyril and Methodius University, Faculty of Civil Engineering-Skopje.

[20] Churilov, S., Dumova-Jovanoska, E. (2013): In-plane shear behaviour of unreinforced and jacketed brick masonry walls, *Soil Dynamics and Earthquake Engineering*, **50**, 85–105, https://doi.org/10.1016/j.soildyn.2013.03.006.

[21] Binda, L., Fontana, A., Frigerio, G. (1988): Mechanical behaviour of brick masonries derived from unit and mortar characteristics, in *8th International Brick and Block Masonry Conference*, Dublin, Ireland, 205–216.

Copyright © 2025 CroCEE
DOI: https://doi.org/10.5592/CO/3CroCEE.2025.24

[22] Kržan, M., Gostič, S., Cattari, S., Bosiljkov, V. (2015): Acquiring reference parameters of masonry for the structural performance analysis of historical buildings, *Bulletin of Earthquake Engineering*, **13**, 203–236, https://doi.org/10.1007/s10518-014-9686-x.

[23] Kaushik, H.B., Durgesh, R.C., Sudhir, J.K. (2007): Stress- strain characteristics of clay brick masonry under uniaxial compression, *Journal of Materials in Civil Engineering*, **19** (9), 728–739, https://doi.org/10.1061/(ASCE)0899-1561(2007)19:9(728).

[24] Tomaževič, M. (2009): Shear resistance of masonry walls and Eurocode 6: shear versus tensile strength of masonry, *Materials and Structures*, **42**, 889-907,, https://doi.org/10.1617/s11527-008-9430-6.

[25] Morandi, P., Magenes, G., Albanesi, L. (2013): Prove Sperimentali per la Valutazione della Risposta Sismica nel Piano di Pareti Murarie in Blocchi di Laterizio a Setti Sottili, in *Proceedings of the XV Convegno Nazionale ANIDIS - "L'ingegneria sismica Italiana"*, Padua, Italy.

[26] Salmanpour, A.H., Mojsilović, N., Schwartz, J. (2015): Displacement capacity of contemporary unreinforced masonry walls: An experimental study, *Engineering Structures*, **80**, 1-16,, https://doi.org/10.1016/j.engstruct.2015.01.052.

[27] Morandi, P., Albanesi, L., Magenes, G. (2014): URM walls with thin shell/web clay units and unfilled head-joints: Cyclic in-plane tests, in *Proceedings of the 2nd European Conference on Earthquake Engineering and Seismology*, Istanbul, Turkey.

[28] Hrasnica, M., Biberkić, F., Medić, S. (2018): Experimental testing of solid brick masonry walls, *Key Engineering Materials*, **747**, 694–701, https://doi.org/10.4028/www.scientific.net/KEM.747.694.

[29] Applied Science International, LLC. (2024): *Extreme loading for Structures, Theoretical Manual, version 01*.

[30] Lourenço, P.B., Gaetani, A. (2022): *Finite Element Analysis for Building Assessment - Advanced Use and Practical Recommendations*, 1st ed. New York, USA: Routledge, Taylor & Francis Group. https://doi.org/10.1201/9780429341564.

[31] Christy, C.F., Tensing, D., Shanthi, R.M. (2012): In-plane shear behaviour of Brick Masonry - A Literature Review on experimental study, *International Journal of Civil and Structural Engineering*, **2** (4), 1144–1152.

[32] Kumar, K.H., Tripathi, R.K. (2024): Damage assessment of infilled frame structures using applied element method, *Bulletin of Earthquake Engineering*, **22**, 1387–1423, https://doi.org/10.1007/s10518-023-01824-6.

[33] Malomo, D., Pinho, R., Penna, A. (2020): Applied element modelling of the dynamic response of a full-scale clay brick masonry building specimen with flexible diaphragms, *International Journal of Architectural Heritage*, **14** (10), 1484–1501, https://doi.org/10.1080/15583058.2019.1616004.

[34] Maekawa, K., Okamura, H. (1983): Deformational Behavior and Constitutive Equation of Concrete using the Elasto-Plastic and Fracture Model, *Journal of the Faculty of Engineering*, **37** (2), 253–328.

[35] Okamura, H., Maekawa, K. (1991): *Nonlinear analysis and constitutive models of reinforced concrete*. Giho-do Press, Tokyo, Japan.

[36] El-Kashif, K.F., Maekawa, K. (2004): Time-dependent nonlinearity of compression softening in concrete, *Journal of Advanced Concrete Technology*, **2** (2), 233–247, https://doi.org/10.3151/jact.2.233.

[37] Lourenço, P.B. (1996): *Computational Strategies for Masonry Structures*. PhD dissertation, Delft University of Technology, Delft, Netherlands.

Proceedings of the 3rd Croatian Conference on Earthquake Engineering - 3CroCEE
19–22 March 2025, Split, Croatia
Copyright © 2025 CroCEE
DOI: https://doi.org/10.5592/CO/3CroCEE.2025.73

BIM APPLICATION IN SEISMIC STRENGTHENING OF REINFORCED CONCRETE BUILDING USING FRP MATERIALS

Goran Chapragoski [(1)], Golubka Nechevska-Cvetanovska [(2)]

[(1)] *Assistant Professor, Institute of Earthquake Engineering and Engineering Seismology, University of Ss. Cyril and Methodious, Skopje, R. N. Macedonia., goran@iziis.ukim.edu.mk*
[(2)] *Professor, Institute of Earthquake Engineering and Engineering Seismology, University of Ss. Cyril and Methodious, Skopje, R. N. Macedonia., golubka@iziis.ukim.edu.mk*

Abstract

With the introduction of 3D graphic representation to improve workflows, communications, collaborations, and data exchange among all members involved in the project, the BIM (Building Information Modelling) methodology is completely transforming the structural industry. In general, BIM is fundamentally based on an information-sharing methodology among all stakeholders, implemented throughout the building's life cycle and materialized using specialized software in the virtual construction of a 3D digital model. In this particular case, the process of seismic assessment and strengthening of RC five storey building will be presented through a series of steps, using BIM methodology. Based on the previously performed analyses of the structure and obtained results, it has been defined which elements of the structure need to be strengthened. In this case, using the BIM platform PlanRadar for organizing and managing the process, it is demonstrated how the seismic assessment of the building and the process of strengthening the elements would be carried out. This methodology, using the PlanRadar platform, allows for the proper planning of all activities that are part of the strengthening procedure of the building. Each defined location in the structure contains its own data card. It specifies the name and type of the task, who defined the task and for whom it is intended, when it should start, the location in the structure, the type of strengthening, details of the strengthening for the structural element, as well as the steps for the gradual installation of the FRP materials. This procedure offers opportunities for complete control of the process, allowing for the review of both models (the architectural and the structural), as well as the ability to control whether the elements requiring strengthening are permissible for architectural reasons or due to other design phases.

Keywords: BIM methodology, strengthening, FRP materials, RC building

1. Introduction

By introducing 3D graphical representation to improve workflows, communication, collaboration, and data exchange among all project participants, BIM methodology completely changes the construction industry [1].

BIM comprises a set of interactive policies, processes, and technologies that create a working methodology capable of managing building design and project data in a digital format throughout the building's lifecycle [2]. It involves the virtual construction of a building in a 3D digital model, known as a Building Information Model. This methodology provides a comprehensive and interactive vision of the project, integrating the interdependencies between various building project phases (architectural, structural, and mechanical, electrical, and plumbing (MEP)) through technological connection of all stakeholders involved [3]. During the virtual construction of the digital model, the stakeholders continuously redefine and optimize their designs, updating the digital model accordingly [4].

In general, BIM is based on a methodology of information sharing among all stakeholders throughout the building lifecycle, using specialized software in the virtual construction of a 3D digital model [5]. The information and its management within BIM models are key aspects of the BIM methodology. The ability to communicate, reuse, and share data efficiently, without loss or misinterpretation among stakeholders using different software applications, is a fundamental requirement. This ensures the integration of collaborative procedures with the technologies inherent to the BIM concept [6].

Copyright © 2025 CroCEE
DOI: https://doi.org/10.5592/CO/3CroCEE.2025.73

Currently, the entire process of seismic assessment of structures is often conducted using BIM methodology. In this specific case, a portion of the BIM methodology is applied to a seismic assessment, the need for strengthening, and the implementation of these measures for an existing reinforced concrete building.

2. Seismic assessment of existing reinforced concrete frame building

The first step in the seismic assessment of an existing structure is defining the structural system of the building as well as the quantity and quality of the materials used in its construction. In this case, since a construction and structural design project exists for the selected reinforced concrete building, most of the fundamental data such as the type of structural system, number of floors, type, quantity, and quality of materials used, are derived from the existing technical documentation.

According to the project documentation, the structure is regular in plan and elevation. It comprises six frames in one direction with spans of 6.00m and four frames in the perpendicular direction with spans of 4.50m. The building consists of five levels, where the ground floor has a floor height of 4.00m, while the height of all other floors is 3.00m. All floors have an identical layout, except for the top floor, which differs in the stairwell area and cantilevered extensions (Figure 1).

When examining the building frame by frame, frames 1 through 7 are identical, as are frames A through E (Figure 1). Structural elements are labeled according to their type, sequence number, and the floor on which they are located. For example, **Sn_f** represents a column, where **n** indicates the column's sequence number, and **f** indicates the floor on which the column is located. Similarly, **Bn_f** denotes a beam, where **n** indicates the beam's sequence number, and **f** indicates the floor on which the beam is situated.

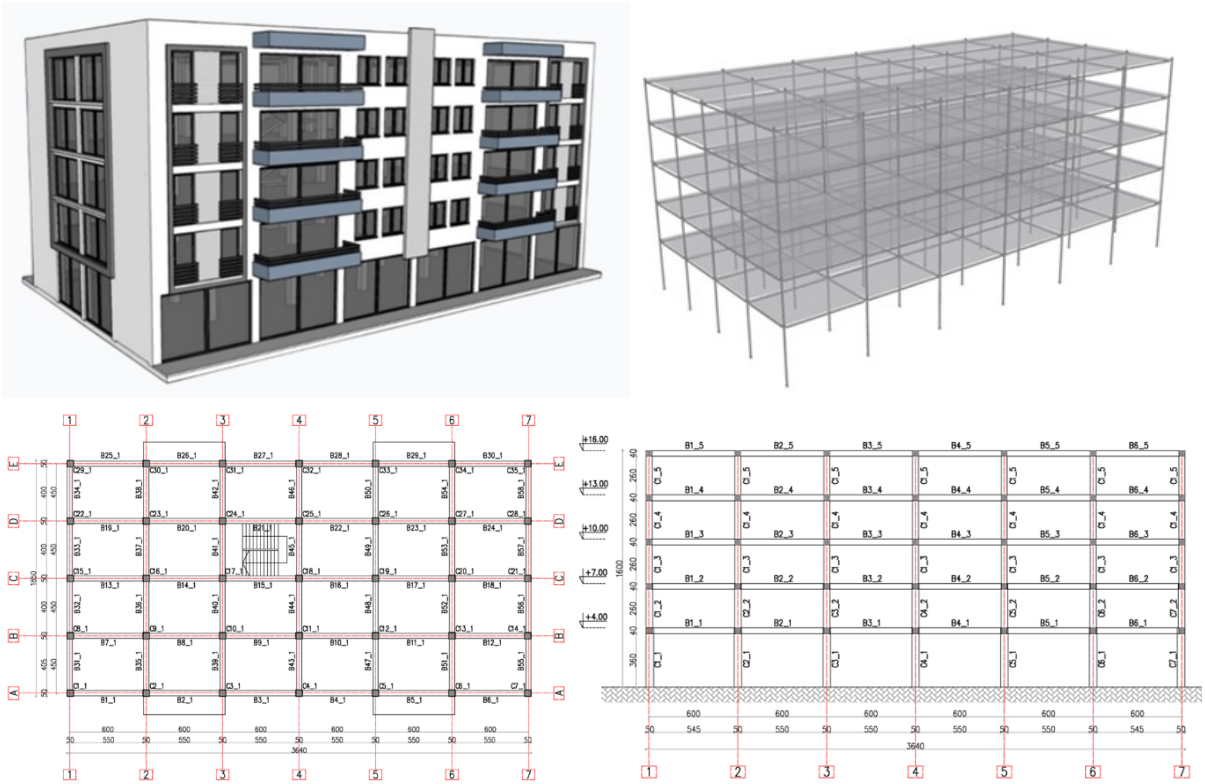


Figure 1. 3D of the building (BIM model) and 2D drawings

Considering the available project documentation, the geometric characteristics of the structural elements have been determined. It has been observed that the columns on the ground floor have dimensions of 50x50 cm, those on the first floor are 45x45 cm, and those on the second, third, and fourth floors are 40x40 cm. On the other hand, all beams on all floors have uniform dimensions of

Proceedings of the 3rd Croatian Conference on Earthquake Engineering - 3CroCEE
19–22 March 2025, Split, Croatia
Copyright © 2025 CroCEE
DOI: https://doi.org/10.5592/CO/3CroCEE.2025.73

40x40 cm. The structural elements have been designed using concrete C25/30 and reinforcement type B500. The dimensions and reinforcement details for the columns and beams are presented in Tables 1 and 2.

Table 1. Embedded reinforcement in the columns

Columns				
Symbol	**Dimensions (cm)**	**Level**	**Longitudinal Reinforcement**	**Stirrups**
C1-1 to C35-1	50/50	Ground floor	8Φ18	Φ8/15cm
C1-2 to C35-2	45/45	First floor	8Φ16	Φ8/15cm
C1-3 to C35-3 C1-4 to C35-4 C1-5 to C35-5	40/40	Second floor Third floor Fourth floor	8Φ16	Φ8/15cm

Table 2. Embedded reinforcement in the beams

Beams						
Symbol	**Dimensions (cm)**	**Level**	**Longitudinal Reinforcement**			**Stirrups**
			Bn_f GL	Bn_f S	Bn_f GD	
B1-n to B30-n	40/40	All	2Φ14+3Φ14	5Φ14	2Φ14+3Φ14	Φ8/10/20cm
B31-n to B58-n	40/40	All	2Φ14+2Φ14	4Φ14	2Φ14+2Φ14	Φ8/10/20cm

Before initiating the process of modeling the structure, detailed geometric and material examinations were carried out to in order to determine the real characteristics and quantities of the embedded materials. Based on these investigations, it was found that the compressive strength of the concrete in some ground-floor columns significantly deviates from the designed strength outlined in the existing project documentation (Figure 2). The concrete strength of the selected columns in the figure 2 is smaller for 7 to 9 MPa than the designed one.

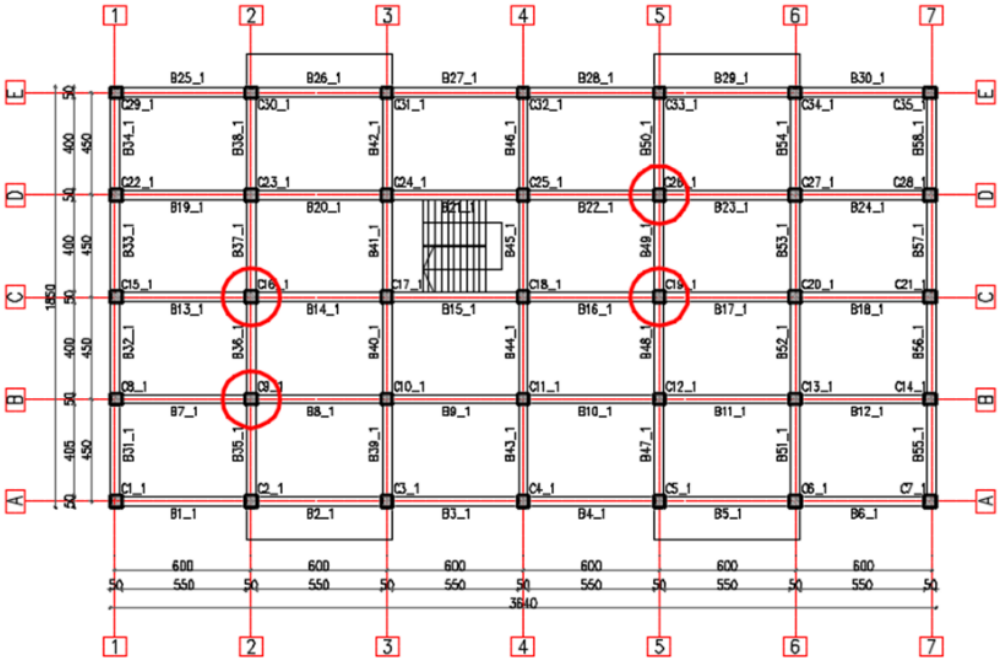


Figure 2. Columns with concrete strength smaller than designed one

Based on these observations, local strengthening of the ground-floor columns using CFRP materials was proposed. CFRP are placed with the fibres perpendicular to the element axis.

Copyright © 2025 CroCEE
DOI: https://doi.org/10.5592/CO/3CroCEE.2025.73

3. Analysis of existing reinforced concrete frame building

Based on the defined element data (geometric characteristics, concrete strength, as well as the type, quantity, and arrangement of reinforcement) and the specified vertical loads (Table 3), structural BIM model was designed.

Table 3. Additional permanent and live load

Level	Permanent load (kN/m²)	Live load (kN/m²)	Snow (kN/m²)
Ground floor	1.50	1.50	/
First floor	1.50	1.50	/
Second floor	1.50	1.50	/
Third floor	1.50	1.50	/
Fourth floor	1.00	/	1.00

After the local strengthening of the structural elements using CFRP was done (Figure 3b), the global load-bearing capacity of the strengthened structure was obtained. For this purpose, a nonlinear static analysis of the structure was performed using the SeismoStruct computer program [7] (Figure 3a).



a) b)

Figure 3. a) 3D model of strengthened structure (Seismostruct computer program), b) Strengthening detail of the columns using CFRP materials

In order to determine the maximum displacements of the structure, according to Eurocode 8 - Part 1 (EN 1998-1, Annex B), the N2 method was selected. In this case, the required displacements were derived using a response spectrum corresponding to a return period of 475 years and a peak ground acceleration of ag = 0.25g (Figure 4).

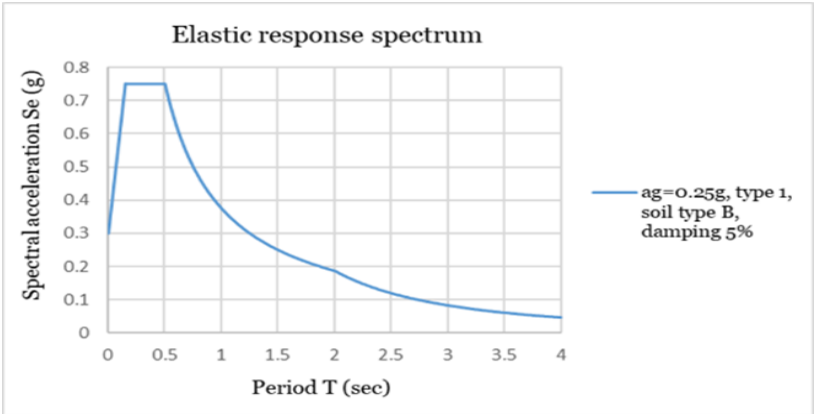


Figure 4. Elastic response spectrum

Copyright © 2025 CroCEE
DOI: https://doi.org/10.5592/CO/3CroCEE.2025.73

To utilize the response spectrum for defining the required displacements, it was transformed into an acceleration-displacement response spectrum (ADRS). This transformation, involving converting the X-axis into a displacement axis, was carried out in accordance with Eurocode 8 - Part 3 (EN 1998-3, Annex B) (Figure 5).

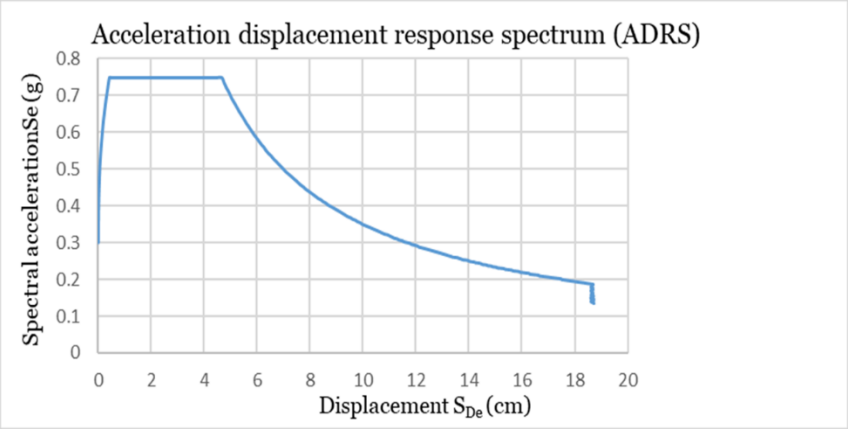


Figure 5. ADRS spectrum

Following the nonlinear static analysis, the obtained results for the structural capacity, along with the performed evaluations of the damage levels and performance criteria of the structural elements, indicate that the deformation capacity of the reinforced structure satisfies the required/target displacements for the selected type of earthquake (Figure 6).

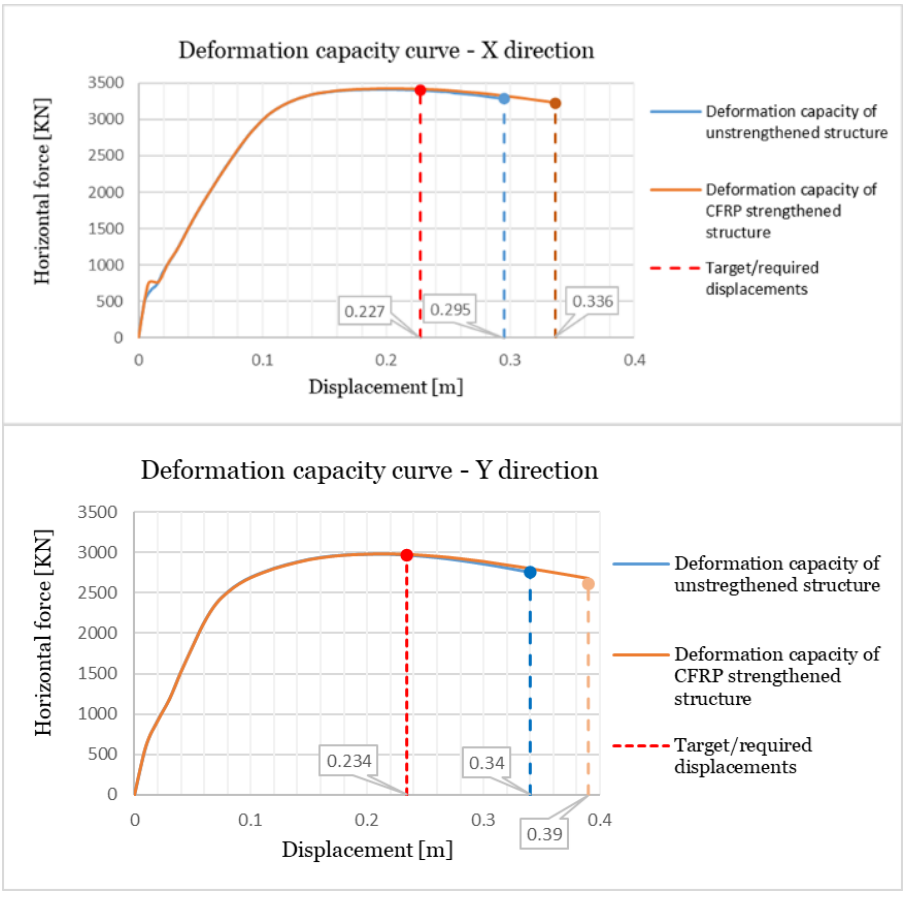


Figure 6. Deformation capacity curve in X and Y direction respectively

Copyright © 2025 CroCEE
DOI: https://doi.org/10.5592/CO/3CroCEE.2025.73

4. BIM (Building information modelling) application in strengthening of the existing building

Based on the project documentation of the existing structure, a 3D model was created, including all architectural elements. This model was then exported as an IFC file, which, in line with BIM methodology, was used for seismic assessment of the structure.

Since prior analyses of the structure had already identified the elements requiring strengthening, the seismic assessment and strengthening process were organized and managed using the BIM platform PlanRadar [8]. This platform facilitates comprehensive control over the entire process, allowing users to review both architectural and structural models. Additionally, it enables verification of whether the proposed strengthening is feasible from an architectural or other project perspective. PlanRadar also supports collaborative teamwork by ensuring that all participants involved in the process have access to updates. Any changes made to the model by an authorized participant are recorded within the platform.

Based on the results of the analyses, key structural elements requiring strengthening were marked (Figure 7). Each marked location and defined task can be viewed by all participants in the process or restricted to specific individuals to whom the task is assigned. Once a task is completed or is in progress, its status is recorded in the program. This ensures seamless tracking and management of the strengthening process.

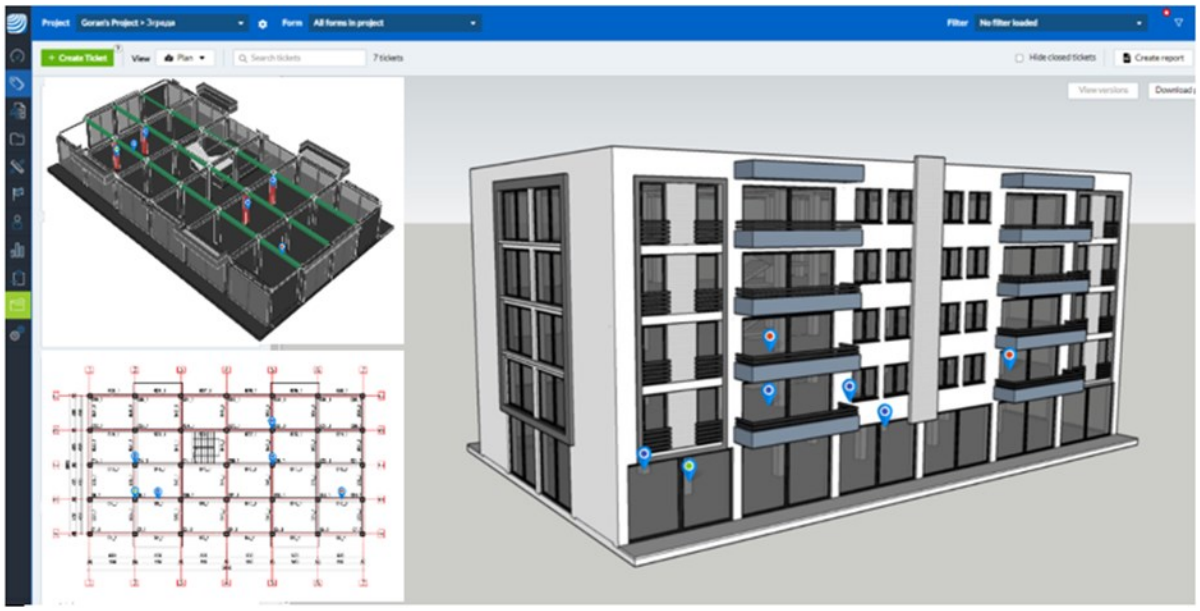


Figure 7. Determining the locations in the structure that require strengthening

Each defined location in the structure contains its own data card. The task's name and type are specified, along with the person who defined the task and the intended recipient. The start date, location within the structure, type of strengthening, and detailed strengthening for the structural element are also outlined. Additionally, the steps for the gradual installation of CFRP materials are defined (Figure 8).

This methodology, using the PlanRadar platform, enables effective planning of all activities involved in the seismic assessment and strengthening procedure.

In this particular case, the sequential approach to each step of the activities outlined in the procedure, along with the specified time frame required for their execution (4D dimension of BIM), is defined within the program (Figure 9). The program specifies the start and end dates for each activity in the procedure, as well as the time needed for its execution.

Proceedings of the 3rd Croatian Conference on Earthquake Engineering - 3CroCEE
19–22 March 2025, Split, Croatia
Copyright © 2025 CroCEE
DOI: https://doi.org/10.5592/CO/3CroCEE.2025.73

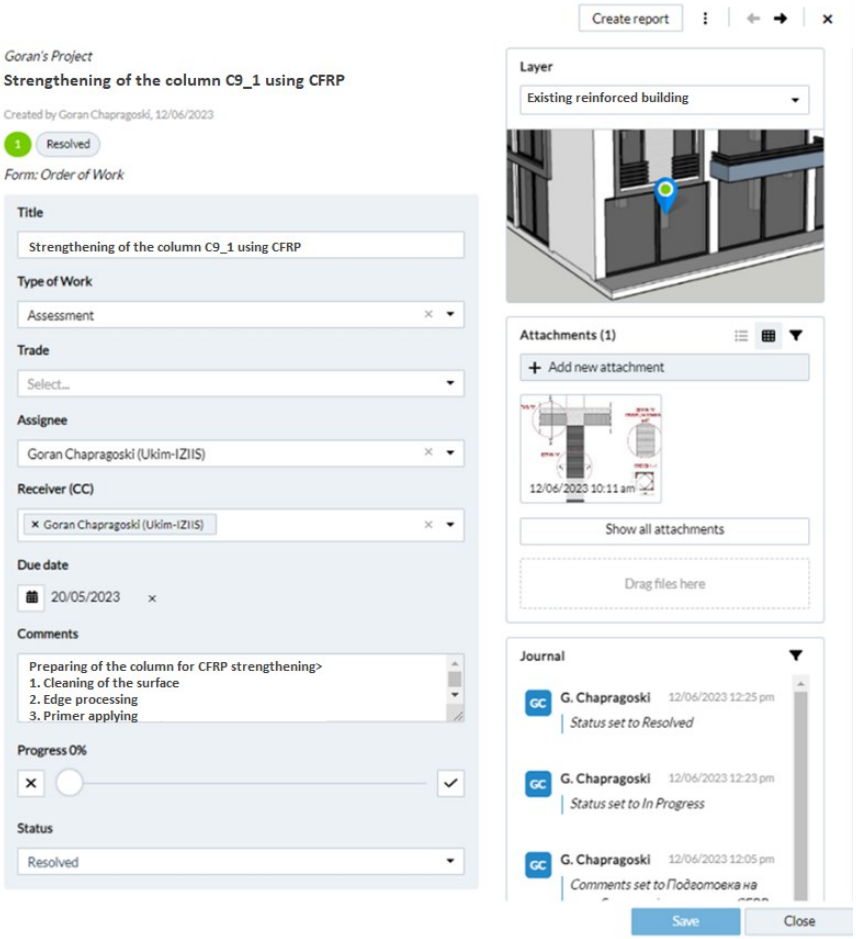
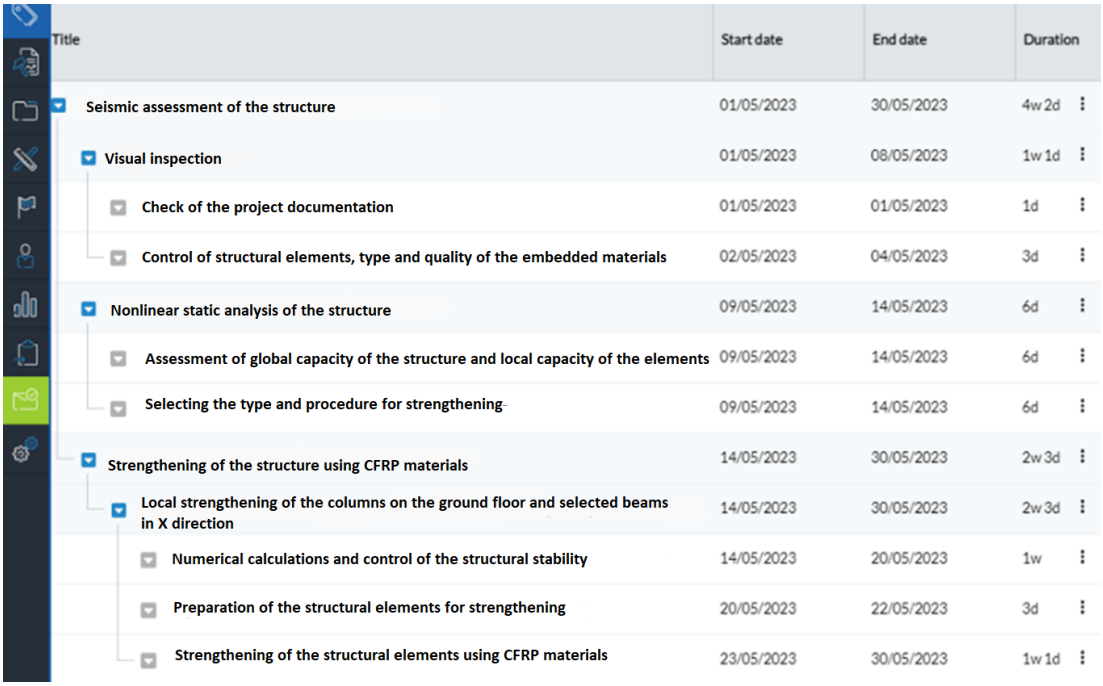


Figure 8. Data card for specific marked location



Title	Start date	End date	Duration
Seismic assessment of the structure	01/05/2023	30/05/2023	4w 2d
Visual inspection	01/05/2023	08/05/2023	1w 1d
Check of the project documentation	01/05/2023	01/05/2023	1d
Control of structural elements, type and quality of the embedded materials	02/05/2023	04/05/2023	3d
Nonlinear static analysis of the structure	09/05/2023	14/05/2023	6d
Assessment of global capacity of the structure and local capacity of the elements	09/05/2023	14/05/2023	6d
Selecting the type and procedure for strengthening	09/05/2023	14/05/2023	6d
Strengthening of the structure using CFRP materials	14/05/2023	30/05/2023	2w 3d
Local strengthening of the columns on the ground floor and selected beams in X direction	14/05/2023	30/05/2023	2w 3d
Numerical calculations and control of the structural stability	14/05/2023	20/05/2023	1w
Preparation of the structural elements for strengthening	20/05/2023	22/05/2023	3d
Strengthening of the structural elements using CFRP materials	23/05/2023	30/05/2023	1w 1d

Figure 9. Each step of the activities outlined in the procedure

Copyright © 2025 CroCEE
DOI: https://doi.org/10.5592/CO/3CroCEE.2025.73

The current work diagram for the required construction activities, showing the duration of each activity and the subsequent or simultaneous activities that follow a specific task, is provided in Figure 10.

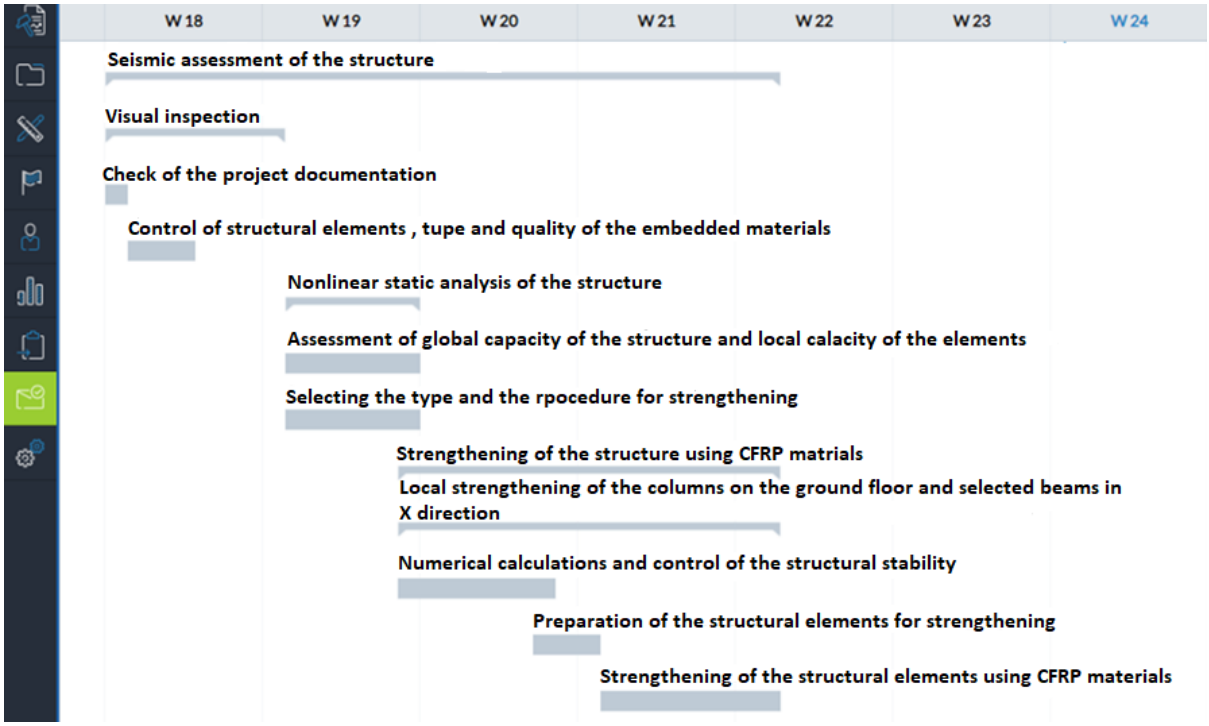


Figure 10. Curren working diagram

5. Conclusion

The entire process of seismic assessment and strengthening of a specific structure using CFRP materials, controlled and enhanced over a defined time period, is demonstrated through an integrated model utilizing the BIM software tool PlanRadar. This showcases that the entire procedure, from the assessment of the structure's seismic resistance to its strengthening with innovative building materials, can be seamlessly and efficiently managed through the Building Information Modeling (BIM) methodology.

The final outcome is a completed project containing comprehensive information about every step executed during the strengthening of the structure with CFRP materials. This data is stored in electronic format, ensuring accessibility for future interventions at any time.

References

[1] Barak, R., Jeong, Y.-S., Sacks, R., & Eastman, C. M. (2009). Unique Requirements of Building Information Modeling for Cast-in-Place Reinforced Concrete. *Journal of Computing in Civil Engineering*, 23(2), 64–74. https://doi.org/10.1061/(ASCE)0887-3801(2009)23:2(64)

[2] Succar, B. (2009). Building information modelling framework: A research and delivery foundation for industry stakeholders. *Automation in Construction*, 18(3), 357–375. https://doi.org/10.1016/j.autcon.2008.10.003

[3] Love, P. E. D., Edwards, D. J., Han, S., & Goh, Y. M. (2011). Design error reduction: toward the effective utilization of building information modeling. *Research in Engineering Design*, 22(3), 173–187. https://doi.org/10.1007/s00163-011-0105-x

[4] Carmona, J. & Irwin, K. (2007). BIM: Who, what, how and why. Building Operation Management. Retrieved August 20, 2018, from https://www.facilitiesnet.com/software/article.aspx?id=7546

Copyright © 2025 CroCEE
DOI: https://doi.org/10.5592/CO/3CroCEE.2025.73

[5] Lino, J. C., Azenha, M., & Lourenço, P. (2012). Integração da Metodologia BIM na Engenharia de Estruturas. Encontro Nacional Betão Estrutural -BE2012, 24–26.

[6] Mienr, M. (2012). Building Information Modeling (BIM). Disponevel em. Retrieved August 1, 2018, from http://www.neuralenergy.info/2009/06/building-information-modeling.html

[7] SeismoStruct (2021): Analysis user's manual. Providence, Seismosoft L.td.

[8] PlanRadar.com

https://www.planradar.com/login#/

Proceedings of the 3rd Croatian Conference on Earthquake Engineering - 3CroCEE
19–22 March 2025, Split, Croatia
Copyright © 2025 CroCEE
DOI: https://doi.org/10.5592/CO/3CroCEE.2025.100

TESTS ON SPECIAL ANCHORS FOR MASONRY INFILLS WITH SPECIAL OPPORTUNITY FOR SEISMIC RETROFITTING

Matthias Roik [(1)], Caroline Piesker [(2)]

[(1)] Research & Development, Leviat GmbH, matthias.roik@leviat.com
[(2)] Research & Development, Leviat GmbH, caroline.piesker@leviat.com

Abstract

Reinforced concrete frame structures are treated as moment resisting frames, with different design options. The bearing capacity of such frames can be significantly increased by masonry infill walls that act as shear walls.

The greatest supporting effect of the wall on the frame is expected in in-plane (IP) direction. The IP loads are introduced into the wall as compressive forces, whereas the Out-of-plane (OoP) loads generate shear forces at the joints between the frame and infill. IP loads can be transferred very well through mortared joints, while additional securing is recommended for OoP direction. Particularly in case of earthquakes, infills must withstand OoP loads to prevent failure, which can endanger people and block escape routes. It should also be possible to quickly refurbish the structure so that it can withstand subsequent impacts.

A good opportunity to improve the OoP performance is to place special ties in the joints between the frame and infill. The action on these ties can be determined from the load carrying capacity and deformation behaviour of the frame structure or by calculation according to EN 1998 or similar.

As the intended anchors are to connect a concrete element to a masonry wall, a system is proposed that consists of an anchor channel cast in concrete into which special masonry anchors engage. This system has the advantage that it is easy to install and can be reinstalled very simply in the event of renovation or damage. This fastening system can also be post-installed in the event of seismic retrofitting.

These fixings have a decisive influence on the interaction between the RC frame and the infill and require a proper design, best to be achieved by tests in different scales.

In this paper, the technical background is explained, and the various experimental results are illustrated and compared.

Keywords: Seismic repair, masonry infill, special fixings, non structural elements.

1. Introduction

Reinforced Concrete (RC) frames with masonry infill walls are widely utilized as an external wall construction system. Under seismic loading, these structures are subjected to forces in both the in-plane (IP) and out-of-plane (OoP) directions. In the IP direction, the masonry infill—if not physically separated from the RC frame—enhances its load-bearing capacity, allowing it to be treated as a structural component. In contrast, OoP forces induce shear stresses at the interface, with the infill often behaving as a non-structural element.

The distinction between structural and non-structural members, as well as corresponding design standards, is critical and has been extensively discussed in the literature (e.g., [1]). Failure of the masonry infill during seismic events, such as falling bricks, poses significant risks to life safety and evacuation. Additionally, such failures adversely affect the IP load-bearing capacity of the structure, increasing deformation demands.

Enhancing the interaction between the RC frame and the infill can mitigate these risks. The incorporation of wall anchors at the frame-infill interface has been shown to improve the overall performance, reducing the likelihood of interface failures and ensuring effective load transfer under varying load directions.

Copyright © 2025 CroCEE
DOI: https://doi.org/10.5592/CO/3CroCEE.2025.100

Traditional unreinforced mortar joints often fail to accommodate large relative displacements induced by seismic loads, necessitating the development of robust anchoring systems. The primary forces on these anchors stem from the relative deformations between the RC frame and the masonry infill, making analytical predictions challenging. Experimental testing provides a more reliable means of evaluating these systems.

This paper explores the behavior of masonry infills in RC frames with specialized anchoring systems, with an emphasis on their performance under IP and OoP seismic loads. The tests are carried out at different scales. This method proved to be particularly effective for obtaining reliable results in a reasonable amount of time and effort [2]. Micro- and macro-scale tests evaluate the effectiveness of these anchors acc. to [3] in improving structural resilience.

2. Micro-scale tests on wall anchors

2.1. Scope

Seismic events often cause RC frame systems with masonry infill walls to fail in the OoP direction due to separation at the mortar joint between the frame and the infill. To improve joint performance, wall ties can be incorporated. This study evaluates the load-bearing behavior of these ties.

2.2. Anchor system for pre-installation

The anchor system analysed here consists of flat anchors placed in the infill wall and a cast-in anchor channel to transfer the connection load into the concrete frame.

The anchor channels consist of a C-shaped channel profile fitted with head bolts. These anchor channels are designed to be inserted into the formwork and cast into the concrete.

Once the concrete frame has been constructed, the infill is masoned in place, with the flat anchors interlocking with the rail profiles to ensure a firm connection between the infill and the concrete, see Figure 1.



Figure 1. a) cast-in anchor channel; b) flat anchor interlocking with the channel.

Copyright © 2025 CroCEE
DOI: https://doi.org/10.5592/CO/3CroCEE.2025.100



Figure 2. a) tested wall anchors; b) anchors installed in the joint of a brick pair.

Micro-scale tests were conducted on individual anchors to determine their horizontal shear capacity, as per EN 846-7 [4], Figure 2. Ten masonry units, each comprising two perforated NF-standard bricks (EN 1998-2 [5]) joined by M2.5 mortar, were constructed. The anchors were embedded in the mortar joints, and the specimens were tested nine days later.

The test load was applied via shear forces on the bricks while the anchoring concrete block remained fixed. Shear forces were induced using a tension rod, as illustrated in Figure 3.

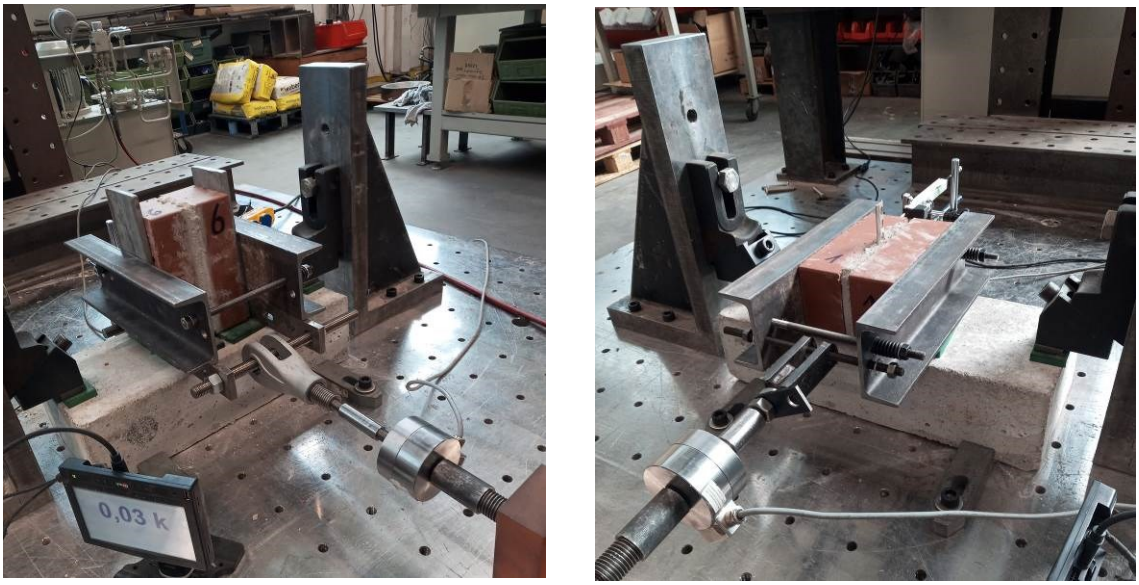


Figure 3. a and b. Test setup for testing the horizontal shear capacity of wall ties in micro scale, a: longitudinal direction of bricks, b: transverse direction of bricks.

For anchors embedded transversely, the mean maximum shear load reached approximately 2900 N, with deflections ranging between 1.50 mm and 3.77 mm. Failure predominantly occurred within the mortar joint.

Copyright © 2025 CroCEE
DOI: https://doi.org/10.5592/CO/3CroCEE.2025.100

2.3. Anchor system for post installation

The fastening system is also suitable for structures that were not fitted directly with the rail system during construction. For subsequent fastening, the rails can be fixed to the concrete using dowels, see Figure 4. As before, the flat anchors are hooked into the rails during the masonry of the infill.



Figure 4. a) post installed anchor channel; b) flat anchor interlocking with the channel.

The resulting gap between the infill and the concrete frame should be grouted.

In contrast to the anchor channels set in concrete, the channel profile cannot transfer the shear force into the concrete with its flanks, but is subjected to bending in the transverse direction.

Appropriate tests - as previously carried out - provide information about the final resistance. These tests could not be carried out by the time this paper was finalised, but the results will be available by the time of the conference.

However, it is to be expected that the final resistances will be similar to those of the concreted-in system, as it is known from preliminary tests that the rails can absorb a higher load and that the failure occurs again in the mortar joint of the bricks.

Proceedings of the 3rd Croatian Conference on Earthquake Engineering - 3CroCEE
19–22 March 2025, Split, Croatia
Copyright © 2025 CroCEE
DOI: https://doi.org/10.5592/CO/3CroCEE.2025.100

3. Macro-scale Tests

3.1. Specimens

The macro-scale specimens replicated a segment of a seven-story RC building at a 1:2.5 scale, see [6] among others. This typical RC frame structure included two-way slabs and unreinforced masonry infill walls, as shown in Figure 5.

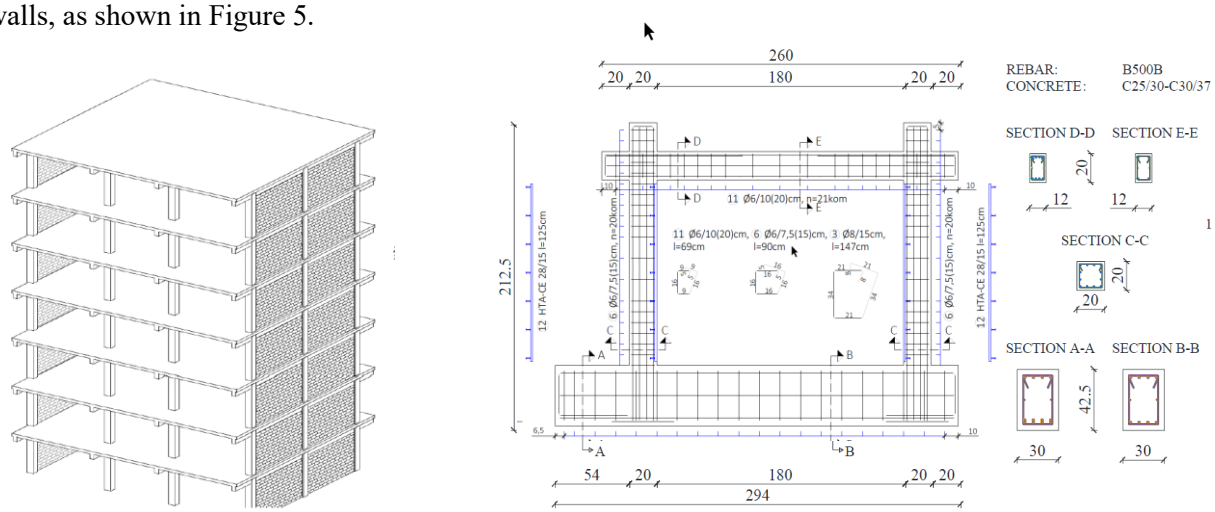


Figure 5. a and b, Representative Building with RC frames, and test frame used for macro scale tests.

Cast-in anchor channels were embedded within the RC columns, allowing anchors to interlock with the masonry joints, see Figure 6.



Figure 6. a and b, Positioning of wall tie anchors: a: clay blocks and b: clay brick masonry

The anchors are distributed like shown in Figure 7, as a result of a pre-calculation, assuming a maximum capacity of 1,5 kN in shear direction (i.e. OoP).

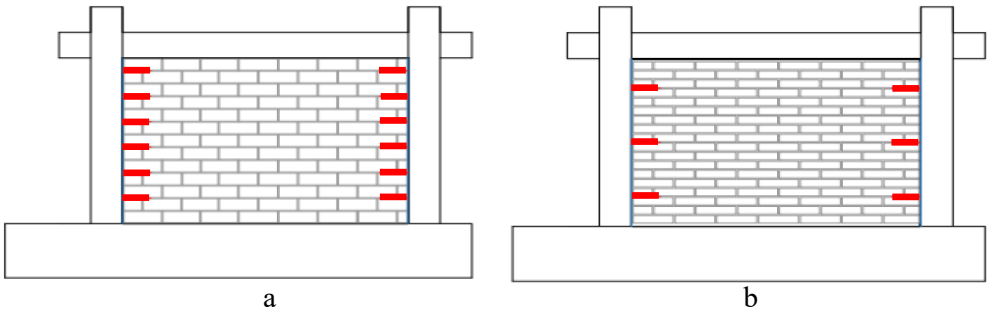


Figure 7. a and b, Distribution of the anchors over the sides of the infill: a: clay blocks and b: clay brick masonry.

Copyright © 2025 CroCEE
DOI: https://doi.org/10.5592/CO/3CroCEE.2025.100

4. Test Setup

The test configuration and procedure followed those described in [7], with the key distinction being the inclusion of wall anchors in the present study. Previous tests omitted such reinforcement at the frame-infill interface. Consequently, the current investigation emphasizes the impact of these ties, particularly on the performance of the connection between the concrete frame and the masonry infill.

4.1. Test Procedure

Out-of-Plane (OoP) Tests

Cyclic quasi-static shear tests were conducted on specimens with cavity walls constructed from hollow clay blocks and solid brick masonry. Each specimen was oriented such that the dotted side faced the ARAMIS optical sensor, enabling precise 3D strain measurement. The specimens were secured with brackets fixed to rails embedded in the reactive floor, while the tops of the columns were left free (see Figure 8).

The load was applied at the intersection of the column centerlines and the top beam using hydraulic jacks, each operated manually through independent hydraulic units. The tests were performed in a single cyclic direction.

Throughout the testing process, crack propagation was marked on the white surface of the specimens until ultimate failure occurred. For safety reasons, crack recording was halted during the final stages of the tests and resumed after specimen unloading to document the residual damage.

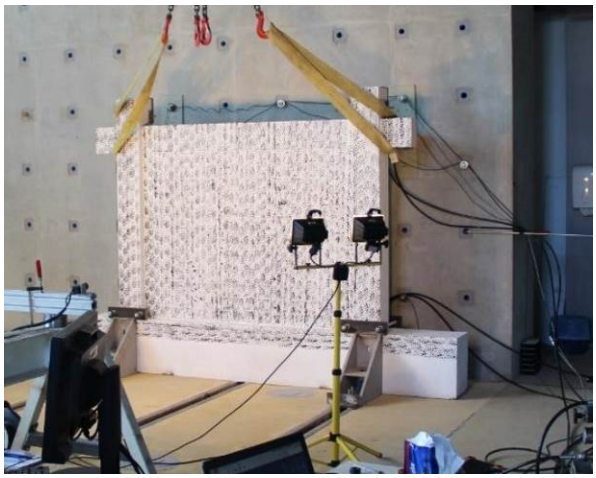


Figure 8. Test setup OoP.

The load was applied incrementally as a quasi-static pulsating cyclic force, with each step executed twice and increasing by 10 kN per increment. Loading continued until the RC frame began yielding, as shown in Figure 9. All deformations were recorded using the ARAMIS optical system. The specimens endured jack displacements up to 140 mm, corresponding to an inter-story drift ratio of approximately 10%. Throughout the tests, the specimens remained stable, and no significant operational issues arose.

Copyright © 2025 CroCEE
DOI: https://doi.org/10.5592/CO/3CroCEE.2025.100



a b c

Figure 9. a, b and c: Load and deflection OoP, a: begin of test, b: medium load level with first cracks in the concrete, c: yielding of the frame.

In-Plane (IP) Tests

The IP tests were conducted on the same infill specimens (hollow clay and solid brick masonry), oriented with the dotted side facing ARAMIS for 3D strain tracking. The specimens were mounted within a reactive frame secured to a reactive slab and wall (see Figure 10). A specialized hood with roller supports was installed atop the columns to allow IP translations.

Vertical gravitational loads of 365 kN were applied to each column using a hydraulic press, maintained manually throughout the tests. This vertical force was combined with lateral loads applied at the ends of the top beam via hydraulic jacks, inducing alternating compression and unloading in the two columns.

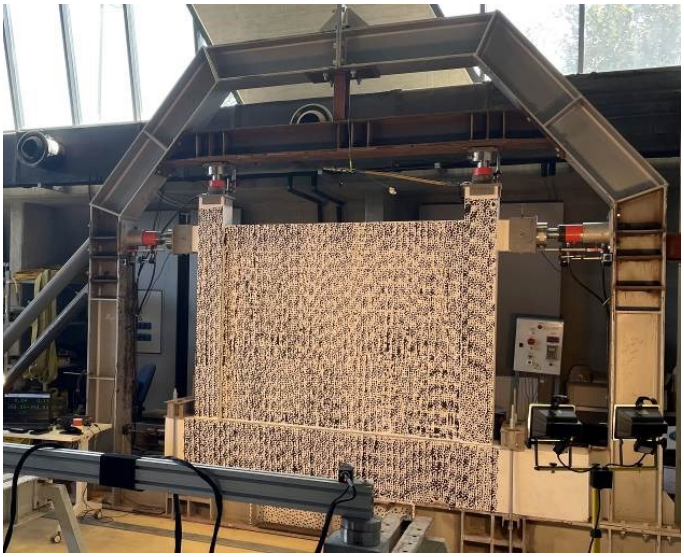


Figure 10. Test setup IP.

Copyright © 2025 CroCEE
DOI: https://doi.org/10.5592/CO/3CroCEE.2025.100

Push-Out Tests

Following each OoP test, push-out tests were performed to evaluate the residual shear capacity of the wall anchors. Load distribution was achieved through steel beams to concentrate forces on the joint interface.

5. Test Results

5.1. Out-of-Plane Tests

The OoP tests aimed to demonstrate the anchoring system's ability to restrain the infill wall under OoP loading while maintaining neutral or positive effects on IP load performance.

Displacement measurements from ARAMIS revealed minimal relative deformation at the column-infill joints (Figure 11). Crack patterns on the tension side (Figure 12) exhibited pronounced horizontal fractures in both concrete and masonry, with negligible vertical cracking, particularly in the joint areas. This suggests that the anchors effectively absorbed loads and maintained structural integrity.

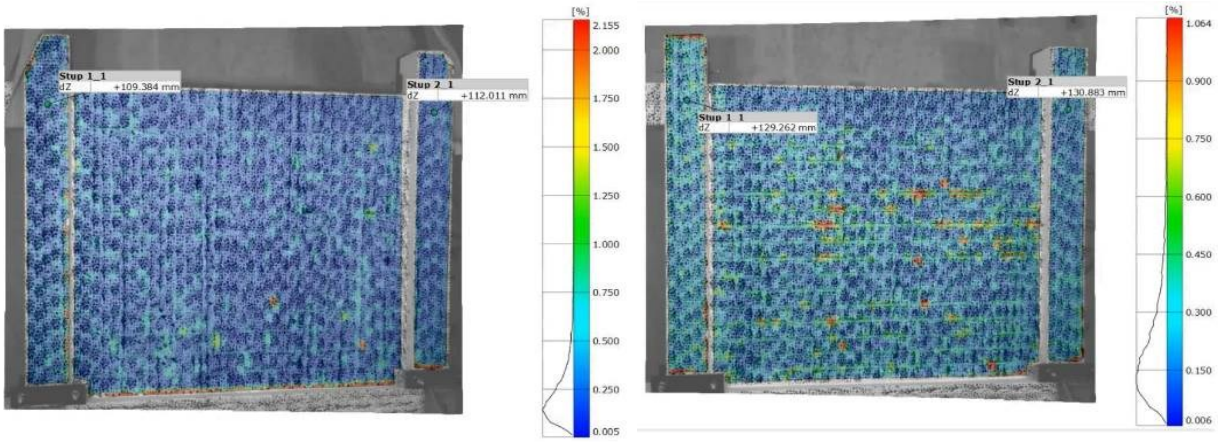


Figure 11. Displacements after OoP tests, a: block masonry, b: brick masonry.

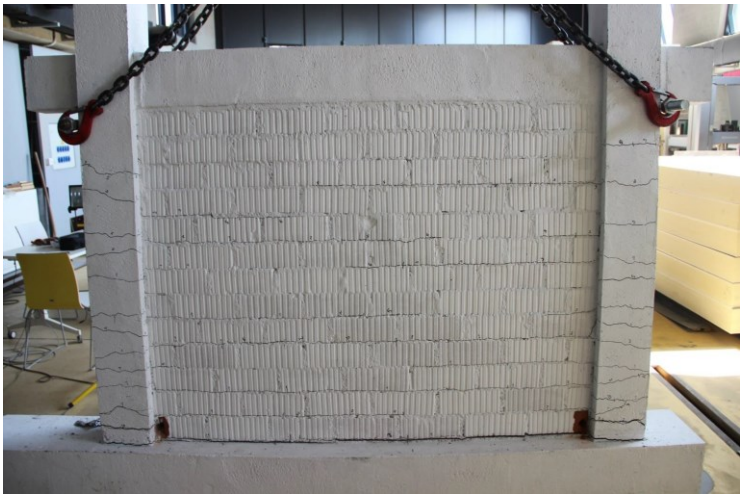
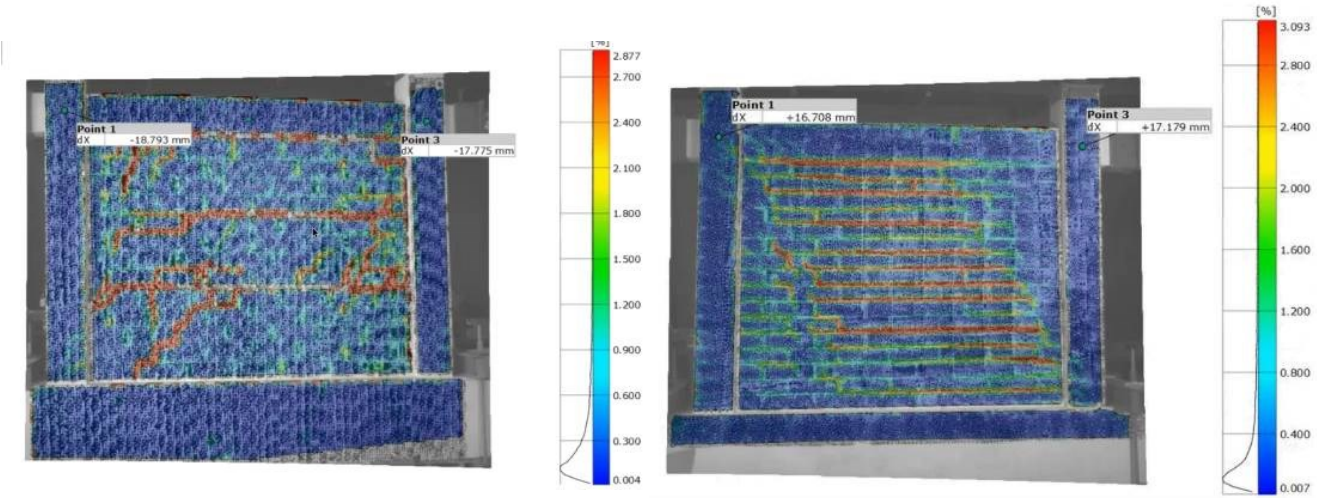


Figure 12. Crack pattern OoP.

Copyright © 2025 CroCEE
DOI: https://doi.org/10.5592/CO/3CroCEE.2025.100

5.2. In-Plane Tests

The IP tests exhibited typical load transfer behavior, with compression forces acting on the infill joints at the applied load side. Shear deformation induced horizontal cracking within the masonry joints, consistent with standard unreinforced masonry failure modes. Figure 13 illustrates displacement



profiles, while Figure 14 highlights final crack patterns.

Figure 13. Displacements after IP tests, a: block masonry, b: brick masonry.

Also in these tests, no relative displacements could be observed in the vertical joints between concrete and masonry. Figure 14 shows the final crack pattern with typical IP (shear) cracks occurring on masonry infills.

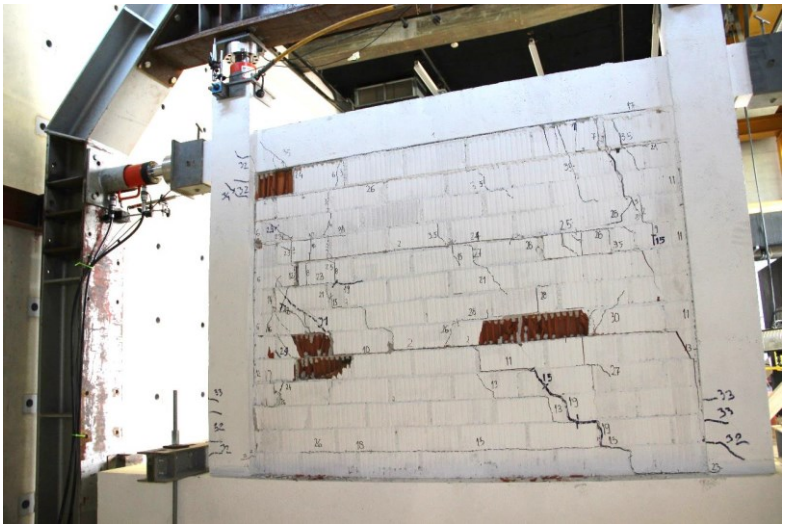


Figure 14. Final crack pattern, IP tests.

Finally, the joints were opened for anchor inspection. It could be observed that neither the anchors nor the channel section in the columns showed significant cracking or deformation during all IP tests.

No relative displacements were observed in the vertical joints between the RC frame and masonry. Post-test inspection revealed no damage to either the anchors or channel sections in the columns (Figure 15).

Proceedings of the 3rd Croatian Conference on Earthquake Engineering - 3CroCEE
19–22 March 2025, Split, Croatia
Copyright © 2025 CroCEE
DOI: https://doi.org/10.5592/CO/3CroCEE.2025.100



Figure 15. Final inspection of the anchors after removing bricks.

5.3. Push out tests.

After each OoP test, a push test was performed on each specimen. These tests were intended to test whether the previous loading has an influence on the horizontal shear capacity of the anchors, the focus here being on the reinforced joint and not on the infill itself. Therefore - instead of the in this case usual airbag test, in which the load is applied to the masonry via inflatable cushions - the load was applied linearly near the joints, see Figure 16. The load was applied with a hydraulic jack, distributed through steel beams so that it was introduced linearly near the column/masonry joint. As before, in the IP and OoP tests no influence of cracking on the vertical joint was observed, the push tests also showed no reduction in the shear strength of the anchors.

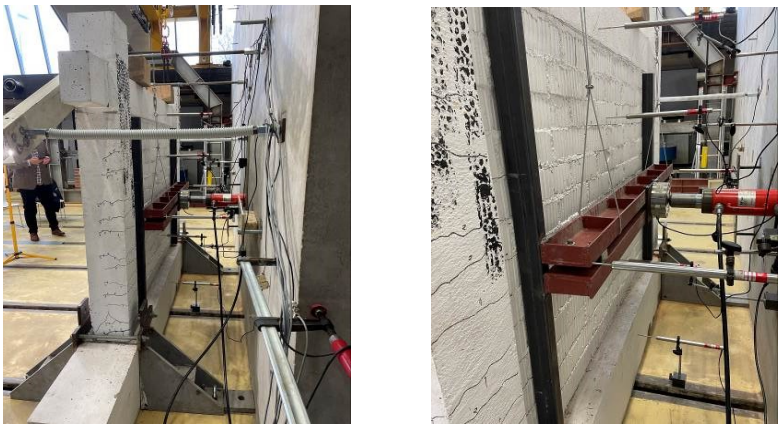


Figure 16. Test setup Push Out.

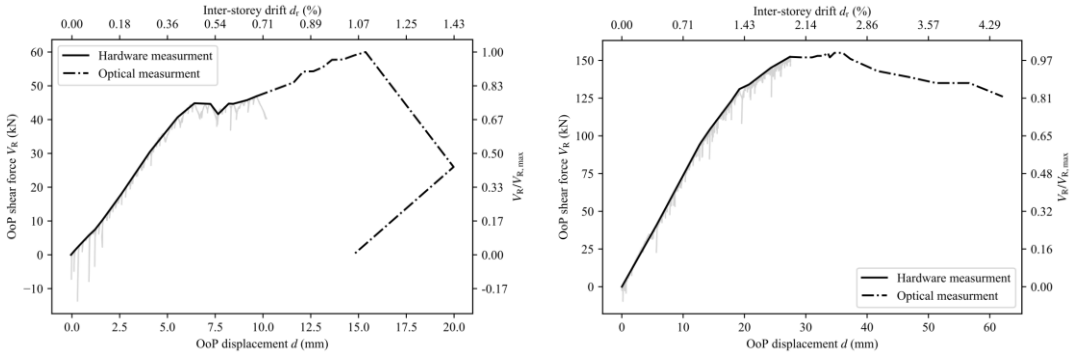


Figure 17. Final load/displacements at Push-Out test.

Proceedings of the 3rd Croatian Conference on Earthquake Engineering - 3CroCEE
19–22 March 2025, Split, Croatia
Copyright © 2025 CroCEE
DOI: https://doi.org/10.5592/CO/3CroCEE.2025.100

6. Summary

This study presents experimental evaluations of masonry infills secured with specialized anchors within RC frames, focusing on seismic load resistance. Tests were performed on masonry infills, placed in reinforced concrete frames, where the joints are secured by flat wall ties to improve the seismic resistance of such a construction. A description of the displacement tests in the IP and OoP directions is presented. For the IP and OoP tests, two sets of specimens with identical RC frames and different infills were used, one consisting of hollow blocks and the other of solid brick masonry.

In a first step, the fixing system, consisting of a channels profile and the flat anchors, were tested in accordance with EN 845 [3] and EN 846 [4] in order to determine the characteristic horizontal shear strength in the longitudinal and transverse directions in so-called micro tests. A distinction was made in these tests between cast-in channels and post-installed channels.

Large tests in a macro scale were carried out on reinforced concrete frames fitted with masonry infills, anchored to the concrete columns with ties. To ensure anchoring, cast-in anchor channels were installed in the concrete columns of the frame, in which the anchors were interlocked and embedded in the masonry joints.

Key findings include:

1. **Micro-scale tests** demonstrated the anchors' substantial horizontal shear capacity.
2. **Macro-scale OoP tests** showed that the anchors maintained the stability of the joint, with no or minimal relative deformation observed.
3. **Post-OoP push-out tests** confirmed that anchors retained full shear capacity, ensuring the system's resilience.

The results emphasise the usefulness of such anchoring systems when using RC frame infill assemblies in cohesive composite structures. It does not necessarily make a difference whether the infill participates in the load-bearing effect of the frame structure, as a shearwall and thus represents a structural element, or whether it is a partition wall without load-bearing effect, i.e. a non-structural element. The anchor system shown - consisting of a rail attached to the concrete and flat anchors that interlock with this rail - can be installed both during the construction of the concrete structure (cast-in) and subsequently (post-installed), e.g. as part of seismic retrofitting.

References

[1] Roik, M., Piesker, C. (2017). A concept for fixing "heavy" façades in seismic zones, *Proceedings of 16th World Conference on Earthquake Engineering*, Santiago de Chile, Chile.

[2] Roik, M., Piesker, C. (2019). Streamlining the Test Methods for Seismic Verification of Façade Anchors, *Fourth International Workshop on the Seismic Performance of Non-structural Elements (SPONSE)*, Pavia, Italy.

[3] CEN (2013). EN 845-1: 2013. Specification for ancillary components for masonry - Part 1: Wall ties, tension straps, hangers and brackets, Comité Européen de Normalisation, Brussels.

[4] CEN (2012). EN 846-7:2012. Methods of test for ancillary components for masonry - Part 7: Determination of shear load capacity and load displacement characteristics of shear ties and slip ties (couplet test for mortar joint connections), Comité Européen de Normalisation, Brussels.

[5] CEN (2010). EN 1998-1:2010. Eurocode 8: Design of structures for earthquake resistance - Part 1: General rules, seismic actions and rules for buildings, Comité Européen de Normalisation, Brussels.

[6] Sigmund V. and Penava D. (2014). Influence of openings, with and without confinement, on cyclic response of infilled R-C frames – An experimental study, *Journal of Earthquake Engineering*., Vol. **18**.

[7] Anić F., Penava D., Guljaš I., Sarhosis V., Abrahamczyk L. (2021). Out-of-plane Cyclic Response of Masonry Infilled RC Frames: An Experimental Study, *Engineering Structures*, Vol. **238**.

Proceedings of the 3rd Croatian Conference on Earthquake Engineering - 3CroCEE
19–22 March 2025, Split, Croatia
Copyright © 2025 CroCEE
DOI: https://doi.org/10.5592/CO/3CroCEE.2025.147

SEISMIC RETROFIT OF MASONRY WALLS USING REPOINTING WITH TRADITIONAL MORTAR AND POLYPROPYLENE STRIPS - TEST RESULTS

Festim ADEMI [(1)], Sergey CHURILOV [(2)], Enis JAKUPI [(3)], Elena DUMOVA - JOVANOSKA [(4)]

[(1)] *PhD student, Ss. Cyril and Methodius University in Skopje, Faculty of Civil Engineering, festim.ademi@unite.edu.mk*
[(2)] *Professor, Ss. Cyril and Methodius University in Skopje, Faculty of Civil Engineering Skopje, curilov@gf.ukim.edu.mk*
[(3)] *Professor, University of Tetovo, Faculty of Applied Sciences, enis.jakupi@unite.edu.mk*
[(4)] *Professor, Ss. Cyril and Methodius University in Skopje, Faculty of Civil Engineering Skopje, dumova@gf.ukim.edu.mk*

Abstract

Seismic strengthening of masonry structures through repointing is recognized as an effective and economical technique for increasing structural stability, especially in regions with high seismic activity. This paper presents results from a research program that includes laboratory tests of the mechanical properties of masonry and its components: bricks, mortar, and polypropylene strips. The aim of the research is to assess the effectiveness of repointing as a method for strengthening existing structures, ensuring greater resistance to compression and dynamic loads.

The results show that repointing, particularly when modern materials are used, significantly increases the compressive strength of masonry structures and their ability to withstand seismic forces. Additionally, this method contributes to preserving the integrity and long-term stability of important cultural and religious buildings, such as churches and mosques. These structures often carry immense historical, spiritual, and architectural significance, and repointing offers a practical solution for their seismic reinforcement, ensuring that they remain safe and enduring symbols of heritage.

Keywords: seismic strengthening, masonry structures, repointing, polypropylene strips, compressive strength, seismic resistance, cultural heritage conservation.

1. Introduction

Unreinforced masonry (URM) structures represent a significant portion of the global building stock, particularly in historic urban centres and cultural heritage sites [1, 2]. These structures, while demonstrating remarkable durability over centuries, exhibit characteristic vulnerabilities to seismic actions due to their low tensile and shear strengths, brittle behaviour, and poor ductility characteristics [2, 3]. The devastating consequences of recent earthquakes, such as the 2020 Zagreb earthquake and the 2023 Turkey-Syria earthquake, have highlighted the critical need for effective seismic strengthening solutions for URM buildings [4-6].

The seismic vulnerability of URM structures originates from several factors, such as the quality of construction materials, structural configuration, and connection details between structural elements [7-8]. During seismic events, these buildings typically exhibit in-plane and out-of-plane failure mechanisms, with damage patterns ranging from diagonal shear cracks to partial or complete collapse of wall elements [9-13]. The heterogeneous nature of masonry structures [14], combined with the degradation of material properties over time, further compounds these vulnerabilities [15-17].

Various strengthening techniques have been developed and implemented to enhance the seismic performance of URM structures. These methods can be broadly categorized into surface treatments, grout injections, external reinforcement, confining using RC ties [18, 19] and structural repointing techniques [19, 20]. Surface treatments, including fibre-reinforced polymer (FRP) applications and ferrocement overlays, primarily enhance the in-plane shear capacity [20-24] and out-of-plane bending resistance [25-26]. Grout injections improve the overall structural integrity by filling voids and cracks,

Proceedings of the 3rd Croatian Conference on Earthquake Engineering - 3CroCEE
19–22 March 2025, Split, Croatia
Copyright © 2025 CroCEE
DOI: https://doi.org/10.5592/CO/3CroCEE.2025.147

thereby increasing compressive strength and homogeneity of the masonry assembly [18, 27-29]. Structural repointing, while less commonly employed, offers advantages in terms of minimal intervention and preservation of architectural authenticity [19, 20, 30-32]. Moreover, structural repointing of masonry enhances structural integrity, by improving compressive and shear strength, enhances ductility, increases weather resistance and durability, and offers cost-effective maintenance while maintaining the building's historical character. Several studies have highlighted the advantages of this method, particularly when combined with innovative materials such as Fiber Reinforced Polymers (FRP). FRP rebars embedded into mortar joints, a technique called FRP Structural Repointing, significantly improved the shear and flexural capacity of hollow clay brick wallets and beams [33-35]. Research on Textile Reinforced Mortar (TRM) strengthening systems, including joint repointing with Near Surface Mounted (NSM) helical rebars, has shown increased in-plane lateral strength and displacement capacity as well as out-of-plane strength of masonry buildings, which are crucial parameters for seismic assessment [36, 37].

Recent advances in strengthening techniques have predominantly focused on modern materials and sophisticated application methods. However, these solutions may not be suitable for all contexts, particularly in regions with limited access to specialized materials or in cases where preservation requirements restrict the use of contemporary materials due to compatibility issues [38, 39]. Additionally, the high cost and technical complexity of modern strengthening systems can present significant barriers to implementation, especially in developing regions or rural areas [40-42].

This research addresses a gap in the current state of practice by investigating the effectiveness of a hybrid strengthening approach that combines traditional lime mortar with polypropylene strips for structural repointing. This method offers several potential advantages: it utilizes readily available materials, maintains compatibility with historic masonry, and can be implemented with basic technical skills. The approach is particularly relevant for situations where modern strengthening solutions are impractical due to economic, technical, or conservation constraints.

The study aims to quantify the improvement in mechanical properties and seismic resistance achieved through structural repointing strengthening technique, focusing specifically on compressive strength, shear capacity, and deformation characteristics. Through comprehensive laboratory testing and analysis, this research seeks to establish the viability of this alternative strengthening method and provide practical guidelines for its implementation in various contexts.

2. Experimental programme for testing the effects of repointing

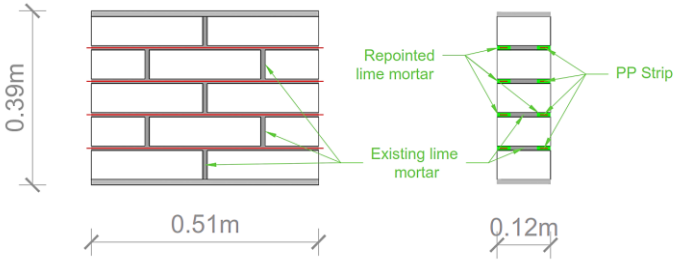
To evaluate the effects of repointing on the behaviour of bearing walls, an experimental program was designed and implemented. The program involved controlled laboratory testing of the bearing capacity of masonry structures with repointing applied in two distinct configurations. These configurations were selected to assess the influence of material properties and reinforcement orientation on structural performance. The repointing techniques tested included:

Strengthened masonry repointed with lime mortar and horizontally placed polypropylene strips: This configuration aims to enhance the tensile capacity of the masonry by introducing horizontal reinforcement to counteract lateral forces, Fig. 1a, Fig. 2a.

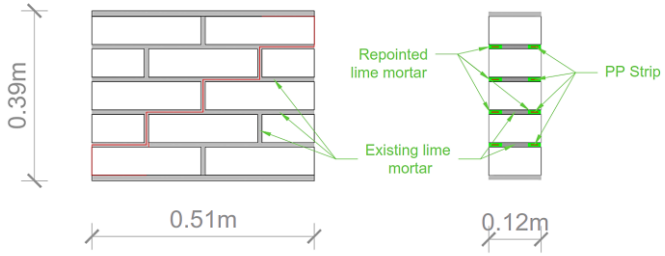
Strengthened masonry repointed with lime mortar and diagonally placed polypropylene strips: This arrangement provides multidirectional reinforcement, improving both shear resistance and the overall stability of the wall under dynamic and static loads, Fig. 1b, Fig. 2b.

Considering that masonry is a composite material, the experimental program was divided into three main phases: assessing the mechanical properties of its constituent materials (bricks and mortar), evaluating the compressive strength, and determining the shear strength of the masonry. To assess the effectiveness of the proposed repointing methods, the results from unreinforced masonry tests were used as baseline values. The following sections provide a concise overview of the tests conducted, the results obtained, and the corresponding conclusions drawn from the analysis.

Proceedings of the 3rd Croatian Conference on Earthquake Engineering - 3CroCEE
19–22 March 2025, Split, Croatia
Copyright © 2025 CroCEE
DOI: https://doi.org/10.5592/CO/3CroCEE.2025.147

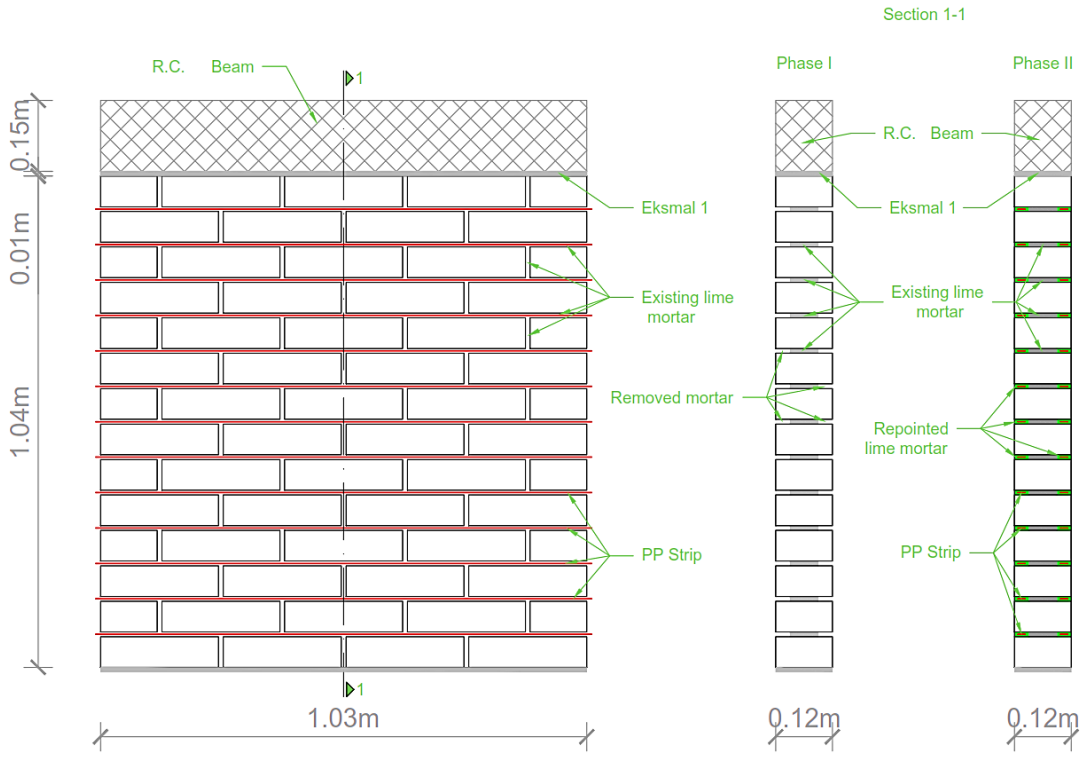


a) Horizontal PP strip and repointing (WS1_AP)



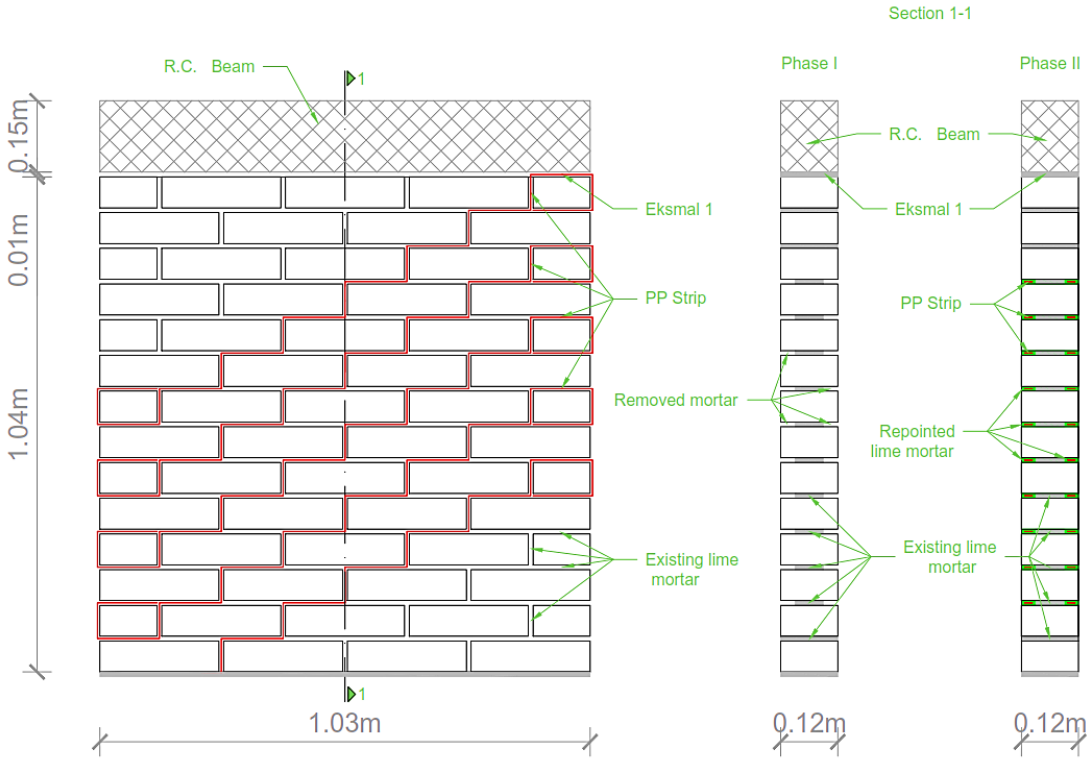
b) Diagonal PP strip and repointing (WS2_AP)

Figure 1. Specimens for compressive strength tests



a) Horizontal PP strip and repointing (WS1_SS)

Copyright © 2025 CroCEE
DOI: https://doi.org/10.5592/CO/3CroCEE.2025.147



b) Diagonal PP strip and repointing (WS2_SS)

Figure 2. Specimens for shear strength tests

2.1. Test of Constituent Materials

Tests on constituent materials are a crucial step in evaluating their durability and suitability for use in engineering structures. The mechanical and physical properties of the materials are determined through various tests, allowing for an analysis of their behaviour under different loads. The research presented involved testing solid clay bricks, mortars, and polypropylene strips to gather data on their strength, density, water absorption, and other characteristics essential for optimizing structural systems and enhancing the safety of structures. Table 1 presents the mechanical properties of the constituent materials obtained from these tests.

2.2. Tests on Masonry as Constituent Material

For the purposes of the investigation, two specialized setups were developed. These setups were designed to test the compressive strength and shear strength of masonry. They enabled precise and controlled analysis of various types of walls, including unreinforced and strengthened structures, to define their mechanical properties and behaviour under different loads. This provided a basis for comparing the results and optimizing strengthening methods in engineering practice.

Table 1. Mechanical characteristics of constituent materials.

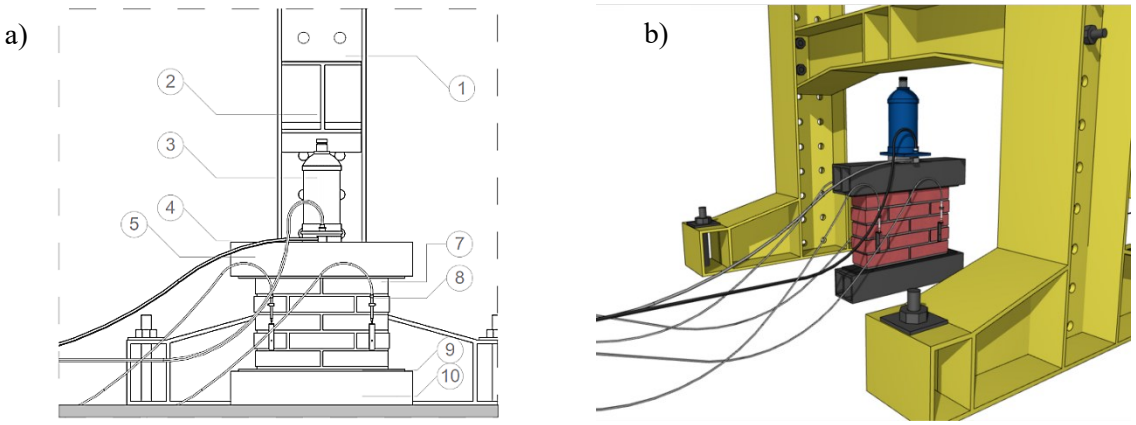
Material	**Density** γ_d (kg/m^3)	**Compressive strength** $f_{m,comp}$ (MPa)	**Flexural tensile strength** $f_{m,flex}$ (MPa)
Clay brick	1750.5	9.54	2.05
Lime mortar		0.73	0.42

Copyright © 2025 CroCEE
DOI: https://doi.org/10.5592/CO/3CroCEE.2025.147

2.2.1. Setup for testing compressive strength of masonry

The compressive strength test was conducted using a custom-built setup consisting of two steel columns firmly anchored to a reinforced concrete floor with steel bolts. These columns were interconnected at the top by a steel beam ("I 160"), providing structural stability and serving as a support frame for the hydraulic actuator, as shown in Fig. 3. The test wall was positioned between the steel columns under a second steel beam ("I 300"), separated by a 10 mm thick rubber layer to ensure uniform contact and force distribution. An additional rubber layer and a steel beam ("I 160") were placed on top of the wall to evenly distribute the applied load to the load cell connected to the hydraulic actuator.

It is important to note that the "I 300" and "I 160" beams, along with the steel columns, form a rigid frame, ensuring that these profiles are aligned and positioned above the test wall. This configuration functions as a stable support structure for the hydraulic actuator, enabling precise compressive strength measurements in a controlled laboratory environment.



1: Steel column
2: Steel beam
3: Force hydraulic actuator
4: Load cell
5: Steel beam "I 160"
6: Rubber pad (10 mm)
7: URM Wall
8: Displacement transducer
9: Rubber pad (10 mm)
10: Steel beam "I 300"

Figure 3. a) Setup for compressive strength testing; b) 3D view of the test setup

This specialized setup enabled precise testing of masonry under compressive stress by minimizing external influences and ensuring controlled conditions for measuring compressive strength. The compressive strength tests conducted on various types of walls using this setup provided accurate and representative results under strictly controlled laboratory conditions. The configuration, which included fixed steel columns and beams along with rubber layers to improve contact and friction, effectively eliminated unwanted movements or deformations that could compromise the testing process.

The construction and positioning of the walls were meticulously executed to ensure their stability and central alignment, facilitating an even distribution of the applied load. The use of a hydraulic press and a load cell allowed for precise control of applied forces and displacements throughout the entire testing process. This setup proved to be an efficient method for testing walls. The introduction of various reinforcement techniques, such as polypropylene (PP) strips and different types of mortar, provided additional data for optimizing the mechanical properties of masonry.

2.2.2. Setup for testing shear strength of masonry

The experimental setup for shear strength testing comprised four steel columns securely anchored to a reinforced concrete floor, interconnected with steel beams to form a rigid frame. The test walls were positioned on a steel beam ("I 200") and stabilized by a reinforced concrete beam. Rubber layers, 10 mm in thickness, were placed at critical contact points to enhance load distribution and minimize localized stress concentrations. Horizontal force was applied using a hydraulic actuator, which transmitted the force to the walls through roller bearings, as depicted in Fig. 4.

Copyright © 2025 CroCEE
DOI: https://doi.org/10.5592/CO/3CroCEE.2025.147

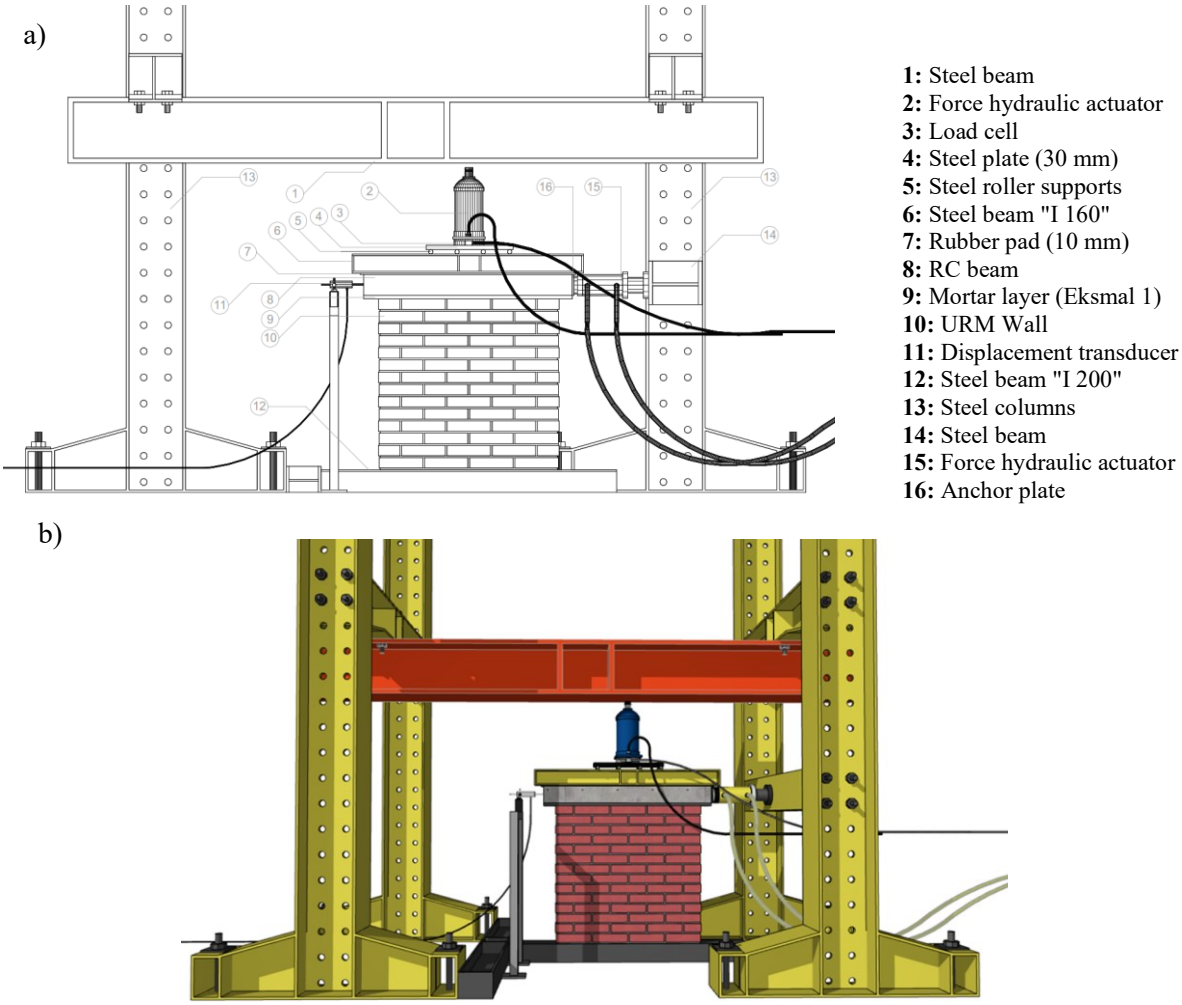


Figure 4. a) Setup for shear strength testing; b) 3D view of the test setup

To facilitate precise measurement of displacements induced by horizontal loading, a displacement transducer was installed. The wall was supported by the I 200 steel beam, ensuring it remained stationary during testing. The horizontal load was applied on the top RC beam. The horizontal force at the base of the specimen was not directly monitored, as the wall base was securely fixed to prevent any displacement. This configuration was specifically designed to accurately assess the transfer and distribution of horizontal forces through the upper portion of the wall, while maintaining stability and eliminating any unintended movement at the base. The testing platform designed for shear strength assessment enabled precise and controlled measurement of the performance of various types of walls. Accurate positioning of the walls, the use of roller supports for the transfer of horizontal forces, and the measurement of displacement with a displacement transducer ensured the reliability of the obtained results. This methodology facilitated the comparison between the shear strength of non-reinforced and reinforced walls, providing data that serves as a valuable contribution to the development of engineering practice. The results also support the optimization of construction materials and structural designs.

These two setups enabled precise and controlled assessment of the performance of different types of walls, including unreinforced and strengthened structures. The comprehensive data collected from these experiments provided valuable insights into the mechanical properties and behaviour of masonry under various loading conditions. This information is instrumental in developing advanced engineering solutions for retrofitting and strengthening existing structures, as well as optimizing the design of new masonry systems to enhance their durability, safety, and resilience against seismic and other dynamic forces.

Copyright © 2025 CroCEE
DOI: https://doi.org/10.5592/CO/3CroCEE.2025.147

2.3. Specimens for testing the compressive strength of masonry

As part of the investigation into the mechanical properties of masonry, several wall specimens were tested to determine their compressive strength, Fig. 5. The specimens consisted of 10 clay bricks and lime mortar, functioning as a composite material. The dimensions of the bricks were 250 x 120 x 60 mm, while the walls measured 510 x 390 x 120 mm. Six walls were tested in total, divided into three categories with two specimens in each category: unreinforced walls, walls strengthened with lime mortar and horizontally placed PP strips, and walls strengthened with lime mortar with diagonally placed PP strips.

a) b)

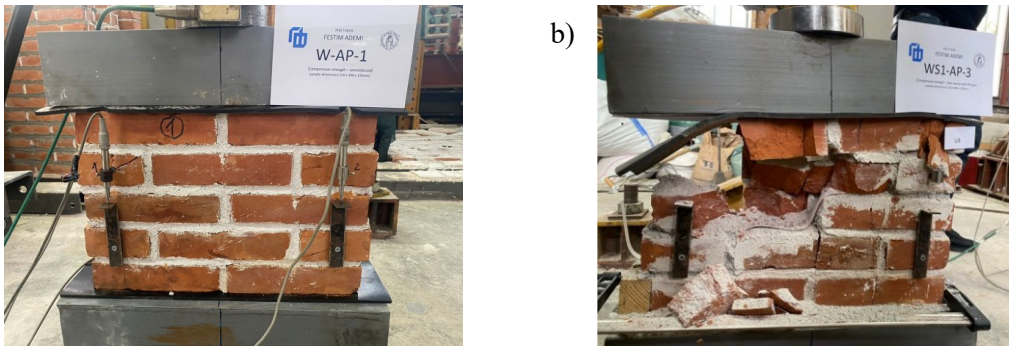


Figure 5. a) Testing the compressive strength of URM specimen; b) Failure mechanism of WS1_AP specimen

2.4. Specimens for testing the shear strength of masonry

As part of the investigation into the mechanical properties of masonry, shear strength tests were conducted in addition to compressive strength tests. Each wall was composed of 56 clay bricks and lime mortar, with brick dimensions 250 x 120 x 60 mm, while the test specimens measured 1030 x 1040 x 120 mm, Fig. 6. A total of six walls were tested, divided into three categories with two specimens in each: unreinforced walls, walls strengthened with lime mortar and horizontally placed PP strips, and walls strengthened with diagonally placed PP strips.

a) б)

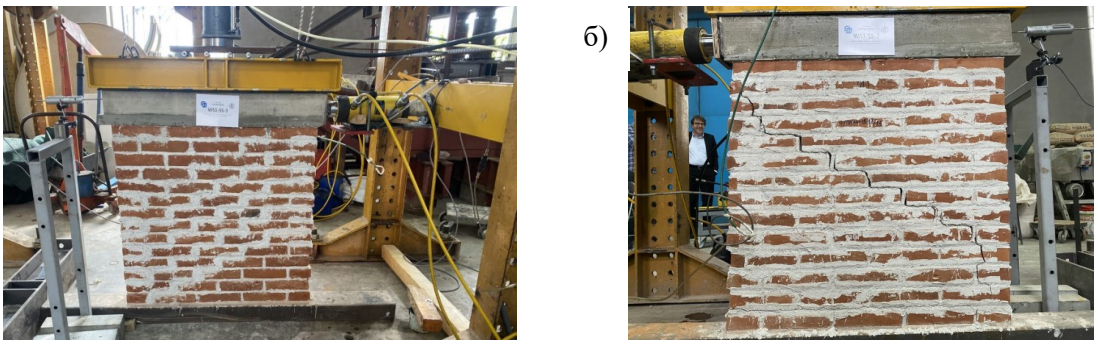


Figure 6. Testing of shear strength of masonry, a) Initial stage b) Failure mechanism

3. Results from experimental tests and discussion

The results from the compressive and shear strength tests of masonry structures provided a comprehensive understanding of the mechanical properties of various types of walls. The experimental findings revealed significant improvements in both compressive and shear strength when masonry walls were strengthened using repointing techniques with lime mortar and polypropylene (PP) strips. The effectiveness of these strengthening methods varied based on the orientation of the strips and the applied loading conditions. Applied force and displacement relationship shown the structural responses of the walls. These results provide valuable insights into the effectiveness of strengthening techniques and their contribution to enhancing the structural stability of masonry walls under both static and dynamic forces.

Copyright © 2025 CroCEE
DOI: https://doi.org/10.5592/CO/3CroCEE.2025.147

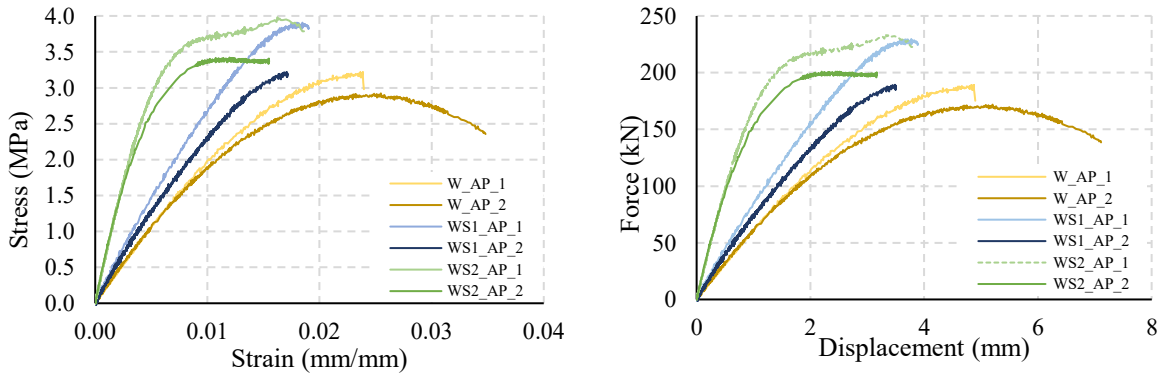
3.1. Compressive Strength of Masonry

The results of the compressive strength tests provide valuable insights into the behaviour of masonry under axial loads. These findings are presented through diagrams and tables, illustrating the force-displacement relationships, peak load capacities, and performance differences between unreinforced and strengthened walls, Fig. 7. The graphical and tabular data serve as a basis for analysing the effectiveness of the applied strengthening techniques and their impact on the structural stability of masonry walls.

For compressive strength, both strengthening configurations showed notable improvements, with diagonal PP strip placement (WS2_AP) yielding slightly better results than horizontal placement (WS1_AP). For WS1_AP, strengthening with lime mortar and PP strips in horizontal joints resulted in an increase in maximum strength by 16.1% and final strength by 31.9%, accompanied by a decrease in displacements of 27.6% and 38.5%. For WS2_AP, the diagonal placement of the PP strips led to an increase in maximum strength by 20.6% and final strength by 34.1, as presented in Table 2. This suggests that the strengthening technique effectively enhances not just peak strength but also post-peak behaviour and ductility. The tests revealed impressive results in reducing wall strain. Diagonal PP strips performed exceptionally well, cutting peak strain by 42.5% and ultimate strain by 41.9%. In comparison, horizontal strips achieved smaller but still significant reductions of 27.6% and 38.5%. These improvements mean the strengthened walls resist displacement much better under axial pressure.

3.2.Shear Strength of Masonry

The results of the shear strength tests offer detailed insights into the performance of masonry under lateral forces. These findings are presented in diagrams and tables, highlighting the force- displacement behaviour, peak shear capacities, and comparative effectiveness of the applied strengthening techniques, Fig. 8. The data provide a clear basis for evaluating the improvements in shear resistance and overall stability of masonry structures, especially under dynamic loading conditions.



a) Shear stress - strain diagram

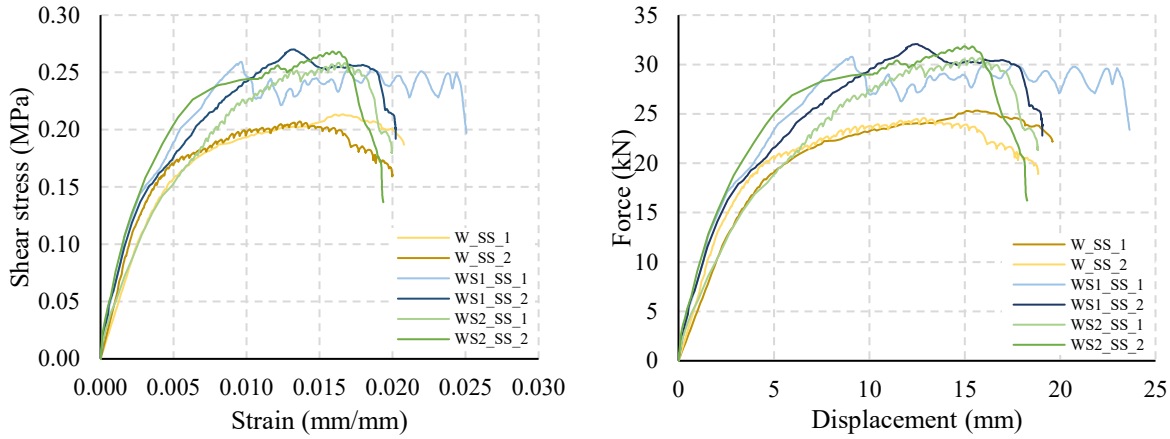
b) Force - displacement diagram

Figure 7. Compressive strength diagrams for URM (W_AP) and strengthened walls (WS1_AP and WS2_AP)

Table 2. Maximum stress and strain at compression for different types of walls

Mean Percentage difference	**Peak compressive stress, $f_{mas,test}$**	Peak stress increase (%)	**Ultimate compressive stress, $f_{mas,ult}$**	Ultimate stress increase (%)	**Peak strain, ε_{max}**	Peak strain decrease (%)	**Ultimate strain, ε_{ult}**	Ultimate strain decrease (%)
W_AP	3.07	0.0%	2.67	0.0%	0.0246	0.0%	0.0294	0.0%
WS1_AP	3.56	16.1%	3.52	31.9%	0.0178	-27.6%	0.0181	-38.5%
WS2_AP	3.70	20.6%	3.58	34.1%	0.0141	-42.5%	0.0171	-41.9%

Copyright © 2025 CroCEE
DOI: https://doi.org/10.5592/CO/3CroCEE.2025.147



a) Shear stress - strain diagram

b) Force - displacement diagram

Figure 8. Shear strength diagrams for URM (W_SS) and strengthened walls (WS1_SS and WS2_SS)

Table 3. Maximum stress and strain at shear for different types of walls

Mean Percentage difference	Peak shear stress, $f_{mas,test}$	Peak shear stress increase (%)	Peak shear strain, ε_{max}	Peak shear strain decrease (%)
W_SS	0.210	0.0%	0.0151	0.0%
WS1_SS	0.265	25.9%	0.0114	-24.5%
WS2_SS	0.263	25.3%	0.0161	6.3%

W_SS_1 and W_SS_2, the unreinforced walls, served as the baseline for comparison. In this case, both strip layouts worked similarly well. Horizontal strips increased the peak shear stress by 25.9%, just slightly better than diagonal strips at 25.3%. However, an interesting difference were noted in how the walls deformed. Horizontal strips reduced shear strain by 24.5%, while diagonal strips actually led to a small increase of the peak shear strain by 6.3%, Table 3. This suggests that horizontal strips may be more effective in controlling lateral deformations, even though both methods effectively strengthen the wall. The force-displacement relationships shown in Figure 8 indicates more stable post-peak behaviour in strengthened specimens compared to unreinforced walls, suggesting improved energy dissipation capacity. This is particularly important for earthquake resistance, as it shows the strengthened walls can better absorb and dissipate energy during repeated (cyclic) shaking.

It is important to emphasize that all graphical and tabular results pertaining to both compressive and shear strength tests are comprehensively presented within this chapter. These visual representations and data tables serve to convey crucial experimental findings, supporting a scientific evaluation of the performance enhancements achieved through the applied strengthening methods. The detailed analysis highlights not only the improvements in peak strength and post-peak response but also the impact on critical structural properties such as deformation capacity, ductility, and load transfer efficiency.

This holistic presentation of results contributes significantly to the scientific understanding of masonry behaviour under different load conditions, thereby offering valuable insights for optimizing structural reinforcement strategies in engineering practice.

4. Conclusions

The experimental investigations confirmed that the application of different techniques for strengthening with structural repointing significantly improved the mechanical characteristics of masonry, particularly in terms of its compressive and shear strength. The experiments were conducted at the Laboratory of the Faculty of Civil Engineering at Ss. Cyril and Methodius University in Skopje, North Macedonia, providing a controlled environment for reliable results. The unreinforced walls were used as a reference

Copyright © 2025 CroCEE
DOI: https://doi.org/10.5592/CO/3CroCEE.2025.147

point for assessing the effectiveness of various strengthening techniques. The structural repointing strengthening technique using lime mortar and PP strips significantly enhances both compressive and shear strength of masonry walls. Compressive strength improvements reached up to 20.6% for maximum strength and 34.1% for ultimate strength, while shear strength increased by approximately 25% for both strengthening configurations. The orientation of PP strips influences the mechanical behaviour differently under various loading conditions. Diagonal placement proves more effective for compressive strength enhancement, while horizontal placement shows slightly better performance in shear strength improvement and displacement control, although in both tests the PP strips were effectively loop-tied in the neighbouring mortar joints. Both strengthening configurations greatly reduce displacements under compressive loading, with diagonal placement achieving up to 42.5% reduction in peak strain. This indicates significantly improved structural stiffness and stability. Moreover, The strengthening demonstrated particular effectiveness in enhancing post-peak behaviour and ductility, crucial characteristics for seismic performance. This is evidenced by the improved ultimate stress values and more stable force- displacement relationships in strengthened specimens.

These findings demonstrate the effectiveness of the applied strengthening methods in enhancing the structural stability of masonry walls. The outcomes of these experiments underline the importance of selecting and applying appropriate strengthening techniques to significantly enhance the bearing capacity, stability, and resistance of masonry structures, especially in seismically active regions. The use of horizontally placed PP strips was identified as a particularly effective solution, providing notable improvements in load-bearing capacity, deformation resistance, overall safety and cost-benefit efficiency. This methodology represents a significant contribution to engineering practice, with practical applications in the design and advancement of structures in high seismic risk zones and a validates a viable solution for improving the seismic resistance of masonry structures, particularly valuable for historical buildings where preservation of architectural authenticity is crucial. The use of traditional materials (lime mortar) combined with modern elements (PP strips) offers an effective compromise between structural enhancement and conservation requirements. Future research could focus on investigating the long-term durability of these strengthening techniques, their performance under cyclic loading conditions and to explore the contemporary applications and adaptations of established methodological frameworks within modern contexts.

Acknowledgements

The authors would like to express their sincere gratitude to several individuals who played crucial roles in the successful completion of this research. First, we want to thank Mr. Borce Jovik, our lab's backbone. His expertise made our experimental tests possible, and his guidance kept us on track throughout the process. We are also deeply grateful to Prof. Toni Arangjelovski who significantly enhanced the quality of our research methodology and analysis. Special appreciation goes to assist. MSc Dejan Janev for helping with the measurements and data collection. A special shoutout goes to the students Marko Gjorgjioski and Petar Janev, for their tireless assistance and valuable input during the experimental phase of the study.

References

[1] Tomaževič, M. (2000): Seismic Rehabilitation of Existing Masonry Buildings. *GRAĐEVINAR*, **52** (11), 683-693, http://www.casopis-gradjevinar.hr/assets/Uploads/JCE-52-2000-11-06.pdf.

[2] D'Ayala, D., Speranza, E. (2003): Definition of Collapse Mechanisms and Seismic Vulnerability of Historic Masonry Buildings. *Earthquake Spectra*, **19** (3), 479-509. doi: https://doi.org/10.1193/1.1599896.

[3] Lourenço, P. B., Mendes, N., Ramos, L. F., Oliveira, D. V. (2011): Analysis of Masonry Structures Without Box Behavior. *International Journal of Architectural Heritage*, ***5*** (4–5), 369–382. doi: https://doi.org/10.1080/15583058.2010.528824.

[4] Markušić, S., Stanko, D., Penava, D., Ivančić I., Bjelotomić Oršulić, O., Korbar, T., Sarhosis, V. (2021): Destructive M6.2 Petrinja Earthquake (Croatia) in 2020 - Preliminary Multidisciplinary Research. *Remote Sensing*, **13** (5), 1095, doi: https://doi.org/10.3390/rs13061095.

Copyright © 2025 CroCEE
DOI: https://doi.org/10.5592/CO/3CroCEE.2025.147

[5] Radnić, J., Grgić, N., Buzov, A., Banović, I., Smilović Zulim, M., Baloević, G., Sunara, M. (2021): Mw 6.4 Petrinja earthquake in Croatia: Main earthquake parameters, impact on buildings and recommendation for their structural strengthening. *GRAĐEVINAR*, **73** (11), 1109-1128, doi: https://doi.org/10.14256/JCE.3243.2021.

[6] Işık, E., Avcil, F., Büyüksaraç, A., İzol, R., Arslan, M.H., Aksoylu, S., Harirchian, E., Eyisüren, O., Arkan, E., Güngür, M.Ş., Günay, M., Ulutaş, H. (2023): Structural damages in masonry buildings in Adıyaman during the Kahramanmaraş (Turkiye) earthquakes (Mw 7.7 and Mw 7.6) on 06 February 2023. *Engineering Failure Analysis*, 151, doi: https://doi.org/10.1016/j.engfailanal.2023.107405.

[7] Sansoni, C. (2021): *Seismic Vulnerability Assessment of Existing URM Structures through a Simplified Analytical Method*. PhD thesis, Sapienza University of Rome, Department of Geotechnical and Structural Engineering.

[8] Koc, A. B., Erberik, M. A., Askan, A., & Karimzadeh, S. (2023): The Sensitivity of Global Structural Parameters for Unreinforced Masonry Buildings Subjected to Simulated Ground Motions. *Buildings*, **13** (8), 2060, doi: https://doi.org/10.3390/buildings13082060.

[9] Gonçalves, M., Ponte, M., & Bento, R. (2024): Seismic Assessment of Existing Masonry Buildings Using Damage Mechanics. *Buildings*, ***14*** (8), 2395, doi: https://doi.org/10.3390/buildings14082395.

[10] Deneko, E., Bilgin, H. (2024): Observed failure modes in existing URM buildings after November 26, 2019 earthquake in Albania. *Research on Engineering Structures & Materials*, **10** (3), 1085-1107, doi: http://dx.doi.org/10.17515/resm2024.106ea1202rs.

[11] Patel, K.P., Dubey, R.N. (2024): Effect of in-plane damage on the out-of-plane strength of masonry walls with openings. *Structures*, **65**, 106708, doi: https://doi.org/10.1016/j.istruc.2024.106708.

[12] Menon, A., Magenes, G. (2008): Out-of-Plane Seismic Response of Unreinforced Masonry. *Research Report No. ROSE-2008/04*, ROSE School, EUCENTRE, Pavia, Italy.

[13] Barbieri, G., Biolzi, L., Bocciarelli, M., Fregonese, L., and Frigeri, A. (2013): Assessing the seismic vulnerability of a historical building. *Engineering Structures*, 57, 523–535, doi: https://doi.org/10.1016/j.engstruct.2013.09.045.

[14] Scamardo, M., Zucca, M., Crespi, P., Longarini, N., Cattaneo, S. (2022): Seismic Vulnerability Evaluation of a Historical Masonry Tower: Comparison between Different Approaches. *Applied Sciences*, **12**, 11254, doi: https://doi.org/10.3390/app122111254.

[15] Binda, L., Saisi, A., Tiraboschi, C. (2000): Investigation procedures for the diagnosis of historic masonries. *Construction and Building Materials*, **14** (4), 199-233, doi: https://doi.org/10.1016/S0950-0618(00)00018-0.

[16] Miedziałowski, C., Walendziuk, A. (2023): Description of Material Properties of Degraded and Damaged Segments of Multi-Leaf Masonry in Analyses of Large Three-Dimensional Structures. *Materials*, ***16*** (11), 4076, https://doi.org/10.3390/ma16114076.

[17] Ceroni, F., Pecce, M., Sica, S., & Garofano, A. (2012): Assessment of Seismic Vulnerability of a Historical Masonry Building. *Buildings*, ***2*** (3), 332-358, doi: https://doi.org/10.3390/buildings2030332.

[18] ElGawady, M., Lestuzzi, P., Badoux, M. (2004): A Review of Conventional Seismic Retrofitting Techniques for URM, *13th International Brick and Block Masonry Conference*, July 4-7, Amsterdam, Nederlands.

[19] Tomaževič, M. (1999): *Earthquake-resistant design of masonry buildings*. Series on Innovation in Structures and Construction: Volume 1, Imperial College press, doi: https://doi.org/10.1142/p055.

[20] Churilov, S., Dumova-Jovanoska, E., Shendova, V., Krstevska, L., Damchevski, B., Janchev, D. (2024): Experimental investigation on masonry structural joint repointing with cement-polymer mortar and polypropylene strips, *GRAĐEVINAR,* **76** (7), 607-620, doi: https://doi.org/10.14256/JCE.3893.2023.

[21] Kałuża, M. (2022): Experimental Analysis of Surface Application of Fiber-Reinforced Polymer Composite on Shear Behavior of Masonry Walls Made of Autoclaved Concrete Blocks. *Buildings*, **12**, 2208, doi: https://doi.org/10.3390/buildings12122208.

[22] Di Tommaso, A., Focacci, F., Micelli, F. (2017): Strengthening Historical Masonry with FRP or FRCM: Trends in Design Approach. *Key Engineering Materials*, **747**, 166–173, doi: https://doi.org/10.4028/www.scientific.net/KEM.747.166.

Copyright © 2025 CroCEE
DOI: https://doi.org/10.5592/CO/3CroCEE.2025.147

[23] Incerti, A., Ferretti, F., Mazzoti, C. (2019): FRCM strengthening systems efficiency on the shear behavior of pre-damaged masonry panels: An experimental study. *Journal of Building Pathology and Rehabilitation*, **4** (14), doi: https://doi.org/10.1007/s41024-019-0053-9.

[24] Hung, C.C, Dai, Y.X., Yen, C.H., Mosalam, K.M. (2024): Comparative studies on in-plane shear behavior of masonry wallettes retrofitted with mortar, UHPC, and ECC ferrocement: Shotcrete and prefabricated panels. *Case Studies in Construction Materials*, **21**, e03801, doi: https://doi.org/10.1016/j.cscm.2024.e03801.

[25] Chen, S. P. (2010): Out-of-Plane Behavior of Masonry Walls Strengthened with Ferrocement. *Advanced Materials Research*, **163–167**, 3545–3550, doi: https://doi.org/10.4028/www.scientific.net/amr.163-167.3545.

[26] Joyklad, P., Ali, N., Verre, S., Magbool, H.M., Elnemr, A., Qureshi, M.I., Hussain, Q., Chaiyasarn, K. (2021): Experimental Study on the Out-of-Plane Behavior of Brick Masonry Walls Strengthened with Mortar and Wire Mesh: A Pioneer Study. *Infrastructures*, 6 (11), 165, doi: https://doi.org/10.3390/infrastructures6110165.

[27] Harvey Jr., D.W., Schuller, M.P., Ruth, W.T. (2012): Internal Strengthening of Historic Clay Brick Masonry Pump Houses in New Orleans, *8th International Conference on Structural Analsyis of Historical Constructions-SAHC 2012*, October 15-17, Wroclaw, Poland.

[28] Oliveira, D.V., Silva, R.A., Garbin, E., Lourenço, P.B. (2012): Strengthening of three-leaf stone masonry walls: an experimental research. *Materials and Structures*, 45 (8), 1259–76. doi: https://doi.org/10.1617/s11527-012-9832-3.

[29] Luso, E., Lourenço, P. B. (2016): Experimental characterization of commercial lime based grouts for stone masonry consolidation. *Construction and Building Materials*, 102 (1), 216-225, doi: https://doi.org/10.1016/j.conbuildmat.2015.10.096.

[30] Damchevski, B., Churilov, S., Dumova-Jovanoska, E. (2018): Mechanical characterisation of polymer fibre-reinforced cement-based mortar for masonry joint repointing, *16th European Conference on Earthquake Engineering*, Thessaloniki, Greece.

[31] Saad, Z.A., Bataineh, M. (2021): Preventive preservation approach for the preservation of unique early neolithic architectural remains of the archaeological site of Beidha-Jordan. *International Journal of Conservation Science*, **12** (2), 493-506, ISSN: 2067-533X.

[32] Kocić, N., Krasić, S., Tomić, J., & Mitrović, I. (2024): Assessment of protective structures for architectural heritage: Case study of Pompeii, Lepenski Vir and Gobekli Tepe. *Journal of the Faculty of Civil Engineering and Architecture*, **39**, doi: https://doi.org/10.62683/ZRGAF39.91-102.

[33] Tinazzi, D., Modena C., Nanni A. (2000): FRP-Structural Repointing of Masonry Assemblages, *3rd International Conference on Advanced Composite Materials in Bridges and Structures*, Ottawa, Canada.

[34] Tumialan, J.G., Micelli, F., Nanni, A. (2001): Strengthening of Masonry Structures with FRP Composites. *Structures 2001: A Structural Engineering Odyssey*, 1-8, doi: https://doi.org/10.1061/40558(2001)130.

[35] Tumialan, J.G., Nanni, A. (2002): Strengthening of Masonry Walls with FRP Bars. *Composites Fabricator Magazine*, Arlington, VA.

[36] Ramonda, L.G. (2020): *Seismic retrofit of masonry with innovative materials for strengthening and repair*. PhD thesis, Universitat Politècnica de Catalunya, Barcelona Tech.

[37] Boem, I. (2022): Masonry Elements Strengthened with TRM: A Review of Experimental, Design and Numerical Methods. *Buildings*, **12**, 1307, doi: https://doi.org/10.3390/buildings12091307.

[38] Binda, L., Penazzi, D., Valluzi, M.R., Cardani, G., Baronio, G., Modena, C. (2000): Behaviour of historic masonry buildings in seismic areas: Lessons learned from the Umbria-Marche earthquake, *12th International Brick/Block Masonry Conference*, Madrid, Spain.

[39] Penazzi, D., Valluzi, M.R., Saisi, A., Binda, L., Modena, C. (2001): Repair and strengthening of historic masonry buildings in seismic areas. International Congress, more than Two Thousand Years in the History of Architecture Safeguarding the Structure of Our Architectural Heritage, Bethlehem, Palestine 10-12 December, Paris: International Council on Monuments and Sites. Vol. 2, Section V, 1-7.

Copyright © 2025 CroCEE
DOI: https://doi.org/10.5592/CO/3CroCEE.2025.147

[40] Shrestha, H., Pradhan, S., Guragain, R. (2012): Experiences on Retrofitting of Low Strength Masonry Buildings by Different Retrofitting Techniques in Nepal, *15th World Conference on Earthquake Engineering*, Lisbon, Portugal.

[41] Ali, A., Mandal, P., Swailes, T. (2016): Strengthening Masonry for Seismic Actions in Developing Communities, *MACE PGR Conference*, University of Manchester, UK.

[42] Tsiavos, A., Sextos, A., Stavridis, A., Dietz, M., Dihoru, L., Di Michele, F., Alexander, N.A. (2021): Low-cost hybrid design of masonry structures for developing countries: Shaking table tests. *Soil Dynamics and Earthquake Engineering*, **146**, 106675, doi: https://doi.org/10.1016/j.soildyn.2021.106675.

Proceedings of the 3rd Croatian Conference on Earthquake Engineering - 3CroCEE
19–22 March 2025, Split, Croatia
Copyright © 2025 CroCEE
DOI: https://doi.org/10.5592/CO/3CroCEE.2025.151

BASE ISOLATION OF AN EXISTING REINFORCED CONCRETE BUILDING

Krešimir Todorić [(1)], Mario Uroš [(2)]

[(1)] *Structural Engineer, Toding Ltd., kresimir.todoric@toding.hr*
[(2)] *Associate Professor, University of Zagreb, Faculty of Civil Engineering, uros@grad.hr*

Abstract

Croatia is located in a seismically active area where moderate to strong earthquakes occur regularly. In addition, the building stock is relatively old and not maintained, so the seismic risk is high. This is evidenced by the damage caused by the earthquakes in Zagreb and Petrinja in 2020. Currently, the reconstruction of earthquake-damaged buildings is mainly carried out using standard structural strengthening methods. However, the application of base isolation has significant potential and could be an effective solution for a specific type of building.
In Croatia, base isolation has not yet been used to increase the seismic safety of buildings. This paper investigates the possibility of applying base isolation system on the existing reinforced concrete frame building from the 1930s. In the paper, the building retrofitting solution with base isolation is compared with the conventional strengthening solution.
The application of base isolation in existing buildings was described and linear and non-linear analyses were carried out using the ETABS software package. Based on results, the construction costs were analyzed and compared. The results show the potential of base isolation as an effective solution for the reconstruction of existing buildings.
Keywords: earthquake, frame structure, numerical model, ETABS, base isolation

1. Introduction

Complex reconstruction works with significant material damage in the area of Zagreb and Sisak-Moslavina County are being carried out on an older building stock that mostly consists of masonry buildings and reinforced concrete frame structures designed before the first seismic codes were used in Croatia. [1]

The ongoing process of reconstruction and strengthening of a large number of buildings still requires a significant amount of financial resources. In order to carry out complex interventions on the structure, it is usually necessary to remove all floor and wall coverings, so relocation and finding a suitable replacement location are necessary. All of the activities above add additional financial costs and make the decision of the reconstruction more difficult. The issue of relocation is particularly prominent in public buildings, and there is a need to increase the building's resistance to seismic action to a sufficient level, if possible without relocation, and to maintain the building in full or partial function during the work.

Public buildings in the Zagreb area were mostly built in the mid-20th century, when reinforced concrete was increasingly used in construction. The structures are constructed as frames, with larger spans and slimmer elements, with ribbed and fine-ribbed ceilings, but without the necessary knowledge of earthquake-resistant construction and adequate seismic design. The biggest initial deficiency due to which buildings do not have sufficient earthquake resistance is lack of adequate details and insufficient resistance of sections to achieve seismic safety, as well as insufficient ductility of reinforced concrete element joints.[2]

In this paper, using the example of an existing public reinforced concrete frame structure, that already implemented retrofitting using the conventional method of inserting walls is compared with a consideration of the alternative option of applying base isolation. Building was renovated in the process of reconstruction after the earthquake using the conventional retrofitting method, which necessitated

Copyright © 2025 CroCEE
DOI: https://doi.org/10.5592/CO/3CroCEE.2025.151

complete relocation and additional financial costs. This paper will present a description of the building, investigative works, parameters and a model of the existing state of the structure, as well as a reconstruction using a base isolation. The results obtained and the necessary interventions were compared with the already implemented reconstruction using conventional methods, and a financial comparison of the solutions used was also made.

2. General Description of Structure

The structure considered in this paper is located in Zagreb and is part of the Faculty of Agriculture complex, called "Pavilion 1", and belongs to the category of public buildings. [3] The building is a reinforced concrete frame structure from the 1930s, built at a time when there were no technical regulations for the design and calculation of structures for earthquakes.

The building's floor plan dimensions are 40.50 x 16.00 m, mostly in rectangular shape, with an annex on the north side measuring 10.50 x 6.50 m. The building consists of a ground floor, first floor, second floor and attic, and the height of the building from the ground level is approximately 17.00 m. In Fig. 1 building is shown before retrofit.



Figure 1. a) South side; b) Main entrance [3]

As part of the available documentation of the building, archival drawings were used, according to which the building was designed in 1932. The original load-bearing structure consists of a system of connected reinforced concrete columns and beams that form transverse frames, while in the longitudinal direction the frames are formed only in the planes of the facades, as shown in Fig. 2. According to the analysis of the archival drawings, it is assumed that the transverse beams were constructed in the main axes at the point of support of the columns (at a distance of 5 meters), at the height of the ribbed ceiling. The column grid is at a distance of 5 meters, the dimensions of the internal columns are variable and decrease in height. The dimensions of the load-bearing elements and the characteristics of the material were determined by investigative works as part of the reconstruction project [3].

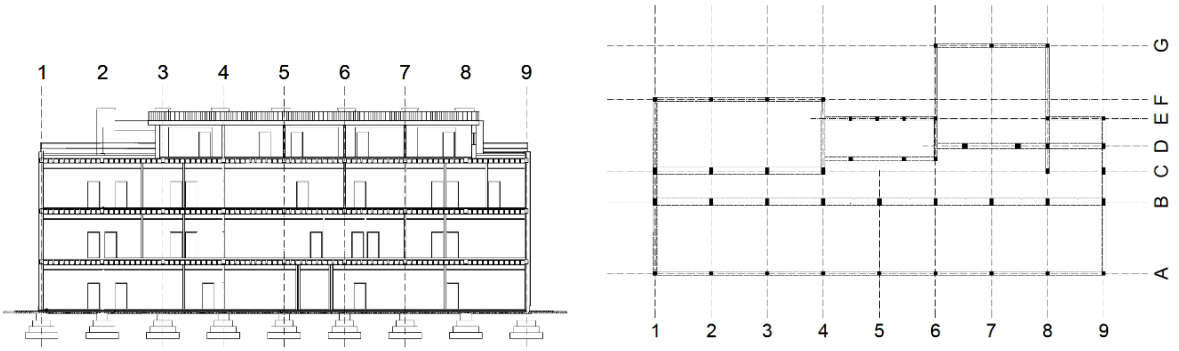


Figure 2. Building plans a) Elevation; b) Floor plan

Copyright © 2025 CroCEE
DOI: https://doi.org/10.5592/CO/3CroCEE.2025.151

According to investigation works [4], the ceiling structure is supported in the transverse direction on longitudinal beams. In the central part of the building there is a reinforced concrete staircase. The foundations of structure are isolated. The inter-story ceiling structure is reinforced concrete, the so-called ribbed ceiling, and the ribs are connected to a 5 cm thick concrete slab. On the underside of the ribs, wooden battens, are installed, on which plaster is applied.

Some of the archival drawings have been preserved, but there is no data about mechanical properties of the used materials. As part of the reconstruction project, investigative work was carried out. According to the Structural investigation report of the structural testing laboratory of the Faculty of Civil Engineering [4], the shear strength of the masonry, the dimensions of the structural elements, as well as the quality of the material were determined. Concrete samples were taken by roller drilling and compressive strength testing of reinforced concrete columns was investigated on the ground floor and upper floors of the building, and non-destructive sclerometer testing was used to assess the quality of the concrete. Fig. 3 shows the reinforcement of the 30/30 cm column.

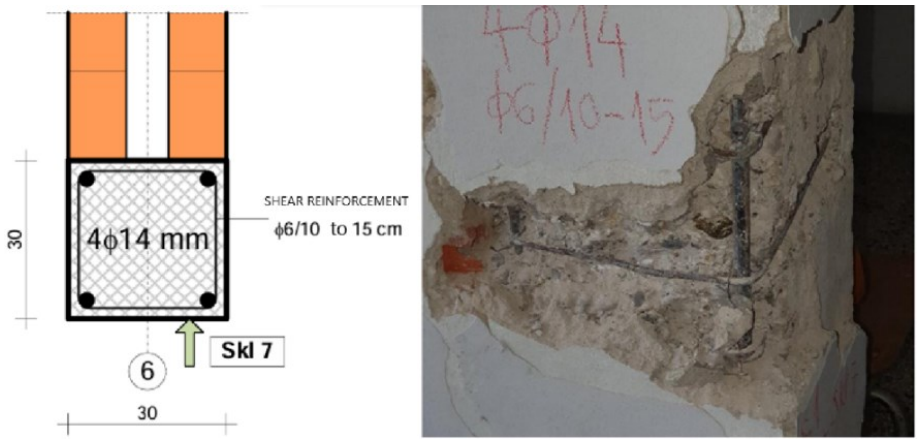


Figure 3. Reinforcement in the column [4]

3. Retrofit using base isolation

3.1. General

The idea is to achieve seismic safety of the building by using base isolation. It is planned to install sliding seismic isolators “Friction Pendulum” isolators. The installation of base isolation ensures the dissipation of energy in a controlled positions and a significant reduction of damage, especially during earthquakes of low intensity where buildings remain undamaged and functional, which is necessary for the operation of important institutions such as hospitals.

Base isolation increases the period of the structure to more than two seconds, which results in a smaller seismic force, but it is necessary to carry out the verification of the structure and the seismic force obtained after the installation of the isolators. The diagram in the Fig. 4 shows the positions of the isolators, where the two types of isolators differ depending on the force. Defined in manufacturer’s data, two types of isolators used, have different horizontal stiffness, which is defined by vertical forces. As shown in Fig. 4 red positions are used to show isolators with greater vertical load, and positions colored blue show isolators with smaller vertical load.

Copyright © 2025 CroCEE
DOI: https://doi.org/10.5592/CO/3CroCEE.2025.151

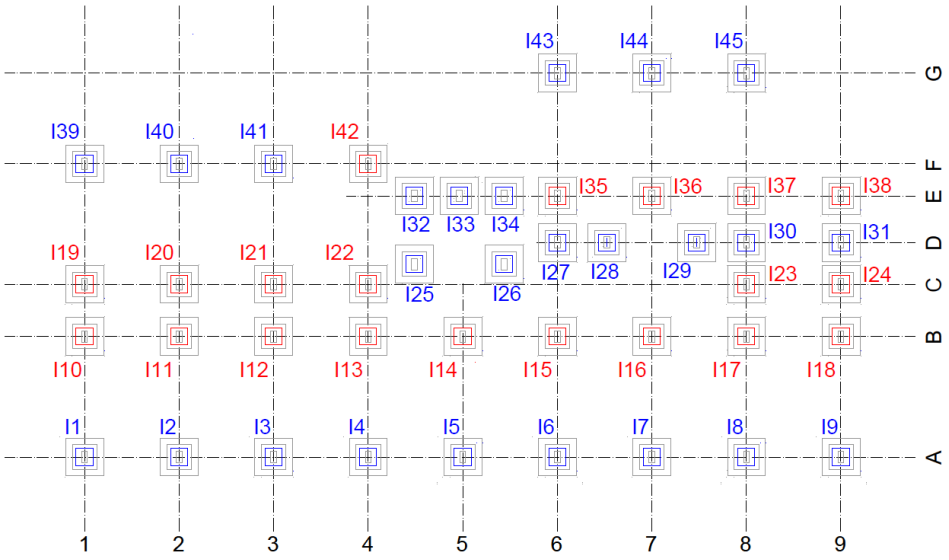


Figure 4. Layout diagram of the base isolation

3.2.Structural analyses

In the ETABS software [5], a numerical model of existing state of the structure was created. The isolators are modelled with "Link elements" with "Friction Pendulum" isolator behavior. An axonometric representation of the model is attached in Fig. 5. Parameters defined for “Friction Pendulum” isolators in ETABS are shown in Table 1.

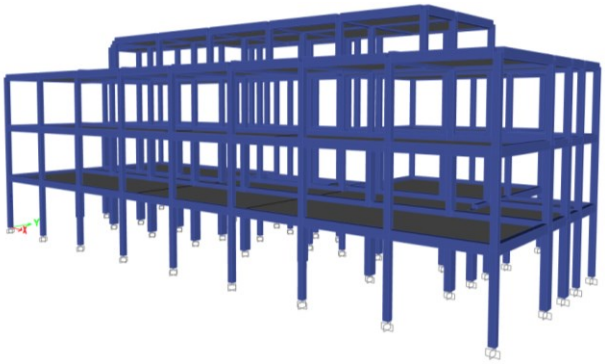


Figure 5. Axonometric view of the model [5]

Table 1. Parameters defined within ETABS

Parameters used in ETABS							
Isolator color	Vertical stiffness (kN/m)	Horizontal linear stiffness (kN/m)	Horizontal nonlinear stiffness (kN/m)	Friction coefficient, slow	Friction coefficient, fast	Rate parameter (sec/m)	Net pendulum radius (m)
Red	1275000	320	20800	0,0182	0,026	50	2,5
Blue	1275000	160	10400	0,0182	0,026	50	2,5

Copyright © 2025 CroCEE
DOI: https://doi.org/10.5592/CO/3CroCEE.2025.151

The non-linear dynamic analyses of the structure is performed. An artificial strong motion record was matched to the elastic spectrum of the response increased by the importance class of the building (1,2). The peak ground acceleration corresponding on the location is 0.254g x 1.2 (importance class) [6], and soil is classified as type C. The damping used is 5%. Fig. 6 shows a 30-second record set in the X and Y directions.

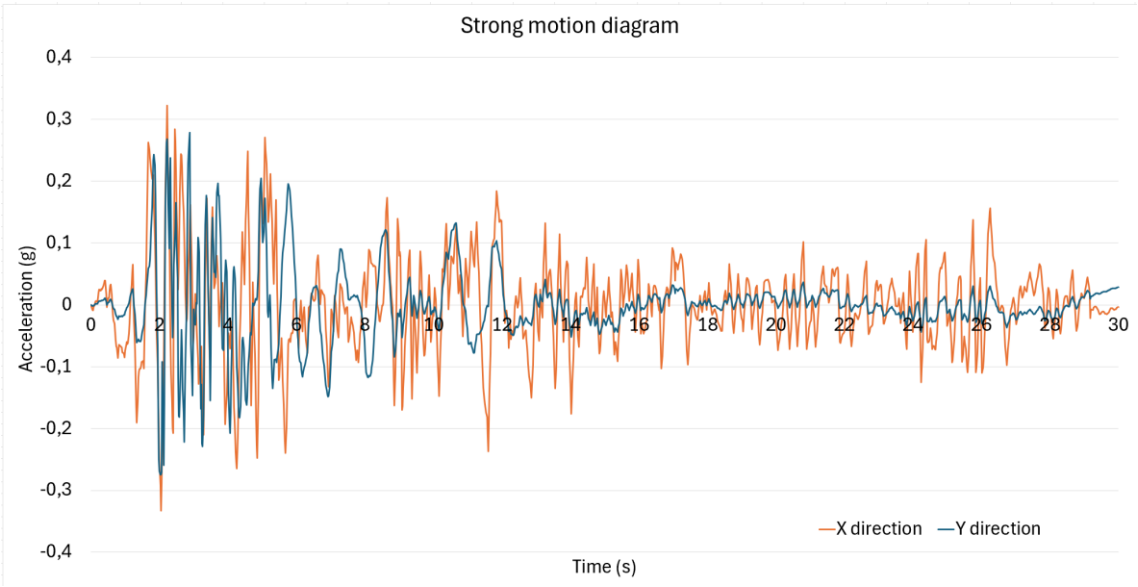


Figure 6. Time History function– X and Y direction

In the bilinear model according to Fig. 7 F_Y defines the critical transverse force required to initiate sliding, equal to the product of the axial force and the coefficient of friction. The ratio of the axial force and the radius of curvature defines the stiffness after yielding. The coefficient of friction depends on the sliding speed and initially increases exponentially, and then reaches a maximum value at a higher speed.

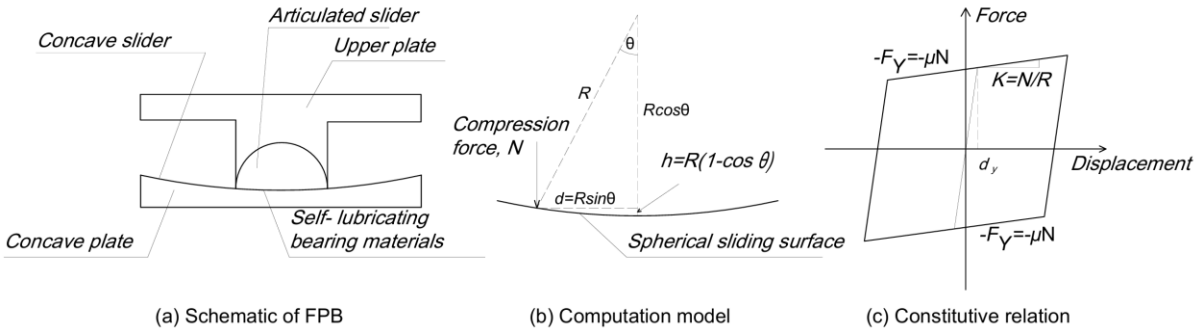


Figure 7. Schematics and behavior of „Friction Pendulum“ isolator [7]

The building is freestanding and separated from neighboring buildings, and as such has the possibility of movement in all directions. For installing isolators, it is necessary to foresee and secure an adequate installation location, in this case it is necessary to construct a technical floor, as shown in Fig. 8.

The planned technical floor would be built at the height of the existing isolated foundations. The floor of the technical floor is planned as a reinforced concrete slab with a thickness of 15 cm. Above the position of the isolators, the installation of HEB 300 steel profiles and trapezoidal sheet metal is planned as lost formwork with a 6-centimeter thick reinforced concrete plate that acts as a

Copyright © 2025 CroCEE
DOI: https://doi.org/10.5592/CO/3CroCEE.2025.151

horizontal diaphragm and ensures uniform structural movements. With this approach, seismic action is distributed to all isolators simultaneously.

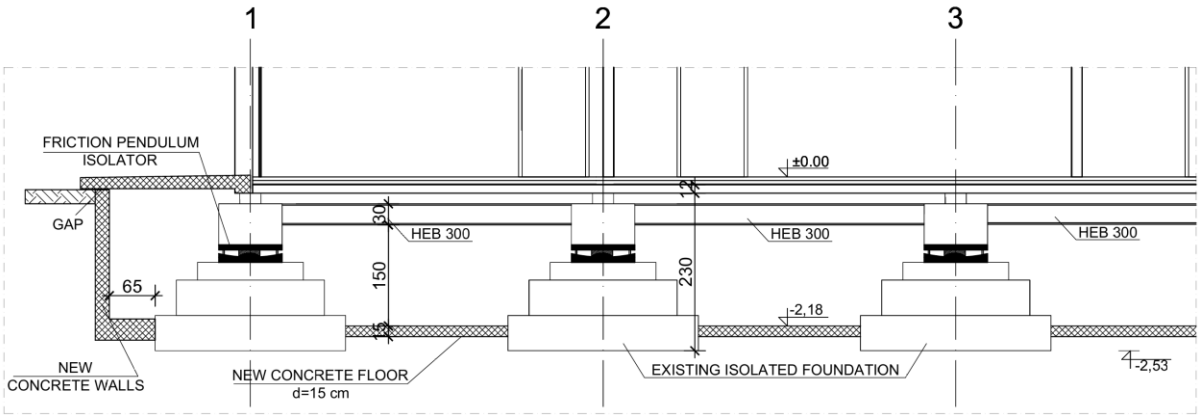


Figure 8. Elevation view of technical floor

3.3. Results

Below are presented the main results of the dynamic nonlinear analysis of the building and isolators. In Table 2. ten isolators with the biggest displacements are shown, with maximal displacement being 10,5 cm. According to the regulations, the displacement results must be increased by a factor of 1.2. Permitted displacement according to the manufacturer's instructions for selected isolators is 17 centimeters.

Table 2. Maximal displacement of isolators

Maximal displacements of Link elements										
Isolator tag	I9	I1	I2	I7	I3	I6	I5	I4	I8	I18
U2 (m)	-0,105	-0,105	-0,105	-0,105	-0,105	-0,105	-0,105	-0,105	-0,105	-0,104
U3 (m)	-0,085	-0,081	-0,082	-0,084	-0,082	-0,083	-0,083	-0,083	-0,085	-0,085

Table 3 shows the maximum forces that occur in isolators. It is important to choose type of isolator depending on maximal displacement and maximal vertical load that occurs on isolators. "Friction Pendulum" isolators cannot transmit tensile stress, so it is necessary to check the forces on the isolators. In table 3. “P” represents Axial force, “V2” force in X axis and “V3” in Y axis.

Table 3. Maximal force in isolators

Maximal forces of Link elements										
Isolator tag	I9	I1	I2	I7	I3	I6	I5	I4	I8	I18
P (kN)	-1180	-1176	-1151	-1145	-1139	-1132	-1122	-1089	-1031	-1022
V2 (kN)	-74,4	-74,7	-73,8	-65,0	-63,0	-72,8	-54,0	-61,8	-36,8	-45,5
V3 (kN)	-55,4	-54,9	-53,7	-51,9	-51,8	-52,4	-47,6	-65,2	-38,3	-44,8

It is important to compare natural periods of the structures. Building before retrofit had first structural period 1,04 s, second period 0,92 s and third period 0,85 s. Base isolated building has first periods 3,53 s, second period 3,50 s, and third period 3,25 s.

Proceedings of the 3rd Croatian Conference on Earthquake Engineering - 3CroCEE
19–22 March 2025, Split, Croatia
Copyright © 2025 CroCEE
DOI: https://doi.org/10.5592/CO/3CroCEE.2025.151

The resulting shear force and horizontal displacement for isolator "I13" in the X and Y directions are shown in the Fig. 9 and correspond to the assumed hysteresis behavior of the isolator.

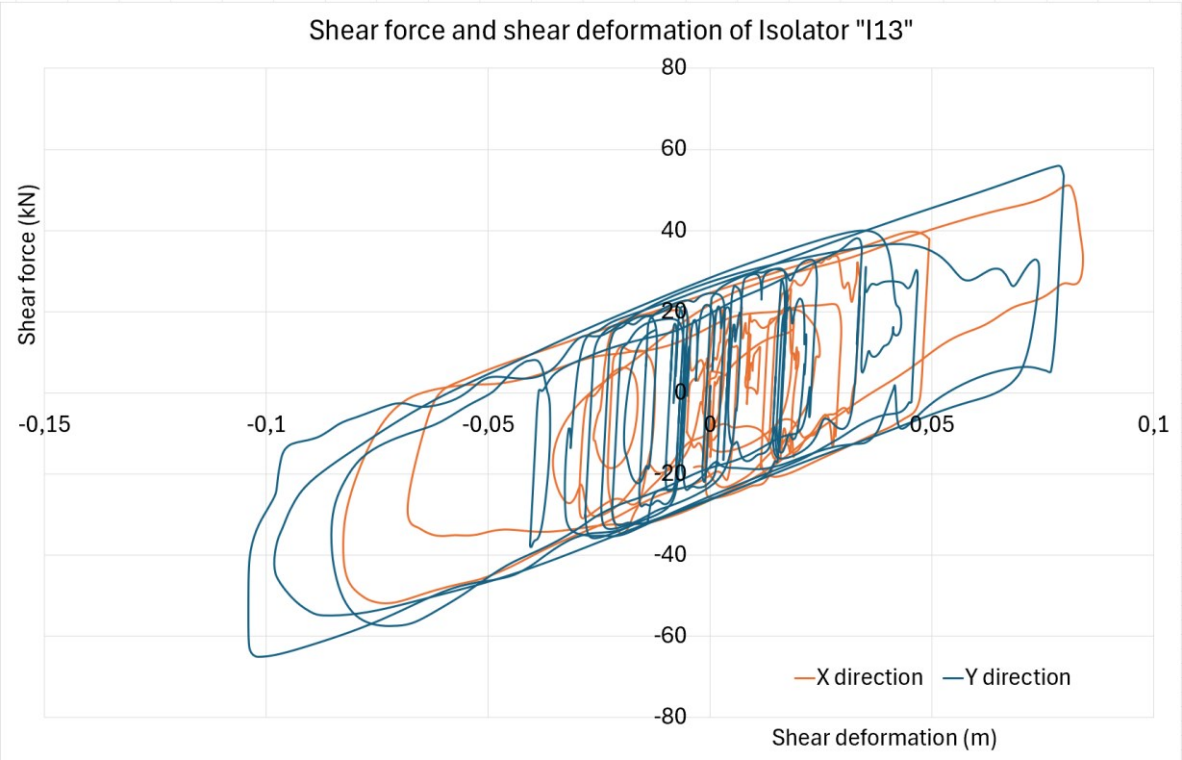


Figure 9. Shear force and deformation of Isolator "I13" in X and Y direction

Horizontal displacement in the X and Y directions for Isolator "I13" during the record is shown in Fig. 10.

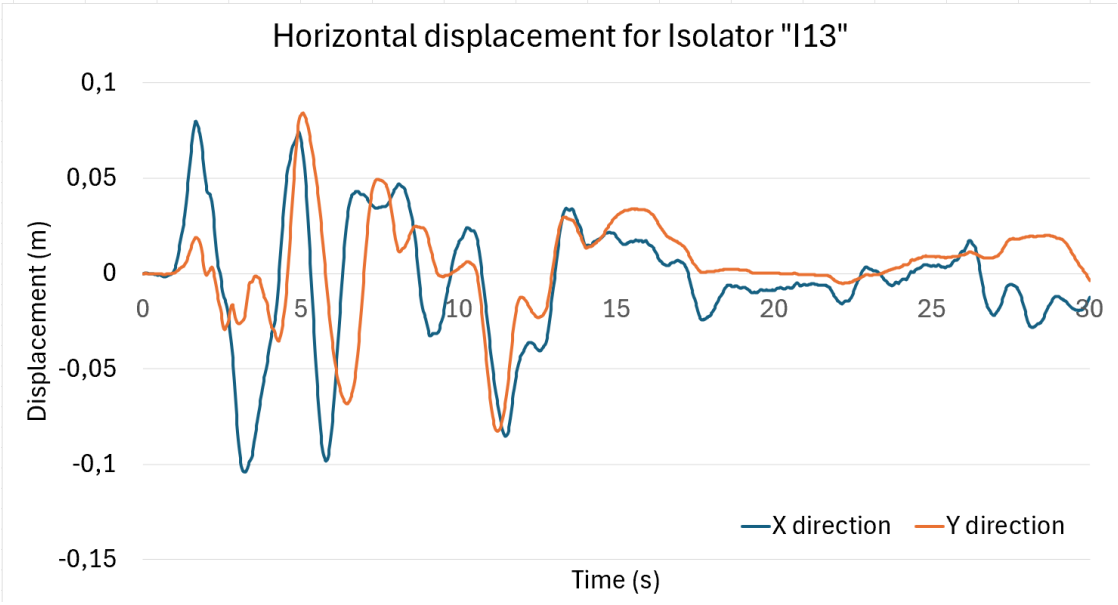


Figure 10. Displacement of Isolator "I13"

Copyright © 2025 CroCEE
DOI: https://doi.org/10.5592/CO/3CroCEE.2025.151

4. Retrofit using conventional method by inserting RC walls

The structure was retrofitted with conventional methods which involves new reinforced concrete walls with new foundations, as shown in Fig. 11. The chosen concept does not require the reinforcement of columns and beams, but rather to minimize the structural displacements and equalize them so that the columns do not exceed the ductility requirements. The new walls relieve the existing frames and achieve greater rigidity of the building, provided that they are constructed continuously from the foundation to the roof and adequately connected to horizontal diaphragms. The connection to the rigid diaphragm was carried out through the existing beams - by drilling the existing beam and pulling the reinforcement through the beam, which also achieved vertical continuity of the walls for force transmission. Due to significant horizontal seismic forces on part of the new reinforced concrete walls, tensile stresses appear at the edge, which cannot be taken over by the existing foundation structure even with reinforcement. Therefore, it was necessary to install ground anchors that transfer the tensile forces to deeper soil.

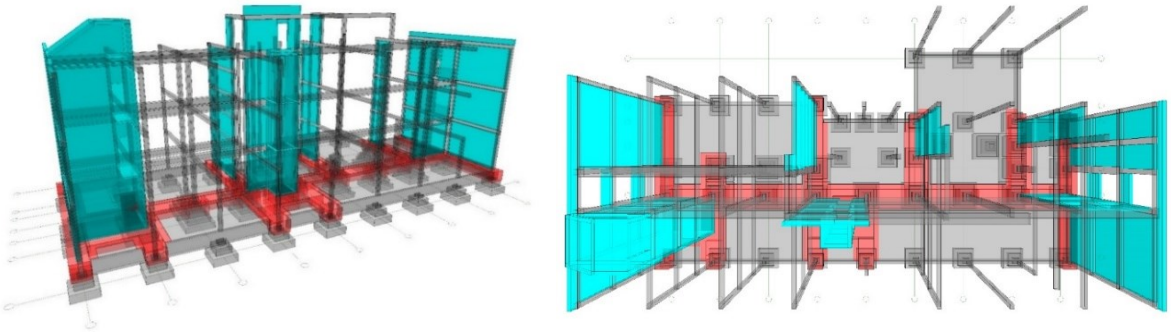


Figure 11. Structural retrofitting according to the reconstruction project [3]

Fig. 12 shows the complexity of the intervention, during reconstruction after the earthquake using the conventional method of inserting walls. The removal of floor and wall coverings on all floors in order to be able to access the reinforcement and new elements of the structure require moving out and the need for a replacement location.



Figure 12. East facade and ground floor during renovation [8]

5. Comparison of results

In this chapter, a comparison of periods, displacements and forces for two cases of reconstruction are shown.

Fig. 13 shows a comparison of the structural periods, the structure achieves a much larger period with base isolation, and thus a significantly lower seismic force. Reconstruction of the building using the conventional method with the insertion of walls adds rigidity to the building and thereby reduces the periods and increases the seismic force.

Copyright © 2025 CroCEE
DOI: https://doi.org/10.5592/CO/3CroCEE.2025.151

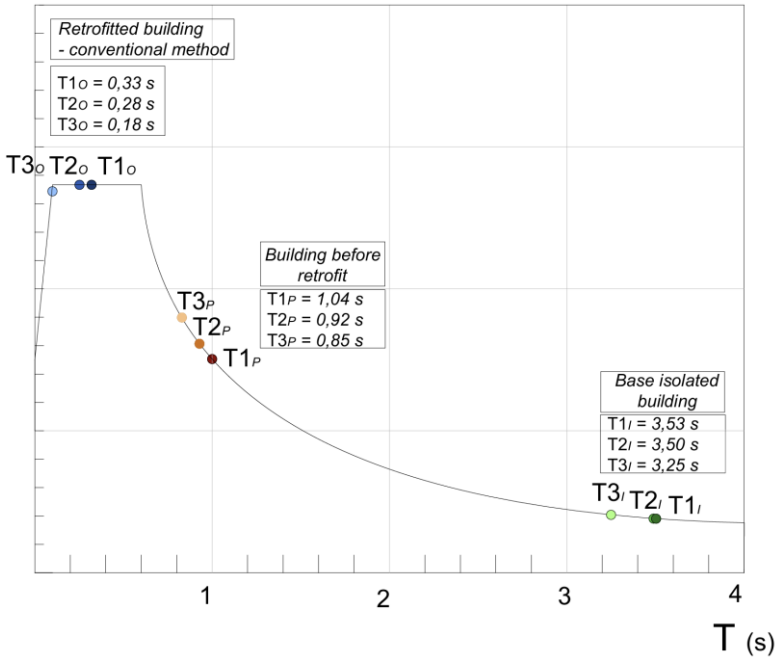


Figure 13. Comparison of construction periods

The Fig. 14 shows the structural displacements for all three models. The structure with base isolation has a large displacement in the isolator, which meets the manufacturer's allowed displacement, and the total displacement of the structure according to dynamic analysis is 17.1 centimeters, as shown in Table 4, so it is important that the building has the ability to move in all directions. Retrofitting by using conventional methods stiffens the structure, and displacements are small. When using base isolation, displacements are concentrated in the isolators.

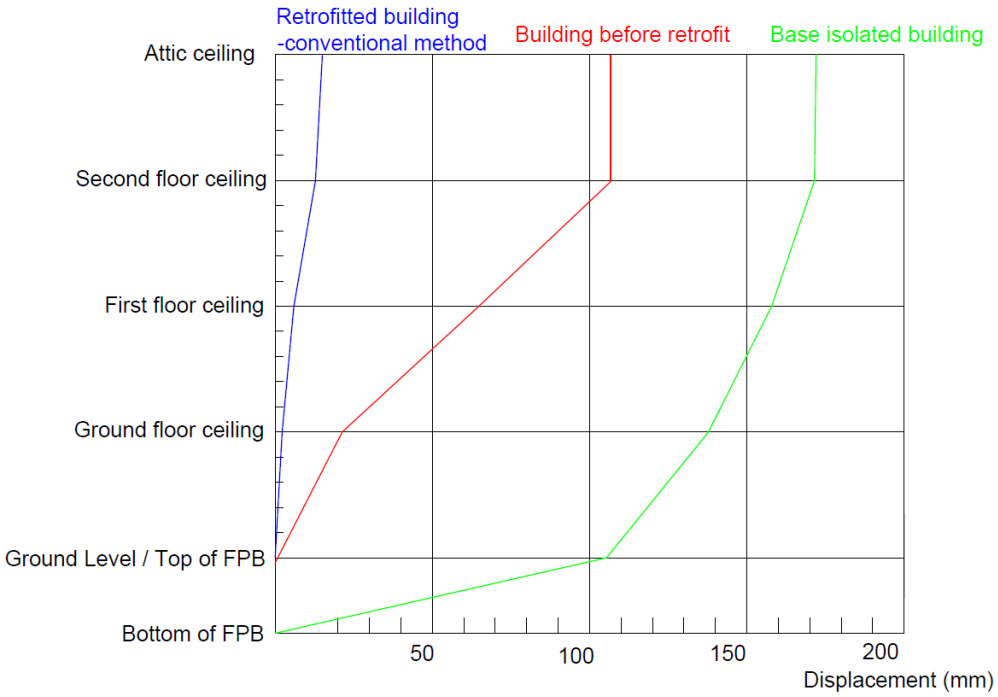


Figure 14. Comparison of displacements

Proceedings of the 3rd Croatian Conference on Earthquake Engineering - 3CroCEE
19–22 March 2025, Split, Croatia
Copyright © 2025 CroCEE
DOI: https://doi.org/10.5592/CO/3CroCEE.2025.151

Table 4. Comparison of maximum story drifts

Displacement of the building before retrofit (earthquake)	10,7 cm
Displacement of the building with base isolation (earthquake) – dynamic analysis	17,1 cm
Displacement of the building after retrofitting by using conventional methods (earthquake)	1,2 cm

The difference between the shear force at the foundation level for the three models is shown in Table 5. As part of Table 5, the Base shear was calculated, which represents the horizontal force as a part of the total weight that is activated by seismic action. It is evident from the results that by using base isolation, we reduce the base shear of structure. Less energy dissipation through structural elements is required, and the structural elements in the model with base isolation have sufficient resistance to new seismic loads.

Table 5. Comparison of Base Shear between models

	Building before retrofit	Base isolated building	Retrofitted building – conventional method
Shear force (kN)	4944	2700	6720
Total weight (kN)	20760	22100	27680
Base shear	24%	12%	24%

5.1. Cost analysis

Building was analyzed based on the prices achieved on the market, as shown in Table 6. Structural reconstruction by inserting new RC walls amounts to only about 30% of the cost of the "complete reconstruction".

- Structural reconstruction costs around 900.000 €
- Other works around 2.100.000 €
- Total reconstruction 3.000.000 €

Table 6. Cost estimate on a building according to the reconstruction project

Recapitulation of construction works – strengthening by conventional method		
1.	Preparatory works	19.400,00
2.	Removal and disassembly works	222.410,00
3.	Renovation of existing structure	138.793,00
4.	Construction of ground anchors	26.160,00
5.	Construction of new foundations	181.093,83
6.	Construction of new reinforced walls and slabs	321.037,69
Construction works total:		**908.894,52**

By analyzing the cost items of other professions, it is estimated that other costs would be significantly reduced to around 40%. Reduction in other costs is achieved because floor and wall coverings on the upper floors are not affected by reconstruction. Removal and assembly of new installation for heating, cooling, gas, water and electricity is avoided, so existing installation remain. There is no need for moving furniture and equipment. The total savings of a complete reconstruction using base isolation would be more significant, as shown in Table 7:

- Structural reconstruction costs around 865.000 €

Proceedings of the 3rd Croatian Conference on Earthquake Engineering - 3CroCEE
19–22 March 2025, Split, Croatia
Copyright © 2025 CroCEE
DOI: https://doi.org/10.5592/CO/3CroCEE.2025.151

- Other works around 840.000 €
- Total reconstruction 1.705.000 €

Table 7. Cost estimate on building with base isolation

Construction works recapitulation – construction with base isolation		
1.	Installation of isolators	308.000,00
2.	Removal and disassembly works	12.078,10
3.	Renovation of existing structure	40.592,00
4.	Construction of steel structure	168.000,00
5.	Excavation and foundation of the technical floor	196.022,00
6.	Construction of reinforced walls and pressure plate of the technical floor	140.437,90
Construction works total:		**865.130,00**

Except achieving resistance to seismic effects by using base isolation, it is necessary to consider other advantages:

- Except on the ground floor (where it is necessary to remove the entire floor covering and floor slab), no structural reinforcement work is carried out on the upper floors, so it is not necessary to remove the floor and wall coverings and subsequently install new and replacement ones.
- It is not necessary to move furniture, dismantle equipment and appliances, dismantle interior and exterior joinery and replace them with new ones, except on part of the ground floor.
- On the upper floors, the existing installations are not damaged during strengthening works.

Looking at the direct and indirect costs, advantages and disadvantages of the application of base isolation, we come to the conclusion that the retrofit using base isolation would be beneficial about 43% compared to the conventional methods of earthquake reconstruction with the addition of new reinforced concrete walls.

6. Conclusion

Until now, base isolation has not had a significant application in Croatia. In the paper, on a example of a building reconstructed after an earthquake, the possibility of ensuring the required seismic resistance according to legal regulations was considered by applying base isolation. In order to obtain realistic financial comparison, data from the realized project with the conventional method were used. The analyzed building typology belongs to the reinforced concrete frame structures built before the first earthquake regulations and which are being widely reconstructed after the recent earthquakes in the Zagreb and Petrinja areas. The reinforcement in the existing columns is insufficient, which is evident from the investigation works and confirmed by the analysis of the existing condition. Accordingly, strengthening measures for such a typology of the building require intervention in the existing structure and the construction of new ductile reinforced concrete elements that will take over the earthquake forces. This strengthening principle has increased the rigidity of the structure, which is evident from the reduced structural periods. The result is increased shear forces that need to be taken over by new reinforcement, continuously carried out and properly founded. After the reconstruction of the building, the significant damage index (IZO factor) met the legally required 0.75 values to achieve Level 3. In this paper, the analysis of the building using base isolation leads to a significant reduction of the shear force, which results in no need for straightening of the existing structure, and therefore no removal of most of the floor and wall coverings and associated installations, which is the main advantage of the reconstruction of frame structures using base isolation.

Furthermore, by applying base isolation, in addition to achieving sufficient seismic safety, damage during future earthquakes would also be reduced, and buildings could remain fully functional.

Copyright © 2025 CroCEE
DOI: https://doi.org/10.5592/CO/3CroCEE.2025.151

This is especially important for critical infrastructure buildings that must remain functional during earthquakes. Base isolation plays an increasingly important role in the construction of new and strengthening existing buildings against seismic action worldwide, and it certainly deserves more significant application in Croatia, as presented in this paper.

Acknowledgments:

This work was created as part of the Master's thesis titled " SEISMIC ISOLATION OF AN EXISTING REINFORCED CONCRETE BUILDING" in collaboration with my mentor, Associate Professor Mario Uroš.

The authors thank Dr. Maria Gabriella Castellano and company FIP MEC Academy, FIP MEC srl, Italy for help while writing this paper.

References

[1] Šavor Novak, M., Uroš, M., Atalić, J., Herak, M., Demšić, M., Baniček, M., Lazarević, D., Bijelić, N., Crnogorac, M., Todorić, M. (2020).: Earthquake in Zagreb on March 22, 2020 - preliminary report on seismological research and damage to buildings, *GRAĐEVINAR, **72*** (10), 843-867, doi: https://doi.org/10.14256/JCE.2966.2020

[2] Crnogorac, M.: Original and acquired defects of building structures, in Earthquake engineering - Reconstruction of masonry buildings, Uroš, M., Todorić, M., Crnogorac, M., Atalić, J., Šavor Novak, M., Lakušić, S. (Eds.), Faculty of Civil Engineering, University of Zagreb, 2021.

[3] Todorić, M., Duvnjak M., Dragičević I., Todorić P., Crnković I., Šešek M.: *Building reconstruction project for the complete renovation of the building,*, Zagreb, 2021.

[4] Krolo, J., Bartolac M., Duvnjak, I.: *Report on investigative works on the construction of the building of the Faculty of Agriculture - Pavilion I in Zagreb*, Zagreb, 2020.

[5] ETABS software, Computers and Structures Inc.

[6] Herak, M., Allegretti, I., Herak, D., Ivančić, I., Kuk, V., Marić, K., Markušić, S., Sović, I. (2011): Croatia. Seizmic Hazard Map, Faculty of Science, University of Zagreb, Department of Geophysics, available online at http://seizkarta.gfz.hr/.

[7] Chen, X., Wu, P., Li, C. (2022) Seismic performance assessment of base-isolated tall pier bridges using friction pendulum bearings achieving resilient design, *Structures, **38***, 618-629 https://doi.org/10.1016/j.istruc.2022.02.032.

[8] Archival Photo Documentation Toding Ltd.

Proceedings of the 3rd Croatian Conference on Earthquake Engineering - 3CroCEE
19–22 March 2025, Split, Croatia
Copyright © 2025 CroCEE
DOI: https://doi.org/10.5592/CO/3CroCEE.2025.161

DYNAMIC ASSESSMENT OF RC BEAMS FLEXURALY STRENGTHENED WITH CFRP STRIPS

Tomislav Brozović [(1)], Tomislav Kišiček [(2)]

[(1)] *Structural Engineer, Institut IGH, Laboratory for materials and structures, tomislav.brozovic@igh.hr*
[(2)] *Full-time professor, University of Zagreb Faculty of Civil Engineering, tomislav.kisicek@grad.unizg.hr*

Abstract

In the last few decades externally bonded FRP strips and sheets have been the most commonly used technique for strengthening of RC structures and bridges. The fact that FRP does not corrode and good mechanical performance have made this material very popular to use. Prior to design and application of FRP strengthening, it is of great interest for design engineers to evaluate condition of deteriorated and damaged RC structures. One of the most popular non-destructive techniques to evaluate structural health is modal testing. In this work Experimental Modal Analysis (EMA) is used as a technique to evaluate loss of beam stiffness due to damage and effectiveness of FRP strengthening in terms of stiffness recovery. This experimental technique is based on fact that changes in local stiffness influence on global dynamic parameters (frequencies, mode shapes and modal damping). This paper presents experimental results of experimental modal analysis carried out on damaged concrete beams strengthened with CFRP strips and sheets. Three RC beams with rectangular cross section were tested. Beams were subjected to monotonic loading with increasing load steps with four-point bending setup in order to generate different damage levels in specimens. CFRP strengthening was applied on the specimens after they were damaged by loading to 50% of their flexural capacity. Modal tests were carried out after each loading-unloading cycle. Beams were excited by the impact hammer. Frequency response functions were processed using Dewesoft software to obtain natural frequencies, mode shapes and damping ratios.

Keywords: FRP strengthening, dynamic parameters, experimental modal analysis, concrete beams

Proceedings of the 3rd Croatian Conference on Earthquake Engineering - 3CroCEE
19–22 March 2025, Split, Croatia
Copyright © 2025 CroCEE
DOI: https://doi.org/10.5592/CO/3CroCEE.2025.161

1. Introduction

Durability is the main issue of old concrete bridges. Exposure to aggressive environment and insufficient maintenance leads to deterioration of concrete and reinforcement corrosion, especially in case of bridge decks with poor waterproofing design and thin concrete layer. Durability issues leads to reliability issue especially in case of very old concrete bridges that are not robust and are designed for lighter traffic, wind and seismic loads in comparison to current Eurocode standards. In order to increase reliability, it is necessary to repair and strengthen old deteriorated and damaged bridges. In the last few decades externally bonded FRP strips and sheets have been used to improve load-bearing capacity and serviceability of RC structures and bridges. FRP material does not corrode, it is much lighter in comparison to steel, and it has very high tensile strength.

Prior to design of FRP strengthening, it is of major interest for designers to evaluate the condition of a deteriorated and damaged concrete structure. One of the non-destructive techniques for evaluation of structural health is modal testing. In this research Experimental Modal Analysis (EMA) is used as a technique to evaluate beam stiffness loss due to damage and effectiveness of FRP strengthening in terms of stiffness recovery. This non-destructive technique is based on fact that changes in local stiffness influence on global dynamic parameters which are: eigen frequencies, mode shapes and modal damping. In general, bridge dynamic testing can be performed either to confirm theoretical values of modal parameters for new bridges or to evaluate condition of existing bridges (Vibration Based Structural Health Monitoring). In combination with static load testing (performed with loaded trucks), modal testing on real bridges is expensive. Also, results from modal tests are very susceptible on boundary conditions and temperature. Instead of testing a real bridge superstructure, numerous laboratory tests have been carried out using smaller beam specimens. In the past decade several laboratory tests were carried out with the goal to evaluate effectiveness of FRP flexural strengthening on RC beams by modal testing. In most experiments testing specimens were RC beams, usually with rectangular cross section. Beams were simply supported during three or four-point bending tests and were suspended during modal tests in order to reduce the influence of boundary conditions on modal test results.

2. Experimental research

2.1 Outline of the experiment

Static and dynamic modal tests were carried out on a total of three specimens. One of the specimens was non-strengthened, while the other two were strengthened with CFRP strip or sheet (Table 2). Specimens were built in the concrete factory with concrete class of C40/50. Steel grade of reinforcement bars was B500B (Table 1).

Table 1 – Cross section properties

Beam type	Cross section dimensions [cm]	Tension reinf.	Shear reinf.
RC beam	b/h = 20/30	3ϕ12	ϕ8/15 cm

Beams, with span of 3.0 m, were submitted to monotonic loading with increasing load steps with symmetric four-point bending setup, and with shear span of 1.0 m. CFRP strengthening was applied on the beam specimens after they were damaged by loading to 50 % of their load-bearing capacity (Figure 1). Modal tests were carried out after each loading-unloading cycle. To avoid the influence of rigid support on the modal test results specimens were suspended (Figure 2). An impact excitation was used to induce free vibrations. Dynamic response was registered with one accelerometer located at the midspan (multi input – single output method). Frequency response functions (FRF) were

Copyright © 2025 CroCEE
DOI: https://doi.org/10.5592/CO/3CroCEE.2025.161

processed using Dewesoft software to obtain natural frequencies, and corresponding damping ratios and mode shapes.

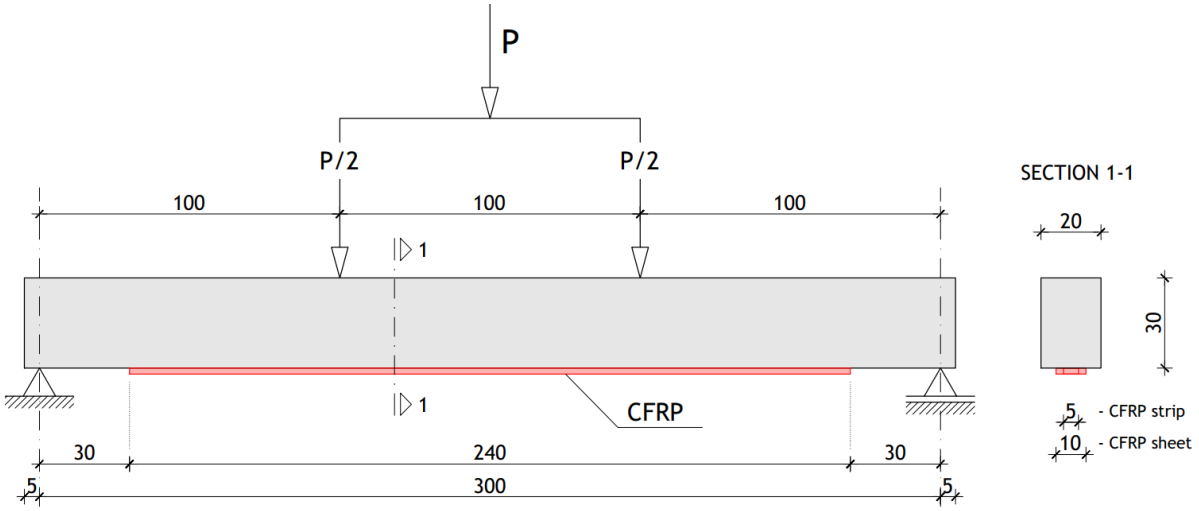


Figure 1. Four point bending test scheme

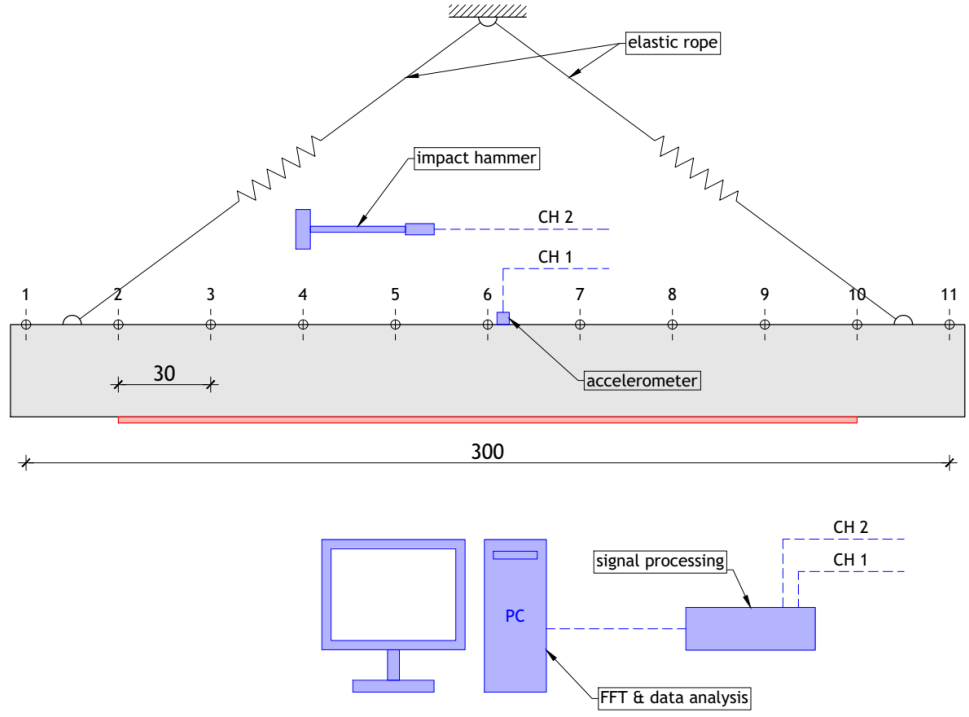


Figure 2. Modal test scheme

2.2 Results and discussion

Results from static and dynamic modal tests are presented on Figure 3 in forms of P-δ diagrams and related P-f diagrams. After strengthening, and after the applied load in phase 3, the first eigen frequency of strengthened specimens 2/3 and 3/3 increased by 6.5 % and 9.2 % respectively. The first eigen frequency of the non-strengthened specimen (1/3), after the load phase 3, remained the same. Higher value of the first eigen frequency indicates that CFRP strengthening increased the flexural stiffness of concrete beams by crack bridging and reducing the crack propagation.

Copyright © 2025 CroCEE
DOI: https://doi.org/10.5592/CO/3CroCEE.2025.161

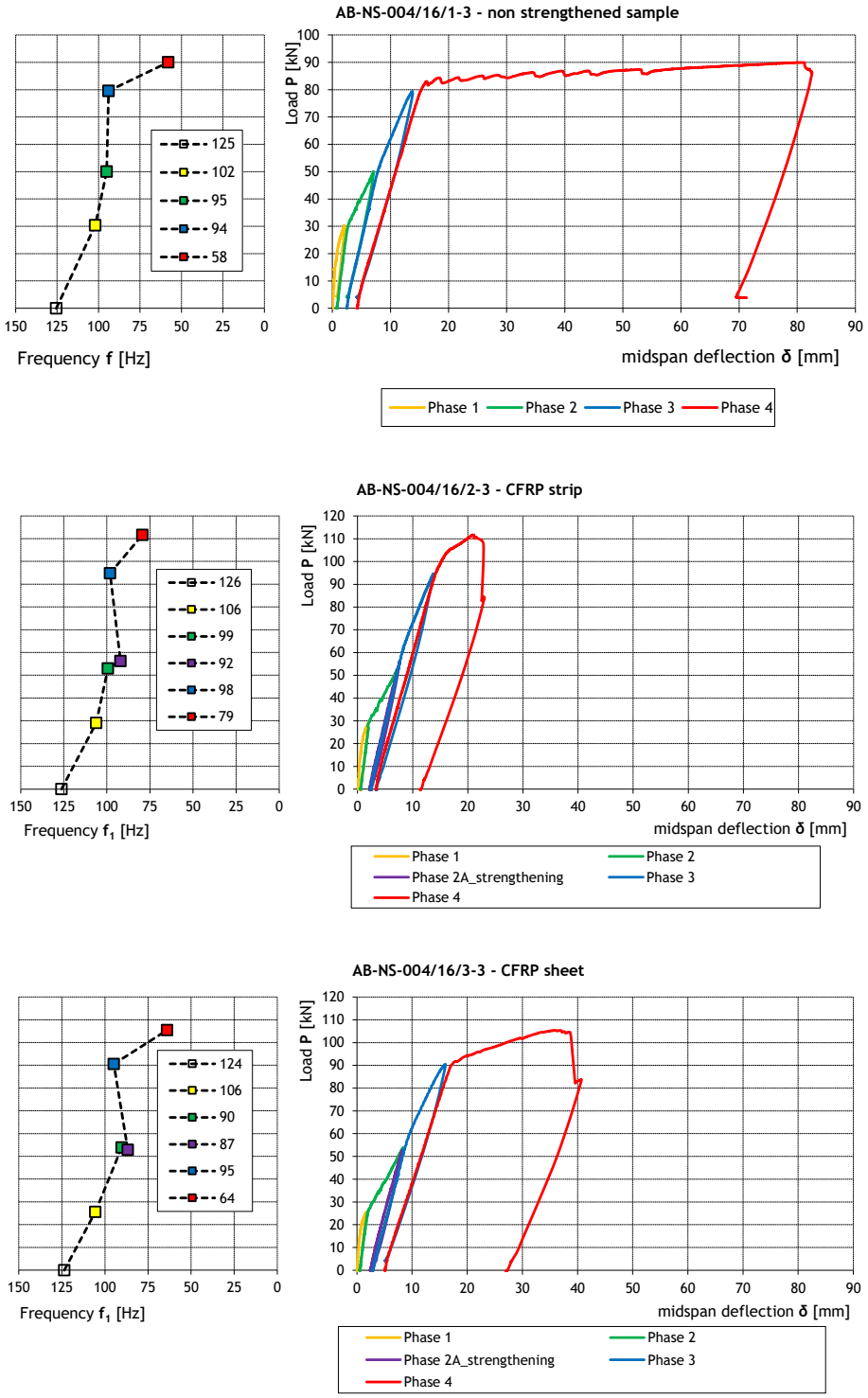


Figure 3. P-δ and P-f relation for RC beams

Proceedings of the 3rd Croatian Conference on Earthquake Engineering - 3CroCEE
19–22 March 2025, Split, Croatia
Copyright © 2025 CroCEE
DOI: https://doi.org/10.5592/CO/3CroCEE.2025.161

Table 2 Results from the static four point bending test

Specimen	Type of strengthening	Failure mode	P_u [kN]	P_u/P_{ref}	δ_u [mm]	δ_u/δ_{ref}
AB-NS-004/16/1-3	-	SY/CC	90.0	-	80.8	-
AB-NS-004/16/2-3	CFRP strip	BL	111.7	1.24	20.9	0.26
AB-NS-004/16/3-3	CFRP sheet	BL	105.4	1.17	36.8	0.46

SY/CC – Steel yielding followed by concrete crushing; BL – bond loss

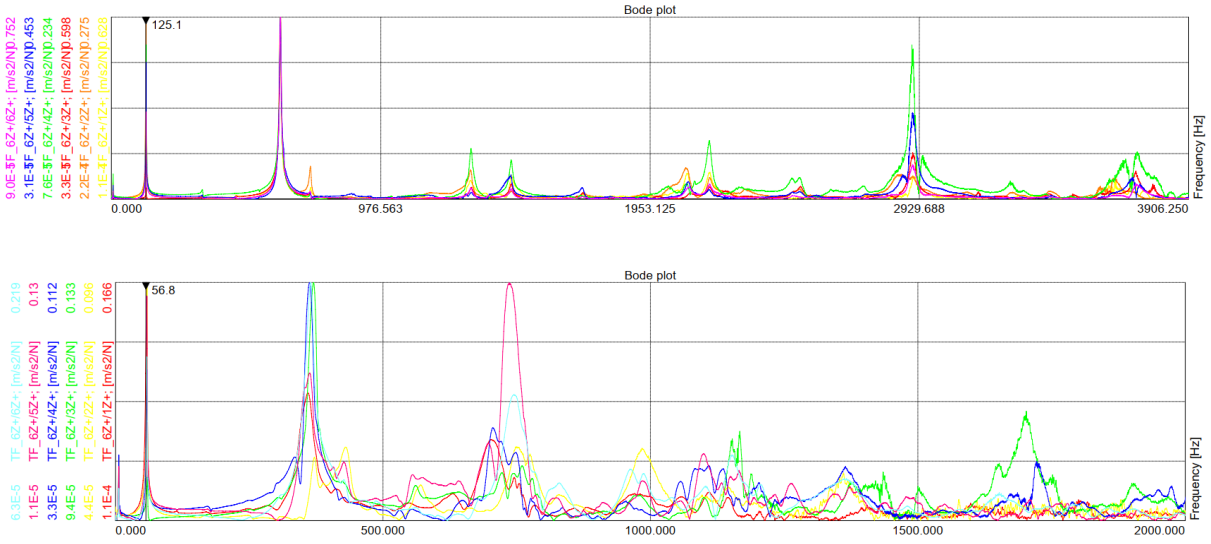


Figure 4. Comparison of the magnitude spectra of the FRF functions n virgin and failure step mode for the non-strengthened specimen

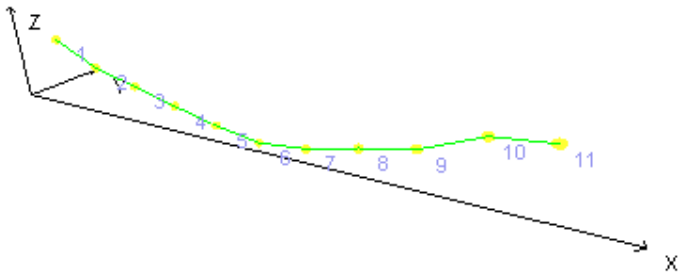


Figure 5. First bending mode shape

From the P-δ diagram of the specimen that was strengthened with CFRP strip (PB-NS-004/16/2-3), deficiency of ductility can be noticed. Bond failure mode in terms of peeling-off in an anchorage zone occurs on both strengthened specimens (Fig 6). Specimen that was strengthened with CFRP sheet had a bigger value of ductility coefficient than the one strengthened with CFRP strip.

Copyright © 2025 CroCEE
DOI: https://doi.org/10.5592/CO/3CroCEE.2025.161

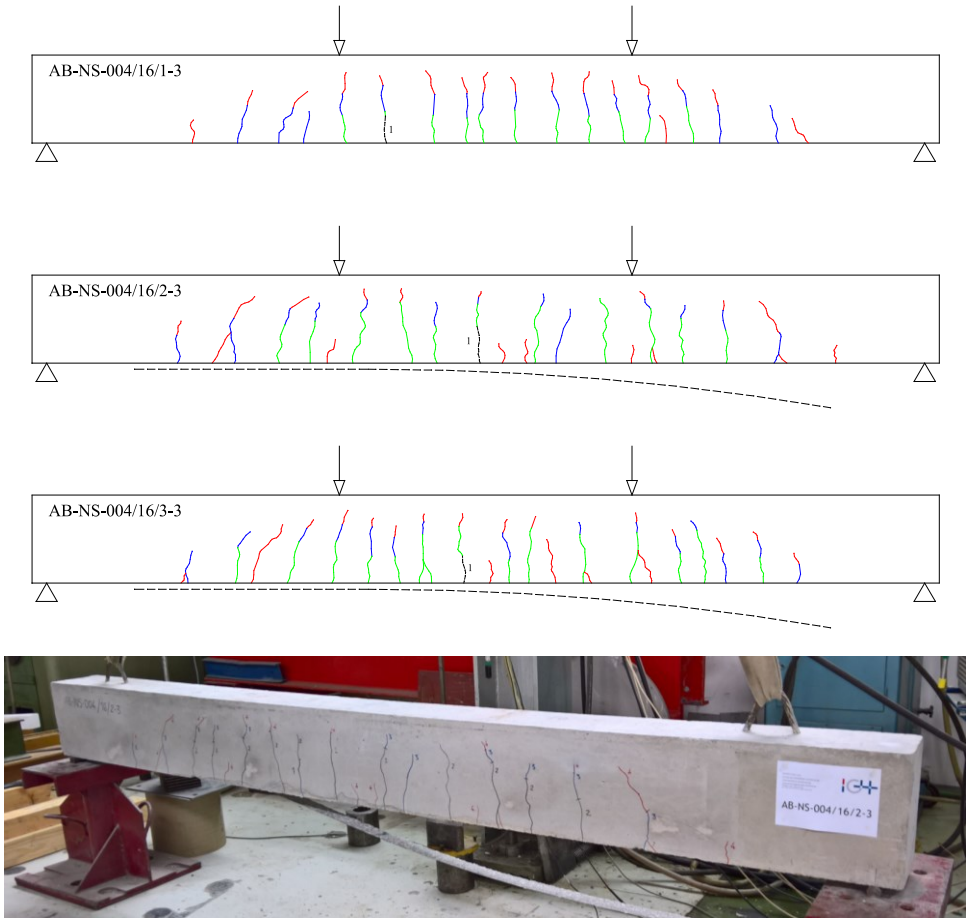


Figure 6. Cracking pattern and failure mode caused by loss of composite action

3. Conclusion

In this paper experimental results of the static and dynamic tests carried out on damaged RC beams flexural strengthened with CFRP are presented.

Static load tests confirmed that flexural strengthening increase load bearing capacity and flexural stiffness; and decreases the ductility of RC beams. Numerous tests have shown that bond failure modes are dominant, and it is very hard to reach full tension strength of the FRP and ULS with full composite action. Therefore, the bond failure modes are well investigated and propositions for anchor length design and other calculations were proposed in a standards and technical reports issued by the fib, ACI and other national committees. Nevertheless, it is obvious that in force transfer between composite and concrete in most of the cases bond failure occur due to shear concrete failure and de-bonding in concrete near the surface. So extra effort must be made to increase the capability of the bond shear force transfer, either with shear connectors or concrete surface preparation before applying FRP strengthening system. These issues will be investigated further.

Dynamic modal test presented in this paper, confirmed previous investigations that with precise measurements it is possible to determine and evaluate decrease of stiffness due to damage caused by static loading and evaluate effectiveness of the FRP flexural strengthening on the stiffness recovery. Modal analysis is a popular and useful non-destructive method for damage detection and structural health monitoring of the bridges and other structures. In the future research activities this method should be proved also on a real case study to evaluate the effectiveness of FRP flexural strengthening on a real bridge superstructure.

Proceedings of the 3rd Croatian Conference on Earthquake Engineering - 3CroCEE
19–22 March 2025, Split, Croatia
Copyright © 2025 CroCEE
DOI: https://doi.org/10.5592/CO/3CroCEE.2025.161

References

[1] Silva, J. M. M. (2001), "Modal Analysis, Experimental/Measurement techniques", Encyclopedia of Vibrations, Pages 813-820, https://doi.org/10.1006/rwvb.2001.0027

[2] fib Bulletin No. 90. "Externally applied FRP reinforcement for concrete structures", Technical report, 2019, fib

[3] Ozturkoglu, Onur & Yucel, Umut & Karademir, Cihan & Durmazgezer, Erkan. (2024), "An Experimental Study on the Effect of GFRP and CFRP Strengthening on the Static and Dynamic Behavior of R/C Beams Under Progressive Damage", Applied Sciences, https://doi.org/10.3390/app14219920

[4] Baghie, N., Esfahani, M. R. and Moslem, K. (2009), "Studies on damage and FRP strengthening of reinforced concrete beams by vibration monitoring", Engineering Structures, Vol. 31, pp. 875-893, http://dx.doi.org/10.1016/j.engstruct.2008.12.009

[5] Bonfiglioli, B. and Pascale, G. (2006), "Dynamic assessment of reinforced concrete beams repaired with externally bonded FRP sheets", Mechanics of Composite Materials, Vol 42, No. 1, pp. 1-12, https://doi.org/10.1007/s11029-006-0012-9

[6] Capozucca, R. (2013), "A reflection on the application of vibration tests for the assessment of cracking in PRC/RC beams", Engineering structures, Vol. 48, pp. 508-518, https://doi.org/10.1016/j.engstruct.2012.09.022

[7] Hamad, W. I., Owen, J. S. and Hussein, M. F. M. (2014), "Modelling the degradation of vibration characteristics of reinforced concrete beams due to flexural damage", Structural Control and Health Monitoring, 2014, https://doi.org/10.1002/stc.1726

Proceedings of the 3rd Croatian Conference on Earthquake Engineering - 3CroCEE
19–22 March 2025, Split, Croatia
Copyright © 2025 CroCEE
DOI: https://doi.org/10.5592/CO/3CroCEE.2025.165

STRUCTURAL RECONSTRUCTION OF THE BELFRY, MONASTERY AND CHURCH OF ST. FRANCIS ON THE KAPTOL IN ZAGREB

Ante Mlinar [(1)], Ante Kelava [(2)], Ante Borovina [(3)], Ante Buzov [(4)]

[(1)] *Spegra d.o.o. Split, Croatia, ante.mlinar@spegra.hr*
[(2)] *Spegra d.o.o. Split, Croatia, ante.kelava@spegra.hr*
[(3)] *Spegra d.o.o. Split, Croatia, ante.borovina@spegra.hr*
[(4)] *Spegra d.o.o. Split, Croatia, ante.buzov@spegra.hr*

Abstract

This paper presents the structural reconstruction process of the St. Francis complex, which includes the belfry, monastery, and church on Kaptol in Zagreb. The complex dates back to the 13th century and is located in the heart of Zagreb's historic center. Constructed entirely in masonry, it reflects the architectural principles and construction techniques of its time, with design solutions tailored to the function of each individual space and structure. Over the centuries, the complex has endured various forms of damage caused by multiple earthquakes, fires, and wartime destruction, necessitating several phases of restoration. The most recent damage resulted from two significant earthquakes in March and December 2020, rendering the complex unfit for use. The company Spegra Ltd. from Split, Croatia, conducted a comprehensive structural rehabilitation, ensuring the building's full static and structural stability in accordance with the restoration project. To address the diverse causes and types of damage, as well as the complex structural behavior of various elements, appropriate technological solutions and materials were applied. Since the complex is a protected cultural heritage site, all restoration work was conducted with the utmost care, in close collaboration with conservation specialists and under their constant supervision.

Keywords: Spegra, Franciscan monastery, rehabilitation, structural reconstruction, earthquake

1. Introduction

The Franciscan monastery, church, and belfry form a harmonious architectural complex at Kaptol 9, in close proximity to Zagreb Cathedral, and are an integral part of the city's historic core (Fig. 1). Characterized by a diverse floor plan and dynamic spatial composition, the complex spans multiple levels, with interiors thoughtfully arranged to accommodate their respective functions. The building's overall dimensions are approximately 77.10 × 45.50 meters, with a registered floor area of 2,582.00 m², as recorded in the Land Registry. The total height, measured from the lowest point of the landscaped terrain to the top of the tower, is approximately 59.55 meters.



Figure 1. Franciscan complex, Zagreb [1]

Proceedings of the 3rd Croatian Conference on Earthquake Engineering - 3CroCEE
19–22 March 2025, Split, Croatia
Copyright © 2025 CroCEE
DOI: https://doi.org/10.5592/CO/3CroCEE.2025.165

The Franciscan presence in Zagreb dates to the 13th century. Initially, the monastery belonged to the Hungarian Province of St. Mary and served as the administrative center of the Zagreb Custody (Fig. 2). In the 17th century, it became the principal house of the newly founded Illyrian Custody of St. Ladislaus the King, which soon evolved into a province. By 1900, the monastery had become the seat of the Provincial Minister of the Croatian Franciscan Province of St. Cyril and Methodius. According to tradition, St. Francis of Assisi, founder of the Order of Friars Minor, is said to have stayed at the monastery during his journey to the Holy Land.

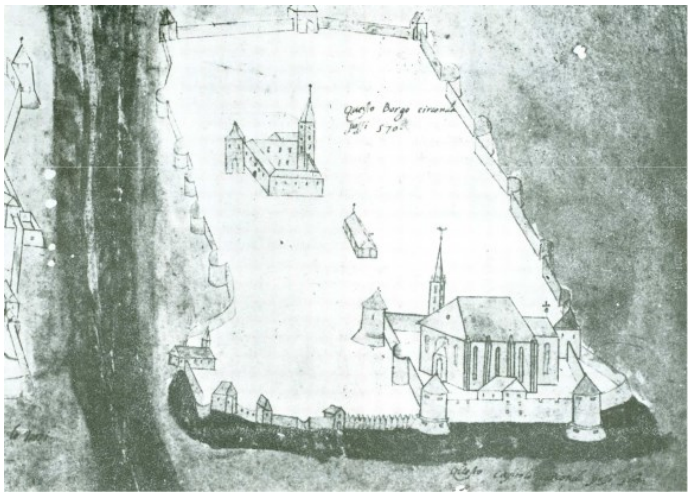


Figure 2. Photo of the plan of Kaptol at the beginning of the 16th century (Zagreb City Museum) [2]

In the 16th century, during the conflict between the supporters of Ferdinand Habsburg and John Zápolya, the monastery sustained significant damage. A few years later, around 1560, due to a dwindling number of friars, it was abandoned. At the beginning of the 17th century, Franciscan Provincial Franjo Drašković led the return of the friars to the monastery and oversaw the restoration of the church.

Throughout its history, the monastery has endured significant damage and destruction. It was devastated by the great fire of 1645, followed by fires in 1674 and 1731, the great earthquake of 1880 (Fig. 3), and heavy destruction during World War II on February 22, 1944. [3].



Figure 3. Removing the cap from the belfry of the Church of St. Francis of Assisi in Zagreb after the earthquake of 1880. [2]

Proceedings of the 3rd Croatian Conference on Earthquake Engineering - 3CroCEE
19–22 March 2025, Split, Croatia
Copyright © 2025 CroCEE
DOI: https://doi.org/10.5592/CO/3CroCEE.2025.165

The most recent damage, which led to the comprehensive structural restoration of the monastery, church, and belfry complex, was caused by the earthquakes of March and December 2020. The first earthquake, measuring M=5.5 on the Richter scale and known as the "Zagreb Earthquake," inflicted initial structural damage, striking Zagreb, and its wider metropolitan area on March 22, 2020, at 6:24 AM (Fig. 4). This main seismic event was followed by a series of aftershocks.

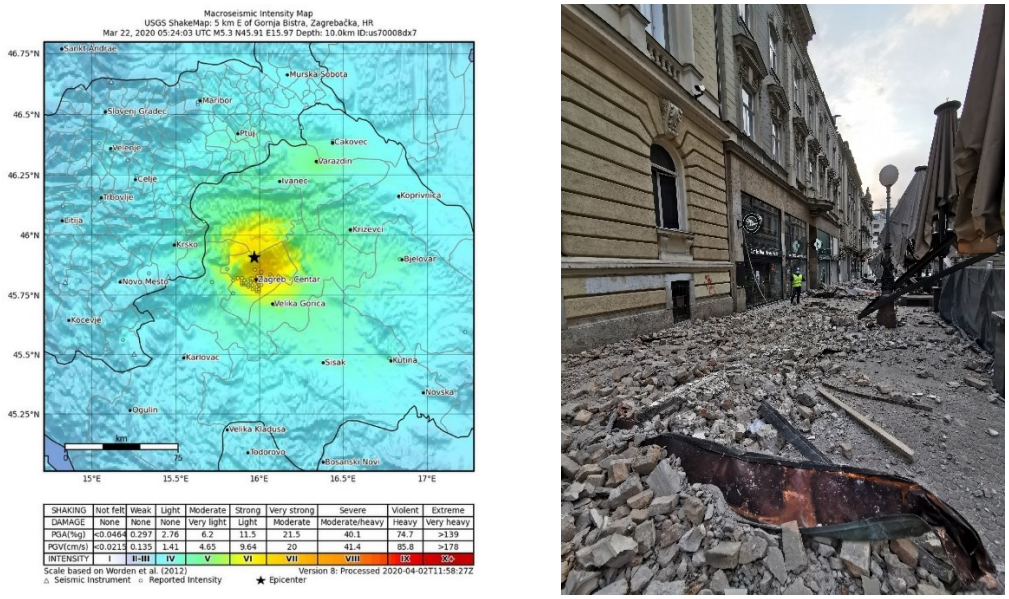


Figure 4. Macroseismic map of the “Zagreb” earthquake (March 22, 2020, at 6:24 a.m.), streets of the city of Zagreb after the earthquake [3, 1]

The second earthquake, measuring M=6.4 on the Richter scale, known as the "Petrinja Earthquake" or the "Banovina Earthquake," struck on December 29, 2020, at 12:19 PM, with its epicenter located 3 km southwest of Petrinja, heavily impacting Sisak-Moslavina County. These earthquakes caused extensive damage to the structural elements of the Franciscan complex, comprising the Church of St. Francis, the monastery building, and the bell tower. Due to the severity of the damage, the complex was taken out of use, as its structural instability posed a serious threat to human safety and a risk of further collapse. Some of the documented damage is shown in Fig. 5.



Figure 5. Photos of some damage to the structural parts of the Franciscan complex [1, 4]

Copyright © 2025 CroCEE
DOI: https://doi.org/10.5592/CO/3CroCEE.2025.165

2. Restoration works conducted in accordance with the project

To repair the damage caused by the earthquakes, a comprehensive restoration and refurbishment was planned, incorporating extensive and high-quality seismic reinforcement of the entire complex, including the church, monastery, and bell tower.

The layout of the Franciscan complex, along with its key structures, is illustrated in Fig. 6.

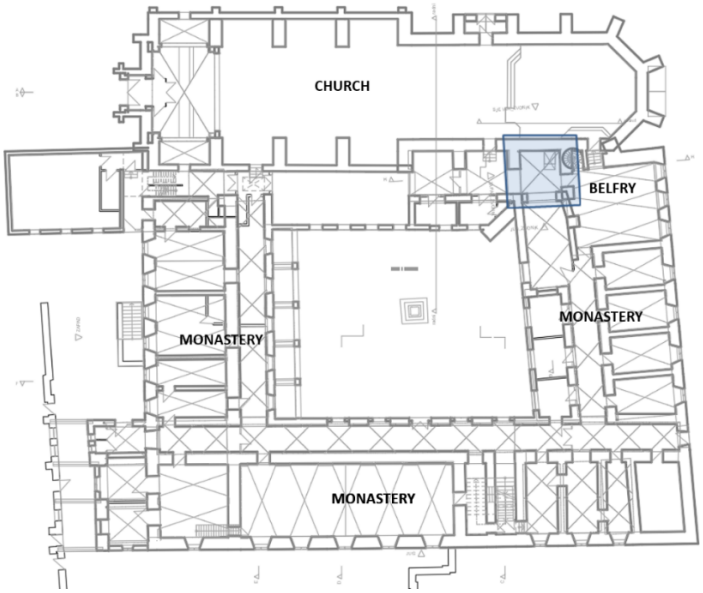


Figure 6. The layout of the Franciscan complex [5]

As per the General Urban Plan (GUP) of the City of Zagreb, the complex is situated within the city's construction zone and is recognized as a protected immovable cultural heritage site (No. Z-202). Given this designation, all planned interventions were conducted with the utmost care and expertise to ensure the preservation of both the authenticity and historical significance of the structure, as well as each of its individual elements and details. The works were conducted under the continuous presence and supervision of conservation specialists.

In accordance with the restoration project [5,6], the structural rehabilitation of the complex was organized into three key areas: the church, the belfry, and the monastery.

Works on the Church of St. Francis of Assisi:

- Installation of geotechnical micropiles adjacent to the church nave buttresses at a depth of 15 meters
- Structural rehabilitation of all walls, buttresses, and vaults of the church
- Repair and enhancement of the mechanical properties of masonry (grouting of discrete and mesh cracks in walls, repointing of masonry joints)
- Strengthening of existing walls (application of reinforced mortar, reinforcement with carbon fiber fabrics at discrete crack locations)
- Integration of existing load-bearing structural elements (installation of tie rods and carbon fiber tendons)
- Dismantling of vaults and installation of LLN arch beams in the western part of the nave
- Replacement of the church roof structure, including all roof elements
- Conservation and restoration of stone elements, paintings, and stained glass windows

Works on the belfry:

- Structural rehabilitation of the bell tower walls
- Installation of an internal lining system (thin-walled reinforced concrete linings and high-performance mortar coatings), structurally connected to the existing church walls and monastery floor structures via short slabs and beams

Proceedings of the 3rd Croatian Conference on Earthquake Engineering - 3CroCEE
19–22 March 2025, Split, Croatia
Copyright © 2025 CroCEE
DOI: https://doi.org/10.5592/CO/3CroCEE.2025.165

- Wrapping of the bell tower with carbon fiber fabrics, particularly in the areas of lintels above large openings
- Repair and enhancement of the mechanical properties of masonry (grouting of discrete and mesh cracks in walls, repointing of masonry joints)
- Installation of a new vertical circulation system within the bell tower and horizontal bracing at monastery floor levels
- Complete conservation and restoration of stone elements, including replacement of deteriorated stone components
- Replacement of the dome structure, along with all associated structural elements

Works on the monastery building:

- Reconstruction, removal, and rebuilding of masonry walls
- Demolition of massive vaults above sections of the second floor
- Removal of massive walls above the refectory, which were supported by vaults spanning the refectory
- Horizontal stiffening through the construction of vertical structural elements, including wall linings and high-performance mortar coatings
- Horizontal stiffening through the installation of floor overlays and new inter-floor slabs
- Repointing and consolidation grouting of masonry walls
- Implementation of FRCM, FRP, and VVM systems using single-sided formwork and thin reinforced concrete diaphragm slabs within inter-floor structures
- Construction of a new roof structure

2.1. Church renovation

The load-bearing walls of the church are built from massive unreinforced masonry, consisting of solid brick bonded with lime mortar. The central part of the church is covered by a masonry vault, which rests upon these walls. Due to the height of the walls and the support reactions generated by the masonry vaults, buttresses were constructed to enhance the structural stability. Given their critical role and their position as the final structural element in the load-bearing system, the buttresses suffered significant damage. Figures 7–9 showcase various rehabilitation works conducted on the buttresses, as well as their final, restored state.



Figure 7. Damage to the church's buttresses [1, 5, 4]

Copyright © 2025 CroCEE
DOI: https://doi.org/10.5592/CO/3CroCEE.2025.165



Figure 8. Renovation of the church's buttresses [1, 5]



Figure 9. The final appearance of the church's buttresses [1]

As previously noted, the vaults of the church are constructed as massive masonry structures. The first earthquake ("Zagreb Earthquake") caused significant structural damage to the vault, necessitating immediate shoring to prevent collapse. This temporary support system proved crucial in preventing further deterioration, not only of the vault itself but also of other structural elements of the church during the second earthquake ("Petrinja Earthquake"). Despite these stabilization efforts, the western section of the vaulted ceiling, having sustained severe initial damage, could not be effectively preserved or repaired. Consequently, it was replaced with a honeycomb-structured system made of glulam (laminated timber), over which prestressed hollow-core slabs were installed to enhance structural integrity. Figures 10–12 illustrate the extent of the vault damage, as well as its final restored condition following rehabilitation.

Copyright © 2025 CroCEE
DOI: https://doi.org/10.5592/CO/3CroCEE.2025.165



Figure 10. Damage to the church vaults [4, 5]

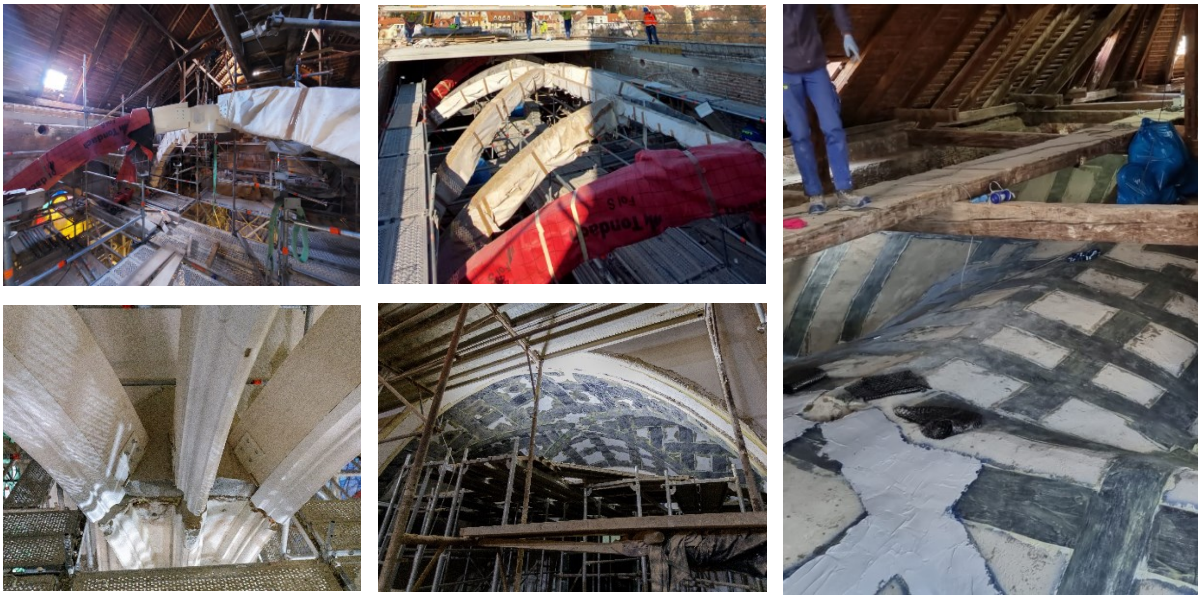


Figure 11. Renovation of church vaults [1]

Copyright © 2025 CroCEE
DOI: https://doi.org/10.5592/CO/3CroCEE.2025.165

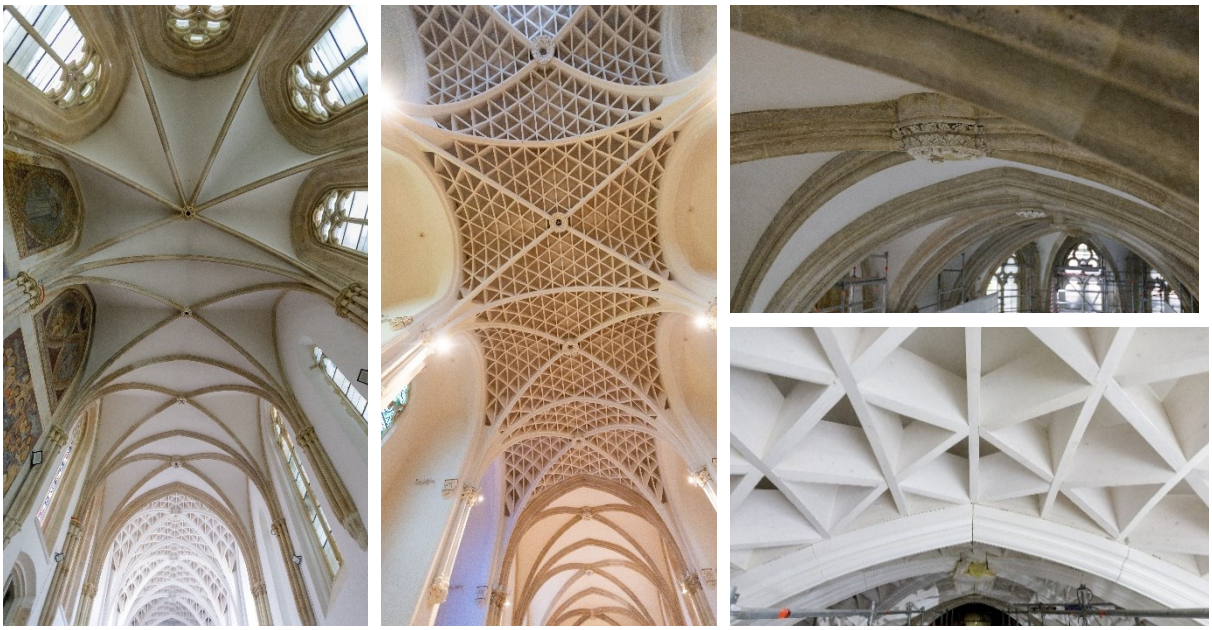


Figure 12. The final appearance of the church vaults [1]

The damage sustained by the church walls, particularly the western gable wall, which suffered the most severe deterioration, along with the rehabilitation measures undertaken, is illustrated in Figures 13–15.



Figure 13. Damage to church walls [1, 5]

Copyright © 2025 CroCEE
DOI: https://doi.org/10.5592/CO/3CroCEE.2025.165



Figure 14. Repair of church walls [1]



Figure 15. The final appearance of the church [1]

2.2. Renovation of the belfry

In plan view, the belfry transitions from a trapezoidal base to a square footprint, measuring 6.0 × 6.6 m, with a total height of 59.55 m. Over the centuries, it has undergone various structural modifications and sustained multiple instances of damage. By the time of the recent earthquakes, it stood as a masonry structure with large openings, featuring wooden staircases and galleries, while the bells were supported by a metal framework. The damage observed in the cantilevered section of the belfry is consistent with its structural frame system with rigid crossbeams, where cracks developed in the lintels due to seismic forces. Figures 16–18 illustrate key damage patterns, the rehabilitation process, and the final restored condition of the belfry.

Copyright © 2025 CroCEE
DOI: https://doi.org/10.5592/CO/3CroCEE.2025.165



Figure 16. Belfry damage [5, 1]



Figure 17. Belfry renovation [1]

Copyright © 2025 CroCEE
DOI: https://doi.org/10.5592/CO/3CroCEE.2025.165



Figure 18. The final appearance of the belfry [1]

2.3. Renovation of the Monastery

The monastery, much like the rest of the Franciscan complex, has endured multiple instances of structural damage and deterioration throughout its history. With a footprint of 55 × 38 m, it comprises a partially underground basement, a ground floor, two upper floors, and an attic. Built as a massive masonry structure, its irregular configuration in both plan and elevation contributed to significant structural distress during the Zagreb and Petrinja earthquakes. Figures 19–21 provide an overview of the damage sustained, the rehabilitation process, and the final restored state of the monastery.



Figure 19. Damage to the monastery [1, 4, 5]

Copyright © 2025 CroCEE
DOI: https://doi.org/10.5592/CO/3CroCEE.2025.165



Figure 20. Monastery renovation [1]



Figure 21. The final appearance of the monastery [1]

3. Conclusion

As a result of the devastating impact of the two recent earthquakes and the structural condition of the Franciscan complex (belfry, monastery, and the Church of St. Francis) significant structural damage was sustained throughout the site. Consequently, the entire complex was deemed unsafe for use and temporarily secured to prevent further deterioration or collapse. A comprehensive structural reconstruction and strengthening project was conducted by Spegra Ltd, Split, Croatia, under the leadership of Chief Site Engineer Ante Mlinar, MCE, and Site Engineer Ante Kelava, MSc. Civ. Eng. The project incorporated conceptual and engineering reinforcement measures in accordance with the design solution developed by lead architect Damir Foretić, MCE, and structural engineer Prof. Dr. Sc. Boris Trogrlić, MCE. The project spanned 34 months, with a total cost of €20,000,000.00. The restoration and strengthening works involved a diverse range of engineering methodologies and advanced technologies, carefully selected to align with the specific needs of each structural intervention. Since the Franciscan complex is a protected cultural heritage site, all work was conducted under strict supervision and in close collaboration with conservators, ensuring the preservation of its historical and

Copyright © 2025 CroCEE
DOI: https://doi.org/10.5592/CO/3CroCEE.2025.165

architectural integrity. Figure 22 provides a selection of views and detailed snapshots capturing various stages of the reconstruction process.



Figure 22. Some views and details [1, 4]

4. References

[1] Own archive of the company Spegra Ltd

[2] https://ika.hkm.hr/novosti/zagrebacka-nadbiskupija-samostanska-crkva-sv-franje-asiskoga-u-zagrebu/

[3] https://hr.wikipedia.org/

[4] Archive of licensed architect Damir Foretić, civil engineer.

[5] Damir Foretić ing.građ., Ivan Foretić d.i.a., Filip Foretić mag.ing.aedif., dr.sc. Boris Trogrlić dipl.ing. građ., Đuro Nižetić dipl.ing. građ., Milko Batinić mag.ing. aedif., Ines Vlahović dipl.ing. građ., dr.sc. Hrvoje Smoljanović dipl.ing. građ., dr.sc. Ivan Balić dipl.ing. građ.: Project for the complete renovation of the building structure – Construction project - Main structural design. Foretić i sinovi d.o.o. June 2021.

Copyright © 2025 CroCEE
DOI: https://doi.org/10.5592/CO/3CroCEE.2025.165

[6] Damir Foretić ing.građ., Ivan Foretić d.i.a., dr.sc. Boris Trogrlić dipl.ing. građ., Dorja Prekratić d.i.a., Nikola Pašalić i.g.: Glavni projekt – Architectural project for the renovation of the Franciscan monastery, church and belfry. Foretić i sinovi d.o.o. July 2021.

Proceedings of the 3rd Croatian Conference on Earthquake Engineering - 3CroCEE
19–22 March 2025, Split, Croatia
Copyright © 2025 CroCEE
DOI: https://doi.org/10.5592/CO/3CroCEE.2025.98

INCREASING STRUCTURAL RESILIENCE: A CASE STUDY OF HOSPITAL RETROFITTING IN ALBANIA

Izet Mehmetaj[(1)], Erjon Çobani[(2)], Armela Kalliri

[(1)] *Assistant Lecturer, Metropolitan Tirana University, imehmetaj@umt.edu.al*
[(2)] *PhD Candidate, Polis University, erjon_cobani@universitetipolis.edu.al*

Abstract

The structural stability of many buildings, including important institutions like hospitals, was seriously affected following the 2019 earthquake in Albania. This paper presents a detailed case study of the retrofitting project undertaken for a hospital in Albania, which experienced significant damage during the earthquake. The primary objective of this project was to restore and improve the hospital's structural stability, ensuring its functionality in future seismic events.

The retrofitting strategy used a combined approach, including reinforced concrete jacketing of the masonry walls, installing steel framing for the masonry openings, and using textile-reinforced mortar (TRM) to strengthen the infill walls. Additionally, new reinforced concrete (R/C) walls were added to improve structural irregularity. These measures are designed to address specific weaknesses identified in the existing hospital structure.

This paper discusses the complete assessment of the hospital's structural condition, the design and implementation of retrofitting solutions, and the challenges encountered during the project. The results demonstrate the effectiveness of these retrofit techniques in increasing the seismic performance of the hospital. The findings provide valuable insights and practical recommendations for similar retrofit projects in earthquake-prone regions.

Keywords: structural resilience, retrofitting, post-earthquake reconstruction, building safety, earthquake-resilient design

1. Introduction

The devastating earthquake that struck northwest Albania on November 26, 2019, had a moment magnitude of Mw 6.4 and revealed significant vulnerabilities in the country's building infrastructure [1]. The earthquake caused extensive damage across at least 11 municipalities, including the populated cities of Tirana and Durrës. It impacted over 200.000 people, resulting in 51 fatalities, over 900 injuries, and substantial displacement of residents. The collapse of 10 buildings in Durrës and Thumanë underscored the urgent need for improved seismic resilience in the housing sector [2].

Additionally, the earthquake exposed critical deficiencies in the seismic design codes and construction practices for essential structures, such as educational institutions and healthcare facilities. Damage was reported in 321 educational institutions and 36 healthcare facilities, with estimated damage costs of approximately 64 million euros and 10 million euros, respectively [3] [4]. The absence of established procedures for retrofitting these vital buildings further magnified the earthquake's impact, highlighting the necessity for standardized retrofitting guidelines and processes [2] [3] [4] [5].

The Earthquake Engineering Field Investigation Team (EEFIT) conducted a mission to assess the damage, primarily focusing on the housing sector [3]. Their findings emphasized the need for comprehensive retrofitting programs that address both residential buildings and critical infrastructure. The earthquake's effects on educational institutions, healthcare facilities, and other essential buildings illustrated the importance of a multi-faceted approach to retrofitting that considers all potential vulnerabilities [5].

Copyright © 2025 CroCEE
DOI: https://doi.org/10.5592/CO/3CroCEE.2025.98

This paper addresses these deficiencies by presenting a thorough assessment of the structural conditions and necessary retrofitting measures for the affected buildings. The study includes detailed documentation of the damages, and advanced seismic performance assessments. The findings and recommendations from this project provide valuable insights for future retrofitting initiatives in earthquake-prone regions, stressing the importance of a holistic approach to retrofitting to ensure the safety and resilience of both residential and critical infrastructure.

2. Assessment of Structural Damage

2.1. Initial condition of the hospital post-earthquake

The building, located at the University Hospital Center "Mother Teresa" (QSUNT) in Tirana, currently functions as a hospital unit. Constructed between 1984-1985, it comprises three independent units: a 2-story load-bearing masonry structure (Unit A), a 4-story reinforced concrete skeleton structure with prefabricated elements and perforated brick walls (Unit B), and a 2-story load-bearing reinforced masonry structure (Unit C).

Over the years, interventions have included expansions and openings of doors and windows for access. On the ground floor, some windows have been converted into doors, and new door/window openings have been created. At higher levels, new window openings are concentrated in the transverse load-bearing walls of the exterior facades. Interventions have also been observed in the internal longitudinal and transverse walls, mainly in the form of new doors or door expansions. The most significant interventions have been observed on the ground floor.

In its current condition, minor structural damages due to seismic activity have been observed in elements such as columns, beam-column joints of prefabricated elements, and load-bearing walls. These damages manifest as fine cracks. Non-structural damages are widespread, primarily affecting infill and partition walls, which have been compromised due to interaction with the main structure, especially at their contact points with structural elements. Another issue is the corrosion of steel bars in reinforced concrete elements caused by moisture presence. Additionally, plaster on the facade and protective layers of reinforced concrete elements have suffered damages in many areas.

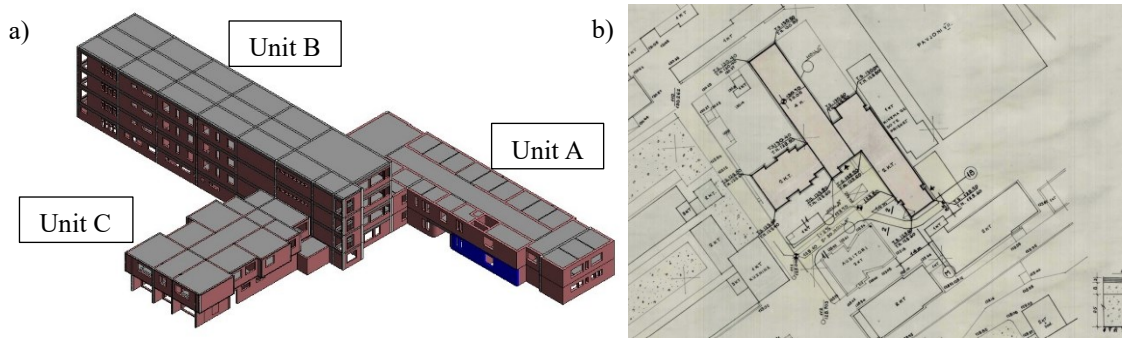


Figure 1. a) The current hospital building in a 3D model; b) Fragment from the original construction project

2.2. Methods used for structural assessment

The seismic assessment of buildings relies on the collection of factual data. This process includes obtaining available documents, field observations, investigations, and photographic documentation. For the building in question, an in-depth expert report has been conducted before, serving as a fundamental basis for understanding the structure and identified issues.

Copyright © 2025 CroCEE
DOI: https://doi.org/10.5592/CO/3CroCEE.2025.98



Figure 2. Observed post-earthquake damages: a), b) corrosion of reinforcement bars; c) Cracks and detachment of plaster layers.

However, in drafting the structural retrofitting project, a detailed field investigation was necessary. The primary objectives of the structural retrofitting project were to ensure the accuracy of the provided drawings and determine the basic information of the buildings. This involved verifying the existing documentation and conducting detailed field investigations to identify any visible structural damages, such as cracks or fractures. These steps were crucial to understanding the current state of the building and planning the necessary interventions.

Additionally, the investigation also aimed to identify potential risks from non-structural elements that could pose a danger if they were to fall. This included assessing ceilings, partition walls, mechanical systems, and other non-structural building elements. Documenting the existing conditions with photographs was also a key objective, providing a visual record to support the findings and recommendations for the retrofitting process.

The data collection process, in addition to field observations and photographic documentation, also includes obtaining existing building documents. For the realization of the structural intervention project, the following documentation was made available:

1. The in-depth expert report conducted for the assessment of the structural capacity, dated 30.04.2020 [6];
2. The implementation project and its specifications for the building, from the Central Technical Archive, including the architectural project, structural project, electrical project, and mechanical project [7].

The collected information and recommendations from the in-depth expert report served as the fundamental basis for the realization of the structural intervention project. Based on the collected data, recommendations from Table 3.1, SSH EN 1998-3, and the conducted in-depth expert report, the level of knowledge KL2 (normal knowledge) has been determined, with a reliability factor CF_{KL2}=1.2 [8].

2.3. Key findings from the previous structural assessments

The in-depth earthquake damage assessment has clearly established the following critical findings.

The 2-story load-bearing reinforced masonry building (Unit C) has sustained corrosion in its reinforced concrete elements and the Unit A displays only minor overall damage. In contrast, the 4-story reinforced concrete skeleton structure (Unit B), which incorporates prefabricated elements and perforated brick walls, shows significant deficiencies including cracks and detachment in plaster layers, minor cracks in beams, corrosion of reinforcement bars, inadequate concrete cover, and voids at column-beam joints.

Material tests confirmed that the concrete grades are C30/37 for the prefabricated structure and C12/16 and C16/20 for the others. Importantly, the reinforcement steel meets the project specifications despite existing corrosion. The masonry characteristics adhere to KTP 9-78 standard [9], utilizing M-75 class bricks and M-25 class mortar.

Proceedings of the 3rd Croatian Conference on Earthquake Engineering - 3CroCEE
19–22 March 2025, Split, Croatia
Copyright © 2025 CroCEE
DOI: https://doi.org/10.5592/CO/3CroCEE.2025.98

Seismic performance assessments, executed per Eurocode 8, Part 3, were comprehensive, employing both linear and nonlinear analyses with a ground acceleration of a_{gR}= 0.240g on type B soil. The assessment rigorously considered significant damage states with a seismic action probability of 10% over 50 years.

The analysis definitively concludes that the load-bearing capacity of the 2-story reinforced masonry building (Unit C) is insufficient, and the two additional buildings fail to meet required performance (Unit A and B). Consequently, retrofitting interventions for all units are not just recommended but essential.

The findings from the in-depth study were crucial for preparing the retrofitting project. They offered a comprehensive understanding of the existing structural conditions, including the identification of damages and material characteristics.

This information was essential for developing effective retrofitting strategies tailored to the specific issues identified in each building unit. In addition to relying on the conclusions from the in-depth study, further investigations were conducted to verify and enhance the recommendations. These additional investigations confirmed the accuracy of the study's findings and provided further insights that were incorporated into the retrofitting plans.

This combined approach ensures that the retrofitting interventions are based on a thorough and accurate assessment of the current structural conditions, leading to more effective and reliable solutions. By integrating the findings from both the in-depth study and the additional investigations, the retrofitting project will address the identified structural deficiencies while also improving the overall safety and resilience of the buildings. This comprehensive strategy is vital for ensuring the long-term stability and functionality of the structures.

3. Retrofitting Strategy

3.1. Challenges encountered during the project

The project faced several significant challenges. Identifying and documenting minor structural damages, such as fine cracks in columns, beam-column joints, and load-bearing walls, required careful field observations and detailed photographic documentation. Widespread non-structural damages in infill and partition walls posed another challenge, necessitating extensive fieldwork to accurately record the affected areas. Corrosion of steel bars in reinforced concrete elements due to moisture presence further complicated the project, impacting the structural integrity of the buildings.

To address these challenges, several solutions and adaptations were implemented. Enhanced documentation efforts, including detailed photographic records and field observations, were undertaken to accurately identify and catalogue both structural and non-structural damages. Advanced seismic performance assessments were conducted using both linear and nonlinear analyses to accurately evaluate the buildings' response to seismic activity. By integrating the findings from the in-depth study with additional investigations, a thorough and accurate assessment was achieved, leading to more effective and reliable retrofitting solutions.

3.2. Overview of the Chosen Retrofitting Techniques

In earthquake-prone regions such as Italy, Greece, and Turkey, structural retrofitting is essential to enhance the resilience of buildings against seismic activity [10] [11] [12]. By strengthening the structural integrity of existing buildings, retrofitting helps ensure that they can withstand seismic forces more effectively [13] [14]. This proactive approach not only preserves the building but also contributes to the overall safety and sustainability of communities in these regions.

Copyright © 2025 CroCEE
DOI: https://doi.org/10.5592/CO/3CroCEE.2025.98

Several advanced techniques are recommended as best practices for the restoration of buildings. Similar methods, extensively utilized across Europe, were chosen as rehabilitative interventions and are described as follows:

1. Jacketing of Masonry Walls: Applying reinforced concrete jacketing with a steel mesh to masonry walls to enhance their strength and stability.
2. Metallic Framing of Masonry Openings: Adding metal profiles to contour openings in masonry walls, such as doors and windows, to improve structural integrity.
3. Textile Reinforced Mortar (TRM) for Infill Wall Reinforcement: Using the TRM system to reinforce infill walls and appropriately connect them to the surrounding reinforced concrete frame.
4. Addition of New Reinforced Concrete (R/C) Walls: Introducing new reinforced concrete walls to create structural regularity and enhance overall stability.

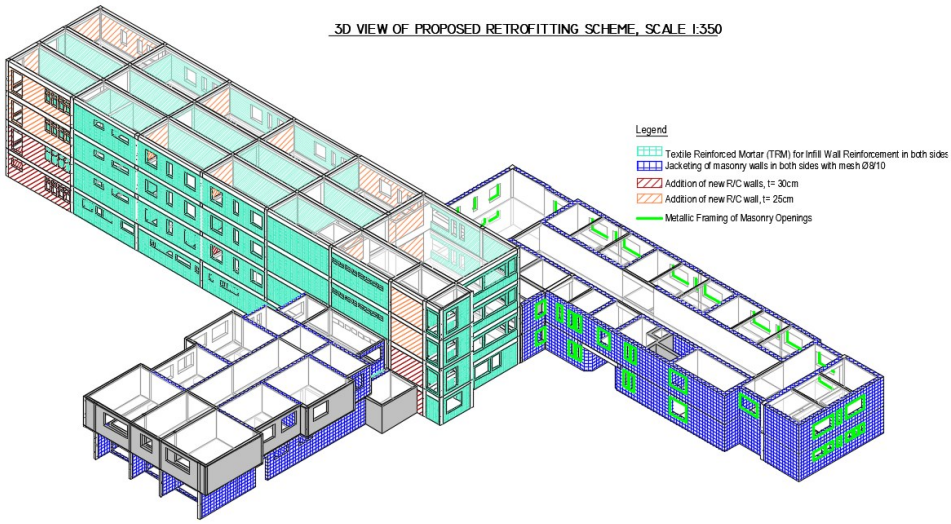


Figure 3. Proposed scheme for implementing the rehabilitation structural interventions.

4. Results and Discussion

A mathematical model was developed to assess the load-bearing capacity of the building in its retrofitting state, following the requirements of SSH EN 1998-3. This model incorporates the geometric dimensions of the structure, the physical and mechanical properties of the materials, permanent and temporary loads, and the proposed retrofitting interventions, which are based on findings from the previously conducted report. The loads used in this analysis were sourced from that same in-depth expert report.

The program 3Muri/TreMuri was utilized for seismic calculations in accordance with Eurocode 8 for the reinforced condition of the two-story units, which features a load-bearing masonry system. For both units, the verification criteria for the building's reinforced condition essentially involve ensuring that the demand, calculated using permitted analysis methods, does not surpass the capacity.

Copyright © 2025 CroCEE
DOI: https://doi.org/10.5592/CO/3CroCEE.2025.98

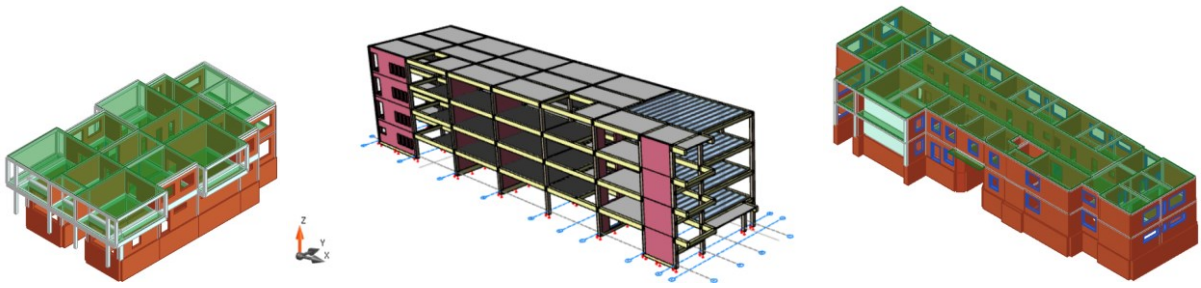


Figure 4. Numerical models of the units: Unit A (right), Unit B (middle), and Unit C (left).

This is assessed by calculating the risk index α (α_{SD}). The seismic vulnerability index (α) serves as an indicator to determine whether the capacity has been exceeded.

The modeling, along with static and dynamic analysis, of the reinforced condition of the four-story unit was conducted using the ProtaStructure calculation program and integrated with OpenSees. According to SSH EN1998-3:2005, Annex A, point A.3.2.3, the structure's capacity assessment for the significant damage limit state is taken as equal to three-fourths of the ultimate displacement capacity of the structure. The ultimate displacement capacity is defined as the displacement at the curve point where the lateral resistance (base shear force) falls below 80% of the peak resistance (the highest point on the curve), due to progressive damage and the failure of elements that resist lateral loads. The target displacement is calculated based on SSH EN 1998-1 (Annex B) for the specified seismic loading.

For each constituent unit, verification is performed according to the significant damage limit state (SD). Additionally, the seismic demand is accepted as increased by an importance factor of 1.4. The seismic loading, per Eurocode standards, relies on the findings of the previous expert report, where the ground acceleration was accepted as a_{gR}=0.240g, with the soil type classified as B.

The seismic vulnerability indices according to SSH EN 1998:1 indicate that the Unit A in its reinforced state, meets the required capacity criterion in both directions. The same conclusion also applies to Unit C.

On the other hand, for the Unit B, there is a high probability of sustaining significant controlled damage if it experiences an earthquake, in reference to the seismic demand and Eurocode requirements.

Table 1. Result details for the Unit A

Unit	Limit state	PGA (m/s^2)	α_{SD}
X direction	SD	4.016	1.706
Y direction	SD	2.528	1.074

Table 2. Result details for the Unit C

Unit	Limit state	PGA (m/s^2)	α_{SD}
X direction	SD	2.938	1.248
Y direction	SD	4.404	1.871

Proceedings of the 3rd Croatian Conference on Earthquake Engineering - 3CroCEE
19–22 March 2025, Split, Croatia
Copyright © 2025 CroCEE
DOI: https://doi.org/10.5592/CO/3CroCEE.2025.98

Table 3. Result details for the Unit B

Unit	Limit state	Defined level of performance	% of members in significant damage region
X direction	SD	Significant damage	97%
Y direction	SD	Significant damage	100%

4.1. Evaluation of the retrofitting effectiveness

The retrofitting effectiveness can be evaluated by examining the improvements in the structural capacity and seismic performance of the buildings. The mathematical calculation model, which includes geometric dimensions, material properties, and proposed interventions, provides a comprehensive assessment of the reinforced condition. The use of advanced programs like 3Muri/TreMuri and ProtaStructure, along with OpenSees integration, ensures accurate modeling and analysis. The findings indicate that the retrofitting interventions have significantly enhanced the load-bearing capacity and seismic resilience of the buildings.

4.2. Comparison of pre- and post-retrofitting structural performance

The comparison of pre- and post-retrofitting structural performance reveals substantial improvements. In the pre-retrofitting condition, the buildings exhibited various structural and non-structural damages, including fine cracks, corrosion of steel reinforcement bars, and insufficient concrete cover. The seismic performance assessment indicated limited capacity to withstand seismic loads. In contrast, for both Unit A and C, the post-retrofitting condition shows enhanced structural integrity, with the buildings meeting the required capacity criteria in both X and Y directions. The reinforced condition of the Unit B building demonstrates a high probability of sustaining significant damages during an earthquake, highlighting the effectiveness of the retrofitting interventions.

4.3. Insights gained and lessons learned

Several insights and lessons have been gained from this project. First, the importance of thorough documentation and field observations in identifying and cataloguing damages cannot be overstated. Accurate data collection is crucial for developing effective retrofitting strategies. This project highlighted the need for thorough attention to detail in documenting both structural and non-structural damages, as even minor issues can significantly impact the overall structural integrity.

Second, advanced seismic performance assessments are essential for ensuring that retrofitting interventions meet the required standards. The use of programs like 3Muri/TreMuri and ProtaStructure, along with OpenSees integration, provided accurate modeling and analysis, leading to reliable solutions. This approach emphasized the value of leveraging advanced technology and software in structural engineering to achieve precise and dependable results.

Third, integrating findings from both in-depth studies and additional investigations leads to more reliable and effective retrofitting solutions. By combining the insights from the expert report with on-site verifications, a more holistic understanding of the building's condition was achieved. This comprehensive approach ensured that the retrofitting interventions were tailored to address the specific needs of each building unit, resulting in more effective and sustainable solutions.

The specific interventions implemented included reinforced concrete jacketing with a steel mesh for load-bearing walls, contouring openings with metal profiles, reinforcing infill walls with the TRM system, adding new reinforced concrete walls for structural regularity, cleaning and removing rust from

Proceedings of the 3rd Croatian Conference on Earthquake Engineering - 3CroCEE
19–22 March 2025, Split, Croatia
Copyright © 2025 CroCEE
DOI: https://doi.org/10.5592/CO/3CroCEE.2025.98

steel bars. These interventions provided valuable lessons on the importance of using appropriate materials and techniques to enhance structural integrity and resilience.

One critical insight gained from these interventions is the necessity of a multi-faceted approach to retrofitting. Each intervention addressed a specific aspect of the building's structural deficiencies, highlighting the need for a comprehensive strategy that considers all potential vulnerabilities. Additionally, the project demonstrated the importance of continuous monitoring and maintenance to ensure the long-term effectiveness of the retrofitting measures. Regular inspections and timely repairs can prevent minor issues from escalating into major structural problems.

Another lesson learned is the significance of collaboration and communication among all stakeholders involved in the project. Effective coordination between engineers, architects, contractors, and other professionals is essential for the successful implementation of retrofitting interventions. Clear communication and a shared understanding of the project's goals and challenges can lead to more efficient and effective solutions.

Finally, the insights gained and lessons learned from this project will be invaluable for future retrofitting efforts. By applying these lessons, future projects can achieve greater structural resilience and safety, ensuring that buildings are better prepared to withstand seismic events.

5. Conclusion

The in-depth study has provided a thorough understanding of the structural conditions and necessary retrofitting measures for the buildings. Key findings include the identification of minor structural damages such as fine cracks in columns, beam-column joints, and load-bearing walls, as well as widespread non-structural damages in infill and partition walls. Corrosion of steel bars in reinforced concrete elements due to moisture presence was a significant issue, impacting the structural integrity. The seismic performance assessment revealed limited capacity for Unit C and insufficient capacity for the other two units, Unit A and Unit B. The retrofitting interventions, including reinforced concrete jacketing, contouring openings, reinforcing infill walls, adding new reinforced concrete walls, cleaning and removing rust from steel bars, have significantly improved the structural integrity and seismic resilience of the buildings.

The findings and interventions from this project have several implications for future retrofitting projects in earthquake-prone regions. First, thorough documentation and field observations are essential for accurately identifying and documenting damages. This ensures that retrofitting strategies are tailored to address specific structural deficiencies. Second, addressing corrosion issues was a critical step in improving structural integrity. The use of protective coatings and corrosion-resistant materials can prevent further deterioration and extend the lifespan of the building. Third, comprehensive material testing and advanced seismic performance assessments are crucial for ensuring that retrofitting interventions meet the required standards. Leveraging advanced technology and software in structural engineering can lead to precise and reliable solutions. Finally, a multi-faceted approach to retrofitting, which considers all potential vulnerabilities, is necessary for achieving greater structural resilience and safety.

Further research is recommended to build on the findings and insights gained from this project. Future studies should focus on developing more advanced and cost-effective retrofitting techniques that can be easily implemented in Albania. Additionally, research should explore the long-term effectiveness of various retrofitting interventions, including their impact on the overall structural integrity and resilience of buildings. Investigating the use of innovative materials and technologies, can provide valuable insights into their potential applications in retrofitting projects. Finally, continuous monitoring and maintenance of retrofitted buildings should be emphasized to ensure the long-term success of the interventions and prevent minor issues from escalating into major structural problems.

Copyright © 2025 CroCEE
DOI: https://doi.org/10.5592/CO/3CroCEE.2025.98

One critical issue highlighted by this project is the lack of established procedures for retrofitting important buildings, such as hospitals, in Albania. The 2019 earthquake in Albania caused considerable damage to many such buildings, underscoring the urgent need for standardized retrofitting guidelines and procedures. Developing and implementing these procedures will be essential for ensuring the safety and resilience of critical infrastructure in future seismic events.

Acknowledgements

We would like to extend our gratitude to Engineer Ardit Bedhia for his invaluable guidance and solid motivation throughout this project. His expertise and encouragement have been instrumental in driving the success of this endeavour. Without his support, this project would not have reached its full potential.

References

[1] Moshou, A., Dushi, E., Argyrakis P.: *A Preliminary Report On The 26 November 2019, Mw=6.4Durres, Albania*, Euro-Mediterranean Seismological Centre, France, https://www.emsc-csem.org/Files/news/Earthquakes_reports/Preliminary_Report_Albania_26112019.pdf?form=MG0AV3, (accessed December 2, 2024)

[2] Lekkas, E., Mavroulis, S., Papa, D., Carydis, P. (2019). The November 26, 2019 Mw 6.4 Durrës (Albania) earthquake. *Newsletter of Environmental, Disaster and Crises Management Strategies*, 15, ISSN 2653-9454, doi: 10.13140/RG.2.2.23801.29281

[3] Andonov, A., Baballëku, M., Baltzopoulos, G., Blagojević, N., Bothara, J., Brûlé, S., Brzev, S., Carydis, P., Duni, L., Dushi, E., Freddi, F., Gentile, R., Giarlelis, C., Greco, F., Guri, M., Isufi, B., Koçi, R., Lekkas, E., Marinković, M., Markogiannaki, O., Mavroulis, S., McKenney, C., Milićević, I., Novelli, V., Sextos, A., Sim, C., Skoulidou, D., Stefanidou, S., Theodoulidis, N., Turner, F., Veliu, E.*: EERI Earthquake Reconnaissance Report: M6.4 Albania Earthquake on November 26, 2019*, https://lfestorage.s3.us-east-2.amazonaws.com/images/earthquakes/2019_Albania_Earthquake/EERI_Earthquake_Reconnaissance_Report_-_M6.4_Albania_Earthquake_on_November_26_2019.pdf, (accessed December 2, 2024)

[4] Andonov, A., Andreev, S., Freddi F., Greco F., Gentile, R.., Novelli, V., Veliu E.: The Mw6.4 Albania Earthquake On The 26th November 2019, A Field Report By EEFIT, Earthquake Engineering Field Investigation Team, The Institution of Structural Engineers International HQ, https://www.istructe.org/IStructE/media/Public/Resources/report-eefit-mission-albania-22102020.pdf, (accessed December 2, 2024)

[5] Sextos, A., Lekkas, E., Stefanidou, S., Baltzopoulos, G., Fragkiadakis, M., Giarlelis, C., Lombardi, L., Markogiannaki, O., Mavroulis, S., Plaka, A., Pnevmatikos, N., Skoulidou, D., Tsiatas, G., Tsopelas, P., Albania earthquake of November 26, 2019, https://www.elekkas.gr/images/stories/pdfdocs/ETAM-Report_Albania2019EQ.pdf, (accessed December 2, 2024)

[6] Polytechnic University of Tirana (2020): Technical Report, In-Depth Structural Analysis, Tirana, Albania.

[7] Central Technical Archive (2023): Original construction project and documentation, Tirana, Albania.

[8] European Committee for Standardization (2005): *Eurocode 8: Design of structures for earthquake resistance-Part 3: Assessment and retrofitting of buildings*, The European Union.

[9] Ministria e Ndërtimit (1978): Kushte teknike projektimi: Llogaritja e mureve dhe themeleve me teorinë e gjendjes kufitare (KTP 9-78), Tirana, Albania.

[10] Fehr M., Baur M., Genesio G., Seismic retrofitting of an existing hospital with external steel brace, SMAR 2024 – 7th International Conference on Smart Monitoring, Assessment and Rehabilitation of Civil Structures, Salerno, Italy, 8 pages.

[11] Bournas, D. (2018): Innovative Materials for Seismic and Energy Retrofitting of the Existing EU Buildings, EUR 29184 EN, Publications Office of the European Union, Luxembourg.

Copyright © 2025 CroCEE
DOI: https://doi.org/10.5592/CO/3CroCEE.2025.98

[12] Pisapia, A., Piluso, V., Montuori, R., Nastri, E., Frattolillo, C. (2023): Seismic Assessment and Structural Retrofitting of the Day-Hospital Building "G. Pascale Foundation", Appl. Sci. 2023, 13, 1663, doi: https://doi.org/10.3390/app13031663

[13] Carofilis, W., Perrone, D., O'Reilly, G. J., Monteiro, R., & Filiatrault, A. (2020): Seismic retrofit of existing school buildings in Italy: Performance evaluation and loss estimation. Engineering Structures, 225, 111243, doi: https://doi.org/10.1016/j.engstruct.2020.111243

[14] Pertile, V., Stella, A., De Stefani, L., Scotta, R. (2021): Seismic and Energy Integrated Retrofitting of Existing Buildings with an Innovative ICF-Based System: Design Principles and Case Studies. Sustainability 2021, 13, 9363, doi: https://doi.org/10.3390/su13169363

Proceedings of the 3rd Croatian Conference on Earthquake Engineering - 3CroCEE
19–22 March 2025, Split, Croatia
Copyright © 2025 CroCEE
DOI: https://doi.org/10.5592/CO/3CroCEE.2025.101

POST-EARTHQUAKE RECONSTRUCTION IN THE ZAGREB SETTLEMENTS MARKUŠEVAC AND ČUČERJE

Svirčić Gotovac, Anđelina [(1)], Zlatar Gamberožić, Jelena [(2)]

[(1)] *Scientific Adviser, Institute for Social Research in Zagreb, svircic@idi.hr*
[(2)] *Senior Research Associate, Institute for Social Research in Zagreb, jelena@idi.hr*

Abstract

The Zagreb settlements of Markuševec and Čučerje were significantly affected by the 2020 Zagreb earthquake, and over the past four years have been undergoing a process of both technical and socio-demographic renewal. The analysis of post-earthquake renovation in these settlements was carried out by qualitative methodology and semi-structured interviews. They were conducted during the year 2024 (from May to September) on a sample of 20 residents and experts (16 residents and 4 experts in the construction profession). The research focus was on reconstruction models of damaged houses and the program for obtaining replacement houses, as well as the secondary accommodation of residents during the process of renovation. The results showed that the majority of residents went through the process of renovation by owners (self-renovation) and independent involvement in the renovation of their houses. They relied only partially on the help of the City of Zagreb and the Ministry of Physical Planning, Construction and State Assets, both in the administrative and financial sense. A smaller part decided for constructive reconstruction in administrative agreement with the Ministry, primarily those whose houses were demolished. The position of residents, who lived in temporary accommodation and in the so-called container houses or in isolated parts of their property that they reconstructed ad hoc, was particularly difficult. According to the different situations in which the residents found themselves we can conclude that they believe that, regardless of the great investment of the state, they were not adequately and on time returned to their own houses. Their expectations were focused on a permanent return to their own houses and to their property, especially because they are mostly elderly and therefore do not want to move out compared to the younger population.

Keywords: Zagreb settlements Markuševec and Čučerje, post-earthquake reconstruction, self-renovation, replacement houses, satisfaction with the reconstruction process

1. Introduction

Two earthquakes hit the City of Zagreb and the areas near Zagreb's northern settlements Markuševec and Čučerje in 2020. The first one occurred on March 22 at 6:24 a.m. with a magnitude of 5.5 on the Richter scale and had its epicentre in Markuševec, 7 kilometres from Zagreb, at a depth of ten kilometres. After the earthquake, some projections show that more than six thousand buildings, public and private, were temporarily unusable (multifamily buildings, kindergartens, primary and secondary schools, faculties and other institutions) [Atalić, 2021]. In 2020, the second and even more devastating earthquake of magnitude 6.2 according to Richter took place on December 29 of the same year. Its epicentre was 3 km southwest of the town of Petrinja in Sisak-Moslavina County. The Petrinja earthquake became one of the two strongest instrumentally recorded earthquakes in the Republic of Croatia (since 1909), and its devastating effects were also felt in Zagreb, where additional damage occurred, especially in the central parts of the city, on the oldest buildings [Svirčić Gotovac et. al. 2021: 138]. The Ministry of Spatial Planning, Construction and State Property adopted The new Reconstruction Act, first in September 2020, half a year after the earthquake, and the new version in February 2023 [*Act on the Renovation of Damaged Buildings*, *2023*]. According to the Ministry, the right to post-earthquake reconstruction is granted to all owners or co-owners of real estates damaged in the earthquakes of March 22, or December 28 and 29 2020, respectively, under the condition that the

Copyright © 2025 CroCEE
DOI: https://doi.org/10.5592/CO/3CroCEE.2025.101

real estates are existent [*Ministry of Physical Planning, Construction and State Assets, 2024*[1]]. In November 2020, the Fund for the Reconstruction of the City of Zagreb, Krapina-Zagorje and Zagreb County was established, and state and city institutions started to participate together in the recovery process. The measures are aimed at residents who are existentially threatened due to the loss of housing security in these areas, especially in the Zagreb region and the Petrinja region, which are threatened the most. Due to a large damage, Croatia was granted funding from the EU Solidarity Fund twice, in a total amount of over a billion euro to recover from the damage. Based on the request from Croatia, and following a thorough examination, the Commission concluded that the circumstances were meeting the criteria justifying an exceptional prolongation of the deadline for the implementation of the EUSF aid for recovering from damage caused by the Zagreb earthquake until June 30 2023 [*Representation of The European Commission in Croatia, 2022*]. The multi-year post-earthquake renewal is primarily led by Ministry of Physical Planning, Construction and State Assets, after the Fund for the Reconstruction of the City of Zagreb, Krapina-Zagorje and Zagreb County has been closed. During these years, the reconstruction of private and public buildings was implemented paralelly in all damaged areas. The renovation of private family houses was much slower than the renovation of public buildings. The problems hindering private renovation are mostly related to property rights, administrative in the sense of applying and waiting for the implementation of the request on the type of reconstruction, and financial in the sense of approval of funding granted to the owners by the Ministry. This will be discussed in more detail in the Results section. Minister Bačić and the Ministry stated at the session of the Expert Council for Reconstruction in June 2024 that the construction of replacement houses started not earlier than 2023, and until that day there were 255 family houses built, while additional 48 replacement houses were built in 2024. It is expected that all the planned replacement houses will be finished until 2027, and the comprehensive reconstruction until 2030.[2] This is definitely not an expected dynamic for the owners of houses, who have now been waiting for already 4 years after the earthquake for the reconstruction and the return to their homes.

The reconstruction of public buildings was much more successful. A large number of schools, kindergartens, churches, museums and similar public institutions were renovated or rebuilt both in the city of Zagreb, and in Petrinja and Sisak. The Ministry's web-site reads: “With regard to the reconstruction of public property and infrastructure, a total of 1,309 projects were agreed for the Zagreb and Petrinja earthquake, amounting to 3.63 billion euro. A total of 997 projects were finished until June 30 2024. Further reconstruction of public purpose buildings will be funded by the National Resilience and Recovery Plan and the state budget. The Government also provided a loan from the World Bank amounting to 200 million dollars“ [*The 4th session of the Expert Council for Reconstruction, held on September 17, 2024, Ministry of Physical Planning, Construction and State Asset*]. Regarding that the current state of the post-earthquake renovation process in Croatia is very complex and includes more counties, cities and villages, as well as private and public objects, and all reconstruction types in line with the most recent Act on Reconstruction of Damaged Buildings 2023, the research presented in this paper analyses only the reconstruction of private family houses and the building of replacement houses.

[1] Also, the right to renovation and co-financing of renovation costs, or the costs of construction of a replacement family house is in more detail regulated by the Act on Reconstruction of Buildings Damaged in the Earthquake and the Programe of Measures for the Renovation of Buildings Damaged by the Earthquake [Ministry of Physical Planning, Construction and State Asset, 2024, https://obnavljamo.hr/obnova-nekretnina-ostecenih-u-potresu/].

[2] „When referring to the very implementation of the renovation, we have renovated 10,847 non-construction objects, and in the very period of those six months we conducted 763 non-construction renovations and in total the whole project of non-construction renovation costed 43.7 million euro. By building family houses we gradually achieve the desired dynamic. Until January of last year, not a single replacement house was built. Today we have a total of 255 replacement family houses. In these six months, additional 48 replacement family houses were finished" reported Minister Bačić to members of the Council. He communicated that the renovation, i.e. the construction of all replacement family houses and buildings, around 900 of them, should be finished until the end of 2026, or the first half of 2027, respectively, while the complete renovation should be finalised until 2030. [The 4th session of the Expert Council for Reconstruction, held on September 17, 2024, https://mpgi.gov.hr/vijesti-8/odrzana-4-po-redu-sjednica-strucnog-savjeta-za-obnovu/17861].

Proceedings of the 3rd Croatian Conference on Earthquake Engineering - 3CroCEE
19–22 March 2025, Split, Croatia
Copyright © 2025 CroCEE
DOI: https://doi.org/10.5592/CO/3CroCEE.2025.101

The paper will also analyse the new model proposed by the Act, the self-renovation model, by which the renovation steps are decided upon faster and more independently, for the owners choose the architect, contractor and the surveillance of the construction work by themselves, as well as the beginning and the end of the construction work [https://obnavljamo.hr/samoobnova/]. In this paper, we analyse the situation four years after the earthquake in the areas of peripheral and rural settlements near Zagreb, Markuševec and Čučerje, which are still in the reconstruction process.

2. Theoretical approaches to post-earthquake reconstruction: putting people first

Post-earthquake reconstruction can be viewed in relation to examples of countries that have already gone through a similar process, and based on that it can be seen which models are currently in use and how applicable they are in the case of the explored settlements near Zagreb. In this sense, some important and newer approaches to post-earthquake reconstruction are distinguished, which also concern the participation of residents and the ways in which reconstruction can be achieved. The literature mentions primarily the process called Postearthquake Recovery and Reconstruction Planning – PERR, which is directed towards many dimensions of reconstruction, among which the construction of housing objects is the most important part and the priority in planning [Johnson, 2007; Wu and Lindell, 2004; Sviršić Gotovac et al., 2021: 142]. It was the construction and renovation of private family houses that was in the explored cases the main goal and need for the citizens who lost their homes in the earthquake, or their homes were severely damaged and in need of reconstruction. The literature thus often points out the principle that people and their houses need to be the priority, i.e. the "people first" principle [Yang et al., 2017:1847], along with warning about the inevitable role of citizens in the renovation process, for their satisfaction will eventually depend on it [Sviršić Gotovac et al., 2021: 142].

In the four-year process of post-earthquake renovation, both in Zagreb and in other parts of the country, it can be pointed out that it has been mostly led institutionally by the state, or the Ministry, respectively, and guided by the so-called top-down model. The involvement of citizens in the decision-making process through the bottom-up model was almost non-existent. The voices and opinions of citizens were noticed only at the level of receiving requests and occasional complaints, which could be heard of in the Ministry's offices' communication with citizens, and in the media. The process of decision-making during post-disaster reconstruction is constantly confronted with tradeoffs between speed and quality, roles of professional and lay people, temporary and permanent housing, to name a few [Pezzica et al., 2021; Davis and Alexander, 2015]. Thus, the rising recognition of traditional construction in the post-disaster context is closely related to a shift in reconstruction schemes from a top-down approach (e.g., donor-driven reconstruction [DDR]) to a participatory approach (e.g., owner-driven reconstruction [ODR] and people-centered reconstruction [PCR] [Wang and Ng, 2023: 2]. The top-down approach has a limitation or weakness that it cannot meet the specific needs of individual communities. The advantages of 'owner-driven reconstruction' - ODR, on the other hand, include, among others, the dweller control of the reconstruction process with customized designs, reduced costs through a short logistic chain of building resources and strengthened community ties through shared participation [Barenstein and Iyengar, 2010; Barakat, 2003; Maly and Iwata, 2019].

In our cases, the principle of participation or PCR was not present, but rather only some critiques and complaints of citizens regarding the renovation process. It was only two years after the adoption of the Act that some of the citizens' demands were accepted, while reducing the pressure on the Ministry, which prior to that used to be much larger. The changes that enabled the self-renovation model and financial aid to citizens have somewhat speeded up the process and enabled more intensive construction. Therefore, a very important renovation principle applicable to the explored cases is the one that the literature labels as *"build back better"*, or BBB, respectively [Maly, 2018]. This phrase became popular for the improvement of recovery. Mannakkara and Wilkinson (2014) have developed a BBB framework that includes: risk reduction, community recovery and implementation. Community participaton as well

Proceedings of the 3rd Croatian Conference on Earthquake Engineering - 3CroCEE
19–22 March 2025, Split, Croatia
Copyright © 2025 CroCEE
DOI: https://doi.org/10.5592/CO/3CroCEE.2025.101

as clear communication during the entire process and also shelter to the residents is vital. Kennedy et al. (2008.) conclude that 'build back to a less vulnerable state than before' or 'building back safer' might be a more appropriate term. In that context it is important to emphasize that the renovation is expected to provide much safer conditions of housing and living, and not just a return to the conditions prior to the catastrophe. Therefore, both the construction models and the self-renovation models are legally obliged to guarantee the reinforcement of construction and greater safety in case of repeating earthquakes, which the type of construction requiring both time and money, and is often slow-paced. Those citizens who did not want this model, would often withdraw and shift to faster and more affordable variants of independent reparation of damage on their houses.

Although the 'People-centered housing recovery' is also one of the approaches that puts people at the center of recovery, in the explored settlements, Markuševec and Čučerje, mostly the "build back better (BBB)" model was employed; and only in the part that is focused on technical safety, whereas less on the needs and preferences of the residents. Compared to the BBB, the People-centered housing recovery could represent a more detailed way to consider and evaluate varied aspects of housing recovery projects [Maly, 2018: 92]. As will be shown in the results, the citizens in the explored settlements were not included in the very process equally. Due to that, as well as the renovation that was not fast enough and the problems that were hindering it, the example of these settlements illustrate that "when citizens are not invited in the process of catastrophe managament, the decisions and activities of those who bring these decisions are often disputed [Pearce, 2003: 217] because even in the results one can see a certain dissatisfaction and contestation of the adopted measures. In this chapter some important and newer approaches to post-earthquake reconstruction are distinguished, which especially concern the participation of residents, and the ways in which reconstruction can be achieved so that the build-back is better and also safer [Kennedy et al., 2008]. It would be advisable to connect the mentioned principles of people-centred reconstruction, people-centered housing recovery and 'build back better' (BBB), to provide a greater participation of residents, and to make their housing construction more satisfactory. However, as shown by the analysis of reconstruction in Čučerje and Markuševec, only a partial BBB principle was implemented, the one implemented in a strictly legal and technical way from the top-down to the local level. This is discussed in more detail in the Results section.

3. Methodology

In the research conducted from May until September 2024 in the Zagreb settlements of Markuševec and Čučerje, the method of semi-structured interviews with the residents and interested actors from Local Committees and City Districts, and civil engineering experts was employed. The research participants were either directly affected by the earthquake as residents of these settlements, or participated as experts in the process of renovation of damaged buildings in the settlements of Markuševec and Čučerje. The total sample consisted of 20 respondents (N=20), of whom 14 men and 6 women. There were 16 residents and 4 experts from the explored settlements (1 member of the Local Committee and 1 member of the City District Council, also an organizer of the construction and an active participant in the renovation, and 2 civil engineers). In the settlement of Markuševec there were 9 respondents, and all were older than 60. In the settlement of Čučerje there were 7 respondents, of whom 4 were older than 60, one older than 50, and two in a younger age category of 25-30 years. The research received approval of the Ethical Committee for conducting the field part of the research. The main aim was to analyse the process of renovation during the past years, and the residents' satisfaction with the repairment of houses and the building of new or replacement houses. Also, an additional aim was to explore how satisfied are the residents affected by the earthquake with the whole process of renovation, both through self-renovation and construction renovation, with regard to the state and city institutions and local government units (Local Committees and City District Councils).

Based on these aims, an a-priori protocol for questions was written according to which the researchers conducted semi-structured interviews by the face-to-face data collection method. The criterion for the

Proceedings of the 3rd Croatian Conference on Earthquake Engineering - 3CroCEE
19–22 March 2025, Split, Croatia
Copyright © 2025 CroCEE
DOI: https://doi.org/10.5592/CO/3CroCEE.2025.101

involvement of interlocutors (tenants) in the sample was ownership over a real estate property and the damage of objects in which they reside (to a smaller or greater extent), and for expert actors it was involvement in the post-earthquake renovation process. The obtained results or transcripts were then transcribed and analysed by NVivo 12 thematic analysis [Boyatzis, 1998]. The interviews lasted for 30–60 minutes. The coding was primarily deductive, and based on the gained insights the codes and topics were identified. The results of semi-structured interviews processed in the thematic analysis were singled out in 3 most important topics that were also, which is important to mention, arranged according to the temporal sequence in which the post-earthquake renovation was taking place: 1) *Help of the local community (Local Committee); 2) Damage repair and types of reconstruction; 3) Satisfaction of residents with the construction of replacement houses.*The obtained results are interpreted further in the text.

4. Results

Most of the residents included in the research had a red sticker after the preliminary static examination, with a lesser part having a yellow sticker. Most often they emphasised that they started the reparation of the occuring damage and the renovation od houses, so that they could return to their homes. A part of them left their place of residence visiting the family or relatives for a certain time, and then returned to the renovated house. A smaller part is still outside their houses. Older residents, prevailing in the sample, mostly stayed in auxilliary objects near their houses, e.g. garages or external kitchens, which were adapted to permanent housing, so that they could be close and work on the main object. To them it was enough, while pointing out that leaving was not a desirable option for them. One part was living in the containers that were provided by the state and the city, but this type of residence was prolonged to 4 years, and it could be inferred that they were particularly unsatisfied with this solution.

1) Help of the local community (Local Committee)

In the days following the earthquake, along with a great shock there was a great engagement of the people and institutions as of how to help the most affected people as quickly and efficiently as possible. In that context, it was important to ask them how did the immediate local authorities react through the Local Committees, whose members themselves reside in the same area. The residents mostly observed that their contribution visible in the cooperation of the Local Committee and the local Voluntary Fire Brigade, who were asking for the provision of various construction material from the City of Zagreb, which was then distributed to the people, which is confirmed by a statement of an expert actor and member of the Local Committee.

It was the main commander of the firemen who was in the crisis staff, and with them I was able to provide help, a load of material for Markuševec, for the renovation, the plankings, the laths, cement, and then we gave it to the people, yes. So, I think that this way the Local Committee did help. For this area, since it was in the epicentre, a load of that material was needed. We gave plenty of the material to the people. (member of the Local Committee, Markuševec, M, 75)

The residents, however, did not point that much to their help, and were more oriented towards themselves. They did not find the work of the Committee that important, but stated that they knew about their agency. The Committee helped them take the things out of their houses or were circling around the area and providing construction material. A part of the residents have never heard of their engagment.

Collaboration with the Local Committee consists only of helping me carry my things from the upper floor. I think it was the guys who organized themeselves on their own. (Vidovec, Ž, 75)

I had no contact with the Local Committee. But I know they were walking around. They were asking about the damage and all. And, what do I know, they gave to the people who had some small damage, some material, roof tiles. (Vidovec, M, 60)

Copyright © 2025 CroCEE
DOI: https://doi.org/10.5592/CO/3CroCEE.2025.101

We did not collaborate with the Local Committee, nor did we hear about their engagement. (Čučerje, M, 28)

Members of the Local Committees were engaged in the obtaining of housing containers for the residents that needed them, and were not able to stay in their houses. According to an actor from the Local Committee, there was extreme dissatisfaction with the containers.

In the beginning, we were even fighting for those housing containers, and we provided quite a few of them, for the people who were in need, who had nowhere or no-one to go to. There are still plenty of them. They were extremely dissatisfied. (member of the Local Committee, Markuševec, M, 75)

2) Damage repair and types of reconstruction

When the renovation of houses started, most residents and involved experts counted on the help of the city or the state. They stated that the financial aid under the public call of the City of Zagreb in 2021 amounting to 50,000 kn was indeed a great help with which the first repairments started on the roofs and walls. Nevertheless, they pointed out that the state and the Ministry did not provide much financially, and that the renovation process started much more complicatedly and for some even administratively very hard. The majority repaired the damage by themselves, because such houses were not labelled with a red sticker, and were able to be renovated within some shorter time, mostly within a year, which was the case for the majority less damaged in the earthquake. For that other part of the houses, which were seriously damaged, the renovation process got prolonged for up to even a few years, while in some it is still taking place. The examples of such houses can be found on the landslides or among the residents who are not satisfied with the attributed model of reconstruction.

I got those 50,000 kn from the city, while the state gave nothing. All right, we used that. So, we were sleeping upstairs on the upper floor, while the ground floor was being repaired. And then, when we got those 50,000, the facade was on the house. (member of the Local Committee, Markuševec, M, 75)

And nobody ever gives us the right answer. And those 50,000 kn, I don't know if you remember, we did not take that because they told us not to take it because our house will be demolished, and that the money was for the construction renovation. I mean, people, I have nothing against them, but they got the option and the money, and we got nothing. I have five kids. We are not here, but down (op.a. in the city). (Čučerje, F, 52)

A part of the residents got and received the aid from the City of Zagreb, and the other did not. Thus a division emerged among those who managed better, and those who navigated worse in the initial repairment of the damage. After initial housing repairments, so that they could serve for residing, particularly for those who could not or did not want to leave them, this aid was especially important, and in this way they would stay and repair them. Some were afterwards involved in the construction renovation, and submitted their requests to the Ministry. The majority of residents, it was only after four years after the earthquake that the administrative request could be brought to the execution phase and the beginning of self-renovation or construction renovation. It was by the new Renovation Act of 2023 that the self-renovation model extended the opportunities of owners who could now classify the demolition of houses under this model, which was not possible by the previous Renovation Act. The implementation is for a part of them expected during 2025 (the project, surveillance, and implementation of the strengthening of housing constructions).

Some residents have thus adapted the initial request for construction renovation to the new self-renovation model, and waited for the state funds, which were then paid to contractors under conducted tenders. As one of the expert actors states, it was the intention of the Ministry to speed up the process of renovation with the self-renovation model, because construction renovation would be much more

Proceedings of the 3rd Croatian Conference on Earthquake Engineering - 3CroCEE
19–22 March 2025, Split, Croatia
Copyright © 2025 CroCEE
DOI: https://doi.org/10.5592/CO/3CroCEE.2025.101

complex and the whole process would in practice be prolonged to a few years, to enable the matching of certain conditions, which was often impossible, and everything was additionally slowed down.

If it is not self-renovation, then the architect is determined following a tender. This also took long. Then an operation coordinator has to be determined, as some kind of a project leader. Then the constructor, and then the surveillance. When all these 4 points match, it lasts 3 years. Also, not every tender succeeds, some of them fail, because they offer prices 100% higher than the planned, or nobody applies (surveillance engineer, M, 62)

In addition, in the whole process of renovation, there were often unclarities regarding the renovation model, and the waiting on the decision on the request. Many took their reconstruction 'in their own hands', and did not create projects with their constructors, and were thus lacking bills for the conducted and authorized works, which was later not regarded in the Ministry's refunding, which caused dissatisfaction.

People were doing self-renovation and some non-construction renovations. Plenty of those did not have their works supported with written documentation. They did not have a project. They started with some initial project, but not by an authorized constructor, they did not register him, and did not have surveillance. (civil engineer, M, 55, Markuševečki Popovec)

In the construction renovation there might be some kind of participation. Later he has to deal with it by himself. He gets paid for the construction part, but has to solve the later phases alone. Construction renovation is construction renovation. Elements will be reconstructed. After that, you won't really be able to live inside. Somewhere, event he finishing floor coverings were not provided. Maybe the bathrooms were, tiles in the bathrooms, but some other places, you don't even have the flooring. (surveillance engineer, M, 62)

An additional problem is that there were multiple constructing sites active at the same time at various places, causing the work to be running late, for there was a lack of both craftsmen and contractors. Also, the Ministry was running late with the payment expected by the owners and contractors, so taht the process was sometimes stuck in one place.

For example, the situation. A friend is here, working, and says: look, there are problems, he i s also doing self-renovation, and is having problems with the sub-contractor. He won't work. He says: I gave him the money. I gave him my part. The state did not give him its part. Because you've made a mistake somewhere in the legal part, and so… (M, 62, organizer of construction and councilor of the City District Council)

...They give you 50 thousand euro, for example… 50, 30, 25 goes for the constructive renovation. The rest goes to the account of the owner who is broke, cannot pay even for the bus ticket. And what happens then? Then it happens that you see scaff here in Gornja Dubrava, in markuševec. Abundance of scaffolding! So, the renovation has started and all of it is going? (M, 62, organizer of construction and councilor of the City District Council)

For such cases it is important to emphasise that they very extremely hard for the residents themselves. Some cases, as the following in Čučerje, would not be finished without the help of expert actors from this area who were involved in the process, and who had the role od so-called construction organizers. The actor mentioned by the interlocutor has significantly helped bring the process to an end, and enable the state to begin with construction renovation of more houses in the area of Čučerje villages.

Yes, we did receive 50,000 kn from the City, and we used it to partialy solve what we were solving, and also by borrowing, friendly help, and so on, and thus we started the self-renovation. In order to function in that object… We our now expecting that stabilization. As Mr says, we need construction renovation and safety, with no more fear when some noise goes under the house that I have to cover my head. (Šuškovićev odvojak street, F, 68)

Copyright © 2025 CroCEE
DOI: https://doi.org/10.5592/CO/3CroCEE.2025.101

The statement of an expert actor who continued to lead the process until the end and was able to get financial aid for the owners in a part of Čučerje, so that the construction and comprehensive renovation would start after four years, speaks of the longlasting process of renovation, particularly for those mostly affected by the earthquake.

I was expecting 30-40 thousand euro. And when we started, I realised that maybe it could be brought to 60 thousand. When the lady sent it to me on Monday, I was thrilled, we got 94 thousand plus the project. About 110 overall. The house is not finished. What the gentleman was doing was painting interventions, that we need to bring down, repair and then return to the state in which it was. This will be the most demanding object I have had untl now, because it involves complete renovation. We can call this comprehensive renovation because we are doing also the construction renovation and we are returning it to the original state. (M, 62, organizer of construction and councilor of the City District Council)

Both the another object in Vidovec is continuing with the construction renvation, to reinforce it. It is implemented by an expert actor, who is helping with the finalisation of the renovation.

This way the construction renovation is done really well, both vertically and horizontally. Upstairs, I now have the walls that are this thick on the upper floor, because the old wall remained which was binded and the new wall was made. As they made these vertical pillars, then connected that with a cornice, and then on the cornice another wall was put next to this wall. (Vidovec, F, 75)

Besides these cases that eventually reached the end of renovation, although through different phases, a parto f residents is extremely unsatisfied for they have still not begun with the renovation of their houses. The example is a resident from Slanovec, who is not satisfied with neither the communication, nor the solution offered by the Ministry, and does not want construction renovation, but demolition of his house and construction of a new one.

They (the Ministry) said that the terrain should be drilled, if it's not all right, then the house should be demolished and built on some other terrain. Then we got a decision to wait for the decision on construction renovation. They said the project was over, and they did not go out in the field. I don't know based on what they made the project, based on photos, they did not conduct a deep measuring of that terrain, they did nothing in the legal sense, and you cannot complain, I am now only waiting for that project, to go sign that project, and then I will not sign it, do you get it? I will ask for my house to be demolished. (Slanovečka street, M, 62)

As with the end of 2023 the Ministry finalised the process of receiving requests for the construction of replacement houses, this case is not simple and creates an impression of neglect towards house owners, who are therefore extremely dissatisfied, and their further communication with the Ministry is lacking. Another case is that of a family whose house is located on a landslide, and does not have a constructing permit anymore, without a solution to a total amount by which the family could buy a house in the Zagreb area, because the Ministry is not providing enough, while not allowing the change of location either. The family was thus unable to solve anything in 4 years, and are still renting a social apartment, which they pay for on their own.

We're down there in Jelkovec for four years already. I don't know what to say. They offered us to buy a house for 150.000 eura, but in the city of Zagreb area. So, not Dugo Selo. I cannot buy it. I buy for 90.000 euro and I found it. The rest of the money cannot be provided by them, but it goes to the state. So, I cannot renovate anything due to the landslide. I cannot do anything. (Čučerje, F, 52)

3) Satisfaction of residents with the construction of replacement houses

According to a statement by a surveillance engineer involved in the renovation process in these settlements from the beginning, the situation is not satisfactory, and according to him many more houses should have been demolished. He points out that the introduction of self-renovation and extension of possibilities of renovation according to this model is a good solution.

Proceedings of the 3rd Croatian Conference on Earthquake Engineering - 3CroCEE
19–22 March 2025, Split, Croatia
Copyright © 2025 CroCEE
DOI: https://doi.org/10.5592/CO/3CroCEE.2025.101

So, it should have been done right away, in those first field visits and afterwards, let go, 100, 200, 500 houses, as now 5 companies have done two years ago, lets bring this down, and later see if replacement is needed, if construction renovation is maybe possible, i fit doesn't need to be domolished, and so on. I think there were 2,800 such objects in the Zagreb area. Surely, half of them would be down until now. For now, we've taken down 80. Now as the latest it has emerged that self-renovation includes demolition, so that the people, if they opt for it, can request the same and look for the contractor. However, something has now slowed it down. (surveillance engineer, M, 62)

Replacement houses grew in the place of those with a red sticker, which were completely unusable, and projects were made on the construction and the location in which the construction will take place. Depending on the number of household members, the so-called typified house was built, with three sized offered by the Ministry and the deadline of 6 months for finishing it.

Here, there were houses that were red, that were unusable. First it was demolished, and then a typified project was noramlly adapted to the terrain. The typified houses are not classical. Each is a little different with regard to the terrain configuration. Our deadline is some 6 months for a house. (civil engineer, M, 55, Markuševečki Popovec)

Some owners are satisfied with the process of construction of new replacement houses. A resident from Čučerje is one such example. To him, the process was fast and he has no objections. Nevertheless, there are divided attitudes on the whole renovation and construction of replacement houses process. A parti s completely satisfied both with the way and the time of construction, and the final outcome, while the second part is extremely dissatisfied.

They started somewhere in September when they put the tables stating that the construction will be done, while they prepared the binding and materials, they started more seriously in October, and in March (2024) it was over, end of March. 74 square metres and I am satisfied. It was really not done in a haste, in some drainages, isolations they put the first, the second, the third, and so on. (Čučerska street, M, 66)

The residents who got a replacement house, for example in Markuševečki Popovec, think that their new typified house is not satisfactory, primarily in size. They used to have a significantly bigger house that they compare to the new one. Nevertheless, as the owners of these houses are mostly the elderly living in two-person housholds, the typified house model that they can get is 55 m2. According to the interlocutor, this is very unfair and they are therefore not satisfied.

Well, I am not satisfied, well relatively yes, but I object that there is some mugging here, where I got too little, in terms of the house. This house was firm, it was larger, and because there is only my wife and me alone, we got what we did, 55 square metres. (Markuševečki Popovec, M, 79)

Besides with the size, they are dissatisfied with the Ministry's relationship towards them in the process of house demolition, because they were not notified about it in due time, but was instead just begun with the demolishing. In that situation, the owners were not allowed to enter their houses, nor to take anything out of them, which was for them, injust and unnecessary.

This is how they brought it down, they brought it down as if I was that F-thing…, I could neither take anything out of it, nor use anything, nothing. (Markuševečki Popovec, M, 79)

5. Conclusion

Our research through interviews with both residents and experts indicate the complexity and long-term nature of post-earthquake reconstruction, as well as the various obstacles they encountered in this process, both administrative, legal and technical. The experts' responses were particularly important in understanding the technical details of the restoration process, as well as the time course in which the reconstruction occured, its different stages and models, and the ways in which it was carried out. In

Proceedings of the 3rd Croatian Conference on Earthquake Engineering - 3CroCEE
19–22 March 2025, Split, Croatia
Copyright © 2025 CroCEE
DOI: https://doi.org/10.5592/CO/3CroCEE.2025.101

some of the thematic units we have singled out, we can notice the division of residents, i.e. their divided satisfaction with the reconstruction process, while in others they are more homogeneous in terms of similar answers and views on the process of post-earthquake reconstruction.

In the first category, which concerns the assistance received by residents from the local community, there is a divided perception of residents of their awareness of the engagement of local committees, especially through their communication with the City of Zagreb in terms of seeking and sharing various construction materials, removing things from houses or visiting the terrain. For a part of them the assistance of the local committee was insufficient, and they were using it very little, while pointing out that some others were using it much more than them, suggesting the relative dissatisfaction with their involvement in the renovation process. The most visible engagement of the local committees is in obtaining housing containers, which was also stated in the answers by the members of the local committees themselves.

In the second category of questions concerning damage repair and types of reconstruction, some residents express dissatisfaction, especially with the slowlyness of the reconstruction, the fact that they did not receive much financially and the complexity of the procedure. The initial request for structural reconstruction by residents was adapted to the new model of self-reconstruction, where funds were expected much faster from the state. A part of the residents thus managed to complete the renovation only through professional help with the construction organization, without which the whole process would not be finished. Some still failed to start or complete their renovation. Such cases are still unsolved and fall into the most difficult category, with the owners in some way pointing out that they are forgotten and that four years are too long for returning to homes, while highlighting a great disappointment. The example are houses on a landslide, for which new construction is not allowed, and demolition is not approved. From what has been said by the residents related to this category, it is possible to conclude that a problem still exist in the communication between the people whose houses were damaged in the earthquake and the Ministry. Nevertheless, it can be argued that the new self-renewal model has finally resulted with some improvements and finalisation of the structural reconstruction.

In the third category of questions, which concerned the residents' satisfaction with the construction of replacement houses, there is perhaps the biggest division between the respondents. A parti s very much satisfied with the construction of a replacement house, both with the size and the quality, while another part is completely dissatisfied. Most often, the most dissatisfied were the elderly residents who previously had a much larger home, and the current typified house does not meet their needs. Thus, the approaches to post-earthquake reconstruction that we have mentioned (putting people first, people-centered reconstruction and recovery and build back better approach) show that these concepts were not implemented and the communication with the residents was missing. Some negative consequences of the top-down approach could be avoided with better communication, especially the dissatisfaction of residents due to insufficient participation [Kennedy et. al., 2008] in the renovation process of building of a replacement house. This type of action on the part of the Ministry indicates a behaviour on the part of the authorities that does not correspond to the stated approaches of community involvement in the decision-making process. According to the results obtained in 2022 on the problems and challenges of post-earthquake renovation in the inner city center of Zagreb, it was also concluded that citizens had much higher expectations from the state and city authorities in the financing and coordination of the complete renovation process: they also expected the setting up of new standards of post-earthquake renovation, which did not happen [Svirčić Gotovac et.al., 2022: 128].

The division of opinions in terms of satisfaction in this category points to the previously mentioned problems of insufficient and unclear communication between residents and the Ministry, but also to an insufficiently planned and implemented renovation process in which it can be said that some residents 'got lucky' while others were largely stuck in the process, both with the bureaucratic part of the process, and in situations they did not expect regarding the finding of construction workers, the poor quality of the renovation, and lack of control over the entire process in general. It can be highlighted that one of the conclusions in the whole process is that priorities were not respected and the residents that were in

Copyright © 2025 CroCEE
DOI: https://doi.org/10.5592/CO/3CroCEE.2025.101

need of assistance were still left without solutions, and that in their relationship institutions-citizens there was little understanding for the finding of the best solution. Institutions have found the best solution for themselves, but not for the citizens, and in these cases the top-down model of managing the renovation process was confirmed. In the cases of Markuševec and Čučerje we can therefore conclude that the previously mentioned top-down approach (DDR) as well as some parts of the BBB approach [Maly, 2018; Maly and Iwata, 2019] are more applicable than the approaches considering 'people first' [Yang, et al., 2017]. In other words, it is possible that this outcome of post-earthquake reconstruction is precisely the result of insufficiently elaborated reconstruction plans and especially of low involvement of residents in the reconstruction process, and for the most severe cases the solution is yet to be found, which has not been done after four years. On the other side, it needs to be pointed out that the technical side of the 'build back better' model although long-lasting for most of the affected citizens, and with the help of the self-renovation model and organized help in managing the process by the experts, has been sucessfully brought to the beginning of the construction renovation, which will for the majority last the next two years. After that, the Ministry will be able to say that the renovation in these Zagreb settlements has been finalised successfully.

Acknowledgements

The research is a part of the ISRZ project *Effects of the Europeanization Process in Selected Urban-Rural Areas of Croatia – HREUURBRUR* financed by the Ministry of Science and Education with the support of the European Union (NextGenerationEU) during the next 4 years (2024-2027). More about the project: https://www.idi.hr/en/projects/competitive-research-projects/effects-of-the-europeanization-process-in-selected-urban-rural-areas-of-croatia.

References

[1] Atalić, J. (2021): Reconstruction Design Models. (Program of Complete Restoration of the Historical Core of Zagreb – First Screening. Zagreb: Institute for Physical Planning of the City of Zagreb.

[2] Svirčić Gotovac, A., Zlatar Gamberožić, J., Adamović, M. (2021): Post-earthquake Renewal of Zagreb's Donji grad from the Perspective of Tenants. *Sociology and Space*, 59 (2), 135-159, doi: https://doi.org/10.5673/sip.59.2.1

[3] Act on the reconstruction of buildings damaged by an earthquake in the area of the City of Zagreb, Krapina-Zagorje County, Zagreb County, Sisak-Moslavina County and Karlovac County. https://www.zakon.hr/z/2656/Zakon-o-obnovi-zgrada-o%C5%A1te%C4%87enih-potresom-na-podru%C4%8Dju-Grada-Zagreba%2C-Krapinsko-zagorske-%C5%BEupanije%2C-Zagreba%C4%8Dke-%C5%BEupanije%2C-Sisa%C4%8Dko-moslava%C4%8Dke%C5%BEupanije-i-Karlova%C4%8Dke-%C5%BEupanije on 5 March, 2022 (accessed December 11th, 2024)

[4] Ministry of Physical Planning, Construction and State Asset, 2024, https://obnavljamo.hr/obnova-nekretnina-ostecenih-u-potresu/].

[5] Representation of the European Commission in Croatia, May 2022. The Commission granted Croatia an extension of the deadline for using funds from the EU Solidarity Fund to mitigate the consequences of the earthquake. Version: 11.12. 2024. https://croatia.representation.ec.europa.eu/news/komisija-odobrila-hrvatskoj-produljenje-roka-za-koristenje-sredstava-iz-fonda-solidarnosti-eu-za-2022-05-20_hr (accessed December 11th, 2024)

[6] The 4th session of the Expert Council for Reconstruction, held on September 17, 2024. Ministry of Physical Planning, Construction and State Assets. https://mpgi.gov.hr/vijesti-8/odrzana-4-po-redu-sjednica-strucnog-savjeta-za-obnovu/17861) (November 29, 2024)

[7] What is Self-Renewal? Version: 11. 12. 2024. Obnavljamo.hr, 2.12. 2024., https://obnavljamo.hr/samoobnova/ (accessed December 11th, 2024)

[8] Johnson, C. (2007): Strategic planning for post-disaster temporary housing. *Disasters*, 31 (4), 435-458., doi: https://doi.org/10.1111/j.1467-7717.2007.01018.x

[9] Wu, J. Y., Lindell, M. K. (2004): Housing Reconstruction after Two Major Earthquakes: The 1994 Northridge Earthquake in the United States and the 1999 Chi-Chi Earthquake in Taiwan. *Disasters*, 28, 63-81. doi: https://doi.org/10.1111/j.0361-3666.2004.00243.x

Copyright © 2025 CroCEE
DOI: https://doi.org/10.5592/CO/3CroCEE.2025.101

[10] Yang, Y., Gao, P., Li, H. (2017). Residents' satisfaction to post-Wenchuan earthquake recovery and reconstruction. *Natural Hazards*, 87, 1847-1858, doi: 10.1007/s11069-017-2852-0
[11] Pezzica C., Cutini V., Bleil de Souza, C. (2021): Mind the gap: State of the art on decision-making related to post-disaster housing assistance. *International Journal of Disaster Risk Reduction,* 53, doi: https://doi.org/10.1016/j.ijdrr.2020.101975
[12] Davis, I., Alexander, D. (2015): *Recovery from disaster.* United Kingdom: Routledge.
[13] Wang, J., Ng, E.Y.Y. (2023): Post-earthquake housing recovery with traditional construction: A preliminary review. *Progress in Disaster Science* 18, 1-17. doi: https://doi.org/10.1016/j.pdisas.2023.100283
[14] Barenstein J. D. and Iyengar, S. (2010): India: From a culture of housing to a philosophy of reconstruction. In: Lyons M., Schilderman T., Boano C. (Eds.). *Building back better*. 163: 183–6.
[15] Barakat, S. (Ed.). (2003). *Housing reconstruction after conflict and disaster,* 43. London: Humanitarian Policy Group, p. 1–40.
[16] Maly, E., Iwata, T. (2019): The Evolution of Localized Housing Recovery in Japan. IOP Conference Series: Earth and Environmental Science 273 (012055). doi:10.1088/17551315/273/1/012055
[17] Maly, E. (2018): Building back better with people centered housing recovery. *International Journal of Disaster Risk Reduction,* 29, 84–93, doi: https://doi.org/10.1016/j.ijdrr.2017.09.005
Maly, E. and Iwata, T. (2019): The Evolution of Localized Housing Recovery in Japan. IOP Conference Series: Earth and Environmental Science 273 (012055). doi:10.1088/17551315/273/1/012055
[18] Mannakkara, S., Wilkinson, S. (2014): Re-conceptualising "Building Back Better" to improve Post-disaster Recovery. *International Journal of Managing Projects in Business*, 7 (3), 327–341, doi: https://doi.org/10.1108/IJMPB-10-2013-0054
[19] Kennedy, J., Ashmore, J., Babister, E., Kelman, I. (2008): The Meaning of 'Build Back Better': Evidence from Post-tsunami Aceh and Sri Lanka. *Journal of Contingencies* and *Crisis Management,* 16 (1), 24–36, doi: https://doi.org/10.1111/j.1468-5973.2008.00529.x
[20] Pearce, L. (2003): Disaster management and community planning, and public participation: How to achieve sustainable hazard mitigation. *Natural Hazards*, 28, 211-228, doi: https://doi.org/10.1023/A:1022917721797
[21] Boyatzis, R. E. (1998): *Transforming Qualitative Information. Thematic Analysis and Code Development*. Sage Publications.
[22] Svirčić Gotovac, A., Adamović, M., Zlatar Gamberožić, J. (2022): Main challenges of post-earthquake renovation in the case of Zagreb City Center. *Journal of Regional and City Planning*, 32 (2), 115-132, doi: https://doi.org/10.5614/jpwk.2022.32.2.7

Proceedings of the 3rd Croatian Conference on Earthquake Engineering - 3CroCEE
19–22 March 2025, Split, Croatia
Copyright © 2025 CroCEE
DOI: https://doi.org/10.5592/CO/3CroCEE.2025.13

COMPUTED BI-DIRECTIONAL COMBINATION COEFFICIENTS FOR STRUCTURES USING THE FEB. 6TH, 2023 KAHRAMANMARAS EARTHQUAKES' GROUND MOTION DATA

Asma YAHIOAUI [(1)], Oguz KOZ [(2)], Oguz C. CELIK [(3)]

[(1)] *Ph.D., University of Sciences and Technology Houari Boumediene (USTHB), Department of Structures and Materials, Built Environmental Research Laboratory, Civil Engineering Faculty, BP 32 El Alia, Bab Ezzouar, 16111, Algiers, Algeria. email: yahiaouiasma14@gmail.com / ayahiaoui1@usthb.dz*
[(2)] *Ph.D. Student, Research Assistant, Istanbul Technical University (ITU) Faculty of Architecture, Structural & Earthquake Engineering Unit, Taskisla, Taksim, 34437, Istanbul, Turkey. email: oguz.koz@itu.edu.tr*
[(3)] *Prof, Istanbul Technical University (ITU) Faculty of Architecture, Structural & Earthquake Engineering Unit, Taskisla, – Taksim, 34437, Istanbul, Turkey. email: celikoguz@itu.edu.tr*

Abstract

The existing seismic design codes consider bi-directional effects by applying the square root sum of squares (SRSS) or the percentage rule; the latter simplified way of design is commonly employed by accounting for the 100% contribution in the assumed principal direction plus 30% or 40% other direction's contribution. Although the potential reasons of widespread building damage and collapses in the Feb. 6th, 2023 Kahramanmaras earthquake doublet have been well documented, there are still questions in mind that whether or not bi-directional effects played a significant role in this devastation. To appropriately address this, bi-directional combination coefficients can be calculated using the strong ground motion records of these earthquakes. The Housner's spectrum intensity values are calculated by using the pseudo-elastic velocity spectrum curves for both directions of the 60 records in locations where destruction was significant. Following the percentage rule, intensities both obtained from the resultant (i.e., bi-directional) and unidirectional velocity spectra are combined, and the corresponding percent values as other direction's contribution are computed. Note that pseudo-velocity spectrum curves cover a wide period range representing various types of structures and are developed for damping ratios ranging from undamped to significantly damped systems (e.g. systems with energy dissipation devices). Numerical results reveal that 50% of the selected stations from both earthquakes suggest combination coefficients in excess of the 30% rule, indicating that the 30% rule may underestimate internal forces and drifts for half of the stations. This would justify and could be one of the reasons for severe damage and collapses observed in several types of structures. Furthermore, most cases satisfied the 40% rule (this is used especially for bridges), but some exceptional cases led to higher combination coefficients, particularly those for undamped (or slightly damped) and 5% damped structures basically assumed for RC framed buildings in design codes.

1. Introduction

During an earthquake shaking, structures are highly influenced by the seismic motion characteristics [1], since they are simultaneously subjected to six ground motion components. Among them, two in the horizontal plane and one in the vertical direction are generally the most destructive for buildings [2]. Since building structures are much more flexible in lateral directions, most seismic design codes require consideration of the two horizontal orthogonal components of ground motion during the design stage. To this end, most seismic design codes allow three main methods for integrating the impact of multiple earthquake components: complete quadratic combination (CQC3), square root sum of squares (SRSS), and the percentage rule. The percentage rule, a widely accepted approach, represents the standard practice accounting for bi-directional effects by designers [3]; it consists of taking into account a 100% contribution from the earthquake's principal direction, along with a 30% or 40% contribution from the other direction. The common 100%-30% combination rule was first introduced by Rosenblueth and Contreras in 1977 [4], and then it has been adopted by the majority of building regulations, such as Eurocode 8 [5], ASCE 7-22 [6], Turkey Building Earthquake Code (TBEC-2018) [7], National Building

Proceedings of the 3rd Croatian Conference on Earthquake Engineering - 3CroCEE
19–22 March 2025, Split, Croatia
Copyright © 2025 CroCEE
DOI: https://doi.org/10.5592/CO/3CroCEE.2025.13

Code of Canada (NBCC-2020) [8], FEMAP (2020) [9], IBC (2018) [10], GB50011-China code [11], ATC 3-06 (1978) [12], Caltrans seismic design criteria version 1.7 (2013) [13], New Zealand (2005) [14], and Iranian code (2008). The rule of 100%-40% is generally dictated by seismic codes for bridges, including ATC-32 (1996) [15] and Seismic Retrofitting Manual for Highway Structures: Part 1–Bridges (Fhwa-Hrt-06-032, 2006) [16].

On February 6th, 2023, two disastrous successive earthquakes, measuring M_w 7.8 and 7.6, struck the southwestern region of the East Anatolian Fault (EAF) [17], causing severe damage to over 2,457,942 different types of structures, including residential buildings, bridges, hospitals, and historical buildings. Note that these earthquakes claimed more than 50,000 lives as well [17]. The primary reasons for these damages were attributed to the substandard material quality of structural members since the safety and structural performance depend on it [18], in addition to the weak soil conditions. However, to date, the impact of orthogonal components has not been investigated yet. Previous studies have been conducted on analyzing various earthquakes ground motion records to predict the bi-directional impact and have concluded that the combination rules proposed by building codes are mostly conservative and sufficient [2,19]. Similar results were observed when analyzing the combination rules to predict the effects of tri-directional earthquake excitation under elastic and inelastic conditions [20–22]. To ascertain whether the combination rules suggested in existing building codes are conservative or not, this research mainly aims to revisit the bi-directional effects from the February 6th Kahramanmaras earthquakes for different structural types, from undamped to highly damped systems.

2. Dataset

From each earthquake, thirty records were downloaded from TADAS AFAD [23] based on the highest PGA values. It should be noted that the data available on AFAD are unprocessed, and using processed data would affect the results slightly. To this end, the dataset was filtered to eliminate noise-contaminated ground motion frequency content from the entire record without modifying the main ground motion characteristics in the predefined frequency band. The applied filtering process was derived from the research conducted by Jinjun Hu et al**.** [24], who investigated the characteristics of the February 6th Kahramanmaras earthquakes. Therefore, the fourth-order Butterworth noncausal filter is adopted with the high-pass and low-pass cutoff frequencies set to 0.07-30 Hz.

It should be noted that the Pazarcik earthquake records with station codes 3146, 0201, and 4632, as well as the Elbistan/Ekinozu earthquake records with station codes 4631, 0213, and 4414, were found to be of poor quality in the study corroborated by Jinjun Hu et al. [24] due to several reasons, such as the significant noise content and incorrect waveform, while Tang et al. [25] determined that the stations 4630, 4629, 4632, 2707, and 2709 were compromised and inaccurate since they sustained damage during the earthquake shaking. Therefore, these stations have been removed from the dataset. Consequently, properties of the constructed dataset to investigate the bi-directional effects of both February 6th Kahramanmaras earthquakes are presented in Table 1 and Table 2. Here, R_{JB} denotes the nearest distance to the surface projection of the fault plane, while R_{rup} indicates the closest distance to the rupture plane.

Table 1. Characteristics of the Pazarcik earthquake

Code station	Province	Longitude	Latitude	R_{JB}	R_{rup}	R_{epi}	R_{hyp}
4614	Kahramanmaras	37.297	37.485	0	8.25	31.42	32.57
3129	Hatay	36.134	36.191	75.71	75.71	146.39	146.64
3126	Hatay	36.138	36.220	72.55	72.55	143.54	143.80
3141	Hatay	36.220	36.373	54.20	54.20	125.42	125.71
3138	Hatay	36.511	36.803	9.70	9.70	71.70	72.21
3125	Hatay	36.133	36.238	70.82	70.82	142.15	142.41
NAR	Kahramanmaras	37.157	37.392	0.00	7.47	15.35	17.60
3135	Hatay	35.883	36.409	66.18	66.18	142.15	142.41
3123	Hatay	36.160	36.214	72.58	72.58	143.00	143.26

Copyright © 2025 CroCEE
DOI: https://doi.org/10.5592/CO/3CroCEE.2025.13

2718	Gaziantep	36.627	37.008	0.00	2.10	48.30	49.06
3142	Hatay	36.366	36.498	38.09	38.09	106.49	106.84
3144	Hatay	36.486	36.757	12.36	12.36	77.04	77.52
4616	Kahramanmaras	36.838	37.375	14.03	22.42	20.54	22.27
3145	Hatay	36.406	36.645	21.68	21.68	91.13	91.54
4615	Kahramanmaras	37.138	37.387	0.00	8.02	13.83	16.28
3139	Hatay	36.414	36.584	28.54	28.54	96.19	96.57
3124	Hatay	36.172	36.239	69.66	69.66	140.11	140.37
2712	Gaziantep	36.733	37.184	2.74	11.58	29.79	31.01
3136	Hatay	36.247	36.116	81.47	81.47	148.38	148.63
3132	Hatay	36.172	36.207	73.08	73.08	143.12	143.38
4625	Kahramanmaras	36.982	37.539	20.83	28.96	28.40	29.67
3137	Hatay	36.489	36.693	18.44	18.44	82.48	82.93
3143	Hatay	36.557	36.849	8.10	8.10	65.13	65.70
4621	Kahramanmaras	36.929	37.593	28.49	36.32	35.42	36.45
3131	Hatay	36.163	36.191	74.95	74.95	144.98	145.23
4624	Kahramanmaras	36.918	37.536	24.02	32.02	29.73	30.95
4611	Kahramanmaras	37.284	37.747	23.28	31.32	55.32	55.98

Table 2. Characteristics of the Elbistan/Ekinozu earthquake

Code station	Province	Longitude	Latitude	R_{JB}	R_{rup}	R_{epi}	R_{hyp}
4612	Kahramanmaras	36.482	38.024	62.18	62.18	66.68	67.05
4406	Malatya	37.974	38.344	60.69	66.64	70.17	70.52
4409	Malatya	37.491	38.561	19.26	27.02	56.86	57.28
3802	Kayseri	36.504	38.478	58.12	58.12	77.41	77.73
4611	Kahramanmaras	37.284	37.747	0.00	6.85	38.21	38.85
4614	Kahramanmaras	37.298	37.485	0.95	7.09	67.35	67.71
4412	Malatya	38.184	38.597	79.75	84.86	99.89	100.14
4405	Malatya	37.940	38.811	60.32	66.23	100.81	101.05
0129	Adana	36.211	38.259	84.76	84.76	91.84	92.11
NAR	Kahramanmaras	37.157	37.392	12.13	10.85	77.85	78.16
4410	Malatya	37.679	38.867	41.23	47.57	94.59	94.84
2703	Gaziantep	37.350	37.058	48.50	49.49	115.06	115.27
5807	Sivas	37.248	38.727	4.52	8.65	70.94	71.28
4613	Kahramanmaras	36.357	37.570	75.34	75.34	96.56	96.82
0130	Adana	35.671	37.252	139.26	21.83	166.46	166.61
4625	Kahramanmaras	36.982	37.539	20.34	20.34	65.22	65.60
0125	Adana	35.796	37.015	136.49	60.84	174.48	174.62
2308	Elazig	39.310	38.451	177.65	180.07	185.23	185.36
4620	Kahramanmaras	36.898	37.586	27.51	27.51	63.46	63.84
8002	Osmaniye	36.562	37.192	66.70	33.24	116.24	116.45
4624	Kahramanmaras	36.918	37.536	26.03	26.03	67.65	68.01
2309	Elazig	38.727	38.799	127.82	131.16	151.77	151.93
3144	Hatay	36.486	36.757	104.09	78.92	162.37	162.52
5809	Sivas	37.382	39.231	61.28	63.39	127.57	127.76
4616	Kahramanmaras	36.838	37.375	35.67	11.62	86.81	87.09
0127	Adana	35.920	37.816	112.56	112.56	119.52	119.73
4617	Kahramanmaras	36.830	37.586	33.53	33.53	66.50	66.87

3. Methodology

After preprocessing the data, the Newmark-beta method [26] for linear systems is employed to compute the elastic response spectrum, namely the velocity spectrum and the pseudo velocity. Therefore, computing the Housner intensity (SI), which best assesses the damage potential of an earthquake [27], is as follows:

$$SI = \int_{0.1}^{2.5} PS_v(\varepsilon, T, dt)dT \quad \text{Eq. 1}$$

Proceedings of the 3rd Croatian Conference on Earthquake Engineering - 3CroCEE
19–22 March 2025, Split, Croatia
Copyright © 2025 CroCEE
DOI: https://doi.org/10.5592/CO/3CroCEE.2025.13

Where PS_v represents the pseudo velocity, T is the fundamental period of a single degree e of freedom system (representing the real building) and ζ is the damping ratio.

In this numerical work, four values of damping ratio (0%, 5%, 20%, and 50%) are considered to demonstrate the impact of damping ratio on various structures ranging from undamped systems to significantly damped systems. Additionally, as explained before, it is known that building codes typically incorporate bi-directional effects through the application of combination rules of 30% or 40%, signifying the total contribution of the principal direction of the earthquake, along with a 30% or 40% contribution from the other direction. These combination rules can be expressed as follows:

$$E_{XY} = E_X + \lambda_1 E_y \quad \text{Eq. 2}$$

$$E_{XY} = \lambda_2 E_x + E_y \quad \text{Eq. 3}$$

Here, λ_1 and λ_2 represent the percentage of the contribution in the other earthquake direction, when two orthogonal records are taken into account. However, combination coefficients proposed in building codes, such as 30% or 40%, are generally calculated based on the principal direction's acceleration record. This study revisits the bi-directional effects using the February 6th Kahramanmaras earthquakes, considering the contributions of other components. Consequently, the α coefficient, as introduced below, is particularly significant for assessing the combination rules in structural codes, and it is expressed as follows:

$$E_{xy} = E_x + \alpha E_x \quad \text{Eq. 4}$$

From the equations given above, λ_1, λ_2, and α can be calculated as follows:

$$\lambda_1 = (SI^{xy} - SI^x)/SI^y \quad \text{Eq. 5}$$

$$\lambda_2 = (SI^{xy} - SI^y)/SI^x \quad \text{Eq. 6}$$

$$\alpha = \frac{SI^{xy}}{SI^x} - 1 \quad \text{Eq. 7}$$

In which x denotes the earthquake's major direction that produces the maximum internal forces. Also, SI^x, SI^y, and SI^{xy} represent the Housner intensities to be calculated for both orthogonal directions and for the resultant alone.

The procedure for obtaining the spectral intensities for each earthquake component and the resultant accounting for the contribution of the two orthogonal directions of the earthquake is illustrated in Figure 1. The methodology to be followed in this work is summarized in Figure 2 in the form of a flowchart.

Proceedings of the 3rd Croatian Conference on Earthquake Engineering - 3CroCEE
19–22 March 2025, Split, Croatia
Copyright © 2025 CroCEE
DOI: https://doi.org/10.5592/CO/3CroCEE.2025.13

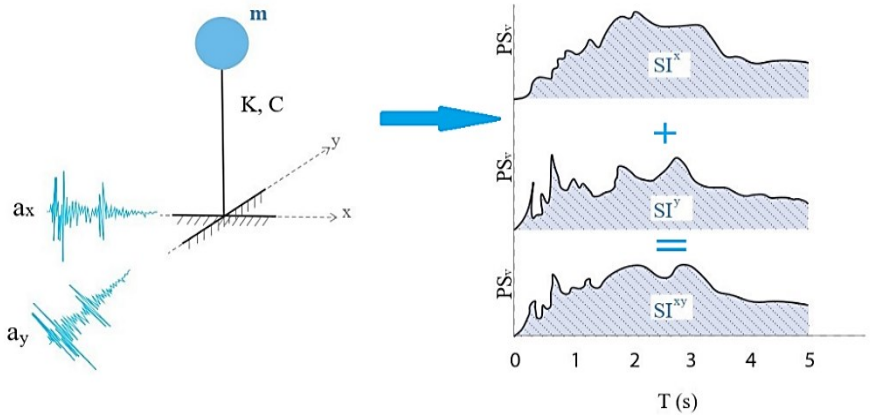


Figure 1. Typical SDOF system subjected to bi-directional seismic excitations and calculated spectral intensities

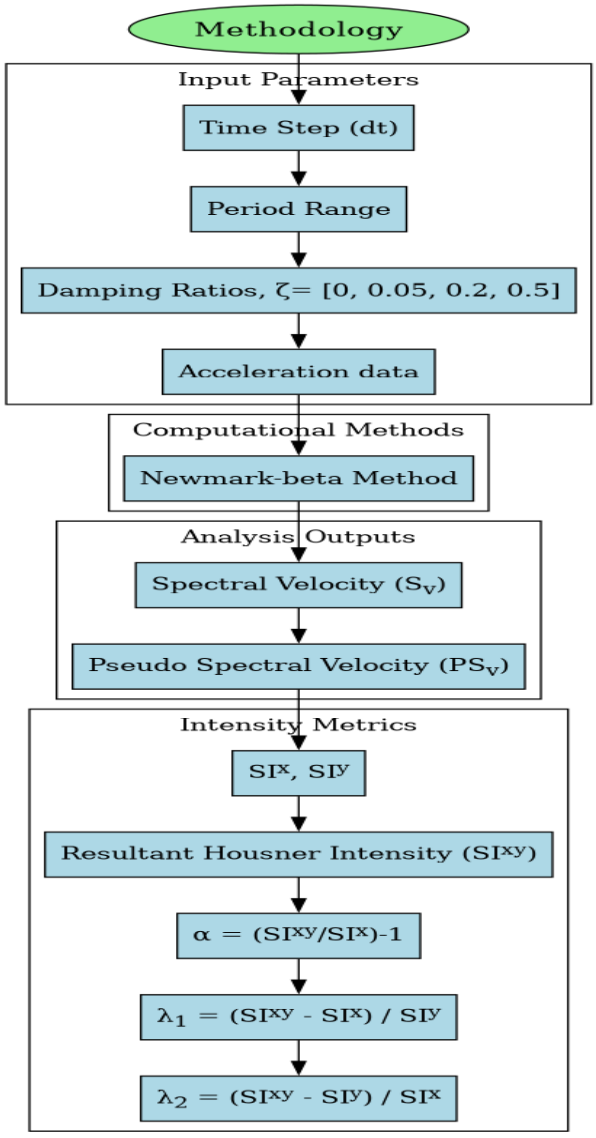


Figure 2. Flowchart of methodology to be followed

Proceedings of the 3rd Croatian Conference on Earthquake Engineering - 3CroCEE
19–22 March 2025, Split, Croatia
Copyright © 2025 CroCEE
DOI: https://doi.org/10.5592/CO/3CroCEE.2025.13

4. Numerical Results and Discussion

4.1. Combination Coefficients for the Feb. 6th, Kahramanmaras (Pazarcik) EQ (M_w 7.8)

Analysis results from the 27 stations selected from the Pazarcik earthquake are illustrated in Table 3. It is clear that nine records for all damping values exhibit α values exceeding 0.3, as suggested by many seismic codes. This data set represents one-third of the total records. For undamped systems, 20 stations surpassed 0.3, while nine stations exceeded 0.4. Moreover, for the damping ratio of 0.05, mainly used for residential RC framed buildings, 14 stations surpassed 0.3, representing over half of the total records, while six records exceeded the value of 0.4. For a damping ratio equal to 20%, the α value surpassed 0.3 in 13 stations, while four records reached or exceeded 0.4. In 11 records, the α values were greater than 0.3, with three stations showing values exceeding 0.4 when the damping ratio is 50%. Therefore, the lower and upper bounds of α for ζ = 0, 0.05, 0.20, and 0.50 are obtained to be 0.20~0.44, 0.14~0.42, 0.16~0.44, and 0.13~0.40, respectively.

Table 3. Computed Housner Intensities and combination coefficients for the February 6th, Kahramanmaras (Pazarcik) earthquake

Stations		ζ = 0%				5%				20%				50%			
		SI (cm/s)	α	λ1	λ2	SI (cm/s)	α	λ1	λ2	SI (cm/s)	α	λ1	λ2	SI (cm/s)	α	λ1	λ2
4614	EW	435.02				162.21				92.38				58.15			
	NS	511.60	**0.34**	0.40	0.49	205.03	0.28	0.35	0.49	120.76	0.26	0.34	0.50	76.81	0.26	0.34	0.50
	R	687.44				262.61				152.38				96.50			
3129	EW	570.06				284.00				166.97				104.98			
	NS	918.08	0.21	0.33	0.58	548.84	0.14	0.28	0.62	334.04	0.13	0.25	0.63	194.70	0.14	0.26	0.60
	R	1106.89				627.00				376.56				221.65			
3126	EW	583.27				268.24				159.48				90.66			
	NS	710.79	**0.32**	0.39	0.50	380.47	0.25	0.35	0.54	222.70	0.24	0.34	0.53	135.13	0.21	0.31	0.54
	R	937.92				474.38				276.73				163.09			
3141	EW	741.73				396.86				236.84				141.89			
	NS	565.88	0.30	0.39	0.54	293.29	0.26	0.36	0.52	164.33	0.23	0.33	0.53	97.19	0.22	0.33	0.54
	R	963.62				501.01				290.78				173.50			
3138	EW	743.78				501.13				314.91				200.18			
	NS	730.49	**0.44**	0.45	0.46	482.27	**0.42**	0.44	0.46	307.89	**0.44**	0.44	0.46	187.82	**0.40**	0.43	0.47
	R	1071.16				713.86				451.90				281.02			
3125	EW	561.39				272.95				164.95				98.40			
	NS	446.59	**0.31**	0.39	0.51	231.51	**0.32**	0.38	0.47	139.74	**0.31**	0.37	0.47	87.90	**0.34**	0.39	0.45
	R	735.50				360.72				216.85				132.29			
NAR	EW	379.10				221.59				147.81				92.44			
	NS	350.79	**0.39**	0.42	0.46	205.17	**0.37**	0.40	0.45	145.09	**0.41**	0.42	0.43	95.97	**0.39**	0.41	0.43
	R	525.19				304.45				208.63				133.45			
3135	EW	400.06				231.25				153.90				91.66			
	NS	326.39	**0.31**	0.38	0.50	181.20	0.28	0.35	0.49	120.62	0.27	0.35	0.49	85.67	**0.37**	0.40	0.44
	R	524.59				294.97				195.83				125.86			
3123	EW	749.90				407.40				212.27				118.32			
	NS	1001.11	0.29	0.38	0.54	581.76	0.25	0.35	0.54	372.74	0.17	0.29	0.60	228.00	0.13	0.26	0.61
	R	1288.69				724.33				434.32				258.24			
2718	EW	419.13				249.33				151.14				105.31			
	NS	352.43	**0.38**	0.45	0.53	210.14	**0.35**	0.42	0.51	125.75	**0.32**	0.39	0.49	74.17	0.23	0.33	0.53
	R	576.49				337.42				199.64				129.99			
3142	EW	385.79				203.70				120.57				70.82			
	NS	375.38	**0.42**	0.43	0.44	212.21	**0.40**	0.42	0.44	140.15	**0.32**	0.38	0.46	90.35	0.27	0.35	0.49
	R	546.43				296.89				185.62				115.19			
3144	EW	442.38	**0.41**	0.43	0.45	260.84	**0.40**	0.42	0.44	166.88	**0.42**	0.42	0.42	101.32	**0.40**	0.41	0.42
	NS	457.38				272.74				166.76				103.92			

Proceedings of the 3rd Croatian Conference on Earthquake Engineering - 3CroCEE
19–22 March 2025, Split, Croatia
Copyright © 2025 CroCEE
DOI: https://doi.org/10.5592/CO/3CroCEE.2025.13

	R	646.40				381.99				237.43				145.38			
	EW	370.63				199.87				110.70				66.04			
4616	NS	420.58	**0.36**	0.41	0.48	220.94	**0.37**	0.40	0.46	158.56	0.22	0.32	0.53	116.56	0.15	0.27	0.58
	R	573.79				301.79				193.99				134.10			
	EW	631.89				410.98				247.41				153.52			
3145	NS	371.84	0.20	0.33	0.61	241.90	0.17	0.30	0.59	151.80	0.18	0.29	0.56	102.84	0.21	0.31	0.54
	R	755.14				482.71				290.98				185.12			
	EW	640.93				315.70				211.22				122.72			
4615	NS	491.27	0.29	0.38	0.52	244.92	0.29	0.37	0.51	163.13	0.27	0.35	0.50	102.52	**0.31**	0.37	0.47
	R	825.79				406.90				268.21				160.22			
	EW	854.12				465.26				232.57				140.29			
3139	NS	803.17	**0.41**	0.43	0.47	517.95	**0.35**	0.39	0.46	323.59	0.23	0.32	0.51	195.07	0.23	0.32	0.51
	R	1201.24				701.28				398.74				240.44			

Table 4 (Continued). Computed Housner Intensities and combination coefficients for the February 6th, Kahramanmaras (Pazarcik) earthquake

Stations		**ζ = 0%**				**5%**				**20%**				**50%**			
		SI (cm/s)	α	λ1	λ2	SI (cm/s)	α	λ1	λ2	SI (cm/s)	α	λ1	λ2	SI (cm/s)	α	λ1	λ2
	EW	710.58				387.95				219.68				128.70			
3124	NS	774.30	**0.41**	0.45	0.49	450.88	**0.37**	0.43	0.51	259.03	**0.33**	0.39	0.49	160.13	0.29	0.36	0.49
	R	1092.11				617.56				345.31				206.62			
	EW	563.42				325.46				215.48				136.20			
2712	NS	380.29	0.23	0.34	0.56	190.83	0.17	0.29	0.58	125.07	0.16	0.27	0.58	91.83	0.21	0.31	0.53
	R	694.38				380.34				249.81				164.33			
	EW	333.28				151.48				81.02				46.96			
3136	NS	406.73	**0.32**	0.40	0.51	211.38	0.24	0.34	0.53	124.90	0.20	0.30	0.55	74.29	0.19	0.30	0.56
	R	538.87				262.90				149.45				88.49			
	EW	412.83				222.60				135.21				77.21			
3132	NS	518.46	**0.32**	0.40	0.52	291.83	0.28	0.37	0.52	173.66	0.28	0.36	0.50	103.62	0.25	0.34	0.51
	R	682.50				374.13				221.68				129.59			
	EW	440.77				177.18				99.38				60.36			
4625	NS	470.78	**0.40**	0.43	0.47	230.17	0.28	0.36	0.51	144.52	0.22	0.33	0.54	95.76	0.19	0.29	0.55
	R	660.18				293.66				176.86				113.48			
	EW	421.42				228.26				133.48				82.68			
3137	NS	388.17	**0.38**	0.41	0.46	209.77	**0.36**	0.40	0.45	115.03	**0.33**	0.38	0.47	72.07	**0.33**	0.38	0.46
	R	582.06				311.50				177.70				110.06			
	EW	403.11				249.73				157.18				96.95			
3143	NS	425.52	**0.41**	0.43	0.46	277.83	**0.35**	0.39	0.46	163.36	**0.40**	0.41	0.44	93.97	**0.40**	0.41	0.43
	R	598.89				376.44				228.32				135.41			
	EW	343.99				150.87				75.82				44.65			
4621	NS	352.11	**0.43**	0.44	0.45	145.42	**0.40**	0.41	0.43	80.01	**0.39**	0.41	0.44	50.63	**0.35**	0.39	0.46
	R	503.10				210.96				111.06				68.18			
	EW	375.73				222.63				128.90				75.74			
3131	NS	272.20	0.27	0.37	0.54	168.84	0.27	0.35	0.51	109.90	**0.32**	0.38	0.47	65.28	**0.33**	0.38	0.47
	R	476.33				282.39				170.62				100.59			
	EW	488.22				202.23				115.95				71.69			
4624	NS	439.02	**0.37**	0.41	0.47	196.92	**0.41**	0.42	0.44	122.58	**0.38**	0.40	0.43	87.57	0.29	0.36	0.47
	R	669.91				285.08				169.21				113.27			
	EW	242.72				121.07				71.43				41.76			
4611	NS	253.15	**0.42**	0.43	0.46	116.98	**0.40**	0.42	0.44	62.78	**0.33**	0.38	0.46	35.67	**0.32**	0.37	0.46
	R	358.24				169.88				95.33				54.99			

Proceedings of the 3rd Croatian Conference on Earthquake Engineering - 3CroCEE
19–22 March 2025, Split, Croatia
Copyright © 2025 CroCEE
DOI: https://doi.org/10.5592/CO/3CroCEE.2025.13

4.2.Combination Coefficients for the Feb. 6th, Kahramanmaras (Elbistan/Ekinozu) EQ (M_w 7.6)

Similarly, analysis results from the 27 stations selected from the Elbistan/Ekinozu earthquake are presented in Table 5; it is observed that 11 records across all damping values exhibit α values exceeding 0.3, accounting for 41% of the total records. For 26 stations, the α value surpassed 0.3 for undamped systems, while in 10 stations, it exceeded 0.4. As for the remaining 16 records and for residential RC framed buildings having a damping value of 0.05, α values surpassed 0.3, representing nearly 60% of the records, and four records exceeded or equaled to 0.4. For damping ratios equal to 20% and 50%, the α value exceeded 0.3 in 12 records and in nine stations, respectively. Consequently, the lower and upper bounds of α for ζ = 0, 0.05, 0.20, and 0.50 are obtained to be 0.27~0.46, 0.22~0.42, 0.18~0.39, and 0.14~0.40, respectively.

Table 5. Computed Housner Intensities and combination coefficients for the February 6th, Kahramanmaras (Elbistan/Ekinozu) earthquake

Stations		ζ = 0%				5%				20%				50%			
		SI (cm/s)	α	λ1	λ2	SI (cm/s)	α	λ1	λ2	SI (cm/s)	α	λ1	λ2	SI (cm/s)	α	λ1	λ2
4612	EW	524.88	**0.32**	0.38	0.49	313.02	0.26	0.35	0.50	174.49	0.18	0.29	0.56	100.49	0.14	0.26	0.59
	NS	630.41				409.58				280.92				183.22			
	R	830.97				517.69				330.96				209.10			
4406	EW	210.55	**0.40**	0.42	0.45	97.95	**0.39**	0.41	0.44	51.04	**0.39**	0.41	0.43	28.82	**0.36**	0.39	0.44
	NS	221.70				92.93				48.77				31.17			
	R	310.78				135.68				70.87				42.48			
4409	EW	94.83	**0.35**	0.41	0.50	45.08	0.27	0.36	0.53	23.15	0.29	0.37	0.50	14.50	0.30	0.36	0.47
	NS	80.62				33.38				18.43				11.93			
	R	127.93				57.20				29.96				18.81			
3802	EW	342.44	**0.39**	0.44	0.51	137.37	**0.32**	0.39	0.50	77.06	0.24	0.34	0.53	44.66	0.24	0.33	0.51
	NS	301.11				113.22				54.69				32.99			
	R	475.13				181.75				95.40				55.57			
4611	EW	169.77	0.27	0.38	0.55	75.41	0.22	0.32	0.55	42.46	0.24	0.33	0.53	25.74	0.22	0.32	0.53
	NS	122.51				50.22				30.17				17.84			
	R	215.88				91.70				52.52				31.52			
4614	EW	75.02	**0.42**	0.43	0.46	34.60	0.25	0.34	0.51	22.00	0.23	0.33	0.53	17.16	0.18	0.29	0.58
	NS	72.13				25.67				15.37				10.28			
	R	106.24				43.38				27.03				20.17			
4412	EW	209.54	**0.43**	0.44	0.45	93.58	**0.37**	0.41	0.45	53.48	**0.38**	0.41	0.46	37.92	**0.33**	0.38	0.47
	NS	214.79				101.88				57.73				32.73			
	R	306.45				139.91				79.78				50.40			
4405	EW	78.32	**0.46**	0.46	0.46	33.16	**0.42**	0.44	0.46	17.14	**0.37**	0.41	0.46	10.11	**0.38**	0.41	0.44
	NS	79.04				34.58				18.72				10.71			
	R	115.02				49.19				25.67				14.81			
129	EW	58.99	**0.41**	0.43	0.45	25.03	**0.36**	0.39	0.44	15.22	**0.39**	0.41	0.43	11.12	**0.31**	0.37	0.46
	NS	61.13				27.25				15.76				9.49			
	R	86.40				37.11				21.94				14.63			
NAR	EW	46.76	**0.35**	0.41	0.49	21.77	0.29	0.36	0.49	14.82	0.24	0.34	0.52	11.62	0.20	0.31	0.55
	NS	40.29				17.46				10.82				7.59			
	R	63.32				28.09				18.45				13.97			
4410	EW	102.01	**0.46**	0.46	0.47	48.41	**0.36**	0.41	0.47	28.42	**0.33**	0.38	0.46	16.37	**0.37**	0.40	0.44
	NS	100.95				43.05				24.66				15.20			
	R	148.52				65.90				37.71				22.37			
2703	EW	97.19	**0.35**	0.41	0.50	39.68	0.29	0.37	0.50	20.73	**0.34**	0.39	0.46	13.45	0.30	0.36	0.47
	NS	82.57				31.43				18.28				11.14			
	R	130.80				51.26				27.80				17.50			

Proceedings of the 3rd Croatian Conference on Earthquake Engineering - 3CroCEE
19–22 March 2025, Split, Croatia
Copyright © 2025 CroCEE
DOI: https://doi.org/10.5592/CO/3CroCEE.2025.13

5807	EW	96.52	**0.34**	0.41	0.49	45.23	0.25	0.34	0.51	25.26	0.24	0.33	0.51	14.02	0.30	0.37	0.47
	NS	82.12				33.16				18.59				11.66			
	R	129.81				56.44				31.45				18.29			
4613	EW	67.85	**0.44**	0.45	0.47	32.97	**0.42**	0.42	0.43	17.98	**0.36**	0.39	0.45	12.14	**0.35**	0.39	0.44
	NS	65.68				32.44				19.71				13.32			
	R	97.54				46.73				26.79				18.04			
0130	EW	148.11	**0.42**	0.43	0.46	65.46	**0.37**	0.40	0.44	38.77	**0.35**	0.39	0.45	24.84	**0.38**	0.40	0.43
	NS	154.12				69.79				43.08				26.06			
	R	218.41				95.94				58.03				36.06			
4625	EW	112.26	**0.33**	0.39	0.49	42.87	**0.31**	0.37	0.47	21.07	0.26	0.34	0.50	12.71	0.24	0.33	0.51
	NS	134.51				51.03				27.93				17.39			
	R	178.50				66.84				35.06				21.55			

Table 6 (Continued). Computed Housner Intensities and combination coefficients for the February 6th, Kahramanmaras (Elbistan/Ekinozu) earthquake

Stations		**ζ = 0%**				**5%**				**20%**				**50%**			
		SI (cm/s)	α	λ1	λ2	SI (cm/s)	α	λ1	λ2	SI (cm/s)	α	λ1	λ2	SI (cm/s)	α	λ1	λ2
0125	EW	192.32	**0.33**	0.40	0.50	78.43	**0.32**	0.37	0.47	40.94	**0.30**	0.36	0.47	25.63	**0.30**	0.36	0.47
	NS	228.93				92.00				49.36				30.70			
	R	306.57				121.21				64.14				40.00			
2308	EW	122.55	**0.39**	0.42	0.46	57.55	**0.42**	0.42	0.42	31.25	**0.38**	0.40	0.44	16.81	**0.31**	0.37	0.47
	NS	113.47				57.06				33.11				19.84			
	R	169.88				81.44				45.72				26.07			
4620	EW	118.05	**0.37**	0.42	0.50	61.26	**0.31**	0.39	0.50	39.72	0.24	0.34	0.52	25.39	0.27	0.35	0.50
	NS	101.96				49.72				28.44				19.37			
	R	161.38				80.52				49.28				32.09			
8002	EW	57.42	**0.37**	0.43	0.50	23.47	**0.33**	0.40	0.51	12.44	**0.37**	0.42	0.48	7.15	**0.39**	0.42	0.46
	NS	65.88				28.58				14.02				7.64			
	R	90.54				37.99				19.19				10.63			
4624	EW	137.18	**0.32**	0.39	0.49	50.85	0.28	0.35	0.49	27.05	0.28	0.36	0.40	16.49	**0.31**	0.37	0.47
	NS	165.27				64.80				33.79				19.63			
	R	218.21				82.64				43.40				25.72			
2309	EW	26.78	**0.42**	0.44	0.47	9.63	**0.40**	0.42	0.45	4.88	**0.34**	0.38	0.46	3.04	0.28	0.35	0.48
	NS	25.52				9.19				5.56				3.81			
	R	38.10				13.48				7.43				4.87			
3144	EW	66.38	**0.32**	0.38	0.49	29.27	0.29	0.36	0.48	17.24	0.29	0.36	0.48	10.82	0.29	0.36	0.49
	NS	55.27				23.62				13.84				8.69			
	R	87.54				37.79				22.20				13.97			
5809	EW	133.96	**0.38**	0.43	0.50	44.24	**0.34**	0.39	0.47	21.91	**0.35**	0.39	0.45	14.34	**0.36**	0.39	0.44
	NS	118.10				38.83				19.75				13.10			
	R	184.59				59.50				29.59				19.43			
4616	EW	42.77	**0.44**	0.45	0.45	17.72	**0.36**	0.39	0.44	11.89	0.28	0.35	0.49	8.51	0.23	0.33	0.52
	NS	42.95				16.27				9.32				6.04			
	R	62.04				24.15				15.18				10.49			
0127	EW	54.77	**0.34**	0.40	0.49	27.11	0.27	0.35	0.50	15.64	0.27	0.35	0.49	9.94	**0.40**	0.41	0.42
	NS	46.36				20.88				12.21				9.77			
	R	73.15				34.38				19.86				13.95			
4617	EW	155.50	**0.34**	0.41	0.50	76.21	0.29	0.37	0.50	46.44	0.26	0.34	0.50	32.11	0.25	0.33	0.50
	NS	130.91				60.28				35.41				24.11			
	R	208.78				98.47				58.56				40.16			

Copyright © 2025 CroCEE
DOI: https://doi.org/10.5592/CO/3CroCEE.2025.13

4.3. Analysis of earthquake damage

The Ministry of Environment, Urbanization, and Climate Change [28,29] reported that Hatay experienced the most extensive destruction, with nearly 20% of 406,849 buildings either collapsed, necessitating urgent demolition, or severely damaged, while approximately 31% sustained so-called slight to moderate damage. Note that no detailed scoring for this classification is available. Notably, of the 27 selected stations for the Pazarcik earthquake based on the highest PGA, seventeen are located in Hatay, while 18 stations from both earthquakes are situated in the province of Kahramanmaras. Table 3, Table 5, and Figure 3 indicate that one-third of the selected stations from the Pazarcik earthquake exhibited an α coefficient exceeding 0.3 across all damping values; six of these stations are located in Hatay, while the others are in Kahramanmaras. The same finding was reached for the Elbistan/Ekinozu Earthquake, wherein the majority of the α coefficient over 0.3 was seen in Kahramanmaras and Malatya. Consequently, it is determined that, alongside soil liquefaction and poor-quality concrete strength [17], the bi-directional impact has also been a contributing factor to the extensive damage sustained during the February 6th, 2023 Kahramanmaras earthquakes.

Note that most stations in the Pazarcik Earthquake are in regions of high seismic hazard, while in the Elbistan/Ekinozu earthquake, some of the stations are located in regions with low to moderate seismic hazard. It is concluded that the damage distribution in the earthquake hit region mostly matched well with the locations of larger computed bidirectional coefficients (Figure 3).

a) The Pazarcik Earthquake

b) The Elbistan/Ekinozu Earthquake

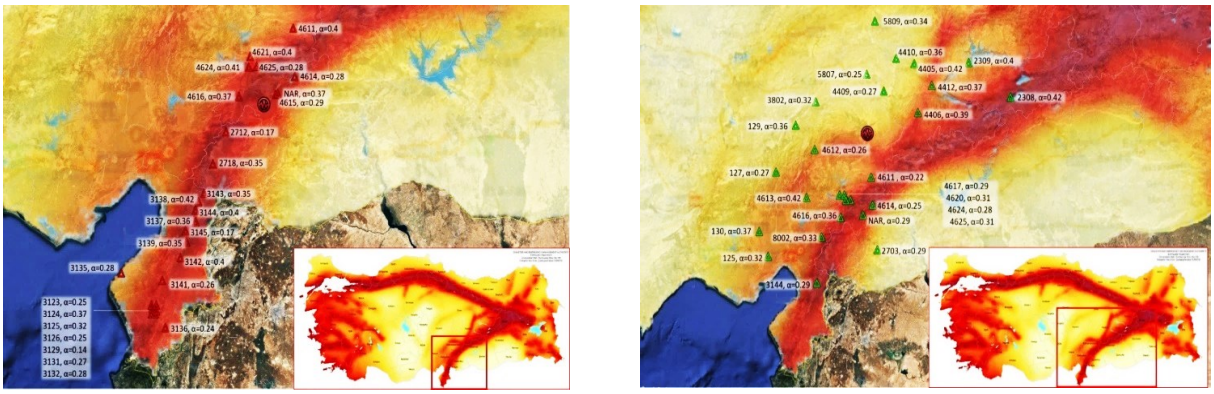


Figure 3. Distribution of α over selected stations for both earthquakes [30]

5. Conclusions

The bi-directional effects of earthquakes on buildings have been revisited. Since building damage is better reflected by the Housner Spectrum Intensity (SI) values of recorded strong ground motions, SI values in X, Y, and XY directions have been numerically computed by using the latest 2023 Kahramanmaras earthquake sequence. To derive the velocity and subsequently, pseudo velocity, the Newmark-beta approach has been followed in computing the Housner intensity. The widely used combination coefficient (i.e., α as introduced in the text) has been computed for different structural types (various damping ratios and fundamental periods). Numerical calculations reveal that one-third of the chosen stations for both earthquakes led to the α coefficients over 0.3. In addition, over half of the stations with damping values set to 5% had contributions from the other orthogonal direction above 30%, justifying the major destructions in residential buildings, while the 40% rule was satisfied in most cases.

It is important to highlight that, for both Pazarcik and Elbistan/Ekinozu earthquakes, the highest α coefficients for undamped systems were obtained to be 0.44 and 0.46, respectively. This value has been obtained to be 0.42 for both earthquakes for damping values equal to 5%, while it reached 0.44 and 0.39, respectively, for damping ratio equal to 20%. For highly damped structures (e.g. systems with

Copyright © 2025 CroCEE
DOI: https://doi.org/10.5592/CO/3CroCEE.2025.13

seismic energy dissipators of any kind), this α coefficient attained 0.40 for both earthquakes. These highest α coefficients reflect the importance of bi-directional effects during the Kahramanmaras earthquakes. Buildings located in Hatay/Antioch, Kahramanmaras, and Malatya were mostly affected from bidirectional effects. Therefore, in addition to other structural and geotechnical problems, it could be concluded that one of the reasons for the widespread damage and collapses was bidirectional effects of the strong ground motion.

Although some exceptions were noticed, it seems that the rule of 40% would be more appropriate for such strong events for most of the structural types. Based on these computed values, it would be judgeable to relate combination coefficients to the building importance factor (i.e., return period). Moreover, some stations that exhibited high PGA values during the Elbistan/Ekinozu earthquake are located in the existing seismic hazard maps with low to moderate seismicity, yielding misleading results in the computation of the seismic forces and corresponding seismic demands during the design stage.

References

[1] Yahiaoui A, Dorbani S, Yahiaoui L. Machine learning techniques to predict the fundamental period of infilled reinforced concrete frame buildings. Structures 2023;54. https://doi.org/10.1016/j.istruc.2023.05.052.

[2] Khaled A, Tremblay R, Massicotte B. Effectiveness of the 30%-rule at predicting the elastic seismic demand on bridge columns subjected to bi-directional earthquake motions. Eng Struct 2011;33:2357–70.

[3] Wang J, Burton H V., Dai K. Combination Rules Used to Account for Orthogonal Seismic Effects: State-of-the-Art Review. J Struct Eng 2019;145:03119001.

[4] Rosenblueth, E., & Contreras H. Approximate design for multicomponent earthquakes. J Eng Mech Div 1977;103:881–93.

[5] Eurocode8. Eurocode 8 : Design of Structures for Earthquake Resistance—Part 1: General Rules. Seismic Actions and Rules for Buildings. 2004.

[6] ASCE. ASCE/SEI 7-16 Minimum Design Loads and Associated Criteria for Buildings and Other Structures. American Society of Civil Engineers; 2017.

[7] TBEC 2018: Turkish Building Earthquake Code 2018:416.

[8] National Building Code of Canada Volume 1. Natl Res Counc Canada 2020.

[9] NEHRP Recommended seismic provisions for new buildings and other structures (FEMAP 2082-1) 2020.

[10] International Code Council. International Building Code (IBC). 2018.

[11] Code for Seismic Design of Buildings (GB 50011-2010) 2010:1–171.

[12] ATC3-06. Applied Technology Council Associated with the Structural Engineers Association of Califorina 1978.

[13] seismic design criteria Version 1.7. Caltrans 2013.

[14] NZS 1170.5. Structural Design Actions Part 5: Earthquake actions – New Zealand. 2004.

[15] Applied Technology Council ATC32. Improved seismic design criteria for California bridges: Provisional recommendations. 1996.

[16] Seismic Retrofitting Manual for Highway Structures : Part 1 – Bridges. Fhwa-Hrt-06-032 2006:658.

[17] Celik OC, Ulker MBC, Gocer C, Guntepe S, Koz O, Eyupgiller MM, et al. Multidisciplinary reconnaissance investigation covering structural, geotechnical, and architectural based damage to mid-rise residential buildings following the February 6th, 2023 Kahramanmaraş, Türkiye earthquake doublets (Mw 7.8, Mw 7.6). Soil Dyn Earthq Eng 2024;182:108738.

[18] Yahiaoui A, Matos J., Dorbani S. Probabilistic forecast of concrete compressive strength using ML. 20th Int. Probabilistic Work. IPW 2024. Cham : Spr, Cham : Springer Nature Switzerland; 2024, p. 281–6. https://doi.org/https://doi.org/10.1007/978-3-031-60271-9_25.

Copyright © 2025 CroCEE
DOI: https://doi.org/10.5592/CO/3CroCEE.2025.13

[19] Sesigur H, Celik OC, Cili F. Review and Evaluation of Combination Rules for Structures under Bi-directional Earthquake Excitations. 13th World Conf Earthq Eng 2004.

[20] Sesigur H, Celik OC, Cili F. Analysis of Code-Defined Combination Rules under Tri-Directional Earthquake Excitation. ECCOMAS Themat Conf Comput Methods Struct Dyn Earthq Eng 2007:13–6.

[21] Sesigur H, Celik OC, Cili F. Determination of orthogonal combination coefficients using inelastic velocity response spectra. ECCOMAS Themat. Conf. Comput. Methods Struct. Dyn. Earthq. Eng., 2009.

[22] Sesigur H, Celik OC, Cili F. Combination coefficients for yielding structures under tri-directional earthquake excitations. ECCOMAS Themat. Conf. Comput. Methods Struct. Dyn. Earthq. Eng., 2011.

[23] AFAD - TADAS n.d. https://tadas.afad.gov.tr/map (accessed December 3, 2024).

[24] Hu J, Liu M, Taymaz T, Ding L, Irmak TS. Characteristics of strong ground motion from the 2023 Mw 7.8 and Mw 7.6 Kahramanmaraş earthquake sequence. Bull Earthq Eng 2023:1–30.

[25] Tang Y, Şeşetyan K, Mai PM. Comprehensive ground-motion characterization of the 6 February 2023 MW 7.8 Pazarcık earthquake in Kahramanmaraş, Türkiye: insights into attenuation effects, site responses and source properties. Bull Earthq Eng 2024;22:6829–57.

[26] Newmark NM. A method of computation for structural dynamics. J Eng Mech Div 1959;85:67–94.

[27] Hussain N, Alam MS, Aman M. Seismic design coefficients verification of regular and vertically irregular high-rise shear wall buildings using bidirectional horizontal ground motions and 3D modeling. Structures 2024;70:107835.

[28] Ministry of Environment Urbanization and Climate Change, Damage Assessment Enquiry 2024. http://hasartespit.csb.gov.tr/ (accessed December 4, 2024).

[29] Damcı E, Temür R, Kanbir Z, Şekerci Ç, Köroğlu EÖ. Comprehensive investigation of damage due to 2023 Kahramanmaraş Earthquakes in Türkiye: Causes, consequences, and mitigation. J Build Eng 2024;99:111420. https://doi.org/https://doi.org/10.1016/j.jobe.2024.111420.

[30] Türkiye Deprem Tehlike Haritası n.d. https://www.afad.gov.tr/turkiye-deprem-tehlike-haritasi (accessed December 4, 2024).

Proceedings of the 3rd Croatian Conference on Earthquake Engineering - 3CroCEE
19–22 March 2025, Split, Croatia
Copyright © 2025 CroCEE
DOI: https://doi.org/10.5592/CO/3CroCEE.2025.14

ANALYSIS OF SGM DATA CHARACTERISTICS FOR BETTER EXPLANATION OF BUILDING DAMAGE DURING THE FEB.6TH, 2023 KAHRAMANMARAS, TURKEY EARTHQUAKES

Oguz Koz [(1)], Sinem Guntepe [(2)], Oguz C. Celik [(3)]

[(1)] *Research Assistant, Structural and Earthquake Engineering Unit, Faculty of Architecture, Istanbul Technical University, Istanbul, Turkey, oguz.koz@itu.edu.tr*
[(2)] *Research Assistant, Structural and Earthquake Engineering Unit, Faculty of Architecture, Istanbul Technical University, Istanbul, Turkey, sinem.guntepe@itu.edu.tr*
[(3)] *Professor, Structural and Earthquake Engineering Unit, Faculty of Architecture, Istanbul Technical University, Istanbul, Turkey; celikoguz@itu.edu.tr*

Abstract

On February 6th, 2023, two massive earthquake doublet, with magnitudes of M_w 7.8 in Pazarcik and M_w 7.6 in Elbistan/Ekinozu, struck the southeastern region of Turkey, causing widespread devastation across multiple cities, resulting in human causalities over fifty thousand, and a total collapse of approximately thirty-three thousand buildings. This study presents a comprehensive analysis of strong ground motion (SGM) data characteristics to explain such extensive structural damage observed during the latest 2023 Kahramanmaras earthquakes. Key ground motion parameters, such as peak ground acceleration, peak ground velocity, peak ground displacement, effective duration, Arias intensity, and Housner intensity, were obtained using the SGM data of the selected stations in the region. Additionally, acceleration-displacement response spectra and inelastic earthquake spectra are generated for various damping ratios and ductility levels for several cities that were primarily affected by these earthquakes. The spectral values are compared with the design earthquake spectra provided by both past and current Turkish Seismic Codes. Relationship between earthquake source parameters and structural damage caused by these earthquakes is investigated. Particularly in regions where reports of substantial building damage were prevalent, the comparison revealed substantial discrepancies between the observed spectrum demands and the code-based design spectra. Results indicate that the recorded ground motions exceeded the recommended seismic reaction limits outlined in the Turkey Building Earthquake Code (TBEC, 2018), particularly for buildings with lower heights and fundamental periods less than 2 seconds. The peak accelerations were considerably high, resulting in considerable structural damage, particularly in structures with substandard columns (i.e. columns with high axial load and shear demands). Inelastic response spectra of buildings with shorter periods showed large fluctuations, suggesting that these structures are vulnerable to severe shaking.

Keywords: Turkey Earthquake Doublet, Strong Ground Motion, Characteristics, Inelastic response spectra.

1. Introduction

The M_w 7.8 and M_w 7.6 Kahramanmaras earthquake doublet (note that these magnitudes are alternatively given to be 7.9, 7.8, 7.7, and 7.5 in some sources) occurred on February 6th, 2023, in SE Turkey and NW Syria where, the Anatolian, Arabian, and African plates meet [1]–[5]. The M_w 7.8 rupture initiated on a previously unmapped splay fault extending southward from the main strand of the East Anatolian Fault Zone (EAFZ) at 04:17:34 local time (37.226°N, 37.014°E, 10 km deep, at 01:17:34.332 UTC). Approximately, nine hours later at 13:24:48 local time (10:24:49.640 UTC), a second large earthquake (Ekinozu earthquake, M_w 7.6), occurred with hypocentral parameters (38.011°N, 37.196°E, 7.4 km deep), along the northern strand of the EAFZ [5]–[7]. Compared to the North Anatolian Fault Zone (NAFZ), another significant fault line in Turkey that has produced major earthquakes for a long time such as the 1999 Kocaeli (M_w=7.4) Earthquake and 1999 Duzce Earthquake (M_w=7.1) and 2022 Duzce (Golyaka) Earthquake (M_w=6.1) while the EAFZ has historically exhibited lower seismic activity, with only a few earthquakes exceeding M_w 7.0 in recent decades. However, it was well known that the EAFZ is capable of producing significant earthquakes, as evidenced by events

Copyright © 2025 CroCEE
DOI: https://doi.org/10.5592/CO/3CroCEE.2025.14

in 1513, 1795, and others that occurred between 1822 and 1905 [8]. The most significant event before the 2023 Kahramanmaras sequence was the M_w 6.8 Doganyol-Sivrice earthquake on January 24th, 2020, which also caused widespread building damage and total collapses in the region [9]. The EAFZ serves as a major plate boundary accommodating the westward extrusion of the Anatolian plate toward the Aegean Sea. Despite its relatively quiet seismic history, this fault system has been the source of destructive earthquakes throughout recorded history, as documented by several studies [8], [10].

The 2023 earthquake sequence is distinguished as the most devastating and recorded event along the EAFZ in recent history, exceeding the impacts of previous earthquakes such as the 1971 Bingol (M_w 6.6), the 2003 Bingol (M_w 6.4), 2010 Kovancilar, Elazig (M_w 6.1), and the 2020 Doganyol-Sivrice earthquakes, as reported by USGS. The region affected by the February 6th, 2023 earthquakes experienced over 50,000 casualties and significant structural devastation across 11 city centers and their districts. Following the mainshock, a series of large aftershocks, including a M_w 6.6 event near Nurdagi, Gaziantep, and more than 30 moderate-sized earthquakes (M_w 5.0~6.0), further damaged already compromised structures. In the three months following the disaster, over 33,000 aftershocks of varying magnitudes were recorded, highlighting the seismic complexity of the region [16].

Structural damage observed during the past earthquakes was influenced by various factors, including poor material quality, inadequate reinforcement, irregular architectural configurations, poor soil conditions, and non-compliance with seismic/building regulations [11]–[15]. Findings from studies on the latest Kahramanmaras earthquake sequence revealed comparable/expected patterns of structural failure in existing buildings [4]. In urban areas, most of the affected structures were reinforced concrete (RC) buildings, while rural regions predominantly comprised masonry (mostly rubble stone) or hybrid constructions incorporating traditional timber frames with mortar binders. The destruction also included cultural and religious landmarks, with many historic mosques, churches, and minarets sustaining severe damage or collapse. Poor soil conditions (amplifications, liquefaction etc.) had also a negative impact in the seismic behavior of buildings especially at Antakya (Antioch), Kahramanmaras, Iskenderun, and Golbasi (Adiyaman).

The aim of this study is to develop a comprehensive analysis of the characteristics of the strong ground motion data in order to possibly explain the widespread structural damage observed during the 2023 Kahramanmaras earthquakes. Spectral characteristics are obtained and compared for the three most affected cities (Kahramanmaras, Hatay, and Malatya) with each city experiencing damage to over 50% of its buildings. The study establishes an evaluation of seismic parameters, offering a deeper understanding of the factors contributing to observed structural damage.

This study underscores the critical role of spectral characteristics in understanding structural damage/collapses observed in buildings during the 2023 Kahramanmaras, Pazarcik and Elbistan/Ekinozu earthquakes. It is concluded that high PGA and PGV values were linked to severe damage as expected, and notable discrepancies are found between spectral demands and the TBEC (2018) design spectra, especially for low-to- midrise structures.

2. Analysis of Strong Ground Motions

2.1.Strong ground motion data

This work delves into earthquake records from the four provinces with the most heavily damaged structures during the 2023 Kahramanmaras earthquakes, including Kahramanmaras, Hatay, Malatya, and Adiyaman. All data were downloaded from TADAS AFAD [16]. Since the available AFAD data were unprocessed, a filtering was applied to remove noise-contaminated frequency content from the records while preserving the primary ground motion characteristics within the predefined frequency band. For this purpose, a fourth-order Butterworth noncausal filter was utilized. The filtering range was determined based on a literature review of studies on the 2023 Kahramanmaras earthquakes and visual inspections of the Fourier Amplitude Spectrum [2]. Strong ground motion records from stations 0201, 3146, and 4632 of the Pazarcik earthquake, as well as 0213, 4414, and 4631 of the Elbistan/Ekinozu earthquake, were found to be interrupted and therefore excluded from the evaluation. Although

Proceedings of the 3rd Croatian Conference on Earthquake Engineering - 3CroCEE
19–22 March 2025, Split, Croatia
Copyright © 2025 CroCEE
DOI: https://doi.org/10.5592/CO/3CroCEE.2025.14

Adıyaman had the highest ratio of collapsed buildings relative to its building stock, the acceleration records from the stations in the region were excluded from the analysis due to interruptions in the data. Processed data were used to compute key parameters, including Peak Ground Acceleration (PGA), Peak Ground Velocity (PGV), Peak Ground Displacement (PGD), Arias Intensity (AI), Housner Intensity (HI or a.k.a. SI), and Effective Duration (5-95%). The definitions and equations of earthquake parameters are summarized in Table 1.

Table 1. Definitions and Equations of Earthquake Characteristics.

Earthquake Characteristic	Definition	Equation
Peak Ground Acceleration PGA	Maximum ground acceleration during an earthquake	$\max\|a(t)\|$
Peak Ground Velocity PGV	Maximum ground velocity during an earthquake.	$\max\|v(t)\|$
Peak Ground Displacement PGD	Maximum ground displacement during an earthquake.	$\max\|d(t)\|$
Arias Intensity AI	A measure of earthquake energy per unit weight absorbed by an idealized oscillator over the earthquake duration (T_d).	$AI = \frac{\pi}{2g}\int_0^{T_d}[a(t)]^2 dt$
Housner Intensity HI	Response spectrum intensity, calculated as the integral of pseudo spectral velocity over the 0.1~2.5s period range for a 5% damping ratio (ξ).	$SI(\xi) = \int_{0.1}^{2.5} S_{pv}(\xi, t)\ dt$
Effective Duration (5-95%)	The time interval between the points at which 5% and 95% of the total energy has been recorded.	$t_{eff} = t_{95} - t_5$

2.2. Earthquake Characteristics and Observations

An earthquake's damage potential can be assessed by using ground motion parameters, each reflecting different physical characteristics of seismic activity. Peak Ground Acceleration (PGA) is one of the most well-known and commonly used indicators in seismic design. However, it does not account for the duration or frequency content of the earthquake and is more suitable for structures with short periods (T < 0.3 s) [17]. Peak Ground Velocity (PGV) represents the maximum ground velocity during an earthquake. It is particularly important for evaluating the dynamic response of flexible structures and provides insights into the earthquake's magnitude and intensity. Peak Ground Displacement (PGD), on the other hand, correlates with damage in long-period structures, including both buildings and infrastructure. Arias Intensity (AI) and Housner Intensity (HI) are energy-based parameters that consider the duration and frequency content of the ground motion. Housner Intensity focuses on dynamic demands in structures with periods between 0.1 and 2.5 seconds. Finally, effective duration represents the time interval during which 5% to 95% of the cumulative energy (Arias Intensity) is released. A longer effective duration indicates that structures are subjected to a greater number of seismic load cycles, which increases the probability of structural damage due to the accumulation of damage caused by repeated loading.

The strong ground motion characteristics from selected stations in the three provinces with the highest damage during the Pazarcik and Elbistan/Ekinozu earthquakes are presented in Tables 2 and 3, respectively. For the Pazarcik earthquake, the analyzed stations include Kahramanmaras (4614), Malatya (4404), and Hatay (3129), while for the Elbistan/Ekinozu earthquake, the selected stations are Kahramanmaras (4612), Malatya (4406), and Hatay (3144).

Proceedings of the 3rd Croatian Conference on Earthquake Engineering - 3CroCEE
19–22 March 2025, Split, Croatia
Copyright © 2025 CroCEE
DOI: https://doi.org/10.5592/CO/3CroCEE.2025.14

Table 2. Ground Motion Characteristics for the M_w 7.8 Pazarcik Earthquake.

Station Code	PGA (cm/sec²)	PGV (cm/sec)	PGD (cm)	PGA_D (cm/sec²)	PGA/PGA_D	AI (m/sec)	HI (cm)	Effective duration 5~95%
3129 E-W	1203.7	68.8	53.3	438.0	2.75	18.3	286.6	15.3
3129 N-S	1366.1	172.5	37.6	438.0	3.12	25.0	545.5	10.7
3129 U-D	797.5	42.9	22.1	350.4	2.28	6.9	165.3	10.6
4614 E-W	2179.8	61.9	26.7	441.4	4.94	58.7	164.6	23.8
4614 N-S	1984.1	85.5	57.9	441.4	4.50	88.2	205.8	23.1
4614 U-D	1602.8	37.4	24.2	353.1	4.54	36.4	97.4	21.0
4404 E-W	139.7	11.4	7.8	495.1	0.28	0.2	39.4	22.0
4404 N-S	132.8	13.6	12.8	495.1	0.27	0.2	42.1	21.2
4404 U-D	96.7	11.9	4.8	396.0	0.24	0.1	34.8	29.3

Table 3. Ground Motion Characteristics for the M_w 7.6 Elbistan/Ekinozu Earthquake.

Station Code	PGA (cm/sec²)	PGV (cm/sec)	PGD (cm)	PGA_D (cm/sec²)	PGA/PGA_D	AI (m/sec)	HI (cm)	Effective duration 5~95%
3144 E-W	76.1	11.3	10.6	464.2	0.16	0.1	29.5	31.4
3144 N-S	59.7	8.1	5.6	464.2	0.13	0.1	23.8	31.3
3144 U-D	27.5	4.1	4.6	371.4	0.07	0.0	15.8	47.7
4406 N-S	471.5	20.2	11.8	419.1	1.13	3.3	94.5	18.4
4406 E-W	409.1	33.8	17.2	419.1	0.98	2.9	97.8	17.4
4406 U-D	303.1	19.9	9.6	335.3	0.90	1.4	62.5	17.0
4612 N-S	637.3	166.7	63.6	377.9	1.69	4.2	410.6	20.2
4612 E-W	523.7	73.3	42.8	377.9	1.39	3.2	315.1	28.8
4612 U-D	488.3	54.3	30.6	302.3	1.62	1.8	129.6	12.0

In the Pazarcik earthquake, the maximum ground acceleration recorded at station 4614 (N-S) exceeded 2000 cm/s², representing a significant seismic event and never recorded in Turkey's history. High vertical acceleration values further increased the axial loads on columns with already high axial force demands (even under gravity loading due to poor concrete quality) and insufficient ductility stemming from poor rebar detailing, contributing to brittle failures in these structures. In Malatya, which experienced significant building damage, the maximum PGA at the 4404 station during the Pazarcik earthquake was relatively low, recorded to be 140 cm/s², with a Housner Intensity of 42.1 cm. However, in the Elbistan/Ekinozu earthquake, the PGA increased significantly to 471.5 cm/s², and the Housner Intensity reached 97.8 cm. These evaluations indicate that the Elbistan/Ekinozu earthquake was more destructive in Malatya in terms of energy release. Long earthquake durations observed across multiple stations, highlight the significant role of prolonged seismic excitation in amplifying cumulative damage (or damage growth), particularly in structures with inadequate detailing or insufficient energy dissipation capacity.

Proceedings of the 3rd Croatian Conference on Earthquake Engineering - 3CroCEE
19–22 March 2025, Split, Croatia
Copyright © 2025 CroCEE
DOI: https://doi.org/10.5592/CO/3CroCEE.2025.14

To better provide a comparative perspective, the Housner Intensity (HI) values from the 1999 Duzce (M_w 7.1), 1999 Kocaeli (M_w 7.4), and 2011 Van (M_w 7.0) earthquakes offer valuable context for evaluating the ground motion characteristics of the 2023 Kahramanmaras earthquakes. For instance, the HI values during the 1999 Kocaeli earthquake reached up to 335 cm, while the 1999 Düzce and 2011 Van earthquakes recorded maximum values of 269 cm and 146 cm, respectively. In contrast, the HI values computed for the 2023 Kahramanmaras earthquakes are significantly higher as shown in Tables 2 and 3. During the Pazarcik event, the HI value at Hatay (3129 N-S component) reached 545.5 cm, while Kahramanmaras (4614 N-S component) recorded 205.8 cm. Similarly, during the Elbistan/Ekinozu event, Malatya (4612 N-S component) resulted in an HI value of 410.6 cm. These remarkable differences highlight the exceptionally high energy demands imposed by the 2023 Kahramanmaras earthquake sequence, particularly on short-to-medium period structures (0.1~2.5 seconds).

3. Spectral Characteristics and Structural Damage Relation

In the earthquake-stricken area, 86.7% of buildings are made with reinforced concrete while 2.4% of the buildings are steel, 3.5% are masonry, and 3.6% are prefabricated [18]. The other category includes timber, mixed or unidentified structural systems and the percentages of other structural systems is quite low. Structural damage classification categorizes buildings based on the severity of earthquake-induced damage, ranging from slight damage to totally collapsed buildings. Slightly damaged buildings exhibit minor cracks on paint, plaster, or walls, with some localized plaster detachment due to the earthquake. Moderately damaged buildings show wall fractures (nonstructural) and minor cracks in structural members, making them uninhabitable without prior repair or structural strengthening. Heavily damaged buildings experience extensive and widespread flexural or shear failures or separation of structural elements, resulting in an irreparable loss of structural integrity, both in terms of strength and economic efficiency. Urgent demolition is required for buildings where substantial permanent deformations have occurred in load-bearing components, leading to partial or total structural collapses. In terms of the building's assessment by Ministry of Environment, Urbanization, and Climate Change of Turkey on 2,457,942 buildings, there were 38,440 collapsed buildings and 20,537 were in need of urgent demolition, 204,745 of them got severe damage, 41,732 experienced moderate damage, and 636,840 were scored as slightly damaged [19]. The number of total and damaged buildings for the most affected 4 cities from these earthquakes is given in Table 4. The distribution of damage to buildings in these four cities is also displayed in Figure 1. Various levels of structural damage observed in buildings in the province of Kahramanmaras are presented in Figure 2.

Table 4. Number of Damaged Buildings for the Most Affected 4 Cities [19].

City	Total Number of Buildings	Slight Damage	Moderate Damage	Severe Damage	Urgent Demolition	Collapsed
Adiyaman	120,496 (100%)	39,888 (33.10%)	4,493 (3.73%)	20,481 (17.00%)	2,271 (1.88%)	6,062 (5.03%)
Hatay	406,849 (100%)	114,566 (28.16%)	12,630 (3.10%)	54,960 (13.51%)	8,839 (2.17%)	13,345 (3.28%)
Kahramanmaras	243,153 (100%)	81,134 (33.37%)	6,036 (2.48%)	35,691 (14.68%)	4,432 (1.82%)	7,480 (3.08%)
Malatya	178,987 (100%)	51,933 (29.01%)	2,323 (1.30%)	35,368 (19.76%)	1,746 (0.98%)	5,545 (3.10%)

Proceedings of the 3rd Croatian Conference on Earthquake Engineering - 3CroCEE
19–22 March 2025, Split, Croatia
Copyright © 2025 CroCEE
DOI: https://doi.org/10.5592/CO/3CroCEE.2025.14

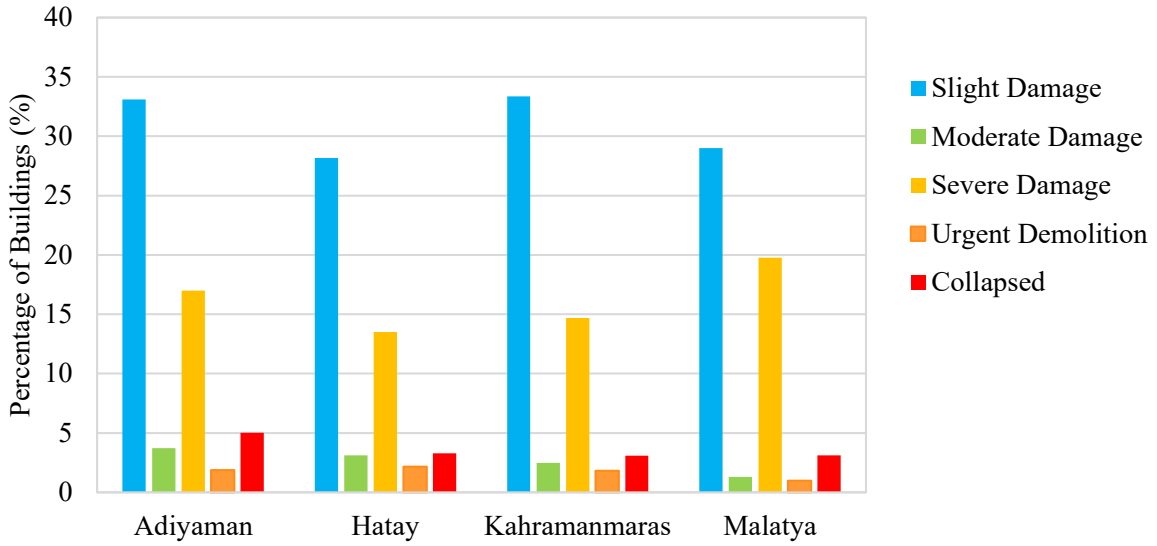


Figure 1. Building Damage Distribution (%) in the Most Affected Cities



Figure 2. Damaged building images from the province of Kahramanmaras

Acceleration, velocity, and displacement spectra were generated for the stations with the maximum recorded accelerations in the three provinces with the highest rate of damaged building stock—Hatay, Kahramanmaras, and Malatya. Horizontal and vertical accelerations, velocity, and displacement spectra were computed for systems with 5% damping and are presented in Figures 3, 4,

Copyright © 2025 CroCEE
DOI: https://doi.org/10.5592/CO/3CroCEE.2025.14

and 5. Additionally, the acceleration spectra corresponding to the ground motion levels with a 2% probability of exceedance in 50 years (return period of 2475 years, DD1) and the design earthquake level with a 10% probability of exceedance in 50 years (return period of 475 years, DD2) are illustrated. These earthquake levels are plotted for the weakest soil conditions, classified as ZE soil class (e.g., loose sand, gravel, or soft to firm clay layers).

In Turkey Building Earthquake Code (2018), the vertical elastic design spectrum is also defined. The design accelerations for DD1 and DD2 earthquake levels are illustrated on the vertical earthquake (U-D) acceleration spectrum. To enhance the clarity of the design spectrum levels, the vertical axis of the acceleration spectra was capped at 3g. However, in the figure illustrating the inelastic spectra (Fig. 7.a), the maximum points are displayed without being capped.

A significant portion (37%) of the existing building stock in the earthquake-affected region was constructed before 1998 and was therefore subjected to the earthquake code in effect at that time [18]. Between 1975 and 1998, Specifications for Structures to be Built in Disaster Zones (SSBDZ, 1975) were in use. Consequently, the design acceleration spectrum from this code has also been included in the acceleration spectra for comparison.

In the elastic response spectrum, within the period range T=0~0.5 s, the spectral acceleration of the 4614 N-S component peaked at 7.4g, while the 3129 N-S component reached its highest value at 5.32g. This highlights the significant impact of high-frequency ground motions on short-period structures (such as single-story or low-rise buildings), which were more vulnerable to these effects.

The spectral values obtained from the acceleration records measured at the Kahramanmaras 4614 and Hatay 3129 stations were found to significantly exceed the design acceleration spectrum, particularly in the short-period range. In Malatya, while the accelerations caused by the Pazarcik earthquake remained below the design spectrum, the accelerations generated during the Elbistan/Ekinozu earthquake exceeded the design spectrum values. High PGA values are indicative of intense shaking and immediate structural demands but are insufficient to comprehensively explain structural damage. Other factors contributing to structural damage include the earthquake's duration, directionality, and frequency content; the characteristics of the building stock; local soil conditions; architectural and structural design flaws in the load-bearing systems; and issues arising from non-compliance with the construction design or errors during the construction phase.

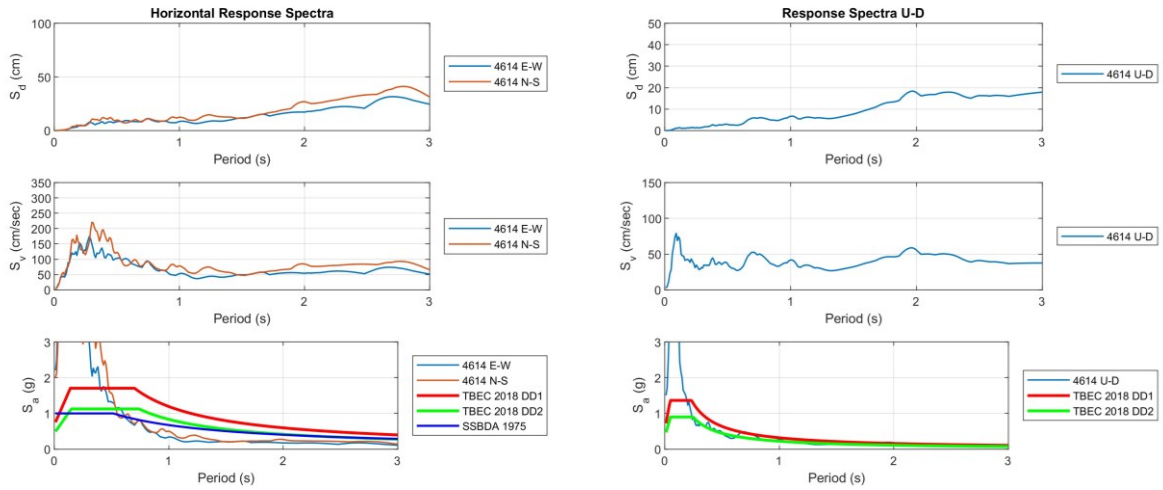


Figure 3. Response spectra for Kahramanmaras stations during the Pazarcik Earthquake:
(a) Horizontal components, (b) Vertical component

Copyright © 2025 CroCEE
DOI: https://doi.org/10.5592/CO/3CroCEE.2025.14

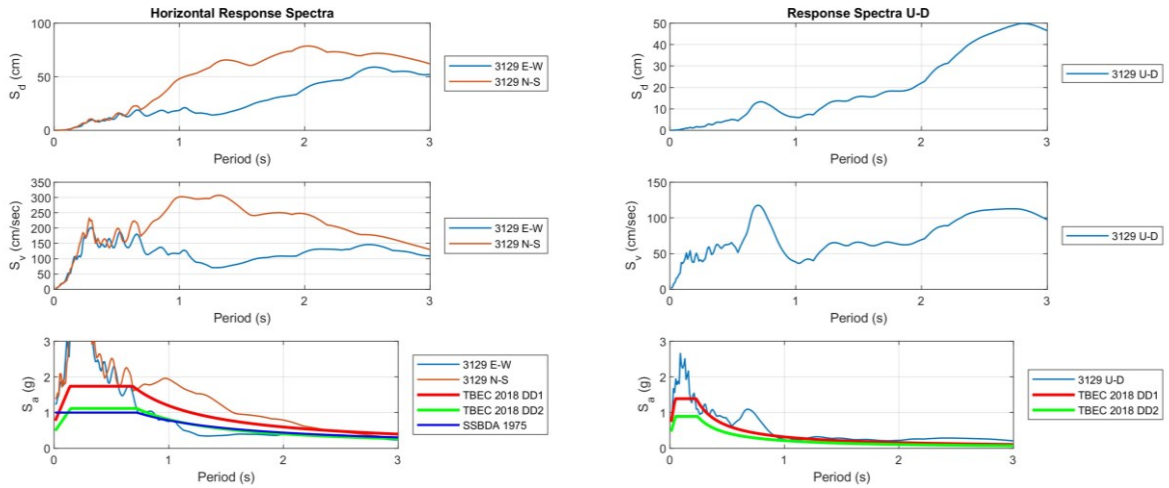


Figure 4. a) Response spectra for Hatay stations during the Pazarcik Earthquake: (a) Horizontal components, (b) Vertical component

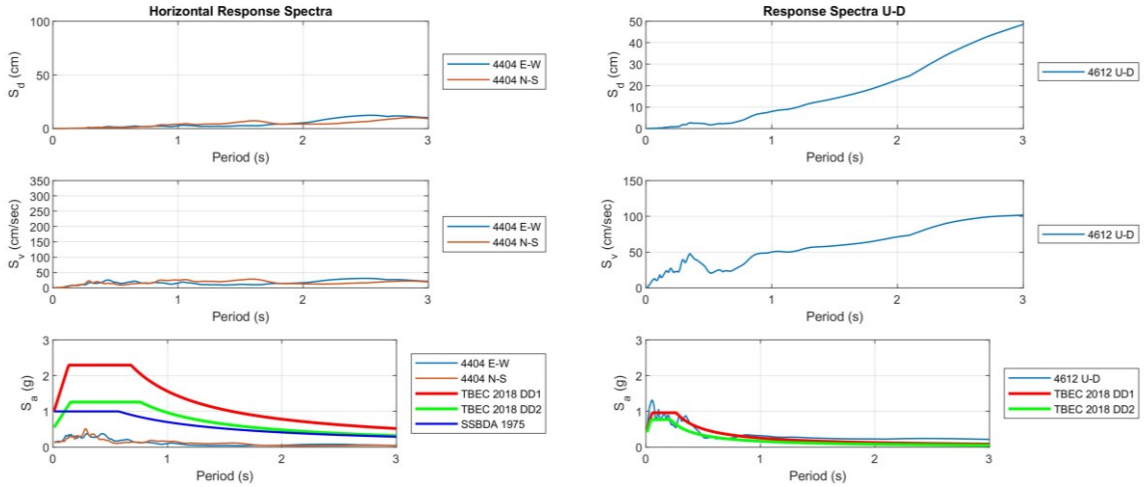


Figure 5. Response spectra for Malatya stations during the Elbistan/Ekinozu Earthquake: (a) Horizontal components, (b) Vertical component

The Acceleration-Displacement Response Spectrum (ADRS) is a tool used in structural engineering to understand how buildings or other structures react to dynamic forces like earthquakes or explosions. It visually compares maximum acceleration and displacement, providing insights into how a structure might behave under different levels of ground motion [20]. By analyzing the intersection of the demand curve (ground motion) and the capacity curve (structural response), engineers identify the structure's performance point. This helps determine if the structure can withstand the applied forces without damage or if it faces a risk of failure. ADRS is crucial in seismic design and performance-based evaluations to ensure structural safety under dynamic loading conditions.

Elastic acceleration-displacement response spectra (bi-spectra) were generated for the Kahramanmaras 4614 and Hatay 3129 stations during the Pazarcik earthquake, as well as the Malatya 4612 station during the Elbistan/Ekinozu earthquake, and are presented in Figure 6.

Copyright © 2025 CroCEE
DOI: https://doi.org/10.5592/CO/3CroCEE.2025.14

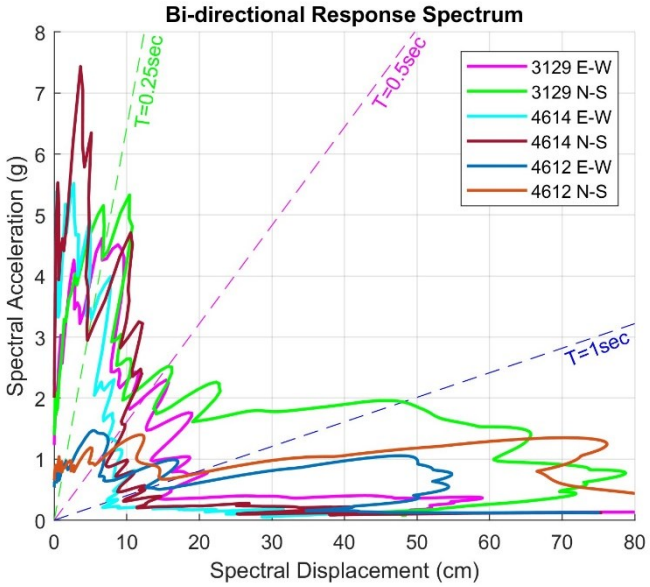


Figure 6. Acceleration-displacement response spectra (bi-spectra)

Constructing inelastic response spectra is useful in seismic engineering to account for yielding in structures during strong shaking. The ductility factor, μ, is defined as the ratio of maximal inelastic deformation to yield deformation, acting as a crucial indicator of a structure's capacity to endure substantial plastic deformation while preserving its stability. The displacement ductility factor (μ) is utilized as a parameter for generating the inelastic response spectrum. Elastic structures are assigned a value of μ=1, whereas systems with high ductility can be considered to have μ=8. The response modification factor (R) is a seismic design parameter and a proportional ductility factor, that represents the inelastic behavior of a structure [21]. The value of R is influenced by various parameters, including the height of the structure, as high-rise and low-rise structures respond differently to seismic forces. Building codes provide well-defined R-values for various structural systems and materials [22]. According to the Turkey Building Earthquake Code (TBEC-2018), the R-value for RC framed buildings with a high level of ductility is specified to be 8. For buildings combining frames with RC shear walls (dual systems), R is given to be 7. Similarly, R is taken to be 8 for steel frame buildings with high ductility, and for reinforced masonry structures, R=4. Figure 7 illustrates the elastic response spectra (μ=1) and inelastic response spectra for ductility levels μ=2, 4, and 8, derived from seismic recordings at three stations (Kahramanmaras (4614), Malatya (4612), and Hatay (3129) [23]). Even with increased ductility ratios, the persistently high acceleration demands observed in the inelastic spectra for short-period structures (T<0.5 s) indicate that these structures dissipate a significant portion of the seismic energy through acceleration, highlighting their limited plastic deformation capacity. The significant reduction in acceleration demands for long-period structures (T>1 s) highlights their ability to effectively dissipate seismic energy through deformation due to their ductile behavior.

Copyright © 2025 CroCEE
DOI: https://doi.org/10.5592/CO/3CroCEE.2025.14

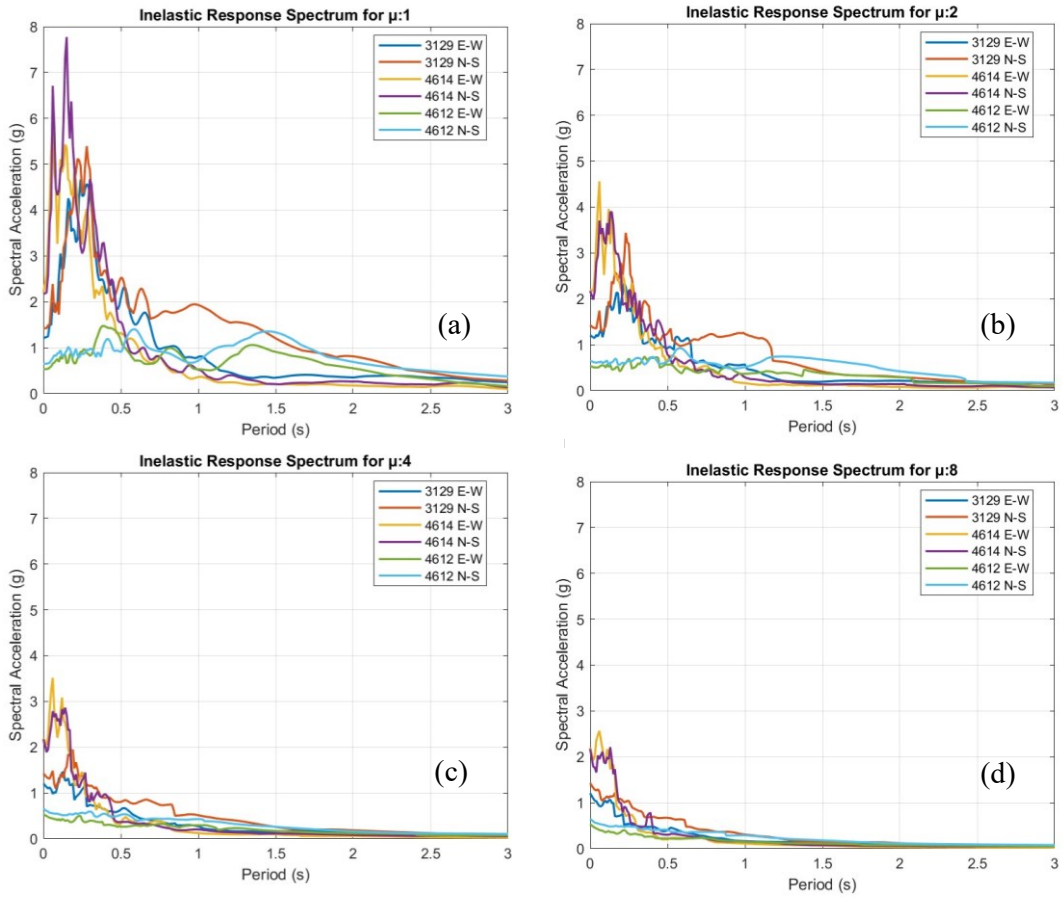


Figure 7. a) Elastic response spectra (μ = 1), b) Inelastic response spectra for μ = 2, c) Inelastic response spectra for μ = 4, and d) Inelastic response spectra for μ = 8

4. Conclusions

This study highlights the significance of strong ground motion characteristics in better explaining the structural vulnerabilities evident during the February 6th, Kahramanmaras (Pazarcik&Elbistan/Ekinozu) earthquake sequence. Ground motion parameters such as PGA, PGV, Arias Intensity, and Housner Intensity, were examined, and their effects on structural damage were evaluated by comparisons with the TBEC (2018) design spectra. The following results can be deduced from this work:

- High PGA values are directly connected with areas of significant building damage.
- Notable differences were identified between the spectral demands and the TBEC (2018) design spectra, particularly in case of low-to-midrise structures.
- The Housner Intensity values revealed a significant energy demand for short-period structures, suggesting potential deficiencies even in code-compliant designs.
- The effective duration of shaking was identified as a contributing factor to cumulative damage and damage growth particularly in structures exhibiting inadequate/nonductile detailing.
- Although the PGA values in some regions exceeded the design earthquake spectra, it is believed that the majority of collapsed buildings (3~5% of the total building stock) were either not constructed in compliance with code requirements or were affected by factors such as structural irregularities and poor material strength.
- Poor soil conditions (amplifications, liquefaction etc.) had also a negative impact in the seismic behavior of buildings especially at Antakya (Antioch), Kahramanmaras, Iskenderun, and Golbasi (Adiyaman).

Copyright © 2025 CroCEE
DOI: https://doi.org/10.5592/CO/3CroCEE.2025.14

References

[1] Wu, F.et al. (2023): Pulse-like Ground Motion Observed during the 6 February 2023 M_w 7.8 Pazarcik Earthquake (Kahramanmaraş, SE Türkiye). Earthq. Sci., 36, 4, 1–12, doi: https://doi.org/10.1016/j.eqs.2023.05.005

[2] Hu, J., Liu, M., Taymaz, T., Ding, L. and Irmak, T. S. (2024): Characteristics of strong ground motion from the 2023 M_w 7.8 and M_w 7.6 Kahramanmaraş earthquake sequence, *Bull. Earthq. Eng.*, doi: https://doi.org/10.1007/s10518-023-01844-2

[3] Goldberg, D. E. et al. (2023): Rapid Characterization of the February 2023 Kahramanmaraş, Türkiye, Earthquake Sequence. *Seism. Rec.*, 3, 2, 156–167, doi: https://doi.org/10.1785/0320230009

[4] Celik, O. C. Ulker MBC, Gocer C, Guntepe S, Koz O, Eyupgiller MM, et al. (2024): Multidisciplinary reconnaissance investigation covering structural, geotechnical, and architectural based damage to mid-rise residential buildings following the February 6th, 2023 Kahramanmaras earthquake doublets (M_w 7.8, M_w 7.6). *Soil Dyn. Earthq. Eng.*, 182, 108738, doi: https://doi.org/10.1016/j.soildyn.2024.108738

[5] Liu, C. et al. (2023): Complex multi-fault rupture and triggering during the 2023 earthquake doublet in southeastern Türkiye. *Nat. Commun.*, 14, 1, pp. 1–14, 2023, doi: https://doi.org/10.1038/s41467-023-41404-5

[6] United States Geological Survey (USGS), *M 7.8 - Pazarcik earthquake, Kahramanmaras earthquake sequence.* https://earthquake.usgs.gov/earthquakes/eventpage/us6000jllz/executive (accessed Aug. 26, 2023).

[7] United States Geological Survey (USGS), *M 7.5 - Elbistan earthquake, Kahramanmaras earthquake sequence.* https://earthquake.usgs.gov/earthquakes/eventpage/us6000jlqa/executive (accessed Aug. 29, 2023).

[8] Wang, Z., Zhang, W., Taymaz, T., He, Z., Xu, T., and Zhang, Z. (2023): Dynamic Rupture Process of the 2023 M_w 7.8 Kahramanmaraş Earthquake (SE Türkiye): Variable Rupture Speed and Implications for Seismic Hazard. *Geophys. Res. Lett.*, 50, 15, 1–11, doi: https://doi.org/10.1029/2023GL104787

[9] Celik, O.C., Bal, A., Atasever, K., Emanet, S., Koca, S. (2020): 24 Ocak 2020 Doğanyol (Malatya)-Sivrice (Elazig) Depreminden Gözlemler (M_w 6.7-Doğu Anadolu Fay Zonu). *Bet. Prefabrikasyon,* 134, April, 5–29.

[10] Emre, Ö. et al. (2018): Active fault database of Turkey. *Bull. Earthq. Eng.*, 16, 8, 3229–3275, 2018, doi: https://doi.org/10.1007/s10518-016-0041-2

[11] Celik, O.C., Cili, F. Ozgen, K. (2000): 17 Agustos 1999 Kocaeli (Izmit) Depremi'nden Gözlemler. *Yapi Dergisi (in Turkish).*

[12] Celep, Z., Erken, A., Taskin, B., and Ilki, A. (2011): Failures of masonry and concrete buildings during the March 8, 2010 Kovancilar and Palu (Elazig) Earthquakes in Turkey. *Eng. Fail. Anal.*, 18, 3, 868–889, 2011, doi: https://doi.org/10.1016/j.engfailanal.2010.11.001

[13] Yazgan, U., Oyguç, R., Ergüven, M. E., and Celep, Z. (2016): Seismic performance of buildings during 2011 Van earthquakes and rebuilding efforts, *J. Earthq. Eng. Eng. Vib.*, 15, 3, 591–606, doi: https://doi.org/10.1007/s11803-016-0346-9

[14] Tapan, M., Comert, M., Demir, C., Sayan, Y., Orakcal, K., and Ilki, A. (2013): Failures of structures during the October 23, 2011 Tabanli (Van) and November 9, 2011 Edremit (Van) earthquakes in Turkey. *Eng. Fail. Anal.*, 34, 606–628, 2013, doi: https://doi.org/10.1016/j.engfailanal.2013.02.013

[15] A. Yakut et al. (2022): Performance of structures in İzmir after the Samos island earthquake. *Bull. Earthq. Eng.*, 20, 14, 7793–7818, 2022, doi: https://doi.org/10.1007/s10518-021-01226-6

[16] Disaster and Emergency Management Presidency (AFAD).: *AFAD TADAS Website*. https://tadas.afad.gov.tr/map (accessed Dec. 14, 2024).

[17] Malcioglu, F.S., O'Kane, A., Donmez, K. and Aktas, Y.D. (2022): Characteristics of Strong Ground Motions in the 30 October 2020, M_W 6.9 Aegean Sea Earthquake. *Front. Built Environ.* 8:870279. doi: https://doi.org/10.3389/fbuil.2022.870279

Copyright © 2025 CroCEE
DOI: https://doi.org/10.5592/CO/3CroCEE.2025.14

[18] Presidency of Strategy and Budget (2023): *2023 Kahramanmaras ve Hatay Earthquakes Report (in Turkish)* [Online]. Available: https://www.sbb.gov.tr/wp-content/uploads/2023/03/2023-Kahramanmaras-ve-Hatay-Depremleri-Raporu.pdf

[19] Damcı, E., Temür, R., Kanbir, Z., Şekerci, Ç., Köroğlu, E.Ö. (2025): Comprehensive Investigation of Damage Due to 2023 Kahramanmaraş Earthquakes in Türkiye: Causes, Consequences, and Mitigation (Pre-print), *J. Build. Eng.,* 99, 111420, doi: https://doi.org/10.1016/j.jobe.2024.111420

[20] Heath, D. J., Wilson, J. L., Gad, E. F. (2015): Acceleration-displacement response spectrum vibration limits for blast vibrations. *Australian Journal of Structural Engineering*, 16(1), 1-16. doi: https://doi.org/10.7158/13287982. 2015.11465175

[21] Heshmatollah, A., Hejazi, F., Jaafar, S.F. (2019): Response Modification Factor: Review Paper. *IOP Conf. Ser.: Earth Environ. Sci. 357 012003*, doi: https://doi.org/10.1088/1755-1315/357/1/012003

[22] Sadjadi, R. and Kianoush, M. R. (2010): Response Modification Factor for reinforced concrete (RC) Liquid Containing Structures. *Proceedings of the 9th U.S. National and 10th Canadian Conference on Earthquake Engineering*, Toronto, Ontario, Canada, pp. 3496–3505.

[23] Seismosoft. *SeismoSignal – A computer program for signal processing of strong-motion data.* 2011. Version 4.3 [software]. https://seismosoft.com/products/seismosignal/ (accessed Dec. 14, 2024).

Proceedings of the 3rd Croatian Conference on Earthquake Engineering - 3CroCEE
19–22 March 2025, Split, Croatia
Copyright © 2025 CroCEE
DOI: https://doi.org/10.5592/CO/3CroCEE.2025.97

RAPID EARTHQUAKE LOSS ASSESSMENT FRAMEWORK: RELAR PROJECT AND ITS APPLICATION ON THE DATA SET FROM THE KRALJEVO (SERBIA) EARTHQUAKE IN 2010

Marko Marinković [(1)], Zoran Stojadinović [(1)], Miloš Kovačević [(1)], Mladen Nikolić [(2)], Dejan Marinković [(1)], Đorđe Nedeljković [(1)], Zoran Babović [(3)], Zoran Pucanović [(1)], Filip Đorđević [(1)], Marija Ivanović [(1)], Nevena Simić [(1)], Božidar Stojadinović [(4)]

[(1)] *Faculty of Civil Engineering, University of Belgrade, Belgrade, Serbia, e-mail address: mmarinkovic@grf.bg.ac.rs*
[(2)] *Faculty of Mathematics, University of Belgrade, Belgrade, Serbia*
[(3)] *Innovation center-School of Electrical Engineering, University of Belgrade, Belgrade, Serbia*
[(4)] *Department of Civil, Environmental and Geomatic Engineering, ETH Zurich, Switzerland*

Abstract

Rapid earthquake damage and loss assessment is a critical process for evaluating the immediate impacts of seismic events on infrastructure and populations. It involves the quick analysis of structural damage and economic losses. The goal is to provide timely information to emergency responders, government agencies, and decision-makers, enabling efficient resource allocation and disaster response. Advanced technologies such as machine learning, remote sensing, and real-time data analytics have improved the accuracy and speed of these assessments, helping to mitigate the effects of earthquakes and support recovery efforts. This paper presents the RELAR project, funded by the Science Fund of the Republic of Serbia, which aims to improve earthquake loss assessment and recovery processes. By integrating Machine Learning and Image Recognition, the project accelerates response times and enhances the accuracy of damage estimation and repair cost assessments. Traditional methods often suffer from delays and inaccuracies due to data limitations and lack of flexibility. RELAR offers innovative solutions for providing reliable, timely information, even in the absence of ground motion data. The project's objectives include developing practical ML algorithms, validating assessment models, and establishing proactive risk mitigation strategies. Within the paper, a brief overview of the first results of the framework applied to the case of Kraljevo 2010 earthquake is given, showing the methodology of the approach.

Keywords: RELAR, Earthquake, Resilience, Preparedness, Recovery

1. Introduction

Earthquakes rank among the most destructive natural hazards, causing extensive damage and significant losses. The processes of evaluating damage and losses are often time-consuming and have a profound impact on the recovery and functionality of affected communities. Current earthquake damage assessment methodologies mainly focus on predicting damage states and are categorized as either pre-event (a priori) or post-event (a posteriori) models.

A priori damage estimation involves creating seismic vulnerability models for different building types (BTs) without referencing any specific earthquake. The classification of buildings is based on factors such as construction materials, structural design, building techniques, and other characteristics affecting seismic performance. These methods include analytical, empirical, and hybrid approaches [1]. Analytical approaches, grounded in dynamic simulations and calculations, predict potential building damage using techniques such as capacity spectrum analysis, collapse mechanism evaluation, or full displacement-based modeling. These approaches have been thoroughly investigated in prior studies [2,3]. While analytical methods deliver measurable and reliable accuracy for specific BTs, challenges arise due to the diversity of real-world building inventories, variations between constructed buildings and theoretical designs, and the effects of aging or insufficient maintenance on seismic resilience. Consequently, applying these models to diverse building inventories can lead to less reliable predictions of earthquake-induced losses.

Proceedings of the 3rd Croatian Conference on Earthquake Engineering - 3CroCEE
19–22 March 2025, Split, Croatia
Copyright © 2025 CroCEE
DOI: https://doi.org/10.5592/CO/3CroCEE.2025.97

Empirical methods, on the other hand, estimate the probability of damage states (DS) for each BT based on data from past earthquake events. These outcomes are typically expressed as damage probability matrices or continuous vulnerability curves specific to the data source [4], as discussed in studies like Buratti et al. [5] and Eleftheriadou and Karabinis [6] However, the effectiveness of empirical methods is constrained by the scarcity of reliable local data, particularly in areas with limited recent seismic activity [5]. Additionally, similar to analytical methods, combining data from various regions to develop vulnerability models introduces uncertainties. These arise from potential differences between the BTs used to construct the models and those being assessed for future earthquake damage.

Unlike a priori models, which depend on vulnerability relationships established before an earthquake, a new class of a posteriori damage prediction models is emerging. These models address the limitations of a priori approaches by adapting to local conditions observed after an earthquake. A posteriori vulnerability relationships are derived based on observed damage states (DSs) from a sample of affected buildings, gathered through remote sensing techniques or on-site surveys. Remote sensing employs various methods to observe damage, such as aerial and satellite imagery [7] or synthetic aperture radar data [8]. Modern advancements in damage assessment increasingly leverage machine learning (ML) algorithms combined with image processing techniques, enabling damage detection at both individual building and neighbourhood levels [9]. However, many studies using remote sensing have categorized buildings simply as either damaged or intact, which may not provide the level of detail required for accurate loss assessments. An alternative approach, proposed by Ci and Wang [10], introduced a model using aerial imagery to classify buildings into four distinct damage categories. This method applied convolutional neural networks (CNNs) integrated with ordinal regression to determine the severity of building damage. However, research by Eleftheriadou and Karabinis [6] highlighted a common tendency for remote sensing methods to underestimate damage, underscoring the importance of conducting detailed ground-truth verification after an earthquake. Another challenge with remote sensing is its inability to assess internal structural damage, which limits the precision of damage estimations. This gap further emphasizes the complementary role of on-site inspections in achieving a more comprehensive understanding of post-earthquake damage.

Recent developments in recovery and resilience have introduced significant advancements. For instance, Terzić and Kolozvari [11] developed a fully probabilistic and comprehensive analytical framework to evaluate the post-earthquake functional recovery of buildings. Similarly, Blagojević et al. [12] proposed an innovative demand/supply-based approach that extends the Re-CoDeS framework, incorporating dynamic component interdependencies to more effectively quantify disaster resilience. Despite these advancements, a critical gap remains in both research and practice regarding a key aspect of loss assessment—monetizing losses. Current methodologies either rely on overly simplistic models or are riddled with uncertainties, leading to reduced accuracy and reliability [13] Financial loss translates physical damage into monetary terms by estimating the costs of repair and reconstruction. Earthquake-related economic impacts are generally categorized into two types: (a) direct losses, stemming from damage to physical structures, and (b) indirect losses, resulting from disruptions to economic activities. Simple models for economic loss typically calculate property values multiplied by damage metric. The HAZUS-MH [13] framework estimates losses with three levels of precision: Level 1 provides rough approximations based on national database data, Level 2 offers improved accuracy by incorporating local details and expert judgment, and Level 3 delivers the highest precision, using detailed engineering analyses and customized methodologies tailored to a specific community's conditions. This project focuses on developing a Level 3 approach for assessing direct losses, ensuring a highly accurate and context-specific evaluation of economic impacts.

This paper introduces the RELAR (Rapid Earthquake Loss Assessment and Recovery) framework, a project launched in January 2024. The proposed research presents a universal, rapid earthquake loss assessment framework based on Machine Learning and Image Recognition technologies, offering a more accurate, cost-effective, and user-friendly solution compared to existing methods. RELAR assigns damage-state-specific tags to buildings, calculates total repair costs for an affected building portfolio, and develops a portfolio-level recovery timeline. The paper outlines the main objectives,

Copyright © 2025 CroCEE
DOI: https://doi.org/10.5592/CO/3CroCEE.2025.97

key tasks, and methodology of the framework. Additionally, practical aspects related to its application and implementations are thoroughly discussed.

2. Framework and approach of the RELAR project

The goal of this research initiative is to create a universal, machine learning (ML)-driven rapid earthquake loss assessment framework, which promises improved accuracy and greater ease of implementation compared to current methods. In this context, "loss assessment" involves quantifying and monetizing the repair work necessary for rebuilding a community's building stock. The project focuses on three key research areas: earthquake engineering, machine learning, and construction project management. It utilizes earthquake datasets to develop and validate the proposed assessment models. Results from the project will be shared through published papers and guidelines, aimed at informing decision-makers and relevant stakeholders. Fig. 1 offers a visual overview of the research's conceptual framework.

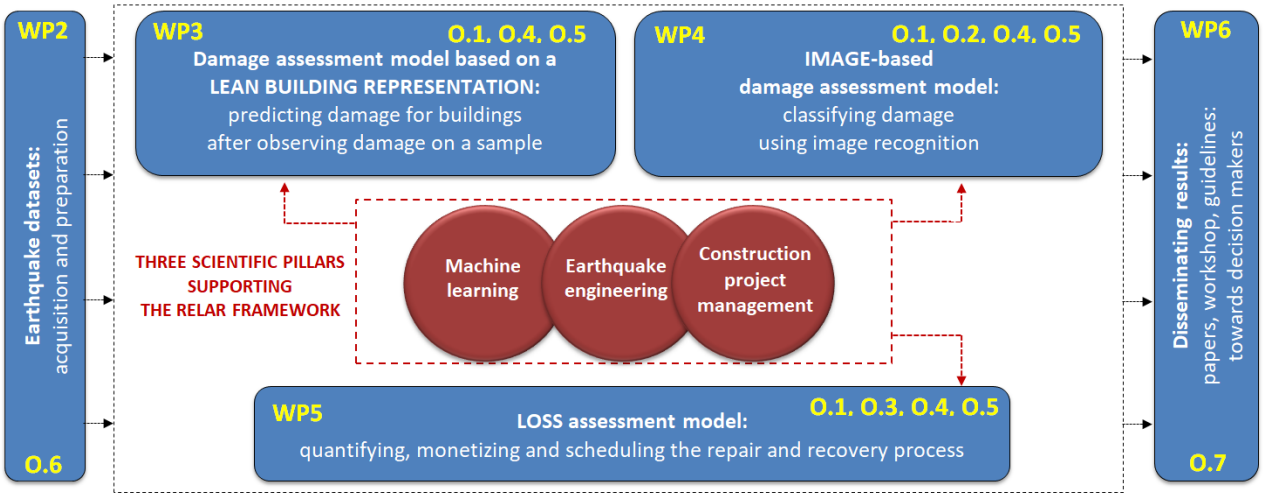


Figure 1. The concept of the project showing work packages (WP), project objectives (O), and scientific research areas supporting the framework

The core component of the proposed framework is a representative set (RS), a carefully selected sample drawn from the local building stock and prepared in advance of an earthquake (Fig. 2). Each building in the portfolio is defined by key characteristics that are linked to potential damage, such as building type or floor count. Immediately after an earthquake, the RS is surveyed to assess the extent of damage. Universal machine learning techniques, including image recognition, are then used to train a local damage assessment model (DAM) based on the RS. This trained model is subsequently applied to predict the damage across the entire building portfolio. Next, a loss assessment model (LAM) uses the damage labels—detailing both the severity and extent of damage—to estimate repair costs and recovery timelines. The proposed sampling strategy, building characterization, and machine learning techniques are designed to be adaptable to any earthquake and region. However, the RS and the DAM are specific to the earthquake in question, ensuring high accuracy in predictions and a swift assessment process using easily accessible resources. A key innovation in this approach is treating an earthquake as a post-event spatial probability distribution of damage, independent of specific ground motion data or building type classifications. This novel methodology is referred to as "Buildings are damage sensors," emphasizing the intrinsic seismic damage information embedded within the buildings themselves.

The proposed implementation protocol for loss assessment is structured into two phases: the pre-earthquake phase and the co-earthquake phase. The pre-earthquake phase begins with the creation of a database derived from raw portfolio data. This step involves defining local building types and

Proceedings of the 3rd Croatian Conference on Earthquake Engineering - 3CroCEE
19–22 March 2025, Split, Croatia
Copyright © 2025 CroCEE
DOI: https://doi.org/10.5592/CO/3CroCEE.2025.97

adopting a streamlined building representation (LBR) that includes easily accessible, damage-related features (such as geographic coordinates, building type (BT), construction year, footprint area, and number of floors), without relying on earthquake-specific data. A representative set (RS) is formed from the portfolio database through a sampling algorithm, with the number of buildings selected as an input parameter. A balance between speed and precision arises in this stage: a larger RS increases observation time but improves accuracy, whereas a smaller RS shortens observation time but may reduce accuracy. In addition to the LBR and sampling algorithm, the universal damage assessment method incorporates an image-based damage assessment model (DAM) that is pre-trained on images of buildings damaged in past earthquakes. A training procedure for developing the local LBR-based DAM is also outlined. The loss assessment model (LAM) is developed during the pre-earthquake phase, utilizing local usage rates and unit costs to estimate repair expenses for various local building types. This comprehensive methodology sets the stage for an efficient and precise earthquake loss assessment process.

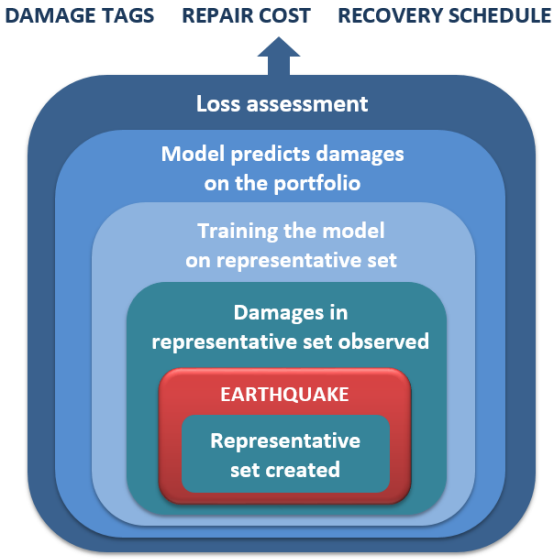


Figure 2. The implementation sequence of the main framework steps

The post-earthquake phase, referred to as the co-earthquake phase, involves the immediate assessment of damage on the representative set (RS). The RS is divided into two segments: expert and non-expert parts. Experts conduct field surveys, capturing photos and assigning damage labels, while non-experts are responsible for taking photos only. The labeled images from experts are then used to update the pre-trained image-based damage assessment model (DAM). This updated model is subsequently used to label the non-expert segment of the RS. Once the RS is fully labeled, it is used to train the lean building representation (LBR)-based DAM. Upon completion of training, the DAM generates damage labels for the entire building portfolio.

The output of the DAM, excluding the green-yellow-red safety tags, is then sent to the loss assessment model (LAM). The safety tags play a critical role in post-earthquake safety measures, with green indicating full access, yellow signaling restricted access, and red marking no access. The LAM, which incorporates damage states (DS), damage extent (DE), and community-specific resource limitations (such as the number of available experts and non-experts, funding, design company availability, licensing speed, and the capacity for rebuilding), predicts the expected repair costs and generates a recovery schedule for the entire portfolio, considering resource constraints. The duration of the co-earthquake phase depends on the resources available within the community and the recovery goals, balancing speed and accuracy. Although this phase typically lasts several days, it is considered rapid. To highlight the framework's adaptability to any region or earthquake, it is important to distinguish between universal and local components. Elements such as the LBR, sampling algorithm,

Copyright © 2025 CroCEE
DOI: https://doi.org/10.5592/CO/3CroCEE.2025.97

pre-trained image-based DAM, the training process for the LBR-based DAM, and the loss assessment procedure are universally applicable to any region and any magnitude of earthquake. The universal approach facilitates the creation of a local RS and locally trained damage and loss assessment models based on damage observed on the RS ("Buildings are damage sensors"). The framework's implementation is both swift and accurate, providing actionable predictions for decision-makers.

The framework operates with basic, readily accessible resources, requiring only a standard computer and an internet connection for storing the portfolio database, training models, and collecting assessor observations in the pre-earthquake phase. During the co-earthquake phase, it relies on a combination of experts and non-experts to assess damage on the RS.

After an earthquake, the proposed framework employs several machine learning (ML)-based classifiers to process each building in a portfolio. These classifiers take a features vector (b) and geo-coordinates (x, y) as input and generate different probability distributions related to damage assessment.

The research plan involves assessing the effectiveness of various classification techniques for each task and across different representative set (RS) sizes. Common classification methods such as ensemble techniques (Random Forest, XGBoost), Neural Networks, and Support Vector Machines will be evaluated. The study will also investigate combining expert-generated labels with those produced by image-based classifiers, aiming to reduce dependence on expert-created labels. This strategy allows for larger RSs to be evaluated quickly by increasing the number of non-expert assessors, ultimately leading to more accurate machine learning-based classification models and, as a result, more precise loss assessments. To determine the most informative representation of a building for each classification task (LBR), various feature selection techniques will be applied to the available datasets. These techniques include univariate methods like Mutual Information, multivariate approaches such as mRMR, wrapper methods that choose features based on their impact on classification performance, and techniques for ranking feature importance in tree-based models. However, it is essential that the selected LBR for each classification task remains easy to acquire and universally accessible.

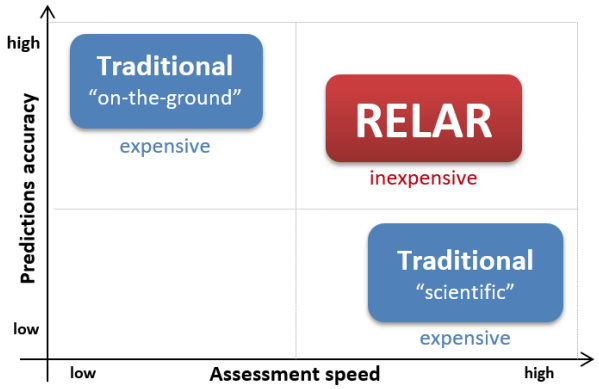


Figure 3. Framework ambition - comparing to other approaches

3. Aim and originality

The proposed framework aims to outperform existing loss assessment methods in terms of speed, accuracy, and cost-efficiency. Traditional "on-the-ground" methods are slow, as they require a detailed inspection of the entire portfolio, and their costs rise significantly due to the time-consuming field surveys conducted by experts. In contrast, the conventional "scientific" approach suffers from inaccuracies due to assumptions and uncertainties, often requiring an expensive network of ground motion sensors. The RELAR framework sets itself apart by being faster than the "on-the-ground" approach, as it relies solely on remote sensing data, and more accurate than the "scientific" approach, as it treats buildings themselves as sensors. This advantage is illustrated in Fig. 3. To achieve these

Proceedings of the 3rd Croatian Conference on Earthquake Engineering - 3CroCEE
19–22 March 2025, Split, Croatia
Copyright © 2025 CroCEE
DOI: https://doi.org/10.5592/CO/3CroCEE.2025.97

goals, the proposed models are aligned with the primary objectives outlined in work packages (WP3, WP4, and WP5).

The upcoming damage assessment model is designed to be trained using observed damage in a representative set of buildings. Its goal is to learn the distribution P(D | b, x, y), which utilizes simplified building features and spatial coordinates. A key innovation of this model is that it does not rely on ground motion data at the specific location of a building, an approach we refer to as "Buildings as damage sensors." As a result, the model can be applied universally across different communities, even in areas without ground motion stations. Additionally, our proposed methodology removes the need for information about previous earthquakes, a ground-breaking feature that distinguishes our approach from existing analytical or empirical methods in seismic damage assessment.

Beyond its independence from ground motion data, the proposed method also departs from the need for buildings (BTs) to fit into predefined categories. Instead, it requires only consistent local-specific building types to be assigned within the affected community. Machine learning-based damage assessment models can effectively understand the seismic behaviour of these locally specific building types based on observed damage in remote sensing (RS) data. This flexibility is particularly significant, as most existing analytical or empirical methods assume rigid building type classifications, which may not align with local construction practices. By accommodating local variations in building types, our approach increases both the applicability and accuracy of seismic assessments in diverse settings.

When two buildings share the same damage state, differences in the damage levels of specific elements, such as walls, may require different amounts of resources for repair. Traditional rapid loss assessment systems often overlook this detail, focusing primarily on damage states without accounting for the variability within specific building elements when estimating monetary losses. As discussed in the Methodology section, our Damage Assessment Model (DAM) is designed to predict the likelihood of various structural and non-structural building elements being at different damage levels (low, medium, high). This prediction is made using a simplified set of building features and spatial coordinates (LBR). By quantifying the damage levels for each building element individually, our approach enhances the precision of repair cost estimations. This leads to a more accurate, resource-constrained recovery schedule at the portfolio level, offering a stronger framework for recovery planning.

To accurately measure the extent of damage, it is crucial to express the required repair quantities as ratios relative to building elements. These ratios represent the percentages of various repair tasks associated with different damage states. Converting qualitative Damage Extent (DE) categories (low, medium, high) into these ratios involves a survey process. Experts with experience in post-earthquake field inspections will complete tables that assign percentages for different repair works based on specific Building Type/Damage State (BT/DS) combinations. The collected data will then be harmonized to ensure consistency. This innovative approach improves the accuracy of loss assessments by providing more precise monetization and ensuring the transferability of the methodology.

By following this process, we can achieve greater accuracy compared to traditional methods that estimate costs per footprint area. Additionally, this system allows for regular updates to the cost matrix, either by adjusting unit prices or by applying local unit prices in different markets. This flexibility ensures that the loss assessment remains relevant and accurate over time, making it adaptable to various regions and evolving conditions.

4. Anticipated effects

The RELAR framework, with its enhanced speed and accuracy, plays a vital role in helping communities manage the aftermath of earthquakes. It supports local and governmental agencies in making informed decisions throughout the recovery phase. By providing immediate, color-coded tags

Proceedings of the 3rd Croatian Conference on Earthquake Engineering - 3CroCEE
19–22 March 2025, Split, Croatia
Copyright © 2025 CroCEE
DOI: https://doi.org/10.5592/CO/3CroCEE.2025.97

(green-yellow-red) right after an earthquake, it improves life safety and facilitates more reliable and precise compensation. This accelerates both functional and social recovery, enabling quicker returns to work, reducing psychological stress, and organizing community events.

Local authorities can use the recovery schedule and resource availability to plan the recovery process efficiently, while government agencies receive a clear estimate of total repair costs soon after the earthquake. The framework also contributes to improving the quality of life by reducing the economic impact of prolonged recovery periods and promoting sustainable economic growth. Furthermore, the proposed framework is particularly beneficial for developing countries and municipalities without extensive ground motion sensor networks, offering an accessible and adaptable solution to earthquake damage assessment.

The successful implementation of the RELAR project has significant potential for advancing various community and societal goals. It introduces an innovative, universally applicable approach to rapid earthquake loss assessment, setting the stage for new research avenues and methodologies in the field.

Municipalities and regions that implement the RELAR framework stand to benefit economically through faster access to accurate data, enabling more informed decision-making. This improves the allocation of funds and financial resources, minimizing wasteful or ineffective spending. The framework's capacity to provide precise quantification and monetization of repair needs fosters collaboration among designers, contractors, and material suppliers, supporting coordinated efforts to rebuild damaged structures. Additionally, quantifying demolished buildings contributes to planning for the recycling and reuse of construction materials, aligning with circular economy principles and benefiting the environment.

Insurance companies will also gain from the RELAR framework by offering better insurance policies to individuals, businesses, and industries, enhancing their competitiveness with more diversified products. The results of the project encourage cross-sector collaborations between associations and companies, extending beyond the core project team and Serbia, and aligning with the European Neighbourhood Regional Policy. Maintaining the project website after its completion will ensure ongoing communication between the scientific community, disaster risk management professionals, insurance providers, and policymakers, increasing the project's visibility and impact. Furthermore, the project’s broader influence includes promoting social and economic cohesion, especially by facilitating the transfer of technology to regions with less advanced infrastructures.

5. Framework application on 2010 Kraljevo, Serbia earthquake dataset

A brief overview of the Framework application on 2010 Kraljevo, Serbia earthquake dataset is here given, with more details presented in [4,14,15].

A rapid earthquake loss assessment framework is introduced, leveraging a machine learning damage classification model combined with a representative sampling algorithm. Using a Random Forest classification approach, the model predicts damage probability distributions, which are then integrated with an expert-curated repair cost matrix. This enables the estimation of expected repair costs for individual buildings and the calculation of direct losses across the affected region. Unlike traditional methods, the proposed framework avoids using explicit earthquake and soil type data. Instead, such factors are inherently represented within the spatial damage distribution. To capture this distribution effectively, a sampling algorithm based on K-means clustering identifies a minimal set of buildings that reflect the seismic risk profile of the area, independent of future seismic events. The model is iteratively refined with each damage observation cycle, progressively improving the precision of the loss assessments.

The M5.4 earthquake that struck Kraljevo, Serbia, in 2010 serves as a representative example of a modern earthquake disaster. This event resulted in 2 fatalities and slightly over 100 injuries requiring medical attention. However, it caused significant structural damage, with nearly 6,000 buildings affected, a quarter of which were deemed unsafe for habitation. Damage inspection and assessment were carried out over several weeks by structural engineers from Kraljevo and other Serbian cities.

Copyright © 2025 CroCEE
DOI: https://doi.org/10.5592/CO/3CroCEE.2025.97

Unfortunately, the collected data on damage and recovery efforts were not centralized, with some records existing only in paper format. Additionally, many damage survey entries were incomplete and could not be utilized. Information on undamaged structures was sourced from the property tax assessor's office of Kraljevo. The finalized dataset comprises 1,979 buildings, of which 652, located in three key districts of the city, experienced damage during the earthquake. The spatial distribution of these buildings and their respective damage states is illustrated in Fig. 4.

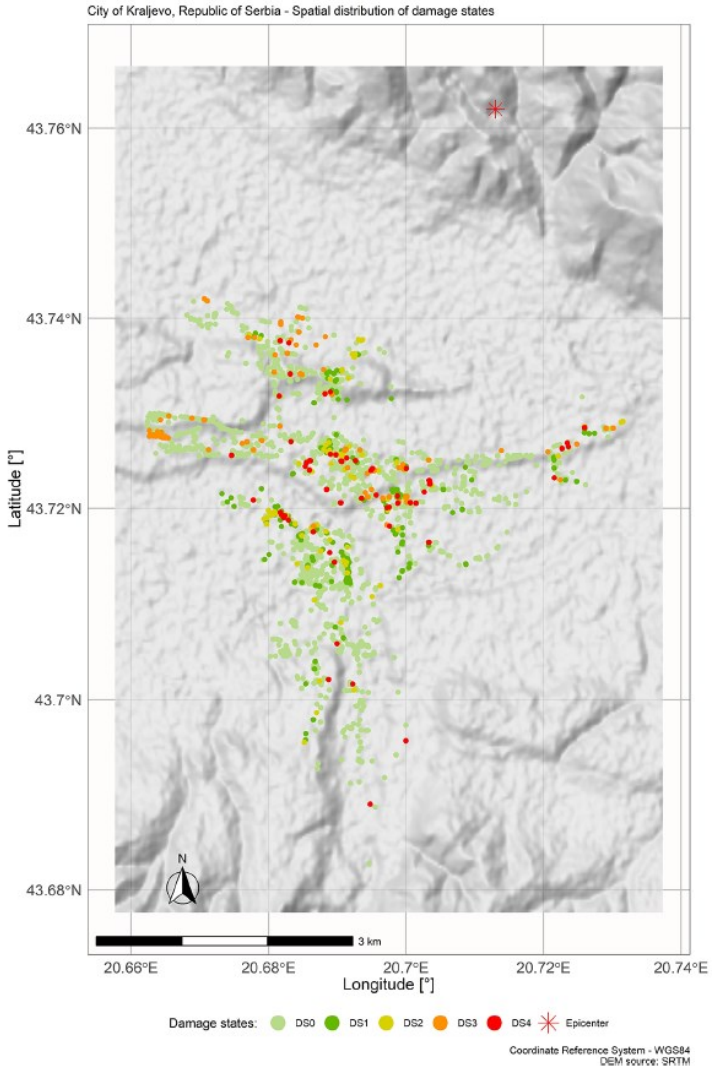


Figure 4. Spatial distribution of database buildings and their damage states after the 2010 Kraljevo earthquake [4]

First an evaluation of the model's performance on two fronts: the accuracy of predicted Damage States (DSs) and the accuracy of Predicted Repair Costs (PRCs), based on an expert-defined repair cost matrix. To validate the model, a square confusion matrix N for k distinct DSs (classes) was constructed iteratively across 10 cross-validation folds. Each element nij in N represents the number of buildings with an actual DSi classified as DSj.

The results, presented in Table 1, demonstrate a high accuracy rate of 85% for the random forest classification model. Precision and recall metrics for DS0 indicate the model's ability to effectively identify undamaged buildings, which constituted the majority class. DS1 and DS3 classifications were moderately accurate, while DS2 and DS4 presented challenges due to the limited number of buildings in these categories within the training set (127 in DS2 and 64 in DS4). This scarcity of data in certain

Proceedings of the 3rd Croatian Conference on Earthquake Engineering - 3CroCEE
19–22 March 2025, Split, Croatia
Copyright © 2025 CroCEE
DOI: https://doi.org/10.5592/CO/3CroCEE.2025.97

DSs significantly impacted the model's classification performance. Increasing the representation of these underrepresented damage classes would likely enhance the model's overall performance.

Table 1. Confusion matrix with accuracy, precision, and recall measures [4]

Actual	Predicted						
	DS0	DS1	DS2	DS3	DS4	Total number of buildings	Recall
DS0	1314	11	0	1	1	1327	0.99
DS1	27	234	38	18	11	328	0.71
DS2	6	64	37	13	7	127	0.29
DS3	7	31	17	69	9	133	0.52
DS4	3	18	14	10	19	64	0.30
Total	1357	358	106	111	47	Accuracy 1673/1979 = 0.85	
Precision	0.97	0.65	0.35	0.62	0.40		

DS: damage state.

To develop the repair cost assessment model, a matrix detailing repair costs for all combinations of Damage States (DS) and Building Types (BT) is essential. Table 2 displays the calculated mean repair costs per unit building footprint area for the dataset of buildings affected by the 2010 Kraljevo earthquake. A statistical analysis of the actual repair costs (ARCs) paid by the Government of Serbia was conducted for all BTs in DS1 and DS2. These ARCs only covered material costs, as homeowners performed the repairs themselves. The resulting cost intervals were broad—approximately 20% of the mean value—highlighting the variability in repairs for buildings with less severe damage.

For DS3, repair scenario analyses were conducted, encompassing both labor and material costs. Due to the engagement of various design and construction firms to plan and execute repairs following the earthquake, a wide range of repair methods was developed for each BT. The scenario analyses revealed significant variation in repair costs per unit footprint area, resulting in wide cost intervals for DS3 as well. The values presented in Table 2 reflect the mean costs of the most frequently used repair methods for each BT, providing a standardized basis for the repair cost assessment model.

Buildings classified as DS4 were demolished and subsequently rebuilt. To estimate the DS4 values presented in Table 2, the costs of reconstructing comparable buildings damaged in recent disasters across Serbia were analyzed. In most instances, the Government of Serbia supplied prefabricated wooden-frame houses as permanent replacements for the destroyed structures. The average cost of constructing this type of building in Serbia is approximately €350 per square meter of gross building area, which is roughly equivalent to the building's footprint area multiplied by the number of floors.

Table 2. Mean repair cost matrix (€/m^2) [4]

	BT1	BT2	BT3	BT4	BT5	BT6
DS1	3.43	12.04	8.36	10.43	9.14	9.14
DS2	13.40	16.04	15.14	18.86	17.54	18.64
DS3	55.69	46.30	44.15	38.87	29.72	32.75
DS4	350.00	350.00	350.00	350.00	350.00	350.00

BT: building type; DS: damage state.

Proceedings of the 3rd Croatian Conference on Earthquake Engineering - 3CroCEE
19–22 March 2025, Split, Croatia
Copyright © 2025 CroCEE
DOI: https://doi.org/10.5592/CO/3CroCEE.2025.97

The subsequent step involved validating the repair cost assessment model. For this purpose, the predicted repair costs (PRCs) for all buildings in the dataset were computed using two distinct approaches: a soft rule and a hard rule. The soft rule incorporates a probability distribution for damage states (DSs), allowing for a weighted calculation of repair costs based on the likelihood of each DS. In contrast, the hard rule utilizes only the most probable DS for each building to determine its repair costs, providing a deterministic estimate.

The total actual repair costs (ARC) paid by the Serbian government were significantly lower than what would have been required for the complete recovery of all damaged buildings due to financial constraints. For buildings in DS1 and DS2, the government covered only the cost of materials, while the homeowners bore the expenses for design (if applicable) and labor. For DS3 buildings, the government funded the repair design, necessary materials, and a nominal amount for labor costs. In the case of DS4 buildings, the government fully financed the construction of replacement houses. The predicted repair costs (PRC) calculated using the soft rule (Equation 1) and the hard rule (Equation 2) were €2,822,640 and €2,160,123, respectively. The relative error, expressed as |PRC – ARC|/ARC, was approximately 20% for the hard rule but reduced to only 5% for the soft rule. This result highlights the advantage of using damage probability distributions (soft rule) over discrete DS labels (hard rule) for repair cost assessment, as it significantly improves accuracy.

The proposed framework was applied to the 2010 Kraljevo earthquake dataset, which included 1,979 buildings, six building types (BTs), and five damage states (DSs). The predicted total repair costs were highly accurate, with a relative error of less than 20%, even after rapidly inspecting only 10% of the building portfolio. This task, which would take the Civil Protection system in Kraljevo approximately two days to complete, demonstrated the framework's efficiency.

Although the framework does not depend on seismological networks, it does require the initial setup and ongoing updates of the building portfolio database, the repair cost matrix, and the training of a local damage assessor network. If these tasks can be implemented in communities exposed to earthquake risks, the framework offers a practical and sustainable solution to improve earthquake risk mitigation and recovery efforts.

6. Conclusions

This paper provides an overview of the necessity and current state of earthquake loss assessment methods, with a particular focus on the RELAR (Rapid Earthquake Loss Assessment and Recovery) project. It offers an in-depth look at the three-year project's goals, plans, and steps to achieve its objectives.

The RELAR project, which will span three years, will involve a team of 10 experts from fields such as earthquake engineering, machine learning, mathematics, big data, construction management, and programming. Alongside publishing the project's results in academic journals and presenting at conferences, the outcomes will also be shared via platforms like Instagram, YouTube, and the project's website. Two sets of guidelines will be developed: one from WP4, which will focus on recommendations for capturing high-quality images with various cameras to optimize spatial information for the image-based Damage Assessment Model (DAM), and the other from WP6, detailing the implementation of the RELAR framework in earthquake-prone communities. These guidelines will cover the necessary resources, algorithms, and procedures for utilizing the DAM and Loss Assessment Model (LAM) in both pre- and co-earthquake phases.

At the project's conclusion, a workshop titled "Rapid Earthquake Loss Assessment for Resilient Societies" will be held at GRFUB to present the key findings and distribute project materials. This workshop will feature lectures from the project team and external collaborators, including simulations and practical demonstrations of case studies. It will target students, engineers, practitioners in the insurance and construction industries, as well as representatives from local municipalities and experts in law and economics.

Copyright © 2025 CroCEE
DOI: https://doi.org/10.5592/CO/3CroCEE.2025.97

The RELAR project has just begun, and with its detailed plan and well-defined tasks, it promises to be an exciting and impactful journey. The project's ultimate aim is to develop a framework for rapid loss assessment after earthquakes, contributing to society and improving the post-disaster situation for local populations affected by future earthquakes.

Acknowledgment

This research was supported by the Science Fund of the Republic of Serbia, #GRANT No 7038, RAPID EARTHQUAKE LOSS ASSESSMENT AND RECOVERY FRAMEWORK - RELAR.

References

[1] Maio R and Tsionis G (2015) Seismic fragility curves for the European building stock: Review and evaluation of analytical fragility curves. JRC technical report no. EUR 27635 EN. Luxembourg: Publications Office of the EU.

[2] Hwang SH, Mangalathu S and Jeon JS (2021) Quantifying the effects of long-duration earthquake ground motions on the financial losses of steel moment resisting frame buildings of varying design risk category. Earthquake Engineering & Structural Dynamics 50(5): 1451–1468.

[3] Martins L, Silva V, Bazzurro P and Marques M (2018) Advances in the derivation of fragility functions for the development of risk targeted hazard maps. Engineering Structures 173: 669–680.

[4] Stojadinović Z., Kovačević M., Marinković D., and Stojadinović B. (2021) Rapid earthquake loss assessment based on machine learning and representative sampling. Earthquake Spectra 38(1), 152-177

[5] Buratti N, Minghini F, Ongaretto E and Savoia M (2017) Empirical seismic fragility for the precast RC industrial buildings damaged by the 2012 Emilia (Italy) earthquakes. Earthquake Engineering & Structural Dynamics 46(14): 2317–2335.

[6] Eleftheriadou AK and Karabinis AI (2008) Damage probability matrices derived from earthquake statistical data. In: Proceedings of the 14th world conference on earthquake engineering, Beijing, China, 12–17 October.

[7] Booth E, Saito K, Spence R, Madabhushi G and Eguchi RT (2011) Validating assessments of seismic damage made from remote sensing. Earthquake Spectra 27: 157–177.

[8] Plank S (2014) Rapid damage assessment by means of multi-temporal SAR—A comprehensive review and outlook to Sentinel-1. Remote Sensing 6: 4870–4906.

[9] Duarte D, Nex F, Kerle N and Vosselman G (2018) Multi-resolution feature fusion for image classification of building damages with convolutional neural networks. Remote Sensing 10: 1636.

[10] Ci T, Liu Z and Wang Y (2019) Assessment of the degree of building damage caused by disaster using convolutional neural networks in combination with ordinal regression. Remote Sensing 11(23): 2858.

[11] Terzić, V., Kolozvari, K. Probabilistic evaluation of post-earthquake functional recovery for a tall RC core wall building using F-Rec framework, Engineering Structures, 253 (2022) 113785

[12] Nikola Blagojević, Fiona Hefti, Jonas Henken, Max Didier & Božidar Stojadinović (2022): Quantifying disaster resilience of a community with interdependent civil infrastructure systems, Structure and Infrastructure Engineering, DOI: 10.1080/15732479.2022.2052912

[13] FEMA, 2020. “HAZUS Earthquake Model Technical Manual”, Washington, D.C.: Federal Emergency Management Agency

[14] Marinkovic, D., Stojadinovic, Z., Kovacevic, M. and Stojadinovic, B. “2010 Kraljevo Earthquake Recovery Process Metrics Derived from Recorded Reconstruction Data”, Proceedings of the 16th European Conference on Earthquake Engineering, 2018, Thessaloniki, Greece

[15] Kovacevic M, Stojadinovic Z, Marinkovic D and Stojadinovic B (2018) Sampling and machine learning methods for a rapid earthquake loss assessment system. In: Proceedings of the 11th US national conference on earthquake engineering, Los Angeles, CA, 25–29 June.

Proceedings of the 3rd Croatian Conference on Earthquake Engineering - 3CroCEE
19–22 March 2025, Split, Croatia
Copyright © 2025 CroCEE
DOI: https://doi.org/10.5592/CO/3CroCEE.2025.110

ENGINEERING EXPERTISE ASPECTS DURING DISASTER RESPONSE – A CASE STUDY OF FLOODS IN FBIH

Ante Pilipović [(1)], Karlo Jandrić [(2)]

[(1)] *Assistant, University of Zagreb Faculty of Civil Engineering, ante.pilipovic@grad.unizg.hr*
[(2)] *Croatian Centre for Earthquake Engineering – Intervention Service, kjandric@hcpi.hr*

Abstract

Heavy rainfall-induced floods, landslides and rockfall that befell Jablanica and Buturović polje regions in Bosnia and Herzegovina in October of 2024 caused widespread damage to buildings, roads, bridges, electrical, water supply and gas distribution networks, along with dozens of victims and hundreds of displaced people. Urban search and rescue operations started immediately, with international teams helping the local authorities and population in mitigating the destructive effects of the disaster. In this work, insights and experiences gained during rescue operations are synthesized and shared regarding behaviour of structures during floods and rockfall, including collapse mechanisms observed, damage to buildings, roads, bridges and infrastructural objects etc. Special focus is given to the unique challenges that floods and rockfall present in comparison with earthquake-induced disasters in terms of structural loads, damage patterns and collapse types, as well as differences in impact on terrain configuration, logistical needs and survivability of victims. While many differences are observed in terms of damage patterns in buildings and infrastructure, similar effects are observed when it comes to landslide and liquefaction occurrences. A review is given of the wide variety of typical tasks that engineers may face in areas affected by floods and rockfall, with attention to different tasks proper to structural, geotechnical, hydraulic and transportation engineers. While structural engineers may have a central role in urban areas after damaging earthquakes, in the case of floods and rockfall hydraulic and geotechnical engineering expertise becomes more important to understand the causes, scale and consequences of the disaster, while transportation engineering provides an important role of maintaining the functionality of roads and railways for efficient and safe disaster mitigation strategies.

Keywords: urban search and rescue, INSARAG, SET module, flash floods, damage assessment

1. Introduction – Roles of Structural engineering teams in disaster response

In the night of October 3rd to 4th 2024 at approximately 3 a.m. heavy torrential rain-induced flash floods, landslides and mudslides devastated the towns of Jablanica, Konjic, Kreševo, Kiseljak, Fojnica and Mostar municipality, causing widespread damage to buildings and infrastructure, taking 27 lives and displacing over 300 people. Over 1000 households were affected by the event, out of which an estimated 55 residential houses were completely destroyed, while more than 800 have been reported damaged [1,2]. The town of Donja Jablanica was affected the most, as the flash flood encountered a defunct quarry in the area above the town and induced a rockfall, causing additional devastation. Alongside residential houses, critical infrastructure has also been damaged in the wider affected area (bridges, roads, railways, electrical grid, water supply etc.), causing additional logistical challenges in the first responder phase, as well as additional requirements in the relief phase.

The Federation of Bosnia and Herzegovina (FBiH) declared a state of national emergency on October 5th 2024, and the European Union Civil Protection Mechanism (EUCPM) was activated. Among other first response capacities deployed through the mechanism, urban search and rescue (USAR) teams from Croatia, Slovenia, Serbia and Montenegro have been deployed. The Croatian USAR team consisted of 37 members and 2 rescue dogs. The team composition included 2 structural engineers of the Croatian Centre for Earthquake Engineering – Intervention Service (HCPI – IS), the authors of this reconnaissance report. The mission lasted from deployment on October 5th until demobilisation on

Copyright © 2025 CroCEE
DOI: https://doi.org/10.5592/CO/3CroCEE.2025.110

October 11th 2024 when most international USAR teams concluded their work and relief phase was initiated.

The specific roles of structural engineers during disaster response operations are a topic of great importance for HCPI – IS as it is a relatively new addition to the Croatian civil protection capacities on the national level, having been established as a result of the key role that structural engineers had during the response to earthquakes in Zagreb and Petrinja in 2020 [3]. The new intervention unit has been fruitfully incorporated into the Croatian civil protection system with the goal of implementing all available structural engineering knowledge in any disaster situations by combining both contemporary scientific research, practicing engineering knowledge and experience to mitigate the consequences of such disasters.

Currently, the Croatian Structural Engineering Team (SET) is in the process of EU certification as an Other response capacity (ORC) within the EUCPM [4], with the capacity to carry out building damage, safety and usability assessments on a large scale, appraisal of buildings to be demolished or repaired, assessment of critical infrastructure, short-term shoring of damaged buildings and assistance to USAR teams in assessment of collapsed buildings. Half the team consists of HCPI – IS engineering experts, while the other half consists of members of the Civil Protection – State intervention unit (DIP CZ) providing technical and tactical support (TAST), logistics and on-site support.

This report aims to analyse the tasks required of the structural engineers that were part of the Croatian USAR team during the mission in FBiH, identify key roles of structural engineering experts in disaster response (particularly in the first responder phase) and recommend further steps within the engineering aspect in order to better prepare the SET module for international deployment.

2. Assessment of collapsed buildings – assisting USAR teams

The most severe structural damage was documented in Donja Jablanica (Fig. 1), with residential buildings primarily consisting of masonry structures of varying construction quality. Older homes were built with stone masonry or earthen walls, whereas newer houses primarily used hollow clay brick, sometimes incorporating reinforced concrete tie beams. Most houses numbered one or two stories with a semi-buried basement. The roofs were typically wooden and often in a deteriorated condition.

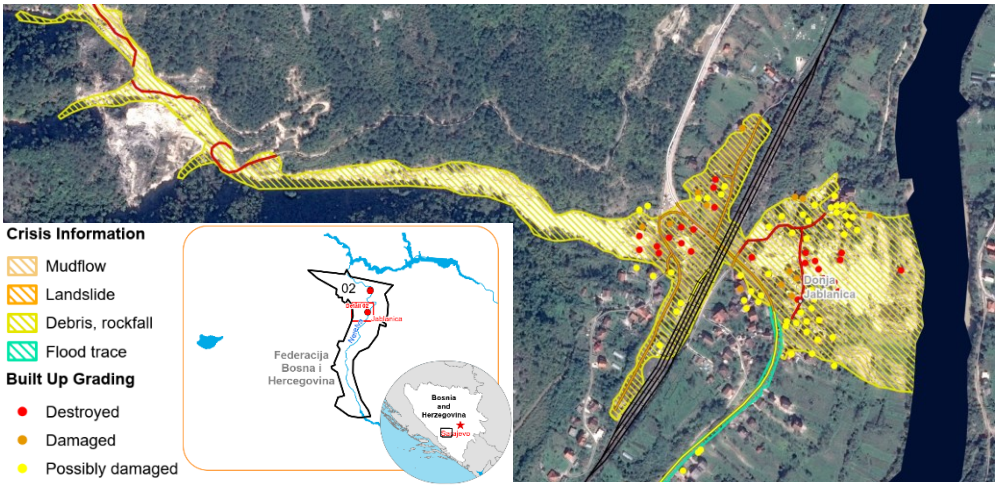


Figure 1. Copernicus emergency management service satellite image of the affected area in Donja Jablanica (source: Copernicus EMS, EU)

The floodwater and rockfall subjected buildings to extreme lateral forces, both from the impact of dislodged boulders originating from a defunct quarry and the stationary dynamic pressure of the flash flood [5]. Structural failure mechanisms varied. In some cases, shear failure at the RC foundation level led to the displacement of entire buildings above the foundation over distances of up to 100 meters. Where foundations were weak or shallow—often consisting of stone or poorly compacted soil—entire

Copyright © 2025 CroCEE
DOI: https://doi.org/10.5592/CO/3CroCEE.2025.110

structures collapsed, with individual building elements carried away by the water current, making identification of original structures difficult. Total structural collapse, where individual elements became fully detached and unrecognizable, can be classified under the *debris heaps* collapse type according to INSARAG (International Search and Rescue Advisory Group) worksite triage categories [6] used by USAR teams for designating potential worksites. Partially collapsed buildings that remained on-site could also be classified under INSARAG as either *debris heaps*, where collapsed structures shifted onto adjacent parcels, or *overhanging elements*, where partial ground-floor collapses left upper floors cantilevered, posing a significant risk of secondary collapse (Fig. 2). Other INSARAG collapse types (*overturning, pancake*, and *inclined layers*) were not observed in Donja Jablanica.



a)



b)

Figure 2. INSARAG collapse types observed in Donja Jablanica; a) debris heaps, b) overhanging elements

Proceedings of the 3rd Croatian Conference on Earthquake Engineering - 3CroCEE
19–22 March 2025, Split, Croatia
Copyright © 2025 CroCEE
DOI: https://doi.org/10.5592/CO/3CroCEE.2025.110

The observed collapse distribution significantly deviates from that of seismic events, such as the 2023 Türkiye earthquake, where *pancake* collapses and overturning of RC frame structures were predominant [7]. Furthermore, the damage patterns of individual elements differed from those typically seen in earthquake-induced failures. No diagonal shear cracks were observed in masonry walls, as these are characteristic of seismic loads. Instead, geotechnical effects, including differential settlement and horizontal cracking, were the primary structural response mechanisms.

In addition to structural failures, widespread infrastructure displacement posed further hazards. Numerous streetlights, electrical poles, retaining walls, and fences were visibly leaning, posing an ongoing risk of overturning. Energy infrastructure was heavily damaged, with displaced electrical cables increasing the risk of electrocution and possibly ruptured water supply pipes raising contamination concerns. Flood debris entered the basements and garages of all houses in the affected area, consisting of a complex mix of materials, including large quarry boulders, stone, sand, gravel, clay, mud, and structural timber fragments, which posed worksite hazards to be avoided during search and rescue operations. The floodwaters ultimately deposited a significant volume of the debris into the Neretva River, raising concerns about sediment accumulation at a dam downstream. A comprehensive risk assessment of the downstream dam's structural integrity requires hydraulic engineers to analyze sediment deposition, potential scouring, and hydrodynamic loads on the structure.

Given the scale of structural collapse, heavy machinery—primarily excavators—played a critical role in clearing debris and assisting in search operations. Structural engineers provided guidance on safe removal of unstable elements. One instance involved lifting a collapsed RC floor to check for survivors, illustrating the effectiveness and practicality of excavators as a short-term shoring solution, especially for medium USAR teams which do not feature their own heavy machinery.

Structural engineers played a critical role in assessing the stability of collapsed buildings and advising on safe search and rescue operations, particularly in mitigating risks associated with secondary collapses, especially in structures where detached roof beams, fractured concrete elements, and freestanding walls or facades remained precariously in place. On the other hand, the complexity of soil movement, landslide and mudslide effects and foundation failures highlighted the necessity of geotechnical expertise in disaster response. Furthermore, a risk assessment of the dam downriver is a task best suited to a hydraulic engineer. The absence of geotechnical and hydraulic engineering specialists on-site limited the ability to fully assess ongoing ground stability risks, particularly in areas prone to further landslides. Integrating specialised engineering assessments alongside structural engineering evaluations into USAR teams would provide a more comprehensive approach to post-disaster reconnaissance, ensuring both immediate responder safety and long-term stabilization of the affected areas.

3. Structural reconnaissance – UAV techniques

The reconnaissance efforts extended to Buturović Polje, a smaller settlement located along a river bend in the area of Jablanica Lake (Fig. 3), characterized by soft sediments. The flash flood significantly reshaped the terrain, eroding an entire stream branch that once extended to the bend and broadening the channel. The flood impact was not confined to Buturović Polje. Upstream settlements, including Trusina, also suffered significant damage, contributing to the mass of debris that was deposited through Buturović Polje into Jablanica Lake.

Several houses were swept away by the flood, while others sustained severe damage, with predominantly overhanging elements collapse type patterns similar to those observed in Donja Jablanica. Victims were carried downstream, buried in mixed debris composed of wood, soil, mud, and other materials. The search for survivors was conducted through a combination of ground teams searching along the riverbanks, water rescue teams using dry suits to navigate the river, and aerial reconnaissance utilizing UAVs (unmanned aerial vehicles).

Copyright © 2025 CroCEE
DOI: https://doi.org/10.5592/CO/3CroCEE.2025.110



a) b)

Figure 3. a) Copernicus emergency management service satellite image of the affected area around Buturović Polje (source: Copernicus EMS, EU); b) photograph of the reshaped terrain along the river bend

While primary responsibilities of structural engineers were limited in this non-urban area, an opportunity arose to evaluate the UAV-assisted search operations techniques. UAVs designed for large-area reconnaissance are valuable to SET modules for broad assessments, especially in the initial phase of sectorization of the affected area. They offer advantages such as joystick-based control interfaces that provide intuitive maneuverability over broad landscapes, longer range and better battery life. However, they could prove less effective for the specific needs of structural engineers when assisting USAR operations, as they cannot inspect the interior of buildings [8]. Instead, the deployment of smaller UAVs with enhanced maneuverability appears as a more viable option (Fig. 4). Such UAVs, equipped with headset controllers, enable precise navigation within confined spaces and allow for structural reconnaissance of the interiors of partially collapsed buildings, providing real-time assessments of internal structural conditions without requiring personnel to enter unsafe areas. This approach would enhance responder safety while improving the accuracy of damage assessments in future urban disaster scenarios. Consequently, integrating both large-area reconnaissance UAVs for sectorization and assessment purposes and compact, high-maneuverability drones for evaluating structural integrity into SET modules could improve operational efficiency and safety assessments in structural reconnaissance efforts.



a) b) c)

Figure 4. a) A large debris-filled area of the Jablanica Lake for large-area reconnaissance; b) Joystick-controlled UAV for large area surveillance; c) Light UAV with a headset controller for building interior reconnaissance

Proceedings of the 3rd Croatian Conference on Earthquake Engineering - 3CroCEE
19–22 March 2025, Split, Croatia
Copyright © 2025 CroCEE
DOI: https://doi.org/10.5592/CO/3CroCEE.2025.110

4. Critical infrastructure assessment

4.1. Access roads

The roads between the locations where our team was deployed were severely impacted by the flash floods, with debris such as rocks, soil, and vegetation obstructing the roadways. Many embankments and roadbeds were displaced by landslides, and in some cases, the roadway was washed away, rendering it impassable. Damage to the pavement surface included Longitudinal cracking of pavement surface and settling of the road edges has been observed (Fig. 5). The priority of the local authorities was to maintain road access, and by the time our team arrived, all main routes had been cleared, although they remained in a compromised condition. This rapid restoration of access was critical, as it enabled the continuation of emergency operations and evacuation efforts. However, the provisional routes were susceptible to further landslides, particularly in the context of anticipated rainfall.



Figure 5. State of the roads in the affected area connecting the main disaster sites

These conditions highlight the importance of transportation engineering expertise in post-disaster assessments, especially as part of a SET module. Transportation experts can evaluate road stability for heavy vehicle use, provide timely and accurate assessments of road conditions, guide the establishment of safe alternative routes, and recommend necessary repairs or reinforcements. Including transportation engineers in SET modules is crucial to ensuring the safety and efficiency of disaster response operations and supporting the host nation's recovery efforts.

4.2. Bridges

Local authorities requested our USAR team to dispatch structural engineers to assess three road RC beam bridges between Buturović Polje and Jablanica (Fig. 6). These bridges were suspected of instability due to erosion and landslides, which had washed away substantial material beneath the bridges and altered the terrain around the foundations of the piers. Despite these concerns, traffic continued to flow across the bridges, making it crucial to ensure that the flow remained safe and uninterrupted, as these are key transportation routes in the area.

Our inspection indicated that the piers were founded on piles extending to bedrock, with adequate anchorage. This conclusion was supported by the absence of visible displacement or damage to the pile caps, as well as to any other structural elements of the bridges, including the pavement surface. Based on these observations, we recommended verifying the pile length and depth from the original construction drawings. Additionally, a geotechnical expert should be engaged to assess the stability of the soil beneath the foundations, with subsequent recommendations for reinforcing measures, if necessary, to ensure the long-term safety and functionality of the bridges.

It is essential to underscore the importance of critical infrastructure assessment, which requires specialized knowledge and expertise. While this case pertains specifically to bridges, the same principles apply to other critical infrastructure such as hospitals, schools, and utilities. In this instance,

Copyright © 2025 CroCEE
DOI: https://doi.org/10.5592/CO/3CroCEE.2025.110

our field engineering team benefited from support provided by our HCPI–IS headquarters in Croatia, where bridge specialists were available to offer guidance and advice. This collaboration highlights the necessity of including a small team of experienced engineers in each mission, ready to provide additional support from the home headquarters when needed. Such a team can gather information from broader sources concerning the affected area and assist field teams with relevant insights, enabling them to better prepare for potential challenges on the ground. This approach has proven invaluable in previous missions as well [7].



Figure 6. Photographs of key structural elements of the inspected bridges and the eroded terrain in the area of pier foundations

Regarding the SET modules, it is crucial to incorporate one or two teams of critical infrastructure experts, consisting of experienced engineers, to ensure that accurate assessments can be made in the field. Critical infrastructure evaluation is one of the top priorities during the early response phase of any disaster. As demonstrated in this case, the host nation may not always have the capacity to conduct these assessments promptly. Therefore, the presence of critical infrastructure specialists is one of the most effective ways to support the host nation and ensure a rapid and informed response.

5. Conclusions – engineering expertise in disaster response operations

An overview of different structural engineering activities during search and rescue operations in the initial response phase after the flash floods of 2024 in Bosnia and Herzegovina has been given in this work. These activities have been conducted by a team of structural engineers that were a part of the Croatian USAR team operating in the affected area. The different engineering aspects have been highlighted in light of a new Croatian Structural engineering team (SET) that is currently in the process of EU certification as an other response capacity (ORC), aiming to offer engineering knowledge, expertise and experience to mitigate the consequences of major natural disasters both domestically and internationally.

The mission in Bosnia and Herzegovina demonstrated the critical role that specialized engineering expertise plays in different disaster response phases. Structural engineers play an important role in ensuring safe and efficient work of USAR teams, but engineering expertise can be offered beyond USAR operations as well. Structural engineers, transportation experts, hydraulic engineers, geotechnical specialists and critical infrastructure assessment experts are all integral to a SET module, each contributing unique insights essential for the rapid and safe assessment of disaster-affected areas. Mission experience underscored the importance of including experts in each of these fields to address a broad range of post-disaster challenges, from assessing collapsed structures and critical infrastructure to evaluating the stability of roads, bridges and soil. The opportunities for using various types of unmanned aerial vehicles (UAVs) in different stages of disaster response have also been explored, both for initial sectorization of large urban areas and enhancing building damage assessment in closed interior spaces.

Copyright © 2025 CroCEE
DOI: https://doi.org/10.5592/CO/3CroCEE.2025.110

Incorporating these diverse engineering roles into SET modules provides a robust framework for effective application of engineering expertise in the aftermath of major disasters. It ensures that not only immediate safety concerns are addressed in the first response phase, but also long-term recovery strategies are effectively planned in the relief phase. The interdisciplinary approach outlined and proposed here strengthens the overall response capacity by offering crucial support to the host nation's efforts both in the critical early response phase and in the long-term.

References

[1] DG ECHO Daily Map, Bosnia and Herzegovina, UCPM response to floods, 14/10/2024, ERCC, Brussels, Belgium, https://erccportal.jrc.ec.europa.eu/API/ERCC/Maps/DownloadPublicMap?fileN=MainFile&forceDownload=False&contentItemID=5027, (accessed 14.2.2025.)

[2] IOM Situation Report: 2024 Flood and Landslide Disaster Response – Focus on displacement (26 December 2024), IOM UN Migration, https://bih.iom.int/sites/g/files/tmzbdl1076/files/documents/2025-02/2025-flood-and-landslide-response-situation-report-6-february_eng.pdf, (accessed 14.2.2025.)

[3] Atalić, J., Uroš, M., Šavor Novak, M., Demšić, M., Baniček, M., Kadić, A., Oreb, J. (2022): The Croatian Centre for Earthquake Engineering: establishment, activities and future opportunities, *Proceedings of the Third European Conference on Earthquake Engineering and Seismology – 3ECEES*, Bucharest, Romania, 10 pages.

[4] DG ECHO (2024): European Civil Protection Pool: Equipping the EU to respond to disasters, Union Civil Protection Knowledge Network , European Union, doi: 10.2795/46443

[5] Milanesi, L., Pilotti, M., Belleri, A., Marini, A., & Fuchs, S. (2018): Vulnerability to flash floods: A simplified structural model for masonry buildings. Water Resources Research, 54, 7177–7197, doi: https://doi.org/10.1029/2018WR022577

[6] International Search and Rescue Advisory Group (2020): INSARAG Guidelines 2020, Volume II: Preparedness and Response, Manual B: Operations, UN OCHA

[7] Pilipović, A., Jandrić, K. (2024): Types of collapse mechanisms in Hatay province after the 2023 Turkey-Syria earthquake, *Proceedings of the 18th World conference on Earthquake engineering*, Milan

[8] Atalić, J., Uroš, M., Šavor Novak, M. et al. (2021): The Mw5.4 Zagreb (Croatia) earthquake of March 22, 2020: impacts and response. *Bulletin of Earthquake Engineering*, 19, 3461–3489. https://doi.org/10.1007/s10518-021-01117-w

Proceedings of the 3rd Croatian Conference on Earthquake Engineering - 3CroCEE
19–22 March 2025, Split, Croatia
Copyright © 2025 CroCEE
DOI: https://doi.org/10.5592/CO/3CroCEE.2025.130

SUZI-SAEE EARTHQUAKE IMAGE DATABASE: A FRAMEWORK FOR TAGGING EARTHQUAKE-INDUCED DAMAGE

Filip Đorđević [(1)], Marko Radišić [(2)], Svetlana Brzev [(3)], Marko Marinković [(4)]

[(1)] *Teaching Assistant, Department of Engineering Mechanics and Theory of Structures, Faculty of Civil Engineering, University of Belgrade, Belgrade, Serbia, fdjordjevic@grf.bg.ac.rs*
[(2)] *Dr, Project Engineer, SDA-solutions GmbH, Herzogerath, Germany, radisic@sda-solutions.de*
[(3)] *Adj. Prof., Department of Civil Engineering, University of British Columbia, Vancouver, Canada, sbrzev@mail.ubc.ca*
[(4)] *Assist. Prof., Department of Engineering Mechanics and Theory of Structures, Faculty of Civil Engineering, University of Belgrade, Belgrade, Serbia, mmarinkovic@grf.bg.ac.rs*

Abstract

The Serbian Association for Earthquake Engineering (SUZI-SAEE) has developed a database platform with images taken during the reconnaissance missions after the earthquakes, with the aim to provide a comprehensive framework for documenting and analyzing earthquake-induced structural damage. This paper presents the main aspects of the database platform with the images of the SAEE team members. The initial database is developed from extensive post-earthquake field investigations carried out by the members of SAEE. This platform tends to gather and label images of damaged buildings from seismic events, incorporating crucial metadata such as structural type, damage level, and failure modes. The importance of this framework also lies in its ability to facilitate the extraction of important statistics, enabling deeper insights into damage patterns, structural vulnerabilities, and responses to seismic forces. Due to its ability to systematically analyse data gathered from past earthquakes, the database is expected to serve as a valuable resource for researchers and practitioners to improve seismic codes, optimize retrofitting strategies, and improve the understanding of the behavior of structures under earthquakes. In addition to providing a direct benefit to earthquake mitigation, the database is expected to serve as an educational and research tool, accessible to the wider community. Due to high seismic risks around the world, the SAEE database also stands as a tool for advancing the field of earthquake engineering and improving the resilience of our built environment, making it a valuable contribution to civil engineering research and practice. By facilitating the study of past seismic events, the SAEE database provides a valuable contribution toward reducing seismic risks.

Keywords: earthquake engineering, post-earthquake analysis, damaged structures, educational tool, suzi-saee tagger, database

1. INTRODUCTION

Earthquakes are among the most destructive natural disasters, causing significant damage to infrastructure and profound social losses, including human casualties [1], [2]. Effective post-earthquake damage assessment is essential for improving building resilience, optimizing retrofitting strategies, and enhancing seismic codes. However, the systematic documentation and analysis of earthquake-induced damage remain challenging due to the diversity of structural systems, materials, failure modes, etc.

The Serbian Association for Earthquake Engineering (SUZI-SAEE) has developed the SUZI-SAEE Earthquake Image Database, associated with a platform designed to address these challenges. This database is supported by the SUZI-SAEE Tagger, a Python-based tool [3] that enables efficient annotation and classification of earthquake damage images. The framework integrates metadata with images, offering a comprehensive resource for researchers, practitioners, and educators. Photographic documentation has long been recognized as important resource in earthquake engineering. The Earthquake Engineering Slide Information System (EASY), developed by Fischinger et al. [4], demonstrated the value of annotated image databases for understanding structural behavior during seismic events. EASY's emphasis on metadata integration and accessibility laid the groundwork for modern systems like the SUZI-SAEE Tagger, which builds on these principles by leveraging

Copyright © 2025 CroCEE
DOI: https://doi.org/10.5592/CO/3CroCEE.2025.130

advancements in digital tools and novel technologies. The SUZI-SAEE Earthquake Image Database also builds on other notable initiatives, such as the Earthquake Image Information System (EqIIS), currently known as the Earthquake Engineering Online Archive [5] which provided access to thousands of images from seismic events worldwide.

The primary objective of the SUZI-SAEE Earthquake Image Database is to streamline the documentation and analysis of post-earthquake damage. The Tagger facilitates this by allowing users to annotate images with selected metadata. This capability enhances the understanding of structural vulnerabilities and promotes informed decision-making in earthquake engineering.

This paper presents the development and current functionalities of the SUZI-SAEE Earthquake Image Database, highlighting its potential role in advancing damage assessment methodologies. Engineers, researchers, and students can benefit greatly from the database's open-access collection of annotated earthquake damage images. In order to promote a more thorough understanding of structural performance under seismic excitations, this framework seeks to close the gap between unprocessed post-earthquake visual data and useful insights.

2. OVERVIEW OF SUZI-SAEE RECONNAISSANCE MISSIONS

In the last 5 years SUZI-SAEE organized several post-earthquake reconnaissance missions, demonstrating its commitment to advancing earthquake engineering and contributing to post-disaster recovery efforts. The teams visited several cities affected by the 26.11.2019. Albania earthquake, the December 29, 2020 Petrinja (Croatia) earthquake, and the February 8, 2023 Türkiye earthquake sequence.

These missions were organized to provide vital assistance to local colleagues in the immediate aftermath of earthquakes, focusing on critical tasks such as assessing the usability of buildings, determining damage states, and prioritizing interventions to ensure public safety. The team members collaborated with local authorities and engineers in tagging buildings according to their usability and safety status. A core aspect of these missions was meticulous documentation of earthquake-induced damage. The teams conducted detailed visual inspections of affected structures and captured extensive photographic records of damaged buildings, and documented various types of structural and non-structural damage. This documentation serves as a valuable dataset for further research aimed at understanding the earthquake damage mechanisms and improving resilience of future construction.

In addition to their field efforts, SUZI-SAEE teams have actively disseminated their findings to both the scientific community and practicing engineers, in the form of presentations which shared lessons learned from the missions, focusing on practical insights into damage patterns, building performance, and the effectiveness of existing design and construction practices. These presentations have been instrumental in bridging the gap between academia and practice, fostering collaboration, and promoting the application of research findings to real-world challenges. Moreover, the knowledge and data gathered during these reconnaissance missions have been formalized in the form of several conference and journal papers [6-13], contributing significantly to the global body of knowledge in earthquake engineering. These publications provided detailed analyses of observed damage patterns, evaluated the performance of different construction techniques, and offered recommendations for improving building design and construction practices in seismically active regions. Also, lessons learned in organizing the SUZI-SAEE's reconnaissance missions were published with the aim of helping other organizations to organize and act after future earthquake events [14].

Through these reconnaissance missions, SUZI-SAEE collaborated with other associations and institutions actively working in the field of earthquake engineering all over the world. This initiative exemplifies the importance of collaboration, both in responding to seismic disasters and in translating lessons learned into actionable strategies for improving resilience, and presents strong basis for activities after future earthquake events.

Images and information collected during these reconnaissance missions present the basis for developing the SUZI-SAEE Earthquake Image Database.

Copyright © 2025 CroCEE
DOI: https://doi.org/10.5592/CO/3CroCEE.2025.130

3. EXISTING EARTHQUAKE IMAGE DATABASES

Although large number of earthquake damage-related images are collected by reconnaissance teams after major earthquakes, usually only a small fraction of all collected images are included in various field reports, journal and conference papers, and presentations. Most frequently, majority of these images are stored in archives by individual researchers, research labs at universities, and/or professional organizations engaged in earthquake engineering. Very few organizations have made an effort to share the images collected during post-earthquake reconnaissance missions with professionals and general public. In this section a few of the existing earthquake image databases will be described to illustrate their organization/structure and the type of information that has been presented.

The most comprehensive earthquake image database, called the Earthquake Engineering Online Archive [5], was developed by the National Information Service for Earthquake Engineering (NISEE) at the University of California (UC) Berkeley, USA (https://nisee.berkeley.edu/elibrary/). The database includes more than 8,000 records from 80 earthquakes from the USA and other countries, and is a valuable repository of earthquake damage information. The same web site also features a special collection of 875 images documenting historic earthquakes called the "Kozak Collection". Access to the NISEE image database is available only to the members of NISEE e-Library (https://nisee.berkeley.edu/elibrary/register.jsp).

Each record in the database consists of an image and the following fields: i) title (type of structure or a structural element), ii) creator (author of the image), iii) date (when the image was taken), iv) location (including city, province/state, and country), v) earthquake (description of the earthquake epicenter, including city and state, date, and magnitude), and vi) a description (characterization of the damage). Besides that, an image has a unique alphanumerical ID, consisting of two letters (abbreviated earthquake name) and a number. Figure 1 illustrates a typical record from the NISEE database related to the January 17, 1994 Northridge, California earthquake (M 6.7), which is a part of the collection comprising 598 records related to that earthquake. The image shows a two-storey unreinforced masonry building in Santa Monica which experienced a failure of out-of-plane walls at the upper floor. The image was taken on January 20, 1994 (3 days after the earthquake) by Božidar Stojadinović, current president of the SUZI-SAEE, who was a PhD student at the UC Berkeley at the time of the earthquake. The database is accessible free of charge, however high-resolution images are available at a nominal fee.

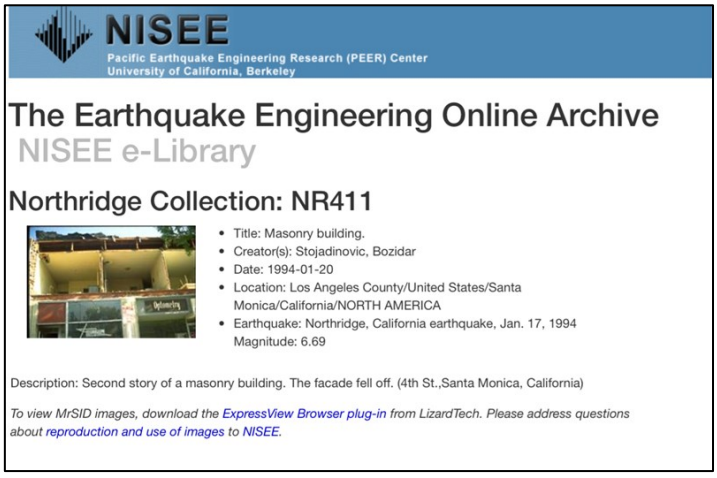


Figure 1. A record from the NISEE's Earthquake Engineering Online Archive (NR411), related to the 1994 Northridge, California earthquake

In terms of the organization/structure and extent of detail, the most relevant database is the Earthquake Engineering Slide Information System (EASY), which was developed in 1997 at the Faculty of Civil and Geodetic Engineering, University of Ljubljana under the leadership of Prof. Matej Fischinger [4]. The database contains 500 images from 4 major earthquakes (1979 Montenegro, 1985 Mexico City,

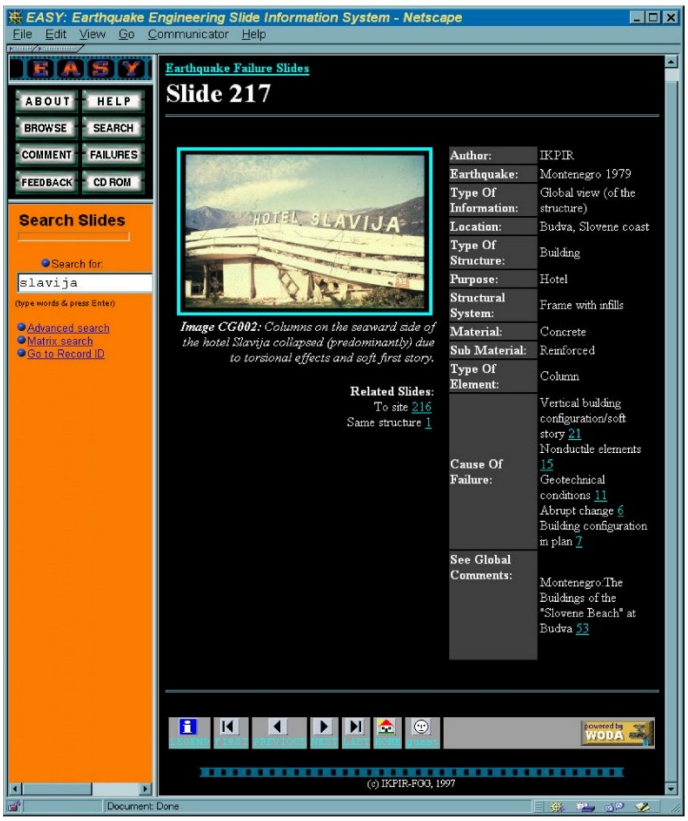
Copyright © 2025 CroCEE
DOI: https://doi.org/10.5592/CO/3CroCEE.2025.130

1994 Northridge, and the 1995 Kobe earthquake). The database used to be accessible free of charge at the web site of the the Faculty of Civil and Geodetic Engineering, University of Ljubljana, and a complementary CD version was also available.

EASY is organized in the form of a relational database. Several fields are assigned to each record, including i) author, ii) earthquake, iii) location (where image was taken), iv) type of structure (e.g. building, bridge, etc.), v) structural system, vi) structural element (e.g. column, beam, wall), vii) material of the structural system (e.g. reinforced concrete), viii) type of failure (failure mode), e.g. flexure, shear, etc. and ix) additional comments. Figure 2a) shows a sample record (Slide 217), which documents the collapse of Hotel "Slavija" in Budva in the 1979 Montenegro earthquake. It can be observed from the figure how various fields were used to explain the image.

Data entry for the records was organized in a user-friendly manner, through drop-down menus which facilitated the selection of appropriate attributes for a specific image. In some cases, e.g. cause of failure, it is possible to select more than one option (e.g. soft storey irregularity, nonductile elements, building configuration in plan, etc.).

A very useful feature of the database is section "Related slides", which contains hyperlinks from specific records to other records (e.g. overall building damage and damage of a structural element in the same building. Also, in some cases there are links to general comments (section "See Global Comments"), which are usually related to several slides. For example, for Slide 217 shown in Figure 2a), a Global Comment is hyperlinked (Slide 53), and it discusses the building and its deficiencies which led to collapse (see Figure 2b).



a)

Copyright © 2025 CroCEE
DOI: https://doi.org/10.5592/CO/3CroCEE.2025.130



b)

Figure 2. A sample record from the EASY image database: a) a record (Slide 217) which documents collapse of Hotel “Slavija” building in the 1979 earthquake, and b) a Global Comment (Slide 53) providing additional information related to the collapsed building.

4. SUZI-SAEE TAGGER TOOL

The SUZI-SAEE Tagger presented in Fig. 3 is a Python-based [3] application developed to support the systematic annotation of earthquake damage images. Built using the Tkinter library, the tool provides a user-friendly interface and a wide range of functionalities, which are described in the following sub-sections.

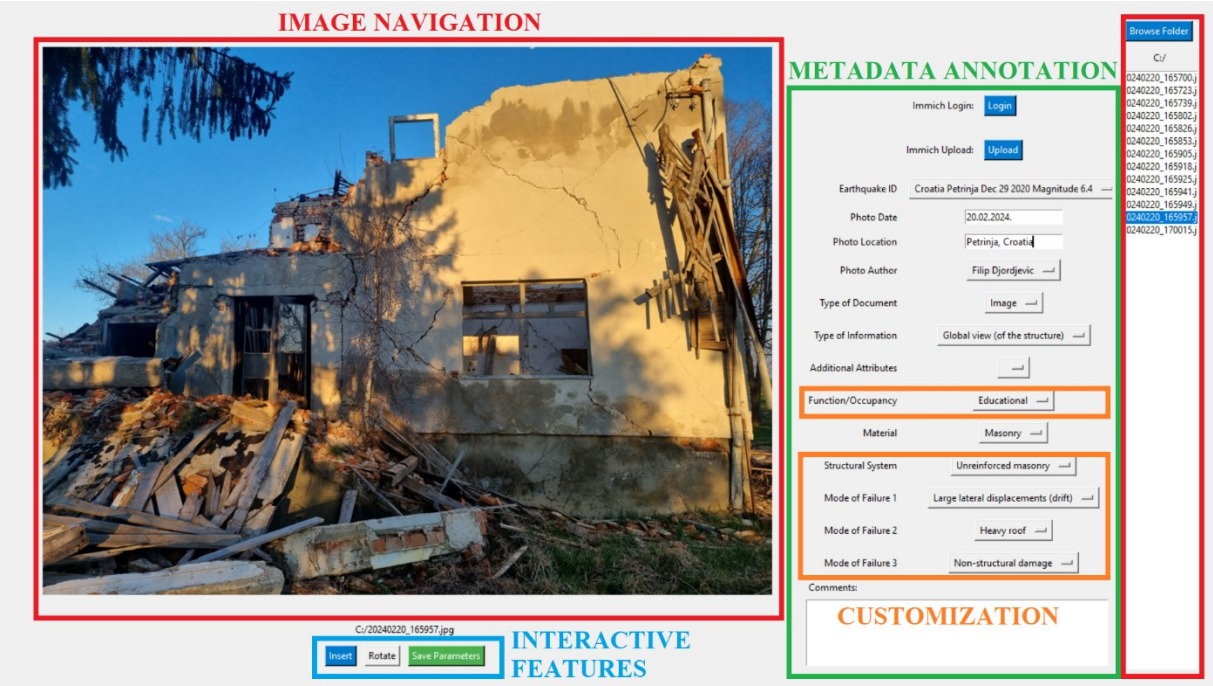


Figure 3. SUZI-SAEE Tagger: data entry screen

Copyright © 2025 CroCEE
DOI: https://doi.org/10.5592/CO/3CroCEE.2025.130

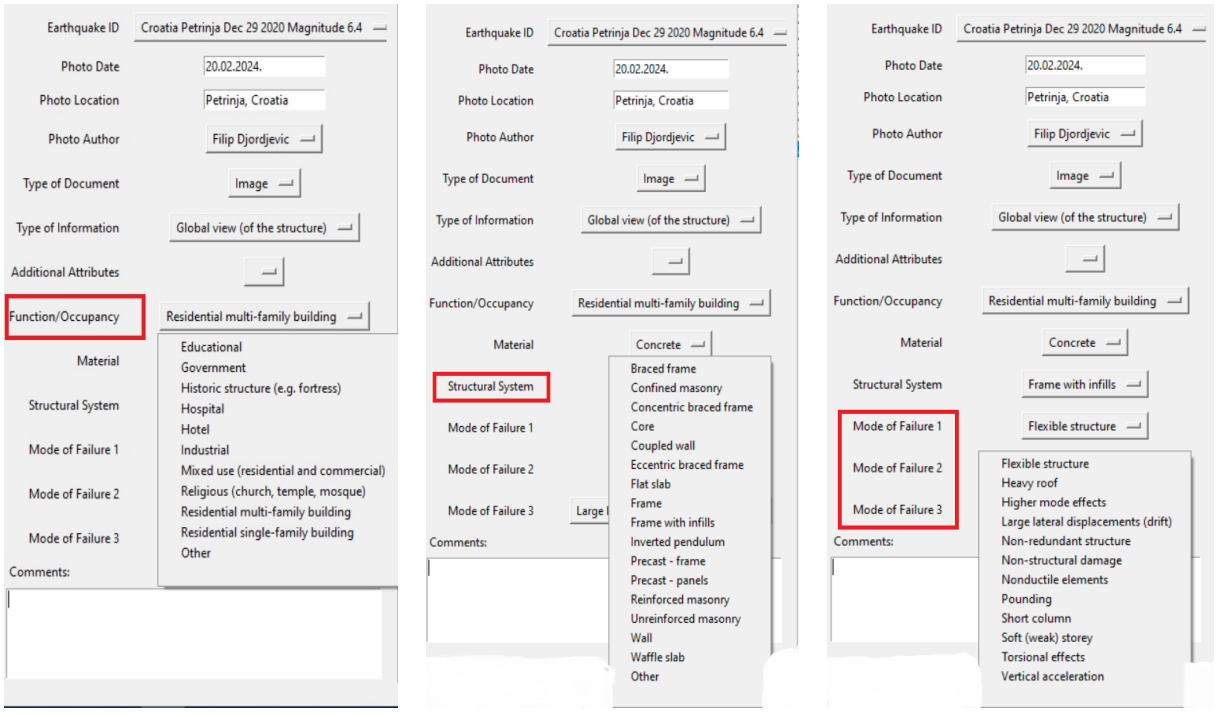
4.1. Image Navigation and Interactive Features

One of the key features of the Tagger is its ability to efficiently navigate through large datasets. Users can browse through folders containing earthquake damage images, select specific documents, and load them onto the main canvas for detailed analysis. The interface also includes a fullscreen mode, which enhances the viewing experience by allowing users to focus on image details without distraction. These navigation capabilities ensure that even extensive datasets remain accessible and manageable.

The tool also incorporates interactive features for detailed image inspection. Users can zoom in and zoom out image to examine specific areas of interest, rotate images for better alignment, and pan across the canvas to explore different sections of an image. These capabilities allow for a comprehensive visual analysis, enabling users to identify and document discrete damage details effectively.

4.2. Metadata Annotation with Customization

At the core of the Tagger's functionality is its metadata annotation system. This feature enables users to systematically document key information about each image, such as earthquake details (e.g. event name and date), structural characteristics (e.g. structural system and material type), and failure modes (e.g., "Flexural failure" and/or "Liquefaction") (see Fig. 4). Additional fields allow for the inclusion of text comments, occupancy types, and retrofitting details. To minimize errors and enhance efficiency, metadata fields are dynamically filtered based on the selected type of information and occupancy. For instance, selecting a specific type of information, such as "Infrastructure" or "Building element," updates the available structural system and failure mode options to reflect relevant categories. This adaptability ensures the tool's applicability to different types of structures, including buildings and bridges (see Fig. 5).



a) b) c)

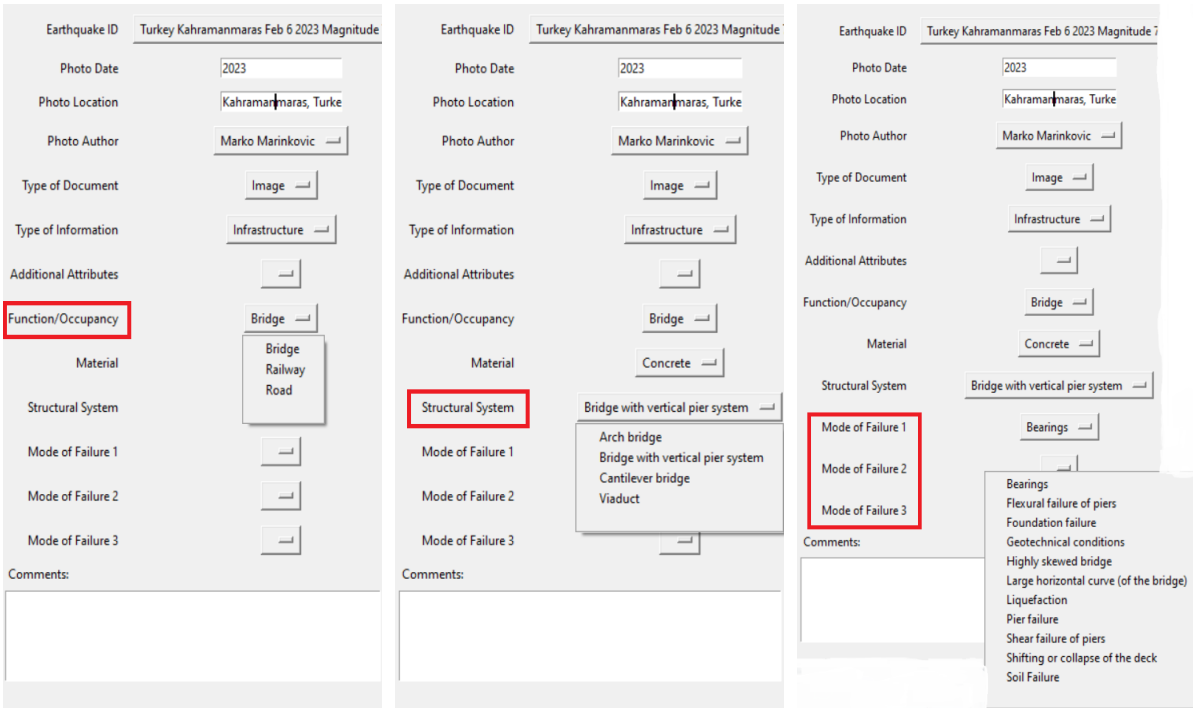
Figure 4. Metadata annotation with dynamic filtering and customization – Example 1 (Building): a) Function/Occupancy; b) Structural System; c) Mode of Failure.

4.3. Technical Implementation

The tool leverages the Python Imaging Library (PIL) for image processing and XML for metadata management. Metadata is saved in XMP format, ensuring compatibility with existing image analysis

Copyright © 2025 CroCEE
DOI: https://doi.org/10.5592/CO/3CroCEE.2025.130

tools. The modular design allows seamless integration with external platforms for data storage and sharing. In its final form the tool is in the form of an executable file; this flexibility makes it a robust solution for post-earthquake damage documentation. Looking ahead, several enhancements are planned for the SUZI-SAEE Tagger. These include the automation of metadata annotation, the expansion of metadata fields, and improvements to the user interface based on feedback from researchers and practitioners.



a) b) c)

Figure 5. Metadata annotation with dynamic filtering and customization – Example 2 (Bridge): a) Function/Occupancy; b) Structural System; c) Mode of Failure.

5. APPLICATIONS AND BENEFITS

The SUZI-SAEE Tagger has important role in advancing earthquake engineering by supporting the identification of structural vulnerabilities through detailed damage classification. This tool provides critical insights into seismic behavior of structures.

The database is a valuable resource for training engineers and conducting advanced research. The repository of labelled images enables the development of predictive models, which are essential for simulating structural response to seismic events. This capability not only advances theoretical understanding but also informs practical decision-making in engineering design and disaster mitigation.

The intuitive interface of the Tagger is expected to attract interest of students and young professionals. By engaging with the tool, users gain hands-on experience in damage assessment and metadata annotation, fostering a new generation of earthquake engineering experts. This educational aspect ensures that the knowledge and skills required for effective seismic resilience are passed on to future practitioners.

The scalability of the overall framework is another significant benefit. The system is designed to accommodate global datasets, allowing for the integration of diverse seismic event records. This adaptability enhances its utility as a universal tool for earthquake damage assessment. Furthermore, the possibilities for integration of machine learning algorithms can automate the tagging process, reducing manual effort and improving the consistency of metadata annotations. These advancements as well as

Copyright © 2025 CroCEE
DOI: https://doi.org/10.5592/CO/3CroCEE.2025.130

interface in English language, have a potential to expand the framework's applicability and efficiency, making it a valuable asset for international collaboration.

Beyond its technical and educational applications, the SUZI-SAEE Tagger has a potential to contribute to disaster preparedness. By analyzing patterns of structural damages and failure modes, the database can inform governmental and institutional strategies for risk reduction. The tool's ability to aggregate and analyze data from multiple seismic events provides a robust foundation for developing targeted interventions that enhance community resilience.

6. CONCLUSIONS

The SUZI-SAEE framework for labelling earthquake-induced damages represents a significant step forward in the field of post-earthquake damage documentation and analysis. By combining systematic tagging with detailed metadata, the framework improves the quality and usability of damage data. This initiative has the potential to enhance seismic resilience by identifying structural vulnerabilities and informing enhanced design and retrofitting practices. The tool's user-friendly interface and customizable metadata fields make it valuable for global community, supporting both advanced research and education.

Future improvements to the framework include expanding its scope to incorporate additional document types and leveraging machine learning for automated tagging by reducing manual effort with increasing the consistency and scalability of metadata annotations, and strengthening international collaborations. These developments are expected to further enhance the database's utility in advancing seismic resilience research and practice. By addressing the challenges of systematic damage documentation, SUZI-SAEE hopes to contribute to the global effort to mitigate seismic risks and improve the resilience of the built environment.

Despite challenges in data consistency and user expertise, the ongoing SUZI-SAEE initiative to create a comprehensive Earthquake Image Database underscores the importance of comprehensive damage documentation for mitigating seismic risk and advancing earthquake engineering research. Its robust functionalities make it a cornerstone of a global effort to mitigate the impact of earthquakes on communities and infrastructure.

Acknowledgements

The authors would like to express their gratitude to their colleagues and members of SUZI-SAEE for their invaluable contribution to the post-earthquake reconnaissance missions, by capturing images that formed the foundation of this image database. Special thanks are also extended to the students of the Faculty of Civil Engineering, University of Belgrade, whose dedication and meticulous work significantly contributed to the labelling process for the database. Their contributions were essential to the success of this research, and the authors deeply appreciate their support and commitment.

References

[1] Coburn, A. and Spence, R., Earthquake Protection. John Wiley & Sons, 2003.

[2] "CRED and UNISDR," 2015. https://www.unisdr.org/we/inform/publications/50589

[3] Van Rossum, G. and Drake, F. L., Python 3 Reference Manual. Scotts Valley, CA: CreateSpace, 2009.

[4] Fischinger, M., Cerovsek, T., and Turk, Z., "Easy: A hypermedia learning tool," Electron. J. Inf. Technol. Constr., pp. 1–10, 1998.

[5] Earthquake Engineering Online Archive, University of California, Berkeley, USA. National Information Service for Earthquake Engineering (https://nisee.berkeley.edu/elibrary/).

[6] Marinković, M., Blagojević, N., Milićević, I., Nikolić-Brzev, S., Main findings of the SUZI-SAEE reconnaissance missions after the November 26, 2019 Albania earthquake (Mw 6.4) and December 29, 2020 Petrinja earthquake (Mw 6.4), 18th World Conference on Earthquake Engineering, Milan, Italy,

Copyright © 2025 CroCEE
DOI: https://doi.org/10.5592/CO/3CroCEE.2025.130

30th June-5th July 2024.

[7] Miranda, E. Brzev, S. Bijelic, N. Arbanas, Ž. Bartolac, M. Jagodnik, V. Lazarević, D. Mihalić Arbanas, S. Zlatović, S. Acosta Vera, A. Archbold, J. Bantis, J. Blagojević, N. Borozan, J. Božulić, I. Cruz, C. Dávalos, H. Fischer, E. Gunay, S. Hadzima-Nyarko, M. Heresi, P. Lignos, D. Lin, T. Marinković, M. Messina, A. Miranda, S. Poulos, A. Scagliotti, G. Tomac, I. Tomić, I. Ziotopoulou, K. Žugić, Ž. Robertson, I. (2021) "JOINT RECONNAISSANCE REPORT (JRR)", in StEER-EERI: PETRINJA, CROATIA DECEMBER 29, 2020, Mw 6.4 EARTHQUAKE. DesignSafe-CI. https://doi.org/10.17603/ds2-1w0y-5080.

[8] M.Marinković, S. Brzev, M. Baballëku, B. Isufi, N. Blagojević, I. Milićević, Ž. Žugić, P. Bursać, Out-of-plane behaviour of loadbearing and non-structural masonry walls during recent earthquakes, 1st Croatian Conference on Earthquake Engineering, Zagreb, Croatia, 22-24 March, 2021.

[9] M. Marinković, M. Baballëku, B. Isufi, I. Milićević, S., Brzev, N. Blagojević, Ž. Žugić, P. Bursać, Performance of reinforced concrete buildings during the November 26, 2019 Albania earthquake (Mw 6.4) and December 29, 2020 Petrinja earthquake (Mw 6.4), 3rd European Conference on Earthquake Engineering & Seismology, Bucharest, Romania, 4-9 September 2022.

[10] Nikolić-Brzev, S., Marinković, M., Milićević, I. i Blagojević, N. (2020). Posledice zemljotresa u Albaniji od 26.11.2019. na objekte i infrastrukturu (Consequences of the November 26, 2019 Albania earthquake on the buildings and infrastructure), Serbian Association for earthquake engineering (SUZI-SAEE), Belgrade, Serbia (in Serbian), 80 p. (ISBN 978-86-7466-843-6)

[11] Andonov, A., Baballëku, M., Baltzopoulos, G., Blagojević, N., Bothara, J., Brûlé, S., Brzev, S., ... & Veliu, E. (2022). EERI earthquake reconnaissance team report: M6.4 Albania Earthquake on November 26, 2019.
http://learningfromearthquakes.org/images/earthquakes/2019_Albania_Earthquake/EERI_Earthquake_Reconnaissance_Report_-_M6.4_Albania_Earthquake_on_November_26_2019.pdf

[12] Marinković, M., Baballëku, M., Isufi, B., Blagojević, N., Milićević, I., Brzev, S., Performance of RC cast-in-place buildings during the November 26, 2019 Albania earthquake, Bulletin of Earthquake Engineering (2022). pp. 1-54. DOI: 10.1007/s10518-022-01414-y

[13] Dilsiz, A., S. Gunay, K. Mosalam, E. Miranda, C. Arteta, H. Sezen, E. Fischer, M. Hakhamaneshi, W. Hassan, B. ALhawamdeh, S. Andrus, J. Archbold, S. Arslanturkoglu, N. BEKTAS, L. Ceferino, J. Cohen, B. Duran, K. Erazo, G. Faraone, T. Feinstein, R. Gautam, A. Gupta, S. Haj Ismail, A. Jana, S. Javadinasab Hormozabad, A. Kasalanati, M. Kenawy, Z. Khalil, I. Liou, M. Marinkovic, A. Martin, Y. Merino, M. Mivehchi, L. Moya, C. Pájaro Miranda, n. quintero, J. Rivera, X. Romão, M. Lopez Ruiz, S. Sorosh, L. Vargas, P. Velani, H. Wibowo, S. Xu, T. YILMAZ, M. Alam, G. Holtzer, T. Kijewski-Correa, I. Robertson, D. Roueche, A. Safiey. (2023) "StEER: 2023 Mw 7.8 Kahramanmaras, Türkiye Earthquake Sequence Preliminary Virtual Reconnaissance Report (PVRR)", in StEER- February 6, 2023, Kahramanmaras, Türkiye, Mw 7.8 Earthquake. DesignSafe-CI. https://doi.org/10.17603/ds2-7ry2-gv66

[14] Marinković, M., Nikolić-Brzev, S., Blagojević, N., Lessons learned from reconnaissance missions of SUZI-SAEE in recent earthquakes, 18th World Conference on Earthquake Engineering, Milan, Italy, 30th June-5th July 2024

Proceedings of the 3rd Croatian Conference on Earthquake Engineering - 3CroCEE
19–22 March 2025, Split, Croatia
Copyright © 2025 CroCEE
DOI: https://doi.org/10.5592/CO/3CroCEE.2025.54

EARTHQUAKE RISK PERCEPTION IN BANJA LUKA: IMPLICATION FOR SEISMIC MANAGEMENT

Vesna Šipka [(1)], Mirjana Landika [(2)], Ljiljana Popović [(3)]

[(1)] *DRR and planning expert, Department for Civil Protection, City of Banja Luka, BiH,vesna_sipka@hotmail.com*
[(2)] *Full Professor, Panevropean University Banja Luka, BiH, mirjana.landika@gmail.com*
[(3)]*Ass.Professor, Faculty of Technical Sciencies, University of Novi Sad, ljiljana.popovic.ns@gmail.com*

Abstract

Seismic risk perception can be considered as critical factor related to citizens behavior during earthquake public risk perceptions had been surveyed in Banja Luka, one of the most earthquake prone risk exposed city in Bosnia and Hercegovina. This study aims to identify various factors influencing people's perceptions of earthquake risk.

This paper presents quantitative research results regarding the influence of socio-demographic factors on the earthquake risk perception of the citizens of Banja Luka. The aim of the research is to determine how much the citizens of Banjaluka are aware of the risk and prepared to react in the event of an earthquake. The relationship between gender, age, level of education, facility ownership and other factors with risk perception have been examined. T-test, Mann Whitney U test, and Pearson correlation coefficient were used to examine the relationship between the variables and the earthquake risk perception.

The questionnaire consists of 16 questions. The first part of the questionnaire was consisted of general questions about the socio-demographic characteristics of the respondents as well as questions in regards to past experience and attitude to earthquakes. The second part of questionnaire consists questions that would determine the level of awareness of the respondents about earthquakes, and the questions for determining the respondents preparedness. Using the snowball sampling technique (online questionnaire) the survey was conducted during August 2024 (N= 415 respondents)

Keywords: disasters, earthquake, risk perception, management, preparedness

1. Introduction

It is widely known that earthquake damage is influenced not only by earthquake parameters, building vulnerability, local soil conditions, and deep geology but also human behavior and actions before, during, and after earthquakes. Resilience, both community and individual, may have a significant impact on level of damage as well as recovery.

Risk is combination at least three variables hazard, exposure and vulnerability. Reducing any of these parameters also diminishes the risk. Understanding that seismic risk hazard cannot be decreased and very often there is no possibility to take any action related to exposures. The only window for certain actions is vulnerability, both material as well as non-material. Non-material resilience might be described as knowledge and preparedness for appropriate actions before, during and after earthquake.

The literature on risk reduction highlights the critical roles that education, families, and the community play in fostering a culture of preparedness and disaster recovery [1]. Risk perception might be important determinant of the behaviour towards risks, e.g. for the decision to take preventive measures. If risk perception and influencing factors of people living in risk prone areas is known, effective information strategies on protective measures can be designed [2]. According to [3] 86 out of 100 Italian citizens, living in the most dangerous zone, do not have a correct perception of seismic hazards. Citizens have scattered ideas and incomplete information regarding risk topic and the civil protection authority (via internet) was the primary source of information [1].

Copyright © 2025 CroCEE
DOI: https://doi.org/10.5592/CO/3CroCEE.2025.54

Earthquakes can result in severe consequences for human communities, infrastructure, and the natural surroundings. Data from the Centre for Research on the Epidemiology of Disasters (CRED) show that earthquakes caused the most widespread devastation, accounting for 58% of total fatalities in natural disasters from 2000 to 2019. Mitigating seismic risks is a diverse process, but it always starts with a precise assessment of seismic hazards [4] but also recognizing interested and affected citizens as legitimate partners in the exercise of risk assessment is not a short-term solution for the challenges of risk management. However, serious attention to participation and process issues may, in the long run, lead to more effective and satisfying ways to manage risk [5].

Numerous global studies have been conducted on the perception of seismic risk; however, local researchers have yet to undertake any investigations in Bosnia and Herzegovina. Researchers in this area have demonstrated a lack of interest in this subject, despite the fact that our country, along with the entire Balkan Peninsula, is seismically active. The seismic activity observed in this region is a result of the subduction of the Adriatic microplate beneath the Eurasian plate. Residents of Banja Luka are at risk from earthquakes originating in the local seismogenic zone, as well as the potential impact of seismic activity in nearby regions. Due to its geographical position, Banja Luka is vulnerable to earthquakes originating from Croatia, which is also a seismically active region.

The 2020 Petrinja earthquake revealed that Banja Luka's citizens, public administration, and institutions lack the knowledge and readiness necessary to withstand even moderate ground shaking. Even when decision-makers are aware of past earthquakes that have resulted in natural disasters in their regions, it can be highly challenging to alert them to the seismic risk issue. Light damage was reported in 85 flats to the local civil protection.

No studies have specifically addressed the population's perception of seismic risk in Banja Luka. However, research focusing on the perception of seismic risk among students in the final years of primary and lower secondary education was conducted as part of a master's thesis [6]. Data for this study were gathered through a closed-ended questionnaire. A total of 812 students from 13 schools participated. The first part of the questionnaire consisted of 5 questions related to knowledge and attitudes towards earthquakes and seismic risk, while the second group of 5 questions evaluated preparedness for earthquake response.

The findings concerning the training and readiness of students are particularly concerning. Just over half of the students indicated that they are familiar with the procedures to follow during and after an earthquake, as well as the designated evacuation routes. Notably, only 40% of the respondents reported having attended lectures on earthquake safety. Furthermore, the participation rate in practical earthquake drills is alarmingly low, with only 19% of students affirming their involvement.

This study aimed to investigate how citizens of Banja Luka perceive seismic risk, despite the lack of data related to building vulnerability and other risk elements. Additionally, the authors intended to analyze the results to draw conclusions about the level of preparedness and knowledge of safety protocols in case of an earthquake. An indicator of trust in the civil protection service can be derived from the responses regarding the source of information about earthquake protection.

The hypothesis is that a significant percentage of Banja Luka's residents perceive seismic risk as high, meaning they are aware of the danger of potential earthquakes. The fear of earthquakes, due to memories of the devastating earthquake, is also strong among many citizens. On the other hand, the level of preparedness, expressed through knowledge of procedures in case of an earthquake, does not match the perceived risk or fear of earthquakes. Statistical analysis of the data will investigate the impact of the respondents' socio-demographic characteristics on the perception of seismic risk.

In this respect, this paper could be considered as the pioneering study of seismic risk perception in Bosnia and Herzegovina, particularly focusing on Banja Luka as one of the most seismically prone city. The aim of this paper is to elaborate on seismic risk perception of populations in a remarkably seismic-prone area of Bosnia and Herzegovina: the Banja Luka area.

Proceedings of the 3rd Croatian Conference on Earthquake Engineering - 3CroCEE
19–22 March 2025, Split, Croatia
Copyright © 2025 CroCEE
DOI: https://doi.org/10.5592/CO/3CroCEE.2025.54

To understand citizens' perception of seismic risk, we analyze psychometric components: (a) awareness of risk, (b) fear, (c) attitude toward the possibility of earthquake protection, and (d) knowledge of safety protocols. This methodology, combined with an assessment of personal traits, might offer comprehensive insight into how individuals perceive earthquake risks and potentially reveal vulnerable populations. By identifying areas of weakness and potential for enhancing community resilience, civil protection authorities can develop focused strategies and policies aimed at fostering a safer and more resilient environment. This study aimed to offer valuable insights into community resilience, thereby assisting decision-makers in strengthening it through strategic initiatives.

Seismic risk assessment requires reliable hazard and vulnerability assessment studies, such studies are inadequate in number in developing countries. In the absence of solid data to accomplish seismic risk assessment, risk perception (perceived risk) may be a good replacement for working out risk reduction measures. This study will be highly helpful for administrative staff, disaster management authorities, and local governments to plan efficient risk reduction policies in the future for disaster risk reduction, particularly in earthquake-prone areas [7].

The paper is organized as follows: Section 1 reviews the literature on seismic risk perception; Section 2 describes the methodology used; Section 3 presents the results; Section 4 discusses the findings and implications; and Section 5 concludes with recommendations for future research.

1.1. Literacy review

The literature review aimed to investigate the similarities and differences in the perception of seismic risk among various societies and its correlation with individual resilience. To accomplish this objective, the authors examined scientific literature concerning seismic risk perceptions and related subjects pertinent to European cities and countries, in addition to Indonesia, Mexico, the USA, Australia, and other regions worldwide. The authors attempted to include not only research for geographically diverse locations but also to cover cities/countries with different levels of seismic hazard and prior earthquake experience.

Social vulnerability is as much a part of risk as building damage, hazard magnitude, and economic loss [8]. By integrating social vulnerability analysis and socio-psychological factors into disaster management, efforts can more effectively prevent, reduce, and respond to the diverse challenges posed by earthquakes [9], [10], [11].

Risk perception is a fundamental element in the definition and adoption of preventive counter-measures [3]. “Risk is the socially constructed sum of hazard and public perceptions” [5]. Risk perception refers to people's judgments and evaluations of hazards they (or their facilities, or environments) are or might be exposed to. Risk attitudes are people's intentions to evaluate a risk situation in a favorable or unfavorable way and to act accordingly [9]. Awareness and perception of risk are among the most crucial steps in the process of taking precautions at individual level for various hazards [12]. Integrating public perception into the decision-making process might bridge the gap between scientific expertise and community values. It can increase the transparency and responsiveness of policy decisions, making them more inclusive and better aligned with the public's needs and concern [13]. A large proportion of people the world over do nothing or very little to adjust to seismic hazards [11]. Some studies have identified fatalistic attitudes, with respondents considering natural disasters as inevitable events [14],[13],[15],[16],[17],[18].

Risk perception studies have identified various determinants that influence individuals’ behaviors and attitudes, The impact of the determinants may be positive and negative. The most commonly examined determinants fall into the following interlinked categories: psychometric, demographic, and socioeconomic [19], [15]. Gender is strongly related to risk judgments and attitudes [5],[8],[20]. Several dozens of studies have documented the finding that men tend to judge risks as smaller and less problematic than do women [5],[20],[19],[15],[22],[23],[24]. On a regular bases the following risk perception determinants were elaborated age, education [20], [19], [21], [15],[12] [22],[23],[24],[18]. Earthquake risk perception varied significantly according to income levels [19], [21],[18]**.** Previous

Copyright © 2025 CroCEE
DOI: https://doi.org/10.5592/CO/3CroCEE.2025.54

earthquake experience also show some impact on seismic risk [21]. Some researches have focus on risk awareneses [25],[26], [23], [27], emphase influence of household structure [12], [28], [24]. Studies conducted in cities that have previously experienced damaging earthquakes reveal that the participants lack a seismic risk prevention culture [29], [24], [18].

The explicit recognition within disaster risk reduction (DRR) activities that socio-psychological factors contribute to human vulnerability can improve the effectiveness of these activities in increasing seismic adjustments in individuals and small groups. Such DRR activities might include [11]. The the serious lack of emergency training perceived, both for adults and children [15], [25], [26], [30].

A region-specific strategy that considers the distinct socio-cultural characteristics of each locality is crucial, rather than implementing a one-size-fits-all methodology to improve resilience**.** The conclusion of the study [31] in this regards is that societies have diverse risk perceptions depending on local framework and cicumstances. Regular community drills, targeted educational campaigns, and the integration of disaster preparedness content into school curricula, have been highlighted as actionable steps to increase public awareness and community resilience [30].

Researchers predominantly assess vulnerability across various structural elements, reflecting a holistic approach to understanding and mitigating the impact of earthquakes on infrastructure and communities [4]. The review found a risk perception paradox related to linkage among risk perception and the likelihood of individuals to take preparedness actions. It is commonly assumed that high risk perception will lead to personal preparedness and, subsequently, to risk mitigation behavior. However, this is not necessarily true. In fact, the opposite can occur if individuals with high risk perception still choose not to prepare themselves personally in the face of a natural hazard [32].

In the absence of solid data for measuring the seismic vulnerability of buildings, risk perception can serve as a valuable proxy for developing earthquake risk reduction strategies [7].Disaster management which used to be more focused on emergency situations needs to be diverted to activities and capacity building [10].

The literature also recognise diverse leading source of information among the respondents such as media that could play an effective role in earthquake preparedness, especially if they act in a more responsive manner [12]. Communication seismic risk in diverse phases of risk management which involves providing technical and scientific information as a priority highlights a dozen of study. Finally, we suggest that further research should be undertaken about the optimal ways of communicating information and their roles in risk perception. [12], [33], [25]. Evidently risk communication is the indispensable link between risk perception and risk management [8]. It is necessary to improve public knowledge about measures for mitigation of damage and preparedness. The results indicate that future preparedness programmes should target people with lower level of risk perception and preparedness.

2. Methodology

The quantitative research aims to examine the influence of socio-demographic factors on the perception of earthquake risk among citizens in Banja Luka and its surrounding areas, and evaluate their preparedness. Given that Banja Luka and surrounding areas are the one of the most seismically active areas in Bosnia and Herzegovina and wider, this research aims to determine how much the citizens of Banja Luka are aware of the risk of earthquakes and how prepared they are to react in the event of an earthquake. The relationship between gender, age, level of education, and facility ownership and some other factors with risk perception were examined.

The paper is based on the central hypothesis that a large percentage of citizens in the study area perceive the seismic risk in Banja Luka as high and experience fear of earthquakes. However, their knowledge about earthquake safety protocols does not align with their perception of the risk. An online survey comprising a questionnaire with 16 closed-ended questions was conducted to evaluate citizens' attitudes and knowledge about seismic risk and protection from earthquakes. The questionnaire was available online from August 9 to September 5, 2024. In total, 415 responses were obtained.

Proceedings of the 3rd Croatian Conference on Earthquake Engineering - 3CroCEE
19–22 March 2025, Split, Croatia
Copyright © 2025 CroCEE
DOI: https://doi.org/10.5592/CO/3CroCEE.2025.54

2.1. Sample

For the purposes of this research, adult citizens of Banja Luka and its vicinity were surveyed, and 415 answers were collected. There was a higher percentage of women (65.5%) than men (34.5%), and the most significant percentage of respondents were in the age group 31-45 years. The percentage of respondents from the group 46-60 years is slightly lower at 33.5%, while the lowest percentage (4.6%) is from the age group of over 60 years. The sample has 13.5% of respondents aged 18-30. The majority of respondents in the sample have higher education, followed by those who have completed high school. The percentage of respondents who have completed postgraduate studies is as follows: master's 12.5%, doctoral 1.4%. The most of respondents are married, 64.1%, followed by single respondents, 25.3%, as well as 8% divorced and 2.7% widowed respondents. The most significant percentage of respondents (50.8%) live in family-owned apartment, 38.3% of the respondents live in its own house and the smallest number of respondents live in a rented building (10.8%).

2.2. Questionnaire Design

The instrument used in the conducted research project was a survey questionnaire, consisting of 16 questions divided into two sections:

- General questions
- Specific questions

The general questions define the personal profile of the respondents and include personal information that may indicate the need for a sense of security, such as gender, age, marital status, educational background, monthly income, place of residence, and type of housing unit.

The specific questions relate to information about natural disasters and the respondents' attitudes towards them. Those questions provide input for assessment of responder's earthquake risk perception and preparedness. Since there is no national papers related to this topic, an examination of international scientific studies that employed questionnaires as research instruments was carried out to refine and develop the questionnaire required for this study.The final questionnaire was crafted using simple language, steering clear of any technical terminology. The questions in the questionnaire were answered by choosing the offered answer.

2.3. Analyses

The data collected from the survey were processed using the statistical software SPSS (Statistical Package for the Social Sciences). In order to eliminate possible errors when entering the answer, the data check was performed. The gathered data were then analyzed using descriptive statistics, and the frequency and percentage were determined. The next step involved comparing the collected data, namely the respondents' demographic traits and their perception of risk, such as the relationship between respondents' educational attainment and knowing safety measures and procedures for earthquakes. The relationship between the variables and earthquake risk perception was examined using a T-test and Mann Whitney U test. The Pearson correlation coefficient has been used for analyzing relationship for different sociodemographic variables. All tests were two-tailed, with a significance level of $p < 0.05$ and $p<0.01$. Statistical analysis was performed using SPSS Statistic 20.0 (IBM SPSS Statistics, New York, United States).

3. Results

With the aim to determine the level of awareness about earthquakes, the first question that have been asked was: " Do you believe that the risk of earthquakes occurring in Banja Luka is high? The most significant percentage of respondents answered affirmatively to this question (68.2%), but 22.9% of respondents answered that they were not sure and 8.9% respondents answered negatively. Regarding previous experience with natural disasters (such as floods, earthquakes, and storms), 52.8% of respondents reported having such experience, while 47.2% answered negatively. Additionally, in response to the question, "What is the source of information about earthquake protection?", 32.8% of

Proceedings of the 3rd Croatian Conference on Earthquake Engineering - 3CroCEE
19–22 March 2025, Split, Croatia
Copyright © 2025 CroCEE
DOI: https://doi.org/10.5592/CO/3CroCEE.2025.54

respondents selected education, 35.7% od decided on the internet, 7.5% chose television, and 24.1% recognized the civil protection service as a source of information related to earthquake safety measures.

Table 1. Responders' attitudes related to earthquake risk perception

	Yes (%)	No (%)	Not sure (%)
Perception of the Banja Luka seismic risk –high	68.2	8.9	22.9
Belief of earthquake protection possibility	43.5	19.3	36.9
Feeling fear of earthquake	65.1	34.9	-
Knowledge of safety protocols	50.6	9.4	40.0
Knowledge of emergency service numbers	81.2	6.7	12.0

The hypothetical framework of the research includes illuminating the following facts: The high percentage of the citizens perceives the seismic risk in Banja Luka as high, but they do not believe that there is a possibility of protection against eartquakes. As a consequence, the level of preparedness in terms of knowledge of earthquake safety protocols is insufficient.

Responder's perception onseismic risk as well as attitudes toward the possibility for earthquake protection are shaped by past experiences, individual characteristics, and knowledge of safety protocols. The examination is conducted using relevant methods of statistical analysis, as follows. The percentage of respondents who believe that the risk in Banja Luka is high and that earthquake protection is possible can be determined using the T-test.

Table 2. Result of T-test related to risk peception in Banja Luka

a) One-Sample Statistics

	N	Mean	Std. Deviation	Std. Error Mean
Do you think that the earthquake risk in Banja Luka is high?	415	1.55	.841	.041

b) One-Sample Test

	Test Value = 1					
	t	df	Sig. (2-tailed)	Mean Difference	95% Confidence Interval of the Difference	
					Lower	Upper
Do you think that the earthquake risk in Banja Luka is high?	13.249	414	.000	.547	.47	.63

The T-test results reveal that 71%-74 % of residents believe that the seismic risk in Banja Luka is high This confirms the fact that citizens are aware that the likelihood of an earthquake occurring in the Banja Luka region is high but there is only 43.5 % responders beliving that earthquake protection is posible. The percentage of repsponders who think negative is 19.3% and significant number 36.9% is not sure about this topic. It means that they do not have information or do not think about this issue at all. The next T-test results reveal there is no correlation between between respondents who perceive the risk as high and the answers to the question about the possibility of protection against earthquakes.

Copyright © 2025 CroCEE
DOI: https://doi.org/10.5592/CO/3CroCEE.2025.54

Table 3. Outcome of T-test, relationship between recognizing earthquake risk and protective measures

a) Paired Samples Statistics

		Mean	N	Std. Deviation	Std. Error Mean
Pair 1	Do you think that the earthquake risk in Banja Luka is high?	1.55	415	.841	.041
	Do you believe that protection against earthquakes is possible?	1.93	415	.897	.044

b) Paired Samples Correlations

		N	Correlation	Sig.
Pair 1	Do you think that the earthquake risk in Banja Luka is high? & Do you believe that protection against earthquakes is possible?	415	-.052	.294

c) Paired Samples Test

		Paired Differences					t	df	Sig. (2-tailed)
		Mean	Std. Deviation	Std. Error Mean	95% Confidence Interval of the Difference				
					Lower	Upper			
Pair 1	Do you think that the earthquake risk in Banja Luka is high? & Do you believe that protection against earthquakes is possible?	-.383	1.261	.062	-.505	-.261	-6.191	414	.000

The survey results indicate that there is a low correlation between the two variables (risk perception and the potential for earthquake protection) at the 95% significance level (0.052). Furthermore, attitudes regarding earthquake protection are influenced by other factors, such as information and knowledge, fatalistic beliefs, and memories of past earthquakes.

The T-test results show no statistically significant difference according to gender in relation to earthquake risk perception and perception of preparedness. Also, Pearson correlation test results between determinants and variables regarding earthquake risk did not reveal any correlation.

The outcomes of the independent samples Mann Whitney U test indicate that gender is the most statistically significant; there is a statistically significant difference between gender and perception of seismic risk and related questions (Table 4).

Table 4. Results test Independent amples Mann Whitney U test

Proceedings of the 3rd Croatian Conference on Earthquake Engineering - 3CroCEE
19–22 March 2025, Split, Croatia
Copyright © 2025 CroCEE
DOI: https://doi.org/10.5592/CO/3CroCEE.2025.54

Gender	
Question	Sig.*
Perception of the Banja Luka seismic risk –high	.012
Belief of earthquake protection possibility	.000
Feeling fear of earthquake	.000
Knowledge of safety protocols	.001
Knowledge of emergency service numbers	.042

*The significance level .05

4. Discussion

The assessment of how socio-demographic factors influence perceptions of seismic risk, as well as attitudes and knowledge regarding earthquake protection, is crucial for effective Disaster Risk Reduction (DRR) activities. These activities include enhancing public awareness, addressing and reducing fatalistic attitudes, increasing the level of individual preparedness, and improving the overall resilience of communities [11]. The high percentage of the citizens perceives the seismic risk in Banja Luka as high, but their belief about potential earthquake protection is not positive. As a consequence, the level of preparedness, in terms of knowledge of earthquake safety protocols, is unsatisfactory.

One possible explanation for this phenomenon is that residents retain memories of the 1969 earthquake, which heightens their perception of risk due to their awareness of the seismic activity in the region. Conversely, the extensive devastation experienced by the city may foster a fatalistic mindset, leading individuals to believe that effective protection against such disasters is unattainable. An analysis of the responses regarding awareness of earthquake response procedures reveals that 50.6% of participants claim to possess knowledge of these protocols, while the remaining respondents either lack knowledge or express uncertainty about their understanding. This uncertainty regarding the appropriate actions to take during an earthquake suggests a significant gap in familiarity with established safety protocols.

This indicates that a significant percentage of the population lacks confidence in their knowledge of earthquake safety measures, which could imply a need for better education and awareness programs about how to act during such events.

Table 5. The distribution responds on the question related to knowledge of safety protocols

Are you familiar with safety protocols in case of an earthquake?					
		Frequency	Percent	Valid Percent	Cumulative Percent
Valid	yes	210	50.6	50.6	50.6
	no	39	9.4	9.4	60.0
	I am not sure	166	40.0	40.0	100.0
	Total	415	100.0	100.0	

These findings are in line with the observed risk perception paradox [32], which reflects that individuals with a perception of high risk still choose not to personally prepare for facing natural hazards. There are three possible reasons according to [32], providing for daily life needs is mentally more important than the perception of natural hazard risks; the influence of trust in the government and public services—both ways; confusion or ignorance about adequate safety protocols.

Considering the historical and political context of the studying region, the authors believe that all the previously mentioned factors are valid. The residents of the surveyed area retain vivid memories of

Copyright © 2025 CroCEE
DOI: https://doi.org/10.5592/CO/3CroCEE.2025.54

wartime devastation and currently experience political instability, alongside the underlying risk of renewed conflict. In conjunction with a challenging economic landscape, it becomes increasingly difficult to encourage the populace to focus on natural disasters, particularly earthquakes, which occur infrequently. The experience of living in a transitional society marked by elevated levels of corruption diminishes the community's confidence in governmental institutions and services, including those related to the management of natural disaster risks. In Montenegro only 37.5% responders reported awareness of basic earthquake response procedures [30].

One of the most consistent findings from research on people's perception of risk is impact of gender, women tend to perceive higher level of risk. The educational attainment of the respondents does not influence this disparity [34]. This research indicated a significant correlation between gender and perceptions of seismic risk in Banja Luka which is consistent with a large number of studies [5], [36], [20], [21], [24] but also reveal larger the level of uncertainty regarding the potential for earthquake protection when compared to male respondents (Figure 1). One potential reason could be a lack of information regarding available protection options, or it could be that women often feel more vulnerable in emergency situations.

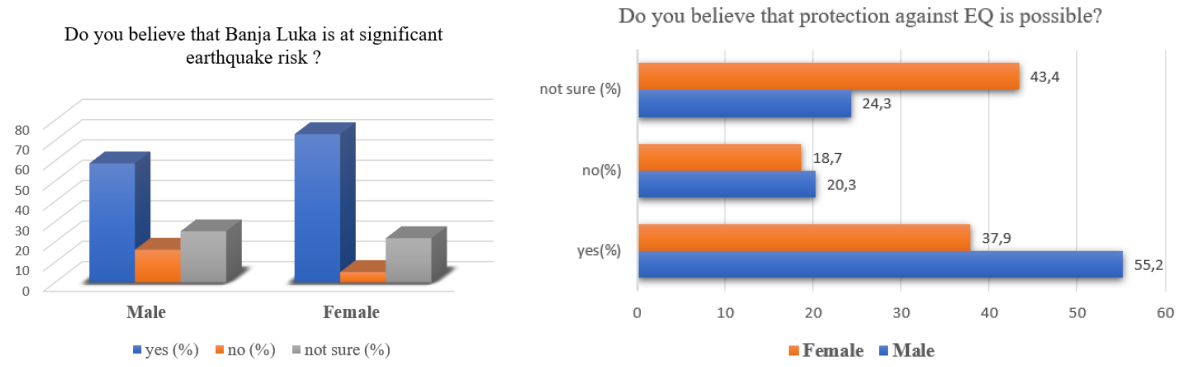


Figure 1. Differences in earthquake risk perception and belief in possibility protection between male and female responders

Besides this, the results further indicate that gender may play a crucial role in shaping attitudes towards familiarity with earthquake safety procedures, and awareness of emergency service contact numbers (Table 5). Other socio-demographic factors such as age, education, montly income, housing do not recognized as statisticall significant factor in seismic risk perception. The findings of study [37] stand in contrast, indicating that at a statistical significance level of 5%, factors such as age, educational attainment, marital status, property ownership, and household income exert an influence. Additionally, study [18] corroborates the effect of age and income, while study [24] demonstrates the impact of the age and housing. The same is with the study [21] revealing that income, and education level also have direct effects on how residents perceive of the risk from an earthquake. Considering that these studies were carried out in Serbia, Pakistan, Myanmar, and China, the observed discrepancies may be attributed to the larger geographical areas involved, which can influence the diversity of the respondents.

The marital status of the respondents indicates a statistically significant difference in only two areas: the perception of earthquake risk in the Banja Luka region and the fear of earthquakes. Additionally, the source of information regarding protective measures demonstrated a statistical correlation with both age and educational level, consistent with the findings of study [38].

The Department of Civil Protection is not highly ranked as a source of information, with only 24.1% of citizens choosing it. This result aligns with a survey in Italy [3] and may indicate a low level of trust or that civil protection is not sufficiently visible on the internet, which is the most frequently chosen source of information related to earthquake safety measures. The fact that only 7.5% of respondents chose television as a source of information can be explained by the lack of DRR contents on TV at all.

Copyright © 2025 CroCEE
DOI: https://doi.org/10.5592/CO/3CroCEE.2025.54

The research conducted is constrained by its focus on a limited geographical scope, the area of Banja Luka. Additionally, electronic surveying method applied in this research has its drawbacks.

The next research will focus on the perception of seismic risk among teaching staff in all educational institutions in the City of Banja Luka. This focus is motivated by findings from a prior study, which revealed an inadequate level of preparedness within primary and secondary schools

The significance of this study lies in the fact that it is a pioneering project not only in the local community but also in Republic Srpska/Bosnia and Herzegovina. Given that this is Banja Luka is earthquake prone city, it is essential to gather data regarding the risk perceptions pf its residents as well as their attitudes and level of preparedness to earthquake.

5. Conclusion

Banja Luka is highly vulnerable to earthquakes. This paper presents findings on the seismic-risk perception and awareness among its residents. The respondents perceive the risks as high but have insufficient knowledge about the appropriate actions related to earthquake protection. According to the survey results, public awareness of seismic risk and mitigation is poor, and citizens' understanding of basic concepts and emergency response needs significant improvement. Reducing damage and increasing preparedness begins with proper and adequate communication of seismic risk to the population. For communication, knowledge of citizens' attitudes is essential. The results show that a considerable challenge to earthquake preparedness exists because of the disparity between the public's awareness of risk and their level of actual preparedness, which is in line with the findings of study [25].

The high percentage of the citizens perceives the seismic risk in Banja Luka as high, but their belief about potential earthquake protection is not positive. As a consequence, the level of preparedness in terms of knowledge of earthquake safety protocols is unsatisfactory. These results confirm the main hypothesis.

This research indicated a significant correlation between gender and perceptions of seismic risk in Banja Luka, in terms of that women mostly perceive risk as high. Other socio-demographic factors such as age, education, monthly income, and housing are not recognized as statistically significant factors in seismic risk perception. The research indicates that, in addition to the disparity between awareness of earthquake hazard exposure and the corresponding level of preparedness, Civil Protection is inadequately represented as an information source. It is necessary for Civil Protection to change its approach and media in communicating risks with the population. Evidently, risk communication is the indispensable link between risk perception and risk management [9]. Additional research and studies are necessary to better identify the risk factors, which will enable the formulation of valuable recommendations for effective risk communication. Researching the perception of seismic risk among people engaged in professions such as educators, first responders, etc., can be useful for creating tailored strategies.

Research of this nature, which focuses on the knowledge and preparedness levels of the population, is becoming increasingly important since there was no seismological research conducted in Banja Luka since 1971, nor analysis of the vulnerability of the housing stock.

Acknowledgements

Authors express their sincere gratitude to the anonymous responders whose insightful feedback and contributions significantly improved this research.The current study's sample was not representative of the entire nation; it focused specifically on participants from Banja Luka and its vicinity. Consequently, the results cannot be applied to the entire population of the Republic of Srpska/Bosnia and Herzegovina.

References

[1] Rego, I. & Pereira, S. & Morro, J.& Adam, M. (2016): Risk Perception and Preparedness for volcanic and seismic events: a study of families' emergency plans. 10.13140/RG.2.2.31762.99522)

Copyright © 2025 CroCEE
DOI: https://doi.org/10.5592/CO/3CroCEE.2025.54

[2] Sjoberg L. (2000): Factors in risk perception. Risk analysis: an official publication of the Society for Risk Analysis, 20 1, 1-11.

[3] Crescimbene, M. & Federica, L. & Romano, C & Alessandro, P. & Peruzza, L. (2014): What's the seismic risk perception in Italy? Conference: IAEG XII, Torino

[4] Ismail A, Rashid ASA, Amhadi T, Nazir R, Irsyam M, Faizal L. (2024): Exploring the Evolution of Seismic Hazard and Risk Assessment Research: A Bibliometric Analysis. *Sustainability*.16(7):2687. https://doi.org/10.3390/su16072687)

[5] Slovic, P. (1999): Trust, Emotion, Sex, Politics, and Science: Surveying the Risk-Assessment Battlefield. *Risk Anal* 19, 689–701 https://doi.org/10.1023/A:1007041821623

[6] Šipka, V. (2022): Upravaljanje seizmičkim rizikom osnovnih i srednjih škola na području Grada Banja Luka, Master teza, Univerzitet u Banjoj Luci, Fakultet bezbjednosnih nauka

[7] Khan, S. U., Qureshi, M. I., Rana, I. A., & Maqsoom, A. (2019): An empirical relationship between seismic risk perception and physical vulnerability: A case study of Malakand, Pakistan. *International Journal of Disaster Risk Reduction,* 41, 101317

[8] Armaş, I. (2008): Social vulnerability and seismic risk perception. Case study: the historic center of the Bucharest Municipality/Romania. *Nat Hazards* 47, 397–410 (2008). https://doi.org/10.1007/s11069-008-9229-3)

[9] Rohrmann, B. (2008): Risk Perception, Risk Attitude, Risk Communication, Risk Management: A Conceptual Appraisal. *15th International Emergency Management Society Annual Conference* (Vol. 2008)

[10] Septia, A.& Indartono, S. (2019): Earthquake Vulnerability in West Nusa Tenggara: Risk Perception, Previous Experience and Preparedness. *Advances in Social Science, Education and Humanities Research, volume 32*3, 10.2991/icossce-icsmc-18.2019.39.).

[11] Rossetto, T., Joffe, H., Solberg, C. (2011): A Different View on Human Vulnerability to Earthquakes: Lessons from Risk Perception Studies. In: Spence, R., So, E., Scawthorn, C. (eds) Human Casualties in Earthquakes. *Advances in Natural and Technological Hazards Research,* vol 29. Springer, Dordrecht. https://doi.org/10.1007/978-90-481-9455-1_20

[12] Yeşil, S., Dedeoğlu, N., Braun-Fahrlaender, C. et al. (2011): Earthquake awareness and perception of risk among the residents of Istanbul. *Nat Hazards* 59, 427–446, https://doi.org/10.1007/s11069-011-9764-1

[13] Renn O. (2024): Perception of risks, *Toxicology Letters,* Volume 149, Issues 1–3,2004, Pages 405-413, ISSN 0378-4274, https://doi.org/10.1016/j.toxlet.2003.12.051.

[14] Kunz-Plapp, T. & Werner, U. (2006): Understanding risk perception from natural hazards: Examples from Germany. 10.1201/9780203963562.ch10),

[15] Armaş J., Cretu R.Z. and Radu Ionescu R. (2017): Selfefficacy, stress, and locus of control: The psychology of earthquake risk perception in Bucharest, Romania, *International Journal of Disaster Risk Reduction,* http://dx.doi.org/10.1016/j.ijdrr.2017.02.018,

[16] Pothon, A., Gueguen, P., Buisine, S., and Bard, P.Y. (2019): California earthquake insurance unpopularity: the issue is the price, not the risk perception, Nat. Hazards Earth Syst. Sci., 19, 1909–1924, https://doi.org/10.5194/nhess-19-1909-2019.

[17] Suwihli, S.S. and Paradise, T.R. (2020): Seismic Risk Perception in Al-Marj, Libya: A Case Study after the 1963 Earthquake. *Open Journal of Earthquake Research*, 9, 349-366;

[18] Qureshi M.I.,Khan S.U,Rana I.A., Babar Ali, Asad ur Rahman, (2021): Determinants of people's seismic risk perception: A case study of Malakand, Pakistan, International Journal of Disaster Risk Reduction,Volume 55,102078, ISSN 2212-4209,https://doi.org/10.1016/j.ijdrr.2021.102078.

[19] Niforatos, S., Panagiotakos, D. & Delladetsimas, P.M. (2024): Socio-demographic determinants of earthquake risk perception: the case of the Corinthiakos Gulf, in Greece. *Nat Hazards* 120, 3847–3864 (2024). https://doi.org/10.1007/s11069-023-06356-5).

[20] Rahman, M.L. (2020): Risk perception and awareness of earthquake: the case of Dhaka, *International Journal of Disaster Resilience in the Built Environment*, Vol. 10 No. 1, pp. 65-82. https://doi.org/10.1108/IJDRBE-04-2018-0020.

Copyright © 2025 CroCEE
DOI: https://doi.org/10.5592/CO/3CroCEE.2025.54

[21] Tian, L., Yao, P., & Jiang, S. J. (2014): Perception of earthquake risk: a study of the earthquake insurance pilot area in China. *Natural hazards*, 74(3), 1595-1611).

[22] Kundak, S. & Türkoğlu H. & Ilki A. (2014): Risk perception in Istanbul: An earthquake-prone city. ITU A|Z. 10. 117-137

[23] Grozdanić, G., Cvetković, V. M., Lukić, T., & Ivanov, A. (2024): Sustainable Earthquake Preparedness: A Cross-Cultural Comparative Analysis in Montenegro, North Macedonia, and Serbia. *Sustainability*, 16(8), 3138. https://doi.org/10.3390/su16083138; .[

[24] Fernandez G., Aye Min Tun, Okazaki K., Saw Htwe Zaw and Kyaw Kyaw, Factors Influencing Fire, Earthquake, and Cyclone Risk Perception in Yangon, Myanmar, *International Journal of Disaster Risk Reduction*, https://doi.org/10.1016/j.ijdrr.2018.02.028)

[25] Rapaport, C. & Dallo, I. & Kligman, Y. & Marti, M. & Komendantova, N. & Ashkenazi, I. (2023): The Same But Different: Cross-Country Comparison of National Earthquake Policies and Societal Perspectives of Seismic Risk in Israel and Switzerland. 10.2139/ssrn.4535332.,

[26] Yang S., Gao H., Liu L., He L, Fan C., Tang W. (2010): analysis on public earthquake risk perception: based on questionnaire 3rd international conference on cartography and GIS 15-20 June, 2010, Nessebar, Bulgaria

[27] Vicente R., Ferreira T.M., Maio R., Koch H., (2014): Awareness, Perception and Communication of Earthquake Risk in Portugal: Public Survey, Procedia Economics and Finance, Volume 18,Pages 271-278, ISSN 2212-5671,https://doi.org/10.1016/S2212-5671(14)00940- X.

[28] Rosetto T, Solberg C, O'Connor C. (2013): Social Representations of Earthquakes: A Study of People Living in Three Highly Seismic Areas. Earthquake Spectra.29(2):367-397. doi:10.1193/1.4000138);

[29] Santos-Reyes J., Gouzeva T., Santos-Reyes G, (2014): Earthquake Risk Perception and Mexico City's Public Safety, Procedia Engineering, Volume 84,Pages 662-671, ISSN 1877- 7058, https://doi.org/10.1016/j.proeng.2014.10.484.

[30] Cvetković, V. & Grozdanić, G. & Milanovic, M.& Markovic, S.& Lukic, T. (2024): Understanding seismic hazard resilience in Montenegro: A qualitative analysis of community preparedness and response capabilities. *Open Geosciences*. 16. 10.1515/geo-2022-0729

[31] Bodas M., Peleg K., Stolero N., Adini B. (2022): Risk Perception of Natural and Human-Made Disasters-Cross Sectional Study in Eight Countries in Europe and Beyond, Frontiers in Public Health, Vol10, https://www.frontiersin.org/journals/public-health/articles/10.3389/fpubh.2022.825985, DOI=10.3389/fpubh.2022.825985, ISSN=2296-2565)

[32] Wachinger, G., Renn, O., Begg, C., & Kuhlicke, C. (2013). The Risk Perception Paradox—Implications for Governance and Communication of Natural Hazards. Risk Analysis, 33.

[33] Savadori, L. & Ronzani, P.& Sillari, G.& Di Bucci, D. & Dolce, M. (2022): Communicating Seismic Risk Information: The Effect of Risk Comparisons on Risk Perception Sensitivity. *Frontiers in Communication*. 7. 743172. 0.3389/fcomm.2022.743172.

[34] Barke, R. P., Jenkins-Smith, H., & Slovic, P. (1997). Risk Perceptions of Men and Women Scientists. Social Science Quarterly, 78(1), 167–176. http://www.jstor.org/stable/42863683

[35] Miranda, C. & Becker, J. & Toma, C. & Vinnell, L. & Johnston, D. (2021). Seismic experience and structural preparedness of residential houses in Aotearoa New Zealand. *International Journal of Disaster Risk Reduction.* 66. 102590. 10.1016/j.ijdrr.2021.102590.

[36] Cvetković, V. & Planić, J. (2022). Earthquake risk perception in Belgrade: implications for disaster risk management. *International Journal of Disaster Risk Management.* International Journal of Disaster Risk Management, 4. 69-88. 10.18485/ijdrm.2022.4.1.5.

[37] Cvetković, V., & Filipović, M. (2019). Percepcija rizika od zemljotresa u Republici Srbiji - teorijskoempirijska studija. Vojno delo

[38] Rüstemli, Ahmet & Karanci, Ayse. (1999). Correlates of Earthquake Cognitions and Preparedness Behavior in a Victimized Population. Journal of Social Psychology - J SOC PSYCHOL. 139. 91-101. 10.1080/00224549909598364.

Proceedings of the 3rd Croatian Conference on Earthquake Engineering - 3CroCEE
19–22 March 2025, Split, Croatia
Copyright © 2025 CroCEE
DOI: https://doi.org/10.5592/CO/3CroCEE.2025.68

DEPLOYING OF SEISMIC ALERT WARNING SYSTEMS IN INDUSTRIAL FACILITY

Igor Gjorgjiev [(1)], Marta Stojmanovska [(2)]

[(1)] *Professor, Ss. Cyril and Methodious University in Skopje, Republic of North Macedonia, Institute of Earthquake Engineering and Engineering Seismology, Skopje, igorg@iziis.ukim.edu.mk*
[(3)] *Associate Professor, Ss. Cyril and Methodious University in Skopje, Republic of North Macedonia, Institute of Earthquake Engineering and Engineering Seismology, Skopje, marta@iziis.ukim.edu.mk*

Abstract

In recent years, advancements in employee safety protocols within production facilities have been steadily progressing. However, seismic events pose significant risks to production facilities, potentially disrupting operations, causing structural damage, and endangering the safety of employees. Such a scenario occurred in January 2022, when the Florina earthquake (M5.3) struck an industrial facility in the Bitola region, North Macedonia, triggering both panic behaviour and minor, non-structural damages. Although post-event inspections identified only damage in infill walls, the incident highlighted the facility's vulnerability and emphasized the urgent need for a more robust warning system. To mitigate these risks, the installation of an early seismic alert system was become a critical safety measure.

This paper explores the implementation of such a system in an industrial production facility, focusing on the integration of seismic sensors, real-time data processing, and automated alerting. The proposed system aims to provide early detection of seismic activity, facilitating the immediate evacuation of employees, shut down of critical operations and structural health monitoring. The initial phase involved determining the optimal placement of sensors through comprehensive noise, vibration, and microtremor measurements. Subsequently, two seismic trigger threshold sets were calibrated based on the region's specific seismic hazards and the structural vulnerability. The final system design incorporated an automated earthquake alert that was fully integrated with the facility's existing alarm system. Key components of the system include a seismic sensor, real-time monitoring software, and a LAN-controlled relay that enables the alert to be trigger across various spots within the plant. The system also supports various notification channels such as email, SMS, client monitoring and relay control, ensuring a rapid and coordinated response to seismic events.

This paper is outlining the technical specifications of the alert system, the anticipated benefits in terms of safety and operational efficiency, and its deployment in a high-risk seismic zone.

Keywords: seismic monitoring, earthquake safety, non-structural damage, seismic sensor, monitoring software.

1. Introduction

Every year, various natural hazards, including earthquakes, cause fatalities and property damage by affecting numerous people worldwide. With technological advancements and data processing speed, risk mitigation tools, such as seismic alert systems, have emerged as life-saving guards in many earthquake prone countries. The primary purpose of these systems is to detect an earthquake in the early stage, estimate the shaking intensity in the target regions, and warn the users before experiencing strong ground motion. Unlike other warning systems (typhoons, tsunamis, volcanoes, floods, etc.), hours- or minutes-long warning time is generally impossible.

The main goals of seismic alert systems are guaranteeing personal safety, preventing malfunctions in critical or important public and private facilities, making sure that infrastructure (such as lifelines) remains intact or can be restored quickly, providing the time needed to evacuate the people or to move them and sensitive items to a safe place, and protecting structures, building elements and equipment. Behind all these goals lies, to a varying extent, the need to avert loss of life, minimize injuries, reduce property damage, and shorten interruptions to public life, business, and production processes. Over the

Copyright © 2025 CroCEE
DOI: https://doi.org/10.5592/CO/3CroCEE.2025.68

last five years, significant progress has been made in developing and implementing earthquake early warning systems. [1][2]. Many earthquake monitoring and warning systems have been designed to detect earthquakes and warn individuals to take appropriate precautions [1][2]. Most seismic instruments on the market are small systems built for offline management. Some of them have built-in applications with limited capabilities for real-time data processing. In many cases, those built-in functionalities are not sufficient to make them applicable to broader requirements. For solving those cases, a special algorithm is needed to be developed as external software solution.

To provide seismic monitoring for buildings and other structures, the earthquake monitoring systems have been extended to compute displacements and drift ratios [3][4]. It is designed to perform a near real-time measurement of the building's seismic performance and to monitor the health of the structure.

A modular structure with specialized toolboxes attached to the main module is the optimal approach to design these systems. Therefore, the developed earthquake monitoring and warning systems consist of main module and attachable additional toolboxes. The first installation of such modular monitoring system was installed for seismic monitoring and alerting of the earthfill dam near Zvornik town [5]. To keep up with the most recent demands, new algorithms are always being introduced, and the system is being updated [6]. Several toolboxes have been developed and deployed over the years [7][8][9]. One of them was real-time monitoring toolbox for experimental in-situ testing which can be connected to the main module of the monitoring system described herein [9]. Its main purpose is to obtain the real-time structures' dynamic properties such as natural frequencies, damping and mode shapes. The capabilities of this module were verified by in-situ testing of a 40-storey residential building using both forced and ambient vibration methods [9]. The other toolbox that is ready for connection to this main module is for real-time measurement and assessment of the impact of blast-induced vibration on buildings and humans [7][8]. The latest request of this system was to implement an automated earthquake alert system in production facility in Macedonia. Furthermore, the automated earthquake alert system must be capable of remotely activating the existing central alarm system. To achieve this goal, several improvements and modifications were made to the existing setup. It is designed to contain several units: (1) instrument, (2) software for monitoring and alerting and (3) LAN controlled relay for remote alarm activation. Since the devices are located in different locations, communication between the units is done in real time over a local area network. The improvement of the main module consisted in obtaining better performance for real-time data streaming, processing, and alerting. The additional alert toolboxes were developed for email and SMS notification, as well as relay control.

The first task for successful installation of the monitoring system was selection of the most favourable location of the strong motion instrument. Therefore, the measurements of noise, microtremors, and vibrations in daily working and idle conditions at three locations were performed. After selection of the most favourable location, the trigger level was defined according to the previously determined seismic potential of the considered terrain. As a final step, the automated earthquake alert system was installed and connected to the existing central alarm system.

Such a designed alert system allows facility employees to prepare for and make an appropriate decision prior to the arrival of the seismic peak. This real-time monitoring system provides a solid foundation for future enhancements such as a structural damage monitoring module.

2. Determination of the alarm level for the structure

The structure is located in the Bitola region and consists of three structural parts that represent one functional unit: (1) Production Building with dimensions in the plan of 180m/200m. The principal structural system represents a reinforced-concrete columns on which spatial steel truss roof structure is placed. (2) Social Building with dimensions in the plan of the structure are 180m/15m. It is steel frame structure with steel columns and beams. (3) Technical building is a one-story RC frame with a total area of 5 450m2.

Due to the action of the earthquake with the epicentre in Florina 2022, damage to buildings in the Bitola region has appeared. After the earthquake, a detailed inspection of the building was carried out where

Copyright © 2025 CroCEE
DOI: https://doi.org/10.5592/CO/3CroCEE.2025.68

damages were detected. The damages that appeared were ascertained and an assessment of the stability of the building was carried out.

From the inspection, the following damages were found:

- Technical building: Non-structural damage was observed in the infill walls was observed within this building. Three locations with large cracks within the walls were noticed. Such damage is insignificant and does not have a specific impact of the overall stability of structure.
- Production building: In the second structure, i.e. the production hall, no damage was observed in the structural or nonstructural elements.
- Social building: In this buildings, vertical cracks were discovered in the walls that are adjacent to the production hall. The cracks are likely the result of a construction mistake, as there is not enough clearance between the cantilevered beams of the frames and the wall.

In order to a rapid structural health check after earthquake event, in this investigation fragility functions are used to obtain the damage level. Fragility curves are essential tools to quantitatively assess the physical vulnerability of structures at risk for a given seismic hazard. Since for the reinforced concrete structures there are no existing fragility curves, fragility curves defined with the SP-BELA method for vulnerability class D (buildings designed according to the seismic codes) have been selected (Fig. 1), [10]. The damages are classified according to the EMS98 scale, which is composed of five damage levels, i.e. slight damage D1, moderate damage D2, extensive damage D3, complete damage D4, and collapse D5.

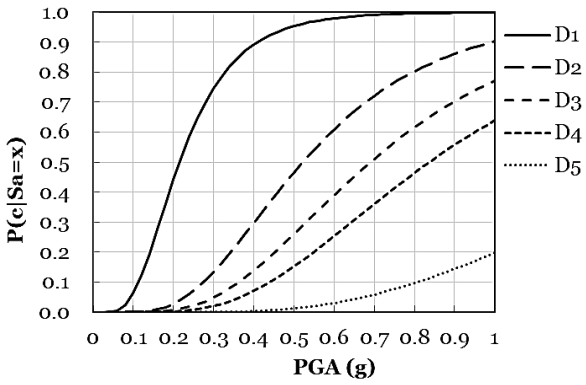


Figure 1. Fragility curves of 2-storey RC frame buildings of vulnerability class D (buildings designed according to the seismic codes)

It is assumed that for peak ground acceleration of 0.21g, there is 50% of probability of exceedance the occurrence the slight damage (D1). This PGA is important parameter that presents the damage level for setting the central alarm system.

3. Trigger level definition

The trigger level is defined in accordance with the previously prepared report for defining the seismic potential of the considered location [11]. Considered location belongs to the Bitola region, which throughout history has been exposed to a large number of earthquakes. The ancient city of Heraclea Linkestis, which is located on the outskirts of Bitola, was destroyed by a catastrophic earthquake. In the last century, the city of Bitola and its wider surroundings were hit several times by earthquakes that occurred in the Bitola-Lerin seismogenic zone: 1920 (M=5.3), 1958 (M = 5.3) and 1994 (M=5.2) (Fig. 1). The Bitola region can be exposed to the effects of earthquakes from neighbouring (Ohrid, Kičevo, Lerin 2022 (M=5.3), Kukuš, Valandovo) and relatively distant (Pehčevo-Kresna) seismogenic zones that might generate significantly stronger earthquakes with seismic intensity in the interval I = 6-7o according to the EMS-98 seismic scale (Fig. 2).

Copyright © 2025 CroCEE
DOI: https://doi.org/10.5592/CO/3CroCEE.2025.68

Neighbouring hotspots are the result of activities on faults of regional character. These hotspots are located within a radius of 40 to 140 km, around the investigated area (Kožani, Ohrid, Kičevo, Lerin, Debar, Valandovo, Pehčevo-Kresna) and the magnitudes of the combined strongest earthquakes in these hotspots in the last 80-100 years are 4-7.8 degrees on the Richter scale. In the last 120 years, only three earthquakes with magnitudes between ML5.2 and ML5.6 occurred in this area. Seismotectonic map of earthquakes from the Bitola-Prespa-Lerin area in the period 1901-2021 (Blue circles are earthquakes from 2022).

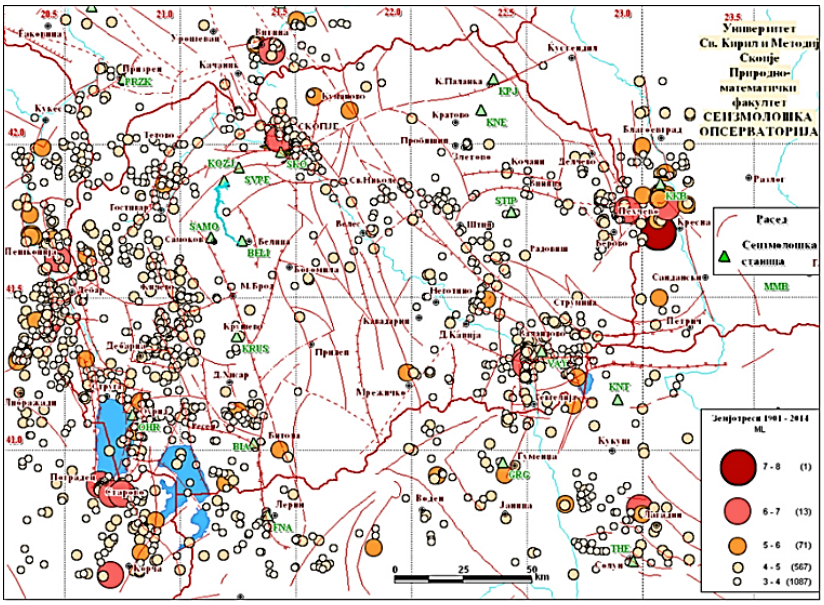


Figure 2. Epicentral map of earthquakes from the territory of the Republic of N.Macedonia and the surrounding areas for the period 1901 – 2014 (source: Seismological Observatory, 2016)

According to the seismic hazard analysis for the considered area [11], the maximum expected acceleration on the bedrock, depending on the return period, ranges between 0.100g to 0.170g. During the earthquake that happened on 09.01.2022, at 21:43, with a magnitude of 5.6 on the Richter scale, the network of instruments for strong ground motion registration installed at the Strezevo dam recorded a maximum acceleration of 22mg on the vertical component to 37mg on the horizontal component, which according to the seismic scale of EMS-98 corresponds to intensity between V and VI degrees.

Following the above data, a trigger level of 1.5% g for the vertical Z axis, and 2.0% g for the X and Y axis, equivalent to a moderate intensity earthquake that would be felt by people inside the buildings, was selected.

4. Determining the location of the instrument

In order to determine the most favorable location for the installation of the instrument, a field survey and microtremor analysis were performed. The Facility Security Officer proposed three possible locations for the device, depending on local technical conditions. The basic technical requirements that the future location would have to satisfy are access to the local area network LAN and power infrastructure. In addition, the site must respond to the absence of an external source of nearby vibrations. The first selected location "Location-1" is located outside the production building and is in the vicinity to "Location-2". The "Location-2" is located in one of the technical buildings, while "Location-3" is located inside the technical room of the production building. For all three locations, microtremor measurements were performed in working conditions.

The results of the measurements are interpretated in the form of frequency-magnitude relationship (Fig. 3 to 5). The conducted visual inspection of the locations and obtained results indicated that "Location-

Copyright © 2025 CroCEE
DOI: https://doi.org/10.5592/CO/3CroCEE.2025.68

2" has the lowest level of noise and it is exposed to the lowest external vibrations. Therefore, it was chosen as the most favorable for the installation of the instrument.

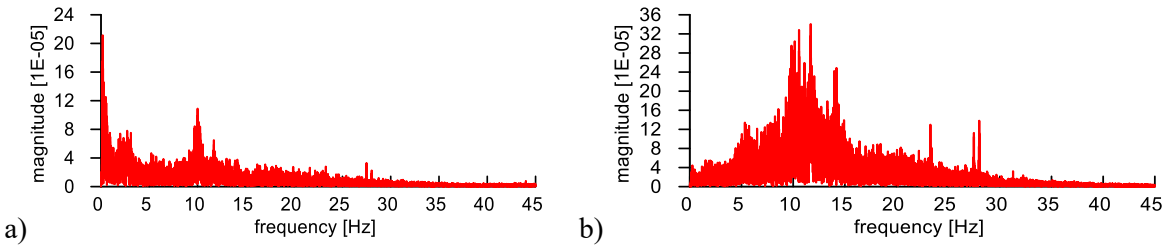


Figure 3. Location-1 a) Horizontal direction b) Vertical direction

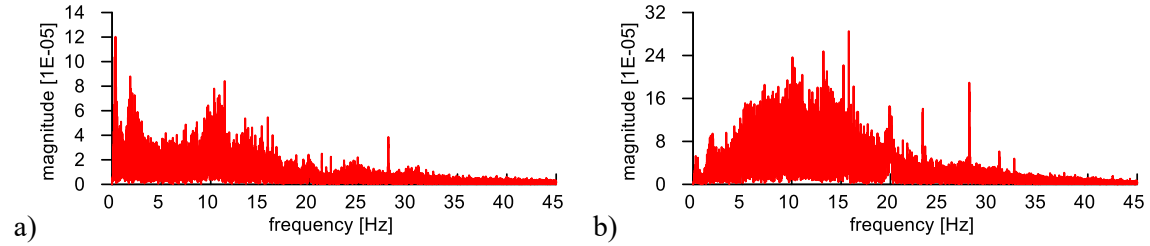


Figure 4. Location-2 a) Horizontal direction b) Vertical direction

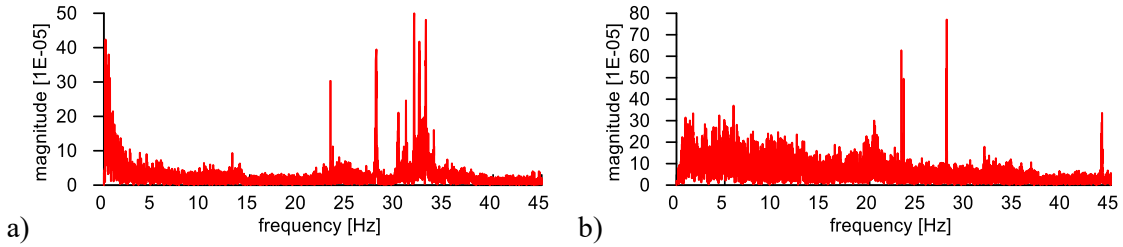


Figure 5. Location-3 a) Horizontal direction b) Vertical direction

5. Description of the seismic monitoring and alert system

The requirement of the safety sector in the industrial complex was to implement a real-time seismic monitoring and warning system that would be connected to the central alarm system. In order to realize this task, it was necessary to create a separate monitoring system, including the purchase of the instrument and developing of special software solution. The basic design parameter was to establish the connection of the newly alert system to the existing local central alarm system. Also, the system needs to be able to perform an automatic real-time activation/deactivation of the central alarm. The input parameters which were taken for the design of the new monitoring system were the locations of the instrument, data center and the location of the central alarm system. Since these three independent connection points are in different locations, the communication is via local area network.

The first step in the implementation of the new alarm system was a review of the existing alarm system and local infrastructure. From the conducted inspection, it was determined that all three proposed locations have access to electricity and LAN. After meeting the project's technical conditions, the design of the seismic monitoring and alert system was completed (Fig. 6).

The monitoring system consists of three devices located in different locations: (1) central alarm system, (2) data center and (3) sensor. The data from the sensor to the software is transmitted in real-time through TCP/IP protocol. The software performs continuous receiving and processing the data and comparing the vibration intensity to the alert threshold. When the alert threshold is exceeded, the software activates the relay and the clients' applications. Clients are additional points (PCs) where the

Copyright © 2025 CroCEE
DOI: https://doi.org/10.5592/CO/3CroCEE.2025.68

current state of the vibration level is presented. By activating the relay, the central alarm system of the industrial complex is activated.

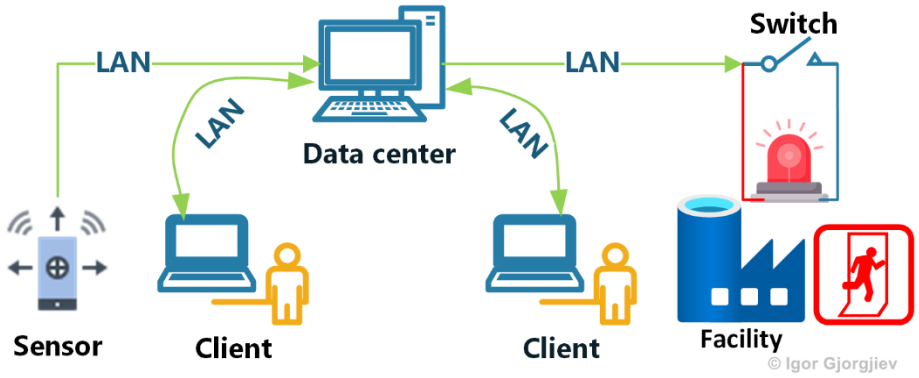


Figure 6. Schematic view of the seismic monitoring and alert system

From the performed site inspection, it was found that the existing alarm system contains a switch that can be used for remote activation/deactivation of the central alarm. Therefore, multi-function LAN/USB two-channel relay controller was used to remotely control the alarm switch. The LAN really uses user datagram protocol (UDP) for communication while USB relay connects to PC using virtual COM port. In order to control the central alarm system, we actually used LAN really, while the client PC uses a USB relay for the local client alarm.

The real-time seismic monitoring and alerting is performed by a tailor-made software solution (Fig. 7). The purpose of the main window is to show the data and status information in real-time (Fig. 7a).

On the right side of the window, the data for all connected instruments is graphically presented. The frequency content of the received data may also be presented. The alert level information along with the reset button are presented on the left side of the main window.

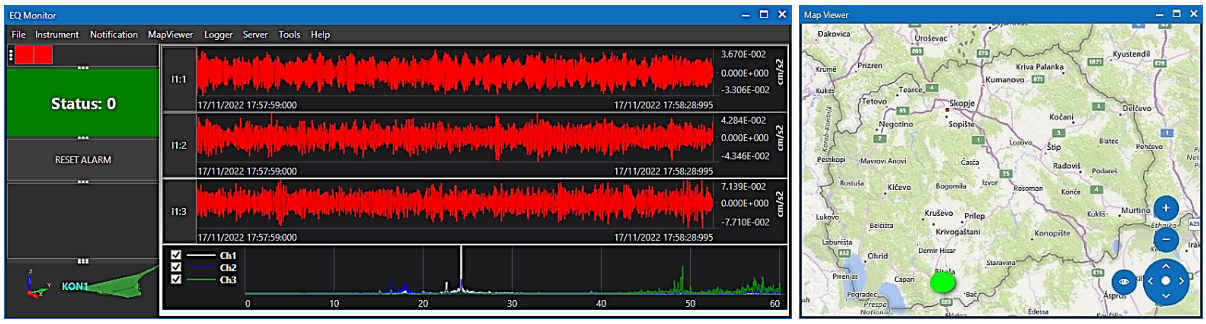


Figure 7. Schematic view of the seismic monitoring and alert system

The intensity of the vibration is presented by four colors. The green color is used for a normal state where no alert level is present. Other colors such as yellow, orange, and red are used for different alert levels. Additionally, a short list of important event messages is also presented in this part of the window. At the button of this window area, a 3D view of the monitored structures and the location with an orientation of the instruments is located (Fig 7a). Furthermore, the alert level of each instrument is presented on a separate map which gives a good quality visualization of multi-instrument monitoring (Fig. 7b). The software package (Fig. 7) consists of several toolboxes (modules): (1) instrument connection, (2) data processing, (3) notification, (4) map viewer, (5) logger and (6) server.

The aim of the instrument connection module is to establish and monitor the connection between the software and the instrument. The automatic reconnection is integrated to handle the connection loss. Also, the alarm reset, retrieving the alert status and the validation of relay connection are part of this module.

Copyright © 2025 CroCEE
DOI: https://doi.org/10.5592/CO/3CroCEE.2025.68

The main purpose of the data processing module is to receive data in real-time and to perform a time synchronization of the data. Additionally, the signal processing and the frequency analysis toolboxes are included (Fig. 8 a, b). The signal processing toolbox contains removing trend together with lowpass, highpass, and bandpass filtering. In the second toolbox, a windowing and frequency analysis are included. As a result of frequency analysis, we can obtain fourier spectra (FS), power spectra (PS), power spectra density (PSD) and singular value of spectral densities (SVD). Additionally, signal averaging can be applied before performing the frequency analysis.

Notification module includes three types of notifications when the alert threshold is reached. The first notification type is sending an email, while the second type is sending an SMS. The last notification type is for controlling the relay status. For each relay type, a different parameter needs to be defined (Fig. 8 c). In the case of LAN relay an IP address and UDP port are required (Fig. 8 c). For USB relay, only COM name is specified. This module monitors whether the alert threshold has been exceeded. In case of alert threshold exceedance, notifications are sent and the central alarm system is turned on. Additionally, an automatic shutdown of the alarm after a particular time interval is supported.

The map viewer module (Fig. 7b) includes real-time graphical presentation of the alert level status on the host PC (data center). There are several view modes: Arial, Roads and Canvas which enable fast and precise monitoring when many instruments are connected.

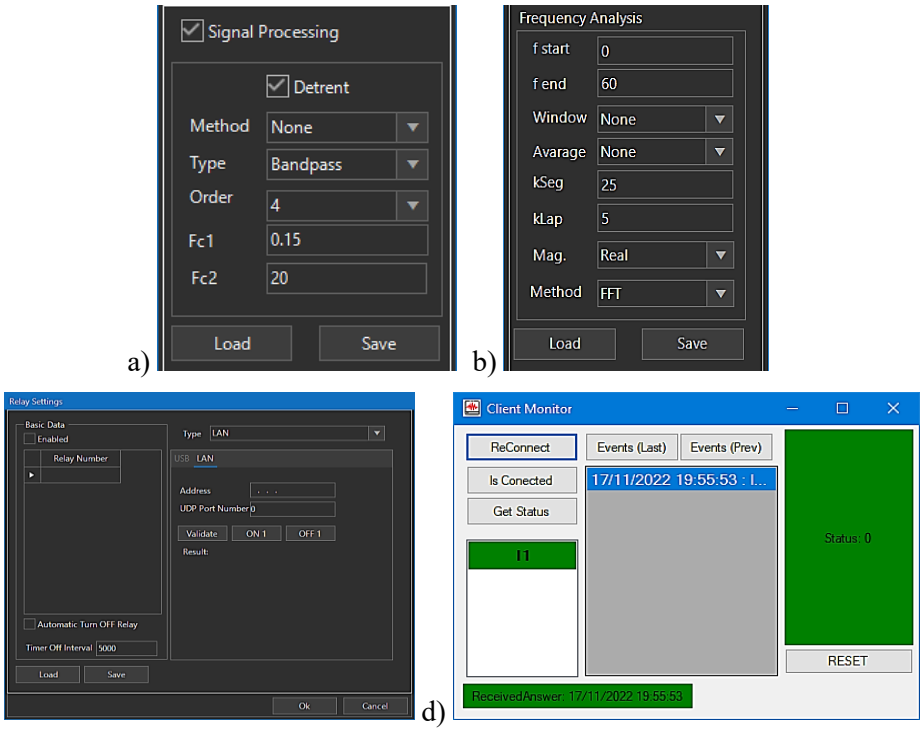


Figure 8. Signal processing (a) and frequency analysis input parameters (b), relay configuration window (c), Client monitor window (d)

The aim of the client monitor module (Fig. 8 d) is real-time monitoring of the alert level status on the client PC side. This module enables viewing the history list of events, getting the alert status on demand, checking the connection of the software to the instrument and doing the reset of the alarm.

The alert module aims to identify the specific earthquake intensity and to activate the notification modules. The alert levels are divided into three earthquake intensities where each earthquake intensity has a threshold for each of the three orthogonal directions. Turning off the alert for any direction is also supported. The control for exceeding the earthquake intensity is set from the highest to the lowest value. When the threshold is exceeded, the central alarm system is turned on and remains active for a defined time interval. The alert level stays active until the higher level is reached or the alert is manually reset. The manual reset can be done from the data center or any connected client.

Copyright © 2025 CroCEE
DOI: https://doi.org/10.5592/CO/3CroCEE.2025.68

Such a designed alert system allows facility employees to prepare for and make an appropriate decision prior to the arrival of the seismic peak. This real-time monitoring system provides a solid foundation for future enhancements such as a structural damage monitoring module.

6. CONCLUSIONS

The Florina earthquake that happened in 2022 with magnitude of 5.3 affected the normal activities of people and lead to uncontrolled crowd panic behavior in the production facility located in the Bitola region. In order to enhance the safety measures, a strong motion instrument has been installed and an earthquake monitoring and warning systems has been developed. The software enables real-time data streaming, processing, and alerting. The alerting consists of three modules: email and SMS notification and remote control of the relay.

A trigger level was defined in each direction separately. The equipment was tested and configured in laboratory conditions, after which it was installed and put into operation. The operability of the strong motion instrument, in laboratory conditions, was confirmed through functional tests, conducted for three trigger levels in each direction individually. In the horizontal direction the alarm level is 2.0%g, while in the vertical direction the level is 1.5%g. The structural slight damage alarm level (D1) was set to 0.21g as the peak ground acceleration.

From the conducted laboratory and field activities, it can be concluded that the installed earthquake alarm system is functional and in working mode. Such alert system designed in this way allows employees to prepare themself and make a proper decision before earthquake peak arrived. Additionally, it presents a good base for adding the next module for structural damage monitoring.

References

[1] Hoque, R., Hassan, S., Sadaf, MD.A., Galib, A., Fahrin, K.T. (2015): Earthquake Monitoring and Warning System, Proceedings of *3rd International Conference on Advancement in Electrical and Electronic Engineering*, Dhaka University of Engineering & Technology (DUET), Gazipur, Bangladesh.

[2] Zhang, M., Qiao, X., Seyler, B. C., Di, B., Wang, Y., Tang, Y. (2021): Effective earthquake early warning systems: appropriate messaging and public awareness roles, *Natural Hazards and Earth System Sciences*, 21, 3243–3250

[3] Celebi, M., Sanli, A., Sinclair, M., Gallant, S., Radulescu, D. (2003): Real-time seismic monitoring needs of a building owner and the solution, Proceedings, *11th FIG Symposium on Deformation Measurements*, Santorini, Greece.

[4] Limongelli, P. M., et al. (2019): S2HM in Some European Countries, *Seismic Structural Health Monitoring*, Chapter 13, Springer

[5] Dojcinovski, D., Stojmanovska, M., Gjorgjiev, I. (2016): Seismic monitoring, maintenance of the accelerograph on the earthfill dam near Zvornik and software maintenance, *IZIIS Report* 2016-50.

[6] Gjorgjiev, I., Dojcinovski, D., Stojmanovska, M. (2022): Installation of earthquake monitoring and alarm system, *IZIIS Report* 2022-52,

[7] Dojcinovski, D., Stojmanovska, M., Gjorgjiev, I. (2022): Measurement of the impact of an explosion in the process of surface exploitation of limestone in the "Dobarski Zeden" located near the village Grupcin, *IZIIS Report* 2022-48,

[8] Gjorgjiev, I., Dojcinovski, D., Stojmanovska, M. (2022): Measurement of the impact of an explosion in the process of surface exploitation in mineral resources at the location "Groot" in the Municipality of Veles, *IZIIS Report* 2022-48.

Proceedings of the 3rd Croatian Conference on Earthquake Engineering - 3CroCEE
19–22 March 2025, Split, Croatia
Copyright © 2025 CroCEE
DOI: https://doi.org/10.5592/CO/3CroCEE.2025.72

BUILDING RESILIENT COMMUNITIES: ADVANCING STEM EDUCATION AND EARTHQUAKE ENGINEERING RESEARCH

Roberta Apostolska [(1)], Vlatko Sheshov [(2)], Marija Vitanova [(2)], Goran Jekic [(2)], Elena Delova [(2)], Ana Nanevska [(2)], Filip Manojlovski [(2)], Dejan Ivanovski [(2)]

[(1)] *Professor, Ss. Cyril and Methodious University in Skopje, Republic of North Macedonia, Institute of Earthquake Engineering and Engineering Seismology, Skopje, beti@iziis.ukim.edu.mk*
[(2)] *Professor, Ss. Cyril and Methodious University in Skopje, Republic of North Macedonia, Institute of Earthquake Engineering and Engineering Seismology, Skopje, vlatko@iziis.ukim.edu.mk*
[(3)] *Associate Professor, Ss. Cyril and Methodious University in Skopje, Republic of North Macedonia, Institute of Earthquake Engineering and Engineering Seismology, Skopje, marijaj@iziis.ukim.edu.mk*
[(4)] *Associate Professor, Ss. Cyril and Methodious University in Skopje, Republic of North Macedonia, Institute of Earthquake Engineering and Engineering Seismology, Skopje, jekic@iziis.ukim.edu.mk*
[(5)] *Research Assistant, Ss. Cyril and Methodious University in Skopje, Republic of North Macedonia, Institute of Earthquake Engineering and Engineering Seismology, Skopje, delova@iziis.ukim.edu.mk*
[(6)] *Research Assistant, Ss. Cyril and Methodious University in Skopje, Republic of North Macedonia, Institute of Earthquake Engineering and Engineering Seismology, Skopje, nanevska@iziis.ukim.edu.mk*
[(7)] *Research Assistant, Ss. Cyril and Methodious University in Skopje, Republic of North Macedonia, Institute of Earthquake Engineering and Engineering Seismology, Skopje, filipmanojlovski@iziis.ukim.edu.mk*
[(8)] *Research Assistant, Ss. Cyril and Methodious University in Skopje, Republic of North Macedonia, Institute of Earthquake Engineering and Engineering Seismology, Skopje, ivanovski@iziis.ukim.edu.mk*

Abstract

QuakeSafe is a transformative initiative, supported by UNESCO and funded by Huawei, aimed at deepening students' understanding of earthquake engineering and its implications for safety and sustainability through an innovative educational model. Implemented by the Ss. Cyril and Methodius University in Skopje, Institute of Earthquake Engineering and Engineering Seismology (IZIIS), this project utilizes specialized expertise to create engaging and impactful learning experiences. In response to the urgent need for proactive strategies in seismically active regions, QuakeSafe actively engages high school students through a blend of interactive workshops, hands-on experiments and immersive virtual reality (VR) simulations. These activities, conducted as pilot case studies in six selected schools, are structured within an inquiry-based, problem-solving learning environment that introduces the principles of seismic science and engineering. The use of digital tools and VR experiences provides students with practical understanding into the complexities of earthquake phenomena, aiming to develop critical thinking and problem-solving skills grounded in scientific knowledge.

This paper presents the methodology and outcomes of the QuakeSafe project, emphasizing its effectiveness in enhancing students' understanding of seismic risks while fostering interest in STEM disciplines. Additionally, it discusses the strategic collaborations with educational institutions and local authorities that have supported the project's successful implementation. The study provides an analysis of pre- and post-assessment surveys measuring the project's influence on students' knowledge, attitudes, and perceptions regarding earthquake safety and STEM engagement. By integrating digital content into a broader STEM educational knowledge hub, QuakeSafe aspires to create a replicable model for other institutions to strengthen disaster preparedness education. The success of the project is reinforced by partnerships and external support, highlighting the significant impact of collaborative efforts in building safer and more resilient communities.

Keywords: STEM, earthquake engineering, VR, hand-on experiments, QuakeSafe, critical skills, resilient communities.

1. Introduction

Through their collaborative project, UNESCO and Huawei Technologies have joined forces to foster the rethinking and revitalisation of the STEM learning model for the next generations, to confront the most pressing societal needs and global challenges. The project, which aims to advance STEM education, contributes to achieving the 2030 Agenda and the Sustainable Development Goals, notably

Copyright © 2025 CroCEE
DOI: https://doi.org/10.5592/CO/3CroCEE.2025.72

SDG 4 – Quality education, SDG 5 – Gender equality, and SDG 9 - Industry, innovation and infrastructure, [1].

Among the five selected projects is the 'Advancing Innovative STEM Education and Research in Earthquake Engineering towards a Sustainable Environment: QUAKESAFE' project, led by Ss. Cyril and Methodius University in Skopje, Institute of Earthquake Engineering and Engineering Seismology (IZIIS). This project focuses on advancing earthquake engineering education and its role in promoting sustainable environmental practices [2], (Fig. 1).

The QuakeSafe project has four main objectives, (Fig. 1):





Figure 1. QuakeSafe project objectives and banner

Within the overall framework of the project, IZIIS conducted the following activities:

1. Develop curriculum and educational materials, including VR stimulation and online applications.
2. Plan and conduct pilot sessions of STEM workshops and hands-on experiments.
3. Evaluate the impact of QUAKESAFE educational activities based on pre-and post-assessment surveys.
4. Scale up STEM educational activities to reach more educational schools and integrate results into STEM educational knowledge hub and regional inventory.

The scientific and educational methodology employed in the QuakeSafe project combines established practices from both STEM education and earthquake engineering. Its goal is to equip students with engineering knowledge and skills and to cultivate proactive mindsets, enabling them to become active contributors to the creation of safe, sustainable, and resilient communities. The methodology is in line with SDG 4, SDG 9, SDG 11 [3] and Guidelines on sustainability science in research and education [4].

Through strategic partnerships with educational institutions and local authorities, the designed innovative educational and research activities are implemented in six selected high/elementary schools in three different cities (Fig.2).

Copyright © 2025 CroCEE
DOI: https://doi.org/10.5592/CO/3CroCEE.2025.72



Elementary schools:

Gjorgjija Pulevski, Skope, ООУ ЃОРЃИЈА ПУЛЕВСКИ (ougpulevski-aerodrom.edu.mk)

Krste Misirkov, Gevgelija - Крсте Мисирков (krstemisirkovgvg.edu.mk)

High schools:

Rade Jovcevski Korcagin, Skopje, СУГС Раде Јовчевски - Корчагин - РЈК (rjk.edu.mk)

Vlado Tasevski, Skopje, СУГС „Владо Тасевски“ - Скопје (sugsvladotasevski.edu.mk)

Josif Josivovski, Gevgelija, СОУ „Јосиф Јосифовски“ – Гевгелија (josifjosifovski.edu.mk)

Josip Broz Tito, СОУ „Јосип Броз-Тито“ – Битола (gimnazija-jbt-bitola.edu.mk)

Figure 2. QuakeSafe project – pilot case studies

2. Educational programme

The educational programme was designed to engage participants in an immersive learning experience about structural engineering and earthquake safety. This chapter outlines the programme's three main components: Interactive Presentation, Activities, and Evaluation, (Fig. 3). Each component is tailored to foster understanding, encourage collaboration, and evaluate the learning outcomes effectively.

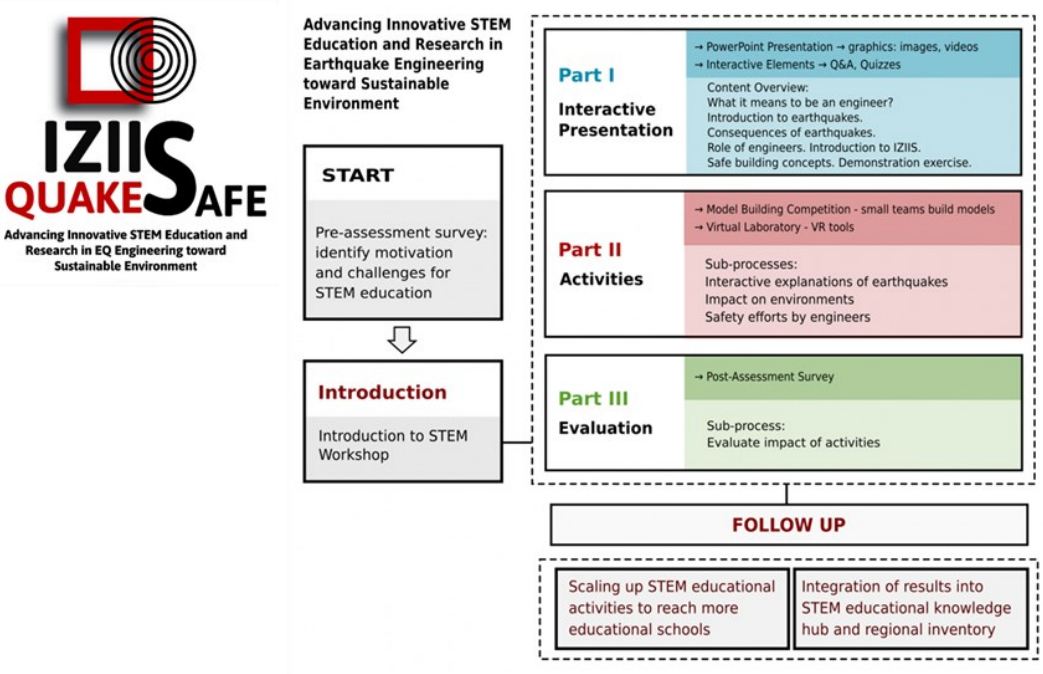


Figure 3. QuakeSafe project in a nutshell

The **Part I** began with an Interactive Presentation, which provides foundational knowledge and sets the stage for deeper engagement. The presentation is delivered using a PowerPoint slideshow enriched with graphic images, videos, and interactive elements like Q&A quizzes to actively involve participants. The content of the presentation covered six key topics:

I) introduction to the role and responsibilities of structural engineers, emphasizing their importance in creating safe and sustainable structures;

Proceedings of the 3rd Croatian Conference on Earthquake Engineering - 3CroCEE
19–22 March 2025, Split, Croatia
Copyright © 2025 CroCEE
DOI: https://doi.org/10.5592/CO/3CroCEE.2025.72

II) a concise explanation of earthquakes, their causes, and the forces they exert on buildings to help participants in understanding the core challenge engineers face in earthquake-prone areas;
III) consequences of earthquakes using real-world examples and visual data, highlighting the devastating effects of earthquakes on structures, communities, and economies;
IV) underscoring the proactive role engineers play in mitigating earthquake impacts, including innovative design and material usage;
V) introduction to IZIIS where the participants were acquainted with the pioneering work of IZIIS in advancing earthquake-resistant engineering solutions and fostering international collaboration and finally
VI) introduction to safe building concepts in which practical principles of safe building design were introduced, showcasing best practices and modern techniques that minimize risks during seismic events.

The interactive elements, such as quizzes and question-answer sessions, enhanced participant engagement, ensuring that the presentation is not just informative but also memorable.

The **Part II** consisted of activities that were meant to translate theoretical knowledge into practical experience. It comprised two key sub-activities designed to challenge participants' creativity and critical thinking: experiencing small laboratory model building challenges and virtual laboratory applying VR tools. The participants were grouped into small teams to design and build structural models. This activity encourages teamwork, innovation, and hands-on application of safe building principles. Each team uses materials to simulate real-world constraints and aims to construct models capable of withstanding simulated seismic forces. Through VR tools, participants explored advanced simulations and scenarios. Details are given in the Chapter 3.

The **Part III**, consisted of evaluation of the overall process and the gained knowledge and interest of the young students in the topic that they participated in. The final component of the programme was designed to assess the effectiveness of the activities and measure participant understanding. Evaluation methods include: (I) team model assessment (the structural models created during the competition were tested for their ability to withstand simulated seismic forces; (II) participant feedback (surveys and questionnaires collected insights about the learning experience, including the interactive presentation, activities, and overall organization of the programme); (III) knowledge testing through a brief quiz on the key concepts of the programme topics, ensuring the educational objectives have been achieved. Details are given in the Chapter 4.

By integrating interactive presentations, hands-on activities, and thorough evaluations, this educational programme was focused not only to inform, but also to inspire young students to appreciate and potentially find themselves in the critical role of structural and earthquake engineers in building a safer, more resilient world.

3. Advance educational resources

Incorporating innovative approaches to STEM education is essential for enhancing student engagement and understanding, particularly when addressing complex scientific and engineering concepts. The educational programme integrates advanced resources, blending hands-on activities with cutting-edge technology to provide a comprehensive learning experience. These resources include the Competition for Building Small Models and the Virtual Laboratory Experience, which combine creativity, critical thinking, and immersive learning to inspire students and foster practical skills. This Chapter highlights these activities, showcasing their role in connecting theoretical knowledge with real-world problem-solving in the fields of earthquake engineering and building resilience.

The small-scale shake table tests provided students with an engaging opportunity to step into the roles of engineers, builders, and researchers. Participants worked in small teams to design and construct models, which they then tested. A total of three models were built and tested simultaneously on a small shake table. Students used Mola Structural Kit 1 models (Fig. 4), which consisted of identical sets of elements that were assembled using magnetic connections. To facilitate the testing, a specially designed

Copyright © 2025 CroCEE
DOI: https://doi.org/10.5592/CO/3CroCEE.2025.72

container (Fig. 4) was constructed to house all three models during dynamic loading. The excitation function applied was a simple sinusoidal signal with varying amplitude and frequency, simulating a realistic earthquake scenario. The APS 400 shaker (Fig. 4) was employed as a mobile shake table due to its lightweight construction and excellent performance.

The tests involved gradually increasing the shaking intensity. One model served as a benchmark, representing a well-designed and well-constructed building, while the other two models had bracing elements intentionally removed to simulate flaws in construction or design. As the shaking intensity increased, students observed the effects of earthquake forces and the comparative responses of well-built versus flawed structures. This hands-on activity fostered innovation and practical application of engineering principles, while highlighting the importance of teamwork, communication, and social skills. By blending creativity with technical challenges, the exercise inspired students to think like engineers and approach real-world problem-solving in a fun and interactive way.



Figure 4. Building and testing engineering models

The Virtual Laboratory Experience offered an immersive interactive journey where students used VR tools to explore the science of earthquakes and the critical role engineers play in ensuring structural safety. The tour utilized three sets of Meta Quest 2 headsets, allowing for efficient rotation and engagement (Fig. 5). With each session lasting 4 minutes, plus an additional minute for setup per student, up to 15 students could participate within a half-hour. This setup was designed to ensure all students had the opportunity to experience the VR tour. The interactive simulations are in eight different scenes, with the journey starting deep within the Earth's interior exploring the layers that drive tectonic plate movement and cause earthquakes. This captivating introduction to geoscience features vivid visualizations and interactive explanations, helping students grasp complex concepts such as fault lines, seismic energy, seismic waves, and the relationship between plate movements and earthquake phenomena. The interactive journey continued in a simulated room setting where the students could visually experience a real earthquake and its impact on objects within the environment. The students also learned how scientists and engineers measure seismic activity and experimentally analyze the structural response. The VR tour concluded at the IZIIS laboratory, where the students could observe videos and images of scaled-down structural models tested on IZIIS' seismic platform. The structured timing and rotational use of headsets ensured accessibility and inclusivity for all participants, maximizing engagement and educational impact.

Copyright © 2025 CroCEE
DOI: https://doi.org/10.5592/CO/3CroCEE.2025.72



Figure 5. The virtual world of the earthquakes

By blending cutting-edge technology with interactive learning the VR Laboratory Experience, were set to not only deepen students' understanding of earthquake science, but also inspire an appreciation for the innovative efforts of engineers in creating a safer built environment.

4. Results from pre- and post- assessment surveys and quizzes

4.1. Survey outcomes

A series of pre-assessment and post-assessment surveys were conducted among students from elementary and high schools participating in the QuakeSafe project. A total of 144 responses were collected to evaluate the effectiveness of the workshops and their impact on students' knowledge and perceptions of STEM disciplines and earthquake engineering[1]. The QuakeSafe project focuses on fostering an innovative STEM education environment, emphasizing earthquake engineering and sustainable practices, particularly for regions prone to seismic activity.

Before the workshops, only 12% of students reported having a clear understanding of STEM disciplines, while 35% indicated some familiarity but lacked detailed knowledge. Another 35% had minimal knowledge, and 18% were entirely unfamiliar with the concept. After the workshops, 78% of students reported a clear understanding of STEM disciplines, 17% indicated some familiarity but not in detail, and only 5% had minimal knowledge. Notably, no students reported being entirely unfamiliar after the workshops (Fig 6).

Regarding their knowledge of earthquakes, 16% of students stated before the workshops that they had a strong understanding of topics such as earthquake causes and measurement scales. Additionally, 48% reported sufficient knowledge, 33% indicated moderate knowledge, and 3% reported insufficient knowledge. Post-workshop results showed a significant improvement, with 69% of students reporting a strong understanding, 27% sufficient knowledge, 5 students indicating moderate knowledge, and only 1 student reporting insufficient knowledge, (Fig. 7).

[1] The response is evaluated based on the five workshops conducted.

Copyright © 2025 CroCEE
DOI: https://doi.org/10.5592/CO/3CroCEE.2025.72

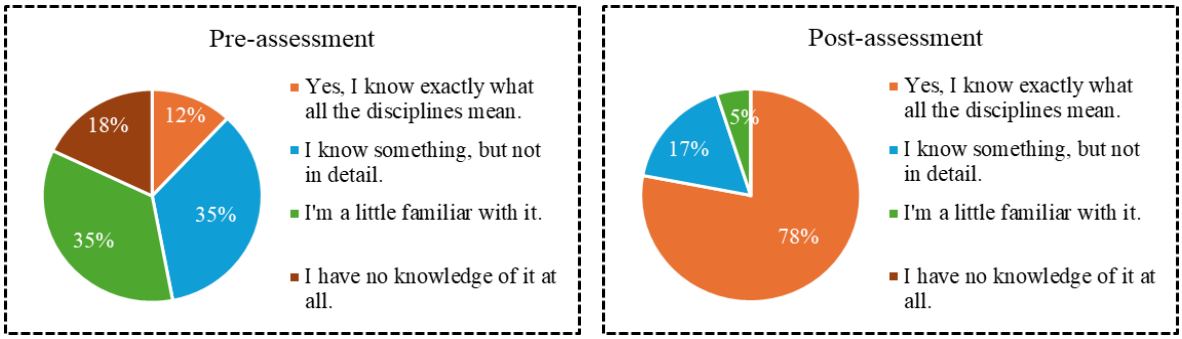


Figure 6. Results from the question: "Are you familiar with what the disciplines in STEM (Science, Technology, Engineering, and Mathematics) mean?"

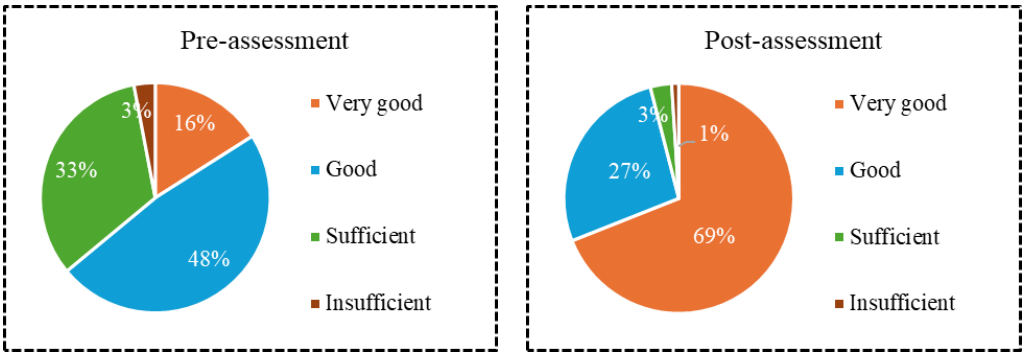


Figure 7. Results from the question: " How extensive is your knowledge of earthquakes (what an earthquake is, where and how it occurs, how it is measured, which scale is used...)?"

Figure 8 shows students' response to the question posed about the role of engineers in ensuring safety against earthquakes. 75% of students reported limited knowledge before the workshops, 8% stated they had extensive knowledge, and 17% indicated no knowledge at all. After the workshops, 74% of students reported extensive knowledge, 25% indicated limited knowledge, and only 1 student reported no knowledge.

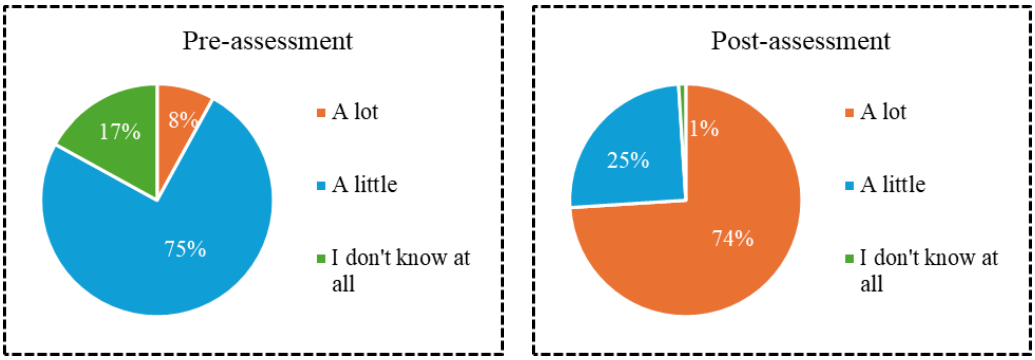


Figure 8. Results from the question: "How much do you know about the role of engineers in protecting people and structures from earthquakes?"

In terms of whether STEM disciplines can help in building safe structures, 88% of students believed they could before the workshops, while 10% were unsure and 2% believed they could not. Post-workshop, 97% of students believed STEM disciplines could contribute to building safe structures, 2% remained unsure, and only 1 student believed they could not (Fig. 9).

Copyright © 2025 CroCEE
DOI: https://doi.org/10.5592/CO/3CroCEE.2025.72

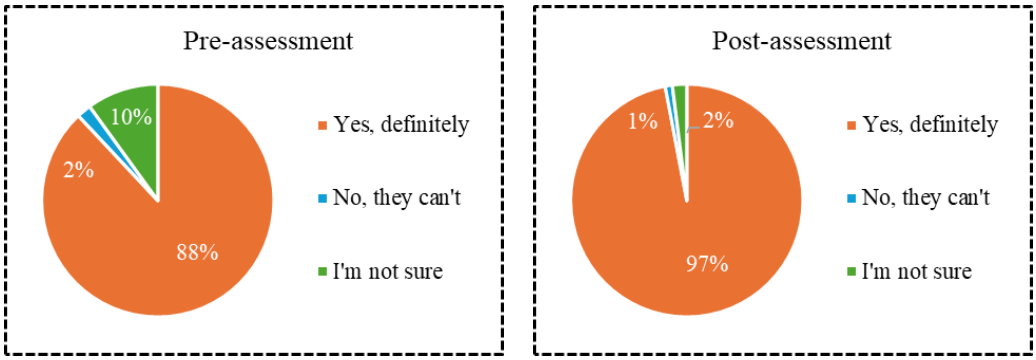


Figure 9. Results from the question: " Do you think that STEM disciplines can help in building safe structures?"

The interactive presentations were also well received (Fig. 10) with 93% of students finding them highly engaging and useful for enriching their knowledge, while 7% found them somewhat useful. Similarly, the VR simulations were considered very engaging and effective by 93% of students for understanding engineering problems. Another 6% found them somewhat effective, and only 1 student was unsure of their usefulness.

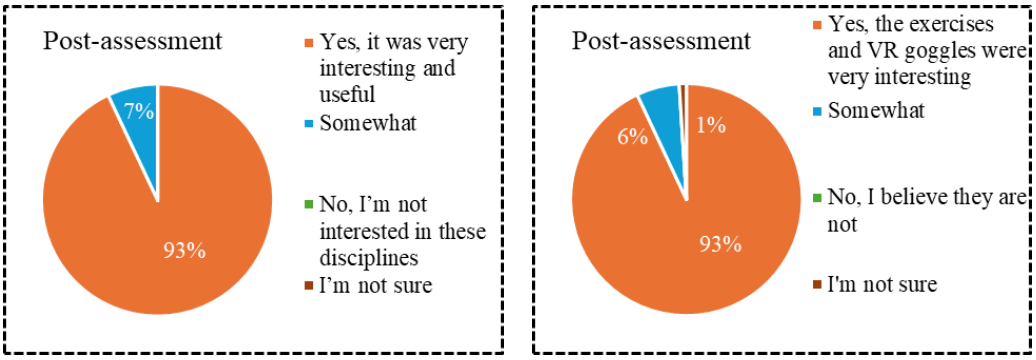


Figure 10. Results from the statements: "The interactive presentation was helpful in enriching my knowledge about earthquakes and how to build safe structures." And “The demonstration exercises with the models and VR goggles are an excellent method for interactive learning and understanding engineering problems”

All these results show that the QuakeSafe project demonstrated a significant improvement in students' understanding of STEM disciplines, earthquake engineering, and the role of engineers in creating safe and sustainable environments. Through the project's innovative approach, students gained deeper insights into complex scientific concepts and their real-world applications. The integration of interactive presentations, model building competitions, and VR simulations proved highly effective in fostering engagement and enhancing learning outcomes. By providing students with immersive experiences and opportunities for creativity, the project successfully bridged the gap between theory and practical application, allowing them to better understand the importance of engineering solutions for natural disaster preparedness.

Moreover, the use of technology-enhanced learning tools encouraged critical thinking, problem-solving, and collaboration among students, preparing them for future challenges in STEM fields. These results underscore the importance of incorporating such innovative and interactive methods into STEM education, particularly for younger generations who will be the leaders in the future of sustainable infrastructure and disaster resilience.

4.2.Quiz outcomes

The online quiz (Fig. 11), an integral part of the QuakeSafe Project workshop, proved to be a highly engaging and successful initiative, effectively reinforcing the knowledge gained during the interactive presentation. With 12 precise designed questions, the quiz challenged students to apply concepts they had learned about earthquake engineering, such as the causes and effects of seismic activity, the role of

Copyright © 2025 CroCEE
DOI: https://doi.org/10.5592/CO/3CroCEE.2025.72

structural engineers, and principles of earthquake-resistant design. The competitive nature of the quiz added an exciting dimension, making the learning process both stimulating and enjoyable for students. This combination of education and entertainment kept the young people highly motivated, ensuring that the knowledge gained during the presentation was retained and understood at a deeper level.

The results demonstrated the workshop's impact on enhancing student understanding. At the high school "Vlado Tasevski" in Skopje, 82% of participants answered correctly, while 81% of students from "Rade Jovchevski Korchagin" in Skopje also achieved impressive accuracy. Similarly, students from the primary school "Gjorgija Pulevski" in Skopje attained a 75% success rate. Schools in Gevgelija also showcased remarkable results, with "Krste Misirkov" achieving 69% and "Josif Josifovski" achieving outstanding 82% accuracy rates. These statistics highlight the students' ability to understand and apply the material, underscoring the effectiveness of the workshop's pedagogical approach. Moreover, the results provided a valuable metric for understanding the areas where students excelled and those requiring further elaboration for future educational applications.



Figure 11. Quiz time

These results clearly demonstrated the success of the initial segment of the workshop, as the interactive presentation received exceptionally positive feedback from the participants. A particularly notable feature was the quiz's competitive character, which brought an added dimension of fun and engagement for the students. This competitive element transformed the quiz into a dynamic and stimulating activity, encouraging students to participate enthusiastically while simultaneously reinforcing the material presented earlier. By fostering a lively and interactive environment, the quiz ensured that learning extended beyond passive listening, actively involving students in applying their knowledge. It became not only an educational tool but also a source of enjoyment and motivation, further deepening their interest in and commitment to understanding earthquake engineering and safety principles. This blend of competition and education proved to be an effective strategy for enhancing engagement and making the learning process both memorable and impactful.

Beyond its educational value, the quiz contributed significantly to raising awareness about earthquake safety and the role of engineering in mitigating seismic risks. Many participants expressed increased confidence in their understanding of the subject, noting that the combination of visuals, interactive discussions, and the quiz solidified their catch of complex concepts. The competitive spirit of the quiz fostered collaboration and healthy rivalry among the students, further enhancing their learning experience. Teachers noted the enthusiasm of the participants, who actively engaged with the questions and demonstrated curiosity about broader applications of the principles discussed.

5. Conclusions

QuakeSafe project is designed to provide students with innovative STEM education and research activities focused on earthquake engineering toward safe and sustainable environment. In response to the pressing need for proactive measures in earthquake-prone regions (including most of South-East

Copyright © 2025 CroCEE
DOI: https://doi.org/10.5592/CO/3CroCEE.2025.72

Europe and Mediterranean), this project seeks to equip students with essential knowledge and skills to enhance their understanding of the earthquakes and their impact on the global environment. Through a series of dynamic and engaging educational and research activities, including interactive workshops, hands-on experiments, online applications, and virtual reality (VR) simulations, in the inquiry-based and problem-solving learning environment, students learn about the basic principles of seismic science and engineering and developed their critical thinking based on scientific facts.

Acknowledgements

This project is funded within the framework of the UNESCO and Huawei collaboration, “Revitalizing STEM education to equip next generations with STEM competency”.

References

[1] https://www.unesco.org/en/articles/revitalizing-stem-education-europe (accessed 15.12.2024)

[2] https://www.iziis.ukim.edu.mk/en/quake-safe/ (accessed 15.12.2024)

[3] https://www.undp.org/sustainable-development-goals (accessed 15.12.2024)

[4] https://unesdoc.unesco.org/ark:/48223/pf0000260600 (accessed 15.12.2024)

Proceedings of the 3rd Croatian Conference on Earthquake Engineering - 3CroCEE
19–22 March 2025, Split, Croatia
Copyright © 2025 CroCEE
DOI: https://doi.org/10.5592/CO/3CroCEE.2025.104

FIELD APPLICATION FOR ASSESSING THE DAMAGE AND USABILITY OF BRIDGES AFTER AN EARTHQUAKE

Anđelko Vlašić [(1)], Marta Šavor Novak [(2)], Ana Mandić Ivanković [(3)], Gordana Hrelja Kovačević [(4)], Mladen Srbić [(5)], Marija Kušter Marić [(6)], Dominik Skokandić [(7)], Jelena Bleiziffer [(8)]

[(1)] *Professor, Faculty of Civil Engineering Zagreb, andjelko.vlasic@grad.unizg.hr*
[(2)] *Associate professor, Faculty of Civil Engineering Zagreb, marta.savor.novak@grad.unizg.hr*
[(3)] *Professor, Faculty of Civil Engineering Zagreb, ana.mandic.ivankovic@grad.unizg.hr*
[(4)] *Professional associate, Faculty of Civil Engineering Zagreb, gordana.hrelja.kovacevic@grad.unizg.hr*
[(5)] *Assistant professor, Faculty of Civil Engineering Zagreb, mladen.srbic@grad.unizg.hr*
[(6)] *Associate professor, Faculty of Civil Engineering Zagreb, marija.kuster.maric@grad.unizg.hr*
[(7)] *Assistant professor, Faculty of Civil Engineering Zagreb, dominik.skokandic@grad.unizg.hr*
[(8)] *Assistant professor, Faculty of Civil Engineering Zagreb, jelena.bleiziffer@grad.unizg.hr*

Abstract

After the last two major earthquakes that shook northwestern Croatia in 2020, field inspections of structures were carried out according to a previously defined methodology, which was implemented through a software application. However, this methodology and application was limited only to typical (multi)storey buildings made of masonry and/or reinforced concrete. A similar approach is now being developed specifically for bridges to create a standardized and straightforward procedure for post-earthquake inspection process. The results of the inspection are entered via a mobile application interface and then uploaded to a central cloud database. This data is divided into three categories: (1) general information about the bridge, its traffic and geometry, information about the structural system, superstructure and substructure definition, information about bearings, expansion joints and equipment; (2) results of the inspection with damage classification grades associated to each bridge element, ranging from slight to moderate to heavy, all according to the proposed methodology; and (3) final assessment of the bridge's usability. The usability of the bridge is assessed as usable, temporarily unusable or unusable according to the previously identified and classified damage. An unusable bridge is to be closed for traffic due to critical structural damage, while a temporarily unusable bridge can further be restricted to a defined traffic speed or vehicle weight, or further inspection or immediate construction work may be recommended to prevent further damage. The benefits of such a bridge usability classification are particularly important in post-earthquake aftermath when search and rescue operations are carried out, demolition crews and heavy machinery are deployed, and mobile temporary housing units are transported. Furthermore, the central database with all the information collected can be used to manage and plan the repair and retrofitting of damaged bridges.

Keywords: bridge, earthquake, damage assessment, usability

1. Introduction – background and project intention

Croatia is a seismically very active area, as was proven by two major earthquakes that struck northwest of the country [1]. The first one was in March 2020 with the epicentre 10 km north of Zagreb with a magnitude of M_L=5.5 [2], and the second stronger one was in December 2020 with the epicentre 50 km southeast of Zagreb near the town of Petrinja with the magnitude of M_L=6.2 [3]. Both earthquakes caused severe structural damage to Zagreb city and nearby settlements, and throughout the whole Sisak-Moslavina County. Recorded structural damage ranged from severe damage including total collapse (about 11% of buildings) to light or moderate damage (65% of buildings) [4,5]. Both earthquakes caused damage to historical masonry and concrete residential buildings, reinforced concrete structures, but also to linear infrastructure (roads, bridges, pipelines) [6] and soil damage (landslides, liquefaction, sinkholes) [7]. After both earthquakes, teams of civil engineers were organized by a Civil Protection Authority and led by experts from the Faculty of Civil Engineering Zagreb to perform a rapid post-earthquake usability assessments. The assessment was carried out according to the methodology which comprised a five-level damage classification system and three-level usability labels [8].

Copyright © 2025 CroCEE
DOI: https://doi.org/10.5592/CO/3CroCEE.2025.104

Problem that was identified during these actions was an inadequate official local and global government platform which would organise civil engineers, give them precise and consistent guidelines for inspection actions, and educate them for assessment procedures. Also, one of the major difficulties was an absence of a framework for collection and processing of gathered inspection data. All these problems were soon to be addressed and solved as the crisis management was established and greatly improved upon since then in the last four years. The post-earthquake inspection system is now well established, with clear procedures, educated engineer personnel rosters, data collection methodologies, digital application tools and cloud databases [9]. However, this framework is still limited to structures which include houses and multistorey buildings (residential or otherwise) with typical structural systems comprising masonry and reinforced concrete. Special engineering structures including bridges are still not covered by these inspection procedures, there are no guidelines, methodology, digital tools or database for collecting information. The post-earthquake rapid damage and usability assessment of bridges and other linear infrastructure during the last two earthquakes in Zagreb and Petrinja in 2020 was limited to an assessment aimed at decision making procedures which resulted in binary answers as to whether the bridge can continue to be operational. There were only a few exceptions where additional actions were prescribed concerning limitations in traffic speed and vehicle weight [10]. The assessment procedures back then did not include systematic gathering of information that would provide additional information about their seismic response or categorize the damage of structural and non-structural parts. Additional problems were recognized where insufficient data was available about the bridge previous state, so some of the damage could not be clearly associated with earthquake actions. Results and conclusions of these inspections were insufficient for later decision-making procedures, such as for the post-earthquake retrofit. There was no data about the urgency for the retrofit of each bridge, nor an estimate about the extent and severity of the damage. In order to get any usable information needed for retrofit projection plans, its financial estimate and funds application, additional inspections were required for each bridge, and for many of them these have not yet been carried out. For the others, there was clear evidence that not all the important damage was recognized during the first rapid post-earthquake inspection. Some of this damage did require immediate actions which were thus not timely performed. It is therefore also crucial that inspections are to be performed by civil engineers experienced in bridge design and maintenance and educated according to adopted assessment methodology.

Motivated by the benefits of the framework that was created for gathering and storing inspection data collected in post-earthquake rapid assessment of houses and buildings, a project was launched to create a similar framework for bridge inspections. In this paper current progress of this project will be presented, discussing some of the challenges of applying the same (or similar) approach as in building inspections. Nevertheless, when fully implemented, this assessment procedure and accompanying digital application and database will become a valuable part of post-earthquake crisis management process, and short-term bridge retrofit estimate.

2. Objectives and agenda

Purpose of the Croatian Centre for Earthquake Engineering is to create a system for organizing engineers in situations after earthquakes, based on their level of education and specific knowledge. Within this agenda, the main objective of this specific project is to establish a framework for conducting post-earthquake bridge inspections, performed by specialist bridge engineers, which would contribute to strengthening of the civil protection system in response to threats to public health and safety, and afterwards recovery and renewal. This objective will increase readiness in managing emergency disaster situations in terms of speed of response, allocation of human and other resources, assessment and reduction of risks, and mitigation of the short and long-term consequences of the disaster.

The secondary objective is to ensure the readiness of civil engineer personnel to perform post-earthquake bridge inspections with sufficient knowledge to recognize important damage that can compromise bridge usability and ultimately its statical and dynamical integrity.

The specific objective of the project is to establish a platform for conducting inspections of bridges after the effects of devastating earthquakes, using specific and standardized forms for the rapid inspection,

Copyright © 2025 CroCEE
DOI: https://doi.org/10.5592/CO/3CroCEE.2025.104

according to standardized and clearly defined procedures. These forms are to be included in the mobile application that can be used on tablets and smartphones directly in the field, and gathered information can be uploaded to the cloud database. The applied model is based on the experiences from 2020, from previous post-earthquake building inspections, but this time adjusted for bridges, taking into account all variations between different bridge types and their possible damage due to earthquake actions. It is important that a uniform methodology is adopted, so that the gathered information is consistent across whole database, to provide accurate overview of the damage. During the rapid bridge inspection, the main goal is to evaluate the possibility and conditions (type of traffic, vehicle weight, speed) for continuation of use of the bridge immediately after the earthquake. The condition of all bridge components is ascertained individually and an overall conclusion about the usability is given, with or without any limitations. Immediate actions can also be prescribed to ensure further usability and/or stability, and in extreme cases when the damage is excessive, full bridge closure can be ordered.

To summarize, all the specific project objectives can be assorted into the following categories:

- development of the standardized forms / application as a digital tool for the input of inspection data according to prescribed methodology,
- availability of a GIS cloud database for storing all relevant bridge information, gathered prior or during bridge inspection, used as a support for extracting needed bridge data during inspections, and inputting post-earthquake inspection conclusions, to be used for decision making process short-term immediately after the earthquake, and also for long-term strategic planning of retrofit,
- education of civil engineers in the specialty of bridge inspection and bridge usability assessment.

3. Previous work and foreign experience

After several strong earthquakes left many bridges in the USA damaged and collapsed, much of the funding and research [11] was dedicated to assessment procedures, retrofitting measures [12–14], design codes upgrades [15], and post-earthquake inspection protocols [16–18]. California implemented a digital web platform ShakeCast [19] which according to recorded ground motions automatically sends warnings about possible damage to certain bridges, calculated from database in which fragility curves are associated with each bridge. Several manuals and guidelines for post-earthquake inspections and assessment/evaluation have been made in the USA [16,17,20–22]. New Zealand published Bridge inspection and maintenance manual [23] which provides a special chapter with guidelines, techniques and procedures for inspections of seismic damage. Several publications by California Department of Transportation (Caltrans) have been issued in order to develop a standard procedure and training program for assessment of earthquake damage. One such publication is a Visual Catalogue of Reinforced Concrete Bridge Damage [24] which documents and classifies earthquake damage into 5 levels and gives guidelines on how to recognize them. Post-earthquake bridge inspection manual from Oklahoma Department of Transportation [16] is intended to prepare and define qualifications for inspection personnel, establish inspection procedures, illustrate typical earthquake damage and provide standard post-earthquake inspection forms. Post-earthquake Bridge Inspection Guidelines for New York State [17] present a course of action in response to an earthquake to assess damage to highway bridge system, in which a bridge can be closed, restricted for traffic, or flagged for further investigation, repair or retrofit. Post-Earthquake Investigation Team (PEQIT) Manual [21] from Caltrans gathers information about the performance of bridges to evaluate current design and retrofit procedures. Post-earthquake investigation field manual for the state of Kentucky [22] provides a rapid and efficient method of inspecting damaged bridges with evaluation forms to be filled out electronically, and damage classified as red, orange and green label. Handbook for the post-earthquake safety evaluation of bridges and roads [20] also uses 3 colour label tags (red, yellow and green) and 2 level inspection protocol for post-earthquake response assessment.

Proceedings of the 3rd Croatian Conference on Earthquake Engineering - 3CroCEE
19–22 March 2025, Split, Croatia
Copyright © 2025 CroCEE
DOI: https://doi.org/10.5592/CO/3CroCEE.2025.104

4. Post-earthquake rapid assessment of bridges

Following a strong earthquake, it is necessary to perform a rapid assessment of traffic infrastructure to detect any significant damage that compromises its usability. Unsafe bridges are to be closed for traffic to avoid their total collapse and casualties. Traffic should be rerouted to bridges that have been assessed as safe. For moderately damaged bridges, where some damage is detected on their structural parts, a limitation of traffic (weight and speed) can be defined. If necessary, temporary emergency immediate measures (supports, stabilization, etc.) for ensuring their further load bearing capacity and integrity are to be prescribed. Priority in rapid assessment is to be given to bridges which are considered as seismically most vulnerable, especially if they are positioned on the traffic routes with high traffic intensity. Certain bridges can also be prioritized if they are to be used for transportation of intervention vehicles such as heavy demolition machinery, construction vehicles, fire vehicles, supply vehicles, temporary housing transportation vehicles, etc. These are the bridges that are located on traffic routes leading directly to the areas most affected by earthquake. Inspection teams must be experienced in bridge design, knowledgeable in all the various bridge types and structural systems, special bridge elements and seismic devices, properly educated so they know which elements are most likely to be damaged during an earthquake, and to be able to identify any critical damage, assessing further usability of the bridge.

Results of the post-earthquake rapid inspections are to be recorded in form fields which are divided into 3 main parts: bridge information, detected damage information and assessment of usability. All inspection information is to be stored in the cloud database, which will be populated with information and accessible in real time, both in-field to all inspection teams, and in-office for coordination and planning purposes. Each bridge can be allocated for inspection to certain team, which will be visible via GIS location mapping. In this manner, an overview of all the bridges in the affected area will show which bridges are to be inspected and by whom, and for which bridges the inspection is already finished. After inspection is finished, awarded usability assessment label will also be visible on a GIS map.

4.1. Bridge information

Bridge information contains data unrelated to earthquake damage. Figure 1 shows all the different categories of this information, relating to bridge location, traffic type, traffic route, geometry, bridge type, structural system, substructure and superstructure elements, foundations, bearings and seismic devices, bridge equipment, etc. Not all of these are mandatory to fill in, some categories can have just one selection, and some multiple selections. Certain choices can ‘lock’ or ‘open’ subsequent categories or inputs, so that the total number of fields is scalable depending on the information already provided.

Most of the information shown in Fig. 1 can be chosen from predefined choices which are presented in the application when selecting each input. To distinguish between these choices, and choose the correct ones, an accompanying manual is to be issued in which all the definitions are given regarding all the inputs. It is important that all the inspection teams abide by the same definitions when making input choices, so that all the information stored in the database is consistent for all the inspected bridges.

All bridge information can be collected during inspection itself, or certain fields can be populated automatically if they are already available in the cloud database. It would certainly be beneficial if the database already contains all (or some) relevant bridge information, for bridges for which such information can be gathered from the design documentation, unrelated to the inspection itself. If present, this information would greatly reduce the time needed for inspection, but it would also provide invaluable help to the inspection engineers by informing them about all the details relevant to bridge seismic behaviour, which are not always accessibly available or reachable in visual inspections. The process of entering this information in the database prior to the inspection is still to be discussed, namely finding an appropriate model for doing it, and companies/personnel responsible for completing this task.

Copyright © 2025 CroCEE
DOI: https://doi.org/10.5592/CO/3CroCEE.2025.104

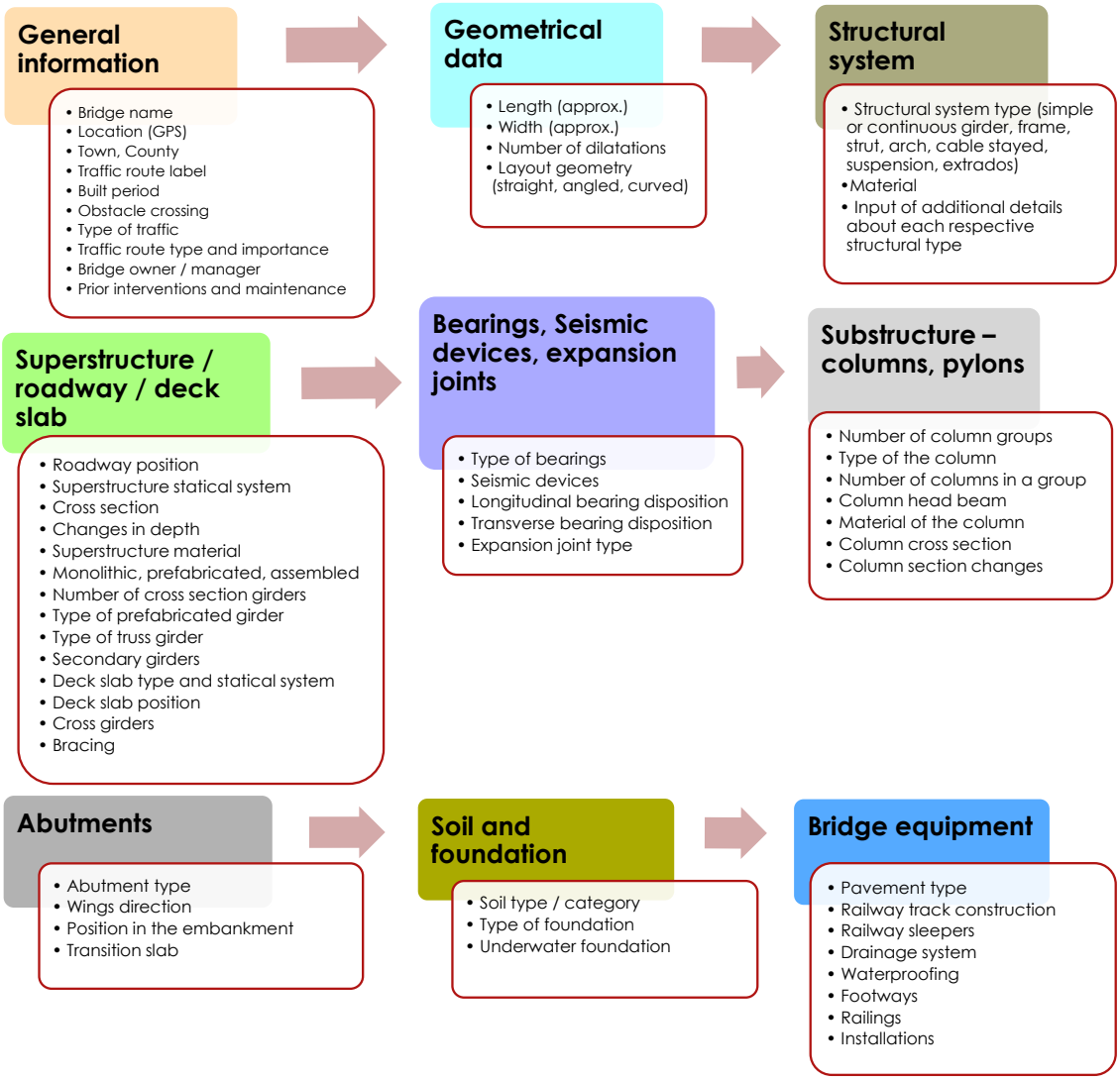


Figure 1. Categories of input of bridge information

4.2.Detected damage information

After bridge information input is completed, inspection team must input damage information. Damage is input according to the bridge elements which can be grouped into soil, foundation and substructure damage, superstructure damage, and equipment damage including seismic devices, bearings and expansion joints. Most of the damage is to be classified into one of 4 categories: 1. very heavy damage; 2. moderate damage; 3. slight damage; or 4. no damage. For some damage (related to soil and foundations), only a binary choice of present/not present is possible.

4.2.1. Soil, foundation and substructure damage

Soil damage or failure is to be detected according to the following occurrences: embankment fracture, liquefaction, landslide activation, settlements, foundation soil fracture, and fault opening. Some of these do not necessarily occur during the earthquake but can also occur in the following days and weeks after the earthquake. If at least some indications for these occurrences are detected, they must be photographed, measured and monitored regularly in the next days/weeks to detect possible progress of damage. Liquefaction can be detected if a dense mixture of sand and water is present on the surface around the bridge foundations [25]. It can result in foundation settlements than can lead to loss of

Copyright © 2025 CroCEE
DOI: https://doi.org/10.5592/CO/3CroCEE.2025.104

stability of the abutments, columns and ultimately superstructure (Fig. 2 a.). Occurrence of liquefaction is only recorded as present/not present. Fractures in the bridge embankments can cause damage to traffic surface and/or loss of stability of bridge abutments (rotation or sliding) (Fig. 2 b.). Fracture of embankment can be recorded as present with visible movements, present with only visible cracks, or not present. Landslide activation can be very dangerous for the bridge integrity (Fig. 2 c.), since it can occur suddenly, with very little warning, so any indication of possible landslide is to be recorded as present with no further damage classification. Fault opening can also cause total bridge collapse (Fig. 2 d.), so if detected, bridge should be closed for traffic with no need for damage classification. Foundation settlements can be the consequence of any previously mentioned occurrences, or any other earthquake related soil damage. Differential settlements are especially dangerous since they can lead to superstructure deflections and rotations (Fig. 2 e.), with possible total loss of support. Most uneven settlements due to earthquake occur between bridge superstructure and embankment behind the abutment with damage to the traffic surface. In this case, limitations to traffic speed should be given accordingly. Foundation settlements are to be recorded during inspection with their approximate movement value in these categories: >15 cm (bridge unusable), 5-15 cm, <5 cm (bridge temporary unusable with at least traffic speed limitation), and none (bridge usable). Foundation soil fracture will occur if the vertical load due to seismic event increased above soil load bearing capacity. This is not often the case, unless liquefaction or uneven settlements also occurs, in which case heavy damage will be present. If such a case of soil fracture is detected, bridge should be closed for traffic.

Damage to the foundation structures due to earthquake can occur on foundation slabs and/or piles if they are present. Most common failure of foundations are pile overload, shear failure of foundation slab or piles, column-foundation anchorage reinforcement failure, pile pullout, reinforcement flexural yielding in foundation plates [17]. Most damage is almost impossible to detect during the rapid assessment since these elements are rarely visible. Only parts of the foundation which are above the ground can be inspected. Nevertheless, if possible, for foundation elements damage can be recorded with 4-degree classification, as stated previously, with an additional option if the state of damage is not visible/unknown. Heavy damage is to be input if foundation failure is detected (Fig. 2 f.), moderate damage for large cracks, and slight damage for small cracks.



Figure 2. Examples of soil damage: a. liquefaction [25]; b. embankment fracture [26]; c. landslide [27]; d. bridge collapse due to fault 7 m upthrust [28]; e. column settlements causing superstructure deflections [26]; f. heavy damage to foundation piles [29]

Copyright © 2025 CroCEE
DOI: https://doi.org/10.5592/CO/3CroCEE.2025.104

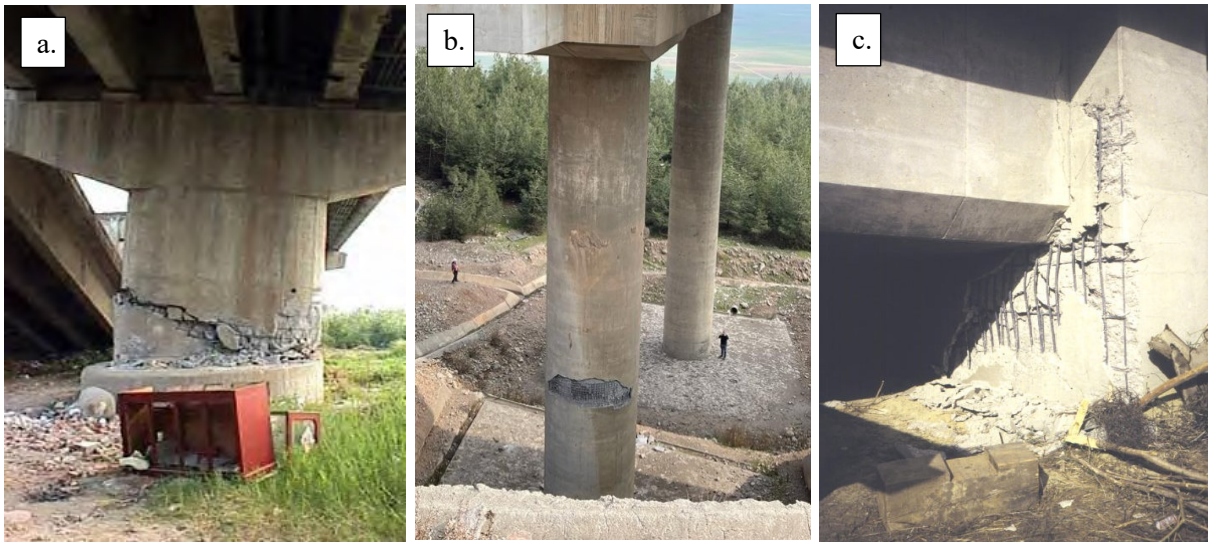


Figure 3. Substructure damage: a. heavy damage to column due to shear failure [16]; b. moderate flexural damage to column [30]; c. moderate damage to abutment wall – cracking and delamination of concrete [20]

Substructure damage is divided into abutment and column (if columns are present) damage. Abutment damage is further divided into categories of abutments movements or rotations, damage to abutment walls and side walls, and damage to wings. Movements or rotations of abutments can be caused by previously mentioned soil or foundation damage. Heavy damage is associated with discontinuation of traffic surface, and with danger of loss of support for superstructure. For moderate damage settlements up to 15 cm can be tolerated. Total failure of abutment wall when superstructure has detached from the wall or bearings is heavy damage, while some cracking (0.5 to 1 mm crack width) and concrete delamination in abutment wall can be classified as moderate damage (Fig. 3 c.). Wing wall failure can lead to landslide of embankment behind the abutment wall, so if this damage is detected, it is to be regarded as heavy damage. Most damage to abutment side walls occur due to impact of the superstructure during earthquake movements, so this damage is often heavy, but it has little consequence to overall usability of the bridge. Typical column earthquake damage comprises shear or flexural damage, compression failure with reinforcement buckling, or any of these combined. For each of these damage types, a damage level can be input. Heavy damage from flexure is considered when yielding of reinforcement occurs, with large concrete crushing and cracking, and detachment of reinforcement from concrete. Moderate flexural damage is considered when concrete compressive strength is reached and delamination of concrete cover occurs (Fig 3 b.). Concrete shear failure occurs when inclined sliding surface has fully developed, with visible slip along this surface, causing reinforcement bending/failure and cracking/crushing of concrete (Fig 3 a.). Smaller shear cracks up to 0.5-2 mm are considered as moderate column shear damage. If steel columns are present, heavy damage is considered when local buckling of the section elements or global buckling of the whole column is present. Damage to column head beams can also be input. Most of this damage occurs due to superstructure impacts, or due to head beam acting as a frame beam element together with the column for lateral earthquake loads.

4.2.2. Superstructure damage

Superstructure can suffer damage due to excessive movements, main girder horizontal or vertical impact into other substructure elements, girder excessive bending or shear force, transverse bending of girders due to lateral seismic action, torsional effects on horizontal or cross bracings, reaction from fixed bearings or seismic devices, etc. Main danger as a consequence of seismic movement of superstructure is slippage of girders from their support which results in total collapse of superstructure. Any damage in which a superstructure has moved excessively, so that any aftershock or other load could cause loss of stability of superstructure, must be classified as heavy and bridge must be closed (Fig 4 a.).

Copyright © 2025 CroCEE
DOI: https://doi.org/10.5592/CO/3CroCEE.2025.104



Figure 4. Superstructure damage: a. excessive movement [18]; b. heavy damage to main girder due to impact in the seismic block and horizontal bending [30]; c. heavy damage – failure of horizontal bracing [31]

For movements that caused damage in traffic surface or deck slab, but adequate support still exists, damage can be classified as moderate (usually this is true for movements up to 15 cm). Heavy damage to main girders is considered when large deflection of plastic deformations are visible (Fig. 4 b.), large cracking due to bending, buckling of steel plates, excessive shear cracking and crushing of concrete in the area of prestressed cables anchorages. If the damage is localized, mainly caused by the impact of the girder into other element, and the bearing capacity of the girder is unchanged, then the damage can be considered moderate. Damage to horizontal or vertical bracings can be substantial since these elements are engaged during horizontal earthquake actions. This can lead to their failure (Fig. 3 c.), fracture or buckling. It is necessary to evaluate if remaining horizontal stabilization is adequate for such a superstructure in case of an aftershock and classify damage as heavy or moderate accordingly.

4.2.3. Bearings, seismic devices, expansion joints and other equipment damage

Damage to bearings and seismic devices are most common types of damage since these elements are engaged during earthquake the most. Causes of damage are excessive displacements of movable or elastomeric bearings, failure of fixed or tension bearings due to excessive earthquake reactions (Fig. 5 a.), inadequate anchorage to substructure or superstructure (Fig 5 b.), excessive in-plane rotations of the superstructure, especially for skewed bridges, lack of boundary movement limitation elements. Heavy damage includes fracture of the bearing body (within neoprene or otherwise), large movements (surpassing the bearing height) and lateral dislocations from the substructure support surface, fracture of the anchorage system, permanent excessive deformations, and damper liquid leakage. Expansion joints usually suffer damage from excessive movements, more than 15 cm can be considered heavy damage, 2.5-15 cm moderate damage, and <2.5 cm slight damage. Traffic speed limit should be set if the traffic surface surrounding the expansion joint is damaged. Bridge equipment damage is to be recorded for drainage, insulation, traffic surface, railings, cornice, installation ducts, etc. This damage will most likely not influence usability assessment of the bridge, except in some cases impose traffic speed limitation.

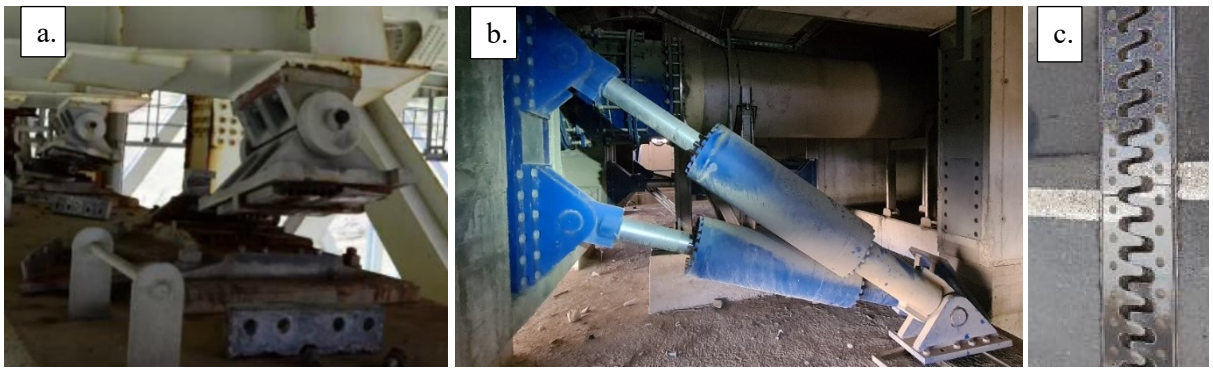


Figure 5. a. Fixed bearing failure [32]; b. Dampers detachment; c. Transverse movement of expansion joint [33]

Copyright © 2025 CroCEE
DOI: https://doi.org/10.5592/CO/3CroCEE.2025.104

4.3. Assessment of usability

Final step of the rapid post-earthquake inspection is to evaluate all the detected damage and assess further usability of the bridge. This assessment is based on the professional judgement of the inspection team, whose members must be sufficiently educated to make such assessment. If there is a heavy structural damage, bridge must be closed for all traffic, and bridge is labelled as 'unusable' (red label). Heavy structural damage is such a damage that threatens the structural integrity of the bridge, or if some parts of the bridge have already collapsed. Most commonly heavy damage may result in sudden bridge collapse by effects of bearing slippage, foundation soil landslide or settlement, column turnover or column shear failure (Fig. 6) [10]. Excessive opening of plastic joints in the column or superstructure sections may also result in collapse if structural system becomes a mechanism. If indications of any of these types of damage have been detected, it is recommended that the bridge is closed for traffic.

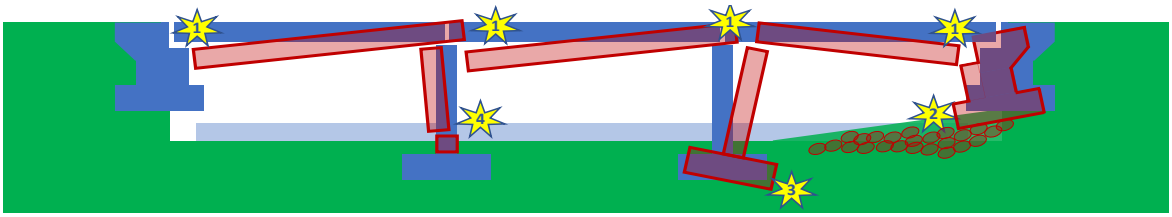


Figure 6. Most common earthquake types of bridge sudden collapses (any or all can occur): 1—bearing slippage; 2—abutment foundation soil landslide; 3—column turnover; 4—column shear failure [10]

If a moderate structural damage is detected, with no risk of total bridge collapse, a designation of 'temporary unusable' is to be assigned in the assessment (yellow label). This assessment leads to further recommendations and/or actions that are required. In any case, for this assessment a detail inspection is required to fully assess the extent of damage, which is to be carried out afterwards. In the meantime, bridge may stay open for traffic if either certain temporary immediate short-term measures are undertaken, or limitations in traffic loads and/or speed are imposed. Short-term measures, if required, must be described in the report in an unambiguous way. They may include temporary supports, stabilization of landslides, repairing of the damage in the traffic surface, alternative traffic regulation – closure of some traffic lanes, etc. Limitation of traffic may be input by closing the bridge for certain types of heavy vehicles, by defining maximum axle load, or by limiting vehicle speed (Fig. 7). For bridges where no damage is detected, or only non-structural damage which does not impair traffic safety, an assessment 'usable' can be assigned (green label), and bridge can be continued for traffic use without any limitations.

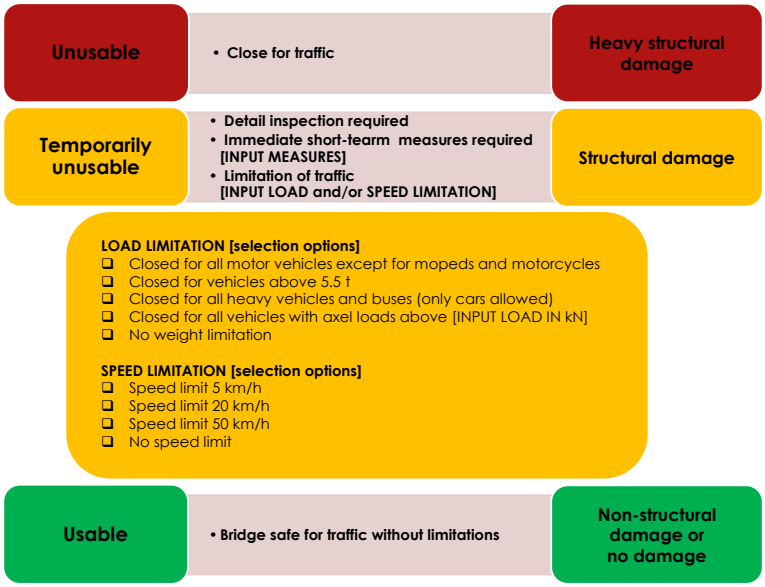


Figure 7. Assessment of usability – labels and additional options / actions

Proceedings of the 3rd Croatian Conference on Earthquake Engineering - 3CroCEE
19–22 March 2025, Split, Croatia
Copyright © 2025 CroCEE
DOI: https://doi.org/10.5592/CO/3CroCEE.2025.104

5. Mobile field application

All the bridge information, damage information, and usability assessment, as discussed in section 4, is to be input during inspection using dedicated mobile application that can be downloaded to mobile phones or tablets. Application is currently in development (Fig. 8) (for now is only available in Croatian language). Input fields in the application can be numerical, textual, or multiple-choice selections where either only one or multiple choices can be selected at the same time. For certain choices, other sections may appear or disappear (for example if the number of bridge columns is zero, then no further information about column types and their damage is asked for), thus reducing the size of the questionnaire to only that information which is relevant and existent for the bridge in question. Photos are to be uploaded from the phone/tablet camera for the damage that is relevant for the final assessment. Mobile application is directly connected to cloud database and live GIS map so assessment information can be accessed from all users in real time. This gives an overview of the usability of all the bridges in the affected area and helps in coordination of teams for further inspections of remaining bridges.

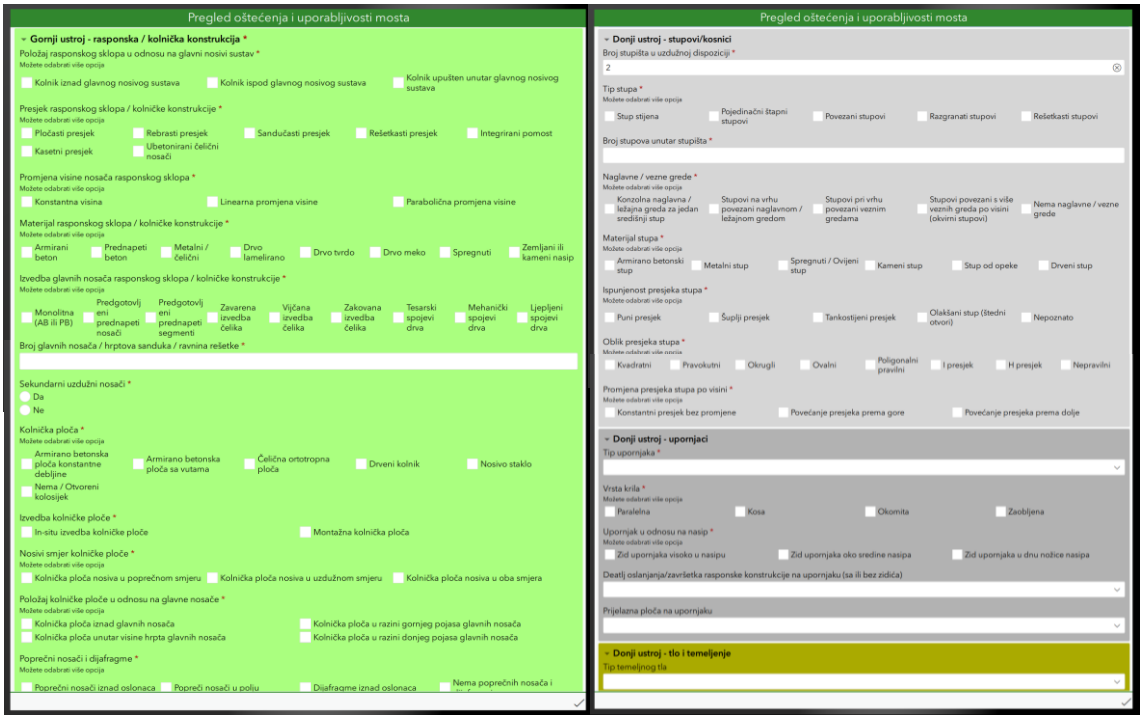


Figure 8. Screenshots of mobile application for assessment inspections (in development, in Croatian)

6. Beneficial parties / users

This project will be beneficial to a wide range of users which are identified as following: general population; Civil protection agency; Ministry of physical planning, construction and state assets; Ministry of the interior; Government of Republic of Croatia (including other state affair bodies); regional and local governments; infrastructure and bridge management and maintenance companies and institutions. General population will benefit from gaining information about the possibility of using safe traffic routes after the earthquake, which is especially important in case of evacuation and/or allocation events. Civil protection agency will have implemented practices for an earthquake event using specialist engineers educated for bridge inspection. It will also have better management of the crisis, for allocating and directing emergency intervention services and their equipment (fireman, search and rescue teams, medical units, heavy machinery transportation and allocation, temporary housing units' transportation, food and water supply, etc.), knowing which bridges are safe to use, and to which extent. If necessary and when possible, immediate measures could be performed on some bridges according to the inspection conclusions, making them short term usable again and mitigating the danger of their total

Copyright © 2025 CroCEE
DOI: https://doi.org/10.5592/CO/3CroCEE.2025.104

collapse, therefore simplifying their afterwords reconstruction. Ministry of physical planning, construction and state assets will gain basis for making key strategic decisions to decrease earthquake consequences. Ministry of the interior will have access to timely information for efficient crisis management which includes traffic regulation and ensured public safety. Government of Republic of Croatia is expected to enhance actions of civil protection agencies, homeland security and strategic planning. Regional and local governments are expected to benefit from gaining basis for taking emergency measures to reduce earthquake consequences, as well as gaining information about the state of their infrastructure network. Infrastructure and bridge management and maintenance companies and institutions will have insight in the usability of their bridges and the demand for retrofit and maintenance work. Along all these parties, benefits are also expected for the civil engineering community, by establishing and educating specialists capable of post-earthquake bridge inspections.

7. Conclusion

An inspection protocol and methodology for post-earthquake rapid assessment of bridges is currently being developed. Field mobile application, cloud database and GIS will enable rapid response, consistent assessment results, ensured public safety, better crisis management and retrofit planning.

References

[1] Vlašić A, Srbić M, Skokandić D, Mandić Ivanković A. Assessment of damage after ML=5.5 and ML=6.2 magnitude earthquakes in Zagreb and Petrinja. 13th Central European Congress on Concrete Engineering CCC 2022 Next Generation of Concrete Engineering for Post-Pandemic Europe, Zakopane: nbi media; 2022, p. 295–308.

[2] Novak MŠ, Uroš M, Atalić J, Herak M, Demšić M, Baniček M, et al. Zagreb earthquake of 22 March 2020 – Preliminary report on seismologic aspects and damage to buildings. Gradjevinar 2020;72:843–67. https://doi.org/10.14256/JCE.2966.2020.

[3] Markušić S, Stanko D, Penava D, Ivančić I, Oršulić OB, Korbar T, et al. Destructive M6.2 Petrinja Earthquake (Croatia) in 2020—Preliminary Multidisciplinary Research. Remote Sens (Basel) 2021;13. https://doi.org/10.3390/rs13061095.

[4] Government of Croatia, World Bank Report. Croatia Earthquake Rapid Damage and Needs Assessment. Zagreb: 2020.

[5] Government of Croatia World Bank report. Croatia December 2020 Earthquake Rapid Damage and Needs Assessment. 2021.

[6] Korbar T, Markušić S, Stanko D, Penava D. Petrinja M6.2 earthquake in 2020 damaged also solid linear infrastructure: are there similar active faults in Croatia? 1st Croatian Conference on Earthquake Engineering1CroCEE, Faculty of Civil Engineering, University of Zagreb; 2021, p. 353–62. https://doi.org/10.5592/co/1crocee.2021.253.

[7] Bacic M, Sasa Kovacevic M, Librić L, Žužul P. Sinkholes induced by the Petrinja M6.2 earthquake and guidelines for their remediation. 1st Croatian Conference on Earthquake Engineering1CroCEE, Faculty of Civil Engineering, University of Zagreb; 2021, p. 341–52. https://doi.org/10.5592/co/1crocee.2021.237.

[8] Uroš M, Novak MŠ, Atalić J, Sigmund Z, Baniček M, Demšić M, et al. Post-earthquake damage assessment of buildings - Procedure for conducting building inspections. Gradjevinar 2021;72:1089–115. https://doi.org/10.14256/JCE.2969.2020.

[9] Croatian Centre of Earthquake Engineering (HCPI - Hrvatski Centar Za Potresno Inˇzenjerstvo) F of CEU of Z. Manual for classification of earthquake building damage. 2020.

[10] Vlašić A, Srbić M, Skokandić D, Mandić Ivanković A. Post-Earthquake Rapid Damage Assessment of Road Bridges in Glina County. Buildings 2022;12. https://doi.org/10.3390/buildings12010042.

[11] Lee GC, Mohan SB, Huang C, Fard BN. A Study of U.S. Bridge Failures (1980-2012), Technical Report MCEER-13-0008. 2013.

Copyright © 2025 CroCEE
DOI: https://doi.org/10.5592/CO/3CroCEE.2025.104

[12] Saini A, Saiid MS. Post-Earthquake Damage Repair of Various Reinforced Concrete Bridge Components, Technical Report CA 13-2180. 2013.

[13] Washington State Department of Transportation. Seismic Design and Retrofit. WSDOT Bridge Design Manual, vol. M 23-50.22, Washington State Department of Transportation; 2023.

[14] Priestley MJN, Seible F, Calvi GM. Seismic Design and Retrofit of Bridges. New York: John Wiley & Sons, Inc.; 1996.

[15] Caltrans. Caltrans Seismic Design Criteria. Sacramento: 2013.

[16] Oklahoma Department of Transportation. Post-Earthquake Bridge Inspection Manual. 2017.

[17] O'connor JS, Alampalli S. Post-Earthquake Bridge Inspection Guidelines for New York State, Technical Report MCEER-12-0003. Buffalo: 2012.

[18] Veletzos M, Panagiutou M, Restrepo J, Sahs S. Visual Inspection & Capacity Assessment of Earthquake Damaged Reinforced Concrete Bridge Elements, Final Report CA08-0284. 2008.

[19] Wald D, Lin KW, Porter K, Turner L. ShakeCast: Automating and improving the use of shakemap for post-earthquake decision-making and response. Earthquake Spectra 2008;24:533–53. https://doi.org/10.1193/1.2923924.

[20] Ramirez JA, Frosch RJ, Sozen MA, Turk AM. Handbook for the Post-Earthquake Safety Evaluation of Bridges and Roads. 2000.

[21] Caltrans. Post Earthquake Investigation Team (PEQIT) Manual 2013.

[22] Sardo AG, Sardo TE, Harik IE. Post Earthquake Investigation Field Manual for the State of Kentucky, Research Report KTC-06-30/SPR-234-01-1F. Lexington: 2006.

[23] Transit New Zealand. Bridge inspection and maintenance manual SP/M/016. New Zealand: Tr; 2001.

[24] California Department of Transportation. Visual Catalog of Reinforced Concrete Bridge Damage. 2006.

[25] Ledezma C, Ashford SA, Hutchinson T, Arduino P. Effects of Liquefaction-Induced Ground Failure on Bridges, Roads, Railroads and Lifeline Systems. Earthquake Spectra 2011;28:119–43.

[26] Stringer ME, Bastin S, McGann CR, Cappellaro C, El Kortbawi M, McMahon R, et al. Geotechnical aspects of the 2016 Kaikōura earthquake on the South Island of New Zealand. Bulletin of the New Zealand Society for Earthquake Engineering 2017;50:117–41. https://doi.org/10.5459/bnzsee.50.2.117-141.

[27] Ding W, Wu Z, Zhan B, Liu J, Bi J. Analysis of seismic damage of a highway bridge during the 2021 Ms 7.4 earthquake in Maduo County, China. Natural Hazards 2023;117:2419–34. https://doi.org/10.1007/s11069-023-05948-5.

[28] Lin Y, Zong Z, Lin J, Li Y, Chen Y. Across-fault ground motions and their effects on some bridges in the 1999 Chi-Chi earthquake. Advances in Bridge Engineering 2021;2. https://doi.org/10.1186/s43251-020-00028-1.

[29] Waldin J, Jennings J, Routledge P. Critically damaged bridges & concepts for earthquake recovery. 2012 NZSEE Conference, 2012.

[30] Dowell RK. Reconnaissance Report of Observed Structural Bridge Damage Mw 7.8 Turkiye (Turkey) Earthquake of 2023. SDSU Structural Engineering Research Project, Report No SERP - 23/03 2023.

[31] Kawashima K. Damage of Bridges due to the 2011 Great East Japan Earthquake. Proceedings of the International Symposium on Engineering Lessons Learned from the 2011 Great East Japan Earthquake, Tokyo, Japan: 2012.

[32] Gimenez JL, Himeno T. Retrofit of a bridge damaged in Kumamoto Earthquake with high energy dissipation devices. 2018 NZSEE Conference 2018.

[33] Tomac I, Zlatović S, Athanasopoulos-Zekkos A, Bleiziffer J, Domitrović D, Frangen T, et al. Geotechnical Reconnaissance and Engineering Effects of the December 29, 2020, M6.4 Petrinja, Croatia Earthquake, and Associated Seismic Sequence 2020. https://doi.org/https://doi.org/10.18118/G63T0S.

Proceedings of the 3rd Croatian Conference on Earthquake Engineering - 3CroCEE
19–22 March 2025, Split, Croatia
Copyright © 2025 CroCEE
DOI: https://doi.org/10.5592/CO/3CroCEE.2025.118

APPLICATION OF THE BAILEY BRIDGES IN POST-EARTHQUAKE INTERVENTIONS

Marko Šimić [(1)], Dražen Brkić [(2)], Marija Kušter Marić [(3)], Anđela Ivanović [(4)]

[(1)] *Lieutenant Colonel, Croatian Military Academy dr. Franjo Tuđman, marko.simic@morh.hr*
[(2)] *Mayor, Croatian Military Academy dr. Franjo Tuđman, drazen.brkic@morh.hr*
[(3)] *Associate professor, University of Zagreb Faculty of civil Engineering, marija.kuster.maric@grad.unizg.hr*
[(4)] *First Lieutenant, Armed Forces of the Republic of Croatia,andjela.ivanovic@morh.hr*

Abstract

After an earthquake, the availability of transport corridors must be guaranteed to allow the evacuation of the population and the unhindered passage of rescue vehicles. Bridges are crucial in any transport network and can be damaged, partially or completely collapsed during an earthquake. On the other hand, in such circumstances, it is important to ensure fast and safe passage of people and goods over obstacles. Bailey bridges are prefabricated systems that enable quick and temporary passage and are used by many armies around the world, including the Croatian army. Possible applications of Bailey bridges after the strong earthquake presented in this paper are: (i) construction of Bailey bridge at the site of an existing bridge that collapsed during the earthquake; (ii) construction of Bailey bridge at an unprepared crossing, (iii) partial bridging of one or more spans of a destroyed bridge, (iv) strengthening of an existing bridge pier with Bailey truss elements, (v) construction of a new support (pier) for the superstructure with Bailey truss elements, (vi) Bailey bridges on barges. In addition to the theoretical possibilities, several case studies – Bailey bridges recently constructed by Armed Forces of the Republic of Croatia will be presented: Bailey bridge in Donja Stubica, Bailey bridge over Korana River near Karlovac, Bailey bridge near Marija Bistrica in Croatia, and Bailey Bridge over Dreta River in Slovenia.

Keywords: Bailey bridge, steel truss, post-earthquake intervention, army.

1. Introduction

The consequences of strong earthquakes are often partially or completely destroyed infrastructures, which ultimately leads to communities being isolated and in urgent need of help. Bailey structures are characterised by their ease of assembly and maintenance, allowing them to be set up and dismantled quickly, making it much easier to provide relief to those at risk, support rescue operations and reconnect communities. Bailey structures were first used on a large scale during the Second World War, where they proved invaluable in situations that required rapid assembly of bridging structures [1, 2].

Bailey structures were invented in the 1940s by Sir Donald Bailey and were primarily intended for military use. The modular design of the Bailey constructions made it possible to quickly and easily build bridges, which allowed the army to quickly cross various types of obstacles. Over time, civilian structures also recognized the advantages of Bailey bridges, therefore their use exceeded only military applications, and they became an indispensable tool in bridging various types of obstacles, especially in dealing with disasters and crises [2, 3].

Bailey bridges are made of prefabricated steel components that can be easily transported and quickly assembled on-site using only manpower, without the need for special tools or heavy machinery. The bridge sections can be connected to each other, allowing the length and load capacity of the bridge to be adjusted to any obstacle. The installation of a Bailey bridge requires minimal or even no preparatory work or site modification for crossing an obstacle, making Bailey bridges ideal for use in emergency and urgent situations [2, 4].

Due to their simplicity and speed of assembly, easy maintenance, and relatively affordable cost, Bailey bridges are used worldwide for both military and civil purposes. They are especially valuable

Copyright © 2025 CroCEE
DOI: https://doi.org/10.5592/CO/3CroCEE.2025.118

in disaster relief efforts following natural catastrophes such as earthquakes, floods, and hurricanes, where rapid infrastructure construction is necessary. Their versatility, durability, and strength make them ideal for both temporary and long-term bridges in both rural and urban areas [2, 5].

2. Possibilities of Bailey bridge

2.1. Purpose of the structure

Bailey structures consist of standardized folding elements, tools, and accessories. The primary function of panel bridge equipment is to assemble fixed bridges, panel crib piers, and towers. Other specialized structures, such as floating bridges, suspension bridges, retractable bridges, and mobile bridges, can be constructed using specialized components. The use of these materials is governed by standard guidelines outlined in the Regulations on the Assembly of Bridges and Scaffolding Made of Bailey Material M-S6 (M-2 and M-1). Beyond their primary function, Bailey materials can also be used to construct a wide range of other structures, including suspension bridges, railway bridges, temporary docks, loading and unloading ramps, auxiliary scaffolding, cable car and electricity pylons, antenna masts, roof structures, and more. Since no standardized solutions exist for these applications, a custom technical solution is developed for each specific case, leveraging the expertise and adaptability of Bailey materials. With minor non-standard modifications, the potential applications of Bailey bridge components are limited only by the user's imagination [5, 6].

2.2. Description of the structure

A Bailey bridge is a type of portable, prefabricated, truss bridge (Fig. 1). Due to the multiple uses and temporary nature of structures made from Bailey material, a key feature of the design is its assembly and disassembly capability. Parts of the same type are identical to ensure interchangeability and possess high strength and durability, allowing for multiple assemblies and disassemblies. Damaged parts can be replaced quickly and easily. The structural design of the elements is based on their primary purpose but also has sufficient properties for a much broader universal application across different types of structures, with or without minor modifications and the addition of new elements. The bridge structure can be easily adapted to the width and depth of an obstacle, required load-bearing capacity and the static system of the designed bridge by adding or removing sections of the superstructure [5, 6].

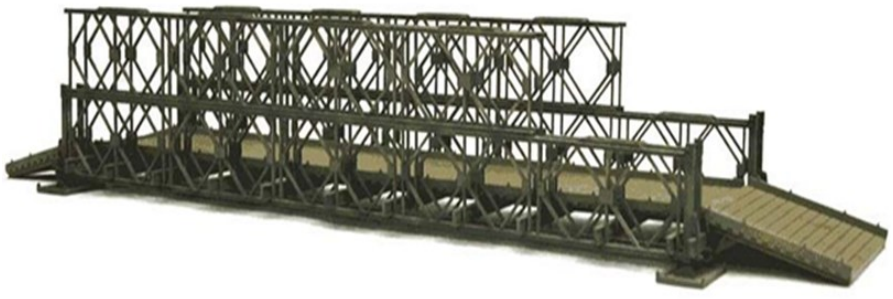


Figure 1. Model of Bailey bridge

The construction is simple to assemble, and the elements are relatively lightweight, allowing them to be transported and assembled manually without the need for heavy machinery. Of course, a crane can be used during assembly to speed up the installation process. No special scaffolding or machinery is required to install the bridge, as it is launched over the obstacle using a launching nose, which is attached to the front of the bridge, and a counterweight,

Copyright © 2025 CroCEE
DOI: https://doi.org/10.5592/CO/3CroCEE.2025.118

which is essentially the mass of the bridge itself. The bridge can be launched manually, with the required number of personnel depending on the bridge dimensions [5, 6].

As a technical system, Bailey material is not used as individual elements but is assembled into specific sets, including: a set for a launching bridge, a set for a pontoon bridge, and a set with additional components for a suspension bridge. Each kit contains the appropriate number of elements to achieve the required load-bearing capacity and bridge length. Additionally, various types of scaffolding can be constructed using elements from the pontoon bridge set [5, 6].

The main components of the bridge structure include (Fig. 2):

- Main girders made of panels,

- Transoms (cross griders),

- Stingers (longitudinal griders) [5, 6 ,7].

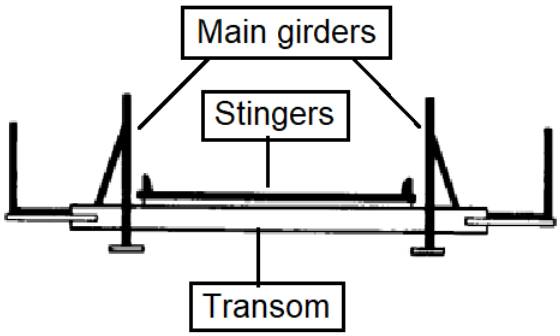


Figure 2. Main parts of Bailey bridge [5, 7]

The main girders are assembled by connecting the trusses to each other, forming walls and stories. The bridge has two main girders. They are interconnected by transoms. The constructions of the main girders allow for different lengths and load-bearing capacities of bridges and spans. They are distinguished by the number of truss walls and stories. The number of truss walls and stories mainly determines the type of main girders, and thus the type of bridge. The prescribed types of main girders are:

- single-truss single-story (SS),
- double- truss single-story (DS),
- triple- truss single-story (TS),
- double- truss double-story (DD),
- double- truss triple- story (DT),
- triple- truss double-story (TD),
- triple- truss triple- story (TT) [5, 6].



Figure 3. Bailey Bridges: single-truss single-story (SS), double-truss double-story (DD) and triple-truss triple-story (TT)

Proceedings of the 3rd Croatian Conference on Earthquake Engineering - 3CroCEE
19–22 March 2025, Split, Croatia
Copyright © 2025 CroCEE
DOI: https://doi.org/10.5592/CO/3CroCEE.2025.118

In addition to the seven types mentioned, it is possible to create other variants of main girders (for example, with 4 stories), but they are rarely used. Instead of adding a wall or story, the main girders can be strengthened by placing additional flanges on the trusses [5, 6].

The transoms connect and stiffen the main girders, support the roadway and transfer the loads received from the roadway to the main girders. In three-story bridges, the transoms are also used to stiffen the upper chords of the main girders, forming the upper part. The transoms determine the distance between the main girders, and thus the fixed width of the bridge and the roadway. The bridge roadway and pedestrian walkways are directly supported on the transoms [5, 6].

The roadway is assembled from stingers, decks and buffers and serves as a surface for vehicle traffic. The basic position of the roadway is on the transoms at the level of the lower chord of the main girders, and the positions of the roadway on the second and third floors are also possible, or above the level of the main girders. The roadway directly receives moving loads and transfers them to the transoms. Unlike the variability of the main girders, the roadway is unchangeable regardless of the length and load capacity of the bridge. It is only possible to add traffic lanes to protect the floors from premature wear [5, 6].

In addition, footpaths can be constructed on the sides of the main girders and ramps are built at the entrances to the bridge [5, 6]. All elements other than the supports (main girders, transoms, carriageway, ramp and footpaths) are referred to as the bridge's superstructure and the supports as the substructure. A superstructure consists of main girders, cross girders and carriageways and the substructure of floating supports.

The bridge rests on the land via supports. Supports are shore or intermediate supports. Shore supports are assembled directly on the shores and the ends of the bridge rest on them. Coastal support consists of two bearing slabs with bearings placed on beams and planks, or other wooden supports, transverse and longitudinal supports or similar in order to increase the bearing capacity of the soil and transfer forces to a larger surface [5, 6].

Inter-support landings are used in multi-span bridges to support the upper part on several supports in an obstacle that cannot or is not optimally bridged in one span. The landings between the supports can be made from Bailey elements of various types or from other types of construction materials, and the existing supports of collapsed bridges are also used [5, 6].

Floating supports are built from pontoons, freighters and logs (Fig. 4). They are only used in scaffolding and pontoon bridges. Bailey pontoons can only be used as three-part supports. Floating supports can consist of one or more three-part pontoons. The ramp consists of special elements that make it possible to enter and leave the bridge. Depending on the purpose of the crossing, the ramp can be one or more bays long. Pedestrian walkways can be installed on the outside of the main girders, regardless of the type of girder. They are supported directly on the ends of the transoms.

The bridge elements are designed so that they can be transported within the construction site and assembled without the use of machines using only human labour. Moreover, single truss in the length of a 3.048 m and corresponding elements create a separate structural unit – one truss field. The ramp at the entrance to the bridge in the length of a 3.048 m ramp is referred to as the ramp field.

Bridges with abutments are built over dry and water obstacles. They are manufactured in all seven types. They are quite stable as they are not dependent on the water level. The fewest types of Bailey elements are installed in them, i.e. only the basic elements of the upper part and coastal supports and, if necessary, additional elements for landing Bailey supports, and the use of pontoons, navigation accessories and anchorages is excluded. The assembly of these bridges is slower than that of pontoon bridges, especially when building between the supports of a larger span bridge.

Bridges with standing supports can be single-span or multi-span. The span is part of the bridge construction between two supports, regardless of whether these supports are on the bank or in the obstacle. A single-span bridge spans the obstacle by supporting the structure of the upper part only at its ends on bank supports. Single-span bridges are built over narrow obstacles where no intermediate

Copyright © 2025 CroCEE
DOI: https://doi.org/10.5592/CO/3CroCEE.2025.118

supports are required due to the short length of the bridge. Due to their short length, such bridges have a simple construction of the main supports and are quickly assembled and placed over the obstacle. A single-span bridge can also be built over a wider obstacle (up to 64 metres) if it is deep and the construction between the supports is not possible or would be very complex (over ravines, in canyons, over deep riverbeds, etc.). In these cases, a larger the width of the barrier requires the use of heavier types of multi-wall and multi-story structures, which are more complex and take longer to build.

A multi-span bridge is assembled on wide barriers and relies not only on the bank supports (like a single-span bridge), but also on intermediate supports in the barrier, creating several spans of the structure between the supports. The bank supports of a multi-span bridge are the same as the bank supports of a single-span bridge. Existing supports from demolished bridges can be used as intermediate supports, or new supports can be built from Bailey elements or local materials, or a combination of these. Multi-span bridges can be permanent or with separate spans.

Bridges with separated spans are such superstructure structures, in which the main girders above the supports are completely separated or connected only in the lower part via external span verticals or directly to the lower truss flanges, forming separate functions of each span or a hinge function of the structure above. between the columns.

The greater or lesser complexity of the construction of a multi-span bridge depends primarily on the complexity of the construction between the supports, and only then on the types of main supports.

In the case of obstacles whose width is within the limits of a single-span bridge, but with a more complex construction, the more optimal solution is to choose between a multi-span bridge with abutments, piers and superstructure of a simpler type, rather than a single-span bridge with a more complex superstructure.



Figure 4. Floating Bailey Bridge

Copyright © 2025 CroCEE
DOI: https://doi.org/10.5592/CO/3CroCEE.2025.118

3. Role of Bailey structures in the post-earthquake period

One of the most vital functions of Bailey bridges following an earthquake is to restore access to areas cut off due to damaged infrastructure. These temporary crossings over rivers, valleys, or collapsed roads provide crucial mobility for people, vehicles, and supplies. In the chaotic aftermath of an earthquake, the priority is to quickly supply the affected population, and Bailey bridges play a critical role in facilitating the transport of essential items like food, water, medical aid, and equipment. By ensuring relief efforts are not impeded by impassable terrain, they are pivotal in the recovery process.

The social and economic impact of an earthquake can be devastating, but Bailey bridges contribute significantly to the rebuilding process. They reconnect isolated communities, allowing residents to reunite with their families, access vital services, and participate in the broader recovery efforts.

Bailey bridges have been applied in post-earthquake interventions worldwide, some example are:

- Japan, 2011: Following the Tōhoku earthquake and tsunami, Bailey bridges were quickly installed to enable access to isolated regions, facilitating relief efforts and aiding the rebuilding process.
- Nepal, 2015: Following the earthquake in Gorkha, Bailey bridges proved crucial in connecting remote mountainous regions to larger urban centres to ensure the timely delivery of aid and support.

4. Case studies – Bailey bridges assembled by Croatian army

4.1. Bailey bridge in Donja Stubica, Croatia

In 2023, the Engineering Regiment of the Croatian Army constructed a "Bailey M-1" bridge in the settlement of Gornja Podgora in the town of Donja Stubica. The bridge was installed to allow the passage of heavy construction machinery and vehicles for the purpose of rebuilding a family house that was severely damaged during the earthquake in March 2020. The bridge construction type is single-truss single-story. The total length of the bridge is 12.19 meters, and the mass of the structure is 7.12 tons. The bridge has a maximum load capacity of 26 tons for tracked vehicles and 30 tons for wheeled vehicles. The installation work lasted for 3 days [8].



Figure 5. Bailey bridge in Donja Stubica, Croatia [9]

Copyright © 2025 CroCEE
DOI: https://doi.org/10.5592/CO/3CroCEE.2025.118

4.2. Bailey bridge over Korana River near Karlovac, Croatia

In June 2020, the Engineering Regiment of the Croatian Army installed the largest "Bailey M-1" bridge in Croatia to date. This bridge is located over the Korana River in the settlement of Turanjski Poloj in the city of Karlovac. The bridge was installed to provide assistance in flood control efforts, specifically to allow the passage of construction machinery and vehicles necessary for building a flood protection embankment along the Korana River. Construction type of the bridge is triple- truss double-story. It is 42.67 meters long, and the structure weighs 74.9 tons. The maximum load capacity of the bridge for tracked vehicles is 40 tons, and for wheeled vehicles, it is 48 tons. The construction of this bridge took 7 days [10]. After the embankment was built, the bridge was disassembled.



Figure 6. Bailey bridge over Korana River near Karlovac, Croatia [10]

4.3. Bailey bridge near Marija Bistrica, Croatia

Over the Krapina River in the settlement of Selnica in the Municipality of Marija Bistrica, the Engineering Regiment of the Croatian Army rebuilt the "Bailey M-2" bridge in September 2024, which was handed over for permanent use to the local community. This bridge was constructed because the original bridge, installed in 1999 by the former "33rd Engineering Brigade of the Croatian Army," was severely damaged in April 2023 when a vehicle much heavier than the allowed weight crossed it This bridge is crucial for the area's transportation connectivity as it facilitates access to agricultural land and the Croatian National Shrine of Our Lady of Bistrica. The bridge features a single-truss single-story construction type. Its total length is 27.43 meters, and the total mass of the structure is 23.58 tons. The bridge's maximum load capacity is 12 tons for tracked vehicles and 14 tons for wheeled vehicles. The bridge structure was installed in two days [11].

Copyright © 2025 CroCEE
DOI: https://doi.org/10.5592/CO/3CroCEE.2025.118



Figure 7. Bailey bridge near Marija Bistrica, Croatia [12]

4.4. Bailey Bridge over Dreta River in Slovenia

In September 2023, the Engineering Regiment of the Croatian Army set up the "Bailey M-1" bridge for the first time outside the borders of Croatia, at the site where a bridge over the Dreta River in the village of Lačja Vas, in the Municipality of Nazarje, Slovenia, collapsed due to severe flooding.The bridge was installed to restore connectivity between Lačja Vas and other parts of Slovenia. The bridge features a double- truss single-story type of construction. It has a maximum load capacity of 36 tons for tracked vehicles and 42 tons for wheeled vehicles. The installation of the bridge was completed in just 4 days [13].



Figure 8. Bailey bridge over Dreta River in Slovenia [13]

5. Conclusion

Bailey bridges are a fascinating engineering invention. Thanks to their modularity, portability, and ease of assembly, Bailey bridges have saved countless lives and facilitated the reconstruction of numerous communities after natural disasters and war. They are a true example of how innovation can have a long-lasting positive impact on the world.

Copyright © 2025 CroCEE
DOI: https://doi.org/10.5592/CO/3CroCEE.2025.118

In order to maximize and properly use Bailey bridges, it is necessary to focus on assessing the affected terrain to define the key points where bridges are urgently needed. Bailey bridges should be installed at the locations we initially selected, such as collapsed road links, key river and stream crossings, or various other types of obstacles, to facilitate the transport of people and aid.

At the very beginning of a crisis event, it is necessary to ensure that bridges of this type are primarily in the service of helping rescue teams and emergency services in order to access the affected areas as easily as possible with the aim of quick evacuation of the injured. Although Bailey bridges are a temporary solution, they need to be included in long-term reconstruction plans to stabilize the situation and begin permanent reconstruction. This approach in an emergency situation ensures that the affected areas get the help they need quickly and that lives return to normal as quickly as possible. As earthquakes continue to pose significant challenges around the world, further development and use of Bailey bridges will be critical in mitigating the effects of such disasters.

Acknowledgements

The authors would like to thank the Croatian Military Academy dr. Franjo Tuđman and Republic of Croatia Ministry of Defence for photos and data used for the article.

References

[1] *The Bailey Bridge*, Explore the past, 2024, https://www.explorethepast.co.uk/2024/03/the-bailey-bridge/ (accessed January 4, 2025).

[2] *What are the key advantages of Bailey bridges in disaster relief?*, Evercross bridge, 2024, https://www.baileybridgesolution.com/what-are-the-key-advantages-of-bailey-bridges-in-disaster-relief.html#What-is-a-Bailey-Bridge? (accessed January 4, 2025)

[3] Ball P.: *Bridge of Wars - The Story of the Bailey Bridge*, The heritage portal, 2016, https://www.theheritageportal.co.za/article/bridge-wars-story-bailey-bridge (accessed January 5, 2025)

[4] *What are Bailey bridges?*, Housing.com, 2023, https://housing.com/news/what-are-bailey-bridges/ (accessed January 5, 2025)

[5] Headquarters, Department of the Army (1986): *Bailey bridge.* Washington, DC.

[6] Pravilo o sklapanju mostova i skela od Bejli materijala M-56 (M1 i M2) – 1966 – DRŽAVNI SEKRETARIJAT ZA NARODNU OBRANU, GENERALŠTAB JNA, UPRAVA INŽENERIJE, Br. 244, 13.VII.1966. god.

[7] Radić J.: *Design of Bailey bridge*, Undergraduate thesis, University of Zagreb, Faculty of Civil Engineering, Zagreb, 2021, https://urn.nsk.hr/urn:nbn:hr:237:231469 (accessed November 15, 2024)

[8] *Ministri Anušić i Bačić obišli gradilišta nakon potresa u Donjoj Stubici te novoizgrađeni most "Bailey"*, Republika Hrvatska, Ministarstvo obrane, 2023, https://www.morh.hr/ministri-anusic-i-bacic-obisli-gradilista-nakon-potresa-u-donjoj-stubici-te-novoizgradeni-most-bailey/ (accessed January 10, 2025)

[9] Galović J.: *Srušena teško dostupna kuća koja je nastradala u potresu, a do koje je vojska sagradila most*, Večernji list, 2023, https://www.vecernji.hr/galleries/gallery-584028/?page=1 (accessed January 10, 2025)

[10] Perković T.: *40 inženjeraca HV-a danas preko Korane lansiralo dosad najveći Bailey most u Hrvatskoj*, Radio Mrežnica, 2021, https://radio-mreznica.hr/40-inzenjeraca-hv-a-danas-preko-korane-lansiralo-dosad-najveci-bailey-most-u-hrvatskoj/ (accessed January 10, 2025)

[11] *Hrvatska vojska izmjestila most Bailey na novu lokaciju u Općini Marija Bistrica*, Republika Hrvatska, Ministarstvo obrane, 2024, https://www.morh.hr/hrvatska-vojska-izmjestila-most-bailey-na-novu-lokaciju-u-opcini-marija-bistrica/ (accessed January 11, 2025)

[12] Vlahović D.: *Bailey na Krapini – 25 godina poslije,* Hrvatski vojnik, 718, 2024, https://hrvatski-vojnik.hr/bailey-na-krapini-25-godina-poslije/ (accessed January 11, 2025)

[13] *Hrvatski vojnici izgradili lansirni most u Sloveniji*, Republika Hrvatska, Ministarstvo obrane, 2023, https://www.morh.hr/hrvatski-vojnici-izgradili-lansirni-most-u-sloveniji/ (accessed January 12, 2025)

Proceedings of the 3rd Croatian Conference on Earthquake Engineering - 3CroCEE
19–22 March 2025, Split, Croatia
Copyright © 2025 CroCEE
DOI: https://doi.org/10.5592/CO/3CroCEE.2025.129

ENHANCING URBAN DISASTER RISK MANAGEMENT: A TRANSNATIONAL ANALYSIS OF SEISMIC RISK ASSESSMENT FRAMEWORKS IN EUROPE

Jelena Pejovic [(1)], Nina Serdar [(2)], Maria Polese[(3)], René Kastner[(4)], Marta Faravelli[(5)], Marco Gaetani d'Aragona[(6)], Paolo Ricci[(7)], Anže Babič[(8)], Neja Fazarinc[(9)], Serena Cattari[(10)], Valerio Poggi[(11)] Marco Lazzati[(12)], Christina Rechberger[(13)], Can Baran Aktaş[(14)], Mehmet Fırat Aydın[(15)], Özkan Kale[(16)], Rıza Secer Orkun Keskin[(17)]

[(1)] *University of Montengro, Faculty of Civil Engineering, jelenapej@ucg.ac.me*
[(2)] *University of Montengro, Faculty of Civil Engineering, ninas@ucg.ac.me*
[(3)] *University of Naples Federico II, Department of Structures for Engineering and Architecture, maria.polese@unina.it*
[(4)] *Disaster Competence Network Austria, rene.kastner@dcna.at*
[(5)] *Eucentre Foundation - European Centre for Training and Research in Earthquake Engineering, marta.faravelli@eucentre.it*
[(6)] *University of Naples Federico II, Department of Structures for Engineering and Architecture, marco.gaetanidaragona@unina.it*
[(7)] *University of Naples Federico II, Department of Structures for Engineering and Architecture, paolo.ricci@unina.it*
[(8)] *University of Ljubljana, Faculty of Civil and Geodetic Engineering, Anze.Babic@ikpir.fgg.uni-lj.si*
[(9)] *University of Ljubljana, Faculty of Civil and Geodetic Engineering, Neja.Fazarinc@fgg.uni-lj.si*
[(10)] *University of Genoa, serena.cattari@unige.it*
[(11)] *National Institute of Oceanography and Applied Geophysics,, vpoggi@ogs.it*
[(12)] *University of Genoa*
[(13)] *Disaster Competence Network Austria, christina.rechberger@dcna.at*
[(14)] *TED University, can.aktas@tedu.edu.tr*
[(15)] *TED University*
[(16)] *TED University, ozkan.kale@tedu.edu.tr*
[(17)] *TED University, secer.keskin@tedu.edu.tr*

Abstract

This paper presents a comparative analysis of seismic risk assessment frameworks within the context of urban disaster risk management (DRM) in European transnational borders, as part of the BORIS2 project. BORIS2 project aims to enhance multi-risk assessment methodologies for emergency conditions at urban scales across country borders in Europe. The project seeks to establish a replicable model of cross-border cooperation in the prevention phase of natural disasters, thereby enhancing the capacity of EU countries to manage and mitigate risks associated with seismic and flood events. In this paper, the synthesis of methodologies from Italy, Slovenia, Austria, Turkey, and Montenegro is presented, highlighting the integration and implementation challenges of DRM strategies in managing seismic risk. The research is focused on the evaluation of current seismic risk assessment methods at urban scale. Each country's approach is reviewed, with special attention to hazard, vulnerability, and exposure models for critical structures and infrastructures. The findings reveal significant variation in seismic risk preparedness and response frameworks, underlining best practices and pinpointing areas needing alignment or improvement. For instance, some countries developed advanced tools for evaluating operational efficiency of DRM based on the concept of emergency limit conditions compared to more basic approaches in other countries. The paper discusses these disparities and suggests recommendations for the harmonization of civil protection systems to enhance cross-border disaster preparedness, contributing to the overall goals of BORIS2 in advancing multi-risk assessments in Europe.

Keywords: disaster risk management, urban scale, seismic risk, seismic hazard, vulnerability, exposure models, damage and impact indicators, emergency limit conditions.

1. Introduction

Building on the foundations laid by the BORIS project [1], project Cross BOrder RISk assessment for increased prevention and preparedness in Europe: way forward (BORIS2) [2] aims to extend and

Proceedings of the 3rd Croatian Conference on Earthquake Engineering - 3CroCEE
19–22 March 2025, Split, Croatia
Copyright © 2025 CroCEE
DOI: https://doi.org/10.5592/CO/3CroCEE.2025.129

enhance multi-risk assessment methodologies for emergency conditions at urban scales across transnational borders in Europe. The project seeks to establish a replicable model of cross-border cooperation in the prevention phase of natural disasters, thereby enhancing the capacity of EU countries to manage and mitigate risks associated with seismic and flood events. This paper presents a comparative analysis of seismic risk assessment frameworks within the context of urban disaster risk management (DRM) in European transnational borders, that has already done within work package 2 of the BORIS2 project [2]. It also reviews and evaluates the diverse DRM frameworks, decision-making processes, and legal and institutional arrangements adopted by different countries, highlighting areas for potential alignment.

The approach undertaken in this paper involved an analysis of methodologies from Italy, Slovenia, Austria, Turkey and Montenegro used for seismic risk assessments at the urban level, focusing on their effectiveness in DRM. This analysis covered the hazard, vulnerability, and exposure models used for structures and infrastructures deemed critical during emergencies. Additionally, this paper scrutinized the DRM frameworks of the countries by examining the coordinated responsibilities, prevention, preparedness, and response plans. Overviews of national assessments are later used for a comparative review, ensuring a comprehensive understanding and highlighting points for further alignment.

2. Comparison of seismic risk assessment procedures at urban scale

This section provides summary of an extensive analysis of seismic risk assessment procedures across Italy, Slovenia, Austria, Turkey, and Montenegro. Each country exhibits unique methodologies tailored to their specific environmental and urban challenges, reflecting diverse approaches to seismic risk management at an urban scale. The analysis conducted for each country covers the hazards, vulnerabilities, exposure, damage and impact indicators and tools (platform) for risk assessment. Special attention is given to the role of seismic risk analysis in effective DRM at urban scale.

Italy's seismic risk assessment at the urban scale integrates probabilistic and scenario-based approaches to inform emergency management and disaster planning. Ground motion scenarios, based on probabilistic seismic hazard analysis (PSHA), consider events with a 10% probability of exceedance in 50 years (475-year return period) as specified in the Italian National Guidelines (DPCM 30/4/2021) [3]. If available, localized seismic microzonation studies refine these assessments by accounting for site-specific factors, such as soil amplification and topographical effects, enabling detailed evaluations of seismic hazards [4]. The exposure model combines census data with municipal inputs to map residential populations, strategic infrastructures, and essential services. For instance, ISTAT (Istituto Nazionale di Statistica, National Institute of Statistics) census data – which is available across the overall country - provide building typology, construction age, and structural material details, enabling vulnerability assessments through classification into EMS-98 vulnerability classes [5]. However, the availability of detailed data varies significantly between municipalities, limiting the granularity of assessments. Vulnerability assessments rely on fragility models, such as EMS-98 and region-specific methodologies like Damage Probability Matrix [6] or fragility curves for residential ([7], [8]) and strategic [9] buildings, such as school, based on a scientific consensus-approach. These models estimate building damage levels and their impact on populations, including injuries, fatalities, and homelessness. For strategic infrastructure, such as hospitals and emergency centers, functionality assessments consider operational performance under earthquake scenarios. Indicators also address cascading effects, such as landslides and service disruptions, although their inclusion varies by municipality. Loss estimation models predict population impacts based on building typology, damage state, and occupancy rates, while functionality assessments use serviceability limit states for infrastructure.

Italy's seismic risk assessment incorporates the concept of Emergency Limit Conditions (ELC), established by the Civil Protection Department to ensure urban resilience during and after disasters. ELC defines thresholds for the physical and functional damage levels of urban systems, aiming to protect residents' safety, preserve essential infrastructures, and maintain urban functionality for emergency operations [10], [11] (Fig. 1). The primary objectives of ELC are to safeguard lives, protect buildings and infrastructures, and preserve the social and environmental identity of urban areas [12].

Copyright © 2025 CroCEE
DOI: https://doi.org/10.5592/CO/3CroCEE.2025.129

Critical components of the ELC system include strategic buildings, emergency areas, road networks, and interfering buildings whose collapse could obstruct emergency operations (Fig. 2). Municipalities are required to identify these elements, collect standardized data, and integrate the information into the SoftCLE platform for emergency planning. To support ELC evaluations, advanced tools like the I.OPà.CLE method [13] assess the operational efficiency of emergency systems, while the SMAV method [14] provides an estimate of the operational condition of strategic assets based on data of dynamic response obtained by ambient vibration tests. These tools aid decision-makers in prioritizing interventions and enhancing disaster preparedness. For example, the schematic representation of Fig. 2 illustrates the identification of some ELC components in the urban environmental as preliminary step for assessing their functionality under seismic events according to the procedure currently established in Italy.

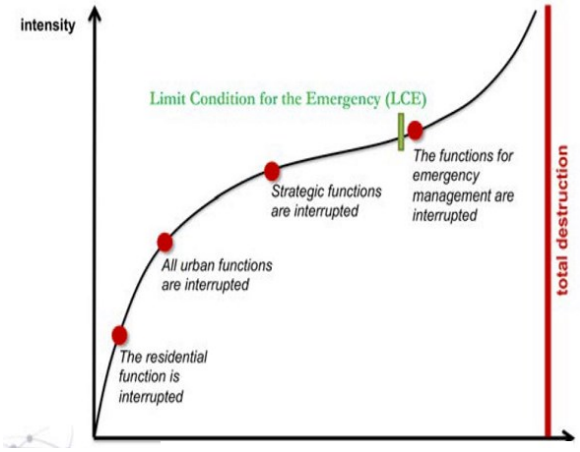


Figure 1. Loss of functionality of the urban system.

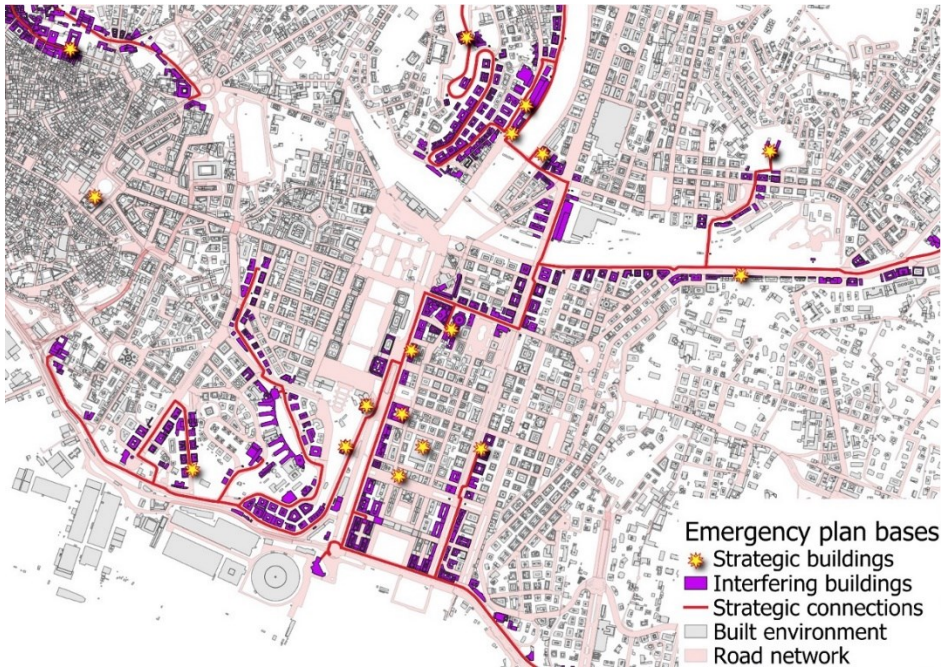


Figure 2. Schematic representation of the ELC components for a portion of the Municipality of Genoa.

In Slovenia, seismic risk assessments for emergency management are carried out at national, regional, and municipal levels, guided by regulatory frameworks such as the Decree on the Content and Elaboration of Protection and Rescue Plans (Official Gazette RS 24/12, 78/16, 26/19) and the Protection Against Natural and Other Disasters Act (Official Gazette RS 51/06, 97/10, 21/18, 117/22). Hazard

Copyright © 2025 CroCEE
DOI: https://doi.org/10.5592/CO/3CroCEE.2025.129

models are based on EMS-98 intensity maps for a 475-year return period, developed using probabilistic spatial smoothing of seismic activity [15]. Vulnerability assessments rely on the POTROG initiative, which categorizes buildings into six vulnerability classes (A to F) using fragility functions derived from the EMS-98 scale [5]. Exposure models integrate data from the Slovenian Real Estate Register, considering buildings, population, and critical infrastructure. While economic losses are primarily based on the value of permanently unusable buildings, indirect losses and repair costs for minor damages are not considered. Additionally, debris volume calculations and road transportability impacts are included, though these indicators are often limited in scope and not consistently integrated into strategic planning. However, limitations include qualitative fragility assessments for infrastructure and the exclusion of indirect economic losses. Scenario-based risk assessments, such as those in Ljubljana [16], incorporate epicenter-specific data and quantitative fragility models but are primarily utilized for post-event response rather than proactive planning. Tools like the POTROG platform [17] support consequence assessment, road transportability analysis, and building damage evaluations, but their integration into strategic DRM planning remains limited (Fig.3).

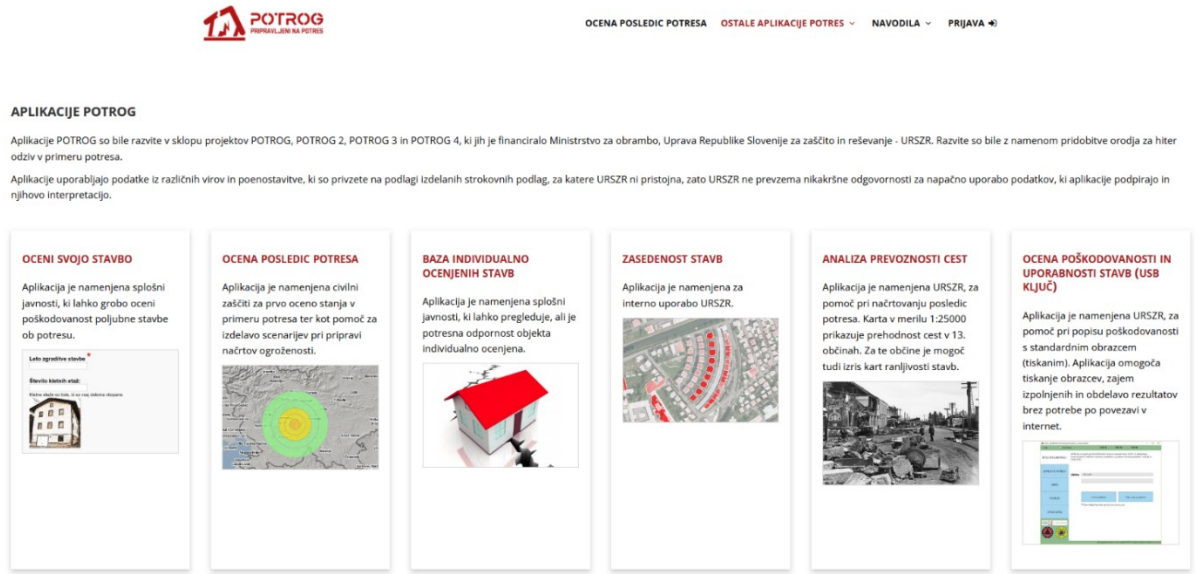


Figure 2. The online POTROG platform [17].

In Austria, seismic risk hazard is governed by Eurocode 8 [18] and its national annexes [19], which define hazard levels. The Austrian seismic hazard map, developed using probabilistic seismic hazard assessment (PSHA), categorizes the country into five zones (0–4) based on peak ground acceleration (PGA) with a 475-year return period. This map accounts for localized geological effects and is complemented by a network of seismological monitoring stations. The new hazard map (2021) incorporates enhanced methodologies, including an updated earthquake catalog and advanced ground motion prediction models [20]. Vulnerability modeling in Austria is in its early stages, focusing on regional data collection for developing exposure and vulnerability profiles. Current seismic assessments use the European Macroseismic Scale (EMS-98) [5] to describe damage intensities, but comprehensive building and infrastructure vulnerability models are not yet implemented. The damage and impact indicators for seismic risk assessment are primarily qualitative and based on historical data, public input, and expert analysis. Tools like the HORA platform visualize hazards for public awareness, while applications like ShakeMaps generate near-real-time intensity distributions following seismic events [21]. Although Austria lacks a detailed risk assessment framework, the integration of seismic hazard maps, real-time monitoring, and public tools provides a robust foundation for disaster preparedness.

Turkey employs advanced seismic risk assessment methodologies at the urban scale, underpinned by the National Earthquake Strategy and Action Plan [22]. The seismic hazard map of Turkey, updated in 2019, incorporates probabilistic approaches to estimate peak ground acceleration (PGA) and spectral accelerations for multiple return periods, including 475 years. This map, accessible through a GIS-based

Copyright © 2025 CroCEE
DOI: https://doi.org/10.5592/CO/3CroCEE.2025.129

application, enables local site adjustments using specific soil factors (e.g., Vs30 values) and supports scenario-based assessments by integrating the active fault map of Turkey [23]. Vulnerability assessments are conducted using fragility curves for damage states (slight, moderate, extensive, complete) based on criteria such as local site conditions and building inventories. The National Disaster Risk Assessment Report [23] defines three main impact criteria: human life and health, economy and environment, and societal functionality. These are further represented by eight indicators, including fatalities, injuries, economic losses, and disruptions to daily life. Impacts are categorized into five levels: limited, significant, severe, very severe, and catastrophic, providing a standardized framework for evaluating disaster consequences.

As an example of urban level assessment, for Istanbul, fragility models are refined using data on building height, structural systems, and construction year, enabling precise district-level risk evaluations. The resulting fragility curves and building inventory data provide insights into damage distribution, as illustrated in the moderately damaged building map for Istanbul under a 475-year return period earthquake [24] (Fig. 4). Exposure models integrate comprehensive building and population datasets alongside infrastructure details, as seen in Istanbul's building inventory maps (Fig. 5).

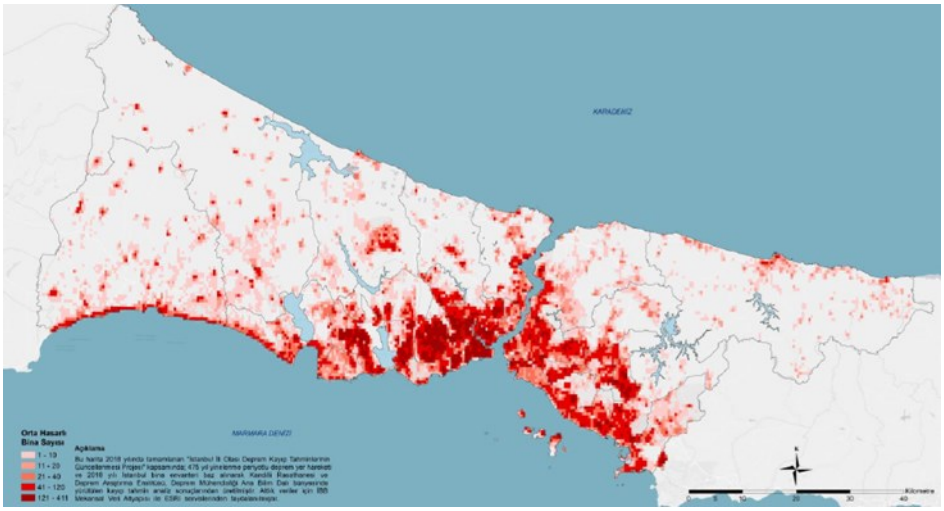


Figure 4. Moderately damaged building distribution estimate for a ground motion with a return period of 475 years (Istanbul, Turkey) [24].

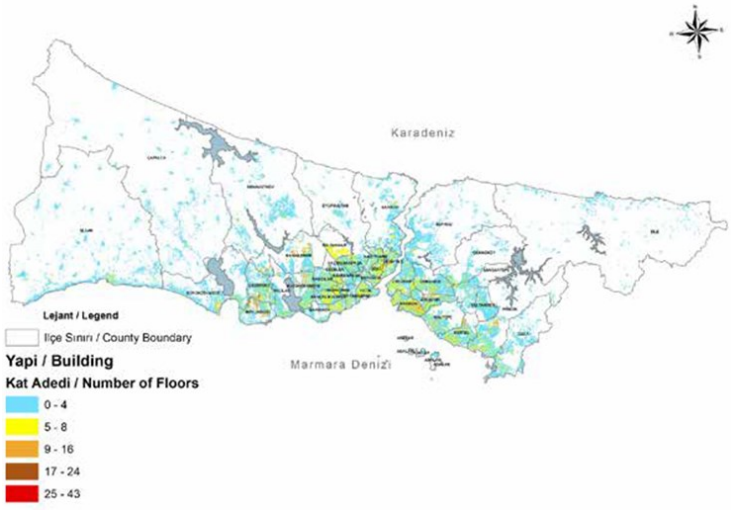


Figure 5. Building stock in Istanbul (Turkey) [24].

AFAD's platforms, such as the Rapid Earthquake Damage and Loss Estimation System (AFAD-RED), facilitate near real-time loss estimations and generate actionable outputs, including damage maps,

Copyright © 2025 CroCEE
DOI: https://doi.org/10.5592/CO/3CroCEE.2025.129

casualty estimates, and lifeline impacts. The system supports the Disaster Management and Decision Support System (DMDS), enhancing response coordination and recovery efforts at provincial and national levels.

In Montenegro, seismic risk assessment methods are integrated into municipal protection and rescue plans, guided by the Rulebook on the Methodology for Developing Protection and Rescue Plans from 2008 [25]. These plans include hazard analyses, vulnerability assessments, and exposure models to inform emergency preparedness and response strategies. Hazard models primarily rely on scenario-based approaches, focusing on credible ruptures and utilizing empirical relationships to estimate peak ground acceleration (PGA) and EMS-98 intensity. Detailed grid analyses refine hazard evaluation, accounting for local soil amplification effects ([26]-[28]). Vulnerability assessments use various models, including the EMS-98 methodology [5], IZIIS model (1984) [29], and ATC-21-1 framework [30], to estimate potential damage across residential buildings and critical infrastructure. Exposure models draw from census data and literature-based distributions of building typologies, incorporating elements like roads, hospitals, and lifelines. While these assessments address critical components of risk, limitations include a lack of unified methodologies and insufficient databases on building characteristics and local geological conditions. The damage and impact indicators focus on economic losses, impacts on people, and structural damages. Economic losses are estimated using simplified methodologies that relate gross national income to regional or municipal budgets. Human impacts are calculated by predicting casualties, injuries, and shelter needs based on building vulnerability and population distribution, using models such as ATC-13 (1985) [31], HAZUS99 [32]. Municipal plans often emphasize response strategies, such as evacuation routes, temporary shelters, and public communication systems, but the direct integration of risk findings into strategic planning remains limited. The absence of dedicated tools or platforms for urban-scale seismic risk assessment further restricts comprehensive analysis and application.

Furthermore, in the following tables, a comparison of seismic risk assessment procedures at urban scale in five countries, is presented. Each component of risk analysis (hazard, vulnerability, exposure and damage and impact indicators) is compared as presented in Tables 1 to 4. Note that the parameters listed in the tables refer to the typical procedures adopted in countries, and these parameters do not necessarily reflect minimum standard requirements.

Table 1. Hazard assessment for seismic risk at urban level: comparison of practices in countries

Description	**ITA**	**SLO**	**AUT**	**TUR**	**MNE**
Scenario(s) developed	✓	✓		✓	✓
Hazard expressed in probabilistic manner	✓	✓	✓	✓	✓
Return period:					
T=475 years	✓	✓	✓	✓	
Other periods considered	✓				✓
Intensity measures:					
I_{MCS}	✓				✓
EMS-98		✓	✓		
PGA	✓		✓	✓	✓
PGV			✓	✓	
PSA	✓		✓	✓	
Local soil effects:					

Proceedings of the 3rd Croatian Conference on Earthquake Engineering - 3CroCEE
19–22 March 2025, Split, Croatia
Copyright © 2025 CroCEE
DOI: https://doi.org/10.5592/CO/3CroCEE.2025.129

From available microzonation	✓			✓	
Identified through soil category (A, B, C,…)		✓	✓		✓
Topographically based	✓				
Multi hazard scenario developed					

Table 2. Vulnerability model for seismic risk: comparison of practices in countries

Description	**ITA**	**SLO**	**AUT**	**TUR**	**MNE**
For residential buildings:					
Model based on EMS-98 scale (5 damage D1-D5, 6 vulnerable classes A to F)	✓	✓			✓
discrete values		✓			
Fragility curves	✓			✓	✓
Additional model in use (e.g. empirical driven)					✓
For infrastructure:					
vulnerability is analyzed					✓
model from literature					✓

Table 3. Exposure model for seismic risk: comparison of practices in countries

Description	**ITA**	**SLO**	**AUT**	**TUR**	**MNE**
Population					
floating population number	✓	✓	✓	✓	
vulnerable population	✓				
civil protection members treated separately		✓			
Scale of available data for population and buildings used in RA:					
building by building			✓		
sub-municipal (settlements, district)	✓	✓		✓	✓
Available residential buildings attributes at sub-municipality scale:					
number of buildings	✓	✓	✓	✓	
number of stories	✓	✓	✓	✓	
material	✓	✓	✓	✓	

Proceedings of the 3rd Croatian Conference on Earthquake Engineering - 3CroCEE
19–22 March 2025, Split, Croatia
Copyright © 2025 CroCEE
DOI: https://doi.org/10.5592/CO/3CroCEE.2025.129

age of construction	✓	✓	✓	✓	
number of dwellings		✓	✓	✓	✓
occupancy	✓	✓			
Infrastructure:					
only listed		✓	✓	✓	
listed with details on attributes	✓		✓		
listed with details on capacities (hospital capacities, shelter capacities)					✓
Types of infrastructure listed:					
hospitals and health care	✓	✓	✓	✓	✓
transportation network	✓	✓	✓	✓	✓
schools	✓		✓	✓	✓
public and strategic buildings	✓		✓	✓	
cultural heritage	✓	✓	✓		✓
sports facilities	✓		✓		
green/protected areas	✓		✓		
lifelines	✓	✓	✓	✓	✓

Table 4. Damage and impact indicators for seismic risk: comparison of practices in beneficiary countries

Description	**ITA**	**SLO**	**AUT**	**TUR**	**MNE**
On people:					
number of death and injured	✓	✓		✓	✓
displaced	✓	✓			✓
lack of fulfillment of basic needs				✓	
people that need to be evacuated				✓	
trapped by collapsed buildings					✓
Economic losses	✓	✓		✓	✓
Impact on buildings:					
collapsed	✓	✓		✓	✓
unusable	✓	✓		✓	✓
damaged	✓	✓		✓	✓
volume of debris		✓			
Infrastructure					
damage grade	✓				✓
functionality of roads	✓			✓	
functionality of hospitals	✓			✓	

Copyright © 2025 CroCEE
DOI: https://doi.org/10.5592/CO/3CroCEE.2025.129

functionality of strategic buildings				✓	

3. The comparative review of the DRM frameworks in different countries

This section provides a comparative analysis of the existing DRM frameworks in the five countries involved in this study. To achieve this, country's procedural frameworks for DRM were reviewed, with a focus on decision-making processes, planning measures, responsibilities, policies, and the legal and institutional arrangements implemented by relevant DRM stakeholders. The objective of this comparative review was to identify and present key aspects related to the Emergency Management preparedness phase. A set of recommendations aimed at harmonizing practices across the countries are highlighted.

Based on the key aspects such as coordination of responsibilities, prevention, preparedness, and response plans, role of real-time monitoring and warning and alerting activities and tools and maps specifically used for emergency management, similarities and differences between the partner countries are recignized.

The organization of DRM responsibilities varies among the countries, reflecting their unique governance structures. In Italy, the National Civil Protection Service oversees DRM at all levels, with regional and municipal coordination centers activated depending on the emergency scale. Slovenia's system is centralized under the Administration for Civil Protection and Disaster Relief, with municipal bodies tasked with local implementation. Austria's federated approach assigns disaster management to provincial authorities, supported by national resources for large-scale events. Turkey operates an integrated system under the Disaster and Emergency Management Presidency (AFAD), which coordinates provincial and district-level efforts. Montenegro, with a more centralized structure, assigns responsibilities to the Directorate for Protection and Rescue, while municipal teams handle local execution.

DRM planning across all five countries emphasizes hazard and risk assessments, though the level of detail and focus varies. Italy's plans are highly detailed, including vulnerability assessments of at-risk populations and critical infrastructure. Slovenia tailors its plans to risk classifications, requiring detailed plans for high-risk municipalities and facilities. Austria emphasizes topographical and infrastructural conditions in its plans, which are reviewed every three years. Turkey's plans integrate risk reduction, response, and recovery, with separate plans at provincial and district levels. Montenegro's plans, while prescriptive, often remain declarative, with some proactive measures informed by risk analysis.

Monitoring and alert systems differ significantly among the countries. Italy has a comprehensive system integrating meteorological, seismic, and hydrological data, managed by national and regional centers. Slovenia relies on its National Meteorological Service for flood alerts but lacks a real-time seismic warning system. Austria's advanced civil protection siren network is complemented by mobile alerts via the AT-Alert system, which covers a range of hazards. Turkey's Flood Forecast and Early Warning System and earthquake monitoring by AFAD provide real-time data to support response measures. Montenegro's systems are more localized, with earthquake warnings issued by the Institute for Hydrometeorology and Seismology and earthquake notifications managed by the Ministry of Interior.

Each country uses different tools to support emergency management. Italy employs the ELC (Emergency Limit Condition) framework and I.OPà.CLE method for evaluating emergency system operability. Slovenia's POTROG platform provides tools for assessing building damage and transportability after seismic events. Austria's provinces use software like the Executive Information System (FÜIS) to coordinate response efforts in real time. Turkey's AFAD-RED system integrates with its Disaster Management and Decision Support System to generate near-real-time loss estimates.

Proceedings of the 3rd Croatian Conference on Earthquake Engineering - 3CroCEE
19–22 March 2025, Split, Croatia
Copyright © 2025 CroCEE
DOI: https://doi.org/10.5592/CO/3CroCEE.2025.129

Montenegro has developed evacuation maps for some municipalities but lacks a comprehensive digital platform for emergency management.

Based on the conducted analysis, the following recommendations for harmonizing national systems have been identified:

- Nationwide templates for the development of disaster management plans and intervention maps should be provided.
- Harmonization of templates, guidelines and terminology across national borders leads to an improved exchange during preparation and the emergency.
- The content of the plans differs depending on the region and country. This is due to the various hazard processes. A harmonization can be achieved, however, including systematically in the plans the following elements: territory description, identification of hazards and risks and definition of risk/impact scenarios with different levels of information/identification of critical points/exposed elements/objects.
- Standardised collection and availability of data as well as the harmonization of individual datasets are required.
- Emergency management requires the development of operational strategies and intervention options to react efficiently in the event of a crisis and to facilitate the prioritization of resources.
- Specialized tools for emergency management such as ELC might be of interest to other countries/ processes. An exchange across process boundaries and country borders would be beneficial.
- Continuous evaluation, revision and updating of plans, procedures, responsibilities and maps as well as corresponding training and exercises are essential.

4. Conclusions

In this paper, a comparative analysis of seismic risk assessment frameworks within the context of urban disaster risk management (DRM) from Italy, Slovenia, Austria, Turkey, and Montenegro is presented. Each country's approach is reviewed, with special attention to hazard, vulnerability, and exposure models for critical structures and infrastructures. The findings reveal diverse methodologies and practices reflecting their unique environmental, urban, and institutional contexts. For instance, Italy's use of advanced tools like the I.OPà.CLE method, which evaluates the operational efficiency of emergency limit conditions compared to more basic approaches in other countries. Italy and Turkey exhibit the most comprehensive approaches, integrating probabilistic hazard models, detailed vulnerability and exposure assessments, and advanced tools into urban DRM frameworks. Slovenia's and Austria's models are limited by a lack of comprehensive infrastructure assessments. Montenegro faces significant gaps in data availability, and standardized methodologies. Standardizing practices across countries, particularly in vulnerability modelling and tool development, could enhance seismic risk assessments and strengthen disaster resilience at the urban scale.

To harmonize national DRM systems, it is essential to establish standardized templates and guidelines for disaster management plans and intervention maps while aligning terminology and methodologies across borders to enhance collaboration. Plans should consistently include key elements, such as hazard and risk identification, impact scenarios, and critical points, supported by standardized data collection and availability. Developing operational strategies and prioritization frameworks, sharing specialized tools like the ELC framework, and fostering cross-border exchanges are crucial for improving efficiency. Regular updates, evaluations, and training are also necessary to ensure adaptability and preparedness across systems.

Copyright © 2025 CroCEE
DOI: https://doi.org/10.5592/CO/3CroCEE.2025.129

Acknowledgements

This study was performed in the framework of EU project "BORIS2 - Cross BOrder RISk assessment for increased prevention and preparedness in Europe: way forward" funded by UCPM-2023-KAPP with grant n. 101140181.

References

[1] *BORIS - cross BOrder RISk assessment for increased prevention and preparedness in Europe*, European Commission project n. 101004882 – UCPM-2020-PP-AG funded by DG-ECHO (2021-2022) https://www.borisproject.eu/ (accessed January 13, 2025).

[2] *BORIS2 - Cross BOrder RISk assessment for increased prevention and preparedness in Europe: way forward*, European Commission project n. 101140181-BORIS2-UCPM-2023-KAPP funded by DG-ECHO (2024-2025), https://www.borisproject.eu/ (accessed January 13, 2025).

[3] DPCM 30/04/21 (2021): Directive of the President of the Council of Ministers of 30 April 2021- *Guidelines for the preparation of civil protection plans at different territorial level* G.U. 06/07/2021 n.160 (in Italian)

[4] Moscatelli, M., Albarello, D., Scarascia Mugnozza, G., Dolce, M. (2020): The Italian approach to seismic microzonation, *Bulletin of Earthquake Engineering*, **18**(12), 5425-5440, doi: https://doi.org/10.1007/s10518-020-00856-6

[5] Grünthal, G. (1998): *European macroseismic scale 1998*, Centre Europèen de Géodynamique et de Séismologie, Musée National d'Histoire Naturelle, Section Astrophysique et Géophysique, Luxembourg.

[6] Zuccaro, G., Cacace, F. (2015): Seismic vulnerability assessment based on typological characteristics. The first level procedure "SAVE", *Soil Dynamics and Earthquake Engineering*, **69**, 262-269, doi: https://doi.org/10.1016/j.soildyn.2014.11.003

[7] Dolce, M., Prota, A., Borzi, B., da Porto, F., Lagomarsino, S., Magenes, G., ... Zuccaro, G. (2021): Seismic risk assessment of residential buildings in Italy, *Bull of Earthquake Eng* **19**(8), pp. 2999-3032. doi: https://doi.org/10.1007/s10518-020-01009-5

[8] Masi A, Lagomarsino S, Dolce M, Manfredi V, Ottonelli D (2021): Towards the updated Italian seismic risk assessment: exposure and vulnerability modelling, *Bull Earthq Eng.* **19**(8):3253-3286. doi: https://doi.org/10.1007/s10518-021-01065-5

[9] Cattari S, Alfano S, Manfredi V, et al. (2024): *National risk assessment of Italian school buildings: The MARS project experience*, *Int J Disaster Risk Reduct*, 113:104822. doi: https://doi.org/10.1016/j.ijdrr.2024.104822

[10] Dolce, M.., Bramerini, F., Castenetto, S., Naso, G. (2019): *The Italian Policy for Seismic Microzonation*. In Earthquake Geotechnical Engineering for Protection and Development of Environment and Constructions, CRC Press, 2019, pp. 925–937.

[11] Bramerini, F., Cavinato, G.P., Fabietti, V. (2013): *Strategie Di Mitigazione Del Rischio Sismico e Pianificazione*, CLE: Condizione Limite per l'Emergenza, 2013.

[12] Cattari, S., Ottonelli, D., Mohammadi, S. (2024): *EQ-DIRECTION Procedure towards an Improved Urban Seismic Resilience: Application to the Pilot Case Study of Sanremo Municipality*, Sustainability 2024, **16**, 2501, doi: https://doi.org/10.3390/su16062501

[13] Dolce, M., Speranza, E., Bocchi, F. et al. (2018): *Probabilistic assessment of structural operational efficiency in emergency limit conditions: the I.OPà.CLE method*, Bull Earthquake Eng **16**, 3791–3818 (2018), doi: https://doi.org/10.1007/s10518-018-0327-7

[14] Spina, D., Acunzo, G., Fiorini, N., Mori, F., Dolce, M. (2021): *A probabilistic simplified Seismic Model from Ambient Vibrations (SMAV) of existing reinforced concrete buildings*, Engineering Structures, **238**, 112255, 2021, doi: https://doi.org/10.1016/j.engstruct.2021.112255

[15] Šket Motnikar, B., Zupančič, P. (2011): *Seismic Intensity Map of Slovenia*, Ujma 25, 226-231. (in Slovenian)

[16] MOL (2015): *Ocena ogroženosti mestne občine Ljubljana zaradi potresov za uporabo v sistemu zaščite, reševanja in pomoči MOL*, Ljubljana.

[17] POTROG (2019): The online platform. https://potrog2.vokas.si/ (accessed April 22, 2024)

Copyright © 2025 CroCEE
DOI: https://doi.org/10.5592/CO/3CroCEE.2025.129

[18] EN1998-1-1 (2004): *Eurocode 8: Design of Structures for Earthquake Resistance — Part 1-1: General rules and seismic action*, CEN European Committee for Standardisation: Brussels, Belgium, 2020.

[19] ÖNORM EN 1998-1 (2013): *Eurocode 8: Auslegung von Bauwerken gegen Erdbeben - Teil 1: Grundlagen, Erdbebeneinwirkungen und Regeln für Hochbauten (konsolidierte Fassung)*, Austrian Standards International, Vienna

[20] Weginger, S., María del Puy, P. I., Hausmann, H., Lenhardt, W. (2021): *Erdbebengefährdungskarte für Österreich*. 2. Wiener Dynamik Tage 2021. Online: https://epub.oeaw.ac.at/0xc1aa5576_0x003cd36e.pdf, (accessed April 24, 2024).

[21] BMLRT (2024): Austrian Federal Ministry of Agriculture, Regions and Tourism, *HORA – Natural Hazard Overview and Risk Assessment Austria* in: Online www.hora.gv.at, (accessed April 24, 2024).

[22] AFAD (2013): *National Earthquake Strategy and Action Plan* (in Turkish), Disaster and Emergency Management Presidency, Ministry of Interior, Republic of Turkey. Available online: https://www.afad.gov.tr/kurumlar/afad.gov.tr/2403/files/udsep_1402013_kitap.pdf (accessed July 18, 2024).

[23] AFAD (2019): *National Disaster Risk Assessment Report of Turkey (*in Turkish), Disaster and Emergency Management Presidency, Ministry of Interior, Republic of Turkey.

[24] Cakti, E., Safak, E., Hancilar, U, Sesetyan, K. (2019): *Istanbul Province Probable Earthquake Loss Estimates Update Project* (in Turkish), Department of Earthquake Engineering, Kandilli Observatory and Earthquake Research Institute, Boğaziçi University, Istanbul, Turkey. Available online: https://depremzemin.mncdn.com/wp-content/uploads/2020/02/DEZiM_KANDiLLi_DEPREM-HASAR-TAHMiN_RAPORU.pdf (accessed July 18, 2024).

[25] Rulebook (2008): *Rulebook on the Methodology for Developing Protection and Rescue Plans*, Ministry of Internal Affairs and Public Administration; Official Gazette of Montenegro, no 44/2008, 22.7.2008.

[26] Glavatovic, B. (1985): *Izvjestaj o seizmicnosti repona Drpe Mandica U Podgorici*, Republicki seizmoloski zavod Crne Gore, strucna arhiva. (in Montenegrin)

[27] Akkar, S., Bommer, J. J. (2010): Empirical equations for the prediction of PGA, PGV, and spectral accelerations in Europe, the Mediterranean region, and the Middle East, *Seismological Research Letters*, **81**(2), 195-206, doi: https://doi.org/10.1785/gssrl.81.2.195

[28] Ambraseys, N. N., Douglas, J., Sarma, S. K., Smit, P. M. (2005): Equations for the estimation of strong ground motions from shallow crustal earthquakes using data from Europe and the Middle East: horizontal peak ground acceleration and spectral acceleration, *Bulletin of earthquake engineering*, **3**, 1-53, https://doi.org/10.1007/s10518-005-0183-0

[29] IZIIS Model (1984): *Primijenjena metodologija za ocjenu povredljivosti I seizmičkog rizika razvijena na osnovu istraživanja efekata zemljotresa od 15. aprila 1979. godine u SR Crnoj Gori (SFR Jugoslavija)*, IZIIS Skoplje, 1984 (In Montenegrin).

[30] ATC-21-1 (1989): *Applied Technology Council Seismic Evaluation of Existing Buildings: Supporting Documentation*, Redwood City, California.

[31] ATC-13 (1985): Earthquake Damage Evaluation Data for California, *Report ATC-13*, Applied Technology Council, Redwood City, California.

[32] HAZUS99 (1999): *FEMA: Technical Manual*, Federal Emergency Management Agency, Washington, DC

Proceedings of the 3rd Croatian Conference on Earthquake Engineering - 3CroCEE
19–22 March 2025, Split, Croatia
Copyright © 2025 CroCEE
DOI: https://doi.org/10.5592/CO/3CroCEE.2025.131

A BUILDING CLASSIFICATION SYSTEM FOR SEISMIC RISK ASSESSMENT OF GOSTIVAR, NORTH MACEDONIA

Shpresim Ibraimi [(1)], Koce Todorov [(2)], Miroslav Nastev [(3)], Stanislav Milovanovic [(4)]

[(1)] *MSc, Institute of earthquake engineering and climate change Skopje, North Macedonia, shpresim@izikp.mk*
[(2)] *Prof, Civil engineering Faculty, University Ss "Cyril and Methodius" Skopje, North Macedonia, todorov@gf.ukim.edu.mk*
[(3)] *Research scientist, Geological Survey of Canada, Québec, Canada, miroslav.nastev@nrcan-mcan.gc.ca*
[(4)] *Prof, ZIM "Skopje" AD Skopje, North Macedonia, info@zimad.com.mk*

Abstract

Seismic risk assessment is central for planning of the emergency response and short- and long-term mitigation efforts in earthquake prone areas. This paper focuses on the classification of the existing building stock as one of the input parameters. With more than 30,000 inhabitants and urban zone characterized with a large portion of older buildings built before the introduction of the first seismic code in 1964, the city of Gostivar, located about 65 km SW from the capital Skopje, was selected as the study area. The proposed classification system was developed collecting information from national census database, municipal and cadastre archives, literature review, rapid visual screening from street surveys and web services such as Google map. The ongoing detailed inventory consist already of a few thousand buildings with assigned attributes including coordinates, footprint, number of stories, structural material, load bearing system, quality of the construction (code level), and occupancy class (residential, commercial, industrial, governmental, agricultural and religious). Particular attention was paid to the inventory of the essential facilities, such as hospitals, police and fire stations, and schools. The proposed classification scheme is based mainly on roundtable discussions with experienced engineers and on existing exposure models for Skopje developed following the 1963 earthquake, EMS-98, Risk-EU project and GEM building taxonomy. It consists of eight main structural types: wooden (1), unreinforced masonry (3), confined masonry (1) and reinforced concrete (3).

Keywords: seismic risk, building classification system, existing buildings, attributes, building taxonomy

Proceedings of the 3rd Croatian Conference on Earthquake Engineering - 3CroCEE
19–22 March 2025, Split, Croatia
Copyright © 2025 CroCEE
DOI: https://doi.org/10.5592/CO/3CroCEE.2025.131

1. Introduction

Strong earthquakes are among the most destructive natural hazards. Although relatively rare, their negative effects must be adequately addressed to allow communities to withstand, respond and recover from earthquakes. The development of building exposure model represents the first step towards community resilience to seismic events. The process of development of an exposure model at municipal or regional level requires comprehensive methodologies and relies on multi-disciplinary and multi-institutional cooperation and constant updating of the collected information. To date, in North Macedonia as well as other countries in the region, databases from the national census or other statistics do not contain data on the characteristics of the structures.

The exposure studies, as a first step in the seismic risk process are very limited in the region. The first exposure model was done following the 1963 Skopje earthquake, where expert committees collected data and statistics on occurred damage to buildings and their classification according to the structural system and the degree of damage [1]. The RISK-EU project [2] developed building taxonomies for cities in Europe, including Bitola in North Macedonia, while in Europe are developed other building taxonomies, i.e. Syner-G [3], GEM [4].

North Macedonia is one of the seismically active regions in the Balkans, south-eastern Europe. Of major importance is the NE-SW seismotectonic zone extending a few hundred kilometres from Kjustendil (Bulgaria), via the capital Skopje to Vlorë (Albania), since it affects the most densely populated areas with about 60% of the total population [5]. The city of Gostivar was selected as the study area for the present research. It is located about 65 km SW from Skopje at the edge of the Polog graben intersected by several active faults [6]. With a population of more than 30.000 inhabitants, the urban area of Gostivar is characterized with a large portion of older buildings built before the introduction of seismic codes. Most of the recent building stock consists of residential buildings built of reinforced concrete.

This paper focuses on the classification system for the existing building stock in the city of Gostivar, North Macedonia, which will consecutively be used for an urban scale risk assessment study. The proposed building classification system is based mainly on roundtable discussions with experienced engineers and on existing exposure models for Skopje following the 1963 earthquake, EMS-98, Risk-EU and GEM building taxonomies. First a brief description of the study area is provided together with seismotectonic settings. Follows the literature review of the past and present seismic codes in North Macedonia and the most important building taxonomies worldwide. The proposed building classification scheme consisting of eight major structural types is given at the end.

2. Study area

Throughout the geological history, the territory of North Macedonia was exposed to multiple tectonic, magmatic, sedimentation and metamorphic processes. As a result, its relief is predominantly hilly to mountainous with relatively narrow valleys. One such depression is the Polog neotectonic graben, where the Gostivar study area is located in its northern (upper) part, Fig. 1a.

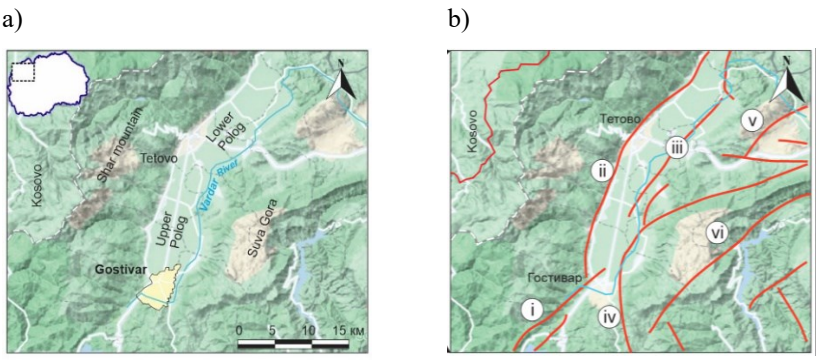


Figure 1. a) location of the Gostivar study area; b) Active fault structures: i) Mavrovo; ii) Shar mountain; iii) Zeden; iv) Suva Gora; v) Rasce; vi) Karsijaka faults. [5]

Proceedings of the 3rd Croatian Conference on Earthquake Engineering - 3CroCEE
19–22 March 2025, Split, Croatia
Copyright © 2025 CroCEE
DOI: https://doi.org/10.5592/CO/3CroCEE.2025.131

The city is located in the Vardar River valley filled with relatively soft geological deposits at the surface with shallow groundwater level. These conditions may contribute to a significant amplification of the amplitude and modification of the frequency of the incoming seismic waves during strong earthquakes.

2.1. Tectonic characteristics

The Polog graben belongs to the Western Macedonian tectonic zone characterized with active radial (vertical) tectonics manifested by increased seismicity. In Fig. 1b are given the confirmed and presumed active faults within the wider study area, given schematically. It can be observed that the main network of approximately parallel faults on both eastern and western sides of Polog, indicated with ii) and iii), dictates the direction of the current flow of the Vardar River. The Shar mountain and Zeden faults extend in the NE-SW direction and belong to the group of normal faults, and located on the foothills of the surrounding mountain chains along the periphery of the valley. Of interest for this study are also the Mavrovo and Suva Gora faults, i) and iv), as the more important faults in the Polog group of faults.

2.2. Seismicity

As a part of the Balkan Peninsula, the territory of North Macedonia belongs to the Eurasian tectonic plate and represents an active seismic area. Therefore, in addition to the seismic hazard from local fault zones within the Polog graben (Tetovo-Gostivar) estimated with a maximum magnitude of M6.1, the potential seismic impacts from more distant and regional zones are also important for the dynamic stability of structures. The most active seismic zones at the regional scale are Skopje M6.5, Ferizaj-Vitina-Kačanik M6.5, Valandovo-Gevgelija M6.9, Mrežičko Kavadarci M6.1, Debar-Peshkopeja M6.9, Struga-Ohrid-Peshtani M6.1, the southern part of Lake Ohrid M6.9, Bitola M6.1 and the most active Pehčevo-Kresna seismic zone M7.9. Among the latest recorded local earthquakes in the Tetovo-Gostivar seismic zone, which can be assumed to be the result of the release of accumulated energy along the Mavrovo Fault, we will mention the earthquakes of: November 11, 2020 with a magnitude of M5.0 and an epicenter 8 kilometers southwest of Vrutok, near Mavrovo Lake; November 11, 2020 with M4.9, 19 kilometers southwest of Gostivar at a depth of 10 km; March 12, 2021 with M4.7 followed by a weaker earthquake M4.2, 18 kilometers southwest of Gostivar. According to the national Annex MKS EN 1998-1/NA:2020, the peak ground acceleration (PGA) and Sa0.2 values for the city of Gostivar are estimated at 0.20-0.25g and 0.55g, respectively, for a return period of 475 years.

3. Building codes, taxonomies and seismic behavior

3.1. Past and current building codes in North Macedonia

In North Macedonia, the building codes evolved gradually with time. Building codes set rules, standards and requirements related to the quality, durability, ductility and safety of structures. Their primary goal is the reduction of damage and losses to buildings from poor construction practices and manmade and natural hazards, such as earthquakes, winds and floods. The first building code on the territory of North Macedonia, then part of ex-Yugoslavia, was introduced with the "Temporary technical guidelines for loading of building structures" in 1948. This code, however, did not contain specific recommendations for reinforced concrete and masonry structures, and eventual dynamic design forces were considered as static loads. The structures were, therefore, designed to withstand the vertical gravity loads only, whereas the resistance to lateral impacts from seismic forces was generally negligible. Still, some of the structures that were designed for wind action suffered minor damage during the devastating 1963 M6.1 Skopje earthquake.

A significant knowledge gain on the potential seismic impacts was acquired following the 1963 Skopje earthquake. Expert committees were formed to collect statistics on occurred damage to buildings and their classification according to the structural system and the degree of damage. This documentation, together with the experiences and regulations of other countries, was used as the basis for the preparation of the new building guidelines, "Temporary regulations for construction in seismic regions" of 1964 (Official Gazette of SFRY No. 39/64). This time the design seismic forces were determined

Copyright © 2025 CroCEE
DOI: https://doi.org/10.5592/CO/3CroCEE.2025.131

based on the assumed seismic shaking intensity, importance of the building, dynamic characteristics of the structure and the soil category. Respective seismic coefficients were recommended according to the seismic zoning map for a return period of 500 years, i.e. zones VII, VIII and IX according to MCS, soil category (weak, moderate and stiff) and the building occupancy. These guidelines contained only basic provisions for reinforced concrete and masonry structures. For example, recommendations and precise guidance were missing for reinforced concrete structures on the reinforcement, anchoring, placement of stirrups and ties in the elements, as well as the use of materials with lower strength was allowed. On the other hand, for masonry structures, no provisions for detailing were prescribed at all, there were only restrictions on the number of storeys depending on the shaking intensity.

Currently, the "Technical regulations for construction of buildings in seismic regions" from 1981 are still in place (Official Gazette of SFRY No. 31/81). According to this code, the equivalent static analysis is mandatory for most of the structures, whereas the dynamic analysis is required for special structures, high-rise buildings over 25 floors and irregular structures. The recommended intensity of seismic shaking is according to the probabilistic seismic hazard analyses (PSHA) for return periods of 50, 100, 200, 500, 1000 and 10000 years through the degree of macro-seismic intensity. A coefficient is introduced that takes into account the importance of the structure, soil category, intensity of seismic shaking, ductility and damping. The ratio of the total lateral force and weight of the structure for buildings of II importance category, built on a medium soil category in a zone with seismic intensity IX varies from 5% for flexible structure, 10% for structures with flexible ground floors, to 13% for rigid masonry structures. Provided are also precise design provisions, details of structural ductility with inclusion of "weak beam-strong columns" failure mechanism, with plastic joints formed at the ends of the elements, details of the reinforcement guidance in all reinforced concrete elements, as well as recommendations for the use of lightweight materials for reinforced concrete frames. These provisions, however, are still descriptive, without specific design guidelines. For masonry structures, provisions are given regarding their spacing, size of openings, thickness and type of element, and mechanical properties. The height of confined masonry structures is limited to 3 floors for zones with seismic intensity IX, to 4 floors for intensity VIII and 5 floors for intensity VII. The allowed height of unreinforced masonry structures is limited to 2 floors for zone VIII and 3 floors for zone VII, whereas this type of structure is not allowed in zones with intensity IX.

New seismic hazard maps were issued with the introduction of the national Annex MKS EN 1998-1/NA: 2020, Fig. 2a and b. These maps were compiled based on the PSHA approach, with the seismic hazard defined with PGA values for return period of 475 yrs ("no-collapse" requirement) and 95 yrs ("damage limitation" requirement). The maps show PGA values for the ground type A, defined as "rock formations", and five and three zones respectively for 475 and 95-year return period. In the calculation of the base-shear force, the PGA value is multiplied by the respective value of the soil factor (S) at the given location, which depends on the spectrum type (1 or 2) and ground type (A to E). Even though MKS EN 1998-1/NA:2020 is in parallel use with current regulations from 1981, almost all designs are done according to the existing code. The next generation probabilistic seismic hazard map with spatial distribution of the spectral acceleration Sa0.2s is given in Fig. 2c [11].

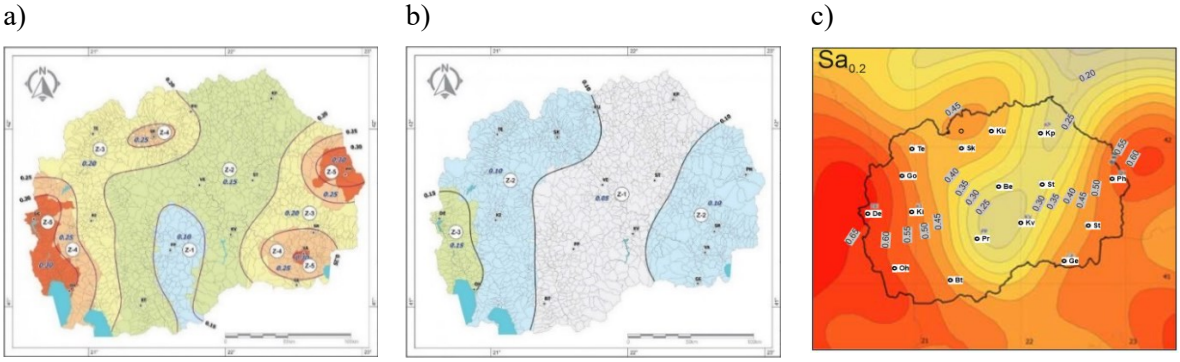


Figure 2. Seizmic hazard maps for PGA for 1/475yrs (a), 95-year return period (b), for soil type A (hard rock) [MKS EN 1998-1/NA: 2020; 11], and (c) for spectral acceleration Sa0.2s for a return period of 475 yrs

Copyright © 2025 CroCEE
DOI: https://doi.org/10.5592/CO/3CroCEE.2025.131

3.2. Existing global and site-specific taxonomies

Creation of a representative exposure model represents the fundamental step in any seismic risk assessment. The most important is the classification of buildings (taxonomy) with respect to their structural system and dynamic behavior during strong seismic motion. Each building class is provided an adequate description with various attributes that cover different characteristics. Depending on the required accuracy and scale of the study area, the exposure model can be based on data collected in-situ with street survey, from municipal databases, from web services such as Google map, and data from national censuses or other statistics. Different taxonomies are currently existing for use at the global and regional levels, which are briefly presented herein.

PAGER-STR is a worldwide taxonomy that classifies buildings into a total of 101 classes based on the construction material, structural system, height, etc [7]. The taxonomy was created by merging existing taxonomies and later supplemented with building typologies collected from a number of countries. This taxonomy is global and is mainly used for real-time first-hand earthquake damage assessment and earthquake risk analysis.

World Housing Encyclopedia (WHE) is a collection of resources related to building practices in seismically active regions. Its mission is to share experience with different construction typologies and to encourage the use of seismically resistant structures. WHE includes more than 170 different building typologies from more than 45 countries.

HAZUS taxonomy is introduced by the DHS Federal Emergency Management Agency [8] to assess the impact of natural disasters, i.e. earthquakes, floods, tsunamis and hurricanes, on buildings in the USA. The taxonomy is characteristic for North American construction practices based on building typologies proposed by a rapid visual inspection in order to assess their occupancy class and safety. It contains 36 building typologies defined based on the structural system, number of stories (low, medium, high) and damage state (five classes).

Several building taxonomies have been developed for the European construction practices. According to the EMS98 - Macroseismic Scale [9] buildings are classified into 15 classes (7 masonry structures, 6 reinforced concrete structures and one steel and one wood structure) based on material and various structural characteristics. Each building class is characterized by an expected vulnerability (six classes). The RISK-EU project proposed building taxonomies for seven selected cities in Europe, including Bitola in North Macedonia. The structures are classified into 23 building classes depending on the structural system, construction material (masonry, reinforced concrete, steel, wood), number of stories (1-2, 3-5, 6+) and quality of construction defined with seismic code level (high, moderate, low and pre code), for a total of 65 building classes [2]. SYNER-G taxonomy includes 15 attributes and is used to classify buildings in a flexible non-hierarchical manner [3]. GEM building taxonomy [4] describes buildings through 13 attributes which are associated with building characteristics that can potentially affect seismic performance.

Although it is a common practice to use taxonomies developed in other regions, this can cause important epistemic uncertainties in the damage model. In addition to this type of uncertainties, it is important to keep in mind that the process of direct classification of buildings into pre-determined classes can be partially biased with respect to the expert experience. In addition, by assigning a given class, some of the information on the structural and non-structural elements is lost. In the phase of data collection, a large number of attributes can be observed and recorded. However, most often only a part of these attributes is used for the actual classification of buildings. Namely, at the application stage, most of this data can be rejected (not used) by using simplified taxonomies that may not fully capture the properties of a building stock. Therefore, it is suggested that the building taxonomy must be sufficiently flexible to allow a classification of the buildings present in the respective study areas that captures the basic characteristic and features that may be used to validate the selected category.

Copyright © 2025 CroCEE
DOI: https://doi.org/10.5592/CO/3CroCEE.2025.131

3.3.Seismic behavior of buildings during the 1963 M6.1 Skopje earthquake

Although it occurred more than 80 years ago, the 1963 M6.1 Skopje earthquake is still the most destructive recent earthquake in North Macedonia. It caused significant human casualties and physical and social damage. It is estimated that a total of 1.500 people died and more than 4.000 were injured. There are unfortunately no seismic records of the earthquake, and according to a few data from seismological stations, the epicenter was located in the northern part of the city, with an estimated depth of 2 - 5 km, and a moment magnitude 9° according to the MCS scale, which corresponds to a moment magnitude M6.1. According to recent analyses [10], the magnitude of the earthquake was estimated at M5.9, the activated fault zone had dimensions of 15x8 km, depth of 2 km, dip of 79°, and strike in the northwest-southeast (NW-SE) direction.

The main reason for the collapse of most of the buildings was that they were designed to withstand vertical gravitational loads only, whereas the resistance to impacts from lateral seismic forces was generally negligible, Fig. 3. Some of the buildings that were designed for wind action suffered minor damage. The most common high damage and collapse states were observed in the older unreinforced masonry buildings (mainly sun-dried bricks), in buildings with weak horizontal and vertical connections between load-bearing elements, in RC buildings with shear walls and infills with poorly reinforced concrete columns and small cross-sectional dimensions. The poor quality of the built-in materials and the poor quality of the construction and maintenance of the buildings contributed to additional weakening of the load-bearing capacity of the structural systems.

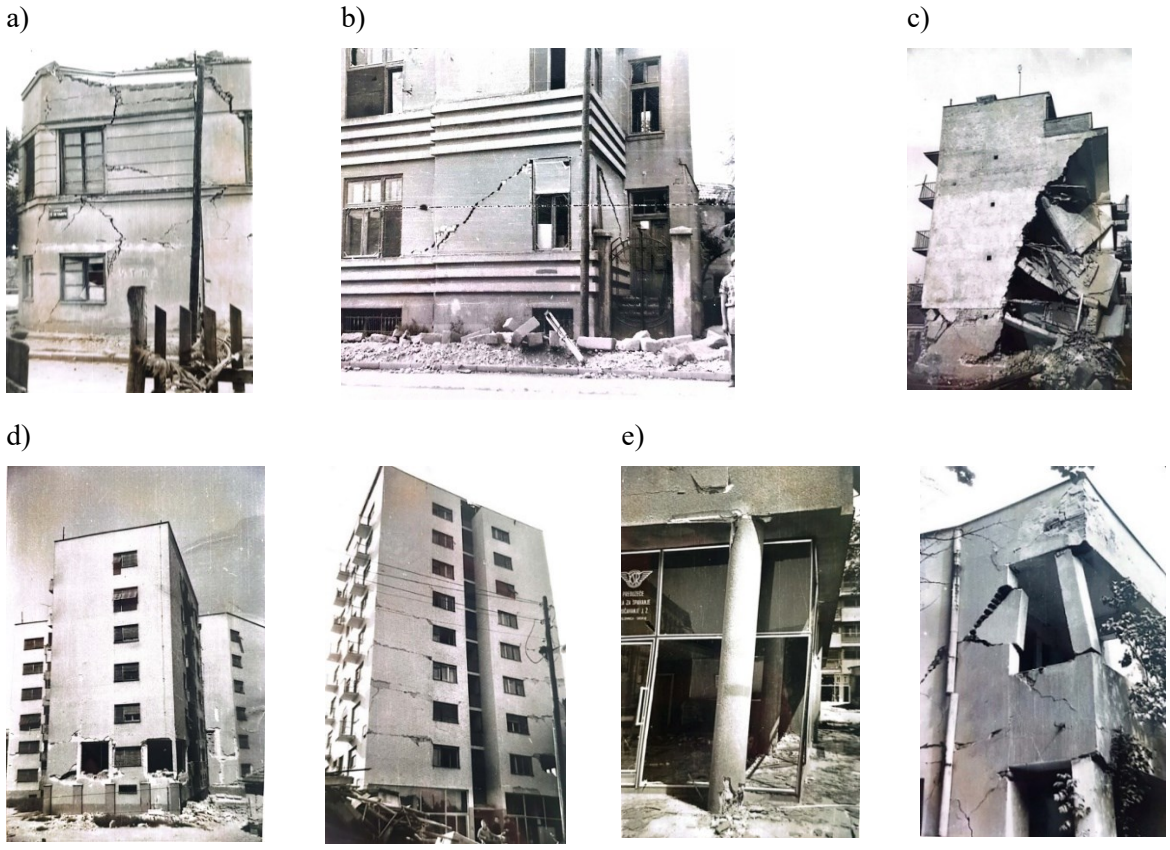


Figure 3. Typical damage during the 1963 Skopje earthquake: a) lack of horizontal/vertical connections, b) diagonal cracks in masonry at ground level; c) collapse of corners and walls due to lack of horizontal/vertical connections; d) separation of walls from the floor structure and partial damage to columns and beams, e) damage to columns due to low stiffness, sparsely placed stirrups and poor horizontal/vertical connections [1].

Buildings with a wooden frame (W) behaved relatively well under seismic loading and large transient deformations. They suffered small permanent deformations and loss of the infill and insignificant displacements of the frame.

Copyright © 2025 CroCEE
DOI: https://doi.org/10.5592/CO/3CroCEE.2025.131

Buildings of unreinforced masonry with flexible diaphragms (URM2) did not behave favorably and, due to the insufficient stiffness along the height, they were partially collapsed or shaken, which posed a problem for reconstruction. The appearance of cracks due to exceeding the in-plane load-bearing capacity of the walls was a common occurrence, Fig. 3a. In the interior, there were partition walls with a smaller thickness, which contributed poorly to the global building stiffness.

Most of the damage to the unreinforced masonry buildings with rigid diaphragms (URM3) occurred in the ground floor. Diagonal cracks were common due to exceedance of the shear strength under alternating horizontal cyclic loading. This type of failure mechanism was often accompanied by cracks along the joints, due to poor mortar quality. In walls with poor stiffness, a tendency for collapse was observed for the corner joints and the joints of the partition walls. There was also frequent damage and separation of the stairs which were supported by the floor structure and the surrounding relatively solid core of thick masonry. At the similar typology (mid-rise), due to the high initial stiffness and low shear resistance, diagonal cracks appeared on the weakened load-bearing walls, corner joints, horizontal cracks at the level of the floor structures, as well as cracks in the partition walls, Fig. 3b and c.

The reinforced concrete frame buildings (RC1) with lightweight partition walls suffered relatively minor damage, while buildings with solid brick infill walls were quite damaged due to the higher mass. In buildings with central core of unreinforced concrete or reinforced concrete supporting the staircase, the seismic forces were absorbed by the rigid cores, which resulted in high damage, whereas the lighter frame structures were less damaged. In the symmetrical buildings, appeared the separation of the walls from the in-plane axe and their collapse, due to the poor structural connections and poor quality of the material, Fig. 3d. In buildings with reinforced concrete frames and shear walls (RC2), failures in columns occurred due to the low stiffness and low number of stirrups. Other reasons for collapse include weak horizontal and vertical connections and asymmetry of the buildings, Fig. 3e.

4. Simplified taxonomy for the existing buildings

According to the 2021 Census data from the State Statistical Office, the total population in the country was 1.836.716 inhabitants. In the city of Gostivar, the total population was 59.770 thousand inhabitants, with a total of 20.054 households. According to the number of households, 9.777 families (32.814 inhabitants) live in urban and 8.145 families (26.956 inhabitants) are in rural areas. According to this data, the approximate number of buildings in urban areas is 10.000, making it one of the larger cities in the country. Unfortunately, these databases do not contain data on the characteristics of the structures.

The proposed simplified taxonomy for the existing buildings in Gostivar, which covers most of the existing building types in North Macedonia, is based on roundtable discussions with experienced engineers and on existing exposure models for Skopje following the 1963 earthquake, EMS-98, Risk-EU project and GEM building taxonomy. The classification was performed based on the following attributes: material of the load-bearing structural system (wood, masonry, reinforced concrete), structural system (masonry, bearing wall system, frame system), type of floor structure (flexible, rigid), height of the structure, year of construction (related to seismic codes), occupancy, building position within a block and building irregularities. Accordingly, 8 main building typologies are proposed for the city of Gostivar: 1 wooden structure, 4 masonry structures and 3 reinforced concrete structures.

4.1. Wooden frame with infill (W) over brick or stone masonry ground floor

Until the beginning of the 20th century, in addition to stone, wood was used as a traditional material for the structural system and architectural design of individual residential buildings, especially in rural settlements. The structural solutions were dictated by the geographical and climatic conditions and the local traditional construction practices. According to the construction technique, the most commonly used were the mixed construction system, i.e., a combination of stone masonry and light wooden construction, so-called bondruk system, Fig. 4. Depending on the type of the used material, there are several types of buildings:

Copyright © 2025 CroCEE
DOI: https://doi.org/10.5592/CO/3CroCEE.2025.131

- Houses where the bearing stone masonry walls are present in most of the ground floor, first and second floors, while the wooden bondruk construction is present in part of the first and second floor, with an open loggia.
- Houses built entirely of stone masonry, where only the cantilever-shaped front part (doxate, chardak) is of the bondruk construction.
- Tower houses are built entirely of stone masonry walls across three levels with wooden floors.

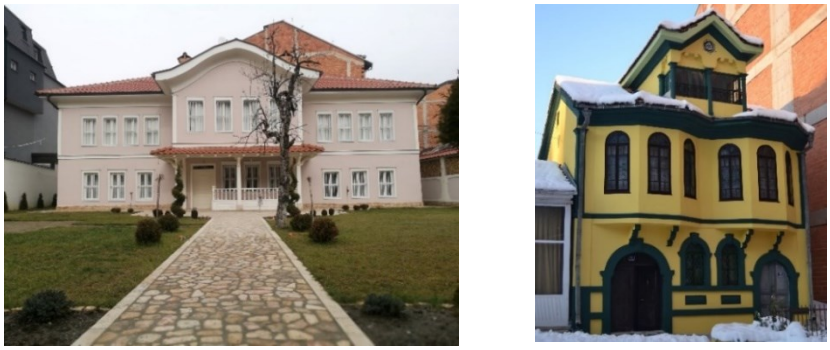


Figure 4. Houses with stone walls on the ground floor and bondruk system on the upper floors, Gostivar (W).

The load-bearing stone masonry walls are usually made of crushed, semi-finished and rarely of finished stone. Hewn stone blocks, in the form of vertical structural elements, are found in the massive ground floors. In stone walls, horizontal wooden strips called "kusacs", visible or built into the thickness of the wall are placed with the function of leveling the stone masonry. Mud is used as a binder for stone walls in older types of buildings, while lime mortar is used in houses from the end of the 19th and first half of the 20th centuries. The frame structure-bondruk consists of a wooden frame made up of columns, horizontal and inclined girders. The filling can be different: wicker, carved planks nailed to both sides of the columns, mud and unbaked bricks. The walls are plastered, and the total thickness varies 18-22 cm. The floor structure consists of a wooden beam system. There are houses without overhang, houses with overhang only on the first or only on the second level, or they can be applied along the entire height. Overhangs are formed by extended beams from the floor structure, supported by a truss, which remain visible or are covered with planks and plastered. The roof structure is in most cases hipped, with a slight slope. The covering is made with slate stone slabs, or with clay tiles (the so-called Turkish type). Mixed structures with wood and stone masonry also belong to this typology. Therefore, the typology could further be break down in subtypes.

4.2. Unreinforced adobe or stone masonry with flexible diaphragms (URM1)

In this typology of structures, several subtypes can be identified. The majority of buildings is built with walls filled with mud or sun-dried bricks, so-called adobe. These buildings are built with a ground floor and an upper floor, with shallow foundations of stone masonry in mud mortar, and a wooden floor structures.

As a representative of the traditional construction of the 19th century is the so-called slamenica (hatched) house, which is characterized mainly as ground-floor buildings with stone walls (60 cm thick) with a mud binder, covered with reeds or straw.

Stone masonry with lime mortar has traditionally been used for the construction of older public buildings, fortresses and religious buildings, such as mosques, churches, monasteries, etc. The vulnerability assessment of these types of structures is usually done on case-by-case basis.

4.3. Unreinforced masonry with flexible diaphragms (URM2)

Constructions of this type were built until the beginning of the 20th century. The buildings were built with a ground floor and two floors, where solid firebricks were used as the structural material for the load bearing walls, Fig. 5. For the construction of the load-bearing walls, “Austrian” type of bricks were

Copyright © 2025 CroCEE
DOI: https://doi.org/10.5592/CO/3CroCEE.2025.131

used with dimensions 14x29 cm with wall thickness 45-60 cm. When smaller brick dimensions were used, the wall thickness was 25-38-51 cm. In the beginning, lime mortar was used as binder, while since 1950, cement/lime mortar was introduced. Similar construction variant was built with stone masonry at the ground floor. The wooden floor structure is composed of a wooden beams with a board formwork. The foundation was made of stone masonry. The roof structure is gable or hipped, covered with tiles.



Figure 5. Unreinforced masonry with solid firebricks and wooden flexible floor, Gostivar (URM2).

4.4. Unreinforced masonry with rigid diaphragms (URM3)

Constructions of this typology can be divided into subtypes depending on the materials used, the period of construction, and the type of floor system, Fig. 6.

Buildings with bearing walls made of baked solid bricks with reinforced concrete floor structure mainly with a ground floor and first floor. The load-bearing walls are 25cm or 38cm thick, while the partition walls are 12cm thick. The floor structures are of semi-prefabricated, type of ribbed RC slab with formed horizontal beams-rings (weakly reinforced) of reinforced concrete on the load-bearing walls. This type was common in the period between the two world wars. The foundations are of unreinforced concrete or stone masonry in cement/lime or cement mortar. The buildings are made of baked brick masonry in lime mortar.

After WW2 are built typical multi-dwelling buildings in urban areas consisted of a ground floor and four floors without an elevator. These structures are with regular and symmetrical footprint. The load-bearing walls are built in two orthogonal directions with solid firebrick with lime or cement/lime mortar. The thickness of the bearing walls is 25 or 38 cm with 12 cm thick partition walls. The foundations are made of unreinforced concrete. The floor structures are of semi-prefabricated ribbed RC slabs with formed horizontal beams-rings (weakly reinforced) of reinforced concrete on the load-bearing walls.

Single-family houses have been built in urban and rural areas after WW2, with a ground floor and one floor on top. The load-bearing walls are built of modular (perforated) bricks or solid bricks in cement/lime mortar. The thickness of the walls varies from 19 to 25 cm. The foundation of these buildings is made of strip foundations made of unreinforced concrete or reinforced strip foundations. In all these types of structures, the concrete strength in the foundations is lower than the above-ground reinforced concrete structure.

Various types of reinforced concrete ribbed floor structures were used. The Herbst system consists of reinforced concrete ribs and a slab of cast concrete with a thickness of 4-5 cm. Another type of semi-prefabricated floor structure is the Avramenko type, with characteristics similar to the Herbst system. In the mid-1960s, a system of semi-prefabricated concrete and brick was used. The “Monta” system consists of hollow brick blocks that constitute the formwork, reinforcement in the ribs (in the space between the blocks) and casting of ribs and a concrete slab with a thickness of 4-5 cm. Another variant is the “Fert” system used since 1980. This system consists of reinforced concrete beams in brick molds with built-in reinforcement, placement of hollow brick blocks between the beams, additional reinforcement and concreting of a rib and a slab with a thickness of 4-5 cm. Following the 1963 Skopje earthquake, the floor structures are most often made as monolith reinforced concrete slabs in both directions. These types of floor structures are used for both masonry and reinforced concrete structures.

Copyright © 2025 CroCEE
DOI: https://doi.org/10.5592/CO/3CroCEE.2025.131

The floor structures in these buildings are treated as rigid horizontal diaphragms, although the behavior of ribbed structures and reinforced concrete monolith slabs is not identical. These structures are covered with gable or hipped wooden roofs made of tiles or as flat terraces.

a) b)



Figure 6. Unreinforced masonry with rigid diaphragms a) single residential house; b) multi-dwelling building, Gostivar (URM3).

4.5. Confined masonry (CM)

This building system dates from 1970. The structure is composed of framed masonry with horizontal and vertical reinforced concrete elements, Fig. 7. These buildings are single or multi-residential built with 1 to 4 floors. The masonry is composed of modular (perforated) or solid clay blocks. The thickness of the walls varies from 19 to 25 cm in cement/lime mortar. The floor structures are executed as reinforced concrete slabs or semi-prefabricated systems (described in the previous section). The roof structures are built as flat reinforced concrete slabs or as sloping wooden roofs. The load-bearing walls are placed above reinforced concrete strip foundation.



Figure 7. Confined masonry with solid bricks or hollow blocks, Gostivar (CM).

4.6. Reinforced concrete frames with masonry infill (RC1)

The first reinforced concrete structures were built only in the 1950s, with a full expansion for residential buildings observed after the 1963 Skopje earthquake. These structures are with rectangular footprint with ground floor usually used for commercial purposes. The number of floors ranges from 6 to 10 floors, whereas it increased to more than 10 floors after 1963, Fig. 8. To increase the rigidity of the structure, reinforced concrete cores is introduced around the staircase and elevator area. The masonry infill was initially made of solid brick and hollow brick after 1963. Characteristic for these buildings is the ground floor with a increased height representing an open space for commercial premises. The foundation is made on single foundations connected with foundation beams or a foundation slab, with concrete of lower strength. The floor structures are constructed with reinforced concrete slabs. For buildings with larger spans, such as business buildings and shopping centers, the construction of floor structures of reinforced concrete cassette slabs is practiced. Following the introduction of the new regulations, “PIOVS 1981”, modern reinforced concrete frame structures are being built, with building materials with stronger strength characteristics.

Copyright © 2025 CroCEE
DOI: https://doi.org/10.5592/CO/3CroCEE.2025.131



Figure 8. Reinforced concrete structures built before and after the 1963 Skopje earthquake, Skopje (photo no.1) and Gostivar (photo no.2, 3) (RC1).

4.7. Reinforced concrete frames with shear walls (RC2)

The application of reinforced concrete shear-walls as a vertical load-bearing system began after 1950. These systems were built with a central core of reinforced concrete walls that were mainly concentrated around the staircase, Fig. 9. The other vertical structural elements consist of reinforced concrete columns or a combination of reinforced concrete columns and walls. The floor structure is of reinforced concrete massive slab, whereas the facade walls are built of non-load-bearing masonry. The main difference between these systems is in the introduction of reinforced concrete core and additional reinforced concrete walls, which contributed to the construction of high-rise structures with more favorable behavior under seismic action. The foundation is most often constructed with a reinforced concrete slab.



Figure 9. Reinforced concrete frames with shear walls, Gostivar (RC2).

4.8. Prefabricated reinforced concrete structures (RC3)

The application of prefabricated reinforced concrete structures began after 1963. There were several different prefabricated systems, mostly the large-panel building system of “Karposh” system, Fig.10.



Figure 10. Prefabricated reinforced concrete structures of the “Karposh” system, Skopje (RC3)

Copyright © 2025 CroCEE
DOI: https://doi.org/10.5592/CO/3CroCEE.2025.131

A large number of residential and industrial buildings have been built in this way due to the shorter construction time and lower costs. The large-panel system consists of reinforced concrete walls and prefabricated floor panels, assembled at the construction site with construction of special connections with steel anchors. The large-panel prefabricated buildings of the "Karposh" type are built usually with 5 to 10 floors, but also for individual residential and industrial buildings.

5. Conclusions

The exposure model is important since it represents the first step in the risk assessment process. It helps to predict and estimate the damage to buildings, social and economic losses. The present study focused on the seismic hazard setting in the study area of the city of Gostivar, North Macedonia, overview of the developed global and regional taxonomies and development of the exposure model for the existing building stock. The building classification system was developed using multiple sources defining attributes that accurately describe the structures. Only buildings of various occupancy categories were taken into account for the classification model. Eight main building categories have been retained: wooden frame with infill (W), unreinforced adobe or stone masonry with flexible diaphragms (URM1), unreinforced masonry with flexible diaphragms (URM2), unreinforced masonry with rigid diaphragms (URM3), confined masonry (CM), reinforced concrete frames with masonry infill (RC1), reinforced concrete frames with shear walls (RC2), prefabricated reinforced concrete structures (RC3). To be included in the risk assessment model under development, each of these categories needs to be further broken down into subtypes with respect to their seismic response and vulnerability.

References

[1] Ibraimi, Sh., Taneski, B., Nastev, M., Milovanovic, S. (2023). 1963 Skopje earthquake: Observed damage to buildings, Macedonian association of structural engineers MASE20, Skopje, North Macedonia

[2] Z. V. Milutinovic and G. S. Trendafiloski. An advanced approach to earthquake risk scenarios with applications to different European towns. Projet europen Risk-UE, 2003.

[3] K. Pitilakis, H. Crowley, and A. M. Kaynia. Syner-g: typology definition and fragility functions for physical elements at seismic risk. Geotechnical, Geological and Earthquake Engineering, 27:1–28, 2014.

[4] S. Brzev, C. Scawthorn, A. W. Charleson, L. Allen, M. Greene, K. Jaiswal, and V. Silva. GEM building taxonomy (Version 2.0). Technical report, GEM Foundation, 2013.

[5] K. Drogreshka, J. Najdovska, and D. Chernih-Anastasovska. Correlation between seismological instruments and seismicity on the territory of the Republic of North Macedonia in the period 1957-2018. Knowledge – International journal Vol.35.3, 2019

[6] R. Salic. (2015). Recent developments of the seismic hazard for N. Macedonia. PhD thesis, Institute of earthquake engineering and engineering seismology, University of Ss. Cyril and Methodius, 316 p. (in Macedonian)

[7] K. Jaiswal and D. J. Wald. Creating a global building inventory for earthquake loss assessment and risk management. Technical report, Geological Survey (US), 2008.

[8] M. HAZUS. Multi-hazard loss estimation methodology. Earthquake Model (HAZUS MH. MR4) Technical Manual. Department of Homeland Security, Emergency Preparedness and Response Directorate, FEMA, 2003.

[9] G. Grünthal. European macroseismic scale 1998 (ems-98). 1998.

[10] Suhadolac, P., Sandron, D., Fitzko, F. et al. (2004). Seismic ground motion estimates for the M6.1 earthquake of July 26, 1963 at Skopje, Republic of Macedonia.Acta Geodaetica et Geophysica39: 319–326

Proceedings of the 3rd Croatian Conference on Earthquake Engineering - 3CroCEE
19–22 March 2025, Split, Croatia
Copyright © 2025 CroCEE
DOI: https://doi.org/10.5592/CO/3CroCEE.2025.139

THE USE OF UAVS IN ASSESSING SEISMIC VULNERABILITY OF EXISTING URM BUILDINGS

Mislav Stepinac[(1)], Lucijano Bajić[(2)], Milan Domazet[(3)]

[(1)] *Faculty of Civil Engineering, University of Zagreb, mstepinac@grad.hr*
[(2)] *ATP Architects Engineers, lucijano.bajic@atp.ag*
[(3)] *AIR-RMLD, milan.domazet@air-rmld.com*

Abstract

This paper explores the use of drones in assessing the seismic resistance of existing buildings. The use of drones, combined with advanced data processing systems, enables remote assessment of structures. The significant advantage of this approach is particularly evident when evaluating hard-to-reach areas, such as roofs and chimneys, reducing the risk to engineers and accelerating the process. The paper provides a critical review of the challenges associated with drone application and proposes further optimization of these methods. In the second part of the paper, a case study is presented to demonstrate the practical application of some of these methods. A drone equipped with an RGB camera and a LIDAR sensor was used to capture and analyze 11 selected buildings, with the data processed using specialized software tools. A macroseismic analysis was also conducted to assess the vulnerability of the analyzed buildings to earthquakes. The results show that drones significantly contribute to seismic risk assessment, providing faster and safer access, especially in urban areas.

Keywords: UAV, drone, assessment, vulnerability, risk, earthquake, URM

1. Introduction

The design, construction, and maintenance of buildings are just some of the areas where unmanned aerial vehicles (UAVs) are applied in the construction industry. The primary advantages of using UAVs compared to traditional methods include time savings, increased efficiency, and enhanced safety. Their application is particularly notable in managing emergency situations, such as earthquakes, where time, efficiency and safety are the top priorities, and UAVs prove to be exceptionally reliable tools in such scenarios. Whether structural resilience is assessed through traditional field inspections or modern technologies, it is crucial to understand the basic typology of damage to the relevant structures to accurately evaluate their actual condition.

In the city of Zagreb, traditional unreinforced masonry buildings dominate the narrow historical center [1–3]. Before the introduction of reinforced concrete floor slabs, inter-story structures were constructed using wooden beams laid on longitudinal walls (walls parallel to the street). The inter-story construction system is generally problematic because it does not provide the desired transfer of horizontal loads, known as the "box effect". Additionally, the main causes of damage include a lack of load-bearing walls in the transverse direction of the building, tall cantilever chimneys, the absence of ties (unconnected masonry), and insufficient load-bearing capacity of roof structures [4]. The most common damages to such buildings typically affect the uppermost parts of the structure, including the collapse or detachment of chimneys and attic gable walls, damage to the roof structure, and issues with other cantilevered elements such as parapets, cornices, projections, and decorative features. The behavior of buildings during earthquakes is a highly complex issue, and studying it requires knowledge of a wide range of scientific fields, including seismology, geology, mathematics, statistics, as well as psychology and related sciences, in addition to civil engineering. Although technology is being implemented in civil engineering very slowly, knowledge in the fields of computer science and programming is increasingly necessary [5].

Proceedings of the 3rd Croatian Conference on Earthquake Engineering - 3CroCEE
19–22 March 2025, Split, Croatia
Copyright © 2025 CroCEE
DOI: https://doi.org/10.5592/CO/3CroCEE.2025.139

Since larger earthquakes expand the scope of the areas that need to be inspected, drones equipped with appropriate equipment significantly accelerate the inspection of large areas in a much shorter time and make the process safer. It should also be noted that, in most cases, the most critical parts of a structure are chimneys and roofs, which gives us another reason to assess their condition using drones [5–8].

Thanks to the extensive efforts of engineers following the Zagreb and Petrinja earthquakes in 2020, guidelines for assessing the usability and condition of buildings after earthquakes are now well-defined [9,10]. However, these procedures rely on visual inspections conducted by engineers, which involve entering buildings and accessing upper floors to evaluate their condition, thereby exposing themselves to immediate hazards. In urban areas, detecting unsafe conditions is further complicated by the limited perspective engineers have from the ground. Data collected by drones provide a comprehensive overview of the situation, making them an indispensable tool for conducting visual inspections of a building's exterior surfaces.

In this paper, preliminary research on using UAVs for vulnerability assessment of unreinforced masonry buildings in urban landscapes is presented. Methodology is presented and parameters often used in macro-seismic vulnerability assessment (like [11,12] are obtained by UAV equipped with LiDAR and RGB camera). The study location was Zagreb, Croatia.

2. Methodology

For the analysis of the seismic resilience of masonry structures, an extended model of the macro-seismic method was applied. This approach has proven effective for evaluating the resilience of a large number of buildings. The assessment of free-standing buildings is based on ten fundamental parameters, while an additional five parameters are considered for buildings in an aggregate [13–18] (Table 1). The influence of each parameter in the analysis is accounted for by applying specific weighting factors. Final results of this method should show seismic vulnerability for different EMS-98 intensity [19].

The DJI Matrice 300 RTK drone, equipped with an RGB camera, a Zenmuse L1 sensor for laser scanning, and an RTK (Real-Time Kinematic) GNSS navigation system, was utilized. Table 1 presents the macro-seismic parameters in relation to the equipment used for their acquisition.

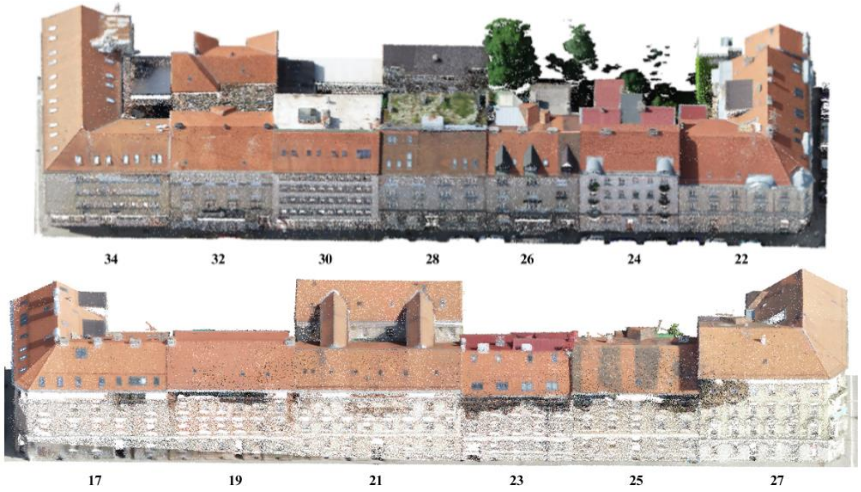
Table 1. Data types based on the drone equipment used

PARAMETER FOR ANALYSIS	DRONE EQUIPMENT
Location of the building	GNSS
Plan irregularity	LIDAR, RGB camera
Vertical regularity	RGB camera
Roofing	RGB camera
Details	RGB camera
Structural condition	RGB camera
Heights of adjacent units	LIDAR
Position of the building within the aggregate	LIDAR, RGB camera
Number of staggered floors	LIDAR, RGB camera
Constructional and structural heterogeneity	RGB camera
Percentage of openings	LIDAR

To examine the practical capabilities of drones in assessing the seismic vulnerability of structures, eleven masonry buildings in aggregate were selected. Parameters for the evaluation were determined based on aerial images obtained by drones. The buildings considered in this case study were constructed in the 19th and the first half of the 20th century and are located within an aggregate, as shown in Figure 1. They are characterized by decorative façade elements and high ceilings. All analyzed buildings are

Copyright © 2025 CroCEE
DOI: https://doi.org/10.5592/CO/3CroCEE.2025.139

masonry structures with wooden floor systems typical of the construction period. The selected buildings serve residential, commercial, or mixed purposes and are part of the historic urban fabric of the city of Zagreb, recognized as protected cultural heritage. RC buildings (street numbers 30 and 34) were not analyzed in this study. However, their influence on adjacent units was considered.



(a).



(b).

Figure 1. (a) LIDAR and (b) RGB (orthophoto) data of the analyzed buildings in the aggregate with indicated street numbers.

As several macro-seismic parameters for the selected regions are often the same [20], here just the ones directly obtained by UAVs are presented.

The parameter “in-plane regularity” is mathematically determined based on the ratios of floor plan dimensions. These dimensions are obtained via a LIDAR sensor on a drone and analyzed in Autodesk Revit 2024 (Figure 1).

Proceedings of the 3rd Croatian Conference on Earthquake Engineering - 3CroCEE
19–22 March 2025, Split, Croatia
Copyright © 2025 CroCEE
DOI: https://doi.org/10.5592/CO/3CroCEE.2025.139

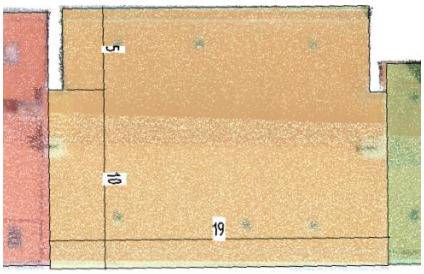


Figure 1. Determination of floor plan dimensions in Revit

The assessment of the building's condition and maintenance was derived from RGB data captured by drones and supplemented with Google Earth analysis (Figure 2). Absolute independence from services such as Google Earth can be achieved by utilizing customized lower flight altitudes.

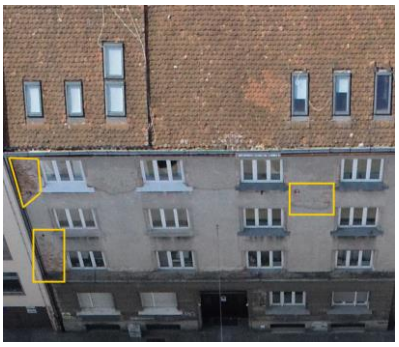
(a)  (b) 

Figure 2. Assessment of the building's condition using (a) an RGB camera mounted on a drone and (b) Google Street View

Presence of adjacent building with different height was easily obtained by LiDAR camera. A model was generated in Revit 2024 based on the imported point cloud (Figure 9), allowing for precise height measurements and the determination of a parameter for macroseismic analysis. As the classification requires only the height ratios of adjacent buildings rather than their exact values, this parameter can also be determined using RGB photogrammetry (Figure 3).

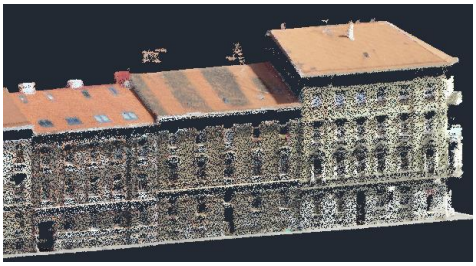
(a)  (b) 

Figure 3. (a) RGB and (b) LIDAR data view of adjacent buildings.

Proceedings of the 3rd Croatian Conference on Earthquake Engineering - 3CroCEE
19–22 March 2025, Split, Croatia
Copyright © 2025 CroCEE
DOI: https://doi.org/10.5592/CO/3CroCEE.2025.139

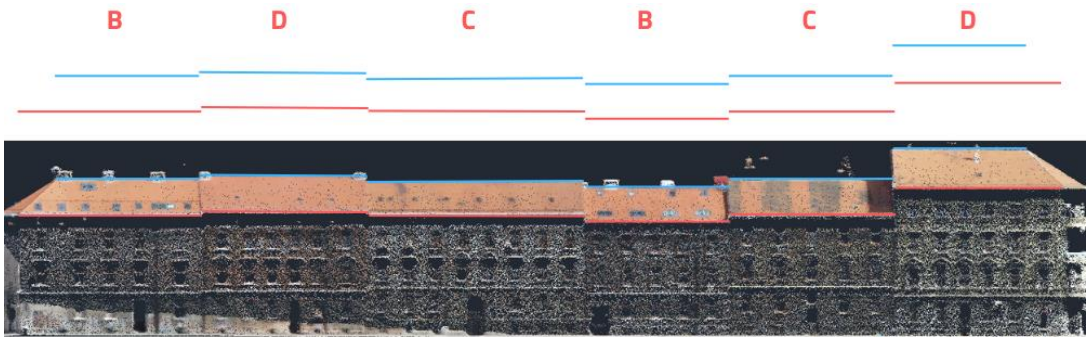


Figure 4. Point cloud classification of buildings with different height (Revit).

The building's position can also have a effect on its seismic response. The position of the analyzed building can be determined using both RGB camera data and LIDAR point clouds (Figure 6).

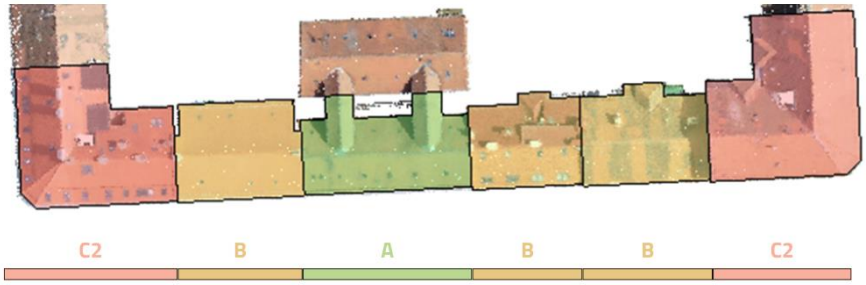


Figure 5. Classification based on building position within the aggregate.

Due to varying construction periods, different buildings were constructed with varying floor heights (older buildings featuring floor-to-ceiling heights exceeding 3.5 meters). This results in staggered floors relative to adjacent buildings. As the number of such instances increases, the adverse effects on the structure are also amplified. One of the consequences is the impact of the intermediate floor structure on the middle of the wall of the adjacent building. For the purposes of this study, the positions of the intermediate floor structures were assumed to be at the balcony levels, which are visible in the point cloud data (LIDAR) and visualized in Revit (Figure 7).

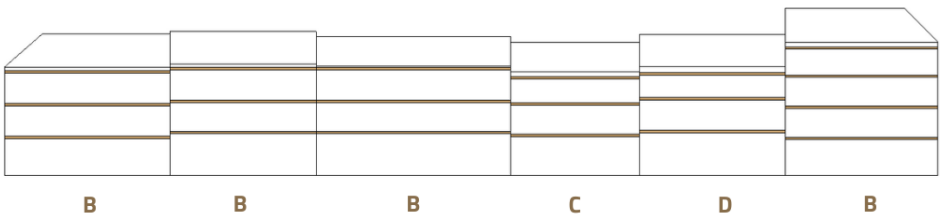


Figure 6. Classification based on number of staggered floors.

3. Results and Conclusion

The preliminary research on the use of UAVs for macro-seismic vulnerability assessment has proven to be valid and offers significant potential for more precise future evaluations. This approach is particularly suitable for urban areas, where flight durations are not excessively time-consuming. In this paper, only a brief overview of the methodology is presented, with vulnerability indices calculated based on knowledge from the literature and data collected using UAVs. Notably, geometrical measurements obtained with LiDAR-equipped UAVs demonstrate exceptional precision. In the following image, the vulnerability assessment of a specific street is illustrated, highlighting parameters that remain consistent or vary due to the similarities among the buildings.

Copyright © 2025 CroCEE
DOI: https://doi.org/10.5592/CO/3CroCEE.2025.139

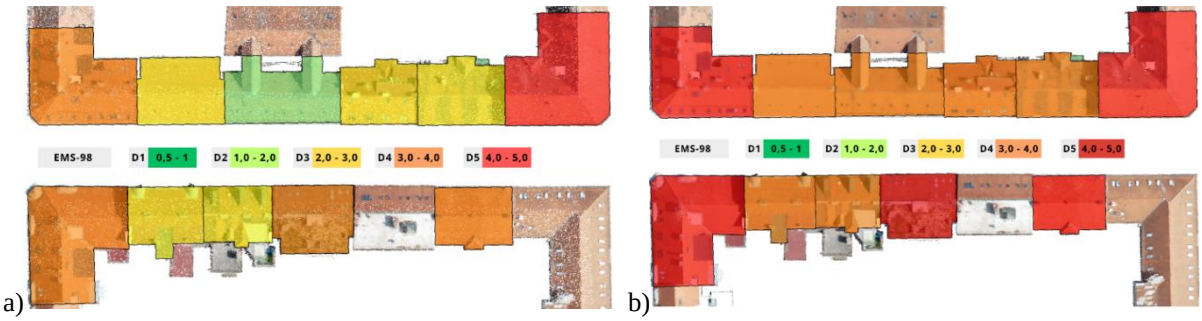


Figure 7. Results of macro seismic analyses for EMS VII and VIII

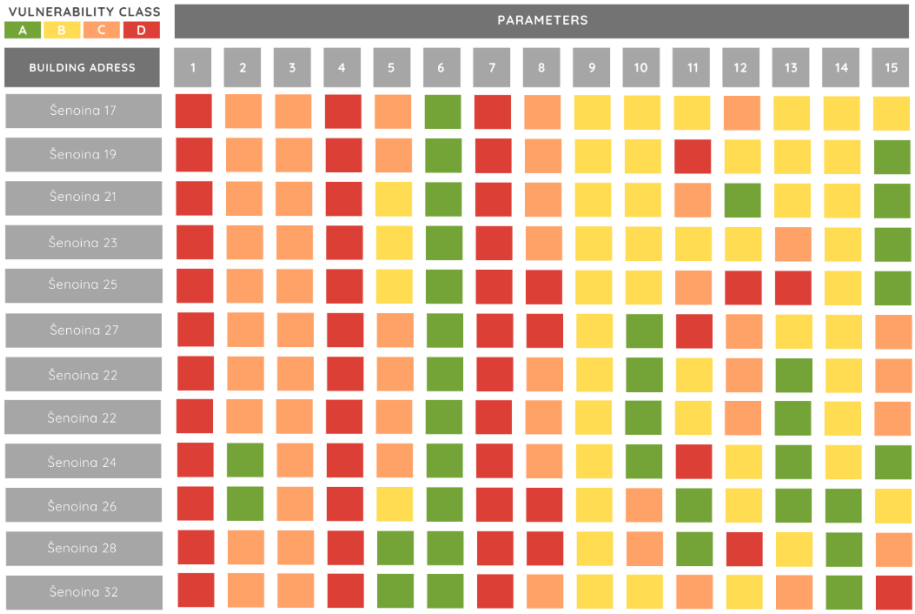


Figure 8. Parameters of macro-seismic analyses for all inspected buildings

In conclusion, this paper addressed the fundamental principles of using drones in the seismic vulnerability assessment of existing buildings, with a particular focus on unreinforced masonry structures constructed prior to the widespread adoption of reinforced concrete systems. The initial hypothesis suggested that drones, equipped with advanced sensors such as LiDAR, and RGB cameras, can significantly enhance the systematic collection and processing of building data, enabling faster and safer assessments, especially in earthquake-affected urban areas. Throughout the study, the importance of utilizing drones in these processes was emphasized, particularly for evaluating hard-to-access and hazardous parts of buildings, such as roofs, chimneys, and tall cantilevered elements.

Data collected with LiDAR and RGB cameras was successfully processed, and seismic vulnerability assessments were conducted using a macro-seismic method. This method was chosen for its ability to evaluate seismic resistance based on geometric and structural parameters of buildings. The selected method considers key factors such as the condition of the structure, the layout and regularity of load-bearing walls, and the type of floor and roof systems. Additionally, the method evaluates the influence of external factors, such as the positioning of buildings within a block and the characteristics of neighboring structures, which is essential for a comprehensive condition assessment. The analysis of selected buildings demonstrated that drones facilitate seismic risk assessments, especially in cases of damage to chimneys, gable walls, and other critical elements that are typically challenging to access using traditional methods.

Copyright © 2025 CroCEE
DOI: https://doi.org/10.5592/CO/3CroCEE.2025.139

Acknowledgements

This research was done in the scope of the HCPI project MZO (IP4) Sustav za brzu detekciju oštećenja nakon potresa na temelju podataka prikupljenih bespilotnim letjelicama (A system for rapid damage detection after earthquakes based on data collected by unmanned aerial vehicles).

References

[1] Stepinac M, Lourenço PB, Atalić J, Kišiček T, Uroš M, Baniček M, et al. Damage classification of residential buildings in historical downtown after the ML5.5 earthquake in Zagreb, Croatia in 2020. International Journal of Disaster Risk Reduction 2021;56:102140. https://doi.org/https://doi.org/10.1016/j.ijdrr.2021.102140.

[2] Hafner I, Lazarević D, Kišiček T, Stepinac M. Post-Earthquake Assessment of a Historical Masonry Building after the Zagreb Earthquake–Case Study. Buildings 2022;12. https://doi.org/10.3390/buildings12030323.

[3] Hafner I, Kišiček T, Gams M. Review of Methods for Seismic Strengthening of Masonry Piers and Walls. Buildings 2023, Vol 13, Page 1524 2023;13:1524. https://doi.org/10.3390/BUILDINGS13061524.

[4] Moretić A, Stepinac M, Lourenço PB. Seismic upgrading of cultural heritage – A case study using an educational building in Croatia from the historicism style. Case Studies in Construction Materials 2022;17. https://doi.org/10.1016/j.cscm.2022.e01183.

[5] Stepinac M, Gašparović M. A Review of Emerging Technologies for an Assessment of Safety and Seismic Vulnerability and Damage Detection of Existing Masonry Structures. Applied Sciences 2020, Vol 10, Page 5060 2020;10:5060. https://doi.org/10.3390/APP10155060.

[6] Haladin I, Stepinac M, Gašparović M, Trifunović N, Domazet M. Rapid post-earthquake damage assessment platform based on UAV and GIS 2021:405–10. https://doi.org/10.5592/CO/1CROCEE.2021.3.

[7] Alsadik B. Crowdsource Drone Imagery – A Powerful Source for the 3D Documentation of Cultural Heritage at Risk. Https://DoiOrg/101080/1558305820201853851 2020;16:977–87. https://doi.org/10.1080/15583058.2020.1853851.

[8] Kucharczyk M, Hugenholtz CH. Remote sensing of natural hazard-related disasters with small drones: Global trends, biases, and research opportunities. Remote Sens Environ 2021;264:112577. https://doi.org/10.1016/j.rse.2021.112577.

[9] Uroš M, Šavor Novak M, Atalić J, Sigmund Z, Baniček M, Demšić M, et al. Post-earthquake damage assessment of buildings – procedure for conducting building inspections. Gradjevinar 2020;72:1089–115. https://doi.org/https://doi.org/10.14256/JCE.2969.2020.

[10] Uroš M, Atalić J, Demšić M, Šavor Novak, Marta Baniček M, Pilipović A, Jevtić Rundek R. Damage to masonry buildings after Petrinja Mw 6.4 earthquake in 2020. Proceedings of the 3rd european conference on Earthquake engineering and seismology, Bucharest: 2022, p. 273–82.

[11] Benedetti D, Benzoni G, Parisi MA. Seismic vulnerability and risk evaluation for old urban nuclei. Earthq Eng Struct Dyn 1988;16:183–201. https://doi.org/https://doi.org/10.1002/eqe.4290160203.

[12] Predari G, Stefanini L, Marinković M, Stepinac M, Brzev S. Adriseismic Methodology for Expeditious Seismic Assessment of Unreinforced Masonry Buildings. Buildings 2023;13:344. https://doi.org/10.3390/buildings13020344.

[13] Chieffo N, Formisano A. Comparative Seismic Assessment Methods for Masonry Building Aggregates: A Case Study. Front Built Environ 2019;5:123. https://doi.org/https://doi.org/10.3389/fbuil.2019.00123.

[14] Maio R, Ferreira TM, Vicente R, Estêvão J. Seismic vulnerability assessment of historical urban centres: Case study of the old city centre of Faro, Portugal. J Risk Res 2016;19:551–80.

[15] Formisano A. Theoretical and Numerical Seismic Analysis of Masonry Building Aggregates: Case Studies in San Pio Delle Camere (L'Aquila, Italy). Journal of Earthquake Engineering 2017;21:227–45. https://doi.org/10.1080/13632469.2016.1172376.

[16] Mallardo V, Malvezzi R, Milani E, Milani G. Seismic vulnerability of historical masonry buildings: A case study in Ferrara. Eng Struct 2008;30:2223–41. https://doi.org/10.1016/J.ENGSTRUCT.2007.11.006.

[17] Ferreira TM, Ortega J, Rodrigues H. Geometrical, constructive, and mechanical characterization of the traditional masonry buildings in the historic city center of Leiria, Portugal. Masonry Construction in Active Seismic Regions 2021:147–74. https://doi.org/10.1016/B978-0-12-821087-1.00004-1.

Copyright © 2025 CroCEE
DOI: https://doi.org/10.5592/CO/3CroCEE.2025.139

[18] Romis F, Caprili S, Salvatore W, Ferreira TM, Lourenço PB. An Improved Seismic Vulnerability Assessment Approach for Historical Urban Centres: The Case Study of Campi Alto di Norcia, Italy 2021. https://doi.org/https://doi.org/10.3390/ app11020849.

[19] Comisión Sismológica Europea. Escala Macro Sísmica Europea EMS - 98. vol. 15. 1998.

[20] Stepinac M, Ožić K, Ninčević A, Funari MF, Lourenço PB. A digital tool based on code indicators to assess the seismic behaviour of existing masonry structures: Application to Croatian residential buildings. Structures 2023;58:105372. https://doi.org/10.1016/J.ISTRUC.2023.105372.

Proceedings of the 3rd Croatian Conference on Earthquake Engineering - 3CroCEE
19–22 March 2025, Split, Croatia
Copyright © 2025 CroCEE
DOI: https://doi.org/10.5592/CO/3CroCEE.2025.142

EMERGE: RAPID MULTI-RISK NEEDS EVALUATION AND PLANNING PLATFORM

Radmila Salic Makreska [(1)], Igor Gjorgjiev [(2)], Julijana Bojadjieva [(3)], Vlatko Sesov [(4)], Roberta Apostolska [(5)], Goran Chapragoski [(6)]

[(1)] *Prof. Dr., Ss. Cyril and Methodius University in Skopje, Institute of Earthquake Engineering and Engineering Seismology (IZIIS), r_salic@iziis.ukim.edu.mk*
[(2)] *Prof. Dr., Ss. Cyril and Methodius University in Skopje, Institute of Earthquake Engineering and Engineering Seismology (IZIIS), igorg@iziis.ukim.edu.mk*
[(3)] *Assoc. Prof. Dr., Ss. Cyril and Methodius University in Skopje, Institute of Earthquake Engineering and Engineering Seismology (IZIIS), jule@iziis.ukim.edu.mk*
[(4)] *Prof. Dr., Ss. Cyril and Methodius University in Skopje, Institute of Earthquake Engineering and Engineering Seismology (IZIIS), vlatko@iziis.ukim.edu.mk*
[(5)] *Prof. Dr., Ss. Cyril and Methodius University in Skopje, Institute of Earthquake Engineering and Engineering Seismology (IZIIS), roberta@iziis.ukim.edu.mk*
[(6)] *Asst. Prof. Dr., Ss. Cyril and Methodius University in Skopje, Institute of Earthquake Engineering and Engineering Seismology (IZIIS), goran@iziis.ukim.edu.mk*

Abstract

The EMERGE project initiative aims to enhance regional disaster management by developing scenario-based and near real-time seismic and landslide risk evaluations. This will enable rapid needs assessments to guide resource allocation at national and regional levels. Building on the achievements of the UCPM CRISIS project, EMERGE seeks to expand CRISIS platform into a tool for rapid needs assessment—a crucial element of civil protection efforts.

The platform to be developed will assist first responders by improving response speed, prioritization, and coordination of resources. EMERGE aligns with Priority 1 of the KAPP-PREV 2024 Call, focusing on risk assessments, anticipation, and planning.

The project is structured into four key areas: (1) defining exposure, resources, and capacities; (2) developing a module for regional multi-hazard real-time scenarios; (3) conducting rapid multi-risk assessments; and (4) creating a web-based platform for needs planning.

EMERGE supports all five 2023 Union Disaster Resilience Goals: anticipate, prepare, alert, respond, and secure. It builds on insights from previous EU UCPM projects, including INFRANAT, CRISIS, and ISRA, leveraging their findings to create a robust and practical framework for disaster management.

Keywords: EMERGE, Multi-Risk, Needs Assessment, Web-based platform, Disaster Resilience Goals.

1. Background and general objectives

Throughout Europe's history and recent past (since year 2000) there have been numerous natural hazards that have had devastating effects on the environment and societies. These include earthquakes, floods, landslides, droughts, extreme temperatures, wildfires, and windstorms, which have caused significant economic, social, and environmental consequences and damages [1]. These events can also impact the emotional and physical well-being of humans and animals, leading to social unrest and homelessness.

The magnitude of these disasters often exceeds the emergency management capacity of a single country, making the multi-country and cross-border (CBR) approaches essential to mitigate their consequences. Unfortunately, the level of prevention and preparedness varies from country to country, and there is usually insufficient regional cooperation to handle the situation effectively. Therefore, it is imperative to establish robust multi-country and CBR collaboration to manage these disasters, which transcend borders and affect the entire region. Without such an effort, their negative impacts will continue to be felt, resulting in long-term economic, social, and environmental consequences.

Copyright © 2025 CroCEE
DOI: https://doi.org/10.5592/CO/3CroCEE.2025.142

Earthquakes and related collateral hazards, such as landslides, are among the greatest natural threat in the wider Balkan region, leading to significant historical losses. For instance, 1962 Fier (Albania, M6.1) earthquake caused 5 deaths, more than 70 injured and 1000 buildings collapsed; Skopje city (North Macedonia) was devastated by a strong earthquake in 1963 (M6.1), resulting in over 1,000 deaths, over 3000 injured and more than 200,000 people homeless; 1967 Debar (North Macedonia, M6.7) earthquake claimed 18 dead and considerable economic loss; in 1969, due to a seismic event Banja Luka (Bosnia and Herzegovina, M6.1) experienced extensive damage, with 86,000 residential units destroyed; 1978 Thessaloniki (Greece, M6.5) earthquake caused 50 victims and more than 220 injured; Montenegrin coastal area earthquake in 1979 (M6.9) resulted in 136 fatalities, more than 1000 people injured, and extensive damage to buildings and infrastructure; 1999 Athens (Greece, M6.0) earthquake 143 claimed victims, more than 1600 injured, and extensive economic loss. The most recent disasters struck Durres (Albania, M6.3) in 2019, causing 51 deaths and €9.8 billion in damages and Zagreb (M5.5) and Petrinja (M6.2) earthquakes in Croatia (2020) causing 8 victims, more than 60 people injured, €10 billion estimated loss. Recent seismic events in Albania (2019) and Croatia (2020) underscore the Balkans' vulnerability to earthquakes and emphasize the need for improved regional cooperation.

Common risk factors across the Balkan region include unplanned urbanization, poor land management, and weak regulations. Thus, the need for reliable seismic risk assessment and post disaster needs planning is therefore evident, recognizing that earthquakes, indifferent to geopolitical boundaries, require a comprehensive understanding of their potential impact across diverse regions. Such assessment should serve as a foundational tool for informed disaster prevention, mitigation strategies, and resilient spatial and urban planning, thus fostering a proactive approach to minimize the societal repercussions of future seismic events.

The European Commission in 2023 published recommendations on Union disaster resilience goals [2] (Fig. 1) with the aim of improving Europe's ability to efficiently respond to various emergencies and disasters. Continuous upgrading of knowledge and capacities to effectively anticipate, respond to, and recover from the impacts of forthcoming or current disasters is fundamental. A crucial precondition for effective crisis and emergency management is having reliable and timely information for the proper allocation of resources and capacities to prioritize disaster measures and activities.

This is the framework for the EMERGE project, with the overall objective of conducting comprehensive multi-country and CBR multi-risk assessment and planning, which involves the rapid identification of needs for early crisis response based on near real-time (NRT) seismic and landslide risk evaluation. The project intends to expand the previously developed CRISIS [3] platform by enhancing speed, prioritization, accuracy, and coordination of post disaster management resources. This expansion will enable first responders in the targeted project cross-border region to provide swift and effective support to those in need following an earthquake and landslide disaster as well as elevate their preparedness to such a future disastrous event. According to the UN 2019 GAR [4] Report, accurate, robust, and near real-time data are needed to effectively guide activities on disaster risk reduction.



Figure 1. EU Disaster Resilience Goals

Copyright © 2025 CroCEE
DOI: https://doi.org/10.5592/CO/3CroCEE.2025.142

Additionally, the project aims to enhance protection against disasters with regional impacts by promoting a culture of prevention and preparedness, facilitating knowledge transfer, and improving cooperation and coordination among civil protection agencies, knowledge providers, and other relevant stakeholders. The project emphasizes the importance of complementarity and interoperability among these entities. It has been structured to operate across four key domains: defining exposure, resources, and capacity portfolios; developing a module for regional multi-hazard NRT scenario analysis; conducting comprehensive multi-risk assessments; and creating a Web-Based Platform (WBP) for rapid multi-risk assessment and needs planning.

The EMERGE project initiative seeks to strengthen knowledge partnerships between civil protection and disaster risk management actors and based on scientific outcomes to inform operational stakeholders. Over the long term, the project aims to continue raising awareness among citizens, local municipalities, businesses, and other relevant stakeholders about the risks they face and the options available to reduce vulnerability, creating synergies and further strengthening the achievements of the ISRA [5] project.

2. Geographic focus and European added value

The EMERGE project is fundamentally aligned with the goals and priorities of the Union Civil Protection Mechanism (UCPM), focusing on enhancing disaster prevention and management capabilities across multiple countries and borders, bridging disparities in disaster preparedness levels, and enhancing the overall European resilience against natural disasters. By conducting thorough multi-risk assessments, improving partnerships based on knowledge, and advocating for a culture of preparedness, the project tackles one of the crucial challenges relevant to the UCPM. It facilitates interaction with primary stakeholders, including civil protection agencies, providers of knowledge, and the wider community.

South-eastern European countries often encounter strong earthquakes that lead to significant economic losses, loss of life, and the destruction of critical infrastructure, public buildings, and cultural heritage. In many instances, these disasters transcend political borders, and not all countries are fully equipped and prepared for a quick and efficient response. Therefore, regional cooperation among countries is crucial for enhancing prevention, preparedness, and response strategies. The successful execution of the planned project activities will further improve the already established cooperation, strengthening the institutional network. This network will continue efficiently to facilitate the exchange of best practices and knowledge in the domain of multi-risk prevention.

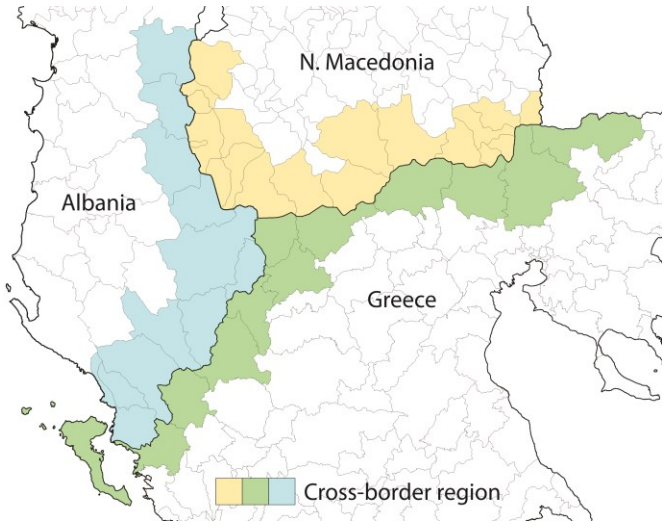


Figure 2. EMERGE pilot region: N. Macedonia-Albania-Greece cross-border region

The geographic focus of the project is the cross-border region of North Macedonia, Albania, and Greece, as indicated in Figure 2. This area includes 18 municipalities in North Macedonia, 11 districts in Albania, and 12 municipalities in Greece. Historically, this region has often been affected by various natural hazards, particularly earthquakes. It is directly influenced by several cross-border seismic sources capable of generating earthquakes with magnitudes even greater than 6. Additionally, this region is prone to landslides due to its topography, lithology, and the distribution of vegetation cover. Triggering factors, such as earthquakes, significantly contribute to the relevance of landslide risks in this area.

Copyright © 2025 CroCEE
DOI: https://doi.org/10.5592/CO/3CroCEE.2025.142

The primary end-users of the project results, CBR National Civil Protection Agencies (NCPAs), are actively engaged as partners in the project. This involvement underscores the importance of the project objectives and ensures both the proper implementation,sustainability and exploitation of the project results.

The EMERGE project is designed to extend its impact beyond a limited regional scope, incorporating a European/transnational dimension. This broader scope is guaranteed by the diversity of the project partners, which include partners from Italy, the Netherlands, and Germany, in addition to primary beneficiaries (institutions coming from North Macedonia, Albania, and Greece). The EMERGE platform to be created will be open-source and modular (multi-risk), enabling re-use and scaling at broader national, regional, and European levels.

Among its various benefits, a direct value added to the EU through EMERGE initiative will be the expansion of the European Integrated Data Archive (ORFEUS-EIDA) [6] network. This expansion will include the integration of the strong motion network of North Macedonia and other CBR strong motion stations not yet connected. As a result, it will enable near-real-time data sharing with the broader EU community and improve seismic monitoring in South-eastern Europe.

Finally, the EMERGE project is set to significantly contribute to the achievement of the EU's 2023 Union disaster resilience goals focusing on effectively anticipating, responding to, and recovering from the impacts of imminent or ongoing disasters. Moreover, on a global scale, the project will support the objectives of Target G of the SFDRR [7], which is dedicated to "Substantially increasing the availability of and access to multi-hazard early warning systems and disaster risk information and assessments to people by 2030" as one of its seven primary targets.

3. Specific objectives

Seismic risk in the Balkan region is continuously increasing due to the growing number and concentration of people and assets in earthquake prone areas. Lessons learned from past, but also recent earthquakes in the targeted CBR (e.g., the latest 2018 Diber, 2019 Korce, and 2022 Florina earthquakes), underscore the need for enhanced regional earthquake prevention, preparedness, and response. It is the primary responsibility of each country to prevent and reduce disaster risk, including through international, regional, subregional, transboundary, and bilateral cooperation. Sustainable and robust CBR, multi-country, and international cooperation can further improve a country's ability to effectively implement national disaster risk reduction policies and measures.

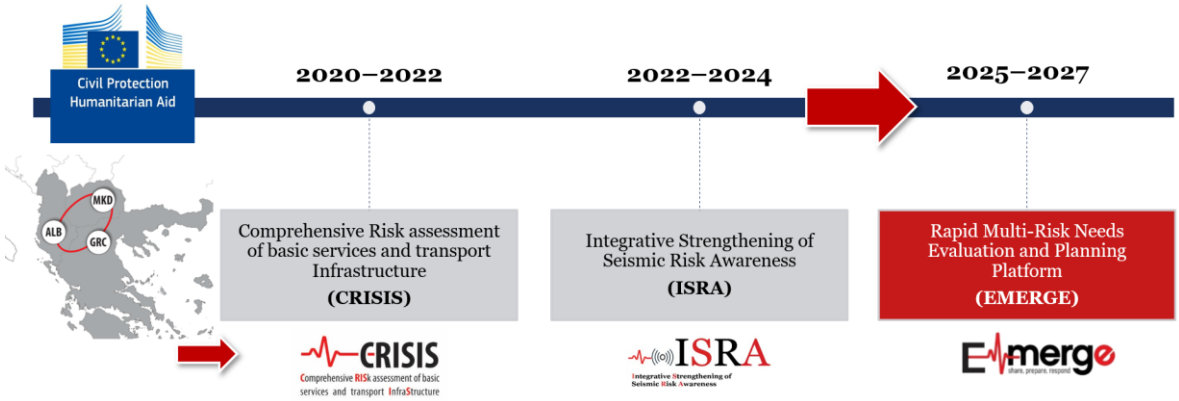


Figure 3. Storyline of recent related UCPM efforts

The establishment of a multi-country and cross-border EMERGE platform is considered necessary, especially to continue what has already been done (Fig. 3) to fill the gaps in several key areas:

1) The need for continuous improved regional prevention, which is still lacking due to insufficient use of best practices, advanced methodologies, and tools in disaster risk management.

Proceedings of the 3rd Croatian Conference on Earthquake Engineering - 3CroCEE
19–22 March 2025, Split, Croatia
Copyright © 2025 CroCEE
DOI: https://doi.org/10.5592/CO/3CroCEE.2025.142

2) A significant gap in multi-risk assessments and preparedness planning, attributed to incomplete exposure models and the limited ability of civil and disaster management bodies to respond effectively.
3) The inadequacy of multi-country and CBR collaboration, highlighted by different levels of prevention and preparedness among cross-border countries and still poor regional cooperation.
4) The necessity to enhance disaster resilience within the region, which falls short of the European Commission's 2023 recommendations for Union disaster resilience objectives.
5) The requirement to further improve culture of prevention and preparedness, due to a lack of knowledge sharing, cooperation, and coordination among civil protection, disaster management agencies, and other essential stakeholders.
6) There is also a noticeable gap in implementing the actions outlined by the EC 2023 Report on Climate Action [8] in addressing the potential effects of climate change on disaster resilience. This includes, for example, not adequately considering how changes in landslide susceptibility as result of climate change might affect the risk of earthquakes-induced landslides.

Having addressed the basic needs for establishment of the EMERGE platform, as further enhancement of CRISIS platform, the specific project objectives are consistent with national civil protection authority's needs, the Call UCPM-2024-KAPP-PV general objectives, and the sustainability of previous UCPM projects (e.g. the CRISIS and ISRA projects), the results of which will be further used and enchased. Following the needs analysis, the objectives of the EMERGE projects can be summarised as:

1) Enhancement of regional prevention through the implementation of best practices and state-of-the-art methodologies and tools in disaster risk reduction.
2) Comprehensive near-real-time multi-risk assessment and needs planning based on a comprehensive exposure model and the coping capacities of civil and disaster management agencies in the region.
3) Robust multi-country and CBR cooperation due to the varying levels of prevention and preparedness across countries and the insufficient regional cooperation.
4) Improvement of disaster resilience in the region through the upgrade of knowledge and capacities based on the EC's 2023 recommendations on Union disaster resilience goals.
5) Strengthening the culture of prevention and preparedness through knowledge transfer, improving cooperation and coordination among civil protection and disaster management agencies, knowledge providers, and other relevant stakeholders.
6) Implement the actions recommended by the EC 2023 Report on Climate Action, specifically addressing the potential impacts of climate change on disaster resilience, including the assessment and mitigation of risks associated with changes in landslide susceptibility and earthquake-induced landslides.

The EMERGE project initiative seeks to address these objectives through a multi-faceted approach that involves comprehensive multi-risk assessment, needs planning, and enhanced coordination among various stakeholders and end-users. This initiative aims not only to mitigate the immediate impacts of earthquake and landslide disasters but also to build a more resilient and prepared region for future challenges.

4. Concept and methodology

The proposed methodology for NRT multi-risk and needs assessment, as outlined in Figure 4, comprises of three main interlinked modules (initially developed under CRISIS Framework) pertinent to CBR of interest as main input for the WBP: (1) Multi-hazard assessment module, which evaluates potential hazards of interest (earthquake & landslides); (2) Multi-risk assessment, which assesses the combined risk of selected hazards; and 3) Needs assessment module, which identifies the specific CBR requirements for efficient crisis management.

EMERGE platform intends to expand the developed CRISIS platform into a comprehensive multi-risk platform for NRT post-disaster needs planning. This enhancement will upgrade all three segments as follows:

Copyright © 2025 CroCEE
DOI: https://doi.org/10.5592/CO/3CroCEE.2025.142

1) Multi-hazard (deterministic and probabilistic) to a NRT multi-hazard assessment.
2) Needs assessment into a rapid NRT post-disaster needs assessment.
3) Expanding the multi-risk assessment focused on basic services and transport infrastructure (CRISIS: schools, hospitals, and bridges) to a more comprehensive assessment, incorporating population and buildings (residential, commercial, and industrial).

The suggested methodology presents an efficient and modular approach for developing the Rapid Multi-Risk Needs Evaluation and Planning Platform - EMERGE. This open-source WBP will be directly utilized by CBR national civil protection and crisis management authorities during real CBR emergencies and disaster scenarios. It will be based on a modular architecture, facilitating future enhancements and the incorporation of additional hazards, assets of interest, and broader spatial coverage.

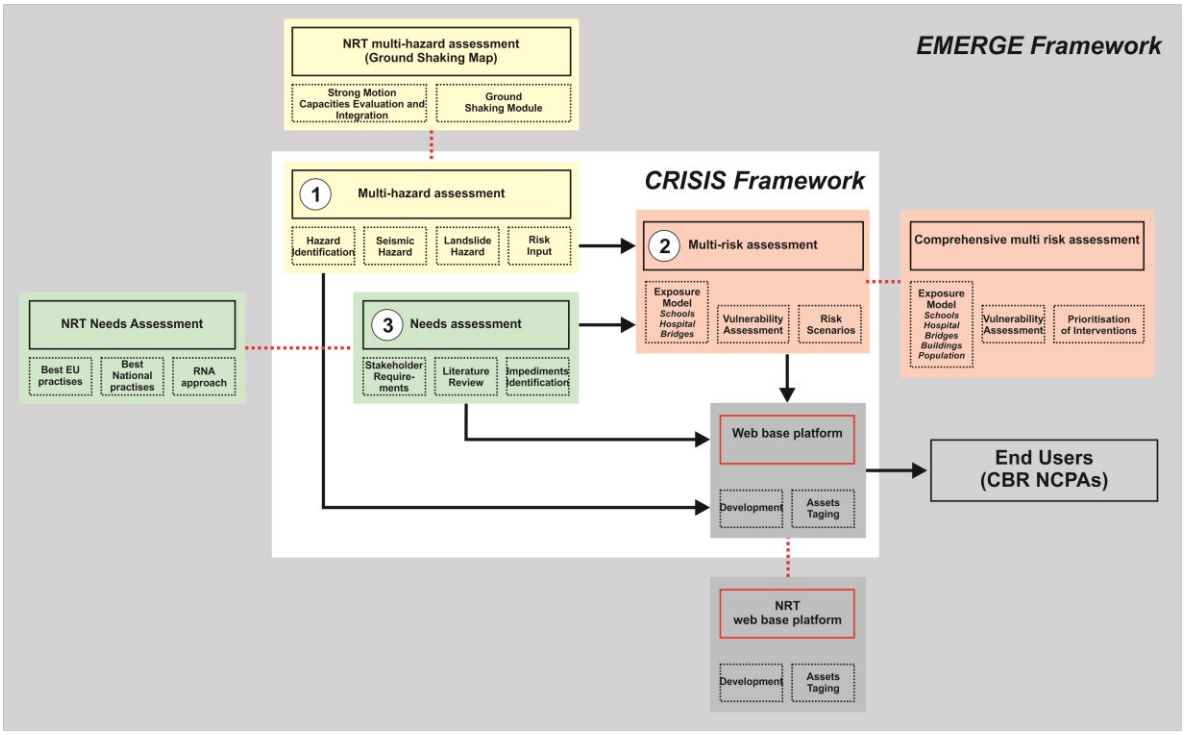


Figure 4. Concept and methodology scheme

5. Outcomes and outputs

To achieve the project objectives, related to a comprehensive assessment of CBR risks and rapid post-disaster needs estimation and planning based on NRT evaluations of seismic and landslide hazards, the following outcomes are expected to be accomplished:

1) Improved understanding and knowledge of current and future disaster risks.
2) EMERGE project proposal emphasizes the importance of a better understanding of the magnitude and potential consequences of present and future disasters in relation to seismic and landslide hazards, underlining the necessity for prevention and preparedness against different emergency scenarios.
3) Harmonised multi-country risk assessments for identified shared risks are developed and/or improved along with the recommendations on the follow-up steps.
4) This involves creating and enhancing unified risk assessment in a pilot region of the CBR countries (North Macedonia, Albania, and Greece) for recognized earthquake and landslide hazards, sharing experiences and strategies to improve CBR preparedness and response, and offering steps towards improvement and better outcomes.
5) Improved sharing of risk data and risk analysis.

Proceedings of the 3rd Croatian Conference on Earthquake Engineering - 3CroCEE
19–22 March 2025, Split, Croatia
Copyright © 2025 CroCEE
DOI: https://doi.org/10.5592/CO/3CroCEE.2025.142

6) EMERGE platform focuses on better distribution and simplification of vital risk assessment parameters and information in the CBR region among civil protection and disaster management agencies, and other stakeholders, thus facilitating more informed operational decisions.
7) Improved cross-border and multi-country cooperation and strengthened exchange of knowledge on risk assessment and risk management planning.
8) Composition of established project consortium highlights the importance of countries working more collaboratively and sharing expertise to effectively assess and manage disaster risks, fostering initiatives that build regional resilience against disasters.
9) Enhanced availability of tools and guidelines on risk assessment and risk management planning.

EMERGE WBP to be established aims to develop and disseminate detailed CBR risk assessment parameters and resources that aid in the assessment and planning for disaster risks, providing stakeholders with essential tools and guidance for efficient regional disaster preparedness and response.

As evidence of the project's progress and efforts, EMERGE project intents achieving the following outputs:

1) Improved risk assessment methodologies of relevance for the UCPM, including to measure and/or enhance the understanding of the impact of current and future disasters.

The EMERGE project activities will enhance risk assessment methodology for a comprehensive multi-risk assessment and needs planning for early crisis/emergency management. This methodology, already applied in the CRISIS project, will be further improved to accommodate the rapid needs planning to efficiently allocate available resources and capacities for an immediate response. The improvement includes: (i) estimating the population distribution and socio-economic vulnerability; (ii) defining/developing/improving an exposure model for buildings (residential, commercial, and industrial), basic services (schools and hospitals), and transport infrastructure (bridges); (iii) conducting a vulnerability assessment and prioritizing interventions for the identified exposure portfolio; and (iv) evaluating the resources, capacities, and capabilities of CBR National Civil Protection Authorities. Undertaking these activities will facilitate the exchange of knowledge and know-how among universities/research institutions (IZIIS, AUTH, UPT-FCE, EUCENTRE, IUSS, NOA), private entities working in civil engineering, disaster preparedness, response, and relief (PPI, JBI and INFRATECH) and the CBR national civil protection and disaster management authorities (PRD, CMC, AKMC and GSCP as well as other stakeholders in risk assessment and risk management planning.

2) Improved or new DRM planning tools.

EMERGE project intents to develop an algorithm that will be integrated into a GIS-oriented tool designed for NRT risk assessment, prioritization, and allocation of resources in the CBR. The tool aims to estimate potential damages and needs, thereby improving the effectiveness of the initial response by relevant CBR emergency and disaster management authorities. Developed tool will be capable of creating NRT scenarios (almost instantly after earthquake detection) but also generate hypothetical (possible) scenarios for prevention and preparedness purposes. These scenarios will aid in planning and refining the actions of first responders. Moreover, it will offer insights on how to prioritize measures and activities to minimize exposure risks to the population, buildings, and critical infrastructure, as well as to mitigate structural vulnerabilities. Furthermore, this tool will prove invaluable in a pre-disaster setting, enabling the conduct of preparedness exercises to identify current shortcomings, enhance knowledge, and improve overall disaster planning strategies.

3) Open-source IT platform for data-sharing.

The EMERGE project will provide an open-source geo-referenced WBP that will be intuitive and user-friendly. The WBP will have to serve well beyond the end of the project. Therefore, it will be designed to be modular, flexible, and expandable, to easily accommodate future updates and

Copyright © 2025 CroCEE
DOI: https://doi.org/10.5592/CO/3CroCEE.2025.142

customizations and to be relevant and useful for dealing with natural or man-made hazards not currently covered in the project. Its design will allow for the continuous refinement and tuning of the exposure and capacity portfolio, ensuring that stakeholders have the tool they need to respond effectively to disasters and emergencies. Through its open-source nature, the developed platform will not only promote innovation and collaboration among users but also ensure that valuable insights and strategies can be developed and shared broadly, benefiting communities and emergency responders.

Acknowledgements

The authors gratefully acknowledge the invaluable contributions and support of all project partners in preparation of the project proposal. This contribution is part of the EMERGE project (GA No. 101193586), financed by the European Union Civil Protection Mechanism under the UCPM-2024-KAPP Call. We thank the funding body for recognizing the value of this idea and enabling its realization in the period Feb 01, 2025 – Jan 31, 2027.

Partner institutions (Fig. 5):

- Ss. Cyril and Methodius university in Skopje, Institute of Earthquake Engineering and Engineering Seismology, N. Macedonia (IZIIS) *Coordinator*
- European Centre for Training and Research in Earthquake Engineering, Pavia, Italy (EUCENTRE)
- Aristotle University of Thessaloniki, Greece (AUTH)
- Polytechnic University of Tirana, Faculty of Civil Engineering, Albania (UPT-FCE)
- University School for Advanced Studies Pavia, Italy (IUSS)
- Crisis Management Centre, Government of Republic of N. Macedonia (CMC)
- Protection and Rescue Directorate, Government of Republic of N. Macedonia (PRD)
- Nacional Civil Protection Agency of Albania (AKMC)
- National Observatory of Athens, Greece (NOA)
- Prepared International, Samerberg, Germany (PPI)
- Janson Bridging International BV, Netherlands (JBI)
- Infratech sh.p.k. Tirana, Albania (INFRATECH)



Figure 5. Partner institutions

References

[1] Overview of natural and man-made disaster risks the European Union may face (2020) Publications Office of the European Union, 2021, ISBN 978-92-76-29303-3; doi:10.2795/1521, KR-03-21-037-EN-N.

[2] European Commission. 2023. Commission Recommendation of 8.2.2023 on Union disaster resilience goals C (2023) 400 final. Brussels. DG ECHO.

[3] CRISIS project: Comprehensive risk assessment of basic services and transport infrastructure (101004830-UCPM-2020-PP-AG).

[4] GAR: Global Assessment Report on Disaster Risk Reduction

[5] ISRA project: Integrative strengthening of seismic risk awareness (101101255-UCPM-2022-PP).

[6] ORFEUS-EIDA: European Integrated Data Archive; https://www.orfeus-eu.org/data/eida/

[7] SFDRR: Sendai Framework for Disaster Risk Reduction, 2015-2023.

[8] COM (2023)653 – Report, EU Climate Action Progress Report 2023.

Proceedings of the 3rd Croatian Conference on Earthquake Engineering - 3CroCEE
19–22 March 2025, Split, Croatia
Copyright © 2025 CroCEE
DOI: https://doi.org/10.5592/CO/3CroCEE.2025.167

EDUCATION OF EXPERTS FOR DAMAGE ASSESSMENT OF BUILDINGS IMMEDIATELY AFTER AN EARTHQUAKE USING XR – PROJECT PROGRESS

Zvonko Sigmund [(1)], Massimo Migliorini [(2)], Karlo Jandrić [(3)], Elios De Maio [(4)], Marina Nadalin [(4)]

[(1)] *Associate professor, University of Zagreb Faculty of Civil Engineering, zsigmund@grad.hr*
[(2)] *Position, affiliation, e-mail address*
[(3)] *Head of response sector, Croatian Centre for Earthquake Engineering – Intervention Service, kjandric@hcpi.hr*
[(4)] *XR Lab Senior Researcher, LINKS Foundation, elios.demaio@linksfoundation.com*
[(5)] *XR Lab Senior Researcher, LINKS Foundation, marina.nadalin@linksfoundation.com*

Abstract

Post-earthquake damage assessment is a critical process carried out by engineers and emergency responders to evaluate structural safety and guide decision-making in the aftermath of seismic events. Traditional training methods face limitations such as restricted access to real damaged structures, safety risks, and high logistical costs. This paper presents the progress of an ongoing project that leverages Extended Reality (XR) technologies to enhance the training of experts in post-earthquake damage assessment. Conducted in collaboration with the University of Zagreb's Faculty of Civil Engineering, the Croatian Centre for Earthquake Engineering (CCEE), and the LINKS Foundation, the project integrates immersive virtual reality (VR) simulations to provide realistic training environments. The development includes high-fidelity 3D models of earthquake-damaged structures, a virtual learning platform, and scenario-based training modules to improve knowledge retention, safety, and decision-making skills. The paper discusses the methodological approach, implementation phases, and preliminary results of the VR-based training pilot, emphasizing its potential to standardize and enhance post-earthquake assessment procedures.

Keywords: XR training, earthquake engineering, damage assessment, virtual reality, expert education.

1. Introduction



Figure 1. Damage to heritage buildings in Petrinja region

Post-earthquake damage assessment is a vital and systematic process conducted by first responders and engineers to evaluate the extent of destruction caused by seismic events on infrastructure and communities. This process is essential not only for ensuring immediate safety and coordination of rescue efforts but also for informing long-term recovery and rebuilding strategies. The assessments typically unfold in multiple phases, starting with rapid initial evaluations that identify visibly damaged structures, followed by more detailed analyses as conditions stabilize and more information becomes available. These activities play a critical role in mobilizing resources and securing federal assistance for affected areas, underscoring their significance in disaster management and recovery efforts.[1][2]. The involvement of diverse teams, including local emergency management agencies, structural engineers, and non-governmental organizations, is crucial for comprehensive damage assessments. First

Proceedings of the 3rd Croatian Conference on Earthquake Engineering - 3CroCEE
19–22 March 2025, Split, Croatia
Copyright © 2025 CroCEE
DOI: https://doi.org/10.5592/CO/3CroCEE.2025.167

responders are typically the first to arrive on the scene, performing rapid inspections to determine the safety of buildings and prioritizing life-saving operations.[3] Engineers complement these efforts by conducting evaluations of structural integrity and advising on safety protocols. Effective communication and collaboration among these groups are essential for overcoming the challenges posed by chaotic post-disaster environments, such as difficulties in documentation and coordination of efforts across different agencies.[4][5]. Despite advancements in technology, including the use of drones and machine learning for real-time data analysis, damage assessment activities still face significant challenges. [6][7].

Traditional training methods for post-earthquake damage assessment have limitations, including restricted access to real damaged structures, safety risks, and logistical challenges. The integration of XR (Extended Reality) technologies offers an innovative approach to overcoming these constraints. By providing immersive and interactive simulations, XR enables experts to experience various earthquake scenarios in a safe, repeatable, and scalable manner.

This paper presents the progress of an ongoing project aimed at utilizing XR for training experts in rapid damage assessment. Conducted in collaboration with CCEE (University of Zagreb, Faculty of Civil Engineering, Croatian Centre for Earthquake Engineering) and the LINKS Foundation, the project involves developing XR-based training modules, creating 3D models of earthquake-damaged structures, and deploying a virtual learning platform to enhance the preparedness and effectiveness of engineers and emergency responders in post-earthquake scenarios.

1.1. Motivation

Engineers play a crucial role in post-disaster response activities, supporting first responders, assessing damage, and assisting in post-earthquake recovery. The immediate post-disaster response phase involves tasks such as rapid structural evaluations to ensure public safety, while the recovery phase includes developing regulatory frameworks to guide reconstruction. In the aftermath of the 2020 earthquakes in Croatia, engineers were deeply engaged in assessing damage to thousands of buildings, establishing vulnerability classifications, and contributing to governmental decision-making regarding financial aid and reconstruction strategies [8].

One of the major challenges encountered during the response to the 2020 Petrinja earthquake was the lack of systematic training for engineers involved in rapid damage assessments. Many engineers had limited prior experience in post-disaster environments, leading to inconsistencies in damage classification and decision-making. Additionally, the high-risk environment of collapsed and unstable structures posed significant safety concerns for assessment teams [9].

To address these challenges, leveraging technological advancements such as Extended Reality (XR) can enhance training programs by providing a safe, immersive, and standardized learning experience. XR allows engineers and emergency responders to engage in realistic simulations of post-earthquake scenarios, enabling them to develop critical decision-making skills and familiarize themselves with damage assessment protocols before working in real disaster zones. Furthermore, digital reconstruction techniques, such as Structure-from-Motion Multi-View Stereo (SfM-MVS) photogrammetry, can create high-fidelity 3D models of damaged structures, offering a valuable resource for training and post-disaster analysis [10].

The integration of XR in expert training is expected to mitigate the limitations of traditional training methods by improving knowledge retention, reducing safety risks, and allowing for repeatable and scalable training exercises. By using XR-based approaches, future engineers and first responders will be better equipped to assess structural damage efficiently, contribute to disaster response efforts, and support the long-term resilience of affected communities.

Proceedings of the 3rd Croatian Conference on Earthquake Engineering - 3CroCEE
19–22 March 2025, Split, Croatia
Copyright © 2025 CroCEE
DOI: https://doi.org/10.5592/CO/3CroCEE.2025.167

2. Why XR/VR for Expert Education

2.1. Limitations of Traditional Training Methods

Traditional training for post-earthquake damage assessment is often conducted in classrooms or through limited hands-on field exercises. These approaches present several challenges:

Earthquake damaged buildings "in use": Conducting field training in real damaged buildings presents numerous dangers, primarily due to the limited controllability of the behaviour both of trainees as well as the limited capability to control the safety of the surroundings in damaged buildings. In addition, most of these damaged buildings do not remain available in the long-term due to their market value or the value of the land on which they are built upon. Thus, they tend to be either demolished or repaired and improved for further use. Additionally, these environments often contain hazardous materials such as asbestos, lead-based paints, and exposed electrical wiring, which pose severe health risks. These risks and limitations make it crucial to develop alternative training methods that provide realistic experiences without endangering the safety of participants.

Cost Related Issues: Implementing in-person training programs often entails significant financial burdens, including travel expenses, accommodation, and equipment procurement. Additionally, securing access to earthquake-damaged structures for training purposes involves high insurance costs and legal considerations. These financial constraints can limit the feasibility of large-scale training initiatives, making it imperative to explore cost-effective alternatives such as XR-based simulations.

Limited Exposure to Scenarios: Traditional theoretical, teacher-led learning methods often fall short in preparing engineers and responders for the unpredictable nature of post-earthquake damage assessment. In such conventional settings, trainees are typically exposed to a limited range of hypothetical case studies, diagrams, and lectures, which may not adequately reflect the complexity and variability of real-world disaster scenarios. As a result, learners may struggle to apply their theoretical knowledge in practical field conditions where unexpected structural failures and diverse damage patterns demand quick, informed decision-making. Without hands-on exposure to a broad range of damage scenarios, professionals may find it challenging to adapt effectively when confronted with unfamiliar or extreme situations in the field.

2.2. Advantages of XR/VR for Training

The integration of Virtual Reality (VR) and Extended Reality (XR) technologies into training for post-disaster damage assessment offers numerous advantages that enhance both the learning experience and the effectiveness of training programs.

Enhanced Learning Experience: One of the primary benefits of VR-based training is its ability to facilitate individualized learning. Trainees can progress at their own pace, allowing for a more thorough understanding of complex disaster-related concepts through asynchronous learning methods [11]. Furthermore, VR applications enable participants to interact with various components of a virtual environment, such as medical interventions and disaster response features, which can mimic real-life scenarios more accurately than traditional methods [11].

Realistic Simulations: VR training provides immersive and realistic scenarios that increase engagement and retention. Participants can experience auditory cues and visual stimuli, which help to recreate the pressure of actual emergency situations, thereby enhancing the learning experience [12] [13]. The realism of these scenarios not only makes training enjoyable but also prepares trainees for the unpredictability and stress of real-world emergencies [12].

Immediate Feedback and Performance Analysis: Another significant advantage is the capability of VR systems to offer immediate feedback and performance analysis. Trainers can observe trainees in real-time, providing corrections and guidance as needed, which fosters a more effective learning environment [14]. Additionally, VR systems can track various metrics, such as response times and

Copyright © 2025 CroCEE
DOI: https://doi.org/10.5592/CO/3CroCEE.2025.167

decision-making processes, allowing for tailored feedback that addresses specific weaknesses in a trainee's performance [14].

Cost-Effectiveness and Logistical Advantages: VR training also presents a cost-effective alternative to traditional training methods. Although the initial investment in VR technology can be substantial, it ultimately leads to long-term savings by reducing the need for expensive physical props and facilities required in live training exercises [14]. Moreover, VR training can be conducted more frequently and with less logistical overhead, enabling regular reinforcement of skills [14].

Long-Term Retention and Skill Development: Long-term retention studies indicate that VR training can significantly enhance knowledge and skill retention over time. This aspect is particularly vital for emergency responders, who must recall critical information and procedures under pressure [14]. The ability to practice in a variety of scenarios also helps to build confidence and improve self-perception among trainees, ultimately contributing to better preparedness in real-life situations [8].

Collaboration and Team Dynamics: Moreover, VR and XR technologies facilitate collaborative training experiences, allowing multiple trainees to engage in discussions and analyses within a shared virtual environment. This capability is essential for training teams on collective decision-making and communication during disaster response scenarios [11] [9].

3. Project Methodology and Progress

A key component of the project is the collaboration with international institutions that specialize in XR-based learning and structural engineering:

- LINKS Foundation (Italy): Provides expertise in XR development, hosting training sessions for engineers, and developing immersive learning environments.
- HCPI (Croatian Centre for Earthquake Engineering): Facilitates data collection of real-world earthquake damage, integrates engineering assessment methodologies into XR training, and ensures alignment with emergency response procedures.
- University of Zagreb Faculty of Civil Engineering: Manages the academic and research aspects of the project, ensuring the integration of XR training into engineering curricula and professional education programs.

The methodology for this project is structured around the development and implementation of XR-based training modules that will be designed to enhance the expertise of engineers and emergency first-responders in post-earthquake damage assessment. The education will be structured to adhere to at least 3 different goals:

- **Education of engineers on assessment of damaged buildings** – so far, the experiences have shown that the so far provided education of engineers usually results with dichotomous results of assessment on site. The assessment methodologies are usually relying on personal live experience of assessors and their subjective explanation of damages.
- **Education of first-responders on initial usability assessment of damaged buildings** – In the immediate post-disaster activities it is relevant to give reliable but safe information to building users on the usability of a building while at the same time not endangering the lives of assessors.
- **Education of first-responders on safe behaviour inside and around the damaged buildings** – this training is most essential for the safety of SAR (Search and Rescue) teams, where a good transfer of relevant and vital information of engineers to rescuers is essential.

The project started in the late 2022 and was structured in 4 phases:

1. Data collection
2. Basic education on VR/XR
3. Creation of the first functional VR environment
4. Cration of the educational platform for engineers and first-responders

Copyright © 2025 CroCEE
DOI: https://doi.org/10.5592/CO/3CroCEE.2025.167

3.1. Data collection

At the outset of the project, the team conducted extensive field surveys to document real-world earthquake damage. This process involved capturing photographic evidence, performing structural assessments, and engaging with local authorities and residents to better understand both the extent of the damage and the challenges faced during emergency response efforts. A crucial element of this phase was the firsthand experience of the project lead and partners, who had been actively involved in post-earthquake activities following the 2020 Petrinja earthquake series.

To enhance data collection, the team employed advanced 3D scanning technology, ensuring a highly detailed and accurate representation of damaged structures. Unmanned Aerial Systems (UAS), including the DJI Matrice 300 and DJI Air 2s, were used for aerial surveys, providing a comprehensive overview of affected areas. For high-precision structural mapping, the FARO Focus M LiDAR scanner was deployed, enabling the capture of intricate building details. Additionally, 360-degree cameras such as the Insta360 X3 were utilized to create immersive visual records, offering a realistic and interactive perspective on the damage conditions.

Through this combination of field expertise and cutting-edge technology, the project established a robust foundation for developing improved post-earthquake damage assessment methods. Utilized 3D scanning technology to capture detailed images of damaged buildings, employing Unmanned Aerial Systems (UAS) such as DJI Matrice 300 and DJI Air 2s for aerial surveys. Additionally, FARO Focus M LIDAR scanner was used for high-precision structural mapping, while 360-degree cameras like Insta360 X3 were deployed to capture immersive visual records of damage conditions.



Figure 2. Damage to a building in Sisak that is about to be demolished

3.2. Basic education on VR/XR

A series of structured training sessions were conducted to educate participants on XR technologies, design thinking, 3D modelling, and XR application development.

Introduction to XR: Participants were introduced to Extended Reality (XR), including Augmented Reality (AR), Virtual Reality (VR), and Mixed Reality (MR) (figure 2). The session covered the evolution of XR from early innovations to modern devices like Oculus Quest and Apple Vision Pro. Applications in education, healthcare, and emergency response were highlighted, alongside interactive demonstrations using AR/VR devices.

Copyright © 2025 CroCEE
DOI: https://doi.org/10.5592/CO/3CroCEE.2025.167

Design Thinking for XR: The focus was on user-centred design and research methods, incorporating qualitative and quantitative techniques such as surveys, focus groups, and SWOT analyses. Participants learned to develop user personas and apply brainstorming methods to refine XR project concepts.

UI/UX Design and Prototyping: This session covered the fundamentals of user interface (UI) and user experience (UX) for XR applications. Key topics included ergonomic design, visual contrast, and interaction elements for VR environments. Participants practiced wireframing, storyboarding, and prototyping to create effective user interactions.



Figure 3. Introduction to XR technology

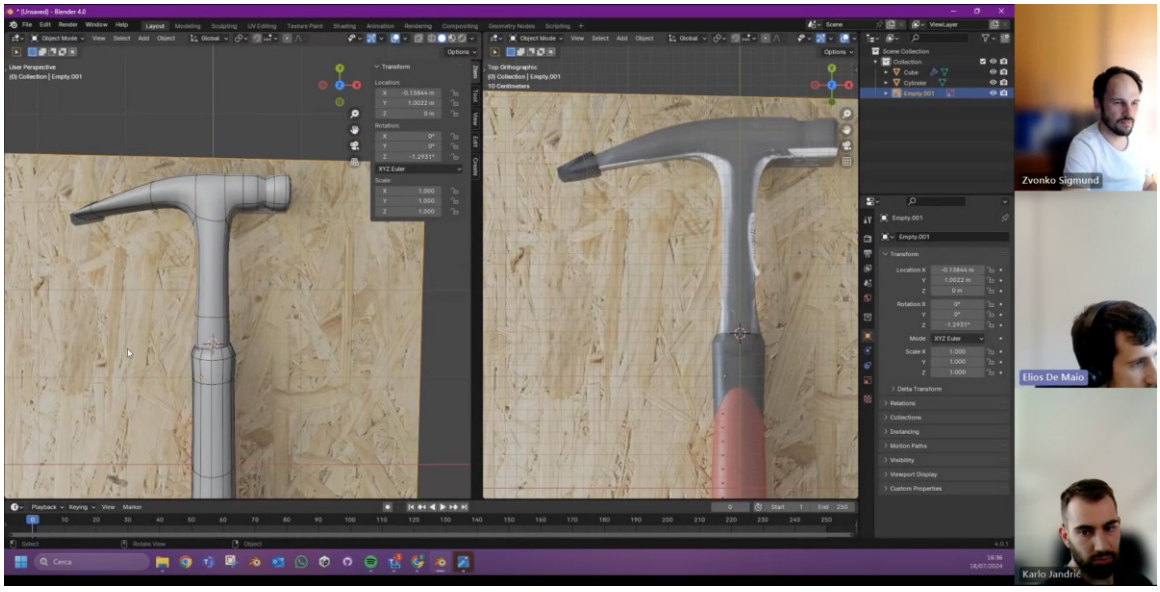


Figure 4. Blender modeling of a hammer

3D Modelling for XR Environments: Participants developed skills in 3D asset creation, including mesh modelling, shading, and texturing (figure 3). UV unwrapping and Physically Based Rendering (PBR) techniques were explored to enhance model realism. The session also introduced animation fundamentals, covering rigging and motion principles for interactive XR applications.

Copyright © 2025 CroCEE
DOI: https://doi.org/10.5592/CO/3CroCEE.2025.167

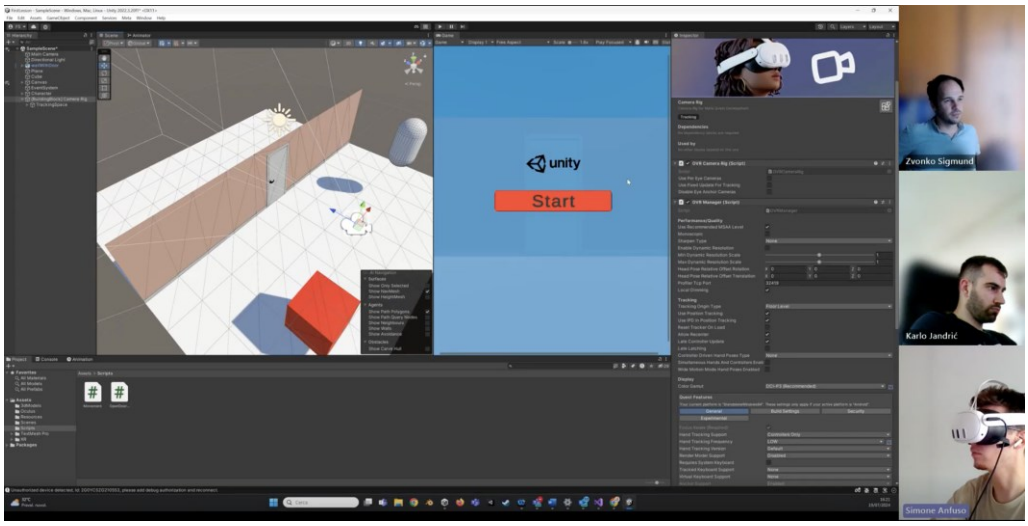


Figure 5. Configure Unity for VR development

Introduction to Unity for XR Development: Participants learned the basics of Unity, a game engine widely used for XR development (figure 4). The session covered Unity's interface, GameObjects, scene management, and animation. Basic scripting in C++ was introduced to enable interactive elements within XR environments. Participants also configured Unity for VR development, integrating the MetaXR SDK and testing their projects with Oculus devices.

3.3. Creation of the first functional VR environment

As part of the collaboration between Fondazione LINKS and HCPI, the project has advanced to the phase of designing and implementing a VR Pilot Demonstrator. This phase is crucial for developing an interactive and immersive training environment for experts in post-earthquake damage assessment. The implementation of the VR demonstrator consists of three key activities:

Storyboard Creation: The first step in the development of the VR Pilot Demonstrator involves transforming the established training concept into a structured storyboard. This storyboard defines the narrative sequences, user interactions, and key visual elements that will guide the virtual experience. By establishing a clear sequence of events and user engagement points, the storyboard ensures that the training module is both pedagogically effective and technically feasible.

3D Modelling: Following the storyboard development, the next phase focuses on creating optimized 3D models of the environments and objects that will be integrated into the VR application. These models replicate real-world earthquake-damaged structures, offering a realistic and interactive setting for training. The modelling process employs state-of-the-art photogrammetry and 3D scanning techniques to enhance the accuracy and fidelity of the virtual environment.

Demonstrator Creation in Unity: Once the 3D assets are developed, they are imported into Unity, a leading game engine used for VR applications. This phase involves programming interactivity, navigation, and user engagement in accordance with the predefined storyboard. The integration of physics-based simulations and user feedback mechanisms ensures that the VR demonstrator provides a dynamic and responsive training experience.

These activities represent a significant milestone in the project's progress, laying the foundation for the implementation and evaluation of the VR-based training program for post-earthquake damage assessment experts.

Copyright © 2025 CroCEE
DOI: https://doi.org/10.5592/CO/3CroCEE.2025.167

4. Conclusions

The integration of Extended Reality (XR) into the training of experts for post-earthquake damage assessment represents a significant advancement in disaster response preparedness. Traditional training methods, which rely on theoretical knowledge and limited field exercises, often fail to provide engineers and first responders with sufficient experience in high-risk, real-world scenarios. By leveraging XR technologies, this project has developed immersive and interactive training environments that enhance skill development, improve knowledge retention, and ensure a safer, more effective learning process.

The project, conducted in collaboration with the University of Zagreb's Faculty of Civil Engineering, the Croatian Centre for Earthquake Engineering (CCEE), and the LINKS Foundation, has successfully progressed through several key phases: data collection from real earthquake-damaged structures, XR training methodology development, creation of high-fidelity 3D models, and implementation of a VR-based learning platform. The use of advanced 3D scanning techniques, drone imagery, and digital reconstruction has enabled the creation of realistic training environments that accurately reflect post-earthquake conditions.

Preliminary findings suggest that XR-based training offers multiple advantages over conventional approaches, including:

- Enhanced safety: Reducing exposure to hazardous conditions while allowing for repeated practice in a risk-free virtual environment.
- Improved decision-making skills: Enabling trainees to experience a variety of structural damage scenarios, reinforcing their ability to assess risks and make critical decisions under pressure.
- Standardization of assessment procedures: Providing a consistent and repeatable learning experience that ensures uniformity in damage classification and usability evaluations.
- Cost-effectiveness and accessibility: Eliminating the need for expensive on-site training and allowing a broader range of professionals to engage in high-quality education.

Despite these benefits, challenges remain, including the need for further validation of XR-based training effectiveness in real emergency conditions and the development of standardized assessment metrics for evaluating trainee performance. Future research will focus on refining the VR training modules, integrating real-time AI-driven assessment tools, and expanding the program to a larger pool of engineers and emergency responders.

Ultimately, the successful implementation of XR in post-earthquake expert education has the potential to revolutionize disaster response training, equipping professionals with the necessary skills to rapidly and accurately assess structural damage. This initiative not only enhances the effectiveness of emergency response efforts but also contributes to the long-term resilience of communities affected by seismic events.

References

[1] Federal Emergency Management Agency (FEMA). (n.d.). IS-559: Local Damage Assessment. Available at: https://emilms.fema.gov/is_0559/groups/210.html (accessed February 18, 2025).

[2] Gen. Antonio. (2023). Post-Earthquake Assessment: Why and How? LinkedIn. Available at: https://www.linkedin.com/pulse/post-earthquake-assessment-why-how-gen-antonio (accessed February 18, 2025).

[3] Envista Forensics. (n.d.). Catastrophe Response: Earthquake Damage Assessment. Available at: https://www.envistaforensics.com/services/catastrophe-response/earthquake/ (accessed February 18, 2025).

[4] Federal Emergency Management Agency (FEMA). (n.d.). IS-559: Damage Assessment Coordination. Available at: https://emilms.fema.gov/is_0559/groups/195.html (accessed February 18, 2025).

Copyright © 2025 CroCEE
DOI: https://doi.org/10.5592/CO/3CroCEE.2025.167

[5] Zhang, Y., Li, X., Wang, J. (2023). Machine Learning Applications in Post-Earthquake Damage Assessments. Buildings, 14(10), 3255. Available at: https://www.mdpi.com/2075-5309/14/10/3255 (accessed February 18, 2025).

[6] Anand-ICE. (2023). The Role of Civil Engineers in Disaster Response and Recovery. Available at: https://anandice.ac.in/blog/the-role-of-civil-engineers-in-disaster-response-and-recovery-infographic/ (accessed February 18, 2025).

[7] BK Engineering. (n.d.). Roles in Earthquake Engineering. Available at: https://www.bk-engineering.in/post/roles-in-earthquake-engineering (accessed February 18, 2025).

[8] Markušić S, Stanko D, Penava D, Ivančić I, Bjelotomić Oršulić O, Korbar T, Sarhosis V (2021). Destructive M6.2 Petrinja Earthquake (Croatia) in 2020—Preliminary Multidisciplinary Research. Remote Sensing 13(6):29.

[9] Government of Croatia; World Bank (2020). Croatia Earthquake Rapid Damage and Needs Assessment. Washington, DC: The World Bank.

[10] Kman NE, Price A, Berezina-Blackburn V, Patterson J, Maicher K, Way DP, McGrath J, Panchal A, Luu K, Oliszewski A, Swearingen S, Danforth D (2023). First Responder Virtual Reality Simulator to Train and Assess Emergency Personnel for Mass Casualty Response. Journal of the American College of Emergency Physicians Open 4(1):8.

[11] Mullins, J., Chen, K., & Weng, Y. (2021). Challenges in preparing for and responding to disasters in Taiwan and the U.S.: Reflections from practice and academia. Trends in International Disaster Management, University of Texas Arlington Press. Available at: https://uta.pressbooks.pub/trendsininternationaldisastermanagement/chapter/challenges-in-preparing-for-and-responding-to-disasters-in-taiwan-and-the-u-s-reflections-from-practice-and-academia/ (accessed February 20, 2025)

[12] Shi, J., Luo, H., Liao, B., Cheng, S., Wu, B., & Xu, Z. (2023). Application of virtual reality technology in post-earthquake emergency response training: A case study of firefighter rescue operations. PLOS ONE, 18(3), e0282698. Available at: https://doi.org/10.1371/journal.pone.0282698

[13] Alfalah, S. F., & Annamalai, N. (2025). The role of virtual reality in medical education: A systematic review and meta-analysis. BMC Medical Education, 25, 66. Available at: https://doi.org/10.1186/s12909-025-06659-0

[14] IFRC (2023). 10 key takeaways from the immersive technologies & digital games for school disaster preparedness report. PrepareCenter. Available at: https://preparecenter.org/story/10-key-takeaways-from-the-immersive-technologies-digital-games-for-school-disaster-preparedness-report/ (accessed February 20, 2025).

[15] Fractales (2024). Can virtual reality simulations improve disaster preparedness and response training? Fractales. Available at: https://fractales.org/news/can-virtual-reality-simulations-improve-disaster-preparedness-and-response-training/ (accessed February 20, 2025).

Proceedings of the 3rd Croatian Conference on Earthquake Engineering - 3CroCEE
19–22 March 2025, Split, Croatia
Copyright © 2025 CroCEE
DOI: https://doi.org/10.5592/CO/3CroCEE.2025.7

CHALLENGES AND CONSIDERATIONS FOR MODULAR CONSTRUCTION SYSTEMS IN SEISMIC PRONE REGIONS: A STATE-OF-THE-ART REVIEW

Vasco Bernardo [(1)], Paulo Candeias [(2)], António A. Correia [(2)]

[(1)] *Researcher, National Laboratory for Civil Engineering (LNEC)*
[(2)] *Senior researcher, National Laboratory for Civil Engineering (LNEC)*

Abstract

Modular construction has been increasingly used worldwide due to its fast assembly, cost-effectiveness, and sustainability; however, the performance of these structures in seismic-prone regions remains a significant engineering challenge.

The seismic behavior of modular buildings varies significantly, depending on the configuration of prefabricated modules and their intra- and inter-connections. In recent years, several modular systems and connection techniques have been developed and are now commercially available. Despite significant advancements, modular construction in seismic-prone regions still encounters major challenges. These include ensuring robust inter-module connections for effective seismic load distribution, addressing differential displacements between stacked units, and improving load redistribution within the modular system. Additionally, variations in material stiffness and structural irregularities can lead to unexpected dynamic responses, increasing their seismic vulnerability.

This paper reviews the main challenges of modular construction in seismic regions, providing insights into key design considerations and recommendations for future research.

Keywords: modular systems, state-of-the-art, seismic vulnerability, design challenges

1. Introduction

Modular construction has emerged in the building industry, promoting a faster construction timeline, cost efficiency, and reduced on-site labor needs. This technique involves the off-site prefabrication of building modules/units, which are then transported and assembled on-site to create complete structures. The implementation of these systems in seismic regions presents significant engineering and design challenges due to the need for structural robustness, efficient energy dissipation capacity, and reliable connections between units. Their seismic behavior is mainly influenced by various factors such as inter-module connections, ductility and system integrity, all of which must be carefully addressed to ensure safety and compliance with seismic design codes [1].

Unlike conventional monolithic structures, which usually provide continuous load paths and stress distributions, modular buildings are composed of prefabricated units connected through (discrete) structural joints. These parts of the system are often the most vulnerable components, requiring careful design to seismic loads, i.e., if not properly designed, inter-module connections can develop stress concentrations, bolt slippage, weld fractures, and inadequate load (re)distribution, leading to structural instability or even progressive collapse [2]. Furthermore, traditional buildings usually incorporate ductile mechanisms into beams, columns, and shear walls to improve seismic performance, whereas modular structures rely on their connections as the main energy dissipation mechanism. Hence, a fundamental challenge in seismic design of modular systems is ensuring that the structure has sufficient ductility and energy dissipation capacity [3].

The distribution of mass and stiffness in modular structures also presents another challenge in seismic regions. The presence of modular joints can introduce irregular stiffness variations throughout the structure, leading to torsional effects, soft-story mechanisms, and dynamic amplification. Various strategies such as base isolation, tuned mass dampers, and hybrid damping systems have been proposed

Proceedings of the 3rd Croatian Conference on Earthquake Engineering - 3CroCEE
19–22 March 2025, Split, Croatia
Copyright © 2025 CroCEE
DOI: https://doi.org/10.5592/CO/3CroCEE.2025.7

to mitigate these effects; however, their integration into modular construction remains an area of ongoing research [4], [5].

This paper provides a comprehensive review of the seismic performance of modular systems, highlighting the best practices and challenges associated with different material systems and connection strategies. Through a literature review of experimental studies, numerical simulations, and case studies, this research explores practical design improvements, innovative connection technologies, and design standards considerations in order to improve the characterization of modular systems in seismic regions.

2. Overview of modular construction systems

Modular construction encompasses a variety of systems distinguished by the materials used and the method of assembly. The most common types include steel, timber, and concrete modular systems, each with its own advantages and challenges, particularly in seismic-prone regions.

2.1. Steel modular systems

Steel modular systems are widely used due to their strength and deformation capacity, durability, and accuracy in fabrication, being particularly suitable for high-rise buildings and industrial applications. These systems also provide a good balance between strength, weight, ductility, and prefabrication efficiency, making them suitable for use in seismic regions. However, their performance depends essentially on the robustness and detailing of connections, as bolted and welded joints can experience fatigue and brittle fractures under cyclic loads. To improve horizontal stability, additional bracings or moment-resisting connections are often needed, namely, in seismic prone areas. Second-order effects, such as P-Δ effects, can also increase deformation and produce instability, sometimes requiring the use of bolted slip-critical joints and post-tensioned frames [6], [7].

In steel modular systems, bolted connections are widely used due to their ease of assembly. They usually consist of high-strength bolts to fix steel plates, brackets, or flanges between modules. The main issue of these connections is slippage and fatigue phenomena under cyclic loads, which can affect structural performance and long-term durability. To reduce these effects, again, slip-critical connections with pre-tensioned bolts can improve stability by transferring forces through friction mechanisms. In addition, full-penetration welds, stiffened plates, and post-weld treatments also minimize stress concentration and improve fatigue resistance and durability [8]. In such cases, regular monitoring plays an important role in order to detect fatigue cracks and bolt loosening, allowing for timely interventions.

One of the major disadvantages of steel modular systems is their susceptibility to corrosion, especially in humid environments, which require proper protective coatings or galvanization. Another challenge is fire, thermal and sound insulation, as steel does not naturally provide the same level of fire protection, heat retention or noise reduction as timber or concrete. Additional materials, such as insulation layers or acoustic panels are often required, increasing overall construction costs.

Although modular steel systems offer durability and efficiency, prefabrication and transportation costs are generally higher than for timber, as well as the complexity of steel connections and the need for specialized labor to assemble the units, which can extend construction timelines [7].

2.2.Timber modular systems

Timber modular systems are increasingly expanding due to their sustainability and increased productivity. The modules are often constructed from cross-laminated timber or *glulam*, providing sustainable and lightweight solutions, particularly in residential and mid-rise constructions. The performance of these systems depends on the connection design and energy dissipation mechanisms.

Timber frame structures have lower ductility compared to steel, and their connections, which often rely on nails, screws, or adhesives, can usually experience slip, pullout, or degradation over the years. In addition, the anisotropic nature of wood, combined with moisture and biological deterioration, can result in long-term durability issues that can affect seismic capacity [9].

The main challenges of timber modular buildings in seismic regions include the conception and design of ductile connections and preventing slip and uplift at inter-module joints to control interstory drifts [10]. The most common type of connections used are based on steel brackets and plates, usually

Copyright © 2025 CroCEE
DOI: https://doi.org/10.5592/CO/3CroCEE.2025.7

embedded in modules to form rigid joints, with bolted or screwed fasteners providing additional shear and tensile strength. In the case of multistory timber modular buildings, post-tensioned connections are frequently used to prevent uplift phenomena and to improve the flexural strength between units. In some cases, namely floor-to-wall joints, glued connections are also combined with mechanical fasteners for added strength and reduced units' deformation. Since timber is susceptible to moisture damage, decay, and material degradation, maintaining the strength of connections over time is critical – the most common techniques employ protective coating, fire-resistant treatments, and ventilation systems to improve material durability [11].

2.3. Concrete modular systems

Concrete modular systems provide structures with high stiffness and durability, which can be beneficial in seismic regions, while the significant mass is not. The main challenge of these constructions is achieving the required ductility for moderate to high seismicity levels, as the presence of discrete units hampers the monolithic behavior, leading to local stresses at the interfaces and resulting in joint failures [12].

Among the various inter-units' connections found in the literature, grouted connections are the most commonly used [13]. This technique involves inserting reinforcing bars or steel dowels between modules and filling the cavities with high-strength grout to improve monolithic behavior. The main drawback of these connections is related to environmental factors, i.e., exposure to aggressive environments, that can cause microcracking and compromising the bond between modules. Thus, regular inspections are needed to maintain the connection durability and functionality. The use of additional reinforcement, such as fiber-reinforced polymers, can also be a solution in these situations, combined with surface treatments [14].

Post-tensioned connections are another widely used technique, proving high strength capacity and structural continuity by using steel tendons tensioned after installation to compress modules, improving their stiffness and seismic performance [13]. However, long-term durability issues, such as tendon corrosion and loss of pre-stress, require periodic monitoring. Mechanical connections, typically using embedded steel plates and bolted joints, allow for easy assembly but are less efficient under cyclic loads [15].

Finally, hybrid connections in concrete modular systems are becoming increasingly common, particularly in seismic regions. These combine different techniques (e.g., grouted connections, post-tensioning, and mechanical fasteners) to improve the inter-modular strength capacity, energy dissipation and durability. The use of hybrid connections is particularly relevant in high-rise modular buildings, bridges, and critical infrastructures. Research studies are being carried out to demonstrate its effectiveness in reducing damage during earthquakes [16], [17].



Figure 1 Examples of modular constructions (steel, timber and concrete, respectively) [13], [18].

3. Prefabrication and assembly of modular systems

Modular construction involves the off-site fabrication of building components in a controlled factory environment, followed by transportation and on-site assembly. This process enhances construction speed, cost efficiency, quality control, and sustainability. The prefabrication and assembly process for modular systems follows several key stages, each one adapted to the material used. In brief, a typical modular construction sequence includes: (i) conception and design, where detailed

Copyright © 2025 CroCEE
DOI: https://doi.org/10.5592/CO/3CroCEE.2025.7

architectural and structural planning is carried out usually using Building Information Models; (ii) manufacturing the structural frame, which includes the modules' construction in a controlled environment, ensuring precision and quality control; (iii) integration of MEP (mechanical, electrical and plumbing) system and interior/exterior finishings within the factory environment, followed by inspections and structural tests to ensure compliance with building standards before transportation to the site; (iv) transportation and logistics of modular units to the construction site; (v) on-site assembly, including modules alignment and inter-module connections to ensure structural continuity; (vi) final MEP and structural integration, where the final remaining connections between units are made and other structural elements are installed (e.g., elevators, staircases, facade elements); (vii) final verification of the modules assembled, which includes inspection and final adjustments before occupancy. These stages, illustrated in Figure *2*, reduce construction time (see Figure *3*), improve quality control, and minimize on-site disruptions.

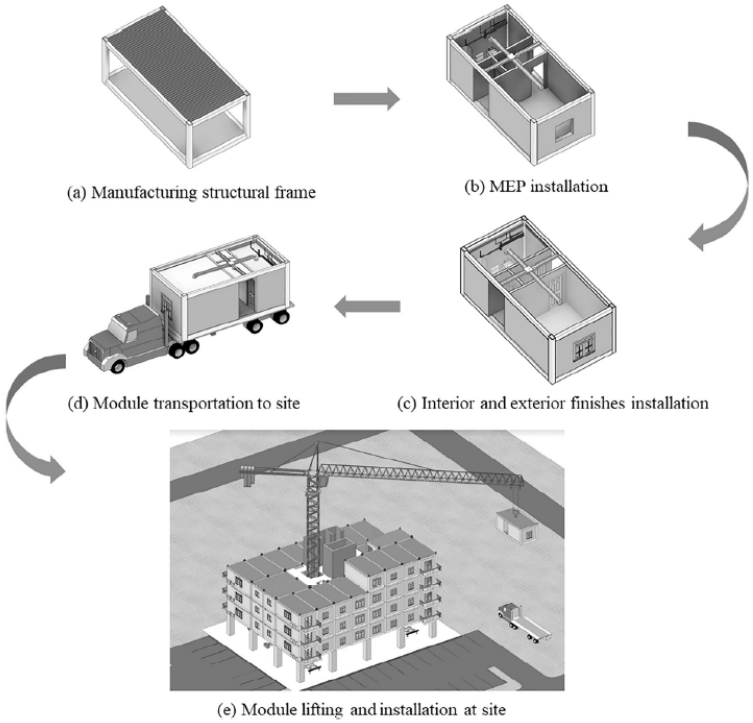


Figure 2 Modular construction from manufacturing to the site of installation [19].

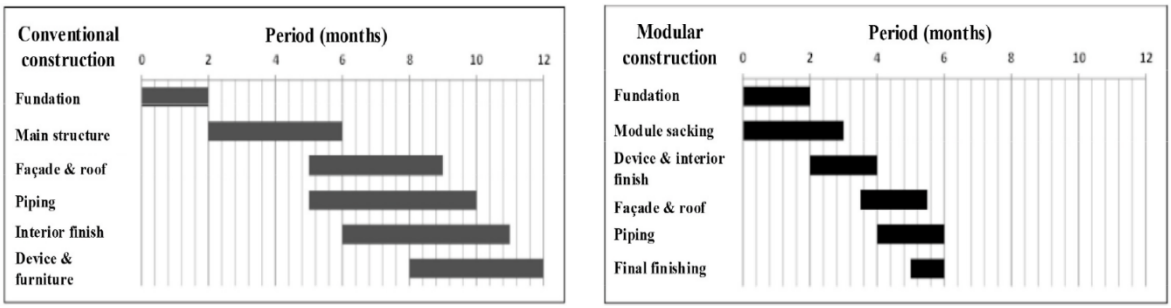


Figure 3 Gantt chart comparison between conventional and modular construction, respectively [20].

Copyright © 2025 CroCEE
DOI: https://doi.org/10.5592/CO/3CroCEE.2025.7

4. Modular systems stability

4.1. Individual modules

Individual modules serve a range of functions and must meet specific demands during construction. During design stage, interconnected assemblies of beams-columns or wall panels are grouped together to form larger components, while the floor cassettes, i.e., flooring systems with structural components, typically remain discontinuous across the same level [21]. This design approach is often preferred in architecture as lighter modular systems reduce interior divisions, creating more open and flexible spaces.

Before being positioned and stacked, the units act as frameworks for installing equipment and interior finishes. Hence, they are designed to have enough capacity to support vertical loads during lifting and transportation. In low-rise buildings, these modules typically handle all lateral loads, transferring them to the foundation system [1]. In some cases, they can also serve other purposes, such as providing blast or fire protection, behaving as cantilevered elements, or being suspended to create unique architectural features. In addition, modular systems can also be used as temporary (emergency or not) structures to be later disassembled [22].

4.2. Modular systems connections

Modular connections can be grouped into four main categories [23]: (i) intra-module or internal connection, which join individual components to create a complete three-dimensional module; (ii) inter-module or external connection, which link adjacent modules and simplify distribution of loads; (iii) connections that serve both intra- and inter-module function; (iv) foundation connections, which transfer lateral and gravity loads from the lowest story to the foundation. Although the connections between modules may be similar to those found in moment-resisting steel frame structures, they face unique challenges due to limited access space, i.e. the pre-installation of partition walls and floor cassettes further restricts access, requiring this consideration in design.

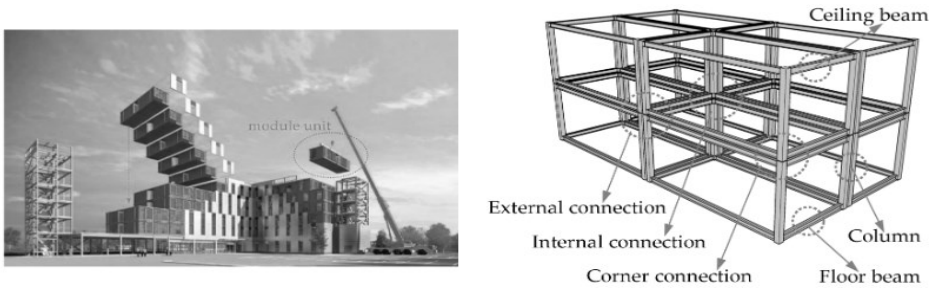


Figure 4 Example of a modular construction and units' assembly, respectively.

Another challenge to module connections is the tendency of individual modules to have their own vertical and horizontal diaphragm effects, which can result in rocking behavior. This effect produces additional forces on the connections, which do not make structural design any easier. For foundation connections, the main challenge is to develop a system that allows quick installation and simple assembly between the upper structure and the substructure. At the same time, it is essential to avoid creating modules with various layouts, since standardization is the key to efficient manufacture and construction. Recent research has explored the structural, construction and manufacturing requirements of modular connections, highlighting the need for innovative solutions in terms of connectivity and structural framework [24].

In terms of seismic loads, horizontal connections are mainly responsible for transferring most of the load and only a small part is distributed downwards to the lower modules and the foundation. Although horizontal connections have less influence on the distribution of vertical loads, compared to other types, they still contribute to vertical rocking behavior, which can create additional vertical loads. A comprehensive state-of-the-art about existing connections can be found in the literature [23], [24].

Copyright © 2025 CroCEE
DOI: https://doi.org/10.5592/CO/3CroCEE.2025.7

4.3. Lateral resistance of modular systems

The structural performance of modular buildings under lateral loads is highly dependent on the connections and specific characteristics of the building, such as its deformation capacity and energy dissipation. To resist seismic loads, buildings require supplemental lateral force resisting systems designed to counteract horizontal forces and enhance lateral stability. The most common solutions include steel bracings, concrete cores, shear walls, and base isolation systems. Steel bracings can be integrated at floor levels and in the walls of the modules to help with the loading distribution and improve torsional capacity. Concrete core and shear walls are often incorporated into stairwells and elevator shafts, providing essential structural support. These can be constructed using either conventional or modular techniques, though integrating concrete cores with non-rigid horizontal diaphragms [25]. Base isolation systems also contribute to minimizing inertia forces and ensuring uniform displacement of the superstructure [26].

The layout of the modules on a single floor significantly influences the distribution of loads to the additional stability units and the distribution of forces between the strongest and weakest modules. The different layout configurations impose different requirements on the stiffness of the horizontal diaphragms and determine the most suitable types of additional stability units needed for structural support. Depending on the configuration, some modules may experience greater load concentrations, requiring connections between modules to distribute the forces effectively. In addition, the alignment and continuity of the load paths between the modules and the stability elements have an impact on the lateral and vertical load capacity of the structure. Hence, the selection of additional stability units must be in accordance with the specific load conditions of the building, ensuring adequate stiffness and strength capacity.

The difference between modular layouts also influences the diaphragm effect. In configurations where the modules are arranged regularly, the horizontal diaphragms can work more efficiently, transferring the forces uniformly [27]. However, in irregular configurations or in cases with large openings, the diaphragms must be strengthened to compensate for discontinuities in the loads' distribution.

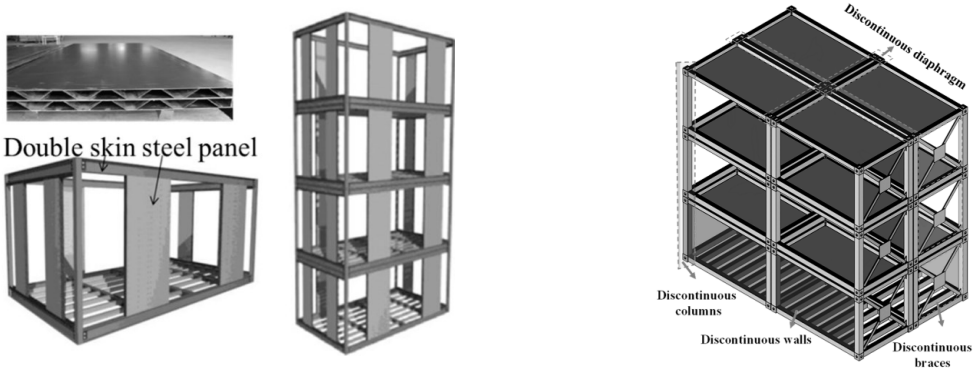


Figure 5 Lateral resistance elements: double skin plate shear wall and bracing system [13], [28].

4.4. Design aspects of modular systems and standards

Emulative and non-emulative designs are two different approaches in modular construction, influencing structural performance and load distribution [29]. The first intends to reproduce the behavior of conventional cast-in-place concrete or steel structures, ensuring reliable and efficient connections between modules, minimizing the impact of discontinuities. In this case, modular group behavior is compared to a conventional structure. On the other hand, if non-emulative design is chosen, some issues including the grouping of beams and columns, behavior of the connections and structural discontinues need to be addressed. In literature review, several investigations have been conducted to address these issues. For instance, Annan *et al*. [30] and Fathieh [21] compared emulative and non-emulative designs through non-linear static and dynamic analysis, assessing the impact of bracing

Copyright © 2025 CroCEE
DOI: https://doi.org/10.5592/CO/3CroCEE.2025.7

systems, diaphragm behavior and the stiffness of connections between steel modules. The studies indicate that modular buildings have greater lateral capacity compared to traditional moment-resisting frames, but lateral drifts and the concentration of forces on the lower floors require special attention in the design. Other studies can be found about the aforementioned approaches including a discussion on beam-column connection effects, floor-cassette discontinuities and individual module behavior (e.g., [31], [32], [33]). Some of these studies are detailed in the next section.

The design of modular systems is subject to requirements in building codes and standards that ideally ensure compliance with the same structural safety and performance criteria as traditional structures. Specific standards have been developed to address particular aspects of modular construction. For instance, ISO 2848:1984, titled "Building construction – Modular coordination – Principles and rules," provides guidelines for modular coordination in design, focusing on dimensional coordination and positioning of building components. The International Building Code (IBC), developed by the International Code Council (ICC), explicitly incorporated off-site modular construction provisions in its 2021 edition, reflecting the increasing adoption of these modular solutions. Additionally, the ICC/MBI standards, introduced by the ICC in collaboration with the Modular Building Institute (MBI), include ICC/MBI Standard 1200-2021, which outlines the planning, design, fabrication, and assembly of off-site construction, and ICC/MBI Standard 1205-2021, which focuses on inspection and regulatory compliance for residential and commercial modular buildings. Recently, ICC/MBI 1210/2023 addresses requirements for mechanical, electrical, and plumbing system elements, energy efficiency, and water conservation in off-site construction projects. In 2024, the handbook “New Prefabricated, modular and offsite construction” was developed in collaboration with the Building 4.0 CRC research program to provide guidance on the use of prefabricated, modular and associated modern construction methods in compliance with the National Construction Code (NCC) in Australia.

In Europe, the Eurocodes serve as a comprehensive set of standards that apply to both traditional and modular buildings. However, design loads in modular construction are different from those in traditional monolithic construction due to the manufacturing process and the introduction of short-term load effects during transportation and on-site assembly. These variations can affect the load transfer mechanism [1]. Therefore, there is a need to develop design standards specifically adapted to modular structures. In this sense, the guideline for European technical approvals of prefabricated Building Units (ETAG 023) will be replaced by an EAD document under the CPR (Construction Products Regulation).

5. Seismic performance of modular systems: case studies

Investigations related to the structural behavior of modular buildings are relatively recent, with very few studies prior to the XXI century, whereas seismic studies of conventional buildings have been widely explored, with extensive research focusing on both historic masonry structures and hybrid structures. The following sections summarize some of the research carried out in the field of modular construction focusing on their seismic performance.

5.1. Steel modular systems

One of the first investigations into the seismic behavior of modular buildings was conducted by Annan *et al*. [34], who analyzed the hysteretic behavior of steel modular buildings under cyclic loads. The analytical model developed successfully captured the inelastic behavior of bracing systems. Expanding on this work, Annan *et al*. [35] later examined the inelastic performance of 2-, 4-, and 6-story modular steel buildings in Vancouver, Canada, through incremental dynamic analysis (IDA) and nonlinear static pushover analysis.

Furthering the understanding of modular structures under seismic conditions, Fathieh *et al*. [21] conducted nonlinear static and incremental dynamic analyses in both two- and three-dimensional models of a four-story modular steel building. Along similar lines, Gunawardena *et al*. [36] employed nonlinear time-history analysis to assess the ductility of modular columns, identifying the formation of

Copyright © 2025 CroCEE
DOI: https://doi.org/10.5592/CO/3CroCEE.2025.7

a plastic hinge at the primary corner column as a critical point of failure. This study highlighted the crucial role of inter-module connections in the seismic behavior of modular steel buildings.

Srisangeerthanan *et al*. [31] introduced new seismic design factors, focusing on force amplification and ductility and based on numerical analysis. Their study examined how diaphragm stiffness and strength influence the seismic performance of multi-story modular steel buildings, concluding that increased diaphragm flexibility leads to larger inter-story displacements and inertia forces.

A performed full-scale cyclic and monotonic load tests on seven corner connections were performed by Deng *et al*. [37]. A new connection design incorporating welded and bolted steel plates was assessed based on seismic performance criteria, including failure modes, stress distribution, stiffness and strength characteristics, ductility, and energy dissipation capacity. A comprehensive review by Deng *et al*. [38] emphasized that, despite ongoing studies, the seismic behavior of modular steel buildings had not yet reached a sufficient level of reliability. The authors argued that the current state of research was not yet advanced enough to facilitate rapid progress toward constructing high-rise modular buildings in seismic-prone regions.

Shan *et al*. [39] presented in 2020 a case study in which they redesigned a real 31-story student housing project in Hong Kong using a modular steel system. They evaluated the elastic behavior of connections through numerical modeling under various loading scenarios. The developed solution was then extended to a hypothetical forty-story building and tested under similar conditions, leading to the establishment of a structural design workflow for high-rise modular steel buildings.

The nonlinear seismic response of medium-rise modular steel buildings located near active fault zones was investigated by Emamikoupaei *et al*. [40]. The study revealed that medium-rise structures exhibited significant stiffness and strength degradation when exposed to high-amplitude and short-duration earthquakes. The increased susceptibility to damage was attributed to the velocity impulse effect observed in forward-directivity ground motion records.

5.2. Timber modular systems

Concerning timber modular systems, Tesfamariam *et al*. [41] evaluates the seismic vulnerability of a hybrid steel moment resisting frame (SMRF) and CLT infill panels in Vancouver, using nonlinear dynamic analysis in OpenSees. Three SMRF models (3-, 6-, and 9-story) were tested with different CLT infill configurations. Results showed that increasing CLT infill reduces the fundamental period and seismic vulnerability.

The ductility factor for an innovative system with hybrid timber-steel structural system was examined by Zhan *et al*. [42], where mass-timber panels act as shear walls connected via steel beams. Results were conducted using nonlinear dynamic analyses, suggesting a ductility factor of 5.0 for safe and efficient seismic design within existing force-based design provisions.

Ganey *et al*. [43] explored a self-centering CLT wall system that combines CLT panels with post-tensioning (PT) provide post-event re-centering. U-shaped flexural plate devices (UFPs) were incorporated to yield under cyclic loading, preserving the PT and CLT components until large inter-story drifts occur. Tests evaluated limit states, strength, and stiffness degradation, showing that CLT walls effectively re-centered after large drifts.

A study conducted by Loss *et al*. [44] introduces an innovative hybrid timber-steel floor diaphragm system, combining CLT panels with cold-formed steel beams for mid- and high-rise buildings. The system was analyzed via numerical modeling calibrated with full-scale tests. Key findings highlight the importance of connection design, shear wall spacing, and floor aspect ratio, emphasizing that unfavorable shear wall layouts should be avoided to prevent excessive in-plane deformations.

Jaramillo *et al*. [45] investigated the structural response of mass timber modular buildings in high-seismic regions, focusing on the role of intermodular connections in diaphragm behavior. A parametric analysis was conducted on 9-, 12-, and 18-story buildings using OpenSees to evaluate how connection stiffness and location affect performance. Results showed that horizontal translational stiffness controls

Proceedings of the 3rd Croatian Conference on Earthquake Engineering - 3CroCEE
19–22 March 2025, Split, Croatia
Copyright © 2025 CroCEE
DOI: https://doi.org/10.5592/CO/3CroCEE.2025.7

diaphragm classification (rigid, semi-rigid, or flexible) and influences column force demands and diaphragm deflections, highlighting the importance of proper connection design in modular construction

Chen *et al*. [46] developed a novel seismic force-resisting system for prefabricated modular mass timber construction, incorporating floor isolation and re-centering techniques to enhance seismic performance. Using finite element modeling in ABAQUS, the seismic performance of the new system and conventional ones was evaluated through nonlinear dynamic time-history analysis showing and improvement in the overall behavior and efficiency of modular construction in high seismic zones.

A comprehensive review of the features of modular CLT construction completed between 2009 and 2021 was carried out by Bhandari *et al*. [10], focusing on architectural and engineering design, manufacturing, and logistics. The implication of these aspects in the use of modular CLT structures in seismic regions and as a solution for temporary housing and rapid mass housing were explored. Additionally, Orozco *et al*. [47] presented an examination of 350 multistory timber projects from 2000 to 2021with the aim to identify the range of morphologies and a better understanding of the design space in current serial and modular multistory mass timber construction.

5.3. Concrete modular systems

Focusing on reinforced concrete modular systems, Chen *et al*. [46] conducted quasi-static cyclic loading tests on a prefabricated concrete module connected *in situ* to other structural elements. Their study provides information to evaluate the seismic performance of modular concrete buildings concerning flexural capacity, initial stiffness, ductility, and energy dissipation.

In the scope of the SAFECAST Project, Negro *et al*. [12] tested a full-scale three-story precast building at ELSA to evaluate different structural configurations under seismic loads. A dual frame-wall system with precast shear walls showed minimal deformation, while removing the walls led to large deformations due to flexible hinged beam-column connections. An innovative connection system was then introduced, significantly improving stability when applied to all beam-column joints, effectively creating a quasi-emulative moment-resisting frame and improving the seismic capacity.

Menegon *et al*. [48] investigated panel-to-panel connections for jointed precast concrete building cores. Three connection types were tested: a baseline welded stitch plate (WSP) connection and two newly developed grouted panel pocket (GPP) and post-tensioned corbel (PTC) connections designed to eliminate wet joints and site welding. Experimental results showed that GPP and PTC connections were stronger and stiffer than the WSP connection.

Pan *et al*. [49] developed an innovative discrete diaphragm system for concrete modular high-rises, eliminating the need for cast-in-situ concrete layers commonly used to ensure rigid diaphragm behavior. A case study in Hong Kong was conducted showing the efficiency of the new system and proved that appropriate flexible horizontal connections are a feasible option for concrete modular structures.

The study of Wang *et al*. [50] developed a new lateral force-resisting system using precast shear walls within modular high-rises, tested on a 40-story public housing building in Hong Kong. A finite element model was generated and validated with cyclic loading tests, then used for nonlinear static and dynamic analyses under seismic loads. The proposed system effectively improves seismic performance, and selecting modes in the multi-modal analysis based on cumulative contributions improves accurately the seismic demands in modular high-rises.

6. Final comments

A review of modular construction systems and the aspects related to structural stability, with a focus on their seismic performance, has been carried out in this study. Despite the well-established knowledge of the materials commonly used in construction, the structural performance of modular buildings remains an area that requires further research, particularly in the context of the behavior of the entire assembled system. The role of inter- and intra-module connections, diaphragm flexibility and the

Copyright © 2025 CroCEE
DOI: https://doi.org/10.5592/CO/3CroCEE.2025.7

redistribution of forces between units remain key to improving structural performance. In addition, gaps in regulation and research highlight the need for more comprehensive and uniform guidelines, particularly adjusted to this type of construction. The growing use of modular systems in seismic regions demands further innovation in connections design and structural integration to ensure safety and efficiency. As research continues to evolve, modular construction has the potential to become an efficient and suitable solution for earthquake-prone areas.

Acknowledgments

This research is funded by project "R2U Technologies – Modular Systems", reference C644876810 - 00000019, financed by the funds from the Recovery and Resilience Plan (RRP), through the NextGenerationEU programme – investment programme no. 48.

References

[1] Lacey, A. W., Chen, W., Hao, H., and Bi, K., Structural response of modular buildings – An overview, *Journal of Building Engineering*. 2018. doi: 10.1016/j.jobe.2017.12.008.

[2] Zhong, X., Chen, A., Chen, Z., and Yu, Y., Research and discussion over seismic performance of modular structure, *Modul. Offsite Constr. Summit Proc.*, 2017, doi: 10.29173/mocs53.

[3] Liu, Y., Chen, Z., Liu, J., and Zhong, X., Experimental study on seismic behavior of two-storey modular structure, *Steel Compos. Struct.*, 2020, doi: 10.12989/scs.2020.37.3.273.

[4] Shang, J., Tan, P., Zhang, Y., Dai, S., and Li, Y., Seismic performance of modular steel frame isolated structures with variable friction pendulum bearings, *Jianzhu Jiegou Xuebao/Journal Build. Struct.*, 2021, doi: 10.14006/j.jzjgxb.2019.0813.

[5] Zhao, X., Wang, G., and Du, B., Standardized Seismic Design of Modular High-rise Steel Structure Equipped with Viscous Dampers, 2022. doi: 10.2749/prague.2022.0395.

[6] Zhang, G., Xu, L. H., and Li, Z. X., Experimental evaluation on seismic performance of a novel plug-in modular steel structure connection system, *Eng. Struct.*, 2022, doi: 10.1016/j.engstruct.2022.115099.

[7] Ding, Y., Deng, E., Zong, L., Dai, X., Li, Y., Wang, H., and Bi, J., State-of-the-art on connection in modular steel construction, *Jianzhu Jiegou Xuebao/Journal of Building Structures*. 2019. doi: 10.14006/j.jzjgxb.2019.03.003.

[8] Wang, C. and Chan, T. M., Seismic design and parametric study of steel modular frames with distributed seismic resistance, *Thin-Walled Struct.*, 2023, doi: 10.1016/j.tws.2022.110325.

[9] Casagrande, D., Sinito, E., Izzi, M., Pasetto, G., and Polastri, A., Structural performance of a hybrid timber wall system for emergency housing facilities, *J. Build. Eng.*, 2021, doi: 10.1016/j.jobe.2020.101566.

[10] Bhandari, S., Riggio, M., Jahedi, S., Fischer, E. C., Muszynski, L., and Luo, Z., A review of modular cross laminated timber construction: Implications for temporary housing in seismic areas, *Journal of Building Engineering*. 2023. doi: 10.1016/j.jobe.2022.105485.

[11] Aquino, C. D. and Branco, J. M., Experimental evaluation of a modular timber unit filled with insulated corkboard, *J. Build. Eng.*, 2020, doi: 10.1016/j.jobe.2020.101725.

[12] Negro, P., Bournas, D. A., and Molina, F. J., Pseudodynamic tests on a full-scale 3-storey precast concrete building: Global response, *Eng. Struct.*, 2013, doi: 10.1016/j.engstruct.2013.05.047.

[13] Ye, Z., Giriunas, K., Sezen, H., Wu, G., and Feng, D. C., State-of-the-art review and investigation of structural stability in multi-story modular buildings, *Journal of Building Engineering*. 2021. doi: 10.1016/j.jobe.2020.101844.

[14] Sharda, A., Manalo, A., Ferdous, W., Bai, Y., Nicol, L., Mohammed, A., and Benmokrane, B., In-plane shear behaviour of prefabricated modular wall system assembled of fibre reinforced polymer composites, *Case Stud. Constr. Mater.*, 2023, doi: 10.1016/j.cscm.2022.e01819.

[15] Psycharis, I. N., Kalyviotis, I. M., and Mouzakis, H. P., Experimental investigation of the response of precast concrete cladding panels with integrated connections under monotonic and cyclic loading, *Eng. Struct.*, 2018, doi: 10.1016/j.engstruct.2017.12.036.

[16] Stanton, J., Stone, W. C., and Cheok, G. S., A hybrid reinforced precast frame for seismic regions, *PCI J.*, 1997, doi: 10.15554/pcij.03011997.20.23.

[17] Zhang, J., Ding, C., Rong, X., Yang, H., Wang, K., and Zhang, B., Experimental seismic study of precast hybrid SFC/RC beam–column connections with different connection details, *Eng. Struct.*, 2020, doi: 10.1016/j.engstruct.2020.110295.

[18] Gunawardena, T., Ngo, T., Mendis, P., and Alfano, J., Innovative Flexible Structural System Using Prefabricated Modules, *J. Archit. Eng.*, 2016, doi: 10.1061/(asce)ae.1943-5568.0000214.

Copyright © 2025 CroCEE
DOI: https://doi.org/10.5592/CO/3CroCEE.2025.7

[19] Liew, J. Y. R., Chua, Y. S., and Dai, Z., Steel concrete composite systems for modular construction of high-rise buildings, *Structures*, 2019, doi: 10.1016/j.istruc.2019.02.010.
[20] Lawson, M., Ogden, R., and Goodier, C., *Design in modular construction*. 2014. doi: 10.1080/10464883.2017.1260969.
[21] Fathieh, A. and Mercan, O., Seismic evaluation of modular steel buildings, *Eng. Struct.*, 2016, doi: 10.1016/j.engstruct.2016.04.054.
[22] Harrison, B. F., Blast resistant modular buildings for the petroleum and chemical processing industries, 2003. doi: 10.1016/S0304-3894(03)00232-2.
[23] Lacey, A. W., Chen, W., Hao, H., and Bi, K., Review of bolted inter-module connections in modular steel buildings, *Journal of Building Engineering*. 2019. doi: 10.1016/j.jobe.2019.01.035.
[24] Srisangeerthanan, S., Hashemi, M. J., Rajeev, P., Gad, E., and Fernando, S., Review of performance requirements for inter-module connections in multi-story modular buildings, *Journal of Building Engineering*. 2020. doi: 10.1016/j.jobe.2019.101087.
[25] Wang, C. and Chan, T. M., Quantifying variation in maximum floor accelerations of modular buildings under earthquakes through stochastic nonlinear structural analysis, *Thin-Walled Struct.*, 2024, doi: 10.1016/j.tws.2023.111454.
[26] Zhao, C., Zeng, C., Witarto, W., wen Huang, H., Dai, J., and Mo, Y. L., Isolation performance of a small modular reactor using 1D periodic foundation, *Eng. Struct.*, 2021, doi: 10.1016/j.engstruct.2021.112825.
[27] Fleischman, R. B. and Farrow, K. T., Dynamic behavior of perimeter lateral-system structures with flexible diaphragms, *Earthq. Eng. Struct. Dyn.*, 2001, doi: 10.1002/eqe.36.
[28] Hong, S. G., Cho, B. H., Chung, K. S., and Moon, J. H., Behavior of framed modular building system with double skin steel panels, *J. Constr. Steel Res.*, 2011, doi: 10.1016/j.jcsr.2011.02.002.
[29] Committee, P. I. H. and Neal, *PCI Design Handbook 7Th Edition Precast and Prestressed Concrete*. 2010.
[30] Annan, C. D., Youssef, M. A., and El Naggar, M. H., Seismic overstrength in braced drames of modular steel buildings, *J. Earthq. Eng.*, 2009, doi: 10.1080/13632460802212576.
[31] Srisangeerthanan, S., Hashemi, M. J., Rajeev, P., Gad, E., and Fernando, S., Numerical study on the effects of diaphragm stiffness and strength on the seismic response of multi-story modular buildings, *Eng. Struct.*, 2018, doi: 10.1016/j.engstruct.2018.02.048.
[32] Deng, E. F., Yan, J. B., Ding, Y., Zong, L., Li, Z. X., and Dai, X. M., Analytical and numerical studies on steel columns with novel connections in modular construction, *Int. J. Steel Struct.*, 2017, doi: 10.1007/s13296-017-1226-5.
[33] Ye, Z., Wu, G., Feng, D. C., and Shafieezadeh, A., Shake table testing and computational investigation of the seismic performance of modularized suspended building systems, *Bull. Earthq. Eng.*, 2020, doi: 10.1007/s10518-020-00902-3.
[34] Annan, C. D., Youssef, M. A., and El Naggar, M. H., Experimental evaluation of the seismic performance of modular steel-braced frames, *Eng. Struct.*, 2009, doi: 10.1016/j.engstruct.2009.02.024.
[35] Annan, C. D., Youssef, M. A., and El Naggar, M. H., Seismic vulnerability assessment of modular steel buildings, *J. Earthq. Eng.*, 2009, doi: 10.1080/13632460902933881.
[36] Gunawardena, T., Ngo, T., and Mendis, P., Behaviour of multi-storey prefabricated modular buildings under seismic loads, *Earthq. Struct.*, 2016, doi: 10.12989/eas.2016.11.6.1061.
[37] Deng, E. F., Zong, L., Ding, Y., Dai, X. M., Lou, N., and Chen, Y., Monotonic and cyclic response of bolted connections with welded cover plate for modular steel construction, *Eng. Struct.*, 2018, doi: 10.1016/j.engstruct.2018.04.028.
[38] Deng, E. F., Zong, L., Ding, Y., Zhang, Z., Zhang, J. F., Shi, F. W., Cai, L. M., and Gao, S. C., Seismic performance of mid-to-high rise modular steel construction - A critical review, *Thin-Walled Structures*. 2020. doi: 10.1016/j.tws.2020.106924.
[39] Shan, S., Looi, D., Cai, Y., Ma, P., Chen, M. T., Su, R., Young, B., and Pan, W., Engineering modular integrated construction for high-rise building: A case study in Hong Kong, *Proc. Inst. Civ. Eng. Civ. Eng.*, 2019, doi: 10.1680/jcien.18.00052.
[40] Emamikoupaei, A., Bigdeli, A., and Tsavdaridis, K. D., Nonlinear seismic response of mid-rise modular buildings subjected to near-field ground motions, *J. Constr. Steel Res.*, 2023, doi: 10.1016/j.jcsr.2022.107696.
[41] Tesfamariam, S., Stiemer, S. F., Dickof, C., and Bezabeh, M. A., Seismic vulnerability assessment of hybrid Steel-Timber structure: Steel moment-Resisting frames with clt infill, *J. Earthq. Eng.*, 2014, doi: 10.1080/13632469.2014.916240.
[42] Zhang, X., Fairhurst, M., and Tannert, T., Ductility Estimation for a Novel Timber–Steel Hybrid System, *J. Struct. Eng.*, 2016, doi: 10.1061/(asce)st.1943-541x.0001296.

Copyright © 2025 CroCEE
DOI: https://doi.org/10.5592/CO/3CroCEE.2025.7

[43] Ganey, R. *et al.*, Experimental investigation of self-centering cross laminated timber walls, 2016. doi: 10.1061/(asce)st.1943-541x.0001877.
[44] Loss, C., Rossi, S., and Tannert, T., In-Plane Stiffness of Hybrid Steel–Cross-Laminated Timber Floor Diaphragms, *J. Struct. Eng.*, 2018, doi: 10.1061/(asce)st.1943-541x.0002105.
[45] Jaramillo, J. S. Z. and Fischer, E. C., THE ROLE OF INTERMODULAR CONNECTIONS IN THE GLOBAL BEHAVIOR OF HIGH-RISE MASS TIMBER BUILDINGS, 2023. doi: 10.52202/069179-0348.
[46] Chen, H., Yang, C., Ou, J., Zhao, B., Li, C., and Li, C., Experimental study on seismic performance of modular cast-in-situ coupled shear wall with LRC infill wall, *J. Build. Eng.*, 2023, doi: 10.1016/j.jobe.2023.106613.
[47] Svatoš-Ražnjević, H., Orozco, L., and Menges, A., Advanced Timber Construction Industry: A Review of 350 Multi-Storey Timber Projects from 2000-2021, *Buildings*, 2022, doi: 10.3390/buildings12040404.
[48] Menegon, S. J., Wilson, J. L., Lam, N. T. K., and Gad, E. F., Experimental testing of innovative panel-to-panel connections for precast concrete building cores, *Eng. Struct.*, 2020, doi: 10.1016/j.engstruct.2020.110239.
[49] Pan, W., Wang, Z., and Zhang, Y., Novel discrete diaphragm system of concrete high-rise modular buildings, *J. Build. Eng.*, 2022, doi: 10.1016/j.jobe.2022.104342.
[50] Wang, Z., Pan, W., and Zhang, Z., High-rise modular buildings with innovative precast concrete shear walls as a lateral force resisting system, *Structures*, 2020, doi: 10.1016/j.istruc.2020.04.006.

Proceedings of the 3rd Croatian Conference on Earthquake Engineering - 3CroCEE
19–22 March 2025, Split, Croatia
Copyright © 2025 CroCEE
DOI: https://doi.org/10.5592/CO/3CroCEE.2025.10

SEISMIC PERFORMANCE EVALUATION OF EXISTING REINFORCED CONCRETE BUILDINGS IN SKOPJE

Elena Delova [(1)], Aleksandar Zlateski [(2)], Marin Grubisic [(3)],
Veronika Shendova [(4)], Zivko Bozinovski [(5)], Kemal Edip [(6)]

[(1)] *Research Assistant, Ss. Cyril and Methodious University in Skopje, Republic of North Macedonia, Institute of Earthquake Engineering and Engineering Seismology, Skopje, delova@iziis.ukim.edu.mk*
[(2)] *Assistant Professor, Ss. Cyril and Methodious University in Skopje, Republic of North Macedonia, Institute of Earthquake Engineering and Engineering Seismology, Skopje, azlate@iziis.ukim.edu.mk*
[(3)] *Assistant Professor, Faculty of Civil Engineering and Architecture, University of Osijek, marin.grubisic@gfos.hr*
[(4)] *Professor, Ss. Cyril and Methodious University in Skopje, Republic of North Macedonia, Institute of Earthquake Engineering and Engineering Seismology, Skopje, veronika@iziis.ukim.edu.mk*
[(5)] *Professor, Ss. Cyril and Methodious University in Skopje, Republic of North Macedonia, Institute of Earthquake Engineering and Engineering Seismology, Skopje, zhivko_bozhinovski747@yahoo.com*
[(6)] *Professor, Ss. Cyril and Methodious University in Skopje, Republic of North Macedonia, Institute of Earthquake Engineering and Engineering Seismology, Skopje, kemal@iziis.ukim.edu.mk*

Abstract

The vulnerability of the built environment to seismic events has been increasingly evident, particularly in the Balkan region, where recent earthquakes have caused significant non-structural damage to both old and new buildings, often leading to restricted use. In North Macedonia, seismic design standards were introduced only after the catastrophic Skopje earthquake in 1963, with the first seismic code implemented in 1964. The construction of reinforced concrete buildings, which began at that time and continues even today, are now regarded as unique monuments of that era. These structures are a significant part of the urban landscape and reflect the evolution of engineering practices in the region. In recent years, there has been a focus on improving building features such as energy efficiency and facade renovations, but seismic evaluation and retrofitting have not been prioritized, as they are not required by national regulations.

This gap highlights the urgent need for guidelines to evaluate the seismic performance of existing buildings, allowing for the estimation of both direct and indirect losses associated with restoring building functionality, as well as the identification of key parameters influencing these losses. To address this, the economic loss prediction method outlined in FEMA-P58 is applied to residential buildings in Skopje's city center, which were constructed after the 1963 earthquake. These buildings serve as prototypes for assessing seismic performance using a scenario-based approach. The findings provide insights into expected repair costs due to earthquake-induced damage. Ultimately, the results of this study contribute to the establishment of performance-based objectives and procedures for assessing the recovery of existing buildings, providing valuable insights for future seismic resilience strategies and building safety improvements.

Keywords: FEMA P-58 methodology, performance-based seismic design, reinforced concrete frame buildings, vulnerability assessment, repair cost estimation, existing building stock.

1. Introduction

The seismic resilience of existing reinforced concrete buildings remains a critical concern, particularly in seismically active regions such as North Macedonia. The devastating 1963 Skopje earthquake marked a turning point in the country's construction practices, leading to the development of the first seismic design codes. [12] Despite the subsequent improvements, many buildings constructed during this transitional period remain vulnerable to seismic events due to their adherence to early code provisions. The need for robust assessment methodologies that can evaluate both direct and indirect earthquake-induced losses has thus become increasingly evident. [10]

To address this challenge, this study proposes an integrated approach combining the established methodology developed at the Institute of Earthquake Engineering and Engineering Seismology (IZIIS) [7] with the FEMA P-58 framework [3]. The IZIIS methodology, widely applied in the region,

Copyright © 2025 CroCEE
DOI: https://doi.org/10.5592/CO/3CroCEE.2025.10

incorporates detailed assessments of the structural system, mainly based on local regulatory requirements. However, it lacks a systematic probabilistic approach for damage and loss estimation analysis. On the other hand, FEMA P-58 provides a performance-based framework that quantifies repair costs, downtime, and safety risks using probabilistic models [5]. By integrating these methodologies, the proposed approach leverages the strengths of both: the contextual specificity of the IZIIS methodology and the systematic loss estimation capabilities of FEMA P-58.

The definition of seismic hazard in this study relies on site-specific investigations of local soil conditions. These investigations provide critical input for developing accurate acceleration response spectra, ensuring that the seismic hazard characterization reflects the unique geotechnical and seismological conditions of the studied locations.

An essential aspect of this integration is the development of fragility curves for structural and non-structural components, as well as loss functions tailored to the local context and the period of construction. These fragility curves and loss functions capture the unique characteristics of Macedonian buildings constructed during the era following the 1963 Skopje earthquake, enabling a more precise evaluation of their seismic vulnerability and potential losses.

This paper applies the integrated methodology to moment resisting reinforced concrete buildings within the "Gradski Zid" complex in Skopje, a representative case study of structures built shortly after the 1963 earthquake. These buildings serve as prototypes for demonstrating the practical application of the integrated approach. The integration allows for a comprehensive evaluation of seismic performance, considering not only immediate structural responses but also basic recovery needs and costs. The findings contribute to advancing performance-based design practices and enhancing resilience strategies tailored to the unique characteristics of Macedonian building stock.

By bridging the gap between local methodologies and international standards, this study aims to provide a robust framework for assessing and improving the seismic resilience of existing buildings in North Macedonia, addressing critical gaps in current reconstruction practices and laying the groundwork for future research in the field.

2. Assessment of the Behavior of Existing Reinforced Concrete Frame Buildings Using the FEMA P-58 Methodology

The previously discussed methodology was applied to existing reinforced concrete buildings constructed during the period between the adoption of the first seismic design standards (1964) and the adoption of the current standards in 1981, in North Macedonia. This period is considered a time of robust construction practices, characterized by structural design carried out by experienced engineers, strict supervision, quality control of construction materials, and mandatory inspection and testing [12].

For prototype buildings, residential structures from the "Gradski Zid" complex in the center of Skopje were selected. These buildings, constructed after the 1963 Skopje earthquake, include a substantial number of structures representative of the buildings of interest. The analysis utilized the integrated approach of combining site-specific seismic hazard characterization with fragility curves and loss functions tailored to the local context and the specific period of construction. To conduct analyses of the prototype buildings, the following input data were prepared:

- Seismic hazard characterization: Developed based on site-specific investigations of local soil conditions, providing critical input for accurate acceleration response spectra. [6]
- Fragility functions and consequence models: Extensive experimental data collected from the database of the Institute of Earthquake Engineering and Engineering Seismology (IZIIS), as well as experimental studies conducted in other European countries, were used to establish these for structural and non-structural components of the buildings.
- Technical documentation and building information: Review of available technical documentation for the buildings and additional required information from building owners were used to develop detailed performance models of the buildings. [13]

Copyright © 2025 CroCEE
DOI: https://doi.org/10.5592/CO/3CroCEE.2025.10

This combination of methodologies ensures a comprehensive evaluation of the seismic behavior of the selected structures, accounting for both immediate structural responses and potential economic losses due to damage, repair costs, and recovery timelines.

2.1. Selection of Ground Motion Time Histories

In accordance with the prescribed methodology defined in FEMA P-58, the seismic excitation is characterized using a target acceleration response spectrum tailored specifically for the studied location. For this site, the seismic potential was rigorously evaluated through detailed site-specific investigations of local soil conditions, ensuring that the acceleration spectrum accurately reflects the unique geotechnical and seismological characteristics of the area [6].

Based on the disaggregation of seismic hazard, two distinct hazard levels were considered.

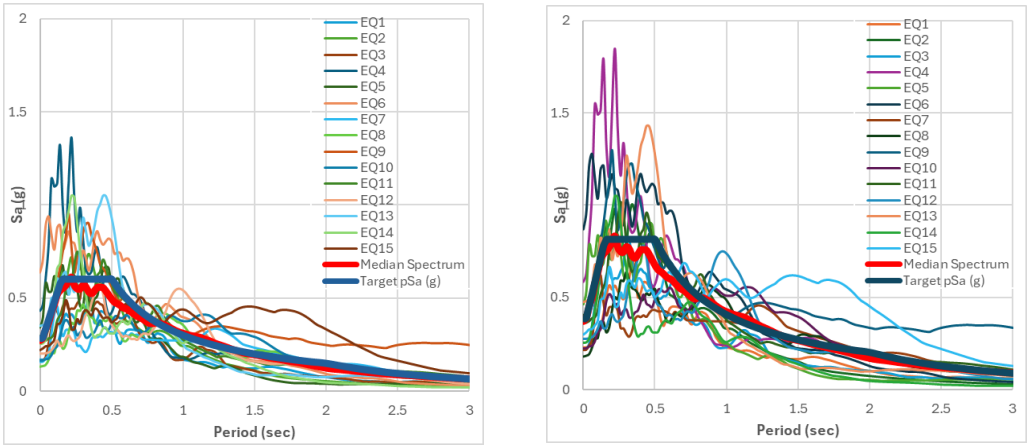


Figure 1. Appropriately selected earthquake spectra according to the considered hazard levels: Design Level Earthquake (DL) – left, Maximum Level Earthquake (ML) – right

The earthquake levels are associated with return periods of 475 and 950 years, referred to as the Design Level (DL) and Maximum Level (ML), respectively. For each level, 15 pairs of ground motion records were selected with spectra matching the target response spectrum for the specific location. Figure 1 illustrates the response spectra of the selected ground motion histories alongside the target response spectrum for the studied location.

2.2. Building Performance Model

The building performance model incorporates several key input parameters: (i) basic data about the building, (ii) data on vulnerable structural and non-structural components, (iii) structural analysis data, (iv) potential residual deformation data, (v) data on the probability of collapse, and (vi) the expected seismic hazard at the building's location.

The basic building data includes the size and geometry of the structure, the total replacement cost, and a loss threshold, which defines the conditions under which repairing the building is deemed uneconomical, prompting a replacement instead.

Vulnerable structural and non-structural components are defined by specific fragility curves and the quantity of components within each performance group. Table 1 presents the considered vulnerable components included in the analysis.

To determine the number of realizations required, preliminary analyses were conducted, varying the number between 100 and 2500. The results indicated minor increases in loss estimates between 100 and 2000 realizations, while increases from 2000 to 2500 were negligible. Consequently, 2000 realizations were adopted. Each realization represents a unique set of simulated building responses, including inter-story drift ratios (IDRs), peak floor accelerations (PFAs), and residual drift ratios.

Copyright © 2025 CroCEE
DOI: https://doi.org/10.5592/CO/3CroCEE.2025.10

Each realization was generated in the "PACT" software using a Monte Carlo simulation process, based on results from a nonlinear response history analysis and the selected dispersion of the model (βm). The dispersion (βm) was calculated as the square root of the sum of the squares of two sources of uncertainty: one related to the definition level of the building and construction quality (βc), and the other associated with the quality and comprehensiveness of the nonlinear structural analysis model (βq). In this study, the values of βc and βq were 0.4 and 0.25, respectively, in accordance with FEMA P-58 recommendations.

Table 1. Fragility Components and Required Parameters

Fragility Components	Demand Parameter
External joints_EWJ	Inter-story drift (%)
Internal joints_IWB	Inter-story drift (%)
Weak foundation columns_DWC	Inter-story drift (%)
Slender columns_BWC	Inter-story drift (%)
Exterior walls without openings	Inter-story drift (%)
Exterior walls with openings	Inter-story drift (%)
Partition walls without openings	Inter-story drift (%)
Partition walls with openings	Inter-story drift (%)
RC stairs with rigid joints	Inter-story drift (%)
Elevator	Floor acceleration (g)

2.3.Case Study Building: “Gradski Zid” Tower

The case study building is a 14-story residential structure located in the center of Skopje, North Macedonia. The building was designed and constructed with a reinforced concrete (RC) frame structural system. The analytical model of the structure is shown in Figure 2 - left, while the layout plan illustrates its symmetrical design along both orthogonal axes (Figure 2, right).

The total floor area is approximately 5830 m², with an average floor area of 370 m². All values for the dimensions of structural elements and material properties were adopted based on the available documentation (Table 2). [13]

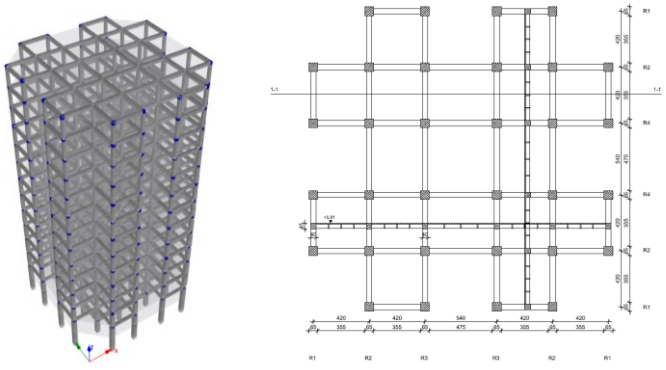


Figure 2. View of the analytical model (left) and the characteristic floor plan (right).

Table 2. Dimensions of Elements and Material Properties

Structural Features	Specifications
Column dimensions [cm]	65/65, 60/60, 55/55, 50/50, 45/45, 40/40
Beam dimensions [cm]	60/65, 65/50, 50/50, 40/45
Floor system	Ribbed slab (rib height 40 cm, slab thickness 8 cm)
Concrete and reinforcement	fc = 30 MPa, GA240/360

Copyright © 2025 CroCEE
DOI: https://doi.org/10.5592/CO/3CroCEE.2025.10

2.4. Description of the Analytical Model

The analytical model for the prototype structures was developed using the SeismoStruct software [9]. The model includes reinforced concrete (RC) structural elements such as columns and beams, while the floor slabs were simulated as diaphragms with constraints at the floor levels. Based on observations of damage manifested during past earthquakes in buildings constructed during the same period, the nonlinear behavior of joints, identified as the weakest points of the structural elements, was incorporated into the model.

The nonlinear behavior of internal joints was simulated using plastic hinges at the ends of the elements, with non-elastic behavior defined according to the designed cross-sectional characteristics of the original construction project. The nonlinear behavior of external joints was modeled using the "Scissors model" [8], which combines beam-column elements and spring connections at the joints. The joint region is represented by a series of rigid links with a central rotational spring to account for shear deformation in the joint region.

Gravitational loads were assigned based on architectural drawings from the available documentation and materials commonly used during the construction period. Live loads were estimated following FEMA P-58 guidelines, as 25% of the designed expected loads [3].

2.5. Results of Nonlinear Time History Analysis

The previously described analytical model was subjected to analysis using two sets of 15 earthquake ground motion records each. Each set corresponds to a specific hazard level: a return period of 475 years, referred to as the Design Level (DL), and a return period of 950 years, referred to as the Maximum Level (ML). For further analysis results for inter-story drift, floor accelerations, residual drift and collapse occurrence are used. The analysis results for inter-story drift and peak floor accelerations along the x and y directions are presented in Figures 3 and 4.

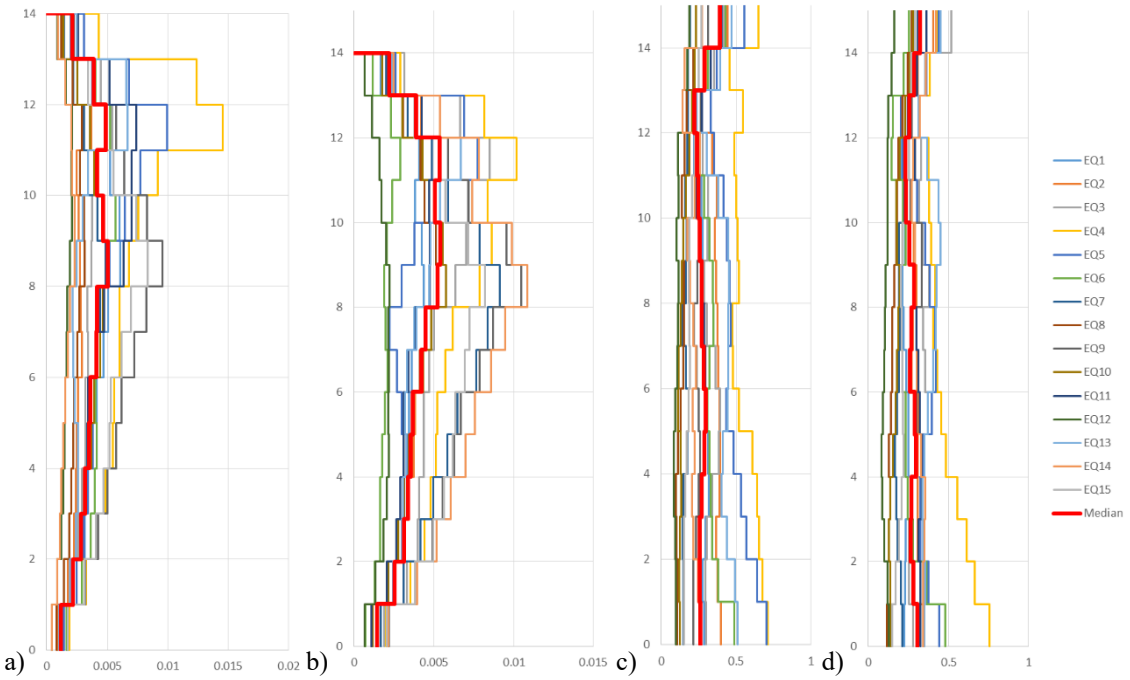


Figure 3. Inter-story drifts (a,b) and peak floor accelerations (c,d) for the x and y directions at the Design Level earthquake.

Copyright © 2025 CroCEE
DOI: https://doi.org/10.5592/CO/3CroCEE.2025.10

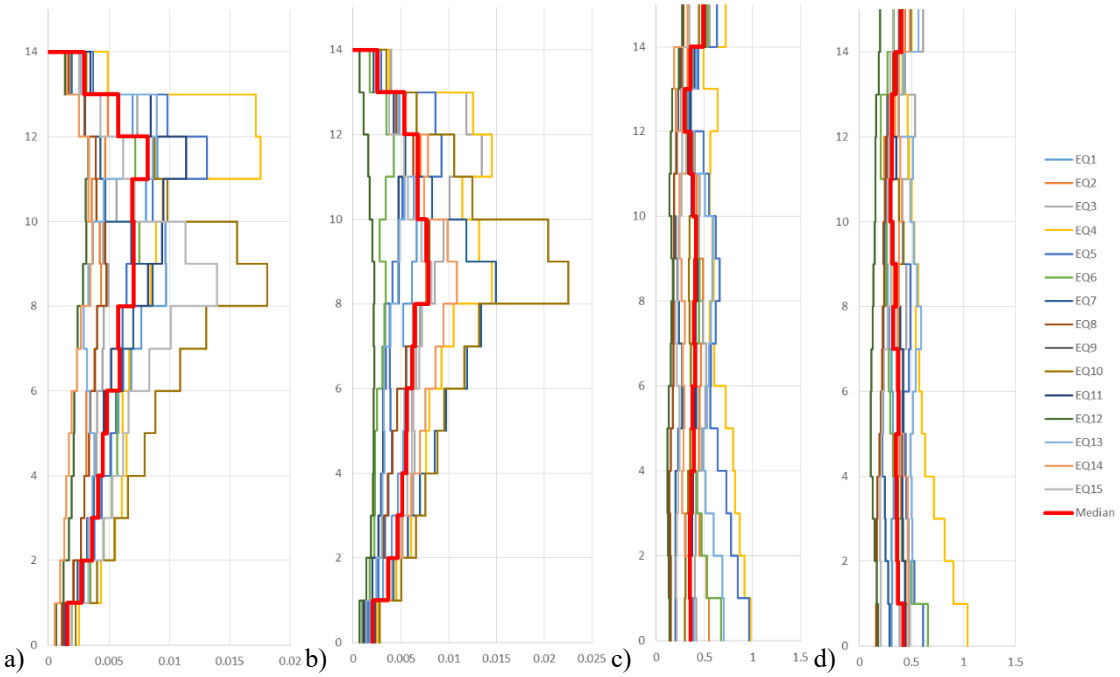


Figure 4. Inter-story drifts (a,b) and peak floor accelerations (c,d) for the x and y directions at the Maximum Level earthquake.

2.6. Results of the Seismic Scenario-Based Assessment of Building Behavior

For the previously defined hazard levels, analyses were performed based on two scenarios. The results are expressed as estimates of potential losses or costs associated with building repairs. In generating these scenarios, the total economic loss was assumed to be equivalent to the replacement cost of the building. The results obtained from the nonlinear analyses determined the economic loss for each defined vulnerable component of the building, correlating with the corresponding fragility functions (Table 2).

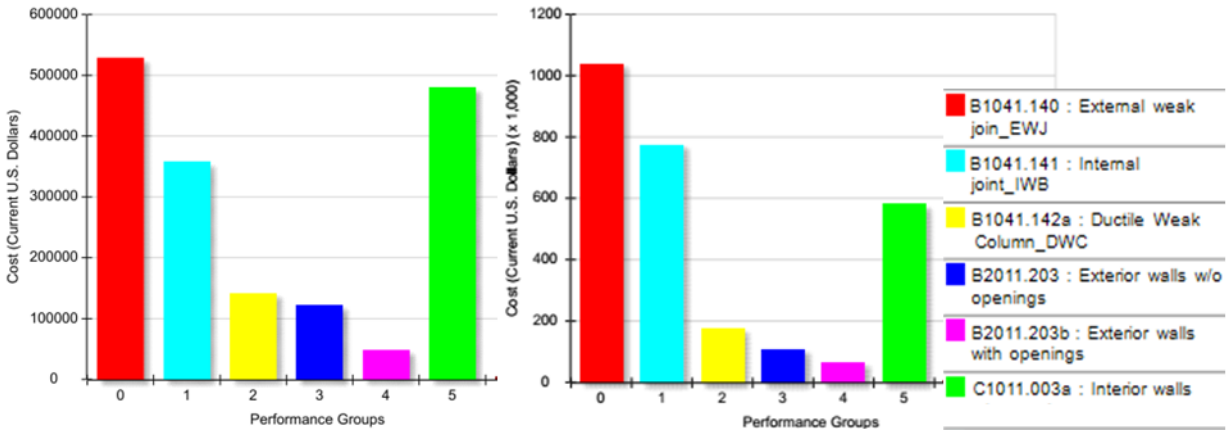


Figure 5. Repair costs distributed by fragility groups: Design Level earthquake (left) and Maximum Level earthquake (right).

Figure 5 illustrates the repair costs derived from 2000 realizations for the evaluated hazard levels and scenarios. For the 475-year return period, designated as the Design Level (DL), and the 950-year return period, designated as the Maximum Level (ML), repair costs are ordered by magnitude and broken down into contributions from each vulnerability group. The results indicate that structural components contribute the most to the building's losses, as repair costs for these components are the highest.

Copyright © 2025 CroCEE
DOI: https://doi.org/10.5592/CO/3CroCEE.2025.10

However, the costs of repairing damage to non-structural elements, such as masonry infills, are also significant.

The expected loss for each scenario represents the anticipated repair cost under a specific seismic intensity scenario. The results reveal a median repair cost of $1,683,545 for the DL scenario and $2,780,618 for the ML scenario.

The repair costs were normalized relative to the replacement cost of the building. Table 3 presents the normalized repair costs in relation to the total replacement cost.

Table 3. Normalized Repair Costs for the Building

Scenario	Replacement Cost [$]	Expected Loss [$]	Loss-to-Replacement Cost Ratio [%]	Repair Cost per m² [$]
DL	4 265 272	1 683 545	39.4%	312.46
ML		2 780 617	65.2%	516.07

Considering the data provided by FEMA P-58 on the expected repair time for potential damage, it becomes evident that the repair timeframe would also be significant. Figure 6 presents the time required for repairs if all floors are repaired simultaneously. However, this type does not provide an accurate picture of the actual repair timeline.

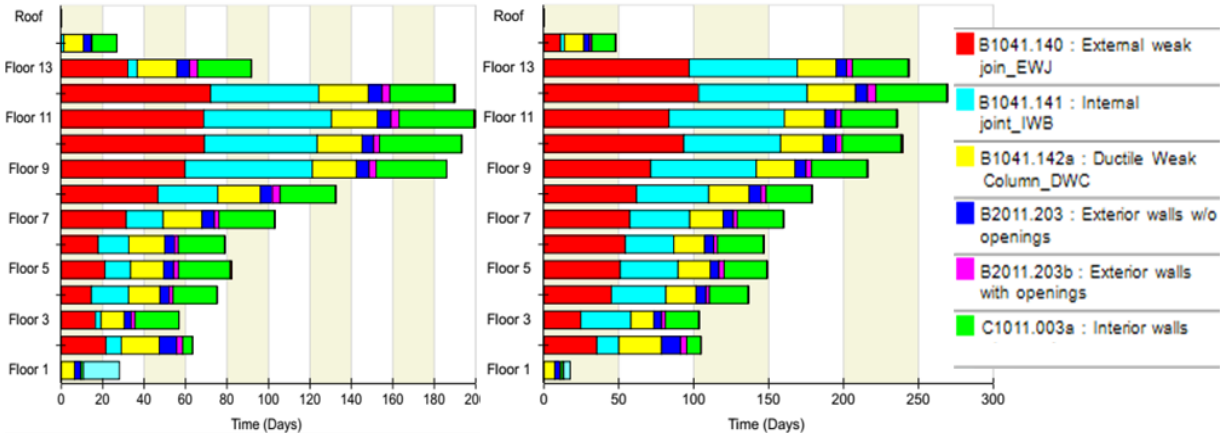


Figure 6. Repair time per floor: Design Level earthquake (left) and Maximum Level earthquake (right).

Certain limitations exist with this method of calculating repair time. The input parameters used in this methodology do not account for flexible allocation of labor, appropriate scheduling of work, and similar factors [14]. To accurately estimate the repair timeline, additional analyses are required to consider a broader range of factors, such as workforce availability and the organization of the repair process. These aspects will be addressed in future research.

3. Conclusions

The integration of the IZIIS methodology with the FEMA P-58 framework represents a significant advancement in the seismic assessment of existing reinforced concrete buildings in North Macedonia. By combining site-specific seismic hazard characterization with fragility curves and loss functions tailored to the local context and construction period, this approach addresses critical gaps in conventional assessment methodologies. The localized investigations, particularly those capturing unique soil characteristics, provide a robust foundation for precise hazard definition and response spectra.

Copyright © 2025 CroCEE
DOI: https://doi.org/10.5592/CO/3CroCEE.2025.10

The application of this integrated methodology to the "Gradski Zid" complex in Skopje demonstrates its practical utility in assessing the vulnerability and recovery potential of buildings constructed after the 1963 Skopje earthquake. The findings underscore the importance of tailoring international frameworks to regional contexts to enhance accuracy in predicting damage, repair costs, and recovery timelines. This integration offers a comprehensive evaluation, bridging immediate structural responses with long-term resilience planning.

This study provides a framework that can guide policymakers and engineers in developing seismic retrofitting strategies and resilience planning specific to the Balkan region. Moreover, it sets a precedent for adapting performance-based methodologies to local conditions, offering valuable insights for other seismically active regions worldwide.

Future research should focus on refining fragility functions and consequence models for non-structural components, as well as improving repair timeline estimations by integrating logistical and resource allocation considerations. Additionally, expanding the application of this methodology to other building typologies and regions within North Macedonia will enhance its generalizability and practical relevance.

By advancing a performance-based approach tailored to the unique characteristics of Macedonian building stock, this study contributes to the global discourse on seismic resilience, highlighting the importance of localized adaptations to international frameworks for improved safety and functionality of the built environment.

References

[1] ASCE (2006) Seismic Rehabilitation of Existing Buildings, ASCE/SEI 41-06, American Society of Civil Engineers, Reston, Virginia

[2] EERC (1996) Performance Based Seismic Design of Buildings, prepared by the Earthquake Engineering Research Center, University of California at Berkeley, for the Federal Emergency Management Agency, Report No. FEMA 283, Washington, D.C.

[3] FEMA (2012) Next-Generation Methodology for Seismic Performance Assessment of Buildings, prepared by the Applied Technology Council for the Federal Emergency Management Agency, Report No. FEMA P-58, Washington, D.C.

[4] FEMA (2009) Quantification of Building Seismic Performance Factors, prepared by the Applied Technology Council for the Federal Emergency Management Agency, Report No. FEMA P-695, Washington, D.C.

[5] Hamburger, R. O., Rojahn, C., Heintz, J. A., Mahoney, M. G. (2012). FEMA P58: Next-Generation Building Seismic Performance Assessment Methodology, 15h World Conference on Earthquake Engineering, Lisbon.

[6] IZIIS Report 2014/23 (2014). Evaluation of the seismic potential of the site, Definition of the seismic design parameters for the Project: MIXED USED CENTER SKOPJE – JUZEN BULEVAR.

[7] Necevska Cvetanovska, G., Apostolska, R., Sendova, V., Bozhinovski, Z. (2012). "Methodology and experiences on repair and strengthening of buildings in Republic of Macedonia compared with Eurocode 8 requirements". Scientific project financed by the Ss Cyryl and Methodious University Skopje. Report: IZIIS 2012-26, June 2012

[8] O'Reilly, G. J., & Sullivan, T. J. (2019). Modeling techniques for the seismic assessment of existing Italian RC frame structures. Journal of earthquake engineering, 2019

[9] SeismoStruct - A computer program for static and dynamic nonlinear analysis of framed structures. Version 7.0, SeismoSoft, 2024, https://www.seismosoft.com

[10] Shendova, V., Zhurovski, A., Zlateski, A., Delova, E., Jekikj, G., Apostolska, R., Bozhinovski, Z. (2023). Seismic Upgrading of Telecommunication Center in Skopje, N. Macedonia, 9th International Conference on Computational Methods in Structural Dynamics and Earthquake Engineering, 12-14 June 2023, Athens, Greece

[11] Shendova, V., Micov, V., Shalikj, R., Vitanova, M., Stojanoski, B., Tomikj, D., Dimitrovski, M., Trajchevski, J., Neziri, Z., Petreski, B., Zafirov, T., Nanevska, A., Zlateski, A., Runevski, K., Delova, E. (2020). Analysis

Copyright © 2025 CroCEE
DOI: https://doi.org/10.5592/CO/3CroCEE.2025.10

of Static and Seismic Stability of the Existing Structure of Office Building "MAKSTIL" in Skopje, Report IZIIS 2020-68, December 2020

[12] Sheshov, V., Apostolska, R., Shendova, V., Bozhinovski, Z., Gjorgiev, I., Bojadjieva, J., Vitanova, M., Jekic, G., Stojanovski, B., Zlateski, A., Zurovski, A., Kitanovski, T., Zafirov, T., Delova, E. (2021). High-level Seismic Screening of the Structures of Medical Facilities in North Macedonia; Public Sector Energy Efficiency Project, consulting services for: Technical Assistance for Seismic Screening and Preparation of Opinion for Healthcare facilities, Report: IZIIS 2021-58, November 2021.

[13] Talevski, Z., Gavrilovic, P., Jurukovski, D. (1967). Gradski ZId – Kula 8, Skopje, MAKEDONIJAPROEKT. VII.1967

[14] Terzic, V., Kolozvari, K. (2020). Evaluation of post-earthquake functional recovery for a 42-story building located in Los Angeles, Proceedings of the 2020 Los Angeles Tall Buildings Structural Design Council Conference.

Proceedings of the 3rd Croatian Conference on Earthquake Engineering - 3CroCEE
19–22 March 2025, Split, Croatia
Copyright © 2025 CroCEE
DOI: https://doi.org/10.5592/CO/3CroCEE.2025.17

RECENT ADVANCES IN SEISMIC VULNERABILITY ASSESSMENT OF CROATIAN COASTAL URBAN AREA

Željana Nikolić [(1)] *, Elena Benvenuti [(2)], Luka Runjić [(3)], Nenad Mladineo [(4)], Marko Mladineo [(5)]

[(1)] *Full Professor, University of Split, Faculty of Civil Engineering, Architecture and Geodesy, zeljana.nikolic@gradst.hr*
[(2)] *Full Professor, University of Ferrara, Engineering Department, elena.benvenuti@unife.it*
[(3)] *Researcher, University of Split, Faculty of Civil Engineering, Architecture and Geodesy, luka.runjic@gradst.hr*
[(4)] *Professor, University of Split, Faculty of Civil Engineering, Architecture and Geodesy, nenad.mladineo@gradst.hr*
[(5)] *Associate Professor, University of Split, Faculty of Electrical Engineering, Mechanical Engineering and Naval Architecture, marko.mladineo@fesb.hr*

Abstract

The seismic vulnerability assessment of existing urban areas provides fundamental information about reducing seismic risk in different phases of planning and emergency management. This contribution presents recent advances in seismic vulnerability assessment in Croatian coastal areas at various scales, starting with a detailed analytical approach at the building scale to large-scale evaluation at the building level and the level of the homogeneous zones. The investigation was performed in the town of Kaštela. This typical coastal settlement has expanded over past centuries, resulting in a heterogeneous distribution of the buildings built in periods with different technical regulations. A detailed nonlinear-linear analysis of important buildings (historical, public) has been performed providing evidence of their collapse behaviour. A comprehensive hybrid approach to large-scale seismic risk assessment, combining seismic vulnerability indices with critical PGAs for different limit states, has been applied to define vulnerability curves that relate vulnerability index, damage index, and peak ground acceleration. The outcome of the present analysis is the large-scale risk representation in terms of the damage and seismic risk indexes at the building level. The level of seismic risk to the community depends on several other parameters whose activation reduces the resilience to extraordinary events. Considering the characteristics of the observed pilot site, additional criteria for the risk assessment of homogenous zones are introduced, such as communal infrastructure, road network, construction density, inhabitation density, importance factor (public building, school, etc.), and status of protected historical buildings. The proposed methodology addresses seismic risk assessment at the level of homogeneous zones and utilizes Spatial Multi-Criteria Decision Making and PROMETHEE method. The presented approach to seismic risk assessment has important operational outcomes in the seismic risk management of the investigated area.

Keywords: seismic vulnerability assessment, hybrid approach, nonlinear-linear analysis, vulnerability index, damage, seismic risk index, PROMETHEE method.

1. Introduction

An insufficient seismic resistance of buildings is a main reason for human losses and material damage during a seismic event. The assessment of seismic performance of buildings, such as seismic vulnerability, structural capacity and damage state, is a demanding task, especially in old cities that have been gradually growing and expanding over the course of centuries. It requires complex nonlinear methods that precisely model the dissipation of energy in earthquake. Analysis of whole buildings is carried out by a non-linear static (pushover) method or an incremental dynamic analysis. Both approaches allow monitoring the level of damage and determining the collapse load.

The assessment of the seismic resistance of most buildings in cities is much more demanding because it is not possible to carry out a nonlinear analysis for all of them. Therefore, to effectively manage earthquake risk, the large-scale seismic vulnerability assessment is usually performed by simplified methods. In this paper, seismic vulnerability is assessed at different scales, starting with analytical approach at the building scale to large-scale assessment at the building level and large-scale assessment at the level of the homogeneous zones.

Copyright © 2025 CroCEE
DOI: https://doi.org/10.5592/CO/3CroCEE.2025.17

The proposed methodology applies a comprehensive hybrid approach to large-scale seismic risk assessment at the building level [1, 2], combining seismic vulnerability indices with critical PGAs for different limit states. The aim is defining vulnerability curves to relate vulnerability index, damage index and peak ground acceleration. The developed methodology combines the advantages of the vulnerability index method, proposed by Benedetti and Petrini [3], in assessing the seismic vulnerability for large-scale datasets of buildings with a detailed analytical approach based on the nonlinear static (pushover) method, implemented in Eurocode 8 [4, 5], which allows the determination of the capacity curves and the specific limit states of the buildings.

The level of risk of the community depends on several other parameters whose activation reduces the "resistance" of the community in seismic event. The most common parameters (criteria) relevant for the influence of the earthquake to the community are grouped into area characteristics (geology, soil, slope, historical earthquake events, fault line, etc.), the characteristics of human intervention in space (land use, built communal infrastructure and roads, etc.) and social characteristics such as housing density, social purpose of buildings (Occupancy Category), social structure, etc.). The large-scale assessment of seismic risk at the level of homogeneous zones has been performed by using the multi-criteria analysis [6] that is commonly used to evaluate and compare quantitative and qualitative criteria in completely different units and the order of magnitude. In this level of processing, the previously analyzed buildings, whose seismic performance has been represented in terms of vulnerability, damage and risk indexes, are grouped into spatial units defined as “homogeneous zones”. Since homogeneous zones have complex characteristics, the parameters for vulnerability and hazard, are coupled with the inclusion of additional criteria in order to assess the level of seismic risk to the community.

The methodology has been applied to a small coastal urban settlement, Kaštel Kambelovac (Fig.1), on the Croatian side of the Adriatic Sea near Split. The settlement consists of a historical core constituted by stonemasonry and the periphery outside of the historical core. The historical core was erected between the 15th and 19th centuries, while the periphery includes mostly modern buildings. In particular, five main categories of construction data of modern buildings have been recognized: before 1948, 1949–1964, 1964–1982, 1982–2005, and modern buildings erected from 2005 onwards. All these buildings exhibit different seismic performances depending on the period of construction and applied technical regulation.



Figure 1. Historical center of Kaštel Kambelovac with typical buildings.

2. Seismic risk assessment at the building level

A comprehensive hybrid approach to large-scale seismic risk assessment, combining seismic vulnerability indices with critical peak ground accelerations (PGA) for different limit states, has been applied to define vulnerability curves that allow to relate vulnerability index, damage index, and PGA.

The vulnerability index method is used to calculate the vulnerability index for the building based on the calculation of 11 geometrical, structural and non-structural vulnerability parameters of the building.

Copyright © 2025 CroCEE
DOI: https://doi.org/10.5592/CO/3CroCEE.2025.17

The parameters consider the influence of the type and quality of the structural system, the shear resistance in two horizontal directions, the position and the foundations, the properties of floors, the configuration in plan and elevation, the maximum wall spacing, the roof's typology and weight, the existence of non-structural elements, and the state of preservation. Four possibilities for each parameter were decided: from "A", indicating an optimal state, to "D", indicating a poor state. Furthermore, the method numerically scores each option. The relative importance of each parameter in the overall vulnerability is computed by using weight coefficients relating to each parameter. Finally, the vulnerability index I_v is calculated in a form $I_V = \sum_i s_{vi} w_i$, where s_{vi} is the numerical score for each class, and w_i is the weight of each parameter. The vulnerability index is normalized in a 0–100% range; a low index indicates high seismic resistance and low vulnerability, while a high vulnerability index is characteristic of the buildings with low seismic resistance and high vulnerability. Vulnerability indexes of the buildings located in the test site are presented in Fig. 2 [2].



Figure 2. Vulnerability index map of the test site.

An important step in seismic risk assessment is representation of seismic risk in terms of the damage index and the index of seismic risk. In this paper a hybrid empirical-analytical procedure that combines seismic vulnerability indices with critical PGA have been developed. For this purpose, detail non-linear pushover analysis for 18 buildings has been performed by 3MURI software [7]. In order to calculate the damage index, the relation between the vulnerability index and the seismic capacity represented by PGA for the sample of 18 buildings has been established. Non-linear static (pushover) analysis has been applied for the calculation of PGA for different limit states of buildings (damage limitation PGA_{DL}, significant damage PGA_{SD}, and near collapse PGA_{NC}). Vulnerability index - PGA relations (Fig. 3) enable the calculation of the damage index of the building, but also the calculation of the index of seismic risk for each limit states.

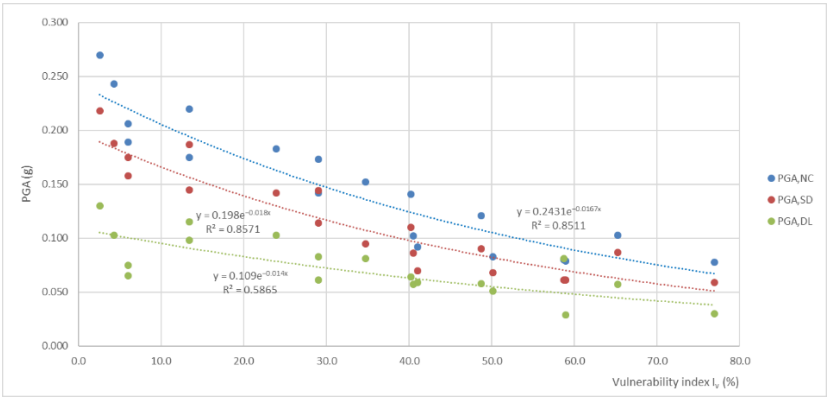


Figure 3. Vulnerability index – PGA relations (I_v–PGA_{DL}, I_v–PGA_{SD}, and I_v–PGA_{NC}).

The vulnerability curves allow to correlate the vulnerability index, damage index and peak ground acceleration. The basis for defining vulnerability curves in the presented investigation are vulnerability indices I_V, yield peak ground acceleration PGA_y, and collapse peak ground acceleration PGA_C, obtained

Copyright © 2025 CroCEE
DOI: https://doi.org/10.5592/CO/3CroCEE.2025.17

by the pushover analysis for 18 analysed buildings. Yield acceleration PGA_y is assigned to PGA_{DL} and collapse acceleration PGA_C to PGA_{NC} limit states, respectively. As PGA_y and PGA_C depend on the vulnerability index I_V, the values of PGA_y, associated with damage d=0, and PGA_C, associated with damage d=1, can be calculated for each value of I_v. Fig. 4 shows the vulnerability curves used for the estimation of the damage index of the buildings at the investigated area [2].

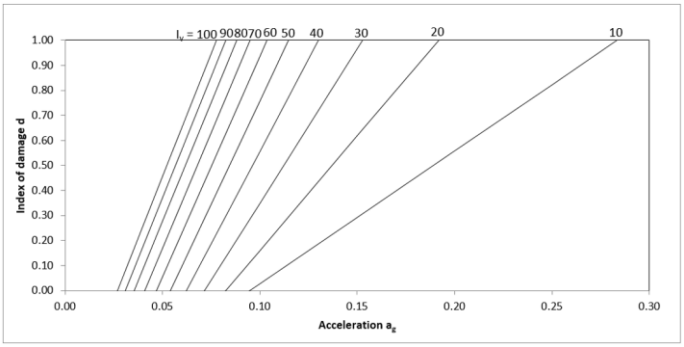


Figure 4. Vulnerability curves for the test site.

The spatial distribution of the damage is represented by the damage index maps of the investigated area for the given intensity of the earthquake. Three seismic scenarios corresponding to return periods of 95, 225, and 475 years and demand PGA of 0.11 g, 0.17 g, and 0.22 g, respectively, have been chosen. The damage to the buildings for different scenarios is presented in Fig. 5.



(a)



(b)

Copyright © 2025 CroCEE
DOI: https://doi.org/10.5592/CO/3CroCEE.2025.17



(c)

Figure 5. Damage index distribution: (a) T=95 years; (b) T=225 years; (c) T=475 years.

The index of seismic risk is calculated as a ratio of the PGA_C associated to the structural capacity and the demand ground acceleration PGA_D in a form $\alpha_{PGA,C} = PGA_C / PGA_D$. PGA_D is obtained from the seismic hazard map for the selected return period as $PGA_D = a_g S$, where a_g represents horizontal PGA on type A soil which also includes importance of the building ($a_g = \gamma_I a_{gR}$) and S is a soil parameter. Indices of seismic risk are used to validate the safety of the structure, $\alpha_{PGA,C} > 1$ refer to safe structures, while the values $\alpha_{PGA,C} < 1$ refer to non-safe structures. The indices of seismic risk for the NC limit state of the buildings for three return periods are presented in Fig. 6.



(a)



(b)

Copyright © 2025 CroCEE
DOI: https://doi.org/10.5592/CO/3CroCEE.2025.17



(c)

Figure 6. Distribution of index of seismic risk: (a) T=95 years; (b) T=225 years; (c) T=475 years.

3. Seismic risk assessment at the level of homogeneous zones

The large-scale assessment of seismic risk at the level of homogeneous zones has been performed to evaluate and compare quantitative and qualitative criteria in completely different units and the order of magnitude. The previously analysed buildings, whose seismic performance has been represented in terms of vulnerability, damage and risk indexes, are grouped into spatial units defined as "homogeneous zones". The homogenous zones are created considering specific urban characteristics, areas surrounded by the main roads and terrain height. The parameters for vulnerability represented by vulnerability index and seismic hazard in each zone are coupled with the inclusion of additional criteria in order to assess the level of seismic risk to the community. Additional criteria are communal infrastructure -electricity supply, communal infrastructure - water supply and drainage, Road network, construction density (distance between buildings), inhabitation density, importance factor of the buildings (public, school, etc.) and existence of protected historical buildings.

A methodology for seismic risk assessment of the area at the level of the homogeneous zones is based on Spatial Multi-Criteria Decision Making based on PROMETHEE method [8], coupled with the Geographic Information System [6].

The advantage of the Spatial Multi-Criteria Decision-Making system is the ability to generate criteria evaluations from GIS analysis. In this research, GIS analyses have been made to aggregate criteria evaluations for each homogenous zone for the following additional criteria: communal infrastructure, road network, construction density, inhabitation density, importance factor (public building, school, etc.), and historical buildings.

Criterion Communal infrastructure can be presented as a unified indicator or, for easier quantification, can be divided into individual content, such as: electricity supply, water supply and sewerage, gas network, telecommunications network, etc. Road network is part of the built infrastructure, but it is also treated as a special criterion due to its importance, because firefighter's accesses are very important element of the system for assessing the vulnerability of urban units. Construction density or distance between buildings as a way of building is an important criterion from the aspect of the organization of the rescue, especially in cases of earthquakes of higher intensity. Inhabitation density is a very common criterion used to have an insight into the expected number of victims or vulnerable persons. Data for this criterion can be generated from a digitized view of the census or from communal databases. The importance factor is a criterion that selects buildings that have social importance (content) such as schools, churches, and kindergartens. Another criterion is dictated by the presence of important historic buildings in a particular homogeneous zone. GIS analysis of these criteria is presented in Fig. 8.

Copyright © 2025 CroCEE
DOI: https://doi.org/10.5592/CO/3CroCEE.2025.17

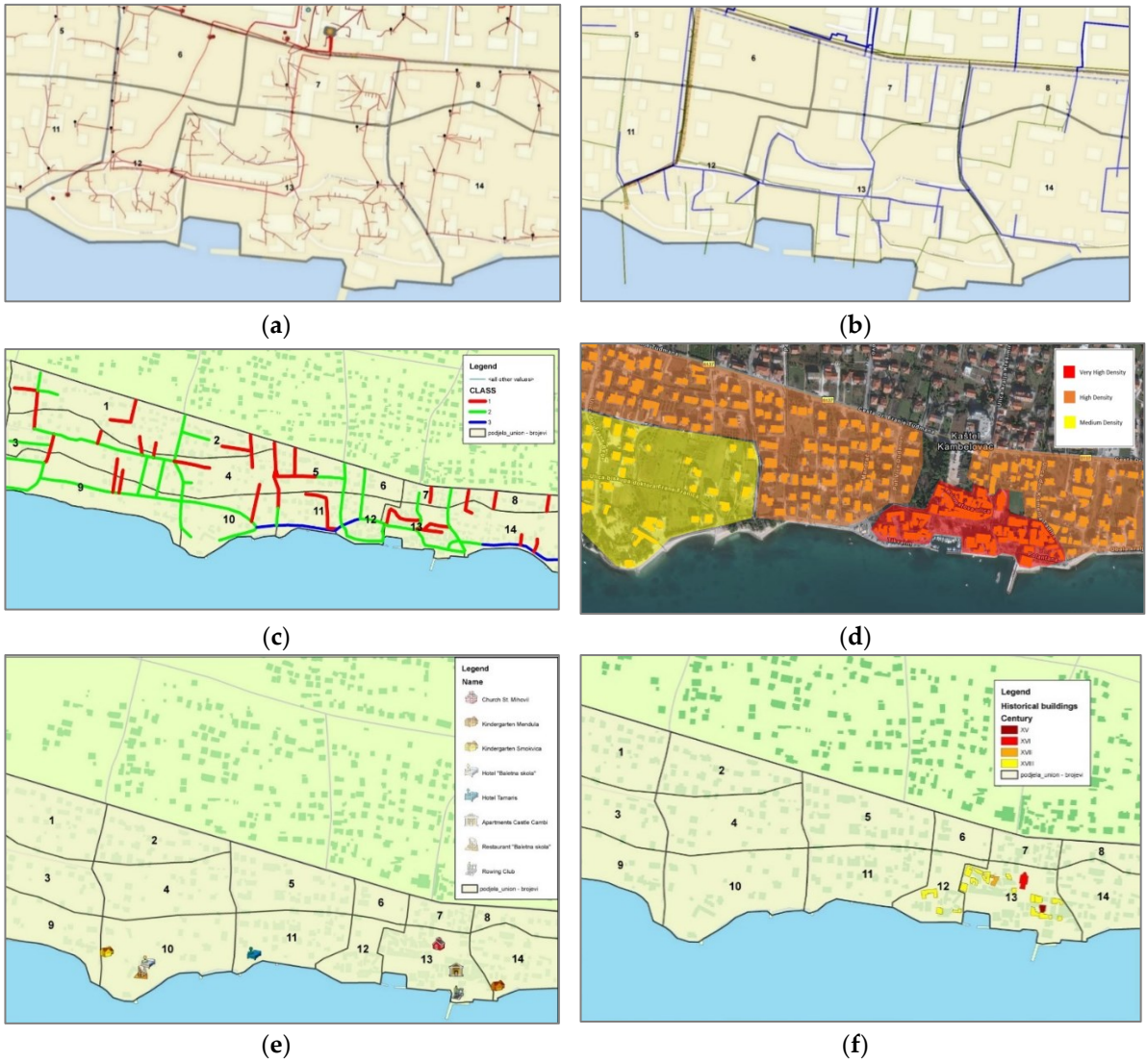


Figure 8. GIS analysis of additional criteria: (a) electricity supply; (b) water supply and drainage; (c) road network; (d) construction density; (e) importance factor (public, school, etc.); (f) historical buildings.

The PROMETHEE method combines all above mentioned criteria with ease, mutually compares homogeneous zones and evaluates the risk for each zone. Visual representation of the results has been made in GIS, where green represents low risk and red represents high risk (Fig. 9).

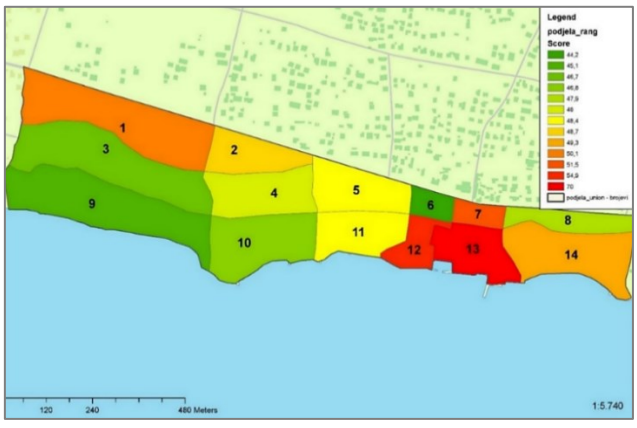


Figure 9. Seismic risk assessment for homogenous zones (green represents low risk, red represents high risk).

Copyright © 2025 CroCEE
DOI: https://doi.org/10.5592/CO/3CroCEE.2025.17

4. Conclusion

This paper presents a methodology for seismic vulnerability assessment at different scales. This methodology utilizes a comprehensive hybrid approach specific for large-scale seismic vulnerability and risk assessment of existing urban area at the building scale. Moreover, vulnerability index method and non-linear static pushover analysis are used for representation of vulnerability index, damage index and index of seismic risk for the Croatian coastal settlement Kaštel Kambelovac. Spatial Multi-Criteria Decision Making based on PROMETHEE method, coupled with the Geographic Information System are used to assess seismic risk to the community at the level of the homogeneous zones introducing additional criteria which influence to the earthquake consequences in the observed zones. Finally, the various homogenous zones are ranked in terms of proneness to seismic risk. The obtained results provide an important basis for systematic take-over and planning of priorities in rehabilitation of vulnerable urban areas. Performed analyses furnish, indeed, useful information for decision makers and public authorities to prioritizing future interventions and planning the operational capacity of civil protection to rescue and recovery after harmful events.

Acknowledgements

This research was funded by: (1) the EUROPEAN UNION, Programme Interreg Italy-Croatia, Project "STRategies for assessing climate change and natural hazards' impact on urban ecosystems, increasing resilience to ENvironmental hazards, and promoting territorial GrowTH" - STRENGTH ID ITHR0200318; (2) the EUROPEAN UNION, Programme Interreg Italy-Croatia, Project "Preventing, managing and overcoming natural-hazards risks to mitigate economic and social impact" - PMO-GATE ID 10046122; (3) the CROATIAN GOVERNMENT and the EUROPEAN UNION through the European Regional Development Fund—the Competitiveness and Cohesion Operational Programme (Project KK.01.1.1.02.0027).

References

[1] Nikolić, Ž., Runjić, L., Ostojić Škomrlj, N., Benvenuti, E. (2021): Seismic vulnerability assessment of historical masonry buildings in Croatian coastal area. *Applied Sciences*, **11**(13), 5997, doi: https://doi.org/10.3390/app11135997

[2] Nikolić, Ž., Benvenuti, E., Runjić, L. (2022): Seismic risk assessment of urban areas by a hybrid empirical-analytical procedure based on peak ground acceleration. *Applied Sciences*, **12**(7), 3585, doi: https://doi.org/10.3390/app12073585

[3] Benedetti, D., Petrini, V. (1984): Vulnerability of masonry buildings: Proposal of a method of assessment (in Italian). *L'industria Delle Costr.*, 149, 66–74.

[4] CEN (2004). EN 1998-1:2004: Eurocode 8: Design of structures for earthquake resistance - Part 1: General rules, seismic actions and rules for buildings, Comité Européen de Normalisation, Brussels.

[5] CEN (2005). EN 1998-3:2005. Eurocode 8: Design of structures for earthquake resistance - Part 3: Assessment and retrofitting of buildings, Comité Européen de Normalisation, Brussels.

[6] Mladineo, N., Mladineo, M., Benvenuti, E., Kekez, T. (2022): Methodology for the Assessment of Multi-Hazard Risk in Urban Homogenous Zones, *Applied Sciences*, **12**(24), 12843, doi: https://doi.org/10.3390/app122412843

[7] 3MURI Software, Professional version, S.T.A. DATA (2019), Torino, Italy.

[8] Brans, J.P., Vincke, P., Mareschal, B. (1986): How to select and how to rank projects: The PROMETHEE method. *European Journal of Operational Research*, 24, 228–238.

Proceedings of the 3rd Croatian Conference on Earthquake Engineering - 3CroCEE
19–22 March 2025, Split, Croatia
Copyright © 2025 CroCEE
DOI: https://doi.org/10.5592/CO/3CroCEE.2025.18

SP-BELA: A STRUCTURAL SEISMIC VULNERABILITY ASSESSMENT METHODOLOGY BASED ON PUSHOVER CURVES

Barbara Borzi [(1)], Antonella Di Meo [(2)], Marta Faravelli [(3)]

[(1)] *Head of research, EUCENTRE, barbara.borzi@eucentre.it*
[(2)] *Researcher, EUCENTRE, antonella.dimeo@eucentre.it*
[(3)] *Researcher, EUCENTRE, marta.faravelli@eucentre.it*

Abstract

SP-BELA (Simplified Pushover-Based Earthquake Loss Assessment) is a method that allows to define the vulnerability of a building taxonomy by associating it with a portfolio of capacity curves. The main advantage of this method is that it keeps the capacity of the buildings separate from the demand imposed by the shaking at the site. This makes SP-BELA highly flexible and applicable to buildings of all structural types whose response to inertial actions can be described by a pushover curve. The method describes the seismic behaviour of a building taxonomy through the simplified mechanical model of a prototype building. The model includes the known data of the taxonomy (e.g., number of floors) and generates a population of buildings using random variables that represent the variability of the buildings belonging to the taxonomy. Therefore, the more data available, the more reliable and accurate the definition of seismic capacity will be because less unknown data will need to be generated.

This article outlines the application of the method to the reinforced concrete (RC) and masonry buildings since these structural types are the most representative of the built environment in Italy and Mediterranean countries. The article also defines the calibration process to which SP-BELA undergoes, testing its ability to numerically replicate the damage scenario of events that occurred in Italy in recent decades. Potential future developments of the methodology are also discussed. Lastly, we briefly document the implementation of SP-BELA in platforms that the Eucentre Foundation developed for the Italian Civil Protection Department (ICPD) to assess the seismic risk of the Italian building assets and calculate the damage scenario due to an earthquake.

Keywords: Seismic assessment, Nonlinear static analysis, Structural vulnerability, Reinforced concrete buildings, Masonry buildings.

1. Introduction

This article presents the SP-BELA (Simplified Pushover-Based Earthquake Loss Assessment) method for seismic vulnerability assessment. When it was first published [1], [2], SP-BELA had all the characteristics to belong to the family of mechanical methods. In fact, it combines the definition of structural capacity through a simplified pushover analysis similar to that proposed in [3], with a displacement-based structural verification method based on displacements according to Direct Displacement Based Assessment (DDBA).

The DDBA defines the nonlinear properties of the building by establishing an equivalent single-degree-of-freedom (SDOF) system that corresponds to the original structure in terms of vibration period, amount of energy dissipated due to nonlinearity, and displacement capacity. The first displacement-based method implemented in a vulnerability model was proposed by Calvi [4]. For reinforced concrete (RC) structures, the method proposed in [4] was further developed by Pinho et al. [5] and Crowley et al. [6], leading to the definition of the DBELA (Displacement-Based Earthquake Loss Assessment) method. In Europe, Tsionis and Fardis [7] developed fragility curves for RC buildings with nonlinear static analysis. The same approach was used by Karantoni et al. [8]for regular masonry buildings considering in-plane and out-of-plane failure mechanisms. For the seismic assessment of Italian buildings there are many approaches in the literature. These include Del Gaudio et al. [9], who

Proceedings of the 3rd Croatian Conference on Earthquake Engineering - 3CroCEE
19–22 March 2025, Split, Croatia
Copyright © 2025 CroCEE
DOI: https://doi.org/10.5592/CO/3CroCEE.2025.18

developed fragility curves for RC buildings using the simplified mechanics-based method applied to an equivalent SDOF system. For masonry buildings, Lagomarsino and Cattari [10] suggest mechanics-based methods referring to non-linear static analyses to describe the building performance.

The fundamental components of SP-BELA are:

- Identification of a building prototype representing the taxonomy;
- Creation of a building dataset through Monte Carlo generation, starting from the building prototype;
- Simulated design of buildings of the aforementioned dataset according to code regulations;
- Definition of a simplified pushover curve for each building in the dataset. The pushover curve should identify displacements characterizing the attainment of specific damage conditions identified by limit states.

Most of the mechanic-based methods published in the technical literature result in the creation of fragility curves that compare the building capacity with the demand imposed by earthquakes for various levels of ground shaking severity. The primary distinctive feature of SP-BELA is the separation between demand and capacity. The capacity of the building taxonomy is compared with the earthquake demand at runtime. This approach makes the method very flexible. Some advantages are listed below:

- It allows for the consideration of the specific ground shaking characteristics during runtime analyses instead of representing the severity of the ground motion using a single parameter (e.g. Peak Ground Acceleration (PGA), Spectral acceleration (Sa), etc.). This makes the method suitable for accounting for different local site conditions and various types of ground shaking, such as crustal, volcanic, and subduction events;
- It allows for the consideration of various building codes, as the design process can be adapted to include different design options. This flexibility enables the description of taxonomies in relation to the specific design code adopted during the construction of the buildings;
- It can be applied to any structural typology, as long as its seismic performance can be represented by a pushover curve.

Although SP-BELA was initially a mechanics-based method, it evolved into a hybrid approach during further development. In fact, the method is calibrated through comparisons between numerically simulated damage scenarios and observed damage data. This innovation allows the method to address some of the limitations inherent in purely mechanics-based approaches, as will be explained in detail in the paper.

Overall, this paper provides a description of the SP-BELA method and its calibration process. Furthermore, the paper shows some practical applications of the method to different assets exposed to risk.

2. Definition pushover curves with SP-BELA

The structural capacity is defined through the pushover curve with a piecewise linear curve. To establish the aforementioned curve, we need the displacement capacities at the control points (i.e., Limit States) and the base shear strength. The latter is then transformed in dimensionless parameter by dividing it by the seismic weight of the building. The Limit States (LSs) under consideration have to be numerical thresholds whose exceedance can be mathematically identified. In SP-BELA, we consider:

- LS1: Slight damage/operational limit condition. After the earthquake, the building is still functional and does not need any structural interventions;
- LS2: Severe damage limit condition. The building cannot be used after the earthquake has occurred and requires structural interventions.

Proceedings of the 3rd Croatian Conference on Earthquake Engineering - 3CroCEE
19–22 March 2025, Split, Croatia
Copyright © 2025 CroCEE
DOI: https://doi.org/10.5592/CO/3CroCEE.2025.18

- LS3: Collapse/life safeguard. Beyond this limit condition, the building is no longer safe because it doesn't withstand the gravity loads for which it was designed. The building will be demolished because structural interventions are either not feasible or cost effective.

In a probabilistic procedure for a large-scale seismic vulnerability assessment, the capacity curve can be derived from a reasonable estimation of the strength and displacement capacities. In simplified methods the capacity curve results from the repetition of the pushover analysis of buildings in a sample generated by varying random variables (i.e., building geometry, loads, and material parameters) according to probabilistic distribution laws. Once the capacity curve is determined, the properties of the SDOF system for each limit state are identified through: (i) the vibration period T, which is calculated based on the secant stiffness and the building mass, and (ii) the equivalent damping ξ, which is determined using relationships linking it to the ductility μ. In SP-BLA the equivalent damping ξ is calculated with the following formula proposed by Priestley et al. [11]:

$$\xi = 0.05 + 0.565\left(\frac{\mu - 1}{\pi\mu}\right) \tag{1}$$

The building taxonomies used to describe the "as built" in Italy are as follows:

- RC buildings, including the effects of infill walls which can be regularly or irregularly (pilotis) distributed along the height. These taxonomies are further divided based on whether the buildings were designed for gravitational or seismic loads. In the former case, only wind actions are considered as lateral loads in the simulated design. In the latter case, lateral forces also include inertial loads for which the building was designed according to the law in force at the time of its construction. Finally, a further subdivision is made into floor classes;
- Masonry buildings. Since SP-BELA relies on defining capacity through a pushover curve, it is capable of describing the behaviour of masonry buildings with global behaviour that triggers a collapse mechanism within the wall plane. This behaviour characterises masonry buildings with low vulnerability. To account for the behaviour of masonry with medium and high vulnerability, capacity correction coefficients have been calculated through a calibration as explained in Chapter 4. Masonry buildings are also divided into various floor classes.

Details on the implementation of SP-BELA for RC and masonry buildings are provided in the following sections.

2.1. RC Buildings

The pushover curves representative of the RC "as built" in Italy [12], [3], [13], in SP-BELA are calculated for the prototype building shown in Figure 1. If buildings are not seismically designed, their frames are generally oriented in only one direction. In the orthogonal direction, frame behaviour is, instead, ensured solely by the collaborating floor width.

Copyright © 2025 CroCEE
DOI: https://doi.org/10.5592/CO/3CroCEE.2025.18

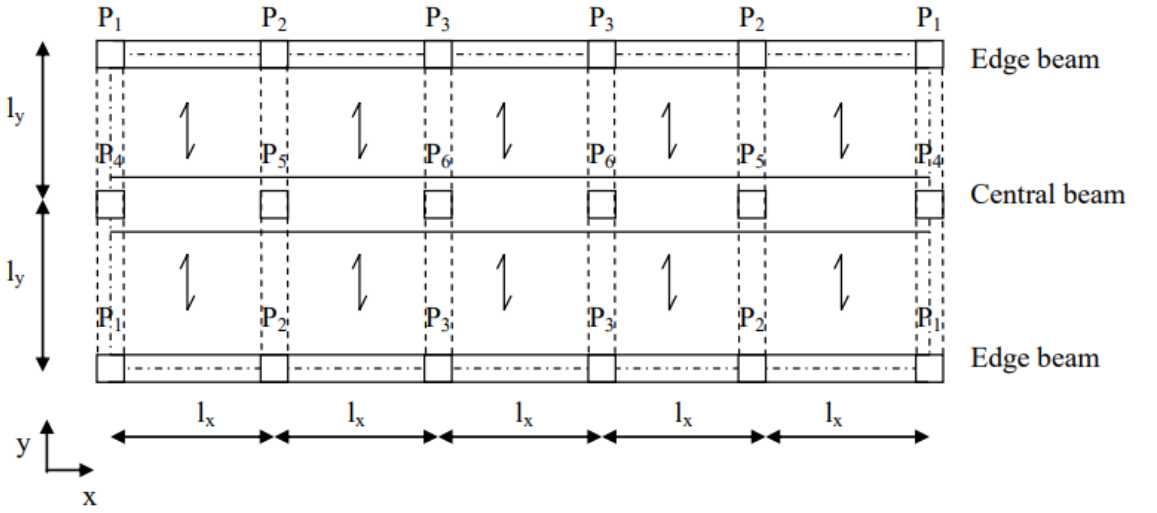


Figure 1. Layout of prototype building considered in SP-BELA as representative of RC buildings taxonomies (Borzi et al. 2008a).

To calculate the collapse multiplier λ, which corresponds to the dimensionless base shear resistance relative to the seismic weight, the distribution of bending moments and shears generated by the combination of gravity and horizontal actions must be defined. It is assumed that the seismic action corresponds to a triangular force distribution. Different distributions could be adopted in SP-BELA to account for higher modes of vibration beyond the first, which could be significant, such as in the case of multi-storey buildings.

The procedure for defining how bending moments and shears are distributed in the building elements is inspired by Priestley et al. [11]. For each column of the structure it calculates the shear resistance as the minimum value among the following:

- The shear strength of the column itself;
- The shear corresponding to the flexural capacity of the columns;
- The shear corresponding to the flexural capacity of the beams supported by the column.

Shear failure of beams collapse is not considered because beams tend to rarely fail in shear due to the shear reinforcement designed to withstand gravitational loads. Further details on the checks performed in SP-BELA for the definition of column shear resistance can be found in [1].

Once the shear resistance of columns is defined for each level, the collapse multiplier is calculated as follows:

$$\lambda_i = \frac{V_C^i}{W_T} \frac{\sum_{j=1}^{n} W_j z_j}{\sum_{k=i}^{n} W_k z_k} \tag{2}$$

where W_T is the total weight of the building, W_i is the weight associated with level i at elevation z_i, and V_{Ci} is the sum of shear resistances of the columns on level i. The collapse multiplier λ is the smallest value among all the λ_i values for each level.

The collapse mechanism is then defined as follows:

- If shear collapse occurs in any of the columns, the analysis stops. This choice is consistent with the fact that shear collapse mechanism is brittle and lacks the ability to dissipate energy.
- After the opening plastic hinges in all beams, if plastic hinges are activated at the base of all columns on a certain level, a global mechanism is considered (Figure 2a).

Copyright © 2025 CroCEE
DOI: https://doi.org/10.5592/CO/3CroCEE.2025.18

- If the columns of a certain level fail in flexure, the activation of a storey mechanism is considered (Figure 2b).

Mixed situations may occur where only some columns are stronger than the beams and vice versa. In such cases, a clear collapse mechanism cannot be identified. Finite element analyses undertaken to validate the procedure implemented in SP-BELA [14] have shown that, in this case, the collapse mechanism is an average between the global mechanism and the storey mechanism.

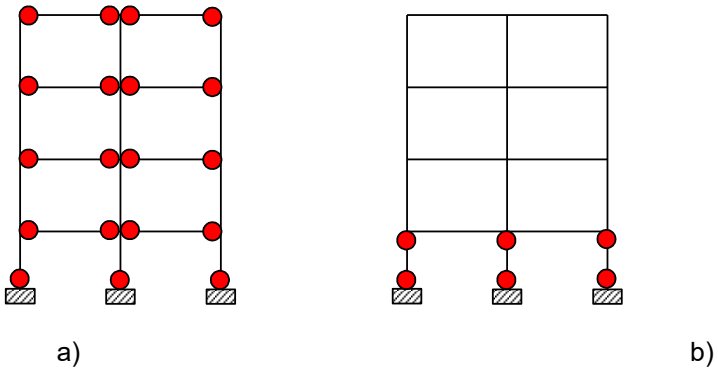


Figure 2. a) global and b) soft storey collapse mechanism (Borzi et al. 2008a).

Given the collapse deformation, the displacements of the equivalent SDOF system are defined at the centre of mass of the buildings based on the inter-story drift values corresponding to the selected limit states. Further details on the application of SP-BELA for reinforced concrete buildings are provided in [1].

2.2. Masonry Buildings

As previously mentioned, the taxonomy of masonry buildings for which the pushover curve is directly calculated includes only those with low vulnerability. These are buildings where masonry walls activate an in-plane failure mechanism and collaborate due to the redistribution of seismic actions associated with the stiff behaviour of the floors. For such buildings, given the presence of rigid diaphragms, a soft storey mechanism is assumed. Therefore, plasticity is concentrated within a storey, i.e. the storey for which the ratio between the resistance to seismic action and shear capacity is the lowest. In SP-BELA, the collapse multiplier at the storeys is calculated with the Equation 3 proposed by Benedetti and Petrini [15]:

$$\lambda_i = \frac{1}{W_T \frac{\sum_{k=i}^{n} h_i \, W_i}{\sum_{j=1}^{n} h_j \, W_j}} A_i \tau_{ki} \left[1 + \frac{\sum_{k=i}^{n} W_k}{1{,}5 \tau_{ki} A_i (1 + \gamma_{AB})} \right]^{1/2} \tag{3}$$

where W_T is the total weight of the building, W_i is the weight associated with the i-th level, τ_{ki} is the reference shear strength at level i for zero axial load, A_i is the area of all the masonry walls resisting at level i in the direction of applied load, n is the total number of storeys, γ_{AB} is the ratio between A_i and B_i, and B_i is the greater between the longitudinal and transverse wall areas. Once λ_i is calculated for each level, the collapse multiplier for the building corresponds to the minimum value assumed by the λ_i values.

Proceedings of the 3rd Croatian Conference on Earthquake Engineering - 3CroCEE
19–22 March 2025, Split, Croatia
Copyright © 2025 CroCEE
DOI: https://doi.org/10.5592/CO/3CroCEE.2025.18

The equation reported in [15] only considers the shear-resistant mechanism and neglects possible three-dimensional effects, such as torsion due to potential eccentricity between the centre of mass and the centre of stiffness. Therefore, Restrepo-Vélez [16] suggested introducing the corrective factor of λ as in Equation 4.

$$\lambda = \Phi_c^{-1} min\{\lambda_i\} \tag{4}$$

The corrective coefficient Φ_c was evaluated by means of the results obtained from 3D finite element analyses conducted using the SAM code, specifically developed for defining capacity curves of masonry buildings. SAM stands for Simplified Analysis of Masonry and was developed at the University of Pavia starting from the late 1990s [17],[18]. Based on a linear regression of the results obtained from analyses conducted by Restrepo-Vélez [16], the following formulation for Φ_c was derived:

$$\Phi_c = 5.5 \frac{\tau_{ki}}{\frac{L_W}{L_T}} + 0.5 \tag{5}$$

where L_T is the length of walls oriented in the direction of load application while L_W is the total length of walls oriented in the direction of load application, excluding openings.

Similarly to RC buildings, once the collapse deformation shape and the inter-story drift values corresponding to the considered limit states are known, the displacements of the equivalent SDOF system can be calculated. Further details on the implementation of SP-BELA for masonry buildings are provided in [2].

3. Definition of Damage Probability with SP-BELA

As outlined in Chapter 2, the points on the pushover curve define the characteristics of an equivalent SDOF system. The assessment of capacity against the demand imposed by the earthquake in SP-BELA aligns with the principles of the DDBA. The probabilities of exceeding a selected limit state is graphically shown on the displacement spectrum (Sd) plotted as a function of the vibration period in Figure 3, where the points represent the SDOF to which the building is reduced. Thus, these points have coordinates of the equivalent vibration period and the equivalent displacement capacity, which is amplified by dividing by the code coefficient η (see Equation 6). The latter coefficient accounts for the equivalent damping ξ and, hence, the portion of energy dissipated due to material hysteresis:

$$\eta = \sqrt{\frac{10}{5 + \xi}} \tag{6}$$

The green points above the displacement spectrum curve represent the buildings in the sample that have a capacity exceeding the demand, satisfying the verification for the reference limit state. On the contrary, the points below the displacement spectrum curve (red points) do not satisfy the verification for the reference limit state since the demand is greater than capacity. Consequently, these buildings evolve into the subsequent damage limit condition. The number of such elements relative to the sample size corresponds to the probability of exceeding the seismic action to which the comparison refers.

Copyright © 2025 CroCEE
DOI: https://doi.org/10.5592/CO/3CroCEE.2025.18

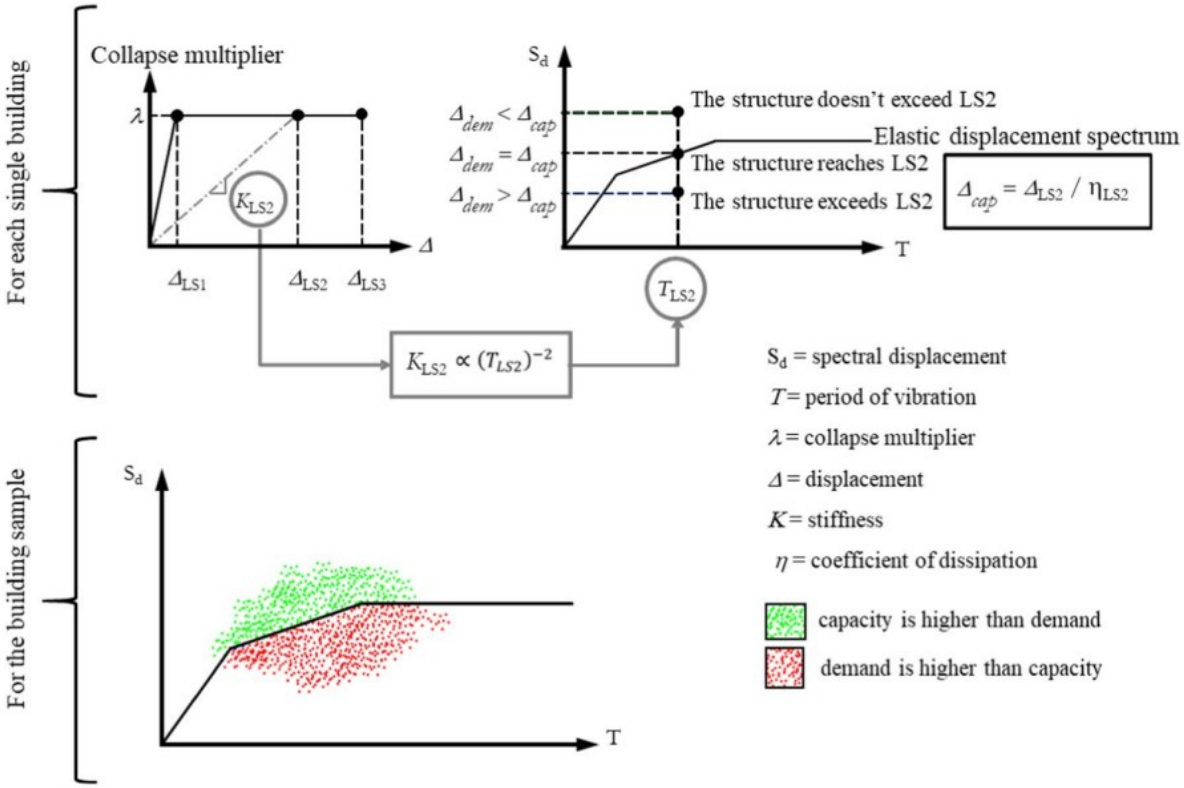


Figure 3. Scheme of the procedure to calculate the probability of exceedance of a selected damage limit state [19].

4. Calibration of SP-BELA

The capacity curves initially obtained from SP-BELA to assess the structural capacity of building classes refer to the three damage limit states (LSs) identified by the current Italian Building Code [20] and described in Chapter 2. Furthermore, as anticipated, masonry capacity curves can only be produced for buildings with low vulnerability. It is therefore necessary to calibrate the capacity resulting from SP-BELA with two different set of coefficients to obtain:

- the capacity of RC and masonry buildings in terms of five damage levels (from DL1 to DL5), the latter defined according to the European Macroseismic Scale 1998 (EMS-98, [21]), starting from LS2 and LS3;
- the capacity of masonry buildings with high and medium vulnerability from those with low vulnerability.

The calibration is based on comparing the actual damage as reported in survey forms due to the specific events happened after 1976 Friuli earthquake onwards with the corresponding damage scenarios calculated with SP-BELA. As Ground Motion Prediction Equation (GMPE), we have adopted the one proposed by Bindi et al. [22], since it performed well for the Italian territory.

The comparison between the actual damage and performed damage scenarios also accounts for the observed damage of non-structural elements, derived from the extent of the reported damage to the infill walls. Since non-structural elements are considered up to damage level DL3, only structural damage is considered for damage levels DL4 and DL5. The earthquakes considered for the calibration process are the mainshocks of: 1980 Irpinia, 1998 Pollino, 2002 Molise-Puglia, and 2009 L'Aquila. We did not consider the 1997 Marche-Umbria and 2012 Emilia sequences because for:

- 1997 Marche-Umbria event, we lacked information about the damage to non-structural elements, due to the lack of specific fields in the survey form used during the inspections;

Proceedings of the 3rd Croatian Conference on Earthquake Engineering - 3CroCEE
19–22 March 2025, Split, Croatia
Copyright © 2025 CroCEE
DOI: https://doi.org/10.5592/CO/3CroCEE.2025.18

- 2012 Emilia event, even if damage to non-structural elements is reported in the survey form used during the inspections, it is likely that it was compromised by the aftershocks.

To convert the reported damage to the infill walls into EMS-98 damage levels [21], we used the approach of Del Gaudio et al. [23] for the events 1998 Pollino, 2002 Molise-Puglia, and 2009 L'Aquila (Table 1). For the 1980 Irpinia earthquake, we have applied a metric developed in Eucentre and reported in Table 2

Table 2. Then, for each building, we compare the non-structural damage level with the structural damage level: the greater of the two is associated with the entire building.

Figure 4 and Figure 5 show the comparison between the observed and calculated damage scenarios for RC and masonry buildings related to the 1980 Irpinia, 1998 Pollino, 2002 Molise-Puglia, and 2009 L'Aquila earthquakes. Based on this comparison, we have derived the two set of calibration coefficients for SP-BELA. These coefficients are reported in [24], where a detailed description of the calibration procedure is also provided.

Table 1. Metric proposed by Del Gaudio et al. (2017) to convert the damage to infill walls reported in the AeDES survey form into the damage levels DLs according to the EMS-98 scale [21]

Damage according to EMS9-8	**Infill walls**	
	Damage levels in the AeDES form	**Damage extension**
DL1	D1	<1/3; 1/3-2/3; >2/3
DL2	D2-D3	<1/3; 1/3-2/3; >2/3
DL3	D4-D5	<1/3; 1/3-2/3; >2/3

Table 2. Metric proposed by EUCENTRE to convert the damage to the infill walls recorded in the 1980 Irpinia survey form into the damage levels DLs of the EMS-98 scale [21]

Damage according to EMS-98	**Infill walls**
	Damage levels in the 1980 Irpinia survey form
DL0 (absence of damage)	D1
DL1	D2 D3
DL2	D4
DL3	D5-D5-D6-D7-D8

Copyright © 2025 CroCEE
DOI: https://doi.org/10.5592/CO/3CroCEE.2025.18

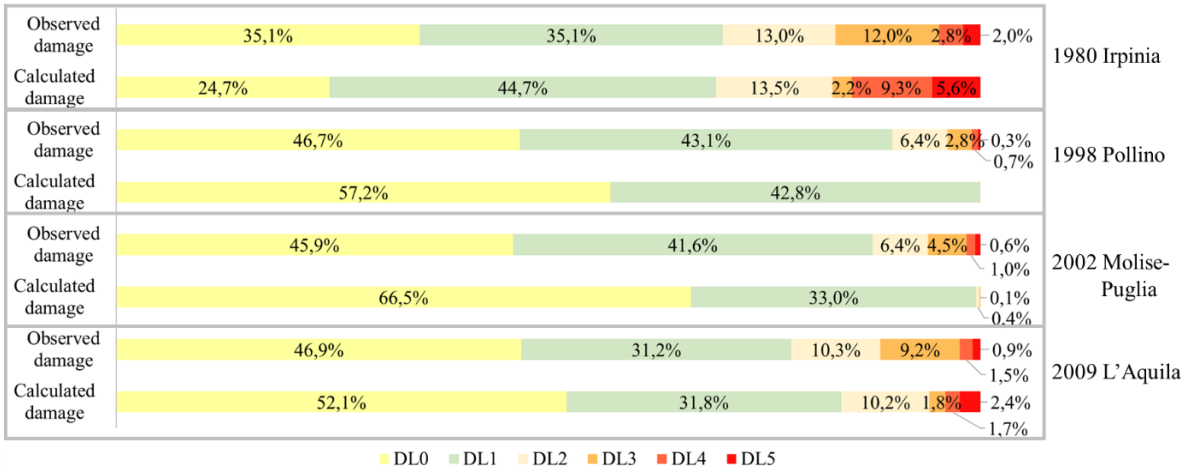


Figure 4. Comparison of real damage scenario (observed scenario) and scenario calculated using the SP-BELA method (calculated scenario) for RC buildings.

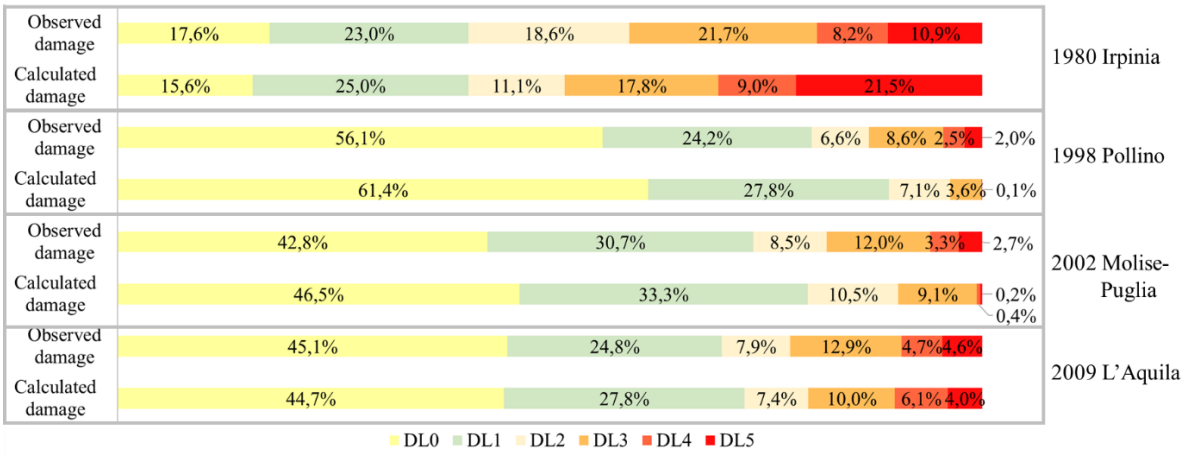


Figure 5. Comparison of real damage scenario (observed scenario) and scenario calculated using the SP-BELA method (calculated scenario) for masonry buildings.

5. Applications of SP-BELA

SP-BELA has been implemented in web-based GIS (WebGIS) tools developed for calculating seismic risk and real-time damage scenarios for buildings. These tools are available in the EUCLIDE (EUCentre for Loss Impact and Damage Evaluation) platform (see the home of EUCLIDE in Figure 6), which also includes tools to calculate seismic risk maps and real-time damage scenarios for infrastructures (e.g., tunnels, bridges, and infrastructures of harbours and airports). The Web-GIS tools for buildings consider:

- Residential buildings;
- Strategic buildings, such as hospitals and schools.

The key distinction between tools dedicated to residential and strategic buildings is that residential buildings are not identified one by one but by referring to the building stock of a given area (e.g., municipality or a sub-portion of a municipality) for which information is available. In contrast, strategic buildings are identified individually. However, even for strategic buildings we need to conduct large-scale vulnerability assessments due to the limited information we have on each of them. With the available information, in fact, we can only classify strategic buildings into taxonomies. Consequently, the results should be considered as averages and not as representative of specific individual buildings.

Copyright © 2025 CroCEE
DOI: https://doi.org/10.5592/CO/3CroCEE.2025.18

Figure 7 provides an overview of the home of EUCLIDE: in the first line there are the three WebGIS tools for residential buildings, schools, and hospitals.



Figure 6. Homepage of EUCLIDE.

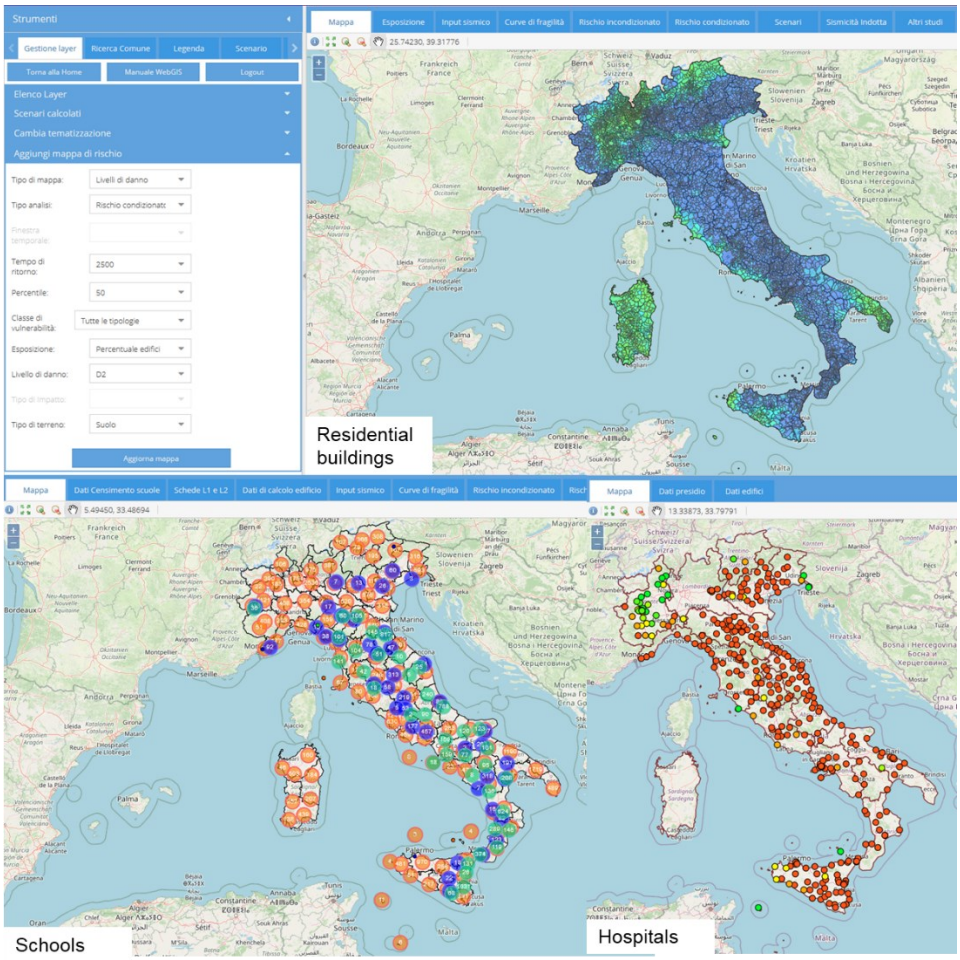


Figure 7. Homepage of the three webtool that have buildings as the exposed asset.

Proceedings of the 3rd Croatian Conference on Earthquake Engineering - 3CroCEE
19–22 March 2025, Split, Croatia
Copyright © 2025 CroCEE
DOI: https://doi.org/10.5592/CO/3CroCEE.2025.18

6. Concluding Remarks

SP-BELA is a method for defining the seismic vulnerability of buildings on a large scale. The method is based on the definition of capacity curves. Originally developed as a mechanical method, it is classified as a hybrid method because damage data from events that have occurred in the Italy over the last 50 years have been used to:

- calibrate the results;
- compensate for the limitations of a purely numerical method, mainly related to situations that cannot be numerically reproduced.

In defining damage probabilities, whether in time-based and event-base analysis, capacity is compared to demand. The SP-BELA approach makes this comparison more straightforward to include effects that alter the frequency content of the earthquake, such as site effects and the different nature of the rupture that provoke the ground shaking.

On the other hand, the damage assessment using fragility curves allows to graph a parameter adopted as a representative measure of shaking severity on the x-axis. However, with a single parameter, it is not equally effective in accounting for all the factors that act and alter the nature of the seismic input.

We plan to further develop the method in the future in order to extend the range of buildings to which SP-BELA can be applied. The first activity in this direction is the integration of the effects of seismic mitigation measures (e.g., building retrofitting), implemented as part of seismic risk mitigation campaigns in earthquake-prone countries.

Acknowledgements

Thanks are due to the Eucentre developers team whose work made possible the calibration of the SP-BELA and the implementation of method in WebGIS tools developed to calculate seismic risk and damage scenario. They are Marco Pagano, Davide Quaroni, Alessio Cantoni and Mauro Onida, who also contributed to create the maps shown in the paper.

The current study has been beneficiary of Italian Department of Civil Protection funds. However, this does not necessarily reflect the ideas and official policy of the Department.

References

[1] Borzi, B., Pinho, R., Crowley, H. (2008a): Simplified pushover-based vulnerability analysis for large scale assessment of RC buildings. *Engineering Structures*, **30**(3), 804-820, doi: https://doi.org/10.1016/j.engstruct.2007.05.021.

[2] Borzi, B., Crowley, H., Pinho, R. (2008b): Simplified Pushover-Based Earthquake Loss Assessment (SPBELA) Method for Masonry Buildings. *International Journal of Architectural Heritage*, **2**(4), 353 – 376, https://doi.org/10.1080/15583050701828178.

[3] Cosenza, E., Manfredi, G., Polese, M., Verderame, G.M. (2005): A multi-level approach to the capacity assessment of existing RC buildings. *Journal of Earthquake Engineering*, **9**(1), 1-22, doi: https://doi.org/10.1080/13632460509350531.

[4] Calvi, G.M. (1999): A displacement-based approach for vulnerability evaluation of classes of buildings, *Journal of Earthquake Engineering*, **3**(3): 411–438, https://doi.org/10.1080/13632469909350353.

[5] Pinho, R., Bommer, J.J., Glaister, S. (2002): A simplified approach to displacement-based earthquake loss estimation analysis. In: *Proceeding of the 12th European conference on earthquake engineering*. Paper no. 738, London, United Kingdom.

[6] Crowley, H., Pinho, R. (2004): Period-height relationship for existing European reinforced concrete buildings. *Journal of Earthquake Engineering*, **8**(1), 93–119, doi: https://doi.org/10.1080/13632460409350522.

[7] Tsionis, G. and Fardis, M.N. (2014). Seismic fragility curves for reinforced concrete buildings and bridges in Thessaloniki. In: *The 2nd European conference on earthquake engineering and seismology*, Istanbul, Turkey.

Copyright © 2025 CroCEE
DOI: https://doi.org/10.5592/CO/3CroCEE.2025.18

[8] Karantoni, F., Tsionis, G., Lyrantzaki, F., Fardis, M.N. (2014): Seismic fragility of regular masonry buildings for in-plane and out-of-plane failure. *Earthq. Struct.*, **6**(6), 689–713, doi: https://doi.org/10.12989/eas.2014.

[9] Del Gaudio, C., Ricci, P., Verderame, G.M., Manfredi, G. (2015): Development and urban-scale application of a simplifed method for seismic fragility assessment of RC buildings. *Eng. Struct.*, **91,** 40–57, doi: https://doi.org/10.1016/j.engstruct.2015.01.031.

[10] Lagomarsino, S., Cattari, S. (2014): Fragility functions of masonry buildings. *In: SYNER-G: Typology definition and fragility functions for physical elements at seismic risk*, Springer, Dordrecht, doi: https://doi.org/10.1007/978-94-007-7872-6_5.

[11] Priestley, M.J.N., Calvi, G.M., Kowalsky, M.J. (2007): *Displacement-based seismic design of structures*. IUSS Press, Pavia, Italy.

[12] Masi, A. (2004): Seismic Vulnerability Assessment of Gravity Load Designed R/C Frames. *Bulletin of Earthquake Engineering*, (**1**)3, 371-395, doi: https://doi.org/10.1023/B:BEEE.0000021426.31223.60.

[13] Iervolino, I., Manfredi, G., Polese, M., Verderame, G.M., Fabbrocino, G. (2006): Seismic risk for Italian type R.C. buildings. *Proceedings of the 1st European Conference on Earthquake Engineering and Seismology*, Geneva, Paper no. 567.

[14] Borzi, B. (2006): Validazione della metodologia semplificata per l'esecuzione di analisi pushover. *Rapporto di Ricerca*. European Centre for Training and Research in Earthquake Engineering (EUCENTRE), Pavia, Italia.

[15] Benedetti, D., Petrini, V. (1984): Sulla vulnerabilità sismica di edifici in muratura: Proposta su un metodo di valutazione. *L' industria delle Costruzioni*, **149**, 66-74.

[16] Restrepo, Vélez L.F. (2003): *A simplified mechanics-based procedure for the seismic risk assessment of unreinforced masonry buildings*. Individual Study, European School for Advanced Studies in Earthquake Engineering, ROSE School, University of Pavia, Italy.

[17] Magenes, G., Della Fontana, A. (1998): Simplified non-linear seismic analysis of masonry buildings, *Proceedings of the British Masonry Society*, **8**, 190-195.

[18] Magenes, G., Braggio, C., Bolognini, D. (2000): *Metodi Semplificati per l'Analisi Sismica Non Lineare di Edifici in Muratura*. Dipartimento di Meccanica Strutturale, Università degli Studi di Pavia, Italy.

[19] Faravelli, M., Borzi, B., Polli, D., Pagano, M. (2019): Calibration of a mechanics-based method for large-scale vulnerability assessment. *Bull. Earthquake Eng.*, **17**, 2485–2508, https://doi.org/10.1007/s10518-019-00560-0.

[20] D.M. 17.01.2018 (2018): *Decreto Ministeriale 17 Gennaio 2018 Aggiornamento delle Norme Tecniche per le Costruzioni (NTC18)* (in Italian), G. U. 20/02/2018 n.42, Italy.

[21] Grünthal, G. (1998). European Macroseismic Scale 1998 (EMS-98). *Council of Europe, Cahiers du Centre Européen de Géodynamique et de Sismologie*, **15**.

[22] Bindi, D., Pacor, F., Luzi, L., Puglia, R., Massa, M., Ameri, G., Paolucci, R. (2011): Ground motion prediction equations derived from the Italian strong motion database. *Bull. Earthq. Eng*., **9**:1899–1920, doi: https://doi.org/10.1007/s10518-011-9313-z.

[23] Del Gaudio. C., De Martino. G., Di Ludovico. M., Manfredi. G., Prota, A., Ricci, P., Verderame, G.M. (2017): Empirical fragility curves from damage data on RC buildings after the 2009 L'Aquila earthquake. B *Earthq. Eng*., **15**, 1425–1450, https ://doi.org/10.1007/s10518-016-0026-1.

[24] Faravelli, M., Di Meo, A., Onida, M., Borzi, B. (2023): Improvement and updating of the SP-BELA method for the vulnerability assessment of masonry and RC buildings. *International Journal of Disaster Risk Reduction*, **98**, 104078, https://doi.org/10.1016/j.ijdrr.2023.104078.

Proceedings of the 3rd Croatian Conference on Earthquake Engineering - 3CroCEE
19–22 March 2025, Split, Croatia
Copyright © 2025 CroCEE
DOI: https://doi.org/10.5592/CO/3CroCEE.2025.19

ON THE IMPACTS OF STRUCTURE-TO-STRUCTURE DAMAGE CORRELATION FOR REGIONAL SEISMIC RISK ASSESSMENT

Tomas Mejia [(1)], Gerard J. O'Reilly [(2)]

[(1)] *PhD Candidate at IUSS Pavia, tomas.mejiasaldarriaga@iusspavia.it*
[(2)] *Associate Professor at IUSS Pavia, gerard.oreilly@iusspavia.it*

Abstract

One of the main challenges of implementing the performance-based earthquake engineering framework and computing risk and associated consequences on a regional scale is incorporating structure-to-structure damage correlation in the analysis. This correlation relates to the expected damage between different structures in a region, considering they were likely built with similar characteristics, resulting in similar strengths or deficiencies when subjected to seismic shaking. While this type of correlation has been largely neglected in risk analysis to date, it can be estimated analytically from non-linear time history analyses (NLTH) when models of all buildings in the region are available, requiring a computationally demanding and time-consuming method. Some strategies, however, can be implemented to simplify the procedure, such as analysing equivalent single degree of freedom (SDOF) oscillators instead of full 3D models of the buildings, an approach commonly found in the literature for similar applications.

To examine the impact of considering such correlation in a regional seismic risk assessment, a case study was conducted, involving the assessment of mid-rise reinforced concrete frame buildings in the Province of Caserta, southern Italy. The correlation was estimated from the results of Incremental Dynamic Analysis (IDA) performed on equivalent SDOF oscillators. Even though it was found that the incorporation of the correlation in the analysis does not significantly alter the estimates of the mean and median number of damaged buildings from a given earthquake scenario, it affects the probability distribution of the data, increasing the estimated risk of low- or widespread damage. Incorporating this aspect into regional risk analysis leads then to more accurate damage and loss estimates, enabling improved strategies for disaster risk preparedness and mitigation.

Keywords: risk analysis, regional assessment, structural damage, correlation

1. Introduction

The quantification of seismic risk has garnered considerable attention from practitioners and researchers in earthquake engineering over the past few decades. A notable advancement in this area is the performance-based earthquake engineering (PBEE) framework, developed by the Pacific Earthquake Engineering Research Center (PEER). Initially introduced in SEAOC's Vision 2000 and subsequently refined in the FEMA P-58 report [1], PBEE has become the leading methodology for assessing the seismic risk of individual structures worldwide.

The PBEE framework systematically addresses uncertainties and variabilities across its modules: earthquake hazard, structural response, damage assessment, and consequence estimation. It begins with a probabilistic approach to the earthquake hazard, which quantifies ground motion intensity measures (IM) such as spectral acceleration or peak ground acceleration at the building site. The outcome is a hazard curve representing the mean annual rate of exceedance for various IM levels.

In the building response module, engineering demand parameters (EDP) like peak story drift or peak floor acceleration are used to describe the structure's response at different IM levels. These are typically estimated through nonlinear time history analyses, using methods such as incremental dynamic analysis (IDA) [2] or multiple stripe analysis (MSA) [3]. The damage module then uses fragility curves to model the likelihood of reaching specific damage states (DS) for each EDP, while the consequence assessment module translates these damage outcomes into economic losses, casualties, or downtime, known as decision variables (DV). The entire framework integrates these components using the total probability theorem, often solved through Monte Carlo simulation for complex cases.

Copyright © 2025 CroCEE
DOI: https://doi.org/10.5592/CO/3CroCEE.2025.19

While PBEE was initially designed for single buildings, extending performance assessment to a regional level is essential for understanding the societal impacts of seismic events. This broader perspective, termed regional performance-based earthquake engineering (RPBEE), requires adjustments to the traditional PBEE methodology, particularly in modelling uncertainties and correlations between variables [4] and the impacts on the broader community. For example, at a regional scale, hazard is treated as a vector representing ground motion intensities at various building sites. These intensities are modelled as random variables following a multivariate lognormal distribution, incorporating a spatial correlation through models such as those developed by Bodenmann et al. [5] and Esposito & Iervolino [6], among others.

The building response module at the regional level often employs taxonomies to group structures with similar characteristics, focusing on overall damage performance rather than individual component behaviour. Fragility curves, that reflect probabilities of observing different global damage states, are used for each taxonomy. Considerable efforts have been made by researchers and organizations to develop fragility curves for commonly used taxonomies worldwide, such as the work of the Global Earthquake Model Foundation (GEM).

Considering regional construction practices, buildings designed and built during similar time periods in a specific geographic area often share structural characteristics, which leads to them having similar strengths or deficiencies during seismic shaking. This results in the fact that damage experienced by one building is likely correlated with damage to nearby, similar structures, a phenomenon known as structure-to-structure damage correlation. Accurately modelling this correlation is crucial, as it significantly influences estimates of large-consequence risks; however, it is either completely neglected or considered in an oversimplified manner by risk modellers in their analysis. A case study in the province of Caserta, Southern Italy, was performed to illustrate the importance of incorporating this correlation in risk analysis, emphasising how its careful estimation is fundamental for a more accurate risk assessment.

2. Structure-to-structure damage correlation

According to Heresi and Miranda [4], one of the main challenges of assessing seismic risk at a regional scale is incorporating the structure-to-structure damage correlation into the analysis. Unlike the spatial correlation of IMs used in seismic hazard analysis, which has been extensively studied with several mathematical models developed to quantify it, damage correlation has received comparatively less attention. This variable is often either completely neglected in the analyses or treated approximately by assigning a constant value for all structures. Some efforts, however, have been made in the last few years to study and understand the problem and make more accurate regional risk models in terms of considering this variable.

One of the first studies on the topic was conducted by Lee and Kiremidjian [7], who analyzed the effects of considering the structure-to-structure damage correlation on spatially distributed systems, primarily focusing on transportation networks. Specifically, the damage correlation was estimated for bridges within the same network, assuming an equi-correlated scenario, in which a value of one was assumed in the diagonal of the correlation matrix (i.e., the structure's damage state is perfectly correlated with itself) and a constant value between 0 and 1 in all the other cases (i.e., the damage to structure i is correlated to structure j by the same amount that structure m is to structure n). The correlation value was considered to be independent of the ground motion intensity level but not on the damage level and was estimated mathematically as an optimisation problem using a least squares adjustment and considering the marginal probabilities of each bridge as constraints. A sensitivity analysis demonstrated that the variation in total loss increases with the estimated value of the correlation.

Other approaches were developed by Kang et al. [8] and Xiang et al. [9]. The first study proposed a model to estimate the correlation between EDPs using the results of IDA's performed on several structures, which in concept, has the same effect as considering the structure-to-structure damage correlation. In the second study, a model was developed to derive the structure-to-structure correlation

Proceedings of the 3rd Croatian Conference on Earthquake Engineering - 3CroCEE
19–22 March 2025, Split, Croatia
Copyright © 2025 CroCEE
DOI: https://doi.org/10.5592/CO/3CroCEE.2025.19

analytically based on the dynamic properties and the spatial distance of the structures, using equivalent SDOF models subjected to consistent and spatially varying white noise.

Heresi and Miranda [10] approached the problem considering that the random variable damage of the structure can be represented by a Bernoulli trial. The correlation between two Bernoulli trials can be derived from their marginal probabilities and the joint probability of both buildings experiencing damage. The authors modelled the joint distribution with a Gaussian Copula, a bivariate normal distribution with a mean vector equal to zero and a given covariance matrix. However, selecting an appropriate correlation factor for the copula remains challenging. The authors proposed an equation inversely proportional to the distance between structures and the difference in their construction years. Although this equation was not validated, it illustrated how different values of structure-to-structure correlation can significantly affect regional risk assessment outcomes.

Among the methods previously discussed, the approach proposed by Heresi and Miranda is the most suitable for the regional seismic risk assessment methodology typically used. It not only allows the use of fragility curves widely accepted in the literature, like the ones derived by GEM, but also acknowledges that the correlation value should not be uniform across all buildings, given their varying characteristics. Additionally, the challenge of selecting the correlation for the Gaussian Copulas can be addressed by developing mathematical models performing regressions with data from real historical events or derived from simulated scenarios. Having this in mind, an extension of this approach was used in the case study to estimate the damage correlation.

2.1. Correlation between Bernoulli trials

A Bernoulli trial is an experiment whose outcome is random but has one of only two possible outcomes: success or failure [11]. The probability of success is typically denoted as p. In the context of seismic events, a structure experiencing a certain damage state can be visualised as a Bernoulli trial, where a successful outcome corresponds to the structure being damaged, and a failure corresponds to the structure remaining undamaged. This probability can be obtained by the fragility curve for a given IM value. Following this assumption, it is possible then to estimate the structure-to-structure damage correlation of two buildings from the equation of the correlation (ρ) between two Bernoulli trials as follows:

$$\rho_{1,2} = \frac{P[D_1=1,D_2=1,]-p_1 p_2}{\sqrt{p_1(1-p_1)p_2(1-p_2)}} \quad (1)$$

where p_1 and p_2 correspond to the marginal probability of buildings 1 and 2 experiencing a given damage state, and $P[D_1=1,D_2=1]$ is the joint probability of both buildings experiencing damage simultaneously.

Even though the marginal probabilities can be easily obtained from the fragility curve of each building, there needs to be more information to estimate the joint probability of damage to the buildings, which is why Heresi and Miranda [10] suggested the use of the Gaussian Copulas. However, in a hypothetical case where sufficient data would exist to perform nonlinear time history analyses on all buildings of the region, it could be possible to determine the joint distribution, and consequently, the structure-to-structure damage correlation for that set of buildings, with a similar procedure to the one used to determine analytical fragility functions.

2.2. Analytical determination of joint probability distribution

The most common approach to estimate fragility functions of buildings is the analytical method [12], in which damage probability distributions are simulated based on statistical results obtained from structural analysis on computational models. The most accurate results are obtained when nonlinear time history analyses are performed, using methods like the IDA or MSA to estimate the seismic response of the building. The IDA, introduced by Vamvatsikos and Cornell [13], involves performing nonlinear time history analyses on a set of ground motion records scaling them incrementally until structural collapse is observed. By using the same records across all IM levels, IDA generates curves

Copyright © 2025 CroCEE
DOI: https://doi.org/10.5592/CO/3CroCEE.2025.19

that relate EDP to IM values, doing a linear interpolation to estimate the values for unperformed analysis points.

However, the method has some limitations, particularly regarding the selection of ground motion records, which can significantly impact the results [14]. Additionally, scaling records heavily may introduce bias, as low and high-intensity motions differ in characteristics, potentially leading to unrealistic outcomes [2]. The MSA, proposed by Jalayer [3], addresses these limitations by using hazard-consistent ground motion records at each IM level (or stripe), thereby minimising the need for extensive scaling and reducing bias. Consequently, MSA is commonly preferred in performance-based earthquake engineering. Although MSA is based on the same underlying principles as IDA, it does not allow for the creation of continuous IM-EDP curves, since different records are used at each stripe.

In the context of the calculation of the structure-to-structure damage correlation, the joint probability distribution can be then determined analytically from the results of either an IDA or MSA of both buildings, in case than some special considerations are accounted for during the analysis. If the same set of records is used for all structures, the probability of two buildings reaching certain damage state can be estimated by counting the records for which the corresponding limit EDP was exceeded for both buildings simultaneously and dividing by the total number of records. It should be noted that the value of the joint probability, and consequently, the correlation factor, is conditioned on the value of the IM experienced by the buildings, since the records are counted for the specific level of the IM experienced by each structure.

Given the limitations of IDA discussed earlier, the ideal approach would involve using the results of MSA on all buildings. However, the impossibility of interpolating the EDP results for IM values other than those corresponding to the one for which the records were selected means that MSA can only be used in a hypothetical scenario where all buildings experience a constant level of ground motion, with an IM corresponding to that of a particular stripe. Considering that the previous case doesn't correspond to a realistic scenario, since each building experiences a different level of intensity, although with some spatial correlation between each site, the only viable alternative is estimating the joint probability by counting the records exceeding the damage threshold for both buildings from the results of IDAs, as presented on Figure 1.

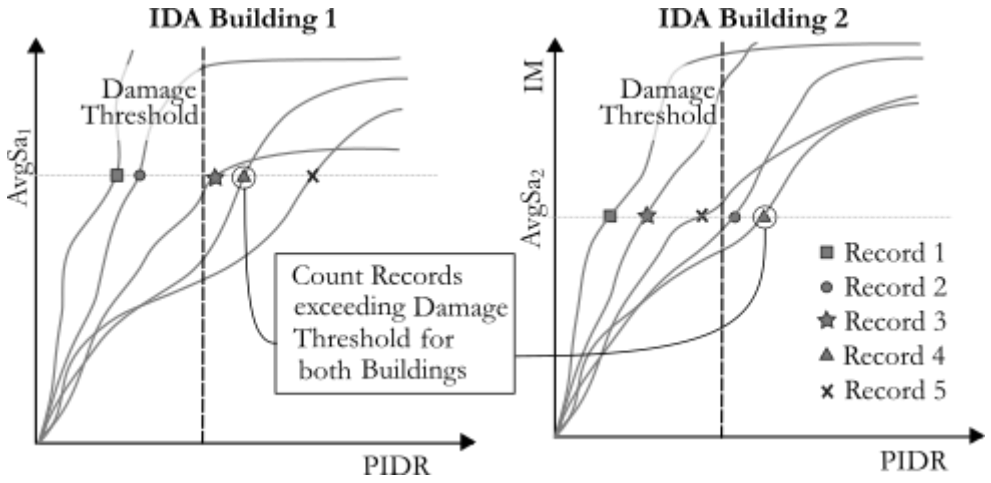


Figure 1. Estimation of joined probability distribution from IDA results

For the marginal probabilities used to estimate the correlation in Eq. (1), it is preferable to derive them directly from the results of the IDA, as shown in Eq. (2) and (3), rather than relying on probabilities from fragility curves, preventing unrealistic mathematical probability distributions. Marginal probabilities from fragility curves are often based on fitted lognormal distributions of the data, which could result in smaller values than the joint probability distribution, leading to inaccurate correlation estimates. Calculating the marginal probability by counting the records where the damage threshold is

Proceedings of the 3rd Croatian Conference on Earthquake Engineering - 3CroCEE
19–22 March 2025, Split, Croatia
Copyright © 2025 CroCEE
DOI: https://doi.org/10.5592/CO/3CroCEE.2025.19

exceeded and dividing by the total number of records ensures consistency with the method used to calculate the joint probability distribution.

$$p_1 = \frac{z_1}{n} \tag{2}$$

$$p_2 = \frac{z_2}{n} \tag{3}$$

where z_i is the number of observations of a given damage state and n is the number of ground motions utilised.

It is important to note, however, that the application of the proposed method is very computationally demanding, as it requires running several records at various IM levels on all buildings of the region under assessment. It is possible, however, to apply in this specific context different approaches commonly used to simplify the process of generating fragility curves, such as using SDOF nonlinear oscillators to approximate the behaviour of a multiple degree of freedom building. This simplification has been previously done in the works of Martins and Silva [15] and Nafeh et al. [16]. The properties of the equivalent oscillator can be estimated considering that the response of the building is dominated by the first mode and based on a linearisation of the pushover curve of the building. This approach was used in the case study to estimate structure-to-structure damage correlation, allowing for an assessment of the impacts of including this variable in a regional seismic risk assessment.

3. Definition of case study

This case study involves a regional seismic risk assessment of mid-rise residential concrete frame structures, using a portfolio generated with the Built Environment Data (BED)'s Design service (https://design.builtenvdata.eu/). This tool simulates building characteristics using Monte Carlo simulation, estimating structural features based on their observed regional proportions. Each building is then designed using the equivalent lateral force method, following European standards and using the lateral force coefficient (β) classification described by Crowley et al. [17]. The resulting building models are compatible with OpenSees, allowing nonlinear time history analyses to be performed in order to estimate specific fragility curves for each of the buildings as well as the structure-to-structure damage correlation with the proposed methodology.

To ensure the simulated buildings reflect realistic conditions, their characteristics were estimated based on real-world data from a study by Corlito and De Matteis [18], in which detailed structural properties of reinforced concrete (RC) buildings across eight municipalities were collected for the Caserta province, Italy. It was decided to focus on three municipalities, Castello del Matese, Gioia Sannitica, and Piedimonte Matese, that share a similar high seismic hazard classification according to the Italian building code, NTC18 [19]. The number and locations of buildings in the analysis were derived from an accurate exposure model, discussed in the next section, reflecting the actual portfolio of buildings of the selected typologies in the studied municipalities.

3.1. Exposure model

The exposure model used for the analysis was the one considered for the European Seismic Risk Model (ESMR20). This model in particular [20] was developed as part of the SERA project for 44 European countries, using publicly available information. It divides the buildings into residential, commercial and industrial use, and categorises them according to the GEM Building Taxonomy v3.1. For the analysis, only the residential buildings with more than four storeys were considered, including all code levels and design lateral force coefficients found in the area. In total there are 62 buildings located in the studied municipalities, distributed into the following taxonomies:

- CR/LFINF+CDL+LFC:0.0/HBET:4-: Low code RC infilled frames with more than four storeys designed for a load factor of 0% (41 Buildings).

Copyright © 2025 CroCEE
DOI: https://doi.org/10.5592/CO/3CroCEE.2025.19

- CR/LFINF+CDL+LFC:7.0/HBET:4-: Low code RC infilled frames with more than four storeys designed for a load factor of 7.0% (15 Buildings).
- CR/LFINF+CDM+LFC:7.0/HBET:4-: Moderate code RC infilled frames with more than four storeys designed for a load factor of 7.0% (6 Buildings).

Since the considered exposure model has all buildings in each municipality lumped in one point, the buildings were spatially disaggregated according to the population distribution within the region. The Python scripts developed by GEM to perform this analysis were used, which can be found in their spatial disaggregation repository available on GitHub [21]. The data on the distribution of the population used for the analysis was obtained from the WorldPop data of Italy for the year 2020, with a resolution of 100m [22]. The spatially disaggregated location of the assets adopted for this study is presented on Figure 2. While these do not necessarily correspond to the actual locations of these typologies, it not envisaged to have any impact on the overall conclusions of the work.

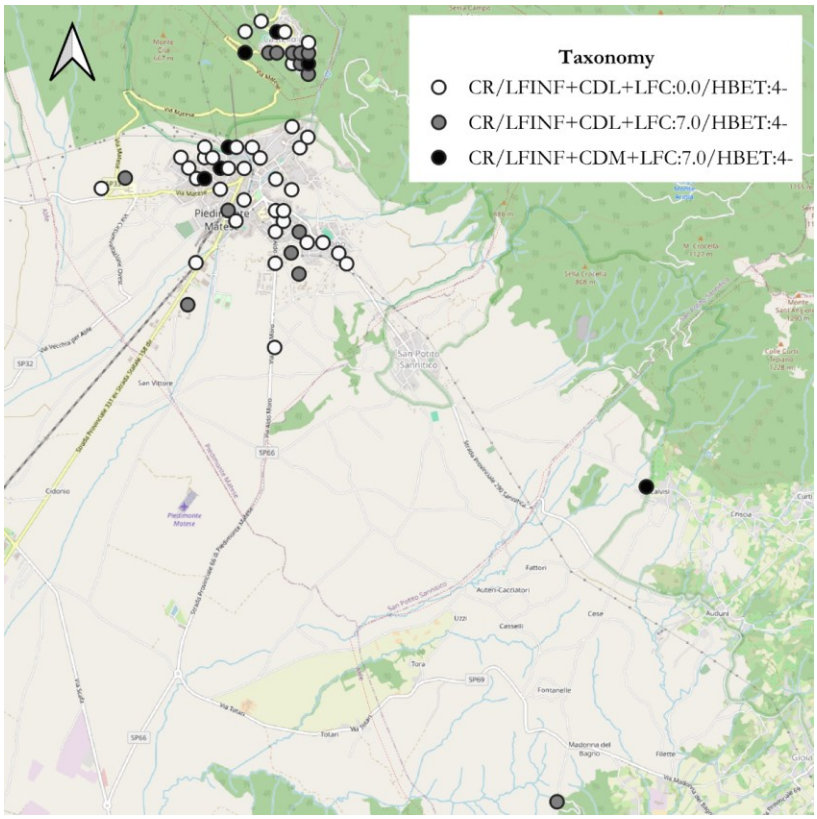


Figure 2 Geographical location of assets

3.2. Modelling of buildings

The portfolio of the 62 buildings found in the exposure model was simulated with the Built Environment Data's Design service based on observed regional proportions of given characteristics, such as slab type, column geometry, number of stories and construction quality. The structural attributes were obtained from a study by Corlito and De Matteis [18] who analysed RC buildings in the province investigated here. Each of the buildings was then designed to its vertical loads and the corresponding lateral force factor, following the design standards in Europe for the desired level of the design code and using the equivalent lateral force coefficient method.

The resulting structural models were developed in OpenSeesPy. Each building was modelled with elastic elements for beams and columns, while zero-length elements were used to simulate nonlinear

Proceedings of the 3rd Croatian Conference on Earthquake Engineering - 3CroCEE
19–22 March 2025, Split, Croatia
Copyright © 2025 CroCEE
DOI: https://doi.org/10.5592/CO/3CroCEE.2025.19

behaviour, capturing plastic deformations under seismic activity. Pushover analyses and modal characteristics were calculated to transform the calculate the properties of the equivalent nonlinear SDOF oscillator. The buildings were distributed geographically across the area, assigning them a random location from the spatially disaggregated exposure model.

3.3. Seismic hazard

The seismic hazard for the case study was quantified performing a probabilistic seismic hazard analysis (PSHA) at the mean coordinates of all the buildings considered in the region. For the analysis the source model developed in the frame of the 2013 European Seismic Hazard Model (ESHM13) was used [23]. The ground motion model (GMM) considered was the one developed by Boore et al. [24], assuming a firm soil to account for the local site effects, $V_{s,30}$=480 m/s, and considering the spatial correlation model from Jayaram and Baker [25]. The IM selected for the analysis was the average spectral acceleration over a period range, $Sa_{avg}(T)$, since it not only accounts for the period lengthening of each individual structure when they start to behave inelastically, but also for the variability of the periods of the different structures analysed. Having that in mind, the period of the range for the analysis was defined based on the limits proposed by Eads et al. [26], considering the average period of both directions of all the 62 buildings under analysis (i.e., 0.12s-1.82s). The $Sa_{avg}(T)$ intensity levels for different return periods is presented in Table 1.

Table 1. $Sa_{avg}(T)$ for different return periods

Return Period [years]	22	42	72	140	224	475	975	2475	4975	9975
PoE in 50 years	0.897	0.696	0.501	0.300	0.200	0.100	0.050	0.020	0.010	0.005
$Sa_{avg}(T)$ [g]	0.021	0.044	0.072	0.123	0.166	0.268	0.383	0.577	0.746	0.945

3.4. Fragility estimation

Fragility curves were derived for each of the buildings by performing a MSA on each of the full 3D models of the buildings for a defined DS. The analysis was performed considering the return periods presented on Table 1, selecting 40 records using the conditional spectrum method described by Lin et al. [27]. The resulting ground motions were therefore hazard consistent with the $Sa(T)$ values at different vibration periods. Then, a lognormal distribution was fitted to the results obtained from the MSA using the maximum likelihood method, as outlined by Baker [27].

3.5. Quantifying structure-to-structure damage correlation

The structure-to-structure damage correlation was estimated with the method previously described by performing IDA on the equivalent nonlinear SDOF oscillators. Since the considered earthquake rupture scenario was selected according to the disaggregation of the 475-year return period, it is expected that the simulated ground motion fields will be centred around the $Sa_{avg}(T)$ value estimated in the PSHA for that intensity. Then, to prevent bias from excessive record scaling in the IDA results, the analysis used the 40 ground motions previously selected for consistency with that hazard level, which were also used to derive fragility functions. For the linearization of the buildings pushover curves required to define the nonlinear SDOF oscillators, maintaining the maximum strength of the buildings over the area beneath both curves was prioritized, as this was considered a more representative parameter of their mechanical behaviour.

4. Scenario analysis

4.1. Estimation of ShakeMap

The total number of damaged buildings was estimated for a given earthquake rupture scenario, corresponding to an event of magnitude 6.25 at 5 km from the point of mean coordinates between all the considered buildings in the study region. The scenario was selected based on the results of the

Copyright © 2025 CroCEE
DOI: https://doi.org/10.5592/CO/3CroCEE.2025.19

disaggregation of the 475-year return period. The intensity of shaking at each building location was simulated for the specified earthquake rupture scenario, using the same GMM and spatial correlation model previously defined for quantifying seismic hazard in the region. Since $Sa_{avg}(T)$ was used for the analysis, and the selected GMM and spatial correlation model estimate spectral ordinates for specific periods, the ground motion fields were calculated indirectly by obtaining spectral acceleration values across different periods, following the method proposed by Kohrangi et al. [28]. This allowed Monte Carlo simulations of multiple earthquake scenario realisations to be performed, both including and neglecting the spatial correlation. An example for two of the realisations is presented in Figure 3, one using the spatial correlation (left), which is the more realistic case, and another neglecting it (right), which is less realistic and more randomised. It can be seen that, even if both realisations have very similar mean values of $Sa_{avg}(T)$ (0.266g for the spatially uncorrelated model and of 0.260 g for the spatially correlated one), the spatially uncorrelated model presents a larger variation of the data, containing the points with both the largest and lowest estimations at random locations. The spatially correlated model, on the other hand, presents a more reasonable estimation of the ground motion intensity, capturing the variability of the results but maintaining a realistic geographical distribution of the data in which similar $Sa_{avg}(T)$ are observed at close locations.

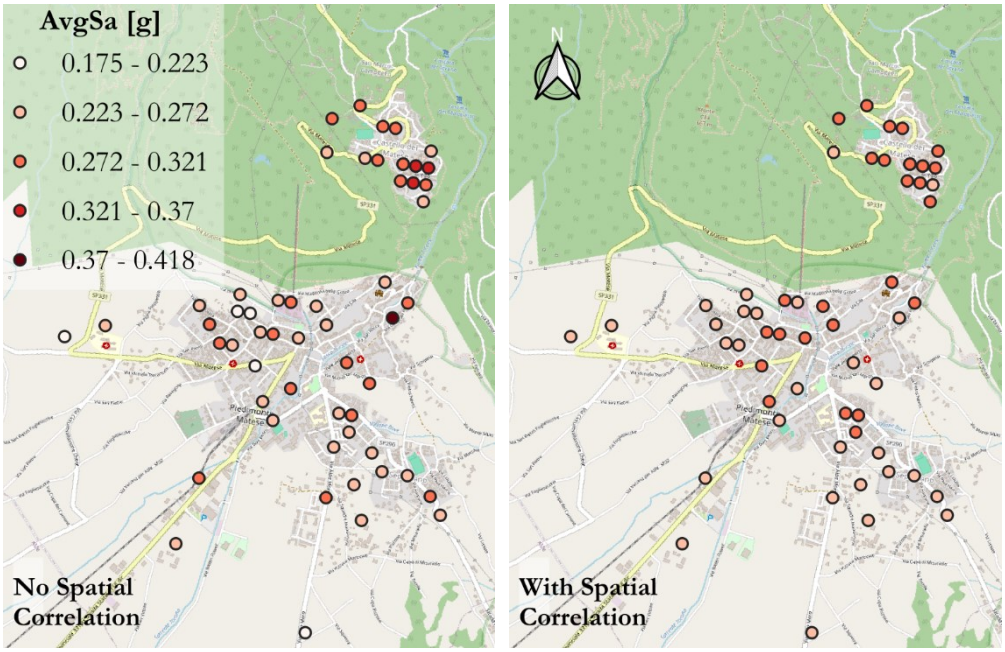


Figure 3 Modelled $Sa_{avg}(T)$ with (left) and without (right) spatial correlation for one realization

4.2. Estimation of building damage scenarios

A DS of light damage was defined as the case in which the peak storey drift (PSD) in any of the two directions of the buildings exceeds a value of 1.0%. Monte Carlo simulation was used to evaluate the impacts of considering or neglecting both the spatial correlation and the structure-to-structure damage correlation in the analysis. Different cases were analysed to see the impact in the results of considering and neglecting both the spatial correlation and the structure-to-structure damage correlation in the model. A summary of the considered cases is presented in Table 2.

Table 2. Considered Cases for Damage Estimation

Case	Spatial correlation, ρ_{sp}	Damage correlation, ρ_{dm}
1	Not Considered	Not Considered
2	Considered	Not Considered
3	Not Considered	Considered
4	Considered	Considered,

Proceedings of the 3rd Croatian Conference on Earthquake Engineering - 3CroCEE
19–22 March 2025, Split, Croatia
Copyright © 2025 CroCEE
DOI: https://doi.org/10.5592/CO/3CroCEE.2025.19

After running 5000 realisations, it was determined that there is not a significant variation of the estimated mean and median number of damaged buildings, as presented on Table 3 and shown in Figure 4. However, there is a substantial difference in the standard deviation, which affects the tails of the distribution and the probability of exceeding a certain number of damaged buildings, as presented in Figure 4.

Table 3. Statistics of results for considered cases

Statistic	Case 1	Case 2	Case 3	Case 4
Mean	30.66	30.56	31.09	30.96
Median	31.00	30.00	32.00	32.00
Standard Deviation	5.72	10.01	17.87	20.04

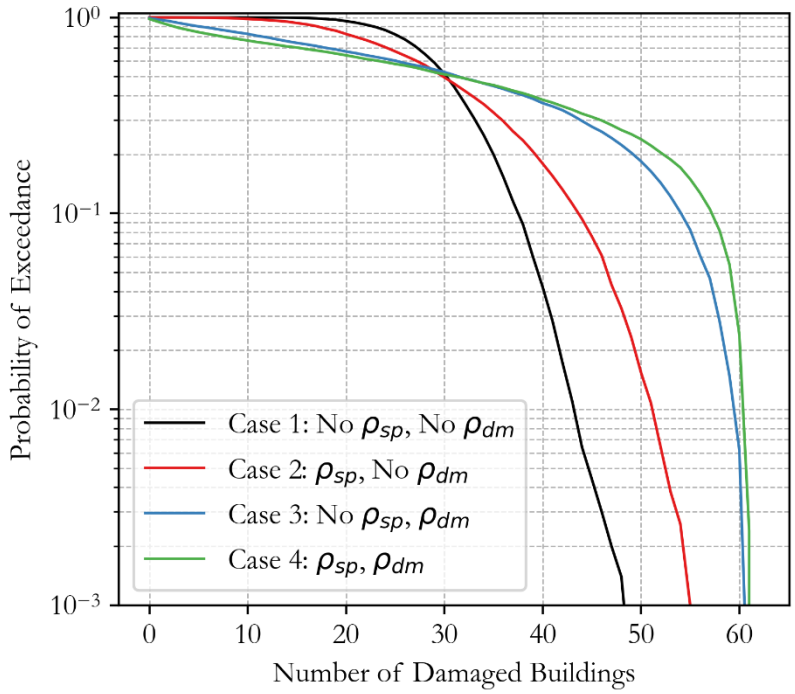


Figure 4 Comparison of probability of exceeding a given number of damaged buildings for the rupture scenario analysed

It can be seen that when considering only spatial or damage correlation, the latter has a more significant impact on the results. It can be deduced then that considering the structure-to-structure damage correlation can be as important as considering the spatial correlation on regional seismic risk assessment, at least for the case study under examination here. On the other hand, the use or not of the spatial correlation also impacts the calculation of the damage correlation itself, since it depends on the values of the simulated ground motion intensities that are derived based on that variable. To observe the results of the figure on a more comparable way the probability of exceeding a range of buildings between 35 and 45 is presented on Table 4.

Table 4 Probability of exceeding a given number of damaged buildings for the rupture scenario investigated

Number of buildings	Case 1	Case 2	Case 3	Case 4
35	20%	33%	45%	45%
40	4%	18%	37%	38%
45	0.4%	8%	28%	31%

Proceedings of the 3rd Croatian Conference on Earthquake Engineering - 3CroCEE
19–22 March 2025, Split, Croatia
Copyright © 2025 CroCEE
DOI: https://doi.org/10.5592/CO/3CroCEE.2025.19

Once again, it can be observed that the differences between the cases increase with the number of damaged buildings. Given that the use of spatial correlation is widely adopted and will likely always be used for this type of analysis, the results were compared using Case 2 as the reference. For instance, focusing on Case 4, which considers both spatial and damage correlation, the probability of exceeding more than 45 damaged buildings increases from 8% to 31%, resulting in a difference of around 300% between the two estimations.

To better understand the real-world implications of this difference, consider a hypothetical scenario in which the local government of the Caserta province plans strategies to finance the reconstruction of the three municipalities analysed in this study in the event of an earthquake. Assuming the earthquake scenario presented here is viewed as a "worst-case scenario," the government might decide to secure funds to repair the number of buildings with a 5% probability of being damaged by such an event. If the analyst only considers spatial correlation in the risk assessment, the government would plan to repair 47 buildings. However, if structure-to-structure damage correlation is also considered, as done in this study, the government would need to finance the repair of 59 buildings, resulting in an increase in the required resources. Obviously, these numbers are case study specific and further studies could be conducted to examine the impacts in other regions, but the fundamental issue is clear.

5. Summary and conclusions

In this study, it was demonstrated how significantly the results of a regional seismic risk assessment can differ when the structure-to-structure damage correlation is either considered or neglected. Using a case study where the probability distribution of the total number of damaged buildings was estimated, it was shown that even if this parameter doesn't affect the average estimates, it does heavily influence the standard deviation and shape of distribution. These parameters heavily impact the probability of exceeding a large number of buildings, which can be a variable of particular interest to government for planning mitigation strategies.

For example, in a hypothetical scenario in the Caserta Province case where the government plans resources based on the number of buildings with a 5% probability of exceeding damage from the earthquake scenario presented here, they would require 21% more resources for building repairs if both damage and spatial correlations are considered. This finding emphasises the importance for decision-makers to incorporate both correlations in risk modelling to ensure accurate resource estimation and efficient allocation of funds for recovery during disaster planning.

It is still important, however, to determine how good are the estimations of the correlation obtained by using the simplification of the equivalent SDOF nonlinear oscillators. A future application of this study could imply comparing the results with the case in which the IDA was performed on full 3D models of the buildings. It would also be ideal to validate the estimations with information from actual events, to assess whether the analytical approach proposed here can be used to develop mathematical models of correlation as a function of different building characteristics that influence their vulnerability. However, doing this validation might be difficult, given that the available data may be sparse and challenging to interpret.

References

[1] ATC, *FEMA P-58*, 2nd ed., vol. Volum 1. 2018.

[2] D. Vamvatsikos and C. A. Cornell, "Incremental dynamic analysis," *Earthq Eng Struct Dyn*, vol. 31, no. 3, pp. 491–514, Mar. 2002, doi: 10.1002/eqe.141.

[3] F. Jalayer, "Direct Probabilistic Seismic Analysis: Implementing Non-Linear Dynamic Assessments," StanfordUniversity, 2003.

[4] P. Heresi and E. Miranda, "RPBEE: Performance-based earthquake engineering on a regional scale," *Earthquake Spectra*, vol. 39, no. 3, pp. 1328–1351, Aug. 2023, doi: 10.1177/87552930231179491.

Copyright © 2025 CroCEE
DOI: https://doi.org/10.5592/CO/3CroCEE.2025.19

[5] L. Bodenmann, J. W. Baker, and B. Stojadinović, "Accounting for path and site effects in spatial ground-motion correlation models using Bayesian inference," *Natural Hazards and Earth System Sciences*, vol. 23, no. 7, pp. 2387–2402, Jul. 2023, doi: 10.5194/nhess-23-2387-2023.

[6] S. Esposito and I. Iervolino, "PGA and PGV Spatial Correlation Models Based on European Multievent Datasets," *Bulletin of the Seismological Society of America*, vol. 101, no. 5, pp. 2532–2541, Oct. 2011, doi: 10.1785/0120110117.

[7] R. Lee and A. S. Kiremidjian, "Uncertainty and Correlation for Loss Assessment of Spatially Distributed Systems," *Earthquake Spectra*, vol. 23, no. 4, pp. 753–770, Nov. 2007, doi: 10.1193/1.2791001.

[8] C. Kang, O.-S. Kwon, and J. Song, "Evaluation of correlation between engineering demand parameters of structures for seismic system reliability analysis," *Structural Safety*, vol. 93, p. 102133, Nov. 2021, doi: 10.1016/j.strusafe.2021.102133.

[9] M. Xiang, J. Shen, Z. Xu, and J. Chen, "Structure-to-structure seismic damage correlation model," *Earthq Eng Struct Dyn*, vol. 53, no. 10, pp. 3205–3229, Aug. 2024, doi: 10.1002/eqe.4172.

[10] P. Heresi and E. Miranda, "Structure-to-structure damage correlation for scenario-based regional seismic risk assessment," *Structural Safety*, vol. 95, p. 102155, Mar. 2022, doi: 10.1016/j.strusafe.2021.102155.

[11] C. Tsokos and R. Wooten, *The Joy of Finite Mathematics*. Elsevier, 2016. doi: 10.1016/C2014-0-02921-8.

[12] Amir M. Kaynia (Editor), Iunio Iervolino (Reviewer), Fabio Taucer (Publishing Editor), and Ufuk Hancilar (Publishing Editor), "Guidelines for deriving seismic fragility functions of elements at risk: Buildings, lifelines, transportation networks and critical facilities," 2013. doi: 10.2788/19605.

[13] D. Vamvatsikos and C. A. Cornell, "Developing efficient scalar and vector intensity measures for IDA capacity estimation by incorporating elastic spectral shape information," *Earthq Eng Struct Dyn*, vol. 34, no. 13, pp. 1573–1600, Nov. 2005, doi: 10.1002/eqe.496.

[14] M. Kohrangi, D. Vamvatsikos, and P. Bazzurro, "Site dependence and record selection schemes for building fragility and regional loss assessment," *Earthq Eng Struct Dyn*, vol. 46, no. 10, pp. 1625–1643, Aug. 2017, doi: 10.1002/eqe.2873.

[15] L. Martins and V. Silva, "Development of a fragility and vulnerability model for global seismic risk analyses," *Bulletin of Earthquake Engineering*, vol. 19, no. 15, pp. 6719–6745, Dec. 2021, doi: 10.1007/s10518-020-00885-1.

[16] A. M. B. Nafeh, G. J. O'Reilly, and R. Monteiro, "Simplified seismic assessment of infilled RC frame structures," *Bulletin of Earthquake Engineering*, vol. 18, no. 4, pp. 1579–1611, Mar. 2020, doi: 10.1007/s10518-019-00758-2.

[17] H. Crowley *et al.*, "Model of seismic design lateral force levels for the existing reinforced concrete European building stock," *Bulletin of Earthquake Engineering*, vol. 19, no. 7, pp. 2839–2865, May 2021, doi: 10.1007/s10518-021-01083-3.

[18] V. Corlito and G. De Matteis, "Caratterizzazione tipologico-strutturale e valutazione della vulnerabilità sismica degli edifici in cemento armato della Provincia di Caserta attraverso i parametri della scheda CARTIS," in *XVIII CONVEGNO ANIDIS "L'Ingegneria Sismica in Italia,"* Pisa: Pisa University Press srl, Sep. 2019, pp. 96–104.

[19] D. Min. Infrastrutture e Trasporti, *Norme tecniche per le costruzioni (NTC 2018)*. 2018.

[20] H. Crowley *et al.*, "European Exposure Model Data Repository (v1.0)." Accessed: Aug. 26, 2024. [Online]. Available: https://zenodo.org/records/5730071

[21] GEM, "Exposure Spatial Disaggregation," GitHub Repository.

[22] U. of S. D. of G. and G. U. of L. D. de G. U. de N. and C. for I. E. S. I. N. (CIESIN), C. U. WorldPop (www.worldpop.org - School of Geography and Environmental Science, "Global High Resolution Population Denominators Project - Funded by The Bill and Melinda Gates Foundation," https://dx.doi.org/10.5258/SOTON/WP00660.

[23] D. Giardini et al., "Seismic Hazard Harmonization in Europe (SHARE): Online Data Resource," 2013.

Copyright © 2025 CroCEE
DOI: https://doi.org/10.5592/CO/3CroCEE.2025.19

[24] D. M. Boore, J. P. Stewart, E. Seyhan, and G. M. Atkinson, "NGA-West2 Equations for Predicting PGA, PGV, and 5% Damped PSA for Shallow Crustal Earthquakes," *Earthquake Spectra*, vol. 30, no. 3, pp. 1057–1085, Aug. 2014, doi: 10.1193/070113EQS184M.

[25] N. Jayaram and J. W. Baker, "Correlation model for spatially distributed ground-motion intensities," *Earthq Eng Struct Dyn*, vol. 38, no. 15, pp. 1687–1708, Dec. 2009, doi: 10.1002/eqe.922.

[26] L. Eads, E. Miranda, and D. G. Lignos, "Average spectral acceleration as an intensity measure for collapse risk assessment," *Earthq Eng Struct Dyn*, vol. 44, no. 12, pp. 2057–2073, Sep. 2015, doi: 10.1002/eqe.2575.

[27] J. W. Baker, "Efficient Analytical Fragility Function Fitting Using Dynamic Structural Analysis," *Earthquake Spectra*, vol. 31, no. 1, pp. 579–599, Feb. 2015, doi: 10.1193/021113EQS025M.

[28] M. Kohrangi, S. R. Kotha, and P. Bazzurro, "Ground-motion models for average spectral acceleration in a period range: direct and indirect methods," *Bulletin of Earthquake Engineering*, vol. 16, no. 1, pp. 45–65, Jan. 2018, doi: 10.1007/s10518-017-0216-5.

Proceedings of the 3rd Croatian Conference on Earthquake Engineering - 3CroCEE
19–22 March 2025, Split, Croatia
Copyright © 2025 CroCEE
DOI: https://doi.org/10.5592/CO/3CroCEE.2025.30

BRIDGING THE GAP: A SOFTWARE TOOL FOR EFFICIENT GROUND MOTION RECORD SELECTION IN EARTHQUAKE ENGINEERING

Davit Shahnazaryan [(1)], Volkan Ozsarac [(2)], Gerard J. O'Reilly [(3)]

[(1)] *Postdoctoral Researcher, Centre for Training and Research on Reduction of Seismic Risk (ROSE Centre), Scuola Universitaria Superiore IUSS Pavia, Pavia, Italy. E-Mail: davit.shahnazaryan@iusspavia.it*
[(2)] *Postdoctoral Researcher, Centre for Training and Research on Reduction of Seismic Risk (ROSE Centre), Scuola Universitaria Superiore IUSS Pavia, Pavia, Italy. E-Mail: volkan.ozsarac@iusspavia.it*
[(3)] *Associate Professor, Centre for Training and Research on Reduction of Seismic Risk (ROSE Centre), Scuola Universitaria Superiore IUSS Pavia, Pavia, Italy. E-Mail: gerard.oreilly@iusspavia.it*

Abstract

With the significant advancements in computational power in recent decades, non-linear response history analysis has become more prevalent in seismic design and assessment. A critical step in these applications is the selection and scaling of appropriate ground motion records. However, state-of-the-art record selection procedures are rarely employed by engineers due to the lack of user-friendly and computationally efficient software tools, despite the advances in know-how in the research community. To address these challenges, a user interface (UI)-based software for ground motion record selection is introduced. In addition to the traditional building code-compliant approaches, the software integrates the generalised conditional intensity measure (GCIM) framework to select hazard-consistent records from harmonised databases, such as the PEER NGA-West2, and to provide corresponding scale factors. This approach allows for a combined consideration of any number of ground motion intensity measure types through cross-correlation matrices. Furthermore, the multiple causal earthquakes and ground motion models (GMMs) can be incorporated, as done in the probabilistic seismic hazard analysis (PSHA). The application of the tool is demonstrated using a generalised GMM to facilitate efficient record selection. The UI is designed for ease of use allowing flexibility for users to switch between the different methods of selection and retention of input and output data. The tool supports the selection of both horizontal and vertical ground motion components. A case study is presented demonstrating the performance of the tool for conditional and unconditional selection.

Keywords: ground-motion record selection, conditional selection, unconditional selection, code-based selection, graphical user interface.

1. Introduction

The selection of ground motion records in seismic design and assessment applications needs to be approached with great care, as it can have direct impact on the accuracy and the reliability of seismic performance evaluations. This process begins with defining a 'target', which, among others, could be the design response spectrum specified in building codes worldwide, a uniform hazard spectrum (UHS) derived from a probabilistic seismic hazard analysis (PSHA) [1], or a weighted average of response spectra from earthquake scenarios conditioned on a specific spectral acceleration ordinate ([2], [3]). Selection algorithms are then employed to identify a suite of records whose response spectra closely match this 'target' based on the specified criteria. Specifically, when the target is a Conditional Spectrum (CS), the selected suite achieves hazard consistency by ensuring that the distributions of response spectra from the selected ground motions are consistent with the hazard curves at all relevant periods. Over the years, numerous ground motion selection methods have been proposed in the literature to account for both the mean and variability of response spectra corresponding to such 'targets' ([4], [5]).

In general, all ground motion record selection methods rely on the elastic spectral accelerations of ground motions. However, it is well understood that the severity of ground motion also depends on

Proceedings of the 3rd Croatian Conference on Earthquake Engineering - 3CroCEE
19–22 March 2025, Split, Croatia
Copyright © 2025 CroCEE
DOI: https://doi.org/10.5592/CO/3CroCEE.2025.30

factors such as intensity, velocity, duration, and frequency content. To address the limitations of these traditional methods, Bradley ([6], [7]) introduced the generalised conditional intensity measure (GCIM) approach, which allows the distribution of a ground motion intensity measure (IM) to be derived based on the values of other IMs. One notable characteristic or 'limitation' (at the time of introduction) of GCIM was the reliance on ground motion models (GMMs) to estimate the distribution of expected ground motion intensities and their associated uncertainties given a set of causal parameters (e.g., magnitude, source-to-site distance). Initially, the GCIM approach could only accommodate a limited number of IMs, such as spectral acceleration, peak ground acceleration, Arias intensity, or significant duration. However, advancements in GMM development in recent years have transformed this perceived limitation into a significant strength. For example, newer GMMs have been developed for cumulative intensity-based IMs (e.g., significant duration) and amplitude-based IMs (e.g., spectral acceleration), with these models predicting the IMs independently ([8]–[11], among others). Recent research has focused on developing GMMs for next-generation IMs, such as filtered incremental velocity (*FIV*3) [12] and average spectral acceleration (Sa_{avg}) [13], which have demonstrated promising efficiency and sufficiency ([14]–[16]). Furthermore, Aristeidou et al. [17] proposed a GMM capable of predicting a wide range of IMs using a single model, further enhancing the applicability of the GCIM framework.

Ground motion selection procedures rely not only on the availability of relevant GMMs but also on the correlations between the IMs (or the spectral ordinates of the same IM). To derive the conditional distribution of one IM with respect to others, these correlations are essential. Addressing this need, Aristeidou et al. [18] developed correlation models that account for both traditional IMs (such as spectral acceleration, peak ground acceleration, peak ground velocity, and significant duration) and next-generation IMs (e.g., *FIV*3, Sa_{avg}).

With substantial advancements in computational power over recent decades, along with progress in GMMs, correlation models, and ground motion record selection procedures, non-linear response history analysis has become increasingly prominent in seismic design and assessment. In fact, it is the preferred method of design verification and assessment for practising engineers worldwide due to its perceived accuracy and insights given into the seismic behaviour of structures. Despite these developments, engineers rarely utilise advanced record selection methods due to the lack of accessible and efficient software tools. To address this gap, this paper presents a user interface (UI)-based software tool for ground motion record selection. Beyond conventional approaches that adhere to building code requirements, the software also allows for vertical component selection and integrates the GCIM framework to select records from harmonised databases such as PEER NGA-West2 [19], while also providing corresponding scale factors. This approach allows for the simultaneous consideration of multiple ground motion IMs using cross-correlation matrices. Furthermore, the tool accommodates multiple causal earthquakes and GMMs, as is standard practice in PSHA. The software's functionality is demonstrated through the application of a generalised GMM [17], facilitating efficient record selection. Finally, a case study compares the performance of unconditional and conditional selection methods.

2. Probabilistic seismic hazard analysis

Before initiating the ground motion selection procedure, it is essential to identify target response spectra for the selection process. A commonly accepted approach for defining these target spectra involves performing PSHA. To conduct PSHA, rupture parameters (*rup*) and GMMs (*gmm*) are required. These inputs form the basis of a logic tree, which is used to capture and quantify epistemic uncertainty associated with the PSHA inputs. Figure 1 illustrates an example of this process, demonstrating how different GMMs are utilised to model two distinct rupture scenarios in constructing a target spectrum. Throughout this document, it is assumed that the rupture parameters and their corresponding GMMs for each IM of interest are predefined and readily available as provided by PSHA disaggregation. Figure 2 illustrates a sample disaggregation output following PSHA for a return period of 4975 years. The disaggregation of hazard from all sources is typically obtained by accumulating magnitude and distance bin contribution to the global hazard. In the example, the highest contribution is controlled by an event

Copyright © 2025 CroCEE
DOI: https://doi.org/10.5592/CO/3CroCEE.2025.30

of magnitude 7.38 and a distance of 1km. This assumption facilitates the consideration of various rupture scenarios and associated GMMs in the calculations, aligning with standard practices in PSHA. For each rupture scenario rup_r, the associated probability p_r is known, such that:

$$\sum_{r=1}^{n_{rup}} p_r = 1 \tag{1}$$

And for each gmm_g used to model this rup_r, its associated weights, $w_{r,g}$, are given:

$$\sum_{g=1}^{n_{gmm}^r} w_{r,g} = 1 \tag{2}$$

where n_{gmm}^r is the number of GMMs used to model rup_r. All *rup* and associated *gmm* are assumed to be considered in the target identification, which is generally referred to in the literature as the *exact* approach, described by Lin et al. [3]. The *approximate* approach, is a special case where one single *rup* is modelled using a single *gmm*, therefore implying that $p_1=w_{1,1}=1.0$.

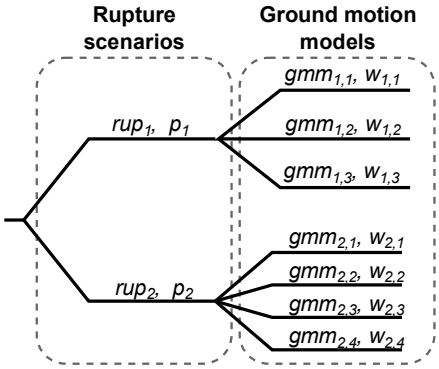


Figure 1. Different rupture scenarios and GMMs that may be considered.

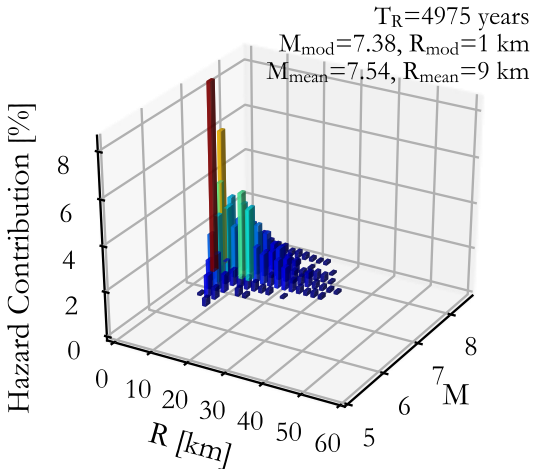


Figure 2. Sample illustration of disaggregation results from PSHA.

3. Target identification

3.1. Unconditional spectrum

Following the setup of the logic tree, first an approximate case with only a single rupture scenario and GMM is employed. In this case, the unconditional mean and variance are computed using Eq. (3) and Eq. (4).

$$\mu_{\ln IM_i} = \mu_{\ln IM_i^g | rup_r} \tag{3}$$

Copyright © 2025 CroCEE
DOI: https://doi.org/10.5592/CO/3CroCEE.2025.30

$$\sigma^2_{\ln IM_i} = \sigma^2_{\ln IM_i^g|rup_r} \tag{4}$$

where $\mu_{\ln IM_i^g|rup_r}$ and $\sigma^2_{\ln IM_i^g|rup_r}$ are the mean and variance of the natural logarithm of a known IM, IM_i, for a single rupture rup_r, and GMM gmm_g. The approximate case may be generalised to consider for many different rupture scenarios and GMMs, as a result the unconditional mean and variance are obtained using Eq. (5) and Eq. (6).

$$\mu_{\ln IM_i} = \sum_{r=1}^{n_{rup}} \sum_{g=1}^{n^r_{gmm}} p_r w_{r,g} \mu_{\ln IM_i^g|rup_r} \tag{5}$$

$$\sigma^2_{\ln IM_i} = \sum_{r=1}^{n_{rup}} \sum_{g=1}^{n^r_{gmm}} p_r w_{r,g} \left(\sigma^2_{\ln IM_i^g|rup_r} + \left(\mu_{\ln IM_i} - \mu_{\ln IM_i^g|rup_r} \right)^2 \right) \tag{6}$$

Lin et al. [3] termed those as *exact* and *approximate* approaches, and presented four different methods to compute a target response spectrum. The different between each method depends on the hazard input cases considered.

- Method 1 involves a single GMM applied to a single rupture scenario (i.e., $n_{rup} = n^r_{gmm} = 1$).
- Method 2 considers multiple GMMs for the same rupture scenario (i.e., $n_{rup} = 1, n^r_{gmm} > 1$). In this approach, the GMM weights, $w_{1,g}$, are derived from the PSHA logic tree (i.e., $p_r = 1, w_{1,g} = w^l_{1,g}$, where l refers to the logic tree).
- Method 3 considers a single rupture scenario for each GMM (i.e., $n_{rup} = n_{gmm} > 1$). Here, the GMM weights, $w_{r,g}$, are obtained from PSHA disaggregation (i.e., $p_r w_{r,g} = p^d_r w^d_{r,g}$, with d signifying disaggregation).
- Method 4 follows a more generalised framework, adhering to the formulations provided in Eq. (5) and Eq. (6).

These methods underscore the varying levels of complexity and the different considerations for hazard inputs in target response spectrum computation. It is crucial to note that the weights derived from PSHA disaggregation (i.e., $p^d_r, w^d_{r,g}$) differ from the logic tree weights (i.e., $p^l_r w^l_{r,g}$). Lin et al. [3] discusses how the logic tree weights are analogous to prior weights in decision analysis, while disaggregation weights correspond to posterior weights. Moreover, disaggregation weights are typically expressed as a single product, $p^d_r w^d_{r,g}$, rather than as separate components, which are still compatible to the formulations given in Eq. (5) and Eq. (6) and correspond to the *exact* approach.

3.2. Conditional spectrum

In the case of conditional response spectrum dependent on a certain IM, *IM**, as the target for record selection, unconditional means and variances transform to $\mu_{\ln IM_i^g|\ln IM^{*h},rup_r}$ and $\sigma^2_{\ln IM_i^g|\ln IM^{*h},rup_r}$, respectively. It is assumed that the value of $\ln IM^{*h}$ will be obtained from another GMM denoted h. Conditional target mean and variance for a given rupture scenario rup_r and GMM pair will be given by the following expressions:

$$\mu_{\ln IM_i^g|\ln IM^{*h},rup_r} = \mu_{\ln IM_i^g|rup_r} + \rho_{\ln IM_i^g,\ln IM^{*h}|rup_r} \sigma_{\ln IM_i^g|rup_r} \epsilon_{\ln IM^{*h}|rup_r} \tag{7}$$

$$\sigma^2_{\ln IM_i^g|\ln IM^{*h},rup_r} = \sigma^2_{\ln IM_i^g|rup_r} \left(1 - \rho^2_{\ln IM_i^g,\ln IM^{*h}|rup_r} \right) \tag{8}$$

$$\epsilon_{\ln IM^{*h}|rup_r} = \frac{\ln IM^* - \mu_{\ln IM^{*h}|rup_r}}{\sigma_{\ln IM^{*h}|rup_r}} \tag{9}$$

Baker [2] describes the term, ρ, as the correlation of the residuals, ϵ, of $\ln IM_i^g$ and $\ln IM^{*h}$, corresponding to two different GMMs, g and h, respectively, and for given rupture parameters rup_r. This definition presumes the availability of a correlation model specific for these two IMs, the

Copyright © 2025 CroCEE
DOI: https://doi.org/10.5592/CO/3CroCEE.2025.30

respective GMMs, and the particular rupture parameters rup_r. However, Baker and Bradley [20] supported the idea of a more practical approach by suggesting the omission of the dependence on specific rupture parameters and GMMs when developing correlation models. This simplification facilitates broader applicability without compromising the utility of the correlation models in practical scenarios. As a result, Eq. (7) and Eq. (8) may be rewritten into Eq. (10) and Eq. (11), respectively.

$$\mu_{\ln IM_i^g|\ln IM^{*h},rup_r} = \mu_{\ln IM_i^g|rup_r} + \rho_{\ln IM_i,\ln IM^*}\sigma_{\ln IM_i^g|rup_r}\epsilon_{\ln IM^{*h}|rup_r} \tag{10}$$

$$\sigma^2_{\ln IM_i^g|\ln IM^*,rup_r} = \sigma^2_{\ln IM_i^g|rup_r}\left(1-\rho^2_{\ln IM_i,\ln IM^*}\right) \tag{11}$$

The combined conditional mean spectrum (CMS) is computed as the weighted sum of each:

$$\mu_{\ln IM_i^g|\ln IM^*,rup_r} = \sum_{h=1}^{n^r_{gmm}} w_h \mu_{\ln IM_i^g|\ln IM^{*h},rup_r} \tag{12}$$

Here, the GMM h is considered individually, meaning that the weights w_h need to be obtained from the logic tree branch for rup_r. For a single rupture scenario, the conditional mean and variance will be given by Eq. (13) and Eq. (14).

$$\mu_{\ln IM_i|\ln IM^*} = \mu_{\ln IM_i^g|\ln IM^*,rup_r} \tag{13}$$

$$\sigma^2_{\ln IM_i|\ln IM^*} = \sigma^2_{\ln IM_i^g|\ln IM^*,rup_r} \tag{14}$$

Extending the conditional approach to include multiple rupture scenarios and GMMs, the resulting mean and variance will be given by Eq. (15) and Eq. (16). This represents the full expansion of the GCIM approach for ground motion record selection as proposed by Bradley [6]. The primary distinction lies in the inclusion of multiple rupture scenarios as opposed to the single rupture scenario originally presented in Bradley [6]. Figure 3 presents an example of a conditional selection, illustrating the means and standard deviations of the target, calculated using Eq. (15) and Eq. (16), respectively. This example involves an application with two rupture scenarios and two Ground Motion Models (GMMs). The individual grey dashed branches represent the results obtained from Eq. (12) for the means and Eq. (11) for the standard deviations.

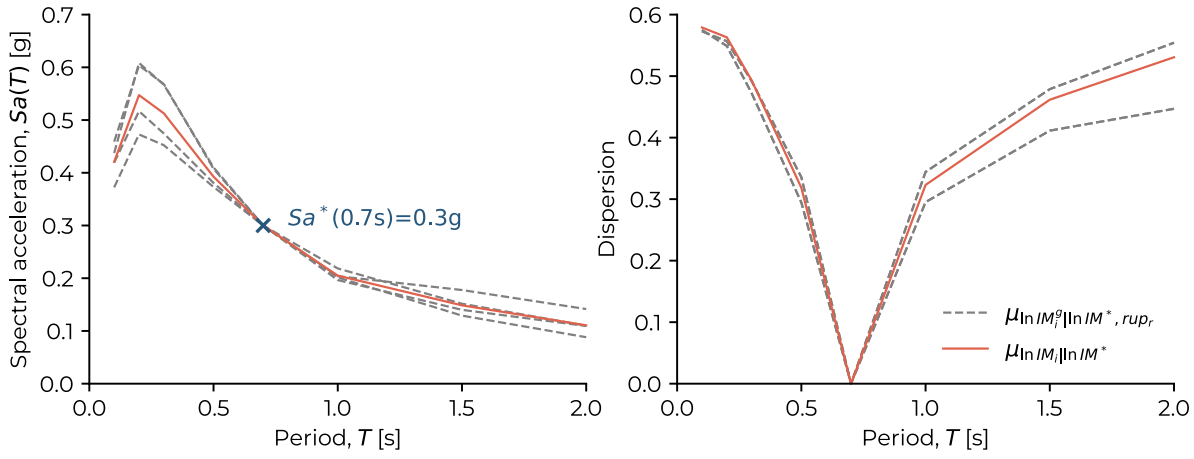


Figure 3. Illustration of (left) means and (right) dispersions computed for a case of two ruptures and two GMMs, where the solid lines represent the mean value and the dashed lines represent the mean plus and minus two standard deviations for a conditional selection

$$\mu_{\ln IM_i|\ln IM^*} = \sum_{r=1}^{n_{rup}}\sum_{g=1}^{n^r_{gmm}} p_r w_{r,g}\mu_{\ln IM_i^g|\ln IM^*,rup_r} \tag{15}$$

Copyright © 2025 CroCEE
DOI: https://doi.org/10.5592/CO/3CroCEE.2025.30

$$\sigma^2_{\ln IM_i|\ln IM^*} = \sum_{r=1}^{n_{rup}} \sum_{g=1}^{n^r_{gmm}} p_r w_{r,g} \left(\sigma^2_{\ln IM_i^g|\ln IM^*, rup_r} + \left(\mu_{\ln IM_i|\ln IM^*} - \mu_{\ln IM_i^g|\ln IM^*, rup_r} \right)^2 \right) \quad (16)$$

3.3. Simulating targets for ground motion record selection

Once the target means and variances are identified, ground motion records may be selected. Ground motions are selected collectively meaning that both the mean and variance of the group must be matched and not in a piecewise fashion. To resolve this, Jayaram and Baker [21] proposed that suitable ground motion records lnIM_i are simulated and actual ground motions with values close to these are looked for. To achieve it, the vector of means, $\mu_{\ln\mathbf{IM}}$, and the covariance, $\Sigma_{\ln\mathbf{IM}}$, of the vector of ln**IM** = {…, lnIM_i, …} is used. Those can be written as:

$$\mu_{\ln\mathbf{IM}} = \begin{bmatrix} \vdots \\ \mu_{\ln IM_i|\ln IM^*} \\ \vdots \end{bmatrix} \quad (17)$$

The standard deviation is written as:

$$\sigma_{\ln\mathbf{IM}} = \begin{bmatrix} \vdots \\ \sigma_{\ln IM_i|\ln IM^*} \\ \vdots \end{bmatrix} \quad (18)$$

The correlation between each of the ln**IM** values conditioned on lnIM* needs to be computed to fully characterise the multivariate normal distribution parameters. Bradley [7] describes this as:

$$\rho = \begin{bmatrix} \ddots & \cdots & \\ \vdots & \rho_{\ln IM_i, \ln IM_j|\ln IM^*} & \vdots \\ & \cdots & \ddots \end{bmatrix} \quad (19)$$

where the individual conditional correlation term is given by:

$$\rho_{\ln IM_i, \ln IM_j|\ln IM^*} = \frac{\rho_{\ln IM_i, \ln IM_j} - \rho_{\ln IM_i, \ln IM^*} \rho_{\ln IM_j|\ln IM^*}}{\sqrt{1-\rho^2_{\ln IM_i|\ln IM^*}} \sqrt{1-\rho^2_{\ln IM_j|\ln IM^*}}} \quad (20)$$

This is then used to construct the covariance matrix between each of the ln**IM** terms conditioned on lnIM* as:

$$\Sigma = \begin{bmatrix} \ddots & \cdots & \\ \vdots & \Sigma_{\ln IM_i, \ln IM_j|\ln IM^*} & \vdots \\ & \cdots & \ddots \end{bmatrix} \quad (21)$$

where the individual conditional covariance term is given by:

$$\Sigma_{\ln IM_i, \ln IM_j|\ln IM^*} = \rho_{\ln IM_i, \ln IM_j|\ln IM^*} \sigma_{\ln IM_i|\ln IM^*} \sigma_{\ln IM_j|\ln IM^*} \quad (22)$$

4. Ground motion record selection tool

This section presents an online toolbox developed to implement the outlined framework. At this stage, the tool, available at https://apps.djura.it/hazard/record-selector, includes several methods, ranging from basic building code requirements to more complex hazard scenarios. However, the building code requirements will not be the focus of this section. The tool enables the selection of records using a set of target spectra for various ground motion IMs, based on specific rupture parameters, a process commonly referred to as scenario-based analysis. Both generalised unconditional and conditional selection options are available. Within the tool, users are required to choose key attributes and functionalities:

1. **IM – GMM Pairs**: IMs must be specified alongside the GMMs required to predict their expected distribution. Figure 4(left) illustrates the interface for this process. For example, when

Copyright © 2025 CroCEE
DOI: https://doi.org/10.5592/CO/3CroCEE.2025.30

spectral acceleration, $Sa(T)$, is selected, a menu of available GMMs is displayed. The graphic below dynamically updates to reflect the chosen GMMs and shows their associated weights, which users can adjust as needed. The following IMs are currently supported: $Sa(T)$, average spectral acceleration, $Sa_{avg}(T)$, peak ground acceleration, *PGA*, peak ground velocity, *PGV*, significant durations, Ds_{575} and Ds_{595}), and filtered incremental velocity, *FIV3*.

2. **Rupture Scenarios**: scenario parameters are defined based on the previously selected IMs and GMMs. The site context, which refers to the characteristics of the site of interest rather than the earthquake rupture itself, is specified separately. The most common parameter to characterise a site is the average shear wave velocity to 30 meters depth, Vs_{30}. Additional fields such as $Z_{2.5}$ and the soil/rock indicator also appear depending on the GMMs employed. Detailed explanations for each parameter are provided within the tool's interface and references are also provided. Next, rupture parameters are specified, typically derived from the disaggregation results of PSHA. Users often define a single dominant rupture scenario for each intensity level, as is customary in the *approximate* selection approach (Lin et al. [3]). A notable feature of the presented record selector is its ability to manage multiple rupture scenarios by assigning relative weights to each scenario based on PSHA results, a method referred to as the *exact* approach by Lin et al. [3]. Figure 4(right) gives the graphical UI for this process.
3. **Conditional IM (only for conditional selection)**: the core concept of conditional ground motion record selection is that the chosen ground motions correspond to a specified value of intensity for a particular IM. This specified value, referred to as the conditioning value, or IM*, is typically obtained from the hazard curve or PSHA. From the previously selected pool of IMs (from Step 1), the user must choose the conditioning IM and specify its conditioning value. The tool then utilises this value to define the target distribution of the ground motions relative to this point.

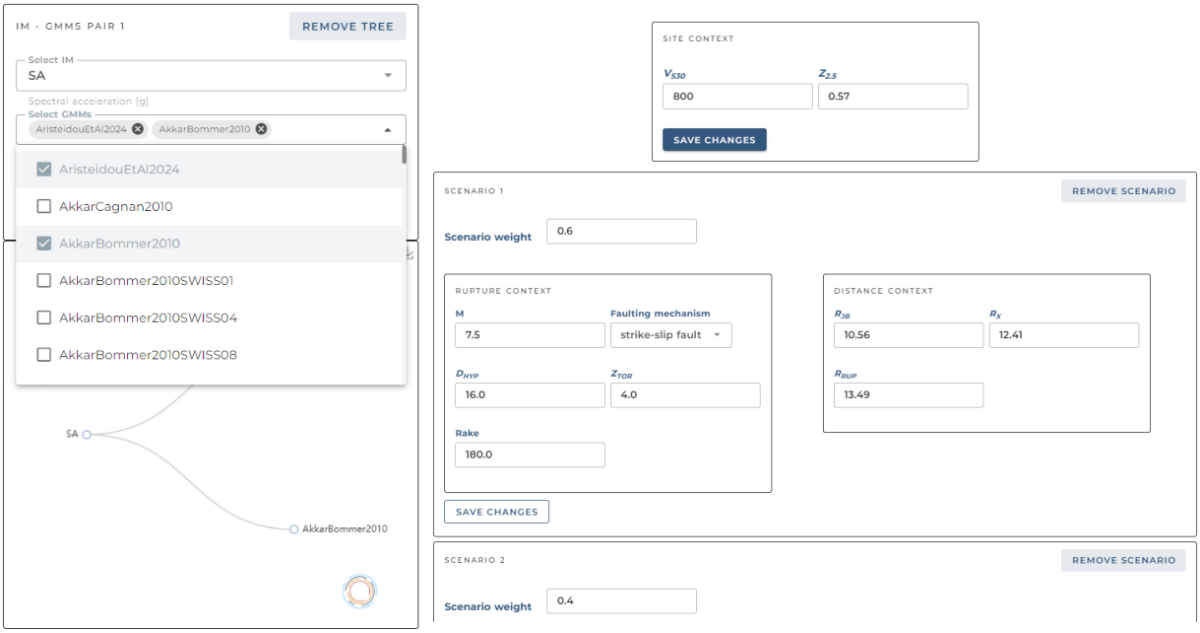


Figure 4. Graphical UI of the proposed tool: (left) IM-GMM pair selection, (right) Rupture scenario definition.

4. **Logic Tree:** after configuring the scenarios and finalising the input, the logic tree can be visualised. This takes the user to a dedicated page where all details about the IMs, GMMs, weights, rupture scenarios, and more are presented in a comprehensive table (Figure 5). This feature ensures that every aspect of the analysis is clearly organised and easily accessible. For a more intuitive overview, an interactive logic tree diagram (Figure 6) provides a global visual representation of the analysis. The diagram breaks down the different elements, beginning with the rupture scenarios (two in the provided example). For each rupture scenario, it illustrates the

Copyright © 2025 CroCEE
DOI: https://doi.org/10.5592/CO/3CroCEE.2025.30

IMs being predicted and the associated GMMs used to estimate their distributions. By hovering over individual elements, users can view specific weights assigned to the IMs and GMMs. The logic tree offers flexibility, allowing users to expand or collapse sections to display the desired level of detail. Additionally, both the full logic tree and the interactive diagram can be downloaded for offline use, providing a convenient way to store and review inputs and results.

5. **Advanced Input:** the software supports configuring several advanced input parameters, with default values pre-set for convenience. These configurations include selecting the number of horizontal components and the method used to define them (geomean, RotD100, RotD50) used to define them. Users can adjust the number of ground motions, set limits on scaling, and define computational settings, such as the number of iterations required to achieve a good match between the target distribution and the selected ground motions. Additionally, users can introduce more IM definitions, such as specifying $Sa(T)$ at a particular period, T, with the option to assign importance weights to each IM. Furthermore, causal earthquake rupture parameter limits can be customised to refine ground motion selections, for instance, by restricting to a particular magnitude range or faulting styles.

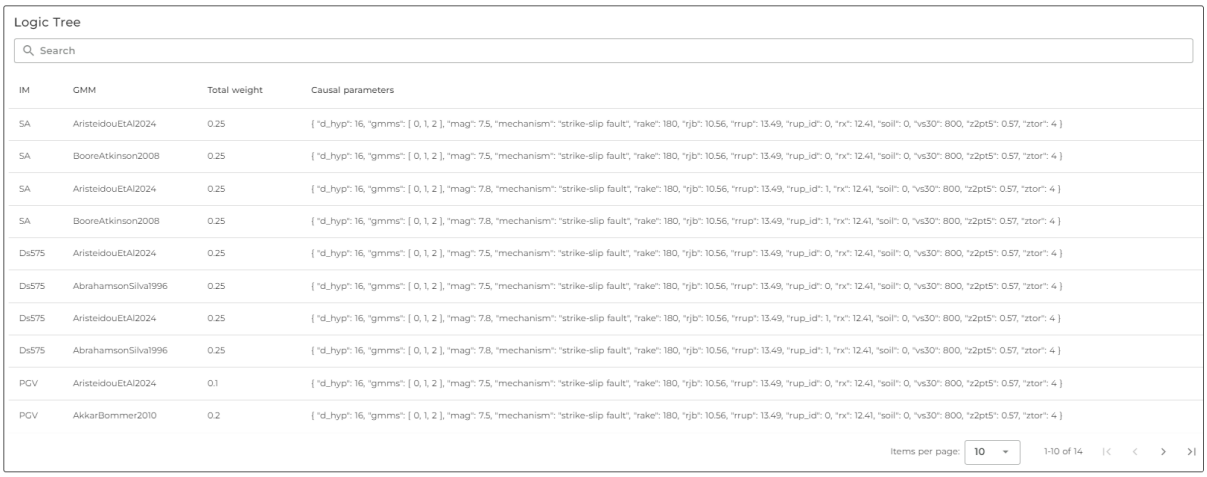


Figure 5. Logic tree table listing relevant data in a structured format.

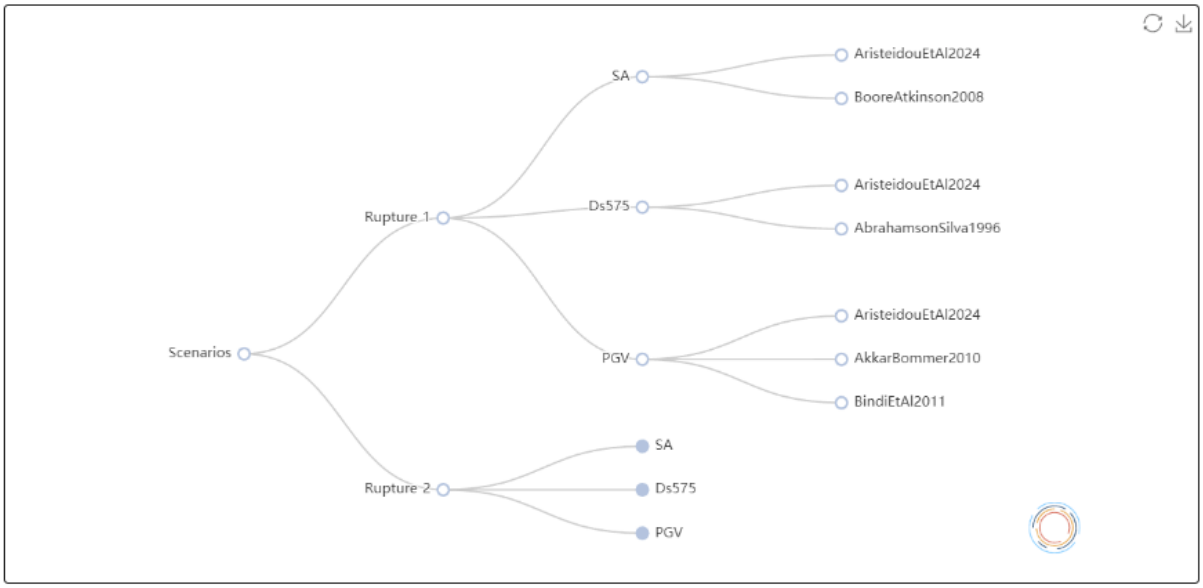


Figure 6. Interactive logic tree diagram.

Copyright © 2025 CroCEE
DOI: https://doi.org/10.5592/CO/3CroCEE.2025.30

It is important to note that at every step of input and output generation, data can be downloaded for use in other applications or analyses. Additionally, within the tool, additional hazard consistency checks may be performed.

5. Example unconditional and conditional record selection

Within this section, an example application of the tool and the framework described in Section 2 are presented. The tool is applied to perform selection following both methods: unconditional and conditional. Once, all input data is defined, the tool is used to generate a target distribution. Figure 7(left) demonstrates an example target unconditional distribution, while Figure 7(right) illustrates an example target conditional distribution, where IM* corresponds to *Sa*(0.7s) with a value of 0.3g. For the sample calculation, the scaling factors of the records were limited to 3.0, and magnitudes of the events were constrained to be 5 or higher.

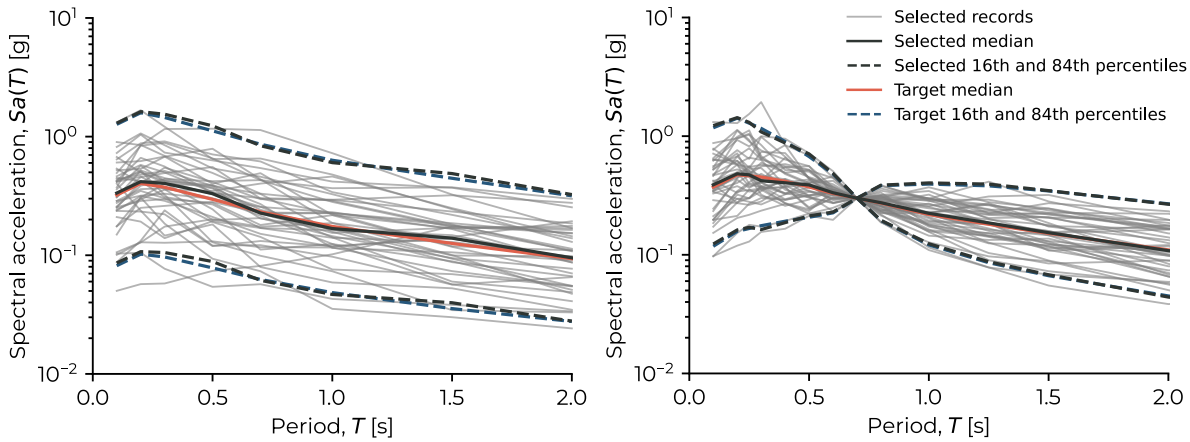


Figure 7. (left) unconditional and (right) conditional target distributions.

In addition to the target distributions, Figure 7 presents the selected record spectra and their median spectra. Each selected ground motion record spectrum is shown alongside the mean and standard deviations, which, as can be observed, correspond to the median and standard deviation of the target distributions. For each IM of interest, Kolmogorov-Smirnov (KS) goodness-of-fit tests are conducted to assess the quality of the selection. The KS test measures the absolute difference between the theoretical and cumulative distribution function (CDF) and the empirical distribution function (EDF) of the sample [22]. Figure 8 illustrates some of the IM tests, showing that the EDFs of the selected ground motions are representative of the target distribution and its KS bounds at a 5% significance level. Finally, the record suite can be downloaded for further analysis.

While it may be obvious, it is important to recall that there is no other software tool widely available that can perform such a ground motion record selection. That is, the ground motion characteristics in terms of the spectral acceleration, velocity, duration and more can all be targeted to be consistent with the seismic hazard of a given site. This essentially means that the chosen records are the more representative ground motions for that site of hazard based on the PSHA results. The benefit is that these ground motions are expected to be much more efficient (i.e., reduced dispersion in the structural response) and also eliminates any possible biasing of the results based on ground motion characteristics that are typically overlooked by practitioners, primarily because the appropriate tools were until now unavailable.

Copyright © 2025 CroCEE
DOI: https://doi.org/10.5592/CO/3CroCEE.2025.30

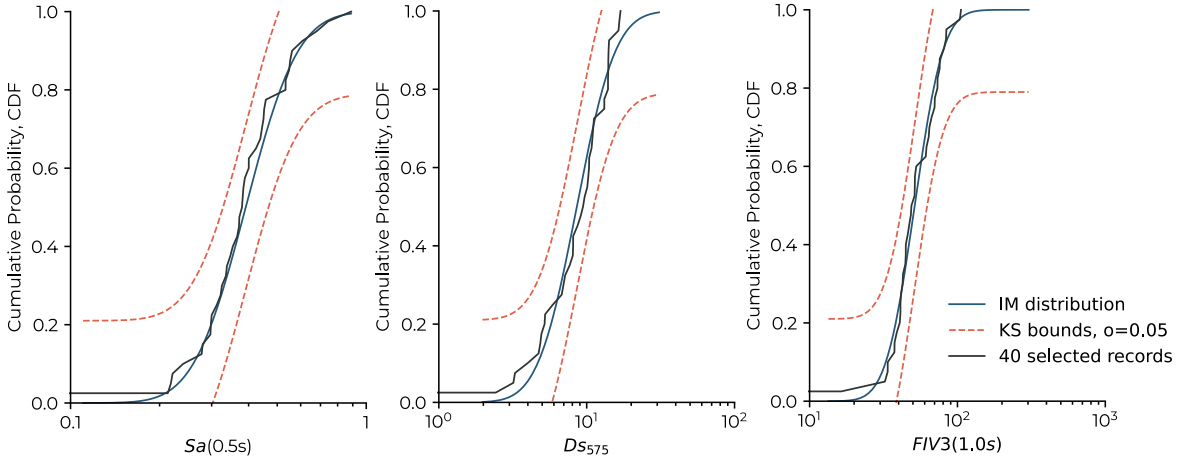


Figure 8. Illustration of the KS tests for a select IMs.

6. Summary

This paper introduced a user-friendly software tool designed to streamline the process of ground motion record selection for seismic design and assessment. By leveraging recent advancements in computational power, the software integrates state-of-the-art methods such as the ground motion conditional intensity measure (GCIM) framework, which allows for efficient record selection from harmonised databases like the PEER NGA-West2. It accommodates the use of multiple ground motion models (GMMs) and intensity measures (IMs) through cross-correlation matrices, mirroring the approach used in probabilistic seismic hazard analysis (PSHA). The tool offers flexibility in selecting both horizontal and vertical ground motion components and features a user interface (UI) that allows seamless switching between various methods of selection and easy retention of input and output data. A case study demonstrated the tool's capabilities for both conditional and unconditional selection of ground motions. The approach was consistent with industry standards and provided a ground motions suite that matches the target distribution and passes all Kolmogorov-Smirnov goodness-of-fit tests for all IMs of interest that are reflected real-world conditions, making it particularly useful for site-specific studies and advanced ground motion selection methods incorporated in design codes.

Acknowledgements

The work presented in this paper has been developed within the framework of the project "Dipartimenti di Eccellenza 2023-2027", funded by the Italian Ministry of Education, University and Research at IUSS Pavia.

References

[1] C. A. CORNELL, "Engineering Seismic Risk Analysis, Bull. Seismol. Soc. Am. 58, 1583–1606.," *Bull. Seismol. Soc. Am.*, vol. 58, no. 5, pp. 1583–1606, 1968, [Online]. Available: http://bssa.geoscienceworld.org/cgi/content/abstract/58/5/1583%5Cnhttp://bssaonline.org/cgi/content/abstract/58/5/1583

[2] J. W. Baker, "Conditional mean spectrum: Tool for ground-motion selection," *J. Struct. Eng.*, vol. 137, no. 3, pp. 322–331, 2011, doi: 10.1061/(ASCE)ST.1943-541X.0000215.

[3] T. Lin, S. C. Harmsen, J. W. Baker, and N. Luco, "Conditional Spectrum Computation Incorporating Multiple Causal Earthquakes and Ground-Motion Prediction Models," *Bull. Seismol. Soc. Am.*, vol. 103, no. 2A, pp. 1103–1116, Apr. 2013, doi: 10.1785/0120110293.

[4] N. Jayaram, T. Lin, and J. W. Baker, "A Computationally Efficient Ground-Motion Selection Algorithm for Matching a Target Response Spectrum Mean and Variance," *Earthq. Spectra*,

Copyright © 2025 CroCEE
DOI: https://doi.org/10.5592/CO/3CroCEE.2025.30

vol. 27, no. 3, pp. 797–815, Aug. 2011, doi: 10.1193/1.3608002.

[5] G. Wang, "A ground motion selection and modification method capturing response spectrum characteristics and variability of scenario earthquakes," *Soil Dyn. Earthq. Eng.*, vol. 31, no. 4, pp. 611–625, Apr. 2011, doi: 10.1016/j.soildyn.2010.11.007.

[6] B. A. Bradley, "A generalized conditional intensity measure approach and holistic ground-motion selection," *Earthq. Eng. Struct. Dyn.*, vol. 39, no. 12, pp. 1321–1342, Oct. 2010, doi: 10.1002/eqe.995.

[7] B. A. Bradley, "A ground motion selection algorithm based on the generalized conditional intensity measure approach," *Soil Dyn. Earthq. Eng.*, vol. 40, pp. 48–61, Sep. 2012, doi: 10.1016/j.soildyn.2012.04.007.

[8] B. A. Bradley, "Empirical equations for the prediction of displacement spectrum intensity and its correlation with other intensity measures," *Soil Dyn. Earthq. Eng.*, vol. 31, no. 8, pp. 1182–1191, Aug. 2011, doi: 10.1016/j.soildyn.2011.04.007.

[9] K. Afshari and J. P. Stewart, "Physically Parameterized Prediction Equations for Significant Duration in Active Crustal Regions," *Earthq. Spectra*, vol. 32, no. 4, pp. 2057–2081, Nov. 2016, doi: 10.1193/063015EQS106M.

[10] K. W. Campbell and Y. Bozorgnia, "Ground Motion Models for the Horizontal Components of Arias Intensity (AI) and Cumulative Absolute Velocity (CAV) Using the NGA-West2 Database," *Earthq. Spectra*, vol. 35, no. 3, pp. 1289–1310, Aug. 2019, doi: 10.1193/090818EQS212M.

[11] H. Zafarani and M. R. Soghrat, "Ground Motion Models for Non-Spectral Intensity Measures Based on the Iranian Database," *J. Earthq. Eng.*, vol. 27, no. 13, pp. 3786–3806, Oct. 2023, doi: 10.1080/13632469.2022.2150334.

[12] H. Dávalos, P. Heresi, and E. Miranda, "A ground motion prediction equation for filtered incremental velocity, FIV3," *Soil Dyn. Earthq. Eng.*, vol. 139, p. 106346, Dec. 2020, doi: 10.1016/j.soildyn.2020.106346.

[13] H. Dávalos and E. Miranda, "A Ground Motion Prediction Model for Average Spectral Acceleration," *J. Earthq. Eng.*, vol. 25, no. 2, pp. 319–342, Jan. 2021, doi: 10.1080/13632469.2018.1518278.

[14] H. Dávalos and E. Miranda, "Filtered incremental velocity: A novel approach in intensity measures for seismic collapse estimation," *Earthq. Eng. Struct. Dyn.*, vol. 48, no. 12, pp. 1384–1405, Oct. 2019, doi: 10.1002/eqe.3205.

[15] L. Eads, E. Miranda, and D. G. Lignos, "Average spectral acceleration as an intensity measure for collapse risk assessment," *Earthq. Eng. Struct. Dyn.*, vol. 44, no. 12, pp. 2057–2073, Sep. 2015, doi: 10.1002/eqe.2575.

[16] G. J. O'Reilly, "Seismic intensity measures for risk assessment of bridges," *Bull. Earthq. Eng.*, vol. 19, no. 9, pp. 3671–3699, Jul. 2021, doi: 10.1007/s10518-021-01114-z.

[17] S. Aristeidou, D. Shahnazaryan, and G. J. O'Reilly, "Artificial neural network-based ground motion model for next-generation seismic intensity measures," *Soil Dyn. Earthq. Eng.*, vol. 184, p. 108851, Sep. 2024, doi: 10.1016/j.soildyn.2024.108851.

[18] S. Aristeidou, D. Shahnazaryan, and G. J. O'Reilly, "Correlation models for next-generation amplitude and cumulative intensity measures using artificial neural networks," *Earthq. Spectra*, Oct. 2024, doi: 10.1177/87552930241270563.

[19] T. D. Ancheta *et al.*, "NGA-West2 database," *Earthq. Spectra*, vol. 30, no. 3, pp. 989–1005, 2014, doi: 10.1193/070913EQS197M.

Proceedings of the 3rd Croatian Conference on Earthquake Engineering - 3CroCEE
19–22 March 2025, Split, Croatia
Copyright © 2025 CroCEE
DOI: https://doi.org/10.5592/CO/3CroCEE.2025.30

[20] J. W. Baker and B. A. Bradley, "Intensity Measure Correlations Observed in the NGA-West2 Database, and Dependence of Correlations on Rupture and Site Parameters," *Earthq. Spectra*, vol. 33, no. 1, pp. 145–156, Feb. 2017, doi: 10.1193/060716eqs095m.

[21] N. Jayaram and J. W. Baker, "Efficient sampling and data reduction techniques for probabilistic seismic lifeline risk assessment," *Earthq. Eng. Struct. Dyn.*, vol. 39, no. 10, pp. 1109–1131, Aug. 2010, doi: 10.1002/eqe.988.

[22] A. H.-S. Ang and W. H. Tang, *Probability Concepts in Engineering: Emphasis on Applications in Civil and Environmental Engineering.* New York, NY: Wiley, 2006.

Proceedings of the 3rd Croatian Conference on Earthquake Engineering - 3CroCEE
19–22 March 2025, Split, Croatia
Copyright © 2025 CroCEE
DOI: https://doi.org/10.5592/CO/3CroCEE.2025.31

ENHANCING FUNCTIONAL RECOVERY ESTIMATIONS THROUGH STOREY LOSS FUNCTIONS

Davit Shahnazaryan [(1)], Gerard J. O'Reilly [(2)]

[(1)] *Postdoctoral Researcher, Centre for Training and Research on Reduction of Seismic Risk (ROSE Centre), Scuola Universitaria Superiore IUSS Pavia, Pavia, Italy. E-Mail: davit.shahnazaryan@iusspavia.it*
[(2)] *Associate Professor, Centre for Training and Research on Reduction of Seismic Risk (ROSE Centre), Scuola Universitaria Superiore IUSS Pavia, Pavia, Italy. E-Mail: gerard.oreilly@iusspavia.it*

Abstract

The computationally intensive nature of performance-based earthquake engineering (PBEE), particularly when implemented through detailed component-based approaches such as FEMA P-58, has limited its use primarily to academic research and specific studies. A more streamlined alternative, favoured by practitioners, employs storey loss functions (SLFs) to estimate expected monetary loss per storey based on seismic demand. This method significantly reduces the data required for analysis, which is particularly beneficial during the design phase when detailed component information may still be unavailable. This paper presents a customisable, user interface (UI)-based tool for use in the seismic design and assessment of buildings. Unlike the FEMA P-58 methodology, which assumes full recovery, where every damaged component must be repaired before the building is considered functional, recent studies have shown that occupants and building managers exhibit varying degrees of tolerance based on the situation. The proposed tool addresses this by targeting specific recovery states (RSs), including functionality recovery, re-occupancy, and full recovery, allowing for a more detailed disaggregation of losses in particular associated with non-structural elements. To make economic loss estimates more reflective of real-world conditions, the concept of RS should be incorporated, and the anticipated RS should be explicitly stated when conducting a loss assessment. This approach provides decision-makers with a more rational and informed strategy for estimating recovery times at different stages of the process.

Keywords: storey loss functions, recovery stages, losses, functional recovery.

1. Introduction

The introduction of the Pacific Earthquake Engineering Research (PEER) Centre's performance-based earthquake engineering (PBEE) framework [1] has enabled seismic engineers to assess damage to various building components in a more probabilistic manner. Building on this, the FEMA P-58 guidelines [2] allow users to translate expected damage into estimates of repair costs, downtime, and potential loss of life in buildings after an earthquake. This approach has gained significant traction in recent years, with numerous studies emphasising the substantial contribution of non-structural elements (NSEs) to monetary losses. Over the past 20 years, engineers have increasingly recognised that using decision variables like monetary loss is a more effective way to convey seismic risk to clients and stakeholders. However, applying a methodology like FEMA P-58 involves making critical assumptions about factors such as seismic hazards and structural modelling.

A simplified alternative to PEER's building-specific loss estimation was proposed by Ramirez and Miranda [3]. This approach introduced engineering demand parameter versus decision variable (EDP–DV) functions, which directly link structural response parameters (EDPs) to economic losses (DVs). These functions, referred to here as storey loss functions (SLFs), typically estimate monetary losses at the building storey level. By offering predefined loss functions that describe repair costs for a generalised inventory of damageable components, SLFs significantly reduce computational complexity and the data requirements for a building's inventory during loss estimation. This simplification is particularly beneficial during the design phase, when detailed information about building components is often unavailable. Generic SLFs help address this limitation by reducing the excessive computational effort associated with component-based approaches. Recent applications of SLFs include their

Copyright © 2025 CroCEE
DOI: https://doi.org/10.5592/CO/3CroCEE.2025.31

implementation by Silva et al. [4] for steel buildings and Shahnazaryan et al. [5] for reinforced concrete buildings in a European context. Significant research has been undertaken to support the development of EDP–DV functions and loss assessment methodologies, focusing on creating fragility and consequence functions for a variety of structural and non-structural components (e.g. [6]–[11]). Perrone et al. [12], for example, introduced a method for estimating the expected annual loss (EAL) of Italian reinforced concrete buildings, which incorporates appropriate SLFs. This further emphasises the necessity of advancing simplified approaches to streamline loss estimation processes.

The objective of this paper is to explore the consideration of level of recovery expected by building managers following post-earthquake repairs and how it impacts the expected losses. Specifically, it investigates whether buildings are expected to be fully restored to their pre-earthquake condition, potentially with improvements, or whether a lower level of repair would be deemed acceptable in the short to medium term. This topic was chosen for detailed exploration due to the valuable insights gained from recent earthquakes in Japan [13],which were informed by structural health monitoring (SHM) data, damage reports, and interviews with commercial building managers and owners. To facilitate this investigation, a toolbox featuring a graphical user interface (UI) is introduced here. This toolbox enables the automated generation of SLFs through regression analysis and accommodates different recovery states (RSs), as escribed in the methodology outlined by Molina Hutt et al. [14], offering a more accurate reflection of real-world conditions.

2. Storey loss function generation tool

The framework incorporated within the toolbox is detailed in this section, as initially presented in Shahnazaryan et al. [5]. Key decisions to be made prior to using the toolbox include characterising the building by defining the component inventory, which is determined by the quantities, fragility, and consequence functions of the components. Additional considerations involve performance grouping of components based on their sensitivity to EDPs, identifying potential interactions between different components, selecting the number of simulations for sampling damage states (DSs), and choosing the type of regression fitting for the analysis. The framework consists of several steps and is depicted in Figure 1.

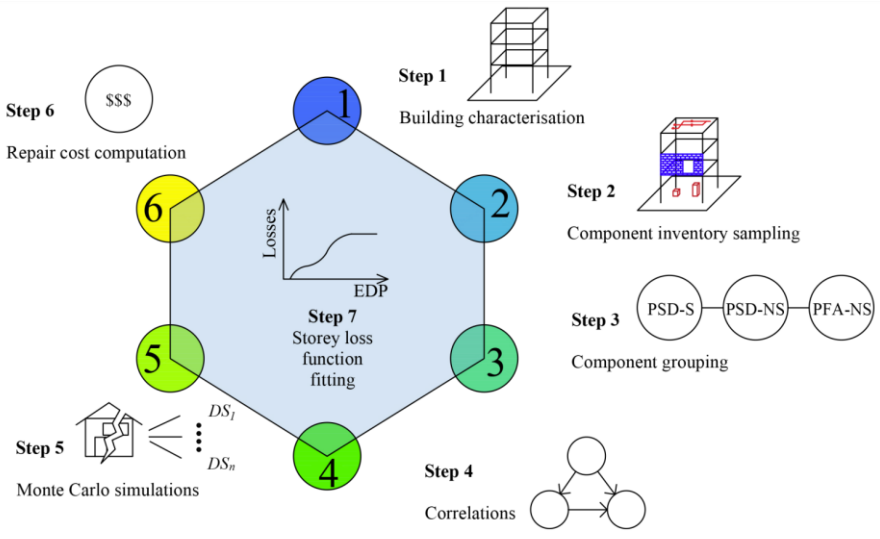


Figure 1. Storey loss function generation framework.

The process starts by identifying the building's characteristics, such as storey count, dimensions, occupancy, and usage. If these are unknown, SLFs can be based on a reference area and adjusted for the building's actual size (e.g., [12], [15]). Once the characteristics are determined, a damageable component inventory is created, considering structural and non-structural components, as well as contents likely to be damaged. The component inventory includes item types, quantities, EDP sensitivity, and whether the component is structural or non-structural. Components are grouped into

Copyright © 2025 CroCEE
DOI: https://doi.org/10.5592/CO/3CroCEE.2025.31

three performance categories, and fragility and consequence functions should be provided, often adapted from sources like the FEMA P-58 database [16]. To apply the framework to 3D buildings, it must be used separately for each direction, with components oriented along those directions. Components can then be grouped and analysed using structural and non-structural demands in the two orthogonal directions. However, interactions between seismic effects in orthogonal directions are not accounted for, and if such interactions are significant, more advanced loss assessment methods should be used but for most practical applications it is sufficient. Once the component inventory is defined, components are classified into groups based on their type (structural or non-structural) and EDP (e.g., peak storey drift (PSD) or peak floor acceleration (PFA)). Components within each performance group are assessed together, with their mutual demand leading to the calculation of the group's SLF. In essence, losses from all components in a performance group are linked to the same EDP. Classifying components into performance groups, alongside separating different component typologies, enables the disaggregation of losses at later stages to identify the key contributors to economic losses, as recently discussed in O'Reilly and Shahnazaryan [17]. This is particularly useful for visualisation, as it allows for easy identification of key loss contributions from collapsing and non-collapsing cases, as well as from individual storeys and performance groups (e.g., structural and non-structural components).

Similar to the studies by Ramirez and Miranda [3], structural and non-structural components sensitive to the same EDP can be grouped to account for potential correlations between their damage states. For instance, a specific intensity level may not directly damage a non-structural component, but it could affect another connected component that does sustain damage. In such cases, repair of the damaged component may require access, which could involve removing part or all of the undamaged non-structural component. Following Monte Carlo simulations and repair cost computations, regression is performed to identify the fitted SLFs.

Figure 2 and Figure 3 display the tool, which features an intuitive graphical UI designed to simplify the creation of SLFs for seismic assessment. Below is a description of the key elements and functionality of the tool's use.

1. **Main dashboard:** allows for the upload and download of inputs and outputs.
2. **Inventory:** where element inventory is defined in a table format. The users are able to perform create, read, update, and delete (CRUD) operations. Here, non-structural, structural elements or content is defined along with their quantities and EDP-sensitivity. The elements may be further categorised into different groups.
3. **Advanced:** element correlation matrix may be set dynamically depending on the updates associated with the element inventory. Additionally further calculation details may be adjusted, such as: number of Monte Carlo simulations, regression functions to be used (as of writing this paper, it supports Weibull [18] and Papadopoulos et al. [15]), and other parameters associated with visualisations.
4. **Visualisations:** allows the users to visualise the SLFs for each performance group, along with error metrics and fitting parameters.

The tool is available here: https://apps.djura.it/structure/edp-dv/standard.

Copyright © 2025 CroCEE
DOI: https://doi.org/10.5592/CO/3CroCEE.2025.31

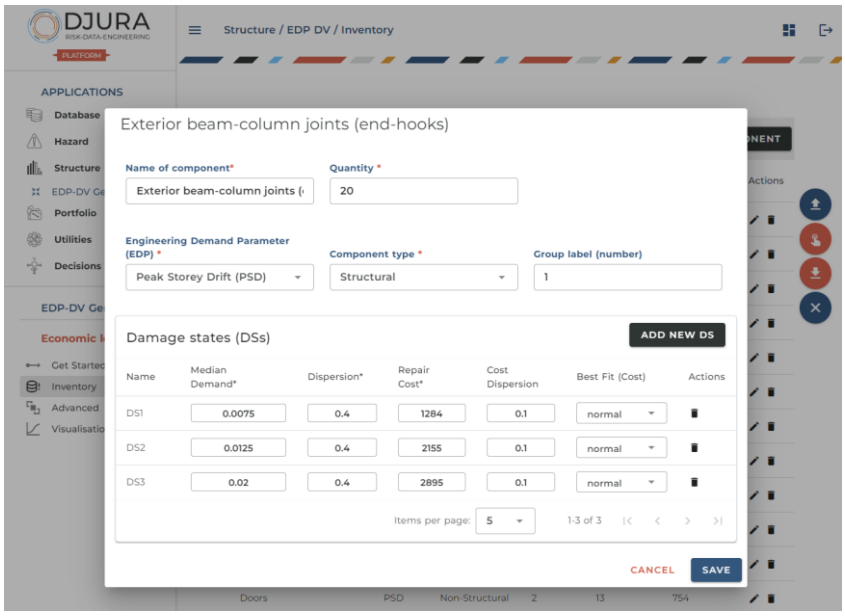


Figure 2. Overview of the graphical UI of the SLF generator.



Figure 3. Sample SLF visualisation.

3. Relative importance of NSEs for functional recovery

In recent decades, seismic engineers have increasingly recognised the importance of NSEs in overall building performance. This understanding traces back to observations made by Engle [19] in the 1920s, who highlighted that a building with significant NSE damage, such as partitions and finishes, is largely unusable after an earthquake, even if the structural frame remains intact. This was later reiterated and popularised by Taghavi and Miranda [20], who examined the monetary investments required for office, hotel, and hospital buildings, breaking them down into structural, non-structural, and building contents contributions. This straightforward illustration (Figure 4) reinforced Engle's earlier points and laid the groundwork for a more integrated approach to evaluating the impacts of NSEs on building performance. Similar findings have also been reported by Dhakal et al. [21] in recent years in New Zealand.

Copyright © 2025 CroCEE
DOI: https://doi.org/10.5592/CO/3CroCEE.2025.31

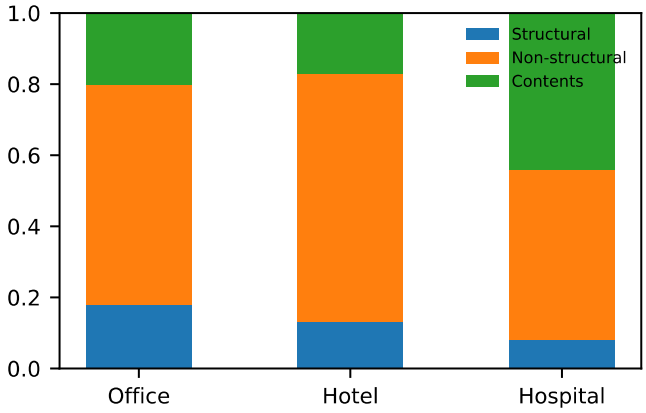


Figure 4. Cost breakdown of typical buildings in the US.

The significant role of NSEs in a building's financial investment was further illustrated by O'Reilly et al. [22], who examined the repair costs needed to fully rehabilitate a school building under increasing levels of ground shaking. The data, developed from surveys and instrumentation of an existing school building in central Italy, is shown in Figure 5 (left), where NSEs clearly dominate the percentage contributions to economic losses up until a return period of around 900 years, at which point their contribution drops to approximately 60%. While Figure 5 (right) demonstrates the importance of NSEs, with their relative contribution to EAL being over 45%.

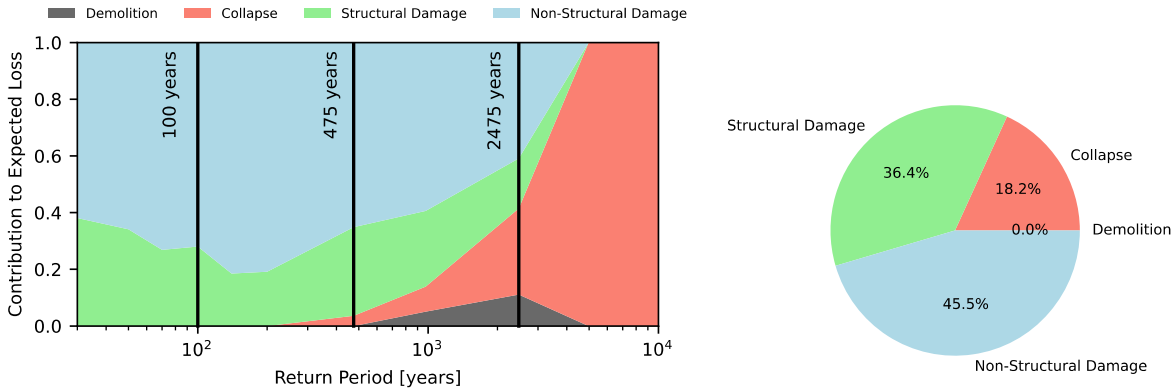


Figure 5. Relative contribution to (left) the expected loss versus return period of ground shaking and (right) to the EAL.

The recent Japanese earthquakes are focused on, specifically the 2018 Osaka and 2018 Hokkaido Eastern Iburi events, to compare research conclusions with actual observations following strong shaking. Data on structural and non-structural damage were collected through the q-NAVI system [23], which is an SHM system deployed in over 500 buildings (as of 2021) in various parts of Japan. Additionally, interviews and reports on the impacts to building functionality were invaluable. These observations focused on commercial buildings with typical office-type NSEs, which is significant because such buildings are usually owned by a single entity responsible for decision-making. This contrasts with residential buildings, where individual units are often owned separately, complicating decision-making for the building as a whole. The q-NAVI system reported no significant structural damage during the 2018 Osaka earthquake, but numerous buildings experienced damage to their NSEs. These included cracks in gypsum partition walls, water leaks from pipes, collapsed tiles from suspended ceiling systems, and the failure of some mechanical devices, representing various NSE types (e.g., drift vs. acceleration sensitive, fixtures vs. mechanical services). Despite the noticeable NSE damage, building maintenance managers, both on-site and at headquarters, along with the building owners,

Proceedings of the 3rd Croatian Conference on Earthquake Engineering - 3CroCEE
19–22 March 2025, Split, Croatia
Copyright © 2025 CroCEE
DOI: https://doi.org/10.5592/CO/3CroCEE.2025.31

concluded that the damage was not critical. They found that in many cases, the damage to NSEs was tolerable for both short- and long-term operations, preventing panic over high repair costs and financial losses often predicted in analytical studies. Many NSEs had relatively minor damage, and when strictly following the FEMA P-58 framework [2], their repair cost implications can be significant.

After the earthquake, partitions often needed full replacement throughout the building, along with repainting and redecorating—processes likely to be expensive and disruptive, especially given the post-earthquake scarcity of materials and labour. Initially, the damage appeared alarming to occupants, but within a few days, it became less concerning. Many occupants regarded the damage as a minor inconvenience, even likening it to an amusing addition to their surroundings. This shift in perception was driven by a desire to clean up and perform quick, ad hoc repairs to return to normal operations once the building was deemed safe. In Japan, this composed response can largely be attributed to effective earthquake safety education, awareness programmes, and frequent earthquake exposure. However, such behaviour may vary significantly in other countries due to differences in preparedness, information dissemination, and experience with seismic events. In some cases, building managers expressed concerns about NSE damage affecting the building's post-earthquake functionality. These issues primarily involved water-related damage, failures in essential mechanical services, and the dislocation or partial collapse of exterior cladding tiles. Water-related damage, such as burst pipes, led to flooding in specific areas, making it impossible for occupants to address the issue immediately. Instead, it required the replacement of damaged items, furnishings, and the piping system itself.

Given those observations in the data collected in Japan regarding the actual impact of NSEs, representation of NSE repair costs in analytical formulation may be an overstatement. Studies like Bonowitz [24] defined RSs as benchmarks for building recovery, including re-occupancy, functional recovery, or full recovery, each representing a compromise on complete restoration. To enhance downtime estimation and model the building recovery process, the REDi rating system by Almufti and Willford [25] introduced the concept that regaining functionality requires a sequence of key repair actions to gradually restore a building to a portion of its original functionality. Molina Hutt et al. [14] expanded on RS concepts with TREADS, defining five RSs ranging from "full recovery" to "stability," as outlined in Table 1.

Table 1. Recovery states by different building recovery frameworks

Recovery state	FEMA P-58	REDi	Molina Hutt et al. [14]
Full recovery (RS1)	x	x	x
Functional recovery (RS2)		x	x
Re-occupancy (RS3)		x	x
Shelter-in-place (RS4)			x
Stability (RS5)			x

To make economic loss estimates more realistic and in line with these observations following major earthquakes around the world, RSs should be integrated into loss assessments, with the targeted RS explicitly stated, and not implicitly assumed to be full recovery (RS1). This involves scrutinising the damageable inventory to determine which components are essential for achieving a specific RS. Each component's DS must be evaluated to decide its impact on the targeted RS. For instance, minor partition wall damage observed in Japan might not hinder "functional recovery" and could be excluded from the loss assessment. In contrast, damaged water pipes would directly affect functionality and must be included in the evaluation. This approach effectively narrows the damageable inventory to only what is essential for the desired RS.

4. Case study application

This case study analyses a four-storey reinforced concrete frame structure previously analysed by Shahnazaryan et al. [26] and designed according to Eurocode 8 provisions [27] for a site in L'Aquila,

Copyright © 2025 CroCEE
DOI: https://doi.org/10.5592/CO/3CroCEE.2025.31

Italy. The structure utilised concrete with a compressive strength of 25 MPa and steel with a yield strength of 415 MPa. It was designed as a regular structure, free of plan or elevation irregularities. The structure was modelled in OpenSees [28] as a single planar frame for simplicity, with floor masses lumped and nodes constrained horizontally to replicate rigid diaphragm behaviour. Nonlinear behaviour in beams and columns was represented using a concentrated plasticity approach, while elastic sections were assigned cracked section stiffness. Beam-column joints were treated as rigid, and capacity design principles ensured no shear mechanisms were included in the model. To characterise non-linear performance, the backbone curves for each structural element were derived from moment-curvature relationships. Plastic hinge lengths were calculated following Priestley et al. [29]. Vertical gravity loads were applied to a leaning column to account for P-Delta effects during nonlinear analysis. Additionally, Rayleigh damping corresponding to 5% of critical damping was implemented. The column bases were modelled as fixed supports to simplify boundary conditions.

Incremental dynamic analysis [30] was performed and losses were calculated using the storey loss function approach as outlined by Shahnazaryan et al. [5]. For the damageable inventory and the specific details regarding component quantities, repair costs, and fragility functions refer to the original study as they are not directly pertinent to the current discussion. To integrate the RS outlined in Table 1, each DS of the components were mapped to a corresponding RS. If a DS occurs, the building cannot be considered within that RS until repairs are completed. For instance, the most severe DS of structural elements, involving rebar fracturing and concrete spalling, was linked to ‘stability’ (RS5), as this condition would compromise the building’s structural stability. Similarly, the first two DSs of internal partitions were tied to ‘full recovery’ (RS1), as their light damage can be tolerated in other RSs but not when full recovery is required. During loss assessments, only the DSs relevant to the targeted RS were included. For instance, targeting ‘full recovery’ necessitates considering all DSs linked to RS1 or higher. Conversely, targeting ‘functional recovery’ would involve DSs linked to RS2 or higher, excluding DSs tied to less severe damage. This approach allows decision-makers to focus on specific damage scenarios and exclude tolerable DSs, refining the loss estimate according to recovery priorities.

The results of loss assessment are shown in Figure 6. When evaluating the ‘full recovery’ state, as commonly assumed in guidelines like FEMA P-58 [2] and in previous studies like O’Reilly et al. [22], the EAL was calculated as 1.42%, with the majority of costs being attributed to repairing NSEs. Although exact EAL varies depending on the specific structure, site conditions, and inventory composition, the result aligns with prior research emphasising the significant role NSEs play in overall losses. However, when the damageable inventory was adjusted to include only the essential repairs for achieving less stringent recovery states, such as 'functional recovery' or 're-occupancy,' the EAL dropped significantly to 0.83% and 0.58%, respectively. This represents a reduction of 42% and 60%, primarily because repairs to non-essential NSEs were excluded, reflecting the more flexible approach seen in Japan, where certain damage could be tolerated without impacting the building’s functionality.

The case study and discussions highlight an improved method for assessing losses, moving beyond the assumption of 'full recovery.' This refined approach offers decision-makers a clearer picture of the expected RS for a given EAL value, along with insights into the primary contributors to the EAL. This approach helps avoid unnecessary focus on non-essential components during retrofitting, preventing the waste of financial resources on repairs that may not be required.

The overarching focus remains on life safety, ensuring a sufficient margin against structural failure while also addressing direct economic losses. This approach is particularly relevant for commercial buildings with centralised ownership, which can prioritise essential repairs over non-critical ones. In contrast, in residential buildings, where ownership is fragmented, coordinating such decisions may be more challenging. Adopting a more measured approach, such as delaying repairs until post-disaster demand and prices have subsided, could help reduce costs. This strategy mirrors the decision-making in Japan, where minor NSE repairs were deferred until the next scheduled refurbishment, avoiding the inflated costs of immediate post-earthquake repairs.

Copyright © 2025 CroCEE
DOI: https://doi.org/10.5592/CO/3CroCEE.2025.31

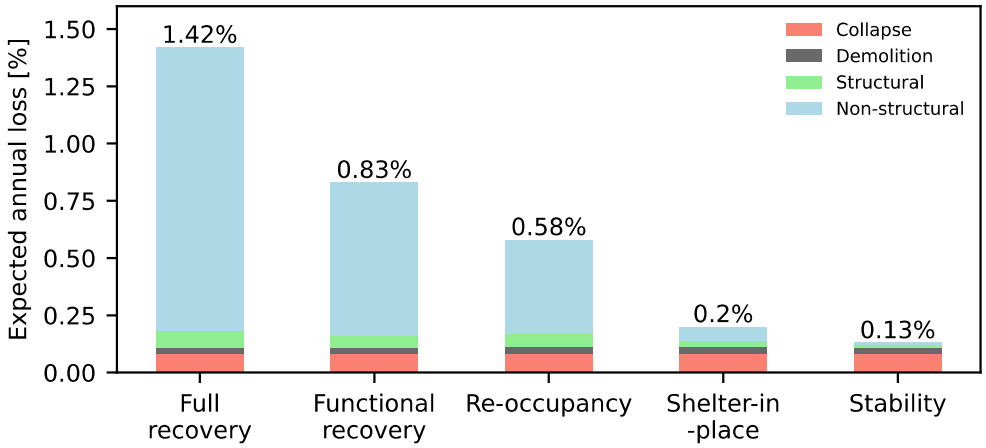


Figure 6. EAL results as a function of RS targeted.

5. Summary

This paper presented a practical tool for preparation of storey loss functions (SLFs) that uses a graphical user interface for ease of its application. This tool allows users to input specific building parameters and assess which components contribute most to economic losses, offering a detailed view of what repairs are necessary for achieving the desired recovery state. Using the presented tool key issues related to estimating damage to non-structural elements (NSEs) in earthquakes were addressed, along with the broader performance implications. Drawing on observations from commercial buildings affected by recent earthquakes in Japan, it offers valuable insights into the realities faced by building managers and owners, contrasting these with recent advancements in research. The findings from Japan underscore a practical approach to earthquake recovery, where functional recovery, rather than full recovery, is often deemed sufficient.

Analysis of interviews with commercial building owners and managers after recent Japanese earthquakes revealed that, in many instances, minor damage to NSEs was not immediately critical, particularly in the context of price and demand surges following major seismic events. This finding contrasts with existing literature, which stresses the significant role of NSEs in the economic impacts of earthquakes, including initial investment costs and potential financial losses, while emphasising the need for improved NSE performance to enhance overall resilience. However, what was considered critical in these cases were issues that directly affected the building's usability, particularly water damage from burst pipes.

These observations align with what is commonly referred to as "functional recovery" in the field, marking a shift from the traditional focus on full recovery to more practical, lower levels of recovery that still meet the needs of building owners and decision-makers. A case study was provided to show how this concept could be incorporated into loss assessments. The key takeaway from this analysis is that by prioritising functional recovery or re-occupancy instead of full recovery, the expected annual losses could be reduced by 42%–60%, as repairs to NSEs deemed non-essential could be postponed. This suggests that a more thoughtful evaluation of the relative importance of various building components should be incorporated into repair and retrofitting decisions, with the anticipated recovery level clearly defined in advance.

Acknowledgements

The work presented in this paper has been developed within the framework of the project “Dipartimenti di Eccellenza 2023-2027”, funded by the Italian Ministry of Education, University and Research at IUSS Pavia.

Copyright © 2025 CroCEE
DOI: https://doi.org/10.5592/CO/3CroCEE.2025.31

References

[1] C. A. Cornell and H. Krawinkler, "Progress and Challenges in Seismic Performance Assessment," *PEER Cent. News*, vol. 3, no. 2, pp. 1–2, 2000.

[2] FEMA, "Seismic performance assessment of buildings, volume 1 - methodology," *Fema P-58-1*, vol. 1, no. December 2018, p. 340, 2018, [Online]. Available: https://femap58.atcouncil.org/%0Ahttps://www.fema.gov/media-library/assets/documents/90380

[3] C. M. Ramirez and E. Miranda, "Building specific loss estimation methods & tools for simplified performance-based earthquake engineering," *Blume Cent. Rep.*, no. 171, 2009.

[4] A. Silva, L. Macedo, R. Monteiro, and J. M. Castro, "Earthquake-induced loss assessment of steel buildings designed to Eurocode 8," *Eng. Struct.*, vol. 208, no. April, pp. 6–7, 2020, doi: 10.1016/j.engstruct.2020.110244.

[5] D. Shahnazaryan, G. J. O'Reilly, and R. Monteiro, "Story loss functions for seismic design and assessment: Development of tools and application," *Earthq. Spectra*, p. 875529302110235, Jul. 2021, doi: 10.1177/87552930211023523.

[6] D. Ottonelli, S. Cattari, and S. Lagomarsino, "Displacement-Based Simplified Seismic Loss Assessment of Masonry Buildings," *J. Earthq. Eng.*, vol. 24, no. sup1, pp. 23–59, 2020, doi: 10.1080/13632469.2020.1755747.

[7] D. Cardone and G. Perrone, "Developing fragility curves and loss functions for masonry infill walls," *Earthq. Struct.*, vol. 9, no. 1, pp. 257–279, 2015, doi: 10.12989/eas.2015.9.1.257.

[8] A. Chiozzi and E. Miranda, "Fragility functions for masonry infill walls with in-plane loading," *Earthq. Eng. Struct. Dyn.*, vol. 46, no. 15, pp. 2831–2850, 2017, doi: 10.1002/eqe.2934.

[9] C. Del Gaudio, M. T. De Risi, P. Ricci, and G. M. Verderame, "Empirical drift-fragility functions and loss estimation for infills in reinforced concrete frames under seismic loading," *Bull. Earthq. Eng.*, vol. 17, no. 3, pp. 1285–1330, 2019, doi: 10.1007/s10518-018-0501-y.

[10] K. Sassun, T. J. Sullivan, P. Morandi, and D. Cardone, "Characterising the in-plane seismic performance of infill masonry," *Bull. New Zeal. Soc. Earthq. Eng.*, vol. 49, no. 1, pp. 98–115, 2016, doi: 10.5459/bnzsee.49.1.98-115.

[11] H. Aslani and E. Miranda, "Fragility assessment of slab-column connections in existing non-ductile reinforced concrete buildings," *Earthq. Spectra*, vol. 31, no. 1, pp. 159–177, 2005, doi: 10.1142/S1363246905002262.

[12] G. Perrone, D. Cardone, G. J. O'Reilly, and T. J. Sullivan, "Developing a Direct Approach for Estimating Expected Annual Losses of Italian Buildings," *J. Earthq. Eng.*, vol. 00, no. 00, pp. 1–32, 2019, doi: 10.1080/13632469.2019.1657988.

[13] G. J. O'Reilly *et al.*, "On the fragility of non-structural elements in loss and recovery: Field observations from Japan," *Earthq. Eng. Struct. Dyn.*, vol. 53, no. 3, pp. 1125–1144, Mar. 2024, doi: 10.1002/eqe.4066.

[14] C. Molina Hutt, T. Vahanvaty, and P. Kourehpaz, "An analytical framework to assess earthquake-induced downtime and model recovery of buildings," *Earthq. Spectra*, vol. 38, no. 2, pp. 1283–1320, May 2022, doi: 10.1177/87552930211060856.

[15] A. N. Papadopoulos, D. Vamvatsikos, and A. Kazantzi, "Development and application of FEMA P-58 compatible story loss functions," *Earthq. Spectra*, vol. 35, no. 1, pp. 39–60, Feb. 2019, doi: 10.1193/020518EQS033M.

[16] FEMA, "FEMA P58-3. Seismic Performance Assessment of Buildings Volume 3 - Performance Assessment Calculation Tool (PACT)," Washington, D.C., 2012.

[17] G. J. O'Reilly and D. Shahnazaryan, "On the utility of story loss functions for regional seismic vulnerability modeling and risk assessment," *Earthq. Spectra*, vol. 40, no. 3, pp. 1933–1955, Aug. 2024, doi: 10.1177/87552930241245940.

[18] Weibull W., *The Statistical Theory of the Strength of Materials*, 151st ed. Stockholm: Generalstabens Litografiska Anstalts Förlag, 1939.

Copyright © 2025 CroCEE
DOI: https://doi.org/10.5592/CO/3CroCEE.2025.31

[19] Engle HM, "The earthquake resistance of buildings from the underwriters' point of view," *Bull Seism. Soc Am*, vol. 19, no. 2, pp. 86–95, 1929.

[20] S. Taghavi and E. Miranda, "Response Assessment of Nonstructural Building Elements," *Rep. PEER 2003/05*, p. 96, 2003.

[21] R. P. Dhakal *et al.*, "Seismic performance of non-structural components and contents in buildings: an overview of NZ research," *Earthq. Eng. Eng. Vib.*, vol. 15, no. 1, pp. 1–17, Mar. 2016, doi: 10.1007/s11803-016-0301-9.

[22] G. J. O'Reilly *et al.*, "System Identification and Seismic Assessment Modeling Implications for Italian School Buildings," *J. Perform. Constr. Facil.*, vol. 33, no. 1, p. 04018089, Feb. 2019, doi: 10.1061/(ASCE)CF.1943-5509.0001237.

[23] K. Kanda, M. Nakashima, Y. Suzuki, and S. Ogasawara, "'q-NAVI': A case of market-based implementation of structural health monitoring in Japan," *Earthq. Spectra*, vol. 37, no. 1, pp. 160–179, Feb. 2021, doi: 10.1177/8755293020935884.

[24] Bonowitz D, *Resilience Criteria for Seismic Evaluation of Existing Building*. 2011.

[25] I. Almufti and M. Willford, *REDi™ Rating System: Resilience-based Earthquake Design Initiative for the Next Generation of Buildings*. 2013.

[26] D. Shahnazaryan, G. J. O'Reilly, and R. Monteiro, "On the seismic loss estimation of integrated performance-based designed buildings," *Earthq. Eng. Struct. Dyn.*, no. January, pp. 1–25, 2022, doi: 10.1002/eqe.3638.

[27] CEN, "Eurocode 8: Design of Structures for Earthquake Resistance - Part 1: General Rules, Seismic Actions and Rules for Buildings (EN 1998-1:2004)," Brussels, Belgium, Comité Européen de Normalisation, 2004.

[28] F. McKenna, M. H. Scott, and G. L. Fenves, "Nonlinear Finite-Element Analysis Software Architecture Using Object Composition," *J. Comput. Civ. Eng.*, vol. 24, no. 1, pp. 95–107, 2010, doi: 10.1061/(asce)cp.1943-5487.0000002.

[29] M. J. N. Priestley, G. M. Calvi, and M. J. Kowalsky, "Displacement based seismic design of structures," 2007.

[30] D. Vamvatsikos and C. A. Cornell, "Incremental dynamic analysis," *Earthq. Eng. Struct. Dyn.*, vol. 31, no. 3, pp. 491–514, Mar. 2002, doi: 10.1002/eqe.141.

Proceedings of the 3rd Croatian Conference on Earthquake Engineering - 3CroCEE
19–22 March 2025, Split, Croatia
Copyright © 2025 CroCEE
DOI: https://doi.org/10.5592/CO/3CroCEE.2025.40

INTEGRATING SEISMIC RISK ASSESSMENT INTO SPATIAL PLANNING: CASE REPUBLIC OF NORTH MACEDONIA

Elena Dumova - Jovanoska [(1)], Kristina Milkova [(2)], Sergey Churilov[(3)] Simona Bogoevska[(4)]

[(1)] prof., Chair of Theory of Structures and Computational Analysis, Department of Structural Analysis and Earthquake Engineering, Faculty of Civil Engineering Skopje, N. Macedonia, dumova@gf.ukim.edu.mk
[(2)] Asst. prof., Chair of Theory of Structures and Computational Analysis, Department of Structural Analysis and Earthquake Engineering, Faculty of Civil Engineering Skopje, N. Macedonia, milkova@gf.ukim.edu.mk,
[(3)] prof., Chair of Theory of Structures and Computational Analysis, Department of Structural Analysis and Earthquake Engineering, Faculty of Civil Engineering Skopje, N. Macedonia, curilov@gf.ukim.edu.mk
[(4)] Assoc. prof., Chair of Theory of Structures and Computational Analysis, Department of Structural Analysis and Earthquake Engineering, Faculty of Civil Engineering Skopje, N. Macedonia, simona.bogoevska@gf.ukim.edu.mk

Abstract

Assessing earthquake risk in regions characterized with moderate to high seismic hazard, such as parts of Republic of North Macedonia, is essential for the development of effective risk management and mitigation strategies [1]. Comprehensive risk assessment enables prediction on most likely locations of high-intensity earthquakes and what their potential impacts might be. In the framework of the Study for Natural and technical risks in the Republic of North Macedonia [2], as one of the background documents for the preparation of the Spatial plan of the country for the period 2021-2040, seismic Risk maps have been created.

The process of assessing earthquake risk involves analyzing three critical components: hazard, exposure, and vulnerability of the exposed structures. A detailed seismic hazard assessment for North Macedonia has been conducted using data on historical earthquake activity, earth crust models, and active fault characterization leading to the development of a seismic hazard map [3]. To evaluate the exposure of objects and people in the Republic of North Macedonia, data from the State Statistical Office, including information from the 2021 population census, households, and dwellings, were utilized. Three authentic research studies were selected as key baseline references, providing vulnerability curves and damage matrices for the most common types of structural systems in the country. Consequently, four sets of vulnerability curves (damage matrices) have been selected for the following structural types: structures constructed with unreinforced masonry prior to 1960, reinforced concrete structures built between 1971 and 1981, reinforced concrete structures with a height of up to 10 stories, built from 1981 to the present, reinforced concrete structures exceeding 10 stories in height, built from 1981 to the present.

Using a methodology that integrates hazard maps, vulnerability curves for the selected structural types, and estimated structural damage, seismic risk maps for Republic of North Macedonia have been developed. The proposed methodology connects the region – specific topologies of buildings and their vulnerability on one hand, and region – specific hazard map on the other.

Keywords: spatial plan, risk analysis, hazard, vulnerability, exposure

1. Introduction

The global community is increasingly confronted with a diverse range of risks, including those arising from natural disasters, technological accidents, climate change, overconsumption of natural resources, poor spatial planning and management, risks associated with modern technologies and processes, and risks related to human activities. Analyzing risks is a complex task and is difficult to predict, with consequences that can be vast and severe [4][5].

To address these challenges in a structured and effective manner, ongoing efforts are being made to enhance capacities and capabilities for the integrated management of contemporary risks, both globally and nationally. The primary goal is to reduce these risks to an acceptable level, preventing them from escalating into crises or disasters [6][7].

Copyright © 2025 CroCEE
DOI: https://doi.org/10.5592/CO/3CroCEE.2025.40

The purpose of this paper is to present the findings from the Study on Natural and Technical Risks in the Republic of North Macedonia, which serves as one of the foundational documents for the preparation of the country's Spatial Plan for the period 2021-2040 [2].

2. Seismic risk assessment

Each year, over one million earthquakes are recorded worldwide. Among the catastrophic events that affect urban areas, high-intensity earthquakes stand out as some of the most destructive. Despite being less frequent than other disasters, these events are highly unpredictable and can trigger secondary natural disasters, amplifying their impact. As a result, earthquakes often lead to severe material damage and significant loss of life [8].

In regions with moderate to high seismic hazard, such as parts of North Macedonia, assessing earthquake risk is essential for effective management and mitigation efforts. Comprehensive risk assessments allow for the identification of areas most likely to experience high-intensity earthquakes and help anticipate their consequences. Modern strategies to reduce earthquake risks prioritize identifying and addressing risks through proactive management. The primary goal is to minimize destruction and safeguard lives. While natural hazards like earthquakes cannot be prevented or reduced, engineering solutions can significantly mitigate their impact on buildings and infrastructure [9].

Earthquake risk assessment typically involves analyzing three critical components: hazard, exposure, and vulnerability, as depicted in Figure 1. By thoroughly evaluating these factors, experts can gain valuable insights into seismic risks in a given region and devise targeted strategies to reduce and manage them effectively.

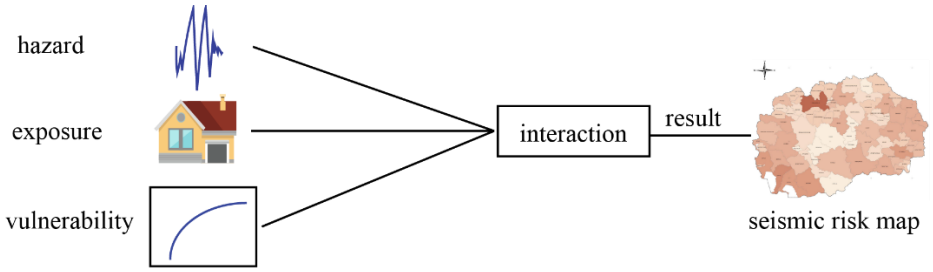


Figure 1. Concept of seismic risk determination

2.1. Seismic hazard assessment

A detailed seismic hazard assessment has been conducted for the territory of Republic of North Macedonia, incorporating data on historical earthquake activity (as shown on Figure 2), crustal models, and the characterization of active faults [10] [11].

The procedure applied based on the application of a complex Poisson-Gamma distribution. This approach allows for the introduction of uncertainties in the time-dependent and variable seismicity. In seismic hazard analyses based on this approach, the parameters of seismic hazard that are assigned to a specific area or local region (which can be referred to as a structural seismic source) are of particular importance. The seismic hazard parameters utilized are: Maximum regional magnitude (the seismic source is a specific structural unit or area with a defined seismic activity), The mean value of the activity coefficient λ within the polygon or seismic source, The coefficient b from the Gutenberg-Richter distribution of earthquake magnitude frequency within the seismic source area [12]. For each surface source, predefined coefficients are introduced to estimate seismic activity, characteristics of acceleration attenuation, and the geographical distribution of epicenters. The final processing of the input data was performed using the R-Crisis software package, where the seismic hazard analysis is based on the full application of the probabilistic approach (PSHA). As a final product, a seismic hazard map (maximum ground acceleration) for a return period of 475 years at national level has been produced [2].

Copyright © 2025 CroCEE
DOI: https://doi.org/10.5592/CO/3CroCEE.2025.40

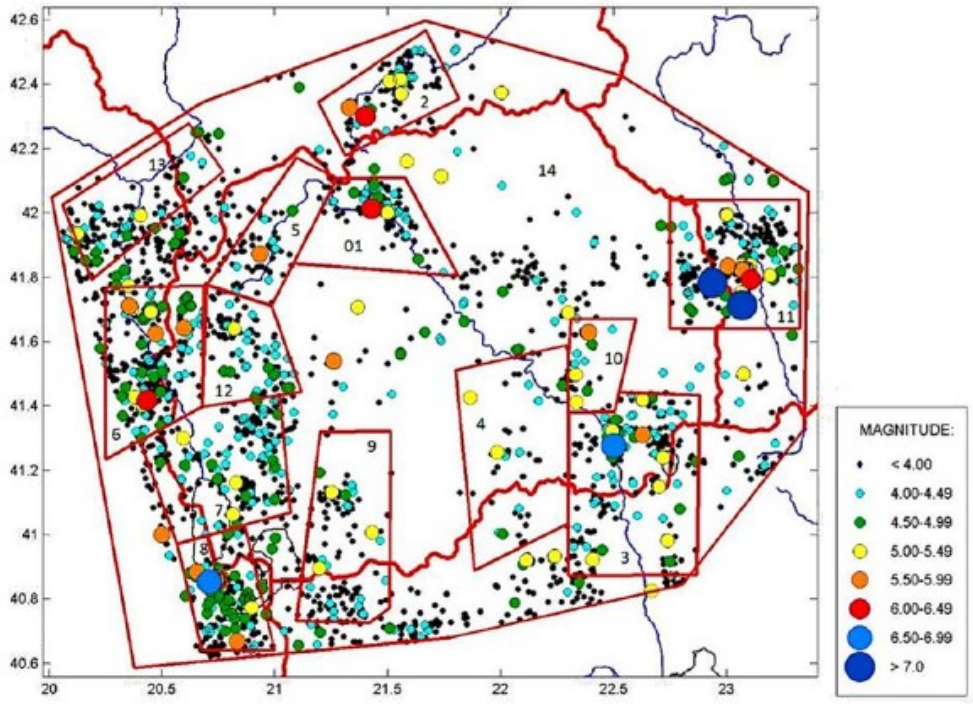


Figure 2. Map of earthquakes in North Macedonia (538-2020) [2]

2.2. Exposure

To assess the exposure of people and structures in the Republic of North Macedonia, data from the State Statistical Office, including the 2021 population census, household, and dwelling data, were utilized. This dataset encompasses all 80 municipalities in the country and includes information such as:

- **Total population**,
- **Year of construction** (categorized as: before 1919; 1919–1945; 1946–1960; 1961–1970; 1971–1980; 1981–1990; 1991–2000; 2001–2010; 2011–2015; 2016 and later; and unknown),
- **Number of floors** (ground floor, G+1, G+3, G+4, G+5–9, G+10–19, G+20 or more, and unknown),
- **Structural materials of buildings** (concrete and reinforced concrete, concrete blocks, steel, bricks, stone, prefabricated wood panels, adobe, and unknown).

Buildings in each municipality were classified based on attributes such as structural materials, year of construction, and number of floors. The classification was initially determined by the seismic design codes under which the buildings were constructed. This classification was performed for every municipality, and the total built-up area was calculated and distributed according to these attributes. The analysis revealed that Skopje has a substantially larger built-up area and higher population density compared to other regions of the country.

The population distribution within buildings is critical for accurate exposure assessments. This includes not only the total population but also how people are distributed across municipalities and structures, categorized by attributes like year of construction, structural material, and number of floors.

Figures 3 and 4 provide insights into the total area of all structures and population distribution, respectively, based on structural materials and the seismic design codes under which the buildings were constructed. The majority of buildings in North Macedonia are made of concrete and reinforced concrete and were constructed according to current codes.

Copyright © 2025 CroCEE
DOI: https://doi.org/10.5592/CO/3CroCEE.2025.40

The exposure maps highlight that an earthquake near Skopje would likely result in far greater impacts compared to other municipalities, even for earthquakes of similar intensity. However, the resilience of the buildings, particularly their capacity to withstand damage without collapsing, is a critical factor in assessing potential hazards.

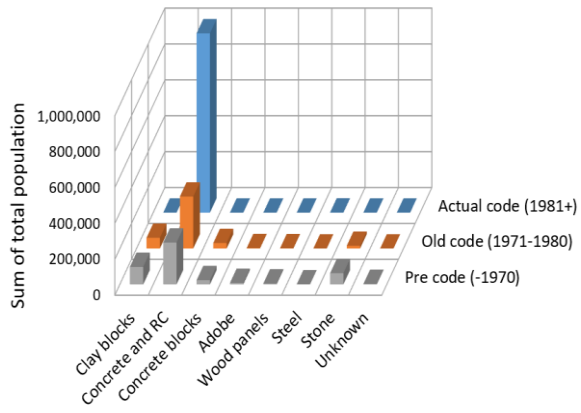


Figure 3. Total population living in buildings from different structural materials and applied codes [2]

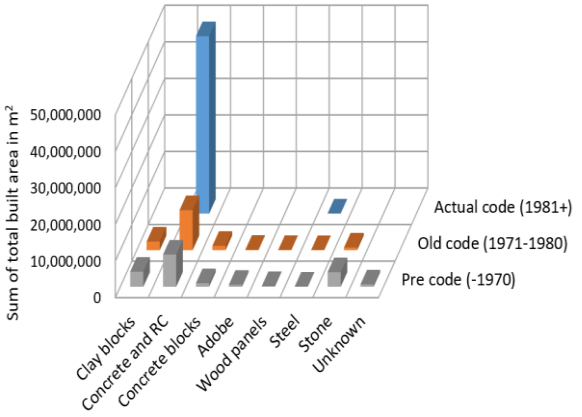


Figure 4. Total built area by structural materials and applied codes [2]

2.3. Vulnerability

The vulnerability of buildings is assessed by analyzing the correlation between earthquake intensity and the likelihood of damage [13]. Different types of buildings, categorized based on predefined attributes, have varying capacities to resist horizontal seismic forces. For example, structures built before 1960 using unreinforced masonry in areas with high seismic hazard are significantly more susceptible to earthquake damage compared to buildings constructed under modern seismic codes.

A detailed analysis of regional research identified three key studies that define vulnerability curves and damage matrices for the most dominant structural systems in the country. Based on these findings and available census exposure data, four sets of vulnerability curves (damage matrices) have been selected for use with the chosen structural types:

- **Unreinforced masonry structures constructed prior to 1960**, Figure 5 [14],
- **Reinforced concrete structures built between 1971 and 1981**, Figure 6[15],
- **Reinforced concrete structures up to 10 stories tall, built from 1981 to the present**, Figure 7 [16],
- **Reinforced concrete structures over 10 stories tall, built from 1981 to the present**, Figure 8 [16].

Fragility curves represent the probability of exceeding specific damage levels for a given earthquake intensity. Defining these curves requires definition of damage indicators and thresholds. The damage levels are generally derived from the computed capacity curve for each construction type and encompass several thresholds, ranging from no damage to total collapse. Due to a lack of information for some damage thresholds, an interpolation process was applied to generate fragility curves for reinforced concrete structures built between 1971 and 1981. These curves were then converted into damage matrices to obtain discrete values, which can be utilized in subsequent steps to define the risk level.

Copyright © 2025 CroCEE
DOI: https://doi.org/10.5592/CO/3CroCEE.2025.40

Table 1. Damage probability matrix for RC frame structures lower than 10 stories [16]

	Damage probability matrix						
	Damage states	Damage index	VII	VIII	IX	X	XI
1	None	<0.05	100.0	99.09	44.37	8.57	1.56
2	Minor	0.05–0.1	**0.00**	0.91	51.65	13.77	2.03
3	Moderate	0.1–0.25	**0.00**	**0.00**	3.97	48.53	8.56
4	Severe	0.25–0.5	**0.00**	**0.00**	**0.00**	28.79	25.32
5	Collapse	>0.5	**0.00**	**0.00**	**0.00**	0.34	62.53

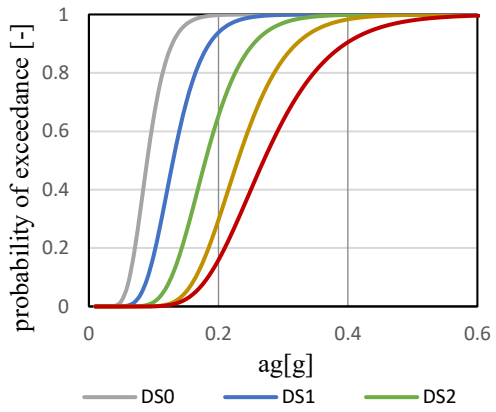


Figure 5. Vulnerability curves for unreinforced masonry structures [15]

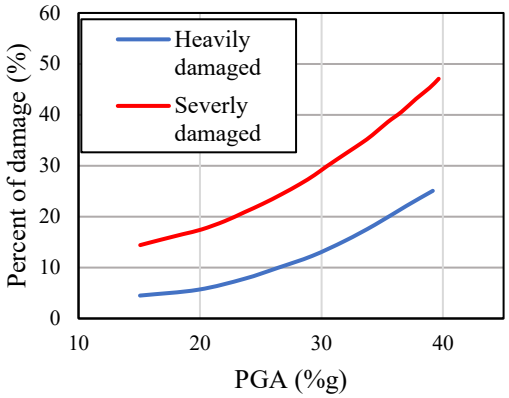


Figure 6. Vulnerability curves for reinforced concrete structures constructed between 1971 and 1981 [14]

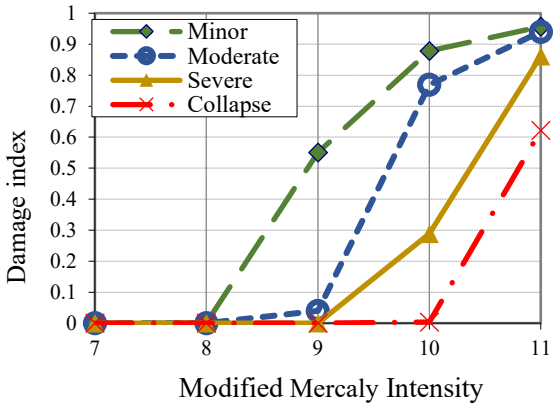


Figure 7. Vulnerability curves for reinforced concrete structures with a height of up to 10 stories [16]

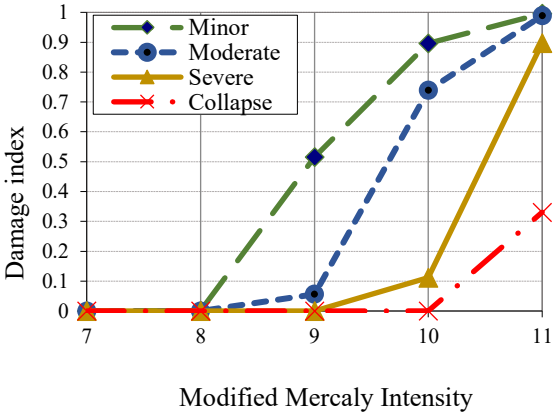


Figure 8. Vulnerability curves for reinforced concrete structures exceeding 10 stories in height [16]

2.4. Methodology for calculation of risk map

The seismic risk calculation, based on the expected damage built area, was conducted at the municipal level. Census data, including population and building area categorized by type, were processed for each municipality. Hazard maps were transformed into municipality-specific maps, allowing for the determination of the maximum expected earthquake intensity for each municipality. This approach enabled the creation of an earthquake scenario for maximum ground acceleration for a return period of 475 years.

Using a methodology that integrates hazard maps, fragility curves for selected structural types, and estimates of structural damage based on damage factors and states (as outlined by Whitman et al. [17]), presented in Table 2, seismic risk maps in terms of expected damaged area for North Macedonia have

Copyright © 2025 CroCEE
DOI: https://doi.org/10.5592/CO/3CroCEE.2025.40

been developed. These maps illustrate the expected extent of damage for the most severe earthquake scenario in each municipality (Figure 9).

Table 2. Correlation - damage level and states Whitman et al. [17]

Damage level	Threshold values (%)
Minor	3.5-7.5
Moderate	7.5-20
Severe	20-65
Collapse	65-100

3. Conclusion

The proper selection and authenticity of all data utilized in the methodology is critical point for ensuring reliable results in seismic risk assessments. This includes the use of accurate data from the census, which provides essential information about the distribution and characteristics of the population and infrastructure. Local hazard calculations, based on historical earthquake activity, earth crust models, and active fault characterization for the country, are critical in determining the seismic risks specific to each region. The use of accurate vulnerability curves, created for specific construction types in North Macedonia, is also a key aspect in defining the seismic risk map. Only by ensuring the authenticity and precision of these data sources a robust and accurate seismic risk map that truly reflects the potential risks and informs effective risk management strategies can be developed at a national level. The presented map is a valuable tool for local governments in preparing strategic documents to define seismic risk mitigation policies.

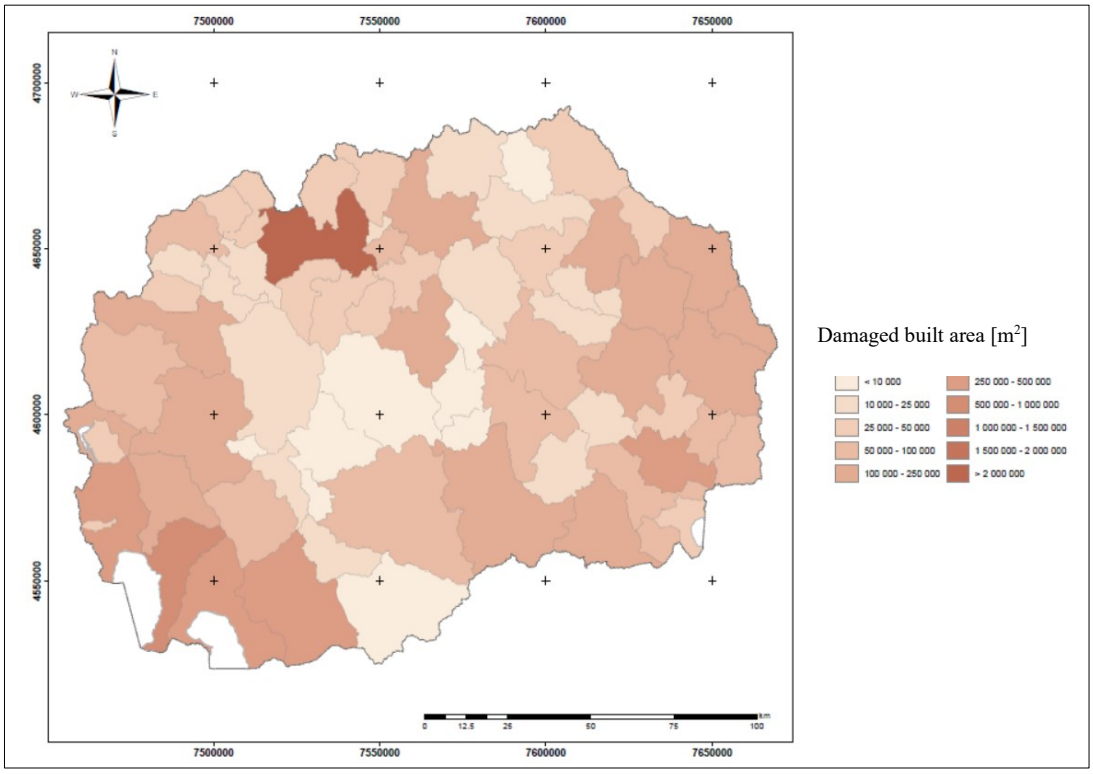


Figure 9. Earthquake risk map for seismic return period of 475 years by municipalities and the city of Skopje (damaged built area) [2]

Copyright © 2025 CroCEE
DOI: https://doi.org/10.5592/CO/3CroCEE.2025.40

References

[1] Milkova, K., Butenweg, C., & Dumova-Jovanoska, E. (2020). Methodology for Development of Seismic Vulnerability Curves for Existing Unreinforced Masonry buildings. In 17th World Conference on Earthquake Engineering, Sendai, Japan.

[2] Dumova – Jovanoska et al, (2024). Report on natural and technical risks in the Republic of North Macedonia.

[3] Dumova-Jovanoska, E., & Milkova, K. (2022). NDSHA-based vulnerability evaluation of precode buildings in Republic of North Macedonia: novel experiences. In Earthquakes and Sustainable Infrastructure (pp. 455-474). Elsevier.

[4] Tesfamariam, S., & Goda, K. (Eds.). (2013). Handbook of seismic risk analysis and management of civil infrastructure systems. Elsevier.

[5] Baker, J., Bradley, B., & Stafford, P. (2021). Seismic hazard and risk analysis. Cambridge University Press.

[6] Sendai Framework for Disaster Risk Reduction 2015-2030., UNISDR/GE/2015-ICLUX EN5000 1st Edition

[7] ISO 31000:2018, Risk Management-Guidelines, https://www.iso.org/standard/65694.html

[8] Crowley, H., Dabbeek, J., Despotaki, V., Rodrigues, D., Martins, L., Silva, V., Romão, X., Pereira, N., Weatherill, G., Danciu, L. (2021). European Seismic Risk Model (ESRM20). EFEHR Technical Report 002, V1.0.0, https://doi.org/10.7414/EUC-EFEHR-TR002-ESRM20.

[9] Milkova, K., Butenweg, C., & Dumova-Jovanoska, E. (2020). Methodology for Development of Seismic Vulnerability Curves for Existing Unreinforced Masonry buildings. In 17th World Conference on Earthquake Engineering, Sendai, Japan.

[10] Jordanovski, Lj., Pekevski, L., Chejkovska, V., Chernih, D., Hristovski, B., and Vasilevski, N. (1998). Basic characteristics of seismology on the territory of the Republic of Macedonia. Seismological Observatory of the Faculty of Natural Sciences and Mathematics, Ss. Cyril and Methodius University in Skopje.

[11] Arsovski, M. and Dumurdžanov, N. (1984). Recent findings of the structure of Pelagonian horst anticlinorium and its relation with the Rhodopean and Serbo-Macedonian massif. GeologicaMacedonica, 1, 3-25.

[12] Kijko, A., Vermeulen, P. J., & Smit, A. (2022). Estimation techniques for seismic recurrence parameters for incomplete catalogues. Surveys in Geophysics, 43(2), 597-617.

[13] Crowley, H., Pinho, R., & Bommer, J. J. (2004). A probabilistic displacement-based vulnerability assessment procedure for earthquake loss estimation. Bulletin of Earthquake Engineering, 2, 173-219.

[14] Nochevski, N. (1993). Definition of empirical and theoretical models for definition of vulnerability level of high-rise structures. Doctoral thesis. Ss. Cyril and Methodius University in Skopje, Institute of Earthquake Engineering and Engineering Seismology (in Macedonian).

[15] Milkova, K. (2021). Methodology for development of seismic vulnerability curves for existing unreinforced masonry buildings. Doctoral thesis, Ss. Cyril and Methodius University in Skopje, Faculty of Civil Engineering-Skopje.

[16] Dumova-Jovanoska, E. (2000) Fragility Curves for Reinforced Concrete Structures in Skopje (Macedonia) Region. Soil Dynamics and 7261(00)00017-8.

[17] Whitman, R. V., Biggs, J. M., Brennan III, J., Cornell, C. A., De Neufville, R., Vanmarcke, E. H. (1974). Methodology and pilot application – Seismic design decision analysis, Report R74-15, Department of Civil Engineering, Massachusetts Institute of Technology.

Proceedings of the 3rd Croatian Conference on Earthquake Engineering - 3CroCEE
19–22 March 2025, Split, Croatia
Copyright © 2025 CroCEE
DOI: https://doi.org/10.5592/CO/3CroCEE.2025.53

A REVIEW OF EXISTING SEISMIC VULNERABILITY FUNCTIONS FOR BUILDINGS IN THE BALKAN REGION

Kristina Milkova [(1)], Marta Šavor Novak [(2)], Marko Marinkovic [(3)], Elena Dumova - Jovanoska[(4)]

[(1)] *Asst. prof., Chair of Theory of Structures and Computational Analysis, Department of Structural Analysis and Earthquake Engineering, Faculty of Civil Engineering Skopje, N. Macedonia, milkova@gf.ukim.edu.mk,*
[(2)] *Assoc. prof., Faculty of Civil Engineering, Department of Engineering Mechanics, University of Zagreb, Croatia, msavor@grad.hr*
[(3)] *Asst. prof., Chair of Engineering Mechanics and Theory of Structures, Faculty of Civil Engineering, University of Belgrade, Serbia; mmarinkovic@grf.bg.ac.rs*
[(4)] *prof., Chair of Theory of Structures and Computational Analysis, Department of Structural Analysis and Earthquake Engineering, Faculty of Civil Engineering Skopje, N. Macedonia, dumova@gf.ukim.edu.mk*

Abstract

This paper provides detailed investigation of the methodologies developed for seismic vulnerability assessment in the area. Empirical, analytical, and hybrid approaches that have been regionally developed and applied are summarized and their similarities and differences are discussed. Having in mind the parallels in existing structural archetypes in the region (N. Macedonia, Serbia, Bosnia and Herzegovina, Croatia, Romania, Greece), the investigation focuses on the most common types: masonry and reinforced concrete structures. A reliable assessment of seismic hazard is essential for effective vulnerability evaluation, and the relevant published methodologies are also summarized. Additionally, the developed risk assessment methodologies are discussed. This overview is expected to guide research at institutions throughout the region and encourage enhanced collaboration among experts in seismic vulnerability.

Keywords: vulnerability functions, Balkan region, hazard, analytical, empirical, hybrid

1. Introduction

The process of seismic risk assessment involves analyzing and precisely determining three key elements: hazard, exposure, and vulnerability. **Hazard** refers to the probability and characteristics of earthquake events in a given area. This includes evaluating factors such as seismic activity, fault lines, historical earthquake data, and seismic hazard analysis to assess the potential intensity and frequency of earthquakes. **Exposure** relates to the assets, population, and infrastructure at risk within the affected region. This involves identifying and quantifying elements such as buildings, critical infrastructure, cultural heritage sites, and the number of people exposed to potential earthquake hazards. **Vulnerability** focuses on the susceptibility of the exposed elements to damage or loss due to an earthquake. This requires evaluating the structural integrity of buildings, the resilience of infrastructure, and the population's preparedness to withstand and recover from an earthquake event.

By thoroughly examining these three factors, experts can gain a comprehensive understanding of the seismic risk in a specific region and develop appropriate strategies for risk reduction and management. In the context of developing a national seismic risk mitigation strategy, the availability of fragility functions for locally defined structural prototypes plays a crucial role. Fragility functions are defined as the probability of exceeding a certain level of damage for a given ground motion intensity, and they serve as a foundation for estimating seismic losses. A multidisciplinary approach, with expertise in hazard and risk estimation, is required for implementing a comprehensive seismic vulnerability evaluation procedure for buildings. The wide range of applications for existing methodologies allows for numerous proposed approaches and categorizations. The available resources and knowledge in construction, as well as local traditions and experiences across different regions, have led to the development of various building typologies since each region can be characterized by its unique buildings, built with specific materials and techniques.

Copyright © 2025 CroCEE
DOI: https://doi.org/10.5592/CO/3CroCEE.2025.53

2. Seismic hazard of Balkan region

The Balkan region is tectonically active, located at the intersection of three major plates: Eurasian, African, and Anatolian, which are further subdivided into smaller plates. The region's geodynamics are influenced by active tectonic processes in the Eastern Mediterranean, including the collision of the Adriatic (Apulian) microplate with the Dinarides, the subduction of the Ionian and Levantine oceanic lithospheres beneath the Hellenic arc-and-trench system, and the collision between Eurasia and Arabia, which drives the westward movement of Anatolia along the North Anatolian dextral strike-slip fault. These processes cause frequent, although generally minor, earthquakes [1].

The most destructive earthquake in the Balkans over the past century occurred in Skopje in July 1963, claiming over a thousand lives and injuring more than 4,000 people [2]. Recent earthquakes in North Macedonia, Albania, and Croatia emphasize the ongoing need for seismic design in new structures and seismic risk assessment of existing ones. The most recent major earthquake in North Macedonia occurred on September 10, 2016, with a magnitude of 5.2 at a depth of 10 km, 2 km northeast of Skopje [3]. The event injured over 50 people and caused significant damage to buildings.

The Croatian coast experiences a range of small to large earthquakes. In 2020, Croatia was struck by a series of significant earthquakes, particularly in the northern part of the country near Zagreb. That year, a magnitude 6.4 earthquake struck Petrinja on December 29, 2020, drawing attention from seismologists. Earlier, in March 2020, Zagreb experienced a 5.4 magnitude earthquake that caused considerable damage and one fatality [4].

Figure 1 illustrates earthquakes with a magnitude greater than 5.5 that have occurred from 1900 to the present.



Figure 1. Map of earthquakes 1900 – 2025, M>5.5, USGS

In Bosnia and Herzegovina, the most significant recent earthquake took place on April 22, 2022. A magnitude 5.7 earthquake struck 42 kilometers southeast of Mostar, causing one fatality and substantial property damage. The earthquake was also felt along the Croatian coast, in Montenegro, and further southeast in Albania [5].

While earthquakes are frequent, significant ones are rare but still happen and can cause minor damage to sturdy homes in Serbia. A notable recent earthquake, with a magnitude of 5.4, struck central Serbia near Kraljevo on November 3, 2010. The shaking was felt throughout the country, including the capital, Belgrade, and in neighboring countries. Many buildings were also damaged, with over 1,500 being deemed unsafe for occupancy [6].

Romania ranks as one of the most affected countries in Europe in terms of the number of fatalities caused by earthquake disasters in the 20th century, including deaths from single events. One significant

Copyright © 2025 CroCEE
DOI: https://doi.org/10.5592/CO/3CroCEE.2025.53

event was the March 4, 1977 earthquake, which resulted in 1,578 deaths, of which 90% occurred in Bucharest [7].

Greece often hosts large magnitude earthquakes, whilst a moderate or small magnitude earthquake is felt every 2-3 days on average. Although most of these earthquakes with low-intensity, a few cases have been recorded as devastating for the human environment or for life loss (e.g. the 1881 Chios, 1953 Kefalonia, 1999 Athens earthquakes). The Great Thessaloniki earthquake occurred on 20 June at 23:03 local time. The shock registered 6.2 on the moment magnitude scale, had a maximum Mercalli intensity of IX (Violent), and was felt throughout northern Greece, former Yugoslavia and Bulgaria [8].

One of the most recent significant studies addressing specifically the seismic hazard in the Western Balkans was conducted as part of the Harmonization of Seismic Hazard Maps in the Western Balkan Countries Project (BSHAP) [9]. The main outcome of BSHAP is the creation of new probabilistic seismic hazard maps for the Western Balkans, developed using the smoothed-gridded seismicity approach. The results are presented in terms of peak horizontal acceleration (PGA) for 95- and 475-year return periods, in accordance with Eurocode 8 requirements.

Considering the seismic hazard in the region and the relatively similar construction practices in the past, it would be highly valuable to establish a database that links structural typologies to vulnerability functions. This would enhance preparedness for future seismic events across a broader area.

3. Existing seismic vulnerability functions in the Balkan Region

This paper's main aim is to present an overview of the seismic vulnerability studies conducted in the Balkan region. Given the shared construction practices across the countries in the region, the objective is to outline the current state of knowledge, which can serve as a foundation for future risk assessments. The classification of seismic vulnerability analysis methods is based on Calvi [10]. Several studies from North Macedonia, Croatia, Serbia, Bosnia and Herzegovina, Romania, and Greece are reviewed, with key findings related to seismic hazard, building types, and the methods used in these studies summarized.

3.1. Republic of N. Macedonia

Researchers in the Republic of North Macedonia have been closely following global advancements in this field since its inception. Specifically, Nochevski, in his PhD research under the supervision of Petrovski, proposed an original methodology for the empirical and analytical calculation of vulnerability curves. Two representative types of **reinforced concrete frames** were analyzed. Peak acceleration of **selected earthquake records** (Ulcinj, Bar, El Centro) have been varied from very low levels up to 0.40g. The integral structure is represented by shear type model. **Vulnerability curves** for structural and nonstructural elements were developed. [11]

Dumova– Jovanoska in her Phd research proposes an analytical methodology for expressing the relationship damage– earthquake intensity in the forms of vulnerability curves and damage probability matrices. A set of **240 synthetic time histories** were generated for local seismic hazard representation. The proposed method is applied on **reinforced concrete frame-wall structures (lower and higher than 10 stories)**. Two sets of **fragility curves** and damage probability matrices were defined. [12]

Within the framework of the RISK-UE Project [13], an approach was proposed for developing the seismic vulnerability of **reinforced concrete structures**, which are the dominant new residential building type in the Republic of North Macedonia. Databases from the **1979 Montenegro earthquake and the 1994 Bitola earthquake** were used as seismic input for the nonlinear dynamic time-history analysis of a 1D shear-type lumped mass model, which was employed to simulate the RC structures. Five damage grades were adopted, and capacity and fragility curves were generated.

Twenty individual **reinforced concrete residential str**uctures for family housing and collective residential buildings were considered, divided into 3 categories according to number of stories in the frame of the research of Jakupi [14]. Nonlinear static “pushover” analysis as a procedure for assessment

Copyright © 2025 CroCEE
DOI: https://doi.org/10.5592/CO/3CroCEE.2025.53

of the seismic response of reinforced concrete buildings was carried out and values of the **vulnerability indices** of the buildings are obtained within the limits of 0,2 to 0,4.

In the research of Milkova, **Scenario-based Neo Deterministic Seismic Hazard Approach** [15] is used. Existing **masonry structures** are selected, each of them chosen to represent a class of similar buildings. The non - linear capacity curves of a single wall are calculated based on the shear and bending resistances according to EC. Sets of **fragility curves** for class of structures were developed [16]

Volchev et al [17] considers six **reinforced concrete three-bay frames** with varying numbers of stories (2, 3, 5, 7, 10, and 13 stories) and two types of infill (strong and weak). Nonlinear dynamic analysis for the defined mathematical models is performed for 14 earthquake records. **Five series of vulnerability curves** are obtained, namely: a series for structures with less than 6 stories, a series for structures with more than 6 stories, a series for structures with weak infill, a series for structures with strong infill, and a series for all analyzed structures.

Research of Zlateski [18] focuses on **unreinforced stone and brick masonry structures** constructed before the introduction of a more demanding seismic design code. The **vulnerability index** is obtained by the calculation of a score as the weighted sum of 14 characteristic parameters related to the building's seismic response and distributed into vulnerability classes, providing initial seismic vulnerability assessment by using simplified scoring method.

3.2. Bosnia and Herzegovina

Research in Bosnia and Herzegovina primarily focuses on methods for rapid building assessment. In [19], the iRapid methodology is employed, considering factors such as building construction age, materials, number of stories, population density, and peak ground acceleration (PGA). Each element is evaluated based on its frequency and represented by a lognormal distribution function. The results indicate that cities with lower PGA and higher population density may face disasters they are unprepared for.

In [20], the macroseismic method derived from the EMS 98 scale is used. This study includes a selection of **unreinforced and confined masonry buildings** in Sarajevo and Banja Luka. The **vulnerability index** is calculated based on the building type, regional vulnerability factor, and behavior modifier factor. Using this index and the proposed ductility index, the average degree of damage for each building is developed for three levels of earthquake intensity, and vulnerability curves are plotted.

The analysis for Tuzla [21] focuses on **earthquake intensities VII and VIII** for seismic risk assessment of structures in the area. The study includes all buildings in Tuzla, **including reinforced concrete, unreinforced masonry with flexible and rigid floors, and confined structures**. The RISK UE category matrix is used to classify the buildings, and the vulnerability index is calculated using the macroseismic method, based on building type, regional vulnerability factors, and behavior modifiers. Damage probability matrices and **vulnerability curves** are generated for all the selected building topologies.

In Visoko [22], **earthquake intensities VI and VII are considered** to determine the seismic risk for buildings. The study analyzes three types **of masonry structures** from a database of 94 buildings. The **vulnerability index** is based on building topology, behavior modifiers, and regional modifiers. The mean damage grade is calculated based on the vulnerability index and macroseismic intensity.

Seismic hazard intensities VII and VIII are applied in an analysis of 105 **unreinforced masonry and concrete buildings** across two municipalities in Sarajevo [23]. The **vulnerability index** here is calculated based on structural behavior modifiers (such as the number of floors, plan irregularity, and type of roof) and regional modifiers. The mean damage grade is calculated based on the vulnerability index, macroseismic intensity, and ductility index.

Proceedings of the 3rd Croatian Conference on Earthquake Engineering - 3CroCEE
19–22 March 2025, Split, Croatia
Copyright © 2025 CroCEE
DOI: https://doi.org/10.5592/CO/3CroCEE.2025.53

3.3.Croatia

An overview of various methodologically diverse risk assessments, including isolated individual initiatives, is provided in [24]. In their 2019 research, it is concluded that the level of awareness regarding Croatia's exposure and vulnerability to earthquakes is insufficiently developed. This lack of awareness undermines efforts to promote institutionalized seismic risk assessment, mitigation, and preparedness activities.

The seismic fragility assessment of **masonry-infilled reinforced concrete frames** was analyzed in research by Grubišić et al. [25]. The study utilized three model structures with different infill configurations. Probabilistic fragility curves were developed and interpreted using Incremental Dynamic Analysis (IDA) with a **set of seven earthquake records**. The results are presented as median values of the **fragility curves for four distinct limit states**, providing insight into the performance of such structural systems under seismic loading.

In the research by Hadzima-Nyarko [26], two methods for earthquake vulnerability assessment are applied and compared. The first method is a relatively simple and fast approach developed by Croatian researchers, which uses the **Damage Index (DI)** as a numerical indicator of structural damage levels. The second method used in the research is the **Macroseismic method**.

A case study on seismic risk assessments is presented using Croatian cities to provide an overview of the **relative seismic risk in Croatia** [27], based on general parameters derived from Census data. The vulnerability of buildings described in this paper is determined by the weighted sum of eight impact factors associated with the construction age, each multiplied by a corresponding weight which reflects the relative significance of each factor.

The methodology proposed in the SERA project for developing fragility and consequence models for European buildings has been applied to the building inventory in Croatia [28]. The framework's basic workflow begins with defining the **Building Class Information Model**, which incorporates all the necessary information to calculate the total variability of the fragility function associated with a specific building class.

The development of fragility curves for fourteen of the **most common structural systems** in Zagreb is detailed in research by Novak et al. [29]. Fragility curves were generated for each building type, including masonry and reinforced concrete buildings, using the macroseismic method in alignment with the RISK-UE Project framework. Seismic hazard data, specifically **peak ground acceleration (PGA)** values for Zagreb, served as input for the vulnerability assessments. The damage probability matrix was initially derived as discrete values and then fitted to a lognormal cumulative probability distribution to obtain **continuous fragility functions**, providing a comprehensive assessment of building vulnerability in the region.

Calculation of seismic vulnerability based on the expected behavior of the building, obtained by overlapping the demand curve and capacity curve applied to **traditional unreinforced masonry buildings** of the city Osijek is done in the research of Pavic et al [30]. The values of spectral displacement obtained for the performance point of a specific building class are used as the input parameters for the **fragility curve** for different levels of damage.

The activities in Croatia following the two earthquakes in 2020 have shown that the seismic vulnerability of the exposed building stock is a major problem.

The research by Demšić et al. [31] evaluates both the in-plane and out-of-plane seismic response of an existing **unreinforced masonry row aggregate located in the historic center of Zagreb's Lower Town**. Particular emphasis is placed on the selection of ground motion records for non-linear dynamic analyses, ensuring they are adapted to the **local seismic hazard**. Fragility curves for each damage mode were generated using the R2R software, applying the least squares fit method to estimate the probability of damage under varying seismic intensities.

Proceedings of the 3rd Croatian Conference on Earthquake Engineering - 3CroCEE
19–22 March 2025, Split, Croatia
Copyright © 2025 CroCEE
DOI: https://doi.org/10.5592/CO/3CroCEE.2025.53

The work of Pilipović [32] contributes to the development of new vulnerability models for typical buildings in Zagreb, Croatia. A representative **unreinforced masonry mid-rise building** with solid brick shear walls was selected as the focus of the study. To generate fragility curves, the multiple stripes analysis approach was employed. On-site seismic hazard was calculated using a **probabilistic seismic hazard assessment** aligned with the national seismic hazard assessment methodology.

These studies ([31] and [32]) were carried out in scope of the 2BESAFE research project (New vulnerability models of typical buildings in urban areas: applications in seismic risk assessment and target retrofitting methodology), funded by the Croatian Science Foundation (https://2besafe.grad.hr/).

3.4.Serbia

In recent research by Blagojevic et al. [33], a novel building classification system was developed for Serbia's residential building stock. This classification is based on **existing building taxonomies** but has been adapted to reflect local building characteristics. Evidence from the performance of common building typologies during past earthquakes in Serbia and the region, along with collective expert knowledge, was utilized to develop **expert-based seismic fragility functions** for these typologies. To derive the fragility functions MCS earthquake intensities were transformed into **peak ground acceleration (PGA)** values. Expert judgments were then statistically analyzed for each PGA value to determine the probabilities of reaching or exceeding specific damage states.

The newly utilized Adriseismic Methodology in Serbia [34] for **Expeditious Seismic Assessment** is developed both for unreinforced masonry and reinforced concrete. Regarding masonry buildings, it focuses on three primary seismic failure mechanisms: masonry disintegration, out-of-plane failure, and in-plane damage or failure. The key parameter for evaluating the seismic behavior of a structure is the **Index of Structural Response**, which is calculated to assess the building's performance under seismic loads. Based on this parameter, seismic risk categories are proposed, offering a framework for classifying the vulnerability of such structures.

The seismic vulnerability of **school buildings** is the focus of research by Marinković et al. [35]. This study introduces a new seismic risk methodology called MM Risk and provides a comparative analysis with the Adriseismic methodology used for seismic risk assessment. Through a review of the existing literature and the application of both methods to a dataset of 213 schools (comprising 367 buildings), the paper evaluates the strengths and limitations of each methodology in terms of accuracy, complexity, and practical usability. A seismic hazard map for Serbia, indicating peak ground acceleration (**PGA) values for earthquakes with a 10% probability of exceedance in 50 years**, was utilized in accordance with Eurocode 8 requirements.

3.5.Romania

The initial data on vulnerability of buildings in Bucharest were obtained from a **post-earthquake survey** conducted following the March 4, 1977, earthquake. This survey analyzed a sample of over **18,000 buildings located in various parts of the city**. The results allowed for the derivation of statistical damage spectra for several sub-areas of Bucharest. These findings were further processed to develop vulnerability functions expressed as conditional damage distributions [36].

One of the first attempt of development of a nationwide seismic vulnerability estimation system, concerning basically the existing building stock was done in frame of two projects, referred to as: AC3, Consultancy services for development of a Vrancea earthquake scenario and AC6, Consultancy services for integrated disaster risk management study [36]. The approach adopted relied primarily on the definition of relevant categories of buildings, that are specific to Romania, categorized according to the material and structural system, height, period of construction.

According to [37], the **seismic risk in Bucharest** is well defined, with the most vulnerable structures identified as mid-and high-rise buildings constructed before the implementation of the 1978 earthquake-resistant design code. Buildings constructed prior to 1941 were designed without accounting for earthquake forces, while those built between 1941 and 1978 were designed using a spectrum that was

Proceedings of the 3rd Croatian Conference on Earthquake Engineering - 3CroCEE
19–22 March 2025, Split, Croatia
Copyright © 2025 CroCEE
DOI: https://doi.org/10.5592/CO/3CroCEE.2025.53

inadequate for mid- and high-rise buildings, given the characteristics of the strong ground motions recorded during the 1977 and 1986 earthquakes. After 1989, the Romanian government and local authorities initiated a national program to evaluate the seismic resistance of vulnerable buildings. This program is later incorporated into a broader national strategy for seismic risk reduction.

HAZUS and ATC-40 methodologies are used for seismic vulnerability assessment of reinforced concrete (RC) in [37]. Five case studies involving **representative residential buildings in Bucharest**, the capital city of Romania, are analyzed and compared. The paper also emphasizes the unique characteristics of the **demand spectra in Bucharest**, which differ significantly from those used in HAZUS.

A seismic vulnerability evaluation of buildings within an urban sector of Timișoara was conducted using the **EMS-98 macroseismic approach** [38]. The typological vulnerability classes of buildings were defined according to the RISK-UE method, allowing for classification from both typological and structural perspectives. A parametric analysis was performed by **varying the seismic magnitude** and the site-source distance to estimate potential seismic losses under different earthquake scenarios.

Another research in Romania is focused on Iași—one of Romania's major cities exposed to earthquakes originating in the Vrancea area—aims to assess seismic vulnerability through a multi-criteria analysis of building infrastructure and social vulnerability. The analysis incorporates several indicators, including physical factors (characteristics of buildings and terrain), social factors (population and economic income), and accessibility to emergency services and hospitals. By summing the weighted values of the standardized indicators, an integrated **seismic vulnerability index** was derived. [39]

A significant new study on the **analytical** derivation of **seismic fragility curves** was conducted in Romania, as shown in [40][41][42]. The seismic fragility assessment in the research of Pavel et al [40] was carried out using **incremental dynamic analysis** for **high-rise reinforced concrete (RC) frame structures**, as well as for **high-rise RC shear wall structures,** which are commonly used in residential buildings. Incremental dynamic analysis was performed with **ground motion datasets specific to the seismic conditions of Romania**.

3.6.Greece

One of the earliest vulnerability assessment methodologies in Greece was introduced in 1998 [43], combining elements of both empirical and analytical approaches. This **hybrid methodology** utilized **probability damage matrices**, which were integrated into a cost-benefit model designed to assess the feasibility of seismic retrofitting for the existing stock **of reinforced concrete buildings in Thessaloniki**, Greece. The losses estimated using the proposed procedure were found to align closely with the actual losses incurred during the 1978 Thessaloniki earthquake.

Seismic vulnerability and collapse probability assessment of buildings in Greece, covering **all common typologies** was done in the research of Pomonis et al [44]. Two distinct methodologies are presented for estimating the collapse probability of various building types **across typical Modified Mercalli Intensity (MMI) levels (VI to IX).** The first approach relies entirely on the statistical analysis of data from past earthquakes in Greece, while the second employs hybrid vulnerability curves that combine analytical and empirical data.

The observational data used in the research of Eleftheriadou and Karabinis [45] were collected from post-earthquake surveys conducted in the region affected by the **September 7, 1999 Athens earthquake**. Following analysis, a unified damage database was compiled, encompassing 180,945 damaged buildings in the earthquake's near-field area. These buildings are categorized into various **structural types based on materials, seismic codes, and construction techniques** characteristic of Southern Europe. **Damage probability matrices (DPMs) and vulnerability curves** were developed for specific structural types, offering valuable insights into their seismic performance.

The **hybrid approach** for seismic vulnerability assessment, developed at Aristotle University of Thessaloniki [46], is characterized by its integration of **statistical data with processed results from**

Proceedings of the 3rd Croatian Conference on Earthquake Engineering - 3CroCEE
19–22 March 2025, Split, Croatia
Copyright © 2025 CroCEE
DOI: https://doi.org/10.5592/CO/3CroCEE.2025.53

nonlinear dynamic or static analyses. This combination enables the extrapolation of statistical data to peak ground accelerations (PGAs) and/or spectral displacements for which direct data is unavailable. The methodology utilizes **two types of earthquake scenarios**. This research addresses **both reinforced concrete (R/C) and unreinforced masonry (URM) buildings,** emphasizing that different analytical methods are more suitable for each type.

A comprehensive database documenting observed damage to Greek reinforced concrete (**RC) and unreinforced masonry (URM) buildings** was used in the research of Pomonis et al [47]. These surveys covered four moderate-magnitude **earthquakes that occurred between 1986 and 2003**, encompassing **data on 28,747 buildings**. This database was used for the derivation of **vulnerability curves based on observed damage**, enabling the relative vulnerability of **10 common structural types in Greece** to be characterized.

Recent studies conducted by a group from the Department of Civil Engineering at Aristotle University, Thessaloniki, Greece, focus on the vulnerability assessment of school buildings [48][49]. Building-specific **fragility and vulnerability curves** were derived for three **reinforced concrete (RC) school buildings** based on **3D incremental dynamic analysis (IDA)** [50] of calibrated numerical models. These curves were then compared with existing generic fragility curves, and the differences were discussed. Given the high computational cost in the process of analytical derivation of fragility curves, a recent paper was published addressing the optimization of ground motions and intensity levels required, without compromising accuracy [51].

4. Summary and Conclusion

A summary of research discussed above is presented in Table 1. This table consolidates key information, offering an overview of the methodologies categorized according to Calvi [10], as referenced in the preceding discussion.

It is worth noting that the first seismic vulnerability functions for buildings in the Balkans were determined as early as the early 1990s in North Macedonia. However, despite this, there followed a period during which such research was absent. Nevertheless, the earthquakes that caused more serious damage in the past decade have reignited researchers' interest in the topic of seismic risk assessment, including the development of vulnerability functions.

4.1. Methodology

When considering the methodologies applied, the dominance of empirical methods in defining vulnerability functions is evident. This is likely due to their practicality: they neither require complex nonlinear analyses nor extensive computational resources, while enabling the assessment of many buildings. Additionally, the availability of earthquake damage data supports the widespread use of empirical methods. These methods are particularly suitable for pre-code structures, which remain prevalent in many Balkan countries.

Examining experiences across individual countries reveals notable trends. In North Macedonia, analytical methods are predominantly used, while Bosnia and Herzegovina and Serbia have relied exclusively on empirical methods to date. In Croatia, the devastating earthquakes in Zagreb and Petrinja have increased efforts to reduce seismic risk, leading to an increasing number of studies on vulnerability functions that employ empirical, analytical, and hybrid methods. Similarly, first research in this subject in Romania explore empirical methods, influenced by the catastrophic 1977 earthquake, later, in beginning of twenties of this century research dealing with RC structures designed according old codes applying analytical methods is performed.

It is worth highlighting the case of Greece, where several earthquakes from the late twenty and early twenty-first centuries, with recorded significant and well-documented damages, enabled the application of empirical methods for defining vulnerability models as early as the 1990s. However, the methodology proposed by researchers from the University of Thessaloniki is particularly valuable, combining the strengths of empirical methods, a large number of well-documented damages to

Copyright © 2025 CroCEE
DOI: https://doi.org/10.5592/CO/3CroCEE.2025.53

buildings from earthquakes, and the possibilities provided by analytical methods (nonlinear analysis) for filling in the gaps in documented damages.

Table 1. Summary of analyzed research

		Republic of North Macedonia	Bosnia and Herzegovina	Croatia	Serbia	Romania	Greece
empirical	index	Zlateski, 2020 [18]	Ademović et al ,2020 [19] Ademović et al, 2022[22] Ademović et al, 2022 [23]	Atalić et al, 2019 [24] Hadzima-Nyarko et al, 2017 [26] Šipoš et al, 2017 [27] Nikolic et al, 2021 [53]	Marinkovic et al. 2023, [35] Predari et al. 2024, [34]	Chieffo et al, 2019 [38] Banica et al, 2017 [39]	
	curves		Ademović et al, 2020 [20] Ademović et al, 2022 [21]	Moretic et al, 2023 [52]	Blagojevic et al, 2023, [33]	Sandi et al, 2007, [36]	Eleftheriadou et al, 2011 [45] Pomonis et al, 2014 [47]
analytical	pushover	Milkova et al, 2020 [16] Jakupi, 2015 [14]		Crowley et al, 2019 [28] Pavic et al, 2019 [30]		Vacareanu et al, 2004 [37]	
	dynamic	Dumova-Jovanoska, E., 2000 [12] Nocevski, 1993 [11] Milutinovic et al., 2003 [13] Volcev, 2024 [17]		Demsic et al, 2024 [31] Grubisicet al, 2013 [25] Novak et al, 2019 [29] Pilipovic et al, 2024 [32]		Pavel et al, 2021 [40] Olteanu et al, 2016 [41] Pavel et al, 2019 [42]	Fotopoulou et al, 2023 [48] Karafagka et al, 2024 [49]
hybrid				Nikolic et al, 2022 [54]			Kappos et al (1998) [43] Pomonis et al, (2009) [44] Kappos, A. J. (2013). [46]

4.2. Hazard

As expected, empirical methods utilize hazard data from macroseismic maps, such as those included in seismic design regulations like MCZ and EMS-98. Conversely, analytical methods based on dynamic analysis rely on records from actual earthquakes, with one notable exception: a study conducted in Skopje that used synthetic earthquakes generated based on local conditions. In one method employing nonlinear static analysis, region-specific response spectra were applied, derived using a neodeterministic approach for selected regions of North Macedonia or the entire country.

Proceedings of the 3rd Croatian Conference on Earthquake Engineering - 3CroCEE
19–22 March 2025, Split, Croatia
Copyright © 2025 CroCEE
DOI: https://doi.org/10.5592/CO/3CroCEE.2025.53

4.3. Constructions classes

Regarding the classes of structures for which vulnerability functions were determined, residential buildings constructed of masonry and reinforced concrete were predominantly analyzed. As expected, empirical methods are mainly applied to pre-code structures and reinforced concrete buildings designed according to older regulations.

4.4. Conclusion

Without claiming to be exhaustive, the authors aim to provide an overview of the existing approaches to defining vulnerability functions that consider the specific hazards and construction practices across the Balkan Peninsula. It is anticipated that this overview will help guide research in various institutions throughout the region, foster greater collaboration among seismic vulnerability experts, and contribute to the creation of a more effective European model for assessing seismic risk.

References

[1] D'Agostino, N., Copley, A., Jackson, J., Koçi, R., Hajrullai, A., Duni, L., & Kuka, N. (2022). Active tectonics and fault evolution in the Western Balkans. Geophysical Journal International, 231(3), 2102-2126.

[2] Abolmasov, B., Jovanovski, M., Ferić, P., & Mihalić, S. (2011). Losses due to historical earthquakes in the Balkan region: Overview of publicly available data. Geofizika, 28(1), 161-181.

[3] Sinadinovski, C., & Cernih, D. (2019, January). Analysis of records from the M5. 2 September 2016 Skopje earthquake. In Geophysical Research Abstracts (Vol. 21).

[4] Government of Croatia, & World Bank. (2021). Croatia December 2020 Earthquake—Rapid Damage and Needs Assessment.

[5] Euronews. 2022. Earthquake in Bosnia Kills One, Causes Significant Damage Across Several Cities. Accessed on 06-Jul-2022. Available at: https://www.euronews.com/2022/04/23/earthquake-in-bosnia-kills-one-causes-significant-damage-across-several-cities

[6] Marinković, D., Stojadinović, Z., Kovačević, M., & Stojadinović, B. (2018). 2010 Kraljevo Earthquake Recovery Process Metrics Derived from Recorded Reconstruction Data. In 16th European Conference on Earthquake Engineering.

[7] Georgescu, E. S., & Pomonis, A. (2008, October). The Romanian earthquake of March 4, 1977 revisited: New insights into its territorial, economic and social impacts and their bearing on the preparedness for the future. In Proceedings of the 14th World Conference on Earthquake Engineering, Beijing, China (pp. 12-17).

[8] Kouskouna, V., & Makropoulos, K. (2004). Historical earthquake investigations in Greece. Annals of Geophysics, 47(2-3).

[9] Salic, R., Sandikkaya, M. A., Milutinovic, Z., Gulerce, Z., Duni, L., Kovacevic, V., ... & Stanko, D. (2017). BSHAP project strong ground motion database and selection of suitable ground motion models for the Western Balkan Region. Bulletin of earthquake engineering, 15, 1319-1343.

[10] Calvi, G. M., Pinho, R., Magenes, G., Bommer, J. J., Restrepo-Vélez, L. F., & Crowley, H. (2006). Development of seismic vulnerability assessment methodologies over the past 30 years. ISET journal of Earthquake Technology, 43(3), 75-104.

[11] Nocevski NK. Definition of empirical and theoretical models for assessment of vulnerability level in high rise buildings. Doctoral thesis. IZIIS, Skopje, 1993.

[12] Dumova-Jovanoska, E. (2000). Fragility curves for reinforced concrete structures in Skopje (Macedonia) region. Soil Dynamics and Earthquake Engineering, 19(6), 455-466.

[13] Milutinovic, Z. V., & Trendafiloski, G. S. (2003). Risk-UE An advanced approach to earthquake risk scenarios with applications to different European towns. Contract: EVK4-CT-2000-00014, WP4: Vulnerability of current buildings, 1-111.

[14] Jakupi, E., Denkovska, L., & Dumova-Jovanoska, E. (2015). Seismic Vulnerability of Rc Buildings in Polog Valley. International scientific jurnal "Micro, Macro & Mezzo Geo Information, 5, 004-0.

Copyright © 2025 CroCEE
DOI: https://doi.org/10.5592/CO/3CroCEE.2025.53

[15] Dumova-Jovanoska, E., & Milkova, K. (2022). NDSHA-based vulnerability evaluation of precode buildings in Republic of North Macedonia: novel experiences. In Earthquakes and Sustainable Infrastructure (pp. 455-474). Elsevier.

[16] Milkova, K., Butenweg, C., & Dumova-Jovanoska, E. (2020). Methodology for Development of Seismic Vulnerability Curves for Existing Unreinforced Masonry buildings. In 17th World Conference on Earthquake Engineering, Sendai, Japan.

[17] Volcev, R., Postolov, N., Milkova, K., Todorov, K., & Dumova-Jovanoska, E. (2024). Seismic vulnerability of masonry infilled rc frames with an open first story, 18WCEE, Milan, Italy

[18] Zlateski, A., & Shendova, V. Harmonization of seismic vulnerability assessment of urban historic centers.

[19] Ademović, N., Kalman Šipoš, T., & Hadzima-Nyarko, M. (2020). Rapid assessment of earthquake risk for Bosnia and Herzegovina. Bulletin of earthquake engineering, 18, 1835-1863.

[20] Ademović, N., Hadzima-Nyarko, M., & Zagora, N. (2020). Seismic vulnerability assessment of masonry buildings in Banja Luka and Sarajevo (Bosnia and Herzegovina) using the macroseismic model. Bulletin of earthquake engineering, 18, 3897-3933.

[21] Ademovic, N., Hadzima-Nyarko, M., & Zagora, N. (2022). Influence of site effects on the seismic vulnerability of masonry and reinforced concrete buildings in Tuzla (Bosnia and Herzegovina). Bulletin of earthquake engineering, 20(5), 2643-2681.

[22] Ademović, N., Hadzima-Nyarko, M., Zagora, N., Piljug, A., & Medanović, Ć. (2022, June). Vulnerability of Residential Buildings in Sarajevo, BIH. In International Symposium on Innovative and Interdisciplinary Applications of Advanced Technologies (pp. 3-14). Cham: Springer International Publishing.

[23] Ademović, N., Hadzima-Nyarko, M., Zagora, N., Piljug, A., & Medanović, Ć. (2022, June). Vulnerability of Residential Buildings in Sarajevo, BIH. In International Symposium on Innovative and Interdisciplinary Applications of Advanced Technologies (pp. 3-14). Cham: Springer International Publishing.

[24] Atalić, J., Šavor Novak, M., & Uroš, M. (2019). Seismic risk for Croatia: Overview of research activities and present assessments with guidelines for the future. Građevinar, 71(10), 923-947.

[25] Grubišić, M., Kalman Šipoš, T., & Sigmund, V. (2013). Seismic fragility assessment of masonry infilled reinforced concrete frames. 50th SE-EEE: Skopje, North Macedonia.

[26] Hadzima-Nyarko, M., & Kalman Sipos, T. (2017). Insights from existing earthquake loss assessment research in Croatia. Earthquakes and structures, 13(4), 365-375.

[27] Šipoš, T. K., & Hadzima-Nyarko, M. (2017). Relative rapid seismic risk assessment. International journal of disaster risk reduction, 24, 348-360.

[28] Crowley, H., Silva, V., Despotaki, V., Martins, L., & Atalić, J. (2019, October). European Seismic Risk Model 2020: Focus on Croatia. In Proceedings of Scientific Symposium "Future Trends in Civil Engineering", Zagreb, Croatia (pp. 83-101).

[29] Novak, M. Š., Atalic, J., Uroš, M., Prevolnik, S., & Nastev, M. (2019, October). Seismic risk reduction in Croatia: mitigating the challenges and grasping the opportunities. In Scientific Symposium FUTURE TRENDS IN CIVIL ENGINEERING Zagreb, Croatia (pp. 72-109).

[30] Pavić, G., Hadzima-Nyarko, M., Plaščak, I., & Pavić, S. (2019). Seismic vulnerability assessment of historical unreinforced masonry buildings in Osijek using capacity spectrum method. Acta Phys. Pol. A, 135(5), 1138-1141.

[31] Demsic, M., Pinasco, S, Pilipović, A., Cattari, S., Lagomarsino, S., Šavor Novak, M. & Uroš, M. (2024), Development of fragility curves of masonry buildings build in a regular row aggregate, 18WCEE, Milan, Italy

[32] Pilipović, A., Jevtić Rundek, R., Uroš M., Šavor Novak, M., Demšić, M., Prevolnik, S., (2024), New vulnerability model of a typical unreinforced masonry building in the urban area of Zagreb, 18WCEE, Milan, Italy.

[33] Blagojević, N., Brzev, S., Petrović, M., Borozan, J., Bulajić, B., Marinković, M., ... & Stojadinović, B. (2023). Residential building stock in Serbia: classification and vulnerability for seismic risk studies. Bulletin of earthquake engineering, 21(9), 4315-4383.

[34] Predari, G., Stefanini, L., Marinković, M., Stepinac, M., & Brzev, S. (2023). Adriseismic methodology for expeditious seismic assessment of unreinforced masonry buildings. Buildings, 13(2), 344.

Copyright © 2025 CroCEE
DOI: https://doi.org/10.5592/CO/3CroCEE.2025.53

[35] Marinković, M., Bošković, M., Đorđević, F., Krtinić, N., & Žugić, Ž. (2024). Seismic Risk Assessment in School Buildings: A Comparative Study of Two Assessment Methods. Buildings, 14(8), 2348.

[36] Sandi, H., Pomonis, A., Francis, S., Georgescu, E. S., Mohindra, R., & Borcia, I. S. (2007). Seismic vulnerability assessment: Methodological elements and applications to the case of Romania.

[37] Vacareanu, R., Radoi, R., Negulescu, C., & Aldea, A. (2004, August). Seismic vulnerability of RC buildings in Bucharest, Romania. In 13thWorld Conference on Earthquake Engineering, Vancouver, Canada.

[38] Chieffo, N., Mosoarca, M., Formisano, A., & Apostol, I. (2019, February). Seismic vulnerability assessment and loss estimation of an urban district of Timisoara. In IOP Conference Series: Materials Science and Engineering (Vol. 471, No. 10, p. 102070). IOP Publishing.

[39] Banica, A., Rosu, L., Muntele, I., & Grozavu, A. (2017). Towards urban resilience: A multi-criteria analysis of seismic vulnerability in Iasi City (Romania). Sustainability, 9(2), 270.

[40] Pavel, F., Vacareanu, R., & Scupin, A. (2021). Seismic fragility assessment for post-1977 high-rise reinforced concrete structures in Romania. *Bulletin of Earthquake Engineering*, *19*, 6521-6544.

[41] Olteanu, P., Coliba, V., Vacareanu, R., Pavel, F., & Ciuiu, D. (2016). Analytical seismic fragility functions for dual RC structures in Bucharest. In *The 1940 Vrancea Earthquake. Issues, Insights and Lessons Learnt: Proceedings of the Symposium Commemorating 75 Years from November 10, 1940 Vrancea Earthquake* (pp. 463-479). Springer International Publishing.

[42] Pavel, F., & Carale, G. (2019). Seismic assessment for typical soft-storey reinforced concrete structures in Bucharest, Romania. *International Journal of Disaster Risk Reduction*, *41*, 101332.

[43] Kappos, A. J., Stylianidis, K. C., & Pitilakis, K. (1998). Development of seismic risk scenarios based on a hybrid method of vulnerability assessment. Natural Hazards, 17, 177-192.

[44] Pomonis, A., Kappos, A., Karababa, F., & Panagopoulos, G. (2009). Seismic vulnerability and collapse probability assessment of buildings in Greece. Second International Workshop on Disaster Casualties 15-16 June 2009, University of Cambridge, UK

[45] Eleftheriadou, A. K., & Karabinis, A. I. (2011). Development of damage probability matrices based on Greek earthquake damage data. Earthquake Engineering and Engineering Vibration, 10, 129-141.

[46] Kappos, A. J. (2013). Seismic vulnerability and loss assessment for buildings in Greece. Seismic Vulnerability of Structures, 111-160.

[47] Pomonis, A., Gaspari, M., & Karababa, F. S. (2014). Seismic vulnerability assessment for buildings in Greece based on observed damage data sets. Bollettino di Geofisica Teorica ed Applicata, 55(2).

[48] Fotopoulou, S., Karafagka, S., Petridis, C., Manakou, M., Riga, E., & Pitilakis, K. (2023). Vulnerability assessment of school buildings: Generic Versus building-specific fragility curves. *Journal of Earthquake Engineering*, *27*(11), 2994-3023.

[49] Karafagka, S., Riga, E., Oikonomou, G., Karatzetzou, A., Fotopoulou, S., Pitilakis, D., & Pitilakis, K. (2024). RiskSchools: a prioritization-based system for the risk assessment of school buildings combining rapid visual screening smartphone app and detailed vulnerability analysis. *Bulletin of Earthquake Engineering*, *22*(6), 2951-2980.

[50] Vamvatsikos, D., & Cornell, C. A. (2002). Incremental dynamic analysis. Earthquake engineering & structural dynamics, 31(3), 491-514.

[51] Sipcic, N., de Quevedo Iñarritu, P. G., Kohrangi, M., Vamvatsikos, D., & Bazzurro, P. (2024). Practical Approach to Hazard-Consistent Fragility Curve Estimates Using Bayesian Updating. Available at SSRN 5033487.

[52] Moretić, A., Chieffo, N., Stepinac, M., & Lourenço, P. B. (2023). Vulnerability assessment of historical building aggregates in Zagreb: implementation of a macroseismic approach. Bulletin of earthquake engineering, 21(4), 2045-2065.

[53] Nikolić, Ž., Runjić, L., Ostojić Škomrlj, N., & Benvenuti, E. (2021). Seismic vulnerability assessment of historical masonry buildings in Croatian coastal area. Applied Sciences, 11(13), 5997.

[54] Nikolić, Ž., Benvenuti, E., Runjić, L., Kozulić, V., & Škomrlj, N. O. (2022). Assessment of seismic vulnerability of existing masonry buildings in urban area Pula.

Proceedings of the 3rd Croatian Conference on Earthquake Engineering - 3CroCEE
19–22 March 2025, Split, Croatia
Copyright © 2025 CroCEE
DOI: https://doi.org/10.5592/CO/3CroCEE.2025.60

BUILDING EXPOSURE MODELLING FOR NATIONAL SEISMIC RISK ASSESSMENT IN MONTENEGRO

Nina Serdar [(1)], Jelena Pejović [(2)]

[(1)] *Assistant professor, University of Montengro, Faculty of Civil Engineering, ninas@ucg.ac.me*
[(2)] *Associate professor, University of Montengro, Faculty of Civil Engineering, jelenapej@ucg.ac.me*

Abstract

Seismic risk assessment in Montenegro has been of critical concern since the devastating earthquake of 1979, which spurred initial studies for the country's spatial planning. In response, significant efforts have been made to mitigate seismic risks and regulate the construction of earthquake-resistant structures. Early vulnerability studies were based on damage observations from the 1979 earthquake. However, since then, seismic risk in Montenegro has increased considerably due to rapid urbanization and intense building construction, particularly in coastal zones with high seismic hazard. In 2021, a comprehensive study was conducted as part of a European Commission-funded project to develop a National Risk Assessment (NRA), led by the Department of Civil Protection. This seismic risk assessment was carried out in accordance with EU guidelines ensuring consistency and comparability in terms of prevention, preparedness, and planning. The development of NRA encountered several challenges primarily due to data gaps, especially in the building exposure modelling. In this paper, the methodology applied for seismic risk assessment is presented, with a focus on the main uncertainties in the existing exposure models from literature. A new refined exposure model is proposed tailored for building typologies in northern Montenegro. Ongoing and future research efforts aimed at continually improving the exposure model are also discussed.

Keywords: seismic risk, exposure model, SERA model, buildings.

1. Introduction

The first seismic risk study in Montenegro was conducted in 1984, in response to the devastating 1979 earthquake, to support the development of the national Spatial Plan. This pioneering study [1] assessed the consequences of the earthquake by examining approximately 40,000 facilities across six coastal and two central municipalities. The analyzed structures included residential buildings, as well as cultural, tourism, and educational facilities. Despite significant social efforts at the time to address seismic risks, no subsequent seismic risk studies were carried out until recently. It is widely recognized that seismic risk assessments has to be regularly updated to account for evolving factors such as population growth, building stock changes, and structural vulnerabilities.

In late 2021, a new National Risk Assessment (NRA) [2] was developed by the Department of Civil Protection (DCP) under the Ministry of Interior to fulfil Montenegro's obligations as an EU candidate country. The NRA aligns with the Strategy for Disaster Risk Reduction (2018–2023) and evaluates nine hazard categories: earthquakes, landslides, climate change, floods, forest fires, epidemics, technical accidents, nuclear incidents, and critical infrastructure failures. This effort benefitted from a collaborative approach involving the DCP, the scientific community (notably the Faculty of Civil Engineering at the University of Montenegro), and the National Seismological Institute, which collectively contributed to the development of Montenegro's seismic risk assessment. The seismic risk assessment, as part of the NRA, adheres to EU guidelines [3], ensuring alignment with the risk assessments of EU member states. This consistency fosters a shared understanding of disaster risks, facilitating cooperative prevention and mitigation efforts across borders.

Proceedings of the 3rd Croatian Conference on Earthquake Engineering - 3CroCEE
19–22 March 2025, Split, Croatia
Copyright © 2025 CroCEE
DOI: https://doi.org/10.5592/CO/3CroCEE.2025.60

The implementation of EU methodologies in Montenegro's seismic risk assessment posed several challenges and raised important questions. This paper outlines the adopted methodology, highlights key uncertainties, and addresses open questions, particularly in relation to exposure modelling using existing building exposure data [4], [5]. It introduces a refined exposure model tailored for building typologies in northern Montenegro. The findings aim to contribute to refining risk assessment practices and improving disaster resilience strategies in the region.

2. Seismic Risk Assessment Methodology

This chapter discusses the conceptual framework and methodology for seismic risk calculation, as outlined in the EU guidelines [3]. According to ISO 31010 [6], risk is defined as the combination of the consequences of an event (hazard) and the probability of their occurrence. A hazard refers to a dangerous phenomenon, substance, human activity, or condition that has the potential to cause loss of life, injury, health impacts, property damage, loss of livelihoods and services, social and economic disruption, or environmental damage. Consequences describe the negative effects of a disaster, which are quantified through impact indicators. These indicators capture dimensions such as human losses, economic damages, environmental degradation, and political or social disruptions.

For natural hazards such as earthquakes, the impacts are often independent of the probability of the hazard occurring. This relationship is mathematically expressed as follows:

$$\text{Risk}=p\times V\times E \tag{1}$$

where p represents the probability of consequences, V denotes vulnerability (expected negative impacts to people and property), and E indicates exposure (assets at risk). Vulnerability refers to the characteristics of assets, properties, or systems that make them susceptible to damage from the hazard. Exposure is defined as the total number of people, properties, systems, and other elements located in hazard-prone areas.

The EU methodology for risk calculation emphasizes the use of quantitative impact indicators wherever possible. However, when the complexity of quantitative calculations does not significantly enhance reliability or robustness, these parameters can be supplemented by qualitative assessments or expert judgment. The EU guidelines categorize impacts into three main types [3]:

- Human Impacts: These include the number of fatalities, severely injured individuals, and permanently displaced persons.
- Economic and Environmental Impacts: These encompass costs related to healthcare, emergency response, restoration of buildings, infrastructure, cultural heritage, and environmental recovery.
- Political and Social Impacts: These consider public anxiety, territorial encroachment, violations of democratic systems, societal psychological effects, disruptions to public order and safety, political repercussions, and damage to cultural assets.

Human impacts are measured numerically, economic and environmental impacts are quantified in monetary terms (Euros), and political and social impacts are expressed semi-quantitatively using categories such as insignificant, minor, moderate, significant, and catastrophic.

Risk is typically visualized using a risk matrix, a two-dimensional chart with the horizontal axis representing the likelihood of impacts and the vertical axis indicating the severity of the impacts. This tool allows for an intuitive comparison of different risks. The seismic risk assessment methodology for Montenegro adopts a scenario-based approach, evaluating risk for specific earthquake events with potentially significant societal consequences. Consequences are categorized from minimal to catastrophic, and when combined with the probability of occurrence, they are depicted in seismic risk matrices. These matrices provide a clear representation of the overall risk level and support decision-making for disaster preparedness and mitigation.

Copyright © 2025 CroCEE
DOI: https://doi.org/10.5592/CO/3CroCEE.2025.60

3. Seismic Risk Assessment Results: Montenegro Overview

The seismic risk assessment from 2021 for Montenegro evaluates two distinct what-if earthquake scenarios:

- Scenario 1: This scenario represents the most likely seismic event, characterized by a return period of 95 years and a magnitude of M=6.
- Scenario 2: This scenario models an event with a return period of 475 years, considered to have the worst possible consequences, with a magnitude of M=7.

Both scenarios assume earthquakes with the same epicenter, located near the municipalities of Bar and Ulcinj, approximately 13 km south of the settlement of Kruce, at a depth of 10 km. The intensity distributions for these scenarios, reflecting the spatial impact and severity, are illustrated in Fig. 1.

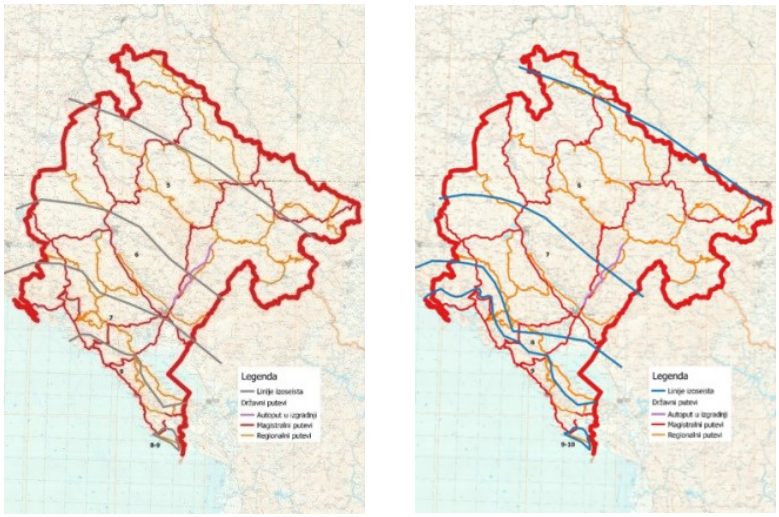


Figure 1. Intensity shaking distribution for a) Scenario 1 and b) Scenario 2 [2].

The damage distribution for the two earthquake scenarios is summarized in Fig.2. In Scenario 1, approximately 0.46% of Montenegro's population and 0.53% of all dwellings are expected to experience the most severe damage levels, categorized as D4 (significant damage) and D5 (collapsed buildings). In contrast, Scenario 2 suggests that as much as 2.7% of inhabitants and 3.11% of dwellings across Montenegro would be subjected to high damage levels D4 and D5.

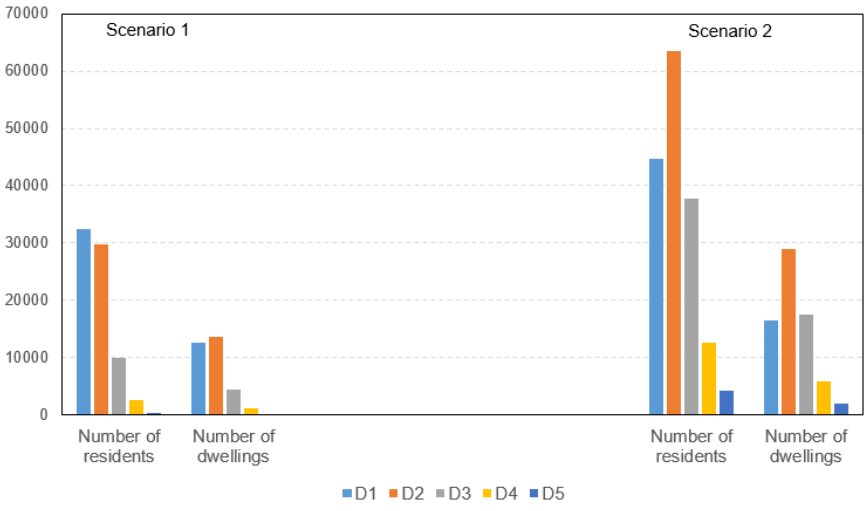


Figure 2. Distribution of damages for Scenario 1 and Scenario 2: number of residents and dwellings for certain damage levels D1-D5.

Copyright © 2025 CroCEE
DOI: https://doi.org/10.5592/CO/3CroCEE.2025.60

Based on the distribution of damages, the impact to people is calculated in terms of fatalities and injuries using two established methodologies: HAZUS [7] and IRMA [8].

- HAZUS Methodology: For Scenario 1, it is estimated that the earthquake will result in 40 fatalities and 169 heavy injuries. In total, 209 residents are projected to be affected, excluding those with minor injuries requiring no to basic medical assistance. For Scenario 2, the estimated impact includes 416 fatalities and 1340 heavy injuries, leading to a total of 1756 affected residents.
- IRMA Methodology: For Scenario 1, the earthquake is projected to cause 65 fatalities and 243 injuries, resulting in a total of 308 affected residents. In Scenario 2, the estimated impact increases significantly, with 543 fatalities and 1,882 injuries, culminating in a total of 2,425 affected residents.

The results highlight small discrepancies between the two methodologies. These findings are illustrated in Fig. 3.

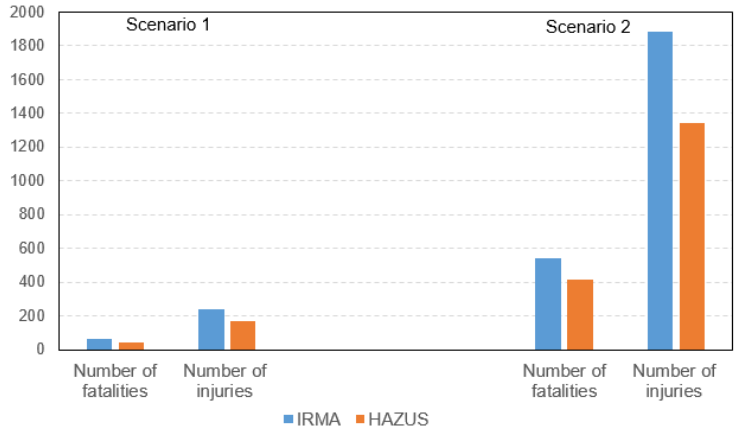


Figure 3. Impact on people according to two methodologies IRMA and HAZUS.

The repair costs for residential buildings are presented in Fig.4. These costs were calculated based on the average construction cost per square meter of dwellings in 2020 and the total area of dwellings corresponding to each damage level. The percentages of repair or replacement costs (Ct) were determined using the methodologies outlined in references [7], [8]. For Scenario 1, the repair costs exhibit minor variations in results from both methodologies, with the maximum estimated cost reaching 10% of GDP. In contrast, for Scenario 2, which accounts for the most severe earthquake scenario, the repair costs are significantly higher, ranging from 25.9% to 40.2% of GDP, depending on the methodology applied.

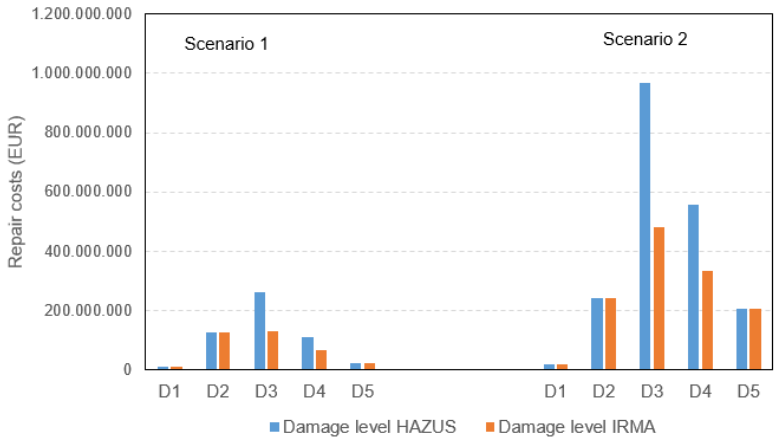


Figure 4. The repair costs for residential buildings for two methodologies IRMA and HAZUS.

Copyright © 2025 CroCEE
DOI: https://doi.org/10.5592/CO/3CroCEE.2025.60

4. Modeling Exposure: Key Challenges

In Montenegro, a systematic database containing essential information about residential and commercial buildings, such as location, structural typology, building materials, and the number of floors, is currently unavailable. These data are critical for accurate seismic risk assessment but are not collected as part of the national census process. The absence of detailed data is a common challenge in many countries and represented a significant obstacle during this research. The only available census information included the number of dwellings categorized by year of construction and population distribution by municipalities.

To address this data gap, the study relied on existing global models, such as the SERA exposure model [4], [5], created based on Montenegro's 2011 census data. The SERA model incorporates assumptions regarding the distribution of common structural systems for residential buildings, categorized by the year of construction. These assumptions were derived from expert opinions and data extrapolated from neighboring countries. In the SERA methodology, the number of dwellings was converted into the number of buildings using assumptions about the average number of dwellings per building typology and the corresponding number of storeys. The distribution of common structural systems by year of construction for urban areas, is illustrated in Fig.5.

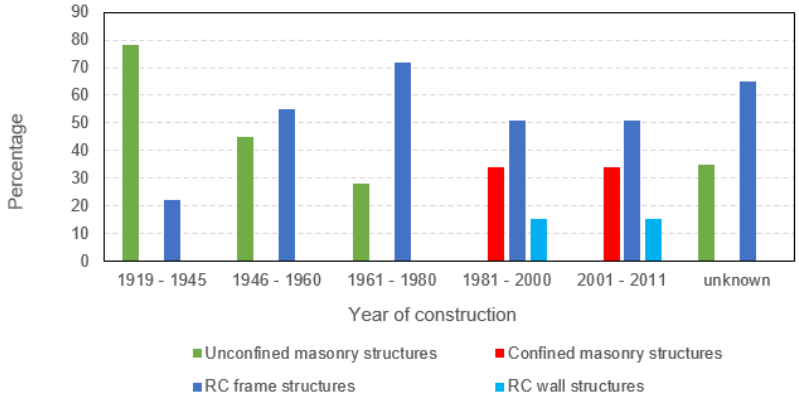


Figure 5. Distribution of common structural systems by year of construction in urban areas.

Based on the authors' expertise and analysis of relevant documents, such as the Protect and Rescue Plans [9]–[12] developed by local civil protection units for specific municipalities, several deficiencies in the SERA exposure model were identified. One significant issue is the model's tendency to overestimate the number of reinforced concrete (RC) buildings as well as the number of dwellings and residents in RC buildings, particularly in the northern part of Montenegro. The distribution of residents by region and structural typology, as represented in the SERA model, is illustrated in Fig.6, highlighting these discrepancies.

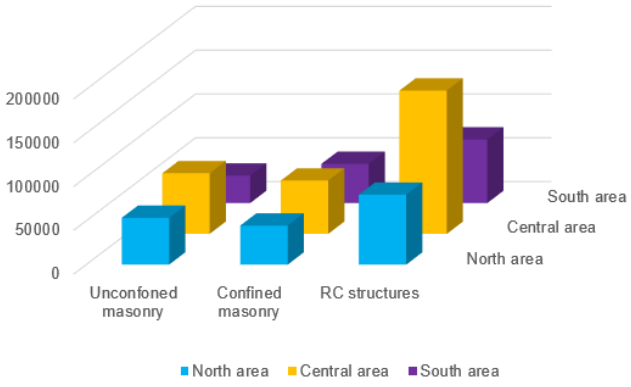


Figure 6. Regional distribution of residents by building typology.

Proceedings of the 3rd Croatian Conference on Earthquake Engineering - 3CroCEE
19–22 March 2025, Split, Croatia
Copyright © 2025 CroCEE
DOI: https://doi.org/10.5592/CO/3CroCEE.2025.60

Earthquake protection and rescue strategies have been specifically tailored for urban areas in the northern municipalities of Montenegro, including Berane, Bijelo Polje, Mojkovac, Pljevlja, Plužine, and Rožaje. Unfortunately, comparable data for municipalities in the southern and central regions were not available. As a result, adjustments to the SERA exposure model were limited to the urban areas of the northern region.

5. Refined SERA exposure model tailored for Montenegro

This chapter provides an in-depth analysis of the refinements made to the SERA exposure model, with a primary focus on the northern municipalities of Montenegro. These adaptations were driven by the lack of comparable data for the southern and central regions, limiting model adjustments to urban areas in the northern region. From the available documents used to refine the SERA model, the existing data from Berane, Bijelo Polje, Mojkovac, and Rožaje proved particularly valuable. These municipalities provided detailed information, including the number of buildings or apartments, construction year, number of floors, and in some cases, even the structural system. This chapter systematically analyzes the available data for each municipality, detailing the adjustments made to the SERA model and their implications.

5.1. Rožaje Municipality

Data analysis for the urban areas of Rožaje were based on the information from 33 collective housing units, predominantly featuring reinforced concrete (RC) structures and reflecting recent construction trends. Individual housing units in this area, by contrast, primarily consist of masonry, adhering to traditional building practices in northern Montenegro. Data collected by local authorities included the number of floors, year of construction, and the number of dwellings. The adjustments were conducted as follows:

- RC Buildings: These were categorized according to the SERA taxonomy, based on the floor count, structural system, and seismic design level (quality of construction). The seismic design levels for buildings were classified as:
  - CDN (no seismic design): built before 1964.
  - CDL (low seismic design): built between 1964 and 1981.
  - CDM (moderate seismic design): built after 1981.
- Masonry Buildings: The relative percentage distribution from the SERA model was maintained, including the assumptions on the number of dwellings per floor (1 dwelling for 1 and 2-storey buildings and 4 dwellings per floor for 3 to 5-storey buildings).

Based on these assumptions, the number of masonry buildings was calculated according to the SERA taxonomy. The final distribution of buildings in specific typologies was derived and expressed in percentages.

5.2. Berane and Bijelo Polje Municipalities

Combined data from 170 collective housing buildings in Berane and Bijelo Polje revealed a prevalence of RC structures in newer constructions and masonry buildings in older ones. The available data included the number of stories and dwellings but lacked construction year details. This missing information was supplemented using data from the 2011 census track. Once the dataset was completed, it was processed in the same manner as for Rožaje municipality.

5.3. Mojkovac Municipality

The dataset for Mojkovac consisted of 38 collective housing buildings but lacked information on the number of floors. To address this issue, floor counts were estimated based on the distribution of apartment numbers and expert opinion. The subsequent data processing followed the same methodology applied to the other municipalities.

Proceedings of the 3rd Croatian Conference on Earthquake Engineering - 3CroCEE
19–22 March 2025, Split, Croatia
Copyright © 2025 CroCEE
DOI: https://doi.org/10.5592/CO/3CroCEE.2025.60

5.4. Aggregate Adjustments

At the end, cumulative adjustments were made to the combined data from the four municipalities. These adjustments were used to recalibrate the SERA model's assumptions on building types and their distribution, aligning the model with the observed construction practices in the northern region. The recalibration also accounted for variations in the seismic design across different construction periods. Table 1 presents the refined distributions of buildings based on the SERA taxonomy. Representations of building types in percentage within the urban areas and for specific time periods were calculated according to the following equation:

$$p_{ti}(\%) = \frac{\sum_{j=1}^{4} p_{ti,j} \cdot d_j}{d_{tot}} \quad (1)$$

p_{ti} corrected percentage of building typology i with taxonomy t

$p_{ti,j}$ corrected percentage of building typology i with taxonomy t for the municipality $j=(1\text{-}4)$

d_j number of dwellings in municipality j

d_{tot} total number of dwellings in analysed municipalities

Table 1. The SERA model refined for Northern Montenegro

Taxonomy	1919-1945	1946-1960	1961-1980	1981-2000	2001-2011
CR/LFINF+CDM/HBET:6-/2.5	0.0	0.0	0.0	1.5	1.2
CR/LFINF+CDN/HBET:6-	0.0	0.0	0.0	0.0	0.0
CR/LFINF+CDN/HBET:3-5	0.0	3.8	0.7	0.0	0.0
CR/LFINF+CDN/H:2	3.3	3.6	0.1	0.0	0.0
CR/LFINF+CDM/HBET:3-5/2.5	0.0	0.0	0.0	5.8	6.8
CR/LFINF+CDM/H:2/2.5	0.0	0.0	0.0	1.9	1.2
CR/LFINF+CDL/HBET:6-/0.0	0.0	0.0	0.2	0.0	0.0
CR/LFINF+CDL/HBET:3-5/0.0	0.0	0.0	0.9	0.0	0.0
CR/LFINF+CDL/H:2/0.0	0.0	0.0	0.3	0.0	0.0
CR/LDUAL+CDM/HBET:6-/2.5	0.0	0.0	0.0	3.2	5.8
MUR/LWAL+CDN/HBET:3-5	5.8	11.1	0.0	0.0	0.0
MUR/LWAL+CDN/H:2	43.5	30.5	35.2	0.0	0.0
MUR/LWAL+CDN/H:1	47.4	51.0	62.6	0.0	0.0
MCF/LWAL+CDN/HBET:3-5	0.0	0.0	0.0	25.8	25.1
MCF/LWAL+CDN/H:2	0.0	0.0	0.0	25.8	25.1
MCF/LWAL+CDN/H:1	0.0	0.0	0.0	36.0	34.8

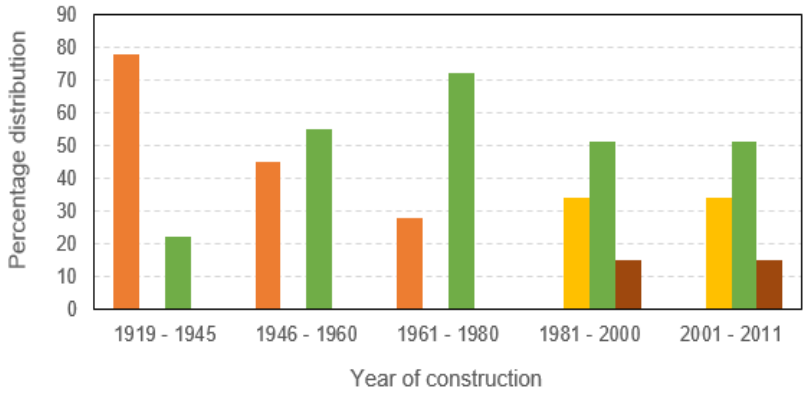
The detailed comparison between the original and revised SERA models highlights significant differences in estimations and categorizations. A key conclusion is that the original SERA model tends to overestimate the number of RC frame buildings, particularly those designed with moderate seismic design. One of the most notable adjustments pertains to the category of RC frame buildings with infill walls (CR/LFINF+CDM/HBET:3-5). In the original SERA model, these buildings were estimated to constitute approximately 28% of the total number of structures during the period 1981–2000. However, the refined model significantly reduces this figure to about 5.8%, reflecting a more accurate assessment

Copyright © 2025 CroCEE
DOI: https://doi.org/10.5592/CO/3CroCEE.2025.60

of the construction practices in the region. Additionally, the refined model introduces a new category for buildings with a dual structural? system with moderate seismic design (CR/LDUAL+CDM/HBET:6), accounting for 3.2% of structures from the same period. This addition represents an enhancement in the current understanding of the building technologies and structural systems likely underrepresented or overlooked in the original SERA assessment.

These revisions underscore the importance of local data and expert input in refining exposure models, ensuring that they better reflect the reality of construction practices and structural diversity in Montenegro's urban areas. The adjusted distribution is illustrated in Fig. 7.

a)



b)

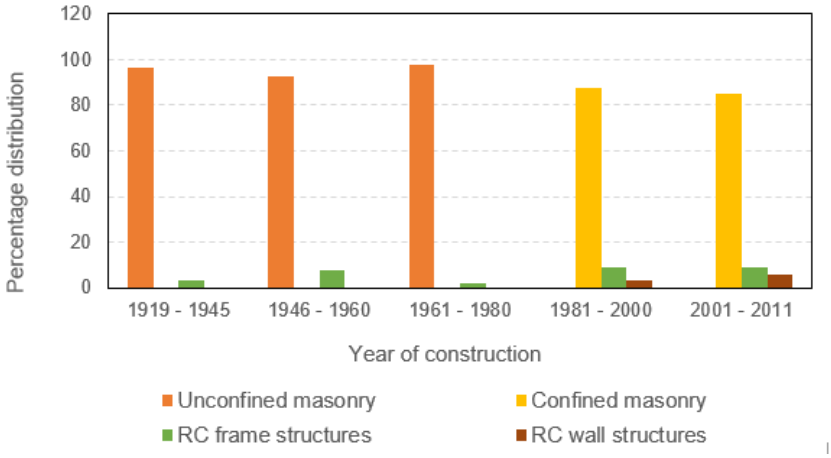


Figure 7. a) Existing SERA model and b) Refined SERA model

6. Conclusions

There were no seismic risk assessment studies conducted in Montenegro since 1979. In 2021, as a part of the European Commission-funded project led by the Department of Civil Protection (DCP) and in collaboration with researchers from the University of Montenegro and the Institute of Seismology, a new National Seismic Risk Assessment (NRA) was developed. The development process faced

Copyright © 2025 CroCEE
DOI: https://doi.org/10.5592/CO/3CroCEE.2025.60

numerous challenges, primarily due to data deficiency, particularly in the building exposure model. This paper discusses the main uncertainties associated with the SERA building exposure data and presents a refined SERA exposure model tailored specifically to the building typologies of northern Montenegro.

An analysis of the SERA model, deemed the most suitable option at the time, concluded that it did not adequately reflect local construction practices. Using the existing rescue and protection plans, a refined model was developed to address these limitations. This refined model, relevant to the northern region of Montenegro, integrates updated data from local assessments, resulting in significant adjustments to the distribution of building types. For instance, the proportion of RC buildings with moderate seismic design was revised to better reflect compliance with updated seismic standards, which were underrepresented in the original model. Moreover, the refined model not only updates previous estimates but also enhances the classification granularity by introducing new building typologies into the existing framework. These revisions underscore the importance of local data and expert input in refining exposure models, ensuring that they better reflect the reality of construction practices and structural diversity in Montenegro's urban areas.

Future research should prioritize systematic data collection in the central and coastal municipalities, addressing the gaps that currently hinder comprehensive national seismic risk assessment. Additionally, advancements in artificial intelligence, image processing, machine learning, digital map analysis, and elevation modeling should be integrated into the analysis of exposure models. These technologies hold the potential to improve data accuracy and achieve more reliable and detailed seismic risk assessment outcomes.

References

[1] Petrovski, J. et al. (1984): Primjenjena metodologija za ocjenu povredljivosti i seizmičkog rizika razvijena na osnovu istraživanja efekata zeljotresa od 15.04.1979. godine u Crnoj Gori. *Report IZIIS*, Skoplje, 1984 (in Montenegrin).

[2] Tmusic, Lj. et al. (2021): Projena Rizika od katastrofa Crna Gora - Disaster Risk Assessment Montenegro, *Report*, Ministry of the Interior, Directorate for Emergency Management Montenegro, 2021, ISBN 978-9940-8815-1-1, https://media.gov.me/media/gov/2021/mup/nacionalna-procjena-rizika-elektronska-publikacija.pdf.

[3] European Commission (2010): Risk Assessment and Mapping Guidelines for Disaster Management, *Guidelines*, Brussels, 21.12.2010, SEC(2010) 1626 final.

[4] SERA (2017-2020): The Seismology and Earthquake Engineering Research Infrastructure Alliance for Europe (http://www.sera-eu.org/en/about/aboutus/)

[5] Crowley, H., Despotaki, V., Rodrigues, D., Silva, V., Toma-Danila, D., Riga, E., Karatzetzou, A., Fotopoulou, S., Zugic, Z., Sousa, L., Ozcebe, S., Gamba, P. (2020): Exposure model for European seismic risk assessment. *Earthquake Spectra* **36**(1_suppl), 252–273, 2020, doi: https://doi.org/10.1177/8755293020919429

[6] ISO 31010 (2019): Risk management –Risk assessment techniques. *International standard,* 2019 ISBN 978-2-8322-6989-3.

[7] HAZUS (2003): HAZUS®MH –MR4 Technical Manual -Multi-hazard loss estimation methodology, Earthquake model, Federal Emergency Management Agency, Washington, DC.

[8] Borzi, B., Onida, M., Faravelli, M., Polli, D., Pagano, M., Quaroni, D., Cantoni, A., Speranza, E., Moroni, C. (2020): IRMA platform for the calculation of damages and risks of Italian residential buildings. *Bulletin of Earthquake Engineering*, 2020, doi: https://doi.org/10.1007/s10518-020-00924-x

[9] Direktorat za vanredne situacije (2018): Nacionalni plan zaštite i spašavanja od zemljotresa, Vlada Crne Gore, 2018.

[10] Opština Berane (2015): Opštinski plan za zaštitu i spasavanje od zemljotresa, novembar 2015. godine.

Copyright © 2025 CroCEE
DOI: https://doi.org/10.5592/CO/3CroCEE.2025.60

[11] Opština Bijelo Polje (2018): Plan zaštite i spašavanja od zemljotresa opštine Bijelo Polje, Bijelo Polje, 2018.

[12] Opština Rožaje (2017): Plana zaštite i spašavanja od zemljotresa opštine Rožaje, Rožaje, 2017.

Proceedings of the 3rd Croatian Conference on Earthquake Engineering - 3CroCEE
19–22 March 2025, Split, Croatia
Copyright © 2025 CroCEE
DOI: https://doi.org/10.5592/CO/3CroCEE.2025.69

SCENARIO-BASED SEISMIC RISK ASSESSMENT OF SCHOOL BUILDINGS IN THE SKOPJE AREA, NORTH MACEDONIA

Lisa Jusufi [(1)], Roberta Apostolska [(2)]

[(1)] *PhD candidate, Institute of Earthquake Engineering and Engineering Seismology in Skopje, lisajusufi3@gmail.com*
[(2)] *D.Sc., Institute of Earthquake Engineering and Engineering Seismology in Skopje, beti@iziis.ukim.edu.mk*

Abstract

The Republic of North Macedonia (RNM) is characterized by a moderate to high seismic hazard. Combined with the vulnerability of the existing building stock, the impact of earthquakes continues to be substantial. The implementation of risk mitigation strategies at regional or national levels includes the seismic assessment of a wide range of buildings. Given the significant social and economic impact of school buildings, especially in the Skopje region, a scenario-based seismic risk assessment of school buildings in this area is presented here.

The RNM is divided into 8 regions and 80 municipalities (urban and rural), 10 of which constitute the City of Skopje, the country's capital. Out of approximately 1119 primary and secondary school buildings, 193 are located in the Skopje region, serving 81,993 students and 8,961 teaching and administrative staff, according to official data from the beginning of the 2022/23 school year.

The ground motion field, representing the shaking intensity in the study area, is defined using the characteristics of the seismic rupture from the July 26, 1963, Skopje earthquake (magnitude 6.1, hypocentral depth 5 km, epicentral intensity IX). The exposure model is developed by utilizing structural attributes from previous studies and current replacement cost estimates. For buildings where structural typology data is unavailable, taxonomies are assigned with weighted values based on statistical analysis and expert judgment. Lastly, for the vulnerability component, taxonomy strings from the GEM vulnerability database are applied through a mapping scheme.

The analysis are carried out using the OpenQuake Engine, and the results are ultimately presented in terms of damages and losses.

Keywords: seismic risk assessment, scenario-based hazard, school buildings, damages, losses

1. Introduction

In recent years, raising awareness about seismic risk has become a critical issue for all seismically active regions, including the Republic of North Macedonia (RNM). The development of earthquake loss models and the implementation of risk mitigation strategies at regional or national levels require comprehensive seismic assessments of different building portfolios. Among these, school buildings hold particular importance due to their critical social and economic roles during and after earthquake events. This research focuses on structuring and implementing a framework for a regional, scenario-based seismic risk assessment of school buildings in the territory of RNM and applying it to a specific region in RNM, the Skopje region.

The Skopje region is the most densely populated among the eight regions of RNM [1]. It accommodates approximately one-third of the country's total population, highlighting the critical importance of seismic risk assessment for buildings in this area. Although there have been several attempts to assess the seismic risk of school buildings across RNM [2, 3, 4, 5, 6], no comprehensive study covering all schools has been conducted to date.

The approach given herein evaluates the potential damages and structural losses to school buildings from a scenario-based hazard modelled after the 1963 Skopje earthquake, the most credible earthquake for this region. All analyses are conducted using the state-of-the-art software, the *OpenQuake engine* [7, 8].

Proceedings of the 3rd Croatian Conference on Earthquake Engineering - 3CroCEE
19–22 March 2025, Split, Croatia
Copyright © 2025 CroCEE
DOI: https://doi.org/10.5592/CO/3CroCEE.2025.69

2. Methodology for regional seismic risk analysis of school buildings

Studies on large building portfolios are generally scarce for the territory of RNM. One notable exception is the recent study focusing on the City of Skopje is [9], which presents a methodology for assessing seismic losses in the aggregated local building inventory. This study considers two hypothetical seismic events as well as a probabilistic hazard approach. Beyond RNM, research on deterministic seismic risk assessment for large building portfolios has explored various aspects of this approach. An example is the study on risk and resilience of Lisbon's school buildings based on seismic scenarios [10], and an analysis of school buildings in two regions of Metro Manila, Philippines [11]. Additionally, in [12] several regional scenario-based assessments are presented, providing valuable insights on the methodology development.

In line with common practice, the proposed framework for the school buildings in RNM consists of the following steps:

1) Scenario-based hazard analysis conducted considering the fault rupture of the 1963 Skopje earthquake and local site conditions;
2) Exposure modelling of the school buildings including a taxonomy mapping scheme;
3) Choosing the appropriate vulnerability/fragility functions;
4) Damage analysis due to the given scenario hazard;
5) Structural loss analysis due to the given scenario hazard.

These steps are applied specifically to the Skopje region but can also be applied to any region of RNM, provided that information on the most credible earthquake and building portfolio is available. This framework represents an initiative of outputting information with potential for their integration into a national seismic risk assessment map in the future.

3. Application of the proposed methodology to the Skopje region

According to the State Statistical Office of the Republic of North Macedonia [1], at the beginning of the 2022/23 academic year, there were 1013 primary and 135 secondary schools (as administrative entities) active, with 252,341 pupils and 30,312 teaching staff.

In general, RNM is comprised of 8 regions and 80 municipalities, 10 of which constitute the City of Skopje, the country's capital. The municipalities are divided into rural and urban municipalities. Information regarding schools for each region is presented in Table 1, in which the information regarding the Skopje region is highlighted in grey.

Table 1. General information on RNM municipalities, population and schools per region.

Region	Number of municipalities	Number of urban municipalities	Number of rural municipalities	Population based on the latest census in 2021 **[1]**	Number of primary schools	Number of secondary schools	Number of primary and secondary school buildings, SY2022/23 [MES]	Number of pupils, SY2022/23 [MES]	Number of teaching staff and administration, SY2022/23 [MES]
Eastern	11	8	3	150,234	94	13	107	17,903	2,573
Northeastern	6	3	3	152,982	99	8	107	22,747	2,693
Pelagonia	9	5	4	210,431	181	16	197	29,798	3,598
Polog	9	2	7	251,552	149	13	162	37,237	4,779
Skopje	**17**	**9**	**8**	**607,007**	**162**	**31**	**193**	**81,904**	**8,909**
Southeastern	10	6	4	148,387	120	7	127	18,412	2,334
Southwestern	9	5	4	177,398	125	10	135	24,286	3,208
Vardar	9	5	4	138,772	82	9	91	20,054	2,218
	80	**43**	**37**	**1,836,713**	**1012**	**107**	**1119**	**252,341**	**30,312**

Proceedings of the 3rd Croatian Conference on Earthquake Engineering - 3CroCEE
19–22 March 2025, Split, Croatia
Copyright © 2025 CroCEE
DOI: https://doi.org/10.5592/CO/3CroCEE.2025.69

As shown in Table 1, this region accounts for approximately 33% of the total population of RNM, while hosting 17% of the total number of school buildings and 32% of the overall number of pupils and staff. This highlights the importance of seismic risk assessment for buildings in this area. Furthermore, according to the zoning map of Macedonia adopted for National Annex to MKS EN 1998-1:2012 Eurocode 8, with a return period of 475 years and a 10% probability of exceedance in 50 years, the expected PGA for this region is 0.25g [13]. The spatial distribution of the school building stock in this region is presented in Figure 1.

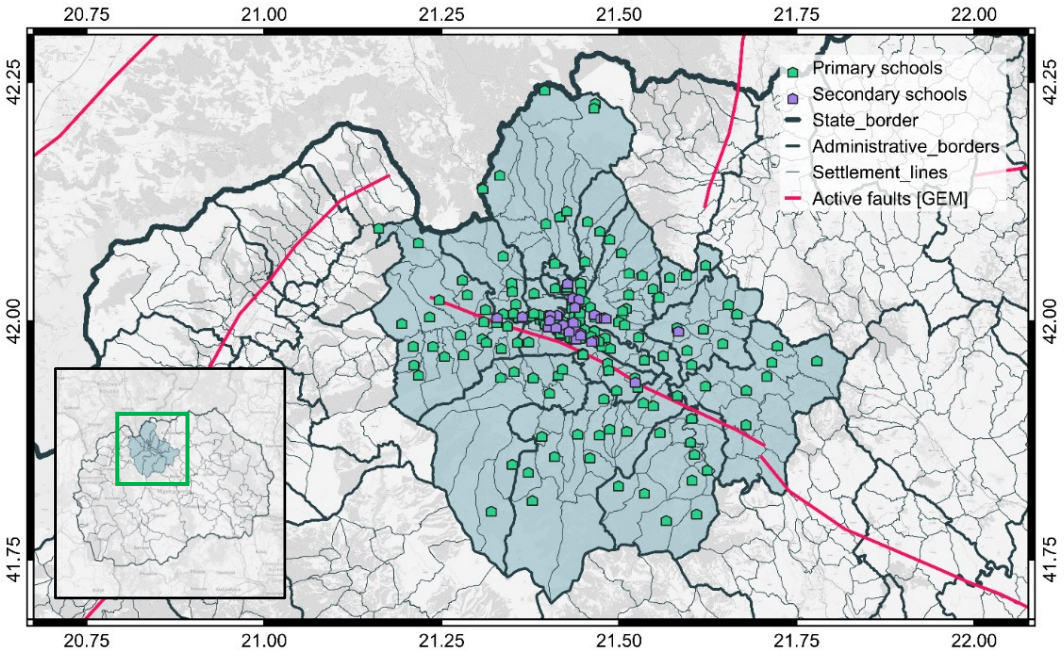


Figure 1. Spatial distribution of primary and secondary school buildings in Skopje region.

3.1. Scenario hazard and site characterisation

The territory of RNM lies on the Eurasian tectonic plate, centrally located within the Balkan Peninsula. Seismic activity in RNM is categorized into three main seismic zones that extend in a north-south direction: the West-Macedonian seismic zone, the Vardar seismic zone, and the East-Macedonian seismic zone, (Figure 2). The neotectonic faults map of RNM is also presented in Figure 2.

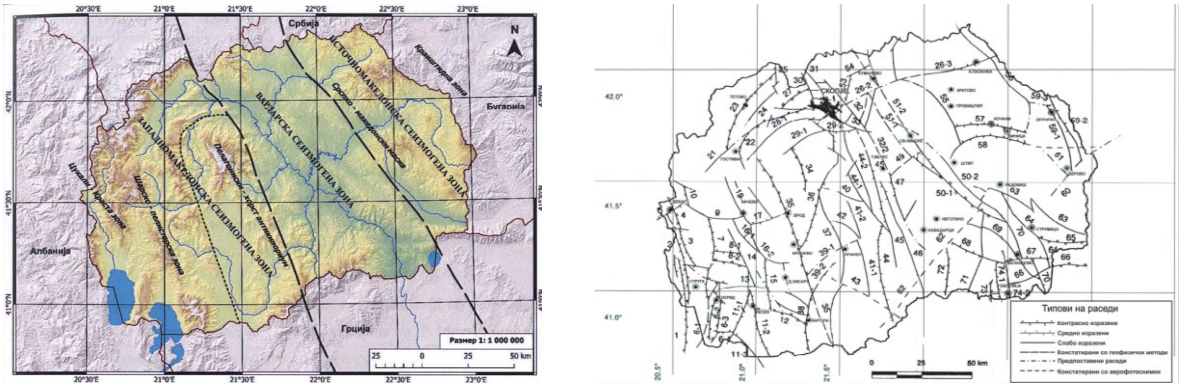


Figure 2. Main seismogenic zones and neotectonic units in RNM [14] (*left*); Map of neotectonic faults in the Republic of Macedonia [15] (*right*).

The Skopje region is located in the Skopje epicentral area and is closely associated with the seismic activity of the Skopje depression. This depression represents a neotectonic feature imposed on older geological structures of the Vardar seismic zone, extending partially into both the West- and East-

Copyright © 2025 CroCEE
DOI: https://doi.org/10.5592/CO/3CroCEE.2025.69

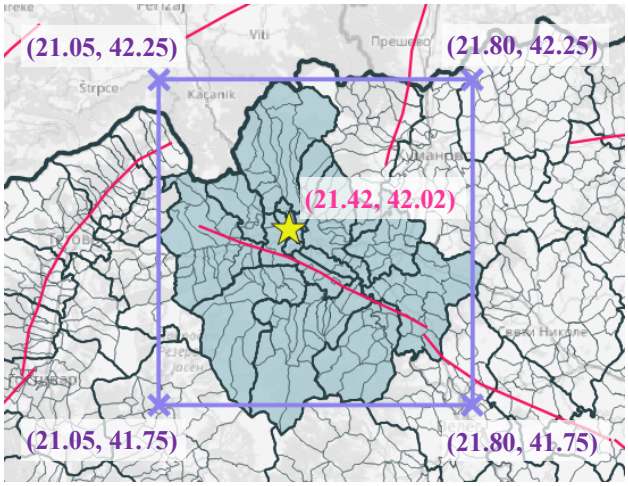
Macedonian zones. The Skopje depression is characterized by the intersection of faults with varying orientations, which has led to significant tectonic activity. The strongest earthquakes in this epicentral area are caused by the uplift and horizontal displacement toward the Skopska Crna Gora Mountain in the northern part of the region, relative to the Vodno mountain in the southern part of the region, along the Skopje-Kyustendil fault [14].

There have been three significant earthquakes with a magnitude of Mw > 6.0 in this region, all causing extensive destruction to the housing and infrastructure in the city of Skopje. The first occurred in the year 518, followed by another in 1555. The most recent earthquake, the one in 1963, will be utilized in this study to determine the hazard of the study area in a deterministic manner. This analysis will later be applied in the seismic risk assessment of damages and losses.

The 1963 Skopje earthquake had a local magnitude 6.10, hypocentral depth 15km and epicentral intensity IX according to [14]. In past studies, the hypocentral depth has also been reported as 5 km [16, 17]. This earthquake caused 1,070 deaths, more than 3,300 seriously injured people and left about 76% of the population without shelter, [18]. In addition to the large number of destroyed and damaged residential buildings, among the most damaged and destroyed typologies were public buildings. According to [19], 8 primary and 11 secondary school buildings were destroyed, and 22 primary and 13 secondary school buildings were severely damaged. All buildings of the University of Skopje were seriously damaged, which led to their forced demolition.

Since its occurrence, many studies have investigated the fault mechanism of this earthquake [16, 17, 20, 14]. The fault is generally considered to be of a strike-slip type, with [16] initially identifying its fault planes as approximately oriented either NW-SE or NE-SW.

In this study, the fault kinematics is modelled according to [14]. Technical information on earthquake and fault, along with the study area polygon, are provided in Figure 3.



Date	26.07.1963
Time	04:17:11.7
Longitude	42.02
Latitude	21.42
Local magnitude	$M_L = 6.10$
Moment magnitude	$M_W = 6.01$
Depth	$h = 15.0km$
Strike	303° WNW
Dip	77° NNE
Rake	-1°
Type of rupture	Normal-left-lateral
Beach ball diagram	

Figure 3. Study area and characteristics of the seismic rupture for 1963 Skopje earthquake according to [14].

To model the local site effects, information on the local site conditions (Vs_{30}), is obtained from USGS [21]. The Vs_{30} values are provided at a resulution of 0.00833° in both longitudonal and latitudonal directions. In total, there are 5,550 data points available for analysis. The *Institute of Earthquake Engineering and Engineering Seismology (IZIIS)* of Skopje has conducted seismic microzonation for several parts of RNM, and Skopje in particular, defining the ground geophysical parameters. The availability of these data will server for a better interpretation of local site effects, however, they will remain as a resource for potential future work for now.

The Ground Motion Prediction Equations (GMPEs) used in this study generally follow the logic tree established by [22]: AkkarBoomer2010 [23] (w=0.3), BooreAttkinson2011 [24] (w=0.25), Bindi2017 [25] (w=0.20) and CauzziFaccioli2008 [26] (w=0.25).

Copyright © 2025 CroCEE
DOI: https://doi.org/10.5592/CO/3CroCEE.2025.69

All the above-mentioned information regarding rupture mechanism, GMPEs and site conditions are input into the *Scenario Calculator* of the OpenQuake engine to compute ground motion fields (GMFs) for several intensity measures (IMs), which indicate the shaking intensity of the study area. To account for the aleatory variability associated with the GMPEs, a truncation level of 5 is utilized and 100 GMFs are generated for each GMPE, resulting in a total of 4000 realizations (4GMPEs*100GMFs). The average GMF for the IM of PGA is presented in Figure 4.

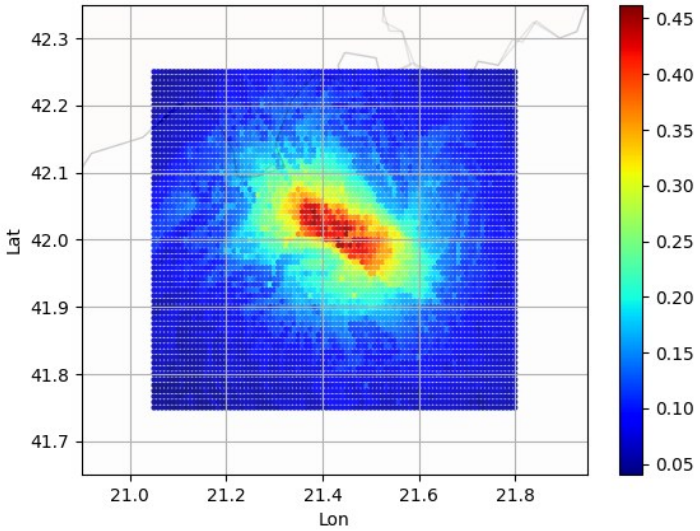


Figure 4. The average ground motion field for IM=PGA.

3.2. Exposure modelling of the school building stock

When conducting a seismic risk analysis, either in general or using the OpenQuake engine, the risk calculator requires an exposure model that includes: a metadata section containing general information about the exposed assets, a taxonomy section, and a cost conversion [27]. The general information on school buildings for the Skopje region is gathered from two sources:

- *Ministry of Education and Science (MES) of RNM* [28] – Provision of administrative information, such as the total number of school facilities, their full names and addresses, level (primary/secondary), status (central/regional), number of pupils, and number of employees at the beginning of the 2022/23 academic year. This information was available upon request.
- *Agency for Real Estate Cadastre (KAT) of RNM* [29] – Provision of the number of stories and net areas for all school buildings located in urban areas, as well as for some located in rural areas. This information is publicly available in.

3.2.1. School building taxonomies

Regarding the taxonomy, to ensure a unified characterization of the considered buildings, they are classified according to the GEM Building Taxonomy v3.2 [30]. It is important to mention the lack of data sources for most school buildings in the country in general, and for the Skopje region in specific. There are no official databases that provide accessible technical information and collecting these data through field and visual inspection on a building-by-building basis is a significant challenge, especially when there is no adequate funding. Therefore, the only available source of technical information is previous research studies and projects focused on school buildings. These available research studies and projects, along with the classification of the school buildings covered in them according to the GEM Building Taxonomy, are presented in [31]. For only Skopje region, the following sources are used for the classification of school buildings:

- The 2001 project of the IZIIS, supported by UNICEF Macedonia: *Physical and psychological management of earthquake related emergency situations in schools in the Republic of Macedonia* [32] [33].

Copyright © 2025 CroCEE
DOI: https://doi.org/10.5592/CO/3CroCEE.2025.69

- *Individual seismic risk assessment of school buildings* at the request of the municipalities or the school administration for one of the following reasons: the school board noticed significant damage in the structural parts of the schools and wanted to ensure that the damage was not structural, or the school board decided to make structural changes to the building (such as floor or story expansion, rearrangement of floor areas, improvement of roof structures, etc.). These individual assessments are all conducted by IZIIS.

These sources provide technical information for only *65* out of 193 school buildings, accounting for approximately *34%* of the total. Some of the attributes that are available for these school buildings include: the lateral load resisting system (LLRS), material type and construction technology; number of stories above ground and below ground, and the height of the ground floor level above grade; year of construction or retrofit; shape of the building plan; structural irregularities in plan and elevation; material of the external walls; roof shape, covering, and system; floor system material and type; and foundation system.

According to [34], the most relevant attributes for seismic risk are considered to be the LLRS and material, date of construction, height and wall material. Less important attributes include roof shape and material, ground floor hydrodynamics and plan orientation, and foundation type. Attributes considered irrelevant in seismic risk assessment include wall openings, presence of basement, and ground floor level.

Initially, in this research, school buildings are classified by systematizing all available attributes, including both the most relevant to seismic risk and some less significant ones. As a result of considering a substantial number of attributes, more than fifty unique building classes were identified. A representation of the identified typologies for the most important attributes is provided in Figure 5.

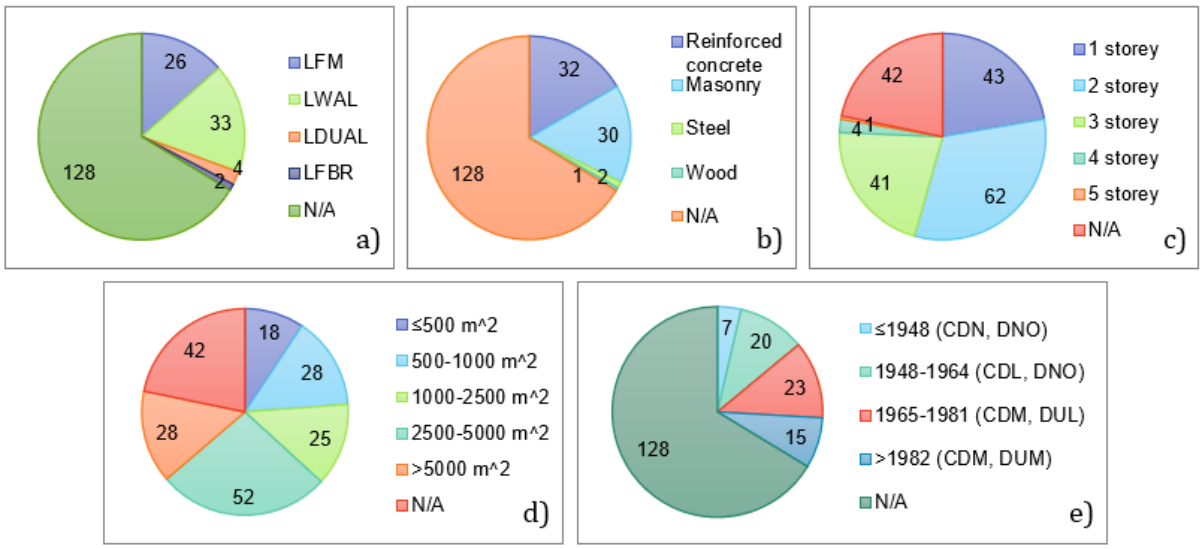


Figure 5. Pie charts representing the identified typologies for each main attribute: a) LLRS; b) Material type; c) Number of stories above ground; d) Area; and e) Date of construction. *Note: Abberivations are as per* [30].

The date of construction attribute is linked to the code and ductility level of the structure. A state-of-the-art concept regarding the genealogy of codification in the territory of RNM is presented in [35]. However, this concept differs from the one proposed in [36], which is considered in [37, 38] for exposure modelling of buildings in the territory of RNM in the European Seismic Risk Model (ESRM20) [39]. The difference lies in the classification of buildings constructed after 1981: they are categorized as *high code* (CDH) by the first source, and as *moderate code* (CDM) by the latter.

Nevertheless, considering that the vulnerability and fragility functions for school buildings utilized here are derived from the ESRM20, the categorization based on [36] is adopted for the code levels of the

Copyright © 2025 CroCEE
DOI: https://doi.org/10.5592/CO/3CroCEE.2025.69

buildings, whereas the categorization for ductility level is taken from [35]. These categorizations are given in Figure 5/e.

Since the exposure model here includes all school buildings in the Skopje region, it is noted that *67%* of the buildings lack information about their structural typology because they have not been studied in previous research. Among these, *86* buildings (roughly *45%* of the total) have only general information available, such as location, area, number of stories, and the number of pupils and staff, as provided by MON and KAT. Additionally, there are *42* buildings (roughly *21%* of the total) for which only partial general information is available, such as location and the number of pupils and staff (MES).

The overall dataset of school buildings is composed of three types of datasets with varying levels of epistemic uncertainty. To address this shortcoming – and considering that not all of the fifty unique building classes in the first group are numerically significant, as some differ only in attributes irrelevant to seismic risk – a taxonomy mapping scheme is utilized.

The step-by-step process of exposure modelling is presented in Figure 6 through a workflow diagram. Data that is automatically read from the resources are shown in green, while actions taken to classify the buildings are marked in blue. Mathematical calculations made during the process are marked in yellow.

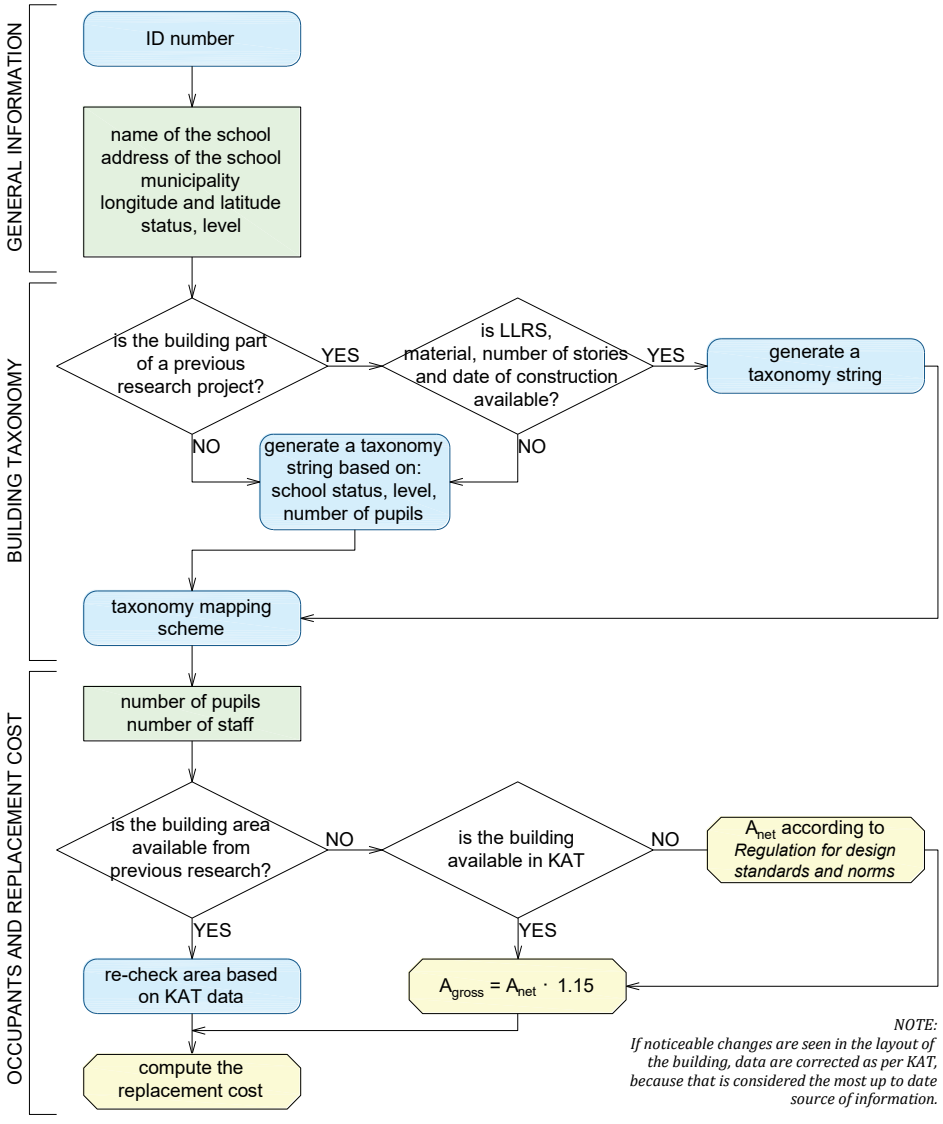


Figure 6. Workflow for exposure modelling of school buildings.

Copyright © 2025 CroCEE
DOI: https://doi.org/10.5592/CO/3CroCEE.2025.69

For buildings with partial taxonomy strings (45%) or those entirely lacking them (21%), assumptions regarding the unavailable data are primarily based on the school status and level, and number of pupils. These assumptions are based on the statistical analysis from the classification of school buildings from previous research and individual assessments and engineering judgement, enabling the assignment of appropriate taxonomy strings. For buildings with already defined strings, the mapping scheme is used only as a connector with a suitable vulnerability/fragility function.

One of the most important types of information that is missing for most structures is the year of construction or retrofit. This will remain an epistemic uncertainty that can be mitigated by conducting more detailed inspections.

3.2.2. Replacement cost

The replacement cost in this research is defined *per asset* and per *unit area*. The area of each school building is determined either through a previous research project, obtained from KAT, or assumed based on the *Regulation for Design Standards and Norms* published in the Official Gazette of RM (no. 60/12, 29/15, 32/16, 114/16) and the Official Gazette of RNM (no. 211/20), as shown in Figure 6.

The structural replacement cost of school buildings is assumed to be 50,220.00MKD/m^2 equivalent to 800€/m^2. This value is taken as a reference value for construction of school buildings, given in the official *Price list for engineering services for building construction*, published in the Official Gazette of RNM (no. 259/22, 2022). The overall area of the school buildings for the Skopje region amounts to *544,225m²*, whereas the total replacement cost is *€435,380,000.*

Although it is well understood that buildings constructed with different materials and technologies, as well as those in different areas, should have varying unit prices per area, this study considers only the most conservative scenario for the sake of simplicity.

3.3. Fragility and vulnerability models

The fragility and vulnerability models considered in this research are those developed for the European Seismic Risk Model (ESRM20) [39]. Notably, these models also serve as the basis for the fragility and vulnerability of Europe employed in the Global Seismic Risk Model [40].

For the fragility models, four damage states are defined: DS1 (slight), DS2 (moderate), DS3 (extensive) and DS4 (complete), where their thresholds are illustrated in Figure 7.

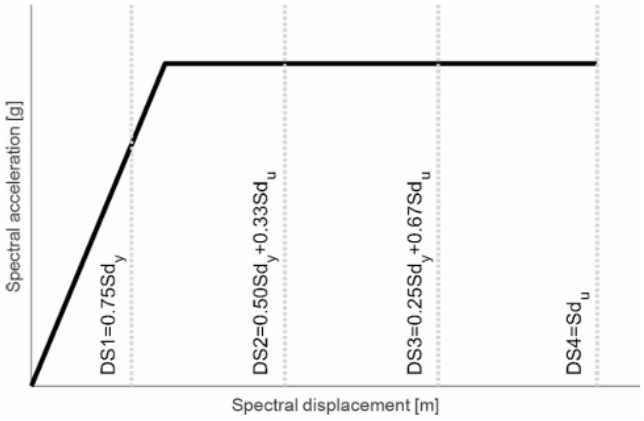


Figure 7. Damage thresholds according to [41].

Using damage-loss models, the fragility functions are converted into vulnerability models. For losses due to damage, the following damage ratios, representing the ratio of repair cost to replacement cost, are adopted: 0.05 for slight damage, 0.15 for moderate damage, 0.6 for extensive damage, and 1.0 for complete damage [39].

Copyright © 2025 CroCEE
DOI: https://doi.org/10.5592/CO/3CroCEE.2025.69

4. Risk analysis of school buildings in Skopje region

Considering the input provided in the previous subsections, scenario damages and losses were computed using the OpenQuake engine for the exposed school buildings of Skopje region.

4.1. Scenario damage

The damage of school buildings was assessed using the *Scenario Damage Calculator* from the OpenQuake engine. The output of this analysis provides the probability (expressed as a fraction) of each building reaching a specific damage state per ground motion field. The mean damage distributions for all the assets, along with the corresponding standard deviations, are presented in Figure 8.

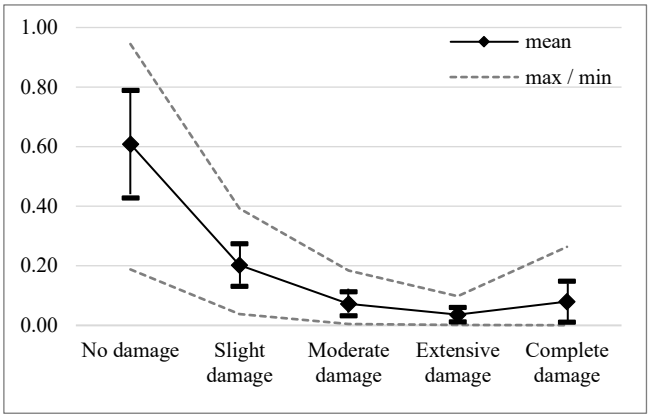


Figure 8. Mean and standard deviation of damage distribution statistics for the current conditions.

From this figure, we can observe that the majority of buildings show *no damage* due to the imposed earthquake. The probability of any asset reaching one of the other damage states is generally less than 20%.

Referring to the observed damage during the 1963 Skopje earthquake, as referenced earlier from [19], 8 primary and 11 secondary school buildings were destroyed, and 22 primary and 13 secondary school buildings were severely damaged. There were also other school buildings that sustained moderate or slight damage state. However, this situation is not reflected in the graph if a similar earthquake were to strike today. The reason for this discrepancy is that the exposure model is primarily based on data from the year 2001, which is 38 years after the earthquake occurred. During these years, school buildings were not only repaired and retrofitted, but two new seismic design building codes were also introduced (JUS39/64 and later JUS31/81). The 1963 Skopje earthquake significantly increased awareness among both the public and governmental authorities, and this is reflected in the results presented in this study.

The damage statistics indicate that the most vulnerable buildings are those located near the earthquake epicenter. This is expected, as Figure 4 shows higher PGA values in that region. Regarding the building taxonomies, the highest probabilities of complete damage (0.20-0.26) are observed in schools primarily belonging to RC and masonry structures with 2 or 3 stories.

4.1.1. Scenario losses

The losses of school buildings were assessed using the *Scenario Loss Calculator* from the OpenQuake engine. In this study, only structural losses were observed, and results are presented in the form of loss maps and statistics.

The mean structural loss of school buildings in the Skopje region is estimated at *€76,054,600*. This represents approximately *17%* of the total area of the schools. While this percentage may not seem very high, it is still significant. The losses are concentrated in only some of the school buildings, as most of the school buildings, as previously noted, do not exceed the no damage and slight damage state.

The aggregated mean losses at the municipality and settlement levels are presented in Figure 9.

Copyright © 2025 CroCEE
DOI: https://doi.org/10.5592/CO/3CroCEE.2025.69

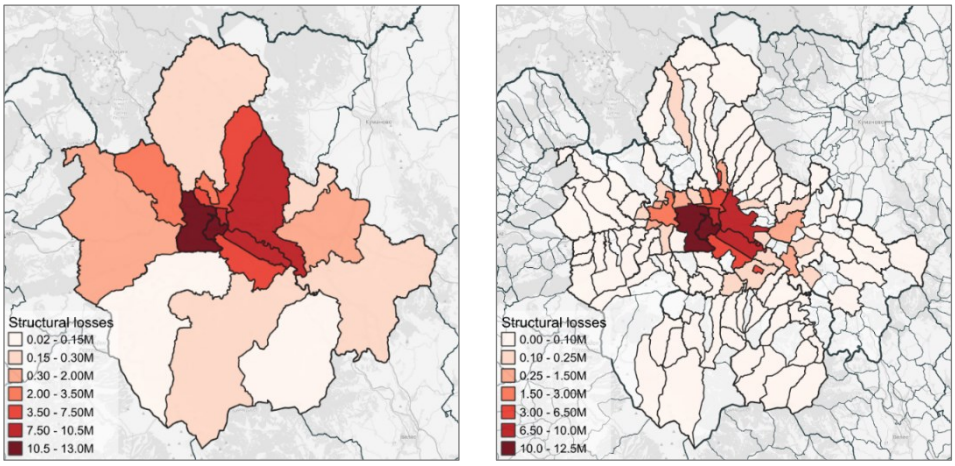


Figure 9. Aggregated structural losses (€) at municipality level (left) and settlement level (right).

The largest structural losses are observed in the municipalities of Karpos and Centar, followed by Cair, Gazi Baba, and Aerodrom. These municipalities are located closer to the epicentre of the earthquake event, and a similar trend was noted during the damage assessment. Located in these municipalities, structural losses exceeding €1 million are observed in 27 school buildings, both RC and masonry structures, primarily with three stories. These buildings typically accommodate more than 200 pupils and have areas exceeding 3500m².

5. Conclusions

This research addressed the scenario-based seismic risk assessment of school buildings in the Skopje region, focusing on the 1963 Skopje earthquake. The total area of school buildings in the amounts to 544,225m², with a total replacement cost of €435,380,000. The study outcomes include damage and loss statistics for individual schools, as well as aggregated data at the municipality level.

The majority of buildings exhibit *no damage* or only *slight damage* due to the imposed hazard. The probability of reaching moderate to severe damage states remained below 20% for most buildings, with a 20-26% probability of complete damage observed in only 12 buildings near the earthquake's epicentre. These were predominantly RC and masonry structures with two or three stories.

The total expected structural loss amounts to approximately 17% of the total school area, equivalent to an estimated €76,054,600.

Finally, it is important to note that significant uncertainties associated with assessing damage and losses based on a single event, as highlighted in [42]. While estimating seismic risk from a single earthquake scenario (deterministic approach) is valuable for raising public awareness and informing decision-makers, a probabilistic seismic risk assessment would be a more proper method for prioritizing risks, planning mitigation, and supporting insurance decisions.

References

[1] State Statistical Office (2022): *Census of population, households and dwellings in the Republic of North Macedonia, 2021*, Republic of North Macedonia, Skopje.

[2] Bozinovski, Z., Stojanovski, B. and Apostolska, R. (1995): Rehabilitation and strengthening of the main structural system and stability analysis of 20 school buildings on the territory of Bitola municipality. *IZIIS Report 1995-26 to 1995-45*, IZIIS, Skopje, North Macedonia.

[3] Milutinovic, Z., Bozinovski, Z., Trendafiloski, G. and Olumceva, T (2001): Seismic risk of school buildings, measures and priorities for its mitigation, recommendations for physical and psychological management of emergency situations. *IZIIS Report 2001-49,* IZIIS, Skopje, North Macedonia.

Copyright © 2025 CroCEE
DOI: https://doi.org/10.5592/CO/3CroCEE.2025.69

[4] Apostolska, R., Necevska-Cvetanovska, G., Shendova, V. and Bojadjieva, J. (2018): Seismic performance assessment of "hybrid" structures using two-level multy group GIS oriented approach: Case studies. *Bulletin of Earthquake engineering,* **16** (10), 4797-4824.

[5] Shendova, V., Apostolska, R. and Sheshov, V. (2022): High level seismic screening of the structures of municipal buildings in North Macedonia. *IZIIS Report*, IZIIS, Skopje, North Macedonia.

[6] Sheshov, V., Apostolska, R., Salic, R., Vitanova, M., Stojmanovska, M., Bogdanovic, A., Jekic, G., Borzi, B., Zuccolo, E., Bozzoni, F., Di Meo, A., Pitilakis, D., Riga, E., Fotopoulou, S., Petridis, Ch., Stefanoski, S., Shkodrani, N. and Baballëku, Sh. (2023): Multi-hazard risk assessment of basic services and transport infrastructure in RN Macedonia, Greece and Albania, cross-border region - CRISIS project. *Building for the future: durable, sustainable, resilient.* Springer, Cham.

[7] Silva, V., Crowley, H. and Pagani, M. (2014): Development of the OpenQuake engine, the Global Earthquake Model's open-source software for seismic risk assessment. *Natural Hazards*, **72**, 1409-1427.

[8] Pagani, M., Monelli, D., Weatherill, G., Danciu, L., Crowley, H., Silva, V., Henshaw, P., Butler, L., Nastasi, M., Panzeri, L., Simionato, M. and Vigano, D. (2014): OpenQuake Engine: An open hazard (and risk) software for the Global Earthquaka Model. *Seismological Research Letters*, **85** (3), 692-702.

[9] Mircevska, V., Abo-El-Ezz, A., Gjorgjeska, I., Smirnoff, A. and Nastev, M. (2019): First-order seismic loss assessment at urban scale: A case study of Skopje, North Macedonia. *Journal of Earthquake Engineering*, **26** (1), 70-88, doi: xxxxxxxxxx

[10] Ribeiro, F. L., Candeias, P. X., Correia, A. A., Carvalho, A. R. and Costa, A. C. (2022): Risk and resilience assessmentt of Lison's school buildings based on seismic scenarios. *Applied Sciences,* **12** (17), 8570.

[11] Jeswani, K., Guo, J. and Christopoulos, C. (2022): Seismic risk assessment and mitigation analysis of large public school building portfolios in Metro Manila. *Earthquake Spectra*, **38** (3), 1946-1971.

[12] Villar-Vega, M. and Silva, V. (2017): Assessment of earthquake damage considering the characteristics of past events in South America. *Soil Dynamics and Earthquake Engineering,* **99,** 86-96.

[13] Milutinovic, Z., Salic, R., Dumurdzanov, V., Cejkovska, V., Pekevski, L. and Tomic, D. (2016): Seismic zoning map with seismic hazard elements, return period 475 years. Institute of earthquake engineering and engineering seismology, Skopje, North Macedonia.

[14] Drogreshka, K (2018): Application of dislocation theory in defining epicentral areas and tectonic conditions on the territory of the Republic of Macedonia. *PhD thesis*, Ss. Cyril and Methodius University in Skopje, North Macedonia.

[15] Arsovski, M. (1997): *Tectonics in Macedonia*. University of Shtip, North Macedonia.

[16] Zatopek, A. (1968): The Skopje earthquake of 26 July 1963 and the seismicity in Macedonia. *UNESCO*.

[17] Anderson, H. and Jackson, J. (1987): Active tectonics of the Adriatic region. *Geophysical Journal International,* **91** (3), 937-983.

[18] Petrovski, J. T. (2003): Damaging effects of July 26 1963, Skopje earthquake, *International Conference in Earthauqke Engineering*, Skopje, North Macedonia, 16 pages.

[19] Jurukovski, D. (1997): Experience from rehabilitation and reconstruction of Skopje after the 1963 earthquake, *WHO Centre for Health Development, Earthquakes and People's Health,* Kobe, Japan, 3 pages.

[20] Suhadolc, P., Sandron, D., Fitzko, F., and Costa, G. (2004): Seismic ground motion estimates for the m6.1 earthquake of July 26, 1963 at Skopje, Republic of Macedonia. *Acta Geodaetica et Geophysica Hungarica,* **39** (2-3), 319-326.

[21] U.S. Geological Survey: *Vs30 Models and Data*. Available at: https://earthquake.usgs.gov.

[22] Salic, R. (2016): A modern approach to determining seismic hazard in the Republic of Macedonia. *PhD thesis*, Ss. Cyril and Methodius University in Skopje, North Macedonia.

[23] Akkar, S. and Boomer, J. (2017): Empirical Equations for the Prediction of PGA, PGV, and Spectral Accelerations in Europe, the Mediterranean Region, and the Middle East. *Seismological Research Letters,* **81** (2), 195-206.

Copyright © 2025 CroCEE
DOI: https://doi.org/10.5592/CO/3CroCEE.2025.69

[24] Atkinson, G. M. and Boore, D. M. (2011): Modifications to existing ground-motion prediction equations in light of new data. *Bulletin of the Seismological Society of America*, **101** (3), 1121-1135.

[25] Bindi, D., Cotton, F., Kotha, S. R., Bosse, C., Stromeyer, D. and Grünthal, G. (2017): Application-driven ground motion prediction equation for seismic hazard assessments in non-cratonic moderate-seismicity areas. *Journal of Seismology*, **21** (5), 1201-1218.

[26] Cauzzi, C. and Fazzioli, E. (2008): Broadband (0.05 to 20s) prediction of displacement response spectra based on worldwide digital records. *Journal of Seismology*, **12**, 453-475.

[27] GEM (2020): The OpenQuake-engine user manual version 3.10.1. GEM Foundatuon, Pavia, Italy.

[28] Ministry of Education and Science of North Macedonia: (2023). Personal correspondace.

[29] Agency of Real Estate Cadastre. Available at: http://www.katastar.gov.mk.

[30] Silva, V., Henshaw, P., Huyck, C., and O'Hara, M. (2018): GED4ALL - Global exposure data for multi-hazard risk analysis. *Technical Report 2018-05,* GEM Foundatuon, Pavia, Italy.

[31] Jusufi, L. and Apostolska, R. (2024): Exposure modeling of school buildings in Republic of North Macedonia, *20th World Conference of Earthquake Engineering*, Milano, Italy, NR pages.

[32] Milutinovic, Z., Bozinovski, Z., Trendafiloski, G., and Olumceva, T. (2001): Catalogue of typical school buildings. *IZIIS Report 2001-46 (Volume II)*, Institute of earthquake engineering and engineering seismology, Skopje, North Macedonia.

[33] Milutinovic, Z., Bozinovski, Z., Olumceva, T. and Trendafiloski, G. (2001): Inspectd school buildings in the municipalities of Berovo, Bitola, Debar, Gevgelija and the city of Skopje. *IZIIS Report 2001-47 (Volume III)*, Institute of earthquake engineering and engineering seismology, Skopje, North Macedonia.

[34] Dabbek, J. and Silva, V. (2021): Modeling the residential building stock in the Middle East for multi-hazard risk assessment. *Natural hazards,* **100** (2), 781-810.

[35] Milutinovic, Z., Salic, R., Tomic, D. and Trajcevski, J. (2022): Genealogy of development and codification of Yugoslavian earthquake resistant design. *Bulletin of Earthquake Engineering,* **20** (13), 7513-7559.

[36] Paz, M. (1994): *International handbook of earthquake engineering practices*, *vol. Chapter 38: (Former) Yugoslavia*, Publisher: Springer New York, USA.

[37] Crowley, H., Despotaki, V., Silva, V., Dabbeek, J., Romão, X., Pereira, N., Castro, J. M., Daniell, J., Veliu, E., Bilgin, H., Adam, C. (2021): Model of seismic design lateral force levels for the existing reinforced concrete European building stock. *Bulletin of Earthquake Engineering,* **19,** 2839-2865.

[38] Romão, X, Pereira, N., Castro, J. M., Crowley, H., Silva, V., Martins, L., De Maio, F. (2021): European building vulnerability data repository (v2.1) [Data set], Zenodo.

[39] Crowley, H., Dabbeek, J., Despotaki, V., Rodrigues, D., Martins, L., Silva, V., Romão, X., Pereira, N., Weatherill, G., Danciu, L. (2021): European Seismic Risk Model (ESRM20), *EFEHR Technical Report 002 V1.0.0*.

[40] Silva, V., Calderon, A., Caruso, M., Costa, C., Dabbeek, J., Hoyos, M. C., Karimzadeh, Z., Martins, L., Paul, N., Rao, A., Simionato, M., Yepes-Estrada, C., Crowley, H., Jaiswal, K. (2023): Global Earthquake Model (GEM) Seismic Risk Map, *V.2023.1*.

[41] Martins, L. and Silva, V. (2020): Development of a fragility and vulnerability model for global seismic risk analysis. *Bulletin of Earthquake Engineering,* **19** (15), 6719-6745.

[42] Silva, V. (2016): Critical issues in earthquake scenario loss modelling. *Journal of Earthquake Engineering,* **20** (8), 1322-1341.

Proceedings of the 3rd Croatian Conference on Earthquake Engineering - 3CroCEE
19–22 March 2025, Split, Croatia
Copyright © 2025 CroCEE
DOI: https://doi.org/10.5592/CO/3CroCEE.2025.75

SEISMIC VULNERABILITY ASSESSMENT OF PART OF HISTORIC CENTER OF SKOPJE

Aleksandar Zlateski [(1)], Elena Delova [(2)], Veronika Shendova [(3)],

[(1)] *Assistant Professor, Ss. Cyril and Methodious University in Skopje, Republic of North Macedonia, Institute of Earthquake Engineering and Engineering Seismology, Skopje, azlate@iziis.ukim.edu.mk*
[(2)] *Research Assistant, Ss. Cyril and Methodious University in Skopje, Republic of North Macedonia, Institute of Earthquake Engineering and Engineering Seismology, Skopje, delova@iziis.ukim.edu.mk*
[(3)] *Professor, Ss. Cyril and Methodious University in Skopje, Republic of North Macedonia, Institute of Earthquake Engineering and Engineering Seismology, Skopje, veronika@iziis.ukim.edu.mk*

Abstract

Urban historic centers, consisting mostly of vulnerable unreinforced stone and brick masonry structures constructed without seismic design considerations, experience significant earthquake damage. This paper uses a vulnerability index method to obtain and discuss a pre-earthquake vulnerability assessment of a representative part of Skopje's Old Bazaar. This method calculates a score for each building based on a weighted sum of key parameters related to its seismic response, categorizing them into different vulnerability classes. The vulnerability index has been previously adapted and calibrated to reflect the unique features of Skopje's urban historic center.

The research aims to create a seismic vulnerability map for the Bazaar, ultimately safeguarding the urban historic center of Skopje and protecting lives through timely structural assessments and the identification of the most at-risk buildings.

The research draws on recent advancements in the field, utilizing calibrated methodologies based on data from past earthquakes and extensive knowledge of the historic buildings in the Old Bazaar. Consequently, the results are sustainable and can be effectively applied to the entire historic center of Skopje, as well as modified for other hazard events in the future.

Keywords: Masonry structures, Historical centers, Vulnerability Assessment, Damage Grade.

1. Introduction

Masonry has been used as a structural material in a wide range of forms for thousands of years. Urban historic centers, almost without exception, consist of complexes of masonry buildings, and stone and brick structures are among the most common, not only in Europe but worldwide. In areas with high seismic activity, masonry structures suffer the most damage during earthquakes. Considering this, it is easy to conclude that the assessment of the vulnerability of masonry buildings in a given urban area directly depends on defining seismic resistance, which is a key condition for assessing overall risk.

The negligible tensile strength, heterogeneity, and anisotropy of the material in masonry are among the main reasons for the weak resistance of masonry structures under seismic actions. Additionally, masonry structures typically have flexible inter-floor diaphragms, often with inadequate connections to the load-bearing walls of the structure. Among the various failure mechanisms in masonry buildings, the most observed is the separation of facade load-bearing walls from other parts of the structure. This type of structural failure is particularly dangerous in densely populated urban areas (historical city centers generally built with masonry structures). First, due to the direct consequences that can result in system collapse, in terms of casualties and economic losses, and second, due to its indirect impact, such as obstructing overall infrastructure due to debris and rubble accumulation.

Given this, it can easily be concluded that assessing the seismic vulnerability of masonry structures is a fundamental step toward defining more effective strategies for their repair and strengthening. To this end, when assessing larger urban areas, it is first necessary to present expected scenarios to identify

Proceedings of the 3rd Croatian Conference on Earthquake Engineering - 3CroCEE
19–22 March 2025, Split, Croatia
Copyright © 2025 CroCEE
DOI: https://doi.org/10.5592/CO/3CroCEE.2025.75

potentially vulnerable buildings or urban areas that require special attention and to determine the most suitable reinforcement methods for them.).

2. Vulnerability Index Method for Urban Historic Centers

The considered vulnerability index method represents an innovative hybrid methodology for bridging the gap between empirical and analytical methods and provides seismic vulnerability assessment by using simplified scoring method. This method has been originally developed by [2], adapted and applied to several historic centres in Portugal [3, 4, 7], and calibrated using post-earthquake damage data, [8]. This methodology also has been successfully calibrated and implemented for vulnerability assessment in order to evaluate, manage and mitigate the earthquake risk in the historical center of Coimbra, Portugal, with the urban configuration very similar to Skopje old Bazar, [11].

The vulnerability index is obtained by the calculation of a score as the weighted sum of 14 parameters,

$$I_{vf}^{*} = \Sigma_{i=1}^{14} c_{vi} p_{vi} \quad (1)$$

Table 1 – Vulnerability index associated parameters classes and weights (according [3] and [8])

Parameters	Class, C_{vi}				Weight, p_i	
	A	B	C	D	Original	Calibrated
1. Structural building system						
P1. Type of resisting system	0	5	20	50	0.75	2.50
P2. Quality of resisting system	0	5	20	50	1.00	2.50
P3. Conventional strength	0	5	20	50	1.50	1.00
P4. Maximum distance between walls	0	5	20	50	0.50	0.50
P5. Number of floors					1.50	0.50
P6. Location and soil condition	0	5	20	50	0.75	0.50
2. Irregularities and interactions						
P7. Aggregate position and interaction	0	5	20	50	1.50	1.50
P8. Irregularity in plan	0	5	20	50	0.75	0.50
P9. Irregularity in height	0	5	20	50	0.75	0.50
3. Floor slabs and roofs						
P10. Alignment of openings	0	5	20	50	0.50	0.50
P11. Horizontal diaphragms	0	5	20	50	1.00	0.75
P12. Roof systems	0	5	20	50	1.00	0.50
4. Conservation status and other elements						
P13. Fragilities and conservation status	0	5	20	50	1.00	1.00
P14. Non-structural elements	0	5	20	50	0.50	0.75

Each parameter shown in Table 1 covers one aspect related to the building's seismic response and is distributed into four vulnerability classes (c_{vi}) of growing vulnerability: A, B, C and D.

The first group includes parameters (P1, P2) that characterize the structural system of the building and define its structural behaviour, including the quality of the masonry through the material (size, shape, and type of masonry), layout, and level of connection between walls. Parameter P3 is one of the most important because it quantitatively assesses shear strength.

The assessment of the vulnerability class for parameter P4 (maximum distance between walls) essentially depends on the ratio L/s and H/s. L/s represents the ratio between the maximum span between load-bearing walls, L, and the average wall thickness, s; H/s represents the ratio between the average inter-story height, H, and the average wall thickness, s. Parameter P4 evaluates the contribution level of walls and implicitly the risk of out-of-plane collapse.

Copyright © 2025 CroCEE
DOI: https://doi.org/10.5592/CO/3CroCEE.2025.75

Parameter P5 assesses the height of the buildings and is directly defined as a function of the number of floors. The vulnerability classes for the parameter related to location and soil condition (P6) are mainly assigned as a function of the specific soil type, based on the definition provided in EN 1998-1.

The second group of parameters mainly focuses on the location and interaction between buildings. Parameter P7 is extremely important for vulnerability because, in dense urban areas, adjacent masonry structures are connected or placed next to each other without space between them. This configuration significantly affects the vulnerability of the building of interest in terms of stiffness, strength, and deformability. This characteristic is not considered in other methodologies but is particularly important because the seismic response of the entire area as a whole differs greatly from the response of a single building.

A drawback of this method is that it does not address so-called "corner buildings," located at the edges or corners of a specific block. According to evidence from past earthquakes, "corner buildings" suffer the most damage compared to other buildings in a given urban block. Therefore, to overcome this limitation of the method, corner buildings are proposed to be classified in the lowest vulnerability class, i.e., for such buildings, the parameter P7 should be assigned the class "D."

Parameters P8 and P9 evaluate irregularities in the building's base and height. Four different configurations are identified as generally representative of many urban areas: square shape, rectangular shape, L-shape, and L-square shape.

The parameter for the layout of openings (P10) identifies the irregularity of openings along the height of the walls. The highest class corresponds to a configuration where the openings are regular and aligned; vulnerability class B is assigned to horizontal misalignment, and vulnerability class C is assigned to both horizontal and vertical irregularities. Finally, vulnerability class D corresponds to situations where openings are misaligned both horizontally and vertically (class C), the presence of a large opening at the ground floor level, a common but erroneous practice observed in many buildings in historical centers.

The remaining two parameters from the third group (P11 and P12) evaluate the horizontal load-bearing substructures and essentially assess the level of connection between the inter-floor structures and the main load-bearing system. Horizontal diaphragms can thus be rigid or flexible and well or poorly connected to the rest of the load-bearing system.

Parameter P13 assesses the level of damage to a specific building, i.e., the current condition of the structure. This includes all observed damages as well as any structural interventions.

The final parameter, P14, considers the presence of external non-structural elements such as balconies, ornaments, chimneys, and so on. Despite their non-structural nature, the presence of such elements must be considered due to the risk associated with their fall or the potential development of localized damage, which could potentially trigger partial collapse mechanisms.

2.1. Harmonized Vulnerability Index for Urban Historic Center of Skopje

The key aspect of this method is determining the vulnerability class for each parameter, ensuring it aligns with the unique features of historic buildings within the urban historic center. A critical component of this process involves identifying the specific independent parameters characteristic of the historic urban area in the old part of Skopje and defining the correlation between these selected structural parameters and their assigned vulnerability classes - levels A, B, C, or D for each parameter.

The available literature on seismic vulnerability assessment of historical centers, related to the collected data that has been accumulated over the past decades about post-earthquake damage surveys and interventions in the historical center of Skopje [1, 5, 6 ,9], opens a unique opportunity to set-up of vulnerability index method, harmonized with the specific characteristics of the specified urban historic center. This was the starting point of the internal IZIIS' project as a contribution to the governmental long-term project on Skopje Old Bazaar revitalization.

Proceedings of the 3rd Croatian Conference on Earthquake Engineering - 3CroCEE
19–22 March 2025, Split, Croatia
Copyright © 2025 CroCEE
DOI: https://doi.org/10.5592/CO/3CroCEE.2025.75

Based on the gathered knowledge about the structures in the Old Bazaar, the relationship between the selected specific independent structural parameters (P - P14) and the vulnerability class levels has been established (as shown in Tables 2, 3, 4, and 5). The content of these tables, along with the corresponding diagrams and detailed explanations provided in Figures 1, 2, and 3, forms part of the harmonized vulnerability index. This index links the independent structural parameters to their associated vulnerability class levels, specifically tailored to the historic buildings of Skopje's Old Bazaar [12].

Table 2 – Harmonized independent parameters associated to vulnerability class, Type of resisting system P1, Quality of resisting system P2 (P3, P13)

Class C_{vi}	**P1 Resisting system**	**P2, Quality of resisting system**						**P3, P13 Cracked stiffness**
		Mortar	**w kN/m³**	**f_c kPa**	**f_t kPa**	**E MPa**	**G MPa**	
A	Confined masonry	Cement	22	800	40	4200	1400	1.00
B	Brick/stone masonry	Lime/cement	20	600	30	3300	1100	0.83
C	Brick/stone masonry	Lime	19	400	20	2100	700	0.67
D	Adobe masonry	Adobe mud	18	100	5	450	150	0.50

Table 3 – Harmonized independent parameters associated to vulnerability class, Distance between walls P4, Number of floors, P5, Location and soil type P6

Class C_{vi}	**P4 Maximum distance between walls (l/d, h_0/d) wall thickness:**	**P5 Number of floors**	**P6 Location and soil condition (according EN 1998-1)**
A	0.60 m	1	A
B	0.50 m	2	B
C	0.40 m	3	C
D	0.30 m	enlarging/ upgrading	D, E

Table 4 – Harmonized independent parameters associated to vulnerability class, Position - interaction P7, Irregularity in plan P8, Irregularity in height P9

Class C_{vi}	**P7**	**P8**	**P9 change in vertical elements' geometry**
A	Figure 1, a	Figure 2, a	0%
B	Figure 1, b	Figure 2, b	up to 10%
C	Figure 1, c, d	Figure 2, c	(10 -20) %
D	Figure 1, e, f	Figure 2, d	(20 – 30) %

Table 5 – Harmonized independent parameters associated to vulnerability class, Alignment of openings P10, Horizontal diaphragms P11, (Roof structure P12)

Class C_{vi}	**P10 Alignment of openings**	**P11, P12 Horizontal diaphragms (Roof structures)**
A	Figure 3, a, regular and aligned	Rigid and well connected
B	Figure 3, b, horizontal misalignment	Flexible and well connected
C	Figure 3, c, horizontal and vertical misalignment	Rigid and poorly connected
D	Figure 3, d, large openings on ground floor	Flexible and poorly connected

Copyright © 2025 CroCEE
DOI: https://doi.org/10.5592/CO/3CroCEE.2025.75

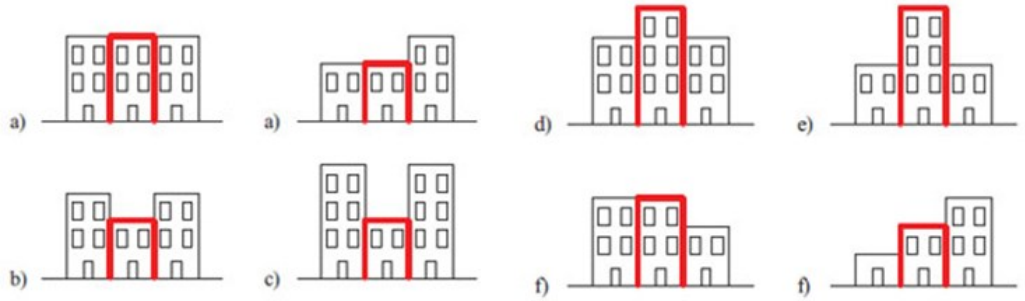


Figure 1. Building position (figure according [10)]

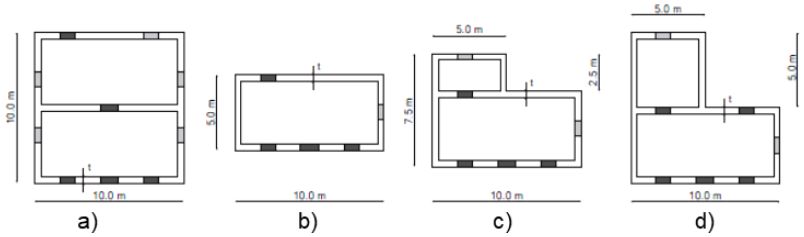


Figure 2. Plan regularity (figure according [10)]

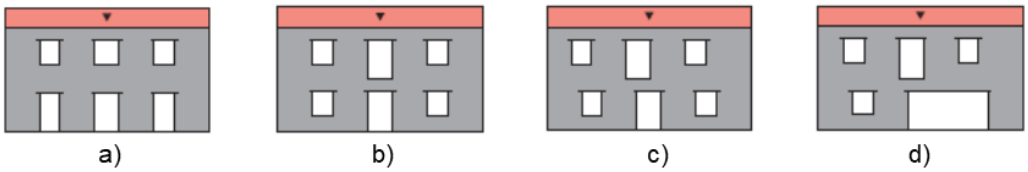


Figure 3. Alignments in openings (figure according [10)]

This section provides a clear and practical guideline for pre-earthquake vulnerability assessment of a specific historic urban center, designed for use by key target groups such as architects and civil engineers involved in the seismic protection of structures with cultural heritage significance. The goal is to develop a vulnerability index method tailored to the specific independent parameters and associated vulnerability class levels unique to the historic buildings in Skopje's Old Bazaar.

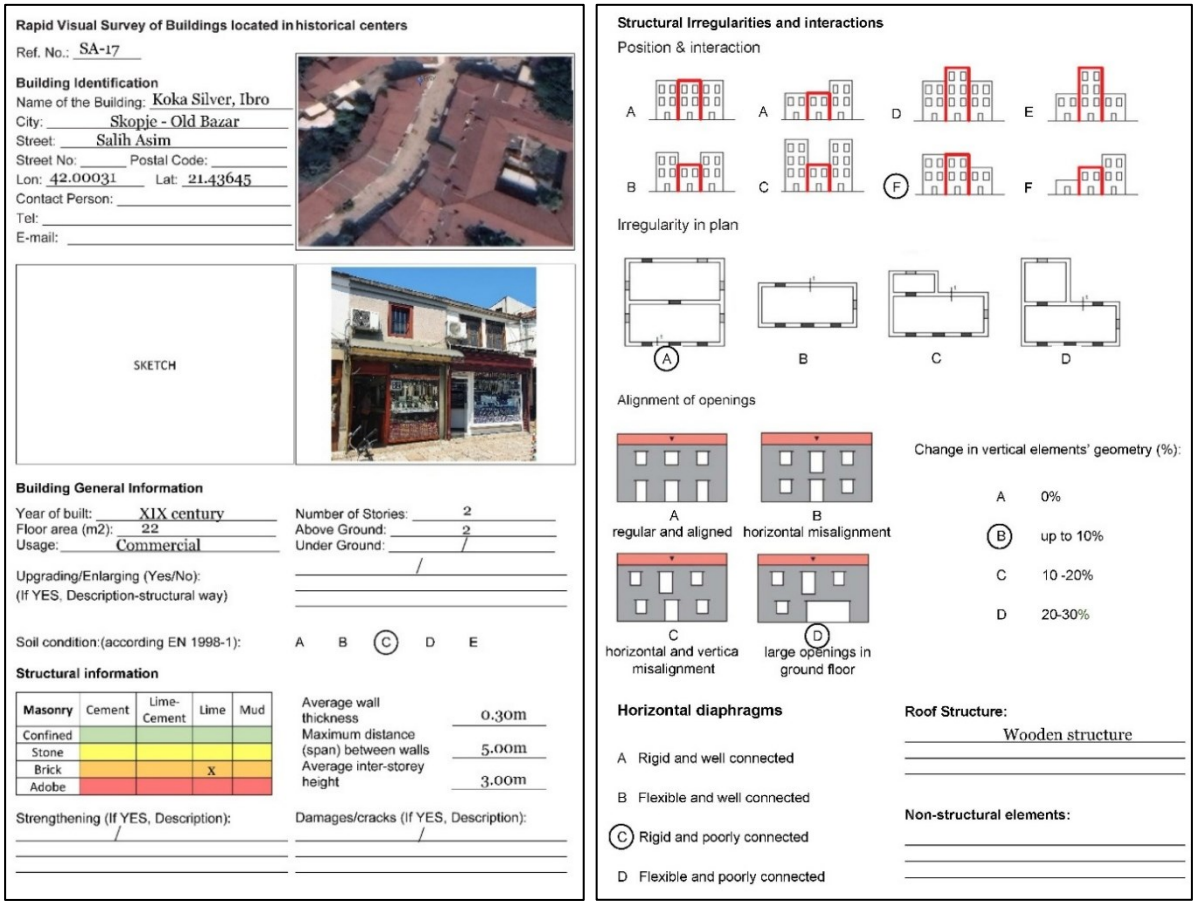
3. Application Of the Harmonized Method to Part Historical City Centre of Skopje

The seismic vulnerability assessment of one representative street of the historical city center of Skopje was carried out by applying the harmonized vulnerability index methodology, shortly presented in section 3. Because the methodology requires accurate knowledge of the building characteristics, which can only be obtained via thorough and detailed inspection, 33 buildings were analysed, in function of the detail of the information available and used on its seismic vulnerability assessment.

It is important to note that during the field assessment and analysis of the buildings, 6 buildings were observed that were reconstructed using reinforced concrete. These buildings were not exempted from the seismic assessment.

To efficiently and quickly collect the large amount of field data, a form for field inspections was created, properly adapted to the characteristics of the historical center of Skopje, which enables the systematic collection of a set of structural parameters needed for the assessment of seismic vulnerability according to the selected and harmonized method. This form consists of four main parts that select the most representative characteristics of the objects: general information, material and structure characteristics and their current condition, structure regularity, non-structural elements, and roof structure. A completed form for a building is shown in Figure 4, as an example.

Proceedings of the 3rd Croatian Conference on Earthquake Engineering - 3CroCEE
19–22 March 2025, Split, Croatia
Copyright © 2025 CroCEE
DOI: https://doi.org/10.5592/CO/3CroCEE.2025.75



Rapid Visual Survey of Buildings located in historical centers

Ref. No.: SA-17

Building Identification

Name of the Building: Koka Silver, Ibro
City: Skopje - Old Bazar
Street: Salih Asim
Street No: ____ Postal Code: ____
Lon: 42.00031 Lat: 21.43645
Contact Person: ____
Tel: ____
E-mail: ____

SKETCH

Building General Information

Year of built: XIX century
Floor area (m2): 22
Usage: Commercial
Number of Stories: 2
Above Ground: 2
Under Ground: /
Upgrading/Enlarging (Yes/No): /
(If YES, Description-structural way)
Soil condition:(according EN 1998-1): A B (C) D E

Structural information

Masonry	Cement	Lime-Cement	Lime	Mud
Confined				
Stone				
Brick			x	
Adobe				

Average wall thickness 0.30m
Maximum distance (span) between walls 5.00m
Average inter-storey height 3.00m

Strengthening (If YES, Description): /
Damages/cracks (If YES, Description): /

Structural Irregularities and interactions

Position & interaction

A A D E
B C (F) F

Irregularity in plan

(A) B C D

Alignment of openings

A regular and aligned
B horizontal misalignment
C horizontal and vertica misalignment
(D) large openings in ground floor

Change in vertical elements' geometry (%):

A 0%
(B) up to 10%
C 10 -20%
D 20-30%

Horizontal diaphragms

A Rigid and well connected
B Flexible and well connected
(C) Rigid and poorly connected
D Flexible and poorly connected

Roof Structure: Wooden structure

Non-structural elements:

Fig. 4 A completed form for quick collection of field data



Fig. 5 The assessed urban area with marked buildings – Salih Asim street (Skopje old Bazaar)

Copyright © 2025 CroCEE
DOI: https://doi.org/10.5592/CO/3CroCEE.2025.75

The proposed data collection method allows for a straightforward process to obtain the required data. It also streamlines and shortens the time needed to process the information and assess the seismic vulnerability of each structure. An additional benefit is that the information collected can be used to create databases for future projects and research.

The methodology applied herein, and results obtained are presented resourcing to a Google Earth application. Figure 5 shows the assessed urban area with marked buildings.

The seismic vulnerability index I_{vf} was calculated according to Equation (1). The values of the I_{vf} are presented in Table 6.

As already mentioned, seismic vulnerability results were mapped using the Google Earth tool, developed to provide a global overview of the vulnerability assessment results and the consequent risk scenarios.

Based on the previous seismic vulnerability values of the buildings within the study area, descriptive damage grades were estimated for seismic scenarios with macroseismic intensity IX.

Tab. 1 vulnerability index values for the whole study area

No.	Ivf	No.	Ivf
SA-1	0	SA-17	320
SA-2	295	SA-18	0
SA-3	325	SA-19	245
SA-4	290	SA-20	275
SA-5	255	SA-21	275
SA-6	255	SA-22	285
SA-7	255	SA-23	275
SA-8	0	SA-24	245
SA-9	275	SA-25	275
SA-10	270	SA-26-A	247.5
SA-11	245	SA-26-B-C	197.5
SA-12	217.5	SA-27	227.5
SA-13	107.5	SA-28	345
SA-14	195	SA-29	0
SA-15	245	SA-30	0
SA-16	275	SA-31	0

Tab. 2 Damage grade, according to vulnerability

Damage - Intensity IX - MSC
Ivf=0-100 - No damage
Ivf =101-200 - Slight / moderate damage
Ivf =201-300 - Severe damage
Ivf >300 - Very severe damage / destruction

The proposed damage for this work, according to the vulnerability, is presented to table 7. Figure 6 presents the spatial distribution of the vulnerability index values for the whole study area and, also presents the damage scenario for seismic intensity IMS-98= IX.

From the results, it is observed that for earthquake intensities IX, 10% of the buildings would collapse, 64% of them would have severe damage, 10% would have minor damage, and 16% would remain undamaged. In this 16 percent, reinforced concrete constructions are placed (Figure 7).

Copyright © 2025 CroCEE
DOI: https://doi.org/10.5592/CO/3CroCEE.2025.75

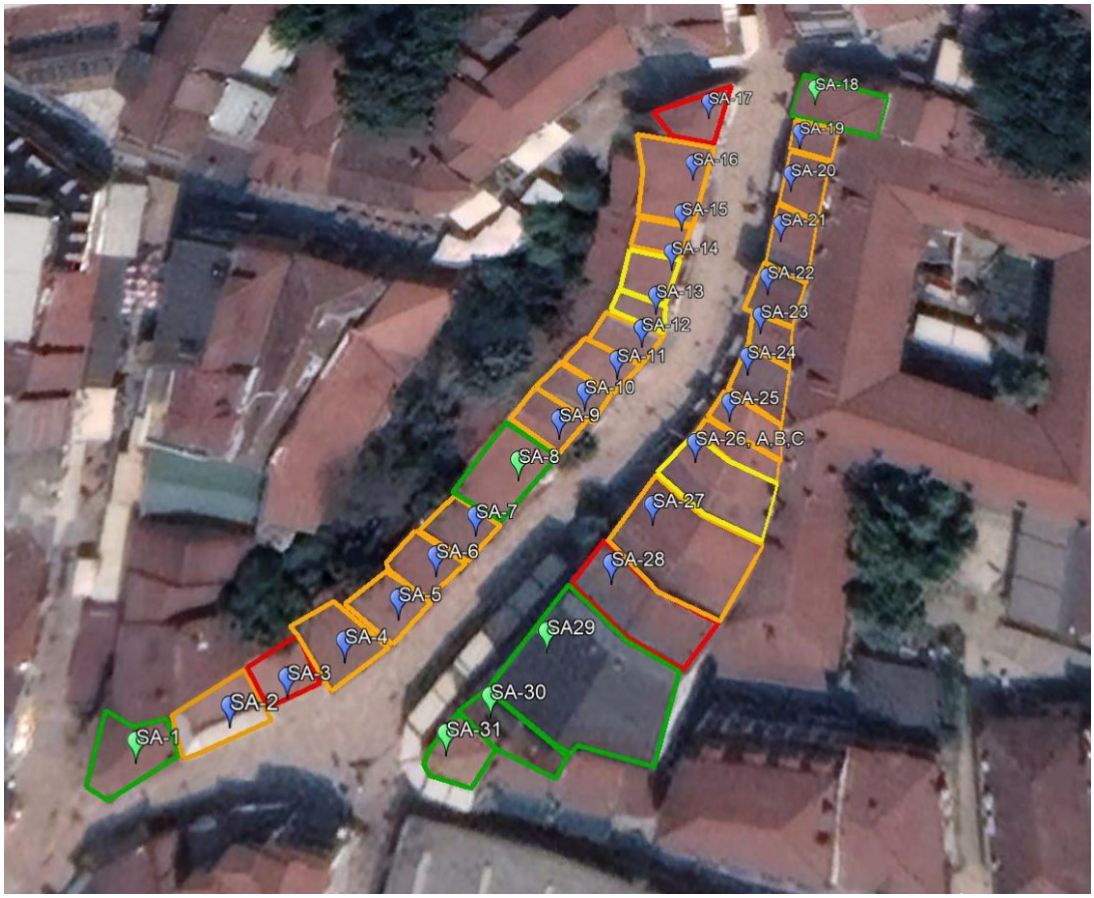


Fig. 6 The assessed urban area with marked buildings – Salih Asim street (Skopje old Bazaar)

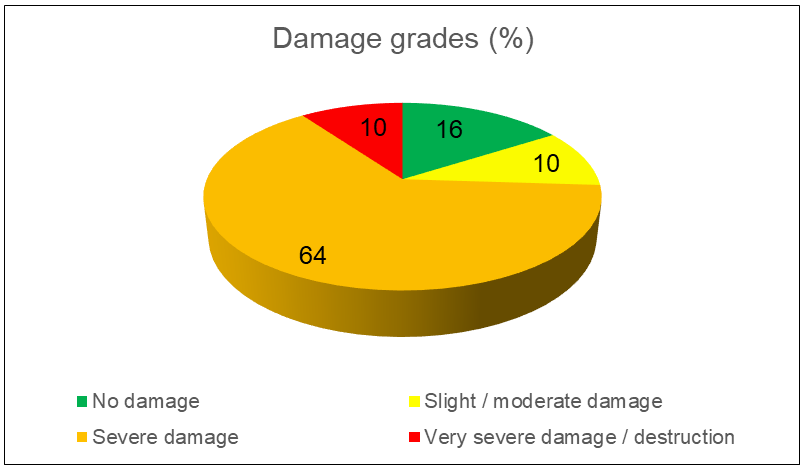


Fig. 1 Percentage representation of different damage grades

4. Conclusions

The vulnerability assessment of masonry buildings in a historical urban area is a fundamental step in evaluating global seismic risk, defined as the likelihood of a seismic event of a certain intensity occurring at a specific location within a given timeframe. This analysis is critical not only due to the physical consequences of potential seismic events but also because of its connection to human safety and evacuation planning—key elements in devising effective risk reduction strategies.

Copyright © 2025 CroCEE
DOI: https://doi.org/10.5592/CO/3CroCEE.2025.75

By integrating vulnerability assessment with the implementation of suitable seismic retrofitting measures and emergency response plans, it becomes possible to mitigate physical damage, reduce human casualties, alleviate critical emergencies, and minimize the economic impact of future seismic events. Specifically, in the context of masonry buildings in historical centers, decades of accumulated knowledge and extensive damage data from post-earthquake surveys provide a unique opportunity to harmonize and refine seismic vulnerability assessment methodologies.

The results achieved through recent advancements in the field, leveraging calibrated methods based on earthquake databases and specific insights into the characteristics of historic buildings in the Old Bazaar, are robust and adaptable. These results can be effectively applied and modified to address the challenges of future seismic events.

The proposed harmonized vulnerability index method, derived by calculating a building's score as a weighted sum of its characteristic parameters, linked to its seismic response and categorized into vulnerability classes, offers an innovative and practical tool. It bridges the gap between empirical and analytical methods, providing a reliable foundation for initial seismic vulnerability assessments.

References

[1] National Conservation Center (1983): Monography marking 20 years of renovation of the Skopje monuments and historic buildings, (in Macedonian).

[2] Benedetti D., Petrini V. (1984): Sulla vulnerabilità sismica di edifici in muratura: Un metodo di valutazione, L'industria delle costruzioni, 149, 66–74, 1984.

[3] Vicente R., S. Parodi, Lagomarsino S., Varum H., Mendes da Silva J.A.R. (2011): Seismic vulnerability and risk assessment: Case study of the historic city centre of Coimbra, Portugal, Bulletin of Earthquake Engineering, 9(4):1067–1096

[4] Ferreira T.M., Maio R., Vicente R. (2013): Seismic vulnerability assessment of historical urban centres: case study of the old city centre in seixal, Portugal, Bulletin of Earthquake Engineering, 15 (5), 1753–1773.

[5] Petrovski J. (2013): Damaging Effects of July 26, 1963 Skopje Earthquake, Proceeding of the International conference Skopje Earthquake – 40 years of European Earthquake engineering, Skopje.

[6] Velkov D. (2013): Skopje 1963 Earthquake, Damages and Reconstruction, Proceeding of the International conference Skopje Earthquake – 40 years of European Earthquake engineering, Skopje

[7] Maio R., Vicente R., Formisano A., Varum H. (2015): Seismic vulnerability of building aggregates through hybrid and indirect assessment techniques, Bulletin of Earthquake Engineering, 13 (10), 2995–3014.

[8] Ferreira T.M., Maio R., Vicente R. (2017): Seismic vulnerability assessment of the old city centre of Horta, Azores: Calibration and application of a seismic vulnerability index method, Bulletin of Earthquake Engineering, 15(7): 2879–2899.

[9] Shendova V., Zlateski A., Delova E. (2018): Skopje 11th September 2016 earthquake: post-earthquake visual screening on cultural heritage buildings, Proc. of the 16ECEE, Thessaloniki.

[10] Maio, R.; Estêvão, J.M.C.; Ferreira, T.M.; Vicente, R. (2020): Casting a new light on the seismic risk assessment of stone masonry buildings located within historic centres. Structures 2020, 25, 578–592. https://doi.org/10.1016/j.istruc.2020.03.008

[11] Zlateski A., Lucesoli M., Bernardini G., Ferreira T. M. (2020): Integrating human behaviour and building vulnerability for the assessment and mitigation of seismic risk in historic centres: Proposal of a holistic human-centred simulation-based approach, International Journal of Disaster Risk Reduction, 43, doi: https://doi.org/10.1016/j.ijdrr.2019.101392

[12] Zlateski A, Shendova V., (2021): Harmonization of seismic vulnerability assessment of urban historic centers, Proc. of the 1CroCEE, Zagreb.

Proceedings of the 3rd Croatian Conference on Earthquake Engineering - 3CroCEE
19–22 March 2025, Split, Croatia
Copyright © 2025 CroCEE
DOI: https://doi.org/10.5592/CO/3CroCEE.2025.89

VULNERABILITY ASSESSMENT AND SEISMIC RISK ANALYSIS OF BUILDINGS IN IRAQ: INSIGHTS FROM BUILDING SURVEYS AND DAMAGE SCENARIOS

Peshawa L. Hasan [(1)], Baban A. Bapir [(2)], Brwa S. Hama Ali [(3)], Lars Abrahamczyk [(4)], Serwan Khurshid [(5)]

[(1)] *Chair of Advanced Structures, Bauhaus-University Weimar, Germany, peshawa.luqman.hasan@uni-weimar.de*
[(2)] *Chair of Advanced Structures, Bauhaus-University Weimar, Germany, baban.bapir@uni-weimar.de*
[(3)] *Department of Civil Engineering, University of Sulaimani, Iraq, brwa.hamahali@univsul.edu.iq*
[(4)] *Chair of Advanced Structures, Bauhaus-University Weimar, Germany, lars.abrahamczyk@uni-weimar.de*
[(5)] *Department of Civil Engineering, University of Sulaimani, Iraq, serwan.rafiq@univsul.edu.iq*

Abstract

Seismic risk analysis of building stocks in earthquake-prone regions builds the entry for any kind of mitigation measures, especially in the case of fast urbanization in developing countries. Iraq, one of such countries, lies in the northern portion of the Arabian plate, bounded in the North-East by the Bitli-Zagros fold and Thrust belt, where the convergent tectonic boundary between the Eurasia and Arabian plates generates intense earthquake activity. In addition, there are no or only very few accurate studies that map out or provide statistics on the number of buildings in Iraq.

This study presents a detailed vulnerability assessment and seismic risk analysis of buildings in Iraq, based on data collected from 4,724 structures through random urbanization methods. Extensive field surveys were conducted to capture key building characteristics, and this data has been digitized to support future research in earthquake engineering, urban planning, and disaster risk management. Each building was classified by vulnerability class and building type using the European Macroseismic Scale (EMS-98) and the Global Earthquake Model (GEM) building taxonomy. These taxonomies enabled a detailed categorization of buildings, helping to assess their expected seismic performance. The validated dataset can be used to develop seismic damage models and conduct risk and loss analyses for the region. Preliminary results from the survey show that 45% of the buildings assessed in Iraq can be classified as non-engineered, primarily constructed using brick masonry and concrete blocks.

Reports of damages in the surveyed buildings were collected from past earthquakes mainly damage reports from the 2017 Iran-Iraq border earthquake with magnitude 7.3, providing valuable insights into the potential impacts of future seismic events. The collection of this data highlights the vulnerabilities of different building types and estimates the economic and human losses that could result from significant earthquakes in Iraq, as well as preparation for future damage scenarios and risk assessment studies. The findings emphasize the importance of targeted interventions, such as retrofitting and emergency preparedness, to reduce seismic risks. In addition to offering insights into potential damage patterns, the digitized data serves as a critical resource for future studies. It supports regional seismic hazard mapping, the improvement of building codes, and the enhancement of emergency response planning. By making this data available, the study promotes collaboration and future research efforts aimed at improving seismic resilience in Iraq and similar regions.

Keywords: Earthquake Response, Vulnerability Assessment, EMS-98, Seismic Risk.

1. Introduction

Seismic risk analysis is an essential component in developing effective mitigation strategies for earthquake-prone regions, particularly in rapidly urbanizing countries like Iraq. Iraq is located at the northern margin of the Arabian Plate, bordered by the tectonically active Bitlis-Zagros Fold and Thrust Belt, where the convergence of the Eurasian and Arabian plates generates intense seismic activity [1,

Copyright © 2025 CroCEE
DOI: https://doi.org/10.5592/CO/3CroCEE.2025.89

2]. This complex tectonic setting subjects Iraq to significant seismic hazards, particularly in its northern regions, where the population density and urban expansion are also high [3]. Recently, the increase in earthquake activity in this region has been observed, with the most recent damaging event being the November 12, 2017, Iran-Iraq border earthquake with a magnitude of 7.3 which caused several damages killing 9 people and injuring 55. Despite the evident risks, comprehensive seismic risk assessments and detailed data on Iraq's building stock remain limited, which are crucial for understanding and mitigating earthquake impacts. Understanding and mitigating these risks is increasingly important as Iraq undergoes rapid urbanization, leading to the expansion of urban settlements and infrastructure development [4]. The unregulated nature of many of these developments results in a substantial increase in non-engineered buildings, which are particularly vulnerable to seismic events [5, 6]. Assessing and mitigating these risks is therefore critical not only for infrastructure protection but also for minimizing the economic and human impact of future seismic events.

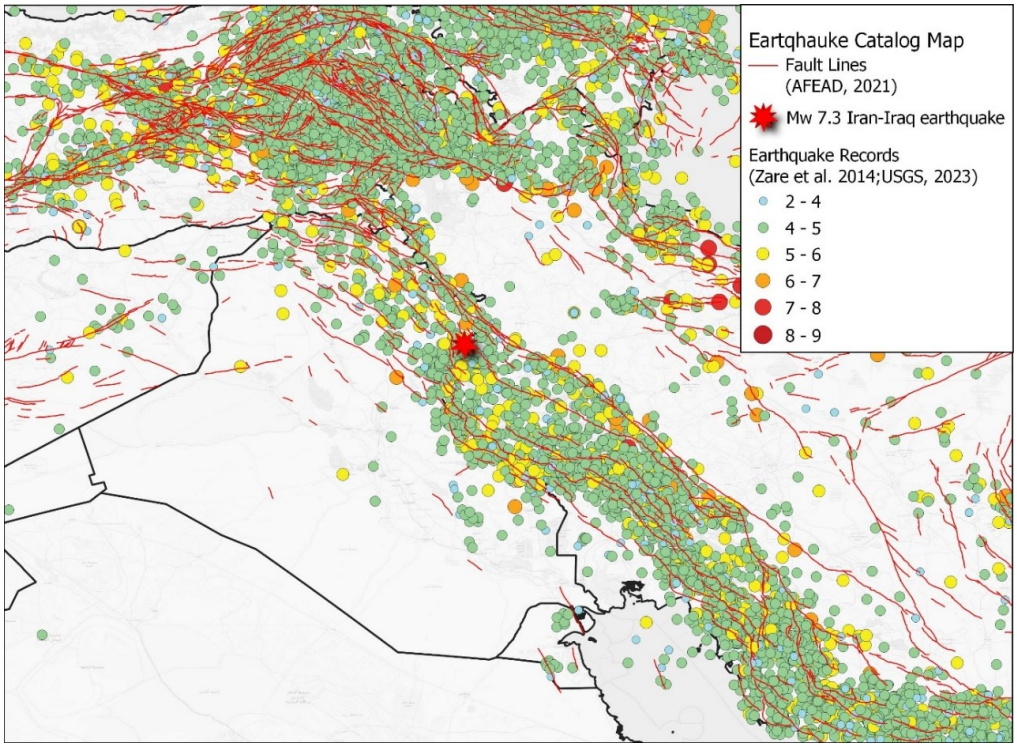


Figure 1. Earthquake catalog between years (0-2020), Zare et al., 2014 [7]; USGS Earthquake Catalog [8]

Despite the pressing need for accurate seismic risk assessments in Iraq, the country currently lacks detailed, comprehensive studies that map the vulnerability of its building stock. Existing research highlights the general geological and seismic characteristics of Iraq but falls short in providing specific, comprehensive data on building inventories and their structural performance during earthquakes [3, 9]. This gap is significant because reliable data on building vulnerability is a fundamental prerequisite for developing effective mitigation strategies, such as retrofitting measures and updating construction codes [4]. The absence of comprehensive and a systematic vulnerability assessment leaves planners and policymakers with limited information, which reduces their ability to adequately prepare for or respond to seismic events.

While regional seismic hazard models such as the Earthquake Model of the Middle East (EMME) have been developed [10, 11], these models often lack the localized data necessary to refine risk estimates for Iraq's unique geological and structural conditions. Previous research has demonstrated the value of integrating local geological conditions and detailed building typologies into seismic risk models to improve accuracy [9, 12]. Addressing these gaps, the present study aims to conduct a detailed vulnerability assessment of buildings in Iraq using data collected from 4,724 structures through field

Copyright © 2025 CroCEE
DOI: https://doi.org/10.5592/CO/3CroCEE.2025.89

surveys. These surveys utilize international standards such as the European Macroseismic Scale (EMS-98) and the Global Earthquake Model (GEM) taxonomy to classify buildings according to their structural characteristics and vulnerability [13–15].

The primary objective of this study is to provide a robust and systematically digitized dataset that supports the development of seismic risk models tailored specifically to Iraq's building stock. By digitizing and categorizing the building data systematically, the research aims to create realistic damage scenarios using past earthquake shake maps to predict potential impacts and economic and human losses. This data-driven and evidence-based approach will inform targeted interventions such as retrofitting programs and emergency preparedness strategies, ultimately enhancing Iraq's resilience to seismic events. Additionally, the study's findings will contribute to improving regional seismic hazard mapping, updating and strengthening building codes, and supporting future disaster risk management efforts in Iraq.

2. Study Area

The city of Sulaimani is a rapidly growing urban center in Iraq, with an estimated population of 823,199 and an annual growth rate of 2.8% [16]. This population increase has led to significant urban development and the planning of new construction projects within the city. While no precise studies currently provide statistics on the total number of buildings in the city, the Microsoft Planetary Computer [17] has identified 86,000 buildings nationwide using high-resolution satellite imagery and deep neural networks (DNNs) to detect building pixels in aerial images. However, the DNN model used for this analysis is trained on datasets derived from international housing imagery, which limits its accuracy in identifying the full scope of buildings in Sulaimani. It is estimated that the actual number of buildings in the city could be a few times higher than the figure provided by Microsoft. This discrepancy highlights the need for localized studies and the development of customized models that reflect Iraq's specific construction types.

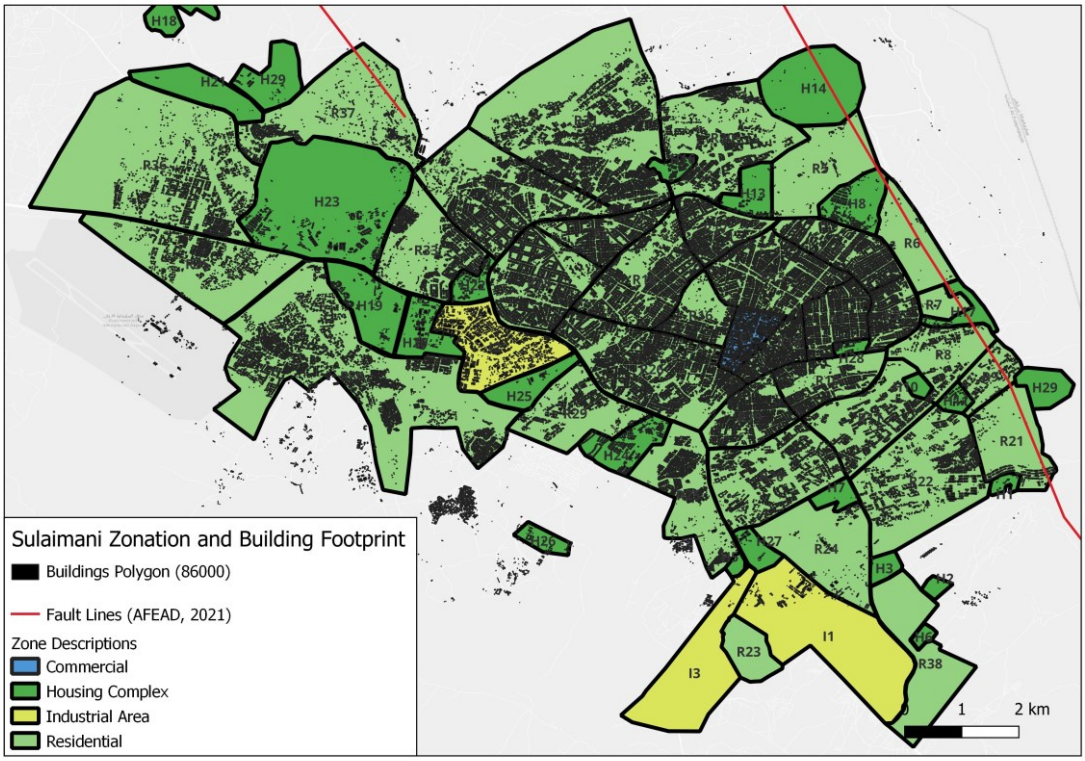


Figure 2. Urban zonation of the study area including building footprints

Copyright © 2025 CroCEE
DOI: https://doi.org/10.5592/CO/3CroCEE.2025.89

The development of Sulaimani has occurred in distinct phases, influenced by different construction styles over time. In recent years, the government has issued permits to several construction companies for the development of housing complexes at multiple stages and locations throughout the city. These projects primarily consist of high-rise residential complexes and standardized structural buildings, typically ranging from one to three stories. These houses are often identical in design, planned, and constructed under the supervision of engineers. However, alongside these planned developments, residential areas have also emerged through the distribution and sale of land to individual homeowners. Many of these houses were constructed by the homeowners themselves, based on varying plans and permits. While government regulations require structural plans for building permits, some houses have been built without full compliance with engineering guidelines, resulting in a high percentage of non-engineered structures. These deviations, including unapproved modifications, make it difficult to ensure that buildings meet safety standards. The survey conducted in this study revealed that 55% of the buildings in Sulaimani are non-engineered, highlighting a major structural risk in the event of an earthquake.

Furthermore, while Sulaimani has only one identified commercial area, commercial buildings are often integrated into residential neighborhoods. The city also contains three primary industrial zones, further contributing to its diverse urban landscape. The locations of these zones are demonstrated in Figure 2, which provides a visual representation of their distribution across the city. The zonation of the city is well-described; however, the building types and their attributes in Sulaimani remain largely undocumented. Previous studies conducted in Erbil [6] have successfully collected building attributes to identify vulnerabilities and classify building types, which offers a valuable basis for this study. Since construction practices across the country share significant similarities, these findings can inform the framework developed for Sulaimani.

In addition to the built environment, subsoil conditions play a crucial role in determining ground motion amplification and directly affect building vulnerability during earthquakes. Studies on site response investigation in Sulaimani [9] have classified the city's subsoil primarily as Class C and Class D, according to Eurocode 8 [18]. Class C soils consist of dense or stiff deposits, while Class D soils represent soft deposits that are more prone to ground motion amplification. In certain areas, particularly those dominated by Class D soils, the presence of soft sediments poses a significant risk, as amplified shaking can increase structural damage during earthquakes. This effect is particularly concerning in the southern parts of the city, where deeper sediment layers further intensify seismic hazards.

Understanding these site-specific soil conditions is essential for seismic risk assessments and can support urban planners and engineers in making informed decisions about building regulations, retrofitting strategies, and land-use planning. By integrating subsoil data with structural assessments, targeted seismic mitigation measures can be developed to enhance earthquake resilience across Sulaimani.

3. Methodology

In order to give a systematic and comprehensive classification of building taxonomies in Sulaimani, this study introduces a modular framework for seismic vulnerability assessment. The framework is designed to work at varying levels of data availability, making it particularly suitable for developing countries where detailed structural inventories may be limited. Unlike traditional classification methods, which often apply fixed or rigid vulnerability classifications, this modular approach allows for incremental refinement of vulnerability classes (VCs) as more structural details become available. The framework integrates structural attributes, soil characteristics, seismic intensity data, and empirical observations, ensuring a more comprehensive and data-driven seismic risk assessment. Through standardization of the assessment process, this framework ensures that buildings are evaluated using globally recognized criteria, which aligns with the European Macroseismic Scale-98 (EMS-98) providing a consistent and reliable understanding of seismic performance across different building types.

Proceedings of the 3rd Croatian Conference on Earthquake Engineering - 3CroCEE
19–22 March 2025, Split, Croatia
Copyright © 2025 CroCEE
DOI: https://doi.org/10.5592/CO/3CroCEE.2025.89

The modular framework is designed specifically to align with the EMS-98 system, offering flexibility and adaptability in classifying building vulnerabilities. Unlike a fixed classification system, this approach operates at varying levels of detail, ensuring that assessments can be performed even with limited data while allowing for progressive refinement depending on the availability of different details.

The framework introduces multiple levels (Level 1, Level 2, and Level 3), which incorporates increasing levels of structural and vulnerability detail, as outlined below:

- Level 1 (Basic Structural Type): In this level the fundamental building parameter material type, is used for an initial vulnerability classification based on EMS-98. This level provides a baseline assessment when only minimal data is available.
- Level 2 (Structural Modifiers & Configuration): Incorporates additional structural and architectural details, these attributes refine the initial classification by incorporating key performance factors that influence seismic response.
- Level 3 (Advanced Seismic & Geotechnical Refinements): Provides a highly detailed classification by integrating seismic code compliance, soil-structure interactions, liquefaction susceptibility, and empirical earthquake impact data, enabling accurate risk assessment.

Table 1: A modular framework for building vulnerability classification, allowing for progressive refinement based on data availability ranging from Level 1 to Level 3.

Level	Category	Attributes
Level 1	Basic Structural Attributes	Material type
	Building Location	Geographic coordinates (latitude, longitude)
	General Building Information	Construction/retrofit date, building height category, building age, primary use/occupancy
	Structural Configuration	Structural system type, material technology, system ductility
	Geometric & Structural Irregularities	Plan irregularity, vertical irregularity, soft story indicators
	Roof System	Roof Cover, Roof Development, Parapet height
Level 2	Foundation & Soil Interaction	Foundation type, foundation-soil interaction, liquefaction susceptibility
	Building Condition & Safety	Retrofitting status, structural integrity (good/poor)
	Non-Structural Components	facade materials, parapet & overhang stability
	Fire & Post-Earthquake Hazards	Fire risk level (post-earthquake hazard), pounding risk between adjacent buildings
	Seismic & Geotechnical Performance	Seismic code compliance, peak ground motion, site-specific soil classification
	Empirical Data & Damage History	Reported earthquake intensity, observed structural & non-structural damage during past earthquakes
Level 3	Heritage & Societal Factors	Cultural or Historical Significance, Proximity to Critical Infrastructure (Hospitals, Lifelines)
	Economic & Recovery Indicators	Ownership Type (Owned vs. Rented), Insurance Coverage, Expected Recovery Time

The attributes associated with each level are outlined in Table 1, showing the progression from fundamental attributes at Level 1 to increasingly detailed characteristics at Level 3. Level 1 gives a basic vulnerability class based on the material type of the building, this could account for a mean vulnerability class of the building giving a preliminary assessment. Level 2 introduces structural modifiers and configuration details, including building height, primary use, irregularities, roof system

Proceedings of the 3rd Croatian Conference on Earthquake Engineering - 3CroCEE
19–22 March 2025, Split, Croatia
Copyright © 2025 CroCEE
DOI: https://doi.org/10.5592/CO/3CroCEE.2025.89

characteristics, foundation type, and non-structural components, refining the initial classification by incorporating key structural and architectural factors that influence seismic response. Level 3 further expands the classification by integrating seismic code compliance, peak ground acceleration (PGA), soil-structure interactions, liquefaction susceptibility, and empirical earthquake impact data, enabling a highly detailed risk assessment. This scalable, modular structure ensures that the EMS-98 classification can be effectively applied in both limited and extensively available data environments, allowing for incremental refinement as more comprehensive data becomes available. By accommodating varying levels of detail, the framework provides a flexible and adaptive methodology suited to the diverse and complex building stock in Sulaimani.

Based on the modular framework, a systematic survey of the building stock in the city of Sulaimani is conducted. For the optimize and efficiency of data collection for this study, senior undergraduate students in their fourth year were trained in the empirical framework developed for assessing buildings in Iraq [19]. This training equipped the students with the necessary skills to evaluate structural parameters and classify buildings according to the proposed modular framework.

After the training phase, the students carried out field surveys across the city. Each zone was allocated to specific groups of students, who were tasked with surveying buildings within their designated areas. During these surveys, students collected essential structural parameters, photographed the buildings, and classified them into types and vulnerability classes in accordance with the EMS-98 classification system [13], following the methodology outlined by [20]. The modular framework guided the data collection process, employing a random selection method to ensure representative sampling and facilitate subsequent verification and adjustments.

In total, data from 4,825 buildings were collected during the survey. After a thorough review and validation process, 4,772 entries (98.9% of the dataset) were approved, while 1.1% of the entries were removed due to unresolvable inaccuracies. Data entries identified as incorrect were adjusted where possible, and uncorrectable entries were excluded from the dataset. The resulting refined dataset reflects the classifications conducted in the field and serves as the foundation for future seismic risk analyses.

The methodology employed for executing the building survey in Sulaimani followed a structured series of steps, ensuring consistency, accuracy, and the reliability of the collected data. These steps included the systematic allocation of zones, the training of data collectors, the use of a modular framework for data collection and classification, and a comprehensive review and validation process to refine the dataset for subsequent analysis. Additional data was collected for each building to enhance the analysis. This included soil data sourced from the study by [6], which evaluated soil conditions in Sulaymaniyah using microtremor measurements, lithological data, and geotechnical datasets. The study classified soil according to EC8 and NEHRP soil classifications, providing critical insights into subsoil characteristics.

Given the distributed nature of soil sampling data in the study, soil data at various locations across the city required testing for interpolation methods to ensure accuracy. Three primary interpolation methods were considered: Inverse Distance Weighting (IDW), Kriging, and Radial Basis Functions (RBF). The performance of these methods was evaluated using metrics such as RMSE, MAE, and R^2, with IDW consistently demonstrating superior results across all tested parameters. This approach ensured the effective integration of soil data for each building.

Table 2. Results of Interpolation Methods for Soil Data

Method	RMSE	MAE	R^2	EVS	Max Error
IDW	0.2773	0.2185	0.7755	0.7786	0.8011
RBF	0.7925	0.5841	-0.8329	-0.7213	2.3468
Kriging	0.5844	0.5378	0.0033	0.0038	1.4814
Natural Neighbor	0.7405	0.4516	-0.6006	-0.4518	2
Spline	0.664	0.5305	-0.2869	-0.2604	1.8158
KNN	0.5917	0.5343	-0.022	-0.0217	1.5325

Copyright © 2025 CroCEE
DOI: https://doi.org/10.5592/CO/3CroCEE.2025.89

The results in Table 2 shows that the selected IDW method performed significantly better than other methods, with the lowest RMSE and MAE and the highest R^2 and EVS values. In contrast, RBF exhibited poor performance, with high RMSE and negative R^2, failing to capture variance effectively. Kriging demonstrated moderate performance but struggled to generalize well, achieving near-zero R^2 and EVS values. The resulting dataset provided a comprehensive understanding of site conditions, facilitating the classification of buildings and enhancing the reliability of vulnerability assessment.

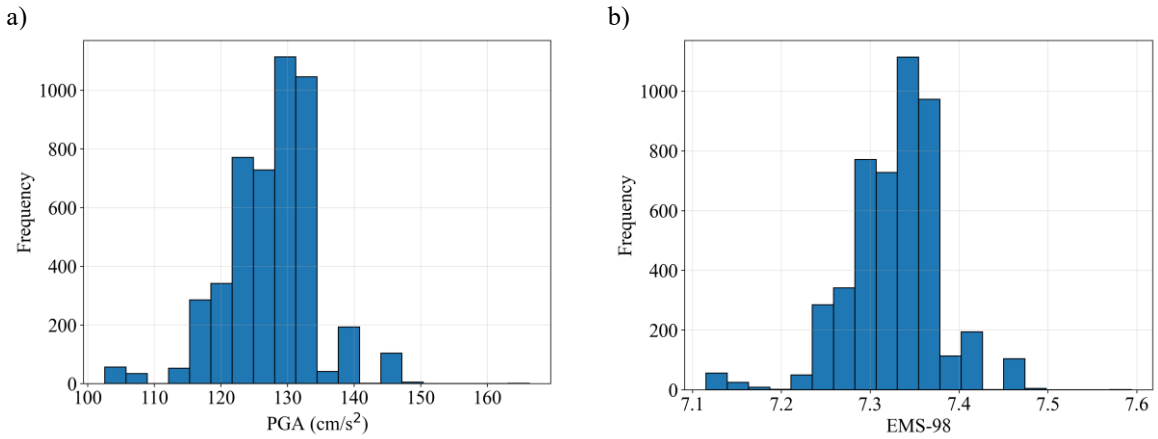


Figure 3. (a) Distribution of Peak Ground Acceleration (PGA) across Sulaimani city during the 2017 Iran-Iraq border earthquake, derived from the USGS ShakeMap [21] (b) Distribution of converted intensity values according to the EMS-98 scale, based on the correlation function of Zanini and Hoffer, 2019 [22]

In addition to the structural and soil data collected, information from past earthquakes was also integrated into the analysis. The survey integrated Peak Ground Acceleration (PGA) values for each building, derived from the USGS ShakeMap [23] model for the event [21]. The PGA values ranged from 100 to 160 cm/s² across the city, reflecting varying levels of ground motion during the earthquake. The distribution of PGA values is presented in Figure 3, which illustrates the frequency of PGA across the study area. This distribution helps in understanding the spatial variability of seismic impacts, forming a crucial input for the creation of damage models and risk assessment strategies.

The survey also included two additional questions aimed at capturing resident's experiences during the 2017 earthquake. Students asked homeowners to report the experienced earthquake intensity according to the EMS-98 scale and whether their houses sustained any damage. For those who reported damage, the survey collected details on the extent and level of damage observed. This firsthand information adds an important layer of empirical data, enhancing the understanding of building performance and community resilience during seismic events. Collection of data from previous earthquakes aids in future damage modeling which is further planned as part of seismic risk assessment in Iraq.

4. Survey Results

Based on the methodology described in the previous section, a detailed survey was conducted in Sulaimani, which resulted in a comprehensive dataset capturing both the structural and usage characteristics of buildings across the city. A total of 36 key attributes were collected, along with 10 supplementary parameters including soil class, soil frequency, and earthquake intensity, which were incorporated to refine the analysis. Figure 4 presents an overview of key parameters such as roof material, construction age, building location, and usage type. The survey revealed that 55% of the buildings are classified as non-engineered, while 45% were identified as engineered structures. Additionally, the majority of buildings were found to be in good (40.38%) or average (38.9%) condition, with a smaller proportion being newly constructed (12.8%) and some in bad condition (7.5%), as shown in Figure 4 (b). Understanding these material distributions is essential for evaluating the structural resilience of buildings against seismic events.

Copyright © 2025 CroCEE
DOI: https://doi.org/10.5592/CO/3CroCEE.2025.89

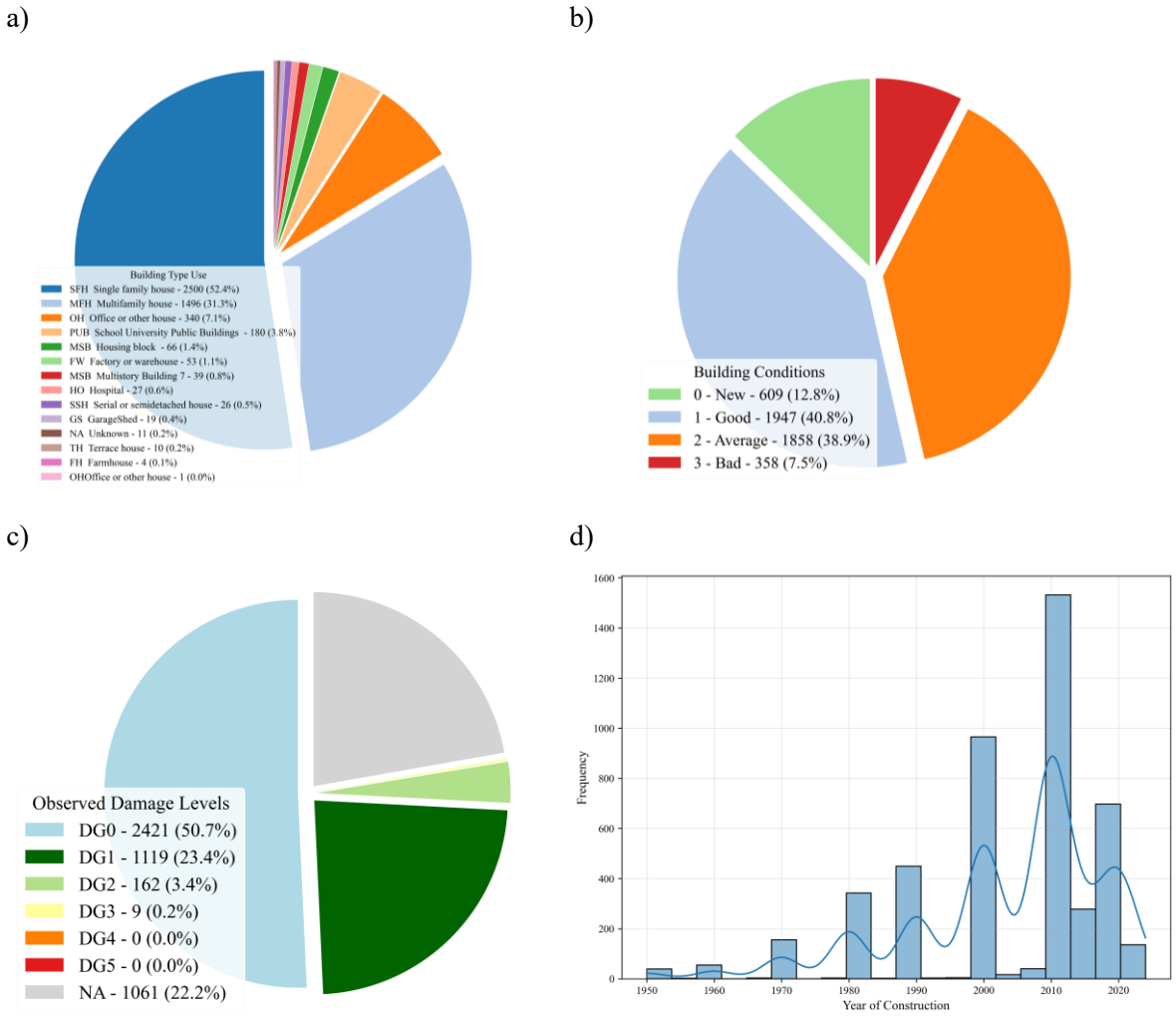


Figure 4. (a) Building types by use; (b) Building conditions; (c) Observed damaged during past earthquakes; (d) Year of construction trends.

The dataset also includes information on the year of construction for each building, Figure 4 (d). According to this dataset, a significant urban growth is observed in the 2000s and 2010s, with peaks in construction activities during these periods. This trend is visually represented in the histogram of construction years, which highlights the evolution of urban development over decades. The damages observed during the 2017 Iran-Iraq border earthquake are presented in Figure 4 (c), showing that at intensity level VII (see Figure 3) on the European Macroseismic Scale (EMS-98), a large number of buildings did not have any cases of damages while a number of buildings sustained minor cracks and negligible damage of damage grade 1, while a small number experiences damage of grade 3, indicating critical structural damages in these building that was later renovated or fixed. This classification provides valuable insights into spatial layouts and the density of residential zones, which are essential for urban planning and seismic risk analysis. Another key parameter recorded in the survey was building use. The results shows that single-family houses make up the majority of the city's building stock, which accounts for over half of the surveyed structures. These are followed by multifamily houses, public buildings, offices, and warehouses, as presented in the Figure 4 (a). This distribution reflects the city's mix of residential and commercial buildings, which are shaped by both planned development and natural growth.

Copyright © 2025 CroCEE
DOI: https://doi.org/10.5592/CO/3CroCEE.2025.89

Additionally, Figure 5 shows the spatial distribution of the building types across different zones, which highlights significant regional variations in urban zoning and building use. According to the shown results, majority of building types are classified as M6 - Unreinforced with RC Floors (74.9%), which represents a common typology across most zones in the city. Other notable types include RC1-L - Frame without ERD (7.9%), M5 - Unreinforced, with manufactured stone unit (6.4%), and M7 - Reinforced or Confined (4.8%). The spatial distribution of the buildings shows that the buildings are scattered across specific zones, which represent local construction practices and architectural trends in different parts of the city.

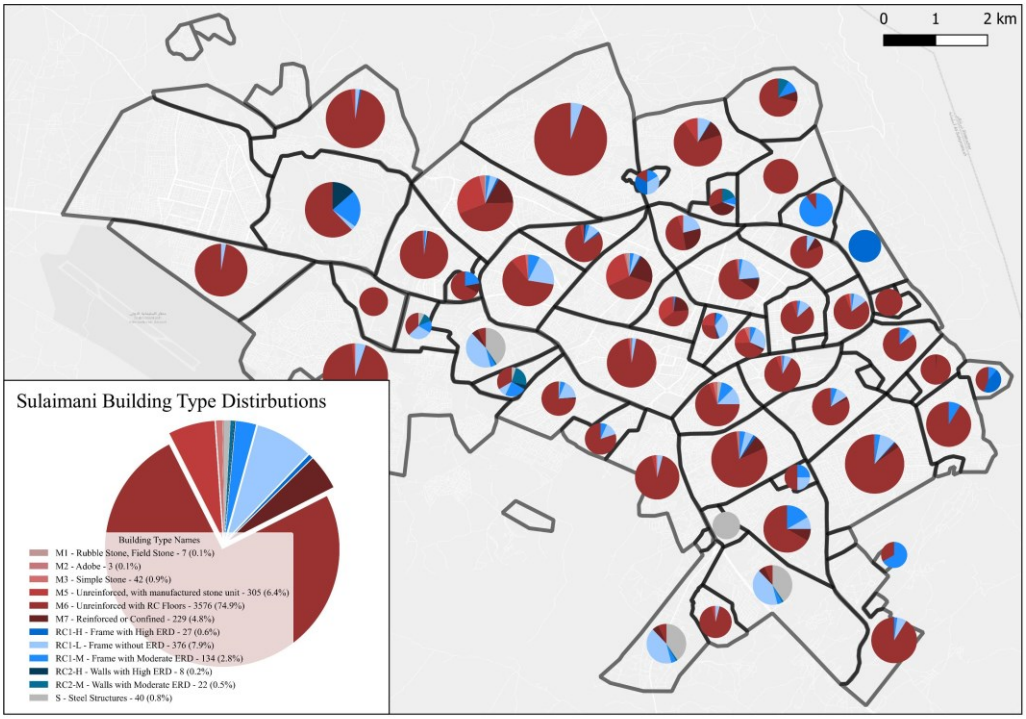


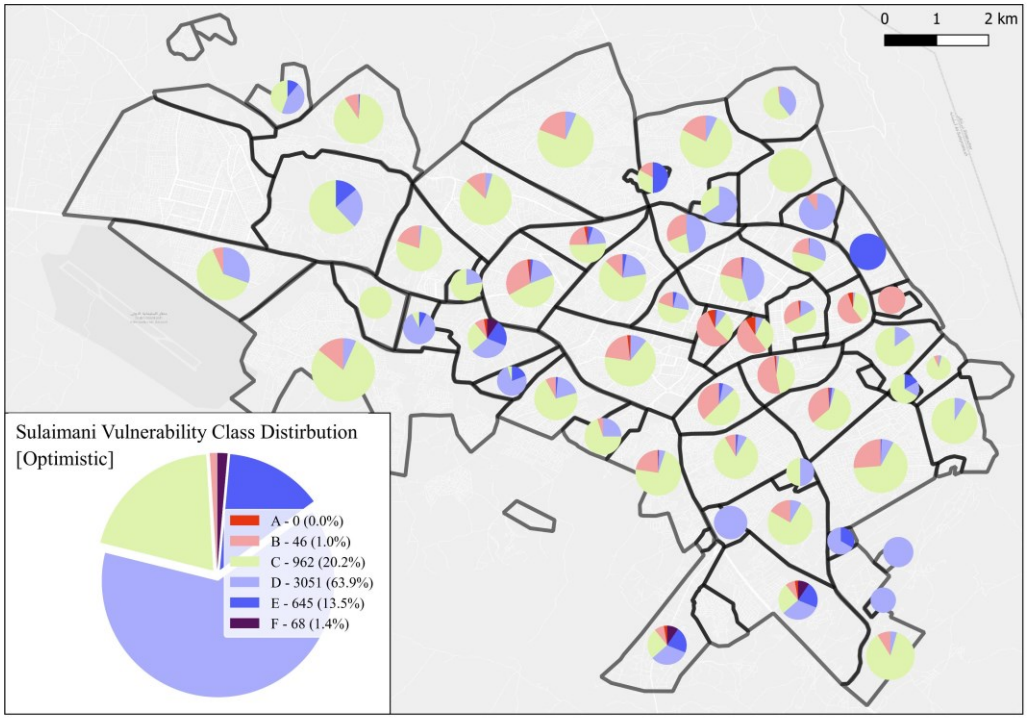
Figure 5. Spatial distribution of building types across zones in Sulaimani

Moreover, Figure 5 shows that some zones exhibit higher proportions of diverse building types, such as RC-M - Frame with Moderate ERD and M3 - Simple Stone, which reflect variations in structural design and urban planning. Conversely, in certain areas, a single typology of buildings is dominant, which is mainly zones of residential complex buildings where the structures are similar. This suggests the uniformity in development and standardized construction within these zones. This distribution provides critical insights into the zoning strategies and construction trends in Sulaimani, revealing areas with concentrated building types and others with a mix of structural designs.

Furthermore, each building was assigned a vulnerability class based on the EMS-98 system. Figure 7 presents the distribution of building vulnerability classes under optimistic and pessimistic scenarios, which provides a clearer picture of structural resilience across the city. In the optimistic scenario, the majority of buildings fall into vulnerability class C, which represents average vulnerability to earthquake actions.

Copyright © 2025 CroCEE
DOI: https://doi.org/10.5592/CO/3CroCEE.2025.89

a)



b)

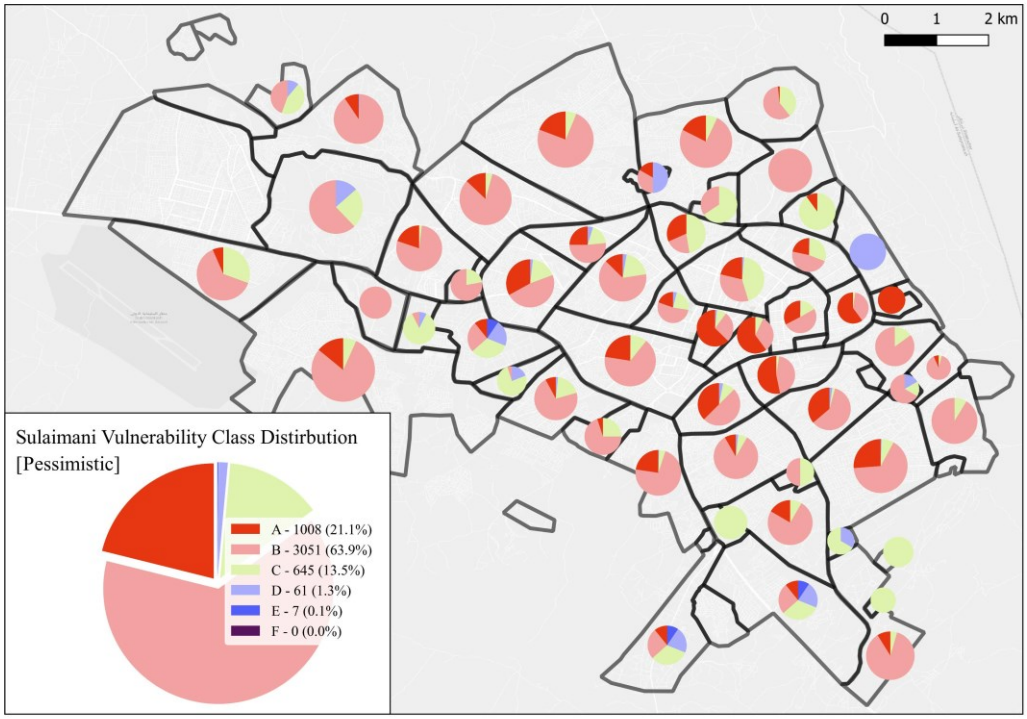


Figure 6. a) Distribution of building vulnerability classes under the optimistic scenario, b) Distribution of building vulnerability classes under the pessimistic scenario

Copyright © 2025 CroCEE
DOI: https://doi.org/10.5592/CO/3CroCEE.2025.89

This classification pattern is mainly due to the high prevalence of masonry buildings, which are the most common building type in the region. Following this, class B and C are the next most common, representing moderate and low vulnerability, respectively. Only a small percentage of buildings are classified as E and F, which are considered very low and extremely low vulnerability structures. These buildings represent well-engineered and designed structures to withstand seismic forces effectively.

In the pessimistic scenario, where weaker construction quality and poor seismic detailing are considered, most buildings fall into vulnerability class B, meaning they have moderate vulnerability to earthquakes. This is followed by class A, which includes the most vulnerable structures, and class C, which remains common but less so than in the optimistic case. The shift in classifications highlights the impact of construction quality and regulatory enforcement on seismic risks, which emphasizes the need for retrofitting strategies and improved building standards to enhance earthquake resilience.

Moreover, the spatial distribution of vulnerability classes reveals notable differences across the city. The pessimistic scenario offers a realistic worst-case perspective and helps to understand which areas are most at risk. These insights are crucial for developing targeted mitigation plans, strengthening disaster preparedness, and reducing the impact of future earthquakes.

5. Conclusion

This study provides a comprehensive vulnerability assessment and seismic risk analysis of the building stock in Iraq, focusing on the city of Sulaimani as a case study. Utilizing an extensive field survey of 4,724 buildings, the study classified building types according to the EMS-98 system, providing a detailed understanding of building typologies and their vulnerabilities to seismic events in Iraq. A key contribution of this study is the modular classification framework, which enables an incremental refinement of vulnerability assessments in region with different level of data availability. This approach improves seismic risk assessment accuracy, especially in regions with limited data availability.

The findings revealed that 55% of the surveyed buildings are non-engineered, constructed with less adherence to engineering standards, thereby highlighting their vulnerability during seismic events. The dominance of unreinforced masonry and concrete block structures, coupled with the widespread use of reinforced concrete as the primary roofing material, underscores the critical need for structural retrofitting and enhanced construction practices. The spatial distribution of building types and vulnerabilities across Sulaimani revealed significant regional variations, reflecting differences in zoning strategies, construction trends, and material quality. By incorporating data from the 2017 Iran-Iraq border earthquake, the study further refines future damage modeling, integrating Peak Ground Acceleration (PGA) values and observed intensity levels into its analysis. This data, coupled with the survey responses on experienced damage and EMS-98 intensities, provides a valuable empirical basis for understanding building performance during seismic events.

The comparison of vulnerability distributions under optimistic and pessimistic scenarios illustrates the potential impact of material quality and construction practices on building resilience. The pessimistic scenario, in particular, serves as a vital tool for worst-case damage modeling, enabling targeted risk mitigation strategies and emergency preparedness measures. This research not only enhances our understanding of the seismic vulnerabilities in Iraq but also provides a systematic and scalable framework for future studies in similar regions. The digitized dataset and the methodology established in this study serve as critical resources for improving building codes, developing targeted retrofitting programs, and informing disaster risk management policies. By addressing the gaps in local data and integrating it into seismic hazard assessments, this study contributes significantly to improving Iraq's resilience to future earthquakes and fostering sustainable urban development in the region.

Acknowledgements

This research is funded by the Ta'ziz short term measures program2024 project entitled "Towards Earthquake Mitigation in Iraq: EMS-98 Adopted Vulnerability Assessment of Existing Buildings", under the grant no. 57727890.

Copyright © 2025 CroCEE
DOI: https://doi.org/10.5592/CO/3CroCEE.2025.89

References

[1] Albusoda B.S.. Engineering Assessments Of Liquefaction Potential Of Baghdad Soil Under Dynamic Loading. Journal of Engineering and Development. 2016;30:59–76.

[2] Al-Taie AJ. Profiles and Geotechnical Properties for some Basra Soils. Al-Khwarizmi Engineering Journal. 2015;11(2):74–85. doi:http://alkej.com/index.php/en/article/view/205

[3] AbdulJaleel Z.A., Taha B.O.. Review of Seismic Characteristics in Erbil City, the Capital of the Kurdistan Region of Iraq. Polytechnic Journal. 2019;9(2):161–170. doi:10.25156/ptj.v9n2y2019.pp161-170

[4] Dabbeek J., Silva V. Modeling the residential building stock in the Middle East for multi-hazard risk assessment. Natural Hazards. 2020;100(2):781–810. doi:10.1007/s11069-019-03842-7

[5] Baytiyeh H, Naja MK. Revolutionising engineering education in the Middle East region to promote earthquake-disaster mitigation. European Journal of Engineering Education. 2014;39(5):573–583. doi:10.1080/03043797.2014.895705

[6] Hasan P.L., Lamadrid L.F.G., Abrahamczyk L., Jamal B., Saeed N.M., Schwartz J. Empirical Seismic Assessment of Urban Settlements In Developing Countries: Case Study Erbil (Iraq). In: World Conference of Earthquake Engineering (WCEE2024). Milan; 2024.

[7] Zare M, Amini H, Yazdi P, Sesetyan K, Demircioglu MB, Kalafat D, Erdik M, Giardini D, Khan MA, Tsereteli N. Recent developments of the Middle East catalog. Journal of Seismology. 2014;18(4):749–772. doi:10.1007/s10950-014-9444-1

[8] United States Geological Survey (USGS). Earthquake Search.

[9] Ibrahim R., Hasan P. L., Saeed B., Hashim H., Omar L., Salih B., Abrahamczyk L. Site Response Investigation in Sulaymaniyah City, Kurdistan Iraq by Microtremor Measurements. In: World Conference on Earthquake Engineering. Milan, Italy; 2024.

[10] Şeşetyan K, Danciu L, Demircioğlu Tümsa M.B., Giardini D., Erdik M., Akkar S., Gülen L., Zare M., Adamia S., Ansari A, et al. The 2014 seismic hazard model of the Middle East: overview and results. Bulletin of Earthquake Engineering. 2018;16(8):3535–3566. doi:10.1007/s10518-018-0346-4

[11] Giardini D, Danciu L, Erdik M, Şeşetyan K, Demircioğlu Tümsa MB, Akkar S, Gülen L, Zare M. Seismic hazard map of the Middle East. Bulletin of Earthquake Engineering. 2018;16(8):3567–70. doi:10.1007/s10518-018-0347-3

[12] Purba J, Restele LO, Hadini LO, Usman I, Hasria H, Harisma H. Spatial study of seismic hazard using classical probabilistic seismic hazard analysis (PSHA) method in the Kendari city area. Indonesian Physical Review. 2024;7(3):300–318. doi:10.29303/ipr.v7i3.325

[13] Grünthal G. European Macroseismic Scale 1998 (EMS-98). Luxembourg: Cahiers du Centre Européen de Géodynamique et de Séismologie; 1998.

[14] Giovinazzi S, Lagomarsino S. A Macroseismic Method for the Vulnerability Assessment of Buildings. In: 13th World Conference on Earthquake Engineering. 2004.

[15] FEMA-P154. Rapid Visual Screening of Buildings for Potential Seismic Hazards. 2015.

[16] World Population Review. Sulaimaniya Population 2025.

[17] Microsoft. Microsoft Planetary Computer. 2023. https://planetarycomputer.microsoft.com

[18] EN 1998-1. Eurocode 8 : Design of structures for earthquake resistance - Part 1. 2004.

[19] Hassan P.L., Bapir B., Saeed B., Muslih H., Abrahamczyk L., Haidar B., Khurshid S., Haidar B.. Guidelines for Empirical Seismic Assessment of Buildings in Iraq. 2024.

[20] Lamadrid LFG, Schwartz J, Abrahamczyk L. Methodological Requests For Transforming Building Stocks Into an Ems-98 Consistent Typology. In: World Conference of Earthquake Engineering (WCEE2024). Milan; 2024.

[21] United States Geological Survey (USGS). M7.3 - Halabjah, Iraq Earthquake Executive Summary.

[22] Zanini M.A., Hofer L., Faleschini F. Reversible ground motion-to-intensity conversion equations based on the EMS-98 scale. Engineering Structures. 2019;180:310–320. doi:10.1016/j.engstruct.2018.11.032

[23] Wald D.J., Worden C.B., Quitoriano V., Pankow K.L.. ShakeMap: A U.S. Geological Survey ground motion and intensity mapping tool. 2005. https://earthquake.usgs.gov/data/shakemap/

Proceedings of the 3rd Croatian Conference on Earthquake Engineering - 3CroCEE
19–22 March 2025, Split, Croatia
Copyright © 2025 CroCEE
DOI: https://doi.org/10.5592/CO/3CroCEE.2025.108

IMPROVEMENT OF THE EXPOSURE MODEL AND PRELIMINARY PHYSICAL RISK ANALYSIS: A PILOT CASE MUNICIPALITY

Daniel Tomic [(1)], Radmila Salic Makreska [(2)], Marija Vitanova [(3)], Zabedin Neziri [(4)], Noah Martin [(5)]

[(1)] *Assistant, IZIIS, danielt@iziis.ukim.edu.mk*
[(2)] *Associate professor, IZIIS, r_salic@iziis.ukim.edu.mk*
[(3)] *Associate professor, IZIIS, marijaj@iziis.ukim.edu.mk*
[(4)] *Assistant, IZIIS, zabedin@iziis.ukim.edu.mk*
[(5)] *Young researcher, SADE, noah.martin2002@icloud.com*

Abstract

Seismic risk encompasses the potential damage and losses resulting from earthquake events. Reliable risk assessment, apart from hazard assessment, requires precise and, as much as possible, accurate definitions of both the exposure and vulnerability models, as these components are interdependent and influence one another. This study focuses on developing an exposure model for the Aerodrom municipality in Skopje, partitioned into three subareas: Blocks A, B, and C. The model integrates data from three sources: Google Street View, the publicly accessible cadastral platform of North Macedonia, and field surveys conducted to fill data gaps not covered by the first two sources. These datasets serve as the foundation for constructing the exposure model and generating the input parameters required for seismic risk analysis. For each building asset, the model encompasses essential definitions, such as geographical coordinates and related taxonomy attributes. The developed exposure model is based on the GEM v2.0 taxonomy, which incorporates 13 attributes. Using the developed exposure model, selected vulnerability curves from the GEM database were applied to quantify the seismic response of different building typologies. The preliminary results highlight differences arising from the use of different vulnerability models and selected Ground Motion Models (GMMs). This study provides a comprehensive overview of potential damage in the pilot region, aiding in the further development of seismic risk input parameters. The results are displayed according to the various damage states identified in the assessment. Values are expressed as a percentage of the total number of buildings, providing insight into the potential impact on the building stock.

Keywords: Scenario calculator, Fragility, OpenQuake, Seismic risk.

1. Introduction

The assessment of seismic risk in urban areas is an active area, the results of which contribute to the definition of the degrees of damage and losses, whether economic or human. The components of seismic risk, i.e. their definition and parameterization, provide a comprehensive picture of the entire process. Components such as exposure, vulnerability curves, definition of seismic hazard and ground motion models are particularly influential in estimating the results arising from the seismic risk itself. This paper focuses on the selection of fragility curves based on a defined exposure model using modern tools and defined seismic conditions-scenarios such as a rapture plane with defined parameters that are associated with previous events that occurred on the territory of Macedonia. Based on the defined exposure model, i.e. part of the territory of the municipality of Aerodrom in Skopje, which consists of a total of 172 reinforced concrete buildings with various storeys. The model combines data from three sources: Google Street View, the publicly available cadastral platform of North Macedonia, and field surveys carried out to address data gaps not covered by the first two sources. Defined ground motion models using OpenQuake, by using 3 attenuation equations that are applicable and adaptable to the subject territory of exposure and the four seismic sources, namely the earthquakes in Skopje 1963, Skopje 2016, Debar 1967 and Pehchevo 1904. The results of the selected 3 fragility curves from the GEM database are presented and discussed. Their diversity indicates the need for classification of buildings according to storeys and development of a fragility function using various methods for nonlinear analysis [1]. In recent years, international codes and the scientific community have emphasized a performance-based design approach for structures. Performance can be measured in terms of mean annual frequency or by the probability conditioned on a specific 'earthquake scenario', which

Copyright © 2025 CroCEE
DOI: https://doi.org/10.5592/CO/3CroCEE.2025.108

could be represented by the worst expected event or the event most likely to occur. Seismic performance should be regarded as uncertain, both in terms of earthquake occurrence and structural behavior [2].

2. Definition of the exposure model with GEM taxonomy

The exposure component describes the collected data on the assets (buildings, infrastructure, lifelines) that are susceptible to be damaged by seismic events [3]. In our case the exposure model is defined with data only for buildings using data sources from the following database:

- Google Street View
- The publicly accessible cadastral platform of North Macedonia
- Field surveys



Figure 1. Pilot case – exposure model

A total of 172 buildings in the subject area shown in Fig. 1 were parameterized, all reinforced concrete built in the eighties on the territory of the municipality of Aerodrom, according to Table 1, 14 reinforce concrete structure taxonomies (RCST) are defined, the number of buildings and their number of storeys are shown. The total estimate for residents of the analyzed exposure model is 15092 residents.

Table 1. RCST assets for exposure model

GEM id.	No. of buildings	Stories	Residents
RCST1	4	2	112
RCST2	9	3	378
RCST3	34	4	1904
RCST4	16	5	1120
RCST5	21	6	1764
RCST6	11	7	1078
RCST7	45	8	5040
RCST8	17	9	2142
RCST9	7	10	140
RCST10	4	11	616
RCST11	1	12	168
RCST12	1	14	196
RCST13	1	15	210

Proceedings of the 3rd Croatian Conference on Earthquake Engineering - 3CroCEE
19–22 March 2025, Split, Croatia
Copyright © 2025 CroCEE
DOI: https://doi.org/10.5592/CO/3CroCEE.2025.108

RCST14 1 16 224

The aim of the Global Earthquake Model (GEM) Building Taxonomy, which is used for the exposure model is to describe and categorize buildings in a standardized way as a crucial step in assessing their seismic risk. The criteria for developing the GEM Building Taxonomy included ensuring its relevance to the seismic performance of various construction types; being comprehensive yet simple; allowing for flexibility; adhering to principles familiar to a wide range of users; and ultimately being adaptable to non-buildings and other hazards. The taxonomy is structured as a series of expandable tables that contain information about various building attributes. Each attribute outlines a specific characteristic of an individual building or a group of buildings that could impact their seismic performance. Typical attributes include materials, lateral load-resisting systems, building height, and more. The proposed taxonomy is adaptable and offers the possibility of adding or modifying attributes based on the level of detail needed and new knowledge gathered through the data collection process, which is a benefit over alternative taxonomy models given the global scope of the GEM initiative. This taxonomy differs from most existing structural taxonomies used for seismic risk assessments [4].

The GEM Building Taxonomy v2.0 characterizes a building or building typology using the following 13 attributes, each linked to specific characteristics that could potentially impact seismic performance:

- Direction - this attribute is used to describe the orientation of building(s) with different lateral load resisting systems in two principal horizontal directions of the building plan which are perpendicular to one another.
- Material of the lateral load-resisting system
- Lateral load-resisting system - the structural system that provides resistance against horizontal earthquake forces through vertical and horizontal structural components
- Height - building height above ground in terms of the number of storeys; this attribute also includes information on number of basements (if present) and the ground slope.
- Date of construction or retrofit - identifies the year when the building construction was completed.
- Occupancy - the type of activity (function) within the building; it is possible to describe a diverse range of occupancies
- Building position within a block - the position of a building within a block of buildings
- Shape of the building plan
- Structural irregularity - a feature of a building's structural arrangement, such as one story significantly higher than other stories, an irregular building shape, or change of structural system or material that produces a known vulnerability during an earthquake.
- Exterior walls - material of exterior walls
- Roof - this attribute describes the roof shape, material of the roof covering, structural system supporting the roof covering, and roof-wall connection.
- Floor - describes floor material, floor system type, and floor-wall connection
- Foundation system – shallow/deep foundation

As a characteristic example of the adopted GEM taxonomy, the example of RCST4, which is for RC buildings with a height of 5 stories, is taken. Table 2 indicates the meaning of each taxonomy component individually.

Table 2. RCS GEM taxonomy

CR+CIP/LFM+DUC/HEX:5+HFEX:3+HD:1/YEX:1983/RES+RES2E/BPD/PLFR/IRRE/EWMA/RSH2+RMT6+RWO+RTDP/FC+FC2+FWCP/FOSSL			
CR	Concrete, reinforced	PLFR	Rectangular, solid
CIP	Cast-in-place concrete	IRRE	Regular structure
LFM	Moment frame	EWMA	Masonry exterior walls
DUC	Ductile	RSH2	Pitched with gable ends

Proceedings of the 3rd Croatian Conference on Earthquake Engineering - 3CroCEE
19–22 March 2025, Split, Croatia
Copyright © 2025 CroCEE
DOI: https://doi.org/10.5592/CO/3CroCEE.2025.108

HEX	Exact number of storeys above ground	RMT6	Metal or asbestos sheets
HFEX	Exact height of ground floor level above grade	RWO	Wood
HD	Slope of the ground	RTDP	Roof tie-down present
YEX	Exact date of construction or retrofit	FC	Concrete floor
RES	Residential	FC2	Cast-in-place beam-supported reinforced concrete floor
RES2E	20-49 Units	FWCP	Floor-wall diaphragm connection present
BPD	Detached building	FOSSL	Shallow foundation, with lateral capacity

3. Ground motion models generated from raptures for a range of magnitudes from past events

For the estimation of the seismic risk of the exposure model defined in this way, four earthquake scenarios shown in a Table 3 have been defined based on earthquakes that have occurred in the territory of Macedonia. The same sources are generated as point sources with defined earthquake parameters and a rapture plane associated with the point source itself.

Table 3. Earthquake scenarios, earthquake and fault parameters

No.	Name	Magnitude Mw	Depth (km)	Lon (◦)	Lat (◦)	Strike (◦)	Dip (◦)	Rake (◦)
1	Skopje EQ1963	6.01	4.8	21.43	42.02	290	70	-55
2	Skopje EQ2016	5.28	15	21.5	42	247	61	-99
3	Debar EQ1967	6.38	20	20.43	41.42	52	60	-155
4	Pehchevo EQ1904	7.58	30	23	41.71	230	55	-105

The point source is the type of elemental source used in the OpenQuake-engine for modeling distributed seismicity. The OpenQuake engine always carries out calculations assuming finite ruptures, even when dealing with point sources. Here are the fundamental assumptions used to generate ruptures with point sources:

- Ruptures take a rectangular form
- The hypocenter of the rupture is positioned at the center of the rupture
- The rupture is constrained at the top and bottom by two planes parallel to sea level, located at two characteristic depths known as the upper and lower seismogenic depths, respectively

Based on the adopted scenarios for scenario damage assessment, 4 attenuation equations applicable to the specified territory [5] with an identical weighting factor of 0.25 have been selected:

Copyright © 2025 CroCEE
DOI: https://doi.org/10.5592/CO/3CroCEE.2025.108

- Akkar et al. 2014 GMPE [6]
- Bindi et al. 2014 GMPE [7]
- Boore et al. 2014 GMPE [8]
- ChiouYoungs2014 GMPE [9]

In relation to local soil conditions, a reference Vs30 value was taken to be 520 m/s.

4. Damage distribution and selection of fragility curves

Fragility curves highlight the probability of exceeding a certain level of damage in relation to a certain intensity measure. In our case, fragility curves from the GEM database with the intensity measure peak ground acceleration PGA were used. Three fragility curves [10, 11, 12] were selected, for low, medium and high-rise buildings, as follows:

- Ahmad et al (2010) - CR_,_DUC_,_IRRE_Low-rise (2storeys)
- Ahmad et al (2010) - CR_,_DUC_,_IRRE_Mid-rise (5storeys)
- Ahmad et al (2010) - CR_,_DUC_,_IRRE_High-rise (8storeys)
- Kappos et al. (2003) - CR_,_LFM LowRise HighCode
- Kappos et al. (2003) - CR_,_LFM MidRise HighCode
- Kappos et al. (2003) - CR_,_LFM HighRise HighCode
- Liao (2006) - Reinforced Concrete, Moment Frame, High Code (1-3 stories)
- Liao (2006) - Reinforced Concrete, Moment Frame, High Code (4-7 stories)
- Liao (2006) - Reinforced Concrete, Moment Frame, High Code (8+ stories)

To carry out scenario damage calculations, it is essential to define a fragility function for every building type present in the exposure model. A fragility model consists of a series of fragility functions, which describe the probability of exceeding a set of limit, or damage, states. These fragility functions can be specified in either a discrete or continuous format, and the fragility model file can contain a combination of both types of fragility functions. The presentation of the fragility curves and their comparative difference are shown in Fig. 2. Regarding the differences, it can be determined that there are differences both in the intensities and in the probabilities of exceeding.

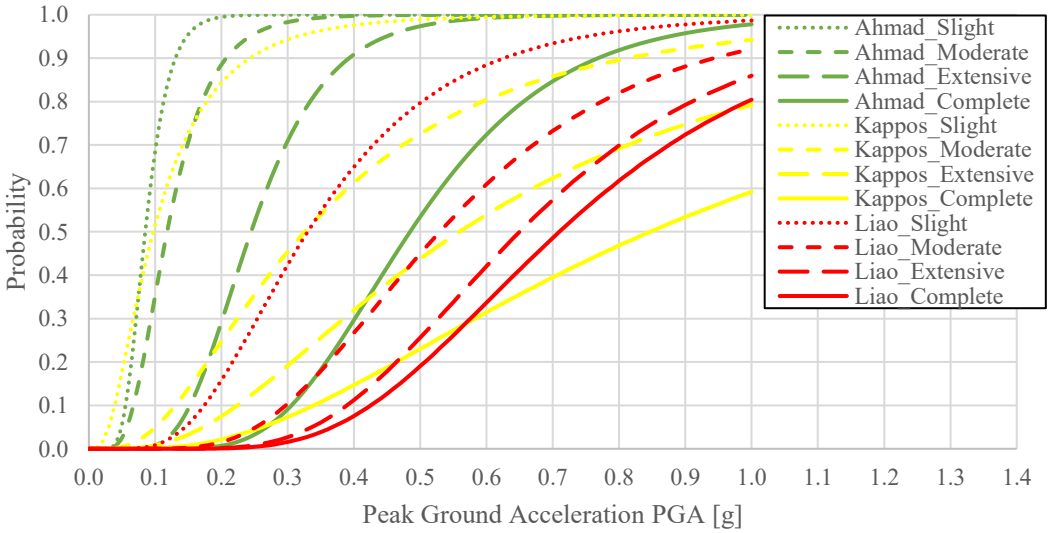


Figure 2. Contribution of fragility curves

The scenario damage calculator used with OpenQuake determines damage distribution statistics for all assets in a given exposure model based on a single specified rupture. These statistics include the mean and standard deviation of damage fractions for various damage states. To operate, this calculator

Copyright © 2025 CroCEE
DOI: https://doi.org/10.5592/CO/3CroCEE.2025.108

requires the definition of a finite rupture model, an exposure model, and a fragility model. An example of the job.ini.file from the scenario damage calculator is shown in Fig. 3. The primary outputs are the damage distribution statistics per asset, aggregated damage distribution statistics per taxonomy, overall damage distribution statistics for the region, and collapse maps, which show the spatial distribution of the number or area of collapsed buildings across the region of interest.

```
[general]
description = Scenario calculation Skopje 1963 ahmad
calculation_mode = scenario_damage
random_seed = 113

[Rupture information]
rupture_model_file = earthquake_rupture_Skopje_1963_cat.xml
rupture_mesh_spacing = 2

[Hazard sites]
region_grid_spacing = 2
region = 18.660643 43.597828, 23.453487 43.441627, 23.588118 40.061431, 18.831175 40.013329

[Exposure model]
exposure_file = exposure_model_Block_A_kor.xml
asset_hazard_distance = {'default': 200}

[Fragility model]
structural_fragility_file = fragility_model_Block_A_kor so ahmad.xml

[Site conditions]
reference_vs30_value = 520
reference_vs30_type = inferred
reference_depth_to_2pt5km_per_sec = 2.0
reference_depth_to_1pt0km_per_sec = 100.0

[Calculation parameters]
gsim_logic_tree_file = gmpe.xml
ground_motion_correlation_model =
truncation_level = 3.0
maximum_distance = 200
number_of_ground_motion_fields = 1000
```

Figure 3. Example of job.ini flie

Based on the conditions defined in this way and the calculation models defined in OpenQuake, a total of 12 analyses were run using the scenario damage calculator. The results are shown in Fig. 4,5,6. The values of the results from the seismic risk estimation are expressed in percentages. The results clearly show the contribution of the fragility curves in the estimation of the distribution of damage levels.

Copyright © 2025 CroCEE
DOI: https://doi.org/10.5592/CO/3CroCEE.2025.108

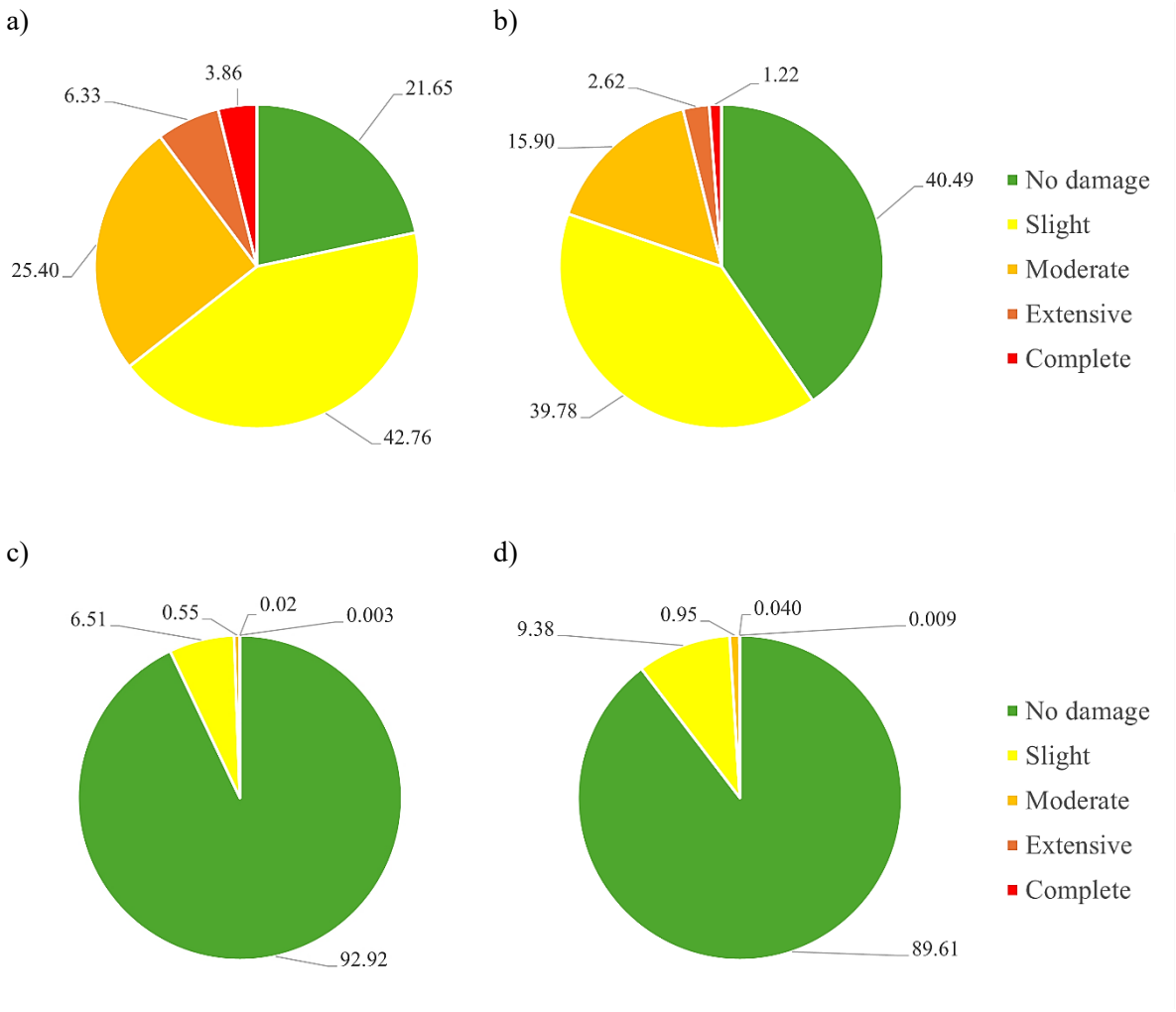
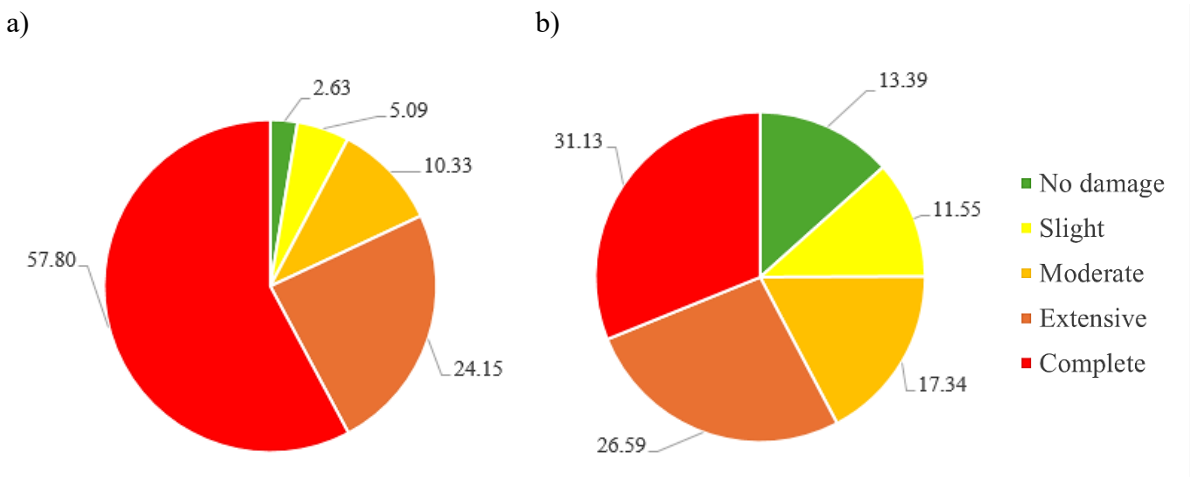


Figure 4. Aggregate Risk Statistics in Percentage FCS1 Kappos et al. 2003 a) Skopje 1963; b) Skopje 2016; c) Debar 1967; d) Pehchevo 1904.



Copyright © 2025 CroCEE
DOI: https://doi.org/10.5592/CO/3CroCEE.2025.108

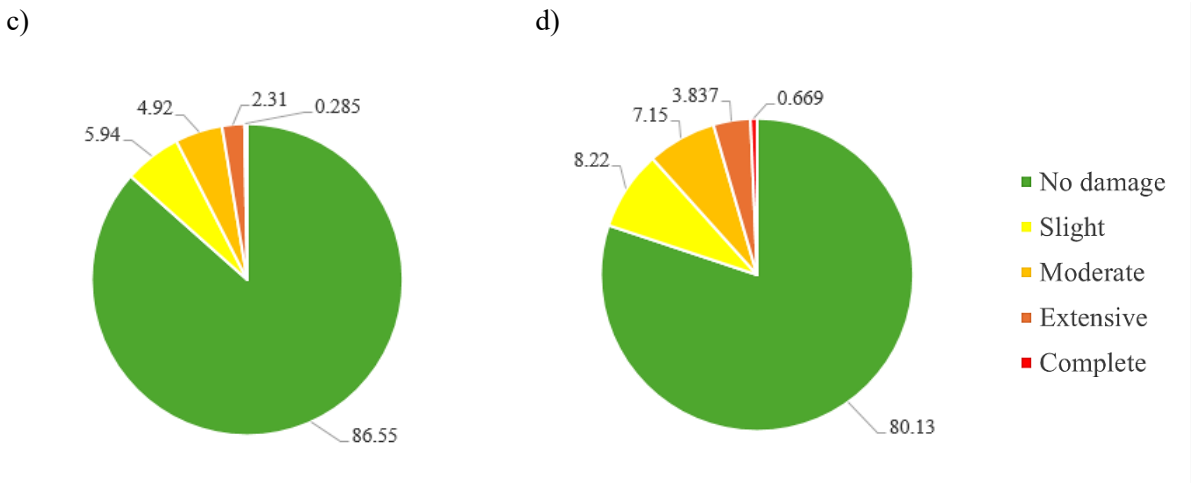


Figure 5. Aggregate Risk Statistics in Percentage FCS2 Ahmad et al. 2006 a) Skopje 1963; b) Skopje 2016; c) Debar 1967; d) Pehchevo 1904.

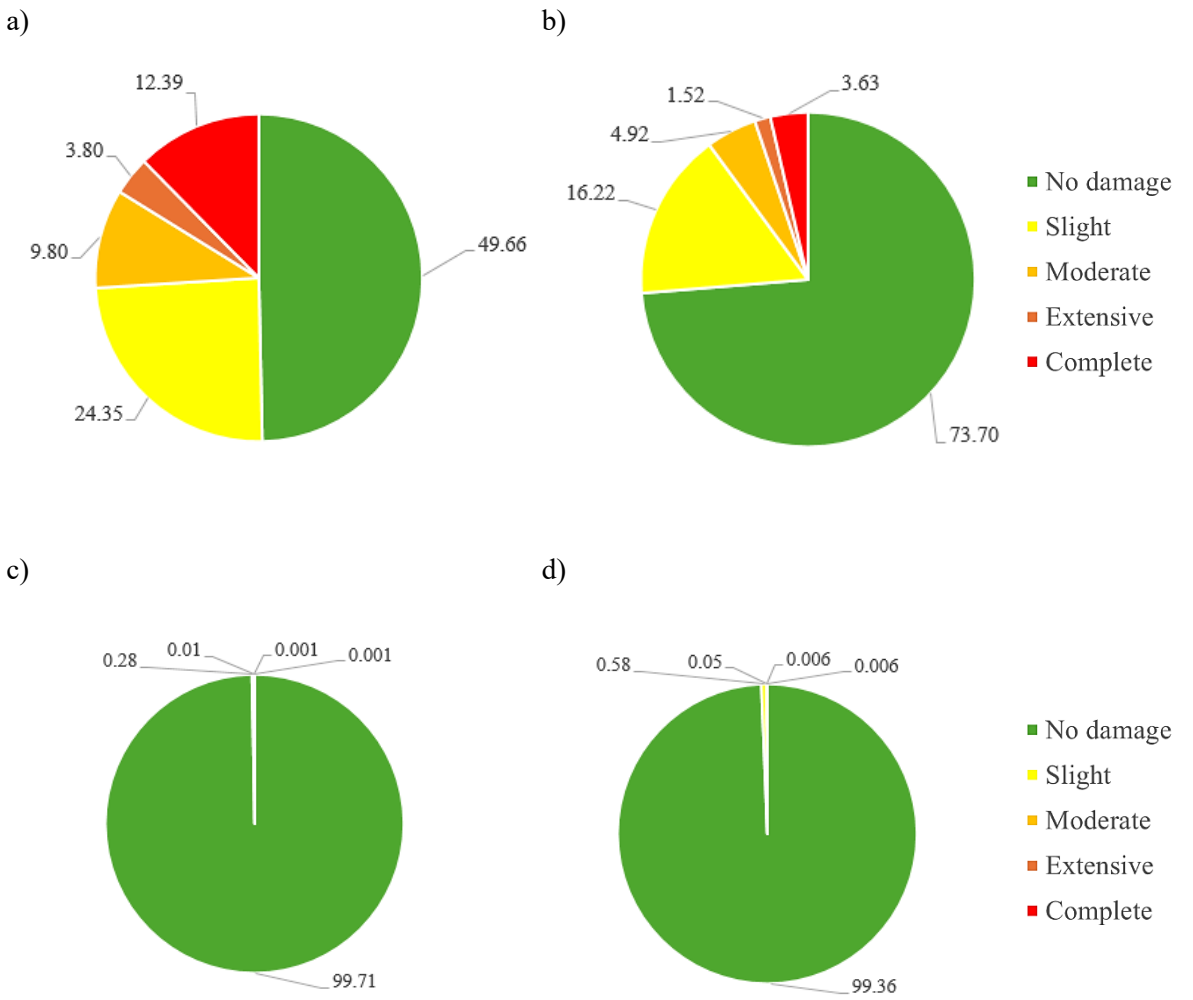


Figure 6. Aggregate Risk Statistics in Percentage FCS3 Liao et al. 2007 a) Skopje 1963; b) Skopje 2016; c) Debar 1967; d) Pehchevo 1904.

Copyright © 2025 CroCEE
DOI: https://doi.org/10.5592/CO/3CroCEE.2025.108

5. Conclusions

The paper generalizes and shows the differences in the selection of fragility curves in relation to the estimation of seismic risk based on a defined exposure model created by obtaining data from three sources. A total of 12 earthquake scenarios were used, four for each of the selected fragility curves. In terms of the results, the most conservative estimate of the damage degrees was obtained with the curves of Ahmad et al. (2010). The curves of Kappos et al. (2003) and Liao (2006) are more uniform despite the fact that all curves are adopted from the GEM database for reinforced concrete structures, moment frame ductile structures.

The differences that originate from the selection of fragility curves indicate the fact that for the estimation of seismic risk, the best results would be obtained by developing fragility curves based on the typology of buildings such as 1 to 3 stories, 4 to 7, over 8 stories. To generate these curves, using various types of nonlinear static and dynamic analyses, curves would be realistically obtained that would be representative of the structures shown in the exposure model.

References

[1] Tomic, D., Salic Makreska, R. (2024): Development of fragility curve for existing RC building. *18th World Conference on Earthquake Engineering (WCEE2024),* Milan, Italy

[2] Giannini R., Paolacci, F., Phan, H.N., Corritore, D., Quinci, G. (2024): A new paradigm in seismic risk assessment of new and existing structures. *18th World Conference on Earthquake Engineering (WCEE2024),* Milan, Italy

[3] Nicodemo, G., Pittore, M., Masi, A., Manfredi, V. (2020): D'Ayala, D., Speranza, E. (2020): Modelling exposure and vulnerability from post-earthquake survey data with risk-oriented taxonomies: AeDES form, GEM taxonomy and EMS-98 typologies. *International Journal of Disaster Risk Reduction*, https://doi.org/10.1016/j.ijdrr.2020.101894

[4] Brzev S., C. Scawthorn, A.W. Charleson, L. Allen, M. Greene, K. Jaiswal, and V. Silva: (2013), GEM Building Taxonomy Version 2.0. *GEM Technical Report 2013-02 V1.0.0, 188 pp*., GEM Foundation, Pavia, Italy, doi:10.13117/GEM.EXP-MOD.TR2013.02

[5] Milutinovic, Z., Salic Makreska, R., Tomic, D. (2016): Seismic zoning maps of the Republic of Macedonia in accordance with the requirements of MKC EN 1998-1:2004 - Eurocode 8 interpretation, *IZIIS report*

[6] Akkar, S., M. A. Sandikkaya and J. J. Bommer (2014): Empirical ground-motion models for point- and extended-source crustal earthquake scenarios in Europe and the Middle East, *Bulletin of Earthquake Engineering,* 12, 359-387.

[7] Bindi, D., M. Massa, L. Luzi, G. Ameri, F. Pacor, R. Puglia, and P. Augliera (2014a): Pan-European ground-motion prediction equations for the average horizontal component of PGA, PGV, and 5%-damped PSA at spectral periods up to 3.0s using the RESORCE dataset. *Bulletin of Earthquake Engineering*, 12(1): 391–430, 2014a. doi: 10.1007/s10518-_013-_9525-_5.

[8] Boore, D. M., J. P. Stewart, E. Seyhan, and G. M. Atkinson (2014): NGA-West 2 equations for predicting PGA, PGV, and 5%-damped PSA for shallow crustal earthquakes. *Earthquake Spectra*, 30(3):1057–1085. doi: 10.1193/070113EQS184M.

[9] Chiou, B. S.-J., Youngs, R. R. (2014): Update of the Chiou and Youngs NGA model for the average horizontal component of peak ground motion and response spectra. *Earthquake Spectra*, 30(3):1117–1153, Aug 2014. doi: 10.1193/072813EQS219M.

[10] Milutinovic, Z., Trendafiloski, G. (2003): An advanced approach to earthquake risk scenarios with applications to different European towns, *WP4: Vulnerability of current buildings, RISK-UE*, Contract EVK4-CT-2000-00014

[11] Liao, WI., Loh, CH. & Tsai, KC. (2006): Study on the Fragility of Building Structures in Taiwan. *Natural Hazards* 37, 55–69, https://doi.org/10.1007/s11069-005-4656-x

[12] Syner D7.1 – Functional Fragility Curve Archive. (2009): Systemic Seismic Vulnerability and Risk Analysis for Buildings, Lifeline Networks and Infrastructures Safety Gain. (2009):, *FP7-ENV-2009-1*

Proceedings of the 3rd Croatian Conference on Earthquake Engineering - 3CroCEE
19–22 March 2025, Split, Croatia
Copyright © 2025 CroCEE
DOI: https://doi.org/10.5592/CO/3CroCEE.2025.143

DEVELOPMENT OF K QUOTIENT METHODOLOGY FOR INTER-CODE LATERAL FORCE COMPARISON

Zoran Milutinovic [(1)], *Radmila Salic Makreska* [(2)], *Jovan Trajchevski* [(3)]. *Daniel Tomic* [(4)]

[(1)] *Professor, IZIIS, † Deceased*
[(2)] *Professor, IZIIS, r_salic@iziis.ukim.edu.mk*
[(3)] *Assistant, IZIIS, jovant@iziis.ukim.edu.mk*
[(4)] *Assistant, IZIIS, danielt@iziis.ukim.edu.mk*

Abstract

The purpose of this paper is to provide clarification to individuals attempting to create models for seismic exposure as well as seismic vulnerability and risk, based on the seismic lateral loads established by the Yugoslavian seismic design codes. The particular focus of the research are the JUS 39/64 and JUS 31/81 seismic design codes, since they were active codes for a significant period of time, in which a lot of the structures still existing today in Macedonia as well as Yugoslavia were built. The main focus of this paper is the development of the K-Quotient method, which aims to provide a direct comparison between the lateral load levels obtained by analysing structures using the mentioned seismic codes.

Keywords: Building codes, Seismic risk, Seismic exposure.

1. Introduction

A building code is a set of minimum regulations intended to safeguard building occupants' public health, safety, and general welfare. The development, adoption, and enforcement of building codes vary widely from one country to another. In some countries, the authority to regulate building construction is delegated to local jurisdictions. In others, building codes are developed by governmental agencies and are enforced nationwide. Former Yugoslavia, of which North Macedonia was a part of, used a combined model by enforcing seismic design codes nationwide but also delegating authority to regulate building construction to Federal units.

The Institute of Earthquake Engineering and Engineering Seismology (IZIIS), in Skopje, with the assistance and the support of the National Coordinator for Implementation of the National Platform for Disaster Risk Reduction, based on the data of last, the 2021 census, intends to develop a high-resolution national exposure model.

Works along this line are already ongoing on the European scale. The European Commission's Horizon 2020 SERA is the first concerted effort among the research community to produce a uniform European risk model (ESRM20). The European seismic risk assessment exposure model is presented in Crowley et al. (2020a and b)[1,2]. In support of Crowley et al., 2020b, Crowley et al., 2021[3] presents the "Model of seismic design lateral force levels for the existing reinforced concrete European building stock," Republic of North Macedonia included.

An understanding of the level of design of a given building class is fundamental for the development of vulnerability models that can represent the features of each design level (Borzi et al. 2008[4]; Verderame et al. 2010[5]; Romao et al. 2020[6]; Crowley et al. 2021) in national seismic risk assessment models.

Yugoslavia enforced the first earthquake design regulations JUS61/48[7] in 1948, Table 1. The second (JUS39/64) was introduced in 1963/1964 following the 1963 Skopje earthquake, at the time when IAEE recorded 25 to 27 seismic design codes worldwide. The third, JUS31/81, was introduced in 1981 (in effect from August 1982). Out of 63 codes currently recorded by IAEE, it is the 31st. By Official Gazette of RNM No. 211 of 02.09.2020, Macedonia adopted the Eurocode Design System MKC EN 1990 –

Proceedings of the 3rd Croatian Conference on Earthquake Engineering - 3CroCEE
19–22 March 2025, Split, Croatia
Copyright © 2025 CroCEE
DOI: https://doi.org/10.5592/CO/3CroCEE.2025.143

MKC EN 1999[10], allowing the parallel use of JUS31/81 and all other related standards for a period of 5 years.

The paper presents in necessary detail the spatial and temporal evolution of seismic design requirements in Yugoslavia over the last 70-75 years. The subject is scarcely treated and published in detail. To the authors' best knowledge, a brief review of Croatian earthquake-resistant design from 1948 to 2021 is presented in Zamolo, 2021 (in Croatian)[11]. However, the subject is not treated in such technical details as this paper does.

Table 1. Evolution of Yugoslavian technical regulations for earthquake resistant design

Regulation	**Abbreviated as**	**Level**
Provisional Technical Regulations for Building Loading (Official Gazette of FNRT No. 61/48)	JUS61/48 (PTP2)	National FNRY
Regulations for Design and Construction of Structures in Seismic Regions (Official Gazette of SRS No. 18/63 of June 13, 1963)	SI18/63	Republic, Slovenia
Regulations for Design and Construction of Structures in Seismic Regions (Official Gazette of SRM No. 33/63 of 24 September 1963) Translation of SI18/63	MK33/63	Republic, Macedonia
Provisional Technical Regulations for Construction in Seismic Regions (Official Gazette of SFRY No. 39/64 of 30 September 1964)	JUS39/64	National SFRY
Technical Regulations for Building Construction in Seismic Regions (Official Gazette of SFRJ No. 31/81 of 5 June 1981, including amendments: No. 49/82 of 13 August 1982, No. 29/83 of 10 June 1983, No. 21/88 of 1 April 1988, and No. 52/90 of 7 September 1990)	JUS31/81	National SFRY
Technical Regulations for Repair, Strengthening and Reconstruction of Building Damaged by Earthquakes, and for Reconstruction and Revitalization of Buildings; (Official Gazette of SFRY No. 52 of 4 October 1985)	JUS52/85 (Not discussed in this contribution)	National SFRY
Regulations on Technical Norms for Design and Calculation of Civil Engineering Facilities in Seismic Regions; (1986, Draft)	JUSxx/86 (Not discussed in this contribution)	National SFRY
Eurocode Design System MKC EN 1990 – MKC EN 1999 (OGoRNM No. 211 of 02.09.2020 Eurocode 8: Design of structures for earthquake resistance - Part 1: General rules, seismic actions and rules for buildings	MKC EN 1998-1	National NRM

The lateral force coefficient K, Eq. 1, follows Crowley et al., 2021[3] formulation that coincides with the JUS31/81 definition.

$$K = K_0 \cdot K_S \cdot K_P \cdot K_D \quad (1)$$

K0 is a coefficient of building importance, Ks is a coefficient of seismic intensity, Kp is a coefficient that considers the energy-dissipation capacity of the structure (in JUS codes termed coefficient of damping and ductility; in other codes very often termed as a structural coefficient) and Kd is a dynamic coefficient or coefficient of dynamic response calculated from the period of vibration of the structure. Adopting the same K formulation enables a direct comparison of findings of this contribution with those presented in Crowley et al., 2021.

The contribution also tends to resolve the “memory hole” effect that generations trained in ongoing Code have inappropriate experience in previous codes. While it is not an issue for design practice, it is of utmost importance for vulnerability and seismic risk modellers and analysts to understand and model the level of design of a given building class in national/regional/European seismic risk assessment

Proceedings of the 3rd Croatian Conference on Earthquake Engineering - 3CroCEE
19–22 March 2025, Split, Croatia
Copyright © 2025 CroCEE
DOI: https://doi.org/10.5592/CO/3CroCEE.2025.143

models. Accordingly, the second primary objective of this contribution is to clarify and save specific evolutionary facts for seismic design in RNM (Republic of North Macedonia) and SFRY (SFR Yugoslavia) from the memory hole.

2. K – Quotient method

Due to conceptual differences between the formats of JUS39/64 and JUS31/81 codes for the definition of base shear, the direct comparison of coefficients constituting the seismic coefficient for flexible buildings (H>20m, or n>5 stories) cannot be made. The comparisons of computer-aided results can be made; however, the insight in behaviour and contribution of some coefficients constituting the seismic coefficient will be lost. For stiff buildings (H≤20m, or n≤5 stories), both codes prescribe the use of a simplified method. JUS39/64 calculates the story shears F_k^{64} according to Eq. 2 and then by sums them as the base shear F_b^{64} using Eq.3. The period of n≤5 story buildings, calculated by T=0.1n, is T≤0.5s and fully corresponds to the JUS39/64 definition of "stiff structure".

$$S_{ik}^{64} = K_i^{64} \cdot w_k = K_S^{64} \cdot S^{64} \cdot S_{ie}^{64} \cdot K_{i\eta}^{64} \cdot w_k \tag{2}$$

$$F_b^{64} = \sum_{k=1}^{n} F_k^{64} \tag{3}$$

Where K_S^{64} is a factor which relates to the site seismicity as well as the importance factor of the structure, S^{64} is a soil amplification factor, S_{ie}^{64} is a dynamic coefficient and $K_{i\eta}^{64}$ is a coefficient which takes into account the modal shape. A more detailed explanation of the JUS39/64[8] and JUS31/81 seismic design codes can be found in Milutinovic et. al. (2022)[12].

The most efficient way to compare or scale the values of base shears defined by two or more codes is taking the appropriate ratio. The ratio, RK_b, defined by Eq. 4 expresses the F_b^{81} base shear in terms of F_b^{64}.

$$RK_b = \frac{F_b^{81}}{F_b^{64}} = \frac{K^{81}}{K^{64}} = \frac{K_O^{81}}{K_O^{64}} \frac{K_P^{81}}{K_P^{64}} \frac{S^{81}}{S^{64}} \frac{S_e^{81}}{S_e^{64}} \frac{K_S^{81}}{K_S^{64}} \frac{K_\eta^{81}}{K_\eta^{64}} = RK_O\ RK_P\ RS\ RS_e\ RK_S\ RK_\eta \tag{4}$$

If, for a particular Seismic Zone (K_s), Building Importance Category (K_0), site Ground Conditions (S), Building Type (K_p) and Number of Stories (n), the RK_b is:

- $RK_b > 1$, JUS31/81 base shear force is larger than that prescribed by JUS39/64; and,
- $RK_b < 1$, JUS31/81 base shear force is smaller than that prescribed by JUS39/64.

It is also true for all RK_b constituents. If the constituent <i> $RK_i > 1$, it will tend to increase the JUS31/81 base shear relative to that prescribed by JUS39/64, and vice versa, if $RK_i < 1$, the constituent <i> will tend to decrease the JUS31/81 base shear relative to that prescribed by JUS39/64.

The RK_b of Eq. 4 is a product of six quotients (ratios). Accordingly, this contribution terms it K – Quotient method.

The method provides a closed-form solution for stiff structures, thus a single value. For flexible structures, it is necessary to conduct structural analysis and then compare the final results.

2.1.Stiff Buildings

According to JUS39/64 Article 2.6, the application of a simplified method is recommended for stiff structures (H≤20 metres, Article 1.3). It is conditioned by: (1) doubling the value of the coefficient of dynamic response (instead 0.75/T use of 1.5/T), and (2) calculation of modal shape factor. For the same structural category (n≤5 storeys), JUS31/81 calculates the F_b^{81} by Eq. 5.

Proceedings of the 3rd Croatian Conference on Earthquake Engineering - 3CroCEE
19–22 March 2025, Split, Croatia
Copyright © 2025 CroCEE
DOI: https://doi.org/10.5592/CO/3CroCEE.2025.143

$$F_b^{81} = K^{81} \cdot W = K_0^{81} \cdot K_P^{81} \cdot K_S^{81} \cdot S^{81} \cdot S_e^{81} \cdot K_{i\eta}^{81} \cdot W \tag{5}$$

The period of n≤5 story buildings is in the range 0-0.5s. It is comprised of all three $S\ e81$ plateaus and the $S\ e64$ plateau. Thus $S_e^{81} = S_e^{64} = 1$. As discussed above, for using a simplified method JUS39/64 (Article 2.6) request that S_e^{64} spectral shape is multiplied by a factor of 1.5. Thus,

$$RS_e = \frac{S_e^{81}}{S_e^{64}} = \frac{1}{1.5} = \frac{2}{3} \tag{6}$$

The coefficient of seismic intensity, irrespectively of its formulation, is the same for both codes, hence

$$RK_S = \frac{K_S^{81}}{K_S^{64}} = \frac{PGA^{81}}{PGA^{64}} = 1 \tag{7}$$

The K_η^{64} shape coefficient is a sum of story shape coefficients $K_{k\eta}^{64}$ and equals to

$$K_\eta^{64} = \sum_{k=1}^{n} K_{k\eta}^{64} = 1.5\ \frac{n\ (n+1)}{2n+1} \tag{8}$$

JUS31/81 base shear is expressed in W (total weight of the structure), not by storey tributary weights $w = wi$ as in JUS39/64. Substituting W with $n \cdot w$ and cancelling out all other ratios except K_η^{81}/K_η^{64} defines $RK_\eta = n/K_\eta^{64}$. The reminder n is de facto the K_η^{81} coefficient, and RK_η ratio is

$$RK_\eta = \frac{K_\eta^{81}}{K_\eta^{64}} = \frac{2}{3}\ \frac{2n+1}{n+1} \tag{9}$$

Defined RK_0, RS, RK_p, and RK_η ratios are displayed in Tables 13 to 16, respectively. Based on Eq. 7 and 8, Eq. 4 reduces to:

$$RK_b = \frac{2}{3}\ RK_O\ RK_P\ RS\ RK_\eta \tag{10}$$

Table 2 JUS39/64-JUS31/81 RK_O ratios

Building Importance Category		I_{MCS} VII	VIII	IX
1	RK_{01}	0.75	0.75	1.00
2	RK_{02}	1.00	1.00	1.00
3	RK_{03}	0.75	1.50	1.50

Table 3 JUS39/64-JUS31/81 RS ratios

Ground Category			S^{64}	S^{81}	RS
I	S_1	Good	1.2	1.0	0.8333
II	S_2	Medium	1.0	1.0	0.6667
III	S_3	Weak	1.2	1.0	0.5556
IV	S_4	Very Weak	2.0	1.0	0.3333

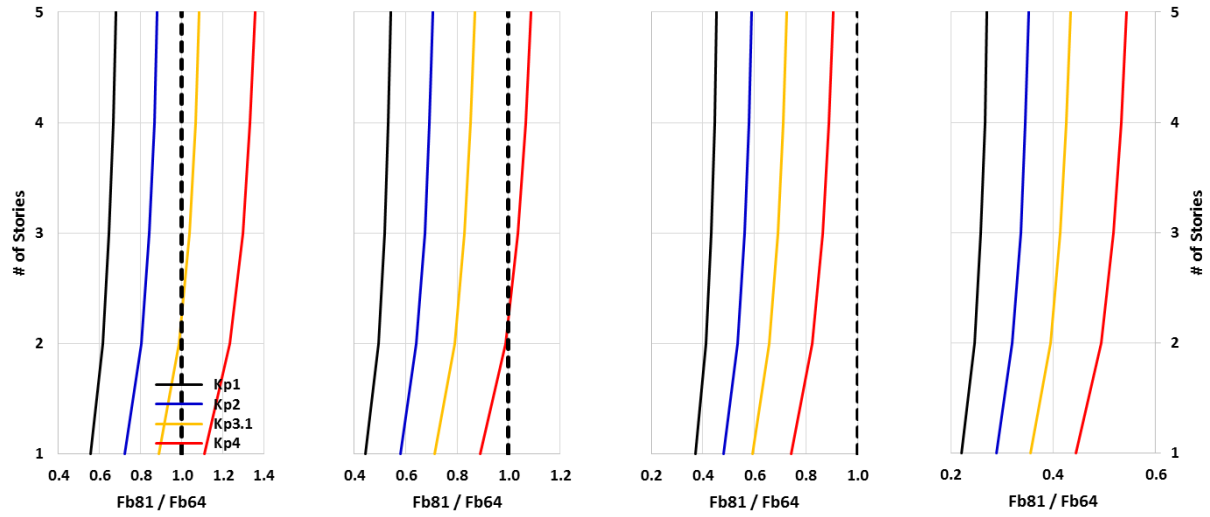
Table 4 JUS39/64-JUS31/81 RK_P ratios

Building Typology		K_P^{64}	K_P^{81}	RK_P
(1)	RK_{P1}	1.0	1.0	1.0
(2)	RK_{P2}	1.0	1.3	1.3
(3.1)	$RK_{P3.1}$	1.0	1.6	1.6
(3.2)	$RK_{P3.2}$	1.6	1.6	1.0
(4)	RK_{P6}	1.0	2.0	2.0

Table 5 JUS39/64-JUS31/81 RK_η ratio

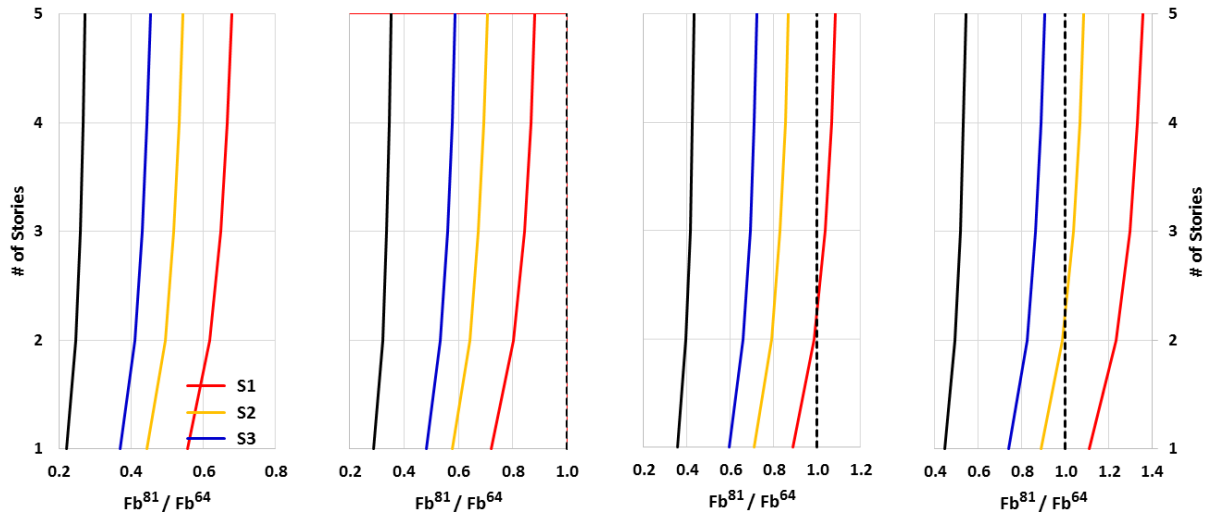
# of stories	K_P^{64}	K_P^{81}	RK_η
6	1.0	0.8077	1.2381	**6**
5	1.0	0.8182	1.2222	**5**
4	1.0	0.8333	1.2000	**4**
3	1.0	0.8571	1.1667	**3**
2	1.0	0.9000	1.1111	**2**
1	1.0	1.0000	1.0000	**1**

Proceedings of the 3rd Croatian Conference on Earthquake Engineering - 3CroCEE
19–22 March 2025, Split, Croatia
Copyright © 2025 CroCEE
DOI: https://doi.org/10.5592/CO/3CroCEE.2025.143



Ground type $GT_1(S_1)$ | Ground type $GT_2(S_2)$ | Ground type $GT_3(S_3)$ | Ground type $GT_4(S_4)$

Fig. 1 Behaviour of K_b by number of stories, ground types, and structural typology; Plots by Ground types



Structural Type K_{p1} | Structural Type K_{p2} | Structural Type $K_{p3.1}$ | Structural Type K_{p4}

Fig. 2 Behaviour of K_b by number of stories, Ground Categories, and structural typology Plots by structural typology

From Tables 2 to 5, it is observable that RK_P and RK_η ratios, both ≥1 tend to increase RK_b. On the other hand, RS and RS_e (Eq. 6) ratios tend to decrease it. RKO ratio, Table 2, for Importance Class I buildings decrease RK_b in $IMCS$ VII and VIII seismic zones whereas stipulate it for Importance Class III buildings in $IMCS$ (Importance class seismicity) VIII and IX zones.

Behaviour of RK_b by ground categories are presented in Figs. 1 and by structural typology in Figs. 2. Data used to generate Figs. 1 and 2 are tabulated in Table 6.

From Figs. 1 and 2, it is evident that JUS31/81 is superior only for all K_{p4} structures on $GT1$ ground category and n=3-5 stories $K_{p3}.1$ structures on $GT2$ ground category.

Proceedings of the 3rd Croatian Conference on Earthquake Engineering - 3CroCEE
19–22 March 2025, Split, Croatia
Copyright © 2025 CroCEE
DOI: https://doi.org/10.5592/CO/3CroCEE.2025.143

Table 6 K conversion coefficient values

VIII	**Soil Factor S**				**Structural Type K_P**			
# of Stories	S_1	S_2	S_3	S_4	K_{P1}	K_{P2}	$K_{P3.1}$	K_{P4}
	$RK_{P1} = 1.0$				**$S_1 = 0.8333$**			
5	0.6790	0.5432	0.4527	0.2713	0.6790	0.8827	1.0864	1.3580
4	0.6666	0.5334	0.4445	0.2664	0.6666	0.8666	1.0666	1.3333
3	0.6481	0.5185	0.4321	0.2590	0.6481	0.8426	1.0370	1.2962
2	0.6173	0.4939	0.4116	0.2467	0.6173	0.8024	0.9876	1.2345
1	0.5555	0.4445	0.3704	0.2220	0.5555	0.7222	0.8889	1.1111
	$RK_{P2} = 1.3$				**$S_2 = 0.6667$**			
5	0.8827	0.7062	0.5885	0.3527	0.5432	0.7062	0.8692	1.0865
4	0.8666	0.6934	0.5778	0.3463	0.5334	0.6934	0.8534	1.0667
3	0.8426	0.6741	0.5618	0.3367	0.5185	0.6741	0.8297	1.0371
2	0.8024	0.6420	0.5350	0.3207	0.4939	0.6420	0.7902	0.9877
1	0.8827	0.7062	0.5885	0.3527	0.4445	0.5778	0.7111	0.8889
	$RK_{P3.1} = 1.6$				**$S_3 = 0.5556$**			
5	1.0864	0.8692	0.7243	0.4341	0.4527	0.5885	0.7243	0.9054
4	1.0666	0.8534	0.7112	0.4262	0.4445	0.5778	0.7112	0.8890
3	1.0370	0.8297	0.6914	0.4144	0.4321	0.5618	0.6914	0.8643
2	0.9876	0.7902	0.6585	0.3947	0.4116	0.5350	0.6585	0.8231
1	0.8889	0.7111	0.5926	0.3552	0.3704	0.4815	0.5926	0.7408
	$RK_{P4} = 2.0$				**$S_4 = 0.3333$**			
5	1.3580	1.0865	0.9054	0.5427	0.2713	0.3527	0.4341	0.5427
4	1.3333	1.0667	0.8890	0.5328	0.2664	0.3463	0.4262	0.5328
3	1.2962	1.0371	0.8643	0.5180	0.2590	0.3367	0.4144	0.5180
2	1.2345	0.9877	0.8231	0.4933	0.2467	0.3207	0.3947	0.4933
1	1.1111	0.8889	0.7408	0.4440	0.2220	0.2886	0.3552	0.4440

JUS31/81 base shear prevail JUS39/64

Cases calculated below

The proposed K-Quotient method is easily applicable for comparing ELF(Equivalent Lateral Force)-based base shears. Fig. 3 is a tabular presentation of the procedure proposed by Eqs. 4 and 10.

$RK_b =$

RS_e
2/3

(Eq. 25)

SZ	RK_S
VII	1.0
VIII	1.0
IX	1.0

(Eq. 26)

RK_O	VII	VIII	IX
RK_{01}	0.75	0.75	1.00
RK_{02}	1.00	1.00	1.00
RK_{03}	0.75	1.50	1.50

(Table 13)

S	RS
S_1	0.8333
S_2	0.6667
S_3	0.5556
S_4	0.3333

(Table 14)

K_P	RK_P
K_{P1}	1.0
K_{P2}	1.3
$K_{P3.1}$	1.6
$K_{P3.2}$	1.0
K_{P4}	2.0

(Table 15)

$K\eta$	RK_η
η_5	1.2222
η_4	1.2000
η_3	1.1167
η_2	1.1111
η_1	1.0000

(Table 16)

Fig. 3 Break down on RS_e, RK_S, RK_O, RS, RK_P and RK_η ratios constituting K transformation coefficient

Copyright © 2025 CroCEE
DOI: https://doi.org/10.5592/CO/3CroCEE.2025.143

For example, for Category II ($RKO1$ = 1.00, Table 2), 5 story (n = 5, η5 = 1.2222, Table 5), RC structure ($KP1$ = 1.00, Table 4), located in the seismic zone of VIII degree intensity (RKS = 1.00), sited on medium ground conditions ($S2$ = 0.6667, Table 3), RKb calculated by order as presented in Fig. 3, is:

RKb = (2/3) · 1.00 · 1.00 · 0.667 · 1.00 · 1.2222 = 0.5432, and $\boldsymbol{Fb81}$= 0.5432 $\boldsymbol{Fb}$64

If the building is with stiffness discontinuity (e.g. soft story, $KP4$ = 2.00), the RKb would be:

RKb = (2/3) · 1.00 · 1.00 · 0.667 · 2.00 · 1.2222 = 1.0865, and $\boldsymbol{Fb81}$= 1.0865 $\boldsymbol{Fb}$64

For four story (n=4, η4 = 1.2000) masonry building strengthened by tie-columns (KP3.1 = 1.6) and all other coefficients as in the previous case, RKb is

RKb = (2/3) · 1.00 · 1.00 · 0.667 · 1.60 · 1.2000 = 0.8534, and $\boldsymbol{Fb81}$ =0.8534 $\boldsymbol{Fb}$64

Relative to JUS31/81, the JUS39/64 simplified method is over-conservative for stiff building. The largest conservativism is associated with lateral force coefficient associated to GT3 and GT4 ground conditions (0.5556 and 0.3333, respectively), then to GT2 (0.6667), and finally to GT1 (0.8333).

2.2. Flexible Buildings

The RK_b ratio (or RK_b-quotient) is calculated for two selected flexible buildings located in $IMCS$ zone of IX degrees with K_S = 0.10. Both are reinforced concrete space moment-resisting frame (skeleton) buildings symmetric in both orthogonal horizontal directions (K_P = 1; RP = 4). They are residential buildings with the ground floor (GF) hosting commercial uses, hence importance category II (K_0 = 1).

DTB (Tomic, 2018) [13] building is 43 metres in height GF+ME+12 story tower with T_x=T_y=1.848s. JTB (Trajcevski, 2018) [14] building is a GF+ME+4 story block type building 19.3 metres in height with T_x =1.108s and T_y=1.048s. ME is the mezzanine story. The floor plan of both buildings is presented in Figs. 4 and 5. Both were designed and executed according to JUS39/64 at the beginning of the 1970s'. In addition, analysed is 10 storey 5 bay (in longitudinal) and 3 bay (in transverse) direction. The building (B10) is a dual RC frame/wall system with a shear wall placed in the middle span of two internal frames.

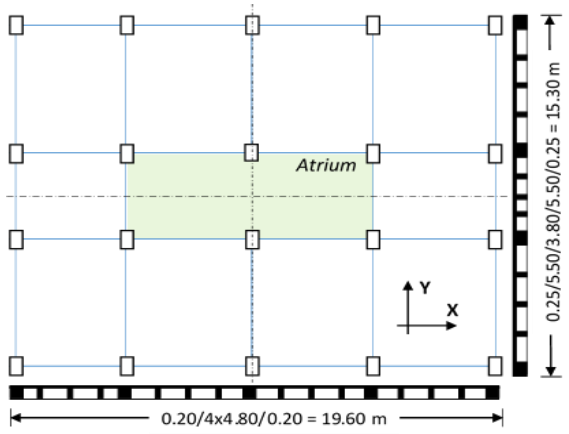


Fig. 4 JTB Building, characteristic floor plan

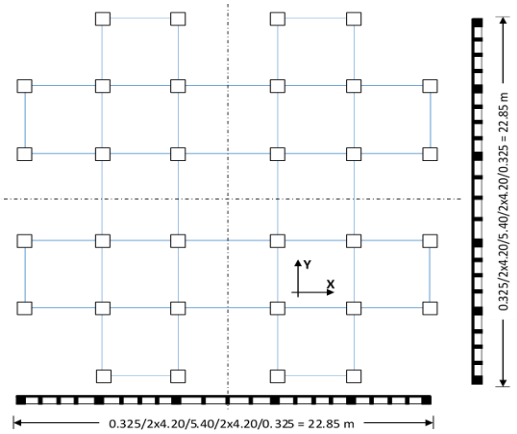


Fig. 5 DTB Building, characteristic floor plan

The analyses are conducted for all three ground types. The results are presented in Table 7. RK_b values are of the same order, irrespective of the fact that JUS39/64 are derived from 3 mode MRS (Modal Response Spectrum) and JUS31/81 by ELF method. Common to both JTB and DTB buildings is the inverse trending of ground type dependent RK_s relative to trends outlined by the simplified method. For $GT1$ ground type, both RK_{bs} are ≤1, hence JUS38/64 did prescribe the higher base shear than JUS31/81. The RK_b≥1.0 are attributed to $GT3$ ground typology demonstrating that JUS31/81 overwhelms the JUS39/64 base shear.

Copyright © 2025 CroCEE
DOI: https://doi.org/10.5592/CO/3CroCEE.2025.143

Comparatively JUS39/64 and JUS31/81 base shears are about the same for $GT2$. However, the results for B10 building, although following the same pattern of GT dependency, are all above the $RK_b \geq 1.0$.

Table 7 Lateral force ratio (RK_b) for JTB and DTB buildings

# of stories	GT	W [t]	Longitudinal Direction LN (X)						Transverse Direction TR (Y)					
			T [s]	JUS39/64		JUS31/81		RK_b	T [s]	JUS39/64		JUS31/81		RK_b
				Fb [kN]	%W	Fb [kN]	%W			Fb [kN]	%W	Fb [kN]	%W	
JTB 6	1	1,802	1.108	92.37	5.13	81.29	4.51	0.880	1.048	95.66	5.31	85.97	4.77	0.899
	2			115.02	6.4	113.81	6.3	0.989		118.79	6.6	120.36	6.7	1.013
	3			138.02	7.7	146.33	8.1	1.060		142.55	7.9	154.76	8.6	1.086
DTB 14	1	6,920	1.848	238.20	3.44	230.67	3.33	0.968						
	2			297.75	4.3	322.93	4.7	1.085						
	3			357.30	5.2	415.20	6.0	1.162						
B10 10	1	2,880	1.069	124.16	4.3	134.70	4.7	1.085	Direction not analysed, Dual system (K_{P1}) symmetric like JTB building					
	2			155.20	5.4	188.58	6.5	1.215						
	3			186.24	6.5	242.45	8.4	1.302						

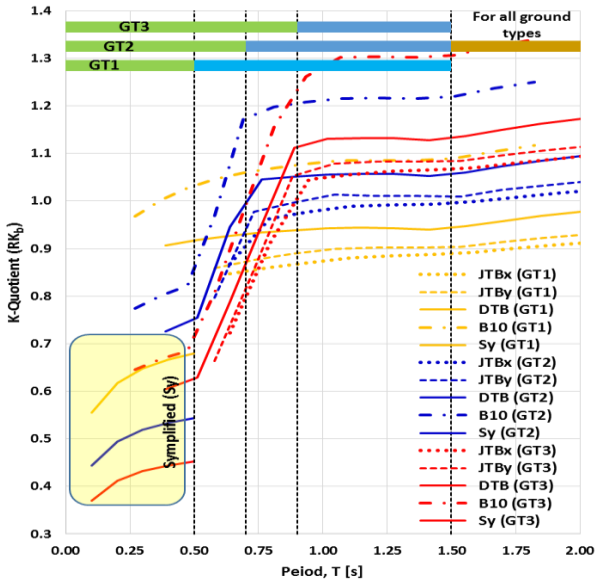


Fig. 6 Spectral behaviour of lateral force ratio (RK_b) for stiff and flexible Buildings

The analyses are conducted for all three ground types. The results are presented in Table 7. RK values are of the same order, irrespective of the fact that JUS39/64 are derived from 3 mode MRS and JUS31/81 by ELF method. Common to both JTB and DTB buildings is the inverse trending of ground type-dependent RKbs relative to trends outlined by the simplified method. For $GT1$ ground type, both RK_{bs} are ≤1, hence JUS38/64 did prescribe the higher base shear than JUS31/81. The $RK_b \geq 1.0$ are attributed to $GT3$ ground typology demonstrating that JUS31/81 overwhelms the JUS39/64 base shear. Comparatively JUS39/64 and JUS31/81 base shears are about the same for $GT2$. However, the results for B10 building, although following the same GT dependency patterns, are all above the $RK_b \geq 1.0$.

To further elucidate the behaviour of RK_b over the velocity and displacement spectral regions, a numerical triage has been performed on JTB, RTB, and B10 buildings. For all three buildings,

Proceedings of the 3rd Croatian Conference on Earthquake Engineering - 3CroCEE
19–22 March 2025, Split, Croatia
Copyright © 2025 CroCEE
DOI: https://doi.org/10.5592/CO/3CroCEE.2025.143

formulated are a number of computational models by simply adding or cancelling out stories. The JTB building from six was upgraded up to 14, DTB from 14 to 20, and B10 to 15 stories by replicating the top story mass and stiffness characteristics of the basic 6, 14, and 10 story computational models. Downscaling of computational models is realized by simply removing stories down to the 3rd story. In such a way, formulated are 43 models in total, 18 for DTB building, 13 for B10, and two times 12 (for each direction separately) computational models that have been analysed for all three ground types. All computations, 165 in total, were conducted by in-house developed Matlab script CodeSDB. The Authors are fully aware that formulation of such computational models influence their Eigenvalue characteristics in general and the behaviour of $K_{\eta 64}$ coefficient in particular. Apart from indicated deficiency of models used, the analyses, Fig. 6:

- Confirmed that in the period range 0.9 - 2.0s+ JUS31/81 overwhelms the JUS39/64 base shear for GT3 ground type. Hence over the entire velocity and displacement spectral regions of GT3 spectral shape the $RKb > 1$ reaching the values of 1.3+ for B10 and 1.2 for the DTB building. The directional values of the JTB building are slightly lower, but both exceed 1.1;
- For GT1 ground type, the trends are inverse. Over the entire TC,($GT2$/$GT3$) - 2.0+ seconds range JUS39/64 overwhelms the JUS81/81 base shear. For DTB building with the first period being in the displacement spectral region (T_1=1.848s), RKb converge to 1, whereas for JTB building (T_{1x}//T_{1y}=1.108/1.048s) it converges to value close to 0.95s. The exception is the B10 building for which $RK_b > 1$ over the entire TC,$GT2 - 2.0s$ period range;
- The order of RKb relations over the TC,($GT2$/$GT3$) - 2.0s+ period range is $\boldsymbol{RK_b,GT3} > RK_b,GT2 > RK_b,GT1$;
- Over the 0.5-TC,($GT2$/$GT3$), the RKb relations reorder themselves so that $\boldsymbol{RKb,GT1} > RKb,GT2 > RKb,GT3$;
- The simplified calculation of base shear for "stiff" buildings is over conservative relative to calculating them by MRS method; and
- The sloping of RKb,GTi,in post TCi velocity and over the entire displacement (TD≥1.5s) regions is influenced by $K\eta 81 = n$ coefficient. The effect is particularly pronounced in TD≥1.5s range where RKb increases monotonically and almost linearly.

Table 8 Computed $RK_{b,GTi,}$ quotients for JTB, DTB, and B10 buildings for closest period larger than 0.5s

Building	T [s]	$R_{P1} = 4$				$R_{P2} = \sim 3.1$	$R_{P3.(1/2)} = 2.5$
		GT_1	GT_2	GT_3	$_{min}GT_i$		
JTB, x	0.640	0.847	0.867	0.723	0.723	0.940	1.157
JTB, y	0.580	0.858	0.796	0.664	0.664	0.863	1.062
DTB	0.514	0.918	0.755	0.629	0.629	0.818	1.006
B10	0.580	1.045	0.970	0.809	0.809	1.052	1.294

All discussed values are relevant only for $KP1$ structural typology ($KP1 = 1$, $RP1 = 4$), which was and still is dominantly implemented RC typology in RNM and Yugoslavia since the 1964 year. The minimum calculated $K - Quotients$ for all ground types at periods slightly over 0.5s are presented in Table 8. $minGTi$ values for $KP1$ structural typology ($KP1 = 1$) are all <1 causing the full prevalence of JUS39/64 over JUS31/81 as well as for three cases of $KP2$ structural typology ($RP2 \approx 3.1$). Irrespective of the ground typology, for one $KP2$ case and all $KP3$ ($RP3 = 2.5$) and $KP4$ ($RP4 = 2$) the JUS31/81 will prevail JUS39/64 base shear.

Proceedings of the 3rd Croatian Conference on Earthquake Engineering - 3CroCEE
19–22 March 2025, Split, Croatia
Copyright © 2025 CroCEE
DOI: https://doi.org/10.5592/CO/3CroCEE.2025.143

As shown, the behaviour of RKb is quite irregular over the analysed spectral range of 0.5-2.0s and does not provide a clear picture to decide on the seismic design level of both codes. RKb is a method of analysis and ground type dependent. For $GT2$ located buildings JUS31/81 consistently overwhelms the JUS39/64 base shear. For other ground types the RKb behaviour is variable. For some of analysed buildings $RKb > 1$ whereas for other $RKb < 1$. The result of this irregularity is that RKb cannot discriminate which code is superior to the other. Hence the irregular behaviour of $K - Quotient$ over the entire analysed spectral range does not allow its exclusive use as a metric for scaling JUS31/81 and JUS39/64 seismic design levels.

3. Challenges for Vulnerability Assessors and Exposure Modellers

Due to discussed irregular behaviour the $Kb - Quotient$ and resulting base shears are not suitable parameters for deciding mutual seismic design levels of JUS39/64 and JUS31/81 codes. The novelty of JUS31/81 relative to JUS39/64 code was that it:

- prescribed the deformation control (Articles 16 and 41). Article 16 limits the maximum lateral elastic deflection of a building top $fmax$ to $H/600$, where H is the height of the building. Article 41 limit the interstory drift di for linear behaviour of the structure to $di \leq hi/350$, and to $di \leq hi/150$ for nonlinear behaviour of the structure subjected to design level earthquake;
- for RC columns and walls prescribes verification of normalised design axial force νd against the following limits: ≤0.35 (for columns, Article 61) and ≤0.20 (for shear walls, Article 73); and
- improved reinforcement detailing to assure better confinement in columns' top and bottom critical regions and prescribes 50% rebar lapping outside the zones of plastic hinges (critical regions) and in areas where the tensile stresses are the least (about the central part of the column).

On this ground, rather than on the value of lateral force coefficients or $K - Quotient$ behaviour, Milutinovic and Trendafiloski, 2003 adopted and assigned four design levels to seismic design codes historically used in Macedonia and Yugoslavia, Table 9.

Table 9 Design and construction eras based on enforcement time of JUS, SZM, & CRC standards

<table>
<tr><th colspan="2">Era</th><th>Enforcement span</th><th>JUS</th><th>SZM</th><th>CRC</th></tr>
<tr><td></td><td>Pre-code</td><td>< 1948</td><td colspan="3">n/a</td></tr>
<tr><td>CDL</td><td>Low code</td><td>1948-1964</td><td>JUS61/48</td><td>SZM1948</td><td rowspan="2">CRC46/47</td></tr>
<tr><td>CDM</td><td>Moderate-code</td><td>1965-1982</td><td>JUS39/64</td><td>SZM1950</td></tr>
<tr><td rowspan="2">CDH</td><td rowspan="2">High code</td><td rowspan="2">1983-2025</td><td rowspan="2">JUS31/81</td><td>SZM1982</td><td rowspan="2">CRC51/71
CRC11/87</td></tr>
<tr><td>SZM1990</td></tr>
<tr><td></td><td>Eurocode system</td><td>≥ 2020</td><td>MKS EN 1998-1</td><td>MKS EN 1998-1/NA</td><td>MKS EN 1992-1-1</td></tr>
</table>

The further complexity that vulnerability assessors and exposure modellers should be aware of is the non-simultaneous enforcement of seismic design codes and codes for Concrete and Reinforced Concrete (CRC). By rule, enforcement of CRCs' was delayed for 6 to 7 years, Table 9. The implication of such non harmonized enforcement timing is that the JUS39/64and JUS31/81 are both associated with two CRC codes, hence with potentially two vulnerability levels dictated solely by their provisions.

Proceedings of the 3rd Croatian Conference on Earthquake Engineering - 3CroCEE
19–22 March 2025, Split, Croatia
Copyright © 2025 CroCEE
DOI: https://doi.org/10.5592/CO/3CroCEE.2025.143

4. Conclusions

The most relevant findings are as summarized below:

- Eq. 5 is not suitable for analysing and comparing Eurocodes wise the lateral force coefficients (K), although for comparing JUS39/64 and JUS31/81, it may be;
- The appropriate K comparison format is the R-code format. In particular, since EN 1998-1 (Eurocode 8) uses it, all lateral force coefficients and its constituents of previous codes can efficiently be compared with it

$$K = \gamma_I \cdot a_{gR} \cdot S \cdot \frac{1}{q} \cdot S_e(T) \tag{11}$$

  where γI is building importance factor, agR reference peak ground acceleration on type A ground, S soil factor, q behaviour factor and, Se (T) elastic horizontal ground acceleration response spectrum shape.
- $K - Quotient$ due to its irregular and ground-type-dependent behaviour over the entire spectral range does not allow its exclusive use as a metric for scaling JUS31/81 and JUS39/64 seismic design levels.
- Proposes and documents K-Quotient method that efficiently compares and intrinsically screens the formulation of all K constituents;
- Both codes allow alternate simplified methods of analysis for stiff buildings. Relative to JUS31/81, the JUS39/64 simplified method is over-conservative. Depending on the ground type, for $KP1$ structural typology it prescribes from 1.2 to 3 times greater base shear;
- K-Quotient behaviour of "flexible" buildings varies with ground typology. For $GT2$ JUS31/81 base shear is consistently greater than of JUS39/64. For other ground conditions, K-Quotient varies in the range of 0.8 to 1.2. The discussed values are relevant only for $KP1$ structural types. For other structural types, JUS31/81 and JUS39/64 base shear prevalence is alternative;
- The minimum calculated $K - Quotients$ for periods slightly over 0.5s (Table 8) and ground types, for $KP1$ structural typology ($KP1 = 1$) are all <1 causing the full prevalence of JUS39/64 over the JUS31/81as well as for three cases of $KP2$ structural typology ($RP2 \approx 3.1$). Irrespective of the ground typology, for one $KP2$ case and all $KP3$ ($RP3 = 2.5$) and $KP4$ ($RP4 = 2$) cases the JUS31/81 prevails JUS39/64 base shear.
- $KP1$ structural types are mostly implemented systems in RNM and Yugoslavia since the 1964 year, hence the irregularity in the behaviour of $K - Quotient$ over the 0.5-2.5s+ period range prevent its exclusive use as a metrics for scaling JUS31/81 and JUS39/64 seismic design levels;
- The development of $K - Quotient$ values is based on actual data from only three buildings and related numerical simulations. The influence of CRC codes on vulnerability and resistance of the exposure is practically unknown. Further research along these two lines is indispensable.

Over the last decade, the SERA Consortium made significant efforts to collect, classify, and analyse building typology across Europe to establish the 2020 exposure model that contains relevant data on approximately 145 million residential, commercial, and industrial buildings in Europe. Recent efforts Crowley et al., 2021, have focused on the spatial and temporal evolution of seismic design across Europe to better understand and classify the seismic design lateral force levels for the existing RC European building stock. Further development of such continent wise model, Russia excluded, is a significant effort exclusively dependent on qualified but also on semi qualified national inputs. Maintenance of such a model is a dynamic issue that requires a permanent update of all information

Copyright © 2025 CroCEE
DOI: https://doi.org/10.5592/CO/3CroCEE.2025.143

controlling the national seismic design lateral force levels. We hope that this contribution provides sufficiently detailed, compact, and valuable technical information on temporal evolution on seismic design models used in Macedonia and Yugoslavia from 1948 until they were replaced by Eurocode Design System EN 1990 – EN 1999.

References

[1] Crowley H, Despotaki V, Rodrigues D, Silva V, Toma-Danila D, Riga E, Karatzetsou A, Sousa L, Ozcebe S, Zugic Z, Gamba P (2020a) Exposure model for European seismic risk assessment. Earthq Spectra.

[2] Crowley H, Despotaki V, Silva V, Dabbeek J, Romao X, Pereira N, Castro JM, Daniell J, Veliu E, Bilgin H, Adam C, Deyanova M, Ademović N, Atalic J, Riga E, Karatzetzou A, Bessason B, Shendova V, Tiganescu A, Toma-Danila D, Zugic Z, Akkar S, Hancilar U (2020b) Evolution of European seismic design levels data (version 1.0). https://doi.org/10.7414/EUC-EVOLUTION-EUROPEAN-SEISMIC-DESIGN-LEVELS-v1.0

[3] Crowley H, Despotaki V, Silva V, Dabbeek J, Romão X, Pereira N, Castro JM, Daniell J, Veliu E, Bilgin H, Adam C, Deyanova M, Ademović N, Atalic J, Riga E, Karatzetzou A, Bessason B, Shendova V, Tiganescu A, Toma-Danila D, Zugic Z, Akkar S, Hancilar U (2021). Model of seismic design lateral force levels for the existing reinforced concrete European building stock. Bull Earthq Eng.

[4] Borzi B, Pinho R, Crowley H (2008) Simplified pushover-based vulnerability analysis for large-scale assessment of RC buildings. Eng Struct 30(3):804–820

[5] Verderame GM, Polese M, Mariniello C, Manfredi G (2010) A simulated design procedure for the assessment of seismic capacity of existing reinforced concrete buildings. Adv Eng Softw 41(2):323–335

[6] Romao X, Pereira N, Castro JM, De Maio F, Crowley H, Silva V, Martins L (2020) European building vulnerability data repository (Version v1.1). https:// doi. org/ 10. 5281/ zenodo. 40878 10

[7] JUS61/48: Provisional Technical Regulations for Building Loading (Official Gazette of FNRY No. 61/48, in Serbo-Croatian)

[8] JUS39/64: Provisional Technical Regulations for Construction in Seismic Regions (Official Gazette of SFRY No. 39/64 of 30 September 1964, in Serbo-Croatian).

[9] Technical Regulations for Building Construction in Seismic Regions (Official Gazette of SFRJ No. 31/81 of 5 June 1981, including amendments: No. 49/82 of 13 August 1982, No. 29/83 of 10 June 1983, No. 21/88 of 1 April 1988, and No. 52/90 of 7 September 1990, in Macedonian)

[10] MKC EN 1998-1: Eurocode 8: Design of structures for earthquake resistance - Part 1: General rules, seismic actions and rules for buildings (Official Gazette of RNM No. 211 of 02.09.2020, in Macedonian)

[11] Zamolo M (2021). Regulations and new legal framework for renewal, Section C.1 of the book Earthquake Engineering –Renewal of masonry structures. 2021 (in Croatian).

[12] Milutinovic et al (2022). Genealogy of Development and Codification of Yugoslavian Earthquake Resistant Design, Bulletin of Earthquake Engineering

[13] Tomic D (2018) Comparative Analysis and Vulnerability of High-Rise Building for Seismic Conditions of Macedonia. University Ss. Cyril and Methodius in Skopje, Institute of Earthquake Engineering and Engineering Seismology, Master Thesis, September 2018.

[14] Trajcevski J (2018) Comparative Analysis and Vulnerability of Six-Story Building for Seismic Conditions of Skopje. University Ss. Cyril and Methodius in Skopje, Institute of Earthquake Engineering and Engineering Seismology, Master Thesis, September 2018 (In MK).

[15] MK33/63: Regulations for Design and Construction of Structures in Seismic Regions

[16] (Official Gazette of SRM No. 33/63 of 24 September 1963, in Macedonian)

[17] SI18/63: Regulations for Design and Construction of Structures in Seismic Regions (Official Gazette of SRS No. 18/63 of June 13, 1963, in Slovenian)

Proceedings of the 3rd Croatian Conference on Earthquake Engineering - 3CroCEE
19–22 March 2025, Split, Croatia
Copyright © 2025 CroCEE
DOI: https://doi.org/10.5592/CO/3CroCEE.2025.164

APPLICATION OF THE PARAMETRIC PUSHOVER CURVE MODEL FOR SEISMIC LOSS ESTIMATION OF A BUILDING STOCK

Neja Fazarinc [(1)], Anže Babič [(2)], Matjaž Dolšek [(3)]

[(1)] *Young researcher, Faculty of Civil and Geodetic Engineering University of Ljubljana, neja.fazarinc@fgg.uni-lj.si*
[(2)] *Assistant Professor, Faculty of Civil and Geodetic Engineering University of Ljubljana, anze.babic@fgg.uni-lj.si*
[(3)] *Professor, Faculty of Civil and Geodetic Engineering University of Ljubljana, matjaz.dolsek@fgg.uni-lj.si*

Abstract

An effective seismic risk assessment of building stock is crucial for informing stakeholders about potential issues in the case of strong earthquakes and enhancing community resilience. Recently, a parametric pushover curve model was introduced, enabling the estimation of building-specific pushover curves and fragility functions even with a low level of knowledge about the building. The model estimates a trilinear pushover curve using twelve parameters assessed for reinforced concrete and masonry buildings in Slovenia, considering limited knowledge about the structures, and can also be used to simulate the pushover curves of an equivalent new building stock. This paper provides an overview of the parametric pushover curve model and its application to the preliminary seismic stress test of the University of Ljubljana building stock. The findings indicate that the seismic capacity of the existing stock, in terms of limit-state peak ground acceleration, is only half of what is expected for new buildings, highlighting significant seismic risk and the urgent need for systematic improvements in seismic safety. Such an underestimation of structural capacity is reflected in the losses. We have shown that the EAL of the existing building stock exceeds the EAL of the equivalent building stock by a factor of 9 and the EAF by a factor of 52. Based on the preliminary seismic stress test results, the University of Ljubljana decided to conduct a second-level seismic stress test, which requires more detailed building data. This ongoing project aims to provide a comprehensive understanding of the seismic resilience of the University of Ljubljana and serves as a foundation for developing a strategic plan to enhance seismic safety.

Keywords: Parametric pushover curve model · Building stock · Seismic performance assessment · Reinforced concrete buildings · Masonry building · Loss estimation

1. Introduction

Seismic risk assessment of a building stock is a complex process, characterized by uncertainties at every stage of analysis (e.g., [1-3]). It begins with establishing both the exposure model and the seismic hazard model. Next, a framework for defining building damage states must be developed, followed by an assessment of the seismic demand model, which can be used to assess the seismic capacity in terms of seismic intensity measures that represent a basis for the building-specific fragility functions. By integrating seismic fragility functions with location-specific seismic hazard data and an appropriate damage-to-loss model, loss estimation can be conducted while considering various seismic risk metrics.

The exposure model includes essential building data used in the analysis, where the level of detail and associated uncertainties depend on the target knowledge level about the buildings and available resources. When assessing larger building stocks, much of the required data can be sourced from publicly available databases or obtained directly from building stock owners or managers. If such data is insufficient, it can be supplemented using various methods, including building inspections, surveys, building stock inventories, or expert judgment. Consequently, buildings with similar characteristics are typically categorized into classes (e.g. [4-6]), allowing for the application of predefined fragility curves ([1, 7-9]), which significantly simplifies the analysis.

In the present study, an alternative approach was implemented using a recently developed parametric pushover curve model [10], which is briefly introduced in Section 2. This model makes it possible to assess building-specific pushover curves based on their fundamental characteristics. The model's

Copyright © 2025 CroCEE
DOI: https://doi.org/10.5592/CO/3CroCEE.2025.164

practical application is demonstrated through the seismic loss estimation of the University of Ljubljana's building stock (Section 3), considering both the existing structures and an equivalent new building stock.

2. Overview of the parametric pushover curve model and its application for Slovenian buildings

The parametric pushover curve (PPC) model [10] allows for the modeling of buildings on a building-by-building basis with minimal knowledge of their characteristics, relying on a set of twelve basic structural parameters. These parameters can be estimated or measured directly, derived from building's design documentation, or determined using additional empirical and theoretical models that account for the construction standards in effect at the time of building. When only limited data is available—a common scenario when utilizing existing databases (e.g., [13])—simplified models can be introduced to estimate the necessary parameters for defining the PPC of a building. The description in the following is directed towards the application to Slovenian buildings and taking into account only a low level of knowledge about the buildings, with particular parameters and models drawn from Slovenian construction practices, highlighting the evolution of building standards and regulations that have been in force in the past. A more general description of the proposed model is available elsewhere [10].

The PPC model represents an idealized tri-linear pushover curve, characterized by at least three key points (e.g., Y – the yield point, M – the capping point, and U – the near-collapse point) or five independent coordinates, determined indirectly. These parameters sufficiently describe the relationship between the displacement at the top of the building and the seismic force (i.e., the force-displacement (F-D) relationship), as illustrated in Fig. 1.

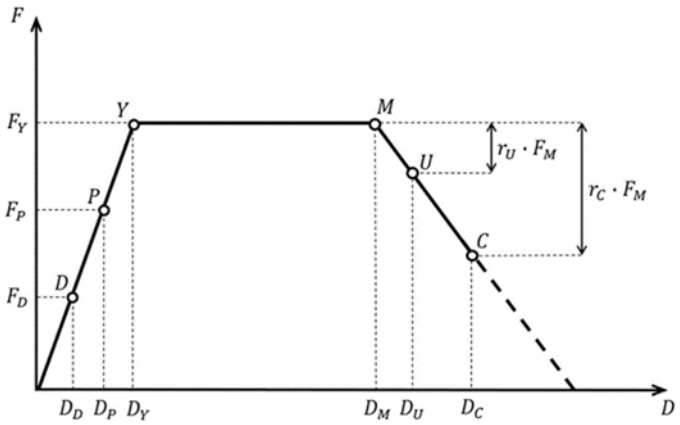


Figure1: The base shear-top displacement relationship of the parametric pushover curve model ([10]).

The F-D relationship is assumed linear until the yield point, Y, where the building reaches its maximum base shear, F_Y, which is defined as the maximum of (i) the value based on the design base shear, F_D, and (ii) the minimum base shear, $F_{Y,min}$, assessed as the capacity of the critical storey of the building, taking into account the possibility that some buildings were not designed for earthquake resistance.

F_D is determined as:

$$F_D = BS_c \cdot \sum m_i \cdot g, \tag{1}$$

where m_i is the mass of the i-th storey of the building, which also represents the i-ih component of the building mass vector $\boldsymbol{m}$. It is calculated as a product of the gross area of the storey A_G and the building typology-specific average mass per unit area m_A, taken as $1.2\,\frac{t}{m^2}$ for RC buildings and $1\,\frac{t}{m^2}$ for masonry buildings [1,14]. In Eq. (1), g is the gravitational acceleration and BS_C is the design base shear coefficient, modelled by considering the development of the regulations for earthquake-resistant design of buildings from past building codes [15, 16], the building location and the construction year CY:

Proceedings of the 3rd Croatian Conference on Earthquake Engineering - 3CroCEE
19–22 March 2025, Split, Croatia
Copyright © 2025 CroCEE
DOI: https://doi.org/10.5592/CO/3CroCEE.2025.164

$$BS_C = \begin{cases} 0{,}01;\ CY \leq 1948 \\ 0{,}011 - 0{,}02;\ 1948 < CY \leq 1963 \\ \begin{cases} 0{,}02 - 0{,}08 \cdot \gamma_{I,1};\ A \\ 0{,}025 - 0{,}1 \cdot \gamma_{I,1};\ B, C \\ 0{,}03 - 0{,}12 \cdot \gamma_{I,1};\ D, E \end{cases};\quad 1963 < CY \leq 1981 \\ K = K_0 \cdot K_s \cdot K_d \cdot K_p;\ 1981 < CY \leq 2008 \\ S_{ad}(PGA_{475}, S, T, T_B, T_C, T_D, q) \cdot \lambda \cdot \gamma_I;\ 2008 < CY. \end{cases} \tag{2}$$

Most of the parameters from Eq. (2) adhere to the standards that were in force during specific periods in the past. Between 1948 and 1981, the values of BS_C are given as intervals because the value for a specific building depends on its location relative to the seismic zones or seismic hazard maps from the relevant construction periods. The letters $A - E$ for the construction period from 1963 to 1981 refer to the soil type at the location of the building, while $\gamma_{I,1}$ and γ_I are the building's importance factors. The parameter K represents the seismic factor, consisting of four components, S_{ad} is the design acceleration at the fundamental period of the building as defined in Eurocode 8 [17], and λ is the proportion of the building's mass considered in the lateral force analysis. The values of these parameters are detailed elsewhere [10, 18].

Considering the low level of knowledge about the buildings, the fundamental period T is estimated using simplified models, taking into account the number of storeys n_e and the predominant structural material. For masonry buildings, the POTROG model [19-21] is adopted. This model is based on measured values of the buildings' fundamental period, so the calculated values are further multiplied by $\sqrt{2}$ to account for the cracking of the elements during the seismic action, while for RC buildings, the HAZUS model [9] for the assumed dual system is adopted.

The minimum base shear $F_{Y,min}$ is modelled as construction period dependent, taking into account the predominant structural material and the assumed critical storey. The load-bearing capacity of RC buildings is determined using a simplified model, grounded in the Japanese standard for seismic evaluation of existing buildings [22] and considering the findings of Sinkovič et al. [23]. The model is based on the horizontal cross-sectional area of columns and walls in the critical storey, their shear strength, τ_j, and the total weight of the building, W. For masonry buildings, the shear failure mechanism is assumed, with the occurrence of the characteristic inclined cracking of the walls, which occurs when the primary tensile stresses exceed the tensile strength of the masonry, f_t [24, 25]. In addition to f_t, the essential parameters for this model are the cross-sectional area of a typical wall oriented in the direction of the earthquake ground motion, A_W, the factor accounting for the uniformity of shear stress distribution across the section, b, and the compressive stress in the walls, σ_0, determined by the weight of the building.

The resulting maximum base shear of the building is:

$$F_Y = \max\{q_R \cdot q_S \cdot F_D; F_{Y,min}\}, \tag{3}$$

where q_R is the component of the overstrength factor, accounting for the structural redundancy and the consequent possibility of the redistribution of the seismic action effects, and q_S is the component of the overstrength factor accounting for all the remaining sources of overstrength (e.g., minimum requirements, material safety factors, etc.). No additional hardening of the building is assumed post-yielding, leading to a constant plastic branch of the PPC. Thus, the base shear at the capping point M, is:

$$F_M = F_Y. \tag{4}$$

The force associated with the third essential characteristic point in the F-D relationship definition corresponds to the near-collapse limit state (point U in Fig. 1) and is defined as a ratio of the maximum base shear. A reduction in load-bearing capacity of 20 % is assumed, modelled by setting the value of r_U to 0.2 (Fig. 1), which results in:

Proceedings of the 3rd Croatian Conference on Earthquake Engineering - 3CroCEE
19–22 March 2025, Split, Croatia
Copyright © 2025 CroCEE
DOI: https://doi.org/10.5592/CO/3CroCEE.2025.164

$$F_U = (1 - r_U) \cdot F_Y = 0.8F_Y. \quad (5)$$

The displacements, corresponding to the three characteristic points, Y, M and U, are defined gradually. To determine the yield displacement, D_Y, an equivalent SDOF system is introduced, assuming it has the same fundamental period as the entire building and a linear F-D relationship until the yield point. Given these assumptions and the conventional relationship between the fundamental period, mass and stiffness of an SDOF system, the displacements corresponding to the design base shear and the yield point, i.e. D_D in D_Y, were determined. The displacement D_U, which is associated with the softening branch of the PPC, determined taking into account the assumed deformation shape of the building at the near collapse limit state, which is reflected in the storey-drift-angle uniformity coefficient C_U and the corresponding storey drift angle of the most deformed storey θ_U:

$$D_U = C_U \cdot \theta_U \cdot \sum_{i=1}^{n_e} h_{e,i}. \quad (6)$$

In Eq. (6), $h_{e,i}$ represents the height of the i-th storey. The storey heights, comprising the storey-height vector $\boldsymbol{h_e}$, are summed up to account for the entire height of the building. Due to the low level of knowledge about the buildings, the term $\sum_{i=1}^{n_e} h_{e,i}$ is replaced by $n_e \cdot h_e$, because all of the storeys are assumed to be of the same height. Parameter C_U can take a value between $\frac{1}{n_e}$, which defines the extreme soft storey effect, and 1 in the case of uniform inter-storey drifts. For this study, it is taken as $\frac{1.2}{n_e}$ for masonry buildings and 1 for RC buildings. Parameter θ_U is modelled considering the predominant structural material and the construction period of the building. The remaining two characteristic displacements, corresponding to the capping point, M, and the collapse point, C, were determined by assuming the linear post-capping branch of the PPC and adopting constant values of $r_U = 0.2$ and $r_C = 0.5$ (Fig. 1) regardless of the building type using Eqs. (7) and (8):

$$D_M = \frac{D_U}{\mu_{0M} - (1 - r_U) \cdot \mu_{0M} + (1 - r_U)} \quad (7)$$

$$D_C = D_M \cdot (1 + \mu_{0M} r_C - r_C). \quad (8)$$

In Eqs. (7) and (8), μ_{0M} represents the post-capping ductility, which defines the ratio between the displacement at the theoretical zero base shear, where the dashed line in Fig. 1 would cross the horizontal axis, and the displacement at the capping point, D_M. This ratio is assumed 1.2 and 3.5 for masonry and RC buildings, respectively.

The presented PPC model is thus defined by twelve structurally dependent parameters, i.e. BS_C, $\boldsymbol{m}$, q_S, q_R, $F_{Y,min}$, $\boldsymbol{\phi}$, μ_{0M}, C_U, θ_U, n_e, $\boldsymbol{h_e}$ and T. The majority of them have been referenced in the preceding part of this section, with the exception of $\boldsymbol{\phi}$, which is the mode shape vector for determining the transformation factor for the introduction of the equivalent SDOF model and taken as an inverted triangle. It should also be noted that some of the models and the values for this set of parameters are region- and time-specific, taking into account the time variation in the local construction practice or based on expert judgement, which should be considered when applying PPC for building stocks elsewhere. More details about the essential models and the values of the corresponding parameters can be found elsewhere (e.g. [10]), as well as the impact of the uncertainties arising from the low level of knowledge about the buildings on the resulting loss estimation ([11-12]).

3. Loss estimation of an existing building stock relative to a new building stock

3.1. Description of the existing building stock and a new building stock scenario

The presented PPC model was applied in the preliminary seismic stress test of a University of Ljubljana's (UL) building stock, consisting of 109 buildings (of which 58 are masonry and 51 RC), with a cumulative net area of over 300,000 m^2, which represents more than 95 % of the entire building stock of the UL. Most of those buildings are located in the capital city of Slovenia, Ljubljana.

Proceedings of the 3rd Croatian Conference on Earthquake Engineering - 3CroCEE
19–22 March 2025, Split, Croatia
Copyright © 2025 CroCEE
DOI: https://doi.org/10.5592/CO/3CroCEE.2025.164

The analysis of the building stock revealed that it is quite outdated, with more than half of the buildings being constructed before 1964, prior to the introduction of Slovenia's first earthquake-resistant building code. Out of 55 buildings constructed in that era, 44 are masonry (referred to as MSN), while 11 are reinforced concrete (RC). Only 6 of the studied buildings, all of them RC, were constructed after 2008, when using Eurocode 8 became obligatory in Slovenia.

The 58 masonry buildings represent about 30% of the building stock area, with the majority built before 1964 and ranging from one to six storeys. The remaining 70% consists of RC buildings, mainly constructed between 1964 and 1981 and ranging from two to 14 storeys. The exposure model, i.e. the building stock, categorized by the predominant structural material, number of storeys, and construction period is presented in Tables 1 and 2, where n represents the number of buildings in each category, N is the nominal number of people in these buildings, and A is the net building area of the category expressed as a percentage of the total building stock area. A more detailed description of the development of the exposure model and the studied building stock can be found elsewhere [10- 12].

Table 1: Number of MSN buildings, the nominal occupation of those buildings, and their net area as % of the total area of the building stock categorized by number of storeys and construction period.

MSN	**≤1963**			**1964-1981**			**1982-2007**			**∑**		
n_e	**n**	**N**	**A [%]**	**n**	**N**	**A [%]**	**n**	**N**	**A [%]**	**n**	**N**	**A [%]**
1 - 3	31	3865	11.8	7	198	0.8	7	400	1.2	45	4463	13.8
4 - 6	13	5271	15.7	/	/	/	/	/	/	13	5271	15.7
∑	**44**	**9136**	**27.5**	**7**	**198**	**0.8**	**7**	**400**	**1.2**	**58**	**9734**	**29.5**

Table 2: Number of RC buildings, the nominal occupation of those buildings, and their net area as % of the total area of the building stock categorized by number of storeys and construction period.

RC	**≤1963**			**1964-1981**			**1982-2007**			**≥2008**			**∑**		
n_e	**n**	**N**	**A [%]**	**n**	**N**	**A [%]**	**n**	**N**	**A [%]**	**n**	**N**	**A [%]**	**n**	**N**	**A [%]**
1 - 3	4	1131	4.1	6	4070	5.3	12	4063	8.8	3	277	1.4	25	9541	19.4
4 - 6	5	5506	8.3	6	7979	10.9	3	3039	6.5	3	917	11.2	17	19730	36.9
≥7	2	503	2.5	6	3647	11.4	1	156	0.4	/	/	/	9	4306	14.3
∑	**11**	**7140**	**14.9**	**18**	**15696**	**27.6**	**16**	**7258**	**15.7**	**6**	**1194**	**12.6**	**51**	**31288**	**70.8**

To facilitate the comparison of seismic performance and the relative evaluation of estimated losses, an equivalent new building stock was also modeled using the PPC. In this hypothetical scenario, the entire building stock would be replaced with equivalent new buildings while maintaining the same geometry and location. However, the new buildings would be designed in compliance with Eurocode 8, with masonry buildings of three or more stories replaced by reinforced concrete (RC) buildings, while those with one or two stories would remain masonry.

This approach aligns with current construction practices in Slovenia, as taller masonry buildings are generally not considered suitable for seismically active areas. Consequently, the equivalent new building stock was modeled using mostly the same input parameters as the existing building stock, except for the CY-dependent parameters, which were updated to comply with Eurocode 8. In some cases, additional modifications were made due to the change in the predominant structural material from masonry to RC.

3.2. Parametric pushover curves

First, the parametric pushover curves of existing and the equivalent new buildings were determined and are presented in Fig. 2 in a normalized manner. The maximum base shear was normalized by the total weight of the building, while the top displacement was normalized with respect to the height of the building. Thus, Fig. 2 represents the F_b/W-D/H relationship for each building and its equivalent new counterpart. The first column of the figure corresponds to the masonry buildings that remain masonry,

Copyright © 2025 CroCEE
DOI: https://doi.org/10.5592/CO/3CroCEE.2025.164

the second column to the masonry buildings, for which the predominant structural material changes in the equivalent new building stock scenario, and the third column to RC buildings. Each row represents a different construction period, i.e. before 1963, from 1964 to 1981 and from 1981 to 2007. The PPCs of existing masonry buildings are depicted in red and those of the equivalent new masonry buildings in orange. The PPCs of existing RC buildings are black, while for the equivalent new RC buildings, they are grey. For buildings, constructed after 2008, such a comparison would be irrelevant, as the PPCs of existing buildings and equivalent new buildings would be the same, and relatively similar to the ones of the equivalent new RC buildings (e. g. in the second and third columns of Fig. 2).

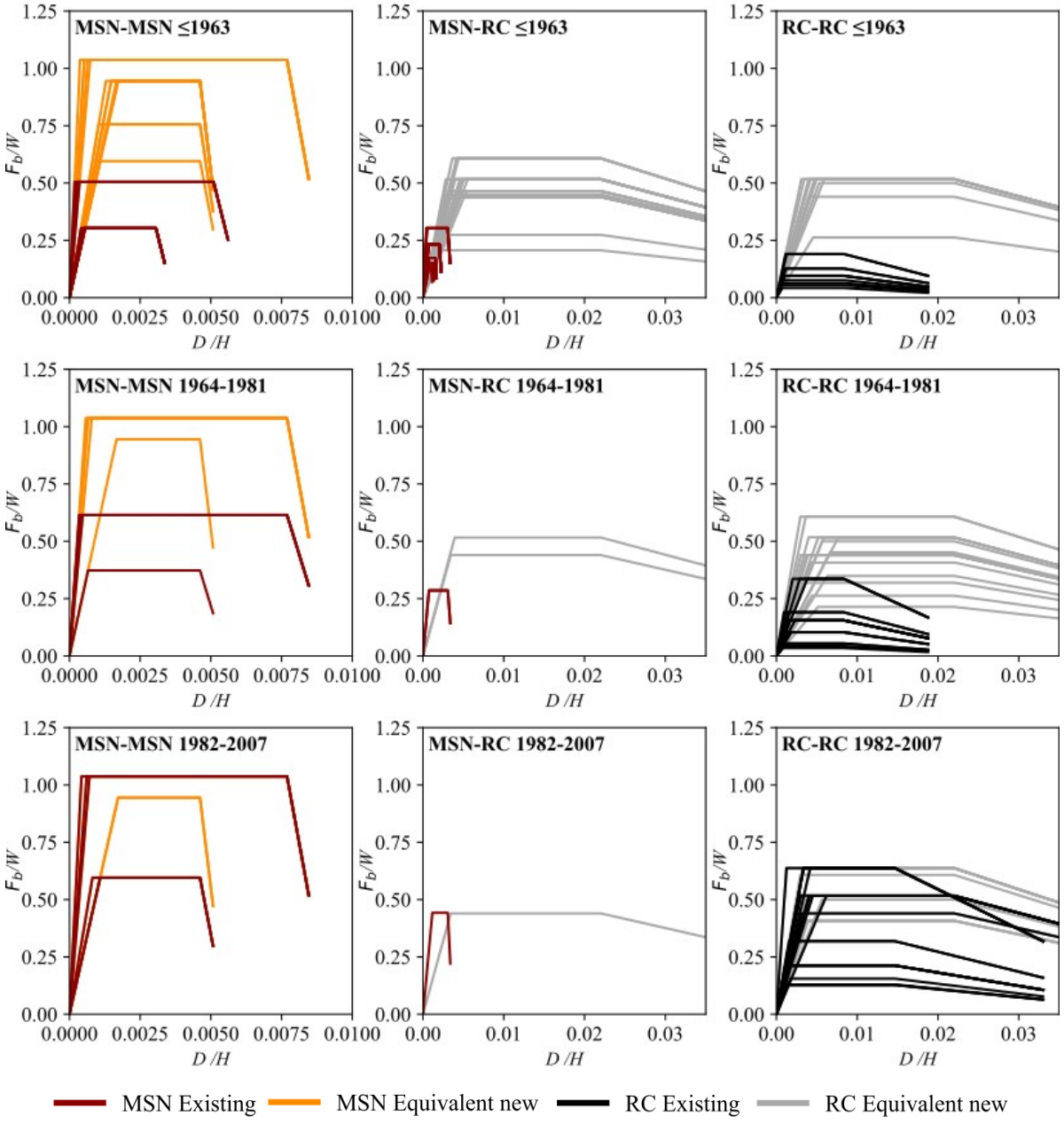


Figure 2: Normalized parametric pushover curves of existing and equivalent new buildings.

Fig. 2 shows that the oldest masonry buildings have the lowest deformation capacity out of all building categories, as well as the lowest normalized load-bearing capacity out of all masonry buildings. For RC buildings, the trend of increasing deformation capacity with respect to construction periods is even more evident, while for the low-bearing capacity, it is less apparent. Nevertheless, the deformation capacity of the RC buildings is significantly larger than that of the masonry buildings regardless of the

Proceedings of the 3rd Croatian Conference on Earthquake Engineering - 3CroCEE
19–22 March 2025, Split, Croatia
Copyright © 2025 CroCEE
DOI: https://doi.org/10.5592/CO/3CroCEE.2025.164

construction period (note also the difference in the limits of the horizontal axis between the first and the remaining two columns of Fig. 2), while the normalized load bearing capacity is mostly larger for masonry buildings. The equivalent new buildings mostly have a larger load bearing as well as deformation capacity than the existing buildings. This is especially significant when existing masonry buildings are replaced with equivalent new RC buildings (second column of Fig. 2).

3.3. Loss estimation

The loss estimation was performed using a conventional seismic risk assessment (e.g. [1]) to estimate two seismic risk measures, i. e. the expected annual loss (EAL) and the expected annual fatalities (EAF). The EAL was determined by taking into account the expected repair costs related to four damage states of the building, DS_1 to DS_4, as:

$$EAL = \sum_{i=1}^{4} c_i C_R \sum_{j=1}^{n} P\left(DS_i \middle| IM = PGA_{j,c}\right) \left(\lambda\left(PGA_{j,a}\right) - \lambda\left(PGA_{j,b}\right)\right) \quad (9)$$

where C_R is the cost of the replacement of the building and c_i defines the relative cost of the repair in the case of the achieved i-th damage state. The latter was modelled in accordance with Dolšek et al. [1] as 0.02, 0.1, 0.4 and 1 for the limit states DS_1 to DS_4. The term $\lambda(PGA)$ represents the mean annual frequency of ground motions with the corresponding intensity of at least PGA, evaluated from the site and soil type-specific seismic hazard curve, while $PGA_{j,a}$, $PGA_{j,b}$ and $PGA_{j,c}$ represent the values of the PGA at the beginning, end and center of each interval, obtained by discretizing the seismic risk integral. The term $P\left(DS_i \middle| IM = PGA_{j,c}\right)$, evaluated using fragility functions, represents the probability that the building reaches damage state DS_i given the ground motion with the maximum peak ground acceleration of $PGA_{j,c}$. The fragility functions were modelled conventionally, using the standardized lognormal distribution, defined by the median ground motion intensity measure, in this case the PGA at a given damage state, i.e. PGA_{DSi}, and the corresponding standard deviation of the logarithmic values of the ground motion intensity, $\beta_{PGA,DSi}$. The values for PGA_{DSi} were determined based on the displacements, corresponding to the four damage states, D_{DSi}, using the N2 method [26]. The displacements D_{DSi} were modelled relative to the characteristic displacements as defined by Fazarinc and Dolšek [12].

The EAF was estimated analogously to the EAL:

$$EAF = E(N)\lambda_{d,C}P(C|DS_4)\sum_{j=1}^{n} P\left(DS_4 \middle| IM = PGA_{j,c}\right)\left(\lambda\left(PGA_{j,a}\right) - \lambda\left(PGA_{j,b}\right)\right), \quad (10)$$

where $E(N)$ represents the equivalent annual number of people in the building, estimated using a model that accounts for fluctuations in building occupancy on a yearly and hourly basis [27], and $\lambda_{d,C}$ represents the proportion of people in the building who would lose their lives if the building collapses, assumed to be 0.1 regardless of the building's structural system [28]. It was also assumed that the building could only collapse upon reaching the limit state DS_4, with the probability of collapse, $P(C|DS_4)$, ranging from 0.05 to 0.15, depending on the predominant structural material and the number of storeys [9].

The losses in terms of EAL and EAF were first estimated for the entire existing building stock. To get a better insight into the contribution of different types of buildings, the results were also analyzed for each predominant structural material and construction period separately and are presented in Table 3. Both EAL in thousands of EUR and EAF are first shown in absolute terms for each category and then in relative terms as a percentage of the losses, estimated for the entire building stock. The analysis revealed that the EAL for the entire existing building stock of Ljubljana is more than 2 million EUR, while EAF is almost 3.9. The masonry buildings contribute more than 60 % of the EAL and more than 90 % to the EAF, although they represent only approximately 30 % of the building stock's net area. Almost all of those losses can be attributed to older masonry buildings, constructed before 1963, which can be almost directly attributed to their low deformation capacity. On the other hand, the EAF for RC buildings is much smaller, contributing only 10 % to the expected risk for the entire building stock. For the EAL, the contribution of RC buildings is almost 40 %, but this percentage decreases if the losses are

Copyright © 2025 CroCEE
DOI: https://doi.org/10.5592/CO/3CroCEE.2025.164

normalized with respect to the net area of buildings. The highest losses for RC buildings are expected for the buildings, constructed between 1964 and 1981 (424,000 EUR), followed by the oldest RC buildings (260,000 EUR). The absolute and relative values for both loss measures for different building categories are presented in more detail in Table 3.

Table 3: Loss measures, i.e. *EAL* and *EAF*, for the existing building stock and different building categories.

		EAL		***EAF***	
MATERIAL	**CY**	**[1000 EUR]**	**[%]**		**[%]**
MSN	**≤1963**	1247	60	3.45E-01	89
	1964-1981	11	1	2.02E-03	1
	1982-2007	5	0	1.04E-03	0
	SUM	**1263**	**61**	**3.48E-01**	**90**
RC	**≤1963**	260	13	1.38E-02	4
	1964-1981	424	21	2.29E-02	6
	1982-2007	81	4	2.31E-03	1
	≥2008	39	2	6.06E-04	0
	SUM	**804**	**39**	**3.96E-02**	**10**
ALL	**SUM**	**2067**	**100**	**3.88E-01**	**100**

To analyze the potential for improvement and risk reduction, the loss measures were then compared on a building-by-building level for the equivalent new and the existing building stock. In addition to EAL and EAF, the third loss measure was added, i.e. the probability of the building reaching or exceeding damage state DS_4 in a given year, denoted as $P(DS_4)$. The values of the loss measures for equivalent new buildings were normalized with respect to the values for the existing buildings and expressed in %, obtaining $\overline{P(DS_4)}$, $\overline{EAL}$ and $\overline{EAF}$, as seen in Table 4. Here, the buildings were first categorised by the construction periods (the three main columns of Table 4) as well as the structural material of existing and the equivalent new buildings (the three main rows of Table 4, i.e. MSN-MSN, MSN-RC and RC-RC) and the number of storeys, n_e. For each loss measure and each such category, the mean value and the corresponding standard deviation were calculated. As expected, older buildings show a higher potential for improvement than newer ones. If older masonry buildings are replaced with masonry buildings, all of the three loss measures for new buildings reduce to about 20-25 % of the values for existing ones, whereas for newer buildings, constructed from 1964 to 1981 and 1982 to 2007 the reduction is less significant, to only 40-60 % and 80-90 %, respectively. For the latter category, i.e. MSN-MSN buildings, constructed from 1982 to 2007 the corresponding standard deviations for all three normalized loss measures are the highest out of all building categories at more than 20 %. As expected, the largest improvement can be observed, if the masonry buildings are replaced with RC buildings (i.e. MSN-RC), where $P(DS_4)$ and EAF reduce to only about 1% of the values for existing buildings, while for EAL, the reduction is less significant. This is the result of the fact that $P(DS_4)$ and EAF are closely related only to DS_4 and thus the deformation capacity, whereas for EAL, all four damage states are taken into account. For RC buildings, constructed before 1963 and from 1964 to 1981, there is a similar potential for improvement regardless of the number of storeys of those buildings. $P(DS_4)$ and the EAF would reduce to only 6-7% of the present value if those buildings were replaced with equivalent new ones, while EAL would reduce to 14-18% of the present values. For the RC buildings constructed from 1982 to 2007, all three loss measures would reduce to approximately 30% of the present value, which means that there is slightly less potential for improvement. Further detail about the relative comparison of the equivalent new and the existing buildings can be observed from Table 4.

Proceedings of the 3rd Croatian Conference on Earthquake Engineering - 3CroCEE
19–22 March 2025, Split, Croatia
Copyright © 2025 CroCEE
DOI: https://doi.org/10.5592/CO/3CroCEE.2025.164

Table 3: The potential for seismic risk reduction, expressed by normalizing the values of seismic risk measures, $P(DS_4)$, EAL and EAF, of equivalent new buildings to the values of existing buildings.

		≤1963						1964-1981						1982-2007					
		$\overline{P(DS_4)}$ [%]		$\overline{EAL}$ [%]		$\overline{EAF}$ [%]		$\overline{P(DS_4)}$ [%]		$\overline{EAL}$ [%]		$\overline{EAF}$ [%]		$\overline{P(DS_4)}$ [%]		$\overline{EAL}$ [%]		$\overline{EAF}$ [%]	
MATERIAL	n_e	**μ**	**σ**	**μ**	**σ**	**μ**	**σ**	**μ**	**σ**	**μ**	**σ**	**μ**	**σ**	**μ**	**σ**	**μ**	**σ**	**μ**	**σ**
MSN-MSN	**1-3**	24	5	21	5	23	5	57	8	44	5	57	9	87	20	85	23	87	21
MSN-RC	**1-3**	1	1	8	3	1	1	1	0	10	0	1	0	1	0	14	0	1	0
	4-6	0	0	4	1	0	0	/	/	/	/	/	/	/	/	/	/	/	/
RC-RC	**1-3**	7	1	15	0	6	1	6	1	16	2	6	1	28	5	46	15	27	5
	4-6	7	1	14	1	6	1	7	1	18	3	7	1	28	1	29	0	28	1
	≥7	7	1	14	1	7	1	8	2	15	1	8	1	29	0	31	0	29	0

The losses of the existing building stock and those of the equivalent new building stock were also compared at the level of building categories, defined by the predominant structural material of existing buildings, construction period and number of storeys. As expected, the highest potential for improvement was observed for older masonry buildings, constructed before 1963, especially those with 4-6 storeys, which would be in hypothetical equivalent new building stock replaced with RC buildings. The EAL for those buildings could be 30 times lower and the EAF almost 530 times lower if they were replaced with equivalent RC buildings, designed according to Eurocode 8. Great potential for improvement was also recognized for the RC buildings constructed before 1981, where the EAL could be reduced by a factor of five and the EAF could be reduced by a factor of 12 to 16. It should be noted, that this improvement seems significant, but since the EAF for existing RC buildings is not as high as for masonry buildings (in absolute terms), the replacement of those buildings would not reduce the overall risk of the building stock as significantly as if replacing the masonry buildings. The overall seismic risk could be reduced almost by a factor of 9 in terms of EAL and almost by a factor of 52 in terms of EAF. This shows a significant potential for better protection of human lives in case of seismic events, which is one of the main goals of seismic-resistant design of buildings.

4. Conclusions

A recently introduced tri-linear parametric pushover curve model implemented for seismic risk assessment of buildings in Slovenia is briefly presented. The model is then demonstrated for the prediction of parametric pushover curves of the existing and equivalent new building stock of the University of Ljubljana, considering only limited knowledge about the buildings. This enabled the comparison between the existing buildings and their equivalent new counterparts designed according to Eurocode 8.

First, the normalized parametric pushover curves of existing and new buildings were analyzed, revealing a very low load-bearing and deformation capacity for buildings constructed in older construction periods. This indicates that the building stock of the University of Ljubljana needs to be strengthened regarding earthquake resistance.

The comparison between the existing and the equivalent new buildings revealed a substantial potential for seismic risk reduction. Replacing older masonry buildings with new RC buildings could reduce the *EAL* on a building level by a factor of 30, while *EAF* by a factor of 530, while for RC buildings, these reduction factors are 5 and 12 to 16, respectively. Overall, the seismic risk for the entire building stock could be reduced nine-fold in terms of *EAL* and 52-fold in terms of *EAF*.

These results highlight the importance of prioritizing the replacement of older, more vulnerable buildings to enhance the seismic resilience of the building stock, thereby improving user safety. The ongoing seismic stress test of the building stock of the University of Ljubljana, incorporating a higher level of knowledge about the buildings, will allow us to refine these assessments further and support

Copyright © 2025 CroCEE
DOI: https://doi.org/10.5592/CO/3CroCEE.2025.164

the development of a strategic plan for improving the seismic safety of the University of Ljubljana. The authors believe the parametric pushover curve model can be used in Croatia with minor adjustments. The demonstrated approach can serve as a model for other institutions and communities aiming to mitigate seismic risk and protect human lives.

Acknowledgements

The results presented in this paper are based on work supported by the Slovenian Research Agency under the research program Earthquake Engineering (P2-0185). This support is gratefully acknowledged.

References

[1] Dolšek M., Žižmond, J., Babič A., Lazar Sinković N., Jamšek A., Gams M., Isaković T. (2020): Seizmični stresni test stavbnega fonda Republike Slovenije (2020–2050). Univerza v Ljubljani, Fakulteta za gradbeništvo in geodezijo, Inštitut za konstrukcije, potresno inženirstvo in računalništvo. (in Slovenian)

[2] Dolšek M., Fazarinc N., Babič A. (2023): Povzetek preliminarnega seizmičnega stresnega testa stavbnega fonda Univerze v Ljubljani. UL FGG, IKPIR (in Slovenian)

[3] Dolšek M., Fazarinc N., Babič A. (2024): Seizmični stresni test stavbnega fonda širšega javnega sektorja na osnovi nizke stopnje poznavanja stavb, UL FGG, IKPIR (in Slovenian)

[4] Sucuoğlu U., Yazgan U., Yakut A. (2007): A screening procedure for seismic risk assessment in urban building stocks, *Earthquake Spectra, 23(2), pp. 441–458*, https://doi.org/10.1193/1.2720931

[5] Dabbeek J., Silva V. (2019): Modeling the residential building stock in the Middle East for multi-hazard risk assessment, *Natural Hazards, 100(2), pp. 781–810*, https://doi.org/10.1007/s11069-019-03842-7

[6] Jamšek A., Babič A., Dolšek M. (2022): Direct seismic loss estimation of predominantly plan-symmetrical frame buildings using simplified nonlinear models, *Earthquake Engineering and Structural Dynamics, 51(15), pp. 3526–3551*, https://doi.org/10.1002/eqe.3734

[7] Silva V., Crowley H., Pagani M., Monelli D., Pinho R. (2013): Development of the OpenQuake engine, the Global Earthquake Model's open-source software for seismic risk assessment, *Natural Hazards. 72(3), pp. 1409–1427*, https://doi.org/10.1007/s11069-013-0618-x

[8] Milutinović Z. V., Trendafiloski G. S. (2003): Risk-UE. An advanced approach to earthquake risk scenarios with applications to different european towns, WP4: Vulnerability of current buildings, http://www.civil.ist.utl.pt/~mlopes/conteudos/DamageStates/Risk%20UE%20WP04_Vulnerability.pdf

[9] FEMA (2022): Hazus Earthquake Model Technical Manual

[10] Fazarinc N., Babič A., Dolšek M. (2023): Parametric pushover curve model for seismic performance assessment of building stock, *Bulletin of Earthquake Engineering*, https://doi.org/10.1007/s10518-023-01821-9

[11] Fazarinc N., Dolšek M. (2024): Evaluating the impact of parametric pushover curve model uncertainties on seismic loss estimation for a specific building stock in Slovenia, *Engineering Structures. 302, p. 117362*, https://doi.org/10.1016/j.engstruct.2023.11736

[12] Fazarinc N., Dolšek M. (2024): The impact of parametric pushover curve uncertainties on seismic loss assessment of building stock, *Proceedings of the 18th World Conference of Earthquake Engineering.*

[13] GURS (2025): *e-prostor*. https://ipi.eprostor.gov.si/jv/

[14] Snoj J., Dolšek M. (2020): Pushover-based seismic risk assessment and loss estimation of masonry buildings, *Earthquake Engineering & Structural Dynamics*, 49(6), 567-588, https://doi.org/10.1002/eqe.3254

[15] Breznik M. (1960): Varnost stavb ob potresih, *Gradbeni Vestnik. Št. 75-86* (in Slovenian)

[16] Fajfar P. (2017): Razvoj predpisov za potresno odporno gradnjo v Sloveniji, *Gradbeni Vestnik. št. 66, pp. 83–96*, http://www.dlib.si/?URN=URN:NBN:SI:doc-NZNQQT6R (in Slovenian)

Copyright © 2025 CroCEE
DOI: https://doi.org/10.5592/CO/3CroCEE.2025.164

[17] SIST EN 1998-1:2005 – Evrokod 8: Projektiranje potresnoodpornih konstrukcij - 1. del: Splošna pravila, potresni vplivi in pravila za stavbe, slovenski standard, Slovenski inštitut za standardizacijo, marec 2005 (in Slovenian)

[18] Fazarinc N. (2024): Modeliranje trajnostne prenove stavbnega fonda na potresnih območjih, *master thesis*, accessable at: https://repozitorij.uni-lj.si/IzpisGradiva.php?lang=slv&id=161673 (in Slovenian)

[19] Lutman M., Weiss P., Klemenc I., Zupančič P., Šket Motnikar B., Banovec P., Cerk M. (2023): POTROG: Potresna ogroženost v Sloveniji za potrebe Civilne zaščite: raziskovalni projekt, zaključno poročilo. Ljubljana, Zavod za gradbeništvo Slovenije: 1318 str (in Slovenian)

[20] Lutman M., Kreslin M., Banovec P., Cerk M. (2016): POTROG 2: Nadgradnja sistema za določanjepotresne ogroženosti in odzivnosti za potrebe zaščite in reševanja v Sloveniji: raziskovalni projekt, zaključno poročilo. Ljubljana, Zavod za gradbeništvo Slovenije: 764 str (in Slovenian)

[21] Lutman M., Banovec P., Cerk M., Šket Motnikar B. (2018): POTROG 3: Nadgradnja sistema za določanjepotresne ogroženosti in odzivnosti za potrebe zaščite in reševanja v Sloveniji. Ljubljana, Zavod za gradbeništvo Slovenije: 370 str (in Slovenian)

[22] JBDPA (2001): Standard for Seismic Evaluation of Existing Reinforced Concrete Buildings, *The Japan Building Disaster Prevention Association*, Tokyo, Japan

[23] Sinkovič K., Peruš I., Fajfar P. (2016): Assessment of the seismic performance of low-rise RC structures by procedures with different levels of complexity, *Bulletin of Earthquake Engineering, 14(1)*, pp. 213–239, https://doi.org/10.1007/s10518-015-9803-5

[24] Turnšek V., Čačovič F. (1971): Some experimental results on the strength of brick masonry walls, *Proceedings of the 2nd International Brick Masonry Conference (pp. 149-156)*, Stoke-on-Trent, UK

[25] Tomaževič M. (2009): Shear resistance of masonry walls and Eurocode 6: shear versus tensile strength of masonry, *Mater Struct 42, 889–907*, https://doi.org/10.1617/s11527-008-9430-6

[26] Fajfar P. (2000): A Nonlinear Analysis Method for Performance Based Seismic Design, *Earthquake Spectra, 16, 573-592*, https://doi.org/10.1193/1.1586128

[27] Lazar Sinković N., Dolšek M. (2020): Fatality risk and its application to the seismic performance assessment of buildings, *Engineering structures, 205: 1-10*

[28] ICPD (2018): National risk assessment, Overview of the potential major disasters in Italy: seismic, volcanic, tsunami, hydro-geological/hydraulic and extreme weather, droughts and forest fire risks, *Presidency of the Council of Ministres Italian Civil Protection Department*

Proceedings of the 3rd Croatian Conference on Earthquake Engineering - 3CroCEE
19–22 March 2025, Split, Croatia
Copyright © 2025 CroCEE
DOI: https://doi.org/10.5592/CO/3CroCEE.2025.22

INFLUENCE OF GROUND MOTION RECORD SELECTION ON HIGHER MODE DEMANDS IN RC WALLS: A COMPARISON OF UHS AND CS APPROACHES

Jose Poveda[(1)], Gerard J. O´Reilly[(2)]

[(1)] *PhD Candidate, Centre for Training and Research on Reduction of Seismic Risk (ROSE Centre), Scuola Universitaria Superiore IUSS di Pavia, jose.poveda@iusspavia.it*
[(2)] *Associate Professor, Centre for Training and Research on Reduction of Seismic Risk (ROSE Centre), Scuola Universitaria Superiore IUSS di Pavia, gerard.oreilly@iusspavia.it*

Abstract

This study examines the influence of code-prescribed methodologies for ground motion record selection on the higher-mode response of structures. Specifically, it compares two conceptually different target spectra: the Uniform Hazard Spectrum (UHS) and the Conditional Spectrum (CS). Using reinforced concrete (RC) shear wall buildings designed following Eurocode 8 provisions, we analysed the non-linear response for different record selection approaches, including a single UHS and distinct CS with conditional periods. The comparison quantifies the differences in key engineering demand parameters (EDPs) in the RC walls, such as peak storey drift, shear demands, and overturning moment. Our results show that the UHS method generally produces a higher envelope for EDPs, while using a single CS often yields a less conservative response. Despite its tendency to overestimate demands and conceptual inconsistency with actual ground shaking, UHS-based selection offers simplicity, requiring fewer inputs and records than the CS, which requires extensive record selection, but provides some benefits for higher-mode response characterisation. Moreover, improper CS selection can result in a misleading reduction of certain EDPs along the wall height, which is a critical issue that practitioners need to be aware of. These findings highlight potential misinterpretations of code guidelines such as Eurocode 8 and the trade-offs between the precision of CS and the simplicity of UHS.

Keywords: RC walls, higher-modes, ground motions, UHS, conditional spectrum

1. Introduction

Reinforced concrete (RC) shear walls play a prominent role in seismic design worldwide, providing essential lateral stiffness, strength, and adaptability, particularly in high-rise buildings. However, events like the 2010 Chile earthquake exposed vulnerabilities in RC shear walls, particularly in lower storeys, due to factors such as high axial stresses, inadequate transverse reinforcement, and vertical irregularities [1]. These issues highlight the limitations of conventional design methods, including pushover analyses, which primarily focus on first-mode responses and fail to account for complex dynamic interactions.

This study revisits some fundamental assumptions in ductile shear wall seismic design and verified through ground motion record selection and non-linear dynamic analysis. It explores methods such as Conditional Spectrum (CS) [2] featured in the new generation of Eurocode 8 [3] and compares them with the well-established Uniform Hazard Spectra (UHS) approach. The research begins with a probabilistic seismic hazard analysis (PSHA) to compute hazard curves and UHS for different return periods. The design phase employs the UHS for a 475-year return period as the elastic design spectrum, guiding the design of shear walls in accordance with the current Eurocode 8 (EC8) guidelines [4]. Once the design is complete, disaggregation analysis is performed to derive CS at each return period, and record selection is performed for both methodologies, enabling multiple-stripe analyses to compare engineering demand parameters (EDPs).

Copyright © 2025 CroCEE
DOI: https://doi.org/10.5592/CO/3CroCEE.2025.22

2. Case study structures

This study considered the seismic response of five RC shear wall buildings with varying heights of 4, 8, 12, 16, and 20 storeys. Each building featured a typical inter-storey height of 3 metres, a floor area of 600m^2 from a 20 by 30 meters plan layout, giving a floor mass of 490 tons, including the roof, and four walls of equal length l_w and thickness t_w as shown in Figure 1(a) and (b). A simple equivalent cantilever model was developed for analysis, as shown Figure 1(c), where the cracked section properties followed the Los Angeles Tall Buildings Structural Design Council (LATBSDC) [5] recommendation of 0.6 factor for cracking in bending and 0.75 in shear with respect to the gross elastic stiffnesses.

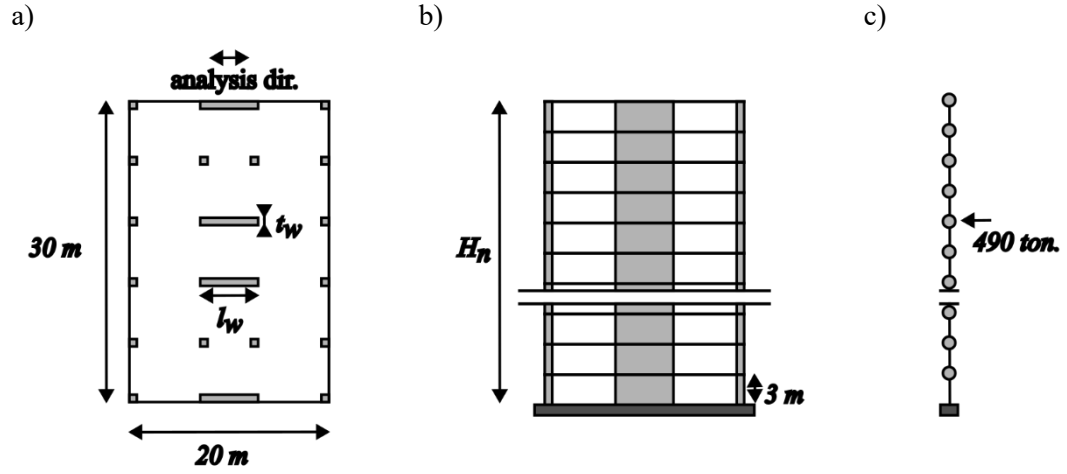


Figure 1. a) Buildings' plan; b) Buildings' elevation; c) Numerical model.

2.1. Seismic design

The buildings were designed as ductile shear walls following EC8 [4]. Response Spectrum Analysis (RSA) using a UHS at 475-year return period spectra was adopted as the design methodology. To estimate the modal properties needed for RSA, the numerical model shown in Figure 1(c) was used. Table 1 shows the modal periods and mass percentage participation for the first three modes of the linear model for the final designs. The gravity load system's contribution to the building's lateral stiffness was not included. When defining the design spectra for the RSA, the EC8 design rules were applied to the UHS determined from PSHA for a site in Duzce, Turkey. That is, the UHS was divided by the design ductility factor $q = 5.4$ and the design forces were determined as prescribed by EC8. The reason the UHS was adopted instead of the simplified spectrum prescribed by EC8 was to ensure consistency between the designs and the ground motion record selection based on PSHA. The lower bound for the design spectral acceleration $\beta = 0.2$ was also applied to ensure minimum lateral resistance criteria were met, as prescribed by the code. The elastic and design spectra are illustrated in Figure 2.

Table 1. Dynamic properties of building model

	4 Storey		8 Storey		12 Storey		16 Storey		20 Storey	
Mode	T (s)	M (%)	T (s)	M (%)	T (s)	M (%)	T (s)	M (%)	T (s)	M (%)
1	0.88	70.3	1.21	65.9	1.41	64.5	1.64	63.7	1.82	63.2
2	0.15	21.9	0.21	21.1	0.24	20.7	0.28	20.3	0.30	20.1
3	0.06	6.32	0.08	7.14	0.09	7.18	0.11	7.13	0.12	7.07

Copyright © 2025 CroCEE
DOI: https://doi.org/10.5592/CO/3CroCEE.2025.22

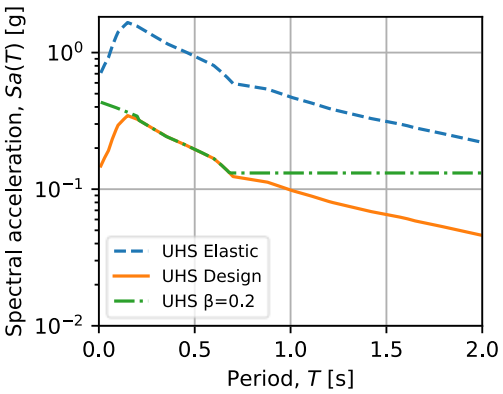


Figure 2. Elastic and design response spectra.

The RSA demands on the buildings, along with the elastic and design spectral acceleration for the first mode, are summarised in Table 2 for the RSA using the CQC modal combination of all modes, even if only three modes were necessary to reach the 90% modal mass participation rules. The maximum peak storey drift (PSD) demand was also evaluated and ensured to be below the design threshold of 2%.

Table 2. Buildings' demand for design UHS-475 years return period.

Building	Sa(T_1) [g]	Sa(T_1)/q ≥ β Sa(T_1) [g]	Base Shear [MN]	Base Moment [MNm]	Drift [%]
4 Storey	0.543	0.13	2.42	17.98	1.62
8 Storey	0.390	0.13	4.46	63.95	1.17
12 Storey	0.331	0.13	6.37	137.63	0.93
16 Storey	0.283	0.13	8.22	239.12	0.82
20 Storey	0.253	0.13	10.05	368.21	0.82

Once the RSA results were available, capacity design envelopes were developed to account for the over-strength of the wall at the base, and the effects of higher modes, and the required reinforcement was subsequently sized. Figure 3 shows the design envelopes for the 20-storey building and the final strength of the wall once the rebar's spacings and diameters were defined. For simplicity, the final design at the base was assumed constant along the buildings high. Still, it is not uncommon for designers to choose to optimise and reduce rebar provisions along the height. The design properties of each building's wall are summarised in Table 3 and the base shear and overturning moment of the walls from the capacity design envelope are shown in Table 4 along with the ε value from code, needed for the base shear capacity envelope ($V_{Ed,b} = \varepsilon \cdot V'_{Ed,b}$) and the shear overstrength ratio ($V_{Ed,b}/V_n$).

Copyright © 2025 CroCEE
DOI: https://doi.org/10.5592/CO/3CroCEE.2025.22

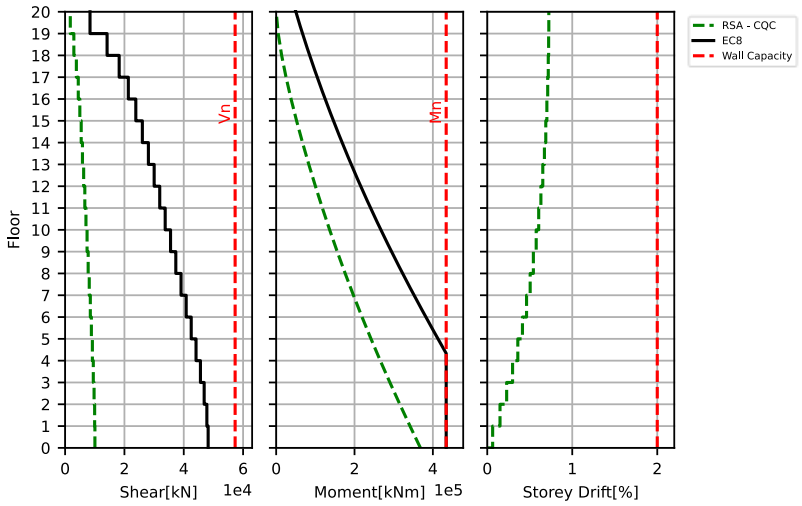


Figure 3. EC8 capacity design envelope for the 20-storey building.

Table 3. Building design properties.

Building	$H_n[m]$	$f_c^{'}\ [MPa]$	$l_w[m]$	$t_w[m]$	$d_{b,l}[mm]$	$s_l[cm]$	ρ [%]	$d_{b,t}[m]$	$s_t[cm]$
4 Storey	12	30	2.50	0.30	12	20	0.37	16	10
8 Storey	24	30	4.50	0.35	12	20	0.32	16	7.5
12 Storey	36	30	6.50	0.40	12	20	0.28	16	7.5
16 Storey	48	50	7.50	0.45	12	20	0.25	20	7.5
20 Storey	60	50	8.50	0.60	14	20	0.25	20	7.5

Table 4. Buildings' walls strength and shear over-strength ratio.

Building	$\boldsymbol{\varepsilon}$	$V_{Ed,b}$[MN]	$V_n[MN]$	$V_{Ed,b}/V_n$	$M_n[MNm]$
4 Storey	2.8	6.9	7.29	1.06	26.5
8 Storey	3.5	15.87	17.70	1.12	90.7
12 Storey	4.0	25.80	26.60	1.03	193.1
16 Storey	4.5	37.21	47.36	1.27	278.8
20 Storey	4.8	48.22	57.32	1.19	434.0

2.2. Non-linear modelling

The non-linear model incorporated a lumped plastic hinge at the base of the wall to represent the flexural yielding, using a simple bi-linear hysteretic model *Steel01* provided in OpenSees [6] with a 1% post-yielding stiffness. The plastic hinge length, l_{pl}, and yield curvature, ϕ_y, were calculated based on wall geometry using the relationship for rectangular walls described in Priestley et al. [7]. The parameters for defining the plastic hinge are summarised in Table 5.

Table 5. Building plastic hinge parameters.

Building	$\phi_y\, m^{-1} * 10^{-3}$	$l_{pl}\ [m]$	$EI_{cr}[kN/m]10^6$
4 Storey	1.8	0.70	14.70
8 Storey	1.0	1.22	90.56
12 Storey	0.7	1.75	278.52
16 Storey	0.6	2.18	163.99
20 Storey	0.5	2.63	818.48

Copyright © 2025 CroCEE
DOI: https://doi.org/10.5592/CO/3CroCEE.2025.22

P-delta effects were incorporated using a corotational element, with the vertical load of each floor's weight applied to the end nodes of the columns. A constant modal damping ratio of $\xi = 5\%$ was assumed for all modes, despite modern recommendations for lower values, such as those in LATBSDC [5]. Finally, the model did not account for shear failure or shear-flexural interaction.

3. Analysis

3.1. Seismic hazard

PSHA was performed using the OpenQuake engine [8] based on the seismic hazard model ESHM13 [9] for a site in Duzce in Turkey. The analysis used a simplified logic tree with just a single ground motion model (AkkarEtAlRjb2014) [10] but kept the three logic tree branches to account for epistemic uncertainties in source characterisation. The analysis was carried out for ten return periods spanning 22 to 19,975 years, including 475 and 2475 years, to align with design code requirements. Outputs include hazard curves, as shown in Figure 4(a), and the UHS previously shown in Figure 2 for 475-years return period. An example of seismic disaggregation is shown in Figure 4(b) for the 475-year return period.

3.2.Ground motion record selection

The record selection procedure involves selecting and scaling natural ground motions to match the target spectrum over the relevant range of periods. When selecting to match the UHS, records must closely match the mean spectrum within a specified tolerance, typically ±10% over the range $0.2(T_1)$ to $2.0(T_1)$ according to EC8 [4], where T_1 is the fundamental period of the structure. The UHS-based selection is deemed to be equivalent to using the code-prescribed response spectrum in this study, as they are conceptually the same. Figure 5 presents the mean of the UHS-based record selection. Since this study encompassed five different buildings, the selection period range was extended from $0.05s$ to $4.0s$ to cover the 90% modal mass participation of the five buildings and the two times the first mode period rule for the 20-storey building, and the same UHS-based ground motions were adopted for all structures.

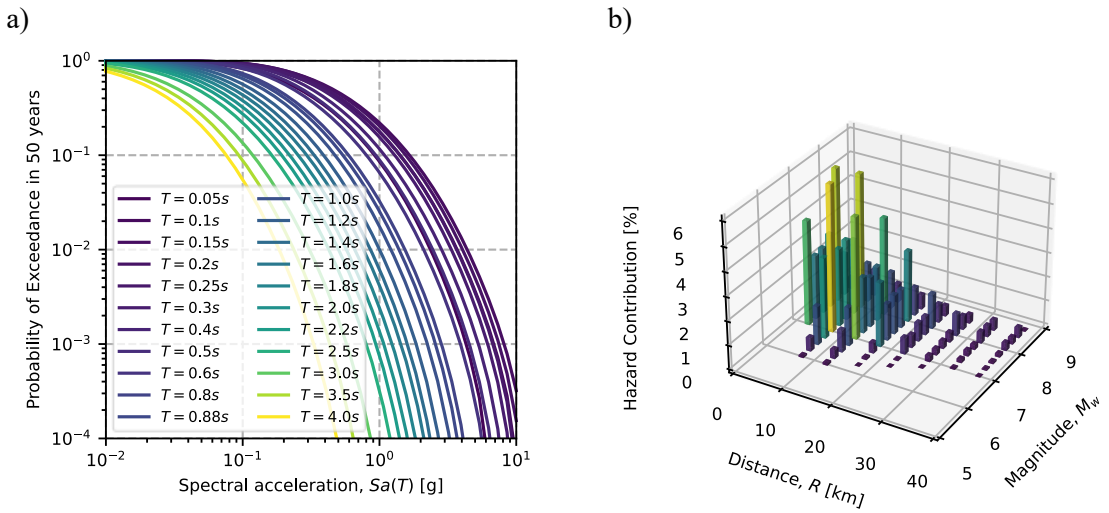


Figure 4. a) Hazard curves; b) 475-year return period disaggregation for *Sa*(*T*=1.0s).

For CS-based selection using *Sa*(*T*), the ground motions are conditioned on a specific spectral acceleration value at a period *Sa*(*T**) for the desired return period and also the variability of the ground motions at periods other than *T**. Unlike the UHS, the CS exhibits lower *Sa*(*T*) at periods farther from the conditioning period. Constructing this spectrum requires PSHA disaggregation outputs and correlation models. Lin et al. [11] described the differences generated in CS when simplifications are applied, and in this case, the "exact" CS was used. For the CS-based selection, a wide range of *T** values from $0.05s$ to $4.0s$ were selected, giving several different CS-based ground motion record sets all selected using slightly different conditioning choices. This is because an essential question in CS-based

Copyright © 2025 CroCEE
DOI: https://doi.org/10.5592/CO/3CroCEE.2025.22

selection is determining the most appropriate conditioning period, T^*, for which several methodologies and recommendations exist in the literature [12], with the most common choice being the first mode period, $T^*=T_1$. This study comprehensively selected various conditioning periods to evaluate trends across different scenarios when periods other than the conditioning one were selected. As an example, Figure 5 shows a record selection for the conditional periods $Sa(T^* = 0.30s)$ and $Sa(T^* = 1.82s)$ alongside the UHS selection for the 475-year return period. It is evident that the spectral demands match between the CS and UHS at the conditioning period T^*, but are lower at other periods. Given the multi-modal nature of RC shear wall response, it is the impact of this different that is of interest in this study.

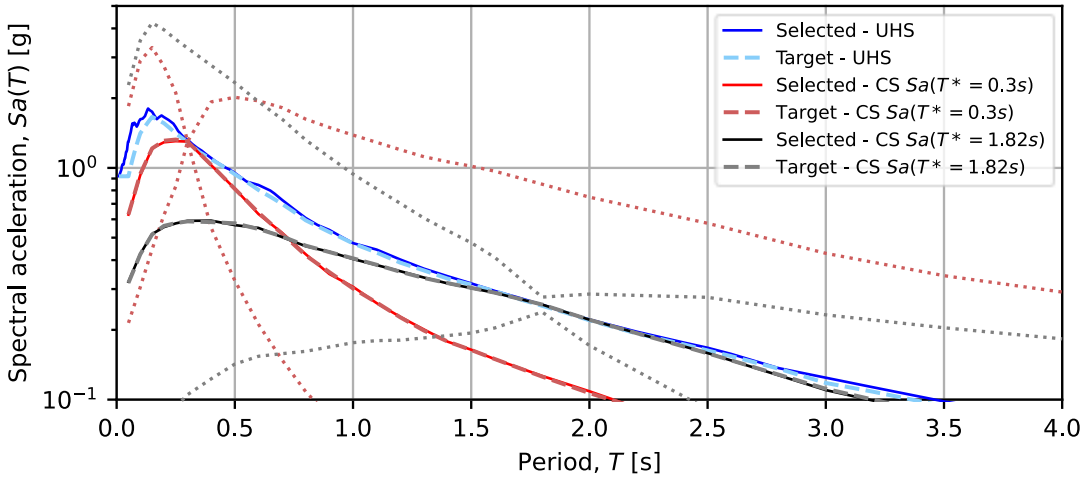


Figure 5. 475-year return period UHS-based selection and CS-based selection for $Sa(T^*=0.30s)$ and $Sa(T^*=1.82s)$, where the target is plotted via dashed lines and the selected ground motions via the solid lines.

The present study considers a single direction of analysis, so only one ground motion record is selected and used. Usually, building codes recommend between 7 and 11 records to assess the median of the structural response; for the present study, 40 ground motion records were selected per return period.

3.3. Multiple stripe analysis

Multiple Stripe Analysis (MSA) is a method in earthquake engineering that involves the analysis of a structural model with multiple ground motion records, each scaled to a specific intensity measure, such as spectral acceleration at a given period. This study analysed 40 ground motion records for the ten return periods analysed in PSHA. In total, 9,200 scaled records were evaluated, derived from 40 records across 10 return periods and 23 target spectra (22 conditional spectra and one uniform hazard spectrum). This comprehensive analysis thus aims to provide insights into the effects of record selection on EDPs used to describe RC shear wall performance subsequent design. For example, Figure 6 illustrates the median (non-collapsed) response for UHS-based and two CS-based selection at the 475-year return period for the 20-storey building and compared to the capacity design envelope. The CS-based selections were done with the first and second mode conditional periods, meaning $Sa(T^*=T_1)$ and $Sa(T^*=T_2)$, respectively.

Examining the storey drift demands, it is evident that the CS conditioned on T_1 quite closely resembles the UHS-based demand, underlining the first-mode dominance of displacement-based EDPs, whereas the CS conditioned on T_2 tends to underestimate the drift demand. Hence, if an analyst wished to move away from the conceptual inconsistencies of the UHS and utilise hazard-consistent ground motions via the CS, conditioning on T_1 appears to be a logical choice.

Examining the shear force and bending moment demands, it is clear that the CS conditioned on T_1 quite closely resembles the UHS-based demand in the lower half of the wall, but underestimates the demands in the upper half because of higher mode contributions. Likewise, the CS conditioned on T_2 underestimates the demands in the lower half but aligns well with the UHS in the upper half of the wall.

Copyright © 2025 CroCEE
DOI: https://doi.org/10.5592/CO/3CroCEE.2025.22

Hence, if an analyst were to choose the CS-based approach, the results would be highly dependent on which conditioning period is selected, with the consequence that the demands will be underestimated in one part of the wall, which would be problematic for ensuring capacity design.

These results refer to a single structure at a single return period intensity. The following section discusses the results for all structures in a more general manner.

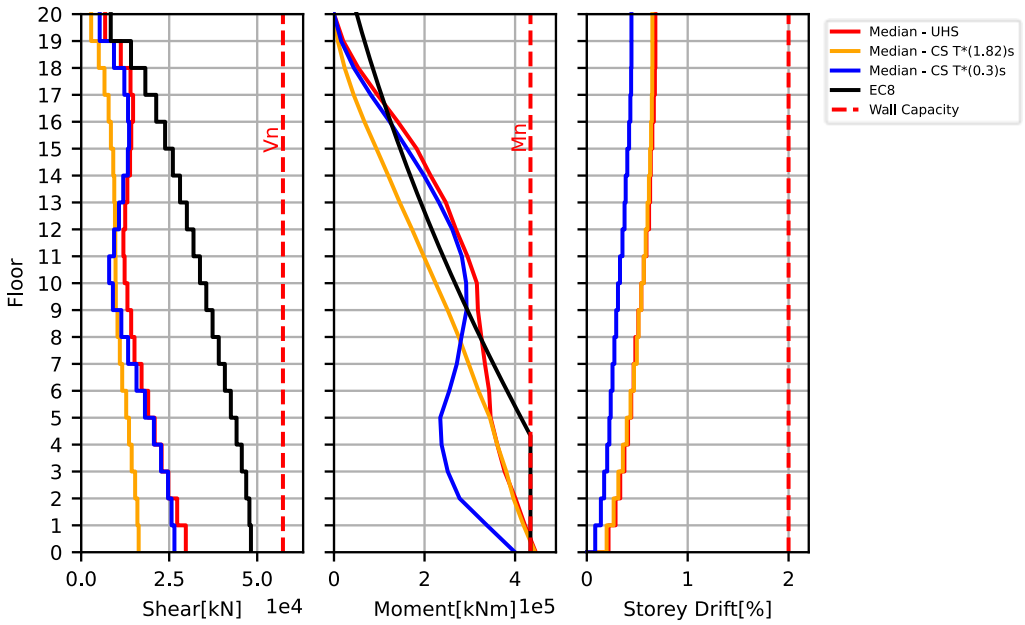


Figure 6. Median (non-collapsed) analysis results at the 475-year return period using UHS-based selection, CS-based selection at $Sa(T^*=1.82s)$ and $Sa(T^*=0.3s)$.

4. Results

The primary objective of this study is to compare key EDP values for RC shear walls obtained using different record selection methods. Figure 7 presents what are termed *EDP spectra* herein for each building by plotting the EDPs of interest as a function of the conditional period used in CS-based selection. For comparison, the UHS-based selection is shown as it is invariant to the conditioning period. To maintain clarity, results are presented for only two return periods: 475 and 2475 years.

For shear demands, the median base shear demand is normalised by the maximum demand from the capacity design envelope ($V_{Ed,b}$ in Table 4). Similarly, for moment demands, the median base overturning moment demand is normalised by the maximum demand from the capacity design envelope (M_n in Table 4). For drifts, the drift at the top of each building is normalised by the 2% drift limit prescribed in the code. These normalisations help illustrate whether the demands exceed the design envelope or the drift limit on relative terms.

The vertical lines in the EDP spectra represent the first three structural modes for each building (i.e., T_1, T_2 and T_3), providing insight into the correlation between structural modes and the corresponding structural responses.

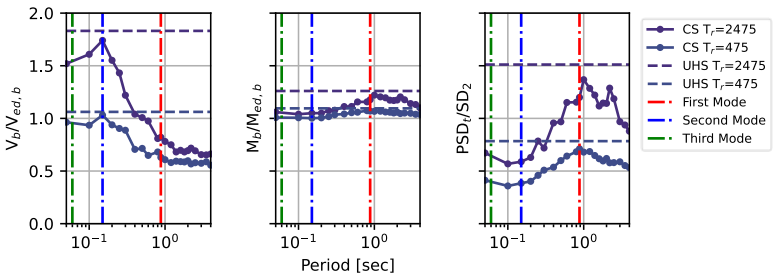
Finally, Table 6 presents the ratio between UHS-based selection and the peak of all CS-based selection at 475- and 2475-year return periods. These ratios helps understand how UHS-selection relates to CS-

Copyright © 2025 CroCEE
DOI: https://doi.org/10.5592/CO/3CroCEE.2025.22

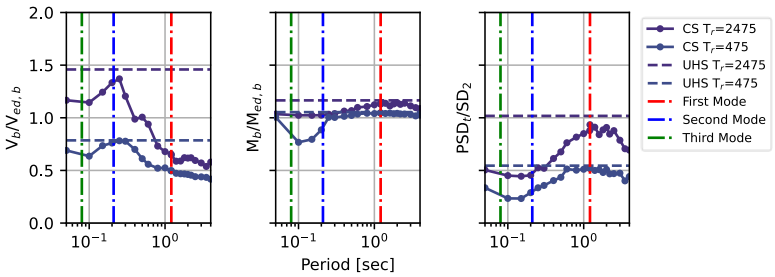
selection for different EDPs. Discussion of these results is presented in the following subsections analysing one EDP at a time.

Table 6. Ratio of the UHS demand to the peak of the CS demands.

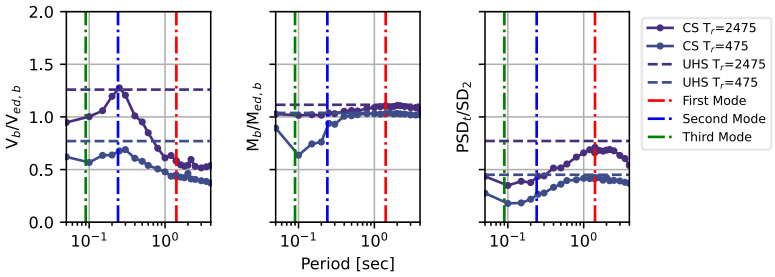
Building	475-year return period			2475-year return period		
	Shear	Moment	Drift	Shear	Moment	Drift
4 Storey	1.03	1.02	1.10	1.05	1.03	1.10
8 Storey	1.01	1.01	1.05	1.07	1.02	1.09
12 Storey	1.12	1.00	1.06	0.99	1.01	1.09
16 Storey	1.02	0.99	0.98	0.99	1.00	1.08
20 Storey	1.12	0.99	0.99	1.04	1.00	1.00



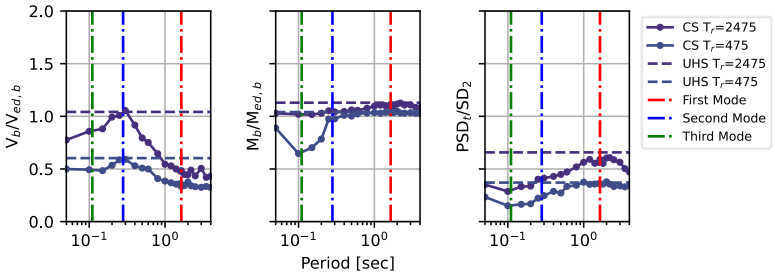
a)



b)

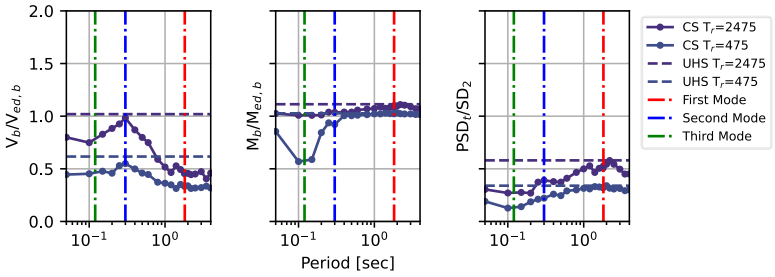


c)



d)

Copyright © 2025 CroCEE
DOI: https://doi.org/10.5592/CO/3CroCEE.2025.22



e)

Figure 7. EDP spectra for 475 and 2475-year return periods, a) 4-storey building; b) 8-storey building; c) 12-storey building; d) 16-storey building; e) 20-storey building

4.1. Shear demands

For the shear demands, Figure 7 shows these ratios in the left column of plots for each building. Starting with the UHS-based assessment, which represents the standard approach adopted in building codes, the capacity design provisions generally provide adequate capacity at the 475-year return period. Only the 4-storey building exhibits a slightly higher ratio of 1.06.

In contrast, the CS-based assessment offers additional insights into shear demand. Peak shear demands at the wall's mid-height are observed at the building's second mode-based selection, $Sa(T^*=T_2)$. On average, the first mode selection, $Sa(T^*=T_1)$, generates 62% of the peak base shear demand for all buildings, from the $Sa(T^*=T_2)$ demand at the 475-year return period, while the third mode selection, $Sa(T^*=T_3)$, generates 85% of the peak base shear demand from the $Sa(T^*=T2)$ base shear demand.

Linking the peak values from CS-based and UHS-based assessments (as shown in Table 6), it is noteworthy that the UHS selection produces demands in the structure that are higher than those of the CS selection by an average ratio of 1.06.

From the CS-based selections, it is evident that the second mode selection contributes most significantly to shear demands in all structures. This indicates that selecting a conditional period based on the first mode T_1 would substantially underpredict shear demands. This is noteworthy because the current EC8 draft [3] fixes the conditional period to the first fundamental mode, T_1. In contrast, ASCE7-22 [13] mandates the use of at least two conditional periods, defined as periods that significantly contribute to the inelastic dynamic response in the two orthogonal directions. Additionally, ASCE7-22 [13] sets a lower bound for the mean of the CS targets at 75% of the UHS, ensuring higher mode effects are reasonably accounted for if the selected conditional periods fail to do so. These issues must be clear to practitioners and governed correctly in the code prescriptions.

While the second mode CS-based selection $T^* = T_2$ captures shear response more realistically than UHS-based selection due to its explicit correlation with spectral intensities, it requires an additional set of ground motions beyond the standard $T^* = T_1$ selection. On the other hand, although UHS-based selection tends to overpredict maximum shear demands by a maximum of 1.12 (as shown in Table 6), it only requires one set of ground motions.

4.2. Moment demands

For overturning moments in Figure 7, the UHS-based selection at the 475-year return period indicates that yielding is achieved. Given the model's 1% post-yielding positive flexural stiffness, further increases in demand, as 2475-year return period, do not increase significantly the ratios.

Similar to shear demands, the CS-based assessment provides additional insights into moment demand behaviour. At the 475-year return period, the conditional period selections capable of inducing flexural yielding range from values near the second mode to periods longer than the first mode. This indicates

Proceedings of the 3rd Croatian Conference on Earthquake Engineering - 3CroCEE
19–22 March 2025, Split, Croatia
Copyright © 2025 CroCEE
DOI: https://doi.org/10.5592/CO/3CroCEE.2025.22

that high moment demands at the base are not solely associated with the first mode or its elongated equivalent.

Notably, a pronounced dip in moment demands is observed near the third mode at the 475-year return period. However, at higher intensities, such as the 2475-year return period, even the third mode can induce yielding at the base.

4.3. Peak storey drift demands

For peak storey drifts in Figure 7, the drift limit of 2% is not exceeded for neither the 475-year nor the 2475-year return periods, except for the 4-storey building. A strong correlation is observed between the drift demands resulting from the ground motions selected to match the UHS and those selected based on the CS at the first mode, $Sa(T^*=T_1)$, and slightly longer periods, $Sa(T^*>T_1)$. This underlines the fact that drift demands in structures tend to be dominated by the first mode of response. This is because the demands of the $Sa(T^*=T_1)$-based selection, whose $Sa(T_2)$ values will be much lower than the UHS-based selection, coincide well with the UHS-based selection, where they are equal (i.e., $Sa(T_1)_{CS} \approx Sa(T_1)_{UHS}$ and $Sa(T_2)_{CS} < Sa(T_2)_{UHS}$). Compared to the previous sections discussed on force-based demands (i.e., shear and moment), it highlights that a CS-based record selection conditioned on the first mode period is likely to give very similar, if not slightly lower, drift demands compared to the UHS-based selection. This is both reassuring for analysts as they would now be using ground motions that are hazard consistent, and not conservative and somewhat unrealistic like the UHS-based ones [14].

The ratio between the demands of the UHS-based selection and the maximum CS-based selection drifts tends to increase for shorter buildings, with the UHS-based selection overpredicting drifts by up to a factor of 1.1. For taller buildings, this discrepancy diminishes, with the ratio approaching 1.0 for the 16- and 20-storey structures.

4.4. Capacity design envelopes

Additionally, apart from the key EDP values, it is noteworthy how the capacity design envelopes align with the actual response of the structures. For example, Figure 6 compares median non collapse demands for the 20-storey building at 475-year return period. This alignment is crucial, as it can inform design optimisations along the height of the structures based on these envelopes.

For the UHS-based selection, which is generally conservative, the shear capacity envelope is higher throughout the height of the building compared with the EC8 capacity design envelope. However, the shapes differ, with the median shear demands spiking at the upper floors due to higher mode effects.

For moments, the UHS-based selection shows median demands exceeding the capacity envelope at mid-height, highlighting a potential yielding location if the design optimisation closely follows the capacity design envelope and ductile detailing required.

Finally, comparing shear and moment shapes for UHS- and CS-based selections, it is evident that UHS selection serves as an envelope for the CS-based selections. Notably, the UHS selection captures higher modes effects, including spikes of shear and moment at higher floors.

5. Conclusions

This study investigated the seismic performance of RC shear wall buildings subjected to ground motion records selected using Uniform Hazard Spectrum (UHS) and Conditional Spectrum (CS) approaches. Key Engineering Demand Parameters (EDPs), including shear, overturning moment, and peak storey drift, were analysed for structures of varying heights at mainly two return periods (475 and 2475 years). The results highlighted the influence of higher modes in shear demands, the limitations and comparative performance of UHS- and CS-based selection. Below is a summary of the key findings:

Copyright © 2025 CroCEE
DOI: https://doi.org/10.5592/CO/3CroCEE.2025.22

- The CS-based assessment reveals that the shear demands in the upper half of the walls occur at the second mode selection, $Sa(T^* = T_2)$, with first mode selection $Sa(T^* = T_1)$, reaching a 62% and third mode selection $Sa(T^* = T_3)$, reaching 85% of the peak demand at the base on average.
- The UHS-based selection captures higher mode effects well but tends to overpredict maximum shear demands compared to $Sa(T^* = T_1)$ selection, with an average overestimation factor of 1.06.
- CS-based assessments show that moment demands capable of inducing yielding range from second mode periods to those longer than the first mode, suggesting that base moments are not exclusively tied to the first mode.
- Drift demands are primarily dominated by the first mode with strong agreement between UHS- and $Sa(T^* = T_1)$ selection.
- UHS-based selection serves as a natural envelope for CS-based selections, effectively capturing higher mode effects, including shear and moment spikes at upper floors, but nevertheless suffer the conceptual issues with its hazard consistency and definition.

This study primarily focused on the provisions of Eurocode 8, as the next generation of the code is set to be published. A notable new feature in the draft is the introduction of CS-based record selection, but the conditional period is currently restricted to the first fundamental mode, T_1. Based on the findings of this study and existing literature [12], it is recommended to at least include a second CS-based record selection associated with the second mode period, $Sa(T^* = T_2)$. Similarly, ASCE 7-22 [13] included similar recommendation, advocating for the use of two or more conditional period selections and stipulating a lower bound of 75% of the UHS for the mean envelope of CS-based selections. While these provisions offer improvements in accuracy, they may introduce significant complexity and potentially discourage the adoption of CS-based record selection methods. Nonetheless, the CS-based selection method should be promoted for its hazard consistency [2] and potential economic benefits [12], as it demonstrated lower shear demands compared to the UHS selection.

Acknowledgements

The work presented in this paper has been developed within the framework of the project ‘‘Dipartimenti di Eccellenza 2023-2027,’’ funded by the Italian Ministry of Education, University and Research at IUSS Pavia.

References

[1] R. Jünemann, J. C. de la Llera, M. A. Hube, J. A. Vásquez, and M. F. Chacón, “Study of the damage of reinforced concrete shear walls during the 2010 Chile earthquake,” in *Earthquake Engineering and Structural Dynamics*, John Wiley and Sons Ltd, Aug. 2016, pp. 1621–1641. doi: 10.1002/eqe.2750.

[2] T. Lin, C. B. Haselton, and J. W. Baker, “Conditional spectrum-based ground motion selection. Part I: Hazard consistency for risk-based assessments,” *Earthq Eng Struct Dyn*, vol. 42, no. 12, pp. 1847–1865, Oct. 2013, doi: 10.1002/eqe.2301.

[3] CEN/TC 250, “Eurocode 8 - Design of structures for earthquake resistance - Part 1-1: General rules and seismic action,” 2023.

[4] CEN, *Eurocode 8, design of structures for earthquake resistance. Part 1, General rules, seismic actions and rules for buildings*. British Standards Institution, 2005.

[5] S. Akelyan and G. Brandow, “AN ALTERNATIVE PROCEDURE FOR SEISMIC ANALYSIS AND DESIGN OF TALL BUILDINGS AN ALTERNATIVE PROCEDURE FOR SEISMIC ANALYSIS AND DESIGN OF TALL BUILDINGS 2023 Edition A consensus document developed by the Council Council Active Members,” 2023.

Copyright © 2025 CroCEE
DOI: https://doi.org/10.5592/CO/3CroCEE.2025.22

[6] F. McKenna, "OpenSees: A Framework for Earthquake Engineering Simulation," 2011.

[7] M. J. N. Priestley, G. M. Calvi, and M. J. Kowalsky, *Displacement Based Seismic Design of Structures*.

[8] M. Pagani *et al.*, "OpenQuake engine: An open hazard (and risk) software for the global earthquake model," *Seismological Research Letters*, vol. 85, no. 3, pp. 692–702, 2014.

[9] J. Woessner *et al.*, "The 2013 European Seismic Hazard Model: key components and results," *Bulletin of Earthquake Engineering*, vol. 13, no. 12, pp. 3553–3596, Dec. 2015, doi: 10.1007/s10518-015-9795-1.

[10] S. Akkar, M. A. Sandıkkaya, and J. J. Bommer, "Empirical ground-motion models for point- and extended-source crustal earthquake scenarios in Europe and the Middle East," *Bulletin of Earthquake Engineering*, vol. 12, no. 1, pp. 359–387, Feb. 2014, doi: 10.1007/s10518-013-9461-4.

[11] T. Lin, S. C. Harmsen, J. W. Baker, and N. Luco, "Conditional spectrum computation incorporating multiple causal earthquakes and ground-motion prediction models," *Bulletin of the Seismological Society of America*, vol. 103, no. 2 A, pp. 1103–1116, Apr. 2013, doi: 10.1785/0120110293.

[12] T. J. Bassman, K. Zhong, and J. W. Baker, "Evaluation of Conditional Mean Spectra Code Criteria for Ground Motion Selection," *Journal of Structural Engineering*, vol. 148, no. 11, Nov. 2022, doi: 10.1061/(asce)st.1943-541x.0003471.

[13] ASCE/SEI, *Minimum Design Loads and Associated Criteria for Buildings and Other Structures*. Reston, VA: American Society of Civil Engineers, 2021. doi: 10.1061/9780784415788.

[14] J. J. Bommer and R. Pinho, "Adapting earthquake actions in Eurocode 8 for performance-based seismic design," *Earthq Eng Struct Dyn*, vol. 35, no. 1, pp. 39–55, 2006, doi: 10.1002/eqe.530.

Proceedings of the 3rd Croatian Conference on Earthquake Engineering - 3CroCEE
19–22 March 2025, Split, Croatia
Copyright © 2025 CroCEE
DOI: https://doi.org/10.5592/CO/3CroCEE.2025.29

ANALYTICAL APPROACH TO SEISMIC BEHAVIOUR ASSESMENT OF RC FRAME STRUCTURES WITH RUBBER JOINTED MASONRY INFILL

Liljana B. Mijalkova[(1)], Aleksandra Bogdanović [(2)], Enrico Tubaldi [(3)], Marko Marinković [(4)], Bartolomeo Pantò [(5)]

(1) *PhD Student, Institute for earthquake engineering and engineering seismology, Skopje, Republic of North Macedonia, e-mail address: liljana.mijalkova84@gmail.com*
(2) *Associate Professor, Institute for earthquake engineering and engineering seismology, Skopje, Republic of North Macedonia, e-mail address: saska@iziis.ukim.edu.mk*
(3) *Professor, Department of Civil and Environmental Engineering, University of Stratchclyde, Glasgow, UK, e-mail address: enrico.tubaldi@strath.ac.uk*
(4) *Assistant Professor, Chair of Engineering Mechanics and Theory of Structures, Faculty of Civil Engineering, University of Belgrade, Belgrade, Serbia, e-mail address: mmarinkovic@grf.bg.ac.rs*
(5) *Assistant Professor, Department of Engineering, Durham University, Durham, UK, e-mail address: bartolomeo.panto@durham.ac.uk*

Keywords: rubber joints, decoupled masonry infill, numerical modelling, in-plane seismic assessment, discrete macro element

1. Introduction

Infilled structures are the most used type of structures in seismic-prone countries and masonry infills are the most vulnerable part of these structures, even under medium-intensity earthquakes. Recent experimental and numerical studies demonstrated that decoupling systems between the infill and the surrounding frame reduce the adverse effects of the frame-infill interaction on the ductility of the system [1].

2. Description of prototype and experimental campaign

Full-scale prototype was subjected to shaking table tests conducted within the ERIES – FLEJOI project by a research group at the Institute of Earthquake Engineering and Engineering Seismology – Skopje, North Macedonia. It consists of one bay, one height reinforced concrete frame structures (as shown in Figure 2a) and masonry infilled wall that is decoupled from the surrounding frame with rubber flexible/ sliding joints with suitable stiffness (Figure 2b).

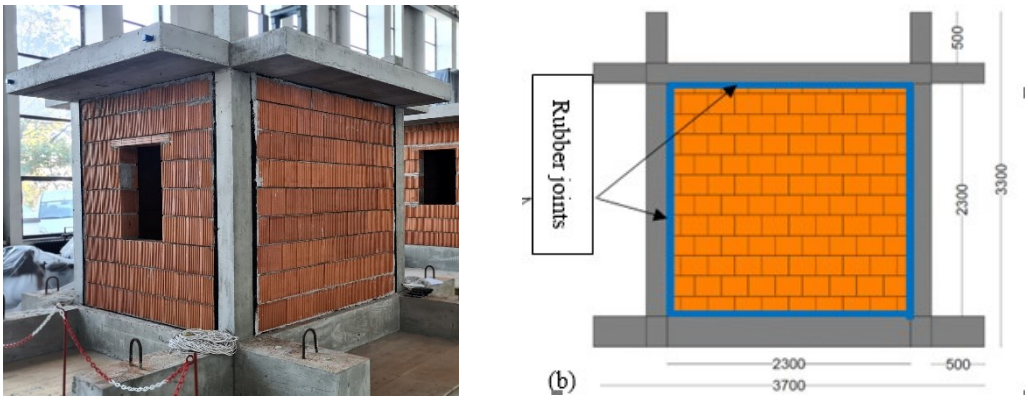


Figure 2. a) Built experimental model; b) Positioning of rubber joints

The following experimental activities were performed by the Dynamic Testing Laboratory of IZIIS [2]: 1) characterisation tests of the constituent materials and components, 2) ambient vibration and impact hammer tests conducted to ascertain the dynamic characteristics and 3) shake table tests aimed to evaluate the dynamic behaviour and seismic response to specific earthquake time histories.

Copyright © 2025 CroCEE
DOI: https://doi.org/10.5592/CO/3CroCEE.2025.29

3. Adopted modelling strategy

The main focus of this paper is to investigate the applicability and accuracy of a discrete macro element as a practical numerical tool for assessment of decoupled RC masonry-infilled frames equipped with rubber joints alongside the frame.

The model (Figure 3b), implemented in OpenSees, can be represented by a simple equivalent mechanical scheme consisting of an articulated quadrilateral panel with a 1D diagonal link simulating the masonry shear deformability and eight 2D perimeter contact links governing the masonry axial and flexural responses and the infill-frame interaction (Figure3.a) [3][4].

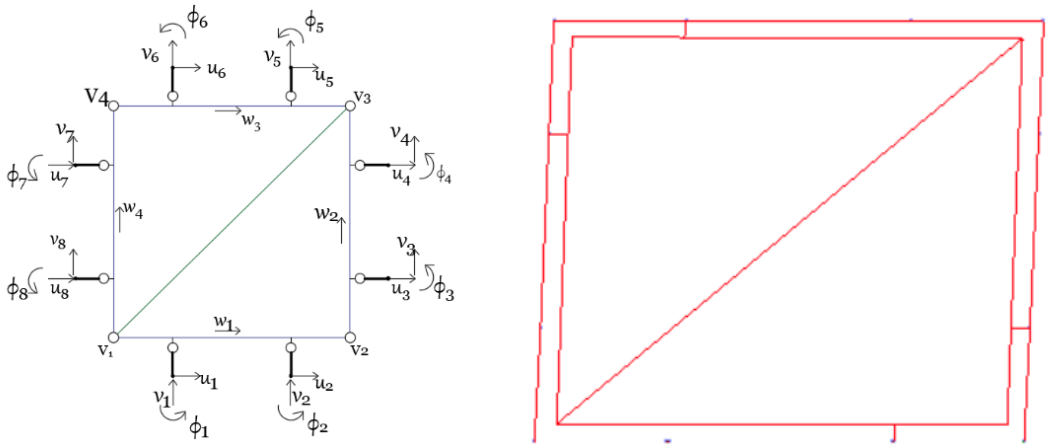


Figure 3. a) Schematic presentation of the discrete macro model; b) Numerical model of one discrete macro element in Open Sees

The experiment results demonstrate that these flexible joints aid in improving and balancing the structure's bearing and ductility capacity and protect the masonry of pre-term damage. The comparisons between the numerical analyses and the experiments, presented in terms of displacement time histories and damage patterns are in the calibration process and to date demonstrate that the macro-element can predict the complex non-linear dynamic response of the system with reasonable accuracy.

Acknowledgements

I would like to express my great appreciation to: my supervisor professor Aleksandra, for the selfless support and motivation, to professors E. Tubaldi and B. Panto for providing me with the discrete macro model so that my research can continue and to professor M. Marinkovic for or day-to-day conversations and his insight into the calibration process of the numerical model.

References

[1] FLEJOI-IZIIS (2024) Data paper ERIES (Engineering Research Infrastructures for European Synergies), FLEJOI (FLExible JOInts for seismic-resilient design of masonry-infilled RC frames), Skopje, North of Macedonia

[2] Dhir, P.K., Tubaldi, E., Ahmadi, H.R., & Gough, J. (2021). Numerical modelling of reinforced concrete frames with masonry infills and rubber joints. *Engineering Structures*. DOI:10.1016/J.ENGSTRUCT.2021.112833

[3] Panto, B., & Rossi, P. P. (2019). A new macromodel for the assessment of the seismic response of infilled RC frames. https://doi.org/10.1002/eqe.3163

[4] Marinković M, Butenweg C,(2022) Numerical analysis of the in-plane behaviour of decoupled masonry infilled RC frames, Engineering Structures, Volume 272, ISSN 0141-0296, https://doi.org/10.1016/j.engstruct.2022.114959.

Proceedings of the 3rd Croatian Conference on Earthquake Engineering - 3CroCEE
19–22 March 2025, Split, Croatia
Copyright © 2025 CroCEE
DOI: https://doi.org/10.5592/CO/3CroCEE.2025.38

EFFECT OF COLUMN BASE ROTATIONAL STIFFNESS ON THE SEISMIC RESPONSE OF STEEL BUILDINGS

Menelaos Papamichelakis [(1)], George Papagiannopoulos [(2)]

[(1)] *Ph.D. Candidate, Laboratory of Applied Mechanics and Structural Technology, Hellenic Open University, Patras, Greece, menelaos.papamichelakis@ac.eap.gr*
[(2)] *Professor, Laboratory of Applied Mechanics and Structural Technology, Hellenic Open University, Patras, Greece, papagiannopoulos@eap.gr*

Abstract

This paper examines in a numerical fashion the, arguably, most critical connection in a steel building: the column base connection under seismic load. It is well-known that failure of this connection can lead to partial or even complete structural collapse. This connection, whether is assumed fixed or pinned, significantly influences the seismic response of a steel building. The rotational stiffness of this connection is determined by several factors, such as the configuration (number of bolts etc.) and type (exposed or embedded). The study presents the results of non-linear time history analyses where the column base connection is modelled by means of a rotational spring. Emphasis is given to the differences in seismic response when different values of rotational stiffness are applied, including cases where the connection is considered completely rigid or pinned. For comparison purposes, three buildings, different in height and essentially in the number of storeys, are studied. Both local (member-level) and global (building-level) response indices, such as column bending moments, the first significant eigenperiods, and the interstory drift ratio (IDR), are employed in order to assess the effect of different values for rotational stiffness. The results indicate that modelling of column base connection, can significantly alter the seismic response, underscoring the need for further investigation to other types of steel buildings.

Keywords: column base connection, steel building, seismic response, time-history analyses.

1. Introduction

The seismic analysis of a steel building, is particularly sensitive to structural modelling assumptions [1],[2], something that have a direct impact on its final design. Traditional modelling practices, such as the widely adopted bare frame centreline approach, have gradually given way to more sophisticated methods mostly inferred by experimental evidence as well as lessons learned from major seismic events. Among these modelling refinements, that of the column base connection has received significant attention due to its critical role in both local (member-level) and global (building-level) seismic response. Modelling of this connection is important in the context of: i) linear seismic (modal response spectrum) analysis, which constitutes the principal analysis method prescribed by modern seismic codes, e.g., EC8 [3], and ii) non-linear seismic analysis, which provides deeper insights into structural behaviour of any building under any seismic motion.

This paper focuses on the inclusion of column base connection modelling as an option within the seismic analysis of realistic 3D steel MRF (moment resisting frame) buildings. More specifically, both linear and non-linear analyses are performed in order to assess the effect of column base connection modelling on some key member- and building-level response indices, such as column bending moments, fundamental periods, and interstorey drift ratios (IDRs). For comparison purposes, three buildings, different in height and essentially in the number of storeys, are studied. This way, one obtains a clear picture about the influence of column base connection modelling on the overall seismic response of a class of steel buildings. It is stressed that modelling of column base-connection is rarely done in practice and one simply relies on assigning a fixed or a pinned column base connection. While broader considerations such as soil-structure interaction and the effects of non-structural elements remain

Copyright © 2025 CroCEE
DOI: https://doi.org/10.5592/CO/3CroCEE.2025.38

outside the scope of this study, the present findings may offer valuable guidance regarding the importance of this modelling aspect in seismic analysis.

2. Model description

Three steel buildings of varying heights (number of storeys), i.e., a 3-storey, a 6-storey, and a 9-storey are employed for the study. Each building consists of five and four moment-resisting frames (MRFs) along the x and y horizontal directions, respectively, as shown in Fig. 1. The orientation of the columns and the span of each frame is common for all three buildings and it is indicatively presented in Fig. 2 for the case of the six-storey building. The grade of steel is S355 for both beams and columns. The beam-column and column base connections are assumed to be rigid, and for each floor, a composite steel/concrete slab with a thickness of 0.14 m is considered. The composite slab is modelled using standard shell elements, providing diaphragmatic action in each floor plane. Gravity loads consist by dead load g_{dead} and live load q_{live}=2.5 kN/m^2. Load g_{dead} is 5.0 kN/m^2 on floors and 3.0 kN/m on walls. The selected beam and column sections are IPE400 and HEM340, respectively. To address lateral buckling, secondary IPE330 beams, pinned to the main IPE400 beams, are placed at intervals of 2.0 m along the x direction of the buildings.

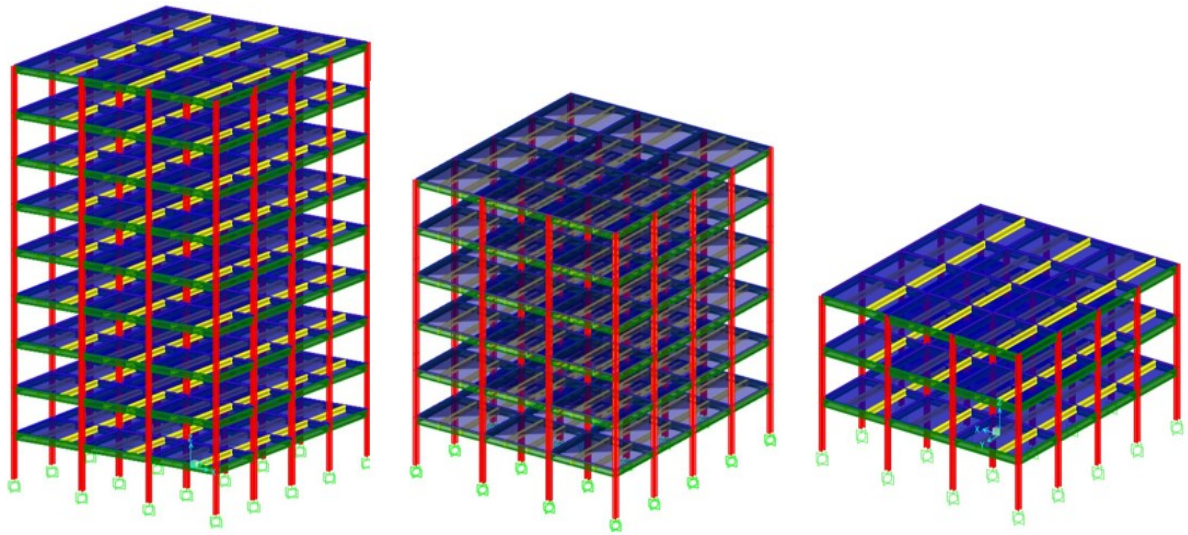


Figure 1. Nine- , six- and three-storey steel buildings (left to right)

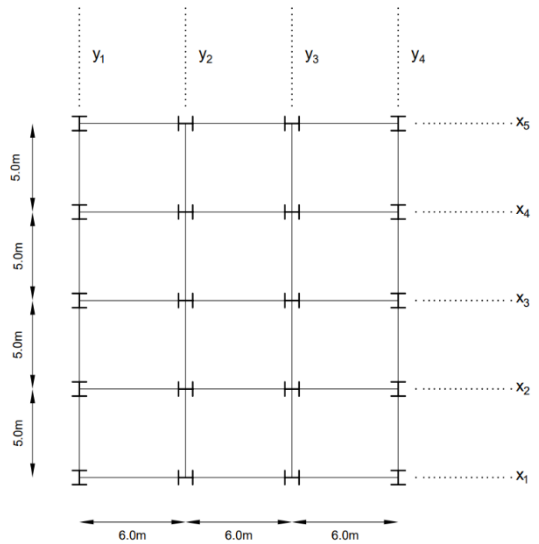


Figure 2. Column orientation along horizontal directions x and y of the steel buildings

Proceedings of the 3rd Croatian Conference on Earthquake Engineering - 3CroCEE
19–22 March 2025, Split, Croatia
Copyright © 2025 CroCEE
DOI: https://doi.org/10.5592/CO/3CroCEE.2025.38

For the linear (modal response spectrum) seismic analysis of the building, the design spectrum of EC8 [3] that corresponds to $a_{gR} = 0.24g$, soil class C, spectrum type 1 is utilized considering an importance factor equal to 1.0 (ordinary building). A value of $q = 4$ for the behavior factor is assumed. Accidental eccentricities of 5% in both horizontal directions are included. For the linear analyses, loading combinations have as follows: $1.35G + 1.5Q$, $G + 0.3Q$, $G + 0.3Q \pm E_x \pm 0.3E_y$ and $G + 0.3Q \pm E_y \pm 0.3E_x$, where E_x, E_y are the seismic loads along directions x and y, respectively. Modal analysis provides the fundamental periods for the 3-storey, 6-storey, and 9-storey buildings, with the first eight modes utilized in modal superposition, satisfying the 90% mass participation requirement of EC8 [3]. The design satisfies EC3 [4] well as the capacity design, inter-storey drift sensitivity coefficient, and damage limitation criteria of EC8 [3], in both directions x and y of the structure.

Then the 3-storey, 6-storey, and 9-storey steel buildings are subjected to non-linear seismic analyses. For the purposes of these analyses, three pairs of seismic motions (accelerograms), appropriately scaled to match the design spectrum of EC8 mentioned above, are utilized.

Several seismic response indices, including maximum interstorey drifts, and bending moments, are derived by both linear and non-linear seismic analyses in order to further discuss the influence of column base connection modelling on the anticipated seismic performance.

A separate comparison of the response indices obtained from the linear and non-linear analyses is presented. This comparison serves in understanding the differences in response results produced by these two analysis methods with respect to column base modelling. While linear analysis provides a simplified approach easily applied in praxis, it cannot capture the real seismic behaviour. Non-linear time-history analysis, on the other hand, having the capability of refined modelling allows for a detailed assessment of the seismic performance of a building. This highlights the importance of conducting non-linear time-history analyses in order to gain deeper insights into the seismic performance of structures, especially when refined modelling assumptions are sought.

3. Column base connection

The column base connection is perhaps the most critical connection of a steel building. Failure of this connection may lead to partial or even complete collapse of the steel building. The rotational stiffness of this connection, i.e., the consideration of a fixed or a pinned connection, affects the seismic response of the steel building. Along the same lines, assigning an erroneous value to the rotational stiffness of this connection, may significantly alter, usually from the non-conservative side, the force and moment demands of the whole building. The rotational stiffness of a column base connection depends essentially on the configuration (base plate, number and placement of anchor rods, vertical stiffeners, footing) and the type (exposed or embedded). A formula that provides the rotational stiffness k_{base} of the column base connection can be found in He et al. [5] and has as follows:

$$k_{base} = \lambda \frac{EI}{L} \tag{1}$$

In Eq.(1), E is the Young's modulus of the material of the steel column, I is the second moment of inertia with respect to the strong axis of the steel column, and L is the height of the steel column, whereas the parameter λ accounts for different k_{base} values. The upper (for a fixed connection) and lower (for a pinned connection) k_{base} value is obtained if $\lambda = 1.67$ and $\lambda = 0.10$ is assumed, respectively. A different procedure to determine k_{base} is summarized in Torres-Rodas et al. [6], however it is not employed herein, in view of the simplicity offered by Eq.(1) in parametric analyses.

On the basis of Eq.(1), the column base connection can be modelled using a rotational spring having a rotational stiffness k_{base}. By varying λ, one may perform seismic analysis for different values of k_{base} in order to investigate their effect on seismic response. The case of not using a rotational spring is indicated as ''Rigid'' in the plots that follow, and essentially corresponds to the analysis of the building described in section 2. The λ values assumed herein are 1.67, 1.50, 1.20, 1.00 and 0.80. The value of $\lambda = 1.67$ provides the maximum rotational stiffness that can be achieved in praxis for a fixed column

Proceedings of the 3rd Croatian Conference on Earthquake Engineering - 3CroCEE
19–22 March 2025, Split, Croatia
Copyright © 2025 CroCEE
DOI: https://doi.org/10.5592/CO/3CroCEE.2025.38

base connection according to He et al. [5], whereas lower λ values represent the case that the actual rotational stiffness of the column base connections is lower than that of the design.

The influence of the rotational stiffness at the column base is examined by considering both the strong and weak axes of the base columns. This consideration acknowledges that the stiffness contribution of the column base can vary significantly between these two axes, depending on the structural design and detailing. The following two cases regarding the assignment of the base rotational stiffness, k_{base}, calculated using Eq. (1), are studied:

- Case 1**:** The rotational stiffness k_{base} is assigned only to the strong axis of the base column, while the weak axis is assumed to be rigid. This case reflects a scenario where the rotational flexibility of the base primarily affects the stronger bending axis of the column, potentially due to construction or design constraints that enhance the rigidity of the weak axis.
- Case 2: The same rotational stiffness value k_{base} is applied to both the strong and weak axes of the base column. This scenario assumes uniform rotational flexibility in both axes, providing a more balanced representation of the behaviour of the base connection.

By exploring these two distinct cases, the study aims to assess how the column base rotational stiffness influences the global and local response of the structure, considering both axes independently. This approach provides insight into whether a simplified assumption (e.g., uniform stiffness for both axes or treating one axis as rigid) is adequate for capturing the structural behavior, or if more detailed modeling is necessary to account for differential stiffness effects between the strong and weak axes. The results of this analysis contribute to understanding the role of base flexibility in the seismic performance of steel building comprised entirely by MRFs.

4. Results

4.1. Modal analysis results

The first three natural periods of the building, corresponding to the various λ values considered, are summarized in Tables 1–6. These results reveal the influence of column base rotational stiffness modelling on the dynamic characteristics of the building.

For the 2 cases mentioned above, it is observed that introducing the rotational stiffness of the column base connection leads to an increase in the fundamental period of the building. This increase can be attributed to the reduced overall stiffness of the building caused by the flexibility at the base connections, which allows greater deformation.

When comparing the periods for the same λ value across the two cases, the differences in periods are relatively small. This suggests that while the additional flexibility of the weak axis in Case 2 slightly influences the dynamic properties, the effect is not pronounced within the range of k_{base} values considered. These findings underscore that while accounting for rotational stiffness is essential for accurately capturing the dynamic behaviour of the building, the distinction between applying stiffness to only the strong axis versus both axes does not significantly alter the global dynamic properties for the studied cases.

Table 1. First three periods (in seconds) - Case 1 - 3-storey building

Mode	*Rigid*	*1.67EI/L*	*1.50EI/L*	*1.20EI/L*	*1.00EI/L*	*0.80EI/L*
1	0.574	0.633	0.636	0.643	0.648	0.655
2	0.569	0.621	0.624	0.630	0.635	0.640
3	0.491	0.553	0.557	0.565	0.571	0.580

Proceedings of the 3rd Croatian Conference on Earthquake Engineering - 3CroCEE
19–22 March 2025, Split, Croatia
Copyright © 2025 CroCEE
DOI: https://doi.org/10.5592/CO/3CroCEE.2025.38

Table 2. First three periods (in seconds) - Case 2 - 3-storey building

Mode	*Rigid*	*1.67EI/L*	*1.50EI/L*	*1.20EI/L*	*1.00EI/L*	*0.80EI/L*
1	0.574	0.652	0.658	0.670	0.681	0.695
2	0.569	0.643	0.648	0.660	0.671	0.685
3	0.491	0.563	0.568	0.579	0.589	0.601

Table 3. First three periods (in seconds) - Case 1 - 6-storey building

Mode	*Rigid*	*1.67EI/L*	*1.50EI/L*	*1.20EI/L*	*1.00EI/L*	*0.80EI/L*
1	1.127	1.188	1.192	1.199	1.205	1.212
2	1.095	1.149	1.152	1.159	1.163	1.170
3	0.965	1.030	1.034	1.043	1.050	1.059

Table 4. First three periods (in seconds) - Case 2 - 6-storey building

Mode	*Rigid*	*1.67EI/L*	*1.50EI/L*	*1.20EI/L*	*1.00EI/L*	*0.80EI/L*
1	1.127	1.209	1.215	1.228	1.240	1.255
2	1.095	1.173	1.178	1.192	1.204	1.219
3	0.965	1.041	1.046	1.059	1.070	1.083

Table 5. First three periods (in seconds) - Case 1 - 9-storey building

Mode	*Rigid*	*1.67EI/L*	*1.50EI/L*	*1.20EI/L*	*1.00EI/L*	*0.80EI/L*
1	1.652	1.712	1.716	1.723	1.729	1.736
2	1.598	1.652	1.655	1.661	1.667	1.673
3	1.410	1.475	1.479	1.488	1.495	1.504

Table 6. First three periods (in seconds) - Case 2 - 9-storey building

Mode	*Rigid*	*1.67EI/L*	*1.50EI/L*	*1.20EI/L*	*1.00EI/L*	*0.80EI/L*
1	1.652	1.733	1.739	1.752	1.764	1.779
2	1.598	1.675	1.681	1.695	1.706	1.722
3	1.410	1.486	1.491	1.504	1.515	1.529

4.2.Interstorey drift (IDR) results

The interstorey drift ratio (IDR) results for the aforementioned two cases of column base rotational stiffness are presented next, comparing outcomes from linear response spectrum analyses and nonlinear time history analyses using three spectrum-compatible accelerograms. These comparisons reveal key insights into the influence of the column base flexibility in conjunction with the analysis method on the IDR values.

For Case 2 (where rotational stiffness is assigned to both the strong and weak axes of the base column), the IDR values are consistently higher than those observed in Case 1 (where rotational stiffness is assigned only to the strong axis, with a rigid assumption for the weak axis). This trend holds true for

Copyright © 2025 CroCEE
DOI: https://doi.org/10.5592/CO/3CroCEE.2025.38

both linear and nonlinear analyses, suggesting that additional flexibility introduced in Case 2 leads to greater deformation across the building height (see Figs. 3-5 for the case of the 9-storey steel building).

A notable observation is that the IDR values obtained from linear response spectrum analyses are higher than those from nonlinear time history analyses for both cases. This indicates that linear analyses may overestimate the IDR, likely due to their reliance on simplified assumptions regarding the seismic demand distribution and seismic displacements induced, whereas nonlinear analyses simulate the realistic dynamic behaviour and the progression of inelastic behaviour under earthquake loading.

Moreover, for both cases and all types of analyses, the IDR value of the 1st story is higher than the one observed in the ‘‘Rigid’’ assumption case, while they tend to converge closer to the ‘‘Rigid’’ case values for the upper floors. This pattern reflects the significant influence of base flexibility at lower stories, which diminishes progressively with height as the global behaviour of the building becomes less dependent on the base conditions.

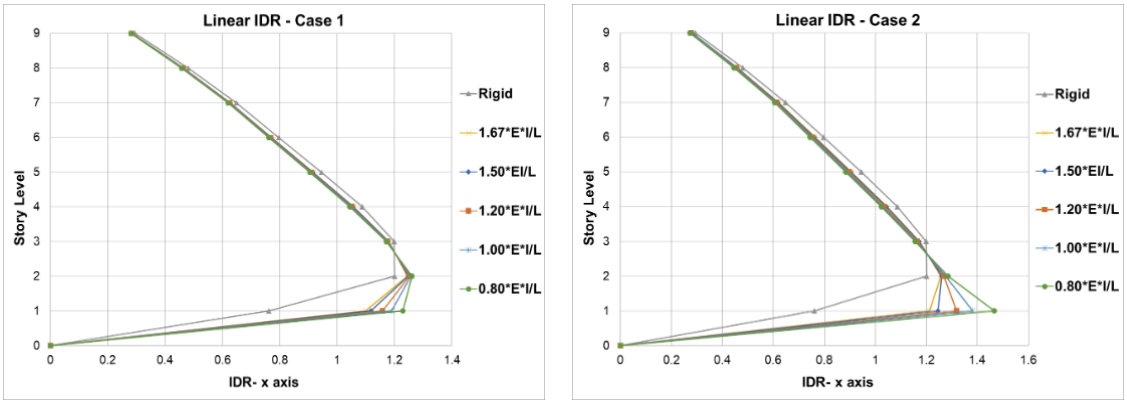


Figure 3. Linear analyses results for the 9-storey building: IDR distribution along direction x for different k_{base} values, Case 1 (left) and Case 2 (right)

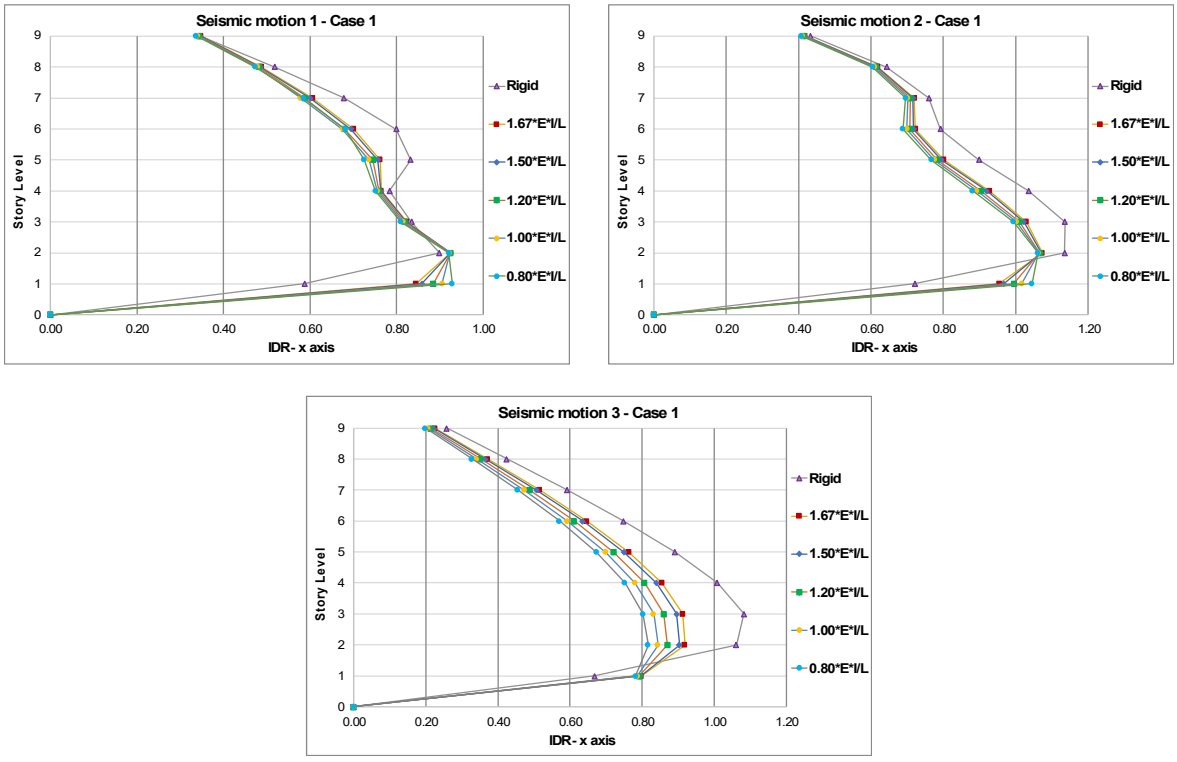


Figure 4. Non-linear analyses results for the 9-storey building: IDR distribution along direction x for different k_{base} values, Case 1

Copyright © 2025 CroCEE
DOI: https://doi.org/10.5592/CO/3CroCEE.2025.38

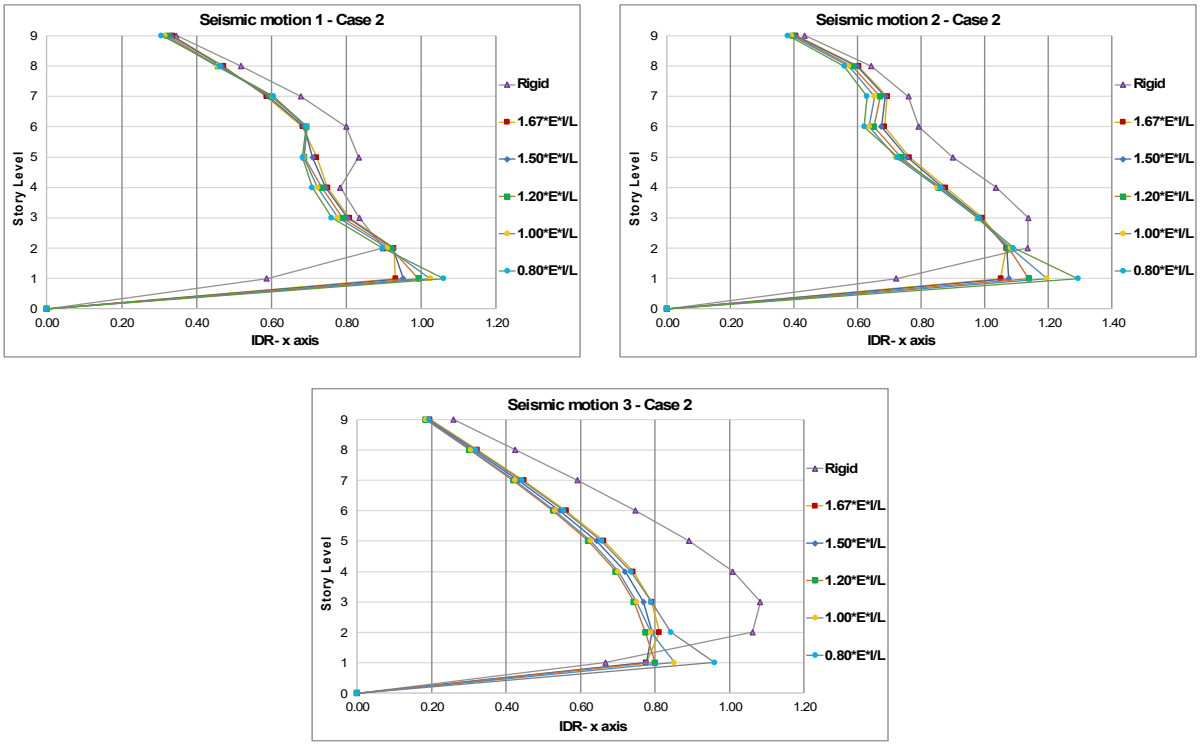


Figure 5. Non-linear analyses results for the 9-storey building: IDR distribution along direction x for different k_{base} values, Case 2

While only the figures for the 9-storey building and the values along the x direction are presented herein, the same observations are identified for the 3-storey and 6-story steel buildings in both horizontal directions, x and y. These results emphasize the importance of considering base flexibility in modelling and demonstrate that nonlinear time history analyses can provide more accurate estimates of interstorey drifts, particularly under flexible base conditions.

4.3. Bending moment results

The bending moments at the base and top of the base column, denoted as M3 (strong axis) and M2 (weak axis), are analysed for the two cases of column base rotational stiffness, presented previously. Comparisons are made between results obtained from linear response spectrum analyses and nonlinear time history analyses using the three spectrum compatible accelerograms, highlighting critical differences in expected behaviour.

The results indicate that for both M3 and M2 bending moments, the bending moments at the base of the most critical base column derived from linear analyses are significantly smaller than those obtained from nonlinear analyses, often underestimating them by, as much as, a factor of four. This stark disparity underscores the limitations of linear analyses in capturing the dynamic inelastic behaviour of the structure under seismic excitation. Nonlinear analyses, which account for material and geometric nonlinearities, provide a more accurate representation of the actual demand on the base columns during earthquakes.

Two notable trends emerge when examining the influence of rotational stiffness on the bending moments:

- Case 1**:** When the rotational stiffness is assigned only to the strong axis (while the weak axis remains rigid), an increase in rotational stiffness leads to a decrease in M3 at the base. This reduction occurs because the greater stiffness along the strong axis redistributes the rotational demands, reducing the bending moment about the strong axis. On the other hand, M2 at the base increases with greater rotational stiffness, indicating an increased demand on this axis.

Copyright © 2025 CroCEE
DOI: https://doi.org/10.5592/CO/3CroCEE.2025.38

This interplay between the axes highlights the sensitivity of bending moment distribution to the modelling assumptions of the base flexibility.

- Case 2: When the rotational stiffness is applied to both the strong and weak axes, increasing the rotational stiffness results in an increase in both M3 and M2 bending moments at the base. This behaviour reflects the overall increase in bending demand as the base flexibility is reduced in both axes, causing the columns to resist greater rotational forces. The simultaneous increase in M3 and M2 bending moments indicates that the flexibility provided by both axes plays a significant role in mitigating bending moment demands at the base.

The remarks above are indicated in the Figs. 6-10, where now the results of the 6-storey steel building are employed for illustration purposes. For the ‘‘Rigid’’ case, the M3 and M2 bending moments at the base, coming from linear analyses, are equal to 320 kNm and 122 kNm, respectively, while for the same indices the values coming from, e.g., the spectrum compatible seismic motion 3, are equal to 1421 kNm and 558 kNm, respectively. A noticeable increase was also identified on the other two seismic motions.

For clarity and ease of interpretation, the remaining results for the 3-storey and the 9-storey steel buildings, are summarized in Tables 7 and 8, rather than being presented as individual figures. Table 7 summarizes the values of the bending moments at the top and the base of the most critical base column for different k_{base} values, along with the percentage difference with the ‘‘Rigid’’ case, allowing for an easy comparison of the influence of base flexibility. Table 8 convey the same information for the 9-storey building. In Tables 7 and 8, a decrease of up to 70% is observed for M3 at the base, when comparing the Rigid base case to the most flexible case (0.80*E*I/L) considered in this paper, for both the 3-storey and 9-storey steel buildings. Moreover, an increase of more than 100% is observed for M3 at the top in Case 2, when comparing the same two limits for rotational stiffness. From the results, Case 2 is presented as the governing one for M3 at the base and the top of the base column and Case 1 as the governing one for M2 at the same locations. Another remark is that for the top of the base column, for both Cases and all seismic motions, the demand is almost always increasing when the rotational stiffness is decreasing.

The results presented in Figures 6-10 and Tables 7 and 8 show the importance of nonlinear time history analyses in providing a more reliable estimation of bending moments under seismic loading, especially in cases where base flexibility and rotational stiffness significantly influence the column response.

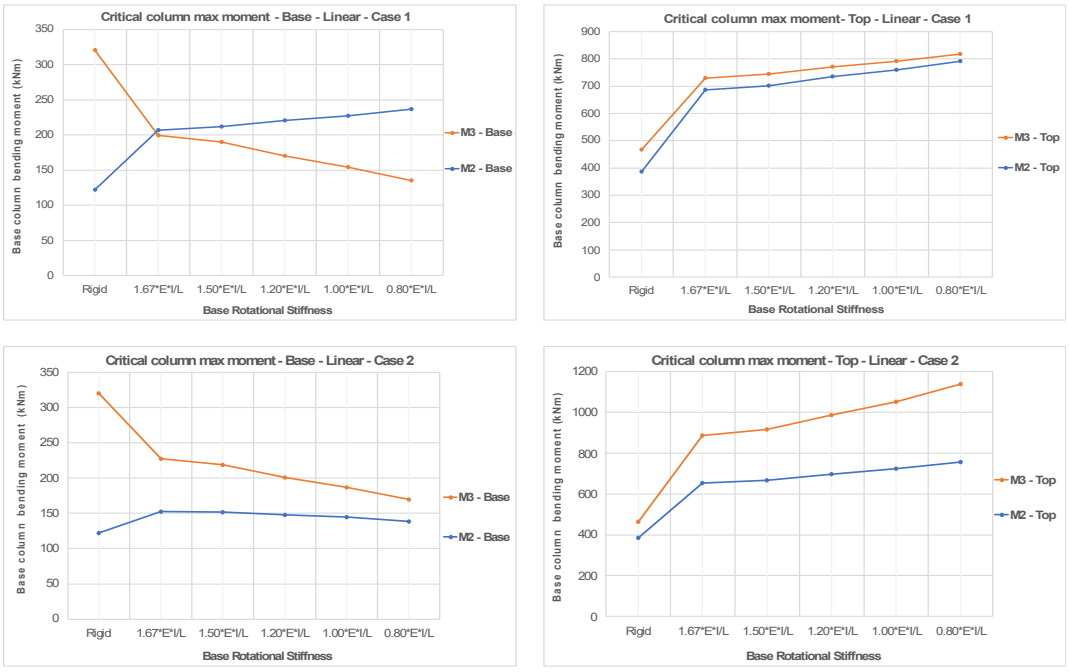


Figure 6. Linear analyses results for the 6-storey building: critical column bending moments for different k_{base} values for Case 1 (top) and Case 2 (bottom)

Proceedings of the 3rd Croatian Conference on Earthquake Engineering - 3CroCEE
19–22 March 2025, Split, Croatia
Copyright © 2025 CroCEE
DOI: https://doi.org/10.5592/CO/3CroCEE.2025.38

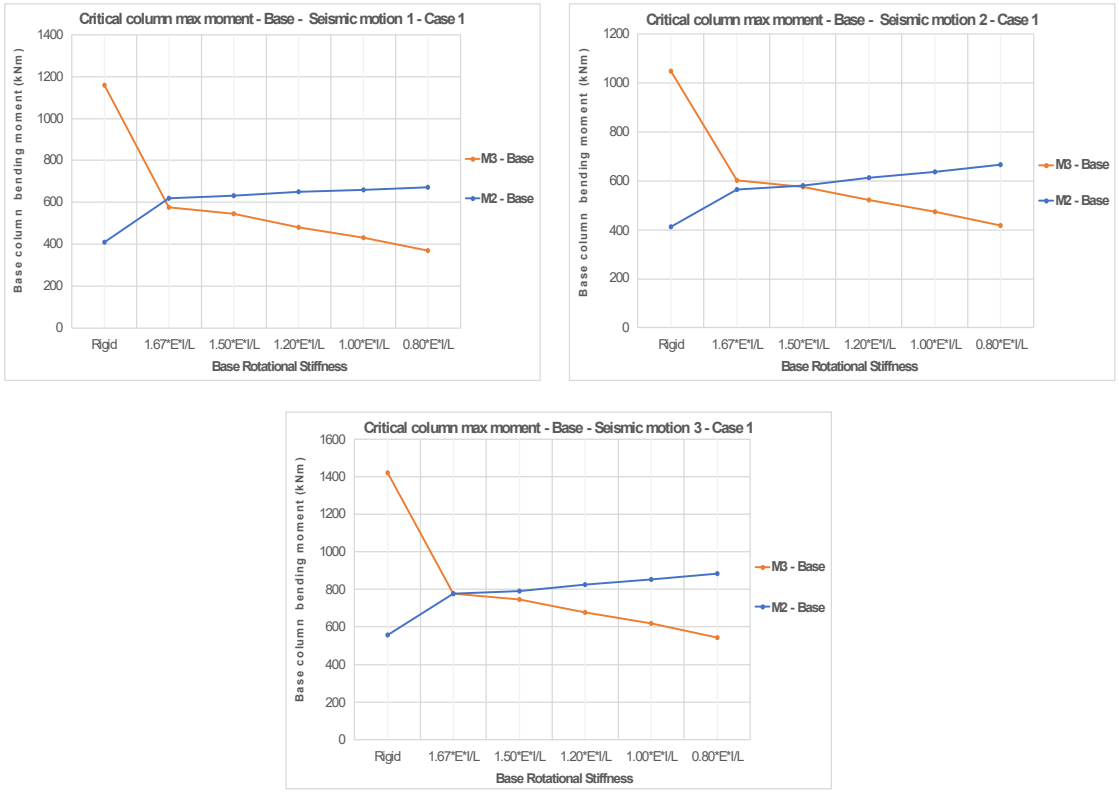


Figure 7. Non-linear analyses results for the 6-storey building: bending moments at the base of the critical column for different k_{base} values, Case 1

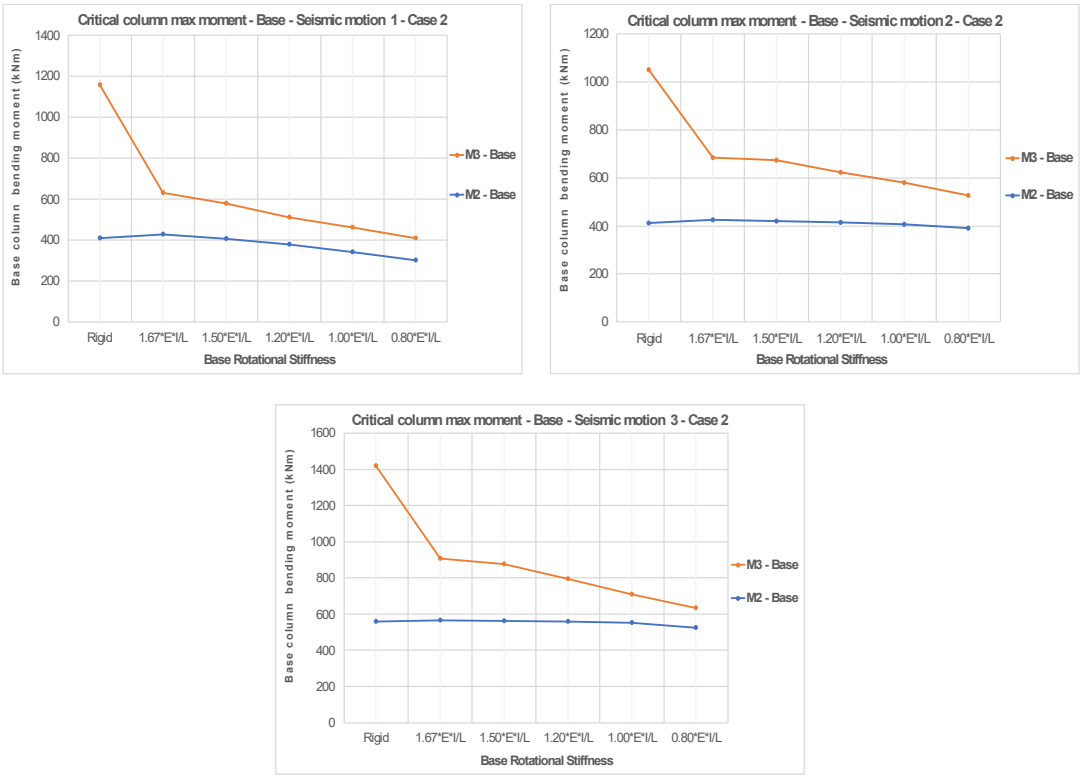


Figure 8. Non-linear analyses results for the 6-storey building: bending moments at the base of the critical column for different k_{base} values, Case 2

Proceedings of the 3rd Croatian Conference on Earthquake Engineering - 3CroCEE
19–22 March 2025, Split, Croatia
Copyright © 2025 CroCEE
DOI: https://doi.org/10.5592/CO/3CroCEE.2025.38

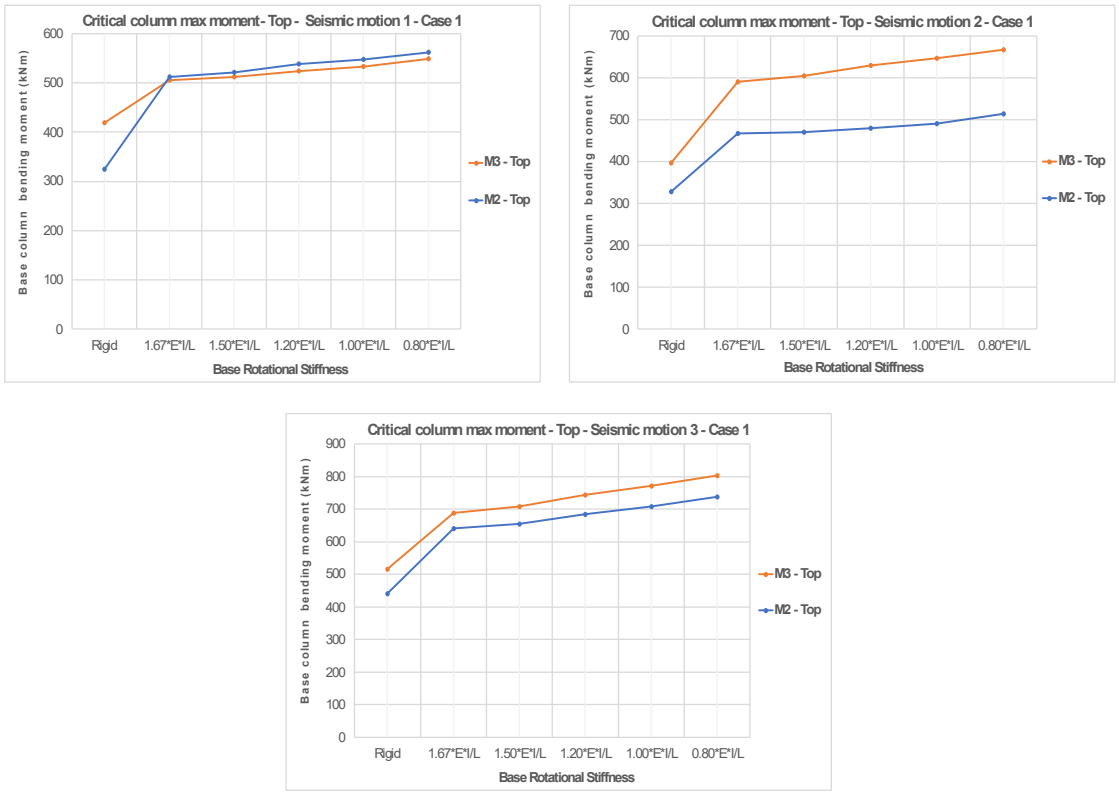


Figure 9. Non-linear analyses results for the 6-storey building - bending moments at the top of the critical column for different k_{base} values, Case 1

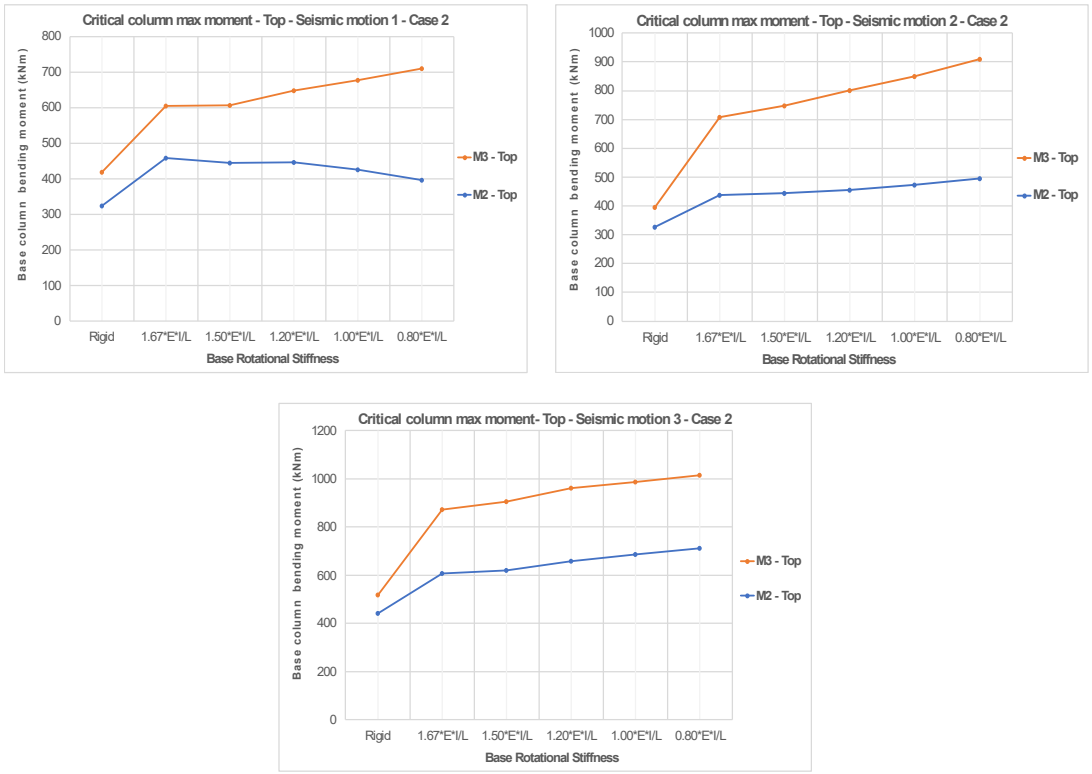


Figure 10. Non-linear analyses results for the 6-storey building - bending moments at the top of the critical column for different k_{base} values, Case 2

Proceedings of the 3rd Croatian Conference on Earthquake Engineering - 3CroCEE
19–22 March 2025, Split, Croatia
Copyright © 2025 CroCEE
DOI: https://doi.org/10.5592/CO/3CroCEE.2025.38

Table 7. Linear and non-linear results for the 3-storey building - Column bending moments (at base and top) for different k_{base} values - % difference from Rigid case

3-storey - Linear	Base Rotational Stiffness										
Base Column Moment (kNm)	*Rigid*	*1.67*E*I/L*	*% Diff.*	*1.50*E*I/L*	*% Diff.*	*1.20*E*I/L*	*% Diff.*	*1.00*E*I/L*	*% Diff.*	*0.80*E*I/L*	*% Diff.*
M3 - Base - Case 1	303.1	165.4	***-45.4***	157.0	***-48.2***	139.4	***-54.0***	125.4	***-58.6***	108.9	***-64.1***
M3 - Base - Case2	303.1	183.1	***-39.6***	175.3	***-42.2***	158.9	***-47.6***	145.4	***-52.0***	129.2	***-57.4***
M2 - Base - Case 1	113.4	170.2	***50.1***	173.1	***52.6***	179.0	***57.8***	183.7	***62.0***	189.2	***66.8***
M2 - Base - Case 2	113.4	120.4	***6.2***	118.7	***4.7***	114.3	***0.8***	109.8	***-3.2***	103.1	***-9.1***
M3 - Top - Case 1	436.4	587.4	***34.6***	594.8	***36.3***	610.0	***39.8***	622.0	***42.5***	635.9	***45.7***
M3 - Top - Case2	436.4	691.0	***58.3***	709.2	***62.5***	749.2	***71.7***	783.7	***79.6***	827.5	***89.6***
M2 - Top - Case 1	329.3	514.6	***56.3***	524.1	***59.2***	543.6	***65.1***	559.1	***69.8***	577.1	***75.3***
M2 - Top - Case 2	329.3	475.8	***44.5***	482.5	***46.5***	495.9	***50.6***	506.2	***53.7***	517.7	***57.2***
3-storey - Seismic motion 1	Base Rotational Stiffness										
Base Column Moment (kNm)	*Rigid*	*1.67*E*I/L*	*% Diff.*	*1.50*E*I/L*	*% Diff.*	*1.20*E*I/L*	*% Diff.*	*1.00*E*I/L*	*% Diff.*	*0.80*E*I/L*	*% Diff.*
M3 - Base - Case 1	1045.8	440.0	***-57.9***	415.2	***-60.3***	364.8	***-65.1***	329.7	***-68.5***	298.5	***-71.5***
M3 - Base - Case2	1045.8	491.9	***-53.0***	489.8	***-53.2***	482.1	***-53.9***	462.8	***-55.7***	419.8	***-59.9***
M2 - Base - Case 1	374.4	473.3	***26.4***	472.0	***26.1***	478.4	***27.8***	489.5	***30.7***	500.3	***33.6***
M2 - Base - Case 2	374.4	317.4	***-15.2***	309.4	***-17.4***	320.5	***-14.4***	326.4	***-12.8***	323.7	***-13.5***
M3 - Top - Case 1	425.3	467.9	***10.0***	463.4	***9.0***	451.3	***6.1***	448.6	***5.5***	458.7	***7.9***
M3 - Top - Case2	425.3	503.7	***18.4***	525.5	***23.6***	593.5	***39.5***	657.7	***54.6***	723.5	***70.1***
M2 - Top - Case 1	285.4	353.5	***23.9***	356.6	***24.9***	360.1	***26.2***	360.1	***26.2***	359.3	***25.9***
M2 - Top - Case 2	285.4	291.2	***2.0***	295.6	***3.6***	327.7	***14.8***	356.1	***24.8***	387.6	***35.8***
3-storey - Seismic motion 2	Base Rotational Stiffness										
Base Column Moment (kNm)	*Rigid*	*1.67*E*I/L*	*% Diff.*	*1.50*E*I/L*	*% Diff.*	*1.20*E*I/L*	*% Diff.*	*1.00*E*I/L*	*% Diff.*	*0.80*E*I/L*	*% Diff.*
M3 - Base - Case 1	1087.2	597.4	***-45.1***	544.8	***-49.9***	500.3	***-54.0***	459.3	***-57.8***	407.2	***-62.5***
M3 - Base - Case2	1087.2	678.3	***-37.6***	659.9	***-39.3***	608.3	***-44.0***	558.1	***-48.7***	490.0	***-54.9***
M2 - Base - Case 1	413.1	642.8	***55.6***	628.6	***52.2***	622.7	***50.7***	626.1	***51.6***	660.5	***59.9***
M2 - Base - Case 2	413.1	426.6	***3.3***	430.8	***4.3***	425.9	***3.1***	415.9	***0.7***	390.5	***-5.5***
M3 - Top - Case 1	446.8	593.9	***32.9***	609.8	***36.5***	642.8	***43.9***	669.9	***49.9***	695.7	***55.7***
M3 - Top - Case2	446.8	747.8	***67.4***	775.6	***73.6***	824.8	***84.6***	857.1	***91.8***	887.6	***98.7***
M2 - Top - Case 1	334.3	536.5	***60.5***	525.6	***57.2***	526.6	***57.5***	530.2	***58.6***	560.5	***67.7***
M2 - Top - Case 2	334.3	454.4	***35.9***	485.1	***45.1***	511.7	***53.1***	529.7	***58.5***	539.4	***61.4***
3-storey - Seismic motion 3	Base Rotational Stiffness										
Base Column Moment (kNm)	*Rigid*	*1.67*E*I/L*	*% Diff.*	*1.50*E*I/L*	*% Diff.*	*1.20*E*I/L*	*% Diff.*	*1.00*E*I/L*	*% Diff.*	*0.80*E*I/L*	*% Diff.*
M3 - Base - Case 1	1276.9	648.1	***-49.2***	612.8	***-52.0***	540.9	***-57.6***	483.9	***-62.1***	417.9	***-67.3***
M3 - Base - Case2	1276.9	704.5	***-44.8***	671.3	***-47.4***	601.9	***-52.9***	554.5	***-56.6***	501.7	***-60.7***
M2 - Base - Case 1	472.6	663.8	***40.5***	673.4	***42.5***	693.6	***46.8***	709.6	***50.1***	728.2	***54.1***
M2 - Base - Case 2	472.6	464.3	***-1.8***	456.3	***-3.4***	436.7	***-7.6***	422.4	***-10.6***	403.3	***-14.7***
M3 - Top - Case 1	525.7	637.5	***21.3***	642.5	***22.2***	652.6	***24.1***	660.9	***25.7***	670.7	***27.6***
M3 - Top - Case2	525.7	731.3	***39.1***	746.0	***41.9***	777.7	***47.9***	822.2	***56.4***	879.8	***67.4***
M2 - Top - Case 1	380.1	553.5	***45.6***	562.3	***47.9***	580.8	***52.8***	595.5	***56.7***	612.5	***61.1***
M2 - Top - Case 2	380.1	503.8	***32.5***	509.3	***34.0***	520.1	***36.8***	536.4	***41.1***	556.7	***46.5***

Table 8. Linear and non-linear results 9-storey building - Column bending moments (at base and top) for different k_{base} values - % difference from Rigid case

9-storey - Linear	Base Rotational Stiffness										
Base Column Moment (kNm)	*Rigid*	*1.67*E*I/L*	*% Diff.*	*1.50*E*I/L*	*% Diff.*	*1.20*E*I/L*	*% Diff.*	*1.00*E*I/L*	*% Diff.*	*0.80*E*I/L*	*% Diff.*
M3 - Base - Case 1	373.2	217.1	***-41.8***	207.3	***-44.5***	186.4	***-50.1***	169.4	***-54.6***	148.9	***-60.1***
M3 - Base - Case2	373.2	249.1	***-33.3***	241.0	***-35.4***	223.8	***-40.0***	209.4	***-43.9***	191.8	***-48.6***
M2 - Base - Case 1	145.6	229.1	***57.3***	234.2	***60.9***	245.0	***68.3***	253.8	***74.3***	264.3	***81.5***
M2 - Base - Case 2	145.6	167.9	***15.3***	167.2	***14.8***	164.8	***13.2***	161.6	***11.0***	156.2	***7.3***
M3 - Top - Case 1	448.5	660.1	***47.2***	673.2	***50.1***	700.8	***56.3***	723.3	***61.3***	750.2	***67.3***
M3 - Top - Case2	448.5	817.5	***82.3***	850.1	***89.5***	924.6	***106.2***	992.1	***121.2***	1085.1	***141.9***
M2 - Top - Case 1	393.6	648.8	***64.8***	664.5	***68.8***	697.6	***77.2***	724.6	***84.1***	756.8	***92.3***
M2 - Top - Case 2	393.6	620.5	***57.6***	635.9	***61.6***	669.4	***70.1***	698.0	***77.3***	734.5	***86.6***
9-storey - Seismic motion 1	Base Rotational Stiffness										
Base Column Moment (kNm)	*Rigid*	*1.67*E*I/L*	*% Diff.*	*1.50*E*I/L*	*% Diff.*	*1.20*E*I/L*	*% Diff.*	*1.00*E*I/L*	*% Diff.*	*0.80*E*I/L*	*% Diff.*
M3 - Base - Case 1	986.5	526.6	***-46.6***	499.0	***-49.4***	441.7	***-55.2***	396.0	***-59.9***	345.3	***-65.0***
M3 - Base - Case2	986.5	588.4	***-40.4***	566.4	***-42.6***	531.1	***-46.2***	496.9	***-49.6***	450.4	***-54.3***
M2 - Base - Case 1	386.7	570.2	***47.5***	579.5	***49.9***	598.6	***54.8***	613.2	***58.6***	629.7	***62.8***
M2 - Base - Case 2	386.7	397.4	***2.8***	390.1	***0.9***	370.8	***-4.1***	351.4	***-9.1***	336.3	***-13.0***
M3 - Top - Case 1	370.0	468.1	***26.5***	474.1	***28.1***	486.1	***31.4***	509.1	***37.6***	535.8	***44.8***
M3 - Top - Case2	370.0	578.3	***56.3***	607.6	***64.2***	668.9	***80.8***	719.6	***94.5***	781.5	***111.2***
M2 - Top - Case 1	306.7	472.4	***54.0***	481.0	***56.8***	498.4	***62.5***	511.7	***66.8***	526.8	***71.8***
M2 - Top - Case 2	306.7	432.1	***40.9***	436.5	***42.3***	443.6	***44.6***	447.4	***45.9***	449.5	***46.6***
9-storey - Seismic motion 2	Base Rotational Stiffness										
Base Column Moment (kNm)	*Rigid*	*1.67*E*I/L*	*% Diff.*	*1.50*E*I/L*	*% Diff.*	*1.20*E*I/L*	*% Diff.*	*1.00*E*I/L*	*% Diff.*	*0.80*E*I/L*	*% Diff.*
M3 - Base - Case 1	1211.7	599.7	***-50.5***	570.1	***-53.0***	511.6	***-57.8***	465.3	***-61.6***	408.7	***-66.3***
M3 - Base - Case2	1211.7	689.1	***-43.1***	667.3	***-44.9***	617.6	***-49.0***	572.1	***-52.8***	515.8	***-57.4***
M2 - Base - Case 1	475.2	643.5	***35.4***	652.8	***37.4***	673.1	***41.6***	689.5	***45.1***	709.2	***49.2***
M2 - Base - Case 2	475.2	448.5	***-5.6***	441.6	***-7.1***	425.9	***-10.4***	410.7	***-13.6***	395.2	***-16.8***
M3 - Top - Case 1	418.9	538.3	***28.5***	550.4	***31.4***	574.6	***37.2***	594.3	***41.9***	616.0	***47.1***
M3 - Top - Case2	418.9	670.2	***60.0***	697.0	***66.4***	753.9	***80.0***	802.1	***91.5***	871.4	***108.0***
M2 - Top - Case 1	375.1	531.1	***41.6***	539.7	***43.9***	558.4	***48.9***	573.5	***52.9***	591.4	***57.7***
M2 - Top - Case 2	375.1	485.6	***29.5***	492.2	***31.2***	507.4	***35.3***	522.6	***39.3***	548.7	***46.3***
9-storey - Seismic motion 3	Base Rotational Stiffness										
Base Column Moment (kNm)	*Rigid*	*1.67*E*I/L*	*% Diff.*	*1.50*E*I/L*	*% Diff.*	*1.20*E*I/L*	*% Diff.*	*1.00*E*I/L*	*% Diff.*	*0.80*E*I/L*	*% Diff.*
M3 - Base - Case 1	1349.3	753.5	***-44.2***	715.8	***-47.0***	637.2	***-52.8***	573.9	***-57.5***	499.2	***-63.0***
M3 - Base - Case2	1349.3	845.5	***-37.3***	812.3	***-39.8***	741.9	***-45.0***	683.5	***-49.3***	611.7	***-54.7***
M2 - Base - Case 1	520.5	745.8	***43.3***	758.8	***45.8***	785.7	***51.0***	806.6	***55.0***	830.1	***59.5***
M2 - Base - Case 2	520.5	525.0	***0.9***	516.8	***-0.7***	506.9	***-2.6***	494.6	***-5.0***	473.8	***-9.0***
M3 - Top - Case 1	515.2	704.8	***36.8***	715.9	***39.0***	739.3	***43.5***	758.0	***47.1***	780.0	***51.4***
M3 - Top - Case2	515.2	849.3	***64.8***	876.9	***70.2***	938.4	***82.1***	992.2	***92.6***	1061.1	***106.0***
M2 - Top - Case 1	409.8	614.1	***49.9***	625.9	***52.7***	650.3	***58.7***	669.2	***63.3***	690.4	***68.5***
M2 - Top - Case 2	409.8	566.9	***38.3***	580.4	***41.6***	609.1	***48.6***	632.9	***54.4***	661.7	***61.5***

Copyright © 2025 CroCEE
DOI: https://doi.org/10.5592/CO/3CroCEE.2025.38

5. Conclusions

This study highlights the critical role of column base rotational stiffness in the seismic response of steel moment-resisting frame (MRF) buildings. By examining the numerical results derived by linear and nonlinear seismic analyses, it is demonstrated that modelling assumptions at the base connection significantly influence key response indices, including interstorey drift ratios (IDRs) and bending moments. Two distinct cases are examined herein: in the first one the variation of the rotational stiffness is applied only to the strong axis (Case 1) and in the second one by applying the same rotational stiffness to both the strong and weak axes (Case 2). The results reveal that Case 2 generally produces larger IDRs and bending moments compared to Case 1, underlining the impact of weak axis flexibility on the response.

Moreover, the study illustrates the limitations of linear response spectrum analyses in estimating seismic demands, as they overestimate IDRs and underestimate bending moments compared to those found by the arguably accurate nonlinear time-history analyses.

The findings of this study underscore the necessity of refined modelling approaches for column base connections, particularly for cases where rotational stiffness significantly influences seismic performance. By assigning different values to the rotational stiffness and by comparing the results for three different buildings, this study provides some insights with respect to the improvement of seismic analysis and design of steel MRFs.

6. References

[1] Swensen D.J., Kunnath S.K. (2018): Consequences of modelling choices in seismic performance assessment of buildings, *Earthquake Spectra*, 34(2): 423-440.

[2] Papamichelakis M., Papagiannopoulos G. (2024): On the effect of modelling in evaluating the seismic response of a steel MRF building, *Proceedings of the 18th World Conference on Earthquake Engineering*, Milan, Italy.

[3] EC8 (2004). *Eurocode 8. Design of Structures for Earthquake Resistance*, Part 1: General Rules, Seismic Actions and Rules for Buildings, EN 1998-1-1, European Committee for Standardization (CEN), Brussels, Belgium.

[4] EC3 (2009). *Eurocode 3. Design of Steel Structures – Part 1-1: General Rules and Rules for Buildings*, EN 1993-1-1, European Committee for Standardization (CEN), Brussels, Belgium.

[5] He J.C.W., Clifton G.C., Ramhormozian S. (2021): Determining the realistic rotational stiffness of column base connections in steel seismic resisting systems, *Proceedings of the 2021 New Zealand Society for Earthquake Engineering Annual Technical Conference*, Christchurch, New Zealand.

[6] Torres-Rodas P., Zareian F., Kanvinde A. (2018): Seismic demands in column base connections of steel moment frames, *Earthquake Spectra*, 34(3): 1383-1403.

Proceedings of the 3rd Croatian Conference on Earthquake Engineering - 3CroCEE
19–22 March 2025, Split, Croatia
Copyright © 2025 CroCEE
DOI: https://doi.org/10.5592/CO/3CroCEE.2025.46

RESPONSE OF THE BUILDING IN AGGREGATES ACCORDING TO THE INTERCONNECTED DIFFERENT PARAMETERS

Maja Mrkonjić [(1)], Josip Atalić [(2)]

[(1)] *Professional associate, Faculty of civil engineering in Zagreb, maja.mrkonjic@grad.unizg.hr*
[(2)] *Associate professor, Faculty of civil engineering in Zagreb, josip.atalic@grad.unizg.hr*

Keywords: earthquake, masonry building aggregates, parameters, vulnerability level

1. Introduction

On March 22, 2020, Zagreb, Croatia, was struck by a devastating earthquake, severely damaging many buildings, particularly those in the city center built during the Austro-Hungarian period (19th century). Standalone family homes near the epicenter also suffered significant damage.

2. Research Objective and Database as an Information Source

The aim of the research is to conclude how the response of a building in aggregate is influenced by neighboring buildings, considering their interconnection (shared or separate gable walls) and the different or identical arrangement of various parameters.

Following the earthquake, volunteer engineers conducted rapid inspections, leading to a crucial database with over 25,000 damage assessments. This database provides essential data for analyzing building damage and usability. It is based on ArcGIS – a Geographic Information System (GIS), a software tools for collecting, managing, analyzing, and visualizing spatial data, developed by the company Esri (Environmental Systems Research Institute).

3. The First Phase of Systematization

Donji Grad, the observed area, spans 3.50 km² of Zagreb. It is bordered by Ulica Republike Austrije to the west, Ulica Vjekoslava Heinzela to the east, Ilica to the north, and a railway line to the south. This district, consisting of 168 blocks composed of buildings in aggregates [1]: Fig. 1 a). Due to damage reports (2,059 buildings out of 6,396) [2] following the earthquake, nearly 3,000 rapid inspections were conducted in this area: Fig. 1 b). Systematization began with Block 19, as existing data [3] enabled a comparative study. This block includes 35 buildings in aggregate. A total of 58 inspections (41 buildings including those in courtyard) were conducted in this block after the Zagreb earthquake (March 2020), with eight additional inspections following the Petrinja earthquake (December 2020).

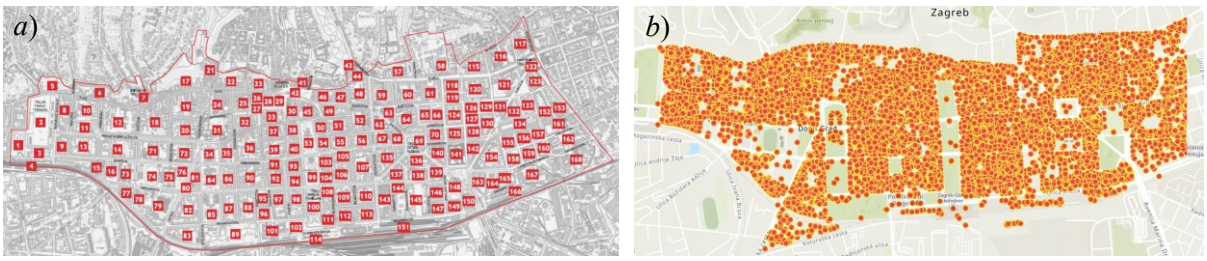


Figure 1. Donji grad a) Block index; b) ArcGIS map showing inspected buildings.

Copyright © 2025 CroCEE
DOI: https://doi.org/10.5592/CO/3CroCEE.2025.46

4. Conclusion

One approach to assessing building vulnerability is the empirical method, which involves analyzing statistical data gathered from damage assessments conducted after earthquake. The goal of this research is to process the collected information (attributes) and adapt it to the available parameters following the methodologies of [4] and [5]. The obtained results will be evaluated based on the criterion of recorded damage.

This paper analyzes the aforementioned parameters and draws conclusions regarding the vulnerability level caused by the same factors. The parameters observed were assigned a certain (different) number of interpolated subcategories: attributes of the structural typology (4), number of storeys (8), height ratio of adjacent buildings (6), floor plan (2) and vertical irregularities (2), height position of the ceiling structure of adjacent buildings (3), and openings arrangement (5). However, the subcategories value is interpolated to compensate those different number for individual attributes. The exception was the typology attribute that was assigned a higher value. The results: Fig. 2 were compared with the position of the building in aggregate (plan interaction classes) and with the detailed inspection conclusions (usability) after the earthquake.

ZGRADA	IME	ULICA	UPORABLJIVOST	POLOŽAJ U BLOKU/NIZU	TIPOLOGIJA	KATNOST	ODNOS VISINA SUSJEDNIH ZGRADA	TLOCRTNA NEPRAVILNOST	VERTIKALNA NEPRAVILNOST	VISINSKI POLOŽAJ STROPNE KONSTRUKCIJE SUSJEDNIH ZGR.	POLOŽAJ I RASPORED OTVORA	ZBROJ OCJENA	PONDIRANA OCJENA
14	Zgrada Zemaljskog	Dalmatinska 12	PN2	U BLOKU	1,00	0,43	1,00	1,00	0,00	1,00	1,00	5,43	0,84
23	Kuća Rossipal	Medulićeva 3	PN2	U BLOKU	1,00	0,43	1,00	1,00	0,00	0,50	0,75	4,68	0,75
7	Dramsko kaz. Gavella	Frankopanska 10	N1	U BLOKU	1,00	0,29	0,33	1,00	1,00	1,00	1,00	5,62	0,75
6	Kuća Kaufmann	Frankopanska 8	PN2	U BLOKU	1,00	0,29	1,00	1,00	1,00	0,50	0,50	5,29	0,75
1	Kuća Honigsberg	Frankopanska 2 / Ilica 41	PN2	UGLOVNICA	1,00	0,43	1,00	1,00	1,00	0,50	0,00	4,93	0,70
25	Kuća Rath	Ilica 55	N2	U BLOKU	1,00	0,29	0,00	1,00	1,00	1,00	1,00	5,29	0,69
3	Kuća Jeršić	Frankopanska 2b	PN2	U BLOKU	1,00	0,29	0,33	0,00	1,00	1,00	1,00	4,62	0,69
2	Kuća Zimmermann	Frankopanska 2a	PN2	U BLOKU	1,00	0,29	0,67	1,00	1,00	0,50	0,50	4,95	0,69
33	Kuća Pelić s tjelarnom K Sveton	Ilica 43	U2	U BLOKU	1,00	0,43	0,00	1,00	1,00	1,00	0,75	5,18	0,68
8	Kuća Hribar-Penić	Frankopanska 12	U2	U BLOKU	1,00	0,29	0,67	0,00	1,00	0,50	0,75	4,20	0,67
11	Kuća Benger	Dalmatinska 6	U2	NA KRAJU NIZA	1,00	0,43	0,00	1,00	0,00	1,00	1,00	4,43	0,66
12	Kuća Kosirnik	Dalmatinska 8	U2	U BLOKU	1,00	0,43	0,67	1,00	0,00	0,50	0,50	4,10	0,66
35	Kuća Friedmann – Švarc	Ilica 41a	U2	U BLOKU	1,00	0,43	0,67	0,00	1,00	0,50	0,50	4,10	0,66
24	Kuća Rossipal	Medulićeva 1 / Ilica 57	N2	UGLOVNICA	1,00	0,29	0,00	1,00	1,00	1,00	0,75	5,04	0,65
34	Radionica i skladište bolničnog rublja	Ilica 43/1 (dvorište)	U2	NA KRAJU NIZA	1,00	0,29	0,00	1,00	0,00	1,00	1,00	4,29	0,63
19	Kuće Grahor	Medulićeva 11–13	PN1	U BLOKU	1,00	0,29	0,67	1,00	0,00	0,50	0,50	3,95	0,63
4	Kuća Schneider	Frankopanska 4	U2	U BLOKU	1,00	0,29	0,00	1,00	1,00	0,50	0,75	4,54	0,61
5	Kuća Uhrl	Frankopanska 6	N1	U BLOKU	1,00	0,29	0,00	1,00	1,00	0,50	0,75	4,54	0,61
9	Kuća Pavelić	Frankopanska 14 / Dalmatinska 2	PN2	UGLOVNICA	1,00	0,43	0,00	1,00	1,00	0,50	0,50	4,43	0,60
16	Kuća Petrko	Dalmatinska 14	U1	U BLOKU	1,00	0,43	0,33	1,00	0,00	0,50	0,50	3,76	0,60
20	Kuća Deutsch	Medulićeva 9	PN2	U BLOKU	1,00	0,43	0,33	1,00	0,00	0,50	0,50	3,76	0,60
10	El.strojarska radionica	Dalmatinska 4	0	NA KRAJU NIZA	1,00	0,00	0,33	0,00	0,00	1,00	1,00	3,33	0,58
32	Hotel »Park 45« (danas)	Ilica 45	0	U BLOKU	1,00	0,29	0,00	1,00	1,00	0,50	0,50	4,29	0,57
17	Kuća Smodek	Dalmatinska 16	U2	U BLOKU	1,00	0,43	1,00	0,00	0,00	0,00	0,00	2,43	0,54
26	Trgovačkoobrtnički zavod Rudolfa Mosingera	Ilica 55/3 (dvorište)	PN1	DVORIŠNA ZGRADA U BLOKU S ANEKSIMA	1,00	0,14	0,33	1,00	1,00	0,00	0,25	3,73	0,52
18	Kuća Grahor	Dalmatinska 18	PN1	UGLOVNICA	1,00	0,43	0,33	1,00	0,00	0,00	0,25	3,01	0,51
13	Kuća Spevec	Dalmatinska 10	PN2	U BLOKU	1,00	0,29	0,33	0,00	0,00	0,50	0,50	2,62	0,51
27	Kuća Honigsberg	Ilica 51–53–53a	PN2	U BLOKU	1,00	0,29	0,33	1,00	1,00	0,00	0,00	3,62	0,51
22	Kuća Šašel nakon rekonstrukcije obrtnika	Medulićeva 5	U2	U BLOKU	1,00	0,29	0,33	1,00	0,00	0,00	0,25	2,87	0,49
29		Ilica 49	U2	U BLOKU	0,00	1,00	0,33	1,00	1,00	0,50	0,50	4,33	0,48
31	Kuća Vulaković	Ilica 47/2 (dvorišna zgrada)	PN1	U BLOKU	1,00	0,43	0,00	1,00	1,00	0,00	0,00	3,43	0,48
30	Kuća Angerer	Ilica 47	N2	U BLOKU	1,00	0,29	0,00	1,00	1,00	0,00	0,00	3,29	0,45
8a	Tiskara - Studij dizajna	Frankopanska 12 (dvorište)		U BLOKU	1,00	0,29	0,33	1,00	0,00	0,00	0,00	2,62	0,45
21	Kuća Balaško	Medulićeva 7	PN2	U BLOKU	1,00	0,29	0,33	0,00	0,00	0,00	0,00	1,62	0,39

Figure 2. Block 19 buildings ranking following analysis.

References

[1] Kiš-Bonačić, K., Žic, D., Bubrić, M., Franjek, I. (2009): Donji grad, Katalog – blokovi, Zavod za prostorno uređenje Grada Zagreba. ZAVOD ZA PROSTORNO UREĐENJE GRADA ZAGREBA, Zagreb, Hrvatska

[2] UHS, GF, HCPI, GDi: Priprema materijala Gradski ured za strategijsko planiranje i razvoj Grada, 3.2021., Potres Zagreb 2020 (accessed January 10, 2025).

[3] Belamarić, J., Bjažić Klarin, T., Damjanović, D., Dundović, B., Horvat-Levaj, K. Horvatinčić, S. Kolešnik, Lj., Kraševac, I. Križić Roban, S., Mance, I., Premerl, D., Šverko, A., Vučetić, R., Želić, D., Žmegač, A. (2021): *Program cjelovite obnove povijesne jezgre Grada Zagreba : Blok 19 - konzervatorski model*, Institut za povijest umjetnosti, Zagreb, Hrvatska.

[4] Benedetti, D. & Petrini, V. 1984. On the seismic vulnerability of masonry buildings: an evaluation method (in Italian), *L'Industria delle Costruzioni* 149: 66-74.

[5] Formisano, A., Florio, G., Landolfo, R., Mazzolani, F. M. (2015): Numerical calibration of an easy method for seismic behaviour assessment on large scale of masonry building aggregates. *Advances in Engineering Software*, 80, 116-138, doi: https://doi.org/10.1016/j.advengsoft.2014.09.013

Proceedings of the 3rd Croatian Conference on Earthquake Engineering - 3CroCEE
19–22 March 2025, Split, Croatia
Copyright © 2025 CroCEE
DOI: https://doi.org/10.5592/CO/3CroCEE.2025.49

OVERVIEW OF THE DEVELOPMENT, APPLICATION AND CHALLENGES OF NATURAL FIBER REINFORCED CEMENTITIOUS MATRIX (NFRCM)

Mario Žigo [(1)], Marina Nikolić [(2)], Marija Smilović Zulim [(3)], Nikola Grgić [(4)]

[(1)] *Teaching and Research Assistant, University of Split (Faculty of Civil Engineering, Architecture and Geodesy), mzigo@gradst.hr*
[(2)] *Assistant Professor, University of Split (Faculty of Civil Engineering, Architecture and Geodesy), msunara@gradst.hr*
[(3)] *Associate Professor, University of Split (Faculty of Civil Engineering, Architecture and Geodesy), msmilovi@gradst.hr*
[(4)] *Associate Professor, University of Split (Faculty of Civil Engineering, Architecture and Geodesy), ngrgic@gradst.hr*

Abstract

Technological development in construction has brought significant advances in the application of materials, particularly composites such as fiber-reinforced polymers (FRP) and textile-reinforced concrete (TRC). These materials are widely used due to their excellent mechanical properties, including high strength and low weight, making them suitable for the refurbishment of damaged structures and the development of new building systems. However, they face challenges such as instability at high temperatures, which can lead to their degradation. In addition, the production of FRP and TRC often involves chemical processes that can have harmful effects on the environment and human health, raising questions about their sustainability and environmental impact.

In response to these challenges, current research is focusing on the development of natural composites, in particular the Natural Fiber Reinforced Cementitious Matrix (NFRCM). These composites use natural fibers as reinforcement in cementitious matrices, reducing the environmental impact while maintaining similar mechanical properties to conventional materials. NFRCMs represent a sustainable alternative to chemically produced materials, and their application can significantly reduce the impact of the construction industry's impact on the environment and human health.

This review aims to synthesize existing knowledge on NFRCMs, evaluate their advantages and limitations relative to conventional composites, and critically examine current research in the field. Particular attention is given to the challenges associated with the development of new matrices based on natural materials, including the evaluation of their mechanical properties and durability. The paper provides an overview of current materials and reinforcement processes using natural fibers, identifies key areas requiring further research and improvement, and offers guidelines for future research and development activities.

Keywords: NFRCM, TRM, FRP, Natural composites, Mechanical properties, Strengthening, Bridging, Ecological

1. Introduction

The development of society brings with it an ecological awareness and the need for sustainable development. Integrating sustainability principles into all sectors, particularly construction, is essential for future advancements. Extending the service life of buildings is one of the most pressing challenges for sustainability in construction, with the potential to prolong the usefulness of both new and historic structures. As a rule, retrofitting and reconstruction must be in line with conservation guidelines and environmental standards.

Many residential areas worldwide are located in seismically active areas. Table 1 shows the earthquakes in Croatia, highlighting the region's seismic activity [1]. Considering the fact that seismic activity can lead to disasters, as was the case in Turkey and Syria in 2023, Japan in 2011, Haiti in 2010, etc., new buildings need to be built according to modern standards. Additionally, inspections and retrofitting of existing buildings are necessary. Most historic buildings were built of natural stone or

Copyright © 2025 CroCEE
DOI: https://doi.org/10.5592/CO/3CroCEE.2025.49

brick, usually without strong mortars or similar binders. However, due to architectural features such as arches, thick walls, and small openings, many of these historic structures are still in use today. Extensive research has focused on retrofitting historic buildings, as detailed in [2–7], with Fig. 1 showing a clear upward trend in publications on masonry strengthening from 2000 to 2023. Over the past four decades, this research has led to the development of numerous principles and materials for structural retrofitting, including micro-reinforced mortars, meshes, fibers, and various composite solutions.

Table 1. The strongest earthquakes in Croatia from the 17th century to 2021 [1]

Date	City	Magnitude (M_L)	Intensity (°MCS)
April 6th 1667.	Dubrovnik		IX-X
November 9th 1880.	Zagreb		VIII
July 2nd 1898.	Trilj		IX
October 8th 1909.	Pokuplje	5.8	VIII
March 12th 1916.	Vinodol	5.8	VIII
March 27th 1938.	Novigrad Podravski	5.6	VIII
December 29th 1942.	Imotski	6.2	VIII-IX
January 11th 1962.	Makarska	6.1	VIII-IX
April 13th 1964.	Dilj Gora	5.7	VIII
September 5th 1996.	Ston-Slano	6.0	VIII
March 22nd 2020.	Zagreb	5.5	VII
December 29th 2020.	Petrinja	6.2	VIII

Reinforcement techniques remain crucial to advancements in construction, necessitating ongoing research to develop innovative concepts and broaden their practical applications.

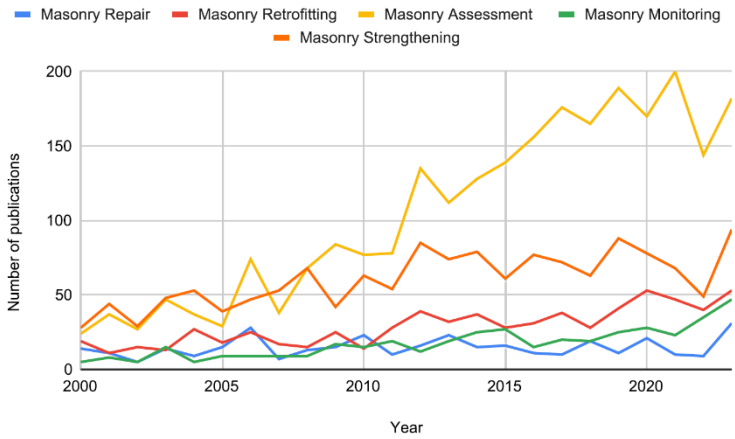


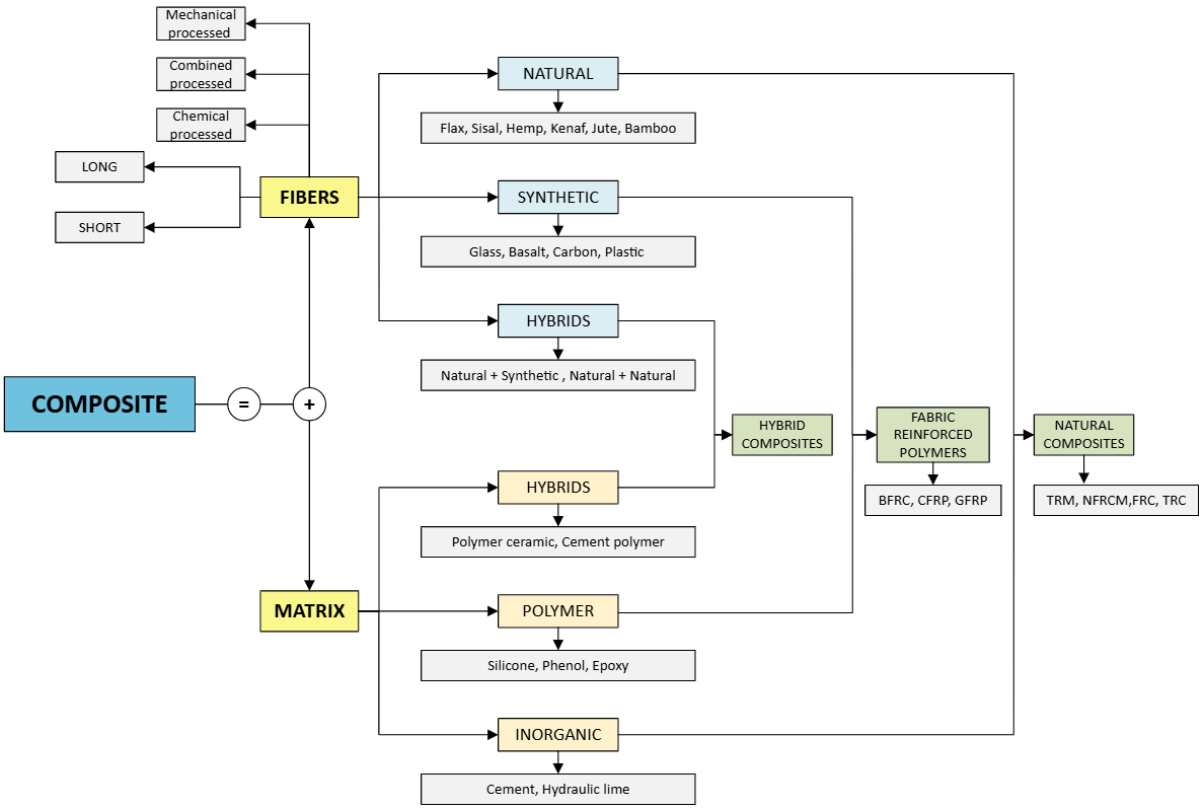
Figure 1. Presentation of the representation of works published from 2000 to 2023 that contain words in the title ‘‘Masonry Repair’’, ‘‘Masonry Retrofitting’’, ‘‘Masonry Assessment’’, ‘‘Masonry Monitoring’’, and ‘‘Masonry Strengthening’’[8]

Copyright © 2025 CroCEE
DOI: https://doi.org/10.5592/CO/3CroCEE.2025.49

With the increasing emphasis on environmental sustainability, the focus is on awareness of the impact of materials on human health. Currently materials such as basalt and glass fibers, carbon tape, and polymer resin are widely used in retrofitting and research [9–13]. Although these materials are widely used, they are synthetic and pose significant challenges in terms of their environmental impact and end-of-life disposal. As a sustainable alternative, composite materials based on natural fibers, such as flax, hemp, sisal, and viscose, are gaining popularity in structural repair [14–20]. Beyond their ecological benefits, the use of natural fibers could have a transformative effect on global economic structures. The economic and ecological benefits of using natural fibers are discussed in [21]. India, for example, which currently has an underdeveloped timber industry, could potentially establish itself as a leading exporter of natural fibers on the world market. This paper presents a comprehensive review of previous research and experimental tests on natural fiber-based composites for retrofitting and repair in the construction industry. It also provides an objective comparison of the mechanical properties of natural fiber-based composites with those of synthetic composites, highlighting their potential as sustainable solutions.

2. Fibers, Matrices and Composites in the Construction Industry

The combination of the matrix and fibers creates a composite material. A composite material consists of a matrix that is either inorganic or chemically processed, strengthened by embedded fibers. The main task of the matrix is to transfer the load to the fibers and bind them together. The most common inorganic matrices include cement-based or hydraulic lime mortars, while chemically synthesized matrices often involve epoxy resins. Unreinforced matrices, especially inorganic ones, are prone to brittle failure due to crack propagation after initial cracking. This challenge has led to the development of composite materials. Fibers are thin filaments introduced into the matrix to improve the mechanical properties. Fig. 2 shows the classification of fibers, partially based on categorizations presented in [22,23]. The most commonly used natural fibers in the construction industry are flax, sisal, viscose, coir, cotton, banana, and hemp, among others. Synthetic fibers such as carbon, steel and plastic, on the other hand, are processed chemically.



Copyright © 2025 CroCEE
DOI: https://doi.org/10.5592/CO/3CroCEE.2025.49

Figure 2. Classification of the composites

The optimization of synthetic fibers has resulted in high tensile strength, low weight, and versatile applications in structural repairs. These fibers are designed to be resistant to corrosion and chemicals proving beneficial across industries such as construction [24], automotive [25], and aerospace [26]. Their production involves chemical processes that ensure stable pricing and consistent availability. The disadvantages of these fibers include susceptibility to high temperatures, decreased permeability in construction, and suboptimal adhesion to bonded surfaces. Furthermore, controlling the distribution and orientation of fibers in micro-reinforced mortars is crucial, as it significantly affects mechanical behavior and failure patterns. Brittle failure is typical for composites with lower fiber content, whereas ductility depends on the fiber amount and spatial distribution, as shown in [27]. On the other hand, natural fibers have high tensile strength and low weight, along with a mesh structure aiding load distribution in orthogonal planes. In addition, they are viable and environmentally friendly with better adhesion and enhanced breathability in construction compared to their synthetic counterparts. Research [28] demonstrated that the use of natural fibers can reduce total construction weight by 10% and production energy requirements by 80%, thereby cutting CO_2 emissions significantly. Ultimately, the most important fact is that work environments with natural fibers have no negative impact on human health. However, natural fibers have inherent limitations, such as susceptibility to biodegradation, thermal limits (around 200 °C for most fibers), pest attacks, and UV-induced deterioration [29].

Additionally, the quality and availability of natural fibers vary with seasonal and climatic factors, causing annual price fluctuations. The global material representation reflects cost trends, although different quantities are required for equivalent performance. Therefore, material cost should not be the sole determinant in overall economic assessments. For example, Fig. 3, based on [21] shows a cost comparison for fibers achieving a tensile load resistance of 100 kN.

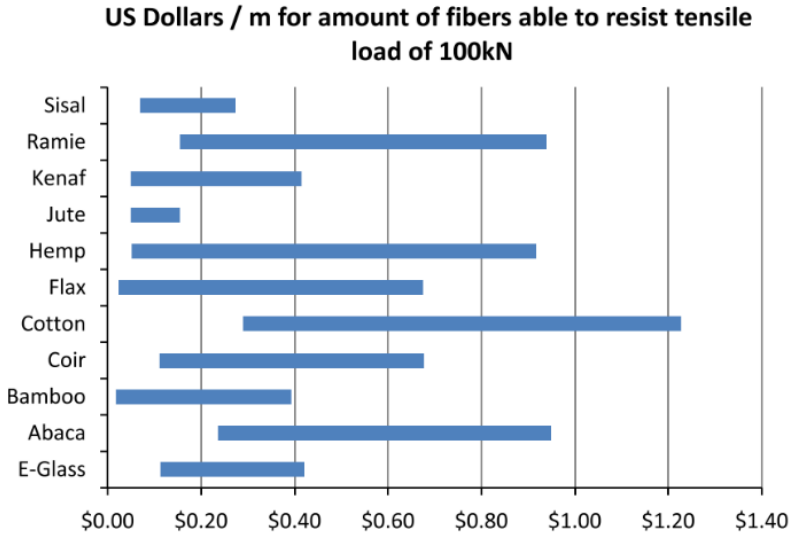


Figure 3. Cost comparison of fibers per unit length [21]

2.1. Selection of Composite

Selecting the optimal combination of fibers and matrix materials can significantly improve both the mechanical properties and durability of composite materials. Fig. 2 illustrates the structural configurations of different composite systems. However, challenges such as fiber length, geometry, and surface adhesion with the matrix remain and require further study. The texture and chemical composition of fibers may impair adhesion at the fiber-matrix interface. (For instance, natural fibers degrade when exposed to alkali in cement-based matrices (C). As a result, composites with a natural hydraulic lime (NHL) matrix show superior resistance, as demonstrated by experimental data [30]. The effects of C

Copyright © 2025 CroCEE
DOI: https://doi.org/10.5592/CO/3CroCEE.2025.49

and NHL matrices on fiber durability were studied in [31]. It was found that fibers embedded in cement matrices exhibited lower durability than fibers embedded in hydraulic lime matrices, leading to significant variations in experimental results. The alkali-induced degradation of fibers in composites can be minimized using fiber impregnation techniques. For example, flax fibers impregnated with curaua fibers reduced the crack width by 20% in tensile tests. Impregnated fibers show better performance due to improved adhesion and a more gradual failure mode, as shown in [32]. The failure mode of a composite depends on its fibers; after an initial crack occurs due to the matrix's limited tensile strength, fibers assume the load-bearing role, deform significantly, and stop crack propagation through "bridging" [33]. Surface adhesion can also be improved by modifying fiber geometry or length. Pull-out tests, as described in [34], have shown that triangular, hollow, and circular cross-sections improve mechanical properties by increasing the force required to dislodge fibers. Moreover, [35] concluded that the performance of Steel Fiber Reinforced Concrete is heavily influenced by the bond between fibers and the concrete matrix. Insufficient fiber length can cause fiber pull-out, diminishing load transfer efficiency. Conversely, optimal fiber length reduces concrete shrinkage and postpones initial cracking [22]. Bonding is often improved by treating fibers mechanically, chemically, or with a combination of methods. As reported in [22] these treatments fall into physical, chemical, or hybrid categories. Treatment intensity is critical since excessive treatment can weaken fibers' mechanical properties [23]. It was also found that mechanical or drying treatments have minimal impact on composites' mechanical properties. Similarly, the fiber-to-matrix ratio is a key determinant of composite performance. In [36], adding 1% curaua fibers by mass improved mortar flexural strength but reduced workability. Raising fiber volume fractions can lower composite compressive strength due to higher pore volume and uneven fiber distribution [22]. Moreover, adjusting fiber content can reduce shrinkage by up to 70%, although it increases surface cracks and decreases their average width.

In summary, the selection of a high-performance composite is an iterative process that involves the optimization of the matrix and fiber combination, supported by experimental testing to verify their mechanical properties and behavior. By varying the matrix and fiber types, several composite variants with distinct properties are developed. The structure of composites varies, and [37] provides a classification based on strengthening systems, such as wet lay-up, prefabricated, and specialized systems. Fiber Reinforced Polymers (FRP) are further subdivided into Glass Fiber Reinforced Polymers (GFRP) and Carbon Fiber Reinforced Polymers (CFRP), which are typically homogeneous composites consisting of short fibers embedded in a polymer matrix. Furthermore, Textile Reinforced Mortars (TRM) are systems composed of an inorganic matrix (e.g., cement or hydraulic lime) reinforced with a knitted mesh of natural fibers. Modern natural composites include Textile Reinforced Concrete (TRC), Textile Reinforced Mortars (TRM), Fabric Reinforced Cementitious Matrix (FRCM), and Natural Fiber Reinforced Matrix (NFRCM).

a) b)

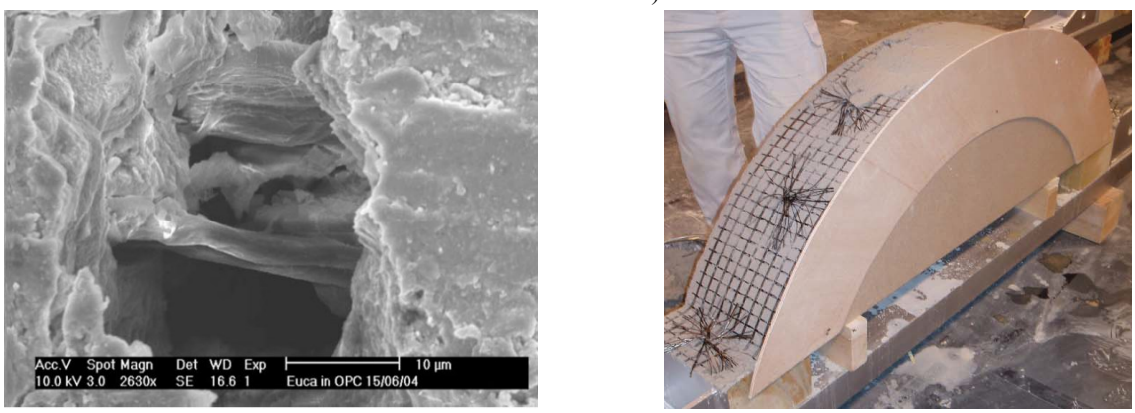


Figure 4. a) Bridging effect [38], b) Application of TRM [39]

Proceedings of the 3rd Croatian Conference on Earthquake Engineering - 3CroCEE
19–22 March 2025, Split, Croatia
Copyright © 2025 CroCEE
DOI: https://doi.org/10.5592/CO/3CroCEE.2025.49

3. Experimental Testing of Composites for Application in Construction

To understand the systems and approaches for strengthening structures, it is important to recognize the possible failure modes. Structural collapse can result from global instability or in-plane shear of walls subjected to significant horizontal loads [37], as well as from local failure of the weakest structural element. The characteristic failure modes of masonry are detailed in [40], concluding that diagonal cracking is typical under moderate compressive forces, whereas stepped cracking occurs in masonry subjected to tensile stresses perpendicular to the face planes and along multiple horizontal planes. Planar failure, on the other hand, results from exceeding the principal tensile stresses within the component. Failure of composite reinforcements can occur within the composite matrix, at the interface between the reinforcement and the substrate, or through fracture of the base material of the structure. To ensure the suitability of a specific composite for application, its effect on the mechanical properties of masonry must be demonstrated through comparisons with unreinforced specimens. To ensure reliable and reproducible results, tests should be conducted on samples with uniform geometric characteristics and boundary conditions. Standardized test methods and guidelines are outlined in various international standards. Test protocols for masonry that comply with European standards can be found on the official website of the Croatian Standards Institute [41]. Croatian standards provide parameters for evaluating of masonry specimens under compression, out-of-plane bending, and shear resistance. For tensile resistance, commonly assessed through diagonal compression tests, studies have primarily adhered to RILEM or ASTM standards [42].

A detailed review of prior experimental research is presented in the following sections, offering critical insights into the state-of-the-art in this field.

3.1. Testing Shear Resistance and Bonding of Composite

Structural reinforcements commonly used in construction today possess significantly higher tensile strength than those of the base structure. For example, unreinforced masonry has a tensile strength of less than 1.0 MPa, while carbon fiber meshes exhibit a tensile strength of approximately 3500 MPa and glass fiber meshes of about 1500 MPa. Failure typically occurs at the interface between the masonry surface and reinforcement, highlighting the importance of determining whether the full potential of the reinforcement can be effectively utilized. To evaluate bond strength, the pull-off test is most commonly used, as it is indirectly correlated with the shear strength between the reinforcement and the base material. Numerous studies have been conducted on this topic [43–47], with variations in matrix composition, fiber types, or loading methods. Furthermore, in [31] it was demonstrated that the high stiffness of PBO (polyparaphenylene benzobisoxazole) fibers relative to the substrate causes delamination of the composite from the substrate. Additionally, it was concluded that flax fibers enhance ductility, causing crack formation in the matrix before delamination from the structure.

Copyright © 2025 CroCEE
DOI: https://doi.org/10.5592/CO/3CroCEE.2025.49

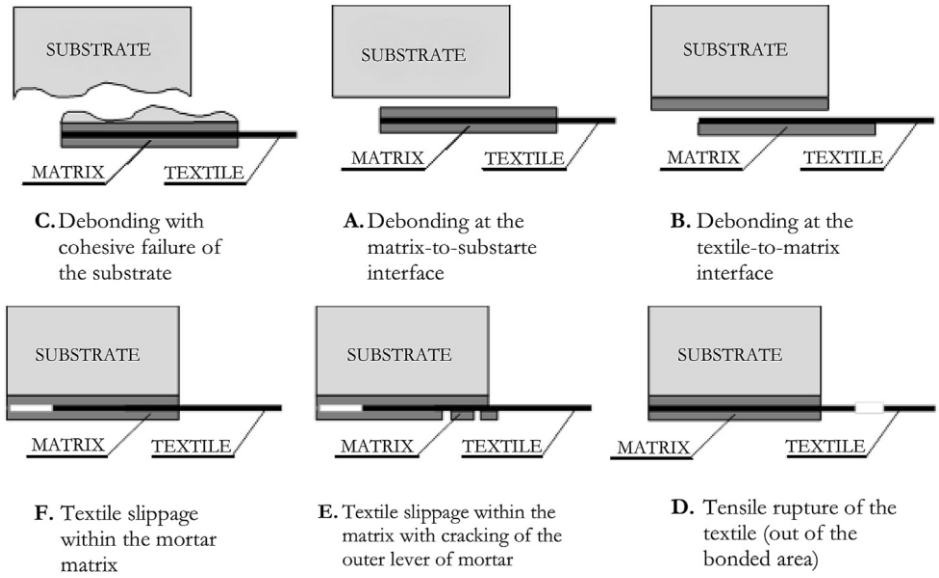


Figure 5. Failure modes of composites subjected to shear testing [48]

3.2. Experimental Testing of Out-of-Plane Bending Resistance

Failure at the interface between the reinforcement and the structure is not the only mode of failure for composites. In [49], experimental tests on reinforced concrete slabs and beams demonstrated various failure modes of composites, such as fiber sliding through the mortar, debonding of the reinforcement from the substrate, partial debonding of the reinforcement from the substrate, and cracking of the TRM due to bending exposure. The same study [49] identified two types of delamination at the concrete-reinforcement interface in concrete beams: from the middle towards the ends and from the ends towards the middle. These failure modes highlight the importance of properly anchoring the reinforcement to prevent premature, ensuring the activation of composite fibers under load. Additionally, bending tests perpendicular to the plane and the comparison of reinforcement contributions to unreinforced specimens were presented in [50–53]. In [54], 27 samples were tested using a simplified procedure to observe out-of-plane bending of walls. In [55] was demonstrated that the use of FRP reinforcement increased bending resistance by 2.5 times, significantly reducing deformability and enhancing structural performance.

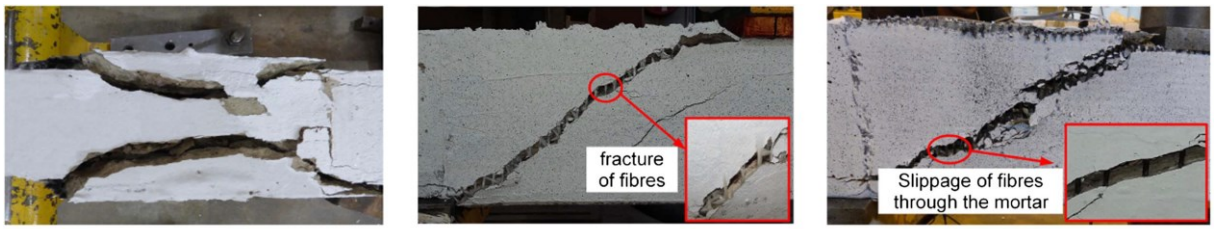


Figure 6. Failure modes of samples subjected to bending load [49]

3.3. In-Plane Testing (Compressive Loading and Diagonal Test)

Diagonal tests are a commonly used technique in experimental research to evaluate the mechanical properties of masonry structures. Specimens subjected to diagonal tests may fail due to exceeding either shear or tensile stresses. Consequently, direct tensile testing of composite materials often precedes diagonal testing to better understand their mechanical behavior. Research presented in [56] investigates the tensile behavior of composites under load, with Fig. 7 illustrating the failure mechanisms identified.

Copyright © 2025 CroCEE
DOI: https://doi.org/10.5592/CO/3CroCEE.2025.49

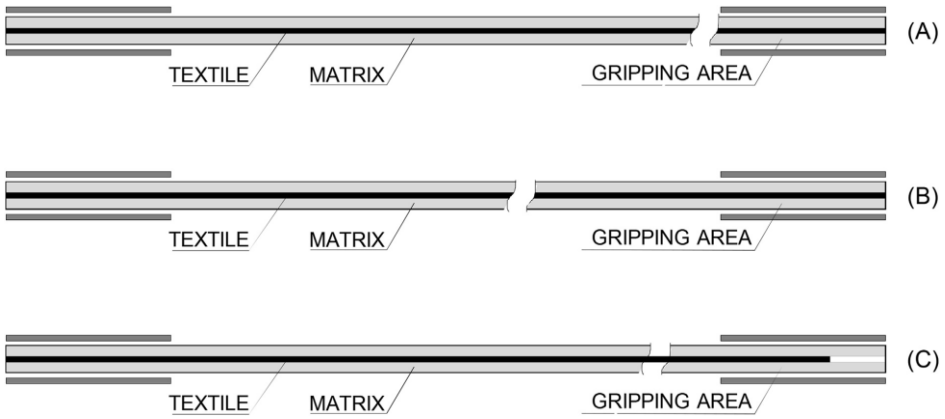


Figure 7. Failure modes of composites subjected to direct tensile testing: (A) tearing failure near the grip surface of the sample, (B) failure at the center of the sample due to exceeding the tensile strength, and (C) slippage of the textile at the grip surface without tensile failure

The failure mechanisms identified in these tests have led to various terminologies in the literature, including terms such as "diagonal shear test," "diagonal tensile test," and "diagonal compressive test," the latter reflecting the specific loading conditions applied during the test. The diagonal test has served as the basis for numerous comparisons and conclusions regarding the contribution of natural-material composite reinforcements to structural performance in masonry. For instance, experimental results in [57] demonstrate that the failure mode of the sample is influenced by factors such as the type of masonry unit (solid bricks of standard format or hollow blocks), mortar strength, and the reinforcement approach (unilateral or bilateral). In [58], a combined analytical and experimental analysis was conducted following RILEM guidelines and certain Italian recommendations. Results from these diagonal tests showed that the load-bearing capacity of samples reinforced with natural-material meshes increased twofold relative to unreinforced ones. Interestingly, there was no significant difference in the load-bearing capacity between samples reinforced with one layer versus two layers of reinforcement. Diagrams further indicated that failure of reinforced elements was not catastrophic, as the fibers within the reinforcement were able to sustain load after initial cracking. In tests conducted on adobe bricks using the diagonal method, it was concluded that the ductility of the masonry primarily depends on the tensile strength of the elements located in the central part of the wall [59]. Additionally, research on masonry samples reinforced with flax fabric and lime-based hydraulic mortar revealed that the composite exhibited ductile behavior in post-peak phase, regardless of the sample configuration [60]. Compression testing, alongside diagonal testing, is one of the most frequently used in-plane evaluation techniques for masonry structures. Compression stresses are ever-present in masonry, either due to self-weight or additional loads, making it critical to monitor stress levels resulting from these forces. In reinforced masonry, failure under in-plane compressive loading occurs when the tensile stresses in the composite fibers exceed their capacity, preventing the propagation of cracks within the structure [61]. Full utilization of textile-reinforced mortar (TRM) fibers occurs only when failure propagates through them [49]. In [62], tests were performed on reinforced and unreinforced masonry samples subjected to compressive loads parallel and perpendicular to the mortar joints. Results indicated that compression parallel to the bed joints leads to brittle failure, producing a single compressive strength value in this direction. Conversely, a relatively linear relationship between axial strain and compressive stress was observed in the perpendicular direction up to approximately 50% of the ultimate load.

These findings collectively highlight the effectiveness of diagonal testing as a diagnostic tool for understanding the mechanical behavior of masonry, particularly when enhanced with natural-material reinforcements. Further, the integration of analytical and experimental approaches offers a robust framework for advancing sustainable and resilient construction practices.

Proceedings of the 3rd Croatian Conference on Earthquake Engineering - 3CroCEE
19–22 March 2025, Split, Croatia
Copyright © 2025 CroCEE
DOI: https://doi.org/10.5592/CO/3CroCEE.2025.49

4. Conclusion

In addition to the widely used synthetic fibers such as steel, glass, carbon, basalt and plastic, natural fibers such as flax, jute, sisal, viscose and cotton are also gaining importance in scientific research. Current findings underline the great potential of natural fiber composites in the construction industry. They offer advantages such as high mechanical performance, rapid biodegradability and environmentally friendly disposal at the end of their service life. To maximize their structural benefits, it is crucial to carefully select the fiber types, optimize their treatment processes and combine them with suitable matrix materials. However, there are still some challenges. Key areas for improvement include enhancing the fiber-matrix interface and improving fire and weathering resistance to meet the stringent requirements of the construction sector. Future research must focus primarily on standardized testing of mechanical properties in compliance with relevant guidelines to establish natural fiber composites as viable, sustainable alternatives to synthetic materials. The use of natural fibers in construction offers additional socio-economic benefits. It promotes the industrial development of underrepresented regions, improves living standards and boosts the local economy. Furthermore, its integration is in line with global efforts to reduce the environmental and health risks associated with synthetic composites. The further development of natural fiber composites requires a multidisciplinary approach. Planned experimental studies will provide crucial insights into their performance in the reinforcement of masonry and provide a basis for reliable and scalable applications. By overcoming these challenges, the construction industry can move towards more sustainable, resilient and environmentally friendly practices.

5. Acknowledgements

This work has been supported through project *"Development of a new technology for strengthening masonry structures with construction quality certification"* [IP.1.1.03.0109], project co-financed by the Croatian Government and the European Union through the European Regional Development Fund-the Competitiveness and Cohesion Operational Programme.

6. References

[1] PRIRODOSLOVNO-MATEMATIČKI FAKULTET n.d. https://www.pmf.unizg.hr/geof/seizmoloska_sluzba/seizmicnost_hrvatske (accessed December 16, 2024).

[2] Radnić J, Grgić N, Buzov A, Banović I, Zulim MS, Baloević G, et al. Mw 6.4 Petrinja earthquake in Croatia: Main earthquake parameters, impact on buildings and recommendation for their structural strengthening. Gradjevinar 2021;73:1109–28. https://doi.org/10.14256/JCE.3243.2021.

[3] Cakir F, Uckan E, Shen J, Seker BS, Akbas B. Seismic damage evaluation of historical structures during Van earthquake, October 23, 2011. Eng Fail Anal 2015;58:249–66. https://doi.org/10.1016/j.engfailanal.2015.08.030.

[4] Latifi R, Rouhi R. Seismic assessment and retrofitting of existing RC structures: Seismostruct and seismobuild implementation. Civil Engineering and Architecture 2020;8:84–93. https://doi.org/10.13189/cea.2020.080206.

[5] Latifi R, Hadzima-Nyarko M, Radu D, Rouhi R. A Brief Overview on Crack Patterns, Repair and Strengthening of Historical Masonry Structures. Materials 2023;16. https://doi.org/10.3390/ma16051882.

[6] Heyman J. THE SAFETY OF MASONRY ARCHES. vol. 11. Pergamon Press; 1969.

[7] Di Tommaso A, Focacci F, Micelli F. Strengthening historical masonry with FRP or FRCM: Trends in design approach. Key Eng Mater, vol. 747 KEM, Trans Tech Publications Ltd; 2017, p. 166–73. https://doi.org/10.4028/www.scientific.net/KEM.747.166.

Copyright © 2025 CroCEE
DOI: https://doi.org/10.5592/CO/3CroCEE.2025.49

[8] Keshmiry A, Hassani S, Dackermann U, Li J. Assessment, repair, and retrofitting of masonry structures: A comprehensive review. Constr Build Mater 2024;442. https://doi.org/10.1016/j.conbuildmat.2024.137380.

[9] Al-Rousan ET, Khalid HR, Rahman MK. Fresh, mechanical, and durability properties of basalt fiber-reinforced concrete (BFRC): A review. Developments in the Built Environment 2023;14. https://doi.org/10.1016/j.dibe.2023.100155.

[10] Sayyad AS, Sayyad RA. A review of research on fiber reinforced concrete. vol. 10. 2023.

[11] Al-Kharabsheh BN, Arbili MM, Majdi A, Alogla SM, Hakamy A, Ahmad J, et al. Basalt Fiber Reinforced Concrete: A Compressive Review on Durability Aspects. Materials 2023;16. https://doi.org/10.3390/ma16010429.

[12] Elkafrawy M, Gowrishankar P, Aswad NG, Alashkar A, Khalil A, AlHamaydeh M, et al. GFRP-Reinforced Concrete Columns: State-of-the-Art, Behavior, and Research Needs. Buildings 2024;14. https://doi.org/10.3390/buildings14103131.

[13] Douadi A, Babba R, Hebbache K, Boutlikht M, Khitas NEH, Messai A, et al. Evaluation of CFRP confinement performance and predictive accuracy of design codes and stress-strain models for concrete. Research on Engineering Structures and Materials 2024. https://doi.org/10.17515/resm2024.435me0906rs.

[14] Monaco A, Baldassari M, D'Anna J, Cornetti P. Effectiveness of Flax-TRM composites under traction. Procedia Structural Integrity, vol. 44, Elsevier B.V.; 2023, p. 2278–85. https://doi.org/10.1016/j.prostr.2023.01.291.

[15] Abbass A, Lourenço PB, Oliveira D V. The use of natural fibers in repairing and strengthening of cultural heritage buildings. Mater Today Proc, vol. 31, Elsevier Ltd; 2019, p. S321–8. https://doi.org/10.1016/j.matpr.2020.02.206.

[16] Illampas R, Oliveira D V., Lourenço PB. Design of Strain-Hardening Natural TRM Composites: Current Challenges and Future Research Paths. Materials 2023;16. https://doi.org/10.3390/ma16134558.

[17] Kamarudin SH, Mohd Basri MS, Rayung M, Abu F, Ahmad S, Norizan MN, et al. A Review on Natural Fiber Reinforced Polymer Composites (NFRPC) for Sustainable Industrial Applications. Polymers (Basel) 2022;14. https://doi.org/10.3390/polym14173698.

[18] Maciel LP, Leão Júnior PSB, Pereira Filho MJM, El Banna WR, Fujiyama RT, Ferreira MP, et al. Experimental Analysis of Shear-Strengthened RC Beams with Jute and Jute–Glass Hybrid FRPs Using the EBR Technique. Buildings 2024;14. https://doi.org/10.3390/buildings14092893.

[19] Attia MM, Olwan MM, Amoush E, Aamer SRRH, Eita MA. Behavior of hybrid natural fiber reinforced polymers bars under uniaxial tensile strength and pull-out loads with UHPC. Case Studies in Construction Materials 2024;21. https://doi.org/10.1016/j.cscm.2024.e03442.

[20] Chandramohan D, Murali B, Vasantha-Srinivasan P, Dinesh Kumar S. Mechanical, Moisture Absorption, and Abrasion Resistance Properties of Bamboo–Jute–Glass Fiber Composites. J Bio Tribocorros 2019;5. https://doi.org/10.1007/s40735-019-0259-z.

[21] Dittenber DB, Gangarao HVS. Critical review of recent publications on use of natural composites in infrastructure. Compos Part A Appl Sci Manuf 2012;43:1419–29. https://doi.org/10.1016/j.compositesa.2011.11.019.

[22] Gamage N, Patrisia Y, Gunasekara C, Law DW, Houshyar S, Setunge S. Shrinkage induced crack control of concrete integrating synthetic textile and natural cellulosic fibres: Comparative review analysis. Constr Build Mater 2024;427. https://doi.org/10.1016/j.conbuildmat.2024.136275.

[23] Ardanuy M, Claramunt J, Toledo Filho RD. Cellulosic fiber reinforced cement-based composites: A review of recent research. Constr Build Mater 2015;79:115–28. https://doi.org/10.1016/j.conbuildmat.2015.01.035.

[24] Böhm R, Thieme M, Wohlfahrt D, Wolz DS, Richter B, Jäger H. Reinforcement systems for carbon concrete composites based on low-cost carbon fibers. Fibers 2018;6. https://doi.org/10.3390/fib6030056.

Copyright © 2025 CroCEE
DOI: https://doi.org/10.5592/CO/3CroCEE.2025.49

[25] Ahmad H, Markina AA, Porotnikov M V., Ahmad F. A review of carbon fiber materials in automotive industry. IOP Conf Ser Mater Sci Eng, vol. 971, IOP Publishing Ltd; 2020. https://doi.org/10.1088/1757-899X/971/3/032011.

[26] Soutis C. Carbon fiber reinforced plastics in aircraft construction. Materials Science and Engineering: A 2005;412:171–6. https://doi.org/10.1016/j.msea.2005.08.064.

[27] Wang X, Lam CC, Iu VP. Comparison of different types of TRM composites for strengthening masonry panels. Constr Build Mater 2019;219:184–94. https://doi.org/10.1016/j.conbuildmat.2019.05.179.

[28] Arpitha GR, Yogesha B. An Overview on Mechanical Property Evaluation of Natural Fiber Reinforced Polymers. Mater Today Proc, vol. 4, Elsevier Ltd; 2017, p. 2755–60. https://doi.org/10.1016/j.matpr.2017.02.153.

[29] Addis LB, Sendekie ZB, Satheesh N. Degradation Kinetics and Durability Enhancement Strategies of Cellulosic Fiber-Reinforced Geopolymers and Cement Composites. Advances in Materials Science and Engineering 2022;2022. https://doi.org/10.1155/2022/1981755.

[30] Cevallos OA, Olivito R, Codispoti R. Experimental analysis of repaired masonry elements with flax-FRCM and PBO-FRCM composites subjected to axial bending loads. Fibers 2015;3:491–503. https://doi.org/10.3390/fib3040491.

[31] Cevallos OA, Olivito RS, Codispoti R, Ombres L. Flax and polyparaphenylene benzobisoxazole cementitious composites for the strengthening of masonry elements subjected to eccentric loading. Compos B Eng 2015;71:82–95. https://doi.org/10.1016/j.compositesb.2014.10.055.

[32] de Carvalho Bello CB, Boem I, Cecchi A, Gattesco N, Oliveira D V. Experimental tests for the characterization of sisal fiber reinforced cementitious matrix for strengthening masonry structures. Constr Build Mater 2019;219:44–55. https://doi.org/10.1016/j.conbuildmat.2019.05.168.

[33] Wang X, Ghiassi B, Oliveira D V., Lam CC. Modelling the nonlinear behaviour of masonry walls strengthened with textile reinforced mortars. Eng Struct 2017;134:11–24. https://doi.org/10.1016/j.engstruct.2016.12.029.

[34] Behdouj Z, Jamshidi M, Latifi M, Halvaei M. Effect of cross sectional shape of polypropylene fibers on flexural toughness of composites and fiber-to-cement matrix adhesion. Adv Mat Res, vol. 687, 2013, p. 485–9. https://doi.org/10.4028/www.scientific.net/AMR.687.485.

[35] Khabaz A. Monitoring of impact of hooked ends on mechanical behavior of steel fiber in concrete. Constr Build Mater 2016;113:857–63. https://doi.org/10.1016/j.conbuildmat.2016.03.142.

[36] Ferrara G, Pepe M, Filho RDT, Martinelli E. Mechanical response and analysis of cracking process in hybrid TRM composites with flax textile and Curauá fibres. Polymers (Basel) 2021;13:1–14. https://doi.org/10.3390/polym13050715.

[37] Kišiček T, Stepinac M, Renić T, Hafner I, Lulić L. Strengthening of masonry walls with FRP or TRM. Gradjevinar 2020;72:937–53. https://doi.org/10.14256/JCE.2983.2020.

[38] Savastano H, Santos SF, Radonjic M, Soboyejo WO. Fracture and fatigue of natural fiber-reinforced cementitious composites. Cem Concr Compos 2009;31:232–43. https://doi.org/10.1016/j.cemconcomp.2009.02.006.

[39] Garmendia L, Larrinaga P, García D, Marcos I. Textile-reinforced mortar as strengthening material for masonry arches. International Journal of Architectural Heritage 2014;8:627–48. https://doi.org/10.1080/15583058.2012.704480.

[40] Angelillo M, Lourenço PB, Milani G. Masonry behaviour and modelling. CISM International Centre for Mechanical Sciences, Courses and Lectures, vol. 551, Springer International Publishing; 2014, p. 1–26. https://doi.org/10.1007/978-3-7091-1774-3_1.

[41] Hrvatski zavod za norme n.d. https://www.hzn.hr/ (accessed October 31, 2024).

[42] Test Method for Diagonal Tension (Shear) in Masonry Assemblages 2022. https://doi.org/10.1520/E0519_E0519M-22.

Copyright © 2025 CroCEE
DOI: https://doi.org/10.5592/CO/3CroCEE.2025.49

[43] Carozzi FG, Poggi C. Mechanical properties and debonding strength of Fabric Reinforced Cementitious Matrix (FRCM) systems for masonry strengthening. Compos B Eng 2015;70:215–30. https://doi.org/10.1016/j.compositesb.2014.10.056.

[44] Gentilini C, Yuan Y, Carloni C, Franzoni E. Adhesion between SRP and masonry: Laboratory simulations of the field moisture and salt conditions. Constr Build Mater 2020;264. https://doi.org/10.1016/j.conbuildmat.2020.120697.

[45] Tamburini S, Natali M, Garbin E, Panizza M, Favaro M, Valluzzi MR. Geopolymer matrix for fibre reinforced composites aimed at strengthening masonry structures. Constr Build Mater 2017;141:542–52. https://doi.org/10.1016/j.conbuildmat.2017.03.017.

[46] Tedeschi C, Kwiecień A, Valluzzi MR, Zając B, Garbin E, Binda L. Effect of thermal ageing and salt decay on bond between FRP and masonry. Materials and Structures/Materiaux et Constructions 2014;47:2051–65. https://doi.org/10.1617/s11527-014-0448-7.

[47] Gentilini C, Carloni C, Santoro R, Franzoni E. CHARACTERIZATION OF FRCM-AND FRP-MASONRY BOND BEHAVIOR. n.d.

[48] Leone M, Aiello MA, Balsamo A, Carozzi FG, Ceroni F, Corradi M, et al. Glass fabric reinforced cementitious matrix: Tensile properties and bond performance on masonry substrate. Compos B Eng 2017;127:196–214. https://doi.org/10.1016/j.compositesb.2017.06.028.

[49] Koutas LN, Tetta Z, Bournas DA, Triantafillou TC. Strengthening of Concrete Structures with Textile Reinforced Mortars: State-of-the-Art Review. Journal of Composites for Construction 2019;23. https://doi.org/10.1061/(asce)cc.1943-5614.0000882.

[50] Pourfalah S, Suryanto B, Cotsovos DM. Enhancing the out-of-plane performance of masonry walls using engineered cementitious composite. Compos B Eng 2018;140:108–22. https://doi.org/10.1016/j.compositesb.2017.12.030.

[51] Gattesco N, Boem I. Characterization tests of GFRM coating as a strengthening technique for masonry buildings. Compos Struct 2017;165:209–22. https://doi.org/10.1016/j.compstruct.2017.01.043.

[52] Munjal P, Singh SB. Out-of-plane response of ECC-strengthened masonry walls. Journal of Structural Integrity and Maintenance 2020;5:18–30. https://doi.org/10.1080/24705314.2019.1692165.

[53] Del Zoppo M, Di Ludovico M, Balsamo A, Prota A. Fibre reinforced mortars for the out-of-plane strengthening of masonry walls. Procedia Structural Integrity, vol. 44, Elsevier B.V.; 2022, p. 2158–65. https://doi.org/10.1016/j.prostr.2023.01.276.

[54] Valluzzi MR, da Porto F, Garbin E, Panizza M. Out-of-plane behaviour of infill masonry panels strengthened with composite materials. Materials and Structures/Materiaux et Constructions 2014;47:2131–45. https://doi.org/10.1617/s11527-014-0384-6.

[55] Hamed E, Rabinovitch O. Lateral Out-of-Plane Strengthening of Masonry Walls with Composite Materials n.d. https://doi.org/10.1061/ASCECC.1943-5614.0000093.

[56] De Santis S, Ceroni F, de Felice G, Fagone M, Ghiassi B, Kwiecień A, et al. Round Robin Test on tensile and bond behaviour of Steel Reinforced Grout systems. Compos B Eng 2017;127:100–20. https://doi.org/10.1016/j.compositesb.2017.03.052.

[57] Giaretton M, Dizhur D, Garbin E, Ingham JM, da Porto F. In-Plane Strengthening of Clay Brick and Block Masonry Walls Using Textile-Reinforced Mortar. Journal of Composites for Construction 2018;22. https://doi.org/10.1061/(asce)cc.1943-5614.0000866.

[58] Ferrara G, Caggegi C, Martinelli E, Gabor A. Shear capacity of masonry walls externally strengthened using Flax-TRM composite systems: experimental tests and comparative assessment. Constr Build Mater 2020;261. https://doi.org/10.1016/j.conbuildmat.2020.120490.

[59] Cassese P, Balestrieri C, Fenu L, Asprone D, Parisi F. In-plane shear behaviour of adobe masonry wallets strengthened with textile reinforced mortar. Constr Build Mater 2021;306. https://doi.org/10.1016/j.conbuildmat.2021.124832.

[60] Ferrara G, Caggegi C, Gabor A, Martinelli E. Mechanical behaviour of masonry panels strengthened by flax TRM systems. Key Eng Mater, vol. 817 KEM, Trans Tech Publications Ltd; 2019, p. 427–34. https://doi.org/10.4028/www.scientific.net/KEM.817.427.

Proceedings of the 3rd Croatian Conference on Earthquake Engineering - 3CroCEE
19–22 March 2025, Split, Croatia
Copyright © 2025 CroCEE
DOI: https://doi.org/10.5592/CO/3CroCEE.2025.49

[61] Ismail N, Ingham JM. In-plane and out-of-plane testing of unreinforced masonry walls strengthened using polymer textile reinforced mortar. Eng Struct 2016;118:167–77. https://doi.org/10.1016/j.engstruct.2016.03.041.

[62] Luccioni B, Rougier VC. In-plane retrofitting of masonry panels with fibre reinforced composite materials. Constr Build Mater 2011;25:1772–88. https://doi.org/10.1016/j.conbuildmat.2010.11.088.

Proceedings of the 3rd Croatian Conference on Earthquake Engineering - 3CroCEE
19–22 March 2025, Split, Croatia
Copyright © 2025 CroCEE
DOI: https://doi.org/10.5592/CO/3CroCEE.2025.86

NEAR-DISTANCE SPECTRAL PARAMETER KAPPA CALCULATIONS FOR STATIONS INSTALLED IN N. MACEDONIA

Marina Poposka [(1)], Davor Stanko [(2)], Radmila Salic Makreska [(3)], Dragi Dojcinovski [(4)] Marta Stojmanovska [(5)]

[(1)] *Research Assistant, Ss. Cyril and Methodius University in Skopje, Institute of Earthquake Engineering and Engineering Seismology, Skopje, R. N. Macedonia, marina@iziis.ukim.edu.mk*
[(2)] *Assistant Professor, Faculty of Geotechnical Engineering, University of Zagreb, Varaždin, Croatia, dstanko@gfv.hr*
[(3)] *Full Professor, Ss. Cyril and Methodius University in Skopje, Institute of Earthquake Engineering and Engineering Seismology, Skopje, R. N. Macedonia, r_salic@iziis.ukim.edu.mk*
[(4)] *Full Professor, Ss. Cyril and Methodius University in Skopje, Institute of Earthquake Engineering and Engineering Seismology, Skopje, R. N. Macedonia, dragidoj1@yahoo.com*
[(5)] *Associate Professor, Ss. Cyril and Methodius University in Skopje, Institute of Earthquake Engineering and Engineering Seismology, Skopje, R. N. Macedonia, marta@iziis.ukim.edu.mk*

Abstract

The objective of this study is to estimate the high-frequency decay parameter – kappa (κ) for stations installed in the regions with highest seismicity in North Macedonia.

Kappa characterizes the attenuation of ground motion at high frequencies, more precisely defines the rate of decrease of the acceleration amplitude spectrum. At higher frequencies ground motions on rock may be larger than those on soil due to lesser damping from impedance contrasts in the near-surface. Thus, site effects on rock are an important topic for structures that are sensitive to high frequencies.

Comparison of kappa estimated values is made using strong motion data obtained from four different locations Pehcevo (PEH), Ohrid (OHR), Debar (DBR), and Valandovo (VAL). Local site condition parameters, specifically V_{S30}, are determined for each station based on conducted geophysical investigations and/or microtremor measurements. The accelerometric data used for analysis are obtained from local earthquake events within a magnitude range (M_w) of 3.0 to 5.5, epicentral distances (R_{epi}) less than 120 km, and focal depths (h) less than 40 km. The data were visually inspected, baseline corrected, and a bandpass filter was applied. Earthquake records with SNR<3 were excluded from the analysis.

The value of kappa is estimated from the acceleration amplitude spectrum of shear waves from the slope of the high-frequency part where the spectrum starts to decay rapidly to a noise level.

Based on the results obtained, conclusions are drawn regarding the impact of this parameter on the attenuation of near-surface crust rock layers, as well as local effects in near-distances.

Keywords: kappa, FAS, near-surface attenuation, strong motion data

1. Introduction

The Republic of North Macedonia is a seismically active region with low to moderate seismicity, though some areas exhibit nearly high levels of seismic activity. In the past, numerous earthquakes struck the country's territory, with some devastating almost entire cities. For instance, in the past century, the most significant earthquakes that occur in the N. Macedonia are Pehchevo earthquake 1904 (M=7.5, I=10), Valandovo earthquake 1931 (M=6.7, I=10), Skopje earthquake 1963 (M=6.1, I=9), Debar earthquake 1967 (M=6.5, I=9). Based on the effects of these events, these regions in North Macedonia are where the expected seismic hazard level is the highest.

Over the years, various studies have been conducted to assess the seismic hazard in this country. However, no study has yet focused on the local attenuation of seismic waves at high frequencies. To

Copyright © 2025 CroCEE
DOI: https://doi.org/10.5592/CO/3CroCEE.2025.86

characterize these effects, Anderson and Hough (1984) introduced the empirical high-frequency decay parameter *kappa* (κ), aiming to explain deviations in the shape of the spectral acceleration curve from the theoretical Brune's model (1970) at frequencies higher than the source corner frequency. Using earthquake records with magnitudes greater than 5, they calculated the spectral parameter kappa for different stations by analyzing log-linear spectral space within constrained frequency ranges. Currently are available many approaches for estimating kappa (Ktenidou et. al 2014), and this parameter is widely used for site characterization, especially given empirical k_0-V_{S30} correlations (Silva et al. 1999, Chandler et al.2005, Drouet et al. 2010, Edwards et al. 2011, Van Heute et al. 2011, Ktenidou et al., 2013, 2014, 2015, Stanko et al. 2017), among other uses such site amplification (Boore et al. 1997), input parameters for creation and calibration of GMPEs, host to target adjustments of GMPEs to different regions (Cotton et al. 2006; Douglas et al. 2006; Biro and Renault 2012), as well as its correlation with engineering parameters like peak ground acceleration (PGA) and Arias intensity (Mena et al. 2010).

Despite its importance, there are no prior studies in North Macedonia focusing on the high-frequency decay parameter to quantify the effect of near-surface geology on seismic waves.

The IZIIS strong motion network with accelerometers installed across N. Macedonia at various locations and on different types of soil types provide valuable data for further research and estimation of the high-frequency decay parameter. In this study, records from earthquakes with magnitudes (M_w) higher than 3 and epicentral distances (R_{epi}) of less than 120 km were analyzed, collected from four locations in North Macedonia

The study begins with an overview of the study area and the description of strong motion records, followed by an evaluation of the method used for kappa calculation. The results are then presented and discussed, with appropriate conclusions drawn.

2. Study area and strong motion records

For this study, the regions with the highest seismicity in North Macedonia were analyzed (Fig. 1). Using information from historical and recent seismic events, along with EC8 seismic hazard zoning maps (Milutinovic at al.2016), four stations—PEH, OHR, DBR, and VAL from the IZIIS strong motion network were selected. These stations, located in the regions where the hazard level is the highest, provided strong motion records obtained from 200 Hz sampling accelerometers (Guralp CMG-5TD and ETNA-2). Site characteristics were determined through geophysical measurements (Seismic Refraction Tomography - SRT or/and Multichannel Analysis of Surface Waves - MASW) for the OHR, PEH and DBR stations (Stojmanovska et al. 2020-2021, Garevski et.al. 2016), while HVSR (horizontal to vertical spectral ratio) from earthquake records using the Konno and Ohmachi [1998] (b-value=20) smoothed Fourier amplitude spectrum was conducted for all four stations to obtain the predominant site frequency and possible site amplifications.

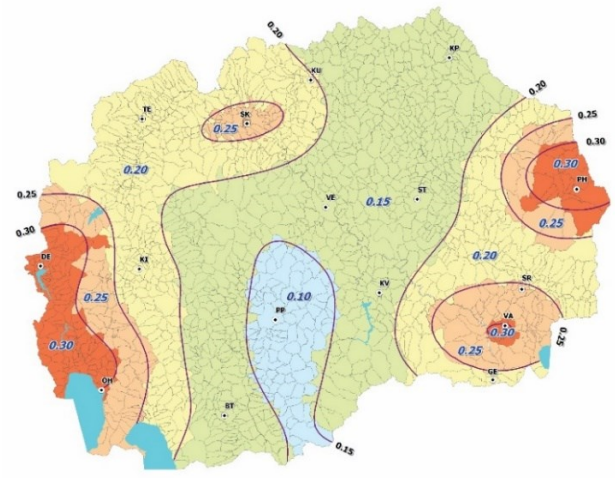


Figure 1. Seismic hazard zoning maps return period T=475 years (Milutinovic at al.2016)

Copyright © 2025 CroCEE
DOI: https://doi.org/10.5592/CO/3CroCEE.2025.86

Between 2011 and 2024, these stations recorded 221 earthquake events with magnitudes ranging from 2.11 to 6.4 and epicentral distances from 1.66 to 430 km. To exclude the possibility of source effects on kappa calculation, only records with magnitudes greater than 3, while for the epicentral distances up to 120 km were considered for this analysis. Fig. 2 presents the spatial distribution of the earthquakes recorded in these stations, and station locations with blue triangles.

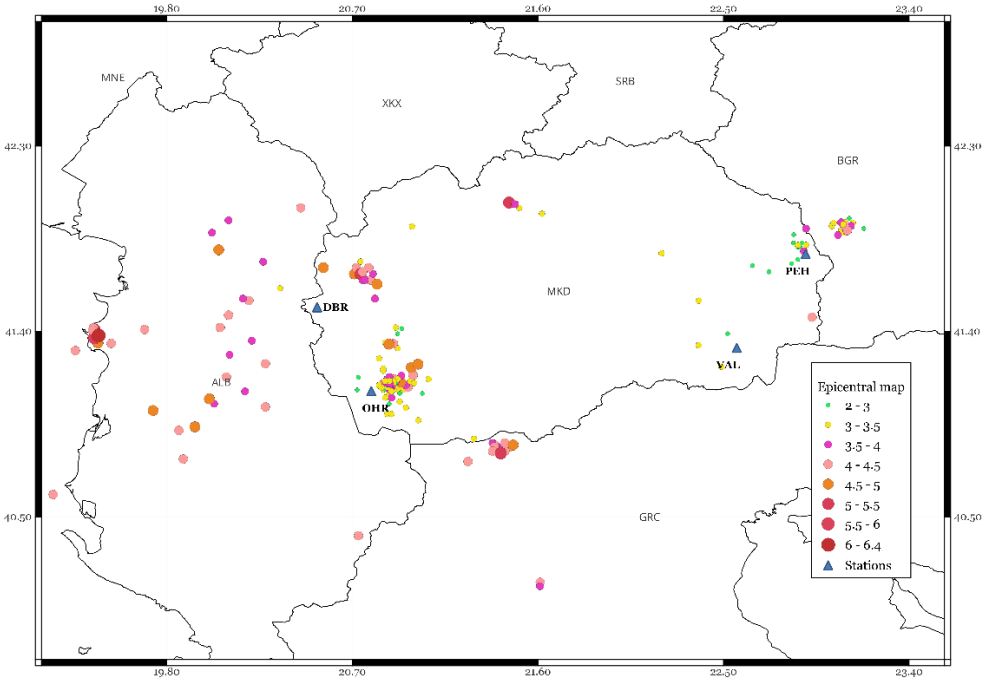


Figure 2. Spatial distribution of earthquake and station locations in the research area.

Table 1 provides station location information, soil type, investigation type, and number of earthquake records included in the analysis. The data included in the analysis are constrained based on the recommendations for higher-quality analysis provided in the following text. Fig. 3 shows the horizontal to vertical spectral ratios (HVSR) derived from earthquakes for the four stations.

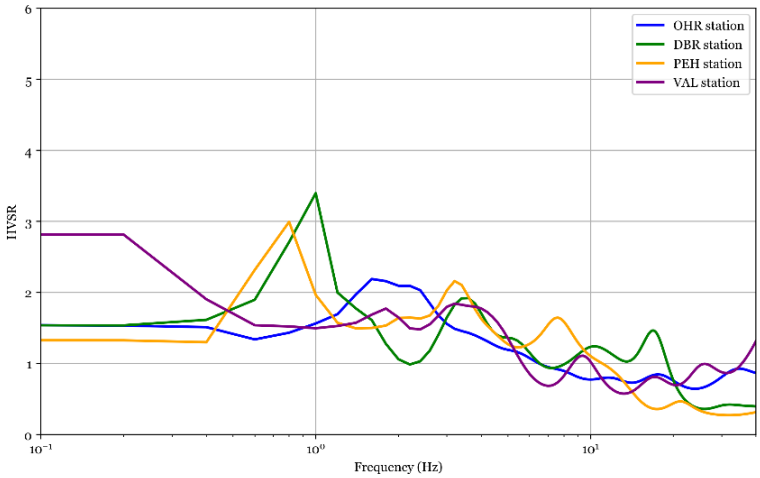


Figure 3. Horizontal to Vertical Spectral Ratios (HVSR) from earthquake records using the Konno and Ohmachi [1998] (b-value=20) smoothed Fourier amplitude spectrum for four stations.

According to Fig. 3 the observed predominant site frequencies fall within the frequency range of 0.6 to 5 Hz. To exclude potential effects on the estimation of kappa (Parolai and Bindi (2004)), the minimum value for boundary frequency f_{1min} is set to 10 Hz.

Proceedings of the 3rd Croatian Conference on Earthquake Engineering - 3CroCEE
19–22 March 2025, Split, Croatia
Copyright © 2025 CroCEE
DOI: https://doi.org/10.5592/CO/3CroCEE.2025.86

Table 1. Station information, investigation type 1- geophysics, type 2 – HVSR, number of earthquake data recorded per station

Station	Latitude [°]	Longitude [°]	V_{s30} [m/s]	Investigation type	Number of earthquake records
OHR	41.111389	20.792222	1000	1, 2	68
DBR	41.518556	20.529361	400-450	1, 2	148
PEH	41.776278	22.897861	380-450	1, 2	50
VAL	41.321528	22.564528	600-800	2	38

3. Signal processing and kappa calculation

The records obtained from the seismic sensors were organized according to the magnitude, epicentral distance, and depth of the earthquake (Fig. 4, green dots representing analyzed data, while blue, yellow, grey, and red dots representing neglected data where M_w<3, R_{epi}>120, and SNR<3). The data were visually inspected, baseline corrected, and a bandpass filter ranging from 0.1 to 100 Hz was applied. Bad quality data, data with SNR < 3, and data with S-window portion less than 4 seconds (to ensure good spectral resolution) were excluded from the analysis.

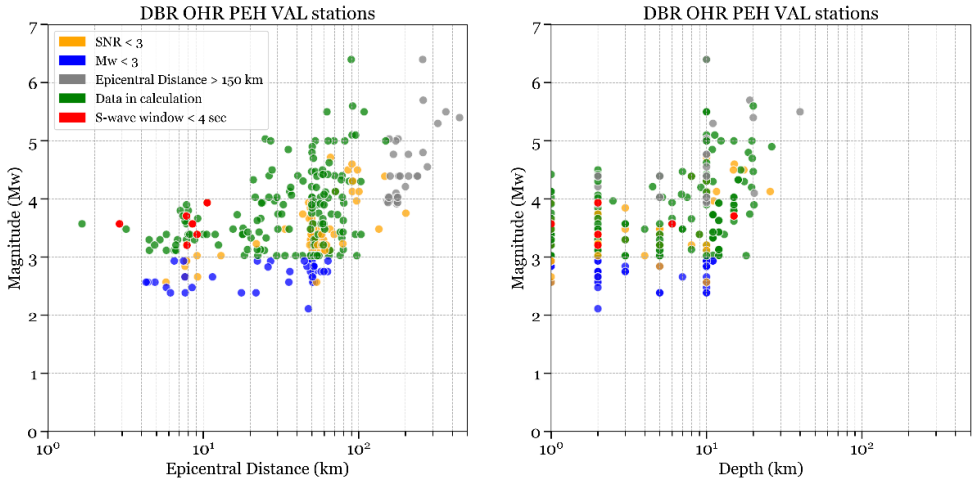


Figure 4. Statistics of the compiled ground motion dataset. (a) R_{epi}-M_W distribution of recordings (b) h-M_W distribution of recordings

As a method for kappa calculation, the original acceleration spectral method (Anderson & Hough, 1984), using the S-wave window and recommended procedure in Ktenidou et al. 2014, was employed. S-wave windows (longer than 4 seconds) and noise windows were manually selected (Fig. 5, first row). A 5% cosine taper was applied to both windows, followed by the calculation of the Fourier Amplitude Spectrum (FAS) (Fig. 5, middle row). Using the earthquake parameters, the corner frequency f_c and the theoretical spectrum, based on Brune's model, were calculated (Fig. 5 – black line). The frequencies f_1 and f_2 were manually selected: f_1 was chosen to be greater than $1.5f_c$ to ensure the source contribution would not bias the kappa calculation, and if f_1<10 Hz, f_1=10 Hz to avoid the influence of possible site resonance. f_2 was selected where the spectrum becomes flat and to ensure that the signal-to-noise ratio (SNR) between the S-wave and noise windows was greater than 3. Kappa was determined from the slope of the FAS in the linear-logarithmic space within the frequency range between f_1 and f_2 (Fig. 5 – blue line). The frequency band Δf was with min value of 10. Spectra with ranges of Δf < 10 Hz were discarded in the interest of the robustness of the slope computation. Depending on the magnitude and distance of the event, the frequency f_1 ranges from 10 to 17 Hz and, while f_2 is between 25 and 40 Hz. The Nyquist frequency based on sampling rate is 100 Hz and the instrument response does not exhibit decay below 60 Hz, so a rather large range of frequencies can be used for κappa computations.

Proceedings of the 3rd Croatian Conference on Earthquake Engineering - 3CroCEE
19–22 March 2025, Split, Croatia
Copyright © 2025 CroCEE
DOI: https://doi.org/10.5592/CO/3CroCEE.2025.86

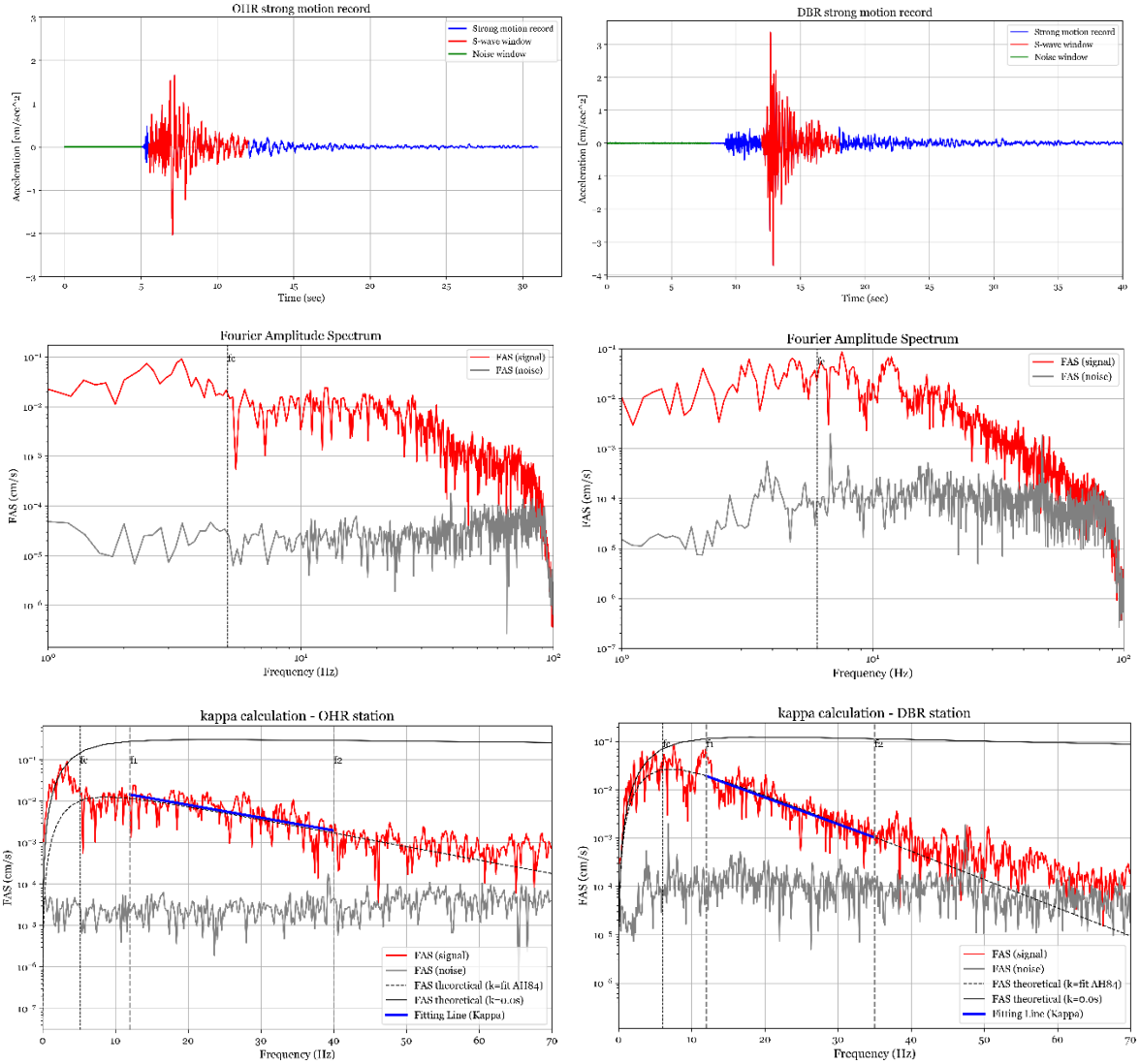


Figure 5. Example of kappa calculation for OHR station - NS component for earthquake event with Mw =3.8, Re = 8.01 km, k = 0.0226s and DBR station – NS component for earthquake event with Mw =3.66, Re = 23.5 km, k= 0.0407s

Fig. 5 presents the procedure for kappa calculation. Two stations are shown: OHR, located on rock (type A according to EC8), and DBR, located on soil type B. The records are horizontal components from earthquakes with magnitude M_w=3.8 and R_{epi}=8.01km for the OHR station, and M_w=3.66 and R_{epi}=23.5 km for the DBR station. The obtained kappa values for these records are k=0.0226s for OHR and k=0.0407s for DBR station. The slope of the FAS is expected to be less steep for OHR (soil type A) and steeper for DBR (soil type B).

4. Results

Using York regression analysis (York et al. 2014) with errors in both variables, kappa for one standard deviation and R_{epi} for 3 km, the high-frequency decay parameter was calculated for four stations. Two of the stations are presented in Fig. 6, while the results for all four stations are provided in Table 2. The site component (k_0) was obtained from the regression line extrapolated to 0 distance, as well as from the mean value of the records up to 25 km for the stations where the majority of the data were from near

Copyright © 2025 CroCEE
DOI: https://doi.org/10.5592/CO/3CroCEE.2025.86

distances. Averaged values for the two horizontal components with a difference of less than 25% were considered, while the others were excluded from the regression. Exceptions were made for stations with a small number of records at close distances, allowing high-quality data with differences larger than 25% to be taken into account.

The regression analysis was performed twice: once using the full dataset (Fig. 6, blue line) and once excluding the outliers in one standard deviation (Fig. 5, red dashed line). There is not a significant difference between the results obtained, except for the coefficient of determination (R^2) for both regressions. The York regression without outliers provides kappa calculation with higher R^2 values, indicating a better fit of the data.

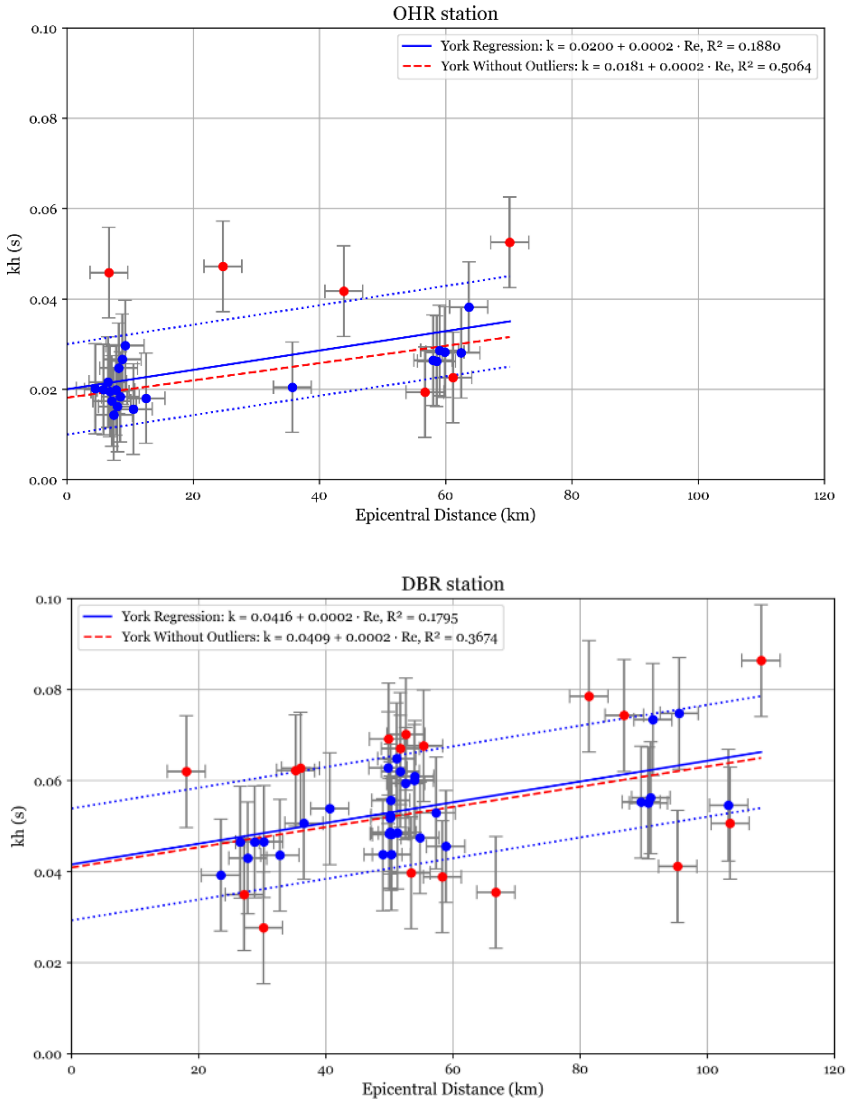


Figure 6. Distribution of individual κappa values and regression with distance for stations (OHR station up) and (DBR station down). Regressed lines plotted ± 1 standard deviation.Vertical error-bars show the uncertainty of κappa values and horizontal error-bars show uncertainty in epicentral distances with standard error set to ± 3 km.

In Fig. 6, the difference in local attenuation due to soil effects is clearly observable. For the station embedded in rock, lower values of local attenuation are observed, whereas higher values are evident for the station located on looser soil. Table 2 presents the site-specific parameter values obtained for the four stations using regression analysis and mean values up to 25 km for each station. If the number of records at close distances was at least 10, the mean value was chosen.

Copyright © 2025 CroCEE
DOI: https://doi.org/10.5592/CO/3CroCEE.2025.86

Table 2. Site component (k_0) values obtained from regression analysis using error-in-variables and mean values for distances up to 25 km, along with the number of records included in each analysis and V_{S30} values for each station

Station	k_0 regression	No. records	k_0 mean up to 25 km	No. records (0-25km)	$V_{s,30}$ [m/s]
OHR	0.0181±0.003	28	0.0232	16	1000
DBR	0.0408±0.006	49	0.0506	2	400-450
PEH	0.0281±0.010	10	0.0396	10	380-450
VAL	0.0317±0.008	9	0.0320	2	600-800

The V_{S30} values for the stations range from 380 to 1000 m/s, corresponding to two soil types, A and B, according to the EC8 classification. Fig. 7 (an updated version based on Ktenidou et al. (2014) and Stanko et al. (2017)) presents the compiled κ_0–V_{S30} values for various global regions where κ_0 was calculated using the AH84 method, alongside the measured κ_0 and V_{S30} values for stations in North Macedonia. This figure demonstrates that the near-site attenuation (κ_0) values observed for North Macedonian stations are closely aligned with the global κ_0 values reported in previous studies.

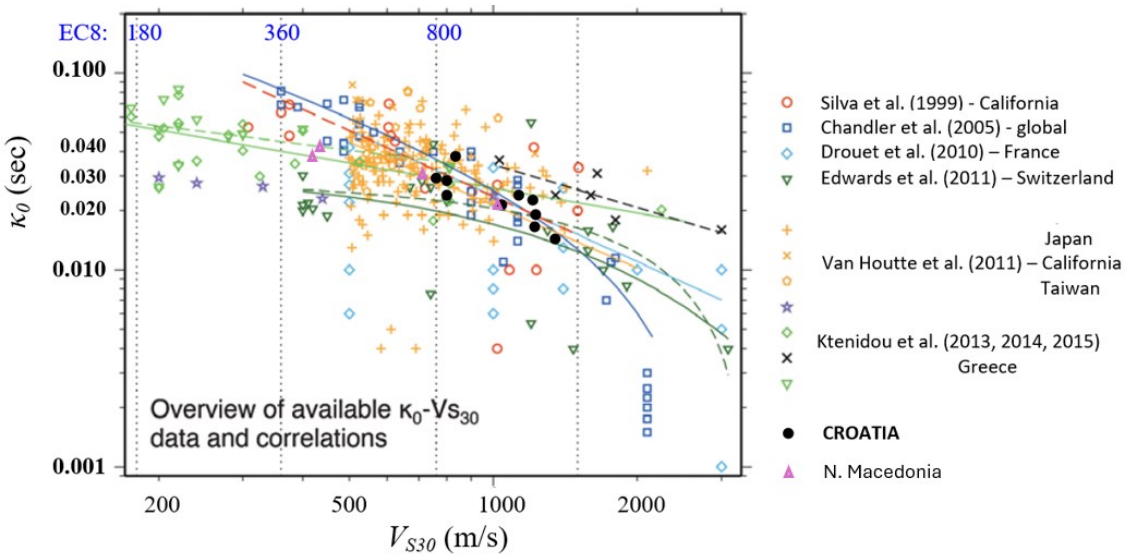


Figure 7. Existing κ_0–V_{S30} correlations in the literature (coloured markers and their fit lines for particular regions are shown in legend). Adapted from Ktenidou et al. (2014) and Stanko et al. (2017). κ_0 and $V_{S,30}$ values for N. Macedonian stations are shown by pink triangles. Site $V_{S,30}$ classes according to EC 8 (blue numbers) are shown above plot.

Fig. 8 shows a 3D plot of kappa values as a function of earthquake magnitude and epicentral distance for station installed on rock (OHR station, Fig.8 left) and for stations on soil (DBR, PEH, VAL stations, Fig.8 right). Lower values for the high - frequency parameter is obtained for OHR – rock station. Fig. 9 presents two 2D plots showing the same correlations for all the stations combined. It is noticeable that the values increase with distance, while there is no particular correlation with magnitude especially for range in 3 to 4. Earthquakes with high magnitudes and close distances are sparse, so it can't be evaluated the magnitude impact on kappa for higher magnitude values in close distance.

Copyright © 2025 CroCEE
DOI: https://doi.org/10.5592/CO/3CroCEE.2025.86

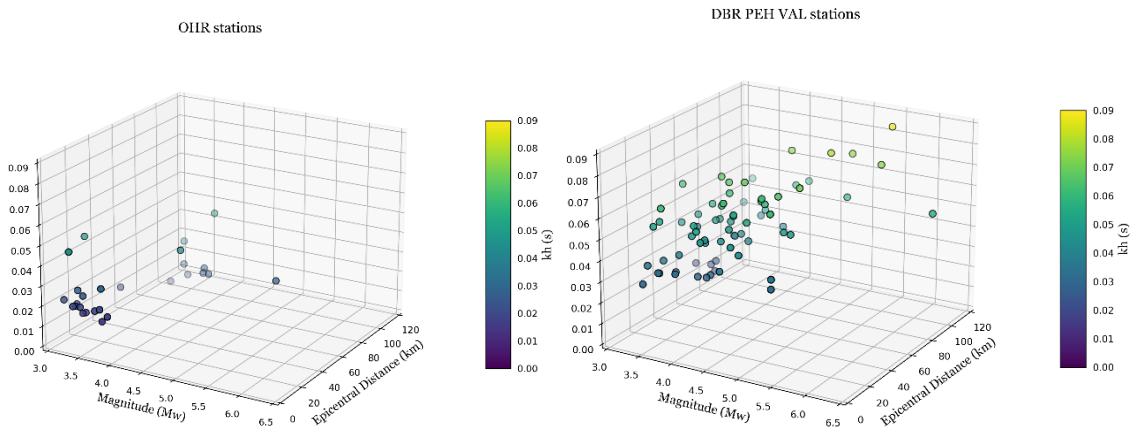


Figure 8. 3D plot of obtained results for kappa in correlation with M_w and R_{epi}

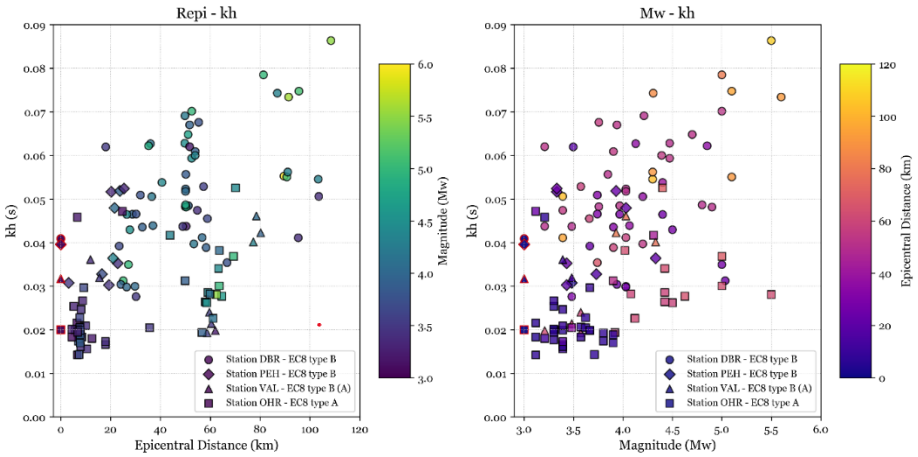


Figure 9. Correlation of kappa parameter with epicentral distance (R_{epi}) and Moment magnitude (M_w), site-specific component k_0 for each station is marked as a symbol with red outline

5. Conclusion

In this article, the kappa parameter and its site–specific component was estimated for four station locations in North Macedonia. For the calculation good – quality earthquake records from the IZIIS strong motion network were used. It was investigated the parameter dependance on epicentral distance, site conditions, and earthquake magnitude. The results from this study could be valuable related to attenuation ground modelling and updating seismic hazard maps in the region.

The observed results provide an estimated correlation with the magnitude and distance of the occurred earthquakes in the region.

It can be seen a suitable correlation with the soil conditions on the analyzed locations. Owing to geological conditions, sites with higher shear wave velocity exhibit lower k_o values, while for lower share wave velocity exhibit higher values corresponding to a region with significant attenuation. The estimated values for the OHR station (V_{s30}=1000m/s) are k_0=0.0232s, while for the VAL (V_{s30} = 600-800m/s), DBR (V_{s30}=400-450m/s), and PEH (V_{s30}=380-450m/s) are k_0=0.0317s, k_0=0.0408s, and k_0=0.0396s, respectively. The obtained results are consistent with the expected range observed in previous studies conducted in other countries.

Copyright © 2025 CroCEE
DOI: https://doi.org/10.5592/CO/3CroCEE.2025.86

References:

[1] Anderson, J., Hough, S. (1984): A model for the shape of the Fourier amplitude spectrum of acceleration at high frequencies. Bulletin of the Seismological Society of America, 74(5), 1969–1993. doi: 10.1785/BSSA0740051969.

[2] Boore, D.M., Joyner, W. (1997): Site amplifications for generic rock sites. Bulletin of the Seismological Society of America, 87(2), 327–341.

[3] Biro, Y., Renault, P. (2012): Importance and impact of host-to-target conversions for ground motion prediction equations in PSHA. Proceedings of the 15th World Conference of Earthquake Engineering, Lisbon, Portugal.

[4] Brune, J.N. (1970): Tectonic stress and the spectra of seismic shear waves from earthquakes. Journal of Geophysical Research, 75, 4997–5009. doi: 10.1029/JB075i026p04997.

[5] Cotton, F., Scherbaum, F., Bommer, J.J., Bungum, H. (2006): Criteria for selecting and adjusting ground-motion models for specific target regions: Application to Central Europe and rock sites. Journal of Seismology, 10, 137–156.

[6] Douglas, J., Bungum, H., Scherbaum, F. (2006): Ground motion prediction equations for southern Spain and southern Norway obtained using the composite model perspective. Journal of Earthquake Engineering, 10, 33–72.

[7] Douglas J, Gehl P, Bonilla LF, Gelis C. (2010): A j model for mainland France. Pure Appl Geophys. 167(11):1303–1315. doi: 10.1007/s00024-010-0146-5.

[8] Edwards, B., Fäh, D., Giardini, D. (2011): Attenuation of seismic shear wave energy in Switzerland. Geophysical Journal International, 185, 967–984. doi: 10.1111/j.1365-246X.2011.04987.

[9] Garevski, M., Gjorgjevska, I., Dojchinovski, D. (2016): Geophysical investigations - Pedestrian bridge in Ohrid (Center-Kaneo), Pangea Inzenering Report No. 08-39, 2016.

[10] Konno K. and T. Ohmachi (1998): Ground motion characteristics estimated from spectral ratio between horizontal and vertical components of microtremor, Bull. Seism. Soc. Am. 88, 228–241.

[11] Ktenidou, O.J., Gelis, C., Bonilla, L.F. (2013): A study on the variability of kappa (κ) in a borehole: Implications of the computation process. Bulletin of the Seismological Society of America, 103(2A), 1048–1068. doi: 10.1785/0120120093.

[12] Ktenidou, O., Cotton, F., Abrahamson, N.A., Anderson, J.G. (2014): Taxonomy of κ: A review of definitions and estimation approaches targeted to applications. Seismological Research Letters, 85, 135–146. doi: 10.1785/0220130027.

[13] Ktenidou, O.J., Abrahamson, N.A., Darragh, R.B., Silva, W.J. (2016): A methodology for the estimation of kappa (κ) from large datasets: Example application to rock sites in the NGA-East database and implications on design motions. PEER Report No. 2016/01.

[14] Milutinovic, Z., Salic, R., Dumurdzanov, N., et al. (2016): Seismic zoning maps for Republic of Macedonia according to the requirements of MKS-EN 1998-1:2004 - Eurocode 8. IZIIS Report, 2016-26.

[15] Palmer, S. M. (2022): Examining κ, the high frequency spectral decay parameter, in Eastern Canada, Electronic Thesis and Dissertation Repository. 8680. https://ir.lib.uwo.ca/etd/8680.

[16] Palmer, S. M., Atkinson G. M. (2020): High frequency decay slope of spectra (kappa) for M≥3.5 earthquakes on rock sites in eastern and western Canada, Bull. Seism. Am. 110(2), 471-488. Doi: 10.1785/0120190206.

[17] Parolai, S., Bindi, D. (2004): Influence of soil-layer properties on κ evaluation. Bulletin of the Seismological Society of America, 94, 349–356.

[18] Silva, W., Darragh, R., Gregor, N., Martin, G., Abrahamson, N., Kircher, C. (1998): Reassessment of site coefficients and near-fault factors for building code provisions. Technical Report Program Element II: 98-HQGR-1010, Pacific Engineering and Analysis, El Cerrito, USA.

[19] Stanko, D., S. Markusic, T. Korbar, and J. Ivancic (2020): Estimation of the high frequency attenuation parameter kappa for the Zagreb (Croatia) seismic stations, Applied Sciences 10, doi: 10.3390/app10248974.

Copyright © 2025 CroCEE
DOI: https://doi.org/10.5592/CO/3CroCEE.2025.86

[20] Stojmanovska, M., Dojcinovski, D., et al. (2020–2021): Development and upgrading of strong motion network, Phase 1: Database, website, and unified approach to signal processing. Report IZIIS 2021-66, financed by the Institute of Earthquake Engineering and Engineering Seismology, UKIM, Skopje, North Macedonia.

[21] Van Houtte, C., Drouet, S., Cotton, F. (2011): Analysis of the origins of κ (kappa) to compute hard rock to rock adjustment factors for GMPEs. Bulletin of the Seismological Society of America, 101(6), 2926–2941. doi: 10.1785/0120100345.

[22] York, D., Evenson, N., Martinez, M., Delgado, J. (2004): Unified equations for the slope, intercept, and standard errors of the best straight line. American Journal of Physics, 72, 367–375.

Proceedings of the 3rd Croatian Conference on Earthquake Engineering - 3CroCEE
19–22 March 2025, Split, Croatia
Copyright © 2025 CroCEE
DOI: https://doi.org/10.5592/CO/3CroCEE.2025.35

A COLLABORATIVE FRAMEWORK TO MODEL THE SEISMIC VULNERABILITY OF RC BUILDINGS USING SIMULATED DESIGN

Volkan Ozsarac[(1)], Nuno Pereira[(2)], Hossameldeen Mohamed[(3)], Xavier Romão[(4)], Gerard O'Reilly[(5)], Helen Crowley[(6)]

[(1)] *Researcher, EUCENTRE Foundation, ozsarac.volkan@eucentre.it*
[(2)] *Researcher, University of Porto, nmsp@fe.up.pt*
[(3)] *Assistant Professor, Aswan University, hossam.ahmed@aswu.edu.eg*
[(4)] *Associate Professor, University of Porto, xnr@fe.up.pt*
[(5)] *Associate Professor, Scuola Universitaria Superiore IUSS Pavia, gerard.oreilly@iusspavia.it*
[(6)] *Secretary General, GEM Foundation, helen.crowley@globalquakemodel.org*

Abstract

The seismic vulnerability assessment of the diverse categories of buildings found across building stocks requires specific methodologies that can capture the wide range of standards, regulations, construction practices, architectural layouts, earthquake design scenarios, and available knowledge. Previous vulnerability models have employed varying assessment approaches, building taxonomies, representations of seismic loading, and, in some instances, relied on a limited number of representative structures to represent an entire building class. Consequently, these models often fail to fully capture building-to-building variability and inadequately address multiple sources of uncertainty, particularly in models intended for large regional applications. Addressing these issues requires a probabilistic approach where seismic vulnerability is assessed using models of building portfolios that are able to reflect, in a unified manner, features related to engineering design practice, as well as construction variability and quality.

In this context, this paper introduces a collaborative framework that performs the simulated design of European reinforced concrete buildings, and presents its integration into the Built Environment Data platform via developed open-source software tools. In particular, it describes how the simulated design approach considers past and current seismic design procedures and how it reflects building-to-building variability. Through the use of open-source software and open data, the structural engineering community in Europe can contribute to the database of design codes covered by the framework. Following the design process, the referred tools generate the *OpenSees* computational models that can then be used to perform nonlinear analyses of the designed buildings and obtain probabilistic seismic demand models. These will ultimately support the development of fragility functions and vulnerability models. The framework's simulated design capabilities are demonstrated through a series of examples that highlight notable distinctions among the building classes under consideration and emphasize the importance of the attributes involved in the analysis.

Keywords: building portfolio, building variability, design codes and regulations, nonlinear model, open-source; seismic design, simulated design, reinforced concrete.

1. Introduction

In seismic risk assessment, physical vulnerability modelling plays a cruicial role in evaluating the seismic performance of buildings during earthquakes. This typically involves developing fragility functions, which describe the probability of a structure reaching or exceeding a certain damage state, given the occurrence of a specific intensity of ground shaking. Several methodologies exist for deriving fragility functions [1], with analytical approaches (e.g., [2,3]) being widely adopted due to their transparency and objectivity, despite high computational demands.

Over the years, several national [4–7] and regional [8–10] initiatives have contributed to the development of fragility functions. While these studies have significantly advanced the field, they often rely on generalized building classes, limited archetype models, or simplified assessment approaches that fail to fully capture building-to-building variability and multiple sources of uncertainty. A systematic approach is needed to integrate diverse construction practices, evolving design codes, and regional seismic demands into vulnerability models.

Proceedings of the 3rd Croatian Conference on Earthquake Engineering - 3CroCEE
19–22 March 2025, Split, Croatia
Copyright © 2025 CroCEE
DOI: https://doi.org/10.5592/CO/3CroCEE.2025.35

To tackle some of these challenges, which are also prevalent across Europe, the European exposure model [11], developed as part of the Horizon 2020 SERA project (http://www.sera-eu.org), introduced an improved taxonomy for RC frame buildings. This approach integrates seismic design code evolution and seismic demand zonation as key classification attributes. Traditional exposure models mainly use morphological characteristics such as construction year, number of storeys, material type. However, these parameters alone do not adequately reflect a building's strength or ductility. Earlier methods attempted to classify ductility levels based on construction era and regional seismicity, but they lacked adaptability across different time periods and geographical areas. To address this, Crowley et al. [12] proposed a novel mapping scheme that separates seismic strength (represented by the design lateral force coefficient, β) from seismic design principles (reflecting ductility-related aspects). In that mapping scheme, the taxonomy is comprised of four design classes, representing the prevalent seismic design practices in Europe during different periods (CDN: absence of seismic design, CDL: designed for lateral resistance using allowable stress design, CDM: designed for lateral resistance with modern limit state design, and CDH: designed for lateral resistance as in CDM coupled with target ductility requirements). The adoption of these categories provided a harmonised classification of seismic design practices across Europe, capturing not only significant changes in seismic zonation but also the evolution of seismic design regulations, structural engineering principles, and construction techniques. While initially developed for RC frame structures in Europe, this framework has the potential to be expanded to include additional building taxonomies tailored to specific national contexts.

While Crowley et al. [12] improved RC building classification, exposure models still lack detailed geometric and structural attributes. In this regard, simulated design procedures, as recognized in Eurocode 8 – Part 3 [13], offer a solution by reconstructing historical design decisions with minimal input variables such as geometry, material properties, and construction quality. Previous studies (e.g., [14–17]) have applied these methods to automate building layout generation and reduce epistemic uncertainty in vulnerability assessments. This methodology was also applied in developing vulnerability curves for low- to mid-rise RC frame buildings, reflecting typical European construction practices, as part of the 2020 European Seismic Risk Model [18]. To account for variability among buildings within the same classification, unknown geometric variables and attributes were stochastically assigned based on statistical distributions.

However, building properties such as span lengths, story heights, and material strengths vary significantly by region, and building codes can evolve differently in response to the seismic events. In fact, a detailed analysis of a specific country's standards (e.g., [19]) can reveal deviations from the generalised building class definitions proposed in Crowley et al. [11]. Current simulated design methods are usually in line with specific design codes, but they lack a broader, adaptable framework. Additionally, despite their influence on seismic performance, many approaches do not incorporate common design practices, such as column uniformity, preferred section dimensions, and reinforcement limits. A further limitation is the discrepancy between real buildings and those strictly modelled using design rules, as construction quality affects material properties, detailing, and geometric configurations. These factors are rarely integrated into seismic design frameworks, reducing the accuracy of risk assessments [20]. Furthermore, no existing framework systematically incorporates modelling strategies to address building class deficiencies identified through experimental (e.g., [21,22]) or post-earthquake reconnaissance studies (see [23,24]).

To address these challenges systematically, this paper briefly introduces a flexible, unified simulated design framework that extends the SERA project's advancements using object-oriented programming in Python. A key innovation is the adoption of composition over inheritance, enabling the development of scalable structural design solutions that accommodate past and present design codes while maintaining the adaptability and generality of the design procedures. The framework generates simulated designs for building portfolios having randomised general characteristics and produces corresponding computational models that account for construction quality effects. These will ultimately support the development of fragility functions and vulnerability models that account for building-to-building variability. While the current focus is RC moment-resisting frame (MRF) buildings, the framework is adaptable to other structural types. As an open-source tool based on widely used

Copyright © 2025 CroCEE
DOI: https://doi.org/10.5592/CO/3CroCEE.2025.35

programming languages, the framework encourages contributions from the engineering community, facilitating the integration of diverse seismic design practices. To further support collaboration, the *SimDesign* framework proposed herein will be incorporated into the Built Environment Data (BED) initiative (www.builtenvdata.eu). To demonstrate its applicability, a series of case studies are carried out based on European design practices, highlighting influence of the variations in building taxonomy attributes and geometry on seismic design and capacity.

2. Methodology

The proposed simulated design framework offers a clear four-step workflow (illustrated in Figure 1) for generating representative structural designs of a building stock within a specific region and their corresponding 3D nonlinear numerical models in *OpenSees* [25]. These models support the development of vulnerability models, ensuring that key variables influencing building behaviour are clearly defined, thereby enabling an accurate description of building taxonomy.

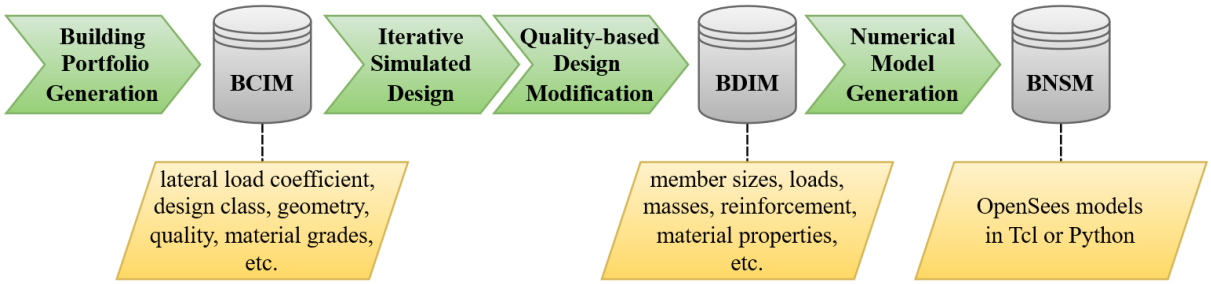


Figure 1. General overview of the workflow defined for the proposed simulated design framework.

The first step of the framework involves generating an information dataset that defines the general characteristics of buildings within a given portfolio. This dataset includes primary attributes, such as the number of storeys, β, and design class, which reflect region-specific seismic design practices in effect. Additionally, secondary attributes, including material grades and construction quality levels, as well as geometry variables like in-plan configurations and storey heights, are assigned to account for building-to-building variability. These attributes are determined through random sampling from probability distributions, which can be derived from existing databases or adjusted to align with regional contexts. The dataset generated at this stage is stored in the *Building Class Information Model (BCIM)* database, serving as the foundation for the subsequent design process.

In the second step, each building realization within the BCIM undergoes a simulated design process that replicates engineering decision-making to produce feasible structural solutions. Accounting for regional seismicity through β, this process iteratively determines structural member dimensions and reinforcement layouts, ensuring compliance with applicable seismic design codes and construction practices. The design methodology is adaptable, allowing for buildings to be modelled using gravity-load-only designs, as in older structures, or seismic load combinations, as in modern seismic-resistant buildings. Likewise, the framework can integrate country-specific design classes while preserving the flexibility of its iterative design algorithms. This adaptability supports the ongoing enhancement of the framework, ensuring its relevance across various regions and its ability to accommodate changing seismic design standards.

The third step introduces construction quality modifications to reflect real-world deviations from idealized designs. Variations in material properties, reinforcement detailing, and potential spatial irregularities are incorporated to capture differences in workmanship and construction standards. These modifications account for construction quality levels categorized as *low*, *moderate*, or *high*, ensuring that the final structural models realistically represent as-built conditions rather than purely theoretical designs. At the end of this stage, the *Building Design Information Model (BDIM)* database is created, storing final building details, such as material properties, reinforcement configurations, and section dimensions.

Copyright © 2025 CroCEE
DOI: https://doi.org/10.5592/CO/3CroCEE.2025.35

The final step involves the development of numerical models in *OpenSees*, utilizing both *.tcl* and *.py* interpreters [26]. These models incorporate structural features associated with both construction quality and design classifications, enabling realistic seismic performance assessment. Specific failure mechanisms, such as shear failure in non-capacity-designed columns and bond-slip effects in low-quality construction, are explicitly modelled. Additionally, along with the generated numerical models, modal and nonlinear static pushover analyses routines are stored in the *Building Nonlinear Structural Model (BNSM)* database.

To support future extensions and facilitate its applicability the framework is implemented in Python [27] using object-oriented programming to ensure modularity and scalability (available at https://github.com/builtenvdata/simulated-design). Its implementation for the RC-MRF systems consists of four core packages: *geometry*, *bcim*, *bdim* and *bnsm*, each contributing to the execution of the described workflow. The following sections provide a detailed explanation of the general steps followed in this implementation while omitting software-specific details for brevity.

3. Building Portfolio Generation

For large-scale seismic risk assessments, buildings within an exposure model are categorized based on key structural attributes [28]. In the SERA project, the primary attributes used for classification include the construction material, lateral load-resisting system, number of storeys, and expected ductility level, which is inferred from the seismic design regulations in place at the time of construction (i.e., the design class) and the hazard level (represented by β). These attributes are combined to generate a taxonomy string [28,29], which serves as an identifier for each building class. When additional data is available, the taxonomy can be further refined to include beam and column types, construction quality levels, and material properties. However, since detailed structural information is often unavailable, the uncertainty associated with these secondary attributes must be incorporated into the building portfolio. Additionally, buildings sharing the same taxonomy string can exhibit significant geometric variations, such as differences in in-plan layouts, bay widths, and storey heights. These variations are inherent to the building stock and must be accounted for to adequately capture the building-to-building variability.

To address these uncertainties, the framework utilizes the primary attributes (i.e., number of storeys, design class, and β coefficient) to generate probabilistic samples of secondary attributes and geometry variables. The secondary attributes include those provided in Table 1, and steel and concrete grades, which are mapped to their respective material properties during the design process. The geometry variables considered in sampling include typical and ground storey heights, bay widths along principal directions (X and Y), staircase bay width along the X axis, and layout configurations. The layout database currently represents each configuration by the number of evenly spaced bays in both horizontal directions and the designated staircase location, though it can be expanded to include irregular plan layouts. The resulting BCIM dataset, generated for a given sample size or portfolio, provides a comprehensive set of attributes and geometric properties for each building, guiding the simulated design process.

Table 1. The secondary taxonomy attributes in BCIM concerning beams, columns and slabs.

Colum Type	Beam Type	Slab Type	Construction Quality
Square	Emergent (EB)	Solid two-way cast-in-situ slabs (SS2)	Low
Rectangular	Wide (WB)	Solid one-way cast-in-situ slabs (SS1)	Moderate
-	-	Composite slabs with pre-fabricated joists and ceramic blocks (HS)	High

The sampling process, managed by the *bcim* package and illustrated in Figure 2, employs random generators and decision trees informed by engineering experience and judgment. The random generators apply probability distributions to model the general characteristics of a given building stock, while the decision trees establish correlations between certain random properties and other structural

Copyright © 2025 CroCEE
DOI: https://doi.org/10.5592/CO/3CroCEE.2025.35

attributes, often incorporating assumptions from the design process. Before initiating the sampling, the framework retrieves probabilistic model parameters from a corresponding data file (a .json[1] file specific to the design class, e.g. CDL). While default values are provided for each parameter, they can be modified by the user to reflect more accurate or region-specific building data.

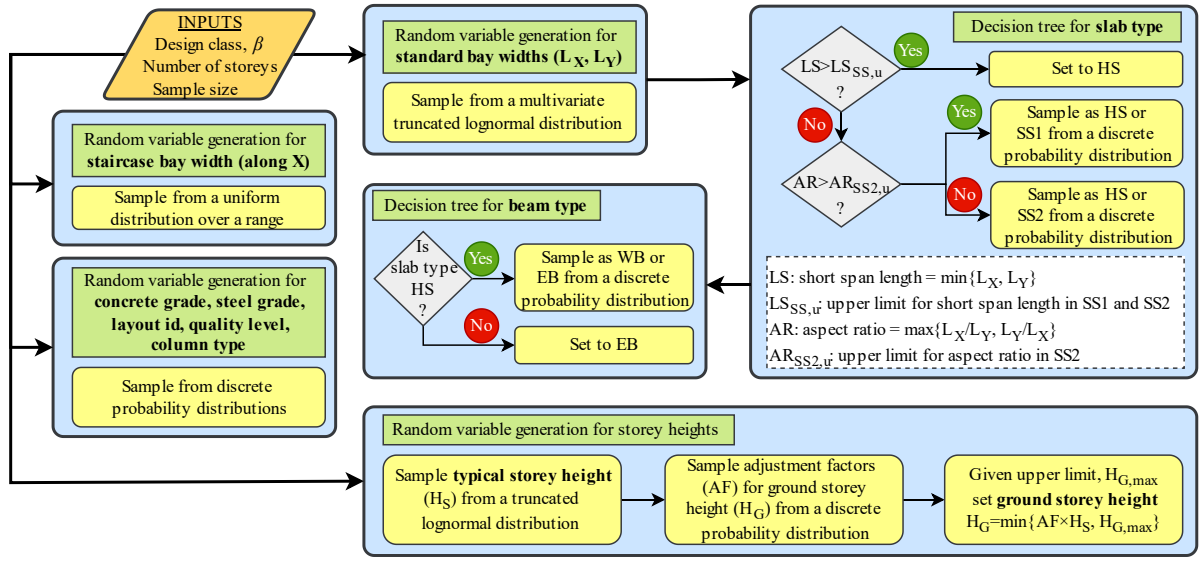
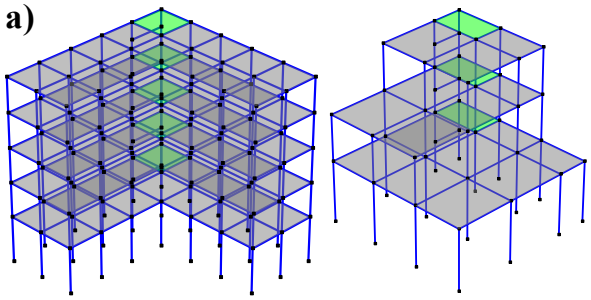


Figure 2. Illustration of the sampling process for BCIM data generation, with sampled data highlighted in bold.

After generating the dataset, the framework utilises the *geometry* package to initialize building geometries as Python objects, defining each building's grid system based on its in-plan layout and number of storeys, with grid spacing determined by bay widths and storey heights. Structural components, i.e., beams, columns, joints, slabs and staircases, are represented as mesh objects, ensuring proper connectivity during design and numerical modelling. While the framework supports irregular geometries, the current layout database is limited to regular, orthogonal configurations (see Figure 3). Moreover, it is worth noting that the buildings feature a single continuous staircase, supported by X-direction beams at mid-storey levels. Once the BCIM dataset and building geometry objects are created, they serve as inputs for the simulated design process, and guide the development of the BDIM dataset.



Layouts Database

Layout ID	Number of bays in X	Number of bays in Y	Staircase grid in X	Staircase grid in Y
B01	3	2	1	0
B02	5	2	2	0
B03	7	2	3	0
B04	3	3	1	0
B04b	3	3	1	1
B05	5	3	2	0
B06	7	3	3	0
B07	3	3	0	0
B08	3	4	0	0
B09	3	5	0	0
B10	3	6	0	0

Figure 3. Example of a-) Irregular and b-) regular frame geometries (green indicates staircase location).

4. Iterative Simulated Design

Regardless of the country or region, the seismic design of RC frame buildings follows a structured sequence of steps based on engineering principles and regulatory building codes. The process begins with defining seismic loads and general building characteristics. Engineers determine the seismic

[1] An example of .json file, available on the following GitHub repository:
https://github.com/builtenvdata/simulated-design/blob/main/simdesign/rcmrf/bcim/data/eu_cdl.json

Copyright © 2025 CroCEE
DOI: https://doi.org/10.5592/CO/3CroCEE.2025.35

hazard level for a given location and return period, typically represented by peak ground acceleration or derived from an elastic acceleration response spectrum. These are then adjusted based on site-specific conditions, building importance, and behaviour factors to determine the design lateral force coefficient or the design acceleration response spectrum. It is worth noting that, herein, the former serve as the seismic hazard input for the framework. Simultaneously, the architectural layout is assessed to identify the placement of key structural components, including beams, columns, and slabs, and to define the lateral load-resisting system. Finally, the initial structural member types and materials are selected, completing the conceptual design phase. As outlined previously, the framework compiles this information in the first step to guide simulated design process, which implements the iterative design algorithm illustrated in Figure 4.

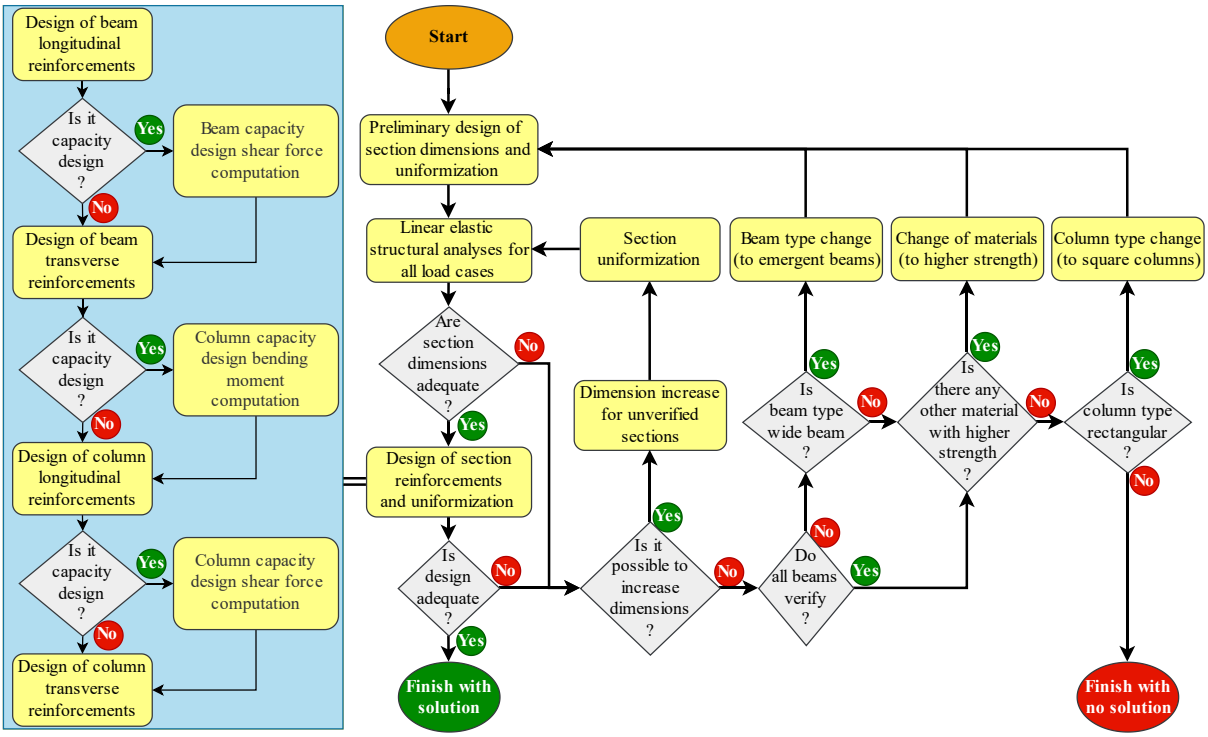


Figure 4. Iterative design algorithm implemented in the framework.

The iterative simulated design procedure begins with the preliminary member sizing, where initial dimensions for columns, beams, and slabs are established based on engineering practice rules, building code requirements, and expected gravity loads. These initial dimensions serve as a baseline for subsequent design iterations. As a common practice, the section dimensions are then standardised to ensure uniformity in beam sections along continuous spans and column sections along the building height. Notably, column dimensions can be uniformised over a specified number of storeys based on the construction practices rather than the entire building height.

Following the preliminary design, an elastic numerical model is developed, and linear elastic analysis is conducted for various loading scenarios. Seismic loads are applied using the equivalent lateral force method, with stiffness adjustments are made to account for cracked section properties where required. The computed member forces are then combined following the load combinations prescribed by building codes. Subsequently, the section dimensions of each member are verified against the design forces. This process includes assessing economic feasibility, verifying admissible stresses, and performing global checks such as drift limits if required by the code.

The next step involves reinforcement design, which follows either working (or allowable) stress design (for older codes) or limit state design (for modern codes). The reinforcement configuration is determined based on available steel diameters and detailing practices. If capacity design principles apply, the procedure also includes:

Copyright © 2025 CroCEE
DOI: https://doi.org/10.5592/CO/3CroCEE.2025.35

- Determining beam longitudinal reinforcement and computing capacity design shear forces for transverse reinforcement.
- Computing capacity design bending moments for columns to define longitudinal reinforcement, followed by deriving capacity design shear forces for transverse reinforcement.

Once the reinforcement layouts are configured for each relevant member section, they are adjusted to align with construction practices. Lastly, the local ductility checks like verification against the maximum longitudinal reinforcement ratio are also performed to verify compliance with reinforcement ratio limits.

If the design fails verification or no suitable reinforcement configuration is found, section dimensions are increased, and the process is repeated. This iterative approach continues until a valid design is achieved. If maximum allowable section dimensions are exceeded without a feasible solution, materials or types of structural members (i.e., beam and column types) must be revised, requiring a restart of the design process. This iterative methodology has been systematically automated within the framework, ensuring efficient convergence toward structural designs compliant with regional or national design practices.

The *bdim* package is structured to align with the iterative design procedure, serving as a key component of the framework that facilitates the simulated design of buildings while ensuring compliance with regional and historical seismic design standards. It consists of multiple sub-packages, each corresponding to a specific building design class, collectively referred to as Design Class Constructors (DCCs). These DCCs implement design methodologies and rules that reflect their respective seismic codes and regional construction practices. At the core of the *bdim* package is a foundational base library, which provides a general interface and shared methods, such as iterative design procedure, for all DCCs. This base library serves as a template, allowing DCCs to inherit general functionalities and modify or extend them as needed to align with specific seismic code requirements and regional practices. This modular design ensures that the *bdim* package remains highly flexible and reusable, enabling the seamless integration of new DCCs into the framework. Developers can focus on implementing specific design rules while leveraging the pre-existing functionalities provided by the base library.

5. Quality-Based Design Modification

Since the degree of conformity between the designed and constructed structure can vary construction quality, quality-based design modifications are added to the structural design solution which is determined by executing the iterative design algorithm. Specifically, spatial variations that commonly arise during the construction process are incorporated into the beam and column designs. This process is carried out using the *bdim* package. Depending on the quality level, the framework adjusts stirrup spacing, concrete cover thickness, concrete strength, and the yield strength of longitudinal and transverse reinforcement, ensuring that the modified design accurately represents expected in-situ conditions for numerical modelling. To determine the modification factors, the framework employs random sampling, considering a uniform distribution for stirrup spacing and lognormal distributions for the remaining parameters.

Additionally, the framework integrates quality-related nonlinear numerical modelling considerations based on the quality level. In particular, it defines bond-slip factors [30] (ranging from 0 to 1) that influence the plastic hinge properties of beams and columns, as well as the selection of the beam-column joint model, which can be *rigid*, *elastic*, or *inelastic*. Accordingly, for all considered quality levels (*low*, *moderate*, and *high*), the bond-slip factors, beam-column joint model type, and distribution parameters for sampling the quality factors are specified within DCC implementations to introduce the corresponding quality-based modifications. Unless modifications to additional design properties or alternative distribution types are necessary, the functionalities inherited from the base library are utilised without alteration.

Copyright © 2025 CroCEE
DOI: https://doi.org/10.5592/CO/3CroCEE.2025.35

6. Numerical Model Generation

Following the adjustments for construction quality, the framework transforms the building design data stored in the BDIM into 3D nonlinear structural models, which can be analysed using *OpenSees* [25]. This is achieved through the *bnsm* package, which organizes structural components, including beams, columns, floors, joints, and foundations, as distinct objects, each encapsulating the necessary parameters for numerical modelling. Additionally, aside from the generation of the numerical models, the package facilitates modal analysis for dynamic characterization and nonlinear static pushover analysis for seismic performance assessment.

The nonlinear behaviour of frame elements is captured using a lumped plasticity approach, where plastic hinges at the ends of beams and columns are modelled using *zero-length* elements while accounting for rigid joint offsets. The in-plane flexural behaviour of beams is represented by a single rotational spring, whereas columns are assigned two rotational springs, one for each orthogonal direction. These springs utilise the *Hysteretic* uniaxial material model in *OpenSees*, with yielding moment and yielding rotation capacity determined according to Panagiotakos and Fardis [30] and Eurocode 8 – Part 3 [13], while other parameters are derived following Haselton et al. [31] and ASCE/SEI – 2017 [32]. The influence of construction quality on the plastic rotation capacity is incorporated through a bond-slip factor [30,31], ensuring that material and detailing deficiencies are accounted for in hinge properties. Additionally, each zero-length element is connected in series with a linear elastic interior element, whose stiffness is adjusted following Zareian and Medina [33] to prevent spurious damping forces from occurring during the dynamic analyses.

To account for shear failure in columns where capacity design principles are not enforced, shear springs are integrated into the *zero-length* elements. The *LimitState* model with a *ThreePoint* limit curve [34] is adopted for modelling shear hinges. In particular, the shear strength degradation model proposed by Sezen and Moehle [35], which defines a trilinear limit curve based on displacement ductility, is considered for shear hinges defined in each orthogonal direction. The shear strength is determined based on ASCE/SEI – 2017 [32], while the initial and degraded stiffness of the shear springs are derived from the expressions by LeBorgne and Ghannoum [36] and Shoraka and Elwood [37], respectively.

Beam-column joints are modelled using *zero-length* elements positioned between the central joint node and floor nodes, both of which share the same location. The central joint node, which carries the structural mass, provides connectivity between beams and columns, while floor nodes are constrained using a rigid diaphragm, simulating the effect of floor slabs. Joint flexibility is considered only in the rotational degrees of freedom along the two horizontal axes. The moment-rotation behaviour of joints is categorized as rigid, elastic, or inelastic, depending on the joint type assigned in the quality model. For inelastic joints, *Hysteretic* uniaxial material models are used, with parameters derived from expressions proposed by O'Reilly and Sullivan [38], accounting for variations in joint locations, such as roof, interior, or exterior joints. The stiffness of *elastic* joints is determined based on the first branches of their respective backbone curves.

7. Case-Study Applications

To demonstrate the framework's applicability, a sample portfolio of 50 buildings was generated. The selected RC frames were assumed to have four storeys, belong to the CDH design class, and be designed for a β value of 0.1, representing high seismicity. The sampled BCIM data exhibit noticeable variability in both secondary attributes and geometric properties, and thus, yielding significant differences in design and seismic performance of buildings. For instance, nonlinear static pushover analyses were performed for each building design using a first-mode load pattern. As shown in Figure 5, the normalized capacity curves reveal substantial differences among the buildings, highlighting the building-to-building variability within the given building class. Although not conducted in this study, further dynamic analysis using ground motion records could help develop fragility and vulnerability models for risk assessment.

Copyright © 2025 CroCEE
DOI: https://doi.org/10.5592/CO/3CroCEE.2025.35

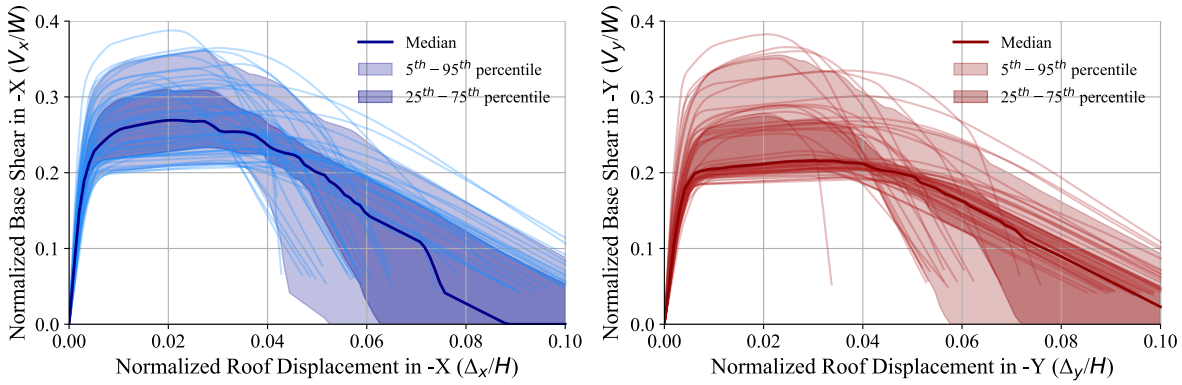


Figure 5. Capacity curves obtained for the sampled building portfolio.

To highlight the framework's simulated design capabilities, identical BCIM data—differing only in material grades specific to each design class—were processed for the design classes proposed in [11] to generate the corresponding BDIM data at various seismic hazard levels (i.e., different β values). In particular, the design classes CDN, CDL, CDM, and CDH represent seismic design practices from different periods: before the 1960s, from the 1960s to the 1970s, from the 1970s to the 2000s, and from the 2000s to the present, respectively. Following the design process, nonlinear static pushover analyses were performed, and the normalized capacity curves, shown in Figure 6, were obtained for each building design. Notably, the curves remain constant for CDN, as it follows only gravity design. In contrast, for the other design classes, the normalized base shear (or strength ratio) systematically increases with β. Moreover, in seismic design cases ($\beta > 0$), the strength ratio values progressively increase from CDN to CDH, reflecting the evolution of seismic design. Regarding ductility, CDH buildings exhibit highly ductile behavior regardless of the β value, as modern capacity design principles are followed in their design. Conversely, buildings in the other design classes demonstrate a similar limited level of ductility in the absence of seismic design. However, as the β value increases, CDL and CDM buildings generally begin to exhibit brittle behavior, with CDL showing a more extreme response, as shear or joint failure mechanisms are more likely to occur in these buildings. Overall, these outcomes show framework's capability to capture the critical differences in the design philosophies, which can be reflected in the generated portfolios.

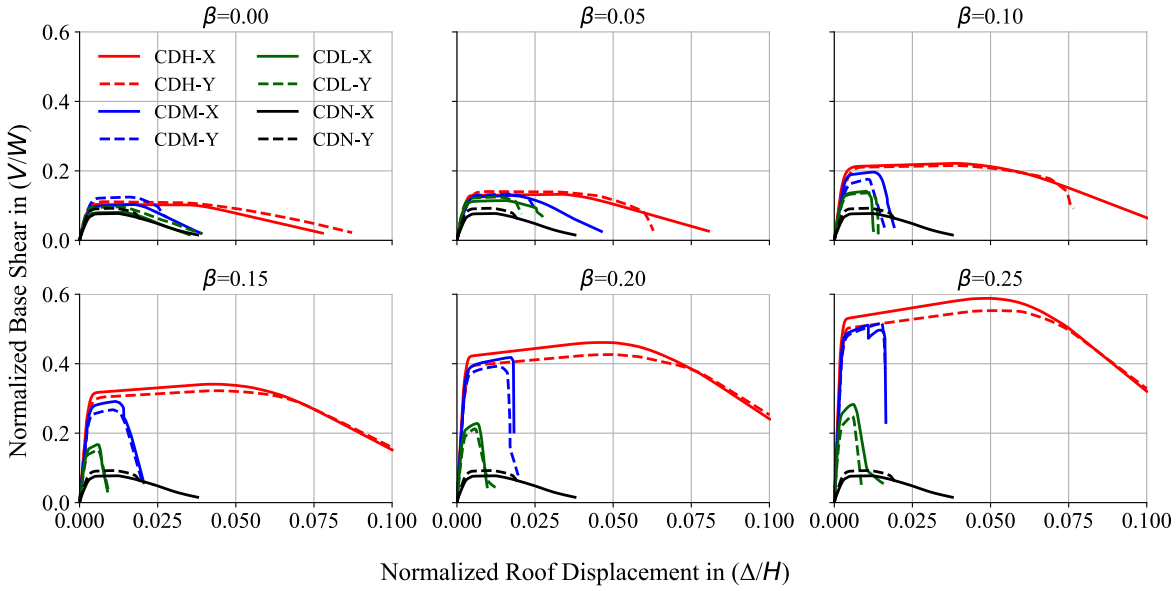


Figure 6. Capacity curves of buildings designed with different seismic design practices and hazard levels.

Proceedings of the 3rd Croatian Conference on Earthquake Engineering - 3CroCEE
19–22 March 2025, Split, Croatia
Copyright © 2025 CroCEE
DOI: https://doi.org/10.5592/CO/3CroCEE.2025.35

8. Conclusions

This article presents an innovative framework for the simulated design of buildings, offering a structured and adaptable approach to capturing building-to-building variability and the evolution of seismic design practices across different regions over time. By integrating probabilistic sampling with iterative design algorithms, the framework enables the generation of realistic building designs and their corresponding numerical models, ensuring alignment with regional or country-specific contexts. These numerical models, in turn, support the development of vulnerability models that accurately reflect the inherent variability within a given building class, thereby enhancing the reliability of large-scale (i.e., regional) seismic risk assessments.

The framework's open-source Python implementation follows object-oriented programming principles, ensuring modularity and extensibility. This allows the earthquake engineering community to seamlessly integrate the framework into existing workflows, customize it for specific regional applications, and expand its capabilities to accommodate different seismic design standards and numerical modelling techniques. The framework's capabilities have been demonstrated through an example that highlights the influence of taxonomy attributes and geometric variables in the design process. The variability captured in the simulated structural designs, as reflected in the capacity curves, effectively illustrates the distinctions between historical and modern design philosophies. These findings validate the framework's ability to generate realistic and regionally representative building portfolios.

Acknowledgements

The feedback and comments provided by Rui Pinho in the development of this framework are gratefully acknowledged as is the input of Serkan Hasanoglu on its implementation in Python. The work presented herein was carried out with financial support from the European Union through the EPOS-ON (Grant Agreement No.101131592) project. The 2nd, 3rd and 4th authors acknowledge the financial support of the Base Funding - UIDB/04708/2020 (https://doi.org/10.54499/UIDB/04708/2020) of CONSTRUCT - Instituto de I&D em Estruturas e Construções, funded by national funds through FCT/MCTES (PIDDAC).

References

1. Calvi GM, Pinho R, Magenes G, Bommer JJ, Restrepo-Vélez LF, Crowley H. Development of seismic vulnerability assessment methodologies over the past 30 years. *ISET Journal of Earthquake Technology* 2006; **43**(3): 75–104.
2. Calvi GM. A displacement-based approach for vulnerability evaluation of classes of buildings. *Journal of Earthquake Engineering* 1999; **3**(3): 411–438. DOI: 10.1080/13632469909350353.
3. Crowley H, Pinho R. Period-height relationship for existing European reinforced concrete buildings. *Journal of Earthquake Engineering* 2004; **8**: 93–119. DOI: 10.1080/13632460409350522.
4. FEMA. *HAZUS-MH MR5, Technical manual, Department of Homeland Security - Federal Emergency Management Agency*. Washington, DC: 2014.
5. Erberik MA. Fragility-based assessment of typical mid-rise and low-rise RC buildings in Turkey. *Engineering Structures* 2008; **30**(5): 1360–1374. DOI: 10.1016/J.ENGSTRUCT.2007.07.016.
6. Borzi B, Crowley H, Pinho R. Simplified pushover-based earthquake loss assessment (SP-BELA) method for masonry buildings. *International Journal of Architectural Heritage* 2008; **2**(4): 353–376. DOI: 10.1080/15583050701828178.
7. Silva V, Crowley H, Varum H, Pinho R, Sousa L. Investigation of the characteristics of Portuguese regular moment-frame RC buildings and development of a vulnerability model. *Bulletin of Earthquake Engineering* 2015; **13**(5): 1455–1490. DOI: 10.1007/s10518-014-9669-

Copyright © 2025 CroCEE
DOI: https://doi.org/10.5592/CO/3CroCEE.2025.35

y.

8. Mouroux P, Le Brun B. Presentation of RISK-UE project. *Bulletin of Earthquake Engineering* 2006; **4**(4): 323–339. DOI: 10.1007/S10518-006-9020-3/METRICS.
9. Calvi GM, Pinho R. LESSLOSS: A European Integrated Project on Risk Mitigation for Earthquakes and Landslides 2004(July).
10. Villar-Vega M, Silva V, Crowley H, Yepes C, Tarque N, Acevedo AB, *et al.* Development of a fragility model for the residential building stock in South America. *Earthquake Spectra* 2017; **33**(2): 581–604. DOI: 10.1193/010716EQS005M.
11. Crowley H, Despotaki V, Rodrigues D, Silva V, Toma-Danila D, Riga E, *et al.* Exposure model for European seismic risk assessment. *Earthquake Spectra* 2020; **36**(1_suppl): 252–273. DOI: 10.1177/8755293020919429.
12. Crowley H, Despotaki V, Silva V, Dabbeek J, Romão X, Pereira N, *et al.* Model of seismic design lateral force levels for the existing reinforced concrete European building stock. *Bulletin of Earthquake Engineering* 2021; **19**(7): 2839–2865. DOI: 10.1007/s10518-021-01083-3.
13. CEN. *Eurocode 8: Design of structures for earthquake resistance - Part 3: Assessment and retrofitting of buildings*. Brussels, Belgium: 2005.
14. Verderame GM, Polese M, Mariniello C, Manfredi G. A simulated design procedure for the assessment of seismic capacity of existing reinforced concrete buildings. *Advances in Engineering Software* 2010; **41**(2): 323–335. DOI: 10.1016/j.advengsoft.2009.06.011.
15. Masi A, Lagomarsino S, Dolce M, Manfredi V, Ottonelli D. Towards the updated Italian seismic risk assessment: exposure and vulnerability modelling. *Bulletin of Earthquake Engineering* 2021; **19**(8): 3253–3286. DOI: 10.1007/s10518-021-01065-5.
16. Del Gaudio C, Ricci P, Verderame GM, Manfredi G. Development and urban-scale application of a simplified method for seismic fragility assessment of RC buildings. *Engineering Structures* 2015; **91**: 40–57.
17. Borzi B, Pinho R, Crowley H. Simplified pushover-based vulnerability analysis for large-scale assessment of RC buildings. *Engineering Structures* 2008; **30**(3): 804–820. DOI: 10.1016/j.engstruct.2007.05.021.
18. Crowley HM, Dabbeek J, Despotaki V, Rodrigues D, Martins L, Silva V, *et al.* European Seismic Risk Model (ESRM20). *EFEHR Technical Report* 2021; **002**.
19. Pavel F, Crowley H, Romão X, Vladut R, Pereira N, Ozsarac V. Evolution of national codes for the design of RC structures in Romania. *Bulletin of Earthquake Engineering* 2024; **22**(3): 911–949. DOI: 10.1007/s10518-023-01791-y.
20. Nafeh AMB, O'Reilly GJ. Fragility functions for non-ductile infilled reinforced concrete buildings using next-generation intensity measures based on analytical models and empirical data from past earthquakes. *Bulletin of Earthquake Engineering* 2024; **22**(10): 4983–5021. DOI: 10.1007/S10518-024-01955-4/METRICS.
21. Calvi GM, Magenes G, Pampanin S. Relevance of beam-column joint damage and collapse in RC frame assessment. *Journal of Earthquake Engineering* 2002; **6**(SPEC. ISS. 1): 75–100. DOI: 10.1142/S1363246902000693.
22. Pampanin S, Calvi GM, Moratti M. Seismic behaviour of R.C. beam-column joints designed for gravity loads. *12th European Conference on Earthquake Engineering* 2002; **726**: 1–10.
23. Sezen H, Whittaker AS, Elwood KJ, Mosalam KM. Performance of reinforced concrete buildings during the August 17, 1999 Kocaeli, Turkey earthquake, and seismic design and construction practise in Turkey. *Engineering Structures* 2003; **25**(1): 103–114. DOI:

Copyright © 2025 CroCEE
DOI: https://doi.org/10.5592/CO/3CroCEE.2025.35

10.1016/S0141-0296(02)00121-9.

24. Ricci P, de Luca F, Verderame GM. 6th April 2009 L'Aquila earthquake, Italy: Reinforced concrete building performance. *Bulletin of Earthquake Engineering* 2011; **9**(1): 285–305. DOI: 10.1007/S10518-010-9204-8/METRICS.

25. McKenna F, Scott MH, Fenves GL. Nonlinear Finite-Element Analysis Software Architecture Using Object Composition. *Journal of Computing in Civil Engineering* 2010; **24**(1): 95–107. DOI: 10.1061/(asce)cp.1943-5487.0000002.

26. Zhu M, McKenna F, Scott MH. OpenSeesPy: Python library for the OpenSees finite element framework. *SoftwareX* 2018; **7**: 6–11. DOI: 10.1016/j.softx.2017.10.009.

27. Rossum G van. *Python tutorial*. Amsterdam, Netherlands: 1995.

28. Brzev S, Scawthorn C, Charleson AW, Allen L, Greene M, Jaiswal K, *et al. GEM Building Taxonomy Version 2.0*. vol. 02. GEM Foundation; 2013. DOI: 10.13117/GEM.EXP-MOD.TR2013.02.

29. Romão X, Castro JM, Pereira N, Crowley H, Silva V, Martins L, *et al. Deliverable Report D26.5 European physical vulnerability models. SERA - Seismology and Earthquake Engineering Research Infrastructure Alliance for Europe*. vol. 26. 2019.

30. Panagiotakos TB, Fardis MN. Deformations of reinforced concrete members at yielding and ultimate. *ACI Structural Journal* 2001; **98**(2): 135–148. DOI: 10.14359/10181.

31. Haselton CB, Liel AB, Taylor-Lange SC, Deierlein GG. Calibration of model to simulate response of reinforced concrete beam-columns to collapse. *ACI Structural Journal* 2016; **113**(6): 1141–1152. DOI: 10.14359/51689245.

32. ASCE. *Seismic Evaluation and Retrofit of Existing Buildings (ASCE/SEI 41-17)*. vol. 41. Reston, Virginia, USA: American Society of Civil Engineers; 2017.

33. Zareian F, Medina RA. A practical method for proper modeling of structural damping in inelastic plane structural systems. *Computers and Structures* 2010; **88**(1–2): 45–53. DOI: 10.1016/j.compstruc.2009.08.001.

34. Elwood KJ. Modelling failures in existing reinforced concrete columns. *Canadian Journal of Civil Engineering* 2004; **31**(5): 846–859. DOI: 10.1139/L04-040.

35. Sezen H, Moehle JP. Shear Strength Model for Lightly Reinforced Concrete Columns. *Journal of Structural Engineering* 2004; **130**(11): 1692–1703. DOI: 10.1061/(asce)0733-9445(2004)130:11(1692).

36. LeBorgne MR, Ghannoum WM. Calibrated analytical element for lateral-strength degradation of reinforced concrete columns. *Engineering Structures* 2014; **81**: 35–48. DOI: 10.1016/j.engstruct.2014.09.030.

37. Shoraka MB, Elwood KJ. Mechanical model for non ductile reinforced concrete columns. *Journal of Earthquake Engineering* 2013; **17**(7): 937–957. DOI: 10.1080/13632469.2013.794718.

38. O'Reilly GJ, Sullivan TJ. Modeling Techniques for the Seismic Assessment of the Existing Italian RC Frame Structures. *Journal of Earthquake Engineering* 2019; **23**(8): 1262–1296. DOI: 10.1080/13632469.2017.1360224.

Proceedings of the 3rd Croatian Conference on Earthquake Engineering - 3CroCEE
19–22 March 2025, Split, Croatia
Copyright © 2025 CroCEE
DOI: https://doi.org/10.5592/CO/3CroCEE.2025.83

SEISMIC RISK AND LOSS ASSESSMENT OF REINFORCED CONCRETE FRAME STRUCTURES STRENGTHENED BY THE ADDITION OF MASONRY INFILL WALLS

Marin Grubišić [1]

[1] *Ass. Prof., University of Osijek, Faculty of Civil Engineering and Architecture Osijek, Croatia, marin.grubisic@gfos.hr*

Abstract

This study addresses the behaviour of bare plane RC frames and RC frames strengthened by the addition of masonry infill in combination with the connection of infill and frame elements for earthquake action. The main objective was to explore the possibilities of using infill walls in RC frames as a strengthening method, observing the in-plane cyclic responses obtained through experimental tests on specific specimens. The experimental part of the study was carried out on 10 single-bay, single-storey specimens of ductile and RC frames strengthened with masonry infill (hollow clay block and solid clay brick units) of which 3 reference samples were used to evaluate the strengthening of the infill and the quality of the interconnection between the infill and the frame. The frame specimens are built to a scale of 1:2.5 and tested under constant vertical and horizontal cyclic loading. The test specimens can be grouped according to the type of infill (hollow clay block and solid clay brick units) and the type of connection between the infill and the frame. The same preliminary simplified calibration with non-linear macro models in OpenSees was performed for all test specimens for which satisfactory responses to cyclic responses were obtained compared to the experiments. The same models were used in the numerical case study for predicting the dynamic response to the application to a case study building through Incremental Dynamic Analysis (IDA), where IDA curves, fragility functions, vulnerability and loss curves, and risk measures such as Expected Annual Loss (EAL) and mean annual frequency of collapse (λ_C) were created separately for each type of strengthening to evaluate the efficiency of a particular strengthening compared to reference models.

Keywords: RC frames, Masonry infill, Seismic strengthening, Numerical modelling, Incremental Dynamic Analysis (IDA), Risk and loss assessment.

1. Introduction

Masonry-infilled reinforced concrete (RC) frames are extensively utilized structural systems, particularly prevalent in Southern and Eastern Europe. They significantly contribute to a structure's lateral stiffness and strength, essential characteristics for resisting seismic loads [1,2]. The complex and highly nonlinear interaction between masonry infill walls and RC frames has been the subject of considerable research. Despite this, accurately capturing this interaction remains a substantial engineering challenge, often resulting in the exclusion of infill contributions during structural design, seismic evaluations, and retrofitting procedures [3,4]. This omission is particularly concerning because masonry infills, when appropriately designed and distributed, can provide beneficial effects like shear walls, enhancing structural performance under seismic conditions. Conversely, their uneven distribution or partial inclusion within a structure may result in detrimental effects, potentially leading to localized structural failures and significant performance degradation [5,6].

Masonry infills are frequently chosen for their advantageous economic and physical characteristics, such as affordability, high thermal and acoustic insulation, fire resistance, and durability [7,8]. However, their inherent brittleness and high stiffness can result in substantial damage even in moderate earthquakes, leading to significant repair costs, building downtime, and increased risk to human safety [9–12]. Post-earthquake assessments repeatedly demonstrate that non-structural elements, especially masonry infills and partition walls, constitute the largest portion of repair and restoration expenses, highlighting their critical role in overall building seismic performance [1–4].

Proceedings of the 3rd Croatian Conference on Earthquake Engineering - 3CroCEE
19–22 March 2025, Split, Croatia
Copyright © 2025 CroCEE
DOI: https://doi.org/10.5592/CO/3CroCEE.2025.83

Consequently, researchers have explored various strategies aimed at improving the seismic performance of masonry-infilled RC frames. Among these strategies, strengthening methods using reinforced masonry infills have gained significant attention due to their potential to enhance both stiffness and ductility of existing structures [13–18]. Such traditional strengthening approaches generally involve reinforcing existing infill walls or constructing new ones that are structurally integrated with the RC frames, thereby optimizing their beneficial properties and reducing vulnerability.

Nonetheless, despite significant advancements in experimental and numerical research, comprehensive probabilistic assessments that integrate seismic risk, reliability, and economic implications remain relatively limited [24–26]. Performance-based earthquake engineering (PBEE) methodologies, particularly incremental dynamic analysis (IDA), offer robust frameworks for evaluating these aspects. IDA-based assessments enable detailed comparison of structural fragility, risk—expressed as mean annual frequency of collapse (λ_C), and associated seismic losses—expressed quantitatively as Expected Annual Loss (EAL)—thus providing critical insights into the benefits and trade-offs associated with different seismic strengthening strategies using masonry infills [24,27,28].

This paper extends the current state-of-the-art by systematically examining the seismic performance of RC frames strengthened using traditional masonry infills. Employing IDA-based methodologies, coupled with comprehensive fragility, hazard, risk, and loss analyses, this study aims to clearly quantify and validate the effectiveness of masonry infills as a seismic retrofitting and strengthening solution.

2. Strengthening techniques

Enhancing seismic resistance of existing reinforced concrete (RC) structures is vital for their safety and operational functionality during earthquakes. Seismic upgrading techniques typically fall into two broad categories: local measures, applied to individual structural elements, and global measures, applied to the structure. Local measures typically involve adding external reinforcement to existing structural elements, enhancing flexural and shear capacities, and ductility. When significant improvements in lateral load capacity or stiffness are needed, local methods alone might be inadequate or economically inefficient. In such cases, global strengthening strategies are employed, aiming either to enhance the structure's overall lateral strength and stiffness or reduce the seismic forces acting on it. Increasing lateral strength and stiffness often involves the introduction of new structural elements, significantly boosting lateral resistance. Alternatively, seismic demand can be mitigated through base isolation systems or energy-dissipating devices. This study specifically focuses on global strengthening approaches involving the addition of masonry infill walls to existing RC frames, as investigated experimentally by Grubišić et al. [29,30]. The effectiveness of these masonry infill walls in strengthening RC frames is assessed in terms of their capacity to enhance structural performance under seismic loading conditions [29,30].

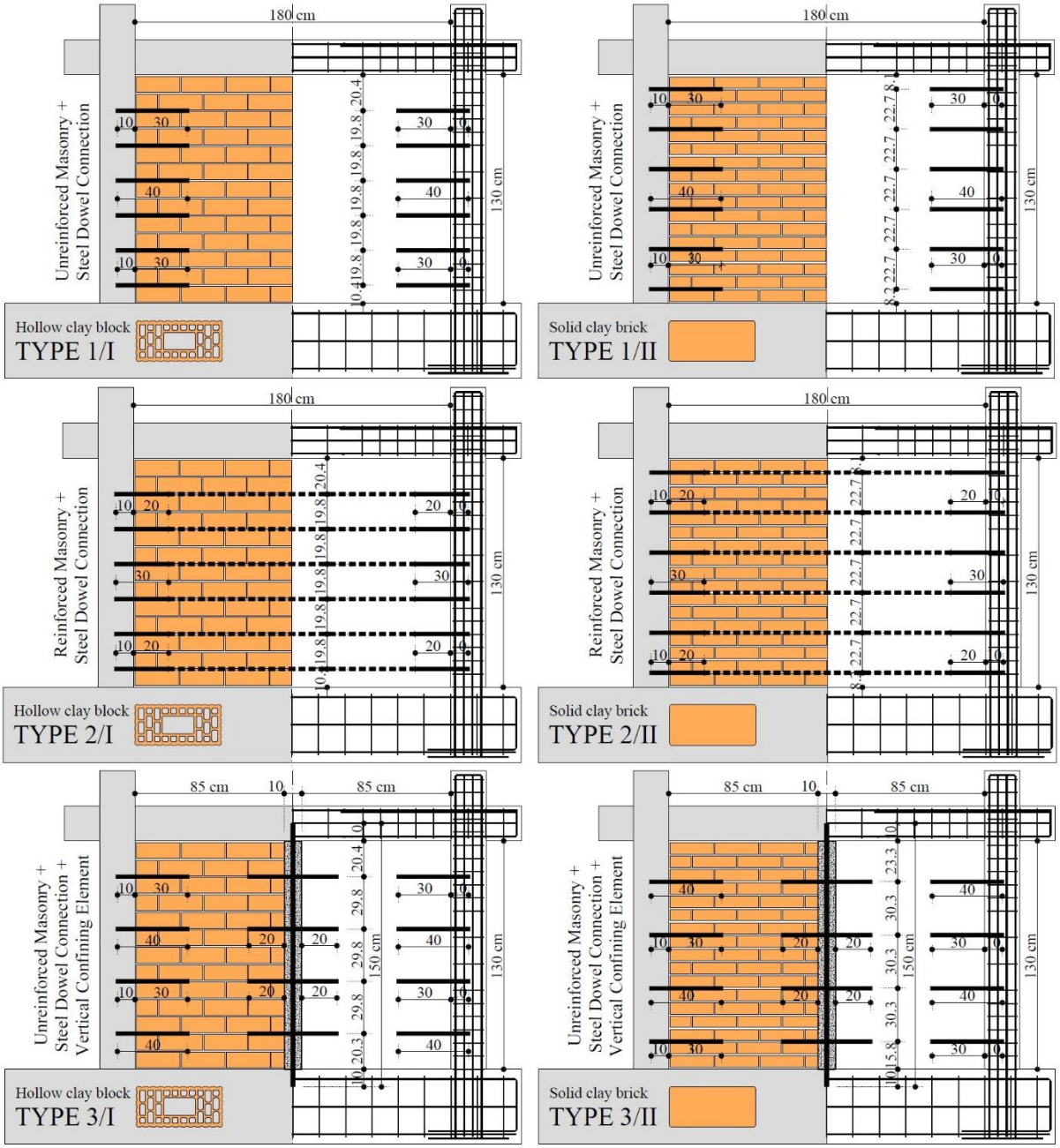
2.1. Test specimens

Experimental tests were performed on RC frame specimens strengthened using masonry infill walls. Specimens were constructed using hollow clay blocks or solid clay bricks with general-purpose cement-lime mortar (strength class M5, minimum compressive strength after 28 days: 5 N/mm²), complying with standard requirements for masonry structures (Eurocode 6). All details regarding the test specimens, testing protocol, material properties, and cyclic static responses are presented and thoroughly explained by Grubišić [30]. The tested specimens included (Figure 1):

- TYPE 1/I – Infilled ductile RC frame, hollow clay blocks with steel dowels.
- TYPE 2/I – Infilled ductile RC frame, reinforced hollow clay blocks with steel dowels.
- TYPE 3/I – Infilled ductile RC frame, hollow clay blocks with vertical confinement and steel dowels.
- TYPE 1/II – Infilled ductile RC frame, solid bricks with steel dowels.
- TYPE 2/II – Infilled ductile RC frame, reinforced solid bricks with steel dowels.

Copyright © 2025 CroCEE
DOI: https://doi.org/10.5592/CO/3CroCEE.2025.83

- TYPE 3/II – Infilled ductile RC frame, solid bricks with vertical confinement and steel dowels.
- TYPE 4 – Infilled ductile RC frame, hollow clay blocks with ECC composite (one side) and steel dowels.
- TYPE 5 – Infilled ductile RC frame, hollow clay blocks with FRP composite (one side) and steel dowels.
- TYPE 6 – Infilled non-ductile RC frame #1, solid bricks with ECC composite (both sides) and steel dowels.
- TYPE 7 – Infilled non-ductile RC frame #2, solid bricks with ECC composite (both sides) and steel dowels.
- TYPE 8/REF – Infilled ductile RC frame, hollow clay blocks (reference specimen).
- TYPE 9/REF – Infilled ductile RC frame, solid bricks (reference specimen).
- TYPE 10/REF – Bare ductile RC frame (reference specimen).



Copyright © 2025 CroCEE
DOI: https://doi.org/10.5592/CO/3CroCEE.2025.83

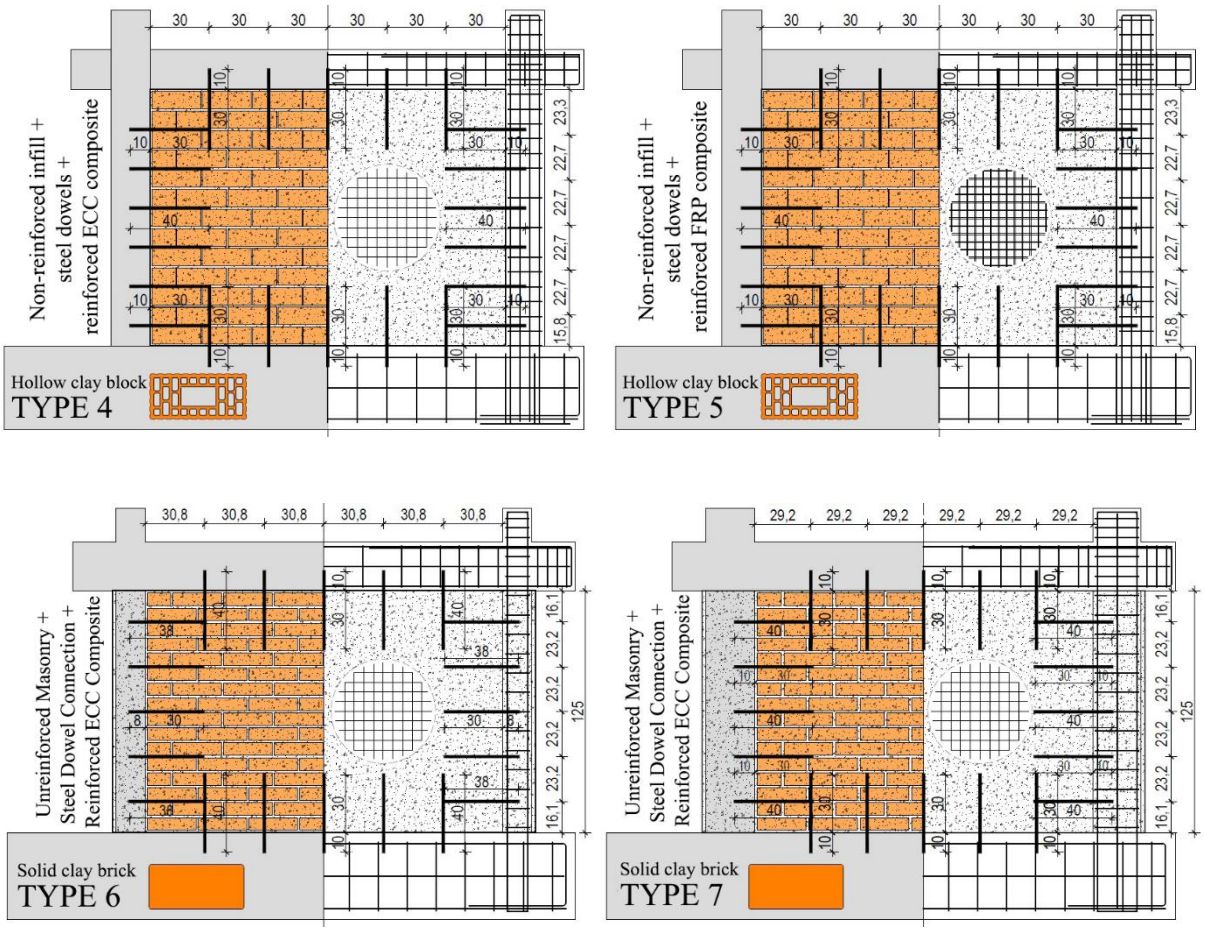


Figure 1. The applied methods of the masonry infill walls. Strengthening methods are shown with and without reinforcement details, i.e., the specimens do not contain any openings.

3. Seismic Risk and Loss Assessment procedure

Performance-Based Earthquake Engineering (PBEE) encompasses a comprehensive framework for the design, evaluation, construction, and maintenance of structures to meet specific performance objectives under seismic conditions. According to Krawinkler and Miranda [32,33], PBEE is based on predicting structural performance with quantifiable confidence, enabling informed decisions and trade-offs considering life-cycle costs rather than initial construction expenses alone. The PBEE methodology integrates seismic hazard assessment, structural response analysis, damage analysis, and loss estimation, explicitly accounting for uncertainties at each stage (Figure 2 and 3).

The FEMA P-58 procedure [34], a widely adopted approach within PBEE, allows clear quantification of seismic performance using comprehensible variables such as economic losses, casualties, and downtime. The inherent uncertainties are explicitly incorporated through Probabilistic Seismic Hazard Analysis (PSHA), structural analysis via Incremental Dynamic Analysis (IDA), damage estimation using fragility curves, and finally loss assessment through specific loss functions. Each step involves distinct performance indicators: Intensity Measure (IM), Engineering Demand Parameters (EDP), Damage Measures (DM), and Decision Variables (DV).

The mathematical formulation of PBEE provided by FEMA P-58 employs the total probability theorem, summarised in Equation 1:

$$\lambda(DV) = \iiint G(DV|\ DM), \mathrm{d}G(DM|\ EDP), \mathrm{d}G(EDP|\ IM), \mathrm{d}\lambda(IM) \tag{1}$$

Copyright © 2025 CroCEE
DOI: https://doi.org/10.5592/CO/3CroCEE.2025.83

where:

- $\lambda(DV)$ is the mean annual frequency of exceeding a specific Decision Variable (DV), such as economic loss, downtime, or casualties.
- $G(DV|\,DM)$, $G(DM|\,EDP)$, and $G(EDP|\,IM)$ represent conditional cumulative distribution functions linking DV to DM, DM to EDP, and EDP to IM, respectively.
- $\lambda(IM)$ denotes the mean annual frequency of exceeding an Intensity Measure (IM) derived from PSHA.

This equation effectively compartmentalises seismic risk assessment into four sequential stages: hazard characterisation, structural response evaluation, damage assessment, and economic loss estimation. Each stage provides a transparent and structured approach to quantify uncertainties and aids engineers and stakeholders in making informed, rational decisions regarding seismic risk management strategies.

Incremental Dynamic Analysis (IDA) quantifies uncertainties in EDP using various seismic excitations. Damage uncertainties are captured via fragility curves, relating the probability of damage states to EDP. Economic losses, casualties, and downtime uncertainties are represented through loss functions conditioned on specific damage states. Mean annual frequencies of decision variables are computed via integration considering IM, EDP, DM, and DV uncertainties, providing robust means to communicate seismic risks clearly.

In this study, the FEMA P-58 methodology is adopted to evaluate and quantify the seismic performance of RC frame structures strengthened using traditional masonry infill walls, contributing significantly to existing research by providing detailed insights into seismic resilience and cost-effectiveness.

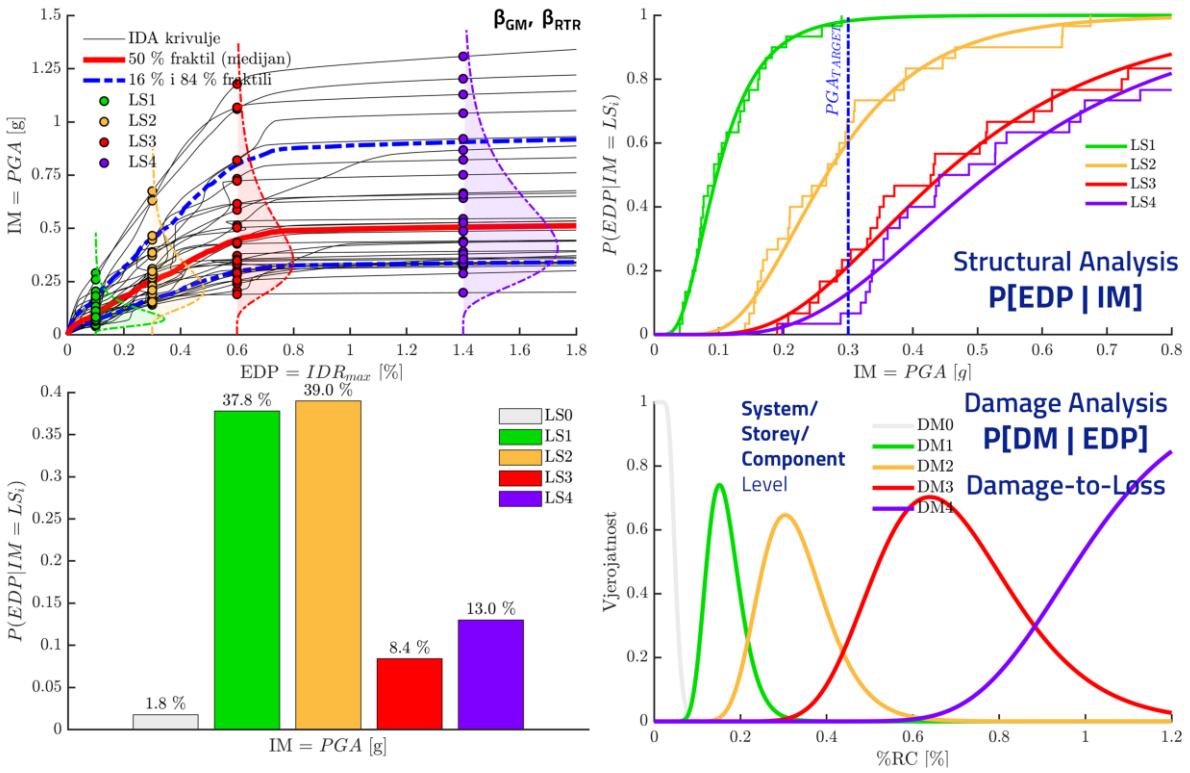


Figure 2. Illustrated steps in probabilistic seismic risk analysis and loss assessment of individual buildings, according to Performance-Based Earthquake Engineering (PBEE) and the FEMA P-58 procedure.

Copyright © 2025 CroCEE
DOI: https://doi.org/10.5592/CO/3CroCEE.2025.83

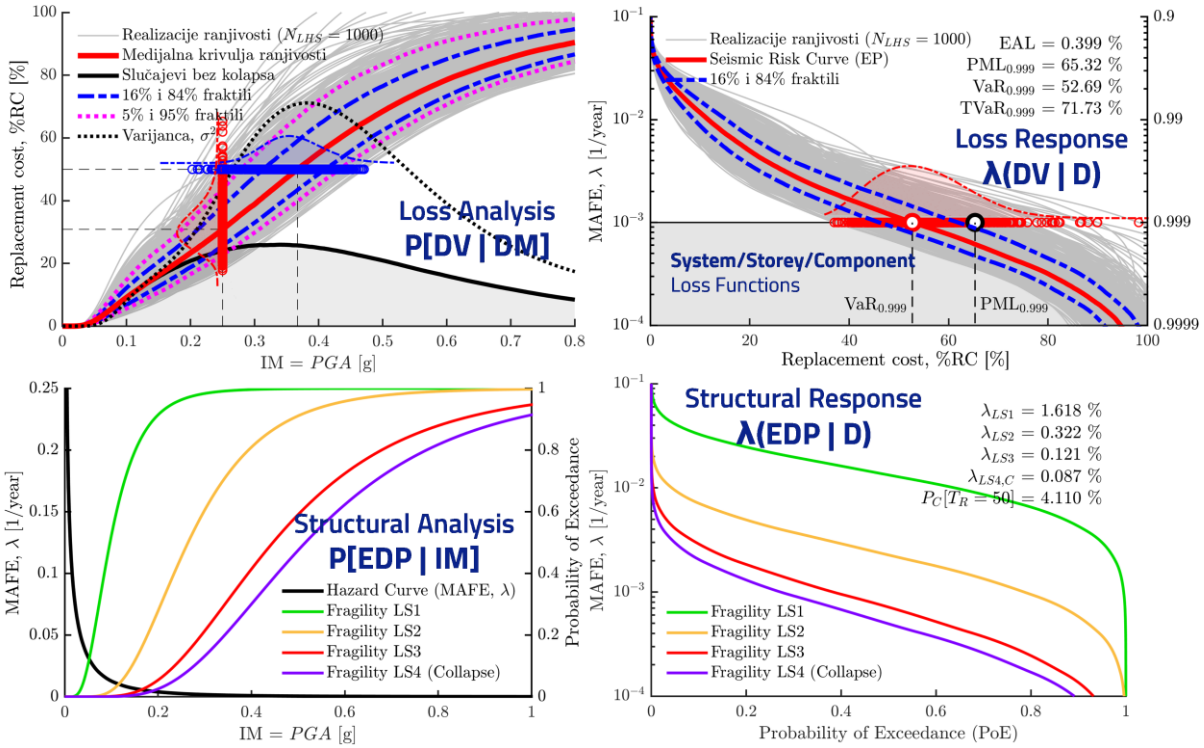


Figure 3. Illustrated steps in probabilistic seismic risk analysis and loss assessment of individual buildings, according to Performance-Based Earthquake Engineering (PBEE) and the FEMA P-58 procedure.

4. Numerical Case Study and Performance Assessment

All numerical models were constructed and analysed in OpenSees and are based on all original calibrated parameters based on previously described experiments, discussed in detail earlier by Grubišić [30]. The structure selected for this numerical case study is a reinforced concrete (RC) frame building designed according to Eurocode 8. The same RC structural configuration was consistently used for all 12 numerical models, differentiated solely by masonry infill and strengthening characteristics. The chosen building replicates the geometry of the Tsukuba building, previously subjected to pseudo-dynamic experimental testing. This building was selected due to the similarity of its geometry and load analysis to the experimental models discussed in previous sections. Detailed information about the basic RC structural system is available in earlier research by Grubišić [30]. From the total of 13 experimental models described previously, 12 numerical models were developed for this study. The numerical models of this case study present the same design properties of the models of the same name described earlier, by means of description and notation.

From the original three-dimensional Tsukuba model, the most heavily loaded representative internal planar frame in the longitudinal direction was isolated for numerical analysis. The selected frame consists of spans measuring 6 m, 5 m, and 6 m, with storey heights of 3.75 m for the ground floor and 3 m for upper floors. RC slabs are 18 cm thick; columns measure 50×50 cm, and beams measure 30×50 cm. Reinforcement detailing for columns and beams is illustrated in Figure 4. Materials used include concrete class C30/37 and reinforcing steel class B500B. All frame elements were designed according to standard vertical and horizontal seismic loading with peak ground acceleration (PGA) of 0.35 g, complying with Eurocode 8 requirements for seismic zone conditions in Croatia.

In terms of dynamic properties, nodal masses were uniformly concentrated at frame nodes, with total values of 16.5 and 27 tonnes at external and internal ground nodes respectively, 18.2 and 28.6 tonnes at upper floors, and 19.3 and 31.7 tonnes at roof nodes. Masonry infill walls were introduced using hollow clay blocks and solid clay bricks bonded by cement-lime mortar (strength class M5) with a

Proceedings of the 3rd Croatian Conference on Earthquake Engineering - 3CroCEE
19–22 March 2025, Split, Croatia
Copyright © 2025 CroCEE
DOI: https://doi.org/10.5592/CO/3CroCEE.2025.83

mortar joint thickness of 1 cm. Detailed material properties for masonry units, mortar, and frame-infill connections were adopted from experimental data. Masonry infills and their connections were implemented consistently across the central bay of each frame.

Numerical modelling adopted a concentrated plasticity approach, defining rotational springs with specific hysteretic behaviour at beam-column joints. Masonry infills were simulated by equivalent diagonal struts representing compression and tension, reflecting their mechanical interaction with the surrounding frame. Beam and column joint details conformed to Eurocode 8. The numerical models were analysed to evaluate displacement capacity, energy dissipation, and fundamental vibration periods. Probabilistic seismic analyses were performed to estimate seismic vulnerability, considering randomness in seismic excitation and calculating exceedance probabilities for specific damage states. A two-dimensional analysis framework was adopted, offering simplicity, robustness, and reliability in seismic performance assessment.

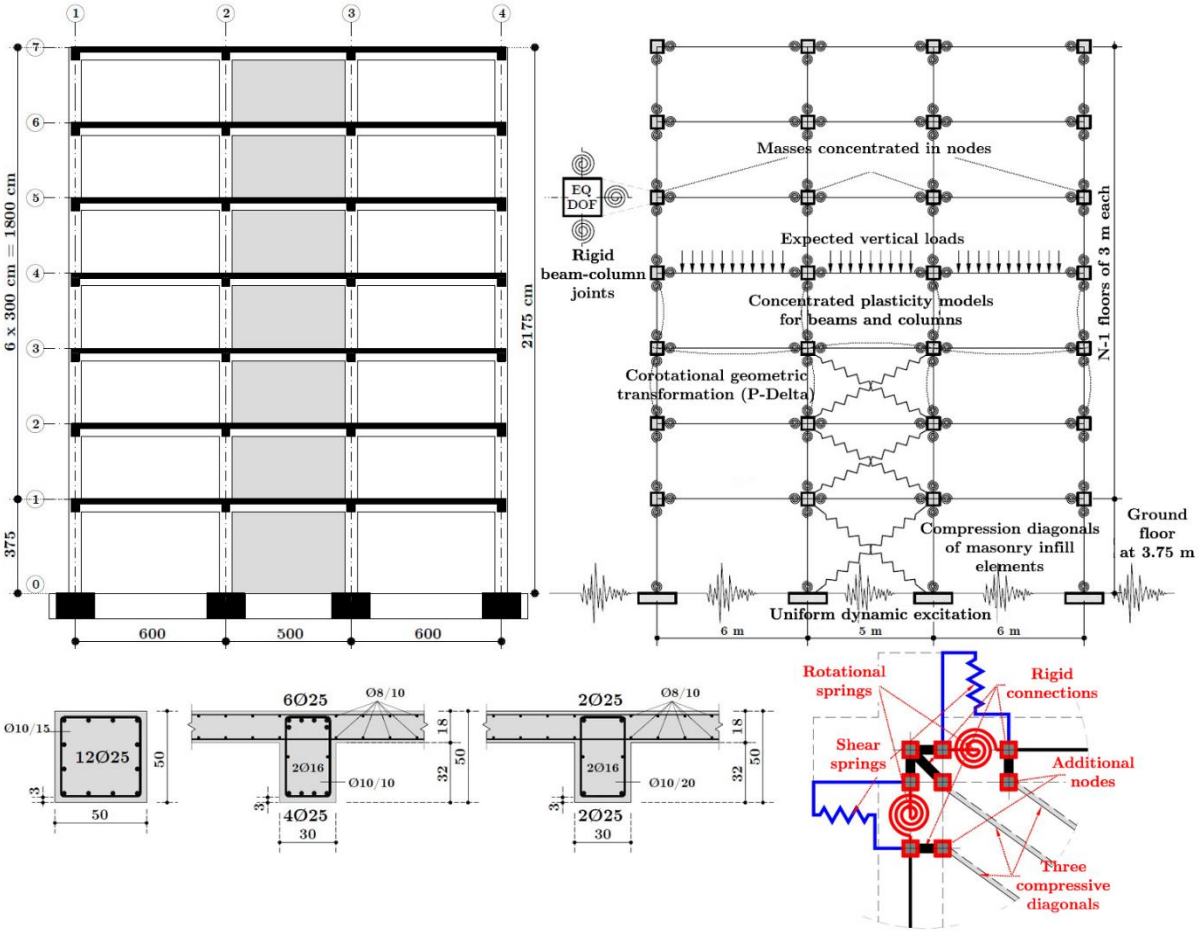


Figure 4. Reinforcement configuration in cross-sections of column ends, or ends and half of beam spans, obtained by designing the structure according to Eurocode 8.

After defining the hazard curve for a selected intensity measure (e.g., spectral acceleration, $S_A(T_1, 5\%)$), the disaggregation of seismic hazard can be analysed for a return period of 475 years (Figure 5, left). For this numerical study, 30 real ground-motion records were selected from the PEER NGA West 2 database. These records were chosen to closely match the mean target spectrum within the expected natural vibration period range of the studied numerical models (Figure 5, right).

Proceedings of the 3rd Croatian Conference on Earthquake Engineering - 3CroCEE
19–22 March 2025, Split, Croatia
Copyright © 2025 CroCEE
DOI: https://doi.org/10.5592/CO/3CroCEE.2025.83

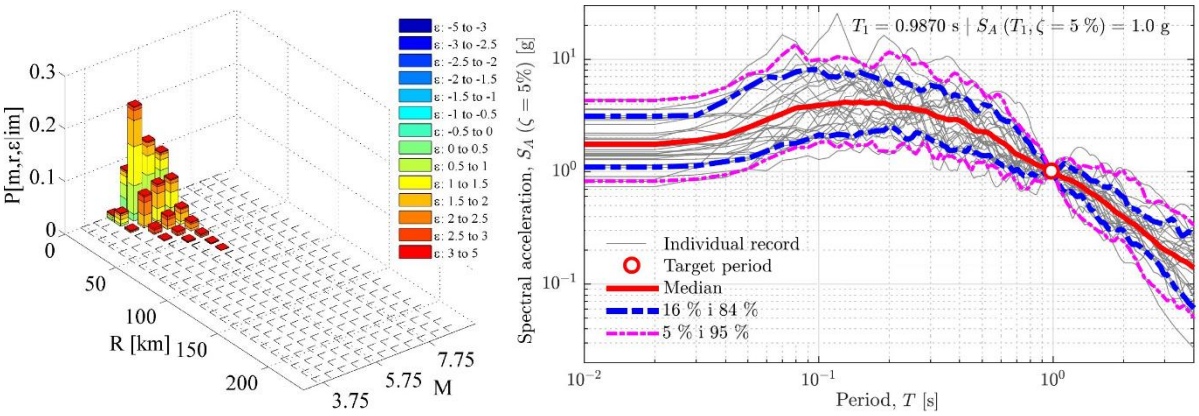


Figure 5. Disaggregation of seismic hazard for the building location (left); 30 real ground-motion records chosen to closely match the mean target spectrum (right).

5. Seismic Risk and Loss Assessment Results

This section presents a brief overview of the key findings derived from the numerical modelling, risk analyses and loss assessment. Figure 6 illustrates the median 5% damped spectral acceleration at the structure's first-mode period, $S_A(T_1, 5\%)$, for all numerical models examined. Specifically, the left figure depicts the median $S_A(T_1, 5\%)$ at the point of structural collapse, providing insight into the seismic intensity required to induce failure. Conversely, the right figure presents the median $S_A(T_1, 5\%)$ corresponding to a 50% loss ratio, indicating the intensity associated with significant, though not complete, structural damage. Figure 7 presents the discrete probability distribution of limit state regions. This distribution is derived from the fragility curve analysis, which quantifies the likelihood of the structure exceeding predefined damage states under varying seismic intensities. The figure visually represents the probabilistic assessment of the structure's vulnerability to different levels of seismic demand. Figure 8 displays the mean annual frequency of collapse, λ_C, on the left. This metric represents the expected number of collapse events per year, providing a crucial measure of the structure's collapse risk. Figure 8 displays the mean annual frequency of collapse (λ_C) on the left, representing the expected number of collapse events per year, and the average annual loss ratio (AAL) on the right, quantifying expected annual economic loss as a fraction of total replacement cost (RC).

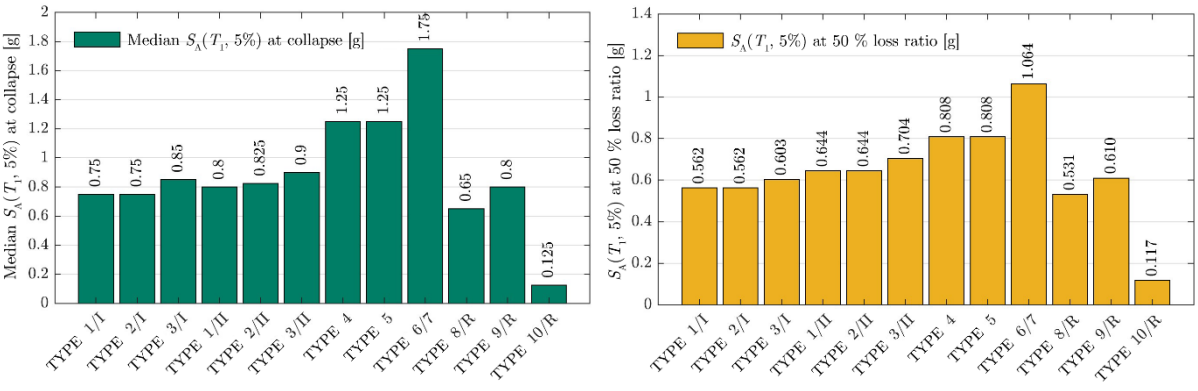


Figure 6. Median $S_A(T_1, 5\%)$ at collapse (left) and $S_A(T_1, 5\%)$ at 50% loss ratio (right) for all numerical models analysed

Based on these analyses, the following conclusions regarding the efficiency of various strengthening techniques can be drawn:

Copyright © 2025 CroCEE
DOI: https://doi.org/10.5592/CO/3CroCEE.2025.83

- The most vulnerable model is clearly the empty RC frame (TYPE 10/REF), as it demonstrates the lowest horizontal load capacity and the highest deformation. This model can sustain the lowest spectral acceleration levels, with nearly a 49% probability of collapse and a 37% probability of reaching the LS4 (near-collapse) limit state, according to the hazard curve based on the set of 30 earthquake records. TYPE 10/REF experiences approximately six times greater average annual losses (AAL) and almost eight times higher mean annual frequency of collapse (λ_C) compared to other models.
- Models TYPE 1/I, 2/I, 3/I, 1/II, 2/II, and 3/II exhibit relatively similar horizontal load capacities and ductilities. Considering spectral acceleration as a measure of intensity at 50% vulnerability, the type of masonry unit (solid brick versus hollow clay block) has a more significant impact than the presence of vertical confinement. Losses and vulnerabilities are quite similar for these six models. However, TYPE 3/II is favoured due to the robustness of the solid brick elements combined with vertical confinement, providing up to 15% higher spectral acceleration capacity and the lowest AAL and λ_C among these models.
- Models TYPE 4 and TYPE 5 show comparable results for most evaluated parameters. The significant difference is observed in TYPE 4, where reinforced ECC composite provides up to 5% higher strength and up to 45% greater ductility compared to the FRP composite used in TYPE 5. Apart from ductility, other results from analyses are nearly identical for both models.
- Model TYPE 6/7 has an identical configuration to TYPE 4, except it utilises double-sided ECC composite strengthening. Double-sided strengthening significantly enhances performance, providing up to 45% higher strength, 15% higher ductility, and resistance to spectral accelerations up to 40% higher compared to TYPE 4. Thus, TYPE 6/7 is identified as the most resilient strengthening system, with ductility comparable to an empty ductile RC frame, along with the lowest AAL and λ_C—up to 35% lower compared to single-sided strengthening (TYPE 4).
- Whenever possible, robust solid clay bricks and commercially available composite materials are recommended for optimal seismic performance enhancement. ECC composites are generally more economical than FRP composites and typically come in easy-to-apply two-component preparations. Applying ECC composites reinforced with galvanized mesh is straightforward, although careful anchoring to the frame and masonry infill walls is necessary. This ECC layer can be integrated into façade layers or applied as an intermediate layer before finishing the wall surfaces.

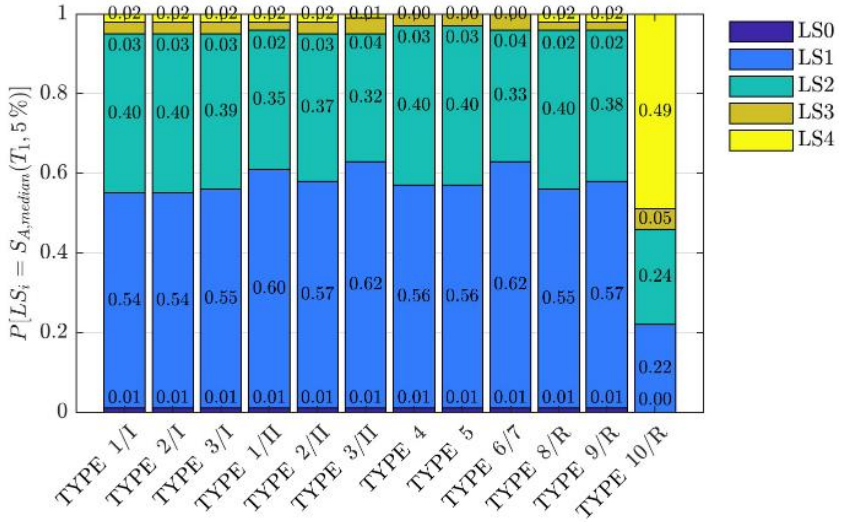


Figure 7. Discrete probability distribution of limit state regions, based on fragility curve analysis.

Copyright © 2025 CroCEE
DOI: https://doi.org/10.5592/CO/3CroCEE.2025.83

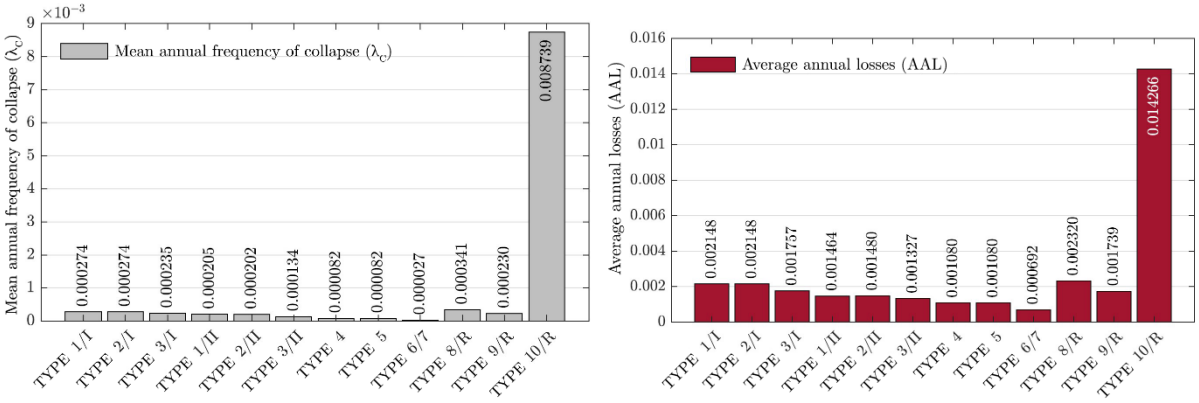


Figure 8. Mean annual frequency of collapse, λ_C (left) and Average annual loss ratio, AAL (right).

6. Conclusions

The results of this study clearly demonstrate the significant benefits of employing simple seismic strengthening techniques, particularly the addition of masonry infill walls, for enhancing the seismic performance of reinforced concrete (RC) frame structures. The detailed numerical analyses highlighted the improved performance of strengthened structures in terms of increased lateral load capacity, ductility, and resilience against seismic-induced damages, compared to bare RC frames.

Empty ductile RC frames (TYPE 10/REF) were identified as notably vulnerable, demonstrating low seismic capacity and significantly higher expected economic losses and collapse risks. Conversely, the introduction of masonry infills substantially improved structural resilience. Specifically, solid brick infills, particularly when combined with vertical confinement and steel dowels (TYPE 3/II), showed a clear advantage over hollow clay block infills. This configuration provided increased strength, reduced expected annual losses, and minimised collapse probabilities, thus indicating a favourable option for seismic retrofitting.

Innovative strengthening approaches involving ECC composites also displayed substantial advantages. Single-sided ECC composite strengthening (TYPE 4) provided moderate improvements in strength and substantial enhancements in ductility compared to FRP composites (TYPE 5). Double-sided ECC strengthening (TYPE 6/7) offered the highest improvement in seismic performance, significantly enhancing both strength and ductility. The findings strongly suggest that ECC composites, due to their cost-effectiveness, ease of application, and substantial performance improvements, should be favoured when practical.

Overall, the application of traditional masonry infill walls combined with targeted composite reinforcement provides a robust, economically viable strategy for enhancing seismic resilience of existing RC frame structures, thus offering a balanced solution between cost-efficiency and seismic performance.

Acknowledgements

This research article is dedicated to the memory of Vladimir Sigmund, who provided the author with invaluable advice, support, and guidance in the fields of profession, science, and philosophy.

Proceedings of the 3rd Croatian Conference on Earthquake Engineering - 3CroCEE
19–22 March 2025, Split, Croatia
Copyright © 2025 CroCEE
DOI: https://doi.org/10.5592/CO/3CroCEE.2025.83

References

[1] Braga, F., Manfredi, V., Masi, A., Salvatori, A., & Vona, M. (2011). Performance of non-structural elements in RC buildings during the L'Aquila, 2009 earthquake. Bulletin of Earthquake Engineering, 9(1), 307–324.

[2] Polese, M., Di Ludovico, M., Marcolini, M., Prota, A., & Manfredi, G. (2015). Assessing reparability: simple tools for estimation of costs and performance loss of earthquake damaged reinforced concrete buildings. Earthquake Engineering & Structural Dynamics, 44(10), 1539–1557.

[3] De Martino, G., Di Ludovico, M., Prota, A., Moroni, C., Manfredi, G., & Dolce, M. (2017). Estimation of repair costs for RC and masonry residential buildings based on damage data collected by post-earthquake visual inspection. Bulletin of Earthquake Engineering, 15(4), 1681–1706.

[4] Del Vecchio, C., Di Ludovico, M., Pampanin, S., & Prota, A. (2018). Repair costs of existing RC buildings damaged by the L'Aquila earthquake and comparison with FEMA P-58 predictions. Earthquake Spectra, 34(1), 237–263.

[5] Cavaleri, L., & Di Trapani, F. (2015). Prediction of the additional shear action on frame members due to infills. Bulletin of Earthquake Engineering, 13(5), 1425–1454.

[6] Di Trapani, F., & Malavisi, M. (2019). Seismic fragility assessment of infilled frames subject to mainshock/aftershock sequences. Bulletin of Earthquake Engineering, 17(1), 211–235.

[7] Mosalam, K. M., & Günay, S. (2015). Progressive collapse analysis of reinforced concrete frames with masonry infill walls. Earthquake Spectra, 31(2), 921–943.

[8] Varum, H., Furtado, A., Rodrigues, H., Dias-Oliveira, J., Vila-Pouca, N., & Arêde, A. (2016). Seismic performance of infill masonry walls after the Ghorka 2015 earthquake. Bulletin of Earthquake Engineering, 15(3), 1185–1212.

[9] Gkournelos, P., Triantafillou, T., & Bournas, D. (2021). Seismic upgrading of existing reinforced concrete buildings: A review. Engineering Structures, 240, 112273.

[10] Anand, P., & Sinha, A. K. (2022). Seismic Strengthening and Retrofitting Techniques for RC Frames. In Ghosh & Kolathayar (Eds.), A System Engineering Approach to Disaster Resilience (pp. 531–539). Springer.

[11] Valente, M., & Milani, G. (2018). Alternative retrofitting strategies for RC frames. Engineering Failure Analysis, 89, 271–285.

[12] Pujol, S., & Fick, D. (2010). Test of a three-story RC structure with masonry infill walls. Engineering Structures, 32, 3112–3121.

[13] Furtado, A., Rodrigues, H., Arêde, A., & Varum, H. (2020). Strengthening strategies for masonry infill walls. Construction and Building Materials, 263, 120520.

[14] Palieraki, V., Zeris, C., Vintzileou, E., & Adami, C. E. (2018). In-plane/out-of-plane response of masonry infills. Engineering Structures, 177, 103–116.

[15] Usta, P., Onat, Ö., & Bozdağ, Ö. (2023). Masonry infill walls' effects on RC structures: İzmir earthquake case. Engineering Failure Analysis, 146, 107081.

[16] Altin, S., Anil, Ö., Kara, M. E., & Kaya, M. (2008). Strengthening infilled RC frames with CFRP strips. Composites Part B: Engineering, 39, 680–693.

[17] Koutas, L., Pitytzogia, A., Triantafillou, T. C., & Bousias, S. N. (2014). Strengthening infilled RC frames with TRM. Journal of Composites for Construction, 18(2), A4013015.

[18] Koutas, L., Triantafillou, T. C., & Bousias, S. N. (2015). Seismic strengthening with TRM. Journal of Composites for Construction, 19(2), 04014048.

[19] Morandi, P., Milanesi, R. R., & Magenes, G. (2018). Seismic-resistant masonry infills with sliding joints. Engineering Structures, 176, 719–733.

[20] Preti, M., Migliorati, L., & Giuriani, E. (2015). Engineered masonry infill walls for structural control. Bulletin of Earthquake Engineering, 13(7), 2029–2049.

[21] Totoev, Y., & Al Harthy, A. (2016). Semi-interlocking masonry as seismic infill walls. Journal of Engineering Research, 13(1), 33–41.

[22] Bolis, V., Stavridis, A., & Preti, M. (2017). Masonry-infilled RC frames with sliding subpanels. Journal of Structural Engineering, 143(2), 04016168.

[23] Bolis, V., & Preti, M. (2019). Infills with sliding joints: parametric study. Bulletin of Earthquake Engineering, 17, 4133–4157.

[24] Manzini, C. F., Morandi, P., Milanesi, R. R., & Magenes, G. (2018). Shaking-table tests on sliding joint infills. 16th ECEE Proceedings.

[25] Preti, M., Bolis, V., & Stavridis, A. (2019). Infill-frame interaction modeling. Journal of Earthquake Engineering, 23(10), 1651–1677.

Copyright © 2025 CroCEE
DOI: https://doi.org/10.5592/CO/3CroCEE.2025.83

[26] Gao, X., Stavridis, A., Bolis, V., & Preti, M. (2018). Seismic performance of RC frames with sliding subpanels. 11th US National Conference on Earthquake Engineering.
[27] Vamvatsikos, D., & Cornell, C. A. (2000). Incremental dynamic analysis. Earthquake Engineering & Structural Dynamics, 31(3), 491–514.
[28] Cornell, C. A., & Krawinkler, H. (2000). Challenges in seismic performance assessment. Center News 3, University of California, Berkeley.
[29] Grubišić, M., Kalman Šipoš, T., Grubišić, A., & Pervan, B. (2023). Testing of Damaged Single-Bay Reinforced Concrete Frames Strengthened with Masonry Infill Walls. Buildings, 13(4), 1021.
[30] Grubišić, M. (2016). Modeli ocjene ojačanja armiranobetonskih okvira dodavanjem ispuna pri potresnom djelovanju. PhD Thesis (In Croatian), Građevinski i arhitektonski fakultet Osijek. Repozitorij GrAFOS. https://repozitorij.gfos.hr/islandora/object/gfos:883
[31] Krawinkler H, Miranda E (2004) Performance-based earthquake engineering, chapter 9. In: Bozorgnia Y,
[32] Bertero V.V. (eds) Earthquake engineering: from engineering seismology to performance-based engineering. CRC Press, Boca Raton
[33] Jalayer, F. (2003) Direct Probabilistic Seismic Analysis: Implementation Non-Linear Dynamic Assessments. PhD Thesis, Stanford University.
[34] Federal Emergency Management Agency (FEMA) (2012) Seismic Performance Assessment of Buildings, Volume 1, Methodology. Report No. FEMA P-58-1, Washington DC.

Proceedings of the 3rd Croatian Conference on Earthquake Engineering - 3CroCEE
19–22 March 2025, Split, Croatia
Copyright © 2025 CroCEE
DOI: https://doi.org/10.5592/CO/3CroCEE.2025.168

EARTHQUAKE RESISTANCE OF POLES ALONG ROADS

Višnja Tkalčević Lakušić [(1)], Iva Crnjac [(2)]

[(1)] *Associate professor, University of Zagreb, Faculty of Civil Engineering, Croatia, visnjat@grad.hr*
[(2)] *Student, University of Zagreb, Faculty of Civil Engineering, Croatia, icrnjac@student.grad.hr*

Abstract

Earthquakes pose a significant threat to roads and infrastructure facilities. The collapse and damage of poles along roads due to earthquakes can pose a danger to road users and an obstacle to rescue services. The paper analyzes the influence of the material of construction and the type of pole foundation on the behavior and damage of poles during an earthquake. The paper first presents the types of poles according to their material of construction. The characteristics of steel, aluminium and composite poles are presented. The behavior of poles and damage during an earthquake depend on the material of the pole, the weight and length of the pole, and other limitations such as the cables carried by the pole. It has been shown that greater damage occurred in concrete poles than in steel poles, and an even better solution is aluminium and composite poles. The following shows the influence of the method of pole foundation (soil and rigid) on the behavior and damage of poles during an earthquake. Finally, an example of increasing the seismic resistance of poles is presented. Past earthquakes have shown that damage to roads and infrastructure facilities can prevent all forms of assistance to the injured. It is crucial that transport infrastructure is functional after an earthquake. Therefore, rapid inspection of affected transport infrastructure (roads, railways, bridges, tunnels, airports and seaports) is essential. The use of earthquake-resistant poles ensures safer transport during and after an earthquake. They can keep key transport routes open for rescue and relief operations and minimize the need for frequent repairs and reconstruction, which reduces maintenance costs. By integrating earthquake-resistant poles made of energy-absorbing materials, cities can build resilient transport networks.

Keywords: earthquake, road infrastructures, poles, materials, damage of poles, energy absorbing, resistance

1. Introduction

Earthquake engineering is an interdisciplinary area aimed at designing and analysing structures that are capable of responding to destructive seismic action. The primary focus of earthquake engineering is on high-rise structures, but no lesser significance is given to infrastructure facilities which must also be designed to withstand seismic action when located in seismically active areas [1].

The earthquake poses a significant threat to roads and infrastructure facilities, such as gas, water and electricity supplies. The impact of earthquake on roads can result in economic losses, delayed emergency responses and reduced connectivity for affected regions, Fig. 1.



Figure 1. Road damages [2]

Copyright © 2025 CroCEE
DOI: https://doi.org/10.5592/CO/3CroCEE.2025.168

After an earthquake, it is very important that the transportation infrastructure is functional within the first 24 hours, and for any damage to be repaired within the first 72 hours. All means of transport must be used to quickly reach people trapped under collapsed and partially collapsed buildings. Injured people pulled from under the rubble must be quickly transported to hospitals. Furthermore, a large number of construction equipment and trucks are being sent to the earthquake-affected area to remove debris. Due to the increased traffic, temporary measures are needed to repair road damage in a short time [2].

Earthquakes can also cause collapse and damage to poles along roads, Fig. 2, which can pose a danger to road users during an earthquake and an obstacle to rescue services after an earthquake. For example, in the 2004 Chuetsu earthquake in Niigata Prefecture, with a recorded maximum seismic intensity of 6.9 on the Richter scale, a total of 3,401 utility poles carrying communication cables were toppled, broken, or tilted [3]. Most of the damage in Niigata occurred because the poles had been installed on weak ground, so they were damaged by ground movement.

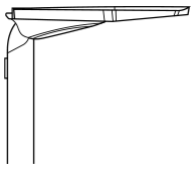
First measure in the restoration of communication and maintenance of safety is the repair of collapsed, broken, or leaning utility poles. Experience has shown that damage to poles after earthquake depends on many parameters, such as the pole material, the purpose of the pole, the location of installation, the type of foundation, etc.



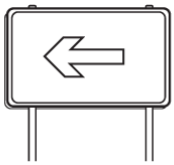
Figure 2. Utility poles damaged by landslide [3]

2. Types of poles along roads

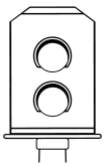
Poles placed along roads play a key role in the traffic system. Their primary function includes traffic safety, navigation, lighting and marking of traffic rules. Among the most common types of columns are those that carry lighting fixtures, traffic signs, traffic lights, navigational markers and cameras, Fig. 3.



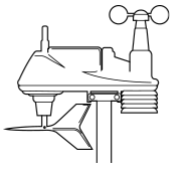
Lighting columns



Traffic sign columns



Traffic signal columns



Columns for monitoring meteorological conditions



Camera columns

Copyright © 2025 CroCEE
DOI: https://doi.org/10.5592/CO/3CroCEE.2025.168

Figure 3. Roadside columns [4]

Poles along roads are usually made of steel, aluminium, steel-reinforced concrete, composite materials and wood [5]. The choice of material depends on the type of road, local conditions, costs, as well as aesthetic and safety requirements.

2.1 Steel poles

Steel is the material most commonly used to make roadside poles. Steel poles are relatively lightweight, durable with appropriate anti-corrosion protection, affordable, and have high resistance to material fatigue [6]. It is important to regularly carry out inspections and maintenance on steel poles to ensure their proper functioning over a longer period. The advantage of steel poles is that they are completely recyclable. Steel recycling is an environmentally friendly and efficient process that reduces the need for new steel production, thereby significantly reducing the negative impact on the environment.

Anti-corrosion protection of steel poles is very important in the event of an earthquake because corrosion can weaken the structure, so the column may not behave as designed during an earthquake.The most commonly used method for protecting poles from corrosion is hot-dip galvanization, in which steel elements are immersed in a molten zinc solution at a temperature of around 449°C to create a strong and resistant coating [7]. Magnelis steel, as an innovative product obtained through the hot-dip galvanizing process with an adjusted composition of the liquid into which the steel elements are immersed, which, in addition to zinc, also includes 3.5% aluminum and 3% magnesium [8], is definitely worth mentioning. This superior coating gives Magnelis exceptional corrosion resistance and self-healing at points of damage, unlike standard galvanized elements. Owing to this characteristic, Magnelis is a long-lasting material and as such becomes a more economical alternative to more expensive materials such as stainless steel and aluminum, which can result in significant savings in the project. As Magnelis contains lower amounts of zinc compared to products obtained through the classic hot-dip galvanizing process, Magnelis is also a better choice for the environment.

In addition to hot-dip galvanization, other processes are used to protect steel poles from corrosion, such as zinc silicate protection, metallization, painting, etc. A good method of anti-corrosion protection is the use of weathering steel, which is produced using alloys such as copper, chromium, nickel, etc., which will oxidize and create its own anti-corrosion protection [9]. Fig. 4 shows the steel poles.



Figure 4. Steel poles [10]

2.2 Aluminium poles

Aluminum poles (Fig. 5) generally have numerous advantages over poles made of steel and concrete. The weight of aluminum poles is 1/3 less than steel poles, which results in lower transportation costs, as well as simpler and faster installation.

Copyright © 2025 CroCEE
DOI: https://doi.org/10.5592/CO/3CroCEE.2025.168

Due to a natural layer of aluminum oxide that creates a protective barrier in contact with oxygen, aluminum is naturally resistant to corrosion. When aluminum poles are scratched or dented, the protective layer re-forms. These poles are the only 'self-maintaining' poles on the market in terms of surface treatment [4]. Due to these characteristics, aluminum poles are an excellent solution for coastal areas where there is a greater possibility of corrosion. Aluminum poles are usually supplied unpainted and retain their natural shiny finish, so no painting or repainting is required during use, which reduces maintenance costs. The designed lifespan of aluminum poles is 50 years, which is twice that of most steel or concrete poles. Since aluminum is fully recyclable and long-lasting, it fulfills many requirements that other materials cannot.



Figure 5. Aluminum lighting poles [11]

2.3 Composite poles

Poles made of composite materials (Fig. 6) are the most expensive alternative to traditional poles, but they have excellent energy absorption properties. By definition, composite materials consist of different materials (metals, ceramics, polymers) firmly bonded together to create a new, different material with physical or chemical properties that exceed those of the individual components [12]. More recently, with the development of polymer materials, composite lighting poles are produced from fiber-reinforced polymer resin [13].

Composite poles have numerous advantages over poles made of other materials, such as higher tensile strength, lower weight, fire resistance, excellent electrical insulators, resistance to adverse environmental influences (water, chemicals, salt). Therefore, they are less susceptible to corrosion and do not require maintenance. The life cycle of composite poles is up to 80 years, which is twice as long as the average life cycle of poles made from other materials [14]. Composite poles do not require carcinogenic protection or other chemicals, which makes them environmentally friendly because there is no leaching of protective coatings, especially in areas near national parks, water sources, etc.

Due to their advantages, composite poles are an excellent choice for areas where extreme conditions such as hurricanes, typhoons, and tornadoes may occur, as well as areas where there is a greater risk of earthquakes, fires and ice storms, etc. The use of this type of pole is desirable in areas where traditional poles are not satisfactory in terms of durability. For example, in areas with high groundwater levels or high average rainfall, rotting and reduced load-bearing capacity of wooden poles may occur. Since the surface of composite poles does not absorb water, such poles are not susceptible to rotting or decay. In coastal areas and on roads where salting is performed in the winter months, there is a high probability of corrosion in steel poles, while in reinforced concrete poles, the steel reinforcement inside the pole may crack due to corrosion. Salt does not permeate composite poles, and owing to the waterproof

Copyright © 2025 CroCEE
DOI: https://doi.org/10.5592/CO/3CroCEE.2025.168

surface, the poles will maintain their characteristics over time. Compared to poles made of other materials, if we look at the initial investment, composites are classified as more expensive alternatives, but their use results in savings over the entire life cycle of the pole.



Figure 6. Composite pole [15]

2.4. The influence of the type of pole on damage after an earthquake

The behavior of a column during an earthquake and the damage after an earthquake depends on the column material, weight and length of the pole and on other constraints such as cables it supports. It has been shown that greater damage occurred in concrete poles than in steel poles. A better solution is aluminum and composite poles due to their ability to deform and absorb more energy.

Most of the damage to concrete poles was attributed to their high weight compared with steel poles. Long and heavy concrete combination poles, which carry communication lines together with electrical lines, suffered greater damage compared to concrete poles carrying communication lines only.

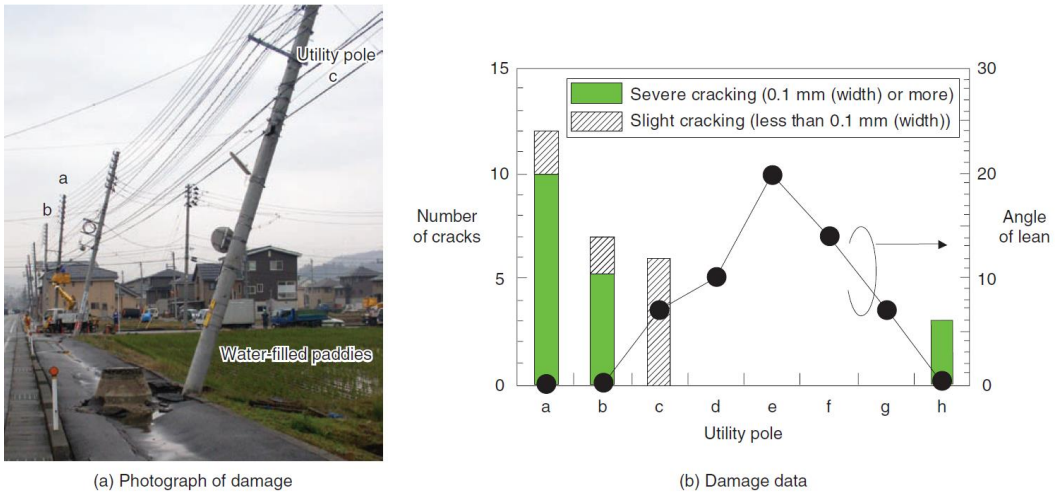
Furthermore, pole damage also depends on the position of the poles. The greatest damage was on utility poles at which lines originate or terminate, then on utility poles along routes where lines curve, and finally on utility poles along routes where lines are straight.

3. Type of foundation

The backfill type of the pole foundation significantly influences pole behavior during an earthquake. When using foundation in the soil, such as for instance in rural areas, toppled and leaning utility poles can be seen after an earthquake [3]. In places where utility poles are installed beside roads and anchored in hard asphalt adjacent to water-filled paddies, the swaying of the pole tops during an earthquake tends to cause leaning toward the softground side, Fig. 7(a). In such areas, a utility pole that leans over more than the others (utility pole e) pulls down on the adjacent poles (a–h) (Fig. 7(b)) to produce a chain-like effect that results in a series of leaning utility poles. Cracks are usually not seen on the pole that is leaning the most, but are seen on surrounding poles that are leaning only slightly.

If the poles are anchored in concrete or asphalt that completely surrounds them, as is common in urban areas, the poles are less likely to lean. In such areas, horizontal cracks will most often appear near the base of the poles, Fig. 8.

Copyright © 2025 CroCEE
DOI: https://doi.org/10.5592/CO/3CroCEE.2025.168



(a) Photograph of damage (b) Damage data

Figure 7. Chain tilting of poles [3]



Figure 8. Horizontal cracking near the base of the poles [3]

4. Increasing the seismic resistance of poles

While seismic resistance of elevated highway bridges (if we looking transportation infrastructure) has been evaluated and upgraded in the seismic codes, most light and utility poles were designed for wind loading and not for earthquake, so their seismic performances were rarely evaluated [16].

Poles along roads are vulnerable to earthquakes due to their slender shapes. They are usually designed to withstand moderate loads at considerable heights [17]. Despite the fact that the loads carried by columns are significantly less than their own weight, the inherent self-weight and thin profile make columns susceptible to lateral forces induced by seismic events [16,18] or wind loads [19,20]. Consequently, various efforts have been made to increase the flexural strength of column structures [21,22].

Traditional base isolation designs configure the bottom of the pole equipment as hinges with restraints. In order to increase traffic safety during and after an earthquake, a solution with use a restrained rocking mechanism at the base of the structure can be applied, Fig. 9. The design leverages the self-centering nature of rocking motion and uses restrainers to control the amplitude of rotation, Fig. 10. Hence, it can effectively avoid tilting of the pole after earthquakes.

Copyright © 2025 CroCEE
DOI: https://doi.org/10.5592/CO/3CroCEE.2025.168

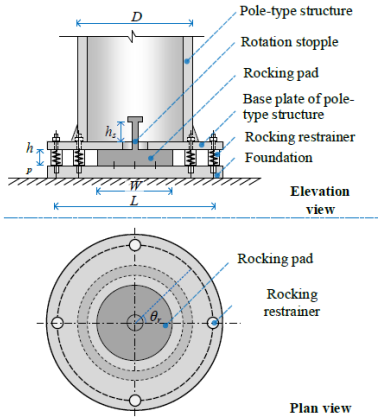


Figure 9. Restrained rocking isolation of pole [16]

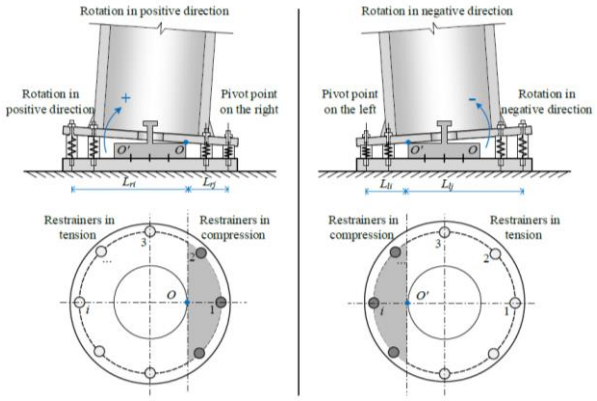


Figure 10. Rocking motion of the isolation device [16]

5. Conclusion

Past earthquakes have shown that damage to transport structures can prevent all kinds of assistance to injured people. It is crucial that transport infrastructure is operational after an earthquake. Therefore, a rapid inspection of the affected transport infrastructure such as roads, railways, bridges, tunnels, airports and seaports is necessary. Collapsed and damaged poles along roads can also pose an obstacle after an earthquake.

The use of earthquake-resistant poles ensures safer transportation during and after earthquakes. They keeps crucial transportation routes open for rescue and relief operations and minimizes the need for frequent repairs and reconstruction, which reduce maintenance costs. Although earthquake-resistant poles cost more due to advanced materials and technology, they save money in the long run by reducing repair and reconstruction costs.

With the increasing frequency of earthquakes around the world, investing in earthquake-resistant road infrastructure is essential. By integrating earthquake-resistant poles made of energy-absorbing materials, cities can build resilient transportation networks. The material used to make the pole has a major impact on the behavior of the poles and their ability to absorb energy during an earthquake.

Adopting earthquake-resistant construction methods will not only protect lives, but will also ensure a more sustainable, disaster-resistant infrastructure for generations to come.

References

[1] Lakušić, S., Haladin, I., Vranešić, K.: Railway infrastructure in earthquake affected areas, GRAĐEVINAR, 72 (2020) 10, pp. 905-922, doi: https://doi.org/10.14256/JCE.2967.2020

[2] Apaydin, N.M. (26 Jun 2024): "Earthquake Response of the Transportation Infrastructure in the Region Affected by the February 6 Türkiye Earthquakes'' Part I-Roads, Railroads and Ports, Journal of Earthquake Engineering, doi: https://doi.org/10.1080/13632469.2024.2370856

[3] A more efficient method of inspecting utility pole damage caused by major earthquakes, https://www.ntt-review.jp/archive/ntttechnical.php?contents=ntr200708sf2.html

[4] Roadside poles, https://www.aluminium-lighting.com/products/highway-lighting/

[5] Crnjac, I.: Roadside columns, Final exam, Supervisor: Tkalčević Lakušić, V., University of Zagreb, Faculty of Civil Engineering, 2023.

[6] Tkalčević Lakušić, V.: Safety of roadside columns of vehicle impact, Građevinar, 64 (2012), 4; 305-313

Copyright © 2025 CroCEE
DOI: https://doi.org/10.5592/CO/3CroCEE.2025.168

[7] Corrosion protection, https://hr.fabmann-jp.com/metal-surface-treatment/hot-dip-galvanizing.html

[8] Magnelis, https://www.laser-ing.hr/blog/sto-je-magnelis-celik/

[9] Tkalčević Lakušić, V.: Analiza stupova uz prometnice iz aspekta sigurnosti u prometu, Projektiranje prometne infrastrukture, Zagreb, University of Zagreb, Faculty of Civil Engineering, Department of Transportation Engineering 2011. pp. 321-346

[10] Steel pole, http://hr.xintongpole.com/8-meter-height-street-light-galvanized-steel-pole-product/

[11] Aluminium pole, https://www.hydro.com/globalassets/01-products--services/poles/product-sheets/pdsenuk.00.02.001-aluminium-lighting-columns.pdf

[12] Composite, https://hr.wikipedia.org/wiki/Kompozit

[13] Krokar J.: Kompozitni rasvjetni stupovi, Diplomski rad, mentor: Skender A., Sveučilište u Zagrebu, Građevinski fakultet, 2018.

[14] Composite column, https://www.rspoles.com/whyusecomposite

[15] Composite column, https://www.mallatite.co.uk/street-lighting/lighting-columns/composite-lighting-poles/

[16] Siringoringo, D. M., Fujino, Y., Nagasaki, A., & Matsubara, T. (2020). Seismic performance evaluation of existing light poles on elevated highway bridges. Structure and Infrastructure Engineering, 17(5), 649–663. https://doi.org/10.1080/15732479.2020.1760894

[17] Li, S., Hu, Y., Lu, Z., Song, B., Guozhong Huang: Seismic Isolation of Fragile Pole-Type Structures by Rocking with Base Restraints, Buildings 2024, 14, 1176, doi: https://doi.org/10.3390/buildings14041176

[18] Baghmisheh, A.G., Mahsuli, M.: Seismic Performance and Fragility Analysis of Power Distribution Concrete Poles. Soil Dynamics and Earthquake Engineering, 2021, 150, 106909., doi: https://doi.org/10.1016/j.soildyn.2021.106909

[19] Ibrahim, A.M., A.E. Damatty, A.A., El Ansary, A.M.: Finite Element Modelling of Pre-Stressed Concrete Poles under Downbursts and Tornadoes, Engineering Structures, 2017, 153, 370–382., doi:10.1016/j.engstruct.2017.10.047

[20] Stephens, M., Xu, Z., Whittaker, C., Wotherspoon, L.: Vulnerability of Power Distribution Utility Poles to Tsunami Bore Impacts. J. Coast. Hydraul. Struct. 2023, 3, doi: https://doi.org/10.48438/jchs.2023.0022

[21] Ju, Y., Zhao, J., Wang, D., Song, Y.: Experimental Study on Flexural Behaviour of Reinforced Reactive Powder Concrete Pole, Construction and Building Materials, 2021, 312, 125399., doi: https://doi.org/10.1016/j.conbuildmat.2021.125399

[22] Sasaki, T., Nozawa, S., Tsukishima, D., Kaneko, A.: Earthquake Damage to Concrete Utility Poles for Shinkansen and Remedial Measure, Concrete Journal, 2015, 53, 622–628., doi:10.3151/coj.53.622

Copyright © 2025 CroCEE

ADVERTISEMENTS



Hrvatska komora
inženjera građevinarstva

HRVATSKA KOMORA INŽENJERA GRAĐEVINARSTVA

Ulica grada Vukovara 271, 10000 Zagreb

Tel.: 01 / 5508 - 447 | E-mail: hkig@hkig.hr | www.hkig.hr

Hrvatska komora
inženjera građevinarstva

Hrvatska komora inženjera građevinarstva osnovana je na temelju Zakona o arhitektonskim i inženjerskim poslovima i djelatnostima u prostornom uređenju i gradnji, kao pravna sljednica Hrvatske komore arhitekata i inženjera u graditeljstvu. HKIG je započela s radom 22. svibnja 2009. godine.

Ustrojstvo, nadležnost i rad Komore uređeni su Zakonom o komori arhitekata i komorama inženjera u graditeljstvu i prostornom uređenju.

Komora je samostalna strukovna organizacija koja čuva ugled, čast i prava ovlaštenih inženjera građevinarstva, promiče, zastupa i usklađuje njihove zajedničke interese pred državnim i drugim tijelima u zemlji i inozemstvu te skrbi da ovlašteni inženjeri građevinarstva savjesno i u skladu sa zakonom i javnim interesom obavljaju svoje poslove i pritom štite i unaprjeđuju hrvatsku graditeljsku baštinu. Osim što promiče i zastupa zajedničke interese svojih članova, stvarajući preduvjete za njihov kvalitetan rad, štititi javni interes i interese ostalih sudionika procesa građenja s ciljem stalnog dizanja kvalitete izgrađenog okoliša.

Komora zastupa i promiče interese struke i na međunarodnom planu, te promiče suradnju i razmjenu iskustava članova Komore.

U Komoru se obvezno učlanjuju ovlašteni inženjeri građevinarstva koji obavljaju stručne poslove projektiranja i stručnog nadzora građenja, a dobrovoljno inženjeri gradilišta i voditelji radova.

Članovi ostvaruju svoje interese i upravljaju Komorom putem svojih izabranih predstavnika u tijelima i radnim tijelima Komore i drugim ustrojstvenim oblicima.

Država je na Hrvatsku komoru inženjera građevinarstva prenijela niz javnih ovlasti.

SPEGRA

SPECIJALNI GRAĐEVINSKI RADOVI
SPLIT, CROATIA

PARTNER OF MODERN RENOVATION
35
YEARS

SPEGRA d.o.o. osnovana je 1989. godine u Splitu, a u svojoj **36-godišnjoj tradiciji** usko se specijalizirala isključivo za izvođenje **spe**cijalnih **gra**đevinskih **r**adova, počevši od izvođenja sanacijskih radova zaštite kulturne baštine do vrlo složenih inženjerskih sanacija. Tvrtka je nastala spontano i igrom slučaja, kao što često svaka velika priča o uspjehu nastane, a pogotovo u svijetu poduzetništva. SPEGRA je osnovana iz praktične potrebe, kada je direktor Berislav Borovina, na samom početku uspješne karijere, pri radu na jednom projektu, uvidio da ne postoji tvrtka koja bi mogla izvesti potrebne radove na sanaciji. Odlučio je odgovoriti na potrebe građevinskog tržišta i osnovati upravo tvrtku kakvu je tražio.

Od nabavke prvog stroja, Hamelmannove visokotlačne pumpe i od svega par zaposlenika, tvrtka je u tri desetljeća narasla do oko **300 zaposlenika** te postala sinonim za radove sanacije građevinskih objekata te nacionalni, ali i internacionalni lider u izvođenju ove vrste radova s najmodernijom opremom i strojevima kakve koriste najbolje svjetske tvrtke iz branše.

Od samog početka, što zbog težnje ka izvrsnosti, a što zbog specifične djelatnosti, SPEGRA d.o.o. prati suvremene, globalne građevinske trendove i materijale. Početkom 90-ih, u vrijeme kada se i na svjetskoj razini počelo ozbiljnije pristupati sanaciji objekata, posebno onih starih s kulturnom i povijesnom vrijednošću, tada je i SPEGRA s jednakom ambicijom krenula u taj posao u Hrvatskoj i do danas postala **mjerilo za kvalitetu i inovaciju**. Upravo su ta dva kriterija ono što krasi svaki projekt izveden od Spegre i zbog čega je SPEGRA angažirana na izvođenju mnogih, velikih i značajnih projekata sanacije.

Izvođenje sanacijskih radova spada u najzahtjevnije i najizazovnije radove na polju građevinarstva. Zahtijeva prvenstveno znanje i izvrsne ljudske kapacitete, a tvrtka SPEGRA tijekom godina postala je upravo baza ovih specifičnih znanja koje je nastalo iz konstantnog učenja i iz ogromnog iskustva uspješno odrađenih projekata.

Svoje projekte SPEGRA je radila uspješno surađujući sa brojnim stručnim autoritetima, od visokoobrazovnih institucija (Fakulteta građevinarstva i arhitekture), konzervatorskih odjela, Ministarstva kulture..., a praktična i teoretska znanja je razmijenjivala i s europskim stručnjacima što dokazuje da razina stručnosti SPEGRA-inih djelatnika ne zaostaje za najboljim stranim stručnjacima. Nerijetko, SPEGRA-ini inženjeri drže predavanja na stručnim skupovima i konferencijama za kolege iz struke.

Za svoj rad SPEGRA je nagrađivana desetke puta, a posljednje, ujedno i najvrjednije postignuće je **nagrada Europske komisije - Europa Nostra**, najprestižnije europsko priznanje u području baštine koje je u kategoriji konzervacije dodijeljeno Hvarskom Arsenalu, a zahtjevan projekt obnove i ojačanja nosive konstrukcije izvela je upravo SPEGRA. Ovo priznanje svrstalo je SPEGRA-u uz bok najboljim europskim tvrtkama koje se bave obnovom spomeničke baštine.

Osim Hvarskog Arsenala, u SPEGRA-inom potrfelju posebno se ističu projekti sanacije na objektima kao što je **Knežev dvor i brojne palače i crkve u Dubrovniku**, Krstionica Sv. Ivana (Jupiterov hram) u Splitu, Biskupova palača u Stonu, dvorac Veliki Tabor... SPEGRA je radila i obnovu Starog mosta u Mostaru, obnovu mostova od Ploča i Pila u Dubrovniku, ali i Krčkog i Paškog mosta.

SPEGRA je u svojoj 31-godišnjoj tradiciji radila i brojne sanacije na hidroelektranama, kao što su HE “Peruča”, HE “Zakučac”, HE “Prančevići”, HE “Orlovac”, HE “Gojak”, a obnavljala je i brojne građevine oštećene u Domovinskom ratu.

Najrecentniji SPEGRA-in projekt je obnova Zagrebačke katedrale koja je značajno oštećena potresima. **Zagrebačka katedrala** predstavlja najveću hrvatsku sakralnu građevinu i jedan od najvrjednijih spomenika hrvatske kulturne baštine.

Mnogi SPEGRA-ini projekti tako ostaju trajan biljeg u prostoru, nadograđujući i uljepšavajući vizure.

Mnoge mlade tvrtke u Hrvatskoj danas su konkurentne na svjetskoj razini i među najboljima su u svojim industrijama, počevši od IT-a, automobilske industrije, farmacije... Spegra je jedan od prvih hrvatskih primjera kako se uz volju, ambiciju i inovativnost i u Hrvatskoj može napraviti svjetska tvrtka, lider u znanju i izvrsnosti.



Arsenal
Hvar ▶



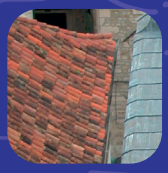












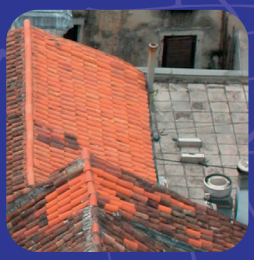
Jupiterov hram
Split ◀





Zagrebačka katedrala
Zagreb ◀













Ninski most
Nin ▶











Knežev Dvor
Dubrovnik ◀

PARTNER OF
MODERN RENOVATION

FT FINANCIAL TIMES
statista
EUROPE'S LONG-TERM GROWTH CHAMPIONS 2025

ZLATNA BILANCA
ZA GRAĐEVINARSTVO

RADNIK
UTEMELJENO 1948.

GRADITE S POVJERENJEM

Preko 75 godina iskustva u graditeljstvu i svim oblicima niskogradnje, visokogradnje i hidrogradnje.







RADNIK GRUPA

HIDRO ING
VODOGRADNJA
HIDRO REGULACIJA
ADRION
RISTRA ĐURĐEVAC
RADNIK-PLIN
vodoprivreda-zagorje d.o.o.

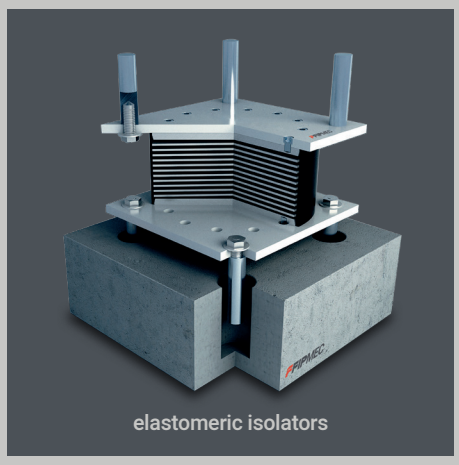
radnik.hr

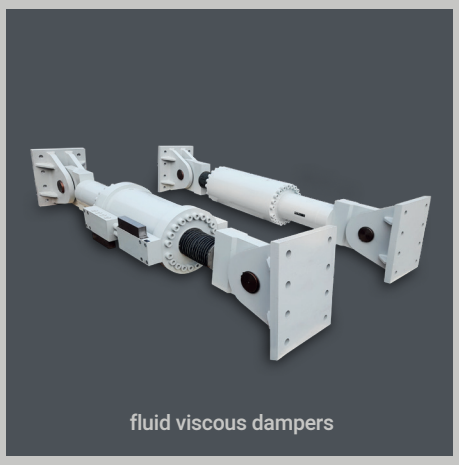
FIPMEC

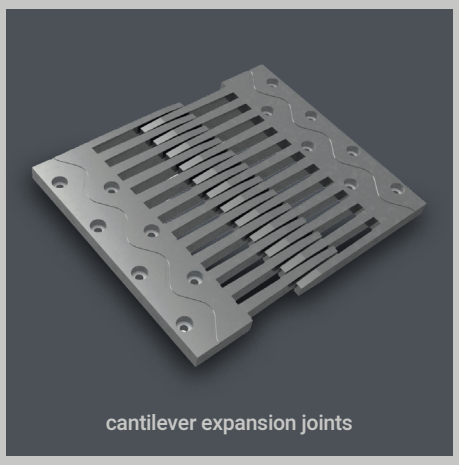
A MARKET LEADER IN INFRASTRUCTURE PROJECTS SINCE 1945

Italian experience and quality in structural devices and anti-seismic devices

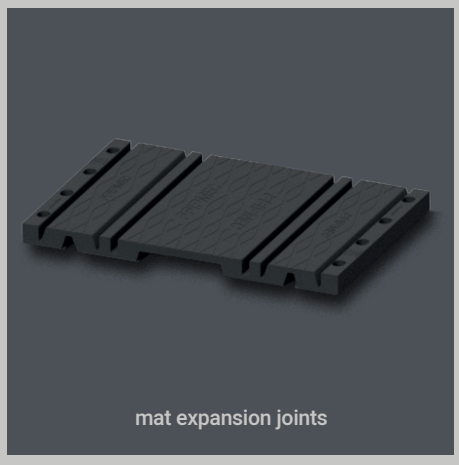
- Anti-seismic devices
- Structural bearings
- Fittings for tunnels
- Expansion joints
- Services, components and special projects


elastomeric isolators


fluid viscous dampers


cantilever expansion joints


pot bearings


mat expansion joints


pendulum isolators

www.fipmec.it



shock transmission units


spherical bearings

BUILDING A **PRESENT** DESIGNED TO HAVE A **FUTURE**



Passion, team spirit and a constant eye on the future. Mapei contributes at a global level to the most important architectural and infrastructure works, residential projects and restoration work on historic buildings. Each and every day, in the name of innovation, we are committed to an increasingly sustainable building industry.

EVERYTHING'S **OK**
WITH **MAPEI**

Learn more on **mapei.com**

MAPEI

ABOUT REGUPOL

Welcome to REGUPOL - tradition and innovation since 1954

REGUPOL is a leading family-owned company specialised in the production of high-quality elastomers since 1954. Originally known for upholstery in seating furniture and elastic floor coverings for sports applications, our company has continued to develop and today, with its **REGUPOL Acoustics** division, has been an expert in the field of vibration and noise protection for more than 30 years.

Our expertise

At **REGUPOL**, we understand the complexity of vibrations and noise. Our elastomers are used worldwide in a broad range of applications, including impact sound insulation, vibration isolation for railway and marine applications, machine isolation and vibration protection for buildings. Our experienced team works closely with customers and engineers to develop solutions that meet their specific requirements.

Our values

As a family-run company in its fourth generation, we are proud to continue the values of our founders: Quality, partnership and sustainability. We are actively committed to a sustainable economy by using recycled elastomers and implementing environmentally friendly manufacturing processes. With a recycling rate of over 85 % and processing more than 90,000 tons of recycled elastomers per year, we make a significant contribution to the circular economy.

REGUPOL Germany GmbH & Co. KG
Head Office: Bad Berleburg
Siegen District Court, HRA 9854
VAT ID no.: DE 360 723 882

Deutsche Bank
IBAN DE82 4607 0090 0362 0259 00
BIC DEUTDEDK460

General Partner:
REGUPOL Germany Verwaltungs GmbH
Head Office: Bad Berleburg
Siegen District Court, HRB 13420

phone +49 2751 803-0
info@regupol.de
www.regupol.com

Managing directors:
Jost Sebastian Pöppel, Sven Christian Pöppel, Niels Pöppel

FREYSSINET

Pioneer in the development of earthquake protection devices, Freyssinet offers a complete range of dedicated products and associated services marketed under the **well-known ISOSISM® brand.**

Wide Range of Solutions



visit our website : www.freyssinet.com

TROMONT

30 YEARS OF ENGINEERING EXCELLENCE

- Civil engineering
- Mechanical engineering
- Electrical engineering
- Production






Visit Our Website
www.tromont.hr

- 230+ COMPLETED CONSTRUCTION PROJECTS
- 300 EMPLOYEES - 60 ENGINEERS
- 2120+ MANUFACTURED PRODUCTS
- 12 YEARS RAIL INDUSTRY EXPORTER

ZIDNI SISTEMI

Porotherm
wienerberger



GZ

GROUND ZERO



Brilliantly simple and versatile system

VST heavy-duty shoring towers for bridges and supporting structures during renovation
(load-bearing capacity up to 720 kN per leg)

The high load-bearing capacity and the structural optimization help to reduce the quantity of required on-site material.
Rentable system solutions fulfil the most varying project requirements.
Fast and simple assembly with fitted bolt connections.

PERI

Formwork
Scaffolding
Engineering

www.peri.com

Lavčević

Graditeljska tvrtka LAVČEVIĆ d.d. osnovana je u Splitu 1948. godine. Od svojih početaka do danas, lista izgrađenih objekata rasla je velikom brzinom i od ove tvrtke stvorila jednog od najvećih graditelja u zemlji. Iako utemeljena i specijalizirana za potrebe visokogradnje, izvodila je i druge vrste objekata (objekte u niskogradnji, kao i pomorske objekte)

Kao renomirana građevinska tvrtka s više od 75 godina i sa našim profesionalnim i stručnim timom, mi čvrsto vjerujemo kako možemo pružiti izvanrednu podršku i dati doprinos u svim fazama procesa izgradnje.

Stoga, navodimo nekoliko ključnih razloga zašto smo prvoklasan i pouzdan partner za izgradnju Vašeg projekta:

1. **Iskustvo-** stekli smo ogromno iskustvo kroz izgradnju vrlo velikog broja raznovrsnih objekata, od stambenih zgrada, hotelskih kompleksa, komercijalnih, industrijskih i infrastrukturnih objekata u Hrvatskoj i u inozemstvu (u monolitnoj i u montažnoj izvedbi). Stekli smo značajno znanje i vještine.
2. **Stručni tim-** imamo tim stručnjaka s različitim specijalizacijama koji su spremni pružiti sveobuhvatnu podršku u svim aspektima realizacije projekta - od projektiranja do gradnje. Ukupno u sustavu Lavčević radi nešto više od 220 zaposlenika od kojih je preko 50 inženjera graditeljstva.
3. **Logistika** – posjedujemo vlastitu proizvodnju i transport svježeg betona, kamenog agregata i montažnih betonskih elemenata na području Južne Hrvatske.
4. **Kvaliteta i poštivanje rokova -** U našem radu posebnu pažnju posvećujemo kvaliteti naših usluga i poštivanju rokova kako bismo osigurali zadovoljstvo naših klijenata.
5. **Integritet** –uspostavljamo najviše etičke i poslovne standarde u našem poslovanju a iste standarde ponašanja prenosimo i na naše podizvođače i dobavljače

55TH ANNIVERSARY

KINEMETRICS

Advancement through Innovation

INNOVATE.
CREATE.
SUSTAIN.
TRUST.



Toding d.o.o.



Projektiranje



Nadzor



Kontrola mehaničke otpornosti i stabilnosti



www.toding.hr





toding@toding.hr

STUDIO ARHING

U.O.I.G.

Tarnik



VIŠE OD 75 GODINA
OSIGURAVAMO STRUČNU
POTPORU GRAĐEVINARSTVU

Building a stable and better future together.

Structural design / Building physics / Architecture
Technical supervision / Project management



stabilnost | info@stabilnost.eu
+385 91 677 0877

Proceedings of the
3rd Croatian Conference on Earthquake Engineering
3CroCEE
19-22 March 2025, Split, Croatia

Engineering Seismology

Geotechnical Earthquake Engineering

Experimental Techniques
for Characterization of Materials and Structures

Historical Structures

Seismic Performance of Structures

Repair and Strengthening of Structures

Post-Earthquake Reconstruction Process

Lessons Learnt from Earthquake Disasters

Preparedness and Emergency Management

Seismic Loss and Risk Analysis

PhD Special Session

ISSN 3043-8071
https://doi.org/10.5592/CO/3CroCEE.2025

